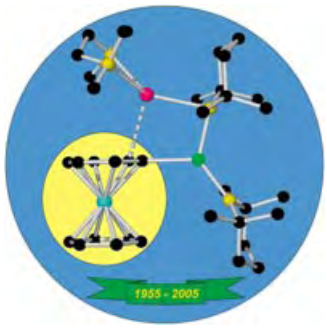
Cover Picture

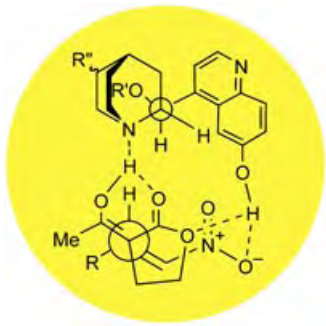


Lei Wang and Peter G. Schultz*

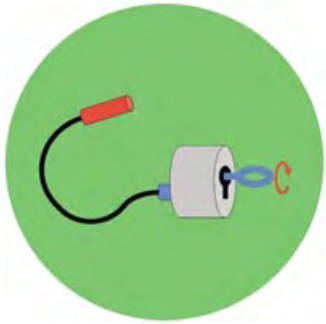
Unnatural amino acids can be incorporated as new building blocks into the genetic codes of both prokaryotic and eukaryotic organisms to facilitate studies of protein structure and function. Over 30 unnatural amino acids with modified side chains have been genetically encoded in response to unique triplet and quadruplet codons. L. Wang and P. G. Schultz describe in their Review on page 34 ff. chemical and biochemical approaches that have been developed to manipulate protein structure and add new amino acids to the genetic code.



Metallocenes
R. E. Mulvey and co-workers report the selective deprotonation of one benzene ring of bis(benzene)chromium by amide bases with Na^{+}/Mg^{2+} or K^{+}/Mg^{2+} as counter ions in their Communication on page 68 ff. No reaction takes place with the monometallic amides.



Asymmetric Catalysis
In their Communication on page 105 ff., L. Deng and co-workers describe the use of chiral organocatalysts for the diastereoselective and enantioselective formation of adjacent tertiary and quaternary stereocenters in Michael additions to nitroalkenes.



Molecular Functional Units
A molecular machine that is based on the redox-coupled exchange of guest molecules in cucurbit[8]uril complexes and functions in a similar way to a chain lock is presented by K. Kim and co-workers in their Communication on page 87 ff.

Open Access and *Angewandte Chemie*

The German Chemical Society (Gesellschaft Deutscher Chemiker, GDCh), the owner of *Angewandte Chemie*, has recently discussed open access and issued an official statement,[1] a summary of which is featured in the box on the right. But what is open access? "Open access to scientific information means the free, unrestricted, and immediate access to data and results of publicly supported scientific work." This definition was given by Robert Schlögl in issue 11/2004 of the German Chemical Society's membership magazine in his plea for open access ("Partnership instead of Monopoly").[2] A counterargument was presented in the same issue by Peter Gregory under the title "All Things to All Men".[3] Elsewhere, the motivation behind the open access movement was recently summarized as follows: "The aim of the open access initiative is to build up a comprehensive, open, and sustainable network of scientific information that supports the self-organization of scientists and the reflection of scientific knowledge in scientific discourse and that allows fair and equal conditions for competition between value-added-service providers."[4] So, free access, is it? Who would oppose such a suggestion, at least as a reflex reaction? However, one suddenly feels that one is perhaps being misled: Partnerships, free access, networking, self-organization, discourse, value-added services, and, of course, sustainability—these words from the vocabulary of the well-meaning conceal much and reveal little. Isn't free access to food, medication, and public transport an even more justifiable goal?

What are the motives behind the open access movement in which a wide spectrum of opinions are represented? The positions portrayed above[2,4] are, however, representative, and I have taken them as a starting point for my discussion as they were presented prominently in the widely read magazines of the German Chemical Society[2] and the German Physical Society.[4] It is often claimed by open access protagonists that renowned big publishers make "fat profits" from their "monopolies".[2,4] Justifiably, many scientists and librarians feel frustrated with the high prices of some, but by no means all, journals, which sometimes are even of a poor quality. However, these journals are—for understandable reasons—provided with articles by scientists (even though there may be more affordable and higher-quality options); they have respectable scientists as editors and advisors, and there are obviously enough customers/libraries who are prepared to pay the price and so contribute to the "fat profits of the big publishers". Is such indignation not hypocritical when one lives in a profit-driven society? What happens when profits are not made can be read about daily in the newspapers! And finally: The cost of all scientific publications has increased in the last two decades (only) in direct proportion to the number of published articles,[5] that is, the increase in the price of journals is only disproportionate when compared with the general cost of living, but that is comparing apples with pears.

The cost of all scientific publications has increased in the last two decades in direct proportion to the number of published articles

"Journals based on the open access model should lead to a higher quality of science and promote scientific discourse"[4] is another argument in favor of open access. One is tempted to ask: Aren't there enough forums for scientific discourse or do the current journals

Summary of a Statement by the GDCh on Open Access

Open access is an interesting and important topic in the discussions on the future of scientific publishing. However, at this point in time there are still risks, open questions, and challenges associated with this model. Further experience must be gained in open access, or indeed any other new models, before a balanced opinion can be made regarding the advantages of these approaches over the traditional processes.

The Gesellschaft Deutscher Chemiker (German Chemical Society, GDCh) will monitor future developments closely and will be open to results from discussions on this issue. The GDCh will participate actively and constructively in such discussions to ensure that any transitions in scientific publishing are carried out fairly so that the needs of all those involved are met and that business models are adopted to reflect the new electronic publishing tools.

Regardless of the open access debate, the GDCh appeals to all its members to avoid submission of their scientific papers to overpriced journals. In particular, members are encouraged to submit their manuscripts to journals that are owned or partly owned by the GDCh and whose price structures have been endorsed by the GDCh.

Of utmost importance to the GDCh and its members is that there be no loss in quality regardless of the publication concept adopted. The scientist must be confident about where he/she can find relevant information. In accordance with its statutes, the GDCh will always strive to maintain these principles.

© 2005 Wiley-VCH Verlag GmbH & Co. KGaA, Weinheim
DOI: 10.1002/anie.200462726

somehow prevent this discourse? Is there insufficient information, or are we actually drowning in it? When the secondary literature or a reference leads one to an article that one wants to read, is it really that difficult to obtain, even when the local library does not have it? Please have your own answers to these questions. Regarding the quality of science, the work is usually complete by the time it is published. Nevertheless, the publication process does, indeed, have a lot to do with the quality, and open access is a threat to the high quality journals (see below).

Open access is a threat to the high quality journals

Regarding the costs involved in open access, R. Schlögl and T. Velden have recently emphasized in the magazine of the Max Planck Society: "However, contrary to popular belief, comprehensive free access to research results is not cheaper than the current system of paper journals".[6] Paper journals sounds defamatorily old-fashioned but the current system has for a number of years now clearly not been one of paper journals—all important journals are electronically available, linked to each other, and provide the opportunity to present additional Supporting Information (raw data, movies, etc.); all this is a result of heavy investments from the slandered publishers of paper journals.

It is too bad that in an open access model with the same costs, users of scientific literature who themselves produce little or no publications, for example, scientists in industry, will not contribute to the expenses. In the open access model the authors should pay for each published article, and amounts between €500 and €10000 per article were mentioned. The authors should obtain the money from sponsoring agencies and institutions, whose coffers would, however, not be getting any fuller through open access. Alternatively, scientists should draw from the library budget, which, after all, would no longer require as much money—but just try asking your librarian! It is clear that the open access model would result in more "information management", "cash-flow control", and blatantly "more bureaucracy".

Open access will lead to more bureaucracy

It is said that the quality of scientific publications should be promoted by open access, through discourse, networking, etc. These are fine "soft words" but, if one wants to produce high-quality scientific journals, money is required more than ever in times of electronic publishing: for hard- and software, as well as for supersoftware, humans, and the words of the Nobel Prize winner in chemistry, Lord Todd, also hold in this case: "Hard work is the minimum requirement—creativity, intelligence, and motivation are also needed". If journal editors are to be paid directly by the authors for each accepted manuscript, then the "economization of the individual article" will be the order of the day. And it is naïve to believe that the fact that editors are paid a determined amount of money by the author for each accepted article will not have an influence on the decision. It is well known that the very good journals invest a much greater amount of editorial effort than the less-good and even bad journals (and they do exist[7]). As authors only have to pay for accepted articles—it is, indeed, difficult to imagine that anyone could be made to pay for a rejection—access to top journals would only be possible for those who are extremely well-funded. Alternatively there will be a leveling of journals: all journals, all articles, all scientists would be equally good. So much regarding the quality of scientific journals in the age of open access.

To maintain and further improve the quality of *Angewandte Chemie*, a dozen and a half chemists and half a dozen colleagues from different backgrounds work together. They are supported by an Editorial Board and an International Advisory Board, both of the highest caliber, as well as by numerous scientists from around the world. Even though access to *Angewandte Chemie* is not free, the number of monthly full-text downloads is phenomenal—far ahead of

Table 1: Country of origin of Communications submitted from 2001–2004 (percentages in brackets). Manuscripts with authors from several countries are assigned to the country of the submitting author.

Country	2001	2002	2003	2004[a]
USA	401 (19)	448 (19)	506 (18)	608 (18)
China (P.R.)	213 (11)	356 (15)	477 (17)	550 (16)
Germany	359 (17)	349 (14)	383 (14)	468 (14)
Japan	296 (14)	366 (15)	429 (15)	466 (14)
Great Britain	112 (5)	127 (5)	171 (6)	183 (5)
France	105 (5)	98 (4)	110 (4)	134 (4)
India	68 (3)	75 (3)	89 (3)	111 (3)
South Korea	71 (3)	82 (4)	83 (3)	105 (3)
Spain	74 (3)	86 (4)	87 (3)	102 (3)
Italy	65 (3)	65 (3)	50 (2)	99 (3)
Switzerland	55 (3)	55 (2)	61 (2)	97 (3)
Canada	52 (2)	51 (2)	52 (2)	63 (2)
Netherlands	32 (2)	32 (1)	50 (2)	52 (2)
Singapore	14 (1)	14 (1)	14 (1)	42 (1)
Israel	27 (1)	27 (1)	28 (1)	37 (1)
Taiwan (R.C.)	27 (1)	36 (1)	31 (1)	34 (1)
Sweden	13 (1)	14 (1)	16 (1)	24 (0.7)
Russia	9 (0.5)	11 (1)	12 (0.4)	16 (0.4)
Poland	11 (1)	16 (1)	9 (0.3)	10 (0.3)
Others	105 (5)	111 (5)	123 (4)	149 (4)
Total	2109	2419 (+14.7%)	2781 (+15%)	3350 (+20.5%)

[a] Projected figures for 2004 based on available data for 10 months.

DOI: 10.1002/anie.200462726
© 2005 Wiley-VCH Verlag GmbH & Co. KGaA, Weinheim

the "second-best" of the over 400 journals in Wiley InterScience. The most important prerequisite to produce a top journal is the receipt of many good manuscripts. *Angewandte Chemie* received more than ever in 2004 (see Table 1 as well as Figures 1 and 2): Approximately 20% more Communications were submitted, 16% more were published (1072 versus 923), and the rejection rate increased from 64% to 65% (during the first six months). Increasingly more chemists outside organic and inorganic chemistry, the fields the journal traditionally focused on, are publishing in *Angewandte Chemie*. The journal is therefore continuously fulfilling the mission to serve chemistry in its entire breadth. Of course, (Mini)Reviews, Highlights, and Essays also contribute to the quality of the journal, and it is especially gratifying that the Essays, a section started in the millennium year 2000, often draw spontaneous praise from our readers. They do not, however, draw a lot of citations. Nevertheless the Impact Factor rose from 7.671 to 8.427 (see Figure 3). Furthermore, it is most pleasing to see how rapidly publications in *Angewandte Chemie* are noticed and bear fruit in the work of others. This is reflected in the extremely high Immediacy Index of 1.655 (see Figure 4). This value implies that each manuscript published in *Angewandte Chemie* in 2003 was on average cited in the same year 1.66 times (papers in the last two or three months of a year have literally no chance of being cited in the same year). Obviously, speed matters: From now on, *all* articles will be published electronically as soon as possible in the Early View mode on Wiley InterScience prior to their appearance in print, usually several weeks later. In 2005, the Editorial team will continue their efforts to fill each issue with the highest quality articles from all fields of chemistry in a most reader-friendly package. The best never rest.



Peter Gölitz

P.S.: Two strong trends of the last few years continue: 1) The productivity of Chinese scientists is rapidly increasing as is the quality of their papers. It is therefore to be expected that more manuscripts from Chinese authors can be seen in the pages of *Angewandte Chemie*. And it is equally important that the *Chinese Journal of Chemistry* will be copublished from 2005 onwards by the Shanghai Institute of Organic Chemistry

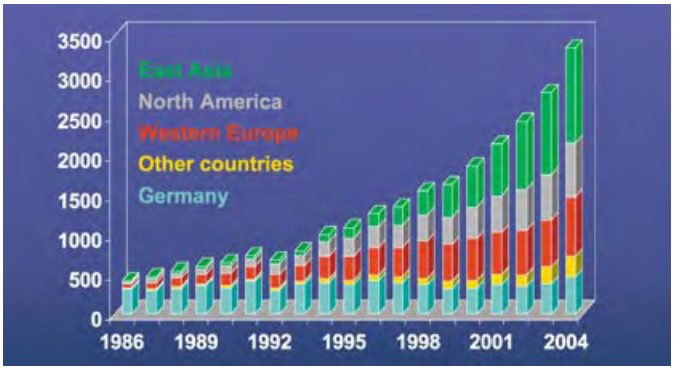


Figure 1. Regional origins of Communications submitted between 1986 and 2004.

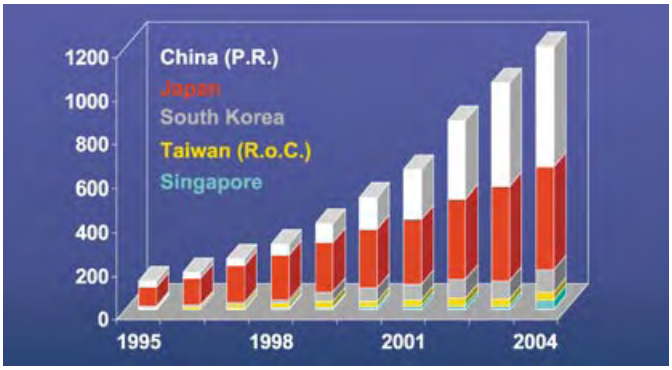


Figure 2. Origins of Communications submitted from East Asia from 1995 to 2004.

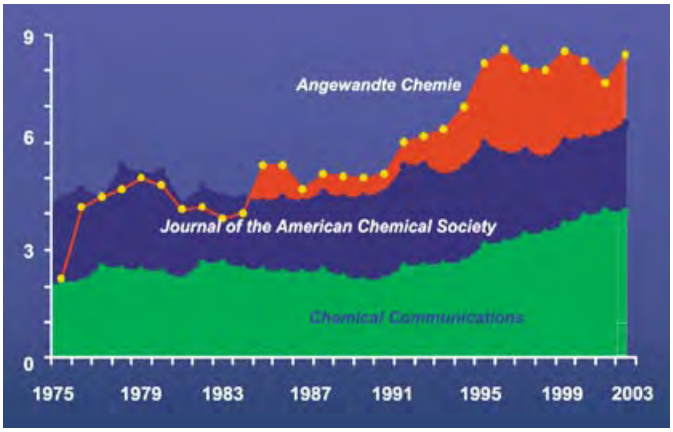


Figure 3. Comparison of the Development of the Impact Factor of *Angewandte Chemie* from 1975 to 2003.

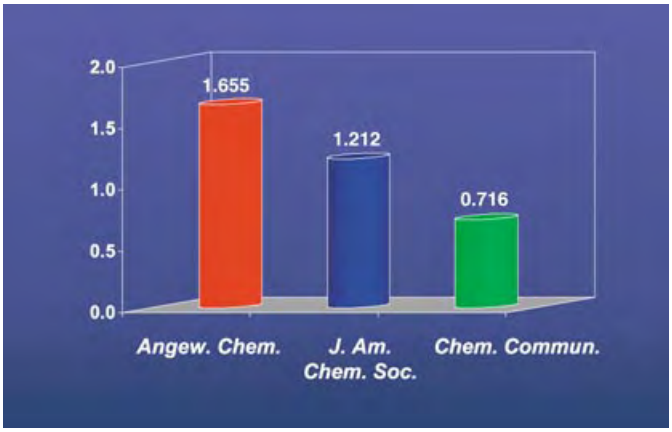


Figure 4. Comparison of the Immediacy Index of *Angewandte Chemie* in 2003.

© 2005 Wiley-VCH Verlag GmbH & Co. KGaA, Weinheim

and Wiley-VCH (see http://www.interscience.wiley.com/journal/cjc) and will be available online in Wiley InterScience. 2) The scientific exploration of nature on the nano- and micrometer scale continues to fascinate biologists, chemists, physicists, engineers, and medical doctors—and their publications now have a new home: The first issue of *Small* is available and was sent to all *Angewandte Chemie* subscribers for information. Please be sure to have a look in case you are interested in "micro & nano" (www.small-journal.com).

PPS: A propos open access: *Chemistry, A European Journal* will be celebrating its 10th anniversary with a one-day symposium in Strasbourg on April 15, 2005 (see box below). The entrance is free, and the "authors" (presenters) also do not have to pay!



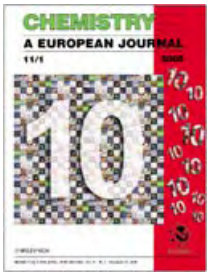
Figure 5. The *Chinese Journal of Chemistry* will be marketed and distributed by Wiley-VCH from 2005 onwards, and the journal will then also be available on Wiley InterScience.



Figure 6. *Small*, the new Wiley-VCH journal for research on the micro- and nanometer scale.

[1] See: www.gdch.de/oearbeit/pospap.htm.
[2] R. Schlögl, *Nachr. Chem.* **2004**, *52*, 1144 (article in German).
[3] P. Gregory, *Nachr. Chem.* **2004**, *52*, 1145 (article in English).
[4] T. Velden, *Physik-Journal*, **2004**, *3*, no. 11, p. 3 (article in German).
[5] L. R. Garson, *Acc. Chem. Res.* **2004**, *37*, 141 – 148. This highly informative article, "Communicating Original Research in Chemistry and Related Sciences", also deals with economic aspects of scientific publishing. The author has 30 years' experience in the "Publications Division" of the American Chemical Society.
[6] R. Schlögl, T. Velden, *MaxPlanckForschung* **2004**, no. 2, p. 15.
[7] See the Correspondence feature: "The Real Dirty Secret of Academic Publishing": V. Svetlov, *Nature*, **2004**, *431*, 897.

Chemistry—A European Journal



To mark the 10th Anniversary of *Chemistry—A European Journal*, a one-day symposium will be held on Friday April 15, 2005, entitled "Chemistry—A European Conference: Stimulating Concepts in Chemistry".

Keynote Speakers:
José Barluenga (Oviedo, Spain), Steve Ley (Cambridge, UK), Frans De Schryver (Leuven, Belgium), Günter Schmid (Essen, Germany), Fraser Stoddart (UCLA, USA), George Whitesides (Harvard, USA)

Location:
Institut de Science et d'Ingénierie Supramoléculaires (ISIS), Université Louis Pasteur, 8, allée Gaspard Monge, 67083 Strasbourg Cedex, www-isis.u-strasbg.fr.

Free Registration:
Registration for the conference is free of charge and can be done preferably directly online through the German Chemical Society (GDCh) at http://10th-anniversary.chemeurj.org.

Organization:
The Symposium has been co-organized by the 14 European Chemical Societies (EU ChemSoc) that jointly own *Chemistry—A European Journal*, and Wiley-VCH. Further details regarding the Program, Registration, and Accommodation are available on the *Chemistry* homepage: http://10th-anniversary.chemeurj.org.

 © 2005 Wiley-VCH Verlag GmbH & Co. KGaA, Weinheim

Contents

VIP *The following Communications have been judged by at least two referees to be "very important papers" and will be published online at www.angewandte.org soon:*

D. Enders, C. Grondal:*
Direct Organocatalytic de novo Synthesis of Carbohydrates

T. Fink, H. Bruggesser, J.-L. Reymond:*
Virtual Exploration of the Small-Molecule Chemical Universe Below 160 Daltons

S. Kobayashi, K. Arai, H. Shimizu, Y. Ihori, H. Ishitani, Y. Yamashita:*
A Bimetallic Chiral Niobium Complex for Lewis Acid Catalyzed Enantioselective Reactions: Design of a Tridentate Ligand and Elucidation of the Catalyst Structure

H. Braunschweig, K. Radacki, D. Rais, G. R. Whittell:*
The First Boryl Bridged Complex: An Unprecedented Coordination Mode of the BR_2 Ligand

C. Whitehouse, J. Fang, A. Aggeli, M. Bell, R. Brydson, C. W. G. Fishwick, J. Henderson, C. M. Knobler, R. W. Owens, N. H. Thomson, D. A. Smith, N. Boden**
Adsorption and Self-Assembly of Peptides on Mica Substrates

*You Seok Seo, C. Lee, K. H. Lee, K. B. Yoon**
1:1 and 2:1 Charge-Transfer Interactions between Aromatic Hydrocarbons and Dry Titanium Dioxide

News

F. Arnold Receives ACS Medal ____ **22**

B. Meunier Becomes President of the CNRS ____ **22**

D. Kurth Accepts Position in Tsukuba **22**

Books

Dithiolene Chemistry — Kenneth D. Karlin, Edward I. Stiefel — *reviewed by G. J. Leigh* ____ ***23***

Synthetic Metal-Containing Polymers — Ian Manners — *reviewed by D. Bergbreiter* ____ ***24***

Highlights

Cycloadditions

B. Niess, H. M. R. Hoffmann* ___ **26–29**

[4+3] Cycloadducts from Lewis Acid Mediated Reactions of Acroleins with Cyclopentadiene



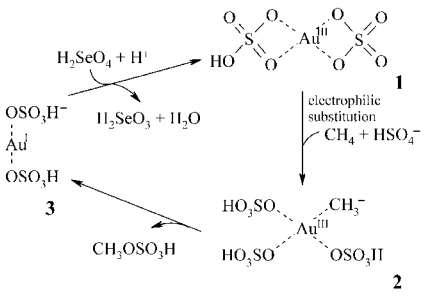
Expect the unexpected: Classic organic chemistry continues to hold surprises. Cyclopentadiene and simple α-alkylated acroleins, in the presence of $AlCl_3$ and Et_2AlCl, furnish unconventional [4+3] cycloadducts (see scheme). The "expected" Diels–Alder adducts are intermediates in the reaction.

Homogeneous Catalysis

D. E. De Vos,* B. F. Sels ____ **30–32**

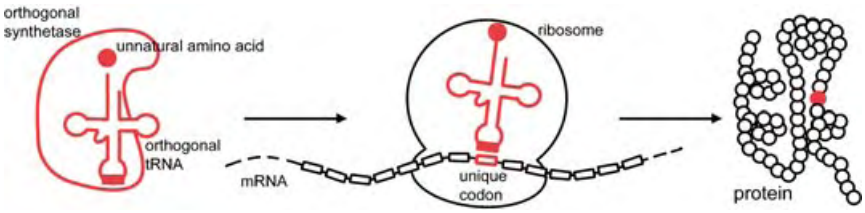
Gold Redox Catalysis for Selective Oxidation of Methane to Methanol

As good as gold: The activation and selective oxygenation of inert C–H bonds, as in methane, is a demanding problem. It is now shown that the combination of gold as a catalyst and H_2SeO_4 as the oxidant results in a 94% selectivity for CH_3OSO_3H at 28% CH_4 conversion (see scheme). These results mean that gold now claims its place alongside the other noble metals as a methane oxidation catalyst.



© 2005 Wiley-VCH Verlag GmbH & Co. KGaA, Weinheim

Reviews



Breaking the code: A large number of novel amino acids have been incorporated into the genetic codes of both prokaryotic and eukaryotic organisms (see schematic representation). These remove the limitations imposed by the existing 20 amino acid codes and should make it possible to generate proteins and perhaps entire organisms with new or enhanced properties.

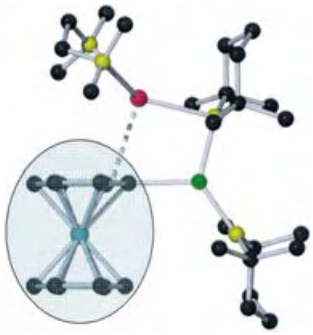
Protein Science

L. Wang, P. G. Schultz* _____ **34 – 66**

Expanding the Genetic Code

Communications

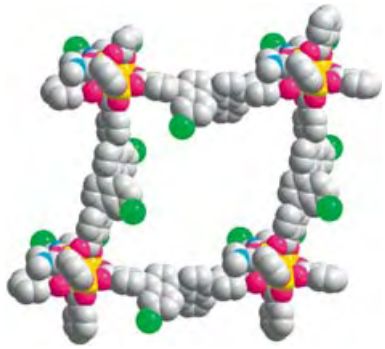
Mixed-metal chemical synergy is strikingly exemplified by the clean, selective deprotonation of one benzene ring of bis(benzene)chromium by bimetallic (Na/Mg or K/Mg) amide base mixtures. The bis(benzene)chromium moiety forms high-yielding crystalline trimetallic products (see picture) with the mixed bases, but it is inert towards the non-synergic, parent monometallic amides. Na/K red; Mg green; Cr light blue; N yellow; C black.



Metalation Reactions

E. Hevia, G. W. Honeyman, A. R. Kennedy, R. E. Mulvey,* D. C. Sherrington **68 – 72**

Synergic Monodeprotonation of Bis(benzene)chromium by Using Mixed Alkali Metal–Magnesium Amide Bases and Structural Characterization of the Heterotrimetallic Products



Packing them in: Based on zinc and aromatic-rich dicarboxylic acids these new coordination networks (see structure; green Cl, red O, yellow Zn, blue N, gray C) have hydrogen uptakes comparable to those of the best carbon nanotubes and metal–organic frameworks. The highly interpenetrating nature of these networks points to a new design strategy for hydrogen-storage materials that employ an entrapment mechanism.

Functional Materials

B. Kesanli, Y. Cui, M. R. Smith, E. W. Bittner, B. C. Bockrath, W. Lin* _____ **72 – 75**

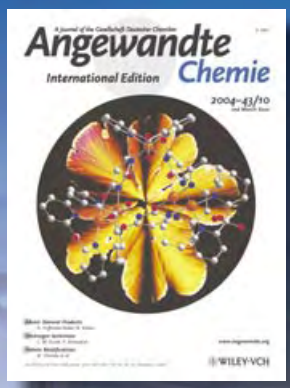
Highly Interpenetrated Metal–Organic Frameworks for Hydrogen Storage

For the USA and Canada:
ANGEWANDTE CHEMIE International Edition (ISSN 1433-7851) is published weekly by Wiley-VCH PO Box 191161, D 69451 Weinheim, Germany. Air freight and mailing in the USA by Publications Expediting Inc. 200 Meacham Ave., Elmont, NY 11003. Periodicals postage paid at Jamaica NY 11431. US POSTMASTER: send address changes to *Angewandte Chemie*, Wiley-VCH, 111 River Street, Hoboken, NJ 07030. Annual subscription price for institutions: US$ 4948.00/4498.00 (valid for print and electronic / print or electronic delivery); for individuals who are personal members of a national chemical society, or whose institution already subscribes, or who are retired or self-employed consultants, print only: US$ 394.00. Postage and handling charges included. All Wiley-VCH prices are exclusive VAT.

 © 2005 Wiley-VCH Verlag GmbH & Co. KGaA, Weinheim

The best in chemistry –

for more than a hundred years



A Journal of the Gesellschaft Deutscher Chemiker

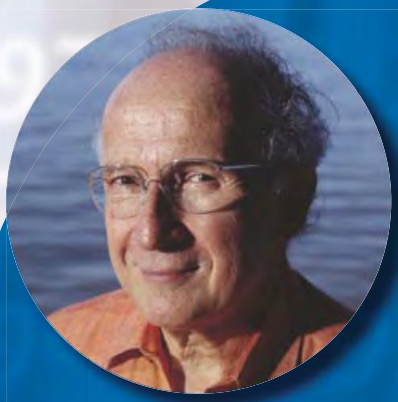
Angewandte International Edition **Chemie**

www.angewandte.org

1888: ***The beginning of a success story***

Constant Innovations

1962: *First issue of the International Edition*
1976: *Graphical abstracts*
1979: *Cover pictures*
1988: *Centenary of Angewandte*
1989: *Routine use of color*
1991: *New section: Highlights*
1992: *Computerized editorial tracking system*
1995: *Internet service for readers*
1998: *Regular press service; full-text online*
2000: *New section: Essays; EarlyView: Communications available online ahead of the printed version*
2001: *New section: Minireviews*
2002: *Online submission of manuscripts*
2003: *Weekly publication; new section: News; new layout*
2004: *Backfiles (1962-1997); ManuscriptXpress: Online system for authors and referees*



Angewandte's advisors...

Roald Hoffmann
Cornell University
(Photo: Lois Anshus)

» *As an applied theoretical chemist, I love it that the best chemical journal in the world has „applied" in its title. It's history, I know. But there is also the implication in this adjective that these sterling accounts of the new, these just-in-time reviews, these incisive essays that* ***Angewandte Chemie*** *contains – that they all are of true utility, and are really used, by the finest chemists of our time.* «

Angewandte Chemie International Edition *is a journal of the German Chemical Society (GDCh)*

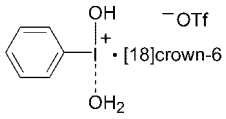
GDCh

WILEY InterScience® DISCOVER SOMETHING GREAT

WILEY-VCH

1195/404_gu

Crown-compound complexation through secondary hypervalent I···O bonding interactions enables stabilization of an aqua(hydroxy)(phenyl)iodonium ion. The resulting aqua complex **1** is stable in the solid state as well as in solution and serves as a versatile oxidizing agent,



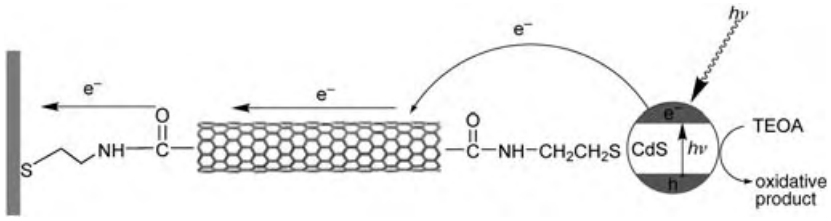
1

especially in water. Tf = trifluoromethanesulfonyl.

Coordination Chemistry

M. Ochiai,* K. Miyamoto, Y. Yokota, T. Suefuji, M. Shiro ——— **75 – 78**

Synthesis, Characterization, and Reaction of Crown Ether Complexes of Aqua(hydroxy)(aryl)iodonium Ions



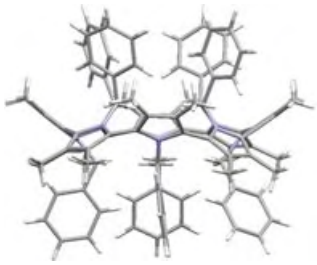
Electric light orchestra! Enhanced photocurrents are generated in an assembly that consists of CdS nanoparticles linked to a gold electrode by carbon nanotubes (see picture, TEOA = triethanolamine). The enhanced photocurrents are attributed to the effective transport of conduction-band electrons through the carbon nanotube to the electrode, a process that competes with electron–hole recombination in the CdS semiconductor nanoparticles.

Nanotechnology

L. Sheeney-Haj-Ichia, B. Basnar, I. Willner* ——— **78 – 83**

Efficient Generation of Photocurrents by Using CdS/Carbon Nanotube Assemblies on Electrodes

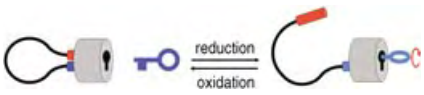
Four up, four down: Reductive alkylation of cyclo[8]pyrrole and its derivatives gives rise to the corresponding reduced per-N-alkylated products, a reaction unknown in the case of porphyrins. These bowl-like molecules are arranged with four substituents up and four substituents down in a well-defined alternating fashion, as observed from their crystal structures (see picture; blue N).



Porphyrin Analogues

T. Köhler, Z. Ou, J. T. Lee, D. Seidel, V. Lynch, K. M. Kadish,* J. L. Sessler* ——— **83 – 87**

Reductive N Alkylation of Cyclo[8]pyrroles



Under lock and key: A molecular machine based on the redox-coupled guest exchange of a cucurbit[8]uril-stabilized charge-transfer complex is reported. It behaves as a molecular loop lock that requires not only a key but also an activation process to open (see graphic).

Host–Guest Chemistry

W. S. Jeon, E. Kim, Y. H. Ko, I. Hwang, J. W. Lee, S.-Y. Kim, H.-J. Kim, K. Kim* ——— **87 – 91**

Molecular Loop Lock: A Redox-Driven Molecular Machine Based on a Host-Stabilized Charge-Transfer Complex

 © 2005 Wiley-VCH Verlag GmbH & Co. KGaA, Weinheim

Contents

Analytical Methods

S.-I. Nishimura,* K. Niikura, M. Kurogochi, T. Matsushita, M. Fumoto, H. Hinou, R. Kamitani, H. Nakagawa, K. Deguchi, N. Miura, K. Monde, H. Kondo ——— **91 – 96**

High-Throughput Protein Glycomics: Combined Use of Chemoselective Glycoblotting and MALDI-TOF/TOF Mass Spectrometry

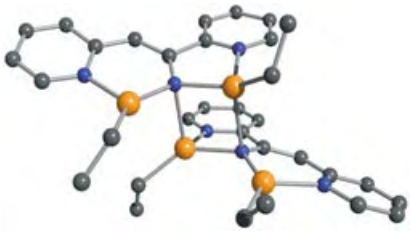


Common oligosaccharides and aldehyde-attached glycoproteins derived from enzymatic modifications can be captured by glycoblotting based on oxylamino-containing polymers. The combination of this glycoblotting and MALDI-TOF/TOF mass spectrometry enabled a high-throughput analytical method to be developed.

C–C Coupling

M. Westerhausen,* A. N. Kneifel, A. Kalisch ——— **96 – 98**

(*Z*)-Bis(alkylzinc)imido-1,2-di(2-pyridyl)-ethene: Intramolecular Stabilization of a Bis(alkylzinc)imide

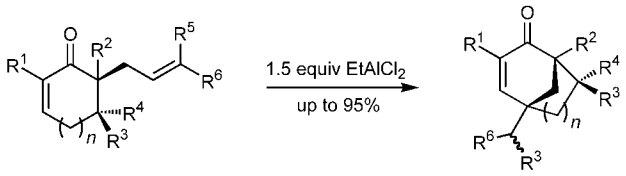


Able to be stable: The reaction of diethylzinc and bis(2-pyridylmethyl)amine yields the title complex by C–C coupling and deamination reactions. This complex is dimeric in the solid state (see structure; orange Zn, blue N, gray C). The pyridyl substituents enable the formation of a rare example of a bis(alkylzinc)imide.

Lewis Acids in Organic Synthesis

A. Goeke,* D. Mertl, G. Brunner **99 – 101**

Alkyl Aluminum Halide Promoted Intramolecular Cyclization of ω-Allyl-cycloalk-2-enones: Access to Bridged Bi- and Tricyclic Compounds

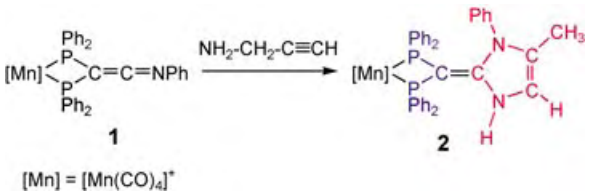


Cyclization makes the scent: A rearrangement of ω-allyl cycloalkenones leads to structurally complex bi- and tricyclic ketones in good yields (see scheme). The method allows efficient access to an olfactorily interesting class of compounds.

Hybrid Carbenes

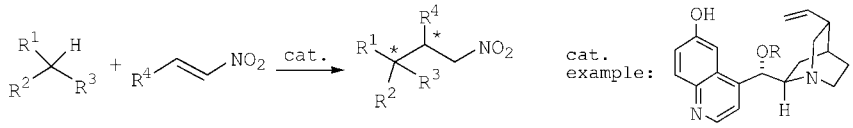
J. Ruiz,* M. E. G. Mosquera, G. García, F. Marquínez, V. Riera ——— **102 – 105**

Imidazoline-Functionalized Diphosphines: Models for N-Heterocyclic Carbene–Diphosphinocarbene Coupling



The next generation: Diphosphinocarbene (Arduengo carbene) and imidazol-2-ylidene (Bertrand carbene) are combined in complex **2**, which was prepared by reaction of the diphosphinoketenimine complex **1** with propargylamine to form a new type of $P_2C{=}CN_2$ electron-rich olefin, which behaves as a strongly basic diphosphine.

© 2005 Wiley-VCH Verlag GmbH & Co. KGaA, Weinheim

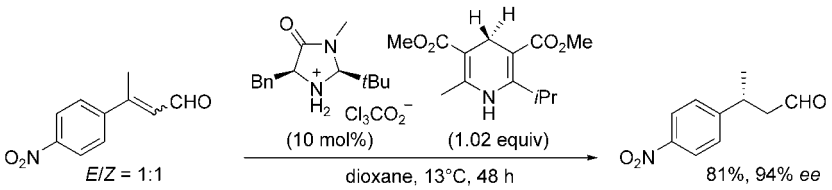


Not too close for comfort: Practical chiral organocatalysts like that shown promote Michael addition reactions of a wide range of trisubstituted carbon nucleophiles to various nitroalkenes, often with nearly perfect stereoselectivity (>99% *ee* and >98:2 d.r.). In one step adjacent carbon- or heteroatom-substituted quaternary and tertiary stereocenters are generated from readily available starting materials.

Asymmetric Catalysis

H. Li, Y. Wang, L. Tang, F. Wu, X. Liu, C. Guo, B. M. Foxman, L. Deng* ——— **105 – 108**

Stereocontrolled Creation of Adjacent Quaternary and Tertiary Stereocenters by a Catalytic Conjugate Addition

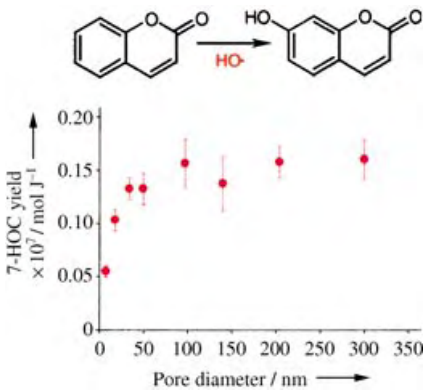


Selective reduction without metals: An imidazolidinone salt effectively catalyzes the highly enantioselective biomimetic transfer hydrogenation of α,β-unsaturated aldehydes to give the saturated analogues using a synthetic dihydropyridine cofactor (see scheme). Remarkably only one enantiomer forms regardless of the configuration of the enal starting material.

Organocatalysis

J. W. Yang, M. T. Hechavarria Fonseca, N. Vignola, B. List* ——— **108 – 110**

Metal-Free, Organocatalytic Asymmetric Transfer Hydrogenation of α,β-Unsaturated Aldehydes

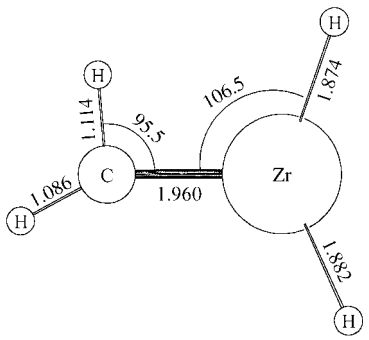


The effect of pore size on the radiolytic production of hydroxyl radicals has been investigated in silica controlled pore glasses (CPGs) by means of the HO•-induced conversion of coumarin into 7-hydroxycoumarin (7-OHC). Production of 7-OHC decreases with decreasing pore size (see plot). This effect is not attributed to the capture of HO• at the water/silica interface but to the modified diffusion regime in such confined environments.

Chemistry in Porous Materials

S. Foley, P. Rotureau, S. Pin, G. Baldacchino, J.-P. Renault,* J.-C. Mialocq ——— **110 – 112**

Radiolysis of Confined Water: Production and Reactivity of Hydroxyl Radicals



Spectrum of zirconium methylidene: Reaction of laser-ablated zirconium with CH_4 in excess neon at 5 K forms [H_2C=ZrH_2], the simplest carbene complex. Density functional theory calculations predict a C_1 symmetry structure (see picture) with agostic C–H···Zr bonding. This structure is confirmed by the match between calculated and observed IR frequencies. Methane activation by [H_2C=ZrH_2] gives [$(CH_3)_2ZrH_2$].

C–H Activation

L. Andrews,* H.-G. Cho, X. Wang ——— **113 – 116**

[H_2C=ZrH_2]: The Simplest Carbene Hydride Complex, Agostic Bonding, and C–H Activation of CH_4 to Form [$(CH_3)_2ZrH_2$]

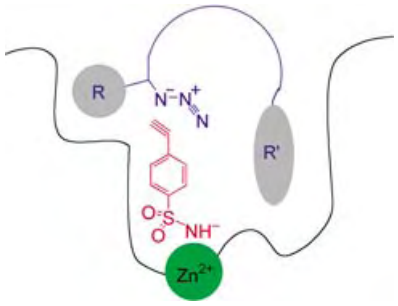
 © 2005 Wiley-VCH Verlag GmbH & Co. KGaA, Weinheim

Contents

Enzyme Inhibitors

V. P. Mocharla, B. Colasson, L. V. Lee, S. Röper, K. B. Sharpless, C.-H. Wong, H. C. Kolb* ——— **116 – 120**

In Situ Click Chemistry: Enzyme-Generated Inhibitors of Carbonic Anhydrase II

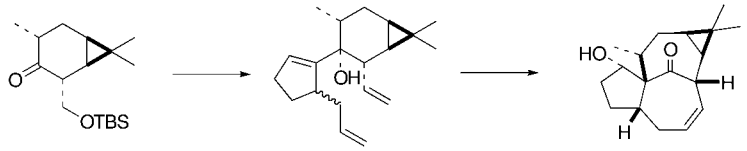


Target-guided synthesis: Rather than making and screening thousands of compounds for lead discovery, in situ click chemistry employs the biological target itself to assemble its inhibitors by selectively binding and interconnecting reagents within the confines of its binding sites. Subnanomolar inhibitors of carbonic anhydrase II were produced by the enzyme from simple azide and acetylene precursors (see picture).

Synthetic Methods

O. L. Epstein, J. K. Cha* ——— **121 – 123**

Rapid Access to the "in,out"-Tetracyclic Core of Ingenol

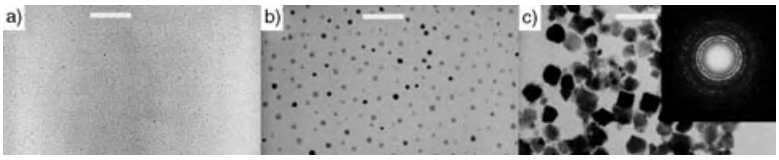


In ... out ... shake it all about! The tetracyclic core of ingenol has been prepared in a convergent synthesis. The pinacol-type rearrangement of an epoxy alcohol provides a simple, expedient solution to the challenging "inside–outside" intrabridgehead stereochemistry of ingenol (see scheme, TBS = *tert*-butyldimethylsilyl).

Magnetic Nanoparticles

Z. Li, Q. Sun, M. Y. Gao* ——— **123 – 126**

Preparation of Water-Soluble Magnetite Nanocrystals from Hydrated Ferric Salts in 2-Pyrrolidone: Mechanism Leading to Fe_3O_4

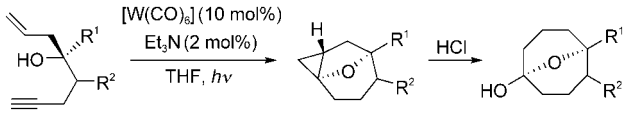


Differently sized and shaped nanocrystals of water-soluble magnetite were prepared by refluxing $FeCl_3 \cdot 6H_2O$ in 2-pyrrolidone for different periods of time. The picture (scale bar: 100 nm) shows how first spherical nanoparticles appear (1 h, a), grow (10 h, b), and finally form cubic particles (24 h, c). The mechanism leading to Fe_3O_4 nanocrystals is discussed.

Medium-Ring Compounds

J. Barluenga,* A. Diéguez, F. Rodríguez, F. J. Fañanás ——— **126 – 128**

Tandem $[W(CO)_5]$-Catalyzed Cycloisomerization–Cyclopropanation Reactions Directed toward the Synthesis of Eight-Membered Carbocycles

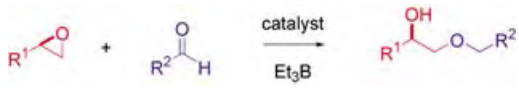


Fischer carbene complexes have been implied as intermediates in a catalytic tandem process for the synthesis of cyclic compounds, including eight-membered carbocycles, in excellent yields from alkynols (see scheme). The method was optimized to avoid the use of large quantities of the metallic species, thus overcoming one of the main limitations of Fischer carbene complexes.

Coupling Reactions

C. Molinaro, T. F. Jamison* ——— **129 – 132**

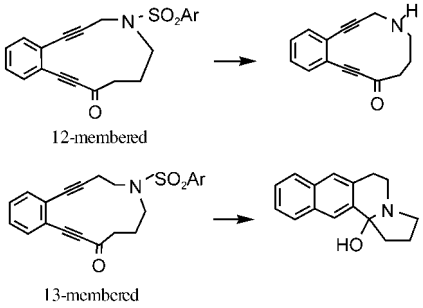
Catalytic Reductive Coupling of Epoxides and Aldehydes: Epoxide-Ring Opening Precedes Carbonyl Reduction



Several lines of evidence suggest that reduction of the carbonyl group occurs *after* epoxide-ring opening in the first examples of catalytic, reductive coupling of epoxides and aldehydes (see scheme). The hydroxyether products are obtained with >95:5 regioselectivity in all cases, independent of the steric and electronic nature of R^1 and R^2.

© 2005 Wiley-VCH Verlag GmbH & Co. KGaA, Weinheim

A question of size: Two N-protected macrocyclic enediynes have been synthesized by intramolecular N-alkylation. The smaller 12-membered enediyne, upon deprotection, yields a stable amine. In contrast, the amine generated from the 13-membered enediyne forms the aminol, which in turn undergoes a spontaneous Bergman cyclization (see scheme).



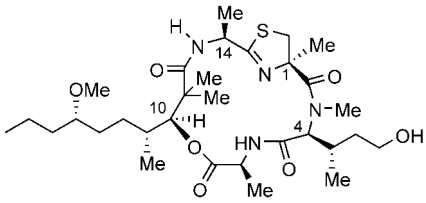
Enediynes

A. Basak,* S. K. Roy, S. Mandal ——— 132 – 135

Activation of Macrocyclic Enediynes by Transannular Cyclization

---

The antiinflammatory drug halipeptin A (**1**) is a 17-membered cyclic depsipeptide made up of L-alanine, α-methylcysteine, decanoic acid, and isoleucine residues. Key steps in its total synthesis, which helped to confirm the stereochemistry of the natural product, include a borane-mediated aldol reaction and an asymmetric aza-Claisen rearrangement.



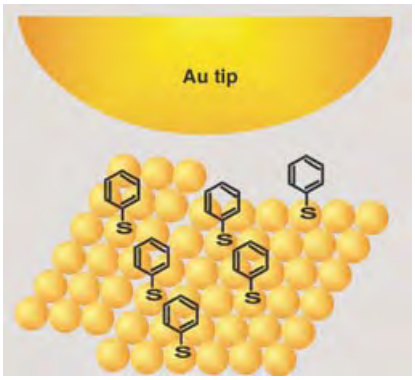
1

Natural Products Synthesis

S. Yu, X. Pan, X. Lin, D. Ma* ——— 135 – 138

Total Synthesis of Halipeptin A: A Potent Antiinflammatory Cyclic Depsipeptide

---



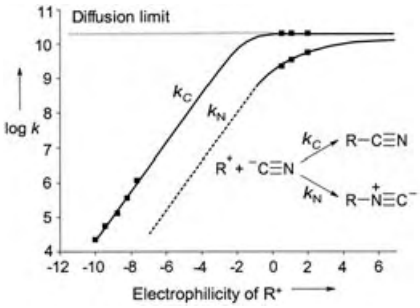
A tip for surface scientists: Tip-enhanced Raman spectroscopy (TERS) was used to record surface Raman spectra of benzenethiol and pyridine-4-thiol adsorbed on Au and Pt single-crystal surfaces (see picture). The benzenethiol spectra on the two surfaces are distinctly different. This result illustrates the power of TERS as a diagnostic tool with high spatial resolution for surface studies.

Surface Analysis

B. Ren,* G. Picardi, B. Pettinger,* R. Schuster, G. Ertl ——— 139 – 142

Tip-Enhanced Raman Spectroscopy of Benzenethiol Adsorbed on Au and Pt Single-Crystal Surfaces

---



Diffusion or activation control: Free CN^- ions are generally alkylated at carbon (see picture). N-attack is only observable in diffusion controlled reactions with carbocations. Since isonitrile formation in reactions with $[Ag(CN)_2]^-$ is due to the change of the nucleophile, the explanation of these regioselectivities by the hard and soft acids and bases principle has to be abandoned.

Reaction Mechanisms

A. A. Tishkov, H. Mayr* ——— 142 – 145

Ambident Reactivity of the Cyanide Ion: A Failure of the HSAB Principle

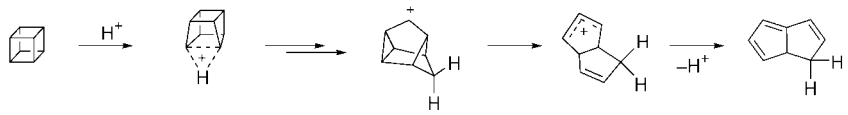
 © 2005 Wiley-VCH Verlag GmbH & Co. KGaA, Weinheim

Contents

Cubane Rearrangements

A. A. Fokin,* B. A. Tkachenko, P. A. Gunchenko, P. R. Schreiner* ____ 146 – 149

The Protonation of Cubane Revisited

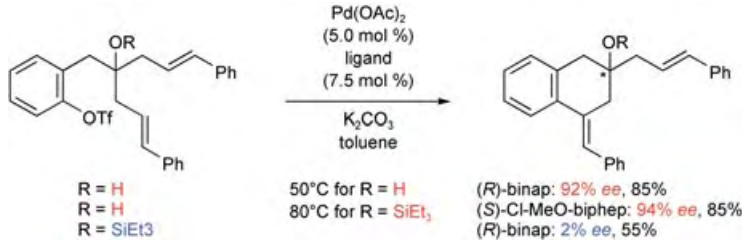


Cubane's proton affinity is now understood! Protonated cubane forms a structure with a protonated C–C bond (see scheme), which undergoes rearrangement along the most favorable reaction path rapidly giving 1,8-dihydropentalene as the final product. The results confirm the experimentally determined proton affinity of cubane.

Asymmetric Heck Reaction

M. Oestreich,* F. Sempere-Culler, A. B. Machotta ____ 149 – 152

Catalytic Desymmetrizing Intramolecular Heck Reaction: Evidence for an Unusual Hydroxy-Directed Migratory Insertion

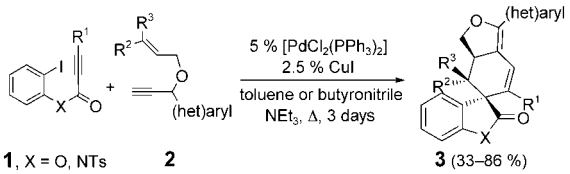


Mild cationic reaction conditions are used for the efficient desymmetrization of prochiral bishomoallylic alcohols in an intramolecular Heck reaction. This is the first example of a group-selective Heck cyclization in which the enantiotopic alkene moieties are not incorporated into a cyclic and, therefore, rigid system (see scheme). The high enantioselectivity is attributed to the hydroxy group functioning as a catalyst-directing group, which could be a novel feature in asymmetric Heck chemistry.

Domino Reactions

D. M. D'Souza, F. Rominger, T. J. J. Müller* ____ 153 – 158

A Domino Sequence Consisting of Insertion, Coupling, Isomerization, and Diels–Alder Steps Yields Highly Fluorescent Spirocycles

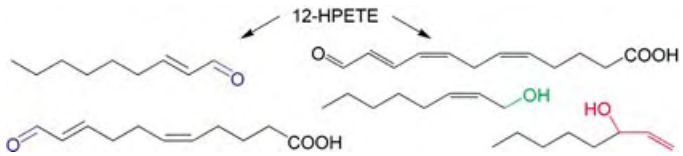


Four bonds at one stroke and products with intensive fluorescence result from a domino sequence consisting of insertion, coupling, isomerization, and Diels–Alder steps (see scheme, Ts = tosyl). Alkynoyl *ortho*-iodophenyl esters or *N*-(iodophenyl)alkynanilides **1** react with propargyl allyl ethers **2** to furnish spirocycles **3**.

Bioorganic Chemistry

T. Wichard, C. Göbel, I. Feussner, G. Pohnert* ____ 158 – 161

Unprecedented Lipoxygenase/Hydroperoxide Lyase Pathways in the Moss *Physcomitrella patens*



Weapons of moss destruction: Previously unknown lipoxygenase biosynthetic pathways in the moss *Physcomitrella patens* transform arachidonic acid into metabolites typical of animals, plants, algae, and mushrooms when the moss is damaged (see scheme). In this way metabolic themes from all these organisms are combined uniquely.

© 2005 Wiley-VCH Verlag GmbH & Co. KGaA, Weinheim

Sources

Product and Company Directory

You can start the entry for your company in "Sources" in any issue of *Angewandte Chemie*.

If you would like more information, please do not hesitate to contact us.

Wiley-VCH Verlag – Advertising Department
Tel.: 0 62 01 - 60 65 65
Fax: 0 62 01 - 60 65 50
E-Mail: MSchulz@wiley-vch.de

Service

Keywords ____ 162

Authors ____ 163

Angewandte's Sister Journals ____ 164

Vacancies ____ 21

Preview ____ 165

Think Macro

Excellence in Specialized Macromolecular Science

Research in the entire field of polymeric materials, engineering, processing, etc.

New ISI Impact Factor 1.170



www.mme-journal.de
ISSN Print 1438-7492
ISSN Online 1439-2054
Volume 290, 12 issues

More Pages – More Content

> Continues the successful section on **Macromolecular Reaction Engineering**, supervised by Prof. Joao B. P. Soares (Waterloo, Canada).
> Presents strictly peer-reviewed Feature Articles/Reviews, Full Papers, Communications.
> Special Issue dedicated to Prof. Karl-Heinz Reichert (TU Berlin).
> "A very effective platform for scientific exchange in the multidisciplinary field of advanced materials research on engineering polymers as well as tailor-made functional polymer systems and new polymer additives."
Rolf Mülhaupt (Freiburg)

Macromolecular Materials and Engineering is available **separately** and as part of the *Macromolecular* Full Package, *Macromolecular Basic* Package + *Macromolecular Materials and Engineering*.



For more details and pricing information please visit
www.mme-journal.de

WILEY InterScience® WILEY WILEY-VCH

John Wiley & Sons, Inc. • Tel.: +1-800-825-7550 (US only) or +1-201-/48-6645 • Fax: +1-201-748-5915 • E-Mail: subinfo@wiley.com
John Wiley & Sons, Ltd. • Tel.: +44 (0) 1243-779777 • Fax: +44 (0) 1243-843232 • E-Mail: cs-journals@wiley.co.uk
Wiley-VCH • Tel.: +49 (0) 6201 606-400 • Fax: +49 (0) 6201 606-184 • E-Mail: service@wiley-vch.de

15433410_ps

 © 2005 Wiley-VCH Verlag GmbH & Co. KGaA, Weinheim



F. Arnold Receives ACS Medal

The Francis P. Garvan–John M. Olin Medal administered by the American Chemical Society has been awarded since 1937 to women in the USA for distinguished service to chemistry. The recipient for 2005 is Frances H. Arnold of the California Institute of Technology (Caltech) in Pasadena. After studying mechanical and aerospace engineering at Princeton University, she first worked at the Solar Energy Research Institute in Golden, CO (USA). In 1980, she decided to continue her studies with a focus on biotechnology and completed her PhD in 1985 in the research group of Henry Blanch at the University of California, Berkeley. She then undertook postdoctoral research with Ignacio Tinoco (Berkeley) and Jack Richards (Caltech), before becoming assistant professor in 1987 at Caltech, where she is now Professor of Chemical Engineering and Biochemistry. She is a member of the US National Academy of Engineering.



F. Arnold

Arnold's research focuses on engineering enzymes, biosynthetic pathways, and genetic regulatory circuits by directed evolution. Her research group also develops software for modeling circuits and networks. Arnold is a member of the Editorial Advisory Board of *ChemBioChem*, where she recently reported on the "Thermostabilization of a Cytochrome P450 Peroxygenase".[1a] In *Angewandte Chemie* she recently described "A Self-Sufficient Peroxide-Driven Hydroxylation Biocatalyst".[1b]

B. Meunier Becomes President of the CNRS

Bernard Meunier has been appointed president of the Centre National de la Recherche Scientifique (CNRS) by the French government. He suceeds the atmospheric researcher Gérard Mégie, who died recently. The CNRS was founded in 1939 on the initiative of several scientists, including the Nobel Prize winner in physics, Jean Perrin, and conducts publicly funded fundamental research in all disciplines. Of its 26000 employees, about 12000 are scientific researchers. Since 1966, the CNRS institutes have been closely linked to university laboratories.



B. Meunier

Meunier studied organometallic chemistry with Robert Corriu and Hugh Felkin. He has worked for the CNRS since 1973: first at the Institute for the Chemistry of Natural Products in Gif-sur-Yvette near Paris, then since 1979 at the Laboratory of Coordination Chemistry in Toulouse, where he has been associate director since 2003. He has also taught at the Ecole Polytechnique in Paris since 1993 and has been a member of the French Academy of Sciences since 1999. His research interests encompass biomimetic catalysis, oxidation reactions, bioinorganic chemistry, and medicinal chemistry. In issue 1/2005 of *ChemBioChem* he reports on "Porphyrin Derivatives for Telomere Bindung and Telomerase Inhibition",[2a] and in a Review in *Advanced Synthesis & Catalysis* he recently described biomimetic catalysts for the oxidative activation of drugs.[2b] Meunier is a member of the Editorial Board of the *European Journal of Inorganic Chemistry* and the Editorial Advisory Board of *ChemBioChem*.

D. Kurth Accepts Position in Tsukuba

From April 2005 the sun will rise earlier for Dirk G. Kurth than it does now: The group leader at the Max-Planck-Institut für Kolloid- und Grenzflächenforschung (MPIKG) in Golm near Potsdam (Germany) will become the first foreign director of a research group at the National Institute for Materials Science (NIMS) in Tsukuba (Ibaraki, Japan). Kurth studied chemistry in Köln, Aachen (Germany), and Albuquerque (NM, USA) and completed his PhD in 1993 at Purdue University in West Lafayette (IN, USA) under the guidance of T. Bein (now at the Universität München (Germany)) on thin organic films on metallic substrates. He then spent two years as a postdoctoral fellow with J.-M. Lehn in Strasbourg (France). In 1996, he moved to join the research group of H. Möhwald at the MPIKG, and at the beginning of 2004 started lecturing at the Universität Potsdam.



D. Kurth

Kurth's research is concentrated on the development of functional modules in hierarchically structured materials for molecular functional units and supramolecular machines. His research group recently reported in *Angewandte Chemie* on directed self-assembly of nanoparticles at oil/water interfaces and in *ChemPhysChem* described the nanoscopic structure of a supramolecular polyelectrolyte–amphiphile complex.[3]

[1] a) O. Salazar, P. C. Cirino, F. H. Arnold, *ChemBioChem* **2003**, *4*, 891; b) P. C. Cirino, F. H. Arnold, *Angew. Chem.* **2003**, *115*, 3421; *Angew. Chem. Int. Ed.* **2003**, *42*, 3299.

[2] a) I. M. Dixon, F. Lopez, J.-P. Estève, A. M. Tejera, M. A. Blasco, G. Pratviel, B. Meunier, *ChemBioChem*, November 18, 2004, DOI: 10.1002/cbic.200400113; b) J. Bernadou, B. Meunier, *Adv. Synth. Catal.* **2004**, *346*, 171.

[3] a) H. Duan, D. Wang, D. G. Kurth, H. Möhwald, *Angew. Chem.* **2004**, *116*, 5757; *Angew. Chem. Int. Ed.* **2004**, *43*, 5639; b) A. Meister, G. Förster, A. F. Thünemann, D. G. Kurth, *ChemPhysChem* **2003**, *4*, 1095.

 © 2005 Wiley-VCH Verlag GmbH & Co. KGaA, Weinheim DOI: 10.1002/anie.200462712

Cycloadditions

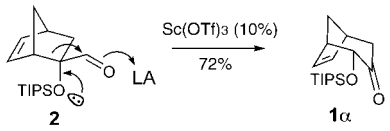
[4+3] Cycloadducts from Lewis Acid Mediated Reactions of Acroleins with Cyclopentadiene

*Barbara Niess and H. Martin R. Hoffmann**

Keywords:
cage expansion · cycloaddition · Diels–Alder reaction · domino reactions · Lewis acids

More than 20 years ago Sasaki et al.[1] reported the Lewis acid promoted cycloaddition of 2-silyloxyacrolein to cyclopentadiene, which led to the isolation of the diastereomeric [4+3] cycloadducts **1α** and **1β** (Scheme 1). A variation of the silyl substituent and of the Lewis acid made little difference (Scheme 1), although starting materials and products were, of course, easier to handle.[2]

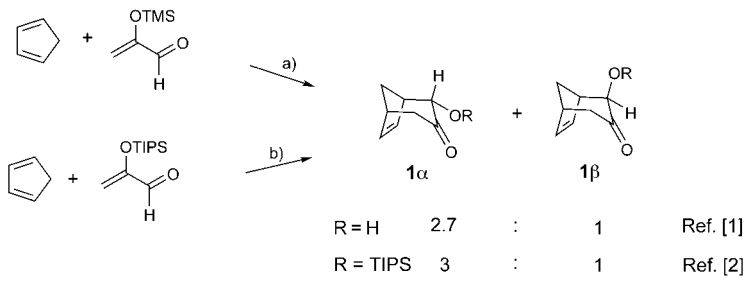
Davies and Dai[3] have now looked more closely at a series of Lewis acid promoted cycloadditions of cyclopentadiene to acroleins and obtained a variety of [4+3] cycloadducts. They also showed that a 5-norbornene-2-carbaldehyde is frequently implicated as an intermediate en route to the final [4+3] cycloadduct. For example, by using a microwave-assisted procedure, they first prepared Diels–Alder adduct **2**, which was then subjected to the original reaction conditions (10% $Sc(OTf)_3$, CH_2Cl_2, 0 °C)[2] to obtain the **1α** adduct (Scheme 2).



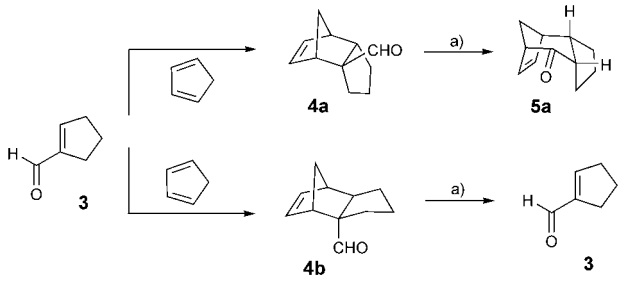
Scheme 2. Scandium triflate mediated rearrangement. LA = Lewis acid.

Tricyclic Diels–Alder adducts **4a** and **4b** were prepared from cyclopentene-1-carbaldehyde (**3**). Adduct **4a** has a sterically accessible formyl group on the *exo* face of the molecule: upon treatment with $AlCl_3$ ring expansion to **5a** occurred. In contrast, the diastereomeric adduct **4b** with a more shielded *endo* formyl group regenerated the substituted acrolein **3** in what appears to be the reverse of the forward reaction, that is, a retro-Diels–Alder reaction (Scheme 3).

Despite the intensive work on Diels–Alder additions of acroleins to cyclopentadiene, Davies and Dai showed that a number of very simple alkylated acroleins, including the parent 2-methacrolein, afford formal [4+3] rather than kinetic [4+2] cycloadducts under appropriate Lewis acid catalysis. For example, the cage-expanded adducts **6α** and **7αα** were formed from 2-methacrolein and 2-methyl-2-butenal, respectively (Scheme 4). Upon subsequent treatment of the respective products with HCl, the more-stable equatorial **6β** was formed predominantly and the diequatorial **7βα** epimer was formed exclusively. The *cis*-decalin system **8** is formed in lower yield (21%) than the five-membered-ring annulated **5a** (92%) (Scheme 3). 2-Butenal, which lacks the α-alkyl group, furnished conventional



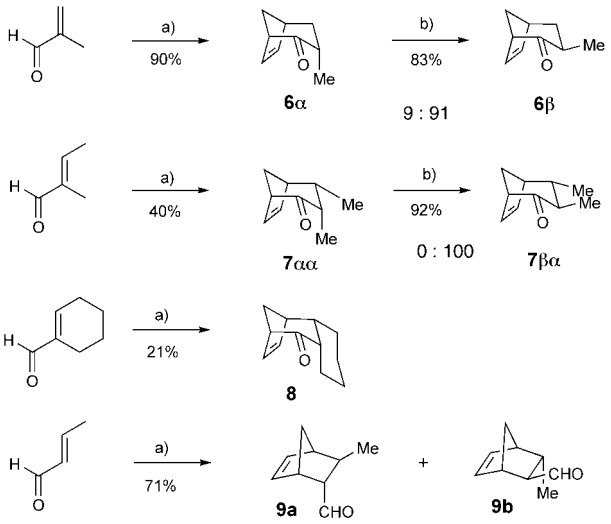
Scheme 1. Reagents and conditions: a) $SnCl_4$, CH_2Cl_2, −78 °C, 72%; b) $Sc(OTf)_3$ (10 mol%), CH_2Cl_2, 0 °C, 72%. TMS = trimethylsilyl; TIPS = triisopropylsilyl.



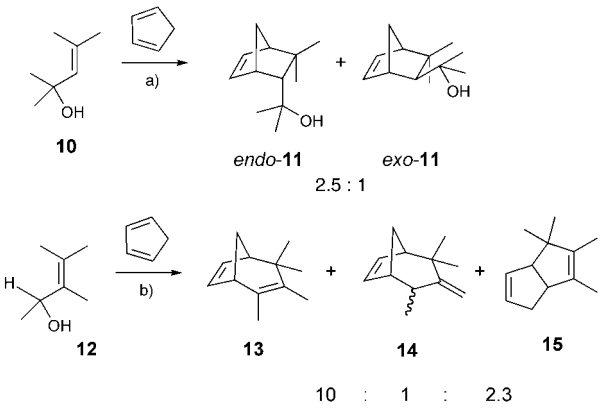
Scheme 3. Reagents and conditions: a) $AlCl_3$ (1.1 equiv), CH_2Cl_2, −78→0 °C, 2 h, 92% **5a**; 84% **3**.

[*] Dipl.-Chem. B. Niess,
Prof. H. M. R. Hoffmann
Institut für Organische Chemie
Universität Hannover
Schneiderberg 1 B
30167 Hannover (Germany)
Fax: (+49) 511-762-3011
E-mail: hoffmann@mbox.oci.uni-hannover.de

© 2005 Wiley-VCH Verlag GmbH & Co. KGaA, Weinheim
DOI: 10.1002/anie.200461313



Scheme 4. Reagents and conditions: a) $AlCl_3$ (1.1 equiv), cyclopentadiene (2.5 equiv), CH_2Cl_2, −78→0°C; b) HCl (1.0 equiv), room temperature, 30 min.



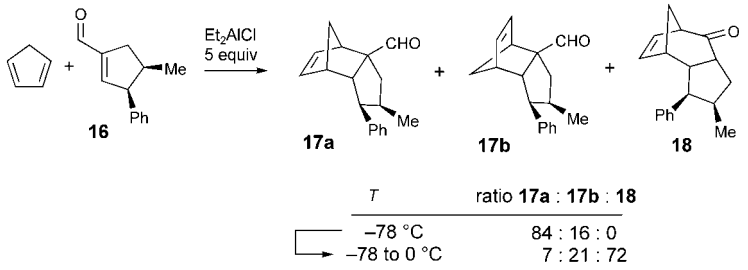
Scheme 5. Reagents and conditions: a) H_2O, TsOH, pentane; b) H_2O, TsOH, pentane, 0°C→RT, 24 h, 69–73%. Ts = *p*-toluenesulfonyl.

Diels–Alder adducts **9a** and **9b** (Scheme 4).

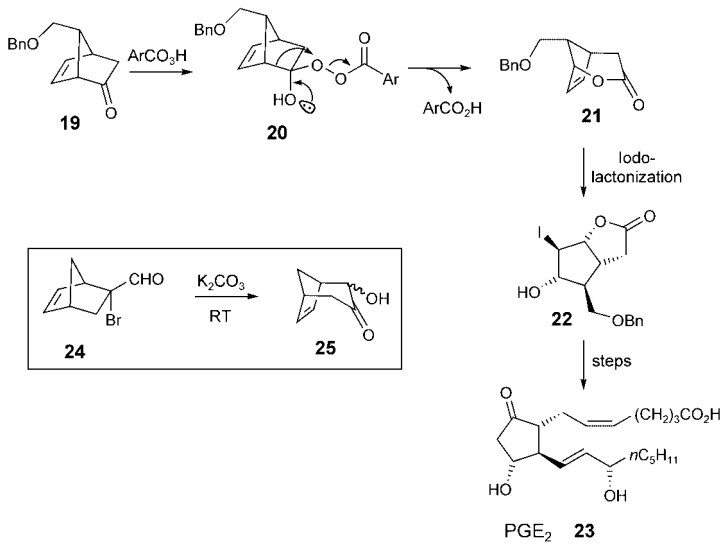
In retracing the possible origins of this unusual behaviour, we note that borderline dienophile/allyl cation reactivity is also encountered for acid-catalyzed cycloadditions of methylated allyl alcohols (Scheme 5). Whereas tetramethylated allyl alcohol **10** gives mainly Diels–Alder adducts *endo*-**11** and *exo*-**11**,[4] placement of one methyl group at the central position of the allyl moiety as in **12** affords unconventional [4+3] adducts **13** and **14**, accompanied by [3+2] adduct **15**, in a dehydrative cycloaddition.[5]

In the presence of Et_2AlCl at −78°C, the more complex cyclopentene aldehyde **16** and cyclopentadiene combined to form diastereomeric annulated norbornenes **17a** and **17b**. Of the four possible primary Diels–Alder adducts, only these two correspond to an attack of the dienophile from the more accessible π face with *exo*-orientated Me and Ph groups. When the reaction mixture was quenched at 0°C, the rearranged adduct **18** with six stereocenters in total was isolated as the major tricyclic product (Scheme 6). Again, product **17a** with the formyl group *syn* to the neighboring methylene bridge rearranged rather than the diastereomeric **17b** (see also Scheme 3).

The observed [3.2.1] cage expansion is driven by the release of ring strain and appears to mimic the isoelectronic Baeyer–Villiger oxidation of norbornenone, which has been known for over three decades: The α-hydroxy peroxy appendage can rotate freely in the *exo* position to adopt a stereoelectronically favorable alignment and conformation for the 1,2-shift to [3.2.1] bicyclic lactone **21** to occur (Scheme 7). Iodinated lactone **22** contains five stereocenters and is a key intermediate in Corey's route to prostaglandins.[6] The α-ketol rearrangement



Scheme 6. Addition of cyclopentene aldehyde **16** to cyclopentadiene.

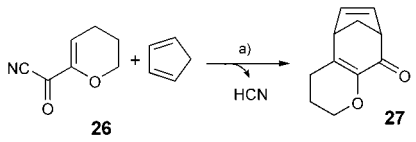


Scheme 7. Baeyer–Villiger and α-ketol rearrangement.

 © 2005 Wiley-VCH Verlag GmbH & Co. KGaA, Weinheim

of an α-bromoaldehyde such as **24** has also been observed to proceed under mild conditions (Scheme 7).[6,7]

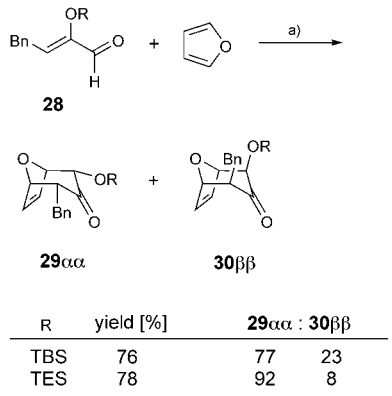
In assessing the scope of the Lewis acid mediated route to bridged seven-membered rings we should bear in mind that not only α,β-unsaturated enals, but also activated α,β-unsaturated enones and push–pull olefins such as **26** give [3.2.1] bicyclic products. In this case, an α,β-unsaturated enone **27** is formed instead of an α-ketol with loss of HCN (Scheme 8).[8] The product is sufficiently stable for isolation under these conditions.



Scheme 8. Reagents and conditions: a) $AlCl_3$, toluene, −78→0°C, 12 h, 70%.

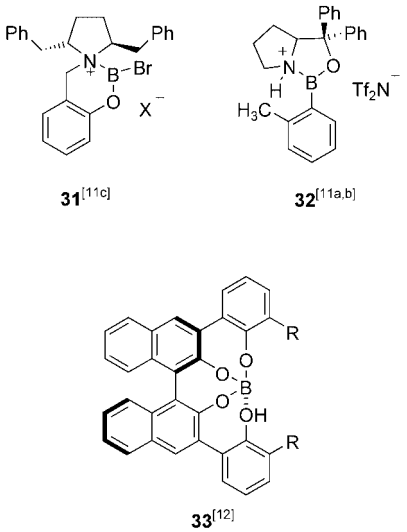
Cyclohexadiene adducts of acroleins are less strained than cyclopentadiene adducts and ring expansion does not occur.[3] Similarly, Diels–Alder adducts with furan are less likely to undergo ring expansion. The reported formation of **29αα** and *syn*-diaxial **30ββ** from furan and enal **28**[9] is characteristic of a W-configured allyl cation equivalent and a compact/extended transition state in a direct [4+3] cycloaddition rather than the [2.2.1] oxabicyclic intermediate (Scheme 9).[10]

It is of special interest that 5-norbornene-2-carbaldehyde derivatives that contain a quaternary center can be obtained in a stereocontrolled fashion.[11–13] In fact, the asymmetric synthesis of these aldehydes has become a benchmark for testing and inventing a host of new chiral Lewis acids. These have been constantly improved and refined over a period of at least one decade. For example, boron-centered **31**–**33** have been shown to be highly efficient in the synthesis of **34** (Scheme 10).[11,12]



R	yield [%]	29αα : 30ββ	
TBS	76	77	23
TES	78	92	8

Scheme 9. Reagents and conditions: Me_2AlCl (1.0 equiv), CH_2Cl_2, −78°C, 12 h. TBS = *tert*-butyldimethylsilyl; TES = triethylsilyl.

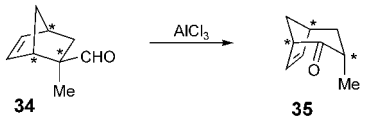


Scheme 10. Chiral Lewis acids for the asymmetric Diels–Alder reaction.

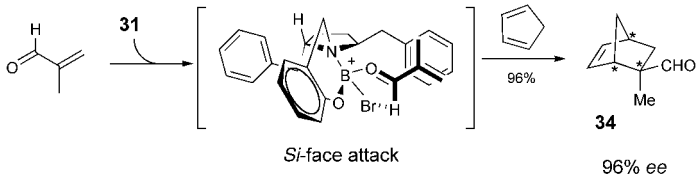
The chiral catalyst **31**, which is based on local C_2 symmetry grafted on bidentate amino phenol, is probably a two-point Lewis acid that involves a bond between the boron atom and the formyl oxygen atom as well as unusual hydrogen bonding of the formyl hydrogen atom. In combination with a suitable "benzenoid wall", the transition state is set up for *exo* addition of cyclopentadiene to the *Si* face (Scheme 11).[11c]

Apart from cationic oxaborolidinium salts such as **32**, various cationic ruthenium species with the transition metal as the stereocenter afford **34** and its enantiomer with high enantiomeric excesses in high chemical yield.[13] Interestingly, these asymmetric catalysts have been so carefully tuned to their task that the potential consecutive [3.2.1] rearrangement appears not to take place. Presumably, the initial Diels–Alder addition has a lower activation energy than the subsequent cage expansion, which requires cleavage of at least one σ bond. However, neighboring oxygen participation (e.g. **2**→**1α**, Scheme 2, and α-ketol rearrangement) lowers the barrier to ring expansion. Whereas α-alkyl substitution is less effective than α-silyloxy substitution, the construction and study of further push–pull olefins, including those with α-sulfur substituents and other heteroatoms, are clearly called for.

Davies and Dai report that the rearrangement of **34** to **35** is feasible with $AlCl_3$ (>1 equiv) and also $Sc(OTf)_3$, which are more electrophilic and sterically more accessible Lewis acids than those in Scheme 10. The [3.2.1] adduct is formed with three stereocenters and complete conservation of chirality (Scheme 12). [4+3] Adducts such as **35** are of continued interest, most recently for constructing chiral cage molecules as drug leads.[14]



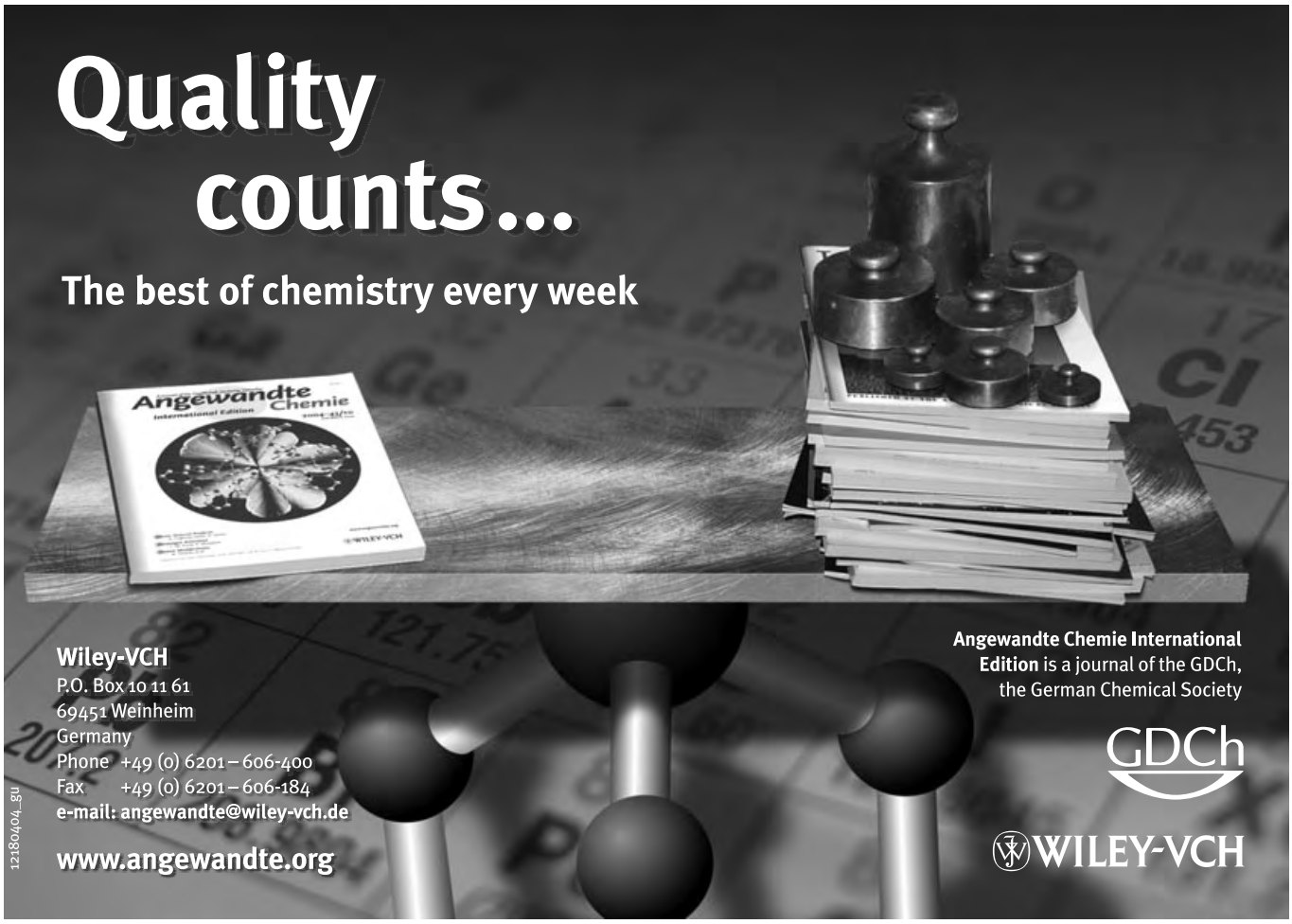
Scheme 12. Lewis acid induced rearrangement of chiral precursor **34**.



Scheme 11. Catalytic asymmetric Diels–Alder reaction of 2-methacrolein with cyclopentadiene.[11c]

© 2005 Wiley-VCH Verlag GmbH & Co. KGaA, Weinheim

[1] T. Sasaki, Y. Ishibashi, M. Ohno, *Tetrahedron Lett.* **1982**, *23*, 1693 – 1696.
[2] M. Harmata, U. Sharma, *Org. Lett.* **2000**, *2*, 2703 – 2705.
[3] H. M. L. Davies, X. Dai, *J. Am. Chem. Soc.* **2004**, *126*, 2692 – 2693.
[4] H. M. R. Hoffmann, H. Vathke-Ernst, *Chem. Ber.* **1981**, *114*, 2898 – 2906.
[5] H. M. R. Hoffmann, H. Vathke-Ernst, *Chem. Ber.* **1980**, *113*, 3416 – 3431; for a further discussion, see: H. M. R. Hoffmann, *Angew. Chem.* **1984**, *96*, 29 – 48; *Angew. Chem. Int. Ed. Engl.* **1984**, *23*, 1 – 19.
[6] E. J. Corey, *Angew. Chem.* **2002**, *114*, 1724 – 1741; *Angew. Chem. Int. Ed.* **2002**, *41*, 1650 – 1667; see also Scheme 7 therein.
[7] X. Creary, P. A. Inocencio, T. L. Underiner, R. Kostromin, *J. Org. Chem.* **1985**, *50*, 1932 – 1938.
[8] H. M. R. Hoffmann, K. Giesel, R. Lies, Z. M. Ismail, *Synthesis* **1986**, 548 – 551.
[9] R. A. Aungst, Jr., R. L. Funk, *Org. Lett.* **2001**, *3*, 3553 – 3555.
[10] I. V. Hartung, H. M. R. Hoffmann, *Angew. Chem.* **2004**, *116*, 1968 – 1984; *Angew. Chem. Int. Ed.* **2004**, *43*, 1934 – 1947.
[11] a) Q.-Y. Hu, P. D. Rege, E. J. Corey, *J. Am. Chem. Soc.* **2004**, *126*, 5984 – 5986; b) E. J. Corey, T. Shibata, T. W. Lee, *J. Am. Chem. Soc.* **2002**, *124*, 3808 – 3809; c) K. T. Sprott, E. J. Corey, *Org. Lett.* **2003**, *5*, 2465 – 2467.
[12] K. Ishihara, H. Kurihara, M. Matsumoto, H. Yamamoto, *J. Am. Chem. Soc.* **1998**, *120*, 6920 – 6930.
[13] a) J. W. Faller, B. J. Grimmond, D. G. D'Alliessi, *J. Am. Chem. Soc.* **2001**, *123*, 2525 – 2529; b) V. Alezra, G. Bernardinelli, C. Corminboeuf, U. Frey, E. P. Kündig, A. E. Merbach, C. M. Saudan, F. Viton, J. Weber, *J. Am. Chem. Soc.* **2004**, *126*, 4843 – 4853.
[14] M. Vidal Pascual, S. Proemmel, W. Beil, R. Wartchow, H. M. R. Hoffmann, *Org. Lett.* **2004**, *6*, 4155 – 4158.



 © 2005 Wiley-VCH Verlag GmbH & Co. KGaA, Weinheim

Homogeneous Catalysis

Gold Redox Catalysis for Selective Oxidation of Methane to Methanol

Dirk E. De Vos and Bert F. Sels*

Keywords:
gold · homogeneous catalysis · methane · oxidation · selenium

The challenge posed by the activation and selective oxygenation of inert C–H bonds, as in methane, has haunted chemists for many years. Gas-phase reactions, such as the oxidative coupling of methane to ethane and ethylene, and the direct conversion of methane into oxygenates, have met with limited success.[1] The need for high selectivity has incited scientists to investigate liquid-phase reactions at more moderate temperatures.

The origins of transition-metal catalyzed CH_4 oxidation chemistry can be traced back to the early work of Snyder and Grosse.[2] They oxidized methane with fuming sulfuric acid at 263 °C employing an $HgSO_4$ catalyst, and obtained oxygenated and sulfonated methane derivatives in a summed yield of 44 %. In an evolved version of this process, it was demonstrated that the reaction is mediated by the Hg^{II}/Hg^{I} redox couple (Table 1).[3] At the same time, Shilov discovered that Pt^{II}/Pt^{IV} is capable of oxidizing alkanes to alcohols;[4] with Pt^{II} chelated by a bipyrimidine ligand and SO_3 as the oxidant, methane was oxidized to a 72 % yield of methanol and its esters.[5] In a recent paper, Periana and co-workers now report that the combination of gold as a catalyst and H_2SeO_4 as the oxidant results in a 94 % selectivity for CH_3O-SO_3H at 28 % CH_4 conversion.[6] As a common feature of all these reactions, the first step is the formation of a M–CH_3 intermediate, possibly by electrophilic substitution on a Hg^{II} or Pt^{II} species.[4b,c,7,8] With this knowledge, the step towards gold then seems straightforward, since Au^{I} is isoelectronic with Hg^{II}, and Au^{III} shares its electronic configuration with Pt^{II}.

This new example of homogeneous gold catalysis joins a series of discoveries made largely in the last decade.[9] Ionic gold, either as Au^{I} or Au^{III}, has been found to catalyze asymmetric aldol reactions and carbonylations.[10] The Lewis acid properties of Au^{n+} have been exploited to promote the addition of oxygen nucleophiles, such as water, to alkynes, or to catalyze C–C bond formations using alkynes.[11] Ionic gold also catalyzes the hydroarylation of alkynes with electron-rich aromatics or furans.[12] This reaction is strongly reminiscent of analogous Pd^{II}-catalyzed couplings, which have been proposed to start with the activation of the aromatic C–H bond by an electrophilic Pd^{II} compound.[13] While it is tempting to propose that with gold, auration of the aromatic compound is the first step, it seems more likely that gold-catalyzed hydroarylation is a classical Friedel–Crafts reaction.

While the previous list is by no means exhaustive, it is clear that none of these reactions involves changes of the gold redox state, even if two redox states of gold, that is, Au^{I} or Au^{III}, are readily accessible. In the case of the coupling of arenes, one might project that, as with Pd^{II}/Pd^{0}, an oxidative coupling of aromatics and olefins to alkenylaromatics might proceed, but attempts to devise such a redox process with gold have not yet been successful.[12a]

Only a small number of homogeneous gold-mediated redox reactions have been reported. Ionic gold catalyzes the oxidation of alkanes with H_2O_2 to alkyl hydroperoxides, for example, but this is probably a free radical process.[14a] $[AuCl_2(NO_3)]$ promotes the oxidation of thioethers to sulfoxides at room temperature and 1 atm of O_2. In this case, the thioether, in a slow step, reduces Au^{III} to Au^{I}, which is quickly reoxidized by O_2 to Au^{III}, without any Au^{0} formation (Scheme 1). This process demonstrates the feasibility of Au^{III}/Au^{I} redox cycling in organic reactions.[14b] In addition, ionic gold catalyzes the oxidative carbonylation of aniline to phenylcarbamates with O_2 as the oxidant.[15] The same reaction is known to be catalyzed by the Pd^{II}/Pd^{0} redox couple;[15c] however, in the gold case, it is not fully clear whether ionic gold or colloidal zerovalent gold is the actual catalyst.

The new successful application of gold in the catalytic methane oxidation critically depends on the use of selenic acid as an oxidant. Periana et al. previously showed that Au^{III} stoichiometrically oxidizes methane to methanol.[3] Only with H_2SeO_4 as the oxidant, the system actually turns over. As selenic acid is one of the few known reagents to dissolve Au^{0}, it may even re-dissolve colloidal Au^{0} particles if these were to form in the drastic reaction conditions. On the other hand, the spontaneous reaction between H_2SeO_4 and methane should not be neglected. Comparison with blank experiments shows that about 20 % of the CH_3OH formation may be due to the background reaction.

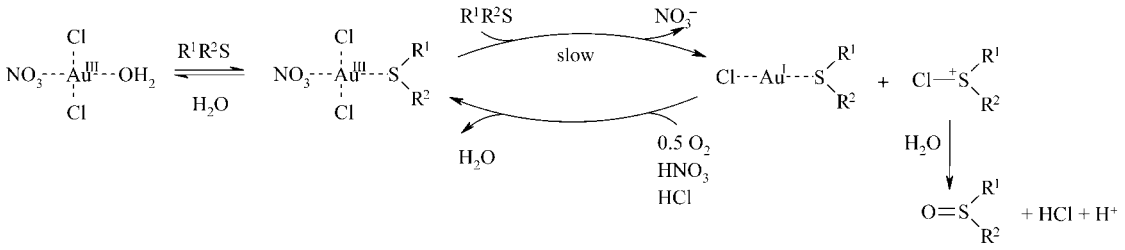
[*] Prof. Dr. D. E. De Vos, Prof. Dr. B. F. Sels
Centre for Surface Chemistry and Catalysis
K.U.Leuven
Kasteelpark Arenberg 23, 3001 Leuven (Belgium)
Fax: (+32) 1632-1998
E-mail: dirk.devos@agr.kuleuven.ac.be

© 2005 Wiley-VCH Verlag GmbH & Co. KGaA, Weinheim
DOI: 10.1002/anie.200461561

Table 1: Reaction characteristics of metal-catalyzed CH_4 oxidation in the liquid phase.

Catalyst	Solvent + oxidant	T [K]	CH_4 conversion [%]	Selectivity [%]	[Oxygenates][a]	CH_4/Cat.[b]	TON[c]	TOF [h^{-1}][d]	Ref.
$Hg(OSO_3H)_2$	100% H_2SO_4	453	50	85% CH_3OSO_3H	≈1.5 M	36	15		[3]
								3.6[e]	[3]
$[Pt(bpym)Cl_2]$[f]	102% H_2SO_4	493	90	81% CH_3OSO_3H	1 M	29	24	10	[5]
							500[e]	36[e]	[5]
Au^0	3 M SeO_3 in 96% D_2SO_4	453	8	77% CH_3OSO_3D	0.18 M	580	32	3.6	[6]
	3 M SeO_3 in 96% D_2SO_4 + 2% SO_3		28	94% CH_3OSO_3D	0.63 M	29	8	2.7	[6]

[a] Eventual concentration of methanol and derivatives. [b] Molar ratio CH_4:catalyst. [c] TON = turnover number = moles of product per mole of catalytic metal. [d] TOF = turnover frequency = moles of product per mole of metal per time. [e] Maximal values, obtained in separate experiments. [f] bpym = 2,2′-bipyrimidine.

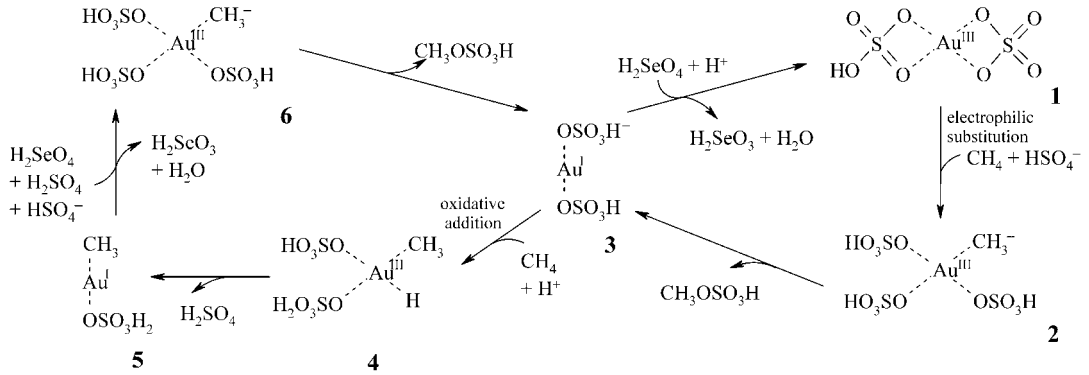


Scheme 1. Au^{III}/Au^{I} redox cycling in organic reactions.

Such a spontaneous reaction does not necessarily decrease the selectivity: protection of methanol as methyl bisulfate greatly reduces the reactivity of the CH_3 group, not only for electrophilic activation, but also for radical processes initiated by hydrogen-atom abstraction.[16]

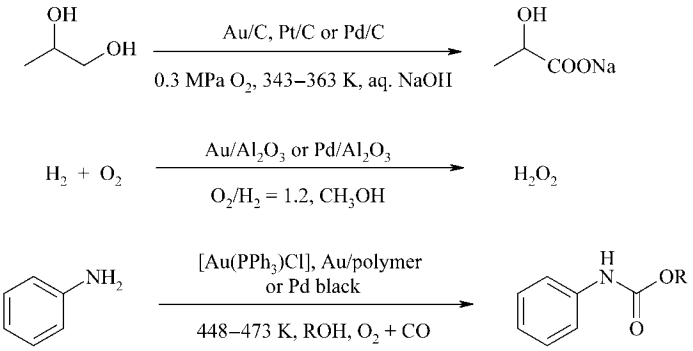
As can be expected based on both experiment and calculation, the catalytic cycle comprises formation of an Au–CH_3 compound, oxidation of the metal, and product elimination, though not necessarily in this order. In the analogous platinum reactions, the oxidation of the metal precedes the product elimination;[4b,5,8] in the case of mercury catalysis, the product is eliminated before reoxidation of Hg^{I}.[3] What will be the order of the steps in case of gold catalysis? This sequence depends on whether methane is activated on Au^{I} (by oxidative addition, **3**→**4** in Scheme 2) or on Au^{III} (by electrophilic substitution, **1**→**2** in Scheme 2). While the majority of gold is present as Au^{III}, a pathway starting with oxidative addition of CH_4 on Au^{I} is energetically favored and therefore should be considered as well.

In evaluating the future applications of this discovery, environmental issues should be considered. While selenium is needed in small quantities in food as a micronutrient, it is quite toxic at high concentrations. This means that the selenium has to be confined to the reactor; selenium leaks, for example, as selenite in waste water or as SeO_2 in offgases must be avoided. Secondly, the reaction is performed in H_2SO_4; methanol recovery implies dilution with water, and next, the sulfuric acid must be concentrated again. It is therefore worthwhile to consider other inert solvents, such as water. Sen and co-workers and Sames and co-workers have demonstrated that catalytic C–H activation on electrophilic Pt^{II} is possible in water,[17] but the very low solubility of methane still needs to be dealt with



Scheme 2. Possible pathways for the gold-catalyzed methane oxidation.

 © 2005 Wiley-VCH Verlag GmbH & Co. KGaA, Weinheim



Scheme 3. Examples of gold-, platinum-, and palladium-catalyzed reactions.

($0.25\ g\,L^{-1}$ at 100 °C and 2 MPa). Finally, it is possible to recycle the selenic acid, by oxidation of the H_2SeO_3 with Cl_2 or H_2O_2. To obtain a commercially viable process, TOFs larger than $3000\ h^{-1}$, and a 5 M concentration of oxygenates would probably be needed (compare values in Table 1). Particularly regarding CH_4 conversion and TON, platinum catalysis seems still more promising than gold catalysis. In any case, major advances are still required before the metal-catalyzed methane oxidations can result in an industrial process.

Strikingly, both in heterogeneous and homogeneous oxidation catalysis, gold is no longer considered inert, but presents itself as an intriguing alternative to platinum and palladium, with often superior characteristics (Scheme 3). Just like metallic supported Pt^0 and Pd^0, Au^0/C oxidizes alcohols to acids, but the gold catalysts are less affected by metal leaching or by poisoning by strong adsorption of acids.[18] In the direct production of H_2O_2 out of H_2 and O_2, supported gold can be used instead of palladium; the formed hydroperoxide can be employed in situ for propene epoxidation.[19] The similar role of palladium and gold in oxidative carbonylation of amines has been discussed before.[15] With the discovery by Periana and co-workers for the Au-catalyzed methane oxidation,[6] gold claims its place in this domain as well, alongside other noble metals.

Published Online: November 26, 2004

[1] a) J. H. Lunsford, *Catal. Today* **2000**, *63*, 165–174; b) O. V. Krylov, *Catal. Today* **1993**, *18*, 209–302; c) D. Wolf, *Angew. Chem.* **1998**, *110*, 3545–3547; *Angew. Chem. Int. Ed.* **1998**, *37*, 3351–3353.

[2] J. C. Snyder, A. V. Grosse, U.S. Patent 2493038, **1950** [*Chem. Abstr.* **1950**, *44*, 20151].

[3] R. A. Periana, D. J. Taube, E. R. Evitt, D. G. Löffler, P. R. Wentrcek, G. Voss, T. Masuda, *Science* **1993**, *259*, 340–343.

[4] a) A. E. Shilov, G. B. Shul'pin, *Chem. Rev.* **1997**, *97*, 2879–2932; b) S. S. Stahl, J. A. Labinger, J. E. Bercaw, *Angew. Chem.* **1998**, *110*, 2298–2311; *Angew. Chem. Int. Ed.* **1998**, *37*, 2180–2192; c) A. Sen in *Applied Homogeneous Catalysis with Organometallic Compounds* (Eds.: B. Cornils, W. A. Herrmann), VCH, Weinheim, **1996**, p. 1081–1092.

[5] R. A. Periana, D. J. Taube, S. Gamble, H. Taube, T. Satoh, H. Fujii, *Science* **1998**, *280*, 560–564.

[6] C. J. Jones, D. Taube, R. A. Periana, *Angew. Chem.* **2004**, *116*, 4726–4729; *Angew. Chem. Int. Ed.* **2004**, *43*, 4626–4629.

[7] A. Sen, *Acc. Chem. Res.* **1998**, *31*, 550–557.

[8] J. A. Labinger, J. E. Bercaw, *Nature* **2002**, *417*, 507–514.

[9] G. Dyker, *Angew. Chem.* **2000**, *112*, 4407–4409; *Angew. Chem. Int. Ed.* **2000**, *39*, 4237–4239.

[10] a) Y. Ito, M. Sawamura, T. Hayashi, *J. Am. Chem. Soc.* **1986**, *108*, 6405–6406; b) A. Togni, S. D. Pastor, *J. Org. Chem.* **1990**, *55*, 1649–1664; c) Q. Xu, Y. Imamura, M. Fujiwara, Y. Souma, *J. Org. Chem.* **1997**, *62*, 1594–1598.

[11] a) J. H. Teles, S. Brode, M. Chabanas, *Angew. Chem.* **1998**, *110*, 1475–1478; *Angew. Chem. Int. Ed.* **1998**, *37*, 1415–1418; b) E. Mizushima, K. Sato, T. Hayashi, M. Tanaka, *Angew. Chem.* **2002**, *114*, 4745–4747; *Angew. Chem. Int. Ed.* **2002**, *41*, 4563–4565; c) R. Casado, M. Contel, M. Laguna, P. Romero, S. Sanz, *J. Am. Chem. Soc.* **2003**, *125*, 11925–11935; d) A. S. K. Hashmi, T. M. Frost, J. W. Bats, *J. Am. Chem. Soc.* **2000**, *122*, 11553–11554; e) C. Nieto-Oberhuber, M. Paz Munoz, E. Bunuel, C. Nevado, D. J. Cardenas, A. M. Echavarren, *Angew. Chem.* **2004**, *116*, 2456–2460; *Angew. Chem. Int. Ed.* **2004**, *43*, 2402–2406.

[12] a) M. T. Reetz, K. Sommer, *Eur. J. Org. Chem.* **2003**, *2003*, 3485–3496; b) A. S. K. Hashmi, L. Schwarz, J.-H. Choi, T. M. Frost, *Angew. Chem.* **2000**, *112*, 2382–2385; *Angew. Chem. Int. Ed.* **2000**, *39*, 2285–2288; c) Z. Shi, C. He, *J. Org. Chem.* **2004**, *69*, 3669–3671.

[13] a) C. Jia, T. Kitamura, Y. Fujiwara, *Acc. Chem. Res.* **2001**, *34*, 633; b) M. Dams, S. Celen, D. E. De Vos, P. A. Jacobs, *Angew. Chem.* **2003**, *115*, 3636–3639; *Angew. Chem. Int. Ed.* **2003**, *42*, 3512–3515.

[14] a) G. B. Shul'pin, A. E. Shilov, G. Süss-Fink, *Tetrahedron Lett.* **2001**, *42*, 7253–7256; b) E. Boring, Y. V. Geletii, C. L. Hill, *J. Am. Chem. Soc.* **2001**, *123*, 1625–1635.

[15] a) F. Shi, Y. Deng, *Chem. Commun.* **2001**, 443–444; b) F. Shi, Y. Deng, *J. Catal.* **2002**, *211*, 548–551; c) F. Ragaini, C. Cognolato, M. Gasperini, S. Cenini, *Angew. Chem.* **2003**, *115*, 2992–2995; *Angew. Chem. Int. Ed.* **2003**, *42*, 2886–2889.

[16] A. Sen, M. A. Benvenuto, M. Lin, A. C. Hutson, N. Basickes, *J. Am. Chem. Soc.* **1994**, *116*, 998–1003.

[17] a) M. Lin, C. Shen, E. A. Garcia-Zayas, A. Sen, *J. Am. Chem. Soc.* **2001**, *123*, 1000–1001; b) B. D. Dangel, J. A. Johnson, D. Sames, *J. Am. Chem. Soc.* **2001**, *123*, 8149–8150.

[18] L. Prati, M. Rossi, *J. Catal.* **1998**, *176*, 552–560.

[19] a) P. Landon, P. J. Collier, A. J. Papworth, C. J. Kiely, G. J. Hutchings, *Chem. Commun.* **2002**, 2058–2059; b) A. K. Sinha, S. Seelan, S. Tsubota, M. Haruta, *Angew. Chem.* **2004**, *116*, 1572–1574; *Angew. Chem. Int. Ed.* **2004**, *43*, 1546–1548.

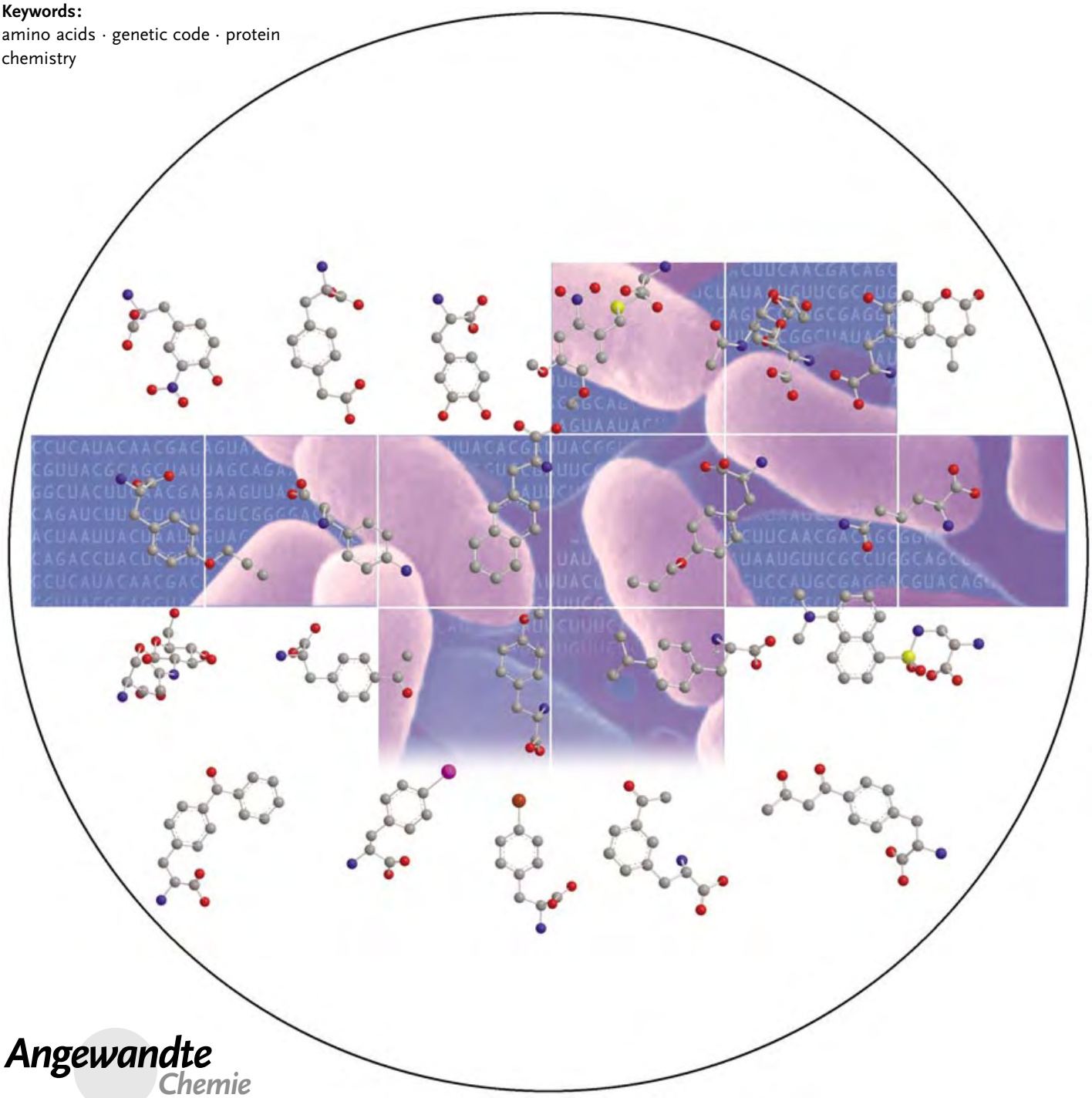
 © 2005 Wiley-VCH Verlag GmbH & Co. KGaA, Weinheim

Protein Science

Expanding the Genetic Code

*Lei Wang and Peter G. Schultz**

Keywords:
amino acids · genetic code · protein chemistry



© 2005 Wiley-VCH Verlag GmbH & Co. KGaA, Weinheim

DOI: 10.1002/anie.200460627

Although chemists can synthesize virtually any small organic molecule, our ability to rationally manipulate the structures of proteins is quite limited, despite their involvement in virtually every life process. For most proteins, modifications are largely restricted to substitutions among the common 20 amino acids. Herein we describe recent advances that make it possible to add new building blocks to the genetic codes of both prokaryotic and eukaryotic organisms. Over 30 novel amino acids have been genetically encoded in response to unique triplet and quadruplet codons including fluorescent, photoreactive, and redox-active amino acids, glycosylated amino acids, and amino acids with keto, azido, acetylenic, and heavy-atom-containing side chains. By removing the limitations imposed by the existing 20 amino acid code, it should be possible to generate proteins and perhaps entire organisms with new or enhanced properties.

From the Contents

1. Introduction 35
2. Chemical Approaches 35
3. In Vitro Biosynthetic Approaches to Protein Mutagenesis 39
4. In Vivo Protein Mutagenesis 43
5. An Expanded Code 46
6. Outlook 61

1. Introduction

The genetic codes of all known organisms specify the same 20 amino acid building blocks. These building blocks contain a limited number of functional groups including carboxylic acids and amides, a thiol and thiol ether, alcohols, basic amines, and alkyl and aryl groups. Although various arguments have been put forth to explain the nature and number of amino acids in the code,[1–3] it is clear that proteins require additional chemical groups to carry out their natural functions. These groups are provided through posttranslational modifications including phosphorylation, methylation, acetylation, and hydroxylation; cofactors; and in rare cases, organisms have evolved novel translational machinery to incorporate either selenocysteine or pyrrolysine.[4,5] The need for additional factors in so many protein-mediated processes suggests that while a code consisting of 20 amino acids is sufficient for life, it may not be ideal. Consequently, the development of a method that makes possible the systematic expansion of the genetic codes of living organisms might enable the evolution of proteins, or even entire organisms, with new or enhanced properties. Moreover, such methodology would dramatically increase our ability to manipulate protein structure and function both in vitro and in vivo. This in turn would allow a more classical chemical approach to the study of proteins, in which carefully defined changes in the steric or electronic properties of an amino acid are correlated with changes in the properties of proteins.[6–8] Herein we provide an overview of both chemical and biochemical approaches that have been developed in the past to manipulate protein structure, and review in depth recent advances that have made it possible to add new amino acids to the genetic codes of both prokaryotic and eukaryotic organisms.

2. Chemical Approaches

2.1. Chemical Modification of Proteins

Reagents that allow the selective chemical modification of amino acid side chains have proven quite useful in assigning functional roles to amino acid residues in proteins. Selectivity depends on the number and reactivity (dependent on both steric and electronic factors) of a particular amino acid side chain. Typical modifications include the oxidation or alkylation of cysteine residues, acylation of either the N-terminal α-amino group or the ε-amino group of lysine, and the condensation of amines with the carboxylate groups of aspartate or glutamate. In some cases it is possible to exploit the unique reactivity of active-site residues for selective chemical modification. For example, treatment of the protease subtilisin with phenylmethanesulfonyl fluoride, followed by reaction with thioacetate and hydrolysis, selectively converts the serine residue at the active site into a cysteine residue (Figure 1 a).[9,10] This mutant thiosubtilisin has diminished proteolytic activity, but still functions as an esterase. Similar approaches have been used to generate a redox-active selenosubtilisin[11,12] and selenotrypsin[13] (Figure 1 b).

Chemical modification has also been used to introduce reactive molecules, biophysical probes, tags, and other non-peptidic groups selectively into proteins. Cysteine is the most commonly used residue for this purpose because of its relatively low abundance in proteins and the increased nucleophilicity of the thio group relative to the side chains of other amino acids. Moreover, site-directed mutagenesis makes it possible to selectively introduce a cysteine residue at any desired site in a protein, in many cases without loss of function. This residue can then be modified, typically by either disulfide bond exchange or alkylation reactions.

[*] Prof. P. G. Schultz
Department of Chemistry and
The Skaggs Institute for Chemical Biology
The Scripps Research Institute
10550 North Torrey Pines Road, La Jolla, CA 92037 (USA)
Fax: (+1) 858-784-9440
E-mail: schultz@scripps.edu
Dr. L. Wang
Department of Pharmacology, University of California
San Diego, 9500 Gilman Drive, La Jolla, CA 92093 (USA)

DOI: 10.1002/anie.200460627
© 2005 Wiley-VCH Verlag GmbH & Co. KGaA, Weinheim

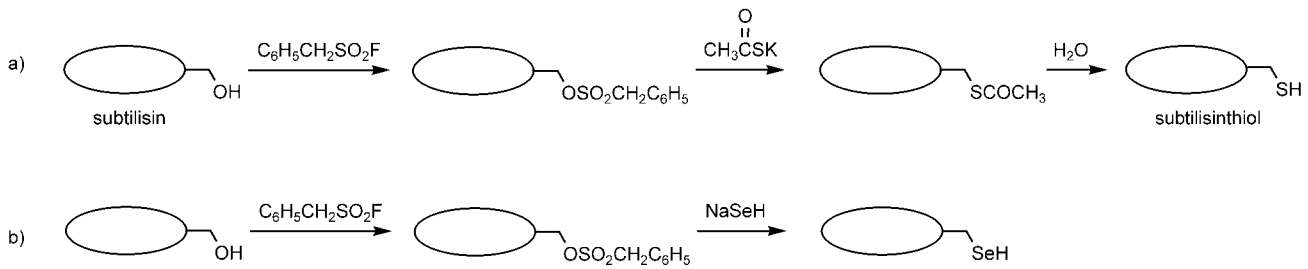


Figure 1. Selective conversion of the hydroxy group of serine to a thio (a) or seleno group (b).

Cysteine modification has been used to alter the catalytic properties of proteins. For example, Kaiser and co-workers conjugated different flavin analogues to the cysteine residue in the active site of papain to generate oxidoreductases that oxidize hydrophobic dihydronicotinamide derivatives (Figure 2a).[14–16] Conversely, an oligonucleotide binding site was introduced into a Lys116→Cys mutant of the nonspecific deoxyribonuclease staphylococcal nuclease to generate a semisynthetic enzyme that selectively cleaves DNA adjacent to the target sequence (Figure 2b).[17]

Cysteine has also been used to introduce a variety of biophysical probes into proteins. For example, a photoactivatable cross-linking agent (Figure 2c) was tethered to an Asp161→Cys mutant of catabolite gene activator protein to probe the interaction of this protein with the α subunit of RNA polymerase during transcriptional activation.[18] Meares and co-workers attached ferric EDTA to proteins through the Cys residue to generate oxidative cleavage reagents that can be used to map protein–protein and protein–nucleic acid complexes (Figure 2d).[19–23] Likewise, Harbury and co-workers have created a powerful chemical footprinting technique termed misincorporation proton–alkyl exchange,[24] which is based upon selective cleavage of the protein backbone at cysteine residues by 2-nitro-5-thiocyanobenzoic acid (Figure 2e).[25] In the related "substituted cysteine accessibility method" (SCAM) the surface accessibility of residues is inferred by the ability of the corresponding cysteine mutant to react with charged or polymeric reagents.[26,27] Nitroxide spin

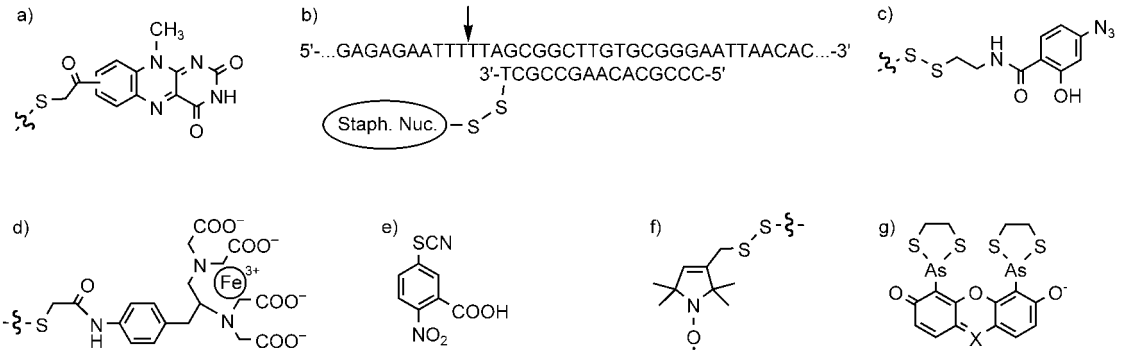


Figure 2. Cysteine residues can be modified with a wide range of nonpeptidic groups: a) flavin, b) oligonucleotide, c) an azido-based photo-cross-linking agent, d) [Fe(babe)], e) 2-nitro-5-thiocyanobenzoic acid, f) a nitroxide spin label, g) biarsenical dyes: FlAsH: X = CC_6H_4COOH, ReAsH: X = N.



Peter Schultz received his B.S. and Ph.D. (1984) from Caltech. He joined the Berkeley faculty in 1985 and moved to the Scripps Research Institute in 1999 where he is currently the Scripps Professor of Chemistry and the Director of the Genomics Institute of the Novartis Research Foundation. His interests focus on catalytic antibodies; the development and application of combinatorial methods in biological chemistry, drug discovery, and materials science; and new building blocks for the genetic code. He is a founder of numerous companies, and his awards include the Alan T. Waterman Award (NSF), the Wolf Prize in Chemistry, the Paul Ehrlich Prize, and membership in the National Academy of Sciences and Institute of Medicine.



Lei Wang received both his BS in organic chemistry (1994) and M.S. in physical chemistry (1997) from Peking University, where he conducted research on nanoparticle properties using scanning probe microscopy. From 1997 to 2002, he pursued graduate studies at the University of California, Berkeley under the guidance of Prof. Peter G. Schultz, where he developed a general method for genetically introducing unnatural amino acids into proteins in live cells. He is currently a postdoctoral fellow in Prof. Roger Y. Tsien's group at the University of California, San Diego.

© 2005 Wiley-VCH Verlag GmbH & Co. KGaA, Weinheim

labels (Figure 2 f) and environmentally sensitive fluorophores have also been conjugated to various proteins through the Cys residue to probe side-chain dynamics and backbone fluctuations.[28–30] Recently, it was shown that biarsenical ligands (FlAsH and ReAsH) can selectively bind to a tetracysteine motif Cys-Cys-Pro-Gly-Cys-Cys in proteins with high affinity and specificity (Figure 2 g).[31,32] The fluorescence of the biarsenical dyes is greatly enhanced after binding to the target site, thus making possible the selective introduction of a fluorophore into proteins in cells.

Another chemical method that has been used to selectively modify proteins involves the oxidation of N-terminal Ser or Thr residues with periodate to form an aldehyde, which can subsequently react with hydrazide or aminooxy groups to form stable conjugates. In one application the reaction of aminoxypentane with the N-terminal aldehyde group of the β-chemokine RANTES yielded a potent inhibitor of HIV-1 infection.[33] Similar chemistry has been used to selectively couple biotin and fluorescent reporters to the N-termini of peptides and proteins,[34] and for the chemoselective ligation of peptides (see Section 2.3).

Chemical modification is clearly a useful method for altering protein properties, including the synthesis of therapeutic proteins conjugated to polyethylene glycol (PEG; for example, Neulasta, PEG-Intron). Nonetheless, this approach relies on the unique reactivity of an amino acid side chain. Thus, the intrinsic selectivity and overall efficiency of the approach is limited.

2.2. Chemical Synthesis

Stepwise solid-phase peptide synthesis (SPPS),[35] pioneered by Merrifield in 1963, has greatly facilitated the synthesis of peptides and small proteins (< 100 amino acids) containing unnatural amino acids.[36] Examples include the substitution of a pyridoxamine phosphate derivative for Phe 8 of the C-peptide to afford a ribonuclease S with transaminase activity,[37] and the incorporation of iminodiacetic acid into the S-peptide which allows the activity of RNase S to be switched on/off by addition of Fe^{III} ions.[38] In other examples, D-amino acids and arginine analogues have been incorporated into luteinizing hormone-releasing hormone to improve affinity,[39–41] and Leu and Val were replaced with their fluorinated analogues (5,5,5-trifluoroleucine and 4,4,4-trifluorovaline, respectively) in the coiled-coil region of the yeast transcription factor GCN4 to increase protein stability.[42] In addition, unnatural amino acids bearing olefinic side chains have been inserted into the C-peptide of RNase A to form cyclic peptides by subsequent metathesis reactions, which resulted in increased resistance to proteases,[43] and 5,5-dimethylproline was substituted for Pro 93 in RNase A to lock the peptide bond into a *cis* conformation as a probe of protein folding.[44]

To overcome the size limitations of SPPS, efficient strategies have been developed to ligate synthetic peptides together to make larger proteins,[45] including a chemoenzymatic strategy[46] (see Section 2.3) and chemical ligation.[47] The latter process takes advantage of chemoselective coupling reactions (for example, thioester,[47] oxime,[48] thiazolidine/oxazolidine,[49,50] thioether,[51] and disulfide[52] bond formation) of unique functional groups incorporated into peptides (Figure 3). Template molecules have also been used to bring together the respective C- and N-termini of the two peptide fragments, thus enabling formation of an amide bond by intramolecular acyl transfer reactions (Figure 3 c).[53] An ingenious strategy termed "native chemical ligation" obviates the need for such a template and allows the direct coupling of peptide fragments to form a native peptide linkage (Figure 3 d).[54,55] In this method, a peptide with an α-thioester at its C-terminus is first ligated to a second peptide with an N-terminal Cys residue through a transthioesterification reaction. The thioester-linked intermediate then undergoes an irreversible S→N acyl rearrangement to form a native peptide bond at the ligation site. This method typically requires an N-terminal Cys residue at the ligation site, but recently it has been shown that an auxiliary sulfhydryl group can be used which is removed after ligation, thus making ligation possible at a non-Cys residue.[56] Native chemical ligation can be routinely used for the preparation of polypeptides comprising over 100 amino acid residues in length.

The emergence of chemical ligation methods has made it possible to incorporate unnatural amino acids into larger proteins. For example, an HIV-1 protease analogue was synthesized in which the amide CONH linkage between Gly 49 and Ile 50 was replaced with a COS linkage by thioester ligation to probe the contribution of this backbone hydrogen bond to catalytic activity.[57] In other studies native chemical ligation has been used to replace Tyr 10 of rubredoxin with tyrosine analogues to modulate the redox properties of this protein,[58] to modify erythropoietin with carbohydrate analogues,[59] and to incorporate fluorophores into chymotrypsin inhibitor 2 for single-molecule studies of protein folding.[60] Intramolecular native chemical ligation has also been used to create cyclic peptides and proteins.[61–63]

Chemical synthesis allows a large variety of unnatural amino acids to be incorporated into peptides and proteins. It is particularly useful for the incorporation of amino acid analogues that are toxic to cells or incompatible with the translational machinery (for example, the synthesis of an all D-amino acid protein[64,65]). Chemical synthesis also allows isotopic labels (for example, ^{2}H-, ^{13}C-, or ^{15}N-labeled amino acids) to be inserted into proteins at specific locations for spectroscopic studies. On the other hand, chemical synthesis can be problematic with peptides or proteins that have poor solubility, and becomes tedious, low yielding, and expensive when applied to larger proteins.

2.3. Semisynthesis

An alternative approach to the generation of larger proteins containing unnatural amino acids involves semisynthesis in which synthetic peptides are ligated to a truncated native protein generated by chemical cleavage, proteolysis, or recombinant methods.[66,67] In comparison to SPPS, much larger peptide fragments can be recombinantly expressed or

 © 2005 Wiley-VCH Verlag GmbH & Co. KGaA, Weinheim

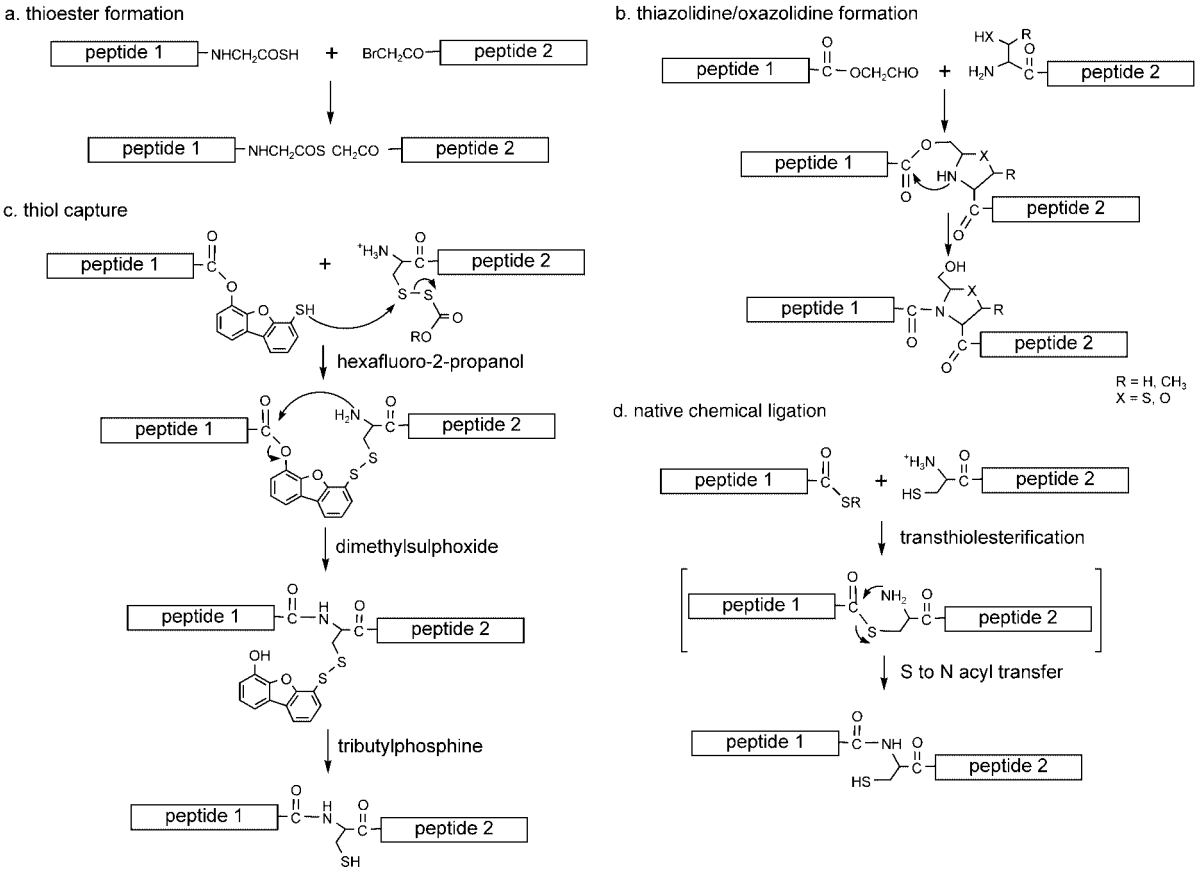


Figure 3. Examples of chemoselective reactions for peptide ligation.

derived from natural proteins, thus allowing access to larger proteins. One such semisynthetic method is based on the autocatalytic re-ligation of peptide fragments generated by cyanogen bromide (CNBr) cleavage of proteins, a phenomenon first noted by Dyckes et al. in 1974.[68] CNBr cleavage results in a C-terminal homoserine lactone, which reacts with a free N-terminus to reform the full-length protein. This approach has been used to insert a number of unnatural amino acids into cytochrome *c*.[69–71]

Enzyme-assisted peptide ligation has also been used for protein semisynthesis.[72] Peptide hydrolysis catalyzed by proteases can be reversed by altering the reaction conditions to favor aminolysis over hydrolysis,[73–76] for example, by adding organic cosolvents to suppress ionization of the α-carboxylic acid group. Alternatively, a peptide with a C-terminal ester can be condensed with the N-terminal amino group of a second peptide to form a ligated protein. Such methods have been used, for example, to incorporate D-Ala into human growth hormone releasing factor to increase protease resistance.[77,78] A significant improvement to this method involves the use of a mutant protease which has decreased hydrolytic activity but can still catalyze amide-bond formation with a C-terminal ester.[79] Kaiser and co-workers were the first to use a subtilisin mutant with a Ser→Cys mutation in the active site[9,10] for peptide ligation.[79] This mutant was further improved by Wells and co-workers to generate a subtiligase, a subtilisin double mutant (Ser221→Cys and Pro225→Ala) that has tenfold higher peptide ligase activity than thiosubtilisin.[80] Subtiligase has been used to assemble a mutant RNase A in which the active-site residues His12 and His119 were independently replaced with 4-fluorohistidine.[46] Similar approaches have also been used to incorporate biotin, heavy atoms, and polyethylene glycol into proteins.[81]

Chemoselective ligation can also be used in semisynthesis as long as an orthogonal functional group can be conveniently included at the terminus of the recombinant peptide. For example, Rose and co-workers enzymatically coupled a hydrazide to the C-terminus of a peptide fragment from human granulocyte colony-stimulating factor (G-CSF), and chemically generated an N-terminal aldehyde on the complementary peptide fragment through oxidation with periodate.[82] These two peptides spontaneously re-ligate to form a G-CSF mutant with a hydrazone linkage.

A technique termed expressed protein ligation (EPL) has greatly facilitated the use of native chemical ligation in protein semisynthesis by generating a recombinant protein with a C-terminal α-thioester for subsequent chemical ligation with a second peptide (Figure 4).[83–86] The C-terminal thioester intermediate is generated from an intein-mediated protein-splicing reaction in which a mutation in the intein blocks the final splicing step. In EPL, a recombinant protein is expressed in-frame with the mutant intein, and exogenous thiol is added to cleave the recombinant protein from the

 © 2005 Wiley-VCH Verlag GmbH & Co. KGaA, Weinheim

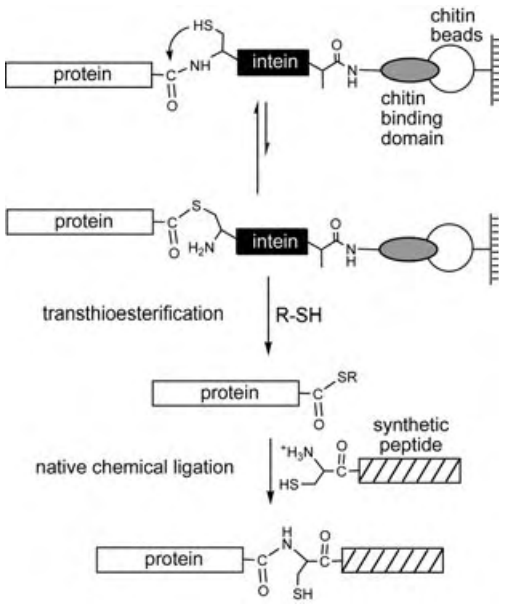


Figure 4. Expressed protein ligation.

partially rearranged splicing intermediate. The resulting α-thioester derivative can subsequently react with an N-terminal Cys peptide (prepared synthetically or enzymatically) to afford the semisynthetic product.[87–89] In addition to an N-terminal cysteine residue, N-terminal homocysteine[90,91] and selenocysteine[92–94] can also be used in native chemical ligation and EPL, thus resulting in the selective incorporation of these amino acids into the semisynthetic protein at the ligation site.

EPL can be used to incorporate fluorophores into the C-terminus,[83,95,96] middle,[97,98] or N-terminus[88] of proteins. In an elegant experiment Muir and co-workers introduced both tetramethylrhodamine and fluorescein into c-Crk-II (a substrate of the Abelson nonreceptor protein tyrosine kinase, c-Abl) to monitor the phosphorylation of c-Crk-II by c-Abl through fluorescence resonance energy transfer (FRET).[99,100] FRET pairs have also been introduced by EPL and/or Cys labeling into different components of the RNA polymerase holoenzyme and RNA polymerase-promoter open complex of *E. coli*.[101,102] In another application, a synthetic fragment of eglin which contained either kynurenine or norvaline at position 25 was ligated to a complementary peptide displayed on phage in which two residues making van der Waals contacts with residue 25 were randomized.[103] After ligation, phage-bearing mutant folded eglins were isolated that accommodate the unnatural side chains in the hydrophobic core. EPL has also been used to introduce posttranslational modifications (for example, glycosylated[104,105] and lipidated amino acids,[106] as well as analogues of phosphorylated amino acids[107–109]) selectively into proteins to study their effects on protein structure and function. Mutations to the protein backbone have also been generated with EPL. For example, Raines and co-workers replaced the Asn 113–Pro 114 residues of RNase A with a reverse-turn mimic composed of the two β-amino acid residues (*R*)-nipecotic acid–(*S*)-nipecotic acid[110] to generate a mutant RNase with the same ribonucleolytic activity as the wild-type enzyme and enhanced thermal stability.

Semisynthesis methods are quite powerful and allow access to larger proteins than does chemical synthesis. The method does, however, require appropriate sites for cleavage and ligation, and becomes cumbersome for internal sites in large proteins or when large amounts of proteins are required. In addition, all of the chemical methods described above are not easily applied to in vivo studies of protein structure and function.

3. In Vitro Biosynthetic Approaches to Protein Mutagenesis

3.1. Methodology

A variety of in vitro (cell-free) methods have been developed to incorporate unnatural amino acids into proteins by using the existing protein biosynthetic machinery of the cell. These methods take advantage of the fact that anticodon–codon recognition between messenger RNA (mRNA) and transfer RNA (tRNA) is largely independent of the structure of the amino acid linked to the 3′-terminus of the acceptor stem of the tRNA. This "adaptor hypothesis"[111,112] was elegantly demonstrated by showing that a cysteinyl-$tRNA^{Cys}$, when converted into an alanyl-$tRNA^{Cys}$ by treatment with H_2/Raney nickel, efficiently incorporates alanine into a polypeptide chain in vitro in response to the cysteine codon UGU.[112] These experiments were extended to derivatives of other common amino acids by the chemical modification of enzymatically aminoacylated tRNAs with synthetic reagents and probes. For example, treatment of Lys-$tRNA^{Lys}$ with *N*-acetoxysuccinimide affords (N^{ε}-acetyl-Lys)-$tRNA^{Lys}$, which can be used to insert N^{ε}-acetyl-Lys into proteins in a cell-free rabbit reticulocyte system.[113] Unfortunately, these methods lead to incorporation of the modified amino acid at all sites in a protein specified by the codon for the modified tRNA. The derivatized amino acid is also inserted in competition with the underivatized amino acid thus leading to heterogeneous protein product. In addition, substitutions are limited to derivatives of the common amino acids which can be generated under reactive conditions that do not hydrolyze the labile aminoacyl ester linkage between the terminal 3′-adenosine group and the amino acid, and do not chemically inactivate the tRNA.

Extension of this approach to a larger variety of amino acids required more general methods for the selective aminoacylation of tRNAs. Misaminoacylation of the tRNA with unnatural amino acids using aminoacyl-tRNA synthetases is problematic because of the high specificity of these enzymes.[114,115] Direct chemical acylation of the tRNA is not practical because of the large number of reactive sites in the tRNA. Consequently, semisynthetic methods were developed in which truncated tRNAs (with the 3′-terminal mono- or dinucleotide removed) are enzymatically ligated to chemically aminoacylated mono- and dinucleotides. For example, Hecht and co-workers developed an approach in which the dinucleotide pCpA is chemically acylated with an N^{α}-

 © 2005 Wiley-VCH Verlag GmbH & Co. KGaA, Weinheim

protected amino acid and then enzymatically ligated to a truncated tRNA ($tRNA^{-CA}$, which is missing the terminal dinucleotide pCpA at the 3′-acceptor stem) with RNA ligase.[116] A number of unnatural amino acids were incorporated into the first position of dipeptides by this method.[117–119] However, this approach suffered a number of limitations: yields of the aminoacylation reaction were quite poor and the N-terminal protecting group of the amino acid could not be efficiently removed without hydrolysis of the aminoacyl ester, thereby limiting substitution to P-site donors and, consequently, the peptide N-terminus (Figure 5). Later,

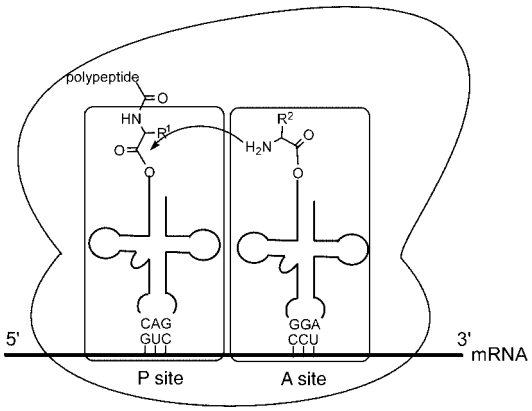


Figure 5. Schematic representation of ribosome and its P site and A site.

Brunner and co-workers developed a method to prepare a fully deprotected aminoacyl-pCpA and ligate it to the truncated tRNA to afford an aminoacyl tRNA which could be used as an A-site donor.[120] Nonetheless, the yields for the synthesis of the acylated dinucleotide were again poor. This method also does not overcome the above limitations associated with use of an endogenous *E. coli* tRNA for delivery of an amino acid including competition with host amino acids and multisite incorporation. Nonetheless, experiments with chemically aminoacylated tRNAs suggested that the natural translational machinery can accept a wide range of unnatural amino acid side chains.

A general in vitro method which allows the site-specific incorporation of a large number of unnatural amino acids into proteins with excellent translational fidelity was reported by us in 1989 (Figure 6).[121] This approach takes advantage of the degeneracy of the three stop codons UAA, UAG, and UGA (termed nonsense codons). These codons do not encode amino acids, but rather signal termination of polypeptide synthesis by binding release factors.[122,123] Since only one stop codon is required for the termination of protein synthesis, two "blank" codons exist in the genetic code which can be used to uniquely specify an unnatural amino acid. Indeed, nonsense suppressor tRNAs (tRNAs that insert one of the common amino acids in response to a stop codon) have been shown to incorporate a number of common amino acids efficiently into proteins both in vivo and in vitro.[124,125] In particular, experiments using [^{3}H]Phe, and later experiments with α-hydroxy

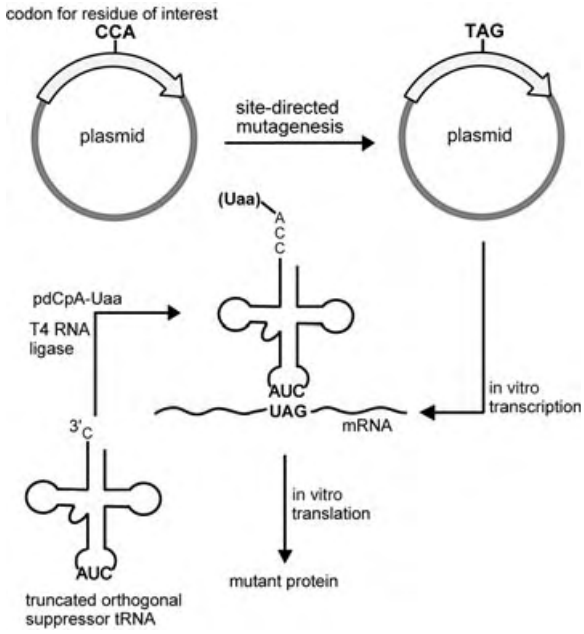


Figure 6. An in vitro biosynthetic method for the site-specific incorporation of unnatural amino acids into proteins. Uaa = unnatural amino acid.

acids, demonstrated that the desired amino acid could be selectively incorporated at the position specified by UAG in an in vitro translation system.[121,126]

Another requirement for the selective incorporation of unnatural amino acids into proteins is a tRNA that uniquely recognizes this blank codon and efficiently incorporates its cognate amino acid into the growing polypeptide chain. Importantly, this tRNA must be orthogonal to the endogenous aminoacyl-tRNA synthetases of the host organism from which the in vitro translation system is derived, that is, it must not be a substrate for any of the aminoacyl-tRNA synthetases present in the in vitro protein-synthesis extract. If the suppressor tRNA were recognized by an endogenous aminoacyl-tRNA synthetase, the tRNA could be subject to proofreading (deacylation of the noncognate amino acid) and/or re-aminoacylation with the cognate amino acid. This would result in either low suppression efficiency or the incorporation of a common amino acid in competition with the desired unnatural amino acid in response to the nonsense codon.

An orthogonal amber suppressor tRNA derived from yeast phenylalanine-tRNA ($tRNA^{Phe}_{CUA}$) was constructed for use in an *E. coli* in vitro protein transcription–translation system.[125,127–130] In this tRNA nucleotides 34–37 in the anticodon loop were replaced by 5′-CUAA-3′ to create an efficient suppressor tRNA. Runoff transcription provided a functional suppressor tRNA in relatively large quantities.[131,132] A modification of the two-step method originally developed by Hecht and co-workers[116] was developed to efficiently aminoacylate the orthogonal tRNA. It was found that the cyanomethyl ester of an N^{α}-protected amino acid selectively monoacylates the 2′,3′-hydroxy groups of the dinucleotide to give the desired aminoacylated product in

 © 2005 Wiley-VCH Verlag GmbH & Co. KGaA, Weinheim

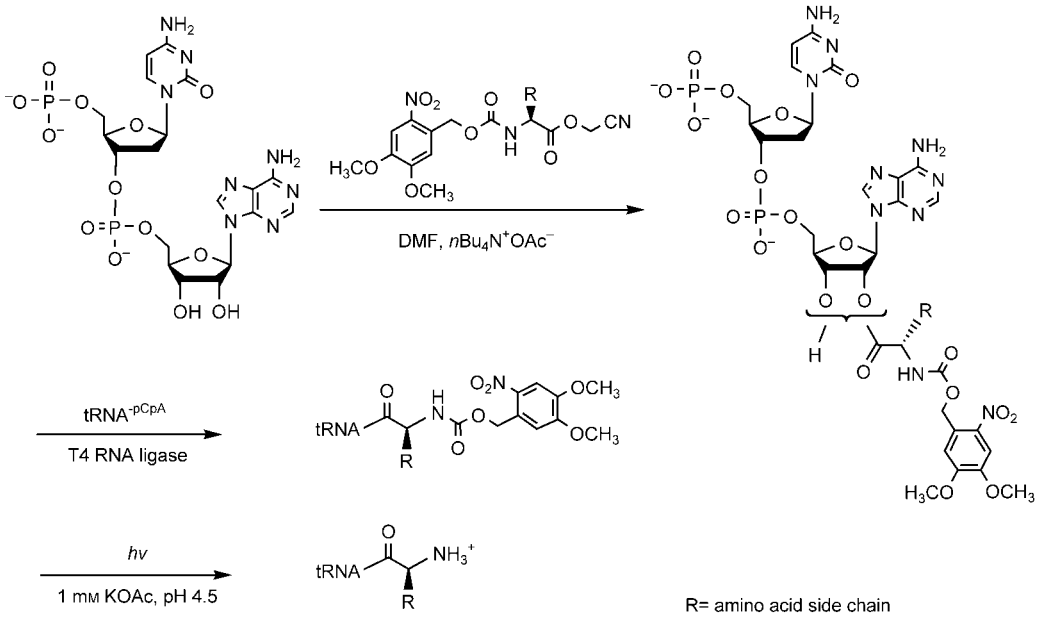


Figure 7. Strategy for the chemical aminoacylation of $tRNA^{Phe}_{CUA}$ using an amino acid cyanomethyl ester protected with a photochemically removable group.

high yield, thereby obviating the need to protect and deprotect the dinucleotide (Figure 7).[133] Replacement of cytidine with deoxycytidine in pCpA simplified the synthesis and eliminated another reactive 2′-OH group without affecting biological activity. The α-amino group of the amino acid and any reactive side-chain groups are protected as their nitroveratryloxy carbamate, ester, or ether derivatives prior to acylation of the dinucleotide.[134,135] These protecting groups can be removed photochemically from the intact aminoacyl-tRNA (after ligation) in high yield under mildly acidic conditions which prevent deacylation of the aminoacyl-tRNA.[133] This aminoacylation protocol is relatively straightforward, proceeds in high yield (both the aminoacylation and ligation reactions), and has been used to incorporate a wide variety of unnatural amino acids into proteins.[136]

The first demonstration of this general approach for the site-specific incorporation of unnatural amino acids into a protein in vitro involved the generation of mutant β-lactamases containing *p*-nitrophenylalanine, *p*-fluorophenylalanine, or homophenylalanine substitutions at Phe66.[121] Mutagenesis with the chemically acylated suppressor tRNA was carried out with an *E. coli* in vitro transcription–translation system consisting of an *E. coli* S-30 extract that contains all of the factors required for transcription and translation, and plasmid DNA containing the gene of interest with a TAG amber codon encoding the unnatural amino acid. Although relatively small quantities of purified protein were obtained (typical yields are 5–30 μg protein per mL), the specificity and fidelity of incorporation were shown to be very high by peptide mapping experiments. Shortly thereafter, a similar approach was reported by Chamberlin and co-workers, in which a suppressor tRNA derived from *E. coli* $tRNA^{Gly}$ was used to incorporate [^{125}I]Tyr site-selectively into a 16-mer peptide.[137]

Over 50 different amino acids and analogues have been incorporated site-specifically into proteins with high fidelity by the above methodology.[136] These include conformationally restricted amino acids (for example, methanoproline, cyclopropylglycine, and α-methyl-L-leucine), amino acids with spin labels and photoaffinity labels as side chains, amino acids with altered acidities and hydrogen-bonding properties, photocaged amino acids, α-hydroxy acids, and amino acids with unusual steric properties (for example, *tert*-butylglycine).

3.2. Applications

In vitro methods for unnatural amino acid mutagenesis have been applied to a large number of problems in protein chemistry, including protein folding, enzyme mechanism, and signal transduction. In addition, this methodology has been used to introduce a variety of biophysical probes into proteins.[138] For example, to determine the degree to which side-chain hydrogen bonding stabilizes the folded state of proteins, Tyr27 in staphylococcal nuclease (SNase) was substituted with several fluorinated tyrosine analogues (Figure 8a).[139] Denaturation studies of the corresponding mutants revealed a free-energy correlation between stability constant K_{app} and the pK_a value of the Tyr27 hydroxy group (Figure 8b), thus providing strong evidence that intramolecular hydrogen bonds between side chains can preferentially stabilize the folded state of a protein relative to the unfolded state in water. To determine the contribution of the main-chain hydrogen bonds to protein stability, several backbone amide linkages in α-helix 39–50 of T4 lysozyme were replaced with ester linkages by incorporating α-hydroxy acids at the N-terminus, the middle, and C-terminus of the helix, respec-

 © 2005 Wiley-VCH Verlag GmbH & Co. KGaA, Weinheim

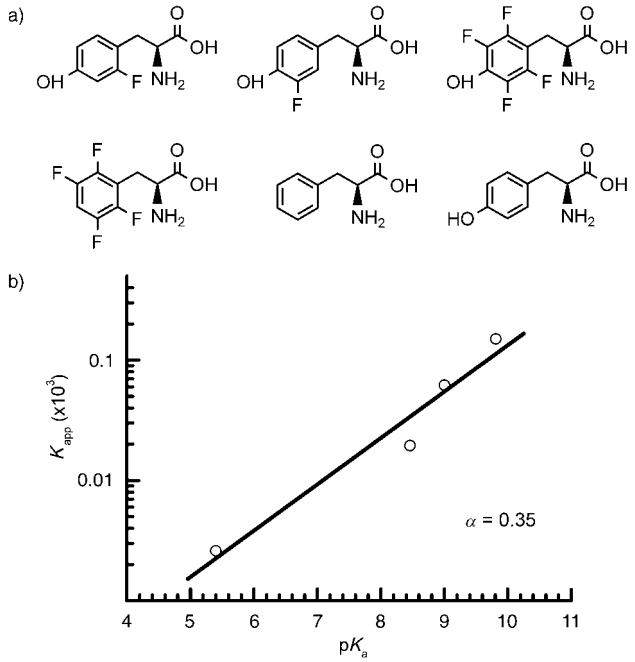


Figure 8. a) Structures of fluorinated amino acids substituted for Tyr 27 in SNase. b) Free energy relationship between the p*K*a value of the Tyr 27 mutant and the stability of SNase.

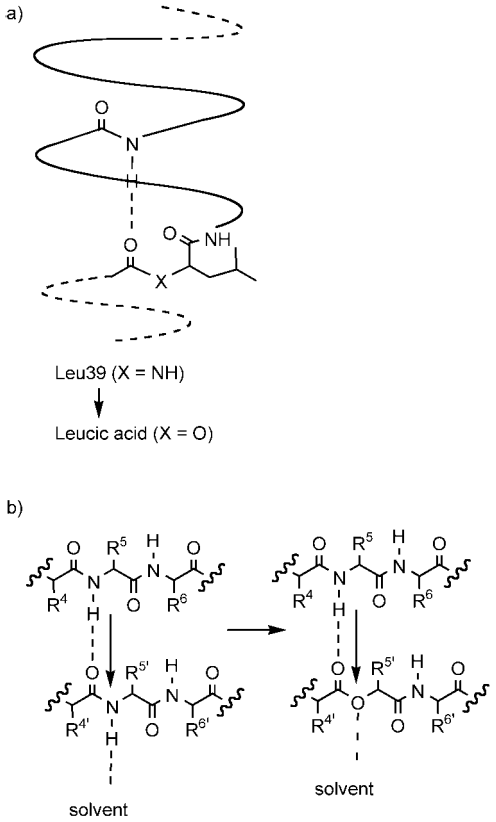


Figure 9. Schematic representation of backbone mutations generated by incorporation of α-hydroxy acids: a) N-terminal mutation of Leu 39 to leucic acid in an α-helix of T4 lysozyme; b) substitution of Leu 14 with leucic acid in a β sheet of SNase.

tively (Figure 9a).[140] The ester group is a conservative replacement for an amide group since both esters and amides are isosteric and exist mainly in the *trans* conformation.[141] These mutations effectively substitute a good hydrogen-bond acceptor (the amide carbonyl group) with a considerably weaker hydrogen-bond acceptor (the ester carbonyl group).[142] It was found that at the N- and C-terminal positions, where only one hydrogen-bonding interaction is perturbed, the ester substitution destabilizes the protein by 0.9 and 0.7 kcal mol^{-1}, respectively. Introduction of ester linkage in the middle of the helix, where two hydrogen-bonding interactions were altered, destabilizes the protein by 1.7 kcal mol^{-1}. Similarly, amide to ester substitutions introduced in antiparallel β sheets were found to decrease the stability by 1.5–2.5 kcal mol^{-1} (Figure 9b).[143] These results provide evidence that backbone hydrogen-bonding interactions involving the amide groups, like side-chain hydrogen bonds, contribute significantly to protein stability.

3.3. Extensions and Improvements of Methodology

A number of improvements have been made to increase the levels of in vitro protein expression. For example, an *E. coli* tRNA^{Asn}-derived suppressor led to a significant improvement in suppression efficiency relative to the yeast $tRNA^{Phe}_{CUA}$ for incorporation of polar unnatural amino acids in the *E. coli* in vitro system.[144] Mild heating of an S-30 extract derived from an *E. coli* release factor 1 (RF1) temperature-sensitive strain increased UAG suppression by decreasing the competition between RF1 and the suppressor tRNA for the amber stop codon.[145] Optimization of the preparation and composition of the *E. coli* S-30 extract, as well as removal of inhibitory by-products generated during the translation reaction, also greatly improved yields of the protein.[146]

Efforts have also focused on encoding unnatural amino acids with codons other than nonsense codons. For example, the rare arginine codon AGG has been used to direct the incorporation of several phenylalanine analogues into a polypeptide using a chemically aminoacylated $tRNA^{Ile}_{CCU}$.[147] In this case, the naturally occurring cognate tRNA, although present in minor amounts, competes with the synthetic tRNA to incorporate Arg and generate heterogeneous full-length protein (in contrast to truncated protein in the case of the nonsense codon). In the case of the rare AGG codon, lowering the arginine concentration in the in vitro protein synthesis reaction mixture decreased such competition.[148] Some organisms do not use all of the triplet codons; these noncoding codons can be used to specify additional amino acids. For example, the unassigned codon AGA in *Micrococcus luteus* has been used to insert Phe in an in vitro transcription/translation extract from *M. luteus*.[149] Recently, a purified in vitro translation system consisting of only ribosomes, initiation factors, and elongation factors was used to simultaneously incorporate several unnatural amino acids into peptides in response to sense codons.[150] If the efficiency can be improved, this system may ultimately allow the synthesis of peptides and proteins containing multiple unnatural amino acids.

 © 2005 Wiley-VCH Verlag GmbH & Co. KGaA, Weinheim

Frameshift suppression of four-base codons can also be used to introduce unnatural amino acids into proteins in vitro. The proper reading frame is maintained only when the extended codon is translated by the suppressor tRNA to afford a full-length protein containing the unnatural amino acid; translation of the triplet codon by an endogenous tRNA results in frameshifting and premature termination. To reduce this competition, the first three nucleotides in most extended codons correspond to either stop or rare codons. In one example, Sisido and co-workers replaced the anticodon of the yeast $tRNA^{Phe}$ with different four-base anticodons, and incorporated a variety of phenylalanine analogues into streptavidin with an in vitro *E. coli* translation system.[151–156] By using two chemically aminoacylated frameshift suppressor tRNAs that recognize either CGGG or AGGU, they were able to simultaneously incorporate 2-naphthylalanine and a 7-amino-4-nitrobenz-2-oxa-1,3-diazole (NBD) derivative of lysine into streptavidin, although the efficiency was quite low (9%).[157] Incorporation efficiency was improved to 64% when efficient four-base codons (CGGG and GGGU) were used.[158] A five-base CGGUA-UACCG codon-anticodon pair was also shown to direct incorporation of unnatural amino acids into streptavidin.[159]

A codon–anticodon pair containing unnatural bases (iso-C)AG-CU(iso-dG) has been used to incorporate iodotyrosine into a short peptide with the rabbit reticulocyte lysate.[160] This study convincingly showed that the ribosome tolerates nucleotides with unnatural bases, and that iso-C and iso-dG can direct translation with reasonable efficiency. However, the mRNA and tRNA containing iso-C and iso-dG must be chemically synthesized, thus making this method impractical for most applications.

Unnatural amino acid mutagenesis has been extended to *Xenopus* oocytes by microinjection of the mutant mRNA and a chemically aminoacylated yeast $tRNA^{Phe}$-derived amber suppressor (Figure 10).[161] The translational machinery of the oocyte inserts the unnatural amino acid at the position specified by UAG. Later, an amber suppressor derived from *Tetrahymena thermophila* $tRNA^{Gln}$ was found to improve the efficiency and fidelity of unnatural amino acid incorporation.[162] This method has been used for structure–function studies of integral membrane proteins, which are generally not amenable to in vitro expression systems.[163,164] For example, fluorinated tryptophan derivatives were incorporated at Trp149 in the binding domain of the nicotinic acetylcholine receptor. A correlation between the receptor activation by acetylcholine (Ach) and the degree of fluorination on tryptophan suggested that the quaternary ammonium center of Ach forms a cation–π interaction with the indole side chain of αTrp149.[165,166] A significant limitation of this method is that the suppressor tRNA has to be chemically aminoacylated with the unnatural amino acid in vitro, and the acylated tRNA is consumed as a stoichiometric reagent during translation and cannot be regenerated. Therefore, yields of proteins are low and highly sensitive techniques, such as patch clamp, are required to characterize the mutant proteins.

The in vitro mutagenesis methodology described above has been used to site-specifically incorporate a large number of unnatural amino acids into various proteins. Mutagenesis studies using unnatural amino acids have provided important insights into protein structure and function. However, the method is technically demanding, the yields of mutant proteins are quite low, and the study of proteins in cells is limited by the need for microinjection and inability to regenerate the aminoacyl tRNA. Moreover, the nature of the amino acid side chain is limited by the aminoacylation chemistry and the stability of the aminoacyl tRNA linkage.

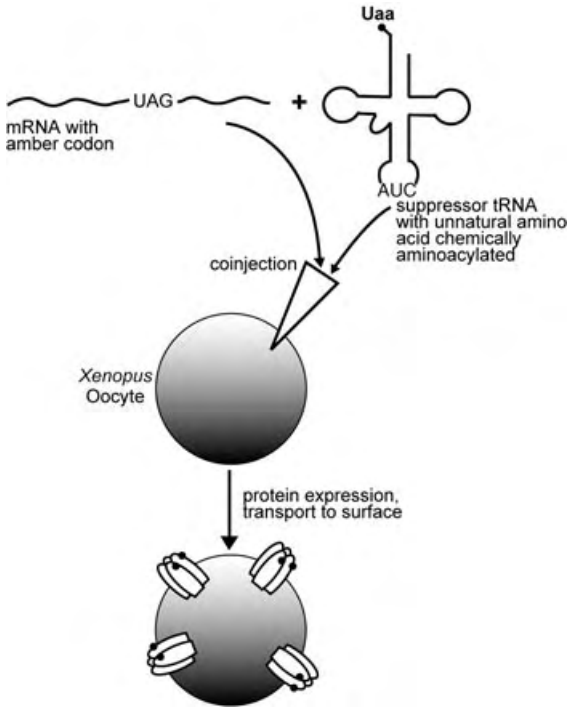


Figure 10. Microinjection of chemically aminoacylated tRNA and mutant mRNA into *Xenopus* oocytes.

4. In Vivo Protein Mutagenesis

The ability to incorporate unnatural amino acids directly into proteins in vivo has several advantages over in vitro methods including high yields of mutant proteins, technical ease, and the potential to study proteins in cells or multicellular organisms. The latter can be accomplished either by substitution of one of the common 20 amino acids with an unnatural amino acid, or by augmenting the genetic code of the host organims with a "21st" unnatural amino acid. In the former case, the unnatural amino acid typically replaces the common amino acid throughout a protein (and the proteome), often in competition with a common amino acid, and results in heterogeneous proteins. In the second approach, unnatural amino acids are *added* to the genetic repertoire without deletion of a common amino acid, thus resulting in an expanded genetic code and the ability to produce proteins consisting of more than 20 building blocks.

 © 2005 Wiley-VCH Verlag GmbH & Co. KGaA, Weinheim

4.1. Site-Directed Mutagenesis

The development of site-directed mutagenesis by Smith and co-workers provided a powerful in vivo method to substitute amino acids in proteins with any of the other common 20 amino acids.[167] Amino acid substitutions are generated by mutating the codon for the amino acid of interest to a codon encoding the desired mutant. This method has dramatically expanded our ability to manipulate protein structure and probe protein structure–function relationships. Notable early examples included studies of β-lactamase,[168,169] tyrosyl-tRNA synthetase (TyrRS),[170] dihydrofolate reductase,[171] trypsin,[172] and subtilisin.[173] Mutagenesis studies of *Bacillus stearothermophilus* TyrRS by the Fersht research group were used to quantify the contributions of various amino acid side chains to the binding of substrates, intermediates, and transition states along the reaction pathway of this enzyme.[174] In other examples, replacement of the complementarity-determining regions of a human antibody with those of a mouse antibody afforded a humanized antibody with the specificity of the latter;[175] site-directed mutagenesis has also been used to modify the specificity of Zn^{2+} finger proteins.[176–183]

Many variants of site-directed mutagenesis have been developed. For example, cassette mutagenesis allows for the rapid generation of all possible mutations at a single site.[184] Homologue- and alanine-scanning mutagenesis provide valuable information about protein function in the absence of structural data.[185,186] Random mutagenesis by error-prone polymerase chain reaction (PCR) or mutator strains allows for a less biased examination of structure–function relationships over a larger sequence space.[7,187–189] Genetic recombination methods, such as DNA shuffling,[190] a recombinative PCR process akin to molecular breeding, can be used to generate libraries of variants from a pool of parent genes. Desired protein properties can be rapidly evolved from these variants with appropriate selections or screens. All of these methods have greatly accelerated our ability to probe protein structure and function and evolve novel protein properties. Unfortunately, all are also limited to substitutions among the common 20 amino acids.

4.2. The Use of Auxotrophic Bacterial Strains To Incorporate Unnatural Amino Acids

More than 50 years ago it was found that many analogues of the common 20 amino acids inhibit the growth of bacteria.[191–193] This observation led to speculation that these analogues are incorporated into proteins by the protein biosynthetic machinery. To test this possibility, Tarver and co-workers fed rats[194] and *Tetrahymena*[195] with the ^{14}C-labeled methionine analogue ethionine. The detection of radioactivity in the isolated protein and peptides from these organisms strongly suggested that unnatural amino acids could in fact be misincorporated into proteins. To efficiently incorporate analogues of the common 20 amino acids into bacterial proteins, Cohen and co-workers used an auxotrophic bacterial strain that cannot biosynthesize the corresponding common amino acid. Induction of protein expression in media in which this common amino acid is replaced with its analogue results in the accumulation of a mutant protein containing the unnatural amino acid (Figure 11).[196]

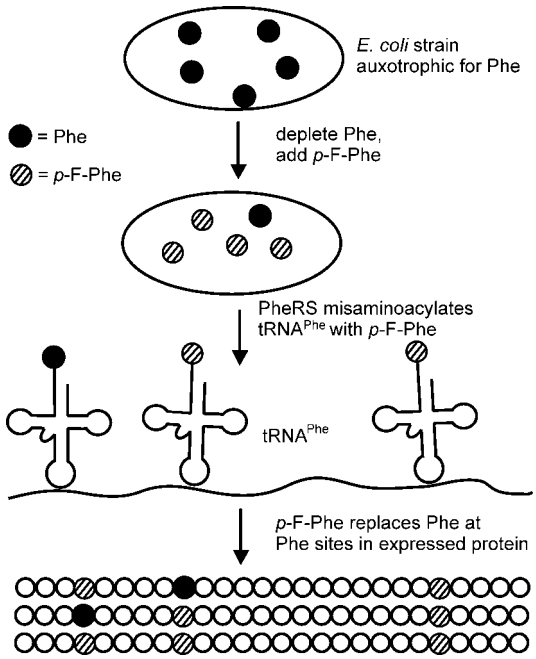


Figure 11. Multiple substitution of phenylalanine by *p*-fluorophenylalanine (*p*-F-Phe) using a phenylalanine auxotrophic strain.

This approach was used to incorporate *p*-fluorophenylalanine into β-galactosidase in an *E. coli* strain auxotrophic for phenylalanine.[196] Fluorophenylalanine was found to partially replace phenylalanine and tyrosine throughout the protein. Selenomethionine was similarly incorporated into β-galactosidase using a methionine auxotroph.[197,198] Over 60 analogues of the common 20 amino acids have subsequently been incorporated into proteins by this method.[193,199] Typical substitutions include replacement of hydrogen with fluorine, methylene with oxygen or sulfur, and ring substitutions. For example, tryptophan has been replaced with tryptazan,[200] arginine with canavanine,[201] methionine with norleucine,[202] leucine with trifluoroleucine,[203] and the phenyl ring of phenylalanine with thioenyl or furyl rings. Most of the early work focused on studies of the effects of amino acid analogues on bacterial growth and protein synthesis and processing.[199] More recently these methods have proven valuable for incorporating NMR and X-ray probes into proteins.

4.2.1. Relaxing the Substrate Specificity of Aminoacyl-tRNA Synthetases

Incorporation of amino acid analogues by the above approach relies on the promiscuity of aminoacyl-tRNA synthetases. However, these enzymes have very high substrate specificity to insure high fidelity in protein translation, which limits substitutions to close structural analogues of the

 © 2005 Wiley-VCH Verlag GmbH & Co. KGaA, Weinheim

common 20 amino acids. For example, although thiaproline can be incorporated quantitatively into proteins, oxaproline and selenaproline cannot.[204] To overcome this limitation, a number of research groups have attempted to relax the substrate specificity of the aminoacyl-tRNA synthetases. Hennecke and co-workers first reported that replacement of Ala294 with Gly in *E. coli* phenylalanyl-tRNA synthetase (PheRS) increases the size of the substrate binding pocket and results in the acylation of $tRNA^{Phe}$ with *p*-chlorophenylalanine (*p*-Cl-Phe).[205] An *E. coli* strain harboring this mutant PheRS allows the substitution of phenylalanine with *p*-Cl-Phe.[206] Tirrell and co-workers later used this mutant synthetase to incorporate *p*-bromo-, *p*-iodo-, *p*-cyano-, *p*-ethynyl-, and *p*-azidophenylalanine as well as pyridylalanine.[207,208] Similarly, a point mutation (Phe130→Ser) near the amino acid binding site of *E. coli* tyrosyl-tRNA synthetase allows azatyrosine to be incorporated more efficiently than tyrosine.[209] In these cases, the isolated protein typically contains a mixture of both the common and unnatural amino acid at the site of substitution.

4.2.2. Attenuating the Proofreading Activity of Aminoacyl-tRNA Synthetases

The fidelity of tRNA aminoacylation is maintained both by substrate discrimination and by proofreading of noncognate intermediates and products. Therefore, synthetases with impaired proofreading activity can also be used to incorporate unnatural amino acids into proteins by allowing close structural analogues of the cognate amino acid to escape the editing function. This approach was first demonstrated with a valyl-tRNA synthetase (ValRS) from *E. coli* (Figure 12).[210] ValRS can misaminoacylate $tRNA^{Val}$ with Cys, Thr, or aminobutyrate (Abu), but these noncognate amino acids are subsequently hydrolyzed by the editing domain. After random mutagenesis of the *E. coli* chromosome, a mutant ValRS was selected that has a mutation in the editing domain, which causes charging of $tRNA^{Val}$ with Cys. Since Abu sterically resembles Cys (the thiol group of Cys is replaced with a methyl group in Abu), the mutant ValRS also incorporates Abu into proteins when this mutant *E. coli* strain is grown in the presence of Abu. Mass spectrometric analysis shows that about 24% of valine is replaced by Abu at each valine position in the native protein. Tirrell and co-workers subsequently used a Thr252→Tyr252 mutant for the partial incorporation of six leucine analogues into proteins.[211]

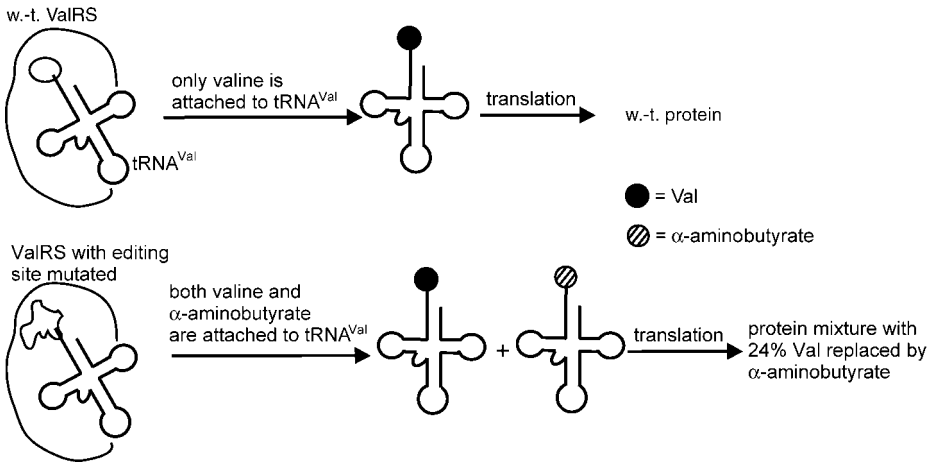


Figure 12. Incorporation of α-aminobutyrate by a ValRS mutant with reduced proofreading activity. w.-t. = wild-type.

4.2.3. Applications

One of the most important applications of the auxotrophic strain method of mutagenesis is the incorporation of amino acid analogues containing heavy atoms for phase determination in X-ray crystallography. Substitution of methionine with selenomethionine is a convenient way to introduce a heavy atom for multiwavelength anomalous diffraction.[212,213] Similarly, telluromethionine[214–216] and β-selenolo[3,2-β]pyrrolylalanine[217] have been incorporated into proteins using methionine and tryptophan auxotrophic *E. coli* strains, respectively.

Isosteric analogues of amino acids have also been incorporated into proteins in *E. coli* to study protein folding, stability, and activity. In one example, norleucine, selenomethionine, and telluromethionine (in which the sulfur atom of methionine is replaced with methylene, Se, and Te, respectively) were incorporated into human annexin V to probe the effects of side-chain packing interactions on protein stability.[218] Similar studies have been carried out with fluorinated amino acids;[219–221] for example, incorporation of trifluoroleucine and hexafluoroleucine in place of leucine resulted in increased thermal and chemical stability of a leucine-zipper protein.[222,223]

Amino acid analogues can also be used as spectroscopic probes. For example, the fluorescence emission maximum and intensity of a barstar mutant containing a tryptophan to aminotryptophan mutation are sensitive to the pH value of the local environment,[224] and replacement of Tyr66 of enhanced cyan fluorescent protein with 4-aminotryptophan significantly red-shifts the emission peak to produce a "gold" fluorescent protein ($\lambda_{max} = 574$ nm).[225] Fluorine-substituted amino acids can be used as NMR probes. For example, fluoromethionine has been substituted for methionine in bacteriophage λ-lysozyme to study ligand binding by ^{19}F NMR spectroscopy,[226–228] and fluorinated tryptophan has been incorporated for ^{19}F NMR studies in cyan fluorescent protein[229] and the chaperone PapD.[230]

Nonproteinogenic functional groups that provide selective handles for further protein modification have also been introduced into proteins by these methods. Examples include the replacement of phenylalanine with electroactive 3-thienylalanine,[231] and the substitution of methionine with alkenes and alkynes.[232–235]

 © 2005 Wiley-VCH Verlag GmbH & Co. KGaA, Weinheim

Azidohomoalanine has been incorporated using a methionine auxotrophic strain, and can be selectively modified with triarylphosphine reagents by Staudinger ligation,[236] or with alkyne reagents by a copper(I)-catalyzed cycloaddition reaction.[237] Finally, a computationally designed *E. coli* PheRS mutant was used to partially incorporate *p*-acetylphenylalanine into proteins; the ketone group was subsequently labeled with biotin hydrazide under mild conditions.[238]

Though very useful, the use of auxotrophic strains for mutagenesis has a number of limitations. This method is not site-specific—all sites corresponding to a particular amino acid throughout a protein (and the entire proteome) are replaced with the amino acid analogue. The extent of incorporation of the unnatural amino acid may also vary—only in rare cases can quantitative substitution be achieved since it is difficult to completely deplete the endogenous amino acids inside the cell. Finally, this method is applicable in general only to close structural analogues of the common amino acids, since substitutions must be tolerated both by the synthetase and at all nonpermissive sites in the proteome in which a particular amino acid is incorporated.

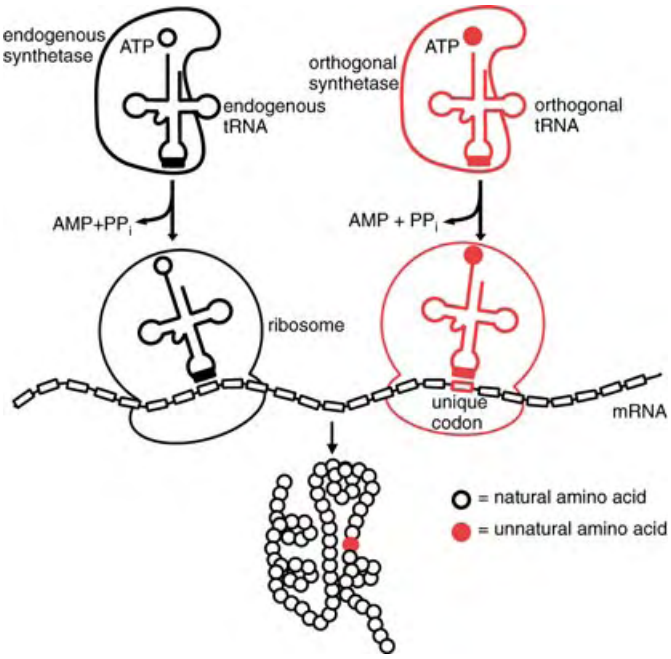


Figure 13. A general approach for the site-specific incorporation of unnatural amino acids into proteins in vivo. PP$_i$ = pyrophosphate.

5. An Expanded Code

Site-directed mutagenesis allows the selective substitution of amino acids in a protein with the other common 20 amino acids. The use of auxotrophic strains allows the substitution of an amino acid with a close structural analogue throughout the proteome, typically in competition with the corresponding common amino acid. Ideally, one would like to be able to carry out the equivalent of site-directed mutagenesis, but with unnatural mino acids. This scenario requires that the unnatural amino acid be genetically encoded by a unique codon in a manner similar to that of the common 20 amino acids.

5.1. Methodology

The "21st" amino acid selenocysteine (Sec) is naturally encoded by an in-frame UGA non-sense codon that is translated by a unique Sec-tRNA^{Sec} (generated by enzymatic modification of seryl-tRNA^{Sec}) in the presence of a special elongation factor and a *cis*-acting element in the mRNA.[4] However, in theory the only requirements to genetically encode unnatural amino acids in vivo are a unique tRNA–codon pair, a corresponding aminoacyl-tRNA synthetase (hereafter referred to as a synthetase), and the unnatural amino acid (Figure 13). The tRNA must be constructed such that it is not recognized by the endogenous aminoacyl-tRNA synthetases of the host, but functions efficiently in translation (an orthogonal tRNA). This tRNA must deliver the novel amino acid in response to a unique codon that does not encode any of the common 20 amino acids. A new aminoacyl-tRNA synthetase (an orthogonal synthetase) is also required that aminoacylates the orthogonal tRNA, but none of the endogenous tRNAs. This synthetase must aminoacylate the tRNA with only the desired unnatural amino acid and no endogenous amino acid. Likewise, the unnatural amino acid cannot be a substrate for the endogenous synthetases. Finally, the amino acid must be efficiently transported into the cytoplasm when added to the growth medium, or biosynthesized by the host.[239]

This potentially general approach to mutagenesis with unnatural amino acids was initially developed using *E. coli*, since it is easily genetically manipulated, has a high transformation efficiency, and many established selections and screens already exist. Initially the amber nonsense codon (UAG) was used to encode the unnatural amino acid since it is the least used of the three stop codons in *E. coli* and *S. cerevisiae*. Moreover, some *E. coli* strains contain natural amber suppressor tRNAs that efficiently incorporate common amino acids without significantly affecting growth rates (most genes essential for normal *E. coli* growth do not end in TAG).[240,241] Amber suppressors can also be engineered, and both natural and engineered amber suppressors have been routinely used for conventional protein mutagenesis in *E. coli*[124,125,242] as well as the in vitro introduction of unnatural amino acids into proteins. In addition, nonsense suppressors have been either identified or generated for use in mammalian cells,[243,244] yeast,[245,246] and *C. elegans*.[247,248] Therefore, it should be possible to use UAG or UGA for the incorporation of unnatural amino acids into proteins in a variety of organisms without adverse effects on the growth of the host organism.

Our initial attempts to generate an orthogonal amber suppressor tRNA/synthetase pair involved modifying the specificity of an existing *E. coli* tRNA/synthetase pair. Key nucleotides at the tRNA/synthetase interface were mutated to reduce the affinity of the tRNA for its cognate synthetase, while maintaining orthogonality to the other endogenous synthetases. A mutant synthetase was then evolved from the

 © 2005 Wiley-VCH Verlag GmbH & Co. KGaA, Weinheim

cognate wild-type synthetase that uniquely recognizes the mutant orthogonal tRNA, but at the same time retains its orthogonality with the endogenous tRNAs in *E. coli*. Based on the X-ray crystal structure of the complex of *E. coli* glutaminyl-tRNA synthetase (GlnRS) and $tRNA_2^{Gln}$,[249] three sites in $tRNA_2^{Gln}$ which make specific contacts with GlnRS were mutated.[250,251] These mutant tRNAs were tested individually in in vitro aminoacylation reactions and in vivo amber codon suppression assays, and an efficient orthogonal amber suppressor tRNA was identified. A library of mutant GlnRSs was then generated and mutants were selected based on their ability to aminoacylate the orthogonal tRNA. Although mutant *E. coli* GlnRSs were evolved that charge the orthogonal tRNA, the best mutant aminoacylates the orthogonal tRNA at approximately 10% the rate of wild-type $tRNA^{Gln}$. An ideal orthogonal synthetase should not acylate any endogenous *E. coli* tRNAs, since even modest misacylation of a wild-type tRNA with an unnatural amino acid will result in misincorporation of the unnatural amino acid at other sites in the protein. The inability to generate an orthogonal glutaminyl tRNA/synthetase pair, together with the finding that mutations within the tRNA interact in complicated, non-additive ways,[250] prompted us to examine alternative strategies.

A second approach to the generation of an orthogonal tRNA/synthetase pair involves the use of a heterologous tRNA/synthetase pair from another organism in *E. coli*. This approach is based on the observation that some prokaryotic tRNA/synthetase pairs do not cross-react to any significant degree with their eukaryotic counterparts, as a result of differences in the tRNA identity elements.[127,252] For example, it has been shown that *E. coli* GlnRS lacks the N-terminal RNA-binding domain present in *S. cerevisiae* GlnRS and does not aminoacylate yeast $tRNA^{Gln}$.[253] We therefore tested and found that the yeast amber suppressor $tRNA^{Gln}$ (*Sc* $tRNA^{Gln}_{CUA}$) is also not a substrate for *E. coli* GlnRS, yet functions efficiently in translation in bacteria. Moreover, whereas the yeast GlnRS does not aminoacylate any *E. coli* tRNAs, it does aminoacylate the amber suppressor *Sc* $tRNA^{Gln}_{CUA}$ in vitro.[254] Therefore, the *S. cerevisiae* $tRNA^{Gln}_{CUA}$/GlnRS is an orthogonal pair in *E. coli*. Unfortunately, no mutant yeast GlnRS could be evolved that aminoacylates the orthogonal tRNA with an unnatural amino acid in *E. coli*, possibly because of the low intrinsic activity of the synthetase in bacteria. Yeast tRNA/synthetase pairs specific for various hydrophobic amino acids were also examined,[255] and attention was focused on the $tRNA^{Tyr}$/TyrRS pair, since TyrRS does not have a proofreading function and the prokaryotic and eukaryotic $tRNA^{Tyr}$s have significant differences (Figure 14). Indeed, in vitro studies have shown that $tRNA^{Tyr}$ of *S. cerevisiae* and *H. sapiens* cannot be aminoacylated by bacterial synthetases, nor do their TyrRS aminoacylate bacterial tRNA.[256,257] Unfortunately, in vivo amber codon suppression assays showed that the amber suppressor $tRNA^{Tyr}_{CUA}$ derived from either *S. cerevisiae* or *H. sapiens* is not orthogonal in *E. coli*.[258]

We then focused our attention on archaea as a source of orthogonal tRNA/synthetase pairs for use in *E. coli*. Archaeal aminoacyl-tRNA synthetases are more similar to their eukaryotic than prokaryotic counterparts in terms of homology and tRNA recognition elements.[115] However, unlike synthetases from eukaryotic cells, which are often expressed poorly or have low activities in *E. coli*, synthetases from archaea can be expressed efficiently in *E. coli* in active form. In addition, the availability of more than 16 archaeal genome sequences, together with the absence of introns in their genomes, facilitates the cloning of archaeal synthetase genes. Finally, it has been shown that almost all the tRNAs of *Halobacterium cutirebrum*, an archaeal halophile, cannot be charged by *E. coli* synthetases.[127]

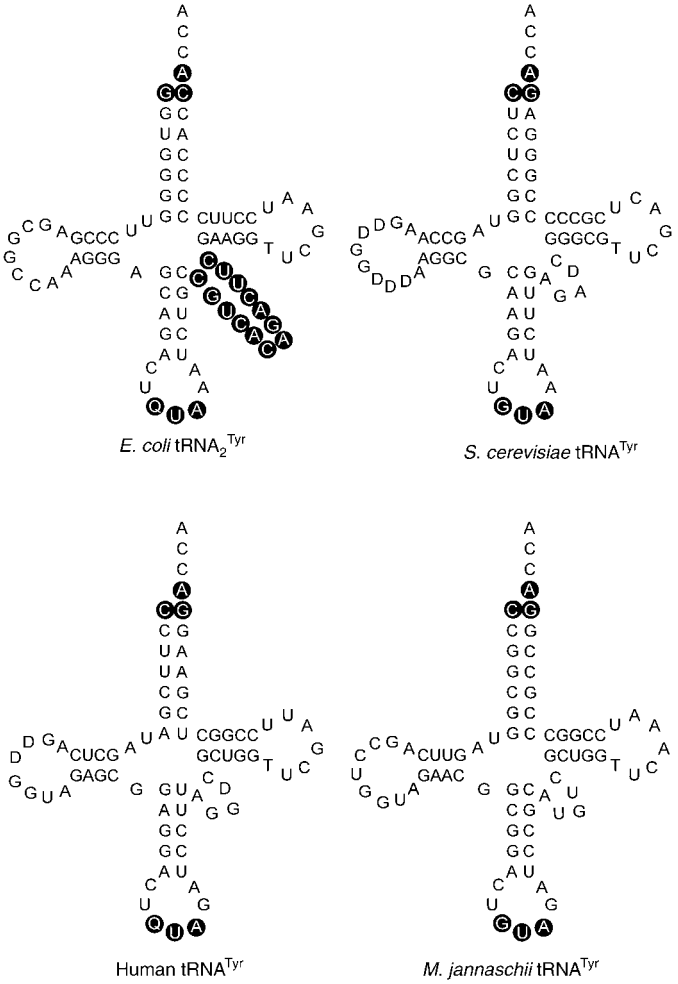


Figure 14. Comparison of $tRNA^{Tyr}$s from different species. Major identity elements are shaded in black. Prokaryotic $tRNA^{Tyr}$ has a long variable arm and a G1:C72 pair, in contrast to the short arm and C1:G72 pair in eukaryotic and archaeal $tRNA^{Tyr}$.

The amber suppressor tyrosyl-tRNA/synthetase pair derived from *Methanococcus jannaschii* was the first orthogonal *E. coli* pair generated from archaea.[258] *M. jannaschii* TyrRS (*Mj*TyrRS) discriminates tRNAs with C1:G72 (an eukaryotic recognition element) from those with G1:C72 (a prokaryotic recognition element), and does not aminoacylate crude tRNA from *E. coli*.[259] In addition, *Mj*TyrRS is missing most of the C-terminal binding domain for the anticodon loop of its $tRNA^{Tyr}$, which suggests that identity elements outside

 © 2005 Wiley-VCH Verlag GmbH & Co. KGaA, Weinheim

the anticodon region are mainly responsible for recognition by TyrRS and the orthogonality of this pair. Mutation of the anticodon loop of this tRNA should therefore have minimal effect on its recognition by other synthetases and its affinity for *Mj*TyrRS. Indeed, when cells expressing a β-lactamase gene with an amber codon at a permissive site are cotransformed with both a suppressor *M. jannaschii* $tRNA^{Tyr}_{CUA}$ ($Mj tRNA^{Tyr}_{CUA}$) and *Mj*TyrRS, they survive in the presence of high concentrations of ampicillin (suppression of the amber mutation results in the production of full-length β-lactamase allowing cells to survive in ampicillin).[258] Unfortunately, while this result shows that the $Mj tRNA^{Tyr}_{CUA}$ is an excellent substrate for *Mj*TyrRS in *E. coli*, we did observe a low but significant level of aminoacylation of this tRNA by endogenous synthetases.

A general strategy for the selection of orthogonal tRNAs in *E. coli* was then developed to further reduce recognition of the $Mj tRNA^{Tyr}_{CUA}$ by endogenous *E. coli* synthetases, while preserving activity with both the cognate synthetase and translational machinery (for example, the ribosomal A site, elongation factor Tu, etc.).[260] This method consists of a combination of negative and positive selections with a mutant suppressor tRNA library in the absence and presence of the cognate synthetase, respectively (Figure 15). In the negative selection, amber nonsense codons are introduced into the barnase gene at sites permissive to substitution by other amino acids. When a member of the suppressor tRNA library is aminoacylated by an endogenous *E. coli* synthetase (that is, it is not orthogonal to the *E. coli* synthetases), the amber codons are suppressed and the ribonuclease barnase is produced, resulting in cell death. Only cells harboring orthogonal or nonfunctional tRNAs can survive. All surviving clones are then subjected to a positive selection in which an amber codon is placed in the β-lactamase gene at a permissive site. tRNAs that are good substrates for the cognate synthetase are selected based on their ability to suppress the amber codon and produce active β-lactamase. Cells harboring nonfunctional tRNAs, or tRNAs that cannot be recognized by their cognate synthetase, will be sensitive to ampicillin. Therefore, only tRNAs that: 1) are not substrates for endogenous *E. coli* synthetases; 2) can be aminoacylated by the synthetase of interest; and 3) function in translation will survive both selections.

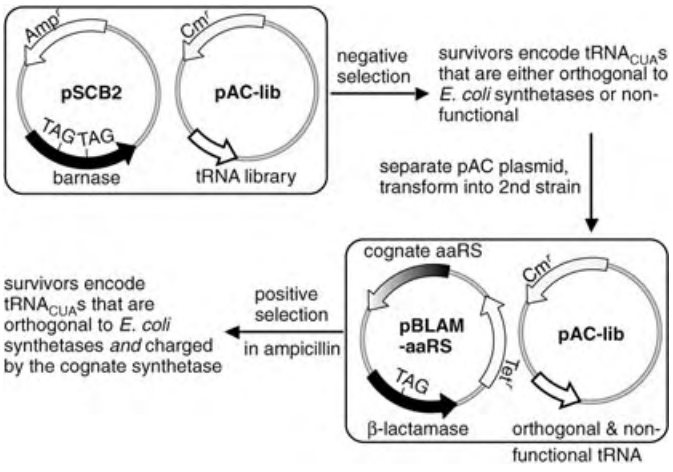
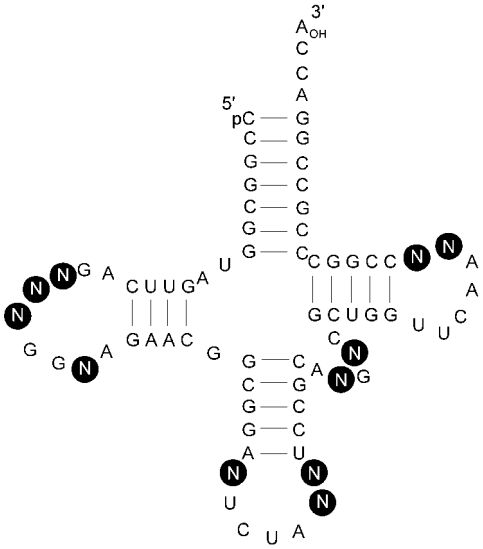


Figure 15. Negative and positive selections used to evolve orthogonal tRNAs.

Eleven nucleotides of the $Mj tRNA^{Tyr}_{CUA}$ that do not interact directly with the *Mj*TyrRS were randomly mutated to generate a suppressor tRNA library (Figure 16). This tRNA



suppressor tRNA	IC_{50} (μg mL^{-1} of amp)	
	with pBLAM	with pBLAM-JYRS
no tRNA	10	10
w.-t. *Mj*Tyr	56	1220
mutRNA^{Tyr}_{CUA}	12	436
mutant 2	20	632
mutant 3	14	459

Figure 16. A mutant tRNA library based on *M. jannaschii* $tRNA^{Tyr}$ with randomized nucleotides indicated with N. The table lists the suppression efficiencies of several selected mutant tRNAs.

library was passed through rounds of negative and positive selection to afford a mutant tRNA ($mutRNA^{Tyr}_{CUA}$) that suppresses the β-lactamase amber mutant at a level comparable to the background level in *E. coli*, thus indicating that this mutant tRNA is a poorer substrate for *E. coli* synthetases than the wild-type $Mj tRNA^{Tyr}_{CUA}$. When the $mutRNA^{Tyr}_{CUA}$ is coexpressed with *Mj*TyrRS, cells survive at high concentration of ampicillin, which indicates that the tRNA is still aminoacylated by its cognate TyrRS and functions efficiently in translation.[260] The low background and high activity of this $mutRNA^{Tyr}_{CUA}$/*Mj*TyrRS pair make it an excellent orthogonal pair in *E. coli*.

Next the substrate specificity of the orthogonal synthetase was altered so that the cognate orthogonal tRNA is charged with only the desired unnatural amino acid and none of the common 20 amino acids. Amino acid promiscuity in the orthogonal synthetase will result in proteins with a mixture of common and unnatural amino acids at the site of mutation. For example, in an attempt to site-specifically incorporate *p*-

© 2005 Wiley-VCH Verlag GmbH & Co. KGaA, Weinheim

fluorophenylalanine (*p*-F-Phe) into proteins, a yeast amber suppressor $tRNA^{Phe}_{CUA}$/PheRS pair was introduced into an *E. coli* strain auxotrophic for Phe and unable to utilize *p*-F-Phe.[261] Since yeast PheRS aminoacylates its cognate tRNA with both Phe and *p*-F-Phe, 64–75% *p*-F-Phe is incorporated at the site of mutation; the remainder is Phe and Lys (even in the presence of an excess of *p*-F-Phe added to the growth media). Moreover, 7% *p*-F-Phe is found at sites encoded by the Phe codon, which indicates that the endogenous *E. coli* PheRS incorporates *p*-F-Phe in addition to Phe.

We have developed a systematic and general approach to evolve mutant synthetases that selectively aminoacylate their cognate orthogonal tRNA with unnatural amino acids.[262] Based on the crystal structure of the homologous TyrRS from *Bacillus stearothermophilus*, five residues (Tyr32, Asn123, Asp158, Ile159, and Leu162) in the active site of *M. jannaschii* TyrRS that are within 6.5 Å of the *para* position of the aryl ring of bound tyrosine were randomized to all possible common amino acids (Figure 17). These residues

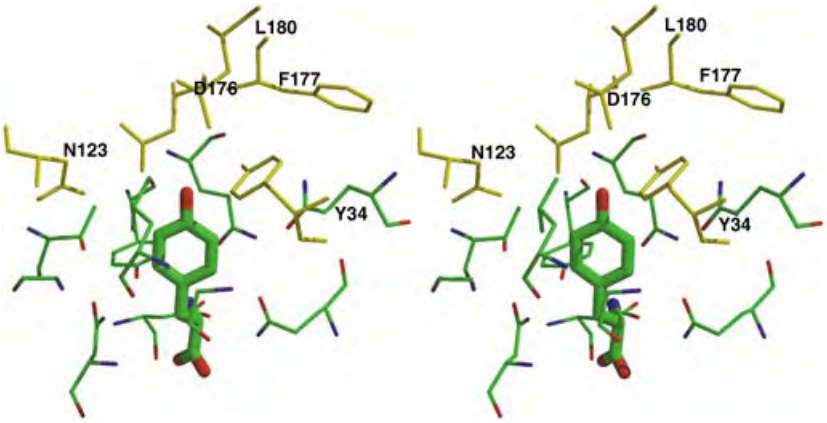


Figure 17. Stereoview of the active site of TyrRS. Residues from *B. stearothermophilus* TyrRS are shown. Corresponding residues from *M. jannaschii* TyrRS are Tyr32 (Tyr34), Glu107 (Asn123), Asp158 (Asp176), Ile159 (Phe177), and Leu162 (Leu180) with residues from *B. stearothermophilus* TyrRS in parentheses; mutated residues are in yellow.[262]

were all initially mutated to alanine to avoid a high background of wild-type TyrRS. The resulting inactive Ala_5 TyrRS was used as a template for PCR mutagenesis to generate the TyrRS library by mutation of the five sites to NNK (N = A, T, G, or C and K = G or T). The size of this library was 1.6×10^9 to ensure complete coverage of all possible mutants. A positive selection was then applied which is based on suppression of an amber stop codon in the chloramphenicol acetyltransferase (CAT) gene in the presence of the unnatural amino acid and chloramphenicol (in contrast to β-lactamase which is secreted into the periplasm, CAT localizes in the cytoplasm). Surviving cells were then grown in the presence of chloramphenicol and in the absence of the unnatural amino acid. Those cells that did not survive were isolated from a replica plate supplemented with the unnatural amino acid. The mutant synthetase genes were isolated from these cells, recombined in vitro by DNA shuffling, and transformed back into *E. coli* for further rounds of selection with increasing concentrations of chloramphenicol (Figure 18).

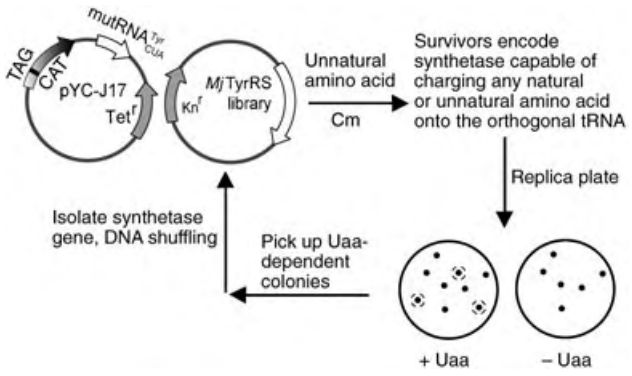


Figure 18. A general positive selection and negative screen scheme for evolving synthetases specific for unnatural amino acids. Cm = chloramphenicol, Uaa = unnatural amino acid.

This selection scheme was first used to generate an *Mj*TyrRS mutant synthetase capable of selectively inserting *O*-methyl-L-tyrosine (OMeTyr) into proteins in response to the amber codon.[262] OMeTyr is structurally similar to tyrosine and phenylalanine and provided an excellent opportunity to test the degree of translational fidelity that can be achieved by this approach. After two rounds of selection and DNA shuffling, a clone was evolved whose survival in chloramphenicol was highly dependent on the addition of 1 mM OMeTyr to the growth media. Cells survived in the presence of chloramphenicol when OMeTyr was added to the growth media, but died in the absence of the amino acid. An OMeTyr mutant of *E. coli* dihydrofolate reductase (DHFR) was generated and characterized to demonstrate that the observed phenotype arises from the site-specific incorporation of OMeTyr by the $mutRNA^{Tyr}_{CUA}$/mutant TyrRS pair in response to an amber stop codon. The third codon of the *E. coli* DHFR gene was mutated to TAG, and a His_6 tag was added to the C-terminus to facilitate protein purification and separation from endogenous DHFR. Full-length DHFR was produced only when the mutant TyrRS, the $mutRNA^{Tyr}_{CUA}$, and OMeTyr were all present (Figure 19). Insertion of OMeTyr in response to the TAG codon was confirmed by mass analysis of both the intact protein and tryptic fragments. No incorporation of tyrosine or other amino acids at the TAG position was observed, and OMeTyr was incorporated only in response to TAG and not any other sites. The growth rate of *E. coli* was not significantly affected and the protein yield was 2 mg L^{-1} in minimal media, which corresponds to 77% of the yield of wild-type DHFR. These results demonstrated for the first time that one could rationally engineer bacteria that genetically encode an unnatural amino acid with high efficiency and translational fidelity.[262]

We then attempted to genetically encode L-3-(naphthyl)-alanine, which represents a significant structural perturbation

 © 2005 Wiley-VCH Verlag GmbH & Co. KGaA, Weinheim

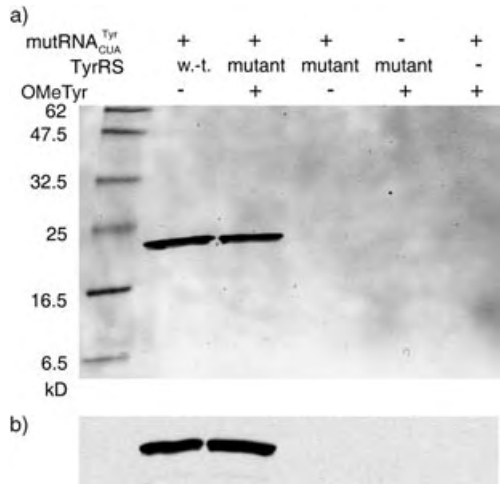


Figure 19. Accumulation of *E. coli* DHFR protein under different conditions. a) Silver-stained sodium dodecylsulfate polyacrylamide gel electrophoresis (SDS-PAGE) of purified DHFR. The left lane is a molecular weight marker. b) Western blot of the protein gel. A penta-His antibody was used to detect the six-histidine tag at the COOH terminus of DHFR.

relative to tyrosine.[263] A slightly different mutant TyrRS library (in which Tyr 32, Asp 158, Ile 159, Leu 162, and Ala167 were randomized) was constructed from which four mutant synthetases were identified that have high activity for this unnatural amino acid. One round of DNA shuffling of these four synthetase genes resulted in a mutant synthetase (SS12) with enhanced activity for L-3-(naphthyl)alanine and greatly reduced activity for endogenous amino acids. An amber codon was introduced in the middle of the gene of mouse DHFR to verify incorporation of the unnatural amino acid. Protein expression and mass-spectrometric analysis confirmed that the mutRNA$_{CUA}^{Tyr}$/SS12 mutant synthetase selectively incorporates L-3-(naphthyl)alanine into proteins with an efficiency and fidelity rivaling that of the common 20 amino acids.[263] This result suggested that the above methodology may be applicable to a large variety of unnatural amino acids.

Alternative selection schemes for evolving the amino acid specificity of the orthogonal *Mj*TyrRS have been developed subsequently. One approach involves passing the mutant synthetase library through a positive selection based on the ability of the mutant synthetase to suppress amber mutations introduced at permissive sites in the CAT gene in the presence of an unnatural amino acid as described above. A negative selection is then applied in which those synthetases that recognize endogenous amino acids are eliminated in the absence of the unnatural amino acid. The negative selection is based on suppression of amber nonsense mutations introduced in the barnase gene.[254] Pilot selections of inactive *Mj*TyrRS and OMeTyr specific mutant synthetases from a large pool of wild-type *Mj*TyrRS were used to optimize the selection conditions for the *M. jannaschii* mutRNA$_{CUA}^{Tyr}$/TyrRS pair.[264] A barnase mutant with three amber codons (encoded in pLWJ17B3) was found to provide optimal selection stringency and enrichment efficiency.[265] Survivors of both the positive and negative selections encode synthetases that charge the orthogonal tRNA with only the unnatural amino acid. More mutations can be introduced by mutagenesis or DNA shuffling into these synthetase genes to generate second-generation synthetase libraries, which can be used for further rounds of selection until a mutant synthetase with a desired activity is evolved. This new scheme (Figure 20) has been used to evolve *M. jannaschii* mutRNA$_{CUA}^{Tyr}$/TyrRS orthogonal pairs for a wide variety of unnatural amino acids (see Section 5.2). By varying the stringency, order, and number of the positive and negative selection steps one can likely affect both the activity and fidelity of the evolved synthetase.[265]

A second method for evolving aminoacyl-tRNA synthetase specificity relies on an amplifiable fluorescent reporter of amber suppression.[266] A T7/GFPuv reporter (pREP) was created in which suppression of amber codons introduced at

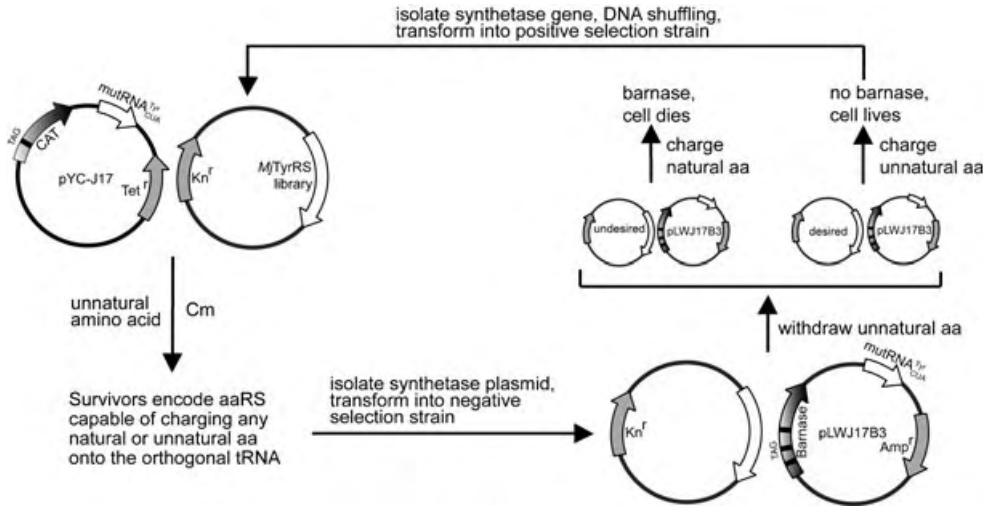


Figure 20. A general positive and negative selection scheme for evolving synthetases specific for unnatural amino acids.

 © 2005 Wiley-VCH Verlag GmbH & Co. KGaA, Weinheim

permissive sites in the gene for T7 RNA polymerase produces full-length protein, which in turn drives the expression of green fluorescent protein (GFPuv). This construct was combined with the above CAT reporter (pYC-J17) to yield pREP(2)/YC-JYCUA which contains the orthogonal mutRNA$^{Tyr}_{CUA}$, the amber mutant of CAT, and the T7/GFPuv reporter genes (Figure 21 a).[266] When *E. coli* containing this reporter are transformed with a mutant *Mj*TyrRS library and grown in the presence of an unnatural amino acid, active synthetases can be identified based on fluorescence and/or chloramphenicol resistance. Cells are subsequently grown in the absence of unnatural amino acid and chloramphenicol, and nonfluorescent cells containing the desired mutant synthetase are collected by fluorescence-activated cell sorting (FACS). The advantages of this method are that a single strain of *E. coli* can be used to perform both positive and negative selections, and cells containing the reporter can be replicated in the presence and absence of amino acid and visually inspected for amino acid dependent fluorescence (Figure 21 b).[266] Alternatively, this chloramphenicol and FACS double-positive selection can also be followed by the barnase negative selection.[265]

A direct positive selection has also been developed in which an antibody specific for an unnatural amino acid (or peptide containing the amino acid) is used to enrich phage into which the unnatural amino acid is incorporated (Figure 22).[267] A C3 peptide with an amber mutation is fused to the N-terminus of the VSCM13 phage coat protein pIII, such that C3TAG phage production requires suppression of the amber stop codon. Cells harboring a phagemid that expresses an orthogonal suppressor tRNA and a synthetase library are infected with the C3TAG phage. An active synthetase results in suppression of C3TAG and display of its cognate amino acid on the phage surface. The phage pool is then incubated with immobilized monoclonal antibodies directed against the unnatural amino acid to isolate only those phage carrying the synthetase specific for the unnatural amino acid. Phage displaying Asp were enriched over 300-fold from a pool of phage displaying Asn in a simulated selection using antibodies raised against the Asp-containing epitope.

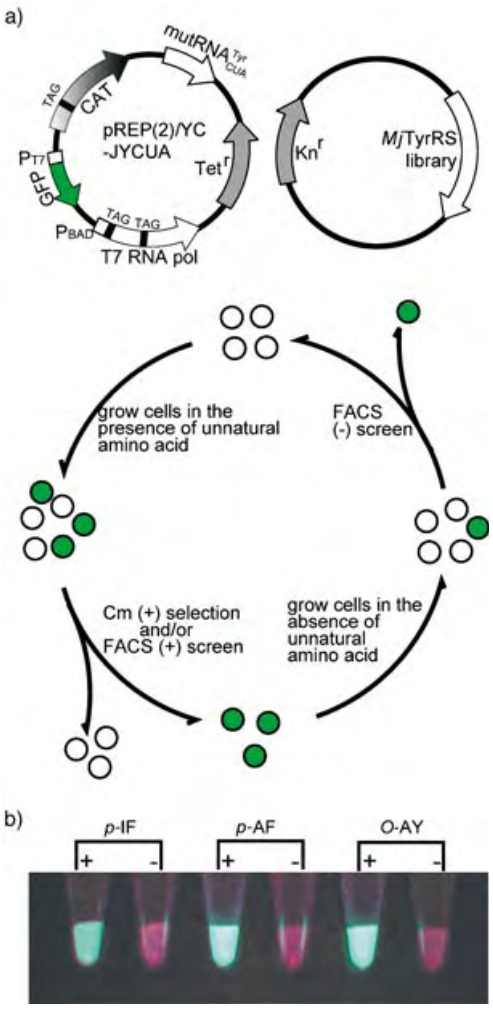


Figure 21. a) A system for evolving synthetase specificity that combines a fluorescent reporter with a chloramphenicol-based selection. b) Green fluorescence can be used to verify unnatural amino acid dependent GFP expression.

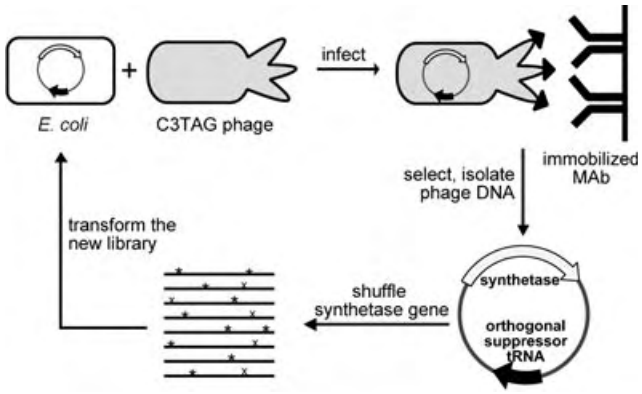


Figure 22. A phage-based selection for the incorporation of unnatural amino acids. *E. coli* are infected by phage with a stop codon in a gene encoding a phage coat protein. Phage containing an active synthetase display the unnatural amino acid on the phage surface and are selected with immobilized monoclonal antibodies.

5.2. A Survey of Genetically Encoded Unnatural Amino Acids

The above selections have been used to add over 30 novel amino acids to the genetic code of *E. coli* (Figure 23).[262,263,266,268–275] These include: 1) various substituted tyrosine and phenylalanine analogues such as *O*-methyl-L-tyrosine (**1**),[262] *p*-amino-L-phenylalanine (**5**),[266] 3-nitro-L-tyrosine (**15**),[276] *p*-nitro-L-phenylalanine (**29**),[276] *m*-methoxy-L-phenylalanine,[276] and *p*-isopropyl-L-phenylalanine (**4**);[266] 2) amino acids with aryl azide (**10**) and benzophenone (**11**) groups that can be photo-cross-linked;[269,270] 3) amino acids that have unique chemical reactivity including *p*-acetyl-L-phenylalanine (**6**) and *m*-acetyl-L-phenylalanine (**9**),[271,273] *O*-allyl-L-tyrosine (**3**),[268] *O*-(2-propynyl)-L-tyrosine

 © 2005 Wiley-VCH Verlag GmbH & Co. KGaA, Weinheim

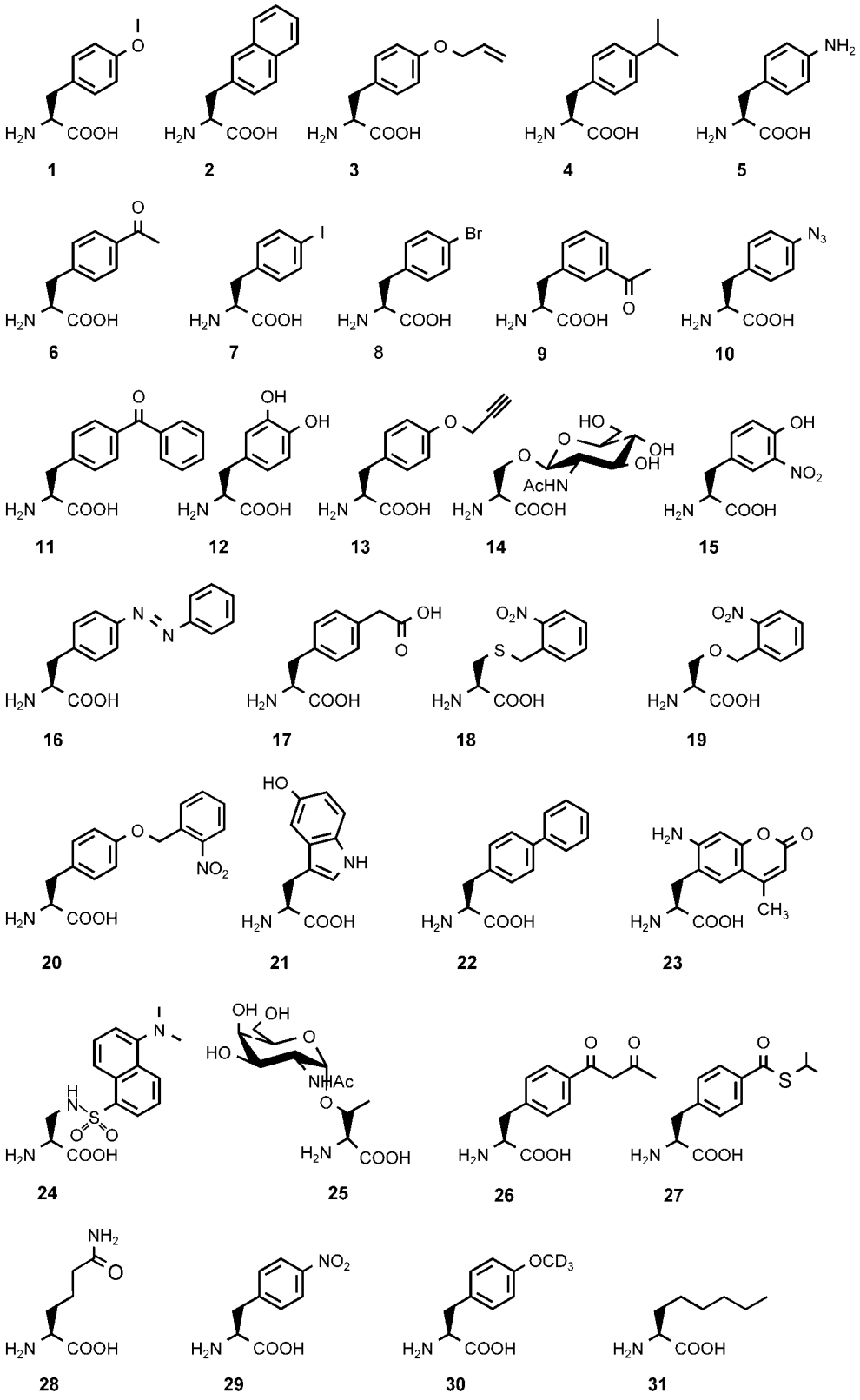


Figure 23. Some structures of unnatural amino acids that have been added to the genetic code of *E. coli*.

(**13**),[276] *p*-ethylthiocarbonyl-L-phenylalanine (**27**), and *p*-(3-oxobutanoyl)-L-phenylalanine (**26**);[276] 4) heavy-atom-containing amino acids for phasing in X-ray crystallography including *p*-iodo (**7**) and *p*-bromo-L-phenylalanine (**8**);[272] 5) the redox-active amino acid dihydroxy-L-phenylalanine (**12**);[274] 6) glycosylated amino acids including β-*N*-acetylglu-

 © 2005 Wiley-VCH Verlag GmbH & Co. KGaA, Weinheim

cosamine-*O*-serine (**14**) and α-*N*-acetylgalactosamine-*O*-threonine (**25**);[275] 7) fluorescent amino acids with naphthyl (**2**), dansyl (**24**), and 7-aminocoumarin (**23**) side chains;[263,276] 8) photocleavable and photoisomerizable amino acids with azobenzene (**16**) and nitrobenzyl Cys, Ser, and Tyr side chains (**18**–**20**);[276] 9) the phosphotyrosine mimetic *p*-carboxymethyl-L-phenylalanine (**17**); 10) the glutamine homologue homoglutamine (**28**);[276] and 11) 2-aminooctanoic acid (**31**). This list suggests that synthetases can be evolved for a large number of structurally diverse amino acid side chains, which range from sugars to extended aromatic groups. Moreover, it appears that the ribosome and elongation factors also tolerate considerable structural diversity, which is consistent with previous in vitro mutagenesis studies.

In general these unnatural amino acids are incorporated with excellent fidelity and efficiency by their cognate tRNA/synthetase pairs. Each pair was characterized by their ability to confer chloramphenicol resistance to cells transformed with the CAT amber mutant gene in the presence and absence of a particular unnatural amino acid.[262] Secondly, each orthogonal tRNA/synthetase pair was used to incorporate the corresponding unnatural amino acid into proteins at permissive sites in the genes for *E. coli* or mouse DHFR,[262,263] the Z domain of protein A,[268,271] or myoglobin.[266] Each protein was tagged with hexahistidine and purified. Milligram quantities of the mutant protein could be purified per liter of minimal media by using the unnatural amino acid and the orthogonal tRNA/synthetase pair. Yields were typically 25–50%, and in some cases greater than 75% that obtained with the wild-type protein.[262,263] High-resolution mass spectrometry was also used to analyze the intact protein and tryptic digests[271] to confirm that only the unnatural amino acid is incorporated in response to the TAG codon and at no other site in the protein.

Many of these unnatural amino acids have novel properties that are useful for a variety of biochemical and cellular studies. For example, two amino acids (*p*-azidophenylalanine (**10**) and *p*-benzoylphenylalanine (**11**)) have side chains that can be photo-cross-linked both in vitro and in vivo.[269,270,277] Benzophenone is a particularly useful photo-cross-linker since it absorbs at relatively long wavelengths (ca. 360 nm), and the excited state inserts efficiently into carbon–hydrogen bonds.[278] Indeed, a mutant homodimeric glutathione S-transferase with *p*-benzoylphenylalanine substituted at the dimer interface could be crosslinked in greater than 50% yield in the cytoplasm of *E. coli* (Figure 24). These amino acids should be useful for studies of protein–protein and protein–nucleic acid interactions in vitro and in vivo, for studies of protein structure and dynamics, and for the identification of receptors for orphan ligands. They should also allow the selective immobilization of proteins and cells on surfaces in defined orientations.

The keto-containing amino acids *p*-acetylphenylalanine (**6**; *p*-Ac-Phe) and *m*-acetylphenylalanine (**9**) can be used for the selective chemical modification of proteins, especially those proteins with multiple cysteine residues.[271,273] The ketone group undergoes a variety of reactions including addition, aldol, transamination, and isomerization reactions. It reacts with hydrazides, alkoxyamines, and semicarbazides

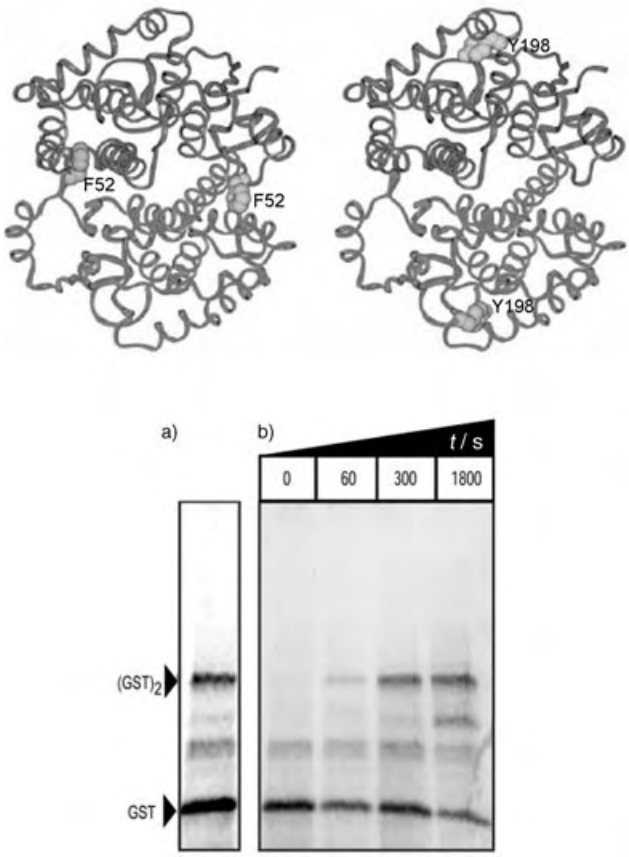


Figure 24. Residues Phe52 (top left) and Tyr198 (top right) of GST were mutated to *p*-benzoylphenylalanine (pBpa). a) Purified GST (Phe52pBpa) was cross-linked in vitro and detected by Western blot with an anti-GST antibody. b) The covalent dimerization of GST (Phe52-pBpa) in *E. coli* as a function of cellular irradiation at 365 nm, detected as in (a). Tyr198-pBpa GST could not be cross-linked.

under aqueous, mild conditions to produce hydrazone, oxime, and semicarbazone linkages that are stable under physiological conditions. For example, the in vitro reaction of a *p*-Ac-Phe mutant of the Z domain protein with 1 mM fluorescein hydrazide at pH 6.5 led to labeling of the protein with fluorescein in a 1:1 molar ratio in greater than 90% yield (Figure 25a).[271] Homogenous glycoprotein mimetics were also generated by labeling *p*-Ac-Phe-containing proteins with aminooxy sugars in $>90\%$ yield (Figure 25b). Oligosaccharides with defined structures were covalently attached to proteins either by adding additional saccharides to the pendant sugar with glycosyltransferases, or by directly coupling an aminooxy-derivatized glycan in one step.[279] Similarly, keto-containing mutants were efficiently labeled with hydrazide derivatives of biotin (Figure 25c) and polyethylene glycol. The latter should allow the generation of homogeneous proteins site-specifically derivatized with PEG with very high chemical purity. In addition, *m*-acetylphenylalanine has been used to efficiently label in vivo a keto-containing mutant of the *E. coli* membrane protein LamB with any of three water soluble fluorophores (Cascade blue, Alexa 568, or Alexa 647).[273] In a related experiment, copper-

 © 2005 Wiley-VCH Verlag GmbH & Co. KGaA, Weinheim

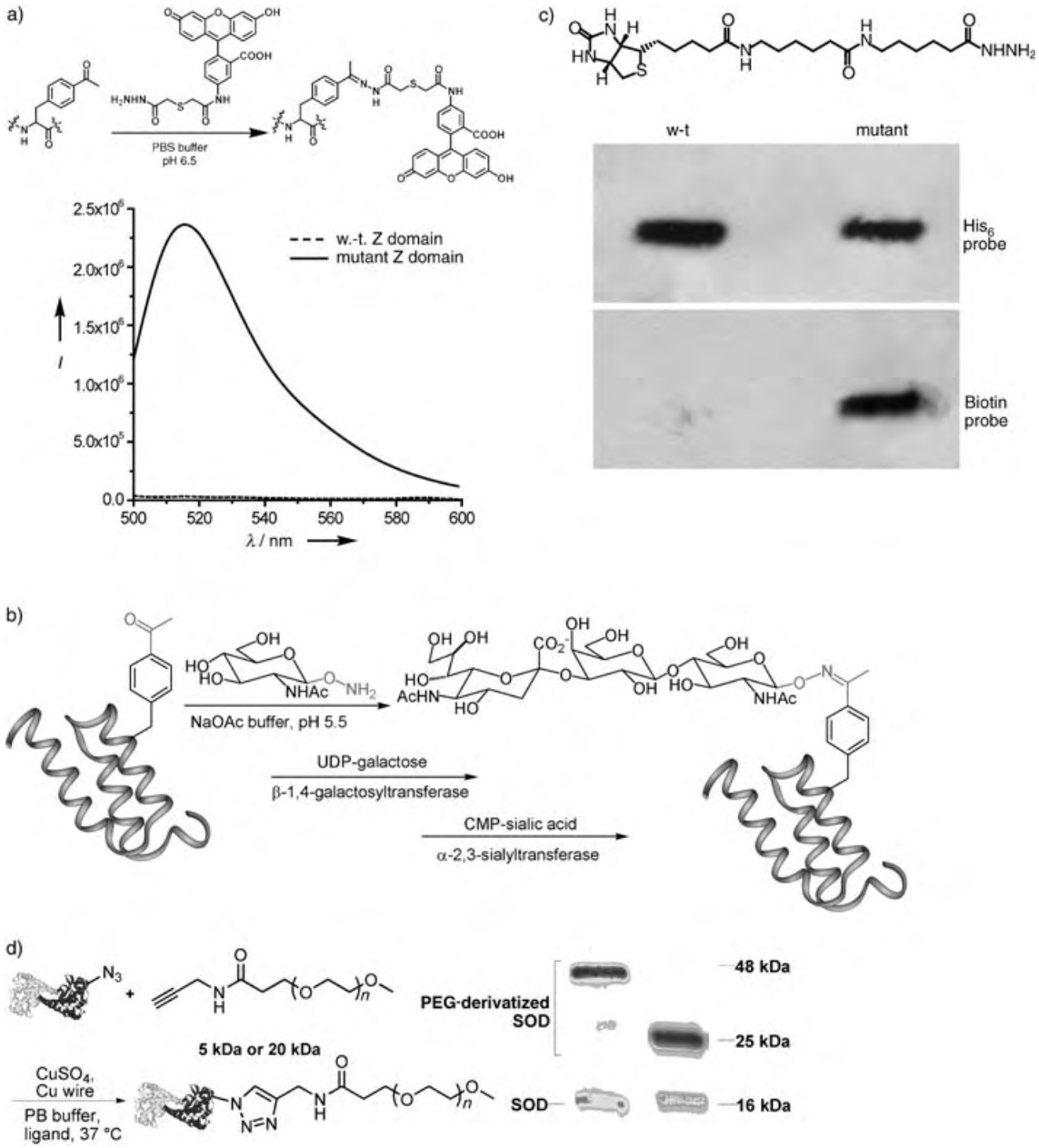


Figure 25. a) In vitro labeling of protein containing *p*-acetyl-L-phenylalanine with fluorescein hydrazide. b) Generation of homogeneous glycoprotein mimetics by conjugating an aminooxy sugar and subsequent extension with glycosyltransferases. c) In vitro labeling of protein containing *p*-acetyl-L-phenylalanine with biotin hydrazide. A His_6 tag was added to the C-terminus of both wild-type and mutant protein and was detected with His_6-specific antibody in Western blot analysis. Only the *p*-acetylphenylalanine-containing protein was labeled with biotin and thus detected by the biotin-specific anitibody. d) Protein derivatization with PEG through a copper-mediated cycloaddition reaction and SDS PAGE analysis.

mediated [2+3] cycloaddition reactions between mutant proteins containing either alkyne or azido unnatural amino acids **10** or **13** and a corresponding azide- or alkyne-derivatized chemical label have been used to selectively modify proteins with fluorophores and polyethylene glycol in high yield (> 75 %, Figure 25 d).[280] In addition, we have recently shown that thioester-containing amino acids can also be used to selectively modify proteins with nonpeptidic groups.[281]

Protein glycosylation is an essential posttranslational modification in eukaryotic cells, which can modulate protein folding and secretion, biological activity, serum half-life, and localization.[282] Although a variety of methods have been developed to obtain pure glycoforms of a protein,[283–286] most impose severe restrictions on the size, quantity, and/or quality of the glycoprotein produced. In an effort to provide a general solution to this problem, we attempted to alter the specificity of the *Mj*TyrRS to accept β-*N*-acetylglucosamine-*O*-serine (β-GlcNAc-Ser, **14**). The esterified amino acid was used to facilitate transport into the cell, where it is subsequently deacetylated by cytosolic esterases. Mutant synthetases were isolated that site-specifically incorporate the glycosylated

 © 2005 Wiley-VCH Verlag GmbH & Co. KGaA, Weinheim

amino acid into myoglobin in response to the amber codon with high translational fidelity and in a yield roughly 20–30% that of wild-type myoglobin. An enzyme-linked immunosorbent assay demonstrated significant binding of the GlcNAc-specific lectin *Bandeiraea simplicifolia* II (BSII) to the β-GlcNAc-Ser mutant myoglobin, whereas no binding was observed for the wild-type myoglobin.[275] Moreover, the *O*-GlcNAc-serine mutant myoglobin could act as a substrate for galactosyltransferases. Incubation of the myoglobin mutant containing the GlcNAc side chain with radioactive UDP[6-H^3]Gal in the presence of β-1,4-galactosyltransferase resulted in radiolabelled product (Figure 26).[275] This approach has also been used to selectively introduce α-GalNAc-Thr into proteins, and is currently being extended to a number of other O- and N-linked sugars.[275] We are also attempting to genetically encode other posttranslationally modified amino acids including methylated and acetylated lysine, as well as phosphorylated tyrosine, serine, and threonine. Recently, an *Mj*TyrRS mutant was evolved that selectively incorporates *p*-carboxylmethyl-L-phenylalanine (**17**), which is a stable mimetic of phosphotyrosine that can be used for studies of signal transduction. In addition, the incorporation of 2-aminooctanoic acid **31** suggests that it may be possible incorporate lipid-modified amino acids directly into proteins.

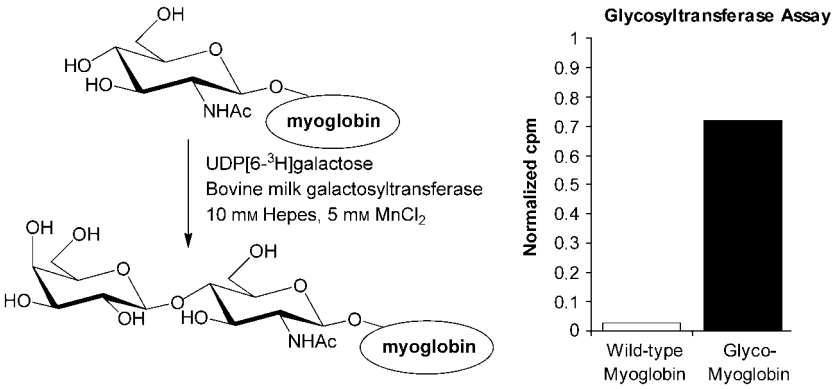


Figure 26. Direct incorporation of β-GlcNAc-Ser into myoglobin in *E. coli* and extension by addition of galactosyltransferase and UDP[6-^{3}H]galactose.

The ability to genetically encode heavy-atom-containing amino acids should facilitate phase determination in X-ray crystallography. To this end, an orthogonal tRNA/synthetase pair has been evolved that selectively incorporates *p*-iodophenylalanine (**7**, *p*-iodo-Phe) in response to the amber codon.[265] The yield of a mutant *p*-iodo-Phe-containing Z domain protein was around 60% of the wild-type protein (5.5 mg L^{-1} versus 9.2 mg L^{-1} in minimal medium). Bacteriophage T4 lysozyme with either residue Ser44 or Phe153 mutated to *p*-iodo-Phe was expressed, purified, and crystallized to determine the utility of *p*-iodophenylalanine for single-wavelength anomalous dispersion (SAD) phasing (the anomalous signal ($\Delta f''$) of iodine at 8 keV is 6.91, six times that of selenium (1.15)). The crystal structure was solved at 1.54-Å resolution by SAD phasing with the incorporated iodine atom using a laboratory $Cu_{K\alpha}$ X-ray source.[287]

Green fluorescent protein (GFP) is a powerful biological tool, which allows protein expression, localization, dynamics, and interactions to be directly visualized in intact cells.[288] However, in many cases the size of GFP and the fact that GFP can only be incorporated as an N- or C-terminal fusion are significant limitations. GFP also requires time for fluorophore maturation. The ability to co-translationally incorporate unnatural amino acids containing relatively small fluorescent side chains would minimize structural perturbations to the host protein, provide a broader range of spectral properties, and allow more control over the location of the fluorescent reporter (namely, at any permissive surface residue, rather than just the N- or C- terminus). To this end, we have evolved *M. jannaschii* TyrRSs that selectively incorporate 7-aminocoumarin (**23**) and 7-hydroxycoumarin into proteins in *E. coli*,[289] as well as an orthogonal *E. coli* leucyl synthetase that incorporates the dansyl-containing amino acid **24** (Figure 23) into proteins in yeast.[290] The environmentally sensitive coumarin-containing amino acid **23** has been used to monitor the unfolding of apo myoglobin and interaction of GroEL with its substrates.

Another novel amino acid that has been incorporated into proteins is dihydroxyphenylalanine (DHP, **12**).[274] DHP can undergo two-electron oxidation to the corresponding quinone (Figure 27), and should be useful to both probe and manipulate electron-transfer processes in proteins. The redox-active amino acid 5-hydroxytryptophan has also been selectively incorporated into proteins in mammalian cells in response to an opal codon (see below). This amino acid undergoes electrochemical oxidation to form an efficient cross-linking agent in vitro. Unnatural amino acids may also be used to perturb the electronic properties of a protein. For example, introduction of several unnatural amino acids in place of Tyr65 in GFP led to blue shifts in the emission spectra and altered quantum yields.[272] In addition, deuterated and ^{15}N-labeled derivatives of OMeTyr have also been site-selectively incorporated into proteins as NMR probes.[327]

Finally, the azobenzene-containing amino acid **16**[291] and the photocaged amino acids nitrobenzyl-Cys, -Ser, and -Tyr **18**–**20**[292] have recently been incorporated into proteins in *E. coli* and/or yeast. These amino acids make possible the in vivo regulation of protein activity by light. For example, mutation of the active site cysteine residue in the proapoptotic protease caspase 3 to nitrobenzylcysteine led to a catalytically inactive enzyme, whose activity could be restored

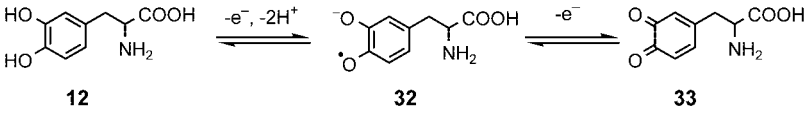


Figure 27. Oxidation of DHP **12** to DHP-semiquinone radical **32**, which is readily oxidized to DHP-quinone **33.**

 © 2005 Wiley-VCH Verlag GmbH & Co. KGaA, Weinheim

by photocleavage of the nitrobenzyl protecting group (Figure 28). The azobenzene-containing amino acid can be photochemically converted from the *trans* into the *cis* isomer and therefore provides an opportunity to photoregulate a variety of biological processes in vivo. For example, this amino acid has been used to photoregulate the binding of cAMP to the catabolite activator protein of *E. coli*.[291]

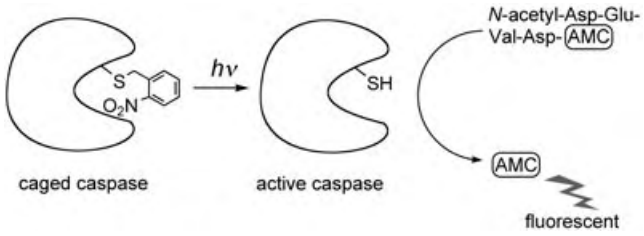


Figure 28. A photocaged caspase with an active-site nitrobenzylcysteine. AMC = 7-amino-4-methylcoumarin.

We have been surprisingly successful in identifying *M. jannaschii* TyrRS mutants with altered specificities, the majority of which are from a library with five active site residues randomized.[239,262] Crystallographic studies of the wild-type and mutant synthetases provide an opportunity to examine the origins of amino acid specificity in this important class of enzymes. A comparison of the active-site structures of bound and unbound wild-type *Mj*TyrRS indicates that there are significant structural changes that occur upon binding of tyrosine (Figure 29).[293,294] Asp 158 moves closer to the active site to bind the tyrosine hydroxy group, while Tyr 32 moves away to accommodate the hydroxy group of the tyrosine residue of the substrate. In addition, the Tyr 151 side chain rotates 60° to form a 2.9-Å hydrogen bond with the α-amino group of tyrosine. Recent determination of the X-ray crystal structure of a *p*-bromophenylalanine-specific synthetase suggests that the structural plasticity evident in the wild-type synthetase plays a major role in the generation of the specificity of this mutant enzyme.[276] This mutant synthetase differs from the wild-type synthetase by five mutations (Y32L, E107S, D158P, I159L, and L162E). Surprisingly, helix α8 of the mutant is disrupted and residues 158, 159, and 162, which line the active site in the wild-type synthetase, are flipped out of the active site in the mutant. Residues H160 and Y161, which are exposed to solvent in the wild-type structure, flip in to form a new binding pocket with extensive van der Waals contacts to *p*-bromophenylalanine. We are constructing new libraries to randomize this entire region (residues 158–162) to take advantage of the observed flexibility in this region to further evolve the activity of this synthetase.

Given the above successes and the availability of additional orthogonal tRNA/synthetase pairs, it is likely that many other unnatural amino acids can be genetically encoded. We are currently attempting to evolve orthogonal tRNA synthetase pairs that selectively incorporate amino acids containing spin labels, *p*-cyanophenylalanine (an IR probe), metal-binding amino acids, and backbone-modified amino acids (for example, *N*-methyl amino acids, β-amino acids, and α-hydroxy acids). In addition, a number of approaches are being explored to further increase the yields of the mutant proteins. These include optimizing the expression levels (and induction protocols) of the orthogonal tRNA and synthetase as well as carrying out selections for synthetases in rich versus minimal media. Indeed, it has been shown by Cho and co-workers that such changes can afford up to 750 mg L^{-1} quantities of mutant proteins.[328] Synthetase and tRNA mutants with increased activities can also be generated by additional rounds of mutagenesis and selection, or by rational design using X-ray crystal structures of mutant synthetase–amino acid complexes. Indeed, it has recently been shown that the affinities of aminoacylated tRNAs for elongation factor Tu (EF-Tu) and the ribosomal A site vary, depending on the attached amino acid and tRNA.[295] We are also beginning to examine the role of endogenous factors in determining the efficiency and fidelity of unnatural amino acid incorporation by using transposon and chemical mutagenesis, and complementation with genomic DNA libraries. For example, transposon mutations in the *fis* gene have been identified that improve the efficiency of amber suppression in some cases. Similar approaches may also increase the transport of some unnatural amino acids and lead to further improvements in suppression efficiency by random mutations in the ribosome, release factors, tRNA genes, etc.

The availability of bacteria with additional genetically encoded amino acids allows one to experimentally test

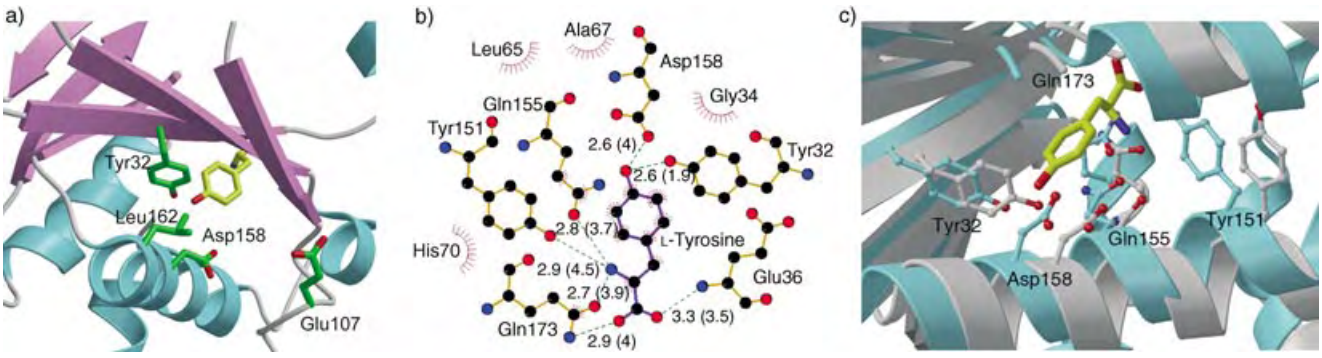


Figure 29. a) The amino acid recognition domain of wild-type *M. jannaschii* TyrRS.[294] b) Hydrogen-bonding interactions between the substrate tyrosine residue and the interacting residues in the binding pocket. The values correspond to the lengths [Å] of the hydrogen bonds in the TyrRS-Tyr-tRNA^{Tyr} complex structure;[294] values in parenthesis are analogous distances from the apo structure.[293] c) Comparison of the *M. jannaschii* TyrRS with (cyan) and without (gray) tyrosine bound in the active site.[293]

© 2005 Wiley-VCH Verlag GmbH & Co. KGaA, Weinheim

whether additional amino acids can lead to proteins with enhanced chemical or biological properties, or provide an evolutionary advantage for an organism.[265] A library of unnatural amino acids can be introduced at all sites in a target protein by using an amber codon walking strategy. Alternatively, mutagenesis can be used to introduce amber codons at random sites in the genome, and the resulting strains grown on media containing each of the above unnatural amino acids. These libraries can then be subjected to a variety of selective pressures, and mutations that provide a growth advantage can be mapped and the resulting protein characterized.

In a related experiment we have shown that unnatural amino acids can be efficiently incorporated into polypeptides fused to the pIII protein of a filamentous phage to generate an infectious phage.[296] This process allows large libraries of phage-displayed peptides and proteins to be created with both natural and unnatural amino acid building blocks, which can subsequently be screened for novel binding and/or catalytic properties.

5.3. Amino Acid Biosynthesis.

In all the above studies the amino acid must be added to the growth media and taken up by the cell in order to be incorporated into a protein in response to the amber codon. There are a large number of amino acid and amine transporters that are relatively nonspecific, and as a consequence, most amino acids we have assayed are transported into *E. coli* cytoplasm from the growth media and accumulate in significant concentrations. In some cases it is necessary to use enzymatically labile derivatives of highly polar amino acids or to mutate/delete enzymes that degrade the amino acid.

An alternative to adding exogenous amino acids to the growth media involves engineering a pathway for the biosynthesis of the unnatural amino acid directly in the host organism. To this end a completely autonomous 21 amino acid bacterium has been generated that contains genes for the biosynthesis of *p*-amino-L-phenylalanine (*p*-AF, **5**) from simple carbon sources,[297] an aminoacyl-tRNA synthetase[266] that uses *p*-AF (and no other endogenous amino acids), and a tRNA[262] that delivers *p*-AF into proteins in response to the amber codon. *p*-AF was biosynthesized from chorismic acid (an intermediate in aromatic amino acid biosynthesis) using the *papA*, *papB*, and *papC* genes from *S. venezuelae* in combination with a nonspecific *E. coli* transaminase (Figure 30). *E. coli* containing *papA–C* produced *p*-AF at levels comparable to those of the other aromatic amino acids and had normal growth rates. In the presence of a *p*-AF-specific, orthogonal mutRNA$^{Tyr}_{CUA}$/synthetase pair, *E. coli* transformed with *papA-C* produced mutant proteins containing *p*-AF at sites encoded by the amber codon with excellent yields and fidelity.[297] In addition to *p*-AF, it should be possible to biosynthesize and genetically encode other amino acids in vivo as well, including methylated, acetylated, and glycosylated amino acids.

5.4. Quadruplet Codons

The ultimate number of unnatural amino acids that can be encoded in any organism is limited by the number of noncoding codons. In addition to nonsense codons, it should be possible to use rare codons to encode unnatural amino acids, although it is likely that some competition with the cognate amino acid will occur. Alternatively, it may be possible to generate a synthetic *E. coli* variant in which rare codons are deleted from the wild-type genome (by replacing them with degenerate codons specifying the same amino acid) and instead used to encode unnatural amino acids.

It should also be possible to use quadruplet codons and cognate suppressor tRNAs with expanded anticodon loops to encode additional amino acids. There are many examples of naturally occurring +1 frameshift suppressors including UAGN (N = A, G, C, or T) suppressors derived from Su7 which encodes glutamine,[298] *sufJ*-derived suppressors of ACCN codons encoding threonine,[299] and CAAA suppressors derived from tRNA^{Lys} and tRNA^{Gln}.[300] Moreover, genetic selections have been used to identify efficient four- and five-base codon suppressor tRNAs from large libraries of mutant tRNAs.[301,302] In these studies, a tRNA library in which the anticodon loop of tRNA$^{Ser}_2$ (positions 31–38) was replaced with all possible eight base-pairing sequences was crossed with a library containing all possible four-base codon sequences encoding Ser70 of β-lactamase. Efficient pairs of suppressor and four-base codon were identified by an in vivo selection strategy,[301] including a mutant tRNA with an anticodon loop sequence of CUUCCUAG that efficiently

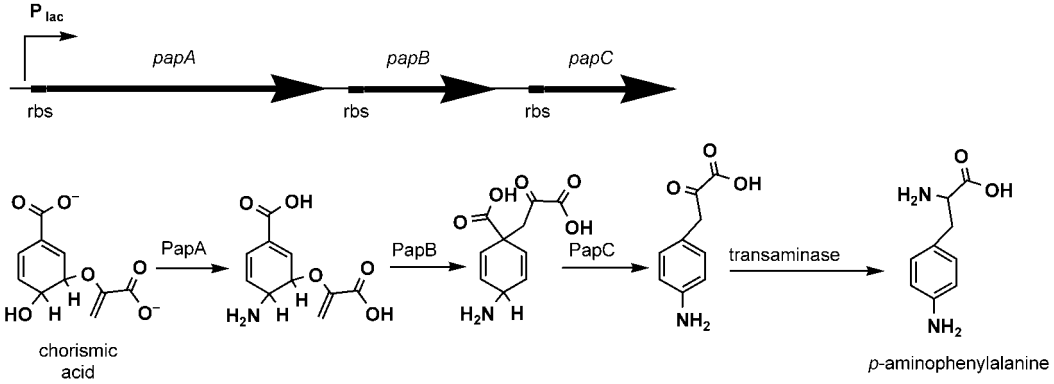


Figure 30. Biosynthesis of *p*-aminophenylalanine in *E. coli* by introducing *papA*, *B*, and *C* genes from *S. venezuelae*.

 © 2005 Wiley-VCH Verlag GmbH & Co. KGaA, Weinheim

suppresses an AGGA codon.[302] In this case, suppression of AGGA is competing with the rare codon AGG, which may account for the efficiency and lack of toxicity of this suppressor tRNA. Frameshift suppressor tRNAs can efficiently incorporate a number of the common 20 amino acids into proteins in vivo,[303] and as described above, chemically aminoacylated frameshift suppressors have also been used to incorporate unnatural amino acids into proteins in in vitro translation systems with four- and five-base codons.

Recently, an orthogonal four-base suppressor tRNA/synthetase pair was generated from archaeal $tRNA^{Lys}$ sequences (see Section 5.5) that efficiently and selectively incorporates the unnatural amino acid homoglutamine into proteins in *E. coli* in response to the quadruplet codon AGGA.[304] Frameshift suppression with homoglutamine does not significantly affect protein yields or cell growth rates, and is mutually orthogonal with amber suppression. This approach allows the simultaneous incorporation of two unnatural amino acids at distinct sites within proteins. For example, orthogonal AGGA-specific and TAG-specific tRNAs were expressed in the presence of a myoglobin with Gly24→AGGA and Ala75→TAG mutations (Figure 31). The corresponding orthogonal *O*-methyl-L-tyrosine-specific and homoglutamine-specific synthetases were combined in a second plasmid. When cells cotransformed with both plasmids were grown in the presence of the two amino acids, 1.7 mg L^{-1} of mutant myoglobin was produced. The overall suppression efficiency was approximately 25%. No protein was produced when either of the two unnatural amino acids was excluded. Electrospray mass spectrometric analysis of the full-length protein confirmed that myoglobin contained both unnatural amino acids.[304] This work suggests that neither the number of available triplet codons nor the translational machinery itself represents a significant barrier to further expansion of the code.

5.5. Other Orthogonal tRNA/Synthetase Pairs in E. coli

A "consensus suppressor strategy" has recently been developed for the rational design of additional orthogonal tRNA/synthetase pairs for use in *E. coli*.[305] In the first application of this strategy an orthogonal synthetase was generated from the *Methanobacterium thermoautotrophicum* leucyl synthetase. The corresponding suppressor tRNA was based on the consensus sequence of multiple archaeal leucyl tRNAs. The anticodon loop of this consensus tRNA was replaced with the sequence CUXXXAA, where XXX is the reverse complement sequence of distinct nonsense codons. To improve suppression efficiency and further reduce recognition of this tRNA by endogenous *E. coli* synthetases, mutations were introduced into the stems of the consensus tRNA sequence and the resulting mutant tRNA library was subjected to the general negative and positive selections described above.[260] The two most significant features identified from these studies for an efficient amber orthogonal suppressor tRNA are a CU(X)XXXAA anticodon loop and the lack of noncanonical or mismatched base pairs in the stem regions.[260,305] An orthogonal tRNA/synthetase pair derived from the archaeal $tRNA^{Glu}$ sequences and the glutamyl tRNA synthetase from *Pyrococcus horikoshii* has also been generated by this strategy (Figure 32).[306] Both orthogonal pairs have comparable suppression efficiencies to the tyrosyl pair derived from *M. jannaschii*. Other orthogonal pairs have also been reported in the literature for use in *E. coli*. An orthogonal $tRNA^{Asp}_{CUA}$/AspRS pair was derived from yeast $tRNA^{Asp}$/AspRS,[307] in which a yeast AspRS E188K mutant was used to improve recognition for the amber suppressor $tRNA^{Asp}_{CUA}$.[307,308] An *E. coli* initiator $tRNA^{fMet}$ amber mutant together with a mutant yeast TyrRS also form an orthogonal pair in *E. coli*.[309] These synthetases have different active sites and may be useful for evolving specificities for other types of amino acids.

5.6. Genetically Encoding Unnatural Amino Acids in Yeast

The same general strategy developed to genetically encode unnatural amino acids in bacteria should also be applicable to higher organisms. This approach requires the generation of orthogonal tRNA/synthetase pairs for each

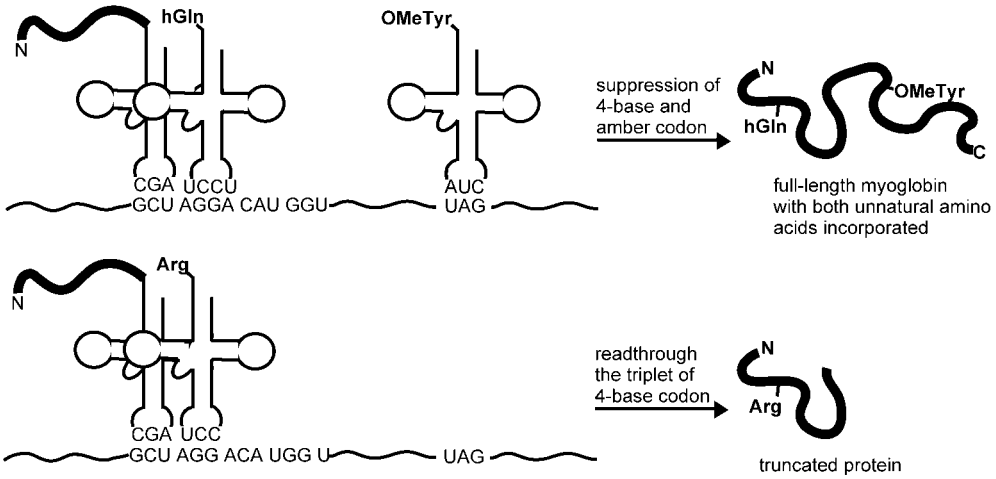


Figure 31. Simultaneous incorporation of the two unnatural amino acids homoglutamine (hGln) and *O*-methyl-L-tyrosine (OMeTyr) into myoglobin by suppression of a four-base codon and an amber nonsense codon.

 © 2005 Wiley-VCH Verlag GmbH & Co. KGaA, Weinheim

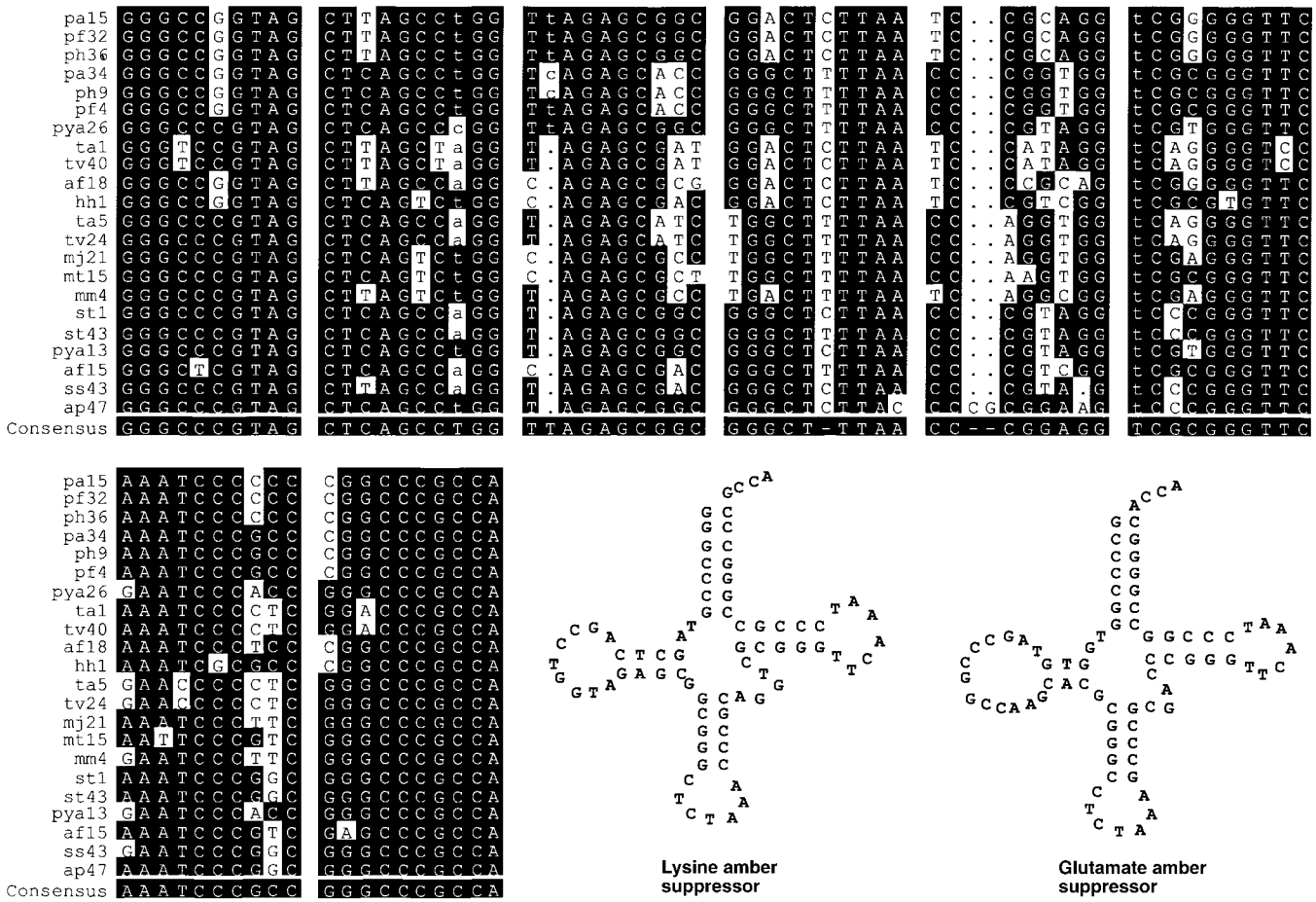


Figure 32. Archaeal lysyl and consensus tRNAs and the derived lysyl and glutamyl amber suppressors.

organism of interest. Most orthogonal tRNA/synthetase pairs that have been reported for eukaryotes are derived from bacterial pairs, reflecting the fact that the divergence of both sequence identity and identity elements of tRNAs from prokaryotes to eukaryotes is greater than that from eukaryotes to archaea and between one eukaryote and another. The transcription of a tRNA gene in eukaryotic cells depends on RNA polymerase III and its associated factors, which recognize A and B box sequences that are internal to the tRNA structural gene.[310] Some bacterial tRNAs that diverge from the eukaryotic A and B box sequence are not efficiently biosynthesized or processed in eukaryotic cells and their sequences need to be modified accordingly.[244,311] While all *E. coli* tRNA genes encode full sequences of tRNAs, many bacterial and archaeal and nearly all eukaryotic tRNAs have the 3′-CCA sequence added enzymatically by tRNA nucleotidyltransferase. Thus, it may also be necessary to delete the 3′-CCA in the tRNA gene imported from *E. coli*.[312] In addition, the generation of a functional tRNA in some cases requires specific 5′ and 3′ flanking sequences, the removal of introns, posttranscriptional nucleotide modifications, as well as export to the cytoplasm through an exportin-tRNA-dependent process.[313–315]

A number of orthogonal tRNA/synthetase pairs have been generated for use in eukaryotic organisms. For example, it has been shown that *E. coli* tyrosyl amber suppressor $tRNA^{Tyr}_{CUA}$ is not aminoacylated by eukaryotic synthetases and acts as an amber suppressor in *S. cerevisiae* in the presence of *E. coli* TyrRS.[316,317] In addition, *E. coli* TyrRS does not aminoacylate yeast tRNAs.[318] Thus, *E. coli* $tRNA^{Tyr}_{CUA}$/TyrRS functions as an orthogonal pair in yeast. A human initiator-tRNA-derived amber suppressor together with *E. coli* GlnRS form another orthogonal pair for use in yeast.[309] In addition, the *E. coli* $tRNA^{Gln}_{CUA}$/GlnRS pair has also been used in mammalian cells for efficient suppression of the amber codon.[244]

To selectively introduce an unnatural amino acid into proteins in eukaryotes, Yokoyama and co-workers screened a small collection of designed active-site variants of *E. coli* TyrRS in a wheat-germ translation system and discovered a mutant synthetase that utilizes 3-iodotyrosine more effectively than tyrosine.[319] This mutant synthetase was used with the *B. stearothermophilus* $tRNA^{Tyr}_{CUA}$ to incorporate 3-iodotyrosine into proteins in mammalian cells.[311]

To develop a general selection scheme in yeast analogous to that used in *E. coli* for evolving synthetases specific for unnatural amino acids, we created a selection strain of *S. cerevisiae* (MaV203:pGADGAL4 (2 TAG)) that contains the transcriptional activator protein GAL4 in which the codons at two permissive sites were mutated to amber

 © 2005 Wiley-VCH Verlag GmbH & Co. KGaA, Weinheim

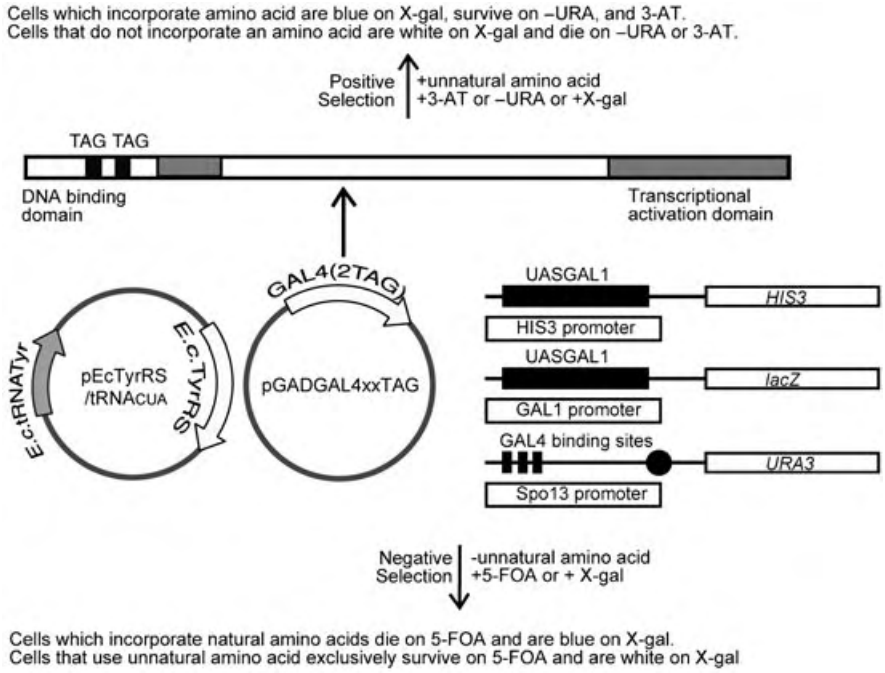


Figure 33. A scheme for selecting mutant synthetases specific for unnatural amino acids in yeast.

nonsense codons (Figure 33). Suppression of these amber codons leads to the production of full-length GAL4, which in turn drives transcription of genomic GAL4 responsive *HIS3*, *URA3*, and *LACZ* reporter genes. Expression of *HIS3* and *URA3* complements the histidine and uracil auxotrophy in this strain and provides a positive selection for clones expressing active tRNA/synthetase pairs. On the other hand, addition of 5-fluoroorotic acid (5-FOA), which is converted into a toxic product by URA3, results in the death of cells expressing active tRNA/synthetase pairs. In the absence of the unnatural amino acid, this serves as a negative selection to remove synthetases specific for endogenous amino acids. Like GFP, the *lacZ* reporter can serve as an additional marker to colormetrically identify active synthetase from inactive ones.

Initially we used the orthogonal *E. coli* $tRNA^{Tyr}_{CUA}$/TyrRS pair[316,317] to incorporate unnatural amino acids into proteins in yeast. A mutant *E. coli* TyrRS library (10^8 in size) was constructed by randomizing five residues in the active site based on the crystal structure of the homologous TyrRS from *Bacillus stearothermophilus* (Figure 17[262]). By using the selection method described above, aminoacyl-tRNA synthetases were identified that incorporate several unnatural amino acids including *p*-acetyl-L-phenylalanine, *p*-azido-L-phenylalanine, *p*-benzoyl-L-phenylalanine, *O*-methyl-L-tyrosine, *p*-iodo-L-tyrosine, and *O*-(2-propynyl)-L-tyrosine.[280,320] To characterize the fidelity and efficiency of unnatural amino acid incorporation an amber mutant of human superoxide dismutase was overexpressed in the presence of each tRNA/synthetase pair with or without the cognate unnatural amino acid. In the presence of the unnatural amino acid, superoxide dismutase could be purified (yields are ca. 0.05 mg L^{-1} corresponding to 20–40 % of wild-type protein); no superoxide dismutase was produced in the absence of added amino acid.[320] The purified superoxide dismutase was shown by mass spectrometry to contain the desired unnatural amino acid and no other amino acid at the specified site. A similar approach has been used to evolve orthogonal *E. coli* leucyl tRNA/synthetase pairs that incorporate long-chain, photocaged, and fluorescent amino acids into proteins in yeast in response to the amber nonsense codon.[276]

5.7. Genetically Encoding Unnatural Amino Acids in Mammalian Cells

While unnatural amino acids have been incorporated into proteins in mammalian cells in the past,[321,322] these efforts have relied primarily on transfection of amber suppressor tRNAs that are acylated in vitro. This approach severely limits the amount of overall protein that can be produced since the suppressor tRNA must be introduced exogenously and cannot be recycled in vivo by an appropriate aminoacyl-tRNA synthetase. Ideally one would like to identify tRNA/synthetase pairs that are orthogonal in mammalian cells, and evolve the substrate specificity of the synthetase such that it can selectively charge a desired unnatural amino acid in vivo.

Since the *E. coli* $tRNA^{Tyr}_{CUA}$/TyrRS pair is orthogonal in mammalian cells (in addition to yeast), and the translational machinery of yeast is similar to that of higher eukaryotes, it should be possible to evolve the specificity of this synthetase in yeast (which is well-suited for genetic selections with large libraries) and transfer the optimized tRNA/synthetase pairs directly to mammalian cells. Unfortunately, *E. coli* $tRNA^{Tyr}_{CUA}$ does not express well in mammalian cells, presumably because of the lack of intact A and B boxes.[311] However, Yokoyama and co-workers showed that the *B. stearothermophilus* $tRNA^{Tyr}_{CUA}$ can function with *E. coli* TyrRS to suppress the TAG codon with tyrosine in vivo. Moreover, this tRNA is not aminoacylated by any endogenous synthetase in mammalian cells.[311] Indeed, coexpression of an *E. coli* mutant TyrRS led to the incorporation of 3-iodo-L-tyrosine into proteins in response to the TAG codon in both Chinese hamster ovarian cells and human embryonic kidney 293 cells with approximately 95 % fidelity.[311] We have shown that several of the *E. coli* TyrRS mutants evolved in yeast can be used in conjunction with a *B. stearothermophilus* $tRNA^{Tyr}_{CUA}$ to incorporate unnatural amino acids into proteins in mammalian cells.[323] However, the suppression efficiencies are low, suggesting that improved synthetases or suppressors, or increased expression levels will be required to generate useful amounts of protein.

An orthogonal *B. subtilis* $tRNA^{Trp}_{UCA}$ ($Bs tRNA^{Trp}_{UCA}$)/tryptophanyl-tRNA synthetase (TrpRS) has also been developed for use in mammalian cells. Wang and co-workers had previously shown that *B. subtilis* $tRNA^{Trp}$ ($Bs tRNA^{Trp}$) is not

 © 2005 Wiley-VCH Verlag GmbH & Co. KGaA, Weinheim

a substrate for TrpRS from yeast and mammalian cells.[324] To test whether the *Bs*tRNA$^{Trp}_{UCA}$ is also orthogonal and can function as an opal suppressor, the codon for Trp68 in a modified bacteriophage T4 fibritin *foldon* gene under control of a CMV promoter[325] was mutated to TGA. Suppression experiments in human 293T cells together with in vitro aminoacylation assays showed that *B. subtilis* TrpRS (*Bs*TrpRS) aminoacylates only *Bs*tRNA$^{Trp}_{UCA}$ and no other endogenous mammalian tRNAs, and that the expressed *Bs*tRNA$^{Trp}_{UCA}$ is charged only by its cognate *Bs*TrpRS and not by other endogenous mammalian synthetases.[326]

The crystal structure of the homologous *Bacillus stearothermophilus* TrpRS was then used to rationally design a synthetase mutant (V144P*Bs*TrpRS) that selectively charges 5-substituted Trp analogues. Val144 points directly towards C5 of tryptophan, thus leading to unfavorable steric interactions with any tryptophan analogue containing a substituent at the C5-position. Mutation of Val144 to a smaller amino acid might be expected to accommodate 5-substituted tryptophan analogues. This mutant was generated and assayed for its ability to suppress the opal nonsense codon in the *foldon* gene in the presence of 5-hydroxytryptophan (5-HTPP). Indeed, expression of full-length protein was seen only in the presence of 5-HTPP (Figure 34).[326] No full-length protein was expressed in the absence of 5-HTPP under otherwise identical conditions, which indicates that this mutant synthetase does not use an endogenous amino acid as a substrate. Electrospray mass spectrometry of the mutant foldon protein verified site-specific incorporation of 5-HTPP at position 68 with a fidelity of $>97\,\%$. The yield of the 5-HTPP mutant protein was approximately 100 $\mu g\,L^{-1}$ of culture, compared to that of about 1 $mg\,L^{-1}$ for wild-type protein. To evolve the *Bs*TrpRS to charge more complex tryptophan analogues, the *Bs*tRNA$^{Trp}_{UCA}$/*Bs*TrpRS can be moved back into the yeast system and the selection scheme described above can be used to isolate desired synthetase mutants from a large library of active-site mutants.

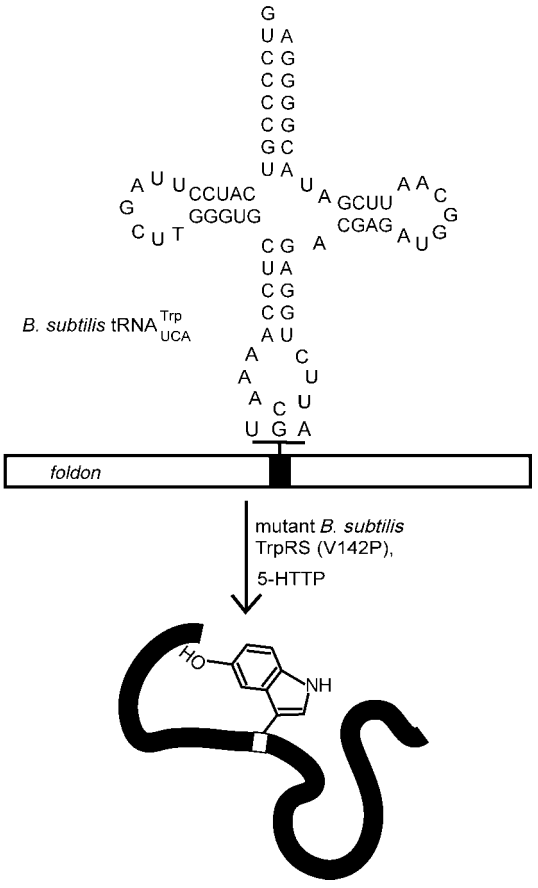


Figure 34. Incorporation of 5-HTTP into the foldon in mammalian cells by suppression of the opal nonsense codon.

6. Outlook

The approach described above has proved remarkably effective in allowing us to add a large number of novel amino acids to the genetic codes of both prokaryotic and eukaryotic organisms. Coincidently, it has recently been shown that nature has evolved a similar strategy (an orthogonal amber suppressor tRNA/synthetase pair) to genetically encode the unnatural amino acid pyrrolysine in *Methanosarcina barkeri*.[5] Future work in this field will likely focus on expanding the nature and number of amino acids that can be genetically encoded in both prokaryotic and eukaryotic organisms, including multicellular organisms. Additional orthogonal pairs that suppress three- and four-base codons are also being developed. It may even be possible to delete rare redundant codons from the *E. coli* genome and use them instead to encode unnatural amino acids. The ability to genetically encode unnatural amino acids should provide powerful probes, both in vitro and in vivo, of protein structure and function. It may also allow the rational design or evolution of proteins with novel properties. Examples might include homogeneous glycosylated or PEG-derivatized therapeutic proteins with improved pharmacological properties, fluorescent proteins that act as sensors of small molecules and protein–protein interactions in the cell, or proteins whose activity can be photoregulated in vivo. It should also be possible to incorporate non-amino acid building blocks into proteins or perhaps even create biopolymers with entirely unnatural backbones. Finally, the ability to add novel amino acids to the genetic codes of organisms will allow us to experimentally test whether there is an evolutionary advantage for organisms with more than 20 amino acid building blocks.

Received: May 11, 2004

[1] J. T. Wong, *Proc. Natl. Acad. Sci. USA* **1975**, *72*, 1909.
[2] M. Di Giulio, M. Medugno, *J. Mol. Evol.* **1999**, *49*, 1.
[3] T. A. Ronneberg, L. F. Landweber, S. J. Freeland, *Proc. Natl. Acad. Sci. USA* **2000**, *97*, 13690.
[4] A. Bock, K. Forchhammer, J. Heider, W. Leinfelder, G. Sawers, B. Veprek, F. Zinoni, *Mol. Microbiol.* **1991**, *5*, 515.
[5] G. Srinivasan, C. M. James, J. A. Krzycki, *Science* **2002**, *296*, 1459.

 © 2005 Wiley-VCH Verlag GmbH & Co. KGaA, Weinheim

[6] A. R. Fersht, J. P. Shi, A. J. Wilkinson, D. M. Blow, P. Carter, M. M. Y. Waye, G. P. Winter, *Angew. Chem.* **1984**, *96*, 455; *Angew. Chem. Int. Ed. Engl.* **1984**, *23*, 467.
[7] M. Smith, *Annu. Rev. Genet.* **1985**, *19*, 423.
[8] J. Pons, A. Rajpal, J. F. Kirsch, *Protein Sci.* **1999**, *8*, 958.
[9] K. E. Neet, D. E. Koshland, Jr., *Proc. Natl. Acad. Sci. USA* **1966**, *56*, 1606.
[10] L. Polgar, M. L. Bender, *J. Am. Chem. Soc.* **1966**, *88*, 3153.
[11] Z. P. Wu, D. Hilvert, *J. Am. Chem. Soc.* **1989**, *111*, 4513.
[12] Z. P. Wu, D. Hilvert, *J. Am. Chem. Soc.* **1990**, *112*, 5647.
[13] J. Q. Liu, M. S. Jiang, G. M. Luo, G. L. Yan, J. C. Shen, *Biotechnol. Lett.* **1998**, *20*, 693.
[14] H. L. Levine, Y. Nakagawa, E. T. Kaiser, *Biochem. Biophys. Res. Commun.* **1977**, *76*, 64.
[15] H. L. Levine, E. T. Kaiser, *J. Am. Chem. Soc.* **1978**, *100*, 7670.
[16] E. T. Kaiser, D. S. Lawrence, *Science* **1984**, *226*, 505.
[17] D. R. Corey, P. G. Schultz, *Science* **1987**, *238*, 1401.
[18] Y. Chen, Y. W. Ebright, R. H. Ebright, *Science* **1994**, *265*, 90.
[19] T. M. Rana, C. F. Meares, *J. Am. Chem. Soc.* **1990**, *112*, 2457.
[20] T. M. Rana, C. F. Meares, *J. Am. Chem. Soc.* **1991**, *113*, 1859.
[21] J. B. Ghaim, D. P. Greiner, C. F. Meares, R. B. Gennis, *Biochemistry* **1995**, *34*, 11311.
[22] J. T. Owens, A. Chmura, K. Murakami, N. Fujita, A. Ishihama, C. F. Meares, *Biochemistry* **1998**, *37*, 7670.
[23] G. M. Culver, H. F. Noller, *Methods Enzymol.* **2000**, *318*, 461.
[24] J. A. Silverman, P. B. Harbury, *J. Biol. Chem.* **2002**, *277*, 30968.
[25] G. R. Jacobson, M. H. Schaffer, G. R. Stark, T. C. Vanaman, *J. Biol. Chem.* **1973**, *248*, 6583.
[26] M. H. Akabas, D. A. Stauffer, M. Xu, A. Karlin, *Science* **1992**, *258*, 307.
[27] A. Karlin, *J. Gen. Physiol.* **2001**, *117*, 235.
[28] A. P. Todd, J. Cong, F. Levinthal, C. Levinthal, W. L. Hubbell, *Proteins Struct. Funct. Genet.* **1989**, *6*, 294.
[29] W. L. Hubbell, C. Altenbach, C. M. Hubbell, H. G. Khorana, *Adv. Protein Chem.* **2003**, *63*, 243.
[30] L. M. Mannuzzu, M. M. Moronne, E. Y. Isacoff, *Science* **1996**, *271*, 213.
[31] B. A. Griffin, S. R. Adams, R. Y. Tsien, *Science* **1998**, *281*, 269.
[32] S. R. Adams, R. E. Campbell, L. A. Gross, B. R. Martin, G. K. Walkup, Y. Yao, J. Llopis, R. Y. Tsien, *J. Am. Chem. Soc.* **2002**, *124*, 6063.
[33] G. Simmons, P. R. Clapham, L. Picard, R. E. Offord, M. M. Rosenklide, T. W. Schwartz, R. Buser, T. N. C. Wells, A. E. I. Proudfoot, *Science* **1997**, *276*, 276.
[34] K. F. Geoghegan, J. G. Stroh, *Bioconjugate Chem.* **1992**, *3*, 138.
[35] R. B. Merrifield, *J. Am. Chem. Soc.* **1963**, *85*, 2149.
[36] S. B. Kent, *Annu. Rev. Biochem.* **1988**, *57*, 957.
[37] R. S. Roy, B. Imperiali, *Protein Eng.* **1997**, *10*, 691.
[38] I. Hamachi, R. Eboshi, J.-I. Watanabe, S. Shinkai, *J. Am. Chem. Soc.* **2000**, *122*, 4530.
[39] J. J. Nestor, Jr., T. L. Ho, R. A. Simpson, B. L. Horner, G. H. Jones, G. I. McRae, B. H. Vickery, *J. Med. Chem.* **1982**, *25*, 795.
[40] J. J. Nestor, Jr., R. Tahilramani, T. L. Ho, G. I. McRae, B. H. Vickery, *J. Med. Chem.* **1988**, *31*, 65.
[41] K. L. Liu, B. L. He, S. B. Xiao, Q. M. Xia, X. Fang, Z. Y. Wang, *Int. J. Pept. Protein Res.* **1990**, *35*, 157.
[42] B. Bilgicer, A. Fichera, K. Kumar, *J. Am. Chem. Soc.* **2001**, *123*, 4393.
[43] C. E. Schafmeister, J. Po, G. L. Verdine, *J. Am. Chem. Soc.* **2000**, *122*, 5891.
[44] V. Cerovsky, E. Welker, H. A. Scheraga, *J. Pept. Res.* **2003**, *61*, 140.
[45] E. T. Kaiser, *Acc. Chem. Res.* **1989**, *22*, 47.
[46] D. Y. Jackson, J. Burnier, C. Quan, M. Stanley, J. Tom, J. A. Wells, *Science* **1994**, *266*, 243.
[47] M. Schnolzer, S. B. Kent, *Science* **1992**, *256*, 221.
[48] K. Rose, *J. Am. Chem. Soc.* **1994**, *116*, 30.
[49] C.-F. Liu, J. P. Tam, *J. Am. Chem. Soc.* **1994**, *116*, 4149.
[50] C.-F. Liu, J. P. Tam, *Proc. Natl. Acad. Sci. USA* **1994**, *91*, 6584.
[51] D. R. Englebretsen, B. G. Garnham, D. A. Bergman, P. F. Alewood, *Tetrahedron Lett.* **1995**, *36*, 8871.
[52] M. Baca, T. W. Muir, M. Schnoelzer, S. B. H. Kent, *J. Am. Chem. Soc.* **1995**, *117*, 1881.
[53] D. S. Kemp, R. I. Carey, *J. Org. Chem.* **1993**, *58*, 2216.
[54] P. E. Dawson, T. W. Muir, I. Clarklewis, S. B. H. Kent, *Science* **1994**, *266*, 776.
[55] P. E. Dawson, S. B. H. Kent, *Annu. Rev. Biochem.* **2000**, *69*, 923.
[56] L. E. Canne, S. J. Bark, S. B. H. Kent, *J. Am. Chem. Soc.* **1996**, *118*, 5891.
[57] M. Baca, S. B. Kent, *Proc. Natl. Acad. Sci. USA* **1993**, *90*, 11638.
[58] D. W. Low, M. G. Hill, *J. Am. Chem. Soc.* **1998**, *120*, 11536.
[59] G. G. Kochendoerfer, S. Y. Chen, F. Mao, S. Cressman, S. Traviglia, H. Shao, C. L. Hunter, D. W. Low, E. N. Cagle, M. Carnevali, V. Gueriguian, P. J. Keogh, H. Porter, S. M. Stratton, M. C. Wiedeke, J. Wilken, J. Tang, J. J. Levy, L. P. Miranda, M. M. Crnogorac, S. Kalbag, P. Botti, J. Schindler-Horvat, L. Savatski, J. W. Adamson, A. Kung, S. B. Kent, J. A. Bradburne, *Science* **2003**, *299*, 884.
[60] A. A. Deniz, T. A. Laurence, G. S. Beligere, M. Dahan, A. B. Martin, D. S. Chemla, P. E. Dawson, P. G. Schultz, S. Weiss, *Proc. Natl. Acad. Sci. USA* **2000**, *97*, 5179.
[61] L. Zhang, J. P. Tam, *J. Am. Chem. Soc.* **1997**, *119*, 2363.
[62] J. A. Camarero, J. Pavel, T. W. Muir, *Angew. Chem.* **1998**, *110*, 361; *Angew. Chem. Int. Ed.* **1998**, *37*, 347.
[63] H. Ishida, Z. Qi, M. Sokabe, K. Donowaki, Y. Inoue, *J. Org. Chem.* **2001**, *66*, 2978.
[64] T. N. Schumacher, L. M. Mayr, D. L. Minor, Jr., M. A. Milhollen, M. W. Burgess, P. S. Kim, *Science* **1996**, *271*, 1854.
[65] D. M. Eckert, V. N. Malashkevich, L. H. Hong, P. A. Carr, P. S. Kim, *Cell* **1999**, *99*, 103.
[66] R. E. Offord, *Protein Eng.* **1987**, *1*, 151.
[67] C. J. Wallace, *Curr. Opin. Biotechnol.* **1995**, *6*, 403.
[68] D. F. Dyckes, T. Creighton, R. C. Sheppard, *Nature* **1974**, *247*, 202.
[69] C. J. Wallace, I. Clark-Lewis, *J. Biol. Chem.* **1992**, *267*, 3852.
[70] C. J. Wallace, *FASEB J.* **1993**, *7*, 505.
[71] D. S. Wuttke, H. B. Gray, S. L. Fisher, B. Imperiali, *J. Am. Chem. Soc.* **1993**, *115*, 8455.
[72] C. H. Wong, K. T. Wang, *Experientia* **1991**, *47*, 1123.
[73] G. A. Homandberg, M. Laskowski, Jr., *Biochemistry* **1979**, *18*, 586.
[74] K. Inouye, K. Watanabe, K. Morihara, Y. Tochino, T. Kanaya, J. Emura, S. Sakakibara, *J. Am. Chem. Soc.* **1979**, *101*, 751.
[75] H. D. Jakubke, P. Kuhl, A. Koennecke, *Angew. Chem.* **1985**, *97*, 79; *Angew. Chem. Int. Ed. Engl.* **1985**, *24*, 85.
[76] V. Schellenberger, H. D. Jakubke, *Angew. Chem.* **1991**, *103*, 1440; *Angew. Chem. Int. Ed. Engl.* **1991**, *30*, 1437.
[77] J. Bongers, T. Lambros, W. Liu, M. Ahmad, R. M. Campbell, A. M. Felix, E. P. Heimer, *J. Med. Chem.* **1992**, *35*, 3934.
[78] J. Bongers, W. Liu, T. Lambros, K. Breddam, R. M. Campbell, A. M. Felix, E. P. Heimer, *Int. J. Pept. Protein Res.* **1994**, *44*, 123.
[79] T. Nakatsuka, T. Sasaki, E. T. Kaiser, *J. Am. Chem. Soc.* **1987**, *109*, 3808.
[80] L. Abrahmsen, J. Tom, J. Burnier, K. A. Butcher, A. Kossiakoff, J. A. Wells, *Biochemistry* **1991**, *30*, 4151.
[81] T. K. Chang, D. Y. Jackson, J. P. Burnier, J. A. Wells, *Proc. Natl. Acad. Sci. USA* **1994**, *91*, 12544.
[82] H. F. Gaertner, R. E. Offord, R. Cotton, D. Timms, R. Camble, K. Rose, *J. Biol. Chem.* **1994**, *269*, 7224.
[83] T. W. Muir, D. Sondhi, P. A. Cole, *Proc. Natl. Acad. Sci. USA* **1998**, *95*, 6705.
[84] K. Severinov, T. W. Muir, *J. Biol. Chem.* **1998**, *273*, 16205.
[85] T. C. Evans, Jr., J. Benner, M. Q. Xu, *Protein Sci.* **1998**, *7*, 2256.
[86] T. W. Muir, *Annu. Rev. Biochem.* **2003**, *72*, 249.

 © 2005 Wiley-VCH Verlag GmbH & Co. KGaA, Weinheim

[87] F. B. Perler, M. Q. Xu, H. Paulus, *Curr. Opin. Chem. Biol.* **1997**, *1*, 292.
[88] T. J. Tolbert, C.-H. Wong, *Angew. Chem.* **2002**, *114*, 2275; *Angew. Chem. Int. Ed.* **2002**, *41*, 2171.
[89] C. J. Noren, J. Wang, F. B. Perler, *Angew. Chem.* **2000**, *112*, 458; *Angew. Chem. Int. Ed.* **2000**, *39*, 450.
[90] J. P. Tam, Q. Yu, *Biopolymers* **1998**, *46*, 319.
[91] R. S. Roy, O. Allen, C. T. Walsh, *Chem. Biol.* **1999**, *6*, 789.
[92] R. J. Hondal, B. L. Nilsson, R. T. Raines, *J. Am. Chem. Soc.* **2001**, *123*, 5140.
[93] M. D. Gieselman, L. Xie, W. A. van der Donk, *Org. Lett.* **2001**, *3*, 1331.
[94] R. Quaderer, A. Sewing, D. Hilvert, *Helv. Chim. Acta* **2001**, *84*, 1197.
[95] J. R. Sydor, M. Mariano, S. Sideris, S. Nock, *Bioconjugate Chem.* **2002**, *13*, 707.
[96] A. Iakovenko, E. Rostkova, E. Merzlyak, A. M. Hillebrand, N. H. Thoma, R. S. Goody, K. Alexandrov, *FEBS Lett.* **2000**, *468*, 155.
[97] G. J. Cotton, B. Ayers, R. Xu, T. W. Muir, *J. Am. Chem. Soc.* **1999**, *121*, 1100.
[98] B. Ayers, U. K. Blaschke, J. A. Camarero, G. J. Cotton, M. Holford, T. W. Muir, *Biopolymers* **2000**, *51*, 343.
[99] G. J. Cotton, T. W. Muir, *Chem. Biol.* **2000**, *7*, 253.
[100] R. M. Hofmann, G. J. Cotton, E. J. Chang, E. Vidal, D. Veach, W. Bornmann, T. W. Muir, *Bioorg. Med. Chem. Lett.* **2001**, *11*, 3091.
[101] J. Mukhopadhyay, A. N. Kapanidis, V. Mekler, E. Kortkhonjia, Y. W. Ebright, R. H. Ebright, *Cell* **2001**, *106*, 453.
[102] V. Mekler, E. Kortkhonjia, J. Mukhopadhyay, J. Knight, A. Revyakin, A. N. Kapanidis, W. Niu, Y. W. Ebright, R. Levy, R. H. Ebright, *Cell* **2002**, *108*, 599.
[103] M. A. Dwyer, W. Lu, J. J. Dwyer, A. A. Kossiakoff, *Chem. Biol.* **2000**, *7*, 263.
[104] D. Macmillan, C. R. Bertozzi, *Tetrahedron* **2000**, *56*, 9515.
[105] T. J. Tolbert, C.-H. Wong, *J. Am. Chem. Soc.* **2000**, *122*, 5421.
[106] K. Alexandrov, I. Heinemann, T. Durek, V. Sidorovitch, R. S. Goody, H. Waldmann, *J. Am. Chem. Soc.* **2002**, *124*, 5648.
[107] M. Huse, M. N. Holford, J. Kuriyan, T. W. Muir, *J. Am. Chem. Soc.* **2000**, *122*, 8337.
[108] M. Huse, T. W. Muir, L. Xu, Y.-G. Chen, J. Kuriyan, J. Massague, *Mol. Cell* **2001**, *8*, 671.
[109] W. Lu, D. Gong, D. Bar-Sagi, P. A. Cole, *Mol. Cell* **2001**, *8*, 759.
[110] U. Arnold, M. P. Hinderaker, B. L. Nilsson, B. R. Huck, S. H. Gellman, R. T. Raines, *J. Am. Chem. Soc.* **2002**, *124*, 8522.
[111] F. H. C. Crick, *Symp. Soc. Exp. Biol.* **1958**, *12*, 138.
[112] F. Chapeville, F. Lipmann, G. von Ehrenstein, B. Weisblum, W. J. Ray, Jr., S. Benzer, *Proc. Natl. Acad. Sci. USA* **1962**, *48*, 1086.
[113] A. E. Johnson, W. R. Woodward, E. Herbert, J. R. Menninger, *Biochemistry* **1976**, *15*, 569.
[114] P. Schimmel, *Annu. Rev. Biochem.* **1987**, *56*, 125.
[115] M. Ibba, D. Soll, *Annu. Rev. Biochem.* **2000**, *69*, 617.
[116] T. G. Heckler, L. H. Chang, Y. Zama, T. Naka, M. S. Chorghade, S. M. Hecht, *Biochemistry* **1984**, *23*, 1468.
[117] T. G. Heckler, Y. Zama, T. Naka, S. M. Hecht, *J. Biol. Chem.* **1983**, *258*, 4492.
[118] J. R. Roesser, M. S. Chorghade, S. M. Hecht, *Biochemistry* **1986**, *25*, 6361.
[119] T. G. Heckler, J. R. Roesser, C. Xu, P. I. Chang, S. M. Hecht, *Biochemistry* **1988**, *27*, 7254.
[120] G. Baldini, B. Martoglio, A. Schachenmann, C. Zugliani, J. Brunner, *Biochemistry* **1988**, *27*, 7951.
[121] C. J. Noren, S. J. Anthony-Cahill, M. C. Griffith, P. G. Schultz, *Science* **1989**, *244*, 182.
[122] F. H. C. Crick, L. Barret, S. Brenner, R. Watts-Tobin, *Nature* **1961**, *192*, 1227.
[123] S. Brenner, A. O. Stretton, S. Kaplan, *Nature* **1965**, *206*, 994.
[124] J. H. Miller, D. Ganem, P. Lu, A. Schmitz, *J. Mol. Biol.* **1977**, *109*, 275.
[125] L. Bossi, J. R. Roth, *Nature* **1980**, *286*, 123.
[126] J. A. Ellman, D. Mendel, P. G. Schultz, *Science* **1992**, *255*, 197.
[127] Y. Kwok, J. T. Wong, *Can. J. Biochem.* **1980**, *58*, 213.
[128] A. G. Bruce, J. F. Atkins, N. Wills, O. Uhlenbeck, R. F. Gesteland, *Proc. Natl. Acad. Sci. USA* **1982**, *79*, 7127.
[129] A. Miller, A. Albertini, *J. Mol. Biol.* **1983**, *164*, 59.
[130] D. Ayer, M. Yarus, *Science* **1986**, *231*, 393.
[131] J. F. Milligan, D. R. Groebe, G. W. Witherell, O. C. Uhlenbeck, *Nucleic Acids Res.* **1987**, *15*, 8783.
[132] C. J. Noren, S. J. Anthony-Cahill, D. J. Suich, K. A. Noren, M. C. Griffith, P. G. Schultz, *Nucleic Acids Res.* **1990**, *18*, 83.
[133] S. A. Robertson, J. A. Ellman, P. G. Schultz, *J. Am. Chem. Soc.* **1991**, *113*, 2722.
[134] S. R. Adams, J. P. Y. Kao, R. Y. Tsien, *J. Am. Chem. Soc.* **1989**, *111*, 7957.
[135] A. Patchornik, B. Amit, R. B. Woodward, *J. Am. Chem. Soc.* **1970**, *92*, 6333.
[136] J. A. Ellman, D. Mendel, S. Anthony-Cahill, C. J. Noren, P. G. Schultz, *Methods Enzymol.* **1992**, *202*, 301.
[137] J. D. Bain, C. G. Glabe, T. A. Dix, A. R. Chamberlin, E. S. Diala, *J. Am. Chem. Soc.* **1989**, *111*, 8013.
[138] V. W. Cornish, D. Mendel, P. G. Schultz, *Angew. Chem.* **1995**, *107*, 677; *Angew. Chem. Int. Ed. Engl.* **1995**, *34*, 621.
[139] J. S. Thorson, E. Chapman, E. C. Murphy, P. G. Schultz, J. K. Judice, *J. Am. Chem. Soc.* **1995**, *117*, 1157.
[140] J. T. Koh, V. W. Cornish, P. G. Schultz, *Biochemistry* **1997**, *36*, 11314.
[141] K. B. Wiberg, K. E. Laidig, *J. Am. Chem. Soc.* **1987**, *109*, 5935.
[142] M. J. Kamlet, J. L. M. Abboud, M. H. Abraham, R. W. Taft, *J. Org. Chem.* **1983**, *48*, 2877.
[143] E. Chapman, J. S. Thorson, P. G. Schultz, *J. Am. Chem. Soc.* **1997**, *119*, 7151.
[144] S. T. Cload, D. R. Liu, W. A. Froland, P. G. Schultz, *Chem. Biol.* **1996**, *3*, 1033.
[145] G. F. Short, S. Y. Golovine, S. M. Hecht, *Biochemistry* **1999**, *38*, 8808.
[146] D. M. Kim, T. Kigawa, C. Y. Choi, S. Yokoyama, *Eur. J. Biochem.* **1996**, *239*, 881.
[147] T. Hohsaka, K. Sato, M. Sisido, K. Takai, S. Yokoyama, *FEBS Lett.* **1994**, *344*, 171.
[148] C. H. Ma, W. Kudlicki, O. W. Odom, G. Kramer, B. Hardesty, *Biochemistry* **1993**, *32*, 7939.
[149] A. K. Kowal, J. S. Oliver, *Nucleic Acids Res.* **1997**, *25*, 4685.
[150] A. C. Forster, Z. Tan, M. N. Nalam, H. Lin, H. Qu, V. W. Cornish, S. C. Blacklow, *Proc. Natl. Acad. Sci. USA* **2003**, *100*, 6353.
[151] T. Hohsaka, Y. Ashizuka, H. Murakami, M. Sisido, *J. Am. Chem. Soc.* **1996**, *118*, 9778.
[152] H. Murakami, T. Hohsaka, Y. Ashizuka, M. Sisido, *J. Am. Chem. Soc.* **1998**, *120*, 7520.
[153] T. Hohsaka, D. Kajihara, Y. Ashizuka, H. Murakami, M. Sisido, *J. Am. Chem. Soc.* **1999**, *121*, 34.
[154] M. Taki, T. Hohsaka, H. Murakami, K. Taira, M. Sisido, *J. Am. Chem. Soc.* **2002**, *124*, 14586.
[155] M. Taki, T. Hohsaka, H. Murakami, K. Taira, M. Sisido, *J. Am. Chem. Soc.* **2002**, *124*, 14586.
[156] T. Hohsaka, M. Sisido, *Curr. Opin. Chem. Biol.* **2002**, *6*, 809.
[157] T. Hohsaka, Y. Ashizuka, H. Sasaki, H. Murakami, M. Sisido, *J. Am. Chem. Soc.* **1999**, *121*, 12194.
[158] T. Hohsaka, Y. Ashizuka, H. Taira, H. Murakami, M. Sisido, *Biochemistry* **2001**, *40*, 11060.
[159] T. Hohsaka, Y. Ashizuka, H. Murakami, M. Sisido, *Nucleic Acids Res.* **2001**, *29*, 3646.

 © 2005 Wiley-VCH Verlag GmbH & Co. KGaA, Weinheim

[160] J. D. Bain, C. Switzer, A. R. Chamberlin, S. A. Benner, *Nature* **1992**, *356*, 537.
[161] M. W. Nowak, P. C. Kearney, J. R. Sampson, M. E. Saks, C. G. Labarca, S. K. Silverman, W. G. Zhong, J. Thorson, J. N. Abelson, N. Davidson, P. G. Schultz, D. A. Dougherty, H. A. Lester, *Science* **1995**, *268*, 439.
[162] M. E. Saks, J. R. Sampson, M. W. Nowak, P. C. Kearney, F. Y. Du, J. N. Abelson, H. A. Lester, D. A. Dougherty, *J. Biol. Chem.* **1996**, *271*, 23169.
[163] D. A. Dougherty, *Curr. Opin. Chem. Biol.* **2000**, *4*, 645.
[164] D. L. Beene, D. A. Dougherty, H. A. Lester, *Curr. Opin. Neurobiol.* **2003**, *13*, 264.
[165] W. G. Zhong, J. P. Gallivan, Y. N. Zhang, L. T. Li, H. A. Lester, D. A. Dougherty, *Proc. Natl. Acad. Sci. USA* **1998**, *95*, 12088.
[166] D. L. Beene, G. S. Brandt, W. Zhong, N. M. Zacharias, H. A. Lester, D. A. Dougherty, *Biochemistry* **2002**, *41*, 10262.
[167] C. A. Hutchison III, S. Phillips, M. H. Edgell, S. Gillam, P. Jahnke, M. Smith, *J. Biol. Chem.* **1978**, *253*, 6551.
[168] G. Dalbadie-McFarland, L. W. Cohen, A. D. Riggs, C. Morin, K. Itakura, J. H. Richards, *Proc. Natl. Acad. Sci. USA* **1982**, *79*, 6409.
[169] I. S. Sigal, B. G. Harwood, R. Arentzen, *Proc. Natl. Acad. Sci. USA* **1982**, *79*, 7157.
[170] G. Winter, A. R. Fersht, A. J. Wilkinson, M. Zoller, M. Smith, *Nature* **1982**, *299*, 756.
[171] J. E. Villafranca, E. E. Howell, D. H. Voet, M. S. Strobel, R. C. Ogden, J. N. Abelson, J. Kraut, *Science* **1983**, *222*, 782.
[172] C. S. Craik, S. Roczniak, C. Largman, W. J. Rutter, *Science* **1987**, *237*, 909.
[173] J. A. Wells, D. A. Estell, *Trends Biochem. Sci.* **1988**, *13*, 291.
[174] A. R. Fersht, *Biochemistry* **1987**, *26*, 8031.
[175] P. T. Jones, P. H. Dear, J. Foote, M. S. Neuberger, G. Winter, *Nature* **1986**, *321*, 522.
[176] J. Nardelli, T. J. Gibson, C. Vesque, P. Charnay, *Nature* **1991**, *349*, 175.
[177] J. R. Desjarlais, J. M. Berg, *Proteins Struct. Funct. Genet.* **1992**, *12*, 101.
[178] J. Nardelli, T. Gibson, P. Charnay, *Nucleic Acids Res.* **1992**, *20*, 4137.
[179] Y. Choo, A. Klug, *Proc. Natl. Acad. Sci. USA* **1994**, *91*, 11163.
[180] M. Isalan, Y. Choo, A. Klug, *Proc. Natl. Acad. Sci. USA* **1997**, *94*, 5617.
[181] M. Isalan, A. Klug, Y. Choo, *Biochemistry* **1998**, *37*, 12026.
[182] Y. Choo, M. Isalan, *Curr. Opin. Struct. Biol.* **2000**, *10*, 411.
[183] S. A. Wolfe, L. Nekludova, C. O. Pabo, *Annu. Rev. Biophys. Biomol. Struct.* **2000**, *29*, 183.
[184] J. A. Wells, M. Vasser, D. B. Powers, *Gene* **1985**, *34*, 315.
[185] B. C. Cunningham, P. Jhurani, P. Ng, J. A. Wells, *Science* **1989**, *243*, 1330.
[186] B. C. Cunningham, J. A. Wells, *Science* **1989**, *244*, 1081.
[187] D. W. Leung, E. Chen, D. V. Goeddel, *Technique* **1989**, *1*, 11.
[188] R. C. Cadwell, G. F. Joyce, *PCR Methods Appl.* **1992**, *2*, 28.
[189] A. Greener, M. Callahan, B. Jerpseth, *Methods Mol. Biol.* **1996**, *57*, 375.
[190] W. P. C. Stemmer, *Nature* **1994**, *370*, 389.
[191] H. K. Mitchell, C. Niemann, *J. Am. Chem. Soc.* **1947**, *69*, 1232.
[192] M. V. Simpson, E. Farber, H. Tarver, *J. Biol. Chem.* **1950**, *182*, 81.
[193] M. H. Richmond, *Bacteriol. Rev.* **1962**, *26*, 398.
[194] M. Levine, H. Tarver, *J. Biol. Chem.* **1951**, *192*, 835.
[195] D. Gross, H. Tarver, *J. Biol. Chem.* **1955**, *217*, 169.
[196] R. Munier, G. N. Cohen, *Biochim. Biophys. Acta* **1956**, *21*, 592.
[197] G. N. Cohen, D. B. Cowie, *C. R. Hebd. Seances Acad. Sci.* **1957**, *244*, 680.
[198] D. B. Cowie, G. N. Cohen, *Biochim. Biophys. Acta* **1957**, *26*, 252.
[199] G. Hortin, I. Boime, *Methods Enzymol.* **1983**, *96*, 777.
[200] G. Brawerman, M. Ycas, *Arch. Biochem. Biophys.* **1957**, *68*, 112.
[201] M. H. Richmond, *Biochem. J.* **1959**, *73*, 261.
[202] D. B. Cowie, G. N. Cohen, E. T. Bolton, H. de Robichon-Szulmajster, *Biochim. Biophys. Acta* **1959**, *34*, 39.
[203] O. M. Rennert, H. S. Anker, *Biochemistry* **1961**, *13*, 471.
[204] N. Budisa, C. Minks, F. J. Medrano, J. Lutz, R. Huber, L. Moroder, *Proc. Natl. Acad. Sci. USA* **1998**, *95*, 455.
[205] M. Ibba, P. Kast, H. Hennecke, *Biochemistry* **1994**, *33*, 7107.
[206] M. Ibba, H. Hennecke, *FEBS Lett.* **1995**, *364*, 272.
[207] N. Sharma, R. Furter, P. Kast, D. A. Tirrell, *FEBS Lett.* **2000**, *467*, 37.
[208] K. Kirshenbaum, S. I. Carrico, A. D. Tirrell, *ChemBioChem* **2002**, *3*, 235.
[209] F. Hamano-Takaku, T. Iwama, S. Saito-Yano, K. Takaku, Y. Monden, M. Kitabatake, D. Soll, S. Nishimura, *J. Biol. Chem.* **2000**, *275*, 40324.
[210] V. Doring, H. D. Mootz, L. A. Nangle, T. L. Hendrickson, V. de Crecy-Lagard, P. Schimmel, P. Marliere, *Science* **2001**, *292*, 501.
[211] Y. Tang, D. A. Tirrell, *Biochemistry* **2002**, *41*, 10635.
[212] W. Yang, W. A. Hendrickson, E. T. Kalman, R. J. Crouch, *J. Biol. Chem.* **1990**, *265*, 13553.
[213] W. Yang, W. A. Hendrickson, R. J. Crouch, Y. Satow, *Science* **1990**, *249*, 1398.
[214] J. O. Boles, K. Lewinski, M. Kunkle, J. D. Odom, B. Dunlap, L. Lebioda, M. Hatada, *Nat. Struct. Biol.* **1994**, *1*, 283.
[215] N. Budisa, B. Steipe, P. Demange, C. Eckerskorn, J. Kellermann, R. Huber, *Eur. J. Biochem.* **1995**, *230*, 788.
[216] N. Budisa, W. Karnbrock, S. Steinbacher, A. Humm, L. Prade, T. Neuefeind, L. Moroder, R. Huber, *J. Mol. Biol.* **1997**, *270*, 616.
[217] J. H. Bae, S. Alefelder, J. T. Kaiser, R. Friedrich, L. Moroder, R. Huber, N. Budisa, *J. Mol. Biol.* **2001**, *309*, 925.
[218] N. Budisa, R. Huber, R. Golbik, C. Minks, E. Weyher, L. Moroder, *Eur. J. Biochem.* **1998**, *253*, 1.
[219] C. Minks, R. Huber, L. Moroder, N. Budisa, *Biochemistry* **1999**, *38*, 10649.
[220] C. Renner, S. Alefelder, J. H. Bae, N. Budisa, R. Huber, L. Moroder, *Angew. Chem.* **2001**, *113*, 949; *Angew. Chem. Int. Ed.* **2001**, *40*, 923.
[221] P. Wang, Y. Tang, D. A. Tirrell, *J. Am. Chem. Soc.* **2003**, *125*, 6900.
[222] Y. Tang, G. Ghirlanda, W. A. Petka, T. Nakajima, W. F. DeGrado, D. A. Tirrell, *Angew. Chem.* **2001**, *113*, 1542; *Angew. Chem. Int. Ed.* **2001**, *40*, 1494.
[223] Y. Tang, D. A. Tirrell, *J. Am. Chem. Soc.* **2001**, *123*, 11089.
[224] N. Budisa, M. Rubini, J. H. Bae, E. Weyher, W. Wenger, R. Golbik, R. Huber, L. Moroder, *Angew. Chem.* **2002**, *114*, 4238; *Angew. Chem. Int. Ed.* **2002**, *41*, 4066.
[225] J. H. Bae, M. Rubini, G. Jung, G. Wiegand, M. H. J. Seifert, M. K. Azim, J.-S. Kim, A. Zumbusch, T. A. Holak, L. Moroder, R. Huber, N. Budisa, *J. Mol. Biol.* **2003**, *328*, 1071.
[226] H. Duewel, E. Daub, V. Robinson, J. F. Honek, *Biochemistry* **1997**, *36*, 3404.
[227] M. D. Vaughan, P. Cleve, V. Robinson, H. S. Duewel, J. F. Honek, *J. Am. Chem. Soc.* **1999**, *121*, 8475.
[228] H. S. Duewel, E. Daub, V. Robinson, J. F. Honek, *Biochemistry* **2001**, *40*, 13167.
[229] M. H. J. Seifert, D. Ksiazek, M. K. Azim, P. Smialowski, N. Budisa, T. A. Holak, *J. Am. Chem. Soc.* **2002**, *124*, 7932.
[230] J. G. Bann, J. Pinkner, S. J. Hultgren, C. Frieden, *Proc. Natl. Acad. Sci. USA* **2002**, *99*, 709.
[231] S. Kothakota, T. L. Mason, D. A. Tirrell, M. J. Fournier, *J. Am. Chem. Soc.* **1995**, *117*, 536.
[232] T. J. Deming, M. J. Fournier, T. L. Mason, D. A. Tirrell, *J. Macromol. Sci. Pure Appl. Chem.* **1997**, *34*, 2143.
[233] J. C. M. van Hest, D. A. Tirrell, *FEBS Lett.* **1998**, *428*, 68.

 © 2005 Wiley-VCH Verlag GmbH & Co. KGaA, Weinheim

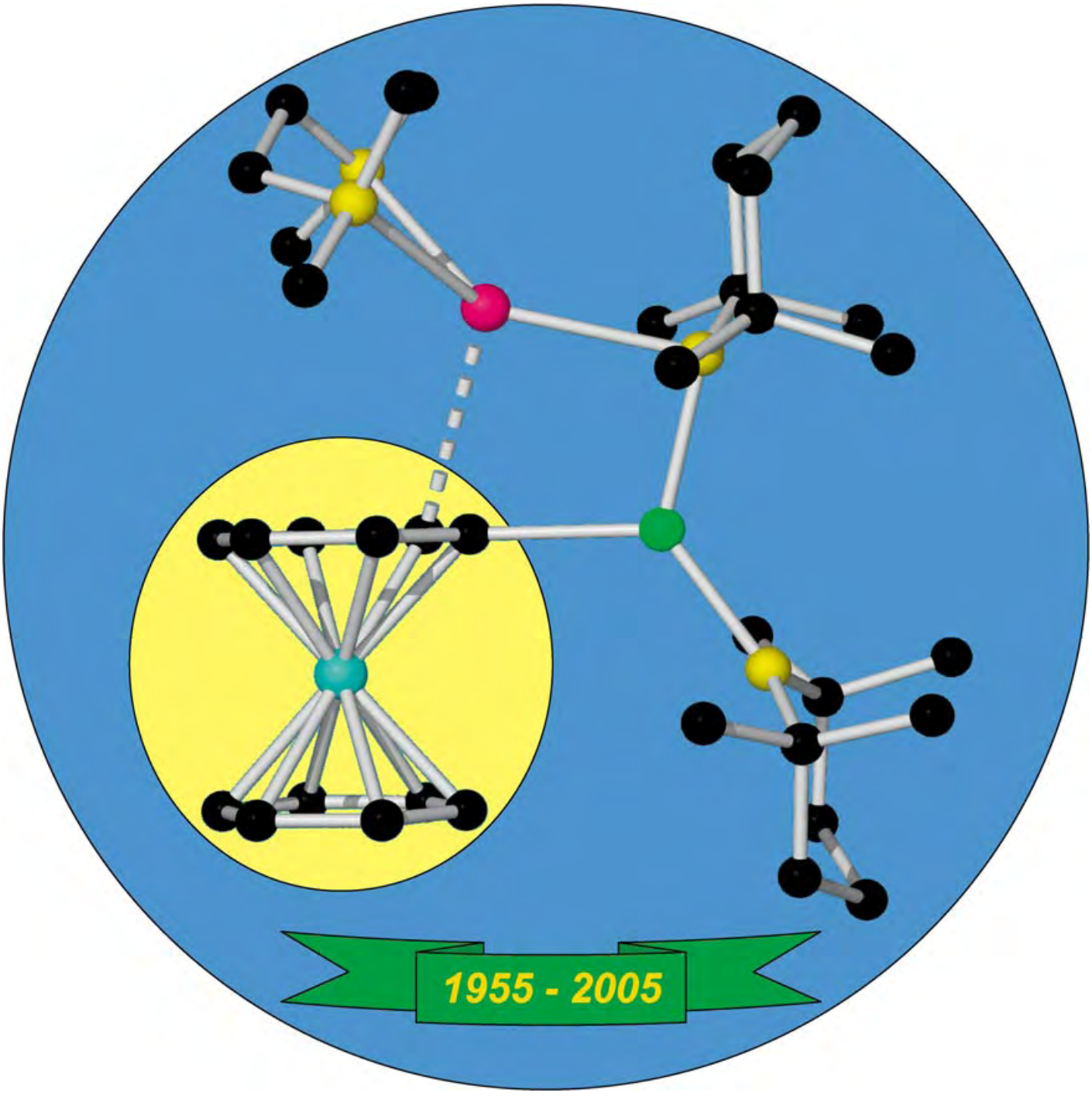
[234] J. C. M. van Hest, K. L. Kiick, D. A. Tirrell, *J. Am. Chem. Soc.* **2000**, *122*, 1282.
[235] K. L. Kiick, J. C. van Hest, D. A. Tirrell, *Angew. Chem.* **2000**, *112*, 2232; *Angew. Chem. Int. Ed.* **2000**, *39*, 2148.
[236] K. L. Kiick, E. Saxon, D. A. Tirrell, C. R. Bertozzi, *Proc. Natl. Acad. Sci. USA* **2002**, *99*, 19.
[237] A. J. Link, D. A. Tirrell, *J. Am. Chem. Soc.* **2003**, *125*, 11164.
[238] D. Datta, P. Wang, I. S. Carrico, S. L. Mayo, D. A. Tirrell, *J. Am. Chem. Soc.* **2002**, *124*, 5652.
[239] L. Wang, P. G. Schultz, *Chem. Commun.* **2002**, 1.
[240] S. Benzer, S. P. Champe, *Proc. Natl. Acad. Sci. USA* **1962**, *48*, 1114.
[241] A. Garen, O. Siddiqi, *Proc. Natl. Acad. Sci. USA* **1962**, *48*, 1121.
[242] J. Normanly, L. G. Kleina, J. M. Masson, J. Abelson, J. H. Miller, *J. Mol. Biol.* **1990**, *213*, 719.
[243] R. M. Hudziak, F. A. Laski, U. L. RajBhandary, P. A. Sharp, M. R. Capecchi, *Cell* **1982**, *31*, 137.
[244] H. J. Drabkin, H. J. Park, U. L. Rajbhandary, *Mol. Cell. Biol.* **1996**, *16*, 907.
[245] F. Sherman in *The Molecular Biology of the Yeast Saccharomyces: Metabolism and Gene Expression* (Eds.: J. N. Strathern, E. W. Jones, J. R. Broach), Cold Spring Harbor Laboratory, Cold Sping Harbor, **1982**, p. 463.
[246] D. Kim, J. Johnson, *J. Biol. Chem.* **1988**, *263*, 7316.
[247] J. Kimble, J. Hodgkin, T. Smith, J. Smith, *Nature* **1982**, *299*, 456.
[248] S. L. Bolten, P. Powell-Abel, D. A. Fischhoff, R. H. Waterston, *Proc. Natl. Acad. Sci. USA* **1984**, *81*, 6784.
[249] M. A. Rould, J. J. Perona, D. Soll, T. A. Steitz, *Science* **1989**, *246*, 1135.
[250] D. R. Liu, T. J. Magliery, P. G. Schultz, *Chem. Biol.* **1997**, *4*, 685.
[251] D. R. Liu, T. J. Magliery, M. Pasternak, P. G. Schultz, *Proc. Natl. Acad. Sci. USA* **1997**, *94*, 10092.
[252] B. P. Doctor, J. A. Mudd, *J. Biol. Chem.* **1963**, *238*, 3677.
[253] E. F. Whelihan, P. Schimmel, *EMBO J.* **1997**, *16*, 2968.
[254] D. R. Liu, P. G. Schultz, *Proc. Natl. Acad. Sci. USA* **1999**, *96*, 4780.
[255] L. Wang, P. G. Schultz, unpublished results **1998**.
[256] K. Wakasugi, C. L. Quinn, N. Tao, P. Schimmel, *EMBO J.* **1998**, *17*, 297.
[257] T. A. Kleeman, D. Wei, K. L. Simpson, E. A. First, *J. Biol. Chem.* **1997**, *272*, 14420.
[258] L. Wang, T. J. Magliery, D. R. Liu, P. G. Schultz, *J. Am. Chem. Soc.* **2000**, *122*, 5010.
[259] B. A. Steer, P. Schimmel, *J. Biol. Chem.* **1999**, *274*, 35601.
[260] L. Wang, P. G. Schultz, *Chem. Biol.* **2001**, *8*, 883.
[261] R. Furter, *Protein Sci.* **1998**, *7*, 419.
[262] L. Wang, A. Brock, B. Herberich, P. G. Schultz, *Science* **2001**, *292*, 498.
[263] L. Wang, A. Brock, P. G. Schultz, *J. Am. Chem. Soc.* **2002**, *124*, 1836.
[264] L. Wang, P. G. Schultz, unpublished results **2001**.
[265] L. Wang, Ph.D. Dissertation, University of California at Berkeley, **2002**.
[266] S. W. Santoro, L. Wang, B. Herberich, D. S. King, P. G. Schultz, *Nat. Biotechnol.* **2002**, *20*, 1044.
[267] M. Pastrnak, P. G. Schultz, *Bioorg. Med. Chem.* **2001**, *9*, 2373.
[268] Z. Zhang, L. Wang, A. Brock, P. G. Schultz, *Angew. Chem.* **2002**, *114*, 2964; *Angew. Chem. Int. Ed.* **2002**, *41*, 2840.
[269] J. W. Chin, S. W. Santoro, A. B. Martin, D. S. King, L. Wang, P. G. Schultz, *J. Am. Chem. Soc.* **2002**, *124*, 9026.
[270] J. W. Chin, A. B. Martin, D. S. King, L. Wang, P. G. Schultz, *Proc. Natl. Acad. Sci. USA* **2002**, *99*, 11020.
[271] L. Wang, Z. Zhang, A. Brock, P. G. Schultz, *Proc. Natl. Acad. Sci. USA* **2003**, *100*, 56.
[272] L. Wang, J. Xie, A. A. Deniz, P. G. Schultz, *J. Org. Chem.* **2003**, *68*, 174.
[273] Z. Zhang, A. C. Smith Brian, L. Wang, A. Brock, C. Cho, P. G. Schultz, *Biochemistry* **2003**, *42*, 6735.
[274] L. Alfonta, Z. Zhang, S. Uryu, J. A. Loo, P. G. Schultz, *J. Am. Chem. Soc.* **2003**, *125*, 14662.
[275] Z. Zhang, J. Gildersleeve, Y.-Y. Yang, R. Xu, J. A. Loo, S. Uryu, C.-H. Wong, P. G. Schultz, *Science* **2004**, *303*, 371; R. Xu,S. R. Hanson, Z. Zhang, P. G. Schultz, C.-H. Wong, *J. Am. Chem. Soc.*, in press.
[276] J. Turner, P. G. Schultz, unpublished results.
[277] J. W. Chin, P. G. Schultz, *ChemBioChem* **2002**, *3*, 1135.
[278] R. E. Galardy, L. C. Craig, M. P. Printz, *Nature New Biol.* **1973**, *242*, 127.
[279] H. Liu, L. Wang, A. Brock, C.-H. Wong, P. G. Schultz, *J. Am. Chem. Soc.* **2003**, *125*, 1702.
[280] A. Deiters, T. A. Cropp, M. Mukherji, J. W. Chin, J. C. Anderson, P. G. Schultz, *J. Am. Chem. Soc.* **2003**, *125*, 11782; A. Deiters, T. A. Cropp, M. Mukherji, D. Summerer, P. G. Schultz, *Bioorg. Med. Chem. Lett.*, in press.
[281] H. Zeng, P. G. Schultz, unpublished results.
[282] R. A. Dwek, *Chem. Rev.* **1996**, *96*, 683.
[283] P. Sears, C. H. Wong, *Science* **2001**, *291*, 2344.
[284] B. G. Davis, *Chem. Rev.* **2002**, *102*, 579.
[285] M. Wacker, D. Linton, P. G. Hitchen, M. Nita-Lazar, S. M. Haslam, S. J. North, M. Panico, H. R. Morris, A. Dell, B. W. Wren, M. Aebi, *Science* **2002**, *298*, 1790.
[286] S. R. Hamilton, P. Bobrowicz, B. Bobrowicz, R. C. Davidson, H. Li, T. Mitchell, J. H. Nett, S. Rausch, T. A. Stadheim, H. Wischnewski, S. Wildt, T. U. Gerngross, *Science* **2003**, *301*, 1244.
[287] J. Xie, L. Wang, N. Wu, A. Brock, G. Spraggon, P. G. Schultz, Nature Biotechnol. **2004**, *22*, 1297.
[288] R. Y. Tsien, *Annu. Rev. Biochem.* **1998**, *67*, 509.
[289] P. G. Schultz, unpublished results.
[290] N. Wu, P. G. Schultz, unpublished results.
[291] M. Bose, D. Groff, P. G. Schultz, unpublished results.
[292] N. Wu, A. Dieters, T. A. Cropp, P. G. Schultz, *J. Am. Chem. Soc.* **2004**, *126*, 14306.
[293] Y. Zhang, L. Wang, I. A. Wilson, P. G. Schultz, unpublished results, **2003**.
[294] T. Kobayashi, O. Nureki, R. Ishitani, A. Yaremchuk, M. Tukalo, S. Cusack, K. Sakamoto, S. Yokoyama, *Nat. Struct. Biol.* **2003**, *10*, 425.
[295] F. J. LaRiviere, A. D. Wolfson, O. C. Uhlenbeck, *Science* **2001**, *294*, 165.
[296] F. Tian, M. Tsao, P. G. Schultz, *J. Am. Chem. Soc.*, in press.
[297] R. A. Mehl, J. C. Anderson, S. W. Santoro, L. Wang, A. B. Martin, D. S. King, D. M. Horn, P. G. Schultz, *J. Am. Chem. Soc.* **2003**, *125*, 935.
[298] J. F. Curran, M. Yarus, *Science* **1987**, *238*, 1545.
[299] L. Bossi, J. R. Roth, *Cell* **1981**, *25*, 489.
[300] M. O'Connor, *Nucleic Acids Res.* **2002**, *30*, 1985.
[301] T. J. Magliery, J. C. Anderson, P. G. Schultz, *J. Mol. Biol.* **2001**, *307*, 755.
[302] J. C. Anderson, T. J. Magliery, P. G. Schultz, *Chem. Biol.* **2002**, *9*, 237.
[303] J. F. Atkins, R. B. Weiss, S. Thompson, R. F. Gesteland, *Annu. Rev. Genet.* **1991**, *25*, 201.
[304] J. C. Anderson, N. Wu, S. W. Santoro, V. Lakshman, G. Schultz Peter, *Proc. Natl. Acad. Sci. USA* **2004**, *101*, 7566.
[305] J. C. Anderson, P. G. Schultz, *Biochemistry* **2003**, *42*, 9598.
[306] S. W. Santoro, J. C. Anderson, V. Lakshman, P. G. Schultz, *Nucleic Acids Res.* **2003**, *31*, 6700.
[307] M. Pastrnak, T. J. Magliery, P. G. Schultz, *Helv. Chim. Acta* **2000**, *83*, 2277.
[308] F. Martin, Dissertation, Université Louis Pasteur (Strasbourg, France), **1995**.
[309] A. K. Kowal, C. Kohrer, U. L. RajBhandary, *Proc. Natl. Acad. Sci. USA* **2001**, *98*, 2268.

 © 2005 Wiley-VCH Verlag GmbH & Co. KGaA, Weinheim

[310] G. Galli, H. Hofstetter, M. L. Birnstiel, *Nature* **1981**, *294*, 626.
[311] K. Sakamoto, A. Hayashi, A. Sakamoto, D. Kiga, H. Nakayama, A. Soma, T. Kobayashi, M. Kitabatake, K. Takio, K. Saito, M. Shirouzu, I. Hirao, S. Yokoyama, *Nucleic Acids Res.* **2002**, *30*, 4692.
[312] F. Li, Y. Xiong, J. Wang, H. D. Cho, K. Tomita, A. M. Weiner, T. A. Steitz, *Cell* **2002**, *111*, 815.
[313] M. P. Deutscher, *Prog. Nucleic Acid Res. Mol. Biol.* **1990**, *30*, 209.
[314] S. L. Wolin, A. G. Matera, *Genes Dev.* **1999**, *13*, 1.
[315] G. J. Arts, S. Kuersten, P. Romby, B. Ehresmann, I. W. Mattaj, *EMBO J.* **1998**, *17*, 7430.
[316] H. Edwards, P. Schimmel, *Mol. Cell. Biol.* **1990**, *10*, 1633.
[317] H. Edwards, V. Trezeguet, P. Schimmel, *Proc. Natl. Acad. Sci. USA* **1991**, *88*, 1153.
[318] Y. Kwok, J. T. Wong, *Can. J. Biochem.* **1980**, *58*, 213.
[319] D. Kiga, K. Sakamoto, K. Kodama, T. Kigawa, T. Matsuda, T. Yabuki, M. Shirouzu, Y. Harada, H. Nakayama, K. Takio, Y. Hasegawa, Y. Endo, I. Hirao, S. Yokoyama, *Proc. Natl. Acad. Sci. USA* **2002**, *99*, 9715.
[320] J. W. Chin, T. A. Cropp, J. C. Anderson, M. Mukherji, Z. Zhang, P. G. Schultz, *Science* **2003**, *301*, 964.
[321] C. Kohrer, J. H. Yoo, M. Bennett, J. Schaack, U. L. RajBhandary, *Chem. Biol.* **2003**, *10*, 1095.
[322] S. L. Monahan, H. A. Lester, D. A. Dougherty, *Chem. Biol.* **2003**, *10*, 573.
[323] T. A. Cropp, P. G. Schultz, unpublished results.
[324] F. Xu, X. Chen, L. Xin, L. Chen, Y. Jin, D. Wang, *Nucleic Acids Res.* **2001**, *29*, 4125.
[325] X. Yang, J. Lee, E. M. Mahony, P. D. Kwong, R. Wyatt, J. Sodroski, *J. Virol.* **2002**, *76*, 4634.
[326] Z. Zhang, L. Alfonta, F. Tian, B. Bursulaya, S. Uryu, D. S. King, P. G. Schultz, *Proc. Natl. Acad. Sci. USA* **2004**, *101*, 8882.
[327] A. Deiters, P. G. Schultz, *Bioorg. Med. Chem. Lett.*, in press.
[328] H. Cho et al., unpublished results.

 © 2005 Wiley-VCH Verlag GmbH & Co. KGaA, Weinheim

Communications



The spotlight is on the classical organometallic molecule bis(benzene)chromium, which this year celebrates its 50th anniversary. Easy to dimetalate, its monometalation on a preparative scale has thus far proved elusive. The synergic action of Na/Mg or K/Mg bases allows its selective deprotonation. For more information, see the Communication by R. E. Mulvey and co-workers on the following pages.

© 2005 Wiley-VCH Verlag GmbH & Co. KGaA, Weinheim
DOI: 10.1002/anie.200460637

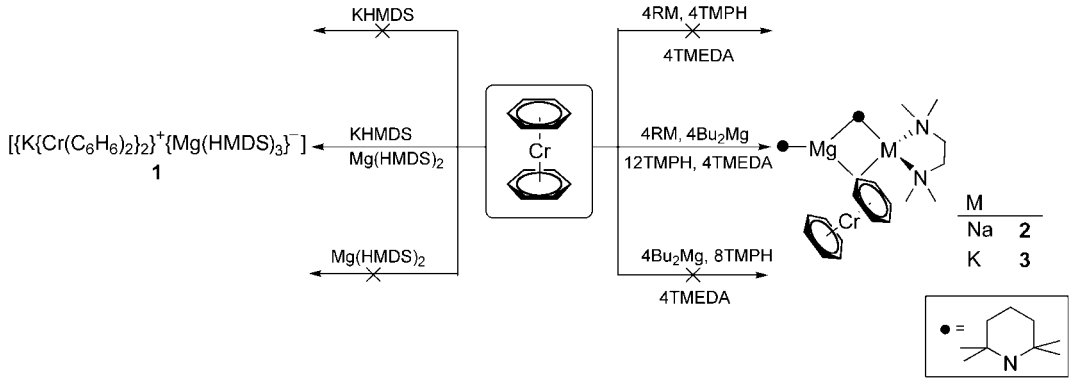
Metalation Reactions

Synergic Monodeprotonation of Bis(benzene)chromium by Using Mixed Alkali Metal–Magnesium Amide Bases and Structural Characterization of the Heterotrimetallic Products**

Eva Hevia, Gordon W. Honeyman, Alan R. Kennedy, Robert E. Mulvey, and David C. Sherrington*

Developed by Elschenbroich in the late 1960s,[1] the reaction of bis(benzene)chromium with TMEDA-activated *n*BuLi still represents today the standard method for metalating the sandwich complex (TMEDA is *N*,*N*,*N*′,*N*′-tetramethylethylenediamine). Metalation plays a pivotal part in the development of bis(benzene)chromium chemistry,[2] which celebrates its 50th anniversary in 2005,[3] as in transforming the parent neutral compound to a more reactive carbanionic form, it opens up a gateway to a plethora of selectively functionalized derivatives.[4] The original lithiation method, which employs a 5:1 molar excess of base, produces mainly the heteroannular dilithio derivative "$[Cr(C_6H_5Li)_2]$" in yields of about 50% at best, as determined indirectly by mass spectrometric studies of D_2O-quenched reaction mixtures. Lithiation of one benzene ring strongly activates the molecule towards a second lithiation (on the other ring), hence the yield of the monolitho derivative "$[Cr(C_6H_5Li)(C_6H_6)]$" is always much poorer (typically 5–20%). A lack of crystallographic evidence means that neither lithio reagent has been structurally authenticated, though an analogy with the TMEDA adduct of heteroannular dilithioferrocene $[\{Fe(C_5H_4)_2\}_3Li_6\cdot(TMEDA)_2]$[5] suggests both could be molecularly complex. Following our recent report[6] that ferrocene can be regioselectively tetrametalated by the synergic action of mixed sodium/magnesium tris(diisopropylamide), manifested in the sixteen-membered inverse crown complex $[\{Fe(C_5H_3)_2\}Na_4Mg_4(i\mathrm{Pr}_2\mathrm{N})_8]$, we posed the question "how would such synergic base mixtures behave towards bis(benzene)chromium?". The surprising and contrasting answers to this question when the π-arene complex is subjected to synergic amide mixtures based on either 1,1,1,3,3,3-hexamethyldisilazide (HMDS) or 2,2,6,6-tetramethylpiperidide (TMP) provides the basis for this Communication. Moreover, all of the metal products synthesized in this study have been successfully characterized crystallographically, thus belatedly revealing the first crystal structures of polar metal complexes of bis(benzene)chromium.[7]

In the first synergic trial, treatment of bis(benzene)chromium with an equimolar mixture of potassium HMDS and magnesium bis(HMDS) afforded $[\{\{K\cdot[Cr(C_6H_6)_2]_2\}^+[Mg(HMDS)_3]^-\}_\infty]$ (**1**; Scheme 1). No metalation has taken place during the synthesis, thus reflecting the relatively weak basic character of HMDS, instead the bis(benzene)chromium acts as a π ligand to the K^+ cation, which forms an ion-pair "-ate" complex with the $[Mg(HMDS)_3]^-$ ion. However, this is still a synergic reaction in the sense that neither homometallic component KHMDS or $Mg(HMDS)_2$ reacts unilaterally with bis(benzene)chromium under similar conditions to those employed in the preparation of **1**. In the molecular structure of **1** (Figure 1)[8] two distinct bis(benzene)chromium molecules π bond to the K^+ ion, which, in turn, engages with the $[Mg(HMDS)_3]^-$ ion through $K\cdots CH_3Si(Me_2)$ agostic interactions. One of the bis(benzene)chromium molecules (labeled Cr2) bridges to



Scheme 1. Comparative reactions of bis(benzene)chromium with homometallic and heterometallic base mixtures.

[*] Dr. E. Hevia, G. W. Honeyman, Dr. A. R. Kennedy, Prof. R. E. Mulvey, Prof. D. C. Sherrington
Department of Pure and Applied Chemistry
University of Strathclyde
Glasgow, G1 1XL (UK)
Fax: (+44) 141-552-0876
E-mail: r.e.mulvey@strath.ac.uk

[**] This work was supported by the UK Engineering and Physical Science Research Council through grant award no. GR/R81183/01, and by the EU through a Marie Curie Fellowship to E.H.

the K^+ ion of a neighboring molecule, thus extending the structure through a metal-rich $\{K(C_6H_6)Cr(C_6H_6)K'\}$ sandwich and making the K^+ ion four-coordinate overall (counting both the anion and neutral ligands as single coordination points). Disorder in one of the bis(benzene)chromium molecules renders the dimensions in which it is involved meaningless, but other key dimensions are listed in the legend to Figure 1. To the best of our knowledge, the cationic moiety of **1** is unprecedented and as such represents with the other

 © 2005 Wiley-VCH Verlag GmbH & Co. KGaA, Weinheim

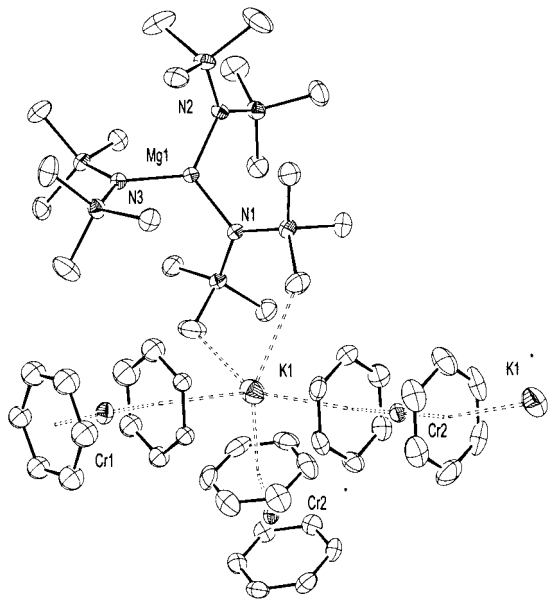


Figure 1. Extended structure of **1** showing the coordination geometry about K1. Hydrogen atoms and disorder components are omitted for clarity. Selected separations [Å] and angles [°]: K1-C33 3.356(3), K1-C34 3.330(3), K1-C38 3.424(3), K1-C39 3.169(4), K1-C40 3.161(3), K1-C41 3.411(3), K1-C1 3.688(3), K1-C4 3.356, C1-K1-Ct2 150.87, C4-K1-Ct2 90.54, Ct1-K1-Ct2 106.42, C1-K1-Ct1 80.03, C4-K1-Ct1 113.59. For the atom labeling scheme refer to cif file.

new complexes reported herein, the first characterized bis(benzene)chromium complexes of any alkali metal. An indirect comparison can be made with the recently reported ferrocene complex $[\{K\cdot[Fe(C_5H_5)_2]_2\cdot(toluene)_2\}^+\{Mg(HMDS)_3\}^-]$.[9]

A distinct change of the reaction solution from brown to deep red gave cause for optimism that metalation had occurred during the synergic trials of the stronger base TMP, as a similar color change accompanies lithiation of bis(benzene)chromium. Composed of butylsodium or benzylpotassium, dibutylmagnesium, TMPH, and TMEDA in a 1:1:3:1 stoichiometry, the synergic base mixture was employed in a 4:1 molar excess with respect to bis(benzene)-chromium (Scheme 1). Each reaction afforded a red crystalline product, namely $[NaMg\{Cr(C_6H_5)(C_6H_6)\}(TMP)_2\cdot(TMEDA)]$ (**2**) or $[KMg\{Cr(C_6H_5)(C_6H_6)\}(TMP)_2\cdot(TMEDA)]$ (**3**). Thus, surprisingly, in contrast to the lithiation precedent, these sodium and potassium congeners show metalation (formally magnesiation) selectively on only one ring, leaving the second benzene ring untouched. Even when the molar excess of base is increased to 10:1, **2** and **3** are still the only isolable products, thus indicating that synergic monometalation deactivates the second benzene ring (and the remaining H sites of the phenyl ring) towards metalation. Moreover, the yields of **2** and **3** of the isolated solids (first batch 64 and 67%, respectively), are unquestionably high for metallo compounds of bis(benzene)chromium, which are usually used in situ without isolation or characterization. Homometallic control reactions that employ the same TMPH/TMEDA mixtures but with only a single metallic reagent (butylsodium, benzylpotassium, or dibutylmagnesium) failed to similarly promote metalation of added bis(benzene)chromium, thus confirming that the selective metalation behind the syntheses of **2** and **3** is also synergic in origin.

The molecular structures of **2** (Figure 2)[10] and **3** (Figure 3)[11] share many common features. These include a central near-planar, four-element MNMgC ring [counting

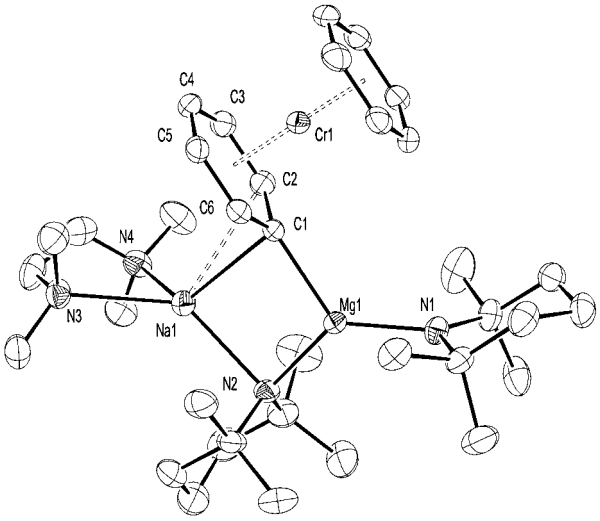


Figure 2. Molecular structure of **2** with hydrogen atoms omitted for clarity. Selected separations [Å] and angles [°]: Na1-N2 2.455(2), Na1-N3 2.515(2), Na1-N4 2.522(2), Na1-C1 2.705(2), Na1-C2 2.910(2), Mg1-N1 2.0032(9), Mg1-N2 2.0825(19), Mg1-C1 2.197(2), N1-Mg1-C1 124.57(8), N1-Mg1-N2 131.09(9), N2-Mg1-Na1 81.83(7), Mg1-N2-Na1 90.51(7), N3-Na1-N4 75.72(7), N2-Na1-N3 133.41(8), N2-Na1-N4 129.66(8), N2-Na1-C1 81.76(7), N3-Na1-C1 119.49(7), N3-Na1-C1 123.17(8).

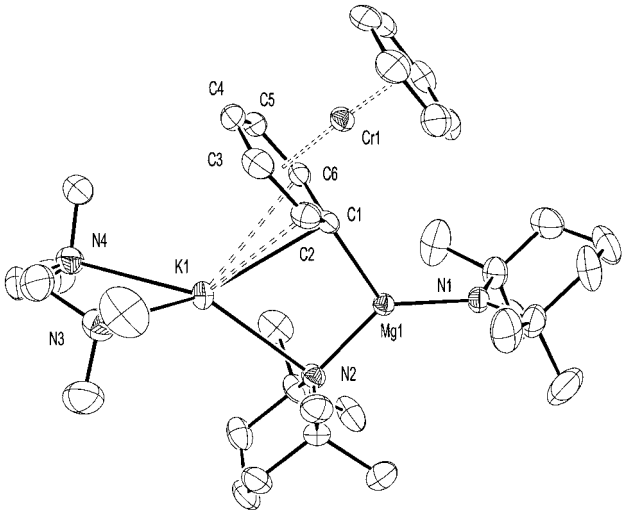


Figure 3. Molecular structure of **3** with hydrogen atoms omitted for clarity. Selected separations [Å] and angles [°]: K1-N2 2.9203(16), K1-N3 2.8313(18), K1-N4 2.8499(18), K1-C1 2.9171(18), K1-C2 3.018(2), K1-C6 3.2279(19) Mg1-N1 2.0018(16), Mg1-N2 2.0857(16), Mg1-C1 2.1720(19),N1-Mg1-N2 132.96(7), N1-Mg1-C1 123.43(7), N2-Mg1-C1 103.54(7), Mg1-N2-K1 94.12(6), Mg1-C1-K1 92.39(6), N3-K1-N4 64.12(5), N3-K1-C1 128.63(5), N4-K1-C1 134.22(5), N4-K1-N2 144.04(5), N3-K1-N2 127.28(5), C1-K1-N2 69.92(5).

 © 2005 Wiley-VCH Verlag GmbH & Co. KGaA, Weinheim

bis(benzene)chromium as formally a ligand that coordinates through a single C atom]; a Mg-attached, terminal TMP ligand; and, bidentate TMEDA chelation of the alkali metal (Na or K). Another salient feature, which has become a distinguishing trademark of inverse crown chemistry[12] is the σ/π distinction of the s-block metal–arene bonding, which reflects the relative size, polarizability, and hardness or softness of the particular type of metal atoms involved. Refilling the position vacated by the H atom, the lower polarity Mg atom forms a stronger, more covalent bond with the anionic C center, the predominately σ character of which can be discerned from its near coplanarity with the plane of the phenyl ring [deviation of Mg from plane: 0.005(3) Å in **2**; 0.290(3) Å in **3**]. In contrast, the higher polarity (and softer) alkali-metal atoms occupy skewed positions above the Ph ring to engage electrostatically with its π face. The closest contact is to the anionic C1 center [2.705(2) Å in **2**; 2.917(2) Å in **3**], where charge is most concentrated, and there are other short contacts to proximate atoms, one for Na [2.910(2) Å to C(2)] and, reflecting the larger cation size and softer character, two for K [3.018(2) Å to C(2); 3.228(2) Å to C(6)]. All other M···C(Ph) distances exceed 3.38 Å and 3.44 Å in **2** and **3** respectively. Dimensions involving Mg atoms vary little between **2** and **3** [e.g., Mg–C1, 2.197(2) Å and 2.172(2) Å, respectively; C1-Mg-N2, 104.39(8)° and 103.54(7)°, respectively], which is consistent with Mg being the anchoring metal center that templates the anionic ligand set into a distorted trigonal planar, pseudoate arrangement about it. The TMEDA-chelated M atoms affix loosely to this template to form a contacted ion pair. Interestingly, the shortest interatomic distance for Na is with the μ-N(TMP) atom [2.455(2) Å; the distance to C1 is 0.250 Å longer], whereas for K the corresponding distances are equally short [to C1, 2.917(2) Å; to μ-N(TMP), 2.920(2) Å]. Furthermore, the K–μ-N(TMP) contact is significantly longer than the K–N(TMEDA) distances (mean, 2.841 Å), which is the reverse of that found for Na [mean Na–N(TMEDA) distance, 2.519 Å, compared with 2.455(2) Å for Na-C1]. Hence it can be deduced that the K center has a greater affinity for binding to the softer areneide than to the harder N anion. The close proximity between the terminal TMP ligand and the non-metalated benzene ring, coupled with the overhanging of the TMEDA molecule above the Ph ring, suggest that the simultaneous attachment of a second TMP-Mg-TMP-M-TMEDA coordination arc (concomitant with a second deprotonation) could possibly be ruled out on steric grounds (though electronic factors may also contribute to the inertness of **2** and **3** towards further deprotonation). It must also be stressed that the synergic Na–Mg/K–Mg bases will themselves be extremely sterically demanding, much more so than *n*BuLi. Thus, in the usual lithium reagent methodology there is no such steric control, hence the selectivity of monometalation is lost and dimetalation readily proceeds.

Further studies will address how different synergic bases will behave towards bis(benzene)chromium and, in view of their ready availability in pure crystalline form, whether **2** and **3** (in the mould of the lithio precedents) can be employed as access reagents to monofunctionalized bis(benzene)chromium derivatives.

Experimental Section

All reactions were carried out under a protective argon atmosphere.

Synthesis of **1**: K(HMDS) (2 mL of a 0.5 M solution in toluene, 2 mmol) was added to a solution of $Mg(HMDS)_2$ in heptane, which was prepared in situ by treating *n*/*s*Bu_2Mg (1 mL of a solution in heptane, 1 mmol) with HMDS(H), (0.422 mL, 2 mmol) at reflux for two hours. The solution was heated at reflux for one hour then left to reach room temperature. Bis(benzene)chromium (0.208 g, 1 mmol) was added and the resulting solution was heated at reflux for another hour. Toluene was added (10 mL) to completely dissolve the dark green precipitate that had formed and the reaction mixture was then heated to reflux for a further hour. The resulting solution was left to cool overnight to facilitate crystallization. A large crop of green/black needle-shaped crystals was obtained. Yield: 34.4% (0.33 g). M.p.: 228 °C. ^{1}H NMR (400.13 MHz, [D_8]toluene, 300 K): $\delta = 0.45$ (s, CH_3, $Mg[N\{Si(CH_3)_3\}_2]_3$), 4.28 ppm (broad s, $Cr(\eta^6\text{-}C_6H_6)_2$). ^{13}C{^{1}H} NMR (100.63 MHz, [D_8]toluene, 300 K): $\delta = 7.35$ (CH_3, $Mg[N\{Si(CH_3)_3\}_2]_2$), 74.74 ppm ($Cr(\eta^6\text{-}C_6H_6)_2$).

Synthesis of **2**: *n*BuNa (0.4 g, 5 mmol) was suspended in hexane (20 mL). *n*/*s*Bu_2Mg (5 mL of a 1 M solution in heptane, 5 mmol) and TMPH (2.5 mL, 15 mmol) were added. The resulting pale yellow solution was stirred for 30 minutes and TMEDA (0.75 mL, 5 mmol) was introduced. The slightly cloudy pale yellow solution was filtered through Celite and $[Cr(C_6H_6)_2]$ (0.26 g, 1.25 mmol) was added. The reaction mixture was heated at reflux for 45 minutes and a change from brown to red was observed. Allowing the solution to cool slowly to room temperature produced a crop of red crystals. Yield: 64% (0.52 g). ^{1}H NMR (400.13 MHz, [D_8]thf, 300 K): $\delta = 4.61$ (d, 2H, H_{ortho}, C_6H_5), 4.16 (t, 2H, H_{meta}, C_6H_5), 4.10 (m, 1H, H_{para}, C_6H_5), 4.03 (s, 6H, C_6H_6), 2.30 (s, 4H, CH_2, TMEDA), 2.15 (s, 12H, CH_3, TMEDA), 1.62 (m, 4H, TMP), 1.30 (s, 24H, CH_3, TMP), 1.18 ppm (m, 8H, TMP). ^{13}C{^{1}H} (100.63 MHz, [D_8]thf, 300 K): $\delta = 105.4$ (C_{para}, C_6H_5), 88.7 (C_{ortho}, C_6H_5), 79.4 (C_{meta}, C_6H_5), 75.9 (C_{ipso}, C_6H_5), 72.2 (C_6H_6), 59.1 (CH_2, TMEDA), 53.2 (N-*C*, TMP), 46.6 (CH_3, TMEDA), 42.8 (TMP), 36.4 (CH_3, TMP), 21.6 ppm (TMP). An as-yet unidentified minor product with signals at 4.71 (d) 4.22 (m), 4.07 (s) was also present in the ^{1}H NMR spectrum.

Synthesis of **3**: BzK (0.65 g, 5 mmol) was suspended in hexane (20 mL). *n*/sBu_2Mg (5 mL of a 1 M solution in heptane, 5 mmol), TMPH (2.5 mL, 15 mmol) and TMEDA (0.75 mL, 5 mmol) were added and the resulting mixture was stirred for 1 h affording a slightly cloudy red solution which was filtered through Celite. $[Cr(C_6H_6)_2]$ (0.26 g, 1.25 mmol) was subsequently added and the reaction mixture was heated under reflux for 45 minutes. Allowing the red solution to cool slowly to room temperature produced a crop of red crystals. Yield: 67% (0.55 g). (400.13 MHz, [D_8]thf, 300 K): $\delta = 4.71$ (d, 2H, H_{ortho}, C_6H_5), 4.16 (t, 2H, H_{meta}, C_6H_5), 4.08 (m, 1H, H_{para}, C_6H_5), 3.98 (s, 6H, C_6H_6), 2.30 (s, 4H, CH_2, TMEDA), 2.15 (s, 12H, CH_3, TMEDA), 1.68 (m, 4H, TMP), 1.28 (s, 24H, CH_3, TMP), 1.23 ppm (m, 8H, TMP). ^{13}C{^{1}H} (100.63 MHz, [D_8]thf, 300 K): $\delta = 107.6$ (C_{para}, C_6H_5), 89.3 (C_{ortho}, C_6H_5), 79.6 (C_{meta}, C_6H_5), 76.2 (C_{ipso}, C_6H_5), 71.7 (C_6H_6), 59.3 (CH_2, TMEDA), 53.2 (N-*C*, TMP), 46.5 (CH_3, TMEDA), 42.8 (TMP), 36.5 (CH_3, TMP), 21.8 ppm (TMP).

Received: May 12, 2004
Published Online: September 7, 2004

Keywords: alkali metals · amides · inverse crown compounds · metalation · metallocenes

[1] C. Elschenbroich, *J. Organomet. Chem.* **1968**, *14*, 157.
[2] For a historical account of the human and chemical story behind bis(benzene)chromium see: D. Seyferth, *Organometallics* **2002**, *21*, 1520; D. Seyferth, *Organometallics* **2002**, *21*, 2800.
[3] E. O. Fischer, W. Hafner, *Z. Naturforsch. B* **1955**, *10*, 665.

 © 2005 Wiley-VCH Verlag GmbH & Co. KGaA, Weinheim

[4] For recent examples of the use of lithio bis(benzene)chromium reagents see: K. C. Hultzch, J. M. Nelson, A. J. Lough, I. Manners, *Organometallics* **1995**, *14*, 5496; C. Elschenbroich, E. Schmidt, B. Metz, K. Harms, *Organometallics* **1995**, *14*, 4043; D. Braga, L. Maini, F. Grepioni, C. Elschenbroich, F. Paganelli, O. Schiemann, *Organometallics* **2001**, *20*, 1875; H. Braunschweig, M. Homberger, C. Hu, X. Zheng, E. Gullo, G. Clentsmith, M. Lutz, *Organometallics* **2004**, *23*, 1968.

[5] I. R. Butler, W. R. Cullen, J. Ni, S. J. Rettig, *Organometallics* ***1985***, *4*, 2196.

[6] W. Clegg, K. W. Henderson, A. R. Kennedy, R. E. Mulvey, C. T. O'Hara, R. B. Rowlings, D. M. Tooke, *Angew. Chem.* **2001**, *113*, 4020; *Angew. Chem. Int. Ed.* **2001**, *40*, 3902.

[7] Examples of structurally authenticated directly metalated bis(benzene)chromium derivatives are extremely rare. For an organotin structure see C. Elschenbroich, E. Schmidt, B. Metz, W. Massa, S. Wocadlo, O. Burghaus, *Z. Anorg. Allg. Chem.* **1999**, *625*, 875; for an organogermanium structure see C. Elschenbroich, E. Schmidt, R. Gondrum, B. Metz, O. Burghaus, W. Massa, S. Wocadlo, *Organometallics* **1997**, *16*, 4589.

[8] Crystal data for **1**: $C_{42}H_{78}Cr_2KMgN_3Si_6$; A yellow tablet of approximate dimensions $0.25\times0.12\times0.05$ mm gave a monoclinic space group $P2_1/n$, $a=16.4987(4)$ $b=14.8080(3)$ $c=22.7857(5)$ Å, $\beta=109.571(1)°$, $V=5245.2(2)$ Å^3, $T=150$ K, $Z=4$, $\rho_{calc}=1.217$ Mg m^{-3}, $2\theta_{max}=54.96°$, $Mo_{K\alpha}$ $\lambda=0.71073$ Å. All structures were solved and refined to convergence on F^2 (SHELXS and SHELXL-97, G. M. Sheldrick, University of Göttingen, Germany, **1997**). $R1=0.0461$ (for 8234 reflections with $I>2\sigma(I)$) $wR2=0.1107$ and S = 1.020 for 562 parameters and 12000 unique reflections. Minimum/maximum residual electron density −0.509/0.624 e Å^{-3}. CCD-238576, 238577 and 238578 contain the supplementary crystallographic data for this paper. These data can be obtained free of charge via www.ccdc.cam.ac.uk/conts/retrieving.html (or from the Cambridge Crystallographic Data Centre, 12 Union Road, Cambridge CB21EZ, UK; fax: (+44) 1223-336-033; or deposit@ccdc.cam.ac.uk).

[9] G. W. Honeyman, A. R. Kennedy, R. E. Mulvey, D. C. Sherrington, *Organometallics* **2004**, *23*, 1197.

[10] *Crystal Data* for **2**: $C_{36}H_{63}CrMgN_4Na$; A red fragment of approximate dimensions $0.30\times0.30\times0.06$ mm gave a triclinic space group $P\bar{1}$, $a=11.8831(5)$, $b=12.0196(3)$, $c=14.7612(6)$ Å, $\alpha=96.602(2)$, $\beta=109.447(2)$, $\gamma=108.630(2)°$, $V=1825.18(12)$ Å^3, $T=123$ K, $Z=2$, $\rho_{calc}=1.185$ Mg m^{-3}, $2\theta_{max}=54.16°$, $Mo_{K\alpha}$ $\lambda=0.71073$ Å. $R1=0.0476$ (for 5304 reflections with $I>2\sigma(I)$) $wR2=0.1064$ and S = 1.012 for 466 parameters and 7991 unique reflections. Minimum/maximum residual electron density −0.412/0.281 e Å^{-3}.

[11] *Crystal Data* for **3**: $C_{36}H_{63}CrKMgN_4$; A red fragment of approximate dimensions $0.35\times0.27\times0.18$ mm gave a monoclinic space group $C2/c$, $a=31.4001(7)$, $b=12.5255(2)$, $c=21.1754(4)$ Å, $\beta=115.787(1)°$, $V=7499.0(2)$ Å^3, $T=123$ K, $Z=8$, $\rho_{calc}=1.182$ Mg m^{-3}, $2\theta_{max}=54.96°$, $Mo_{K\alpha}$ $\lambda=0.71073$ Å. $R1=0.0413$ (for 6373 reflections with $I>2\sigma(I)$) $wR2=0.1034$ and S = 1.035 for 488 parameters and 8590 unique reflections. Minimum/maximum residual electron density −0.388/0.437 e Å^{-3}.

[12] R. E. Mulvey, *Chem. Commun.* **2001**, 1049.

 © 2005 Wiley-VCH Verlag GmbH & Co. KGaA, Weinheim

Functional Materials

Highly Interpenetrated Metal–Organic Frameworks for Hydrogen Storage**

*Banu Kesanli, Yong Cui, Milton R. Smith, Edward W. Bittner, Bradley C. Bockrath, and Wenbin Lin**

Metal–organic frameworks (MOFs) provide an interesting avenue to novel materials through fine-tuning their structures by a modular construction approach.[1] A variety of MOFs have recently been explored for potential applications, such as nonlinear optics, size-, shape-, and functional-group-selective sorptions, and catalysis.[2] Many of the perceived applications for MOFs require accessible large pores, which presents a significant challenge owing to a strong tendency of interpenetration in such very open frameworks. In contrast to a vast number of porous non-interpenetrated MOFs, only a few examples of porous interpenetrated MOFs have been reported.[3]

Kitagawa et al. have pioneered the studies on the adsorption of small molecules (such as methane and oxygen) by microporous MOFs.[4] More recent results by Rosi et al. further suggested that microporous MOFs are able to store hydrogen at a capacity unmatched by other materials.[5] It was believed that favorable interactions exist between aromatic rings of MOFs and hydrogen molecules.[6] We hypothesize that microporous interpenetrated MOFs would be ideal candidates for the sorption of small gaseous molecules. Interpenetration can be utilized to strengthen the interaction between the gaseous molecule and the framework by an entrapment mechanism in which a hydrogen molecule is in close proximity with several aromatic rings from interpenetrating networks.[7] Herein we report the design of highly interpenetrated aromatic-rich MOFs and preliminary data on their hydrogen and methane sorption capacities.

New aromatic-rich, dicarboxylic acids 6,6′-dichloro-2,2′-diethoxy-1,1′-binaphthyl-4,4′-dibenzoic acid (L_1-H_2) and 6,6′-dichloro-2,2′-dibenzyloxy-1,1′-binaphthyl-4,4′-dibenzoic acid (L_2-H_2) were prepared by Suzuki coupling reactions between

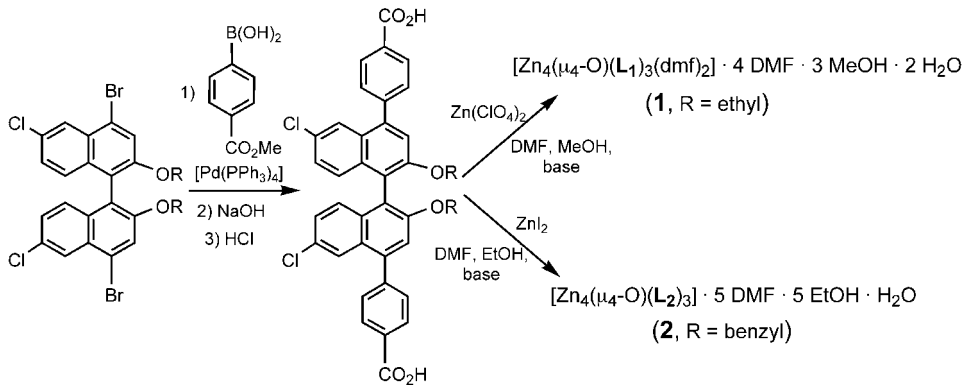
[*] Dr. B. Kesanli, Dr. Y. Cui, Prof. W. Lin
Department of Chemistry, CB#3290
University of North Carolina
Chapel Hill, NC 27599 (USA)
Fax: (+1) 919-962-2388
E-mail: wlin@unc.edu

Dr. M. R. Smith, Dr. E. W. Bittner, Dr. B. C. Bockrath
National Energy Technology Laboratory
United States Department of Energy
P.O. Box 10940, Pittsburgh, PA 15236 (USA)

[**] We acknowledge financial support from NSF. W.L. is an Alfred P. Sloan Fellow, an Arnold and Mabel Beckman Young Investigator, a Cottrell Scholar of Research Corp, and a Camille Dreyfus Teacher-Scholar. We thank Dr. C. Wu for help with X-ray structure determinations.

Supporting information for this article is available on the WWW under http://www.angewandte.org or from the author.

 © 2005 Wiley-VCH Verlag GmbH & Co. KGaA, Weinheim DOI: 10.1002/anie.200461214



Scheme 1.

4-methoxycarbonylphenylboronic acid and previously reported 6,6′-dichloro-4,4′-dibromo-1,1′-binaphthyl starting materials followed by hydrolysis (Scheme 1).[8] Single crystals of $[Zn_4(\mu_4\text{-}O)(L_1)_3(dmf)_2]\cdot 4\,DMF\cdot 3\,CH_3OH\cdot 2\,H_2O$ (**1**) and $[Zn_4(\mu_4\text{-}O)(L_2)_3]\cdot 5\,DMF\cdot 5\,C_2H_5OH\cdot H_2O$ (**2**) were obtained by treating $Zn(ClO_4)_2$ with L_1-H_2 in DMF and MeOH or ZnI_2 with L_2-H_2 in DMF and EtOH in the presence of dimethylaniline at 50 °C for two days. The formulations of **1** and **2** were supported by IR, microanalysis, and thermogravimetric analysis (TGA) results.

Compound **1** adopts a 3D interpenetrating network structure that is built from two distinct $[Zn_4(\mu_4\text{-}O)(L_1)_3(dmf)_2]$ clusters (Figure 1a).[9] While one of the L_1 ligands adopts an *exo*-tridentate coordination mode, the other L_1 ligands adopt *exo*-tetradentate coordination mode. One of the two $[Zn_4(\mu_4\text{-}O)(L_1)_3(dmf)_2]$ clusters contains three Zn^{II} centers in tetrahedral and one in a trigonal bipyramidal coordination geometry that are bridged by a μ_4-O atom and five carboxylate groups of L_1 ligands, while the other contains three Zn^{II} centers in tetrahedral and one in an octahedral coordination geometry that are bridged by a μ_4-O atom and six carboxylate groups of L_1 ligands. Each of the two $[Zn_4(\mu_4\text{-}O)(L_1)_6(dmf)_2]$ clusters is completed by the coordination of two DMF molecules. Each type of $[Zn_4(\mu_4\text{-}O)(L_1)_6(dmf)_2]$ cluster in **1** is interlinked by the carboxylate groups of L_1 ligands to generate an extended neutral 3D network of a cubic topology that is built upon six-connected nodes. The 3D network of **1** thus possesses very large cubic cavities of approximately $19\times19\times19$ Å (Figure 1b). However, **1** avoids extremely large void space by forming a fourfold interpenetrated structure (Figure 1c). Even after fourfold interpenetration, **1** still possesses significant void space that is occupied by disordered DMF, MeOH, and H_2O guest molecules.[10] These void spaces can be accessed from open channels (Figure 1d) of approximately 4.1×5.0 Å along the *a* axis, of 3.2×4.0 Å and 2×2.5 Å along the *b* axis, and of 4.7×5.4 Å and 1.8×3.4 Å along the *c* axis. The effective free volume of **1** was calculated by PLATON analysis as 46.1% of the crystal volume (15168 $Å^3$ out of the 32912 $Å^3$ unit cell volume).

Compound **2** adopts a similar fourfold 3D interpenetrating network structure that is built from C_3-symmetric $[Zn_4(\mu_4\text{-}O)(L_2)_3]$ clusters.[9] All the Zn centers in the $[Zn_4(\mu_4\text{-}O)(L_2)_3]$ cluster have tetrahedral geometry through coordination to a

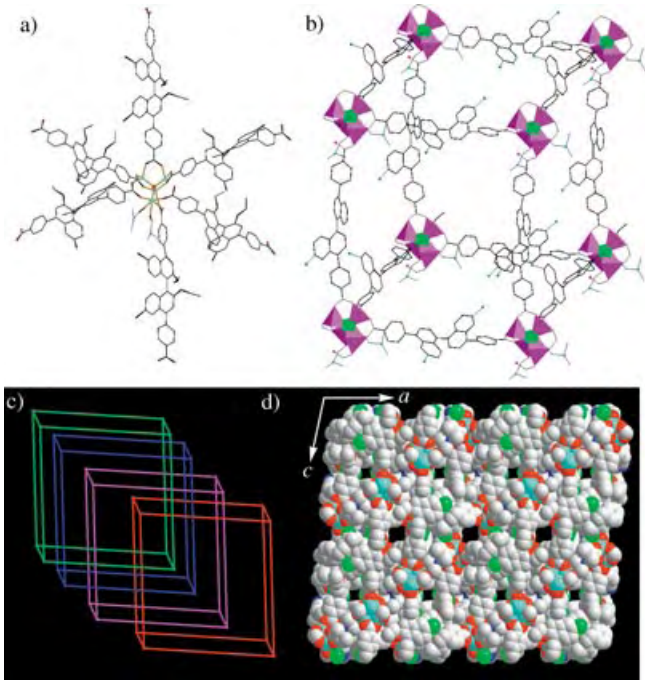


Figure 1. a) A view of the one of the $[Zn_4(\mu_4\text{-}O)(L_1)_6(dmf)_2]$ clusters of **1** b) A view of the cubic cavity formed by the 3D network (ethoxy groups have been omitted for clarity; the purple and green polyhedra represent the cluster building unit. c) A schematic presentation of the fourfold interpenetration in **1**. d) A space-filling model of **1** as viewed down the *b* axis (solvent molecules have been omitted); gray C, red O, blue N, green Cl, turquoise Zn.

μ_4-oxygen atom and three oxygen atoms of the bridging carboxylate groups of the L_2 ligands. There are no coordinating solvent molecules in the structure of **2**. Just like **1**, the $[Zn_4(\mu_4\text{-}O)(L_2)_3]$ clusters in **2** are linked by L_2 ligands to form an extended 3D network structure of a cubic topology. The 3D network structure of **2** contains cubic cavities of approximately $19\times19\times19$ Å. The porosity of **2** is drastically reduced by adopting fourfold interpenetration, and the void space in **2** is filled with five DMF, one H_2O, and five ethanol guest molecules as established by TGA and elemental analysis. PLATON analysis indicated that the effective free volume of **2** was 41.4% of the crystal volume (5257 $Å^3$ out of the

 © 2005 Wiley-VCH Verlag GmbH & Co. KGaA, Weinheim

12699 Å^3 unit cell volume). A smaller percent effective free volume of **2** compared to **1** is consistent with the presence of larger benzyloxy groups in **2**. The void space of **2** is only accessible along the *c* axis by open channels of approximately 1.3×4.5 Å.

Single-crystal X-ray diffraction studies, TGA, and elemental analyses demonstrated the inclusion of disordered guest molecules in **1** and **2**. Powder X-ray diffraction studies further indicated that the long-range order of the framework structures of **1** and **2** was retained upon complete removal of the guest molecules (see Supporting Information). Permanent microporosity of **1** and **2** was unambiguously established with CO_2 adsorption measurements at 0 °C. Samples of **1** and **2** were soaked in CH_2Cl_2 overnight and then evacuated at 85 °C for 12 h before CO_2 adsorption measurements. Type 1 behavior was observed for the CO_2 adsorption isotherms of both **1** and **2**, which is characteristic of solids with micropores. Compounds **1** and **2** possess a BET surface area of 502 and 396 $m^2 g^{-1}$, respectively. The micropore volume for **1** is 0.20 $mL g^{-1}$ and for **2** is 0.13 $mL g^{-1}$.[11] Smaller surface area observed for **2** is consistent with its percent effective free volume calculated with PLATON.

We have examined gas storage behaviors of **1** and **2** at room temperature. Hydrogen adsorption isotherms were taken using a pulse mass analyzer[12] in the 0.9–48 bar pressure range on samples of **1** and **2** that had been heated at 150 °C for 1 h to remove the included solvent molecules. The H_2 uptakes are calculated to be 1.12 wt % for **1** and 0.98 wt % for **2** at 48 bar (Figure 2, Table 1), which corresponds to H_2 storage capacity of 124.7 $mL g^{-1}$ for **1** and 109.6 $mL g^{-1}$ for **2**.[12] The H_2 uptake of **1** and **2** is reversible for at least six times. For comparison, MOF-5 reported by Rosi et al.[5] exhibits a H_2 uptake of 1.65 wt % ($\approx$1.5 times that of **1**) using our procedures under the same conditions. These hydrogen uptake results for **1** and **2** are comparable to H_2 storage capacities of purified single-walled carbon nanotubes and only slightly inferior to the best MOFs (which have surface areas of 5–10 times those of **1** and **2**).[5,12,13] Methane-adsorption measurements indicated a room-temperature methane uptake of 11.0 wt % (154 $mL g^{-1}$) for **1** and 9.5 wt % (133 $mL g^{-1}$) for **2**. These methane storage capacities are lower than those of the best MOFs, which is consistent with the smaller microporous surface areas of **1** and **2**.

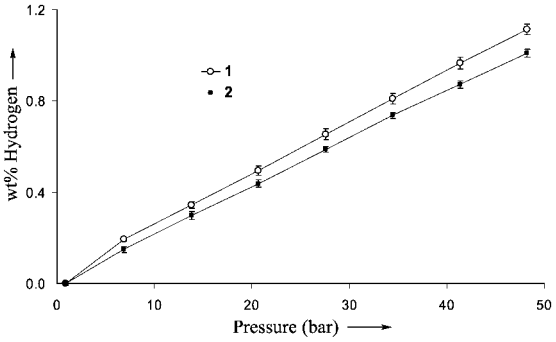


Figure 2. Hydrogen adsorption isotherms of **1** and **2** at 25 °C. The data points represent averages of six consecutive runs and the error bars indicate run-to-run variations.

Table 1: Porosity and gas storage capacity of **1** and **2**.

Sample	Surface area $m^2 g^{-1}$[a]	Pore volume $mL g^{-1}$[b]	Void volume %[c]	wt% H_2	wt% CH_4
1	502	0.20	46.1	1.12	11.0
2	396	0.13	41.4	0.98	9.5

[a] Determined from fits of adsorption data to the BET equation. [b] Calculated using the DR equation. [c] Estimated from PLATON calculations

Our results agree with an earlier observation that large surface area and pore volume are not the only recipe for the attainment of H_2 storage materials.[13a] That significant H_2 uptake is detected in the highly interpenetrated networks of **1** and **2** points to new directions for the design of efficient H_2 storage materials by utilizing interpenetration to strengthen the interaction between H_2 molecules and the framework by multiple contacts with several aromatic rings from the interpenetrating networks. Similar to triple-junction sites in carbon nanotube bundles,[6] such storage sites would have higher H_2 binding energy which is another key to the development of practical H_2 storage materials.

In summary, we have synthesized and characterized two novel fourfold interpenetrated MOFs of cubic topology that exhibit significant H_2 uptake at 25 °C. The ready tunability of these MOFs should allow the optimization of both H_2 storage capacity and H_2 binding energy in future generations of MOFs.

Experimental Section

1: A mixture of $Zn(ClO_4)_2 \cdot 6H_2O$ (3.7 mg, 0.01 mmol) and L_1-H_2 (0.01 mmol) was placed in a small vial containing DMF (0.5 mL), MeOH (0.2 mL), and *N*,*N*′-dimethylaniline (5 μL). The vial was sealed, heated at 50 °C for 48 h, and allowed to cool to room temperature. The crystals suitable for X-ray diffraction were collected by filtration, washed with diethyl ether, and dried in air. Yield: 81 %. Elemental analysis calcd (%) for $C_{135}H_{136}Cl_6Zn_4N_6O_{30}$, C 57.97, H 4.86, N 3.00; found: C 57.96, H 4.85, N 3.79, IR: $\tilde{\nu}$ = 3487 (m), 2978 (w), 2924 (w), 1660 (m), 1603 (s), 1552 (m), 1508 (m), 1411 (s), 1373 (m), 1343 (s), 1324 (m), 1213 (w), 1189 (w), 1155 (w), 1088 (m), 1059 (w), 1019 (m), 948 (w), 866 (w), 816 (w), 788 (w), 723 (w), 699 (w), 625 cm^{-1} (w).

Carbon dioxide adsorption studies were carried out at 0 °C on a Quantachrome-1C surface-area analyzer. Details of hydrogen adsorption studies were described in ref. [12].

Received: July 6, 2004
Revised: August 12, 2004

Keywords: coordination networks · crystal engineering · functional materials · hydrogen storage · zinc

[1] a) B. Moulton, M. Zaworotko, *Chem. Rev.* **2001**, *101*, 1629–1658; b) M. Eddaoudi, D. B. Moler, H. Li, B. Chen, T. M. Reineke, M. O'Keeffe, O. M. Yaghi, *Acc. Chem. Res.* **2001**, *34*, 319–330; c) N. G. Pschirer, D. M. Ciurtin, M. D. Smith, U. H. F. Bunz, H. C. zur Loye, *Angew. Chem.* **2002**, *114*, 603–605; *Angew. Chem. Int. Ed.* **2002**, *41*, 583–585.

[2] a) O. R. Evans, W. Lin, *Acc. Chem. Res.* **2002**, *35*, 511–522; b) B. Kesanli, W. Lin, *Coord. Chem. Rev.* **2003**, *246*, 305–326.

 © 2005 Wiley-VCH Verlag GmbH & Co. KGaA, Weinheim

[3] a) T. M. Reineke, M. Eddaoudi, D. Moler, M. O'Keeffe, O. M. Yaghi, *J. Am. Chem. Soc.* **2000**, *122*, 4843 – 4844; b) O. R. Evans, Z. Wang, R.-G. Xiong, B. M. Foxman, W. Lin, *Inorg. Chem.* **1999**, *38*, 2969 – 2973.
[4] a) S. Kitagawa, R. Kitaura, S.-i. Noro, *Angew. Chem.* **2004**, *116*, 2388 – 2430; *Angew. Chem. Int. Ed.* **2004**, *43*, 2334 – 2375; b) S. i. Noro, S. Kitagawa, M. Kondo, K. Seki, *Angew. Chem.* **2000**, *112*, 2161 – 2164; *Angew. Chem. Int. Ed.* **2000**, *39*, 2081 – 2084.
[5] N. L. Rosi, J. Eckert, M. Eddaoudi, D. T. Vodak, J. Kim, M. O'Keeffe, O. M. Yaghi, *Science* **2003**, *300*, 1127 – 1129.
[6] Y. S. Nechaev, O. K. Alexeeva, *Int. J. Hydrogen Energy* **2003**, *28*, 1433 – 1443.
[7] J. Li, T. Furuta, H. Goto, T. Ohashi, Y. Fujiwara, S. Yip, *J. Chem. Phys.* **2003**, *119*, 2376 – 2385.
[8] Y. Cui, O. R. Evans, H. L. Ngo, P. S. White, W. Lin, *Angew. Chem.* **2002**, *114*, 1207 – 1210; *Angew. Chem. Int. Ed.* **2002**, *41*, 1159 – 1162.
[9] X-ray single-crystal diffraction data for both **1** and **2** were collected on a Siemens SMART CCD diffractometer. Crystal data for **1**: monoclinic, space group *C*2, with $a = 32.768(7)$, $b = 39.312(8)$, $c = 25.680(5)$ Å, $b = 95.79(3)°$, $V = 32\,912(11)$ Å^3, $Z = 8$, $\rho_{calcd} = 1.13$ g cm^{-3}. Least-squares refinement based on 21 943 reflections with $I > 2\sigma(I)$ and 1358 parameters led to convergence, with a final $R1 = 0.131$, $R_w2 = 0.373$, and GOF = 1.38. Flack parameter = 0.17(2). Crystal data for **2**: trigonal, space group *R*3, with $a = 36.649(1)$, $c = 10.918(1)$ Å, $V = 12\,699.1(8)$ Å^3, $Z = 3$, $\rho_{calcd} = 1.24$ g cm^{-3}. Least-squares refinement based on 3671 reflections with $I > 2\sigma(I)$ and 163 parameters led to convergence, with a final $R1 = 0.125$, $R_w2 = 0.308$, and GOF = 1.38. The crystal of **2** is refined as a twin structure. CCDC-243787 (**1**) and CCDC-243788 (**2**) contain the supplementary crystallographic data for this paper. These data can be obtained free of charge via www.ccdc.cam.ac.uk/conts/retrieving.html (or from the Cambridge Crystallographic Data Centre, 12 Union Road, Cambridge CB2 1EZ, UK; fax: (+44) 1223-336-033; or deposit@ccdc.cam.ac.uk).
[10] Although the exact locations of the included solvent molecules cannot be unambiguously determined from single crystal X-ray diffraction studies owing to their highly disordered nature, we have resorted to TGA and elemental analyses to establish the formulations of **1** and **2**.
[11] The micropore volume was calculated by fitting the adsorption data to the Dubinin–Radushkevich (DR) equation.
[12] M. R. Smith, E. W. Bittner, W. Shi, J. K. Johnson, B. C. Bockrath, *J. Phys. Chem. B* **2003**, *107*, 3752 – 3760.
[13] a) L. Pan, M. B. Sander, X. Huang, J. Li, M. Smith, E. Bittner, B. Bockrath, J. K. Johnson, *J. Am. Chem. Soc.* **2004**, *126*, 1308 – 1309; b) D. N. Dybtsev, H. Chun, S. H. Yoon, D. Kim, K. Kim, *J. Am. Chem. Soc.* **2004**, *126*, 32 – 33; c) G. Férey, M. Latroche, C. Serre, F. Millange, T. Loiseau, A. Percheron-Guégan, *Chem. Commun.* **2003**, 2976 – 2977.

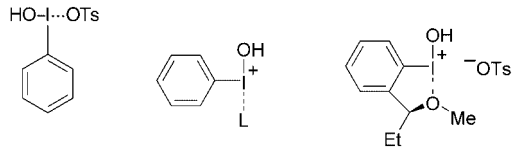
 © 2005 Wiley-VCH Verlag GmbH & Co. KGaA, Weinheim

Coordination Chemistry

Synthesis, Characterization, and Reaction of Crown Ether Complexes of Aqua(hydroxy)(aryl)iodonium Ions

Masahito Ochiai, Kazunori Miyamoto, Yukie Yokota, Takashi Suefuji, and Motoo Shiro*

The Koser reagent, [hydroxy(tosyloxy)iodo]benzene (**1**; Ts = *p*-toluenesulfonyl), is a useful oxidizing agent for a range of organic substrates.[1] It has been reported that upon dissolution in water the λ^3-iodane undergoes complete ionization to give the hydroxy(phenyl)iodonium cation (PhI^+OH).[2] The hydroxy(phenyl)iodonium ion does not form an ion pair with a tosylate ion and is presumed to be ligated with at least one water molecule at an apical site of the iodine(III) center. This aqua(hydroxy)(phenyl)iodonium ion **2** ($L = H_2O$) is highly soluble in water with a pK_a value of 4.30 at 20 °C.



1 **2** **3**

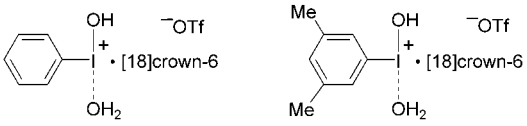
Iodosylbenzene is a polymer bridged by secondary I···O hypervalent interactions,[3] and hence is essentially insoluble in both nonreactive organic solvents and water at near neutral pH conditions;[4] however, at pH < 2.3 iodosylbenzene is highly soluble in water, in which **2** ($L = H_2O$) was also assumed to be a primary monomeric species.[2]

Aqua complexes of λ^3-iodanes with a water molecule coordinated to an iodine(III) center are unique, and there are no well-established precedents. Therefore, direct evidence supporting the proposed structure of **2** ($L = H_2O$) is highly desirable. Recently, Wirth and co-workers synthesized an interesting chiral hydroxyiodonium ion **3**, in which the oxygen atom of the *ortho* methoxymethyl group replaces the tosylate ligand of the Koser reagent with a near-linear O–I···O triad.[5] We have reported the isolation and characterization of the crown ether complex **2**·BF_4^- (L = [18]crown-6) of hydroxy(phenyl)iodonium ion. In this complex, an oxygen atom of the crown ether is tightly bound to the iodine(III) center at the apical site and forms a T-shaped structure with linear O–I···O hypervalent bonding.[6] Herein, we report the first synthesis

[*] Prof. M. Ochiai, K. Miyamoto, Y. Yokota, T. Suefuji
Faculty of Pharmaceutical Sciences
University of Tokushima
1-78 Shomachi, Tokushima 770-8505 (Japan)
Fax: (+81) 88-633-9504
E-mail: mochiai@ph.tokushima-u.ac.jp
M. Shiro
Rigaku Corporation
3-9-12 Matsubara, Akishima
Tokyo 196-8666 (Japan)

 DOI: 10.1002/anie.200461375 © 2005 Wiley-VCH Verlag GmbH & Co. KGaA, Weinheim

and characterization of the aqua complexes **4** (Tf = trifluoromethanesulfonyl) of (hydroxy)(aryl)iodonium ions, which are stabilized by the coordination of [18]crown-6 through secondary I···O bonding. The crystalline crown ether complex **4a** is stable at ambient temperature and oxidizes a variety of functional groups under mild conditions, especially in water.



4a **4b**

The exposure of (diacetoxyiodo)benzene to trimethylsilyl trifluoromethanesulfonate (1.1 equiv) in the presence of [18]crown-6 (1 equiv) in dichloromethane at −50 to 0 °C under nitrogen resulted in ligand exchange at the iodine(III) center. The aqua crown ether complex **4a** was obtained in 91 % yield as a white powder after repeated decantation with hexane and diethyl ether at −40 °C. Complex **4b** was prepared in a similar way from 3,5-dimethyl(diacetoxyiodo)benzene[7] in 92 % yield. The aqua complex **4a** is soluble in dichloromethane, chloroform, acetonitrile, acetone, and methanol, but not in the less polar solvents diethyl ether and hexane. Interestingly, complex **4a** is stable in the solid state as well as in solution: No decomposition was detected when it was left standing in air at room temperature for 10 days. As a solution in $CDCl_3$, the half-life ($t_{1/2}$) of **4a** at room temperature was found to be approximately 2 weeks, whereas that of the crown ether complex **2**·BF_4^- (L = [18]crown-6) is only 6 hours as a solution in dichloromethane.[6]

In the ^{1}H NMR spectrum of **4a** in CD_3CN, the signals for the aromatic hydrogen atoms are comparable to those reported for hydroxy(phenyl)(triflato)-λ^3-iodane.[8] The observed downfield shift (0.05 ppm) of a methylene singlet for **4a** relative to that for [18]crown-6 suggests the formation of a crown ether complex in solution. The ^{13}C NMR signal for [18]crown-6 (δ = 71.2 ppm in CD_3CN) is shifted to higher field (δ = 70.8 ppm) in the complex.

Recrystallization from acetone/diethyl ether/hexane at −30 °C afforded single crystals of **4a** suitable for X-ray crystallographic analysis.[9] Figure 1 illustrates a T-shaped structure, ligated with one water molecule at the apical site of the iodine(III) center of hydroxy(phenyl)iodonium ion with a near-linear O1-I1-O2 triad (173.96°). Including the close contact between one of the crown ether oxygen atoms, O7, and the iodine center, the complex adopts a distorted square-planar geometry around the iodine atom. A rms deviation of 0.082 Å was observed for I1, O1, O2, O7, and C1 from their least-squares plane, and the sum of the iodine-centered bond angles is Σ°I = 360.1°.

The linear O1-I1-O2 hypervalent bonding[10] is highly unsymmetrical, as observed in polymeric iodosylbenzene

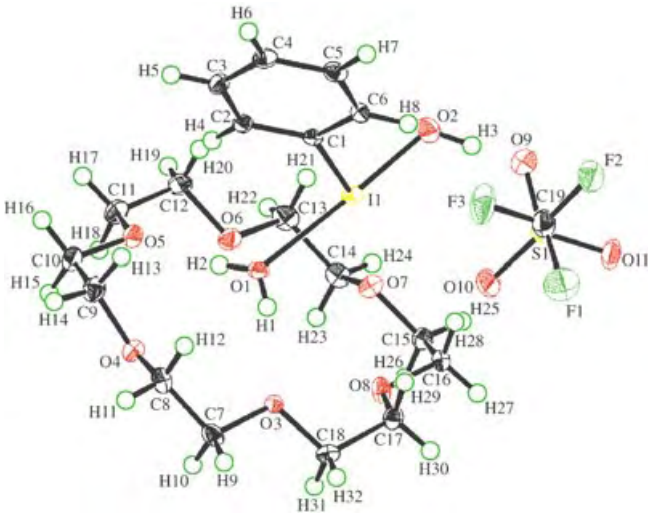
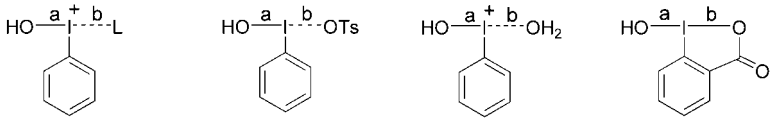


Figure 1. ORTEP drawing of **4a**. Selected bond lengths [Å] and angles [°]: I1–C1 2.117(2), I1–O2 1.967(2), I1–O1 2.392(2), I1···O7 2.942(2), O3···H1 2.04(4), O5···H2 1.91(4), O9···H3 1.9582, C1-I1-O2 92.32(3), C1-I1-O1 81.80(8), O2-I1-O1 173.96(7).

(2.04 and 2.38 Å).[3] The hydroxy ligand in **4a** is tightly bound to the iodine(III) center with an O2–I1 distance of 1.967 Å, which is slightly shorter than that predicted for covalent radii (1.99 Å), whereas the water ligand is loosely bound (O1–I1, 2.392 Å). Scheme 1 depicts the varying degrees of the unsymmetrical nature of the hypervalent bonding in the known hydroxy-λ^3-iodanes, in which HO–I bond distances (a) increase in the order shown from left to right. Interestingly, the other I–O distances (b) decrease in this order. It is noteworthy that the hypervalent bonding of a neutral water molecule to the iodine(III) center in **4a** is much stronger than that of the tosylate anion in the Koser reagent (**1**).



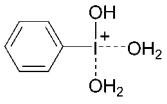
2 (L = [18]crown-6) **1** **4a** **5**

2 (L = [18]crown-6)	**1**	**4a**	**5**
a: 1.937(2)	a: 1.940(4)	a: 1.967(2)	a: 2.00
b: 2.598(2)	b: 2.473(3)	b: 2.392(2)	b: 2.30

Scheme 1. Distances of hypervalent O–I–O bonding interactions in hydroxy-λ^3-iodanes.

The ligated water molecule is in firm contact with [18]crown-6 through two hydrogen-bonding interactions, O3···H1 and O5···H2. Furthermore, the highly acidic nature of the hydroxy ligand (pK_a 4.3)[2] results in another hydrogen-bonding interaction with the triflate anion (O9···H3, 1.9582 Å). All of these close contacts are responsible for the enhanced thermal stability of complex **4a**. Based on the structure of **4a**, a monomeric iodosylbenzene species in an aqueous acidic medium is proposed to be a tetracoordinate square-planar iodonium ion **6**, in which two water molecules

 © 2005 Wiley-VCH Verlag GmbH & Co. KGaA, Weinheim



6

coordinate to the iodine center through hypervalent interactions.

The aqua complexes **4** serve as versatile oxidizing agents, especially in water, which is, of course, a safe, cheap, and environmentally benign solvent. The reactions shown in Scheme 2 illustrate the broad range of their applications. The exposure of phenyltrimethylstannane to **4a** in water at room temperature resulted in facile ligand exchange at the iodine center and afforded the diphenyl-λ^3-iodane·[18]crown-6 complex **7**.[11] Similarly, borate–λ^3-iodane exchange of 1-alkenyl and 1-alkynyl trifluoroborates produced the corresponding 1-alkenyl λ^3-iodane and 1-alkynyl λ^3-iodane complexes with [18]crown-6 (e.g. **8** and **9**) in high yields.[12,13] On the other hand, the reaction with alkyl trifluoroborates resulted in the introduction of a hydroxy group to yield primary alcohols **10**. All of these reactions proceed smoothly without further activation of **4a** by adding an external acid catalyst.

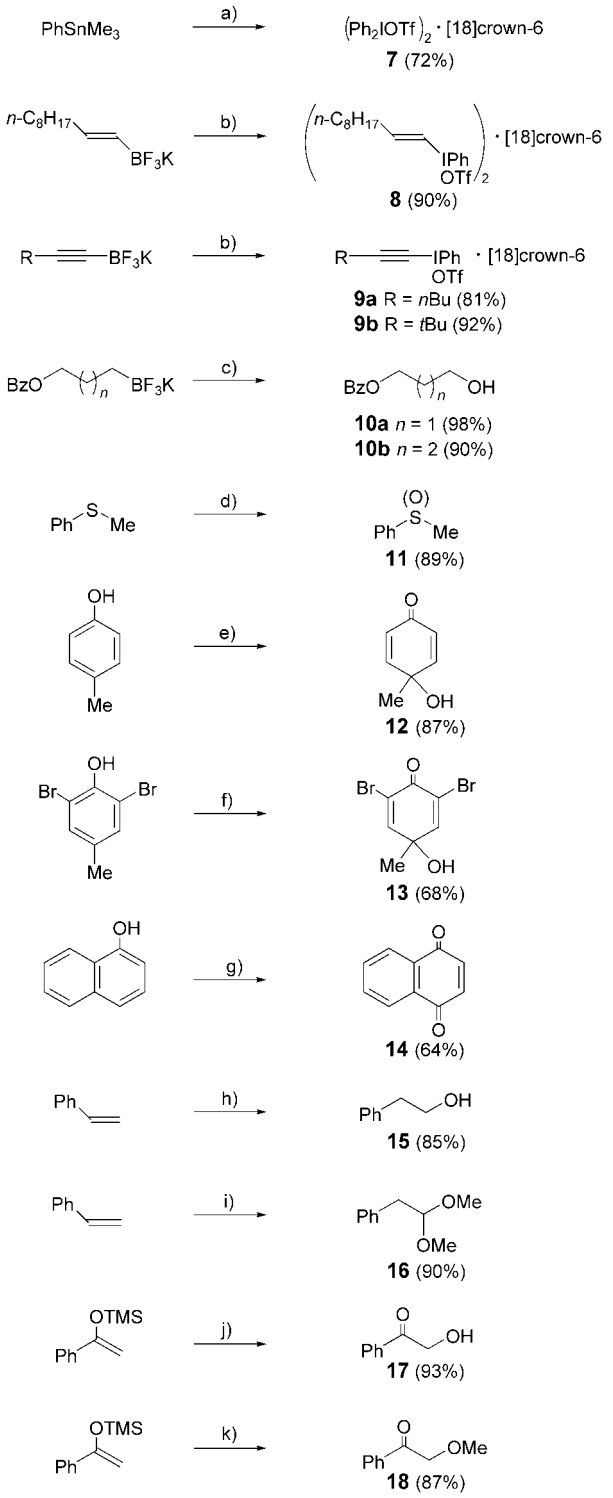
The oxidation of sulfides and *p*-substituted phenols in water produced sulfoxides and *p*-quinols, respectively. The yield of 2,6-dibromo-*p*-quinol **13** increased to 68% when the aqua complex **4b** was used instead of **4a** (55%). 1-Naphthol gave naphthoquinone (**14**) in good yield. The oxidation of styrene in water produced phenylacetaldehyde, and after reduction with $NaBH_4$ 2-phenylethanol was obtained in 85% yield. The use of methanol as a solvent afforded the dimethyl acetal **16**.[14] The α-hydroxy ketone **17** was obtained by the oxidation of a silyl enol ether in the presence of water, whereas in methanol a methoxy group was introduced at the α position to give **18**.

We have presented the synthesis and characterization of a crown ether complex of aqua(hydroxy)(phenyl)iodonium ion, which is assumed to be a primary monomeric iodosylbenzene species in an acidic aqueous medium. The complex is stable in the solid state as well as in solution and serves as a versatile oxidant in water.

Experimental Section

4a: Trimethylsilyl trifluoromethanesulfonate (152 mg, 0.69 mmol) was added dropwise at −50 °C under nitrogen to a solution of (diacetoxyiodo)benzene (200 mg, 0.62 mmol) and [18]crown-6 (164 mg, 0.62 mmol) in CH_2Cl_2 (6.7 mL). The mixture was gradually warmed to 0 °C over 4 h. The solvent was evaporated under an aspirator vacuum at 0 °C to give a yellow oil, which was washed several times with hexane and diethyl ether by decantation at −40 °C to give **4a** (368 mg, 0.56 mmol, 91%) as a white powder. Recrystallization of **4a** (100 mg) from acetone/diethyl ether/hexane at −30 °C gave colorless prisms (35 mg): m.p. 61–63 °C; ^{1}H NMR (400 MHz, CD_3CN): $\delta = 8.24$ (d, $J = 8.0$ Hz, 2H), 7.78 (t, $J = 7.3$ Hz, 1H), 7.64 (dd, $J = 8.0$, 7.3 Hz, 2H), 3.56 ppm (s, 24H); ^{13}C NMR (75 MHz, CD_3CN): $\delta = 136.3$, 134.4, 132.4, 123.3, 70.8 ppm; IR (nujol): $\tilde{\nu} = 3564$, 3485, 1354, 1285, 1109, 1038, 965, 842, 638 cm^{-1}; elemental analysis calcd (%) for $C_{19}H_{32}F_3IO_{11}S$ (652.42): C 34.98, H 4.94; found: C 35.22, H 4.88.

4b: Colorless prisms (recrystallized from acetone/diethyl ether/hexane at −30 °C): m.p. 59–61 °C; ^{1}H NMR (400 MHz, $CDCl_3$): $\delta =$ 7.75 (br s, 2H), 7.21 (br s, 1H), 3.69 (s, 24H), 2.36 ppm (s, 6H); ^{13}C NMR (75 MHz, CD_3CN): $\delta = 142.6$, 135.9, 133.6, 123.3, 70.8, 21.2 ppm; IR (nujol): $\tilde{\nu} = 3515$, 1354, 1258, 1107, 1032, 961, 838,



Scheme 2. Reaction of the aqua complexes **4** with nucleophiles under nitrogen. a) **4a** (1.5 equiv), H_2O, room temperature, 6 h; b) **4a** (1.5 equiv), H_2O, RT, 3 h; c) **4a** (1.2 equiv), H_2O, room temperature, 3 h; d) **4a** (1 equiv), H_2O, 0 °C, 3 h; e) **4a** (1.2 equiv), H_2O, 0 °C→RT, 3 h; f) **4b** (1.5 equiv), H_2O, room temperature, 6 h; g) **4a** (2.1 equiv), H_2O, 0 °C→RT, 3 h; h) 1. **4a** (1.1 equiv), H_2O, room temperature, 3 h; 2. $NaBH_4$ (2.2 equiv), MeOH, room temperature, 0.5 h; i) **4a** (1.1 equiv), MeOH, room temperature, 26 h; j) **4a** (1.1 equiv), H_2O/MeCN 2:5, 0 °C, 1 h; k) **4a** (1.1 equiv), MeOH, −78 °C→RT, 7 h. Bz = benzoyl, TMS = trimethylsilyl.

 © 2005 Wiley-VCH Verlag GmbH & Co. KGaA, Weinheim

639 cm^{-1}; elemental analysis calcd (%) for $C_{21}H_{37}F_3IO_{11.5}S$ (689.50): C 36.58, H 5.41; found: C 36.29, H 5.14.

8: Potassium *trans*-1-decenyl trifluoroborate (9.9 mg, 0.04 mmol) was added at room temperature under nitrogen to a solution of **4a** (39 mg, 0.059 mmol) in H_2O (2.5 mL), and the mixture was stirred for 3 h. The mixture was extracted with CH_2Cl_2 four times. The combined organic phases were filtrated and evaporated under an aspirator vacuum to give an oil, which was washed several times with hexane and then with hexane/diethyl ether by decantation at 0 °C to give a 1:1.3 mixture of *trans*-1-decenyl(phenyl)(trifluoromethanesulfonato)-λ^3-iodane and [18]crown-6 (30.6 mg, 0.036 mmol, 90 %) as a white powder. Recrystallization from dichloromethane/ethyl acetate/hexane at −30 °C gave **8** as colorless needles: m.p. 71.5–72 °C; ^{1}H NMR (400 MHz, $CDCl_3$): $\delta = 7.95$ (d, $J = 8.2$ Hz, 4H), 7.70 (t, $J = 7.3$ Hz, 2H), 7.54 (dd, $J = 8.2$, 7.3 Hz, 4H), 6.85–6.72 (m, 4H), 3.69 (s, 24H), 2.34 (q, $J = 7.3$ Hz, 4H), 1.44 (quint, $J = 7.3$ Hz, 4H), 1.32–1.19 (m, 20H) 0.88 ppm (t, $J = 6.8$ Hz, 6H); IR (nujol): $\tilde{\nu} = 3042$, 1563, 1265, 1223, 1152, 1101, 1031, 956, 838, 754, 638 cm^{-1}; elemental analysis calcd (%) for $C_{46}H_{72}F_6I_2O_{12}S_2$ (1249.03): C 44.23, H 5.81; found: C 44.55, H 5.93.

Received: July 21, 2004

Keywords: crown compounds · hypervalent compounds · iodine · Koser reagent · oxidation

[1] a) G. F. Koser, *Aldrichimica Acta* **2001**, *34*, 89; b) R. M. Moriarty, R. K. Vaid, G. F. Koser, *Synlett* **1990**, 365; c) V. V. Zhdankin, P. J. Stang, *Chem. Rev.* **2002**, *102*, 2523; d) A. Varvoglis, *The Organic Chemistry of Polycoordinated Iodine*, VCH, New York, **1992**; e) For hypervalent iodine chemistry, see: T. Wirth, *Top. Curr. Chem.* **2003**, *224*.

[2] H. W. Richter, B. R. Cherry, T. D. Zook, G. F. Koser, *J. Am. Chem. Soc.* **1997**, *119*, 9614.

[3] C. J. Carmalt, J. G. Crossley, J. G. Knight, P. Lightfoot, A. Martin, M. P. Muldowney, N. C. Norman, A. G. Orpen, *J. Chem. Soc. Chem. Commun.* **1994**, 2367.

[4] We measured the solubility of iodosylbenzene (2.3×10^{-3} M) in water at 25 °C by ^{1}H NMR spectroscopy. The ylide-type structure $PhI^+(OH_2)O^-$ was proposed for monomeric iodosylbenzene dissolved in water at near pH 7.[2]

[5] a) T. Wirth, U. H. Hirt, *Tetrahedron: Asymmetry* **1997**, *8*, 23; b) U. H. Hirt, M. F. H. Schuster, A. N. French, O. G. Wiest, T. Wirth, *Eur. J. Org. Chem.* **2001**, 1569.

[6] M. Ochiai, K. Miyamoto, M. Shiro, T. Ozawa, K. Yamaguchi, *J. Am. Chem. Soc.* **2003**, *125*, 13006.

[7] K. S. Daub, B. Habermann, T. Hahn, L. Teich, K. Eger, *Eur. J. Org. Chem.* **2004**, 894.

[8] T. Kitamura, R. Furuki, H. Taniguchi, P. J. Stang, *Tetrahedron* **1992**, *48*, 7149.

[9] Crystal data for **4a**: $C_{19}H_{32}F_3IO_{11}S$, colorless block of dimensions $0.20 \times 0.15 \times 0.07$ mm^3, triclinic, $P\bar{1}$ (No. 2), $a = 9.058(5)$, $b = 10.820(7)$, $c = 13.99(1)$ Å, $\beta = 93.95(2)°$, $V = 1307(1)$ $Å^3$, $Z = 2$, $\rho_{calcd} = 1.657$ $g\,cm^{-3}$. Data collected on a Rigaku RAXIS-RAPID imaging plate diffractometer with $Mo_{K\alpha}$ radiation ($\lambda = 0.71075$ Å) at $T = 93$ K, $2\theta_{max} = 59.8°$, 14070 reflections measured, of which 7318 unique ($R_{int} = 0.023$), $\mu = 13.80$ cm^{-1}. The structure was solved by direct methods[15a] and expanded by using Fourier techniques,[15b] $R = 0.042$, $R_w = 0.090$. Some hydrogen atoms were refined isotropically, some were refined by using the riding model, and the rest were included in fixed positions. CCDC-242208 contains the supplementary crystallographic data for this paper. These data can be obtained free of charge via www.ccdc.cam.ac.uk/conts/retrieving.html (or from the Cambridge Crystallographic Data Centre, 12, Union Road, Cambridge CB21EZ, UK; fax: (+44) 1223-336-033; or deposit@ccdc.cam.ac.uk).

[10] a) N. W. Alcock, *Adv. Inorg. Chem. Radiochem.* **1972**, *15*, 1; b) J. Starbuck, N. C. Norman, A. G. Orpen, *New J. Chem.* **1999**, *23*, 969; c) G. A. Landrum, R. Hoffmann, *Angew. Chem.* **1998**, *110*, 1989; *Angew. Chem. Int. Ed.* **1998**, *37*, 1887.

[11] M. Ochiai, T. Suefuji, K. Miyamoto, N. Tada, S. Goto, M. Shiro, S. Sakamoto, K. Yamaguchi, *J. Am. Chem. Soc.* **2003**, *125*, 769.

[12] a) M. Ochiai, M. Toyonari, T. Sueda, Y. Kitagawa, *Tetrahedron Lett.* **1996**, *37*, 8421; b) M. Ochiai, M. Toyonari, T. Nagaoka, D.-W. Chen, M. Kida, *Tetrahedron Lett.* **1997**, *38*, 6709.

[13] a) M. Ochiai, K. Miyamoto, T. Suefuji, S. Sakamoto, K. Yamaguchi, M. Shiro, *Angew. Chem.* **2003**, *115*, 2241; *Angew. Chem. Int. Ed.* **2003**, *42*, 2191; b) M. Ochiai, K. Miyamoto, T. Suefuji, M. Shiro, S. Sakamoto, K. Yamaguchi, *Tetrahedron* **2003**, *59*, 10153.

[14] R. M. Moriarty, J. S. Khosrowshahi, O. Prakash, *Tetrahedron Lett.* **1985**, *26*, 2961.

[15] a) SHELXS86: G. M. Sheldrick in *Crystallographic Computing 3* (Eds.: G. M. Sheldrick, C. Kruger, R. Goddard), Oxford University Press, Oxford, **1985**, p. 175; b) DIRDIF99: P. T. Beurskens, G. Admiraal, G. Beurskens, W. P. Bosman, R. de Gelder, R. Israel, J. M. M. Smits, *The DIRDIF-99 program system*, Technical Report of the Crystallography Laboratory, University of Nijmegen, The Netherlands, **1999**.

 © 2005 Wiley-VCH Verlag GmbH & Co. KGaA, Weinheim

Nanotechnology

Efficient Generation of Photocurrents by Using CdS/Carbon Nanotube Assemblies on Electrodes**

*Laila Sheeney-Haj-Ichia, Bernhard Basnar, and Itamar Willner**

The organization of functional semiconductor nanoparticles (NPs) on surfaces, and specifically electrodes, attracts substantial research efforts.[1] Semiconductor NP architectures on surfaces have been used to assemble photoelectrochemical cells,[2,3] to tailor light-emitting diodes,[4] to fabricate electrochromic devices,[5] and to organize sensor systems.[6,7] The photochemical excitation of semiconductor NPs to form an electron–hole pair is the primary event for the photocurrent generation. However, the transfer of conduction-band electrons to the electrode (or the supply of electrons from the electrode to the valence-band holes)—the processes that lead to the photocurrents—are hampered by the competing electron–hole recombination process, which degrades the

[*] L. Sheeney-Haj-Ichia, Dr. B. Basnar, Prof. I. Willner
Institute of Chemistry
The Hebrew University of Jerusalem
Jerusalem 91904 (Israel)
Fax: (+972) 2-652-7715
E-mail: willnea@vms.huji.ac.il

[**] This research is supported by the Israel Science Foundation (Project 101/00).

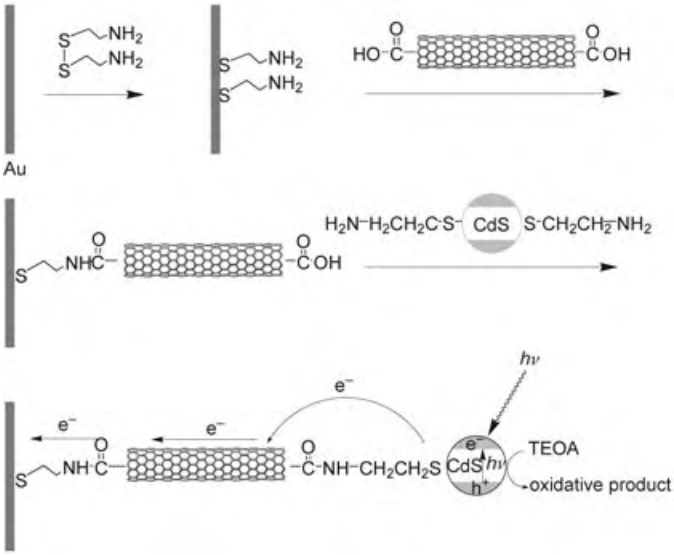
 © 2005 Wiley-VCH Verlag GmbH & Co. KGaA, Weinheim DOI: 10.1002/anie.200461666

photogenerated species and prohibits the generation of the photocurrent. To enhance the photocurrent, the retardation of the recombination of the electron–hole species is essential. Different approaches to maximize charge separation in semiconductor NP architectures have been suggested. These include the use of molecular electron-relay semiconductor NP structures, in which the electron–hole is spatially separated by trapping the electrons in the relay units.[8,9] Conductive polymer films, which contact CdS nanoparticles with electrodes, act as efficient electron-transport matrices that retard the recombination reactions.[10] Hybrid composite semiconductor nanoclusters[11] or hybrid metal/semiconductor NP systems[12] were used for the enhanced generation of photocurrent. There the coupling of the two semiconductors CdS and SnO_2 resulted in improved photoelectrochemical properties of the hybrid material which were attributed to improved charge separation. The transfer of the CdS conduction-band electrons to the SnO_2 conduction band resulted in the separation of the electron–hole pair onto two different semiconductor particles. Similarly, the enhanced photocurrents[12] and photocatalytic properties[13] of metal/semiconductor composite nanostructures were attributed to the spatial separation of the electron–hole pair in the two nanoparticles.

Carbon nanotubes are an attractive material for application in electronic or sensor devices.[14] Carbon nanotubes (CNTs) are formed by the folding of graphite sheets, and the formation of conductive or semiconductive CNTs depends on the folding angle of the graphite sheets.[15] Conductive CNTs usually reveal high values of conductivity.[16] Different electronic applications of CNTs have been reported in recent years which include the organization of memory devices[17] or transistors.[18] Also, CNTs have been used as active sensing elements[19] and as building blocks of biosensors.[20] Numerous methods to functionalize the edges or ends of CNTs with chemical groups that enable the binding of the CNTs to other units or surfaces have been developed.[21,22] The organization of assemblies of CNT and semiconductor NP on electrodes might provide a new structure for improved photoelectrochemistry. To our knowledge, only one study has been reported on the assembly of a CNT/ZnO NP hybrid system,[23] but no function or photoelectrochemical properties of the system were addressed. Here we report the assembly of CdS NP/CNT hybrid systems on electrode surfaces. The system reveals efficient photoelectrochemical functions.

Fullerenes were previously employed as a carbon-based nanomaterial for photoelectrochemical applications.[24] The C_{60} nanostructure exhibits electron-acceptor properties. Its reversible redox activity was studied in detail,[25] and different photoelectrochemical studies have used C_{60} as an electron acceptor for mediated electron transport and the generation of photocurrents. For example, photoexcited polyphenylenevinylene polymers were used as electron donors for C_{60}, and the resulting composites resulted in the effective formation of photocurrents.[26] In stark contrast to C_{60}, CNTs do not display reversible electrochemistry and do not exhibit electron-acceptor features. The documented high conductivity of CNTs (1.0×10^{6}–$3.0\times10^{6}\,S\,m^{-1}$)[16] renders them conductive nanowires rather than charge traps. Thus, the enhanced photocurrents in the present system originate from improved electron transport through the conductive wires in contrast to the mediated electron transfer in the C_{60} systems.

Scheme 1 depicts the method to assemble the CdS/CNT monolayer on a Au electrode. The CNTs were purified and



Scheme 1. The assembly of the CdS NP/CNT system on a Au electrode, and the photoinduced charge transport in the system. TEOA = triethanolamine, h^+ = hole.

"cut" by using a mixture of concentrated sulfuric and nitric acids (3:1, 98 % and 70 %, respectively) to yield CNTs with an average length of $\approx$10–100 nm as determined by TEM experiments. This procedure introduces carboxylic acid functionalities at the ends of the CNTs as well as some carboxylic acid units at the CNT sidewalls. The Au electrode was functionalized with a primary monolayer of cysteamine to which the CNTs were then coupled. The CdS NPs (5 nm, protected a capping monolayer of cysteamine and 2-thioethanesulfonic acid) were then coupled to the ends of the CNTs.

Microgravimetric quartz crystal microbalance (QCM) analyses allowed the surface coverage of the components to be characterized. The modification of the surface with the CNTs is controlled by the duration of the coupling process. Figure 1 shows the frequency changes (Δf) that occurred upon modification of the cysteamine monolayer-functionalized Au surface with the CNTs that were cut for a period of 4 h in acid solution. After $\approx$4 h of coupling, the frequency change reaches a constant value that translates to a weight coverage of $\approx3.14\times10^{-6}\,g\,cm^{-2}$ ($\Delta f=-575$ Hz). The CNT-functionalized surface was then modified with the CdS NPs. The absorbance spectrum of the CdS NPs revealed a shoulder at $\approx$400 nm which is consistent with the size of the NPs. The CdS NPs were then coupled to the CNTs associated with the electrode in the presence of 1-ethyl-3-(3-dimethyaminopropyl)carbodiimide (EDC). The microgravimetric analysis of the coupling of the CdS NPs to the CNTs assembled on a Au/quartz crystal (2 h of coupling) indicated a frequency change of -270 Hz that corresponds to a surface coverage of $\approx4.7\times$

 © 2005 Wiley-VCH Verlag GmbH & Co. KGaA, Weinheim

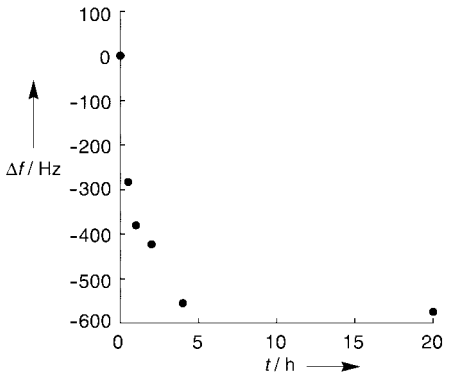


Figure 1. Time-dependent frequency changes (Δf) of a cysteamine-functionalized Au/quartz crystal upon the coupling of CNTs that had undergone oxidative digestion for 4 h. The coupling was performed with dicyclohexylcarbodiimide (0.01 M) in DMF in the presence of the CNT (5 mg mL^{-1}). Frequencies were recorded in air.

10^{12} particles cm^{-2}. Further evidence for the coupling of the CdS NPs to the surface was obtained from X-ray photoelectron spectroscopic (XPS) measurements. After the modification of the CNT interface with the CdS NPs for 2 h, the electrons characteristic of Cd(3d), C(1s), and Au(4f) at 404, 283.8, and 82.65 eV, respectively, were observed in a ratio of 4.1:48.9:21.0%. After 4 h of modification, the coverage of the CdS NPs increased as seen by the ratio of the intensities 4.3:50.1:15.9% for the Cd(3d), C(1s), and Au(4f) electrons, respectively.

The assembly of the CdS NPs and CNTs on the surface was also characterized by AFM. Figure 2a shows the image of the CNTs that were covalently linked to a Au surface during a modification time of 10 minutes (CNTs generated by acidic digestion for 4 h were used in this experiment). Vertically aligned (standing) CNTs are observed with a maximum height of $\approx$20 nm. By allowing longer durations for the modification step, high-density coverage of the surface by the CNTs was observed. Figure 2b shows the AFM image of the surface after the covalent attachment of the CdS NPs. Higher objects ($\approx$25 nm) are observed which suggests that the semiconductor NPs are linked to the ends of the CNTs (it is impossible to exclude the binding of the CdS NPs to the sidewalls of the CNTs). Figure 2c shows the AFM image of a surface modified with CdS NPs which was obtained after coupling to the CNT-modified Au surface during 4 h. From the surface area of the electrode and the size of the CdS NPs, a random and densely packed monolayer of NPs was observed with a surface coverage of $\approx 4.5 \times 10^{12}$ particles cm^{-2}. The microgravimetric analyses of the surface revealed a surface coverage of $\approx 4.7 \times 10^{12}$ particles cm^{-2}. This value, taken together with the AFM image, suggests that a densely packed monolayer of the semiconductor NPs is associated with the electrode. The AFM images of the CNTs that were linked to the surface during short modification periods (Figure 2a and b) show heights of 10 to 30 nm, whereas the TEM image reveals a substantially higher dispersity of 10 to 100 nm. This may originate from the relatively low concentration of longer CNTs in the mixture and the lower reactivity of the longer CNTs in the coupling process. In fact, similar

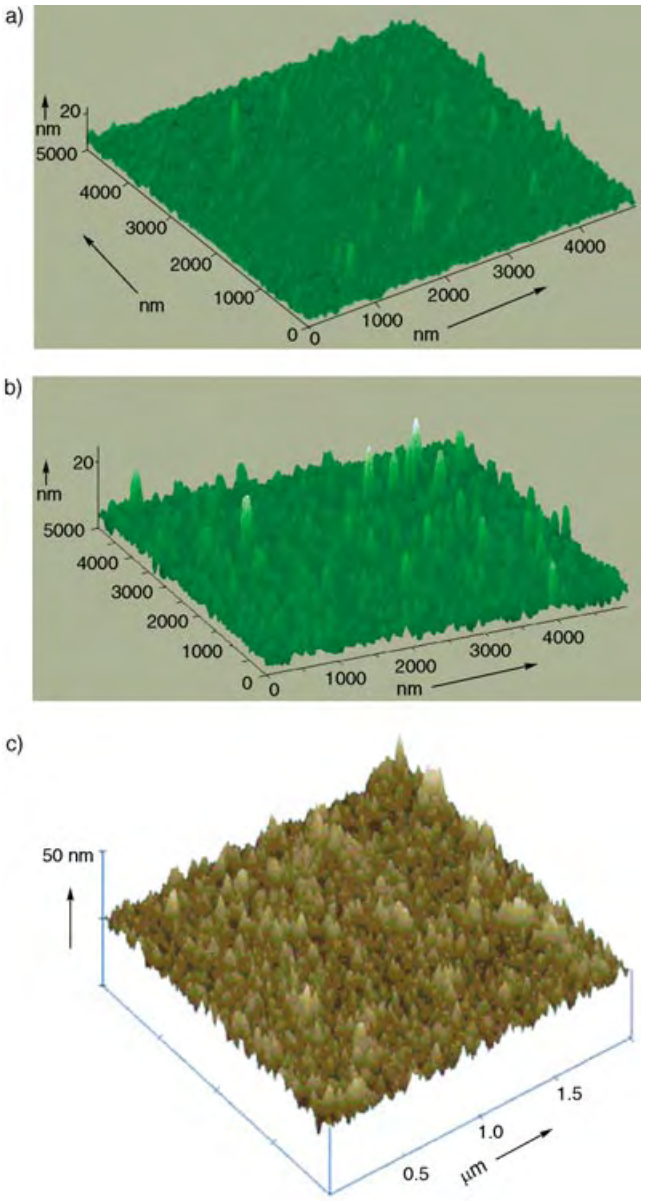


Figure 2. AFM images of the cysteamine-functionalized Au surface upon a) the coupling of CNTs (reaction time: 10 min; oxidative digestion: 4 h), b) after the subsequent coupling of the modified CdS NPs (reaction time:2 h), and c) after the coupling of the CNTs (oxidative digestion: 4 h) to the surface (reaction time: 4 h) and the subsequent binding of the CdS NPs (reaction time: 2 h).

AFM results were previously reported for CNT-modified surfaces that employed CNT prepared by an analogous procedure to the present study.[21]

The photoelectrochemical properties of the CdS NP/CNT-functionalized electrodes, which were generated from CNTs that were digested in the acidic solution for 4 h, were examined. The photocurrent generated by the functionalized electrode in the presence of triethanolamine as a sacrificial electron donor was examined in an electrolytic aqueous phosphate buffer solution (0.1 M, pH 10). The resulting photocurrent action spectrum is depicted in Figure 3, curve (a). The photocurrent spectrum follows the profile of the absorption

 © 2005 Wiley-VCH Verlag GmbH & Co. KGaA, Weinheim

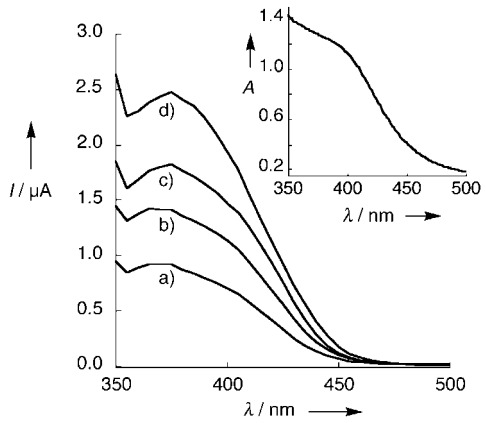


Figure 3. Photocurrent action spectra observed with Au electrodes modified with CdS NP/CNT systems, in which the CNTs were allowed to undergo oxidative digestion during a) 4 h, b) 6 h, c) 8 h, or d) 10 h. In all of the experiments, the resulting CNT interfaces were treated with the CdS NPs during 2 h. Photocurrent spectra were recorded in phosphate buffer solution (0.1 M, pH 10) that contained triethanolamine (0.02 M). Inset: Absorbance spectrum of the CdS nanoparticles (5 nm) capped with cysteamine/2-thioethanesulfonic acid (1:10).

spectrum of the CdS NPs which indicates that it originates from the excitation of the semiconductor NPs. No photocurrent is generated in the absence of triethanolamine. In a control experiment, no photocurrent was observed upon irradiation of a CNT-functionalized electrode that lacked the CdS NPs in the presence of triethanolamine. This result indicates that the photocurrent originates from the CdS NPs and that the CNTs are not photoactive in the process. The generated photocurrent is, however, impressively high, $I(\lambda_{390}) = 0.83\ \mu A$, for the CNT/CdS NP monolayer. From the intensity of the light absorbed by the sample, we estimate that the quantum efficiency for the photon-to-electron conversion is 25%.

In a further control experiment, a monolayer of CdS NPs was assembled on a Au electrode by the covalent coupling of the NPs to an electrode functionalized with a monolayer of cysteic acid. The microgravimetric characterization of the assembly of the monolayer on a Au/quartz crystal indicated a surface coverage of 5.1×10^{12} particles cm^{-2}. Although the surface coverage of the NPs in the monolayer assembly is very similar to that observed in the CdS NPs/CNT system, the photocurrent generated by the system that lacks the CNT connectors is substantially lower, $I(\lambda_{390}) = 0.05\ \mu A$, and the photon-to-electron quantum efficiency is $\approx 1.5\%$. Thus, we conclude that the CNTs which bridge the CdS NPs to the electrode play a major role in the enhanced generation of photocurrents.

We further examined the effect of the lengths of the CNTs on the resulting photocurrent. It is established that the longer time intervals of acidic digestion of the CNTs yields shorter tubes. Accordingly, we digested the CNTs for different lengths of time and used the resulting CNTs to assemble the bridged CdS NP-functionalized electrodes. Unfortunately, we were unable to determine the lengths of the CNTs obtained upon the acidic digestion process owing to a broad dispersity. Thus, we assume that prolongation of the digestion time leads to a decrease in the length of the CNTs (without actual quantification of the length of the bridging units). Figure 3 shows the photocurrents generated by the CdS NP/CNT-functionalized electrodes, which consist of CNTs that were acid-digested for different lengths of time, as bridging units. The photocurrent action spectra follow the profile of the absorbance spectrum of the CdS NPs (see Figure 3, Inset) which implies that the photocurrent originates from the excitation of the semiconductor NPs. The photocurrents obtained reveal that the photocurrent is enhanced as the digestion time of the CNTs is increased (shorter linking CNTs). Table 1 summarizes the surface coverage, the photocurrent intensities at $\lambda = 390$ nm, and the photon-to-electron quantum efficiencies of the CdS NPs in the systems with the different CNTs. The quantum efficiencies increase as the digestion time increases (shorter CNTs), and for CNTs digested for 4, 6, 8, and 10 h, the quantum yields correspond to 25, 39, 51, and 70%. From the data in Table 1 we see that the surface coverages of the CdS NPs in the different systems are comparable.

Table 1: Microgravimetric quartz-crystal-microbalance analyses of the CdS/CNT systems assembled on Au/quartz crystals and the respective surface coverage values.

System[a]	Δf [Hz] SWCNT	Δm [$g\,cm^{-2}$]	Δf [Hz] CdS NP	Particles [cm^2]
a	−575	3.14×10^{-6}	−270	4.66×10^{12}
b	−520	2.83×10^{-6}	−310	5.34×10^{12}
c	−450	2.45×10^{-6}	−238	4.12×10^{12}
d	−320	1.74×10^{-6}	−287	4.96×10^{12}
CdS monolayer[b]			−294	5.07×10^{12}

[a] The different systems comprise CNTs that were subjected to oxidative digestions during a) 4 h, b) 6 h, c) 8 h, or d) 10 h. [b] The surface loading of a CdS NP system directly coupled to the electrode is provided for comparison.

The results clearly demonstrate the very efficient generation of photocurrents in the CNT-bridged CdS NP assemblies. Although we have no firm explanation for the enhanced photocurrents, we speculate and suggest a possible origin for these observations on the basis of the known properties of CNTs. The photocurrent originates from the photoexcitation of the semiconductor NPs which yields an electron–hole pair. The injection of the conduction-band electrons into the electrode yields the photocurrent, whereas the electron donor (in solution) provides the electrons to the valence-band holes to thus complete the photocurrent generation cycle (see Scheme 1). The electron–hole recombination is a competing process to the electron-injection mechanism, and thus the photocurrent efficiency is low. The CNT connectors which bridge the CdS NPs to the electrode may then facilitate the photocurrent generation by trapping the conduction-band electrons, a process that results in charge separation and retardation of the recombination process. That is, the conductive CNT wires provide efficient paths for the transport of the conduction-band electrons to the electrode. This

 © 2005 Wiley-VCH Verlag GmbH & Co. KGaA, Weinheim

explanation, based on the conductance of the CNT connector is, however, contradicted by the observation of a dependence on the length of the CNT. Whereas charge-transport rates in ideal CNTs should be almost length-independent, the CNTs employed in the present study are far-from-ideal wrapped graphite sheets. The oxidative acidic digestion of the CNTs not only shortens the CNTs, but it introduces defects into the sidewalls, which consist of phenolic, ketone, or carboxylic acid functionalities. These units disrupt the conjugation within the graphite sheets and act as local defect sites for charge transport.

The effect of defects in CNTs on the charge-transport properties has been considered theoretically by using a "back-scattering" model.[27] According to this model, as the electron reaches a defect site, it is back-scattered to find an alternative conjugated path to be transported along the CNT. As the number of defects in the CNT increases with its length, charge transport along the CNT will be dominated by its length. That is, the charge injection of the conduction-band electrons to the CNTs, leads to charge separation by entrapment of the electrons in the CNT wire. The chemically generated local defects in the CNTs affect, however, the efficiency of the charge separation. As the CNTs are longer, more defects exist in the connecting wires and thus the back-scattering process retards the conductance of the trapped electrons to the electrode. The trapped electrons in the CNTs can then recombine with the valence-band holes to result in lower quantum yields for the photon-to-electron conversion process as the CNTs become longer.

An alternative mechanism for the observed enhanced photocurrent in the system is based on the semiconductive properties of the CNTs. The band-gap structure of CNTs has been studied,[28] and interparticle–CNT electron transfer could lead to charge separation and enhanced photocurrents. The low population of semiconductive CNTs in the carbon nanotube mixture, and particularly the enhanced photocurrents observed with shorter CNTs, probably exclude any function of the semiconductive CNTs in the enhanced generation of photocurrents. For shorter CNTs, larger band gaps are formed which would perturb the interparticle–CNT electron-transfer process. Thus, if semiconductive CNTs participate in the generation of photocurrents, one would anticipate to observe lower yields of photocurrents for shorter CNTs, in contrast to the experimental observations.

In conclusion, the present study has demonstrated unprecedented high quantum yields for the generation of photocurrents by using semiconductor nanoparticles/carbon nanotubes as a hybrid system. The results suggest that the length of the CNTs plays a major role in the formation of photocurrents and probably the defects in the CNT affect the extent of charge separation that follows the photoexcitation of the CdS NPs. More experiments which employ CNTs of low length dispersity are underway to further characterize the system.

Experimental Section

Single-walled CNTs (SWCNTs; Carbolex, Sigma) were purified by heating the as-received nanotubes in nitric acid (3 M) at reflux for 48 h. The resulting CNTs were isolated by centrifugation and rinsed with NaOH solution (1 mM) until pH 7.0. The purified long SWCNTs were then chemically shortened by oxidation in a mixture (3:1) of concentrated sulfuric acid (98%) and nitric acid (70%): the samples were sonicated in an ice/water bath during 4, 6, 8, or 10 h. The solutions containing the SWCNTs were centrifuged, then the samples were washed with NaOH solution (1 mM) until pH 7.0, and the CNTs were then dissolved in DMF (*N*,*N*-dimethylformamide). This procedure yielded shortened SWCNTs with terminal carboxylate groups.

Cysteamine-protected CdS nanoparticles were prepared according to a reported procedure.[12b] The surface of a Au electrode was modified with a monolayer of a mixture of 2-thioethanol and cystamine (3:1 ratio), and the shortened SWCNTs were covalently linked to the amino groups of the cysteamine monolayer-functionalized Au surface in the presence of dicyclohexylcarbodiimide (DCC; 1×10^{-2} M) in DMF (2-thioethanol was incorporated in the mixed monolayer to prevent nonspecific adsorption of the SWCNTs onto the electrode surface and also to prevent the coupling of the SWCNTs through their sidewalls to the surface). The modified electrodes were treated with a solution of cysteamine-stabilized CdS nanoparticles (1 mg mL^{-1}, 2 mL) in HEPES buffer, which included 1-ethyl-3-(3-dimethyaminopropyl)carbodiimide (EDC), for 2 h. The assembly of the CdS monolayer on the Au surface was prepared according to the published procedure.[12b]

Microgravimetric QCM measurements were performed with a QCM analyzer (Fluke) by using Au/quartz crystals (AT-cut, 10 MHz). Photoelectrochemical experiments were performed with a home-built photoelectrochemical system that includes a 300W Xe lamp (Oriel, model 5258), a monochromator (Oriel, model 74000, 2-nm resolution), and a chopper (Oriel, model 76994). XPS analyses were performed with a Kratos AXIS-HS spectrometer equipped with a monochromatic $Al_{K\alpha}$ source. Usually scans were run at 45 or 75 W. All data acquisitions were performed in a hybrid mode by using electrostatic and magnetic lenses and detection pass energies of 40–80 eV. AFM images were recorded in the tapping mode in air with a Smena B instrument (NT-MDT, Russia), with a 30-μm scanner, NCS-16 cantilevers (resonance frequency 180 KHz), a scan rate of 1.5–2.5 Hz, and a cantilever oscillation amplitude of the order of 20–40 nm.

Received: August 16, 2004
Revised: September 1, 2004

Keywords: electrochemistry · electron transport · monolayers · nanotubes · semiconductors

[1] a) A. N. Shipway, E. Katz, I. Willner, *ChemPhysChem* **2000**, *1*, 18–52; b) M.-C. Daniel, D. Astruc, *Chem. Rev.* **2004**, *104*, 293–346.
[2] a) S. G. Hickey, D. J. Riley, E. J. Tull, *J. Phys. Chem. B* **2000**, *104*, 7623–7626; b) M. Miyake, T. Torimoto, T. Sakata, H. Mori, H. Yoneyama, *Langmuir* **1999**, *15*, 1503–1507.
[3] H. Jensen, D. J. Fermin, J. E. Moser, H. H. Girault, *J. Phys. Chem. B* **2002**, *106*, 10908–10914.
[4] a) B. O. Dabbousi, M. G. Bawendi, O. Onitsuka, M. F. Rubner, *Appl. Phys. Lett.* **1995**, *66*, 1316–1318; b) H. Mattoussi, L. H. Radzilowski, B. O. Dabbousi, E. L. Thomas, M. G. Bawendi, M. F. Rubner, *J. Appl. Phys.* **1998**, *83*, 7965–7974; c) N. Tessler, V. Medvedev, M. Kazes, S. H. Kan, U. Banin, *Science* **2002**, *295*, 1506–1508.
[5] C. Bechinger, S. Ferrer, A. Zaban, J. Sprague, B. A. Gregg, *Nature* **1996**, *383*, 608–610.
[6] F. Patolsky, R. Gill, Y. Weizmann, T. Mokari, U. Banin, I. Willner, *J. Am. Chem. Soc.* **2003**, *125*, 13918–13919.
[7] a) V. Pardo-Yissar, E. Katz, J. Wasserman, I. Willner, *J. Am. Chem. Soc.* **2003**, *125*, 622–623; b) I. Willner, F. Patolsky, J.

 © 2005 Wiley-VCH Verlag GmbH & Co. KGaA, Weinheim

Wasserman, *Angew. Chem.* **2001**, *113*, 1913 – 1916; *Angew. Chem. Int. Ed.* **2001**, *40*, 1861 – 1864.
[8] L. Sheeney-Haj-Ichia, J. Wasserman, I. Willner, *Adv. Mater.* **2002**, *14*, 1323 – 1326.
[9] L. Sheeney-Haj-Ichia, I. Willner, *J. Phys. Chem. B* **2002**, *106*, 13094 – 13097.
[10] E. Granot, F. Patolsky, I. Willner, *J. Phys. Chem. B* **2004**, *108*, 5875 – 5881.
[11] a) A. Zaban, S. G. Chen, S. Chappel, B. A. Gregg, *Chem. Commun.* **2000**, 2231 – 2232; b) P. A. Sant, P. V. Kamat, *Phys. Chem. Chem. Phys.* **2002**, *4*, 198 – 203; c) C. Nasr, S. Hotchandani, W. Y. Kim, R. H. Schmehl, P. V. Kamat, *J. Phys. Chem. B* **1997**, *101*, 7480 – 7487.
[12] a) V. Subramanian, E. Wolf, P. V. Kamat, *J. Phys. Chem. B* **2001**, *105*, 11439 – 11446; b) L. Sheeney-Haj-Ichia, S. Pogorelova, Y. Gofer, I. Willner, *Adv. Funct. Mater.* **2004**, *14*, 416 – 424.
[13] V. Subramanian, E. E. Wolf, P. V. Kamat, *J. Am. Chem. Soc.* **2004**, *126*, 4943 – 4950.
[14] a) E. Katz, I. Willner, *ChemPhysChem* **2004**, *5*, 1084 – 1104; b) J. J. Davis, K. S. Coleman, B. R. Azamian, C. B. Bagshaw, M. L. H. Green, *Chem. Eur. J.* **2003**, *9*, 3732 – 3739.
[15] a) A. Hirsch, *Angew. Chem.* **2002**, *114*, 1933 – 1939; *Angew. Chem. Int. Ed.* **2002**, *41*, 1853 – 1859; b) S. Iijima, *Physica B* **2002**, *323*, 1 – 5.
[16] a) J. E. Fischer, H. Dai, A. Thess, R. Lee, N. M. Hanjani, D. L. Dehaas, R. E. Smalley, *Phys. Rev. B* **1997**, *55*, R4921 – R4924; b) D. H. Cobden, M. Bockrath, P. L. McEuen, A. G. Rinzler, R. E. Smalley, *Phys. Rev. Lett.* **1998**, *81*, 681 – 684.
[17] a) T. Rueckes, K. Kim, E. Joselevich, G. Y. Tseng, C. L. Cheung, C. M. Lieber, *Science* **2000**, *289*, 94 – 97; b) N. Mason, M. J. Biercuk, C. M. Marcus, *Science* **2004**, *303*, 655 – 658.
[18] a) S. J. Tans, A. R. M. Verschueren, C. Dekker, *Nature* **1998**, *393*, 49 – 52; b) R. Martel, T. Schmidt, H. R. Shea, T. Hertel, P. Avouris, *Appl. Phys. Lett.* **1998**, *73*, 2447 – 2449.
[19] a) J. Wang, M. Musameh, *Anal. Chem.* **2003**, *75*, 2075 – 2079; b) J. Wang, S. B. Hocevar, B. Ogorevc, *Electrochem. Commun.* **2004**, *6*, 176 – 179; c) K. Bradley, M. Briman, A. Star, G. Grüner, *Nano Lett.* **2004**, *4*, 253 – 256; d) A. Star, J.-C. P. Gabriel, K. Bradley, G. Grüner, *Nano Lett.* **2003**, *3*, 459 – 463.
[20] a) F. Patolsky, Y. Weizmann, I. Willner, *Angew. Chem.* **2004**, *116*, 2165 – 2169; *Angew. Chem. Int. Ed.* **2004**, *43*, 2113 – 2117; b) K. Besteman, J.-O. Lee, F. G. M. Wiertz, H. A. Heering, C. Dekker, *Nano Lett.* **2003**, *3*, 727 – 730.
[21] a) P. Diao, Z. Liu, B. Wu, X. L. Nan, J. Zhang, Z. Wei, *ChemPhysChem* **2002**, *3*, 898 – 901; b) Z. Liu, Z. Shen, T. Zhu, S. Hou, L. Ying, Z. Shi, Z. Gu, *Langmuir*, **2000**, *16*, 3569 – 3573; c) J. J. Gooding, R. Wibowo, J. Liu, W. Yang, D. Losic, S. Orbons, F. J. Mearns, J. G. Shapter, D. B. Hibbert, *J. Am. Chem. Soc.* **2003**, *125*, 9006 – 9007.
[22] a) K. Jiang, L. S. Schadler, R. W. Siegel, X. Zhang, H. Zhang, M. Terrones, *J. Mater. Chem.* **2004**, *14*, 37 – 39; b) M. J. Moghaddam, S. Taylor, M. Gao, S. Huang, L. M. Dia, M. J. H. McCall, *Nano Lett.* **2004**, *4*, 89 – 93; c) M. Hazani, R. Naaman, F. Hennrich, M. M. Kappes, *Nano Lett.* **2003**, *3*, 153 – 155; d) H. Peng, L. B. Alemany, J. L. Margrave, V. N. Khabasheku, *J. Am. Chem. Soc.* **2003**, *125*, 15174 – 18182.
[23] a) J. Sun, L. Gao, M. Iwasa, *Chem. Commun.* **2004**, 832 – 833; b) B. R. Azamian, K. S. Coleman, J. J. Davis, N. Hanson, M. L. H. Green, *Chem. Commun.* **2002**, 366 – 367.
[24] a) S. Licht, O. Khasclev, P. A. Ramakrishnan, D. Faiman, E. A. Katz, A. Shames, S. Goren, *Solar Energ. Mater. Solar Cells* **1998**, *51*, 9 – 19; b) P. V. Kamat, M. Gavaert, K. Vinodgopal, *J. Phys. Chem. B* **1997**, *101*, 4422 – 4427.
[25] R. E. Hauflter, J. Conceicao, L. P. F. Chibamte, Y. Chai, N. E. Byrne, S. Flanagan, M. M. Haley, S. C. O'Brien, C. Pan, Z. Xiao, W. E. Billups, M. A. Ciufolini, R. H. Hauge, J. L. Margrave, L. J. Wilson, R. F. Curl, R. E. Smalley, *J. Phys. Chem.* **1999**, *103*, 8634 – 8636.
[26] a) C. H. Lee, G. Yu, D. Moses, K. Pakbaz, C. Zhang, N. S. Sariciftci, A. J. Heeger, F. Wudl, *Phys. Rev. B* **1993**, *48*, 15425 – 15433; b) L. Smilowitz, N. S. Sariciftci, R. Wu, C. Gettinger, A. J. Heeger, F. Wudl, *Phys. Rev. B* **1993**, *47*, 13835 – 13842.
[27] V. Mujica, A. Nitzan, Y. Mao, W. Davis, M. Kemp, A. Roitberg, M. A. Ratner, *Physics* **1997**, *107*, 403 – 429.
[28] a) T. Nakanishi, A. Bachtold, C. Dekker, *Phys. Rev. B* **2002**, *66*, 073307; b) L. C. Venema, J. W. Janssen, M. R. Buitelaar, J. W. G. Wildöer, S. G. Lemay, L. P. Kouwenhoven, C. Dekker, *Phys. Rev. B* **2000**, *62*, 5238 – 5244.

 © 2005 Wiley-VCH Verlag GmbH & Co. KGaA, Weinheim

Porphyrin Analogues

Reductive N Alkylation of Cyclo[8]pyrroles**

Thomas Köhler, Zhongping Ou, Jeong Tae Lee, Daniel Seidel, Vincent Lynch, Karl M. Kadish, and Jonathan L. Sessler**

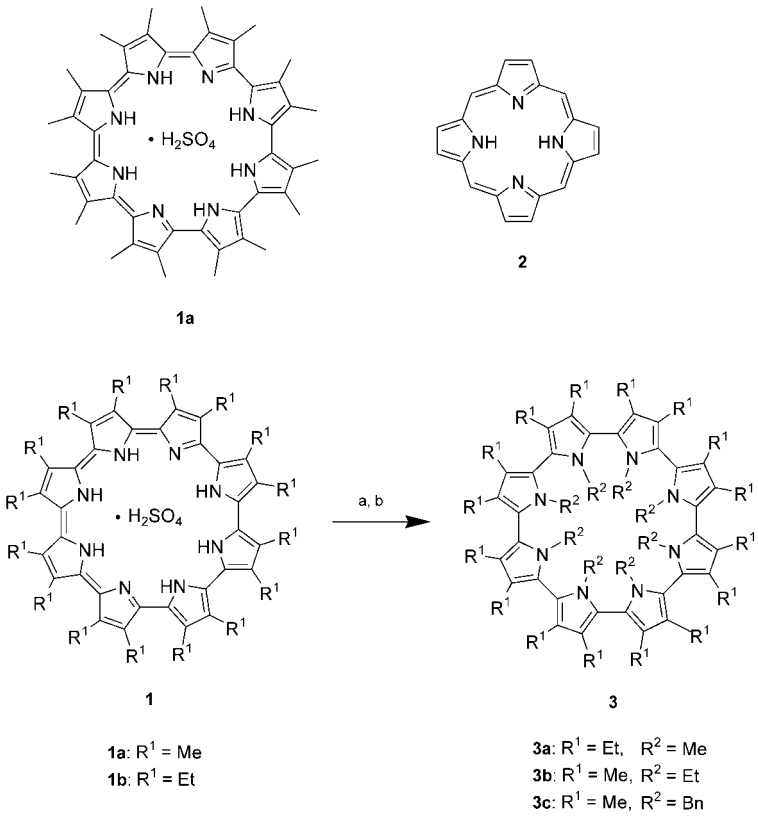
Cyclo[8]pyrrole (**1**), although lacking bridging meso carbon atoms, may be considered as a larger analogue of porphyrin (**2**) in that it is flat and aromatic (see Scheme 1).[1] For this reason, we have been interested in exploring the chemical behavior of cyclo[8]pyrrole and contrasting it to that of the porphyrins. In previous work, we have found that cyclo[8]-pyrrole in its diprotonated form may be reduced electrochemically to produce a formally antiaromatic 32-π-electron species under conditions that are much less forcing than those needed to reduce typical porphyrins.[2] Here we report that cyclo[8]pyrrole, upon treatment with NaH and an alkyl halide, undergoes chemical reduction to produce an octa-N-

[*] Dr. T. Köhler, J. T. Lee, Dr. D. Seidel, Dr. V. Lynch, Prof. J. L. Sessler
Department of Chemistry and Biochemistry
Institute for Cellular and Molecular Biology
The University of Texas
1 University Station—A5430
Austin, TX 78712-0165 (USA)
Fax: (+1) 512-471-7550
E-mail: sessler@mail.utexas.edu
Dr. Z. Ou, Prof. K. M. Kadish
Department of Chemistry
University of Houston
Houston, TX 77204 (USA)
Fax: (+1) 713-743-2745
E-mail: kkadish@uh.edu

[**] This work was supported by the National Science Foundation (Grant CHE 0107732 to J.L.S.) and the Robert A. Welch Foundation (Grant E-680 to K.M.K. and Grant F-1018 to J.L.S.).

Supporting information for this article (experimental details describing the synthesis of **3a** and **3b** and spectroelectrochemical/ESR/X-ray diffractions results) is available on the WWW under http://www.angewandte.org or from the author.

 DOI: 10.1002/anie.200461801 © 2005 Wiley-VCH Verlag GmbH & Co. KGaA, Weinheim



Scheme 1. Reaction sequence used to effect the reduction and N alkylation of cyclo[8]pyrroles **1**. a) NaH, THF, Ar, room temperature; b) R^2X, Ar, reflux, 12 h. R^2 = Me, Et, or Bn, Bn = benzyl.

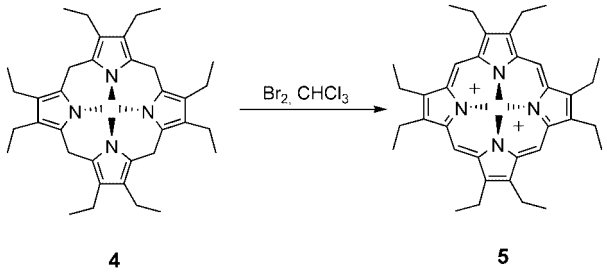
alkylated product, **3**. This reaction sequence is to the best of our knowledge without precedent in the literature regarding porphyrins. Furthermore, in the case of larger substituents, the synthesized products, namely **3b** and **3c**, are without direct analogy in the case of simple porphyrins/porphyrinogens.[3]

N,*N*′,*N*″,*N*‴-(tetramethyl)octaethylporphyrinogen (**4**), the porphyrin analogue of **3a**, was reported in a doctoral dissertation from the group of Professor Franck in 1986.[4] However, in contrast to **3a** (see below), **4** was not produced through reductive alkylation, but rather it was generated by the cyclization of N-substituted diethylpyrrole. Compound **4** is not only a direct analogue of **3a**, but it is also a historically important intermediate in porphyrin chemistry. In particular, Vogel et al. used it to produce the long-sought-after *N*,*N*′,*N*″,*N*‴-(tetramethyl)octaethylporphyrin dication (**5**) in 1989 (Scheme 2).[5]

Nonetheless, our own efforts to produce this nonaromatic, tetrapyrrolic macrocycle by using the reductive alkylation procedure to generate **3** failed to give isolable quantities of product.[6] This difference in reaction behavior thus highlights an important difference between porphyrin (**2**) and cyclo[8]-pyrrole (**1**). It also underscores the fact that compounds **3** represent a new, potentially interesting class of functionalized oligopyrroles. Scheme 1 summarizes the chemistry involved in the conversion of **1** into **3**. Briefly, treatment of **1** with NaH under an inert atmosphere, followed by addition of an alkylating agent (methyl iodide, ethyl iodide, and benzyl bromide in the case of **3a**, **3b**, and **3c**, respectively), and heating the mixture at reflux for 12 h produces the corresponding N-alkylated derivatives **3** in 64–70% yield. In contrast to the diprotonated form of **1**, which dissolves in organic solvents to produce solutions that are yellow–brown in color, the products obtained in this way were essentially colorless. Such a lack of color is consistent with the absence of an extended conjugation pathway. Evidence for the proposed lack of aromaticity came from the ^{1}H NMR spectroscopic data. In contrast to the observations reported by Vogel for **5** ($\delta = -4.59$ ppm for the protons of the CH_3 group—a result of the diamagnetic ring current),[5] the signals of the N-alkylated fragments were not shifted upfield (e.g. for **3a**, the signals for the protons from CH_3 appear at $\delta = 2.65$ ppm).

Further support for the nonaromatic and unconjugated nature of **3** comes from solid-state X-ray diffraction structural analyses (Figure 1, A–C).[7–9] The structures of **3a**, **3b**, and **3c** reveal that the eight nitrogen substituents adopt an alternating up–down orientation. As a result, the macrocycle as a whole is highly distorted from planarity and appears to be almost bowl-like in nature. Whereas **3a** shows N_1-$C_{\alpha1}$-$C_{\alpha2}$-N_2 torsional angles of 67° (average), **3b** and **3c** are both characterized by smaller torsional angles (61° and 58°, respectively). Nonetheless, the alkyl fragments in **3b** and **3c** are located almost perpendicular to the mean plane of the heterocyclic ring. The compounds reveal bond lengths of approximately 1.37 Å for the C_α–C_β bonds in all three cases, whereas the C_β–$C_{\beta'}$ bond lengths are in the range of 1.40–1.42 Å. This nonequivalence in bond lengths is consistent with localized pyrrole aromaticity and stands in contrast to what is seen in the aromatic precursor **1** in which the pyrrolic C–C bond lengths are much more similar.[1] Furthermore, the C–C distances between adjacent pyrrole units in **3** are of the order of 1.46 Å, as expected for an electron-localized system that lacks extensive conjugation.

The hallmark of porphyrinogen systems is their ability to undergo oxidation to the corresponding aromatic systems: for example, the conversion of porphyrinogen **4** to the dication **5**. To test whether this might be possible with the reduced



Scheme 2. Oxidation of the N-tetramethylated porphyrinogen **4** to the aromatic dication **5**. For details, see reference [5].

 © 2005 Wiley-VCH Verlag GmbH & Co. KGaA, Weinheim

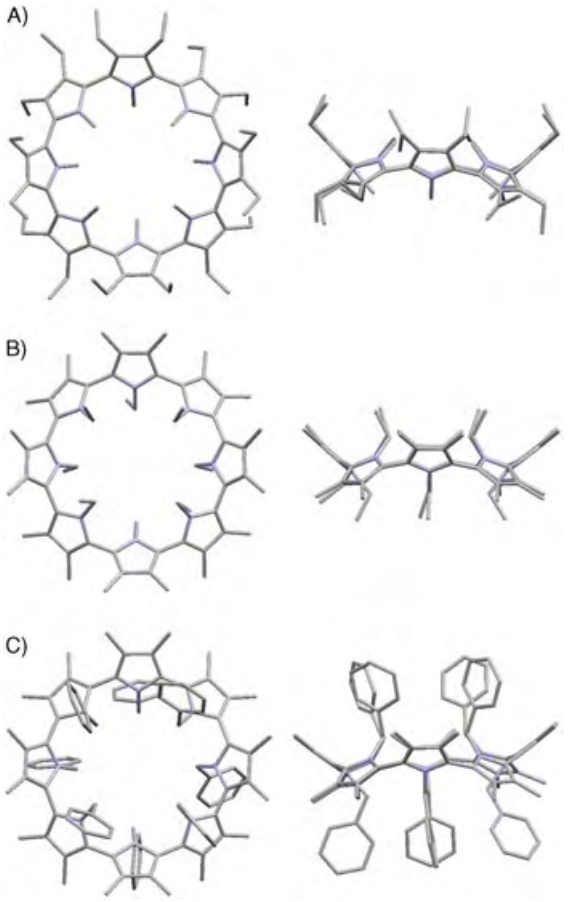


Figure 1. Single crystal X-ray diffraction analyses. Top and side views of mercury-rendered wire-frame structures of A) **3a**,[7] B) **3b**,[8] and C) **3c**.[9] Hydrogen atoms are removed for clarity; half a molecule of methylene chloride (**3a**) and one molecule of methylene chloride and half a molecule of benzene (**3c**) have also been omitted. Blue N.

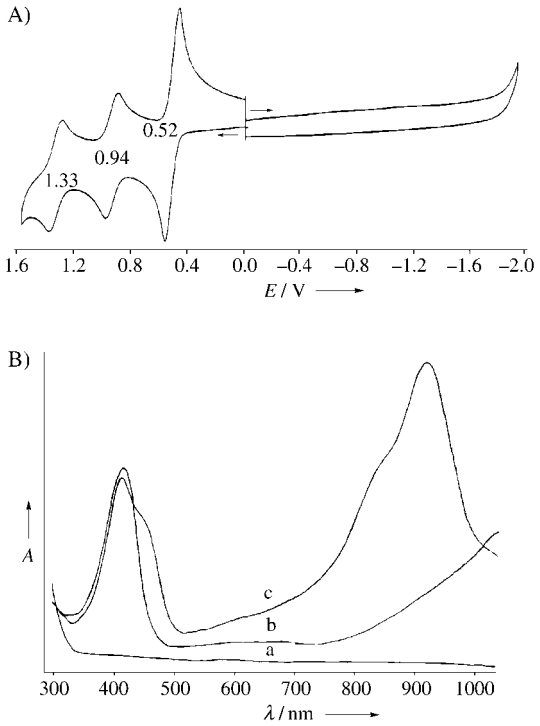


Figure 2. A) Cyclic voltammograms (vs SCE) of **3a** (in CH_2Cl_2 with TBAP (0.1 M)) and B) UV/Vis spectra of **3a** a) before and b) after the first two-electron oxidation at 0.70 V and c) after the second one-electron oxidation at 1.10 V (in CH_2Cl_2 with TBAP (0.2 M)).

cyclo[8]pyrrole derivative **3a**, a series of electrochemical and spectroelectrochemical studies were carried out in CH_2Cl_2 containing tetra-*n*-butylammonium perchlorate (TBAP, 0.1 or 0.2 M). Three reversible oxidations are observed at $E_{1/2} = 0.52$, 0.94, and 1.33 V, the first of which is a two-electron-transfer process. No reductions are seen under these experimental conditions up to a potential of −2.0 V vs SCE (saturated calomel electrode; see Figure 2A).

The N-alkylated macrocycle **3a** displays no significant absorption bands in the region $\lambda = 325$–1100 nm. However, upon two-electron oxidation of this species at 0.70 V in a thin-layer spectroelectrochemical cell, an initial product was observed and is assigned as the dication $\mathbf{3a}^{2+}$, which is characterized by a spectrum with two bands at $\lambda = 415$ and 1036 nm, respectively (see curve b in Figure 2B). The λ_{max} of these bands correspond to the Soret and Q-type bands seen for the diprotonated form of the 30-π-electron cyclo[8]pyrrole (**1a**). Upon further oxidation of $\mathbf{3a}^{2+}$ in a thin-layer cell at 1.10 V, a high intensity Q type band at $\lambda = 917$ nm is observed (see curve c in Figure 2B). This spectrum is assigned to the π-cation radical, $\mathbf{3a}^{3+}$, which has one unpaired electron as inferred from ESR measurements. Similar spectra were obtained upon bulk controlled-potential electrolysis. A summary of the spectral data is given in Table 1.[11]

Table 1: UV/Vis spectral data of 30-π-electron systems, determined from thin-layer spectroelectrochemistry in CH_2Cl_2.

compound	λ_{max} [nm]	
	Soret band	Q band
cyclo[8]pyrrole **1a**	431[a]	1112[a]
N-methylated cyclo[8]pyrrole dication $\mathbf{3a}^{2+}$	415	>1040[b]
radical π cation $\mathbf{3a}^{3+}$	415[c]	917[c]
N-benzylated cyclo[8]pyrrole dication $\mathbf{3c}^{2+}$	450	>1040[b]

[a] Taken from reference [1]. [b] Lower limit: the exact determination was limited by the spectral response of the instrument. [c] Shoulders are also observed at 447 nm and 845 nm.

Upon bulk controlled-potential electrolysis of **3a** at 0.70 V in CH_2Cl_2 containing TBAP (0.2 M) for 15 min, a strong signal in the ESR spectrum at $g = 2.004$ was observed (see Supporting Information). However, when the controlled-potential electrolysis was carried out for a longer time (45 min), the intensity of the signal of the ESR spectrum decreased and became negligible. This leads us to suggest that a comproportionation reaction occurs between the neutral compound, **3a**, and the oxidized species, presumably $\mathbf{3a}^{2+}$,

 © 2005 Wiley-VCH Verlag GmbH & Co. KGaA, Weinheim

which is produced as the result of a two-electron oxidation. This comproportionation reaction gives rise to $\mathbf{3a}^{+}$, which exhibits an ESR signal. The final product, $\mathbf{3a}^{2+}$, is expected to be ESR-inactive provided that the two holes (unpaired spins), which are produced upon oxidation, are paired. Further oxidation at 1.10 V leads to the formation of a species with a strong ESR signal at $g = 2.007$ and $\Delta H = 7.8$ G (see Supporting Information). Such values are consistent with a π-cation radical and leads us to propose that the product of this oxidative process is the triply oxidized species, $\mathbf{3a}^{3+}$.

Currently, we are working to affirm the results of spectroelectrochemistry by chemical oxidation. We have found, for instance, that treatment of colorless solutions of **3a** in methylene chloride with perchloric acid, acidic aqueous solutions of chromate and bromate under heterogeneous conditions, or with bromine (but not with iodine) under homogeneous conditions gives rise to a compound (or a mixture of compounds) whose spectrum also resembles that of the acid salt **1a**. Unfortunately, the spectral features ascribed to the presumed compound produced in this way, namely $\mathbf{3a}^{2+}$, begin to fade over the course of 0.5 h which leads us to infer that the product is not stable under these conditions at ambient temperature. Nonetheless, these findings, when considered in conjunction with the results of the bulk electrolysis experiments described above, suggest that it might be possible to isolate dicationic products of general structure $\mathbf{3}^{2+}$ or even their more-oxidized radical-cation analogues $\mathbf{3}^{3+}$ under appropriate conditions. Efforts are currently directed to this end. We are also working to test the generality of the reductive alkylation procedure of Scheme 1 by applying it, for example, to other expanded porphyrin systems.[12] Besides this, we are exploring the use of **3**, with its unique "four up, four down" orientation, as a possible scaffold for further synthetic elaboration, such as in the construction of self-assembled arrays and polytopic receptor systems.

Experimental Section

Unless otherwise noted, solvents and reagents were reagent-grade and were used without further purification. Tetrahydrofuran (THF) was dried by passage through two columns of activated alumina. The bipyrrolic precursors were prepared as described previously.[13] ^{1}H and ^{13}C NMR spectra were measured at 25 °C on a Varian Unity Innova at 300 and 400 MHz, respectively. UV/Vis spectra were recorded on a Beckman DU 640B spectrophotometer. High-resolution CI and FAB mass spectra were measured with a VG ZAB2-E mass spectrometer.

3c: Under an argon atmosphere, sodium hydride (60% suspension in mineral oil; 95 mg, 2.38 mmol) was added to a solution of cyclo[8]pyrrole **1a** (49.2 mg, 58.5 μmol) in dry THF (20 mL), and the mixture was stirred at room temperature for 30 min. Then, benzyl bromide (335 μL, 2.8 mmol) was added, and the solution was heated under reflux for 12 h. The solution was allowed to cool to room temperature, then aqueous NaOH solution (1M, 10 mL) was added along with CH_2Cl_2 (20 mL). After stirring this mixture for 20 min, the phases were separated, and the aqueous phase was extracted further with CH_2Cl_2 (10 mL). The combined organic phases were dried over anhydrous sodium sulfate, and the solvent was removed in vacuo. The residue was passed through a short plug of silica gel using CH_2Cl_2 as the eluent. Compound **3c** was isolated as a white–amber-colored crystalline product (66 mg, 70%). ^{1}H NMR (300 MHz, $CDCl_3$): $\delta =$ 1.68 (s, 48H, CH_3), 5.09 (s, 16H, benzyl-CH_2), 6.34–6.37 (m, 16H, phenyl-*H*), 6.83–6.88 (m, 16H, phenyl-*H*), 6.94–6.99 ppm (m, 8H, phenyl-*H*); ^{13}C NMR (75 MHz, $CDCl_3$): $\delta = 9.82$, 48.91, 121.08, 123.96, 126.50, 126.67, 127.76, 138.17 ppm. HRMS (FAB); *m*/*z*: calcd for $C_{104}H_{104}N_8$: 1464.8384; found: 1464.8410 ([M^+]).

Received: August 26, 2004

Keywords: aromaticity · electrochemistry · nitrogen heterocycles · porphyrinoids · redox chemistry

[1] D. Seidel, V. Lynch, J. L. Sessler, *Angew. Chem.* **2002**, *114*, 1480–1483; *Angew. Chem. Int. Ed.* **2002**, *41*, 1422–1425.
[2] T. Köhler, D. Seidel, V. Lynch, F. O. Arp, Z. Ou, K. M. Kadish, J. L. Sessler, *J. Am. Chem. Soc.* **2003**, *125*, 6872–6873.
[3] During the course of this work, the preparation and full structural characterization of a tetra-N-benzylated *meso*-tetrakis(3,5-di-*tert*-butyl-4-oxocyclohexa-2,5-dienylidene)porphyrinogen, obtained from the four-fold N alkylation of the parent *meso*-tetra(oxocyclohexadienylidene)porphyrinogen (generated by oxidation of the corresponding *meso*-substituted (4-hydroxyphenyl)porphyrin), was reported. However, this procedure apparently cannot be successfully applied to produce the corresponding unoxidized (that is, "normal") porphyrinogen starting from, for example, *meso*-unsubstituted porphyrins. See J. P. Hill, I. J. Hewitt, C. E. Anson, A. K. Powell, A. L. McCarty, P. A. Karr, M. E. Zandler, F. D'Souza, *J. Org. Chem.* **2004**, 69, 5861–5869. For a recent review about hydroporphyrins and reduced species, see: a) M. O. Senge, J. Richter, *J. Porphyrins Phthalocyanines* **2004**, *8*, 934–953; b) L. R. Milgrom, *Tetrahedron* **1983**, *39*, 3895–3898; c) L. R. Milgrom, J. P. Hill, G. Yahioglu, *J. Heterocycl. Chem.* **1995**, *32*, 97–101; d) E. Dolusic, S. Toppet, S. Smeets, L. van Meervelt, B. Tinant, W. Dehaen, *Tetrahedron* **2003**, *59*, 395–400.
[4] M. Gosmann, PhD Thesis, Universität Münster (Germany) **1986**.
[5] E. Vogel, P. Röhrig, M. Sicken, B. Knipp, A. Herrmann, M. Pohl, H. Schmickler, J. Lex, *Angew. Chem.* **1989**, *101*, 1683–1687; *Angew. Chem. Int. Ed. Engl.* **1989**, *28*, 1651–1655; .
[6] That porphyrins may be reduced to produce porphyrinogens (and other reduced species) is historically well appreciated. See, for instance: H. Fischer, H. Orth, *Die Chemie des Pyrrols*, Band *II, II.* Haelfte, Akad. Verlagsgesellschaft, Leipzig, **1940**. However, conversion of these species to **4** and its analogues is apparently problematic. For instance, our attempts to N alkylate calix[4]pyrrole (*meso*-octamethylporphyrinogen) by treatment with excess *n*-butyllithium followed by ethyl bromoacetate did not result in an N-alkylated product analogous to **4**. Rather, very effective β-pyrrolic C alkylation was observed. See P. A. Gale, J. L. Sessler, W. E. Allen, N. A. Tvermoes, V. Lynch, *Chem. Commun.* **1997**, 665–666.
[7] Structural data for compound **3a**: Single crystals suitable for X-ray diffraction studies of compound $\mathbf{3a}\cdot 0.5\,CH_2Cl_2$ were obtained by slow evaporation of its solution in methylene chloride and methanol. Data were collected on a Nonius Kappa CCD diffractometer by using a graphite monochromator with $Mo_{K\alpha}$ radiation ($\lambda = 0.71073$ Å). $C_{72.50}H_{105}ClN_8$, $M_r = 1124.09$, monoclinic, space group $P21/n$, $a = 16.7530(5)$ Å, $b = 24.4090(6)$ Å, $c = 18.3380(9)$ Å, $\alpha = 90.000(2)°$, $\beta = 112.488(2)°$, $\gamma = 90.000(11)°$, $V = 6928.6(4)$ Å^3, $Z = 4$. Full matrix least-squares on F^2 was used as the refinement method. Final $R1$ ($I > 2\sigma(I)$) = 0.1093; $wR2$(all data) = 0.1932.[10]
[8] Structural data for compound **3b**: Single crystals suitable for X-ray diffraction studies of compound **3b** were obtained by vapor diffusion of methylene chloride into a solution of the macrocycle in methanol. Data were collected on a Nonius Kappa CCD

 © 2005 Wiley-VCH Verlag GmbH & Co. KGaA, Weinheim

diffractometer by using a graphite monochromator with $Mo_{K\alpha}$ radiation ($\lambda = 0.71073$ Å). $C_{64}H_{88}N_8$, $M_r = 969.42$, orthorhombic, space group *Pbcn*, $a = 12.6903(1)$ Å, $b = 28.1058(3)$ Å, $c = 17.2872(2)$ Å, $\alpha = 90°$, $\beta = 90°$, $\gamma = 90°$, $V = 6165.84(11)$ Å^3, $Z = 4$. Full matrix least-squares on F^2 was used as the refinement method. Final $R1$ ($I > 2\sigma(I)$) = 0.1445; $wR2$(all data) = 0.1534.[10]

[9] Structural data for compound **3c**: Single crystals suitable for X-ray diffraction studies of compound **3c**·CH_2Cl_2·0.5 C_6H_{14} were obtained by vapor diffusion of *n*-hexane into a solution of the macrocycle in methylene chloride. The data were collected on a Nonius Kappa CCD diffractometer by using a graphite monochromator with $Mo_{K\alpha}$ radiation ($\lambda = 0.71073$ Å). $C_{108}H_{113}Cl_2N_8$, $M_r = 1593.96$, orthorhombic, space group *Pbca*, $a = 26.5693(3)$ Å, $b = 24.2573(3)$ Å, $c = 28.3957(2)$ Å, $\alpha = 90°$, $\beta = 90°$, $\gamma = 90°$, $V = 18301.0(4)$ Å^3, $Z = 8$. Full-matrix-block least-squares on F^2 was used as the refinement method. Final $R1$ ($I > 2\sigma(I)$) = 0.0560; $wR2$ (all data) = 0.1462.[10]

[10] For further details on the crystal-structure data and structure refinements for **3a**, **3b**, and **3c**, see the Supporting Information. CCDC-248431 (**3a**), CCDC-248429 (**3b**), and CCDC-248430 (**3c**) contain the supplementary crystallographic data for this paper. These data can be obtained free of charge via www.ccdc.cam.ac.uk/conts/retrieving.html (or from the Cambridge Crystallographic Data Centre, 12, Union Road, Cambridge CB21EZ, UK; fax: (+44) 1223-336-033; or deposit@ccdc.cam.ac.uk).

[11] Spectral features similar to those seen in the case of the thin-cell spectroelectrochemical studies are observed after carrying out both the first two-electron and second one-electron oxidations by bulk electrolysis. However, the shoulder at 447 nm seen in Figure 2B was not seen in the case of the latter experiments. We are currently exploring the significance of this finding.

[12] In preliminary work, we have found that the reaction sequence used to produce **3a** from **1a** could be successfully applied to cyclo[6]pyrrole[2] to produce the corresponding reduced hexa-N-methylated macrocycle—the smaller homologue of **3a**.

[13] J. L. Sessler, M. C. Hoehner, *Synlett* **1994**, 211.

 © 2005 Wiley-VCH Verlag GmbH & Co. KGaA, Weinheim

Host–Guest Chemistry

Molecular Loop Lock: A Redox-Driven Molecular Machine Based on a Host-Stabilized Charge-Transfer Complex**

*Woo Sung Jeon, Eunju Kim, Young Ho Ko, Ilha Hwang, Jae Wook Lee, Soo-Young Kim, Hee-Joon Kim, and Kimoon Kim**

Dedicated to Professor Dong H. Kim

Artificial molecular machines have received much attention in recent years because of their potential application in the creation of nanometer-scale molecular devices.[1,2] A wide variety of molecular machines such as shuttles,[3a] rotors,[3b] muscles,[3c] ratchets,[3d] pistons and cylinders,[3e] scissors,[3f] and elevators[3g] have been reported. Nevertheless, the design and synthesis of new molecular machines that are reminiscent of macroscopic machines would further widen the scope of this area of chemistry.

Cucurbit[8]uril (CB[8]),[4] a member of the host family cucurbit[*n*]uril, which has a cavity that is similar to that of γ-cyclodextrin, exhibits remarkable host–guest properties including the encapsulation of a hetero-guest-pair inside the cavity.[5] For example, it encapsulates methyl viologen (MV^{2+}) and 2,6-dihydroxynaphthalene ($Np(OH)_2$) inside the cavity to form the stable 1:1:1 complex $\mathbf{1}^{2+}$. Formation of the complex is driven by the markedly enhanced charge-transfer (CT) interaction between the electron-deficient and electron-rich guest molecules inside the hydrophobic cavity of CB[8].[5a] This discovery led us to build several novel supramolecular assemblies such as supramolecular amphiphiles that led to

[*] Dr. W. S. Jeon, E. Kim, Dr. Y. H. Ko, I. Hwang, Dr. J. W. Lee,[+] Dr. S.-Y. Kim, Dr. H.-J. Kim,[++] Prof. Dr. K. Kim
National Creative Research Initiative Center
for Smart Supramolecules and
Department of Chemistry
Division of Molecular and Life Sciences
Pohang University of Science and Technology
San 31 Hyojadong, Pohang 790-784 (Republic of Korea)
Fax: (+82) 54-279-8129
E-mail: kkim@postech.ac.kr

[+] Current address: Department of Chemistry
Dong-A University
840 Hadan-dong, Busan 604-714 (Republic of Korea)

[++] Current address: Department of Applied Chemistry
Kumoh National Institute of Technology
188 Shinpyung-dong, Gumi, Gyeongbuk 730-701 (Republic of Korea)

[**] We gratefully acknowledge the Creative Research Initiative Program and the International R&D Cooperation Program of the Korean Ministry of Science and Technology for support of this work, and we thank the Korean Ministry of Education (BK 21 Program) for graduate studentships to W.S.J., E.K., and I.H. This paper is dedicated to Professor Dong H. Kim, a founding father of Pohang University of Science and Technology, on his retirement.

Supporting information for this article is available on the WWW under http://www.angewandte.org or from the author.

 DOI: 10.1002/anie.200461806 © 2005 Wiley-VCH Verlag GmbH & Co. KGaA, Weinheim

vesicles,[5b] molecular loops,[5c] supramolecular polymers on surfaces,[5d] and molecular necklaces[5e] by exploiting the host-stabilized CT interactions. Despite the progress in the construction of self-assembly systems, the redox properties of the host-stabilized CT complexes, in particular, the interplay between the redox process and the exchange of the guest within the host-stabilized CT complexes have not been reported. These properties may provide a novel operating principle of molecular machines or stimuli-responsive materials. Herein we report the redox-coupled guest-exchange properties of CB[8]-stabilized CT complexes which demonstrate the interconversion of hetero- and homo-guest-pair inclusion in a molecular host triggered by an external stimulus (Scheme 1). We also report a molecular loop lock, a novel redox-driven molecular machine based on this phenomenon.

Treatment of a mixture of methyl viologen (MV^{2+}) and the ternary complex $\mathbf{1}^{2+}$ (1:1) with a reducing agent such as sodium dithionite ($Na_2S_2O_4$) results in a drastic change in the UV/Vis spectrum. The appearance of new absorption bands at $\lambda = 365$, 540, and 884 nm (see Supporting Information) supports the near-quantitative formation of the 2:1 inclusion complex $(MV^{+\bullet})_2\subset CB[8]$ $(\mathbf{2}^{2+})$[6] and free $Np(OH)_2$ (Scheme 1). Introduction of O_2 into the solution regenerates $\mathbf{1}^{2+}$ and MV^{2+}. This behavior is confirmed by UV/Vis and NMR spectroscopy, and this result demonstrates the reversible conversion of hetero- and homo-guest-pair inclusion inside CB[8] triggered by a redox stimulus.

The redox-coupled guest-exchange process was further investigated by cyclic voltammetry (Figure 1). Methyl viologen (MV^{2+}) shows two reversible waves that correspond to the redox couples $MV^{2+}/MV^{+\bullet}$ and $MV^{+\bullet}/MV^0$ (Figure 1a). Compared to MV^{2+}, $\mathbf{1}^{2+}$ exhibits a moderate negative shift of the first reduction peak and a large negative shift of the second reduction peak (Figure 1b). Furthermore, the oxidation process that corresponds to the first reduction process of $\mathbf{1}^{2+}$ shows two peaks at −0.71 V and −0.50 V (vs SCE—saturated calomel electrode), the latter of which is almost the same as that for the oxidation of $\mathbf{2}^{2+}$.[6] With increasing scan rates the oxidation peak at −0.71 V increases, whereas the peak at −0.50 V decreases (see Supporting Information), as often seen in processes that involve electron transfer followed by a chemical reaction. The addition of MV^{2+} (1 equiv) results in a small positive shift of the first reduction wave, disappearance of the oxidation peak at −0.71 V, and concomitant increase of the peak at −0.50 V (Figure 1c).[7] A spectroelectrochemical study shows that the absorption spectrum of the species generated by the electrolysis of $\mathbf{1}^{2+}$ (applied potential, −0.85 V vs SCE, in the presence or absence of MV^{2+} (1 equiv)) is essentially identical to that of $\mathbf{2}^{2+}$ (see Supporting Information). Taken together, these results suggest that the reduction of $\mathbf{1}^{2+}$ initially generates the one-electron-reduced species $\mathbf{1}^{+\bullet}$, which contains $MV^{+\bullet}$ and $Np(OH)_2$ encapsulated in CB[8], and then reacts with free $MV^{+\bullet}$ to undergo the rapid guest exchange that leads to $\mathbf{2}^{2+}$ and free $Np(OH)_2$ (see Supporting Information). Note that the regeneration of $\mathbf{1}^{2+}$ and MV^{2+} by the oxidation of $\mathbf{2}^{2+}$ and $Np(OH)_2$ probably does not follow the reverse pathway because the 1:1 mixture of $\mathbf{2}^{2+}$ and $Np(OH)_2$ is thermodynamically far more stable than the 1:1 mixture of $\mathbf{1}^{+\bullet}$ and $MV^{+\bullet}$. Instead, it is more likely to occur through another pathway that involves the initial generation of the 1:1 complex $MV^{2+}\subset CB[8]$ by the oxidation of $\mathbf{2}^{2+}$, as we

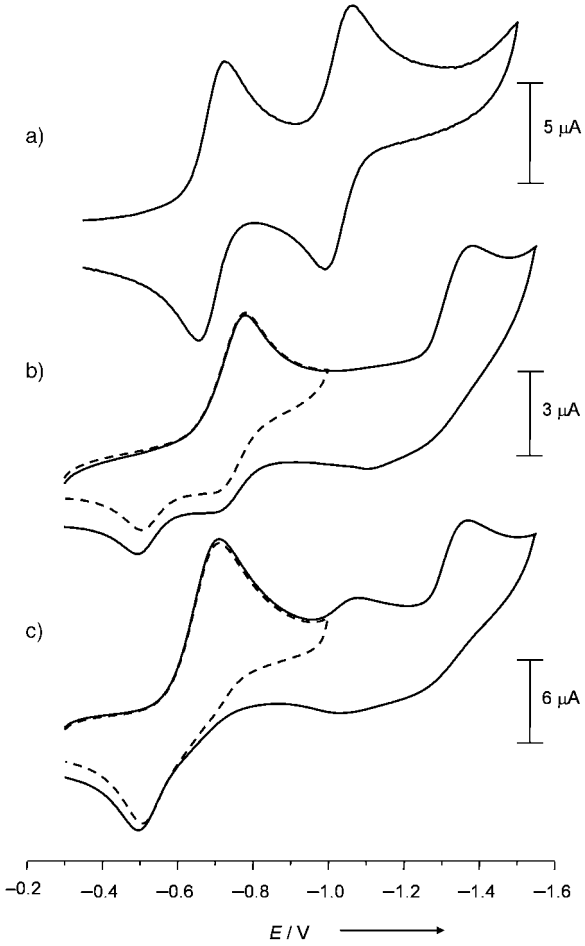
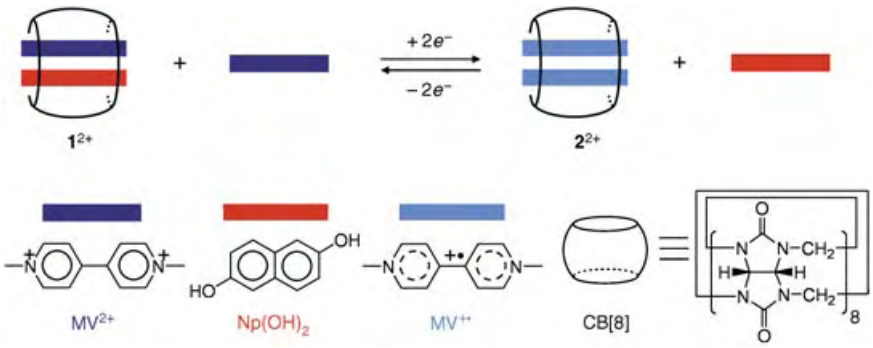


Figure 1. Cyclic voltammograms of a) MV^{2+} (0.5 mM) and b) $\mathbf{1}^{2+}$ (0.5 mM) in the absence of free MV^{2+}, and c) $\mathbf{1}^{2+}$ (0.5 mM) in the presence of free MV^{2+} (1 equiv) in phosphate buffer solution (0.1 M, pH 7.0). Scan rate = 100 mV s^{-1}; – – – different scan rate.

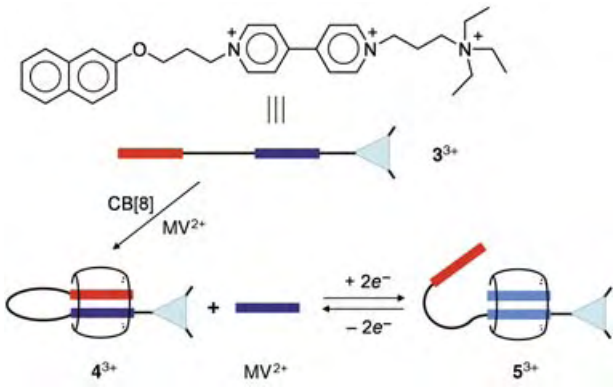


Scheme 1. Interconversion of hetero- and homo-guest-pair inclusion in CB[8] triggered by a redox stimulus. MV = methyl viologen, $Np(OH)_2$ = 2,6-dihydroxynaphthalene, CB[8] = cucurbit[8]uril.

 © 2005 Wiley-VCH Verlag GmbH & Co. KGaA, Weinheim

demonstrated previously,[6] which then reacts with free $Np(OH)_2$ to produce $\mathbf{1}^{2+}$ (see Supporting Information).

The discovery of the redox-coupled guest-exchange process prompted us to design and synthesize a redox-driven molecular machine that behaves as a molecular loop lock, which can be switched on and off (locked and unlocked) by means of a key and a redox stimulus (Schemes 2 and 3). The guest molecule $\mathbf{3}^{3+}$, which contains a naphthalen-2-yloxy (Np) unit and a viologen unit linked to each other by a flexible



Scheme 2. Formation of the molecular loop lock $\mathbf{4}^{3+}$ (folded "locked" state) through the formation of an intramolecular CT complex inside CB[8], and the redox-induced formation of ternary complex $\mathbf{5}^{3+}$ (open "unlocked" state).

tether as well as a bulky cationic unit at the terminal,[8] was synthesized in four steps (see Supporting Information). Treatment of $\mathbf{3}^{3+}$ with CB[8] (1 equiv) in water resulted in the exclusive formation of the stable 1:1 complex $\mathbf{4}^{3+}$ through the formation of the intramolecular CT complex between the Np and viologen units inside CB[8], as confirmed by ESI-MS and UV/Vis and NMR spectroscopy analyses (see Supporting Information). In particular, the upfield-shifted signals for the protons of the Np and viologen units and the downfield-shifted signals for the protons of the linker and cationic terminal in the ^{1}H NMR spectrum of $\mathbf{4}^{3+}$ (see Supporting Information) are consistent with the formation of a molecular loop[5c] with a "closed" or "locked" conformation as illustrated in Scheme 2.

The ^{1}H NMR spectrum of $\mathbf{4}^{3+}$ is not affected by the addition of MV^{2+} (1 equiv) which indicates that the 1:1 host–guest complex formed by the intramolecular CT interaction is much more stable than the ternary complex formed by the intermolecular CT interaction between the Np unit of $\mathbf{4}^{3+}$ and MV^{2+} inside CB[8]. However, treatment of a solution containing $\mathbf{4}^{3+}$ and MV^{2+} (1 equiv) with $Na_2S_2O_4$ results in the formation of the ternary complex $\mathbf{5}^{3+}$ (Scheme 2) in which the one-electron-reduced viologen unit of $\mathbf{3}^{2+\bullet}$ interacts with $MV^{+\bullet}$ inside CB[8]. The formation of this complex was confirmed by the appearance of new absorption bands at $\lambda =$ 368, 550, and 890 nm, which are characteristic of a CB[8]-stabilized viologen radical-cation dimer (Figure 2).[9,10] Owing to the paramagnetic nature of $\mathbf{5}^{3+}$, the signals for the Np unit are broad, but are clearly observed by NMR spectroscopy (Figure 3).[10] Furthermore, the chemical shift values ($\delta \approx 7$–

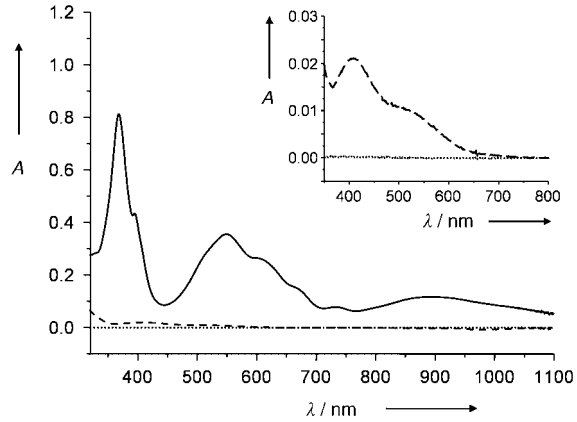


Figure 2. Absorption spectra of $\mathbf{4}^{3+}$ (0.25 mM) before (----- and inset) and after (——) reduction with $Na_2S_2O_4$ in the presence of MV^{2+} (1 equiv) in carbonate buffer (pH 10.0). Optical path = 1 mm; ••••• zero absorption.

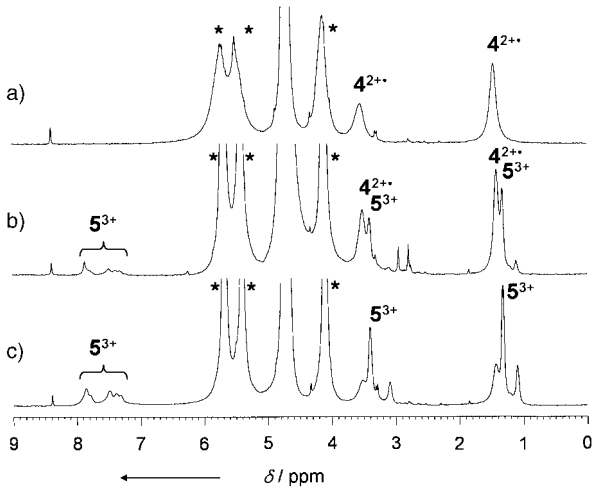
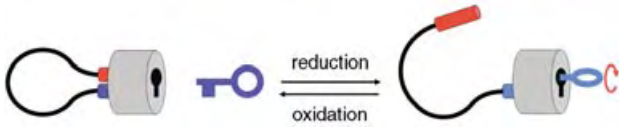


Figure 3. ^{1}H NMR spectra obtained after reduction of $\mathbf{4}^{3+}$ with $Na_2S_2O_4$ in carbonate buffer (pH 10.0) a) in the absence of MV^{2+}, b) in the presence of MV^{2+} (0.5 equiv), and c) in the presence of MV^{2+} (1.0 equiv). The signals labeled with * correspond to the CB[8] host.

8 ppm) for the protons of $\mathbf{5}^{3+}$ are close to those for free $\mathbf{3}^{3+}$ which indicates that the Np unit is now located outside CB[8] and that $\mathbf{5}^{3+}$ has an open or "unlocked" conformation as schematically shown in Scheme 2. Introduction of O_2 into the solution of $\mathbf{5}^{3+}$ regenerates $\mathbf{4}^{3+}$ and MV^{2+} as confirmed by UV/Vis and NMR spectroscopy. Thus, $\mathbf{4}^{3+}$ with a "closed" conformation is converted into $\mathbf{5}^{3+}$ with an "open" conformation upon reduction in the presence of MV^{2+}, and the process can be reversed by oxidation.[11] This system thus behaves as a molecular loop lock that can be locked and unlocked with a key and a redox stimulus (Scheme 3): The two species $\mathbf{4}^{3+}$ and $\mathbf{5}^{3+}$ represent the locked and unlocked states, respectively, and MV^{2+}, which is activated by reduction, plays the role of the key. It may be regarded as a "safeguarded" lock that requires not only a key but also an activation process to open.[10,12,13]

In summary, we have demonstrated the redox-coupled guest-exchange of CB[8]-stabilized CT complexes which illustrates unprecendented interconversion, triggered by an

 © 2005 Wiley-VCH Verlag GmbH & Co. KGaA, Weinheim



Scheme 3. Illustration of the working mode of a molecular loop lock with a key.

external stimulus, of hetero- and homo-guest-pair inclusion in a molecular host. Furthermore, we have synthesized a redox-driven molecular machine based on this phenomenon that behaves as a molecular loop lock, which requires both a key and an activation process to open. Further studies on the novel molecular machine and its applications are in progress.

Experimental Section

3·3Br**:** The tribromide salt of *N*-(3-(naphthalen-2-yloxy)propyl)-*N*′-(3-(trimethylamino)propyl-4,4′-bipyridinium) ($\mathbf{3}^{4+}\cdot 3\,Br^-$) was prepared according to a reported procedure[5c] with a minor modification. Detailed procedures are described in Supporting Information.

4·3Br**:** CB[8]·H_2SO_4·16H_2O (20.0 mg, 11.6 μmol) was added to a solution of **3**·3Br (7.0 mg, 9.7 μmol) in D_2O (4 mL), and the resulting mixture was sonicated for 1 min. Undissolved solid was filtered off, and the filtrate was slowly evaporated under reduced pressure to yield the title product (18.2 mg, 92%). ^{1}H NMR (500 MHz, D_2O, 25 °C, TMS): $\delta = 8.84$ (d, J(H,H) = 6.3 Hz, 1H; Py), 8.79 (d, J(H,H) = 6.6 Hz, 2H; Py), 8.76 (d, J(H,H) = 6.3 Hz, 1H; Py), 6.85–6.78 (m, 2H; Py, Np), 6.74 (d, J(H,H) = 6.5 Hz, 3H; Py, Np), 6.65 (d, J(H,H) = 8.9 Hz, 1H; Np), 6.62 (d, J(H,H) = 4.8 Hz; Np), 6.56 (d, J(H,H) = 8.1 Hz, 1H; Np), 6.51 (d, J(H,H) = 3.4 Hz, 2H; Np), 6.06 (d, J(H,H) = 1.9 Hz, 1H; Np), 5.72 (dd, J(H,H) = 9.2, 15.3 Hz, 16H; CB[8]), 5.47 (s, 16H; CB[8]), 5.08–5.02 (m, 2H; Py-CH_2), 4.91–4.88 (m, 2H; Py-CH_2), 4.62–4.57 (m, 2H; OCH_2), 4.21–4.16 (dd, J(H,H) = 9.2, 15.3 Hz, 16H; CB[8]), 3.66 (t, J(H,H) = 9.1 Hz, 2H; NCH_2), 3.57–3.56 (m, 6H; NCH_2), 2.99–2.66 (m, 4H; CH_2), 1.46 ppm (t, J(H,H) = 7.11 Hz, 9H; CH_3); HRMS (ESI-MS): m/z: calcd for $C_{80}H_{90}N_{35}O_{17}$ [M-3Br]$^{3+}$: 604.2418; found: 604.2411.

Received: August 27, 2004
Revised: September 25, 2004

Keywords: charge transfer · electrochemistry · molecular devices · self-assembly · supramolecular chemistry

[1] For reviews, see: a) V. Balzani, A. Credi, F. M. Raymo, J. F. Stoddart, *Angew. Chem.* **2000**, *112*, 3484; *Angew. Chem. Int. Ed.* **2000**, *39*, 3348; b) "Molecular Machines Special Issue": *Acc. Chem. Res.* **2001**, *34*, 409–522.

[2] Electronic devices based on molecular machines have been reported, see: a) C. P. Collier, E. W. Wong, M. Belohradský, F. M. Raymo, J. F. Stoddart, P. J. Kuekes, R. S. Williams, J. R. Heath, *Science* **1999**, *285*, 391; b) C. P. Collier, G. Mattersteig, E. W. Wong, Y. Luo, K. Beverly, J. Sapaio, F. M. Raymo, J. F. Stoddart, J. R. Heath, *Science* **2000**, *289*, 1172.

[3] For representative examples, see: a) P. L. Anelli, N. Spencer, J. F. Stoddart, *J. Am. Chem. Soc.* **1991**, *113*, 5131; b) T. R. Kelly, H. De Silva, R. A. Silva, *Nature* **1999**, *401*, 150; c) M. C. Jiménez, C. O. Dietrich-Buchecker, J.-P. Sauvage, *Angew. Chem.* **2000**, *112*, 3484; *Angew. Chem. Int. Ed.* **2000**, *39*, 3284; d) L. Mahedevan, P. Matsudaira, *Science* **2000**, *288*, 95; e) A. M. Brouwer, C. Frochot, F. G. Gatti, D. A. Leigh, L. Mottier, F. Paolucci, S. Roffia, G. W. H. Wurpel, *Science* **2001**, *291*, 2124; f) T. Muraoka, K. Kinbara, Y. Kobayashi, T. Aida, *J. Am. Chem. Soc.* **2003**, *125*, 5612; g) J. D. Badjić, V. Balzani, A. Credi, S. Silvi, J. F. Stoddart, *Science* **2004**, *303*, 1845.

[4] a) J. Kim, I.-S. Jung, S.-Y. Kim, E. Lee, J.-K. Kang, S. Sakamoto, K. Yamaguchi, K. Kim, *J. Am. Chem. Soc.* **2000**, *122*, 540; b) J. W. Lee, S. Samal, N. Selvapalam, H.-J. Kim, K. Kim, *Acc. Chem. Res.* **2003**, *36*, 621.

[5] a) H.-J. Kim, J. Heo, W. S. Jeon, E. Lee, J. Kim, S. Sakamoto, K. Yamaguchi, K. Kim, *Angew. Chem.* **2001**, *113*, 1574; *Angew. Chem. Int. Ed.* **2001**, *40*, 1526; b) Y. J. Jeon, P. K. Bharadwaj, S. W. Choi, J. W. Lee, K. Kim, *Angew. Chem.* **2002**, *114*, 1574; *Angew. Chem. Int. Ed.* **2002**, *41*, 4474; c) J. W. Lee, K. Kim, S. W. Choi, Y. H. Ko, S. Sakamoto, K. Yamaguchi, K. Kim, *Chem. Commun.* **2002**, 2692; d) K. Kim, D. Kim, J. W. Lee, Y. H. Ko, K. Kim, *Chem. Commun.* **2004**, 848; e) Y. H. Ko, K. Kim, J.-K. Kang, H. Chun, J. W. Lee, S. Sakamoto, K. Yamaguchi, J. C. Fettinger, K. Kim, *J. Am. Chem. Soc.* **2004**, *126*, 1932.

[6] We previously demonstrated that the 1:1 inclusion complex MV^{2+}⊂CB[8] undergoes disproportionation to form an equal mixture of the 2:1 complex $\mathbf{2}^{2+}$ (($MV^{+\cdot}$)$_2$⊂CB[8]) and free CB[8] upon chemical or electrochemical reduction and that the reaction is reversible: W. S. Jeon, H.-J. Kim, C. Lee, K. Kim, *Chem. Commun.* **2002**, 1828.

[7] The small, reversible wave at −1.1 V in Figure 1c, which increases with increasing scan rates, corresponds to the $MV^{+\cdot}$/MV^0 redox couple of free $MV^{+\cdot}$. The subsequent spectroelectrochemical study revealed no absorption bands that correspond to free monomeric $MV^{+\cdot}$ after electrolysis of $\mathbf{1}^{2+}$ in the presence of MV^{2+} (1 equiv, see Supporting Information) which implies that the reaction between $\mathbf{1}^{+\cdot}$ and $MV^{+\cdot}$ that leads to $\mathbf{2}^{2+}$ is relatively slow on the timescale of cyclic voltammetry experiments. The second reduction wave of $\mathbf{1}^{2+}$ in the absence (Figure 1b) or presence (Figure 1c) of MV^{2+} is apparently related to the reduction of the 2:1 complex $\mathbf{2}^{2+}$ generated in the first reduction step, but we do not clearly understand this process at the moment.

[8] The bulky cationic unit was introduced at the terminal to prevent the formation of intermolecular CT complexes and intermolecular viologen radical-cation dimers inside CB[8] upon reduction. Another role of the cationic terminal unit is to improve the solubility of the complex after reduction.

[9] The bands at $\lambda = 368$, 550, and 890 nm can also be attributed to $\mathbf{2}^{2+}$ (($MV^{+\cdot}$)$_2$⊂CB[8]), which may be generated during the reduction process. However, the intensity of the band at $\lambda =$ 368 nm increases linearly with increasing concentrations of MV^{2+} (0–1.0 equiv) and is almost twice as high as that of $\mathbf{2}^{2+}$ generated by the reduction of a 1:1 mixture of MV^{2+} and CB[8] at the same concentration (see Supporting Information). These results thus indicate that the amount of $\mathbf{2}^{2+}$ generated during this reduction process is insignificant. Besides the bands that are assigned to $\mathbf{5}^{3+}$, shoulders at $\lambda = 395$ and 610 nm are observed (Figure 2) which can be attributed to the one-electron-reduced species $\mathbf{4}^{2+\cdot}$ and $MV^{+\cdot}$ that are in equilibrium with $\mathbf{5}^{3+}$. It also suggests that the reduction of a 1:1 mixture of $\mathbf{4}^{3+}$ and MV^{2+} first generates $\mathbf{4}^{2+\cdot}$ and $MV^{+\cdot}$, which further react to produce $\mathbf{5}^{3+}$ (see Supporting Information).

[10] Treatment of $\mathbf{4}^{3+}$ with $Na_2S_2O_4$ in the absence of MV^{2+} produces the one-electron-reduced species $\mathbf{4}^{2+\cdot}$, whose UV/Vis spectrum is similar to that of $MV^{+\cdot}$ which indicates that the viologen unit of the guest molecule exists in its radical-cation form. Owing to the paramagnetic nature of the species, the signals for the protons from the stopper unit ($\delta \approx 1.4$ and ≈ 3.5 ppm) are broad. However, the signals are clearly observed in the ^{1}H NMR spectrum of $\mathbf{4}^{2+\cdot}$ whereas those for the Np unit are not, which indicates that the Np unit is still in close proximity to the viologen radical-cation unit. This result in turn suggests that $\mathbf{4}^{2+\cdot}$ maintains the same "locked" conformation with the one-

 © 2005 Wiley-VCH Verlag GmbH & Co. KGaA, Weinheim

electron-reduced viologen and Np units located inside CB[8]. Thus, the molecular loop lock does not open in the absence of the key (MV^{2+}) and the activation process (reduction).
[11] Preliminary electrochemical studies confirmed that this reversible process can also be triggered by electrochemical stimuli. Details of the electrochemical behavior of $\mathbf{4}^{3+}$ and related compounds will be published elsewhere in due course.
[12] A "safeguarded" switch has been reported: J. W. Lee, K. Kim, K. Kim, *Chem. Commun.* **2001**, 1042.
[13] It may also be viewed as a reversibly operating molecular AND logic gate: F. M. Raymo, S. Giordani in *Encyclopedia of Nanoscience and Nanotechnology*, *Vol. 5* (Ed.: H. S. Nalwa), American Scientific, California, **2004**, pp. 677 – 692.

 © 2005 Wiley-VCH Verlag GmbH & Co. KGaA, Weinheim

Analytical Methods

High-Throughput Protein Glycomics: Combined Use of Chemoselective Glycoblotting and MALDI-TOF/TOF Mass Spectrometry**

Shin-Ichiro Nishimura, Kenichi Niikura, Masaki Kurogochi, Takahiko Matsushita, Masataka Fumoto, Hiroshi Hinou, Ryousuke Kamitani, Hiroaki Nakagawa, Kisaburo Deguchi, Nobuaki Miura, Kenji Monde, and Hirosato Kondo*

Glycosylation is one of the posttranslational modifications of proteins in eukaryotes. This step is thought to modulate a wide range of protein functions both on the cellular surfaces and within the cells.[1] This highly dynamic process in which rapid changes in the carbohydrate structures occur in response to cellular signals or cellular stages result in the key informational markers of some serious human diseases. For example, it is known that carbohydrates of IgG can be drastically altered to form unusual structures in patients with rheumatoid arthritis[2] and specific carbohydrates are used as tumor-associated markers in pancreatic and colon cancers.[3] Recently, it has also been reported that the oligosaccharides of the therapeutic human IgG play a critical role of enhancing antibody-dependent cellular cytotoxicity.[4] Glycosylation of nuclear and cytoplasmic proteins with a GlcNAc residue is ubiquitous in nearly all eukaryotes and is a crucial event in posttranslational modifications for regulating protein functions within the cells.[1b] Dynamic perturbations in *O*-GlcNAc regulation have been implicated in the etiology of type II diabetes, cancer, and neurodegenerative diseases.[5]

Although there have been substantial advances in our understanding of the effects of glycosylation on some biological systems, we still do not fully understand the specific functional roles of carbohydrates and the relationship between their structures and functions. The major difficulty in carbohydrate sequencing is a consequence of the fact that the purification of trace amounts of oligosaccharides requires extremely tedious multistep processes. This is because crude sample mixtures prepared by enzymatic digestion from cells, organs, serum, etc. usually contain large amounts of impurities such as peptides, lipids, and salts. These technical problems in the sequencing of carbohydrates make it impossible to achieve high-throughput protein glycomics. We report herein that the combined use of two novel techniques, chemoselective glycoblotting and MALDI-TOF/TOF mass spectrometry,[6] allows for both facile purification and precise analysis of common oligosaccharides and glycopeptides from native glycoproteins.

The concept of the "sugar family tree," constructed by Fischer,[7] motivated us to use the chemoselective "glycoblotting" technique, which has become a key feature in the efficient isolation of carbohydrates in this study. Fischer found that the reaction of glucose, mannose, and major oligosaccharides with phenylhydrazine proceeds smoothly to give the corresponding stable phenylhydrazone derivatives under mild basic and aqueous conditions. Once oligosaccharides are released from glycoconjugates, they can be regarded as a general class of the compound library which have an aldehyde or ketone group at each reducing terminal. As indicated in Scheme 1a, aldehydes preferentially react with reagents bearing hydrazine-like functional groups. Fischer-type reagents do not need any catalyst or reducing agent to accelerate the reaction with sugars and the reactions usually proceed under mild conditions. However, the reactions of aldehydes with primary amino groups require some activating reagent for the formation of stable products. As a result, carbohydrates preferentially react with Fischer-type reagents even in the presence of large amounts of peptides or amino acids with primary amino groups.

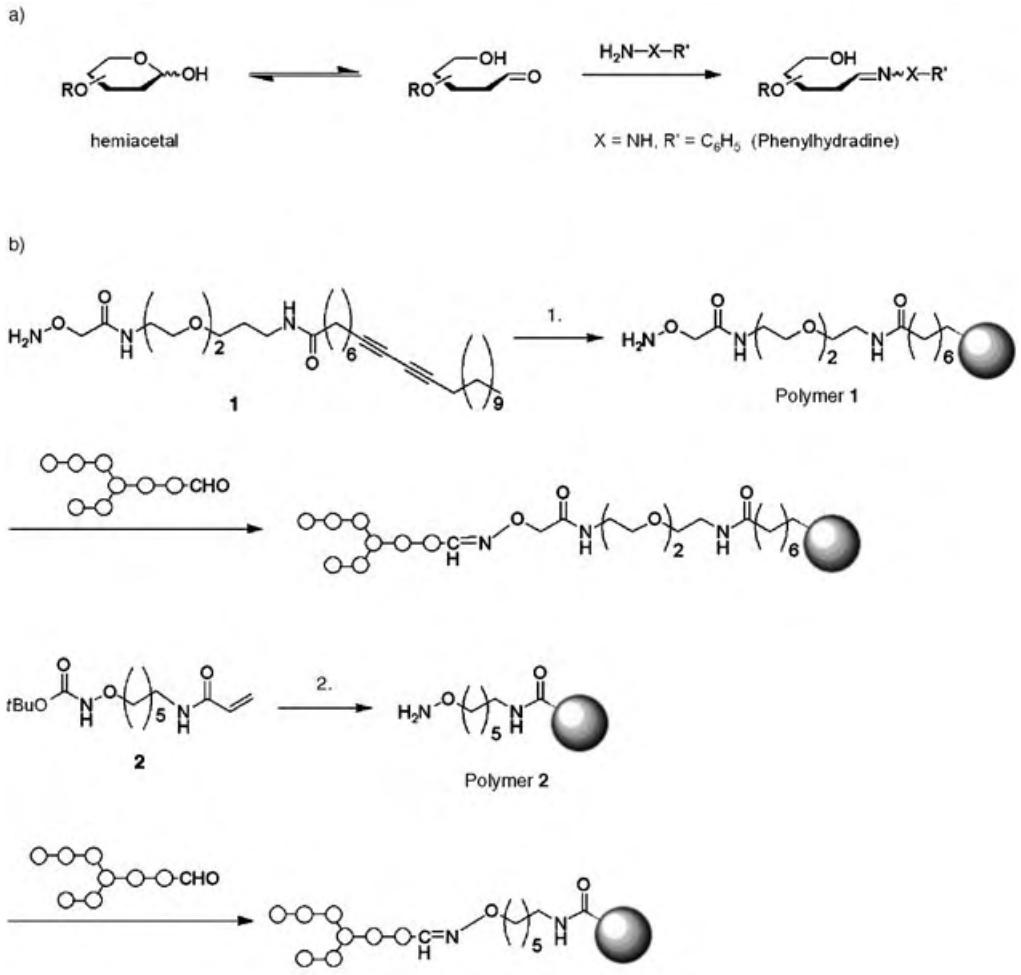
The unique chemical characteristics of the sugar family encouraged us to design novel polymers for capturing only carbohydrates from crude samples on the basis of the

[*] Prof. S.-I. Nishimura, Dr. K. Niikura, Dr. M. Kurogochi, T. Matsushita, R. Kamitani, Dr. H. Nakagawa, Dr. K. Deguchi, Dr. N. Miura, Dr. K. Monde
Division of Biological Sciences
Graduate School of Science
Frontier Research Center for Post-Genome Science and Technology
Hokkaido University
N21, W11, Sapporo 001-0021 (Japan)
Fax: (+81) 11-706-9042
E-mail: shin@glyco.sci.hokudai.ac.jp
Prof. S.-I. Nishimura, M. Fumoto, Dr. H. Hinou
Research Center for Glycoscience
National Institute of Advanced Industrial Science and Technology (AIST)
Sapporo 062-8517 (Japan)
Dr. H. Kondo
Discovery Research Laboratories
Shionogi & Co. Ltd.
Osaka 553-0002 (Japan)

[**] This work was partly supported by a grant for the National Project on "Functional Glycoconjugate Research Aimed at Developing for New Industry" from the Ministry of Education, Science, and Culture of Japan. Part of this study was presented at the Annual Conference of the Society for Glycobiology, December 3–6, 2003, San Diego, CA (USA).

Supporting information for this article is available on the WWW under http://www.angewandte.org or from the author.

 DOI: 10.1002/anie.200461685 © 2005 Wiley-VCH Verlag GmbH & Co. KGaA, Weinheim



Scheme 1. Fischer's concept and glycoblotting by Fischer-type polymer reagents. a) Reactions of carbohydrates with Fischer's reagents. b) Syntheses and reactions of Fischer-type polymer reagents: 1) liposomes prepared with phosphatidylcholine-related monomer, then UV (254 nm) irradiation, 2) radical copolymerization (ammonium persulfate) with acrylamide, followed by deprotection with 4 N HCl.

chemoselective ligation strategy. From considerations of the chemical stability, the handling of reagents, and the feasibility to the general synthesis of versatile polymer materials, we have developed several Fischer-type polymer reagents with reactive and stable oxylamino functional groups by polymerization of a diacetylene-containing lipid derivative **1** or an acrylamide-type derivative **2** (Scheme 1b). Liposomes composed of diacetylene-containing reagent **1** and phospholipid derivatives can be readily polymerized by UV irradiation to produce polymer-based nanoparticles having a mean diameter of 200–300 nm. Compound **2** gives a water-soluble polymer on radical copolymerization with acrylamide. We evaluated the feasibility of the polymers displaying oxylamino functional groups as a useful platform for the "trap and release" of the target oligosaccharides and glycopeptides.

The general protocol for the isolation and analysis of carbohydrates proposed here is simple and easy: a) Trapping carbohydrates by mixing polymers with unpurified proteolytic digest; b) collecting polymers by spin filtration from a crude mixture of peptides, salts, and other impurities; and c) releasing and subsequent MALDI-TOF MS analysis of the target carbohydrates (Figure 1). In this study we selected the *N*-glycans of human IgG to test the efficiency of protein glycomics in the strategy, since the importance of substantial structural alteration of IgG *N*-glycans has been extensively investigated,[3,8] The structural characterization of human IgG *N*-glycans was carried out using crude IgG samples obtained from human serum (100 μL, Figure 1). The merits of glycoblotting are evident since MALDI-TOF MS analysis of oligosaccharides trapped on the polymer has proven to be remarkably improved by using trapping and spin filtration (Figure 2b). When the crude digest was directly subjected to MALDI-TOF MS analysis we obtained an extremely complex spectrum (Figure 2a). The precursor ion peaks, which correspond to the *N*-glycans, cannot be distinguished from numerous other signals in the spectrum because of an excess amount of peptide impurities. As anticipated, highly sensitive and singly charged precursor ion peaks were generated in the presence of α-cyano-4-hydroxycinnamic acid (CHCA) and these greatly facilitated the subsequent sequencing and quantitative analysis of the oligosaccharides. In addition, it was found that the fragmentation of the precursor ions by the

 © 2005 Wiley-VCH Verlag GmbH & Co. KGaA, Weinheim

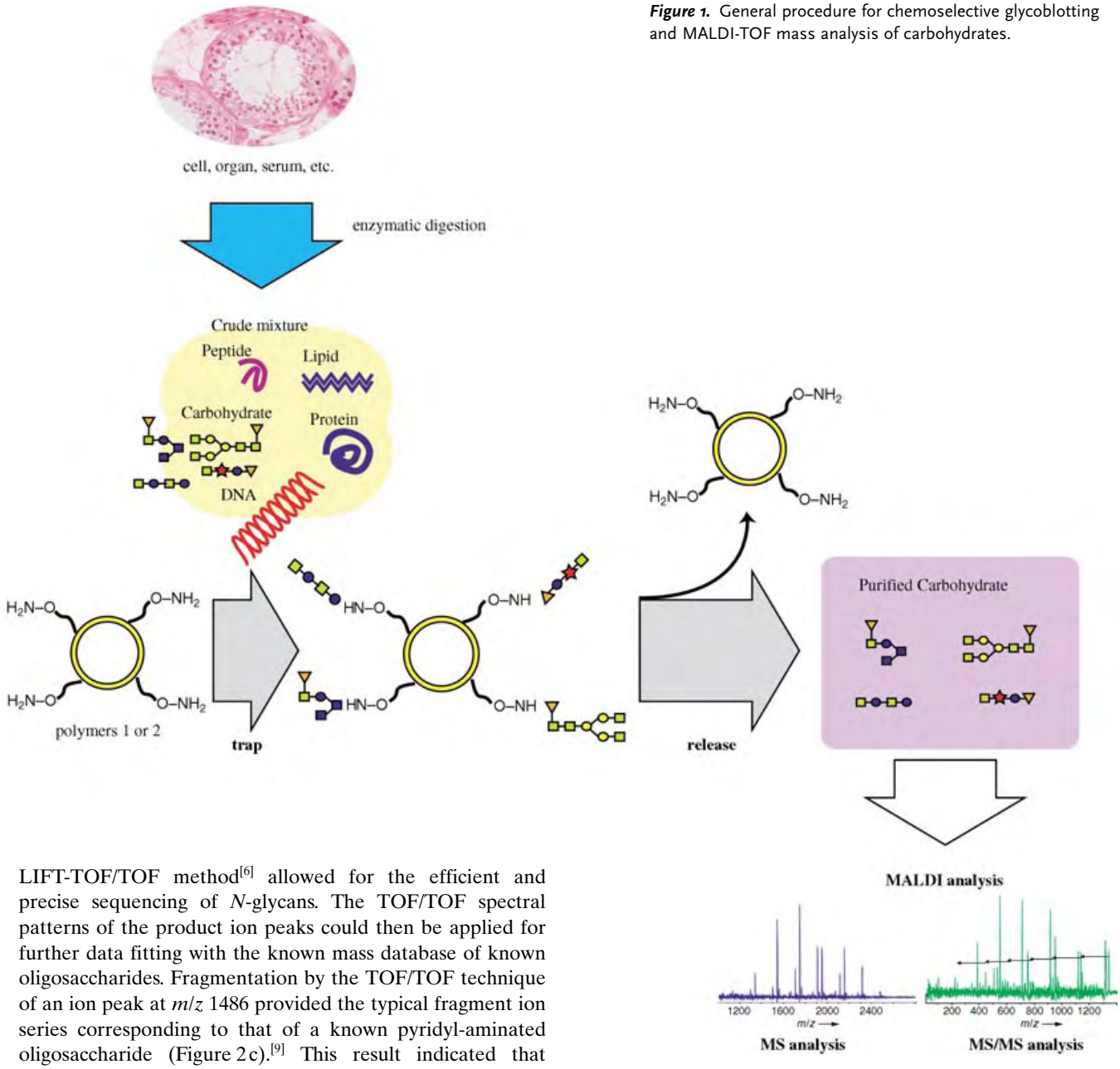


Figure 1. General procedure for chemoselective glycoblotting and MALDI-TOF mass analysis of carbohydrates.

LIFT-TOF/TOF method[6] allowed for the efficient and precise sequencing of *N*-glycans. The TOF/TOF spectral patterns of the product ion peaks could then be applied for further data fitting with the known mass database of known oligosaccharides. Fragmentation by the TOF/TOF technique of an ion peak at *m*/*z* 1486 provided the typical fragment ion series corresponding to that of a known pyridyl-aminated oligosaccharide (Figure 2c).[9] This result indicated that carbohydrate mass fingerprinting (CMF) analysis by the MALDI-TOF/TOF method allows for the precise structural identification of oligosaccharides captured from glycoproteins by glycoblotting.

It was clearly suggested that the structure of each oligosaccharide measured by the MALDI-TOF instrument was in good agreement with the data obtained by a conventional HPLC-based analysis of the corresponding pyridyl-aminated derivatives prepared from human IgG.[10] The relative intensity of each carbohydrate response given by the two methods exhibited quite similar results (see the Supporting Information), which suggests that the polymer captures carbohydrates with a reaction efficiency in proportion to the amount of each oligosaccharide existing in the sample mixtures. This result means that glycoblotting is a general and versatile method for trapping a variety of carbohydrates bound to proteins.

The CMF analysis based on TOF/TOF can also be used to determine the ratio of oligosaccharide isomers, as shown in the analysis of the ion peak at *m*/*z* 1648 (see Figure 3). The observed fragmentation of this precursor ion peak was found to be a mixture of two structural isomers and the analysis using the correlation coefficient calculated by using the known compounds enabled the ratio of the two isomers to be estimated as 62:38.

Our attention was next directed toward the application of the glycoblotting strategy for the identification of the *O*-GlcNAc site present in abundance in nucleocytoplasmic glycoproteins.[1b] Recently, we succeeded in the high-throughput identification of *O*-glycosylation (*O*-GalNAc) sites by high-speed analysis in the LIFT-TOF/TOF mode of the ion peaks of the glycosylated products in the presence of 2,5-

 © 2005 Wiley-VCH Verlag GmbH & Co. KGaA, Weinheim

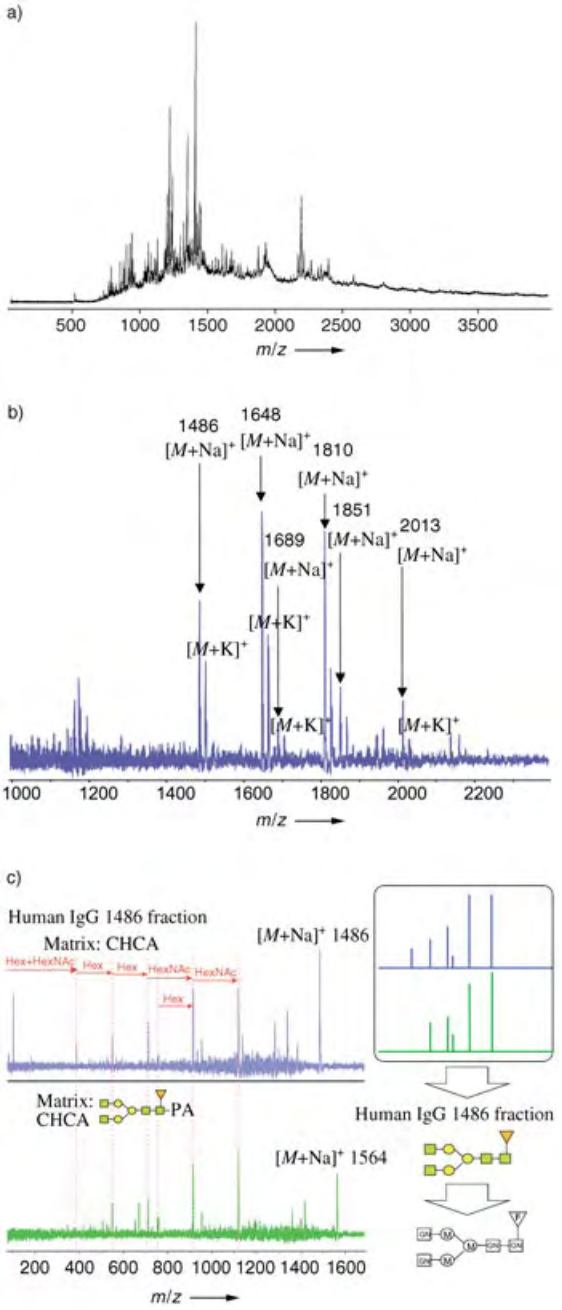
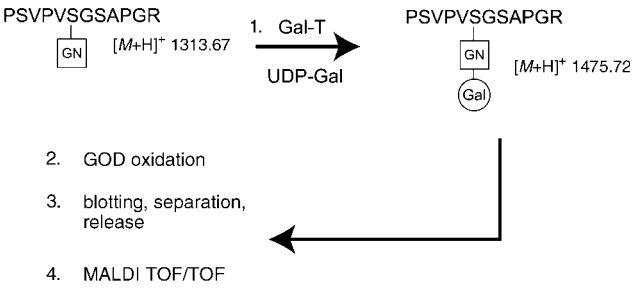


Figure 2. MALDI-TOF analysis of human IgG *N*-glycans. a) MALDI-TOF mass spectrum of crude *N*-glycans before glycoblotting. b) Major precursor ion peaks of *N*-glycans obtained by glycoblotting. c) Fragmentation by MALDI-LIFT-TOF/TOF tandem mass spectroscopy. Fragmentation of the precursor ion at *m*/*z* 1486 was performed according to the conditions reported previously in the presence of CHCA as a matrix.[11] Precise structural identification was carried out by comparing the fragmentation pattern of the known pyridyl-aminated oligosaccharide. All measurements were performed using an Ultraflex TOF/TOF mass spectrometer equipped with a reflector, and controlled by the Flexcontrol 1.2 software package (Bruker Daltonics GmbsH, Bremen, Germany). Ions generated by a pulsed UV laser beam (nitrogen laser, $\lambda = 337$ nm) were accelerated to a kinetic energy of 23.5 kV. Metastable ions generated by laser-induced decomposition of the selected precursor ions were analyzed without any additional collision gas. Precursor ions were accelerated to 8 kV and selected in a timed ion gate. The fragments were further accelerated by 19 kV in the LIFT cell, and their masses were analyzed after the ion reflector passage. Masses were automatically annotated by using XMASS 5.1.2 NT.

dihydroxybenzoic acid (DHB).[6a] To test the feasibility of glycoblotting and the subsequent TOF/TOF analysis of glycopeptides, we preliminarily investigated the enzymatic modification of a synthetic glycopeptide (PSVPVS(*O*-GlcNAc)GSAPGR) which was identified as the *O*-GlcNAc-modified peptide derived from basic phosphoprotein.[11] This glycopeptide was subjected to: a) Galactosylation with galactosyl transferase (GalT)[12] and b) oxidation with galactose oxidase (GOT) to generate a terminal aldehyde group at the C-6 position of the modified galactose residue (Scheme 2). A



Scheme 2. Strategy for the analysis of *O*-GlcNAc modified peptides.

crude glycopeptide mixture was directly used for further blotting with polymer reagent **2** and the subsequent analysis by MALDI-TOF mass spectrometry. Since peptide fragments bearing oligosaccharides prepared by tryptic digestion often exhibited poor solubility in water, water-soluble Fischer-type reagents may be a useful alternative to nanoparticles in terms of the efficiency. The TOF/TOF MS spectrum of the precursor ion at *m*/*z* 1473.71 measured with DHB gave highly sensitive and ideal fragmentation patterns because of the glycopeptide containing a (CHO)Galβ→4GlcNAcβ→Ser residue (Figure 4b). As anticipated, fragmentation in the presence of the DHB matrix occurred preferentially at peptide bonds without serious de-*O*-glycosylation (elimination) or fragmentation (cleavage) in the carbohydrate moiety. This characteristic greatly facilitated the identification of the O-glycosylation site in the target molecule (Figure 4c). This result suggests that the aldehyde attachment by enzymatic derivatization of the *O*-GlcNAc-modified peptide enables a high-throughput identification of O-glycosylation sites based on the glycoblotting method.[13] The merit of the present strategy is evident because the identification of new *O*-GlcNAc-modified proteins and the sites of modification would facilitate more global studies of the regulatory role of this posttranslational modification.

In conclusion, this study demonstrated that glycoblotting based on oxylamino-containing polymers (Fischer-type polymer reagents) could generally be used for capturing both common oligosaccharides and aldehyde-attached glycopeptides derived by enzymatic modifications. It should be noted that the efficiency and versatility in the capturing of carbohydrates from the crude proteolytic digests is crucial for ideal and practical protein glycomics. Therefore, the combined use of glycoblotting and high-performance MALDI-TOF/TOF analysis provides us with a new promising

 © 2005 Wiley-VCH Verlag GmbH & Co. KGaA, Weinheim

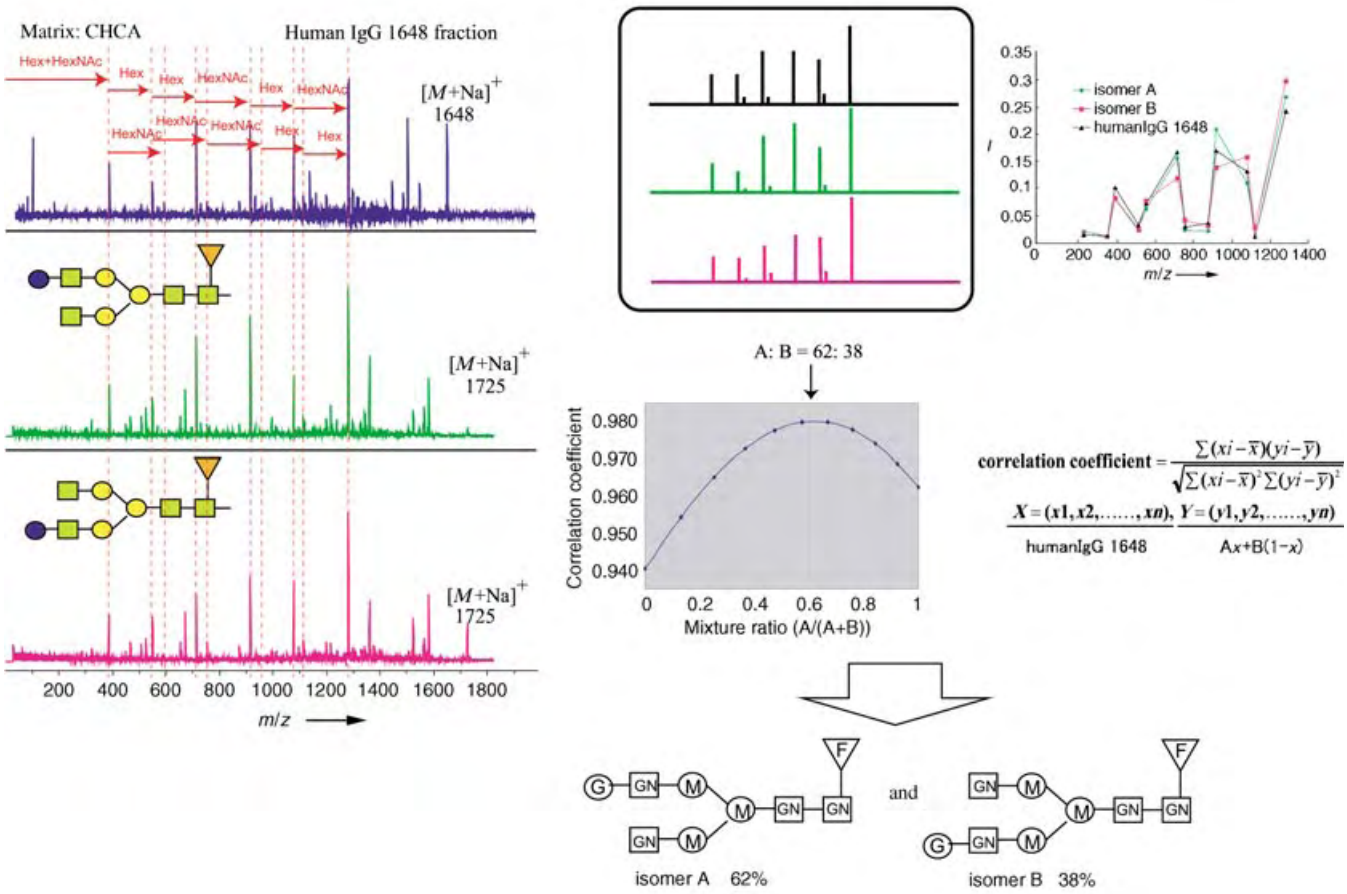


Figure 3. Identification of the ratio between isomers A and B found in the molecular ion peak at *m/z* 1648 by using carbohydrate mass fingerprinting (CMF) analysis recorded in LIFT-TOF/TOF mode. The relative intensities of LIFT-TOF/TOF product ion peaks of unknown carbohydrate structure were subjected to matching simulation with the correlation coefficient analysis. Two known oligosaccharide derivatives were used for achieving the standard CMF data.

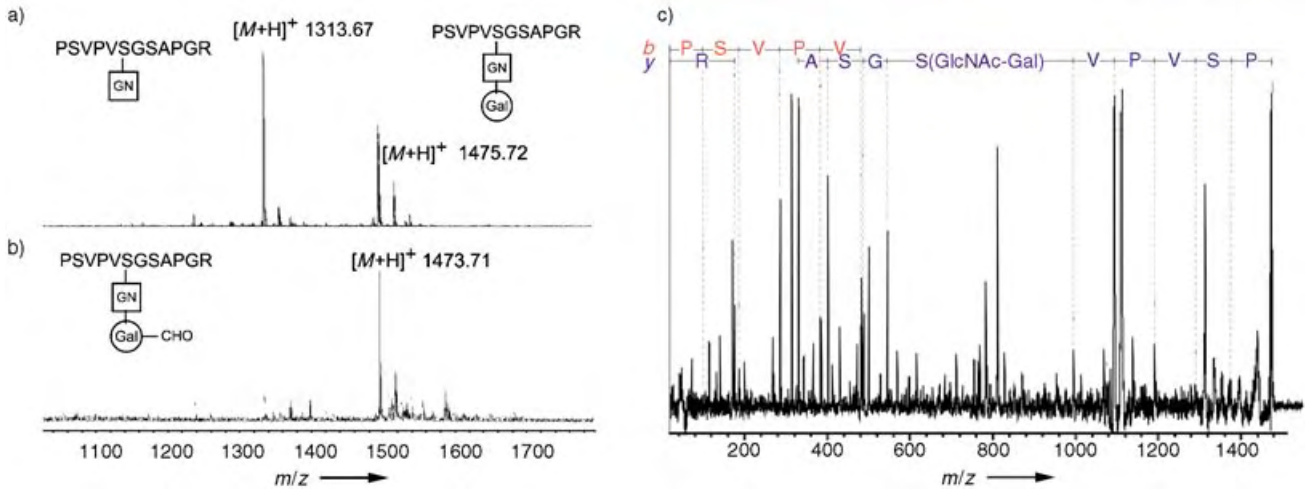


Figure 4. Identification of the *O*-GlcNAc modified peptides by MALDI-TOF mass spectrometry. a) MALDI-TOF MS of the reaction mixture after enzymatic galactosylation of glycopeptide, b) MALDI-TOF MS of an isolated glycopeptide derivative by glycoblotting method, and c) MALDI-LIFT-TOF/TOF tandem mass analysis of the precursor ion peak at *m/z* 1473.71.

 © 2005 Wiley-VCH Verlag GmbH & Co. KGaA, Weinheim

strategy for early diagnoses and tailored treatments of a variety of diseases, as well as high-throughput protein glycomics.

Received: August 17, 2004

Keywords: carbohydrates · chemoselectivity · glycoproteins · high-throughput screening · mass spectrometry

[1] a) R. A. Dwek, *Chem. Rev.* **1996**, *96*, 683; b) N. E. Zachara, G. W. Hart, *Chem. Rev.* **2002**, *102*, 431.
[2] R. B. Parekh, R. A. Dwek, B. J. Sutton, D. L. Fernandes, A. Leung, D. Stanworth, B. T. W. Rademacher, *Nature* **1985**, *316*, 452.
[3] A. Varki in *Essentials of Glycobiology* (Eds.: A. Varki, R. Cummings, J. Esko, H. Freeze, G. Hart, J. Marth), Cold Spring Harbor Laboratory Press, New York, **1999**, pp. 537–549.
[4] R. L. Shields, J. Lai, R. Keck, L. Y. O'Connell, K. Hong, Y. G. Meng, S. H. A. Weikert, L. G. Presta, *J. Biol. Chem.* **2002**, *277*, 26733.
[5] F. I. Comer, G. W. Hart, *J. Biol. Chem.* **2000**, *275*, 29179.
[6] a) M. Kurogochi, T. Matsushita, S.-I. Nishimura, *Angew. Chem.* **2004**, *116*, 4163–4167; *Angew. Chem. Int. Ed.* **2004**, *43*, 4071–4075; b) M. Kurogochi, S.-I. Nishimura, *Anal. Chem.* **2004**, in press; c) M. Kurogochi, S.-I. Nishimura, Y. C. Lee, *J. Biol. Chem.* **2004**, in press.
[7] a) E. Fischer, *Ber. Dtsch. Chem. Ges.* **1884**, *17*, 579; b) E. Fischer, *Ber. Dtsch. Chem. Ges.* **1887**, *20*, 821.
[8] J. S. Axford, *Biochim. Biophys. Acta* **1999**, *1455*, 219.
[9] D. Suckau, A. Resemann, M. Schuerenberg, P. Hufnagel, J. Franzen, A. Holle, *Anal. Bioanal. Chem.* **2003**, *376*, 952.
[10] H. Nakagawa, Y. Kawamura, K. Kato, I. Shimada, Y. Arata, N. Takahashi, *Anal. Biochem.* **1995**, *226*, 130.
[11] K. D. Greis, W. Gibso, G. W. Hart, *J. Virol.* **1994**, *68*, 8339.
[12] K. Kamemura, B. K. Hayes, F. J. Comer, G. W. Hart, *J. Biol. Chem.* **2002**, *277*, 19229.
[13] An aldehyde group generated at the C-8 position of the terminal sialic acid of a glycoprotein can also be trapped by this method. The feasibility of this strategy was preliminarily demonstrated by trapping the tryptic digest of fetuin in which the diols at the C-8 and C-9 positions of sialic acids were selectively converted into aldehyde groups by treating with 1 mM $NaIO_4$ solution at 0 °C for 30 min (data not shown). The present method can not be used for the analysis of glycopeptides displaying high mannose-type oligosaccharides, since it seems that specific conversion of a terminal mannose residue into an appropriate aldehyde derivative is difficult.

 © 2005 Wiley-VCH Verlag GmbH & Co. KGaA, Weinheim

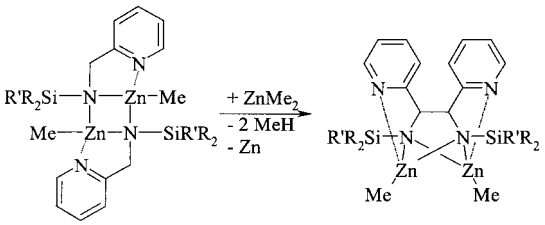
C–C Coupling

(Z)-Bis(alkylzinc)imido-1,2-di(2-pyridyl)ethene: Intramolecular Stabilization of a Bis(alkylzinc)imide**

Matthias Westerhausen, Alexander N. Kneifel, and Alexander Kalisch*

Dedicated to Professor Nils Wiberg on the occasion of his 70th birthday

The oxidative metal-mediated C–C coupling reaction of (2-pyridylmethyl)(trialkylsilyl)amines succeeds smoothly with dialkylzinc [Eq. (1)] or tin(II) bis[bis(trimethylsilyl)amide].[1] The influence of the standard potential as well as the role of the steric demand of the nitrogen-bonded trialkylsilyl and zinc-bonded alkyl groups have been investigated.[2] The N-bonded trialkylsilyl substituent is obligatory to prevent side reactions. The reaction of dialkylzinc with 2-py-CH_2NH_2 (py = pyridyl) yields several products which can be explained by a combination of oxidative C–C coupling and transamination reactions. After protolysis of this reaction mixture a small amount of *cis*-1,2-di(2-pyridyl)aminoethene (**1**; Scheme 1) can be isolated in a reproducible procedure.[3] However, we were not able to detect the zincated 1,2-di(2-pyridyl)aminoethene during the reaction. Amine **1** crystallized as the eneamine tautomer, an equilibrium with the imine tautomer was not detectable with spectroscopic methods.



(1)

Even 30 years ago, doubly zincated primary amines of the type $[RN(ZnR')_2]$ were of interest as catalysts for polymerization reactions,[4] however, these compounds were poorly characterized and more recent attempts to prepare bis(alkylzinc)alkyl- and -arylimides by zincation of primary alkylamines failed.[5,6] The polymerization reactions are also

[*] M. Westerhausen,[+] A. N. Kneifel, A. Kalisch
Department Chemie und Biochemie
Ludwig-Maximilians-Universität München
Butenandtstrasse 9 (Haus D), 81377 Munich (Germany)
Fax: (+49) 89-2180-77867
E-mail: maw@cup-uni-muenchen.de

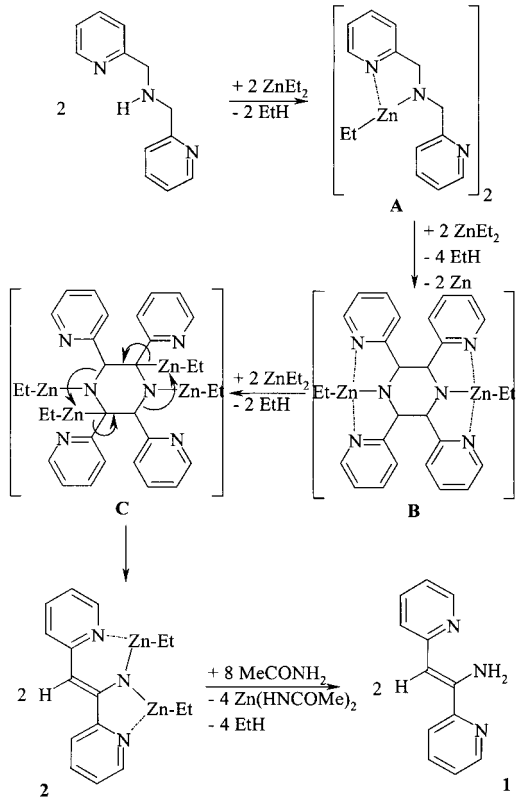
[+] Current address:
Institut für Anorganische und Analytische Chemie
Friedrich-Schiller-Universität Jena
August-Bebel-Strasse 2, 07743 Jena (Germany)

[**] We thank the Deutsche Forschungsgemeinschaft (DFG, Bonn-Bad Godesberg) for financial support.

 © 2005 Wiley-VCH Verlag GmbH & Co. KGaA, Weinheim DOI: 10.1002/anie.200461356

explainable under the assumption that monozincated amines and dialkylzinc coexist during the polymerization reaction, unequivocal data for the biszincated amines were not reported.[4] With stronger metalating reagents imides were synthesized successfully. Thus magnesium phenylimides and related compounds were prepared by Power and co-workers.[7] Similar observations were reported for geminal carbdianions; whereas geminal doubly magnesiated[8] and lithiated[9] carbdianions were characterized by X-ray crystallography, the corresponding zinc derivatives tend to avoid the formation of two Zn–C bonds to one carbon atom.[10] Therefore, to date, only one zinc derivative, which was prepared by a rather complex reaction, has been reported.[11]

The reaction of an excess of diethylzinc with bis(2-pyridylmethyl)amine in toluene yields **2** (Scheme 1). The first



Scheme 1. Proposed mechanism for the formation of **2**

reaction step is the zincation of $(2\text{-pyCH}_2)_2$NH, the resulting compound **A** was identified by NMR spectroscopy.[12] Heating of this reaction solution under reflux for more than twenty hours led to the C–C coupling product **B** under elimination of zinc metal. The excess of dialkylzinc metalated the intermediate **B** at the endocyclic CH moieties giving compound **C** and ethane. Finally, a subsequent deamination (rearrangement) reaction gives **2**. A complex similar to **B** which has $AlMe_2$ fragments instead of the ZnEt moieties has been observed by Trepanier and Wang[13] as a minor dark-brown product in the reaction of $AlMe_3$ and $(2\text{-pyCH}_2)_2$NH. However, a concise mechanism for its formation was not proposed.

The protolysis of **2** with acetamide led to a nearly quantitative formation of *cis*-1,2-dipyridylaminoethene (**1**). The NMR spectroscopic parameters of **1**[3] and **2** (Table 1) differ remarkably little. This observation can be understood by taking into account that in both compounds the eneamine tautomer is formed and stabilized by N···Zn (**2**) and N···H (**1**) contacts to the pyridyl moieties, respectively.

Table 1: NMR spectroscopic data for **2** (solvent: $[D_8]$THF).[a]

Assignment	^{1}H NMR δ[ppm]	^{13}C{^{1}H} NMR δ[ppm]
δ(pyr 1)	8.23, 7.84–7.80	146.6, 145.9
δ(pyr 2)	7.08–7.01, 6.26	120.5, 111.6
δ(pyr 3)	7.51, 7.08–7.01	138.1, 134.6
δ(pyr 4)	7.84–7.80, 6.67	123.0, 122.5
δ(pyr 5)	–	161.0, 158.9
δ(CH)	5.84	91.0
$\delta(C_q)$	–	128.7
$\delta(NH_2)$	–	–
$\delta(ZnCH_2CH_3)$	0.30	−1.9
$\delta(ZnCH_2CH_3)$	1.25	12.9

[a] The assignment of the pyridyl (pyr) resonances signals to a specific pyridyl group was not possible.

The asymmetric unit of **2** is represented in Figure 1. The zinc atoms are both bonded to the imide nitrogen atom N2 and fixed by additional bonds to the pyridyl bases which leads

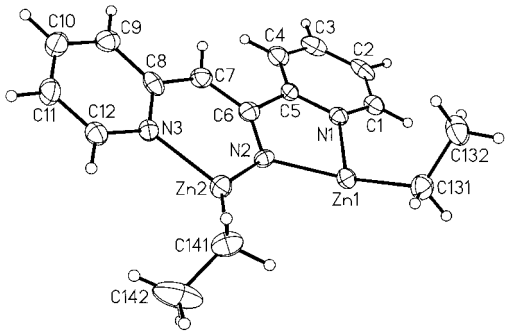


Figure 1. Molecular structure of **2**. Thermal ellipsoids set at 30% probability, the H atoms are drawn with arbitrary radii. Selected bond lengths [pm]: Zn1-N1 209.0(5), Zn1-N2 200.0(4) (Zn1-N2′ 225.4(4)), Zn1-C131 198.1(6), Zn2-N2 192.5(5), Zn2-N3 204.9(4), Zn2-C141 197.4(8), N2-C6 134.2(7), N1-C1 132.4(7), N1-C5 133.3(7), C1-C2 138(1), C2-C3 140(1), C3-C4 136.3(9), C4-C5 134.9(8), C5-C6 156.6(8), C6-C7 138.1(8), C7-C8 141.7(8), C8-C9 141.5(8), C9-C10 136.4(9), C10-C11 136(1), C11-C12 133.7(8), N3-C8 136.9(7), N3-C12 135.9(7).

to a nearly planar molecule. In the solid state **2** is a dimer (Figure 2) with a crystallographically imposed C_2 axis ($-x$, $-y$, z).

In **1** an isolated eneamine fragment with characteristic C–C single bonds to the attached pyridyl fragments was found[3] whereas in **2** the ligand's anionic charge is partly delocalized within the neighboring pyridyl moiety (Scheme 2). The consequence of the delocalization is a shortening of the C6–N2 bond of the imide moiety (**1**: 137.8(6) pm;[3] **2**: 134.2(7) pm) and a lengthening of the adjoining C6–C7 double bond (**1**: 129.5(6) pm;[3] **2**: 138.1(8) pm). The C7-C8 bond length of **2** is 141.7(8) pm which supports a multiple-

 © 2005 Wiley-VCH Verlag GmbH & Co. KGaA, Weinheim

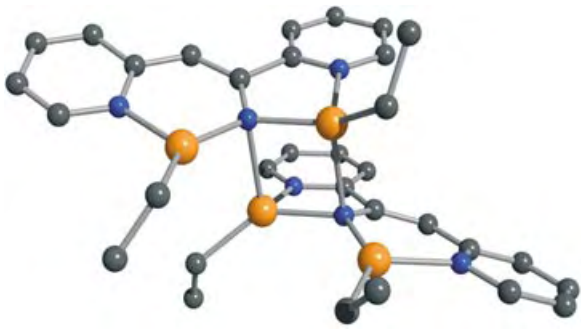
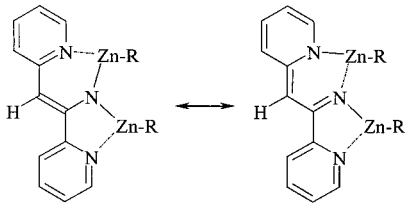


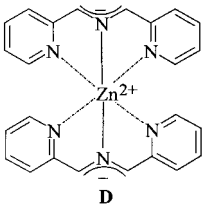
Figure 2. Perspective representation of dimeric **2** (Zn orange, N blue, C black). The hydrogen atoms are omitted for clarity.



Scheme 2. Mesomeric forms of **2**.

bond character and a delocalization of the anionic charge into the pyridyl moiety. This situation weakens the aromaticity of this pyridyl ligand which gives rise to bond lengthening within this heterocycle (N3, C8–C12).

Owing to the dimer formation in which Zn1 and N2 are the bridging atoms the zinc atom Zn1 is four-coordinate whereas Zn2 is in a distorted trigonal planar environment. Owing to the additional electrostatic attraction the Zn1–N2 and Zn2–N2 bond lengths to the imide function are smaller than the Zn1–N1 and Zn2–N3 values of the pyridyl substituents. The intermolecular Zn1–N2′ separation of 225.4(4) pm is large and can be interpreted as an interaction between the occupied nitrogen-centered p orbital with the empty p orbital at the zinc atom. The trans-annular nonbonding Zn1···Zn1′ separation is 290.4(1) pm whereas the Zn1···Zn2′ separation is larger (305.24(9) pm).



Scheme 3. Schematic representation of **D**.

The reaction conditions, such as temperature, substituents at N, and stoichiometry play a key role during the formation of **2**. At low temperatures the C–C coupling reaction is extremely slow and **D** (Scheme 3) forms from **A** in an unstirred toluene solution.[14] At elevated temperatures the C–C coupling reaction is favored and **2** becomes the major product.

Experimental Section

All manipulations were carried out in an anhydrous argon atmosphere. The solvents were thoroughly dried and distilled under argon.

Synthesis of **2**: Diethylzinc in n-hexane (20 mL of a 1.0 M solution, 20 mmol) was added slowly to a solution of bis(2-pyridylmethyl)-amine (1.8 mL; 10.0 mmol) in toluene (20 mL). The solution turned red-brown. After stirring at room temperature for 1 day the solution was heated under reflux for 22 h. During this time zinc metal precipitated. The hot solution was filtered and the filtrate collected and cooled to room temperature. Then the volume was reduced to a few milliliters. At room temperature 1.24 g of red prisms of **2** (3.2 mmol, 32 %) precipitated. M.p. 264 °C. Elemental analysis calcd (%) for $C_{16}H_{19}N_3Zn_2$, 384.12 g mol^{-1}: C 50.03, H 4.99, N 10.94; found C 50.16, H 4.99, N 10.74. MS (EI, *m*/*z*): 383 (M^+–H, 2), 355 (383-Et, 14). NMR data see Table 1.

Crystal data for **2**:[15] red cubes, $C_{16}H_{19}N_3Zn_2$, $M_r = 384.08$, orthorhombic, space group *Fdd*2 (no. 43), $a = 1339.73(7)$, $b = 4211.6(2)$, $c = 1150.00(5)$ pm, $V = 6.4888(5)$ nm^3, $\rho_{calcd} = 1.573$ g cm^{-3}, $\mu(Mo_{K\alpha}) = 2.953$ mm^{-1}, $Z = 16$ (8 dimers), 5736 reflections were collected on a Siemens P4 diffractometer with a CCD area detector at 193(2) K using graphite monochromated $Mo_{K\alpha}$ radiation, 1797 independent reflections ($R_{int} = 0.0490$), 196 refined parameters, $wR_2 = 0.0743$ (on F^2), $R1 = 0.0293$ (on 1748 reflections with $I > 2\sigma(I)$), $s = 1.079$, residual electron density 426/–332 e nm^{-3}.

Received: July 19, 2004

Keywords: anions · C–C coupling · imides · metalation · zinc

[1] M. Westerhausen, T. Bollwein, N. Makropoulos, T. M. Rotter, T. Habereder, M. Suter, H. Nöth, *Eur. J. Inorg. Chem.* **2001**, 851–857.
[2] M. Westerhausen, T. Bollwein, N. Makropoulos, S. Schneiderbauer, M. Suter, H. Nöth, P. Mayer, H. Piotrowski, K. Polborn, A. Pfitzner, *Eur. J. Inorg. Chem.* **2002**, 389–404.
[3] M. Westerhausen, T. Bollwein, P. Mayer, H. Piotrowski, A. Pfitzner, *Z. Anorg. Allg. Chem.* **2002**, *628*, 1425–1432.
[4] a) H. Tani, N. Oguni, *J. Polym. Sci. Part B* **1969**, *7*, 769–773; b) N. Oguni, H. Tani, *J. Polym. Sci.* **1973**, *11*, 573–586; for an example of zinc compounds in catalysis see: D. J. Darensbourg, M. W. Holtcamp, *Coord. Chem. Rev.* **2004**, *153*, 155–174.
[5] M. M. Olmstead, W. J. Grigsby, D. R. Chacon, T. Hascall, P. P. Power, *Inorg. Chim. Acta* **1996**, *251*, 273–284.
[6] M. Westerhausen, T. Bollwein, A. Pfitzner, T. Nilges, H.-J. Deiseroth, *Inorg. Chim. Acta* **2001**, *312*, 239–244.
[7] a) T. Hascall, K. Ruhlandt-Senge, P. P. Power, *Angew. Chem.* **1994**, *106*, 350–351; *Angew. Chem. Int. Ed. Engl.* **1994**, *33*, 356–357; b) T. Hascall, M. M. Olmstead, P. P. Power, *Angew. Chem.* **1994**, *106*, 1056–1057; *Angew. Chem. Int. Ed. Engl.* **1994**, *33*, 1000–1001; c) W. J. Grigsby, T. Hascall, J. J. Ellison, M. M. Olmstead, P. P. Power, *Inorg. Chem.* **1996**, *35*, 3254–3261.
[8] F. Bickelhaupt in *Grignard Reagents: New Developments* (Ed.: H. G. Richey), Wiley, Chichester, **2000**, chap. 11, pp. 367–393.
[9] A. Maercker in *Lithium Chemistry: A Theoretical and Experimental Overview* (Eds.: A.-M. Sapse, P. v. R. Schleyer), Wiley, New York, **1995**, chap. 11, pp. 477–577.
[10] T. Bollwein, M. Westerhausen, A. Pfitzner, *Z. Naturforsch. B* **2003**, *58*, 493–495.
[11] P. C. Andrews, C. L. Raston, B. W. Skelton, A. H. White, *Organometallics* **1998**, *17*, 779–782.
[12] M. Westerhausen, A. N. Kneifel, I. Lindner, J. Grèiæ, H. Nöth, *Z. Naturforsch. B* **2004**, *59*, 161–166.
[13] S. J. Trepanier, S. Wang, *Can. J. Chem.* **1996**, *74*, 2032–2040.
[14] M. Westerhausen, A. N. Kneifel, *Inorg. Chem. Commun.* **2004**, *7*, 763–766.
[15] CCDC-244839 (**2**) contains the supplementary crystallographic data for this paper. These data can be obtained free of charge via www.ccdc.cam.ac.uk/conts/retrieving.html (or from the Cambridge Crystallographic Data Centre, 12 Union Road, Cambridge CB21EZ, UK; fax: (+44) 1223-336-033; or deposit@ccdc.cam.ac.uk).

 © 2005 Wiley-VCH Verlag GmbH & Co. KGaA, Weinheim

Lewis Acids in Organic Synthesis

Alkyl Aluminum Halide Promoted Intramolecular Cyclization of ω-Allyl-cycloalk-2-enones: Access to Bridged Bi- and Tricyclic Compounds

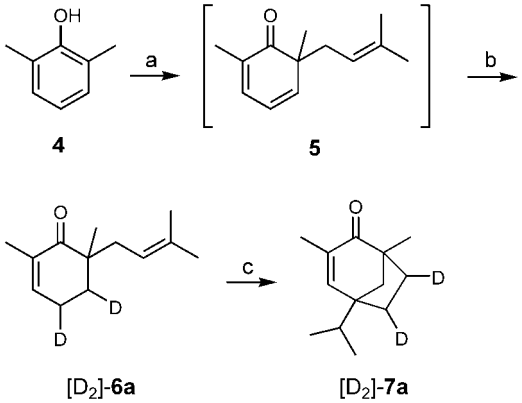
Andreas Goeke, Daniel Mertl, and Gerhard Brunner*

Dedicated to Professor Günter Helmchen

The cationic cyclization of olefins has been developed as an important methodology in organic synthesis.[1] Since Stork and Burgstahler and Eschenmoser et al. rationalized the proton-catalyzed biological cyclization of polyprenoids,[2] a variety of different initiators of this and related reactions have been developed.[3] Intramolecular Lewis acid promoted conjugate additions of olefins to α,β-unsaturated ketones or aldehydes belong to this category,[4] although, depending on the Lewis acid, the course of such cyclizations can be different. Snider et al. demonstrated that cyclohexenone **1** reacted in the presence of $SnCl_4$ to compound **2** which is the product of a concerted Lewis acid induced ene reaction,[5] while treatment of **1** with two equivalents of $MeAlCl_2$ (or $EtAlCl_2$) resulted in naphthalenone **3** (Scheme 1).[6] It was deduced that this compound was generated by two consecutive 1,2-H shifts of zwitterionic intermediates **A** and **B** rather than by one 1,3-H shift as the relative configuration of the stereogenic centers C4a and C8 was determined to be *anti*.

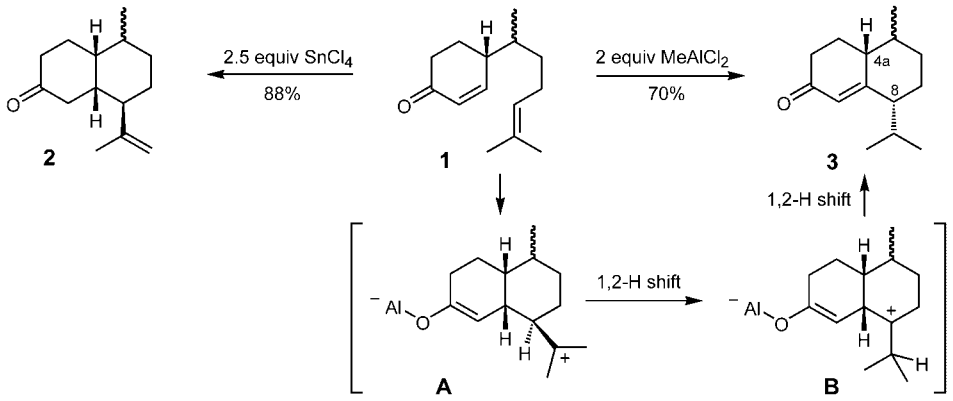
This unique behavior of alkyl aluminum halides as Lewis acids was partially explained by their Brønsted base-like character: Any adventitious water will be scavenged by forming an alkane and a new Lewis acid.[7]

While investigating novel syntheses of functionalized odorants,[8] we observed a novel and unexpected $EtAlCl_2$ promoted cyclization of cyclohexenone **6a** to bicyclo[3.2.1]octenone **7a** (see Table 1, entry 1) which displays a pleasant woody vetiver-like odor.[9] To better understand this reaction, labeled substrate [D_2]-**6a** was prepared by a selective deuteration of unstable trienone **5**[10] which was accessible by C-alkylation of phenol **4** (Scheme 2).[11] After cyclization,



Scheme 2. Synthesis of [D_2]-**7a** by deuteration of trienone **5**. Conditions: a) NaH, toluene, prenyl chloride; b) MeOH, Pd/C, D_2; c) 1.5 equiv $EtAlCl_2$, toluene.

the overall deuterium incorporation of [D_2]-**6a** was retained in [D_2]-**7a**, which indicates a) the methylene-bridge in **7a** stems from the prenyl group and b) the deuterated positions of the cyclohexenone unit of **6a** are not the locations of intermediate zwitterions.



Scheme 1. Ene reaction versus cationic cyclization of **1**.[6]

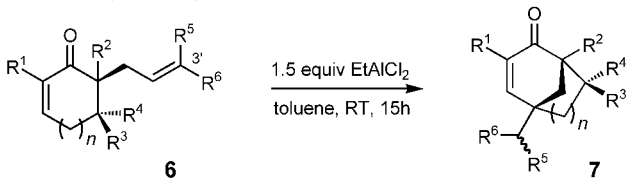
[*] Dr. A. Goeke, D. Mertl, Dr. G. Brunner
Givaudan Schweiz AG, Fragrance Research
Überlandstrasse 138
8600 Dübendorf (Switzerland)
Fax (+41) 44-824-2926
E-mail: andreas.goeke@givaudan.com

Supporting information for this article is available on the WWW under http://www.angewandte.org or from the author.

Further investigation (Table 1) revealed that the cyclization tolerates cycloalkenones of different substitution at R^1–R^6 and also of different ring sizes, although yields decrease with increasing steric strain (entries 3,4) and increasing ring size (entries 8,9). Additional unsaturation in substituents R^2,R^4, and R^6 (entries 5,6,7) neither disturbed the cationic cyclization, nor was a competitive or subsequent cyclization observed in these cases.[12] The yields dramatically decreased

 DOI: 10.1002/anie.200461207 © 2005 Wiley-VCH Verlag GmbH & Co. KGaA, Weinheim

Table 1: Cyclization of allyl cycloalkenones **6** to bicyclic compounds **7**.



6 **7**

Entry	R^1	R^2	R^3	R^4	R^5	R^6	*n*	d.r.	Product [%][a]
1	Me	Me	H	H	Me	Me	1	-	**7a** 95
2	Me	H	H	H	Me	Me	1	-	**7b** 86
3	Me	H	Me	Me	Me	Me	1	-	**7c** 67
4	Me	Me	H	H	Me	*c*-C_6H_{13}	1	-	**7d** 54
5	Me	Me	H	H	Me	$CHC(CH_3)_2$	1	1.6:1	**7e** 90
6	Me	prenyl	H	H	Me	Me	1	-	**7f** 75
7	Me	H	H	$C(CH_2)CH_3$	Me	Me	1	7:3[b]	**7g** 71
8	H	H	H	H	Me	Me	2	-	**7h** 64
9	H	H	H	H	Me	Me	3	-	**7i** 45
10	Me	Me	H	H	H	Me	1	-	**7j** 30[c]
11	Me	Me	H	H	Me	$(CH_2)_2CO_2Me$	1	1.5:1	**7k** 86[c,d]

[a] Products isolated by chromatography. [b] *Endo:exo*-isomers at 7-position. [c] Reaction was carried out at 80 °C. [d] 3 equiv $EtAlCl_2$, 8 h.

with R^5 or $R^6 = H$, which reflects the necessity of cation stabilization at the 3′ position of the allylic substituent in ketone **6** (Table 1, entry 10). Entry 11 shows that an additional ester group in substrate **6k** consumes at least one equivalent of the Lewis acid by a competitive complexation, although esters were shown to be less basic than ketones.[13]

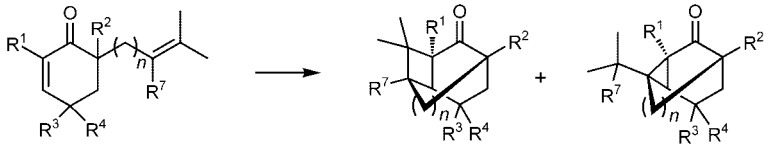
The outcome of the cyclization does change completely with different substitution patterns of ketones **8**[10] (Table 2). In these cases, mixtures of tricyclic compounds **9** and **10** were usually obtained, in ratios not very much influenced by varying steric demand of the substituents R^3 and R^4. However, cyclization of compound **8a** (R^3, $R^4 = H$) led to a mixture of **9a** and **11a** (see Scheme 3) while the transformation of homoallylic derivative **8f** provided compound **10f** exclusively.

These observations are in accordance with the proposed mechanism in Scheme 3. It can be explained by a sequence of 1,2-H and alkyl shifts that were proposed by Snider et al.[6,7]

The conversion of compounds **6** (and **8a**) follows path A. The initially formed zwitterion results from cyclization of the enone–$EtAlCl_2$ complex with the allyl side chain being in an *s-trans* conformation. Subsequent 1,2-H (or methyl) shift followed by intramolecular alkyl migration generates compounds **7** (**11a**). In path B, the allyl side chain of compounds **8** may be sterically (R^3,R^4 = alkyl, $R^7 = Me$) pushed into a *s-cis* conformation which gives, after the initial cyclization, the cation close to the enolate. This effect may also be caused by angular strain that occurs during the cyclization of homoallylic derivative **8f**. The quenching of charges in the zwitterionic intermediate at this stage results in compounds **9**. However, the 1,2-R^7 shift is rapid enough to allow path B to be partially terminated by the formation of compounds **10**.

In summary, the novel $EtAlCl_2$-induced cyclization of 6-allyl cyclohexenones is a flexible tool for the synthesis of bi- and tricyclic compounds. The scope and limitations were investigated with respect to substitution patterns.

Table 2: Cyclization of cyclohexenones **8** to tricyclic compounds **9**, **10**, and **11**.

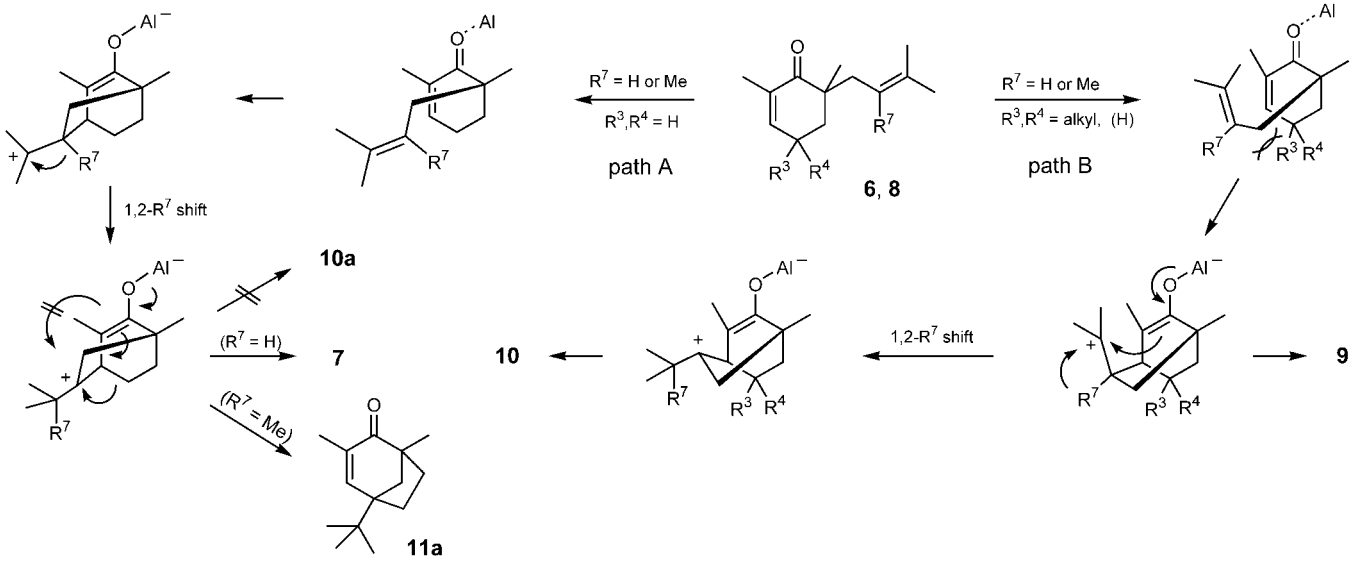


8 **9** **10**

Entry	Compound	R^1	R^2	R^3	R^4	R^7	*n*	Ratio	Yield [%][a]
1	**8a**	Me	Me	H	H	Me	1	**9a**:**11a**[b] (1:1)	61
2	**8b**	H	Me	Me	Me	H	1	**9b**:**10b** (1.4:1)	74
3	**8c**	Me	Me	Me	Me	Me	1	**9c**:**10c** (1:1.4)	52
4	**8d**	H	Me	$CH_2(CH_2)_3CH_2$		H	1	**9d**:**10d** (1.1:1)	78
5	**8e**	Me	Me	$CH_2(CH_2)_2CH_2$		H	1	**9e**:**10e** (1.5:1)	86
6	**8f**	Me	Me	H	H	H	2	only **10f**	60

[a] Products isolated by chromatography. [b] For compound **11a** see Scheme 3; **10a** was not detected.

 © 2005 Wiley-VCH Verlag GmbH & Co. KGaA, Weinheim

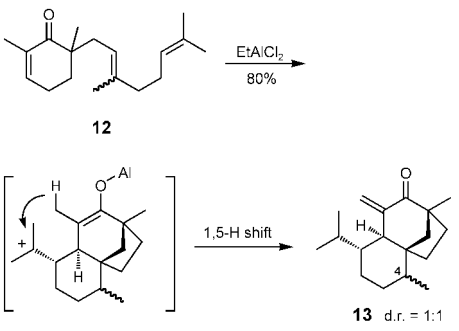


Scheme 3. Mechanistic considerations.

Received: July 6, 2004
Revised: August 13, 2004

Keywords: aluminum · cyclization · hydride shifts · Lewis acids · rearrangement

[1] T.-L. Ho in *Carbocycle Construction in Terpene Synthesis*, Wiley-VCH, Weinheim, **1987**, pp. 256 – 328.
[2] a) G. Stork, A. W. Burgstahler, *J. Am. Chem. Soc.* **1955**, *77*, 5068; b) A. Eschenmoser, L. Ruzicka, O. Jeger, D. Arigoni, *Helv. Chim. Acta* **1955**, *38*, 1890.
[3] a) W. S. Johnson, *Angew. Chem.* **1976**, *88*, 33; *Angew. Chem. Int. Ed. Engl.* **1976**, *15*, 9; b) for a recent example see: K. Ishihara, H. Ishibashi, H. Yamamoto, *J. Am. Chem. Soc.* **2002**, *124*, 3647, and references therein.
[4] Some classical cycloalkylations of enones: a) J. L. Cooper, K. E. Harding, *Tetrahedron Lett.* **1977**, *18*, 3321; b) P. Naegeli, M. Wetli, *Tetrahedron* **1981**, *37*, 247.
[5] For reviews of the Lewis acid mediated ene reaction see: a) W. Oppolzer, V. Snieckus, *Angew. Chem.* **1978**, *90*, 506; *Angew. Chem. Int. Ed. Engl.* **1978**, *17*, 476; b) B. B. Snider, *Acc. Chem. Res.* **1980**, *13*, 426; c) M. Santelli, J.-M. Pons, *Lewis Acids and Selectivity in Organic Synthesis*, CRC, Boca Raton, **1996**, pp. 21 – 90.
[6] B. B. Snider, D. J. Rodini, J. van Straten, *J. Am. Chem. Soc.* **1980**, *102*, 5872.
[7] a) B. B. Snider, D. J. Rodini, M. Karras, T. C. Kirk, E. A. Deutsch, R. Cordova, R. T. Price, *Tetrahedron* **1981**, *37*, 3927; b) B. B. Snider, M. Karras, R. T. Price, D. J. Rodini, *J. Org. Chem.* **1982**, *47*, 4538.
[8] For a recent review of fragrance chemistry see: P. Kraft, J. A. Bajgrowicz, C. Denis, G. Fráter, *Angew. Chem.* **2000**, *112*, 3106; *Angew. Chem. Int. Ed.* **2000**, *39*, 2980.
[9] The odor descriptions of compounds **7**, **8**,and **10** are given in the Supporting Information.
[10] Selective hydrogenation of trienones **5** to compounds **6** and **8**: A. Goeke (Givaudan Schweiz AG) EP 1213276, **2002**[Chem. Abstr. **2002**, *137*, 19737].
[11] For C-alkylation of phenols see: H. Greuter, H. Schmid, G. Fráter, *Helv. Chim. Acta* **1977**, *60*, 1701.
[12] A single case of a domino-cyclization of geranylcyclohexenone **12** to tricyclic ketone **13** was observed. The terminating step is a 1,5-hydride shift leading to an exo-methylene group [Eq. (1)].



(1)

[13] I. R. Hunt, C. R. Rogers, S. Woo, A. Rauk, B. A. Keay, *J. Am. Chem. Soc.* **1995**, *117*, 1049.

 © 2005 Wiley-VCH Verlag GmbH & Co. KGaA, Weinheim

Hybrid Carbenes

Imidazoline-Functionalized Diphosphines: Models for N-Heterocyclic Carbene–Diphosphinocarbene Coupling**

Javier Ruiz, Marta E. G. Mosquera, Gabriel García, Fernando Marquínez, and Víctor Riera*

N-Heterocyclic carbenes **I** derived from imidazol-2-ylidene, also referred to as Arduengo carbenes, are important compounds whose isolation as stable, free molecules has greatly contributed to the development of carbene chemistry in recent years.[1] They show no tendency to dimerize to afford tetraazafulvalenes **II**, except under special circumstances,[2] unlike the corresponding saturated N-heterocyclic carbenes. In contrast, related diphosphinocarbenes **III** are not isolable, and have been reported in the literature only as transient species,[3,4] whereas their corresponding dimers **IV** are known to be stable.[5] As far as we are aware, no example of coupling of both types of carbenes (**V** in Figure 1) has been described.

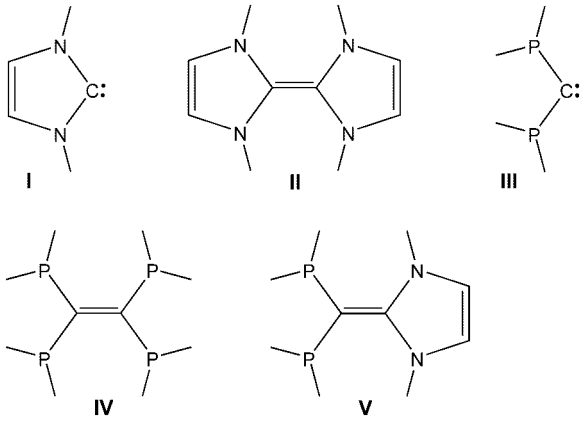


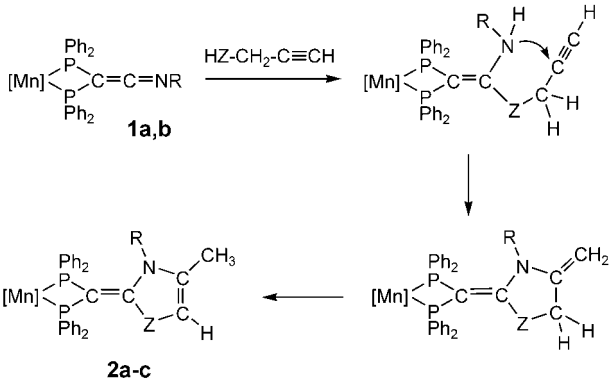
Figure 1. Schematic representation of imidazol-2-ylidenes and diphosphinylcarbenes, and their coupling products.

We report here the metal-assisted synthesis of new diphosphine ligands bearing an imidazoline residue that can serve as models of N-heterocyclic carbene–diphosphinocarbene coupling. The synthesis of analogous oxazoline-functionalized diphosphines is also described.

[*] J. Ruiz, G. García, F. Marquínez, V. Riera
Departamento de Química Orgánica e Inorgánica
Facultad de Química, Universidad de Oviedo
Oviedo (Spain)
Fax: (+34) 98-5103-446
E-mail: jruiz@fq.uniovi.es
M. E. G. Mosquera
Departamento de Química Inorgánica
Edificio de Farmacia, Universidad de Alcalá
Alcalá de Henares (Spain)

[**] This work was supported by the Spanish Ministerio de Ciencia y Tecnología (PGE and FEDER funding, Project BQU2003-01011) and by the Principado de Asturias (Project PR-01-GE-7).

The diphosphinoketenimine ligand coordinated in the cationic complex $[Mn(CO)_4\{(PPh_2)_2C{=}C{=}NPh\}]^+$ (**1a**)[6] reacts with propargylamine in refluxing toluene to afford **2a** (Scheme 1), which is a diphosphine complex containing an



Scheme 1. Proposed mechanism for the formation of complexes **2a–c**. [Mn] = $[Mn(CO)_4]^+$. **1a**: R = Ph; **1b**: R = *p*-tolyl. **2a**: R = Ph, Z = NH; **2b**: R = Ph, Z = O; **2c**: R = *p*-tolyl, Z = NMe.

imidazoline functionality. This complex is formed in a cycloaddition process involving the ketenimine fragment of the ligand. This result is in sharp contrast to the reaction of free diphosphinoketenimines with propargylamines, which affords phosphinine derivatives due to the additional involvement of a phosphorus atom in the cycloaddition process.[7] As proposed in Scheme 1, a likely mechanism for the formation of **2a** implies, in a first step, nucleophilic attack of the amine to the ketenimine to afford an enediamine derivative. Then, a 5-*exo*-dig addition of the phenylamino moiety to the alkyne leads to the formation of an imidazolidine cycle, which is converted into the corresponding imidazoline residue by a 1,3 proton shift from the endocyclic methylene group to the exocyclic one. This results in a change of the C=C bond position and the formation of a conjugated six-π-electron system. The reaction of **1a** with propargyl alcohol proceeds similarly to give the corresponding diphosphine complex **2b** bearing an oxazoline functionality (Scheme 1).

It is well known that the reaction of ketenimines with amines and alcohols usually gives the corresponding amidine and imidate derivatives, respectively.[8] However, as far as we are aware, no reaction of organic ketenimines with propargylic amines or alcohols has been reported thus far. The reaction described here therefore represents a completely new method for the formation of imidazoline and oxazoline functionalities by a new cyclization process.

The spectroscopic data of **2a**,**b** (see the Experimental Section) are in agreement with the proposed formulation. Moreover, their solid-state structures were confirmed by X-ray analysis (Figure 2 and Figure 3).[9] The most important feature in the structures of **2a** and **2b** is the presence of the imidazoline and oxazoline cycle, respectively, which is coplanar with the PCP skeleton of the diphosphane. The C1–C2 bond lengths in **2a** (1.429(4) Å) and **2b** (1.385(6) Å) are, to varying degrees, intermediate between single and double bonds, as are the P1–C1 and P2–C1 distances and the

 © 2005 Wiley-VCH Verlag GmbH & Co. KGaA, Weinheim DOI: 10.1002/anie.200461120

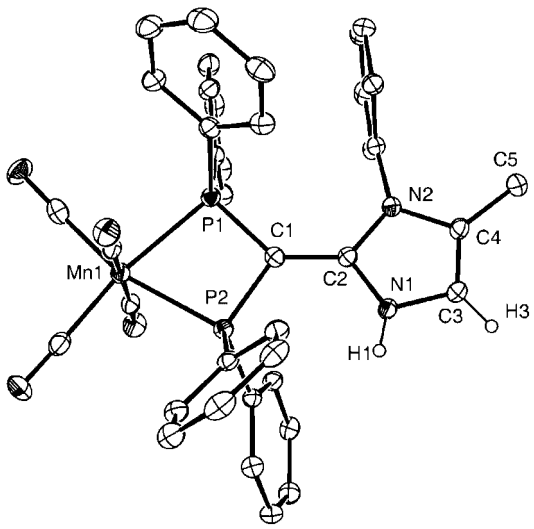


Figure 2. A view of the structure of the cation of **2a**. Selected bond lengths [Å] and angles [°]: P1-C1 1.749(3), P2-C1 1.761(3), C1-C2 1.429(4), N1-C2 1.342(3), N1-C3 1.382(4), N2-C2 1.371(3), N2-C4 1.416(3), C3-C4 1.333(4); P1-Mn-P2 69.84(2), P1-C1-P2 99.23(13), N1-C2-N2 105.4(2), N1-C2-C1 125.0(2), N2-C2-C1 129.5(2).

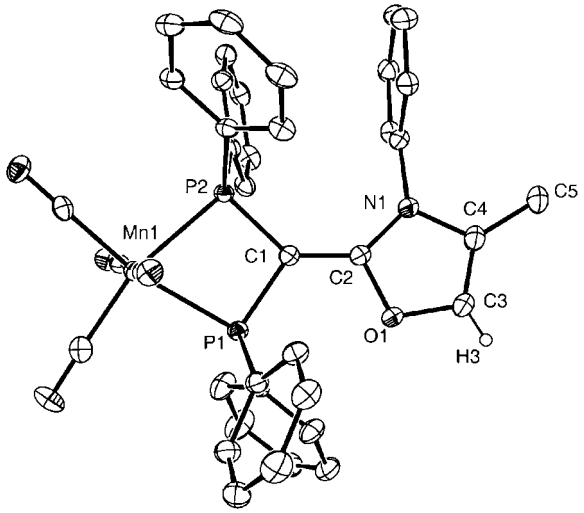


Figure 3. A view of the structure of the cation of **2b**. Selected bond lengths [Å] and angles [°]: P1-C1 1.781(4), P2-C1 1.770(4), C1-C2 1.385(6), N1-C2 1.338(6), N1-C4 1.422(5), O1-C2 1.364(5), O1-C3 1.398(6), C3-C4 1.335(7); P1-Mn-P2 71.09(4), P1-C1-P2 99.7(2), N1-C2-O1 107.9(3), N1-C2-C1 135.4(4), O1-C2-C1 116.7(4).

different interatomic distances in the imidazoline and oxazoline cycles (see the legends for Figure 2 and Figure 3). These data are consistent with a bond description in the diphosphine ligand resulting from the contribution of two resonance structures, as illustrated in Figure 4 for the imidazoline case (olefinic form **a** and imidazolium ylide form **b**). Obviously, in the ylidic form the negative charge of the diphosphinomethanide fragment is stabilized by charge delocalization through the metallacycle, whereas the positive one is stabilized by π-donation from the nitrogen lone-pairs. If we consider complexes **2a** and **2b** as models for carbene–carbene coupling, the structural data described here are in agreement with the well-

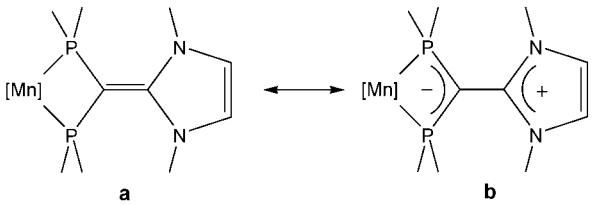


Figure 4. Resonance structures of imidazoline-functionalized diphosphane complexes. [Mn] = $[Mn(CO)_4]^+$.

known nucleophilic character of N-heterocyclic carbenes[10] and the electrophilic character of transient metalladiphosphinocarbenes,[11] whose coupling should lead to a net charge-transfer from the former to the latter, thus justifying the contribution of structure **b** in Figure 4. The IR spectra of **2a** and **2b** in the ν_{CO} region (see the Experimental Section), which show absorptions at values intermediate between those of diphosphine complexes and diphosphinomethanide derivatives,[12] support the above interpretation and indicate that the new diphosphines are strongly basic. Note that these absorptions occur at lower frequency in **2a** than in **2b**. This reflects the fact that the imidazoline fragment is a better electron donor than the oxazoline fragment, which also explains why the C1–C2 bond in **2b** is shorter than that in **2a**.

The $^{31}P\{^1H\}$ NMR spectra of **2a**,**b** at room temperature in CD_2Cl_2 show a single resonance, which suggests free rotation around the C1–C2 bond. For **2a**, this single signal is maintained when the spectrum is recorded at −80 °C, whereas it splits into two resonances, corresponding to the two inequivalent phosphorus atoms, in the case of **2b**. This observation agrees with the proposal outlined above that C1–C2 bond in **2b** has higher multiple-bond character than in **2a**.

Substituted propargylamine also reacts with coordinated diphosphinoketenimines in a similar manner. Thus, reaction of $[Mn(CO)_4\{(PPh_2)_2C{=}C{=}N\text{-}p\text{-tolyl}\}]^+$ (**1b**) with methylpropargylamine affords **2c** (Scheme 1), whose spectroscopic data are similar to those of **2a**. However, the structural data derived from the X-ray analysis (Figure 5) show appreciable changes that deserve comment. Thus, the plane of the imidazoline ring in **2c** is orthogonal to the PCP plane, with the methyl substituent of the nitrogen atom apparently locked between two phenyl groups of different phosphorus atoms. Consequently, the C1–C2 bond in **2c** (1.461(9) Å) is clearly longer than in **2a** (1.429(4) Å) and **2b** (1.385(6) Å), which suggests that the imidazolium ylide resonance form is dominant for **2c**.

The structural and spectroscopic data of complexes **2a–c** discussed above allow us to conclude that the degree of charge transfer from the five-membered heterocycle to the metallacycle through the C1–C2 bond, and therefore the basicity of the new diphosphines, can be modulated by changing either the heteroatoms in the cycle (imidazoline or oxazoline), the substituents at these heteroatoms, or the extent of molecular motion around the C1–C2 bond.

To summarize, we have described a new cycloaddition reaction for the formation of imidazoline and oxazoline functionalities, which consists of the treatment of coordinated

 © 2005 Wiley-VCH Verlag GmbH & Co. KGaA, Weinheim

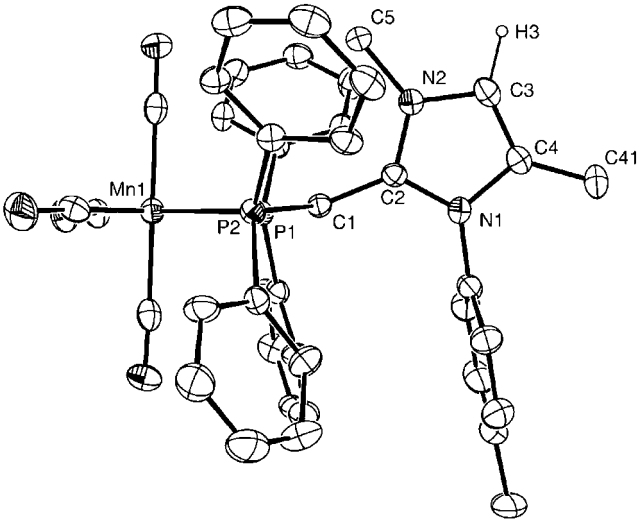


Figure 5. A view of the structure of the cation of **2c**. Selected bond lengths [Å] and angles [°]: P1-C1 1.755(7), P2-C1 1.744(7), C1-C2 1.461(9), N1-C2 1.351(8), N1-C4 1.404(9), N2-C2 1.346(8), N2-C3 1.385(9), C3-C4 1.356(9); P1-Mn-P2 69.90(7), P1-C1-P2 99.9(), N1-C2-N2 105.9(6), N2-C2-C1 124.9(6), N1-C2-C1 129.2(6).

diphosphinoketenimines with propargylamines or propargyl alcohol. The resulting functionalized diphosphine ligands can be considered as models for the coupling of either N-heterocyclic carbenes or N,O-heterocyclic carbenes with diphosphinocarbenes. These models raise the experimental challenge of coupling imidazol-2-ylidenes (Arduengo-type carbenes) with phosphinocarbenes (Bertrand-type carbenes) to yield new types of electron-rich olefins, which should behave as strongly basic phosphines.

Experimental Section

All reactions and manipulations were performed under an atmosphere of dry nitrogen by using standard Schlenk techniques. Solvents were distilled from appropriate drying agents under dry nitrogen prior to use. Chemical shifts of the NMR spectra are referenced to internal $SiMe_4$ (^1H and ^{13}C) or external H_3PO_4 (^{31}P).

2a·ClO_4: $[Mn(CO)_4\{(PPh_2)_2C{=}C{=}NPh\}]ClO_4$ (**1a**·ClO_4; 0.05 g, 0.066 mmol) was dissolved in 20 mL of toluene, and $NH_2CH_2C{\equiv}CH$ (10 μL, 0.13 mmol) was added to this solution. The mixture was then refluxed for 30 min. Cooling the solution to room temperature led to the formation of yellow crystals that were suitable for X-ray analysis. Yield: 0.04 g, 76%. Elemental analysis (%) calcd for $C_{39}H_{30}ClMnN_2O_8P_2$: C 58.04, H 3.75, N 3.47; found: C 57.87, H 4.03, N 3.53; IR (CH_2Cl_2): $\tilde{\nu}$ = 2081(s), 2009 (sh), 1999 (vs), 1979 (s) cm^{-1}. ^1H NMR (300 MHz, CD_2Cl_2): δ = 8.28 (s, 1H, NH), 7.8–6.6 (m, 26H, Ph + =CH), 1.60 (s, 3H, CH_3) ppm; $^{31}P\{^1H\}$ NMR (121.5 MHz, CD_2Cl_2): δ = 3.7 (br) ppm.

2b·ClO_4: $HOCH_2C{\equiv}CH$ (20 μL, 0.33 mmol) was added to a solution of **1a**·ClO_4 (0.05 g, 0.066 mmol) in 10 mL of toluene. The mixture was then refluxed for 15 min. A solid precipitated out of the solution upon cooling, which was isolated and dried under vacuum. Crystals suitable for X-ray analysis were obtained from a mixture of $CHCl_3$ and hexane (1:1.5). Yield: 0.03 g, 57%. Elemental analysis (%) calcd for $C_{39}H_{29}ClMnNO_9P_2$: C 57.97, H 3.62, N 1.73; found: C 57.75, H 3.62, N, 1.58; IR (CH_2Cl_2): $\tilde{\nu}$ = 2083 (s), 2014 (s), 2001 (vs), 1985 (s) cm^{-1}. ^1H NMR (300 MHz, $CDCl_3$): δ = 6.6–8.0 (m, 26H, Ph + =CH), 1.26 (s, 3H, CH_3) ppm; $^{13}C\{^1H\}$ NMR (75.5 MHz, CH_2Cl_2/D_2O): δ = 8.1 (s, CH_3), 50.4 (t, $^1J_{C,P}$ = 47 Hz, P_2C), 156.8 (s, OCN), 212.3 (br, 4 × CO) ppm; $^{31}P\{^1H\}$ NMR (121.5 MHz, CD_2Cl_2): δ = 8.7 (br) ppm.

2c·ClO_4: $NH(CH_3)CH_2C{\equiv}CH$ (13 μL, 0.16 mmol) was added to a solution of $[Mn(CO)_4\{(PPh_2)_2C{=}C{=}N\text{-}p\text{-}tolyl\}]ClO_4$ (**1b**·ClO_4; 0.10 g, 0.13 mmol) in 40 mL of toluene. The mixture was then refluxed for 50 min. A solid precipitated out of the solution on cooling, which was isolated and dried under vacuum. Crystals suitable for an X-ray diffraction study were obtained from crystallization from a $CHCl_3$/hexane mixture (1:1.5). Yield: 0.09 g, 83%. Elemental analysis (%) calcd for $C_{41}H_{34}ClMnN_2O_8P_2$: C 58.97, H 4.10, N 3.35; found: C 59.09, H 4.08, N 3.58; IR (CH_2Cl_2): $\tilde{\nu}$ = 2079 (s), 2010 (m), 1990 (vs) cm^{-1}; ^1H NMR (300 MHz, $CDCl_3$): δ = 7.6–6.9 (m, 24H, Ph), 2.63 (s, 3H, NCH_3), 2.22 (s, 3H, $PhCH_3$), 1.91 (s, 3H, CH_3) ppm; $^{13}C\{^1H\}$ NMR (75.5 MHz, CH_2Cl_2/D_2O): δ = 11.7 (s, CH_3), 22.3 (s, $PhCH_3$), 27.7 (t, $^1J_{C,P}$ = 45 Hz, P_2C), 35.6 (s, NCH_3), 213 (s, 4 × CO) ppm; $^{31}P\{^1H\}$ NMR (121.5 MHz, $CDCl_3$): δ = 16.1 (br) ppm.

Received: June 29, 2004

Keywords: carbenes · cyclizations · manganese · nitrogen heterocycles · phosphines

[1] For recent reviews see: a) A. J. Arduengo, *Acc. Chem. Res.* **1999**, *32*, 913; b) D. Bourissou, O. Guerret, F. P. Gabbaï, G. Bertrand, *Chem. Rev.* **2000**, *100*, 39–91; c) W. A. Herrmann, *Angew. Chem.* **2002**, *114*, 1326; *Angew. Chem. Int. Ed.* **2002**, *41*, 1290.

[2] T. A. Taton, P. Chen, *Angew. Chem.* **1996**, *108*, 1098–1100; *Angew. Chem. Int. Ed. Engl.* **1996**, *35*, 1011–1013.

[3] a) A. Baceiredo, A. Igau, G. Bertrand, M. J. Menu, Y. Dartiguenave, J. J. Bonnet, *J. Am. Chem. Soc.* **1986**, *108*, 7868; b) M. Soleilhavoup, A. Baceiredo, G. Bertrand, *Angew. Chem.* **1993**, *105*, 1245; *Angew. Chem. Int. Ed. Engl.* **1993**, *32*, 1167.

[4] Their protonated phosphonium phosphinocarbene derivatives $[(R_2P)(R_2PH)C{:}]^+$ are known to be stable: M. Soleilhavoup, A. Baceiredo, O. Treutler, R. Ahlrichs, M. Nieger, G. Bertrand, *J. Am. Chem. Soc.* **1992**, *114*, 10959.

[5] D. M. Anderson, P. B. Hitchcock, M. F. Lappert, *J. Organomet. Chem.* **1989**, *363*, C7–C11.

[6] This complex was prepared by simple substitution of iodide by CO, in the presence of $AgClO_4$, in the compound *fac*-$[MnI(CO)_3\{(PPh_2)_2C{=}C{=}NPh\}]$: J. Ruiz, V. Riera, M. Vivanco, M. Lanfranchi, A. Tiripicchio, *Organometallics* **1998**, *17*, 3835.

[7] J. Ruiz, F. Marquínez, V. Riera, M. Vivanco, S. García-Granda, M. R. Díaz, *Chem. Eur. J.* **2002**, *8*, 3872–3878.

[8] a) "The Chemistry of Ketenes, Allenes and Related Compounds": M. W. Barker, W. E. McHenry, in *The Chemistry of Functional Groups*, *Part* 2 (Ed.: S. Patai), Interscience, New York, **1980**, chapter 17, pp. 701–720; b) G. Tennant, in *Comprehensive Organic Chemistry. The Synthesis and Reactions of Organic Compounds*, *Vol. 2* (Eds.: D. Barton, W. D. Ollis, I. O. Sutherland), Pergamon, Oxford, **1979**, pp. 21–527.

[9] Crystal data for **2a**·ClO_4 ($C_{39}H_{30}ClMnN_2O_8P_2$): M_r = 806.98, monoclinic, space group $P2_1/a$, a = 17.3936(5), b = 11.2150(3), c = 19.5595(6) Å, β = 106.637(2)°, V = 3655.73(18) Å^3, Z = 4, ρ_{calcd} = 1.466 g cm^{-3}, $F(000)$ = 1656, $Cu_{K\alpha}$ radiation (λ = 1.5418 Å), μ = 4.913 mm^{-1}; crystal dimensions 0.25 × 0.12 × 0.05 mm. Data collection was performed at 120(2) K on a Nonius Kappa CCD diffractometer. The structure was solved by direct methods and refined using full-matrix least-squares techniques on F^2. Non-hydrogen atoms were refined anisotropically. Hydrogen atoms were placed geometrically and left riding on their parent atoms, except for H1 and H3, which were found in the difference map and refined isotropically. The final cycle of full-matrix least-squares refinement based on 6890 reflections

 © 2005 Wiley-VCH Verlag GmbH & Co. KGaA, Weinheim

and 486 parameters converged to R_1 ($F^2 > 2\sigma(F^2)$) = 0.0426 and wR_2 ($F^2 > 2\sigma(F^2)$) = 0.1106. Crystal data for **2b**·(ClO_4)·$CHCl_3$ ($C_{40}H_{30}Cl_4MnNO_9P_2$): M_r = 927.33, triclinic, space group $P\bar{1}$, a = 11.1996(3), b = 11.9095(2), c = 16.1366(3) Å, α = 74.9480(10), β = 79.413(2), γ = 74.0010(10)°, V = 1983.34(7) Å^3, Z = 2, ρ_{calcd} = 1.553 g cm^{-3}, $F(000)$ = 944, $Cu_{K\alpha}$ radiation (λ = 1.5418 Å), μ = 6.438 mm^{-1}; crystal dimensions 0.32 × 0.30 × 0.10 mm. Data collection was performed at 120(2) K on a Nonius Kappa CCD diffractometer. The structure was solved by direct methods and refined using full-matrix least-squares techniques on F^2. All non-hydrogen atoms were refined anisotropically. Hydrogen atoms were placed geometrically and left riding on their parent atoms except for H3 and H1D, which were found in the difference map and refined isotropically. The final cycle of full-matrix least-squares refinement based on 7427 reflections and 523 parameters converged to R_1 ($F^2 > 2\sigma(F^2)$) = 0.0727 and wR_2($F^2 > 2\sigma(F^2)$) = 0.2075. Crystal data for **2c**·(ClO_4)·($CHCl_3$)$_2$ ($C_{43}H_{36}Cl_7MnN_2O_8P_2$): M_r = 1073.77, triclinic, space group $P\bar{1}$, a = 11.6701(16), b = 11.733(2), c = 18.812(3) Å, α = 107.144(10), β = 92.229(7), γ = 99.475(10)°, V = 2417.3(6) Å^3, Z = 2, ρ_{calcd} = 1.475 g cm^{-3}, $F(000)$ = 1092, $Cu_{K\alpha}$ radiation (λ = 1.5418 Å), μ = 6.843 mm^{-1}; crystal dimensions 0.17 × 0.10 × 0.03 mm. Data collection was performed at 200(2) K on a Nonius Kappa CCD diffractometer. The structure was solved by direct methods and refined using full-matrix least-squares techniques on F^2. All non-hydrogen atoms were refined anisotropically except for one oxygen atom in the counteranion, which is disordered over two positions. Hydrogen atoms were placed geometrically and left riding on their parent atoms, except for H3, H7, H8, H10, and H11, which were found in the difference map and refined isotropically. The final cycle of full-matrix least-squares refinement based on 7386 reflections and 590 parameters converged to R_1 ($F^2 > 2\sigma(F^2)$) = 0.0868 and wR_2($F^2 > 2\sigma(F^2)$) = 0.2437. CCDC-241569 (**2a**), -241570 (**2b**), and -241571 (**2c**) contain the supplementary crystallographic data for this paper. These data can be obtained free of charge via www.ccdc.cam.ac.uk/conts/retrieving.html (or from the Cambridge Crystallographic Data Centre, 12, Union Road, Cambridge CB21EZ, UK; fax: (+44) 1223-336-033; or deposit@ccdc.cam.ac.uk).

[10] Y. Kim, A. Streitwieser, *J. Am. Chem. Soc.* **2002**, *124*, 5757–5761, and references cited therein.

[11] J. Ruiz, M. E. G. Mosquera, G. García, E. Patrón, V. Riera, S. García-Granda, F. Van der Maelen, *Angew. Chem.* **2003**, *115*, 4915–4919; *Angew. Chem. Int. Ed.* **2003**, *42*, 4767–4771.

[12] IR (CH_2Cl_2) data for representative tetracarbonyl complexes of Mn^I are as follows: $\tilde{\nu}$[$Mn(CO)_4${$(PPh_2)_2CH_2$}]$^+$ = 2094 (m), 2027 (m), 2014 (s), 1999 (sh) cm^{-1}; $\tilde{\nu}$[$Mn(CO)_4${$(PPh_2)_2CH$}] = 2071 (m), 1990 (s), 1955 (m) cm^{-1}: J. Ruiz, V. Riera, M. Vivanco, S. García-Granda, A. García-Fernández, *Organometallics* **1992**, *11*, 4077–4082.

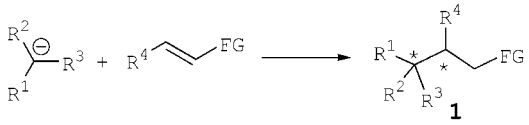
 © 2005 Wiley-VCH Verlag GmbH & Co. KGaA, Weinheim

Asymmetric Catalysis

Stereocontrolled Creation of Adjacent Quaternary and Tertiary Stereocenters by a Catalytic Conjugate Addition**

*Hongming Li, Yi Wang, Liang Tang, Fanghui Wu, Xiaofeng Liu, Chengyun Guo, Bruce M. Foxman, and Li Deng**

Adjacent quaternary and tertiary stereocenters as in structure **1** are common structural motifs in complex natural products. In principle, the stereocontrolled conjugate addition of a prochiral trisubstituted carbon nucleophile to a prochiral β-substituted Michael acceptor with a chiral catalyst could provide a one-step construction of such highly congested motifs from simple precursors [Eq. (1)]. However, this



(1)

requires the catalyst to impart both high enantioselectivity and diastereoselectivity in a sterically demanding, intermolecular C–C bond formation that simultaneously creates both the quaternary and tertiary stereocenters. This task has proven to be a formidable challenge. Among numerous literature examples,[1–3] to our knowledge there are only two catalytic asymmetric conjugate additions that afford the 1,4-adducts containing adjacent carbon-substituted quaternary and tertiary stereocenters in excellent enantioselectivity and with a diastereomeric ratio (d.r.) of greater than 10:1 for a substantial number of trisubstituted carbon Michael donors.[2] Herein, we report an asymmetric conjugate addition mediated by a chiral bifunctional organocatalyst that affords high enantioselectivity and diastereoselectivity for several structurally distinct classes of trisubstituted carbon nucleophiles. This reaction allows the direct and stereocontrolled construction of a wide variety of adjacent carbon- or heteroatom-substituted quaternary and tertiary stereocenters.

Readily accessible cinchona alkaloids **2** have been identified recently as effective catalysts for the enantioselective conjugate addition of dimethyl malonate and ethyl acetoacetate to nitroalkenes.[4,5] These results prompted us to examine

[*] H. Li, Dr. Y. Wang, L. Tang, F. Wu, X. Liu, C. Guo, Prof. B. M. Foxman, Prof. L. Deng
Department of Chemistry, Brandeis University
Waltham, MA 02454-9110 (USA)
Fax: (+1) 781-736-2516
E-mail: deng@brandeis.edu

[**] This work was supported financially by the National Institutes of Health (GM-61591) and by a Sloan Research Fellowship (L.D.).

Supporting information for this article is available on the WWW under http://www.angewandte.org or from the author.

 DOI: 10.1002/anie.200461923 © 2005 Wiley-VCH Verlag GmbH & Co. KGaA, Weinheim

conjugate additions involving trisubstituted carbon nucleophiles, especially those that could be conveniently generated in situ from readily available racemic carbonyl compounds. Screening of catalysts **2** for the addition of cyclic ketoester **3A** to nitroalkene **4a** in THF at room temperature revealed that Q-**2b** affords excellent enantioselectivities (94 and 95% *ee*) for both diastereomers of the 1,4-adducts, which were, however, generated in only a 4.5:1 ratio (Scheme 1). Interestingly, the reaction temperature was found to have a dramatic impact on the diastereoselectivity. Conjugate addition at −60°C afforded a d.r. of 18:1 with 99% *ee* for the major diastereomer.

Following this encouraging result, we examined a wide variety of trisubstituted carbon Michael donors in conjugate additions to nitroalkenes **4** mediated by Q-**2** (Table 1, Figure 1). Outstanding diastereoselectivity and enantioselectivity were obtained with various cyclic and acyclic β-ketoesters (**3A–D**). Similarly high enantioselectivity was also observed for the 2-substituted 1,3-diketone **3E**; the diastereoselectivity decreased noticeably but is yet of synthetic utility. Importantly, high diastereoselectivity and enantioselectivity can also be attained with trisubstituted carbon Michael donors that are not 1,3-dicarbonyl compounds (**3F–H**), including even those bearing a heteroatom substituent (**3F–G**). It is noteworthy that catalysts Q-**2** accept this unprecedented scope of trisubstituted carbon Michael donors and still tolerate a wide range of nitroalkenes (**4a–f**) bearing aryl, heteroaryl, and alkyl groups with varying electronic and steric properties.

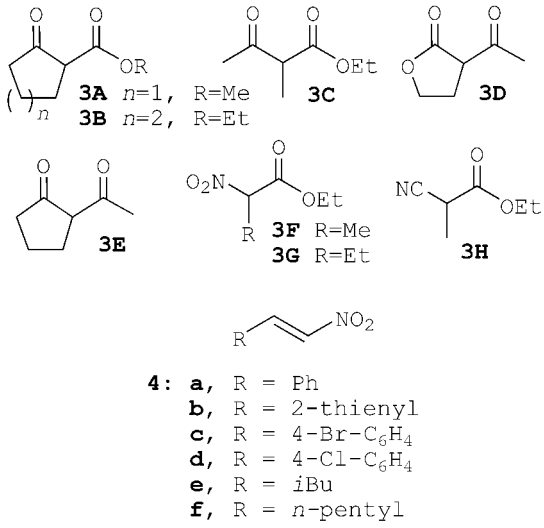
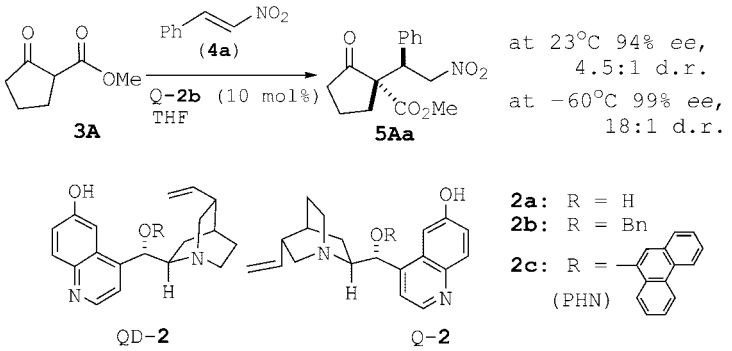
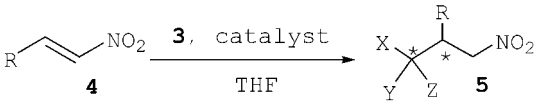


Figure 1. Carbon nucleophiles **3** and Michael acceptors **4** from Table 1.



Scheme 1. Michael addition of **3A** to **4a**.

Table 1: Diastereoselective and enantioselective 1,4-addition catalyzed by Q-**2**.[a]



Entry	3	4	Cat.	*T* [°C]	*t*	Yield [%][b]	d.r.[c]	*ee* [%][d]
1	**3A**	**4a**	Q-**2b**	−60	48 h	94	95:5	99
2	**3A**	**4e**	Q-**2b**	−60	4 d	87	>98:2	99
3	**3B**	**4a**	Q-**2a**	−20	72 h	93	>98:2	99
4	**3B**	**4b**	Q-**2a**	−20	74 h	91	>98:2	99
5	**3B**	**4c**	Q-**2a**	−20	74 h	95	>98:2	>99
6	**3B**	**4e**	Q-**2c**	23	4 d	83	>98:2	99
7	**3C**	**4a**	Q-**2c**[e]	−20	63 h	73[g]	91:9	>99
8	**3D**	**4d**	Q-**2b**	−60	44 h	87	98:2	99
9	**3D**	**4e**	Q-**2c**	−60	48 h	82	98:2	99
10	**3E**	**4a**	Q-**2b**	−60	48 h	76[g]	86:14	99
11	**3F**	**4a**	Q-**2a**	−20	60 h	78[g]	92:8	92
12	**3F**	**4f**	Q-**2a**	−20	84 h	78[g]	93:7	92
13	**3G**	**4a**	Q-**2a**[f]	−50	6 d	77	95:5	96
14	**3H**	**4a**	Q-**2b**[f]	−50	6 d	77[g]	>98:2	>99
15	**3H**	**4f**	Q-**2a**	−20	84 h	75	93:7	98

[a] Unless noted, reactions were conducted on a 0.2-mmol scale in 0.2 mL THF with 10 mol% Q-**2**. [b] Yield of isolated product. [c] Determined by ^{1}H NMR analysis of crude product. [d] Determined by HPLC analysis. [e] Here 15 mol% catalyst was used. [f] Here 20 mol% catalyst was used. [g] Yield of the pure major diastereomer.

Mechanistic studies were carried out to gain insight into the transition-state assembly of this reaction. The absolute configuration of **5Dd** generated using Q-**2b** and the relative configuration of **5De** has been determined by X-ray crystallography.[6] We established that the asymmetric Michael addition follows a first-order dependence on the catalyst, the donor, and the acceptor.[6] We also found that the reaction proceeds at significantly higher stereoselectivities in aprotic solvents (THF, ether, and toluene) rather than protic solvents (MeOH, EtOH), which could form hydrogen bonds with either the catalyst or the substrates. To delineate the active conformer for the flexible catalysts **2** in the transition state, we compared their stereoselectivities with those of **6** (Figure 2),[7] a conformationally rigid catalyst, in Michael additions utilizing a variety of combinations of donors and acceptors. The remarkably similar d.r. and *ee* profiles thus exhibited by QD-**2** and **6** provide powerful evidence to support a *gauche*-open active conformer for catalysts **2** in the transition state (Table 2).[8–9] These results are also noteworthy for establishing QD-**2** and **6** as efficient catalysts for the asymmetric Michael addition.

 © 2005 Wiley-VCH Verlag GmbH & Co. KGaA, Weinheim

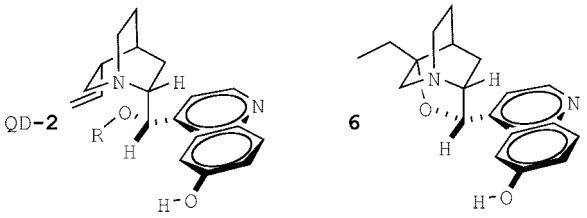
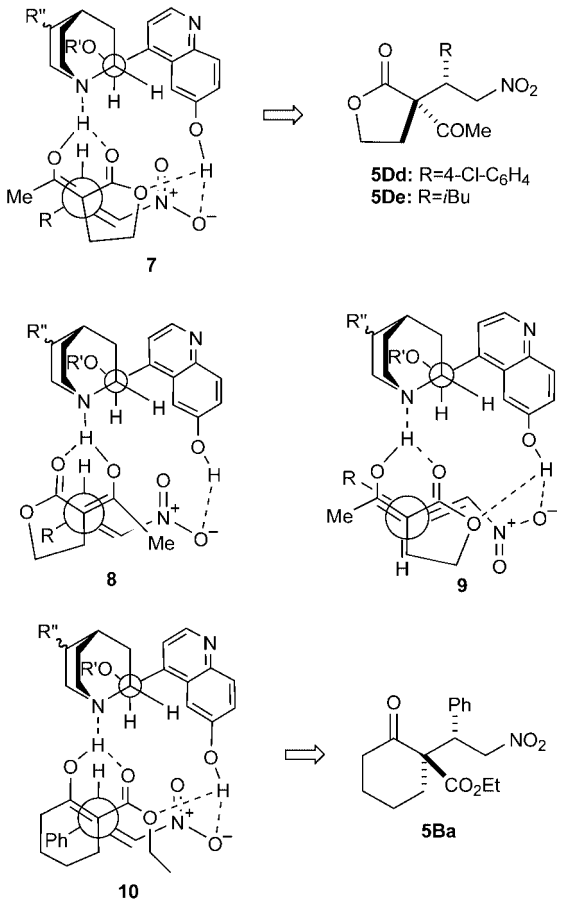


Figure 2. Catalyst QD-**2** shown as its *gauche*-open conformer and catalyst **6**.

With this key insight into the active conformer of the catalysts **2**, the kinetic results consistent with an acid–base bifunctional catalysis mode, and the observed solvent effect indicating an important role played by hydrogen-bond interactions between the catalyst and the substrates, we propose the transition-state model **7** to rationalize the stereochemical outcome of the asymmetric Michael addition (Scheme 2). In this model cinchona alkaloids **2** and **6** adopt a *gauche*-open conformer to simultaneously activate and orient the Michael donor and the acceptor by means of a network of hydrogen-bonding interactions. The substituents of the two bond-forming carbons are in a staggered rather than eclipsed arrangement. Alternative transition states generating the other stereoisomers are relatively disfavored due to either the loss of hydrogen-bond interaction between the chiral catalyst and the substrates (as in **8**) or the engagement of unfavorable eclipsed interactions between the substitutents of the bond-forming carbons (as in **9**). Application of this model (as in **10**) predicts that the adduct **5Ba** should have the relative configuration shown in Scheme 2. Gratifyingly, this was confirmed by X-ray structure analysis.[6]



Scheme 2. Stereochemical model for Michael additions catalyzed by QD-**2** or **6**.

Table 2: Asymmetric Michael additions catalyzed by QD-**2** and **6** (in brackets).[a]

Entry	3	4	Cat.	*T* [°C]	Yield [%]	d.r.	*ee* [%]
1	**3A**	**4a**	QD-**2c** (**6**)	−60	97 (97)	94:6 (97:3)	>99 (98)
2	**3B**	**4c**	QD-**2a** (**6**)	−20	96 (97)	>98:2 (>98:2)	99 (98)
3	**3C**	**4a**	QD-**2c** (**6**)	−20	70 (75)	82:18 (89:11)	99 (96)
4	**3D**	**4d**	QD-**2c** (**6**)	−60	92 (92)	97:3 (97:3)	98 (98)
5	**3E**	**4a**	QD-**2c** (**6**)	−60	70 (80)	88:12 (90:10)	98 (96)
6	**3F**	**4a**	QD-**2a** (**6**)	−20	74 (80)	89:11 (95:5)	89 (88)
7	**3H**	**4a**	QD-**2a** (**6**)	−20	76 (74)	86:14 (86:14)	95 (88)

[a] Reactions were run under the same conditions as described in Table 1 (see the Supporting Information).

In summary, we have developed a highly enantioselective and diastereoselective catalytic conjugate addition for a direct, stereocontrolled construction of adjacent carbon- or heteroatom-substituted quaternary and tertiary stereocenters from readily available starting materials. With exceptionally wide scopes for both the trisubstituted carbon Michael donors and the Michael acceptors, this experimentally simple new method should be useful for the synthesis of many multifunctional chiral building blocks containing adjacent quaternary and tertiary stereocenters that were previously not easily accessible. The stereochemical outcome of the reaction can be rationalized by a transition-state model, which is derived from mechanistic studies that clarify the active conformer of the bifunctional cinchona alkaloid catalyst in the transition state.

Received: September 8, 2004
Published Online: November 26, 2004

Keywords: asymmetric catalysis · cinchona alkaloids · hydrogen bonding · Michael addition · nitroalkenes

[1] For reviews see: a) M. P. Sibi, S. Manyem, *Tetrahedron* **2000**, *56*, 8033; b) N. Krause, A. Hoffmann-Röder, *Synthesis* **2001**, 171; c) O. M. Berner, L. Tedeschi, D. Enders, *Eur. J. Org. Chem.* **2002**, 1877; d) J. Christoffers, A. Baro, *Angew. Chem.* **2003**, *115*, 1726; *Angew. Chem. Int. Ed.* **2003**, *42*, 1688; e) J. Christoffers, *Chem. Eur. J.* **2003**, *9*, 4862; f) C. J. Douglas, L. E. Overman, *Proc. Natl. Acad. Sci. USA* **2004**, *101*, 5363; g) M. Yamaguchi in *Comprehensive Asymmetric Catalysisis* (Eds.: E. N. Jacobsen, A. Pfaltz,

 © 2005 Wiley-VCH Verlag GmbH & Co. KGaA, Weinheim

H. Yamamoto), Springer, Heidelberg, **2003**, Suppl. 1, Supplement to chap. 31.2, p. 151.
[2] a) M. S. Taylor, E. N. Jacobsen, *J. Am. Chem. Soc.* **2003**, *125*, 11204; b) J. F. Austin, S.-G. Kim, C. J. Sinz, W.-J. Xiao, D. W. C. MacMillan, *Proc. Natl. Acad. Sci USA*, **2004**, *101*, 5482.
[3] For other notable studies of intermolecular, diastereoselective, and enantioselective catalytic conjugate additions for the construction of vicinal quaternary and tertiary stereocenters see: a) Y. Hamashima, D. Hotta, M. Sodeoka, *J. Am. Chem. Soc.* **2002**, *124*, 11240; b) M. Mase, R. Thayumanavan, F. Tanaka, C. F. Barbas III, *Org. Lett.* **2004**, *6*, 2527.
[4] H. Li, Y. Wang, L. Tang, L. Deng, *J. Am. Chem. Soc.* **2004**, *126*, 9906.
[5] For other recent examples of highly enantioselective Michael additions catalyzed by cinchona alkaloid derivatives see: a) P. McDaid, Y. Chen, L. Deng, *Angew. Chem.* **2002**, *114*, 348; *Angew. Chem. Int. Ed.* **2002**, *41*, 348; b) M. Bella, K. A. Jørgensen, *J. Am. Chem. Soc.* **2004**, *126*, 5672.
[6] See the Supporting Information for details.
[7] Catalyst **6** was first reported by Hatakeyama et al. See: a) Y. Iwabuchi, M. Nakatani, N. Yokoyama, S. Hatakeyama, *J. Am. Chem. Soc.* **1999**, *121*, 10219; b) S. Kawahara, A. Nakano, T. Esumi, Y. Iwabuchi, S. Hatakeyama, *Org. Lett.* **2003**, *5*, 3103.
[8] For the use of conformationally rigid cinchona alkaloids to probe the active conformer of cinchona alkaloids as ligands for Os-catalyzed Sharpless asymmetric dihydroxylations see: a) E. J. Corey, M. C. Noe, *J. Am. Chem. Soc.* **1993**, *115*, 12579; b) E. J. Corey, M. C. Noe, *J. Am. Chem. Soc.* **1996**, *118*, 11038.
[9] For a study of the active conformer of cinchona alkaloids in applications as an organic catalyst see: G. S. Cortez, S. H. Oh, D. Romo, *Synthesis* **2001**, 1731.

 © 2005 Wiley-VCH Verlag GmbH & Co. KGaA, Weinheim

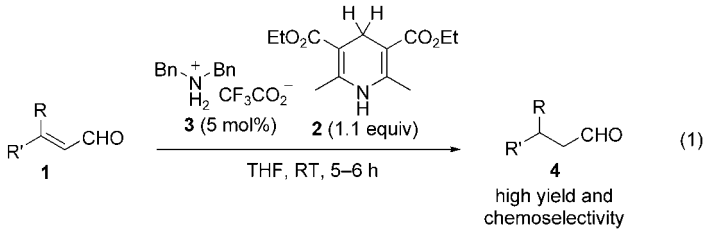
Organocatalysis

Metal-Free, Organocatalytic Asymmetric Transfer Hydrogenation of α,β-Unsaturated Aldehydes**

*Jung Woon Yang, Maria T. Hechavarria Fonseca, Nicola Vignola, and Benjamin List**

Asymmetric catalytic hydrogenations are used in the large-scale industrial production of pharmaceuticals and fine chemicals and also by all living organisms. While chemical hydrogenations require metal catalysts or the use of stoichiometric amounts of metal hydrides,[1] living organisms typically rely on organic cofactors such as nicotinamide adenine dinucleotide (NADH) in combination with metalloenzymes.[2] Until now, metal-free catalytic asymmetric hydrogenations have been unknown in chemical synthesis and seem to be rare in nature.[3] Here we show that a small organic molecule effectively catalyzes a highly enantioselective biomimetic transfer hydrogenation of α,β-unsaturated aldehydes using a synthetic dihydropyridine cofactor.

Industrially, metal-catalyzed hydrogenations are the most often used catalytic asymmetric processes. The complete removal of metal impurities from the reaction product, though difficult, is generally required in the production of pharmaceutical intermediates because of toxicity concerns.[4] Organocatalysis is a rapidly growing area of research, and one of its advantages is the general lack of metals.[5] We have recently developed an amine-catalyzed nonasymmetric transfer hydrogenation of α,β-unsaturated aldehydes **1** with Hantzsch ester **2** [Eq. (1)].[6]



(1)

This reaction is the first example of a completely metal-free transfer hydrogenation of olefins.[7] We could also show that enantioselective iminium catalysis of the reaction is in principle possible. Iminium catalysis has recently been introduced as a powerful organocatalytic method for carbonyl transformations such as conjugate additions and cycloadditions.[8] We have now completed an extensive screening of several synthetic and commercially available Hantzsch dihydropyridines and chiral ammonium salt catalysts and report here on an efficient enantioselective variant of our transfer hydrogenation.

We found that upon treating aromatic, trisubstituted α,β-unsaturated aldehydes **5** with a slight excess of dihydropyridine **6** and a catalytic amount of MacMillan imidazolidinone salt **7** at 13 °C in dioxane, the corresponding saturated aldehydes **8** were obtained in high yields and excellent enantioselectivities [Eq. (2), Table 1].

Like our nonasymmetric variant, the enantioselective reactions are generally clean and highly chemoselective, and carbonyl reduction or aldolization products were not detected. We also investigated the influence of the stereochemistry at the double bond. Remarkably, when we subjected both the isolated pure *E* or *Z* isomers of 4-nitro-substituted derivative **5c** to our reaction conditions, the same *R* enantiomer of product **8c** was obtained and with the same enantiomeric ratio of 97:3. Similarly, (*E*)/(*Z*)-**5c** mixtures always gave the same result and, independent of their exact ratio, all furnished (*R*)-**8c** in 97:3 e.r. Thus, our process is *enantioconvergent*, a highly desirable yet rare feature of a catalytic asymmetric reaction, where a mixture of stereoisomers furnishes only one product enantiomer. As a practical

[*] Dr. J. W. Yang, Dr. M. T. Hechavarria Fonseca, Dr. N. Vignola, Prof. Dr. B. List
Max-Planck-Institut für Kohlenforschung
Kaiser-Wilhelm-Platz 1, 45470 Mülheim an der Ruhr (Germany)
Fax: (+49) 208-306-2999
E-mail: list@mpi-muelheim.mpg.de

[**] We thank Degussa for donation of chemicals and the analytical departments of the Max-Planck-Institut für Kohlenforschung for technical assistance.

 © 2005 Wiley-VCH Verlag GmbH & Co. KGaA, Weinheim DOI: 10.1002/anie.200462432

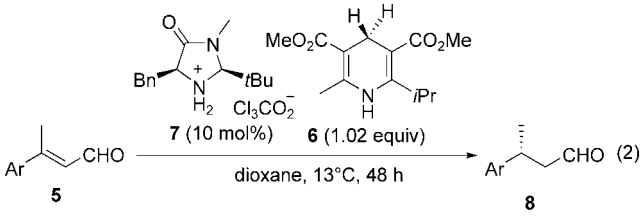
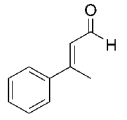
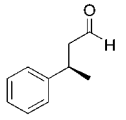
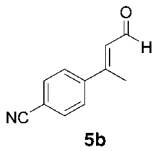
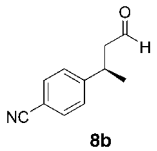
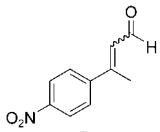
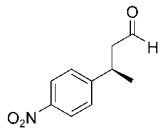
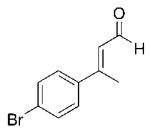
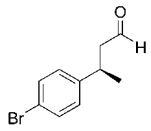
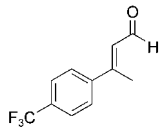
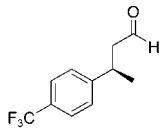
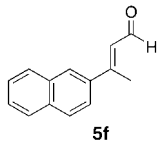
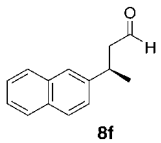


Table 1: Organocatalytic asymmetric transfer hydrogenation of α,β-unsaturated aldehydes.

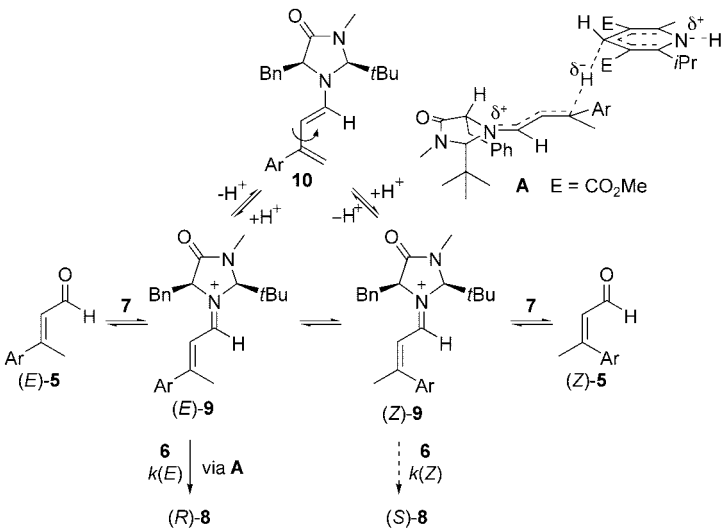
Entry	Starting material	Product	Yield [%]	e.r.
1	 **5a**	 **8a**	77[a]	95:5
2	 **5b**	 **8b**	89	98:2
3	 **5c**	 **8c**	83 (from (*E*)-**5c**) 80 (from (*Z*)-**5c**) 81 (from (*E*)/(*Z*)-**5c** (1:1))	97:3 97:3 97:3
4	 **5d**	 **8d**	90	97:3
5	 **5e**	 **8e**	85	97:3
6	 **5f**	 **8f**	86	96:4

[a] Yield of the 2,4-dinitrophenylhydrazone derivative.

consequence of this feature, the unsaturated aldehyde starting material of our reaction may be used as a mixture of *E* and *Z* isomers as obtained from common synthetic procedures such as the Wittig reaction.

Mechanistically, we assume the reaction to proceed by formation of iminium ion **9**, which presumably isomerizes quickly via dienamine **10** (Scheme 1). The following rate-determining hydride transfer from dihydropyridine **6** to enal (*E*)-**9** via transition state **A** proceeds faster than to (*Z*)-**9** [$k(E) > k(Z)$] and, as a result, saturated aldehyde (*R*)-**8** is formed predominantly.

In summary we have described the first completely metal-free catalytic asymmetric transfer hydrogenation. In our



Scheme 1. Proposed mechanism of the organocatalytic asymmetric transfer hydrogenation.

iminium catalytic reaction α,β-unsaturated aldehydes are highly efficiently reduced by means of transfer hydrogenation from a dihydropyridine. Attractive features of the process are 1) its high yields, chemo-, and enantioselectivities, 2) its enantioconvergence, and 3) its simplicity and practicability. Applications in the synthesis of natural products, pharmaceuticals, and fine chemicals may be envisioned.

Experimental Section

General procedure for the asymmetric transfer hydrogenation reaction: To a stirred solution of α,β-unsaturated aldehyde **5** (0.5 mmol) in dioxane (7 mL) at 13 °C was added catalyst **7** (20.4 mg, 0.05 mmol, 10 mol %) and, after five minutes, crystalline dihydropyridine **6** (129.2 mg, 0.51 mmol). After a reaction time of 48 h the mixture was poured into distilled water (20 mL) and extracted with dichloromethane (2 × 15 mL). The combined organic layers were dried ($MgSO_4$), filtered, and concentrated. The product was isolated by flash chromatography (SiO_2, ethyl acetate/hexane) to give the saturated aldehyde product **8**. Aldehydes **5a–f** were synthesized according to previously reported methods and their analytical data as well of those of aldehydes **8** match literature values.[9] The absolute configuration of (*R*)-**8f** was determined by measurement of its optical rotation and comparision to the literature value.[10] Enantiomeric ratios were determined by chiral stationary phase GC-analysis.

Received: October 26, 2004

Keywords: asymmetric catalysis · chemoselectivity · enantioselectivity · hydrogenation · organocatalysis

[1] a) R. Noyori, *Angew. Chem.* **2002**, *114*, 2108–2123; *Angew. Chem. Int. Ed.* **2002**, *41*, 2008–2022; b) W. S. Knowles, *Angew. Chem.* **2002**, *114*, 2096–2107; *Angew. Chem. Int. Ed.* **2002**, *41*, 1998–2007.
[2] F. Dickinson, K. Dalziel, *Nature* **1967**, *214*, 31–33.
[3] For mechanistic studies on the base-catalyzed and transition-metal-free hydrogenation of ketones, see: a) A. Berkessel, T. J. S. Schubert, T. N. Müller, *J. Am. Chem. Soc.* **2002**, *124*,

 © 2005 Wiley-VCH Verlag GmbH & Co. KGaA, Weinheim

8693 – 8698; Also see: b) J. H. Teles, S. Brode, A. Berkessel, *J. Am. Chem. Soc.* **1998**, *120*, 1345 – 1346; c) E. J. Lyon, S. Shima, G. Buurman, S. Chowdhuri, A. Batschauer, K. Steinbach, R. K. Thauer, *Eur. J. Biochem.* **2004**, *271*, 195 – 204.
[4] C. E. Garrett, K. Prasad, *Adv. Synth. Catal.* **2004**, *346*, 889 – 900.
[5] P. I. Dalko, L. Moisan, *Angew. Chem.* **2001**, *113*, 3840 – 3864; *Angew. Chem. Int. Ed.* **2001**, *40*, 3726 – 3748.
[6] J. W. Yang, M. T. Hechavarria Fonseca, B. List, *Angew. Chem.* **2004**, *116*, DOI: 10.1002/ange. 200461816; *Angew. Chem. Int. Ed.* **2004**, *43*, DOI: 10.1002/anie.200461816.
[7] For examples of transition-metal-catalyzed asymmetric conjugate reductions of amides, esters, ketones, and nitroalkenes, see: a) U. Leutenegger, A. Madin, A. Pfaltz, *Angew. Chem.* **1989**, *101*, 61 – 62; *Angew. Chem. Int. Ed. Engl.* **1989**, *28*, 60; b) D. H. Appella, Y. Moritani, R. Shintani, E. M. Ferreira, S. L. Buchwald, *J. Am. Chem. Soc.* **1999**, *121*, 9473 – 9474; c) B. H. Lipshutz, J. M. Servesko, *Angew. Chem.* **2003**, *115*, 4937 – 4940; *Angew. Chem. Int. Ed.* **2003**, *42*, 4789 – 4792; d) C. Czekelius, E. M. Carreira, *Angew. Chem.* **2003**, *115*, 4941 – 4943; *Angew. Chem. Int. Ed.* **2003**, *42*, 4793 – 4795.
[8] a) K. A. Ahrendt, C. J. Borths, D. W. C. MacMillan, *J. Am. Chem. Soc.* **2000**, *122*, 4243 – 4244; b) B. List, *Synlett* **2001**, 1675 – 1686; c) J. F. Austin, D. W. C. MacMillan, *J. Am. Chem. Soc.* **2002**, *124*, 1172 – 1173.
[9] a) R. Martin, I. Islas, A. Moyano, M. A. Pericas, A. Riera, *Tetrahedron* **2001**, *57*, 6367 – 6374; b) M. I. Al-Hassan, *Gazz. Chim. Ital.* **1985**, *115*, 441; c) M. Akhtar, L. Jallo, A. Johnson, *J. Chem. Soc. Chem. Commun.* **1982**, *1*, 44 – 46; d) A. I. Meyers, A. Nabeya, H. W. Adickes, I. R. Politzer, *J. Am. Chem. Soc.* **1969**, *91*, 764 – 765.
[10] T. Lee, J. B. Jones, *J. Am. Chem. Soc.* **1997**, *119*, 10260 – 10268.

 © 2005 Wiley-VCH Verlag GmbH & Co. KGaA, Weinheim

Chemistry in Porous Materials

Radiolysis of Confined Water: Production and Reactivity of Hydroxyl Radicals**

Sarah Foley, Patricia Rotureau, Serge Pin, Gérard Baldacchino, Jean-Philippe Renault, and Jean-Claude Mialocq*

As technology progresses to the nanoscale, the question of how chemical reactions are perturbed by the size of the environment needs further consideration. Such supramolecular steric effects provide new strategies to orientate reactivity towards desired functionality.[1,2] Confinement and interfacial phenomena are expected to have dramatic effects on reaction rates and mechanisms.[3] However, studies on these effects are still very limited, as most kinetic methods are difficult in a nanometer-confined environment.[2,4] Radiolysis of liquids is an efficient tool which can be used to investigate chemical reactivity in complex environments. As ionizing radiation induces reactions throughout the entire sample, whatever its complexity, information on the chemical reactivity at the microscopic scale can be obtained from macroscopic analytical strategies. Such studies of radiation-induced chemical processes in nanostructured materials have mostly been concerned with the effects on the solid material itself[5] or the reactivity of molecules adsorbed at the solid surface.[6] The present study aims to establish how radiation affects the reactivity of radiolytically produced radicals within nanometric water-filled pores in comparison to that in homogeneous solutions.

Radiation chemists have thus typically sought a target that can trap radicals in order to generate a change in some easily measurable property, as in chemical dosimeters.[7] Such traps are useful since they can probe cavities of any size and shape. High sensitivity can be achieved by choosing a system in which radiolysis results in the formation of a fluorescent compound and thus can be detected by spectrofluorimetry.[8,9] One of these profluorescent compounds is coumarin, which has the advantage of only measuring the formation of the $HO^{\bullet}$ radical whilst disregarding other primary radiolysis species. In aqueous solution, nonfluorescent coumarin is converted on irradiation into fluorescent 7-hydroxycoumarin (7-OHC).[10–14] The fluorescence intensity is proportional to the number of 7-OHC molecules formed, and this in turn is proportional to the locally available $HO^{\bullet}$ concentration down to 10^{-8} mol dm^{-3}. Such a selectivity and sensitivity with respect to $HO^{\bullet}$ can not be achieved by measuring the bleaching of a dye under irradiation.

We have determined the concentration of 7-OHC produced in a variety of controlled pore glasses (CPGs) with pore sizes ranging from 8 to 300 nm[15,16] to ascertain the influence of pore size on radiolytic radical production and reaction in a confined space. Figure 1 shows the fluorescence of 7-OHC

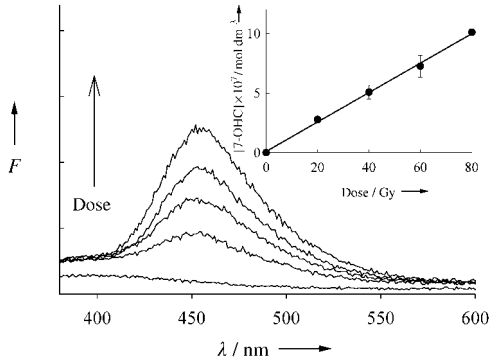


Figure 1. Fluorescence spectra of 7-OHC extracted from irradiated CPG of 200 nm pore size (excitation wavelength 332 nm, excitation and emission slits 0.5 mm, gamma irradiation with ^{137}Cs, 2 Gy min^{-1}). The inset shows the concentration of 7-OHC produced as a function of dose.

[*] Dr. S. Foley, Dr. P. Rotureau, Dr. S. Pin, Dr. G. Baldacchino, Dr. J.-P. Renault, Dr. J.-C. Mialocq
CEA/Saclay
DSM/DRECAM/SCM/URA 331 CNRS
91191 Gif-sur-Yvette, Cedex (France)
Fax: (+33) 1-6908-3466
E-mail: jrenault@drecam.cea.fr

[**] The authors thank the Direction de L'Energie Nucléaire (CEA/Saclay) for financial support and Hervé Coffigny of the Direction des Sciences du Vivant (CEA/Fontenay aux Roses) for use of the gamma irradiator.

Supporting information for this article is available on the WWW under http://www.angewandte.org or from the author.

 © 2005 Wiley-VCH Verlag GmbH & Co. KGaA, Weinheim DOI: 10.1002/anie.200460284

produced when 1 mM coumarin was irradiated in a CPG with a pore size of 200 nm. To ensure that all the 7-OHC produced in the CPG was extracted, control experiments were performed in which aqueous solutions of coumarin containing varying concentrations of 7-OHC were mixed with the CPGs. The amount of 7-OHC that could be extracted from these glasses was measured by using a fluorescence calibration curve down to 2×10^{-8} mol dm^{-3}; $95\pm5\%$ of the 7-OHC introduced could be recovered, irrespective of the CPG used. The concentration of 7-OHC produced in the pore was determined from the extraction coefficient of 95% and the fluorescence calibration curve. The results for a CPG with a pore size of 200 nm are shown in the inset of Figure 1. The concentration of 7-OHC produced remains proportional to the dose, as in aerated homogeneous solutions. Similar results were obtained for all the CPGs. The concentration of 7-OHC produced was also measured for CPGs with pore sizes of 8, 50, and 300 nm filled with solutions flushed by N_2O. Under these conditions, the reducing hydrated electrons e^-_{aq} are converted into HO$^\bullet$ radicals. Thus, in homogeneous solution, N_2O induces a 40% increase in the production of 7-OHC.[11] After exposure of the porous material to N_2O, the concentration of 7-OHC is increased by a factor of 1.5 relative to that obtained under Ar, a value which is in good agreement with that obtained by Makrigiorgos et al.,[11] and which shows that HO$^\bullet$ radicals are responsible for the formation of 7-OHC. The similarities between the behavior of coumarin in homogeneous solutions and in porous glasses and the possibility to efficiently quantify the 7-OHC produced allowed us to apply the capture of HO$^\bullet$ radicals by coumarin to the case of confined water.

Figure 2 shows how the concentration of 7-OHC in CPGs varies as a function of the pore size of the glass. The amount of solution added was equal to the available pore volume. The concentration of 7-OHC produced per Gy absorbed by water (the radiolytic yield) increases with increasing pore size of the CPGs. When the pore diameter decreases from 100 to 8 nm, the radiolytic yield of 7-OHC is divided by three, and thus we can assume that the radiolytic yield of HO$^\bullet$ radicals decreases by the same amount. Above a pore diameter of 150 nm, the behavior of confined coumarin solutions is similar to that of homogenous solutions.[10,17]

Such results can be attributed either to a cagelike effect which favors radical recombination in the pores[2] or to an enhanced surface reaction of HO$^\bullet$ at the water/silica interface.[18] To identify a possible role of this interface, CPGs with pore sizes of 8, 50, and 300 nm were filled with various amounts of 1 mM coumarin solution and irradiated as described above. In hydrophilic porous materials such as CPGs and Vycor glasses, when the amount of solution decreases, first the center of the pore empties leaving a layer of water on the silica surface, after which the thickness of this layer gradually diminishes.[19] The concentration of 7-OHC produced per Gy absorbed by water was determined as described above. The radiolytic yield of 7-OHC was found to increase when the amount of solution in the pores was decreased but the coumarin concentration was kept constant, that is, the thickness of the water layer on the silica decreased and the relative amount of silica surface available for a possible capture reaction of the HO$^\bullet$ radical on the surface increased (Figure 3a). The increase in the 7-OHC radiolytic yield shows that the capture of HO$^\bullet$ radicals at the surface is not efficient. At constant coumarin concentration, the only explanation for this increase is thus enhancement of radiolytic production of HO$^\bullet$ radicals.

Figure 3b shows the 7-OHC production per gram of glass and per Gray when the degree of pore saturation is increased. This value increases linearly with respect to the amount of water confined in the pores, but has a positive intercept. The linear increase with respect to the filling of the pore is due to

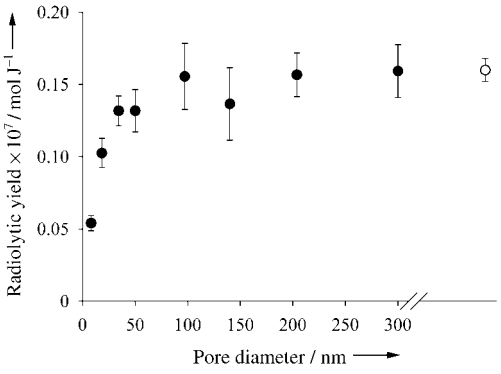


Figure 2. Effect of pore size on the yield of 7-OHC in CPGs. The empty circle refers to the yield in solution taken from Louit et al.[10]

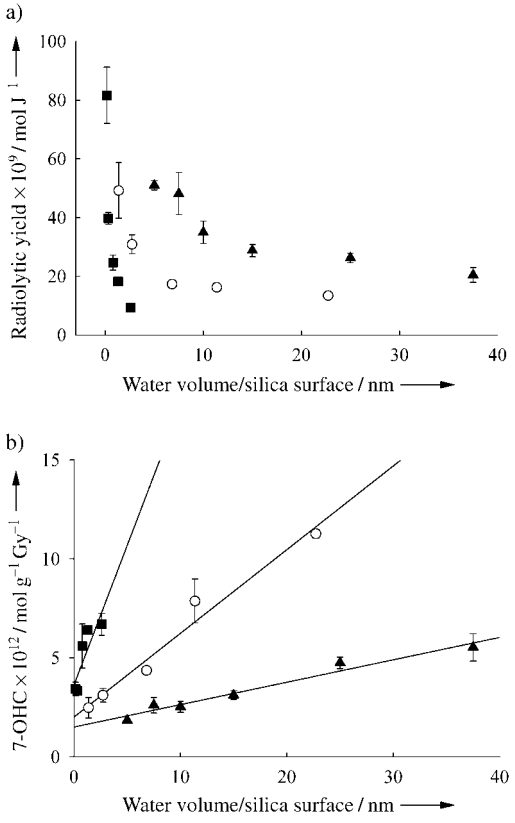


Figure 3. a) Yield of 7-OHC as a function of the ratio of introduced coumarin solution volume with respect to the wetted silica surface area for CPGs with pore sizes of 8 (■), 50 (○), and 300 nm (▲). b) Total amount of 7-OHC produced per gram of CPG and per Gray directly received by the glasses as a function of this ratio.

 © 2005 Wiley-VCH Verlag GmbH & Co. KGaA, Weinheim

the direct radiation–water interaction, that is, to the direct production of hydroxyl radicals in water. On the other hand, the intercept is linked to an overproduction of oxidative species at the water/silica interface. Such an overproduction can be associated with energy transfer from the oxide to the adsorbed water.[20] As expected, this energy transfer is more efficient for materials with a large specific surface area, that is, for smaller pores. Therefore, the contribution of water to the production of HO• radicals can be separated from the surface contribution. A more accurate determination of the effects of confinement on 7-OHC production inside the pores can be obtained by subtracting the surface contribution. When this is done for the data in Figures 2 and 3b, the amount of HO• available for reaction with coumarin is decreases by a factor of almost 6 for 8 nm pores and by a factor of 1.5 for 50 nm pores with respect to the amount for 300 nm pores.

To explain this effect, we must take into account that the quantity of 7-OHC produced is the result of competition between recombination of radiolytic radicals and their capture by coumarin. In the 8 nm pores the hydroxyl radicals cannot migrate as far apart as in bulk water, and thus they recombine faster with radicals produced in the same radiolytic track than they can react with a solute such as coumarin.[21] This recombination is reminiscent of the recombinations of both the primary and secondary geminate radical pairs resulting from photolysis of ketones in the "void space" of MFI zeolites, although the diameters of the cylindrical channels and their spherical intersections are smaller (5.5 and 9 Å, respectively).[2] This acceleration of the reaction induced by confinement has been theoretically described by Tachiya in micelles.[22] From this model, such cage effects are not expected to be effective for pore sizes as large as 50 nm. A complementary explanation for the observed results can be provided by the model of Barzykin and Tachiya which was developed for gels.[23] In porous media, reactions on long timescales are expected to be slowed down by local depletion and impaired diffusion, especially for low concentrations of reactants. We assume that this slowing down of the capture of HO• radicals by coumarin can explain part of the decrease in radiolytic yield of 7-OHC in porous glasses.

These results show that the effects of confinement, clearly identified at the nanopore scale, are important even at the mesopore scale, and this suggests the need to completely reevaluate our knowledge of reactivity in this type of environment. Experiments are underway to better understand the effects of confinement on the rates of radical reactions.

Received: April 9, 2004
Revised: September 6, 2004

Keywords: confinement effects · fluorescence spectroscopy · mesoporous materials · radical reactions · radiolysis

[1] a) N. K. Mal, M. Fujiwara, Y. Tanaka, *Nature* **2003**, *421*, 350; b) P. J. A. Kenis, R. F. Ismagilov, G. M. Whitesides, *Science* **1999**, *285*, 83; c) B. H. Barretz, N. J. Turro, *J. Am. Chem. Soc.* **1983**, *105*, 1309; d) J. M. Drake, P. Levitz, N. J. Turro, K. S. Nitsche, K. F. Cassidy, *J. Phys. Chem.* **1988**, *92*, 4680; e) N. J. Turro, S. Jockusch, X. G. Lei, *J. Org. Chem.* **2002**, *67*, 5779.

[2] N. J. Turro, *Acc. Chem. Res.* **2000**, *33*, 637.

[3] a) J. Ahn, R. Kopelman, P. Argyrakis, *J. Chem. Phys.* **1999**, *110*, 2116; b) A. L. Lin, R. Kopelman, P. Argyrakis, *Phys. Rev. E* **1997**, *56*, 6204; c) A. L. Lin, R. Kopelman, P. Argyrakis, *J. Phys. Chem. A* **1997**, *101*, 802; d) A. L. Lin, R. Kopelman, P. Argyrakis, *Phys. Rev. E* **1996**, *54*, R5893.

[4] a) P. Hunt, D. R. Worrall, F. Wilkinson, S. N. Batchelor, *J. Am. Chem. Soc.* **2002**, *124*, 8532; b) S. N. Batchelor, A. I. Shushin, *J. Phys. Chem. B* **2001**, *105*, 3405.

[5] S. C. Chemirisov, A. D. Trifunac, *Chem. Phys. Lett.* **2001**, *347*, 65.

[6] J. K. Thomas, *Chem. Rev.* **1993**, *93*, 301.

[7] J. W. T. Spinks, R. J. Woods, *An Introduction to Radiation Chemistry*, 3rd ed., Wiley-Interscience, New York, **1990**.

[8] a) W. A. Armstrong, R. A. Facey, D. W. Grant, W. G. Humphreys, *Can. J. Chem.* **1963**, *41*, 1575; b) W. A. Armstrong, D. W. Grant, *Nature* **1958**, *182*, 747.

[9] a) R. W. Matthews, *Radiat. Res.* **1980**, *83*, 27; b) J. C. Baretto, G. S. Smith, N. H. P. Strobel, P. A. McQuillin, T. A. Miller, *Life Sci.* **1995**, *54*, 89; c) X. Fang, G. Mark, C. von Sonntag, *Ultrason. Sonochem.* **1996**, *3*, 57.

[10] G. Louit, S. Foley, J. Cabillic, H. Coffigny, F. Taran, A. Valleix, J. P. Renault, S. Pin, *Rad. Phys. Chem.*, in press.

[11] G. M. Makrigiorgos, J. Baranowska-Kortylewicz, E. Bump, S. K. Sahu, R. M. Berman, A. I. Kassis, *Int. J. Radiat. Biol.* **1993**, *63*, 445.

[12] S. C. Ashawa, U. R. Kini, U. Madhvanath, *Int. J. Appl. Radiat. Isot.* **1979**, *30*, 7.

[13] K. Gopakumar, U. R. Kini, S. C. Ashawa, N. S. Bhandari, G. U. Krishnan, D. Krishnan, *Radiat. Eff.* **1977**, *32*, 199.

[14] J. A. R. Mead, J. N. Smith, R. T. Williams, *Biochem. J.* **1958**, *68*, 61.

[15] W. Haller, *Nature* **1965**, *206*, 693.

[16] A table listing pore size distributions and mean values for the various materials used, a SEM image of CPG 300 nm, and experimental details are available as Supporting Information.

[17] A. K. Collins, G. M. Makrigiorgos, G. K. Svenson, *Med. Phys.* **1994**, *21*, 1741.

[18] M. Suh, P. S. Bagus, S. Pak, M. P. Rosynek, J. H. Lunsford, *J. Phys. Chem. B* **2000**, *104*, 2736.

[19] a) M. Rovere, P. Gallo, *J. Phys. Condens. Matter* **2003**, *15*, S145; b) P. Gallo, M. Rapinesi, M. Rovere, *J. Chem. Phys.* **2002**, *117*, 369; c) P. Gallo, M. A. Ricci, M. Rovere, *J. Chem. Phys.* **2002**, *116*, 342.

[20] a) J. A. LaVerne, L. Tandon, *J. Phys. Chem. B* **2003**, *107*, 13623; b) J. A. LaVerne, L. Tandon, *J. Phys. Chem. B* **2002**, *106*, 380; c) N. G. Petrik, A. B. Alexandrov, A. I. Vall, *J. Phys. Chem. B* **2001**, *105*, 5935.

[21] A simple way to understand the confinement effect of 8 nm pores is to evaluate whether HO• reacts with coumarin before reaching the pore wall. Taking $D = 2.3 \times 10^{-9}\ m^2 s^{-1}$ for the diffusion constant of HO• (G. V. Buxton, C. L. Greenstock, W. P. Helman, A. B. Ross, *J. Phys. Chem. Ref. Data* **1988**, *17*, 513) one can estimate the average time needed for a hydroxyl radical to reach the pore wall as 5 ns. If the reaction constant between hydroxyl radical and coumarin is taken as $k = 8.2 \times 10^9\ mol^{-1} dm^3 s^{-1}$ (K. Gopakumar, U. R. Kini, S. C. Ashawa, N. S. Bhandari, G. U. Krishnan, D. Krishnan, *Radiat. Eff.* **1977**, *32*, 199) the half-life of HO• in 10^{-3} mol dm^3 coumarin solution is about 85 ns. According to this analysis, confinement in 8 nm pores can effectively prevent diffusion of HO• out of their production site and increase their recombination with their parent radicals prior to reaction with coumarin.

[22] M. Tachiya in *Kinetics of Nonhomogeneous Processes* (Ed.: G. R. Freeman), Wiley, New York, **1987**, p. 575.

[23] A. V. Barzykin, M. Tachiya, *J. Phys. Chem. B* **2003**, *107*, 2953.

 © 2005 Wiley-VCH Verlag GmbH & Co. KGaA, Weinheim

C–H Activation

$[H_2C{=}ZrH_2]$: The Simplest Carbene Hydride Complex, Agostic Bonding, and C–H Activation of CH_4 to Form $[(CH_3)_2ZrH_2]$**

Lester Andrews, Han-Gook Cho, and Xuefeng Wang*

High oxidation state transition-metal complexes with a carbon–metal double bond have proven important for understanding the nature of metal coordination and for catalysts in alkene-metathesis and alkane-activation reactions.[1–3] Several early transition-metal alkylidenes are agostic,[1] and these compounds provide the opportunity to characterize the agostic interaction of hydrogen to a transition-metal center in a simple carbene complex (most agostic interactions involve much more complicated systems) and to help understand the important alkane C–H bond-activation process (a key step in many transition-metal catalyzed reactions).[4–8]

The simplest compound of this type is the methylidene complex, $[H_2C{=}MH_2]$, which is an ideal model system to examine substituent effects and the agostic interaction. Such Group 4 compounds have been investigated by electronic-structure calculations using small basis sets and shown to have symmetrical structures without agostic interactions.[9–11] Recently we have treated laser-ablated Ti, Zr, and Hf atoms with CH_3F and prepared the fluorine substituted $[H_2C{=}MHF]$ derivatives.[12–14] These methylidene species result from α-hydrogen migration in the initial $[CH_3MF]$ intermediate. Our electronic-structure calculations using basis sets with polarization functions reveal a tilted CH_2 group and provide evidence for agostic interaction in the $[H_2C{=}MHF]$ molecules.

The simple $[H_2C{=}MH_2]$ analogues contain two intense infrared chromophores, namely the CH_2 and MH_2 groups, which are sensitive to the distortion associated with intramolecular agostic bonding. Hence the IR spectrum of $[H_2C{=}ZrH_2]$ can provide evidence for agostic interaction through symmetry lowering in the molecule, as can computations using large basis sets. In particular, a simple count of [CHD=ZrHD] isotopomers provides a ready method to confirm agostic interactions in this simplest possible carbene complex, as only two isotopomers (*cis* and *trans*) will be formed if there is no agostic interaction (C_{2v} or C_s symmetry), but four isotopomers (*cis* and *trans* for H and for D in the agostic position) if there is agostic interaction (C_1 symmetry). We report herein the first experimental characterization of $[H_2C{=}ZrH_2]$ and demonstrate the agostic C–H···Zr interaction from the IR spectrum in solid neon and from density functional structure and frequency calculations.

The laser-ablation matrix-IR experiment has been described elsewhere.[15,16] Briefly, laser-ablated zirconium atoms (Johnson–Matthey) reacted with CH_4 (Matheson), $^{13}CH_4$, CD_4, CH_2D_2 (Cambridge Isotopic Laboratories) in excess neon (Spectra Gases) during condensation on a CsI window at 5 K. IR spectra were recorded at 0.5 cm^{-1} resolution on a Nicolet 750 spectrometer with HgCdTe detector. Samples were irradiated by a mercury arc lamp (175 W, globe removed), were annealed, and more spectra were recorded.

Complementary density functional theory (DFT) calculations were performed using the Gaussian 98 package,[17] B3LYP density functional, 6-311++G(2d,p) basis sets for C and H atoms, and SDD pseudopotential and basis set for the Zr atom to provide a consistent set of vibrational frequencies for the reaction products. Geometries were fully relaxed during optimization, and the optimized geometry was confirmed via vibrational analysis. All the vibrational frequencies were calculated analytically.

IR spectra are illustrated in Figure 1 in the Zr–H stretching region for laser-ablated Zr and CH_4 (0.4% in neon). Four new product absorptions are observed at 1546.2 and 1581.0 cm^{-1} (labeled **1**) and at 1587.5 and 1617.2 cm^{-1} (labeled **di**). The bands increased on $\lambda > 530$ nm and 240–380 nm irradiations. Annealing to 10 K sharpened and slightly increased these absorptions, and produced a new 1551.0 cm^{-1} satellite feature (labeled **1′**). Further annealing to 11 K increased the 1587.5, 1617.2 cm^{-1} set, decreased the 1546.2, 1581.0 cm^{-1} pair (**1**), and increased the satellite (**1′**). Continued annealing to 12 K increased the high-wavenumber set (**di**) another 10%, almost destroyed the low-wavenumber pair (**1**), markedly increased the 1551.0 cm^{-1} satellite and an associ-

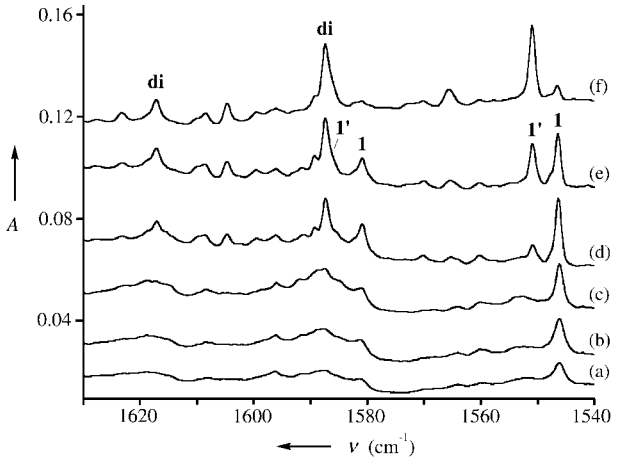


Figure 1. IR spectra in the 1630–1540 cm^{-1} region for laser-ablated zirconium co-deposited with CH_4 in excess neon at 5 K. a) 0.4% CH_4 in neon deposited for 45 min, b) after $\lambda > 530$ nm irradiation for 20 min, c) after 240–380 nm irradiation for 20 min, d) after annealing to 10 K, e) after annealing to 11 K, and f) after annealing to 12 K. For a discussion of the bands **1** (assigned to $[H_2C{=}ZrH_2]$), **1′**, and **di** (assigned to $[(CH_3)_2ZrH_2]$) see the text.

[*] Prof. Dr. L. Andrews, Prof. Dr. H.-G. Cho, Dr. X. Wang
Department of Chemistry
University of Virginia
P.O. Box 400319, Charlottesville, VA 22904-4319 (USA)
Fax: (+1) 434-924-3710
E-mail: lsa@virginia.edu

[**] We gratefully acknowledge financial support for this work from N.S.F. Grant CHE 00-78836 and CHE 03-53487, and sabbatical leave support (H.-G.C.) from the Korea Research Foundation (KRF-2003-013-C00044).

 DOI: 10.1002/anie.200461526 © 2005 Wiley-VCH Verlag GmbH & Co. KGaA, Weinheim

ated 1586 cm^{-1} shoulder absorption (also labeled **1′**). Subsequent visible and UV irradiation (not shown) decreased the 1586, 1551.0 cm^{-1} (**1′**) features in favor of the original 1581.0 and 1546.2 cm^{-1} bands (**1**) and slightly decreased the 1617.2 and 1587.5 cm^{-1} absorptions (**di**).

Table 1 lists these frequencies, their unshifted $^{13}CH_4$ counterparts, and analogous displaced CD_4 reaction product bands. These absorptions have H/D frequency ratios of 1.389–1.396, which characterize Zr–H stretching vibrations. Figure 2 shows spectra in the Zr–H and Zr–D stretching regions for reactions with CH_4, CH_2D_2, and CD_4 after UV irradiation. The important new information is that two new mixed H, D absorptions (marked **4**,**6** and **3**,**5**) appear between the low-wavenumber pair (**1**) in each region and one new mixed H, D band (marked **di**) appears between the high-wavenumber pair (**di**) in each region. Finally, all the **di** bands increase markedly on annealing.

Table 1: IR bands [cm^{-1}] observed for laser-ablated zirconium atom reactions with methane in excess neon.

CH_4	$^{13}CH_4$	CD_4	CH_2D_2	CH_2D_2	Identity
1617.2	1617.2	1158.1	1616.2	–	$[(CH_3)_2ZrH_2]$
			1602.2	1150.5	$[(CH_3)_2ZrHD]$
1587.5	1587.5	1142.6	1587.5	1142.5	$[(CH_3)_2ZrH_2]$
1586 sh	1586 sh	1136.9			$[H_2C{=}ZrH_2]$[a]
1581.0	1581.0	1133.1	1580.7	1132.7	$[H_2C{=}ZrH_2]$
1551.0	1551.0	1115.2	1550.1	1115.5	$[H_2C{=}ZrH_2]$[a]
1546.2	1546.2	1112.3	1545.5[b]	1112.5[c]	$[H_2C{=}ZrH_2]$
1375.1	1372.0	1009.0			$[(CH_3)_2ZrH_2]$
1125.0	1114.8	895.9	949.4		$[(CH_3)_2ZrH_2]$
757.0	737.4	687.0	750	718	$[H_2C{=}ZrH_2]$
634.5	629.8	499.4			$[H_2C{=}ZrH_2]$
593.4	592.2	–			$[(CH_3)_2ZrH_2]$
564.2	559.2	469.7			$[(CH_3)_2ZrH_2]$

[a] Bands owing to different neon packing configuration. [b] Additional bands at 1554.4 and 1571.0 cm^{-1} with annealing counterparts at 1558.7 and 1573.3 cm^{-1} for [CHD=ZrHD] isotopomers. [c] Additional bands at 1116.2 and 1129.2 cm^{-1} with annealing counterparts at 1118.9 and 1133.0 cm^{-1} for [CHD=ZrHD] isotopomers.

The lower frequency region contains four associated weaker absorptions at 757.0, 634.5, 593.4, and 564.4 cm^{-1} (not shown). On photolysis and annealing the 757.0, 634.5 cm^{-1} bands track with the low-wavenumber pair in the Zr–H stretching region (1581.0 and 1546.2 cm^{-1} (**1**)), and the 593.4 and 564.4 cm^{-1} absorptions follow the 1617.2, 1587.5 cm^{-1} pair (**di**). A weak 1375.1 cm^{-1} band and the 1125.0 cm^{-1} absorption (Figure 2c, **di**) also track with the **di** bands. The $^{13}CH_4$ and CD_4 isotopic counterparts are given in Table 1.

Calculations were performed for $[H_2C{=}ZrH_2]$ using the B3LYP density functional, and the global minimum energy C_1 structure with no symmetry is illustrated in Figure 3. The CH_2 group is tilted owing to the agostic C–H···Zr interaction. Additional calculations using the BPW91 functional and the MP2 method[17] gave similar skewed structures. When C_{2v} symmetry was imposed, the resulting planar structure which gives two imaginary frequencies is 0.8 kcal mol^{-1} higher in energy. Clearly, the planar form is unstable and relaxes along the imaginary CH_2 rocking and ZrH_2 wagging motions to the stable C_1 structure.

The C–H···Zr separation computed for the C_1 structure, 2.345 Å, is slightly longer

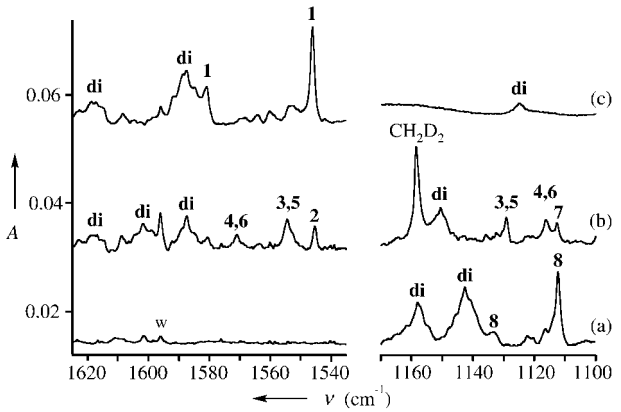


Figure 2. IR spectra in the 1620–1540 cm^{-1} Zr–H stretching and 1170–1100 cm^{-1} Zr–D stretching regions for laser-ablated Zr co-deposited with CH_4, CH_2D_2, and CD_4 in excess neon at 5 K for 45 min and subjected to $\lambda > 530$ and 240–380 nm irradiations. a) 0.4% CD_4 in neon, b) 0.6% CH_2D_2 in neon, and c) 0.4% CH_4 in neon. For discussion of the spectra see text; **1**–**8** indicate bands from the correspondingly numbered isotopmers in Scheme 1 **di** = isotopomers of $[(CH_3)_2ZrH_2]$, w = water.

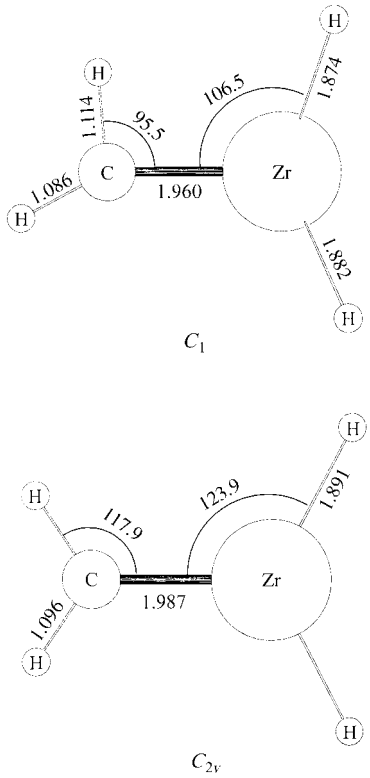


Figure 3. Minimum energy C_1 and C_{2v} symmetry structures computed for $[H_2C{=}ZrH_2]$ at the B3LYP/6-311++G(2d,p)/SDD level of theory.

 © 2005 Wiley-VCH Verlag GmbH & Co. KGaA, Weinheim

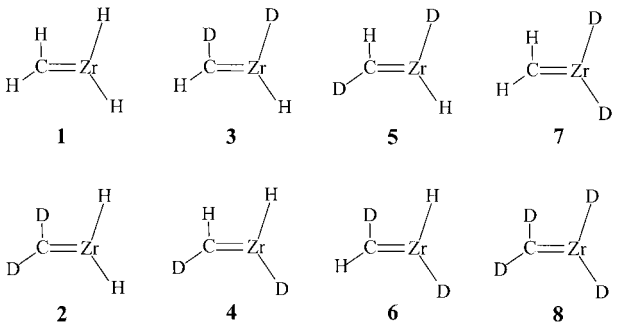
than agostic bonds measured for Cr and W complexes in crystals (2.24 and 2.27 Å),[6] but shorter than the agostic bond length computed (2.379 Å) for a model Ir complex using basis sets with polarization functions.[7] Since agostic bond energies in the 10–15 kcal mol^{-1} range have been determined for the Group 6 complexes,[6] our slightly longer agostic bond in [H_2C=ZrH_2] is probably almost as strong.

Computed frequencies listed in Table 2 provide the basis to identify agostic [H_2C=ZrH_2] from four observed frequencies and [CHD=ZrHD] isotopic modifications. The 1581.0 and 1546.2 cm^{-1} absorptions are due to symmetric and antisymmetric stretching modes of a ZrH_2 group: [ZrH_2] itself has been observed at 1519 cm^{-1} in solid argon and at 1530 cm^{-1} in solid neon.[18,19] The related satellite features at 1586 and 1551.0 cm^{-1} are due to a different neon packing configuration around the Zr center that is formed on annealing and destroyed on photolysis. The observed ZrH_2 modes are just below computed ZrH_2 modes for both structures, and these discrepancies are in line with that expected for the B3LYP density functional,[20] but structural assignment cannot be made on this basis. However, a definitive choice can be made from the [CHD=ZrHD] isotopomers since the symmetrical form has two and the agostic form has four such variants. Our calculations for *cis* and *trans* planar [CHD=ZrHD] predict the same ZrHD stretching modes ($\pm$0.1 cm^{-1}) for each isomer so only one DZr–H and one HZr–D mode would be observed in each region. However four such bands are found (Figure 2b **3**,**4**,**5**,**6**). Our calculations describe four distinct [CHD=ZrHD] isotopmers (**3**, **4**, **5**, and **6** in Scheme 1), and two of these isotopmers have Zr–H and Zr–D stretching modes that are different from those of the other two isotopmers. Our calculations predict **3** and **5** to have a Zr–H stretching mode 9.2 cm^{-1} above the strong antisymmetric stretching mode of **1** and a Zr–D stretching mode 13.3 cm^{-1} above the strong antisymmetric stretching mode of **8** (compare Figure 2 a–c). These bands are observed 8.3 and 17.0 cm^{-1} higher, respectively. In like manner our calculations find **4** and **6** to have strong Zr–H and Zr–D stretching modes 21.6 cm^{-1} above **1** and 4.2 cm^{-1} above **8**, and these bands are observed 24.8 and 4.0 cm^{-1} higher, respectively. The bands labeled **2** and **7** in Figure 2 arising from [D_2C=ZrH_2] and [H_2C=ZrD_2] are predicted to be shifted 0.1 cm^{-1} from **1** and **8**, and 0.7 and 0.2 cm^{-1} differences are found.

Table 2: Harmonic vibrational frequencies [cm^{-1}] computed for the C_1 and C_{2v} structures of [H_2C=ZrH_2] shown in Figure 3.

Mode Description	C_1		C_{2v}	
	Freq.	Int.[a]	Freq.	Int.[a]
CH_2 str	3172	(1)	3096	(8)
CH_2 str	2876	(6)	3014	(1)
ZrH_2 str	1640	(303)	1625	(379)
ZrH_2 str	1610	(574)	1582	(755)
CH_2 *scis*	1316	(17)	1314	(9)
C=Zr str	762	(134)	742	(130)
CH_2 wag	661	(151)	720	(206)
ZrH_2 *scis*	643	(91)	561	(16)
ZrH_2 rock	520	(9)	643	(0)
CH_2 twist	415	(22)	524	(0)
CH_2 rock	278	(131)	131 i	(0)
ZrH_2 wag	227	(95)	196 i	(471)

[a] IR intensities [km mol^{-1}]; i = imaginary frequencies.



Scheme 1. Isotopmers of [H_2C=ZrH_2].

The excellent agreement between experiment and theory for Zr–H and Zr–D stretching modes in four different CHD=ZrHD isotopomers (**3**, **4**, **5**, and **6**) with H or D in the agostic bonding position confirms the identification and the C_1 symmetry agostic structure for [H_2C=ZrH_2]. Although [H_2C=ZrH_2] is isoelectronic in the valence shell with the fundamentally and industrially important symmetrical, planar ethylene molecule, H_2C=CH_2, the d orbitals on zirconium support agostic bonding to one methylene hydrogen and reduce the symmetry in the [H_2C=ZrH_2] molecule.

Additional spectroscopic evidence for the C_1 structure is found in the lower frequency C–Zr stretching and CH_2 wagging modes, whose vibrational character and thus isotopic shifts depend heavily on molecular symmetry. The C_{2v} structure has a strong mixed C–Zr stretching, CH_2 bending mode computed at 742 cm^{-1} with an 8.9 cm^{-1} ^{13}C shift, whereas the C_1 structure has a strong mostly C–Zr stretching mode computed at 762 cm^{-1} with a 17.4 cm^{-1} ^{13}C shift. A pure ^{12}C–Zr diatomic oscillator would shift 26 cm^{-1} for ^{13}C–Zr in this region. Hence the observed 757.0 cm^{-1} absorption with 19.6 cm^{-1} ^{13}C shift fits the C_1 frequency prediction very well and the C_{2v} prediction very poorly. Our calculation for the C_1 structure slightly under estimates the ^{13}C shift and over estimates the D shift for this mode. The C_{2v} structure has a strong CH_2 wagging mode computed at 720 cm^{-1} whereas for the C_1 structure this mode is computed at 661 cm^{-1}. The associated absorption observed at 634.5 cm^{-1} is clearly in line with the C_1 and not the C_{2v} results, and the isotopic shifts are appropriate for this assignment.

The 1617.2 and 1587.5 cm^{-1} absorptions (labeled **di** in Figure 1) are assigned to dimethyl zirconium dihydride, [$(CH_3)_2ZrH_2$]. These frequencies may be compared to the antisymmetric stretching mode for [ZrH_4] observed at 1623 cm^{-1} in solid argon and at 1648 cm^{-1} in solid neon.[18,19] Our calculations predict a very stable molecule with effectively C_{2v} symmetry and strong Zr–H_2 stretching modes at 1673 and 1642 cm^{-1}, which are only 3.4% higher than the observed values, which is slightly better agreement than found above for [CH_2=ZrH_2]. The [$(CD_3)_2ZrD_2$] counterparts at 1158.1 and 1142.6 cm^{-1} and single intermediate -ZrHD species bands at 1602.2 and 1150.5 cm^{-1} confirm this assign-

 © 2005 Wiley-VCH Verlag GmbH & Co. KGaA, Weinheim

ment (Figure 2b). The next strongest lower frequency ZrH_2 bending and deformation modes predicted at 612 and 569 cm^{-1} are observed at 593.4 and 564.2 cm^{-1}, and weaker CH_3 bending and deformation modes computed at 1419 and 1166 cm^{-1} are found at 1375.1 and 1125.0 cm^{-1}. This is the first report of a Group 4 dimethyl dihydride. The $[(CH_3)_2TiF_2]$ analogue has been observed in similar Ti reactions with CH_3F.[12]

The zirconium atom reaction with methane apparently proceeds with excited zirconium atoms produced in the laser ablation process[16] or by irradiation,[21] this is because the C–H activation to form the $[CH_3ZrH]$ intermediate requires activation energy.[22] Then α-hydrogen transfer[23] gives $[H_2C{=}ZrH_2]$, Equation (1).

$$Zr^* + CH_4 \rightarrow [CH_3ZrH]^* \rightarrow [H_2C{=}ZrH_2] \quad (1)$$

Our calculations show that $[CH_3ZrH]$ ($^3A''$) and $[H_2C{=}ZrH_2]$ (^1A) have comparable energies.[24] However, the reaction with a second CH_4 molecule to form $[(CH_3)_2ZrH_2]$ appears to be spontaneous on annealing in solid neon. The $[(CH_3)_2ZrH_2]$ molecule is computed to be 65 kcal mol^{-1} more stable than $Zr(^3F)$ and two methane molecules, and the reaction in Equation (2) is exothermic by 44 kcal mol^{-1}. Alkylidene complexes are also known for their roles in C–H activation processes,[2] and the reaction in Equation (2) provides a simple example of the C–H activation process for methane.

$$[H_2C{=}ZrH_2] + CH_4 \rightarrow [(CH_3)_2ZrH_2] \quad (2)$$

Herein we have demonstrated how matrix IR spectroscopy and electronic structure calculations can work together to identify novel molecules with unique bonding interactions.

Received: August 3, 2004

Keywords: agostic interactions · C–H activation · density functional calculations · IR spectroscopy · matrix isolation

[1] R. R. Schrock, *Chem. Rev.* **2002**, *102*, 145.
[2] P. Legzdins, E. Tran, *J. Am. Chem. Soc.* **1997**, *119*, 5071.
[3] M. R. Buchmeiser, *Chem. Rev.* **2000**, *100*, 1565.
[4] R. H. Crabtree, *Chem. Rev.* **1985**, *85*, 245.
[5] R. H. Crabtree, D. G. Hamilton, *Adv. Organomet. Chem.* **1988**, *28*, 299.
[6] K. Zhang, A. A. Gonzalez, S. L. Mukerjee, S.-J. Chou, C. D. Hoff, K. A. Kubat-Martin, D. Barnhart, G. J. Kubas, *J. Am. Chem. Soc.* **1991**, *113*, 9170.
[7] G. Ujaque, A. C. Cooper, F. Maseras, O. Eisenstein, K. G. Caulton, *J. Am. Chem. Soc.* **1998**, *120*, 361.
[8] K. Wada, B. Craig, C. B. Pamplin, P. Legzdins, B. O. Patrick, I. Tsyba, R. Bau, *J. Am. Chem. Soc.* **2003**, *125*, 7035.
[9] M. M. Franci, W. J. Pietro, R. F. Hout, Jr., W. J. Hehre, *Organometallics* **1983**, *2*, 281.
[10] M. M. Franci, W. J. Pietro, R. F. Hout, Jr., W. J. Hehre, *Organometallics* **1983**, *2*, 815.
[11] T. R. Cundari, M. S. Gordon, *J. Am. Chem. Soc.* **1992**, *114*, 539.
[12] H.-G. Cho, L. Andrews, *J. Phys. Chem. A* **2004**, *108*, 6294.
[13] H.-G. Cho, L. Andrews, *J. Am. Chem. Soc.* **2004**, *126*, 10485.
[14] H.-G. Cho, L. Andrews, *Organometallics* **2004**, *23* 4357.
[15] G. V. Chertihin, L. Andrews, *J. Phys. Chem.* **1995**, *99*, 6356.
[16] L. Andrews, A. Citra, *Chem. Rev.* **2002**, *102*, *885*.
[17] Gaussian 98 (Revision A.7), M. J. Frisch, G. W. Trucks, H. B. Schlegel, G. E. Scuseria, M. A. Robb, J. R. Cheeseman, V. G. Zakrzewski, J. A. Montgomery, R. E. Stratmann, J. C. Burant, S. Dapprich, J. M. Millam, A. D. Daniels, K. N. Kudin, M. C. Strain, O. Farkas, J. Tomasi, V. Barone, M. Cossi, R. Cammi, B. Mennucci, C. Pomelli, C. Adamo, S. Clifford, J. Ochterski, G. A. Petersson, P. Y. Ayala, Q. Cui, K. Morokuma, D. K. Malick, A. D. Rabuck, K. Raghavachari, J. B. Foresman, J. Cioslowski, J. V. Ortiz, B. B. Stefanov, G. Liu, A. Liashenko, P. Piskorz, I. Komaromi, R. Gomperts, R. L. Martin, D. J. Fox, T. Keith, M. A. Al-Laham, C. Y. Peng, A. Nanayakkara, C. Gonzalez, M. Challacombe, P. M. W. Gill, B. G. Johnson, W. Chen, M. W. Wong, J. L. Andres, M. Head-Gordon, E. S. Replogle, J. A. Pople, Gaussian, Inc., Pittsburgh, PA, **1998**.
[18] G. V. Chertihin, L. Andrews, *J. Phys. Chem.* **1995**, *99*, 15004.
[19] Similar experiments with Zr and H_2 in excess neon give 1648 cm^{-1} for $[ZrH_4]$ and 1530 cm^{-1} for $[ZrH_2]$.
[20] I. Bytheway, M. W. Wong, *Chem. Phys. Lett.* **1998**, *282*, 219.
[21] A host of Zr* metastable states are observed below 2 eV: C. E. Moore, *Atomic Energy Levels*, Nat. Bur. Stds, Circular 467, Washington, D.C, **1952**.
[22] M. R. A. Bloomberg, P. E. M. Siegbahn, M. Swensson, *J. Am. Chem. Soc.* **1992**, *114*, 6095.
[23] R. H. Crabtree, *The Organometallic Chemistry of the Transition Metals*, Wiley, New York, **2001**, p. 190.
[24] We find $[CH_3ZrH]$ bound by 25.0 kcal mol^{-1} and $[H_2C{=}ZrH_2]$ bound by 21.3 kcal mol^{-1} relative to $Zr(^3F_2) + CH_4$.

 © 2005 Wiley-VCH Verlag GmbH & Co. KGaA, Weinheim

Enzyme Inhibitors

In Situ Click Chemistry: Enzyme-Generated Inhibitors of Carbonic Anhydrase II**

*Vani P. Mocharla, Benoit Colasson, Lac V. Lee, Stefanie Röper, K. Barry Sharpless, Chi-Huey Wong, and Hartmuth C. Kolb**

Traditional lead discovery approaches often rely on synthesizing and screening large numbers of compounds to identify the few inhibitor molecules that these libraries contain. In

[*] V. P. Mocharla, B. Colasson, L. V. Lee, S. Röper,
Prof. Dr. K. B. Sharpless, Prof. Dr. C.-H. Wong, Prof. Dr. H. C. Kolb
Department of Chemistry
The Scripps Research Institute
10550 North Torrey Pines Road, SP-227
La Jolla, CA 92037 (USA)
Fax: (+1) 858-784-7723
E-mail: hckolb@scripps.edu

[**] We thank the National Institute of General Medical Sciences, the National Institutes of Health (K.B.S., C.H.W.), the Skaggs Institute for Chemical Biology (H.C.K., K.B.S.; V.M. is a Skaggs Postdoctoral Fellow), and the W. M. Keck Foundation (K.B.S.) for financial support. We also thank Professor M. G. Finn and Professor V. V. Fokin for valuable discussions.

Supporting information for this article is available on the WWW under http://www.angewandte.org or from the author.

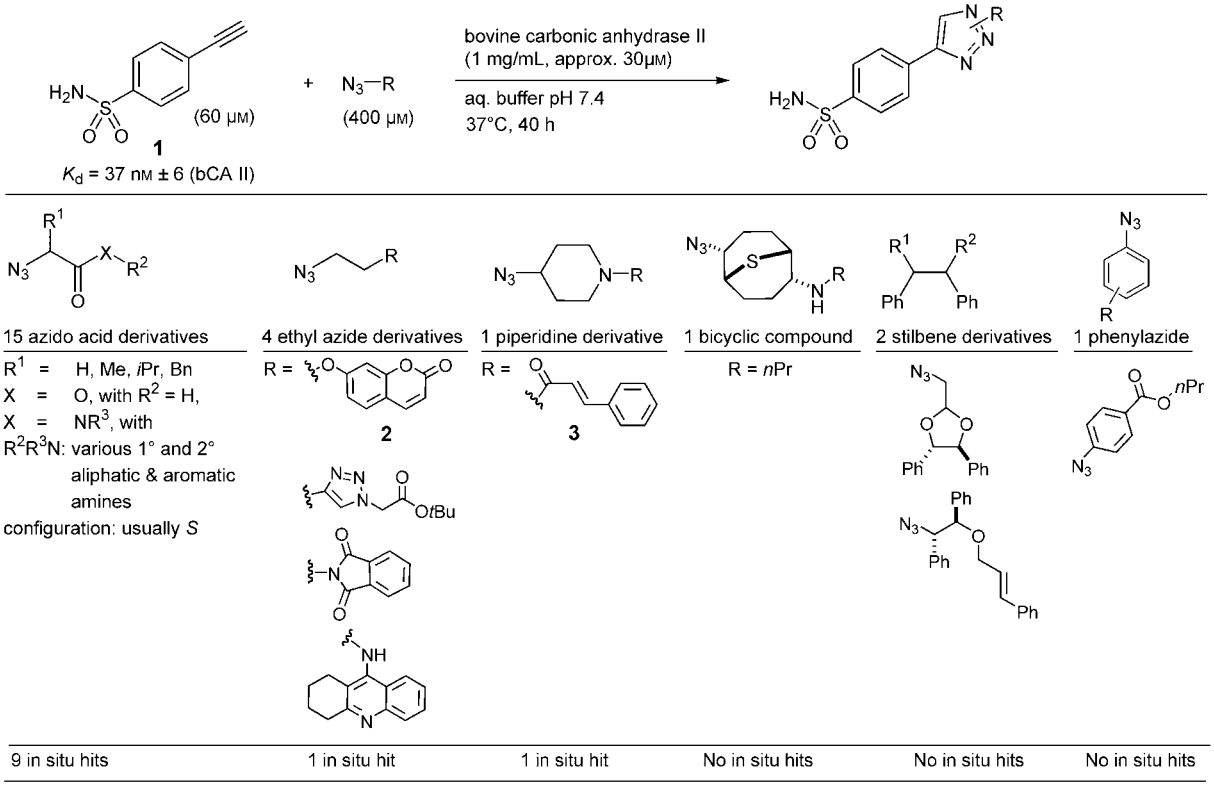
 © 2005 Wiley-VCH Verlag GmbH & Co. KGaA, Weinheim DOI: 10.1002/anie.200461580

contrast, target-guided synthesis (TGS) approaches employ the target proteins themselves for assembling potent inhibitors from reactive building blocks within the confines of their binding sites. In principle, hit discovery by TGS becomes independent of the actual function of the target because it relies solely on its ability to bind reagents and hold them in close proximity until they become connected through the "arranged" chemical reaction. Since the initial report of TGS by Rideout et al. 20 years ago,[1,2] several approaches have been developed: dynamic combinatorial chemistry,[3–12] stepwise target-guided synthesis,[13,14] and kinetically controlled target-guided synthesis.[15–23] The latter approach employs irreversible reactions to assemble highly reactive reagents (strong electrophiles or nucleophiles, metathesis catalysts etc.), which can cause side reactions or even destroy the enzymic target. In contrast, the in situ click chemistry approach to TGS[15,24] employs the completely bioorthogonal [1,3]-dipolar cycloaddition reaction between azides and acetylenes which was pioneered by Rolf Huisgen.[25] This process is self-contained, hence there are no external reagents, catalysts, or byproducts that might interfere, and the reactants themselves are "invisible" in biological milieu. Most importantly, the cycloaddition reaction, which is slow at room temperature, is accelerated tremendously when azide and acetylene groups are held together in close proximity to lead to irreversible formation of triazoles.[26–28] Previously, we have employed this approach to assemble acetylcholinesterase (AChE) inhibitors with subpicomolar binding affinities from reagents that carried known active- and peripheral-site binders.[15,24]

We now report the identification of novel carbonic anhydrase (CA) inhibitors using in situ click chemistry. Carbonic anhydrases are zinc-containing enzymes that catalyze the interconversion of HCO_3^- and CO_2. They are involved in key biological processes connected with respiration and the transport of CO_2/HCO_3^-, acid secretion and pH control, bone resorption, calcification, tumorigenicity, and many others.[29,30] Systemically and topically administered carbonic anhydrase inhibitors have long been used to control the elevated intraocular pressure associated with glaucoma.[31,32] Most inhibitors are aromatic or heteroaromatic sulfonamides[30,33,34] whose anion coordinates to the Zn^{2+} ion in the active site.[35]

Inspired by the work of Whitesides and co-workers on 4-carboxybenzenesulfonamide-derived carbonic anhydrase inhibitors,[33,36–39] we selected the acetylenic benzenesulfonamide **1** as a reactive scaffold for capturing complementary azide reagents to form "divalent" CA inhibitors in situ (see Scheme 1).[40] Scaffold **1** binds to bovine carbonic anhydrase II (bCA II) with nanomolar affinity ($K_d = 37$ nM ± 6), as determined by a competition assay with 5-(dimethylamino)-1-napthalenesulfonamide (dansyl amide, DNSA).[33,41] A total of 24 azide reagents, which cover 6 different structural themes, were employed as complementary reagents for in situ click chemistry screening. α-Azido carboxamide derivatives were best represented as we intended to probe for analogues of the peptidic carboxybenzenesulfonamide-derived inhibitors reported by Whitesides.[33,36–39]

The in situ click chemistry experiments were conducted in parallel by using 96-well microtiter plates. Each well con-



Scheme 1. In situ screening protocol and reagents. Control experiments to test for false-positive results were performed under identical conditions either in the absence of enzyme or in the presence of bCA II and ethoxazolamide (200 μM; see Figure 1).

 © 2005 Wiley-VCH Verlag GmbH & Co. KGaA, Weinheim

tained a mixture of bCA II (30 μM), the acetylene (60 μM), and a given azide reagent (400 μM) in phosphate buffer solution (pH 7.4).[41] The formation of the product was monitored by HPLC analysis and mass spectrometric detection through electrospray ionization and selected ion mode monitoring (LC/MS-SIM).[24] Under these conditions, over 99% of the active sites are occupied by ethynyl benzenesulfonamide (**1**), whereas the formation of triazole product from the enzyme-free background reaction remains below the LC/MS-SIM detection limit after 40 h at 37°C. In fact, the acetylene concentration can be raised to as high as 400 μM without producing detectable amounts of triazoles which demonstrates that the uncatalyzed reaction is extremely slow. Two sets of control experiments were conducted in parallel to test for false positives: Each acetylene/azide combination was incubated with mixtures of enzyme and the known active-site inhibitor ethoxazolamide (200 μM) (see Figure 1 and Table 2) and with bovine serum albumin (BSA) in place of bCA II.

Analysis of each reaction mixture by LC/MS-SIM revealed that 12 out of 24 reagent combinations had led to the formation of triazole products in the presence of the enzyme. Of these, 11 combinations did not form triazoles in the corresponding control experiments in the presence of BSA or enzyme/inhibitor, thereby validating these compounds as in situ hits and demonstrating that their formation required the enzyme active site to be accessible. Figure 1 illustrates the results for the acetylene/azide pair **1**/**4**. Most of the in situ hits are derived from α-substituted azido acid amides. The two exceptions are reagents **2** and **3**, which are azide derivatives of a coumarin and a piperidine, respectively. Conversely, 9 out of 12 azides that do not react in situ are not based on α-substituted azido acid platforms.

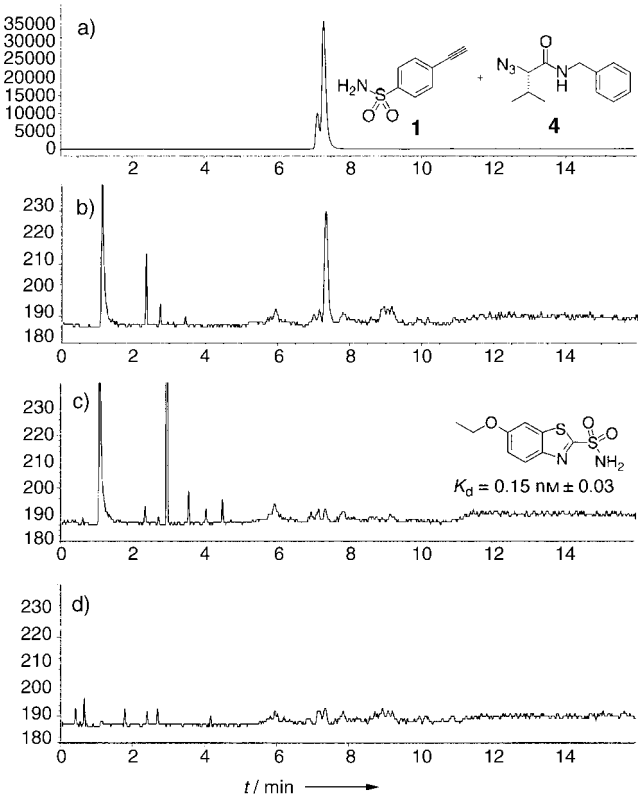


Figure 1. Results of in situ click chemistry between acetylene **1** and azide **4**, monitored by HPLC. a) Thermal reaction (85°C, 6 d): triazole products between 7.1 and 7.3 min; b) Reaction with bCA II (1 mg mL^{-1}; 37°C, 40 h): product at 7.3 min; c) bCA II (1 mg mL^{-1}), ethoxazolamide (200 μM; 37°C, 40 h); d) Bovine serum albumin (1 mg mL^{-1}) instead of bCA II (37°C, 40 h).

A comparison of the in situ reaction products with pure 1,4-disubstituted ("*anti*") triazoles, which were prepared by the Cu^{I}-catalyzed reaction of the precursor azides and acetylenes,[42,43] and *syn*/*anti*-triazoles, which were prepared by thermal cycloaddition, by LC/MS-SIM reveals the enzyme reaction to be highly *anti*-selective, in contrast to the thermal cycloaddition (see Supporting Information). The great *anti* selectivity further supports the notion that the formation of the product is enzyme controlled.

For the determination of inhibition constants at 25°C, all 24 *anti*-triazoles were synthesized from their respective acetylene/azide precursors under the copper-catalyzed reaction conditions recently developed in the laboratories of Sharpless/Fokin and Meldal.[42,43] The dissociation constants for these compounds were measured with a fluorescence-based assay,[39,44] which uses DNSA as a reporting ligand that is displaced by the test compound.[41]

Without exception, the in situ hit compounds display significantly higher binding affinities for bCA II (K_d = 0.2–7.1 nM) than the acetylene scaffold **1** (K_d = 37 nM ± 6) or the azide reagents (high micromolar affinities and above) from which they are derived (Table 1 and Table 2). These results demonstrate that the azide/acetylene in situ click chemistry can be used to produce enzyme inhibitors in which only one of the components binds well to the target. The dissociation constants of the triazoles prepared in situ compare favorably with those of the drugs acetazolamide (K_d = 6.4 nM) and ethoxazolamide (K_d = 0.15 nM; see Table 2). Of the six azide chemotypes in this initial screen (see Scheme 1), α-azido acid derived triazolyl benzenesulfonamides gave the most potent inhibitors with subnanomolar dissociation constants (Table 1). The amide residue can vary over a wide range without leaving the subnanomolar regime which suggests that the azido acid residues, and not the amide substituents, are responsible for high activity. From the reagents that were not derived from azido acids (Table 2), only the hydrophobic stilbene derivative **7** gave a product with low nanomolar activity. The other structural types were much less active: the runners-up were the coumarin and piperidine derivatives **8** and **9**, which displayed a 5 to 7.5 times higher affinity than the starting acetylene **1**.

Interestingly, six out of ten compounds that were not formed by the enzyme were also highly active with dissociation constants of less than 7.5 nM. These results demonstrate that compounds that are formed in situ are very likely to be potent inhibitors—in this case without exception—whereas the reverse is not true which leads to "false negatives" from the perspective of in situ screening. We do not regard this as a drawback because the in situ hits invariably display high binding affinities, that is, there are no "false positives". The best in situ hits (Table 1) have a 185-times higher binding

 © 2005 Wiley-VCH Verlag GmbH & Co. KGaA, Weinheim

Table 1: Summary of in situ click chemistry experiments and dissociation constants of azido acid derived triazolyl benzenesulfonamides with K_d values of less than 7.5 nM.

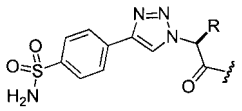
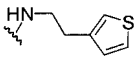
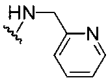
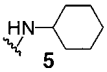
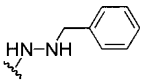
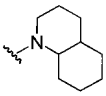
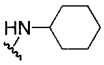
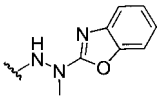
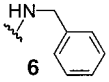
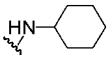
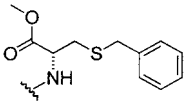
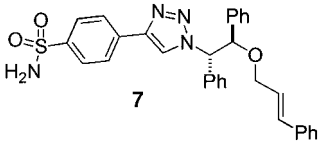
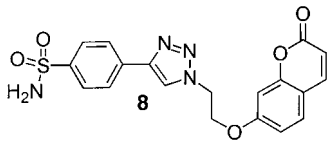
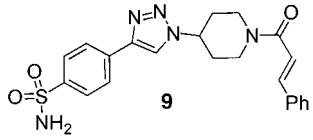
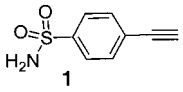
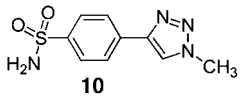
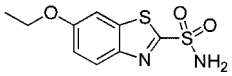
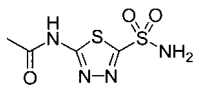
	R	In situ hit	K_d [nM]	
				high affinity
	*i*Pr	Yes	0.2–0.5	
	Bn	Yes	0.2–0.4	
	*i*Pr	Yes	0.4–0.5	
 **5**	Bn	Yes	0.5–0.9	
	Bn	No	0.5 ± 0.1	
	Bn	No	0.5 ± 0.1	
	*i*Pr	Yes	0.8 ± 0.2	
	Bn	Yes	0.9 ± 0.1	
	H	No	1.1–1.4	
 **6**	*i*Pr	Yes	1.9–2.3	
	*i*Pr	Yes	2.4 ± 0.4	
	*i*Pr	No	2.6 ± 0.2	
	H	No	7.0 ± 0.5	
				low affinity

Table 2: Summary of in situ click chemistry experiments and dissociation constants.

Reagent	In situ hit	K_d [nM]
 **7**	No	1.0–1.5
 **8**	Yes	4.9 ± 0.7
 **9**	Yes	7.1 ± 0.4
 **1**	N/A	37 ± 6
 **10**	N/A	38 ± 10
 ethoxazolamide	N/A	0.15 ± 0.03
 acetazolamide	N/A	6.4 ± 0.9

affinity to bCA II than the scaffold **1**, and the worst in situ hits are still more than five times as potent.

Even though the inhibitors were formed by bovine CA II, they also strongly inhibit the human enzyme (hCA II). Compounds **5** and **6** have dissociation constants of 1.2 nM (± 0.3) and 0.9 nM (± 0.2), respectively; that is, their potency is comparable to acetazolamide ($K_d = 0.9$ nM ± 0.05).[45]

Interested to what extent the binding affinities of the in situ products are influenced by the newly-formed triazole moiety, for example, by changing the pK_a value of the sulfonamide, we prepared *N*-methyltriazole **10** (Table 2). Its dissociation constant ($K_d = 38$ nM ± 10) is almost identical to that of the parent acetylene **1** which demonstrates that the triazole does not affect the binding affinity significantly and suggests that the increased affinity of the hit compounds formed in situ is largely provided by favorable binding interactions with substituents that are more remote on the azide component. Furthermore, a lack of direct triazole–protein interactions would indicate that the [3+2] cycloaddition reaction in this system is more dependent on entropic stabilization of the transition state, in contrast to the AChE system, in which the presence of strong protein–triazole attractive interactions suggests that the rate enhancement is partially due to enthalpic stabilization effects.[16] All in all, the triazole-containing linker appears to be suboptimal in the bCA II system as the observed dissociation constants are much larger than the theoretical optimum of approximately 50 pM, which is calculated based on the known affinities of scaffold **1** ($K_d = 37$ nM) and the azide reagents (high micromolar to low millimolar) and assumes the complete absence of positive or negative linker effects.[46] We are currently optimizing the linker with the aid of in situ click chemistry and investigating the ligand/protein interactions on a molecular level by X-ray crystallography.

Received: August 9, 2004
Revised: September 27, 2004

 © 2005 Wiley-VCH Verlag GmbH & Co. KGaA, Weinheim

Keywords: azides · enzymes · high-throughput screening · inhibitors · template synthesis

[1] D. Rideout, *Science* **1986**, *233*, 561 – 563.
[2] D. Rideout, T. Calogeropoulou, J. Jaworski, M. McCarthy, *Biopolymers* **1990**, *29*, 247 – 262.
[3] I. Huc, J.-M. Lehn, *Proc. Natl. Acad. Sci. USA* **1997**, *94*, 2106 – 2110.
[4] O. Ramström, J.-M. Lehn, *ChemBioChem* **2000**, *1*, 41 – 48.
[5] J.-M. Lehn, A. V. Eliseev, *Science* **2001**, *291*, 2331 – 2332.
[6] T. Bunyapaiboonsri, O. Ramström, S. Lohmann, J.-M. Lehn, L. Peng, M. Goeldner, *ChemBioChem* **2001**, *2*, 438 – 444.
[7] A. V. Eliseev, *Pharm. News* **2002**, *9*, 207 – 215.
[8] O. Ramström, J.-M. Lehn, *Nat. Rev. Drug Discovery* **2002**, *1*, 26 – 36.
[9] S. Otto, *Curr. Opin. Drug Discovery Dev.* **2003**, *6*, 509 – 520.
[10] D. A. Erlanson, A. C. Braisted, D. R. Raphael, M. Randal, R. M. Stroud, E. M. Gordon, J. A. Wells, *Proc. Natl. Acad. Sci. USA* **2000**, *97*, 9367 – 9372.
[11] D. A. Erlanson, J. W. Lam, C. Wiesmann, T. N. Luong, R. L. Simmons, W. L. DeLano, I. C. Choong, M. T. Burdett, W. M. Flanagan, D. Lee, E. M. Gordon, T. O'Brien, *Nat. Biotechnol.* **2003**, *21*, 308 – 314.
[12] O. Ramström, S. Lohmann, T. Bunyapaiboonsri, J.-M. Lehn, *Chem. Eur. J.* **2004**, *10*, 1711 – 1715.
[13] D. J. Maly, I. C. Choong, J. A. Ellman, *Proc. Natl. Acad. Sci. USA* **2000**, *97*, 2419 – 2424.
[14] J. W. Kehoe, D. J. Maly, D. E. Verdugo, J. I. Armstrong, B. N. Cook, Y.-B. Ouyang, K. L. Moore, J. A. Ellman, C. R. Bertozzi, *Bioorg. Med. Chem. Lett.* **2002**, *12*, 329 – 332.
[15] W. G. Lewis, L. G. Green, F. Grynszpan, Z. Radić, P. R. Carlier, P. Taylor, M. G. Finn, K. B. Sharpless, *Angew. Chem.* **2002**, *114*, 1095 – 1099; *Angew. Chem. Int. Ed.* **2002**, *41*, 1053 – 1057.
[16] Y. Bourne, H. C. Kolb, Z. Radić, K. B. Sharpless, P. Taylor, P. Marchot, *Proc. Natl. Acad. Sci. USA* **2004**, *101*, 1449 – 1454.
[17] J. Inglese, S. J. Benkovic, *Tetrahedron* **1991**, *47*, 2351 – 2364.
[18] D. L. Boger, N.-E. Haynes, P. A. Kitos, M. S. Warren, J. Ramcharan, A. E. Marolewski, S. J. Benkovic, *Bioorg. Med. Chem.* **1997**, *5*, 1817 – 1830.
[19] S. E. Greasley, T. H. Marsilje, H. Cai, S. Baker, S. J. Benkovic, D. L. Boger, I. A. Wilson, *Biochemistry* **2001**, *40*, 13538 – 13547.
[20] R. Nguyen, I. Huc, *Angew. Chem.* **2001**, *113*, 1824 – 1826; *Angew. Chem. Int. Ed.* **2001**, *40*, 1774 – 1776.
[21] K. C. Nicolaou, R. Hughes, S. Y. Cho, N. Winssinger, C. Smethurst, H. Labischinski, R. Endermann, *Angew. Chem.* **2000**, *112*, 3981 – 3986; *Angew. Chem. Int. Ed.* **2000**, *39*, 3823 – 3828.
[22] K. C. Nicolaou, R. Hughes, S. Y. Cho, N. Winssinger, H. Labischinski, R. Endermann, *Chem. Eur. J.* **2001**, *7*, 3824 – 3843.
[23] A. T. Poulin-Kerstien, P. B. Dervan, *J. Am. Chem. Soc.* **2003**, *125*, 15811 – 15821.
[24] R. Manetsch, A. Krasinski, Z. Radić, J. Raushel, P. Taylor, K. B. Sharpless, H. C. Kolb, *J. Am. Chem. Soc.* **2004**, *126*, 12809 – 12818.
[25] R. Huisgen in *1,3-Dipolar Cycloaddition Chemistry*, *Vol. 1* (Ed.: A. Padwa), Wiley, New York, **1984**, pp. 1 – 176.
[26] W. L. Mock, T. A. Irra, J. P. Wepsiec, T. L. Manimaran, *J. Org. Chem.* **1983**, *48*, 3619 – 3620.
[27] W. L. Mock, T. A. Irra, J. P. Wepsiec, M. Adhya, *J. Org. Chem.* **1989**, *54*, 5302 – 5308.
[28] W. L. Mock, *Top. Curr. Chem.* **1995**, *175*, 1 – 24.
[29] S. J. Dodgson in *Carbonic Anhydrases* (Ed.: S. J. Dodgson), Plenum, New York, **1991**, pp. 3 – 14.
[30] C. T. Supuran, A. Scozzafava, A. Casini, *Med. Res. Rev.* **2003**, *23*, 146 – 189.
[31] M. F. Sugrue, P. Gautheron, C. Schmitt, M. P. Viader, P. Conquet, R. L. Smith, N. N. Share, C. A. Stone, *J. Pharmacol. Exp. Ther.* **1985**, *232*, 534 – 540.
[32] M. F. Sugrue, R. L. Smith, *Annu. Rep. Med. Chem.* **1985**, *20*, 83 – 91.
[33] J. Gao, X. Cheng, R. Chen, G. B. Sigal, J. E. Bruce, B. L. Schwartz, S. A. Hofstadler, G. A. Anderson, R. D. Smith, G. M. Whitesides, *J. Med. Chem.* **1996**, *39*, 1949 – 1955.
[34] M. T. DuPriest, P. W. Zinke, R. E. Conrow, D. Kuzmich, A. P. Dantanarayana, S. J. Sproull, *J. Org. Chem.* **1997**, *62*, 9372 – 9375.
[35] J. Y. Liang, W. N. Lipscomb, in *Carbonic Anhydrase, Proc. Int. Workshop* (Eds.: F. Botre, G. Gros, B. T. Storey), VCH, Weinheim, **1990**, pp. 50 – 64.
[36] B. A. Grzybowski, A. V. Ishchenko, C.-Y. Kim, G. Topalov, R. Chapman, D. W. Christianson, G. M. Whitesides, E. I. Shakhnovich, *Proc. Natl. Acad. Sci. USA* **2002**, *99*, 1270 – 1273.
[37] G. B. Sigal, G. M. Whitesides, *Bioorg. Med. Chem. Lett.* **1996**, *6*, 559 – 564.
[38] P. A. Boriack, D. W. Christianson, J. Kingery-Wood, G. M. Whitesides, *J. Med. Chem.* **1995**, *38*, 2286 – 2291.
[39] A. Jain, S. G. Huang, G. M. Whitesides, *J. Am. Chem. Soc.* **1994**, *116*, 5057 – 5062.
[40] D. F. Hayman, G. B. Jackman, V. Petrow, O. Stephenson, A. M. Wild, *J. Pharm. Pharmacol.* **1964**, *16*, 677 – 689.
[41] See Supporting Information for experimental details.
[42] V. V. Rostovtsev, L. G. Green, V. V. Fokin, K. B. Sharpless, *Angew. Chem.* **2002**, *114*, 2708 – 2711; *Angew. Chem. Int. Ed.* **2002**, *41*, 2596 – 2599.
[43] C. W. Tornøe, C. Christensen, M. Meldal, *J. Org. Chem.* **2002**, *67*, 3057 – 3064.
[44] R. F. Chen, J. C. Kernohan, *J. Biol. Chem.* **1967**, *242*, 5813 – 5823.
[45] The fluorometric assay was performed as described in the Supporting Information for bovine CA II. The dissociation constant K_d of DNSA and human CA II was determined to be 0.43 μM by titration of hCA II with DNSA.
[46] If it is assumed that the linker, that is, the triazole, does not participate in any way in binding, the free energy of binding for the divalent inhibitor can be calculated as the sum of the free energies of the individual components which in turn provides approximate values for the corresponding dissociation constant (see Ref. [39]).

 © 2005 Wiley-VCH Verlag GmbH & Co. KGaA, Weinheim

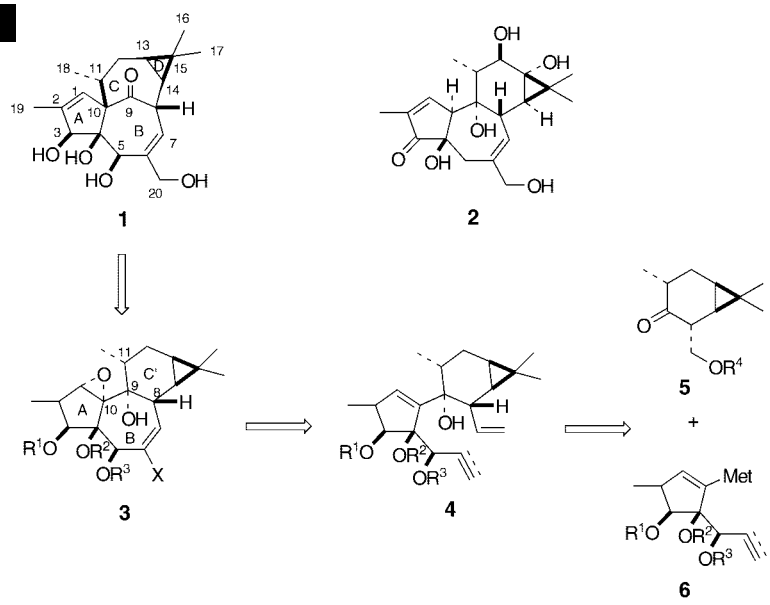
Synthetic Methods

Rapid Access to the "in,out"-Tetracyclic Core of Ingenol**

*Oleg L. Epstein and Jin Kun Cha**

Ingenol (**1**), a prototypical diterpene of ingenanes, was first isolated from *Euphorbia ingens* by Hecker and co-workers.[1] Along with esters of the structurally related phorbol (**2**), the naturally occurring C3-monoesters of **1** are known to be among the most potent tumor promoters. The mode of action of these esters at the molecular level is believed to be associated with binding to protein kinase C, a key enzyme involved in cell signal transduction, and with mimicking the function of 1,2-diacylglycerol, the endogenous activator of the enzyme.[2] Surprisingly, certain ester derivatives of **1** were reported to possess anti-leukemic and anti-HIV activity.[3] Biological activity of this class of natural products is thus significantly altered by subtle, yet little-understood, structural modifications. For more than two decades these structurally complex molecules have attracted many studies directed toward total syntheses.[4,5] The highly strained "inside–outside" intrabridgehead stereochemistry of the BC ring system of **1** presents a particularly taxing synthetic challenge.[6] Several attractive solutions were developed by several groups,[7,8] culminating in an elegant total synthesis of (±)-**1** by Winkler et al.[9] followed by another by Kuwajima and co-workers.[10] Nonetheless, an efficient, convergent approach to **1** remains highly desirable. To this end, we report herein a rapid assembly of the carbocyclic core of **1** by a pinacol rearrangement.

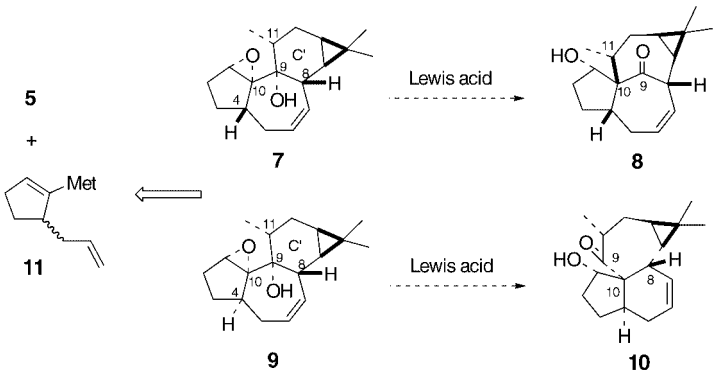
Our key strategy for addressing the requisite inside–outside *trans* stereochemistry of **1** with concomitant, diastereoselective construction of the quaternary C10 center was based on a 1,2-alkyl shift (**3**→**1**) at a late stage by adaptation of the Tsuchihashi–Suzuki rearrangement of 2,3-epoxy alcohols or silyl ethers (Scheme 1).[11–13] We speculated that a related 1,2-alkyl shift may well be involved in the biosynthesis of **1** for the conversion of its ABC′D ring system into the ABCD ring system.[14,15] Among several possible variations within this approach (A + C′D→ABC′D), a most expedient route to **3** seemed available by ring-closing olefin metathesis of **4** for the formation of the rigid, yet relatively strain-free, seven-membered ring B.[16] In turn, **4** could be prepared by straightforward coupling of two fragments of comparable complexity, **5** and **6**. Particularly attractive was the innate



Scheme 1. Retrosynthetic analysis of **1**. X = alkyl or alkenyl group, Met = metal.

convergence of the overall approach which could provide a most expeditious route to **1** and its analogues.

For our preliminary study, we chose to employ a simplified derivative of **6**, namely **11**, which is devoid of oxygen and remaining functionalities, to establish the feasibility of a convergent synthesis of the complete tetracyclic core of **1** (Scheme 2). According to molecular models, the stereochemistry about C4 was considered to be of principal importance to the key Lewis acid catalyzed rearrangement of **3** with respect to the antiperiplanar stereoelectronic requirements to ensure the desired migration of the C9–C11 (ingenol numbering) bond. With the natural configuration at C4 (e.g. **7**), the epoxide C10–O bond is antiperiplanar to the C9–C11 bond as required for the conversion of **7**→**8**, whereas the C8–C9 bond is nearly orthogonal. However, in the case of the opposite configuration at C4 (e.g. **9**), migration of only the undesired C8–C9 bond that occupies the antiperiplanar alignment could occur. These considerations prompted us to utilize racemic **11**



Scheme 2. Met = metal.

[*] Dr. O. L. Epstein, Prof. J. K. Cha
Department of Chemistry
Wayne State University
Detroit, MI 48202 (USA)
Fax: (+1) 313-577-8822
E-mail: jcha@chem.wayne.edu

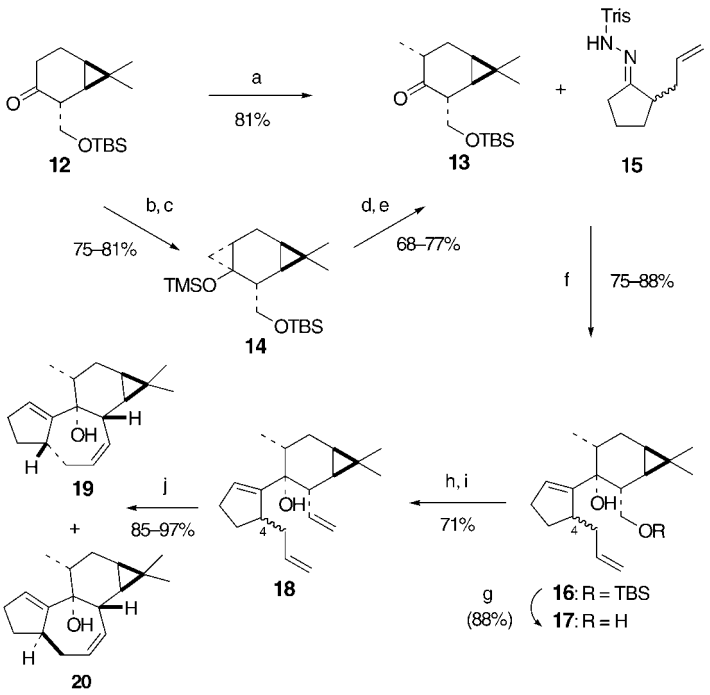
[**] This work was supported by the National Institutes of Health (GM35956).

Supporting information for this article is available on the WWW under http://www.angewandte.org or from the author.

 DOI: 10.1002/anie.200461807 © 2005 Wiley-VCH Verlag GmbH & Co. KGaA, Weinheim

so that the stereochemical outcomes of both C4 epimers could be assessed simultaneously.

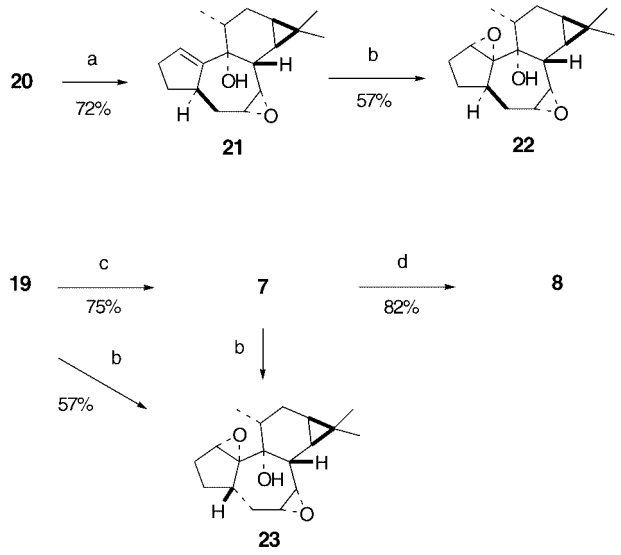
Our study began with the ketone **12**, which was readily prepared in large quantities from (+)-3-carene according to the method of Paquette et al. (Scheme 3).[17] Formation of the



Scheme 3. Reagents and conditions: a) LiHMDS, MeI, −78 to 0 °C; b) LiHMDS, TMSCl; c) Et_2Zn, CH_2I_2; d) K_2CO_3, MeOH; e) $[Pt_2Cl_4(C_2H_4)_2]$; f) *t*BuLi (2 equiv); g) TBAF; h) SO_3Py, DMSO, *i*Pr_2NEt; i) Ph_3PCH_3Br, NaHMDS; j) RCM. HMDS = hexamethyldisilazide, TBS = *tert*-butyldimethylsilyl, Tris = 2,4,6-triisopropylbenzenesulfonyl, TMSCl = trimethylsilyl chloride, TBAF = tetra-*n*-butylammonium fluoride, Py = pyridine, DMSO = dimethylsulfoxide, RCM = ring-closing metathesis.

kinetic enolate of **12** with LiHMDS (lithium hexamethyldisilazide) followed by alkylation with methyl iodide yielded **13** as a single diastereomer in 81% yield. Alternatively, **13** was obtained through subsequent ring opening of **14** with $[Pt_2Cl_4(C_2H_4)_2]$. This served to corroborate the α stereochemistry of the C11 methyl group in **13** from NOE measurements (interaction between the hydrogen atom at C13 and the hydrogen atoms of the methyl group at C18 in **13**). Addition of the 5-allylcyclopentenyl subunit to **13** was best achieved by means of the lithium reagent of **15**, which was prepared in situ by the Shapiro reaction,[18] to yield **16** in 75–88% yield. To set the stage for the construction of the seven-membered ring B, **16** was then converted into **18** by standard methods to give an inseparable 1:1 mixture of the two C4 epimers in 62% overall yield. Ring-closing olefin metathesis of **18** (5 mM in CH_2Cl_2) with Grubbs' second-generation catalyst (10 mol%) and heating at reflux proceeded smoothly to give **19** and **20** in excellent yield.

Following chromatographic separation of **19** and **20**, treatment of the less-polar isomer **20** with MCPBA (*m*-chloroperbenzoic acid) or *t*BuOOH–$VO(acac)_2$ resulted in regioselective epoxidation at the C6–C7 double bond to furnish **21** (Scheme 4). Upon prolonged exposure to MCPBA, the latter was converted into bisepoxide **22**. In sharp contrast, epoxidation of the more-polar isomer **19** with *t*BuOOH–$VO(acac)_2$ afforded the desired C1–C10 epoxide **7** in 75% yield. The bisepoxide **23** was obtained by treating **7** with MCPBA. On the basis of these conspicuous differences in the epoxidation of **19** and **20**, their C4 configuration was assigned as shown in Scheme 3. Inspection of molecular models clearly reveals that the hydroxy group at C9 in **20** is located in closer proximity to the C6–C7 double bond. Finally, upon exposure of epoxide **7** to $AlMe_3$ (3 equiv), the key Lewis acid mediated semipinacol rearragement proceeded cleanly to afford the desired ingenane **8** as the sole isomer (82% yield) which contains the complete skeleton of ingenol (**1**). The "inside–outside" stereochemistry of **8** was in accord with mechanistic considerations and difference-NOE measurements. Irradiation of the hydrogen atom at C8 ($\delta = 3.85$ ppm) showed diagnostic nuclear Overhauser enhancements at C(4)–H, C(11)–H, C(12)–H_β, and C(16)–Me.[7b] The indicated stereochemistry was subsequently confirmed by single crystal X-ray analysis of **8**.[19] Note that under identical conditions, bisepoxide **22** produced a complex mixture of polar products presumably owing to ring opening of epoxide(s), whereas bisepoxide **23** was found to be relatively inert to rearrangement conditions.



Scheme 4. Reagents and conditions: a) MCPBA or *t*BuOOH/$VO(acac)_2$; b) MCPBA; c) *t*BuOOH/$VO(acac)_2$; d) $AlMe_3$, CH_2Cl_2, −78 to 0 °C.

In conclusion, the demanding "inside–outside" stereochemistry of ingenol (**1**) and the stereoselective construction of the quaternary center at C10 have been successfully addressed by the pinacol-type rearrangement of an epoxy alcohol to develop a convergent synthesis of the fully assembled tetracyclic core of **1**. Thus, **8** was prepared in 8 steps from the known, readily available ketone **12**. We believe our approach holds promise in completing a concise, convergent synthesis of ingenol itself and its analogues by preinstallation of all the necessary functionalities in fragment

 © 2005 Wiley-VCH Verlag GmbH & Co. KGaA, Weinheim

6 prior to its coupling to **5**. A unified approach to the syntheses of the ingenane, tigliane, and daphnane diterpenes is also anticipated to be forthcoming and will be reported in due course.

Received: August 27, 2004

Keywords: epoxidation · natural products · rearrangement · ring-closing metathesis · terpenoids

[1] a) K. Zechmeister, F. Brandl, W. Hoppe, E. Hecker, H. J. Opferkuch, W. Adolf, *Tetrahedron Lett.* **1970**, *11*, 4075; b) H. J. Opferkuch, E. Hecker, *Tetrahedron Lett.* **1974**, *15*, 261; c) E. Hecker, *Pure Appl. Chem.* **1977**, *49*, 1423.

[2] a) Y. Nishizuka, *Science* **1986**, *233*, 305; b) A. M. Jeffery, R. M. J. Liskamp, *Proc. Natl. Acad. Sci. USA* **1986**, *83*, 241; c) P. A. Wender, K. F. Koehler, N. A. Sharkey, M. L. Dell'Aquila, P. M. Blumberg, *Proc. Natl. Acad. Sci. USA* **1986**, *83*, 4214; d) H. Nakamura, Y. Kishi, M. A. Pajares, R. R. Rando, *Proc. Natl. Acad. Sci. USA* **1989**, *86*, 9672.

[3] a) S. M. Kupchan, I. Uchida, A. R. Branfman, R. G. Dailey, Jr., B. Y. Fei, *Science* **1976**, *191*, 571; b) M. Fujiwara, K. Ijichi, K. Tokuhisa, K. Katsuura, S. Shigeta, K. Konno, G. Y. S. Wang, D. Uemura, T. Yokota, M. Baba, *Antimicrob. Agents Chemother.* **1996**, *40*, 271; c) M. Fujiwara, K. Ijichi, K. Tokuhisa, K. Katsuura, G.-Y.-S. Wang, D. Uemura, S. Shigeta, K. Konno, T. Yokota, M. Baba, *Antiviral Chem. Chemother.* **1996**, *7*, 230.

[4] For a total synthesis of **2**, see: a) P. A. Wender, H. Kogen, H. Y. Lee, J. D. Munger, Jr., R. S. Wilhelm, P. D. Williams, *J. Am. Chem. Soc.* **1989**, *111*, 8957; b) P. A. Wender, F. E. McDonald, *J. Am. Chem. Soc.* **1990**, *112*, 4956; c) P. A. Wender, K. D. Rice, M. E. Schnute, *J. Am. Chem. Soc.* **1997**, *119*, 7897.

[5] For a formal synthesis of **2**, see: K. Lee, J. K. Cha, *J. Am. Chem. Soc.* **2001**, *123*, 5590.

[6] For excellent reviews, see: a) S. Kim, J. D. Winkler, *Chem. Soc. Rev.* **1997**, *26*, 387; b) R. W. Alder, S. P. East, *Chem. Rev.* **1996**, *96*, 2097.

[7] a) R. L. Funk, T. A. Olmstead, M. Parvez, *J. Am. Chem. Soc.* **1988**, *110*, 3298; b) R. L. Funk, T. A. Olmstead, M. Parvez, J. B. Stallman, *J. Org. Chem.* **1993**, *58*, 5873; c) J. H. Rigby, V. de Sainte Claire, S. V. Cuisiat, M. J. Heeg, *J. Org. Chem.* **1996**, *61*, 7992; d) J. H. Rigby, B. Bazin, J. H. Meyer, F. Mohammadi, *Org. Lett.* **2002**, *4*, 799; e) H. Kigoshi, Y. Suzuki, K. Aoki, D. Uemura, *Tetrahedron Lett.* **2000**, *41*, 3927; f) H. Tang, N. Yusuff, J. L. Wood, *Org. Lett.* **2001**, *3*, 1563.

[8] For stereocontrolled construction of an ingenol prototype that has *cis* stereochemistry, see: L. A. Paquette, R. J. Ross, J. P. Springer, *J. Am. Chem. Soc.* **1988**, *110*, 6192.

[9] J. D. Winkler, M. B. Rouse, M. F. Greaney, S. J. Harrison, Y. T. Jeon, *J. Am. Chem. Soc.* **2002**, *124*, 9726.

[10] K. Tanino, K. Onuki, K. Asano, M. Miyashita, T. Nakamura, Y. Takahashi, I. Kuwajima, *J. Am. Chem. Soc.* **2003**, *125*, 1498.

[11] a) K. Maruoka, M. Hasegawa, H. Yamamoto, K. Suzuki, M. Shimazaki, G.-i. Tsuchihashi, *J. Am. Chem. Soc.* **1986**, *108*, 3827; b) T. Saito, T. Suzuki, M. Morimoto, C. Akiyama, T. Ochiai, K. Takeuchi, T. Matsumoto, K. Suzuki, *J. Am. Chem. Soc.* **1998**, *120*, 11633; c) T. Nagasawa, K. Taya, M. Kitamura, K. Suzuki, *J. Am. Chem. Soc.* **1996**, *118*, 8949, and references therein.

[12] For a general review, see: a) D. J. Coveney, "*The Semipinacol and Other Rearrangements*" in *Comprehensive Organic Synthesis*, *Vol. 3* (Eds.: B. M. Trost, I. Fleming), Pergamon, Oxford, UK, **1991**, Chap. 3.4, pp. 777–801; For recent studies from other laboratories, see: b) C. M. Marson, A. J. Walker, J. Pickering, A. D. Hobson, R. Wrigglesworth, S. J. Edge, *J. Org. Chem.* **1993**, *58*, 5944; c) M. E. Jung, D. C. D'Amico, *J. Am. Chem. Soc.* **1995**, *117*, 7379; d) C.-A. Fan, B.-M. Wang, Y.-Q. Tu, Z.-L. Song, *Angew. Chem.* **2001**, *113*, 4020; *Angew. Chem. Int. Ed.* **2001**, *40*, 3877.

[13] For reviews on enantioselective construction of quaternary centers, see: a) K. Fuji, *Chem. Rev.* **1993**, *93*, 2037; b) E. J. Corey, A. Guzman-Perez, *Angew. Chem.* **1998**, *110*, 402; *Angew. Chem. Int. Ed.* **1998**, *37*, 388; c) J. Christoffers, A. Mann, *Angew. Chem.* **2001**, *113*, 4725; *Angew. Chem. Int. Ed.* **2001**, *40*, 4591.

[14] a) A recent total synthesis of **1** by Kuwajima and co-workers also utilized a Tsuchihashi–Suzuki rearrangement, but in a different ring system (see ref [10]; b) A retropinacol rearrangement of ingenol to a tigliane derivative was known (see also ref [1c]): G. Appendino, G. C. Tron, G. Cravotto, G. Palmisano, R. Annunziata, G. Baj, N. Surico, *Eur. J. Org. Chem.* **1999**, 3413; c) See also: L. A. Paquette, Z. Zhao, F. Gallou, J. Liu, *J. Am. Chem. Soc.* **2000**, *122*, 1540.

[15] It may be noted that our successful synthesis of (+)-asteltoxin evolved from a biosynthetic postulate that featured a related 1,2-alkyl shift: a) K. D. Eom, J. V. Raman, H. Kim, J. K. Cha, *J. Am. Chem. Soc.* **2003**, *125*, 5415; b) J. V. Raman, H. K. Lee, R. Vleggaar, J. K. Cha, *Tetrahedron Lett.* **1995**, *36*, 3095.

[16] For reviews, see: a) R. H. Grubbs, S. J. Miller, G. C. Fu, *Acc. Chem. Res.* **1995**, *28*, 446; b) A. Fürstner, K. Langemann, *Synthesis* **1997**, 792; c) D. S. La, J. B. Alexander, D. R. Cefalo, D. D. Graf, A. H. Hoveyda, R. R. Schrock, *J. Am. Chem. Soc.* **1998**, *120*, 9720, and references therein.

[17] a) L. A. Paquette, R. J. Ross, Y. J. Shi, *J. Org. Chem.* **1990**, *55*, 1589; b) A. Sekine, N. Kumagai, K. Uotsu, T. Ohshima, M. Shibasaki, *Tetrahedron Lett.* **2000**, *41*, 509.

[18] For a review, see: A. R. Chamberlin, S. H. Bloom, *Org. React.* **1990**, *39*, 1.

[19] a) The crystal structure of **8** can be found in the Supporting Information; b) We thank Dr. Fook Tham at the University of California, Riverside for X-ray crystallographic analysis.

 © 2005 Wiley-VCH Verlag GmbH & Co. KGaA, Weinheim

Magnetic Nanoparticles

Preparation of Water-Soluble Magnetite Nanocrystals from Hydrated Ferric Salts in 2-Pyrrolidone: Mechanism Leading to Fe_3O_4**

*Zhen Li, Qiao Sun, and Mingyuan Gao**

Magnetic nanoparticles of iron oxides (γ-Fe_2O_3 and Fe_3O_4) and their suspensions have extensive applications in magnetic sealing, oscillation damping, and position sensing,[1] ultrahigh-density magnetic storage media,[2] clinical diagnosis and

[*] Z. Li, Q. Sun, Prof. M. Y. Gao
Key Laboratory of Colloid, Interface Science and Chemical Thermodynamics
Institute of Chemistry, Chinese Academy of Sciences
Zhong Guan Cun, Bei Yi Jie 2, Beijing 100080 (P.R. China)
Fax: (+86) 10-8261-3214
E-mail: gaomy@iccas.ac.cn

[**] The authors thank Prof. D.-X. Wang for his assistance with PES measurements. Funding was provided by an 863 project (2002AA302201) and NSFC projects (20225313, 90206024, 90201006).

 DOI: 10.1002/anie.200460715 © 2005 Wiley-VCH Verlag GmbH & Co. KGaA, Weinheim

treatment,[3] and biological labeling, tracking, imaging, detection, and separations.[4] For these applications, major efforts have recently been devoted to the synthesis of magnetic iron oxide nanoparticles.[5] Generally, magnetic iron oxide nanoparticles can be prepared by co-precipitating ferrous and ferric ions in aqueous solution. However, variations in the molar ratio of Fe^{3+} and Fe^{2+} often lead to rather complicated changes in the crystalline structures of the iron oxides obtained.[6] Both pH and the ionic strength, which play critical roles in the preparations, also affect the surface chemical composition of the magnetite nanoparticles.[5] Furthermore, the relatively poor size uniformity and low crystallinity of magnetic iron oxide nanoparticles obtained to some extent limit their use in many applications. Although sol–gel and hydrothermal methods were proven to be effective in increasing the crystallinity, the magnetic nanoparticles obtained exhibit poor solubility or dispersibility.[7] Recently, Alivisatos et al. reported a thermal decomposition approach to synthesize nearly monodisperse maghemite nanocrystals.[8] Sun et al. succeeded in preparing monodisperse magnetite nanocrystals by decomposition of [Fe(acac)$_3$](acac = acetylacetonate) in the presence of 1,2-hexadecanediol, oleic acid, and oleylamine.[9] Hyeon et al. obtained high-quality maghemite nanocrystals by thermal decomposition of [Fe(CO)$_5$] followed by oxidation with $(CH_3)_3NO$.[10] However, the direct products of the thermal decomposition method are generally soluble in organic solvents. Sophisticated post-preparative approaches are required to make those magnetic nanocrystals water-soluble,[11] and this limits their applications in biomedical fields. Furthermore, the mechanisms for the formation of magnetic nanocrystals by thermal decomposition are far from clear.[8–10]

Recently, we demonstrated the possibility of producing water-soluble magnetite nanocrystals by the thermal decomposition method using strong polar 2-pyrrolidone as a coordinating solvent.[12] Here we report the preparation of magnetite nanocrystals by using hydrated ferric salts as iron precursors instead of costly [Fe(acac)$_3$]. In addition, the mechanism leading to Fe_3O_4 in 2-pyrrolidone is discussed.

$FeCl_3{\cdot}6H_2O$ was used as a single iron source in the preparation of magnetic nanocrystals. Figure 1 shows TEM images of three typical samples of iron oxide nanoparticles obtained after refluxing a certain amount of $FeCl_3{\cdot}6H_2O$ in 2-pyrrolidone for 1, 10, and 24 h. Their average particle sizes are 4, 12, and 60 nm, respectively. In addition to the difference in size, the nanoparticles also change their shape with increasing reflux time. During the early stages, spherical nanoparticles appear and then grow larger and larger, and finally they lose the original shape and form cubic particles after 24 h. The crystalline structure of the samples shown in Figure 1 was determined by powder XRD. The diffraction patterns and relative intensities of all diffraction peaks match well with those of JCPDS card 19-0629 for magnetite. The electron diffraction pattern inserted in Figure 1c also supports the magnetite crystal structure. In addition, FT-IR spectra of the particles exhibit characteristic peaks of magnetite at around $\tilde{\nu} = 589\ cm^{-1}$.[13]

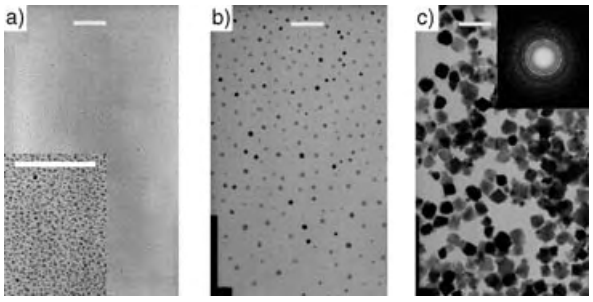


Figure 1. TEM images of nanoparticles obtained after $FeCl_3{\cdot}6H_2O$ was refluxed in 2-pyrrolidone for 1, 10, and 24 h, respectively. The inset in a) is an enlarged part. The scale bar corresponds to 100 nm.

The magnetic properties of the as-prepared magnetite nanoparticles were investigated with a vibrating sample magnetometer (VSM). Figure 2 presents the magnetic hysteresis curves of the nanocrystals shown in Figure 1. The saturation magnetization increases from 3 to 59 to 84 emu g^{-1} with increasing reflux time, which can be attributed to the growth of particle size and enhancement in crystallinity. Samples a and b in Figure 1 are superparamagnetic at room temperature, while the cubic particles exhibit a magnetic coercivity of 85 Oe. This is because their size already exceeds the critical size of single magnetic domains.[14]

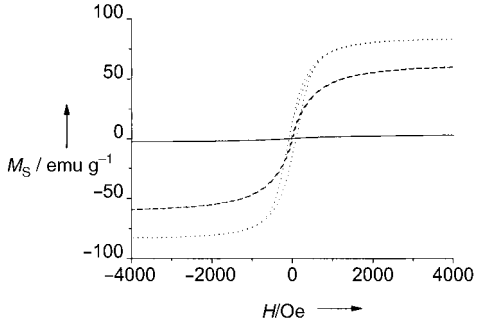


Figure 2. Room-temperature magnetization curves of the magnetic nanocrystals shown in Figure 1: 4 nm (solid line), 12 nm (dashed line), and 60 nm (dotted line) magnetite nanocrystals.

Similar to our previous report, the as-synthesized magnetite nanocrystals reported here can also be dissolved in water under both acidic and alkaline conditions, especially when the particles are smaller than 10 nm. This makes our investigation significant since $FeCl_3{\cdot}6H_2O$ is a very inexpensive iron source. To the best of our knowledge, the current synthetic approach is the first example using $FeCl_3{\cdot}6H_2O$ as a single iron source to prepare water-soluble Fe_3O_4 nanocrystals by the high-temperature wet-chemical approach. Therefore, nearly nothing is known about the mechanism leading to Fe_3O_4 nanocrystals in this reaction system. To investigate the formation of Fe_3O_4 nanocrystals in 2-pyrrolidone, photoelectron spectroscopy (PES) was used to analyze the small molecules released during the reaction. A stream of nitrogen carried these small molecules through a glass U-tube whose bottom was immersed in liquid nitrogen in a Dewar flask. Then the U-tube was connected to a double-chamber UPS machine-II for PES measurements.

 © 2005 Wiley-VCH Verlag GmbH & Co. KGaA, Weinheim

He I photoelectron spectroscopy is a powerful tool for characterizing unstable, metastable, and transient species.[15] The gaseous species entrapped in the glass U-tube were released on slow addition of alcohol to the Dewar flask. Gases with different boiling points were released successively. The photoelectron spectrum of the early released gas is shown in Figure 3a. The peaks centered at 13.78, 17.59, 18.08, and

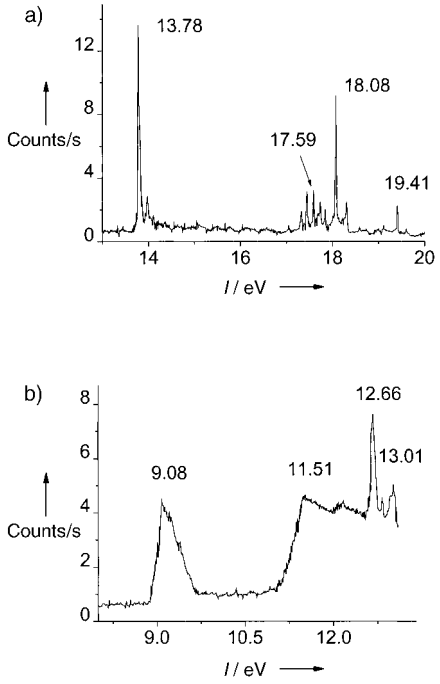
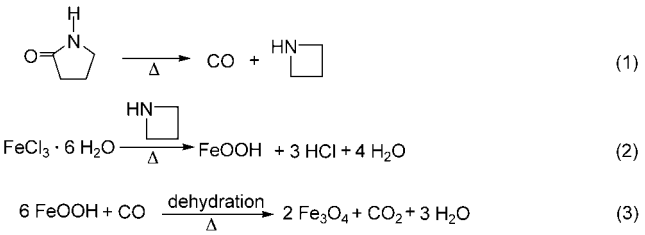


Figure 3. Photoelectron spectra of gaseous species released during the preparation of magnetite nanocrystals. Spectra a) and b) were recorded in sequence with increasing temperature.

19.41 eV are characteristic for carbon dioxide.[16] The generation of carbon dioxide during reflux indicates that 2-pyrrolidone is not stable at its boiling point even in an oxygen-free environment. The photoelectron spectrum of the gaseous species released at higher temperature is shown in Figure 3b. The PES peaks at 12.66 and 13.01 eV can be attributed to water,[16] and those at 9.08 and 11.51 eV can be assigned to the first and second bands of azetidine according to a previous report.[17] In addition, hydrogen chloride was also detected when the initial concentration of $FeCl_3{\cdot}6H_2O$ was relatively high.

In accordance with these results, a possible mechanism leading to magnetite nanocrystals is proposed in Scheme 1. In fact, the thermal decomposition of 2-pyrrolidone is rather complex. We observed that prolonged reflux of 2-pyrrolidone also generated fluorescent species in solution. Therefore, Scheme 1 does not depict all decomposition reactions that take place. Only those related to the formation of magnetite nanocrystals are shown. Since carbon dioxide and azetidine were released during reflux, it can be deduced that thermal decomposition of 2-pyrrolidone produces carbon monoxide and azetidine by cleavage of the acylamide bond. Azetidine catalyzes the hydrolysis of $FeCl_3{\cdot}6H_2O$ to form ferric oxide hydroxide (FeOOH) which is then partially reduced by CO.



Scheme 1. Chemical reactions involved in the formation of magnetite nanoparticles. Equation (2) is a process involving dissolution of $FeCl_3{\cdot}6H_2O$ in 2-pyrrolidone and azetidine-catalyzed hydrolysis of $FeCl_3$.

Upon dehydration it forms magnetite and carbon dioxide is released as a by-product. The thermal decomposition of 2-pyrrolidone and the formation of intermediate CO also explains why only magnetite was produced even when $[Fe(cup)_3]$ (cup = *N*-nitrosophenylhydroxylamine) or $[Fe(acac)_3]$ was used instead of $FeCl_3{\cdot}6H_2O$ in the preparation.

To provide direct proof for the generation of carbon monoxide, a typical identification reaction was used to determine CO. At room temperature CO can reduce Pd^{2+} to give black precipitates of Pd metal. We purged the reaction system with nitrogen during reflux and allowed the N_2 flow to pass successively through a glass tube filled with KOH powder and a flask with H_2SO_4 solution. At the end of this gas line, a fine glass tube was used to introduce the N_2 flow into an aqueous solution of $PdCl_2$. Black precipitates were observed after long enough time and shown to be Pd metal by TEM measurements. The *d* spacings of 0.2244, 0.1945, 0.1391, 0.1190, and 0.0894 nm calculated from selected-area electron diffraction on the black precipitates match well with the *d* values for (111), (200), (220), (311), and (331) lattice planes of Pd metal, respectively.

In summary, we have presented a simple route to synthesize water-soluble magnetite nanocrystals by refluxing inexpensive $FeCl_3{\cdot}6H_2O$ in 2-pyrrolidone. Differently sized and shaped magnetite nanocrystals can be obtained simply by varying the reaction time. Carbon monoxide generated during the reaction plays a critical role in the formation of magnetite nanocrystals, since it partly reduces Fe^{3+} to Fe^{2+}. We believe this novel synthetic approach will not only pave a new way for the preparation of water-soluble magnetite nanocrystals but also provide a new route for mass production of high-quality magnetic nanocrystals, since much more concentrated colloidal solutions can be directly obtained by the current method.

Experimental Section

In a typical synthesis of magnetite nanocrystals, a solution of 10 mmol $FeCl_3{\cdot}6H_2O$ in 100 mL 2-pyrrolidone was first purged with nitrogen to remove oxygen and then heated to the boiling point of 2-pyrrolidone. Samples were taken after the mixture was refluxed for 1, 10, and 24 h, and then cooled to room temperature. A threefold volume of methanol/diethyl ether (1:3) was added to precipitate the nanoparticles. The resultant black precipitate was washed with acetone several times and then dried for characterization.

The magnetite nanocrystals were characterized by TEM, XRD, FTIR, and VSM. TEM images were obtained on a JEM-2010

 © 2005 Wiley-VCH Verlag GmbH & Co. KGaA, Weinheim

microscope. XRD patterns were obtained with a Rigaku D/Max-2500 diffractometer equipped with a rotating anode and a $Cu_{K\alpha 1}$ radiation source ($\lambda = 1.54056$ Å). FT-IR spectra were recorded on a Bruker EQUINOX55 FT-IR spectrometer. VSM spectra were collected on a homemade magnetometer.

PES measurements were performed on a double-chamber UPS machine-II. Argon and methyl iodide were used as internal standards for measurements.

Received: May 19, 2004
Revised: September 9, 2004

Keywords: iron · magnetic properties · magnetite · nanostructures · photoelectron spectroscopy

[1] K. Raj, R. Moskowitz, *J. Magn. Magn. Mater.* **1990**, *85*, 233 – 245.
[2] H. Zeng, J. Li, J. P. Liu, Z. L. Wang, S. H. Sun, *Nature* **2002**, *420*, 395 – 398.
[3] A. Jordan, R. Scholz, K. Maier-Hauff, M. Johannsen, P. Wust, J. Nadobny, H. Schirra, H. Schmidt, S. Deger, S. Loening, W. Lanksch, R. Felix, *J. Magn. Magn. Mater.* **2001**, *225*, 118 – 126.
[4] a) J. W. M. Bulte, T. Douglas, B. Witwer, S. C. Zhang, E. Strable, B. K. Lewis, H. Zywicke, B. Miller, P. V. Gelderen, B. M. Moskowitz, L. D. Duncan, J. A. Frank, *Nat. Biotechnol.* **2001**, *19*, 1141 – 1147; b) J. M. Nam, C. S. Thaxton, C. A. Mirkin, *Science* **2003**, *301*, 1884 – 1886.
[5] P. Tartaj, M. P. Morales, S. Veintemillas-Verdaguer, T. González-Carreño, C. J. Serna, *J. Phys. D* **2003**, *36*, R182 – R197.
[6] E. Tronc, P. Belleville, J. P. Jolivet, J. Livage, *Langmuir* **1992**, *8*, 313 – 319.
[7] a) K. Woo, H. J. Lee, J. P. Ahn, *Adv. Mater.* **2003**, *15*, 1761 – 1763; b) J. Wang, J. J. Sun, Q. Sun, Q. W. Chen, *Mater. Res. Bull.* **2003**, *38*, 1113 – 1118.
[8] J. Rockenberger, E. C. Scher, P. A. Alivisatos, *J. Am. Chem. Soc.* **1999**, *121*, 11595 – 11596.
[9] a) S. H. Sun, H. Zeng, *J. Am. Chem. Soc.* **2002**, *124*, 8204 – 8205; b) S. H. Sun, H. Zeng, D. B. Robinson, S. Raoux, P. M. Rice, S. X. Wang, G. X. Li, *J. Am. Chem. Soc.* **2004**, *126*, 273 – 279.
[10] T. Hyeon, S. S. Lee, J. Park, Y. Chung, H. B. Na, *J. Am. Chem. Soc.* **2001**, *123*, 12798 – 12801.
[11] a) Y. Wang, J. F. Wong, X. W. Teng, X. Z. Lin, H. Yang, *Nano Lett.* **2003**, *3*, 1555 – 1559; b) L. E. Euliss, S. G. Grancharov, S. O. Brien, T. J. Deming, G. D. Stucky, C. B. Murry, G. A. Held, *Nano Lett.* **2003**, *3*, 1489 – 1493.
[12] Z. Li, H. Chen, H. B. Bao, M. Y. Gao, *Chem. Mater.* **2004**, *16*, 1391 – 1393.
[13] U. Schwertmann, R. M. Cornell, *Iron Oxides in the Laboratory: Preparation and Characterization*, 2nd ed., Wiley, New York, **2000**.
[14] R. E. Dunin-Borkowski, M. R. McCartney, R. B. Frankel, D. A. Bazylinski, M. Pósfai, P. R. Buseck, *Science* **1998**, *282*, 1868 – 1870.
[15] J. Wang, Z. Sun, X. J. Zhu, X. J. Yang, M. F. Ge, D. X. Wang, *Angew. Chem.* **2001**, *113*, 3145 – 3147; *Angew. Chem. Int. Ed.* **2001**, *40*, 3055 – 3057.
[16] K. Kimura, S. Katsumata, Y. Achiba, T. Yamazaki, S. Iwata, *Handbook of He I Photoelectron Spectra of Fundamental Organic Molecules*, Japan Scientific Societies, Tokyo, **1981**.
[17] K. Yoshikawa, M. Hashimoto, I. Morshima, *J. Am. Chem. Soc.* **1974**, *96*, 288 – 289.

 © 2005 Wiley-VCH Verlag GmbH & Co. KGaA, Weinheim

Medium-Ring Compounds

Tandem $[W(CO)_5]$-Catalyzed Cycloisomerization–Cyclopropanation Reactions Directed toward the Synthesis of Eight-Membered Carbocycles**

José Barluenga, Alejandro Diéguez, Félix Rodríguez, and Francisco J. Fañanás*

Dedicated to Professor José Elguero on the occasion of his 70th birthday

The development of new metal-catalyzed reactions for the formation of carbon–carbon bonds is a major research area in organic chemistry.[1] Of particular significance are those tandem processes which allow the formation of several new bonds in a single step from readily available starting materials, thus increasing efficiency and minimizing the amount of waste generated.[2] The potential of Group 6 Fischer carbene complexes to undergo unusual reactions has been widely demonstrated since their discovery almost 40 years ago.[3] However, one of the most important drawbacks of these complexes is that a stoichiometric amount has to be used. Only very few examples of catalytic processes in which a Group 6 Fischer carbene complex is implied have been reported.[4,5] Moreover, for several years we have pursued a program related to the development of new methodologies for the synthesis of medium-sized rings promoted by Fischer carbene complexes.[6] Thus, recently we reported a new one-pot process for the synthesis of eight-membered carbocycles by the use of ketone enolates and alkenyl carbene complexes.[7] To avoid the use of stoichiometric amounts of metallic species and to extend the scope of this method, we initiated an investigation directed toward the design of a catalytic version of this process. These studies culminated with the discovery of a tandem $[W(CO)_5]$-catalyzed cycloisomerization–cyclopropanation reaction, which has been used as the key step for the synthesis of eight-membered carbocycles.

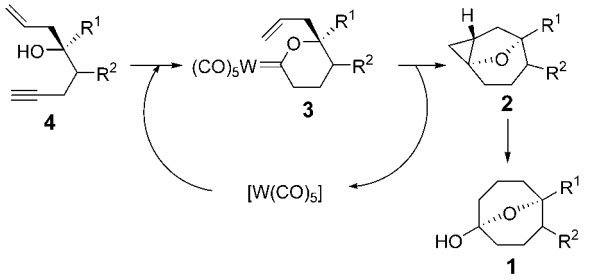
In our previous studies in this field we demonstrated that eight-membered rings **1** were readily available from tricyclic compounds **2** generated from cyclic Fischer carbene complexes **3** (Scheme 1).[7] We envisaged that these complexes **3** could be obtained through a cycloisomerization reaction of 4-alkyn-1-ol derivatives **4** promoted by pentacarbonyltungsten

[*] Prof. Dr. J. Barluenga, A. Diéguez, Dr. F. Rodríguez, Dr. F. J. Fañanás
Instituto Universitario de Química Organometálica "Enrique Moles"
Unidad Asociada al C.S.I.C.
Universidad de Oviedo
Julián Clavería, 8, 33006 Oviedo (Spain)
Fax: (+34) 98-5103-450
E-mail: barluenga@uniovi.es

[**] We gratefully acknowledge financial support from the DGICYT (BQU-2001-3853), FICYT (grant to A.D.), and MCYT ("Ramón y Cajal" contract to F.R.).

Supporting information for this article is available on the WWW under http://www.angewandte.org or from the author.

 © 2005 Wiley-VCH Verlag GmbH & Co. KGaA, Weinheim DOI: 10.1002/anie.200461414

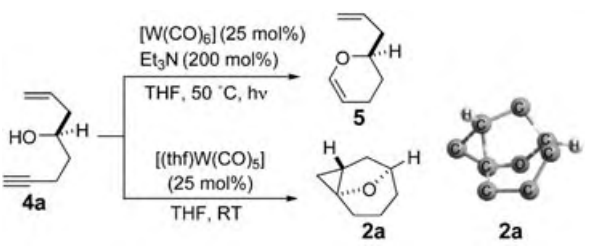


Scheme 1. Proposed catalytic cycle for the synthesis of tricyclic compounds **2**, and further transformation into eight-membered carbocycles **1**.

complexes.[8] The subsequent cyclopropanation reaction of complexes **3** should generate the tricyclic compounds **2**, with regeneration of the pentacarbonyltungsten species. Thus, a catalytic process as shown in Scheme 1 could be feasible.

Our initial attempts to promote the tandem sequence described above employed the method developed by McDonald et al. for the synthesis of cyclic enol ethers from 4-alkyn-1-ol derivatives.[4c] The established conditions for this cycloisomerization are treatment with triethylamine or 1,4-diazabicyclo[2.2.2]octane (dabco, 200 mol%) in the presence of $[W(CO)_6]$ (5–25 mol%) under constant irradiation, with THF as the solvent.

Unfortunately, when we employed this method with the starting alkynol derivative **4a**, the reaction did not lead to the expected tricyclic compound **2a**; instead the cyclic enol ether **5** was obtained exclusively (Scheme 2). This result indicates



Scheme 2. Different reaction conditions for the cycloisomerization reaction of the alkynol derivative **4a**.

that the carbene complex **3a** ($R^1 = R^2 = H$) formed does not undergo cyclopropanation of the double bond of the allylic moiety, but instead reacts with the triethylamine present in the reaction medium to give the enol ether **5**. It was clear at this point that an alternative method to generate the catalytic $[W(CO)_5]$ species in the absence of an amine was required. We next turned our attention to the use of preformed $[(thf)W(CO)_5]$. To our delight, when we treated the alkynol derivative **4a** with $[(thf)W(CO)_5]$ (25 mol%) in THF at room temperature for 24 h, the tricyclic compound **2a** was obtained in 90% yield (Scheme 2; for clarity, a 3D representation of compound **2a** has been included).[9]

To check the scope of the reaction, a number of allyl-substituted 4-alkynol derivatives **4** were tested. As summarized in Table 1 (method A), the reaction gave the expected tricyclic compounds **2** in very high yield starting from both

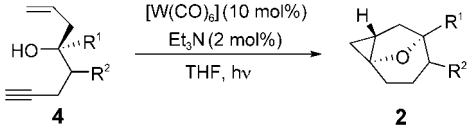
Table 1: Tricyclic compounds **2** from the catalytic cycloisomerization reaction of alkynol derivatives **4**.

4	R^1	R^2	2	Method A[a] Yield [%][c]	Method B[b] Yield [%][c]
4a[d]	H	H	**2a**	90	–
4b[d]	Me	H	**2b**	69	70
4c[d]	Bu	H	**2c**	85	87
4d[d]	allyl	H	**2d**	74	80[e]
4e[d]	*c*-C_3H_5	H	**2e**	60	61
4f[d]	Ph	H	**2f**	82	83
4g[d]	4-$MeOC_6H_4$	H	**2g**	84	84
4h[d]	(*E*)-PhCH=CH	H	**2h**	80	82
4i[f]	$-(CH_2)_4-$		**2i**	88	86
4j[g]	H	OBn	**2j**[h]	91	–

[a] The alkynol **4** was stirred as a solution in THF with preformed $[(thf)W(CO)_5]$ (25 mol%) at room temperature for 24 h. [b] A solution of the alkynol **4** in THF was irradiated with $[W(CO)_6]$ (10 mol%) and Et_3N (2 mol%) for 12 h. [c] Yield of the isolated product based on the starting alkynol **4**. [d] Racemic mixture. [e] In this case the amount of $[W(CO)_6]$ can be decreased to 5 mol% without any observed decrease in the yield of the reaction. [f] The racemic 1*S**,2*S** diastereoisomer was used. [g] The 4*S*,5*S* enantiomer was used. [h] The 1*R*,3*S*,5*S*,6*S* enantiomer was obtained; $[\alpha]_D^{20} = -26.7$ ($c = 0.45$, CH_2Cl_2).

secondary and tertiary alcohol derivatives **4**. The reaction is completely diastereoselective, and a single diastereoisomer of the product was observed in all cases.[9] It should be noted that the alternative diastereoisomer would be significantly more strained. The enantiopure tricyclic compound **2j** was isolated when the reaction was performed with the alkynol derivative **4j**.

A minor drawback of this method for the catalytic synthesis of tricyclic compounds **2** is the fact that the catalyst has to be generated in a separate vessel by irradiation of a solution of $[W(CO)_6]$ in THF and then added to the solution of the corresponding alkynol derivative. However, the conditions described by McDonald et al.[4c] for the in situ generation of $[W(CO)_5]$ species were shown not to be applicable to our substrates as a result of the amine-promoted formation of enol ethers analogous to **5** (see Scheme 1). We reasoned that we could find appropriate catalytic conditions if we were able to lower the amount of amine used to such an extent that the amine could only act to stabilize the $[W(CO)_5]$ species. With this idea in mind, we carried out a set of experiments with different $[W(CO)_6]$/triethylamine ratios under a variety of reaction conditions. We were delighted to find that constant irradiation at 350 nm of a solution of the corresponding alkynol **4** in THF in the presence of 10 mol% of $[W(CO)_6]$ and only 2 mol% of triethylamine gave similar results to those obtained when preformed $[(thf)W(CO)_5]$ was used (Scheme 3 and Table 1, method B). As before, the



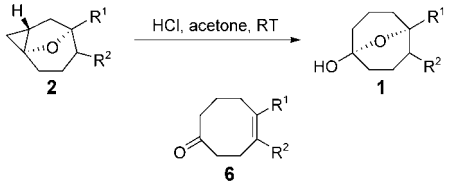
Scheme 3. Cycloisomerization reactions of alkynols **4** with catalytic amounts of $[W(CO)_6]$ and Et_3N to give compounds **2**.

 © 2005 Wiley-VCH Verlag GmbH & Co. KGaA, Weinheim

reaction led to a single diastereoisomer of the products in all cases studied.[9]

To illustrate the synthetic utility of the tungsten-catalyzed process described, we further transformed the tricyclic compounds **2** into eight-membered carbocycles **1** following the protocol developed previously by our research group.[7] Thus, the treatment of compounds **2** with hydrochloric acid in acetone at room temperature yielded the corresponding eight-membered carbocycles **1** (Table 2).[9] Under the same

Table 2: Eight-membered carbocycles **1** or **6** from tricyclic compounds **2**.



2	R^1	R^2	Product	Yield [%][a]
2a	H	H	**1a**	98
2b	Me	H	**1b**	97
2c	Bu	H	**1c**	97
2d	allyl	H	**1d**	95
2e	*c*-C_3H_5	H	**1e**	98
2f	Ph	H	**1f**	98
2g	4-$MeOC_6H_4$	H	**6a**	95
2h	(*E*)-PhCH=CH	H	**6b**	97
2i	$(CH_2)_4$		**1g**	96
2j	H	OBn	**1h**[b]	97

[a] Yield of the isolated product based on the starting cyclic ether **2**. [b] The 1*R*,4*S*,5*S* enantiomer was obtained; $[\alpha]_D^{20} = -13.0$ ($c = 1.15$, CH_2Cl_2).

reaction conditions, dehydrated compounds **6** were obtained when the R^1 group of the starting compound **2** was an electron-rich aryl group (i.e. **2g**) or an alkenyl group (i.e. **2h**). Interestingly, compounds with structures analogous to that of **1h** ($R^1 = H$, $R^2 = OBn$, 1*R*,4*S*,5*S* enantiomer) have shown remarkable activity as herbicides. The methodology described herein provides straightforward access to such compounds.[10]

In summary, we have developed an effective and general method for the synthesis of eight-membered carbocycles based on a new tandem tungsten-catalyzed cycloisomerization–cyclopropanation reaction. This process is one of very few examples of a catalytic reaction in which a heteroatom-stabilized Fischer carbene complex is implied. The method described herein opens the door to the development of new catalytic methods which avoid the use of large quantities of metallic species, thus overcoming one of the main limitations of Fischer carbene complexes. Moreover, as the procedure has been shown to be applicable to the synthesis of functionalized and biologically active compounds from very simple starting materials, it is expected to find wide application in organic synthesis.

Received: July 23, 2004

Keywords: alkynols · medium-ring compounds · synthetic methods · tandem reactions · tungsten

[1] a) *Transition Metal Reagents and Catalysts: Innovations in Organic Synthesis* (Ed.: J. Tsuji), Wiley, Chichester, **2000**; b) *Catalytic Asymmetric Synthesis* (Ed.: I. Ojima), Wiley-VCH, Weinheim, **2000**.

[2] L. F. Tietze, F. Hautner in *Stimulating Concepts in Chemistry* (Eds.: F. Vögtle, J. F. Stoddart, M. Shibasaki), Wiley-VCH, Weinheim, **2000**, p. 38; c) K. C. Nicolaou, E. W. Yue, T. Oshima in *The New Chemistry* (Ed.: N. Hall), Cambridge University Press, Cambridge, **2001**, p. 168; d) L. F. Tietze, *Chem. Rev.* **1996**, *96*, 115; e) L. F. Tietze, U. Beifuss, *Angew. Chem.* **1993**, *105*, 103; *Angew. Chem. Int. Ed. Engl.* **1993**, *32*, 131.

[3] a) J. Barluenga, J. Santamaría, M. Tomás, *Chem. Rev.* **2004**, *104*, 2259; b) A. de Meijere, H. Schirmer, M. Duetsch, *Angew. Chem.* **2000**, *112*, 4124; *Angew. Chem. Int. Ed.* **2000**, *39*, 3964; c) W. D. Wulff in *Comprehensive Organometallic Chemistry II*, *Vol. 12* (Eds.: E. W. Abel, F. G. A. Stone, G. Wilkinson), Pergamon, Oxford, **1995**, p. 470; d) W. D. Wulff in *Comprehensive Organic Synthesis*, *Vol. 5* (Eds.: B. M. Trost, I. Fleming), Pergamon, Oxford, **1991**, p. 1065.

[4] a) P. Wipf, T. H. Graham, *J. Org. Chem.* **2003**, *68*, 8798; b) F. E. McDonald, K. S. Reddy, *Angew. Chem.* **2001**, *113*, 3765; *Angew. Chem. Int. Ed.* **2001**, *40*, 3653; c) F. E. McDonald, K. S. Reddy, Y. Díaz, *J. Am. Chem. Soc.* **2000**, *122*, 4304.

[5] For some examples in which Group 6 nonstabilized Fischer carbene complexes are proposed as intermediates in the catalytic cycle, see: a) K. Miki, T. Yokoi, F. Nishino, Y. Kato, Y. Washitake, K. Ohe, S. Uemura, *J. Org. Chem.* **2003**, *68*, 1557; b) T. Miura, K. Kiyota, H. Kusama, K. Lee, H. Kim, S. Kim, P. H. Lee, N. Iwasawa, *Org. Lett.* **2003**, *5*, 1725; c) N. Iwasawa, T. Miura, K. Kiyota, H. Kusama, K. Lee, P. H. Lee, *Org. Lett.* **2002**, *4*, 4463; d) H. Kusama, H. Yamabe, N. Iwasawa, *Org. Lett.* **2002**, *4*, 2569; e) H. Kusama, J. Takaya, N. Iwasawa, *J. Am. Chem. Soc.* **2002**, *124*, 11592; f) K. Miki, F. Nishino, K. Ohe, S. Uemura, *J. Am. Chem. Soc.* **2002**, *124*, 5260; g) K. Ohe, T. Yokoi, K. Miki, F. Nishino, S. Uemura, *J. Am. Chem. Soc.* **2002**, *124*, 526; h) T. Miura, N. Iwasawa, *J. Am. Chem. Soc.* **2002**, *124*, 518; i) N. Iwasawa, K. Maeyama, H. Kusama, *Org. Lett.* **2001**, *3*, 3871; j) N. Iwasawa, M. Shido, H. Kusama, *J. Am. Chem. Soc.* **2001**, *123*, 5814; k) K. Maeyama, N. Iwasawa, *J. Org. Chem.* **1999**, *64*, 1344; l) K. Maeyama, N. Iwasawa, *J. Am. Chem. Soc.* **1998**, *120*, 1928; m) J. Pfeiffer, K. H. Dötz, *Angew. Chem.* **1997**, *109*, 2948; *Angew. Chem. Int. Ed. Engl.* **1997**, *36*, 2828.

[6] For some leading references from our research group on the synthesis of seven- and eight-membered rings, see: a) J. Barluenga, P. Barrio, L. A. López, M. Tomás, S. García-Granda, C. Alvarez-Rúa, *Angew. Chem.* **2003**, *115*, 3116; *Angew. Chem. Int. Ed.* **2003**, *42*, 3008; b) J. Barluenga, F. Aznar, M. A. Palomero, *Angew. Chem.* **2000**, *112*, 4514; *Angew. Chem. Int. Ed.* **2000**, *39*, 4346; c) J. Barluenga, J. Alonso, F. Rodríguez, F. J. Fañanás, *Angew. Chem.* **2000**, *112*, 2555; *Angew. Chem. Int. Ed.* **2000**, *39*, 2460; d) J. Barluenga, M. Tomás, E. Rubio, J. A. López-Pelegrin, S. García-Granda, M. Pérez-Priede, *J. Am. Chem. Soc.* **1999**, *121*, 3065; e) J. Barluenga, M. Tomás, A. Ballesteros, J. Santamaría, F. López-Ortiz, R. Carbajo, S. García-Granda, P. Pertierra, *Chem. Eur. J.* **1996**, *2*, 180; f) J. Barluenga, F. Aznar, A. Martín, J. T. Vázquez, *J. Am. Chem. Soc.* **1995**, *117*, 9419.

[7] J. Barluenga, A. Diéguez, F. Rodríguez, J. Flórez, F. J. Fañanás, *J. Am. Chem. Soc.* **2002**, *124*, 9056.

[8] For some recent reviews, see: B. Weyershausen, K. H. Dötz, *Eur. J. Inorg. Chem.* **1999**, 1057; b) F. E. McDonald, *Chem. Eur. J.* **1999**, *5*, 3103.

[9] The relative configuration of the chiral centers was ascertained unequivocally by NMR spectroscopic experiments (including HMQC, HMBC, COSY, and NOESY).

[10] M. F. Schlecht (du Pont de Nemours, E. I., and Co., USA), PCT Int. Appl. **1992**, WO 9203440; [*Chem. Abstr.* **1992**, *116*, 255482].

 © 2005 Wiley-VCH Verlag GmbH & Co. KGaA, Weinheim

Coupling Reactions

Catalytic Reductive Coupling of Epoxides and Aldehydes: Epoxide-Ring Opening Precedes Carbonyl Reduction**

*Carmela Molinaro and Timothy F. Jamison**

Transition-metal-catalyzed reductive coupling reactions have attracted considerable interest for several decades since the development of reductive polymerization of carbon monoxide by Fischer and Tropsch.[1] Hydroformylation[2] and the Nozaki–Hiyama–Kishi reaction[3] are other important examples, and in the past decade dozens of nickel- and rhodium-catalyzed reductive coupling reactions have also been described.[4] Represented among these transformations are diverse coupling partners, catalysts, and mechanisms, yet what they have in common is the formation of a carbon–carbon bond. In contrast, with the exception of reductive etherification of carbonyl groups and acetals,[5] catalytic reductive C–O bond formation has remained largely unexplored,[6,7] despite the recent emergence of transition-metal-catalyzed carbon–oxygen bond-forming methods[8] and the importance of oligosaccharides, ribonucleic acids, epoxy resins, natural products, and pharmaceuticals. We now report the first example of such a transformation that employs epoxides (Table 1). Several lines of evidence suggest, perhaps counterintuitively, that carbonyl reduction occurs after epoxide-ring opening.

Recently we reported that a species derived from $[Ni(cod)_2]$ and Bu_3P catalyzes the inter- and intramolecular reductive coupling of alkynes and terminal epoxides to give homoallylic alcohols.[4a,9] To account for several observations, we proposed that epoxide-ring opening occurred prior to carbon–carbon bond formation, possibly by way of a metallaoxetane.[9a,10–11] We reasoned that this species would likely have very different reactivity patterns to those of the epoxide itself, and accordingly we have begun to investigate catalytic reductive coupling reactions of epoxides with other functional groups, including aldehydes.

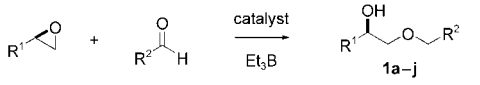
[*] Dr. C. Molinaro, Prof. Dr. T. F. Jamison
Department of Chemistry
Massachusetts Institute of Technology
Cambridge, MA 02139 (USA)
Fax: (+1) 617-324-0253
E-mail: tfj@mit.edu

[**] Postdoctoral support was provided by the Fonds Québécois de la Recherche sur la Nature et les Technologies (FQRNT, fellowship to C.M.) and Boehringer-Ingelheim (New Investigator Award to T.F.J.). We thank Engelhard-CLAL for a generous donation of $[(Ph_3P)_3RhCl]$ and the National Institute of General Medical Sciences (GM-063755), the NSF (CAREER CHE-0134704), Amgen, Bristol-Myers Squibb, GlaxoSmithKline, Johnson & Johnson, Merck Research Laboratories, Pfizer, the Sloan Foundation, and MIT for generous financial support. The NSF (CHE-9809061 and DBI-9729592) and NIH (1S10RR13886-01) provide partial support for the MIT Department of Chemistry Instrumentation Facility.

Supporting information for this article is available on the WWW under http://www.angewandte.org or from the author.

We initially examined a number of nickel(II) and nickel(0) complexes and found that, at room temperature and without added solvent, both $[Ni(cod)_2]/PBu_3$ and $[NiCl_2(PBu_3)_2]$ catalyzed a reductive ring-opening reaction between 1,2-epoxybutane and benzaldehyde in the presence of Et_3B, giving the 1-benzyl ether of 1,2-butanediol with high selectivity (Table 1, entries 1–2). Superior results (Table 1, entries 3–11) were obtained with $[(Ph_3P)_3RhCl]$ (also without added solvent), representing the first use of Et_3B as reductant in a reaction promoted by the Wilkinson catalyst. Sterically

Table 1: Transition-metal-catalyzed reductive coupling of epoxides and aldehydes.[a]



Entry	R^1	R^2	Catalyst	Product	Yield [%]
1	Et	Ph	$[Ni(cod)_2]$, Bu_3P	**1a**	64
2	Et	Ph	$[(Bu_3P)_2NiCl_2]$	**1a**	62
3	Et	Ph	$[(Ph_3P)_3RhCl]$	**1a**	90
4	Ph	Ph	$[(Ph_3P)_3RhCl]$	**1b**	74
5	*i*Pr	Ph	$[(Ph_3P)_3RhCl]$	**1c**	26
6	*t*Bu	Ph	$[(Ph_3P)_3RhCl]$	**1d**	12
7	*i*Pr	Ph	$[(Ph_3P)_3RhCl]$, Et_3N	**1c**	96
8	*t*Bu	Ph	$[(Ph_3P)_3RhCl]$, Et_3N	**1d**	90
9	Et	2-naphthyl	$[(Ph_3P)_3RhCl]$, Et_3N	**1e**	70
10	*n*-hexyl	*p*-anisyl	$[(Ph_3P)_3RhCl]$, Et_3N	**1f**	67
11	*n*-hexyl	2-furyl	$[(Ph_3P)_3RhCl]$, Et_3N	**1g**	57
12	*n*-hexyl	*i*Pr	$[(Ph_3P)_3RhCl]$, Et_3N	**1h**	15

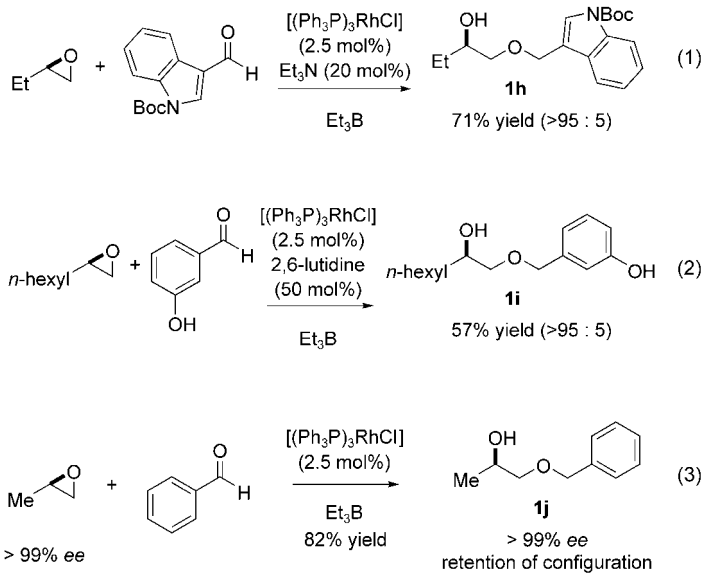
[a] Standard procedure: To the catalyst specified and, where indicated, Et_3N (20 mol%) at room temperature were added the epoxide, aldehyde, Et_3B (200 mol%, dropwise). The mixture was stirred for 16 h and purified by silica-gel chromatography. See Supporting Information for details. cod = cycloocta-1,5-diene.

encumbered epoxides such as *tert*-butyloxirane and isopropyloxirane underwent near-quantitative reductive coupling when a substoichiometric amount of Et_3N was included (Table 1, entries 5–8). Other aromatic and heteroaromatic aldehydes were also effective (Table 1, entries 9–11). The reaction between isobutyraldehyde and 1,2-epoxyoctane proceeded in 15% yield (Table 1, entry 12).[12] Several ketones (benzophenone, acetophenone, cyclohexanone, and 2-octanone) underwent catalytic reductive coupling in 10–25% yield. Despite the large variation in steric and electronic properties of the epoxides in the above examples, the regioselectivity of the ring-opening reaction was universally $>95:5$, a significant observation as aryl and alkyl oxiranes often undergo ring opening with the opposite sense of regioselectivity.[13–14]

Three examples are worthy of further comment. The one-step Rh-catalyzed reductive coupling shown in Equation (1) demonstrates the tolerance of acid-labile functional groups that would be problematic in a more traditional two-step approach, for example, reduction with $NaBH_4$ and acid-promoted epoxide opening. Complementarity to Jacobsen's methods of enantioselective epoxide opening by oxygen-centered nucleophiles[15] is demonstrated in Equation (2)

 DOI: 10.1002/anie.200461705 © 2005 Wiley-VCH Verlag GmbH & Co. KGaA, Weinheim

(Boc = *tert*-butoxycarbonyl). Phenolic hydroxy groups are typically more reactive than aliphatic hydroxy groups in [(salen)Co]-catalyzed ring openings,[15e–f] yet in the Rh/Et_3B system the former are unreactive which allows the aldehyde to function as a masked hydroxymethyl group. Finally, as shown in Equation (3), the stereochemical integrity of the epoxide is preserved in these transformations.

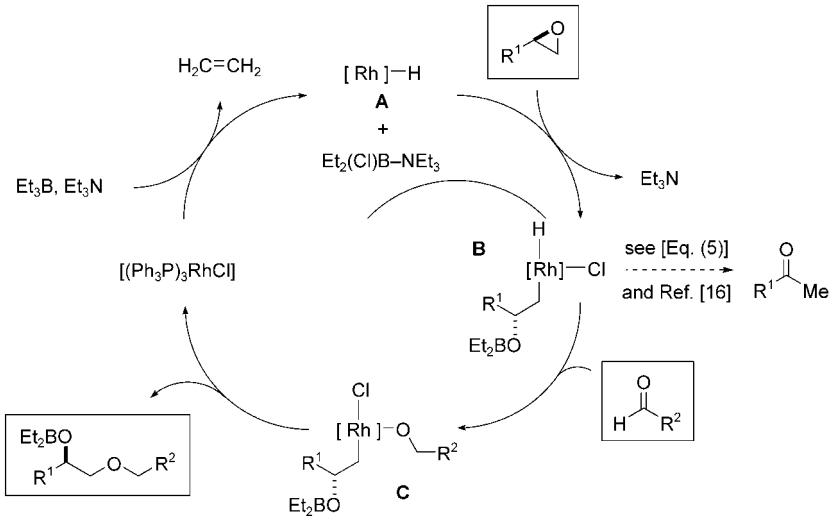


It might be expected that reduction of the aldehyde would initiate these reactions, giving a nucleophilic metal alkoxide that would then open the epoxide. However, we have found no evidence whatsoever to support this mechanistic framework. Reduction of the aldehyde does not occur in the absence of epoxide, even with 50 mol% catalyst [Eq. (4)], and isomerization of the epoxide to a methyl ketone[16] occurs in the absence of aldehyde [Eq. (5)]. It is unlikely that this process is a Lewis acid promoted 1,2-H shift as a terminal epoxide would generally rearrange to an aldehyde.[13b,17]

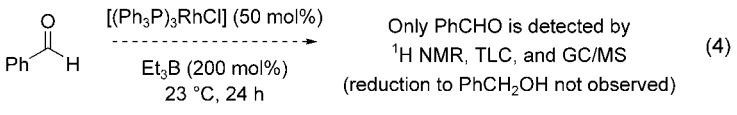
The reactivity of epoxides toward Rh complexes[16,18] [Eq. (5)] and the fact that the aldehyde is not reduced in the absence of epoxide [Eq. (4)] can both be explained by a catalytic cycle in which reduction of the carbonyl follows epoxide opening (Scheme 1).[19] A combination of $[(Ph_3P)_3RhCl]$, Et_3B, and Et_3N affords ethylene, $Et_2(Cl)B\text{-}NEt_3$ and species **A**, which opens the epoxide,[16] possibly assisted by Et_2BCl, leading to **B** and the regeneration of Et_3N. In other words, Et_3N may serve to temper the Lewis acidity of Et_2BCl.[20] Coordination of the aldehyde to **B**[21] and formal reduction of the carbonyl could occur at this stage to provide **C**, and C–O bond formation through reductive elimination of the product as a borinate ester would complete the catalytic cycle. A similar mechanism involving nickel (Table 1, entries 1–2) can also be envisioned.[9a,10]

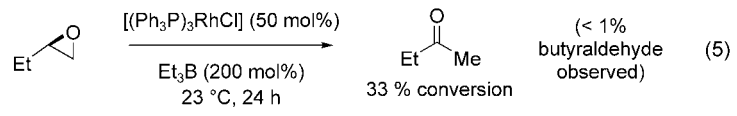
Several other experiments and observations also support this proposal. Ethylene is present in the atmosphere above the reaction mixture (^{1}H NMR spectroscopic analysis of head gas samples). In support of **B** (or a related species), ^{11}B NMR spectra of a mixture of all reaction components except for the aldehyde show the appearance of a new signal at $\delta = 53$ ppm (see Supporting Information), representative of $Et_2B\text{-}OR$.[22]

One could also imagine a mechanism in which a Rh species undergoes addition to the aldehyde,[23] the resulting alkoxide opens the epoxide, and then the Rh–C bond is reduced thereafter. To account for the results in Equation (4), therefore, the carbonyl addition would have to be reversible, and the results of Equation (5) and several ^{11}B NMR spectroscopy experiments (see above) would necessarily have to originate from a process not directly involved in the catalytic cycle. Nevertheless, as in the mechanism shown in Scheme 1, epoxide-ring opening still precedes carbonyl reduction in this alternate framework.



Scheme 1. Proposed mechanism for the catalytic reductive coupling of epoxides and aldehydes.





In summary, only off-the-shelf reagents and catalysts are required to effect both a reduction and a carbon–oxygen bond formation in the reductive coupling of two of the most readily available functional groups to provide differentially modified, synthetically useful 1,2-diols in a single catalytic operation. The regioselectivity of this process is very high; none of the

 © 2005 Wiley-VCH Verlag GmbH & Co. KGaA, Weinheim

minor regioisomer can be detected by ^{1}H NMR spectroscopic analysis of the unpurified product mixtures. This method circumvents one of the key problems of catalytic C–O bond formation, β-elimination of a carbinol hydrogen atom to give an aldehyde (or ketone) and an M–H species that is often catalytically inactive.[8d] Moreover, as all evidence suggests that epoxide-ring opening occurs prior to reduction of the aldehyde, other functional groups might also undergo reductive coupling with epoxides by way of proposed intermediate **B**. Thus, these first examples of metal-catalyzed reductive C–O bond formation of epoxides not only are of inherent utility, but also provide a starting point for the development of other useful catalytic reductive C–X coupling methods.

Received: August 18, 2004

Keywords: aldehydes · coupling reactions · epoxides · nickel · rhodium

[1] a) F. Fischer, H. Tropsch, DR Patent 411 416, **1922**; b) R. B. Anderson, *The Fischer-Tropsch Synthesis*, Academic Press, New York, **1984**.

[2] P. W. N. M. van Leeuwen, *Homogenous Catalysis: Understanding the Art*, Kluwer, Dordrecht, **2004**, chap. 5–6.

[3] a) Y. Okude, S. Hirano, T. Hiyama, H. Nozaki, *J. Am. Chem. Soc.* **1977**, *99*, 3179 – 3181; b) H. Jin, J. Uenishi, W. J. Christ, Y. Kishi, *J. Am. Chem. Soc.* **1986**, *108*, 5644 – 5646.

[4] For recent reviews, see: a) K. M. Miller, C. Molinaro, T. F. Jamison, *Tetrahedron: Asymmetry* **2003**, *14*, 3619 – 3625; b) S.-i. Ikeda, *Angew. Chem.* **2003**, *115*, 5672 – 5678; *Angew. Chem. Int. Ed.* **2003**, *42*, 5120 – 5122; c) J. Montgomery, *Angew. Chem.* **2004**, *116*, 3980 – 3998; *Angew. Chem. Int. Ed.* **2004**, *43*, 3890 – 3908; d) H.-Y. Jang, M. J. Krische, *Acc. Chem. Res.* **2004**, *37*, DOI: 10.1021/ar020108e.

[5] For reviews, see: a) J. H. Brewster in *Comprehensive Organic Synthesis*, *Vol. 8* (Eds.: B. M. Trost, I. Fleming), Pergamon Press, Oxford, **1991**, pp. 211 – 234; b) K. Miura, H. Hosomi in *Lewis Acid Reagents* (Ed.: H. Yamamoto) Oxford University Press, Oxford, **1999**, pp. 159 – 168.

[6] Reductive C–O bond formation (but no net reduction of the coupling partners) occurs in the Sm^{II}-catalyzed Evans–Tishchenko reaction: D. A. Evans, A. H. Hoveyda, *J. Am. Chem. Soc.* **1990**, *112*, 6447 – 6449.

[7] For C–O bond formation in the presence of Ph_3P as promoter and reductant, see: C.-K. Jung, J.-C. Wang, M. J. Krische, *J. Am. Chem. Soc.* **2004**, *126*, 4118 – 4119.

[8] a) M. Palucki, J. P. Wolfe, S. L. Buchwald, *J. Am. Chem. Soc.* **1996**, *118*, 10333 – 10334; b) G. Mann, J. F. Hartwig, *J. Am. Chem. Soc.* **1996**, *118*, 13109 – 13110; c) J. F. Hartwig, *Acc. Chem. Res.* **1998**, *31*, 852 – 860; d) A. R. Muci, S. L. Buchwald, *Top. Curr. Chem.* **2002**, *219*, 131 – 209.

[9] a) C. Molinaro, T. F. Jamison, *J. Am. Chem. Soc.* **2003**, *125*, 8076 – 8077, and references therein; b) K. M. Miller, T. Luanphaisarnnont, C. Molinaro, T. F. Jamison, *J. Am. Chem. Soc.* **2004**, *126*, 4130 – 4131.

[10] Nickella(II)oxetanes have not been isolated in pure form but have been proposed as intermediates in catalytic reactions: a) R. J. De Pasquale, *J. Chem. Soc. Chem. Commun.* **1973**, 157 – 158; b) J.-E. Bäckvall, O. Karlsson, S. O. Ljunggren, *Tetrahedron Lett.* **1980**, *21*, 4985 – 4988; c) A. Miyashita, T. Shimada, A. Sugawara, H. Nohira, *Chem. Lett.* **1986**, 1323 – 1326; For computational studies, see: d) J.-E. Bäckvall, F. Bökman, M. R. A. Blomberg, *J. Am. Chem. Soc.* **1992**, *114*, 534 – 538; e) M. Mavrikakis, D. J. Doren, M. A. Barteau, *J. Phys. Chem. B* **1998**, *102*, 394 – 399; f) J. W. Medlin, M. Mavrikakis, M. A. Barteau, *J. Phys. Chem. B* **1999**, *103*, 11169 – 11175; g) For gas-phase studies (Ni), see: E. Kline, R. H. Hauge, J. L. Margrave, H. Zakya, *High Temp. Sci.* **1990**, *30*, 69 – 82.

[11] For X-ray crystal structures of Group 10 metallaoxetanes and related complexes, see: Pd^{II} and Pt^{II} metallaoxetanes: a) R. Schlodder, J. A. Ibers, M. Lenarda, M. Graziani, *J. Am. Chem. Soc.* **1974**, *96*, 6893 – 6900; b) M. Lenarda, R. Ros, O. Traverso, W. D. Pitts, W. H. Baddley, M. Graziani, *Inorg. Chem.* **1977**, *16*, 3178 – 3182; c) K.-T. Aye, L. Gelmini, N. C. Payne, J. J. Vittal, R. J. Puddephatt, *J. Am. Chem. Soc.* **1990**, *112*, 2464 – 2465; d) Nickella(II)azetidine: B. L. Lin, C. R. Clough, G. L. Hillhouse, *J. Am. Chem. Soc.* **2002**, *124*, 2890 – 2891.

[12] For decarbonylation of aldehydes in the presence of $[ClRh(PPh_3)_3]$, see: a) J. P. Collman, L. S. Hegedus, J. R. Norton, R. G. Finke, *Principles and Applications of Organotransition Metal Chemistry*, University Science Books, Sausalito, **1987**, pp. 768 – 775; b) K. Ohno, J. Tsuji, *J. Am. Chem. Soc.* **1968**, *90*, 99 – 107.

[13] a) S. Winstein, R. B. Henderson, in *Heterocyclic Compounds*, *Vol. 1* (Ed.: R. C. Elderfield), Wiley, New York, **1950**; b) R. E. Parker, N. S. Isaacs, *Chem. Rev.* **1959**, *59*, 737 – 799; c) R. A. Wohl, *Chimia* **1974**, *28*, 1 – 5.

[14] In contrast to the regioselectivity trends we observe in the work reported herein, asymmetric allylic alkylation of alcohols by alkenyl oxiranes favors epoxide-ring opening through cleavage of the more substituted C–O bond of the epoxide: B. M. Trost, E. J. McEachern, F. D. Toste, *J. Am. Chem. Soc.* **1998**, *120*, 12702 – 12703.

[15] Water: a) M. Tokunaga, J. F. Larrow, F. Kakiuchi, E. N. Jacobsen, *Science* **1997**, *277*, 936 – 938; b) S. E. Schaus, B. D. Brandes, J. F. Larrow, M. Tokunaga, K. B. Hansen, A. E. Gould, M. E. Furrow, E. N. Jacobsen, *J. Am. Chem. Soc.* **2002**, *124*, 1307 – 1315; c) D. E. White, E. N. Jacobsen, *Tetrahedron: Asymmetry* **2003**, *14*, 3633 – 3638; d) L. P. C. Nielsen, C. P. Stevenson, D. G. Blackmond, E. N. Jacobsen, *J. Am. Chem. Soc.* **2004**, *126*, 1360 – 1362; phenols and aliphatic alcohols: e) J. M. Ready, E. N. Jacobsen, *J. Am. Chem. Soc.* **2001**, *123*, 2687 – 2688; f) J. M. Ready, E. N. Jacobsen, *Angew. Chem.* **2002**, *114*, 1432 – 1435; *Angew. Chem. Int. Ed.* **2002**, *41*, 1374 – 1377; g) carboxylic acids: E. N. Jacobsen, F. Kakiuchi, R. G. Konsler, J. F. Larrow, M. Tokunaga, *Tetrahedron Lett.* **1997**, *38*, 773 – 776.

[16] a) D. Milstein, *J. Am. Chem. Soc.* **1982**, *104*, 5227 – 5228; b) M. J. Calhorda, A. M. Galvão, C. Ünaleroglu, A. A. Zlota, F. Frolow, D. Milstein, *Organometallics* **1993**, *14*, 3316 – 3325.

[17] B. Rickborn in *Comprehensive Organic Synthesis*, *Vol. 3* (Eds.: B. M. Trost, I. Fleming), Pergamon Press, New York, **1991**, pp. 733 – 775.

[18] a) M. Farmer, M. A. Khan, K. M. Nicholas, *J. Chem. Soc. Chem. Commun.* **1988**, 1384 – 1385; b) K.-T. Aye, G. Ferguson, A. J. Lough, R. J. Puddephatt, *Angew. Chem.* **1989**, *101*, 765 – 767; *Angew. Chem. Int. Ed. Engl.* **1989**, *28*, 767 – 768; c) K.-T. Aye, L. Gelmini, N. Payne, J. J. Vittal, R. J. Puddephatt, *J. Am. Chem. Soc.* **1990**, *112*, 2464 – 2465; d) Y. Fukumoto, N. Chatani, S. Murai, *J. Org. Chem.* **1993**, *58*, 4187 – 4188.

[19] Rhodium is required for catalysis. Neither reductive coupling (i.e. product formation) nor reduction of the aldehyde occurs when $[(Ph_3P)_3RhCl]$ is omitted from the reaction. Similarly, when $[(Ph_3P)_3RhCl]$ is omitted but Ph_3P is included in the reaction, neither product formation nor aldehyde reduction is observed.

[20] For acceleration of Rh-catalyzed reactions by bases, see: a) hydrogenation: W. S. Knowles, M. J. Sabacky, B. D. Vineyard, *Ann. N. Y. Acad. Sci.* **1970**, *172*, 232 – 237; b) reductive C–C bond formation: H.-Y. Jang, R. R. Huddleston, M. J. Krische, *J. Am. Chem. Soc.* **2002**, *124*, 15156 – 15157.

 © 2005 Wiley-VCH Verlag GmbH & Co. KGaA, Weinheim

[21] In the absence of aldehyde, a β-H abstraction by Rh in **B** would give a boron enolate and, upon workup, a methyl ketone, accounting for the results in Equation (5).
[22] "Nuclear Magnetic Resonance Spectroscopy of Boron Compounds Containing Two-, Three-, and Four-Coordinate Boron": B. Wrackmeyer in *Annual Reports on NMR Spectroscopy*, *Vol. 20* (Ed.: G. A. Webb), Academic Press, San Diego, **1988**, pp. 61 – 204.
[23] a) B. B. Wayland, B. A. Woods, V. M. Minda, *J. Chem. Soc. Chem. Commun.* **1982**, 634 – 635; b) X. Fu, L. Basickes, B. B. Wayland, *Chem. Commun.* **2003**, 520 – 521.

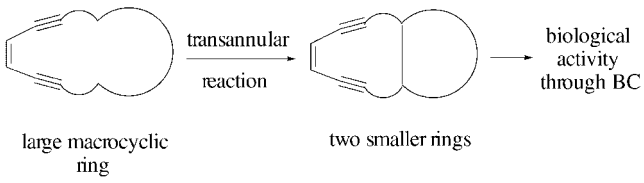
 © 2005 Wiley-VCH Verlag GmbH & Co. KGaA, Weinheim

Enediynes

Activation of Macrocyclic Enediynes by Transannular Cyclization**

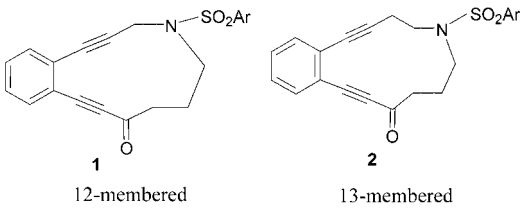
Amit Basak, Sandip Kumar Roy, and Subrata Mandal*

Species containing single electrons were long known to possess cytotoxic activity through DNA damage; however, this property could not be utilized in the development of antitumor agents because methods to generate radicals under mild conditions were not known until Mother Nature revealed how it could be done through the chemistry of naturally occurring enediynes.[1] Although these enediynes possess potent antitumor activity, their extreme toxicity acted as a deterrent for their direct medical use. This prompted chemists to synthesize analogous molecules with the hope of reducing the toxicity without sacrificing the antitumor activity to a great extent. Designed enediynes can be broadly classified into two groups: one comprising intrinsically reactive enediynes stabilized by the use of a locking device. Fusion of small strained rings,[2] incorporation of sp^2-carbon atoms,[3] tuning of redox characteristics,[4] and the ability to undergo allylic rearrangement[5] are some examples of locking devices. The other group comprises ambiently unreactive enediynes, usually acyclic, that are made active in situ by a suitable triggering reaction such as isomerization to eneyne allenes,[6] and ligation to metal ions.[7] Examples are also known in which a reactive enediyne core has been generated from a prodrug. As macrocyclic enediynes[8] with 11-membered rings or higher are stable at physiological temperature, it would be possible to broaden the scope of the second approach if an intramolecular transannular reaction were carried out to reduce the ring size of a large macrocyclic enediyne, which in turn should enhance the rate of the Bergman cyclization (Scheme 1).[9] Herein, we report the synthesis of two novel macrocyclic N-substituted enediynyl



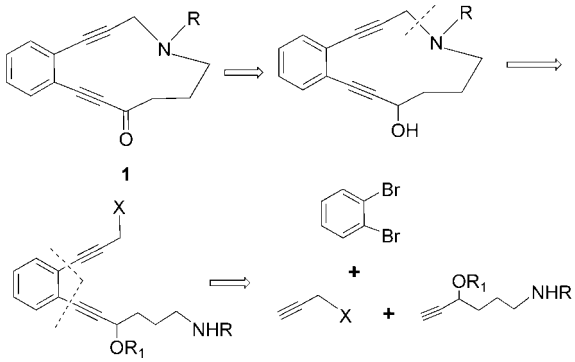
Scheme 1. Design of macrocyclic enediynes.

ketones **1** and **2**. Ways to control their chemical and biological activity are also reported. To our knowledge, this is the first



example of the use of a transannular reaction for enediyne activation,[10] although transannular reactions have been used to activate promitosene, a precursor to mitosene, under photoirradiation conditions.[11]

The retrosynthesis of the enediyne **1** (Scheme 2) involves three critical bond-forming reactions, namely the construction



Scheme 2. Retrosynthesis of enediyne **1**.

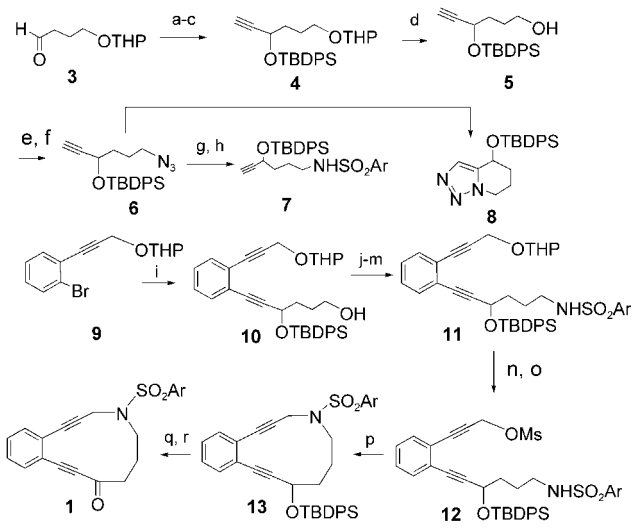
of the enediyne framework by two successive Sonogashira couplings,[12] followed by macrocyclization by intramolecular N-alkylation.[13] The actual synthesis was, however, executed with a slight modification. Azide **6**, the precursor for the protected amine **7** proved to be unstable as it undergoes facile intramolecular cycloaddition with the alkyne functionality.[14] This forced us to do the second palladium(0)-mediated coupling with protected hydroxy alkyne **5** instead of **7** (Scheme 3). The resulting enediyne **10** was converted into the 4-nitrosulfonamide **11** by the following sequence of

[*] Dr. A. Basak, S. K. Roy, S. Mandal
Bioorganic Laboratory, Department of Chemistry
Indian Institute of Technology, Kharagpur 721 302 (India)
Fax: (+91) 3222-282252
E-mail: absk@chem.iitkgp.ernet.in

[**] Support has been provided by Council of Scientific and Industrial Research, Goverment of India, Grant No. 01(1745)/02/EMR-II.

Supporting information for this article is available on the WWW under http://www.angewandte.org or from the author.

 © 2005 Wiley-VCH Verlag GmbH & Co. KGaA, Weinheim DOI: 10.1002/anie.200460831

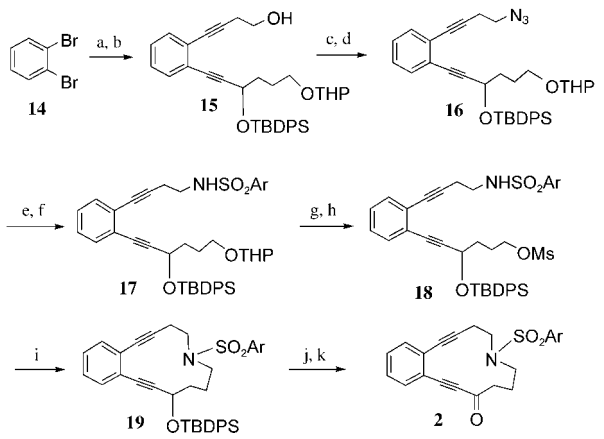


Scheme 3. Synthesis of enediyne **1**. a)TMS-acetylene, nBuLi, THF, 0°C; b) CsF, MeOH, RT; c) TBDPS-Cl, imidazole, DMAP, CH_2Cl_2, RT; d) PPTS, EtOH, 50°C; e) MsCl, Et_3N, CH_2Cl_2, 0°C; f)NaN_3, DMF, RT; g) PPh_3, moist THF, RT; h) $ArSO_2Cl$, Et_3N, CH_2Cl_2, 0°C; i) **5**, $[Pd(Ph_3)_4]$, nBuNH$_2$, reflux; j) MsCl, Et_3N, CH_2Cl_2, 0°C; k) NaN_3, DMF, RT; l) PPh_3, moist THF, RT; m) $ArSO_2Cl$, Et_3N, CH_2Cl_2, 0°C; n) PPTS, EtOH, 50°C; o) MsCl, Et_3N, 0°C; p) K_2CO_3, DMF, RT; q) MeOH, 3% HCl, RT; r) PCC, CH_2Cl_2, RT. Ar = 4-nitrophenyl; THP = tetrahydropyranyl; TBDPS = *tert*-butyldiphenylsilyl; PCC = pyridinium chlorochromate.

reactions: mesylation, displacement with NaN_3,[15] reduction into the amine,[16] and protection with 4-nitrobenzene sulfonyl chloride. Removal of THP followed by treatment with mesyl chloride and Et_3N furnished the mesylate **12**. Intramolecular N-alkylation in K_2CO_3/DMF under high dilution worked quite well to give the 12-membered enediyne **13** as the only isolable product in about 60% yield.[17] This was then converted into the ketone **1**.

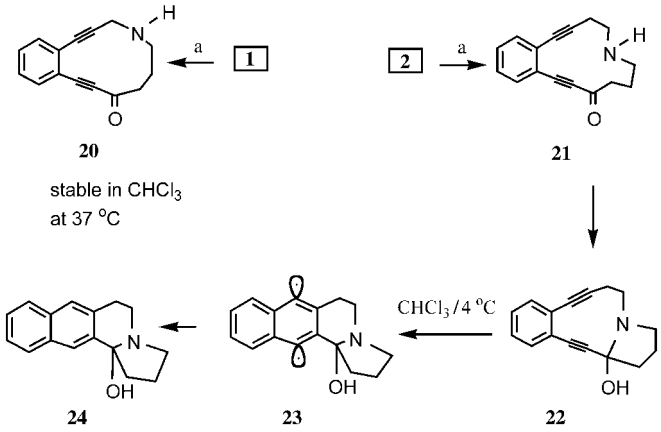
The synthesis of the 13-membered enediyne **2** could not be achieved in a similar way as intramolecular N-alkylation at a homopropargylic center is known to produce only the elimination product.[18] The synthesis was completed by intramolecular N-alkylation in the reverse direction (Scheme 4). As expected, this step was free from any elimination. The structures of the cyclic enediynes were confirmed by NMR and mass spectral studies. The appearance of peaks at m/z 431 [$M-Na^+$] for **1** and at m/z 423 [$M-H^+$] and 445 [$M-Na^+$] for **2** in the mass spectrum (ES+ mode) confirmed that only intramolecular N-alkylation has occurred and ruled out the formation of any dimeric or oligomeric products during cyclization.

The sulfonamido ketone **1** was then deprotected by using thiophenol and K_2CO_3 in DMF[19] to generate the 12-membered free amino ketone **20**.[20] Compound **20** proved to be stable at room temperature and no significant decomposition was observed when a solution of **20** in $CHCl_3$ was kept at 37°C for seven days. Moreover, **20** could be converted back to the starting sulfonamide **1** upon treatment with 4-nitrobenzenesulfonyl chloride and triethylamine, thus demonstrating the inherent stability of **20**. Attempts to induce transannular cyclization to the aminol with catalytic amounts of *p*-toluenesulfonic acid (PTSA) also failed. On the contrary,



Scheme 4. Synthesis of enediyne **2**. a) 3-butyn-1-ol, $[Pd(PPh_3)_4]$, nBuNH$_2$, reflux; b) **4**, $[Pd(PPh_3)_4]$, nBuNH$_2$, reflux; c) MsCl, Et_3N, CH_2Cl_2, 0°C; d) NaN_3, DMF, RT; e) PPh_3, moist THF, RT; f) $ArSO_2Cl$, Et_3N, CH_2Cl_2, 0°C; g) PPTS, EtOH, 50°C; h) MsCl, Et_3N, CH_2Cl_2, 0°C; i) K_2CO_3, DMF, RT; j) 3% HCl, MeOH/THF (4:1), RT; k) PCC, CH_2Cl_2, RT. Ar = 4-nitrophenyl; PPTS = pyridinium *p*-toluenesulfonate.

deprotection of the sulfonamido group in ketone **2** gave the product amine **21**, which remained mostly in the unstable aminol form **22** (as indicated by its inability to be reconverted to the starting sulfonamide **2**). The aminol, being a 10-membered enediyne, decomposes in $CHCl_3$ even at 4°C ($t_{1/2}$ ~ 40 h) to give the new product **24**.[21] The occurrence of a Bergman cyclization was indicated by the disappearance of all four acetylenic carbon atoms, which are now replaced by signals for aromatic carbon atoms. The probable mechanism of formation of **24** is shown in Scheme 5. That the mechanism



Scheme 5. Fate of aminoenediynes. a) PhSH, K_2CO_3, DMF, RT.

involves the generation of the diradical **23** is also supported by the interaction of the enediyne with supercoiled DNA. Thus **22** showed single-strand cuts to generate form II when incubated with double-stranded plasmid DNA (pBR 322) in the supercoiled form (Figure 1). The corresponding sulfonamido ketone **2**, under similar conditions, did not show any DNA damage, thus ruling out a possible cleavage mechanism by the Michael addition of nucleophilic bases of DNA to the

 © 2005 Wiley-VCH Verlag GmbH & Co. KGaA, Weinheim

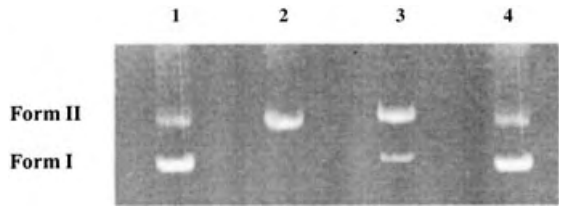


Figure 1. DNA cleavage studies. Lane 1: DNA in TAE buffer (pH 8, 0.4 μM/bp) (5 μL) + acetonitrile (15 μL) at 37°C; lane 2: DNA in TAE buffer (pH 8, 0.4 μM/bp) (5 μL) + aminol (**22**) (40 μM, 48 h) in acetonitrile (15 μL) at 37°C; lane 3: DNA in TAE buffer (pH 8, 0.4 μM/bp) (5 μL) + aminol (**22**) (40 μM, 24 h) in acetonitrile (15 μL) at 37°C; lane 4: DNA in TAE buffer (pH 8, 0.4 μM/bp) (5 μL) + sulfonamide (**2**) (40 μM, 48 h) in acetonitrile (15 μL) at 37°C.

unsaturated carbonyl system. The stability of the 12-membered amino ketone **20** is ascribed to its inability to undergo the transannular reaction, as it involves the formation of a nine-membered enediyne, which is a kinetically disfavored reaction.[22]

In conclusion, we have synthesized two novel N-based macrocyclic enediynes and have been able to activate one of these by a transannular reaction. The use of a 4-nitrophenylsulfonyl group as a deactivating device that renders the nitrogen non-nucleophilic has been demonstrated. Thiol-mediated deprotection can act as a triggering mechanism that activates the enediyne through an intramolecular cyclization reaction. When the protected amino ketone **2** was incubated with supercoiled DNA in the presence of glutathione, a biological thiol, at a pH of 8.0, it was able to cleave supercoiled DNA (Figure 2). This observation has proven

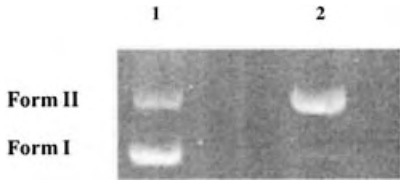


Figure 2. DNA cleavage studies. Lane 1: DNA in TAE buffer (pH 8, 0.4 μM/bp) (5 μL) + acetonitrile (15 μL) at 37°C; lane 2: DNA in TAE buffer (pH 8, 0.4 μM/bp) (7 μL) + glutathione (25 μM) in TAE buffer (pH 8, 20 μL) + sulfonamido ketone (**2**) (20 μm, 48 h) in acetonitrile (40 μL) at 37°C.

our design; namely, the activation by way of a biological thiol-mediated triggering of enediyne towards Bergman cyclization. Considering the repertoire of amine-protecting groups and different methods for their deprotection, our design offers a wide array of triggering mechanisms for the development of antitumor agents that work through generation of diradicals.

Received: May 30, 2004
Revised: July 29, 2004

Keywords: cyclization · DNA damage · enediynes · macrocycles

[1] a) K. C. Nicolaou, A. L. Smith in *Modern Acetylene Chemistry* (Eds.: P. J. Stang, F. Diederich), VCH, Weinheim, **1995**, p. 203; b) M. E. Maier, *Synlett* **1995**, 13; c) *DNA and RNA Cleavers and Chemotherapy of Cancer and Viral Diseases* (Ed.: B. Meunier), Kluwer, Dordrecht, **1996**, p. 1; d) Z. Xi, I. H. Goldberg in *Comprehensive Natural Product Chemistry*, *Vol. 7* (Eds.: D. H. R. Barton, K. Nakanishi), Pergamon, Oxford, **1999**, p. 553; e) W.-M. Dai, K. C. Nicolaou, *Angew. Chem.* **1991**, *103*, 1453; *Angew. Chem. Int. Ed. Engl.* **1991**, *30*, 1387; f) H. Lhermite, D. Grierson, *Contemp. Org. Synth.* **1996**, *3*, 93; g) J. W. Grisom, G. U. Gunawardena, D. Klingberg, D. Huang, *Tetrahedron* **1996**, *52*, 6453.

[2] a) K. C. Nicolaou, E. J. Sorensen, R. Discordia, C.-K. Hwang, R. E. Minto, K. N. Bharucha, R. G. Bergman, *Angew. Chem.* **1992**, *104*, 1094; *Angew. Chem. Int. Ed. Engl.* **1992**, *31*, 1044; b) L. Banfi, G. Guanti, *Angew. Chem.* **1995**, *107*, 2613; *Angew. Chem. Int. Ed. Engl.* **1995**, *34*, 2393; c) L. Banfi, G. Guanti, *Eur. J. Org. Chem.* **1998**, 1543; d) A. Basak, U. K. Khamrai, U. K. Mallick, *Chem. Commun.* **1996**, 749; e) K. C. Nicolaou, W.-M. Dai, S.-C. Tsay, V. A. Estevez, W. Wrasidlo, *Science* **1992**, *256*, 1172.

[3] a) P. Magnus, R. A. Fairhurst, *J. Chem. Soc. Chem. Commun.* **1994**, 1541; b) J. P. Snyder, *J. Am. Chem. Soc.* **1990**, *112*, 5367; c) P. Magnus, P. Carter, J. Elliott, R. Lewis, J. Harling, T. Patterna, W. E. Butta, S. Fortt, *J. Am. Chem. Soc.* **1992**, *114*, 2544.

[4] a) M. F. Semmelhack, T. Neu, F. Foubelo, *J. Org. Chem.* **1994**, *59*, 5038; b) K. C. Nicolaou, A. Liu, Z. Zheng, S. McComb, *J. Am. Chem. Soc.* **1992**, *114*, 9279; c) M. E. Maier, T. Brandstetter, *Tetrahedron Lett.* **1991**, *32*, 3679; d) A. D. Myers, P. S. Dragovich, *J. Am. Chem. Soc.* **1992**, *114*, 20.

[5] a) W.-M. Dai, K. W. Lai, A. Wu, W. Hamaguchi, M. Y. H. Lee, L. Zhou, A. Ishii, S. Nishimoto, *J. Med. Chem.* **2002**, *45*, 758; b) W.-M. Dai, *Curr. Med. Chem.* **2003**, *10*, 2265.

[6] a) W.-M. Dai, K. C. Fong, H. Danjo, S.-I. Nishimoto, *Angew. Chem.* **1996**, *108*, 821; *Angew. Chem. Int. Ed. Engl.* **1996**, *35*, 779; b) M. Wakayama, H. Nemoto, M. Shibuya, *Tetrahedron Lett.* **1996**, *37*, 5397; c) I. Suzuki, M. Wakayama, A. Shigenaga, H. Nemotoo, M. Shibuya, *Tetrahedron Lett.* **2000**, *41*, 10019; d) I. Suzuki, A. Shigenaga, H. Nemoto, M. Shibuya, *Heterocycles* **2001**, *54*, 571; e) M. J. Wu, C.-F. Lin, J.-S. Wu, H.-T. Chen, *Tetrahedron Lett.* **1994**, *35*, 1879.

[7] a) A. Basak, S. Mandal, S. S. Bag, *Chem. Rev.* **2003**, *103*, 4077; b) B. Konig, *Eur. J. Org. Chem.* **2000**, 381.

[8] K. C. Nicolaou, G. Zuccarello, Y. Oogawa, E. J. Schweiger, T. Kumazawa, *J. Am. Chem. Soc.* **1988**, *110*, 4866.

[9] a) R. G. Bergman, *Acc. Chem. Res.* **1973**, *6*, 25; b) T. P. Lockhart, R. G. Bergman, *J. Am. Chem. Soc.* **1981**, *103*, 4091.

[10] The closest conceptually similar example is the activation of a maduropeptin artifact by aziridine formation involving attack by a nucleophilic nitrogen atom (D. Schroeder, K. L. Colson, S. E. Klohr, N. Zein, D. R. Langley, M. S. Lee, J. A. Matson, T. W. Doyle, *J. Am. Chem. Soc.* **1994**, *116*, 935; N. Zein, W. Solomon, K. L. Colson, D. R. Schroeder, *Biochemistry* **1995**, *34*, 11591; C. Roger, D. S. Grierson, *Tetrahedron Lett.* **1998**, *39*, 27). However, this may be considered to be activation by an allylic rearrangement for which the ring size of the parent system remains the same.

[11] S. B. Rollins, R. M. Williams, *Tetrahedron Lett.* **1997**, *38*, 4033.

[12] a) K. Sonogashira, Y. Tohoda, N. Hagihara, *Tetrahedron Lett.* **1975**, *16*, 4467; b) S. Takahashi, Y. Kuroyama, K. Sonogashira, N. Hagihara, *Synthesis* **1980**, 627.

[13] A. Basak, U. K. Khamrai, J. C. Shain, *Tetrahedron Lett.* **1997**, *38*, 6067.

[14] a) W. Lwowski in *1,3-Dipolar Cycloaddition Chemistry*, *Vol. 1* (Ed.: A. Padwa), Wiley Interscience, New York, **1984**, p. 559;

 © 2005 Wiley-VCH Verlag GmbH & Co. KGaA, Weinheim

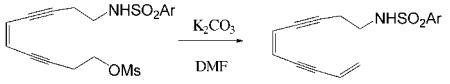
b) P. K. Kadaba, B. Stanovnik, M. Tisler in *Advances in Heterocyclic Chemsitry*, *Vol. 37* (Ed.: A. R. Kartrizsky), Academic Press, New York, **1984**, p. 217.

[15] The azide derived from **10** is stable and does not undergo intramolecular cycloaddition as the actylene is now part of the enediyne system.

[16] N. Knozvi, M. Vaultier, L. Toupet, R. Carrie, *Tetrahedron Lett.* **1987**, *28*, 1757.

[17] Experimental procedure for the intramolecular N-alkylation: Anhydrous K_2CO_3 (5 equiv) was added to a solution of acyclic enediyne **12**/**18** (0.35 mmol) in dry DMF (80 mL) under argon, and the mixture was stirred at room temperature for 13 h. The mixture was then partitioned between EtOAc and water (2 × 200 mL each). The combined organic layers were washed with water (3 × 150 mL), dried (Na_2SO_4), and evaporated under vacuum at room temperature. The cyclized product was isolated by column chromatography by using hexane–EtOAc (4:1) as eluent (yield ~60%). Selected ^{1}H NMR data: For **1** (200 MHz, [D$_6$]DMSO): $\delta = 8.16$ (d, ^3J(H,H) = 8.8 Hz, 2H; nitroaryl-H), 7.92 (d, ^3J(H,H) = 8.8 Hz, 2H; nitroaryl-H), 7.49 (m, 1H; aryl-H), 7.28 (m, 3H; aryl-H), 4.28 (s, 2H; NCH_2CC), 3.19 (m, 2H; NCH_2CH_2), 2.46 (m, 2H; $COCH_2$), 2.01 ppm (m, 2H; NCH_2CH_2). For **2** (200 MHz, [D$_6$]DMSO): $\delta = 8.40$ (d, ^3J(H,H) = 8.6 Hz, 2H; nitroaryl-H), 8.11 (d, ^3J(H,H) = 8.6 Hz, 2H; nitroaryl-H), 7.68 (d, ^3J(H,H) = 7.5 Hz, 1H; aryl-H), 7.57–7.41 (m, 3H; aryl-H), 3.28 (m, 4H; $CH_2NCH_2CH_2CC$), 2.92 (m, 2H; NCH_2CH_2CC), 2.60 (m, 2H; $NCH_2CH_2CH_2$), 2.30 ppm (m, 2H; $NCH_2CH_2CH_2$).

[18] J. C. Shain, Ph.D. Thesis, IIT, Kharagpur, **2000**, [Eq. (1)].



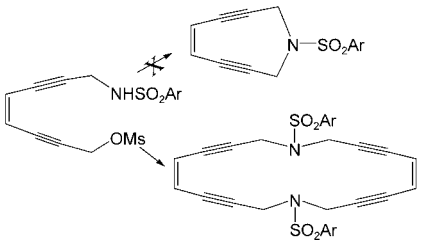
(1)

[19] T. Fukuyama, C.-K. Jow, M. Cheung, *Tetrahedron Lett.* **1995**, *36*, 6373.

[20] Experimental procedure for the deprotection of the 4-nitrosulfonamido group: Thiophenol (1.1 equiv) and K_2CO_3 (2.2 equiv) were added to a solution of **1** or **2** (0.12 mmol) in DMF (5 mL), and stirred under argon for 1 h. The mixture was then partitioned between EtOAc and water (2 × 25 mL each). The combined organic layers were washed with water (3 × 25 mL), dried (Na_2SO_4), and evaporated under vacuum at room temperature. The free amine **20** or the aminol **22** was isolated by column chromatography using CH_2Cl_2–MeOH (10:1) as eluent (yield ~75%). Selected ^{1}H NMR data: For **20** (200 MHz, $CDCl_3$): $\delta = 7.22$–7.18 (bm, 1H; aryl-H), 7.04–6.90 (m, 3H; aryl-H), 6.87 (bs, 1H; NH), 3.74 (s, 2H; NCH_2CC), 2.95 (t, ^3J(H,H) = 6.3 Hz, 2H; NCH_2CH_2), 2.65 (t, ^3J(H,H) = 6.1 Hz, 2H; $COCH_2$), 2.05 ppm (m, 2H; NCH_2CH_2). For **22** (200 MHz, $CDCl_3$): $\delta = 7.46$ (m, 1H; aryl-H), 7.25–6.84 (m, 3H; aryl-H), 6.59 (bs, 1H; OH), 3.04–2.85 (m, 4H; $CH_2NCH_2CH_2CC$), 2.75 (m, 2H; NCH_2CH_2CC), 2.60 (m, 2H; $C(OH)CH_2$), 2.04 ppm (m, 2H; $NCH_2CH_2CH_2$).

[21] Cyclization of aminol **22**: The solution of aminol (40 mg) in $CHCl_3$ was kept at 4°C for seven days and periodically monitored by TLC. After evaporation of the solvent, the cyclized product **24** was isolated by column chromatography over silica gel using hexane–EtOAc (5:1) as eluent (17 mg, ~45%). ^{1}H NMR (500 MHz, $CDCl_3$): $\delta = 7.70$ (dd, ^3J(H,H) = 8.5, 1.1 Hz, 1H; aryl-H), 7.69 (dd, ^3J(H,H) = 8.5, 1.1 Hz, 1H; aryl-H), 7.15 (m, 4H; aryl-H), 6.45 (s, 1H; OH), 3.03 (m, 3H; $CHNCH_2$), 2.82 (m, 2H; ArCH, NCH), 2.23 (m, 1H; ArCH), 1.95 (m, 1H; C(OH)CH), 1.68 ppm (m, 3H; C(OH)CH, $C(OH)CH_2CH_2$); ^{13}C NMR (125 MHz, $CDCl_3$): $\delta = 135.9$ (quaternary C), 133.7 (quaternary C), 133.4 (quaternary C), 133.1 (quaternary C), 129.5 (CH), 129.3 (CH), 128.3 (CH), 127.4 (CH), 126.6 (CH), 125.4 (CH), 68.9 (quaternary C), 50.6 (CH_2), 45.4 (CH_2), 36.9 (CH_2), 29.7 (CH_2), 22.8 ppm (CH_2); Mass (ES+): m/z: 239 [M^+], 221 [M^+-H_2O]. Keeping a solution of the amine **22** in $CDCl_3$ gave a mixture of deuteriated as well as monochloro products.

[22] Attempted intramolecular N-alkylation to produce a nine-membered enediyne failed. The reaction produced only the dimer [Eq. (2)] as shown below. (A. Basak, J. C. Shain, U. K. Khamrai, K. Rudra, A. Basak, *J. Chem. Soc. Perkin Trans. 1* **2000**, 1955).



(2)

 © 2005 Wiley-VCH Verlag GmbH & Co. KGaA, Weinheim

Natural Products Synthesis

Total Synthesis of Halipeptin A: A Potent Antiinflammatory Cyclic Depsipeptide**

*Shouyun Yu, Xianhua Pan, Xianfeng Lin, and Dawei Ma**

The halipeptins A (**1**) and B (**2**) are two cyclic depsipeptides that were isolated from the sponge *Haliclona* species by Gomez-Paloma and co-workers.[1,2] Initially, their structures were misassigned as the 17-membered cyclic depsipeptides containing an unusual oxazetidine.[1] One year later the same group reported the revised structures of these two compounds

[*] S. Yu, Prof. Dr. D. Ma
State Key Laboratory of Bioorganic and Natural Products Chemistry
Shanghai Institute of Organic Chemistry
Chinese Academy of Sciences
354 Fenglin Lu, Shanghai 200032 (China)
Fax: (+86) 21-6416-6128
E-mail: madw@mail.sioc.ac.cn

X. Pan
Department of Chemistry, Fudan University
Shanghai 200433 (China)

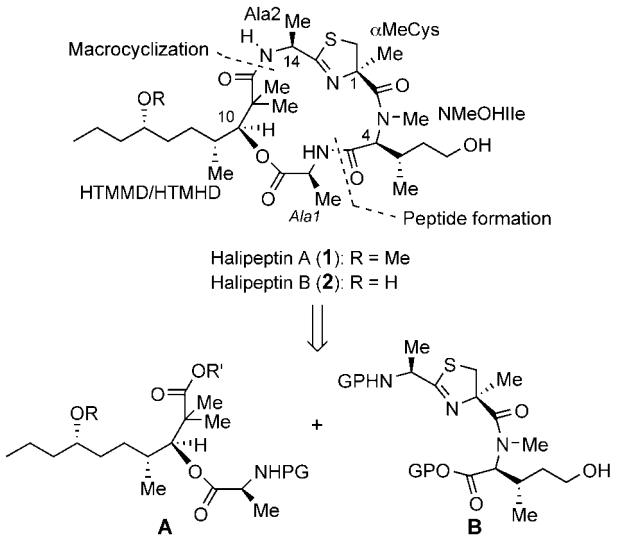
X. Lin
Department of Chemistry, Lanzhou University
Lanzhou 730000 (China)

[**] The authors are grateful to the Chinese Academy of Sciences (grant KGCX2-SW-209), the National Natural Science Foundation of China (grant 20321202), and the Science and Technology Commission of Shanghai Municipality (grants 02JC14032 & 03XD14001) for financial support.

Supporting information for this article is available on the WWW under http://www.angewandte.org or from the author.

 DOI: 10.1002/anie.200461239 © 2005 Wiley-VCH Verlag GmbH & Co. KGaA, Weinheim

as those shown in Scheme 1 which bear two L-alanine residues, an α-methylcysteine unit connected to one of the L-alanine residues through a methylthiazoline ring, and two new residues that had not been discovered from natural

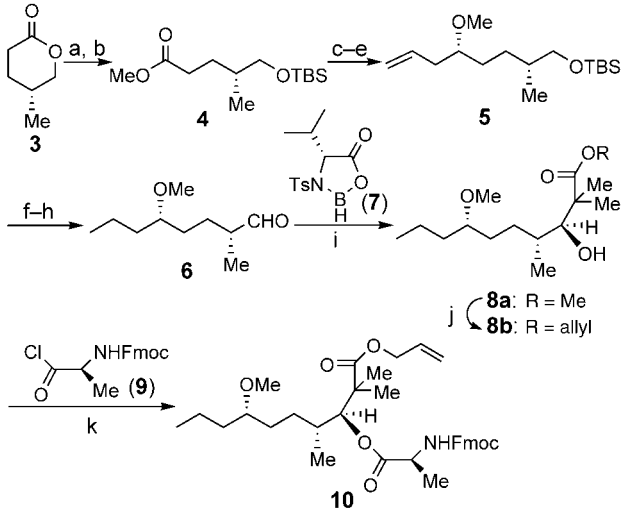


Scheme 1. Structures and retrosynthetic analysis of halipeptins A (**1**) and B (**2**). PG = protecting group.

sources:[2] 3-hydroxy-2,2,4-trimethyl-7-methoxy (or hydroxy) decanoic acid (HTMMD or HTMHD) and *N*-methyl-δ-hydroxyisoleucine (NMeOHIle). Preliminary pharmacological tests revealed that halipeptin A has potent antiinflammatory activity (60% reduction of carrageenan-induced edema at an intraperitoneal dose of 0.3 mg kg^{-1} in mice).[1] The unique structures and important biological characteristics of halipeptins A and B have attracted considerable synthetic attention.[3] As part of the continuing efforts to synthesize of cyclic peptides,[4] we report herein the first total synthesis of halipeptin A and the confirmation of its stereochemistry.

Our retrosynthetic analysis of halipeptin A is outlined in Scheme 1. As this molecule is highly methylated, the most critical problem in its assembly is the connection of the sterically hindered units with other amino acid residues. We envisaged that two less hindered positions could be reserved for late-stage connections, namely the Ala1–NMeOHIle and HTMMD–Ala2 sites. Our plan therefore required the assembly of an ester part **A** and an amide unit **B**, and hence the stereoselective synthesis of the HTMMD, NMeOHIle, and methylthiazoline residues. Because the configurations of C7 of the HTMHD and Cα of the two alanine residues were all established as *S*, the ring system of halipeptin A might have a 1*R*,4*S*,7*S*,10*S*,14*S* configuration, and hence the residues with the corresponding stereochemistry were considered as primary targets. Furthermore, ready racemization at C14 directed by the methylthiazoline group would be another critical problem,[5,6] and therefore the protecting groups for the above two units should be removable under mild conditions.

As depicted in Scheme 2, our assembly of the HTMMD unit started from (*R*)-4-methyl-5-valerolactone (**3**), an oxidative degradation product of diosgenin.[7] Ring opening of **3** with methanolic sodium methoxide followed by protection of the hydroxy group as a silyl ether provided **4**. After the ester **4** was reduced to an aldehyde with DIBAL-H, the chain was extended through an asymmetric allylboration based on the procedure of Brown and Racherla[8] to deliver a homoallylic alcohol, which was treated with NaH/MeI to produce ether **5**. Cleavage of silyl ether **5** with TBAF, hydrogenation of the terminal C-C double bond, and Swern oxidation afforded aldehyde **6**. At this stage we planned to build the β-hydroxy-α,α-dimethyl ester part in the HTMMD by an enantioselective chiral borane-mediated aldol reaction.[9] Accordingly, treatment of a mixture of the aldehyde **6** and 1-(trimethylsiloxy)-1-methoxy-2-methyl-1-propene with the borane **7** at −78 °C produced methyl ester **8a** in 95% yield as a single isomer, which was transformed into allyl ester **8b** through hydrolysis and subsequent alkylation. Esterification of the alcohol **8b** with an *N*-protected L-alanine group proved to be challenging. The method of Yamaguchi and co-workers[10] and other activated ester procedures were unsuccessful. However, we found that coupling of **8b** with acyl chloride **9**[11] at −15 °C in the presence of DMAP (0.5 equiv) gave our desired product **10** in good yield. Notably, both the amount of DMAP used and the reaction temperature are critical, as extensive racemization occurred at Cα of the L-alanine residue when this reaction was conducted at 0 °C in the presence of 0.5 equivalents of DMAP or at −15 °C in the presence of 1 equivalent of DMAP, and low conversion was attained when

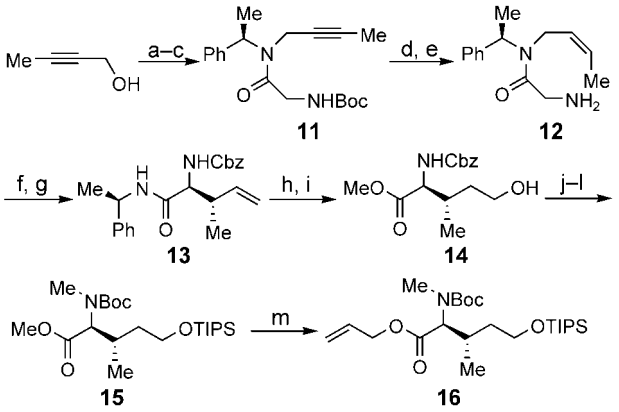


Scheme 2. a) NaOMe, MeOH, 0 °C→RT, 82%; b) TBSCl, imidazole, DMF, 98%; c) DIBAL-H, diethyl ether, −100→−90 °C; d) D-B-allyldiisopinocampheylborane; then H_2O_2, NaOH, 90% over three steps; e) NaH, MeI, DMF, room temperature, 91%; f) TBAF, THF, room temperature, 90%; g) Pt/C, H_2, EtOAc, room temperature, 99%; h) Swern oxidation, 85%; i) **7**, 1-(trimethylsiloxy)-1-methoxy-2-methyl-1-propene, −78 °C, 95%; j) aqueous LiOH, THF, MeOH; then allyl bromide, K_2CO_3, DMSO, 92%; k) **9**, DMAP (0.5 equiv), iPr_2NEt, CH_2Cl_2, −15 °C, 95% yield based on 90% conversion of **8b**. TBS = *tert*-butyldimethylsilyl, DMF = *N*,*N*-dimethylformamide, DIBAL-H = diisobutylaluminum hydride, DMSO = dimethyl sulfoxide, TBAF = tetrabutylammonium fluoride, DMAP = 4-dimethylaminopyridine.

 © 2005 Wiley-VCH Verlag GmbH & Co. KGaA, Weinheim

the coupling was carried out at 0 °C in the presence of 0.2 equivalents of DMAP.

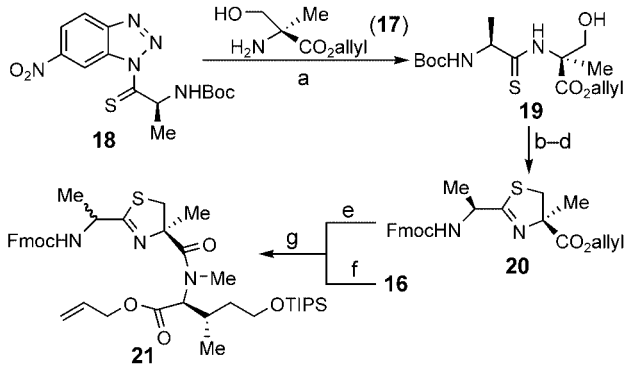
The construction of the NMeOHIle unit relied on an asymmetric aza-Claisen rearrangement developed by Tsunoda et al.[12] Although in their report only diastereoselective rearrangement of *N*-substituted *N*-(*E*)-2-butenylpropanamides to *syn* products was mentioned, based on related studies[13] we reasoned that if olefin (*Z*)-**12** was used, the desired *anti* compound would be the major product. To this end, mesylation of 2-butyn-1-ol followed by introduction of the chiral auxiliary (*R*)-α-methylbenzylamine and subsequent condensation with *N*-Boc-Gly yielded amide **11** (Scheme 3).



Scheme 3. a) MsCl, Et_3N, 82%; b) (*R*)-α-methylbenzylamine, 80%; c) $BocNHCH_2CO_2H$, EDCI, HOBT, *i*Pr_2NEt, 96%; d) Lindlar catalyst, H_2, diethyl ether, 91%; e) CF_3CO_2H, CH_2Cl_2, 96%; f) LiHMDS, THF; g) benzyl chloroformate, Et_3N, 52% over two steps; h) HCl (5 M), MeOH, reflux; then CH_2N_2, diethyl ether, 76%; i) BH_3·THF complex; then H_2O_2, pH 7 buffer, 72%; j) TIPSCl, imidazole, DMAP, 89%; k) Pd/C, H_2, $(Boc)_2O$, MeOH; l) Ag_2O, MeI, DMF, 50 °C, 94% over two steps; m) aqueous LiOH, THF, MeOH; then allyl bromide, K_2CO_3, DMSO, 92%. Ms = methanesulfonyl, Boc = *tert*-butoxycarbonyl, EDCI = ethyl dimethylaminopropyl carbodiimide chloride; HOBT = 1-hydroxy-1*H*-benzotriazole, HMDS = hexamethyldisilazide, TIPS = triisopropylsilyl.

Hydrogenation of **11** with Lindlar catalyst and subsequent deprotection with trifluoroacetic acid delivered the **12**. Exposure of **12** to LiHMDS afforded the aza-Claisen rearrangement products,[12] which were masked with Cbz to give a mixture of diastereomers. ^{1}H NMR spectroscopic analysis revealed that the ratio of the major isomer **13** to other isomers was about 3:1, and pure **13** was isolated in 52% overall yield by recrystallization. Next, removal of the chiral auxiliary from **13** followed by treatment with CH_2N_2 provided a methyl ester, which was then elaborated into the alcohol **14** through a hydroboration–oxidation reaction. After the hydroxy group of **14** was masked as a silyl ether and the *N*-protecting group was changed, methylation was carried out to give **15**. Finally, the methyl ester of **15** was saponified and the resulting acid was treated with allyl bromide to furnish **16**. Notably, Izzo and co-workers recently reported a method to elaborate the NMeOHIle unit through a similar strategy.[3c]

In a parallel procedure, treatment of (*S*)-α-methylserine allyl ester (**17**) with the thioacylating agent **18**[14] produced the thioamide **19**. The Boc protecting group was exchanged for a Fmoc group, and subsequent exposure to DAST[15] afforded the methylthiazoline **20** (Scheme 4). Removal of the allyl protecting group from **20** by a Pd^0-catalyzed reaction[16] gave



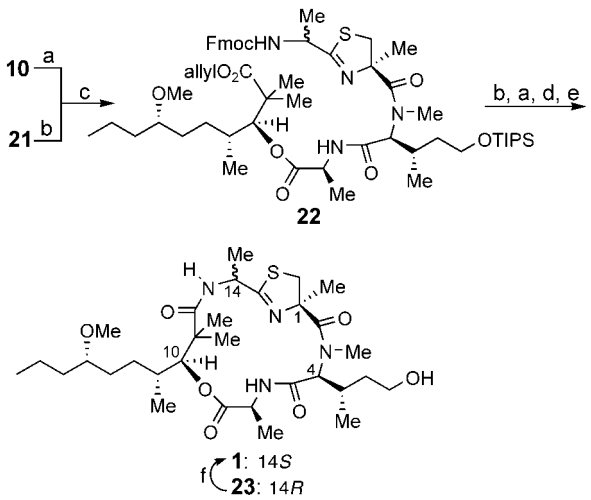
Scheme 4. a) Et_3N, CH_2Cl_2, 50%; b) CF_3CO_2H, CH_2Cl_2; c) FmocOSu, Na_2CO_3, dioxane, H_2O, 75% for two steps; d) DAST, CH_2Cl_2, −78 °C, 89%; e) $[Pd(PPh_3)_4]$, *N*-methylaniline, CH_2Cl, room temperature; f) $AlCl_3$, CH_2Cl_2; g) BEP, *i*Pr_2NEt, CH_2Cl_2, 71% from **16**. Fmoc = 9-fluorenylmethyloxycarbonyl, Su = succinimide; DAST = (diethylamino)sulfur trifluoride; BEP = 2-bromo-1-ethyl pyridinium tetrafluoroborate.

the corresponding acid, which was coupled with the amine liberated from **16**[17] in the presence of BEP[18] as an activating agent to deliver the dipeptide part **21**. Partial racemization at Cα of the L-alanine residue still occurred, even under the very mild conditions, and two isomers (3:1) were determined by ^{1}H NMR spectroscopy. Clearly, installation of the methylthiazoline ring at the ultimate stage of this total synthesis might avoid the racemization problem.[5] Toward this goal, we attempted to link the NMeOHIle residue to various *N*-substituted (*S*)-α-methylserines, but failed to obtain any coupling products as a result of steric hindrance.

The final steps of the synthesis of halipeptin A are described in Scheme 5. Deprotection of **10** with diethylamine and of **21** through palladium-mediated reactions liberated the amine and acid, respectively, which were coupled to afford **22**. Sequential deprotection of **22** provided an amino acid, which was subjected to macrocyclization. To our delight, this transformation worked well in the presence of HATU[19] as the coupling agent and delivered **1** (27% yield from **22**) and its 14-epimer **23** (5% yield from **22**) after cleavage of the silyl ether with TBAF. The 5:1 ratio for **1** to **23** indicated that isomerization at C14 occurred after cyclization because the ratio for two isomers in **21** was only 3:1. Indeed, partial conversion of **23** into **1** (≈2.4:1) was seen by exposure **23** to TBAF in THF. A similar phenomenon was observed by the groups of Wipf[5b] and Pattenden.[5c] The analytical data of **1** were identical with those reported and thus confirmed the stereochemistry of halipeptin A proposed by Gomez-Paloma and co-workers.

Today, the vast majority of antiinflammatory drugs are cyclooxygenase (COX) enzyme inhibitors and lead to several side effects. The unique structures of the halipeptins imply that their mechanism of action is different to that of current drugs, thus making them ideal leads for the discovery of novel

 © 2005 Wiley-VCH Verlag GmbH & Co. KGaA, Weinheim



Scheme 5. a) Et_2NH, MeCN; b) $[Pd(PPh_3)_4]$, *N*-methylaniline, CH_2Cl_2, room temperature; c) BEP, iPr_2NEt, CH_2Cl_2, 71% from **21**. d) HATU, iPr_2NEt, DMF/CH_2Cl_2 (1:4); e) TBAF, THF; 27% (for **1**) and 5% (for **23**) overall yield from **22**; f) TBAF, THF, 2.4:1 ratio for **1** and **23** determined by HPLC. HATU = *N*-[(dimethylamino)-1*H*-1,2,3-triazolo[4,5-*b*]pyridin-1-ylmethylene]-*N*-methylmethanaminium hexafluorophosphate *N*-oxide.

antiinflammatory agents.[20] The total synthesis and structure confirmation of halipeptin A presented herein should represent a significant step in this campaign. Further structure–activity relationship studies are actively being pursued in this laboratory and will be reported in due course.

Received: July 8, 2004

Keywords: amino acids · macrocyclization · natural products · peptides · total synthesis

[1] A. Randazzo, G. Bifulco, C. Giannini, M. Bucci, C. Debitus, G. Cirino, L. Gomez-Paloma, *J. Am. Chem. Soc.* **2001**, *123*, 10870.
[2] C. D. Monica, A. Randazzo, G. Bifulco, P. Cimino, M. Aquino, I. Izzo, F. De Riccardis, L. Gomez-Paloma, *Tetrahedron Lett.* **2002**, *43*, 5707.
[3] a) B. B. Snider, J. R. Duvall, *Tetrahedron Lett.* **2003**, *44*, 3067; b) C. D. Monica, N. Maulucci, F. De Riccardis, I. Izzo, *Tetrahedron: Asymmetry* **2003**, *14*, 3371; c) I. Izzo, E. Avallone, L. D. Corte, N. Maulucci, F. De Riccardis, *Tetrahedron: Asymmetry* **2004**, *15*, 1181; d) S. Hara, K. Makino, Y. Hamada, *Tetrahedron* **2004**, *60*, 8031.
[4] a) J. Zhu, D. Ma, *Angew. Chem.* **2003**, *42*, 5506; *Angew. Chem. Int. Ed.* **2003**, *42*, 5348; b) B. Zou, J. Wei, G. Cai, D. Ma, *Org. Lett.* **2003**, *5*, 3503; c) D. Ma, Q. Wu, *Tetrahedron Lett.* **2001**, *42*, 5279; d) D. Ma, Q. Wu, *Tetrahedron Lett.* **2000**, *41*, 9089.
[5] a) P. Wipf, P. C. Fritch, *J. Am. Chem. Soc.* **1996**, *118*, 12358; b) P. Wipf, P. C. Fritch, S. J. Geib, A. M. Sefler, *J. Am. Chem. Soc.* **1998**, *120*, 4105; c) B. McKeever, G. Pattenden, *Tetrahedron* **2003**, *59*, 2713.
[6] For other studies on the synthesis of thiazoline-containing cyclopeptides, see: a) K. C. Nicolaou, M. Nevalainen, M. Zak, S. Bulat, M. Bella, B. S. Safina, *Angew. Chem.* **2003**, *42*, 3540; *Angew. Chem. Int. Ed.* **2003**, *42*, 3418; b) J. Chen, C. J. Forsyth, *J. Am. Chem. Soc.* **2003**, *125*, 8734; c) B. McKeever, G. Pattenden, *Tetrahedron* **2003**, *59*, 2701; d) J. M. Caba, I. M. Rodriguez, I. Manzanares, E. Giralt, F. Albericio, *J. Org. Chem.* **2001**, *66*, 7568; e) P. Wipf, Y. Uto, *J. Org. Chem.* **2000**, *65*, 1037.
[7] a) W. F. Johns, *J. Org. Chem.* **1967**, *32*, 4086; b) W. S. Tian, Chinese patent ZL 96116304.6.
[8] U. S. Racherla, H. C. Brown, *J. Org. Chem.* **1991**, *56*, 401.
[9] S.-I. Kiyooka, Y. Kaneko, M. Komura, H. Matsuo, M. Nakano, *J. Org. Chem.* **1991**, *56*, 2276.
[10] J. Inanaga, K. Hirata, H. Saeki, T. Katsuki, M. Yamaguchi, *Bull. Chem. Soc. Jpn.* **1979**, *52*, 1989.
[11] L. A. Carpino, B. J. Cohen, K. E. Stephens, S. Y. Sadat-Aalaee, J.-H. Tien, D. C. Langridge, *J. Org. Chem.* **1986**, *51*, 3732.
[12] T. Tsunoda, S. Tatsuki, Y. Shiraishi, M. Akasaka, S. Itô, *Tetrahedron Lett.* **1993**, *34*, 3297.
[13] a) U. Kazmaier, *Angew. Chem.* **1994**, *106*, 1046; *Angew. Chem. Int. Ed. Engl.* **1994**, *33*, 998; b) T. Tsunoda, M. Sakai, O. Sasaki, Y. Sako, Y. Hondo, S. Itô, *Tetrahedron Lett.* **1992**, *33*, 1651.
[14] M. A. Shalaby, C. W. Grote, H. Rappoport, *J. Org. Chem.* **1996**, *61*, 9045.
[15] P. Lafargue, P. Guenot, J. P. Lellouche, *Synlett* **1995**, 171.
[16] M. Ciommer, H. Kunz, *Synlett* **1991**, 593.
[17] D. S. Bose, V. Lakshminarayana, *Synthesis* **1999**, 66.
[18] P. Li, J.-C. Xu, *Tetrahedron* **2000**, *56*, 8119.
[19] L. A. Capino, A. El-Faham, F. Albericio, *Tetrahedron Lett.* **1994**, *35*, 2279.
[20] A. Winter, B. B. Jarvis, *Chemtracts: Org. Chem.* **2003**, 688.

 © 2005 Wiley-VCH Verlag GmbH & Co. KGaA, Weinheim

Surface Analysis

Tip-Enhanced Raman Spectroscopy of Benzenethiol Adsorbed on Au and Pt Single-Crystal Surfaces**

Bin Ren, Gennaro Picardi, Bruno Pettinger,* Rolf Schuster, and Gerhard Ertl*

Raman spectroscopy (RS) provides rich spectral and structural information on gaseous, liquid, and solid samples. However, the Raman process usually exhibits a very low cross section of the order of $(d\sigma/d\Omega)_{RS} \sim 10^{-31}$–$10^{-28}\,cm^2\,sr^{-1}$. This hampers its wide application, particularly when only a small number of scatterers can be probed, as is the case for adsorbate systems on (smooth) interfaces. This situation changed in the mid-1970s with the discovery of surface-enhanced Raman spectroscopy (SERS) on rough silver surfaces. The tremendous enhancement arises from cooperative "electromagnetic" and "chemical" enhancement mechanisms.[1,2] In the course of the 30 years of research on SERS, the height of the surface enhancement and the efficiency of the Raman instrumentation have improved substantially, permitting the study of monolayers and submonolayers of adsorbates. Recently, Raman spectroscopy of even single molecules has been achieved on Ag and Au nanoparticles.[3,4]

Initially, only noble metals were known to exhibit SERS. In the meantime SERS has also been observed for adsorbates on rough transition-metal surfaces.[5] Further applications have been found by using UV light to excite the SERS, and in some cases even surface-enhanced resonance Raman scattering of adsorbates, for example, for SCN^- and CO adsorbed on roughened rhodium surfaces, has been observed.[6] Most applications of SERS are, however, limited to rough surfaces, in which typically a variety of different adsorption sites are exposed, often hampering the assignment of spectral features to specific vibrational modes. It is therefore highly desirable to record Raman spectra of flat single-crystal surfaces, which would allow the identification of the adsorbed species and the determination of their bonding sites and molecular orientation. This knowledge could then be transferred to more complex systems, such as roughened surfaces and supported catalysts. However, Raman studies on single-crystal surfaces have been extremely difficult so far because of insufficient intensity due to the absence of or only minor level of SERS enhancement for smooth interfaces. Thus, only very few investigations have been reported in this field, and they were performed in vacuum,[7] in an electrochemical environment,[8] or in a special attenuated total reflection (ATR) cell, which makes use of the resonant excitation of surface plasmons leading to a rather moderate enhancement of electromagnetic fields at the interface.[9]

Recently, a new approach has been developed to enhance the Raman scattering intensity, by combining Raman microscopy with scanning probe microscopy such as atomic force microscopy (AFM), scanning near-field optical microscopy (SNOM), or scanning tunneling microscopy (STM). Its central element consists of an illuminated AFM, SNOM, or STM tip (either covered with Ag or Au film or made from a silver or gold wire) placed in close vicinity to a sample surface; in other words, the tip is operated either in contact or tunneling mode.[10–16] Upon illumination, localized surface plasmons are excited in the tip–metal gap, producing a large, local increase of the electromagnetic field relative to that of the incident light. This results in a tremendous increase of the Raman intensity (which is proportional to the 4th power of the field enhancement).[10–18] Moreover, the enhanced signal stems from a subwavelength region having the size of the tip apex or an even smaller diameter; in other words, its extension is only of a few tens of nanometers. Since the enhancement is restricted to the tip–substrate gap, there is no surface roughness needed, and (if the proper tip is chosen) the enhancement can be created also on flat transition-metal surfaces. In this way, Raman spectroscopy and scanning probe microscopy (SPM) can be combined to take advantage of the high spatial resolution of SPM and the rich chemical information of Raman spectroscopy. This approach is known as tip-enhanced Raman spectroscopy (TERS) and is sometimes referred to as apertureless SNOM.

In a previous paper, we presented mainly TERS results for malachite green isothiocyanate on gold single-crystal surfaces. Its absorption band is well centered at the excitation wavelength; therefore, for the adsorbed dye a resonance Raman scattering (RRS) process occurs, yielding a weak, but measurable RRS signal in the absence of the gold tip. The approach of the tip to the Au(111) surface causes a tremendous increase of the Raman scattering by many orders of magnitude.[16] In addition, we presented the spectra of malachite green isothiocyanate on a Pt(110) substrate as well as of CN^- on Au(111. Here we further demonstrate the general power of TERS.

The test system we employed was a self-assembled monolayer of benzenethiol on Pt(110). The TERS spectra are shown in Figure 1. As spectrum a shows, no Raman signal can be detected if the STM tip is retracted by about 1 μm or if it is completely absent. When, however, the Au tip is moved into the tunneling position above the Pt(110) substrate (at a distance of about 1 nm above the surface), high-quality spectra can be obtained (spectra b–f in Figure 1). The Raman signal of the most intense peak is about 20 counts

[*] Prof. Dr. B. Ren
Department of Chemistry
State Key Laboratory for Physical Chemistry of Solid Surfaces
Xiamen University
361005 Xiamen (China)
Fax: (+86) 592-208-5349
E-mail: bren@xmu.edu.cn
Dr. G. Picardi, Dr. B. Pettinger, Dr. R. Schuster, Prof. Dr. G. Ertl
Department of Physical Chemistry
Fritz-Haber-Institut der Max-Plank-Gesellschaft
Faradayweg 4–6, 14195 Berlin (Germany)
Fax: (+49) 30-8413-5106
E-mail: pettinger@fhi-berlin.mpg.de

[**] B.R. thanks the Alexander von Humboldt Foundation for a fellowship, the National Science Foundation of China (grant no. 90206039), and the 973 project (2001CB610506). G.P. thanks the Max Planck Society for a scholarship.

 DOI: 10.1002/anie.200460656 © 2005 Wiley-VCH Verlag GmbH & Co. KGaA, Weinheim

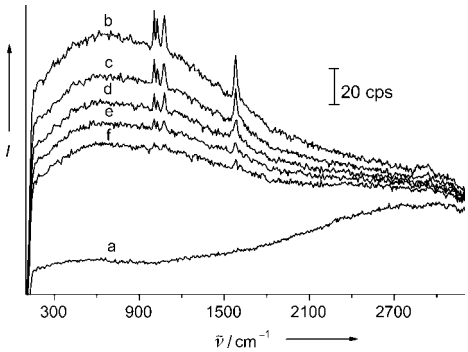


Figure 1. TERS for benzenethiol at Pt(110). Spectrum a was measured with a retracted tip. Spectra b–f were recorded in the tunneling mode and were recorded sequentially. Laser power: 5 mW.

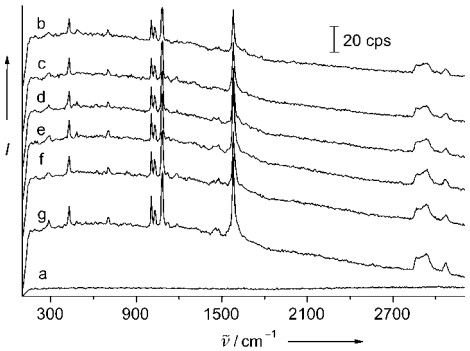


Figure 2. TERS for benzenethiol at Au(110) at reduced laser power. Spectrum a was recorded with a retracted tip. Spectra b–f were recorded in the tunneling mode and were recorded sequentially. Laser power: 0.5 mW.

per second (cps) and decreases slightly with time, showing a decay process reminiscent of the bleaching of dye molecules upon illumination. However, adsorbed benzenethiol is not expected to have an appropriate absorption band in the wavelength region of the excitation laser we used. Thus, the intensity decay must be attributed to the very high electromagnetic field generated in the close vicinity of the tip apex, possibly leading to the photodesorption or photodecomposition of benzenethiol. This conclusion was confirmed by decreasing the laser power by a factor of ten and probing a new patch on the surface. Under these conditions the signal became fairly stable; the three most prominent bands are clearly visible with a signal-to-noise ratio of 3:1, and the intensity of the strongest band was then about 3.4 cps (not shown). If one considers the signal intensity of 24 cps found with full laser power, this indicates that even for the first spectrum, a part of the surface benzenethiol had already been decomposed, leading to a decreased signal intensity.

To exclude SERS created by surface defect sites and to produce an ideally flat substrate, the Pt(110) surface was flame-annealed. In the absence of the tip, no Raman signals from benzenethiol adsorbed on a smooth Pt(110) surface were observable. In the presence of the tip, the TERS signal obtained from this Pt surface was reasonably intense. Although it takes 60 s to acquire a spectrum with a sufficiently high signal-to-noise ratio, the recording of a Raman spectrum of optically nonresonant species adsorbed at a smooth Pt(110) surface represents a breakthrough in the field of surface Raman spectroscopy.

For comparison, a Au(110) substrate was used, which was also flame-annealed to produce a smooth, well-defined surface and to exclude any contribution of roughness-induced SERS. When the tip was in the retracted position, only a low-intensity, flat background signal was observed without spectral features from adsorbed benzenethiol (Figure 2). When the tip was brought into the tunneling mode, very strong peaks of benzenethiol could be observed over a broad, curved baseline, similar to the case of Pt. The maximum peak intensity is about 64 cps with the reduced laser power, which is about twenty times higher in intensity than that measured for the Pt(110) surface. In both experiments (Figure 1 and Figure 2) the same gold tip was used and the relative positions of the gold tip to the laser beam and substrate were essentially unchanged. Therefore, both experiments can be compared quantitatively. Obviously, the use of a gold substrate leads to an excellent optical coupling between tip and substrate, thus better meeting the conditions for surface plasmon excitation and generation of a strong enhancement in the tip–substrate gap. The 20-fold difference in the Raman intensities on Au and Pt, though surprisingly low, is due to the optically different nature of the two samples, causing a different reflectivity, absorption, and tip–substrate coupling.[17]

In general, different substrates will exhibit different interactions with the adsorbate, which can lead to (slightly) different vibrational frequencies and relative intensities. This accounts for the power of vibrational spectroscopies as analytical tools. A careful examination of Figure 1 and Figure 2 shows that there is a 7-cm^{-1} blue shift for the benzenethiol band at around 1070 cm^{-1} having an a_1-type symmetry.[19] The Raman frequency is about 1068 cm^{-1} on Pt and shifts to 1075 cm^{-1} on Au. For clarity, we expanded the spectra in this frequency region and displayed them as Figure 3. In addition to the frequency shifts we observe a distinct change of the relative intensities in the frequency region from 950 to 1150 cm^{-1}. Since there are only small frequency shifts and changes of the relative intensities upon adsorption, the typical spectroscopic pattern of benzenethiol is preserved. Thus, the assignment of the benzenethiol bands,

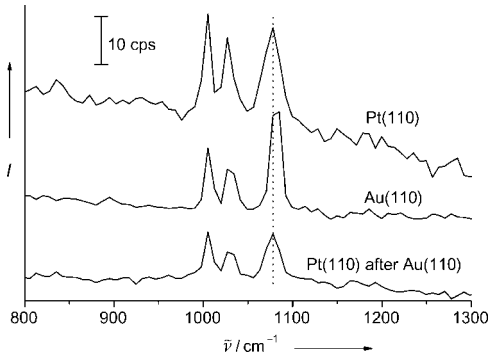


Figure 3. Expanded TERS spectra for sequential experiments, performed at first on Pt(110), then on Au(110), and finally on a Pt(110) surface again. All other experimental conditions were the same as those in Figure 2.

 © 2005 Wiley-VCH Verlag GmbH & Co. KGaA, Weinheim

as given in ref. [19], can be transferred to the TERS spectra. Note the large baseline in all spectra. Presumably, it arises mainly from the surface plasmon continuum of the tip–substrate gap and to a minor extent from the contamination of tip or substrate. To prove that the frequency shift is not an artifact, spectra on Pt(110) were recorded before and after the Au(110) spectrum, using the same tip. Both Pt spectra exhibit the same spectral features, which are clearly different from those of Au(110).

TERS provides, therefore, a diagnostic tool for determining to which surface the observed benzenethiol is bound. Furthermore, the experimental results in Figure 3 prove that the vibrational frequency at 1068 cm^{-1} arises from benzenethiol bound to a Pt surface, and not to the Au tip. Hence, the observed TERS signals seen in the spectra a–c stem from benzenethiol bound to the substrates. Additional evidence is provided by the change of the relative intensities. In the spectrum of liquid benzenethiol the 998-cm^{-1} band is the strongest, and the 1075-cm^{-1} band is relatively weak. [19] However, in both cases of Pt and Au substrates the 1075 cm^{1} peak becomes stronger than the 998 cm^{1} band. This situation is more pronounced in the Au system, where the intensity of the 1075-cm^{-1} band is much higher than that of the 998-cm^{-1} band. Since both bands are assigned to the vibrations having the same a_1 symmetry, the differences in the peak intensity ratios cannot be explained by different orientations of benzenethiol on the surface. In a recent report on pyridine adsorption on transition-metal surfaces, it was pointed out that the change in relative intensity may be due to the different interactions of pyridine with the metal surfaces;[20] similar reasons may apply in the case of benzenethiol on Pt and Au, as discussed here. It should be noted at this point that the substrate sensitivity of the spectra proves that the signal stems from (sub)monolayers.

To demonstrate the general applicability of TERS, spectra were also recorded for other adsorbates, for instance, 4-pyridine-4-thiol (4-PT, Figure 4). The four Raman bands appearing at 1011, 1099, 1207, and 1617 cm^{-1} present the essential spectral features of 4-PT on metal surfaces. The peak intensities are even stronger than in the case of benzenethiol. However, during our study of 4-PT we noticed that the Au tip can be contaminated easily by the 4-PT. The signal of 4-PT on the Au tip is weaker than on Au(110) and, hence, does not alter spectroscopically the TERS signal of 4-PT on Au(110). However, on Pt(110) the signal from the tip becomes comparable with the TERS of 4-PT from the substrate and, hence, the two spectra will mix. A possible reason for the easy contamination may be that the S and N atom of 4-PT can form strong bonds to the substrate. When the tip approaches the tunneling position, it may pick up some 4-PT molecules from the substrate, because the Au atoms of the tip form strong bonds with the N atoms of the 4-PT molecules. At the same time S–Au bonds with the substrate are weakened. Apparently, molecules with multiple bonding sites have an inherent tendency to contaminate the tip.

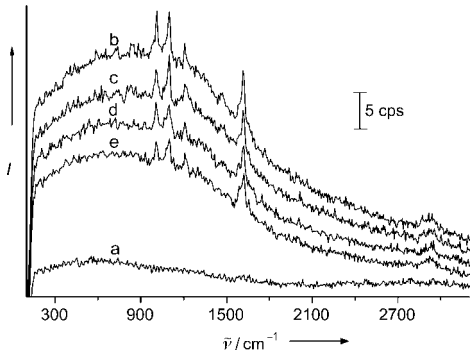


Figure 4. TERS for pyridine-4-thiol on Au(110) at reduced laser power. Spectrum a was recorded with a retracted tip. Spectra b–f were recorded in the tunnelling mode and were recorded sequentially. Laser power: 0.5 mW.

From earlier estimates on the lateral extension of the enhanced field[16] we conclude that the spatial resolution of TERS corresponds roughly to the size of the tip used, which in the present case had a radius of about 30 nm. On the other hand, theoretical predictions point to an even stronger confinement of the electromagnetic field, down to a tiny spot 9 nm in diameter for 30-nm tip radius and a tunneling distance of 1 nm.[21] These two values may be seen as upper and lower limits of the actual extension of the enhanced field, highlighting the enormous power and resolution of this technique for (sub)wavelength microscopy.

Our present study illustrates that the detection of species adsorbed in (sub)monolayer quantities on smooth single-crystal metal surfaces is no longer a difficult task, even if the adsorbates exhibit moderate or weak Raman cross sections. For adsorbates on single-crystal surfaces, additional information (such as on molecular orientation) can be achieved by choosing appropriate light polarization in TERS and analyzing the response with respect to surface selection rules. With the high spatial resolution of TERS applied to the study of probe molecules having a high sensitivity to the binding site, it might become possible to reveal the role of terraces, steps, and different facets during the adsorption process or in the course of chemical reactions in catalytic and electrochemical processes. The surface structure might be varied continuously from atomically flat to mildly and highly roughened surfaces, in order to smoothly bridge the gap between model single-crystal surfaces and real catalyst surfaces. Even TERS studies on single catalyst particles are within reach. Additionally, TERS may provide clues to the nature of SERS-active sites, a still unresolved issue. In contrast to SERS, where the chemical enhancement provides an important contribution to the overall enhancement, TERS does not require this type of chemical interaction between the adsorbed molecule and the substrate. TERS will be developed as a valuable analytical tool, providing simultaneous spectroscopic and microscopic information in the nanometer region, which ultimately may include single-molecule detection and investigation, an aspect that has been addressed previously.[14,16]

Experimental Section

The STM tip was fabricated by electrochemically etching a gold wire 0.25 mm in diameter at 2.4 V DC in a mixture of fuming hydrochloric acid and ethanol (1:1).[22] The tip was cleaned with Milli-Q water immediately after etching. Tip radii obtained with this method were

 © 2005 Wiley-VCH Verlag GmbH & Co. KGaA, Weinheim

around 30 nm. Before every experiment, the Pt and Au single crystals were flame-annealed in order to produce atomically flat surfaces. Monolayer adsorption of benzenethiol was accomplished by dipping freshly flame-annealed single-crystal electrodes into a 0.01 M solution of benzenethiol in ethanol for 3 to 4 min and then rinsing with copious amounts of ethanol to remove adsorbed multilayers. A similar procedure was used to prepare pyridine-4-thiol monolayers except that a shorter time, ca. 2–3 min, sufficed.

The TERS experiment was conducted using an Olympus microscope attached to a Raman spectrograph (LabRam 1000 from DILOR) together with a homemade adapter to redirect the incident laser beam and to collect the Raman signal at an angle of roughly 60° to the surface normal of the single-crystal surface.[16] The microscope objective was an Olympus ×50 long-working-distance objective with an numerical aperture of 0.5. The laser power (He–Ne, 632.8 nm) on the sample was about 5 mW, which can be reduced through a set of neutral density filters. The STM was an in-house built instrument, which was solidly connected to the sample stage of the microscope through an extended arm.[14] Sample and tip were placed in the laser focus with an *x*–*y* translation stage, while the beam was focused using the vertical translation stage of the microscope. The focusing as well as the coarse approach of the tip toward the sample were monitored by means of the microscope and an auxiliary CCD camera. The acquisition time for each spectrum in the sequential acquisition mode was 60 s, and the time interval between each spectrum was about 1 s. Tunneling current and voltage (referenced to sample) were 1 nA and −150 mV, respectively, resulting in a tunneling gap in the order of 1 nm, which is slightly larger than that in vacuum due to the presence of a thin layer of water between the tip and the surface.

Received: May 14, 2004

Keywords: gold · platinum · Raman spectroscopy · scanning probe microscopy · surface analysis

[1] M. Moskovits, L. L. Tay, J. Yang, T. Haslett, *Top. Appl. Phys.* **2002**, *82*, 215 – 226.
[2] A. Otto, *J. Raman Spectrosc.* **2002**, *33*, 593 – 598.
[3] K. Kneipp, Y. Wang, H. Kneipp, L. T. Perelman, I. Itzkan, R. Dasari, M. S. Feld, *Phys. Rev. Lett.* **1997**, *78*, 1667 – 1670.
[4] S. M. Nie, S. R. Emory, *Science* **1997**, *275*, 1102 – 1106.
[5] Z. Q. Tian, B. Ren, D. Y. Wu, *J. Phys. Chem. B* **2002**, *106*, 9463 – 9483.
[6] B. Ren, X. F. Lin, Z. L. Yang, G. K. Liu, R. F. Aroca, B. W. Mao, Z. Q. Tian, *J. Am. Chem. Soc.* **2003**, *125*, 9598 – 9599.
[7] S. S. Perry, S. R. Hatch, A. Campion, *J. Chem. Phys.* **1996**, *104*, 6856 – 6859.
[8] K. Sakamoto, H. Hashizume, M. Nagafusa, H. Sato, S. Ushioda, *Surf. Sci.* **1996**, *368*, 292 – 295.
[9] A. Bruckbauer, A. Otto, *J. Raman Spectrosc.* **1998**, *29*, 665 – 672.
[10] R. Zenobi, V. Deckert, *Angew. Chem.* **2000**, *112*, 1814 – 1825; *Angew. Chem. Int. Ed.* **2000**, *39*, 1746 – 1756.
[11] R. M. Stoeckle, Y. D. Suh, V. Deckert, R. Zenobi, *Chem. Phys. Lett.* **2000**, *318*, 131 – 136.
[12] M. S. Anderson, *Appl. Phys. Lett.* **2000**, *76*, 3130 – 3132.
[13] N. Hayazawa, T. Yano, H. Watanabe, Y. Inouye, S. Kawata, *Chem. Phys. Lett.* **2003**, *376*, 174 – 180.
[14] B. Pettinger, G. Picardi, R. Schuster, G. Ertl, *Electrochemistry* **2000**, *12*, 942 – 949; B. Pettinger, G. Picardi, R. Schuster, G. Ertl, *Single Mol.* **2002**, *3*, 285 – 294; B. Pettinger, G. Picardi, R. Schuster, G. Ertl, *J. Electroanal. Chem.* **2003**, *554–555*, 293 – 299.
[15] A. Hartschuh, E. J. Sanchez, X. S. Xie, L. Novotny, *Phys. Rev. Lett.* **2003**, *90*, 095503-1-4.
[16] B. Pettinger, B. Ren, G. Picardi, R. Schuster, G. Ertl, *Phys. Rev. Lett.* **2004**, *92*, 096101-1-4.
[17] S. Klein, T. Witting, K. Dickmann, P. Geshev, M. Hietschold, *Single Mol.* **2002**, *3*, 281 – 284.
[18] M. Micic, N. Klymyshyn, Y. D. Suh, H. P. Lu, *J. Phys. Chem. B* **2003**, *107*, 1574 – 1584.
[19] K. T. Carron, L. G. Hurley, *J. Phys. Chem.* **1991**, *95*, 9979 – 9984.
[20] D. Y. Wu, M. Hayashi, Z. Q. Tian, S. H. Lin, *Spectrochim. Acta Part A* **2004**, *60*, 137 – 146.
[21] D. L. Mills, *Phys. Rev. B* **2002**, *65*, 125419-1-11.
[22] B. Ren, G. Picardi, B. Pettinger, *Rev. Sci. Instrum.* **2004**, *75*, 837 – 841.

 © 2005 Wiley-VCH Verlag GmbH & Co. KGaA, Weinheim

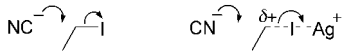
Reaction Mechanisms

Ambident Reactivity of the Cyanide Ion: A Failure of the HSAB Principle**

*Alexander A. Tishkov and Herbert Mayr**

Dedicated to Professor Christoph Rüchardt on the occasion of his 75th birthday

The ambident reactivity of the cyanide ion is one of the classical examples used to illustrate the application of the Klopman–Salem equation and the hard and soft acids and bases (HSAB) principle. According to Fleming, *"alkyl halides in simple S_N2 reactions are soft electrophiles; thus it is appropriate for cyanide to react from the soft end of the ion. When a silver ion is present (other Lewis acids like zinc and mercuric ion behave similarly), the halide ion is assisted in leaving the carbon atom, and in the transition state there is now a greater development of charge on the carbon atom undergoing substitution. Carbonium ions are hard electrophiles, and therefore it is again appropriate that on this occasion cyanide ion should react from the harder end of the ion."*[1]



Comparable statements are found in many textbooks, including the latest edition of March's Organic Chemistry.[2] Although Pearson had already indicated problems of the HSAB principle in explaining the ambident reactivity of the

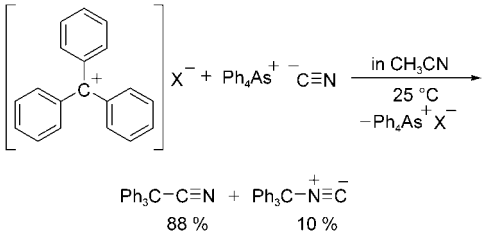
[*] Dr. A. A. Tishkov, Prof. Dr. H. Mayr
Department Chemie und Biochemie
Ludwig-Maximilians-Universität München
Butenandtstrasse 5–13 (Haus F), 81377 München (Germany)
Fax: (+49) 89-2180-77717
E-mail: herbert.mayr@cup.uni-muenchen.de

[**] We thank the Alexander von Humboldt foundation (stipend to A.A.T.) and the Deutsche Forschungsgemeinschaft for financial support of this work. HSAB = hard and soft acids and bases.

Supporting information for this article is available on the WWW under http://www.angewandte.org or from the author.

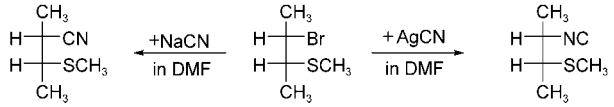
 © 2005 Wiley-VCH Verlag GmbH & Co. KGaA, Weinheim DOI: 10.1002/anie.200461640

cyanide ion,[3] experimental evidence that cast doubt on this interpretation has largely been ignored. For example, the report by Songstad and co-workers[4a] that trityl chloride and perchlorate react with unassociated cyanide ions to form predominantly triphenylacetonitrile and only 10% of isocyanotriphenylmethane received little attention (Scheme 1).



Scheme 1. Reaction of trityl chloride and perchlorate with cyanide ions (Songstad and co-workers).[4a]

In 1985, Carretero and Ruano reported the retention of configuration in the reaction of *erythro*- and *threo*-2-bromo-3-methylthiobutanes (Scheme 2) and found that "*the observed*



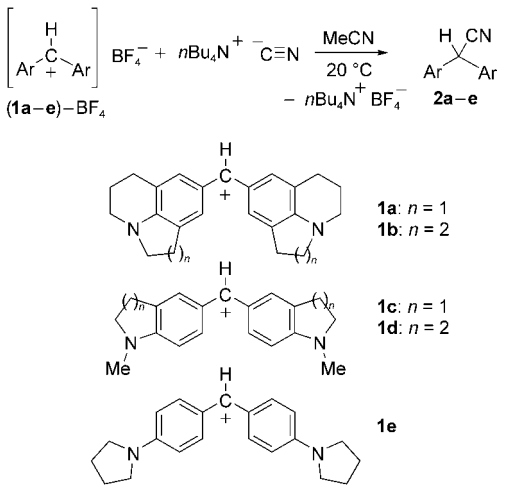
Scheme 2. Reaction of 2-bromo-3-methylthiobutane with cyanide ions (Carretero and Ruano).[4b]

regioselectivity with both metal cyanides cannot be explained as variations in the hardness of the electrophilic carbon induced by the interactions between the metal cation and the halogen."[4b] Their clear conclusion, "*that the reactions between alkyl halides and metal cyanides … are not a good example for illustrating the Klopman–Salem equation*" also found little resonance.

We recently reported that the HSAB principle cannot explain the ambident reactivity of the thiocyanate ion in alkylation reactions, since hard carbocations as well as soft haloalkanes preferentially attack the soft sulfur terminus.[5] Only when diffusion control is reached, can the attack of carbocations at the nitrogen atom compete with attack at the sulphur atom. We now report that the knowledge of the diffusion control limit is also key to understanding the ambident reactivity of the cyanide ion.

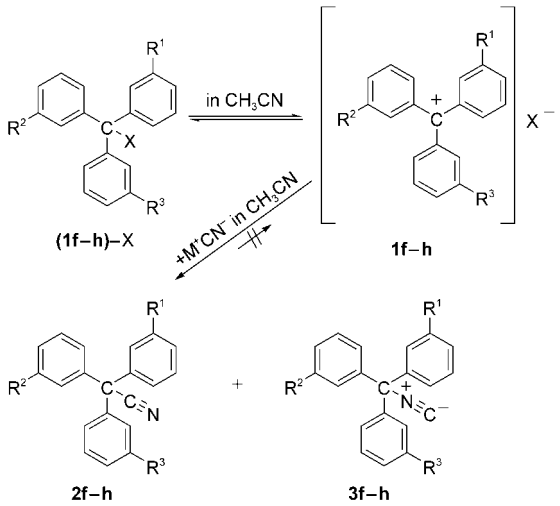
Scheme 3 shows that the highly stabilized benzhydrylium ions (**1a**–**e**)–BF_4 react with nBu$_4$N$^+$CN$^-$ in acetonitrile to give the corresponding diaryl acetonitriles **2a**–**e**.[6] As any produced isocyanomethanes would reionize and successively yield the thermodynamically more stable nitriles **2a**–**e**, the outcome of the reaction presented in Scheme 3 does not give information about the site of the kinetically controlled attack.[7]

Treatment of 3-chlorophenyldiphenylmethyl chloride (**1g**–Cl) with nBu$_4$N$^+$CN$^-$ under the same conditions as shown in Scheme 3 yields a mixture of nitrile **2g** and isonitrile **3g**, as revealed by the presence of absorptions at $\tilde{\nu} = 2240$



Scheme 3. Reaction of the benzhydrylium ions (**1a**–**e**)–BF_4 with nBu$_4$N$^+$CN$^-$.

(**2g**) and 2126 cm^{-1} (**3g**) in the IR spectrum of the crude reaction product (Scheme 4). The **2g**/**3g** ratio was derived from the ^{1}H NMR signals of 2-H in the chloro-substituted



	R^1	R^2	R^3	X	M	**2**/**3** ratio
f	H	H	H	Cl	Ph_4As	8.8[a]
g	Cl	H	H	Cl	nBu$_4$N	5.7
h	Cl	Cl	Cl	Br	nBu$_4$N	3.6

[a] From ref. [4a]

Scheme 4. Product distribution in the reaction of (**1f**–**h**)–X with cyanide ions.

arene rings which absorb as doublets ($J = 0.4$ Hz) of triplets ($J = 2.0$ Hz) and can be assigned to **2g** and **3g** by comparison with the NMR spectra of the pure compounds (Figure 1). An analogous experiment with tris-(3-chlorophenyl)methyl bromide (**1h**–Br) showed a decrease in the nitrile/isonitrile ratio (Scheme 4, see also the Supporting Information). In accord with previous reports on the **3f**→**2f** rearrangement[7a] the isomerizations **3g,h**→**2g,h** are slow under the chosen reac-

 © 2005 Wiley-VCH Verlag GmbH & Co. KGaA, Weinheim

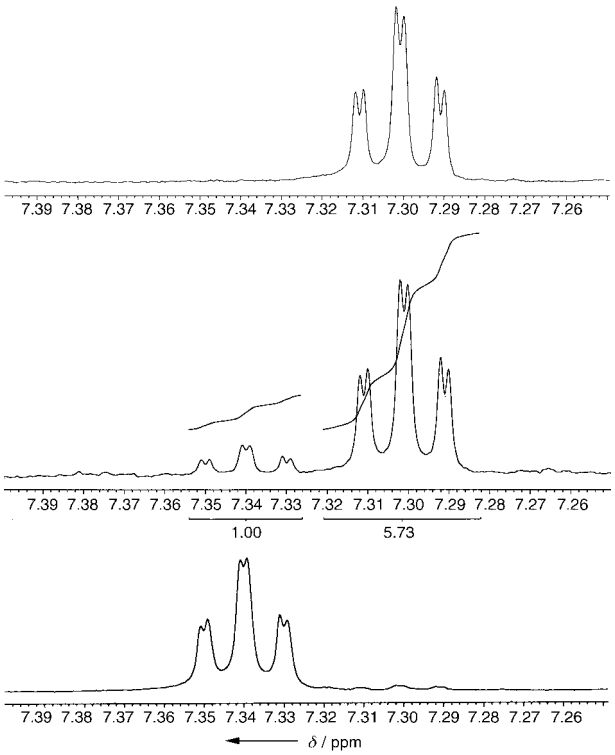
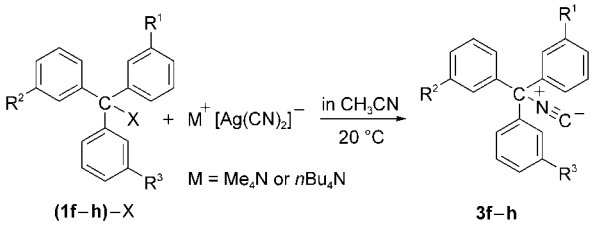


Figure 1. Comparison of the ^{1}H NMR spectrum (200 MHz, C_6D_6) of the product obtained from the reaction of **1g**–Cl with tetra-*n*-butylammonium cyanide (middle) with the spectra of nitrile **2g** (top) and isonitrile **3g** (bottom), respectively.

tion conditions, indicating that the product ratios listed in Scheme 4 are the result of kinetic control.

The reactions of (**1f–h**)–X with $[Ag(CN)_2]^-$ lead to the selective formation of the isonitriles **3f–h** (Scheme 5).[8] Since



Scheme 5. Selective isonitrile formation in the reaction of (**1f–h**)–X with $[Ag(CN)_2]^-$; X = Cl or Br.

the nucleophilic substitutions of trityl halides described in Scheme 4 and 5 generally follow the S_N1 mechanism, it is clear that the observed reversal of regioselectivity is not due to a change in mechanism from S_N2 to S_N1, but to modification of the cyanide ion by coordination with silver.

How can the C/N ratios, reported in Scheme 4, be explained? We recently showed that the correlation Equation (1) also describes the rates of reactions of stabilized carbocations with anions (*k* is the second-order rate constant at 20 °C, *E* is a nucleophile-independent electrophilicity parameter, and *N* and *s* are electrophile-independent nucleophilicity parameters).[9,10]

$$\log k_{20^\circ C} = s(E + N) \quad (1)$$

When the reactions of (**1a–e**)–BF_4 with $nBu_4N^+CN^-$ were monitored photometrically in acetonitrile by using previously described methodology,[10] second-order kinetics were observed with the rate constants listed in Table 1.

Table 1: Rate constants for the reactions of the benzhydrylium ions **1a–e** with tetra-*n*-butylammonium cyanide (CH_3CN, 20 °C).

	Electrophilicity *E*[a]	k_C [$M^{-1}s^{-1}$]
1a	−10.04	2.42×10^4
1b	−9.45	5.50×10^4
1c	−8.76	1.31×10^5
1d	−8.22	3.58×10^5
1e	−7.69	1.12×10^6

[a] From reference [9].

From the linear part of the $\log k_C$ versus *E* correlation (Figure 2) one can derive $N = 16.3$ and $s = 0.70$ for the C nucleophilicity of CN^- in acetonitrile. Extrapolation indicates that k_C reaches diffusion control for carbocations with

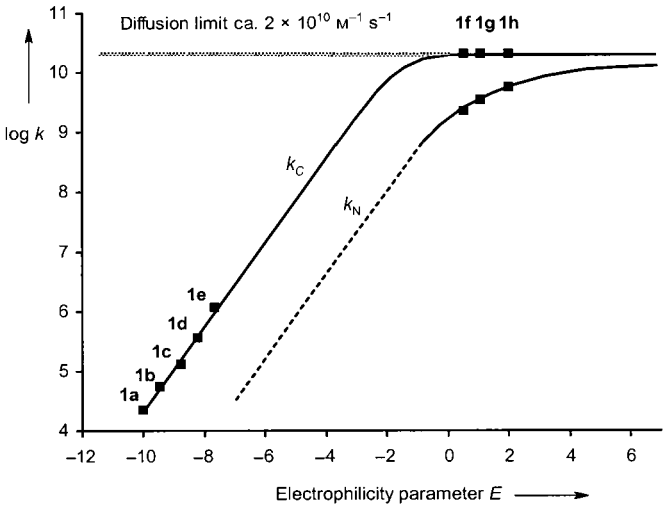


Figure 2. Plot of $\log k$ for the reactions of the benzhydrylium ions **1a–e** and the tritylium ions **1f–h** with the cyanide ion versus the electrophilicity parameters *E* of these carbocations.[9,10a]

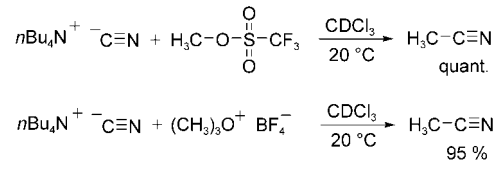
$E > 0$.[11] As all carbocations with $E > 0$ can thus be assumed to react with CN^- with the same rate constant of $2\times10^{10}M^{-1}s^{-1}$ (C attack), the product ratios reported in Scheme 4 can be used to estimate k_N, that is, the rate constants for attack at the cyanide nitrogen atom. Figure 2 illustrates that the decrease in the **2**/**3** ratio ($= k_C/k_N$) as the electrophilicities of the carbocations **1f–h**[10a] grow from 0.5 to 2.0 can be explained by the fact that C attack has already reached diffusion control while N attack approaches the diffusion limit. Even when the exact location of these borders is problematic, it is clear from Figure 2 that carbocations that

 © 2005 Wiley-VCH Verlag GmbH & Co. KGaA, Weinheim

are less stabilized than Ph_3C^+ undergo barrierless combination reactions with free CN^- in acetonitrile. Attempts to explain C/N ratios by traditional transition-state models must, therefore, be obsolete.

S_N1 reactions with participation of the cyanide anion are problematic in protic solvents. As the nucleophilicity of CN^- decreases significantly in protic solvents (e.g., in water $N = 9.19$ and $s = 0.60$),[10a] carbocations generated under such conditions usually react faster with the solvent than with CN^-.[12] Thus, the reaction of 1-chloro-1-(4-methoxyphenyl)-ethane with KCN in ethanolic solution yields the corresponding ethyl ether in almost quantitative yield.[13] Reactions of *tert*-haloalkanes with alkali-metal cyanides in alcohols give particularly low yields of substitution products owing to the high basicity of CN^-. Depending on the reaction conditions, small amounts of *tert*-cyanoalkanes are formed along with tertiary ethers and elimination products.[14]

In summary, C attack is generally preferred whenever carbocations react with free CN^-. Let us now turn to S_N2 reactions of the cyanide ion: It has long been known that haloalkanes react with alkali-metal and onium cyanides with preferential formation of nitriles.[15] Even in the reaction of KCN with the relatively hard methylating agent dimethyl sulfate, the preferential formation of acetonitrile was observed.[16,17] We have now studied the reactions of tetra-*n*-butylammonium cyanide with the even harder S_N2 alkylating agents methyl triflate and trimethyloxonium tetrafluoroborate in $CDCl_3$ and observed the exclusive formation of acetonitrile in both cases (^1H and ^{13}C NMR spectroscopy, Scheme 6).



Scheme 6. Exclusive formation of acetonitrile in the reactions of tetra-*n*-butylammonium cyanide with the hard S_N2 alkylating agents methyl triflate and trimethyloxonium tetrafluoroborate.

In conclusion, electrophilic alkylations at free CN^- occur preferentially at carbon, regardless of whether the S_N1 or S_N2 mechanism is involved and whether hard or soft electrophiles are employed. Preferred N attack, as postulated for hard electrophiles by the HSAB principle, could not be observed with any alkylating agent. Isocyano compounds are only formed with highly reactive electrophiles that react without an activation barrier because the diffusion limit is approached (Figure 2). We therefore claim that the knowledge of absolute rate constants and not of the hardness of the reaction partners is needed to predict the outcome of alkylations of the cyanide ion.

Received: August 13, 2004

Keywords: ambident anions · HSAB principle · Klopman–Salem equation · Kornblum rule · reaction kinetics

[1] I. Fleming, *Frontier Orbitals and Organic Chemical Reactions*, Wiley, Chichester, **1976**, pp. 40–41.
[2] M. B. Smith, J. March, *March's Advanced Organic Chemistry. Reactions, Mechanisms, and Structure*, 5th ed., Wiley, New York, **2001**, p. 460.
[3] R. G. Pearson, *Chemical Hardness*, Wiley-VCH, Weinheim, **1997**, p. 7.
[4] a) T. Austad, J. Songstad, L. J. Stangeland, *Acta Chem. Scand.* **1971**, *25*, 2327–2336; b) J. C. Carretero, J. L. G. Ruano, *Tetrahedron Lett.* **1985**, *26*, 3381–3384.
[5] R. Loos, S. Kobayashi, H. Mayr, *J. Am. Chem. Soc.* **2003**, *125*, 14126–14132.
[6] For analogous reactions of 4-amino-substituted tritylium ions with KCN, see: M. L. Herz, *J. Am. Chem. Soc.* **1975**, *97*, 6777–6785.
[7] a) The rearrangement of isocyanotriphenylmethane (**3f**) into cyanotriphenylmethane (**2f**) is described in: T. Austad, J. Songstad, *Acta Chem. Scand.* **1971**, *26*, 3141–3147; b) for a change in mechanism in isocyanide→cyanide rearrangements, see: C. Rüchardt, M. Meier, K. Haaf, J. Pakusch, E. K. A. Wolber, B. Müller, *Angew. Chem.* **1991**, *103*, 907–915; *Angew. Chem. Int. Ed. Engl.* **1991**, *30*, 893–901.
[8] The synthesis of isocyanotriphenylmethane (**3f**) from trityl chloride **1f**–Cl and $Me_4N^+[Ag(CN)_2]^-$ was described in reference [4a].
[9] a) H. Mayr, T. Bug, M. F. Gotta, N. Hering, B. Irrgang, B. Janker, B. Kempf, R. Loos, A. R. Ofial, G. Remennikov, H. Schimmel, *J. Am. Chem. Soc.* **2001**, *123*, 9500–9512; b) H. Mayr, B. Kempf, A. R. Ofial, *Acc. Chem. Res.* **2003**, *36*, 66–77.
[10] a) S. Minegishi, H. Mayr, *J. Am. Chem. Soc.* **2003**, *125*, 286–295; b) R. Lucius, R. Loos, H. Mayr, *Angew. Chem.* **2002**, *114*, 97–102; *Angew. Chem. Int. Ed.* **2002**, *41*, 91–95; c) T. Bug, H. Mayr, *J. Am. Chem. Soc.* **2003**, *125*, 12980–12986; d) T. Bug, T. Lemek, H. Mayr, *J. Org. Chem.* **2004**, *69*, 7565–7576.
[11] This conclusion is in accord with results obtained by Ritchie who reported $N_+ = 8.64$ for CN^- (in DMSO) and a rate constant $\log k = 6.72$ for the reaction of the tritylium ion with HO^-, from which $\log k_0(Ph_3C^+) = 1.97$ can be derived: C. D. Ritchie, *Can. J. Chem.* **1986**, *64*, 2239–2250
[12] For solvent nucleophilicities, see: S. Minegishi, S. Kobayashi, H. Mayr, *J. Am. Chem. Soc.* **2004**, *126*, 5174–5181.
[13] R. Quelet, *Bull. Soc. Chim. Fr.* **1940**, 205–215.
[14] R. N. Lewis, P. V. Susi, *J. Am. Chem. Soc.* **1952**, *74*, 840–841.
[15] a) D. T. Mowry, *Chem. Rev.* **1948**, *42*, 189–283; b) C. Grundmann, *Methoden Org. Chem. (Houben-Weyl)*, *Vol. E5*, **1985**, pp. 1448–1488.
[16] a) R. Walden, *Ber. Dtsch. Chem. Ges.* **1907**, *40*, 3214–3217; b) it has been claimed that traces of malodorous isocyanides can form in this reaction; however, measurable amounts of isocyanides (≈5%) are formed only when the reactions are conducted at higher temperatures (>100 °C): J. Wade, *J. Chem. Soc.* **1902**, *81*, 1596–1617.
[17] Exclusive C attack was also reported for the reactions of KCN/[18]crown-6 with methyl methanesulfonate in ethanol, acetonitrile, THF, and benzene: H. Lemmetyinen, L. Lehtinen, J. Koskikallio, *Finn. Chem. Lett.* **1979**, 72–75.

 © 2005 Wiley-VCH Verlag GmbH & Co. KGaA, Weinheim

Cubane Rearrangements

The Protonation of Cubane Revisited**

Andrey A. Fokin, Boryslav A. Tkachenko, Pavel A. Gunchenko, and Peter R. Schreiner**

Dedicated to Professor A. G. Yurchenko on the occasion of his 70th birthday

Protonation of saturated hydrocarbons is the simplest and practically most important electrophilic reaction.[1] Small alkanes like methane, ethane, and isobutane[2] form well-defined protonated species, and their experimental proton affinities (PAs) are excellently reproduced computationally.[3–5] However, the current data on the protonations of strained hydrocarbons are rather controversial, and facile rearrangements are thought to account for the difficulties encountered in measuring the PAs.[6] Cyclopropane (strain energy(E_{str}) = 27.2 kcal mol^{-1}) is an exception because the number of energetic downhill paths is very limited and the barrier for the ring opening of corner-protonated $C_3H_7^+$ to the 2-propyl cation is high. The experimental PA of cyclopropane (179.4 kcal mol^{-1} [7]) is well reproduced computationally (179.3 kcal mol^{-1} at CCSD(T)/cc-pVTZ//CCSD(T)/cc-pVDZ for corner-protonated $C_3H_7^+$).[8] In contrast to cyclopropane which displays secondary C–H bonds only, a surprisingly small range of PAs is characteristic for a number of hydrocarbons with tertiary C–H bonds. These hydrocarbons differ considerably in their strain energies, for example, dodecahedrane (PA = 201.7 kcal mol^{-1},[9] E_{str} = 65.4 kcal mol^{-1} [10]), adamantane (PA = 175.7 kcal mol^{-1},[11] E_{str} = 6.3 kcal mol^{-1} [12]), and cubane[13] (PA = ca 200 kcal mol^{-1},[7,9] E_{str} = 161 kcal mol^{-1} [14]). For these systems the question remains: How much does the strain energy affect the proton affinity of a saturated hydrocarbon and to what extent should isomerizations be considered? The experimental PA of cubane (**1**) measured by ion-cyclotron resonance spectroscopy[9] is surprisingly low and was recently questioned by Koppel et al.[15] on the basis that **1** rearranges rapidly to cuneane so that the PA is attributed to the energy change of the entire protonation/rearrangement/deprotonation process. However, cuneane is also highly strained, so where one does stop? Are there any other rearrangement paths for protonated cubane? Herein we address both computationally and experimentally the question to what extent the cubane cage is able to survive electrophilic attack[16] and what the most favorable paths for the reaction of **1** with a proton are.

Despite enormous strain, cubane[15,17,18] is kinetically quite stable because breaking just one C–C bond causes only minor structural changes and hence only little relief of strain. However, cleavage of a second C–C bond is highly exothermic and followed by rapid rearrangements. For instance, thermolysis[16,19] and single-electron oxidation[20] of **1** leads to cyclooctatetraene. In contrast, mild radical reagents[21] lead to substitution products with conservation of the cubane cage.[22] Electrophilic cubane conversions are limited to reactions of soft electrophiles like metal ions,[18] and a number of fascinating rearrangements (e.g., to *syn*-tricyclooctadiene (**2**) with Pd^{2+} and to cuneane (**3**) with Ag^+ and Li^+) are preparatively useful.[18,23]

The attack of a proton on cubane is highly exergonic and all of our and previous[9,15,16,24] attempts to locate $C_8H_9^+$ protonated minima retaining the cubane cage at various levels of density functional theory (DFT) failed. When DFT methods are used, edge-protonated cubane (**4**, Scheme 1) is not a minimum and converges to the tetracyclo[4.2.0^{2,4}.0^{3,8}]oct-5-yl cation (**5**)[25] upon optimization without symmetry constrains. This structure is energetically much too low to account for the "experimental" gas-phase basicity of **1** (ca. 200 kcal mol^{-1}).[7,9] The explanation for this discrepancy was proposed[15] to lie in the rapid conversion of **1** to **3** via **5** followed by deprotonation. However, our computations[26] at this level indicate that there is a low-energy path from **5** via transition structure (TS) **6** to the lower-lying cation **7**, which can subsequently rearrange to the more stable bicyclo[3.3.0]octadienyl **8** via TS **9**. The discrepancies between experiment and theory are simply unacceptable and require careful scrutiny of both the high-energy part of the $C_8H_9^+$ potencial enery surface (PES) and the theoretical treatment.

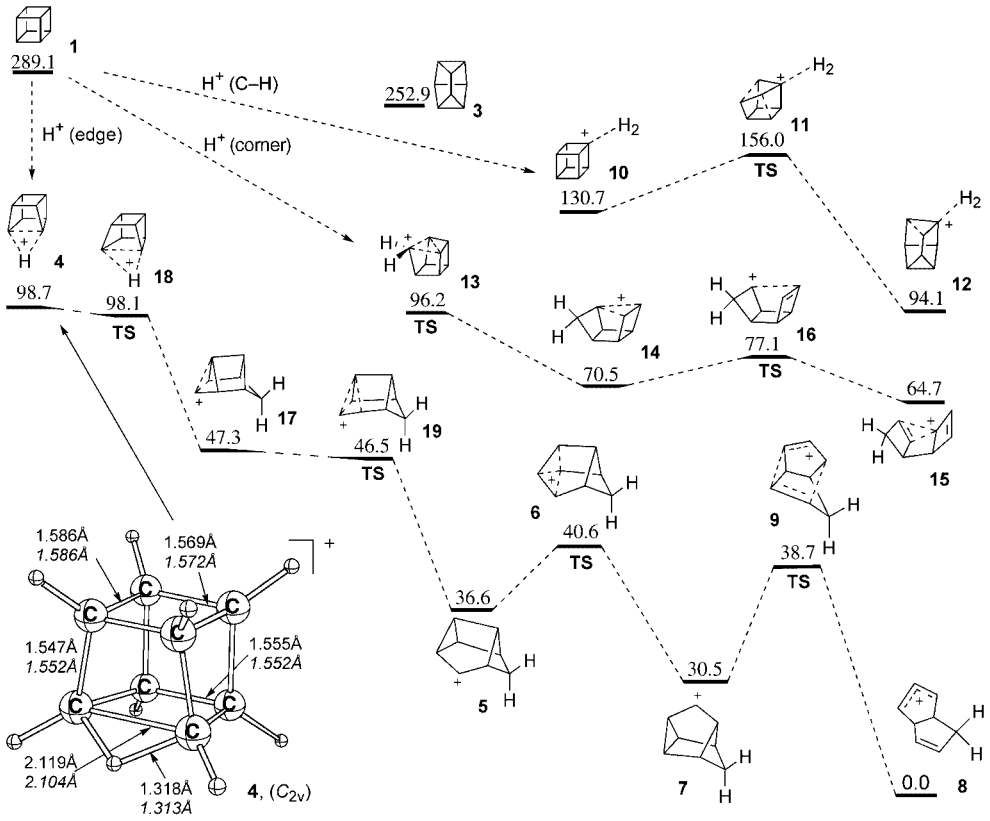
First of all, the gas-phase protonation of hydrocarbons with tertiary C–H bonds results in weakly bound complexes ($R^+\cdots H_2$) as shown both experimentally[2] and computationally[5] for isobutane as well as computationally for adamantane;[11] the situation for cubane is expected to be similar. Small, strained hydrocarbons like cyclopropane[8] and cyclobutane[4] form structures protonated at a C–C bond. To test the DFT findings we used Møller-Plesset perturbation theory (MP2) utilizing a correlation-consistent Dunning basis set (cc-pVDZ) and considered (Scheme 1) the attack of a proton on **1** at a C–H bond (top), corner (middle), and edge (bottom); MP2 is known to be very suitable for the description of highly delocalized carbocations, even when DFT approaches fail.[27] As the formation of the cubyl cation in the condensed phase is well documented,[28] we also searched for the products of the

[*] Prof. A. A. Fokin, Dr. P. A. Gunchenko
Department of Organic Chemistry
Kiev Polytechnic Institute
pr. Pobedy 37, 03056 Kiev (Ukraine)
Fax: (+038) 44-236-97-74
E-mail: aaf@xtf.ntu-kpi.kiev.ua
Dr. B. A. Tkachenko, Prof. Dr. P. R. Schreiner
Institute of Organic Chemistry
Justus-Liebig University
Heinrich-Buff-Ring 58, 35392 Giessen (Germany)
Fax: (+49) 641-99-34309
E-mail: prs@org.chemie.uni-giessen.de
and
Department of Chemistry
The University of Georgia
Athens, GA 30602-2556 (USA)
Fax: (+1) 706-542-9454
E-mail: prs@chem.uga.edu

[**] This work was supported by the Volkswagenstiftung, the Ukrainian Science Foundation, and the NATO Science Program. We thank A. G. Marshall for helpful discussions.

Supporting information for this article is available on the WWW under http://www.angewandte.org or from the author.

 © 2005 Wiley-VCH Verlag GmbH & Co. KGaA, Weinheim DOI: 10.1002/anie.200461042



Scheme 1. The computed paths for the protonation of cubane (**1**) (ΔH_0 in kcal mol^{-1} at CCSD(T)/cc-pVDZ//MP2/cc-pVDZ + ΔZPVE) and the structure of edge-protonated cubane **4** at MP2/cc-pVDZ and CCD/cc-pVDZ (in italics).

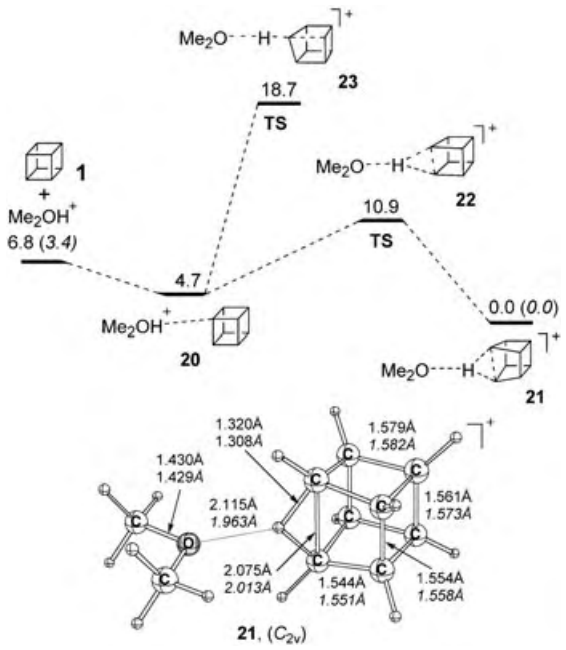
formal "hydride" abstraction with H^+. Similar to isobutane and adamantane, **1** forms a weakly bound complex with H_2 (**10**) upon protonation.[29] The absolute value of the reaction enthalpy[30] ($\Delta H_0 = -158.0$ kcal mol^{-1}) is approximately 40 kcal mol^{-1} higher than the "experimental" gas-phase basicity and proton affinity of **1**; in other words, **10** cannot be the high-energy $C_8H_9^+$ species resulting from protonation. Complex **10** is connected via TS **11** with the complex of the 2-cuneyl cation with H_2 (**12**), which is 195.0 kcal mol^{-1} lower in energy than **1**. Although this value is only slightly lower than the "experimental" PA[7,9] of cubane, the barrier for the rearrangement of **10** to **12** is too high (25.3 kcal mol^{-1}) for it to occur in a weakly bound complex such as **10**.

Corner-protonated cubane **13** in not a minimum and converges upon optimization without symmetry constrains to **14**, which is connected with protonated *syn*-tricyclooctadiene **15** via TS **16**. Cation **14** is also too stable ($\Delta\Delta H_0 = 219$ kcal mol^{-1}) to stand for the "experimental" PA of cubane. In contrast, edge-protonated cubane **4** *is* a true minimum that is 190.4 kcal mol^{-1} below **1** + H^+ (Scheme 1) at MP2/cc-pVDZ. Reoptimization at the coupled cluster CCD/cc-pVDZ as well as at the decisive CCSD(T)/cc-pVDZ levels of theory also identifies **4** as a minimum. The cubane cage opening to the "boat" structure **17** through TS **18** is barrierless. As the ZPVE correction is larger than the difference in electronic energies, the TSs appear to have a lower energy than the starting minima. This simply means that the reaction is barrierless and highly exothermic; **17** is connected with cation **5** via another low-lying TS **19**.

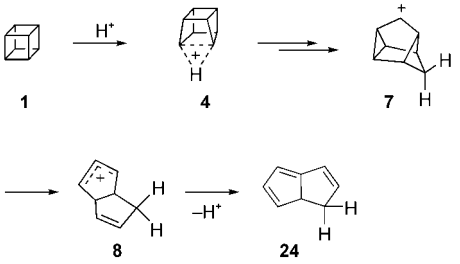
The PA of **1** previously was determined with a bracketing experiment in which the equilibrium reaction between cubane and protonated 2-propyl ether was examined using the FT/ICR technique.[9] Computations show that edge-protonated cubane **4** is not able to survive under these experimental conditions (155 °C, time from 0.1 to 25 s),[9] as its rearrangement is barrierless. To define the most favorable path for the proton transfer, we modeled the reaction of cubane with protonated dimethyl ether. Because of the size of the system we employed both DFT (B3LYP/6-311 + G**) and MP2/cc-pVDZ (for selected highly symmetrical structures), which both gave very similar results for this part of the PES (Scheme 2). Encounter complex **20** forms mildly exergonically (−2.1 kcal mol^{-1}, B3LYP/6-311 + G**) and proceeds to a complex of edge-protonated cubane with methyl ether **21** via TS **22**.[31] The barrier for the alternative corner attack (TS **23**) is 7.8 kcal mol^{-1} larger. The geometry of the hydrocarbon moiety of **21** is virtually identical to that of **4**.

Thus, in the FT-ICR experiment the protonation of cubane should give cation **8** (Scheme 1 and Scheme 3).[32] This is followed by deprotonation to give 1,8-dihydropentalene (**24**) after back proton transfer to the base,[33] and this hydrocarbon probably forms in the ICR chamber. The proton affinity of **24** computed at different levels is about 200 kcal mol^{-1}, which is in perfect agreement with the experimental

 © 2005 Wiley-VCH Verlag GmbH & Co. KGaA, Weinheim



Scheme 2. The proton transfer from protonated dimethyl ether to cubane (ΔG_{298} in kcal mol^{-1}, B3LYP/6-311+G**, MP2/cc-pVDZ, in italics) and the structure of edge-protonated cubane in the complex with dimethyl ether (**21**) at B3LYP/6-311+G** and MP2/cc-pVDZ (in italics).

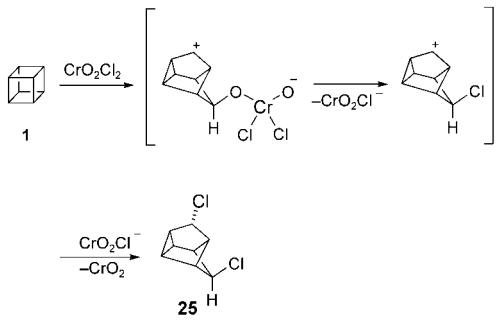


Scheme 3. The rearrangement of cubane in the protonation/deprotonation process.

value obtained previously for the reaction of cubane with protonated bases.[7,9]

The key conclusion derived from Scheme 1 is that the most favorable follow-up transformation of **4** is the rearrangement to **5** and further to the low-lying cation **7**. Thus, the reaction of cubane with electrophiles should first give a derivative of the tetracyclic cation **7**, which is stable towards deprotonation (to the anti-Bredt olefin) and may be stabilized in solution due to more effective solvation relative to that of cation **8**. These conclusions are fully supported by our experimental observation that the reaction of cubane with the electrophile CrO_2Cl_2 (Scheme 4) gives a single diastereomer of dichloride **25**.[34] This product forms through trapping of the *exo*-4-substituted tetracyclo[3.3.0.0^{2,8}.0^{3,6}]oct-7-yl cationic structure with the reagent.

In summary, we find that both H^+ and $(CH_3)_2OH^+$ favor an edge attack on **1** leading to C–C bond protonated minima (**4** and **21**, respectively) where the positive charge is delocalized over the entire σ cage. However, under the experimental gas-phase conditions protonated cubane **4** can only survive the early protonation stages very briefly because the barriers for rearrangements are simply too low. Careful scrutiny of the $C_8H_9^+$ PES starting from cubane gives 1,8-dihydropentalene (**24**) as the final product along the most favorable protonation/isomerization/deprotonation downhill path. We suggest that hydrocarbon **24** is responsible for the "experimental" proton affinity of cubane measured previously by the ICR technique.



Scheme 4. The experimentally found rearrangement of cubane in its reaction with CrO_2Cl_2.

Received: June 22, 2004

Keywords: computational chemistry · cubane · proton affinity · rearrangements

[1] G. A. Olah, A. Molnár, *Hydrocarbon Chemistry*, Wiley, New York, **1995**; J. Sommer, J. Bukala, *Acc. Chem. Res.* **1993**, *26*, 370–376.
[2] K. Hiraoka, P. Kebarle, *J. Am. Chem. Soc.* **1976**, *98*, 6119–6125.
[3] P. R. Schreiner, *Angew. Chem.* **2000**, *112*, 3375–3377; *Angew. Chem. Int. Ed.* **2000**, *39*, 3239–3241.
[4] S. Sieber, P. Buzek, P. von R. Schleyer, W. Koch, J. W. D. Carneiro, *J. Am. Chem. Soc.* **1993**, *115*, 259–270.
[5] C. J. A. Mota, P. M. Esteves, A. Ramírez-Solís, R. Hernández-Lamoneda, *J. Am. Chem. Soc.* **1997**, *119*, 5193–5199.
[6] F. Cacace, A. Guarino, E. Possagno, *J. Am. Chem. Soc.* **1969**, *91*, 3131–3134.
[7] E. P. Hunter, S. G. Lias, *J. Phys. Chem. Ref. Data* **1998**, *27*, 413.
[8] B. Chiavarino, M. E. Crestoni, A. A. Fokin, S. Fornarini, *Chem. Eur. J.* **2001**, *7*, 2916–2921.
[9] I. Santos, D. W. Balogh, C. W. Doecke, A. G. Marshall, L. A. Paquette, *J. Am. Chem. Soc.* **1986**, *108*, 8183–8185.
[10] C.-Y. Zhao, Y. Zhang, X.-Z. You, *J. Phys. Chem. A* **1997**, *101*, 5174–5182.
[11] P. M. Esteves, G. G. P. Alberto, A. Ramirez-Solis, C. J. A. Mota, *J. Phys. Chem. A* **2001**, *105*, 4308–4311.
[12] A. A. Fokin, P. R. Schreiner, P. von R. Schleyer, P. A. Gunchenko, *J. Org. Chem.* **1998**, *63*, 6494–6502.
[13] D. R. Kirklin, K. L. Churney, E. S. Domalski, *J. Chem. Thermodyn.* **1989**, *21*, 1105–1113.
[14] As pointed out by one of the referees, the strain energy of cubane is suspect. An indication of this is the fact that the newest measurement of the enthalpy of sublimation of cubane differs by some 5 kcal mol^{-1} from that measured earlier (A. Bashir-Hashemi, J. S. Chickos, W. Hanshaw, H. Zhao, B. S. Farivar, J. F. Liebman, *Thermochim. Acta* **2004**, *424*, 91–97).

 © 2005 Wiley-VCH Verlag GmbH & Co. KGaA, Weinheim

[15] J. L. M. Abboud, I. A. Koppel, J. Z. Davalos, P. Burk, I. Koppel, E. Quintanilla, *Angew. Chem.* **2003**, *115*, 1074 – 1076; *Angew. Chem. Int. Ed.* **2003**, *42*, 1044 – 1945.
[16] Z. Li, S. L. Anderson, *J. Phys. Chem. A* **2003**, *107*, 1162 – 1174.
[17] P. E. Eaton, T. W. Cole, Jr., *J. Am. Chem. Soc.* **1964**, *86*, 3157 – 3158.
[18] G. W. Griffin, A. P. Marchand, *Chem. Rev.* **1989**, *89*, 997 – 1010.
[19] H.-D. Martin, T. Urbanek, P. Pföhler, R. Walsh, *J. Chem. Soc. Chem. Commun.* **1985**, 964.
[20] P. R. Schreiner, A. Wittkopp, P. A. Gunchenko, A. I. Yaroshinsky, S. A. Peleshanko, A. A. Fokin, *Chem. Eur. J.* **2001**, *7*, 2739 – 2744.
[21] E. W. Della, N. J. Head, P. Mallon, J. C. Walton, *J. Am. Chem. Soc.* **1992**, *114*, 10730 – 10738.
[22] a) D. S. Reddy, M. Maggini, J. Tsanaktsidis, P. E. Eaton, *Tetrahedron Lett.* **1990**, *31,* 805 – 806; b) A. A. Fokin, P. R. Schreiner, *Chem. Rev.* **2002**, *102*, 1551 – 1593; c) A. A. Fokin, O. Lauenstein, P. A. Gunchenko, P. R. Schreiner, *J. Am. Chem. Soc.* **2001**, *123*, 1842 – 1847.
[23] S. Moss, B. T. King, A. de Meijere, S. I. Kozhushkov, P. E. Eaton, J. Michl, *Org. Lett.* **2001**, *3*, 2375 – 2377.
[24] D. Moran, H. L. Woodcock, Z. Chen, H. F. Schaefer III, P. von R. Schleyer, *J. Am. Chem. Soc.* **2003**, *125*, 11442 – 11451.
[25] The endohedral O_h-symmetrical complex of cubane with H^+ is a high-order stationary point (NIMAG = 3, ref. [24]).
[26] Geometry optimizations, frequency analysis of stationary points, and IRC calculations were carried out as implemented in Gaussian 03 (Revision B.04), M. J. Frisch,. G. W. Trucks, H. B. Schlegel, G. E. Scuseria, M. A. Robb, J. R. Cheeseman, J. A. Montgomery, Jr., T. Vreven, K. N. Kudin, J. C. Burant, J. M. Millam, S. S. Iyengar, J. Tomasi, V. Barone, B. Mennucci, M. Cossi, G. Scalmani, N. Rega, G. A. Petersson, H. Nakatsuji, M. Hada, M. Ehara, K. Toyota, R. Fukuda, J. Hasegawa, M. Ishida, T. Nakajima, Y. Honda, O. Kitao, H. Nakai, M. Klene, X. Li, J. E. Knox, H. P. Hratchian, J. B. Cross, C. Adamo, J. Jaramillo, R. Gomperts, R. E. Stratmann, O. Yazyev, A. J. Austin, R. Cammi, C. Pomelli, J. W. Ochterski, P. Y. Ayala, K. Morokuma, G. A. Voth, P. Salvador, J. J. Dannenberg, V. G. Zakrzewski, S. Dapprich, A. D. Daniels, M. C. Strain, O. Farkas, D. K. Malick, A. D. Rabuck, K. Raghavachari, J. B. Foresman, J. V. Ortiz, Q. Cui, A. G. Baboul, S. Clifford, J. Cioslowski, B. B. Stefanov, G. Liu, A. Liashenko, P. Piskorz, I. Komaromi, R. L. Martin, D. J. Fox, T. Keith, M. A. Al-Laham, C. Y. Peng, A. Nanayakkara, M. Challacombe, P. M. W. Gill, B. Johnson, W. Chen, M. W. Wong, C. Gonzalez, J. A. Pople, Gaussian, Inc., Pittsburgh, PA, **2003**.
[27] D. H. Aue in *Encyclopedia of Computational Chemistry*, *Vol. 1* (Eds.: P. von R. Schleyer, N. L. Allinger, T. Clark, J. Gasteiger, P. A. Kollman, H. F. Schaefer III, P. R. Schreiner), Wiley, Chichester, **1998**, pp. 210 – 220.
[28] a) P. E. Eaton, C.-X. Yang, Y. Xiong, *J. Am. Chem. Soc.* **1990**, *112*, 3225 – 3226; b) G. A. Olah, C. S. Lee, G. K. S. Prakash, R. M. Moriarty, M. S. C. Rao, *J. Am. Chem. Soc.* **1993**, *115*, 10728 – 10732.
[29] Formation of tight $C_8H_7^+\cdots H_2$ complexes is in agreement with the experimental observation of an ion at *m*/*z* 103 derived from protonated cubane [**1**+H^+ – H_2] in the low-temperature chemical ionization mass spectra.[16]
[30] We use ΔH_0 values at CCSD(T)/cc-pVDZ//MP2/cc-pVDZ + ΔZPVE because these are closely related to the experimental proton affinities (PAs). The relative energies ΔG_{298} (Supplementary Information) differ only by ± 1.5 kcal mol^{-1}.
[31] A sizable imaginary mode (150*i*), which still present at B3LYP/6-311 + G** for **21** in C_1 (even with tight convergence criteria) show that this method still does not handle this flat part of the PES properly; however, at MP2/6-31G* this structure is a true minimum.
[32] Further rearrangement of cation **8** to the more stable homotropylium cation (protonated cyclooctatetraene) is precluded by a high barrier (ca. 30 kcal mol^{-1}).
[33] Deprotonation of **8** may lead to semibullvalene, which, however, is ca. 10 kcal mol^{-1} less stable than **24**.
[34] NMR ^{1}H ($CDCl_3$): $\delta = 1.75$ (m, 1H), 1.89 (m, 1H), 2.12 (m, 1H), 2.62 (m, 1H), 2.87 (br s, 1H), 3.05 (m, 1H), 4.06 (s, 1H), 4.13 ppm (m, 1H); NMR ^{13}C ($CDCl_3$): $\delta = 17.4$, 18.8, 33.5, 47.8, 48.0, 49.1, 63.5, 64.7 ppm; MS (*m*/*z*): 174, 139, 125, 103 (100%), 77, 63, 51.

 © 2005 Wiley-VCH Verlag GmbH & Co. KGaA, Weinheim

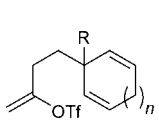
Asymmetric Heck Reaction

Catalytic Desymmetrizing Intramolecular Heck Reaction: Evidence for an Unusual Hydroxy-Directed Migratory Insertion**

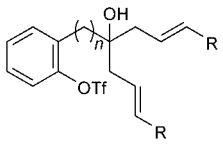
Martin Oestreich, Fernando Sempere-Culler, and Axel B. Machotta*

As reflected by a remarkable number of beautiful applications to the synthesis of structurally intriguing natural products,[1] the asymmetric intramolecular Heck reaction[2] has evolved as a prominent carbon–carbon bond-forming process.[3] The invention of asymmetric variants of Heck cyclizations has been approached by two distinct strategies: by indirect[4] and by direct[5] formation of stereogenic carbon centers.

Indirect construction of stereogenic carbons was realized by asymmetric Heck cyclization of prochiral precursors **A** (PG = protecting group), which emerged as privileged substrates for these so-called group-selective cyclizations. How-



A
(R = CO_2Me, CH_2OPG; n = 0, 1)



B
(R = H, aryl; n = 0, 1)

[*] Dr. M. Oestreich, Dipl.-Chem. F. Sempere-Culler, A. B. Machotta
Institut für Organische Chemie und Biochemie
Albert-Ludwigs-Universität
Albertstrasse 21, 79104 Freiburg im Breisgau (Germany)
Fax: (+49) 761-203-6100
E-mail: martin.oestreich@orgmail.chemie.uni-freiburg.de

[**] The research was supported by the Fonds der Chemischen Industrie and the Wissenschaftliche Gesellschaft in Freiburg im Breisgau. M.O. is indebted to the Deutsche Forschungsgemeinschaft for an Emmy Noether Fellowship (2001–2005) and to Prof. Reinhard Brückner for his continuous support. The authors thank Ilona Hauser for skillful technical assistance and Gerd Fehrenbach and Dr. Richard Krieger for performing the HPLC analyses. Generous donation of palladium precatalysts and (*S*)-Cl-MeO-biphep by Bayer Chemicals AG (Germany) is gratefully acknowledged.

 DOI: 10.1002/anie.200460921 © 2005 Wiley-VCH Verlag GmbH & Co. KGaA, Weinheim

ever, despite elegant investigations by Shibasaki et al.,[6] this methodology appears to be restricted to systems **A** in which the enantiotopic groups are incorporated into a cyclic framework.[7,8] Interestingly, desymmetrizing Heck cyclizations of less rigid systems **B** have not been reported so far.[9]

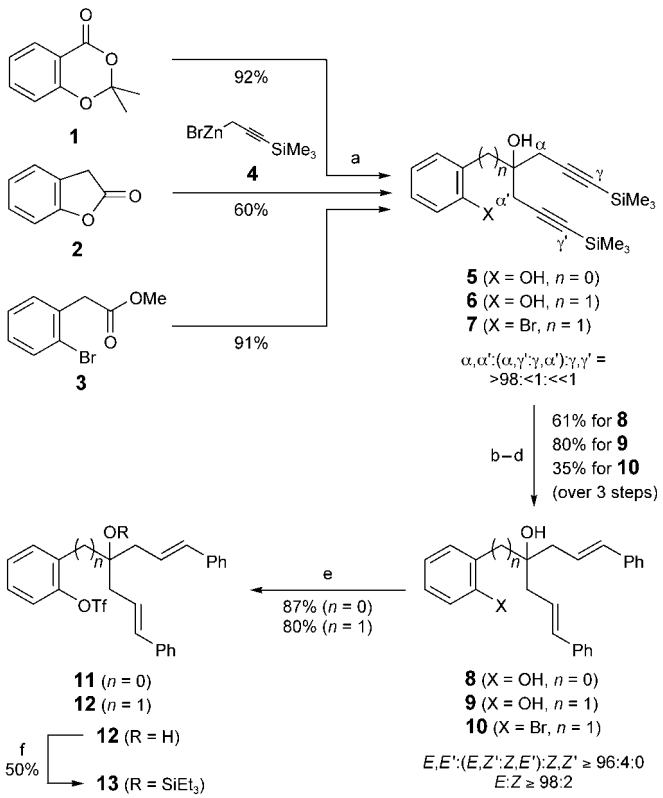
We envisioned compounds **B** as attractive substrates for an exploratory analysis of such desymmetrization reactions. In this paper, we wish to communicate the first catalytic desymmetrizing intramolecular Heck reaction of open-chain precursors **B** as well as experimental evidence for an unusual catalyst-directing hydroxy group[10] in these ring closures.

In the initial phase of the project, we extensively surveyed reaction conditions for the desymmetrization of prototype **B** (R = H, $n = 1$), but the enantiomeric excesses obtained were only moderate ($\leq 40\%$ *ee*).[11] These findings led us to consider the introduction of aryl groups at the terminal positions of the allyl moieties in **B** (R = Ph, $n = 1$). We anticipated that such a modification would have two beneficial effects: 1) prevention of post-Heck double-bond migration on account of the styrene unit and 2) improvement of enantioselectivity due to increased steric hindrance and aryl–aryl interactions.

The requisite cyclization precursors **11** and **12** were prepared starting from acetonide **1** and lactone **2**, respectively (Scheme 1). The direct synthesis of bishomoallylic alcohols from esters by twofold allylation employing γ-substituted allyl metal reagents is rather delicate since there is no general methodology available for controlling regio- and diastereoselectivity. We developed a reliable reaction sequence consisting of regioselective bispropargylation using zinc reagent **4** and diastereoselective reduction with aluminum hydrides.[12] Application of this procedure to **1** and enolizable **2** provided **5** ($n = 0$) and **6** ($n = 1$), respectively, in excellent regio- (**1**→**5** and **2**→**6**) and diastereoselectivities (**5**→**8** and **6**→**9**). Chemoselective triflation of final diol **8** was rather capricious due to the proximity of the hydroxy groups, whereas triflation of **9** proceeded smoothly (**8**→**11** and **9**→**12**, Scheme 1). The preparation of the corresponding aryl bromide **10** was accomplished by the identical protocol (**3**→**7**→**10**, Scheme 1).

When we subjected diene **12** to standard Heck reaction conditions (5.0 mol% $Pd(OAc)_2$, 7.5 mol% (*R*)-binap (**L1**), K_2CO_3, 80 °C) in various solvents,[13a] we were pleased to find exclusive formation of a single isomer **14**[14] with substantially improved enantioselectivity (Table 1, entry 1).[13b] Replacing **L1** by its cognate derivative **L2** resulted in slightly diminished selectivity (Table 1, entry 2); conversely, the novel binap surrogate (*S*)-Cl-MeO-biphep (**L3**),[15] for which applications in asymmetric Heck chemistry are unprecedented,[16] gave the best enantioselectivity (Table 1, entry 3).[17]

Complete conversion accompanied by enhanced enantioselectivity was achieved even at 60 °C and 50 °C (Table 1, entries 4–6). Though, intramolecular migration of the triflyl group (transtriflation) became a competing reaction pathway at temperatures below 50 °C and the prolonged reaction times required. In an attempt to prevent this undesired side reaction, we prepared the silyl ether of **12** (**12**→**13**, Scheme 1). Unexpectedly, cyclization of **13** under reaction conditions identical to those for **12** provided **15** in almost racemic form (Table 1, entry 7). Similarly, the deoxygenated substrate **17** furnished **18** with poor enantioselectivity (Scheme 2).[18]



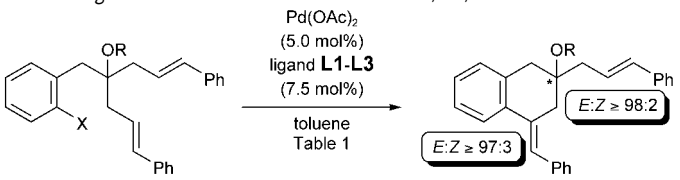
Scheme 1. Preparation of cyclization precursors **10**–**13**. Reaction conditions: a) **4**, THF, RT; b) TBAF·3 H_2O, THF, RT; c) PhI, $[Pd(PPh_3)_2Cl_2]$, CuI, Et_3N; d) Red-Al ($n = 0$) or $LiAlH_4$ ($n = 1$), THF, RT; e) Tf_2O, 2,6-lutidine, DMAP, CH_2Cl_2, −30 °C→RT ($n = 0$) and $PhNTf_2$, Cs_2CO_3, DMF, RT ($n = 1$); f) Et_3SiOTf, 2,6-lutidine, CH_2Cl_2, 0 °C. DMAP = 4-*N*,*N*-dimethylaminopyridine, DMF = *N*,*N*-dimethylformamide, Red-Al = sodium bis(2-methoxyethoxy)aluminum dihydride, TBAF = tetra-*n*-butylammonium fluoride, Tf = trifluoromethanesulfonyl.

This pronounced effect (88 vs. 0–18% *ee*) indicated that the unprotected hydroxy group plays the pivotal role in the stereochemistry-determining step of the ring closure of **12**. A plausible assumption is that the free hydroxy group acts as a catalyst-directing group. We verified this further by conducting Heck cyclizations of **12** in the presence of equimolar amounts of an alcohol additive (MeOH or *t*BuOH).[19] Consistently, cyclization of **12** furnished **14** in merely moderate enantiomeric excess (Table 1, entries 8 and 9). Obviously, the external hydroxy group interferes with intramolecular coordination of the catalyst by the tertiary hydroxy group of **12**.

Moreover, ring closures of **17** and **12** occur at markedly different rates. Whereas the cyclization of **12** is complete after 20 h at 50 °C, conversion of **17** is low. This accelerating effect also supports the hypothesis that these Heck cyclizations involve intramolecular coordination of the catalyst.[20] Changing the position of the unprotected hydroxy group relative to the aryl triflate moiety had a similar effect. Bishomoallylic alcohol **11**, which produces a five-membered carbocycle, cyclized in low yield and poor enantioselectivity (**11**→**19**, Scheme 3).

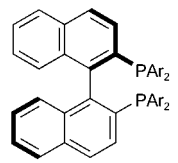
 © 2005 Wiley-VCH Verlag GmbH & Co. KGaA, Weinheim

Table 1: Desymmetrizing intramolecular Heck reactions of **10**, **12**, and **13**.[a]

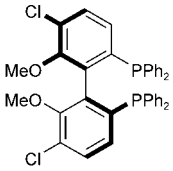


10 (X = Br, R = H)
12 (X = OTf, R = H)
13 (X = OTf, R = $SiEt_3$)

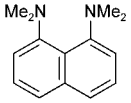
14 (R = H)
15 (R = $SiEt_3$)



L1 (Ar = Ph): (*R*)-binap
L2 (Ar = Tol): (*R*)-Tol-binap



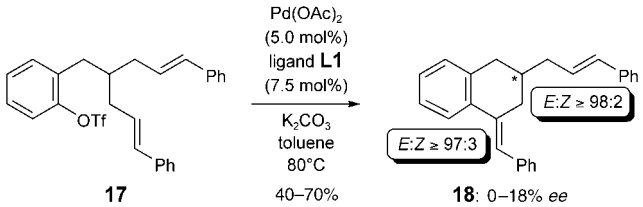
L3: (*S*)-Cl-MeO-biphep



16
proton sponge

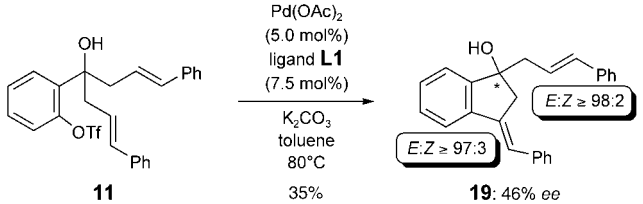
Entry	Precursor	Base, Additive	L	*T* [°C]	*t* [h]	Prod.	*ee* [%][b]	Yield [%][c]
1	**12**	K_2CO_3	**L1**	80	15	**14**	88	74
2	**12**	K_2CO_3	**L2**	80	15	**14**	80	81
3	**12**	K_2CO_3	**L3**	80	15	**14**	90[d]	81
4	**12**	K_2CO_3	**L1**	60	20	**14**	92	85
5	**12**	K_2CO_3	**L3**	60	20	**14**	94[d]	85
6	**12**	K_2CO_3	**L1**	50	20	**14**	92	85
7	**13**	K_2CO_3	**L1**	80	15	**15**	2[e]	55
8	**12**	K_2CO_3, MeOH[f]	**L1**	80	15	**14**	42	85
9	**12**	K_2CO_3, *t*BuOH[f]	**L1**	80	15	**14**	54	85[g]
10	**12**	TMP	**L1**	80	15	**14**	78	65
11	**12**	NaOAc	**L1**	80	15	**14**	86	85
12	**12**	**16**	**L1**	80	15	**14**	90	54
13	**12**	Cs_2CO_3	**L1**	80	15	**14**	–	–[h]
14	**10**	K_2CO_3	**L1**	80	15	**14**	12[d]	25[i]

[a] All reactions were conducted with a substrate concentration of 0.1 M in toluene with 4.0 equiv of the respective base. [b] Enantiomeric excess of the depicted *E*,*E*-configured diastereomer were measured by HPLC using a Daicel Chiralcel AD column (*n*-heptane:*i*PrOH = 90:10 at 15 °C). [c] Yield of analytically pure product isolated by flash chromatography on silica gel. [d] Absolute configuration opposite to that obtained for the cyclization of **12** using **L1** (Table 1, entry 1). [e] Enantiomeric excess was measured by HPLC using a Daicel Chiralcel AD column (*n*-heptane:*i*PrOH = 100:1 at 20 °C). [f] 1.0 equiv of anhydrous and degassed alcohol. [g] Approximately 80% conversion. [h] No product detected. [i] Reaction performed under conditions identical to those for **12**; yield not optimized. TMP = 2,2,6,6-tetramethylpiperidine.



17 40–70% **18**: 0–18% *ee*

Scheme 2. Desymmetrizing intramolecular Heck reaction of **17**.



11 35% **19**: 46% *ee*

Scheme 3. Desymmetrizing intramolecular Heck reaction of **11**.

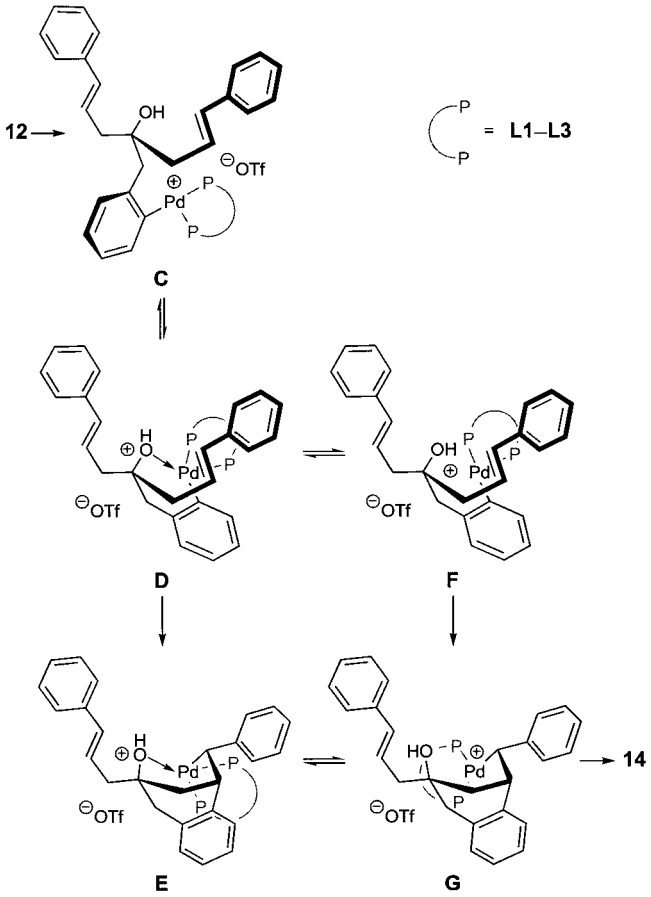
To clarify whether the free hydroxy or the corresponding alkoxy group functions as the directing group we screened several bases (Table 1, entries 10–13). Except for strong inorganic bases, all other bases tested had only minor influence on the enantiomeric purity of **14**. In particular, the enantioselectivity is unaffected when NaOAc is added, which implies that the free hydroxy group is possibly operating as a weak ligand for the palladium catalyst.

Coordination of the hydroxy group requires a free coordination site at the palladium center which, in principle, is available under so-called cationic reaction conditions.[2,3] In a control experiment, we performed the Heck cyclization under neutral conditions[21] employing the appropriate aryl bromide **10**. As expected, the level of enantioselectivity was low (Table 1, entry 14). Based on these observations, we propose a mechanism in which the cationic arylpalladium species **C** is reversibly coordinated by the tertiary hydroxy group to form a six-membered ring (**C** and **D**, Scheme 4). The fate of key intermediate **D** is unclear since migratory alkene insertion involving pentacoordinate palladium complexes is not completely understood (**D**→**E**).[21,22]

In our case, a modified scenario appears to be likely: coordination of the hydroxy group in **D** generates a highly ordered transition state which allows for efficient differentiation of the formerly enantiotopic branches. Either a dissociative (**D**→**F**→**G**) or an associative (**D**→**E**→**G**) migratory insertion is a plausible reaction pathway providing **14**. The high enantioselectivity observed for **12** could stem from the ideal proximity of the hydroxy group and the palladium center.[23]

In summary, we have elaborated a catalytic desymmetrizing intramolecular Heck reaction of a structurally novel substrate class. These investigations have revealed a conceptually interesting role of a hydroxy group as a catalyst-directing group in an asymmetric Heck reaction.[10] In addition to further studies directed towards a more refined mechanistic understanding, we are currently exploring the use of chiral alcohols as additional ligands in asymmetric Heck reactions. Application of this methodology to the formal total synthesis of anthracyclines will be reported in due course.[24]

 © 2005 Wiley-VCH Verlag GmbH & Co. KGaA, Weinheim



Scheme 4. Catalyst-directing hydroxy group.

Received: June 9, 2004

Keywords: asymmetric catalysis · asymmetric synthesis · C–C coupling · palladium

[1] A. B. Dounay, L. E. Overman, *Chem. Rev.* **2003**, *103*, 2945–2964.
[2] a) M. Shibasaki, F. Miyazaki in *Handbook of Organopalladium Chemistry for Organic Synthesis*, *Vol. 1* (Eds.: E.-i. Negishi, A. de Meijere), Wiley, New York, **2002**, pp. 1283–1315; b) Y. Donde, L. E. Overman in *Catalytic Asymmetric Synthesis* (Ed.: I. Ojima), 2nd ed., Wiley, New York, **2000**, pp. 675–697.
[3] a) J. T. Link in *Organic Reactions*, *Vol. 60* (Ed.: L. E. Overman), Wiley, New York, **2002**, pp. 157–534; b) I. P. Beletskaya, A. V. Cheprakov, *Chem. Rev.* **2000**, *100*, 3009–3066.
[4] Y. Sato, M. Sodeoka, M. Shibasaki, *J. Org. Chem.* **1989**, *54*, 4738–4739.
[5] N. E. Carpenter, D. J. Kucera, L. E. Overman, *J. Org. Chem.* **1989**, *54*, 5846–5848.
[6] a) Y. Sato, S. Watanabe, M. Shibasaki, *Tetrahedron Lett.* **1992**, *33*, 2589–2592; b) K. Ohrai, K. Kondo, M. Sodeoka, M. Shibasaki, *J. Am. Chem. Soc.* **1994**, *116*, 11737–11748.
[7] For the desymmetrization of bicyclodienes, see: M. Lautens, V. Zunic, *Can. J. Chem.* **2004**, *82*, 399–407.
[8] For a different desymmetrization strategy for a cyclic substrate, see: S. Bräse, *Synlett* **1999**, 1654–1656.
[9] For a review of enantioselective desymmetrization, see: M. C. Willis, *J. Chem. Soc. Perkin Trans. 1* **1999**, 1765–1784.
[10] For other chelate-controlled Heck reactions, see: a) P. Nilsson, M. Larhed, A. Hallberg, *J. Am. Chem. Soc.* **2001**, *123*, 8217–8225; b) K. Itami, T. Nokami, Y. Ishimura, K. Mitsudo, T. Kamei, J.-i. Yoshida, *J. Am. Chem. Soc.* **2001**, *123*, 11577–11585; c) P. Nilsson, M. Larhed, A. Hallberg, *J. Am. Chem. Soc.* **2003**, *125*, 3430–3431; d) for regioselective vinylation of allylic alcohols, see: E. Bernocchi, S. Cacci, P. G. Ciattini, E. Morera, G. Ortar, *Tetrahedron Lett* **1992**, *33*, 3073–3076.
[11] As a result of alkene migration, formation of two isomers was yet another issue. Nevertheless, identical enantiomeric excesses were measured for both isomers.
[12] M. Oestreich, F. Sempere-Culler, *Chem. Commun.* **2004**, 692–693, and references therein.
[13] a) Of the standard solvents utilized in asymmetric Heck chemistry, THF and toluene worked equally well; however, the enantioselectivity was slightly better in toluene. b) Interestingly, catalyst loadings as low as 1.0 mol% $Pd(OAc)_2$ precatalyst and 1.5 mol% **L1** did not affect the enantioselectivity of the reaction.
[14] The absolute configuration of **14** has not been determined yet since all attempts to derivatize and crystallize or chemically correlate **14** have failed so far.
[15] C. Laue, G. Schröder, D. Arlt (Bayer AG), DE-A1 19522293, **1995**.
[16] Asymmetric Heck reactions using MeO-biphep have been reported: a) G. Trabesinger, A. Albinati, N. Feiken, R. W. Kunz, P. S. Pregosin, M. Tschoerner, *J. Am. Chem. Soc.* **1997**, *119*, 6315–6323; b) M. Tschoerner, A. Albinati, P. S. Pregosin, *Organometallics* **1999**, *18*, 670–678; c) L. F. Tietze, K. Thede, R. Schimpf, F. Sannicolò, *Chem. Commun.* **2000**, 583–584.
[17] A brief survey of oxazoline-containing P,N ligands showed that axially chiral diphosphines were the optimal choice for this intramolecular Heck reaction. For successful applications of P,N ligands, see: a) D. Kiely, P. J. Guiry, *Tetrahedron Lett.* **2002**, *43*, 9545–9547; b) L. Ripa, A. Hallberg, *J. Org. Chem.* **1997**, *62*, 595–602; c) For a review on P,N-ligands, see: O. Loiseleur, M. Hayashi, M. Keenan, N. Schmess, A. Pfaltz, *J. Organomet. Chem.* **1999**, *576*, 16–22.
[18] Cyclization precursor **17** was prepared by a twofold palladium(0)-catalyzed, Et_3B-promoted C-allylation of 2-hydroxyacetophenone with cinnamic alcohol followed by deoxygenation: Y. Horino, M. Naito, M. Kimura, S. Tanaka, Y. Tamaru, *Tetrahedron Lett.* **2001**, *42*, 3113–3116.
[19] It should be noted that Shibasaki et al. employed *t*BuOH as a cosolvent in an asymmetric Heck reaction in order to suppress oxidation of a secondary-alcohol-containing substrate without affecting the level of enantioselectivity: K. Kondo, M. Sodeoka, M. Mori, M. Shibasaki, *Synthesis* **1993**, 920–930. For a general overview on alcohols as cosolvents, see ref. [3b].
[20] For an excellent review on substrate-directed reactions, see: A. H. Hoveyda, D. A. Evans, G. C. Fu, *Chem. Rev.* **1993**, *93*, 1307–1370.
[21] A. Ashimori, B. Bachand, M. A. Calter, S. P. Govek, L. E. Overman, D. J. Poon, *J. Am. Chem. Soc.* **1998**, *120*, 6488–6499.
[22] However, Wolfe et al. have recently presented evidence for an alkene insertion into an arylpalladium alkoxide intermediate: J. P. Wolfe, M. A. Rossi, *J. Am. Chem. Soc.* **2004**, *126*, 1620–1621.
[23] In contrast, intramolecular coordination in the cyclization of **11** would require formation of a virtually planar (and strained) five-membered ring, which could potentially account for the distinctly diminished enantioselectivity.
[24] M. Oestreich, F. Sempere-Culler, manuscript in preparation.

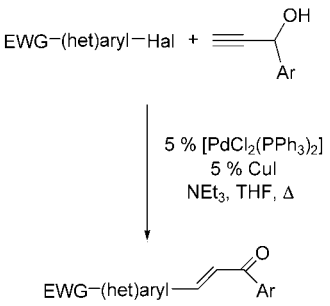
 © 2005 Wiley-VCH Verlag GmbH & Co. KGaA, Weinheim

Domino Reactions

A Domino Sequence Consisting of Insertion, Coupling, Isomerization, and Diels–Alder Steps Yields Highly Fluorescent Spirocycles**

*Daniel M. D'Souza, Frank Rominger, and Thomas J. J. Müller**

The coupling–isomerization reaction[1] (CIR, [Eq. (1)], EWG = electron-withdrawing group) of electron-deficient (hetero)aryl halides and (hetero)arylpropargyl alcohols



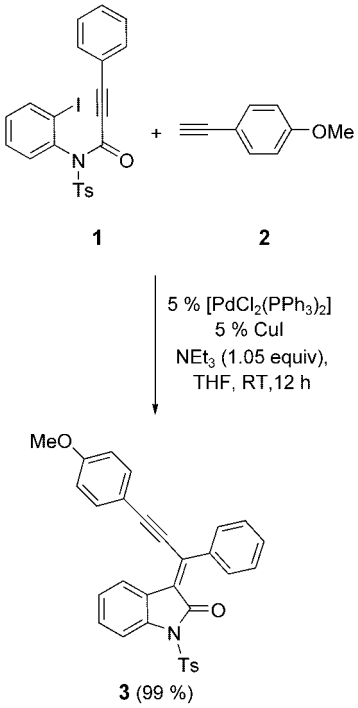
(1)

under the conditions of the Sonogashira coupling[2] is a mild and efficient route to enones, in particular, to 1,3-di(hetero)arylpropenones, known as chalcones. In the past years this new chalcone synthesis has been applied to novel consecutive one-pot multicomponent syntheses of pharmaceutically relevant heterocycles.[1,3] Mechanistically, the CIR can be rationalized as a rapid palladium/copper-catalyzed alkynylation reaction followed by the slow base-catalyzed isomerization of a propargyl alcohol into an enone. Although the proposed allenol intermediate is elusive and highly reactive, the major potential of the CIR clearly lies in selectively addressing allenol derivative intermediates by thermodynamically and kinetically favored intramolecular trapping reactions. Conceptually, the installation of the electron-withdrawing functionality required for the isomerization step by means of an organometallic elementary step such as the insertion of an alkyne into a carbon–palladium bond[4] followed by a CIR would be more than a methodological extension of the CIR; it could also provide access to heterodomino reactions.[5,6] Here, we describe a new domino reaction based upon a sequence of CIR and the Diels–Alder reaction.

[*] Dipl.-Chem. D. M. D'Souza, Dr. F. Rominger, Prof. Dr. T. J. J. Müller
Organisch-Chemisches Institut
Ruprecht-Karls-Universität Heidelberg
Im Neuenheimer Feld 270, 69120 Heidelberg (Germany)
Fax: (+49) 6221-546-579
E-mail: thomas_j.j.mueller@urz.uni-heidelberg.de

[**] This work was supported by the Deutsche Forschungsgemeinschaft (Graduate College 850). Financial support by the Fonds der Chemischen Industrie and the Dr.-Otto-Röhm Gedächtnisstiftung is gratefully acknowledged. The authors also thank Benjamin Willy for experimental assistance and the BASF AG for the generous donation of chemicals.

Intramolecular Heck reactions[7] have been developed into a widely applied method and have culminated in impressive domino sequences like the Negishi "zipper" reactions;[4] however, the termination of insertion cascades by Sonogashira alkynylation[2] has remained unexplored to date.[8] Therefore, we first tested a Sonogashira sequence with an intermediate alkyne insertion. Upon reaction of *N*-(iodophenyl)alkynamide **1**[9] and *p*-methoxyphenylacetylene (**2**) in THF at room temperature and in the presence of one equivalent of triethylamine and catalytic amounts of $[PdCl_2(PPh_3)_2]$ and CuI the bright yellow dihydroindolone **3**[10] was obtained in quantitative yield [Eq. (2), Ts = tosyl].



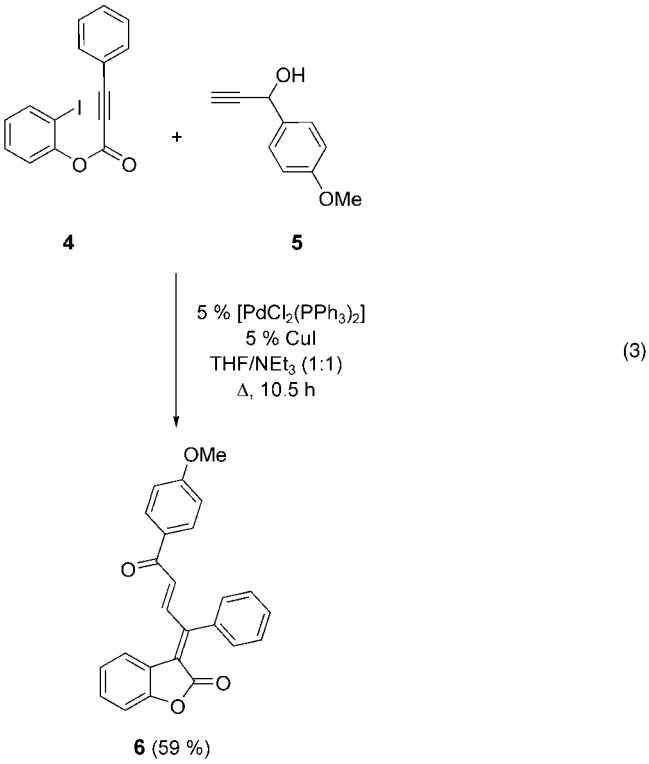
(2)

The *E* configuration of the double bond of the newly formed enyne functionality is unambiguously supported by the characteristic crosspeaks in the NOESY spectrum for interactions between the anisyl protons and the benzo protons in the 4- and 5-positions of the indolone moiety. Mechanistically, this stereospecific formation of the enyne can be rationalized by a sequence of oxidative addition of a palladium(0) species into the carbon–iodine bond of **1** followed by coordination and intramolecular *syn* insertion of the arylpalladium species to furnish a configurationally stable *E*-vinylpalladium derivative. Finally, the terminating intermolecular cross-coupling by transmetalation of the in situ formed copper acetylide and reductive elimination produces the enyne product **3**.

Analogously, the CIR of the *ortho*-iodophenyl alkynoate **4**[9] and the *p*-anisylpropargylalcohol (**5**) in a 1:1 mixture of THF and triethylamine heated at reflux and in the presence of catalytic amounts of $[PdCl_2(PPh_3)_2]$ and CuI furnishes benzofuranone **6**[10] in 59% yield [Eq. (3)]. Thorough NMR spectroscopic analysis (^1H, ^{13}C, DEPT, COSY, NOESY, HETCOR, and HMBC experiments) unequivocally supports

 DOI: 10.1002/anie.200461489 © 2005 Wiley-VCH Verlag GmbH & Co. KGaA, Weinheim

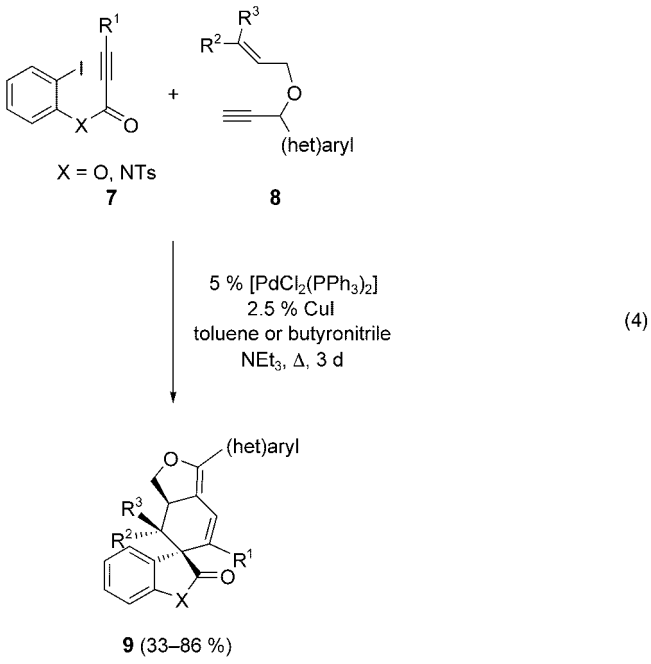
the *E* configurations of the disubstituted enone ($\delta = 6.76$, 9.20, doublets, $^3J = 15.5$ Hz) and the tetrasubstituted double bond generated by the insertion, coupling, and isomerization steps.



(3)

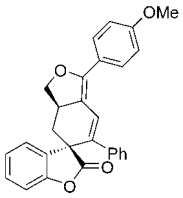
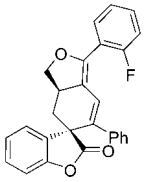
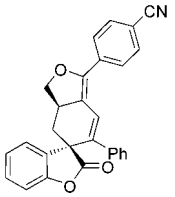
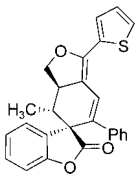
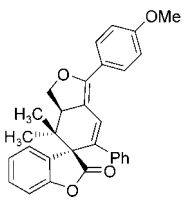
As a consequence of the insertion–CIR an electron-deficient diene can be readily constructed. For a highly reactive allenol intermediate in the CIR (see above), the transient should be an enallene, a class of particularly reactive dienes in Diels–Alder reactions. Hence, we set out to conduct the insertion–CIR with a propargyl allyl ether, not only to shut off the irreversible allenol–enone tautomerism but also to employ a tethered dienophile functionality as a trap for an intramolecular [4+2] cycloaddition with inverse electron demand. The reaction of alkynoyl *ortho*-iodo ester or amide **7**[9] and propargyl allyl ether **8**[9] in the presence of catalytic amounts of $[PdCl_2(PPh_3)_2]$ and CuI in a mixture of toluene or butyronitrile and triethylamine heated at reflux produces the hitherto unknown class of spiro[benzofuranon-tetrahydroisobenzofurans] and spiro[dihydroindolone-tetrahydroisobenzofurans] **9**[10] in moderate to excellent yields [Eq. (4), Table 1]. In this process the formation of four new carbon–carbon bonds leads to a complex tetracyclic framework with high efficiency.

The structures of the spirocycles **9** were unambiguously supported by spectroscopic (^{1}H, ^{13}C and DEPT, COSY, NOESY, HETCOR and HMBC NMR experiments, IR, UV/Vis, mass spectrometry) and combustion analyses. Additionally, the molecular structure was corroborated by X-ray structure analyses of the benzofuranone **9d** and the dihydroindolone **9h** (Figure 1).[11] Most interestingly, in the crystal structure the thienyl (**9d**) and the phenyl substituents (**9h**) in the 3-position of the isobenzofuran moiety are almost



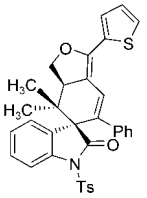
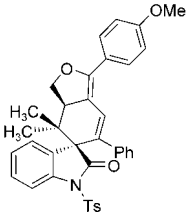
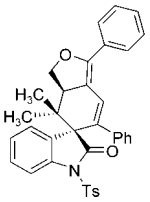
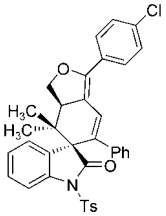
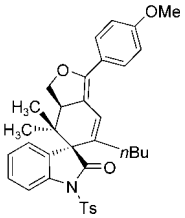
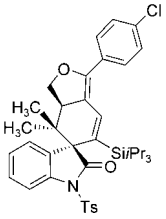
(4)

Table 1: Domino reaction consisting of insertion, CI, and Diels–Alder steps yielding spirocycles **9**.[a]

Entry	Aryl iodide **7**	Propargyl allyl ether **8**	Spirocycles **9** (yield)[b]
1	**7a** X = O, R^1 = Ph	**8a** $R^2 = R^3 = H$, (het)aryl = *p*-$MeOC_6H_4$	 **9a** (66 %)
2	**7a**	**8b** $R^2 = R^3 = H$, (het)aryl = *o*-FC_6H_4	 **9b** (50 %)
3	**7a**	**8c** $R^2 = R^3 = H$, (het)aryl = *p*-NCC_6H_4	 **9c** (51 %)
4	**7a**	**8d** $R^2 = CH_3$, $R^3 = H$, (het)aryl = 2-thienyl	 **9d** (49 %)
5	**7a**	**8e** $R^2 = R^3 = CH_3$, (het)aryl = *p*-$MeOC_6H_4$	 **9e** (33 %)

 © 2005 Wiley-VCH Verlag GmbH & Co. KGaA, Weinheim

Table 1: (Continued)

Entry	Aryl iodide **7**	Propargyl allyl ether **8**	Spirocycles **9** (yield)[b]
6	**7b** X = NTs R^1 = Ph	**8f** $R^2 = R^3 = CH_3$ (het)aryl = 2-thienyl	 **9f** (72%)
7	**7b**	**8e**	 **9g** (79%)
8	**7b**	**8g** $R^2 = R^3 = CH_3$ (het)aryl = Ph	 **9h** (86%)
9	**7b**	**8h** $R^2 = R^3 = CH_3$ (het)aryl = *p*-ClC_6H_4	 **9i** (86%)
10	**7c** X = NTs R^1 = *n*Bu	**8e**	 **9j** (77%)
11	**7d** X = NTs R^1 = *i*Pr_3Si	**8h**	 **9k** (79%)

[a] Reaction conditions: A mixture of 1.0 equiv of **7**, 1.1 equiv of **8** (0.1 M in toluene/triethylamine 1:1 for **9a–e**, in butyronitrile/triethylamine 1:1 for **9f–k**), 0.05 equiv of $[PdCl_2(PPh_3)_2]$, and 0.025 equiv of CuI was heated at reflux for 48–36 h. [b] Yields refer to yields of compounds **9** isolated after flash chromatography on silica gel and crystallization and estimated to 95% pure by NMR spectroscopy and elemental analysis.

addition of the aryl halide **7** to the Pd^0 species generated in situ, the arylpalladium halide **10** intramolecularly coordinates and inserts the tethered triple bond by means of *syn*-carbopalladation to furnish stereospecifically the cyclized vinylpalladium species **11** with a β-acceptor substitution. Transmetalation of the copper acetylide **12** generated in situ gives rise to the palladium complex **13**, which readily undergoes reductive elimination and liberates the electron-poor vinylpropargyl allyl ether **14**. The triethylamine-catalyzed propargyl–allene isomerization furnishes the electron-poor enallene **15**, which reacts in an intramolecular [4+2] cycloaddition to conclude the sequence with the formation of the spirocycle **9** via an *anti-exo* transition state in the Diels–Alder step (as deduced from the X-ray structure analysis of **9d**, entry 4).

Most distinctively, upon irradiation with UV light all members of this new class of spirocycles display a pronounced and intense blue to yellow-green fluorescence with large Stokes shifts in solution and in the solid state (see Figures 2, 3, and 4, Table 2). Therefore, they are promising candidates for a new class of fluorophores with a rigid spirocyclic framework. In the emission spectra of **9** around the same energies a maximum is always accompanied by a shoulder either blue-shifted (**9a**, **9c**, **9f**, and **9g**) or red-shifted (**9h** and **9i**). For the lower energy emission maxima (**9a**, **9c**, and **9f**) the apparent fluorescence color is yellow-green to green, whereas the higher energy bands (**9g**, **9h**, and **9i**) cause a bright blue fluorescence. In a first approximation as derived from the absorption and emission behavior, the excited state structure of **9** shows only a minor dependence of the substitution pattern. In contrast, the absorption properties, as reflected by the longest wavelength maxima, strongly depend on the electronic nature of and the substituents on the conformationally fixed (1*Z*,3*Z*)-1-phenyl-4-(hetero)arylbutadiene chromophor (comparable to *trans-cis*-1,4-diphenylbutadiene). Hence, the Stokes shifts range from 5900 to 7500 cm^{-1}. Most interestingly, upon photoexcitation the model *trans-cis*-1,4-diphenylbutadiene does not fluoresce at

Table 2: Absorption and emission maxima of selected spirocycles **9** (recorded in CH_2Cl_2, $T = 298$ K).

Cmpd.	$\lambda_{max,abs}$ [nm] (ε)[a]	$\lambda_{max,em}$ [nm][b]	$\Delta\tilde{\nu}$ [cm^{-1}][c]	Fluorescence color
9a	256 (17500), 348 (26700)	470sh, 507	7500	green
9c	246 (11000), 368 (12700)	471sh, 504	5900	green
9f	246 (19600), 362 (18600)	470sh, 510	6300	yellow-green
9g	242 (25500), 350 (20900)	470sh, 506	7300	blue
9h	244 (27600), 348 (24900)	471, 506sh	7500	blue
9i	242 (27000), 350 (22900)	472, 506sh	7400	blue-green

[a] Recorded at $c = 10^{-4}$ M. [b] Recorded at $c = 10^{-7}$ M. [c] Stokes shift $\Delta\tilde{\nu} = \lambda_{max,abs} - \lambda_{max,em}$ [cm^{-1}].

coplanar with the conformationally fixed butadienyl system, whereas the 5-phenyl substituent is twisted out of the plane by 50° for steric reasons.

Mechanistically, this new domino sequence consisting of insertion, coupling, isomerization, and Diels–Alder steps can be rationalized as follows (Scheme 1): After the oxidative

 © 2005 Wiley-VCH Verlag GmbH & Co. KGaA, Weinheim

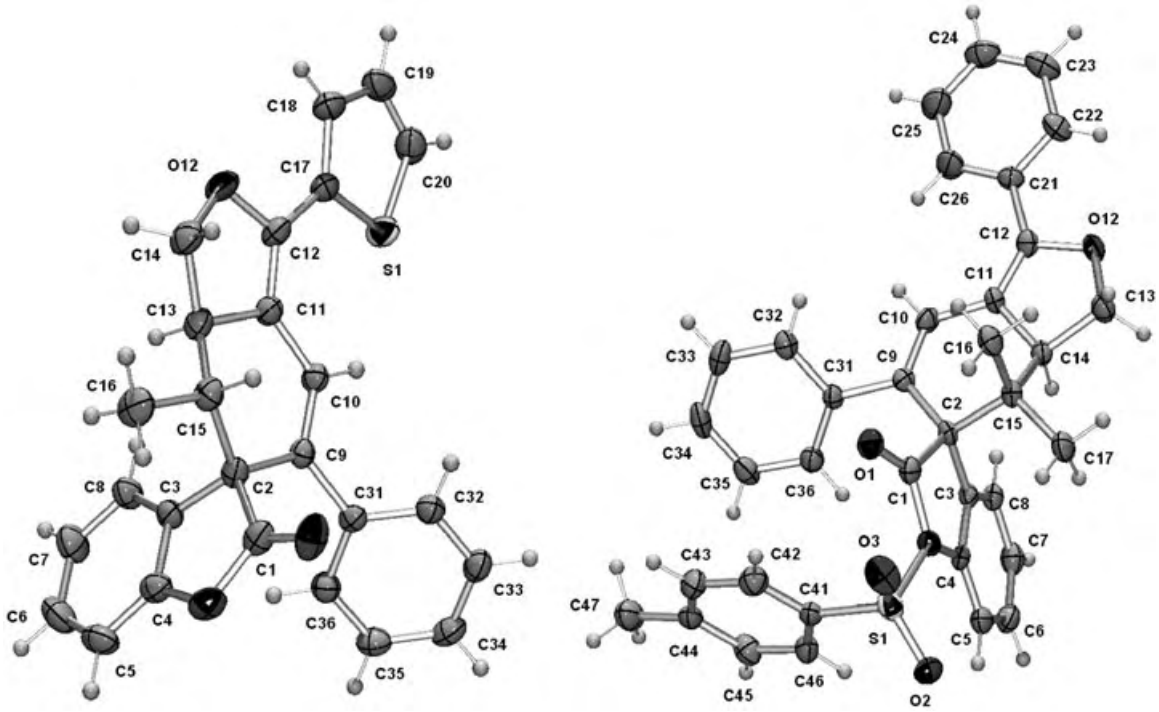
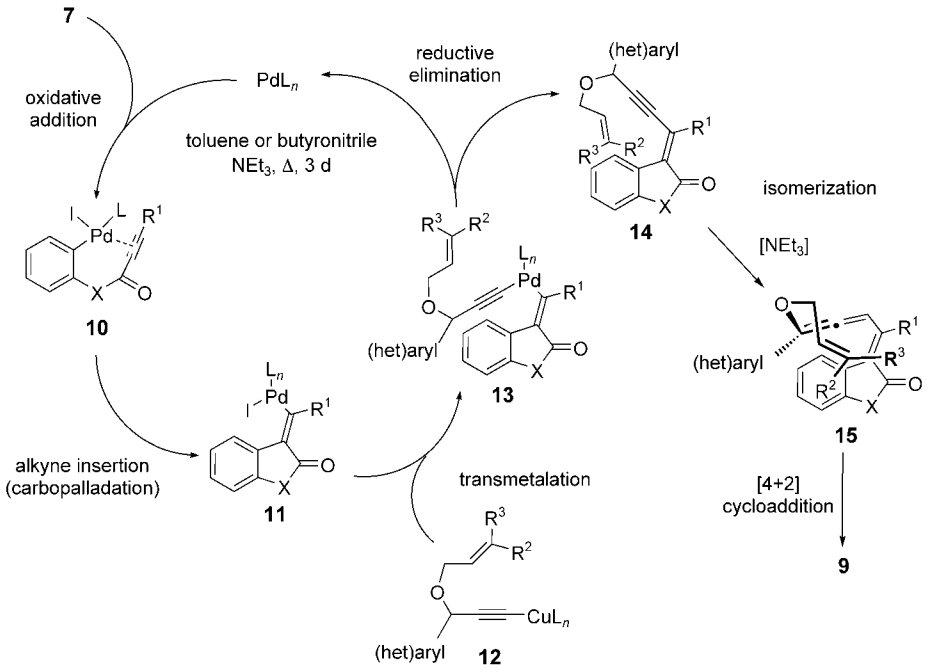


Figure 1. ORTEP plots of spirocycles **9d** (left) and **9h** (right). Selected bond lengths [Å] and angles [°]: **9d**: C31-C9 1.489, C9-C10 1.351, C10-C11 1.435, C11-C12 1.354, C12-C17 1.441, plane (C32-C31-C36)-plane(C2-C9-C10) 50.88, plane(C11-C12-O12)-plane(S1-C17-C18) 9.42. **9h**: C31-C9 1.500, C9-C10 1.336, C10-C11 1.435, C11-C12 1.349, C12-C21 1.465, plane(C36-C31-C32)-plane(C2-C9-C10) 49.00, plane(C12-C12-O12)-plane(C22-C21-C26) 5.73.



Scheme 1. Mechanism of the domino sequence yielding spirobenzofurans and spirodihydroindolones **9**.

all but undergoes conformational twisting and an efficient internal conversion to return to the ground state.[12] This peculiar behavior of the spirocyclic 1-phenyl-4-(hetero)aryl-butadienes **9** can be attributed unequivocally to a structurally fixed ground-state conformation.

In conclusion, we have developed a new domino reaction consisting of insertion, CI, and Diels–Alder reactions that furnishes spirocyclic benzofuranones and dihydroindolones **9** in moderate to excellent yields. Furthermore, this hitherto known class of spirocycles displays an intense blue to green

 © 2005 Wiley-VCH Verlag GmbH & Co. KGaA, Weinheim



Figure 2. Fluorescence of the spirocycles **9f** (left) and **9h** (right) in solution ($T = 298$ K, $c = 10^{-7}$ M in CH_2Cl_2, irradiation at $\lambda_{max} = 360$ nm).

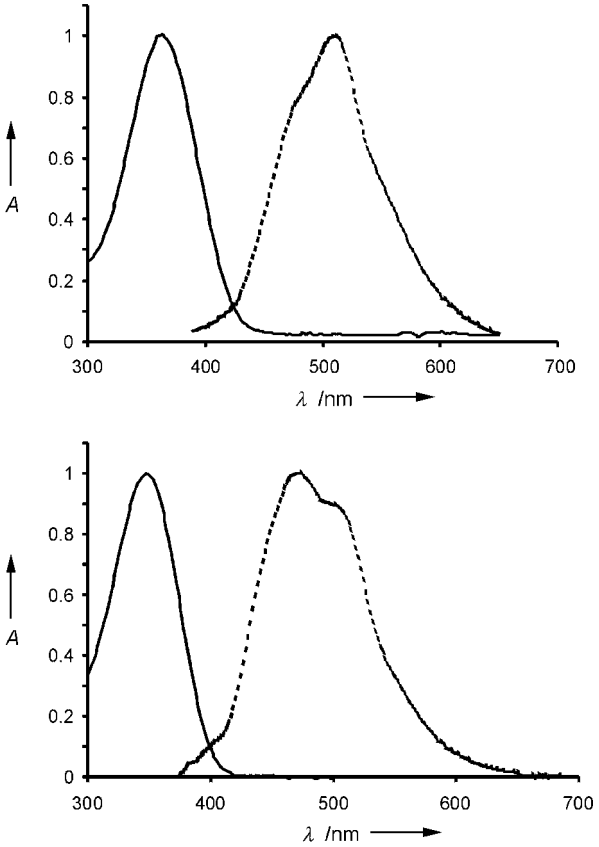


Figure 3. Absorption (solid lines, $c = 10^{-4}$ M) and emission spectra (dotted lines, $c = 10^{-7}$ M) of the spirocycles **9f** (top) and **9h** (bottom) ($T = 298$ K, in CH_2Cl_2, irradiation at $\lambda_{max} = 372$ and 358 nm, respectively).

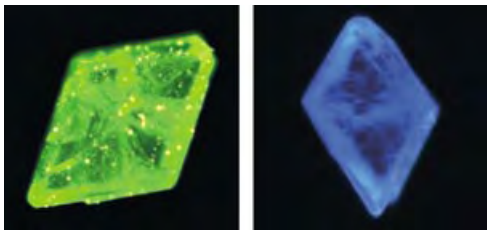


Figure 4. Solid-state fluorescence of single crystals of the spiroindolones **9f** (left) and **9h** (right).

fluorescence. Studies addressing the synthetic scope of the domino reaction and the photophysical and pharmacological properties of these new poly(hetero)cyclic entities are currently underway.

Experimental Section

9h: To a deaerated mixture of 6 mL of butyronitrile and 6 mL of triethylamine in an oven-dried screw-cap vessel were added successively **7b** (752 mg, 1.50 mmol), **8g** (330 mg, 1.65 mmol), $[PdCl_2(PPh_3)_2]$ (53 mg, 0.08 mmol), and CuI (14 mg, 0.07 mmol). This mixture was stirred at room temperature for 2.5 h and then heated at reflux temperature for 48 h. The reaction mixture was allowed to cool to room temperature, the solvents were removed in vacuo, and the residue was chromatographed on silica gel (hexane/ethyl acetate, 2:1) and crystallized from pentane/diethylether to give 740 mg (86%) of **9h** as colorless crystals with blue fluorescence, m.p. 219 °C. ^{1}H NMR (500 MHz, $CDCl_3$, 25 °C, TMS): $\delta = 0.73$ (s, 3H; CH_3), 1.21 (s, 3H; CH_3), 2.44 (s, 3H; CH_3), 3.91 (dd, $J = 10.0$, 12.4 Hz, 1H; CH), 4.23 (dd, $J = 8.7$, 12.4 Hz, 1H; CH), 4.53 (dd, $J = 8.7$, 9.7 Hz, 1H; CH), 6.44 (dd, $J = 1.2$, 8.3 Hz, 2H; CH), 6.68 (dd, $J = 7.5$, 8.2 Hz, 2H; CH), 6.90 (tt, $J = 1.1$, 7.4 Hz, 2H; $CH_{arom.}$), 7.01 (s, 1H; $CH_{olef.}$), 7.19 (m, 2H; $CH_{arom.}$), 7.23 (dd, $J = 1.0$, 7.6 Hz, 1H; $CH_{arom.}$), 7.29 (dd, $J = 1.3$, 7.6 Hz, 1H; $CH_{arom.}$), 7.34–7.45 (m, 4H; $CH_{arom.}$), 7.67 (m, 2H; $CH_{arom.}$), 7.85 (d, $J = 8.4$ Hz, 2H; $CH_{arom.}$), 8.04 ppm (d, $J = 8.2$ Hz, 1H; $CH_{arom.}$); ^{13}C NMR (125 MHz, $CDCl_3$, 25 °C, TMS): $\delta = 16.8$ (CH_3), 21.6 (CH_3), 21.9 (CH_3), 39.9 ($C_{quat.}$), 47.7 (CH), 62.3 ($C_{quat.}$), 70.2 (CH_2), 109.5 ($C_{quat.}$), 112.8 (CH), 122.8 (CH), 124.4 (CH), 126.1 (CH), 126.2 (CH), 127.2 (CH), 127.9 (CH), 128.0 (CH), 128.5 (CH), 129.0 (CH), 129.1 (CH), 129.5 (CH), 129.6 (CH), 130.7 ($C_{quat.}$), 131.6 ($C_{quat.}$), 134.1 ($C_{quat.}$), 134.9 ($C_{quat.}$), 139.0 ($C_{quat.}$), 141.1 ($C_{quat.}$), 145.1 ($C_{quat.}$), 152.8 ($C_{quat.}$), 174.9 ppm ($C_{quat.}$); EI MS (70 eV): *m*/*z* (%): 573 (M^+, 100), 418 ($M^+ - SO_2C_6H_4CH_3$, 32), 267 (10), 201 (10); HRMS calcd for $C_{36}H_{31}NO_4S$: 573.1974, found: 573.1957; Elemental analysis calcd for $C_{36}H_{31}NO_4S$ (573.7): C 75.37, H 5.45, N 2.44, S 5.59; found: C 75.04, H 5.33, N 2.65, S 5.63.

Received: July 30, 2004

Keywords: C–C coupling · cycloaddition · domino reactions · fluorescence · spiro compounds

[1] T. J. J. Müller, M. Ansorge, D. Aktah, *Angew. Chem.* **2000**, *112*, 1323–1326; *Angew. Chem. Int. Ed.* **2000**, *39*, 1253–1256.

[2] For lead reviews on Sonogashira couplings, see, for example, a) S. Takahashi, Y. Kuroyama, K. Sonogashira, N. Hagihara, *Synthesis* **1980**, 627–630; b) K. Sonogashira in *Metal-Catalyzed Cross-Coupling Reactions* (Eds.: F. Diederich, P. J. Stang), Wiley-VCH, Weinheim, **1998**, p. 203–229; c) K. Sonogashira, *J. Organomet. Chem.* **2002**, *653*(1–2), 46–49; d) E.-I. Negishi, L. Anastasia, *Chem. Rev.* **2003**, *103*, 1979–2018.

[3] a) T. J. J. Müller, R. Braun, M. Ansorge, *Org. Lett.* **2000**, *2*, 1967–1970; b) R. U. Braun, K. Zeitler, T. J. J. Müller, *Org. Lett.* **2000**, *2*, 4181–4184; c) R. U. Braun, K. Zeitler, T. J. J. Müller, *Org. Lett.* **2001**, *3*, 3297–3300; d) N. A. M. Yehia, K. Polborn, T. J. J. Müller, *Tetrahedron Lett.* **2002**, *43*, 6907–6910; e) O. G. Dediu, N. A. M. Yehia, T. J. J. Müller, *Z. Naturforsch. B* **2004**, *59*, 443–450.

[4] For an excellent review on cyclic carbopalladations, see, for example, E.-I. Negishi, C. Copéret, S. Ma, S.-Y. Liou, F. Liu, *Chem. Rev.* **1996**, *96*, 365–393.

[5] For excellent reviews and classifications of domino reactions, see, for example, a) L. F. Tietze, *J. Heterocycl. Chem.* **1990**, *27*, 47–69; b) L. F. Tietze, U. Beifuss, *Angew. Chem.* **1993**, *105*, 137–

 © 2005 Wiley-VCH Verlag GmbH & Co. KGaA, Weinheim

170; *Angew. Chem. Int. Ed. Engl.* **1993**, *32*, 131 – 163; c) L. F. Tietze, *Chem. Rev.* **1996**, *96*, 115 – 136.
[6] For recent reviews on transition-metal-assisted sequential transformations and domino processes, see, for example, a) G. Kirsch, S. Hesse, A. Comel, *Curr. Org. Synth.* **2004**, *1*, 47 – 63; b) I. Nakamura, Y. Yamamoto, *Chem. Rev.* **2004**, *104*, 2127 – 2198, and references therein; c) G. Balme, E. Bossharth, N. Monteiro, *Eur. J. Org. Chem.* **2003**, 4101 – 4111; d) G. Battistuzzi, S. Cacchi, G. Fabrizi, *Eur. J. Org. Chem.* **2002**, 2671 – 2681.
[7] J. T. Link, L. E. Overman in *Metal-Catalyzed Cross-Coupling Reactions* (Eds.: F. Diederich, P. J. Stang), Wiley-VCH, Weinheim, **1998**, pp. 231 – 269.
[8] For two very recent examples, see, for example, a) M. Pal, K. Parasuraman, V. Subramanian, R. Dakarapu, K. Rao Yeleswarapu, *Tetrahedron Lett.* **2004**, *45*, 2305 – 2309; b) L. R. Pottier, J.-F. Peyrat, M. Alami, J.-D. Brion, *Synlett* **2004**, 1503 – 1508.
[9] Compound **7a** (= **4**) was synthesized from *ortho*-iodophenol and the corresponding 3-phenylpropynoyl chloride. Compounds **7b** (= **1**), **7c**, and **7d** were prepared according to H. Sashida, *Heterocycles* **1998**, *48*, 631 – 634 and S. A. Brunton, K. Jones, *J. Chem. Soc. Perkin Trans. 1* **2000**, 763 – 768. The syntheses of compounds **8** were performed according to K. Brickmann, F. Hambloch, J. Suffert, R. Brückner, *Liebigs Ann.* **1996**, *4*, 457 – 472. The detailed protocols will be described elsewhere.
[10] All new compounds have been fully characterized spectroscopically and have given correct elemental analysis and HRMS.
[11] CCDC-246090 (**9d**) and CCDC-246089 (**9h**) contain the supplementary crystallographic data for this paper. These data can be obtained free of charge via www.ccdc.cam.ac.uk/conts/retrieving.html (or from the Cambridge Crystallographic Data Centre, 12, Union Road, Cambridge CB21EZ, UK; fax: (+44) 1223-336-033; or deposit@ccdc.cam.ac.uk).
[12] W. A. Yee, S. J. Hug, D. S. Kliger, *J. Am. Chem. Soc.* **1988**, *110*, 2164 – 2169.

 © 2005 Wiley-VCH Verlag GmbH & Co. KGaA, Weinheim

Bioorganic Chemistry

Unprecedented Lipoxygenase/Hydroperoxide Lyase Pathways in the Moss *Physcomitrella patens***

*Thomas Wichard, Cornelia Göbel, Ivo Feussner, and Georg Pohnert**

Lipoxygenase (LOX) pathways are involved in the production of important signal and defensive metabolites in mammals, higher plants, and algae.[1–4] In these pathways molecular oxygen is introduced into a polyunsaturated fatty acid to form an intermediate hydroperoxide, which may then be cleaved to give shorter chain-length oxygenated products. Interestingly, different principles of transformations have been identified. While plants use almost exclusively C_{18} fatty acids for the production of oxylipins,[1] algae and animals rely predominantly on the transformation of C_{20} fatty acids.[3,5] In animals cleavage of the intermediate hydroperoxy fatty acids is achieved by a dual function of LOXes, while plants and algae rely often on hydroperoxide lyases (HPLs) to produce shorter chain oxylipins.[1–3] Due to their central importance, LOX/HPL pathways have been well investigated in these organisms, but nearly nothing is known about related transformations in mosses. Since mosses are located phylogenetically between higher plants and algae, the biosynthetic pathways are of special interest.

Certain mosses are known to release unbranched unsaturated C_8 and C_9 alcohols and aldehydes, but until now the pathways to and function of these metabolites have not been addressed.[6,7] We report here that the moss *Physcomitrella patens* releases volatile oxylipins upon tissue damage. These include (*E*)-non-2-enal (**4**) known from higher plants, which has a cucumberlike odor, (*R*)-1-octen-3-ol (**1**) (94% *ee*),[8] a major aroma compound from mushrooms, (*E*)-oct-2-en-1-ol (**2**), and (*E*)-oct-2-enal (**3**; Figure 1). In mushrooms (*R*)-**1** is derived from linoleic acid, which is transformed by a 10-LOX and a lyase activity to give (*E*)-10-oxodec-8-enoic acid as a second fragment.[9–11] In higher plants linoleic acid is also a precursor for the generation of (*E*)-non-2-enal (**4**) and (*Z*)-non-3-enal (**8**). There, a 9-LOX and a 9-HPL produce the C_9 aldehyde **8** and 9-oxononanoic acid.[2,12]

[*] T. Wichard, Dr. G. Pohnert
Max-Planck-Institut für Chemische Ökologie
Hans-Knöll-Strasse 8, 07745 Jena (Germany)
Fax: (+49) 3641-571-256
E-mail: pohnert@ice.mpg.de
Dr. C. Göbel, Prof. Dr. I. Feussner
Georg-August-Universität Göttingen
Albrecht-von-Haller-Institut für Pflanzenwissenschaften
Justus-von-Liebig-Weg 11, 37077 Göttingen (Germany)

[**] We thank Prof. Dr. W. Boland for his support during the preparation of this work. The DFG (G.P.) and the EC (I.F.) are acknowledged for funding.

Supporting information for this article is available on the WWW under http://www.angewandte.org or from the author.

 © 2005 Wiley-VCH Verlag GmbH & Co. KGaA, Weinheim DOI: 10.1002/anie.200460686

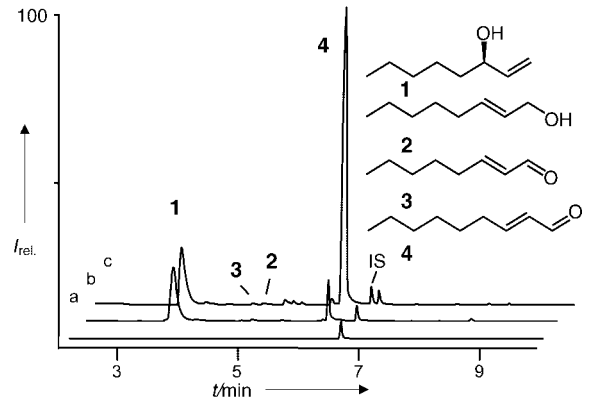


Figure 1. a) GC/MS of the SPM-extract of volatiles from *P. patens*; b) same as a) from the wounded moss; c) same as b) in the presence of 200 μg arachidonic acid (**5**)/~100 mg *P. patens*. IS = internal standard 2-decanone.

In our investigations on the biosynthesis of the volatile oxylipins from *P. patens* we found that external application of linoleic or α-linolenic acid did not result in significantly increased production of **1**–**4** or related higher unsaturated metabolites. Moreover, neither 10-oxodec-8-enoic acid nor 9-oxononanoic acid, metabolites formed from analogous pathways in plants and mushrooms, were detected. These results imply that mosses rely on other precursors for the generation of **1**–**4**. In contrast to higher plants, *P. patens* is also rich in arachidonic acid (**5**),[13] which could, judging from the position of the double bonds, also be a possible precursor for these volatile oxylipins. Indeed, externally applied arachidonic acid (**5**) was transformed with high efficiency into **1**–**4**. This could be shown impressively by administration of [D_8]arachidonic acid to *P. patens* cell preparations, which resulted in deuterated **1** (>400% labeled), **2**, **3**, and **4** (>1100% labeled) (Figure 1). This surprising fact—arachidonic acid (**5**) has not been identified as a precursor for **1**–**4** in any other organisms—prompted us to investigate the pathways in more detail. Trapping experiments with dimethyl sulfide revealed that an arachidonate 12-LOX is involved in the transformations. Using this reagent, intermediate hydroperoxy fatty acids are transformed into the corresponding alcohols, which are not further metabolized by HPL.[3] In intact moss we found no endogenous hydroxylated fatty acids after reduction; however, after only a few seconds after tissue damage, (*S*)-12-hydroxyarachidonic acid ((*S*)-12-HETE, 83% *ee*), (*S*)-15-HETE (56% *ee*), and minor amounts of nearly racemic 11-HETE were detected. The related 11-hydroperoxide, 11-HPETE, could also be a precursor for the C_9 volatiles, but since it is found only in minor amounts as a racemate, it is most likely an autoxidation product of arachidonic acid and not involved in enzymatic pathways. In the presence of **5** the amount of 12-hydroperoxyeicosatetraenoic acid (12-HPETE, **6**) increased drastically within 30 seconds after wounding and decreased over the next 16 minutes—the time required for the formation of **1**–**4** and oxo-acids (see the Supporting Information). Accordingly, (*S*)-12-HPETE, which arises from the LOX-mediated oxidation of arachidonic acid (**5**), is an intermediate in the biosynthesis of **1**–**4**.

To further investigate the mechanism of fatty acid transformation in *P. patens* we identified the fragments generated from **6** in addition to **1**–**4**. The HPLC-MS chromatograms obtained from *P. patens* preparations before and after tissue damage were used to identify two dominant metabolites derived from fatty acids. The UV spectrum ($\lambda_{max} = 279$ nm) of the less polar metabolite is characteristic for an α,β,γ,δ-unsaturated carbonyl compound, and the mass spectrum suggested an oxidized C_{12} carboxylic acid (Figure 2). These

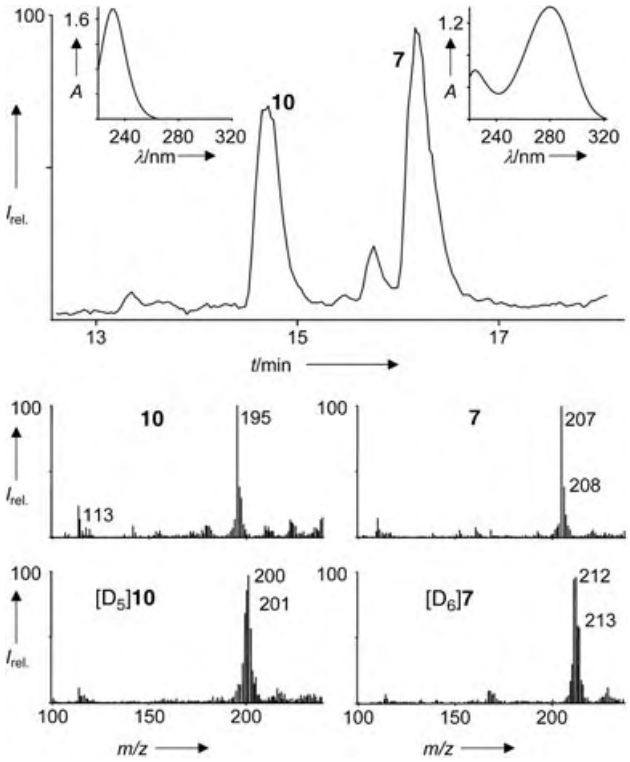
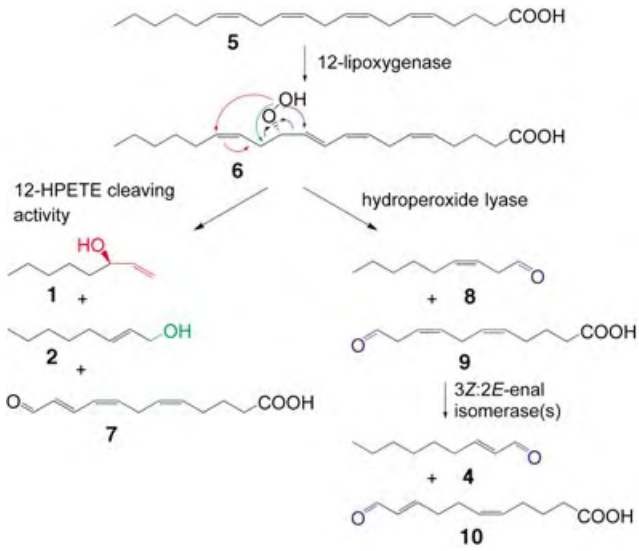


Figure 2. Top: LC/MS of wounded *P. patens* in the presence of 200 μg arachidonic acid (**5**)/~100 mg *P. patens*. The inserts show the UV-spectra of the metabolites **7** and **10**, respectively. Bottom: Negative ionization mass spectra for the unlabeled (above) and labeled (below) oxo-acids after transformation of **5** or [D_8]-**5**.

data matched those of (5*Z*,8*Z*,10*E*)-12-oxododeca-5,8,10-trienoic acid (12-ODTE, **7**) and co-injection with synthetic **7**[14] finally proved the structure. The other metabolites could be identified as 11-oxoundeca-5,9-dienoic acid (11-OUDE, **10**).[15]

These assigned structures are in accordance with biosynthetic considerations on the generation of the oxylipins shown in Scheme 1. The identified structures suggest that **5** is transformed without prior degradation by, for example, β-oxidation, into the hydroperoxide **6**, which then undergoes cleavage to give the oxo-acids and volatiles. This biosynthetic path was further supported by incubations of damaged moss with [D_8]arachidonic acid. Mass spectra of **6**, **7** and **10** showed mass shifts of +8, +6 and +5, respectively, when the labeled acid was present (see Figure 2 and the Supporting

 © 2005 Wiley-VCH Verlag GmbH & Co. KGaA, Weinheim



Scheme 1. Proposed arachidonate 12-LOX/HPL pathways in *P. patens*. After administration of [D_8]-arachidonic acid (**5**) [D_8]-HPETE (**6**) can be trapped as intermediate. [D_2]-C8-fragments and [D_6]-**7** as well as [D_3]-**4** and [D_5]-**10** are formed in the subsequent reactions. All 8 deuterium labels of **5** are thus found in the respective intermediates and break down products.

Information). The corresponding high degree of labeling of **6** and the shorter chain oxylipins indicates that **5** is the precursor of all the oxylipins shown in Scheme 1.

These results show that *P. patens* employs hitherto unknown pathways for the production of known LOX/HPL products. The biosynthesis of **1**, **2**, and **4** is initiated by a 12-LOX, which provides **6** as a substrate for HPL or other fatty acid cleaving enzymes. Further transformation of **6** results in the C_8 metabolites **1** and **2** together with **7** as the second fragment (Scheme 1). Interestingly, **7** has been detected previously in arachidonic acid stimulated human platelets.[16] It acts as an agonist towards human neutrophils, presumably interacting with the leukotriene B4 binding site.[17] Compound **7** is also known as deleterious metabolite from diatoms,[18,19] but there (1*E*,3*E*)-octa-1,3-diene results as the second fragment from a 12HPETE.[14] In *P. patens* **6** can also be transformed into (*Z*)-non-3-enal (**8**) and (5*Z*,8*Z*)-11-oxoundeca-5,8-dienoic acid (**9**), presumably by an HPL. In analogy to well-known transformations in higher plants, these intermediates may be transformed quickly by a 3*Z*:2*E*-enal isomerase to give **4** and **10** (Scheme 1).[12,20]

Our findings show that hitherto unknown LOX pathways are involved in the biosynthesis of a multitude of oxylipins in *P. patens*. The moss produces metabolites typical for animals, plants, algae, and mushrooms by new transformations of arachidonic acid, combining in a unique way metabolic themes from all these organisms. Mosses are known to be highly resistant to herbivores and pathogens, and in higher plants this type of resistance is often mediated by lipoxygenases.[21] We are particularly interested in determining if and how the newly identified biosynthetic pathways contribute to the production of putative signal or defensive metabolites involved in this remarkable resistance.

Experimental Section

General: Cultures of *P. patens* were obtained from Prof. Dr. Ralf Reski, Freiburg, and were cultivated as described.[22] Preparation of samples for MS analysis: A 5-mL aliquot of a dense culture was left to settle, and the medium was removed by pipetting. The resulting pellet with a wet weight of 100–200 mg was resuspended in 1 mL of fresh medium and used directly or treated with 20 μL of 10 mg mL^{-1} solutions of fatty acids in EtOH. The suspension was sonicated and cooled in an ice bath for 2 min. For SPME analysis the vial was sealed with a Teflon septum, and a polydimethyldiloxane-coated fiber (Supelco, Taufkirchen, Germany) was inserted for 15 min in the gas phase. Analysis by GC/MS was performed as described.[14] Commercially available reference compounds were used for the identification of **1**–**4**. For LC/MS analysis, the moss preparation was treated 30 s or 16 min after sonication with the same volume of MeOH. The sample was centrifuged for 5 min (12000 rpm), and the supernatant was used directly for analysis on an Agilent HP1100/Finnigan LCQ.

The intermediate hydroperoxy fatty acids were trapped by addition of a 10% solution of dimethyl sulfide in methanol to preparations previously treated with arachidonic acid (**5**). The *ee* value was determined by a known method.[23] For calculation, means of measurements after 30 s, 2 min, 8 min, 15 min, and 30 min were used.

Received: May 17, 2004
Revised: July 30, 2004

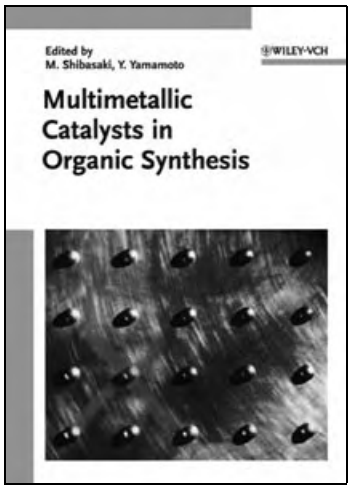
Keywords: biosynthesis · fatty acids · mass spectrometry · oxylipins · UV/Vis spectroscopy

[1] I. Feussner, C. Wasternack, *Annu. Rev. Plant Biol.* **2002**, *53*, 275–297.
[2] M. A. Noordermeer, G. A. Veldink, J. F. Vliegenthart, *ChemBioChem* **2001**, *2*, 494–504.
[3] G. Pohnert, W. Boland, *Nat. Prod. Rep.* **2002**, *19*, 108–122.
[4] A. R. Brash, *J. Biol. Chem.* **1999**, *274*, 23679–23682.
[5] W. H. Gerwick, *Biochim. Biophys. Acta* **1994**, *1211*, 243–255.
[6] M. Toyota, T. Saito, J. Matsunami, Y. Asakawa, *Phytochemistry* **1997**, *44*, 1265–1270.
[7] V. M. Dembitsky, *Prog. Lipid Res.* **1993**, *32*, 281–356.
[8] The optical purity of (3*R*)-**1** was determined by GC in comparison with a commercially available standard after derivatisation with trifluoroacetic acid anhydride/pyridine (GC-column: Macherey-Nagel (Düren, Germany) Hydrodex-β-3P, 25 m, id 0.25 mm).
[9] K. Matsui, S. Sasahara, Y. Akakabe, T. Kajiwara, *Biosci. Biotechnol. Biochem.* **2003**, *67*, 2280–2282.
[10] M. Wurzenberger, W. Grosch, *Biochim. Biophys. Acta* **1984**, *794*, 18–24.
[11] M. Wurzenberger, W. Grosch, *Z. Lebensm.-Unters. Forsch.* **1982**, *175*, 186–190.
[12] M. A. Noordermeer, G. A. Veldink, J. F. G. Vliegenthart, *FEBS Lett.* **1999**, *443*, 201–204.
[13] N. H. Grimsley, J. M. Grimsley, E. Hartmann, *Phytochemistry* **1981**, *20*, 1519–1524.
[14] G. Pohnert, *Angew. Chem.* **2000**, *112*, 4506–4508; *Angew. Chem. Int. Ed.* **2000**, *39*, 4352–4354.
[15] The mass spectrum of **10** is in accordance with an oxidised C-11 fatty acid and the UV-maximum at 230 nm suggests the presence of an α,β-unsaturated aldehyde (Figure 2). This structure was further supported by GC/MS investigation of the derivatized extract of the moss (Supporting Information).
[16] W. C. Glasgow, T. M. Harris, A. R. Brash, *J. Biol. Chem.* **1986**, *261*, 200–204.

 © 2005 Wiley-VCH Verlag GmbH & Co. KGaA, Weinheim

[17] P. H. Naccache, Y. Leblanc, J. Rokach, P. Patrignani, B. F. Delaclos, P. Borgeat, *Biochim. Biophys. Acta* **1991**, *1133*, 102 – 106.
[18] S. Adolph, S. A. Poulet, G. Pohnert, *Tetrahedron* **2003**, *59*, 3003 – 3008.
[19] G. Pohnert, O. Lumineau, A. Cueff, S. Adolph, C. Cordevant, M. Lange, S. Poulet, *Mar. Ecol. Prog. Ser.* **2002**, *245*, 33 – 45.
[20] D. R. Phillips, J. A. Matthew, J. Reynolds, G. R. Fenwick, *Phytochemistry* **1979**, *18*, 401 – 404.
[21] P. Kenrick, P. R. Crane, *Nature* **1997**, *389*, 33 – 39.
[22] T. Girke, U. Schmidt, R. Reski, E. Heinz, *Plant J.* **1998**, *15*, 39 – 48.
[23] A. R. Brash, D. J. Hawkins, *Methods Enzymol.* **1990**, *187*, 187 – 195.

Unique – New - Fascinating



2004. XV, 295 pages, 173 figures, 66 tables. Hardcover.
ISBN 3-527-30828-8
€ 129.- /£ 90.- /US$ 185.-

MASAKATSU SHIBASAKI and YOSHINORI YAMAMOTO, (eds.)

Multimetallic Catalysts in Organic Synthesis

This first book to comprehensively cover this hot topic presents the information hitherto scattered throughout smaller reviews or single book chapters to provide an introduction to this rapidly expanding field.
In ten chapters, the international team of expert authors treats asymmetric syntheses, new transformations, and organometallic reactions using homo- and hetero-bimetallic catalysts. Written for advanced researchers, this very timely publication is of significant benefit to organic and organometallic chemists in both academia and industry.

15711411_kn

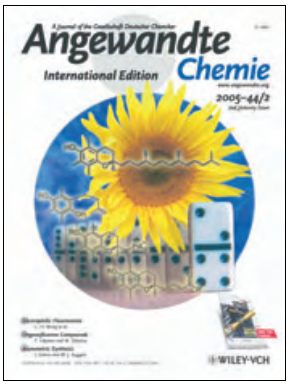
Register now for the free
WILEY-VCH Newsletter!
www.wiley-vch.de/home/pas

WILEY-VCH • P.O. Box 10 11 61 • D-69451 Weinheim, Germany
Fax: +49 (0) 62 01 - 60 61 84
e-mail: service@wiley-vch.de • http://www.wiley-vch.de

WILEY-VCH

 © 2005 Wiley-VCH Verlag GmbH & Co. KGaA, Weinheim

Cover Picture

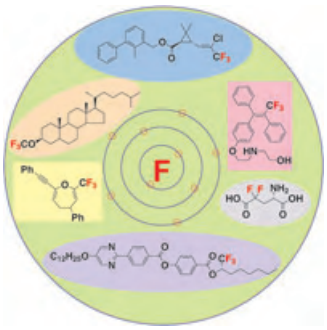


Lutz F. Tietze,* Konrad M. Sommer, Julia Zinngrebe, and Florian Stecker

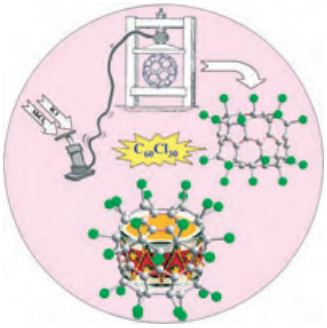
A domino reaction consists of several consecutive transformations in which the functions required for one reaction are generated in the preceding bond-formation or fragmentation step. L. F. Tietze et al. applied this concept to the synthesis of vitamin E described on page 257 ff. They developed an enantioselective palladium-catalyzed process for the construction of the chiral chroman framework with 96% *ee* and concomitant introduction of part of the side chain.



Fluorination
The demand for an electrophilic fluorinating agent that is easy to handle, stable, and highly reactive ultimately led to the development of selectfluor. C.-H. Wong and co-workers discuss the applications and reaction mechanisms of this reagent in their Review on page 192 ff.



Organofluorine Compounds
Fluorine substitution can have a dramatic effect on the properties of organic compounds, including pharmaceuticals and materials. Methods for the synthesis of organofluorine compounds are reviewed by T. Hiyama and M. Shimizu on page 214 ff.



Fullerenes
In their Communication on page 234 ff. P. A. Troshin, S. I. Troyanov et al. describe a highly chlorinated stable fullerene consisting of a cylinder-shaped carbon cage.

Contents

VIP ***The following Communications have been judged by at least two referees to be "very important papers" and will be published online at www.angewandte.org soon:***

D. Enders, C. Grondal:*
Direct Organocatalytic de novo Synthesis of Carbohydrates

T. Fink, H. Bruggesser, J.-L. Reymond:*
Virtual Exploration of the Small-Molecule Chemical Universe Below 160 Daltons

S. Kobayashi, K. Arai, H. Shimizu, Y. Ihori, H. Ishitani, Y. Yamashita:*
A Bimetallic Chiral Niobium Complex for Lewis Acid Catalyzed Enantioselective Reactions: Design of a Tridentate Ligand and Elucidation of the Catalyst Structure

H. Braunschweig, K. Radacki, D. Rais, G. R. Whittell:*
The First Boryl-Bridged Complex: An Unprecedented Coordination Mode of the BR_2 Ligand

C. Whitehouse, J. Fang, A. Aggeli, M. Bell, R. Brydson, C. W. G. Fishwick, J. Henderson, C. M. Knobler, R. W. Owens, N. H. Thomson, D. A. Smith, N. Boden*:*
Adsorption and Self-Assembly of Peptides on Mica Substrates

You Seok Seo, C. Lee, K. H. Lee, K. B. Yoon:*
1:1 and 2:1 Charge-Transfer Interactions between Aromatic Hydrocarbons and Dry Titanium Dioxide

Web Sites

http://invention.swmed.edu/etblast/	eTBlast—It's Only Words, and Words Are All I Have ...	*C. Weise*	**182**

Books

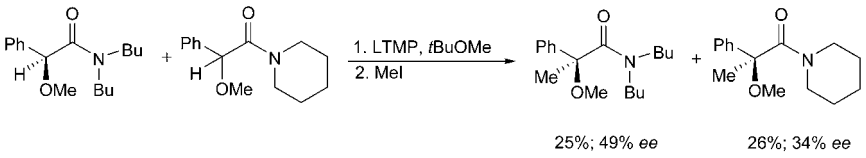
Protecting Groups	Philip J. Kocieński	*reviewed by C. Vogel*	**183**
Principles of Chemical Separations with Environmental Applications	Richard D. Noble, Patricia A. Terry	*reviewed by F. H. Frimmel*	**183**
Nucleic Acids	Shawn Doonan	*reviewed by R. Cosstick*	**184**

Highlights

Asymmetric Synthesis

J. Eames,* M. J. Suggate — **186–189**

Recent Developments in the Transfer of Chirality within Enolate Alkylation Reactions



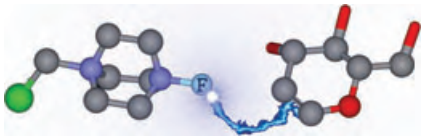
Remarkable asymmetric induction is observed in the alkylation of enolates derived from enantiomerically pure amides, even though these enolates seem to have no apparent chirality (see scheme). The proposed origin and mechanism for this transfer of chirality is discussed. LTMP = lithium tetramethylpiperidide.

Reviews

Fluorination Reagents

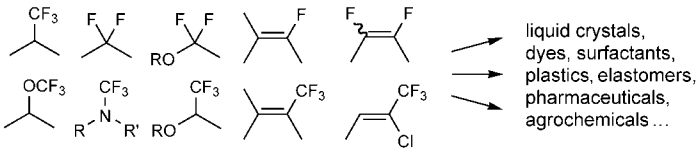
P. T. Nyffeler, S. G. Durón, M. D. Burkart, S. P. Vincent, C.-H. Wong* — **192–212**

Selectfluor: Mechanistic Insight and Applications



A versatile reagent: The search for more efficient and readily available sources of electrophilic fluorine culminated in the development of selectfluor (see scheme), which is both highly reactive and safe to handle. This Review presents the myriad of applications of selectfluor and discusses possible reaction mechanisms. The perspectives for fluorinated compounds in medicine and biology are also investigated.

© 2005 Wiley-VCH Verlag GmbH & Co. KGaA, Weinheim



The incorporation of fluorine into organic molecules is a powerful strategy for the discovery of potent biologically active agents and versatile materials that exhibit unique functions (see scheme). The availability of such fluorinated compounds is critically dependent on synthetic fluorine chemistry. Novel synthetic methods for the preparation of a variety of organofluorine target molecules are described.

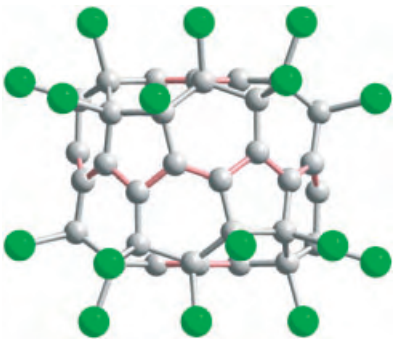
Organofluorine Compounds

M. Shimizu, T. Hiyama* ——— **214 – 231**

Modern Synthetic Methods for Fluorine-Substituted Target Molecules

Communications

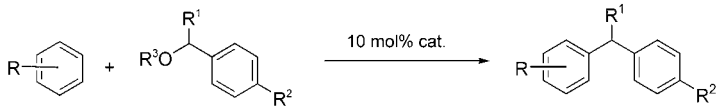
Chlorination of C_{60} with $SbCl_5$, ICl, or ICl_3 at 220–250 °C gives the highly chlorinated fullerene $C_{60}Cl_{30}$. The carbon cage of the $C_{60}Cl_{30}$ molecule has a unique cylindrical shape (see picture), composed of two aromatic six-membered rings located opposite each other and one equatorial aromatic 18π trannulene belt. DFT calculations suggest that $C_{60}Cl_{30}$ is the final product of [60]fullerene chlorination.



Fullerenes

P. A. Troshin,* R. N. Lyubovskaya, I. N. Ioffe, N. B. Shustova, E. Kemnitz, S. I. Troyanov* ——— **234 – 237**

Synthesis and Structure of the Highly Chlorinated [60]Fullerene $C_{60}Cl_{30}$ with a Drum-Shaped Carbon Cage

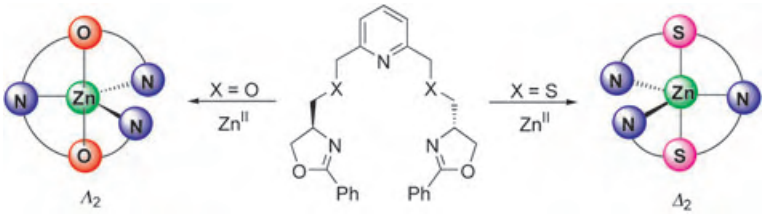


Friedel–Crafts-type benzylation of various aromatic and heteroaromatic compounds with benzylic acetates, alcohols, and carbonates was promoted under mild reaction conditions by a series of Rh, Ir, Pd, and Pt catalysts (see scheme; R^1 = H, Me; R^2 = H, Cl, MeO; R^3 = H, Ac, CO_2Me). The desired products were obtained in high yields and with high selectivities.

Homogeneous Catalysis

K. Mertins, I. Iovel, J. Kischel, A. Zapf, M. Beller* ——— **238 – 242**

Transition-Metal-Catalyzed Benzylation of Arenes and Heteroarenes



Δ_2 or Λ_2, that is the question! Depending on the heteroatom X, the pentadentate bis(oxazoline) ligand will fold around a zinc(II) ion exclusively in the Δ_2 or Λ_2 configuration, both in solution and in the solid state.

Stereogenic Metal Centers

M. Seitz, S. Stempfhuber, M. Zabel, M. Schütz, O. Reiser* ——— **242 – 245**

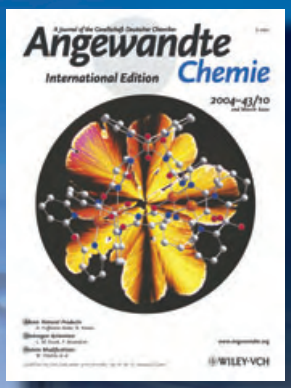
Helical Chirality in Pentacoordinate Zinc Complexes—Selective Access to Both Pseudoenantiomers with One Ligand Configuration

For the USA and Canada:
ANGEWANDTE CHEMIE International Edition (ISSN 1433-7851) is published weekly by Wiley-VCH PO Box 191161, D 69451 Weinheim, Germany. Air freight and mailing in the USA by Publications Expediting Inc. 200 Meacham Ave., Elmont, NY 11003. Periodicals postage paid at Jamaica NY 11431. US POSTMASTER: send address changes to *Angewandte Chemie*, Wiley-VCH, 111 River Street, Hoboken, NJ 07030. Annual subscription price for institutions: US$ 4948.00/4498.00 (valid for print and electronic / print or electronic delivery); for individuals who are personal members of a national chemical society, or whose institution already subscribes, or who are retired or self-employed consultants, print only: US$ 394.00. Postage and handling charges included. All Wiley-VCH prices are exclusive VAT.

 © 2005 Wiley-VCH Verlag GmbH & Co. KGaA, Weinheim

The best in chemistry –

for more than a hundred years



A Journal of the Gesellschaft Deutscher Chemiker

Angewandte International Edition **Chemie**

www.angewandte.org

1888: ***The beginning of a success story***

Constant Innovations

1962: *First issue of the International Edition*
1976: *Graphical abstracts*
1979: *Cover pictures*
1988: *Centenary of Angewandte*
1989: *Routine use of color*
1991: *New section: Highlights*
1992: *Computerized editorial tracking system*
1995: *Internet service for readers*
1998: *Regular press service; full-text online*
2000: *New section: Essays; EarlyView: Communications available online ahead of the printed version*
2001: *New section: Minireviews*
2002: *Online submission of manuscripts*
2003: *Weekly publication; new section: News; new layout*
2004: *Backfiles (1962-1997); ManuscriptXpress: Online system for authors and referees*



Angewandte's advisors...

Colin L. Raston
University of Leeds

»Why would you not want to publish in ***Angewandte Chemie*** *and be part of the 'action'? The cutting edge papers hitting the community on a weekly basis keep you up to date on the major development across the chemical sciences and beyond.«*

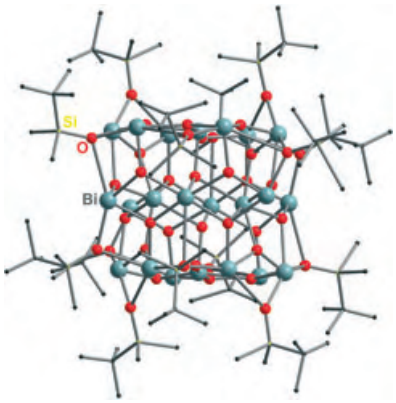
Angewandte Chemie International Edition *is a journal of the German Chemical Society (GDCh)*

GDCh

WILEY InterScience® DISCOVER SOMETHING GREAT

WILEY-VCH

11941104_gu



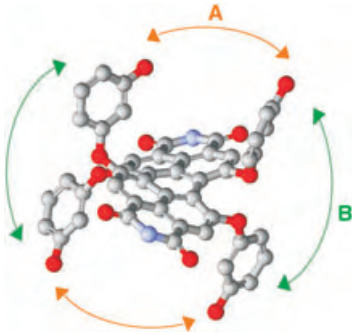
The high-nuclearity bismuth oxo cluster $[Bi_{22}O_{26}(OSiMe_2tBu)_{14}]$ (see structure) was obtained by partial hydrolysis of $Bi(OSiMe_2tBu)_3$. A hydrophobic layer of silanolate groups covers the bismuth oxo core, the structure of which is closely related to that of β-Bi_2O_3. Both the bismuth oxo cluster and the bismuth silanolate precursor decompose to give the sillenite-type compound $Bi_{12}SiO_{20}$.

Cluster Compounds

D. Mansfeld, M. Mehring,* M. Schürmann ——— 245 – 249

From a Monomeric Bismuth Silanolate to a Molecular Bismuth Oxo Cluster: $[Bi_{22}O_{26}(OSiMe_2tBu)_{14}]$

Conformation-dependent tuning of color: Starting from aryloxy-substituted perylene bisimides two isomeric diagonally (A) and laterally (B) bridged macrocycles were synthesized (see picture) for three different bridge lengths. These isomers comprise different conformational features and can, therefore, be used as molecular probes to deduce the conformational influence on the optical properties of this important class of fluorophores in solution.

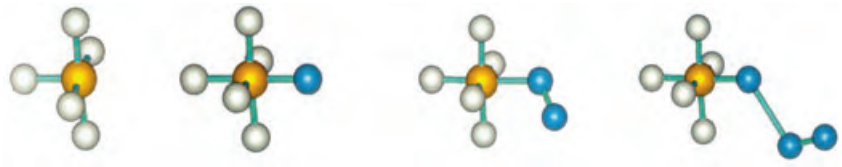


Macrocyclic Perylene Bisimides

P. Osswald, D. Leusser, D. Stalke, F. Würthner* ——— 250 – 253

Perylene Bisimide Based Macrocycles: Effective Probes for the Assessment of Conformational Effects on Optical Properties

---

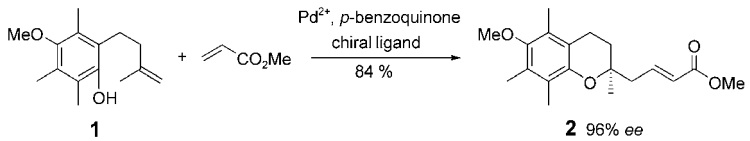


No longer up in the air: The radicals SF_5O_x ($x = 0$–3) were isolated in a matrix and characterized by IR and UV spectroscopy, photolysis experiments, and quantum chemical calculations. They are probably involved in the atmospheric oxidation of SF_6, a gas commonly used in the electric-power industry.

Atmospheric Chemistry

M. Kronberg, S. von Ahsen, H. Willner,* J. S. Francisco* ——— 253 – 257

The SF_5O_x Radicals, $x = 0$–3



A new route to vitamin E: The palladium-catalyzed enantioselective domino reaction of the unsaturated phenol derivative **1** with acrylate provides efficient access to the chiral chroman **2** with 96% *ee* and in 84% yield (see scheme). Intermediate **2** can then be converted into vitamin E in a few steps.

Domino Reactions

L. F. Tietze,* K. M. Sommer, J. Zinngrebe, F. Stecker ——— 257 – 259

Palladium-Catalyzed Enantioselective Domino Reaction for the Efficient Synthesis of Vitamin E

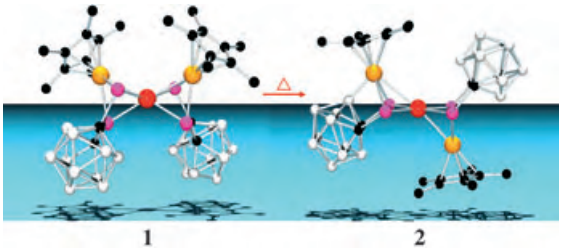
 © 2005 Wiley-VCH Verlag GmbH & Co. KGaA, Weinheim

Contents

Cluster Synthesis

G.-X. Jin,* J.-Q. Wang, C. Zhang, L.-H. Weng, M. Herberhold ___ **259 – 262**

Formation of Ir–Rh and Ir–Mo Bonds by Using an Ancillary *ortho*-Carborane-1,2-diselenolato Ligand

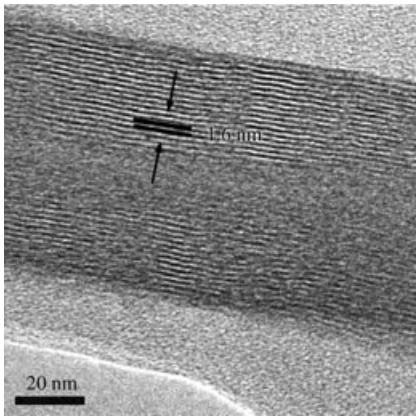


Trinuclear clusters containing heteronuclear Ir–M bonds, for example $[\{Cp^*Ir[Se_2C_2(B_{10}H_{10})]\}_2Rh]$ (**1**), were obtained from the reactions of the 16-electron complex $[Cp^*Ir\{Se_2C_2(B_{10}H_{10})\}]$ and characterized by X-ray crystallography. Compound **1** is thermally converted into **2** by generation of an additional Ir–B bond (see picture: Ir yellow; Rh red; Se magenta; C black; B white). $Cp^* = \eta^5\text{-}C_5Me_5$.

Nanotubes

H. A. Therese, F. Rocker, A. Reiber, J. Li, M. Stepputat, G. Glasser, U. Kolb, W. Tremel* ___ **262 – 265**

VS_2 Nanotubes Containing Organic-Amine Templates from the NT-VO_x Precursors and Reversible Copper Intercalation in NT-VS_2

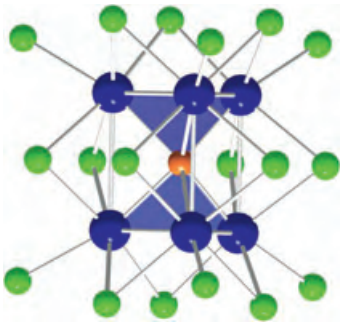


Softly, softly: VS_2 nanotubes (see electron micrograph, layer separation 1.6 nm) are prepared from vanadium oxide nanotubes by a "chimie douce" process. The VS_2 nanotubes are remarkably stable; the corresponding bulk compound is unstable unless it is intercalated with alkali-metal atoms. The nanotubes reversibly intercalate copper with high capacity and thus could serve as precursors for conductors or contacts in electronic circuitry.

Cluster Compounds

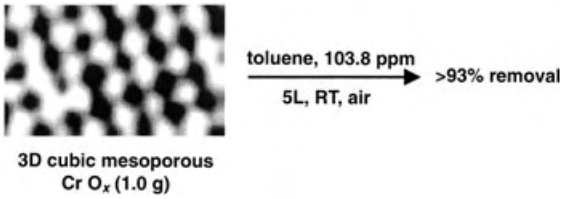
R. Burgert, K. Koch, H. Schnöckel,* M. Weisser, H.-J. Meyer,* H. G. von Schnering ___ **265 – 269**

Mass Spectrometric Investigations of the Dissociation of $[C@W_6Cl_{17}]^-$ Ions in the Gas Phase



A clean break: A carbon-centered tungsten cluster $[C@W_6Cl_{18}]^{2-}$ (see picture: C orange, Cl green, W blue) was examined by mass spectrometry and its decomposition studied by collisionally activated dissociation experiments. A retrosynthesis-type dissociation sequence which gives indications about the mechanism of formation is observed. The bonding of the carbon atoms in the center of the tungsten framework shows parallels to the bonding in tungsten carbide.

© 2005 Wiley-VCH Verlag GmbH & Co. KGaA, Weinheim



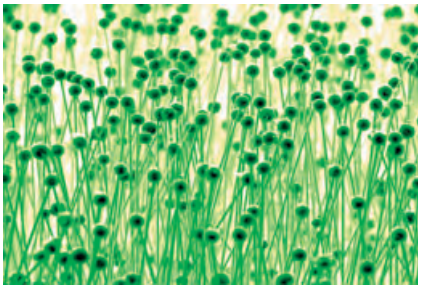
An exceptionally high capacity for the elimination of volatile organic compounds (VOCs) is displayed by a three-dimensional mesoporous chromium oxide (see picture). Under ambient conditions the material acts as a selective sorbent for VOCs (e.g., toluene), whereas at higher temperatures it is an effective and selective deep oxidation catalyst for these compounds.

Mesoporous Materials

A. K. Sinha,* K. Suzuki ——— **271 – 273**

Three-Dimensional Mesoporous Chromium Oxide: A Highly Efficient Material for the Elimination of Volatile Organic Compounds

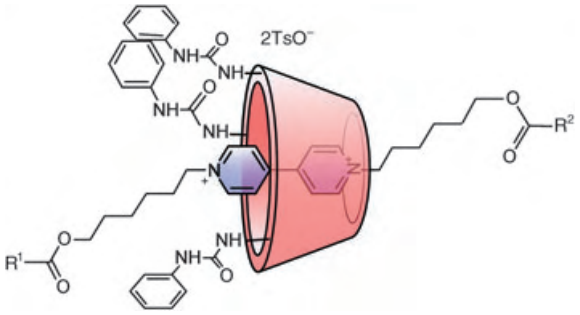
Green fields of nanowires: Germanium, a Group IV semiconductor, can act as an efficient catalyst for high-rate (up to 400 $\mu m\,h^{-1}$) growth of very long (up to 200 μm), extremely straight, and quasi-aligned arrays of single-crystalline ZnO nanowires (see picture). The diameter of the Ge particles (0.5–4 μm) is about 5–15 times that of the associated nanowires (50–400 nm). The patterned growth of ZnO nanorods was achieved on photolithographically prepared Ge-dot patterns.



Nanostructures

Z. W. Pan, S. Dai, C. M. Rouleau, D. H. Lowndes* ——— **274 – 278**

Germanium-Catalyzed Growth of Zinc Oxide Nanowires: A Semiconductor Catalyst for Nanowire Synthesis



Only in apolar media is the calix[6]arene wheel threaded from its upper rim by asymmetric bipyridinium axles. This leads to the formation of oriented pseudorotaxanes. Their stoppering with a different stopper yields rotaxanes characterized by the unequivocal orientation of the wheel rims with respect to the two different stoppers (see picture, $R^1 = CHPh_2/CHCy_2$, $R^2 = CHCy_2/CHPh_2$, Cy = cyclohexyl, Ts = toluene-4-sulfonyl).

Rotaxane Synthesis

A. Arduini,* F. Ciesa, M. Fragassi, A. Pochini, A. Secchi ——— **278 – 281**

Selective Synthesis of Two Constitutionally Isomeric Oriented Calix[6]arene-Based Rotaxanes

 © 2005 Wiley-VCH Verlag GmbH & Co. KGaA, Weinheim

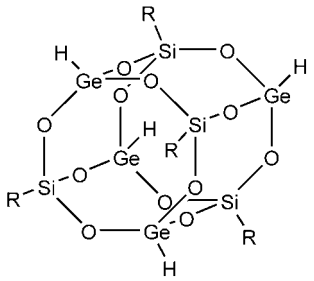
Contents

Cluster Compounds

U. N. Nehete, V. Chandrasekhar, H. W. Roesky,* J. Magull ——— **281 – 284**

The Formal Conversion of SiOH Protons into Hydrides by Germanium(II) Species Leads to the Formation of the Germanium(IV) Hydride Cluster $[(RSiO_3GeH)_4]$

Germanium cubed: Addition of $[Ge\{N(SiMe_3)_2\}_2]$ to a suspension of $RSi(OH)_3$ ($R = (2,6\text{-}iPr_2C_6H_3)N(SiMe_3)$) in hexane/THF affords the germanium siloxane **1** with terminal Ge–H units in good yield. Compound **1** contains a $Ge_4O_{12}Si_4$ cubic polyhedron core in which the corners of the cube are alternately occupied by germanium and silicon atoms. Each of the twelve edges of the cube contains one bridging oxygen atom.

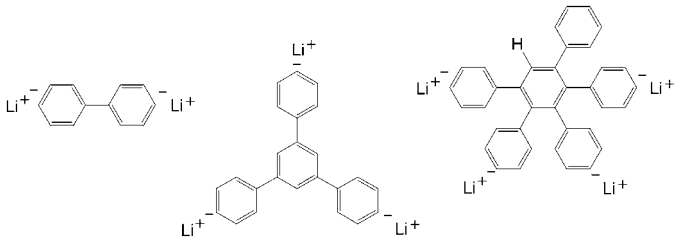


1

Living Polymerization

R. Matmour, A. Lebreton, C. Tsitsilianis, I. Kallitsis, V. Héroguez, Y. Gnanou* ——— **284 – 287**

Tri- and Tetracarbanionic Initiators by a Lithium/Halide Exchange Reaction: Application to Star-Polymer Synthesis

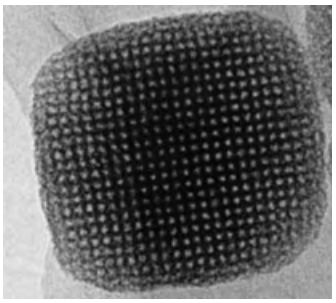


A family of polycarbanionic initiators: Bis-, tris-, and tetrakisaryl lithium compounds (see scheme) were synthesized from the corresponding aryl halides by simple halogen/lithium exchange reactions. These polylithiated species were used to prepare telechelic and three- and four-armed star polystyrene and polybutadiene homopolymers, as well as poly(styrene-*block*-butadiene-*block*-methyl methacrylate) star block terpolymers.

Mesoporous Silica Nanoparticles

Y. Han, J. Y. Ying* ——— **288 – 292**

Generalized Fluorocarbon-Surfactant-Mediated Synthesis of Nanoparticles with Various Mesoporous Structures

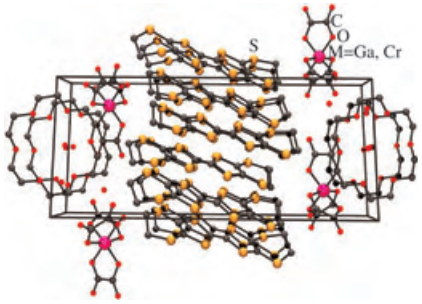


Tunable mesostructures and ultrafine particle sizes were achieved by means of triblock-copolymer and fluorocarbon surfactants, respectively, in the hydrothermal synthesis of mesoporous silica nanoparticles. The TEM image shows one such nanoparticle with a diameter of approximately 300 nm.

Conducting Materials

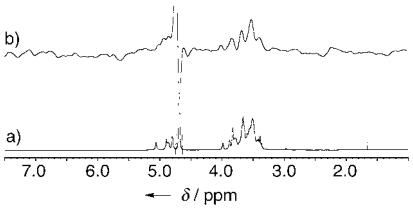
A. Akutsu-Sato, H. Akutsu, S. S. Turner, P. Day,* M. R. Probert, J. A. K. Howard, T. Akutagawa, S. Takeda, T. Nakamura, T. Mori ——— **292 – 295**

The First Proton-Conducting Metallic Ion-Radical Salts



Any old ion? Two bis(ethylenedithio)-tetrathiafulvalene (BEDT-TTF) radical salts with ion channels of stacked [18]crown-6 and Cat/H_2O molecules ($Cat = H_3O^+$ or NH_4^+) are described. The structures contain alternating BEDT-TTF layers, $[(Cat)M(C_2O_4)_3]^{2-}$ ($M = Ga, Cr$) layers, and the [18]crown-6 ion channels (see picture). The salts are metallic electrical conductors, and they show high protonic conductivity.

© 2005 Wiley-VCH Verlag GmbH & Co. KGaA, Weinheim



SIGN of the times: Receptor–ligand interactions in which integral membrane proteins are involved can be detected directly by 1D saturation transfer difference (STD) NMR experiments on living cells (see ^{1}H NMR (a) and STD (b) spectra of mannan with K562-CD209 cells). The technique can be used for molecular recognition in drug-screening processes and is demonstrated for the DC-SIGN receptor.

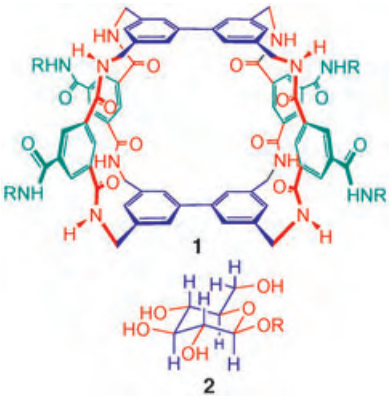
Molecular Recognition

S. Mari, D. Serrano-Gómez, F. J. Cañada, A. L. Corbí,* J. Jiménez-Barbero* ——— **296 – 298**

1D Saturation Transfer Difference NMR Experiments on Living Cells: The DC-SIGN/Oligomannose Interaction

---

A sweet center: Most carbohydrates are supremely comfortable in water. Can they be tempted to leave? Yes, if their new home satisfies all their needs. The water-soluble receptor **1** (R = polycarboxylate) provides hydrophobic surfaces (purple) for CH groups and amide groups (red) for polar substituents. Equatorial substitution is especially well accommodated, and the system duly favors β-glucosyl (**2**).

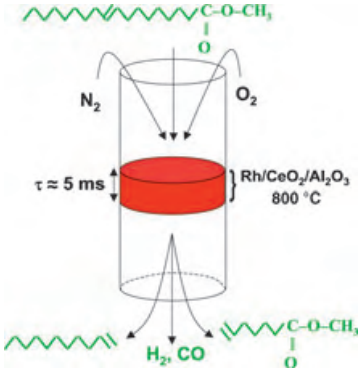


Molecular Recognition

E. Klein, M. P. Crump, A. P. Davis* ——— **298 – 302**

Carbohydrate Recognition in Water by a Tricyclic Polyamide Receptor

---



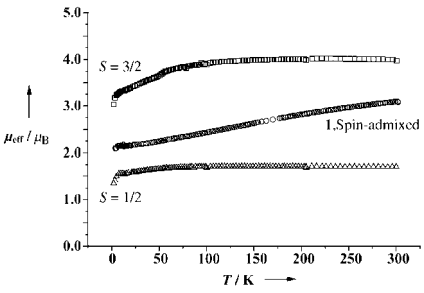
Not just a fuel: Renewable olefins, olefinic esters, and hydrogen are synthesized by the partial oxidation of biodiesel (methyl esters derived from vegetable oils) with air on a Rh–Ce catalyst in an autothermal reactor (see scheme). The availability and prices of vegetable oils suggest that this process could replace much of chemical production from fossil fuels.

Green Heterogeneous Catalysis

R. Subramanian, L. D. Schmidt* ——— **302 – 305**

Renewable Olefins from Biodiesel by Autothermal Reforming

The unusual magnetic behavior of $[Ru_2(\mu\text{-}O_2CMe)(\mu\text{-}DPhF)_3(H_2O)]BF_4 \cdot 0.5\,CH_2Cl_2$ (**1**; DPhF = *N*,*N*′-diphenylformamidinate), which is intermediate between that of compounds with spin states $S = 1/2$ and $S = 3/2$, is attributed to a quantum mechanical spin admixture. This phenomenon results from a multiple bond between the metal atoms which permits an appropriate disposition of molecular orbitals.



Diruthenium Complex

M. C. Barral, S. Herrero, R. Jiménez-Aparicio,* M. R. Torres, F. A. Urbanos ——— **305 – 307**

A Spin-Admixed Ruthenium Complex

 © 2005 Wiley-VCH Verlag GmbH & Co. KGaA, Weinheim

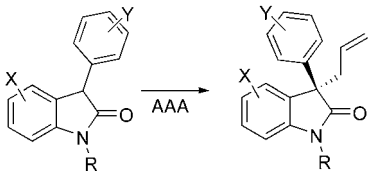
Contents

Allylations

B. M. Trost,*
M. U. Frederiksen _____ **308 – 310**

Palladium-Catalyzed Asymmetric Allylation of Prochiral Nucleophiles: Synthesis of 3-Allyl-3-Aryl Oxindoles

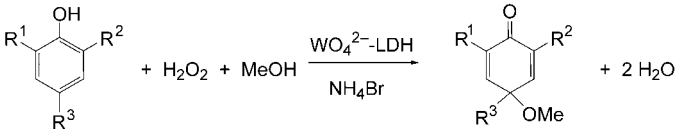
Excellent yields and enantioselectivities are attained in the synthesis of 3-alkyl-3-aryl oxindoles based on the Pd-catalyzed asymmetric allylic alkylation (AAA) reaction. This approach utilizes a nonbasic hydroxylic additive in the transformation of 3-aryl oxindoles into complex, synthetically valuable oxindoles (see scheme).



Synthetic Methods

B. F. Sels, D. E. De Vos,
P. A. Jacobs* _____ **310 – 313**

Bromide-Assisted Oxidation of Substituted Phenols with Hydrogen Peroxide to the Corresponding *p*-Quinol and *p*-Quinol Ethers over WO_4^{2-}-Exchanged Layered Double Hydroxides



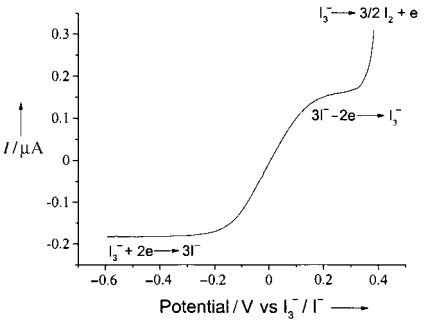
A simple and efficient one-pot synthesis of *p*-quinols and their ethers occurs over tungstate-exchanged layered double hydroxides (WO_4^{2-}-LDHs), which catalyze the bromide-assisted oxidation of substituted phenols to the corresponding 4-alkoxy- and 4-hydroxycyclohexa-2,5-dienones in high yields (see scheme).

Solid Electrolytes

Q. Dai,* D. R. MacFarlane, P. C. Howlett, M. Forsyth _____ **313 – 316**

Rapid I^-/I_3^- Diffusion in a Molecular-Plastic-Crystal Electrolyte for Potential Application in Solid-State Photoelectrochemical Cells

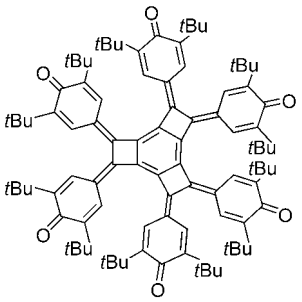
High current-carrying capacity and rapid, liquidlike diffusion were achieved in a dye-sensitized solar cell (DSSC) based on the plastic-crystalline electrolyte succinonitrile and the I^-/I_3^- redox couple (see diagram). This could lead to the development of true solid-state DSSCs without conventional organic-liquid electrolytes, which can cause problems with long-term device stability.



Conjugated Systems

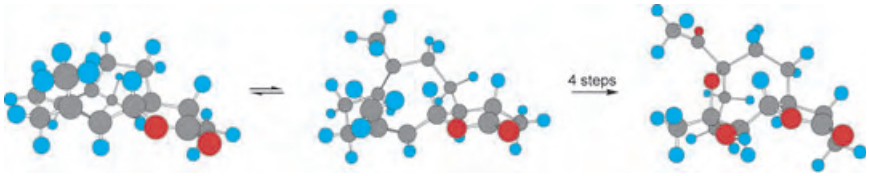
T. Kawase,* Y. Minami, N. Nishigaki, S. Okano, H. Kurata, M. Oda* **316 – 319**

A Hexapentaene-Extended Quinocumulene Cyclotrimerized to a Tricyclobutabenzene Derivative



Rings around rings: Cyclotrimerization of a hexapentaene-extended quinocumulene led to the novel tricyclobutabenzene derivative shown. Its molecular structure reveals a considerably distorted propeller configuration that deviates largely from the ideal C_3 symmetry. Moderate bond alternation is evident in the central benzene ring.

© 2005 Wiley-VCH Verlag GmbH & Co. KGaA, Weinheim



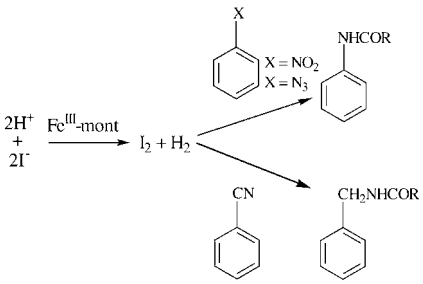
From conformational flexibility to rigidity: The straightforward synthesis of rigid molecules with a transannular oxygen bridge starting from flexible germacrolides, which are easily obtained from renewable sources, is described (see scheme). Transannular cyclization of medium-sized rings enhances molecular rigidity and structural complexity, two properties often associated with biological activity in small molecules.

Tandem Reactions

A. Rosales, R. E. Estévez, J. M. Cuerva, J. E. Oltra* ——— 319 – 322

Enantiospecific Strategy Towards Oxygen-Bridged Terpenoids: Tandem Transannular-Cyclization and Ring-Contraction Processes

---



The production of hydrogen by the relay of electrons from I^- to H^+ in an acidic, aqueous medium and the consumption of hydrogen by reductive N acylation open up enormous opportunities in hydrogen chemistry (see scheme).

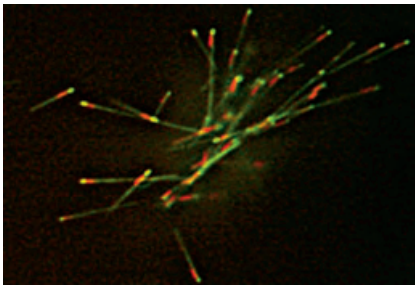
Geochemistry

B. M. Choudary,* M. L. Kantam, K. V. S. Ranganath, K. K. Rao ——— 322 – 325

Hydrogen Processing by Fe^{III}-Exchanged Montmorillonite: A Unique Geochemical Protocol

---

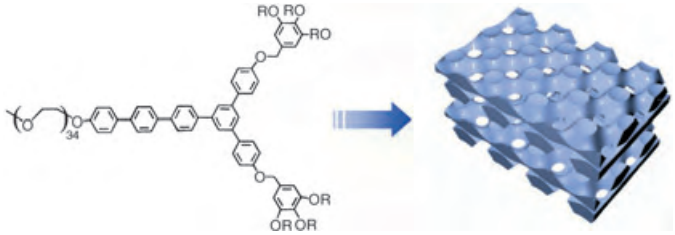
Bioinspiration: Polar assembly (a feature of many natural protein-based fibrous structures, such as actin, microtubules, intermediate filaments, and collagens) is demonstrated in a straightforward, synthetic, peptide-based fiber system of de novo design (see false-color confocal-microscope image of fibers). This finding opens up possibilities for engineering self-assembling soft materials from the bottom up and with nano-to-microscale precision.



Protein Self-Assembly

A. M. Smith, S. F. A. Acquah, N. Bone, H. W. Kroto, M. G. Ryadnov, M. S. P. Stevens, D. R. M. Walton, D. N. Woolfson* ——— 325 – 328

Polar Assembly in a Designed Protein Fiber



Shape sorting: The incorporation of a flexible coil of variable length into a rigid wedge-shaped building block leads to the spontaneous formation of a rich variety of supramolecular structures. These include a bilayer lamellar structure with in-plane hexagonally ordered perforations (see picture, $R = (CH_2)_{13}CH_3$).

Supramolecular Chemistry

J.-K. Kim, M.-K. Hong, J.-H. Ahn, M. Lee* ——— 328 – 332

Liquid-Crystalline Assembly from Rigid Wedge–Flexible Coil Diblock Molecules

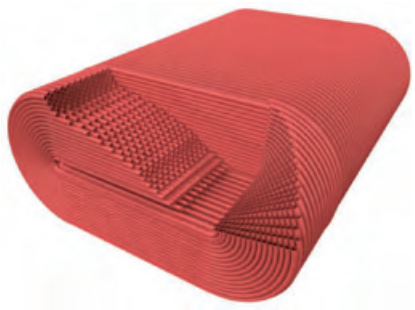
 © 2005 Wiley-VCH Verlag GmbH & Co. KGaA, Weinheim

Contents

Mesoporous Materials

J. Wang, C.-K. Tsung, R. C. Hayward, Y. Wu, G. D. Stucky* ——— **332 – 336**

Single-Crystal Mesoporous Silica Ribbons



Take a length of ribbon: Mesoporous silica ribbons that are typically 50–250 nm thick, 0.4–1.5 μm wide, and hundreds of micrometers long were prepared by a one-phase approach with cationic surfactants as templates under acidic conditions, and their cross-sections were studied by SEM and TEM techniques (see picture).

Deadline for recruitment adverts

6/2004	January 13	Publication date: January 28
7/2005	January 20	Publication date: February 4

Angewandte Chemie International Edition
Advertising Sales Department:
Marion Schulz
Phone: 0 62 01 – 60 65 65
Fax: 0 62 01 – 60 65 50
E-Mail: MSchulz@wiley-vch.de

Place an advert in the printed version
and have it made available online for 1 month, free of charge!

Service

Keywords ——— *338*

Authors ——— *339*

Vacancies ——— *191*

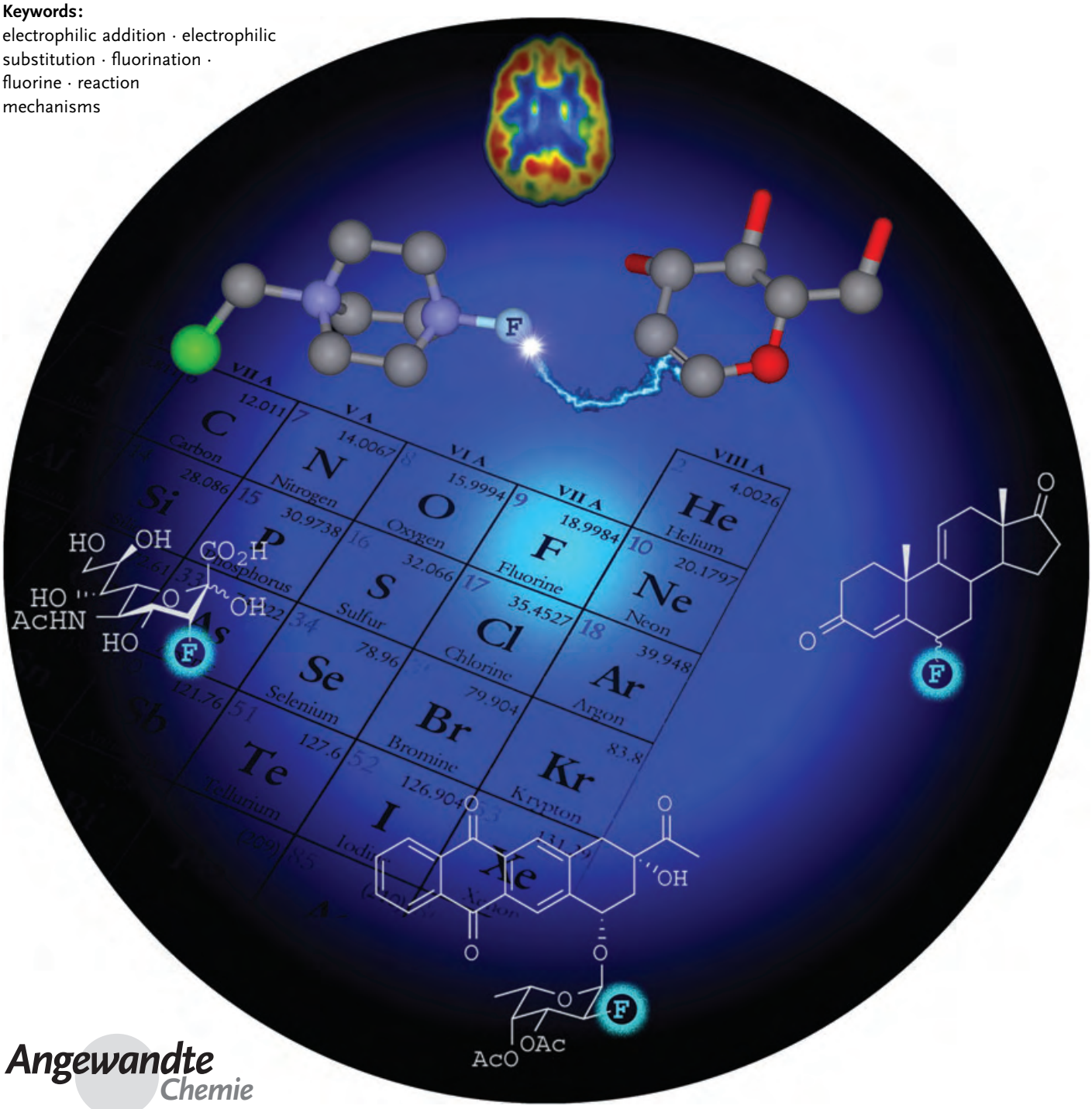
Preview ——— *341*

Fluorination Reagents

Selectfluor: Mechanistic Insight and Applications

*Paul T. Nyffeler, Sergio Gonzalez Durón, Michael D. Burkart, Stéphane P. Vincent, and Chi-Huey Wong**

Keywords:
electrophilic addition · electrophilic substitution · fluorination · fluorine · reaction mechanisms



© 2005 Wiley-VCH Verlag GmbH & Co. KGaA, Weinheim
DOI: 10.1002/anie.200400648

The replacement of hydrogen atoms with fluorine substituents in organic substrates is of great interest in synthetic chemistry because of the strong electronegativity of fluorine and relatively small steric footprint of fluorine atoms. Many sources of nucleophilic fluorine are available for the derivatization of organic molecules under acidic, basic, and neutral conditions. However, electrophilic fluorination has historically required molecular fluorine, whose notorious toxicity and explosive tendencies limit its application in research. The necessity for an electrophilic fluorination reagent that is safe, stable, highly reactive, and amenable to industrial production as an alternative to very hazardous molecular fluorine was the inspiration for the discovery of selectfluor. This reagent is not only one of the most reactive electrophilic fluorinating reagents available, but it is also safe, nontoxic, and easy to handle. In this Review we document the many applications of selectfluor and discuss possible mechanistic pathways for its reaction.

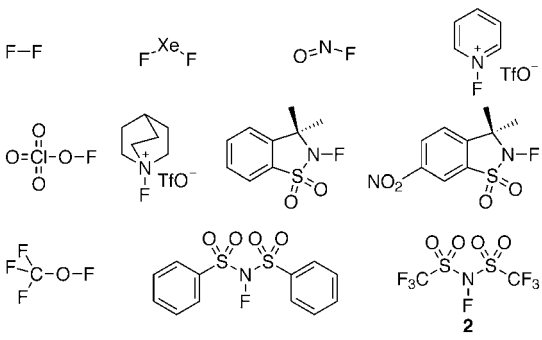
From the Contents

1. Introduction 193
2. Selectfluor: Properties and Preparation 194
3. Electrophilic Fluorination with Selectfluor 196
4. Other Transformations with Selectfluor 201
5. Enantioselective Transformations 203
6. Mechanism of Fluorination with Selectfluor: Electron Transfer or S_N2 Reaction? 204
7. Selected Applications of Fluorinated Compounds 208
8. Conclusion 211

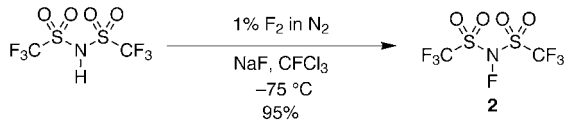
1. Introduction

The introduction of fluorine substituents into organic molecules has a long history of development. In particular, the development of (diethylamino)sulfur trifluoride (DAST)[1] set the standard by which all nucleophilic fluorinating reagents are compared. Though many sources of nucleophilic fluorine existed, fewer sources of electrophilic fluorine were available. Initially, molecular fluorine was the sole source for electrophilic fluorinations, but because of the ease of $F^{\cdot}$ formation and the extremely dangerous properties of F_2 (highly toxic, strong oxidant with little or no specificity, potential runaway free-radical reactions), the development of alternate sources of electrophilic fluorine was essential. The first electrophilic fluorine reagent, fluoroxytrifluoromethane (CF_3OF), was reported by Barton et al.[2] The introduction of other reagents followed, including perchloryl fluoride ($FClO_3$),[3,4] xenon difluoride (XeF_2),[5] nitrogen oxide fluorides,[6] and several other hypofluorides[7,8] (Scheme 1). Although these reagents served as a safer alternative to fluorine gas and found widespread application in research and industry, the need for a stable and nontoxic form of electrophilic fluorine still remained.

Recently, a new class of electrophilic fluorinating reagents with the general structure $R_2N{-}F$ or $R_3N^+{-}F$ began to gain popularity. In comparison to the previous reagents, these compounds were milder, safer, more stable, and less expensive to produce. Furthermore, some of these compounds proved to be as reactive as established reagents in some cases, while also capable of a degree of selectivity that was previously unattainable. Efforts by Umemoto et al. led to the first isolatable *N*-fluoropyridinium salts, which had good activity and were amenable to commercial production.[9] The important role of the counteranion, which influences the reactivity, selectivity, and stability of the reagent, was also demonstrated.[10] DesMarteau and co-workers later reported the discovery of *N*-fluorobis[(trifluoromethyl)sulfonyl]imide (**2**), accessed by the reaction of bis[(trifluoromethyl)sulfonyl]-imide with fluorine gas (Scheme 2).[11,12] The synthesis of this compound, which is still one of the most powerful sources of



Scheme 1. Electrophilic fluorinating reagents.

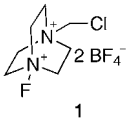


Scheme 2. Synthesis of **2** by DesMarteau and co-workers.[11,12]

[*] P. T. Nyffeler, Dr. S. G. Durón, Dr. M. D. Burkart, Dr. S. P. Vincent, Prof. C.-H. Wong
Department of Chemistry and
The Skaggs Institute for Chemical Biology
The Scripps Research Institute
10550 North Torrey Pines Road, BCC 357
La Jolla, California 92037 (USA)
Fax: (+1) 858-784-2409
E-mail: wong@scripps.edu

 DOI: 10.1002/anie.200400648 © 2005 Wiley-VCH Verlag GmbH & Co. KGaA, Weinheim

electrophilic fluorine, was a step forward in the identification of a stable source of electrophilic fluorine with desirable physical properties. One major drawback of **2** is that it is not commercially available, so that the use of fluorine gas for its preparation in the laboratory is ultimately required. More recently, the development of the reagent selectfluor (**1**, Figure 1) presented a major advance for electrophilic fluorination, as it is a reliable, mild, stable, and effective source of electrophilic fluorine that lends itself to large-scale synthesis and is commercially available. A number of reagents, each with its advantages and disadvantages, currently exist for the electrophilic incorporation of fluorine and have been the subject of several reviews.[13–16] This Review focuses on the versatility of the selectfluor reagent and its applications, and includes some mechanistic insight into plausible reaction pathways.



1

Figure 1. Selectfluor, 1-chloromethyl-4-fluorodiazoniabicyclo[2.2.2]octane bis(tetrafluoroborate).

2. Selectfluor: Properties and Preparation

Selectfluor,[15,17] an exceptionally stable, virtually nonhydroscopic crystalline solid, represents a significant improvement on traditional electrophilic fluorinating agents, which require special handling and tend to be synonymous with danger. In an extreme experiment to demonstrate its stability (and to satisfy the United States Department of Transportation regarding the risks associated with transporting a potentially dangerous compound), a self-accelerating decomposition temperature (SADT) test was performed, in which a 55-gallon drum filled with selectfluor was heated to 56 °C for 7 days; during this time the temperature remained constant within ±5 °C.[18] Selectfluor has been found to be stable at temperatures up to 195 °C, although the inventors warn that bulk samples should only be heated above 80 °C with caution.[15] Therefore, a significant advantage of the selectfluor reagent remains its remarkable stability, as a result of which it has become a commercially available, hazard-free source of fluorine.

Compared to F_2, which is extremely toxic, selectfluor is relatively harmless. Toxicology studies revealed an oral LD_{50} (dose needed to kill 50% of the subjects) of 640 mg kg^{-1} for male adult rats; skin exposure up to 2.0 g kg^{-1} led to no lethality in rats.[15,18] Only mild eye and skin irritation was observed in studies with rabbits and guinea pigs. Selectfluor also failed to demonstrate any signs of mutagenic or carcinogenic activity. Studies showed that the ecological and environmental effects of selectfluor were also minor: Its impact on algal growth, sewage-sludge respiration, and the toxicity of several species were found to be within acceptable levels.



Paul T. Nyffeler was born in Stromsburg, Nebraska in 1976. He received his BA in 1999 from Carleton College, where he studied the stereochemistry of enolate reactions under the tutelage of Prof. Jerry Mohrig. He then moved to The Scripps Research Institute, where his ongoing research in the laboratory of Chi-Huey Wong includes the diazotransfer reaction, regioselective azide reductions, fluorinated glycolipids, and the study of dihydrogen trioxide.



Sergio G. Durón received his BS in chemistry from the University of Texas at Austin in 1995. After a year at Hoechst-Celanese, he moved to the University of Illinois at Urbana-Champaign, where he carried out research on the total synthesis of batzelladine A with David Y. Gin. After completing his PhD he pursued postdoctoral studies at The Scripps Research Institute with Chi-Huey Wong on new methods for the one-pot synthesis of complex oligosaccharides and the synthesis of fluorinated carbohydrates. He is currently at Kalypsys, Inc. in San Diego.



Mike Burkart was born in Arlington, Texas in 1972 and received his BA in chemistry from Rice University. During his graduate studies with Chi-Huey Wong at The Scripps Research Institute, he explored the synthetic chemistry of fluorinated carbohydrates and their application as enzyme inhibitors. Following postdoctoral studies with Chris Walsh at Harvard Medical School, he initiated his own research group in 2002 at the University of California, San Diego. His current research interests include natural product biosynthesis and antibiotic design.



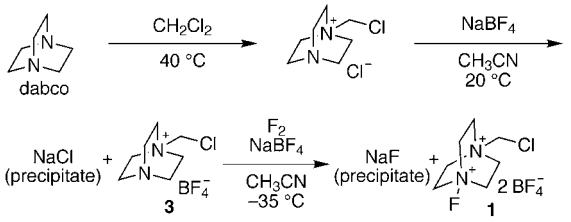
Stéphane Vincent received his PhD in bioorganic chemistry from the Université Louis Pasteur (Strasbourg, France) with Charles Mioskowski. After postdoctoral studies first at The Scripps Research Institute in the research group of Chi-Huey Wong and then in Strasbourg with Jean-Marie Lehn, he took up a permanent position as a CNRS researcher in 2001 in the laboratory of Pierre Sinaÿ (Ecole Normale Supérieure, Paris). His research interests include the glycosciences, biocatalysis, and mechanistic enzymology.



Chi-Huey Wong received his BS and MS from the National Taiwan University, and his PhD in chemistry from the Massachusetts Institute of Technology. After a year as a postdoctoral fellow at Harvard University, he moved to Texas A&M University in 1983. He became Professor of Chemistry in 1989 at The Scripps Research Institute (Ernest W. Hahn Chair). His research interests encompass organic and chemoenzymatic methods in synthesis with a specific focus on the study of carbohydrate-mediated biological recognition.

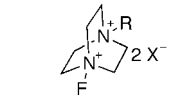
 © 2005 Wiley-VCH Verlag GmbH & Co. KGaA, Weinheim

The preparation of selectfluor, which is produced in multiton quantities per year, was designed to be simple, flexible, and efficient.[18,19] The most practical procedure for the production of selectfluor involves the preparation of the precursor **3** by initial alkylation of 1,4-diazabicyclo[2.2.2]octane (dabco, also known as triethylenediamine (TEDA)) with the dichloromethane solvent (Scheme 3). After counterion exchange with sodium tetrafluoroborate and subsequent precipitation of sodium chloride from the acetonitrile solution, fluorination with F_2 provides **1**. Variations on this scheme allow not only the synthesis of commercial selectfluor on industrial scales, but also the preparation of a variety of derivatives with different characteristics and reactivities.



Scheme 3. Method for preparing **1**.[18,19]

The choice of the peripheral alkyl group on the dabco moiety has the greatest impact upon the reactivity and cost of production of the general class of F-TEDA-X reagents, which includes **1**.[15] Derivatives that have been made range from the simple methyl derivative **4a** to the highly reactive 2,2,2-trifluoroethyl derivative **4j** (Figure 2). The most powerful variant of the F-TEDA-X reagents is **4j**, which even fluorinates benzene. In general, the more electron withdrawing the alkyl substituent is, the more electrophilic the fluorine group will be. From an economic standpoint, the chloromethyl derivative **1** is an ideal reagent, as it has the second-highest reactivity and can be synthesized conveniently. The least reactive compounds are those with methyl, ethyl, or octyl substituents. However, all F-TEDA-X derivatives are reactive enough to fluorinate both pyridine and quinuclidine, demonstrating their superior reactivity over *N*-fluoropyridinium and *N*-fluoroquinuclidinium reagents.

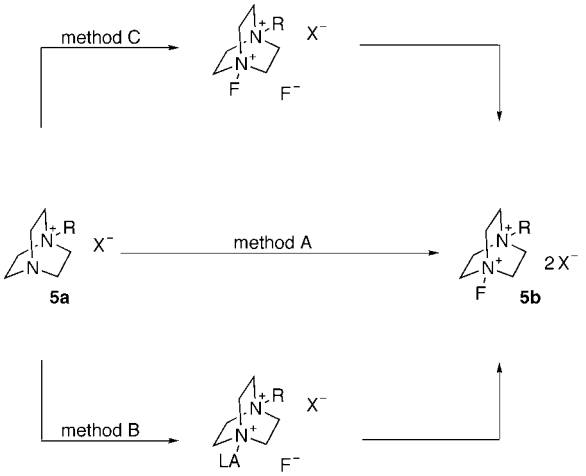


4a R=Me, X=TfO$^-$
b R=Me, X=BF_4^-
c R=Me, X=PF_6^-
d R=Me, X=TfO$^-$, X'=BF_4^-
e R=Me, X=TfO$^-$, X'=PF_6^-
f R=Me, X=TfO$^-$, X'=FSO_3^-
g R=CH_2Cl, X=TfO$^-$
h R=CH_2Cl, X=PF_6^-
i R=Et, X=TfO$^-$
j R=CF_3CH_2, X=TfO$^-$
k R=C_8H_{17}, X=TfO$^-$

Figure 2. F-TEDA-X derivatives. Tf = trifluoromethanesulfonyl.

The counterion employed with selectfluor can have an impact on both the reactivity and the cost of the final compound. In earlier studies, no obvious effect of the counterion on the reactivity had been observed, leading to the commercialization of the tetrafluoroborate salt.[15] However, recent studies demonstrated that the use of the trifluoromethanesulfonate (triflate) salt **4g** for the fluorination of glycals led to decreased side-product formation and higher yields of the desired product than with **1**.[20] This outcome was rationalized by the greater solubility of the triflate salt of selectfluor in the desired solvent (nitromethane) and the fact that no bisfluorinated by-products are formed, a side reaction that occurs with **1**.

The desired counteranion can be introduced by exploiting the low solubility of metal halides in various solvents (Scheme 4).[15,17,18] The procedure involves initial alkylation with dichloromethane, which also serves as the solvent, followed by the addition of lithium tetrafluoroborate, yielding **5a** upon filtration. A different counterion can be incorporated during fluorination by using one of three methods. The first method (Scheme 4, method A), primarily used for small-scale reactions, involves fluorination of **5a** at −35 °C in acetonitrile, then addition of the desired counteranion in the form of the lithium or sodium adduct, filtration, and evaporation. In the second method (Scheme 4, method B), used for industrial-scale production, fluorine is added to a solution of **5a** and the appropriate lithium salt in acetonitrile. This process does not require the separate addition of the salt after fluorination, but does introduce the complication of precipitate formation during the reaction. The third method involves the formation of a Lewis acid (LA) adduct with **5a** prior to fluorination (Scheme 4, method C). On small scales this method is ideal, since no precipitate is formed, and therefore no filtration is needed to provide the pure product. As F_2 gas is used in all methods, either at reduced pressures or diluted with an inert gas such as N_2, any attempts to produce these types of reagents should be undertaken by trained people who are fully aware of the dangers associated with molecular fluorine. Fortunately, because of the efficiency and economic feasibility of this process, selectfluor is commercially available, precluding the need for its preparation.



Scheme 4. Methods for synthesizing F-TEDA-X derivatives.[15]

 © 2005 Wiley-VCH Verlag GmbH & Co. KGaA, Weinheim

3. Electrophilic Fluorination with Selectfluor

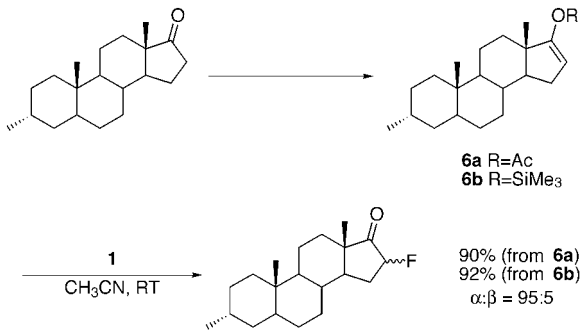
Since the publication of the original patent[19] that described the discovery of selectfluor, the scope of its application has become vast, thus demonstrating the necessity for reagents with the electrophilic fluorination potential of selectfluor. In fact, in a rather remarkable case, Chambers et al. showed that selectfluor is capable of fluorinating unfunctionalized hydrocarbons.[21] Taken together with the examples to follow, there seems to be virtually no end to the number of substrates amenable to transformation by selectfluor.

3.1. Solvent Requirements and Restrictions

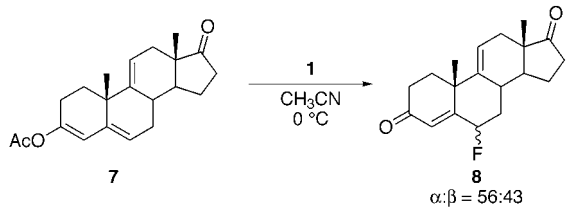
As a dication, selectfluor is soluble in only a few polar solvents, namely, acetonitrile, *N*,*N*-dimethylformamide (DMF), and water.[15] Nitromethane may also be used, since it is inert and sufficiently polar to dissolve the reagent.[20,22] Such a solvent is particularly effective when solvent participation, such as that by acetonitrile in glycosylations, is not desired. The use of nitromethane may also be advantageous when acidic conditions have to be avoided, as it precludes the need for a base or proton sponge. Recently, the use of ionic liquids, such as triflate, tetrafluoroborate, and phosphorous hexafluoride salts of 1-ethyl-3-methylimidazolium or 1-butyl-3-ethylimidazolium, for reactions with **1** has received attention.[23,24] As reaction efficiencies are higher for many substrates in these reusable and environmentally friendly media, these studies have opened an interesting avenue for further investigation.

3.2. α Fluorination of Carbonyl Functionalities

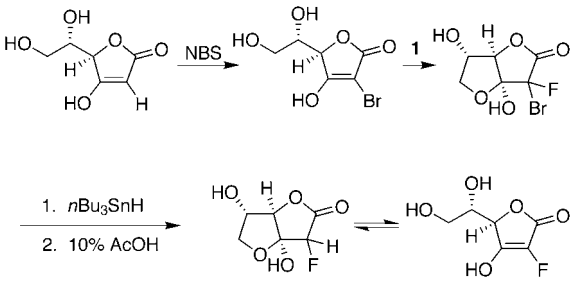
The incorporation of a fluorine substituent adjacent to a carbonyl group is a common reaction motif. This transformation can be carried out by initial conversion of the carbonyl functionality into an enol ester (e.g. **6a**) or a silyl enol ether (e.g. **6b**) prior to reaction with selectfluor (Scheme 5).[25] Fluorinated glucocorticoid derivatives are of great interest in the field of medicinal chemistry, and Herrinton and co-workers reported that selectfluor was the best reagent for converting **7** into **8** (Scheme 6).[26] In a further investigation into the effects of fluorine substituents on the behavior of bioactive compounds, Ge and Kirk reported the synthesis of fluorinated derivatives of L-ascorbic acid (Scheme 7) and tetronic acid (Scheme 8).[27,28] The tetronic acid group is found in many important biologically active compounds. By protecting the carbonyl group as a silyl enol ether, Hoffman and Tao were able to synthesize fluorinated peptide analogues with high diastereo- and enantioselectivity.[29] The incorporation of fluorine into β-diketones is readily accomplished by the reaction of selectfluor with the corresponding enolate salts.[25,30] This transformation is not limited to enolates: The sodium salts of some phosphonates have also been fluorinated in moderate yield. Alternatively, α,α-difluoroketones can be formed regioselectively by the reaction of selectfluor with alkynes.[31]



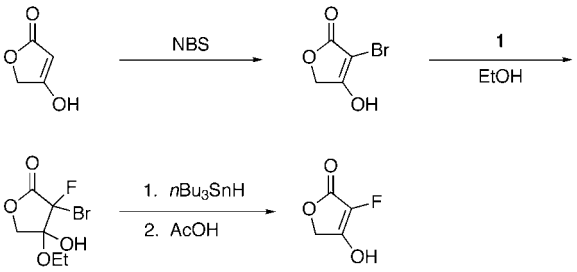
Scheme 5. α Fluorination of ketones via an enol ester or a silyl enol ether.[25]



Scheme 6. Glucocorticoid fluorination.[26]



Scheme 7. Synthesis of a fluorinated derivative of L-ascorbic acid.[28]



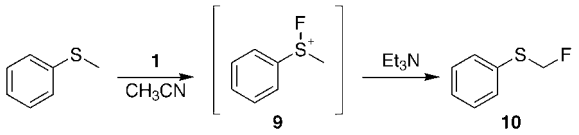
Scheme 8. Synthesis of a fluorinated tetronic acid derivative.[27]

3.3. α Fluorination and Oxidation of Thioethers

Reactions of thioether-containing compounds with selectfluor lead to interesting synthetic products. For example,

 © 2005 Wiley-VCH Verlag GmbH & Co. KGaA, Weinheim

thioethers with α protons can be converted into α-fluorosulfides in reasonable yields (Scheme 9).[25] This process occurs by initial reaction of the sulfide with selectfluor in acetonitrile

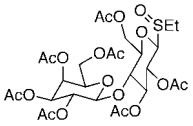
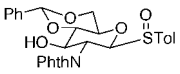
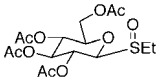
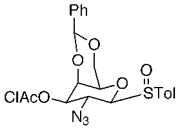
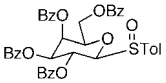
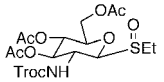
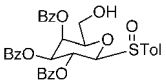
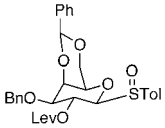
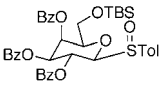
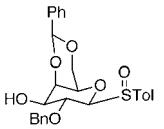


Scheme 9. α Fluorination of thioethers.[25]

at room temperature to form a fluorosulfonium salt (e.g. **9**). It was proposed that this intermediate undergoes a Pummerer-like rearrangement upon treatment with a base, such as triethylamine or 1,8-diazabicyclo[5.4.0]undec-7-ene (DBU), providing the α-fluorosulfide product **10**.

Selectfluor is also an excellent reagent for the conversion of thioglycosides into the corresponding glycosyl sulfoxides (Table 1).[20] These reactions are typically complete within 20 min at 0 °C in acetonitrile/water mixtures. Essentially quantitative yields were observed for all substrates examined.

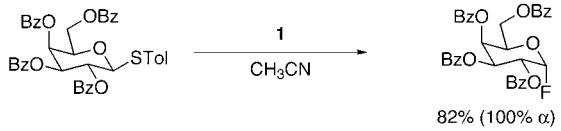
Table 1: Oxidation of thioglycosides to sulfoxides.[20]

Product[a]	Yield [%]	Product[a]	Yield [%]
	99		99
	99		99
	99		99
	99		99
	95		99

[a] Bn = benzyl, Bz = benzoyl, Lev = levulinyl, Tol = tolyl, Troc = 2,2,2-trichloroethoxycarbonyl.

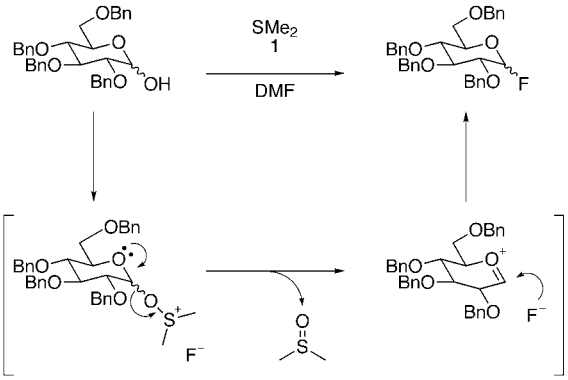
3.4. Synthesis of Glycosyl Fluorides

The inherent thiophilic properties of electrophilic fluorine provide a useful avenue for accessing fluorinated compounds. One possible route is the conversion of thioglycosides into the corresponding glycosyl fluorides with selectfluor (Scheme 10).[32] This method is an improvement on previous methods with DAST, which was successfully used by Nicolaou et al. to synthesize glycosyl fluoride donors.[33]



Scheme 10. Direct conversion of thioglycosides into α-fluoro sugars.[32]

Glycosyl fluorides can be accessed directly from anomeric hemiacetals in one step by using the reagent combination of selectfluor and dimethylsulfide (Scheme 11). This reaction



Scheme 11. Proposed mechanism for the substitution of an anomeric hydroxy group for a fluorine substituent in the presence of methyl sulfide and **1**.[20,32]

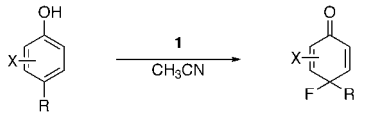
demonstrates the potential of this combination as a safe alternative to potentially explosive DAST for the conversion of alcohols into fluorides.[20,32] Selectfluor was also shown to promote glycosylation with thioglycoside donors in high yields.[20,32] Its application in the glycosylation of 2-deoxy-thioglycosides is exceptional, as other methods of activation fail as a result of the high reactivity of the glycosyl donors.[34]

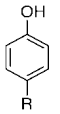
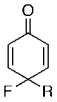
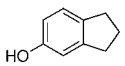
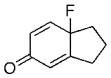
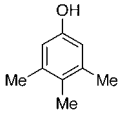
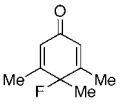
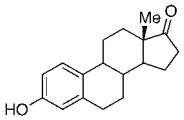
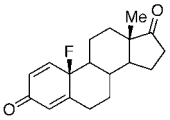
3.5. Fluorination of Aromatic Compounds

Selectfluor has proven to be a competent reagent for the fluorination of substituted aromatic systems. Banks et al. reported that of all the F-TEDA series (Figure 2) only the 2,2,2-trifluoroethyl derivative **4j** fluorinates benzene, albeit in very low yields when aqueous acetonitrile is used (3.5 % after 48 h at 80 °C).[15] Higher yields, up to 20 % conversion, were observed when trifluoroacetic acid (10 % *v*/*v*) was added. Many substituted aromatic compounds could readily be fluorinated with selectfluor.[15] Electron-donating substituents are known to increase the rate of formation and yield of the fluorinated compounds. For example, when methoxybenzene was exposed to **1**, a 1:1 mixture of 2- and 4-fluoro(methoxy)-benzene was obtained in high yield (72 % conversion). Stavber et al. found that substituted phenols are fluorinated by **1**, in an efficient synthesis of 4-fluorocyclohexadienone derivatives (Table 2).[35] Flanagan et al. employed **1** in the synthesis of aromatic fluorescent dyes, which were used in DNA-sequencing.[36]

 © 2005 Wiley-VCH Verlag GmbH & Co. KGaA, Weinheim

Table 2: Synthesis of 4-fluorocyclohexadienones from 4-substituted phenol derivatives.[35]



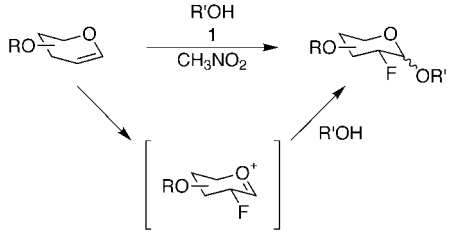
Substrate	Product	Yield [%][a]
		R = Me: 60 (52) R = *i*Pr: 55 (44)
		84 (77)
		93 (82)
		90 (79)

[a] Yield of the crude product by ^{19}F NMR spectroscopy; the values in brackets refer to the yield of the isolated product.

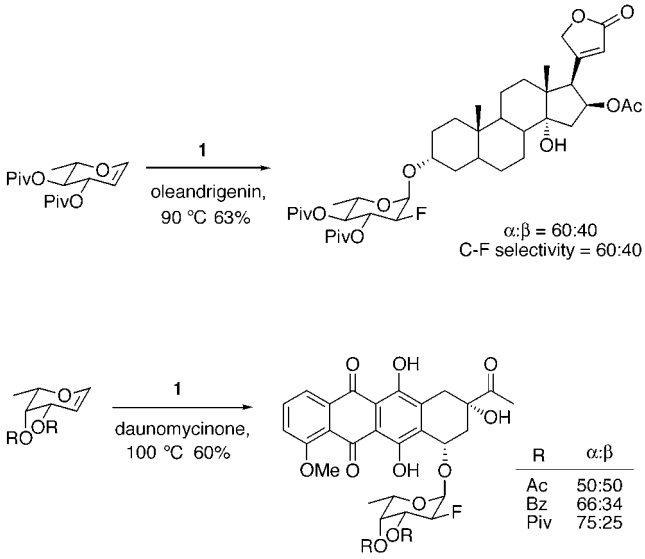
3.6. Fluorination of Alkenes

The susceptibility of alkenes to functionalization with electrophilic species provides a convenient handle for fluorination with selectfluor. Lal,[25] as well as Stavber et al.,[37] demonstrated that 1,2-fluoroethers can be prepared from alkenes by treatment with **1** in the presence of alcohols. Stavber et al. studied the kinetics of this reaction[38] and reported that the transformation was not limited to alcohols, but that 1,2-fluoroamides could also be made efficiently with various amines.[39] Castro et al. selectively introduced fluorine into 3-[3-(piperidin-1-yl)propyl]indoles with **1** in excellent yields. One fluorinated analogue had a higher oral absorption than the corresponding nonfluorinated derivative.[40]

Alkenes contained within the enol ether moiety of glycals are also susceptible to fluorination by **1**. Selectfluor is capable of converting glycals into the corresponding 2-deoxy-2-fluoroglycosides in excellent yield (Scheme 12).[20,22,32,41] Many alcohols, including other protected sugars, can be used as acceptors in this reaction. The fluorination and subsequent glycosylation occur as a two-step one-pot reaction. By employing this methodology, 2-fluoroglycosyl derivatives of the cardiotonic oleandrigenin and the antibiotic daunorubicin were accessed in good yields (Scheme 13). The synthesis of fluorinated analogues of current pharmaceuticals

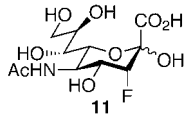


Scheme 12. Proposed mechanism for the fluorination and glycosylation of glycals.[20,22,32,41]



Scheme 13. 2-Fluoroglycosyl derivatives of oleandrigenin and daunomycinone.[20] Piv = pivaloyl.

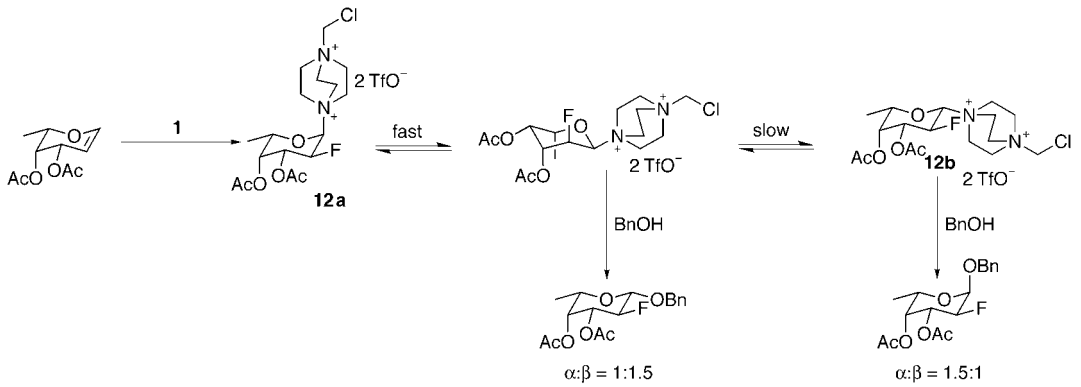
represents a potential avenue for the design of more potent inhibitors.[20] This transformation is not limited to the use of alcohols as acceptors; glycosyl azides, bromides, fluorides, and acetamides can also be formed in high yields starting from glycal precursors. Although pyranosyl glycals are generally employed, furanosyl glycals can also be used successfully. A potential application of this strategy may be the derivatization of 3-fluorosialic acid (**11**) starting from glycal precursors. The resulting products have been shown to be potent selective inhibitors of the influenza virus. They bind to hemagglutinin and neuraminidase, thus limiting the infectious ability of the virus.[42,43]



11

Detailed ^{19}F NMR spectroscopic studies were undertaken to gain insight into the stereoselectivity of anomer formation and fluorination in glycals.[20] These studies demonstrated that **1** adds to the alkene functionality of the glycal in a *syn* fashion, yielding an intermediate of the type **12a**, which then slowly anomerizes to the more thermodynamically stable intermediate **12b** (Scheme 14). Thus, α selectivity is observed if the *syn* adduct has sufficient time to epimerize to the thermodynamically more stable intermediate. Furthermore, it was demonstrated that the steric demands of both the nucleophile and the glycal also play an important role in the anomeric selectivity, with increasing steric bulk favoring α selectivity. Several factors were also shown to influence the efficiency of the reaction. The use of nitromethane as the solvent in lieu of acetonitrile and the replacement of tetrafluoroborate as the counteranion with triflate led to

 © 2005 Wiley-VCH Verlag GmbH & Co. KGaA, Weinheim

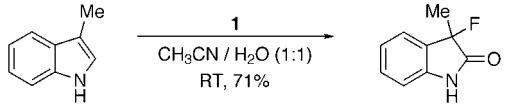


Scheme 14. The conformation and configuration at the anomeric center of the intermediates determine the anomeric selectivity in reactions of glycals.[20]

increased yields, decreased reaction times, and a dramatic decrease in the formation of side products. The choice of protecting groups on the glycal and the steric hindrance of the alcohol acceptor had a significant influence on the selectivity of the reaction.

3.7. Electrophilic Fluorination of Indoles

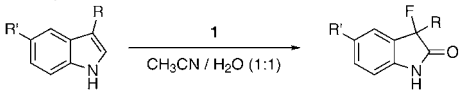
Indoles are convenient precursors in the synthesis of many biologically active molecules, and their derivatives are also useful probes for the study of enzymatic mechanisms and metabolic pathways. Fluorinated analogues containing indole moieties can be useful tools for the elucidation of various biological processes. Indole derivatives can be fluorinated efficiently by using selectfluor to provide various fluorooxindole derivatives (Scheme 15).[44] This method takes advantage of the nucleophilic character of the enamine functionality contained within the indole moiety. The choice of solvent was crucial, as the products decomposed when only acetonitrile was used. Although mixtures of acetonitrile with either methanol or trifluoroethanol were tolerated, the best results were obtained with a 1:1 mixture of acetonitrile and water. The generality of this method was further demonstrated by the successful electrophilic fluorination of other indoles (Table 3, entries 1 and 2), including biologically relevant indoles, such as tryptophan (entry 3), tryptamine (entry 4), and serotonin (entry 5) derivatives. In all cases, their conversion into the fluorooxindoles was efficient.



Scheme 15. Fluorination of an indole.[44]

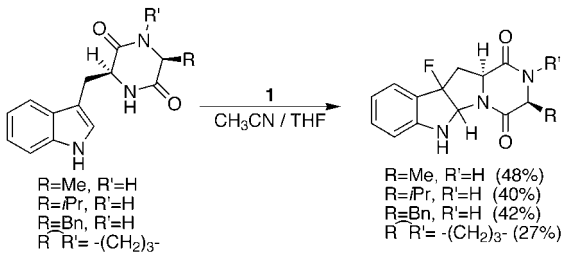
The functionalization of indoles with selectfluor was further extended to the synthesis of some hexahydropyrazino[1′,2′-1,5]pyrrolo[2,3-*b*]indole-1,4-dione derivatives. This indole moiety is present in a wide variety of natural products, including gypsetin[45,46] and brevianamide E.[47] The synthesis of the fluorinated core of these biologically relevant molecules by using **1** is illustrated in Schemes 16 and 17).[48]

Table 3: Electrophilic fluorination of indoles.[44]

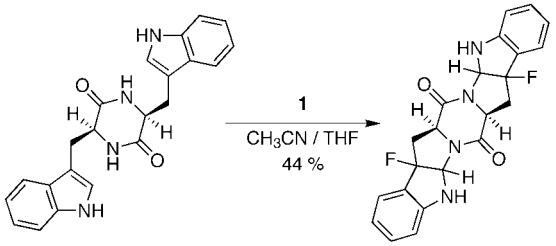


R	R′	Yield [%]
$(CH_2)_2CO_2Me$	H	82
$(CH_2)_3CO_2Me$	H	77
$(CH_2)_2CH(NHpNB)CO_2Me$[a]	H	92
$(CH_2)_2NPhth$[b]	H	82
$(CH_2)_2NPhth$[b]	OAc	82

[a] *p*NB = *para*-nitrobenzyl. [b] Phth = phthaloyl.



Scheme 16. Fluorination of gypsetin derivatives.[52]

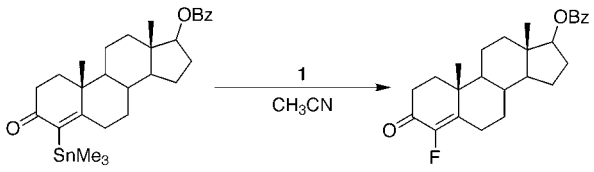


Scheme 17. Synthesis of the fluorinated core of brevianamide E.[48]

 © 2005 Wiley-VCH Verlag GmbH & Co. KGaA, Weinheim

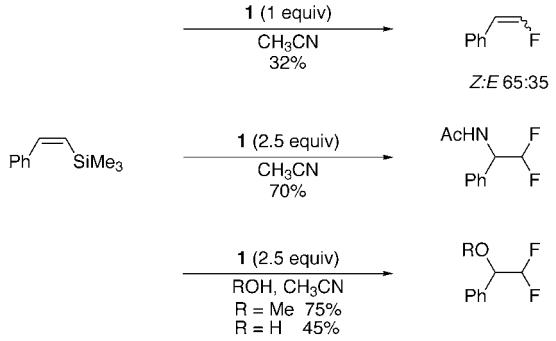
3.8. Synthesis of Vinyl and Alkyl Fluorides

Selectfluor is a versatile reagent for the synthesis of alkenyl and alkyl fluorides. McCarthy and co-workers reported the electrophilic fluorination of vinyl stannanes with selectfluor.[49] Widdowson and co-workers applied this strategy to steroid derivatives containing vinyl stannane groups to prepare fluorinated steroid products (Scheme 18),[50] thus providing a potentially useful method for the synthesis of ^{18}F-labeled steroids for applications in



Scheme 18. Conversion of a vinyl stannane into a fluoride.[50]

positron emission tomography (PET). Greedy and Gouverneur showed that this transformation is not limited to tin-containing species, but that vinyl silanes are also suitable substrates (Scheme 19).[51] The use of 1 equivalent of **1** leads to fluoroalkene products. Interestingly, in the presence of an excess of **1** in acetonitrile, solvent participation in the formation of α,α-difluoro-substituted products was observed. Furthermore, the addition of methanol or water to the reaction mixture led to the incorporation of alcohol and ether groups in the α,α-difluoro-substituted products.



Scheme 19. Conversion of vinyl silanes into fluoroalkanes or α,α-difluoroethers.[51]

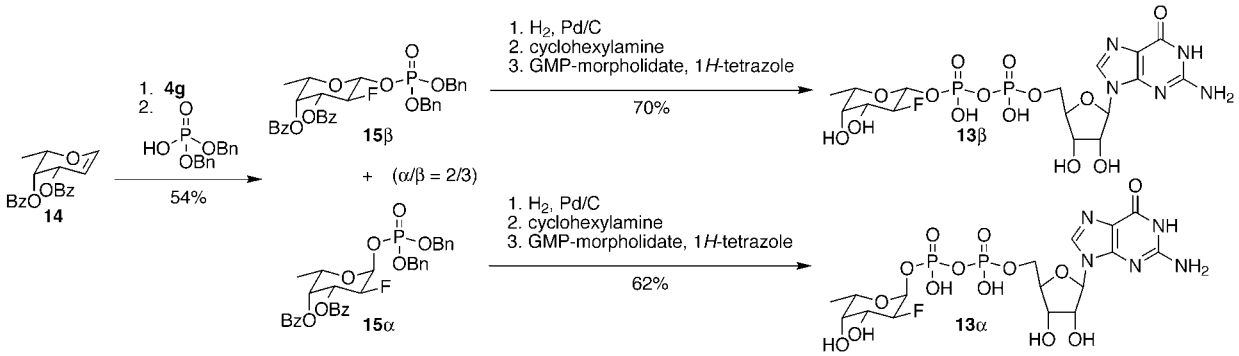
3.9. Oxidative Phosphorylation: Synthesis of 2-Fluoro Sugar Nucleotides

The substitution of the 2-hydroxy group of monosaccharides with fluorine provides useful analogues with which to probe enzyme mechanisms. However, to be introduced into a biological system, the corresponding nucleotide diphosphate must be synthesized, which usually requires many tedious steps involving selective protecting-group manipulations. Recently, new methods for the synthesis of 2-fluoro sugar diphosphates and nucleotide diphosphates with selectfluor have simplified the preparation of these valuable substrates.

The direct oxidative fluorophosphorylation of glycals with selectfluor provides protected 2-fluoroglycosyl phosphates in a one-pot procedure.[20] The synthesis of α- and β-2-fluorofucosylguanine diphosphate (GDP-2F-Fuc; **13**α and **13**β, respectively) is a demonstrative example of this general strategy (Scheme 20). The electrophilic fluorination of 3,4-di-*O*-benzoylfucal (**14**) with **4g**, followed by the addition of dibenzyl phosphate, provided the protected 2-fluorofucosyl phosphate **15** in 54% yield and an α/β ratio of 2:3. After chromatographic resolution, deprotection, and subsequent coupling to GMP-morpholidate, both anomers of **13** were obtained in moderate yield.[52]

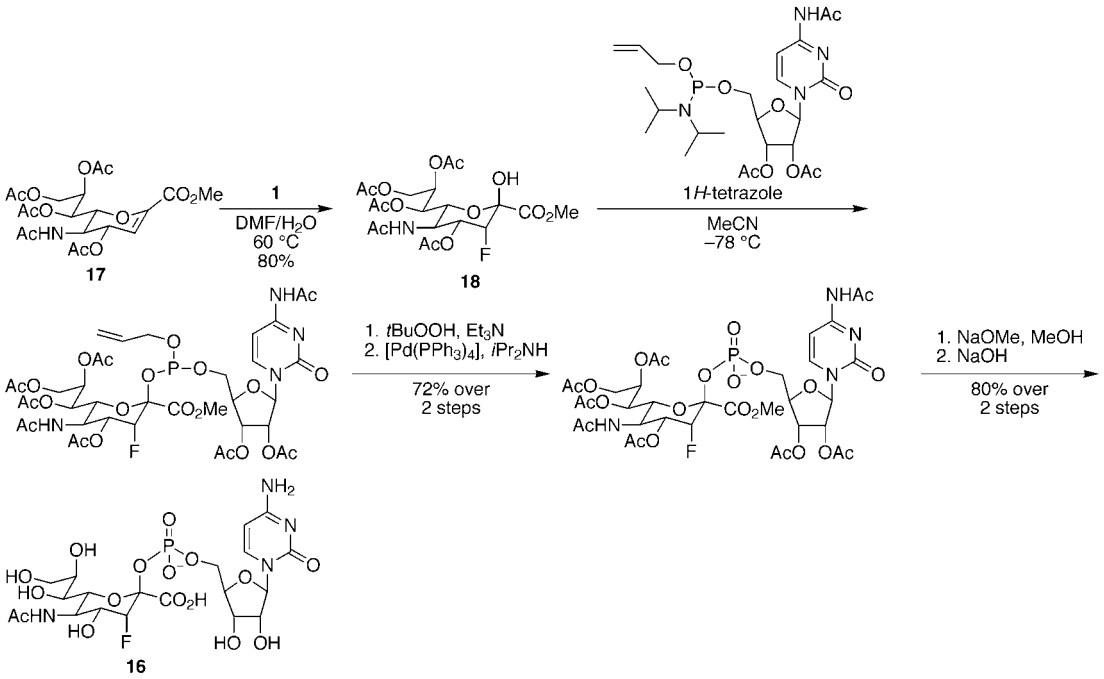
N-Acetylneuraminic acid (NeuAc), also known as sialic acid, is a structurally unique carbohydrate involved in many recognition processes of cell surfaces, including viral infection, inflammation, and cell signaling.[42] Synthetic analogues of this monosaccharide have been utilized to probe cell-surface recognition,[53] and could be useful in other areas of research. As the synthesis of CMP-3F-NeuAc (**16**; CMP = cytidine monophosphate) was hindered by the ester group adjacent to the anomeric center, a three-step fluorophosphorylation was employed (Scheme 21).[42] The glycal derivative **17** of sialic acid was treated with **1** in the presence of water to form the hemiacetal **18**, which was phophitylated by using standard phosphoramidite chemistry. Oxidation and palladium-catalyzed deallylation, deacetylation, and saponification then provided the desired product in good yield.

The use of selectfluor to prepare fluorinated monosaccharides is also amenable to the one-pot chemoenzymatic synthesis of sugar nucleotide diphosphates (Scheme 22).[52] The electrophilic fluorination of galactal with **1** was conducted in water to provide 2-fluorogalactose, which, after pH

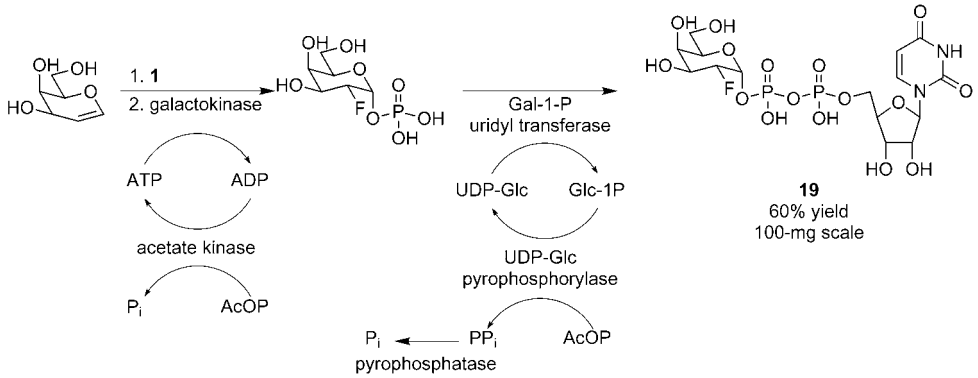


Scheme 20. Synthesis of α-GDP-2F-Fuc (**13**α) and β-GDP-2F-Fuc (**13**β).[20,52]

 © 2005 Wiley-VCH Verlag GmbH & Co. KGaA, Weinheim



Scheme 21. Synthesis of CMP-3F-sialic acid.[42]



Scheme 22. Chemoenzymatic synthesis of UDP-2F-Gal.[52]

adjustment, was phosphorylated by galactokinase. Adenosine triphosphate (ATP), the phosphate source for this transformation, was generated economically in situ with an ATP synthase and a stoichiometric amount of acetyl phosphate. Upon completion of the reaction, the pH was again adjusted, and galactose-1-phosphate uridyltransferase was added. The desired product **19** is formed in good yield, and the procedure can be carried out on a preparative scale.

4. Other Transformations with Selectfluor

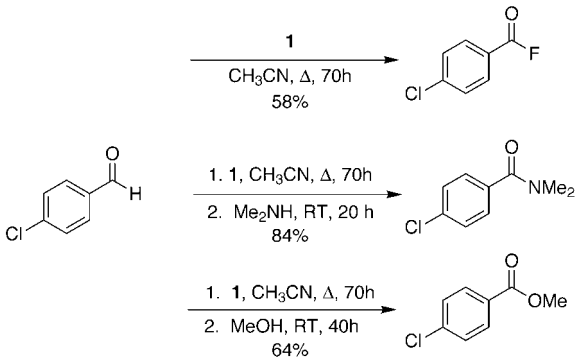
4.1. Oxidation of Benzylic Alcohols

Alongside numerous examples of the use of selectfluor for the electrophilic fluorination of organic molecules, reactions with selectfluor that lead to nonfluorinated products have also been discovered. Banks et al. capitalized on the oxidative properties of selectfluor for the synthesis of benzaldehyde derivatives from benzylic alcohols in moderate yields.[54] The authors postulated that the reaction most likely proceeds through radical fluorination at the benzylic position initiated by a single-electron transfer (SET), followed by the rapid loss of HF to yield the aldehyde product. They also found that **1** could oxidize benzaldehyde derivatives to the corresponding benzoic acids in good to excellent yields via a benzoyl fluoride intermediate (Scheme 23). Furthermore, they demonstrated that aldehydes can be converted into amides and esters in good yields.

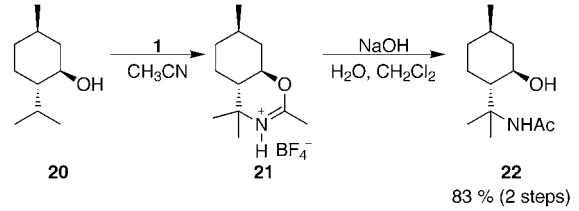
4.2. Oxidation of Tertiary Carbon Centers

In an interesting transformation of (−)-menthol (**20**), remote functionalization of alcohols in the presence of excess selectfluor was demonstrated (Scheme 24).[55] The reaction

 © 2005 Wiley-VCH Verlag GmbH & Co. KGaA, Weinheim



Scheme 23. Oxidative functionalization of *p*-chlorobenzaldehyde.[54]

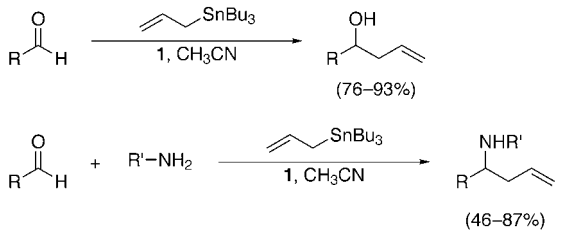


Scheme 24. Remote functionalization of (−)-menthol.[55]

proceeds through initial formation of a tertiary carbocation, which subsequently reacts with the solvent (in this case acetonitrile), and the resulting intermediate is trapped intramolecularly by the alcohol group through a Ritter-like mechanism. The oxazinium salt **21** formed is then hydrolyzed under basic conditions to provide the functionalized menthol derivative **22**. The presence of a tertiary carbon center β to the alcohol group is a prerequisite for this reaction. This method was found to be general, as a similar reaction occurs in propionitrile and butyronitrile, albeit in lower yields. The authors also proposed an SET mechanism to account for the observed transformation.

4.3. Selectfluor-Mediated Allylstannation of Aldehydes and Imines

A unique application of selectfluor as a promoter for the allylstannation of aldehydes and imines was reported recently.[56] Generally, strong Lewis acids, such as aluminum trichloride and titanium tetrachloride, which require the exclusion of moisture and strict maintenance of an inert atmosphere, are employed in this reaction. With selectfluor the desired homoallylic alcohols and amines are produced in good yields with excellent tolerance of moisture and air (Scheme 25). The reactions of aromatic and aliphatic aldehydes usually proceed to completion within hours when a stoichiometric amount of **1** is used. With a catalytic amount of **1** (0.05 equiv) longer reaction times (24 h) are required and yields are lower (≈60% conversion). In the absence of selectfluor no product formation was observed. Although the mechanism for this transformation is not well understood, it can be speculated that **1** may act as a Lewis acid to activate the



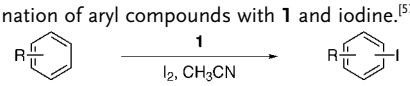
Scheme 25. Allylstannation of aldehydes and imines.[56]

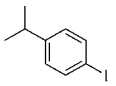
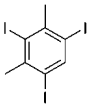
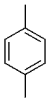
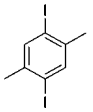
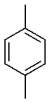
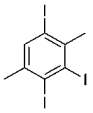
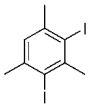
aldehyde for nucleophilic addition. However, one can also imagine that the effective Lewis acid may be the tri-*n*-butyltin cation, formed in conjunction with allyl fluoride from the reaction between allyl(tri-*n*-butyl)tin and **1**.

4.4. Selectfluor-Mediated Functionalization of Aromatic Systems

Although selectfluor is most often used as an electrophilic reagent for the introduction of fluorine substituents, it can also mediate the electrophilic addition of other common anions. The inherent electrophilic activity of **1** has been exploited recently for the conversion of nucleophilic compounds into electrophilic reagents. It has been known for some time that selectfluor decomposes in the presence of iodide ions,[15] but when mixed with molecular iodine it forms a potent iodonium source. Stavber et al. reported that alkylated aromatic rings can be iodinated in excellent yield in acetonitrile by using iodine and **1** (Table 4).[57] The reaction

Table 4: Iodination of aryl compounds with **1** and iodine.[57]



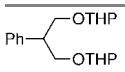
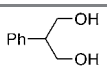
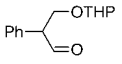
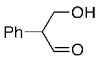
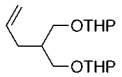
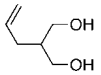
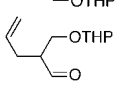
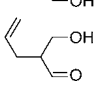
Substrate	Aryl/**1**/I_2	Product	Yield [%]
	1:0.75:0.75		95
	1:0.6:0.6		93
	1:5:5		72
	1:1.5:1.5		89
	1:5:5		73
	1:0.6:0.6		96
	1:1.1:1.1		87

is usually carried out with substoichiometric quantities of the reagents, but when excess I_2 and **1** were used, bis- and trisiodinated products were formed. This transformation is not limited to activated benzene derivatives, as aryl alkyl ketones could be converted into aryl α-iodoketones in excellent yields.[58] A solvent effect was noted in this reaction: With methanol the α-iodoketones were formed, whereas the use of acetonitrile led to aryl iodide species. A three-component mixture of the alkyl aryl ketone, iodine, and **1** was required for any reaction to occur. Selectfluor also proved useful for the conversion of common anions into electrophilic reagents. The reaction of **1** with the sodium or potassium salts of Cl^-, Br^-, SCN^-, and NO_2^- converts the anions into the corresponding electrophilic cations, which are capable of the electrophilic functionalization of a variety of activated benzene derivatives.[59] In general, the potassium salts are more reactive than the sodium salts, and the reactivity decreases in the order $Cl^+ > Br^+ > SCN^+ > NO_2^+$. The reaction is substrate dependent and proceeds faster for some nucleophiles in DMF and for others in acetonitrile. Acetate and trifluoroacetate could be converted into the corresponding electrophilic species for a limited number of substrates, but with other anions (CN^-, OCN^-, CH_3O^-, CH_3S^-) no reaction occurred under any conditions investigated.

4.5. Protecting-Group Removal

Selectfluor is a useful reagent for the removal of some common protecting groups. The protection of alcohols as their tetrahydropyranyl (THP) ethers was reported as early as 1934.[60,61] This protecting group still sees widespread application as a result of its low cost, ease of introduction, and stability. The addition of stoichiometric amounts of selectfluor leads to the selective, mild cleavage of THP ethers in high yields (Table 5).[62] Under these mild conditions, aldehydes and olefins are tolerated. The protecting group *p*-methoxybenzylidene, commonly employed for the protection of 1,3-diols, can also be removed easily in high yields with an excess amount of **1** (Table 6).

Table 5: Deprotection of THP ethers with **1**.[62]

Substrate	Product	Yield [%]
		94
		92
		95
		89

The most useful deprotection by **1** is arguably the cleavage of dithianes (Table 7). Dithianes have found wide application in synthesis as a result of their stability and accessibility. They

Table 6: Deprotection of *p*-methoxybenzylidene with **1**.[62]

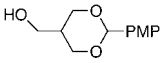
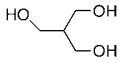
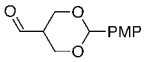
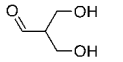
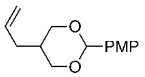
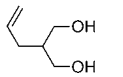
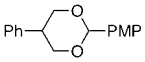
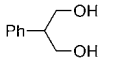
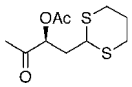
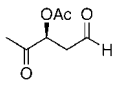
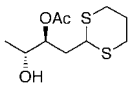
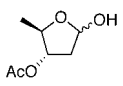
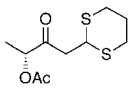
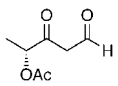
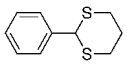
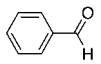
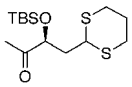
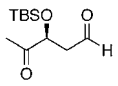
Substrate	Product	Yield [%]
		90
		87
		92
		90

Table 7: Deprotection of 1,3-dithianes with **1**.[62]

Substrate	Product	Yield [%]
		95
		85
		95
		85
		80

are commonly used as umpoled synthons and for the protection of aldehydes and ketones.[63] However, one major drawback to the use of dithiane groups is that mercury salts, which are highly toxic and an environmental hazard, are required for their removal. Selectfluor is capable of cleaving 1,3-dithianes in excellent yields in less than 5 min, with the formation of innocuous by-products.[62] It has been proposed that **1** acts as a Lewis acid in this process, but various other reaction pathways are imaginable, including oxidation.

5. Enantioselective Transformations

Selectfluor has been utilized, either directly or indirectly, in many types of enantioselective reactions. Enders et al. described the regio- and enantioselective electrophilic fluorination of enantiopure α-silylketones, but selectfluor found limited success in this reaction.[64] Although indirect and substrate-directed enantioselective reactions with selectfluor can be useful, the enantioselective fluorination of nucleophilic substrates has been studied the most intensively.

The first report of an asymmetric α fluorination was by Differding and Lang, who described the enantioselective fluorination of an enolate with camphor-based *N*-fluoro sultams.[65] These chiral electrophilic sources of fluorine provided the anticipated α-fluorocarbonyl compounds upon treatment with various metal enolates. Depending on the substrate, enantioselectivities of up to 70% *ee* were observed.

 © 2005 Wiley-VCH Verlag GmbH & Co. KGaA, Weinheim

Improved enantioselective fluorinations were observed with a new class of charged $[N-F]^+$ reagents. Selectfluor was used to prepare the *N*-fluoroammonium derivatives **23a–d** of cinchona alkaloids by transfer fluorination (Figure 3, Scheme 26).[66–68] The fluorinated reagents **23a–d** were

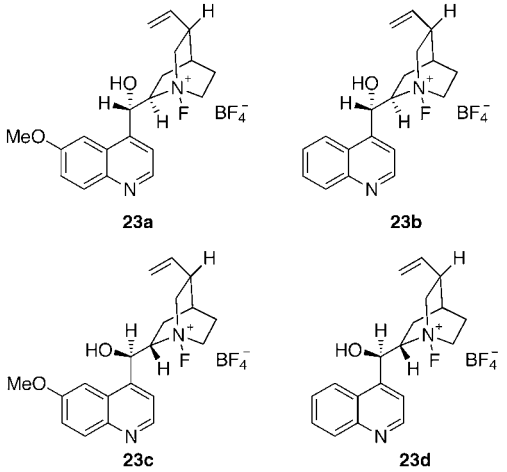
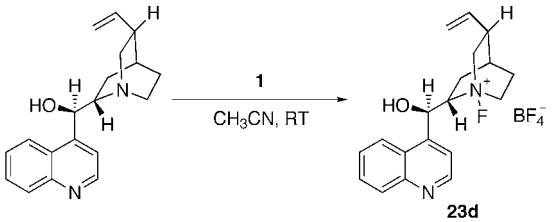


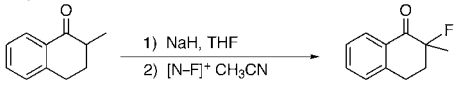
Figure 3. *N*-Fluoroammonium derivatives of cinchona alkaloids for enantioselective electrophilic fluorination.[66–68]



Scheme 26. Synthesis of the fluorinated cinchona alkaloid F-CD-BF_4.[66–68]

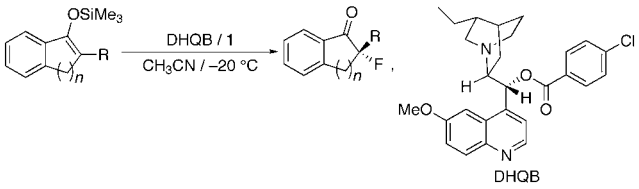
tested in the enantioselective fluorination of the sodium enolate of 2-methyl-1-tetralone, providing the product in up to 98% yield and with up to 50% *ee* (Table 8). Higher enantioselectivities (up to 94% *ee*) were later observed with modified *N*-fluoro cinchona alkaloids.[69] In a similar manner, enantioselective fluorinations with a reagent combination of a cinchona alkaloid derivative and **1** were demonstrated (Table 9).[70] This method bypasses the isolation of the *N*-fluoroammonium salt and therefore constitutes a one-pot

Table 8: Enantioselective fluorination with $[N-F]^+$ cinchona alkaloids (see Figure 3).[66–68]



$[N-F]^+$	*ee* [%]	Configuration	Yield [%]
23a	50	*S*	98
23b	40	*R*	70
23c	27	*R*	87
23d	20	*S*	98

Table 9: Enantioselective fluorination with a combination of DHQB and **1**.[70]



R	*n*	*ee* [%]	Configuration	Yield [%]
Me	1	53	*R*	93
Et	1	73	*R*	100
Bn	1	91	*R*	86
Me	2	40	*R*	94
Et	2	67	*R*	71
Bn	2	71	*S*	95

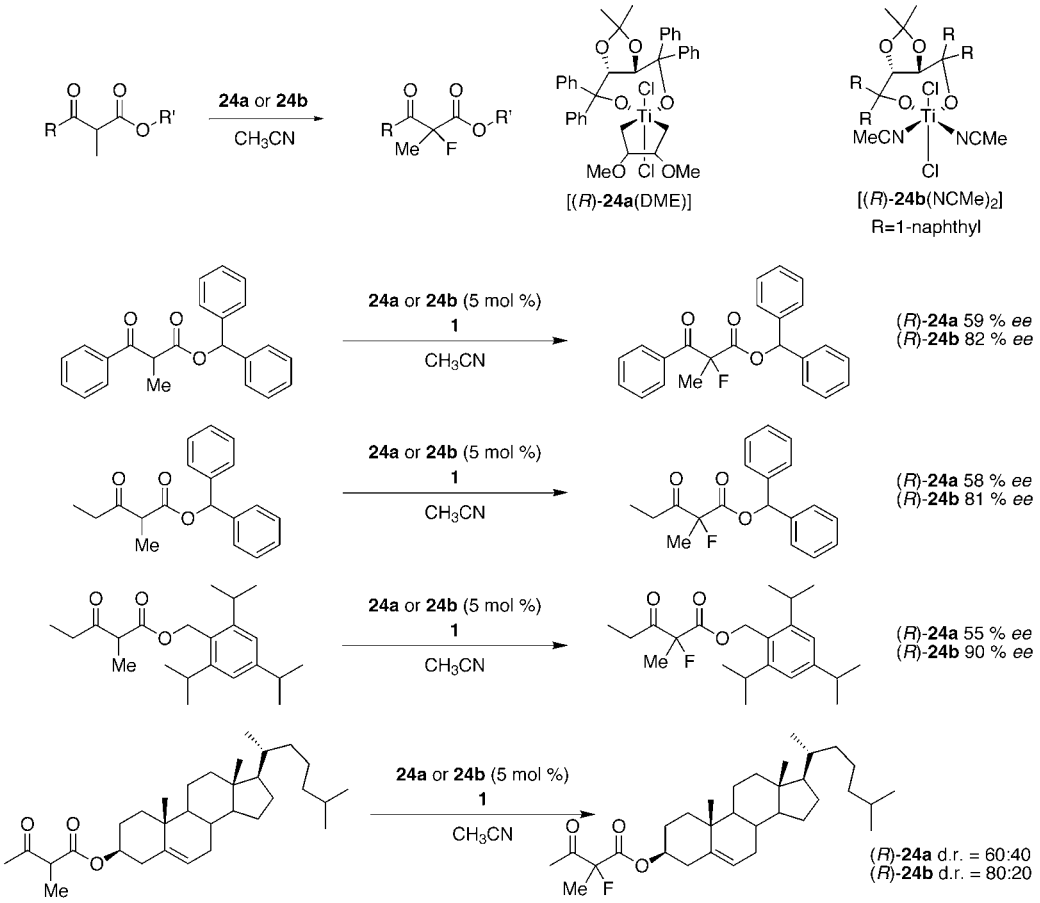
procedure, in which a mixture of the cinchona alkaloid and **1** can be added to a variety of substrate types, including silyl enol ethers. Both cyclic and acyclic carbonyl compounds were fluorinated in good to excellent yields with selectivities sometimes greater than 90% *ee* by this method, which is also useful for β-keto esters (up to 80% *ee*) and acyclic β-cyano esters (up to 87% *ee*). Significant progress has been made in the development of an enantioselective electrophilic fluorination method. In most cases cinchona alkaloids and selectfluor have been used in a transfer fluorination to access the corresponding chiral electrophilic fluorination reagents. This strategy has proved to be very practical, especially because of the commercial availability of the cinchona alkaloid derivatives.

A major breakthrough would be the development of catalytically active enantioselective fluorination reagents. The systematic investigation of the catalytic activity of various transition-metal complexes in the electrophilic fluorination of ketones led to the discovery that the taddol-modified (taddol = α,α,α′,α′-tetraaryl-2,2-dimethyl-1,3-dioxolan-4,5-dimethanol) titanium complexes **24a** and **24b** are highly efficient catalysts for the enantioselective fluorination of β-keto esters (Scheme 27).[71] It was hypothesized that the interaction of the ketoester with the Lewis acidic catalyst induces enolization, and that the resulting enol is then fluorinated enantioselectively with **1**. This mechanistic rationalization is supported by previous reports of a rate enhancement in the fluorination of ketones with *N*-fluoropyridinium salts in the presence of zinc(II) chloride.[10] Further mechanistic details[72] were reported.

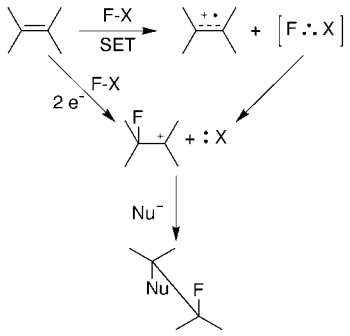
6. Mechanism of Fluorination with Selectfluor: Electron Transfer or S_N2 Reaction?

The mechanism of fluorination with N–F reagents has been a subject of debate since their introduction. There are two possible mechanistic pathways: single-electron transfer (SET) or nucleophilic S_N2 substitution. As shown in Scheme 28, both SET and S_N2 pathways lead to the same product, in this case a fluorinated carbocation. Banks and coworkers initially voiced support for a SET mechanism to

 © 2005 Wiley-VCH Verlag GmbH & Co. KGaA, Weinheim



Scheme 27. Catalytic enantioselective electrophilic fluorination with chiral titanium complexes.[71] DME = 1,2-dimethoxyethane.



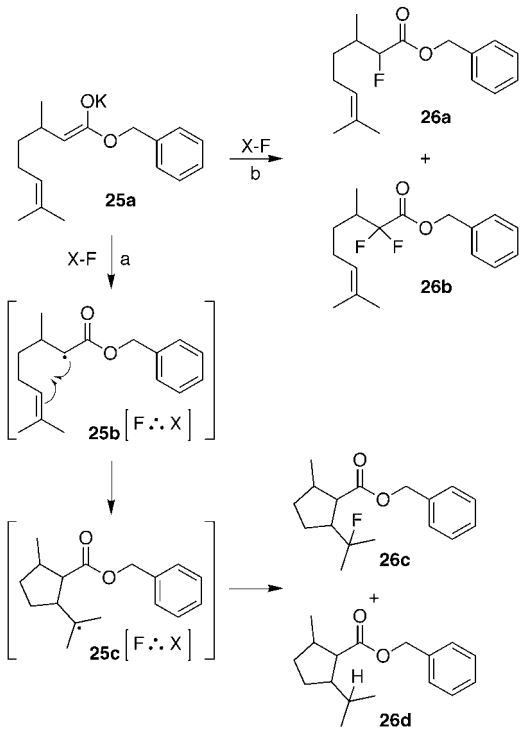
Scheme 28. Single- and two-electron processes in the presence of **1** can result in identical products.

explain reactions with selectfluor,[54] but later spoke of "… a substrate-dependent mechanistic continuum [S_N2(F)↔fully developed SET process] …"[15] As discussed below, the difference between the two mechanisms is probably smaller than it appears, and the limits of current methods to study extremely fast reactions inhibit the definitive elucidation of the operative mechanism.

Supporters of the nucleophilic-substitution theory have undertaken creative and elegant experiments to refute the intermediacy of discrete radical species. Differding and co-workers were the first to use radical clocks to monitor the reaction for the presence of intermediate radicals.[73,74] Their experiment was based on the following logic: If the potassium enolate **25a** were to react in an SET process, the resulting radical **25b** would undergo cyclization to the radical **25c** (Scheme 29). The recombination of **25c** and atomic fluorine would produce some amount of **26c** and **26d**, thus proving the existence of radicals in the reaction. Their results clearly demonstrated that no products of cyclization were formed in the reaction, providing support for the notion that electrophilic fluorination does not involve SET (Table 10).

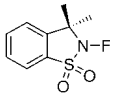
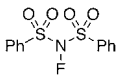
However, other issues have to be taken into account. The cyclization of a 5-hexenyl radical has been shown definitively to occur at a rate of approximately $1 \times 10^5\ s^{-1}$;[75] however, according to Differding and Rüegg, **25b** is not a pure alkyl radical, but is subject to the electronic effects of the adjacent ester group. Furthermore, it was determined by laser flash photolysis that the absolute rate constant for the reaction of atomic fluorine (F•) with a solvent is between 10^9 and $10^{11}\ s^{-1}$,[76] some four to six orders of magnitude faster than the fastest possible closing of a 5-hexenyl radical. Since the reactivity of F• was studied by the abstraction of a hydrogen atom from the solvent and found to be diffusion controlled,[76] the recombination of F• with any alkyl radical should proceed at an equal or greater rate.

The arguments for an SET pathway for fluorination by N–F reagents are quite compelling, but they must be interpreted



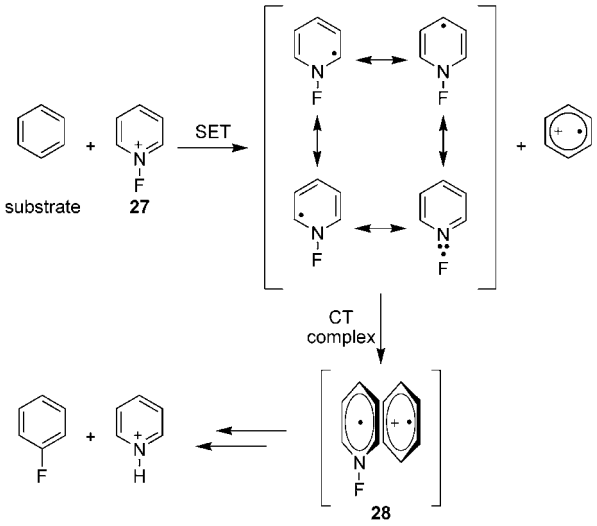
Scheme 29. Experimental attempt to differentiate between SET (a) and two-electron-transfer (b) reactions with **25a**.[73,74]

Table 10: Yields of products (in %) from reactions of fluorinating reagents with **25a** (see Scheme 29).[73,74]

	26a	26b	26c	26d	25a
	59	23	0	0	<10
	21	31	0	0	20
	64	23	0	0	13
XF_2	11	3	0	10	10

transition state for the SET reaction with organolithium compounds occurs in such an early phase of the reaction that F· reacts with the solvent preferentially, with no formation of the desired product. Kochi and co-workers later suggested that the stability of the organic radicals has a strong influence upon whether fluorinated product is generated, or HF from the reaction of F· with the solvent and numerous other organic side products.[79] In the end, Umemoto may have been correct in his interpretation of the data,[10] but until this question is addressed further, caution should be employed when invoking this argument to support an SET mechanism with N–F reagents.

Much stronger evidence for the SET mechanism was found first by Umemoto et al.[10] and later by Kochi and co-workers.[79,80] Umemoto et al. commented on a color change that occurred when **27** reacted with 2-napthol and a disappearance of the color as the reaction proceeded further. They surmised that the color change was caused by the formation of a π complex between the reagent and the substrate (Scheme 30).[10] Later, Kochi and co-workers attrib-

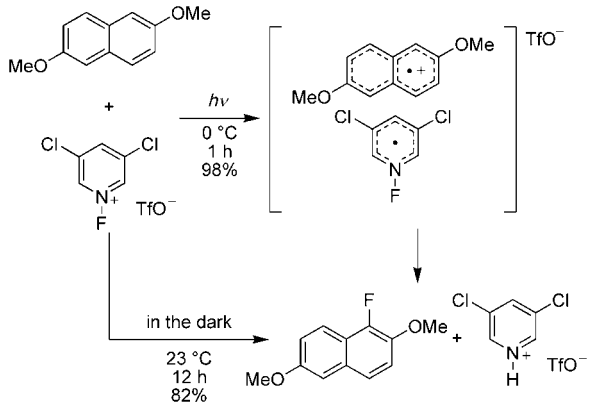


Scheme 30. Electrophilic fluorination via a charge-transfer (CT) complex as an intermediate.[10]

with caution. Umemoto et al. observed that the reaction of *N*-fluoropyridinium salts with Grignard reagents provided alkyl fluorides, whereas their reaction with the related organolithium reagents did not.[10] They used this finding to justify the notion that N–F reagents react through SET, since Grignard reagents were shown to react in such a manner. However, work by Holm and Crossland showed that Grignard reagents can react by an S_N2 mechanism.[77] Thus, the degree of SET versus S_N2 character of reactions of Grignard reagents depends on several factors. Furthermore, Yamataka et al. reported that organolithium reagents react almost exclusively by SET. They suggested that the rate-determining step is the electron transfer, unlike for Grignard reagents, in which case the recombination of the radicals is the rate-determining step.[78] If both studies are taken together, one possible interpretation of the finding of Umemoto et al. is that the uted this color change to a charge-transfer complex, thus relating the mechanism of electrophilic aromatic fluorination with that of electrophilic aromatic nitration.[79,80] The latter was elegantly shown by Perrin to proceed by SET.[81] Single-electron transfer from the substrate to **27** results in a complex between F· and pyridine, which could be stabilized by the donation of a π electron from pyridine to yield the charge-transfer complex **28**. Kochi and co-workers also found evidence for the participation of the charge-transfer complex as a reaction intermediate by demonstrating that photoexcitation at the CT band led to a dramatic increase in the rate of fluorination and the yield relative to the corresponding thermochemical reaction (Scheme 31).[79]

Selectfluor and the other compounds of this general class are the only electrophilic fluorination reagents for which no clear evidence has been found for the intermediacy of radical

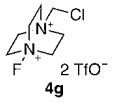
 © 2005 Wiley-VCH Verlag GmbH & Co. KGaA, Weinheim



Scheme 31. Comparison of photochemical and thermochemical reaction products.[79]

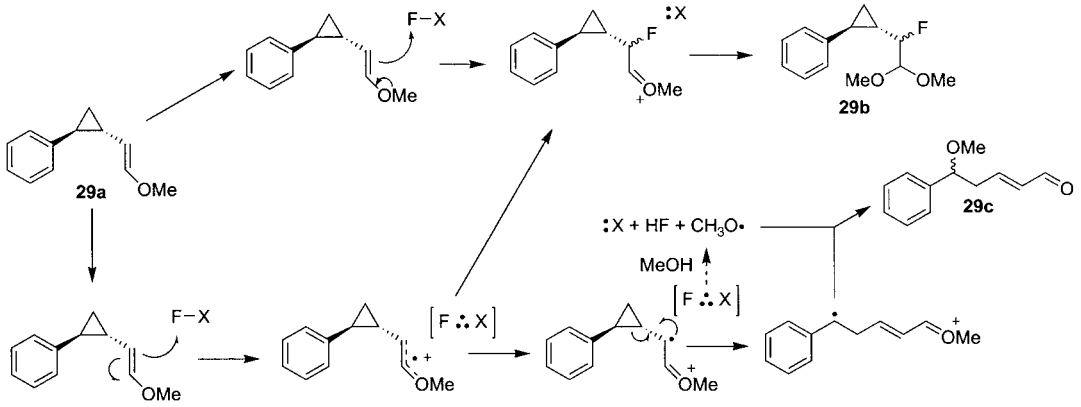
intermediates. The DesMarteau reagent (**2**, Scheme 2) is inhibited by *p*-dinitrobenzene,[12] an efficient electron-transfer quencher, and *N*-fluoropyridinium reagents display CT bands indicative of SET, as described previously.[10] No evidence for radical intermediates was identified in reactions of **1** with **29a** (Scheme 32),[20] a derivative of a phenylcyclopropyl radical trap that was shown to undergo ring opening at rates as high as $2\times10^{11}\ s^{-1}$.[82] Comparison of the fluorinating reagents **4g** and **30**, which is known to react by the SET mechanism, led to inconclusive results, as **29b** was formed from **29a** in virtually identical yield in the two reactions (Table 11). Furthermore, the findings of Horner et al. indicate that numerous other factors, such as solvent polarity and the choice of nucleophile, may complicate the use of enol ether

Table 11: Yields of isolated products from reactions of electrophilic fluorinating reagents with **29a**.[20]

	Mechanism	**29b** [%]	**29c** [%]
 **4g**	???	45	not detected
 **30**	SET	40	5

radical traps to detect radical intermediates.[83] However, the fact that 2,2,6,6-tetramethylpiperidine *N*-oxide (TEMPO), which is oxidized by a suitable oxidant (Cl_2, Br_2, XeF_2, etc.) by liberation of a single electron,[84] reacts rapidly with selectfluor[20] strongly suggests that selectfluor can participate in SET reactions. Based on this evidence and on additional data supporting SET with other N–F reagents, it is probable that SET also occurs with selectfluor, but that the radical intermediates are strongly destabilized and therefore unlikely to be detected. As **1**, unlike **2** and **27**, lacks a polarizable p-electron-donor center to stabilize F•, the unstabilized fluorine radical would react immediately with the radical cation formed from the substrate by SET. Thus, the use of radical traps, such as the phenylcyclopropyl radical system,[82] would be inappropriate, since they only measure rates below the diffusion limit. This hypothesis was supported by molecular dynamics calculations performed by Togni and co-workers on a simplified system. Their results indicated that the lifetime of the intermediate radicals is approximately 3×10^{-15} s:[72] roughly 1000 times shorter than the time required for phenylcyclopropylmethyl radical to rearrange. If an SET mechanism were operative in the case of selectfluor, then only the first of two distinct reactions could be monitored: the SET from the substrate to **1**, and not the subsequent recombination of the proximal radicals. As the reaction of F• with the solvent occurs at the rate of diffusion (see above),[76] the reaction of F• with an existing radical must also be at least as fast as diffusion. Hence, the recombination of the carbon-centered radical and F• would most likely occur faster than the rearrangement of the solvent, making solvent interaction, and therefore rates of diffusion, irrelevant. These arguments suggest why selectfluor only displays net S_N2 reactivity.

An explanation for the greater electrophilic reactivity of selectfluor over other R_3N^+–F reagents can most readily be derived from the unique orbital configuration of dabco and from an X-ray crystallographic analysis. Recently, electron momentum spectroscopy[85] confirmed a long-standing theoretical prediction by Hoffmann et al.[86] that the lone pairs of electrons on the two nitrogen atoms of dabco do not occupy the expected orbitals according to classic valence bond theory,[87–89] but instead are delocalized throughout the entire molecule. The discovery that the radical cation of dabco was exceptionally stable[90] was directly attributed by

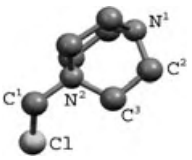
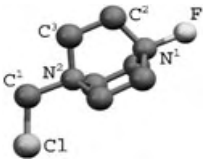


Scheme 32. Proposed mechanisms for the electrophilic fluorination of **29a**.[20]

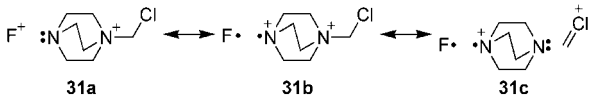
 © 2005 Wiley-VCH Verlag GmbH & Co. KGaA, Weinheim

Hoffmann et al. to a through-bond interaction in the molecule.[86] Theoretical calculations suggest that "F^+" is ten times more unstable than atomic fluorine.[91] The structural changes that occur upon the fluorination of **31** to give selectfluor (see X-ray crystal structures)[92] suggest that the fluorine center has more radical than "fluoronium" character, as the electron density in the rest of the molecule decreases (Table 12).

Table 12: Structural comparison of the nonfluorinated cation **31** and **1**.[92]

	31	**1**
Structure		
Bond lengths/ interatomic distances [Å]		
N^1–N^2	2.559	2.477
N^2–C^1	1.491	1.525
C^1–Cl	1.760	1.715
Bond angles [°]		
N^1-C^2-C^3	108.61	107.79
N^2-C^3-C^2	108.65	110.59

Compensation occurs through a shortening of the C–C bonds, in agreement with the through-bond (not through-space) interactions postulated by Hoffmann et al.,[86] and a simultaneous lengthening of the N–CH_2Cl bond and contraction of the CH_2–Cl bond. The contraction of the CH_2–Cl bond is suggestive of partial double-bond character between the methylene and chlorine centers. Therefore, the resonance structure **31c**, with fluorine as a radical, a double bond between the methylene and chlorine groups, and dabco as a radical cation, is perhaps a more realistic interpretation of the molecular structure of selectfluor (Scheme 33). These results



Scheme 33. Possible resonance structures for **1**.

are consistent with the high reactivity of **1** and its ability to react in an SET process, since the addition of a single electron to this system would allow the formation of F· and restore the electronic state of **31** to that prior to fluorination. Rearrangement of the bonds of **31** would follow, returning it to the more stable configuration determined by crystallography and leaving unstabilized F· to react immediately with the newly formed carbon radical.

Despite extensive research into the possible reaction mechanisms of N–F reagents, a definitive answer has not been found and may remain undiscovered as a result of the difficulty of assessing reactions in this timeframe. Even if a reaction were known to proceed exclusively by SET followed by radical recombination, the two reactions might occur in such rapid succession that the intermediate is not detected. William Jencks once wrote, "An intermediate is, therefore, defined as a species with a significant lifetime, longer than that of a molecular vibration of $\sim 10^{-13}$ s, that has barriers for its breakdown to both reactants and products."[93] When reactions proceed at rates greater than 10^{11} s^{-1}, arguments for or against an SET mechanism become pointless. In our view selectfluor is capable of reacting through an SET mechanism, as evident by its reaction with TEMPO, but in the case of electrophilic fluorination the radicals, if formed at all, react too quickly to be detected. Thus, based on our previous work,[20] the only definitive answer is that if SET is occurring, the radicals involved react faster than rates of diffusion, and anything beyond that will probably remain unproven.

7. Selected Applications of Fluorinated Compounds

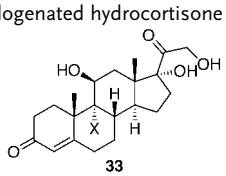
The fluorination of molecules has many applications in organic chemistry. For example, the high electronegativity of fluorine can be used to modulate the electronic properties of a molecule, and ultrasensitive ^{19}F NMR spectroscopy is a useful analytical technique for monitoring reactions and obtaining molecular information (e.g. by Mosher ester analysis for the determination of enantiomeric excess).[94,95] However, the applications of fluorinated molecules in biology are even more intriguing. Perhaps the oldest examples of fluorinated biologically relevant molecules are salts of fluoroacetate, the active component of the poison derived from the South African gifblaar plant (*Dichapetalum cymosum*).[96] Biochemically, fluoroacetate is converted into fluoroacetyl CoA, which enters the tricarboxylic acid (TCA) cycle. Fluoroacetyl CoA condenses with oxaloacetate to form fluorocitrate (an effective inhibitor of aconitase), which shuts down the TCA cycle, resulting in convulsions, ventricular fibrillation, and death.

7.1. Fluorinated Glucocorticoids

The first reported use of fluorination to enhance the activity of a medicinally useful compound was by Fried and Sabo in 1954.[97] A year earlier, they had described the synthesis of derivatives of the glucocorticoid hydrocortisone (**33a**), a steroid hormone with anti-inflammatory and thymolytic activity. Substitution of the 9-αH atom of hydrocortisone acetate for an iodine, bromine, or chlorine atom resulted in an increase in activity relative to that of the natural compound only in the case of the chlorine derivative **33c**.[98] The general trend in this series suggested that the activity was inversely proportional to the size of the halogen substituent, thus prompting the synthesis of the fluorinated derivative.[97] As can be seen in Table 13, **33b** is more than ten times as active as naturally occurring hydrocortisone; more importantly, these studies established fluorination as a promising method for improving the activity of pharmacologically relevant compounds. Several examples of fluorinated glucocorticoids and their corresponding activities can be found in Figure 4.[99] As

 © 2005 Wiley-VCH Verlag GmbH & Co. KGaA, Weinheim

Table 13: Activity of halogenated hydrocortisone derivatives.[97,98]



33

Compound	X	Activity[a]
33a	H	1
33b	F	10.7
33c	Cl	4
33d	Br	0.28
33e	I	0.1

[a] Assay of glycogen from rat liver.

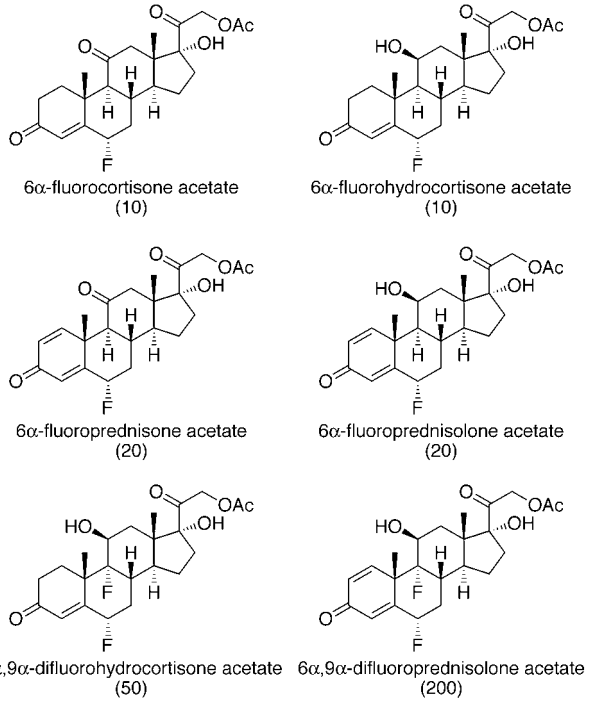


Figure 4. Biological activities of fluorocorticoids;[99] in each case the anti-inflammatory activity in rats relative to hydrocortisone acetate is given.

stated previously, Herrinton and co-workers determined that **1** is a highly efficient fluorinating reagent for the synthesis of **8**.[26]

7.2. Fluorinated Glycosyltransferase Inhibitors

Carbohydrates with a fluorine atom adjacent to the anomeric center demonstrate inhibitory activity towards some glycosyltransferases and allow insight into enzyme mechanisms.[100] Given the important role of oligosaccharides in biological processes, the selective inhibition of certain mammalian glycosyltransferases could be a potential strategy against cancer proliferation, xenotransplant rejection, and tissue inflammation. Fucose, sialic acid, and galactose moieties in particular are essential components of oligosaccharides and determinant structural motifs for specific biological phenomena.

The inhibition of several glycotransferases by fluorinated sugars has been investigated by our research group.[52,101] Four different fucosyltransferases were chosen for this inhibition study (FucT-III, V, VI, and VII), as well as α-2,6-sialyltransferase and two galactosyltransferases (the configuration-inverting bovine β-1,4-GalT and the configuration-retaining α-1,3-GalT). For FucT, the fluorinated fucose analogues **13α**, **13β**, and **34** displayed K_i values that were similar to or less than the K_M value for GDP-Fuc (Table 14). Similar results were obtained for the inhibition of sialyltransferase with **16** (Table 15). The K_i value for the inhibition of β-1,4-GalT by α-

Table 14: Inhibition of four human fucosyltransferases.[52,101]

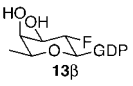
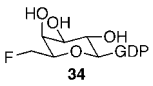
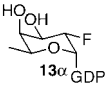
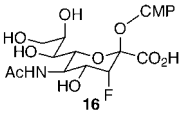
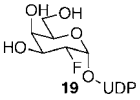
	GDP-Fuc	 **13β**	 **34**	 **13α**
	K_M [μM]	K_i [μM]	K_i [μM]	K_i [μM]
FucT-III	33.6	38 ± 4	22 ± 10	–
FucT-V	18.8	4 ± 0.6	3.4 ± 1	36 ± 4
FucT-VI	9	10 ± 2.4	1 ± 0.5	2 ± 1
FucT-VII	8	21 ± 2	11 ± 2	–

Table 15: Inhibition of a sialyl- and two galactosyltransferases.[52]

Glycosyltransferase	Inhibitor	K_i [μM]
α-2,6-SialylT (K_M = 15 mM)	 **16**	5.7 ± 2
β-1,4-GalT (K_M = 3 ± 6 mM)	 **19**	2.0 ± 0.3
α-1,3-GalT (K_M = 17 ± 3 mM)		245

UDP-2F-Gal (**19**) is approximately equal to the K_M value for the enzyme with the natural substrate, but for the inhibition of α-1,3-GalT, the only configuration-retaining enzyme in the study, a K_i value was observed that was 14-fold lower than the K_M value with the natural substrate.

Earlier mechanistic studies with FucT-V demonstrated a secondary isotope effect with deuteriated GDP-[1-^{2}H]-fucose and competitive inhibition by **12β**.[101] Similar inhibition patterns were found for FucT-III, VI, and VII.[52] Given the 90% homology between these enzymes, it was proposed that they may share a considerable number mechanistic features, including the formation of an oxycarbenium-like transition state. These considerations also took into account the inhibition of fucosyl transferases by **34**. Evidence suggests that the replacement of the hydroxy groups at the 6- or 2-position, equidistant from the endocyclic oxygen atom, leads to similar electronic effects—a potentially valuable result for future inhibitor design. The good inhibition observed with the anomerically nonnatural **13α** indicates that the binding

 © 2005 Wiley-VCH Verlag GmbH & Co. KGaA, Weinheim

domain of fucosyltransferases allows stereochemical flexibility.

Recent syntheses of potent inhibitors of α-2,6-sialyltransferase have elucidated important conformational parameters of the transition-state structure, including sp^2 character at the anomeric position.[102–106] However, a cationic transition state, predicted based on the quaternary structure at the anomeric carbon atom, has not yet been demonstrated. CMP-3F-sialic acid (**16**) has been found to be a competitive inhibitor (K_i = 5.7 μM), thus supporting the involvement of an oxycarbenium intermediate in the transition state.[42]

Interesting results were obtained with galactosyltransferases.[52] The configuration-inverting β-1,4-GalT was as susceptible to competitive inhibition by **19** as other inverting glycosyltransferases (Figure 5), whereas the configuration-

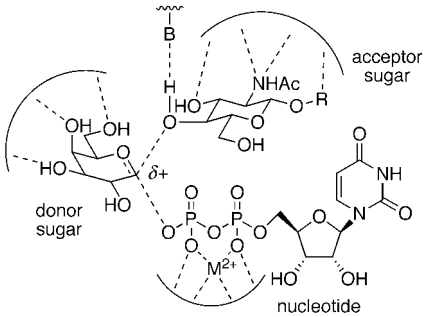


Figure 5. Putative transition state for configuration-inverting β-galactosyltransferase.[52]

retaining α-1,3-GalT was only weakly inhibited (K_i = 245 μM, K_M = 17 μM). These results suggest that the mechanisms by which these two galactosyltransferases catalyze the glycosylation may be strikingly different. This would be consistent with the differences observed for the glycosidases as a function of their inverting or retaining nature.[107] Since a double displacement mechanism could rationally be invoked for the retaining α-1,3-GalT, experiments were conducted to determine whether **19** was a slow inactivator of this enzyme. On the time scale of the experiments performed, no inactivation was observed, demonstrating that the enzyme does not form a covalent adduct with the fluorinated substrate **19**. In the case of various retaining glycosidases, 2-fluoroglycosides had been shown to form covalent adducts, which is evidence of the nucleophilic role of carboxylate groups present in the vicinity of the anomeric center. Indeed, some 5-fluoroglycosides proved to be better, albeit very unstable, inactivators than the corresponding derivatives fluorinated at the 2-position.[108]

7.3. Electrophilic Fluorination for ^{18}F Positron Emission Tomography

The use of radioactive isotopes for chemotherapy and the elucidation of reaction pathways is well established. Another useful application for certain nuclei that decay through positron (β^+) emission is positron emission tomography (PET).[109] For some nuclei of small atomic mass, radioactive decay occurs by the emission of a positron, which is a positively charged particle with the mass of an electron. Collision of a positron with an electron results in annihilation and the release of a gamma-ray photon. The radiation can be analyzed by a photomultiplier in similar way to the detection of X-rays. A substance containing a β^+ emitter can be introduced into a living organism and then localized noninvasively by detecting the emitted gamma rays in a 3D image of the organism.

Common positron-emitting nuclei include ^{11}C, ^{15}O, ^{13}N, and ^{18}F (Table 16). ^{18}F has a relatively long half-life of almost

Table 16: Physical properties of β^+-emitting radionuclides.[109]

Radionuclide	$t_{1/2}$ [min]	β^+ decay [%]	Maximum specific activity[a]	Maximum energy [MeV]	Maximum linear range in H_2O [mm]
^{11}C	20.40	99	3.4×10^{11}	0.96	4.12
^{13}N	9.96	99	6.9×10^{11}	1.19	5.39
^{15}O	2.07	99.9	3.4×10^{12}	1.72	8.2
^{18}F	109.70	97	6.3×10^{10}	0.635	2.39

[a] Defined as the number of decay events per second per mole.

2 h, which makes it possible to carry out synthetic manipulations on substrates without significant loss of activity. The other nuclei must be used immediately upon formation (usually occurs in a cyclotron) because of their shorter half-lives. ^{18}F-labeled reagents can be delivered to nearby sites, such as hospitals and universities, making research more practical. Finally, the positrons emitted from ^{18}F have much lower kinetic energy than those from the other nuclei, which translates to shorter distances between emission and annihilation, and thus to higher resolution.

Fluorination with ^{18}F is limited by the small number of labeled reagents that can be made. The bombardment of ^{18}O-labeled water with high-energy protons results in the absorption of a proton by each ^{18}O nucleus, followed by the emission of a neutron, to provide nucleophilic ^{18}F ions, which can be separated by ion exchange. Alternatively, the absorption of a high-energy deuteron by a ^{20}Ne nucleus in a gas mixture of Ne with 0.1 % F_2, followed by the emission of an α particle, gives $^{18}F_2$ gas for electrophilic fluorination. Labeled molecular fluorine has been used directly for electrophilic fluorinations, but it has also been converted into other electrophilic fluorinating reagents, such as acetyl [^{18}F]fluoride ($AcO^{18}F$),[110,111] [^{18}F]fluoropyridones,[112,113] [^{18}F]fluoro-*N*-sulfonamides,[114] and labeled xenon difluoride ($Xe^{18}F_2$).[115,116]

The use of ^{18}F and other positron-emitting nuclei necessitates fast and simple chemistry, as well as safeguards against the dangers of handling radioactive material. All manipulations for the synthesis of ^{18}F-labeled compounds (including purification) must be completed in approximately 1–2 h to ensure sufficient active material for clinical use. The use of automated synthesizers and robotics has shortened the length of time needed to synthesize compounds and eliminates the dangers associated with the handling of radioactive material.

Many different applications of ^{18}F-labeled compounds in PET have been described. The first ^{18}F-labeled compound to

 © 2005 Wiley-VCH Verlag GmbH & Co. KGaA, Weinheim

be used in PET was [2-^{18}F]fluoroglucose for monitoring glucose metabolism in organs.[117–119] This method is still the most popular use of PET, with applications in oncology, cardiology, and neurology. Dopamine metabolism can be monitored by ^{18}F-labeled L-DOPA, a technique that is useful in neurological diseases, such as schizophrenia and Parkinson's disease (DOPA = 3-(3,4-dihydroxyphenyl)alanine).[120] Steroids labeled with ^{18}F have been used to image breast and prostate tumors.[121]

The development of ^{18}F-labeled selectfluor would revolutionalize electrophilic fluorination in much the same way as the development of the unlabeled reagent, and would enable the synthesis of labeled compounds with more complex structures by existing methodologies. For example, the synthesis of the fluorinated daunorubicin analogue in Scheme 13 can be carried out quickly enough that ^{18}F could be introduced.[122] As the use of PET as a noninvasive imaging technique becomes more widespread, there will be increased demand for new methodology for the incorporation of ^{18}F into molecules of interest in a safe, efficient, and selective manner. Because of its general applicability, high reactivity, and safety, selectfluor is a reagent with great potential for the development of new fluorination methods.

8. Conclusion

Electrophilic fluorination is an extremely useful and viable method for the incorporation of fluorine into organic molecules and a natural complement to nucleophilic fluorination. Although initially molecular fluorine was the only available reagent, the demand for a safe alternative has led to a plethora of reagents that deliver fluorine effectively under electrophilic conditions. Over the years the development of safer and milder reagents ultimately led to the discovery of selectfluor, which now represents the hallmark for stability, reactivity, and mildness within the realm of electrophilic fluorinations. Furthermore, the unique reactivity of selectfluor enables deeper insight into complex reactions and demands new experiments and methods to probe the underlying mechanisms.

This work was supported by the NIH. P.T.N. acknowledges a fellowship from the Skaggs Foundation.

Received: January 8, 2004
Published Online: December 1, 2004

Please note: Unfortunately the authors omitted to cite an important review on fluorination with selectfluor in the version of their article published online in *Angewandte Chemie* Early View.[123] The authors apologize for this oversight.

[1] W. J. Middleton, *J. Org. Chem.* **1975**, *40*, 574.
[2] D. H. R. Barton, L. S. Godinho, R. H. Hesse, M. M. Pechet, *Chem. Commun.* **1968**, 804.
[3] D. H. R. Barton, A. K. Ganguly, R. H. Hesse, S. N. Loo, M. M. Pechet, *Chem. Commun.* **1968**, 806.
[4] C. J. Schack, K. O. Christe, *Inorg. Chem.* **1979**, *18*, 2619.
[5] M. A. Tius, *Tetrahedron* **1995**, *51*, 6605.
[6] R. Schmutzler, *Angew. Chem.* **1968**, *80*, 466; *Angew. Chem. Int. Ed. Engl.* **1968**, *7*, 440.
[7] S. Rozen, *Chem. Rev.* **1996**, *96*, 1717.
[8] W. Navarrini, V. Tortelli, A. Russo, S. Corti, *J. Fluorine Chem.* **1999**, *95*, 27.
[9] T. Umemoto, K. Kawada, K. Tomita, *Tetrahedron Lett.* **1986**, *27*, 4465.
[10] T. Umemoto, S. Fukami, G. Tomizawa, K. Harasawa, K. Kawada, K. Tomita, *J. Am. Chem. Soc.* **1990**, *112*, 8563.
[11] G. Resnati, D. D. DesMarteau, *J. Org. Chem.* **1991**, *56*, 4925.
[12] D. D. DesMarteau, Z.-Q. Xu, M. Witz, *J. Org. Chem.* **1992**, *57*, 629.
[13] M. Zupan, S. Stavber, *Trends Org. Chem.* **1995**, *57*, 629.
[14] R. E. Banks, *J. Fluorine Chem.* **1998**, *87*, 1.
[15] R. E. Banks, M. K. Besheesh, S. N. Mohialdin-Khaffaf, I. Sharif, *J. Chem. Soc. Perkin Trans. 1* **1996**, 2069.
[16] G. S. Lal, G. P. Pez, R. G. Syvret, *Chem. Rev.* **1996**, *96*, 1737.
[17] R. E. Banks, S. N. Mohialdin-Khaffaf, G. S. Lal, I. Sharif, R. G. Syvret, *J. Chem. Soc. Chem. Commun.* **1992**, 595.
[18] J. J. Hart, R. G. Syvret, *J. Fluorine Chem.* **1999**, *100*, 157.
[19] R. E. Banks (Air Products and Chemicals, Inc., USA), US 5,086,178, **1992**, p. 9.
[20] S. P. Vincent, M. D. Burkart, C.-Y. Tsai, Z. Zhang, C.-H. Wong, *J. Org. Chem.* **1999**, *64*, 5264.
[21] R. D. Chambers, M. Parsons, G. Sandford, R. Bowden, *Chem. Commun.* **2000**, 959.
[22] M. Albert, K. Dax, J. Ortner, *Tetrahedron* **1998**, *54*, 4839.
[23] K. K. Laali, G. I. Borodkin, *J. Chem. Soc. Perkin Trans. 2* **2002**, 953.
[24] J. Baudoux, A.-F. Salit, D. Cahard, J.-C. Plaquevent, *Tetrahedron Lett.* **2002**, *43*, 6573.
[25] G. S. Lal, *J. Org. Chem.* **1993**, *58*, 2791.
[26] V. Reydellet-Casey, D. J. Knoechel, P. M. Herrinton, *Org. Process Res. Dev.* **1997**, *1*, 217.
[27] P. Ge, K. L. Kirk, *J. Fluorine Chem.* **1997**, *84*, 45.
[28] P. Ge, K. L. Kirk, *J. Org. Chem.* **1997**, *62*, 3340.
[29] R. V. Hoffman, J. Tao, *J. Org. Chem.* **1999**, *64*, 126.
[30] R. E. Banks, N. J. Lawrence, A. L. Popplewell, *J. Chem. Soc. Chem. Commun.* **1994**, 343.
[31] M. Zupan, J. Iskra, S. Stavber, *J. Org. Chem.* **1995**, *60*, 259.
[32] M. D. Burkart, Z. Zhang, S.-C. Hung, C.-H. Wong, *J. Am. Chem. Soc.* **1997**, *119*, 11743.
[33] K. C. Nicolaou, R. E. Dolle, D. P. Papahatjis, J. L. Randall, *J. Am. Chem. Soc.* **1984**, *106*, 4189.
[34] J. Jaunzems, E. Hofer, M. Jesberger, G. Sourkouni-Argirusi, A. Kirschning, *Angew. Chem.* **2003**, *115*, 1198; *Angew. Chem. Int. Ed.* **2003**, *42*, 1166.
[35] S. Stavber, M. Jereb, M. Zupan, *Synlett* **1999**, *9*, 1375.
[36] J. H. Flanagan, Jr., C. V. Owens, S. E. Romero, E. Waddel, S. H. Kahn, R. P. Hammer, S. A. Soper, *Anal. Chem.* **1998**, *70*, 2676.
[37] S. Stavber, T. Sotler, M. Zupan, *Tetrahedron Lett.* **1994**, *35*, 1105.
[38] S. Stavber, T. Sotler-Pecan, M. Zupan, *Bull. Chem. Soc. Jpn.* **1996**, *69*, 169.
[39] S. Stavber, T. Sotler Pecăn, M. Papež, M. Zupan, *Chem. Commun.* **1996**, 2247.
[40] J. L. Castro, I. Collins, M. G. N. Russell, A. P. Watt, B. Sohal, D. Rathbone, M. S. Beer, J. A. Stanton, *J. Med. Chem.* **1998**, *41*, 2667.
[41] J. Ortner, M. Albert, H. Weber, K. Dax, *J. Carbohydr. Chem.* **1999**, *18*, 297.
[42] M. D. Burkart, S. P. Vincent, C.-H. Wong, *Chem. Commun.* **1999**, 1525.
[43] X.-L. Sun, Y. Kanie, C.-T. Guo, O. Kanie, Y. Suzuki, C.-H. Wong, *Eur. J. Org. Chem.* **2000**, 2643.

 © 2005 Wiley-VCH Verlag GmbH & Co. KGaA, Weinheim

[44] Y. Takeuchi, T. Tarui, N. Shibata, *Org. Lett.* **2000**, *2*, 639.
[45] C. Shinohara, K. Hasumi, Y. Takei, A. Endo, *J. Antibiot.* **1994**, *47*, 163.
[46] B. Nuber, F. Hansske, C. Shinohara, S. Miura, K. Hasumi, A. Endo, *J. Antibiot.* **1994**, *47*, 168.
[47] A. J. Birch, J. J. Wright, *Chem. Commun.* **1969**, 644.
[48] N. Shibata, T. Tarui, Y. Doi, K. L. Kirk, *Angew. Chem.* **2001**, *113*, 4593; *Angew. Chem. Int. Ed.* **2001**, *40*, 4461.
[49] D. P. Matthews, S. C. Miller, E. T. Jarvi, J. S. Sabol, J. R. McCarthy, *Tetrahedron Lett.* **1993**, *34*, 3057.
[50] H. F. Hodson, D. J. Madge, D. A. Widdowson, *J. Chem. Soc. Perkin Trans. 1* **1995**, 2965.
[51] B. Greedy, V. Gouverneur, *Chem. Commun.* **2001**, 233.
[52] M. D. Burkart, S. P. Vincent, A. Duffels, B. W. Murray, S. V. Ley, C. H. Wong, *Bioorg. Med. Chem.* **2000**, *8*, 1937.
[53] E. Saxon, C. R. Bertozzi, *Science* **2000**, *287*, 2007.
[54] R. E. Banks, N. J. Lawrence, A. L. Popplewell, *Synlett* **1994**, 831.
[55] R. E. Banks, N. J. Lawrence, M. K. Besheesh, A. L. Popplewell, R. G. Pritchard, *Chem. Commun.* **1996**, 1629.
[56] J. Liu, C.-H. Wong, *Tetrahedron Lett.* **2002**, *43*, 3915.
[57] S. Stavber, P. Kralj, M. Zupan, *Synlett* **2002**, 598.
[58] S. Stavber, M. Jereb, M. Zupan, *Chem. Commun.* **2002**, 488.
[59] R. G. Syvret, K. M. Butt, T. P. Nguyen, V. L. Bulleck, R. D. Rieth, *J. Org. Chem.* **2002**, *67*, 4487.
[60] R. Paul, *Bull. Soc. Chim. Fr.* **1934**, *1*, 971.
[61] G. F. Woods, D. N. Kramer, *J. Am. Chem. Soc.* **1947**, *69*, 2246.
[62] J. Liu, C.-H. Wong, *Tetrahedron Lett.* **2002**, *43*, 4037.
[63] T. W. Greene, P. G. M. Wuts, *Protective Groups in Organic Synthesis*, 3rd ed., Wiley, New York, **1999**.
[64] D. Enders, S. Faure, M. Potthoff, J. Runsink, *Synthesis* **2001**, *15*, 2307.
[65] E. Differding, R. W. Lang, *Tetrahedron Lett.* **1988**, *29*, 6087.
[66] D. Cahard, C. Audouard, J.-C. Plaquevent, N. Roques, *Org. Lett.* **2000**, *2*, 3699.
[67] D. Cahard, C. Audouard, J.-C. Plaquevent, L. Toupet, N. Roques, *Tetrahedron Lett.* **2001**, *42*, 1867.
[68] N. Shibata, E. Suzuki, Y. Takeuchi, *J. Am. Chem. Soc.* **2000**, *122*, 10728.
[69] B. Mohar, J. Baudoux, J.-C. Plaquevent, D. Cahard, *Angew. Chem.* **2001**, *113*, 4339; *Angew. Chem. Int. Ed.* **2001**, *40*, 4214.
[70] N. Shibata, E. Suzuki, T. Asahi, M. Shiro, *J. Am. Chem. Soc.* **2001**, *123*, 7001.
[71] L. Hintermann, A. Togni, *Angew. Chem.* **2000**, *112*, 4530; *Angew. Chem. Int. Ed.* **2000**, *39*, 4359.
[72] S. Piana, I. Devillers, A. Togni, U. Rothlisberger, *Angew. Chem.* **2002**, *114*, 1021; *Angew. Chem. Int. Ed.* **2002**, *41*, 979.
[73] E. Differding, G. M. Rüegg, *Tetrahedron Lett.* **1991**, *32*, 3815.
[74] E. Differding, M. Wehrli, *Tetrahedron Lett.* **1991**, *32*, 3810.
[75] D. Griller, K. U. Ingold, *Acc. Chem. Res.* **1980**, *13*, 317.
[76] G. Bucher, J. C. Scaiano, *J. Am. Chem. Soc.* **1994**, *116*, 10076.
[77] T. Holm, I. Crossland, *Acta. Chem. Scand.* **1971**, *25*, 59.
[78] H. Yamataka, Y. Kawafuji, K. Nagareda, N. Miyano, T. Hanafusa, *J. Org. Chem.* **1989**, *54*, 4706.
[79] T. M. Bockman, K. Y. Lee, J. K. Kochi, *J. Chem. Soc. Perkin Trans. 2* **1992**, 1581.
[80] K. Y. Lee, J. K. Kochi, *J. Chem. Soc. Perkin Trans. 2* **1992**, 1011.
[81] C. L. Perrin, *J. Am. Chem. Soc.* **1977**, *99*, 5516.
[82] M. Newcomb, M. B. Manek, *J. Am. Chem. Soc.* **1990**, *112*, 9662.
[83] J. H. Horner, E. Taxil, M. Newcomb, *J. Am. Chem. Soc.* **2002**, *124*, 5402.
[84] J. M. Bobbitt, M. C. L. Flores, *Heterocycles* **1988**, *27*, 509.
[85] S. Wolfe, Z. Shi, C. E. Brion, J. Rolke, Y. Zheng, G. Cooper, D. P. Chong, C. Y. Hu, *Can. J. Chem.* **2002**, *80*, 222.
[86] R. Hoffmann, A. Imamura, W. J. Hehre, *J. Am. Chem. Soc.* **1968**, *90*, 1499.
[87] L. Pauling, *J. Am. Chem. Soc.* **1931**, *53*, 1367.
[88] L. Pauling, *J. Chem. Educ.* **1992**, *69*, 519.
[89] L. C. Pauling, *The Nature of the Chemical Bond*, 3rd ed., Cornell University Press, Ithaca, **1960**.
[90] T. M. McKinney, D. H. Geske, *J. Am. Chem. Soc.* **1965**, *87*, 3013.
[91] M. Cartwright, A. A. Woolf, *J. Fluorine Chem.* **1981**, *19*, 101.
[92] R. E. Banks, I. Sharif, R. G. Pritchard, *Acta Crystallogr. Sect. C* **1993**, *49*, 492.
[93] W. P. Jencks, *Acc. Chem. Res.* **1980**, *13*, 161.
[94] J. A. Dale, D. L. Dull, H. S. Mosher, *J. Org. Chem.* **1969**, *34*, 2543.
[95] J. A. Dale, H. S. Mosher, *J. Am. Chem. Soc.* **1973**, *95*, 512.
[96] *The Merck Index*, 13th ed., Merck&Co., Whitehouse Station, NJ, **2001**.
[97] J. Fried, E. F. Sabo, *J. Am. Chem. Soc.* **1954**, *76*, 1455.
[98] J. Fried, E. F. Sabo, *J. Am. Chem. Soc.* **1953**, *75*, 2273.
[99] A. Bowers, E. Denot, M. Blanca Sanchez, H. J. Ringold, *Tetrahedron* **1959**, 153.
[100] T. Hayashi, B. W. Murray, R. Wang, C.-H. Wong, *Bioorg. Med. Chem.* **1997**, *5*, 497.
[101] B. W. Murray, V. Wittmann, M. D. Burkart, S.-C. Hung, C.-H. Wong, *Biochemistry* **1997**, *36*, 823.
[102] Y. Kajihara, H. Hashimoto, H. Kodama, T. Wakabayashi, K.-i. Sato, *J. Carbohydr. Chem.* **1993**, *12*, 991.
[103] Y. Kajihara, H. Kodama, T. Wakabayashi, K.-i. Sato, H. Hashimoto, *Carbohydr. Res.* **1993**, *247*, 179.
[104] B. Müller, T. J. Martin, C. Schaub, R. R. Schmidt, *Tetrahedron Lett.* **1998**, *39*, 509.
[105] B. Müller, C. Schaub, R. R. Schmidt, *Angew. Chem.* **1998**, *110*, 3021; *Angew. Chem. Int. Ed.* **1998**, *37*, 2893.
[106] C. Schaub, B. Müller, R. R. Schmidt, *Glycoconjugate J.* **1998**, *15*, 345.
[107] S. G. Withers, *Can. J. Chem.* **1999**, *77*, 1.
[108] D. L. Zechel, S. G. Withers, *Acc. Chem. Res.* **2000**, *33*, 11.
[109] M.-C. Lasne, C. Perrio, J. Rouden, L. Barré, D. Roeda, F. Dolle, C. Crouzel, *Top. Curr. Chem.* **2002**, *222*, 201.
[110] C.-Y. Shiue, P. A. Salvadori, A. P. Wolf, J. S. Fowler, R. R. MacGregor, *J. Nucl. Med.* **1982**, *23*, 899.
[111] R. E. Ehrenkaufer, J. F. Potocki, D. M. Jewett, *J. Nucl. Med.* **1984**, *25*, 333.
[112] S. T. Purrington, W. A. Jones, *J. Org. Chem.* **1983**, *48*, 761.
[113] F. Oberdorfer, E. Hofmann, W. Maier-Borst, *Appl. Radiat. Isot.* **1988**, *39*, 685.
[114] N. Satyamurthy, G. T. Bida, M. E. Phelps, J. R. Barrio, *Appl. Radiat. Isot.* **1990**, *41*, 733.
[115] M. Constantinou, F. I. Aigbirhio, R. G. Smith, C. A. Ramsden, V. W. Pike, *J. Am. Chem. Soc.* **2001**, *123*, 1780.
[116] R. Cirakal, G. Firnau, G. J. Schrobilgen, J. McKay, E. S. Garnett, *Int. J. Appl. Radiat. Isot.* **1984**, *35*, 401.
[117] T. Ido, C.-N. Wan, V. Casella, J. S. Fowler, A. P. Wolf, M. Reivich, D. E. Kuhl, *J. Labelled Compd. Radiopharm.* **1978**, *14*, 175.
[118] H. H. Coenen, V. W. Pike, G. Stöcklin, R. Wagner, *Appl. Radiat. Isot.* **1987**, *38*, 605.
[119] B. Beuthien-Baumann, K. Hamacher, F. Oberdorfer, J. Steinbach, *Carbohydr. Res.* **2000**, *327*, 107.
[120] A. Luxen, M. Guillaume, W. P. Melega, V. W. Pike, O. Solin, R. Wagner, *Int. J. Radiat. Appl. Instrum. Part B* **1992**, *19*, 149.
[121] J. A. Katzenellenbogen, *J. Fluorine Chem.* **2001**, *109*, 49.
[122] Unpublished results.
[123] R. P. Singh, J. M. Shreeve, *Acc. Chem. Res.* **2004**, *37*, 31.

 © 2005 Wiley-VCH Verlag GmbH & Co. KGaA, Weinheim

Asymmetric Synthesis

Recent Developments in the Transfer of Chirality within Enolate Alkylation Reactions

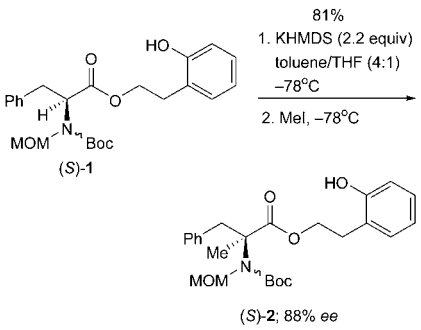
Jason Eames and Michael J. Suggate*

Keywords:
alkylation · asymmetric synthesis · conformational chirality · enantioselectivity · enolates

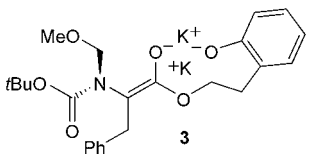
The transfer of chirality within asymmetric synthesis is very well documented.[1] Over the last 25 years, a significant number of these reports have focused on the transfer of chirality from covalently bound chiral auxiliaries to prochiral enol(ate)s.[2] Since 1990,[3] the use of chiral enolate complexes (obtained through complexation of chiral Lewis acids to achiral enol(ate)s) has become more commonplace.[4] However, recent studies have revealed that the use of such an additional chiral component bound to the enolate may not be required for an enolate to be intrinsically chiral.[5]

Kawabata, Fuji, and co-workers elegantly showed[6] that an enantiomerically pure α-amino ester (*S*)-**1** can be alkylated enantioselectively by simple treatment with KHMDS at −78 °C, followed by addition of a suitable S_N2-active electrophile, such as methyl iodide, to give the required substituted ester (*S*)-**2** with 88 % *ee* (Scheme 1). This process is believed to occur via a chelated enolate **3**, which contains axial chirality along the C2–N axis of the enolate owing to the differential substitution pattern of the amino substituent (Scheme 2). This chirality is evidently dynamic, as the enolate is known to racemize at −40 °C over a period of 80 min. The use of a tethered phenol in (*S*)-**1** was found to be particularly important as this group additionally stabilized the enantiomerically pure chiral conformer **3** by at least one order of magnitude relative to that of the ethyl ester,[6] and consequently gave better levels of enantioselectivity. For this chiral enolate conformer, there appear to be two elements of stereogenicity: 1) the oxygen atom of the ester (C–O–CH_2-) motif and 2) the nitrogen atom of the amino group. Both these dynamic components have the potential to enhance the conformational stability of the enolate and to improve the levels of enantioselectivity.

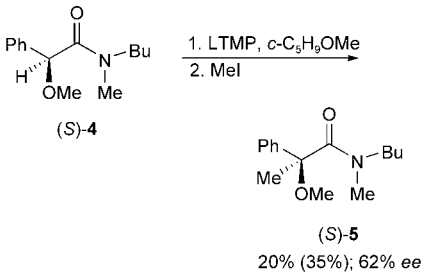
This approach has been extended towards the synthesis of enantiomerically enriched amides such as (*S*)-**5** (Scheme 3).[5] This strategy is similar to that used for the ester in that it relies on an unsymmetrically substituted amino group present within the amide (*S*)-**4** to induce conformational chirality within the corresponding enolate **6** (Scheme 4). The origin of chirality in this enolate is slightly different to that of the enolate **3**,[6] as there only appears to be axial chirality along the C2–N bond. (This



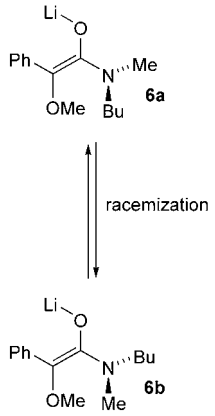
Scheme 1. Enantioselective alkylation of amide (*S*)-**1** with methyl iodide. KHMDS = potassium bis(trimethylsilyl)amide, Boc = *tert*-butoxycarbonyl, MOM = methoxymethyl.



Scheme 2. Formation of conformationally chiral potassium enolate **3**.



Scheme 3. Enantioselective alkylation of unsymmetrically substituted amide (*S*)-**4** with methyl iodide. In brackets yield based on recovered starting material. LTMP = lithium tetramethylpiperidide.



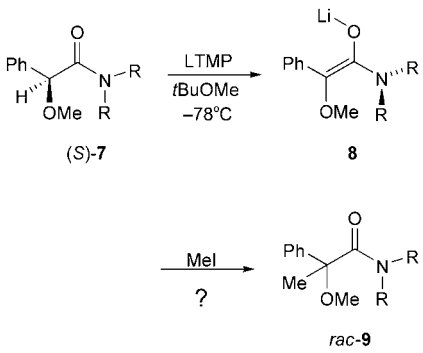
Scheme 4. Interconversion of enantiomeric lithium enolates **6a** and **6b**.

[*] Dr. J. Eames, M. J. Suggate
Department of Chemistry
Queen Mary, University of London
London, E1 4NS (UK)
Fax: (+44) 20-7882-7794
E-mail: j.eames@qmul.ac.uk

 © 2005 Wiley-VCH Verlag GmbH & Co. KGaA, Weinheim DOI: 10.1002/anie.200461617

refers to enolate **6**.) Deprotonation of the amide (*S*)-**4** with LTMP in cyclopentyl methyl ether and subsequent C-alkylation of the intermediate lithium enolate **6**[7] with MeI gave the required substituted amide (*S*)-**5** with moderate levels of enantioselectivity (Scheme 3).

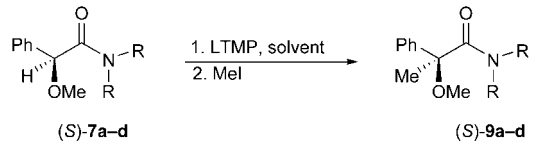
At a glance, this study undoubtedly suggests that the formation of an enolate **8** derived from a chiral symmetrically N,N-disubstituted amide (*S*)-**7**, which has no axial chirality (owing to the substitution pattern of the amino group), and subsequent alkylation would almost certainly lead to the racemic product *rac*-**9** (Scheme 5). However, Kawabata, Fuji, and co-workers recently disproved this idea.[5] They discovered that alkylation of a lithium



Scheme 5. Proposed alkylation of enolate **8**.

enolate derived from a symmetrically N,N-disubstituted amide (*S*)-**7** can lead to an enantiomerically enriched amide (*S*)-**9** with moderate, but significant, enantioselectivity (up to 64% *ee*) (Scheme 6). These results suggest that there is a less clear element of asymmetry present within the lithium enolate aggregate (surrounding the lithium enolate **8**) to account for this enantioselectivity. It is particularly noteworthy that the levels of enantioselectivity are evidently dependent on the levels of diastereoselective C-alkylation of the intermediate chiral lithium enolate **8**, and consequently the relative amount of enantiomerically pure enolate may be significantly underestimated.

The levels of stereocontrol were found to be dependent on the structural nature of the alkyl substituents in (*S*)-**7** and independent on whether the amide was unsymmetrically or symmetrically

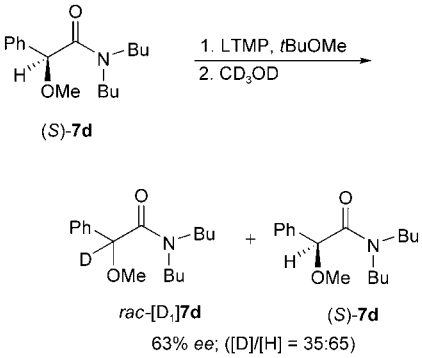


Entry	Starting Material	R	R	Solvent	Product	Yield [%][a]	*ee* [%]
1	**7a**	-$(CH_2)_4$-		*t*BuOMe	(*S*)-**9a**	34 (82)	44
2	**7b**	-$(CH_2)_5$-		*t*BuOMe	(*S*)-**9b**	27 (68)	41
3	**7c**	Me	Me	*t*BuOMe	(*S*)-**9c**	27 (68)	44
4	**7d**	*n*Bu	*n*Bu	*t*BuOMe	(*S*)-**9d**	25[b] (71)	56
5	**7d**	*n*Bu	*n*Bu	THF	(*S*)-**9d**	72 (95)	0
6	**7d**	*n*Bu	*n*Bu	*c*-C_5H_9OMe	(*S*)-**9d**	30[c] (90)	64

Scheme 6. Enantioselective alkylation of amides (*S*)-**7a–d** with methyl iodide. [a] In brackets yields based on recovered starting material. [b] Recovered amide (*S*)-**7d** was isolated with 86% *ee*. [c] Recovered amide (*S*)-**7d** was isolated with 89% *ee*.

N,N-disubstituted; both types of amides, (*S*)-**4** and (*S*)-**7a–d**, gave similar enantioselectivities (62 and 44–56% *ee*, respectively) under identical conditions (Scheme 3 and Scheme 6, entries 1–4). The structural nature of the solvent was found to be very important for the level of enantioselectivity; a symmetric ether such as THF gave no enantioselectivity, whereas unsymmetric ethers such as *tert*-butyl methyl ether and cyclopentyl methyl ether gave moderate stereocontrol (Scheme 6, entries 4–6).

A weakness of this approach appears to be the low conversion of the amides (*S*)-**7** into the required enantiomerically enriched methylated amides (*S*)-**9**. The yields were consistently low (25–34%; Scheme 6, entries 1–4). The starting amides were easily recovered in good yield, and in some cases there was some loss of enantiomeric purity (Scheme 6, entries 4 and 6). To determine the amount of enolate formation, Kawabata, Fuji, and co-workers[5] chose to deprotonate the amide (*S*)-**7d** with LTMP and quench the resulting lithium enolate with CD_3OD; the D-labeled amide (*S*)-[D_1]**7d** was obtained in quantitative yield with moderate D incorporation ([D]/[H] = 35:65; Scheme 7). The enantiomeric excess of this mixture ((*S*)-**7d** and [D_1]**7d**) was found to be 63% *ee*. This presumably shows that deprotonation of amide (*S*)-**7d** and subsequent formation of enolate **8d** occurs in approximately 35% yield. As this virtually mirrors the loss in enantiomeric excess (37%), it appears that stereorandom



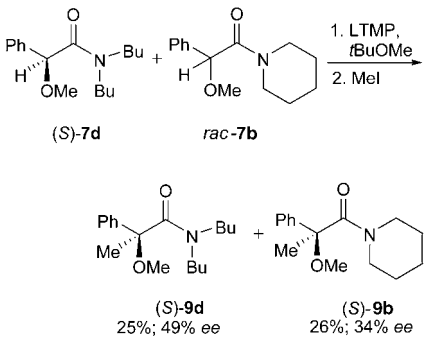
Scheme 7. Deprotonation and *C*-deuteriation of amide (*S*)-**7d**.

deuteration of the enantiomerically pure/enriched enolate **8d** may have occurred.

In an attempt to gain further insight into and comprehension of the origin of this stereocontrol, amides (*S*)-**7d** and *rac*-**7b** (equimolar mixture) were deprotonated with LTMP (1.1 equiv) in *tert*-butyl methyl ether at −78°C, and the resulting enolates were methylated with methyl iodide to give the required amide (*S*)-**9d** in 25% yield with 49% *ee* and the enantiomerically enriched amide (*S*)-**9b** in 26% yield with 34% *ee* (Scheme 8). This intermolecular transfer of chirality from the amide (*S*)-**7d** to *rac*-**7b** is particularly intriguing and suggests the possibility of mixed aggregates.[5]

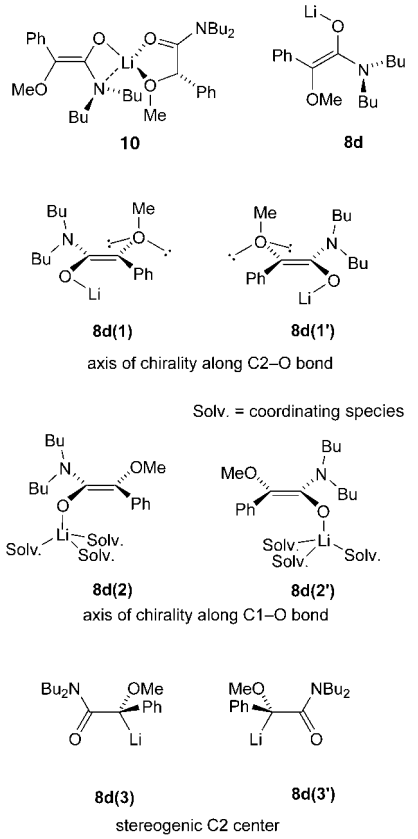
Kawabata, Fuji, and co-workers argued[5] that the chirality transfer may occur from the remaining enantiomerically pure parent amide (*S*)-**7d** within

 © 2005 Wiley-VCH Verlag GmbH & Co. KGaA, Weinheim



Scheme 8. Intermolecular transfer of chirality from amide (*S*)-**7d** to amide (*S*)-**9b**. 59% of (*S*)-**7d** and 67% of *rac*-**7b** were recovered.

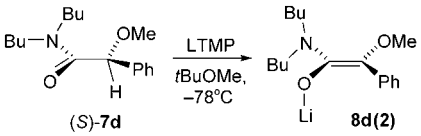
10, the lithium aggregate of the enolate (Scheme 9). Diastereoselective alkylation of the intermediate enolate present in **10** with methyl iodide could potentially lead to the required methylated amide **9d**.[8] They also noted that the original enolate **8d** could potentially have a plane of chirality as a result of restricted rotation around the C2–OMe bond in **8d(1)**, but argued that this rotational barrier would be too small



Scheme 9. Proposed intermediates in the enantioselective alkylation of amide **7d**.

to prevent racemization of this enolate at −78 °C (Scheme 9). However, the rotational barrier of the C1–OLi bond in enolate **8d(2)** may be larger owing to the presence of additional aggregation (to the residual tetramethylpiperidine, solvent, and parent amide). Other possibilities include the formation of chiral C-lithiated intermediates (e.g., **8d(3)**); however, this could be discounted, as related enolates are known to be O-lithiated.[9]

In principle, initial formation of the lithium enolate **8d(2)** may be preferred as a result of the stereospecific deprotonation of the amide (*S*)-**7d** with the lithium amide LTMP (Scheme 10). This

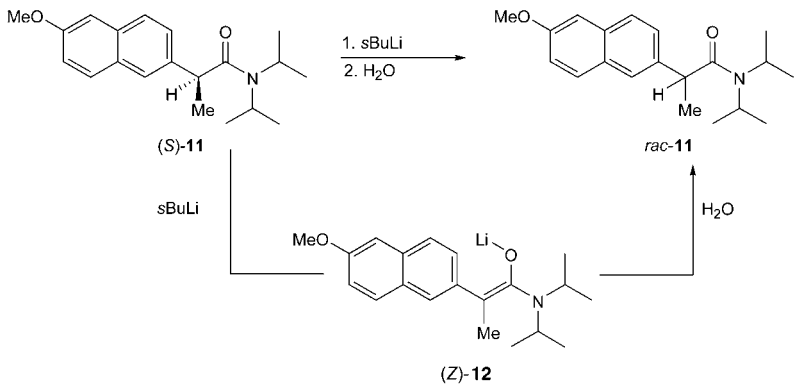


Scheme 10. Proposed deprotonation of amide (*S*)-**7d** to give conformationally chiral enolate **8d**.

deprotonation process was previously shown to occur via a chelated six-membered transition state,[9,10] and intrinsically the resulting enolate would appear to be enantiomerically pure irrespective of its configuration. It was noted that incorporation of additives such as tetramethylethylenediamine, which are known to promote deaggregation by favoring the formation of more-defined mono- or dimeric enolates, only served to lower the overall enantioselectivity from 64 to 33% *ee*; in both cases, the (*S*)-amide **9b** was favored.

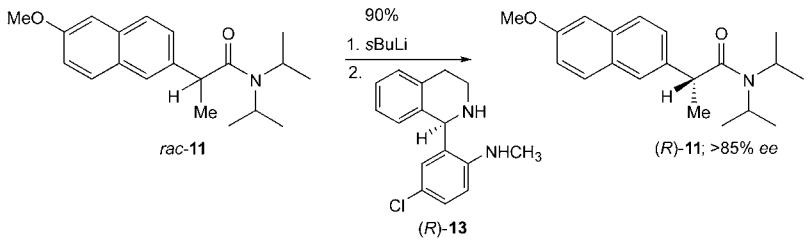
The structures of related prochiral lithium enolates have been determined by single-crystal X-ray diffraction.[9] These lithium enolates were shown to exist as tetra- or dimeric aggregates that contain a plane or point of symmetry. It appears that simple fragmentation of these aggregates to form a combination of monomeric enolates, however, has the potential to lead to (conformationally) chiral intermediates.[11]

The consequence of dynamic enolate chirality has wider implications for other stereoselective processes, for example in the enantioselective C-protonation of enolates to give enantiomerically enriched carbonyl derivatives.[12] Within this area, the intermediate enolate ideally needs to be achiral. However, if the resulting enolate is conformationally chiral, both enantiomeric enolates need to interconvert faster than the rate of stereoselective proton transfer in order to give the required carbonyl derivatives with moderate enantiomeric purity under kinetic control. Vedejs and co-workers[13] reported efficient racemization of a related amide (*S*)-**11** by deprotonation with *s*BuLi followed by C-protonation with H_2O to give the corresponding racemic amide **11** (Scheme 11). In light of findings by Kawabata, Fuji, and co-workers,[5] this suggests that the resulting enolate **12**, if chiral, either racemizes rapidly or is not facially selective C-protonated; in both cases the racemic amide **11** would be formed. However, the racemization would have to be rapid to allow access to both enantiomeric enolates, as protonation with an enantiomerically pure acid, for example, amine (*R*)-**13**, leads to the complementary enantiomerically



Scheme 11. Indirect racemization of amide (*S*)-**11** through deprotonation and reprotonation.

 © 2005 Wiley-VCH Verlag GmbH & Co. KGaA, Weinheim



Scheme 12. Enantioselective synthesis of amide (*R*)-**11**.

enriched amide (*R*)-**11** in high yield (90%) with greater than 85% *ee* (Scheme 12).

In conclusion, Kawabata, Fuji, and co-workers reported[5] an unprecedented transfer of chirality during the alkylation of amides derived from mandelic acid and achiral amines. These reactions proceed by the formation of an intermediate chiral enolate **8** by deprotonation of amides (*S*)-**7** with a lithium amide. Subsequent alkylation of these enolates with MeI leads to the required enantiomerically enriched methylated amides (*S*)-**9**. The origin of this remarkable stereoselective process is thought to be the formation of mixed lithium aggregates such as **10**. However, there could potentially be other forms of hidden chirality present within the enolate substructure and associated aggregates that could assist in this type of enantioselective C-alkylation.

[1] a) T. Kawabata, K. Fuji, *Top. Stereochem.* **2003**, *23*, 175; b) D. Seebach, A. R. Sting, M. Hoffmann, *Angew. Chem.* **1996**, *108*, 2880; *Angew. Chem. Int. Ed. Engl.* **1996**, *35*, 2708; c) S. D. Bull, S. G. Davies, D. J. Fox, A. C. Garner, T. G. R. Sellers, *Pure Appl. Chem.* **1998**, *70*, 1501.

[2] a) D. A. Evans in *Asymmetric Synthesis*, *Vol. 3* (Eds.: J. D. Morrison), Academic Press, New York, **1984**, p. 1; b) D. A. Evans, *Aldrichimica Acta* **1982**, *53*, 23; c) G. Procter, *Asymmetric Synthesis*, Oxford University Press, New York, **1996**; d) D. A. Evans, M. D. Ennis, D. J. Mathre, *J. Am. Chem. Soc.* **1982**, *104*, 1737.

[3] For a recent review, see: P. Arya, H. Qin, *Tetrahedron* **2000**, *56*, 917.

[4] a) E. J. Corey, S. S. Kim, *J. Am. Chem. Soc.* **1990**, *112*, 4976; b) K. Furuta, T. Maruyama, H. Yamamoto, *J. Am. Chem. Soc.* **1991**, *113*, 1041; c) E. Carreira, R. A. Singer, W. Lee, *J. Am. Chem. Soc.* **1994**, *116*, 8837; d) D. A. Evans, M. C. Kozlowski, C. S. Burgey, D. W. C. MacMillan, *J. Am. Chem. Soc.* **1997**, *119*, 7893.

[5] T. Kawabata, O. Ozturk, J. Chen, K. Fuji, *Chem. Commun.* **2003**, 162.

[6] T. Kawabata, S. Kawakami, K. Fuji, *Tetrahedron Lett.* **2002**, *43*, 1465.

[7] The chirality of the intermediate enolate **6** is unknown—for additional information, see reference [5].

[8] The enantioselectivity was found to be independent of the conversion. Consequently, increasing concentrations of the product have no effect on the overall level of enantioselectivity.

[9] For an elegant and comprehensive account of the structure and chemistry of enolates, see: D. Seebach, *Angew. Chem.* **1988**, *100*, 1685; *Angew. Chem. Int. Ed. Engl.* **1988**, *27*, 1624.

[10] R. E. Ireland, P. Wipf, J. D. Armstrong III, *J. Org. Chem.* **1991**, *56*, 650.

[11] For example, fragmentation of a *meso* dimer can potentially lead to a racemic pair of conformationally chiral enolates. Whereas, fragmentation of an achiral dimer can potentially give two chiral enolates of the same absolute configuration. The absolute sense of configuration is dependent on the position of fragmentation.

[12] a) J. Eames, N. Weerasooriya, *Tetrahedron: Asymmetry* **2001**, *12*, 1; b) C. Fehr, *Angew. Chem.* **1996**, *108*, 2726; *Angew. Chem. Int. Ed. Engl.* **1996**, *35*, 2566, and references therein.

[13] a) E. Vedejs, A. W. Kruger, N. Lee, S. T. Sakata, M. Stec, E. Suna, *J. Am. Chem. Soc.* **2000**, *122*, 4602; b) E. Vedejs, A. W. Kruger, E. Suna, *J. Org. Chem.* **1999**, *64*, 7863; c) E. Vedejs, N. Lee, S. T. Sakata, *J. Am. Chem. Soc.* **1994**, *116*, 2175; d) E. Vedejs, N. Lee, *J. Am. Chem. Soc.* **1991**, *113*, 5483.

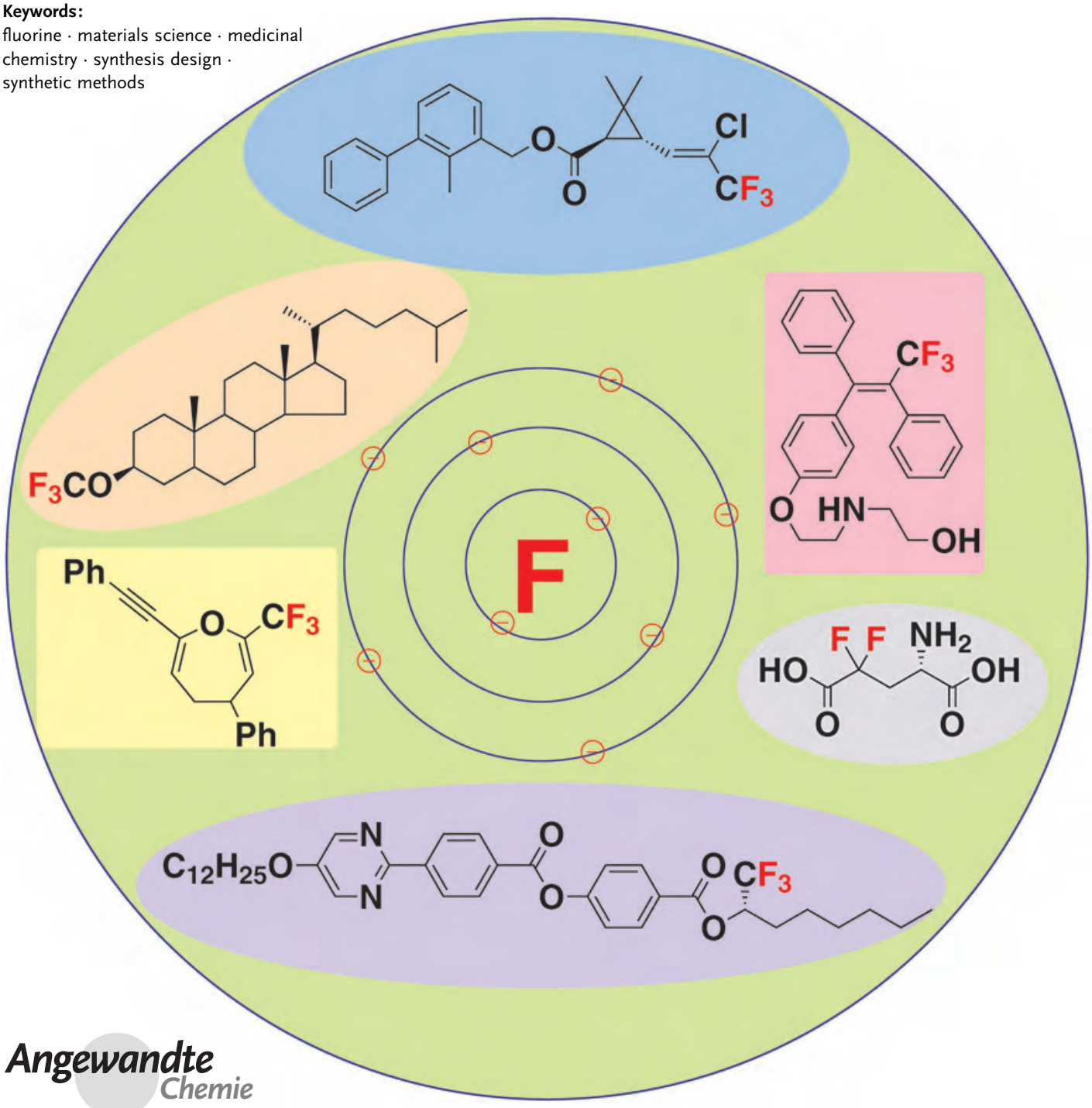
 © 2005 Wiley-VCH Verlag GmbH & Co. KGaA, Weinheim

Organofluorine Compounds

Modern Synthetic Methods for Fluorine-Substituted Target Molecules

*Masaki Shimizu and Tamejiro Hiyama**

Keywords:
fluorine · materials science · medicinal chemistry · synthesis design · synthetic methods



© 2005 Wiley-VCH Verlag GmbH & Co. KGaA, Weinheim
DOI: 10.1002/anie.200460441

Fluorine has come to be recognized as a key element in materials science: in heat-transfer agents, liquid crystals, dyes, surfactants, plastics, elastomers, membranes, and other materials. Furthermore, many fluorine-containing biologically active agents are finding applications as pharmaceuticals and agrochemicals. Progress in synthetic fluorine chemistry has been critical to the development of these fields and has led to the invention of many novel fluorinated molecules as future drugs and materials. As a result of the electronic effects of fluorine substituents, fluorinated substrates and reagents often exhibit unusual and unique chemical properties, which often make them incompatible with established synthetic methods. Thus, the problem of how to control the unusual properties of compounds with fluorine substituents deserves much attention, so as to promote the design of facile, efficient, and environmentally benign methods for the synthesis of valuable organofluorine targets.

From the Contents

1. Introduction 215
2. Classification of Synthetic Methods 216
3. Oxidative Desulfurization–Fluorination 216
4. Fluorine-Containing Polyhaloalkyl Metal Reagents 219
5. Trifluoromethyl-Substituted Oxiranyl Lithium Reagents 223
6. A Facile Route to Seven-Membered Oxacycles 224
7. Stereoselective Synthesis of CF_3-Containing Tetrasubstituted Alkenes 225
8. Asymmetric Synthesis of 1,1,1-Trifluoro-2-alkanols 227
9. Summary 228

1. Introduction

As the most electronegative element, fluorine has played a key role in recent pharmaceutical, agrochemical, and materials science. As the incorporation of fluorine and/or fluorine-containing groups into an organic molecule often drastically perturbs the chemical, physical, and biological properties of the parent compound (Figure 1), it is thought that the synthesis of desired fluorinated compounds should lead to the invention of novel agents and materials endowed with prerequisite functions.[1] Since a basic discussion of such fluorine effects is found in many books and reviews,[1,2] we do not cover them in detail herein. Instead we draw your attention to the very recent special issue of *ChemBioChem* on "Fluorine in the Life Sciences", which provides a very comprehensive and up-to-date picture of fluoroorganic compounds and fluorine effects.[3]

Because naturally occurring organofluorine compounds are rare, target organofluorine compounds are accessible solely by organic synthesis. With respect to chemical reactivity and stability, fluorinated compounds behave in a unique manner owing to so-called inductive and resonance effects caused by fluorine.[4] For example, fluorine-substituted carbocations are stabilized by the donation of nonbonding electron pairs on the fluorine atom, whereas electrostatic p–n repulsion between an anionic center and the lone pairs of electrons on the fluorine atom destabilizes a fluorine-substituted anionic center (Figure 2). Similarly, n–π repulsion between the lone pairs and a π-electron system pushes the π electrons far apart. Furthermore, a resonance effect operates in which the lone pairs participate in conjugation with the π system.

Like various other fluorine-containing groups, trifluoromethyl groups at C(sp^2) and C(sp^3) centers always withdraw electrons to destabilize cations and to stabilize anions (Figure 3). This anion stabilization can also be understood to be a result of negative hyperconjugation, an overlap of an anionic p orbital with the σ* orbital of a C–F bond.[5]

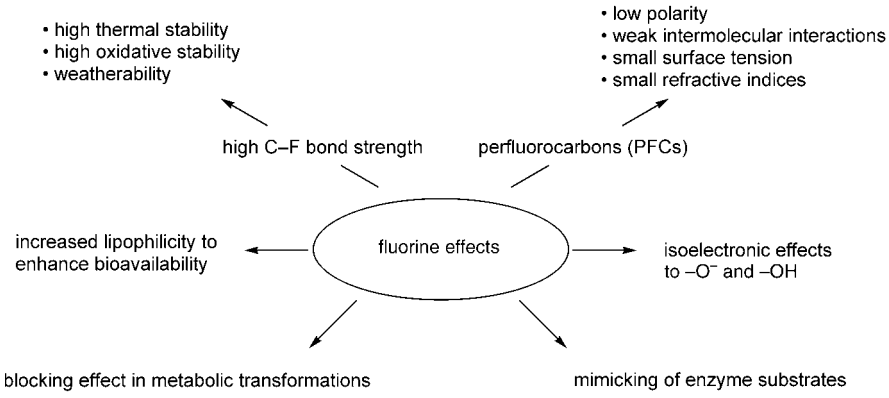


Figure 1. Fluorine effects in biologically active agents and materials.

[*] Dr. M. Shimizu, Prof. Dr. T. Hiyama
Department of Material Chemistry
Graduate School of Engineering
Kyoto University, Nishikyo-ku, Kyoto 615-8510 (Japan)
Fax: (+81) 75-383-2445
E-mail: thiyama@npc05.kuic.kyoto-u.ac.jp

DOI: 10.1002/anie.200460441
© 2005 Wiley-VCH Verlag GmbH & Co. KGaA, Weinheim

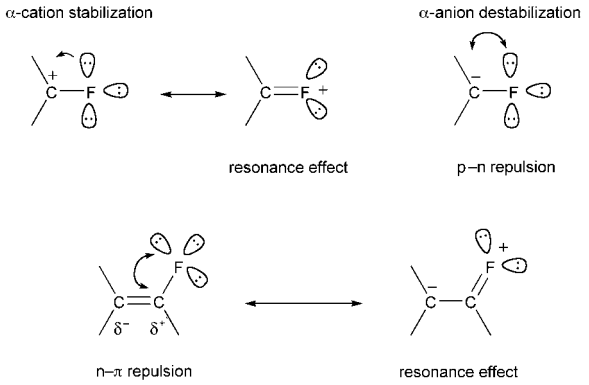


Figure 2. α-Fluorine effects.



Figure 3. α-CF_3 effects on carbocations and carbanions.

Trifluoromethyl groups also strongly affect chemical reactivity. For example, nucleophilic substitution at a trifluoromethyl-substituted carbon atom is not an easy process. The difficulty is attributed to destabilization of the transition state by fluorine and also to electrostatic repulsion between a nucleophile and the lone pairs of electrons on the fluorine atoms. There are many phenomena that can be understood in terms of C–H···F or C–M···F interactions, although such interactions are still a topic of controversy.[6]

In view of the unique characteristics of fluorine, it is easy to recognize that conventional synthetic methods are not always applicable to the synthesis of organofluorine compounds. Thus, a deep understanding of the nature of reaction mechanisms, reagents, and synthetic strategies based on the unique chemical and physical properties of fluorine is essential.[7] Herein we describe some novel synthetic methods, particularly those we have developed over the last two decades for the preparation of fluorine-substituted target molecules, focusing on oxidative desulfurization–fluorination, synthetic reactions based on fluorine-containing polyhaloalkyl metal reagents and CF_3-substituted oxiranyl lithium reagents, and the asymmetric synthesis of 1,1,1-trifluoro-2-alkanols.

2. Classification of Synthetic Methods

Synthetic methods for the synthesis of organofluorine compounds are roughly classified into two basic strategies: the fluorination method and the building-block method. Fluorination includes C–F bond formation through the transformation of a C–H bond or a functional group by treatment with a fluorinating reagent, such as elemental fluorine (F_2), hydrogen fluoride (HF), or derivatives thereof.[8] This is a straightforward method for the introduction of fluorine atoms into target molecules, especially when the fluorination can be carried out with high regio- and chemoselectivities. However, the handling of such fluorinating reagents requires special apparatus, techniques, and care, as the reagents are usually extraordinarily reactive and toxic, often as a result of corrosive HF that is released. Hence, methods that employ reagents with moderate reactivity under mild conditions are needed for the facile synthesis of fluorine-containing target molecules.

The building-block method involves appropriate chemical transformations starting from fluorinated small molecules (building blocks).[9] Since standard experimental procedures are applicable, this approach is more familiar to synthetic chemists. The ready availability and easy handling of fluorine-containing building blocks are essential for the success of this approach. However, fluorine substitution very often causes abnormal behavior with regard to the reactivity and/or selectivity of these building blocks relative to that of their nonfluorinated counterparts, thus providing a challenge to synthetic chemists to overcome these fluorine effects.

3. Oxidative Desulfurization–Fluorination

Many reagents for nucleophilic fluorination are now available. Representative examples are hydrogen fluoride (HF, b.p. 19.54 °C), its aqueous solution (hydrofluoric acid), sulfur tetrafluoride (SF_4), and diethylaminosulfur trifluoride (DAST); these reagents are, however, very reactive, corro-



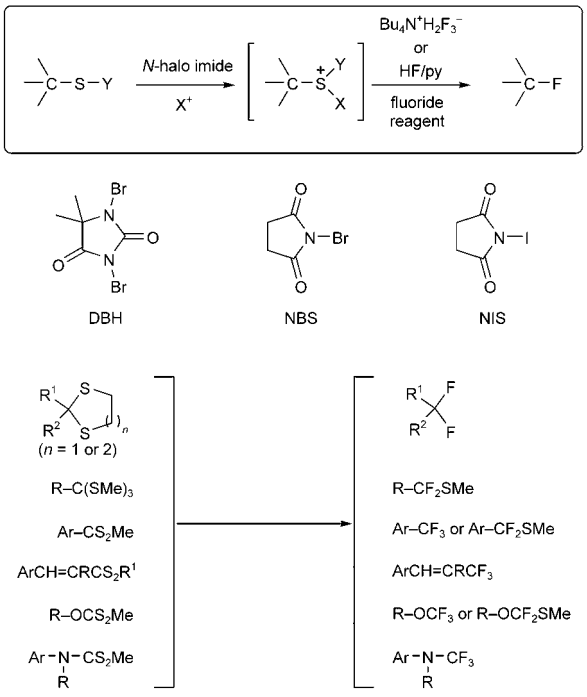
Born in Osaka in 1946, Tamejiro Hiyama completed his PhD in engineering at Kyoto University in 1975 (mentor: Hitoshi Nozaki). He undertook postdoctoral research at Harvard University with Yoshito Kishi, received the Young Chemist Award of the Chemical Society of Japan in 1980, and in 1981 started his own research team at Sagami Chemical Research Center. He moved in 1992 to Tokyo Institute of Technology as Professor, and since 1997 has been Professor of Organic Materials at Kyoto University. His research interests include organofluorine and organosilicon chemistry, as well as the synthesis of biologically active substances and materials with novel functionality.



Masaki Shimizu was born in 1965 in Tokyo. He completed his PhD at Tokyo Institute of Technology in 1994 (Takeshi Nakai and Koichi Mikami). He was a research associate at Mitsubishi Chemical Co., then from 1995 at Tokyo Institute of Technology. In 1998, he moved to Kyoto University as Assistant Professor. He spent one year at Massachusetts Institute of Technology as a postdoctoral fellow (S. L. Buchwald) and was promoted to Associate Professor at Kyoto University in 2003. His research interests focus on synthetic methods with organofluorine compounds and organometallic reagents, and functional organosilicon materials.

 © 2005 Wiley-VCH Verlag GmbH & Co. KGaA, Weinheim

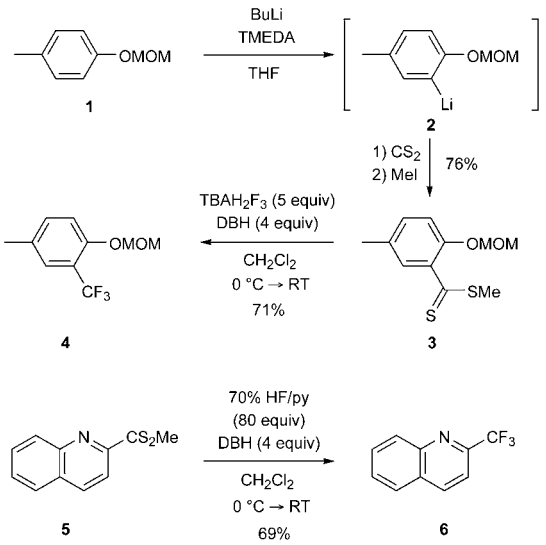
sive, and toxic. When they are modified for more convenient handling, their nucleophilicity often decreases. To facilitate nucleophilic attack of a substrate by the modified reagent, electrophilic substrate activation by an oxidant is quite effective, as exemplified in the halofluorination of alkenes and alkynes,[10] the thio- and selenofluorination of alkenes,[11] and nitrofluorination.[12] We have applied this concept to organosulfur compounds, a readily accessible class of organic compounds (Scheme 1).[13] The basic idea involves activation



Scheme 1. Oxidative desulfurization–fluorination. py = pyridine.

of a C–S bond by a positive halogen generated from *N*-iodosuccinimide (NIS), *N*-bromosuccinimide (NBS), or 1,3-dibromo-5,5-dimethylhydantoin (DBH), followed by nucleophilic substitution with a fluoride ion from HF/pyridine (Olah reagent) or tetrabutylammonium dihydrogen trifluoride ($TBAH_2F_3$). This methodology is called oxidative desulfurization–fluorination and is applicable to the preparation of various types of organofluorine compounds. The scope is summarized in Scheme 1. The following paragraphs present some representative examples that demonstrate the versatility of this method.

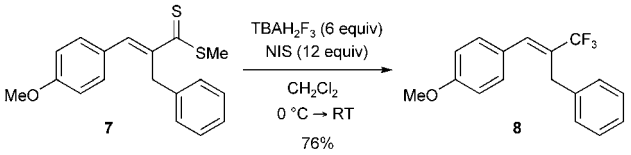
Trifluoromethyl-substituted aromatic compounds can be prepared from the corresponding arenedithiocarboxylates with $TBAH_2F_3$ and DBH.[14] For example, the *ortho* lithiation of *p*-cresol methoxymethyl (MOM) ether (**1**), followed by trapping of the resulting anion **2** with carbon disulfide and then with iodomethane, produces the dithiocarboxylate **3**, which is smoothly converted into the trifluoromethyl-substituted *p*-cresol derivative **4** in good overall yield (Scheme 2). The trifluorination of dithiocarboxylates is applicable to heteroaromatic compounds, such as the quinoline derivative **5**: A combination of DBH and 70% HF/pyridine as the



Scheme 2. Synthesis of trifluoromethyl-substituted aromatic compounds. TMEDA = *N*,*N*,*N*′,*N*′-tetramethylethylenediamine.

fluoride source was the best system for the transformation of electron-deficient heteroaromatic compounds.

The α,β-unsaturated dithiocarboxylate **7** undergoes trifluoromethylation with a combination of $TBAH_2F_3$ and NIS, giving rise to the 1-aryl 3,3,3-trifluoropropene **8** (Scheme 3).[14] Other combinations (HF/pyridine in place of $TBAH_2F_3$; DBH or NBS in lieu of NIS) were ineffective for this transformation.

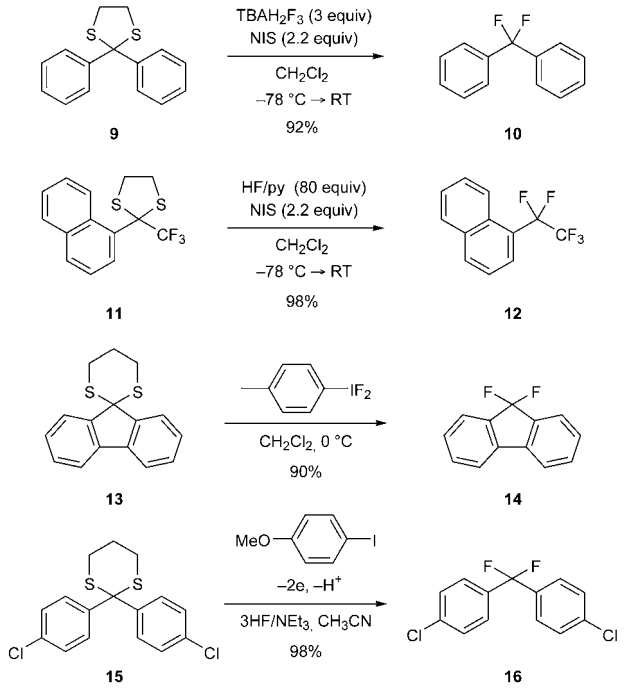


Scheme 3. Synthesis of the 1-aryl 3,3,3-trifluoropropene **8**.

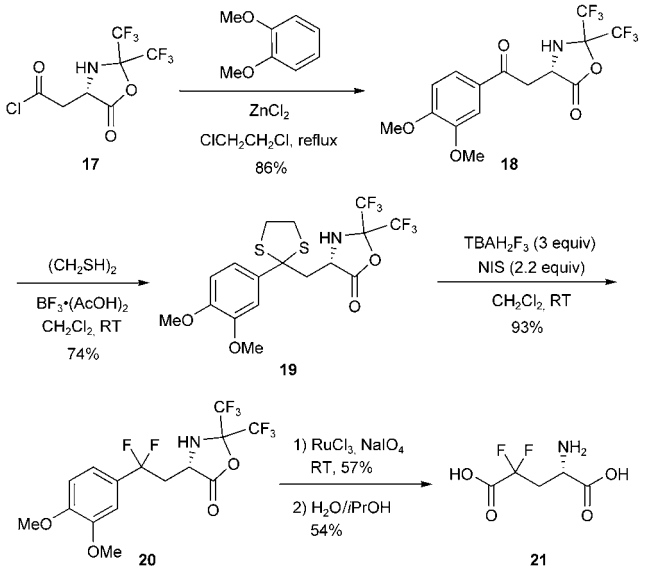
Since the introduction of a *gem*-difluoromethylene moiety into biologically active but unstable agents considerably improves their biostability, there is a need for facile and versatile methods for the construction of difluoromethylene groups.[15] Upon treatment with NIS and $TBAH_2F_3$ or HF/pyridine, the dithioacetals of benzophenone **9** and 1-naphthyl trifluoromethyl ketone **11** afford **10** and **12**, respectively, in high yields (Scheme 4).[16] When DBH is employed as the oxidant, the difluorination is sometimes accompanied by halogenation of the aromatic ring. The same type of transformation can be performed with *p*-$CH_3C_6H_4IF_2$ and electrochemically generated *p*-$(MeO)C_6H_4IF_2$ (Scheme 4).[17] The synthetic utility of this strategy is demonstrated by the synthesis of the difluoroglutamic acid **21** (Scheme 5).[18]

Difluoroalkyl ethers and difluoromethylenedioxy compounds can be prepared from thione esters and thione carbonates, which are in turn readily accessible from esters and carbonates by treatment with the Lawesson reagent ((*p*-$(MeO)C_6H_4P(=S)S)_2$).[19] For example, in the presence of

 © 2005 Wiley-VCH Verlag GmbH & Co. KGaA, Weinheim



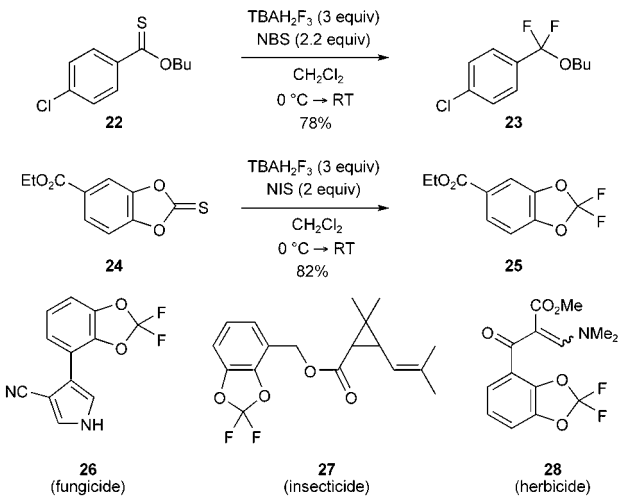
Scheme 4. Oxidative desulfurization–fluorination of dithioacetals derived from aryl ketones.



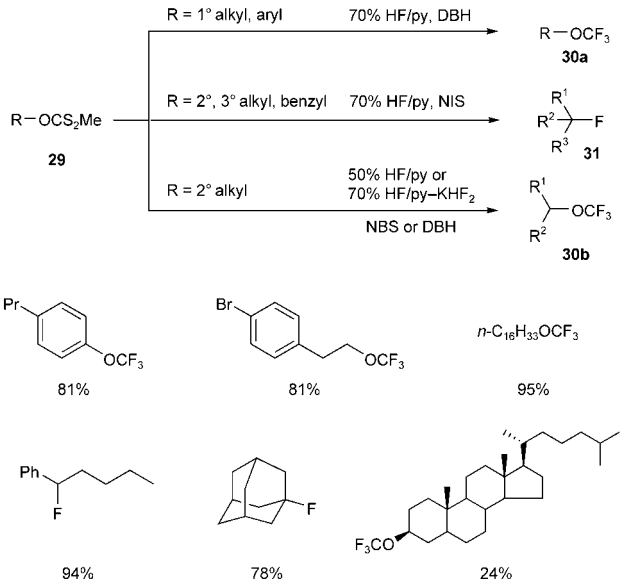
Scheme 5. Synthesis of the difluoroglutamic acid **21**.

$TBAH_2F_3$ and NBS (or NIS) the thione ester **22** and carbonate **24** are converted into **23** and **25**, respectively, in good yields (Scheme 6). This approach is useful for the preparation of biologically active substances containing a difluoromethylenedioxy moiety, such as **26**, **27**, and **28**.

Trifluoromethyl ethers **30a** of primary alcohols and phenols can be prepared from the corresponding xanthates **29** with 70% HF/pyridine and DBH (Scheme 7).[20] In contrast, the treatment of xanthates derived from secondary or tertiary alcohols with 70% HF/pyridine and NIS results in



Scheme 6. Preparation of difluoroalkyl ethers and difluoromethylenedioxy compounds.



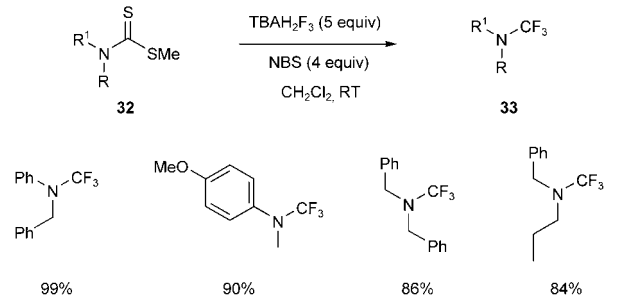
Scheme 7. Synthesis of trifluoromethyl ethers and alkyl fluorides from dithiocarbonates.

fluorination, giving rise to secondary or tertiary fluorides **31**, respectively. However, the use of milder fluorinating reagents, such as 50% HF/pyridine or 70% HF/pyridine with KHF_2, for the reaction of secondary xanthates **29** allows the isolation of secondary alkyl trifluoromethyl ethers **30b**. This reaction is in sharp contrast with that carried out in the presence of $TolIF_2$ in which only fluorination products are formed.[21] 3β-Trifluoromethoxycholestane prepared by this method was found to act as a chiral dopant for twisted-nematic liquid-crystal displays.[22] Cyclohexyl trifluoromethyl ethers prepared in a similar way are potential future materials for TFT (thin-film transistor for active matrix) displays.[23]

Dithiocarbamates **32**, readily available from secondary amines, carbon disulfide, and methyl iodide, are converted

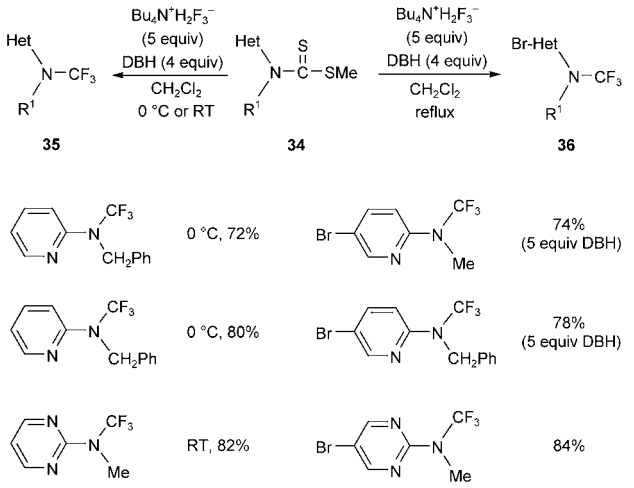
 © 2005 Wiley-VCH Verlag GmbH & Co. KGaA, Weinheim

into trifluoromethyl amines **33** by treatment with $TBAH_2F_3$ and NBS (Scheme 8).[23] This protocol is applicable to both aromatic and aliphatic amines. Aryl trifluoromethylamines are stable to moisture, whereas dialkyl trifluoromethylamines are easily hydrolyzed. The presence of a trifluoromethyl group on the nitrogen atom retards oxidation of the amino group.



Scheme 8. Synthesis of trifluoromethylamines.

The trifluoromethylation of heteroarenedithiocarbamates **34** with DBH at 0 °C or room temperature gives trifluoromethylamines **35**, whereas the same reaction in CH_2Cl_2 at reflux causes selective bromination of the aromatic ring at the *para* position as well as trifluorination to produce **36** (Scheme 9).[23]



Scheme 9. Oxidative desulfurization–fluorination of heteroaryl dithiocarbamates.

4. Fluorine-Containing Polyhaloalkyl Metal Reagents

Since halogen–metal exchange is a relatively facile process, the reduction of commercially available fluorine-containing polyhaloalkanes, so-called halons, with a metal or an organometallic reagent would be a versatile method for the generation of fluorine-containing carbenoids, if the stability and reactivity of the reagents could be controlled.[24]

The artificial pyrethroids bifenthrin and cyhalothrin, both of which contain $CH{=}C(Cl)CF_3$ in lieu of $CH{=}CMe_2$ or $CH{=}CCl_2$, are highly potent, exhibiting remarkably enhanced activity relative to nonfluorinated congeners (Figure 4).[25] We have established a practical and stereocontrolled approach to

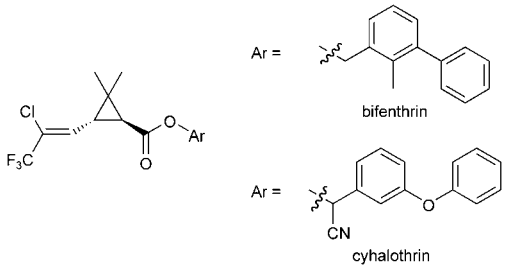
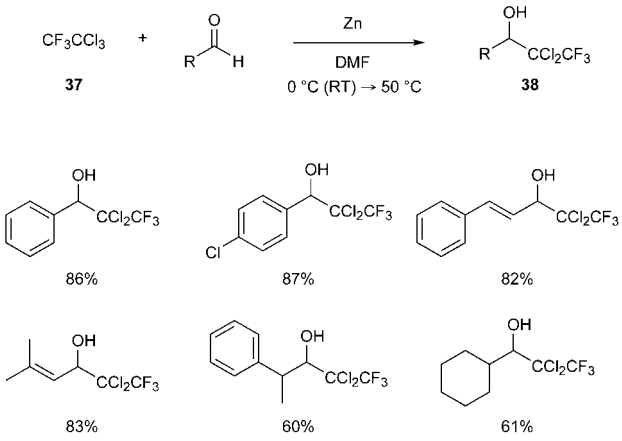


Figure 4. Examples of artificial pyrethroids.

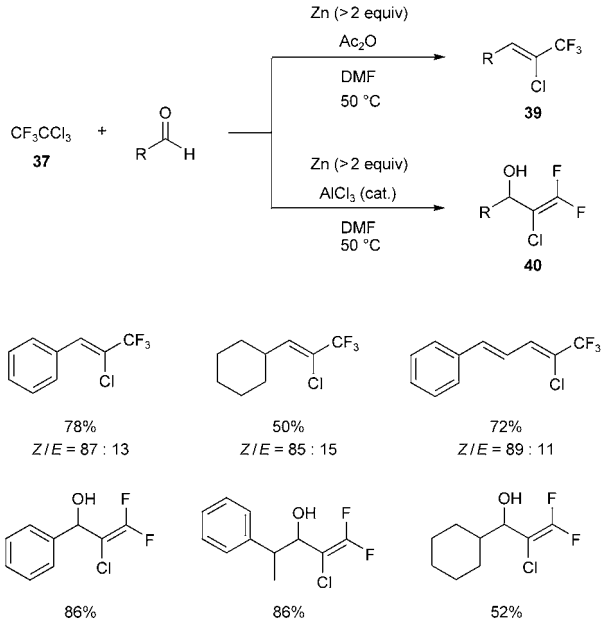
di- and trifluorinated synthetic pyrethroids based on the addition of CF_3CCl_2ZnCl to aldehydes and reductive olefination of the adducts.[26] The two-step transformation can also be carried out in one pot. The reduction of CF_3CCl_3 (**37**) with zinc metal in DMF at 50 °C generates the thermally stable zinc carbenoid CF_3CCl_2ZnCl, which reacts with various aldehydes, including aromatic, aliphatic, and α,β-unsaturated aldehydes, to give alcohols **38** in good yields (Scheme 10). A similar transformation was disclosed independently by Lang and coworkers, who were successful in isolating the carbenoid and showed it to be monomeric in the solid state by single-crystal X-ray diffraction.[27,28]



Scheme 10. Generation of CF_3CCl_2ZnCl and addition to aldehydes. DMF = *N*,*N*-dimethylformamide.

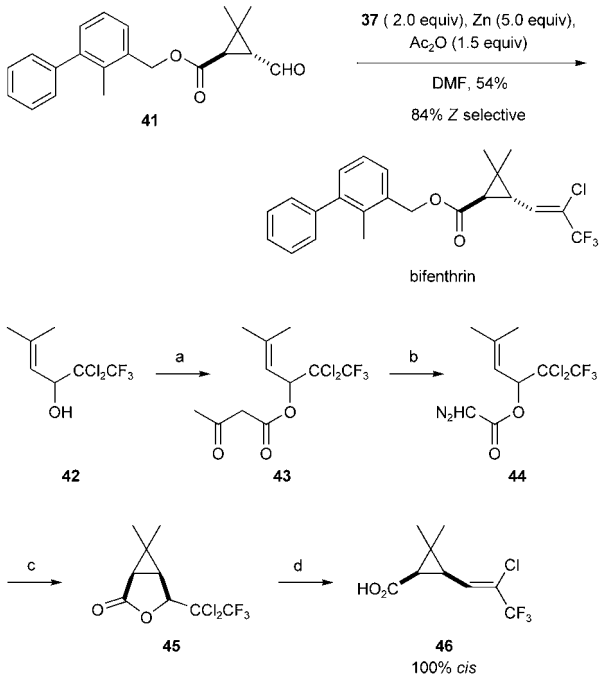
The use of zinc in excess (> 2 equiv) in the presence of acetic anhydride in DMF at 50 °C induces reductive β elimination of chloride and acetate ions to afford 2-chloro-1,1,1-trifluoro-2-alkenes **39** in one pot with *Z* selectivity. 2-Chloro-1,1-difluoro-1-alken-3-ols **40** are obtained conveniently by the 1,2-elimination of chloride and fluoride when a catalytic amount of aluminum chloride is employed instead of acetic anhydride (Scheme 11).[29]

 © 2005 Wiley-VCH Verlag GmbH & Co. KGaA, Weinheim



Scheme 11. One-pot synthesis of polyfluorinated alkenes **39** and **40** from CF_3CCl_3.

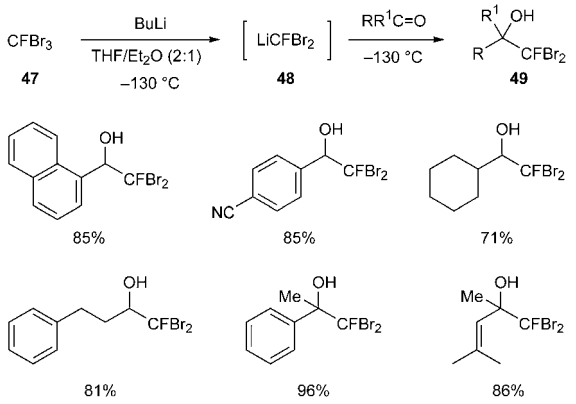
The synthetic versatility of this method is demonstrated by a one-step synthesis of bifenthrin, in which the non-methyl substituents on the cyclopropane ring are in a *trans* relationship (Scheme 12).[30] In a complementary sequence, the *cis* cyclopropanecarboxylic acid **46** can be formed stereoselectively from the adduct **42** through diazoacetylation,



Scheme 12. Synthesis of bifenthrin and the *cis* cyclopropane **46**: a) diketene, K_2CO_3 (88%); b) TsN_3, NEt_3, then NaOH (82%); c) [Cu(acac)$_2$], dioxane (75%); d) Zn, DMF (84%). acac = acetylacetonate, Ts = *p*-toluenesulfonyl.

intramolecular cyclopropanation, and reduction with zinc. The present method constitutes a practical approach to the preparation of 3,3,3-trifluoroprop-1-enyl-substituted cyclopropanecarboxylic acids, a key fragment of highly potent artificial pyrethroids.

In contrast to that of perfluoroalkyl metal reagents, the chemistry of monofluoroalkyl metal reagents still remains to be explored. We succeeded in generating dibromofluoromethyllithium (**48**), which underwent addition to carbonyl derivatives as shown in Scheme 13.[31] The carbenoid reagent



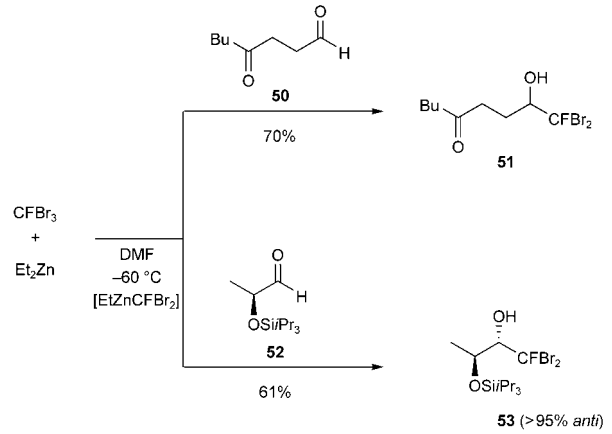
Scheme 13. Generation of $LiCFBr_2$ (**48**) and addition to carbonyl compounds.

48 is prepared by the treatment of tribromofluoromethane (**47**) with butyllithium at −130 °C in a solvent mixture of THF/Et_2O (2:1) in the presence of the aldehyde or ketone substrate. A variety of dibromofluoromethylated alcohols **49** were prepared in high yields in this way. Since **48** reportedly undergoes decomposition through α elimination leading to :CFBr even at −116 °C,[32] its generation at −130 °C in the presence of an electrophile is essential for the success of the transformation.

An alternative reagent to **48** is a zinc carbenoid prepared by bromine–zinc exchange of tribromofluoromethane with diethylzinc in DMF at −60 °C. The zinc carbenoid makes it possible to perform the whole transformation at higher temperatures with high chemoselectivity: Aldehydes are favored significantly over ketones.[33] For example, the ketoaldehyde **50** reacts with the carbenoid to give only the aldehyde adduct **51** (Scheme 14). Diastereoselective addition to the lactaldehyde silyl ether **52** is also possible with the zinc reagent.

Fluoroolefins play essential roles in liquid-crystalline materials as well as peptide isosteres and enzyme inhibitors.[34] Since the physical properties and biological activity of fluoroolefins greatly depend on configuration, their stereocontrolled synthesis is indispensable. For the stereoselective synthesis of various types of fluoroolefins, stereodefined bromofluoroolefins serve as valuable precursors, as the cross-coupling of bromofluoroolefins with various organometallic reagents in general proceeds to give the target molecules with retention of configuration.[35] Therefore, any new method for

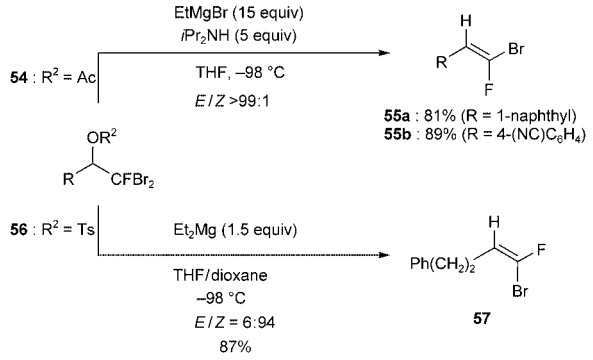
 © 2005 Wiley-VCH Verlag GmbH & Co. KGaA, Weinheim



Scheme 14. Chemoselective and stereoselective addition of $EtZnCFBr_2$ to aldehydes.

the facile and stereoselective synthesis of bromofluoroolefins[36] leads to a versatile entry to fluoroolefins.

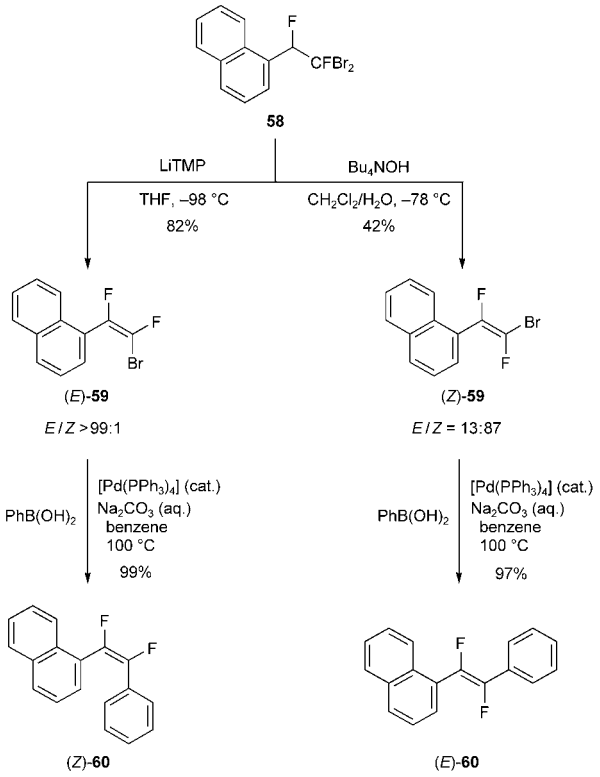
To this end, dibromofluoromethylated alcohols **49** serve as the precursors of bromofluoro- and bromodifluoroolefins. Acetates **54** derived from **49** ($R^1 = H$) are converted into (*E*)-1-bromo-1-fluoro-1-alkenes **55** stereoselectively upon treatment with EtMgBr (15 equiv) and iPr_2NH (5 equiv), as shown in Scheme 15. On the other hand, bromine–magnesium exchange of the tosylate **56** ($R = Ph(CH_2)_2$) with Et_2Mg (1.5 equiv) provides **57** with high *Z* selectivity.



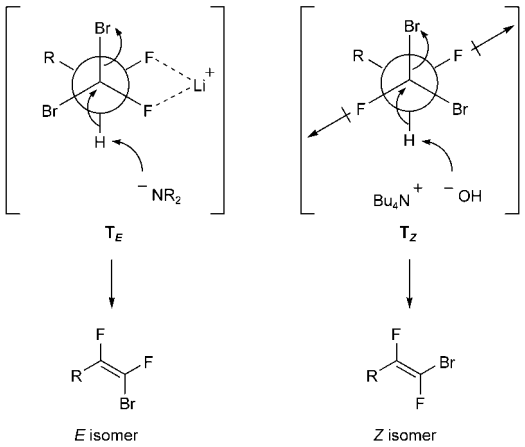
Scheme 15. Stereoselective synthesis of bromofluoroolefins.

The synthesis of 1-bromo-1,2-difluoro-1-alkenes was carried out by dehydrobromination of 1,1-dibromo-1,2-difluoroalkanes, which can be readily prepared from **49** by fluorination with DAST at −78 °C. The treatment of **58** with lithium 2,2,6,6-tetramethylpiperidide (LiTMP) produces (*E*)-**59** as a single diastereomer, whereas (*Z*)-**59** forms preferentially when the metal-free base tetrabutylammonium hydroxide is employed (Scheme 16). These bromides couple with various aryl metal reagents (metal = B, Si, Sn, or Zn): The reaction with $PhB(OH)_2$ is illustrated in Scheme 16.

The stereoselectivity observed in the base-dependent elimination of **58** can be rationalized by a transition-state model that involves chelation of a metal center for *E*-selective elimination and dipole–dipole repulsion of C–F bonds for *Z*-selective elimination with a metal-free base (Scheme 17). In other words, dehydrobromination with LiTMP should proceed via $\mathbf{T}_E$, in which two fluorine atoms are in a synclinal arrangement as a result of Li–F chelation, to produce the



Scheme 16. Stereodivergent synthesis of difluoroolefins.



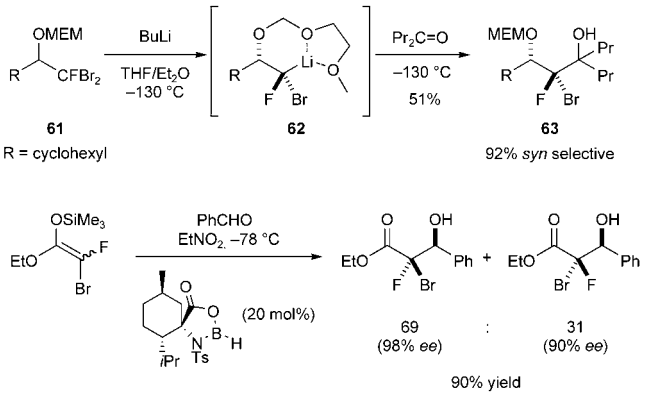
Scheme 17. Transition-state models for stereoselective dehydrobromination.

E isomer. On the other hand, the elimination of HBr takes place with Bu_4NOH via $\mathbf{T}_Z$, wherein two C–F bonds prefer to adopt an antiperiplanar arrangement owing to dipole–dipole repulsion, thus giving the *Z* isomer.

Treatment of the MEM (methoxyethoxymethyl) ether **61** with BuLi in THF/Et_2O (2:1) at −130 °C generates the

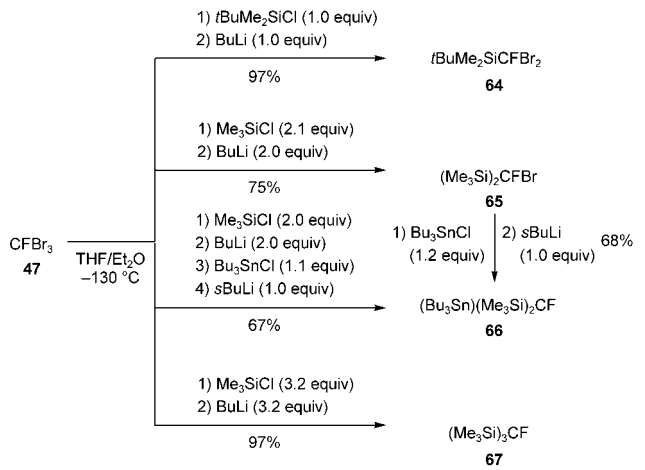
 © 2005 Wiley-VCH Verlag GmbH & Co. KGaA, Weinheim

corresponding lithium carbenoid **62**, which can be trapped selectively with 4-heptanone to give the 2-bromo-2-fluoro-1,3-alkanediol derivative **63**.[37] The stereochemical outcome can be explained by the stereoselective generation of the carbenoid **62** through chelation of the lithium ion by the oxygen atoms of the MEM group. The enantioselective synthesis of 2-bromo-2-fluoro-1-hydroxy derivatives is possible by aldol reactions of bromofluoroketene ethyl silyl acetals with aldehydes catalyzed by a chiral Lewis acid (Scheme 18).[38]



Scheme 18. Diastereoselective and enantioselective construction of 2-bromo-2-fluoro-1-alcohols.

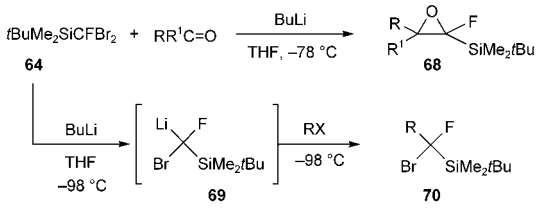
One possibility to improve the thermal stability of fluorine-substituted carbenoids derived from tribromofluoromethane is the introduction of a silyl group at the carbenoid carbon atom, as silyl groups can stabilize an anionic center. Furthermore, the silyl group in the product offers opportunities for functional-group transformations.[39] The fluoromethanes **64**, **65**, and **67** substituted with one, two, or three silyl groups, respectively, are readily prepared by the treatment of $CFBr_3$ (**47**) at −130 °C with appropriate stoichiometric amounts of butyllithium in the presence of a chlorosilane (Scheme 19).[40] The fluorobis(silyl)stannylmethane **66** is accessible from **65** through lithiation followed by stannylation. The mixed fluorometallomethane **66** can alternatively



Scheme 19. Preparation of poly(triorganosilyl)methanes from **47**.

be prepared directly from **47** by stepwise silylation and stannylation of the corresponding carbenoids.

The generation of the *tert*-butyldimethylsilyl-substituted carbenoid **69** and its addition to carbonyl compounds is possible at −78 °C, thus clearly demonstrating, as expected, that **69** is more stable than **48**, which should be handled at −130 °C (Scheme 20). When the reaction mixture is warmed to room temperature, 1-fluoro-1-silyloxiranes **68** are produced in good to excellent yields. No product resulting from

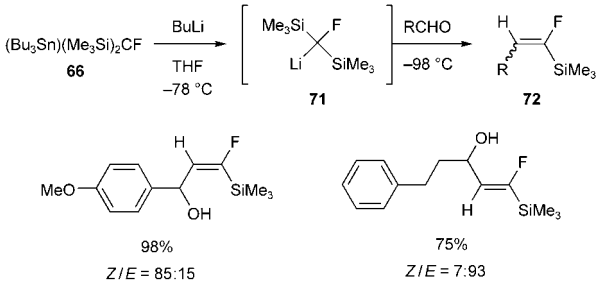


Scheme 20. Addition to carbonyl compounds and alkylation of the silicon-substituted carbenoid **69**.

the Peterson elimination or the Brook rearrangement is formed. The Darzens-type substitution proceeds at the fluorine-substituted carbon atom, a reaction that is thought to be difficult to achieve in an intermolecular sense.[41] Thus, it is evident that the accelerating effect of silicon surpasses the retarding effect of fluorine for the nucleophilic substitution at the α carbon atom.[42] Furthermore, the anion stabilization by silicon allows the addition of an electrophile after the generation of **69** at −98 °C, so that alkylation of **69** with alkyl halides is possible.

Whereas bromine–lithium exchange of **65** to generate fluorobis(trimethylsilyl)methyllithium (**71**) in the presence of aldehydes is unsuccessful, tin–lithium exchange of **66** with butyllithium can be performed successfully at −78 °C to give **71**, which then reacts with aldehydes to produce 1-fluoro-1-trimethylsilyl-1-alkenes **72** through addition to the carbonyl group followed by a Peterson elimination (Scheme 21).[43] The stereochemical outcome depends on R in the aldehyde RCHO.

The activation of a carbon–silicon bond by a fluoride ion is a highly useful strategy in organic synthesis with organosilicon reagents.[44] This strategy is also highly effective in synthetic fluorine chemistry. For example, trimethyl(trifluoromethyl)-silane reacts with a wide variety of electrophiles upon treatment with Bu_4NF (TBAF). Similarly, the treatment of



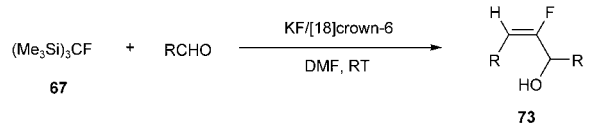
Scheme 21. Synthesis of 1-fluoro-1-silyl-1-alkenes **72**.

 © 2005 Wiley-VCH Verlag GmbH & Co. KGaA, Weinheim

(polyfluoroethenyl)silanes with a catalytic amount of tris-(diethylamino)sulfonium difluoro(trimethyl)silicate generates the corresponding naked polyfluoroethenyl anions, which react with aldehydes to produce polyfluorinated allylic alcohols conveniently.[45]

We have found that fluoro(tris(trimethylsilyl))methane (**67**) reacts with 2 molar equivalents of an aromatic aldehyde in the presence of an equimolar amount of KF/[18]crown-6 in DMF at room temperature to give 2-fluoro-1,3-diaryl-2-propen-1-ols **73** in *E*/*Z* ratios of roughly 2:1 (Table 1). The

Table 1: Fluoride-mediated addition of **67** to aldehydes.



Entry	R	Yield [%]	*E*/*Z*
1	Ph	74	65:35
2	*p*-tolyl	70	68:32
3	*p*-(MeO)C_6H_4	78	65:35
4	1-naphthyl	65	61:39
5	*p*-PhC_6H_4	68	67:33

one-pot transformation involves the generation and addition to an aldehyde of the fluorine-substituted naked anion, a Peterson elimination leading to an α-fluoroalkenyl silane, generation of an α-fluoroalkenyl anion, and final aldehyde addition, and thus allows the conversion of three carbon–silicon bonds into a C–C single bond and a C=C double bond in a single operation.

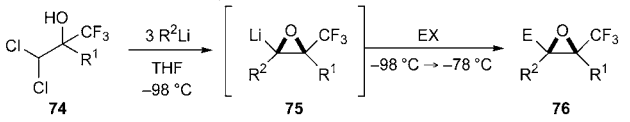
5. Trifluoromethyl-Substituted Oxiranyl Lithium Reagents

Oxiranyl lithium reagents have recently emerged as a highly versatile class of reagents for the stereoselective synthesis of functionalized oxiranes and alkenes.[46] However, fluorine-containing oxiranyl lithium compounds remained unexplored until 2001, when we reported our results on trifluoromethyl-substituted oxiranyl lithium reagents.[47a]

The synthetic elaboration of CF_3-substituted β-oxido carbenoids derived from 3,3-dichloro-1,1,1-trifluoroalkan-2-ols **74** has led to the discovery that oxiranyl lithium intermediates **75** are efficiently produced at −98 °C with 3 equivalents of R^2Li and react with such electrophiles as chlorotrimethylsilane, isopropoxy(pinacolato)borane, and carbonyl compounds, to afford tri- and tetrasubstituted oxiranes **76** in good yields (Table 2).[47] Worthy of emphasis are: 1) the simultaneous nature of oxirane formation and the introduction of the substituent R^2, 2) the high diastereoselectivities observed (d.r. > 95:5) in the formation of **76**, 3) the *cis* arrangement of CF_3 and Li in **75**, and 4) the diastereotopic discrimination between the two chlorine substituents in the acyclic substrate **74**.

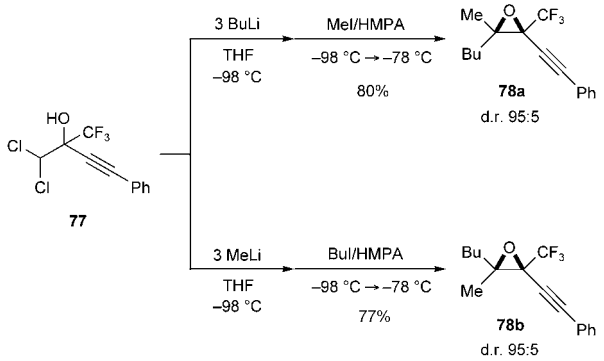
With an alkyl halide as the electrophile E–X, the stereodivergent synthesis of tetrasubstituted oxiranes is achieved

Table 2: Stereoselective synthesis of CF_3-substituted oxiranes.



Entry	R^1	R^2	E	Yield [%]	d.r.
1	Ph$(CH_2)_2$	Bu	H	85	> 95:5
2	(*E*)-PhCH=CH	Bu	H	74	83:17
3	PhC≡C	Bu	H	84	> 95:5
4	Ph	Bu	H	83	89:11
5	Ph$(CH_2)_2$	Ph	H	93	> 95:5
6	PhC≡C	Ph	H	95	> 95:5
7	PhC≡C	Bu	$SiMe_3$	79	> 95:5
8	PhC≡C	Ph	B$(OCMe_2)_2$	76	> 95:5
9	Ph$(CH_2)_2$	Bu	$Ph_2C(OH)$	57	> 95:5

through the proper choice of R^2Li and E–X. For example, the treatment of **77** with BuLi and then with a solution of iodomethane in HMPA afforded **78a**, whereas the other diastereomer **78b** was obtained by the methyllithium-mediated generation of **75** followed by trapping with 1-iodobutane in HMPA (Scheme 22).

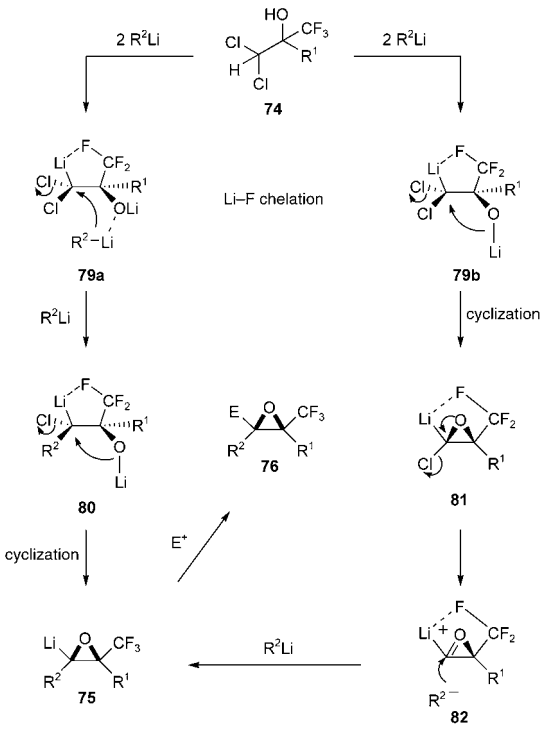


Scheme 22. Stereodivergent synthesis of tetrasubstituted oxiranes. HMPA = hexamethyl phosphoramide.

A proposed mechanism for the stereoselective generation of **75** is shown in Scheme 23. At first, it is thought that **74** reacts with 2 equivalents of R^2Li to produce the β-oxido carbenoid **79a** (or **79b**).[48] The assumption of a favored Li–F-chelated conformation as shown in **79a** (or **79b**) leads to two possible pathways: One pathway is the substitution of chlorine in **79a** by R^2Li through coordination with OLi to produce **80**, which should undergo intramolecular cyclization to generate **75**. Intermediate **75** should be stable enough at −98 °C to react with an electrophile and produce **76**. Alternatively, the cyclization of **79b** first gives the chlorolithiooxirane **81**, which might liberate a chloride ion to form the oxyrenium ion **82** by participation of the lone pair of electrons on the oxygen atom. The intermediate **82** is apparently unstable and is trapped immediately by another molecule of R^2Li from the face opposite to Li–F chelation to afford **75**.

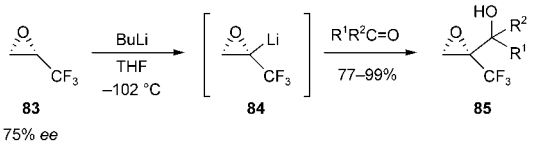
Very recently, the trifluoromethyl-substituted oxiranyl anion **84** was generated successfully from optically active 2,3-

 © 2005 Wiley-VCH Verlag GmbH & Co. KGaA, Weinheim



Scheme 23. Proposed mechanism for the stereoselective generation of **75**.

epoxy-1,1,1-trifluoropropane (**83**, 75% *ee*) and BuLi in THF at −102 °C (Scheme 24).[49] The configuration of **84** was reported to be stable below −78 °C. Its reaction with aldehydes and ketones gives alcohols **85**.

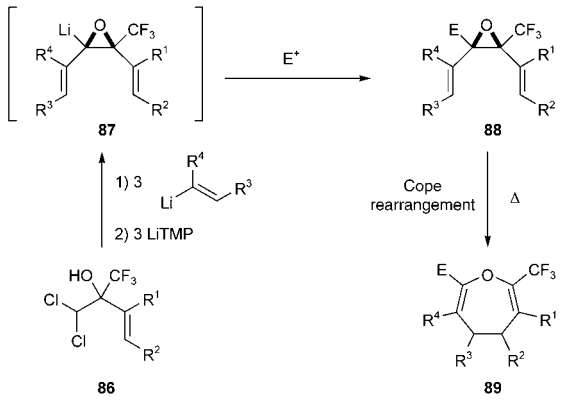


Scheme 24. Generation and reactions of α-CF_3-substituted oxiranyl lithium.

6. A Facile Route to Seven-Membered Oxacycles

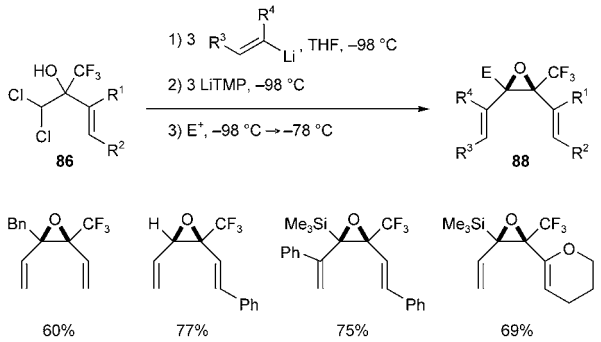
Much attention is focused on seven-membered oxacycles, such as oxepanes and oxepins, owing to their occurrence in biologically active natural products and to valence-bond isomerization between oxepin and benzene oxide.[50] As the incorporation of a CF_3 group into biologically active compounds can alter their properties, facile methods for the synthesis of CF_3-substituted seven-membered oxacycles, a novel class of CF_3-containing compounds, is of particular interest in the quest for potent biologically active substances.

The Cope rearrangement of 2,3-bis(alkenyl)oxiranes would appear to be an attractive approach to the construction of such oxacycles. However, this strategy has remained unrealized, mainly because 1) bis(alkenyl)oxiranes with the essential *cis* arrangement are hard to construct, 2) the rearrangement requires relatively high reaction temperatures, and 3) available disubstituted oxiranes are limited to precursors of 2,7-unsubstituted oxepins. Thus, tri- and tetrasubstituted oxiranes have remained unexplored because of the lack of efficient and stereoselective access routes.[51] We envisaged that it would be possible to prepare 2-CF_3-substituted 2,3-*cis*-bis(alkenyl)oxiranes **88** readily if the protocol for the stereoselective generation of CF_3-substituted oxiranyl lithium compounds was applicable to alkenyl-substituted dichlorohydrins **86** and alkenyl lithium intermediates (Scheme 25).



Scheme 25. Synthetic plan for the preparation of 2-trifluoromethyl-4,5-dihydrooxepins.

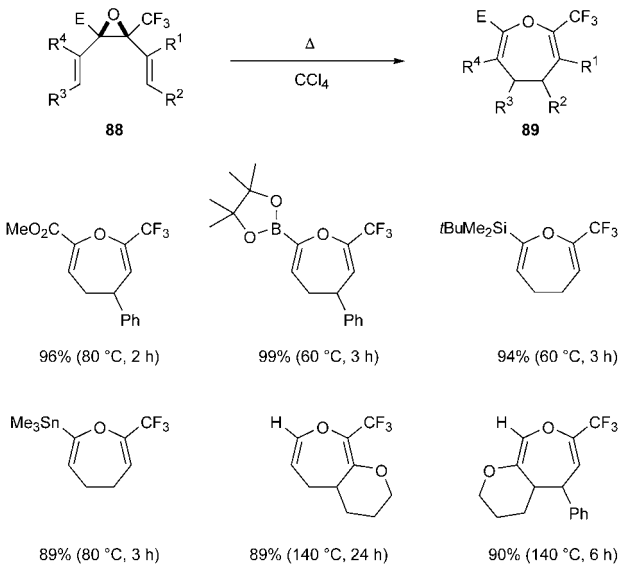
Regretfully, however, no trace of the desired reaction took place under the original conditions, probably as a result of the low basicity of the alkenyl lithium intermediates and/or the low acidity of a methine proton of **86**. After many trials, we found that the addition of LiTMP (3 equiv) to a solution of **86** and an alkenyl lithium compound is a highly effective way to generate oxiranyl lithium intermediates **87**, which can be trapped with a variety of electrophiles (E^+) to give **88** with excellent *cis* selectivity (Scheme 26).[52]



Scheme 26. Synthesis of *cis* bis(alkenyl)oxiranes **88**.

The Cope rearrangement of **88** proceeded smoothly upon heating at 60–140 °C to afford **89** in good to excellent yields (Scheme 27).[52] The rate of the reaction depends on the substituent E. If E is bulky, it appears to force the two

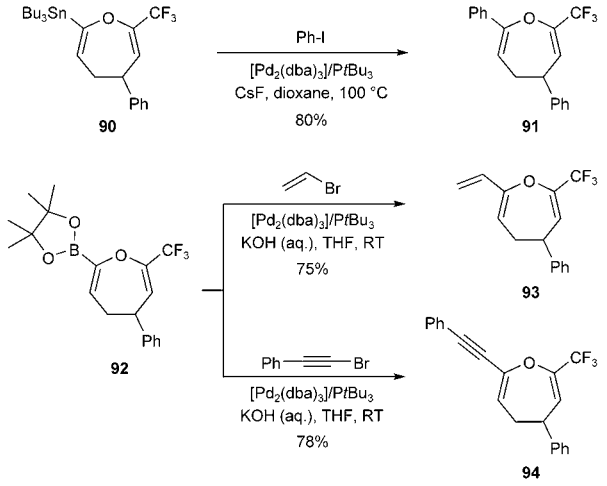
 © 2005 Wiley-VCH Verlag GmbH & Co. KGaA, Weinheim



Scheme 27. Cope rearrangement of **88**.

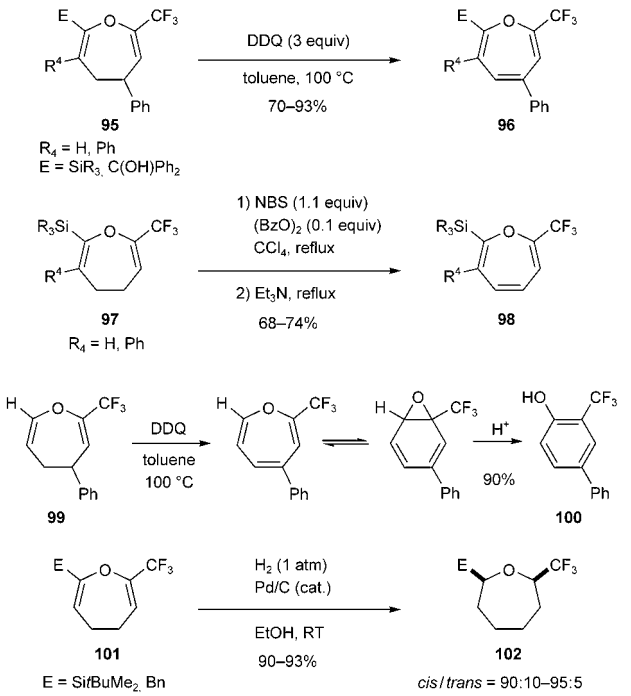
terminal C(sp^2) atoms close together, thus accelerating the rearrangement. If the starting substrate contains a cyclic olefin, oxepins with a fused framework, which are otherwise difficult to prepare, are obtained.

An additional feature of the present approach is the versatility of products containing metalloid elements introduced during the preparation of oxiranes **88**. Thus, a tin or boron substituent is readily converted into an aryl, alkenyl, or alkynyl group by a Pd-catalyzed cross-coupling reaction with an aryl, alkenyl, or alkynyl halide, respectively (Scheme 28).



Scheme 28. Coupling reaction of metal-substituted oxepins.

Dihydrooxepins **95** and **97** are readily converted into oxepins **96** (by oxidation with DDQ) and **98** (by allylic bromination–dehydrobromination with NBS and NEt_3), respectively, as illustrated in Scheme 29.[52] Oxidation of the 7-unsubstituted 4,5-dihydrooxepin **99** with DDQ produces **100** through equilibration of the oxepin to a benzene oxide,



Scheme 29. Oxidation and reduction of 2-CF_3-4,5-dihydrooxepins. Bn = benzyl, Bz = benzoyl, DDQ = 2,3-dichloro-5,6-dicyano-1,4-benzoquinone.

followed by acid-induced isomerization. Finally, 2-CF_3-substituted oxepanes **102** are readily available through the catalytic hydrogenation (1 atm) of **101** in the presence of 5% Pd/C.

7. Stereoselective Synthesis of CF_3-Containing Tetrasubstituted Alkenes

The regio- and stereoselective synthesis of tetrasubstituted alkenes is always a challenging issue in organic synthesis.[53] In particular, fluorine-containing tetrasubstituted alkenes are crucial in the search for potential fluorinated drugs. For example, panomifene is reported to exhibit antiestrogenic activity superior to that of tamoxifen, a widely used drug for the treatment of breast cancer (Figure 5).[54]

As oxiranyl lithium compounds are known to react with organometallic reagents, such as RLi, R_3Al, R_2Zn, and R_4CeLi, to give alkylated alkenes,[55] we first attempted unsuccessfully to apply this methodology to **103**. Fortunately,

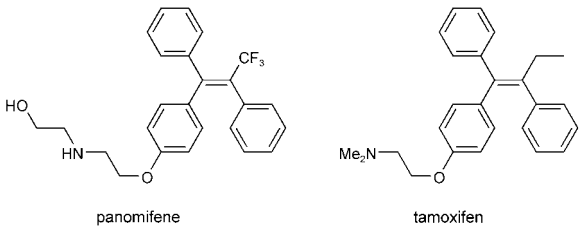
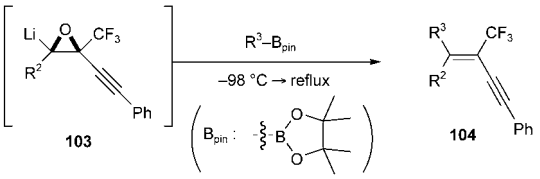


Figure 5. Examples of nonsteroidal antiestrogens.

 © 2005 Wiley-VCH Verlag GmbH & Co. KGaA, Weinheim

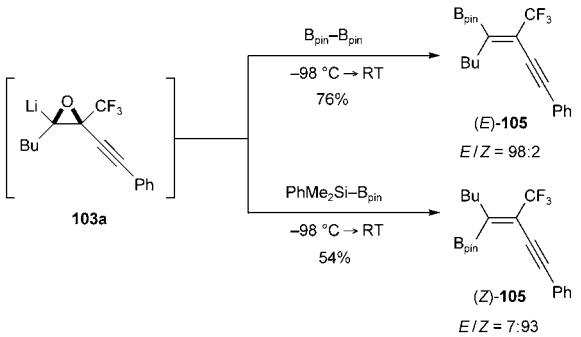
we have since found that the treatment of **103** with organo(-pinacolato)borane reagents R^3–B_{pin} (pin = pinacolato) affords tetrasubstituted alkenes stereoselectively in good yields, with CF_3 and R^3 in a *cis* relationship (Table 3). An

Table 3: Stereoselective synthesis of CF_3-containing tetrasubstituted alkenes.



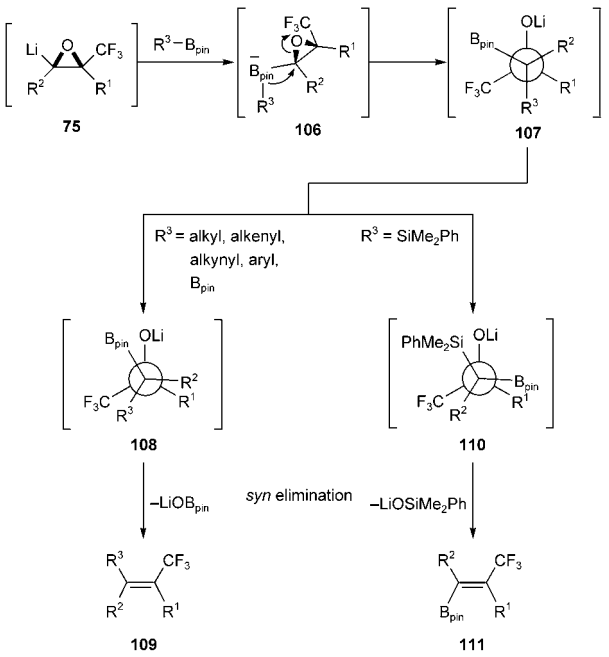
Entry	R^2	R^3	Yield [%]	d.r.
1	Bu	PhC≡C	74	>95:5
2	Bu	(*E*)-BuCH=CH	56	>95:5
3	Bu	Ph	66	97:3
4	Ph	Bu	84	96:4

appropriate combination of R^2 and R^3 allows the preparation of either stereoisomer at will (entries 3 and 4 of Table 3). The stereodivergent synthesis of β-CF_3-substituted alkenyl boronates **105** is also possible when bis(pinacolato)diboron or dimethylphenylsilyl(pinacolato)boron is employed with **103**. The stereochemical outcome with the diboron reagent is opposite to that observed with the silylborane and the same as that with R^3–B_{pin} (Scheme 30).



Scheme 30. Stereoselective synthesis of CF_3-containing tetrasubstituted alkenes.

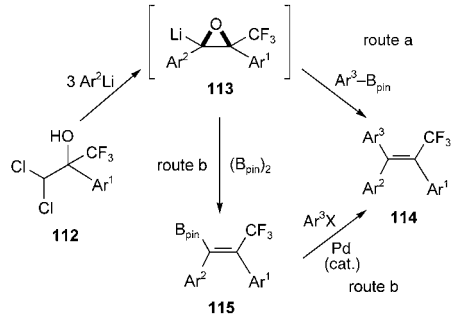
The stereoselective and stereodivergent formation of (*E*)- or (*Z*)-**105** can be explained by assuming that a *syn* elimination of $LiOB_{pin}$ or $LiOSiPhMe_2$ takes place in the last step, as illustrated in Scheme 31. First, **75** reacts with the borane reagent R^3–B_{pin} to give the borate **106**, which undergoes 1,2-migration of the substituent R^3 and opening of the oxirane to generate the lithium alkoxide **107**.[56] If R^3 is an alkyl, alkenyl, alkynyl, aryl, or boryl group, minimal rotation is required to attain the conformation **108**, in which the carbon–boron and carbon–oxygen bonds are eclipsed. The alkene **109** is then produced by the *syn* elimination of $LiOB_{pin}$.[57] When the silylborane is employed (i.e. R^3 in **106** is the silyl group), a rotation of 180° would be required for $LiOSiMe_2Ph$ to be eliminated in a *syn* fashion to give **111**. The elimination of



Scheme 31. Mechanism for stereoselective alkene formation.

$LiOSiMe_2Ph$ rather than $LiOB_{pin}$ might be expected, as a $PhMe_2Si$ group is more oxophilic than a B_{pin} group.

Based on these results, it seemed that various CF_3-substituted triaryl ethenes **114**, including panomifene, would be accessible if diaryl-substituted oxiranyl lithium intermediates **113** are generated successfully from Ar^1-substituted dichlorohydrins in the presence of Ar^2Li and react with Ar^3–B_{pin} smoothly (route a in Scheme 32).[58] However, this



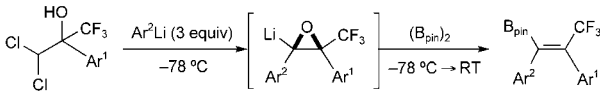
Scheme 32. Synthetic plan for the preparation of CF_3-substituted triaryl ethenes.

expectation was not fulfilled, although it was shown that intermediate **113** was generated quite efficiently even at −78 °C. Hence, we took another approach (route b), which involves the preparation and cross-coupling of β-CF_3-substituted alkenyl boron reagents **115**.[59] Thus, the lithiooxirane **113** is first generated from **112** with Ar^2Li at −78 °C and then allowed to react with the diboron reagent to produce **115** in good yields with high *E* selectivities (Table 4).

The Pd-catalyzed cross-coupling reaction of **115** (route b in Scheme 32) with a variety of aryl iodides was carried out

 © 2005 Wiley-VCH Verlag GmbH & Co. KGaA, Weinheim

Table 4: Stereoselective preparation of β-CF_3-substituted alkenyl boronates.

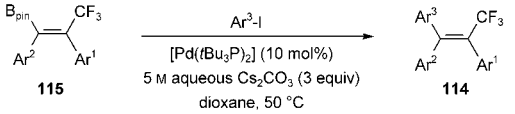


112 **113** **115**

Ar^1	Ar^2	Yield [%]	*E*/*Z*
Ph	Ph	63	98:2
Ph	*p*-ClC_6H_4	73	97:3
Ph	*p*-$(MeO)C_6H_4$	78	94:6
Ph	*p*-$(MOMO)C_6H_4$	75	92:8
p-ClC_6H_4	Ph	80	99:1
p-$(MeO)C_6H_4$	Ph	63	99:1

successfully in the presence of a 5 M aqueous solution of Cs_2CO_3 to give **114** as a single stereoisomer in high to excellent yields (Table 5).[59] The coupling reaction under anhydrous conditions causes deborylation of **115** to some extent. Neither electron-donating nor electron-withdrawing groups on Ar^1 or Ar^2 affect the reaction. The demethylation of **114d** with NaOEt followed by the introduction of a 2-(2-hydroxyethyl)aminoethyl moiety completed a facile synthesis of panomifene.[59]

Table 5: Cross-coupling reaction of β-CF_3-substituted alkenyl boronates.



	Ar^1	Ar^2	Ar^3	Yield [%]
114a	Ph	Ph	*p*-$(EtO_2C)C_6H_4$	92
114b	Ph	Ph	*p*-FC_6H_4	91
114c	Ph	Ph	*p*-ClC_6H_4	96
114d	Ph	*p*-$(MeO)C_6H_4$	Ph	90
114e	Ph	*p*-ClC_6H_4	*p*-$(MeO)C_6H_4$	89
114f	Ph	*p*-$(MOMO)C_6H_4$	Ph	92
114g	*p*-$(MeO)C_6H_4$	Ph	*p*-FC_6H_4	94

8. Asymmetric Synthesis of 1,1,1-Trifluoro-2-alkanols

In recent years, many optically active organofluorine compounds have been employed in the pharmaceutical, agrochemical, and materials sciences. For example, many antiferroelectric liquid crystals contain optically active 1,1,1-trifluoro-2-alkanols as key fragments that contribute to the stabilization of the SmC_A phase (Figure 6). Accordingly, the enantioselective synthesis of such fluorinated alcohols has been a target in organic synthesis.[60] We have designed novel methods for the efficient synthesis of 1,1,1-trifluoro-2-alkanols, including the asymmetric synthesis of trifluoromethyl-substituted hemiacetals and their stereospecific nucleophilic substitution.[61]

In our studies on asymmetric hemiacetal synthesis we found that bubbling gaseous trifluoroacetaldehyde, generated from 1-ethoxy-2,2,2-trifluoroethanol (**118**) and polyphosphoric acid (PPA), into a solution of an alcohol in toluene in the presence of a preprepared (*R*)-binol–Ti(O*i*Pr)$_2$ catalyst yielded the optically active hemiacetal **119**, which then underwent acylation with an acid chloride or sulfonyl chloride at low temperatures to give the optically active mixed acetal (*S*)-**120** (Table 6).[62] Alternatively, optically pure 1-alkoxy-2,2,2-ethyl tosylates are accessible by the optical resolution of racemic tosylates by chiral preparative HPLC (Daicel chiralpak AD or chiralcel OD).[63] The presence of the CF_3 group makes it possible to isolate otherwise unstable α-alkoxyalkyl tosylates.

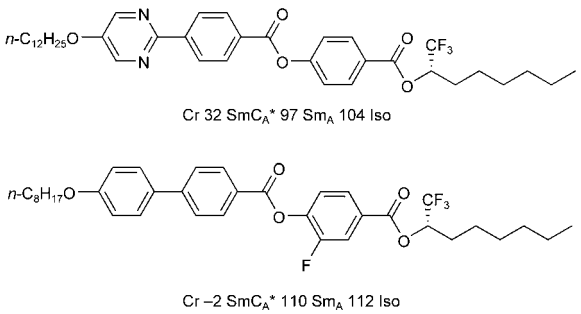
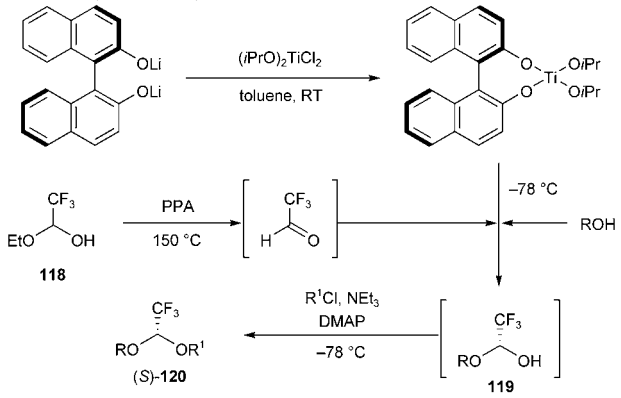


Figure 6. Examples of antiferroelectric liquid crystals.

Table 6: Asymmetric synthesis of CF_3-substituted hemiacetals.



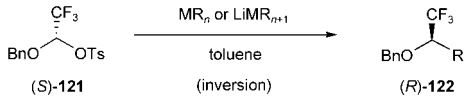
Entry	R	R^1	Yield [%]	*ee* [%]
1	Bu	PhCO	65	65
2	$Ph(CH_2)_2$	PhCO	57	78
3	*i*Pr	PhCO	85	85
4	Et_2CH	PhCO	54	73
5	$PhCH_2$	PhCO	54	91
6	$PhCH_2$	$MeSO_2$	35	79

DMAP = 4-dimethylaminopyridine.

Hemiacetal tosylates (*S*)-**121** react with organoaluminum, organoboron, and organozinc reagents to give substitution products with inversion of configuration.[64] The best overall results with respect to the yields and *ee* values of the isolated products were obtained with aluminate reagents (Table 7). This study demonstrated for the first time that intermolecular nucleophilic substitution is possible at a CF_3-substituted carbon atom to form a carbon–carbon bond. We should emphasize at this point that the alkoxy substituent in **121** assists in this process by increasing the reactivity of the

 © 2005 Wiley-VCH Verlag GmbH & Co. KGaA, Weinheim

Table 7: Nucleophilic substitution of hemiacetal **121** with organometallic reagents.



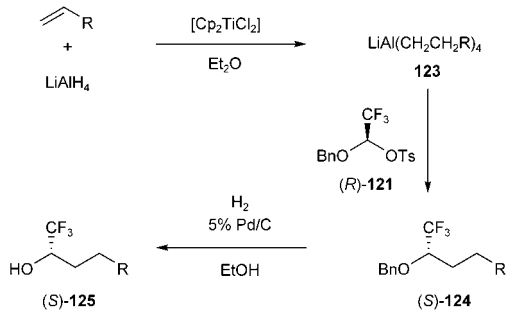
(*S*)-**121**
100% *ee*

(*R*)-**122**

Entry	MR_n or $LiMR_{n+1}$	*T* [°C]	Yield [%]	*ee* [%]
1	$AlEt_3$	−20	75	82
2	$LiAlEt_4$	0	69	98
3	$LiAlBu_4$	RT	62	90
4	$LiAl(iBu)_4$	0	46	93
5	$LiBEt_4$	RT	32	95
6	$LiZnEt_3$	RT	30	96

otherwise unreactive CF_3-substituted alkyl tosylates. Thus, the presence of the substituent OCH_2Ph α to a CF_3 group in **121** is essential for the success of the nucleophilic substitution. The intramolecular nucleophilic substitution of 1,1,1-trifluoro-2-alkanol derivatives with an amino group or a cyano-stabilized carbanion is reported to take place with inversion of configuration, giving rise to trifluoromethyl-substituted aziridines and cyclopropanes, respectively.[65]

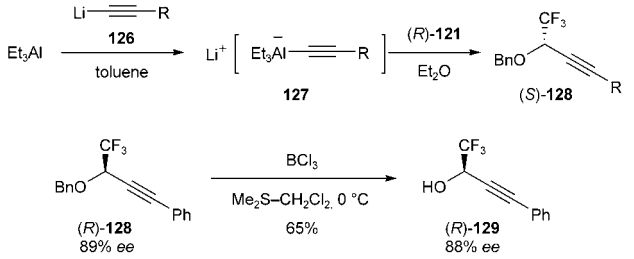
The versatility of the present approach is demonstrated by the preparation of 1,1,1-trifluoro-2-alkanols (Scheme 33).



Scheme 33. Efficient route to optically active 1,1,1-trifluoro-2-alkanols.

Thus, the titanocene-catalyzed hydroalumination of 1-alkenes with $LiAlH_4$ produces regioselectively lithium tetraalkyl aluminates **123**, which undergo stereospecific substitution with (*R*)-**121** to give (*S*)-**124**. The hydrogenolysis of (*S*)-**124** under a hydrogen atmosphere in the presence of 5% Pd/C gives optically active alcohols (*S*)-**125**. Any alkanol of the type **125** can be prepared from the corresponding readily available 1-alkene and the tosylate **121** by this sequence.[66]

As only one alkyl group in aluminates takes part in the substitution, the use of mixed aluminates that transfer a required moiety to the exclusion of the less reactive groups is more practical. Indeed, 1-alkynyl trialkyl aluminum compounds are appropriate for this purpose.[67] Thus, mixed aluminates **127**, prepared from commercially available triethylaluminum and the requisite alkynyl lithium reagent **126**, undergo reaction with (*R*)-**121** selectively and stereospecifically to afford alkynylated products (*S*)-**128** with inversion of configuration (Scheme 34). The catalytic hydrogenation of (*R*)-**128** at 1 atm with PtO_2 furnishes the benzyl ether (*R*)-**124**



Scheme 34. Alkynylation of the optically active tosylate (*R*)-**121** with the mixed aluminate **127**.

(R = Ph), whereas debenzylation of (*R*)-**128** with BCl_3 and Me_2S gives the alcohol (*R*)-**129**, leaving both the CF_3 and C≡C functional groups untouched.

9. Summary

Herein we have reviewed our progress during the last two decades in synthetic fluorine chemistry. A fluorination method (oxidative desulfurization–fluorination) has been developed, as well as building-block methods in which readily available CF_3CCl_3, $CFBr_3$, $CF_3COCHCl_2$, $CF_3CH(OH)OEt$, and their derivatives are used in combination with organometallic reagents. These novel synthetic methods have allowed the convenient preparation of a variety of fluorine-containing target molecules. The presence of fluorinated or perfluorinated substituents often induces unusual phenomena, which may be ascribed ultimately to the strong electron-withdrawing effect of these substituents. From this point of view, insight into synthetic fluorine chemistry opens possibilities for the design of new reactions/reagents not only in organofluorine chemistry but also in general organic synthesis and organometallic chemistry. We hope this Review may foster research in related fields.

The authors sincerely thank their colleagues, whose names are listed in the references, for their continuing efforts and devotion, and acknowledge financial support from the Ministry of Education, Culture, Sports, Science, and Technology of Japan, The Japan Society of the Promotion of Science, and Asahi Glass Foundation. In particular, T.H. acknowledges the support of COE Research on Elements Science, no. 12CE2005, from the Ministry of Education, Culture, Sports, Science, and Technology of Japan.

Received: April 26, 2004

[1] a) T. Hiyama, *Organofluorine Compounds: Chemistry and Applications*, Springer, Berlin, **2000**; b) *Houben-Weyl, Vol. E10a* (Eds.: B. Baasner, H. Hagemann, J. C. Tatlow), Thieme, Stuttgart, **2000**; c) *Biomedical Frontiers of Fluorine Chemistry, ACS Symposium Series 639* (Eds.: I. Ojima, J. R. McCarthy, J. T. Welch), American Chemical Society, Washington, **1996**; d) *Chemistry of Organic Fluorine Compounds II: A Critical Review, ACS Monograph 187* (Eds.: M. Hudlicky, A. E.

 © 2005 Wiley-VCH Verlag GmbH & Co. KGaA, Weinheim

Pavlath), American Chemical Society, Washington, **1995**; e) *Organofluorine Chemistry—Principles and Commercial Applications* (Eds.: R. E. Banks, B. E. Smart, J. C. Tatlow), Plenum Press, New York, **1994**; f) *Chemistry of Organic Fluorine Compounds*, 2nd ed. (Ed.: M. Hudlicky), Ellis Horwood, New York, **1992**; g) *Selective Fluorination in Organic and Bioorganic Chemistry*, *ACS Symposium Series 456* (Ed.: J. T. Welch), American Chemical Society, Washington, **1991**; h) *Fluorine-containing Molecules: Structure, Reactivity, Synthesis, and Applications* (Eds.: J. F. Liebman, A. Greenberg, J. W. R. Dolbier), VCH, New York, **1988**; i) J. T. Welch, *Tetrahedron* **1987**, *43*, 3123; j) M. Schlosser, *Tetrahedron* **1978**, *34*, 3; k) P. Kirsch, *Modern Fluoroorganic Chemistry*, Wiley-VCH, Weinheim, **2004**.

[2] B. E. Smart, *J. Fluorine Chem.* **2001**, *109*, 3.

[3] Special issue on "Fluorine in the Life Sciences", *ChemBioChem* **2004**, *5*, 557 – 726.

[4] M. Schlosser, *Angew. Chem.* **1998**, *110*, 1538; *Angew. Chem. Int. Ed.* **1998**, *37*, 1496.

[5] D. A. Dixon, T. Fukunaga, B. E. Smart, *J. Am. Chem. Soc.* **1986**, *108*, 4027.

[6] For C–H···F interactions, see: a) J. A. K. Howard, V. J. Hoy, D. O'Hagan, G. T. Smith, *Tetrahedron* **1996**, *52*, 12613; b) J. D. Dunitz, R. Taylor, *Chem. Eur. J.* **1997**, *3*, 89; c) I. Hyla-Kryspin, G. Haufe, S. Grimme, *Chem. Eur. J.* **2004**, *10*, 3411; d) J. D. Dunitz, *ChemBioChem* **2004**, *5*, 614; for C–M···F interactions, see: e) H. Plenio, *Chem. Rev.* **1997**, *97*, 3363; f) H. Plenio, *ChemBioChem* **2004**, *5*, 65.

[7] a) Reference [1b]; b) *Houben-Weyl*, *Vol. E10b/1* (Eds.: B. Baasner, H. Hagemann, J. C. Tatlow), Thieme, Stuttgart, **2000**; c) *Houben-Weyl*, *Vol. E10b/2* (Eds.: B. Baasner, H. Hagemann, J. C. Tatlow), Thieme, Stuttgart, **2000**; d) T. Kitazume, T. Yamazaki, *Experimental Methods in Organic Fluorine Chemistry*, Kodansha, Tokyo, **1998**; e) *Top. Curr. Chemi.* **1997**, *192*; f) *Top. Curr. Chem.* **1997**, *193*; g) *Synthetic Fluorine Chemistry* (Eds.: G. A. Olah, R. D. Chambers, G. K. S. Prakash), Wiley, New York, **1992**.

[8] a) Reference [7a,b]; b) J. Hutchinson, G. Sandford, *Top. Curr. Chem.* **1997**, *193*, 1; c) J. A. Wilkinson, *Chem. Rev.* **1992**, *92*, 505.

[9] a) Reference [7b,c]; b) J. M. Percy, *Top. Curr. Chem.* **1997**, *193*, 131.

[10] For a review on halofluorination, see: a) *Houben-Weyl*, *Vol. E10a* (Eds.: B. Baasner, H. Hagemann, J. C. Tatlow), Thieme, Stuttgart, **2000**, p. 122; b) G. A. Olah, J. T. Welch, Y. D. Vankar, M. Nojima, I. Kerekes, J. A. Olah, *J. Org. Chem.* **1979**, *44*, 3872; c) C. York, G. K. S. Prakash, G. A. Olah, *J. Org. Chem.* **1994**, *59*, 6493; d) M. Kuroboshi, T. Hiyama, *Bull. Chem. Soc. Jpn.* **1995**, *68*, 1799.

[11] a) G. Haufe, *Tetrahedron Lett.* **1988**, *29*, 2311; b) C. Saluzzo, G. Alvernhe, D. Anker, G. Haufe, *Tetrahedron Lett.* **1990**, *31*, 663.

[12] See reference [10b].

[13] M. Kuroboshi, K. Kanie, T. Hiyama, *Adv. Synth. Catal.* **2001**, *343*, 235.

[14] S. Furuta, M. Kuroboshi, T. Hiyama, *Bull. Chem. Soc. Jpn.* **1999**, *72*, 805.

[15] For a review on the synthesis of *gem*-difluoromethylene compounds, see: M. J. Tozer, T. F. Herpin, *Tetrahedron* **1996**, *52*, 8619.

[16] M. Kuroboshi, T. Hiyama, *Synlett* **1991**, 909.

[17] a) W. B. Motherwell, J. A. Wilkinson, *Synlett* **1991**, 191; b) T. Fuchigami, T. Fujita, *J. Org. Chem.* **1994**, *59*, 7190.

[18] M. Kuroboshi, T. Hiyama, unpublished results. The Friedel–Crafts acylation of 1,2-dimethoxybenzne with **17**, leading to **18**, is reported independently: K. Burger, M. Rudolph, H. Neuhauser, *Liebigs Ann. Chem.* **1991**, 1365.

[19] a) M. Kuroboshi, T. Hiyama, *Synlett* **1994**, 251; see also: b) G. S. Lal, E. Lobach, A. Evans, *J. Org. Chem.* **2000**, *65*, 4830.

[20] K. Kanie, Y. Tanaka, K. Suzuki, M. Kuroboshi, T. Hiyama, *Bull. Chem. Soc. Jpn.* **2000**, *73*, 471.

[21] M. J. Koen, F. I. Guyader, W. B. Motherwell, *J. Chem. Soc. Chem. Commun.* **1995**, 1241.

[22] K. Kanie, S. Takehara, T. Hiyama, *Bull. Chem. Soc. Jpn.* **2000**, *73*, 1875.

[23] a) K. Kanie, K. Mizuno, M. Kuroboshi, T. Hiyama, *Bull. Chem. Soc. Jpn.* **1998**, *71*, 1973; b) P. Kirsch, M. Bremer, *Angew. Chem.* **2000**, *112*, 4384; *Angew. Chem. Int. Ed.* **2000**, *39*, 4216.

[24] For reviews on fluorinated organometallic compounds, see: a) D. J. Burton, Z.-Y. Yang, *Tetrahedron* **1992**, *48*, 189; b) D. J. Burton, Z.-Y. Yang, P. A. Morken, *Tetrahedron* **1994**, *50*, 2993; c) D. J. Burton, L. Lu, *Top. Curr. Chem.* **1997**, *193*, 45.

[25] For a Review on the synthesis of pyrethroid acids, see: D. Arlt, M. Jautelat, R. Lantzsch, *Angew. Chem.* **1981**, *93*, 719; *Angew. Chem. Int. Ed. Engl.* **1981**, *20*, 703.

[26] a) M. Fujita, T. Morita, T. Hiyama, *Tetrahedron Lett.* **1986**, *27*, 2135; b) M. Fujita, T. Hiyama, *Bull. Chem. Soc. Jpn.* **1987**, *60*, 4377.

[27] a) R. W. Lang, *Helv. Chim. Acta* **1986**, *69*, 881; see also: b) R. W. Lang, *Helv. Chim. Acta* **1988**, *71*, 369.

[28] D. Bellus, B. Klingert, R. W. Lang, G. Rihs, *J. Organomet. Chem.* **1988**, *339*, 17.

[29] a) M. Fujita, T. Hiyama, *Tetrahedron Lett.* **1986**, *27*, 3655; b) M. Fujita, K. Kondo, T. Hiyama, *Bull. Chem. Soc. Jpn.* **1987**, *60*, 4385.

[30] a) M. Fujita, T. Hiyama, K. Kondo, *Tetrahedron Lett.* **1986**, *27*, 2139; b) reference [29b].

[31] a) M. Kuroboshi, N. Yamada, Y. Takebe, T. Hiyama, *Synlett* **1995**, 987; b) M. Shimizu, N. Yamada, Y. Takebe, T. Hata, M. Kuroboshi, T. Hiyama, *Bull. Chem. Soc. Jpn.* **1998**, *71*, 2903.

[32] D. J. Burton, J. L. Hahnfeld, *J. Org. Chem.* **1977**, *42*, 828.

[33] a) T. Hata, M. Shimizu, T. Hiyama, *Synlett* **1996**, 831; b) T. Hata, H. Kitagawa, M. Shimizu, T. Hiyama, *Bull. Chem. Soc. Jpn.* **2000**, *73*, 1691.

[34] a) O. Yokokoji, T. Shimizu, S. Kumai, JP 08040952, **1996** [*Chem. Abstr.* **1996**, *124*, 316586]; b) T. Allmendinger, E. Felder, E. Hungerbühler in *Selective Fluorination in Organic and Bioorganic Chemistry* (Ed.: J. T. Welch), American Chemical Society, Washington, **1991**, p. 186; c) P. Bey, J. R. McCarthy, I. A. McDonald in *Selective Fluorination in Organic and Bioorganic Chemistry* (Ed.: J. T. Welch), American Chemical Society, Washington, **1991**, p. 105.

[35] a) *Metal-catalyzed Cross-coupling Reactions* (Eds.: F. Diederich, P. J. Stang), Wiley-VCH, Weinheim, **1998**; b) *Top. Curr. Chem.* **2002**, *219*.

[36] a) V. A. Petrov, C. G. Krespan, B. E. Smart, *J. Fluorine Chem.* **1996**, *77*, 139; b) J. Weber, L. Xu, U. H. Brinker, *Tetrahedron Lett.* **1992**, *33*, 4537; c) S. Eddarir, C. Francesch, H. Mestdagh, C. Rolando, *Tetrahedron Lett.* **1990**, *31*, 4449; d) T. Gouyon, R. Sauvetre, J. F. Normant, *J. Organomet. Chem.* **1990**, *394*, 37; e) M. Shimizu, G.-H. Cheng, H. Yoshioka, *J. Fluorine Chem.* **1988**, *41*, 425; f) T. Fuchikami, I. Ojima, *J. Organomet. Chem.* **1981**, *212*, 145.

[37] a) M. Shimizu, Y. Takebe, M. Kuroboshi, T. Hiyama, *Tetrahedron Lett.* **1996**, *37*, 7387; b) reference [31b].

[38] K. Iseki, Y. Kuroki, Y. Kobayashi, *Tetrahedron Lett.* **1997**, *38*, 7209.

[39] a) A. R. Bassindale, P. G. Taylor in *The Chemistry of Organic Silicon Compounds*, *Vol. 2* (Eds.: S. Patai, Z. Rappoport), Wiley, New York, **1989**, p. 893; b) J. S. Panek in *Comprehensive Organic Synthesis*, *Vol. 1* (Eds.: B. M. Trost, I. Fleming), Pergamon, London, **1991**, p. 579.

[40] a) M. Shimizu, T. Hata, T. Hiyama, *Tetrahedron Lett.* **1997**, *38*, 4591; b) M. Shimizu, T. Hata, T. Hiyama, *Tetrahedron Lett.* **1999**, *40*, 7375; c) M. Shimizu, T. Hata, T. Hiyama, *Heterocycles* **2000**, *52*, 707; d) M. Shimizu, T. Hata, T. Hiyama, *Bull. Chem. Soc. Jpn.*

 © 2005 Wiley-VCH Verlag GmbH & Co. KGaA, Weinheim

2000, *73*, 1685; see also: e) H. Burger, P. Moritz, *Organometallics* **1993**, *12*, 4930.

[41] B. E. Smart in *Organofluorine Chemistry—Principles and Commercial Applications* (Eds.: R. E. Banks, B. E. Smart, J. C. Tatlow), Plenum, New York, **1994**, p. 57.

[42] a) I. Fleming in *Comprehensive Organic Chemistry*, *Vol. 3* (Eds.: D. Barton, W. D. Ollis), Pergamon, Oxford, **1979**, p. 541; b) A. R. Bassindale, P. G. Taylor, in *The Chemistry of Organic Silicon Compounds*, *Vol. 2* (Eds.: S. Patai, Z. Rappoport), Wiley, New York, **1989**, p. 951.

[43] For examples of vinylsilane products from bis- or tris(triorganosilyl)methanes, see: a) H. Sakurai, K.-i. Nishiwaki, M. Kira, *Tetrahedron Lett.* **1973**, 4193; b) B.-T. Gröbel, D. Seebach, *Angew. Chem.* **1974**, *86*, 102; *Angew. Chem. Int. Ed. Engl.* **1974**, *13*, 83; c) B.-T. Grobel, D. Seebach, *Chem. Ber.* **1977**, *110*, 852; d) D. Seyferth, J. L. Lefferts, J. R. L. Lambert, *J. Organomet. Chem.* **1977**, *142*, 39; e) I. Fleming, C. D. Floyd, *J. Chem. Soc. Perkin Trans. 1* **1981**, 969; f) D. J. Ager, *J. Org. Chem.* **1984**, *49*, 168; g) P. F. Hudrlik, E. L. O. Agwaramgbo, A. M. Hudrlik, *J. Org. Chem.* **1989**, *54*, 5613; h) C. Palomo, J. M. Aizpurua, J. M. Garcia, I. Ganboa, F. P. Cossio, B. Lecea, C. Lopez, *J. Org. Chem.* **1990**, *55*, 2498.

[44] a) G. G. Furin, O. A. Vyazankina, B. A. Gostevsky, N. S. Vyazankin, *Tetrahedron* **1988**, *44*, 2675; b) T. Hiyama, E. Shirakawa, *Top. Curr. Chem.* **2002**, *219*, 61; c) T. Hiyama in *Metal-catalyzed Cross-coupling Reactions* (Eds.: F. Diederich, P. J. Stang), Wiley-VCH, Weinheim, **1998**, p. 421.

[45] a) G. K. S. Prakash in *Synthetic Fluorine Chemistry* (Eds.: G. A. Olah, R. D. Chambers, G. K. S. Prakash), Wiley, New York, **1992**, p. 227; b) G. K. S. Prakash, A. K. Yudin, *Chem. Rev.* **1997**, *97*, 757; c) M. Fujita, M. Obayashi, T. Hiyama, *Tetrahedron* **1988**, *44*, 4135.

[46] For reviews on oxiranyl anions, see: a) T. Satoh, *Chem. Rev.* **1996**, *96*, 3303; b) Y. Mori, *Rev. Heteroat. Chem.* **1997**, *17*, 183; c) D. M. Hodgson, E. Gras, *Synthesis* **2002**, 1625; see also: d) G. A. Molander, K. Mautner, *Pure Appl. Chem.* **1990**, *62*, 707; e) E. Doris, L. Dechoux, C. Mioskowski, *Synlett* **1998**, 337.

[47] a) M. Shimizu, T. Fujimoto, H. Minezaki, T. Hata, T. Hiyama, *J. Am. Chem. Soc.* **2001**, *123*, 6947; b) M. Shimizu, T. Fujimoto, X. Liu, H. Minezaki, T. Hata, T. Hiyama, *Tetrahedron* **2003**, *59*, 9811.

[48] It is widely known that β-oxido carbenoids undergo 1,2-rearrangement of a substituent β to the oxygen atom, giving rise to carbonyl compounds; for reviews, see: a) P. M. Wockulich, in *Comprehensive Organic Synthesis*, *Vol. 1* (Eds.: B. M. Trost, I. Fleming), Pergamon, Oxford, **1991**, p. 873; b) G. Boche, J. C. W. Lohrenz, *Chem. Rev.* **2001**, *101*, 697; for examples, see: c) J. Villieras, C. Bacquet, J. F. Normant, *J. Organomet. Chem.* **1972**, *40*, C1; d) G. Köbrich, J. Grosser, *Tetrahedron Lett.* **1972**, 4117; e) H. Taguchi, H. Yamamoto, H. Nozaki, *Tetrahedron Lett.* **1972**, 4661; f) G. Köbrich, J. Grosser, *Chem. Ber.* **1973**, *106*, 2626; g) J. Villieras, C. Bacquet, J. F. Normant, *J. Organomet. Chem.* **1975**, *97*, 325; h) H. Taguchi, H. Yamamoto, H. Nozaki, *Bull. Chem. Soc. Jpn.* **1977**, *50*, 1592.

[49] Y. Yamauchi, T. Katagiri, K. Uneyama, *Org. Lett.* **2002**, *4*, 173.

[50] For reviews on oxepanes and oxepins, see: a) D. R. Boyd in *Comprehensive Heterocyclic Chemistry*, *Vol. 7* (Eds.: A. R. Katritzky, C. W. Rees), Pergamon, Oxford, **1984**, p. 547; b) W. Tochtermann, G. Olsson, *Chem. Rev.* **1989**, *89*, 1203; c) L. I. Belen'kii in *Comprehensive Heterocyclic Chemistry II*, *Vol. 9* (Eds.: A. R. Katritzky, C. W. Rees, E. F. V. Scriven), Pergamon, Oxford, **1996**, p. 45; d) D. R. Boyd, N. D. Sharma, *Chem. Soc. Rev.* **1996**, *25*, 289; e) S. von Angerer, W. Tochtermann in *Methods of Organic Chemistry*, *Vol. E9 (Houben-Weyl)*, Thieme, Stuttgart, **1998**, p. 1.

[51] For a review on the Cope rearrangement of bis(alkenyl)oxiranes, see: a) T. Hudlicky, R. Fan, J. W. Reed, K. G. Gadamasetti, *Organic Reactions*, *Vol. 41*, Wiley, New York, **1992**, p. 1; for examples, see: b) T. Hudlicky, A. Fleming, T. C. Lovelace, *Tetrahedron* **1989**, *45*, 3021; c) D. L. Clark, W.-N. Chou, J. B. White, *J. Org. Chem.* **1990**, *55*, 3975; d) W.-N. Chou, J. B. White, *Tetrahedron Lett.* **1991**, *32*, 157; e) W.-N. Chou, J. B. White, W. B. Smith, *J. Am. Chem. Soc.* **1992**, *114*, 4658; f) P. von Zezschwitz, K. Voigt, A. Lansky, M. Noltemeyer, A. de Meijere, *J. Org. Chem.* **1999**, *64*, 3806.

[52] M. Shimizu, T. Fujimoto, X. Liu, T. Hiyama, *Chem. Lett.* **2004**, *33*, 438.

[53] *Preparation of Alkenes: A Practical Approach* (Ed.: J. M. J. Williams), Oxford University Press, Oxford, **1996**, p. 1.

[54] a) *Drugs Fut.* **1985**, *10*, 395; b) *Drugs Fut.* **1990**, *15*, 532; c) G. Abraham, T. Horvath, L. Toldy, J. Borvendeg, E. Csanyi, E. Kiss, I. Hermann, S. K. Tory (Gyogyszerkutato Intezet), US 763078, **1989** [*Chem. Abstr.* **1989**, *111*, 77630]; for biological properties, see: d) J. Borvendeg, I. Hermann, O. Csuka, *Acta Physiol. Hung.* **1996**, *84*, 405 [*PubMed ID*, **1996**, 9328614]; e) V. Erdelyi-Toth, F. Gyergyay, I. Szamel, E. Pap, J. Kralovanszky, E. Bojti, M. Csorgo, S. Drabant, I. Klebovich, *Anti-Cancer Drugs* **1997**, *8*, 603 [*Chem. Abstr.* **1997**, *127*, 287616]; for the synthesis of panomifene, see: f) G. Nemeth, R. Kapiller-Dezsofi, G. Lax, G. Simig, *Tetrahedron* **1996**, *52*, 12821.

[55] a) Y. Ukaji, T. Fujisawa, *Tetrahedron Lett.* **1988**, *29*, 5165; b) Y. Ukaji, A. Yoshida, T. Fujisawa, *Chem. Lett.* **1990**, 157; c) M. Taniguchi, K. Oshima, K. Utimoto, *Tetrahedron Lett.* **1991**, *32*, 2783; d) B. Santiago, C. Lopez, J. A. Soderquist, *Tetrahedron Lett.* **1991**, *32*, 3457; e) J. A. Soderquist, C. Lopez, *Tetrahedron Lett.* **1991**, *32*, 6305; f) E. Doris, L. Dechoux, C. Mioskowski, *Tetrahedron Lett.* **1994**, *35*, 7943; g) E. Doris, L. Dechoux, C. Mioskowski, *Tetrahedron Lett.* **1994**, *35*, 7943; h) A. N. Kasatkin, R. J. Whitby, *Tetrahedron Lett.* **2000**, *41*, 5275.

[56] a) T. Hata, H. Kitagawa, H. Masai, T. Kurahashi, M. Shimizu, T. Hiyama, *Angew. Chem.* **2001**, *113*, 812; *Angew. Chem. Int. Ed.* **2001**, *40*, 790; b) M. Shimizu, H. Kitagawa, T. Kurahashi, T. Hiyama, *Angew. Chem.* **2001**, *113*, 4283; *Angew. Chem. Int. Ed.* **2001**, *40*, 4413; c) M. Shimizu, T. Kurahashi, T. Hiyama, *Synlett* **2001**, 1006; d) T. Kurahashi, T. Hata, H. Masai, H. Kitagawa, M. Shimizu, T. Hiyama, *Tetrahedron* **2002**, *58*, 6381; e) M. Shimizu, T. Kurahashi, H. Kitagawa, T. Hiyama, *Org. Lett.* **2002**, *4*, 225; f) M. Shimizu, T. Kurahashi, H. Kitagawa, K. Shimono, T. Hiyama, *J. Organomet. Chem.* **2003**, *686*, 286.

[57] a) M. W. Rathke, R. Kow, *J. Am. Chem. Soc.* **1972**, *94*, 6854; b) D. S. Matteson, *Synthesis* **1975**, 147.

[58] Triaryl alkenes are one of the key structures of antiestrogens; for reviews on antiestrogens, see: a) R. A. Magarian, L. B. Overacre, S. Singh, K. L. Meyer, *Curr. Med. Chem.* **1994**, *1*, 61; b) V. C. Jordan, *J. Med. Chem.* **2003**, *46*, 883; c) V. C. Jordan, *J. Med. Chem.* **2003**, *46*, 1081.

[59] X. Liu, M. Shimizu, T. Hiyama, *Angew. Chem.* **2004**, *115*, 897; *Angew. Chem. Int. Ed.* **2004**, *43*, 879.

[60] a) *Asymmetric Fluoroorganic Chemistry: Synthesis, Applications, and Future Directions*, *ACS Symposium Series 746* (Ed.: P. V. Ramachandran), American Chemical Society, Washington, **2000**; b) *Enantiocontrolled Synthesis of Fluoro-Organic Compounds* (Ed.: V. A. Soloshonok), Wiley, Chichester, **1999**; c) K. Iseki, *Tetrahedron* **1998**, *54*, 13887; d) T. Kitazume, T. Yamazaki, *Top. Curr. Chem.* **1997**, *193*, 90; e) P. Bravo, G. Resnati, *Tetrahedron: Asymmetry* **1990**, *1*, 661.

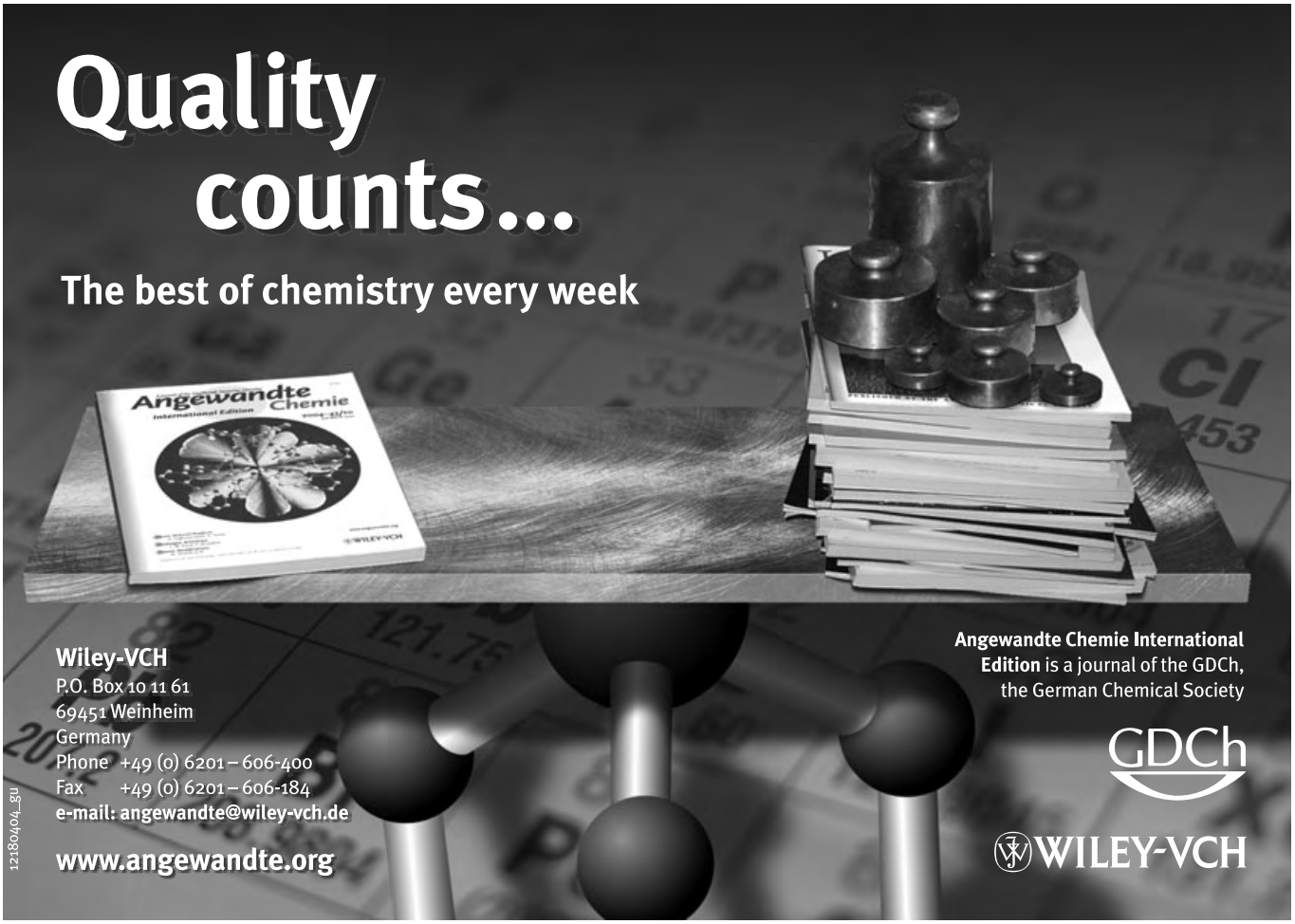
[61] T. Hiyama, T. Kusumoto, H. Matsutani in *Asymmetric Fluoroorganic Chemistry: Synthesis, Applications, and Future Directions*, *ACS Symposium Series 746* (Ed.: P. V. Ramachandran), American Chemical Society, Washington, **2000**, p. 226.

[62] H. Poras, H. Matsutani, J. Yaruva, T. Kusumoto, T. Hiyama, *Chem. Lett.* **1998**, 665.

[63] H. Matsutani, H. Poras, T. Kusumoto, T. Hiyama, *Chem. Commun.* **1998**, 1259.

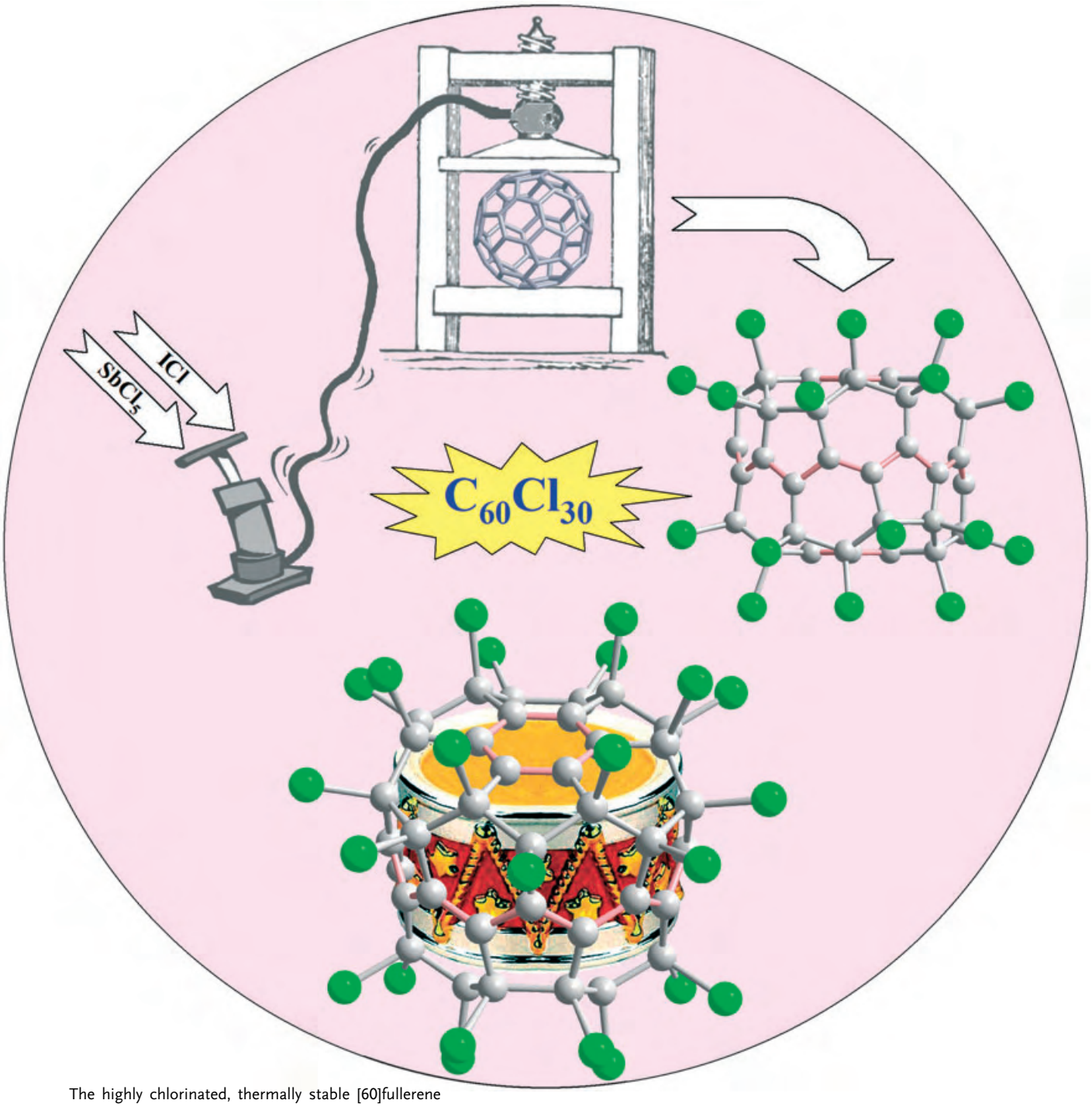
 © 2005 Wiley-VCH Verlag GmbH & Co. KGaA, Weinheim

[64] H. Matsutani, S. Ichikawa, J. Yaruva, T. Kusumoto, T. Hiyama, *J. Am. Chem. Soc.* **1997**, *119*, 4541.
[65] a) T. Katagiri, H. Ihara, M. Takahashi, S. Kashino, K. Furuhashi, K. Uneyama, *Tetrahedron: Asymmetry* **1997**, *8*, 2933; b) T. Katagiri, M. Irie, K. Uneyama, *Tetrahedron: Asymmetry* **1999**, *10*, 2583.
[66] H. Matsutani, H. Poras, T. Kusumoto, T. Hiyama, *Synlett* **1998**, 1353.
[67] H. Matsutani, T. Kusumoto, T. Hiyama, *Chem. Lett.* **1999**, 529.



 © 2005 Wiley-VCH Verlag GmbH & Co. KGaA, Weinheim

Communications



The highly chlorinated, thermally stable [60]fullerene $C_{60}Cl_{30}$ contains a cylinder-shaped carbon cage consisting of two aromatic six-membered rings and one equatorial 18π-trannulene belt separated by two 15-membered belts of sp^3 carbon atoms bearing Cl substituents. Find out more about the synthesis and properties of $C_{60}Cl_{30}$ in the Communication by P. A. Troshin, S. I. Troyanov et al. on the following pages.

© 2005 Wiley-VCH Verlag GmbH & Co. KGaA, Weinheim
DOI: 10.1002/anie.200461531

Fullerenes

Synthesis and Structure of the Highly Chlorinated [60]Fullerene $C_{60}Cl_{30}$ with a Drum-Shaped Carbon Cage**

Pavel A. Troshin, Rimma N. Lyubovskaya, Ilya N. Ioffe, Natalia B. Shustova, Erhard Kemnitz, and Sergey I. Troyanov**

Halogenated fullerenes are versatile precursors for the synthesis of various complex derivatives, some of which exhibit promising properties for material science applications.[1] To date, considerable success has been achieved in preparation and structural characterization of fullerene bromides[2] and fluorides.[3] Despite numerous reports on chlorination of C_{60} by different reagents,[4] only two individual compounds have been isolated so far. The structure of $C_{60}Cl_6$ formed in the reaction of ICl with C_{60} in benzene was deduced from the ^{13}C NMR and IR spectra.[4b] $C_{60}Cl_{24}$ was synthesized using VCl_4 and $SbCl_5$; a tetrahedral structure similar to that of $C_{60}Br_{24}$[2a,d] was assigned to this chloride on the basis of a comparison between the experimental and theoretically calculated IR spectra.[5]

Here we report the synthesis and structural characterization of the novel, highly chlorinated fullerene $C_{60}Cl_{30}$. This chlorofullerene can be prepared using chlorinating agents such as ICl, ICl_3, and $SbCl_5$. Typically, 50–100 mg of C_{60} and a large excess (~2 g) of chlorinating agents were sealed in glass ampules and heated at 220–250 °C for one to three days. Then, the ampules were opened, and the excess of the chlorinating agents and their decomposition products were removed in vacuo at 150 °C. Pure $C_{60}Cl_{30}$ (**1**) was formed in the reaction of C_{60} with $SbCl_5$, whereas chlorination by ICl yielded the $C_{60}Cl_{30}\cdot 2\,ICl$ solvate (**2**), both as dark-orange crystals stable in air. The IR spectrum of $C_{60}Cl_{30}$ is presented in Figure 1. The most prominent bands are observed at $\tilde{\nu} = 439$, 450, 471, 479, 730, 775, 822, 854, 895, 903, 918, 958, 993, and 1447 cm^{-1}.[6]

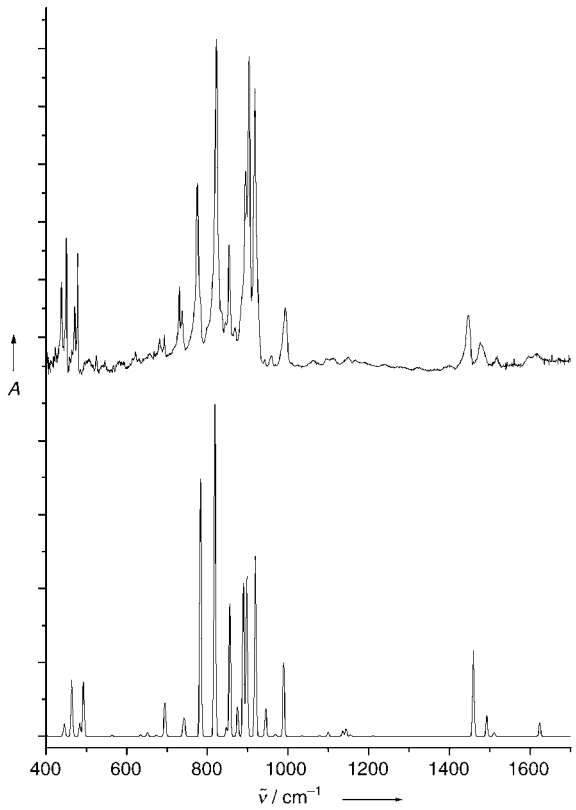


Figure 1. The experimental (top) and calculated (bottom) IR spectra of $C_{60}Cl_{30}$.

$C_{60}Cl_{30}$ is insoluble in most common organic solvents such as diethyl ether, 1,4-dioxane, CH_2Cl_2, $CHCl_3$, and CCl_4; it is poorly soluble in CS_2, toluene, and chlorobenzene; and its solubility in 1,2-dichlobenzene was estimated at roughly 0.2 mg mL^{-1}. The thermal stability of $C_{60}Cl_{30}$ appears to be remarkably high: its decomposes into C_{60} and Cl_2 at 450–500 °C (Figure 2), which is about 120 °C higher than the temperature ranges previously reported for $C_{60}Cl_{24}$.[4b,5] The mass loss for $C_{60}Cl_{30}$, 60.1 %, corresponds well to the calculated value of 59.75 %.

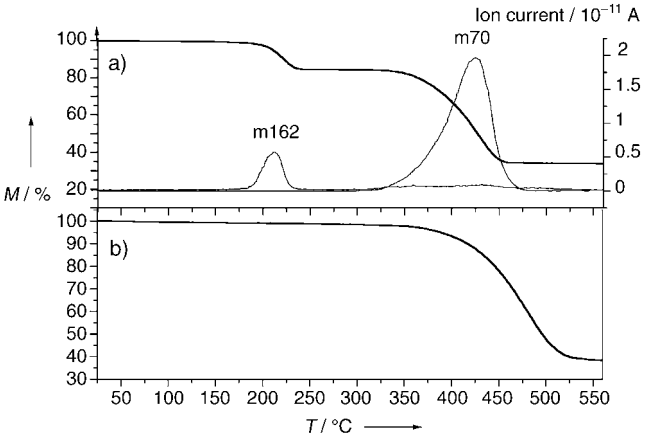


Figure 2. Thermoanalytical data for $C_{60}Cl_{30}\cdot 2\,ICl$ (a) and $C_{60}Cl_{30}$ (b).

[*] P. A. Troshin, Prof. R. N. Lyubovskaya
Institute of Problems of Chemical Physics of RAS
142432 Chernogolovka, Moscow Region (Russia)
Fax: (+7) 096-2521852
E-mail: troshin@cat.icp.ac.ru
Dr. I. N. Ioffe, N. B. Shustova, Prof. Dr. S. I. Troyanov
Chemistry Department
Moscow State University
119992 Moscow (Russia)
Fax: (+7) 095-9391240
E-mail: troyanov@thermo.chem.msu.ru
Prof. Dr. E. Kemnitz
Institut für Chemie
Humboldt-Universität zu Berlin
12489 Berlin (Germany)

[**] This work was supported in part by the Deutsche Forschungsgemeinschaft (KE 489/20-1) and by the Russian Foundation for Basic Research (03-03-04006 and 04-03-32870a). We are grateful to A. A. Popov for his help in scaling the calculated IR spectrum, and to M. Feist and N. V. Chelovskaya for thermoanalytical measurements.

 © 2005 Wiley-VCH Verlag GmbH & Co. KGaA, Weinheim

X-ray single-crystal structures of both $C_{60}Cl_{30}$ (**1**) and $C_{60}Cl_{30}\cdot 2\,ICl$ (**2**) were determined with good accuracy.[7] While the isolated molecule of $C_{60}Cl_{30}$ should possess D_{3d} symmetry, crystallographically imposed symmetry in **1** and **2** becomes reduced to C_i and C_{2h}, respectively. There are two planar aromatic six-membered rings on the opposite sides of the cage and an equatorial 18π all-*trans* annulene (*trannulene*) belt in the chlorofullerene molecule (Figure 3). $C_{60}Cl_{30}$ is the first molecule in which the trannulene belt is separated from the benzenoid rings by two 15-membered rings of sp^3 carbons bearing chlorine atoms. Such a structural arrangement results in the unique cylindrical, drumlike shape of the carbon cage.

The fluorofullerene molecule $C_{60}F_{18}$ contains one six-membered planar aromatic fragment which is surrounded by the fluorinated belt of 15 sp^3 carbons.[8] The S_N2' substitution of three additional outlying fluorine atoms by various malonate groups yields compounds having the composition $C_{60}F_{15}[CX(COOR)_2]_3$, which also contain [18]annulene belts. These subunits satisfy the magnetic and geometric criteria of aromaticity, even though they are not completely isolated from the rest of the π system.[1,9]

The IR spectroscopic and mass spectrometric study of the products collected before the completion of the reaction revealed that tetrahedral $C_{60}Cl_{24}$ is an intermediate in the synthesis of $C_{60}Cl_{30}$. Noteworthy, the formation of D_{3d} $C_{60}Cl_{30}$ from T_h $C_{60}Cl_{24}$ requires rearrangement of at least 18 Cl atoms over the fullerene cage. The analogous migration of fluorine atoms yielding the most thermodynamically stable structures is called the "fluorine dance" and is known for the fluorination of $C_{60}F_{36}$ to give $C_{60}F_{48}$[10a] and for the transformation of C_1 $C_{60}F_{36}$ into C_3 $C_{60}F_{36}$ by fluorine rearrangement.[10b] The formation of $C_{60}Cl_{30}$ from $C_{60}Cl_{24}$ is the first observation of the "chlorine dance". The thermally induced "chlorine dance" appears to be slow enough for other possible intermediates to be isolated by termination of the reaction at a certain stage.

Quantum chemical calculations at the DFT level of theory were performed to examine the relative stability of various higher chlorides of C_{60}.[11] Two main factors were found to influence the stability of chlorofullerenes beyond $C_{60}Cl_{24}$: destabilizing van der Waals repulsions between the adjacent chlorine atoms and the stabilizing effect of the aromatic fragments such as benzenoid rings. Particularly high steric strain was observed for the structures containing chlorine atoms surrounded by three others ("triple contacts"). Ruling out the "triple contacts" results in a maximum of two isolated benzenoid rings in the closed-shell chlorofullerene molecules. One of two possible structures containing two aromatic six-membered rings and no "triple contacts" corresponds exactly to the presently found isomer of $C_{60}Cl_{30}$. It is approximately 110 kJ mol^{-1} more stable than the second possible $C_{60}Cl_{30}$ isomer, which is characterized by nonparallel arrangement of two aromatic six-membered rings. The remarkable thermal stability of $C_{60}Cl_{30}$ might have a kinetic origin since detachment of any chlorine atom would perturb the stable aromatic fragments. $C_{60}Cl_{30}$ probably represents the terminal stage of C_{60} chlorination since further chlorine attachment would involve a strongly unfavorable destruction of the aromatic rings.

The averaged experimental and calculated molecular structures of $C_{60}Cl_{30}$ are in very good agreement (Table 1). The aromatic six-membered rings are almost perfectly planar; the sum of the valence angles involving aromatic carbons exceeds 359.9°; and the 6/6 (*a'*) and 5/6 (*a''*) C–C bonds in these rings are virtually equal. Similar equalization of the 6/6 (*h*) and 5/6 (*i*) bonds is seen in the equatorial trannulene ring, which serves as additional evidence of its aromatic character. The sp^3–sp^3 C–C bonds appear to be strongly elongated, reaching a value of 1.70 Å (*e*). For comparison, similar bonds in $C_{60}F_{18}$ and $C_{60}F_{36}$ are "only" 1.67 Å long.[9,12] The calculated IR spectrum of $C_{60}Cl_{30}$ is in a good agreement with the experimental one (Figure 1).

It is known that oxygen can attack the elongated C–C bonds in $C_{60}F_{18}$, which results in their cleavage and formation of intramolecular ethers.[13] Impurities of $C_{60}F_{18}O$ in some $C_{60}F_{18}$ samples have been observed by means of X-ray single-crystal diffraction.[9b] In these cases, the presence of oxygen was manifested in the characteristic maxima near the elongated C–C bonds on electron density maps. Similar peaks were found for **1a** (synthesized with nonpurified $SbCl_5$),[7] where one of the *e* bonds was elongated up to

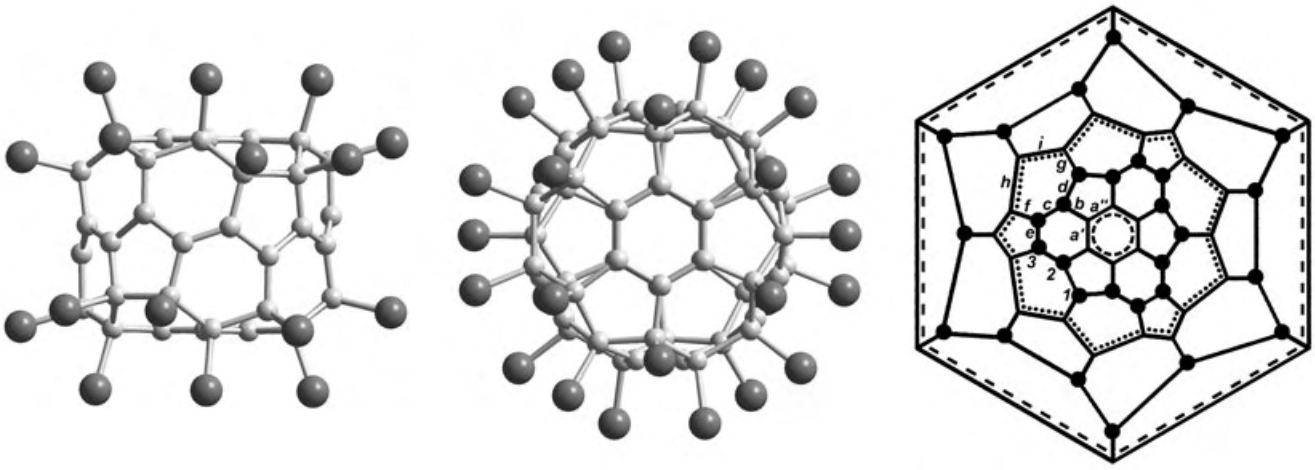


Figure 3. The top and side views and the Schlegel diagram of the $C_{60}Cl_{30}$ molecule.

 © 2005 Wiley-VCH Verlag GmbH & Co. KGaA, Weinheim

Table 1: C–C and C–Cl bonds [Å] in $C_{60}Cl_{30}$ according to the averaged data[a] for structures **1** and **2** and DFT calculations.

Bond type[b]	**1**	**2**	Calcd
C–C			
a′, sp^2–sp^2, 6/6	1.367	1.372	1.372
a″, sp^2–sp^2, 5/6	1.377	1.374	1.380
b, sp^2–sp^3, 5/6	1.476	1.476	1.479
c, sp^3–sp^3, 6/6	1.576	1.582	1.582
d, sp^3–sp^3, 5/6	1.622	1.620	1.628
e, sp^3–sp^3, 5/6	1.693	1.699	1.699
f, sp^2–sp^3, 5/6	1.509	1.509	1.509
g, sp^2–sp^3, 6/6	1.494	1.494	1.496
h, sp^2–sp^2, 6/6	1.381	1.386	1.381
i, sp^2–sp^3, 5/6	1.391	1.392	1.391
C–Cl			
1	1.776	1.772	1.800
2	1.788	1.786	1.815
3	1.787	1.779	1.811

[a] Estimated standard deviations of individual bond lengths in **1** and **2** are 0.002 Å and 0.003–0.004 Å, respectively. [b] Bond labels are defined in the Schlegel diagram in Figure 3.

1.722 Å, as compared to 1.690 Å for the rest two *e* bonds. Taking into account a statistical averaging with the parent $C_{60}Cl_{30}$, this additional elongation indicates the presence of the $C_{60}Cl_{30}O_2$ ether (about 7 %) with two cleaved C–C bonds.

The chemical properties of $C_{60}Cl_{30}$ may be rather versatile. Firstly, the weak elongated C–C bonds can be regarded as a convenient site for further derivatization of this molecule. The benzenoid moieties can allow organometallic η^6-coordination, as it was previously observed for $C_{60}F_{18}$.[14] Our preliminary experiments showed that $C_{60}Cl_{30}$ can undergo nucleophilic substitution reactions though significantly slower than $C_{60}Cl_{24}$. Detailed investigation of $C_{60}Cl_{30}$ reactivity is a subject for further studies.

Received: August 4, 2004
Published Online: November 12, 2004

Keywords: chlorination · density functional calculations · fullerenes · structure elucidation

[1] G. A. Burley, A. G. Avent, I. V. Gol'dt, P. B. Hitchcock, H. Al-Matar, D. Paolucci, F. Paolucci, P. W. Fowler, A. Soncini, J. M. Street, R. Taylor, *Org. Biomol. Chem.* **2004**, *2*, 319.

[2] a) F. N. Tebbe, R. L. Harlow, D. B. Chase, D. L. Thorn, G. C. Campbell, J. C. Calabrese, N. Herron, R. J. Young, E. Wasserman, *Science* **1992**, *256*, 822; b) P. R. Birkett, P. B. Hitchcock, H. W. Kroto, R. Taylor, D. R. M. Walton, *Nature* **1992**, *357*, 479; c) P. A. Troshin, D. Kolesnikov, A. V. Burtsev, R. N. Lubovskaya, N. I. Denisenko, A. A. Popov, S. I. Troyanov, O. V. Boltalina, *Fullerenes Nanotubes Carbon Nanostruct.* **2003**, *11*, 47; d) S. I. Troyanov, P. A. Troshin, O. V. Boltalina, E. Kemnitz, *Fullerenes Nanotubes Carbon Nanostruct.* **2003**, *11*, 61.

[3] R. Taylor, *J. Fluorine Chem.* **2004**, *125*, 359.

[4] a) G. A. Olah, I. Bucsi, C. Lambert, R. Aniszfeld, N. J. Trivedy, D. K. Sensharma, G. K. S. Prakash, *J. Am. Chem. Soc.* **1991**, *113*, 9385; b) P. R. Birkett, A. G. Avent, A. D. Darwish, H. W. Kroto, R. Taylor, D. R. M. Walton, *J. Chem. Soc. Chem. Commun.* **1993**, 1230; c) D. Heymann, F. Cataldo, R. Fokkens, N. M. M. Nibbering, R. Vis, *Fullerene Sci. Technol.* **1999**, *7*, 159; d) P. A. Troshin, O. Popkov, R. N. Lyubovskaya, *Fullerenes Nanotubes Carbon Nanostruct.* **2003**, *11*, 163.

[5] S. I. Troyanov, N. B. Shustova, A. A. Popov, M. Feist, E. Kemnitz, *Zh. Neorg. Khim.* **2004**, *49*, 1413.

[6] IR spectra were recorded for KBr pellets on a NICOLET-200 FT spectrometer; 128 scans were averaged and the resolution was 0.5 cm^{-1}.

[7] The data for crystals of $C_{60}Cl_{30}\cdot 0.09\,Cl_2$ (**1**) and $C_{60}Cl_{30}\cdot 2\,ICl$ (**2**) were collected on an IPDS diffractometer (Stoe) at 170 K and 150 K, respectively (graphite-monochromated $Mo_{K\alpha}$ radiation, $\lambda = 0.71073$ Å). **1**: monoclinic, $P2_1/n$, $a = 12.539(1)$, $b = 13.507(1)$, $c = 17.106(2)$ Å, $\beta = 99.98(1)°$, $V = 2853.3(5)$ Å^3, $Z = 2$; 19414 reflections collected, 6347independent. Structure solution with SHELXS-97. The final anisotropic LS refinement (SHELXL-97) with 416 parameters converged to $wR_2 = 0.054$ and $R_1 = 0.021$. In structure **1a**, additional peaks detected after location of all atoms in $C_{60}Cl_{30}$ were treated as one O and two Cl atoms with refined site occupancy 0.067(2). **2**: tetragonal, $P4_2/m$, $a = 13.492(2)$, $c = 17.027(3)$ Å, $V = 3099.5(9)$ Å^3, $Z = 2$; 30901 reflections collected, 3818 independent. Both ICl molecules are disordered over several positions. Anisotropic LS refinement with 257 parameters gave the final values of $wR_2 = 0.098$ and $R_1 = 0.035$. CCDC 246573–246575 contain the supplementary crystallographic data for this paper. These data can be obtained free of charge via www.ccdc.cam.ac.uk/conts/retrieving.html (or from the Cambridge Crystallographic Data Centre, 12, Union Road, Cambridge CB21EZ, UK; fax: (+44) 1223-336-033; or deposit@ccdc.cam.ac.uk).

[8] a) I. S. Neretin, K. A. Lyssenko, M. Yu. Antipin, Yu. L. Slovokhotov, O. V. Boltalina, P. A. Troshin, A. Yu. Lukonin, L. N. Sidorov, R. Taylor, *Angew. Chem.* **2000**, *112*, 3411; *Angew. Chem. Int. Ed.* **2000**, *39*, 3273; b) S. I. Troyanov, O. V. Boltalina, I. V. Kuvytchko, P. A. Troshin, E. Kemnitz, P. B. Hitchcock, R. Taylor, *Fullerene Sci. Technol.* **2002**, *10*, 243.

[9] G. A. Burley, P. W. Fowler, A. Soncini, J. P. B. Sandall, R. Taylor, *Chem. Commun.* **2004**, 3042.

[10] a) A. A. Gakh, A. A. Tuinman, *Tetrahedron Lett.* **2001**, *42*, 7137; b) A. Avent, R. Taylor, *Chem. Commun.* **2002**, 2726.

[11] DFT calculations were carried out with the use of the Priroda code (D. N. Laikov, *Chem. Phys. Lett.* **1997**, *281*, 151), which employs fast implementation of the RI technique. PBE exchange-correlation functional (J. P. Perdew, K. Burke, M. Ernzerhof, *Phys. Rev. Lett.* **1996**, *77*, 3865) and a basis set of TZ2P quality were used.

[12] P. B. Hitchcock, R. Taylor, *Chem. Commun.* **2002**, 2078.

[13] O. V. Boltalina, B. de La Vaissière, P. W. Fowler, P. B. Hitchcock, J. P. B. Sandall, P. A. Troshin, R. Taylor, *Chem. Commun.* **2000**, 1325.

[14] M. D. Francis, O. V. Boltalina, J. F. Nixon, R. Taylor, *Fullerenes Nanotubes Carbon Nanostruct.* **2003**, *11*, 115.

 © 2005 Wiley-VCH Verlag GmbH & Co. KGaA, Weinheim

Homogeneous Catalysis

Transition-Metal-Catalyzed Benzylation of Arenes and Heteroarenes**

*Kristin Mertins, Irina Iovel, Jette Kischel, Alexander Zapf, and Matthias Beller**

Dedicated to Professor Rüdiger Selke on the occasion of his 70th birthday

The majority of known fine chemicals, pharmaceuticals, agrochemicals, dyes, etc. contain aromatic and/or heteroaromatic substructures. To vary and improve the properties of these compounds functionalization reactions of the aromatic core are of fundamental importance to organic chemistry. In the past and still today most aromatic products are prepared on the industrial level by well-known classic transformations such as Friedel–Crafts alkylations, Friedel–Crafts acylations, nitrations, and halogenations.[1] Although these methods work reliably with a variety of substrates, they often have major drawbacks such as drastic reaction conditions (high temperature, strong acidic conditions), low regioselectivity, and large amounts of (salt) by-products. In addition it is common that the construction of specific C–C bonds on the aromatic core requires several steps including introduction of activating groups and protection and deprotection steps. Therefore, the development of new direct C–C coupling reactions of arenes has become an important topic in organometallic chemistry and catalysis. Recent elegant examples of such catalytic functionalization reactions include the addition of olefins to acetophenones (Murai reaction)[2] and aromatic imines,[3] novel additions of olefins to electron-rich arenes[4] and heterocycles,[5] the addition of arenes to alkynes,[6] the carbonylation of heterocycles,[7] the intramolecular cyclization of arylalkynes,[8] and the C-arylation of heteroarenes.[9]

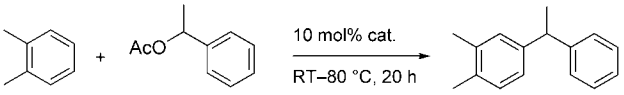
In the past we have mainly focused on transformations of aryl chlorides using the C–Cl bond as an activating and directing functionality.[10] Because of the obvious advantages of direct C–H transformations over palladium-catalyzed reactions of aryl halides, we initiated a program to search for new catalysts for C–C coupling reactions of arenes. Herein, we report our first results and show that various transition-metal catalysts are capable of benzylating activated and nonactivated arenes and heteroarenes with high yield and selectivity under mild conditions.

[*] Dipl.-Chem. K. Mertins, Dr. I. Iovel, J. Kischel, Dr. A. Zapf, Prof. Dr. M. Beller
Leibniz-Institut für Organische Katalyse
Universität Rostock e.V. (IfOK)
Buchbinderstrasse 5–6, 18055 Rostock (Germany)
Fax: (+49) 381-466-9324
E-mail: matthias.beller@ifok.uni-rostock.de

[**] This work was supported by the State of Mecklenburg-Western Pomerania and the Bundesministerium für Bildung und Forschung ("Nachhaltige Aromatenchemie"). We thank Prof. Dr. M. Michalik, Dr. W. Baumann, Dr. C. Fischer, H. Baudisch, and S. Buchholz (all IfOK) for excellent assistence with the analyses.

Initially we were attracted by the reaction of benzyl alcohol and its derivatives with arenes leading to diarylmethane-type compounds. The diarylmethane motif is found in a number of biologically active compounds such as piritrexim,[11a] trimethoprim,[11a] avrainvilleol,[11b] papaverine,[11c] beclobrate,[11d] and anastrozole[11e] and in a precursor in the synthesis of letrozole.[11e] Diarylmethane derivatives are used to prepare electroactive and photoactive oligomers and polymers based on fluorenes.[12] Friedel–Crafts reactions of benzylic alcohols and halides have been studied with traditional Brønsted and Lewis acids,[13] more recently with lanthanide and actinide triflates,[14] and also with heterogeneous catalysts.[15] Surprisingly few transition-metal catalysts based on palladium and ruthenium have been described to date for this type of reaction.[16] While palladium complexes have been used only on a stoichiometric basis for this reaction,[17] ruthenium complexes required high temperatures (200 °C) and gave the corresponding diarylmethanes generally in low to moderate yield (22–77 %).[18]

In our search for new and improved catalysts we studied the benzylation of *o*-xylene with 1-phenylethyl acetate as a model reaction (Scheme 1). A variety of Brønsted acids, transition-metal salts, and organometallic complexes were tested under mild conditions (80 °C). Selected results are given in Table 1. In the presence of catalytic amounts



1

Scheme 1. Benzylation of *o*-xylene with 1-phenylethyl acetate.

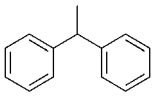
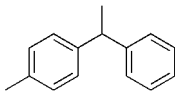
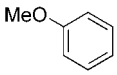
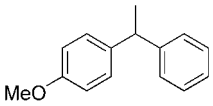
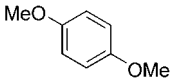
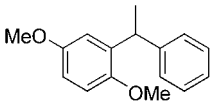
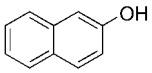
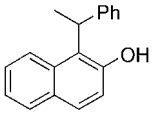
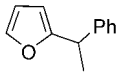
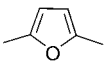
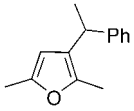
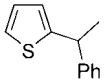
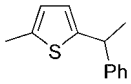
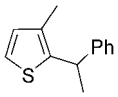
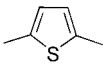
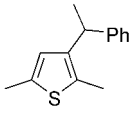
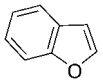
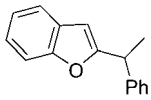
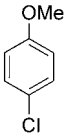
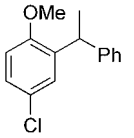
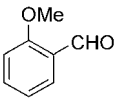
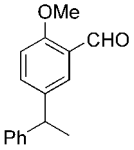
Table 1: Screening of catalysts for the model reaction.[a]

Entry	Catalyst	*T* [°C]	Conv. [%][b]	Yield [%][c]
1	HCl	80	5	0
2	*p*-TSA	80	52	2
3	H_2SO_4	80	9	0
4	HOAc	80	8	0
5	$[W(CO)_6]$	80	18	6
6	$[MesW(CO)_3]$	80	100	61
7	$MnCl_2 \cdot 4\,H_2O$	80	0	0
8	$Co(OAc)_2 \cdot 4\,H_2O$	80	0	0
9[d]	$RhCl_3 \cdot n\,H_2O$	50	100	79
10[d]	$RhCl_3 \cdot n\,H_2O$	RT	83	48
11	$[Rh(cod)Cl]_2$	80	0	0
12[d]	$IrCl_3 \cdot n\,H_2O$	80	100	99
13[d]	$IrCl_3 \cdot n\,H_2O$	50	100	99
14[d]	$IrCl_3 \cdot n\,H_2O$	RT	100	75
15	$IrBr_3 \cdot 4\,H_2O$	80	19	16
16	$[\{Ir(cod)Cl\}_2]$	80	0	0
17	$H_2[PdCl_4] \cdot 6\,H_2O$	80	100	99
18	$H_2[PdCl_4] \cdot 6\,H_2O$	50	75	65
19	$H_2[PdCl_4] \cdot 6\,H_2O$	RT	0	0
20	$[Pd(PPh_3)_4]$	80	0	0
21	$H_2[PtCl_6] \cdot 6\,H_2O$	80	100	99
22	$H_2[PtCl_6] \cdot 6\,H_2O$	50	100	99
23	$H_2[PtCl_6] \cdot 6\,H_2O$	RT	100	99
24	$PtCl_2$	80	8	7
25	$[Pt(cod)Cl_2]$	80	0	0

[a] Reaction conditions: 10 mL *o*-xylene, 0.5 mmol 1-phenylethyl acetate, 10 mol % catalyst, 20 h. Mes = mesitylene, cod = cycloocta-1,5-diene. [b] GC conversion based on 1-phenylethyl acetate. [c] GC yield. [d] 8 mol % catalyst.

 © 2005 Wiley-VCH Verlag GmbH & Co. KGaA, Weinheim DOI: 10.1002/anie.200460666

Table 2: Benzylation of different substrates.[a]

Entry	Substrate	Main product	Catalyst	*T* [°C]	*t* [h]	Conv.[b] [%]	Yield[c] [%]	Regiosel. (*o*/*m*/*p*)
1[d]			$H_2[PtCl_6]\cdot 6H_2O$	140	20	100	62	–
2[d]			$H_2[PtCl_6]\cdot 6H_2O$	RT	24	76	57	87
3[d]			$H_2[PtCl_6]\cdot 6H_2O$	50	24	100	87	83
4[d]			$IrCl_3\cdot n H_2O$	50	24	100	79	84
5[d]			$H_2[PtCl_6]\cdot 6H_2O$	50	24	100	99	17:0:83
6[d]			$IrCl_3\cdot n H_2O$	50	24	100	99	17:0:83
7[e]			$H_2[PtCl_6]\cdot 6H_2O$	80	24	100	92	–
8[f]			$H_2[PtCl_6]\cdot 6H_2O$	120	23	100	96	<1:99
9[f]			$H_2[PtCl_6]\cdot 6H_2O$	120	24	100	62	<1:99
10[f]			$H_2[PtCl_6]\cdot 6H_2O$	120	24	100	85	–
11[f]			$H_2[PtCl_6]\cdot 6H_2O$	120	20	100	84	82:18[g]
12[f]			$H_2[PtCl_6]\cdot 6H_2O$	120	20	100	96	77
13[f,h]			$IrCl_3\cdot n H_2O$	80	20	100	92	63:5:32[i]
14[f]			$H_2[PtCl_6]\cdot 6H_2O$	120	24	100	94	–
15[d,h]			$H_2[PtCl_6]\cdot 6H_2O$	80	20	100	91	77
16[j]			$H_2[PtCl_6]\cdot 6H_2O$	50	20	100	99	<1:99
17[d,h]			$H_2[PtCl_6]\cdot 6H_2O$	80	20	100	67	<1:99

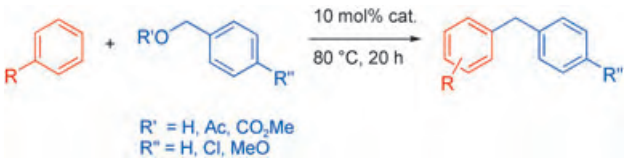
[a] Reaction conditions: 0.5 mmol 1-phenylethyl acetate, 10 mol% catalyst, 20–24 h. [b] GC conversion based on 1-phenylethyl acetate. [c] GC yield. [d] In 10 mL substrate. [e] 10 mmol substrate in 8 mL benzene. [f] 10 mmol substrate in 8 mL dioxane. [g] 2-/3-. [h] 8 mol% catalyst. [i] 2-/4-/5-. [j] 10 mmol substrate in 8 mL CH_2Cl_2.

 © 2005 Wiley-VCH Verlag GmbH & Co. KGaA, Weinheim

(10 mol%) of various Brønsted acids (HCl, H_2SO_4, HOAc, *p*-toluenesulfonic acid) the benzylated product 1-(3,4-dimethylphenyl)-1-phenylethane (**1**) was obtained at best in low yields (≤2%; Table 1, entries 1–4); however, to our surprise a variety of Rh, Ir, Pd, and Pt salts proved to be suitable catalysts for the test reaction. In addition, also [(mesitylene)-$W(CO)_3$] gave a significant yield (61%) of the desired product (Table 1, entry 6). At 80°C excellent results (99% yield of **1**) were obtained in the presence of hydrated $IrCl_3$, $H_2[PdCl_4]$, and $H_2[PtCl_6]$ (Table 1, entries 12, 17, and 21, respectively).[19] Good to quantitative yields of **1** (up to 99%) were observed even at room temperature using $IrCl_3$ and $H_2[PtCl_6]$ (Table 1, entries 14 and 23, respectively). Although for convenience most of the screening were conducted for 20 h, it is noteworthy that the reaction with $H_2[PtCl_6]$ at 80°C is complete within 1 h. In some cases a significant difference between the conversion and yield of **1** is observed (e.g., Table 1, entries 2, 6, 10). Here, side reactions of 1-phenylethyl acetate such as elimination, oligomerization, and polymerization of the resulting styrene take place.

With reliable catalysts for the benzylation of *o*-xylene in hand, we were interested in the benzylation of other arenes and heteroarenes (Table 2) and in the use of different benzylating agents (Table 3). Although a number of the active transition-metal salts listed in Table 1 also catalyze these reactions, only the results with the most active and selective catalysts ($IrCl_3$ and $H_2[PtCl_6]$) are listed in Tables 2 and 3. As expected, a variety of electron-rich arenes such as toluene (87%), anisole (>99%), 1,4-dimethoxybenzene (92%), and 2-naphthol (96%) gave the corresponding benzylated products in good to excellent yield. In addition, heteroarenes, for example, 2,5-dimethylfuran (85%), benzofuran (91%), and 2-methylthiophene (96%) react very well. Interestingly, even nonactivated substrates such as benzene (62%) and more challenging starting materials such as 4-chloroanisole (99%)[20] and 2-methoxybenzaldehyde (67%) gave the corresponding products selectively. It is important to note that the last example constitutes one of the very rare cases of a selective Friedel–Crafts reaction in the presence of an aldehyde group!

Finally, we set out to study the scope and limitation of the benzylating agent in more detail (Scheme 2). As shown in

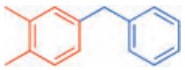
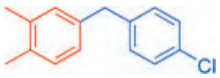
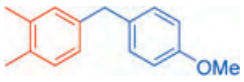
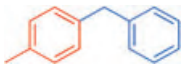
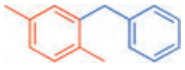
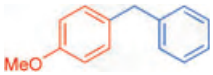
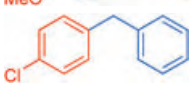


Scheme 2. Benzylation of arenes with different benzylation reagents. cat. = $H_2[PdCl_6]\cdot 6H_2O$, $IrCl_3\cdot n H_2O$.

Table 3 apart from 1-phenylethyl acetate also benzyl acetate and 4-chlorobenzyl acetate react with *o*-xylene in the presence of $H_2[PtCl_6]$ at 80°C (Table 3, entries 1, 4). In addition, benzyl methyl carbonate (66%) and benzyl alcohol (48%) also gave the desired product in moderate yields (Table 3, entries 2, 3). More interestingly, the reaction of benzyl acetate and chlorobenzene proceeded in good yield (57%). It is important to note that this latter reaction is one of the few successful Friedel–Crafts benzylations that work well also with deactivated arenes.

With regard to the mechanism, the presented reactions clearly operate by means of electrophilic aromatic substitu-

Table 3: Reactions with different benzylation reagents.[a]

Entry	Product	R′	Catalyst	*T* [°C]	Conv.[b] [%]	Yield[c] [%]	Regiosel. (*o*/*m*/*p*)
1		Ac	$H_2[PtCl_6]\cdot 6H_2O$	80	100	45	<1:99
2		CO_2Me	$H_2[PtCl_6]\cdot 6H_2O$	80	100	66	<1:99
3		H	$H_2[PtCl_6]\cdot 6H_2O$	80	100	48	<1:99
4		Ac	$H_2[PtCl_6]\cdot 6H_2O$	80	100	65	28:0:72
5		CO_2Me	$H_2[PtCl_6]\cdot 6H_2O$	80	100	42	1:99
6		Ac	$H_2[PtCl_6]\cdot 6H_2O$	140	100	79	–
7		Ac	$H_2[PtCl_6]\cdot 6H_2O$	80	100	80	40:7:53
8		Ac	$IrCl_3\cdot n H_2O$	80	100	88	40:7:53
9		Ac	$H_2[PtCl_6]\cdot 6H_2O$	80	100	80	–
10		Ac	$H_2[PtCl_6]\cdot 6H_2O$	80	93	93	35:0:65
11		Ac	$IrCl_3\cdot n H_2O$	80	80	76	38:0:62
12		Ac	$H_2[PtCl_6]\cdot 6H_2O$	100	100	57	42:1:57

[a] Reaction conditions: 10 mL substrate, 0.5 mmol benzylating agent, 10 mol% catalyst, 20–24 h. [b] GC conversion based on benzylating agent. [c] GC yield.

 © 2005 Wiley-VCH Verlag GmbH & Co. KGaA, Weinheim

tion. Thus, different regioisomers can be formed; however, in a number of cases (Table 2, entries 1, 7–10, 14, 16, 17) the benzylation proceeds regioselectively to produce only one product. By comparing the results in the presence of simple Brønsted acids and our transition-metal catalysts we propose that the active benzylation reagent is not a protonated benzyl acetate. In addition, we exclude the existence of a "free" benzylic carbocation because labeled $Ph^{13}CH_2OH$ does not lead to a scrambling of the ^{13}C atom by tropylium ion formation. However, reaction of enantiomerically pure 1-phenylethyl acetate with *o*-xylene results in a racemic mixture of **1**. Basically, the transition-metal center should stabilize the carbocation intermediate and prevent unproductive formation of styrene and subsequent polymerization. Based on the reactivity of the applied catalysts we rule out both a transition-metal-based C–H activation pathway as well as a simple oxidative addition to the benzyl acetate.

In summary, we have developed a new general benzylation reaction of aromatics. Arenes and heteroarenes can be easily benzylated in the presence of several transition-metal compounds, of which $IrCl_3$ and $H_2[PtCl_6]$ are the most active catalysts. Often the reactions proceed under mild conditions (RT–80 °C; no strong acid or base) with high selectivity. Interestingly, even nonactivated arenes and substituted benzyl alcohol derivatives can be applied successfully in this reaction.

Experimental Section

All reactions were carried out in air without any special precautions. ^1H and ^{13}C NMR spectra were recorded on a Bruker ARX 400 spectrometer. Chemical shifts (δ) are given in ppm and the residual solvent served as the internal standard. Gas chromatography was performed on a Hewlett Packard HP 6890 chromatograph with a HP5 column. Mass spectra were recorded on an AMD 402/3 mass spectrometer. Chemicals and solvents were purchased from Fluka and Aldrich and used as received.

General procedure for benzylation of *o*-xylene: In a pressure tube, 1-phenylethyl acetate (0.50 mmol) and catalyst (10 mol%, 0.050 mmol) were dissolved in *o*-xylene (10 mL). Hexadecane (50 μL) was added as internal GC standard. The reaction mixture was stirred 20 h before aliquots were removed and analyzed by GC to determine the yield and conversion. For isolation of the products the reaction was quenched with water. The aqueous phase was extracted with dichloromethane. The combined organic layers were dried over $MgSO_4$, and the solvents were removed under reduced pressure. The product was purified by column chromatography on silica gel (70–230 mesh, *n*-heptane/ethyl acetate (50:1)). ^1H NMR (400 MHz, $CDCl_3$, 25 °C): $\delta = 1.5$ (d, $J(H,H) = 7.2$ Hz, 3H; CH_3), 2.1 (s, 6H; $2\,ArCH_3$), 4.0 (q, $J(H,H) = 7.2$ Hz, 1H; CH), 6.9–7.2 ppm (m, 8H; CH arom.); ^{13}C NMR (101 MHz, $CDCl_3$, 25 °C): $\delta = 18.3$, 18.8, 20.9, 43.2, 123.8, 124.8, 126.5, 127.3, 127.9, 128.6, 133.1, 135.4, 142.8, 145.6 ppm; MS (70 eV): *m/z* [%]: 210 (40) [M^+], 195 (100) [$C_{15}H_{15}^+$], 91 (10) [$C_7H_7^+$].

Received: May 14, 2004
Revised: July 20, 2004

Keywords: arenes · benzylation · Friedel–Crafts reaction · iridium · platinum

[1] K. Weissermel, H.-J. Arpe, *Industrielle Organische Chemie*, VCH, Weinheim, **1988**.

[2] a) S. Murai, F. Kakiuchi, S. Sekine, Y. Tanaka, A. Kamatami, M. Sonoda, N. Chatani, *Nature* **1993**, *366*, 529–531; b) F. Kakiuchi, S. Sekine, Y. Tanaka, A. Kamatami, M. Sonoda, N. Chatani, S. Murai, *Bull. Chem. Soc. Jpn.* **1995**, *68*, 62–83; c) F. Kakiuchi, S. Murai, *Acc. Chem. Res.* **2002**, *35*, 826–834; d) F. Kakiuchi, T. Uetsuhara, Y. Tanaka, N. Chatani, S. Murai, *J. Mol. Catal.* **2002**, *182*, 511–514; e) Y. Guari, A. Castellanos, S. Sabo-Etienne, B. Chaudret, *J. Mol. Catal.* **2004**, *212*, 77–82.

[3] a) F. Kakiuchi, M. Yamauchi, N. Chatani, S. Murai, *Chem. Lett.* **1996**, 111–112; b) C.-H. Jun, J.-B. Hong, Y.-H. Kim, K.-Y. Chung, *Angew. Chem.* **2000**, *112*, 3582–3584; *Angew. Chem. Int. Ed.* **2000**, *39*, 3440–3442; c) C.-H. Jun, C. W. Moon, J.-B. Hong, S.-G. Lim, K.-Y. Chung, Y.-H. Kim, *Chem. Eur. J.* **2002**, *8*, 485–492; d) Y.-G. Lim, J.-S. Han, B. T. Koo, J.-B. Kang, *J. Mol. Catal.* **2004**, *209*, 41–49.

[4] For a recent review on stereoselective Friedel–Crafts-type reactions see: M. Bandini, A. Melloni, A. Umani-Ronchi, *Angew. Chem.* **2004**, *116*, 560–566; *Angew. Chem. Int. Ed.* **2004**, *43*, 550–556.

[5] a) R. K. Thalji, K. A. Ahrendt, R. G. Bergman, J. A. Ellman, *J. Am. Chem. Soc.* **2001**, *123*, 9692–9693; b) K. A. Ahrend, R. G. Bergman, J. A. Ellman, *Org. Lett.* **2003**, *5*, 1301–1303.

[6] a) F. Kakiuchi, Y. Yamamoto, N. Chatani, S, Murai, *Chem. Lett.* **1995**, 681–682; b) C. G. Jia, W. T. Lu, J. Oyamada, T. Kitamura, K. Matsuda, M. Irie, Y. Fujiwara, *J. Am. Chem. Soc.* **2000**, *122*, 7252–7263; c) T. Kitamura, K. Yamamoto, M. Kotani, J. Oyamada, C. Jia, Y. Fujiwara, *Bull. Chem. Soc. Jpn.* **2003**, *76*, 1889–1895.

[7] a) E. J. Moore, W. R. Pretzer, T. J. O'Connell, J. Harris, L, Labounty, L. Chou, S. S. Grimmer, *J. Am. Chem. Soc.* **1992**, *114*, 5888–5890; b) N. Chatani, T. Fukuyama, F. Kakiuchi, S. Murai, *J. Am. Chem. Soc.* **1996**, *118*, 493–494.

[8] a) S. J. Pastine, S. W. Youn, D. Sames, *Tetrahedron* **2003**, *59*, 8859–8868; b) S. J. Pastine, D. Sames, *Org. Lett.* **2003**, *5*, 4053–4055; c) S. J. Pastine, S. W. Youn, D. Sames, *Org. Lett.* **2003**, *5*, 1055–1058.

[9] a) B. Sezen, D. Sames, *Org. Lett.* **2003**, *5*, 3607–3610; b) B. Sezen, D. Sames, *J. Am. Chem. Soc.* **2003**, *125*, 5274–5275; c) B. Sezen, D. Sames, *J. Am. Chem. Soc.* **2003**, *125*, 10580–10585.

[10] For recent examples see: a) F. Rataboul, A. Zapf, R. Jackstell, S. Harkal, T. Riermeier, A. Monsees, U. Dingerdissen, M. Beller, *Chem. Eur. J.* **2004**, *10*, 2983–2990; b) A. Zapf, R. Jackstell, F. Rataboul, T. Riermeier, A. Monsees, C. Fuhrmann, N. Shaikh, U. Dingerdissen, M. Beller, *Chem. Commun.* **2004**, 38–39; c) A. Frisch, A. Zapf, O. Briel, B. Kayser, N. Shaikh, M. Beller, *J. Mol. Catal.* **2004**, *214*, 231–239; d) K. Kumar, D. Michalik, I. Garcia Castro, A. Tillack, A. Zapf, M. Arlt, T. Heinrich, H. Böttcher, M. Beller, *Chem. Eur. J.* **2004**, *10*, 746–757; e) M. Sundermeier, A. Zapf, M. Beller, *Angew. Chem.* **2003**, *115*, 1700–1703; *Angew. Chem. Int. Ed.* **2003**, *42*, 1661–1664; f) K. Selvakumar, A. Zapf, M. Beller, *Org. Lett.* **2002**, *4*, 3031–3033; g) A. Ehrentraut, A. Zapf, M. Beller, *J. Mol. Catal.* **2002**, *182–183*, 515–523; h) A. Zapf, M. Beller, *Top. Catal.* **2002**, *19*, 101–109; i) W. Mägerlein, A. F. Indolese, M. Beller, *J. Organomet. Chem.* **2002**, *641*, 30–40.

[11] a) M. G. -Nordberg, K. Kolmodin, J. Aquist, S. F. Queener, A. Hallberg, *J. Med. Chem.* **2001**, *44*, 2391–2402; b) H. H. Sun, V. J. Paul, W. Fenical, *Phytochemistry* **1983**, *22*, 743–745; c) H. Hoshina, K. Maekawa, K. Taie, T. Igarashi, T. Sakurai, *Heterocycles* **2003**, *60*, 1779–1786; d) C. Manzoni, M. R. Lovati, A. Bonelli, G. Galli, C. R. Sirtori, *Eur. J. Pharmacol.* **1990**, *190*, 39–49; e) C. Rose, O. Vtoraya, A. Pluzanska, N. Davidson, M. Gershanovich, R. Thomas, S. Johnson, J. J. Caicedo, H. Gervasio, G. Manikhas, F. B. Ayed, S. B. -Radoux, H. A. C. Ross, R. Lang, *Eur. J. Cancer* **2003**, *39*, 2318–2327.

 © 2005 Wiley-VCH Verlag GmbH & Co. KGaA, Weinheim

[12] a) J. Jacob, L. Oldridge, J. Y. Zhang, M. Gaal, E. J. W. List, A. C. Grimsdale, K. Mullen, *Curr. Cancer Drug Targets* **2004**, *4*, 339 – 342; b) M. S. Khan, M. R. A. Al-Mandhary, M. K. Al-Suti, B. Ahrens, M. F. Mahon, L. Male, P. R. Raithby, C. E. Boothby, A. Kohler, *J. Chem. Soc. Dalton Trans. 1* **2003**, 74 – 84; c) P. J. Skabara, I. M. Serebryako, I. F. Perepichka, *Synth. Met.* **1999**, *102*, 1336 – 1337.

[13] a) G. A. Olah, R. Krishnamurti, G. K. S. Prakash in *Comprehensive Organic Synthesis*, *Vol. 3* (Eds.: B. M. Trost, I. Fleming), Pergamon, Oxford, **1991**, pp. 293 – 339; b) R. M. Roberts, A. A. Khalaf, *Friedel–Crafts Alkylation Chemistry*, Marcel Dekker, New York, **1984**; c) *Friedel–Crafts Chemistry* (Ed.: G. A. Olah), Wiley, New York, **1973**.

[14] a) M. Noji, T. Ohno, K. Fuji, N. Futabe, H. Tajima, K. Ishii, *J. Org. Chem.* **2003**, *68*, 9340 – 9347; b) T. Mukaiyama, H. Kamiyama, H. Yamanaka, *Chem. Lett.* **2003**, *32*, 814 – 815; c) I. Shiina, M. Suzuki, *Tetrahedron Lett.* **2002**, *43*, 6391 – 6394; d) G. V. M. Sharma, A. K. Mahalingam, *J. Org. Chem.* **1999**, *64*, 8943 – 8944; e) T. Tsuchimoto, K. Tobita, T. Hiyama, S.-I. Fukuzawa, *J. Org. Chem.* **1997**, *62*, 6997 – 7005; f) S.-I. Fukuzawa, T. Tsuchimoto, T. Hiyama, *J. Org. Chem.* **1997**, *62*, 151 – 156; g) M. T. E. Gihani, H. Heaney, K. F. Shuhaibar, *Synlett* **1996**, 871 – 872.

[15] Selected recent examples: a) M. Salavati-Niasari, J. Hasanalian, H. Najafian, *J. Mol. Catal.* **2004**, *209*, 209 – 214; b) V. R. Choudhary, S. K. Jana, V. S. Narkhede, *Appl. Catal. A* **2002**, *235*, 207 – 215; c) V. R. Choudhary, S. K. Jana, *J. Mol. Catal. A* **2002**, *180*, 267 – 276; d) X. Hu, G. K. Chuah, S. Jaenicke, *Appl. Catal. A* **2001**, *217*, 1 – 2; e) V. R. Choudhary, S. K. Jana, *J. Catal.* **2001**, *201*, 225 – 235; f) A. B. Deshpande, A. R. Bajpai, S. D. Samant, *Appl. Catal. A* **2001**, *209*, 229 – 235.

[16] A special exception is the cyclization of substituted benzyl alcohols with pyrrole see: a) G. Dyker, D. Hildebrandt, J. Liu, K. Merz, *Angew. Chem.* **2003**, *115*, 4536 – 4538; *Angew. Chem. Int. Ed.* **2003**, *42*, 4399 – 4402; see also: b) Y. Nishibayashi, M. Yoshikawa, Y. Inada, M. D. Milton, M. Hidai, S. Uemura, *Angew. Chem.* **2003**, *115*, 2663 – 2666; *Angew. Chem. Int. Ed.* **2003**, *42*, 2681 – 2684; c) Y. Nishibayashi, Y. Inada, M. Yoshikawa, M. Hidai, S. Uemura, *Angew. Chem.* **2003**, *115*, 1533 – 1536; *Angew. Chem. Int. Ed.* **2003**, *42*, 1495 – 1498.

[17] E. Mincione, P. Bovicelli, *Gazz. Chim. Ital.* **1982**, *112*, 437 – 440.

[18] a) T. Kondo, S. Kajiya, S. Tantayanon, Y. Watanabe, *J. Organomet. Chem.* **1995**, *489*, 83 – 91; b) T. Kondo, S. Tantayanon, Y. Tsuji, Y. Watanabe, *Tetrahedron Lett.* **1989**, *30*, 4137 – 4140.

[19] When 5 mol% (1 mol%) of $H_2[PtCl_6]$ was used, the yield of **1** was 81% (43%).

[20] The use of 5 mol% (1 mol%) $H_2[PtCl_6]$ at 80 °C afforded 97% (42%) yield of 4-chloro-1-methoxy-2-(1-phenylethyl)benzene.

 © 2005 Wiley-VCH Verlag GmbH & Co. KGaA, Weinheim

Stereogenic Metal Centers

Helical Chirality in Pentacoordinate Zinc Complexes—Selective Access to Both Pseudoenantiomers with One Ligand Configuration**

*Michael Seitz, Sabine Stempfhuber, Manfred Zabel, Martin Schütz, and Oliver Reiser**

The controlled construction of complexes with stereogenic metal centers ("chiral-at-metal complexes") is an important task because of the potential impact on various areas of chemical research, for example, supramolecular chemistry, asymmetric catalysis, or biological recognition. Since the first separation of the enantiomers of an inorganic coordination compound in 1911 by Werner,[1] the area of inorganic stereochemistry has emerged as a rapidly growing field, especially over the last years. In particular, the transfer of chirality from chiral, nonracemic organic ligands to metal centers with a variety of coordination geometries has attracted great interest.[2,3]

Predetermined chirality around a trigonal-bipyramidal-coordinated metal center is rather rare and normally favored with tripodal ligands.[4] Except for the complexes described herein, only three other examples with topologically linear ligands exist.[4a–c] To date, only the employment of enantiomeric (trivial) or diastereomeric[4b] ligands is suitable to enforce the formation of opposite chiral configurations.

In our case, only two achiral donor atoms are exchanged in an otherwise isosteric ligand to complete this task. To the best of our knowledge, this is the first time that this phenomenon is observed. The closest analogy can be seen in the cobalt complexes of ligand **1**:[5] Whereas **1a** forms an octahedral complex with Δ_2 configuration upon complexation

[*] Dr. M. Seitz, Prof. Dr. O. Reiser
Institut für Organische Chemie
Universität Regensburg
Universitätsstrasse 31, 93053 Regensburg (Germany)
Fax: (+49) 941-943-4121
E-mail: oliver.reiser@chemie.uni-regensburg.de

S. Stempfhuber, Dr. M. Zabel
Insititut für Anorganische Chemie
Universität Regensburg
Universitätsstrasse 31, 93053 Regensburg (Germany)

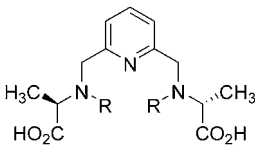
Prof Dr. M. Schütz[+]
Institut für Theoretische Chemie
Universität Stuttgart (Germany)
Pfaffenwaldring 55, 70569 Stuttgart (Germany)

[+] Current address: Institut für Theoretische Chemie
Universität Regensburg
Universitätsstrasse 31, 93053 Regensburg (Germany)

[**] This work was supported by the Deutsche Forschungsgemeinschaft (SP 1118, RE-948-5/2 and SCHU 1456/2), the Fonds der Chemischen Industrie, and through generous gifts of chemicals by Degussa AG.

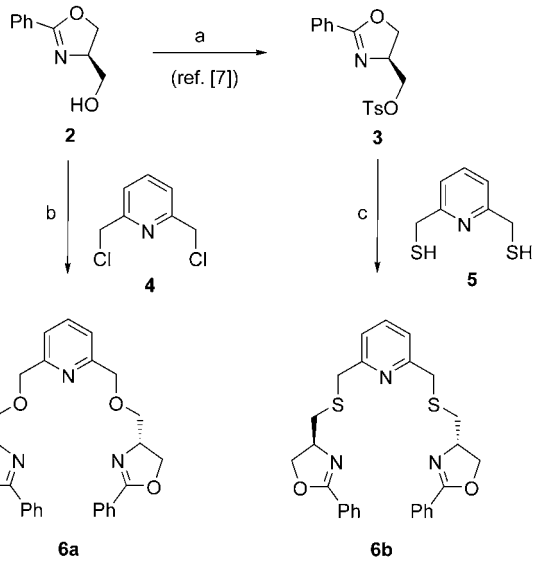
Supporting information for this article is available on the WWW under http://www.angewandte.org or from the author.

 © 2005 Wiley-VCH Verlag GmbH & Co. KGaA, Weinheim DOI: 10.1002/anie.200460843

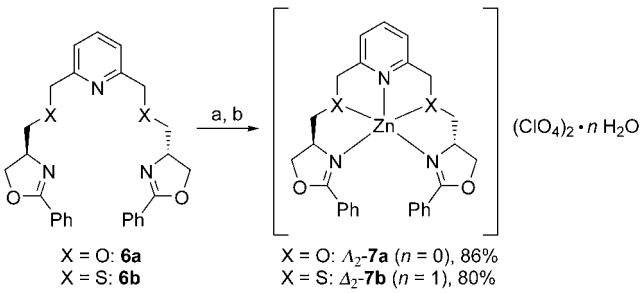


with Co^{III}, ligand **1b** gives rise to a mixture of two complexes, one of which was identified as the Λ_2-configured species.

We recently reported the novel pentadentate bis(oxazoline) ligand **6b** (Scheme 1), which forms octahedral Co^{II} or



Scheme 1. Synthesis of **6a** and **6b**. Reagents and conditions: a) **2** (1.0 equiv), TsCl (1.1 equiv), NEt_3 (2.2 equiv), $CHCl_3$, 0 °C→RT, 20 h, 78%; b) **2** (2.2 equiv), **4** (1.0 equiv), NaH (2.3 equiv), DMF, 0 °C→RT, 20 h, 88%; c) **3** (2.1 equiv), **5** (1.0 equiv), NaH (2.1 equiv), DMF, 0 °C→RT, 20 h, 72%. Ts = *p*-toluenesulfonyl; DMF = *N*,*N*-dimethylformamide.



Scheme 2. Reagents and conditions: a) $Zn(ClO_4)_2 \cdot 6H_2O$, THF, room temperature, 1 h; b) CH_3CN, Et_2O.

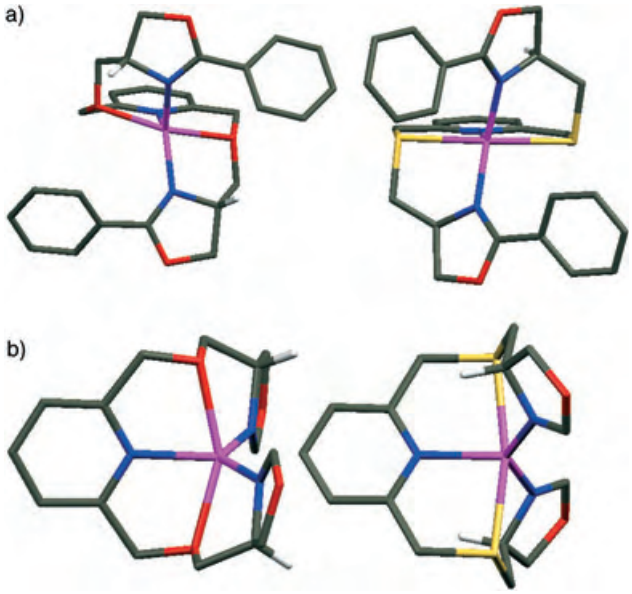


Figure 1. Crystal structures of the cations of the complexes Λ_2-**7a** and Δ_2-**7b**.[16] Hydrogen atoms have been omitted for clarity, except for the ones at the stereocenters of the oxazolines. a) Front view. b) Top view (phenyl rings have been omitted for clarity). C gray, H white, N blue, O red, S yellow, Zn pink.

Ru^{II} complexes with exclusive Δ_2 configuration.[6] Herein we describe trigonal-bipyramidal Zn^{II} complexes of **6a** and **6b**,[7] which differ only in the heteroatom at the benzylic position of the pyridine (O versus S).

Ligands **6** were readily assembled from the known oxazoline **2**[8] in a modular fashion. After deprotonation of **2** with NaH, the resulting anion was trapped with the pyridine dielectrophile **4**[9] to give **6a** in 88% yield. Analogously, tosylation of **2** resulted in **3**,[6] which was treated with the pyridine dinucleophile **5**[6,10] to yield **6b** in 72% yield.

The zinc complexes[11] were prepared by mixing equimolar amounts of zinc(II) perchlorate hexahydrate and the corresponding ligand **6** in THF at ambient temperature (Scheme 2). The precipitated complexes **7** were recrystallized from acetonitrile/diethyl ether to give colorless crystals that were suitable for X-ray crystallographic analysis.

The crystal structures of **7a** and **7b** show two pentacoordinate zinc complexes with distorted trigonal-bipyramidal geometry (Figure 1, Table 1). The complexes each have a single but opposite configuration at the metal center: Λ_2 for **7a** and Δ_2 for **7b**. This remarkable reversal in helical folding around the metal center is not easy to understand. The N_{py}–Zn and N_{oxaz}–Zn distances are approximately equal in both complexes, and the Zn–O (2.22 and 2.27 Å) and the Zn–S (2.53 Å) distances are within normal limits. The most pronounced difference is the stronger distortion of the oxygen (O-Zn-O = 153°) atoms towards the pyridine moiety relative to that of the sulfur atoms (S-Zn-S = 169°), which is dictated by the fact that the benzylic C–O bond (1.44 Å) is shorter than the corresponding C–S (1.81 Å) bond.

To assess the energy difference between the particular helical folding of ligands **6a** and **6b** in the zinc complexes, ab initio calculations at the second-order Møller–Plesset perturbation theory (MP2) level were performed. Geometry optimizations were carried out for the two complex cations Λ_2-**7a** and Δ_2-**7b** and the corresponding pseudoenantiomers Δ_2-**7a** and Λ_2-**7b**.[12] The geometry optimizations reflect well the geometries found in the X-ray crystal structure of Λ_2-**7a**

 © 2005 Wiley-VCH Verlag GmbH & Co. KGaA, Weinheim

Table 1: Selected bond lengths [Å], angles [°], and dihedral angles [°] of the cations of Λ_2-**7a** and Δ_2-**7b**.[a]

	Λ_2-**7a** (X = O)	Δ_2-**7b** (X = S)
N_{py}–Zn [Å]	2.031	2.096
N_{oxaz1}–Zn [Å]	1.961	1.981
N_{oxaz2}–Zn [Å]	1.953	1.981
X_1–Zn [Å]	2.220	2.530
X_2–Zn [Å]	2.275	2.530
N_{py}-Zn-N_{oxaz1} [°]	113.74	110.12
N_{py}-Zn-N_{oxaz2} [°]	116.44	110.12
N_{py}-Zn-X_1 [°]	76.93	84.43
N_{py}-Zn-X_2 [°]	76.07	84.43
N_{oxaz1}-Zn-N_{oxaz2} [°]	129.62	139.76
N_{oxaz1}-Zn-X_1 [°]	115.31	83.84
N_{oxaz1}-Zn-X_2 [°]	80.43	100.02
N_{oxaz2}-Zn-X_1 [°]	80.64	100.02
N_{oxaz2}-Zn-X_2 [°]	107.30	83.84
X_1-Zn-X_2 [°]	152.56	168.86
-CH_2-X_1-CH_2- [°]	112.87	104.19
-CH_2-X_2-CH_2- [°]	113.51	104.19
N_{py}-CH-CH_2-X_1 [°]	24.92	−3.77
N_{py}-CH-CH_2-X_2 [°]	22.88	−3.77

[a] py = pyridine, oxaz = oxazoline.

and Δ_2-**7b**; the bond lengths and angles found for the pseudoenantiomers Δ_2-**7a** and Λ_2-**7b** are all in the normal range and are similar to their counterparts.[11]

Two different steric interactions can be identified which work in opposite directions for the Λ_2 and Δ_2 configuration of each complex. In the Λ_2 configuration, the phenyl substituents of the oxazoline rings point toward the pyridine backbone, as manifested in the especially close distance between the *ortho* carbon atom of the phenyl ring and the heteroatom X (Figure 2a). This interaction is especially severe for Λ_2-**7b**

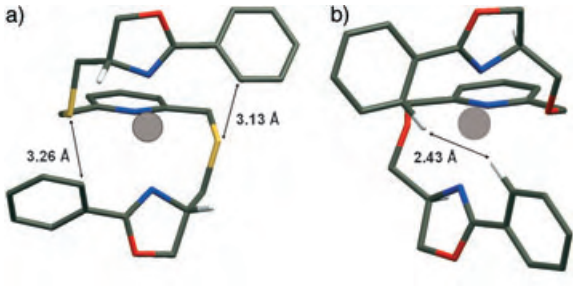


Figure 2. Calculated structures of Δ_2-**7a** and Λ_2-**7b**. C gray, H white, N blue, O red, S yellow, Zn gray ball.

(C–S distance 3.13 and 3.26 Å, sum of van der Waals radii for C and S = 3.50 Å), clearly favoring Δ_2-**7b** (C–S distance 3.43 Å). The same trend is seen for **7a** (Λ_2-**7a**: C–O distance 3.01 and 3.19 Å; Δ_2-**7a**: C–O distance 3.77 Å), but still acceptable in Λ_2-**7a** owing to the smaller van der Waals radius of oxygen (C+O = 3.22 Å).

The second steric interaction that must be considered is the distance between the two phenyl rings (Figure 2b). In the Λ_2 configuration, these phenyl rings are especially close to each other as manifested in the distance between two of the *ortho*-hydrogen atoms (Δ_2-**7a**: 2.43 Å; Δ_2-**7b**: 2.46 Å), whereas in the corresponding Λ_2 configuration the phenyl rings are far away from each other. This interaction seems to be particularly unfavorable in Δ_2-**7a** (sum of van der Waals radii of two hydrogen atoms is 2.40 Å), resulting in the exclusive formation of Λ_2-**7a**. In agreement with this analysis, the calculations predict a decrease in energy on going from the pseudoenantiomers Δ_2-**7a** and Λ_2-**7b** to the experimentally confirmed structures Λ_2-**7a** and Δ_2-**7b** of 2–4 kcal mol^{-1} (X = O) and 6–8 kcal mol^{-1} (X = S), respectively.

Remarkably, the Δ_2 configurations exhibit perfect C_2 point-group symmetry, whereas this symmetry is distorted to C_1 for the Λ_2 conformers. The ab initio calculations and the measured X-ray structures both agree with this distortion. As a consequence, the Λ_2 conformers exist in two isometric versions on their higher symmetric potential-energy surfaces, which in the present case correspond to the molecular symmetry group C_2(M).[13] The Λ_2 configurations of C_2 point-group symmetry are likely to be saddle points (transition structures) on the interconversion pathways connecting the two related C_1 versions. Hence, the vibrational ground state splits for the Λ_2 conformers.

The solution behavior of **7a** and **7b** was investigated by means of NMR and CD spectroscopic analysis of the bulk material obtained in the complexation experiments. The ^{1}H and the ^{13}C NMR spectra[11] in CD_3CN show a single species for each complex. As expected, the signals for the complexed ligands are shifted downfield with respect to the free ligands. In particular, the ^{13}C NMR spectra clearly show the C_2 symmetry of the complexes in both cases, as well as the pentacoordination of the ligand, indicated by the strong downfield shift of the signals for the quaternary carbon atom of the oxazolines (**6a**→**7a**: 164.9 to 175.4 ppm; **6b**→**7b**: 164.6 to 172.7 ppm). Therefore, both species must be either Δ_2 or Λ_2.

CD spectroscopic analysis of the complexes in CH_3CN solution showed a quasi-mirror image of the n→π* transition (Figure 3), which indicates a quasi-enantiomeric relationship between the two zinc complexes. Application of the sector rules for C_2-symmetric pyridines put forward by Palmer and co-workers[14] predicts the configuration around the zinc atom

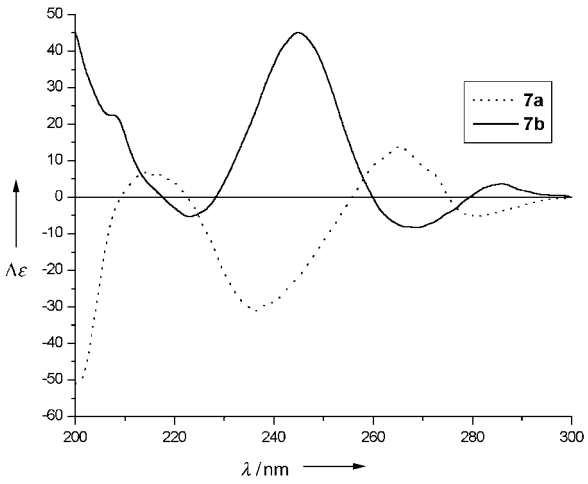


Figure 3. CD spectra of the complexes Λ_2-**7a** and Δ_2-**7b** in CH_3CN.

 © 2005 Wiley-VCH Verlag GmbH & Co. KGaA, Weinheim

as Λ_2 for **7a** and Δ_2 for **7b**, in complete agreement with the crystal structures.

In summary, a new ligand system is introduced that allows the completely stereoselective transfer of chirality from the pentadentate bis(oxazolines) to a trigonal-bipyramidal coordinated central metal atom in the solid state as well as in solution. For the first time, two opposite, pseudoenantiomeric configurations were observed with a single ligand design, that is, **6a** and **6b** differ only by two single atoms and are otherwise stereochemically identical.

Received: June 1, 2004
Revised: September 15, 2004

Keywords: bisoxazoline ligands · coordination chemistry · helical chirality · stereogenic metal centers · zinc

[1] A. Werner, *Ber. Dtsch. Chem. Ges.* **1911**, *44*, 1887 – 1898.
[2] Reviews: a) U. Knof, A. von Zelewsky, *Angew. Chem.* **1999**, *111*, 312 – 333; *Angew. Chem. Int. Ed.* **1999**, *38*, 302 – 322; ; b) H. Brunner, *Angew. Chem.* **1999**, *111*, 1248 – 1263; *Angew. Chem. Int. Ed.* **1999**, *38*, 1194 – 1208.
[3] For selected recent examples, see: a) C. Hamann, A. von Zelewsky, A. Neels, H. Stoeckli-Evans, *Dalton Trans.* **2004**, 402 – 406; b) H. Brunner, F. Henning, M. Weber, M. Zabel, D. Carmona, F. J. Lahoz, *Synthesis* **2003**, *7*, 1091 – 1099; c) I. J. Munslow, A. J. Clarke, R. J. Deeth, I. Westmoreland, P. Scott, *Chem. Commun.* **2002**, 1868 – 1869; d) G. Muller, J. P. Riehl, K. J. Schenk, G. Hopfgartner, C. Piguet, J.-C. G. Bünzli, *Eur. J. Inorg. Chem.* **2002**, 3101 – 3110; e) G. Muller, J.-C. G. Bünzli, J. P. Riehl, D. Suhr, A. von Zelewsky, H. Mürner, *Chem. Commun.* **2002**, 1522 – 1523; f) D.-R. Ahn, T. W. Kim, J.-I. Hong, *J. Org. Chem.* **2001**, *66*, 5008 – 5011; g) S. Fraysse, A. von Zelewsky, H. Stoeckli-Evans, *New J. Chem.* **2001**, *5*, 1374 – 1375; h) R. S. Dickins, J. A. K. Howard, C. L. Maupin, J. M. Moloney, D. Parker, J. P. Riehl, G. Siligardi, J. A. G. Williams, *Chem. Eur. J.* **1999**, *5*, 1095 – 1105.
[4] a) C. J. Sanders, P. N. O'Shaughnessy, P. Scott, *Polyhedron* **2003**, *22*, 1617 – 1625; b) O. Mamula, A. von Zelewsky, T. Bark, H. Stoeckli-Evans, A. Neels, G. Bernardinelli, *Chem. Eur. J.* **2000**, *6*, 3575 – 3585; c) L. Casella, M. E. Silver, J. A. Ibers, *Inorg. Chem.* **1984**, *23*, 1409 – 1418; d) Y.-H. Chiu, O. dos Santos, J. W. Canary, *Tetrahedron* **1999**, *55*, 12069 – 12078; e) A. Abufarag, H. Vahrenkamp, *Inorg. Chem.* **1995**, *34*, 3279 – 3284; f) J. W. Canary, C. S. Allen, J. M. Castagnetto, Y. Wang, *J. Am. Chem. Soc.* **1995**, *117*, 8484 – 8485; g) W. A. Nugent, R. L. Harlow, *J. Am. Chem. Soc.* **1994**, *116*, 6142 – 6148.
[5] K. Bernauer, H. Stoeckli-Evans, D. Hugi-Cleary, H. J. Hilgers, H. Abd-el-Khalek, J. Porret, J.-J. Sauvain, *Helv. Chim. Acta* **1992**, *75*, 2327 – 2339.
[6] M. Seitz, A. Kaiser, D. R. Powell, A. S. Borovik, O. Reiser, *Adv. Synth. Catal.* **2004**, *346*, 737 – 741.
[7] M. Seitz, A. Kaiser, S. Stempfhuber, M. Zabel, O. Reiser, *J. Am. Chem. Soc.* **2004**, *126*, 11426 – 11427.
[8] A. I. Meyers, W. Schmidt, M. J. McKennon, *Synthesis*, **1993**, 250 – 262.
[9] E. V. Dehmlow, J. Vor der Brüggen, *J. Prakt. Chem.* **2000**, *342*, 502 – 503.
[10] B. Nock, H.-J. Pietsch, F. Tisato, T. Maina, P. Leibnitz, H. Spies, E. Chiotellis, *Inorg. Chim. Acta* **2000**, *304*, 26 – 32.
[11] See Supporting Information.
[12] The ab initio energy-minimization calculations were performed with the new analytic local MP2 gradient based on density fitting (DF-LMP2).[15a] The SVP AO basis set by Schäfer et al.[15b] together with the SVP/MP2FIT and TZVP/MP2FIT fitting basis sets[15c] (the former for the LMP2, the latter for the Hartree–Fock specific parts of the gradient[15a]) was used. For zinc, a quasi-relativistic energy-adjusted pseudopotential based on the Ne-like Zn^{20+} core together with the related 6s5p3d AO basis set[15d] was employed. At the minimum-energy geometries of Λ_2-**7a** and Δ_2-**7a**, single-point energy calculations were also performed with the TZVP basis set by Schäfer et al.[15e] in conjunction with the TZVP-MP2FIT and TZVPPMP2FIT fitting basis sets,[15c] and an additional set of f functions with exponent 3.22 on the Zn center.
[13] P. R. Bunker, P. Jensen, *Molecular Symmetry and Spectroscopy*, NRC Research, Ottawa, **1998**.
[14] R. B. Dyer, R. A. Palmer, R. G. Ghirardelli, J. S. Bradshaw, B. A. Jones, *J. Am. Chem. Soc.* **1987**, *109*, 4780 – 4786.
[15] a) M. Schütz, H.-J. Werner, R. Lindh, F. R. Manby, *J. Chem. Phys.* **2004**, *121*, 737; b) A. Schäfer, H. Horn, R. Ahlrichs, *J. Chem. Phys.* **1992**, *97*, 2571; c) F. Weigend, M. Häser, H. Patzelt, R. Ahlrichs, *Chem. Phys. Lett.* **1998**, *294*, 14; d) M. Dolg, U. Wedig, H. Stoll, H. Preuss, *J. Chem. Phys.* **1987**, *86*, 866; e) A. Schäfer, C. Huber, R. Ahlrichs, *J. Chem. Phys.* **1994**, *100*, 5829.
[16] CCDC-236253 and 236254 contain the supplementary crystallographic data for this paper. These data can be obtained free of charge via www.ccdc.cam.ac.uk/conts/retrieving.html (or from the Cambridge Crystallographic Data Centre, 12, Union Road, Cambridge CB21EZ, UK; fax: (+44) 1223-336-033; or deposit@ccdc.cam.ac.uk).

 © 2005 Wiley-VCH Verlag GmbH & Co. KGaA, Weinheim

Cluster Compounds

From a Monomeric Bismuth Silanolate to a Molecular Bismuth Oxo Cluster: $[Bi_{22}O_{26}(OSiMe_2tBu)_{14}]$**

Dirk Mansfeld, Michael Mehring, and Markus Schürmann*

Recent interest in bismuth oxide based materials including heterometallic phases, such as Bi/Mo/O,[1,2] Bi/Ti/O,[3] Bi/Nb/O,[4] Bi/Sr/Ta/O,[5] and Bi/V/O[6] stems from their use as catalysts, ferroelectric devices, oxide ion conductors, and non-toxic pigments. In addition, bismuth oxide (doped with 4 atom% of a transition metal) was suggested to serve as a

[*] D. Mansfeld, Dr. M. Mehring, Dr. M. Schürmann
Universität Dortmund
Lehrstuhl für Anorganische Chemie II
44221 Dortmund (Germany)
Fax: (+49) 231-755-5048
E-mail: michael.mehring@uni-dortmund.de

[**] This work was supported by the Deutsche Forschungsgemeinschaft, the Fonds der Chemischen Industrie, and the Fachbereich Chemie der Universität Dortmund. For support of our work Prof. K. Jurkschat is gratefully acknowledged.

Supporting information for this article (molecular structure of **2** and a view of the $[Bi_{22}O_{26}]^{14+}$ unit with selected bond lengths and angles) is available on the WWW under http://www.angewandte.org or from the author.

 DOI: 10.1002/anie.200461476 © 2005 Wiley-VCH Verlag GmbH & Co. KGaA, Weinheim

selective sensing material for the detection of NO.[7] Traditionally, the synthesis of bulk bismuth oxide materials is carried out at high temperature starting from compounds such as bismuth nitrate or bismuth subcarbonate. However, homo- and heterometallic bismuth alkoxides have been shown to be potential precursors for the synthesis of bismuth oxide materials by the sol–gel process and chemical vapor deposition (CVD).[8,9] Thus, in recent years several homo- and heterometallic bismuth alkoxides including a few bismuth oxo alkoxide clusters with up to nine bismuth atoms have been fully characterized,[2,9–13] however there is little information on their siloxide counterparts. Single examples of bismuth silanolates have been reported,[11,14,15] but to date $Bi(OSiPh_3)_3(thf)_3$[11] and $Bi(OSiPh_2tBu)_3$[15] are the only ones characterized by single-crystal X-ray diffraction. We have sought to use compounds of the type $Bi(OSiR_3)_3$ for the preparation of bismuth oxide based materials, because the thermally induced decomposition of bismuth silanolates was expected to give Bi_2O_3 and $R_3SiOSiR_3$. Our assumption was supported by the observations, that heterometallic bismuth and antimony alkoxides are able to either partially eliminate ethers (ROR), with formation of low-nuclearity metal oxo clusters, or to eliminate an alkene, to give MOH and subsequent condensation to give oxo clusters.[13,16] For example, partial elimination of hexamethyldisiloxane occurs when $Sb(OSiMe_3)_3$ is treated with $NaOSiMe_3$ to give the cluster $[Na_4Sb_2(O)(OSiMe_3)_8]$.[17] Bismuth silanolates are expected to react in this way as the heat of formation of a siloxane is significantly higher than that of the corresponding ether and elimination of a silaethene from a silanyloxide is not very likely. Another advantage of bismuth silanolates compared with simple bismuth alkoxides is their higher solubility, which is crucial for solution-based approaches to novel materials. Herein we report the synthesis, characterization, and thermally induced decomposition of $Bi(OSiMe_2tBu)_3$ (**1**), and the partial hydrolysis of **1** to give the novel high-nuclearity metal oxo cluster $[Bi_{22}O_{26}(OSiMe_2tBu)_{14}]$ (**2**).

The bismuth silanolate $Bi(OSiMe_2tBu)_3$ (**1**) was prepared in high yield by the reaction of $Bi(OtBu)_3$ with $tBuMe_2SiOH$ [Eq. (1)]. The low-melting-point solid is easily purified by Kugelrohr-distillation under reduced pressure.

$$Bi(OtBu)_3 + 3\,Me_2tBuSiOH \rightarrow Bi(OSiMe_2tBu)_3\,(\mathbf{1}) + 3\,tBuOH \quad (1)$$

Single crystals of compound **1** were obtained after the neat compound was warmed to give an oil then cooled to −20 °C. The molecular structure of **1** is given in Figure 1. The coordination geometry of **1** is best described as a trigonal pyramid with three oxygen atoms and the bismuth atom occupying the apical positions. The Bi–O bonds are in the range 2.003(14)–2.054(16) Å which is comparable with the values reported for $Bi(OSiPh_3)_3(thf)_3$ (2.04(1) Å)[11] and $Bi(OSiPh_2tBu)_3$ (2.041(4)–2.062(4) Å).[15] The O-Bi-O angles are between 94.0(5)° and 99.6(6)° and thus, indicate a strong s-character of the lone-pair. In contrast to bismuth alkoxides that associate through intermolecular Bi···O bonds, the bulky organic groups in monomeric **1** prevent such secondary interactions. Note, that in $Bi(OSiPh_3)_3(thf)_3$ three solvent molecules complete the coordination sphere at the bismuth atom and $Bi(OSiPh_2tBu)_3$ forms a dimer as a result of intermolecular bismuth–π interactions. Compound **1** can be evaporated at 150 °C in vacuum (10^{-2} Torr) without decomposition and it is highly soluble in common organic solvents, such as THF, $CHCl_3$, diethyl ether, benzene, and hexane.

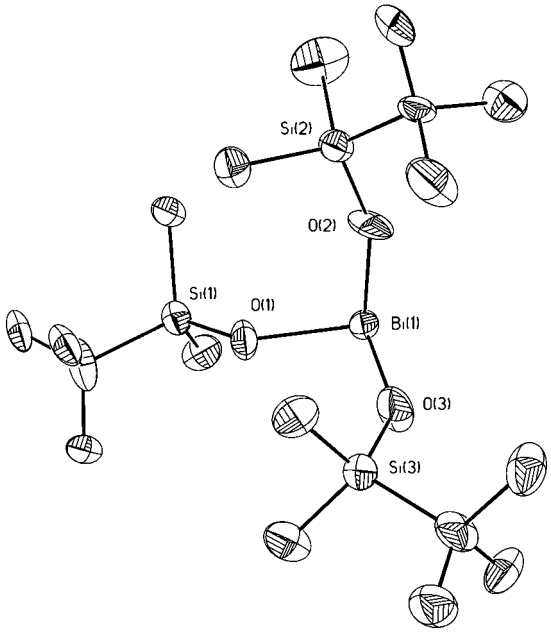


Figure 1. Molecular structure of **1** (thermal ellipsoids set at 30% probability); two crystallographically independent but structurally similar molecules are found in the crystal lattice. Selected bond lengths [Å] and angles [°]: Bi(1)-O(1) 2.054(10), Bi(1)-O(2) 2.006(15), Bi(1)-O(3) 2.018(12), Si(1)-O(1) 1.615(12), Si(2)-O(2) 1.596(16), Si(3)-O(3) 1.595(13); O(1)-Bi(1)-O(2) 97.0(5), O(1)-Bi(1)-O(3) 96.9(5), O(2)-Bi(1)-O(3) 97.9(7), Si(1)-O(1)-Bi(1) 134.0(7), Si(2)-O(2)-Bi(1) 156.6(8), Si(3)-O(3)-Bi(1) 144.3(8).

Hydrolysis of **1** in benzene occurs slowly upon contact with air moisture to give the bismuth oxo cluster $[Bi_{22}O_{26}(OSiMe_2tBu)_{14}]$ (**2**) [Eq. (2)]. If the benzene is evaporated slowly the yield is almost quantitative and only crystals are formed. When the rate of hydrolysis is increased by the addition of water or by fast evaporation of the solvent a, to date uncharacterized, amorphous material is obtained. Note that, single crystals of **2** together with amorphous material were also isolated upon hydrolysis of **1** in *i*PrOH.

$$22\,Bi(OSiMe_2tBu)_3\,(\mathbf{1}) \xrightarrow[\text{benzene}]{\text{air moisture}} [Bi_{22}O_{26}(OSiMe_2tBu)_{14}]\,(\mathbf{2}) + 52\,HOSiMe_2tBu \quad (2)$$

The ^1H NMR spectrum of a solution of compound **1** in $[D_6]$benzene which had been exposed to air moisture to give a significant amount of single crystals of **2** showed exclusively signals assigned to $tBuMe_2SiOH$ and the starting material **1**. Apparently, a rapid and clean conversion of the bismuth silanolate **1** into the bismuth oxo cluster **2** takes place. The high-nuclearity cluster **2** ($M_r = 6851\ g\,mol^{-1}$) is almost insoluble in all common solvents but can be dispersed in organic media without decomposition.

 © 2005 Wiley-VCH Verlag GmbH & Co. KGaA, Weinheim

The molecular structure of **2** is best described as being composed of a $[Bi_{22}O_{26}]^{14+}$ core which is covered by a hydrophobic layer of 14 tBuMe$_2$SiO$^-$ ligands (Figure 2). Eight of the silanolate oxygen atoms are μ_2-bridging to

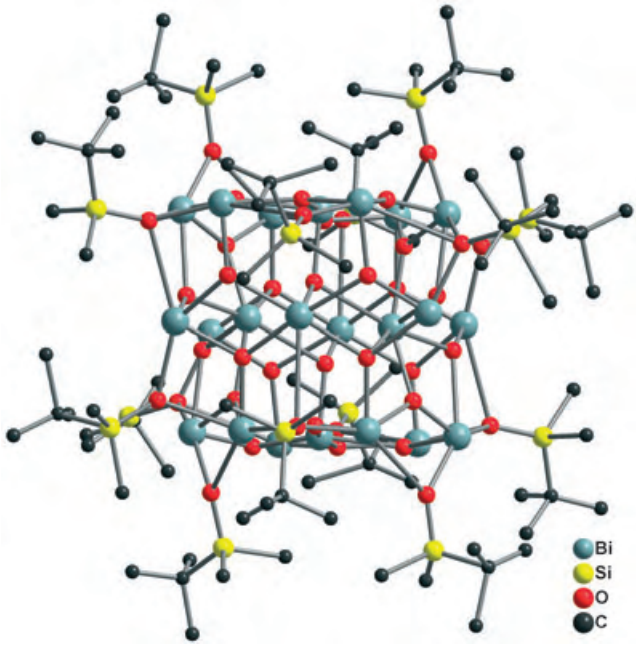


Figure 2. Molecular structure of **2**; hydrogen atoms are omitted for clarity.

bismuth and six silanolate oxygen atoms have a μ_3-coordination mode. The corresponding Bi–O bonds lie between 2.126(9) and 3.347(11) Å. These bonds are significantly shorter than the sum of the van der Waals radii of bismuth (r_{vdW}(Bi) = 2.40 Å)[18] and oxygen (r_{vdW}(O) = 1.50 Å).[19] The $[Bi_{22}O_{26}]^{14+}$ core is composed of the layers A, A′, and B (Figure 3). The symmetry-related layers A and A′ are

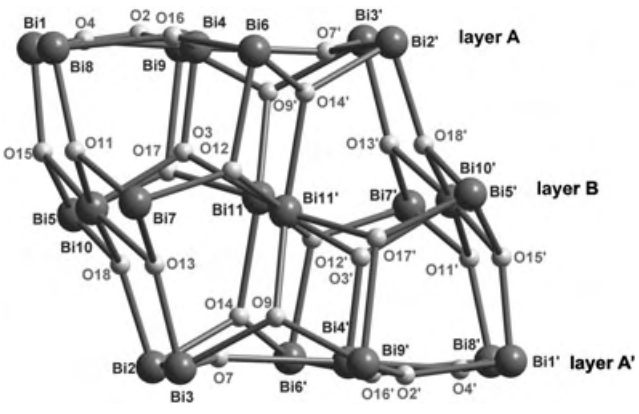


Figure 3. View of the $[Bi_{22}O_{26}]^{14+}$ core structure of **2**; the structure is composed of three layers containing 7 (layer A and A′) and 8 bismuth atoms (layer B); symmetry transformation used to generate equivalent atoms: $a = -x+{}^1/_2, -y+{}^1/_2, -z$; typical bond lengths and angles are found in the ranges: Bi-O 2.037(8)–2.655(8) Å; Bi-O-Bi 93.6(3)–138.2(4)°; O-Bi-O: 67.5(3)-171.8(3)° (details are given in the Supporting Information).

composed of seven bismuth atoms and six μ_3-bridging oxygen atoms. Two of these oxygen atoms (O9 and O14) are coordinated to two bismuth atoms of layer A and to one bismuth atom of layer B. The other oxygen atoms of layer A are exclusively coordinated to bismuth atoms of layer A. The bismuth–μ_3-oxygen atom bonds are in the range 2.037(8)–2.655(8) Å and the sums of the bond angles amount to 355.8–358.4° assuming a μ_3-coordination. Notably, several additional bismuth–oxygen separations that are slightly smaller than the sum of the van der Waals radii are present, but these do not significantly disturb the μ_3-coordination. Layer B is built from eight bismuth atoms and fourteen oxygen atoms. All the oxygen atoms of this layer are coordinated to two bismuth atoms of layer B and to one bismuth atom of layers A or A′. Assuming μ_3-coordination the deviation of the sum of the bond angles (Bi-O-Bi 342.9–356.2°) from the ideal value of 360° is significantly larger than the corresponding sum of bond angles associated with layers A and A′. The oxygen atoms O3 and O3′ show the largest deviation (Bi-O-Bi 342.9°), which is also reflected by the bond lengths. For these atoms, two short Bi–O bonds of 2.112(9) and 2.157(7) Å, a significantly longer Bi–O bond of 2.835(8) Å, and an additional bismuth–oxygen separation of 3.036(9) Å all of which are smaller than the sum of the van der Waals radii of bismuth and oxygen are found. Thus, the coordination geometry of these oxygen atoms might alternatively be described to be between a μ_3- and μ_4-coordination. The Bi–O bonds involving the other μ_3-oxygen atoms of layer B are in the range 2.039(9)–2.481(9) Å. Notably, the oxygen atoms O13 and O18 also have additional Bi–O separations that are below the sum of the van der Waals radii (O18–Bi11 3.121(3) Å and O13–Bi11′ 2.768(3) Å) but the sum of their bond angles is close to 360° (Bi-O13-Bi 354.0°, Bi-O18-Bi 356.2°).

The bismuth–oxygen core structure of the cluster built from the bismuth atoms Bi7, Bi10, Bi11 and their symmetry related counterparts in layer B resembles the structure of β-Bi_2O_3[20] although the bond lengths and angles show large deviations. The core structure of **2** is best described as a $[Bi_2O_2]_n$ ladder-type arrangement which is also found in β-Bi_2O_3 and α-Bi_2O_3 (Figure 4). However, the structural fragment in **2** might alternatively be described as being composed of two dimerized heterocubane-like subunits in which one vertex is not occupied. This Bi_3O_4 building unit is observed in β-Bi_2O_3 but not in α-Bi_2O_3. The mean Bi–O bond lengths in the $[Bi_2O_2]_n$ units of **2** (2.42 Å) and β-Bi_2O_3 (2.40 Å) are comparable, but individual bond lengths deviate by 0.11–0.96 Å between the two structures. Similarly, large deviations are observed for corresponding Bi-O-Bi bond angles.

We have initiated preliminary studies on the thermally induced decomposition of both **1** and **2**. Thermolysis in the temperature range 25–700 °C gave $Bi_{12}SiO_{20}$ (JCPDS 80–0627) as the final material.[21] In both cases, the content of residual carbon was negligible. However, decomposition in the temperature range 25–350 °C gave β-Bi_2O_3 (JCPDS 78-1793) as the only crystalline product apart from small quantities of amorphous SiO_2. At temperatures slightly above 400 °C the metastable β-Bi_2O_3 reacts with SiO_2 to give the sillenite phase $Bi_{12}SiO_{20}$.[22] In the differential thermal analysis (DTA) diagram this process is indicated by an

 © 2005 Wiley-VCH Verlag GmbH & Co. KGaA, Weinheim

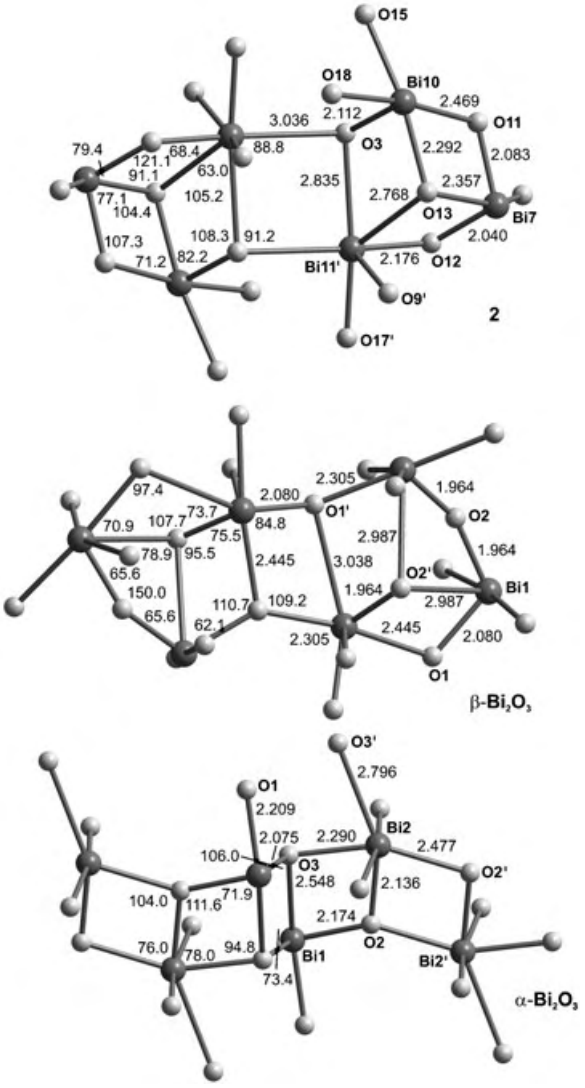


Figure 4. Comparison of bond lengths [Å] and angles [°] within the typical $[Bi_2O_2]_n$ ladder-type arrangements in **2**, β-Bi_2O_3, and α-Bi_2O_3.

exothermic peak which is not accompanied by a weight loss. The thermolysis of the layered compounds $(BiO)_2(CO_3)$ and BiO(OMe) is also reported to give metastable β-Bi_2O_3 whereas hydrolysis of $Bi(OEt)_3$ in benzene gives α-Bi_2O_3.[20,23,24]

In conclusion, we have reported the synthesis and characterization of $Bi(OSiMe_2tBu)_3$ (**1**) which is volatile and highly soluble in polar as well as in non-polar solvents. With these properties, compound **1** is a potential precursor for bismuth oxide based materials prepared by the sol–gel process and the CVD technique. The high-nuclearity cluster $[Bi_{22}O_{26}(OSiMe_2tBu)_{14}]$ (**2**) results from partial hydrolysis of **1**. This cluster has a diameter close to 2 nm and can be regarded as a silanolate capped "molecular bismuth oxide". It has potential as a model compound with which to study the formation and surface chemistry of metal oxide nanoparticles. Thermolysis of compounds **1** and **2** below 350 °C gave metastable β-Bi_2O_3. An explanation on the molecular level for the formation of β-Bi_2O_3 is offered by the molecular structure of **2** which contains the basic structural motif of β-Bi_2O_3 within its $[Bi_{22}O_{26}]^{14+}$ core. Decomposition of both **1** and **2** at higher temperatures gave the sillenite-type compound $Bi_{12}SiO_{20}$ which is of interest because of its electro-optical properties and potential use as holographic storage material.[25]

Experimental Section

1: A solution of $tBuMe_2SiOH$[26] (15.47 g, 117.20 mmol) in toluene (50 mL) was added dropwise to a solution of $Bi(OtBu)_3$[12] (16.68 g, 38.88 mmol) in toluene (100 mL) at room temperature. The solution was stirred at room temperature overnight. After removal of the solvent and *t*BuOH in vacuo at 40 °C the residue was dissolved in *n*-pentane. The solid material was removed by filtration, the filtrate was collected and the solvent was removed in vacuo (10 mbar) at 40 °C. Kugelrohr distillation of the crude product (150 °C, 1.4×10^{-2} mbar) gave colorless **1** (21.30 g, 91 %) m.p. 63 °C. ^{1}H NMR (200.13 MHz, C_6D_6): $\delta = 0.24$ (s, 6H, $SiCH_3$), 1.06 ppm (s, 9H, CCH_3); ^{13}C NMR (50.33 MHz, C_6D_6): $\delta = 0.85$ ($SiCH_3$), 19.84 (CCH_3), 26.37 ppm (CCH_3); ^{29}Si NMR (59.63 MHz, C_6D_6): $\delta = 13.7$ ppm; Elemental analysis calcd (%) for $C_{18}H_{45}Bi_1O_3Si_3$ (602.8): C 35.9, H 7.5; found: C 35.6, H 8.0; IR (KBr): $\tilde{\nu} = 2952$ (s), 2928 (s), 2893 (s), 2884 (s), 2855 (s), 2821 (w), 2799 (w), 2767 (w), 2735 (w), 2708 (w), 2645 (w), 1471 (s), 1463 (s), 1443 (w), 1434 (w), 1407 (m), 1387 (m), 1360 (m), 1254 (s), 1213 (w), 1091 (w sh.), 1040 (w sh.), 1006 (m sh.), 939 (s sh.), 880 (vs b.), 830 (s sh.), 769 (s), 671 (s), 666 (s), 576 (m sh.), 554 (s), 499 (s), 470 (m) cm^{-1}.

2: Slow evaporation of the solvent under air moisture from a solution of $Bi(OSiMe_2tBu)_3$ (**1**, 10.20 g, 16.92 mmol) in benzene almost quantitatively gave $\mathbf{2}\cdot2C_6H_6$ with m.p. 108 °C (decomp). Elemental analysis calcd (%) for $C_{96}H_{222}Bi_{22}O_{40}Si_{14}$ (7007.56): C 16.5, H 3.2; found: C 16.4, H 3.1. IR (KBr): $\tilde{\nu} = 3090$ (w), 3071 (w), 3034 (w), 2946 (s), 2922 (s), 2879 (s), 2851 (s), 2805 (w sh.), 2796 (w sh.), 2765 (w sh.), 2731 (w sh.), 2704 (w sh.), 2645 (w sh.), 1470 (s), 1462 (s), 1443 (m), 1429 (m), 1403 (m), 1386 (m), 1357 (m), 1327 (m), 1250 (s), 1209 (m), 1036 (w sh.), 1005 (m sh.), 909 (s b.), 826 (s), 813 (s), 784 (m sh.), 764 (s), 681 (m), 660 (s), 540 (vs b.), 475 (s b.) cm^{-1}.

Single crystal X-ray diffraction analyses were carried out at 173 K with a Nonius Kappa CCD for a colorless plate of dimensions $0.02\times0.08\times0.04$ mm^3 (**1**) and a colorless block of dimensions $0.12\times0.10\times0.06$ mm^3 ($\mathbf{2}\cdot2C_6H_6$). Crystal data for **1**: $C_{18}H_{45}BiO_3Si_3$, $M_r = 602.79$, monoclinic, $P2_1/n$, $a = 13.452(3)$, $b = 10.0431(18)$, $c = 39.891(6)$ Å, $\beta = 90.891(6)°$, $V = 5335.2(17)$ Å^3, $Z = 8$, $\mu(Mo_{K\alpha}) = 6.757$ mm^{-1}, 9758 unique data ($\theta_{min} = 2.95°$, $\theta_{max} = 25.50°$), 5141 data with $I \geq 2\sigma(I)$, R (obs) = 0.0817, wR (all data) = 0.2344. The residual peaks in the final difference Fourier map range between 4.692 and -1.964 e Å^{-3}. The high residual peak is located at a distance of 0.918 Å from Bi1. After merging the equivalent reflections and after corrections for Lorentz, polarization, and absorbtion effects using SCALEPACK[27] ($T_{min} = 0.774$, $T_{max} = 0.341$), an internal R value of 0.128 was obtained. Crystal data for $\mathbf{2}\cdot2C_6H_6$: $C_{96}H_{222}Bi_{22}O_{40}Si_{14}$, $M_r = 7007.56$, monoclinic, $C2/c$, $a = 30.8244(10)$, $b = 22.4631(15)$, $c = 24.9469(5)$ Å, $\beta = 91.739(7)°$, $V = 17265.1(17)$ Å^3, $Z = 4$, $\mu(Mo_{K\alpha}) = 22.484$ mm^{-1}, 15700 unique data ($\theta_{min} = 2.92°$, $\theta_{max} = 25.45°$), 7399 data with $I \geq 2\sigma(I)$, R (obs) = 0.0465, wR (all data) = 0.0829. The residual peaks in the final difference Fourier map range between 2.308 and -1.899 e Å^{-3}. After merging the equivalent reflections and after corrections for Lorentz, polarization, and absorbtion effects using SCALEPACK[27] ($T_{min} = 0.346$, $T_{max} = 0.164$), an internal R value of 0.069 was obtained. Two $SiMe_2tBu$ (C21–C36) and two *t*Bu (C65, C66, C73–C76) groups were refined isotropically. CCDC-243439 and CCDC-243440 contain the supplementary crystallographic data for this paper. These data can be obtained free of charge via www.ccdc.cam.ac.uk/conts/retrieving.html (or from the Cambridge Crystallographic Data

 © 2005 Wiley-VCH Verlag GmbH & Co. KGaA, Weinheim

Centre, 12 Union Road, Cambridge CB21EZ, UK; fax: (+44) 1223-336-033; or deposit@ccdc.cam.ac.uk).

Received: July 29, 2004

Keywords: bismuth · cluster compounds · hydrolysis · materials science · silanolates

[1] a) C. Limberg, *Angew. Chem.* **2003**, *115*, 6112 – 6136; *Angew. Chem. Int. Ed.* **2003**, *42*, 5932 – 5954; b) C. Limberg, M. Hunger, W. Habicht, E. Kaifer, *Inorg. Chem.* **2002**, *41*, 3359 – 3365; c) R. K. Grasselli, J. D. Burrington, *Adv. Catal.* **1981**, *30*, 133 – 163; d) A. Castro, P. Begue, B. Jimenez, J. Ricote, R. Jimenez, J. Galy, *Chem. Mater.* **2003**, *15*, 3395 – 3401; e) A. M. Beale, G. Sankar, *Chem. Mater.* **2003**, *15*, 146 – 153.

[2] M. Hunger, C. Limberg, P. Kircher, *Angew. Chem.* **1999**, *111*, 1171 – 1174; *Angew. Chem. Int. Ed.* **1999**, *38*, 1105 – 1108.

[3] a) B. H. Park, B. S. Kang, S. D. Bu, T. W. Noh, J. Lee, W. Jo, *Nature* **1999**, *401*, 682 – 684; b) M. Schuisky, K. Kukli, M. Ritala, A. Harsta, M. Leskelä, *Chem. Vap. Deposition* **2000**, *6*, 139 – 145; c) W. F. Su, Y. T. Lu, *Mater. Chem. Phys.* **2003**, *80*, 632 – 637; d) Y. Kageyama, T. Yoshida, Y. Mitsushima, K. Suzuki, K. Kato, *Integr. Ferroelectr.* **2001**, *36*, 173 – 181.

[4] J. H. Thurston, K. H. Whitmire, *Inorg. Chem.* **2003**, *42*, 2014 – 2023.

[5] a) C. A. Paz de Araujo, J. D. Cuchiaro, L. D. McMillan, M. C. Scott, J. F. Scott, *Nature* **1995**, *374*, 627 – 629; b) Y. Tsunoda, W. Sugimoto, Y. Sugahara, *Chem. Mater.* **2003**, *15*, 632 – 635.

[6] a) J. H. Thurston, T. O. Ely, D. Trahan, K. H. Whitmire, *Chem. Mater.* **2003**, *15*, 4407 – 4416; b) J. W. Pell, K. M. Delak, H. C. zur Loye, *Chem. Mater.* **1998**, *10*, 1764 – 1770; c) *High Performance Pigments* (Ed.: H. M. Smith), Wiley-VCH, Weinheim, **2001**.

[7] A. Cabot, A. Marsal, J. Arbiol, J. R. Morante, *Sens. Actuators B* **2004**, *99*, 74 – 89.

[8] a) K. H. Whitmire, *Chemtracts: Inorg. Chem.* **1995**, *7*, 167 – 181; b) S. Parola, R. Papiernik, L. G. Hubert-Pfalzgraf, S. Jagner, M. Hakansson, *J. Chem. Soc. Dalton Trans.* **1997**, 4631 – 4635; c) Y. Kim, H. K. Chae, K. S. Lee, W. I. Lee, *J. Mater. Chem.* **1998**, *8*, 2317 – 2319; d) Y. T. Kim, C. Hwang, H. K. Chae, Y. K. Lee, W. I. Lee, Y. W. Dong, H. Yun, *J. Sol-Gel Sci. Technol.* **2000**, *19*, 301 – 304; e) E. P. Turevskaya, V. B. Bergo, K. A. Vorotilov, A. S. Sigov, D. Benlian, *J. Sol-Gel Sci. Technol.* **1998**, *13*, 889 – 893; f) F. Soares Carvalho, P. Thomas, J. P. Mercurio, B. Frit, S. Parola, *J. Sol-Gel Sci. Technol.* **1997**, *8*, 759 – 763.

[9] a) J. H. Thurston, K. H. Whitmire, *Inorg. Chem.* **2002**, *41*, 4194 – 4205; b) P. A. Williams, A. C. Jones, M. J. Crosbie, P. J. Wright, J. F. Bickley, A. Steiner, H. O. Davies, T. J. Leedham, G. W. Critchlow, *Chem. Vap. Deposition* **2001**, *7*, 205 – 209.

[10] a) M. A. Matchett, M. Y. Chiang, W. E. Buhro, *Inorg. Chem.* **1990**, *29*, 358 – 360; b) C. M. Jones, M. D. Burkart, K. H. Whitmire, *Angew. Chem.* **1992**, *104*, 466 – 467; *Angew. Chem. Int. Ed. Engl.* **1992**, *31*, 451 – 452; c) C. M. Jones, M. D. Burkart, R. E. Bachman, D. L. Serra, S. J. Hwu, K. H. Whitmire, *Inorg. Chem.* **1993**, *32*, 5136 – 5144; d) T. J. Boyle, D. M. Pedrotty, B. Scott, J. W. Ziller, *Polyhedron* **1998**, *17*, 1959 – 1974; e) M.-C. Massiani, R. Papiernik, L. G. Hubert-Pfalzgraf, J.-C. Daran, *J. Chem. Soc. Chem. Commun.* **1990**, 301 – 302; f) A. Haaland, H. P. Verne, H. V. Volden, R. Papiernik, L. G. Hubert-Pfalzgraf, *Acta Chem. Scand.* **1993**, *47*, 1043 – 1045; g) R. C. Mehrotra, A. K. Rai, *Indian J. Chem.* **1966**, *4*, 537; h) V. G. Kessler, N. Y. Turova, E. P. Turevskaya, *Inorg. Chem. Commun.* **2002**, *5*, 549 – 551; i) T. A. Hanna, G. Keitany, C. Ibarra, R. D. Sommer, A. L. Rheingold, *Polyhedron* **2001**, *20*, 2451 – 2455; j) C. M. Jones, M. D. Burkart, K. H. Whitmire, *J. Chem. Soc. Chem. Commun.* **1992**, 1638 – 1639; k) M. Hunger, C. Limberg, P. Kircher, *Organometallics* **2000**, *19*, 1044 – 1050; l) S. Parola, R. Papiernik, L. G. Hubert-Pfalzgraf, C. Bois, *J. Chem. Soc. Dalton Trans.* **1998**, 737 – 739; m) J. W. Pell, W. C. Davis, H. C. zur Loye, *Inorg. Chem.* **1996**, *35*, 5754 – 5755; n) N. N. Sauer, E. Garcia, R. Ryan, *Mater. Res. Soc. Symp. Proc.* **1990**, *180*, 921 – 924; o) K. H. Whitmire, C. M. Jones, M. D. Burkart, J. C. Hutchinson, A. L. McKnight, *Mater. Res. Soc. Symp. Proc.* **1992**, *271*, 149 – 154; p) S. C. James, N. C. Norman, A. G. Orpen, M. J. Quayle, U. Weckenmann, *J. Chem. Soc. Dalton Trans.* **1996**, 4159 – 4161.

[11] M.-C. Massiani, R. Papiernik, L. G. Hubert-Pfalzgraf, J.-C. Daran, *Polyhedron* **1991**, *10*, 437 – 445.

[12] W. J. Evans, J. J. H. Hain, J. W. Ziller, *J. Chem. Soc. Chem. Commun.* **1989**, 1628 – 1629.

[13] a) J. L. Jolas, S. Hoppe, K. H. Whitmire, *Inorg. Chem.* **1997**, *36*, 3335 – 3340; b) K. H. Whitmire, S. Hoppe, O. Sydora, J. L. Jolas, C. M. Jones, *Inorg. Chem.* **2000**, *39*, 85 – 97; c) M. Veith, E.-C. Yu, V. Huch, *Chem. Eur. J.* **1995**, *1*, 26 – 32.

[14] a) H. Schmidbaur, M. Bergfeld, *Z. Anorg. Allg. Chem.* **1968**, *363*, 84 – 88; b) K. W. Terry, K. Su, T. D. Tilley, A. L. Rheingold, *Polyhedron* **1998**, *17*, 891 – 897.

[15] D. Mansfeld, M. Mehring, M. Schürmann, *Z. Anorg. Allg. Chem.* **2004**, *630*, 1795 – 1797.

[16] K. G. Caulton, L. G. Hubert-Pfalzgraf, *Chem. Rev.* **1990**, *90*, 969 – 995.

[17] M. Baier, P. Bissinger, J. Blümel, H. Schmidbaur, *Chem. Ber.* **1993**, *126*, 947 – 950.

[18] N. C. Norman, *Chemistry of Arsenic, Antimony and Bismuth*, 1st ed., Blackie, London, **1998**.

[19] A. Bondi, *J. Phys. Chem.* **1964**, *68*, 441 – 451.

[20] S. K. Blower, C. Greaves, *Acta Crystallogr. Sect. C* **1988**, *44*, 587 – 589.

[21] DTA-thermogravimetry (TG) experiments of **1** and **2** were performed under argon with a heating rate of 6 K min^{-1} in two temperature ranges and the final materials were analyzed; 1) 25–350 °C (X-ray diffraction (XRD), energy dispersive X-ray spectroscopy (EDX)) and 2) 25–700 °C (XRD, EDX, elemental analysis (%) calcd for $Bi_{12}SiO_{20}$ Bi 87.8, Si 1.0; found (from **1**): Bi 87.2, Si 1.0; found (from **2**): Bi 86.3, Si 0.8; for both materials no residual carbon was detected).

[22] a) B. Aurivillius, L. G. Sillen, *Nature* **1945**, *155*, 305 – 306; b) H. S. Horowitz, A. J. Jacobson, J. M. Newsam, J. T. Lewandowski, M. E. Leonowicz, *Solid State Ionics* **1989**, *32*/33, 678 – 690.

[23] F. Reifler, H. R. Oswald, R. A. Gubser, C. Baerlocher, A. Reller, *Solid State Ionics* **1996**, *84*, 283 – 291.

[24] E. P. Turevskaya, V. B. Bergo, M. I. Yanovskaya, N. Ya. Turova, *Russ. J. Inorg. Chem.* **1996**, *41*, 695 – 699.

[25] a) H. Vogt, K. Buse, H. Hesse, E. Kratzig, R. R. Garcia, *J. Appl. Phys.* **2001**, *90*, 3167 – 3173; b) M. Valant, D. Suvorov, *J. Am. Ceram. Soc.* **2001**, *84*, 2900 – 2904; c) P. S. Aithal, P. P. Kiran, D. N. Rao, *J. Nonlinear Opt. Phys. Mater.* **2000**, *9*, 217 – 225.

[26] S. Sieburth, W. Mu, *J. Org. Chem.* **1993**, *58*, 7584 – 7586.

[27] Z. Otwinowski, W. Minor in *Macromolecular Crystallography, Part A*, *Vol. 276* (Eds.: C. W. Carter, Jr., R. M. Sweet), Academic, New York, **1997**, pp. 307 – 326.

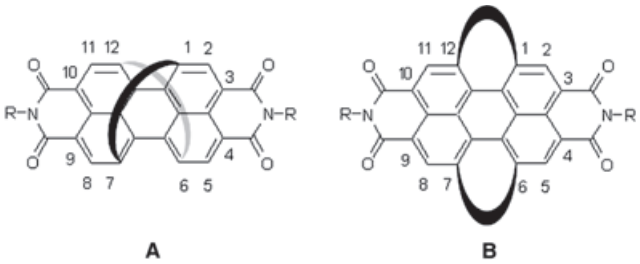
 © 2005 Wiley-VCH Verlag GmbH & Co. KGaA, Weinheim

Macrocyclic Perylene Bisimides

Perylene Bisimide Based Macrocycles: Effective Probes for the Assessment of Conformational Effects on Optical Properties**

*Peter Osswald, Dirk Leusser, Dietmar Stalke, and Frank Würthner**

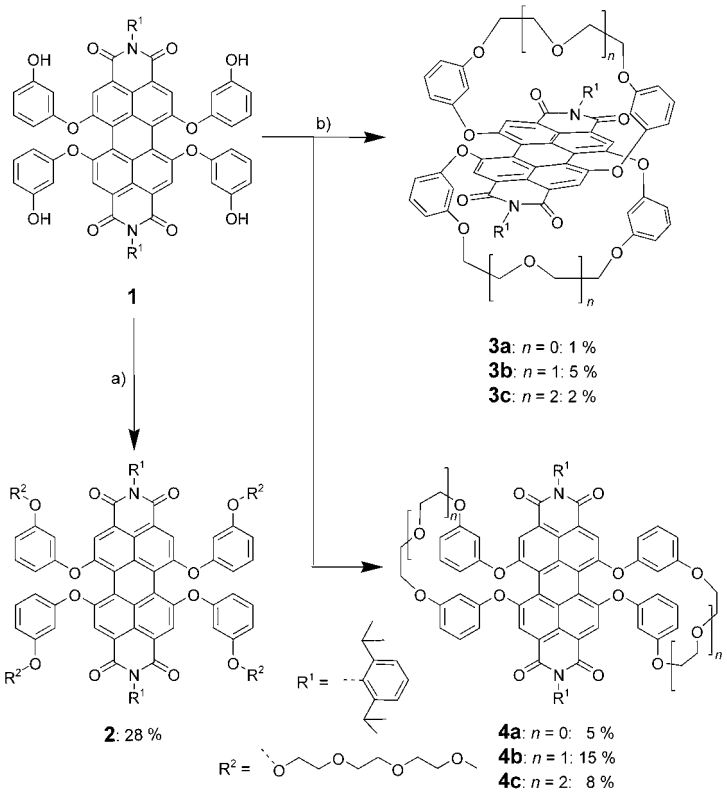
Dedicated to Professor Johann Weis on the occasion of his 60th birthday



Scheme 1. Schematic presentation of diagonally bridged (A) and laterally bridged (B) macrocyclic perylene bisimides.

During the last few years, perylene bisimides bearing phenoxy substituents in the bay positions have been developed to become one of the most useful classes of fluorophores. They can be diversely functionalized at the imide and the bay phenoxy units to achieve desired optical and electrochemical properties.[1] Indeed, in multichromophoric dendritic perylene bisimides[2] as well as in self-organized metallosupramolecular squares[3] or mesoscopic assemblies[4] highly efficient energy- and electron-transfer processes have been demonstrated—such supramolecular arrays based on phenoxy-substituted perylene bisimides (PPBIs) may serve as artificial light-harvesting systems.[5] Furthermore, PPBIs show potential for application in solar cells,[4b,6] polymeric light-emitting diodes,[7] and as molecular probes in biological systems.[8] Despite this remarkable versatility of PPBIs, the effect of different conformations on the optical properties of this class of fluorophores has been barely explored. Single-molecule spectroscopic studies revealed that different conformations—that is, the twist of the perylene bisimide chromophore and the orientation of the phenoxy groups—have an effect on the photophysical properties of *immobilized* PPBIs.[9] Nevertheless, conformational effects on the optical properties of perylene bisimides in solution have not been reported yet.[1b]

To identify the conformational effect on the optical properties of PPBI chromophores, conformationally restricted macrocyclic perylene bisimides, which are diagonally bridged through 1,7- and 6,12-linkages (Scheme 1, A) seem to be properly suited since the conformational freedom of the perylene core should be restricted in these systems and a particular conformation of the phenoxy substituents can be achieved through variation of the length of the bridging unit. Oligo(ethylene glycol) units were chosen as the bridging unit because, on the one hand, this functionality can be introduced in perylene bisimide by etherification of the resorcin groups in the bay positions and, on the other hand, the chain length can be varied through the appropriate choice of ditosylates. Herein we present the synthesis (Scheme 2) of diagonally bridged macrocyclic perylene bisimides **3a–c** as well as the corresponding laterally bridged isomers **4a–c**, and report on their optical properties in comparison to those of the open-chain reference compound **2**, which confirm a pronounced conformational effect on the optical properties of perylene bisimides.



Scheme 2. a) H_3C-$(OCH_2CH_2)_3$-O-*p*-Tos, Cs_2CO_3, DMSO, argon, 80°C, 5 h; b) *p*-Tos-O-CH_2CH_2O-$(CH_2CH_2O)_n$-*p*-Tos (n = 0–2), Cs_2CO_3, DMSO, argon, 100°C, 5 h. Tos = tosyl, DMSO = dimethyl sulfoxide.

[*] P. Osswald, Prof. Dr. F. Würthner
Institut für Organische Chemie
Bayerische Julius-Maximilians-Universität Würzburg
Am Hubland, 97074 Würzburg (Germany)
Fax: (+49) 931-888-4756
E-mail: wuerthner@chemie.uni-wuerzburg.de
Dr. D. Leusser, Prof. Dr. D. Stalke
Institut für Anorganische Chemie
Bayerische Julius-Maximilians-Universität Würzburg
Am Hubland, 97074 Würzburg (Germany)

[**] This work was supported by the Deutsche Forschungsgemeinschaft and the Fonds der Chemischen Industrie.

Supporting information for this article is available on the WWW under http://www.angewandte.org or from the author.

 © 2005 Wiley-VCH Verlag GmbH & Co. KGaA, Weinheim DOI: 10.1002/anie.200461585

As shown in Scheme 2, compound **2** was synthesized by etherification of **1** with 2-[2-(2-methoxyethoxy)ethoxy]ethyl tosylate and cesium carbonate in DMSO at 80 °C in 28 % yield. The macrocyclic perylene bisimides **3a–c** were synthesized by employing batch cyclization as a convenient one-pot macrocyclization method with a perylene bisimide concentration of 6×10^{-3} M.[10] For this purpose **1** was treated with the corresponding oligo(ethylene glycol) ditosylates and cesium carbonate in DMSO at 100 °C. After purification by column chromatography the diagonally bridged macrocyclic perylene bisimides **3** were isolated in 1–5 % yield and the laterally bridged isomers **4** were obtained in 5–15 % yield for mono-, di-, and tri(ethylene glycol) chains.[11]

The presence of four resorcin units in the precursor bisimide **1** causes formation of isomeric bis(macrocycles) by etherification. Only based on spectroscopic data, in particular ^{1}H NMR data, reliable assignment of the isolated macrocycles to a particular isomer is not possible. Therefore, crystallization of the macrocycles has been carried out and single crystals suitable for X-ray diffraction were obtained in the case of **3b** and **4a** by dissolving the compounds in dichloromethane, subsequent addition of equal amounts of methanol, and slow evaporation of dichloromethane at room temperature.

Figure 1 shows the molecular structures of **3b** and **4a** in the crystal.[12] Compound **3b** possesses the envisioned macrocyclic structure with the bridging units lying above and below the perylene core. A further characteristic feature of this diagonally bridged isomer is an almost perpendicular orientation of the phenoxy substituents relative to the perylene core which resembles a conformation suggested based on molecular modeling studies of related noncyclic compounds.[9] For the macrocyclic systems **3** an interconversion between the conformational enantiomers (*M*⇄*P*) as observed for nonrigid twisted perylene bisimides[13] is not possible because in the case of **3** a bond cleavage is required. Thus, these systems possess favorable structural features to assess the conformational effect of the bay phenoxy substituents on the optical properties of this class of chromophores. The twist angle between the two naphthalene units of the perylene core of **3b** was determined to 33° and is thus higher than that known for a phenoxy-substituted diazadibenzoperylene derivative,[14] which underlines the rigid character of these isomers.

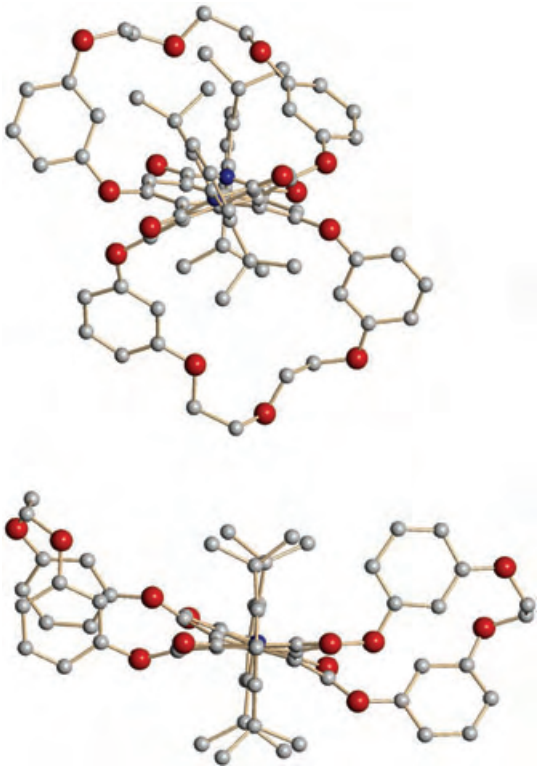


Figure 1. Molecular structures of **3b** (top, *P* enantiomer) and **4a** (bottom, *P* enantiomer). View along the N–N axis of the perylene bisimide showing the twisted nature and the cyclic structure of both isomers. Note that both centrosymmetric crystal structures contain *P* and *M* enantiomers (for crystal packing see the Supporting Information).

The molecular structure of **4a** shows that the phenoxy groups are connected laterally through the ethylene glycol groups and that the twist angle between the two naphthalene units is 25°. Whereas the phenoxy groups in **3b** are orthogonally orientated, in **4a**, they are horizontally orientated to the perylene core.

Although single crystals could not be obtained for all compounds, the structures of **3a**,**c** and **4b**,**c** could be unequivocally assigned by comparison of their ^{1}H NMR data with those of **3b** and **4a**. For this purpose, the resonance of the proton situated between the two oxygen atoms of the resorcin substituents is particularly informative, because this proton is differently shielded by the aromatic ring current in lateral and diagonal isomers (see the Supporting Information).

The optical properties of the macrocyclic perylene bisimides were investigated by UV/Vis, steady-state, and time-resolved fluorescence spectroscopy. The absorption spectra of laterally bridged macrocycles **4** (Figure 2) show typical patterns for PPBIs with a maximum around 580 nm assigned to the $S_0 \rightarrow S_1$ transition, a shoulder of the second vibronic transition, and a broad maximum at 450 nm belonging to the $S_0 \rightarrow S_2$ transition. For the derivatives **4b** and **4c**, the absorption maxima as well as the molar absorption coefficients are in good agreement with that of the reference compound **2**; thus, **2** may possess a similar conformation to that of the lateral isomers. Only the smallest macrocycle **4a**

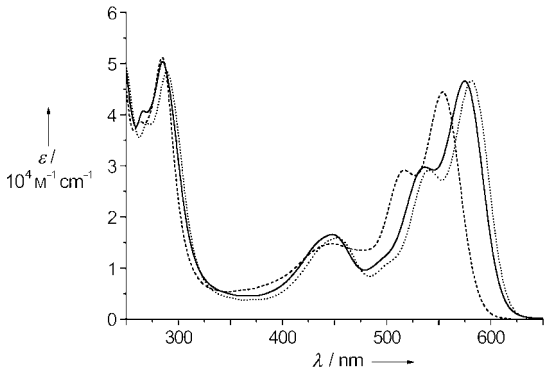


Figure 2. Absorption spectra of **4a** (dashed line), **4c** (dotted line), and the reference compound **2** (solid line) in dichloromethane.

 © 2005 Wiley-VCH Verlag GmbH & Co. KGaA, Weinheim

adopts an exceptional position because the maximum of the $S_0 \rightarrow S_1$ transition is hypsochromically shifted by 20 nm compared to that of **4b** and a decrease of the molar absorption coefficient is observed. This shift is presumably due to the conformational restriction imposed by the short spacer units.

For the diagonally bridged macrocycles **3** significant spectral differences were observed compared to those of the reference compound **2**. The absorption maxima of the $S_0 \rightarrow S_1$ transition are shifted up to 41 nm towards shorter wavelength from 575 nm (**2**) to 545 nm (**3a**,**c**) and 534 nm (**3b**) (Figure 3).

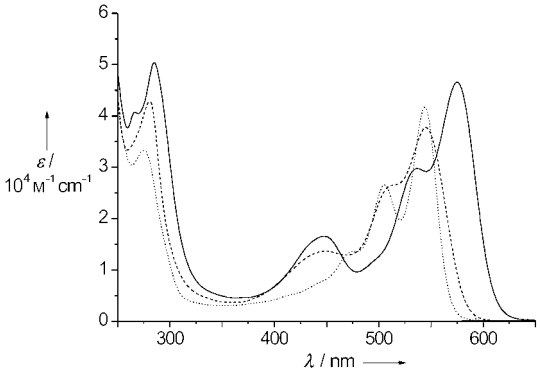


Figure 3. Absorption spectra of **3a** (dotted line), **3c** (dashed line), and the reference compound **2** (solid line) in dichloromethane.

This hypsochromic shift and the observed pronounced hypochromicity may be attributed to the formation of a conformer with less conjugation between the phenoxy groups (+M effect) and the electron-deficient perylene bisimide.[15]

The fluorescence properties of the reference compound **2**, diagonal isomers **3**, and lateral isomers **4** are given in Table 1 (emission spectra are shown in the Supporting Information). As the data reveal, fluorescence quantum yields and lifetimes of the lateral isomers **4a–c** are indistinguishable with that of the reference compound **2**, which again indicates that the behavior of these isomers is similar to that of the open-chain PPBI derivatives. In contrast to the situation with the lateral isomers **4**, the fluorescence quantum yields of the diagonally bridged macrocycles **3** are much lower than that of the reference compound **2**. This effect is clearly related to an increase of the nonradiative rate constants k_{nr} (**2** < **3c** < **3b** < **3a**), whereas the radiative rate constants k_r are almost identical for all compounds presented here.

Table 1: Emission properties of macrocyclic perylene bisimides in dichloromethane.

	λ_{max} [nm]	ϕ_{fl}[a]	τ_{fl} [ns][b]	k_r [s^{-1}][c]	k_{nr} [s^{-1}][d]
2	609	0.89	5.6	1.6×10^8	2.0×10^7
3a	562	< 0.02	< 0.5	$> 4.0\times10^7$	$> 2.0\times10^9$
3b	573	0.09	0.8	1.1×10^8	1.1×10^9
3c	582	0.43	2.7	1.6×10^8	2.1×10^8
4a	588	0.78	5.4	1.4×10^8	4.1×10^7
4b	605	0.82	5.3	1.6×10^8	3.4×10^7
4c	606	0.84	5.6	1.5×10^8	2.9×10^7

[a] $\phi_{fl} \pm 0.03$. [b] $\tau \pm 0.5$. [c] $k_r = \phi_{fl}\tau^{-1}$. [d] $k_{nr} = (1-\phi_{fl})\tau^{-1}$.

Based on the fact that the spectroscopic data of the diagonally bridged isomers **3** differ significantly from those of the reference compound **2**, it can be concluded that non-macrocyclic PPBIs do not exhibit a perpendicular orientation of the phenoxy residues in solution. Instead, based on the observed optical properties of the macrocyclic perylene bisimides **4**, which are similar to the non-macrocyclic reference **2**, a conformation with horizontal orientation of the phenoxy groups is most likely for non-macrocyclic PPBI dyes such as **2** in solution. These results establish for the first time the conformational effect on the optical properties of these chromphores in solution. The question to what extent the charge-density distribution and, hence, the optical properties of the perylene core correlate to the various conformations will further be investigated. The results of the current study will be of major impact to the development of improved molecular probes for biological systems,[8] applications of these dyes in single-molecule spectroscopy,[9] and the development of PPBI based fluorescence sensors.[16] In this context the isolation of enantiopure macrocyclic dyes **3a–c** is one of our particular goals.

Received: August 9, 2004

Keywords: conformational effects · dyes/pigments · fluorescent probes · macrocycles

[1] For reviews on perylene bisimides see: a) H. Langhals, *Heterocycles* **1995**, *40*, 477–500; b) F. Würthner, *Chem. Commun.* **2004**, 1564–1579.

[2] a) J. M. Serin, D. W. Brousmiche, J. M. J. Fréchet, *Chem. Commun.* **2002**, 2605–2607; b) D. Liu, S. De Feyter, M. Cotlet, A. Stefan, U.-M. Wiesler, A. Herrmann, D. Grebel-Koehler, J. Qu, K. Müllen, F. C. De Schryver, *Macromolecules* **2003**, *36*, 5918–5925; c) J. Qu, N. G. Pschirer, D. Liu, A. Stefan, F. C. De Schryver, K. Müllen, *Chem. Eur. J.* **2004**, *10*, 528–537.

[3] a) F. Würthner, A. Sautter, D. Schmid, P. J. A. Weber, *Chem. Eur. J.* **2001**, *7*, 894–902; b) F. Würthner, A. Sautter, *Org. Biomol. Chem.* **2003**, *1*, 240–243; c) C.-C. You, F. Würthner, *J. Am. Chem. Soc.* **2003**, *125*, 9716–9725; d) B. K. Kaletas, R. Dobrawa, A. Sautter, F. Würthner, M. Zimine, L. De Cola, R. M. Williams, *J. Phys. Chem. A* **2004**, *108*, 1900–1909.

[4] a) F. Würthner, C. Thalacker, A. Sautter, W. Schärtl, W. Ibach, O. Hollricher, *Chem. Eur. J.* **2000**, *6*, 3871–3886; b) T. van der Boom, R. T. Hayes, Y. Zhao, P. J. Bushard, E. A. Weiss, M. R. Wasielewski, *J. Am. Chem. Soc.* **2002**, *124*, 9582–9590; c) K. Sugiyasu, N. Fujita, S. Shinkai, *Angew. Chem.* **2004**, *116*, 1249–1253; *Angew. Chem. Int. Ed.* **2004**, *43*, 1229–1233.

[5] M. J. Ahrens, L. E. Sinks, B. Rybtchinski, W. Liu, B. A. Jones, J. M. Giaimo, A. V. Gusev, A. J. Goshe, D. M. Tiede, M. R. Wasielewski, *J. Am. Chem. Soc.* **2004**, *126*, 8284–8294.

[6] a) M. Thelakkat, P. Pösch, H.-W. Schmidt, *Macromolecules* **2001**, *34*, 7441–7447; b) A. S. Lukas, Y. Zhao, S. E. Miller, M. R. Wasielewski, *J. Phys. Chem. B* **2002**, *106*, 1299–1306; b) A. P. H. J. Schenning, J. van Herrikhuyzen, P. Jonkheijm, Z. Chen, F. Würthner, E. W. Meijer, *J. Am. Chem. Soc.* **2002**, *124*, 10252–10253.

[7] C. Ego, D. Marsitzky, S. Becker, J. Zhang, A. C. Grimsdale, K. Müllen, J. D. MacKenzie, C. Silva, R. H. Friend, *J. Am. Chem. Soc.* **2003**, *125*, 437–443.

 © 2005 Wiley-VCH Verlag GmbH & Co. KGaA, Weinheim

[8] a) J. Qu, C. Kohl, M. Pottek, K. Müllen, *Angew. Chem.* **2004**, *116*, 1554 – 1557; *Angew. Chem. Int. Ed.* **2004**, *43*, 1528 – 1531; b) M. A. Abdalla, J. Bayer, J. O. Rädler, K. Müllen, *Angew. Chem.* **2004**, *116*, 4057 – 4060; *Angew. Chem. Int. Ed.* **2004**, *43*, 3967 – 3970.
[9] J. Hofkens, T. Vosch, M. Maus, F. Köhn, M. Cotlet, T. Weil, A. Herrmann, K. Müllen, F. C. De Schryver, *Chem. Phys. Lett.* **2001**, *333*, 255 – 263.
[10] U. Lüning, M. Müller, M. Gelbert, K. Peters, H. G. von Schnering, M. Keller, *Chem. Ber.* **1994**, *127*, 2297 – 2306.
[11] The compounds have been characterized by NMR spectroscopy and MALDI-TOF mass spectrometry. Synthetic details, spectroscopic and analytical data will be published elsewhere.
[12] Details of the X-ray structure determination of compounds **3b** and **4a** are given in the Supporting Information. CCDC-246746 and CCDC-246747 contain the supplementary crystallographic data for this paper. These data can be obtained free of charge via www.ccdc.cam.ac.uk/conts/retrieving.html (or from the Cambridge Crystallographic Data Centre, 12, Union Road, Cambridge CB21EZ, UK; fax: (+44) 1223-336-033; or deposit@ccdc.cam.ac.uk)..
[13] Z. Chen, M. G. Debije, T. Debaerdemaeker, P. Osswald, F. Würthner, *ChemPhysChem* **2004**, *5*, 137 – 140.
[14] F. Würthner, A. Sautter, J. Schilling, *J. Org. Chem.* **2002**, *67*, 3037 – 3044.
[15] Electron-donating substituents cause a bathochromic shift of the $S_0 \rightarrow S_1$ transition in perylene bisimide dyes (see Table 1 in ref. [1b]).
[16] L. Zang, R. Liu, M. W. Holman, K. T. Nguyen, D. M. Adams, *J. Am. Chem. Soc.* **2002**, *124*, 10640 – 10641.

 © 2005 Wiley-VCH Verlag GmbH & Co. KGaA, Weinheim

Atmospheric Chemistry

The SF_5O_x Radicals, $x = 0$–3**

Marc Kronberg, Stefan von Ahsen, Helge Willner, and Joseph S. Francisco**

Sulfur hexafluoride, SF_6, has found widespread use beyond its original application as an insulator gas in electrical high-voltage equipment and switchgear boxes.[1] It is a major plasma etching gas now commonly used in the semiconductor industry.[2] Because SF_6 is an excellent source of fluorine atoms upon strong excitation and contains no carbon, it leaves no carbonaceous deposits in the plasma etching process.[3–5] An attractive feature of SF_6 is its nonflammability and chemical inertness. Surprisingly, the environmental concerns of the long-term usage of SF_6 have become an issue only recently as a result of its increasing abundance in the atmosphere.[6,7] Because SF_6 is a greenhouse gas with a global-warming potential that is 23900 times higher than that of CO_2, this also has contributed to the growing concern about its atmospheric impact.[8] Recent studies of the environmental consequences of the decomposition of SF_6 have attempted to characterize the breakdown products that result from electrical discharges.[9–12] The main products observed under various spark arc and corona discharge conditions are SF_2O, SF_2O_2, and SF_4O. Detailed mechanisms to describe their formation remain unclear.[13,14] The observation of the even stronger greenhouse gas SF_5CF_3, chemically related to SF_6, in stratospheric air samples has further raised questions of the atmospheric consequence of these species.[15] At present the molar ratio of SF_5CF_3 relative to SF_6 amounts to about 4%. Here we report on the spectroscopic characterization of the key radical species SF_5, a product of the photodissociation of SF_6 and SF_5CF_3, and the radicals SF_5O, SF_5OO, and SF_5OOO, which form in the oxidation reactions of the SF_5 radical.

The SF_5 radical: Smardzewski et al.[16] found two new IR bands at 812 and 552 cm^{-1} from the photodissociation of SF_5X compounds (X = F, Cl, Br, SF_5). The same bands were observed in reactions of F atoms with SF_4, which confirmed the presence of the SF_5 radical. Andrews et al.[17] also isolated the SF_5 radical in an Ar matrix and observed an additional IR band at 885 cm^{-1}. Since these studies, other bands of SF_5 have not been reported nor has the UV spectrum of SF_5 been published.

The SF_5 radical belongs to the symmetry point group C_{4v}. Hence, the nine normal modes are represented by three A_1, two B_1, one B_2, and three E modes, of which only the A_1- and E-type vibrations are IR active. In order to measure all six IR-active modes, a much more efficient synthesis for matrix-isolated SF_5 radicals was needed. For this purpose the thermally labile precursors S_2F_{10},[18] SF_5NO_2,[19] and $N(SF_5)_3$[20,21] highly diluted in Ne or Ar were flash thermolyzed at low pressures and subsequently quenched as matrices. All three precursors resulted in the same set of IR matrix bands with three additional weak bands at 633.0, 524.7, and 387.2 cm^{-1} (Ne matrix). In Table 1 the bands are assigned by comparison with the calculated band positions and intensities. The UV spectrum of SF_5 was obtained from the matrix-isolated thermolysis products of SF_5NO_2 diluted in Ne. Because a 1:1 mixture of SF_5 and NO_2 is present in the matrix, the cross sections of SF_5 were determined by calibration[22] using the UV spectrum of the by-product NO_2, and a reference spectrum of NO_2 could be used in turn for subtraction. The UV spectrum of SF_5 shows a structureless weak absorption beginning at about 235 nm ($\sigma < 10^{-20}$ cm^2) and ending at 200 nm with an absorption cross section of 1.1×10^{-18} cm^2 (see the Supporting Information). Hence, SF_5 should be photostable in the stratosphere, as the

[*] Dr. M. Kronberg, Dr. S. von Ahsen, Prof. Dr. H. Willner
Fachbereich C, Anorganische Chemie
Bergische Universität Wuppertal
Gaussstrasse 20, 42097 Wuppertal (Germany)
Fax: (+49) 202-439-3053
E-mail: willner@uni-wuppertal.de
Prof. Dr. J. S. Francisco
Department of Chemistry, Earth and Atmospheric Sciences
Purdue University
1393 H. C. Brown Building, West Lafayette IN 47907 (USA)
Fax: (+1) 765-494-0239
E-mail: francisc@purdue.edu

[**] This work was supported by the Deutsche Forschungsgemeinschaft. J.S.F. expresses his thanks to the Alexander von Humboldt Foundation for a research award for senior U.S. scientists.

Supporting information for this article is available on the WWW under http://www.angewandte.org or from the author.

 DOI: 10.1002/anie.200461235 © 2005 Wiley-VCH Verlag GmbH & Co. KGaA, Weinheim

Table 1: Calculated [B3LYP/6–311++G(3df,3pd)] and observed IR band positions [cm^{-1}] and relative intensities of the matrix-isolated radicals SF_5 and SF_5OO.

SF_5							SF_5OO				
Ne		Ar	Calcd[a,b]				O_2		Calcd[a,b]		
$\tilde{\nu}$ [cm^{-1}]	Rel. int.	$\tilde{\nu}$ [cm^{-1}]	$\tilde{\nu}$ [cm^{-1}]	Rel. int.			$\tilde{\nu}$ [cm^{-1}]	Rel. int.	$\tilde{\nu}$ [cm^{-1}]	Rel. int.	
891.7	15	887	862	16	$\nu_1 A_1$		1135	6.1	1217	14	$\nu_1 A'$
817.8	100	797	778	100	$\nu_7 E$		929	81	892	94	$\nu_2 A'$
633.0	2.4	631	601	0.90	$\nu_2 A_1$		919	100	880	100	$\nu_{13} A''$
			553	–	$\nu_5 B_2$		870	65	855	71	$\nu_3 A'$
553.4	6.6	552	522	2.9	$\nu_3 A_1$		693	2.0	653	0.88	$\nu_4 A'$
524.7	1.1	524	494	0.01	$\nu_8 E$				622	0.09	$\nu_5 A'$
			437	–	$\nu_4 B_1$				606	0.01	$\nu_6 A'$
387.2	0.6	384	339	0.01	$\nu_9 E$		602	17	582	12	$\nu_7 A'$
			226	–	$\nu_6 B_2$		555	1.6	551	3.0	$\nu_{14} A''$

[a] A relative intensity of 100 corresponds to 918 km mol^{-1} for SF_5 and 397 km mol^{-1} for SF_5OO. [b] Low-frequency modes in cm^{-1}, (rel. int.), assignment: 530 (2.4), $\nu_8 A'$; 488 (0.03), $\nu_9 A'$; 426 (0.25), $\nu_{15} A''$; 408 (0.35), $\nu_{10} A'$; 329 (0.13), $\nu_{11} A'$; 315 (0.00), $\nu_{16} A''$; 282 (0.05), $\nu_{17} A''$; 218 (0.09), $\nu_{12} A'$; 82 (0.01), $\nu_{18} A''$.

reaction with oxygen is expected to be its dominant fate. This is similar to the known atmospheric fate of the radical CF_3, which is converted rapidly into CF_3OO in the presence of O_2.[23]

The SF_5O radical: Merill and Cady postulated that the SF_5O radical results from irradiation of bis(pentafluorosulfur) peroxide, F_5SOOSF_5.[24] Czarnowski and Schumacher[25,26] also suggested the formation of SF_5O from the thermal decomposition of the peroxide. Neither of these studies identified the radical, although a study by Feliz and Schumacher,[27] in which CO was added to F_5SOOSF_5 during photolysis, showed that carbon monoxide was oxidized to CO_2 providing indirect evidence for the existence of SF_5O.

Quantum chemical calculations predict the SF_5O radical to have C_{2v} symmetry (and not C_{4v}) as an SO bond with participation of an oxygen sp or p orbital results in a p-type singly occupied molecule orbital (SOMO) mainly located at the O atom. This orbital geometry is inconsistent with a fourfold axis. Our observed IR spectrum of SF_5O isolated in Ne matrix obtained by flash thermolysis of SF_5OOSF_5 and SF_5OOOSF_5 is consistent with this finding. The observed IR band positions are presented in Table 2 and Figure 1 and are in accordance with the computational data. From the 15 fundamentals (six A_1, one A_2, four B_1, four B_2 modes) only the A_2 mode is IR inactive. Six fundamentals were observed while for the missing modes the calculations predict either a low frequency (not yet measured) and/or a very low intensity. Photolysis of SF_5O in a Ne matrix with full radiation of a xenon or mercury high-pressure lamp resulted in a slow decrease of its IR bands, yielding mainly SF_4O and fluorine atoms, and as a minor channel $SF_4 + OF$ (see Figure 1). Hence, SF_5O is a weak UV absorber (for its Ne matrix UV spectrum, see the Supporting Information).

The SF_5OO radical: The existence of the SF_5OO radical was first postulated by Czarnowski and Schumacher[25,26] in the mechanism for formation of the trioxide $F_5SOOOSF_5$. The trioxide is accessible by photolysis of SF_5Cl in the presence of a large excess of oxygen at low temperatures. Feliz and Schumacher[27] suggested that the SF_5 radicals, the primary photolysis products together with chlorine atoms, rapidly add molecular oxygen. Schumacher and co-workers could not identify the SF_5OO radicals directly in their experiment. They argued that SF_5OO is unstable and the bimolecular self reaction yielding SF_5O and O_2 is very fast.

Indeed, in our experiments conducted in an oxygen matrix, SF_5 adds O_2. However, flash thermolysis of the trioxide SF_5OOOSF_5 in excess of noble gas yields $SF_5O + SF_5 + O_2$, although a mixture of SF_5O and SF_5OO is expected.

Table 2: Calculated [B3LYP/6-311++G(3df,3pd)] and observed IR band positions and relative intensities of the matrix-isolated radicals SF_5O and SF_5OOO.

SF_5O							SF_5OOO				
Ne		Ar	Calcd[a,b]				O_2		Calcd[a,b]		
$\tilde{\nu}$ [cm^{-1}]	Rel. int.	$\tilde{\nu}$ [cm^{-1}]	$\tilde{\nu}$ [cm^{-1}]	Rel. int.			$\tilde{\nu}$ [cm^{-1}]	Rel. int.	$\tilde{\nu}$ [cm^{-1}]	Rel. int.	
937.7	47	933	912	66	$\nu_1 A_1$		1513	18	1637	46	ν_1
915.6	30[d]	912	883	81	$\nu_8 B_1$		899	88	891	100	ν_2
905.9	100	899	877	100	$\nu_{12} B_2$		897	48	876	74	ν_3
			730	1.1	$\nu_2 A_1$		884	100	869	81	ν_4
			621	0.42	$\nu_3 A_1$		755	1.9	726	4.8	ν_5
			597	0.84	$\nu_4 A_1$				612	0.42	ν_6
609.0	1.0	604	587	4.4	$\nu_{13} B_2$		614	3.9	592	1.7	ν_7
602.3	12	601	587	7.9	$\nu_5 A_1$				585	3.2	ν_8
575.1	5.4	571	550	4.4	$\nu_9 B_1$		600	16	579	19	ν_9
			520	0.05	$\nu_{14} B_2$		592	1.6	558	2.8	ν_{10}

[a] A relative intensity of 100 corresponds to 407 km mol^{-1} for SF_5O and 499 km mol^{-1} for SF_5OOO. [b] Low-frequency modes of SF_5O in cm^{-1}, (rel. int.), assignment: 475 (inactive), $\nu_7 A_2$; 416 (0.74), $\nu_{10} B_1$; 350 (0.00), $\nu_{15} B_2$; 324 (0.00), $\nu_6 A_1$; 289 (0.09), $\nu_{11} B_1$. [c] Low-frequency modes of SF_5OOO in cm^{-1} (rel. int.): 518 (0.04), 477 (0.00), 458 (0.81), 346 (0.00), 328 (0.42), 320 (1.0), 193 (1.3), 67 (1.6), 63 (0.30), 44 (0.02), 22 (0.01). [d] Intensity affected by overlap with SF_4O bands.

The $F_5S–O_2$ bond in SF_5OO must be weaker than the O–O bonds in the trioxide. For the trioxide a bonding energy of 106 kJ mol^{-1} and for $SF_5–OO$ a dissociation energy of about 55 kJ mol^{-1} were estimated.[25,26] Our observations are in agreement with these data. DFT calculations [B3LYP/6-311++G(3df,3pd)] predict a dissociation energy of 19.1 kJ mol^{-1}, which represents a lower limit as the bond strengths of weak bonds are generally underestimated.

SF_5OO is expected to show C_s symmetry, like many other peroxy radicals. Hence, all 18 fundamentals (twelve A′ and six A″) should be observable in the IR spectrum. The typical feature in the IR spectrum of matrix-isolated SF_5OO is the

 © 2005 Wiley-VCH Verlag GmbH & Co. KGaA, Weinheim

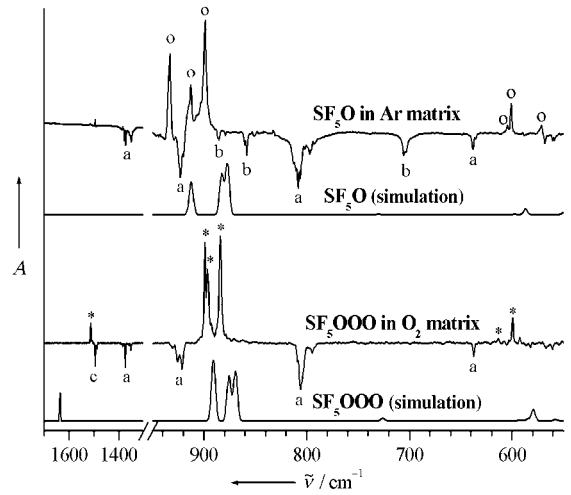


Figure 1. Upper half: IR spectrum of SF_5O radicals isolated in an Ar matrix; bands of the SF_5O radical are labeled with (o). The simulated spectrum of SF_5O is shown underneath. Lower half: IR spectrum of SF_5O radicals isolated in an O_2 matrix; bands of the product SF_5OOO are labeled with (*). The simulated spectrum of SF_5OOO is shown underneath. Both experimental IR spectra are difference spectra from spectra measured before and after photolysis. The photolysis products show negative bands while the absorptions of the photolyzed radicals are positive. The assigned absorptions of the photolysis products belong to SF_4O (a), SF_4 (b), and FOO (c).

presence of an absorption at 1135 cm^{-1}, which is assigned to the O–O stretching mode. The seven most intensive fundamentals were observed while the eleven missing modes have low intensities and/or are outside the experimental spectral range. Band positions and intensities are in good agreement with the calculated data (see Table 1).

The SF_5OOO radical: Trioxy radicals are formed when a highly electronegative oxy radical interacts with molecular oxygen. In analogy to CF_3OOO[28] the radical SF_5OOO is observed in an oxygen matrix. The IR-matrix spectrum of SF_5OOO has several dominant features that distinguish the trioxy radical from SF_5O (see Table 2 and Figure 1): 1) a strong band at 1513 cm^{-1}, assigned as ν(OO) of the terminal OO bond; 2) a strong red shift of the stretching modes of the SF_5O moiety; 3) significant differences in the intensities of the SF_5O fundamentals when recorded with O_2 or Ar as matrix materials; 4) the rapid UV photolysis of O_2-matrix-isolated SF_5OOO while SF_5O photolyzes one order of magnitude slower when isolated in Ne matrix. In oxygen matrix photolysis produces SF_4O and FOO.

The computations predict a structure with C_1 symmetry, close to C_s, and a SF_5O–OO bond length of 2.36 Å. Table 3 presents the (calculated) structural data and some properties of the SF_5O_x radicals, $x = 0$–3. The calculated structures are shown in the Supporting Information.

With the characterization of the SF_5O_x ($x = 0$–3) radicals, their existence is now proven. Nevertheless, their significance in atmospheric chemistry has to be considered. A summary of the important oxidation reactions in the atmosphere is shown in Figure 2. SF_6 photolysis is possible only in the upper stratosphere as the solar flux in the high-energy UV region is significant only above the ozone layer. The formed SF_5 radicals react with O_2 rather than degrade photochemically due to the high concentration of molecular oxygen in the atmosphere. The peroxy radical is probably in equilibrium with the SF_5 radical as the calculations and experiments predict only a weak F_5S–O bond. However, the peroxy radical can be reduced by reaction with NO, CO, or O_3 forming the oxy radical SF_5O. The oxy radical is expected to be photostable but, in equilibrium with the SF_5OOO radical, it will be photolyzed much faster. SF_5O is expected to oxidize atmospheric trace compounds like NO. Independent of the degradation process—thermal or photochemical—SF_5O is

Table 3: Calculated [B3LYP/6-311++G(3df,3pd)] structures, partial charges, and dipole moments of the SF_5O_x radicals ($x = 0$–3).[a]

	SF_5	SF_5O	SF_5OO	SF_5OOO
Symmetry	C_{4v}	C_{2v}	C_s	C_1
r(SF)[b]	1.623	1.585	1.585	1.591 (avg)
	1.554	1.591	1.588	1.585
		1.580	1.567	
r(SO)		1.612	1.805	1.605
r(OO)[c]			1.276	2.362
				1.192
α(FSF)[d]	91.8	87.6	90.8	87.4 (avg)
		92.0	90.8	91.1 (avg)
α(OSF)[e]		92.4	91.2	92.6 (avg)
		90.1	87.2	90.5 (avg)
α(OOS)			114.5	120.4
α(OOO)				107.4
τ			45.0	180.0
				180.0
q(S)	+1.20	+1.05	+1.17	+0.88
$q(F)_{eq,avg}$	−0.26	−0.18	−0.16	−0.17
$q(F)_{ax}$	−0.17	−0.26	−0.29	−0.25
q(O)[f]		−0.05	−0.10	−0.05
			−0.12	+0.08
				0.00
μ	0.28	0.05	0.63	1.56

[a] Bond lengths r are given in Å, bond angles α and dihedral angles τ in °, charges q in units of e, and dipole moments μ in Debye. [b] F_{eqs}, F_{ax}: last value. [c] SO–OO and OO–O. [d] $F_{ax}SF_{eq}$. [e] OSF_{eq}. [f] In order of $SF_5O^1O^2O^3$.

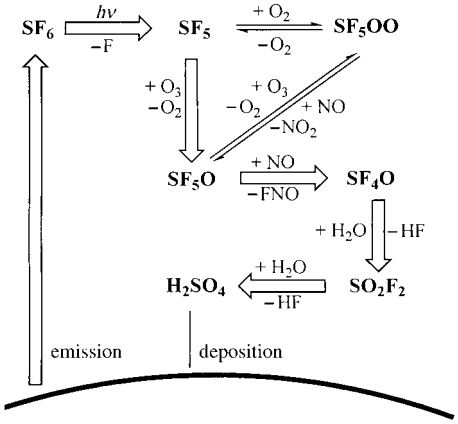


Figure 2. Reaction scheme for SF_5O_x species in the atmosphere.

 © 2005 Wiley-VCH Verlag GmbH & Co. KGaA, Weinheim

converted to SF_4O, which is thermally and photochemically stable. The latter compound undergoes hydrolysis to form SO_2F_2, which is even more stable. Because hydrolysis requires significant water concentration, a downward diffusion of SF_4O and/or SO_2F_2 from the stratosphere into more humid air should be observable. Finally, SO_2F_2 hydrolyzes very slowly (yields sulfuric acid and HF) which makes it suitable as a tracer for SF_6 or SF_5CF_3 degradation in the atmosphere.

Experimental Section

Precursors for the thermal radical generation: The compounds S_2F_{10}, $N(SF_5)_3$, and SF_5NO_2 were used as sources for SF_5 radicals. S_2F_{10}[29] and $N(SF_5)_3$[20] were prepared as described in the literature. SF_5NO_2 was provided by N. Lu (group J. S. Thrasher).[19] For SF_5O generation the compounds SF_5OOSF_5[25] and SF_5OOOSF_5[26] were used and prepared according to literature procedures.

Generation of the radicals in matrix: SF_5 or SF_5O radicals were generated by low-pressure flash thermolysis of the respective precursors diluted 1:1000 with Ne or Ar and subsequent quenching of the reaction products in a noble-gas matrix. The stable precursors S_2F_{10} and SF_5NO_2 were mixed with the excess noble gas in a 1-L stainless-steel storage container. The labile precursors $N(SF_5)_3$, SF_5OOSF_5, and SF_5OOOSF_5 were placed in a U-trap mounted directly in front of the matrix support and cooled to temperatures of −65 °C, −125 °C, −120 °C, respectively (maintaining the respective vapor pressures are in the 10^{-3}-mbar range). A flow of nobel gas passed the cooled samples achieving a mixing ratio of noble gas to host close to 1:1000. Finally, the gas mixture passed the thermolysis device that was mounted directly in front of the matrix support and heated to 400 °C for S_2F_{10}, 340 °C for SF_5NO_2, 400 °C for $N(SF_5)_3$, 420 °C for SF_5OOSF_5, and 200 °C for SF_5OOOSF_5. The matrix support (Cu block) was held under high vacuum, and the matrices were formed at 16 K (Ar) or 6 K (Ne). About 1 mmol of noble gas was used in a typical experiment and deposited within 10–20 min.

SF_5OO and SF_5OOO were generated by isolating SF_5 or SF_5O in O_2 matrix at 16 K. Photolysis experiments on the matrix-isolated species were carried out with UV light from a 150-W Xe (AMKO) or Hg high-pressure lamp (TQ 150, Heraeus) or from a Hg low-pressure lamp (TK 15, Heraeus)—in some cases in combination with a 235-nm cutoff filter (Schott). Details of the matrix apparatus are given elsewhere.[30]

IR spectra of the matrix-isolated species were recorded with a FT-IR spectrometer (IFS 66 v/S, Bruker) with a resolution of 1 cm^{-1} (Ar, O_2 matrix) or 0.25 cm^{-1} (Ne matrix) in reflection mode. A KBr (or a 6-μm Mylar/Ge for SF_5 far-IR) beamsplitter was used together with a DTGS detector, and 64 scans were co-added. UV spectra of Ne-matrix-isolated compounds were measured in reflection mode using a quartz fiber optic (Hellma) with a Lambda 900 spectrometer (Perkin Elmer). An integration time of 1 s per data point, a data point spacing of 1 nm, and a slit width of 0.5 nm were applied.

All calculations were performed using the Gaussian98 software package.[31] For accurate structures, energies, and vibrational frequencies the density functional[32] method B3LYP[33,34] and a 6-311++G(3df,3dp) basis set was used. Within the IR simulation procedure for each normal mode a Gaussian function was derived which is characterized by three parameters: calculated band position, calculated total (integrated) intensity as given in the G98 output file, and a half height width set to 4 cm^{-1}. Integrated intensity and absorption differ only by a constant factor for a Gaussian band profile.

Received: July 8, 2004

Keywords: atmospheric chemistry · matrix isolation · radicals · sulfur fluorides · vibrational spectroscopy

[1] V. N. Maller, M. S. Naidu, *High Voltage Insulation and Arc Interruption in SF_6 and Vacuum*, Pergamon, Oxford, **1981**.
[2] D. M. Manos, D. L. Flamm, *Plasma Etching: An Introduction*, Academic Press, Boston, **1989**.
[3] A. Picard, G. Turban, B. Grolleau, *J. Phys. D* **1986**, *19*, 991.
[4] R. Pinto, K. W. Ramonathan, R. S. Baba, *J. Electrochem. Soc.* **1987**, *134*, 165.
[5] K. R. Ryan, I. C. Plumb, *Plasma Chem. Plasma Process.* **1988**, *8*, 263.
[6] M. Maiss, C. A. M. Brenninkmeijer, *Environ. Sci. Technol.* **1998**, *32*, 3077.
[7] J. W. L. Goodwin, A. G. Salway, T. P. Murrels, C. J. Dove, H. S. Eggleston, *UK Emissions of Air Pollutants 1970–1997: A Report of the National Atmospheric Emissions Inventury*, AEA Technology, Harwell, **1999**.
[8] *Scientific Assessment of Ozone Depletion: 1998*, *Global Ozone Research and Monitoring Project*, *Rep. 44*, World Meteorological Organization, Geneva, **1999**.
[9] G. D. Griffin, C. E. Easterly, I. Sauers, H. W. Elles, L. G. Christopherous, *Toxicol. Environ. Chem.* **1984**, *9*, 139.
[10] F. Y. Chu, *IEEE Trans. Electr. Insul.* **1986**, *E1–21*, 693.
[11] A. Derodouri, J. Casanovas, R. Grob, J. Mathieu, *IEEE Trans. Electr. Insul.* **1989**, *24*, 1147.
[12] R. J. van Brunt, J. T. Herron, *IEEE Trans. Electr. Insul.* **1990**, *25*, 75.
[13] O. Toubert, J. Pelletiev, C. Fiori, T. A. N. Tan, *J. Appl. Phys.* **1990**, *67*, 4291.
[14] K. R. Ryan, I. C. Plumb, *Plasma Chem. Plasma Process.* **1990**, *10*, 207.
[15] W. T. Sturges, T. J. Wallington, M. D. Hurley, K. P. Shine, K. Sihra, A. Engel, D. E. Oram, S. A. Penkett, R. Mulvaney, C. A. M. Brenninkmeijer, *Science* **2000**, *289*, 611.
[16] R. R. Smardzewski, W. B. Fox, *J. Chem. Phys.* **1977**, *67*, 2309.
[17] P. Hassanzadeh, L. Andrews, *J. Phys. Chem.* **1992**, *96*, 79.
[18] H. L. Roberts, *J. Chem. Soc.* **1962**, 3183.
[19] N. Lu, J. S. Thrasher, S. von Ahsen, H. Willner, D. Hnyk, H. Oberhammer, D. Lentz, *224th ACS Fluorine Division National Meeting*, ACS Meeting Abstracts 224:044-FLUO Part 1, Boston, USA, **2002**.
[20] J. S. Thrasher, J. B. Nielsen, *J. Am. Chem. Soc.* **1986**, *108*, 1108.
[21] M. R. Choudhury, J. W. J. Harrell, J. B. Nielson, J. S. Thrasher, *J. Chem. Phys.* **1988**, *89*, 5353.
[22] S. Sander, H. Pernice, H. Willner, *Chem. Eur. J.* **2000**, *6*, 3645.
[23] M. K. W. Ko, N. D. Sze, J. M. Rodriguez, D. K. Weistenstein, C. W. Heisey, R. P. Wayne, P. Biggs, C. E. Canosa-Mas, H. W. Sidebottom, J. Treacy, *Geophys. Res. Lett.* **1994**, *21*, 101.
[24] C. I. Merrill, G. H. Cady, *J. Am. Chem. Soc.* **1961**, *83*, 298.
[25] J. Czarnowski, H. J. Schumacher, *J. Fluorine Chem.* **1978**, *12*, 497.
[26] J. Czarnowski, H. J. Schumacher, *Int. J. Chem. Kinet.* **1978**, *10*, 111.
[27] M. Feliz, H. J. Schumacher, *J. Photochem.* **1981**, *15*, 109.
[28] S. von Ahsen, H. Willner, J. S. Francisco, *Angew. Chem.* **2003**, *115*, 4838; *Angew. Chem. Int. Ed.* **2003**, *42*, 4690.
[29] G. Brauer, *Handbuch der präparativen Anorganischen Chemie*, 3rd ed., Ferdinand Enke, Stuttgart, **1975/1981**.
[30] H. Schnöckel, H. Willner in *Infrared and Raman Spectroscopy: Methods and Applications* (Ed.: B. Schrader), VCH, Weinheim, **1994**, p. 297.
[31] Gaussian 98 (Revision A.7), M. J. Frisch, G. W. Trucks, H. B. Schlegel, G. E. Scuseria, M. A. Robb, J. R. Cheeseman, V. G. Zakrzewski, J. A. Montgomery, R. E. Stratmann, J. C. Burant, S. Dapprich, J. M. Millam, A. D. Daniels, K. N. Kudin, M. C. Strain, O. Farkas, J. Tomasi, V. Barone, M. Cossi, R. Cammi, B. Mennucci, C. Pomelli, C. Adamo, S. Clifford, J. Ochterski, G. A. Petersson, P. Y. Ayala, Q. Cui, K. Morokuma, D. K. Malick, A. D. Rabuck, K. Raghavachari, J. B. Foresman, J. Cioslowski, J.

 © 2005 Wiley-VCH Verlag GmbH & Co. KGaA, Weinheim

V. Ortiz, B. B. Stefanov, G. Liu, A. Liashenko, P. Piskorz, I. Komaromi, R. Gomperts, R. L. Martin, D. J. Fox, T. Keith, M. A. Al-Laham, C. Y. Peng, A. Nanayakkara, C. Gonzalez, M. Challacombe, P. M. W. Gill, B. G. Johnson, W. Chen, M. W. Wong, J. L. Andres, M. Head-Gordon, E. S. Replogle, J. A. Pople, Gaussian, Inc., Pittsburgh, PA, **1998**.
[32] W. Kohn, L. J. Sham, *Phys. Rev.* **1965**, *140*, 1133.
[33] A. D. Becke, *Phys. Rev. A* **1988**, *38*, 3098.
[34] A. D. Becke, *J. Chem. Phys.* **1993**, *98*, 5648.

 © 2005 Wiley-VCH Verlag GmbH & Co. KGaA, Weinheim

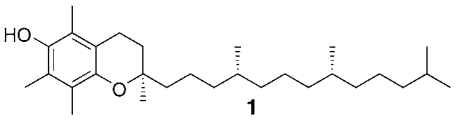
Domino Reactions

Palladium-Catalyzed Enantioselective Domino Reaction for the Efficient Synthesis of Vitamin E**

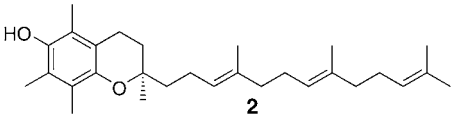
Lutz F. Tietze, Konrad M. Sommer, Julia Zinngrebe, and Florian Stecker*

Dedicated to Professor Hiriyakkanavar Ila on the occasion of her 60th birthday

Vitamin E is one of the fat-soluble vitamins and a collective term for all tocopherols and tocotrienols. The vitamin E family consists of eight natural compounds which, depending upon the degree of methylation of their aromatic ring, are specified as α, β, γ and δ. All possess a chroman framework with a stereogenic center at C2 with *R* configuration (examples: α-tocopherol: **1**, α-tocotrienol: **2**).[1] Natural α-tocopherol (**1**) with the *R* configuration at all stereogenic centers has the most pronounced biological activity. Vitamin E acts as an antioxidant and is considered an essential protective factor against lipid peroxidation; in particular, it protects polyunsaturated fatty acids essential for animal and human metabolism by capturing highly reactive free radicals formed in the body as by-products of normal oxidative metabolism and which cause irreversible destruction of cell membranes.[2]



1

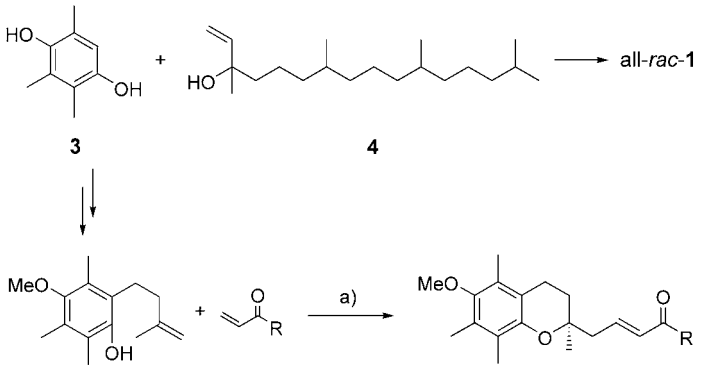


2

Industrially α-tocopherol (**1**) is produced on a large scale by the acid-catalyzed reaction of trimethylhydroquinone (**3**) with all-*rac*-isophytol (**4**; see Scheme 1), whereby a mixture of eight stereoisomers is formed. However, in this reaction compounds with an *S* configuration in the chroman framework and thus of far lower antioxidant action are also formed.[3] Thus, from the point of view of industry there is considerable interest in the development of a process for the efficient enantioselective construction of α-tocopherol (**1**); this applies especially to the stereoselective formation of the stereogenic center on the chroman ring, if possible with the concomitant introduction of the side chain.

There are already a number of enantioselective synthetic methods for **1**, which are not suitable, however, for industrial use.[4] Here we describe a new enantioselective palladium-catalyzed method[5] which allows not only the formation of the chiral chroman framework[6] with an enantioselectivity of 96% *ee* but also the simultaneous introduction of part of the side chain of vitamin E within the context of a domino reaction.[7]. This sequence comprises an enantioselective Wacker oxidation[8] and a subsequent Heck reaction (Scheme 1).[9]

The substrate for the domino reaction, alkene **5**, was obtained in an overall yield of 60% from trimethylhydroquinone (**3**) in a few steps by acid-catalyzed condensation with methyl vinyl ketone and reaction with the Lombardo reagent.[10] The reaction of **5** with methyl acrylate in dichloro-



Scheme 1. Top: Industrial production of racemic α-tocopherol (**1**) by the reaction of trimethylhydroquinone (**3**) with all-*rac*-isophytol (**4**). Bottom: Domino reaction for the preparation of **7** with BOXAX ligands **6a–c**. Bn = Benzyl.

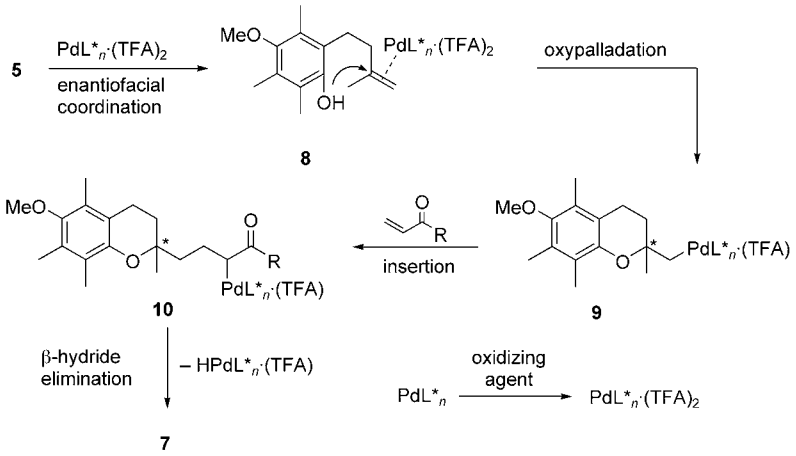
[*] Prof. Dr. L. F. Tietze, Dr. K. M. Sommer, Dipl.-Chem. J. Zinngrebe, Dipl.-Chem. F. Stecker
Institut für Organische und Biomolekulare Chemie
Georg-August-Universität Göttingen
Tammannstrasse 2, 37077 Göttingen (Germany)
Fax: (+49) 551-39-9476
E-mail: ltietze@gwdg.de

[**] This research was supported by the Deutsche Forschungsgemeinschaft (SFB 416) and the Fonds der Chemischen Industrie. We thank Roche Vitamins (now DSM Vitamins) for reference samples and Symrise for (*R*)-citronellol.

 DOI: 10.1002/anie.200461629 © 2005 Wiley-VCH Verlag GmbH & Co. KGaA, Weinheim

methane in the presence of catalytic amounts of $Pd(TFA)_2$ (TFA = trifluoroacetate), the chiral ligand (*S*,*S*)-*i*Pr-BOXAX **6a**,[11] and *p*-benzoquinone afforded the desired chroman **7a** with 96% *ee* in 84% yield;[12] comparably good selectivities were obtained with (*S*,*S*)-Bn-BOXAX (**6b**). The selectivity was significantly lower with the use of **6c** as ligand which was obtained from (*L*)-*t*leucine; similar effects have already been observed in other catalytic processes.[13] The domino reaction was also carried out with methyl vinyl ketone to provide **7b**; however, in this case the yield and the selectivity (84% *ee*) were lower. The reaction with simple alkenes such as 3-methyl-1-pentene failed to yield the desired product.

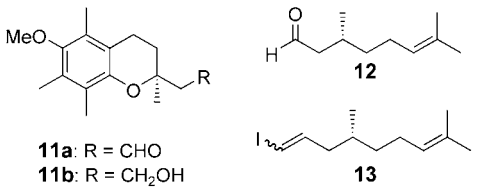
We assume that in the first step of the domino reaction **5** coordinates enantiofacially through its double bond to the chiral catalyst generated from $Pd(TFA)_2$ and the enantiomerically pure **6**. The resulting intermediate **8** reacts further by oxypalladation to give **9** with formation of the chroman framework and construction of the stereogenic center (Scheme 2). The palladium species can then form the intermediate **10** in a subsequent Heck reaction with acrylate or methyl vinyl ketone, which leads to the final product **7** and Pd^0 in a β-hydride elimination. It is necessary for the catalytic



Scheme 2. Mechanism of the palladium-catalyzed domino reaction of **5**.

cycle that Pd^0 is reoxidized to Pd^{2+}; this is achieved by the addition of *p*-benzoquinone, which does not interfere with the course of the reaction.

Numerous possibilities are plausible for the further conversion of **7a** or **7b** to α-tocopherol (**1**). Thus the unsaturated ester **7a** was converted into the respective diol by dihydroxylation[14] with AD-mix-β. Subsequent oxidative cleavage with sodium periodate afforded aldehyde **11a**, which can be converted into α-tocopherol (**1**) in a few steps by known methods.[15] Direct cleavage of **7a** by ozonolysis to give



11a was not successful. We reduced aldehyde **11a** to alcohol **11b** so that the absolute configuration of the stereogenic center in **7a** could be determined by comparison of the data with known values.[16] Alternatively we prepared vitamin E from ketone **7b** by reaction with the vinyl iodide **13** readily obtained from (*R*)-citronellal (**12**) followed by subsequent dehydration and hydrogenation.

The enantioselective domino reaction described here facilitates the efficient and stereoselective construction of the chroman framework of vitamin E with concomitant introduction of part of the side chain in high yield with very good *ee* values.

Received: August 12, 2004
Published Online: November 26, 2004

Keywords: asymmetric catalysis · domino reactions · Heck reactions · palladium · vitamins · Wacker oxidation

[1] a) T. Netscher, *Chimia* **1996**, *50*, 563–567; b) M. K. Horwitt, *Am. J. Clin. Nutr.* **1986**, *44*, 973–985; c) H. M. Evans, K. S. Bishop, *Science* **1922**, *56*, 650–651.

[2] a) G. T. Vatessary, W. E. Smith, H. T. Quach, *Lipids* **1989**, *24*, 1043–1047; b) H. N. Jacobson, *Free Radical Biol. Med.* **1987**, *3*, 209–213; c) G. W. Burton, A. Joyce, K. U. Ingold, *Arch. Biochem. Biophys.* **1983**, *221*, 281–290; d) G. W. Burton, A. Joyce, K. U. Ingold, *Lancet* **1982**, *2*, 327–328; e) J. E. Packer, T. F. Slater, R. L. Willson, *Nature* **1979**, *278*, 737–738; f) E. J. Simon, C. S. Gross, A. T. Milhorat, *J. Biol. Chem.* **1956**, *221*, 797–805.

[3] a) J. Kreimayer, M. Schmidt, *Pharm. Ztg.* **1998**, *143*, 823–828; b) R. V. Acuff, R. G. Dunworth, L. W. Webb, J. R. Lane, *Am. J. Clin. Nutr.* **1998**, *67*, 459–464; c) C. Kiyose, R. Maramatsu, Y. Kameyama, T. Ueda, O. Igarashi, *Am. J. Clin. Nutr.* **1997**, *65*, 785–789; d) *Ullmans Encyclopedia of Industrial Chemistry*, *vol A27*, VCH, Weinheim, **1996**, p. 478–488; e) K. U. Ingold, G. W. Burton, D. O. Foster, L. Hughes, D. A. Lindsay, A. Webb, *Lipids* **1987**, *22*, 163–172; f) S. C. Cheng, G. W. Burton, K. U. Ingold, D. O. Foster, *Lipids* **1987**, *22*, 469–473; g) G. Leibold, *Vitamin E*, ECON Taschenbuchverlag, **1986**.

[4] a) B. M. Trost, N. Asakawa, *Synthesis* **1999**, 1491–1494; b) L. F. Tietze, J. Görlitzer, A. Schuffenhauer, M. Hübner, *Eur. J. Org. Chem.* **1999**, 1075–1084; c) B. M. Trost, D. F. Toste, *J. Am. Chem. Soc.* **1998**, *120*, 9074–9075; d) J. A. Hyatt, C. Skelton, *Tetrahedron: Asymmetry* **1997**, *8*, 523–526; e) L. F. Tietze, J. Görlitzer, *Synlett* **1996**, *11*, 1041–1042; f) E. Mizuguchi, T. Suzuki, K. Achiwa, *Synlett* **1994**, 929–930; g) K. Takabe, K. Okisaka, Y. Uchiyama, T. Katagiri, H. Joda, *Chem. Lett.* **1985**, 561–562; h) H. Mayer, P. Schudel, R. Rüegg, O. Isler, *Helv. Chim. Acta* **1963**, *46*, 650–671.

[5] L. F. Tietze, H. Ila, H. P. Bell, *Chem. Rev.* **2004**, *104*, 3453–3516.

[6] Y. Uozumi, K. Kato, T. Hayashi, *J. Am. Chem. Soc.* **1997**, *119*, 5063–5064.

[7] a) L. F. Tietze, A. Modi, *Med. Res. Rev.* **2000**, *20*, 304–322; b) L. F. Tietze, F. Haunert in *Stimulating Concepts in Chemistry* (Eds.: F. Vögtle, J. F. Stoddart, M. Shibasaki), Wiley-VCH, Weinheim, **2000**, p. 39–64; c) L. F. Tietze, M. Lieb, *Curr. Opin. Chem. Biol.* **1998**, *2*, 363–371; d) L. F. Tietze, *Chem. Rev.* **1996**, *96*, 115–136; e) L. F. Tietze, U. Beifuss, *Angew. Chem.* **1993**, *105*, 137–170; *Angew. Chem. Int. Ed. Engl.* **1993**, *32*, 131–163; f) M. F. Semmelhack, W. R. Epa, *Tetrahedron Lett.* **1993**, *34*, 7205–7208.

[8] a) R. M. Trend, Y. K. Ramtohul, E. M. Ferreira, B. M. Stoltz, *Angew. Chem.* **2003**, *115*, 2998–3001; *Angew. Chem. Int. Ed.*

 © 2005 Wiley-VCH Verlag GmbH & Co. KGaA, Weinheim

2003, *42*, 2892 – 2895; b) M. A. Arai, M. Kuraishi, T. Arai, H. Sasai, *J. Am. Chem. Soc.* **2001**, *123*, 2907 – 2908.

[9] a) A. B. Dounay, L. E. Overman, *Chem. Rev.* **2003**, *103*, 2945 – 2963; b) I. P. Beletskaya, A. V. Cheprakov, *Chem. Rev.* **2000**, *100*, 3009 – 3066; c) A. de Meijere, E. F. Meyer in *Metal-Catalyzed Cross-Coupling Reactions* (Eds.: F. Diederich, P. J. Stang), Wiley-VCH, Weinheim, **1998**; d) M. Beller, T. H. Riermeir, G. Stark in *Transition Metals for Organic Synthesis* (Eds.: M. Beller, C. Bolm), Wiley-VCH, Weinheim, **1998**.

[10] L. Lombardo, *Tetrahedron Lett.* **1982**, *23*, 4293 – 4296.

[11] a) H. Hocke, Y. Uozumi, *Synlett* **2002**, 2049 – 2053; b) T. Furutani, M. Hatsuda, R. Imashiro, M. Seki, *Tetrahedron: Asymmetry* **1999**, *10*, 4763 – 4768; c) F. Dubois, M. Gingras, *Tetrahedron Lett.* **1998**, *39*, 5039 – 5040; d) M. B. Andrus, D. Asgari, J. A. Sclafani, *J. Org. Chem.* **1997**, *62*, 9365 – 9368; e) Y. Uozumi, H. Kyota, E. Kishi, K. Kitayama, T. Hayashi, *Tetrahedron: Asymmetry* **1996**, *7*, 1603 – 1606; f) T. D. Nelson, A. I. Meyers, *J. Org. Chem.* **1994**, *59*, 2655 – 2658; g) J. I. Kim, G. B. Schuster, *J. Am. Chem. Soc.* **1992**, *114*, 9309 – 9317; h) A. Miyashita, H. Takaya, T. Souchi, R. Noyori, *Tetrahedron* **1984**, *40*, 1245 – 1253.

[12] A mixture of palladium trifluoroacetate (7.1 mg, 0.0214 mmol, 0.1 equiv) and (*S*,*S*)-*i*Pr-BOXAX **6a** (40.7 mg, 0.0856 mmol, 0.4 equiv) in CH_2Cl_2 (0.1 mL, degassed) was stirred for 30 min at room temperature, then treated with *p*-benzoquinone (93.1 mg, 0.855 mmol, 4.0 equiv), and stirred for a further 10 min. A solution of **5** (50 mg, 0.214 mmol, 1.0 equiv) and methyl acrylate (91.9 mg, 1.07 mmol, 5.0 equiv) in CH_2Cl_2 (0.20 mL, degassed) was added to the suspension, and the mixture was stirred at room temperature for 3.5 d (TLC control). At the end of the reaction the mixture was treated with 1N HCl (5 mL) and the aqueous phase extracted with Et_2O (3 × 5 mL). The combined organic phases were washed with 1N NaOH solution (3 × 5 mL) and dried over $MgSO_4$, and the solvent was removed under reduced pressure. The crude product was purified by column chromatography (*n*-pentane/diethyl ether). Chroman **7a** (57 mg, 0.181 mmol, 84 %) was obtained as a clear oil. The enantiomeric excess was determined by HPLC on a chiral phase (OD-Chiracel, hexane/isopropanol) and gave a value of 96 % *ee*. The absolute configuration was determined by conversion into the alcohol **11b** and comparison of the optical rotation with known literature values.[16] ^{1}H NMR (300 MHz, $CDCl_3$): $\delta = 1.23$ (s, 3H, 2′-CH_3), 1.77 (dd, 1H, $J = 7.1$, 14.2 Hz, 3′-H_a), 1.85 (dd, 1H, $J = 7.1$, 14.1 Hz, 3′-H_b), 2.09, 2.14, 2.19 (3 × s, 9H, 5′-CH_3, 7′-CH_3, 8′-CH_3), 2.45 (ddd, 1H, $J = 1.2$, 8.2, 14.1 Hz, 4-H_a), 2.53 (ddd, 1H, $J = 1.2$, 8.2, 14.1 Hz, 4-H_b), 2.60 (t, 2H, $J = 7.1$ Hz, 4′-H_2), 3.63 (s, 3H, 6′-OCH_3), 3.74 (s, 3H, 1-OCH_3), 5.88 (dt, 1H, $J = 1.2$, 15.9 Hz, 2-H), 7.05 ppm (dt, 1H, $J = 7.8$, 15.9 Hz, 3-H); ^{13}C-NMR (50.3 MHz, $CDCl_3$): $\delta = 11.66$, 11.76, 12.52 (5′-CH_3, 7′-CH_3, 8′-CH_3), 20.43 (C4′), 24.38 (2′-CH_3), 31.20 (C4), 42.31 (C3′), 51.44 (1′-OCH_3), 60.36 (6′-OCH_3), 74.22 (C2′), 117.1 (C4a′), 123.1 (C8′), 123.8 (C2), 125.8 (C7′), 128.1 (C5′), 144.7 (C3), 147.1 (C8a′), 149.7 (C6′), 166.7 ppm (C1); $[\alpha]_D^{20} = +15.4$ ($c = 0.52$, $CHCl_3$); IR (KBr): $\tilde{\nu} = 2977$ cm^{-1} (CH), 2936, 1725 (C=O); UV (CH_3CN): λ_{max} (lgε): 202.5 nm (5.609), 287.0 (1.558); MS (70 eV, EI): *m*/*z* (%) = 179 (30), 219 (60), 318 (100) $[M]^+$. $C_{19}H_{26}O_4$ (318.41): calcd: 318.1831; found: 318.1831 (HRMS).

[13] L. F. Tietze, J. K. Lohmann, *Synlett* **2002**, 2083 – 2085.

[14] H. C. Kolb, M. S. VanNieuwenhze, K. B. Sharpless, *Chem. Rev.* **1994**, *94*, 2483 – 2547.

[15] a) N. Cohen, C. G. Scott, C. Neukom, R. J. Lopresti, G. Weber, G. Saucy, *Helv. Chim. Acta* **1981**, *64*, 1158 – 1173; b) N. Cohen, W. F. Eichel, R. J. Lopresti, C. Neukom, G. Saucy, *J. Org. Chem.* **1976**, *41*, 3505 – 3511.

[16] (*S*)-(−)-6-benzyloxy-2,5,7,8-tetramethylchroman-2-ethanol: S. Takano, Y. Shimazaki, Y. Iwabuchi, K. Ogasawara, *Tetrahedron Lett.* **1990**, *31*, 3619 – 3622: $[\alpha]_D^{20} = -15.99$ ($c = 1.15$, $CHCl_3$).

 © 2005 Wiley-VCH Verlag GmbH & Co. KGaA, Weinheim

Cluster Synthesis

Formation of Ir–Rh and Ir–Mo Bonds by Using an Ancillary *ortho*-Carborane-1,2-diselenolato Ligand**

Guo-Xin Jin, Jian-Qiang Wang, Chen Zhang, Lin-Hong Weng, and Max Herberhold*

Since the discovery of 1,2-dicarba-*closo*-dodecaborane(12), the chemistry of this exceptionally stable carborane and its 1,7- and 1,12-isomers has aroused considerable interest.[1] 1,2-Dicarba-*closo*-dodecaborane-1,2-dichalcogenolates (*ortho*-carborane dichalcogenolates) can be used as the voluminous and chemically robust chelate ligands to form half-sandwich complexes of the type $[Cp^*M\{E_2C_2(B_{10}H_{10})\}]$ ($Cp^* = \eta^5$-C_5Me_5, M = Co, Rh, Ir; E = S, Se).[2] These sterically congested, mononuclear coordination compounds can be stored conveniently and used for further transformations in a controlled way under various conditions. In particular, addition reactions at the metal atom have been accomplished,[3] and formation of a metal-to-boron bond and/or substitution of the carborane cage in the positions B(3)/B(6) have been achieved.[4] Another attractive possibility, the formation of heteronuclear metal–metal bonds through bridge support by an ancillary *o*-carboranyl dichalcogenolato ligand has not been explored so far, to our knowledge.

We have previously described the 16-electron "pseudo-aromatic" iridium complex $[Cp^*Ir\{Se_2C_2(B_{10}H_{10})\}]$ (**1**),[5] and suggested that this species may undergo further transformations owing to its electron deficiency at the iridium center. In exploring the reactivity of the 16-electron iridacycle **1** towards various transition-metal complexes, we discovered the formation of heterometallic clusters in which carborane 1-2-diselenolates act as bridging chelate ligands. We report here the first trinuclear cluster complexes, which have been obtained from the half-sandwich iridium complex **1** by reactions with $[\{RhCl(cod)_2\}]$ and $[Mo(CO)_3(py)_3]$. The products, *cis*-$[\{Cp^*Ir[Se_2C_2(B_{10}H_{10})]\}_2Rh]$ (**2**), *trans*-$[\{Cp^*Ir[Se_2C_2(B_{10}H_9)]\}Rh\{[Se_2C_2(B_{10}H_{10})]IrCp^*\}]$ (**3**), and $[\{Cp^*Ir[Se_2C_2(B_{10}H_{10})]\}_2Mo(CO)_2]$ (**4**), were characterized by X-ray crystallography.

[*] Prof. Dr. G.-X. Jin, Dr. J.-Q. Wang, C. Zhang, Prof. Dr. L.-H. Weng
Laboratory of Molecular Catalysis and Innovative Material
Department of Chemistry
Fudan University
Shanghai 200433 (P.R. China)
Fax: (+86) 21-6564-3776
E-mail: gxjin@fudan.edu.cn
Prof. Dr. M. Herberhold
Anorganische Chemie II
Universitat Bayreuth
95440 Bayreuth (Germany)

[**] This work was supported by the National Science Foundation of China for Distinguished Young Scholars (29925101, 20274008) and by the Key Project of Science and Technology of the Education Ministry of China.

 DOI: 10.1002/anie.200461348 © 2005 Wiley-VCH Verlag GmbH & Co. KGaA, Weinheim

The 16-electron complex **1**, which was synthesized from $[\{Cp^*IrCl_2\}_2]$ and dilithium carborane 1,2-diselenolate,[5] reacts with $[\{Rh(cod)Cl\}_2]$ (cod = cycloocta-1,5-diene) in THF to give the dark red trinuclear complex **2** together with a violet trinuclear derivative **3** (Scheme 1). Complex **3** can be obtained in higher yield when longer reaction times are applied. In refluxing toluene solution, the *cisoid* complex **2** is converted in more than 90% yield to the *transoid* complex **3** which contains a boron–iridium bond. Both **2** and **3** are diamagnetic. In **2**, the iridium atoms have been reduced from Ir^{III} to Ir^{II}, apparently by $[\{Rh^{I}(cod)Cl\}_2]$. In **3**, one of the two *ortho*-carborane groups is drawn sufficiently close to the iridium center to initiate B–H activation, affording the corresponding cyclometalated ligand species. This kind of metal-induced B–H activation has also been observed in other cases.[4,6] The first indication of cyclometalation in **3** is the appearance of a singlet in the ^{11}B NMR spectrum at $\delta = -19$ ppm, which is characteristic of metal-bonded boron atoms.[7] The Ir–B bond formation causes the molecule to become unsymmetrical, as confirmed by two singlets at $\delta = 2.17$, 2.21 ppm in the ^{1}H NMR spectrum of **3**. The NMR data are consistent with the results of an X-ray structure analysis of **3**, which proves beyond doubt the existence of the Ir–B and of the two nonequivalent Ir–Rh bonds.

The molecular structures of **2** and **3** are shown in Figure 1.[8] In the molecule **2** the four selenium atoms of the two *ortho*-carborane diselenolato ligands surround the central rhodium atom in a distorted tetrahedral arrangement; the two Se-Rh-Se planes are twisted by 63.1° with respect to one other. The two Cp* rings and the two carborane 1,2-diselenolato ligands are in *cisoid* arrangements. The diselenairidacycles in **2** are nonplanar as a result of the coordination of the Se atoms to rhodium. The Ir–Rh distances in **2** (2.7097(11), 2.6630(11) Å) may therefore be compared with the corresponding distances in the *trans*-trinuclear complex **3** (2.663(3) Å), in $[RhIr(CO)_3(dppm)_2]$ (2.7722(7) Å),[9] $[RhIr(CH_3)(CO)_3(dppm)_2](CF_3SO_3)$ (2.743(1) Å),[10] and in $[(Cp^*IrS)_2Rh(cod)][RhCl_2(cod)]$ (2.906(1) and 2.913(9) Å).[11] The Ir–Se distances (2.4280(12)–2.4637(13 Å) in **2** are in the normal range of Ir–Se single bonds, but significantly longer than those in the "pseudo-aromatic" $IrSe_2C_2$ ring in **1** (2.3753(9) and 2.3656(9) Å).[5]

In complex **3** the iridium atoms of the Ir_2Rh backbone have retained their Cp* rings in a *transoid* arrangement (Figure 1b). The Rh center is six-coordinate with a distorted

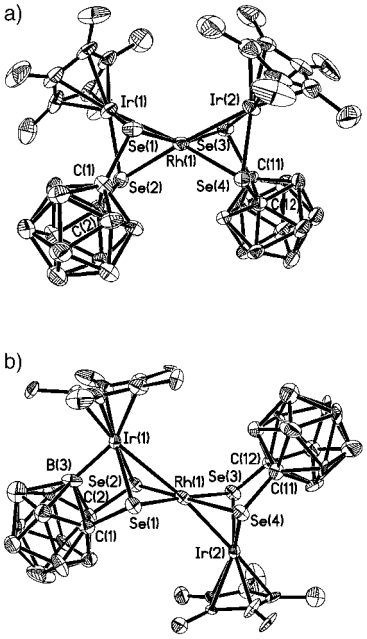
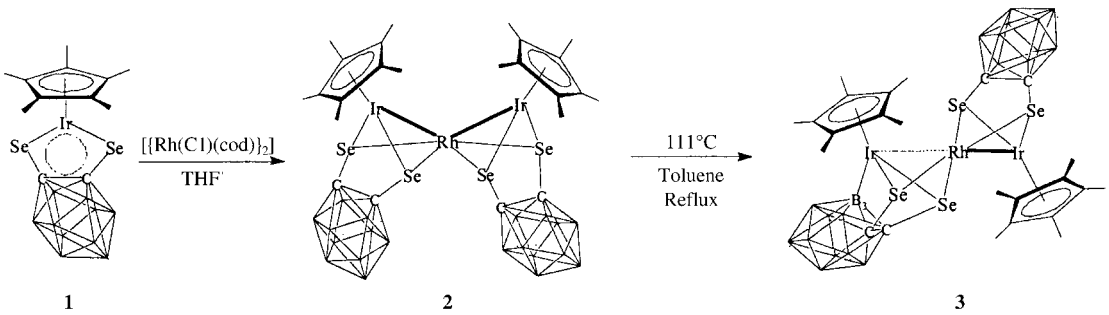


Figure 1. Molecular structures of **2** and **3**. Selected bond lengths [Å] and angles [°]: a) **2**: Ir(1)-Rh(1) 2.7097(11), Ir(2)-Rh(1) 2.6630(11), Ir(1)-Se(1) 2.4637(13), Ir(1)-Se(2) 2.4556(13), Rh(1)-Se(1) 2.4605(16), Rh(1)-Se(2) 2.5616(15), Rh(1)-Se(3) 2.4505(16), Rh(1)-Se(4) 2.4821(15), Se(1)-C(1) 1.987(10), C(1)-C(2) 1.613(14); Ir(1)-Rh(1)-Ir(2) 128.83(4), Se(1)-Ir(1)-Se(2) 82.43(4), Se(1)-Ir(1)-Rh(1) 56.56(4), Se(1)-Rh(1)-Se(2) 80.37(5), Se(1)-Rh(1)-Se(3) 157.40(5), Se(1)-Rh(1)-Se(4) 108.13(5), Se(1)-Rh(1)-Ir(1) 56.67(3); b) **3**: Ir(1)-Rh(1) 3.074(3), Ir(2)-Rh(1) 2.663(3), Ir(1)-Se(1) 2.539(3), Ir(1)-Se(2) 2.562(3), Ir(1)-B(3) 2.02(4), Ir(2)-Se(3) 2.415(3), Ir(2)-Se(4) 2.395(3), Rh(1)-Se(1) 2.335(4), Rh(1)-Se(2) 2.355(4), Rh(1)-Se(3) 2.477(4), Rh(1)-Se(4) 2.481(4), C(1)-C(2) 1.66(4), C(11)-C(12) 1.68(4); Ir(1)-Rh(1)-Ir(2) 172.95(10), B(3)-Ir(1)-Se(1) 71.4(11), B(3)-Ir(1)-Se(2) 72.6(9), B(3)-Ir(1)-Rh(1) 97.4(11), Se(1)-Ir(1)-Se(2) 78.10(10), Se(1)-Rh(1)-Se(2) 86.52(13), Se(1)-Rh(1)-Se(4) 96.03(13), Se(1)-Rh(1)-Se(3) 176.85(15), Se(3)-Rh(1)-Se(4) 81.39(13), Se(3)-Ir(2)-Se(4) 84.46(11).

trigonal-prismatic geometry. The central Rh atom and the four Se atoms form a plane (deviations 0.015 Å). The Ir(1) atom adopts a three-legged piano-stool configuration with two Se and one B atom, and owing to the cyclometalation of the diselenolato ligand at Ir(1) it participates in two four-membered metallacyclic rings, the dihedral angle between the planes (Ir(1)-B(3)-C(2)-Se(2) and Ir(1)-B(3)-C(1)-Se(1)) of which is 100°. Owing to the formation of the Ir(1)–B(3) bond



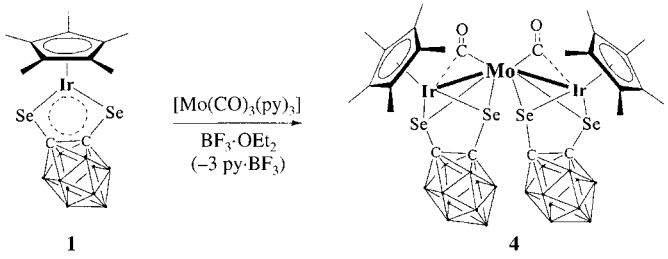
1 2 3

Scheme 1. Synthesis of **2** and **3**.

 © 2005 Wiley-VCH Verlag GmbH & Co. KGaA, Weinheim

(2.02(4) Å), the dihedral angle at the Se(1)···Se(2) vector in the Ir(1)Se_2C_2 ring is 78.4°, in contrast to the angle of 123.8° at the Se(3)···Se(4) vector in the Ir(2)Se_2C_2 ring. The Ir(1)–Rh(1) bond (3.074(3) Å) is longer than the Ir(2)–Rh(1) bond(2.663(3) Å), which can be rationalized by the fact that the formal oxidation ("valence") state is +3 for Ir(1) and +2 for Ir(2).

Complex **1** reacts with $[Mo(CO)_3(py)_3]$ (py = pyridine) in the presence of more than three equivalents of BF_3 in diethyl ether to give the red, mixed-metal complex **4**. The combination of $[Mo(CO)_3(py)_3]$ and BF_3 can be used as an effective way to generate a reactive $[Mo(CO)_3]$ fragment.[12] Complex **4** comprises two diselenairidacycles bridged by a molybdenum dicarbonyl unit; consistent with this, two strong bridging carbonyl absorptions are observed in the IR spectrum of **4** at 1859 and 1794 cm^{-1}.



1 **4**

The iridium atoms of the Ir_2Mo backbone in **4** have retained their Cp* rings (Figure 2). The Mo center is eight-coordinate with a dodecahedral geometry; the two Se-Mo-Se planes are twisted by 36.8° with respect to one another. The two Ir–Mo single bonds (2.7820(19), 2.8189(17 Å) are each supported by a symmetrically bridging *ortho*-carborane-1,2-diselenolato ligand. The Ir–Se bond lengths (2.4827(16), 2.4458(18)) are close to those in the complexes **2** and **3**, with an Ir(1)-Mo(1)-Ir(2) angle of 144.46(4)°. The planar pseudo-aromatic system of the iridadiselenolene heterocycle **1** is no longer present in **4**; the dihedral angles at the Se···Se vector in the $IrSe_2C_2$ rings are 134.8° and 135.9°, respectively.

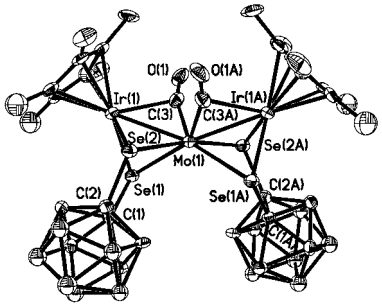


Figure 2. Molecular structure of **4**. Selected bond lengths [Å] and angles [°]: Ir(1)-Mo(1) 2.7820(19), Ir(2)-Mo(1) 2.8189(17), Ir(1)-Se(1) 2.4827(16), Ir(1)-Se(2) 2.4458(18), Ir(1)-C(3) 2.557(12), Mo(1)-Se(1) 2.687(2), Mo(1)-Se(2), 2.5972(18), Mo(1)-Se(3) 2.6520(19), Mo(1)-Se(4) 2.6519(18), Mo(1)-C(3) 1.978(11), C(1)-C(2) 1.611(15); Ir(1)-Mo(1)-Ir(2) 144.46(4), Se(1)-Ir(1)-Se(2) 82.63(5), Se(1)-Ir(1)-Mo(1) 61.06(5), Se(2)-Ir(1)-Mo(1) 59.16(4), Se(1)-Mo(1)-Se(2) 76.00(5), Se(1)-Mo(1)-Se(3) 105.39(5), Se(1)-Mo(1)-C(3) 79.2(3), Ir(1)-Se(1)-Mo(1) 64.98(5), Ir(1)-Se(2)-Mo(1) 66.88(6), Mo(1)-C(3)-Ir(1) 74.5(4).

The formation of heteronuclear metal–metal bonds in complexes **2**–**4** by reactions of the 16-electron complex **1** involves redox processes, during which Ir is partially reduced by low-valent transition-metal complexes, such as the fragments [RhCl(cod)] and $[Mo(CO)_3]$. The synthesis of the Ir_2M (M = Rh, Mo) clusters **2**–**4** demonstrates that complex **1** can serve as a useful building block for heteronuclear complexes.

Experimental Section

All manipulations were carried out under an argon atmosphere by using standard Schlenk techniques; all solvents were dried and deoxygenated before use.

Preparation of **2** and **3**: $[\{Rh(cod)Cl\}_2]$ (49 mg, 0.1 mmol) was added to the green solution of **1** (251 mg, 0.4 mmol) in THF (30 mL). The mixture was stirred for three days; the color changed first to black and then gradually to deep red. After removal of the solvent, the residue was chromatographed on silica gel. Elution with toluene/hexane (2:1) gave **3** as a violet zone, yield 32% (86 mg). Recrystallization from toluene/hexane afforded air-stable dark red crystals. Elemental analysis calcd (%) for $C_{24}H_{49}B_{20}Se_4Ir_2Rh$: C 21.24, H 3.64; found: C 21.11, H 3.62; ^1H NMR (500 MHz, $CDCl_3$, 25 °C, TMS): δ = 2.17(s, 15H; C_5Me_5), 2.21 ppm (s, 15H; C_5Me_5); ^{11}B NMR (160 MHz; $CDCl_3$, 25 °C): δ = −2.23, −5.05, −6.27, −8.32, −10.43, −11,72, −13.50, −14.68, −19.15 ppm (Ir–B); IR (KBr disk): $\tilde{\nu}$ = 2583 cm^{-1}(ν_{B-H}). The second red zone was eluted with CH_2Cl_2/hexane (1:4), yield 38% (103 mg). Recrystallization from benzene/hexane afforded air-stable red crystals of **2**. Elemental analysis calcd (%) for $C_{24}H_{50}B_{20}Se_4Ir_2Rh$: C 21.23, H 3.71; found: C 21.08, H, 3.68; ^1H NMR (500 MHz, $CDCl_3$, 25 °C, TMS): δ = 2.06 (s, 30H; C_5Me_5); ^{11}B NMR (160 MHz; $CDCl_3$, 25 °C): δ = −4.42, −6.51, −8.32, −10.95 ppm; IR (KBr disk): $\tilde{\nu}$ = 2569 cm^{-1}(ν_{B-H}).

Preparation of **4**: $BF_3{\cdot}OEt_2$ (0.26 mL, 47%, 1.0 mmol) was added dropwise at room temperature to a mixture of **1** (125 mg, 0.20 mmol) and $[Mo(CO)_3(py)_3]$ (42 mg, 0.10 mmol) in diethyl ether (50 mL). The deep blue suspension was stirred for 8 h, then the solvent was removed and the residue chromatographed on silica gel. The component in the first band was eluted with toluene/hexane (1:4) and recrystallized from toluene/hexane at −18 °C to give red crystals of **4**, yield 56% (78 mg). Elemental analysis calcd (%) for $C_{26}H_{50}B_{20}Se_4O_2Ir_2Mo$: C 22.19, H 3.58; found: C 21.80, H 3.52; ^1H NMR (500 MHz, $CDCl_3$): δ = 1.91(s, 30H; C_5Me_5); ^{11}B NMR (160 MHz, CD_3Cl): δ = −4.28, −7.13, −8.90, −10.91; IR (KBr disk): $\tilde{\nu}$ = 2580 cm^{-1}(ν_{B-H}), 1859, 1794 cm^{-1}(ν_{CO}).

Received: July 18, 2004

Keywords: carboranes · diselenolato ligands · iridium · molybdenum · rhodium

[1] a) M. F. Hawthorne, Z. P. Zheng, *Acc. Chem. Res.* **1997**, *30*, 267–276; b) G.-X. Jin, *Coord. Chem. Rev.* **2004**, *248*, 587–602.

[2] a) D. H. Kim, J. Ko, K. Park, S. Cho, S. O. Kang, *Organometallics* **1999**, *18*, 2738–2740; b) J. Y. Bae, Y. I. Park, J. Ko, K. I. Park, S. I. Cho, S. O. Kang, *Inorg. Chim. Acta* **1999**, *289*, 141–148; c) Q. Kong, G.-X. Jin, S.-Y. Cai, L.-H. Weng, *Chin. Sci. Bull.* **2003**, *48*, 1733–1736; d) X-F. Hou, X. Wang, J. Q. Wang, G.-X. Jin, *J. Organomet. Chem.* **2004**, *689*, 2228–2235.

[3] a) M. Herberhold, G.-X. Jin, H. Yan, W. Milius, B. Wrackmeyer, *J. Organomet. Chem.* **1999**, *587*, 252–257; b) M. Herberhold, H. Yan, W. Milius, B. Wrackmeyer, *J. Chem. Soc. Dalton Trans.* **2001**, 1782–1789.

[4] a) M. Herberhold, H. Yan, W. Milius, B. Wrackmeyer, *Angew. Chem.* **1999**, *111*, 3888–3890; *Angew. Chem. Int. Ed.* **1999**, *38*,

 © 2005 Wiley-VCH Verlag GmbH & Co. KGaA, Weinheim

3689 – 3691; b) M. Herberhold, H. Yan, W. Milius, B. Wrackmeyer, *Chem. Eur. J.* **2000**, *6*, 3026- 3032; c) M. Herberhold, H. Yan, W. Milius, B. Wrackmeyer, *Chem. Eur. J.* **2002**, *8*, 388 – 395.

[5] M. Herberhold, G.-X. Jin, H. Yan, W. Milius, B. Wrackmeyer, *Eur. J. Inorg. Chem.* **1999**, 873 – 875.

[6] a) J.-Y. Bae, Y.-J. Lee, S.-J. Kim, J. Ko, S. Cho, S. O. Kang, *Organometallics* **2000**, *19*, 1514 – 1521; b) Y.-J. Lee, J.-D. Lee, S.-J. Kim, J. Ko, I.-H. Suh, M. Cheong, S. O. Kang, *Organometallics* **2004**, *23*, 135 – 143.

[7] E. L. Hoel, M. F. Hawthorne, *J. Am. Chem. Soc.* **1974**, *96*, 6770 – 6771.

[8] Crystal structure data for **2**: $C_{27}H_{53}B_{20}Ir_2RhSe_4$ ($M_r = 1397.04$), monoclinic, space group $C2/c$, $a = 25.264(7)$, $b = 19.004(5)$, $c = 20.884(6)$ Å, $\beta = 103.077(4)°$, $V = 9766(5)$ Å^3, $Z = 8$, $\rho_{calcd} = 1.900$ Mg m^{-3}, 20255 measured, 8591 unique, 502 variables, GOF = 1.028, $R1 = 0.0471$ ($I > 2\sigma(I)$), $wR2 = 0.1129$ (all unique reflections); for **3**: $C_{24}H_{49}B_{20}Ir_2RhSe_4$ ($M_r = 1356.98$), monoclinic, space group $P2(1)$, $a = 9.955(3)$, $b = 13.223(4)$, $c = 16.864(5)$ Å, $\beta = 104.205(5)°$, $V = 2151.9(12$ Å^3, $M_r = 2$, $\rho_{calcd} = 2.094$ Mg m^{-3}, 9074 measured, 6793 unique, 479 variables, GOF = 1.029, $R1 = 0.0760$ ($I > 2\sigma(I)$), $wR2 = 0.1710$ (all unique reflections); for **4**: $C_{26}H_{50}B_{20}Ir_2MoO_2Se_4$ ($M_r = 1407.04$), monoclinic, space group $P2(1)/c$, $a = 14.247(9)$, $b = 21.447(14)$, $c = 15.495(10)$ Å, $\beta = 109.281(9)°$, $V = 4469(5)$ Å^3, $Z = 4$, $\rho_{calcd} = 2.091$ Mg m^{-3}, 18386 measured, 7853 unique, 516 variables, GOF = 1.029, $R1 = 0.0487$ ($I > 2\sigma(I)$), $wR2 = 0.1057$ (all unique reflections). Diffraction data of **2**–**4** were collected at 293 K on a Bruker Smart APEX CCD diffractometer ($Mo_{K\alpha}$ radiation). The structures were solved by direct methods and subsequently refined on F^2 by using full-matrix least-squares techniques (SHELXL-97), All non-hydrogen atoms were refined anisotropically, and hydrogen atoms were located at calculated positions. CCDC-241962(**2**), CCDC-241963(**3**), and CCDC-241964(**4**) contain the supplementary crystallographic data for this paper. These data can be obtained free of charge via www.ccdc.cam.ac.uk/conts/retrieving.html (or from the Cambridge Crystallographic Data Centre, 12, Union Road, Cambridge CB21EZ, UK; fax: (+44)1223-336-033; or deposit@ccdc.cam.ac.uk).

[9] R. McDonald, M. Cowie, *Inorg. Chem.* **1990**, *29*, 1564 – 1571.

[10] F. H. Antwi-Nsiah, O. Oke, M. Cowie, *Organometallics* **1996**, *15*, 1042 – 1054.

[11] Z. Tang, Y. Nomura, Y. Ishii, Y. Mizobe, M. Hidai, *Organometallics* **1997**, *16*, 151 – 154.

[12] a) A. N. Nesmeyanov, V. V. Krivykh, V. S. Kaganovich, M. I. Rybinskaya, *J. Organomet. Chem.* **1975**, *102*, 185 – 193; b) M. Nihei, T. Nankawa, M. Kurihara, H. Nishihara, *Angew. Chem.* **1999**, *111*, 1174 – 1176; *Angew. Chem. Int. Ed.* **1999**, *38*, 1098 – 1100.

 © 2005 Wiley-VCH Verlag GmbH & Co. KGaA, Weinheim

Nanotubes

VS_2 Nanotubes Containing Organic-Amine Templates from the NT-VO_x Precursors and Reversible Copper Intercalation in NT-VS_2**

*Helen Annal Therese, Frank Rocker, Andreas Reiber, Jixue Li, Michael Stepputat, Gunnar Glasser, Ute Kolb, and Wolfgang Tremel**

Dedicated to Professor Philipp Gütlich on the occasion of his 70th birthday

Soon after the discovery of carbon nanotubes[1] the layered chalcogenides WS_2 and MoS_2 were reported as the first inorganic analogues of these hollow-cage structures.[2] Subsequently, more fullerene-type structures of inorganic compounds have been made, among them BN,[3] V_2O_5,[4] Tl_2O[5] as well as layered metal chalcogenides, such as TiS_2,[6] $NbSe_2$,[7] or ReS_2.[8] A common feature of most cage-forming compounds are their layered 2D-structures, which are able to bend or curl and to avoid vacant bonding sites through the formation of intralayer linkages. Meanwhile a number of methods for the synthesis of chalcogenide nanotubes have been devised. The most successful among them are the reductive sulfidization of oxide nanoparticles using H_2S,[9] the reduction of trichalcogenides with H_2,[7] chemical transport with iodine,[10] and the sulfidization of reactive metal halide precursors on a carbon nanotube template.[11] A conversion of preformed oxide nanotubes into their respective sulfide counterparts with preservation of the tubelike structures, however, has not been observed to date. Herein we report the first synthesis of chalcogenide VS_2 nanotubes with intercalated organic molecules by the sulfidization of a tubelike VO_x precursor. The VS_2 nanotubes are remarkable, as bulk VS_2[12] (and the VSe_2 analogue[13]) can only be obtained as A_xVS_2 (A = alkali metal, Cu) or self-intercalated non-stoichiometric (metal-excess $V_{1+x}S_2$) compounds.[14]

The starting material for the synthesis of the VS_2 nanotubes (NT-VS_2) were vanadium oxide nanotubes (NT-VO_x, $x \approx 2.3$), their synthesis is given in the Experimental Section. A representative low-resolution transmission electron micro-

[*] Dr. H. A. Therese, F. Rocker, A. Reiber, Prof. Dr. W. Tremel
Institut für Anorganische Chemie und Analytische Chemie
Johannes Gutenberg-Universität
Duesbergweg 10–14, 55099 Mainz (Germany)
Fax: (+49) 6131-39-25605
E-mail: tremel@mail.uni-mainz.de
Dr. J. Li, M. Stepputat, Dr. U. Kolb
Institut für Physikalische Chemie
Johannes Gutenberg-Universität
Welderweg 11, 55099 Mainz (Germany)
G. Glasser
Max Planck-Institut für Polymerforschung
Ackermannweg 10, 55128 Mainz (Germany)

[**] This work was supported by the Bundesministerium für Bildung und Forschung (BMBF) and by the Deutsche Forschungsgemeinschaft (DFG). NT = nanotube.

 © 2005 Wiley-VCH Verlag GmbH & Co. KGaA, Weinheim DOI: 10.1002/anie.200461326

scopic (TEM) image of NT-VO_x is given in Figure 1a. It shows that the NT-VO_x is the main product; the tubes are 0.5–5 μm long and have an outer diameter between 50 and 150 nm. Upon sulfidization of NT-VO_x with H_2S at 225 °C, VS_2 nanotubes (NT-VS_2) are formed. A scanning electron micrograph (SEM) of a typical NT-VS_2 obtained after sulfidization (Figure 1b), shows that the structure and the morphology of the VO_x tubes are preserved during the oxide into sulfide conversion. The SEM micrograph also indicates the high yield of NT-VS_2 obtained by this method. Full conversion into NT-VS_2 was observed for NT-VO_x intercalated with dodecyl amine (C_{12}-amine) but not with hexadecyl amine (C_{16}-amine). Reaction temperatures higher than 250 °C lead to a total collapse of the VS_2 tube structure.

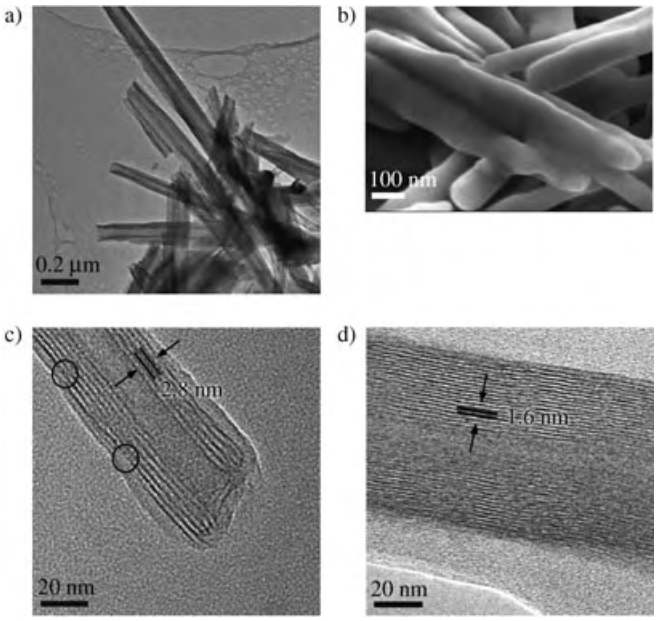


Figure 1. a) Low-resolution overview TEM image of VO_x nanotubes used as a starting material for the synthesis of NT-VS_2. b) Overview SEM image of NT-VS_2 obtained after sulfidization of NT-VO_x. c) HRTEM image of a single VS_2 nanotube with a layer separation of 2.8 nm, a flat cap, and a partially crystalline or amorphous coating. Imperfections are marked by a circle. d) HRTEM image of a NT-VS_2 obtained from NT-VO_x intercalated with C_{12}-amine. The layer separation is 1.6 nm.

That NT-VO_x has been sulfidized to produce NT-VS_2 is evidenced by the high-resolution TEM images (HRTEM) in Figure 1c. All the NT-VS_2 tubes are hollow, most of them are open, around 20% have flat caps, which make a 90° connection with the outer wall of the cylinder. The flat caps give an additional indication that structure of the NT-VO_x precursor is preserved during the sulfidization. Although the inner VS_2 layers of the tubes are smooth and almost free of defects, the outermost VS_2 layer is partially incomplete (Figure 1c), and each VS_2 tube is surrounded by a coating of amorphous VS_2. In addition, the outermost VS_2 layer exhibits a number of defects, this could be due to an incomplete reconstruction of the outer shell of the oxide precursor during the sulfidization step.

Figure 1c and d show HRTEM images of a partially and a fully sulfidated VS_2 nanotube with lattice fringes corresponding to a layer separation of approximately 2.8 nm (partially sulfidated) and 1.6 nm (fully sulfidated), values which are significantly larger than the layer separation in bulk VS_2 (0.57 nm). The observed layer spacing corresponds to the separation of the VO_x layers in the starting material, which in turn was determined by the chain length of the template molecules used in the synthesis of NT-VO_x. This result indicates that the template layer is partially intact in the VS_2 product, a hypothesis which is supported by the IR spectra of NT-VO_x before and after sulfidization (Figure 2). The IR spectra of alkylamine-templated NT-VO_x, given in Figure 2a (C_{16}-amine) and Figure 2b (C_{12}-amine), show strong vibrational bands characteristic of alkyl C–C stretching mode at 2920 cm^{-1} and 2850 cm^{-1}. The vibrational bands characteristic of V–O bond appear at 991, 791, 721, 575, and 480 cm^{-1}. The bands corresponding to V=O stretching and V-O-V deformation modes are shifted to lower frequencies compared to the crystalline V_2O_5.[15,16] A new band at 721 cm^{-1}, which can be attributed to V–NH_2 vibration, indicates that the amine groups of the templates are bound to the vanadium atoms in NT-VO_x. Chemical analysis of the NT-VS_2 samples show that the C_{16}-amine intercalated NT-VO_x does not convert fully, as also indicated by the characteristic broad V–O band at 990 cm^{-1} in the IR spectrum of the corresponding NT-VS_2. The products also tend to retain part of the intercalated templates, which can be deduced from the vibrational absorption bands at 2920 cm^{-1} and 2850 cm^{-1} (Figure 2c). On the other hand, complete sulfidization was achieved when C_{12}-amine templated NT-VO_x was reduced, as indicated by the absence of all V–O bands from the IR spectrum, while retaining part of the templates (see Figure 2d). Furthermore, the results of elemental analyses indicate a partial thermolysis (NH_3 loss) of the template during the sulfidization step.

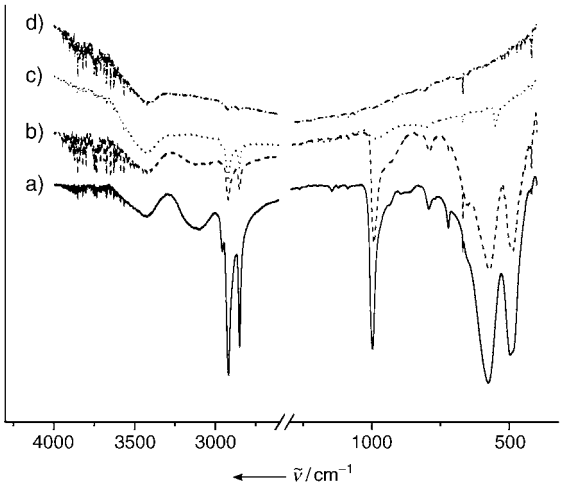


Figure 2. The FT-IR spectra of NT-VO_x samples before and after sulfidization. a) NT-VO_x with C_{16}-amines and b) NT-VO_x with C_{12}-amines, before conversion, c) NT-VS_2 with C_{16}-amines and d) NT-VS_2 with C_{12}-amines, after conversion.

 © 2005 Wiley-VCH Verlag GmbH & Co. KGaA, Weinheim

To ascertain whether the $VO_x \rightarrow VS_2$ conversion was complete, we performed additional energy dispersive X-ray (EDX) analyses of the products. Figure 3a shows the EDX spectrum of a partially sulfidized product (C_{16}-amine template). The EDX analyses show high sulfur content for the outermost regions of the tube, whereas significant oxygen content is found in the interior. This result demonstrates that the VO_x nanotubes are converted layer by layer to NT-VS_2. Figure 3b shows the EDX spectrum of a fully sulfidized VS_2 nanotube (C_{12}-amine). The V:S ratio of 1:2 (accuracy $\pm 1\%$) is almost constant over the wall cross section, independent of the beam position. The results indicated that for C_{12}-amine-intercalated NT-VO_x the conversion is almost complete whereas for C_{16}-amine-intercalated NT-VO_x the sulfidization is incomplete.

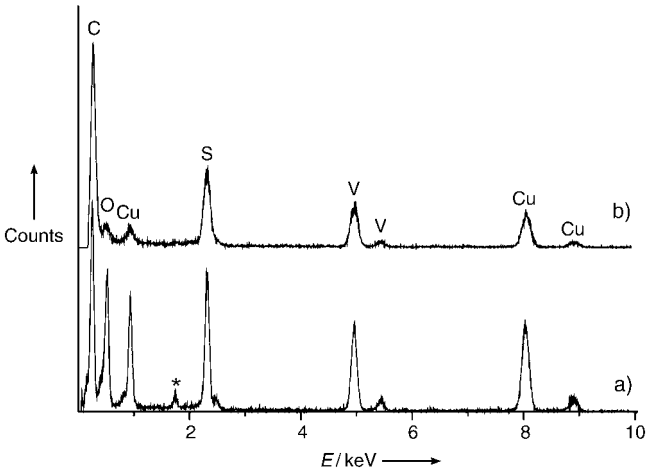


Figure 3. EDX spectra of isolated hollow VS_2 tubes. The spectra show signals arising from V, O, and S atoms. Incomplete reaction of C_{16}-amine-templated nanotube is indicated by the much greater intensity of the peak arising from oxygen in (a) than that in the spectrum of the VS_2 nanotube shown in (b) in which the C_{12}-amine template was used. The peak marked by * is due to the detector.

Studies on electrochemical intercalation of copper into a partially sulfidized NT-VS_2 have revealed that the intercalation of copper up to a composition $Cu_{0.77}VS_2$ can be achieved. NT-VO_x intercalates alkali, alkaline-earth, and a number of transition metals.[17] Studies on copper intercalation of NT-VO_x by chemically methods, through exchanging the intercalated templates with copper ions in a liquid medium, show that a small fraction (0.08 mole) of copper could be intercalated, and that the exchange resulted in considerable changes in the structure and the morphology of the starting material.[18] In contrast, no electrochemical copper intercalation was possible in NT-VO_x. The discharge/charge voltage profile of copper intercalation into 4.4 mg of NT-VS_2 is shown in Figure 4. The voltage of the working electrode dropped gradually with the insertion of copper until a limiting composition, $Cu_{0.77}VS_2$, is reached. This result corresponds to a total capacity of 360 mA h g^{-1}. The copper is reversibly deintercalated in the subsequent oxidation to regain a composition of VS_2. The cycle can be repeated, although there is a small degree of irreversibility. The capacity of the reversible copper intercalation corresponds to a specific capacity of 314 mA h g^{-1}, in comparison, graphite has a theoretical capacity of 372 mA h g^{-1}.[19]

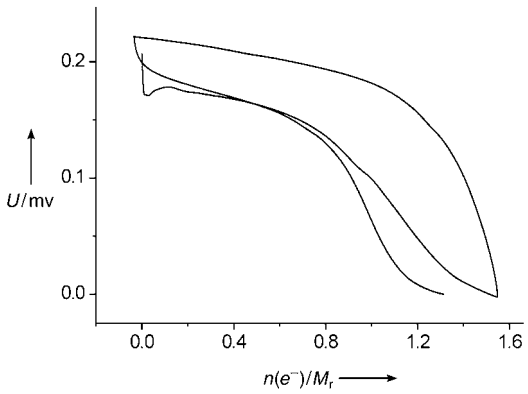


Figure 4. Plot of discharge/charge potential (U) versus the amount of electrons in mol ($n(e^-)$)intercalated per formula weight of VS_2 (M_r) during copper-intercalation studies.

The reason for the easy copper intercalation and high capacity value of NT-VS_2 in comparison with the other non-carbon nanotubes could be due to the defects that form during the conversion of NT-VO_x into NT-VS_2. This situation is in line with reports of chemically etched single-walled nanotubes (SWNTs)[20] and ball-milled MoS_2 nanotubes[21] showing better storage capacity than their untreated (unactivated) starting counterparts. The etching and ball-milling processes greatly increase the number of defects in the nanotube structures. In contrast, chemical intercalation of silver and gold was not possible with NT-VS_2, whereas VO_x nanotubes could easily be filled with gold colloids and were always heterogeneous, irrespective of their diameter and length. The gold colloids could chemically be connected to linear chains with the aid of dithiols and mechanically recovered from the VO_x tubes.

In summary, we have demonstrated that oxide nanotubes containing template molecules intercalated between the layers can be converted into sulfide nanotubes under retention of the tubelike structure. The amine-intercalated NT-VS_2 is the first layered chalcogenide nanotube in which organic molecules are inserted between the layers. In addition, we have demonstrated the reversible copper intercalation in these chalcogenide nanotubes.

Experimental Section

Vanadium oxide nanotubes (NT-VO_x) were prepared from vanadium(v) alkoxides and primary monoamines ($C_nH_{2n+1}NH_2$; with $n =$ 12 or 16) by a sol–gel reaction[4] and subsequent hydrothermal treatment. After washing and drying, the NT-VO_x was subjected to H_2S treatment in a tubular furnace at 225 °C for 22 h.

The resulting products were characterized by X-ray powder diffraction in reflection geometry, (Siemens D8 powder diffractometer, $Cu_{K\alpha}$ radiation), scanning electron microscopy (LEO 1530 field-emission SEM, 6 kV extraction voltage), and by high-resolution transmission electron microscopy (Philips TECNAIF F30 electron microscope; field-emission gun, 300 kV extraction voltage) equipped

 © 2005 Wiley-VCH Verlag GmbH & Co. KGaA, Weinheim

with a high-angle annular dark-field detector (HAADF), a Gatan imaging filter (GIF), and an energy dispersive X-ray analysis (EDX) system. IR studies of the samples were carried out using a Mattson Instruments 2030 Galaxy FT-IR spectrometer. Elemental analysis was performed with an Elemental Analyser Vario EL (Elementar Analysensyteme). The X-ray powder patterns are almost featureless, which indicates a low degree of long-range order. The elemental analysis of NT-VS_2 revealed that only a fraction (~25%) of the template is preserved.

VS_2 nanotubes were electrochemically intercalated with copper. For intercalation studies 4–7 mgs of the NT-VS_2 sample was ground well with Teflon powder, pressed between a platinum mesh and used as a working electrode. A copper ring and a copper wire were used as counter and reference electrodes. The cell was discharged and charged in galvanostatic mode, in an aqueous electrolyte under air (1 mol L^{-1} $CuSO_4$) and at a current density $j_c = 50\ \mu A\,cm^{-2}$.

Received: July 16, 2004
Revised: October 6, 2004

Keywords: nanotubes · sol–gel processes · template synthesis · vanadium

[1] S. Iijima, *Nature* **1991**, *354*, 56.
[2] a) R. Tenne, L. Margulis, M. Genut, G. Hodes, *Nature* **1992**, *360*, 444; b) L. Margulis, G. Salitra, R. Tenne, M. Talianker, *Nature* **1993**, *365*, 113; c) Y. Feldman, E. Wasserman, D. L. Srolovitz, R. Tenne, *Science* **1995**, *267*, 222.
[3] a) M. L. Cohen, *Solid State Commun.* **1994**, *92*, 45; b) E. J. M. Hamilton, S. E. Dolan, C. M. Mann, H. O. Colijn, C. A. McDonald, S. G. Shore, *Science* **1993**, *260*, 659.
[4] M. E. Spahr, P. Bitterli, R. Nesper, M. Müller, F. Krumeich, H.-U. Nissen, *Angew. Chem.* **1998**, *110*, 1339; *Angew. Chem. Int. Ed. Engl.* **1998**, *37*, 1263.
[5] S. Avivi, Y. Mastai, A. Gedanken, *J. Am. Chem. Soc.* **2000**, *122*, 4331.
[6] J. Chen, S.-L. Li, Z.-L. Tao, F. Gao, *Chem. Commun.* **2003**, *8*, 980.
[7] a) C. N. R Rao, M. Nath, *Dalton Trans.* **2003**, 1; b) M. Nath, S. Kar, A. Raychaudhuri, C. N. R. Rao, *Chem. Phys. Lett.* **2003**, *368*, 690.
[8] a) K. S. Coleman, J. Sloan, N. A. Hanson, G. Brown, G. P. Clancy, M. Terrones, H. Terrones, M. L. H. Green, *J. Am. Chem. Soc.* **2002**, *124*, 11580; b) M. Brorson, T. W. Hansen, C. J. H. Jacobsen, *J. Am. Chem. Soc.* **2002**, *124*, 11582.
[9] M. Homyonfer, B. Alperson, Y. Rosenberg, L. Sapir, S. R. Cohen, G. Hodes, R. Tenne, *J. Am. Chem. Soc.* **1997**, *119*, 2693.
[10] M. Remskar, A. Mrzel, Z. Skraba, A. Jesih, M. Ceh, J. Demšar, P. Stadelmann, F. Lévy, D. Mihailovic, *Science* **2001**, *292*, 479.
[11] R. L. D. Whitby, W. K. Hsu, P. K. Fearon, N. C. Billingham, I. Maurin, H. W. Kroto, D. R. M. Walton, C. B. Boothroyd, S. Firth, R. J. H. Clark, D. Collison, *Chem. Mater.* **2002**, *14*, 2209.
[12] G. A. Wiegers, R. van der Meer, H. van Heiningen, H. J. Kloosterboer, A. J. A. Albernik, *Mater. Res. Bull.* **1974**, *9*, 1261.
[13] L. F. Schneemeyer, A. Stacy, M. J. Sienko, *Inorg. Chem.* **1980**, *19*, 2659.
[14] a) D. W. Murphy, F. J. DiSalvo, G. W. Hull, J. V. Waszczak, *Inorg. Chem.* **1976**, *15*, 17; b) N. Le Nagard, A. Katty, G. Collin, O. Gorochov, A. Willig, *J. Solid State Chem.* **1979**, *27*, 267; c) F. Hulliger in *Physics and Chemistry of Materials with Layered Structures*, 5th ed. (Ed.: F. Lévy), D. Reidel, Dordrecht, **1977**.
[15] C. Sanchez, J. Livage, G. Lucazeau *J. Raman Spectros.* **1982**, *12*, 68.
[16] J. Ryczkowski, *Catal. Today* **2001**, *68*, 263.
[17] J. M. Reinoso, H.-J. Muhr, F. Krumeich, F. Bieri, R. Nesper, *Helv. Chim. Acta* **2000**, *83*, 1724.
[18] B. Azambre, M. J. Hudson, *Mater. Lett.* **2003**, *57*, 3005.
[19] B. Gao, A. Kleinhammes, X. P. Tang, C. Bower, L. Fleming, Y. Wu, O. Zhou, *Chem. Phys. Lett.* **1999**, *307*, 153.
[20] H. Shimoda, B. Gao, X. P. Tang, A. Kleinhammes, L. Fleming, Y. Wu, O. Zhou, *Phys. Rev. Lett.* **2002**, *88*, 015502.
[21] J. Chen, N. Kuriyama, H. Yuan, H. T. Takeshita, T. Sakai, *J. Am. Chem. Soc.* **2001**, *123*, 11813.

 © 2005 Wiley-VCH Verlag GmbH & Co. KGaA, Weinheim

Cluster Compounds

Mass Spectrometric Investigations of the Dissociation of $[C@W_6Cl_{17}]^-$ Ions in the Gas Phase**

Ralf Burgert, Katharina Koch, Hansgeorg Schnöckel, Martina Weisser, Hans-Jürgen Meyer,* and Hans Georg von Schnering*

Dedicated to Professor Martin Jansen on the occasion of his 60th birthday

The first steps into the field of metal-cluster compounds with endohedral hetero atoms were the planned synthesis and structural characterization of $[HNb_6I_{11}]$ by Simon[1] as well as the identification of $[Ru_6C(CO)_{17}]$.[2–4] Since then, the $[M_6X_{12}]$ clusters of the transition elements and their substituted variants have been discussed in particular detail.[5–7] In recently published experiments on the synthesis of octahedral tungsten halogenide clusters, the carbon-centered compounds $[C@W_6Cl_{16}]$ (**1**) and $[C@W_6Cl_{18}]$ (**2**), formed as by-products, have been detected for the first time; their formation can be put down to the fact that the commercially available educt WCl_4, besides containing WCl_5 und $WOCl_4$, was also soiled with 1,2,4,5 tetrachlorobenzene which provided a source of carbon atoms.[8] Based on this knowledge, the synthesis of **1**

[*] R. Burgert, K. Koch, Prof. Dr. H. Schnöckel
Institut für Anorganische Chemie
Universität Karlsruhe (TH)
Engesserstrasse 15, 76128 Karlsruhe (Germany)
Fax: (+49) 721-608-4854
E-mail: schnoeckel@chemie.uni-karlsruhe.de

M. Weisser, Prof. Dr. H.-J. Meyer
Institut für Anorganische Chemie
Universität Tübingen
Auf der Morgenstelle 18, 72076 Tübingen (Germany)
Fax: (+49) 7071-29-5702
E-mail: Juergen.Meyer@uni-tuebingen.de

Prof. Dr. H. G. von Schnering
Max-Planck-Institut für Festkörperforschung
Heisenbergstrasse 1, 70569 Stuttgart (Germany)

[**] This publication was financially supported by the Deutsche Forschungsgemeinschaft and the Fonds der Chemischen Industrie. Part of the results was presented on March 29, 2004 at the EFTMS 2004 (Seventh European Workshop On Fourier Transform Ion Cyclotron Resonance Mass Spectrometry) in Konstanz.

Supporting information for this article is available on the WWW under http://www.angewandte.org or from the author.

 DOI: 10.1002/anie.200460972 © 2005 Wiley-VCH Verlag GmbH & Co. KGaA, Weinheim

und **2** was optimized and the bonding properties were described in detail based on the crystal-structure examination.[8,9] Now we have developed an improved synthesis, in which the lithium as well as the calcium salts of the ion $[C@W_6Cl_{18}]^{2-}$ ($\mathbf{2}^{2-}$) are generated.[10,11] Independent from our findings, the generation of the $\mathbf{2}^{2-}$ during the synthesis of **1** from WCl_6 and CCl_4 with elemental bismuth as the reducing agent was described recently.[12] Cyclovoltametric experiments in addition to structural data helped to examine the stability of the various ions $[C@W_6Cl_{18}]^{n-}$ ($\mathbf{2}^{n-}$ $n = 1, 2, 3$) and formed the basis for the discussion of the bonding properties of these clusters.[12]

Herein we describe for the first time investigations on a structurally characterized endohedral cluster species by FT-ICR-MS (ion cyclotron resonance mass spectrometry). In these experiments $\mathbf{2}^{2-}$ and the cluster ion $[C@W_6Cl_{17}]^-$ ($\mathbf{3}^-$; which is formed after loss of Cl^-) are transferred into the gas phase entirely, without any initial decomposition. Thus, the decomposition of $\mathbf{3}^-$ can be observed step by step in different isolation and collisionally activated dissociation (CAD) experiments.[13]

First, a polycrystalline $[Li_2(\mathbf{2}^{2-})]$ sample was analyzed by laser desorption ionization (LDI). A multitude of tungsten chloride clusters (many of them C-bearing) could be identified, however none of them had the composition of $\mathbf{2}^{2-}$ or $\mathbf{3}^-$.[14]

Electrospray ionization (ESI) proved to be more efficient.[15–17] In accordance with earlier experiments[12] even sensitive compounds, such as heavy cluster ions,[18] can be transferred into the gas phase without disintegration and subsequently investigated. Figure 1 a shows the anion spectrum of a freshly prepared green solution of $[Li_2(\mathbf{2}^{2-})]$ in methanol. Along with small traces of $[C@W_6Cl_{18}]^-$ ($\mathbf{2}^-$) only the isotope pattern of $\mathbf{3}^-$ can be detected. The ESI mass spectrum of the same solution about 30 min later, shows new signals (Figure 1 b) which can be assigned to the ion $\mathbf{2}^{2-}$ as well as to the dissociation products $\mathbf{4}^-$ and $\mathbf{5}^-$ described below.[19]

To examine the stepwise fragmentation of this cluster in the gas phase, several isolation and dissociation experiments were performed. First, the most intensive signal (m/z 1718) out of the great number of isotopomers of $\mathbf{3}^-$ could be isolated (Figure 2). The fragmentation of $\mathbf{3}^-$ takes place after collisionally activated dissociation by radio frequency (RF) irradiation and admission of argon (SORI-CAD).[20] Three new signal groups are observed which can be assigned to the compounds $[C@W_5Cl_{13}]^-$ ($\mathbf{4}^-$), $[C@W_4Cl_9]^-$ ($\mathbf{5}^-$), and $[C@W_3Cl_6]^-$ ($\mathbf{6}^-$). To confirm experimentally that the dissociation of $\mathbf{3}^-$ proceeds by a consecutive mechanism in which two WCl_4 and one WCl_3 fragment are sequentially split from the parent cluster, each of the species $\mathbf{4}^-$, $\mathbf{5}^-$, and $\mathbf{6}^-$ was isolated once more and dissociated by collisional activation. The resulting fragments proved to be both $\mathbf{5}^-$ and $\mathbf{6}^-$ (from $\mathbf{4}^-$) and $\mathbf{6}^-$ (from $\mathbf{5}^-$; Figure 2). During the fragmentation of $\mathbf{6}^-$ only the appearance of Cl^- is observed. Based on these experimental findings the reaction channel shown in Equation (1) is deduced.

$$[C@W_6Cl_{17}]^-\ (\mathbf{3}^-) \xrightarrow[\Delta E_1]{-WCl_4} [C@W_5Cl_{13}]^-\ (\mathbf{4}^-) \xrightarrow[\Delta E_2]{-WCl_4} [C@W_4Cl_9]^-\ (\mathbf{5}^-) \xrightarrow[\Delta E_3]{-WCl_3} [C@W_3Cl_6]^-\ (\mathbf{6}^-) \quad (1)$$

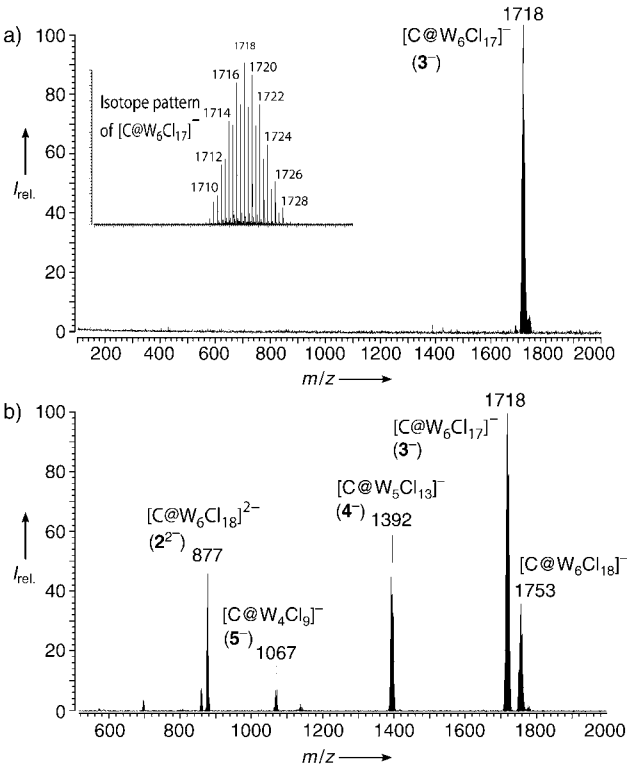


Figure 1. a) Mass spectrum (by electrospray ionization, ESI) of a freshly prepared solution of $[Li_2(\mathbf{2}^{2-})]$ in methanol. b) Mass spectrum (by electrospray ionization, ESI) of an aged solution of $[Li_2(\mathbf{2}^{2-})]$ in methanol (the experiment was performed under identical conditions to those used to obtain Figure 1 a, in particular the skimmer voltages (−20 V) were similar).

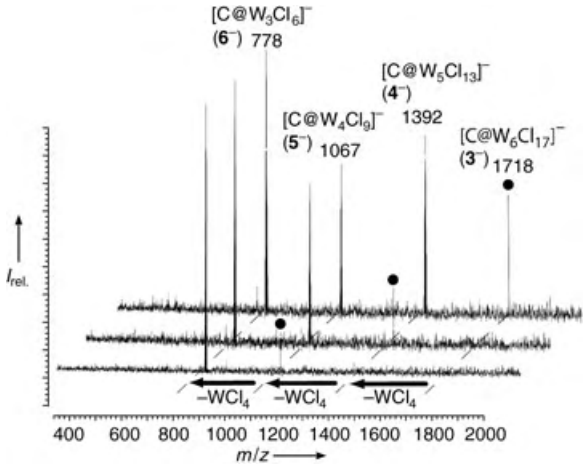


Figure 2. SORI-CAD experiments: The products after the collisionally activated dissociation of $\mathbf{3}^-$, $\mathbf{4}^-$, and $\mathbf{5}^-$. The marked signals (●) were previously isolated isotope selectively.

These fragmentation processes are of note as both WCl_4 and WCl_3 are used as starting compounds for the synthesis of $\mathbf{2}^{n-}$.[21]

However, determination of the dissociation pathway of $\mathbf{6}^-$ by mass spectrometric methods is not possible, because no further fragmentation of $\mathbf{6}^-$ into smaller ionic $[C@W_xCl_y]^-$

 © 2005 Wiley-VCH Verlag GmbH & Co. KGaA, Weinheim

units is detected. Moreover, no conclusions can be made regarding the stabilizing function of carbon or about the structures of the fragments involved in the dissociation process. In experiments with our apparatus configuration the energy amounts ΔE_1, ΔE_2, ΔE_3, which are necessary for the dissociation, can not be determined by CAD.

To find answers to these questions concerning the structure of the intermediates as well as the energy balance during the dissociation processes, we performed density functional theory (DFT) calculations.[22,23] To check the reliability of the energetic aspect of these calculations we examined the isodesmic disproportionation reaction given in Equation (2).

$$2\,WCl_{4(g)} \rightarrow WCl_{6(g)} + WCl_{2(g)} \quad (2)$$

Using highly correlated CCSD(T)/TZVPP methods[24] a ΔE value of 337 kJ mol^{-1} is obtained which is close to the values calculated by the DFT methods mentioned above (334 kJ mol^{-1}).[25,26] Therefore, the dissociation energies determined by DFT methods in equation (1) should be an adequate basis for the discussion of the experimentally found results: $\Delta E_1 = 196$ kJ mol^{-1}, $\Delta E_2 = 63$ kJ mol^{-1}, and $\Delta E_3 = 256$ kJ mol^{-1}.

In Figure 3 a–d the calculated structures of $\mathbf{3}^-$, $\mathbf{4}^-$, $\mathbf{5}^-$, and $\mathbf{6}^-$ are displayed. Detailed information and interatomic distances of all the ions calculated by this method can be found in the Supporting Information.

The mass spectrometric methods used here cannot answer the question of the fragmentation of $[C@W_3Cl_6]^-$ ($\mathbf{6}^-$), since no further fragmentation to smaller $[C@W_xCl_y]^-$ units is observed. A plausible reaction channel could be a simple electron loss from $\mathbf{6}^-$, since for $[C@W_3Cl_6]$ an electron affinity of 332 kJ mol^{-1} was calculated. However, the exclusive detection of Cl^- ions from the dissociation $\mathbf{6}^-$ suggests a different reaction channel. Under preparative conditions, as in the synthesis of $\mathbf{2}^{2-}$ (see above) a reduction could be possible where, apart from Cl^- ions, only the neutral starting compounds emerge [Eq. (3)]. For this hypothetical mode of dissociation we calculated an energy amount of +306 kJ mol^{-1}.[27]

$$[C@W_3Cl_6]^- \rightarrow Cl^- + {}^1/_4\,WCl_4 + CCl_4 + {}^{11}/_4\,W_{(s)} \quad (3)$$

The hypothesis of this reaction path is supported by approximate calculations, for alternative dissociation pathways giving products such as $[C@W_2]$, $[C@W_2Cl_2]$, and $[ClW_3]$, they predict a significantly higher energy requirement. Thus, the reaction in Equation (3) seems to be a plausible suggestion, especially after consideration of retrosynthesis. The results obtained experimentally and by quantum chemical methods for the dissociation of $\mathbf{3}^-$ via $\mathbf{6}^-$ demonstrate that the smallest carbon-containing tungsten cluster $[C@W_3Cl_6]^-$ detected in experiments is possibly one of the first clusters generated in syntheses that start from solid tungsten, WCl_4, and CCl_4 [Eq. (3)].

The results reported herein raise the principle questions, to what extent the insertion of a carbon atom in these clusters is reflected in the energy balance and how strongly a carbon

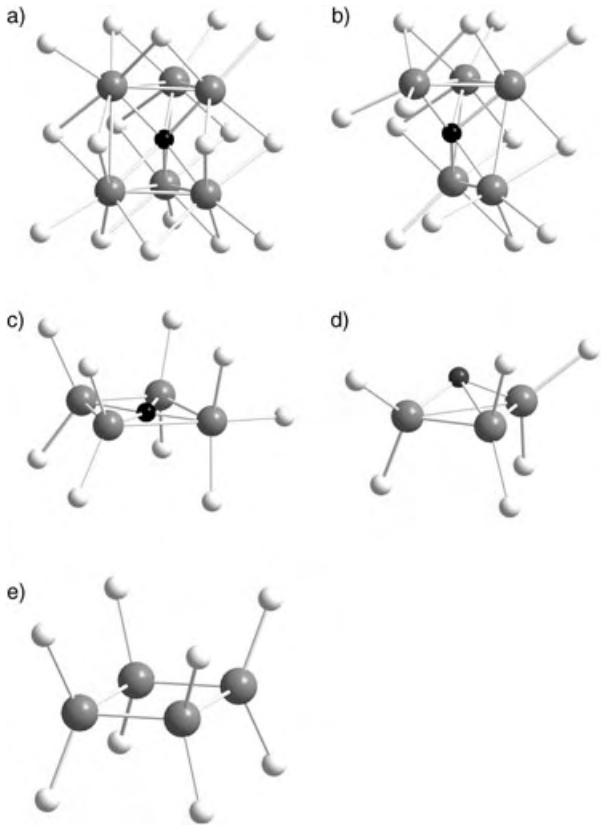


Figure 3. Calculated DFT structures of the fragment ions $\mathbf{3}^-$ (a), $\mathbf{4}^-$ (b), $\mathbf{5}^-$ (c), $\mathbf{6}^-$ (d), and of the hypothetical $[W_4Cl_8]$ molecule **8** (e).

atom is bound? Since with the neutral cluster $[C@W_4Cl_8]$ (**7**), which is derived from $[C@W_4Cl_9]^-$ ($\mathbf{5}^-$), our experiments provide a good model compound with which to try and answer these questions, we investigated the following DFT-supported idea: the removal of a carbon atom from **7** to generate the hypothetical $[W_4Cl_8]$ molecule (**8**; Figure 3 e) requires 699 kJ mol^{-1}.[28] This calculated energy gain for the insertion of a carbon atom into a molecular tungsten-atom framework corresponds to the experimentally determined energy gain which results from the formation of solid tungsten carbide WC from tungsten metal and carbon (752 kJ mol^{-1}).[29] Thus, carbon-centered metal clusters such as **1** are suitable molecular models for the topological and energetic situation in the appropriate solid-state compounds.[30]

In addition to the results for the bonding energy of carbon in the endohedral tungsten clusters reported herein, the dissociation experiments in the gas phase of $\mathbf{3}^-$, $\mathbf{4}^-$, and $\mathbf{5}^-$ as well as the accompanying quantum-chemical calculations make it seem plausible that the recently presented synthesis of **2** and $\mathbf{2}^{2-}$ also proceeds over the observed intermediates, in particular because the educts WCl_4/WCl_3 of the synthesis were released. This conclusion is also based on the fact that the intermediate products $\mathbf{4}^-$ and $\mathbf{5}^-$ can be detected in a methanol solution of $[Li_2(\mathbf{2}^{2-})]$ after ageing.

Since, to date, only **2** and $\mathbf{2}^{n-}$ ($n = 1,2,3$) can be obtained in the crystalline state, it is a challenge for future preparative investigations to isolate and characterize the cluster frag-

 © 2005 Wiley-VCH Verlag GmbH & Co. KGaA, Weinheim

ments presented herein. Furthermore, through the comparison of the experimental data with quantum-chemical calculations (see Supporting Information) the accuracy of the simple bonding descriptions[31,32] of the mostly open-shelled structures presented could be verified.

Experimental Section

The experiments presented here were performed on an Ionspec ULTIMA FT-ICR mass spectrometer with a 7.0 T magnet, equipped with both a MALDI and an electrospray (Analytica) ion source.

For the electrospray ionization a solution of $[Li_2(\mathbf{2}^{2-})]$ in methanol (approximately 10 mg mL^{-1}) was sprayed slowly (2 μL min^{-1}) through a stainless steel capillary (with an internal diameter of 100 μm) into an inert gas atmosphere (nitrogen). The ions lose their solvent and arrive over several intermediate stages in an ultrahigh vacuum area, which is generated with a differential pump system (consisting of a rotary vane pump, a turbo molecular pump, and two cryo pumps). The ions are transferred into a hexapole through a glass capillary (with voltages of 3900 V, and −140 V on their nickel coated ends) and a skimmer (−20 V), wherein they are stored for 1500 ms. Within the hexapole the pressure is approximately 10^{-6} mtorr. The ions finally arrive at the ICR cell (at 10^{-10} mtorr) through a quadrupole.

For the SORI-CAD experiments ions were selected by SWIFT-isolation (SWIFT = stored wave inverse Fourier transformation) and accelerated by a RF-pulse in the presence of a collision gas (argon) at 10^{-8} mtorr.[33] The excitation frequency is about 200 Hz higher than the cyclotron frequency, with a amplitude of 5–15 V and a duration of 1000 ms.

Received: June 15, 2004
Revised: July 23, 2004

Keywords: carbon · cluster compounds · density functional calculations · mass spectrometry · tungsten

[1] A. Simon, *Z. Anorg. Allg. Chem.* **1967**, *355*, 295.
[2] B. F. G. Johnson, R. D. Johnston, J. Lewis, *Chem. Commun.* **1967**, 1057.
[3] A. Sirigu, M. Bianchi, E. Benedetti, *J. Chem. Soc. D* **1969**, 596.
[4] "Clusters with Interstitial Atoms from the p-Block: How do Wade's Rules Handle Them ?": C. E. Housecroft in *Structural and Electronic Paradigms in Cluster Chemistry* (Ed.: D. M. P. Mingos), Springer, Heidelberg, **1997**, p. 138.
[5] H. Schaefer, H. G. von Schnering, *Angew. Chem.* **1964**, *76*, 833.
[6] F. Brian, G. Johnson, C. M. Martin in *Metal Clusters in Chemistry*, *Vol. II* (Ed.: P. Braunstein), Wiley-VCH, Weinheim, **1998**, p. 877.
[7] J. Robert, J. Goudsmit, D. H. Farrar in *Metal Clusters* (Ed.: M. Moskovits), Wiley, New York, **1986**, p. 29.
[8] Y.-Q. Zheng, H. G. von Schnering, J.-H. Chang, Y. Grin, G. Engelhardt, G. Heckmann, *Z. Anorg. Allg. Chem.* **2003**, *629*, 1256.
[9] In particular the structures of the cluster units with and without endohedral C-atoms, as well as the dramatic changes in the symmetry (from quasi-octahedral to trigonal prismatic) were described in detail and discussed therein (see ref [8]). In agreement with the observation, our own DFT calculations show that $[W_6Cl_{18}]$ with octahedral W_6-framework is favored over the trigonal-prismatic arrangement by around 70 kJ mol^{-1}. In addition we found that for the C-centered cluster $[C@W_6Cl_{18}]$ the trigonal-prismatic arrangement is more favored than the octahedral by around 260 kJ mol^{-1}.
[10] M. Weisser, H.-J. Meyer, unpublished results.
[11] M. Weisser, Diploma thesis, Tübingen, **2003**.
[12] E. J. Welch, N. R. M. Crawford, R. G. Bergman, J. R. Long, *J. Am. Chem. Soc.* **2003**, *125*, 11464.
[13] The stabilizing function of centred carbon atoms in metal clusters could also be demonstrated recently by reactions at naked metal clusters with CH_4 by FT-ICR-MS: C. P. G. Butcher, A. Dinca, P. J. Dyson, B. F. G. Johnson, P. R. R. Langridge-Smith, J. S. McIndoe, *Angew. Chem.* **2003**, *115*, 5930; *Angew. Chem. Int. Ed.* **2003**, *42*, 5752.
[14] The disadvantage of this kind of ionization is that numerous fragmentations and side reactions are induced by the UV laser (337 nm) energy, and thus no more parent ions can be detected.
[15] J. B. Fenn, *Angew. Chem.* **2003**, *115*, 3999; *Angew. Chem. Int. Ed.* **2003**, *42*, 3871.
[16] The compound is dissolved in a polar solvent and atomized in a strong electrical field. Depending on the sign of their charge, ions accumulate on the surface of the solvent droplets. A heated nitrogen counter current lets the solvent droplets shrink until they burst through the electrostatic repulsion of the ions. In this way no "new" ions are produced, on the contrary solvated ions are released from their solvent.
[17] D. Schroeder, *Angew. Chem.* **2004**, *116*, 1351; *Angew. Chem. Int. Ed.* **2004**, *43*, 1329.
[18] K. Weiss, H. Schnöckel, *Z. Anorg. Allg. Chem.* **2003**, 629, 1175.
[19] In all the experiments the skimmer potential was kept at a constant −20 V. The comparison of Figure 1a and Figure 1b shows that fragmenting reactions caused by the difference of potential between capillary exit and skimmer can be excluded. These findings can be interpreted that $\mathbf{3}^-$ (and Cl^-) arises during the dissolving of $\mathbf{2}^{2-}$, see Figure 1a. We explain the presence of $\mathbf{2}^{2-}$ in an aged solution by the following equilibrium reaction: at the beginning the equilibrium is exclusively on the side of $\mathbf{3}^-$ and the Cl^- ions. By a substantial increase of the Cl^- concentration (also experimentally observed) the equilibrium is shifted in favor of $\mathbf{2}^{2-}$. These additionally needed Cl^- ions are released during the aging processes, which also yields the fragments $\mathbf{4}^-$ and $\mathbf{5}^-$. This conclusion could be confirmed by the fact that after addition of Cl^- (as tetrabutylammonium chloride), $\mathbf{3}^-$ was no longer detected while $\mathbf{2}^{2-}$ could still be observed.
[20] SORI-CAD (sustained off-resonance irradiation collision activated dissociation). A small shift in the excitation frequency compared to the cyclotron frequency ensures that excitation only occurs with the flank of the RF pulse. The kinetic energy of the system is raised moderately over 1000 ms to give an energy distribution of the particles according to Boltzmann statistics. By collision-induced conversion into internal energy the weakest bonds in the cluster molecule finally break. J. W. Gauthier, T. R. Trautman, D. B. Jacobson, *Anal. Chim. Acta* **1991**, *246*, 211.
[21] The appearance of $\mathbf{4}^-$ and $\mathbf{5}^-$ (however not $\mathbf{6}^-$) in an aged methanol of $[Li_2(\mathbf{2}^{2-})]$ solution shows clearly that they represent intermediate stages in the decomposition of $\mathbf{3}^-$, and probably also in the assembly. The absence of $\mathbf{6}^-$ in this context demonstrates that the spectrum in Figure 1b actually shows the composition of the aged solution, and the decomposition products $\mathbf{4}^-$ and $\mathbf{5}^-$ are not the results of fragmenting reactions caused by differences of potential between glass capillary and skimmer within the medium pressure range.
[22] a) R. Ahlrichs, M. Bär, M. Häser, H. Horn, C. Kölmel, *Chem. Phys. Lett.* **1989**, *162*, 165–169; b) O. Treutler, R. Ahlrichs, *J. Chem. Phys.* **1995**, *102*, 346–354; c) J. C. Slater, *Phys. Rev.* **1951**, *81*, 385; d) S. H. Vosko, L. Wilk, M. Nusair, *Can. J. Phys.* **1980**, *58*, 1200; e) A. D. Becke, *Phys. Rev. A* **1988**, *38*, 3098; f) J. P. Perdew, *Phys. Rev. B* **1986** *33*, 8822; g) A. D. Becke, *J. Chem. Phys.* **1993**, *98*, 5648; h) A. Schäfer, C. Huber, R. Ahlrichs, *J. Chem. Phys.* **1994**, *100*, 346; h) W: E. D. Andrae, U. Haeussermann, M. Dolg, H. Stoll, H. Preuss, *Theor. Chim. Acta* **1990**, *77*,

 © 2005 Wiley-VCH Verlag GmbH & Co. KGaA, Weinheim

123; i) Cl: A. Bergner, M. Dolg, W. Kuechle, H. Stoll, H. Preuss, *Mol. Phys.* **1993**, *80*, 1431.

[23] Although compounds of heavy transition metals can be described only to a limited extent correctly in this way, Schimmelpfennig et al. recently reported on DFT calculations for different tungsten chlorides, which are in agreement with the experimental data.[26] We therefore oriented ours approach towards these methods (B3LYP-functional, with quasirelativistic core potential (ecp) in combination with the TZVPP basic set), and thus confirmed bond lengths from the crystallographic data of $[C@W_6Cl_{18}]$.

[24] Gaussian 98 (Revision A.7), M. J. Frisch, G. W. Trucks, H. B. Schlegel, G. E. Scuseria, M. A. Robb, J. R. Cheeseman, V. G. Zakrzewski, J. A. Montgomery, R. E. Stratmann, J. C. Burant, S. Dapprich, J. M. Millam, A. D. Daniels, K. N. Kudin, M. C. Strain, O. Farkas, J. Tomasi, V. Barone, M. Cossi, R. Cammi, B. Mennucci, C. Pomelli, C. Adamo, S. Clifford, J. Ochterski, G. A. Petersson, P. Y. Ayala, Q. Cui, K. Morokuma, D. K. Malick, A. D. Rabuck, K. Raghavachari, J. B. Foresman, J. Cioslowski, J. V. Ortiz, B. B. Stefanov, G. Liu, A. Liashenko, P. Piskorz, I. Komaromi, R. Gomperts, R. L. Martin, D. J. Fox, T. Keith, M. A. Al-Laham, C. Y. Peng, A. Nanayakkara, C. Gonzalez, M. Challacombe, P. M. W. Gill, B. G. Johnson, W. Chen, M. W. Wong, J. L. Andres, M. Head-Gordon, E. S. Replogle, J. A. Pople, Gaussian, Inc., Pittsburgh, PA, **2001**..

[25] Unfortunately, there exists only imprecise data for the chemical energy of our experimental reaction: In ref. [29], ΔH_R is quoted with a value of 166 kJ mol^{-1} at a tolerance of $\pm$190 kJ mol^{-1} (!) and therefore can not be used to judge the quality of the calculation methods. All energy values calculated herein relate to the respective molecular structures at 0 K. We abstained from a correction with respect to the zero-point vibrational energy, this contribution for the educts and products is almost identical so that according to our approximate calculations the energy difference is only about (5 ± 5) kJ mol^{-1}.

[26] B. Schimmelpfennig, U. Wahlgren, O. Gropen, A. Haaland, *J. Chem. Soc. Dalton Trans.* **2001**, 1616.

[27] For $W_{(s)}$ in Equation (3) we have used the evaporation heat (850 kJ mol^{-1}) from ref. [29], and thus corrected the calculated reaction energy for Equation (3) with $W_{(g)}$.

[28] In cooperation with H.-J. Himmel a study of the cluster molecules $[W_2Cl_4]$, $[W_4Cl_8]$, and $[W_6Cl_{12}]$ is in preparation where the possibility of multiple bonding is discussed in comparison to organic compounds with aromatic bonding relations.

[29] M. Binnewies, E. Milke, *Thermochemical Data of Elements and Compounds*, *Vol. 2*, Wiley-VCH, Weinheim, **2002**; M. W. Chase, Jr., C. A. Davies, J. R. Downey, Jr., D. J. Frurip, R. A. McDonal, A. N. Syverend, *JANNAF-Thermodynamical Tables*, 3rd ed., American Chemical Society, American Institute of Physics, US National Bureau of Standards, Midland, MI, **1985**.

[30] As demonstrated by our experiments and calculations, the significant energy gain from the insertion of carbon atoms is already obtained with the generation of the smallest clusters (e.g. $C@W_3$ units in $\mathbf{6}^-$).

[31] D. M. P. Mingos, *Structural And Electronic Paradigms In Cluster Chemistry*, Springer, Heidelberg, **1997**.

[32] D. M. P. Mingos, *Acc. Chem. Res.* **1984**, 311.

[33] A. G. Marshall, T. C. L. Wang, T. L. Ricca, *J. Am. Chem. Soc.* **1985**, *107*, 7893.

 © 2005 Wiley-VCH Verlag GmbH & Co. KGaA, Weinheim

Mesoporous Materials

Three-Dimensional Mesoporous Chromium Oxide: A Highly Efficient Material for the Elimination of Volatile Organic Compounds**

Anil K. Sinha and Kenichirou Suzuki*

Increasingly strict legislation for controlling the atmospheric emission of industrial volatile organic compounds (VOCs), which contribute to photochemical smog, ground-level ozone, and toxic air emissions,[1–4] has made the catalytic combustion of hydrocarbons a vital topic of research for the development of new processes for limiting air pollution by VOCs.[5] Oxides of transition metals such as Mn, Cr, Cu, and Co are the most commonly used, cost-effective catalysts for complete oxidation of VOCs,[6–9] and crystalline chromium oxide, which favors the formation of CO_2, is the most promising candidate for the total oxidation of organics.[10]

Ordered mesostructures of transition-metal oxides[11,12] are of immense interest in areas such as catalysis, sorption, chemical and biological separation, photonic and electronic devices, and drug delivery,[13] and well-ordered mesoporous oxides of Mn,[14] Ti,[15,16] V,[17] Zr,[18] W,[15] Nb,[15,17] and Ta[15,18] have been reported. However, the preparation of three-dimensionally (3D) ordered mesoporous oxides of Cu, Co, Cr, Ni, and Fe is more difficult, although it has been possible to prepare unstable lamellar phases of these materials. Recently, hexagonally ordered mesoporous nickel oxide[19] and wormhole-like mesoporous iron oxide[20] have been reported. However, nanoporous 3D structure of oxides are more suitable for application as catalysts or adsorbents as they do not suffer from mass-transfer limitations and therefore allow the easier diffusion of reactants.[21] Transitional-metal oxides are more susceptible to hydrolysis, redox reactions, or phase transitions and possess a number of different coordination numbers and oxidation states, which makes it rather difficult to prepare mesoporous structures from them, unlike silica and aluminosilicates, which can easily form stable mesoporous structures. A neutral templating route has been successfully used for the synthesis of metal-oxide mesostructures[11,15] that are less readily accessible by electrostatic-templating pathways.[12,16]

Herein we demonstrate for the first time that a 3D mesoporous chromium oxide material, prepared by a neutral templating route, shows an exceptionally high removal/oxidation ability for VOCs (toluene, acetaldehyde) after calcination. For transition-metal oxides, control of the rates of precursor hydrolysis, condensation of metal species, and precipitation of mesostructured oxides, for example by slow crystallization, is an important prerequisite for the enhanced framework cross-linking[22,23] that leads to a stable mesoporous structure. We therefore used a metal nitrate salt precursor, a mixed nonaqueous, ethylene glycol/propanol medium, and poly(alkylene oxide) block copolymers as template to prepare a very stable 3D mesoporous structure. The mixed nonaqueous medium allows a very slow crystallization (gelation) process, which favors the formation of a stable mesostructure by enhanced framework cross-linking. Our intention was to exploit such a material with 3D mesoporosity, large surface area, high oxidizing power, and probable ready evolution of active lattice oxygen, to prepare a commercially viable, cost-effective catalyst/sorbent system for the efficient removal of VOCs at low temperatures.

The as-synthesized mesoporous chromium oxide samples were transparent, and formed a fluffy, foamlike material after heating in air at 150 °C. Thermogravimetric experiments indicated that the template molecules could be completely removed by calcinating the samples at 400 °C; this was confirmed by C,H analysis.

Typical X-ray diffraction (XRD) patterns for the mesostructured chromium oxide before and after organic-template removal are shown in Figure 1a. The as-made chromium

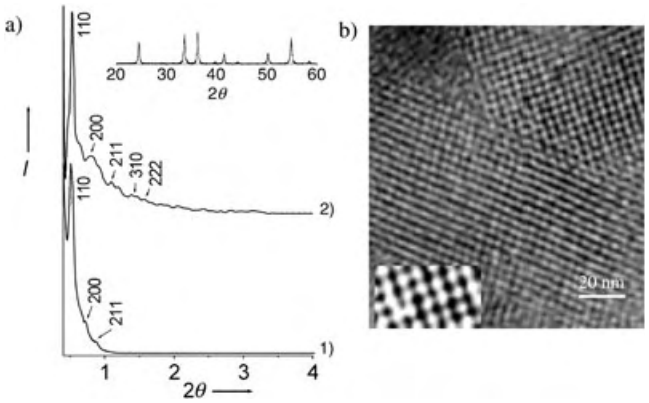


Figure 1. a) XRD pattern of mesoporous chromium oxide: 1) as-made and 2) template-free (heated to 150 °C and extracted with ethanol); b) TEM image of the template-free mesoporous chromium oxide. Inset: the reconstructed image of a selected region.

inorganic/polymer mesostructure shows diffraction peaks with lattice spacings, d, of 173, 122, and 100 Å. The d-value ratios for these peaks are $\sqrt{2}:\sqrt{4}:\sqrt{6}$, and they are indexable as (110), (200), and (211) reflections, respectively, in the cubic $Im3m$ space group. Five major XRD peaks, with d spacings of 150, 106, 87, 67, and 61 Å and d-value ratios $\sqrt{2}:\sqrt{4}:\sqrt{6}:\sqrt{10}:\sqrt{12}$, are observed after removal of the organic block-copolymer template. They are similarly indexable as the (110), (200), (211), (310), and (222) reflections of the cubic $Im3m$ space group. The basal spacing is observed to decrease by 23 Å upon removal of the template due to lattice contraction. The wide-angle X-ray diffraction pattern of the

[*] Dr. A. K. Sinha, K. Suzuki
Toyota Central R&D Labs Inc.
41-1, Aza, Yokomichi, Nagakute-cho
Aichi-gun, Aichi-ken 480-1192 (Japan)
Fax: (+81) 561-63-6137
E-mail: sinha-anil@mosk.tytlabs.co.jp

[**] We thank Mr. N. Suzuki and Ms. N. Takahashi of Toyota CRDL Inc. for transmission electron microscopy (TEM) and X-ray photoelectron spectroscopy (XPS) analyses, respectively.

Supporting information for this article is available on the WWW under http://www.angewandte.org or from the author.

 DOI: 10.1002/anie.200461284 © 2005 Wiley-VCH Verlag GmbH & Co. KGaA, Weinheim

template-free calcined sample (Figure 1a, inset) clearly shows peaks that can be indexed according to the rhombohedral phase of crystalline Cr_2O_3, thus indicating the presence of trivalent Cr in the sample. However, the presence of other mixed-valent Cr species cannot be ruled out because X-ray photoelectron spectroscopy (XPS; vide infra) revealed the presence of Cr species with different oxidation states.

The XRD peak assignment was further confirmed by transmission electron microscopy (TEM). The TEM image of the mesopore arrangement is shown in Figure 1b, where a regular arrangement of bright spots and ordered channels is observed that is attributed to the three-dimensional cubic ordered arrangement of mesopores.

The N_2 adsorption–desorption isotherm and Barret–Joyner–Halenda (BJH) pore-size distribution for the 3D mesoporous chromium oxide are presented in Figure 2. The

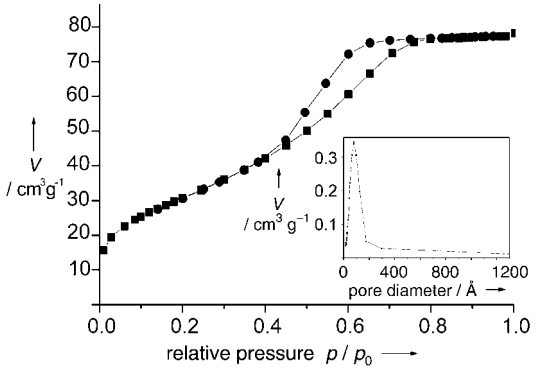


Figure 2. N_2 sorption isotherm and pore-size analysis (inset) of the mesoporous chromium oxide calcined at 400 °C.

sample exhibits a type-IV isotherm that is typical of mesoporous materials, with a well-defined step in the adsorption curve between partial pressures, p/p_o, of 0.4 to 0.8, and a large hysteresis loop due to capillary condensation in the mesoporous channels and/or cages. BJH analysis of the adsorption data, assuming cylindrical pores, shows that the calcined mesoporous chromium oxide has a mean pore-size of 7.9 nm and a wall thickness of 13.3 nm, as estimated from the XRD unit-cell parameter (a_o) value of 21.2 nm. The absence of textural mesoporosity is indicated by a plateau at a relative pressure of about 0.8 to 1.0. The template-free sample (after ethanol extraction) has a surface area of 212 $m^2 g^{-1}$, which decreases to 96 $m^2 g^{-1}$ after calcination at 400 °C and to 78 $m^2 g^{-1}$ after calcination at 500 °C.

A sample (0.4 g) of the 3D mesoporous chromium oxide calcined at 500 °C showed the highest toluene removal ability among all these materials, with 52% toluene removal and 11 ppm CO_2 formation (2% conversion) after 25 h at room temperature (sample 3 in Figure 3). The toluene-removal ability increased to 65%, with 66 ppm CO_2 formation (12% conversion), when the temperature was increased to 85 °C (sample 4). An increase in toluene-removal ability with increasing temperature is an indication of catalytic oxidation of toluene at low temperatures. This is the first report of partial catalytic decomposition of VOCs by mesoporous transition-metal oxides at low temperature. In comparison,

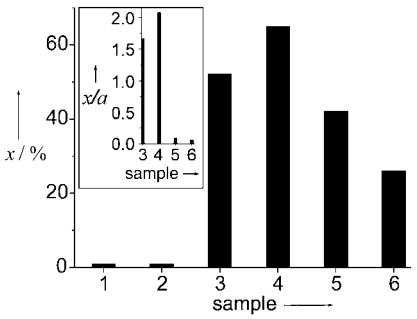


Figure 3. Toluene removal (x) over various chromium oxide samples: 1) commercial Cr_2O_3, 2) commercial CrO_3, 3) mesoporous CrO_x (at room temperature), 4) mesoporous CrO_x (at 85 °C), 5) mesoporous SiO_2 (room temperature), 6) mesoporous SiO_2 (at 85 °C). The inset shows the toluene removal per unit area of the samples (x/*a*).

mesoporous silica with a surface area of 1120 $m^2 g^{-1}$ showed 42% toluene removal at room temperature (sample 5), which decreased to 26% when the reaction temperature was increased to 85 °C (sample 6). Even though the 3D mesoporous chromium oxide has a surface area about 10 times lower than that of mesoporous silica, it still shows a much higher toluene-removal ability. The toluene-removal ability per unit area is about 18 times higher at room temperature, and about 35 times higher at 85 °C, for mesoporous chromium oxide than for mesoporous silica (Figure 3, inset). It was possible to achieve 94% toluene removal with 1.0 g of 3D mesoporous chromium oxide (see Supporting Information). Commercial hexavalent and trivalent chromium oxide (Wako Chemicals) samples (samples 1 and 2) gave less than 1% toluene removal. A high-surface-area amorphous chromia aerogel (278 $m^2 g^{-1}$),[24] which contains mostly trivalent chromium species (from XPS analysis), also showed a low toluene-removal performance (< 10%).

The X-ray photoelectron spectrum of the mesoporous chromium oxide sample shows a broad band, which indicates the presence of Cr in multiple oxidation states from +2 to +6 (see Supporting Information) with about 75% of the Cr present in the +3, or lower, oxidation state. This implies that the mixed oxidation state of the 3D mesoporous chromium oxide sample, as well as its high surface area and 3D mesoporosity, is probably responsible for the exceptionally high toluene-removal ability. Strong π–d[25] and d–σ interactions,[26] the possibility of ready evolution of active lattice oxygen species, as well as the high oxidizing power of higher valent Cr species favored by lattice strain, is probably responsible for the excellent toluene-removal ability of this mesoporous chromium oxide. In fact, when the toluene combustion reaction was evaluated in a flow reactor the toluene decomposition was found to start well below 100 °C, and it was possible to achieve 100% toluene combustion at temperatures of 280–300 °C (see Supporting Information).

These 3D mesoporous oxides could therefore be excellent materials for the sorption of VOCs at room temperature. The adsorbed VOCs can then be directly decomposed by the same catalyst at higher temperatures, thereby eliminating the need for the elimination of VOCs from the sorbent as is required for conventional VOC-removal materials such as activated

 © 2005 Wiley-VCH Verlag GmbH & Co. KGaA, Weinheim

carbon or porous silica. We were able to completely decompose the toluene adsorbed on the surface of the catalyst by thermal treatment at around 350 °C, and the regenerated catalyst could be reused without any loss in activity. XPS analysis did not show any change in the oxidation state of Cr after regenerating the 3D mesoporous oxide. There was also little change in the surface area of the regenerated catalysts. Further work on the long-term use of these catalysts is still underway to determine the total catalyst lifetime and coking behavior.

The 3D mesoporous chromium oxide catalyst (0.4 g) also removed 94% of the acetaldehyde from a 27 ppm acetaldehyde feed in air after reaction at room temperature for 25 h.

In summary, we have reported a commercially viable 3D mesoporous chromium oxide sorbent/catalyst with an exceptionally high VOC elimination ability. We expect to be able to develop a novel, dual-function sorbent/catalyst material—under ambient conditions the material acts as a selective sorbent for the VOCs, then, when it is heated to higher temperature, it acts as an effective and selective deep-oxidation catalyst for the VOCs so that the recovery and/or incineration step required in the case of currently available commercial VOC adsorbents can be eliminated. These mesoporous oxides also have potential applications as catalysts for various organic transformations, as supports, adsorbents, and separation materials, and in sensors, porous electrodes or electrolytes, and electromagnetic and electronic devices.

Experimental Section

Triblock copolymer F-127 ($HO(CH_2CH_2O)_{106}(CH_2CH(CH_3)O)_{70}(CH_2CH_2O)_{106}H$) and chromium nitrate were used as the template and inorganic source, respectively. The typical molar gel composition was 134 Cr:1115 propanol:1080 EG:1 F-127 (or P-123). In a typical synthesis, F-127 block copolymer (1 g) was dissolved in a mixture of propanol (5 g) and ethylene glycol (EG; 5 g). $Cr(NO_3)_2{\cdot}3H_2O$ (2.42 g) was added to this solution with vigorous stirring over 30–40 min. The resulting sol solution was then aged at 40–50 °C for 7–14 days and then heated gradually (1 °C min^{-1}.) to 150 °C. Finally, the organic template molecules were removed by extracting with ethanol. The samples were further calcined by heating gradually (1 °C min^{-1}) to 300–500 °C.

A gas mixture containing 103.3 ppm toluene, 20% oxygen, and the balance as nitrogen was used as the evaluation gas. A 0.4-g sample of each of the aforementioned catalysts and the evaluation gas were put in a 5-L gas container. The gas was analyzed after different time intervals by GC (Shimadzu, column Sp-1000) and a CO_2 analyzer (LI-6262, LI-COR, Inc.). The toluene conversion was determined from the equation: toluene removal (%) = [{(toluene concentration in gas container without catalyst) − (toluene concentration in gas container with catalyst)}/toluene concentration in gas container without catalyst] × 100.

A packed-bed reactor was used to evaluate the catalysts' activity in the complete oxidation of toluene (space velocity 30000 h^{-1}; toluene: 100 ppm; oxygen: 18%; and the balance of nitrogen). At the onset of the reaction the catalyst was pretreated with reactant mixture at 180 °C for 1.5 h to prevent over-estimation of toluene conversion caused by adsorption of toluene during the initial stages of the test.

Received: July 13, 2004

Keywords: adsorption · chromium · environmental chemistry · mesoporous materials · oxidation

[1] J. J. Spivey, *Ind. Eng. Chem. Res.* **1987**, *26*, 2165.
[2] W. Chu, H. Windawi, *Chem. Eng. Prog.* **1996**, *92*, 37.
[3] B. K. Hodnett, *Heterogeneous Catalytic Oxidation, Fundamentals and Technological Aspects of the Selective and Total Oxidation of Organic Compounds*, Wiley, Chichester, **2000**, p. 191.
[4] G. Centi, P. Ciambelli, S. Perathoner, P. Russo, *Catal. Today* **2002**, *75*, 3.
[5] M. F. M. Zwinkels, S. G. Jaras, P. G. Menon, *Catal. Rev. Sci. Eng.* **1993**, *35*, 319.
[6] D.-C. Kim, S.-K. Ihm, *Environ. Sci. Technol.* **2001**, *35*, 222.
[7] Y. Moro-oka, A. Ozaki, *J. Catal.* **1966**, *5*, 116.
[8] D. L. Trimm, *Appl. Catal.* **1983**, *7*, 249.
[9] *Catalytic Control of Air Pollution* (Eds.: R. G. Silver, J. E. Sawyer, J. C. Summers), American Chemical Society, Washington DC, **1992**.
[10] C. M. Pradier, F. Rodrigues, P. Marcus, M. V. Landau, M. L. Kaliya, A. Gutman, M. Herskowitz, *Appl. Catal. B* **2000**, *27*, 23; H. Rotter, M. V. Landau, M. Carrera, D. Goldfarb, M. Herskowitz, *Appl. Catal. B* **2004**, *47*, 111.
[11] P. Yang, D. Zhao, D. I. Margolese, B. F. Chmelka, G. D. Stucky, *Nature* **1998**, *396*, 152.
[12] F. Schüth, *Chem. Mater.* **2001**, *13*, 3184.
[13] X. He, D. Antonelli, *Angew. Chem.* **2002**, *114*, 222; *Angew. Chem. Int. Ed.* **2002**, *41*, 214.
[14] Z.-R. Tian, W. Tong, J.-Y. Wang, N.-G. Duan, V. V. Krishnan, S. L. Suib, *Science* **1997**, *276*, 926.
[15] P. Yang, D. Zhao, D. I. Margolese, B. F. Chmelka, G. D. Stucky, *Chem. Mater.* **1999**, *11*, 2813.
[16] D. M. Antonelli, J. Y. Ying, *Angew. Chem.* **1995**, *107*, 2202; *Angew. Chem. Int. Ed. Engl.* **1995**, *34*, 2014.
[17] P. Liu, I. L. Moudrakovski, J. Liu, A. Sayari, *Chem. Mater.* **1997**, *9*, 2513.
[18] D. M. Antonelli, J. Y. Ying, *Chem. Mater.* **1996**, *8*, 874.
[19] S. Banerjee, A. Santhanam, A. Dhathathreyan, P. M. Rao, *Langmuir* **2003**, *19*, 5522.
[20] D. N. Srivastava, N. Perkas, A. Gedanken, I. Felner, *J. Phys. Chem. B* **2002**, *106*, 1878.
[21] A. K. Sinha, S. Seelan, S. Tsubota, M. Haruta, *Angew. Chem.* **2004**, *116*, 1572; *Angew. Chem. Int. Ed.* **2004**, *43*, 1546.
[22] J. Livage, M. Henry, C. Sanchez, *Prog. Solid State Chem.* **1988**, *18*, 259.
[23] C. F. Baes, Jr., R. E. Mesmer, *The Hydrolysis of Cations*, Wiley, New York, **1976**.
[24] M. Abecassis-Wolfovich, H. Rotter, M. V. Landau, E. Korin, A. I. Erenburg, D. Mogilyansky, E. Gartstein, *J. Non-Cryst. Solids* **2003**, *318*, 95.
[25] A. A. Davydov, *Infrared Spectroscopy of Adsorbed Species on the Surface of Transition Metal Oxides*, Wiley, New York, **1990**, p. 195; A. A. Davydov, V. G. Mikhaltchenko, V. D. Sokolvskii, G. K. Boreskov, *J. Catal.* **1978**, *55*, 299.
[26] M. R. Albert, J. T. Yates, *The Surface Scientist's Guide to Organometallic Chemistry*, American Chemical Society, Washington DC, **1987**.

 © 2005 Wiley-VCH Verlag GmbH & Co. KGaA, Weinheim

Nanostructures

Germanium-Catalyzed Growth of Zinc Oxide Nanowires: A Semiconductor Catalyst for Nanowire Synthesis**

*Zheng Wei Pan, Sheng Dai, Christopher M. Rouleau, and Douglas H. Lowndes**

The vapor–liquid–solid (VLS) crystal growth mechanism, first proposed by Wagner and Ellis in 1964 for Si-whisker growth,[1] has been widely used to guide the growth of a wide range of nanowires, such as Group IV (such as Si and Ge),[2–7] III–V (such as GaAs and InP),[5,6] and II–VI (such as ZnS and ZnSe)[5,7] semiconductors, and oxides (such as ZnO and SiO_2).[8–10] In this mechanism, a catalyst nanoparticle serves as a preferential site for the absorption and dissolution of reactants from the vapor phase, directs the nanowire's growth direction, and defines the diameter of the nanowire. A common morphological feature of VLS-grown nanowires is that each nanowire is terminated at one end by a catalyst nanoparticle with a diameter similar to that of the nanowire. The catalysts used so far are usually metals, with the most popular ones being gold[3–9] and iron.[2]

ZnO is recognized as a promising photonic material in the blue-ultraviolet (UV) region due to its wide bandgap (3.37 eV) and large exciton binding energy (60 meV). Stimulated by recent reports of room-temperature UV lasing from ZnO nanowires,[9] ZnO, in the form of nanowires, nanorods, and nanobelts, is attracting a great deal of attention from the research community. Various methods have been developed for synthesizing these one-dimensional ZnO nanostructures, such as metal-catalyzed VLS growth,[8,9,11] physical vapor deposition,[12–14] chemical vapor deposition (CVD),[15] metal-organic vapor-phase epitaxy,[16] metalorganic CVD,[17] template-assisted growth,[18] and various solution methods.[19,20] Among these techniques, metal-catalyzed VLS growth has the advantage of allowing the controlled and patterned growth of ZnO nanowires,[8,9,11] and yields nanowires from well-defined and/or patterned sites on surfaces that could facilitate the integration of ZnO nanowires for characterization and their use in devices.

We report here that Ge, a Group IV semiconductor, can be used as an efficient catalyst for high-yield growth of very long (up to several hundred micrometers), extremely straight, and quasi-aligned arrays of single-crystalline ZnO nanowires in a VLS process. The Zn source was generated by carbothermal reduction of ZnO powder. The Ge catalyst was provided either by the vapor, generated by carbothermal reduction of GeO_2 powder, or by patterning Ge dots on a SiO_2-coated Si wafer by photolithography. Several kinds of substrates were used for nanowire growth, such as alumina plates, sapphire wafers, silicon wafers, and copper grids.

Figure 1a shows a low-magnification scanning electron microscopy (SEM) image of the ZnO nanowires grown on an alumina substrate. A white layer of high-density ZnO nanowires with a uniform thickness of about 150 μm has formed on the substrate surface. The nanowires tend to grow normal to the substrate surface to form a quasi-aligned nanowire array (Figure 1b). They are well-faceted with hexagonal cross-sections (Figure 1c, d), which indicates that the Wurtzite-type

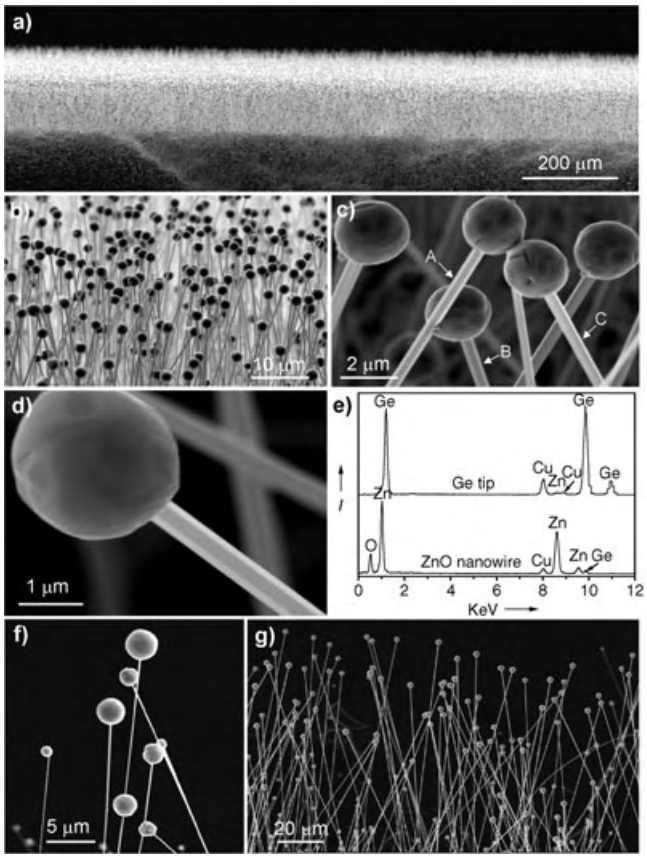


Figure 1. SEM and EDS characterization of Ge-catalyzed ZnO nanowires. a–d) SEM images of a long, straight ZnO nanowire array grown on an alumina substrate. The nanowires are terminated at their upper ends with large Ge particles. e) EDS spectra recorded at the tip and trunk of the Ge-particle-terminated ZnO nanowires. The spectra were recorded with a TEM. The Cu peaks are from the copper TEM grid. f) An SEM image showing similar-sized nanowires catalyzed by different-sized Ge particles. g) Straight ZnO nanowire arrays grown on a sapphire substrate.

[*] Dr. Z. W. Pan, Dr. C. M. Rouleau, Dr. D. H. Lowndes
Condensed Matter Sciences Division
Oak Ridge National Laboratory
Oak Ridge, TN 37831-6056 (USA)
Fax: (+1) 865-576-5235
E-mail: lowndesdh@ornl.gov
Dr. S. Dai
Chemical Sciences Division
Oak Ridge National Laboratory
Oak Ridge, TN 37831-6201 (USA)

[**] This research was sponsored by the Office of Basic Energy Science of the US Department of Energy (DOE) and the Laboratory Directed Research and Development Program of Oak Ridge National Laboratory (ORNL). The research was carried out at the ORNL, managed by UT-Battelle, LLC, for the US DOE under contract no. DE-AC05-00OR22725. We thank the ORNL SHaRE Collaborative Research Center for the use of their electron facilities. We are also grateful to Dr. D. B. Beach and Dr. N. D. Evans for helpful discussions.

 © 2005 Wiley-VCH Verlag GmbH & Co. KGaA, Weinheim DOI: 10.1002/anie.200460043

ZnO nanowires grow along the ⟨0001⟩ direction. One unique feature of our nanowires is that they are terminated at their growing ends by very large spherical particles with diameters of up to several micrometers. The presence of particles at the ends of the nanowires is suggestive of a VLS growth process.[1–3] Indeed, as shown in Figure 1c, the fact that wire A slices the tip of wire B, and that the tips of wire A and wire C are stuck together, strongly suggests that the large particles were in the liquid or semi-solid state during the growth. Energy-dispersive X-ray spectroscopy (EDS) analyses conducted with a transmission electron microscope (TEM) show that the particles are Ge with traces of Zn, whereas the nanowires contain Zn and O with traces of Ge (< 1 atom %) (Figure 1e). This indicates that the particles atop the nanowires are Ge and that the nanowires are Ge-doped ZnO. We therefore conclude that our ZnO nanowires grow by a Ge-catalyzed VLS process. To the best of our knowledge, this is the first example of a nonmetal catalyzing nanowire growth. (Note that Ge has been used before as a growth medium in the synthesis of millimeter-scale GaAs whiskers, but it was subsequently found to be present in the core and throughout the entire length of the whisker.[21])

The Ge-catalyzed ZnO nanowires are very straight and very little curvature was observed over the full length of some of the hundreds-of-micrometers-long nanowires. Detailed SEM investigations across the entire nanowire growth region showed that, within the nanowire formation regime (500–650 °C), the sizes of both the nanowires and the Ge particles increase with temperature. After 30 min of growth, the diameters and lengths of the nanowires are in the ranges 50–400 nm and 50–200 μm, respectively. The diameters of the Ge particles, however, vary from 0.5 to 4 μm, about 5–15 times those of the associated nanowires. These Ge-particle diameters are much larger than for metal-catalyzed nanowire growth, for which the diameters of the catalyst particles are similar to those of the nanowires.[2–6] The present nanowires grow very rapidly, with rates of up to 400 μm h^{-1} at a growth temperature of about 600 °C; this is about one order of magnitude faster than Au-catalyzed ZnO nanowire growth.[8,9] Unlike metal-catalyzed nanowire growth, in which the diameter of the nanowires is mainly determined by the size of the catalyst particles,[2–6] it seems that the diameter of the Ge-catalyzed ZnO nanowires is less influenced by the Ge particle size. For example, as shown in Figure 1f, the nanowires that result from a 3.5-μm-diameter Ge particle (the largest one) and a 1-μm-diameter Ge particle (the smallest one) have essentially the same diameter (~100 nm). This may explain the fact that even though the Ge particle grows up with time by continuously absorbing Ge species from the vapor, the diameter of each nanowire is almost constant over most of its length. (Note that a tapered morphology can be observed over the first few micrometers of the nanowires, probably due to the significant increase of the size of the Ge particle at the initial growth stage.)

The Ge-catalyzed ZnO nanowire growth is substrate independent. Besides alumina substrates, ZnO nanowires were also grown on sapphire and silicon wafers, and even on copper TEM grids. Figure 1g is an SEM image of ZnO nanowires grown on a sapphire wafer. It shows long (up to 100 μm), very straight, and quasi-aligned ZnO nanowires that terminate in large Ge particles. Figure 2a is a low-magnification SEM image of ZnO nanowires grown on the bars of a copper TEM grid consisting of hexagonal windows. In each

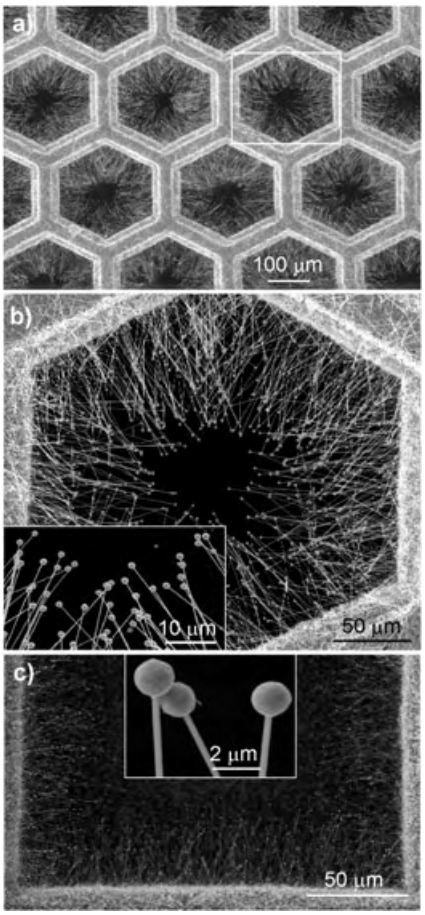


Figure 2. SEM images of Ge-catalyzed ZnO nanowires grown on copper TEM grids. a) Low-magnification SEM image of ZnO nanowires grown on a copper grid with hexagonal windows. b) An enlargement of the boxed region in Figure 2a. The inset shows a high-magnification image of the nanowires. c) An SEM image of ZnO nanowires grown on a copper grid with square windows. The inset shows a high-magnification image of the nanowires.

hexagonal window straight ZnO nanowires tend to grow along the surface normal of each edge of the hexagon; they converge upon the window center (Figure 2b). Such a growth phenomenon was also observed on a TEM grid consisting of square windows (Figure 2c).

TEM studies of the ZnO nanowires provide further insight into the morphology of these materials. Figure 3a and b show the TEM images of the ZnO nanowires grown directly on TEM grids. It is clear that the nanowires are very straight, have a uniform diameter along their axes, and terminate in large spherical Ge particles. High-resolution TEM investigations show that the ZnO nanowires are structurally uniform and single crystalline. Figure 3c is a high-resolution TEM image of a thin, single-crystalline ZnO nanowire, and Figure 3d is an atomic-resolution image of the surface of a nanowire. These images clearly show the (0001) atomic planes

 © 2005 Wiley-VCH Verlag GmbH & Co. KGaA, Weinheim

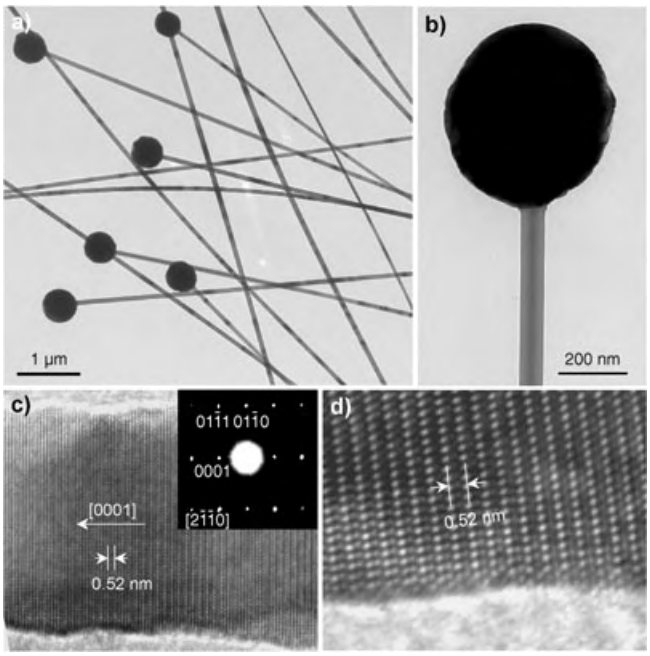


Figure 3. TEM and high-resolution TEM images of Ge-catalyzed ZnO nanowires. a,b) TEM images of ZnO nanowires grown directly on the TEM grid, showing straight and uniform nanowires terminating in large Ge particles. c) High-resolution TEM image of a thin ZnO nanowire. The inset is an electron-diffraction pattern of the crystalline nanowire recorded along the $[2\bar{1}\bar{1}0]$ zone axis. d) An atomic-resolution image showing a clean and structurally perfect nanowire surface.

(separation: 0.52 nm) perpendicular to the nanowire axis, thus indicating that $\langle 0001 \rangle$ is the preferred growth direction of these Wurtzite-type ZnO nanowires. The single-crystal nature of the nanowires and their $\langle 0001 \rangle$ growth direction were confirmed by the electron-diffraction pattern recorded perpendicular to the nanowire's long axis, as shown in the inset of Figure 3c, which could be indexed as the $[2\bar{1}\bar{1}0]$ zone axis of crystalline ZnO. The surfaces of the nanowires are clean, atomically sharp, and without any amorphous sheathed phase (Figure 3d).

In metal-catalyzed semiconductor nanowire growth, binary or pseudobinary phase diagrams are usually used to predict catalysts and growth conditions.[2,5] Although no Ge–ZnO phase diagram is available, this principle can be rationally applied to the present Ge-catalyzed ZnO nanowire growth by considering both the conventional Ge–Zn binary phase diagram[22] and the in-situ oxidation of Zn into ZnO during growth.[8] The Ge–Zn phase diagram is characterized by a eutectic reaction at 394 °C and 94.2 atom % Zn. This implies that a Ge-catalyzed VLS-type process can take place if the concentration of Zn is higher than 94.2 atom %. Such high-Zn-content Ge–Zn droplets can be readily formed since in the source materials the amount of ZnO present is about 10 times that of GeO_2 (molar ratio). When the droplets become supersaturated, ZnO nanowires are formed, possibly by the in situ reaction between Zn and a small amount of CO/O_2 present in the reaction chamber, as happens in Au-catalyzed ZnO nanowire growth.[8] The CO gas is formed by the carbothermal reduction of ZnO and GeO_2, whereas the oxygen mainly originates from leaks in our reaction system.[10]

For the Ge-catalyzed ZnO nanowire growth reported above, Ge was fed from the vapor, and the Ge catalyst particles formed on the substrate surface at the initial growth stage were randomly distributed. However, recent studies on metal-catalyzed VLS nanowire growth have shown that the controlled growth of nanowires at certain locations can be achieved from well-defined metal-catalyst particles on substrate surfaces.[4,8,9] To achieve such controlled growth from Ge, and to verify the catalytic effect of Ge on ZnO growth, we patterned uniformly sized Ge dots (~0.5 μm in diameter and 75 nm thick), with a spacing of about 5 μm, on a SiO_2-coated Si wafer by photolithography (Figure 4, upper inset), and

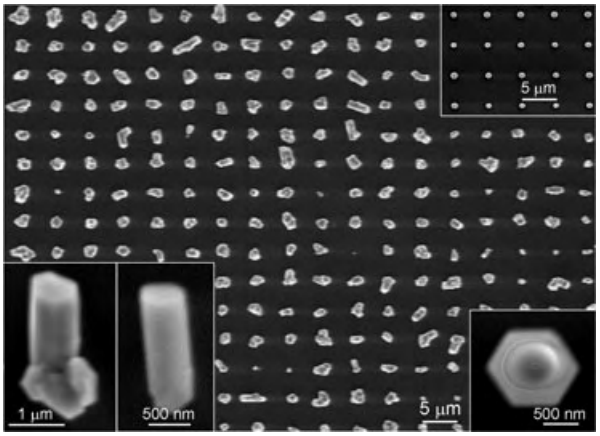


Figure 4. SEM images of a ZnO nanorod pattern grown on a Ge-dot pattern. The top-right inset shows the Ge-dot pattern. The bottom-left insets show two typical morphologies of the nanorods. The bottom-right inset is the top view of a hexagonal nanorod, showing a hemispherical hollow at the upper end of the nanorod.

carried out ZnO growth. Subsequent SEM studies (Figure 4) revealed the formation of a ZnO nanorod array that conforms to the Ge-dot pattern with high fidelity; the region without Ge dots remains completely clean. These observations clearly demonstrate the feasibility of highly deterministic control of ZnO nanowire growth at predetermined Ge-dot locations, as well as the catalytic capability of Ge for ZnO nanorod array synthesis. However, the nanorods in Figure 4 are much shorter (< 2 μm) than the nanowires described above, and no Ge particles were observed at the nanorod tips after the growth experiment at 900 °C for 1 h. This may be explained by considering the different sources of Ge and evolution of Ge particle sizes in these two kinds of syntheses. For the growth shown in Figure 1–3, the Ge particles can grow (up to 4 μm) by continuously absorbing Ge species from the vapor, so that they have sufficient volume to absorb Zn and O species to sustain fast growth of long ZnO nanowires. In contrast, for the Ge-dot pattern the Ge dots' initial volume is only about 3 % of that of even a 1-μm-diameter Ge particle, and therefore the Ge dots decrease in size, and finally disappear, due to the continuous evaporation of Ge without replenishment. This process results in a much lower growth rate and short ZnO nanorods. Indeed, hemispherical hollows with diameters

 © 2005 Wiley-VCH Verlag GmbH & Co. KGaA, Weinheim

similar to those of the original Ge dots were usually observed at the top ends of the nanorods (Figure 4, bottom right inset). These are possibly left by the evaporated Ge dots, thus confirming this model. Further work is underway to deterministically grow ZnO nanowires with controllable lengths and locations using a variety of well-defined Ge dots.

The photoluminescence (PL) spectra of the Ge-catalyzed ZnO nanowires were measured by using a Xe lamp (325 nm) as the excitation source. Figure 5 shows a room-temperature

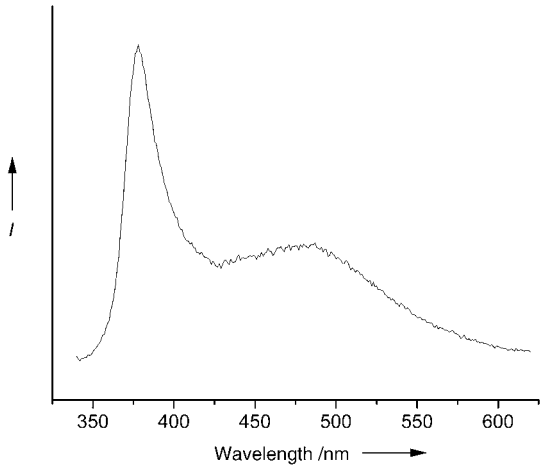


Figure 5. Photoluminescence spectrum of ZnO nanowires showing an intense UV emission at 378 nm and a weak green emission peaking at about 490 nm.

PL spectrum recorded from the ZnO nanowires grown on an alumina substrate. An intense UV emission at 378 nm and a weak, broader green emission peaking at about 490 nm were detected. While the UV-band emission corresponds to the near-band-edge free excitonic emission, the green-band emission is commonly referred to as deep-level or trap-state emission.[8] The observation of an intense free-exciton peak at room temperature strongly suggests that the Ge-catalyzed ZnO nanowires are of high optical quality. The origin of the deep-level emission in ZnO is not yet clearly understood, but is generally attributed to singly ionized oxygen vacancies[23] and extrinsic impurities.[24,25] Since our ZnO nanowires are structurally uniform and single crystalline, the weak green emission presumably arises mainly from the trace amount of Ge present in the nanowires, which could provide the green luminescence by either donor–acceptor pair or donor–hole recombination.[24,25]

Taken together, the above results show that semiconductor Ge can act as an efficient catalyst for high-yield growth of very long, extremely straight, and quasi-aligned arrays of single-crystalline ZnO nanowires by a VLS process. The use of Ge as the catalyst enriches and broadens the current understanding of the conventional VLS nanowire growth mechanism in which metals have generally been used as the catalysts. Our results suggest that it should be possible to prepare nanowires of other oxides or of compound semiconductors by using Ge or other nonmetallic elements as the catalysts. Moreover, the ZnO nanowires and synthesis methods reported here could offer opportunities for further fundamental research as well as technological applications. For example, it should be readily possible to apply electrodes to these straight and long nanowires for transport measurements, and the deterministic growth may have important practical implications, for example, for near-UV light emitting arrays.

Experimental Section

Nanowire synthesis: The ZnO nanowires were synthesized in a tube furnace system[10] by carbothermal reduction of ZnO powder in the presence of semiconductor Ge as the catalyst. The Ge catalyst was provided either from the vapor generated by carbothermal reduction of GeO_2 powder or by patterning Ge dots on a SiO_2-coated silicon wafer by photolithography. For the syntheses in which Ge was provided from the vapor, ZnO powder, carbon black, and GeO_2 powder (1:1:0.1 molar ratio) were ground together and transferred into an alumina boat. The boat was then positioned at the center of an alumina tube that was inserted into a horizontal tube-furnace. Several alumina (or silicon wafer or sapphire wafer) strips ($30 \times 10\ mm^2$) were placed downstream one-by-one to act as nanowire-growth substrates. The starting materials were then heated to 900 °C under an argon atmosphere at a flow rate of 50 sccm and a pressure of about 250 Torr for 30 min. The reactant vapors (Zn, Ge, CO, and O species) generated by carbothermal reduction of ZnO and GeO_2 were carried and transported by the argon flow to the substrates, where ZnO nanowires grew. After the furnace had cooled down to room temperature, ZnO nanowires were found on all exposed surfaces (including the top surface and four side surfaces) of the substrates located in the region at temperatures of about 500–650 °C.

For the patterned growth of ZnO nanowires, the Ge-dot patterns were prepared by photolithography using a GCA Autostep 200 *i*-line stepper system.[26] A 4-inch Si wafer coated with a 1-μm-thick SiO_2 layer was used as the substrate. The wafer was spin-coated with approximately 500 nm of photoresist (Shipley Megaposit 955-CM 0.9) at 6000 rpm for 30 s. After baking at 90 °C for 90 s, the wafer was exposed using a step size of 15 mm and a 25×25 mm aperture. At $5\times$ reduction, we obtained a 5×5 array of 5×5 mm die on a 15 mm pitch. After exposure, the wafer was baked at 120 °C for 90 s, developed for 60 s (Shipley Microposit MF-CD-26), and then reactive-ion-etched for 30 s ($308\ mW\,cm^{-2}$ with 0.1 Torr O_2 at 50 sccm) to eliminate the photoresist residue. At this stage, the wafer had many small windows (~0.5 μm in diameter on a 5 μm pitch) within the photoresist and was ready for metallization. A 75-nm-thick layer of Ge was then deposited onto the patterned substrate at room temperature by electron-beam evaporation. Finally, liftoff was performed by soaking the wafer in acetone to remove all the unnecessary Ge, leaving a 5×5 array of 5×5 mm squares on a 15 mm pitch. Within each square there was an array of Ge dots with a diameter of 0.5 μm, a thickness of 75 nm, and a spacing of 5 μm, as shown in the upper inset of Figure 4.

The Ge-dot-patterned substrates were then loaded onto a 20-cm-long graphite crucible filled with equal amounts of ZnO powder and carbon black, with the catalyst side facing down and a vertical distance between the Zn source and substrates of about 3–5 mm. The growth was conducted at 900 °C for 1 h in an argon flow. During these experiments, we noted that rodlike ZnO nanostructures were grown only on the Ge-dot patterns located in the region at a temperature of about 650–800 °C, about 150 °C higher than the nonpatterned growth described above. Below about 650 °C, no ZnO nanorods were grown, and the Ge-dot patterns seemed unchanged. Above about 800 °C, however, the Ge dots evaporated completely and thus no nanorods were formed.

Characterization: The morphology of the as-synthesized nanowires was examined with a Philips XL-30 SEM operating at 10 kV.

 © 2005 Wiley-VCH Verlag GmbH & Co. KGaA, Weinheim

The microstructure was characterized with a Philips CM200 high-resolution TEM operating at 200 kV. The composition of the nanowires was analyzed by an energy-dispersive X-ray spectrometer attached to the TEM. The photoluminescence study was carried out at room temperature on a SPEX Fluorolog-3 spectrofluorometer using a Xe lamp as the excitation source. The excitation wavelength was 325 nm.

Received: March 18, 2004
Revised: September 23, 2004

Keywords: catalyst · germanium · nanostructures · semiconductors

[1] R. S. Wagner, W. C. Ellis, *Appl. Phys. Lett.* **1964**, *4*, 89.
[2] A. M. Morales, C. M. Lieber, *Science* **1998**, *279*, 208.
[3] J. Westwater, D. P. Gosain, S. Tomiya, S. Usui, H. Ruda, *J. Vac. Sci. Technol. B* **1997**, *15*, 554.
[4] D. W. Wang, H. J. Dai, *Angew. Chem.* **2002**, *114*, 4977; *Angew. Chem. Int. Ed.* **2002**, *41*, 4783.
[5] X. F. Duan, C. M. Lieber, *Adv. Mater.* **2000**, *12*, 298.
[6] M. S. Gudiksen, J. F. Wang, C. M. Lieber, *J. Phys. Chem. B* **2001**, *105*, 4062.
[7] Y. W. Wang, L. D. Zhang, C. H. Liao, G. Z. Wang, S. S. Peng, *Chem. Phys. Lett.* **2002**, *357*, 314.
[8] M. H. Huang, Y. Y. Wu, H. Feick, N. Tran, E. Weber, P. D. Yang, *Adv. Mater.* **2001**, *13*, 113.
[9] M. H. Huang, S. Mao, H. Feick, H. Q. Yan, Y. Y. Wu, H. Kind, E. Weber, R. Russo, P. D. Yang, *Science* **2001**, *292*, 1897.
[10] Z. W. Pan, Z. R. Dai, C. Ma, Z. L. Wang, *J. Am. Chem. Soc.* **2002**, *124*, 1817.
[11] H. T. Ng, J. Li, M. K. Smith, P. Nguyen, A. Cassell, J. Han, M. Meyyappan, *Science* **2003**, *300*, 1249.
[12] Z. W. Pan, Z. R. Dai, Z. L. Wang, *Science* **2001**, *291*, 1947.
[13] Y. C. Kong, D. P. Yu, B. Zhang, W. Fang, S. Q. Feng, *Appl. Phys. Lett.* **2001**, *78*, 407.
[14] S. C. Lyu, Y. Zhang, H. Ruh, H. J. Lee, H. W. Shim, E. K. Suh, C. J. Lee, *Chem. Phys. Lett.* **2002**, *363*, 134.
[15] J. J. Wu, S. C. Liu, *Adv. Mater.* **2002**, *14*, 215.
[16] W. I. Park, D. H. Kim, S. W. Jung, G. C. Yi, *Appl. Phys. Lett.* **2002**, *80*, 4232.
[17] B. P. Zhang, N. T. Binh, Y. Segawa, K. Wakatsuhi, N. Usami, *Appl. Phys. Lett.* **2003**, *83*, 1635.
[18] Y. Li, G. W. Meng, L. D. Zhang, F. Phillipp, *Appl. Phys. Lett.* **2000**, *76*, 2011.
[19] Z. R. Tian, J. A. Voigt, J. Liu, B. Mckenzie, M. J. Mcdermott, M. A. Rodriguez, H. Konishi, H. F. Xu, *Nat. Mater.* **2003**, *2*, 821.
[20] L. Vayssieres, *Adv. Mater.* **2003**, *15*, 464.
[21] S. Iida, Y. Sugita, *Appl. Phys. Lett.* **1964**, *8*, 77.
[22] T. B. Massalski, *Binary Alloy Phase Diagrams*, *Vol. 2*, 2nd ed., ASM International, New York, **1990**, p. 2023.
[23] K. Vanheusden, W. L. Warren, C. H. Seager, D. R. Tallant, J. A. Voigt, B. E. Gnade, *J. Appl. Phys.* **1996**, *79*, 7983.
[24] R. Dingle, *Phys. Rev. Lett.* **1969**, *23*, 579.
[25] N. Y. Garces, L. Wang, L. Bai, N. G. Giles, L. E. Halliburton, G. Cantwell, *Appl. Phys. Lett.* **2002**, *81*, 622.
[26] M. A. Guillorn, M. L. Simpson, G. J. Bordonaro, V. I. Merkulov, L. R. Baylor, D. H. Lowndes, *J. Vac. Sci. Technol. B* **2001**, *19*, 573.

 © 2005 Wiley-VCH Verlag GmbH & Co. KGaA, Weinheim

Rotaxane Synthesis

Selective Synthesis of Two Constitutionally Isomeric Oriented Calix[6]arene-Based Rotaxanes**

Arturo Arduini, Flavio Ciesa, Marcello Fragassi, Andrea Pochini, and Andrea Secchi*

Rotaxanes are key compounds for the construction of synthetic molecular machines.[1,2] In spite of the remarkable achievements in their synthesis, as well as in the control of the movement of the wheel along the dumbbell component,[3] the synthesis of rotaxanes endowed with an unequivocal and predetermined relative orientation of the wheel/dumbbell systems still represents a relatively unexplored field.[4] In fact, the structure of the cyclic component employed is often related to that of a two-dimensional macrocycle, such as a crown ether, or three-dimensional symmetrical hosts, such as cucurbitols,[5] and thus have degenerate properties on the two sides of the wheel that face the two identical[6] or different[7] stoppers of the dumbbell. In the cases where the three-dimensional and nonsymmetrical cyclodextrins are used as the wheel, an axle can thread the cyclodextrin from both rims, thus leading to a mixture of orientational pseudorotaxane isomers[8] in which the orientation of the cyclodextrin along the axle is virtually unpredictable.[9] It could, however, be foreseen that a predetermined orientation of the components within these interlocked systems could endow devices with new properties.

A relatively new type of wheel that can be used in this context is the calix[6]arene platform. We have shown that triphenylureidocalix[6]arene derivatives can act as heteroditopic receptors and form remarkably stabile pseudorotaxanes with dioctylviologen salts ($K_s = 1.3 \times 10^6\,\text{M}^{-1}$)[10] as well as a calixarene-based rotaxane based on this axle/wheel dyad.[11] The binding properties of triphenylureidocalix[6]arene (**1**) were used to address the threading of an asymmetrical dipyridinium axle that threads the wheel exclusively from the upper rim in the apolar solvent C_6D_6 to yield an oriented pseudorotaxane.[12]

Herein it is demonstrated that the binding features of **1** can be exploited to control the orientation of the pseudorotaxane stoppers by using two different stoppers to yield an asymmetric [2]rotaxane having an unequivocal orientation of the wheel with respect to the different stoppers, and that an

[*] Prof. Dr. A. Arduini, F. Ciesa, Dr. M. Fragassi, Prof. Dr. A. Pochini, Dr. A. Secchi
Dipartimento di Chimica Organica ed Industriale dell'Università
Parco Area delle Scienze 17/a, 43100 Parma (Italy)
Fax: (+39) 0521-905-472
E-mail: arturo.arduini@unipr.it

[**] This research was partly supported by MIUR (Supramolecular Devices Project) and FIRB (Manipolazione Molecolare per Macchine Nanometriche). We thank the Centro Interdipartimentale di Misure "G. Casnati" for NMR measurements.

Supporting information for this article is available on the WWW under http://www.angewandte.org or from the author.

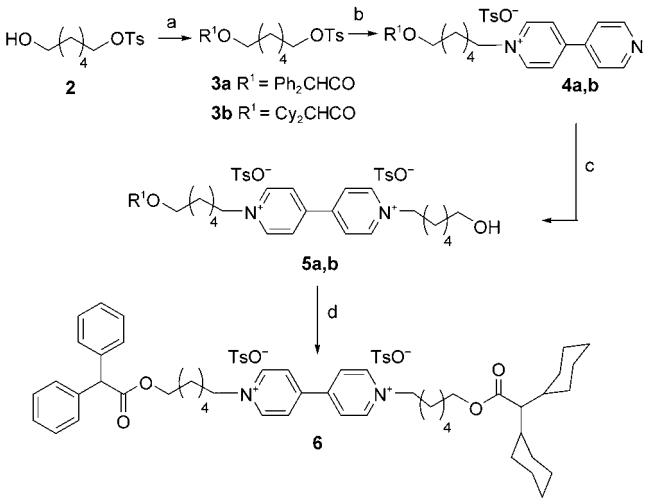
 © 2005 Wiley-VCH Verlag GmbH & Co. KGaA, Weinheim DOI: 10.1002/anie.200461336

axle based on the 4,4′-bipyridyl group can also thread through the wheel from its lower rim.

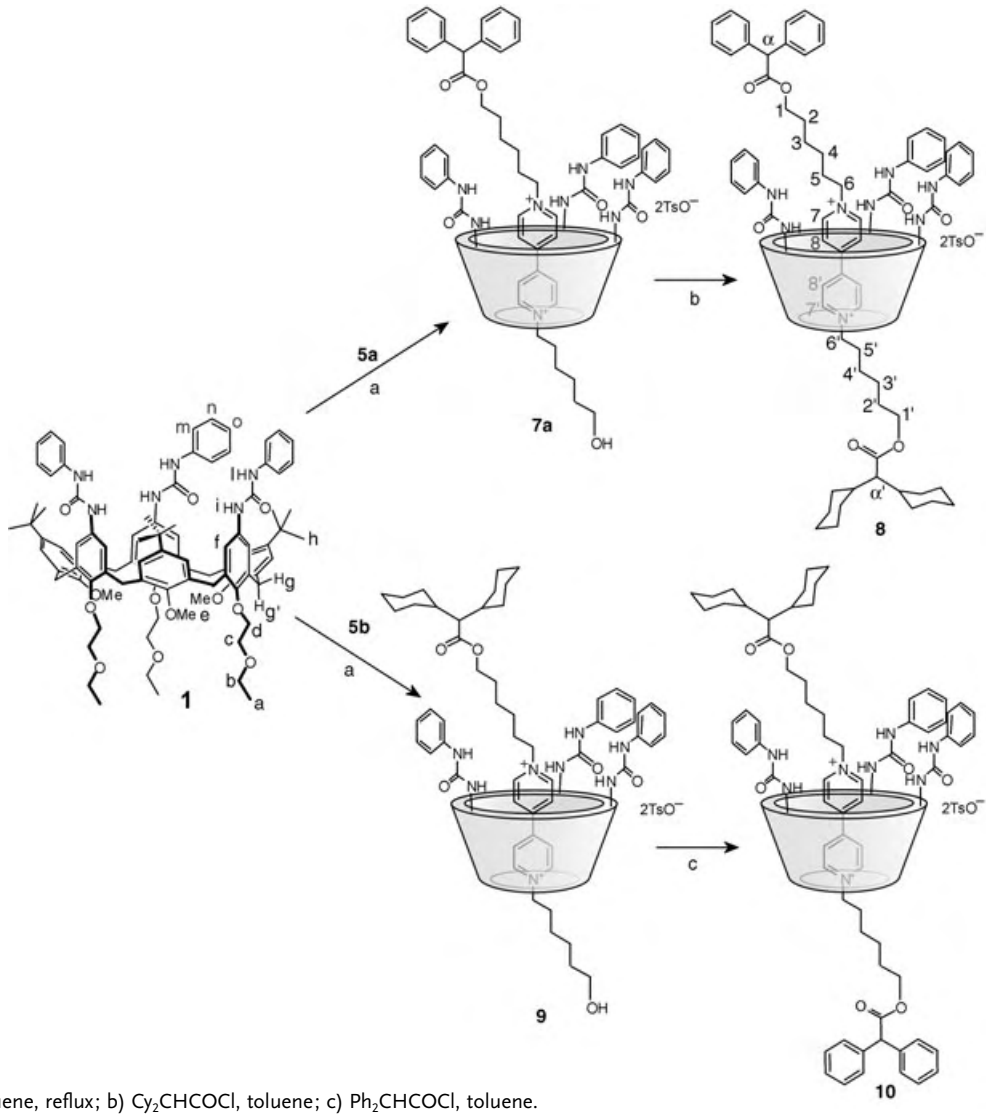
The design of the axial component was based on the observations that the position of the two identical diphenylacetyl stoppers of a calix[6]arene-based rotaxane with respect to the calixarene rims can be established by NMR techniques.[12]

Axle **5a**, in which the 4,4′-bipyridyl unit is functionalized with two C_6 alkyl chains, one of which bears a diphenylacetyl stopper at one side and the other an alcoholic OH group to be used for further stoppering, was synthesized from 6-hydroxyhexyl tosylate **2** in 12% overall yield according to Scheme 1. Wheel **1** was added to a solution of **5a** in toluene to effect the threading reaction. An excess of dicyclohexylacetyl chloride was added to the homogeneous deep red solution thus obtained to stopper the alcoholic OH group of the pseudorotaxane **7a** (Scheme 2). Rotaxane **8** was isolated in 25% yield after chromatographic separation.

Dumbbell **6** was also synthesized for comparison and enable the structure of **8** to be established (Scheme 1). The ^{1}H NMR spectrum of **8** in C_6D_6 shows that the calixarene



Scheme 1. a) R^1Cl, CH_2Cl_2, reflux, 2 h; b) 4,4′-dipyridine, CH_3CN, reflux, 24 h; c) **2**, CH_3CN, reflux, 48 h (11 and 8% overall yield for **5a** and **5b**, respectively); d) **4b**, **3a**, CH_3CN, reflux, 8 h. Cy = cyclohexyl, Ts = toluene-4-sulfonyl.



Scheme 2. a) Toluene, reflux; b) $Cy_2CHCOCl$, toluene; c) $Ph_2CHCOCl$, toluene.

 © 2005 Wiley-VCH Verlag GmbH & Co. KGaA, Weinheim

wheel rearranges and assumes a more-stiffened cone structure. The downfield shift of almost $\Delta\delta = 2$ ppm of the resonances of the six NH protons indicates their involvement in hydrogen bonding with the two tosylate anions of **5a**, as also shown by X-ray structural data.[13] The position of the calixarene along the axle was established by looking at the variation in the chemical shifts of the protons of the dumbbell portion between C1 and C1′ relative to those of **6** (see Scheme 2 for numbering). In particular, the protons from C2 to C6′ in **8** undergo a substantial upfield shift, while those from C5′ to α′ are downfield shifted to a much smaller extent. The relative orientation of the dumbbell C_6 spacers with respect to the calixarene rims were established through ROESY experiments, which showed cross peaks between protons 4 and 5 of the axle and protons m, n, and o of the wheel (see Supporting Information).

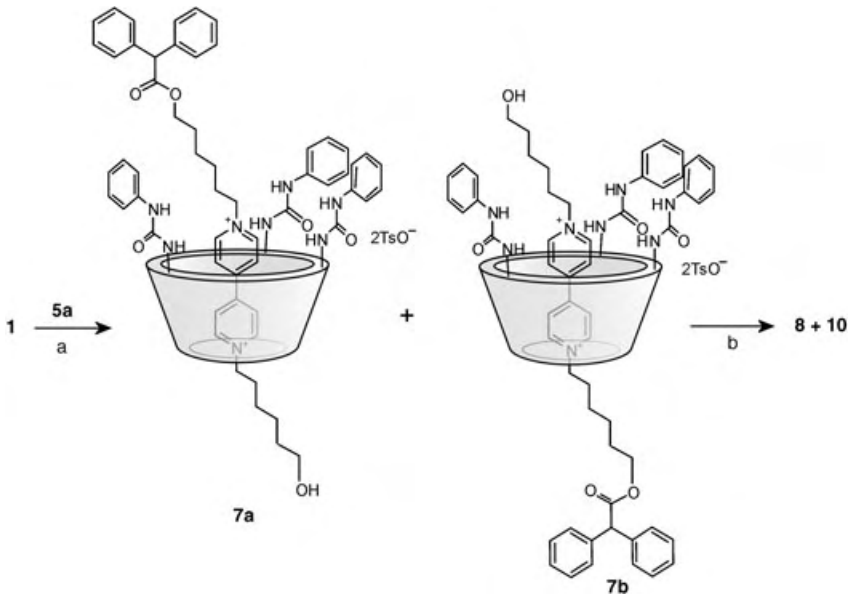
The lack of ROE cross peaks between the two different stoppers and the corresponding hexyl chains, or with protons of the wheel, precluded the existence of equivalent matching spacer—stopper groups. Nevertheless, the presence of only one signal for proton α at $\delta = 5.24$ ppm in the NMR spectrum of **8**[12] enables it to be assumed that the diphenylacetyl stopper is positioned at the upper rim of the wheel, while the dicyclohexyl one points toward the lower rim of the calixarene.

To confirm the structure of **8**, and also to exclude the presence of other rotaxanes in the reaction mixture, the rotaxane isomer **10** (see Scheme 2) was also synthesized (in 18% yield) by employing the new axle **5b**, which is characterized by the presence of a dicyclohexylacetic stopper (see Scheme 1). As expected, the ^{1}H NMR spectrum of **10** shows that the conformation of the calix[6]arene is almost exactly the same as that observed in **8**. However, the protons of the dumbbell portion between C3′ to C6 in **10** are substantially shifted upfield, while those from C5 to C1 are shifted downfield. The presence of only one singlet at $\delta =$ 5.23 ppm strongly suggests that the diphenylacetyl stopper is in proximity to the lower rim in **10**, while the dicyclohexyl stopper is oriented toward the upper rim of the calixarene (see the Supporting Information).

These data can be tentatively explained if it is considered that axles **5a** and **5b** are present as tight ion pairs during the initial formation of the pseudorotaxane in toluene and as such can not fit into the calixarene cavity. These conditions maximize the hydrogen-bonding ability of the ureido NH groups toward the axle counteranion(s) that thus pivot the cationic portion of the axles to thread through the wheel exclusively from the upper rim. The high kinetic stability of the oriented pseudorotaxane that forms favors the stoppering of the OH group that protrudes from the lower rim of the wheel, without any detectable axle–wheel isomerization.

At this point a question came apparent: are these results sufficient to exclude the threading of some of the axles **5a** or **5b** from the lower rim, or is this direction of threading prevented because of the insufficient size of the calix[6]arene annulus for these guests? Acetonitrile should decrease the extent of ion pairing of the axle and hence limit the magnitude of the pivoting role exerted by the ureido groups of the wheel during threading.

Pseudorotaxane formation in CD_3CN was thus studied by ^{1}H NMR spectroscopy by equilibrating **1** and **5a** in a 1:1 molar ratio. In the spectrum of the solution thus obtained, most of the signals appeared as broad peaks and this prevents accurate assignment. However, the presence of three singlets at $\delta = 5.11$, 5.13, and 5.14 ppm (relative ratio 9:59:32) in the region where the proton α of the diphenylacetyl moiety resonates suggested that this proton existed in three different environments. In particular, the signal at $\delta = 5.11$ ppm was easily assigned to the free axle while the other two were tentatively assigned to the two isomeric pseudorotaxanes **7b** and **7a**. A similar distribution of products was also observed by dissolving the oriented pseudorotaxane **7a** that had formed in C_6D_6 in CD_3CN. This observation shows that the oriented pseudorotaxane **7a** can dissociate into its components in acetonitrile and that the threading/dethreading processes can occur from both calix[6]arene rims, thus yielding both pseudorotaxanes isomers (see the Supporting Information). This result clearly indicates that the calix[6]-arene annulus is also large enough to thread on to the axle from the lower rim, and that indeed, in acetonitrile, the control elements governing the exclusive threading from the upper rim operate—if at all—only to a limited extent. Both rotaxanes **8** and **10** were obtained in 24% yield as unique chromatographic fractions by treating **1**, axle **5a**, and dicyclohexylacetyl chloride in acetonitrile (Scheme 3). Their ^{1}H NMR spectra in C_6D_6 correspond exactly to the sum of rotaxanes **8** and **10**, and thus indirectly demonstrate that only



Scheme 3. a) CH_3CN, reflux; b) $Cy_2CHCOCl$.

 © 2005 Wiley-VCH Verlag GmbH & Co. KGaA, Weinheim

one of the two constitutionally isomeric rotaxanes had formed in the apolar toluene (see the Supporting Information).

The study of the unidirectional movement of the wheel along the axle of the new oriented calix[6]arene-based rotaxanes under the action of electrochemical stimuli is under investigation.

Received: July 16, 2004

Keywords: calixarenes · rotaxanes · self-assembly · solvent effects · supramolecular chemistry

[1] V. Balzani, A. Credi, M. Venturi, *Molecular Devices and Machines—A Journey into the Nano World*, VCH, Weinheim, **2003**.
[2] V. Balzani, A. Credi, F. M. Raymo, J. F. Stoddart, *Angew. Chem.* **2000**, *112*, 3486; *Angew. Chem. Int. Ed.* **2000**, *39*, 3348.
[3] J. D. Badjic, V. Balzani, A. Credi, S. Silvi, J. F. Stoddart, *Science* **2004**, *303*, 1845.
[4] H. R. Tseng, S. A. Vignon, P. C. Celeste, J. F. Stoddart, A. J. P. White, D. Williams, *Chem. Eur. J.* **2003**, *9*, 543.
[5] J. W. Lee, S. Samal, N. Selvapalam, H.-J. Kim, K. Kim, *Acc. Chem. Res.* **2003**, *36*, 621.
[6] H. R. Tseng, S. A. Vignon, P. C. Celeste, J. Perkins, J. O. Jeppesen, A. Di Fabio, R. Ballardini, M. T. Gandolfi, M. Venturi, V. Balzani, J. F. Stoddart, *Chem. Eur. J.* **2004**, *10*, 155.
[7] a) G. W. H. Wurpel, A. M. Brouwer, I. H. M. Stokkum, A. Farran, D. A. Leigh, *J. Am. Chem. Soc.* **2001**, *123*, 11327; b) J. O. Jeppesen, K. A. Nielsen, J. Perkins, S. A. Vignon, A. Di Fabio, R. Ballardini, M. T. Gandolfi, M. Venturi, V. Balzani, J. Becher, J. F. Stoddart, *Chem. Eur. J.* **2003**, *9*, 2982.
[8] B. C. Gibb, *J. Supramol. Chem.* **2002**, *2*, 123.
[9] For examples of cyclodextrin-based oriented pseudorotaxanes, see: a) H. Yonemura, M. Kasahara, H. Saito, H. Nakamura, T. Matsuo, *J. Phys. Chem.* **1992**, *96*, 5765; b) M. R. Craig, M. G. Hutchings, T. D. W. Claridge, H. L. Anderson, *Angew. Chem.* **2001**, *113*, 1105; *Angew. Chem. Int. Ed.* **2001**, *40*, 1071; c) R. Isnin, A. E. Kaifer, *J. Am. Chem. Soc.* **1991**, *113*, 8188.
[10] A. Credi, S. Dumas, S. Silvi, M. Venturi, A. Arduini, A. Pochini, A. Secchi, *J. Org. Chem.* **2004**, *69*, 5881.
[11] A. Arduini, R. Ferdani, A. Pochini, A. Secchi, F. Ugozzoli, *Angew. Chem.* **2000**, *112*, 3595; *Angew. Chem. Int. Ed.* **2000**, *39*, 3453.
[12] A. Arduini, F. Calzavacca, A. Pochini, A. Secchi, *Chem. Eur. J.* **2003**, *9*, 793.
[13] F. Ugozzoli, C. Massera, A. Arduini, A. Pochini, A. Secchi, *CrystEngComm* **2004**, *6*, 227.

 © 2005 Wiley-VCH Verlag GmbH & Co. KGaA, Weinheim

Cluster Compounds

The Formal Conversion of SiOH Protons into Hydrides by Germanium(II) Species Leads to the Formation of the Germanium(IV) Hydride Cluster $[(RSiO_3GeH)_4]$**

Umesh N. Nehete, Vadapalli Chandrasekhar, Herbert W. Roesky, and Jörg Magull*

Dedicated to Professor Manfred Meisel on the occasion of his 65th birthday

We have been interested for some time in the synthesis and characterization of metallosiloxanes containing the Si-O-M motif[1] (M = main-group or transition-metal atom). Utilizing the multifunctional N-bonded silanetriol $RSi(OH)_3$ (R = (2,6-iPr$_2$C$_6$H$_3$)N(SiMe$_3$)) we have successfully assembled a number of polyhedral metallosiloxanes with a high metal/silicon ratio.[1] Many such compounds have been shown to be structural models for complex, naturally occurring metallosilicates or synthetic metal-containing zeolites.[2] Some compounds, such as $[(RSiO_3TiOR^1)_4]$ (R = (2,6-iPr$_2$C$_6$H$_3$)N(SiMe$_3$), R^1 = Et, iPr)[3] have been shown to be catalysts for the epoxidation of olefins.[4] Recently we have been intrigued by the varied products obtained in the reaction of $RSi(OH)_3$ with tin substrates. Thus, while tin(IV) reagents, such as $PhSnCl_3$, react with $RSi(OH)_3$ to afford the cubic compound $[(RSiO_3SnPh)_4]$ or the bicyclic compound $[(RSiO_3)_2(PhSn)_3]$[5] analogous reaction with $[Sn\{N(SiMe_3)_2\}_2]$ proceeds in an entirely different manner. The product of this reaction is a hexatin(II) assembly $[(SnO)_6(R_2Si_2O_3)_2]$ which is formed as a result of an in situ generated disiloxanetetrol $[(RSi(OH)_2)_2O]$.[6] In view of this unusual reactivity, it was of interest to probe analogous germanium compounds. It is also noted that only a handful of structurally characterized compounds containing the Ge-O-Si linkage are known $[(Ph_2Ge)_2(Ph_2Si)_2O_4]$,[7a] $[(Me_2Ge)_2(Ph_2Si)_2O_4]$,[7a] $[(Cl_2Ge)_2(t$BuSi$)_2O_4]$,[7b] $[(Et_2Ge)_2(Ph_2Si)_2O_4]$,[7c] $[(Ph_2Ge)_2(Ph_2Si)_2O_3]$,[7d] $[(t$Bu$_2$Ge)(Ph$_2$Si)$\{[(CH_2)_3NMe_2]_2Sn\}O_3]$.[7e] Herein, we report the first polyhedral germanium siloxane $[(RSiO_3GeH)_4]$ (R = (2,6-iPr$_2$C$_6$H$_3$)N(SiMe$_3$)). This species also is the first example of a Ge-O-Si containing compound with terminal functional Ge–H units. Although other Group 14 species, such as

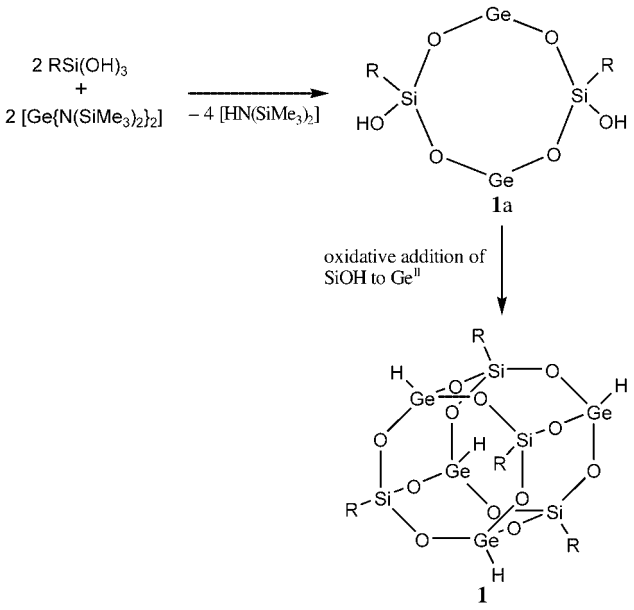
[*] U. N. Nehete, Prof. Dr. H. W. Roesky, Prof. Dr. J. Magull
Institut für Anorganische Chemie
Universität Göttingen
Tammannstrasse 4, 37077 Göttingen (Germany)
Fax: (+49) 551-393-373
E-mail: hroesky@gwdg.de
Prof. Dr. V. Chandrasekhar
Department of Chemistry
IIT-Kanpur, Kanpur-208 016 (India)

[**] This work was supported by the Deutsche Forschungsgemeinschaft and the Göttinger Akademie der Wissenschaften. V.C. thanks the Alexander von Humboldt Foundation, Bonn (Germany), for the Friedrich Wilhelm Bessel Research Award. R = (2,6-iPr$_2$C$_6$H$_3$)N(SiMe$_3$).

 DOI: 10.1002/anie.200460849 © 2005 Wiley-VCH Verlag GmbH & Co. KGaA, Weinheim

$[(HSiO_3)_4]$, are known,[8] the corresponding germanium or germanium siloxane analogues have not been reported. The synthesis of $[(RSiO_3GeH)_4]$ also involves an unprecedented oxidative addition of an SiO–H bond to a germanium(II) center, which leads to the formal conversion of the OH proton into a hydride. The oxidative addition of an alcohol to an alkylgermanium(II) compound is known.[9]

The reaction of the germanium(II) amide[10] $[Ge\{N(SiMe_3)_2\}_2]$ with $RSi(OH)_3$[11] in a 1:1 molar ratio afforded $[(RSiO_3GeH)_4]$ (**1**) in about 64% yield (Scheme 1). The



Scheme 1. Synthesis of compound **1**.

colorless crystals of **1** were obtained at room temperature from its saturated solution in hexane. Compound **1** is soluble in a large number of common organic solvents including hydrocarbons such as hexane and pentane. Compound **1** has been characterized by analytical, spectroscopic, and X-ray crystallographic techniques (see Figures 1 and 2).[12] Compound **1** is thermally quite stable and is also stable under the conditions of the EI mass spectrometry. The EI-mass spectrum of **1** shows the molecular ion peak at 1592.5 (100%) $[M^+]$.

The presence of the Ge–H motif is also detected in the ^{1}H NMR spectrum as a singlet at $\delta = 5.83$ ppm.[13] The ^{29}Si NMR spectrum shows a single resonance ($\delta = -87.4$ ppm) for the core of **1** indicating the equivalence of the silicon atoms, while the IR spectrum exhibits the characteristic Ge–H stretching frequency ($\tilde{\nu} = 2211$, 2184 cm^{-1}).[13] The formation of **1** involves the oxidation of germanium(II) to germanium(IV). We assume that the first step of the reaction involves the intermediate $[\{RSi(OH)O_2Ge\}_2]$ (**1a**; Scheme 1) which can result from a condensation of the germanium amide with the silanetriol. The next step is the fusion of two molecules of **1a** through an intermolecular oxidative addition reaction of SiO–H with germanium(II) centers. Such a process leads to a concomitant Ge-O-Si bond formation. Alternatively it may be possible that first an oxidative addition of $RSi(OH)_3$ to $[Ge\{N(SiMe_3)_2\}_2]$ occurs with an elimination of $H[N(SiMe_3)_2]$ resulting in the formation of **1**. Although oxidative addition reactions are common in organometallic chemistry, we have found no precedence for an oxidative addition reaction involving the SiOH group. Moreover, during the course of this reaction the proton of the SiOH group is formally converted into a hydride.

Compound **1** crystallizes in the monoclinic space group *C*2/*c* (Figure 1and Figure 2).

The structure of **1** can be described as a polyhedral cubic cage where the alternate corners of the cube are occupied by germanium and silicon atoms. The edges of the cube contain

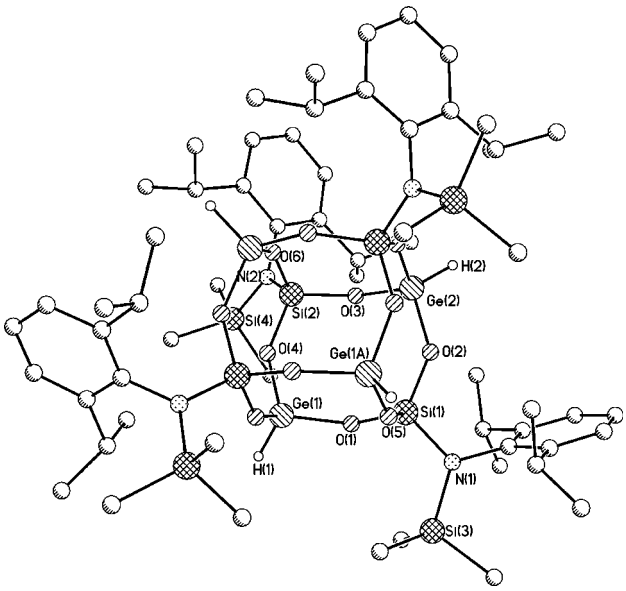


Figure 1. Molecular structure of **1**.

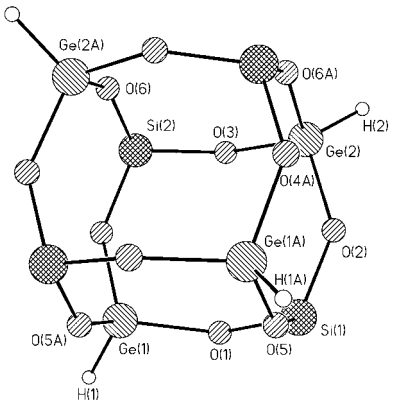


Figure 2. Core structure of **1**. The substituents on the silicon atoms have been omitted for clarity. Selected bond lengths [Å] and angles [°]: Ge(1)-O(5A) 1.737(1), Ge(2)-O(6A) 1.738(1), Ge(1)-O(1) 1.740(1), Ge(2)-O(2) 1.745(1), Ge(1)-O(4) 1.741(1), Ge(2)-O(3) 1.742(1), Ge(1)-H(1) 1.40(2), Ge(2)-H(2) 1.38(2), Si(2)-O(6) 1.623(1), Si(2)-O(4) 1.623(2), Si(2)-O(3) 1.628(1), Si(1)-O(2) 1.620(2), Si(1)-O(5) 1.628(2), Si(1)-O(1) 1.628(1); Si(2)-O(4)-Ge(1) 142.78(9), Si(1)-O(5)-Ge(1A) 142.55(10), Si(1)-O(1)-Ge(1) 140.74(9), Si(1)-O(2)-Ge(2) 142.52(9), Si(2)-O(3)-Ge(2) 140.05(9), Si(2)-O(6)-Ge(2A) 142.55(9).

 © 2005 Wiley-VCH Verlag GmbH & Co. KGaA, Weinheim

oxygen atoms which act as bridging atoms between germanium and silicon. Each of the six-faces of the cube is made up of a puckered eight-membered $Ge_2O_4Si_2$ ring. The average bond lengths in **1** are Ge–O 1.7405 Å, Si–O 1.625 Å, and Ge–H (1.39 Å). The Ge-O-Si bond angle (av. 141.86°) indicates the bent nature of this bond. In the eight-membered rings $[(Me_2Ge)_2(Ph_2Si)_2O_4]$,[7a] $[(Cl_2Ge)_2(t\mathrm{BuSi})_2O_4]$,[7b] and $[(Et_2Ge)_2(Ph_2Si)_2O_4]$,[7c] the Ge–O and Si–O bonds are 1.77(6) and 1.60(7), 1.69(4) and 1.63(4), 1.75(5) and 1.61(6) Å, respectively. The Ge-O-Si bond angles observed for these compounds are 136.9(3), 158.8(2), and 142.0(3)°. These parameters compare well with those observed for **1**. The Ge–H bond length in **1** (1.39(2) Å) is similar to that in *p*-anisylgermane (1.40 Å).[13a]

In conclusion, we have prepared the first cubic polyhedral cage compound that contains Ge-O-Si linkages. The formation of this compound occurs by an unprecedented oxidative addition reaction involving the SiOH unit to a germanium(II) center.

Experimental Section

1: $[Ge\{N(SiMe_3)_2\}_2]$ (1.2 g, 3.06 mmol) was slowly added to a stirred suspension of the silanetriol (1.0 g, 3.06 mmol) in hexane (20 mL) and THF (3 mL). During the addition the milky suspension of silanetriol changes to a colorless clear solution. This clear solution was stirred for 12 h at room temperature. The volatile components were removed in vacuo to obtain a white product. To this hexane (9 mL) was added. Colorless crystals of **1** were obtained from the concentrated solution after two days at room temperature. Yield: 0.78 g (64 %), m.p. 251 °C (decomp), ^{1}H NMR (300 MHz, C_6D_6, TMS): $\delta = 0.19$ (s, 36 H, $Si(CH_3)_3$), 1.22, 1.24 (d, $J = 6.85$ Hz, 48 H, $CH(CH_3)_2$), 3.55 (sept, $J = 6.85$ Hz, 8 H, $CH(CH_3)_2$), 5.83 (s, 4 H, Ge*H*), 7.04 ppm (s, 12 H, aromatic); ^{29}Si NMR (99 MHz, C_6D_6, TMS): $\delta = 6.55$ ($SiMe_3$), −87.4 ppm (SiO_3); IR (Nujol, KBr): $\tilde{\nu} = 2211$ (m), 2184 (m, GeH), 1439 (m), 1318 (m), 1248 (s), 1183 (m), 1079 (s), 1045 (s), 1022 (s), 976 (s), 904 (s), 878 (m), 840 (s), 799 (s), 752 (s), 738 (s), 685 (w), 611 (m), 545 (m) cm^{-1}; EIMS (70 eV): *m*/*z* (%) 1592.5 (100) [M^+]; Elemental analysis (%) calcd for $C_{60}H_{108}Ge_4N_4O_{12}Si_8$ (1592.58) C 45.25, H 6.84, N 3.52; found: C 44.80, H 6.94, N 4.05.

Received: June 2, 2004

Keywords: cluster compounds · germanium · hydrides · oxidative addition · silicon

[1] a) V. Chandrasekhar, R. Murugavel, A. Voigt, H. W. Roesky, *Organometallics* **1996**, *15*, 918–922; b) R. Murugavel, A. Voigt, M. G. Walawalkar, H. W. Roesky, *Chem. Rev.* **1996**, *96*, 2205–2236; c) R. Murugavel, V. Chandrasekhar, H. W. Roesky, *Acc. Chem. Res.* **1996**, *29*, 183–189; d) H. J. Gosink, H. W. Roesky, H.-G. Schmidt, M. Noltemeyer, E. Irmer, R. Herbst-Irmer, *Organometallics* **1994**, *13*, 3420–3426.

[2] a) M. L. Montero, A. Voigt, M. Teichert, I. Usón, H. W. Roesky, *Angew. Chem.* **1995**, *107*, 2761–2763; *Angew. Chem. Int. Ed. Engl.* **1995**, *34*, 2504–2506; b) A. Voigt, R. Murugavel, E. Parisini, H. W. Roesky, *Angew. Chem.* **1996**, *108*, 823–825; *Angew. Chem. Int. Ed. Engl.* **1996**, *35*, 748–750; c) A. Voigt, M. G. Walawalkar, R. Murugavel, H. W. Roesky, E. Parisini, P. Lubini, *Angew. Chem.* **1997**, *109*, 2313–2315; *Angew. Chem. Int. Ed. Engl.* **1997**, *36*, 2203–2205; d) G. Anantharaman, V. Chandrasekhar, U. N. Nehete, H. W. Roesky, D. Vidovic, J. Magull, *Organometallics* **2004**, *23*, 2251–2256; e) U. N. Nehete, G. Anantharaman, V. Chandrasekhar, R. Murugavel, M. G. Walawalkar, H. W. Roesky, D. Vidovic, J. Magull, K. Samwer, B. Sass, *Angew. Chem.* **2004**, *116*, 3920–3923; *Angew. Chem. Int. Ed.* **2004**, *43*, 3832–3835; f) U. N. Nehete, V. Chandrasekhar, V. Jancik, H. W. Roesky, R. Herbst-Irmer, *Organometallics* **2004**, *23*, 5372–5374.

[3] a) N. Winkhofer, A. Voigt, H. Dorn, H. W. Roesky, A. Steiner, D. Stalke, A. Reller, *Angew. Chem.* **1994**, *106*, 1414–1416; *Angew. Chem. Int. Ed. Engl.* **1994**, *33*, 1352–1354; b) A. Voigt, R. Murugavel, V. Chandrasekhar, N. Winkhofer, H. W. Roesky, H.-G. Schmidt, I. Usón, *Organometallics* **1996**, *15*, 1610–1613.

[4] a) M. Fujiwara, H. Wessel, H.-S. Park, H. W. Roesky, *Tetrahedron* **2002**, *58*, 239–243; b) M. Fujiwara, H. Wessel, H.-S. Park, H. W. Roesky, *Chem. Mater.* **2002**, *14*, 4975–4981.

[5] A. Voigt, R. Murugavel, H. W. Roesky, *Organometallics* **1996**, *15*, 5097–5101.

[6] U. N. Nehete, V. Chandrasekhar, G. Anantharaman, H. W. Roesky, D. Vidovic, J. Magull, *Angew. Chem.* **2004**, *116*, 3930–3932; *Angew. Chem. Int. Ed.* **2004**, *43*, 3842–3844.

[7] a) H. Puff, M. P. Böckmann, T. R. Kök, W. Schuh, *J. Organomet. Chem.* **1984**, *268*, 197–206; b) A. Mazzah, A. Haoudi-Mazzah, M. Noltemeyer, H. W. Roesky, Z. *Anorg. Allg. Chem.* **1991**, *604*, 93–103; c) M. Akkurt, T. R. Kök, P. Faleschini, L. Randaccio, H. Puff, W. Schuh, *J. Organomet. Chem.* **1994**, *470*, 59–66; d) H. Puff, T. R. Kök, P. Nauroth, W. Schuh, *J. Organomet. Chem.* **1985**, *281*, 141–148; e) J. Beckmann, K. Jurkschat, N. Pieper, M. Schürmann, *Chem. Commun.* **1999**, 1095–1096.

[8] a) F. J. Feher, K. J. Weller, J. J. Schwab, *Organometallics* **1995**, *14*, 2009–2017; b) J. N. Greeley, L. M. Meeuwenberg, M. M. Banaszak Holl, *J. Am. Chem. Soc.* **1998**, *120*, 7776–7782; c) M. A. Said, H. W. Roesky, C. Rennekamp, M. Andruh, H.-G. Schmidt, M. Noltemeyer, *Angew. Chem.* **1999**, *111*, 702–705; *Angew. Chem. Int. Ed.* **1999**, *38*, 661–664.

[9] M. F. Lappert, S. J. Miles, J. L. Atwood, M. J. Zaworotko, A. J. Carty, *J. Organomet. Chem.* **1981**, *212*, C4–C6.

[10] M. J. S. Gynane, D. H. Harris, M. F. Lappert, P. P. Power, P. Rivière, M. Rivière-Baudet, *J. Chem. Soc. Dalton Trans.* **1977**, *20*, 2004–2009.

[11] N. Winkhofer, A. Voigt, H. Dorn, H. W. Roesky, A. Steiner, D. Stalke, A. Reller, *Angew. Chem.* **1994**, *106*, 1414–1416; *Angew. Chem. Int. Ed. Engl.* **1994**, *33*, 1352–1354.

[12] Crystal data for compound **1** $C_{60}H_{108}Ge_4N_4O_{12}Si_8$, $M_r = 1592.58$, monoclinic, space group *C*2/*c*, $a = 26.4229(12)$, $b = 12.5692(6)$, $c = 26.1702(12)$ Å, $\alpha = 90$, $\beta = 112.945(4)°$, $V = 8003.8(6)$ Å^3, $Z = 4$, $\rho_{calcd} = 1.322$ mg m^{-3}, $F(000) = 3328$, $T = 133(2)$ K, $\mu(Mo_{K\alpha}) = 1.660$ mm^{-1}. The data was collected using the ω scan mode in the range of $-31 \le h \le 31$, $-14 \le k \le 14$, $-30 \le l \le 30$. Of 41571 reflections collected, 6890 were unique. Final *R*1 ($I > 2\sigma(I)$) = 0.0252; *wR*2 (all data) = 0.0622. Maximum and minimum heights in the final Fourier difference map were 0.296 and −0.380 e A^{-3}. The colorless single crystals suitable for X-ray diffraction studies of compound **1** were obtained from hexane at room temperature. Diffraction data was collected on a IPDS II Stoe image-plate diffractometer with graphite-monochromated $Mo_{K\alpha}$ radiation ($\lambda = 0.71073$ Å). The structure was solved by direct methods (SHELX-97)[14] and refined against F^2 on all data by full-matrix least squares with SHELX-97.[15] The heavy atoms were refined anisotropically. Hydrogen atoms were included using the riding model with U_{iso} tied to the U_{iso} of the parent atoms. CCDC-236577 (**1**) contains the supplementary crystallographic data for this paper. These data can be obtained free of charge via www.ccdc.cam.ac.uk/conts/retrieving.html (or from the Cambridge Crystallographic Data Centre, 12 Union Road, Cambridge CB2 1EZ, UK; fax: (+44) 1223-336-033; or deposit@ccdc.cam.ac.uk).

 © 2005 Wiley-VCH Verlag GmbH & Co. KGaA, Weinheim

[13] a) F. Riedmiller, G. L. Wegner, A. Jockisch, H. Schmidbaur, *Organometallics* **1999**, *18*, 4317 – 4324; b) C. Brelière, F. Carré, R. J. P. Corriu, G. Royo, *Organometallics* **1988**, *7*, 1006 – 1008; c) A. Castel, P. Riviere, J. Satgé, H. Y. Ko, *Organometallics* **1990**, *9*, 205 – 210.
[14] G. M. Sheldrick, *Acta Crystallogr. Sect. A* **1990**, *46*, 467 – 473.
[15] G. M. Sheldrick, SHELX-97, *Program for Crystal Structure Refinement*, University of Göttingen, Göttingen (Germany), **1997**.

 © 2005 Wiley-VCH Verlag GmbH & Co. KGaA, Weinheim

Living Polymerization

Tri- and Tetracarbanionic Initiators by a Lithium/Halide Exchange Reaction: Application to Star-Polymer Synthesis**

*Rachid Matmour, Arnaud Lebreton, Constantinos Tsitsilianis, Ioannis Kallitsis, Valérie Héroguez, and Yves Gnanou**

Although well described by a mechanism involving the formation of ate complex intermediates, especially in the case of aryl halides, and routinely used for the preparation of simple organolithium reagents, lithium/halogen exchange reactions could never be successfully applied to the synthesis of precisely defined polylithium organic compounds.[1] Indeed polylithiations of multihalide organic molecules by reagents such as *tert*-butyllithium or *sec*-butyllithium are reported to result at best in moderate yields and to afford products with different degrees of substitution.[2–6] The reasons that are generally held responsible for the impracticality of polylithiation, especially when the halogen atoms to be substituted are attached to the same carbon atom or to adjacent carbon atoms, are twofold. α-Lithium halide eliminations and intermolecular couplings between the lithiated reagent and the halide-substituted species are two important competing reactions that have long prevented polylithiation reactions being considered practical. Another reason for the lack of attention paid to multiple metal/halide exchange is the fact that polylithiated compounds have limited solubility in most organic solvents, since they form rather insoluble aggregates.[7]

For instance, in polymer chemistry polylithiation has never been contemplated for the reasons mentioned above; had it been mastered and the experimental conditions worked out, polylithiation would be a viable and straightforward route to prepare multicarbanionic initiators for the synthesis of star-shaped polymers. So far the only possibility of generating such multicarbanionic initiators was lithiation by addition to multivinyl compounds, but the very small number of reports on this synthetic strategy indicates that it is not a convenient route. Indeed it requires the prior synthesis of multivinyl compounds that would not homopolymerize on addition of organolithium reagents.[8] These constraints explain why the only initiator of precise functionality ever synthesized by this method is the tricarbanionic compound of Quirk et al., which was obtained by addition of *sec*-butyllithium to a molecule containing three 1,1-diphenylethylene-type unsaturated moieties.[9]

We report here a novel approach to the preparation of polylithium organic compounds by lithium/halogen exchange and their use as initiators for the synthesis of miscellaneous star polymers by anionic means. This method relies on the metalation of poly(aryl halide)s whose halogen atoms are carried by separate aryl rings and not by adjacent carbon atoms as in previous cases. Unlike regular halogen/metal exchanges, metalation in our case could be conducted at room temperature and in apolar medium, since the polylithiated species formed were unexpectedly found to be soluble in the presence of σ/μ-coordinating ligands; this remarkable feature could be further exploited for star polymer synthesis.

To successfully demonstrate the viability of our method, we utilized commercially available bis(aryl halide) **1** and also designed two poly(aryl halide)s carrying respectively three (**2**) and four (**3**) halo groups, which were synthesized by using reported procedures.[10,11] Compound **2** was obtained from 4-bromoacetophenone diethyl ketal and acetyl chloride with samarium trichloride as catalyst, and **3** was prepared in excellent yields (>90%) by Diels–Alder reaction of 2,3,4,5-tetrakis(*p*-bromophenyl)cyclopentadienone and phenylacetylene with extrusion of carbon monoxide (see Supporting Information for the ^{1}H NMR spectra of **2** and **3**). Next, **1**, **2**, and **3** were treated with stoichiometric amounts of *sec*-butyllithium in benzene to generate **1′**, **2′**, and **3′**, the corresponding di-, tri-, and tetracarbanionic initiators (Scheme 1).

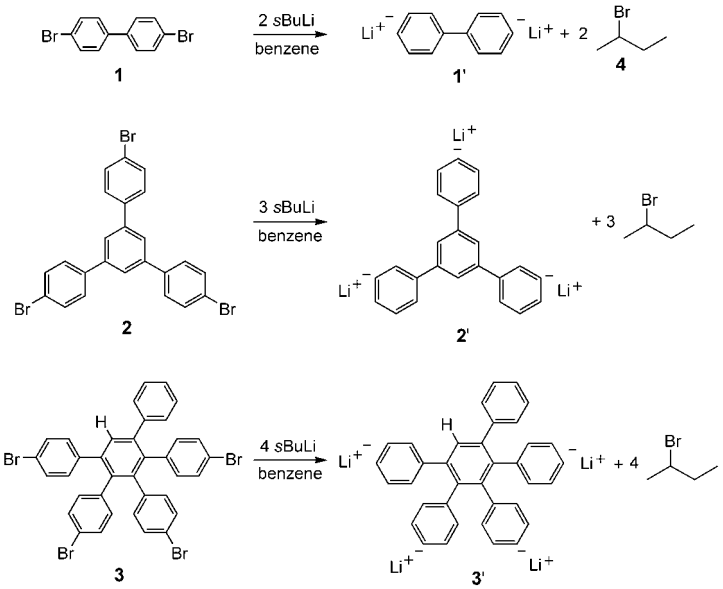
The formation of 2-bromobutane (**4**) was monitored by GC (see Supporting Information). In all three cases the yields were quantitative, and only 2-bromobutane and the corresponding protonated polyaryl compounds were formed as products. No coupling between 2-bromobutane and the polycarbanionic species **1′**, **2′**, or **3′** was ever detected, that is, in apolar medium no such side reactions occurred. However, the resulting polylithiated species were insoluble in benzene and therefore could not be used as such for

[*] R. Matmour, Dr. A. Lebreton, Dr. V. Héroguez, Prof. Y. Gnanou
Laboratoire de Chimie des Polymères Organiques
École Nationale Supérieure de Chimie et Physique de Bordeaux
Université Bordeaux 1
16 Avenue Pey-Berland, 33607 Pessac (France)
Fax: (+33) 5-4000-8487
E-mail: gnanou@enscpb.fr
Prof. I. Kallitsis
Department of Chemistry
University of Patras
26504 Patras (Greece)
Prof. C. Tsitsilianis
Department of Chemical Engineering
University of Patras
26504 Patras (Greece)

[**] The authors thank the CNRS and the French Ministry of Research for support of this research.

Supporting information for this article is available on the WWW under http://www.angewandte.org or from the author.

 © 2005 Wiley-VCH Verlag GmbH & Co. KGaA, Weinheim DOI: 10.1002/anie.200461056



Scheme 1. Synthesis of dilithiated (**1′**), trilithiated (**2′**), and tetralithiated (**3′**) initiators.

initiation purposes; the investigated monomers (styrene, butadiene, 1,1-diphenylethylene) failed to react with these aggregates. Various additives were therefore employed to solubilize the polycarbanionic species. The ligand that proved most efficient at solubilizing these carbanionic aggregates regardless of their functionality was lithium 2-methoxyethoxide (**5**). This σ/μ ligand was previously employed by Teyssié et al. to prevent lithium enolates from aggregating in apolar medium and thus bring about a living anionic polymerization of methacrylic monomers.[12] A ratio of [lithium 2-methoxyethoxide] to [C_6H_4Li groups] of four was necessary to obtain fully soluble initiators in benzene (see Supporting Information). In these attempts at solubilizing **1′**, **2′**, and **3′**, **5** was prepared separately by reaction of *sec*-butyllithium with 2-methoxyethanol, but in the subsequent polymerization experiments **5** was simply generated in situ by addition of *sec*-butyllithium prior to lithium/halide exchange by **1**, **2**, or **3**.

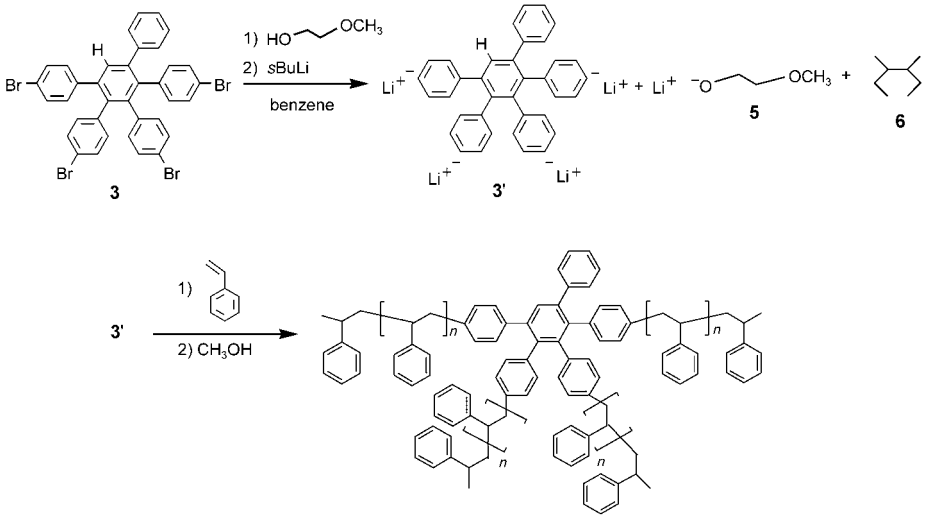
Before triggering polymerization by monomer addition, we managed to neutralize **4** that resulted from the lithium/halide exchange reaction; even though **4** is inert enough not to react with poly(aryl lithium)s **1′**, **2′**, and **3′**, it is sufficiently electrophilic to deactivate the growing carbanionic chains of polystyrene or polybutadiene. Indeed, in a separate experiment conducted under stoichiometric conditions in benzene, we observed such deactivation of polystyryllithium anions by **4** in the presence of *N*,*N*,*N′*,*N′*-tetramethyethylenediamine, when **4** completely disappeared within less than 30 min. To neutralize **4** prior to monomer addition one equivalent of *sec*-butyllithium was added and the formation of 3,4-dimethylhexane (**6**) was monitored by GC (see Supporting Information). After checking that the neutralization of **4** was complete, the polymerization of styrene or butadiene could be triggered by addition of the corresponding monomer (Scheme 2). On deactivation of the living carbanionic chains by ethylene oxide after complete monomer consumption, ω-hydroxy three- and four-armed polystyrene and polybutadiene stars could be isolated from **2′**, **3′** as initiators. α,ω-Dihydroxy telechelic polymers were obtained from **1′**.

Analysis by GC and size exclusion chromatography (SEC) indicated the complete consumption of initiators. No peak attributable to residual **1**, **2**, or **3** could be detected in the low molar mass region, and the only trace seen was a narrow and monomodal peak corresponding to the expected star or linear polymer in the high molar mass region (Figure 1).

Such narrow molar mass distribution ($\bar{M}_w/\bar{M}_n < 1.1$) reflects a rate of initiation by **1′**, **2′**, or **3′** comparable to that of propagation (Table 1). The structure of the polymer formed and specially the star character could be established first by ^{1}H NMR analysis on polybutadiene samples with low degrees of polymerization (see Supporting Information). From the ratio of the integrals of the signal for the aromatic core ($\delta = 6.8$–7.3 ppm) to that for the methylene protons of the $-CH_2OH$ chain ends ($\delta = 3.7$ ppm) the actual functionality of the various samples prepared could be determined: functionalities close to three and four for the three- and four-arm polybutadiene stars, respectively, and close to two for the telechelics were obtained.

Characterization of both linear and star polystyrene and polybutadiene samples by SEC with a light-scattering detector (SEC-LS) also showed an excellent agreement between experimental and expected values of molar masses.

Further evidence for the three- and four-arm star structures was obtained by comparing the intrinsic viscosity [η] of our samples with that of linear polymers. Indeed, a classical



Scheme 2. Synthesis of four-armed polystyrene stars.

 © 2005 Wiley-VCH Verlag GmbH & Co. KGaA, Weinheim

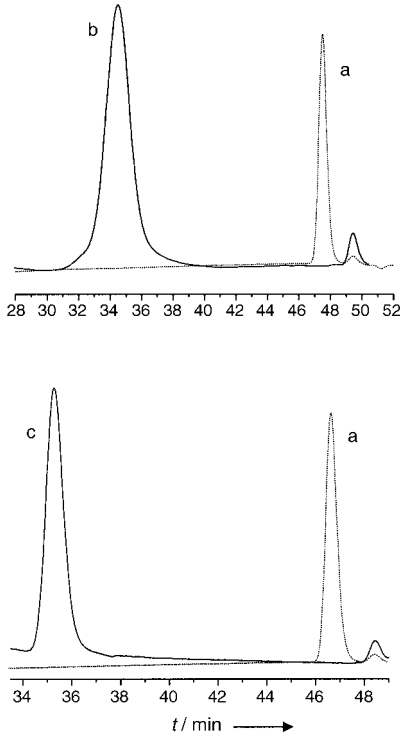
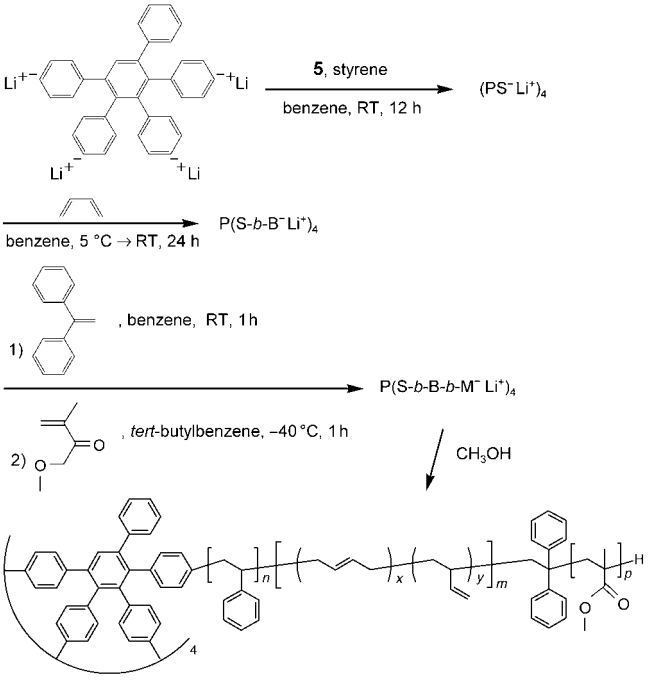


Figure 1. SEC eluograms of $(PS)_4$ polystyrene and $(PB)_4$ polybutadiene stars. a) Protonated version of **3′**. b) Polystyrene star. c) Polybutadiene star.

means to probe starlike architectures and their actual functionality is to determine $g' = [\eta]_{star}/[\eta]_{linear}$. As can be seen in Table 1, the calculated g' values are close to those predicted by theoretical models.[13] These results thus confirm that the target structures were actually obtained and validate the pertinence of our novel approach to star synthesis by anionic means.

After demonstrating the efficiency of these di-, tri-, and tetracarbanionic initiators for the synthesis of polystyrene and polybutadiene telechelics and stars, $(ABC)_n$ ($n = 2$–4) linear and star block terpolymers were derived by sequential anionic polymerization of styrene (S), butadiene (B), and methyl methacrylate (M) with **1′**, **2′**, or **3′** as initiator. These novel architectures—P(S-*b*-B-*b*-M)$_2$ pentablock terpolymers from **1′**, P(S-*b*-B-*b*-M)$_3$ and P(S-*b*-B-*b*-M)$_4$ star block terpolymers from **2′** and **3′**, respectively—were prepared by the same sequence of monomer addition as for the synthesis of P(S-*b*-B-*b*-M) linear block terpolymers (Scheme 3).[14]



Scheme 3. Reaction scheme for the synthesis of SBM star block terpolymers.

Since lithium 2-methoxyethoxide (**5**) was present as an additive to solubilize **1′**, **2′**,or **3′**, methyl methacrylate could be polymerized under living conditions, as disclosed by Teyssié et al.,[12] from polybutadienyllithium anions. Prior to the addition of M, polybutadienyllithium anions were end-capped with 1,1-diphenylethylene (DPE) to reduce the probability of side reactions at the ester group of M while initiating its polymerization. The reaction medium was also diluted with *tert*-butylbenzene and the temperature decreased to −40 °C to further prevent the above-mentioned side reactions. Upon addition of M, the color of the medium changed from the characteristic red of diphenylethyllithium carbanions to colorless. By taking an aliquot before introduction of each type of monomer, the formation of these SBM-based architectures could be easily followed by SEC (see Supporting Information).

The absolute molar mass of the first PS block could be determined by SEC-LS; as for PB and PM blocks their respective molar masses were deduced by ^{1}H NMR spectroscopy, given the known molar masses of their precursors (Table 2,

Table 1: Characterization of PS and PB samples synthesized from initiators **1′**, **2′**, and **3′**.

	$\bar{M}_w$[a]	$\bar{M}_w/\bar{M}_n$[b]	$\bar{M}_{n(theo)}$[c]	f[d]	g'[e]	$g'_{(theo)}$ Zimm–Stockmayer[f]	$g'_{(theo)}$ Berry[g]	$g'_{(theo)}$ Grest[h]
PS_2	11200	1.12	12000	1.9	–	–	–	–
PS_3	90800	1.08	89000	3.0	0.805	0.91	0.88	0.99
	131000	1.13	128000	3.0	0.846	0.91	0.88	0.99
PS_4	38400	1.08	39500	3.9	0.75	0.83	0.79	0.79
	98600	1.08	120000	3.9	0.79	0.83	0.79	0.79
PB_3	32500	1.03	30000	3.0	–	–	–	–
PB_4	16400	1.05	17200	3.9	–	–	–	–

[a] Determined by SEC in THF with a multiangle laser light scattering detector. The dn/dc value was taken equal to that of linear polystyrene (dn/dc = 0.183 cm^3 g^{-1} in THF). [b] Derived from refractometric detector. [c] $\bar{M}_{n(theo)} = M_{styrene} \times$ ([Styrene]/[C_6H_4Li groups]) $\times n$ (n = 2, 3, or 4). [d] Average functionality of the samples as determined by ^{1}H NMR spectroscopy. [e] Experimental values of $g' = [\eta]_{star}/[\eta]_{linear}$. [f] $g'_{R.W.} = (2/f)^{1.5}[0.396(f-1) + 0.196]/0.586$[13a] (R.W. = random walk). [g] $g' = g'^{0.5}_{R.W.} = [(3f-2)/f^2]^{0.5}$.[13b] [h] $g' = K'F^{\beta}$ ($K = 2.37$, $\beta = -0.789$).[13c]

 © 2005 Wiley-VCH Verlag GmbH & Co. KGaA, Weinheim

Table 2: Characterization of P(S-*b*-B-*b*-M)$_2$ pentablock and P(S-*b*-B-*b*-M)$_3$ and P(S-*b*-B-*b*-M)$_4$ star block terpolymer samples.

	PS		P(S-*b*-B)		P(S-*b*-B-*b*-M)		Microstructure
	$\bar{M}_w$[a]	$\bar{M}_w/\bar{M}_n$[b]	$\bar{M}_n$[c]	$\bar{M}_w/\bar{M}_n$[b]	$\bar{M}_n$[c]	$\bar{M}_w/\bar{M}_w$[b]	[%1,2-(B)][d]
(SBM)$_2$	30000	1.09	35000	1.1	41000	1.2	60
(SBM)$_3$	2800	1.08	5700	1.1	7500	1.1	75
(SBM)$_4$	6100	1.05	12100	1.1	16100	1.2	70

[a] Determined by SEC in THF by using a multiangle laser light scattering detector. The d*n*/d*c* value of PS was 0.183 cm^3 g^{-1} in THF. [b] Derived from refractometric detector. [c] Determined by ^{1}H NMR spectroscopy from the molar mass of the polystyrene block, assuming 100% efficiency in the initiation of the second and third blocks. [d] Calculated from ^{1}H NMR spectra.

Figure 2). In all cases narrow molar mass distributions were observed for the three types of structures, that is, the growth of the three blocks occurred under living conditions. In some instances, P(S-*b*-B-*b*-M)$_{3,4}$ star block terpolymers were contaminated with P(S-*b*-B)$_{3,4}$ precursors (less than 10%) but the latter could be easily removed by fractionation through a silica column.

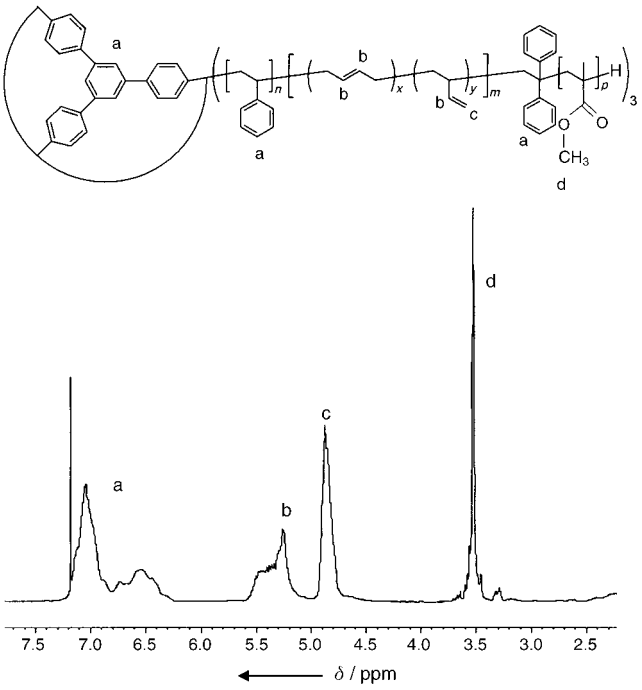


Figure 2. ^{1}H NMR spectrum ($CDCl_3$, 400 MHz) of P(S-*b*-B-*b*-M)$_3$ star block terpolymer.

In summary, halogen/lithium exchange reactions have been successfully applied to generate di-, tri-, and tetracarbanionic species from bis-, tris- and tetrakis-bromoaryl compounds. The use of a σ/μ ligand was instrumental in obtaining polycarbanionic initiators soluble in apolar medium, and the subsequent preparation of various well-defined star-shaped (co)polymers. These are the first examples of three and four-armed polystyrene and polybutadiene stars synthesized by the "core-first" method using anionic polymerization. Analysis of the macromolecular architectures obtained by SEC-LS, ^{1}H NMR spectroscopy, and viscometry all endorse the star character and functionalities of three and four for the samples derived from **2′** and **3′**, respectively. The efficiency of the latter was even exploited to synthesize P(S-*b*-B-*b*-M)$_3$ and P(S-*b*-B-*b*-M)$_4$ star block terpolymers. The phase separation and morphologies that develop in such materials are currently under investigation and will be compared with those reported for linear SBM copolymers.[15] The synthesis of a compound carrying ten bromoaryl moieties by Diels–Alder reaction between a diarylacetylene and a tetraphenylcyclopentadienone is contemplated. Such halogen/metal exchange chemistry is ripe to be applied for the derivatization and/or the selective "construction" of C–C bonds in polycyclic aromatic hydrocarbons.[16]

Received: June 23, 2004
Revised: September 7, 2004

Keywords: carbanions · copolymerization · living polymerization · metalation · star polymers

[1] a) H. Gilman, F. W. Moore, *J. Am. Chem. Soc.* **1940**, *62*, 1843–1846; b) G. Wittig, *Angew. Chem.* **1958**, *70*, 65.
[2] a) R. West, P. C. Jones, *J. Am. Chem. Soc.* **1969**, *91*, 6156–6161; b) R. West, P. A. Carney, I. C. Mineo, *J. Am. Chem. Soc.* **1965**, *87*, 3788–3789.
[3] a) R. West, E. G. Rochow, *J. Org. Chem.* **1953**, *18*, 1739–1742; b) C. Chung, R. J. Lagow, *J. Chem. Soc. Chem. Commun.* **1972**, 1078–1079.
[4] a) F. J. Landro, J. A. Gurak, J. W. Chinn, R. M. Newman, R. J. Lagow, *J. Am. Chem. Soc.* **1982**, *104*, 7345–7346; b) J. A. Gurak, J. W. Chinn, R. J. Lagow in *Chemistry for the Future* (Ed.: H. Grünewald), Pergamon, New York, **1982,** pp. 107–113.
[5] a) J. R. Baran, R. J. Lagow, *J. Am. Chem. Soc.* **1990**, *112*, 9415–9416; b) J. R. Baran, C. Hendrickson, D. A. Laude, R. J. Lagow, *J. Org. Chem.* **1992**, *57*, 3759–3760.
[6] C. Tsitsilianis, G. Vogiagis, J. K. Kallitsis, *Macromol. Rapid Commun.* **2000**, *21*, 1130–1135.
[7] A. W. Kleij, H. Kleijn, J. T. B. H. Jastrzebski, W. J. J. Smeets, A. L. Spek, G. van Koten, *Organometallics* **1999**, *18*, 268–276.
[8] N. G. Vasilenko, E. A. Rebrov, A. M. Muzafarov, B. Eßwein, B. Striegel, M. Möller, *Macromol. Chem. Phys.* **1998**, 199, 889–895.
[9] R. P. Quirk, Y. Tsai, *Macromolecules* **1998**, *31*, 4372–4375.
[10] K. J. Cheng, Z. B. Ding, S. H. Wu, *Synth. Commun.* **1997**, *27*, 11.
[11] J. F. Wolfe, F. E. Arnold, *Macromolecules* **1981**, *14*, 909.
[12] J. S. Wang, R. Jérôme, P. Bayard, M. Patin, P. Teyssié, *Macromolecules* **1994**, 27, 4635.
[13] a) B. H. Zimm, W. H. Stockmayer, *J. Chem. Phys.* **1949**, *17*, 1301; b) G. C. Berry, *J. Polym. Sci. Polym. Phys. Ed.* **1971**, *9*, 687; c) G. S. Grest, L. J. Fetters, J. S. Huang, D. Richter, *Advances in Chemical Physics*, Wiley, New York, **1996**, 94.
[14] V. Krappe, R. Stadler, I. Voigt-Martin, *Macromolecules* **1995**, *28*, 4558.
[15] R. Stadler, C. Auschra, J. Beckman, U. Krappe, I. Voigt-Martin, L. Leibler, *Macromolecules* **1995**, *28*, 3080.
[16] M. Watson, A. Fechtenkötter, K. Müllen, *Chem. Rev.* **2001**, *101*, 1267.

 © 2005 Wiley-VCH Verlag GmbH & Co. KGaA, Weinheim

Mesoporous Silica Nanoparticles

Generalized Fluorocarbon-Surfactant-Mediated Synthesis of Nanoparticles with Various Mesoporous Structures**

*Yu Han and Jackie Y. Ying**

Research on the synthesis of mesoporous materials has mainly focused on mesostructural diversity,[1–4] compositional flexibility,[5–8] and morphological control.[9–12] The ability to obtain mesoporous particles with a controlled particle size would be important for many practical applications. For example, ultrafine mesoporous particles would be very useful in catalysis and gas adsorption, since they would provide greater pore accessibility and facilitate molecular diffusion. They could also act as the host matrix for the synthesis of quantum dots and magnetic nanoparticles in functional materials and bio-imaging applications.[13] Ultrafine mesoporous particles could also act as carriers for drugs, genes, and proteins for novel biomedical applications.[14,15] Some examples of ultrafine mesoporous particles have been sporadically reported,[16–23] but the type of mesostructure, the degree of structural ordering, and the range of pore sizes are limited. Herein we describe a simple wet-chemical method that enables the synthesis of nanometer-sized particles (50–300 nm) with tunable pore sizes in the range 5–30 nm. This fluorocarbon-surfactant-mediated synthesis can be generalized to achieve various pore structures, including 3D cubic $Im\bar{3}m$, 3D cubic $Fm\bar{3}m$, 2D hexagonal $p6m$, foamlike, and disordered pores, as well as different material compositions.

Our syntheses were carried out in a weakly acidic medium (pH 1.6–1.8), in which a homogeneous solution was formed by mixing a soluble silica precursor, a nonionic triblock copolymer surfactant $EO_xPO_yEO_x$ (EO = ethylene oxide, PO = propylene oxide), and the cationic fluorocarbon surfactant FC-4 ($C_3F_7O(CFCF_3CF_2O)_2CFCF_3CONH(CH_2)_3N^+(C_2H_5)_2-CH_3I^-$). In some cases, the organic swelling agent 1,3,5-trimethylbenzene (TMB) was also added to adjust the pore size or vary the mesostructure. Fluorocarbon surfactants have much higher surface activity than common surfactants. Moreover, unlike the hydrocarbon chains of common surfactants, which are hydrophobic but lipophilic, fluorocarbon chains are hydrophobic and lipophobic. Therefore, hydrocarbon and fluorocarbon surfactants are either immiscible or only partially miscible under most conditions.[24]

In our synthetic strategy, the triblock copolymer surfactant would act as the supramolecular template for the periodic mesostructure, whereas the fluorocarbon surfactant would be used to control the growth of mesoporous particles. The process could be described as follows: The weakly acidic conditions would promote a slow hydrolysis of silica precursors, and the hydrolyzed silica species would co-assemble with triblock copolymer surfactants to form well-defined mesophases, whose structures and pore sizes would depend on the type of copolymer and the amount of organic additives. Simultaneously, fluorocarbon surfactants would surround the silica particles through $S^+X^-I^+$ interactions, thereby limiting the growth of silica particles. By this approach, five different mesoporous structures were successfully obtained with nanometer particle sizes (denoted IBN-1 to IBN-5 in Table 1).

Table 1: Mesoporous nanoparticles obtained with the fluorocarbon-surfactant-mediated synthesis.[a]

Sample	Mesostructure	Template	BET surface area [$m^2 g^{-1}$]	Pore volume [$cm^3 g^{-1}$]	Pore size [nm][b]
IBN-1	3D cubic ($Im\bar{3}m$)	F127	779	0.73	5.8
IBN-2	3D cubic ($Fm\bar{3}m$)	F127 + TMB	804	0.65	9.5
IBN-3	mesocellular foam	P65 + TMB	821	0.72	19.5
IBN-4	2D hexagonal ($p6m$)	P123	709	0.88	6.4
IBN-5	disordered	F108	575	0.54	5.2

[a] Fluorocarbon surfactant FC-4 was used in all syntheses to limit the particle size. [b] Calculated from the adsorption branch of the N_2 sorption isotherm by using the BJH method.

Figure 1a shows an SEM image of calcined IBN-1 that was prepared with Pluronic F127 triblock copolymer ($EO_{106}PO_{70}EO_{106}$) and fluorocarbon surfactant FC-4 by using the synthetic approach described above (see Experimental Section for details). IBN-1 was composed of relatively uniform particles of 100–300 nm. A TEM image (Figure 1a, inset) revealed that these particles are well dispersed with little aggregation. The XRD pattern of calcined IBN-1 (Figure 1e) showed two well-resolved peaks with d spacings of 116 and 82 Å, which could respectively be indexed as the 110 and 200 diffractions of cubic symmetry with a lattice constant of $a = 164$ Å. The high-resolution TEM (HRTEM) images of this material taken at [100], [110], and [111] incidences and the corresponding Fourier transforms (FT) are shown in Figure 1b–d, respectively. IBN-1 particles displayed morphologies that were in good accordance with their cubic symmetry (for example, square and hexagonal particle morphologies were observed in [100] and [111] directions, respectively). The highly ordered arrangement of mesopores that could be observed over the entire particle in all cases indicated the high quality of the sample. The reflections in the FT patterns could be indexed as 110, 200,

[*] Dr. Y. Han, Prof. J. Y. Ying
Institute of Bioengineering and Nanotechnology
31 Biopolis Way, The Nanos, #04-01
Singapore 138669 (Singapore)
Fax: (+65) 6478-9020
E-mail: jyying@ibn.a-star.edu.sg

[**] This work was supported by the Institute of Bioengineering and Nanotechnology (Agency for Science, Technology and Research, Singapore). The authors would like thank Dr. Su Seong Lee and Dr. Yiyan Yang for helpful discussions. They are grateful to BASF Corporation and BASF Singapore for providing the Pluronic triblock copolymer surfactants.

Supporting information for this article is available on the WWW under http://www.angewandte.org or from the author.

 © 2005 Wiley-VCH Verlag GmbH & Co. KGaA, Weinheim DOI: 10.1002/anie.200460892

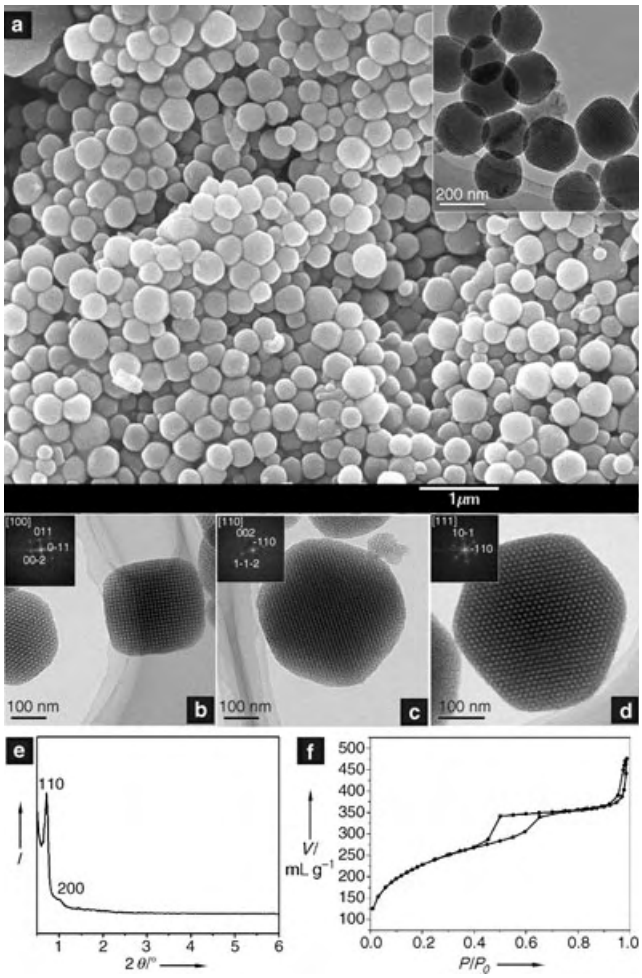


Figure 1. Calcined IBN-1. a) SEM image (inset: TEM image). b)–d) HRTEM images taken at [100], [110], and [111] incidences (insets: the corresponding FT patterns). e) XRD pattern. f) N_2 adsorption/desorption isotherm.

211, and 220 of a cubic phase ($Im\bar{3}m$ space group) with a large lattice constant of $a = 165$ Å, consistent with the XRD findings. IBN-1 has a type IV N_2 adsorption/desorption isotherm with a type-H_2 hysteresis loop (Figure 1 f), which suggests that the mesopores are cagelike. The average pore diameter was calculated to be 5.8 nm from the adsorption branch of the isotherm by using the Barrett–Joyner–Halenda (BJH) method. Besides the well-defined mesopores, this material showed interparticle (textural) porosity (as evidenced by the adsorption step at high relative pressures of > 0.9), which constituted a quarter of the total pore volume of 0.73 $cm^3 g^{-1}$. IBN-1 has a high BET surface area of 779 $m^2 g^{-1}$.

IBN-2 was synthesized under conditions similar to those for IBN-1, except that a large amount of TMB was added (see Table 1). It is composed of well-dispersed particles of 50–300 nm (Figure 2 a). The N_2 sorption isotherm (Figure 2 a, inset) showed that IBN-2 has cage-type pores averaging 9.5 nm in size, which are much larger than those of IBN-1 due to the addition of TMB as swelling agent. High-resolution TEM images taken at various incidences (Figure 2 b–d) showed well-ordered large pores in IBN-2. The spots in the

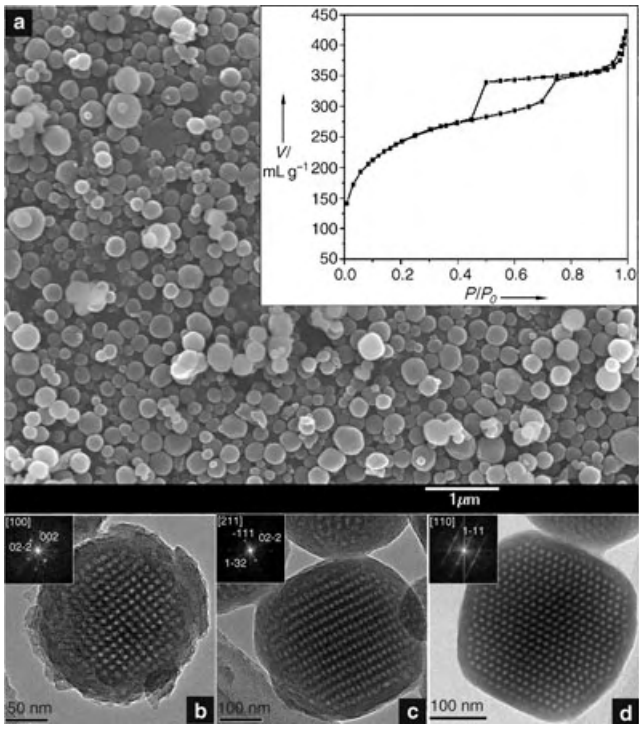


Figure 2. Calcined IBN-2. a) SEM image (inset: N_2 adsorption/desorption isotherm). b)–d) HRTEM images taken at [100], [211], and [110] incidences (inset: corresponding FT patterns).

FT patterns (Figure 2 b–d, insets) were indexed as 111, 200, 220, 311, and 222 reflections of a cubic system with a large lattice constant of $a = 220$ Å. According to extinction rules and previous studies,[25,26] IBN-2 could be assigned to a face-centered cubic structure ($Fm\bar{3}m$). Notably, the FT pattern for [110] incidence showed strong diffuse streaks along the $[1\bar{1}1]$ direction, which suggest the presence of mixed phases. This was confirmed by the corresponding TEM image (Figure 2 d), which illustrated narrow cubic close-packed (ccp, ABCABC…) bands with periodicity in twin relation. In addition, some 3D hexagonal domains with the cages arranged in hexagonal close-packed (hcp, ABAB…) mode were also observed between the cubic twins as a transitional phase (see Supporting Information). This is the first report of an intergrowth of cubic and 3D hexagonal phases in such a small particle; similar intergrowth has been observed in bulk mesoporous silicas such as FDU-1[25] and SBA-12.[26]

Mesocellular foam (MCF) is a novel mesostructured silica material templated by oil-in-water microemulsions.[27,28] The ultralarge mesopores (25–40 nm) have made MCF particularly useful as catalyst support and separation medium for processes involving large substrates. Conventional MCF has a cauliflower-type morphology with a particle size of tens of micrometers.[27] Using our fluorocarbon-surfactant-mediated synthesis, we obtained spherical MCF nanoparticles (50–300 nm), denoted IBN-3 (Figure 3 a). In this synthesis, Pluronic P65 ($EO_{20}PO_{30}EO_{20}$) and TMB were used as the surfactant and oil, respectively, for the formation of a microemulsion template. The ultralarge foamlike pores in the particles obtained could be easily seen by TEM, even at

 © 2005 Wiley-VCH Verlag GmbH & Co. KGaA, Weinheim

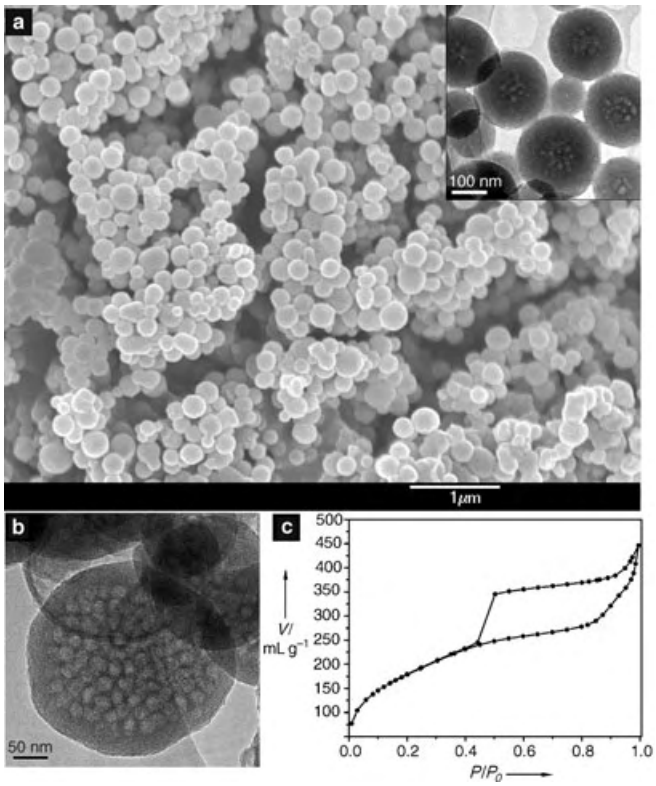


Figure 3. Calcined IBN-3. a) SEM image (inset: TEM image). b) HRTEM image. c) N_2 adsorption/desorption isotherm.

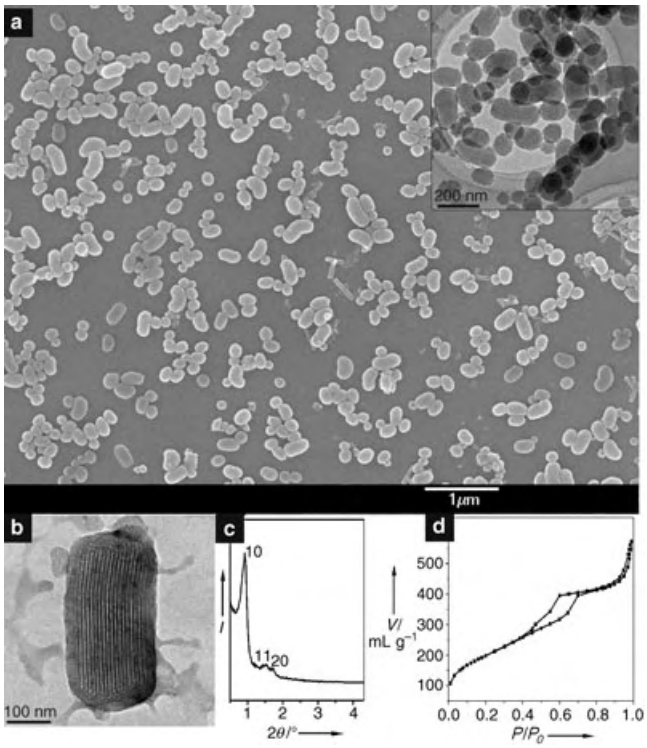


Figure 4. Calcined IBN-4. a) SEM image (inset: TEM image). b) HRTEM image. c) XRD pattern. d) N_2 adsorption/desorption isotherm.

relatively low magnification (Figure 3a, inset). The HRTEM image showed that the pores are about 20 nm in diameter (Figure 3b), consistent with the average adsorption BJH pore size (19.5 nm; Table 1). The pore diameter of IBN-3 could be tailored in the range 15–30 nm, without changing the particle size and morphology, by varying the amount of TMB added in the synthesis.

IBN-1, IBN-2, and IBN-3 all have cage-type mesopores, as evidenced by the type-H_2 hysteresis loops in their sorption isotherms. The fluorocarbon-surfactant-mediated synthesis could also be used to obtain nanoparticles with channel-like mesopores. For example, IBN-4, which was templated by Pluronic P123 ($EO_{20}PO_{70}EO_{20}$), exhibited a mesostructure typical of a 2D hexagonal phase (*p6m*) with a lattice constant of $a = 105$ Å (Figure 4b and c). IBN-4 showed channel-type mesopores with a uniform diameter of 6.4 nm, as calculated from the N_2 sorption isotherm, which has a type-H_1 hysteresis loop (Figure 4d). Most of the IBN-4 particles have a rodlike morphology (200–400 nm long and 50–150 nm wide; Figure 4a), in good accordance with their 2D hexagonal mesostructure.

Periodic mesoporous organosilicas (PMOs) were reported independently in 1999 by three groups.[29–31] We employed 1,2-bis(trimethoxysilyl)ethane and F108 ($EO_{132}PO_{50}EO_{132}$) as precursor and surfactant template, respectively, in our fluorocarbon-surfactant-mediated synthesis to prepare nanoparticles of PMO (IBN-5). The ^{29}Si MAS and ^{13}C CP/MAS NMR spectra (Figure 5d and e) showed that all of the Si atoms in the material are bonded covalently to C atoms and the framework consists of $SiO_{1.5}CH_2CH_2SiO_{1.5}$ structural units. Both SEM and TEM images (Figure 5a and inset) showed that IBN-5 consisted of fairly uniform particles of about 100 nm in size. However, unlike the pure silica materials discussed above, IBN-5 nanoparticles are not well-dispersed. The mesopores in IBN-5 could be observed by TEM, but the contrast was relatively weak (Figure 5a, inset) due to the disordered pore arrangement. Only one peak appeared in the XRD pattern (Figure 5b), a further indication of the lack of long-range order in IBN-5. Nevertheless, the pore size distribution in IBN-5 (centered at ca. 5.2 nm) was still narrow, as illustrated by the sharp step (at $P/P_0 \sim 0.6$) in the adsorption isotherm (Figure 5c). The presence of substantial textural porosity, as judged from the isotherm, revealed that the interparticle voids were still accessible despite the particle agglomeration.

Fluorocarbon surfactant FC-4 was used in all syntheses described above, without which large, irregular mesoporous particles were obtained instead of well-defined nanoparticles. On the other hand, no precipitates were formed if only FC-4 was used without copolymer surfactant. These results illustrate that the use of fluorocarbon surfactant is essential for forming ultrafine particles, while the mesostructures are templated by copolymer surfactant. The function of fluorocarbon surfactant in controlling the particle size is believed to be associated with its special surface activity and immiscibility with copolymer surfactant, which allows them to be enriched at the particle periphery during the particle formation which consequently limits the particle growth. This mechanism is supported by a recent publication which reported the use of a

 © 2005 Wiley-VCH Verlag GmbH & Co. KGaA, Weinheim

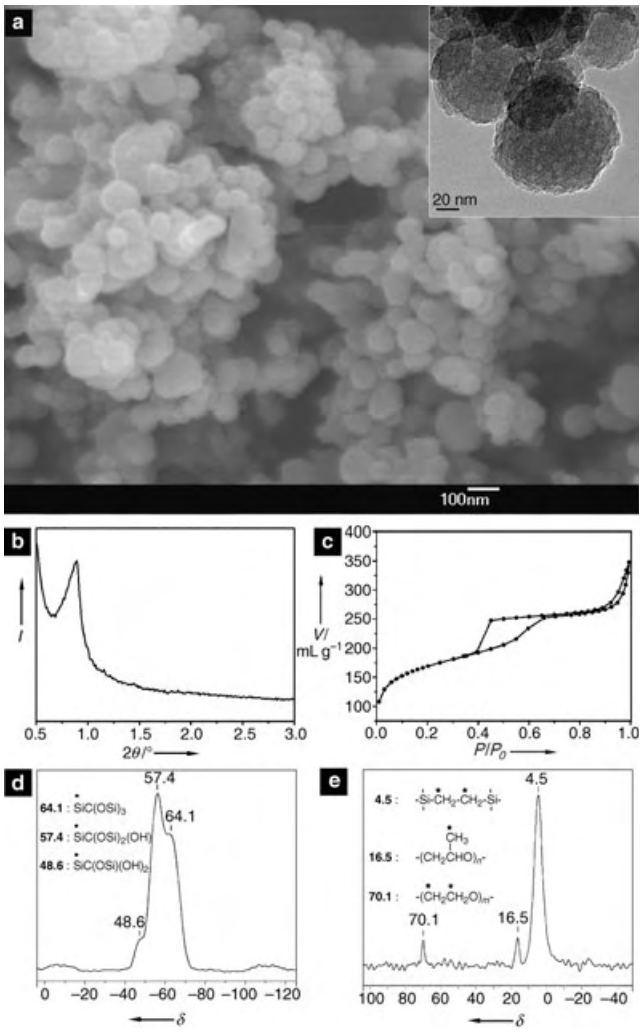


Figure 5. Surfactant-extracted IBN-5. a) SEM image (inset: HRTEM image). b) XRD pattern. c) N_2 adsorption/desorption isotherm. d) ^{29}Si MAS NMR spectrum. e) ^{13}C CP/MAS NMR spectrum (note: the two small peaks at $\delta = 16.5$ ppm and 70.1 ppm were due to C species from residual triblock copolymer surfactant).

mixture of copolymer F127 and cationic fluorocarbon surfactant IC-11 to obtain a new core–shell structure in silica particles.[22] In that study, IC-11 and F127 gave rise to the mesoporosity in the shell and the mesoporosity in the core, respectively, due to the phase separation of fluorocarbon surfactant from copolymer surfactant, with ordered packing of fluorocarbon surfactant around the silica particles. In our case, however, the FC-4 micelles were most likely packed around the silica particles in a disordered manner, since no ordered pattern was observed at the edge of the particles.

The optimal ratio of FC-4 to copolymer surfactant for nanoparticle synthesis depends on the nature of the copolymer. For example, when the concentration of FC-4 was kept within 2.0–2.5 wt%, as used in our syntheses, the triblock copolymers with relatively long hydrophilic EO segments [for example, F127 ($EO_{106}PO_{70}EO_{106}$) and F108 ($EO_{132}PO_{50}EO_{132}$)] could be used over a wide range of concentrations (0.5–3 wt%) to produce IBN-1 and IBN-5, respectively. In contrast, the triblock copolymer with low EO/PO ratio [for example, Pluronic P123 ($EO_{20}PO_{70}EO_{20}$)] had to be used at low concentrations (0.5–1 wt%) in the synthesis of IBN-4, or large particles with an irregular morphology were obtained. This was possibly because different copolymers have different miscibilities with FC-4.[32–34] In general, the longer its hydrophobic PO segment, the more solubilizing power the triblock copolymer has, and therefore the more likely it would form mixed micelles with fluorocarbon surfactant.[32] Thus, a copolymer surfactant with a large hydrophobic volume (for example, P123), would involve most of the FC-4 molecules in forming mixed micelles at relatively high concentrations, but when its concentration was kept low, excess FC-4 molecules would still contribute to controlling particle growth.[34] For cases that involve TMB addition (for example, IBN-2 and IBN-3), low concentrations of copolymer should be used, since TMB will increase the hydrophobic volume of the copolymer micelles, and consequently increase the tendency to form mixed micelles with FC-4.

Moreover, mildly acidic conditions (pH 1.6–1.8) and a moderate reaction temperature (25–30 °C) were necessary for the syntheses. Stronger acidity or higher temperature would promote a rapid, uncontrolled hydrolysis/condensation of silica species which would not lead to the formation of ultrafine particles with a regular morphology. Weaker acidity with a pH value above 2.0 would not promote the co-assembly of surfactant and silica species, and lower reaction temperature would result in materials with poorly ordered mesostructures.

Experimental Section

IBN-1: 0.65 g of Pluronic F127 and 0.8 g of FC-4 were dissolved in 40 mL of aqueous HCl solution (0.02 M), and 2.2 g of tetraethyl orthosilicate (TEOS) was added. The solution was stirred at 30 °C for 20 h, and then transferred to an autoclave for further condensation at 100 °C for 1 d. The product was collected by centrifugation, dried in air, and calcined at 550 °C for 5 h for surfactant removal. Details on the syntheses of other mesoporous nanoparticles are described in the Supporting Information.

XRD patterns were obtained with a Siemens D5005 diffractometer by using $Cu_{K\alpha}$ radiation. SEM images were obtained on a JEOL JSM-6700F electron microscope. TEM experiments were performed on a JEOL JEM-3010 electron microscope with an acceleration voltage of 300 kV. The nitrogen sorption isotherms were obtained with a Micromeritics ASAP 2020M system; the samples were degassed for 10 h at 150 °C before the measurements. ^{29}Si and ^{13}C CP/MAS NMR spectra were recorded with a Bruker AV500WB system with a 4 mm DVT CP/MAS probe; chemical shifts for both spectra were referenced to tetramethylsilane (TMS) at 0 ppm.

Received: June 7, 2004

Keywords: hydrothermal synthesis · mesoporous materials · nanoparticles · silica

[1] Q. Huo, D. I. Margolese, U. Ciesla, P. Feng, T. E. Gier, P. Sieger, R. Leon, P. M. Petroff, F. Schüth, G. D. Stucky, *Nature* **1994**, *368*, 317.

[2] Y. Sakamoto, M. Kaneda, O. Terasaki, D. Zhao, J.-M. Kim, G. D. Stucky, H. J. Shin, R. Ryoo, *Nature* **2000**, *408*, 449.

 © 2005 Wiley-VCH Verlag GmbH & Co. KGaA, Weinheim

[3] D. Zhao, Q. Huo, J. Feng, B. F. Chmelka, G. D. Stucky, *J. Am. Chem. Soc.* **1998**, *120*, 6024.
[4] J. Y. Ying, C. P. Mehnert, M. S. Wong, *Angew. Chem.* **1999**, *111*, 58; *Angew. Chem. Int. Ed.* **1999**, *38*, 56.
[5] B. Tian, X. Liu, B. Tu, C. Yu, J. Fan, L. Wang, S. Xie, G. D. Stucky, D. Zhao, *Nat. Mater.* **2003**, *2*, 159.
[6] D. M. Antonelli, J. Y. Ying, *Angew. Chem.* **1996**, *108*, 461; *Angew. Chem. Int. Ed. Engl.* **1996**, *35*, 426.
[7] F. Schüth, *Chem. Mater.* **2001**, *13*, 3184.
[8] R. Ryoo, S. H. Joo, S. Jun, *J. Phys. Chem. B* **1999**, *103*, 7743.
[9] S. Schacht, Q. Huo, I. G. Voigt-Martin, G. D. Stucky, F. Schüth, *Science* **1996**, *273*, 768.
[10] P. J. Bruinsma, A. Y. Kim, J. Liu, S. Baskaran, *Chem. Mater.* **1997**, *9*, 2507.
[11] H. Yang, N. Coombs, I. Sokolov, G. Ozin, *Nature* **1996**, *381*, 589.
[12] I. A. Aksay, M. Trau, S. Mann, I. Honma, N. Yao, L. Zhou, P. Fenter, P. M. Eisenberger, S. M. Gruner, *Science* **1996**, *273*, 892.
[13] J. Y. Ying, *Sci. Spectra* **1999**, *18*, 56.
[14] C.-Y. Lai, B. G. Trewyn, D. M. Jeftinija, K. Jeftinija, S. Xu, S. Jeftinija, V. S.-Y. Lin, *J. Am. Chem. Soc.* **2003**, *125*, 4451.
[15] Y.-J. Han, G. D. Stucky, A. Butler, *J. Am. Chem. Soc.* **1999**, *121*, 9897.
[16] K. Suzuki, K. Ikari, H. Imai, *J. Am. Chem. Soc.* **2004**, *126*, 462.
[17] S. Sadasivan, F. E. Fowler, D. Khushalani, S. Mann, *Angew. Chem.* **2002**, *114*, 2255; *Angew. Chem. Int. Ed.* **2002**, *41*, 2151.
[18] Q. Cai, Z.-S. Luo, W.-Q. Pang, Y.-W. Fan, X.-H. Chen, F.-Z. Cui, *Chem. Mater.* **2001**, *13*, 258.
[19] R. I. Nooney, D. Thirunavukkarasu, Y. Chen, R. Josephs, A. E. Ostafin, *Chem. Mater.* **2002**, *14*, 4721.
[20] W. Zhao, Q. Li, *Chem. Mater.* **2003**, *15*, 4160.
[21] Y. Lu, H. Fan, A. Stump, T. L. Ward, T. Rieker, C. J. Brinker, *Nature* **1999**, *398*, 223.
[22] S. Areva, C. Boissière, D. Grosso, T. Asakawa, C. Sanchez, M. Lindén, *Chem. Commun.* **2004**, 1630.
[23] D. Grosso, E. L. Crepaldi, B. Charleux, C. Sanchez, *Adv. Funct. Mater.* **2003**, *13*, 37.
[24] M. Almgren, K. Wang, *Langmuir*, **1997**, *13*, 4535.
[25] J. R. Matos, M. Kruk, L. P. Mercuri, M. Jaroniec, L. Zhao, T. Kamiyama, O. Terasaki, T. J. Pinnavaia, Y. Liu, *J. Am. Chem. Soc.* **2003**, *125*, 821.
[26] Y. Sakamoto, I. Diaz, O. Terasaki, D. Zhao, J. Perez-Pariente, J. Kim, G. D. Stucky, *J. Phys. Chem. B* **2002**, *106*, 3118.
[27] P. Schmidt-Winkel, P. Yang, D. I. Margolese, J. S. Lettow, J. Y. Ying, G. D. Stucky, *Chem. Mater.* **2000**, *12*, 686.
[28] J. S. Lettow, Y. J. Han, P. Schmidt-Winkel, P. Yang, D. Zhao, G. D. Stucky, J. Y. Ying, *Langmuir* **2000**, *16*, 8291.
[29] T. Asefa, M. J. MacLachlan, N. Coombs, G. A. Ozin, *Nature* **1999**, *402*, 867.
[30] S. Inagaki, S. Guan, Y. Fukushima, T. Ohsuna, O. Terasaki, *J. Am. Chem. Soc.* **1999**, *121*, 9611.
[31] B. J. Melde, B. T. Holland, C. F. Blanford, A. Stein, *Chem. Mater.* **1999**, *11*, 3302.
[32] N. Funasaki, S. Hada, *J. Phys. Chem.* **1983**, *87*, 342.
[33] Y. Muto, K. Esumi, K. Meguro, R. Zana, *J. Colloid Interface Sci.* **1987**, *120*, 162.
[34] Y. Han, D. Li, L. Zhao, F.-S. Xiao, *Angew. Chem.* **2003**, *115*, 3761; *Angew. Chem. Int. Ed.* **2003**, *42*, 3633.

 © 2005 Wiley-VCH Verlag GmbH & Co. KGaA, Weinheim

Conducting Materials

The First Proton-Conducting Metallic Ion-Radical Salts**

Akane Akutsu-Sato, Hiroki Akutsu, Scott S. Turner, Peter Day, Michael R. Probert, Judith A. K. Howard, Tomoyuki Akutagawa, Sadamu Takeda, Takayoshi Nakamura, and Takehiko Mori*

Metallic materials that also conduct protons are being sought because of their potential as components in solid-state electrochemical devices, such as batteries and fuel cells.[1] To date, the search has concentrated mainly on purely inorganic materials, and in particular continuous lattice oxides. In fact, there is a clear lack of candidates among electronically conducting organic molecular crystals, despite the existence of proton-conducting polymers, such as perfluorinated Nafion. Recently a 2,2′-[2,5-cyclohexadiene-1,4-diylidene]-bis(propanedinitrile) (TCNQ) charge transfer complex of benzimidazolyl–benzimidazole was shown to exhibit coupled protonic and electronic conductivity, and a TCNQ complex of 1,4-diazabicylo[2.2.2]octane also exhibited proton transfer.[2] Herein we report what we believe to be the first molecular ion-radical salts that are metallic conductors at room temperature, and also show a high proton conductivity. We provide evidence that the mobility of both protons and electrons is

[*] Dr. A. Akutsu-Sato, Dr. H. Akutsu, Dr. S. S. Turner, Prof. P. Day
Davy–Faraday Research Laboratory (DFRL)
Royal Institution of Great Britain
21 Albemarle Street, London, W1S 4BS (United Kingdom)
Fax: (+44) 20-7629-3569
E-mail: pday@ri.ac.uk

Dr. S. S. Turner
School of Biological and Chemical Sciences
Department of Chemistry, University of Exeter
Exeter, EX4 4QD (United Kingdom)

M. R. Probert, Prof. J. A. K. Howard
Department of Chemistry, University of Durham
South Road, Durham, DH1 3LE (United Kingdom)

Dr. H. Akutsu
Graduate School of Material Science
University of Hyogo, Hyogo, 678-1297 (Japan)

Dr. A. Akutsu-Sato, Prof. T. Mori
Department of Organic and Polymeric Materials
Tokyo Institute of Technology
O-okayama, Megaru-ku, Tokyo, 113-0033 (Japan)

Prof. T. Akutagawa, Prof. T. Nakamura
Research Institute for Electronic Science
Hokkaido University, Sapporo, 060-0812 (Japan)

Prof. S. Takeda
Division of Chemistry, Graduate School of Science
Hokkaido University, Sapporo, 060-0812 (Japan)

[**] This work was supported by the Engineering and Physical Sciences Research Council, EPSRC, (UK), and Monbukagakusho (Japanese Ministry for Education, Culture, Sports, Science and Technology). H.A. and A.A.-S. wish to thank the Japanese Society for the Promotion of Science (JSPS) for postdoctoral fellowships at the DFRL. JAKH thanks the EPSRC for a Senior Research Fellowship.

 © 2005 Wiley-VCH Verlag GmbH & Co. KGaA, Weinheim DOI: 10.1002/anie.200461686

high in these lattices because of a unique crystal structure consisting of layers of organic donor molecules interleaved with arrays of stacked crown ether molecules. The crown ether molecules form "pipes" filled with water molecules. The crystal structure, resolved from X-ray data recorded at 30 K,[3] gives strong indication of a hydrogen-bonding network, which gives rise to the protonic conductivity.

The series of cation-radical salts (BEDT-TTF)$_4$[(Cat)M-(C_2O_4)$_3$]G, where BEDT-TTF = bis(ethylenedithio)tetrathiafulvalene, has proven to be an exceptionally fruitful source of different collective electronic ground states, promoted by the ease with which the monocation Cat, 3d metal M^{3+}, and neutral guest molecule G can be varied. Thus we found the first examples of paramagnetic superconductors (Cat = H_3O; M = Cr, Fe; G = PhCN, $PhNO_2$)[4] and the first case of polymorphism, in the whole realm of solid-state chemistry, that arose from different spatial distributions of chiral enantiomers $[M(C_2O_4)_3]^{3-}$ in a racemic lattice.[5] By inserting asymmetrically substituted aromatic G molecules in cavities within the anion sublattice, it has also been possible to synthesize unique conducting salts containing a superlattice of two different packing types (α and β'') of the BEDT-TTF cations.[6] The present salts also contain superlattices of cation layers but, instead of being made up from two different arrangements of the BEDT-TTF molecules, they consist of BEDT-TTF and crown ether molecules that incorporate both H_2O and H_3O^+ or NH_4^+ ions.

β''-(BEDT-TTF)$_4$[(Cat)M^{III}(C_2O_4)$_3$]$_2$[(Cat)$_2$([18]crown-6 ether)]·5H_2O, where M^{III} is Cr or Ga (**1** and **2**, respectively) and Cat is H_3O^+ or NH_4^+, were synthesized by electrochemical crystallization. Both **1** and **2** crystallized in the triclinic space group ($P\bar{1}$). From single-crystal X-ray diffraction data recorded at 150 K,[7] the structure of the Cr salt has been resolved, with all Cat molecules assigned to H_3O^+. X-ray data recorded at 30 K on the Ga salt established the molecular structure, but in addition enabled many of the protons to be resolved.[8] The crystal structure consists of successive layers of BEDT-TTF with a β'' packing motif (layer A), Δ-[(Cat)M(C_2O_4)$_3$] (layer B), (Cat/H_2O)·[18]crown-6 (layer C), and Λ-[(Cat)M(C_2O_4)$_3$] (layer D) arranged in the sequence …ABCDA… (Figure 1). Within experimental error the C–C and C–S bond lengths of the crystallographically inequivalent BEDT-TTF are equal and from the correlation between bond length and charge in BEDT-TTF salts,[9] these identify a mean charge on each cation of +0.5, as seen in the β'' phase paramagnetic superconductors.

Considering the stoichiometry of **1** and **2** and the known charges of the molecular species, overall charge neutrality requires four monocations (Cat), which could be H_3O^+ or NH_4^+. The 30 K structure refinement of **2** confirms the Cat molecules, embedded in the anionic oxalate layers, are all well ordered NH_4^+ ions. In this case there is a marginal improvement in the residual factors for occupancy by nitrogen as compared to oxygen. The remaining cations are predicted to be located in the channels formed by the stack of crown ether molecules. The water molecules found in the channels, refined with a fixed 50% occupancy, form zigzag hydrogen-bonded chains that align with the axis of the crown ether stacks. Additional electron density is located, off the stack axis between adjacent crown ether molecules. Refinements were carried out to try to distinguish between the preferred occupancy of these sites as oxygen or as nitrogen atoms, but these refinements were inconclusive. Despite the very low-temperature diffraction data, there is not sufficient information therein to identify individual atomic sites for occupancy by nitrogen or oxygen in these channel regions. Figure 2 shows the zigzag hydrogen-bonded network within the crown ether stacks, with these atoms assigned as oxygen.

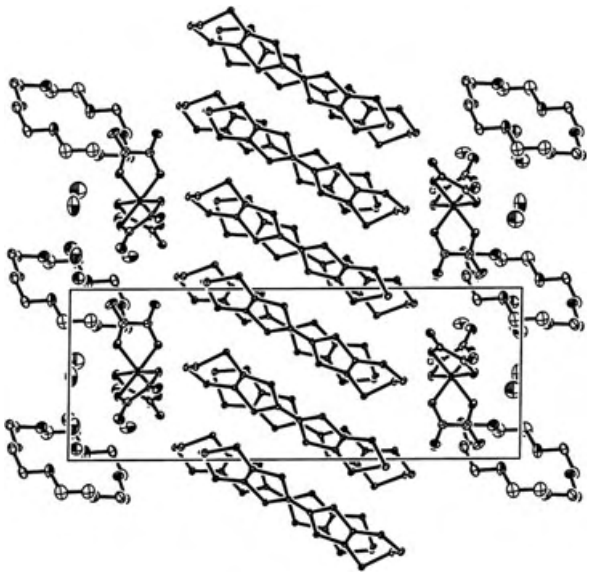


Figure 1. The crystal structure of **2** at 30 K, showing the sequence of BEDT-TTF, [(Cat)Ga(C_2O_4)$_3$], and crown ether layers. Protons have been removed for clarity.

Four-probe DC electrical conductivity measurements on single crystals of **1** and **2** with current flow parallel to the layers reveals high electronic conductivities at room temperature (300 $S\,cm^{-1}$ for **1** and 200 $S\,cm^{-1}$ and **2**) with temperature dependence characteristic of a metal. However, in each case the resistance shows an upturn at lower temperature, which occurs at 190 K for **1** and 240 K and **2** (Figure 3). These metal–semiconductor transitions contrast with the behavior of other BEDT-TTF salts of tris(oxalato)metallates, which have metal–superconducting transitions.[4]

Measurements of proton conductivity of **1** and **2** from 260–297 K made on pellet samples, show specific conductivities varying from 10^{-6} to 10^{-3} $S\,cm^{-1}$ over this temperature range (Figure 4a). For each compound the conductivity is activated, as anticipated, but does not follow a simple Arrhenius Law. Instead the measured activation energies change slightly for **1** from 1.06–1.59 eV and for **2** from 1.01–1.92 eV with the lower activation energy at higher temperatures and a gradual change across approximately 280 K. For a similar measurement on Nafion 117 (Figure 4a) there is a constant activation energy of 0.27 eV. A slight discontinuity in protonic conductivity at about 280 K can be seen clearly in Figure 4a for **1** and to a lesser extent for **2**. Typical complex impedance plots are shown for **1** in Figure 4b. The relatively high values of the room-temperature specific conductivity are comparable to those found in polymeric electrolytes of the polyethylene oxide type.[10] The mechanism of the proton

 © 2005 Wiley-VCH Verlag GmbH & Co. KGaA, Weinheim

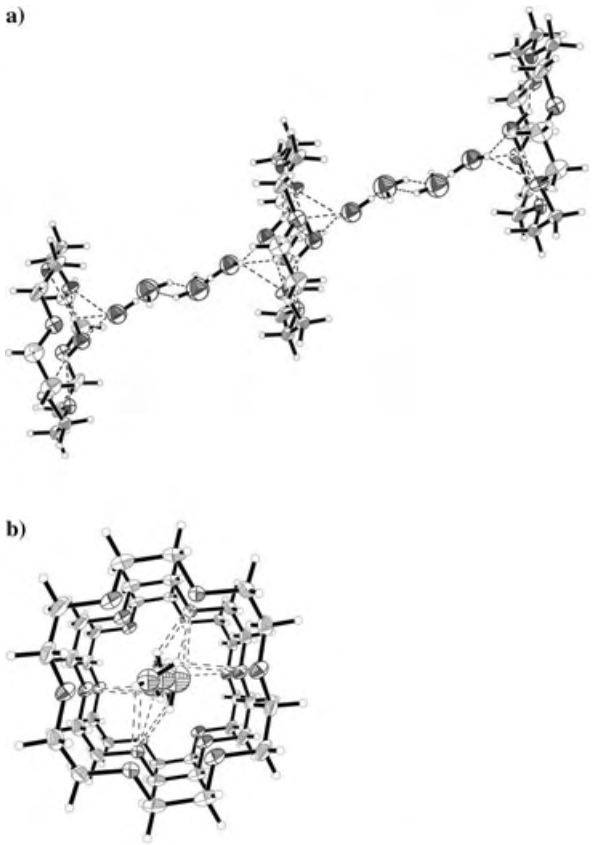


Figure 2. Hydrogen-bonding (broken lines) of water molecules within the crown ether stacks of **2** a) perpendicular and b) parallel to the stacks. O black ellipsoids, H small gray circles, C gray ellipsoids.

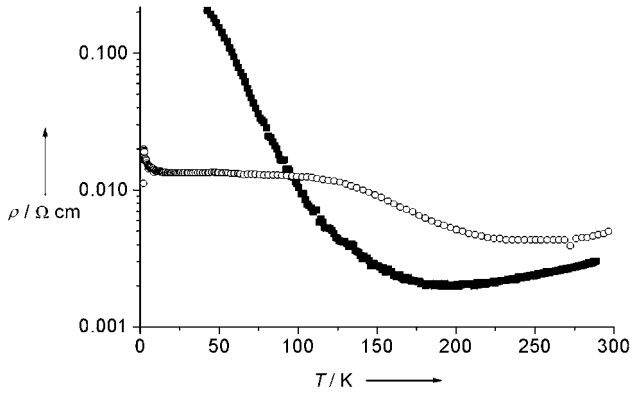


Figure 3. Four-probe single-crystal electronic conductivity of **1** (■) and **2** (○).

conductivity is not known. However, it has been established that significant proton conductivity can be mediated by a diffusion mechanism involving NH_4^+/H_2O or NH_4^+/H_3O^+ species. The former has been found in $(NH_4)_4[Fe(CN)_6]\cdot 1.5\,H_2O$ and the latter in the polytungstate $(NH_4)_{10}[W_{12}O_{41}]\cdot 5\,H_2O$,[13] albeit with smaller absolute conductivities than the compounds presented herein.

Solid-state NMR spectra were studied as a function of the temperature in the diamagnetic salt **2**, under magic-angle spinning (MAS) and static conditions. At room temperature, the high-resolution ^1H spectrum of a fully protonated sample

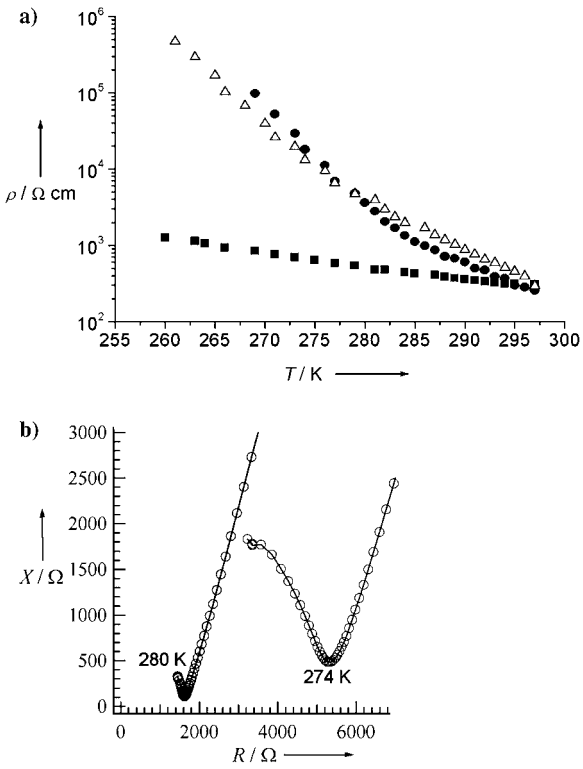


Figure 4. a) Proton conductivity of **1** (△), **2** (●), and Nafion 117 (■) from 260–297 K with logarithmic y axis; b) typical complex impedance plots for **1** at 274 and 280 K.

consisted of three resonance signals A ($\delta = 7.7$ ppm), B ($\delta = 4.3$ ppm), and C ($\delta = 4.8$ ppm) with intensity ratio 1:0.3:>2 and widths of 1.6, 0.6, and 7.4 ppm, respectively. Signal A can be assigned to H_2O, H_3O^+ (and/or NH_4^+) since it corresponds to a signal, found in the ^2H NMR spectrum, which appears when a sample is prepared with D_2O. A separate experiment indicates that the chemical shift of ND_4 is $\delta = 7.4$ ppm, similar to the shift of signal A. It is difficult to distinguish between deuterated water and this species since the details of hydrogen bonding, not known from crystallography, could affect the chemical shifts. Signal C is assigned to the $-CH_2-$ group of BEDT-TTF and the [18]crown-6 ether. The assignment of signal C is supported by its behavior at low temperature; in the wide-line ^1H NMR spectrum at 130 K it splits into a doublet with a separation of approximately 30 kHz, which is typical for the nuclear dipole interaction between the two protons in a $-CH_2-$ group. Furthermore, the signal is absent in the ^2H NMR spectrum of the sample when exchanged with D_2O. Signal B, which is much weaker and narrower than the other two, is tentatively assigned to water molecules adsorbed on the surface of the crystallites. The increasing line width of signal C in the wide-line ^1H NMR spectrum of the fully protonated sample (Figure 5) clearly indicates freezing of the thermal fluctuations of the $-CH_2-$ on lowering the temperature. In contrast, the width of signal A, remains relatively constant and small (11 kHz) between 130 and 250 K before decreasing further between 250 and 300 K. The ^2H NMR spectrum of the D_2O sample further confirms an almost isotropic and rapid rotation of those molecules producing signal A, at least down to 195 K.

 © 2005 Wiley-VCH Verlag GmbH & Co. KGaA, Weinheim

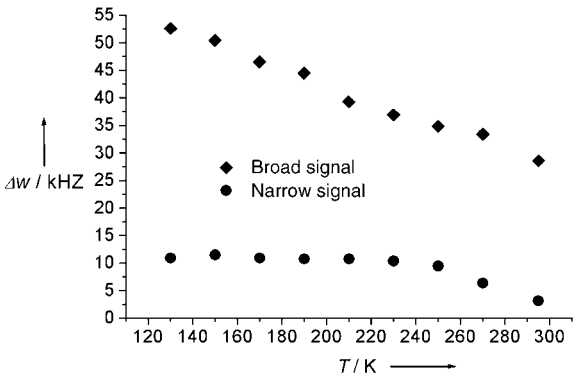


Figure 5. Temperature dependence of the spectral width (Δw) of the wide-line ^{1}H NMR spectra of a fully ^{1}H substituted sample of **2**. The spectral width of BEDT-TTF and [18]crown-6 $-CH_2-$ groups (◆) and of H_2O (●) including the weak signal (signal B, see text) are shown.

In summary, we have identified the first molecular ion-radical salts that are both protonic and metallic conductors. The high values of both the ionic and electronic conductivities at room temperature are especially noteworthy and are attributed to the presence of discrete conducting layers in the crystal consisting of either organosulfur molecules or of crown ether stacks containing disordered H_2O, H_3O, and/or NH_4. This discovery expands the search for other mixed ionic-electronic conductors among the large and versatile family of TTF and BEDT-TTF ion-radical salts.

Experimental Section

The BEDT-TTF salts were prepared by in situ oxidation of BEDT-TTF (12 mg) in an H-shaped electrochemical cell in the presence of a racemic solution of $(NH_4)_3[M(C_2O_4)_3]$ (M = Cr, Ga; 120 mg), [18]crown-6-ether (250 mg) and four drops of distilled H_2O in a mixture of freshly distilled CH_3CN (10 mL) and CH_2Cl_2 (10 mL). A constant current of 1 μA was applied across the cell and thin dark brown elongated plates of the product grew on the Pt anode in 2–3 days. Elemental analysis calcd (%) for (BEDT-TTF)$_4$[$(NH_4)M(C_2O_4)_3$]$_2$[$(NH_4)_2$([18]crown-6)]·5H_2O): **1** C 29.58, H 3.18, N 2.16; found: C 29.48, H 2.91, N 1.70; **2** C 29.30, H 2.77, N 2.14; found: C 29.47, H 2.82, N 2.17

Single-crystal DC conductivity were made using four contacts (15 μm diameter Au wires attached to the crystals with Au paste) and an Oxford Instruments Maglab 2000 cryostat with EP probe.

Temperature-dependent protonic conductivity was measured by the AC impedance method in the frequency range $100–5\times10^6$ Hz using an HP4194A impedance analyzer. The sample, prepared as a compressed pellet with a diameter of 3 mm, was enclosed by a Teflon ring to avoid short circuit, this pellet was then sandwiched by proton-conducting Nafion 117 (Aldrich). The sample was clamped by metal electrodes, and was inserted into a Daikin PS24SS cryogenic refrigerating system. The conductivity was measured in vacuo ($<10^{-3}$ torr).

Solid-state high-resolution ^{1}H and ^{2}H NMR spectra were measured by a magic-angle spinning technique with spinning speed of 25 (^{1}H NMR) and 7 kHz (^{2}H NMR) using a Bruker DSX 300 spectrometer. Echo pulse sequence synchronized with spinning speed was used for ensuring the phase of all spinning side-band signals. The thermometers of the NMR probes were calibrated by standard samples. Wide-line ^{1}H NMR spectrum under static conditions was measured by the solid echo pulse sequence $\pi/2_x$-τ-$\pi/2_y$; the $\pi/2$ pulse width and τ were 1.5 μs and 15 μs, respectively.

Received: August 17, 2004

Keywords: conducting materials · electron transport · ion channels · proton transport

[1] For example see W. R. M. Kinnon in *Solid State Electrochemistry* (Ed.: P. G. Bruce), Cambridge University, **1994**, pp. 163–178.

[2] a) T. Akutagawa, T. Hasegawa, T. Nakamura, T. Inabe, G. Saito, *Chem. Eur. J.* **2002**, *8*, 4402–4411; b) T. Akutagawa, S. Takeda, T. Hasegawa, T. Nakamura, *J. Am. Chem. Soc.* **2004**, *126*, 291–294.

[3] A. E. Goeta, L. K. Thompson, C. L. Sheppard, S. S. Tandon, C. W. Lehmann, J. Cosier, C. Webster, J. A. K. Howard, *Acta. Cryst.* **1999**, *C5*, 1243–1246.

[4] a) M. Kurmoo, A. W. Graham, P. Day, S. J. Coles, M. B. Hursthouse, J. L. Caulfield, J. Singleton, F. L. Pratt, W. Hayes, L. Ducasse, P. Guionneau, *J. Am. Chem. Soc.* **1995**, *117*, 12209–12217; b) S. Rashid, S. S. Turner, P. Day, J. A. K. Howard, P. Guionneau, E. J. L. McInnes, F. E. Mabbs, R. J. H. Clark, S. Firth, T. Biggs, *J. Mater. Chem.* **2001**, *11*, 2095–2101.

[5] a) L. Martin, S. S. Turner, P. Day, K. M. A. Malik, S. J. Coles, M. B. Hursthouse, *Chem. Commun.* **1999**, 513–514; b) L. Martin, S. S. Turner, P. Day, P. Guionneau, J. A. K. Howard, K. M. A. Malik, M. B. Hursthouse, M. Uruichi, K. Yakushi, *Inorg. Chem.* **2001**, *40*, 1363–1371.

[6] H. Akutsu, A. Akutsu-Sato, S. S. Turner, P. Day, E. Canadell, S. Firth, R. J. H. Clark, J. Yamada, S. Nakatsuji, *Chem. Commun.* **2004**, *1*, 18–19.

[7] S. Rashid, S. S. Turner, P. Day, M. E. Light, M. B. Hursthouse, S. Firth, R. J. H. Clark, *Chem. Commun.* **2001**, 1462–1463.

[8] Crystallographic data for **2**: $C_{64}H_{79}Ga_2N_2O_{37}S_{32}$, $M_r = 2633.65$, dark red crystal, crystal size $= 0.3\times0.25\times0.02$ mm^3, triclinic, $P\bar{1}$, $a = 10.2070(3)$, $b = 11.2012(3)$, $c = 24.2433(6)$ Å, $\alpha = 88.4170(10)$, $\beta = 24.2433(6)$, $\gamma = 63.4470(10)°$, $V = 2478.15(12)$ Å^3, $Z = 1$, $\rho_{calcd} = 1.766$ g cm^{-3}, $\mu = 1.302$ mm^{-1}, graphite monochromated $Mo_{K\alpha}$ radiation ($\lambda = 0.71073$ Å), $T = 30(2)$ K, 10910 independent reflections of which 9167 with $F_0 > 4\sigma(F_0)$ were included in the refinement, $R_{int} = 0.026$, max residual density $= 0.859$ e Å^{-3}, $R_1 = 0.0357$, $wR_2 = 0.0794$. Data were collected through ω-scans, at 30 K, using an Oxford Cryosystems HELIX,[3] on a Bruker SMART 1K diffractometer. A numerical absorption correction was applied using SADABS.[11] The structure was solved by direct methods and refined using full-matrix least-squares methods (SHELX97),[12] with all fully occupied atoms having position and thermal-displacement parameters refined. Hydrogen atoms were placed by Fourier and geometric methods, and refined as riding atoms. Multiple refinements were attempted to definitively determine the cations between adjacent crown ether molecules. The final model was chosen as it give the best residual Fourier map. CCDC-234609 (**2**) contains the supplementary crystallographic data for this paper. These data can be obtained free of charge via www.ccdc.cam.ac.uk/conts/retrieving.html (or from the Cambridge Crystallographic Data Centre, 12 Union Road, Cambridge CB2 1EZ, UK; fax: (+44) 1223-336-033; or deposit@ccdc.cam.ac.uk).

[9] a) P. Guionneau, C. J. Kepert, D. Chasseau, M. R. Truter, P. Day, *Synth. Met.* **1997**, *86*, 1973–1974; b) P. Guionneau, PhD thesis, Université de Bordeaux I (France), **1996**.

[10] M. F. Daniel, B. Desbat, J. C. Lassegues, *Solid State Ionics* **1988**, *28–30*, 632.

[11] G. M. Sheldrick, *SADABS* Empirical absorption correction program, University of Göttingen, Göttingen, **1997**.

[12] *SHETXTL* version 5.1, Bruker Analytical X-ray instruments, Madison, Wisconsin, U.S.A., **1999**.

[13] *Proton Conductors, Solids, Membranes and Gels: Materials and Devices* (Ed.: P. Colomban), CUP, Cambridge, **1992**, p. 25.

 © 2005 Wiley-VCH Verlag GmbH & Co. KGaA, Weinheim

Molecular Recognition

1D Saturation Transfer Difference NMR Experiments on Living Cells: The DC-SIGN/ Oligomannose Interaction**

Silvia Mari, Diego Serrano-Gómez, F. Javier Cañada, Angel L. Corbí, and Jesús Jiménez-Barbero**

Dedicated to Professor Luis Castedo on the occasion of his 65th birthday

Molecular recognition by specific targets is at the heart of the drug discovery process. Recently, it has been demonstrated that NMR screening is ideal for finding ligands that bind to a receptor.[1] Although modern NMR experiments and technologies permits the exploration of the interaction process using nanomole quantities of the receptor, in some cases the availability of the target protein might pose a problem in the detection of the molecular recognition event, especially in the case of membrane-bound proteins. On this basis, we hypothesized that receptor-rich living cells could be used as a first step to screen the binding of different molecules to some types of receptors. The study of the role of the carbohydrate-binding C-type lectin and lectin-like receptors in the immune system is a topic of current interest. In particular, the dendritic-cell-specific ICAM-3-grabbing non-integrin (DC-SIGN) receptor[2] mediates the binding and internalization of a large array of pathogens including HIV,[3] Ebola virus,[4] SARS-CoV,[5] *Leishmania* amastigotes,[6] *Mycobacterium tuberculosis*,[7] *Schistosoma mansoni*, *Helicobacter pylori*,[8] and *Candida*[9] in a Man- or Fuc-dependent manner.[10] Moreover, DC-SIGN plays an important role in the establishment of the initial contact between the dendritic cell and naive T lymphocytes through recognition of ICAM-3,[2] and also mediates dendritic cell trafficking through interactions with endothelial ICAM-2.[11] In this context, *Saccharomyces cerevisiae* mannan has been shown to compete with most of these DC-SIGN-dependent pathogen recognitions.[12] Herein, we demonstrate that the direct interaction between the DC-SIGN receptor and *S. cerevisiae* mannan may be easily detected by simple 1D saturation transfer difference (STD) NMR experiments[13] that employ living cells directly, without the necessity for isolating the protein receptor. This evidence may open new avenues in the drug discovery process, since NMR spectroscopy may also provide key structural information.

The cell line K562 transfected with the prototype DC-SIGN, namely K562-CD209 (DC-SIGN+),[12] and mock-transfected K562 (DC-SIGN−) were employed. These two cell types differ only in the expression of the receptor DC-SIGN on the cell surface. Thus, the untransfected cells were used as a control. The K562-CD209 DC-SIGN expression level was determined by flow cytometric analysis (see the Supporting Information). The *S. cerevisiae* mannan was obtained from Sigma and its average molecular weight was estimated to be 100 kDa by DOSY NMR experiments[14] (see the Supporting Information).

To perform the STD NMR experiments, about 5×10^6 cells were counted, washed, and dissolved in deuterated phosphate-buffered saline (PBS), and mannan (5 mg) was dissolved in the same deuterated PBS. Typical NMR tube volumes were 600 μL. Additional experiments with a commercial beta-glucan preparation, which does not bind to DC-SIGN, were also performed as blank experiments. All the experiments were repeated three times, and carried out using different batches. The estimated concentration of DC-SIGN in the NMR tube was approximately 0.1 μM.[15,16]

NMR control experiments were recorded in all cases. As illustrated in Figure 1, the STD control spectrum (Figure 1 d) of mannan confirmed that the on-resonance irradiation ($\delta =$ 6.8 ppm, aromatic region) did not affect the mannan signals.

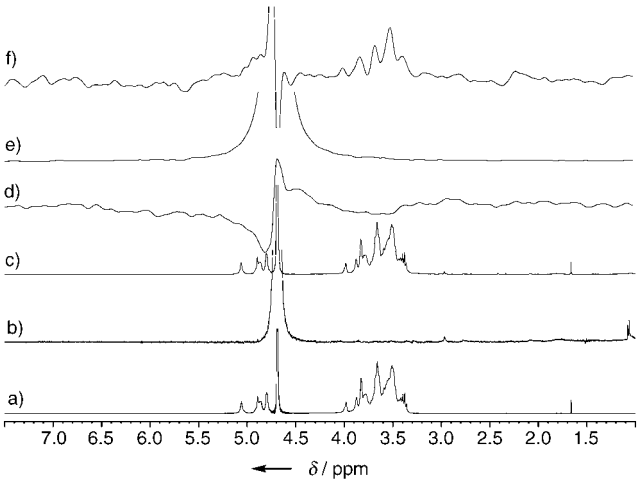


Figure 1. a) ^{1}H NMR spectrum of mannan in PBS; b) ^{1}H NMR spectrum of K562-CD209 cells in PBS, enhanced 20×; c) ^{1}H NMR spectrum of mannan with K562-CD209 cells in PBS; d) STD reference spectrum of mannan: number of scans (NS) = 256, on-resonance frequency = 6.8 ppm, off-resonance frequency = 100 ppm, total saturation time = 2 s, enhanced 100×; e) STD reference spectrum of K562-CD209 cells under the same experimental conditions as (d), enhanced 600×, signals enhanced 16×; f) STD spectrum of mannan with K562-CD209 cells: NS = 64, on-resonance frequency = 6.8 ppm, off-resonance frequency = 100 ppm, signals enhanced 800×. All the samples (cells and mannan) were dissolved in deuterated PBS at pH 7.3 containing $CaCl_2$ (1 mM). Total sample volumes were 600 μL.

[*] S. Mari,[+] D. Serrano-Gómez,[+] Dr. F. J. Cañada, Prof. Dr. A. L. Corbí, Prof. Dr. J. Jiménez-Barbero
Centro de Investigaciones Biológicas
Departamentos de Inmunología y de Estructura de Proteínas
C.S.I.C., c/Ramiro de Maeztu 9, 28040 Madrid (Spain)
Fax: (+34) 91-5360-432
E-mail: acorbi@cib.csic.es
jjbarbero@cib.csic.es

[+] S. Mari and D. Serrano-Gómez have contributed equally to this work and the order of authors is arbitrary.

[**] We thank the Ministerio de Educación y Ciencia of Spain (grants BQU2003-03550-C03-01 and SAF2002-04615-CO2-01) and the European Union (HPRN-CT2002-0173) for financial support. We thank Dr. Antonio Leal for the gift of the mannan sample and Dr. Leal and Dr. P. Groves for helpful discussions. DC-SIGN = dendritic-cell-specific ICAM-3-grabbing non-integrin.

Supporting information for this article is available on the WWW under http://www.angewandte.org or from the author.

 © 2005 Wiley-VCH Verlag GmbH & Co. KGaA, Weinheim DOI: 10.1002/anie.200461574

Identical results were obtained with saturation at $\delta = 1.3$ ppm (aliphatic side-chain region). Control NMR data of the living cells were acquired in an analogous manner (Figure 1 b and e). The cells used to obtain these spectra were then centrifuged and the pellet was dissolved in the mannan solution used to generate the spectra in Figure 1 a and d.[17] The resulting reference spectrum is shown in Figure 1 c, while its corresponding STD NMR spectrum is displayed in Figure 1 f. The mannan signals are observed unambiguously. Thus, irradiation at the aromatic or aliphatic regions protons of the DC-SIGN receptor protein expressed in living cells results in transfer of magnetization to the polysaccharide protons. The control spectra support the notion that the observed process is specific for the interaction of living cells of K562-CD209 (DC-SIGN+) with mannan. Indeed, when the same set of experiments was repeated with mock-transfected K562 cells (DC-SIGN−) instead of K562-CD209 (DC-SIGN+) cells, no mannan signals were detected in the STD NMR experiment (Figure 2 f). Additional reference experiments were performed using beta-glucan as the ligand. In this case, and as expected for a molecule that does not bind to DC-SIGN, no STD signals were observed with either cell line (data not shown), which supports the NMR-based detection of the specific interaction between the K562-CD209 cells and mannan.

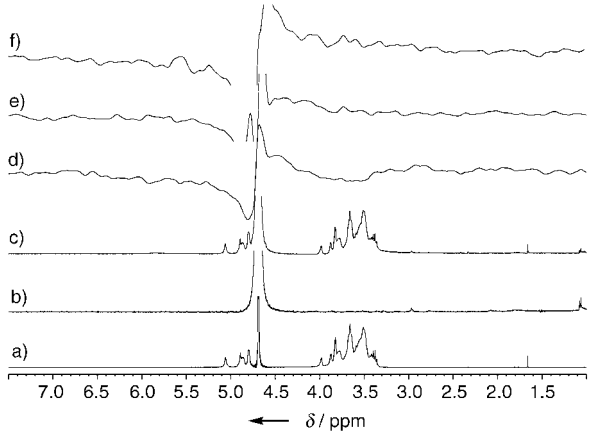


Figure 2. a) ^{1}H NMR spectrum of mannan in PBS; b) ^{1}H NMR spectrum of K562 (DC-SIGN−) cells in PBS enhanced 4×; c) ^{1}H NMR spectrum of mannan with K562 (DC-SIGN−) cells in PBS enhanced 10×; d) STD reference spectrum of mannan: NS = 256, on-resonance frequency = 6.8 ppm, off-resonance frequency = 100 ppm, total saturation time = 2 s, enhanced 600×; e) STD reference spectrum of K562 (DC-SIGN−) cells under the same experimental conditions as (d), signals enhanced 400×; f) STD spectrum of mannan with K562 (DC-SIGN−) cells: NS = 64, on-resonance frequency = 6.8 ppm, off-resonance frequency = 100 ppm, signals enhanced 800×.

Direct detection of interactions between a ligand and a membrane protein by employing living cells could open new possibilities in the screening of compound libraries in a fast and efficient way. By using our current experimental setup for this K562-CD209/mannan system robust data have been obtained with 32 scans, which correspond to a total experimental time of 3 minutes, and includes a recycling of the mannan solution from a previous experiment. The cells were checked by optical microscopy before and after the NMR experiments to determine their biological stability, and cell viability was also evaluated by the Trypan Blue exclusion method. Both assays demonstrated that cell viability was not significantly affected during the NMR experiments (see the Supporting Information).

In conclusion, receptor–ligand interactions with integral membrane proteins may be investigated by 1D STD NMR spectroscopy as the initial step in screening processes, which use living cells directly in a manner similar to that previously reported for detecting virus–ligand and platelet–ligand interactions.[16] This protocol represents a significant advance in molecular recognition studies, since it eliminates time-consuming purification processes, especially in the case of receptors that are difficult to isolate.[18]

Experimental Section

Cells: K562 cells were cultured in RPMI media supplemented with 10% fetal calf serum (FCS), 2-[4-(2-hydroxyethyl)-1-piperazinyl]-ethanesulfonic acid (HEPES, 25 mM), and glutamine (2 mM; complete medium). DC-SIGN-expressing K562 transfectants (K562-CD209) have been previously described,[12] and were cultured in complete medium supplemented with G418 (300 μg mL^{-1}, Gibco).

NMR experiments: All the experiments were recorded on a Bruker 500-MHz instrument at 283 K. A basic STD sequence was used, with the on-resonance frequency variable between $\delta = 6.8$ and 1.3 ppm.[13] The off-resonance frequency was maintained at 100 ppm. A train of 40 Gaussian-shaped pulses of 50 ms each was employed, with a total saturation time of the protein envelope of 2 s. All the samples (cells and mannan) were dissolved in deuterated PBS at pH 7.3 containing $CaCl_2$ (1 mM) previously exchanged with D_2O. Total sample volumes were 600 μL.

Flow cytometry and antibodies: Cellular phenotypic analysis was carried out by indirect immunofluorescence. Monoclonal antibodies used for cell-surface staining included 9E10 (anti-c-Myc) and MR-1 (anti-DC-SIGN, CD209).[12] All incubations were performed in the presence of human immunoglobulin G (50 μg mL^{-1}) to prevent binding through the Fc portion of the antibodies. Flow cytometric analysis was performed with an EPICS-CS instrument (Coulter Científica, Madrid, Spain) using log amplifiers.

Received: August 7, 2004

Keywords: drug design · molecular recognition · NMR spectroscopy · proteins · receptors

[1] B. Meyer, T. Peters, *Angew. Chem.* **2003**, *115*, 890; *Angew. Chem. Int. Ed.* **2003**, *42*, 864.
[2] T. B. Geijtenbeek, R. Torensma, S. J. van Vliet, G. C. van Duijnhoven, G. J. Adema, Y. van Kooyk, C. G. Figdor, *Cell* **2000**, *100*, 575.
[3] T. B. Geijtenbeek, D. S. Kwon, R. Torensma, S. J. van Vliet, G. C. van Duijnhoven, J. Middel, I. L. Cornelissen, H. S. Nottet, V. N. KewalRamani, D. R. Littman, C. G. Figdor, Y. van Kooyk, *Cell* **2000**, *100*, 587.
[4] C. P. Alvarez, F. Lasala, J. Carrillo, O. Muniz, A. L. Corbi, R. Delgado, *J. Virol.* **2002**, *76*, 6841.
[5] Z. Y. Yang, Y. Huang, L. Ganesh, K. Leung, W. P. Kong, O. Schwartz, K. Subbarao, G. J. Nabel, *J. Virol.* **2004**, *78*, 5642.

 © 2005 Wiley-VCH Verlag GmbH & Co. KGaA, Weinheim

[6] M. Colmenares, A. Puig-Kroger, O. M. Pello, A. L. Corbi, L. Rivas, *J. Biol. Chem.* **2002**, *277*, 36766.
[7] L. Tailleux, O. Schwartz, J. L. Herrmann, E. Pivert, M. Jackson, A. Amara, L. Legres, D. Dreher, L. P. Nicod, J. C. Gluckman, P. H. Lagrange, B. Gicquel, O. Neyrolles, *J. Exp. Med.* **2003**, *197*, 121.
[8] B. J. Appelmelk, I. van Die, S. J. van Vliet, C. M. Vandenbroucke-Grauls, T. B. Geijtenbeek, Y. van Kooyk, *J. Immunol.* **2003**, *170*, 1635.
[9] A. Cambi, K. Gijzen, J. M. de Vries, R. Torensma, B. Joosten, G. J. Adema, M. G. Netea, B. J. Kullberg, L. Romani, C. G. Figdor, *Eur. J. Immunol.* **2003**, *34*, 532.
[10] A. Cambi, C. G. Figdor, *Curr. Opin. Cell Biol.* **2003**, *15*, 539.
[11] T. B. Geijtenbeek, D. J. Krooshoop, D. A. Bleijs, S. J. van Vliet, G. C. van Duijnhoven, V. Grabovsky, R. Alon, C. G. Figdor, Y. van Kooyk, *Nat. Immunol.* **2000**, *1*, 353.
[12] M. Relloso, A. Puig-Kroger, O. M. Pello, J. L. Rodriguez-Fernandez, G. de la Rosa, N. Longo, J. Navarro, M. A. Munoz-Fernandez, P. Sanchez-Mateos, A. L. Corbi, *J. Immunol.* **2002**, *168*, 2634.
[13] M. Mayer, B. Meyer, *Angew. Chem.* **1999**, *111*, 1902; *Angew. Chem. Int. Ed.* **1999**, *38*, 1784. The success of the STD NMR experiments depends on the kinetics of the dissociation process and the molar ratio of ligand versus receptor. For a seminal discussion, see ref. [1].
[14] P. Groves, M. O. Rasmussen, M. D. Molero, E. Samain, F. J. Canada, H. Driguez, J. Jimenez-Barbero, *Glycobiology* **2004**, *14*, 451.
[15] F. Baribaud, S. Pöhlmann, G. Leslie, F. Mortari, R. W. Doms, *J. Virol.* **2002**, *76*, 9135.
[16] a) A. Benie, R. Moser, E. Bäuml, D. Blaas, T. Peters, *J. Am. Chem. Soc.* **2003**, *125*, 14; b) B. Meyer, personal communication.
[17] The NMR solution stays relatively clear for about 10 minutes. After this time, the cells start to sediment. However, the high sensitivity of the STD NMR experiment[1] allows one to overcome this point without major problems.
[18] The use of the STD technique together with high-resolution magic angle spinning may even open the window of applicability of the protocol described herein; see J. Klein, R. Meinecke, M. Mayer, B. Meyer, *J. Am. Chem. Soc.* **1999**, *121*, 5336.

 © 2005 Wiley-VCH Verlag GmbH & Co. KGaA, Weinheim

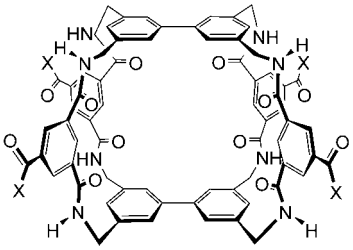
Molecular Recognition

Carbohydrate Recognition in Water by a Tricyclic Polyamide Receptor**

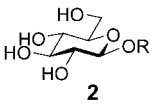
*Emmanuel Klein, Matthew P. Crump, and Anthony P. Davis**

Carbohydrate recognition in aqueous solution remains an important challenge in supramolecular chemistry.[1] Saccharides are complex, irregular, and multifunctional, while their hydroxylated exteriors blend well with water. Even nature has difficulty; binding constants of proteins with monosaccharides peak at approximately $10^7\,M^{-1}$, a remarkably low value for biological molecular recognition.[1a,2] Synthetic receptors that exploit covalent B–O bonds have been relatively successful,[1b,3] but there are still few reports of binding in water through noncovalent interactions.[1a,4] Such systems are of special interest as they shed light on natural carbohydrate recognition, a process of fundamental biological significance.[5]

A few years ago, we reported the octa-amide **1a** as a receptor for octyl glycosides in organic media.[6] The tricyclic



1a: X = OC_5H_{11}
1b: X = O^-
1c: X = NH(OBn)(OBn)(OBn)
1d: X = NH(CH$_2$CO$_2^-$)$_3$



2

core **1** was specifically targeted at β-glucosyl derivatives **2**. It was supposed that the axial hydrogens in **2** would make C–H–π contacts with the biphenyl surfaces, while the equatorial substituents would form hydrogen bonds to the isophthalamide spacers. Accordingly, **1a** showed high affinities for **2**

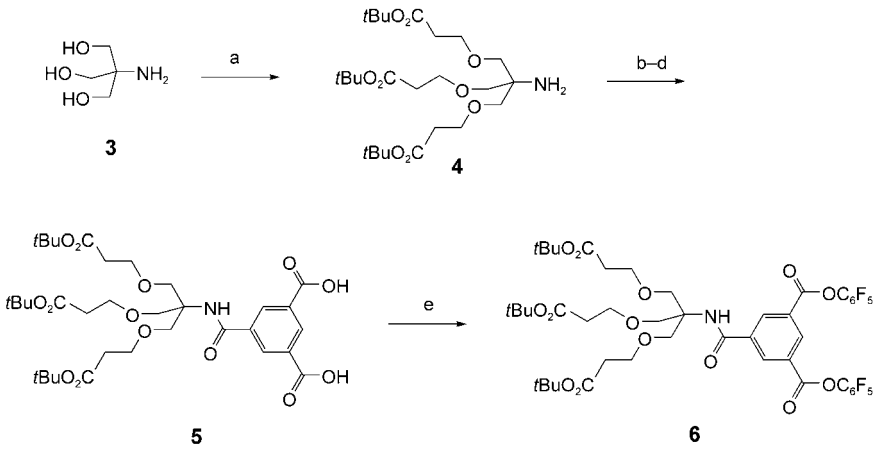
[*] Dr. E. Klein, Dr. M. P. Crump, Prof. A. P. Davis
School of Chemistry
University of Bristol
Cantock's Close
Bristol BS8 1TS (UK)
Fax: (+44) 117-929-8611
E-mail: anthony.davis@bristol.ac.uk

[**] Financial support was provided by the European Commission (network contract HPRN-CT-2002-00190). Assistance from Dr. C. Dempsey (Department of Biochemistry, University of Bristol) and the EPSRC National Mass Spectrometry Service Centre, Swansea, is gratefully acknowledged.

Supporting information for this article is available on the WWW under http://www.angewandte.org or from the author.

 © 2005 Wiley-VCH Verlag GmbH & Co. KGaA, Weinheim DOI: 10.1002/anie.200461409

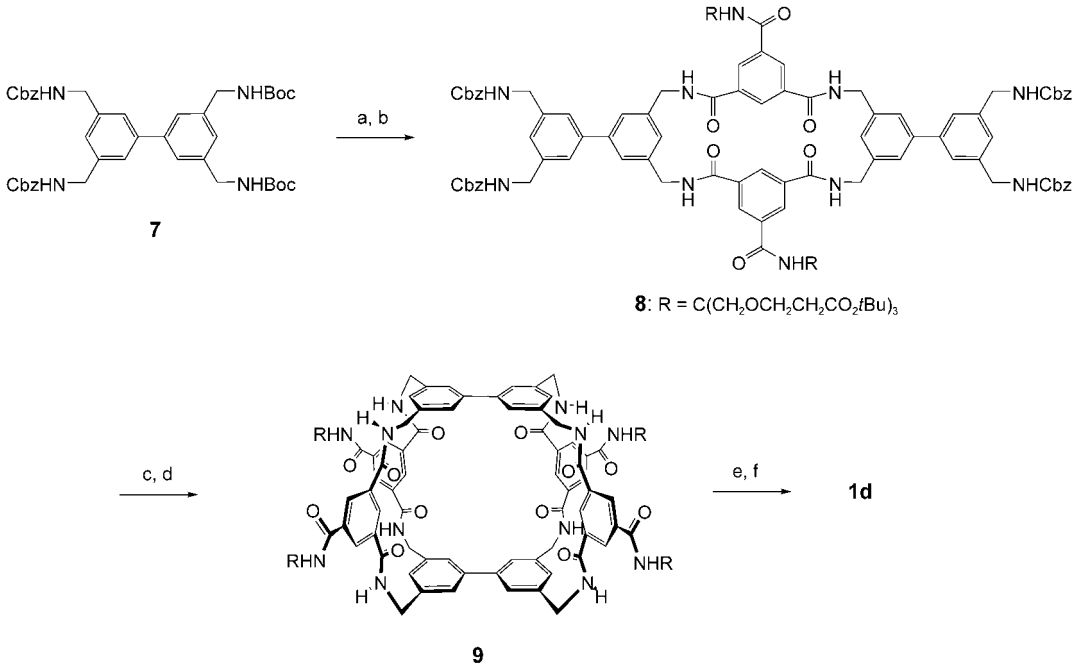
(R = octyl) and was less effective for the α anomer or octyl β-D-galactoside. Our prime objective, however, was recognition in water. In this more-challenging medium, hydrogen bonding would provide less (if any) impetus for binding, but, in compensation, the C–H–π interactions should be reinforced by the hydrophobic effect. Tetracarboxylate **1b** could not be employed owing to aggregation in water. Attempts to use a tris(hydroxymethyl)methyl solubilizing group also foundered, although precursor **1c** proved useful for phase-transfer experiments.[7] We now describe the synthesis of dodecacarboxylate **1d** and report that this polyanion provides, at last, an opportunity to study carbohydrate recognition by **1** in homogeneous aqueous solution.



Scheme 1. Synthesis of **6**: a) *tert*-butyl acrylate, NaOH, DMSO, H_2O; b) 1,3,5-benzenetricarbonyl trichloride (excess), *i*Pr_2NEt, THF; c) aq. NaOH (2 M); d) aq. HCl (3.5 M); e) C_6F_5OH, DCC, THF. DMSO = dimethylsulfoxide, DCC = *N*,*N*′-dicyclohexylcarbodiimide.

Receptor **1d** was prepared as shown in Schemes 1 and 2. The active ester **6** was synthesized from tris(hydroxymethyl)aminomethane **3** through the aminotriester **4**[8] and diacid **5** (Scheme 1). The biphenyl unit **7** was prepared as previously reported.[7] Acid deprotection of **7** followed by cyclization with **6** under high dilution gave macrocycle **8** (Scheme 2). Hydrogenolysis of **8** followed by a second [2+2] macrolactamisation gave the protected macrocycle **9**. The sodium salt of dodecacarboxylate **1d** was obtained through deprotection of **9** with trifluoroacetic acid followed by treatment with sodium hydroxide. ^{1}H NMR spectra of solutions in D_2O/H_2O consisted of sharp signals (Figure 1) and did not vary with concentration in the range 1–4 mM. Receptor **1d** was therefore assumed to be monomeric in aqueous solution at approximately 1 mM.

Preliminary NMR titration studies on the dodeca-*tert*-butyl ester **9** confirmed that, as expected, this macrocycle binds carbohydrates in the organic solvent system $CDCl_3$/CD_3OD (92:8). The K_a value for octyl β-D-glucopyranoside was 600 M^{-1}, which is similar to those obtained previously for **1a**[6] and **1c**.[7] Variations in the chemical shifts were also similar to those for the earlier systems. More significantly, the addition of glucose **10** to **1d** in D_2O/H_2O yielded qualitatively similar NMR effects. In particular, the signal for the inward-directed spacer protons, B (for labeling, see Figure 1), moved downfield, whereas that for the annular amide protons, NH^a, moved upfield and split into two (Figure 2). The signal for the protons C of the biphenyl group also split and moved



Scheme 2. Synthesis of **1d**: a) TFA, CH_2Cl_2; b) **6**, *i*Pr_2NEt, THF, high dilution; c) H_2, 10% Pd/C, THF/methanolic ammonia (1:1); d) **6**, *i*Pr_2NEt, THF, high dilution; e) TFA, CH_2Cl_2; f) aq. NaOH (1 M). Boc = *tert*-butoxycarbonyl, Cbz = benzyloxycarbonyl, TFA = trifluoroacetic acid.

 © 2005 Wiley-VCH Verlag GmbH & Co. KGaA, Weinheim

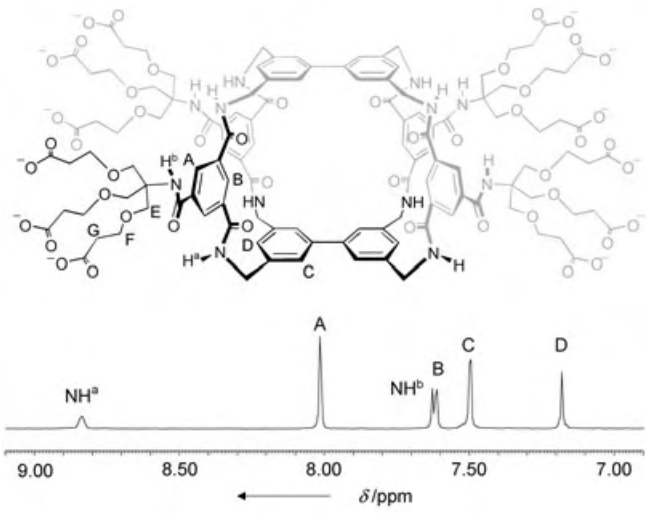


Figure 1. Partial ^{1}H NMR spectrum (600 MHz, 93:7 H_2O/D_2O) of receptor **1d**.

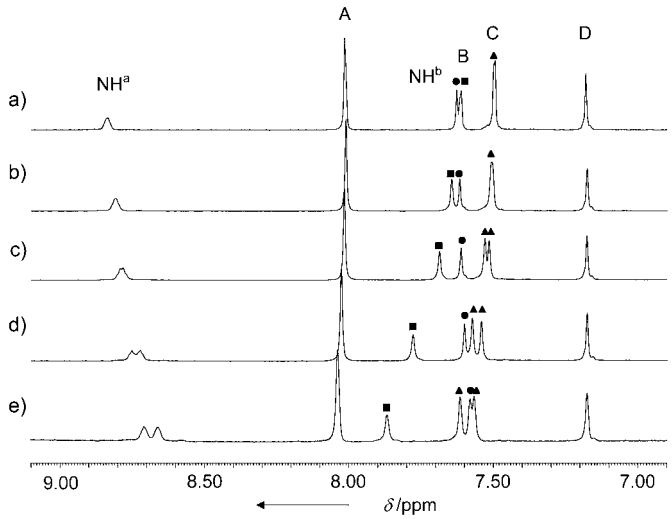


Figure 2. ^{1}H NMR spectra (600 MHz, 93:7 H_2O/D_2O) of receptor **1d** after addition of increasing amounts of D-glucose **10**: a) 0, b) 20, c) 50, d) 200, and e) 1000 equivalents. ● = NH^b, ■ = protons B, ▲ = protons C.

downfield. The splitting of the eight equivalent NH^a and C protons into groups of 4 is expected for a D_{2h} receptor that interacts with an asymmetrical substrate.[6] As illustrated in Figure 3a the motions could be fitted, to high accuracy, to a 1:1 binding model. The resulting binding constants varied according to the history of the glucose solution. For freshly dissolved glucose with an anomeric ratio α/β of 72:28 a K_a value of 4.6 M^{-1} was obtained in D_2O. For glucose that had been equilibrated overnight (α/β = 40:60), the binding constant was 9.2 M^{-1}. The figures imply substantial selectivity for the β anomer; indeed, they are consistent with $K_a \approx 14\,M^{-1}$ for β-glucopyranose and $< 1\,M^{-1}$ for the α anomer.[9]

Binding to other carbohydrates (**11**–**24**) was followed by NMR spectroscopy to yield the association constants shown in Table 1, page 301. Errors may be high for the smaller K_a

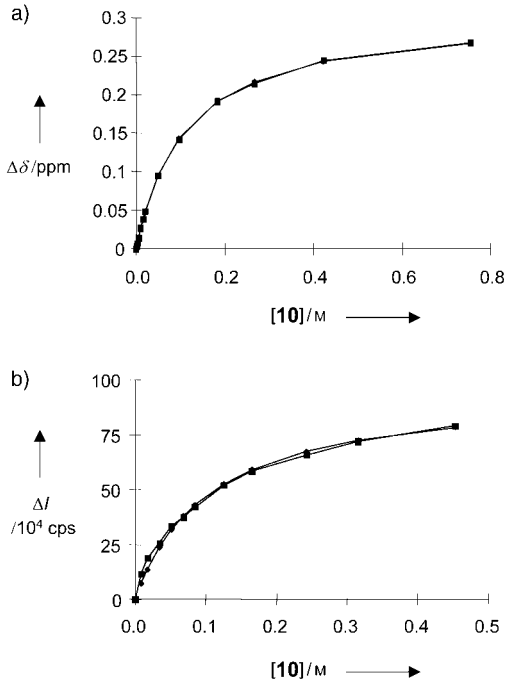


Figure 3. Theoretical (◆) and experimental (■) binding curves for a) NMR titration of **1d** + **10** (proton B) and b) fluorescence emission titration of **1d** + **10** (cps = counts per second; λ_{ex} = 266 nm, λ_{em} = 475 nm).

values (especially when $K_a \approx 2\,M^{-1}$), but selectivities are clearly significant. The receptor shows a notable preference for β-glucosyl units in accordance with the original design and with previous work on **1a** and **1c**. Thus the highest K_a values are to methyl β-D-glucoside **15** and cellobiose **22**. The selectivity for **22** relative to lactose **23** and maltose **24** is especially striking and mirrors the results in organic media for an "extended", terphenyl-based analogue of **1a**.[10] Other units with all-equatorial substitution (2-deoxy-D-glucose **17** and D-xylose **18**) are also bound well by the receptor. Remarkably, the removal of hydroxyl groups does not enhance binding—**17** is no more strongly bound than glucose, while rhamnose **20** and fucose **21** are poor substrates.

The formation of the complexes was also detected by means of fluorescence spectroscopy. On addition of substrates to **1d**, the fluorescence emission was enhanced and shifted slightly in wavelength (see Supporting Information). Analysis by curve fitting (see Figure 3b) yielded the binding constants shown in Table 2 which are in good agreement with the values obtained through ^{1}H NMR titrations.

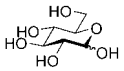
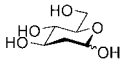
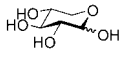
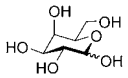
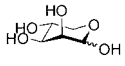
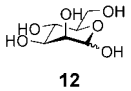
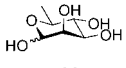
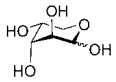
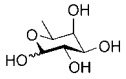
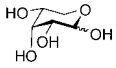
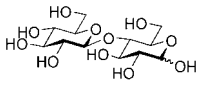
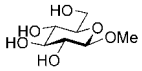
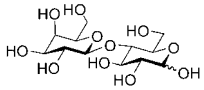
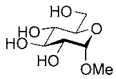
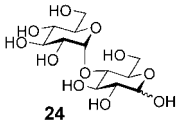
Table 2: Association constants (K_a) between receptor **1d** and carbohydrates as measured in H_2O by fluorescence titration.[a]

Carbohydrate	K_a [M^{-1}]	Carbohydrate	K_a [M^{-1}]
D-glucose (**10**; α/β 40:60)	9.5	methyl α-D-glucoside (**16**)	5.7
methyl β-D-glucoside (**15**)	32	D-xylose (**18**)	3.8

[a] T = 298 K. For binding curves and further details, see Supporting Information.

 © 2005 Wiley-VCH Verlag GmbH & Co. KGaA, Weinheim

Table 1: Association constants (K_a) between receptor **1d** and carbohydrates as measured in D_2O by ^1H NMR titration.[a]

Carbohydrate		K_a [M^{-1}]	Carbohydrate		K_a [M^{-1}]
 **10** (α/β 72:28)[b]	D-glucose	4.6	 **17**	2-deoxy-D-glucose[c]	7.2
10 (α/β 40:60)[c]	D-glucose	9.2	 **18**	D-xylose[c]	4.6
 **11**	D-galactose[c]	2.1	 **19**	D-lyxose[c]	v.s.[d]
 **12**	D-mannose[c]	v.s.[d]	 **20**	L-rhamnose[c]	v.s.[d]
 **13**	D-arabinose[c]	2.2	 **21**	L-fucose[c]	2.1
 **14**	D-ribose[c]	3.1	 **22**	D-cellobiose[c]	16.6
 **15**	methyl β-D-glucoside	27.3	 **23**	D-lactose[c]	v.s.[d]
 **16**	methyl α-D-glucoside	6.9	 **24**	D-maltose[c]	v.s.[d]

[a] $T = 296$ K. Data were analyzed by using a nonlinear least-squares curve-fitting program implemented within MS Excel 2000. Quoted figures were derived from the peak for proton B (see Figure 1); peaks for protons C and (sometimes) A could also be followed and gave closely consistent results. For binding curves and further details, see Supporting Information. [b] Freshly dissolved in D_2O. Anomeric ratio was monitored by ^1H NMR spectroscopy and was found to remain roughly constant throughout the titration. [c] Solution in D_2O allowed to equilibrate before use. For further information on anomeric ratios, see Supporting Information. [d] Very small. Minor signal movements, almost linear with substrate concentration.

Information on the geometry of the **1d**·glucose complex was provided by NOESY experiments. A portion of the spectrum is shown in Figure 4. Cross-peaks are observed between glucose protons (β anomer only) and receptor protons B, C, and NH^a, whereas connections from substrate to externally directed protons A, NH^b, and D are weak or

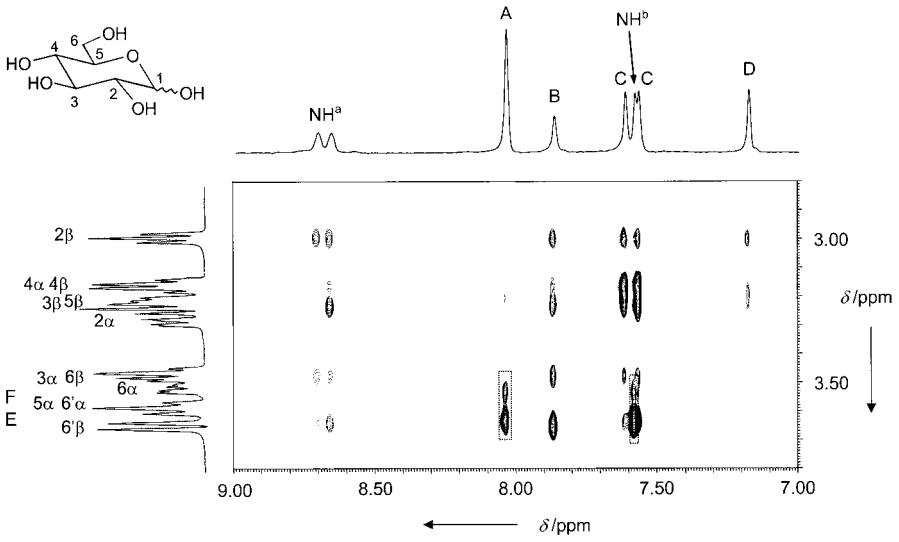


Figure 4. Partial NOESY spectrum of receptor **1d** and 1000 equivalents of D-glucose (**10**) in H_2O/D_2O 93:7 (600 MHz). The horizontal axis covers the region 7.0–9.0 ppm, which includes aromatic and NH protons of the receptor (for atom labeling, refer to Figure 1). The vertical axis covers 2.8–3.8 ppm, which includes protons 2–6 of glucose. The region plotted vertically also includes protons F and E of the receptor which are invisible in the 1D spectrum owing to the disparity in concentrations. Intramolecular cross-peaks that involve these signals are framed by dotted lines (•••••). All other cross-peaks represent intermolecular contacts. For further details see Supporting Information.

 © 2005 Wiley-VCH Verlag GmbH & Co. KGaA, Weinheim

nonexistent. These data provide strong evidence that the carbohydrate is bound in the interior of the macrotricyclic structure. Both protons B and C appear to show cross-peaks with all of the carbohydrate protons, but the cross-peaks between protons B and proton H^6 of glucose, and those between proton C and the axial protons H^3, H^4, and H^5, are especially strong. Our proposed binding geometry, with "axial→biphenyl" and "equatorial→isophthaloyl" orientations, thus receives some support.

In conclusion we have shown that, in the form of **1d**, the tricyclic cage **1** can bind carbohydrates in water. Affinities are low, but selectivities are significant. The designed preference for β-glucosyl which was previously demonstrated in organic solvents is retained in the saccharides' natural environment. The formation of complexes has been characterized by ^{1}H NMR spectroscopy and confirmed by a second, independent technique, namely fluorescence spectroscopy. Tricycle **1** is thus established as a carbohydrate receptor with consistent behavior across a wide range of media. This property should allow its use in studies which complement those on natural receptors and further elucidate the principles underlying biological carbohydrate recognition.

Received: July 23, 2004

Keywords: carbohydrates · hydrophobic effect · molecular recognition · receptors · supramolecular chemistry

[1] a) A. P. Davis, R. S. Wareham, *Angew. Chem.* **1999**, *111*, 3160; *Angew. Chem. Int. Ed.* **1999**, *38*, 2978; b) T. D. James, K. R. A. S. Sandanayake, S. Shinkai, *Angew. Chem.* **1996**, *108*, 2038; *Angew. Chem. Int. Ed. Engl.* **1996**, *35*, 1911; c) S. Striegler, *Curr. Org. Chem.* **2003**, *7*, 81.

[2] F. A. Quiocho, *Pure Appl. Chem.* **1989**, *61*, 1293.

[3] For recent examples, see: W. Q. Yang, J. Yan, H. Fang, B. H. Wang, *Chem. Commun.* **2003**, 792; C. J. Ward, P. Patel, T. D. James, *Org. Lett.* **2002**, *4*, 477; Z. L. Zhong, E. V. Anslyn, *J. Am. Chem. Soc.* **2002**, *124*, 9014; J. N. Camara, J. T. Suri, F. E. Cappuccio, R. A. Wessling, B. Singaram, *Tetrahedron Lett.* **2002**, *43*, 1139; H. S. Cao, D. I. Diaz, N. DiCesare, J. R. Lakowicz, M. D. Heagy, *Org. Lett.* **2002**, *4*, 1503; W. Yang, H. He, D. G. Drueckhammer, *Angew. Chem.* **2001**, *113*, 1764; *Angew. Chem. Int. Ed.* **2001**, *40*, 1714.

[4] R. D. Hubbard, S. R. Horner, B. L. Miller, *J. Am. Chem. Soc.* **2001**, *123*, 5810; V. Král, O. Rusin, F. P. Schmidtchen, *Org. Lett.* **2001**, *3*, 873; N. Sugimoto, D. Miyoshi, J. Zou, *Chem. Commun.* **2000**, 2295. For leading references to studies in nonaqueous media, see ref [1a] and: T. Ishi-i, M. A. Mateos-Timoneda, P. Timmerman, M. Crego-Calama, D. N. Reinhoudt, S. Shinkai, *Angew. Chem.* **2003**, *115*, 2402; *Angew. Chem. Int. Ed.* **2003**, *42*, 2300; M. Segura, B. Bricoli, A. Casnati, E. M. Munoz, F. Sansone, R. Ungaro, C. Vicent, *J. Org. Chem.* **2003**, *68*, 6296; K. Wada, T. Mizutani, S. Kitagawa, *J. Org. Chem.* **2003**, *68*, 5123; R. Welti, F. Diederich, *Helv. Chim. Acta* **2003**, *86*, 494; M. Mazik, W. Radunz, W. Sicking, *Org. Lett.* **2002**, *4*, 4579; Y. H. Kim, J. I. Hong, *Angew. Chem.* **2002**, *114*, 3071; *Angew. Chem. Int. Ed.* **2002**, *41*, 2947; K. Ladomenou, R. P. Bonar-Law, *Chem. Commun.* **2002**, 2108; J. H. Liao, C. T. Chen, H. C. Chou, C. C. Cheng, P. T. Chou, J. M. Fang, Z. Slanina, T. J. Chow, *Org. Lett.* **2002**, *4*, 3107; J. Bitta, S. Kubik, *Org. Lett.* **2001**, *3*, 2637; S. Tamaru, M. Yamamoto, S. Shinkai, A. B. Khasanov, T. W. Bell, *Chem. Eur. J.* **2001**, *7*, 5270.

[5] R. A. Dwek, T. D. Butters, *Chem. Rev.* **2002**, *102*, 283 (and succeeding articles); C. R. Bertozzi, L. L. Kiessling, *Science* **2001**, *291*, 2357; T. Feizi, B. Mulloy, *Curr. Opin. Struct. Biol.* **2001**, *11*, 585 (and succeeding articles).

[6] A. P. Davis, R. S. Wareham, *Angew. Chem.* **1998**, *110*, 2397; *Angew. Chem. Int. Ed.* **1998**, *37*, 2270.

[7] T. J. Ryan, G. Lecollinet, T. Velasco, A. P. Davis, *Proc. Natl. Acad. Sci. USA* **2002**, *99*, 4863.

[8] C. M. Cardona, R. E. Gawley, *J. Org. Chem.* **2002**, *67*, 1411.

[9] This estimate is subject to large errors, and is therefore tentative.

[10] G. Lecollinet, A. P. Dominey, T. Velasco, A. P. Davis, *Angew. Chem.* **2002**, *114*, 4267; *Angew. Chem. Int. Ed.* **2002**, *41*, 4093.

 © 2005 Wiley-VCH Verlag GmbH & Co. KGaA, Weinheim

Green Heterogeneous Catalysis

Renewable Olefins from Biodiesel by Autothermal Reforming**

*Ramanathan Subramanian and Lanny D. Schmidt**

Olefins are the largest volume chemical intermediates produced in the chemical industry, with global annual production over 300 billion lbs per year (1 lb = 0.454 kg).[1] Olefins are produced almost exclusively from ethane or other light alkanes (naphtha) in a process called steam cracking. This process involves homogeneous pyrolysis at approximately 800 °C in a tube furnace with a residence time of about 1 s. It has been estimated that 30 % of all pollution from chemical plants comes from steam cracking owing to NO_x emissions and unburned hydrocarbons in the flame required to heat the tube furnace.

Approximately 10 % of petroleum is consumed in the production of olefins and related chemicals. To reduce our reliance on fossil fuels, it would be desirable to produce olefins from renewable fuels that produce no net CO_2 emissions to contribute to global warming. To reduce pollution in olefins production, it would also be desirable to use partial oxidation rather than steam cracking. This possibility is discussed herein.

Biodiesel is the methyl ester formed by the reaction of triglyceride vegetable oils with methanol. From soy oil, there are five major ester compounds with the typical composition: methyl palmitate (12 %), methyl stearate (5 %), methyl oleate (25 %), methyl linoleate (52 %), and methyl linolenate (5 %).

[*] R. Subramanian, Prof. L. D. Schmidt
Department of Chemical Engineering and Materials Science
University of Minnesota
Minneapolis, MN 55455 (USA)
Fax: (+1) 612-626-7246
E-mail: schmidt@cems.umn.edu

[**] This research was partially sponsored by grant No. 518-6651 from the National Science Foundation. We gratefully acknowledge discussions with Christopher J. Cramer regarding reaction mechanisms. We thank Gregg A. Deluga for reviews and discussions.

 © 2005 Wiley-VCH Verlag GmbH & Co. KGaA, Weinheim DOI: 10.1002/anie.200460790

Double bonds (all in the *cis* configuration) occur exclusively after carbon atoms 9, 12, and 15 for fatty acids containing one, two, and three double bonds, respectively.

We[2] and others[3] have shown that the partial oxidation of ethane or other light alkanes (naphtha) can be used to produce olefins in autothermal reactors with as high as 85% selectivity for ethylene. We recently showed that higher alkanes, such as *n*-decane and *n*-hexadecane, can also be converted into olefins in high selectivity.[4] However, olefinic esters, such as those contained in biodiesel, are not expected to be reformed under autothermal oxidation because of the carbon formation that is expected from the presence of double bonds. Moreover, the oxidation of aliphatic esters could result in substantial decarboxylation giving low-value products.

The apparatus and procedures reported herein have been described elsewhere for experiments with *n*-decane, *n*-hexadecane, and diesel fuel.[4–6] Liquid fuels were injected into the reactor (Figure 1, inset) by using an automotive fuel injector that sprayed droplets onto the wall of a quartz tube heated to approximately 300 °C. The catalyst was a mixture of 2.5% Rh and 2.5% Ce deposited on α-Al_2O_3 ceramic foam from nitrate salt solutions, which was then dried and heated in an oven to 600 °C. Experiments were conducted at several flow rates, but only results at 4 standard litres min^{-1} are shown herein. Products were analyzed by dual column gas chromatography (GC) and by GC-mass spectrometry.

Figure 1 shows conversions of biodiesel and O_2 along with the back-face temperature of the catalyst plotted versus the carbon to oxygen (C/O) ratio, calculated assuming 18.8 carbon atoms per molecule. C/O = 1 represents one oxygen atom from O_2 per carbon atom in the biodiesel. It is seen that the conversions of biodiesel and of O_2 are $>90\%$ for most conditions.

Figure 2 shows the selectivities for the major products formed in the partial oxidation of biodiesel. The selectivities are based on H atoms for H_2 and C atoms for all other species. All H and C containing products add to 100%. At C/O = 0.9, the selectivity for H_2 is 85% and for CO is 80%, as the C/O ratio increases, the selectivity towards these species decrease rapidly as the "total hydrocarbons" (that is, all products C_2 through C_{15}) increase. The total-combustion products CO_2 (not shown) remain $<13\%$ for all C/O ratios. Species C_2 through C_5 are almost exclusively olefins, and larger species comprise both olefins and olefinic esters.

Figure 3 shows the selectivity for the production of ethylene, propylene, 1-butene, and 1-pentene versus C/O ratio for biodiesel. Ethylene dominates the small olefins with a maximum of approximately 25%, followed by propylene and smaller amounts of higher olefins.

Since biodiesel contains exclusively linear C_{16} and C_{18} fatty acids, its molecular weight and isomers should correspond closely to *n*-hexadecane which has been studied with rhodium catalysts.[4] Since the catalyst used herein was Rh–Ce, we repeated all of the experiments reported above on this catalyst using *n*-hexadecane. These results are shown as open symbols and dashed curves in Figure 1, Figure 2, and Figure 3. It is seen that conversions and selectivities correspond closely between biodiesel and *n*-hexadecane. The maximum H_2

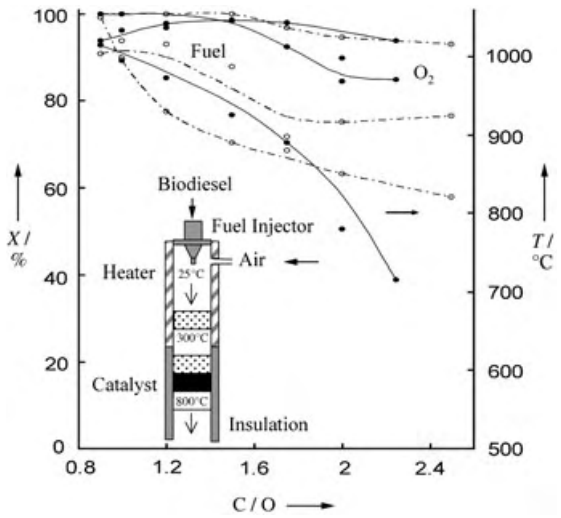


Figure 1. Fuel and oxygen conversions (*X*) and reactor temperature (*T*) versus C/O ratio for the partial oxidation of biodiesel (closed symbols and solid curves) and *n*-hexadecane (open symbols and broken lines). From the bottom, the first two curves indicate the temperatures (right-hand scale) for the partial oxidation of biodiesel (solid line) and *n*-hexadecane (broken line), the next two curves indicate fuel conversion (left-hand scale) for biodiesel (solid line) and *n*-hexadecane (broken line), and the top two curves indicate oxygen conversion (left-hand scale) for the partial oxidation of biodiesel (solid line) and *n*-hexadecane (broken line). The catalyst was a mixture of 2.5% Rh and 2.5% Ce deposited on an α-Al_2O_3 ceramic foam and the total flow rate was 4 standard litres min^{-1}, which corresponds to a catalyst contact time of approximately 5 ms. Liquid fuels were injected into the reactor using an automotive fuel injector. Cold air, admitted near the injector, rapidly mixed with the vaporized fuel with temperature and concentration gradients that minimized the potential for autothermal ignition before the reactor. Inset: schematic representaion of the reactor.[4–6]

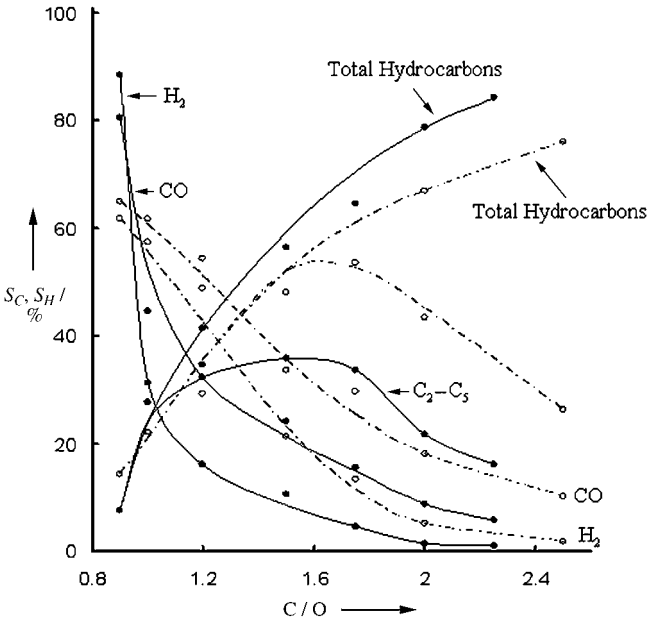


Figure 2. Selectivities *S* for the major products (H_2, CO, C_2–C_5 hydrocarbons, and total hydrocarbons) obtained from the autothermal oxidation of biodiesel with an Rh–Ce catalyst (closed symbols and solid curves) and from *n*-hexadecane over the same catalyst (open symbols and broken lines); see text for details.

 © 2005 Wiley-VCH Verlag GmbH & Co. KGaA, Weinheim

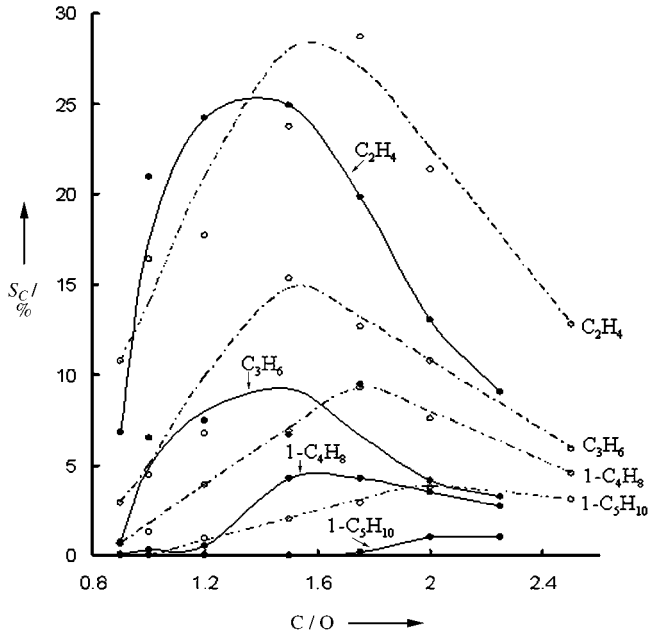


Figure 3. Selectivity *S* for the formation of ethylene, propylene, 1-butene, and 1-pentene versus C/O ratio from the partial oxidation of biodiesel (closed symbols and solid curves) and *n*-hexadecane (open symbols and broken lines). Methane is the only significant saturated alkane for which the selectivity is less than 8% (not shown).

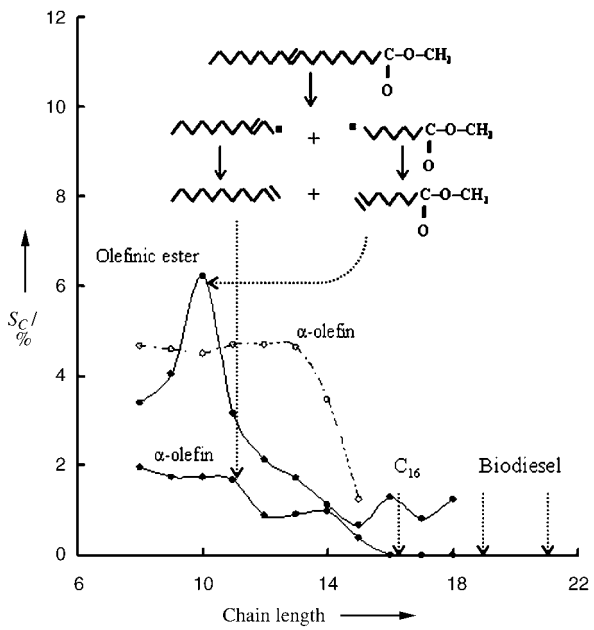


Figure 4. Plots of selectivities *S* for different species versus the chain length of the products observed at C/O = 2.25. 90% of the molecules present in biodiesel have a double bond between the ninth and tenth carbon atoms. Dissociation occurs mostly near this double bond because the allylic radical thus formed is resonance stabilized, this leads to a large amount of olefinic ester with a chain length of C_{10}. In contrast, *n*-hexadecane undergoes random C–C scission, which leads to nearly equal amounts of all α-olefins up to C_{14} (open symbols and broken line).

selectivity appears to be higher for biodiesel, but this is sensitive to the exact C/O ratio and reactor temperatures. The GC chromatograms of the products from biodiesel and *n*-hexadecane indicate that α-olefins and olefinic esters are formed from biodiesel, but only α-olefins are formed from *n*-hexadecane. Figure 4 shows plots of selectivities for different species versus the chain length of the products.

All of these processes are initiated by surface oxidation reactions on the rhodium surface that produces primarily H_2, H_2O, CO, and CO_2. These reactions occur near the entrance of the catalyst (probably within the first millimeter) where the surface is nearly free of carbon.[4] Most or all of the other products including olefins and olefinic esters arise from homogeneous reactions that occur after most O_2 has been consumed,[4] and rapid quenching within 20 ms prevents secondary reactions that would make many products. Further, most of the ester linkages survive the 800 °C of the reactor.

We never observed deactivation or extinction of the reaction under any conditions up to C/O = 3 for at least 50 h and this strongly indicates that carbon in the catalyst is not forming in sufficient quantities to block the rhodium surface sites that are required for oxidation reactions. Once all the O_2 has been consumed, we believe that the rhodium sites are carbon covered (up to 5% carbon by weight of the monolith), but this does not cause time-dependent results, so a steady state is rapidly obtained.

For *n*-hexadecane the process is fitted quite well assuming a very simple mechanism, dissociation of the parent molecule into two radicals [Eq. (1)] followed by the elimination of the H atom on the carbon atom in the position β to the radical [Eq. (2)] to produce the corresponding α-olefins.

$$n\text{-}C_{16}H_{34} \rightarrow C_mH_{2m+1}^{\bullet} + C_{16-m}H_{33-2m}^{\bullet} \quad (1)$$

$$C_mH_{2m+1}^{\bullet} \rightarrow C_mH_{2m} + H^{\bullet} \quad (2)$$

The alternative to β-H elimination is β-scission of C–C bond [Eq. (3)] which produces ethylene and a smaller alkyl radical.

$$C_mH_{2m+1}^{\bullet} \rightarrow C_{m-2}H_{2m-3}^{\bullet} + C_2H_4 \quad (3)$$

This reaction can continue producing ethylene until the final radical is ethyl or propyl which dehydrogenates to form ethylene or propylene. Since β-H elimination has a lower activation energy than the elimination of the alkyl to form ethylene, it is predicted that high temperature (lower C/O ratio) favors small olefins and low temperature (high C/O ratio) favors longer-chain olefins (Figure 2 and Figure 3).

Biodiesel is of course more complex than *n*-hexadecane because of the ester group and because there is at least one double bond in 90% of the molecules (shown in Figure 4 for methyl oleate). Dissociation should occur mostly at C–C bonds because the C=C and C–O bonds are stronger. The most likely C–C bond dissociation occurs where the activation is lowest and, this is where the allylic radical stabilizes one of the radicals as a resonance structure, R = C–C• and R-C=C•.

Since in soy oil the first double bond always occurs between the ninth and tenth carbon atom in the fatty acid, the most likely dissociation location in 90% of biodiesel mole-

 © 2005 Wiley-VCH Verlag GmbH & Co. KGaA, Weinheim

cules occurs between the eighth and ninth carbon atoms (Figure 4).

From these radicals, the ester radical will undergo β-H elimination to produce an olefinic ester with a chain length of ten carbon atoms. The allylic radical will eliminate H to form an α-olefin with 11 carbon atoms.

This simple argument predicts that the dominant olefinic ester will have a chain length of C_{10}. Note from Figure 4 that this is exactly the maximum selectivity observed in the olefinic ester. Since the olefin side of the dissociated radicals can continue to dissociate, it is predicted that α-olefins with 11 carbon atoms or less but seldom more are produced, as shown in Figure 4.

Vegetable oils are widely produced throughout the world, and their production is increasing rapidly.[7] These supplies are probably adequate to replace production of most small olefins with renewable sources instead of petroleum. The short-chain-olefin selectivities we obtain from biodiesel are only around 40%, but all the other products (H_2, CO, α-olefins, and olefinic esters) all have considerable value. Only the CO_2 produced is irretrievably lost as a valuable chemical, so 90% of the carbon in vegetable oils can in principle be converted into chemicals and fuels by autothermal reforming. Olefins typically are priced at about \$0.25 per lb, so vegetable oil below \$3 per gallon should be a competitive source of olefins (\$0.20 per lb). An industrial olefins plant is capable of producing up to 1 billion lb per year by steam cracking. Our process produces about 1 lb per day from a 3 cm^2 reactor, 1 cm in depth, so a reactor would have to be approximately 4.5 meters diameter to match the output of the industrial olefin plant. We have not optimized flow rates, catalyst, preheat, or other variables, so it is likely that improvements in efficiency and yield will be possible. The H_2 selectivity was approximately 85% at the lowest C/O ratio (0.9). Higher H_2 selectivities can be obtained by using H_2O dilution to lower the temperature and increase the CO_2/CO ratio by promoting the water gas shift reaction in staged reactors.[8,9]

Ultimately, it will be necessary to replace fossil fuels by renewable fuels because of issues of supply, global warming, and pollution. The constraints on using renewable fuels as an energy source are considerable because of their limited supply and the need to produce energy at low cost. However, chemicals have a much higher value and require smaller amounts of material than fuels, so the production of chemicals from renewable fuels appears to be less difficult.

The simplicity of the products and product distribution obtained from biodiesel indicates that the mechanism could be as simple as that outlined in Figure 4. The process produces both short-chain and longer-chain olefins and olefinic esters. Since both short-chain olefins and short-chain olefinic esters have considerable value in polymer and copolymer production, this process could be quite attractive as an alternative to making polymers from fossil fuels.

Received: May 26, 2004
Revised: September 14, 2004

Keywords: alkenes · fatty acids · green chemistry · heterogeneous catalysis · oxidation

[1] R. Deng, F. Wei, Y. Jin, Q. Zhang, Y. Jin, *Chem. Eng. Technol.* **2002**, *25*, 711 – 716.
[2] A. S. Bodke, D. A. Olschki, L. D. Schmidt, E. Ranzi, *Science* **1999**, *285*, 712 – 715.
[3] A. Beretta, P. Forzatti, E. Ranzi, *J. Catal.* **1999**, *184*, 469 – 478.
[4] J. J. Krummenacher, K. N. West, L. D. Schmidt, *J. Catal.* **2003**, *215*, 332 – 343.
[5] D. A. Hickman, L. D. Schmidt, *Science* **1993**, *259*, 343 – 346.
[6] D. A. Goetsch, L. D. Schmidt, *Science* **1996**, *271*, 1560 – 1562.
[7] A. Demirbas, *Energy Sources* **2003**, *25*, 721 – 728.
[8] G. A. Deluga, J. R. Salge, L. D. Schmidt, X. E. Verykios, *Science* **2004**, *303*, 993 – 997.
[9] C. Wheeler, A. Jhalani, E. Klein, S. Tummala, L. D. Schmidt, *J. Catal.* **2004**, *123*, 191 – 199.

 © 2005 Wiley-VCH Verlag GmbH & Co. KGaA, Weinheim

Diruthenium Complex

A Spin-Admixed Ruthenium Complex**

M. Carmen Barral, Santiago Herrero, Reyes Jiménez-Aparicio, M. Rosario Torres, and Francisco A. Urbanos*

Ruthenium complexes attract great attention because of their potential use in electronic and magnetic devices.[1] Multiply bonded diruthenium compounds, in particular, have been investigated as models or building blocks to construct magnets, wires, switches, and other molecular devices.[2] Among this type of compounds the diruthenium(II,III) complexes are the most widely studied owing to their unusual stability.[3,4] In general, they have three unpaired electrons in accordance with a ground state electronic configuration of $\sigma^2\pi^4\delta^2(\pi^*\delta^*)^3$ owing to close spacing of the π^* and δ^* orbitals, as predicted by the theoretical studies of Norman et al.[5] This electronic configuration has been observed in all complexes containing the $[Ru_2(\mu\text{-}L)_4]^+$ unit with L = carboxylate, amidate, hydroxypyridinate, or aminopyridinate.[3,4] When L is a triazenide or formamidinate ligand, the energy difference between the π^* and δ^* levels is larger, and the electronic structure $\sigma^2\pi^4\delta^2\pi^{*3}$ is favored.[6] However, only a few examples of low-spin diruthenium(II,III) complexes with this

[*] Dr. M. C. Barral, Dr. S. Herrero, Dr. R. Jiménez-Aparicio, Dr. F. A. Urbanos
Departamento de Química Inorgánica
Universidad Complutense
Ciudad Universitaria, 28040 Madrid (Spain)
Fax: (+34) 91-394-4352
E-mail: qcmm@quim.ucm.es
Dr. M. R. Torres
Centro de Asistencia a la Investigación de Rayos X
Facultad de Ciencias Químicas
Universidad Complutense
Ciudad Universitaria, 28040 Madrid (Spain)

[**] We are grateful to the Ministerio de Ciencia y Tecnología (Dirección General de Investigación, project no. BQU2000-0643) for financial support.

 DOI: 10.1002/anie.200461463 © 2005 Wiley-VCH Verlag GmbH & Co. KGaA, Weinheim

electronic configuration are known.[6,7] Moreover, $[Ru_2Cl(\mu\text{-}O_2CMe)(\mu\text{-}DPhF)_3]$ (DPhF = *N*,*N*′-diphenylformamidinate)[8] has three unpaired electrons, whereas the derivative $[Ru_2(NCS)(\mu\text{-}O_2CMe)(\mu\text{-}DPhF)_3]$ is a low-spin complex with only one unpaired electron.[7] Chen and Ren also reported high- and low-spin diruthenium(III) complexes with the same core but different axial ligands.[9]

The high sensitivity of the magnetic moment to the nature of the axial ligand in this class of compounds challenged us to find the limit at which the difference in energy between the π* and δ* levels becomes similar to the electron-pairing energy. The aim was to design compounds whose magnetic properties are very sensitive to small changes in the environment.

To facilitate the search for a suitable axial ligand we prepared in good yield an air-stable compound with a labile water molecule at the axial position, namely, $[Ru_2(\mu\text{-}O_2CMe)(\mu\text{-}DPhF)_3(H_2O)]BF_4{\cdot}0.5\,CH_2Cl_2$ (**1**). Crystals of **1** were used for all measurements, including an X-ray diffraction study.[10]

The crystal structure of **1** (Figure 1) shows an eclipsed paddle-wheel disposition of the equatorial acetate and diphenylformamidinate ligands with a torsion angle of less

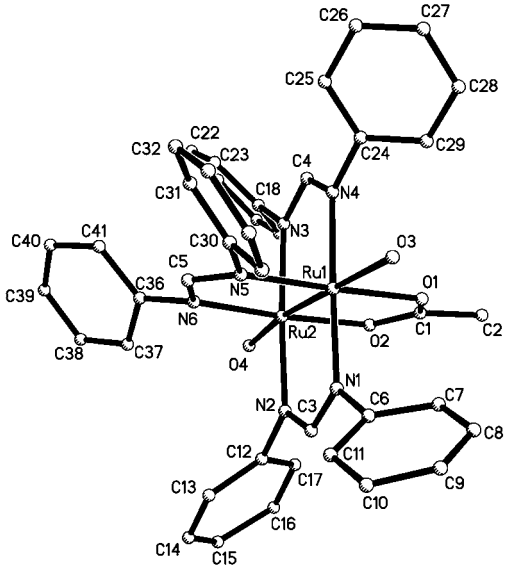


Figure 1. PLUTO view of the cationic unit $[Ru_2(\mu\text{-}O_2CMe)(\mu\text{-}DPhF)_3(H_2O)]^+$ in **1**. Hydrogen atoms are omitted for clarity.

than 0.5°. The water molecule is coordinated to the axial positions of the diruthenium units with 50% occupancy. The metal–metal bond (2.3503(9) Å) is longer than in the parent compounds $[Ru_2Cl(\mu\text{-}O_2CMe)(\mu\text{-}DPhF)_3]$ (2.3203(5) Å)[8] and $[Ru_2(NCS)(\mu\text{-}O_2CMe)(\mu\text{-}DPhF)_3]$ (2.3182(11) Å).[7]

Complex **1** shows exceptional magnetic behavior (Figure 2), intermediate between those observed for the chloro and the isothiocyanato derivatives. The μ_{eff} value at room temperature corresponds to the presence of two unpaired electrons (3.09 μ_B). Similar values for the magnetic moment (between $S = 1/2$ and $S = 3/2$) were also found at room temperature for diosmium(II,III) complexes such as

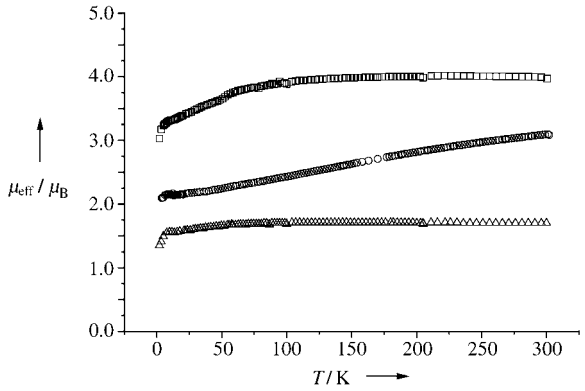


Figure 2. Magnetic moment curves versus temperature for $[Ru_2Cl(\mu\text{-}O_2CMe)(\mu\text{-}DPhF)_3]$ (□), $[Ru_2(NCS)(\mu\text{-}O_2CMe)(\mu\text{-}DPhF)_3]$ (△), and $[Ru_2(\mu\text{-}O_2CMe)(\mu\text{-}DPhF)_3(H_2O)]BF_4{\cdot}0.5\,CH_2Cl_2$ (**1**; ○).

$[Cp_2Co][Os_2Cl_2(\mu\text{-}O_2CPr)_4]$[11] and $[Os_2Cl(\mu\text{-}chp)_4]$ (chp = 6-chloro-2-hydroxypyridinate)[12]: 2.73 and 2.90 μ_B, respectively. However, $[Os_2Cl(\mu\text{-}fhp)_4]$ (fhp = 6-fluoro-2-hydroxypyridinate) has a magnetic moment of 3.70 μ_B.[13] at room temperature. These intermediate values were ascribed to some important contributions of the $S = 1/2$ and $S = 3/2$ spin states.[11–14] Unfortunately, the absence of magnetic data for a wide temperature range prevented the authors from providing a more satisfactory explanation.

Our attempts to simulate the experimental curve of μ_{eff} versus T for **1** as a thermal spin equilibrium (spin crossover) between the $S = 1/2$ and $S = 3/2$ spin states or as a physical spin mixture were unsuccessful. However, this magnetic behavior can be explained by considering a quantum mechanical spin admixture which generates a new discrete spin state by mixing of the $S = 1/2$ and $S = 3/2$ spin states. This mixing of states takes place through spin–orbit coupling[15] when both spin configurations are close in energy (with a difference comparable to or less than the spin–orbit coupling constant).

Such spin admixtures have been observed in several first-row transition-metal complexes, mainly for low-symmetry iron compounds in which high, low, and intermediate spin states are possible.[15] To our knowledge, there is no example of complexes of metals of the second and third transition series that show this type of magnetic behavior. This is not surprising given the usually large energy gap between the different spin states for these type of compounds. However, in complexes with a $[Ru_2(\mu\text{-}O_2CMe)(\mu\text{-}DPhF)_3]^+$ core, the $S = 1/2$ and $S = 3/2$ spin states are sufficiently close in energy that either can be obtained by variation of the axial ligand. Furthermore, ruthenium is a second-row transition metal, for which significant spin–orbit interactions can be expected. Indeed, in compounds of this kind with three unpaired electrons, the drop in magnetic moment at low temperatures indicates the presence of zero-field splitting, the magnitude of which is related to the strength of the spin–orbit coupling. Therefore, these diruthenium compounds could form spin-admixed ground states with an appropriate axial ligand, as observed in complex **1**. This finding and the potential of

 © 2005 Wiley-VCH Verlag GmbH & Co. KGaA, Weinheim

compound **1** to be used as a building block open the door to designing supramolecular materials with special magnetic properties.

Experimental Section

1 was prepared by adding $AgBF_4$ (0.118 g, 0.606 mmol) to a suspension of $[Ru_2Cl(\mu\text{-}O_2CMe)(\mu\text{-}DPhF)_3]$[8] (0.526 g, 0.596 mmol) in 10 mL of THF. The mixture was protected from light and stirred for 1 day. The bluish solution was filtered though Celite, and the solvent was removed by evaporation. The residue was dissolved in 10 mL of dichloromethane (hydrous), and the resulting solution was layered with 80 mL of hexane. When the diffusion was complete, the crystals were collected. Yield: 81 %. Elemental analysis (%) calcd for **1**: C 50.14, H 3.95, N 8.45; found: C 50.16, H 4.03, N 8.44; IR (KBr): $\tilde{\nu}$ = 3058, 3036, 2959, 1626, 1592, 1531, 1488, 1439, 1316, 1216, 1083, 1057, 1027, 1001, 940, 842, 777, 739, 696, 659, 619, 519 cm^{-1}; UV/Vis (MeOH): λ_{max} (ε) = 495 (5900), 564 nm (6000 $M^{-1}cm^{-1}$); Λ = 118.6 $\Omega^{-1}cm^2mol^{-1}$; ESI-MS ($CHCl_3$): *m/z*: 848 [M^+-H_2O].

Magnetic susceptibility was measured on a Quantum Design MPMSXL SQUID susceptometer and corrected for diamagnetic contributions. The differences in the magnetic behavior for samples prepared directly from crystals to those prepared by crushing the crystals to form disks under pressure are insignificant.

Received: July 28, 2004
Revised: September 21, 2004

Keywords: magnetic properties · metal–metal interactions · N ligands · ruthenium

[1] For example, see: a) G. R. Newkome, T. J. Cho, C. N. Moorefield, P. P. Mohapatra, L. A. Godínez, *Chem. Eur. J.* **2004**, *10*, 1493 – 1500; b) H.-W. Lin, X.-H. Wang, X.-J. Zhao, J. Li, F.-S. Wang, *Synth. Met.* **2003**, *135–136*, 239 – 240; c) M. Shiotsuka, Y. Yamamoto, S. Okuno, M. Kitou, K. Nozaki, S. Onaka, *Chem. Commun.* **2002**, 590 – 591; d) A. Beyeler, P. Belser, *Coord. Chem. Rev.* **2002**, *230*, 29 – 39; e) J.-P. Launay, *Chem. Soc. Rev.* **2001**, *30*, 386 – 397.

[2] For example, see: a) W.-Z. Chen, T. Ren, *Organometallics* **2004**, *23*, 3766 – 3768; b) G.-L. Xu, M. C. DeRosa, R. J. Crutchley, T. Ren, *J. Am. Chem. Soc.* **2004**, *126*, 3728 – 3729; c) P. Angaridis, J. F. Berry, F. A. Cotton, P. Lei, C. Lin, C. A. Murillo, D. Villagrán, *Inorg. Chem. Commun.* **2004**, *7*, 9 – 13; d) P. Angaridis, J. F. Berry, F. A. Cotton, C. A. Murillo, X. Wang, *J. Am. Chem. Soc.* **2003**, *125*, 10327 – 10334; e) K.-T. Wong, J.-M. Lehn, S.-M. Peng, G.-H. Lee, *Chem. Commun.* **2000**, 2259 – 2260.

[3] F. A. Cotton, R. A. Walton, *Multiple Bonds Between Metal Atoms*, *2nd ed.*, Oxford University Press, Oxford, **1993**.

[4] M. A. S. Aquino, *Coord. Chem. Rev.* **1998**, *170*, 141 – 202.

[5] J. G. Norman, G. E. Renzoni, D. A. Case, *J. Am. Chem. Soc.* **1979**, *101*, 5256 – 5267.

[6] a) F. A. Cotton, L. R. Falvello, T. Ren, K. Vidyasagar, *Inorg. Chim. Acta* **1992**, *194*, 163 – 170; b) F. A. Cotton, A. Yokochi, *Inorg. Chem.* **1998**, *37*, 2723 – 2728.

[7] M. C. Barral, R. González-Prieto, S. Herrero, R. Jiménez-Aparicio, J. L. Priego, E. C. Royer, M. R. Torres, F. A. Urbanos, *Polyhedron* **2004**, 20, 2637 – 2644.

[8] M. C. Barral, S. Herrero, R. Jiménez-Aparicio, M. R. Torres, F. A. Urbanos, *Inorg. Chem. Commun.* **2004**, *7*, 42 – 46.

[9] W.-Z. Chen, T. Ren, *Inorg. Chem.* **2003**, *42*, 8847 – 8852.

[10] Crystal data for **1**: $BC_{41.5}ClF_4H_{39}N_6O_3Ru_2$, M_r = 994.209, thin violet plate (0.04 × 0.30 × 0.38 mm), triclinic, space group $P\bar{1}$, a = 11.8028(8), b = 12.1149(9), c = 16.5002(12) Å, α = 100.1500(10), β = 99.0910(10), γ = 109.4040(10)°, V = 2130.1(3) $Å^3$, Z = 2, ρ_{calcd} = 1.481 $g\,cm^{-3}$, μ = 0.770 mm^{-1}, $2\theta_{max}$ = 57.7°, $\lambda(Mo_{K\alpha})$ = 0.71073 Å, T = 293(2) K, 9653 unique reflections (R(int) = 0.0342), $R1$ = 0.0821, $wR2$ = 0.2572 [$I > 2\sigma(I)$], $R1$ = 0.1370, $wR2$ = 0.2966 (all data), GOF (F^2) = 0.956, N_0/N_v = 9653/494, highest residual electron density 3.571 $e^- Å^{-3}$. X-ray diffraction data were measured on a Bruker Smart CCD diffractometer. The structure was solved by direct methods and refined by full-matrix least-squares techniques using the SHELX system of programs: G. M. Sheldrick, SHELXS-97, program for the solution of crystal structures, University of Göttingen, Göttingen, **1997**. All non-hydrogen atoms were refined anisotropically except for those of the anion and the dichloromethane of crystallization. The presence of this solvent was confirmed by elemental analysis and NMR and IR spectroscopy. In the crystal structure, dichloromethane is severely disordered about an inversion center, and no coordinates were retained. The BF_4^- ion was refined with geometrical constraints (B–F fixed at 1.43 Å). The hydrogen atoms attached to carbon atoms in the complex were generated and assigned isotropic thermal parameters, riding on their parent carbon atoms. CCDC-245747 (**1**) contains the supplementary crystallographic data for this paper. These data can be obtained free of charge via www.ccdc.cam.ac.uk/conts/retrieving.html (or from the Cambridge Crystallographic Data Centre, 12, Union Road, Cambridge CB2 1EZ, UK; fax: (+44) 1223-336-033; or deposit@ccdc.cam.ac.uk). The powder diffractogram of **1** was registered on a Philips X'Pert diffractometer to be sure that the samples contained only one phase. All reflections were indexed with the cell parameters obtained from the single-crystal X-ray study on **1**.

[11] S. M. Tetrick, V. T. Coombe, G. A. Heath, T. A. Stephenson, R. A. Walton, *Inorg. Chem.* **1984**, *23*, 4567 – 4570.

[12] F. A. Cotton, K. R. Dunbar, M. Matusz, *Inorg. Chem.* **1986**, *25*, 1585 – 1589.

[13] F. A. Cotton, M. Matusz, *Polyhedron* **1987**, *6*, 1439 – 1443.

[14] F. A. Cotton, K. R. Dunbar, M. Matusz, *Polyhedron* **1986**, *5*, 903 – 905.

[15] a) M. M. Maltempo, T. H. Moss, *Q. Rev. Biophys.* **1976**, *9*, 181 – 215; b) C. A. Reed, F. Guiset, *J. Am. Chem. Soc.* **1996**, *118*, 3281 – 3282; c) G. Mund, R. J. Batchelor, R. D. Sharma, C. H. W. Jones, D. B. Leznoff, *J. Chem. Soc. Dalton Trans.* **2002**, 136 – 137; d) M. J. Carney, G. C. Papaefthymiou, R. B. Frankel, R. H. Holm, *Inorg. Chem.* **1989**, *28*, 1497 – 1503.

 © 2005 Wiley-VCH Verlag GmbH & Co. KGaA, Weinheim

Allylations

Palladium-Catalyzed Asymmetric Allylation of Prochiral Nucleophiles: Synthesis of 3-Allyl-3-Aryl Oxindoles**

Barry M. Trost and Mathias U. Frederiksen*

The generation of quaternary centers with control of absolute stereochemistry represents a fundamental challenge in synthetic organic chemistry.[1] In this area, we have examined the ability of asymmetric allylic alkylation (AAA) to control stereochemistry at prochiral nucleophiles, a particularly daunting challenge given its direct attack at the face of the allyl fragment opposite to that bound to the metal. Our success with a few classes of nucleophiles exemplified by β-ketoesters,[2] ketones,[3] among others,[4–6] encouraged us to examine new classes of nucleophiles of particular significance such as lactam enolates.

The 3-alkyl-3-aryl oxindole structural motif is a prominent feature in a number of biologically active natural products, for example, diazonamide A[7] and leptosin D,[8] as well as several pharmaceutically active compounds.[9] In spite of the importance of this structural motif, few general methods exist for its construction. Aside from the elegant asymmetric intramolecular Heck reaction developed by Overman and co-workers,[10] only scattered examples based on Pd-catalyzed α arylation[11] and asymmetric acyl transfer have been reported.[12] Pd-catalyzed AAA represents a conceptually novel and flexible approach to this important structural class, especially when combined with the powerful Pd-catalyzed α-arylation protocols for the synthesis of 3-aryl oxindoles developed by Hartwig and co-workers.[11,13] When used in concert, these processes would readily give access to structurally complex oxindoles endowed with a quaternary stereocenter from simple and readily available starting materials [Eq (1)]. Herein we report the successful development of this strategy.

Our studies commenced with a comprehensive matrix screen of bases in the presence of our standard set of ligands **5**–**7** in the Pd-catalyzed AAA reaction of oxindole **8** to form **9** (Table 1).[14] These experiments revealed large variations in yield and enantioselectivity, for example, the use of potassium carbonate in conjunction with ligands **5**–**7** showed a dramatic increase in both yield and *ee* values (Table 1, entries 1–3) relative to other counterions (results not shown). Weaker bases showed better compatibility with this reaction (Table 1, entries 4 and 5). Interestingly, 10 mol% KF gave essentially identical results to the stoichiometric reaction (Table 1, entries 5 and 6). This trend was also observed when nonmetal bases such as Et_3N (Table 1, entries 7 and 8) were used. When BSA was utilized, a spectacular increase in the *ee* value by 36% (from 40 to 76% *ee*) was observed when the base loading was lowered from 1 to 0.1 equivalent (Table 1, entries 9 and 10).

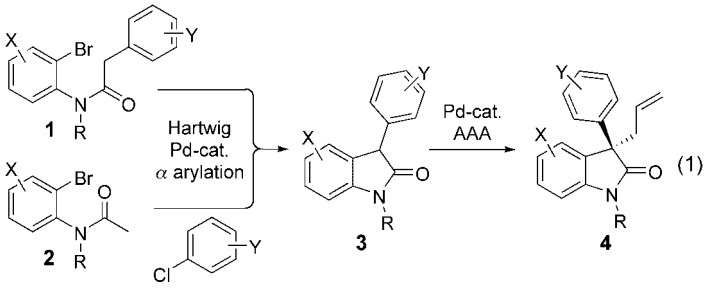
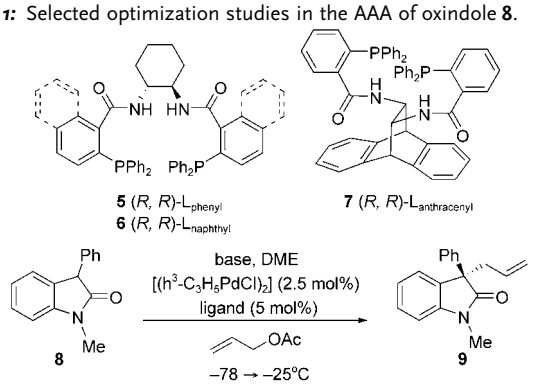


Table 1: Selected optimization studies in the AAA of oxindole **8**.



Entry	Ligand	Base (equiv)	Yield [%][a]	*ee* [%][b]
1	**5**	K_2CO_3 (1.1)	68	19
2	**6**	K_2CO_3 (1.1)	81	28
3	**7**	K_2CO_3 (1.1)	83	56
4	**7**	AcOK (1.1)	92	47
5	**7**	KF (1.1)	86	64
6	**7**	KF (0.1)	84	65
7	**7**	Et_3N (1.1)	66	73
8	**7**	Et_3N (0.1)	66	78
9	**7**	BSA[c] (1.1)	91	40
10	**7**	BSA[c] (0.1)	59	76

[a] Yield of isolated product after chromatography. In all cases, the yields based on recovered starting material are nearly quantitative (>98%). [b] Determined by chiral HPLC. [c] BSA = *N*,*O*-bis(trimethylsilyl)acetamide.

These observations combined with the proficiency of AcOK in this reaction suggested that the addition of only a catalytic amount of base was necessary to initiate the enolization, as ionization of allyl acetate maintained the catalytic concentration of base. However, either the enolate or enol may function as the nucleophile. As oxindoles tautomerize to hydroxyindoles, it seemed reasonable to probe whether it was in fact the latter that acted as the

[*] Prof. B. M. Trost, Dr. M. U. Frederiksen
Department of Chemistry
Stanford University
Stanford, CA 94305-5080 (USA)
Fax: (+1) 650-725-0002
E-mail: bmtrost@stanford.edu

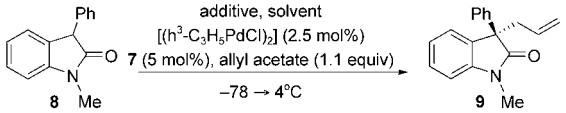
[**] We thank the National Science Foundation and the Institute of General Medical Sciences of the NIH (GM 13598) for their generous support of our programs and GlaxoSmithKline Research and Development (M.U.F.) for partial postdoctoral fellowship support.

Supporting information for this article is available on the WWW under http://www.angewandte.org or from the author.

 © 2005 Wiley-VCH Verlag GmbH & Co. KGaA, Weinheim DOI: 10.1002/anie.200460335

nucleophile. In this case, the reaction should proceed without any external base. It was expected that the rate of tautomerization, and thus the rate of reaction, would be influenced by the polarity of the solvent (Table 2).

Table 2: Selected additive effects in the AAA of oxindole **8**.



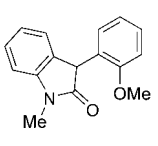
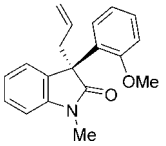
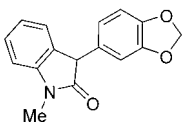
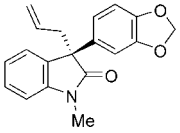
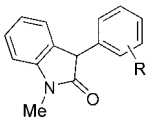
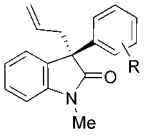
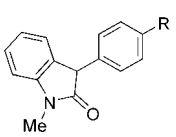
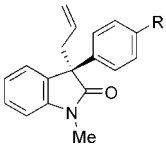
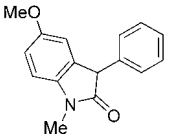
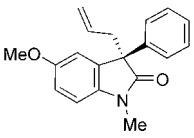
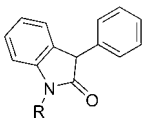
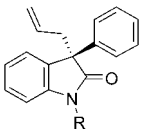
Entry	Solvent	*t* [h]	Yield [%][a]	*ee* [%][b]
1	DME	2	95	61
2	THF	2	75	72
3	CH_2Cl_2	12	31	61
4	PhMe	12	72	78
5[c]	PhMe	12	93	81

[a] Yield of isolated product after chromatography. In all cases, the yields based on recovered staring material are quantitative. [b] Determined by chiral HPLC. [c] *t*BuOH (4 equiv) was used as an additive in this reaction.

In accord with our predictions, the reaction proceeded when carried out in DME (1,2-dimethoxyethane) in the absence of any additives. The reaction was completed in 2 h at 4 °C and afforded **9** in excellent yield with 61 % *ee* (Table 2, entry 1). The reactions in THF occurred with higher enantioselectivity than the reactions in DME (Table 2, entry 2). Further optimization with respect to solvent showed that toluene allowed the highest enantioselectivity, albeit in lower yield (Table 2, entry 4). Reasoning that the oxindole–hydroxindole tautomerization would be significantly faster in hydroxylic media, we next examined the effect of various polar additives in their ability to promote the key tautomerization. After much experimentation, we found that the addition of 4 equivalents of *t*BuOH was optimal and provided the desired product **9** in 93 % yield with 81 % *ee* (Table 2, entry 5).[15] Notably, the yields based on returned starting material are always nearly quantitative, which serves as a testament to the extraordinary selectivity of this reaction. In summary, the use of *t*BuOH (4 equiv), $[(\eta^3\text{-}C_3H_5PdCl)_2]$ (2.5 mol %), and **7** (5 mol %) in toluene at 4 °C under neutral conditions became our standard reaction conditions for the synthesis of 3-aryl oxindoles.

With the optimized procedure established, we sought to examine the scope of the reaction. Thus a number of different aryl oxindoles were prepared and subjected to the standard conditions (Table 3).[16] Significant structural variation in the oxindole system can be accommodated in this reaction.[17] For example, an *ortho*-methoxy group is tolerated (Table 3, entry 1) and the sterically demanding product is obtained in good yield (72 %) with excellent enantioselectivity (97 % *ee*). Otherwise, the method is compatible with electron-rich (Table 3, entries 2–5 and 7) and electron-poor (Table 3, entry 6) aryl groups as well as aryl chloride substituents (Table 3, entry 8). The oxindole core may also be modified. Thus, both the benzo moiety (Table 3, entry 9) and the N-protecting group may be changed as well (Table 3, entries 10–14), for example, the trimethylsilylmethyl group (TMSM) can

Table 3: Scope of Pd-catalyzed AAA of 3-aryl oxindoles.

Entry	Substrate	Product	R	Yield [%][a]	*ee* [%][b]
1				72	97
2				68	79
3			*p*-Me	75	80
4			*m*-Me	96	77
5			*o*-Me	75	70
6			F	73	75
7			Ph	90	73
8			Cl	81	70
9				83	74
10			Me	93	81
11			TMSM[c]	76	80
12			Bn	75	70
13			SEM	81	68
14			MOM	96	66

[a] Yield of isolated product after chromatography. [b] Determined by chiral HPLC analysis, see Supporting Information for details. [c] TMSM = trimethylsilylmethyl.

be used (Table 3, entry 11). This group is interesting owing to the known propensity of such substrates to undergo dipolar cycloadditions,[18] and as such should give access to structurally diverse scaffolds. Other protecting groups may be incorporated, although at a slight detriment to the enantioselectivity. The lower *ee* values attained are intriguing: In the case of aromatic protecting groups (Table 3, entry 12), the lower enantioselectivity may be due to favorable interactions with the phenylphosphino moiety of the ligands which alter the approach of the nucleophile. MOM and SEM aminals (Table 3, entries 13–14) are likely to form stable hydrogen-bonded chelates that confer higher steric demands on the hydroxyindole nucleophile. Simple substituents (e.g. TMSM) may place their sterically demanding groups "outside" the chiral pocket, thereby allowing an ideal approach of the nucleophile to the Pd–allyl complex.

In summary, we have developed an enantioselective palladium-catalyzed AAA reaction for the synthesis of 3-alkyl-3-aryl oxindoles. The salient features of this approach

 © 2005 Wiley-VCH Verlag GmbH & Co. KGaA, Weinheim

are: 1) extraordinarily mild reaction conditions, 2) good to excellent enantioselectivity in the generation of sterically congested quaternary stereocenters, 3) broad substrate scope, and 4) enantioselective access to important structural motifs from readily available and cheap starting material through two Pd-catalyzed processes.

Received: April 15, 2004
Revised: June 1, 2004

Keywords: allylation · asymmetric synthesis · heterocycles · homogenous catalysis · palladium

[1] For a review, see: J. Christoffers, A. Baro, *Angew. Chem.* **2001**, *113*, 4725; *Angew. Chem. Int. Ed.* **2003**, *42*, 1688.
[2] B. M. Trost, R. Radinov, E. M. Grenzer, *J. Am. Chem. Soc.* **1997**, *119*, 7879.
[3] a) B. M. Trost, G. M. Schroeder, *J. Am. Chem. Soc.* **1999**, *121*, 6759; b) B. M. Trost, G. M. Schroeder, J. Kristensen, *Angew. Chem.* **2002**, *114*, 3642; *Angew. Chem. Int. Ed.* **2002**, *41*, 3492.
[4] For a review, see: B. M. Trost, M. L. Crawley, *Chem. Rev.* **2003**, *103*, 2921.
[5] For other examples of Pd-catalyzed asymmetric allylic substitution, see: a) R. Kuwano, Y. Ito, *J. Am. Chem. Soc.* **1999**, *121*, 3236; b) S. L. You, X. Z. Zhu, Y. M. Luo, X. L. Hou, L. X. Dai, *J. Am. Chem. Soc.* **2001**, *123*, 7471; c) S. L. You, X. L. Hou, L. X. Dai, X. Z. Zhu, *Org. Lett.* **2001**, *3*, 149; d) for a review, see: U. Kazmaier, *Curr. Org. Chem.* **2003**, *7*, 317.
[6] For examples of other metal-catalyzed asymmetric allylic substitutions, see: a) Mo: B. M. Trost, K. Dogra, *J. Am. Chem. Soc.* **2002**, *124*, 7256; b) Pt: A. J. Blacker, M. L. Clarke, M. S. Loft, M. F. Mahon, M. E. Humphries, J. M. J. Williams, *Chem. Eur. J.* **2000**, *6*, 353; c) Ir: T. Kanayama, K. Yoshida, H. Miyabe, Y. Takemoto, *Angew. Chem.* **2003**, *115*, 2100; *Angew. Chem. Int. Ed.* **2003**, *42*, 2054; d) W: G. C. Lloyd-Jones, A. Pfaltz, *Angew. Chem.* **1995**, *107*, 534; *Angew. Chem. Int. Ed. Engl.* **1995**, *34*, 462; e) Ni: E. Gomez-Bengoa, N. M. Heron, M. T. Didiuk, C. A. Luchaco, A. H. Hoveyda, *J. Am. Chem. Soc.* **1998**, *120*, 7649.
[7] K. C. Nicolaou, P. B. Rao, J. L. Hao, M. V. Reddy, G. Rassias, X. H. Huang, D. Y. K. Chen, S. A. Snyder, *Angew. Chem.* **2003**, *115*, 1795; *Angew. Chem. Int. Ed.* **2003**, *42*, 1753, and references therein.
[8] C. Takahashi, A. Numata, Y. Ito, E. Matsumura, H. Araki, H. Iwaki, K. Kushida, *J. Chem. Soc. Perkin Trans. 1* **1994**, 1859.
[9] R. R. Goehring, Y. P. Sachdeva, J. S. Pisipati, M. C. Sleevi, J. F. Wolfe, *J. Am. Chem. Soc.* **1985**, *107*, 435.
[10] a) A. B. Dounay, K. Hatanaka, J. J. Kodanko, M. Oestreich, L. E. Overman, L. A. Pfeifer, M. M. Weiss, *J. Am. Chem. Soc.* **2003**, *125*, 6261; b) for a review, see: A. B. Dounay, L. E. Overman, *Chem. Rev.* **2003**, *103*, 2945.
[11] S. Lee, J. F. Hartwig, *J. Org. Chem.* **2001**, *66*, 3402.
[12] a) I. D. Hills, G. C. Fu, *Angew. Chem.* **2003**, *115*, 4051; *Angew. Chem. Int. Ed.* **2003**, *42*, 3921; b) S. A. Shaw, P. Aleman, E. Vedejs, *J. Am. Chem. Soc.* **2003**, *125*, 13368.
[13] K. H. Shaughnessy, B. C. Hammann, J. F. Hartwig, *J. Org. Chem.* **1998**, *63*, 6546.
[14] The depicted configuration is based on the absolute stereochemistry of products derived from the Pd-catalyzed AAA of the closely related 3-alkyl oxindoles, which were converted into known compounds: B. M. Trost, M. U. Frederiksen, unpublished results.
[15] The rate of tautomerization does not seem to be influenced by the addition of *t*BuOH alone, as preliminary ^{1}H NMR spectroscopic analyses of a solution of **8** in [D_8]toluene in the presence or absence of *t*BuOD do not differ appreciably. The addition of tetrabutylammonium acetate (5 mol%) shows significant exchange, whereas catalytic amounts of tetrabutylammonium chloride does not. We attribute this to a general acid–general base catalyzed enolization effected by *t*BuOH in combination with the acetate anion generated in situ.
[16] 3-Aryl oxindoles were prepared by α arylation; see Supporting Information for details.
[17] Despite the efficiency of this process, we have so far been unable to expand the scope with respect to other electrophiles.
[18] L. M. Harwood, R. J. Vickers in *Synthetic Applications of 1,3-Dipolar Cycloaddition Chemistry Toward Heterocycles and Natural Products* (Eds.: A. Padwa, W. H. Pearson), Wiley, New York, **2002**.

 © 2005 Wiley-VCH Verlag GmbH & Co. KGaA, Weinheim

Synthetic Methods

Bromide-Assisted Oxidation of Substituted Phenols with Hydrogen Peroxide to the Corresponding *p*-Quinol and *p*-Quinol Ethers over WO_4^{2-}-Exchanged Layered Double Hydroxides**

*B. F. Sels, D. E. De Vos, and P. A. Jacobs**

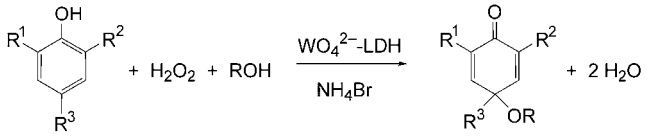
The selective oxidation of substituted phenols to yield 4-hydroxycyclohexa-2,5-dienones (*p*-quinols) and their ethers has been intensely investigated in view of their applications as antioxidants, antibiotics, and antitumor agents.[1,2] Besides electrolytic[3] and photosensitized[4] approaches, procedures for quinol preparation require stoichiometric amounts of oxidants, such as Bi^{III} or Tl^{III} salts,[5,6] oxygen at high pressure,[7] hydrogen peroxide,[8] or particularly electrophilic halogens,[9] such as I^{III} reagents, chlorine, or bromine. In view of the risks associated with handling such reactive species, much attention has recently been devoted to the in situ generation of halonium species from harmless halides by using oxygen or hydrogen peroxide.[10] As with haloperoxidase enzymes, this halide oxidation requires a catalyst. Most haloperoxidase mimics reported until now are only effective at extremely low pH values. However, we developed a heterogeneous haloperoxidase-like catalyst based on WO_4^{2-}-exchanged layered double hydroxides (WO_4^{2-}-LDH), which strongly accelerates the halide oxidation with hydrogen

[*] Prof. B. F. Sels, Prof. D. E. De Vos, Prof. P. A. Jacobs
Department of Interphase Chemistry
Centre for Surface Chemistry and Catalysis
Katholieke Universtiteit Leuven
Kasteelpark Arenberg 23, 3001, Heverlee (Belgium)
Fax: (+32) 16-321-998
E-mail: bert.sels@agr.kuleuven.ac.be

[**] The authors thank the FWO-Vlaanderen (BFS) for a postdoctoral fellowship and Roeland Vancutsem for skilful technical assistance. This work was performed in the frame of the IAP program "Supramolecular Chemistry and Catalysis" of the Belgian Federal government.

 © 2005 Wiley-VCH Verlag GmbH & Co. KGaA, Weinheim DOI: 10.1002/anie.200461555

peroxide even at mild pH values.[11] Based on this method, we anticipated the overall transformation of substituted phenols to quinol ethers with hydrogen peroxide in the presence of a bromide salt, the WO_4^{2-}-LDH catalyst, and the appropriate alcohol. If successful, this one-pot synthesis could provide a new route towards the highly valuable *p*-quinol ethers:

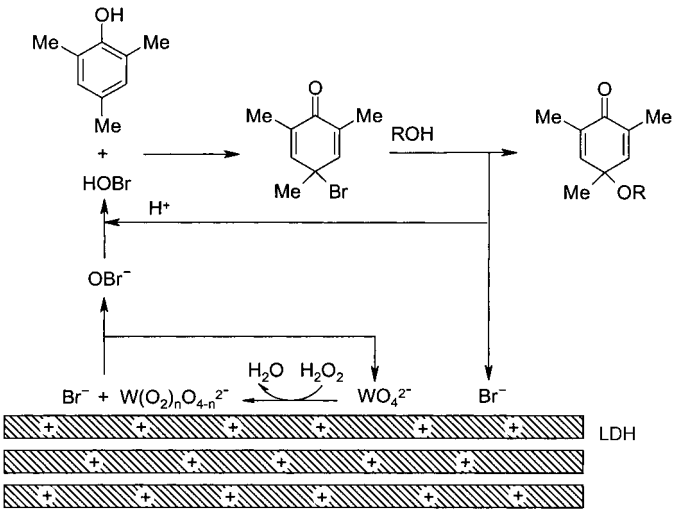


Initial investigations focused on the oxidative methoxylation of mesitol (**1**) with hydrogen peroxide in methanol in the presence of a bromide source and 1 mol% WO_4^{2-} exchanged on LDH (Table 1). Hydrogen peroxide was added slowly to the reaction mixture. We employed LDHs as supports with varying compositions $M^{II}_{1-x}M^{III}_x(OH)_2[(WO_4^{2-})_{xy/2}(A^-)_{x(1-y)}]\cdot m H_2O$ ($M^{II} = Zn^{II}$, Ni^{II}, Mg^{II}; $M^{III} = Al^{III}$, Ga^{III}; $A^- = Cl^-$, NO_3^-).[12] In our experience, the oxidative bromination proceeds fastest with LDHs with a large degree of isomorphous substitution ($x = 0.37$) and with tungstate contents of 20–25% of the total anion exchange capacity ($y = 0.25$–0.30). Ni^{II}- and NO_3^--containing LDHs have especially high productivities: quinol ether **1a** was produced in 87% yield within 30 min (Table 1, entry 1). With Mg^{II} in the hydroxide layers or with Cl^- as the counterion, the yield of **1a** is only slightly lower (Table 1, entries 2–3). In contrast, with the homogeneous catalyst Na_2WO_4, only 21% of **1a** is formed after 6 h (Table 1, entry 4). This result highlights the importance of the LDH support in facilitating the bromide oxidation (Scheme 1). Indeed, the cationic surface, decorated with peroxotungstate anions, attracts bromide anions and thus compensates for the repulsion between the negatively charged reaction partners Br^- and peroxotungstate. As a result, the bromide-oxidation rate is increased tremendously. In the absence of either WO_4^{2-}-LDH or Br^-, no product was observed after 12 h (Table 1, entries 5–6). As a solvent, a methanol/ethyl acetate mixture proved suitable, though satisfactory yields were also obtained in pure methanol or other methanol-containing mixtures (73–85%, data not shown). However, when acetone is used or when the water content is too high, the yields of **1a** drastically drop to lower values (32 and 72%; Table 1, entries 7–8).

Table 1: Br^--assisted oxidation of mesitol (**1**) to 4-methyoxy-4-methylcyclohexa-2,5-dienone (**1a**).[a]

Entry	Catalyst, conditions	Yield[b] (Conversion) [%]	*t* [h]	*p*/*o*[c]
1	NiAl[NO_3^-, WO_4^{2-}]	91 (100)	0.5	25:1
2	NiAl[Cl^-, WO_4^{2-}]	84 (97)	0.5	24:1
3	MgAl[NO_3^-, WO_4^{2-}]	86 (92)	0.5	21:1
4	$Na_2WO_4\cdot 2H_2O$	21 (28)	6	23:1
5	no WO_4^{2-} catalyst	0 (<1)	12	–
6	no NH_4Br	0 (<1)	12	–
7	5 vol% water	72 (95)	1	24:1
8	acetone instead of ethyl acetate	32 (34)	1	24:1

[a] Conditions, unless mentioned otherwise: WO_4^{2-}-LDH ($Ni_{0.64}Al_{0.36}(OH)_2[(WO_4^{2-})_{0.045}(NO_3^-)_{0.27}]\cdot 0.6\,H_2O$) (17 mg), MeOH/EtOAc/$H_2O$ (10 mL; 30:68.5:1.5 vol%), NH_4Br (0.15 M), **1** (0.06 M), aqueous H_2O_2 (35 wt%; added at 2.8 mmol h^{-1}), 60°C. Product yields and identities were determined by GC and GC–MS, and, after product extraction with diethyl ether, by ^1H and ^{13}C NMR spectroscopic analysis. [b] Yield of *p*- and *o*-quinol ethers. [c] Molar ratio of *p*- and *o*-quinol ethers.



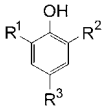
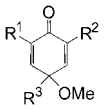
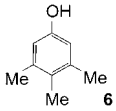
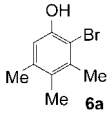
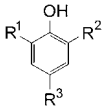
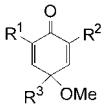
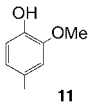
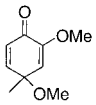
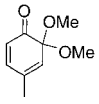
Scheme 1. Bromide-assisted oxidation of mesitol with H_2O_2 to the corresponding *p*-quinol (ether) over WO_4^{2-}-exchanged layered double hydroxide.

The synthetic utility of this heterogeneous tungstate-catalyzed oxidation was evaluated with a wide range of variously substituted phenols (Table 2). Alkylated phenols undergo the Br^--assisted oxidative methoxylation in moderate to excellent yields, especially when the *ortho* and *para* positions are substituted (Table 2, **1–4**; 81–91%). However, when the *ortho* or *para* positions are unsubstituted, stable brominated phenols are the main products (**5–6**). This limitation does not hold for the *p*-alkoxylated phenols (**7–10**), and high yields of the *p*-benzoquinone monoketals are obtained, irrespective of the substitution pattern. A considerable benefit of the catalytic procedure is that the products are not transketalized. Thus, the WO_4^{2-}-LDH can be used for the synthesis of mixed ketal 4-ethoxy-4-methoxycyclohexa-2,5-dienone (**8a**). When Tl salts are used as the oxidant, **8a** is not accessible because of Tl^{III}-induced transketalization.[6,13] Reactions with *o*-alkoxylated phenols, **11**, are less selective and give rise to a mixture of products, including the *o*-quinone monoketal **11b**. The latter is unstable and dimerizes through a Diels–Alder mechanism.[9f]

Finally, the use of various alcohol nucleophiles was evaluated in Table 3. If the bromide salt is sufficiently soluble in the solvent mixture and the alcohol is not too bulky (as for example, *tert*-butyl alcohol), many alcohol reagents lead to the quinol ether products in good yields (75–91%). The oxidative alkoxylation is highly *para*-selective, with *p*/*o* ratios >20:1, in contrast to most existing procedures.[9,14]

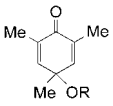
 © 2005 Wiley-VCH Verlag GmbH & Co. KGaA, Weinheim

Table 2: Oxidation of substituted phenols to quinol ethers.[a]

Substrate	Product	R^1	R^2	R^3	H_2O_2 [equiv]	Yield (Conv.) [%]
						
1	**1a**	Me	Me	Me	2.3	91 (100)
2	**2a**	*i*Pr	*i*Pr	Me	3.0	88 (100)
3	**3a**	*t*Bu	*t*Bu	Me	3.2	87 (96)
4	**4a**	*t*Bu	*t*Bu	*t*Bu	6.0	81 (94)
5	**5a**	H	Me	Me	4.0	21 (100)[b]
 **6**	 **6a**				2.3	71 (100)[c]
						
7	**7a**	H	H	OMe	2.3	94 (100)
8	**8a**	H	H	OEt	2.3	92 (100)
9	**9a**	H	Cl	OMe	2.3	92 (99)
10	**10a**	Me	Me	OMe	2.3	89 (100)
 **11**	 **11a**  **11b**				4.0	56 (96)[d]

[a] Conditions as in Table 1; 0.5–1 h. [b] 2-Brominated product (m/z = 200–202): 59% yield. [c] m/z = 214–216. [d] $p/o \approx 8{:}1$; to be taken with caution because of considerable dimerization of the *ortho* product.

Table 3: WO_4^{2-}-LDH-catalyzed oxidative alkoxylation of mesitol (**1**) with various alcohols.[a]

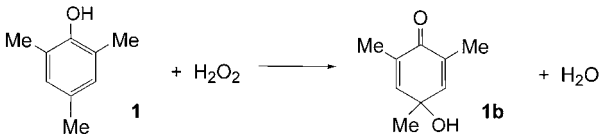
Entry	Alcohol (ROH)	Products	H_2O_2 [equiv]	*p*/*o*	Yield (Conv.) [%]
1	MeOH		2.3	25:1	91 (100)
2	EtOH		2.3	26:1	89 (100)
3	*n*PrOH		2.3	24:1	86 (100)
4	*n*BuOH		3.2	25:1	84 (100)
5	*n*HexOH		3.2	n.d.	21 (68)
6	AllylOH		3.2	n.d.	81 (100)
7	AmylOH		3.2	n.d.	82 (98)
8	*i*PrOH		3.2	27:1	75 (99)
9	*i*BuOH		3.2	30:1	78 (95)
10	*t*BuOH		3.2	n.d.	3 (85)

[a] Conditions as in Table 1, except that methanol is replaced by other alcohols.

As is known from previous mechanistic work,[11b] hydrogen peroxide is activated by the tungstate to give peroxotungstates, which in turn oxidize Br^- into hypobromite. As shown in Scheme 1 and in agreement with literature reports,[15,16] subsequent electrophilic bromination of mesitol (**1**) by HOBr generates the 4-bromocyclohexa-2,5-dienone intermediate, which in some reactions was detected as a transient product in small amounts by GC–MS. Under neutral conditions, this compound rapidly reacts with the alcohol to form the quinol ether,[15,17] and the eliminated HBr can participate in a new catalytic cycle. Under acidic conditions, the same 4-Br compound rearranges into the stable 3-bromomesitol.[9e] Clearly, for the success of the overall transformation, it is essential to avoid acidity, which underlines again the need for a haloperoxidase mimic capable of halide oxidation under neutral conditions.

Regarding the efficiency of hydrogen peroxide, it is important to avoid the unproductive reduction of OBr^- by excess hydrogen peroxide, which yields singlet oxygen. Whether this occurs depends on the hydrogen peroxide concentration, the pH value of the reaction conditions, and the reactivity of the phenol. In the case of **1** in 0.15 M NH_4Br, dropwise addition of hydrogen peroxide at a maximum rate of 500 mol (mol W)$^{-1}$ h^{-1} resulted in reasonable yields based on the concentration of hydrogen peroxide.

Careful analysis of the products from **1** showed that the *p*-quinol 4-hydroxy-2,4,6-trimethylcyclohexa-2,5-dienone (**1c**) was always formed in small amounts. Since **1b** is a drug and vitamin E precursor,[2] we briefly investigated its formation. In reaction conditions similar to those given in Table 3, and in a water/THF solvent mixture (9:1), **1c** is produced in 91% yield, with only 2,6-dimethylquinone as a minor byproduct.



In conclusion, we have designed a one-pot metal-catalyzed procedure for the synthesis of 4-alkoxy- or 4-hydroxy-substituted cyclic 2,5-dienones in good yields from a broad range of phenol substrates. Although this particular class of phenol oxidations has often been performed with stoichiometric oxidants, we propose a metal-catalyzed route based on the clean oxidant hydrogen peroxide. A unique feature of the WO_4^{2-}-LDH/NH_4Br/H_2O_2 catalytic system is that high bromide-oxidation rates are decoupled from strong acidity which allows a high chemoselectivity for the desired quinol products to be reached.

Received: August 5, 2004
Revised: September 2, 2004

Keywords: heterogeneous catalysis · hydroxycyclohexadienones · oxidation · peroxides · tungsten

 © 2005 Wiley-VCH Verlag GmbH & Co. KGaA, Weinheim

[1] a) A. G. Schultz, S. O. Myong, S. Puig, *Tetrahedron Lett.* **1984**, *25*, 1011; b) T. Matsuura, K. Ogura, *J. Am. Chem. Soc.* **1978**, *100*, 2834; c) D. Liotta, M. Saindane, C. Barnum, *J. Am. Chem. Soc.* **1981**, *103*, 3224; d) Y. Ito, H. Ito, M. Ino, T. Matsuura, *Tetrahedron Lett.* **1988**, *29*, 3091; e) M. C. Pirrung, D. S. Nunn, *Tetrahedron Lett.* **1992**, *33*, 6591; f) K. Blades, G. S. Cockerill, H. J. Easterfield, T. Lequeux, J. M. Percy, *Chem. Commun.* **1996**, 1615; g) V. Caprio, J. Mann, *J. Chem. Soc. Perkin Trans. 1* **1998**, *19*, 3151; h) S. Large, N. Roques, B. R. Langlois, *J. Org. Chem.* **2000**, *65*, 8848; i) M.-E. Tran-Huu-Dau, R. Wartchow, E. Winterfeldt, Y.-S. Wong, *Chem. Eur. J.* **2001**, *7*, 2349; j) M. C. Carreno, M. Ribagorda, A. Somoza, A. Urbano, *Angew. Chem.* **2002**, *114*, 2879; *Angew. Chem. Int. Ed.* **2002**, *41*, 2755; k) G. Wells, J. M. Berry, T. D. Bradshaw, A. M. Burger, A. Seaton, B. Wang, A. D. Westwell, M. F. G. Stevens, *J. Med. Chem.* **2003**, *46*, 532; l) R. W. Van De Water, C. Hoarau, T. R. R. Pettus, *Tetrahedron Lett.* **2003**, *44*, 5109.

[2] a) *Ullmann's Encyclopedia, 6th ed.*, **2000** (Electronic release); b) Y. Ichikawa, Y. Yamanaka, N. Suzuki, T. Naruchi, O. Kobayashi, H. Tsuruta, *Ind. Eng. Chem. Prod. Res. Dev.* **1979**, *18*, 473; c) J. Jono, T. Tomita, US 4477682, **1984** [*Chem. Abstr.* **1983**, *99*, 194488]; d) M. Costantini, F. Igersheim, L. Krumenacker, US 4612401, **1986** [*Chem. Abstr.* **1986**, *104*, 129540]; e) V. Nardello, S. Bogaert, P. L. Alsters, J. M. Aubry, *Tetrahedron Lett.* **2002**, *43*, 8731.

[3] A. Nilsson, U. Palmquist, T. Pettersson, A. Ronlán, *J. Chem. Soc. Perkin Trans. 1* **1987**, 708.

[4] N. Homs, P. R. de la Piscina, F. Borrull, *J. Chem. Soc. Chem. Commun.* **1988**, 1075.

[5] E. Adler, K. Holmberg, *Acta Chem. Scand. Ser. B* **1974**, *28*, 883.

[6] A. McKillop, D. H. Perry, M. Edwards, S. Antus, L. Farkas, M. Nógrádi, *J. Org. Chem.* **1976**, *41*, 282.

[7] Y. Ichikawa, N. Suzuki, H. Tsuruta, Y. Yamanaka, US 3975441 [*Chem. Abstr.* **1975**, *83*, 9307].

[8] M. Shimizu, H. Orita, T. Hayakawa, Y. Watanabe, K. Takehira, *Bull. Chem. Soc. Jpn.* **1990**, *63*, 1835.

[9] a) C. Elston, A. T. Peters, F. M. Rowe, *J. Chem. Soc.* **1948**, 367; b) K. Ley, DE 1 200 810, **1965** [*Chem. Abstr.* **1968**, *68*, 104614]; c) J. H. Atkinson, D. Clark, US 3895069, **1975** [*Chem. Abstr.* **1973**, *79*, 146194]; d) K.-E. Bergquist, A. Nilsson, A. Ronlán, *Acta Chem. Scand. Ser. B* **1982**, *36*, 675; e) A. Fischer, G. N. Henderson, *Can. J. Chem.* **1983**, *61*, 1045; f) E. Adler, G. Andersson, E. Edman, *Acta Chem. Scand. Ser. B* **1975**, *29*, 909; g) A. Pelter, S. Elgendy, *J. Chem. Soc. Perkin Trans. 1* **1993**, 1891; h) H. Togo, S. Abe, G. Nogami, M. Yokoyama, *Bull. Chem. Soc. Jpn.* **1999**, *72*, 2351.

[10] a) A. Butler, J. V. Walker, *Chem. Rev.* **1993**, *93*, 1937; b) J. V. Walker, M. Morey, H. Carlsson, A. Davidson, G. D. Stucky, A. Butler, *J. Am. Chem. Soc.* **1997**, *119*, 6921; c) A. G. J. Ligtenbarg, R. Hage, B. L. Feringa, *Coord. Chem. Rev.* **2003**, *237*, 89; d) R. Ben-Daniel, S. P. de Visser, S. Shaik, R. Neumann, *J. Am. Chem. Soc.* **2003**, *125*, 12116; e) B. M. Choudary, T. Someshwar, M. Lakshmi Kantam, Ch. Venkat Reddy, *Catal. Commun.* **2004**, *5*, 215.

[11] a) B. F. Sels, D. De Vos, M. Buntinx, F. Pierard, F. Kirsch-De Mesmaeker, P. Jacobs, *Nature* **1999**, *400*, 855; b) B. F. Sels, D. De Vos, P. Jacobs, *J. Am. Chem. Soc.* **2001**, *123*, 8350; c) B. F. Sels, D. De Vos, M. Buntinx, P. Jacobs, *J. Catal.* **2003**, *216*, 288.

[12] B. F. Sels, D. E. De Vos, P. A. Jacobs, *Catal. Rev.* **2001**, *43*, 443.

[13] An alternative synthesis of these 4,4-dialkoxycyclohexa-2,5-dienones is the ketalization of the quinones: A. Kaji, R. Saito, Y. Hata, N. Kiriyama, *Chem. Pharm. Bull.* **1999**, *47*, 77.

[14] Reaction of **1** with *N*-(phosphonomethyl)iminodiacetic acid (PIDA; $PhI(OAc)_2$) and H_5IO_6 in methanol gave the *p*- and *o*-quinol ethers in a ratio of 5:1 and 1:1, respectively.

[15] A. F. Hegarty, J. P. Keogh, *J. Chem. Soc. Perkin Trans. 2* **2001**, *5*, 758.

[16] L. A. Paquette, G. J. Hefferon, R. Samodral, Y. Hanzawa, *J. Org. Chem.* **1983**, *48*, 1262.

[17] M. Tashiro, G. Fukata, H. Yoshiya, *Synthesis* **1979**, 988.

 © 2005 Wiley-VCH Verlag GmbH & Co. KGaA, Weinheim

Solid Electrolytes

Rapid I^-/I_3^- Diffusion in a Molecular-Plastic-Crystal Electrolyte for Potential Application in Solid-State Photoelectrochemical Cells**

Qing Dai, Douglas R. MacFarlane, Patrick C. Howlett, and Maria Forsyth*

A molecular plastic crystal based electrolyte is described which has almost liquidlike diffusion properties for I^-/I_3^-, a redox couple of interest in photoelectrochemical cells. These cells, which are typically composed of TiO_2 photoanodes covered with dye molecules or a conducting polymer and a liquid-based electrolyte, are currently under intense investigation because of their relatively low-cost materials and extremely simple fabrication techniques.[1] Although dye-sensitized nanocrystalline solar cells (DSSCs) offer high efficiency, comparable to that of amorphous silicon solar cells, a major disadvantage of such devices is the necessity of using a liquid-based electrolyte which includes the dissolved I^-/I_3^- redox couple.[2] A number of difficulties in encapsulation of this liquid electrolyte considerably hinder the long-term stability of these devices. Thus hole-transporting organic materials,[3,4] *p*-type semiconductors,[5] and polymers incorporating the redox couple have been investigated to replace the organic solvent-based liquid electrolytes for solid-state DSSCs.[6–8] Wang et al. have succeeded in employing quasi-solid-state electrolytes based on room-temperature ionic liquids, which yielded up to 7% efficiency in AM 1.5 sunlight.[9,10] However, so far, true solid-state DSSCs have still shown much lower efficiency because of the mass transport limitation of current electrolytes.

In the past we have investigated a family of ionic plastic crystals[11–13] and molecular plastic crystals[14,15] for potential application in Li batteries and fuel cells. In the present study,

[*] Dr. Q. Dai, Prof. D. R. MacFarlane, Dr. P. C. Howlett
School of Chemistry, Monash University
Clayton, Victoria 3800 (Australia)
Fax: (+61) 3-9905-4597
E-mail: qing.dai@sci.monash.edu.au
Prof. M. Forsyth
School of Physics & Material Engineering
Monash University
Clayton, Victoria 3800 (Australia)

[**] We are grateful to Australia Research Council for financial support under the Discovery Project (No. DP02102260).

 DOI: 10.1002/anie.200460871 © 2005 Wiley-VCH Verlag GmbH & Co. KGaA, Weinheim

succinonitrile, a molecular plastic crystal, was chosen for investigation as a solvent with potential application in solid-state photoelectrochemical cells. This material was chosen because of its similarity to acetonitrile and glutaronitrile, which are commonly used as solvents for DSSCs. Succinonitrile displays the typical behavior of a molecular plastic crystal and has potentially good solvent properties.[16–19] The plastic phase is stable between 233 and 331 K in a body-centered cubic (bcc) structure.[15–20] In this phase the molecules exist in three isomeric conformations: two (identical) *gauche* and one *trans* isomer,[15–19] which are interrelated by a 120° rotation around the central C–C bond.[15–20,22] The bcc unit cell contains two molecules with the C–C bonds oriented along the diagonals of the cube.[16,19,21,23] Below 233 K the molecules exist exclusively in the *gauche* conformation.[16,20] At 233 K the material undergoes a phase change to a plastic phase. The disorder in this phase is related to *trans–gauche* isomerization (involving rotation about the central C–C bond) of the molecules and molecular jumps from one diagonal position of the cubic structure to another.[19,23] Hawthorne and Sherwood suggested that the availability of three possible conformers in succinonitrile has a major effect on the diffusion capability of the molecules, whereby the *trans* isomers act as "impurities" that create monovacancies in the lattice[16,23] and hence lead to high molecular diffusivity. These properties triggered our interest in the concept of fast I^-/I_3^- diffusion in a molecular plastic crystal. Here we communicate our preliminary results which support this concept. The materials described are the first examples of electrolytes based on molecular plastic crystals and exhibit mass transport rates high enough to be of relevance to applications such as DSSC.

The plastic crystal based electrolyte is composed of 0.375 M tetrabutylammonium iodide and 0.225 M iodine in succinonitrile. The redox couple showed good miscibility with succinonitrile, and the electrolyte was a waxy solid at ambient temperature. Typical thermal traces are presented in Figure 1 (left axis). Apparently, the solid–solid transition temperature does not change significantly on addition of the redox couple, as would be expected if the transition is an equilibrium thermodynamic phase change related to structural changes of the matrix phase. The melting behavior is complex, but it is apparent that the material is in a completely solid state below 45 °C. This is still low enough to allow fabrication of a DSSC with the electrolyte in the liquid state, which ensures good penetration into the pores of the nanocrystalline TiO_2. Comparing the enthalpy of the solid–solid transition of succinonitrile in the mixture (65.3 $J\,g^{-1}$) with the expected value (66.5 $J\,g^{-1}$) indicates that the physical properties of succinonitrile itself are not changed after addition of the solutes. Figure 1 (right axis) shows the ionic conductivity. There is a significant step in the conductivity at the melting point, as compared with the pure material, which is consistent with the presence of a significantly greater number of mobile ionic species. The NMR diffusivities and the apparent transport numbers of the cation and the anions are also listed in Table 1. The NMR data suggest that mobile succinonitrile molecules diffusing in the matrix do so at a faster rate (1.3×10^{-6} cm^2s^{-1}) than the cation. The calculated transport numbers further indicate that the mobilities of both I^- and I_3^- are much higher than that of the cation in the succinonitrile electrolyte system.

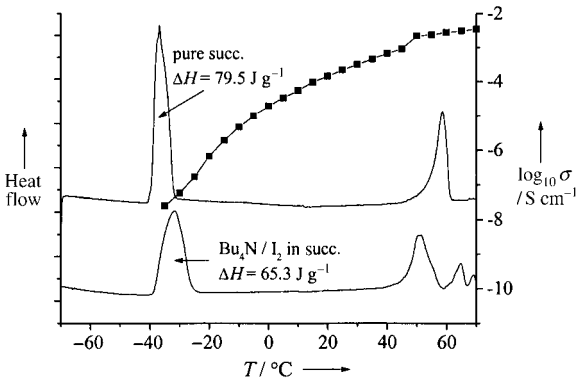


Figure 1. Conductivity (■, right axis) versus temperature for succinonitrile doped by 0.375 M Bu_4NI/0.225 M I_2 and its DSC thermogram (left axis). The thermogram of pure succinonitrile is shown for comparison.

Table 1: Diffusion properties of a molecular plastic crystal based electrolyte at 25 °C (error: ±5%).

	D_{app} [10^{-6} cm^2s^{-1}]		D_{PFG} [10^{-6} cm^2s^{-1}]		Transport number[a]		
	I_3^-	I^-	succ.	Bu_4N^+	I_3^-	I^-	Bu_4N
Bu_4NI/I_2	1.6	6.5	1.3	0.53	0.23	0.64	0.13

[a] The transport number t was calculated from the formula: $t(I_3^-) = [I_3^-]D_{app}(I_3^-)/\{[I_3^-]D_{app}(I_3^-)+[I^-]D_{app}(I^-)+[Bu_4N]D_{PFG}(Bu_4N)\}$.

Figure 2 shows the linear sweep of the molecular plastic crystal based electrolyte. The apparent diffusion coefficients

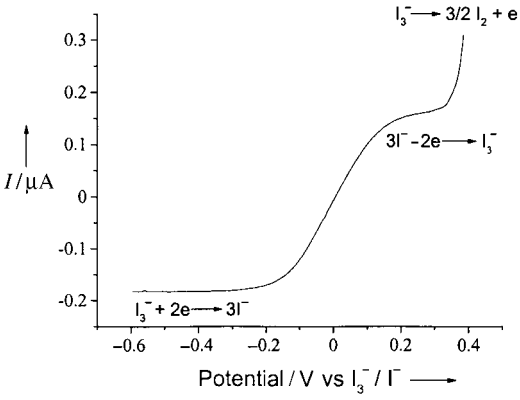


Figure 2. Linear sweep of molecular plastic crystal based electrolyte with Pt ultramicroelectrode at 25 °C. Scan rate: 50 $mV\,s^{-1}$.

D_{app} of iodide and triiodide (Table 1) were calculated from the anodic and cathodic limiting current I_{lim} by using Equation (1)[24] where n is the number of electrons per molecule, F

$$I_{lim} = 4nFDCr \qquad (1)$$

the Faraday constant, C the concentration, and r the radius of the electrode. Comparable data for a commonly used liquid

 © 2005 Wiley-VCH Verlag GmbH & Co. KGaA, Weinheim

solvent (acetonitrile) were reported by Matsumoto et al.[25] and recently for a gelled ionic liquid by Wang et al.[10] The results indicate that the diffusivity of I_3^- in the plastic solid is higher than in the gelled ionic liquid. Diffusivities that are higher in the solid state than in the corresponding liquid state have been observed previously[26] and are related to defect motion in the ordered crystalline lattice. Moreover, $D_{app}(I^-)$ in the plastic crystal based electrolyte is 4.7 times larger than in the gel electrolytes.[9,10] The high diffusivity of the iodide ion may reflect the formation of polyiodide species, so that iodide transport is facilitated in a Grotthus-type mechanism. A spectroscopic investigation of these species is underway.

Figure 3 presents short-circuit current densities J_{sc} as a function of light intensity for the plastic crystal electrolyte. For comparison, J_{sc} of the conventional organic liquid electrolyte system under 1 Sun illumination is also shown.

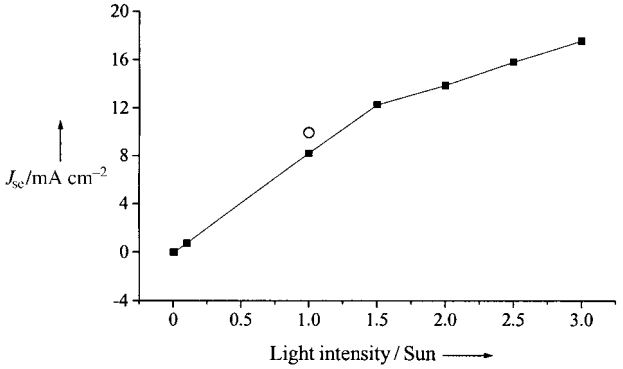


Figure 3. Short-circuit current J_{sc} as a function of light intensity for plastic crystal (■) and organic liquid (○) electrolytes. Photoelectrode size: 5×5 mm.

As described in the Experimental Section, these cells did not contain optimized photoanodes, and the standard thin electrolyte layer (25-μm thick Surlyn) was unavailable; therefore, J_{sc} for the conventional organic liquid electrolyte system is not as high as some published data at 1 Sun illumination. Nevertheless, the data in the figure also show that the electrolyte is capable of carrying currents as high as 18 mA cm^{-2} in the solid state, which corresponds to some of the highest published 1 Sun currents. Furthermore, under 1 Sun conditions, J_{sc} of the plastic crystal electrolyte system reaches 82.8% of that of the conventional liquid electrolyte system. All these values are of sufficient magnitude to be of interest for photoelectrochemical cells. Further increases in short-circuit current for both electrolyte systems are possible by optimizing the electrolyte systems, the TiO_2 working electrode, and the thickness of the electrolyte layer.

This is the first example of a DSSC based on a plastic crystalline electrolyte with high current-carrying capacity. Although the melting point of about 45 °C of the succinonitrile electrolyte system is somewhat low for practical devices for outdoor applications, it is high enough for devices for indoor application. More important, the new concept established here will be very helpful in developing other types of plastic crystal systems with rapid I^-/I_3^- mobility and higher melting points for potential application in photoelectrochemical cells. Further work to optimize the electrolyte composition and cell construction, to characterize the device performance of the succinonitrile electrolyte in photoelectrochemical cells, and to explore better plastic crystal electrolyte systems for application in photoelectrochemical devices are underway.

Experimental Section

Analytical grades of succinonitrile, tetrabutylammonium iodide, and iodine were used. Tetrabutylammonium iodide was recrystallized and iodine was sublimed prior to use. The sample was prepared in an N_2-filled glove box and dried under vacuum at 65 °C for at least 48 h before the measurements. The thermal properties were measured on a Perkin Elmer DSC7 at a scanning rate of 20 °C min^{-1}. Solid–solid phase transition temperatures T_{s-s} and melting/liquid points T_m were determined as a function of composition. Conductivity measurements were carried out in a locally designed conductance cell. During the measurements, the temperature was raised at a steady rate of 0.3 °C min^{-1}. An electrochemical cell equipped with a Pt ultramicroelectrode of 6.4 μm radius as the working electrode, a Pt wire as the counterelectrode, and a Pt wire pseudoreference electrode were used to study mass transport in the electrolyte at 25 °C. ^{1}H NMR pulsed field gradient (PFG) diffusion experiments were used to determine the diffusion coefficients of the doped species in the sample on a Bruker Advance 300 spectrometer at 25 °C.

DSSCs were constructed from TiO_2-coated transparent conducting oxide (TCO) plates (purchased from STA Ltd, Australia), $[Ru(dcbpy)_2(SCN)_2]$ (dcbpy = 2,2′-bipyridyl-4,4′-dicarboxylate), and a Pt-catalyzed TCO counterelectrode. Prior to dye adsorption, electrodes were heated at 450 °C for 15 min to remove any adsorbed water. The electrodes underwent chemical adsorption in the dye solution at 80 °C for 12 h. A 200-μm thick Surlyn gasket was then cut to fit around the TiO_2 film on the electrodes and seal the cells during heating. The plastic electrolyte was sandwiched between the electrodes by filling the cell with the molten electrolyte under vacuum. For comparison, the conventional volatile electrolyte (0.5 M LiI and 0.04 M I_2 in acetonitrile) was then administered by capillary force into the open sandwich cell. The TiO_2 electrodes were soaked in a solution of 0.1 M 4-*tert*-butylpyridine (Aldrich) in acetonitrile (BDH) just before constructing the cells. The current–voltage curves were determined under illumination with an 80-W halogen lamp (Phillips). Labview 6.1 (National Instruments) drove a Keithley 2400 source meter to record the current across a linear voltage sweep from −0.2 to 0.8 V. Light intensity corresponding to 1 Sun was determined by a luxmeter (RS Components, 180–7133). The cells were tested by using an externally calibrated photodiode. Cells were mounted on a heat sink and measurements were limited to less than 1 min to minimize temperature rises.

Received: June 4, 2004
Revised: September 4, 2004

Keywords: conducting materials · electrochemistry · iodine · photoelectrochemical cells · solid electrolytes

[1] M. Grätzel, *Nature* **2001**, *414*, 338–344.
[2] M. K. Nazeeruddin, P. Pechy, T. Renouard, S. M. Zakeeruddin, R. Humphry-Baker, P. Comte, P. Liska, L. Cevey, E. Costa, V. Shklover, L. Spiccia, G. B. Deacon, C. A. Bignozzi, M. Graetzel, *J. Am. Chem. Soc.* **2001**, *123*, 1613–1624.
[3] B. O'Regan, D. T. Schwartz, *Chem. Mater.* **1998**, *10*, 1501–1509.

 © 2005 Wiley-VCH Verlag GmbH & Co. KGaA, Weinheim

[4] G. R. A. Kumara, S. Kaneko, M. Okuya, K. Tennakone, *Langmuir* **2003**, *19*, 10493 – 10495.
[5] U. Bach, D. Lupo, P. Comte, J. E. Moser, F. Weissortel, J. Salbeck, H. Spreitzer, M. Grätzel, *Nature* **1998**, *395*, 583 – 585.
[6] F. Cao, G. P. C. Oskam, Searson, *J. Phys. Chem.* **1995**, *99*, 17071 – 17073.
[7] A. F. Nogueira, J. R. Durrant, M. A. De Paoli, *Adv. Mater.* **2001**, *13*, 826 – 830.
[8] E. Stathatos, P. Lianos, U. Lavrencic-Stangar, B. Orel, *Adv. Mater.* **2002**, *14*, 354 – 357.
[9] P. Wang, S. M. Zakeeruddin, I. Exnar, M. Graetzel, *Chem. Commun.* **2002**, *24*, 2972 – 2973.
[10] P. Wang, S. M. Zakeeruddin, P. Comte, I. Exnar, M. Graetzel, *J. Am. Chem. Soc.* **2003**, *125*, 1166 – 1167.
[11] D. R. MacFarlane, M. Forsyth, *Adv. Mater.* **2001**, *13*, 957 – 966.
[12] D. R. MacFarlane, J. Huang, M. Forsyth, *Nature* **1999**, *402*, 792 – 794.
[13] D. R. MacFarlane, P. Meakin, N. Amini, M. Forsyth, *J. Phys. Condens. Matter* **2001**, *13*, 8257 – 8267.
[14] S. Long, D. R. MacFarlane, M. Forsyth, *Solid State Ionics*, **2004**, in press.
[15] S. Long, D. R. MacFarlane, M. Forsyth, *Solid State Ionics* **2003**, *161(1-2)*, 105 – 112.
[16] H. M. Hawthorne, J. N. Sherwood, *Trans. Faraday Soc.* **1970**, *66*, 1792 – 1798.
[17] G. Dosseh, C. Fressigne, B. Rousseau, N. Wilding, A. H. Fuchs, *J. Chim. Phys. Phys.-Chim. Biol.* **1990**, *87*, 1821 – 1833.
[18] T. Bischofberger, E. Courtens, *Phys. Rev. Lett.* **1974**, *32*, 163 – 166.
[19] G. Cardini, R. Righini, S. Califano, *J. Chem. Phys.* 1991, *95*, 679 – 685.
[20] A. Masui, S. Yoshioka, S. Kinoshita, *Chem. Phys. Lett.* **2001**, *341*, 299 – 305.
[21] P. Derollez, J. Lefebvre, M. Descamps, W. Press, H. Fontaine, *J. Phys. Condens. Matter* **1990**, *2*, 6893 – 6903.
[22] M. Brissaud-Lancin, C. Marhic, A. Riviere, *Philos. Mag. A* **1986**, *53*, 61 – 72.
[23] R. E. Wasylishen, B. A. Pettitt, *Mol. Phys.* **1978**, *36*, 1459 – 1467.
[24] B. M. Quinn, Z. Ding, R. Moulton, A. J. Bard, *Langmuir* **2002**, *18*, 1734 – 1742.
[25] H. Matsumoto, T. Matsuda, T. Tsuda, R. Hagiwara, Y. Ito, Y. Miyazaki, *Chem. Lett.* **2001**, 26 – 27.
[26] H. A. Every, A. G. Bishop, D. R. MacFarlane, G. Oraedd, M. Forsyth, *J. Mater. Chem.* **2001**, *11*, 3031 – 3036.

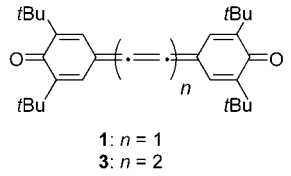
 © 2005 Wiley-VCH Verlag GmbH & Co. KGaA, Weinheim

Conjugated Systems

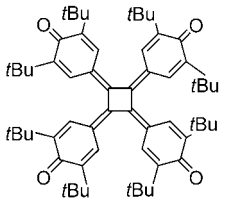
A Hexapentaene-Extended Quinocumulene Cyclotrimerized to a Tricyclobutabenzene Derivative**

Takeshi Kawase, Yuichiro Minami, Naoki Nishigaki, Satoshi Okano, Hiroyuki Kurata, and Masaji Oda**

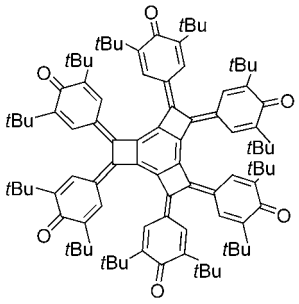
Quinocumulenes are extended biphenoquinones in which two quinoid rings are linked through a cumulenic π system. In 1967 West and Zecher reported the synthesis of the butatriene-extended quinocumulene **1**.[1] Later, this quinocumulene was shown to undergo thermal or metal-catalyzed dimerization to form [4]radialene derivative **2**.[2] However, a further extension of conjugation had not been explored to



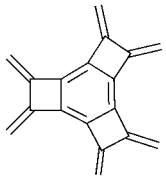
1: *n* = 1
3: *n* = 2



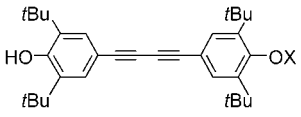
2



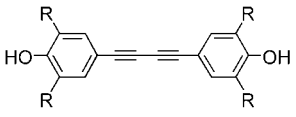
4



5



6: X = H, **12**: X = $COCH_3$



7: R = H, **8**: R = CH_3, **9**: R = Ph

[*] Prof. Dr. T. Kawase, Y. Minami, N. Nishigaki, S. Okano, Dr. H. Kurata, Prof. Dr. M. Oda
Department of Chemistry
Graduate School of Science, Osaka University
Toyonaka, Osaka 560-0043 (Japan)
Fax: (+81) 6-6850-5387
E-mail: tkawase@chem.sci.osaka-u.ac.jp
moda@chem.sci.osaka-u.ac.jp

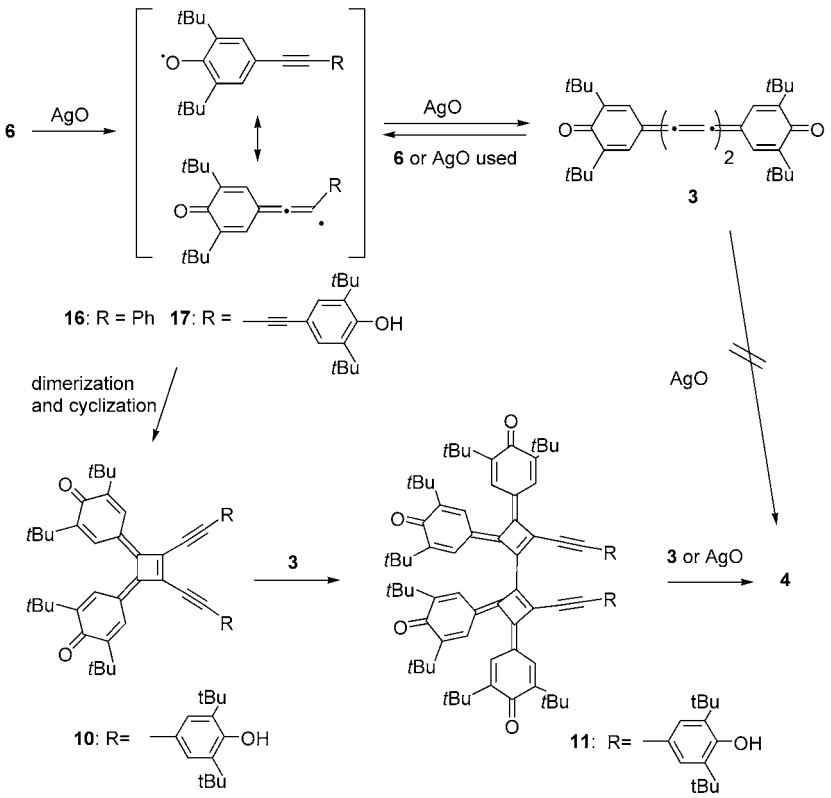
[**] This work was supported by a Grant-in-Aid for Scientific Research (No.16655057 and 16350073) from the Ministry of Education, Culture, Sports, Science, and Technology (Japan).

Supporting information for this article (selected physical data for **3**, **4**, **6**, **8**–**13**, selected NMR spectra, absorption spectra, and a cyclic voltammogram of **4**.) is available on the WWW under http://www.angewandte.org or from the author.

 © 2005 Wiley-VCH Verlag GmbH & Co. KGaA, Weinheim DOI: 10.1002/anie.200461608

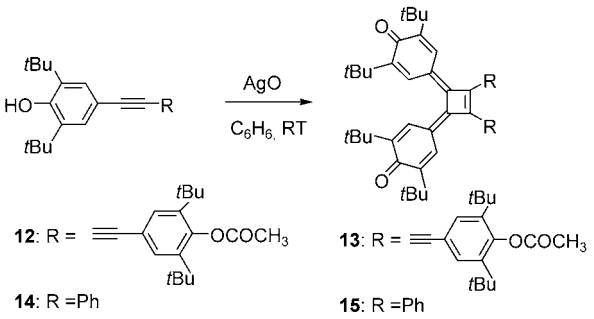
date. We have synthesized a new hexapentaene-extended quinocumulene **3** from the corresponding extended 4,4′-biphenol, and found that **3** underwent cyclotrimerization to form the novel tricyclobutabenzene derivative **4**. Tricyclobutabenzene derivatives have been extensively studied from synthetic[3] and theoretical[4] points of view. Although hexamethylenetricyclobutabenzene (**5**) has been regarded as a key model compound concerning the bond alternation of the central benzene ring,[4,5] no derivative has been prepared so far. We describe herein the mechanism of formation, the molecular structure, and physical properties of **4** as a first derivative of **5**.

A biphenol **6** as a promising precursor of **3** was synthesized from 1-acetoxy-2,6-di-*tert*-butyl-4-ethynylbenzene[6] by Eglinton coupling and deprotection of the acetyl groups under weak alkaline conditions in 77% total yield. The new quinocumulene **3** was readily prepared by treatment of **6** with silver oxide (AgO) in benzene at room temperature for 15 min in 72% yield. The presence of *tert*-butyl groups at C2 and C6 is critical to the formation of **3**, because oxidative treatment of the biphenols **7**–**9**[7] with AgO gave polymeric materials, probably owing to the high reactivity of the corresponding quinocumulenes. Actually, even **3** is thermally labile; when heated at 100 °C in the absence of solvent, **3** was converted into an insoluble material.



Scheme 1. Proposed mechanism for the formation of **4**.

A reaction mixture of **6** and AgO was allowed to stand at room temperature for 3.5 h which led to the disappearance of the generated **3** and the appearance of new products in the mixture. The highly symmetrical cyclotrimer **4** was isolated as a sole product in 54% yield. On the other hand, treatment of **3** with freshly prepared AgO even for 3 days afforded unchanged **3**. Notably, even in the absence of AgO, **4** was obtained almost quantitatively by mixing a solution of **3** and **6** (3:1) in chloroform. The reaction process can be monitored by ^{1}H NMR spectroscopy (see Supporting Information). NMR spectroscopic experiments revealed the stepwise formation of dimer **10**, an acyclic trimer **11**, and **4** (Scheme 1). The reaction of **6** with **3** afforded **10**, and the reaction of **10** and **11** with **3** led to **11** and **4**, respectively. The quinone **3** acts as an oxidizing agent toward these biphenols. In fact, the reaction stopped when **3** is no longer present in the solution. The high lability of **10** and **11** to silica gel chromatography has so far prevented their isolation and further characterization; however, the structures can be deduced from the ^{1}H NMR spectra. Treatment of monoacetate **12** (prepared by partial deprotection of the diacetate of **6**) with AgO afforded the corresponding dimer **13** in 60% yield (Scheme 2). Moreover, when exposed to air or heated at 60 °C, **11** was readily converted into **4**. These results support the assignments. It was already known that oxidation of 2,6-di-*tert*-butyl-4-phenylethynylphenol (**14**) with appropriate oxidizing agents led to the formation of the bismethylenecyclobutene **15** in good yield (Scheme 2).[8] A radical species **16** (Scheme 1) is postulated as a reactive intermediate of the reaction. The intermediate **16** could dimerize through the allenic resonance structure to yield a conjugated bisallene.



Scheme 2. Oxidative dimerization of **12** and **14**.

This, in turn, could cyclize to **15**.[9] In analogy with the mechanism, the cyclotrimerization of **3** would start with the oligomerization of the corresponding monoradical **17** generated by redox reaction of **3** with **6** or AgO used as shown in Scheme 1.

Good single crystals of **4** (with solvent molecules in a 2:1 ratio) were collected from a solution in dioxane.[10] Figure 1 reveals that the molecule has a considerably distorted propeller structure largely deviated from the ideal C_3 symmetry; the torsion angles between the exo methylene double bonds on the same cyclobutane ring are 11.7°, 60.4°, and 62.2°. In particular, the two quinomethide rings involving C27 and C69 carbons are largely curved and slightly twisted from the central benzene plane, probably as a result of steric repulsion of the bulky *tert*-butyl groups. Table 1 shows the

 © 2005 Wiley-VCH Verlag GmbH & Co. KGaA, Weinheim

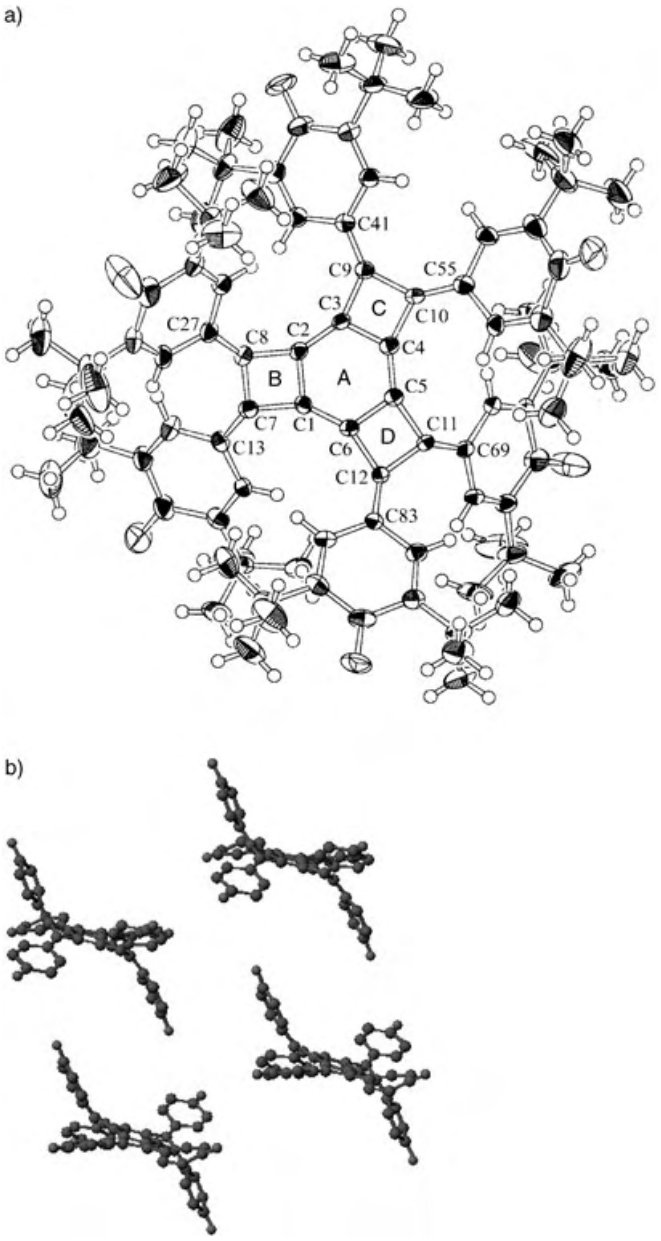
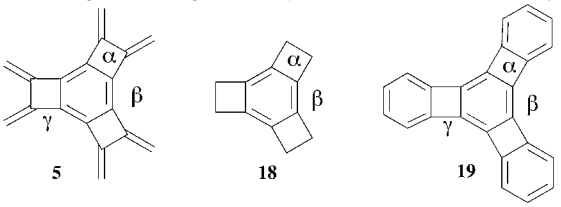


Figure 1. Single crystal structure of **4**: a) ORTEP drawing with 50% probability; b) molecular packing; *tert*-butyl groups and hydrogen atoms are omitted for clarity. Selected bond lengths [Å] and angles [°]: C1–C2 1.441(5), C2–C3 1.373(5), C3–C4 1.426(5), C4–C5 1.381(5), C5–C6 1.435(4), C6–C1 1.371(5), C1–C7 1.483(5), C2–C8 1.477(5), C3–C9 1.489(5), C4–C10 1.478(4), C5–C11 1.487(5), C6–C12 1.487(5), C7–C8 1.507(5), C9–C10 1.515(5), C11–C12 1.499(5), C7–C13 1.362(5), C8–C27 1.370(5), C9–C41 1.360(5), C10–C55 1.372(5), C11–C69 1.357(5), C12–C83 1.357(6); C41-C9-C10-C55 11.7(10), C69-C11-C12-C83 60.4(7), C13-C7-C8-C27 62.2(8); torsion angles between least squares planes: AB 9.4(2), AC 4.3(2), AD 11.1(2), BC 12.1(2), BD 15.4(2), CD 14.7(2).

observed bond lengths of the central benzene rings of **4**, tricyclobutabenzene **18**,[3d] and triangular [4]phenylene **19**[3b] together with the calculated values of **5**.[4b] Despite its nonplanarity, the values of **4** are similar to those of **5**. The degree of bond alternation of these compounds is in the order **19** ≫ **4** > **18**. In conclusion, the present results have experimentally proven that the aromatic character of the outer benzene rings of **19** plays an important role in the high degree of bond alternation of the central benzene ring.

Table 1: Average bond lengths of tricyclobutabenzene derivatives (Å).



	4	5	18	19
α	1.434	1.430	1.413	1.494
β	1.375	1.385	1.390	1.336
γ	1.484	1.484	–	1.500

Selected spectral data for **3** and **4** are shown in Table 2. The longest absorption maximum of **3** is considerably longer than those of **1** (486 nm in C_6H_6) and biphenoquinone **20** (426 nm in CH_2Cl_2). The trimer **4** shows intense absorptions in the visible region of about 400–600 nm which is responsible for its deep coloration. The absorption curve is similar to that of **2**; the longest absorption band of **4** is 20–30 nm shorter and the second-longest absorption band is ≈50 nm longer than

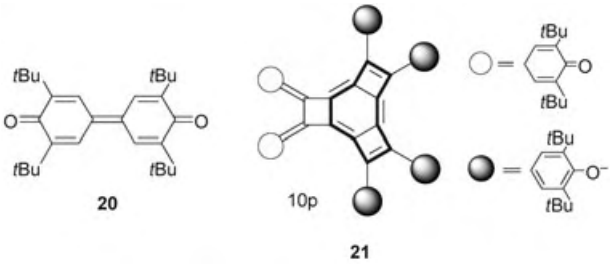
Table 2: Selected spectral data for new extended quinones **3**, **4**, **10**, **11**.

3: IR (KBr): $\tilde{\nu}$2954 s, 1586 s (C=O), 1456 m, 1357 m, 1250 m, 1220 w, 1082 m, 921 cm^{-1} (m); ^1H NMR (270 MHz, $CDCl_3$): $\delta = 1.26$ (s, 36H), 7.06 ppm (s, 4H); ^{13}C NMR (67.8 MHz, $CDCl_3$): $\delta = 29.71$, 35.96, 118.82, 123.83, 130.26, 140.34, 150.32, 185.84 ppm; UV/Vis (CH_2Cl_2): λ_{max} (log ε) = 301 (3.84), 351 (3.96), 477 (4.54), 491 (4.58), 531(5.24), 614 nm (sh) (4.18)

4: IR (KBr): $\tilde{\nu} = 2958$ s, 1617 s (C=O), 1458 m, 1363 s, 1091 m, 884 cm^{-1} (m); ^1H NMR (270 MHz, $CDCl_3$): $\delta = 1.31$ (s, 54H), 1.35 (s, 54H), 7.38 (d, $J = 2.4$ Hz, 6H), 7.53 ppm (d, $J = 2.4$ Hz, 6H): ^{13}C NMR (67.8 MHz, $CDCl_3$): $\delta = 29.16$, 29.66, 36.06, 36.13, 124.21, 127.79, 128.92, 137.49, 146.70, 150.65, 151.50, 185.87 ppm; UV/Vis (CH_2Cl_2): λ_{max} (log ε) = 348 (4.83), 424 (5.14), 447 (5.38), 517 (4.76), 558 nm (4.76)

10: ^1H NMR (270 MHz, $CDCl_3$): $\delta = 1.33$ (s, 18H), 1.41 (s, 18H), 1.47 (s, 36H), 5.66 (s, 2H), 7.38 (d, $J = 2.3$ Hz, 2H), 7.45 (s, 4H), 8.09 ppm (d, $J = 2.3$ Hz, 2H)

11: ^1H NMR (270 MHz, $CDCl_3$): $\delta = 1.11$ (s, 18H), 1.25 (s, 36H), 1.32 (s, 18H), 1.37 (s, 18H), 1.49 (s, 18H), 5.60 (s, 2H), 7.24 (d, $J = 2.3$ Hz, 2H), 7.34 (s, 4H), 7.44 (d, $J = 2.3$ Hz, 2H), 7.46 (d, $J = 2.3$ Hz, 2H), 8.16 ppm (d, $J = 2.3$ Hz, 2H)



 © 2005 Wiley-VCH Verlag GmbH & Co. KGaA, Weinheim

those of **2**.[2] The carbonyl stretching of **3** (1586 cm^{-1}) is almost similar to that of **1** (1590 cm^{-1}), despite the extension of conjugation. On the other hand, the relatively high values of **2** (1630 cm^{-1}), **4** (1617 cm^{-1}), **13** (1608 cm^{-1}), and **15** (1609 cm^{-1})[11] are consistent with the order of distortion of the biphenoquinone structures. Because the average twist angle between the quinomethide rings of **2**[2] (36°) is the largest in these compounds.

The electrochemical properties of **3** and **4** as new electron acceptors were examined by cyclic voltammetry. The reduction potentials of **1**–**4** and **20** are summarized in Table 3.

Table 3: Reduction potentials of extended quinones **1**–**4**, **20**.

	$^1E_{1/2}$	$^2E_{1/2}$	$^3E_{1/2}$	$^4E_{1/2}$
1	−0.65	−0.85		
2	−0.52	−0.85		
3	−0.42	−0.76		
4	−0.61	−0.89	−1.03	−1.35
20	−0.96	−1.29		

V vs. Ag/Ag^+ ($Fc/Fc^+ = +0.26$ V) in 0.1 M nBu_4NClO_4/CH_2Cl_2, sweep rate 100 $mV s^{-1}$.

Quinocumulene **3** shows two sets of highly reversible one-electron reduction waves together with one irreversible oxidation wave (1.40 V). The longest conjugation of **3** in these compounds would account for the highest electron affinity. Moreover, **4** exhibits four sets of highly reversible one-electron reduction waves within the measurable range (1.5 to −2.4 V). The results suggest the facile formation of the tetraanion **21**, which has a 10π electronic periphery.

These results suggest that 2,6-di-*tert*-butyl-4-ethynylphenol derivatives would act as versatile building blocks for the construction of extended diphenoquinone derivatives with novel structure and redox properties.

Received: August 11, 2004

Keywords: aromaticity · cumulenes · quinones · redox chemistry · strained molecules

[1] R. West, D. C. Zecher, *J. Am. Chem. Soc.* **1967**, *89*, 153–155.
[2] K. S. Roster, R. West, *J. Org. Chem.* **1975**, *40*, 2300–2305.
[3] a) W. Nutakul, R. P. Thuummel, A. D. Tagger, *J. Am. Chem. Soc.* **1979**, *101*, 770–771; b) R. Diercks, K. P. C. Vollhardt, *J. Am. Chem. Soc.* **1986**, *108*, 3150–3152; c) R. Boese, A. J. Matzger, D. L. Mohler, K. P. C. Vollhardt, *Angew. Chem.* **1995**, *107*, 1630–1633; *Angew. Chem. Int. Ed. Engl.* **1995**, *34*, 1478–1481; d) A. Stanges, N. Ashkenazi, R. Boese, *J. Org. Chem.* **1998**, *63*, 247–253; e) S. Kumaraswamy, S. S. Jalisatgi, A. J. Marzger, O. S. Miljanic, K. P. C. Vollhardt, *Angew. Chem.* **2004**, *116*, 3797–3801; *Angew. Chem. Int. Ed.* **2004**, *43*, 3711–3715.
[4] a) R. Faust, E. D. Glendenling, A. Streitwieser, K. P. C. Vollhardt, *J. Am. Chem. Soc.* **1992**, *114*, 8263–8268; b) A. Stanger, E. Tkachenko, *J. Comput. Chem.* **2001**, *22*, 1377–1386.
[5] H. Hopf, *Classics in Hydrocarbon Chemistry*, Wiley-VCH, Weinheim, **1999**.
[6] H. Nishide, N. Yoshioka, K. Inagaki, E. Tsuchida, *Macromolecules* **1992**, *25*, 569–575; T. Kawase, N. Nishigaki, H. Kurata, M. Oda, *Eur. J. Org. Chem.* **2004**, 3090–3096.
[7] Among the extended biphenols **7**–**9**, only **7** is known: B. Grant, *Mol. Cryst. Lig. Cryst.* **1978**, *48*, 175–182.
[8] S. Hauff, A. Rieker, *Tetrahedron Lett.* **1972**, 1451–1452.
[9] H. Hopf, F. T. Lenich, *Chem. Ber.* **1973**, *106*, 3461–3462; K. Kleveland, L. Skattebøl, *J. Chem. Soc. Chem. Commun.* **1973**, 432–433; F. Toda, *Eur. J. Org. Chem.* **2000**, 1377–1386.
[10] Crystal data for **4**·(dioxane)$_{1/2}$ ($C_{98}H_{124}O_7$): $M_w = 1413.93$, dark red prisms, crystal dimension: $0.2 \times .0.2 \times 0.1$ mm^3, triclinic, space group $P\bar{1}$ (#2), $a = 13.765(6)$ Å, $b = 17.568(9)$ Å, $c = 19.722(9)$ Å, $\alpha = 77.18(4)°$, $\beta = 83.21(4)°$, $\gamma = 73.62(4)°$, $V = 4453(14)$ $Å^3$, $Z = 2$, $\rho_{calcd} = 1.111$ $g cm^{-1}$, $Mo_{K\alpha}$ ($\lambda = 0.71075$ Å), $2\theta_{max} = 55.0°$; intensity data were collected on a Rigaku RAXIS-RAPID imaging-plate diffractometer at 200 K. The structure was solved with direct methods on F^2 with SHELXS-97. A total of 41147 reflections were collected, 19274 unique reflections were measured and used in the refinement, 946 parameters, $R1 = 0.056$, $Rw = 0.206$ for 4615 reflections with $I > 2\sigma(I)$, GOF = 0.58, max. peak in final diff. map 0.20 e $Å^{-3}$; all non-hydrogen atoms were refined anisotropically, hydrogen atoms (except the disordered dioxane protons) were placed geometrically and refined by using a rigid model. CCDC-241621 contains the supplementary crystallographic data for this paper. These data can be obtained free of charge via www.ccdc.cam.ac.uk/conts/retrieving.html (or from the Cambridge Crystallographic Data Centre, 12, Union Road, Cambridge CB21EZ, UK; fax: (+44) 1223-336-033; or deposit@ccdc.cam.ac.uk).
[11] Our result; the reported value (1650 cm^{-1})[8] was not reproducible.

 © 2005 Wiley-VCH Verlag GmbH & Co. KGaA, Weinheim

Tandem Reactions

Enantiospecific Strategy Towards Oxygen-Bridged Terpenoids: Tandem Transannular-Cyclization and Ring-Contraction Processes**

*Antonio Rosales, Rosa E. Estévez, Juan M. Cuerva, and J. Enrique Oltra**

The transannular cyclization of medium-sized rings contributes to the enhancement of molecular rigidity and structural complexity, two properties often associated with biological activity in small molecules.[1] In fact, there are several naturally occurring terpenoids with a transannular oxygen

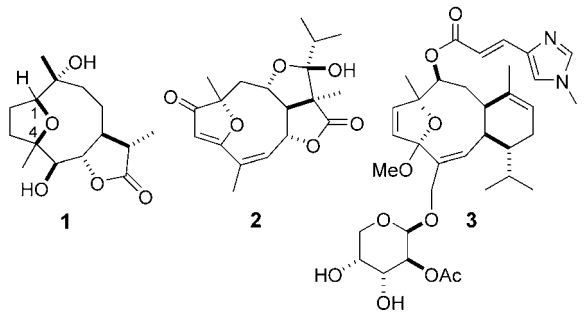
[*] Dr. A. Rosales, R. E. Estévez, Dr. J. M. Cuerva, Dr. J. E. Oltra
Department of Organic Chemistry
Faculty of Sciences
Campus Fuentenueva s/n
University of Granada
18071 Granada (Spain)
Fax: (+34) 958-248-437
E-mail: joltra@ugr.es

[**] This work was supported by the "Junta de Andalucía" (PAI group FQM339). We also thank Dr. A. F. Barrero for his collaboration during the early stage of the work as well as our English colleague Dr. J. Trout for revising our text.

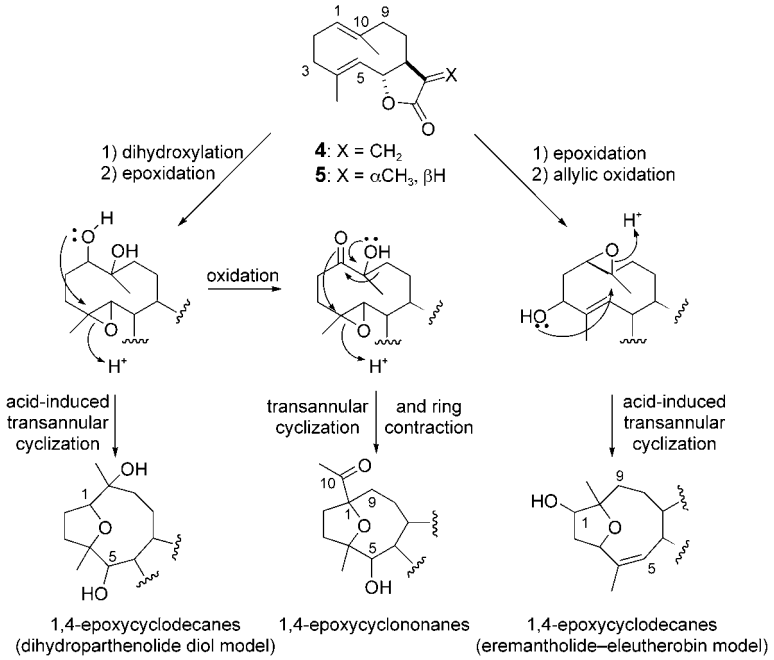
Supporting information for this article is available on the WWW under http://www.angewandte.org or from the author.

 DOI: 10.1002/anie.200461210 © 2005 Wiley-VCH Verlag GmbH & Co. KGaA, Weinheim

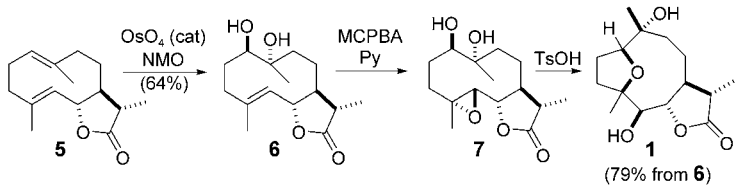
bridge in their 1,4-epoxycyclodecane system, such as dihydroparthenolide diol (**1**),[2] eremantholide A (**2**),[3] and eleutherobin (**3**),[4] all of which show interesting pharmacological properties. The 1,4-epoxycyclononane system, however, is considerably less widespread among natural products, although some examples have been reported.[5] Bioactive terpenoids with the 1,4-epoxycyclodecane motif have attracted the attention of chemists, and different total syntheses of **2**[6] and **3**[7] have been described. Moreover, some procedures for the synthesis of 1,4-epoxycyclononanes have been developed,[8] and other tetrahydrofuran derivatives have recently been prepared by radical tandem reactions.[9] These total syntheses, however, are generally restricted to the preparation of only one or a few specific compounds, require numerous steps and generally give low overall yields.



Hemisynthesis can be a valuable alternative to total synthesis, especially when nature provides sufficient quantities of homochiral raw materials that can easily be isolated from renewable sources. This is true of germacrolides (+)-costunolide (**4**) and (+)-11β,13-dihydrocostunolide (**5**, see Scheme 1), which can be obtained in (multi)-gram quantities from the commercially available extract Costus Resinoid.[10] Additional amounts of these compounds can also be obtained by chemical synthesis.[11] We therefore deemed that accessible germacrolides might well be a suitable starting material for the enantiospecific synthesis of both 1,4-epoxycyclodecanes and 1,4-epoxycyclononanes as they require relatively simple but selective chemical transformations based on the different reactivity shown by the double bonds located at $\Delta^{1(10)}$ and Δ^{4} of the cyclodecadiene ring (Scheme 1).[12]



Scheme 1. Hypothetical strategy for the synthesis of oxygen-bridged terpenoids from accessible germacrolides.



Scheme 2. Enantiospecific synthesis of **1** from **5**. NMO = *N*-methylmorpholine *N*-oxide, MCPBA = *m*-chloroperbenzoic acid, Py = pyridine, Ts = *p*-toluenesulfonyl.

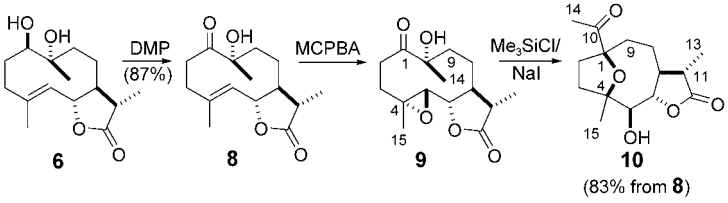
To prove our hypothesis, we selected (+)-dihydroparthenolide diol (**1**) as the first synthetic target. To determine the absolute stereochemistry of natural **1**, we started the synthesis with homochiral (+)-11β,13-dihydrocostunolide (**5**), which was obtained from commercial Costus Resinoid.[10b] Selective dihydroxylation of **5** by using the Upjohn procedure[13] allowed us to obtain diol **6**[14] with a yield of 64%. Treatment of **6** with MCPBA (*m*-chloroperbenzoic acid) in the presence of pyridine furnished epoxide **7**, which was submitted to the next step without further purification. Thus the acid-induced transannular cyclization of crude **7** provided (+)-dihydroparthenolide diol (**1**) in 79% yield (from **6**). The spectroscopic data for synthetic **1** as well as optical rotation measurements[15] agreed with those reported for natural (+)-dihydroparthenolide diol, thus confirming the chemical structure of this metabolite. As the absolute stereochemistry of (+)-11β,13-dihydrocostunolide (**5**) is known,[16] the chemical synthesis of **1** from **5** suggests that the absolute configuration of natural **1** is that as depicted in Scheme 2.

We subsequently approached the second part of our hypothesis, that is, a tandem reaction combining transannular-cyclization and ring-contraction processes that we hoped would lead to 1,4-epoxycyclononanes. Owing to both entropy and enthalpy factors, the synthesis of nine-membered carbocycles by ring-closing procedures is rendered quite difficult.[8a,17] Nine- and ten-membered rings, however, have similar total strain levels,[18] and therefore ring-contraction processes from cyclodecanes to cyclononanes should not be

 © 2005 Wiley-VCH Verlag GmbH & Co. KGaA, Weinheim

seriously hindered by thermodynamic phenomena. Surprisingly, synthetic chemists have not yet exploited this procedure probably owing to the lack of a suitable technique.[19] Within this context we considered that with the anchimeric assistance provided by an OH group located at C-10, an epoxyketone such as **9** might undergo acid-induced transannular cyclization followed by a ring-contraction process that leads to 1,4-epoxycyclononanes (see Scheme 1), and thus open a novel synthetic way towards nine-membered carbocycles.

To this end we prepared crude **9** (Scheme 3) and treated it without further purification with a substoichiometric quantity of Me_3SiCl/NaI. In this manner, we obtained oxygen-bridged cyclononane **10** with a yield of 83% (from **8**).[20] Analysis of HRMS and ^{13}C NMR spectra of **10** supported the tricyclic nature of this product, and the IR spectrum showed bands assignable to alcohol, ketone, and γ-lactone groups. Moreover, in the ^{1}H NMR spectrum, signals at $\delta = 3.75$ (d, $J = 8.9$ Hz, H-5) and 4.30 (t, $J = 9.0$ Hz, H-6) indicated that the



Scheme 3. Enantiospecific synthesis of **10** from **6**. DMP = Dess–Martin periodinane.

OH group was equatorially juxtaposed to the *trans*-fused γ-lactone. The signal for the hydrogen atoms of a methyl ketone unit also appeared in this spectrum at $\delta = 2.19$ (s, 3H, H-14) together with those of two other methyl groups at $\delta = 1.36$ (s, 3H, H-15) and 1.20 (d, $J = 6.9$ Hz, 3H, H-13). The chemical shifts and multiplicities of the protons of these two methyl groups indicate that the former ($\delta = 1.36$) is attached to an oxygenated quaternary carbon center and that the latter ($\delta = 1.20$) is coupled to H-11 ($\delta = 2.32$, dq, $J = 6.9$, 12.0 Hz). The ^{13}C NMR spectrum showed signals for quaternary oxygenated carbon centers at $\delta = 86.0$ (C-4) and 89.0 (C-1), which correspond to the heads of the oxygenated bridge. Furthermore, the HMBC (heteronuclear multiple-bond correlation) spectrum showed correlations between H-5 and C-4, between H-15 and C-4, and between H-14 and C-1, and firmly support structure **10**. Finally, the NOE observed between H-15 and H-6 may be explained by assuming a 1*S*,4*S*,6*S* stereochemistry in which H-6 and the oxygen bridge are situated on the same side of the cyclononane ring (see Figure 1).[21]

The chemical transformation of **9** into **10** represents an unprecedented tandem reaction that provides a straightforward synthetic means of obtaining the otherwise elusive nine-membered carbocycles. This method works well at room temperature under mild conditions, needs only catalytic proportions of Me_3SiCl/NaI, and conforms to the principles of selectivity and atom- and step-economy required in contemporary chemistry.[22] The reaction also produces a substantial increase in molecular rigidity and structural

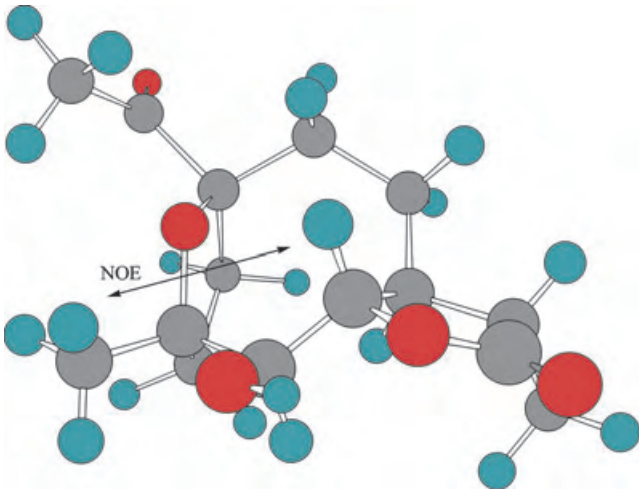


Figure 1. Minimized energy conformation of **10.** NOE between H-6 and H-15. O = red, C = gray, H = blue.

complexity in only one step, thus proving itself to be a potentially useful tool for diversity-oriented synthesis.[1]

Finally, we embarked upon the preparation of (−)-1β,10α-epoxy-11β,13-dihydrocostunolide (**11**) by the selective epoxidation of **5**.[10b] The results obtained in the synthesis of **1** (Scheme 2) suggest that the allylic oxidation at C-3 of **11** followed by the acid-induced transannular cyclization of the corresponding epoxy-alcohol (see Scheme 1) will give the 1,4-epoxycyclodecane model shown by eremantholide A (**2**) and eleutherobin (**3**), a task we are currently engaged on.

In summary, we present an enantiospecific strategy for the synthesis of oxygen-bridged terpenoids from accessible germacrolides. This method has proved to be useful for obtaining antimycobacterial (+)-dihydroparthenolide diol (**1**) and 1,4-epoxycyclononane **10**. The synthesis of **10** employs a novel tandem reaction that combines a transannular cyclization with a ring-contraction process and opens up a new approach to nine-membered carbocycles.

Received: July 6, 2004

Keywords: carbocycles · cyclization · epoxidation · ring contraction · synthetic methods

[1] S. L. Schreiber, *Science* **2000**, *287*, 1964–1969.
[2] Dihydroparthenolide diol, a scarce metabolite from the Chinese plant *Carpesium longifolium*, has antimycobacterial activity: a) C. Yang, C. Yuan, Z. Jia, *J. Nat. Prod.* **2003**, *66*, 1554–1557; b) J. K. Rugutt, F. R. Fronczek, S. G Franzblau, I. M. Warner, *Acta Crystallogr. Sect. E* **2001**, *57*, 323–325.
[3] For an exhaustive review on furanoheliangolides, including eremantholide A and other bioactive oxygen-bridged sesquiterpenoids, see: D. S. Brown, L. A. Paquette, *Heterocycles* **1992**, *34*, 807–834.
[4] Eleutherobin, isolated from an Australian soft coral of the genus *Eleutherobia*, showed antitumor properties closely related to

 © 2005 Wiley-VCH Verlag GmbH & Co. KGaA, Weinheim

those of Taxol; see: a) I. Ojima, S. Chakravarty, T. Inoue, S. Lin, L. He, S. B. Horwitz, S. D. Kuduk, S. J. Danishefsky, *Proc. Natl. Acad. Sci. USA* **1999**, *96*, 4256 – 4261; b) T. Lindel, *Angew. Chem.* **1998**, *110*, 806 – 808; *Angew. Chem. Int. Ed. Engl.* **1998**, *37*, 774 – 776; c) T. Lindel, P. R. Jensen, W. Fenical, B. H. Long, A. M. Casazza, J. Carboni, C. R. Fairchild, *J. Am. Chem. Soc.* **1997**, *119*, 8744 – 8745.

[5] a) R. Durán-Patrón, J. Aleu, R. Hernández-Galán, I. G. Collado, *J. Nat. Prod.* **2000**, *63*, 44 – 47; b) J. Jakupovic, F. Jeske, T. Morgenstern, F. Tsichritzis, J. A. Marco, W. Berendsohn, *Phytochemistry* **1998**, *47*, 1583 – 1600.

[6] Total synthesis of eremantholide A: a) K. Takao, H. Ochiai, K. Yoshida, T. Hashizuka, H. Koshimura, K. Tadano, S. Ogawa, *J. Org. Chem.* **1995**, *60*, 8179 – 8193; b) J. R. Boeckman Jr., S. K. Yoon, D. K. Heckendorn, *J. Am. Chem. Soc.* **1991**, *113*, 9682 – 9684; Other synthetic studies on furanoheliangolides: c) D. S. Brown, L. A. Paquette, *J. Org. Chem.* **1992**, *57*, 4512 – 4521.

[7] Total synthesis of eleutherobin: a) X. T. Chen, S. K. Bhattacharya, B. Zhou, C. E. Gutteridge, T. R. R. Pettus, S. J. Danishefsky, *J. Am. Chem. Soc.* **1999**, *121*, 6563 – 6579; b) S. K. Bhattacharya, X. T. Chen, C. E. Gutteridge, S. J. Danishefsky, *Tetrahedron Lett.* **1999**, *40*, 3313 – 3316; c) K. C. Nicolaou, T. Ohshima, S. Hosokawa, F. L. van Delft, D. Vourloumis, J. Y. Xu, J. Pfefferkorn, S. Kim, *J. Am. Chem. Soc.* **1998**, *120*, 8674 – 8680; d) X. T. Chen, B. Zhou, S. K. Bhattacharya, C. E. Gutteridge, T. R. R. Pettus, S. J. Danishefsky, *Angew. Chem.* **1998**, *110*, 835 – 838; *Angew. Chem. Int. Ed. Engl.* **1998**, *37*, 789 – 792; e) K. C. Nicolaou, F. van Delft, T. Ohshima, D. Vourloumis, J. Xu, S. Hosokawa, J. Pfefferkorn, S. Kim, T. Li, *Angew. Chem.* **1997**, *109*, 2630 – 2634; *Angew. Chem. Int. Ed. Engl.* **1997**, *36*, 2520 – 2524; More recent approaches: f) R. Beumer, P. Bayón, P. Bugada, S. Ducki, N. Mongelli, F. R. Sirtori, J. Telser, C. Gennari, *Tetrahedron* **2003**, *59*, 8803 – 8820; g) K. P. Kaliappan, N. Kumar, *Tetrahedron Lett.* **2003**, *44*, 379 – 381; h) C. Sandoval, E. Redero, M. A. Mateos-Timoneda, F. A. Bermejo, *Tetrahedron Lett.* **2002**, *43*, 6521 – 6524.

[8] a) G. A. Molander, C. Köllner, *J. Org. Chem.* **2000**, *65*, 8333 – 8339; b) J. L. Mascareñas, A. Rumbo, L. Castedo, *J. Org. Chem.* **1997**, *62*, 8620 – 8621.

[9] a) A. Gansäuer, B. Rinker, N. Ndene-Schiffer, M. Pierobon, S. Grimme, M. Gerenkamp, C. Mück-Lichtenfeld, *Eur. J. Org. Chem.* **2004**, 2337 – 2351; b) A. Gansäuer, B. Rinker, M. Pierobon, S. Grimme, M. Gerenkamp, C. Mück-Lichtenfeld, *Angew. Chem.* **2003**, *115*, 3815 – 3818; *Angew. Chem. Int. Ed.* **2003**, *42*, 3687 – 3690.

[10] a) A. F. Barrero, A. Rosales, J. M. Cuerva, J. E. Oltra, *Org. Lett.* **2003**, *5*, 1935 – 1938; b) A. F. Barrero, J. E. Oltra, J. M. Cuerva, A. Rosales, *J. Org. Chem.* **2002**, *67*, 2566 – 2571; c) A. F. Barrero, J. E. Oltra, M. Álvarez, A. Rosales, *J. Org. Chem.* **2002**, *67*, 5461 – 5469.

[11] For a review on the synthesis of costunolide, 11β,13-dihydrocostunolide, and other germacrane sesquiterpenoids, see: A. J. Minnaard, B. P. A. W. Joannes, A. de Groot, *Tetrahedron* **1999**, *55*, 2115 – 2146.

[12] Owing to both steric and electronic factors, the double bond at Δ^4 is considerably less reactive than that at $\Delta^{1(10)}$. Carbon-atom numbering corresponds to the germacrane system.

[13] a) K. Bergstad, S. Jonson, J. E. Bäckvall, *J. Am. Chem. Soc.* **1999**, *121*, 10424 – 10425; b) V. VanRheenen, R. C. Kelly, D. Y. Cha, *Tetrahedron Lett.* **1976**, 1973 – 1976.

[14] All of the products obtained, except **7** and **9**, were isolated by flash chromatography and characterized by spectroscopic techniques including high resolution mass spectrometry and NMR spectroscopy.

[15] Data for synthetic **1**: gold-colored syrup; $[\alpha]_D^{20} = +9.1$ ($c = 0.90$, CH_2Cl_2); HR(FAB)MS: m/z: calcd. for $C_{15}H_{24}O_5Na$: 307.1521; found: 307.1516 $[M+Na]^+$; ^1H and ^{13}C NMR spectra matched those reported for the natural product.[2a]

[16] The absolute stereochemistry of (+)-11β,13-dihydrocostunolide (**5**) was established by chemical correlation with (+)-costunolide (**4**).[10b]

[17] A. Deiters, R. Fröhlich, D. Hoppe, *Angew. Chem.* **2000**, *112*, 2189 – 2192; *Angew. Chem. Int. Ed.* **2000**, *39*, 2105 – 2107.

[18] E. L. Eliel, S. H. Wilen, M. P. Doyle, *Basic Organic Stereochemistry*, Wiley, New York, **2001**, pp. 429 – 433.

[19] For a rare example of ring contraction reactions from ten- to nine-membered carbocycles, see: X. Lei, C. Doubleday, Jr., N. J. Turro, *Tetrahedron Lett.* **1986**, *27*, 4675 – 4678.

[20] For experimental details, see Supporting Information.

[21] The interatomic distance between H-6 and H-15 of **10** is 3.789 Å in the minimized energy conformation shown in Figure 1 (CS Chem3D Pro, MOPAC).

[22] a) B. M. Trost, *Angew. Chem.* **1995**, *107*, 285 – 307; *Angew. Chem. Int. Ed. Engl.* **1995**, *34*, 259 – 281; b) B. M. Trost, *Science* **1991**, *254*, 1471 – 1477.

 © 2005 Wiley-VCH Verlag GmbH & Co. KGaA, Weinheim

Geochemistry

Hydrogen Processing by Fe^{III}-Exchanged Montmorillonite: A Unique Geochemical Protocol**

Boyapati M. Choudary, Mannepalli L. Kantam, Kalluri V. S. Ranganath, and Kottapalli K. Rao*

Hydrogen processing, such as the production of hydrogen by the reduction of protons and consumption of hydrogen by oxidation, is of renewed interest since hydrogen is regarded as a fuel for the future. Hydrogen has long been known as a biofuel—it can be produced by many microbes under anaerobic conditions and then consumed later on as a fuel[1]—and [Fe]-hydrogenase is known to produce hydrogen, whereas [NiFe]-hydrogenase consumes it.[1–4] During hydrogen production by [Fe]-hydrogenase, the electrons are relayed by hydride clusters. Hydrogenase model compounds, developed from complex and tedious synthetic protocols, are known to facilitate heterolytic H_2 activation and H/D exchange reactions or produce hydrogen catalytically in cyclic voltammetry.[5] Initial results from divergent approaches to the production of hydrogen by photoreduction of protons[6] or by water cleavage[7–9] are quite encouraging.

[*] Dr. B. M. Choudary, Dr. M. L. Kantam, K. V. S. Ranganath, Dr. K. K. Rao
IICT Commun NO:040923
Indian Institute of Chemical Technology
Hyderabad 500 007 (India)
Fax: (+91) 40-2716-0921
E-mail: choudary@iict.res.in

[**] K.V.S.R thanks the Council of Scientific and Industrial Research, India, for a research fellowship.

Supporting information for this article is available on the WWW under http://www.angewandte.org or from the author.

 © 2005 Wiley-VCH Verlag GmbH & Co. KGaA, Weinheim DOI: 10.1002/anie.200461070

The Earth's crust has abundant reserves of hydrogen buried in it. Besides dehydrogenation of minerals, such as $Mg(OH)_2$ and silanols of silicates, the interaction of water with the reduced form of Fe^{II}, which is available in the subsurface of the Earth, is thought to contribute to the production and existence of such huge reserves of hydrogen.[10,11] However, the presence of only low quantities of this reduced form of Fe^{II}, which produces hydrogen stoichiometrically, brings into question the extent to which this process contributes to hydrogen production in the Earth's crust.[11] Another geochemically important reaction is the formation of dihydrogen and pyrite from FeS and H_2S under anaerobic conditions.[12]

Despite several attempts, the classical, stoichiometric production of hydrogen in situ by the reduction of protons with Fe^0 powder and acids, which is currently used in industry for the reduction of nitroarenes to anilines and acetanilides,[13] has not yet been transformed into a catalytic reaction. We therefore conceived a nonbiological and nonphotochemical catalytic system for the production of hydrogen by a simple electron-transfer protocol with I^- as the electron source and metal-ion-exchanged montmorillonite clay as the catalyst. This clay is known to promote electron transfer and is abundant in the Earth's crust.[14] The standard Gibbs energy change of reaction for the formation of H_2 and I_2 from H^+ and I^- at room temperature, $\Delta G°$, is $+25.79\ kJ\,mol^{-1}$. Even though the free-energy change ($\Delta G°$) is positive, the above "uphill" reaction has been realized previously by choosing a suitable catalyst and reaction conditions.[15,16] We report herein a unique geochemical protocol for the effective, catalytic electron-transfer from I^- to H^+ to generate I_2 and H_2, two products of commercial importance. The reaction occurs at room temperature, employs carboxylic acids as proton source, iodide ions as electron source, and is catalyzed by recyclable Fe^{III}-exchanged montmorillonite (Fe^{III}-mont) [Eq. (1)].

$$2\,H^+ + 2\,I^- \xrightarrow{Fe^{III}\text{-mont}} H_2 + I_2 \qquad (1)$$

The superiority of Fe^{III}-mont over the other catalysts in terms of turnover number in hydrogen production is clearly evidenced by the results summarized in Table 1 (see also Supporting Information). The activity is correlated to the higher number of acidic sites, which increase with the increased valence state of the cation.[17] Furthermore, the production of hydrogen increases as the percentage of iron in the montmorillonite increases (Figure 1). This result unambiguously demonstrates that iron is the active ingredient in the clay support.

Table 1: Production of hydrogen gas catalyzed by Fe^{III}-mont at different temperatures using water/carboxylic acids as the proton source.

Entry	Proton Source	T [°C]	H_2 evolution (μmol)	Turnover number[a]
1	acetic acid	25	1562.5	8.0, 8.0[b]
2	acetic acid	60	2700.0	13.8
3	acetic acid	150	3370.0	17.3, 17.2[b]
4	propionic acid	150	5400.0	27.7
5	hexanoic acid	150	9370.0	48.0
6	water	25	446.0	2.3
7	water	60	713.8	3.7, 3.7[c]

[a] The calculation is given in the Supporting Information. [b] HI was used in place of NaI. [c] Fourth recycle of the catalyst.

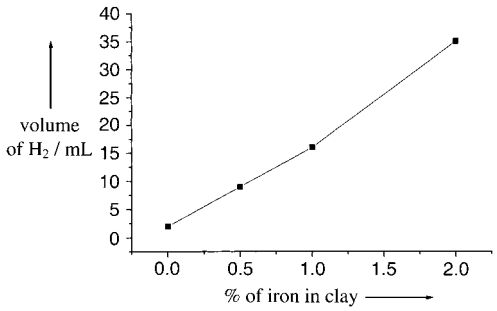


Figure 1. A plot of volume of hydrogen liberated (mL) versus the amount of iron (%) in the clay.

Hydrogen production is enhanced when higher homologues of organic acids or higher temperatures are used (Table 1). The maximum production of hydrogen was found to be 9.37 mmol per g of catalyst using hexanoic acid (Table 1, entry 5). When the production of hydrogen was attempted under identical conditions, but with water as the proton source, no reaction was observed. However, the reaction proceeded well after the addition of a small amount of I_2 as initiator. This result indicates that I_2 reacts initially with I^- to form I_3^- in situ, as determined spectrometrically;[18] it is known that I_3^- is a better electron source to induce proton reduction.[19] The formation of both H_2 and I_3^- at identical rates in an aqueous medium, plotted in Figure 2 as a function of time, further reinforces the proposal that I_3^- is indeed the electron source here. These results are impressive when compared with other examples of electron transfer from I^- to H^+, which require temperatures of 300–400 °C and employ either expensive, noble-metal catalysts or an iodine–sulfur thermochemical process.[15,16] There was no oxygen evolution from the reaction, which further confirms that the electron transfer occurs from the iodide only. Moreover, deactivation of the catalyst was not noticed even after the fifth cycle in the production of hydrogen; the XRD pattern of the catalyst recovered after the fourth recycle remains unchanged (Table 1, entries 1, 5, 7).

In an effort to extend the scope of this reaction and to demonstrate the production and consumption of hydrogen in the reaction catalyzed by Fe^{III}-exchanged montmorillonite, the reductive N-acylation of azo-, cyano-, and nitroarenes was accomplished, in a one-pot reaction, under reflux conditions (Table 2). The selective reduction of azo-, cyano-, and nitroarenes in the presence of other susceptible functional groups, such as carbonyl and chloro groups, is a significant achievement. The catalyst, used for four cycles, shows a slight decrease in activity after each run (Table 2, entry 7). These catalytic reactions effected by the cheap and readily available Fe^{III}-mont are superior to the nonregenerable, stoichiometric hydride reagents or the expensive catalysts needed to reduce azo-[20,21] or cyanoarenes[22–24] under hydrogen pressure. Sim-

 © 2005 Wiley-VCH Verlag GmbH & Co. KGaA, Weinheim

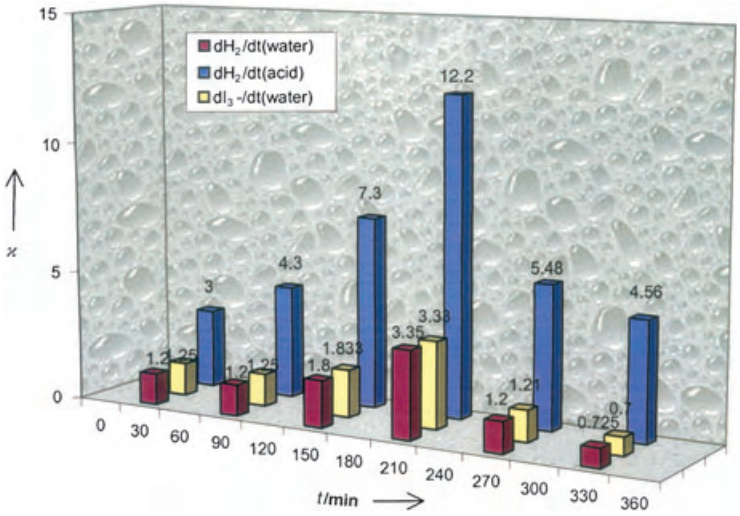


Figure 2. The activity profile diagram for the formation of both H_2 and I_3^- at identical rates in aqueous medium at 60 °C as a function of time. A mixture of catalyst (1.0 g), sodium iodide (40 mmol), and carboxylic acid/water (50 mL) (when water is used as proton source 0.0250 g of iodine was added initially) was heated to 60 °C. x = formation rate of d/dt H_2 or I_3^- [μmol min^{-1} g cat^{-1}].

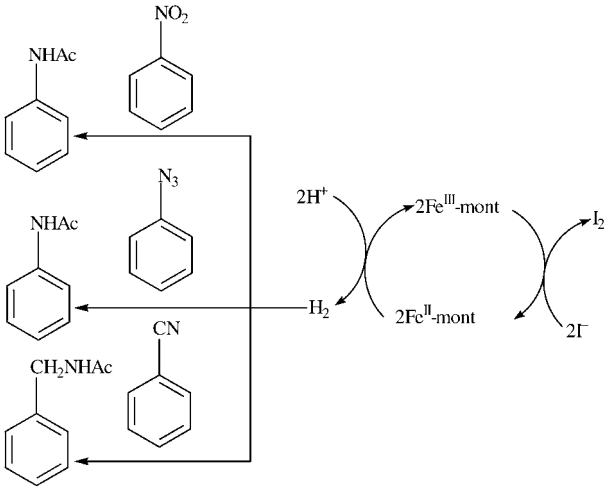
Table 2: Reductive N-acylation of azo-, cyano-, and nitroarenes catalyzed by Fe^{III}-mont.[a]

Entry	Substrate	t [h]	Yield [%]
1	2-azidoanisole	0.50	98, 92[b]
2	4-azidonitrobenzene	0.50	98
3	4-azidochlorobenzene	0.50	100
4	2-azidobenzoic acid	0.50	92
5	benzonitrile	20.0	60
6	benzyl cyanide	20.0	80
7	nitrobenzene	12.0	82, 70,[c] 5[d]
8	*p*-nitroanisole	12.0	74
9	*p*-chloronitrobenzene	16.0	63
10	1-nitronaphthalene	12.0	70

[a] For azoarenes: NaI/acetic acid under reflux; for cyano- and nitroarenes: NaI/propionic acid under reflux. [b] HI/acetic acid under reflux. [c] Fourth recycle of the catalyst. [d] $FeCl_3/FeSO_4$.

ilarly, the reduction of nitroarenes[25–28] is usually performed by nonregenerable, stoichiometric carbonyl complexes or by expensive catalysts under hydrogen or CO pressure.

Fe^{III}-mont was obtained by following a reported procedure.[29] The X-ray photoelectron spectrum ($Fe\,^{2p}_{3/2}$ band) of a catalyst sample generated by the treatment of freshly prepared Fe^{III}-mont with NaI highlights the predominance of Fe^{II} species. However, the heterogeneous catalyst obtained after reductive acylation of nitrobenzene shows larger amounts of Fe^{III} in the montmorillonite (Figure 1 in the Supporting Information). These results provide strong evidence that, upon treatment with NaI, the Fe^{III} centers in Fe^{III}-mont are predominantly reduced to Fe^{II}, which is, in turn, reoxidized to Fe^{III} during the reductive acylation of nitrobenzene. The redox cycle Fe^{III}/Fe^{II}, involving the relay of two electrons from I_3^- to H^+ to form hydrogen, is thus established in the present system (Scheme 1). Conversely, the reductive acylation of nitroarenes conducted in the presence of an



Scheme 1. Fe^{II}/Fe^{III} redox cycle in the production and consumption of hydrogen.

equimolar ratio of $FeCl_3$ or $FeSO_4$ instead of Fe^{III}-mont, under otherwise identical conditions, afforded the desired products in less than 5% yield. These results reinforce our observation that the montmorillonite is an excellent support that facilitates the redox reaction.

In conclusion, the geochemical approach presented here, which provides unambiguous evidence for the production of hydrogen by reduction of protons with the iodide anion as an electron source, even at room temperature, opens up enormous opportunities in hydrogen chemistry. Production of hydrogen by geochemicals, as described here, provides evidence that the vast quantities of hydrogen found in the Earth's crust may be formed by a similar process. The cogeneration of H_2 and I_2 by simple electron transfer has great potential for the economical production of iodine and hydrogen. This methodology has also been used for the catalytic and selective reductive N-acylation of a variety of functional groups.

Experimental Section

General procedure for the production and consumption of hydrogen in the reductive N-acylation of azo-, cyano-, and nitroarenes: A mixture of carboxylic acid (acetic acid for azoarenes and propionic acid for cyano- and nitroarenes; 40 mmol), sodium iodide (40 mmol), substrate (10 mmol), and Fe^{III}-montmorillonite (1.0 g) was placed in a 100-mL, two-necked, round-bottomed flask, which was sealed with a rubber septum and fitted with a reflux condenser. The reaction mixture was then heated to reflux. After completion of the reaction (as monitored by GC), the reaction mixture was filtered. The filtrate was taken up in ethyl acetate (50 mL) and quenched with a 1% $Na_2S_2O_3$ solution (20 mL) to remove the iodine. It was then washed with a 5% sodium bicarbonate solution to remove the unreacted carboxylic acid. The resulting mixture was concentrated under vacuum and the crude product was purified by column chromatography using ethyl acetate/hexane (1:5) as eluent to yield the pure product.

Received: June 24, 2004

Keywords: acylation · clays · geochemistry · hydrogen · iodine

 © 2005 Wiley-VCH Verlag GmbH & Co. KGaA, Weinheim

[1] R. Cammack, *Nature* **1999**, *397*, 214 – 215.
[2] H. Li, T. B. Rauchfuss, *J. Am. Chem. Soc.* **2002**, *124*, 726 – 727.
[3] M. W. W. Adams, E. I. Stiefel, *Science* **1998**, *282*, 1842 – 1843.
[4] M. Schmidt, S. M. Contakes, T. B. Rauchfuss, *J. Am. Chem. Soc.* **1999**, *121*, 9736 – 9737.
[5] a) D. Sellmann, T. G. -Gaudig, F. W. Heinemann, *Inorg. Chem.* **1998**, *37*, 3982 – 3988; b) X. Zhao, I. P. Georgakaki, M. L. Miller, R. M. Rodriguez, C.-Y. Chiang, M. Y. Darensbourg, *Inorg. Chem.* **2002**, *41*, 3917 – 3928; c) F. Gloaguen, J. D. Lawrence, T. B. Rauchfuss, *J. Am. Chem. Soc.* **2001**, *123*, 9476 – 9477.
[6] A. F. Heyduk, D. G. Nocera, *Science* **2001**, *293*, 1639 – 1640.
[7] a) Z. Zou, J. Ye, K. Sayama, H. Arakawa, *Nature* **2001**, *414*, 625 – 628; b) K. Sayama, K. Mukasa, R. Abe, Y. Abe, H. Arakawa, *Chem. Commun.* **2001**, 2416.
[8] G. B. Saupe, T. E. Mallouk, *J. Phys. Chem. B* **1997**, *101*, 2508 – 2513.
[9] J. Kim, D. W. Hwang, H. G. Kim, S. W. Bae, S. M. Ji, J. S. Lee, *Chem. Commun.* **2002**, 2488.
[10] F. Freund, J. T. Dickinson, M. Cash, *Astrobiology* **2002**, *2*, 83 – 92.
[11] R. T. Anderson, F. H. Chapelle, D. R. Lovley, *Science* **1998**, *281*, 976 – 977.
[12] E. Drobner, H. Huber, G. Wächtershauser, D. Rose, K. O. Stetter, *Nature* **1998**, *396*, 742 – 744.
[13] D. C. Owsley, J. J. Bloomfield, *Synthesis* **1977**, 118 – 120.
[14] P. Laszlo, *Science* **1987**, *235*, 1473 – 1480.
[15] a) G. J. Hwang, K. Onuki, *J. Membr. Sci.* **2001**, *194*, 207 – 215; b) L. C. Brown, R. D. Lentsch, G. E. Besenbruch, K. R. Schultz, *General Atomics Report* **GA-A24266**; c) M. Sakurai, H. Nakajima, K. Onuki, S. Shimizu, *Int. J. Hydrogen Energy* **2000**, *25*, 605 – 611; d) M. Sakurai, H. Nakajima, R. Amir, K. Onuki, S. Shimizu, *Int. J. Hydrogen Energy* **2000**, *25*, 613 – 619; e) G.-J. Hwang, K. Onuki, *J. Membr. Sci.* **2001**, *194*, 207 – 215.
[16] a) P. A. Kittle, US 3,995,016, **1976**. For some other "uphill" reactions, see: b) W. Leitner, *Angew. Chem.* **1995**, *107*, 2391 – 2405; *Angew. Chem. Int. Ed. Engl.* **1995**, *34*, 2207 – 2221; c) E. Graf, W. Leitner, *J. Chem. Soc. Chem. Commun.* **1992**, 623 – 624.
[17] K. Higuchi, M. Onaka, Y. Izumi, *Bull. Chem. Soc. Jpn.* **1993**, *66*, 2016.
[18] D. Meyerstein, A. Treinin, *Trans. Faraday Soc.* **1963**, *59*, 1114.
[19] T. Ohno, S. Saito, K. Fujihara, M. Mitsumura, *Bull. Chem. Soc. Jpn.* **1996**, *69*, 3059.
[20] A. Capperucci, A. D. Innocenti, M. Funicello, G. Mauriello, P. Scafato, P. Spangnolo, *J. Org. Chem.* **1995**, *60*, 2254 – 2256.
[21] A. Kamal, E. Laxman, M. Arifuddin, *Tetrahedron Lett.* **2000**, *41*, 7743 – 7746.
[22] F. E. Gould, G. S. Johnson, A. F. Ferris, *J. Org. Chem.* **1960**, *25*, 1658 – 1660.
[23] C. Jellimann, M. M. Allainmat, J. Andrieux, S. Kloubert, J. A. Boutin, J. P. Nicolas, C. Bennejean, P. Delagrange, M. Langlois, *J. Med. Chem.* **2000**, *43*, 4051 – 4062.
[24] H. C. Brown, Y. M. Choi, S. Narasimhan, *Synthesis* **1981**, 605 – 606.
[25] K. Nomura, *J. Mol. Catal. A* **1998**, *130*, 1 – 28.
[26] a) B. H. Kim, R. Han, F. Piao, Y. M. Jun, W. Baik, B. M. Lee, *Tetrahedron Lett.* **2003**, *44*, 77 – 79; b) A. Kamal, K. V. Ramana, H. B. Ankati, A. V. Ramana, *Tetrahedron Lett.* **2002**, *43*, 6861 – 6863; c) A. Kamal, P. S. M. M. Reddy, D. R. Reddy, *Tetrahedron Lett.* **2002**, *43*, 6629 – 6631.
[27] J. M. Landesberg, L. Katz, C. Olsen, *J. Org. Chem.* **1972**, *37*, 930 – 936.
[28] Y. Wantanabe, Y. Tsuji, T. Kondo, R. Takeuchi, *J. Org. Chem.* **1984**, *49*, 4451 – 4455.
[29] P. Laszlo, A. Mathy, *Helv. Chim. Acta* **1987**, *70*, 577 – 586.

 © 2005 Wiley-VCH Verlag GmbH & Co. KGaA, Weinheim

Protein Self-Assembly

Polar Assembly in a Designed Protein Fiber**

*Andrew M. Smith, Steve F. A. Acquah, Neil Bone, Harold W. Kroto, Maxim G. Ryadnov, Marryat S. P. Stevens, David R. M. Walton, and Derek N. Woolfson**

Self-assembling systems are found extensively in biology.[1] An improved understanding of these systems would fuel efforts to engineer novel, bioinspired assemblies through de novo design. Interest in the area is intense because an ability to engineer or design water-soluble self-assembling systems offers routes to novel biomaterials with potential applications in nanobiotechnology.[2–6]

Self-assembling systems based on peptides, proteins, DNA, and RNA are all being explored.[2–6] Furthermore, "living templates", namely fungal hyphae, are being used to direct the hierarchical assembly of nanoparticles.[7] Our focus has been on peptide-based assemblies.[8–10] Specifically, we are interested in making self-assembling fibers and networks from straightforward, synthetically accessible peptide building blocks.

Considerable work has been done to mimic fibrous protein assemblies by using predominantly β-structured peptides that form amyloid-like fibrils.[2,11,12] Relatively less has been done with α-helix-based assemblies.[3,8,13] We have focused on fibrous assemblies based on the α-helical coiled coil, which is a widespread and well-understood protein–protein interaction motif.[14–16]

Specifically, we have combined rules for coiled-coil assembly to design a self-assembling-fiber (SAF) system comprising two complementary peptides, SAF-p1 and SAF-p2.[8] Unlike natural and previously designed coiled coils, which form blunt-ended structures,[14,17] the SAF peptides were engineered to make offset dimers with complementary sticky ends to promote longitudinal assembly into fibers (Figure 1). Helical assembly was confirmed by using circular dichroism spectroscopy and X-ray fiber diffraction,[8] and

[*] Dr. A. M. Smith,[+] N. Bone, Dr. M. G. Ryadnov, M. S. P. Stevens, Prof. D. N. Woolfson
Department of Biochemistry
School of Life Sciences, University of Sussex
Falmer, BN1 9QG (UK)
Fax: (+44) 1273-678-433
E-mail: dek@sussex.ac.uk

S. F. A. Acquah, Prof. Sir H. W. Kroto, Dr. D. R. M. Walton
Department of Chemistry
School of Life Sciences, University of Sussex
Falmer, BN1 9QJ (UK)

[+] Current address:
School of Biochemistry and Molecular Biology
University of Leeds
Leeds, LS2 9JT (UK)

[**] We thank the EPSRC for studentships to A.M.S. and S.F.A.A., and the BBSRC for a studentship to M.S.P.S. and grant support (reference B10280).

 DOI: 10.1002/anie.200461599 © 2005 Wiley-VCH Verlag GmbH & Co. KGaA, Weinheim

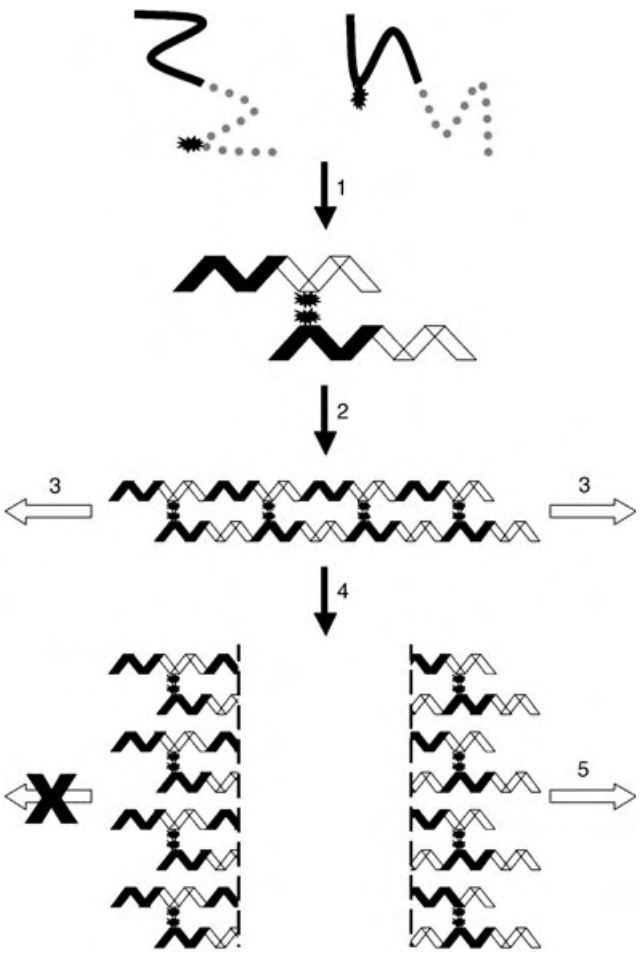


Figure 1. A model for SAF fibrillogenesis. Each SAF peptide is represented by a polar strand with a basic (solid lines) N-terminal half, an acidic (broken/hollow lines) C-terminal half, and a single asparagine residue (starred). These features direct the assembly of a sticky-ended heterodimer (step 1). These heterodimers then assemble longitudinally to give double-stranded coiled-coil protofibrils (step 2). We assume that, at this stage, extension occurs by the addition of peptide building blocks to either end of the protofibril (step 3). At some point the protofibrils have enough affinity for one another to assemble laterally and thicken (step 4). These thickened fibers are polar; that is, when one type of the SAF peptide is added to matured fibers it is selectively recruited to just one end of the fibers (step 5).

more recently by FTIR spectroscopy (unpublished data). Fiber formation was confirmed by electron microscopy (EM), which revealed that the fibers were linear, extended many microns, and were $\approx$45 nm thick:[8] approximately 20 times thicker than expected for coiled-coil dimers.[18] One explanation for thickening is that two-chain assemblies form nascent structures (protofibrils) that assemble further laterally to form the matured, thick fibers (Figure 1). Herein we describe experiments initially conceived to follow lateral assembly directly in water. We also show that this relatively straightforward system displays the unexpected and potentially exploitable feature of polar assembly.

To follow the process of lateral assembly directly in solution we performed the following experiment: A cysteine residue was introduced into SAF-p2a—a variant of SAF-p2—to make SAF-p2aCys (Table 1). This peptide was used to make two fluorescently labeled peptides: one containing fluorescein and the other rhodamine. Each labeled peptide was incorporated separately and at low levels (0.05% total peptide) into otherwise standard SAF-p1:SAF-p2a fiber preparations. When visualized by confocal fluorescence microscopy, the resulting fibers appeared green and red, respectively, and otherwise normal. By mixing these fibers and recording images over time we observed the formation of matured fibers through the emergence of thickened yellow structures (Figure 2a–c). The yellowing did not result from subunit exchange between the solution and fibers, however,

Table 1: SAF peptide sequences.

Peptide	Sequence[a]
SAF-p1	K IAALKQK IASLKQE IDALEYE NDALEQ
SAF-p2	K IRALKAK NAHLKQE IAALEQE IAALEQ
SAF-p2a	K IR***R***LK***Q***K NA***R***LKQE IAALE***Y***E IAALEQ
SAF-p2a-Cys	K IRRLK***C***K NARLKQE IAALEYE IAALEQ
SAF-p2a-Lys	K IRRLK***K***K NARLKQE IAALEYE IAALEQ

[a] Successive mutations are highlighted in bold, italic font.

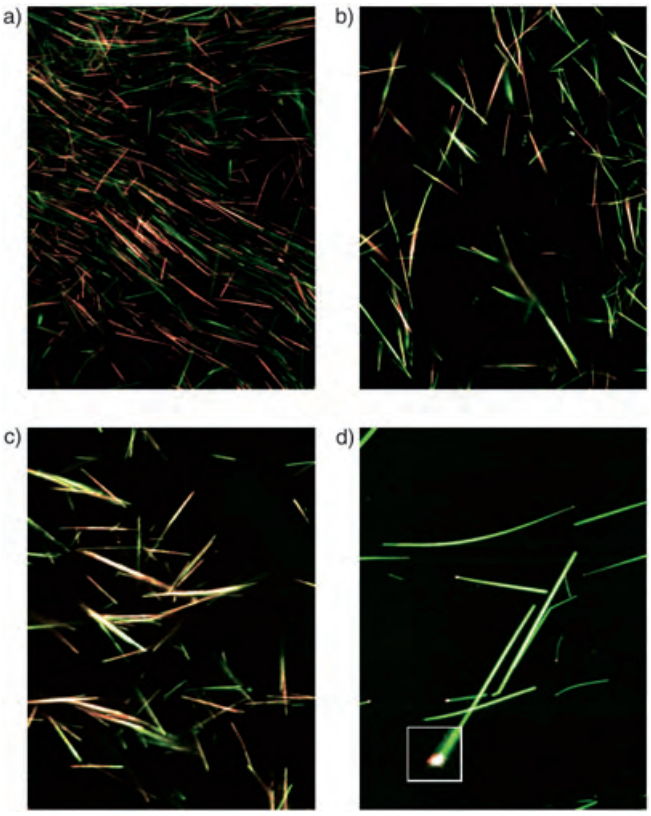


Figure 2. False-color images of merged red- and green-filtered confocal microscope data: a) recorded immediately after mixing two separately prepared samples of rhodamine- and fluorescein-labeled fibers; b and c) for samples prepared as described in A, but left to mix for 24 and 48 h, respectively; d) for a matured fluorescein-labeled sample, which was treated subsequently with rhodamine-labeled SAF-p2a. The inset shows an approximately fourfold further magnification of one fiber tip. The short axis of each of these panels is approximately 100 μm.

 © 2005 Wiley-VCH Verlag GmbH & Co. KGaA, Weinheim

because some of the fibers showed distinct red and green halves and yellow central regions, thus indicating that red and green fibers must have merged in a manner consistent with our model for fibrillogenesis (Figure 1).

We conducted the following additional experiment to probe how individual (or at least small numbers of) peptides were recruited to matured fibers: Fibers containing the fluorescein-labeled peptide were assembled as described above and matured for 16 h, after which time fiber formation had essentially ceased, and the concentration of free monomers had fallen to the critical concentration for fibrillogenesis ($\approx$30 μM).[19] At this point, rhodamine-labeled SAF-p2a was added. Intriguingly, as shown in Figure 2d, the rhodamine-labeled monomers appeared to be selectively recruited to just one end of the matured fibers.

To examine this finding further, and to test the possibility of making nano-to-micron-scale barcodes,[20] but from self-assembling biomolecules, we conducted a further experiment: First, unlabeled fibers were grown for 24 h. Rhodamine-labeled SAF-p2a was then added, and the sample was left to mature for 24 h, followed by the addition of fluorescein-labeled SAF-p2a and further maturation for 24 h. The result was fibers with one end labeled red followed by green (Figure 3). Although there was some background staining of the unlabeled fibers, it was clear that only one end of each fiber was labeled and, moreover, that labeling was in the correct (red–green) order as prescribed in the experiment.

What gives rise to polar assembly in our system? The SAF peptides themselves are polar: They each have a positively charged N-terminal half and a negatively charged C-terminal half (Figure 1).[8] As a result, the designed heterodimeric building block for the fibers, in which the C-terminal half of SAF-p1 binds to the N-terminal half of SAF-p2a and vice versa, will be polar. Thus, the longitudinally extended coiled-coil protofibrils will be polar. On this basis, there may be preferred protofibril–protofibril arrangements that could lead to polar matured fibers. In turn, the different ends of these matured fibers could be distinguished by new incoming peptides (Figure 1), as observed. Indeed, a theory for this type of polar assembly has been advanced,[21] although examples of this type of assembly for soft materials appear to be restricted to natural protein fibers, such as microtubules, intermediate filaments, and collagens,[1,22,23] and, most recently, the fibril form of the yeast prion protein Ure2p.[24] This unexpected mimicry in our relatively simple, designed binary peptide system is intriguing and may shed light on both natural and synthetic self-assembly processes in general. Furthermore, and in view of current attention being given to the generation of bioinspired materials for applications in nanobiotechnology,[2,3,11,25–28] our findings offer promise for nano-to-micron-scale engineering of self-assembling systems from the bottom up in water; for example, the directed incorporation of functionalized peptides—that is, either regularly spaced along the fibers, or specifically located at one end of the fibers—can be envisaged based on the observations presented herein.

Experimental Section

Peptide synthesis: Peptides were made chemically on a pioneer peptide synthesis system (PE Applied Biosystems, CA, USA) by using standard Fmoc-based solid-phase protocols (Fmoc = 9-fluorenylmethoxycarbonyl). Two approaches were taken to introduce the fluorescent labels: For our initial experiments (Figure 2), labeled peptides were prepared by conjugating SAF-p2a-Cys (Table 1) with either fluorescein-5-maleimide or tetramethylrhodamine-5-maleimide (Molecular Probes) by the protocols of the supplier. The labeled peptides were purified on PD 10 columns (Amersham Biosciences, Buckinghamshire, UK) by using the protocol of the supplier. For the later experiments (Figure 3), succinimidyl esters of 5- (and 6-)carboxyfluorescein and 5- (and 6-)carboxytetramethylrhodamine were used to label the lysine residue introduced into SAF-p2a-Lys (Table 1), which was specifically deprotected and subjected to reaction during peptide synthesis by analogous procedures to those published elsewhere.[10] Peptides were purified by semipreparative reversed-phase HPLC and, when necessary for dye–peptide conjugates, beforehand by using PD-10 columns. The final constructs were identified by MALDI-TOF mass spectrometry (Micromass Ltd, Manchester, UK): *m/z*: calcd for SAF-p1: 3174, found: 3175 $[M+H]^+$; calcd for SAF-p2: 3128, found: 3129 $[M+H]^+$; calcd for SAF-p2a: 3325, found: 3326 $[M+H]^+$; calcd for SAF-p2a-Cys: 3300, found: 3301 $[M+H]^+$. Mass increases of 359, 413, 427, and 481 Da were detected for carboxyfluorescein-, carboxytetramethylrhodamine-, fluorescein-5-maleimide-, and tetramethylrhodamine-5-maleimide-labeled SAFs, respectively.

Fluorescence microscopy: For the "kinetic-mixing" experiments (Figure 2a--c), the unlabeled peptides SAF-p1 (100 μM) and SAF-p2a (100 μM) were mixed with the labeled peptide (0.1 μM) in MOPS (3-

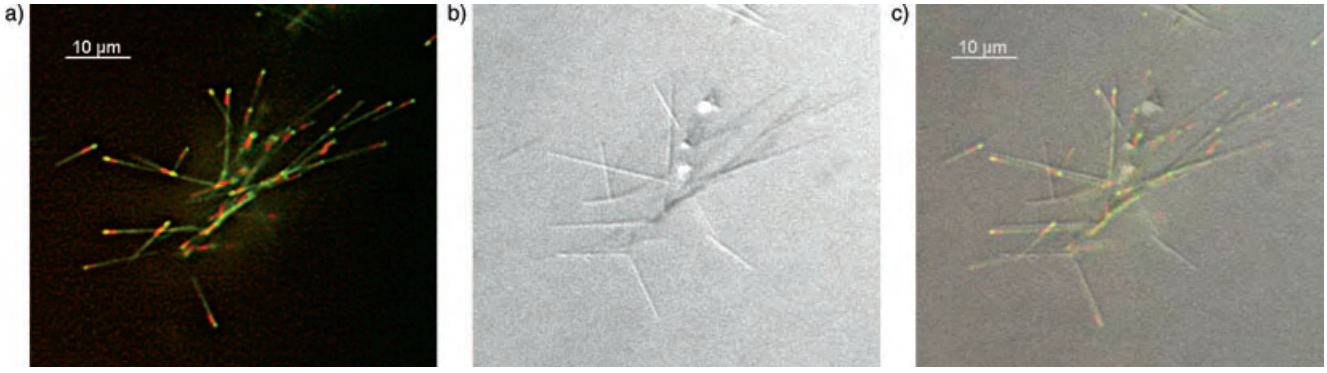


Figure 3. a) Merged false-color image showing unlabeled fibers treated first with rhodamine-labeled peptide, and then with fluorescein-labeled peptide. b) The corresponding DIC image highlighting the full lengths of the fibers. c) Merge of A and B showing that the fluorescent labels are located predominantly at the fiber tips and in the correct order.

 © 2005 Wiley-VCH Verlag GmbH & Co. KGaA, Weinheim

(*N*-morpholino)propanesulfonic acid; 10 mM, pH 7). The sample was allowed to mature for 16 h at 20 °C prior to each experiment. The matured solutions were then mixed and either visualized immediately or incubated for a further 24 or 48 h before examination. In the first "polar-assembly" experiment (Figure 2d), fluorescein-labeled fibers were prepared as described above. After the 16-hour incubation the rhodamine-labeled peptide (0.1 μM) was added, and the solution was left for 24 h before examination. For these experiments, samples were visualized by using an x60 oil-immersion lens on a BioRad MRC 600 confocal microscope with a krypton/argon mixed-gas laser, dual-excitation filter, and K1 (520 nm, fluorescein) and K2 (585 nm, rhodamine) filter-block set. Data were collected by using COMOS (BioRad). Images were contrast stretched and false colored red or green before overlaying the two halves.

For the experiments presented in Figure 3, unlabeled fibers were formed first by using our standard protocol (100-μL samples, 100 μM in each of SAF-p1 and SAF-p2a, MOPS (10 mM, pH 7), incubation at 20 °C for 24 h); the sample was then made up to 1 μM in rhodamine-labeled SAF-p2a and incubated for a further 24 h; finally, the sample was made up to 1 μM in fluorescein-labeled SAF-p2a and incubated for a further 24 h. The experiment was repeated with the introduction of the labels in the opposite order (data not shown). Fluorescence and differential interference contrast (DIC) images were recorded on a Carl Zeiss Vision widefield microscope fitted with x10 and x40 LD lenses, a krypton/argon mixed-gas laser, a dichromic mirror, and two light filters (520 nm (filter set 10) for fluorescein and 585 nm (set 15) for rhodamine). Data were collected by using an ORCA ER camera. Images were false colored red or green before they were overlayed by using the Carl Zeiss Vision imaging software.

Received: August 10, 2004

Keywords: fibrous proteins · nanostructures · peptides · protein design · self-assembly

[1] T. D. Pollard, W. C. Earnshaw, *Cell Biology*, Saunders, London, **2002**.
[2] S. G. Zhang, D. M. Marini, W. Hwang, S. Santoso, *Curr. Opin. Chem. Biol.* **2002**, *6*, 865.
[3] T. O. Yeates, J. E. Padilla, *Curr. Opin. Struct. Biol.* **2002**, *12*, 464.
[4] C. M. Niemeyer, *Curr. Opin. Chem. Biol.* **2000**, *4*, 609.
[5] N. C. Seeman, *Biochemistry* **2003**, *42*, 7259.
[6] L. Jaeger, N. B. Leontis, *Angew. Chem.* **2000**, *112*, 2576; *Angew. Chem. Int. Ed.* **2000**, *39*, 2521.
[7] Z. Li, S. W. Chung, J. M. Nam, D. S. Ginger, C. A. Mirkin, *Angew. Chem.* **2003**, *115*, 2408; *Angew. Chem. Int. Ed.* **2003**, *42*, 2306.
[8] M. J. Pandya, G. M. Spooner, M. Sunde, J. R. Thorpe, A. Rodger, D. N. Woolfson, *Biochemistry* **2000**, *39*, 8728.
[9] M. G. Ryadnov, D. N. Woolfson, *Nat. Mater.* **2003**, *2*, 329.
[10] M. G. Ryadnov, D. N. Woolfson, *Angew. Chem.* **2003**, *115*, 3129; *Angew. Chem. Int. Ed.* **2003**, *42*, 3021.
[11] C. E. MacPhee, C. M. Dobson, *J. Am. Chem. Soc.* **2000**, *122*, 12707.
[12] T. Scheibel, R. Parthasarathy, G. Sawicki, X. M. Lin, H. Jaeger, S. L. Lindquist, *Proc. Natl. Acad. Sci. USA* **2003**, *100*, 4527.
[13] S. A. Potekhin, T. N. Melnik, V. Popov, N. F. Lanina, A. A. Vazina, P. Rigler, A. S. Verdini, G. Corradin, A. V. Kajava, *Chem. Biol.* **2001**, *8*, 1025.
[14] A. Lupas, *Trends Biochem. Sci.* **1996**, *21*, 375.
[15] W. D. Kohn, R. S. Hodges, *Trends Biotechnol.* **1998**, *16*, 379.
[16] P. Burkhard, J. Stetefeld, S. V. Strelkov, *Trends Cell Biol.* **2001**, *11*, 82.
[17] J. Walshaw, D. N. Woolfson, *J. Mol. Biol.* **2001**, *307*, 1427.
[18] E. K. O'Shea, J. D. Klemm, P. S. Kim, T. Alber, *Science* **1991**, *254*, 539.
[19] A. M. Smith, DPhil thesis, University of Sussex (Brighton), **2003**.
[20] S. R. Nicewarner-Pena, R. G. Freeman, B. D. Reiss, L. He, D. J. Pena, I. D. Walton, R. Cromer, C. D. Keating, M. J. Natan, *Science* **2001**, *294*, 137.
[21] J. Hulliger, *Chem. Eur. J.* **2002**, *8*, 4579.
[22] D. J. Prockop, A. Fertala, *J. Struct. Biol.* **1998**, *122*, 111.
[23] K. E. Kadler, D. F. Holmes, H. Graham, T. Starborg, *Matrix Biol.* **2000**, *19*, 359.
[24] N. Fay, Y. J. Inoue, L. Bousset, H. Taguchi, R. Melki, *J. Biol. Chem.* **2003**, *278*, 30199.
[25] A. Aggeli, M. Bell, N. Boden, J. N. Keen, P. F. Knowles, T. C. B. McLeish, M. Pitkeathly, S. E. Radford, *Nature* **1997**, *386*, 259.
[26] J. D. Hartgerink, E. Beniash, S. I. Stupp, *Science* **2001**, *294*, 1684.
[27] J. E. Padilla, C. Colovos, T. O. Yeates, *Proc. Natl. Acad. Sci. USA* **2001**, *98*, 2217.
[28] T. C. Holmes, *Trends Biotechnol.* **2002**, *20*, 16.

 © 2005 Wiley-VCH Verlag GmbH & Co. KGaA, Weinheim

Supramolecular Chemistry

Liquid-Crystalline Assembly from Rigid Wedge–Flexible Coil Diblock Molecules**

*Jung-Keun Kim, Min-Ki Hong, Jong-Hyun Ahn, and Myongsoo Lee**

There is a growing interest in the rational design of new self-assembling molecules that possess various chemical or biological functionalities and self-assemble into tunable and predictable supramolecular structures.[1] Among self-assembling molecular systems, a dendritic molecular architecture has proved to be a promising scaffold for nanometer-sized aggregation structures including spheres and cylinders.[2–6] Rod–coil block molecules represent another class of self-assembling systems that are increasingly used for the construction of supramolecular architectures with well-defined shape.[7] The supramolecular structures can be precisely controlled by systematic variation of the type and relative length of the respective blocks.[8,9]

Incorporation of a rigid wedge-shaped building block into a diblock molecular architecture gives rise to a novel class of self-assembling systems consisting of a rigid wedge and a flexible coil because the molecule shares certain general characteristics of both dendrons and block copolymers.

[*] J.-K. Kim, M.-K. Hong, J.-H. Ahn, Prof. M. Lee
Center for Supramolecular Nanoassembly and
Department of Chemistry
Yonsei University
Shinchon 134, Seoul 120-749 (Korea)
Fax: (+82) 2-393-6096
E-mail: mslee@yonsei.ac.kr

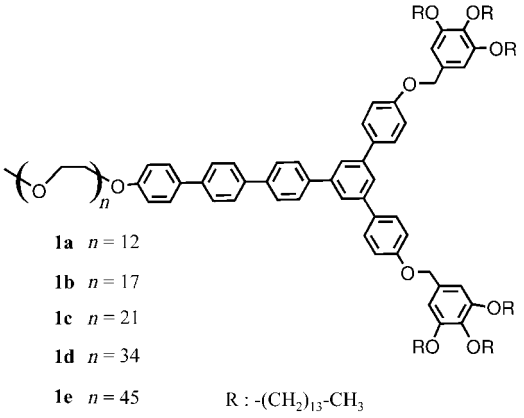
[**] This work was supported by the Creative Research Initiative Program of the Ministry of Science and Technology, Korea, and Pohang Accelerator Laboratory, Korea (use of synchrotron radiation).

Supporting information for this article is available on the WWW under http://www.angewandte.org or from the author.

 © 2005 Wiley-VCH Verlag GmbH & Co. KGaA, Weinheim DOI: 10.1002/anie.200461623

Wedge-shaped molecules based on a short flexible coil should self-assemble into discrete supramolecular structures with a highly curved surface, similar to self-assembling dendron molecules. As the length of the flexible coil increases, however, supramolecular structures with a flatter interface might be formed as a result of the increased effective area of the flexible coil and consequent space-filling requirement. Therefore, a combination of the organizing principles of dendritic wedges and block copolymers may open up new possibilities for the design of unique supramolecular arrangements from wedge-shaped dendritic building blocks.

This work focuses on a novel combination of the above perspectives, in which wedge–coil diblock molecules consisting of a rigid wedge and a flexible poly(ethylene oxide) (PEO) coil were investigated. The self-assembling behavior of



these diblock molecules in the melt state was studied by optical polarized microscopy, differential scanning calorimetry (DSC), and X-ray scattering measurements. The molecules self-assembled successively, as the length of the PEO chain increased, into 3D micellar cubic (with *Im3m* and *Pm3n* lattices), 2D hexagonal columnar, 3D perforated lamellar, and smectic-like lamellar structures in the melt state.

The synthesis of rigid wedge–flexible coil diblock molecules, which consisted of the wedge-shaped rigid aromatic segment containing peripheral tetradecyloxy groups and a flexible PEO chain, started with the preparation of an aromatic scaffold with a tetradecyloxy periphery according to the procedures described previously.[10] The final wedge–coil diblock molecules were synthesized by an etherification reaction of a phenolic precursor with the appropriate tosyl-terminated PEO chains. The resulting block molecules were purified by column chromatography on silica gel with ethyl acetate as the eluent and then further purified by preparative gel-permeation chromatography (prep. GPC, see the Experimental Section). The resulting molecules were characterized by NMR spectroscopy, elemental analysis, GPC, and MALDI-TOF mass spectroscopy, and the data were shown to be in full agreement with the structures presented.

As shown in Table 1, all of the molecules had a thermotropic liquid-crystalline structure after melting. The wide-angle X-ray diffraction patterns of all the molecules in the melt state are characterized by a diffuse scattering, which confirms their liquid-crystalline nature. However, a significant structural variation in the melt state was observed as the length of the PEO segment was varied, as evidenced by optical microscopic textures and small-angle X-ray diffraction scattering (SAXS, Figure 1). Compounds **1a** and **1b**, which are based on a short PEO chain, exhibited a lack of birefringence between crossed polarizers, thus indicating the presence of a 3D cubic liquid-crystalline phase. The SAXS study of **1a** revealed a number of well-resolved reflections corresponding to a body-centered cubic structure with *Im3m* symmetry and a lattice parameter of 11.6 nm. However, the SAXS pattern of **1b** appeared to correspond to a 3D cubic structure with a *Pm3n* space group symmetry with a lattice constant of 20.3 nm. These results indicate that the symmetry change in the 3D cubic phase, from an *Im3m* to a *Pm3n* symmetry, occurs with increasing chain length. This symmetry change was also observed for the 3D micellar cubic phase of other dendritic molecules on changing the temperature.[11] The number of molecules per sphere in spherical supramolecular structures is estimated to be 200 and 237 for **1a** and **1b**, respectively.

In contrast, compound **1c** displayed a birefringent mesophase upon melting of the crystalline phase. SAXS studies confirmed the formation of a 2D hexagonal columnar structure with a lattice constant $a = 10.3$ nm, which is in accordance with the phase assignment made by optical microscopy (Figure 2a). Remarkably, further cooling from the hexagonal structure gave rise to a metastable perforated lamellar structure. On cooling from the hexagonal columnar mesophase, arc-shaped striations appeared on the pseudo-focal conic domains at 45 °C (see Supporting Information), which was indicative of transformation into a 3D hexagonal structure. This finding was confirmed by SAXS experiments that showed a number of reflections with low intensity in addition to a strong reflection at a lower angle, which can be

Table 1: Thermal transitions of **1a–e** (data from heating and cooling scans).

	M_w/M_n[b]	Phase transition[a] [°C] and corresponding enthalpy changes [kJ mol^{-1}]	
		Heating	Cooling
1a	1.08	cr 60.8 (31.5) cub(*Im3m*) 78.4 (0.14) i	i 74.5 (0.08) cub(*Im3m*) 18.5 (12.5) cr
1b	1.04	cr 60.2 (32.0) cub(*Pm3n*) 88.4 (0.80) i	i 83.9 (0.09) cub(*Pm3n*) 22.4 (14.9) cr
1c	1.04	cr 56.5 (18.1) col 93.2 (0.99) i	i 91.5 (0.34) col 50.7 (0.23) L_{hex} 21.0 (36.3) cr
1d	1.05	cr 57.5 (29.6) L_{hex} 115.6 (1.90) i	i 112.9 (0.26) L_{hex} 36.1 (3.65) cr 28.8 (13.5) cr
1e	1.05	cr 48.0 (49.6) s_A 143.7 (0.36) i	i 142.1 (0.38) s_A 32.4 (4.07) cr 24.0 (1.75) cr 10.3 (49.0) k

[a] cr: crystalline phase, cub: cubic phase, col: hexagonal columnar phase, L_{hex}: hexagonal perforated lamellar phase, s_A: smectic A phase, i: isotropic phase. [b] Determined by GPC.

 © 2005 Wiley-VCH Verlag GmbH & Co. KGaA, Weinheim

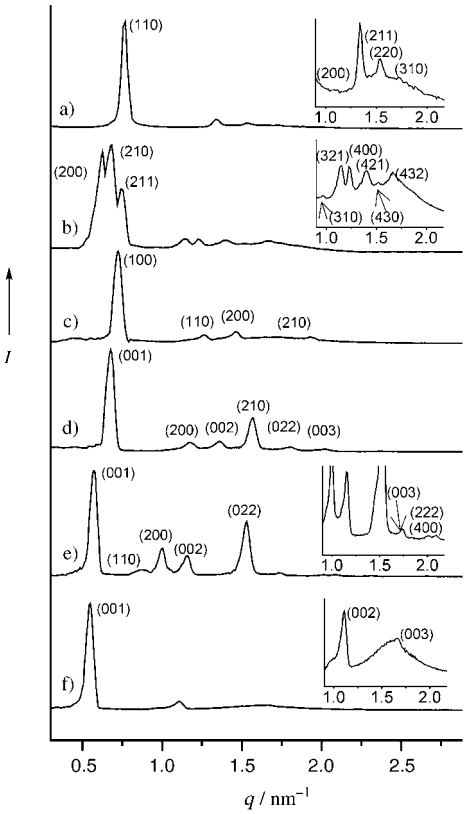


Figure 1. Small-angle X-ray diffraction patterns of **1a**–**e** plotted against q. a) The *Im3m* cubic lattice exhibited by **1a** at 65 °C; b) the *Pm3n* cubic lattice exhibited by **1b** at 65 °C; c) the hexagonal columnar lattice exhibited by **1c** at 70 °C; d) the hexagonal perforated layer lattice exhibited by **1c** at 40 °C; e) the hexagonal perforated layer lattice exhibited by **1d** at 70 °C; and f) the lamellar lattice exhibited by **1e** at 70 °C.

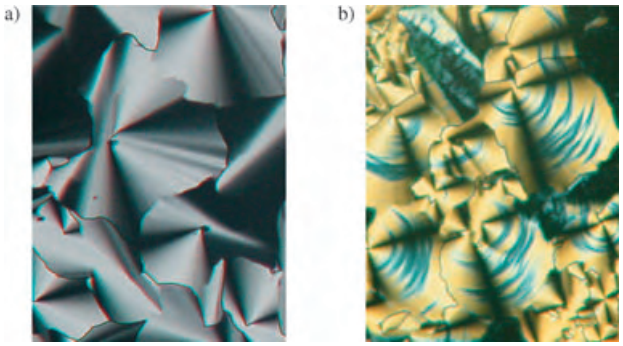


Figure 2. Representative optical micrographs (100×) of: a) the texture exhibited by the hexagonal columnar mesophase of **1c** at 80 °C in the cooling scan; and b) the texture exhibited by the hexagonal perforated lamellar mesophase of **1d** at 90 °C in the cooling scan.

indexed as a 3D hexagonal close-packed structure with lattice constants of $a = 12.3$ nm and $c = 9.2$ nm (Figure 1 d). The peak intensity associated with the (001) reflection appeared to be the most intense, which suggests that the fundamental structure is lamellar, similar to that of the perforated lamellar structure reported previously.[9,12] Thus, this 3D hexagonal structure can be considered as a system of perforated aromatic layers with in-plane hexagonal packing of coil perforations. The consequent layers are stacked in a bilayer AB–AB arrangement to generate 3D order. The tendency of a hexagonal columnar phase to transform into a perforated lamellar phase on cooling is consistent with the results from rod–coil systems described previously.[9c,13]

Compound **1d** displayed a stable perforated lamellar mesophase. Small-angle X-ray scattering revealed a similar diffraction pattern to that of the lower-temperature mesophase of **1c**, which indicates the presence of a bilayer lamellar structure with in-plane hexagonally ordered coil perforations ($a = 14.5$ nm and $c = 11.0$ nm). This phase identification is further supported by transmission electron microscopy (TEM) and optical microscopic observations. The TEM images stained with RuO_4 showed a layered structure with in-plane light-colored coil domains in a matrix of dark rod segments (Figure 3 a). An arc-shaped pseudofocal conic

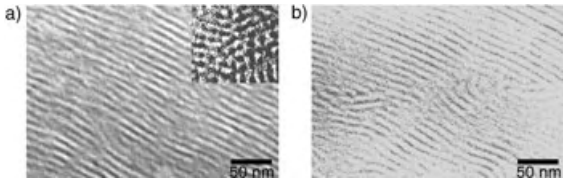


Figure 3. Representative TEM images of a) an ultramicrotomed film of **1d** stained with RuO_4 revealing an ordered array of alternating light-colored PEO layers and dark aromatic layers. The inset shows an in-plane hexagonally ordered array of PEO perforations. b) An ultramicrotomed film of **1e** stained with RuO_4 exhibiting alternating dark aromatic layers and light PEO layers.

texture was observed on an optical polarized microscope (Figure 2 b) on cooling from the isotropic liquid, which supports the formation of a 3D hexagonal structure.[9b] In contrast, compound **1e** exhibited a smectic A phase, as confirmed by optical microscopic texture and X-ray diffraction studies. The layer thickness obtained from the X-ray diffraction pattern appeared to be 11.5 nm, that is, much smaller than the estimated molecular length (17.1 nm by CPK models), and suggests that the molecules are packed with a monolayer lamellar structure in which the rigid wedge segments are interdigitated. This result is further supported by TEM experiments that showed much thinner dark aromatic layers compared to those of **1d** (Figure 3 b). These findings indicate that increasing coil length leads to transformation of a bilayer to an interdigitated monolayer structure.

The results described above demonstrate the capability of manipulating the supramolecular structure by grafting flexible PEO chains of different lengths to the apex of the same wedge-shaped rigid building block (Figure 4). The variation in the supramolecular structure can be rationalized by considering the microphase separation between the dissimilar parts of the molecule and the space-filling requirement of the flexible PEO chains. The molecules based on a short PEO chain can be packed with a radial arrangement to fill the space efficiently, which results in a spherical supramolecular

 © 2005 Wiley-VCH Verlag GmbH & Co. KGaA, Weinheim

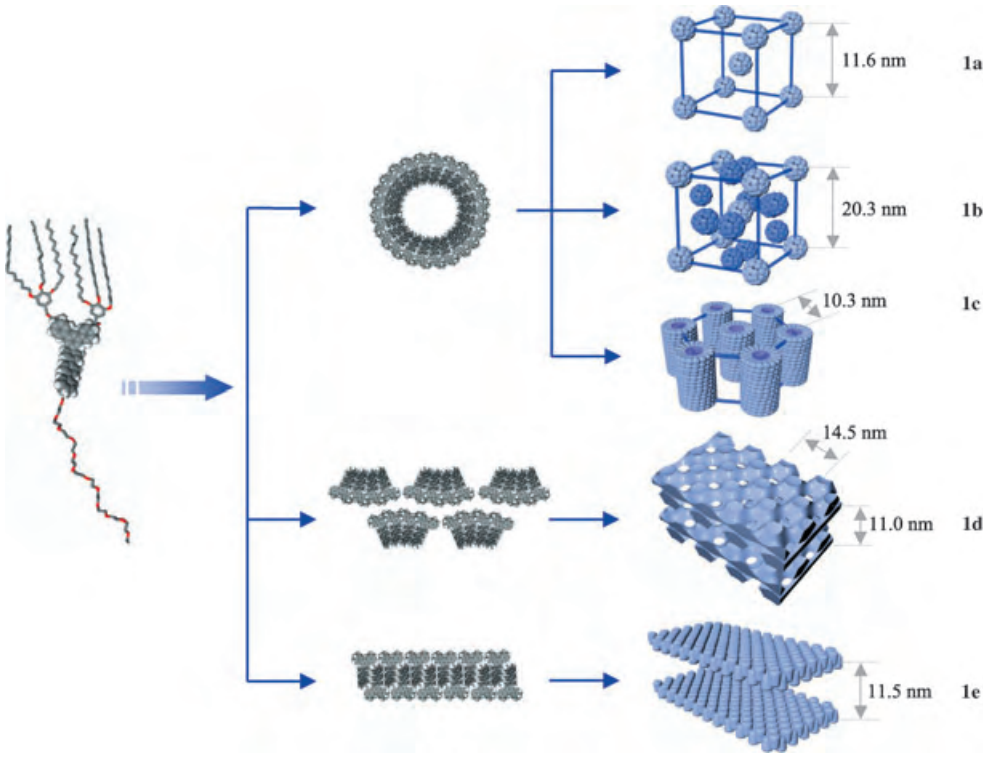


Figure 4. Schematic representation of supramolecular structures formed by wedge-shaped molecules.

structure. Increasing the length of the PEO chain results in more space for the chains being required while maintaining the radial arrangement of the rigid segments. Consequently, the discrete PEO domains will be extended to an infinitely long cylindrical domain in which the coils are less confined, which results in the formation of a 2D hexagonal columnar structure. Further increasing the length results in the rigid wedge-shaped segments assembling into a perforated lamellar structure with a radial arrangement of rigid segments, which allows a greater volume for the PEO chains to explore compared to that of the columnar structure. The radial arrangement of the wedge-shaped rigid segments eventually transforms into a parallel arrangement with interdigitation, to produce a flat interface while maintaining a constant density of the rigid hydrophobic domain. This transformation results in a monolayer lamellar structure as in the case of **1e**.

The self-organization phenomena of the series of rigid wedge–flexible coil diblock molecules demonstrate that systematic variation in the coil length can regulate the supramolecular structure, from 3D micellar cubic with different lattices, 2D hexagonal columnar, and perforated lamellar to smectic-like liquid crystalline assemblies. The primary force responsible for this structural change is believed to be the combination of shape complementarity and microphase separation between rigid and flexible segments. Compared to other self-assembling systems based on dendritic molecules,[2–6,11,14] the remarkable feature of the wedge-shaped building blocks investigated here is their ability to self-assemble not only into spherical cubic and columnar structures, but also into an unusual bilayer lamellar structure with in-plane hexagonally ordered coil perforations. These results demonstrate that this approach of controlling supramolecular structures using wedge-shaped building blocks and only a small variation in the length of grafted coils allows unexpectedly complex superstructures to be produced.

Received: August 12, 2004

Keywords: liquid crystals · nanostructures · polymers · self-assembly · supramolecular chemistry

[1] a) J.-M. Lehn, *Supramolecular Chemistry: Concepts and Perspectives*, VCH, Weinheim, **1995**; b) J. A. A. W. Elemans, A. E. Rowan, R. J. M. Nolte, *J. Mater. Chem.* **2003**, *13*, 2661; c) T. Kato, *Science* **2002**, *295*, 2414.

[2] a) G. Ungar, Y. Liu, X. Zeng, V. Percec, W.-D. Cho, *Science* **2003**, *299*, 1208; b) V. Percec, C. M. Mitchell, W.-D. Cho, S. Uchida, M. Glodde, G. Ungar, X. Zeng, Y. Liu, V. S. K. Balagurusamy, P. A. Heiney, *J. Am. Chem. Soc.* **2004**, *126*, 6078.

[3] a) T. Kato, T. Matsuoka, M. Nishii, Y. Kamikawa, K. Kanie, T. Nishimura, E. Yashima, S. Ujiie, *Angew. Chem.* **2004**, *116*, 2003; *Angew. Chem. Int. Ed.* **2004**, *43*, 1969; b) M. Enomoto, A. Kishimura, T. Aida, *J. Am. Chem. Soc.* **2001**, *123*, 5608; c) M. Suarez, J.-M. Lehn, S. C. Zimmerman, A. Skoulios, B. Heinrich, *J. Am. Chem. Soc.* **1998**, *120*, 9526.

[4] J. C. M. van Hest, D. A. P. Delnoye, M. W. P. L. Baars, M. H. P. van Genderen, E. W. Meijer, *Science* **1995**, *268*, 1592.

[5] a) M. R. Leduc, W. Hayes, J. M. J. Fréchet, *J. Polym. Sci. Polym. Chem.* **1998**, *36*, 1; b) J. Iyer, K. Fleming, P. T. Hammond, *Macromolecules* **2004**, *37*, 2490; c) A. R. Hirst, D. K. Smith, M. C. Feiters, H. P. M. Geurts, A. C. Wright, *J. Am. Chem. Soc.* **2003**, *125*, 9010.

[6] a) S. Lecommandoux, H.-A. Klok, M. Sayar, S. I. Stupp, *J. Polym. Sci. Polym. Chem.* **2003**, *41*, 3501; b) E. R. Zubarev,

 © 2005 Wiley-VCH Verlag GmbH & Co. KGaA, Weinheim

M. U. Pralle, E. D. Sone, S. I. Stupp, *J. Am. Chem. Soc.* **2001**, *123*, 4105.
[7] Recent reviews: a) M. Lee, Y.-S. Yoo, *J. Mater. Chem.* **2002**, *12*, 2161; b) M. Lee, B.-K. Cho, W.-C. Zin, *Chem. Rev.* **2001**, *101*, 3869; c) H.-A. Klok, S. Lecommandoux, *Adv. Mater.* **2001**, *13*, 1217; d) S. I. Stupp, *Curr. Opin. Colloid Interface Sci.* **1998**, *3*, 20.
[8] a) M. Lee, B.-K. Cho, H. Kim, J.-Y. Yoon, W.-C. Zin, *J. Am. Chem. Soc.* **1998**, *120*, 9168; b) M. Lee, D.-W. Lee, B.-K. Cho, J.-Y. Yoon, W.-C. Zin, *J. Am. Chem. Soc.* **1998**, *120*, 13258; c) M. Lee, B.-K. Cho, N.-K. Oh, W.-C. Zin, *Macromolecules* **2001**, *34*, 1987; d) M. Lee, J.-W. Kim, I.-W. Hwang, Y.-R. Kim, N.-K. Oh, W.-C. Zin, *Adv. Mater.* **2001**, *13*, 1363; e) M. Lee, B.-K. Cho, Y.-G. Jang, W.-C. Zin, *J. Am. Chem. Soc.* **2000**, *122*, 7449.
[9] a) M. Lee, B.-K. Cho, K. J. Ihn, W.-K. Lee, N.-K. Oh, W.-C. Zin, *J. Am. Chem. Soc.* **2001**, *123*, 4647; b) B.-K. Cho, M. Lee, N.-K. Oh, W.-C. Zin, *J. Am. Chem. Soc.* **2001**, *123*, 9677; c) J.-H. Ryu, N.-K. Oh, W.-C. Zin, M. Lee, *J. Am. Chem. Soc.* **2004**, *126*, 3551.
[10] a) M. Lee, Y.-S. Yoo, M.-G. Choi, *Bull. Korean Chem. Soc.* **1997**, *18*, 1067; b) Y.-S. Yoo, J.-H. Choi, J.-H. Song, N.-K. Oh, W.-C. Zin, S. Park, T. Chang, M. Lee, *J. Am. Chem. Soc.* **2004**, *126*, 6294.
[11] a) V. Percec, M. N. Holerca, S. Uchida, W.-D. Cho, G. Ungar, Y. Lee, D. J. P. Yeardley, *Chem. Eur. J.* **2002**, *8*, 1106; b) Y. Li, S.-T. Lin, W. A. Goddard III, *J. Am. Chem. Soc.* **2004**, *126*, 1872.
[12] It should be noted that this is in contrast to that of the 3D hexagonal lattice based on discrete particles; see T. Kenichi, *Phys. Rev. Lett.* **1995**, *75*, 1807.
[13] N.-K. Oh, W.-C. Zin, J.-H. Im, J.-H. Ryu, M. Lee, *Chem. Commun.* **2004**, 1092.
[14] a) D. J. Pesak, J. S. Moore, *Angew. Chem.* **1997**, *109*, 1709; *Angew. Chem. Int. Ed. Engl.* **1997**, *36*, 1636; b) I. M. Saez, J. W. Goodby, *Chem. Commun.* **2003**, 1726; c) A. R. A. Palmans, J. A. J. M. Vekemans, E. E. Havinga, E. W. Meijer, *Angew. Chem.* **1997**, *109*, 2763; *Angew. Chem. Int. Ed. Engl.* **1997**, *36*, 2648; d) J. M. J. Fréchet, *Proc. Natl. Acad. Sci. USA* **2002**, *99*, 4782; e) C. Tschierske, *J. Mater. Chem.* **2001**, *11*, 2647.

 © 2005 Wiley-VCH Verlag GmbH & Co. KGaA, Weinheim

Mesoporous Materials

Single-Crystal Mesoporous Silica Ribbons**

*Jianfang Wang, Chia-Kuang Tsung, Ryan C. Hayward, Yiying Wu, and Galen D. Stucky**

Mesoporous materials have many present and potential future applications for catalysis, chemical and biological separations, chromatography, photonic and electronic devices, drug delivery, and energy storage.[1] They are typically synthesized with amphiphilic organic molecules as templates through the cooperative assembly between these molecules and inorganic species. Since their discovery, control of ordered mesoporous structures and pore sizes has been widely investigated by changing synthetic conditions and by using different types of amphiphiles, including small charged surfactant molecules and large block copolymers. Meanwhile, progress has also been made in the assembly of surfactant molecules and inorganic species into mesoporous materials with a wealth of morphological shapes and internal pore architectures, such as spheres,[2] gyroids,[3] fibers,[4–6] tubules,[7] and thin films,[8] for a variety of applications. Furthermore, cooperative assembly between inorganic and organic components has recently become an exciting approach for the development of novel multifunctional materials.[9]

Ribbon-shaped one-dimensional nanostructures made of transition metals,[10] transition metal oxides,[11] and II–VI semiconductor compounds[12] have been extensively investigated owing to their distinctive geometries, novel physical and chemical properties, and potential applications in magnetic, electronic, and photonic devices. These inorganic ribbons are prepared by using either a vapor–solid or a solution–solid process. They exhibit the same crystallographic structures as the corresponding bulk materials and are usually enclosed by low-index facets with rectangular cross sections. Here, we report the synthesis of single-crystal mesoporous silica ribbons by using small cationic surfactant molecules. These ribbons have tracklike pore channels that are oriented perpendicular to the length of the ribbon and are hexagonally

[*] Dr. J. Wang, C.-K. Tsung, Dr. Y. Wu, Prof. G. D. Stucky
Mitsubishi Chemical Center for Advanced Materials
Department of Chemistry and Biochemistry
University of California
Santa Barbara, CA 93106 (USA)
Fax: (+1) 805-893-4120
E-mail: stucky@chem.ucsb.edu
R. C. Hayward
Department of Chemical Engineering
University of California
Santa Barbara, CA 93106 (USA)

[**] This work was supported by Mitsubishi Chemical Center for Advanced Materials, the National Science Foundation (award No. DMR 01-20967), and an IBM faculty award to G. D. Stucky and made use of MRL Central Facilities supported by the MRSEC Program of the National Science Foundation (award No. DMR 00-80034). We gratefully acknowledge the assistance provided by Peter Allen in the artistic illustration of the internal pore architecture of the mesoporous ribbons.

 © 2005 Wiley-VCH Verlag GmbH & Co. KGaA, Weinheim DOI: 10.1002/anie.200461296

packed together. The internal pore architecture of these ribbons is significantly different from the two-dimensional hexagonal mesostructure. Previously, helically twisted silica ribbons were prepared with a chiral phospholipid, but they have a lamellar mesostructure that collapses upon calcination.[13] Furthermore, silica ribbons with hexagonal mesoporous structures have been prepared with electrospinning, but the organization of their pore channels is polycrystal-like with the pore channels in different domains oriented randomly.[14] To the best of our knowledge, there have been no reports on the formation of single-crystal-like mesostructured silica ribbons with highly organized pore channels remaining after calcination.

In the past, a two-phase route has been used to synthesize one-dimensional mesostructured silica materials with silica precursor molecules dissolved in an oil phase and surfactant molecules dissolved in a separate water phase.[4,15] The morphologies and internal pore architectures of the resulting mesostructured products depend strongly on the supply of silica precursor molecules that diffuse from the oil phase through the interface to the water phase.

In contrast, we believe that a one-phase synthesis procedure carried out in dilute aqueous solutions of surfactant molecules and hydrolyzed silica species might be used to reduce the nucleation and growth rates of mesostructured products. By this procedure, their morphological shapes and internal pore architectures would be largely determined by the cooperative assembly between silica species and surfactant molecules in a single aqueous growth solution. With this in mind, we have developed a one-phase route to synthesize one-dimensional mesostructured silica materials with cationic hexadecyltrimethylammonium or hexadecylpyridinium surfactants as templates and tetraethyl orthosilicate (TEOS) as a silica precursor under acidic conditions. This approach has been used to selectively synthesize either mesostructured silica nanofibers that have hexagonal fiber cross sections with pore channels aligned parallel to the fiber axis or mesostructured silica fibers that have circular fiber cross sections with pore channels wound circularly around the fiber axis with an acid concentration of approximately 4.0 M.[6] The one-phase route can readily expand the kinetic control range of synthetic parameters, including the concentration of the acid, temperature, concentrations of the surfactant and the silica precursor, and the type of surfactant, and it has the potential to allow the synthesis of more complicated mesostructured configurations. Indeed, we found that the one-phase synthesis with an acid concentration in the range of 1.0–2.0 M led to the formation of one-dimensional mesostructured silica materials that were all in the form of ribbons.

After the one-phase synthesis, fiberlike flocculates were seen suspended in the growth solutions. Scanning electron microscopy (SEM) images taken of the flocculates, which were isolated, washed with distilled water, and dried, indicate that they consist of a large quantity of fiberlike structures with typical lengths of the order of several hundreds of micrometers (Figure 1a). SEM imaging at higher magnifications reveals that the geometrical shape of the silica fiberlike structures is a ribbon (Figure 1a, inset), which is clearly distinct from the shape of the previously reported mesostructured fibers.[4–6] Each silica ribbon has a relatively uniform width along its entire length, and the typical widths of the ribbons are in the range of 0.4–1.5 μm. Some ribbons were seen twisted along both their length and width axes, which suggests that as-synthesized mesostructured silica ribbons have a low bending stiffness. Low-angle X-ray diffraction (XRD) measurements show that the as-synthesized ribbon sample exhibits two diffraction peaks, which remain after calcination (Figure 1b), indicating that these ribbons are ordered mesostructures. The diffraction patterns can be indexed according to a two-dimensional hexagonal lattice. The determined lattice constant for the as-synthesized ribbons is $a = 4.7$ nm, which reduces to $a = 4.3$ nm after calcination.

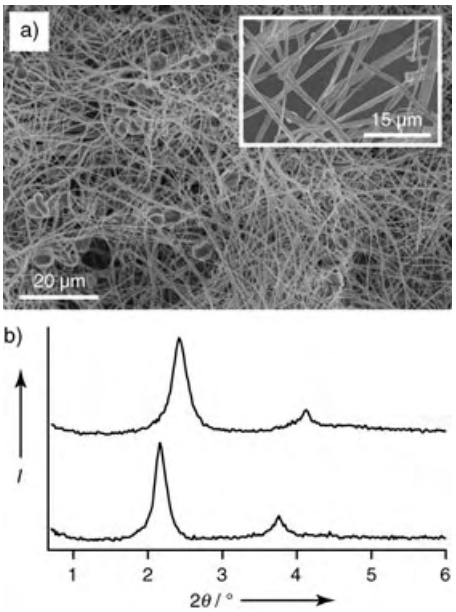


Figure 1. Mesoporous silica ribbons. a) SEM image of the mesostructured ribbons synthesized with hexadecylpyridinium bromide (C_{16}PB) surfactant. Inset: a magnified SEM image showing clearly the ribbon shape of the synthesized products. b) Low-angle XRD patterns recorded on the as-synthesized (lower; $d(100) = 4.09$ nm, $d(110) = 2.35$ nm, $a = 4.7$ nm) and calcined (upper; $d(100) = 3.65$ nm, $d(110) = 2.15$ nm, $a = 4.3$ nm) ribbons.

Low-magnification transmission electron microscopy (TEM) images confirm that the geometrical shape of the fiberlike structures is a ribbon (Figure 2a) and that each ribbon has a uniform width along its length (Figure 2b). From the TEM images taken at high magnifications of the individual ribbons that are flat and straight, hexagonally packed pore channels are observed at the edge of each ribbon, whereas parallel fringes oriented perpendicular to the length of the ribbon are observed in the central region of the ribbon (Figure 2c). In fact, the hexagonally packed pore channels are visible at both the left and right edges of each ribbon. Moreover, the hexagonally packed pore channels at the edges and the parallel fringes in the central region can be seen over the entire length of the individual ribbons that are straight and untwisted, which demonstrates that these ribbons are structurally uniform.

 © 2005 Wiley-VCH Verlag GmbH & Co. KGaA, Weinheim

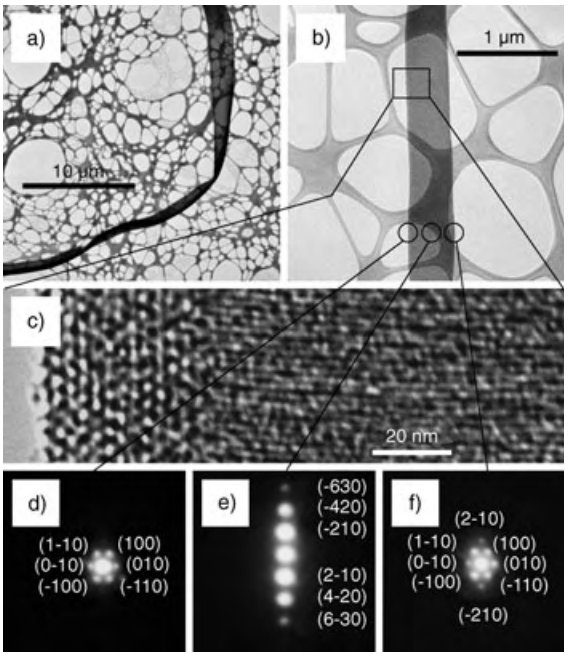


Figure 2. TEM images of mesoporous silica ribbons showing their geometrical shape and internal pore architecture. The ribbons were synthesized with C_{16}PB surfactant and calcined. a) TEM image of a twisted ribbon that shows the characteristic ribbon shape. b) TEM image of a straight ribbon that shows a uniform width along its length. c) Zoomed-in TEM image of the boxed area in Figure 2b that shows hexagonally packed pore channels at the edge and parallel fringes oriented perpendicular to the length of the ribbon in the central region of the ribbon. d)–f) Selected-area electron diffraction patterns taken at the left edge, in the central region, and at the right edge, respectively, of the ribbon shown in Figure 2b. The diffraction patterns are indexed according to a two-dimensional hexagonal lattice. The zone axes for Figure 2, d–f, are [001], [120], and [001], respectively.

The organization of the pore channels in the mesoporous silica ribbons is also revealed by the selected-area electron diffraction patterns recorded at the edges and in the central region of the individual ribbons. Hexagonal diffraction patterns are observed at the edges (Figure 2, d and f) and a string of diffraction spots are obtained in the central region (Figure 2e) which indicates that each mesoporous ribbon is single-crystalline. The diffraction patterns recorded at the edges and in the central region can be indexed separately according to a two-dimensional hexagonal lattice, with zone axes [001] and [120], respectively.

To further verify the morphological characteristics and ascertain the internal pore architecture of the mesoporous silica ribbons, we performed microtoming to cut thin cross-sectional slices of the ribbons. Figure 3, a and c show the TEM images of the cross sections that are perpendicular to the length of the ribbon. These cross sections are semicircular at the edges and rectangular in the central region. The cross-sectional TEM images at higher magnifications reveal that the pore channels in the central region are aligned parallel to the width of the ribbon (Figure 3b) and those at the edges curve around semicircularly (Figure 3d). These pore channels appear to be tracklike, and the curvatures of the pore channels from outside to inside at the edges become increasingly larger. The pore channels that are close to the central region curve back to make sharp turns of 180° and the innermost channel becomes a single straight pore channel. Furthermore, we also observed cross sections that are parallel to the length of the ribbon (Figure 3, e and f) as judged on the basis of the cross-sectional size and the organization of the pore channels. With this viewing configuration, hexagonally packed pore channels aligned parallel to the width of the ribbon are observed.

Taking together all of the structural observations of the mesoporous ribbons, including selected-area electron diffraction patterns and high-magnification TEM images recorded from different viewing directions, we have constructed a three-dimensional model of the internal pore architecture of the mesoporous silica ribbons (Figure 4). Each ribbon is composed of a large number of tracklike pore channels that are oriented perpendicular to the length of the ribbon and are hexagonally packed together. For a ribbon with a thickness of 120 nm, a width of 800 nm, and a length of 100 μm, which are the typical dimensions of these mesoporous ribbons, it is estimated that there are about 4×10^5 tracklike pore channels with perimeters in the range of 1 to 2 μm. It is remarkable that such a large number of the pore channels with a uniform pore size and varying perimeters can assemble together with such high order to form a mesoporous ribbon.

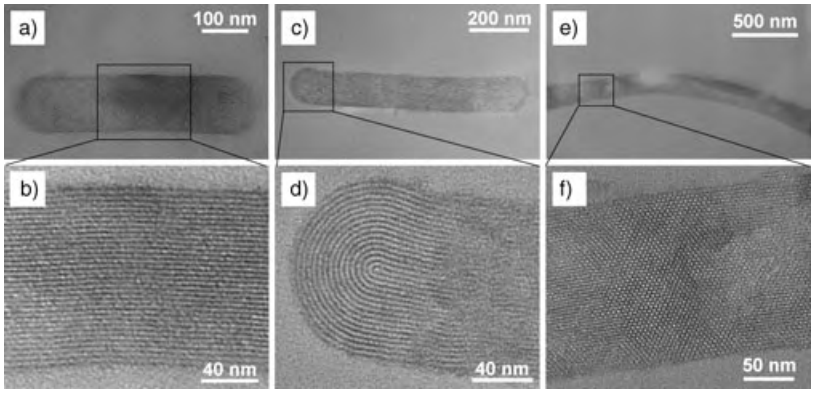


Figure 3. Cross-sectional TEM images of mesoporous silica ribbons showing their geometrical shape and internal pore architecture. The ribbons were synthesized with C_{16}PB surfactant and calcined. a) TEM image of a cross section that is perpendicular to the length of the ribbon. The ribbon has a width-to-thickness ratio of approximately 4.3. b) Zoomed-in TEM image of the boxed area in Figure 3a that shows parallel pore channels in the central region of the ribbon. c) TEM image of a cross section that is perpendicular to the length of the ribbon. The ribbon has a width-to-thickness ratio of about 7.0. d) Zoomed-in TEM image of the boxed area in Figure 3c that shows pore channels curving back at the edge of the ribbon. e) TEM image of a cross section that is parallel to the length of the ribbon. Only a short segment is shown here: the actual length of the ribbon is more than 10 μm. f) Zoomed-in TEM image of the boxed area in Figure 3e that shows hexagonally packed pore channels. The occurrence of blurred lattice structures in some regions of the ribbons is probably due to the nonuniform distribution of strain induced by microtoming.

 © 2005 Wiley-VCH Verlag GmbH & Co. KGaA, Weinheim

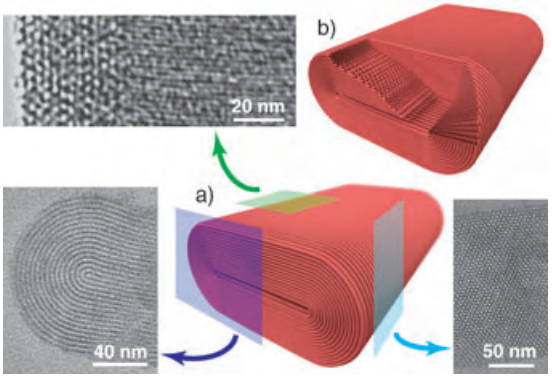


Figure 4. Three-dimensional model of the pore structure of individual mesoporous silica ribbons. a) Overview with overlapping planes showing the relationship between recorded TEM images and different viewing directions relative to the ribbon. b) A portion is cut away to show the internal pore architecture.

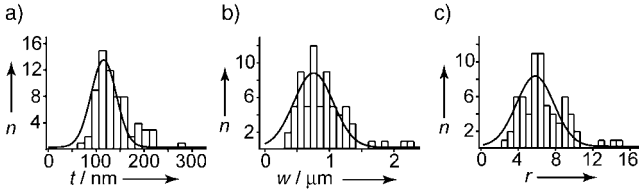


Figure 5. Size distributions of the calcined mesoporous silica ribbons synthesized with C_{16}PB surfactant: a) thickness (t), b) width (w), and c) width-to-thickness ratio (r). The number of counted ribbons is 68.

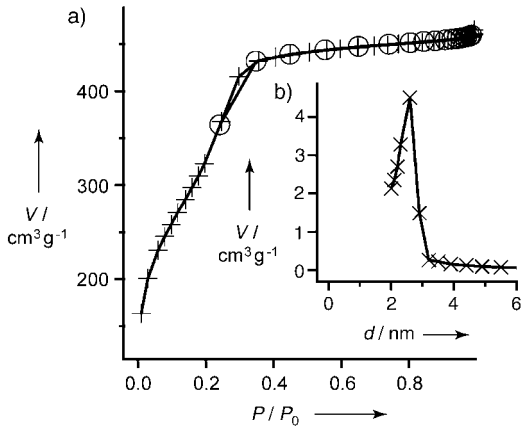


Figure 6. Nitrogen adsorption–desorption measurements of mesoporous silica ribbons obtained with C_{16}PB surfactant. a) Sorption isotherms (+ = adsorption, ○ = desorption). b) BJH pore size distribution obtained from the adsorption branch (d = diameter).

According to the three-dimensional model, hexagonally packed pore channels at the edges and parallel fringes in the central region are visible under TEM imaging when a mesoporous ribbon that stays flat and straight is viewed normal to its flat portion. The top and bottom surfaces of the flat portion of the ribbon are enclosed by ±(010) facets. On the basis of the organization of the pore channels as shown in Figure 4, the spacing between the neighboring parallel fringes in the central region should be half of the hexagonal lattice constant at the edges, which is in excellent agreement with the measurements made by using the TEM images as shown in Figure 2c. Furthermore, it can be seen from the model that tracklike pore channels are visible on the cross sections that are perpendicular to the length of the ribbon, and hexagonally packed pore channels are visible on the cross sections that are parallel to the length of the ribbon, which is also in agreement with our observations from TEM.

The internal pore architecture of the mesoporous silica ribbons is not a simple truncation of the two-dimensional hexagonal mesostructure. As described above, the pore channels in the mesoporous ribbons are curved at the edges with a tracklike conformation. Unlike the transition metal oxide ribbons, which are enclosed by low-index facets and have rectangular cross sections,[11] the mesoporous silica ribbons have smooth external surfaces without sharp edges. There have been no reported materials that exhibit such structures. The closest structural analogy are ribbons obtained from the spontaneous hierarchical self-assembly of highly charged cytoskeletal filamentous actin and cationic lipid membranes.[16] These ribbons also exhibit tracklike cross sections, but are composed of folded two-dimensional lipid bilayers sandwiched between two layers of actin.

The size distributions of the mesoporous silica ribbons were measured from the cross-sectional TEM images taken on microtomed samples (Figure 5). The ribbons have an average thickness of (120 ± 30) nm, an average width of (0.8 ± 0.3) μm, and an average width-to-thickness ratio of (6 ± 2).

The nitrogen adsorption–desorption isotherms measured at −196 °C for the calcined mesoporous silica ribbons are shown in Figure 6a. The isotherms can be classified as type IV isotherms without hysteresis. The ribbons exhibit a nitrogen Brunauer–Emmett–Teller (BET) surface area of 1200 $m^2 g^{-1}$, and the single-point total desorption pore volume at a relative pressure of 0.98 is 0.71 $cm^3 g^{-1}$. The Barrett–Joyner–Halenda (BJH) pore size distribution plot (Figure 6b) determined from the adsorption branch shows a sharp peak at 2.6 nm with a full width at half maximum (FWHM) of 0.8 nm.

In summary, single-crystal mesoporous silica ribbons that are 50–250 nm thick, 0.4–1.5 μm wide, and hundreds of micrometers long have been synthesized by using a one-phase route in dilute aqueous solutions of surfactants and silica species under acidic conditions. The mesoporous ribbons have excellent long-range order with tracklike pore channels oriented perpendicular to the length of the ribbon and hexagonally organized. Our one-phase route to the selective synthesis of one-dimensional mesostructured silica ribbons, together with our previously reported mesostructured silica nanofibers with controlled cross-sectional shapes and internal pore architectures,[6] provides a relatively simple reaction system for further developing theoretical models for the cooperative assembly between inorganic and organic components. Understanding the thermodynamics and growth kinetics involved in the formation of the mesostructured materials of particular morphological shapes and internal pore architectures can further help in creating novel inorganic–organic hybrid functional materials with desired hierarchical structures through the cooperative assembly between inorganic and organic building components.[9]

 © 2005 Wiley-VCH Verlag GmbH & Co. KGaA, Weinheim

Experimental Section

Mesostructured silica ribbons were prepared with cationic hexadecyltrimethylammonium or hexadecylpyridinium surfactants and TEOS (tetraethyl orthosilicate) silica precursor. In a typical synthesis batch with C_{16}PB (hexadecylpyridinium bromide) surfactant, a 37 wt% solution of HCl (6.51 g) was mixed with distilled water (43.49 g), and C_{16}PB (0.21 g) was dissolved into this mixture. The resulting solution was stirred until the surfactant molecules were dissolved completely. TEOS (177 μL) was then added. After the solution was stirred at room temperature for 10 min, it was transferred to a 60 mL glass vessel. The vessel was closed and kept in an isothermal oven at approximately 65 °C for 2 days. Within this period of time, fiberlike flocculates suspended in the solution were observed. The flocculates were removed after growth, washed with distilled water, and dried at 100 °C in air. The yield of mesostructured ribbons from each synthesis was estimated to be about 25 wt%. To remove cationic surfactants, dried ribbon samples were calcined in a box furnace in air at 500 °C for 5 h, with a ramp rate of 1 °C min^{-1}. We found that mesostructured silica ribbons can only be synthesized within a certain range of concentration of HCl. The reaction composition with which ribbons can be obtained for C_{16}PB is 100 H_2O:2.0–3.5 HCl:0.02 C_{16}PB:0.03 TEOS (in molar ratio). Furthermore, mesostructured ribbons can also be obtained from the syntheses with hexadecyltrimethylammonium chloride (C_{16}TMAC), hexadecyltrimethylammonium bromide (C_{16}TMAB), and hexadecylpyridinium chloride (C_{16}PC) surfactants. The reaction compositions using C_{16}TMAC, C_{16}TMAB, and C_{16}PC for producing mesostructured ribbons are 100 H_2O:1.5–2.5 HCl:0.02 C_{16}TMAC:0.03 TEOS, 100 H_2O:1.5–2.5 HCl:0.02 C_{16}TMAB:0.03 TEOS, and 100 H_2O:2.0–3.5 HCl:0.02 C_{16}PC:0.03 TEOS, respectively. In contrast, ribbons were not obtained from syntheses that involved trimethylammonium surfactants with dodecyl, tetradecyl, or octadecyl hydrophobic tails. Low-angle XRD patterns with a step of 0.02° and time-per-step of 2 s were obtained on a Scintag PADX diffractometer by using Cu K_α radiation. SEM studies were performed on a JEOL 6340F microscope operating at 2–5 keV. TEM studies were carried out on a JEOL 2010 microscope operating at 200 keV. Silica ribbon samples were dispersed into ethanol and then deposited onto either silicon wafers or copper grids coated with carbon-stabilized lacey formvar for SEM or TEM imaging, respectively. To obtain cross-sectional TEM images, ribbon samples were embedded into a thermocurable resin (Eponate 12 kit, Ted Pella) and kept at 60 °C overnight. The embedded ribbon samples were then microtomed into thin slices of around 70 nm thickness, which were transferred onto bare copper grids for TEM observations. Nitrogen adsorption and desorption isotherms were measured using a Micromeritics TriStar 3000 system at liquid nitrogen temperature (−196 °C) after the samples were degassed with flowing nitrogen at 200 °C overnight.

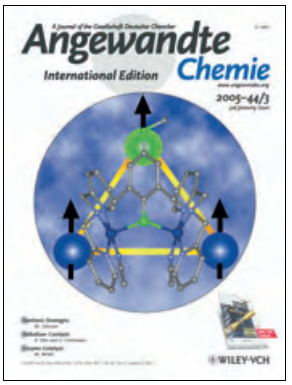
Received: July 13, 2004

Keywords: cooperative effects · mesoporous materials · silicates · surfactants · template synthesis

[1] M. E. Davis, *Nature* **2002**, *417*, 813 – 821.
[2] a) Y. F. Lu, H. Y. Fan, A. Stump, T. L. Ward, T. Rieker, C. J. Brinker, *Nature* **1999**, *398*, 223 – 226; b) C. E. Fowler, D. Khushalani, B. Lebeau, S. Mann, *Adv. Mater.* **2001**, *13*, 649 – 652.
[3] H. Yang, N. Coombs, G. A. Ozin, *Nature* **1997**, *386*, 692 – 695.
[4] a) Q. S. Huo, D. Y. Zhao, J. L. Feng, K. Weston, S. K. Buratto, G. D. Stucky, S. Schacht, F. Schüth, *Adv. Mater.* **1997**, *9*, 974 – 978; b) F. Marlow, B. Spliethoff, B. Tesche, D. Y. Zhao, *Adv. Mater.* **2000**, *12*, 961 – 965; c) F. Kleitz, F. Marlow, G. D. Stucky, F. Schüth, *Chem. Mater.* **2001**, *13*, 3587 – 3595.
[5] Z. L. Yang, Z. W. Niu, X. Y. Cao, Z. Z. Yang, Y. F. Lu, Z. B. Hu, C. C. Han, *Angew. Chem.* **2003**, *115*, 4333 – 4335; *Angew. Chem. Int. Ed.* **2003**, *42*, 4201 – 4203.
[6] J. F. Wang, J. P. Zhang, B. Y. Asoo, G. D. Stucky, *J. Am. Chem. Soc.* **2003**, *125*, 13966 – 13967.
[7] H.-P. Lin, C.-Y. Mou, *Science* **1996**, *273*, 765 – 768.
[8] a) H. Yang, N. Coombs, I. Sokolov, G. A. Ozin, *Nature* **1996**, *381*, 589 – 592; b) Y. F. Lu, R. Ganguli, C. A. Drewien, M. T. Anderson, C. J. Brinker, W. L. Gong, Y. X. Guo, H. Soyez, B. Dunn, M. H. Huang, J. I. Zink, *Nature* **1997**, *389*, 364 – 368.
[9] a) S. Park, J.-H. Lim, S.-W. Chung, C. A. Mirkin, *Science* **2004**, *303*, 348 – 351; b) H. Y. Fan, K. Yang, D. M. Boye, T. Sigmon, K. J. Malloy, H. F. Xu, G. P. López, C. J. Brinker, *Science* **2004**, *304*, 567 – 571; c) J. F. Wang, G. D. Stucky, *Adv. Funct. Mater.* **2004**, *14*, 409 – 415.
[10] Z. P. Liu, S. Li, Y. Yang, S. Peng, Z. K. Hu, Y. T. Qian, *Adv. Mater.* **2003**, *15*, 1946 – 1948.
[11] a) Z. W. Pan, Z. R. Dai, Z. L. Wang, *Science* **2001**, *291*, 1947 – 1949; b) X. Y. Kong, Z. L. Wang, *Nano Lett.* **2003**, *3*, 1625 – 1631; c) X. Y. Kong, Y. Ding, R. Yang, Z. L. Wang, *Science* **2004**, *303*, 1348 – 1351; d) J. G. Yu, J. C. Yu, W. K. Ho, L. Wu, X. C. Wang, *J. Am. Chem. Soc.* **2004**, *126*, 3422 – 3423; e) M. Law, D. J. Sirbuly, J. C. Johnson, J. Goldberger, R. J. Saykally, P. D. Yang, *Science* **2004**, *305*, 1269 – 1273.
[12] C. Ma, Y. Ding, D. Moore, X. D. Wang, Z. L. Wang, *J. Am. Chem. Soc.* **2004**, *126*, 708 – 709.
[13] A. M. Seddon, H. M. Patel, S. L. Burkett, S. Mann, *Angew. Chem.* **2002**, *114*, 3114 – 3117; *Angew. Chem. Int. Ed.* **2002**, *41*, 2988 – 2991.
[14] G. Larsen, S. Noriega, R. Spretz, R. Velarde-Ortiz, *J. Mater. Chem.* **2004**, *14*, 2372 – 2373.
[15] S. Schacht, Q. Huo, I. G. Voigt-Martin, G. D. Stucky, F. Schüth, *Science* **1996**, *273*, 768 – 771.
[16] G. C. L. Wong, J. X. Tang, A. Lin, Y. L. Li, P. A. Janmey, C. R. Safinya, *Science* **2000**, *288*, 2035 – 2039.

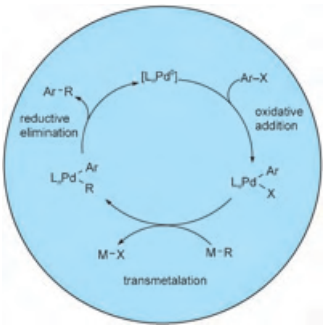
 © 2005 Wiley-VCH Verlag GmbH & Co. KGaA, Weinheim

Cover Picture

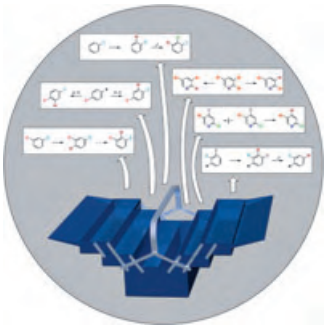


Fabien Michel, Stéphane Torelli, Fabrice Thomas,* Carole Duboc, Christian Philouze, Catherine Belle, Sylvain Hamman, Eric Saint-Aman, and Jean-Louis Pierre

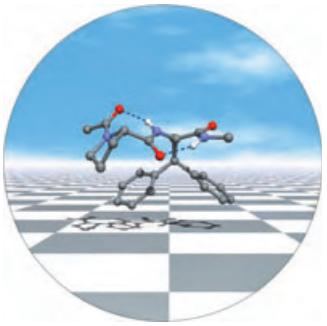
Metal–radical interactions are at the heart of many biocatalysts that contain transition metals. The cover picture shows the structure of a dicopper(II) complex in which a phenoxyl radical bridges the metal centers. The three spins are ferromagnetically coupled, as the black arrows indicate. In their Communication on page 438 ff., F. Thomas and co-workers describe the synthesis, structure, and properties of this type of complex. The stability and reactivity are dictated by the nuclearity of the complex and the nature of the coordinating solvent.



Palladium Catalysts
In the Minireview on page 366 ff., R. Vilar and U. Christmann summarize the latest advances in the development of Pd complexes, in particular with carbenes and phosphines as supporting ligands, as catalytic systems for cross-coupling reactions.



Synthesis Strategies
A "toolbox of methods" based on halogen–metal exchange of aromatic substrates leads to the regiochemically exhaustive functionalization of valuable building blocks. This concept is introduced by M. Schlosser in his Review on page 376 ff.



Peptide Structures
A. I. Jiménez et al. report in their Communication on page 396 ff. their observation of two consecutive γ turns in a crystalline linear dipeptide through analysis of the solid-state conformations.

Contents

VIP ***The following Communications have been judged by at least two referees to be "very important papers" and will be published online at www.angewandte.org soon:***

D. Enders, C. Grondal*
Direct Organocatalytic de novo Synthesis of Carbohydrates

*T. Fink, H. Bruggesser, J.-L. Reymond**
Virtual Exploration of the Small-Molecule Chemical Universe Below 160 Daltons

S. Kobayashi, K. Arai, H. Shimizu, Y. Ihori, H. Ishitani, Y. Yamashita*
A Bimetallic Chiral Niobium Complex for Lewis Acid Catalyzed Enantioselective Reactions: Design of a Tridentate Ligand and Elucidation of the Catalyst Structure

H. Braunschweig, K. Radacki, D. Rais, G. R. Whittell*
The First Boryl-Bridged Complex: An Unprecedented Coordination Mode of the BR_2 Ligand

C. Whitehouse, J. Fang, A. Aggeli, M. Bell, R. Brydson, C. W. G. Fishwick, J. Henderson, C. M. Knobler, R. W. Owens, N. H. Thomson, D. A. Smith, N. Boden**
Adsorption and Self-Assembly of Peptides on Mica Substrates

*You Seok Seo, C. Lee, K. H. Lee, K. B. Yoon**
1:1 and 2:1 Charge-Transfer Interactions between Aromatic Hydrocarbons and Dry Titanium Dioxide

News

S. John and G. Ozin Receive Brockhouse Canada Prize ——— **358**

Polymer Award to C. J. Hawker ——— **358**

Noyori Prize to D. Seebach ——— **358**

Books

Catalysis and Electrocatalysis at Nanoparticle Surfaces — Andrzej Wieckowski, Elena R. Savinova, Constantinos G. Vayenas — *reviewed by R. Imbihl* ——— ***359***

Calculation of NMR and EPR Parameters — Martinin Kaupp, Michael Bühl, Vladimir G. Malkin — *reviewed by C. Ochsenfeld* ——— ***359***

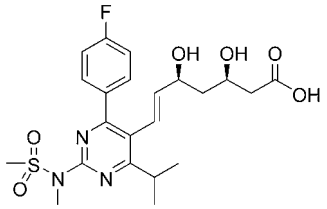
Organometallics in Process Chemistry — Robert D. Larsen — *reviewed by M. Bröring* ——— ***360***

Highlights

Enzyme Catalysis

M. Müller* ——— **362 – 365**

Chemoenzymatic Synthesis of Building Blocks for Statin Side Chains



Biocatalysis: Enzymatic transformations have become competitive methods for the synthesis of complex organic compounds. The wide range of possibilities offered by biocatalysis for the synthesis of target molecules are highlighted based on the example of the statins. This class of compounds, which includes rosuvastatin (see picture), are good inhibitors of cholesterol synthesis and dominate the market for cholesterol-lowering drugs.

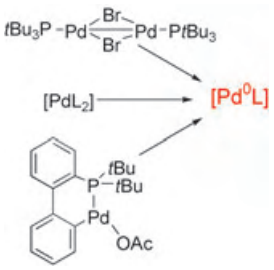
Minireviews

Palladium Catalysts

U. Christmann, R. Vilar* ——— **366 – 374**

Monoligated Palladium Species as Catalysts in Cross-Coupling Reactions

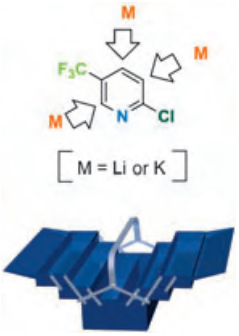
A matter of size: Lately, new catalysts based on complexes of palladium with electron-rich and bulky ligands have been developed for the activation of less-reactive aryl chlorides in cross-coupling reactions to generate C–E bonds (E = C, N, O, S). The enhanced reactivity of the catalysts is attributed to the formation of unsaturated [Pd^0L] species (see scheme; L = phosphines or carbenes).



© 2005 Wiley-VCH Verlag GmbH & Co. KGaA, Weinheim

Reviews

Like a wildcard in a card game, the introduction of a metal into aromatic or heterocyclic building blocks ensures a maximum of target flexibility in the synthesis (see scheme). It can be replaced with a wide range of electrophiles and thus offers a convenient access to virtually any functionalized derivative. The ultimate objective of this "toolbox" approach is not to miss any structural opportunity inherent in a new substituent pattern.

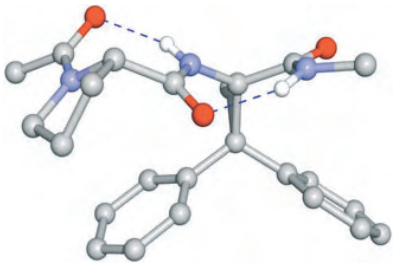


Synthesis Strategies

M. Schlosser* ——— **376 – 393**

The 2×3 Toolbox of Organometallic Methods for Regiochemically Exhaustive Functionalization

Communications

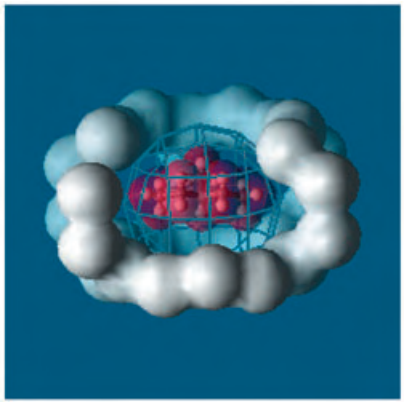


Which way to turn? For the very first time, a linear dipeptide has been shown to accommodate two consecutive γ turns in the solid state. An aminocyclopropane carboxylic acid has overridden the tendency of proline to induce a β-turn conformation in Pro-Xaa dipeptides (see X-ray crystal structure; blue: N, red: O, dashed lines show H bonds).

Peptide Structures

A. I. Jiménez,* G. Ballano, C. Cativiela ——— **396 – 399**

First Observation of Two Consecutive γ Turns in a Crystalline Linear Dipeptide



Yanking chains and rattling cages: Depending on their radius of gyration, molecules either retain or lose their ability to rotate inside zeolite cages (see picture). Such differences in rotational adsorption entropy result in a preferential uptake of branched alkanes over their linear structural isomers in zeolites such as MCM-22 which allows the separation of the two types of molecules.

Molecular Separations

J. F. M. Denayer,* R. A. Ocakoglu, I. C. Arik, C. E. A. Kirschhock, J. A. Martens, G. V. Baron —— **400 – 403**

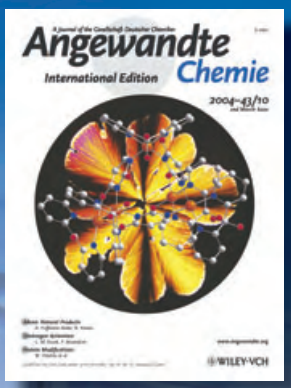
Rotational Entropy Driven Separation of Alkane/Isoalkane Mixtures in Zeolite Cages

For the USA and Canada:
ANGEWANDTE CHEMIE International Edition (ISSN 1433-7851) is published weekly by Wiley-VCH PO Box 191161, D 69451 Weinheim, Germany. Air freight and mailing in the USA by Publications Expediting Inc. 200 Meacham Ave., Elmont, NY 11003. Periodicals postage paid at Jamaica NY 11431. US POSTMASTER: send address changes to *Angewandte Chemie*, Wiley-VCH, 111 River Street, Hoboken, NJ 07030. Annual subscription price for institutions: US$ 4948.00/4498.00 (valid for print and electronic / print or electronic delivery); for individuals who are personal members of a national chemical society, or whose institution already subscribes, or who are retired or self-employed consultants, print only: US$ 394.00. Postage and handling charges included. All Wiley-VCH prices are exclusive VAT.

 © 2005 Wiley-VCH Verlag GmbH & Co. KGaA, Weinheim

The best in chemistry –

for more than a hundred years



A Journal of the Gesellschaft Deutscher Chemiker

Angewandte International Edition **Chemie**

www.angewandte.org

1888: ***The beginning of a success story***

Constant Innovations

1962: *First issue of the International Edition*
1976: *Graphical abstracts*
1979: *Cover pictures*
1988: *Centenary of Angewandte*
1989: *Routine use of color*
1991: *New section: Highlights*
1992: *Computerized editorial tracking system*
1995: *Internet service for readers*
1998: *Regular press service; full-text online*
2000: *New section: Essays; EarlyView: Communications available online ahead of the printed version*
2001: *New section: Minireviews*
2002: *Online submission of manuscripts*
2003: *Weekly publication; new section: News; new layout*
2004: *Backfiles (1962-1997); ManuscriptXpress: Online system for authors and referees*



Angewandte's advisors...

Seiji Shinkai
Kyushu University, Fukuoka

» ***Angewandte Chemie*** *is my favorite journal and I am honored to serve on its International Advisory Board. The research essence of an article can be understood rapidly because text and illustrations are finely harmonized. Furthermore, the high quality contents, which have a strong impact, are published very quickly.* «

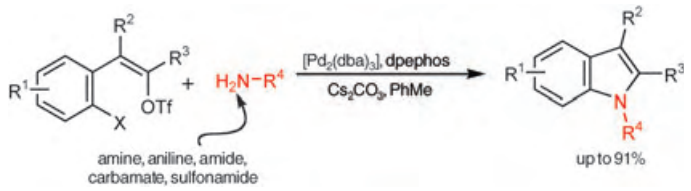
Angewandte Chemie International Edition *is a journal of the German Chemical Society (GDCh)*

GDCh

WILEY InterScience® DISCOVER SOMETHING GREAT

WILEY-VCH

1190104_gu

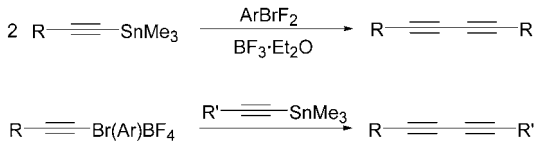


A single tandem operation allows rapid access to a variety of substituted N-functionalized indoles. The nitrogen atom of the indole nucleus is incorporated through Pd-catalyzed aryl and alkenyl C–N bond-forming reactions (see scheme; dba = dibenzylideneacetone). Amine, aniline, amide, carbamate, and sulfonamide functional groups can be introduced efficiently.

Nitrogen Heterocycles

M. C. Willis,* G. N. Brace, I. P. Holmes ——— 403 – 406

Palladium-Catalyzed Tandem Alkenyl and Aryl C–N Bond Formation: A Cascade N-Annulation Route to 1-Functionalized Indoles



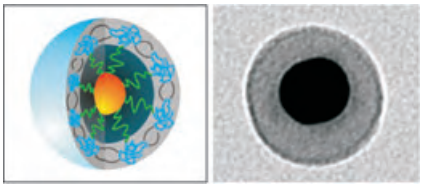
Symmetrical 1,3-diynes result from the oxidative homocoupling reaction of alkynylstannanes with an aryldifluoro-λ^3-bromane in the presence of $BF_3 \cdot Et_2O$ (see scheme, Ar = *p*-$CF_3C_6H_4$). The reaction involves a Michael addition of alkynylstannanes to the initially formed alkynyl-λ^3-bromanes. Cross-coupling of alkynyl-λ^3-bromanes with alkynylstannanes affords unsymmetrical 1,3-diynes (see scheme).

Synthetic Methods

M. Ochiai,* Y. Nishi, S. Goto, H. J. Frohn ——— 406 – 409

1-Alkynyl(aryl)(tetrafluoroborato)-λ^3-bromanes as Highly Efficient Michael Acceptors: Uncatalyzed Conjugate Addition of 1-Alkynyl(trialkyl)stannanes To Yield Symmetrical and Unsymmetrical 1,3-Butadiynes

Plated gold: Self-assembly of core/shell nanostructures occurs spontaneously when gold nanoparticles are combined with amphiphilic block copolymers. Polymer cross-linking then topologically fixes the composite nanostructure (see picture). The thickness of the polymer shell, as well as the optical and chemical properties of the composite nanostructure, are precisely determined by the

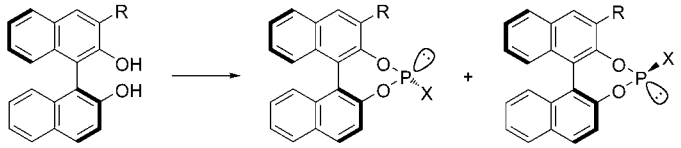


molecular characteristics of the assembled block copolymer.

Nanoparticles

Y. Kang, T. A. Taton* ——— 409 – 412

Core/Shell Gold Nanoparticles by Self-Assembly and Crosslinking of Micellar, Block-Copolymer Shells



Buried in the symmetry: Phosphorylation of *ortho*-substituted binol derivatives leads to monodentate phosphites (X = OR) or phosphoramidites (X = NR_2) having stereogenic centers at phosphorus (see scheme). Such compounds are excellent ligands in rhodium-catalyzed olefin-hydrogenation (95–99% *ee*) surpassing the C_2-symmetric parent ligands.

Asymmetric Catalysis

M. T. Reetz,* J.-A. Ma, R. Goddard ——— 412 – 415

Binol-Derived Monodentate Phosphites and Phosphoramidites with Phosphorus Stereogenic Centers: Novel Ligands for Transition-Metal Catalysis

 © 2005 Wiley-VCH Verlag GmbH & Co. KGaA, Weinheim

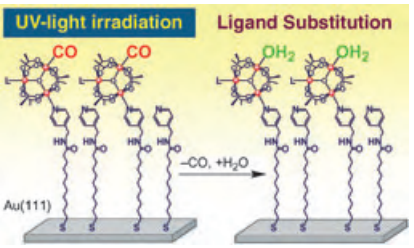
Contents

SAM Photochemistry

M. Abe,* T. Masuda, T. Kondo, K. Uosaki,* Y. Sasaki* ——— **416 – 419**

Photoconversion of a Redox-Active Self-Assembled Monolayer: In Situ Probing of Photoinduced CO Dissociation from a Triruthenium Cluster Center on Gold

Photoresponsive self-assembled monolayers (SAMs): Photoexcitation of a CO-bearing trinuclear ruthenium cluster assembled on an Au(111) electrode results in dissociation of CO to form a H_2O-terminated SAM (see picture). This is the first well-defined example of clean conversion of a redox-active molecular film by using light stimulus.

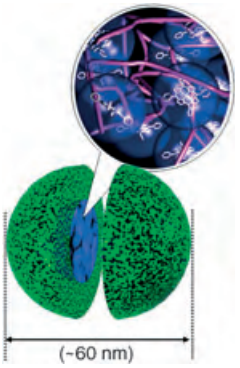


Drug Delivery

W.-D. Jang, N. Nishiyama, G.-D. Zhang, A. Harada, D.-L. Jiang, S. Kawauchi, Y. Morimoto, M. Kikuchi, H. Koyama, T. Aida, K. Kataoka* ——— **419 – 423**

Supramolecular Nanocarrier of Anionic Dendrimer Porphyrins with Cationic Block Copolymers Modified with Polyethylene Glycol to Enhance Intracellular Photodynamic Efficacy

Photo finish: A polymeric micelle system is formed in aqueous media by electrostatic assembly of an anionic dendrimeric porphyrin and a poly(ethylene glycol)–poly(L-lysine) block copolymer (see picture). The micelles exhibit high photocytotoxicity and stability. The hydrodynamic size (ca. 60 nm) makes this polymeric micelle system suitable for intravenous administration in photodynamic tumor therapy.

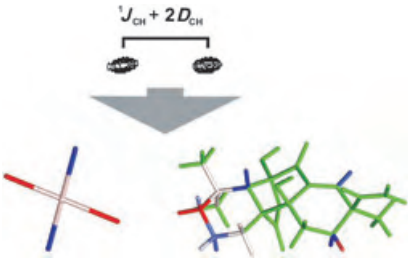


NMR Spectroscopic Methods (1)

J. C. Freudenberger, S. Knör, K. Kobzar, D. Heckmann, T. Paululat, H. Kessler, B. Luy* ——— **423 – 426**

Stretched Poly(vinyl acetate) Gels as NMR Alignment Media for the Measurement of Residual Dipolar Couplings in Polar Organic Solvents

Partial alignment of molecules in polar organic solvents for the measurement of residual dipolar couplings (RDCs) in high-resolution NMR spectroscopy can be achieved by stretched poly(vinyl acetate) gels. The method opens the door of RDC-derived structural information (e.g. from D_{CH} couplings, see picture) to new classes of molecules by closing the existing gap between apolar and aqueous solutions.

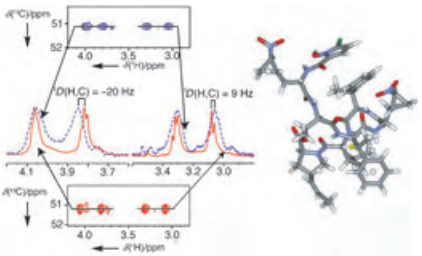


NMR Spectroscopic Methods (2)

P. Haberz, J. Farjon, C. Griesinger* ——— **427 – 429**

A DMSO-Compatible Orienting Medium: Towards the Investigation of the Stereochemistry of Natural Products

Organic molecules of different complexity are aligned by a DMSO-compatible gel in such a way that C–H dipolar couplings up to 29 Hz are observed. This paves the way to the simultaneous determination of conformation and configuration of organic compounds by NMR spectroscopy and thus enables the determination of the stereochemistry of natural products (e.g. hormaomycin, see picture) that cannot be crystallized.



Catalytic emulsion polymerization with a hydrophilic catalyst afforded extraordinarily small polyethylene particles of <20 nm size in the form of aqueous dispersions. The small size of the particles renders the dispersions transparent (see picture).

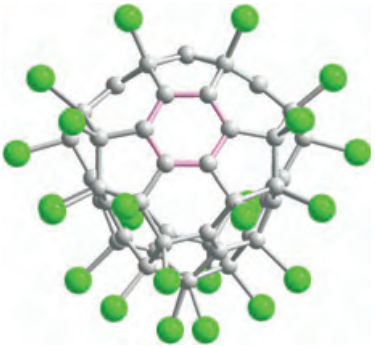


Polymers

L. Kolb, V. Monteil, R. Thomann, S. Mecking* ——— 429 – 432

Aqueous Dispersions of Extraordinarily Small Polyethylene Nanoparticles

On the way: Chlorination of C_{60} with ICl or VCl_4 results in the formation of two novel chlorofullerenes, C_1-$C_{60}Cl_{28}$ and C_2-$C_{60}Cl_{30}$, respectively, which comprise two aromatic rings and two chains of sp^3-hybridized carbon atoms that bear chlorine atoms (the picture shows $C_{60}Cl_{30}$; Cl green). These molecules are kinetically stable intermediates on the way from $C_{60}Cl_{24}$ to the thermodynamically stable D_{3d}-$C_{60}Cl_{30}$.

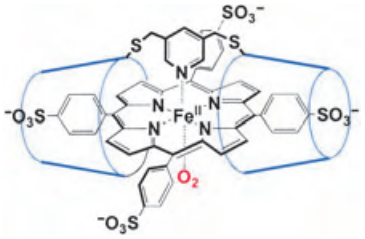


Fullerenes

S. I. Troyanov,* N. B. Shustova, A. A. Popov, L. N. Sidorov, E. Kemnitz ——— 432 – 435

Preparation and Structural Characterization of Two Kinetically Stable Chlorofullerenes, $C_{60}Cl_{28}$ and $C_{60}Cl_{30}$

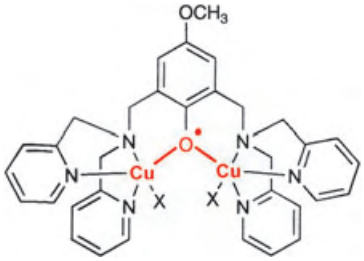
Reversible binding of dioxygen occurs in aqueous solution to a myoglobin model composed of a porphinato iron(II) compound and a per-*O*-methylated β-cyclodextrin dimer with a pyridine linker (see picture). The dioxygen affinity of this system is 17.5 ± 1.7 Torr and the half-life of the O_2 adduct is 30.1 h in phosphate buffer at pH 7 and 25 °C.



Supramolecular Chemistry

K. Kano,* H. Kitagishi, M. Kodera, S. Hirota ——— 435 – 438

Dioxygen Binding to a Simple Myoglobin Model in Aqueous Solution



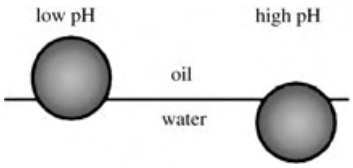
Cooperativity between metal centers and a bridging radical ligand, reflected by ferromagnetic exchange coupling, was studied with the dicopper complex shown. The stability, and thus the reactivity of the complex, is finely tuned by both the nuclearity of the complex and the nature of the coordinating solvent X.

Metal–Radical Complexes

VIP

F. Michel, S. Torelli, F. Thomas,* C. Duboc, C. Philouze, C. Belle, S. Hamman, E. Saint-Aman, J.-L. Pierre —— 438 – 441

An Unprecedented Bridging Phenoxyl Radical in Dicopper(II) Complexes: Evidence for an $S = \frac{3}{2}$ Spin State



Getting the right mix: Controlling the extent of the charge on the surfaces of carboxy-coated latex nanoparticles enables ultrastable oil-in-water and water-in-oil emulsions to be prepared. Emulsion inversion is simply achieved by changing the pH value (see picture) or salt concentration.

Nanostructures

B. P. Binks,* J. A. Rodrigues — 441 – 444

Inversion of Emulsions Stabilized Solely by Ionizable Nanoparticles

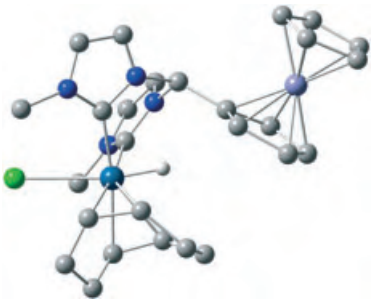
 © 2005 Wiley-VCH Verlag GmbH & Co. KGaA, Weinheim

Contents

Carbene Ligands

M. Viciano, E. Mas-Marzá, M. Poyatos, M. Sanaú, R. H. Crabtree, E. Peris* ——— 444 – 447

An N-Heterocyclic Carbene/Iridium Hydride Complex from the Oxidative Addition of a Ferrocenyl–Bisimidazolium Salt: Implications for Synthesis



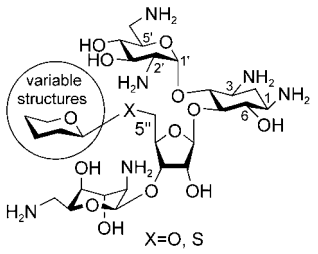
A ferrocenyl–imidazolium salt can be employed as a precursor to a stable [Ir^{III}(H)(biscarbene)] complex (see X-ray crystal structure) under very mild conditions. The study shows that the role of the base in the activation of the imidazolium salt may not just be a simple deprotonation of the precursor.

Aminoglycosides

M. Fridman, V. Belakhov, L. V. Lee, F.-S. Liang, C.-H. Wong,* T. Baasov* ——— 447 – 452

Dual Effect of Synthetic Aminoglycosides: Antibacterial Activity against *Bacillus anthracis* and Inhibition of Anthrax Lethal Factor

Defence against bioterrorism: Recent events have created an urgent need for therapeutic strategies to treat anthrax, an infectious disease caused by the toxigenic bacterium *Bacillus anthracis*. A new class of aminoglycosides (see picture) are powerful inhibitors under physiological conditions of the anthrax lethal factor, which has a major role in the disease, and function simultaneously as antibiotics against *B. anthracis*.

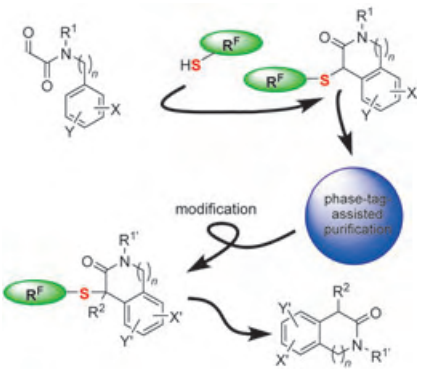


Fluorous-Phase Synthesis

L. A. McAllister, R. A. McCormick, S. Brand, D. J. Procter* ——— 452 – 455

A Fluorous-Phase Pummerer Cyclative-Capture Strategy for the Synthesis of Nitrogen Heterocycles

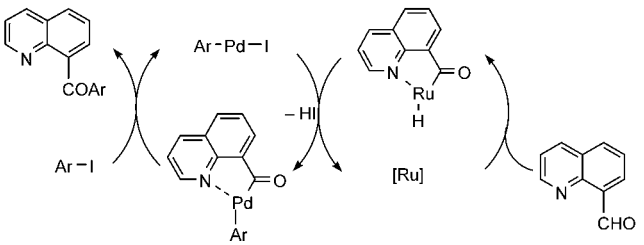
Catching on: Fluorous-tagged heterocyclic frameworks accessed rapidly through a Pummerer cyclative-capture approach can then be modified conveniently, for example, by Pd-catalyzed cross-coupling. Traceless, reductive cleavage of the fluorous phase tag completes a strategy for the high-throughput, fluorous-phase synthesis of N heterocycles (see scheme, $R^F = C_8F_{17}CH_2CH_2$).



Homogeneous Catalysis

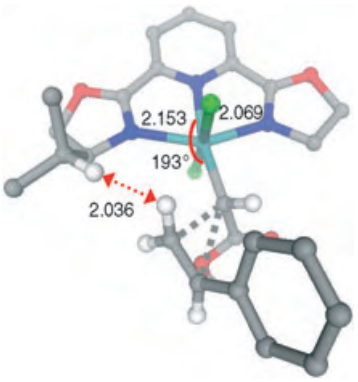
S. Ko, B. Kang, S. Chang* ——— 455 – 457

Cooperative Catalysis by Ru and Pd for the Direct Coupling of a Chelating Aldehyde with Iodoarenes or Organostannanes



Two is better than one: The combination of two metallic catalyst systems effects transformations that are difficult to carry out with any single-catalyst systems. This is demonstrated by the coupling of 8-quinolinecarboxaldehyde with a range of iodoarenes to give diaryl ketones (see picture) and its reaction with organostannanes to afford ketones.

© 2005 Wiley-VCH Verlag GmbH & Co. KGaA, Weinheim



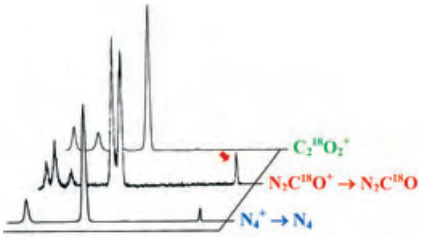
One stereogenic center suffices in pyridinebis(oxazoline) (pybox) ligands for efficient ruthenium-catalyzed cyclopropanation. A molecular-modeling study reveals the main origin of the enantioselectivity to be unfavorable steric interactions between the substituent on pybox and styrene in a *Si* approach to the carbene intermediate (see picture).

Molecular Modeling

A. Cornejo, J. M. Fraile, J. I. García,* M. J. Gil, V. Martínez-Merino, J. A. Mayoral, L. Salvatella — **458 – 461**

Asymmetric versus C_2-Symmetric Ligands: Origin of the Enantioselectivity in Ruthenium–Pybox-Catalyzed Cyclopropanation Reactions

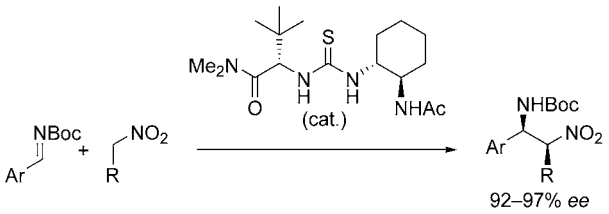
The missing link in the 28-electron family of open-chain N_4, N_2CO, and C_2O_2 molecules has been detected in the gas phase as an isolated, intact N_2CO species, whose lifetime exceeds 0.8 μs. The new metastable molecule has been prepared by neutralization–reionization mass spectrometry of labeled N_2CO^+ ions, which were generated in various N_2/CO ionized mixtures (see picture).



Metastable Molecules

G. de Petris,* F. Cacace, R. Cipollini, A. Cartoni, M. Rosi, A. Troiani — **462 – 465**

Experimental Detection of Theoretically Predicted N_2CO

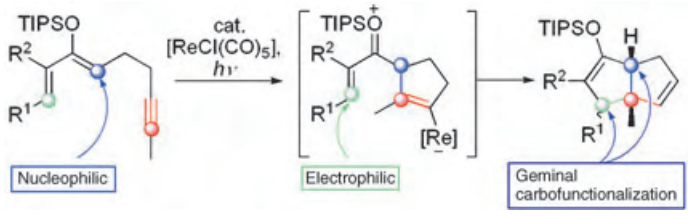


Approaching "privileged" status? A new and highly effective enantioselective catalyst for the nitro-Mannich reaction was identified by modification of thiourea-based Strecker catalysts (see scheme). Products are obtained in high enantiomeric purity and up to 16:1 diastereoselectivity.

Asymmetric Catalysis

T. P. Yoon, E. N. Jacobsen* — **466 – 468**

Highly Enantioselective Thiourea-Catalyzed Nitro-Mannich Reactions



Bicycle production: The low-valent rhenium complex $[ReCl(CO)_5]$ catalyzes a tandem intramolecular cyclization reaction of ω-acetylenic dienol silyl ethers. The alkyne undergoes a geminal carbofunctionalization in the presence of 0.5–3.0 mol% $[ReCl(CO)_5]$ under photoirradiation to give bicyclic enol silyl ethers in high yields (see scheme, TIPS = triisopropylsilyl).

Homogeneous Catalysis

H. Kusama, H. Yamabe, Y. Onizawa, T. Hoshino, N. Iwasawa* — **468 – 470**

Rhenium(I)-Catalyzed Intramolecular Geminal Carbofunctionalization of Alkynes: Tandem Cyclization of ω-Acetylenic Dienol Silyl Ethers

 © 2005 Wiley-VCH Verlag GmbH & Co. KGaA, Weinheim

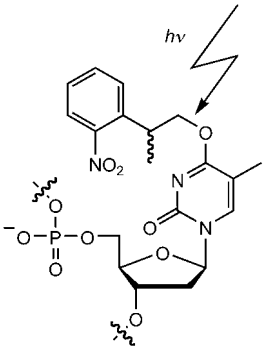
Contents

Bioorganic Chemistry

L. Kröck, A. Heckel* ——— **471 – 473**

Photoinduced Transcription by Using Temporarily Mismatched Caged Oligonucleotides

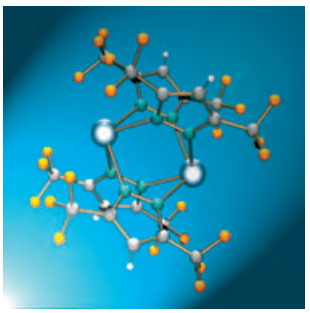
Spatial and temporal control of the function of DNA with light: In oligonucleotides, protected ("caged") thymidine can act as a temporary mismatch in base pairing and, for example, prevent transcription. The photolabile caging group can be removed by light (see picture), fully restoring an intact DNA strand.



Tin Complexes

F. Breher,* H. Rüegger ——— **473 – 477**

Distannenes Turned Inside Out: Bis(stannylenes) with an Unusual Structural Motif

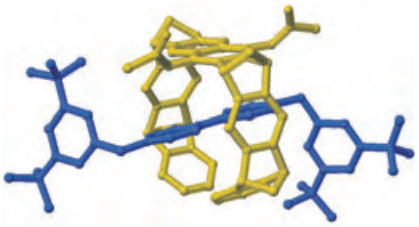


Alkene analogues: Simple acid–base reactions of $[Sn\{N(SiMe_3)_2\}_2]$ with 3,5-substituted pyrazoles, H(3,5-R_2pz) ($R = CF_3$ and CMe_3), give the homoleptic tin(II) pyrazolyl compounds, $[\{Sn(3,5\text{-}R_2pz)_2\}_2]$. Owing to additional N-donor functionalities in the tin-bound ligand the two stannylene entities dimerize in a head-to-tail fashion (see structure) and not through a covalent Sn–Sn bond. Thus, the title compounds can be described as analogues of quadruply R-bridged alkenes.

Dendritic Effects

C. A. Schalley,* C. Verhaelen, F.-G. Klärner, U. Hahn, F. Vögtle ——— **477 – 480**

Gas-Phase Host–Guest Chemistry of Dendritic Viologens and Molecular Tweezers: A Remarkably Strong Effect on Dication Stability

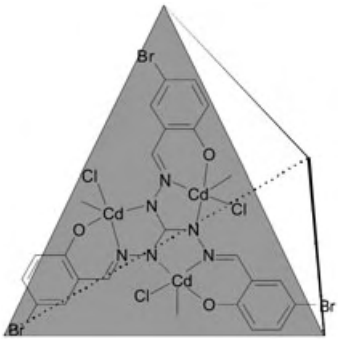


Size does matter: Viologen dications (blue) substituted with dendrons form strong host–guest complexes with molecular tweezers (yellow) in solution and in the gas phase (see picture). Complexation even stabilizes dications which are intrinsically unstable as "naked" species in the high vacuum of a mass spectrometer. A remarkably pronounced effect of dendrimer size on the stability of these dications switches their fragmentation between two mechanisms.

Cage Compounds

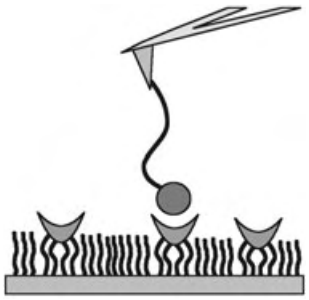
I. M. Müller,* D. Möller, C. A. Schalley ——— **480 – 484**

Rational Design of Tightly Closed Coordination Tetrahedra that are Stable in the Solid State, in Solution, and in the Gas Phase



No way out: Small guest cations, such as $[Et_4N]^+$ template the formation of stable and tightly closed octaanionic metallosupramolecular tetrahedra (see picture). Since $[Et_3NH]^+$ is co-encapsulated with exactly one water molecule, the filling of space seems to be a more pivotal factor for the templation than the symmetry of the cation. X-ray crystallography excellently agrees with NMR spectroscopy and ESI-FT-ICR mass spectrometry data.

© 2005 Wiley-VCH Verlag GmbH & Co. KGaA, Weinheim



Pulling power: The specific interaction of individual (alkyl) ammonium residues with a resorc[4]arene cavitand that is attached to a gold surface are investigated. Measurements are made by attaching the residue to the cantilever of an atomic force microscope (AFM; see picture). The results confirm that the affinity of the guest for the host depends of their mutual steric compatibility.

Single-Molecule Studies

R. Eckel, R. Ros, B. Decker, J. Mattay,* D. Anselmetti* ——— **484 – 488**

Supramolecular Chemistry at the Single-Molecule Level

Looking for outstanding employees?

Do you need another expert for your excellent team?
... Chemists, PhD Students, Managers, Professors, Sales Representatives...

Place an advert in the printed version and have it made available online for 1 month, free of charge!

Angewandte Chemie International Edition
Advertising Sales Department: Marion Schulz
Phone: 0 62 01 - 60 65 65
Fax: 0 62 01 - 60 65 50
E-Mail: MSchulz@wiley-vch.de

Service

Keywords ——— *490*

Authors ——— *491*

Preview ——— *493*

 © 2005 Wiley-VCH Verlag GmbH & Co. KGaA, Weinheim



S. John and G. Ozin Receive Brockhouse Canada Prize

Sajeev John and Geoffrey Ozin of the University of Toronto (Canada) have received the first Brockhouse Canada Prize of the Natural Sciences and Engineering Research Council of Canada (NSERC). The prize, accompanied by a research grant of CAN$ 250000, is to be awarded annually for outstanding results in an interdisciplinary NSERC-funded project. It is named after the Canadian physicist Bertram N. Brockhouse, who was awarded the 1994 Nobel Prize for the development of neutron spectroscopy.



S. John



G. Ozin

Theoretical physicist Sajeev John and materials chemist Geoffrey Ozin have together developed photonic crystals in which light can be trapped. These crystals, which are based on inverse silicon opals, should form the basis of optical microchips that operate at the speed of light. After John's concept had been rejected by many scientists around the world, he came across Ozin at his own university in 1998. Ozin had 30 years of experience in zeolite chemistry, also on a nanometer scale. The collaboration of theory and experiment of these two researchers is as fruitful as their backgrounds are different.[1a] Ozin's article on nanocrystallinity in anatase thin films is highlighted on the cover of issue 2/2005 of *Small*.[1b]

Ozin completed his PhD at the University of Oxford (UK) and since 1969 has been at the University of Toronto, where he currently holds the Canada Research Chair in Materials Chemistry. John completed his PhD in physics at Harvard University (USA). From 1986 to 1989 he was assistant professor at Princeton University, where he co-invented the concept of photonic band gap materials. He now holds the Canada Research Chair in Physics at the University of Toronto.

Polymer Award to C. J. Hawker

Craig J. Hawker is to receive the 2005 ACS Award in Applied Polymer Science. Hawker studied chemistry in Queensland (Australia) and completed his PhD in 1988 at the University of Cambridge (UK) with A. R. Battersby on the biosynthesis of vitamin B12. Following postdoctoral research with J. M. J. Fréchet at Cornell University (USA), he returned in 1990 to the University of Queensland. Since 1993 he has worked at the Almaden Research Center of IBM in San José, California and since 2001 has also been adjunct professor at the University of Queensland.



C. J. Hawker

Hawker's research encompasses synthetic polymer chemistry and materials for nanotechnology (microelectronics and biotechnology). For example, he is interested in the structuring of surfaces on the nanometer scale. To overcome the disadvantages of top-down and bottom-up approaches, he works on methods based on imprinting and subsequent polymerization. In both 2003 and 2004 he was the co-author of cover-picture articles in *Angewandte Chemie*: on the synthesis of triazole dendrimers, and on the structured cross-linking of silsesquioxanes.[2]

Noyori Prize to D. Seebach

The Ryoji Noyori Prize is awarded by the Society of Synthetic Organic Chemistry, Japan and sponsored by the company Takasago. The prize of US$ 10000 is awarded in recognition of outstanding contributions to asymmetric synthetic chemistry. The recipient for 2004, selected by a committee composed of four people from Japan and three from abroad, is Dieter Seebach of the ETH Zürich (Switzerland).

Seebach, a former member of the Editorial Board of *Angewandte Chemie*, completed his PhD at the Universität Karlsruhe (Germany) with R. Criegee, then undertook postdoctoral research with E. J. Corey at Harvard University. In 1971 he became professor in Giessen (Germany), and then in 1977 at the ETH Zürich. His research is broadly concerned with the development of methodology in organic chemistry. One of his current projects focuses on β-peptides; he recently reported on their secondary structure in *Angewandte Chemie*.[3a] A comprehensive review on this topic appeared in 2004 in *Chemistry & Biodiversity*.[3b] Over a period of almost 30 years *Angewandte Chemie* has published 11 Reviews by Seebach on a wide range of topics, including umpolung, Ti and Zr nucleophiles, and asymmetric synthesis. His Review on the future of organic synthesis is legendary.[3c]



D. Seebach

[1] a) N. Tétreault, H. Míguez, G. A. Ozin, *Adv. Mater.* **2004**, *16*, 1471; b) S. Y. Choi, M. Mamak, S. Speakman, N. Chopra, G. A. Ozin, *Small* **2005**, *1*, 226.

[2] a) P. Wu, A. K. Feldman, A. K. Nugent, C. J. Hawker, A. Scheel, B. Voit, J. Pyun, J. M. J. Fréchet, K. B. Sharpless, V. V. Fokin, *Angew. Chem.* **2004**, *116*, 4018; *Angew. Chem. Int. Ed.* **2004**, *43*, 3928; b) E. F. Connor, L. K. Sundberg, H.-C. Kim, J. J. Cornelissen, T. Magbitang, P. M. Rice, V. Y. Lee, C. J. Hawker, W. Volksen, J. L. Hedrick, R. D. Miller, *Angew. Chem.* **2003**, *115*, 3915; *Angew. Chem. Int. Ed.* **2003**, *42*, 3785.

[3] a) K. Gademann, A. Häne, M. Rueping, B. Jaun, D. Seebach, *Angew. Chem.* **2003**, *115*, 1573; *Angew. Chem. Int. Ed.* **2003**, *42*, 1534; b) D. Seebach, A. K. Beck, D. J. Bierbaum, *Chem. Biodiv.* **2004**, *1*, 1111; c) D. Seebach, *Angew. Chem.* **1990**, *102*, 1363; *Angew. Chem. Int. Ed. Engl.* **1990**, *29*, 1320.

© 2005 Wiley-VCH Verlag GmbH & Co. KGaA, Weinheim
DOI: 10.1002/anie.200462890

Dateiname: G462890E
Seite: 1 te von 1
Status Neusatz
Sprache
Pagina: 358
Umfang (Seiten): 1
Datum: 53 KW., 28. Dezember 2004 (Dienstag)
Zeit: 12:05:56 Uhr

Enzyme Catalysis

Chemoenzymatic Synthesis of Building Blocks for Statin Side Chains

*Michael Müller**

Keywords:
enzyme catalysis · inhibitors · natural products · statins · steroids

Dedicated to Heinz G. Floss on the occasion of his 70th birthday

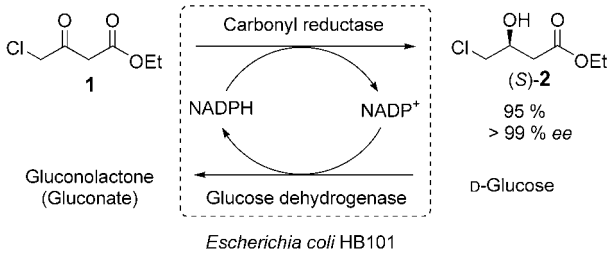
Statins[1] inhibit the enzyme HMG-CoA reductase (HMG = 3-hydroxy-3-methylglutaryl), which catalyzes the reductive conversion of HMG-CoA into mevalonate, an early and rate-limiting step in cholesterol biosynthesis. This inhibition leads to decreased levels of LDL cholesterol (LDL = low-density lipoprotein). Large-scale clinical trials with the statin class of cholesterol-lowering drugs have shown the relationship between diminished levels of LDL cholesterol and decreased morbidity and mortality from coronary heart disease.[2] Moreover, statins also decrease levels of triglycerides and increase levels of HDL cholesterol (HDL = high-density lipoprotein).

The market for cholesterol-lowering drugs, valued at more than US$20 billion and thus the largest in the pharmaceutical sector, is dominated by the statins. In 2003, revenues of US$9.2 billion (2002: US$8.0 billion) and US$6.1 billion (2002: US$6.2 billion) were recorded for atorvastatin and simvastatin, respectively, which means that these pharmaceuticals are the two top-selling drugs in the world. Relative to simvastatin, pravastatin (2003: US$2.8 billion), and lovastatin (the first statin marketed in 1987), which are all derived from microorganisms through partial synthesis, the synthetic HMG-CoA reductase inhibitors atorvastatin,[3] fluvastatin, and rosuvastatin (approved by the US Food and Drug Administration in August 2003)[4] are increasing in value.[5] With pitavastatin (NK 104) the next candidate is in phase III clinical trials.[2b] All statins have in common a homochiral side chain pharmacophore in the form of a 3,5-dihydroxy acid[6] and a (hetero)aromatic or cyclic residue (Scheme 1).

As a result of their extremely high market value and the requirement for high chemical and stereochemical purity (> 99.5 % *ee*, > 99 % *de*), immense effort has been invested in the production of synthetic statins by competing research groups. Pharmaceutical, chemical, and biotechnological companies have recently developed various chemoenzymatic strategies in which different biocatalysts are used for the stereoselective synthesis of the 3,5-dihydroxy acid side chain (Scheme 2). Several remarkable achievements have been made in the optimization of the biocatalytic step for application on an industrial scale. These examples nicely demonstrate that for the synthesis of a specific target molecule many different enzymatic transformations are applicable.

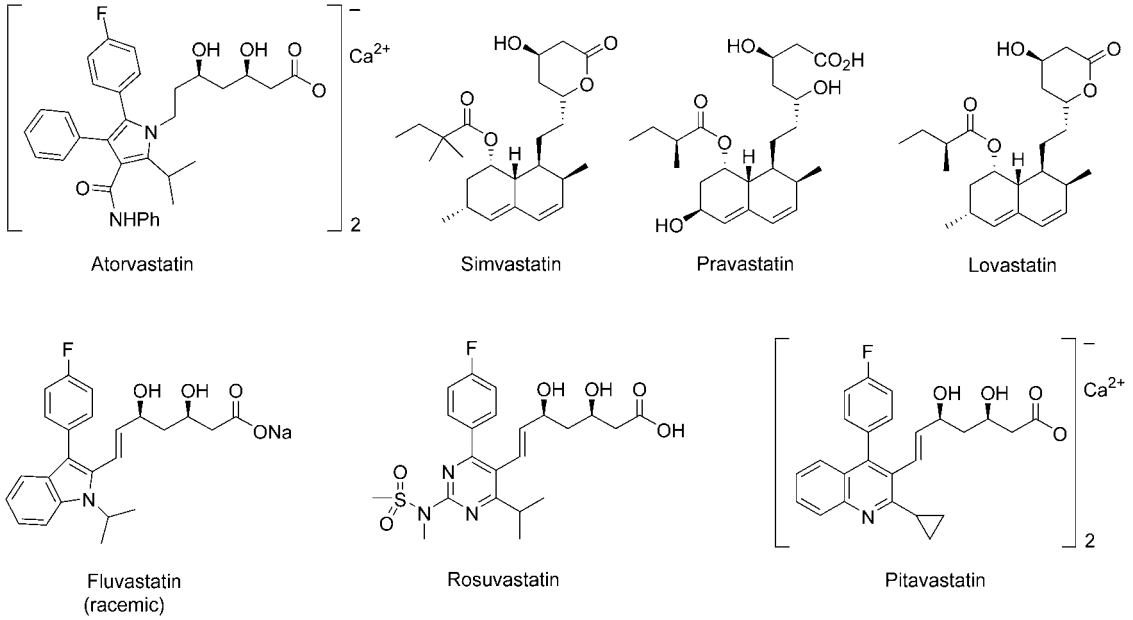
The established strategy of enantioselective reduction of alkyl 4-chloroacetoacetates (Scheme 2 A), such as **1**, has been optimized by Shimizu and coworkers in collaboration with scientists at Kaneka. Permeabilized cells of a recombinant *E. coli* strain that overproduces both an alcohol dehydrogenase (ADH, in the form of carbonyl reductase from *Candida magnoliae*) and glucose dehydrogenase from *Bacillus megaterium* were used in a biphasic organic solvent/aqueous buffer system for the production of ethyl (*S*)-4-chloro-3-hydroxybutanoate ((*S*)-**2**) in enantiopure form. Product concentrations of 63 g L^{-1} were observed in the organic phase, and the product was isolated in 95 % yield,[7] but much higher product concentrations might also be attainable.[7c] The main disadvantages of this system are the high concentration of the coproduct gluconate and the utilization of nonliving cells. The use of living organisms that express both the catalyst and the cofactor-regenerating enzyme might enable continuous production with high total turnover numbers for the catalyst and the cofactor NAD(P)H.[8]

Chemists at Avecia Pharmaceuticals (formerly Zeneca, formerly ICI) have developed a biocatalytic alternative to the problematic diastereoselective reduction of 3-hydroxyketones **3**, which is

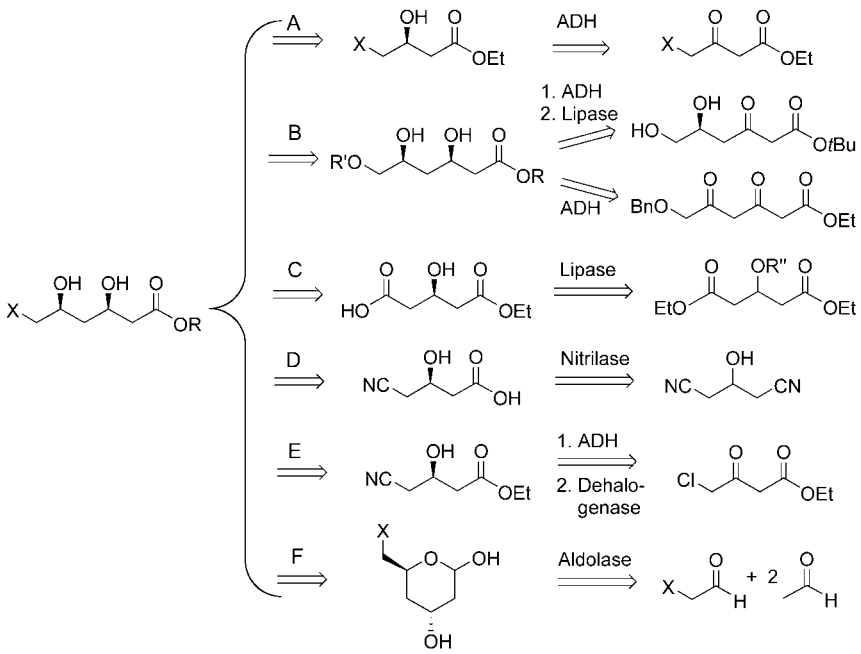


[*] Prof. Dr. M. Müller[+]
Institut für Biotechnologie 2
Forschungszentrum Jülich GmbH
52425 Jülich (Germany)
Fax: (+49) 2461-613-870
E-mail: mi.mueller@fz-juelich.de
[+] Present address: Institut für Pharmazeutische Wissenschaften
Lehrstuhl für Pharmazeutische und Medizinische Chemie
Albert-Ludwigs-Universität Freiburg
Albertstrasse 25, 79104 Freiburg (Germany)

© 2005 Wiley-VCH Verlag GmbH & Co. KGaA, Weinheim
DOI: 10.1002/anie.200460852



Scheme 1. HMG-CoA reductase inhibitors.



Scheme 2. Biocatalytic transformations for the synthesis of (3*R*,5*S*)-dihydroxyhexanoates. Bn = benzyl.

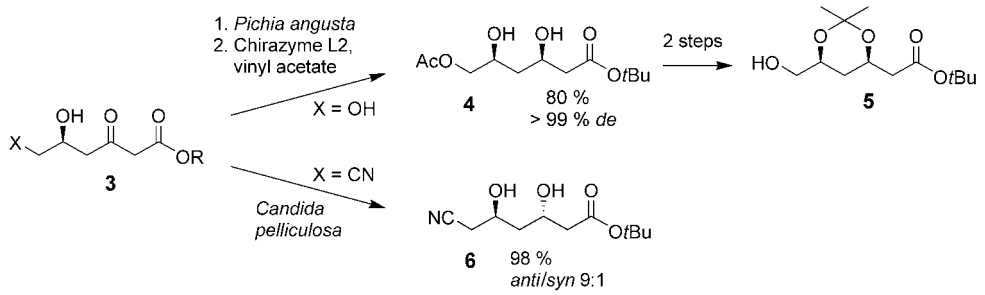
a price-limiting factor on an industrial scale because of ecological and economic concerns. The bioreduction of (*S*)-**3** with cells of *Pichia angusta* resulted in the formation of the desired diastereomerically pure triol in 80% yield (substrate concentration 25 g L^{-1}). Immobilized lipase from *Candida antarctica* (Chirazyme L2) provided access in very high yield to regioselectively acetylated **4**, which was used in the synthesis of the important building block **5**.[9] Depending on the strain and on the substituent at C6, either the *syn* or the *anti* 1,3-diol (e.g. **6**) is obtained.[10b] A similar approach has been developed by scientists at Kaneka, for example with *Candida magnoliae*.[10]

The research group of Patel (Bristol-Myers Squibb) used cell suspensions of *Acinetobacter calcoaceticus* for the stereoselective direduction of ethyl 6-benzyloxy-3,5-dioxohexanoate. The corresponding diol was isolated in 85% yield with 97% *ee* (Scheme 2B).[11]

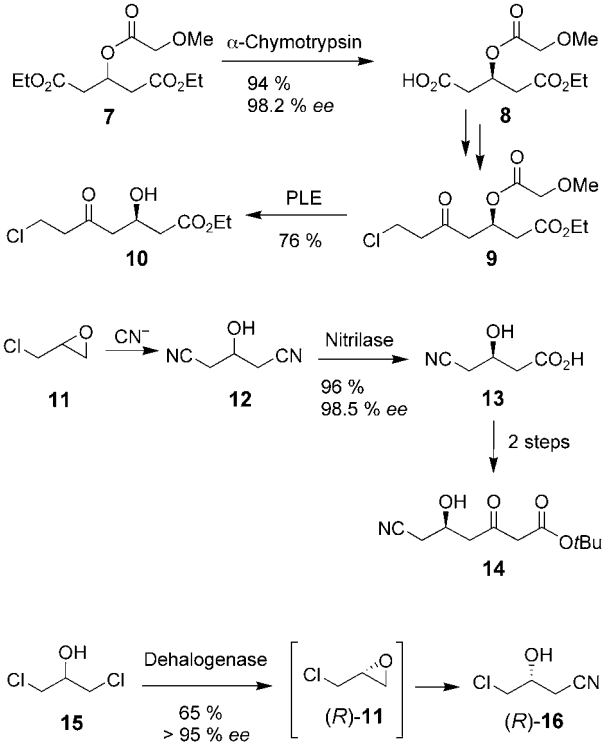
The known desymmetrization of prochiral 3-substituted glutarates by enzymatic hydrolysis (Scheme 2C)[12] has been optimized by chemists at Ciba Speciality Chemicals for the synthesis of **8** on a kilogram scale.[13] α-Chymotrypsin, an extremely cheap and robust biocatalyst, is used in the selective hydrolysis of the triester **7**. The process is characterized by a high substrate concentration (285 g L^{-1})[14] and a 94% yield of the isolated product with 98.2% *ee*. After chain elongation, the methoxyacetyl ester is removed selectively by hydrolysis in the presence of pig-liver esterase (PLE) (**9**→**10**); the ethyl ester is left untouched.[14] Because of the potential for flexible functionalization of the monoprotected glutarate **8**,[13] this strategy, like the following, in principle allows access to both enantiomers of 3-hydroxy-5-oxohexanoates and 5-hydroxy-3-oxohexanoates.

Burk and co-workers (Diversa) identified more than 200 new nitrilases by using large genomic libraries created by extracting DNA directly from environmental samples. Four of the enzymes

 © 2005 Wiley-VCH Verlag GmbH & Co. KGaA, Weinheim



identified were employed successfully in the desymmetrization of 3-hydroxyglutaronitrile (**12**), which is readily available from epichlorohydrin (**11**; Scheme 2D). Subsequently, a highly enantioselective nitrilase was created through site-saturation mutagenesis. The optimized efficient enzymatic transformation, which was performed on a gram scale with a substrate concentration of 3 M, is characterized by a high volumetric productivity. After a reaction time of 15 h, the product (98.5% *ee*) was isolated in 96% yield, which corresponds to a space–time yield of 619 $g L^{-1} d^{-1}$.[15]



The dehalogenase-catalyzed racemic resolution of *rac*-**2** was described by Kasai and co-workers (Daiso).[16] Prochiral 1,3-dichloro-2-propanol was used in the synthesis of (*R*)-4-chloro-3-hydroxybutyrontrile ((*R*)-**16**) via (*R*)-epichlorohydrin ((*R*)-**11**). The dehalogenase enzyme catalyzes both the reversible removal of HCl from 1,3-dichloro-2-propanol and the introduction of the cyano group.[17] The enantiomer (*S*)-**16** can be obtained in two steps starting either from racemic epichlorohydrin or from prochiral 1,3-dichloro-2-propanol.[18]

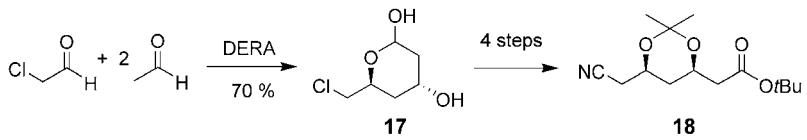
Recently, scientists at Codexis together with Roger Sheldon described the combination of a ketoreductase- and a dehalogenase-catalyzed one-pot transformation (Scheme 2E).[19] Although this is an interesting approach, the published data are not yet adequate for the application of this two-step transformation on a larger scale.

Another highly attractive approach has been developed by scientists at DSM[20] based on a transformation introduced by Wong and co-workers.[21] The 2-deoxyribose-5-phosphate aldolase (DERA) catalyzed formation of the pyran **17** proceeds through asymmetric C–C bond formation starting from the cheap bulk chemicals acetaldehyde and chloroacetaldehyde. Although the reaction characteristics published in the initial article were not very promising (low substrate concentration, high catalyst loading, 7-day reaction time), this biotransformation is now in operation on an industrial scale.[20c] The optimized enzymatic transformation, which is performed at low temperature (2–4 °C), is characterized by a high final product concentration (> 100 $g L^{-1}$).[20a]

Recently, scientists at Diversa applied the strategy of screening genomic libraries prepared from environmental DNA, as mentioned in the case of nitrilases, for the identification of improved DERA enzymes.[22] More than 15 DERA enzymes were discovered, one of which was used to optimize the process on a 100-g scale. By using a fed-batch strategy, which is necessary because of substrate inhibition, Burk and co-workers obtained **17** (> 99.5% *ee*, 96.6% *de*) in a final concentration of 93 $g L^{-1}$ and were able to decrease the amount of enzyme used to 2 wt%. In addition, Wong and co-workers recently reported the DERA S238D mutant catalyzed transformation of 3-azidopropionaldehyde with two molecules of acetaldehyde.[21d] Thus, the building block **18** for the atorvastatin side chain is accessible through a straightforward chemoenzymatic five-step synthesis starting from cheap bulk chemicals.

These examples demonstrate that state-of-the-art enzymatic transformations have reached an extraordinary level, making them valuable and competitive methods for use in the chemical and pharmaceutical industry. Clearly,

 © 2005 Wiley-VCH Verlag GmbH & Co. KGaA, Weinheim



17 18

biocatalysis is "growing up" in terms of its acceptance by chemists. Biocatalytic strategies offer innovative solutions to problems such as crossed-aldol reactions, the regio- and stereoselective reduction of 1,3-diketones, the stereoselective formation of 1,3-diols, and the desymmetrization of prochiral compounds. These approaches will also have an impact on the development and elucidation of non-enzymatic transformations, as well as on the training of chemistry, pharmacy, and biology students.

Published Online: December 9, 2004

[1] According to the Anatomical Therapeutic Chemical (ATC) classification of the World Health Organization, the International Nonproprietary Names (INN) of the so-called "statins" are assigned the root "-vastatin".

[2] Coronary heart disease is a leading cause of death and morbidity in the developed world; a) J. A. Tobert, *Nat. Rev. Drug Discovery* **2003**, *2*, 517 – 526; b) H. Stark, *Pharm. Unserer Zeit* **2003**, *32*, 464 – 470; c) D. Manns, *Pharm. Unserer Zeit* **1999**, *28*, 147 – 152.

[3] B. D. Roth, *Prog. Med. Chem.* **2002**, *42*, 1 – 22.

[4] a) J. Quirk, M. Thornton, P. Kirkpatrick, *Nat. Rev. Drug Discovery* **2003**, *2*, 769 – 770; b) C. I. Carswell, G. L. Plosker, B. Jarvis, *Drugs* **2002**, *62*, 2075 – 2085; c) M. Watanabe, H. Koike, T. Ishiba, T. Okada, S. Seo, K. Hirai, *Bioorg. Med. Chem.* **1997**, *5*, 437 – 444.

[5] Cerivastatin, marketed by Bayer, was withdrawn from the market in 2001 because of reported cases of rhabdomolysis (severe muscular toxicity).

[6] Fluvastatin is marketed as a racemate.

[7] a) Y. Yasohara, N. Kizaki, J. Hasegawa, M. Wada, M. Kataoka, S. Shimizu, *Tetrahedron: Asymmetry* **2001**, *12*, 1713 – 1718; b) N. Kizaki, Y. Yasohara, J. Hasegawa, M. Wada, M. Kataoka, S. Shimizu, *Appl. Microbiol. Biotechnol.* **2001**, *55*, 590 – 595; c) M. Kataoka, L. P. S. Rohani, K. Yamamoto, M. Wada, H. Kawabata, K. Kita, H. Yanase, S. Shimizu, *Appl. Microbiol. Biotechnol.* **1997**, *48*, 699 – 703.

[8] a) M. Ernst, B. Kaup, M. Müller, S. Bringer-Meyer, H. Sahm, *Appl. Microbiol. Biotechnol.* **2005**, DOI: 10.1007/s00253-004-1765-5; b) T. Endo, S. Kiozumi, *Adv. Synth. Catal.* **2001**, *343*, 521 – 526.

[9] a) A. J. Blacker, R. A. Holt, C. D. Reeve (Avecia Pharmaceuticals), WO 01/85975, **2001**; b) C. D. Reeve (Avecia Pharmaceuticals), WO 97/00968, **1997**.

[10] N. Kizaki, Y. Yamada, Y. Yasohara, A. Nishiyama, M. Miyazaki, M. Mitsuda, T. Kondo, N. Ueyama, K. Inoue (Kaneka), WO 00/08011, **2000**.

[11] a) R. N. Patel, A. Banerjee, C. G. McNamee, D. Brzozowski, R. L. Hanson, L. J. Szarka, *Enzyme Microb. Technol.* **1993**, *15*, 1014 – 1021; b) R. N. Patel, C. G. McNamee, A. Banerjee, L. J. Szarka (Squibb & Sons, Inc.), Eur. Pat. Appl. EP 569,998, **1993** [*Chem. Abstr.* **1994**, *120*, 52826q].

[12] F.-C. Huang, L. F. H. Lee, R. S. D. Mittal, P. R. Ravikumar, J. A. Amigo, C. J. Sih, E. Caspi, C. R. Eck, *J. Am. Chem. Soc.* **1974**, *96*, 4144 – 4145.

[13] R. Öhrlein, G. Baisch, *Adv. Synth. Catal.* **2003**, *345*, 713 – 715.

[14] See also: S. J. C. Taylor, R. C. Brown, P. A. Keene, I. N. Taylor, *Bioorg. Med. Chem.* **1999**, *7*, 2163 – 2168.

[15] a) G. DeSantis, K. Wong, B. Farwell, K. Chatman, Z. Zhu, G. Tomlinson, H. Huang, X. Tan, L. Bibbs, P. Chen, K. Kretz, M. J. Burk, *J. Am. Chem. Soc.* **2003**, *125*, 11476 – 11477; b) G. DeSantis, Z. Zhu, W. A. Greenberg, K. Wong, J. Chaplin, S. R. Hanson, B. Farwell, L. W. Nicholson, C. L. Rand, D. P. Weiner, D. E. Robertson, J. Burk, *J. Am. Chem. Soc.* **2002**, *124*, 9024 – 9025; c) see also: S. J. Maddrell, N. J. Turner, A. Kerridge, A. J. Willetts, J. Crosby, *Tetrahedron Lett.* **1996**, *37*, 6001 – 6004.

[16] a) N. Kasai, T. Suzuki, *Adv. Synth. Catal.* **2003**, *345*, 437 – 455; b) T. Suzuki, H. Idogaki, N. Kasai, *Enzyme Microb. Technol.* **1998**, *24*, 13 – 20.

[17] T. Nakamura, T. Nagasawa, F. Yu, I. Watanabe, H. Yamada, *Tetrahedron* **1994**, *50*, 11821 – 11826.

[18] E. J. de Vries, D. B. Janssen, *Curr. Opin. Biotechnol.* **2003**, *14*, 414 – 420.

[19] S. C. Davis, J. H. Grate, D. R. Gray, J. M. Gruber, G. W. Huisman, S. K. Ma, L. M. Newman, R. Sheldon, L. A. Wang (Codexis Inc.), WO 2004/015132.

[20] a) J. G. T. Kierkels, D. Mink, S. Panke, F. A. M. Lommen, D. Heemskerk (DSM), WO 03/006656; b) J. M. H. H. Kooistra, H. J. M. Zeegers, D. Mink, J. M. C. A. Mulders (DSM), WO 02/06266; c) M. Wubbolts, *Screening and biocatalyst development for custom manufacturing of fine chemicals*, Biocat, Barcelona, Spain, **2003**.

[21] a) H. J. M. Gijsen, C.-H. Wong, *J. Am. Chem. Soc.* **1994**, *116*, 8422 – 8423; b) C.-H. Wong, E. Garcia-Junceda, L. Chen, O. Blanco, H. J. M. Gijsen, D. H. Steensma, *J. Am. Chem. Soc.* **1995**, *117*, 3333 – 3339; c) G. DeSantis, J. Liu, D. P. Clark, A. Heine, I. A. Wilson, C.-H. Wong, *Bioorg. Med. Chem.* **2003**, *11*, 43 – 52; d) J. Liu, C.-C. Hsu, C.-H. Wong, *Tetrahedron Lett.* **2004**, *45*, 2439 – 2441.

[22] W. A. Greenberg, A. Varvak, S. R. Hanson, K. Wong, H. Huang, P. Chen, M. J. Burk, *Proc. Natl. Acad. Sci. USA* **2004**, *101*, 5788 – 5793.

 © 2005 Wiley-VCH Verlag GmbH & Co. KGaA, Weinheim

Palladium Catalysts

Monoligated Palladium Species as Catalysts in Cross-Coupling Reactions

*Ute Christmann and Ramón Vilar**

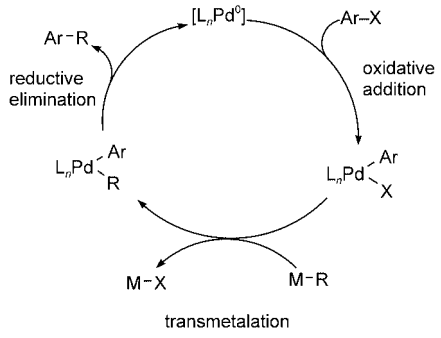
Keywords:
amination · carbenes · cross-coupling · palladium · phosphines

Palladium-mediated cross-coupling reactions are attractive organometallic transformations for the generation of C–C, C–N, C–O, and C–S bonds. Despite being widely employed in small-scale syntheses, cross-coupling reactions have not found important industrial applications because until recently, only reactive aryl bromides and iodides could be used as substrates. These substrates are generally more expensive and less widely available than their chloride counterparts. Over the past few years, new catalytic systems with the ability to activate unreactive and sterically hindered aryl chlorides have been developed. The new catalysts are based on palladium complexes that contain electron-rich and bulky phosphine or carbene ligands. The enhanced reactivity observed with these new systems has been attributed to the formation of unsaturated and reactive [PdL] species which can readily undergo oxidative addition reactions with ArX to yield [Pd(Ar)X(L)].

1. Introduction

Palladium-mediated cross-coupling reactions to form C–C, C–N, C–O, and C–S bonds are among the most powerful organometallic transformations employed in organic synthesis. These reactions are generally thought to proceed through a mechanism that involves three distinctive steps (see Scheme 1). First, an aryl halide reacts with the palladium(0) center through an oxidative addition reaction. This is followed by a transmetalation reaction to yield a palladium(II) complex that contains the two moieties to be coupled. The final step is the reductive elimination of the product with the concomitant regeneration of the active palladium(0) catalyst. In this mechanism, the nature of the aryl halide substrate is very important in the determination of the rate-limiting step. For example, for aryl chlorides and unactivated aryl bromides, it is often found that the oxidative addition is the rate-limiting step.

Initially, cross-coupling reactions had an important limitation: only reactive aryl bromides and iodides could be used as substrates. However, as aryl chlorides are more widely available and generally less expensive than their bromide and iodide counterparts, there has been a growing interest to find catalytic systems that can successfully catalyze cross-coupling reactions with these substrates. The past few years have seen important advances in this direction, with part of this success owed to the development of new palladium complexes which contain electron-rich and bulky ligands (namely phosphines and carbenes) that improve their catalytic activity in coupling



Scheme 1. General mechanism for cross-coupling reactions.

[*] Dr. R. Vilar
Institution of Research and Advanced Studies (ICREA) and
Institute of Chemical Research of Catalonia (ICIQ)
43007 Tarragona (Spain)
Fax: (+34) 977-920-228
E-mail: rvilar@iciq.es

U. Christmann
Department of Chemistry
Imperial College London
London SW7 2AZ (UK)

© 2005 Wiley-VCH Verlag GmbH & Co. KGaA, Weinheim
DOI: 10.1002/anie.200461189

reactions. The enhanced reactivity observed with these new systems has been attributed to the formation of unsaturated [PdL] species, which can readily undergo oxidative addition reactions to yield [Pd(Ar)X(L)].

Herein we present the most important advances that have been made over the past few years in the development of catalytic systems that use bulky and electron-rich ligands for cross-coupling reactions. As several excellent reviews[1–16] and books[17,18] on palladium-catalyzed coupling reactions have already been published, we limit our discussion to examples in which monoligated palladium species have been implicated in the catalytic process.

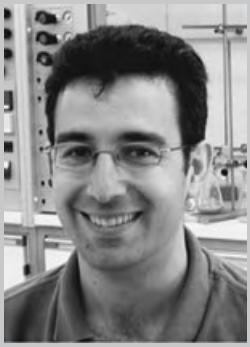
2. Palladium Catalysts Supported by Bulky and Electron-Rich Ligands

2.1. Phosphines

Several groups have established that the combination of bulky and electron-rich phosphines with different sources of palladium generate species that show high catalytic activity in cross-coupling reactions. In 1998, Nishiyama and co-workers showed that mixtures of $P t Bu_3$ and either $Pd(OAc)_2$ or $[Pd_2(dba)_3]$ (dba = dibenzylideneacetone) had unusually high activities in amination reactions.[19] The same year, Littke and Fu reported that a mixture which contained $[Pd_2(dba)_3]$ and $P t Bu_3$ was highly active as a catalyst for the Suzuki coupling reaction of a broad spectrum of aryl halides.[20] A more detailed study by Fu and co-workers, in which the catalytic properties of palladium complexes with different phosphines as ligands were compared by using different aryl halides as substrates, gave further insight into the catalytic mechanism.[21] In these studies, it was shown that a mixture of $[Pd_2(dba)_3]$ and $P t Bu_3$ catalyzed the Suzuki cross-coupling of vinyl and aryl halides (including chloride) with arylboronic acids, whereas $Pd(OAc)_2$ in the presence of PCy_3 (Cy = cyclohexyl) generated a good catalyst for the cross-coupling reaction of vinyl and aryl triflates with arylboronic acids. The system with $P t Bu_3$ showed high selectivity with the order of reactivity $I > Br > Cl \gg OTf$. Interestingly, it was shown that the optimal palladium/phosphine ratio for high catalytic activity was between 1 and 1.5, which suggested that a monophosphine–palladium complex may be the catalytically active species. It was observed that $[Pd(P t Bu_3)_2]$ was a very poor catalyst for the Suzuki coupling of 3-chloropyridine and *o*-tolylboronic acid (7% conversion). However, addition of the phosphine-free species $[Pd_2(dba)_3]$ to $[Pd(P t Bu_3)_2]$ to generate the $[Pd(P t Bu_3)]$ species produced an important increase in activity (91% conversion).

These studies were followed by various reports which showed that other types of cross-coupling reactions occur readily in the presence of a range of palladium sources and bulky phosphine ligands. Littke and Fu also demonstrated that a mixture of $[Pd_2(dba)_3]$ and $P t Bu_3$ yields a general catalyst system for Stille cross-coupling[22] and Heck reactions.[23] Hartwig and co-workers, on the other hand, reported that this palladium/phosphine combination produces an excellent catalyst for the arylation of ketones and malonates.[24,25] They also studied in detail the formation of C–N bonds catalyzed by palladium in the presence of bulky and electron-rich phosphines such as $P t Bu_3$, PCy_3, $PAd(t Bu_2)$ (Ad = 1-adamantyl), and $(Ph_5Fc)P t Bu_2$ (Q-phos; Fc = ferrocenyl).[26–28] In most cases, standard palladium sources such as $[Pd_2(dba)_3]$ and $Pd(OAc)_2$ were employed to generate the catalytic species in the presence of the corresponding phosphine. Further studies by Hartwig and co-workers showed that the previously reported palladium(I) dimer $[Pd_2(\mu\text{-}Br)_2(P t Bu_3)_2]$[29,30] could be used as a novel single-source precatalyst for cross-coupling reactions.[31] Unparalleled rates for amination and Suzuki–Miyaura cross-coupling reactions of aryl chlorides and bromides were observed with this complex. The high reactivity of this compound was attributed to the formation of the monoligated species $[Pd(P t Bu_3)]$ by either a disproportionation reaction or by the direct reduction of the dipalladium complex in the presence of the substrate and a base.

Beller and co-workers reported an efficient catalytic system for cross-coupling reactions based on the sterically demanding phosphine, $PAd_2(n Bu)$.[32] A mixture of $Pd(OAc)_2$ and this phosphine generates catalysts for the amination of aryl chlorides, the Suzuki coupling of aryl halides and boronic acids, and the α-arylation of ketones. In these reports, a detailed comparison of the activity of several catalytic systems was carried out that highlighted the influence of the supporting phosphine, the palladium/phosphine ratio, and the quantity (mol%) of the catalyst in the corresponding cross-coupling reactions. Furthermore, Beller and co-workers isolated the monophosphine–palladium(0) complexes **1** and **2** (see Scheme 2) which were used as efficient catalysts for Suzuki cross-coupling reactions.[33] The effectiveness of these complexes as catalysts is directly related to their ability to

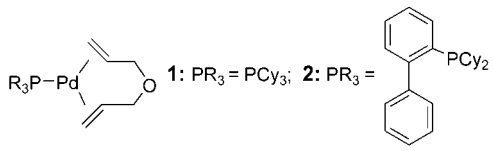


Ramón Vilar, born in Mexico City in 1969, completed his PhD (1996) on the synthesis and catalytic properties of palladium cluster compounds in the group of Prof. D. M. P. Mingos at Imperial College London. He remained at Imperial College as a lecturer and was appointed Senior Lecturer in 2003. Since April 2004, he is an ICREA Research Professor at the Institute of Chemical Research of Catalonia (ICIQ). His current research interests include the organometallic chemistry of palladium and supramolecular chemistry of metal complexes.



Ute Christmann, born in Peine (Germany), studied chemistry at the University of Hamburg. After completing her diploma with Prof. D. Rehder, she started her PhD (2002) in the group of Dr. R. Vilar at Imperial College, London (currently at ICIQ, Tarragona). Her research interests include the activation of small molecules by palladium(I) dimers and organometallic catalysis.

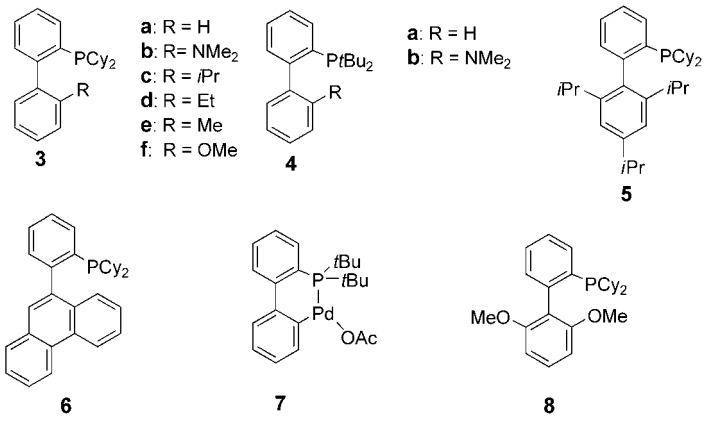
© 2005 Wiley-VCH Verlag GmbH & Co. KGaA, Weinheim



Scheme 2. Monophosphine–palladium complexes.

liberate the coordinated diene to generate the corresponding 12-electron species [PdL].

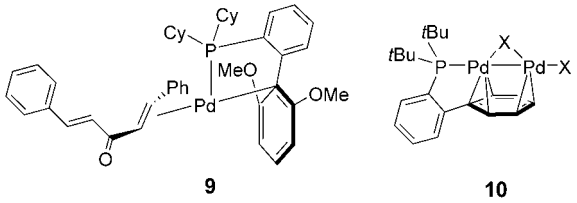
In the late 1990's, Buchwald and co-workers reported an important set of phosphines which proved to be excellent supporting ligands for the palladium-catalyzed formation of C–C, C–N, and C–O bonds with substrates such as aryl chlorides and bromides (see Scheme 3).[34–36] The effective-



Scheme 3. Buchwald's biaryl phosphine ligands and a cyclometallated palladium complex, **7**, of one such ligand (see References [6, 37]).

ness of these systems was attributed to a combination of electronic and steric properties of the ligands that favor both the oxidative addition and reductive elimination steps in the catalytic cycle. The formation of monoligated palladium species with biaryl phosphines was also invoked to be responsible for the rapid oxidative addition of the aryl halide substrates to the palladium(0) center. More recently, Buchwald's group reported a second generation of phosphines (see **5** and **8** in Scheme 3) with improved activities that demonstrate the generality of the catalyst system for a wide range of cross-coupling reactions.[37] As part of these studies, it was shown that the source of palladium and the phosphine/palladium ratio had an important impact on the catalytic performance of the system.

Besides the use of common palladium sources such as $Pd(OAc)_2$ and $[Pd_2(dba)_3]$, a single-component precatalyst based on a cyclometallated biaryl phosphine **7** was reported as a convenient air- and moisture-stable complex for aryl amination reactions.[38] It has been suggested that the biaryl group in Buchwald's phosphines may contribute to the stabilization of monophosphine–palladium complexes by establishing π interactions with the palladium(0) center. This is supported by the recent isolation of the complexes [Pd(dba)(L)] (where L = **4a**, **6**, or **8**) in which there is indeed a π interaction between the metal center and the aromatic system of the biaryl group (see **9**, Scheme 4).[39–41] The ability of this type of phosphine to stabilize unusual coordinations around metal centers can also be seen in the palladium dinuclear complex **10** in which $PtBu_2(bph)$ (bph = biphenyl)

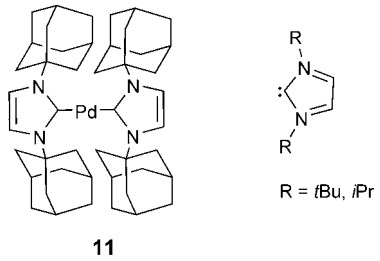


Scheme 4. Representation of a monometallic palladium(0) complex and a dinuclear palladium(I) compound with the π interactions between the metal center and the corresponding biaryl phosphine shown. X = Br, Cl.

bridges the two palladium centers through a μ_2-η^3:η^3-coordinated phenyl group (see Scheme 4).[41] This species catalyzed the amination reaction of aryl chlorides and bromides. The system is phosphine-deficient, thus it is likely that $[Pd\{PtBu_2(bph)\}]$ species are generated and these act as the true catalysts.

2.2. N-Heterocyclic Carbenes

Palladium complexes of N-heterocyclic carbenes (NHCs) can also be used as catalysts to activate aryl chlorides for cross-coupling reactions. For this type of reaction to occur at low temperatures and with reasonable yields, sterically demanding NHCs need to be employed (see Scheme 5). Some of these bulky ligands were successfully prepared and used in catalytic coupling reactions by the groups of Herrmann,[42] Beller,[43] Nolan,[44–46] Glorius,[47] and Cloke.[48]



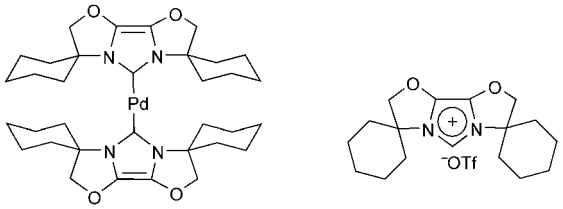
Scheme 5. General N-heterocyclic carbenes (NHC) that are commonly used as ligands in cross-coupling reactions and a palladium(0) homoleptic NHC complex **11**.

The ratios of ligand/palladium, the steric bulk of the ligand, and the source of palladium were shown to be very important in defining the catalytic activity of the system. Furthermore, mechanistic studies suggested that monoligated palladium(0) complexes are implicated in the catalysis. Herrmann and co-workers reported that homoleptic palladium complexes $[Pd(NHC)_2]$ are good catalysts for the Suzuki

 © 2005 Wiley-VCH Verlag GmbH & Co. KGaA, Weinheim

coupling of aryl chlorides.[49] The activity of this type of complex is highly dependent on the steric bulk of the carbene ligand. In particular, the complex $[Pd(NHC)_2]$ **11**, in which the NHC is the very sterically demanding 1,3-bisadamantylimidazolin-2-ylidene (see Scheme 5), proved to be an excellent catalyst for the Suzuki coupling of aryl chlorides at ambient temperature.

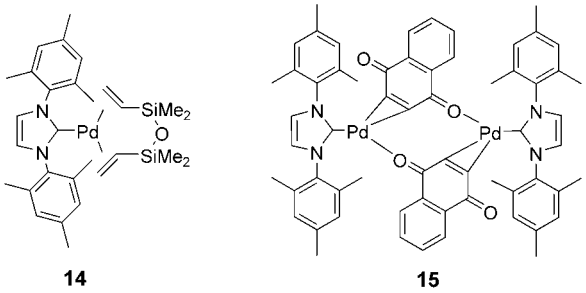
More recently, Glorius and co-workers reported the new homoleptic palladium complex **12**, which comprised the sterically demanding but flexible NHC ligand derived from **13** (see Scheme 6).[47] In contrast to the complexes described by Herrmann,[49] complex **12** proved to be catalytically inactive in the Suzuki coupling reaction at room temperature. However, a catalyst prepared from $Pd(OAc)_2$ and only one equivalent of the imidazolium salt **13** showed excellent catalytic activity for Suzuki cross-coupling reactions of aryl chlorides and even of sterically demanding substrates at room temperature. The authors attributed the high activity of this catalyst system to the formation of monoligated palladium–carbene complexes.



12 13

Scheme 6. Palladium(0) complex **12** with a geometrically flexible N-heterocyclic carbene ligand derived from the imidazolium salt **13**. OTf = trifluoromethylsulfonyl.

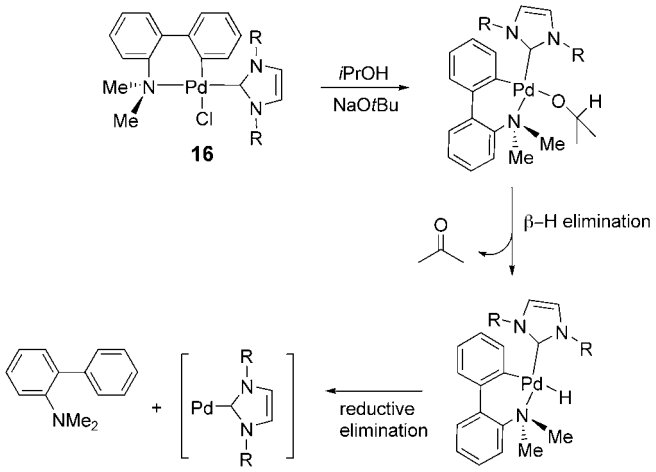
The potential role played by monoligated palladium–carbene complexes in cross-coupling reactions has also been studied by Beller and co-workers, who reported that the monocarbene–palladium(0) complexes **14** and **15** (see Scheme 7) act as good catalysts for Heck reactions of aryl chlorides (above 140 °C).[43] It was suggested that these complexes can generate the active 12-electron [PdL] species under the catalytic conditions. Interestingly, compound **14** has shown remarkable productivities and selectivities for the telomerization of 1,3-dienes with alcohols.[50,51] The good catalytic properties of this complex were attributed to the presence of unsaturated [PdL] species.



14 15

Scheme 7. Monocarbene–palladium(0) complexes.

Nolan and co-workers reported that the monocarbene–palladium(II) complex **16** (see Scheme 8) generated good catalytic species for Suzuki–Miyaura coupling reactions and Heck reactions of sterically hindered aryl chlorides at room temperature.[44,52] The isolation and identification of the organic fragments liberated in the initial steps of these reactions led the authors to propose a mechanism in which [Pd(NHC)] species, which act as the true catalysts, were generated (see Scheme 8).



Scheme 8. Representation of the reaction pathway to produce a catalytically active palladium(0)–monocarbene complex from **16**. R = 2,6-diisopropylphenyl.

3. Mechanistic Studies

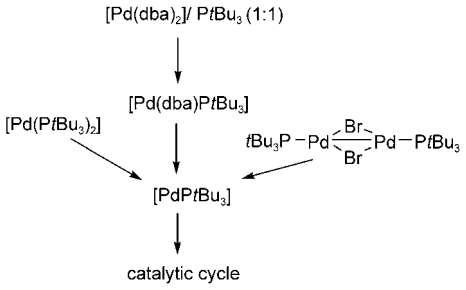
The experimental evidence described in the previous sections indicates that palladium in the presence of bulky and electron-rich ligands (either phosphines or carbenes) yields active catalytic systems for a wide range of cross-coupling reactions. The experimental observations also indicate that the source of palladium and the ratio of palladium/ligand employed have a great impact on the catalytic activity of the corresponding system. Some detailed mechanistic studies have now appeared which support the important catalytic role that monoligated palladium complexes play in cross-coupling reactions. To understand the mechanism of action of the catalytic species (and to optimize consequently conditions to enhance their catalytic properties), it is important to consider the different steps involved in the process. First, the generation of the catalytically active species from the corresponding palladium precursor needs to be considered; this step has demonstrated to be rate-limiting in several cases. After the "true" catalyst is generated, the oxidative addition of the aryl halide to the palladium(0) center takes place (which is favored by electron-rich ligands). Following a transmetalation reaction, the final step is the reductive elimination of the product,

 © 2005 Wiley-VCH Verlag GmbH & Co. KGaA, Weinheim

the rate of which is usually increased by the coordination of bulky ligands to the palladium center. Furthermore, the mechanism of the catalysis can also be significantly influenced by the nature of the base added to the system.

3.1. Formation of Catalytically Active Species from Palladium Precursors

It is first necessary to address the step in which the catalytically active species are generated from the corresponding palladium precursors. Several authors have shown that even when the same phosphine or carbene ligand is used in a particular reaction, the source of palladium employed has an important influence on the catalytic rates. For example, Hartwig and co-workers recently published a study on the palladium-catalyzed amination of five-membered heterocyclic halides in which various combinations of palladium precursors and P*t*Bu$_3$ were tested as catalysts for the reaction of 3-bromothiophene with *N*-methylaniline (see Scheme 9).[28] The fastest reactions were observed with the



Scheme 9. Scheme showing the different potential routes employed by Hartwig and co-workers to generate the catalytically active [Pd(P*t*Bu$_3$)] species.[28]

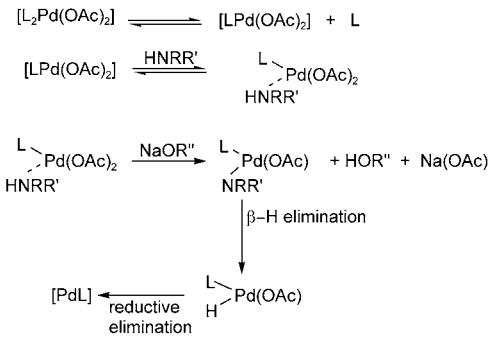
palladium(I) dimer [Pd$_2$(μ-Br)$_2$(P*t*Bu$_3$)$_2$], whereas those conducted with [Pd(P*t*Bu$_3$)$_2$] were very slow. If [Pd(dba)$_2$] was added to the latter, the reaction was faster than with the homoleptic diphosphine compound. Interestingly, the rate of reactions catalyzed by 1:1 mixtures of [Pd(dba)$_2$] and P*t*Bu$_3$ depended on the mixing time: Catalytic reactions conducted after allowing [Pd(dba)$_2$] and P*t*Bu$_3$ to mix for five minutes proceeded approximately three times faster than those conducted after mixing the two components for one hour. Note: the formation of [Pd(P*t*Bu$_3$)$_2$] from [Pd(dba)$_2$] and P*t*Bu$_3$ takes approximately one hour. These investigations strongly suggest that the efficiency of the formation of the monophosphine complex [Pd(P*t*Bu$_3$)] controls the rates of the amination reaction.

Analogous observations were reported by Littke and Fu, who used P*t*Bu$_3$ in palladium-catalyzed C–C bond formation,[4] by Glorius and co-workers, who used bulky carbenes as supporting ligands,[47] and by Buchwald and co-workers, who used (biphenyl)phosphines in C–N and C–C bond-forming reactions.[6,40,53,54] In these reports, the ability of the system to generate monoligated [PdL] species was proposed to be very important in the rate of catalysis.

Strieter, Blackmond, and Buchwald recently reported that the bulkiness of the phosphine group controls not only the catalytic activity of palladium complexes in amination reactions, but also the rate of the activation of the catalyst.[53] They used reaction calorimetry to study the amination of *p*-chlorotoluene with morpholine in the presence of catalytic systems, which comprised mixtures of Pd(OAc)$_2$ and different biaryl phosphines. With the trisubstituted isopropyl biaryl phosphine **5** (see Scheme 3), higher initial rates were observed relative to those observed with the less sterically demanding P*t*Bu$_2$(bph) phosphine (**4a**). In an additional experiment, the reactivities of the catalyst systems with the *ortho*-substituted biaryl phosphines **3c**–**3e** were compared with the reactivity of the trisubstituted biaryl phosphine **5**. Across the series **5**, **3c, 3d**, and **3e**, a 10-fold difference in the reaction rate was observed, and the highest activity was shown for the bulkier phosphine **5**.

In these studies, it was also demonstrated that the amine has an important effect on the activation of the catalyst. When the catalyst system derived from **3c**–**3e** was preincubated with the amine, although the initial rate was increased in comparison to the corresponding system without preincubation, the subsequent reactions displayed a decrease in the rate. In contrast, the preincubation of the phosphine **5** with the amine did not seem to influence the initial rates of consecutive reactions. This implicates the amine in the activation of the catalyst and indicates that the less bulky ligands **3c**–**3e** require longer exposure to the amine to reach a steady-state concentration of the active catalyst.

The sensitivity of the activation of the catalyst to the size of the phosphine suggests that dissociation of the phosphine from a diphosphine–palladium(II) species takes place. On the basis of the results described above, Strieter, Blackmond, and Buchwald proposed a mechanism in which monophosphine–palladium species are formed by the dissociation of [PdX$_2$(PR$_3$)$_2$] (see Scheme 10).[53] Slow dissociation (observed



Scheme 10. Mechanism for the generation of [PdL] catalytically active species (L = biaryl phosphine) proposed by Strieter, Blackmond, and Buchwald on the basis of calorimetric studies (see Reference [53]).

for the less bulky phosphines) of the palladium(II) complexes resulted in slower activation of the catalyst. This clearly indicates the important relationship between the steady-state concentration of the palladium catalysts and the size of the supporting phosphine.

 © 2005 Wiley-VCH Verlag GmbH & Co. KGaA, Weinheim

3.2. The Oxidative Addition Step

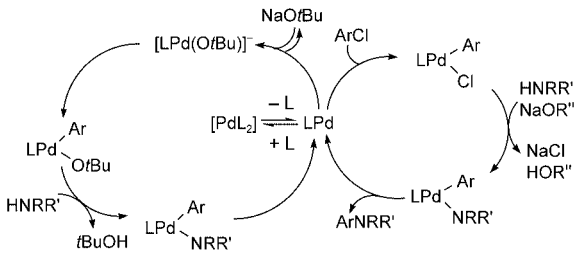
Several studies have been carried out to establish the effect of different ligands on the oxidative addition step of the catalytic cycle. Sterically demanding ligands have the ability to stabilize low-coordination palladium complexes (in particular monoligated species) which, owing to their low electron count, are more reactive. On the other hand, electron-donating ligands generate an electron-rich metal complex which undergoes faster oxidative addition reactions.

In a series of papers published in the mid 1990's, Hartwig and co-workers proposed monoligated palladium species as important intermediates in the catalytic amination of aryl halides using P(*o*-tolyl)$_3$ as a supporting ligand.[55] The oxidative addition of various aryl halides to [Pd{P(*o*-tolyl)$_3$}$_2$] generated the palladium(II) dimer [Pd$_2$Ar$_2$(μ-X)$_2${P(*o*-tolyl)$_3$}$_2$] where only one phosphine per palladium was present. Kinetic data demonstrated that this dimetallic compound was formed by oxidative addition to the monoligated species [Pd{P(*o*-tolyl)$_3$}] through a dissociative mechanism.[56–58]

More recently, Brown and co-workers[59] showed the mechanism of oxidative addition to [Pd(PR$_3$)$_2$] complexes to be highly sensitive to the bulkiness of PR$_3$ (where PR$_3$ = PCy$_n$*t*Bu$_{3-n}$, n = 0, 1, 2, 3). Complexes with PR$_3$ = P*t*Bu$_3$ or PCy*t*Bu$_2$ undergo oxidative addition with aryl halides by a dissociative mechanism, whereas [Pd(PR$_3$)$_2$] complexes with the less bulky phosphines PCy$_2$*t*Bu and PCy$_3$ follow an associative mechanism. The dissociative mechanism for the bulkier phosphines has been substantiated by the recent isolation by Hartwig and co-workers of a series of tricoordinated palladium(II) compounds with general formula [Pd(Ph)X(PR$_3$)] (PR$_3$ = PAd*t*Bu$_2$, P*t*Bu$_3$, or (Ph$_5$Fc)P*t*Bu$_2$; X = Br, I, or OTf).[60,61] These complexes were obtained in good yields by treating the phenyl halides with either [Pd(PR$_3$)$_2$] or with mixtures of [Pd(dba)$_2$] and one equivalent of the corresponding phosphine. This suggests that the tricoordinated products are formed through oxidative addition of the phenyl halide to monophosphine–palladium(0) complexes. The rates of oxidative addition reactions to generate the [Pd(Ph)X(PR$_3$)] complexes correlate well with the catalytic rates observed for the corresponding systems in cross-coupling reactions.

The X-ray crystal structures of [Pd(Ph)X(PR$_3$)] revealed that these species have a T-shaped monomeric geometry with the phenyl ring located in a position *trans* to the open coordination site of the metal. The structural characterization also showed weak agostic interactions between the palladium center and a C–H bond from a ligand—this was suggested to be the interaction that stabilizes the unusual geometry of these complexes. More recently, the palladium(II) complexes [Pd(*p*-anisyl)(NAr$_2$)(PR$_3$)] (PR$_3$ = (Ph$_5$Fc)P*t*Bu$_2$, FcP*t*Bu$_2$; Ar = 3,5-(CF$_3$)$_2$C$_6$H$_3$) were reported and their crystal structures revealed the absence of agostic interactions although they also have T-shaped geometries around the palladium center.[62] In the context of palladium-catalyzed coupling reactions, these tricoordinated species are very important because they demonstrate the possibility to obtain monophosphine complexes in which both of the substrates to be coupled are attached to the metal center.[63]

In 2001, Hartwig and co-workers proposed that the catalytic reaction of aryl chlorides with amines in the presence of alkoxide bases occurs by two concurrent mechanisms (see Scheme 11).[64] In one of these mechanisms, the alkoxide base



Scheme 11. Proposed concurrent catalytic cycles for the amination of aryl halides; the left-hand cycle depicts the anionic path.[64]

participates directly in the oxidative addition step to generate a monophosphine anionic active species.[65] This proposed mechanism could explain the observation that several cross-coupling reactions with the same aryl halide substrate and catalyst system required different conditions and reaction times. This is also consistent with the experimental observation that the amination of aryl halides with weak or strong bases require very different temperatures and catalyst loadings.

Despite the increasing interest in the use of palladium–NHC complexes as catalysts in cross-coupling reactions (see Section 2.2), their mechanism of action remains unclear. To gain a better understanding of this process, Caddick, Cloke, and co-workers carried out mechanistic investigations into the catalytic amination of aryl chlorides using [Pd(NHC)$_2$] (where NHC = *cyclo*-C{N(*t*Bu)CH}$_2$).[48] Their studies indicated that the oxidative addition of the aryl chloride is the rate-limiting step, and that the reaction takes place through a dissociative mechanism—as also observed with palladium complexes that contain bulky phosphines. Variable-temperature NMR spectroscopy experiments showed the dissociation of [Pd(Ar)Cl(NHC)$_2$] into the monoligated [Pd(Ar)Cl(NHC)] complex upon heating. Under conditions typical of catalytic amination, it was proposed that this dissociation of the complex into monocarbene–palladium species is the rate-determining step.

3.3. Reductive Elimination of the Final Product

The final step in the catalytic cycle corresponds to the reductive elimination of the coupled product from the metal center (see Scheme 1). It is generally accepted that this step is faster when palladium is coordinated to electron-withdrawing and sterically demanding ligands. It has also been shown that for very bulky ligands, the steric properties dominate over the electronic properties and even electron-donating ligands (such as the phosphines and carbenes discussed so far) accelerate the reductive elimination reaction. Although there are several studies which discuss the reductive elimination step of "classical" cross-coupling catalysts, only a few reports

 © 2005 Wiley-VCH Verlag GmbH & Co. KGaA, Weinheim

have appeared in which this process is analyzed for catalyst systems with bulky and electron-rich ligands that favor monoligated palladium species. This is probably because the reductive elimination step is rarely rate-limiting when these bulky ligands are used.

The reductive elimination of different organic partners to generate C–C, C–N, C–O, and C–S bonds can proceed through different mechanistic pathways.[66–68] The supporting ligands, the ability of the metal complex to dissociate, and the nature of the substrates to be coupled have an important influence on which of the paths is followed. Three-coordinated palladium(II) complexes have often been postulated as the intermediate species that form the coupled product by reductive elimination. Until recently, the implication of such species was postulated mainly from kinetic and computational data. Early kinetic studies by Stille and Loare on C–C bond-forming reactions already suggested that the dissociation of a phosphine group from the palladium(II) complex was required prior to the reductive elimination step.[67] More recently, it was suggested that three-coordinated palladium(II) complexes (with bulky biaryl phosphines) are involved in the formation of diaryl ethers.[34,69] Although the exact mechanism of the reductive elimination step in these reactions is still unknown, Buchwald and co-workers proposed some hypotheses and found that for electron-deficient aryl halides, the most likely mechanism for the reductive elimination involves the transfer of a phenolate group from palladium to the *ipso*-carbon atom of the aryl halide. This intermediate is then converted into the diaryl ether to regenerate the palladium(0) species. In contrast, for electron-rich and electronically neutral aryl halides, the most likely mechanism involves a three-centered transition state.

The importance of three-coordinated palladium(II) intermediates in the reductive elimination step has been recently confirmed by Hartwig and co-workers, who reported the first fully characterized three-coordinated aryl–palladium amido complexes (see Section 3.2).[62] The reaction of 2-thienyl bromide with $[Pd(P\mathit{t}Bu_3)_2]$ in the presence of $KNAr_2$ yielded $[Pd(thienyl)(NAr_2)(P\mathit{t}Bu_3)]$, which was isolated and structurally characterized (analogous complexes with $(Ph_5Fc)P\mathit{t}Bu_2$ and $FcP\mathit{t}Bu_2$ were prepared by treating $[Pd(Ar)Br(PR_3)]$ with $KNAr_2$). Upon heating these complexes in toluene, reductive elimination reactions took place and the corresponding amine was formed. The rate of reductive elimination from the three-coordinated palladium complex $[Pd(p\text{-anisyl})(NAr_2)(P\mathit{t}Bu_3)]$ was compared with the rate of the analogous reaction from the four-coordinated complex $[Pd(p\text{-anisyl})(NAr_2)(dppf)]$ (dppf = 1,1′-bis(diphenylphosphino)ferrocene). The three-coordinated complex underwent reductive elimination at −10 °C to form the triarylamine product in 91% yield and with a half-life of 10 minutes. In contrast, the four-coordinated complex eliminated the triarylamine with a half-time of 55 minutes at 75 °C. These results strongly point toward three-coordinated palladium complex intermediates in the reductive elimination step of the catalytic cycle.

Hartwig and co-workers also recently presented a detailed mechanistic study of the reductive elimination of aryl halides from the dimeric arylpalladium(II) halide complexes $[Pd_2Ar_2(\mu\text{-}X)_2\{P(o\text{-tolyl})_3\}_2]$ (X = Cl, Br, I) upon addition of the hindered alkylphosphines $P\mathit{t}Bu_3$.[72] As stated earlier, it is generally accepted that reductive elimination is faster for complexes with weakly electron-withdrawing ligands because these ligands can remove some electron density from the metal center to generate favorable conditions for the reduction. Consequently, it would be expected that electron-rich phosphines such as $P\mathit{t}Bu_3$ would not favor the reductive elimination step. However, this recent study showed that coordination of $P\mathit{t}Bu_3$ to the palladium center induces reductive elimination of the aryl halide and indicates that the steric properties of this phosphine override its electronic effects.This is an important observation in the context of cross-coupling reactions as it suggests that $P\mathit{t}Bu_3$ indeed has a unique combination of steric and electronic properties to favor both the oxidative addition of the aryl halide (owing to its highly electron-donating properties) and the reductive elimination of the coupled product (owing to its steric bulk).

4. Conclusions and Outlook

The past few years have seen important advances in the development of highly-active catalysts to carry out cross-coupling reactions with unreactive and sterically hindered aryl halide substrates (with particular emphasis on aryl chlorides). To develop these new catalytic systems, a series of sterically demanding and electron-rich phosphine and N-heterocyclic carbene ligands have been employed. As shown throughout this review, there is increasing evidence to suggest that the ability of these ligands to stabilize monoligated palladium species is responsible for their enhanced reactivity. The generation of the catalytically active [PdL] species and the oxidative addition of the aryl halide onto the palladium(0) center are generally considered the rate-limiting steps. The steric bulk of the ligands discussed here has proved to be very important in the stabilization of the unsaturated [PdL] species, which is needed to initiate the catalytic cycle. Also, the electron-rich properties of the ligands favor the oxidative addition of the aryl halide onto the palladium(0) center even when the substrate is sterically hindered and unreactive. Besides their implication in cross-coupling reactions, unsaturated [PdL] complexes have also been invoked as the catalytically active species in some highly selective and efficient telomerization reactions.

The success of the systems described here provides a good basis for a more rational approach to the design and development of new catalytic systems for cross-coupling reactions. Important structure–activity relationships have been already established which open possibilities for the design of more-active and general catalytic systems. An important challenge remains the search for catalytic systems that not only activate unreactive aryl halides but also C–H bonds. Furthermore, the knowledge that has already been generated should stimulate the investigation of other organometallic transformations that could benefit from these ligand/metal systems.

 © 2005 Wiley-VCH Verlag GmbH & Co. KGaA, Weinheim

The authors thank the ICIQ Foundation for financial support and the EPSRC for a project studentship (U.C.).

Received: July 5, 2004

[1] R. R. Tykwinski, *Angew. Chem.* **2003**, *115*, 1604 – 1606; *Angew. Chem. Int. Ed.* **2003**, *42*, 1566 – 1568.
[2] K. Tamao, N. Miyaura, *Top. Curr. Chem.* **2002**, *219*, 1 – 9.
[3] J. F. Hartwig, *Acc. Chem. Res.* **1998**, *31*, 852 – 860.
[4] A. F. Littke, G. C. Fu, *Angew. Chem.* **2002**, *114*, 4350 – 4386; *Angew. Chem. Int. Ed.* **2002**, *41*, 4176 – 4211.
[5] J. P. Wolfe, S. Wagaw, J.-F. Marcoux, S. L. Buchwald, *Acc. Chem. Res.* **1998**, *31*, 805 – 818.
[6] A. R. Muci, S. L. Buchwald, *Top. Curr. Chem.* **2002**, *219*, 131 – 209.
[7] N. Miyaura, A. Suzuki, *Chem. Rev.* **1995**, *95*, 2457 – 2483.
[8] D. J. Cárdenas, *Angew. Chem.* **2003**, *115*, 398 – 401; *Angew. Chem. Int. Ed.* **2003**, *42*, 384 – 387.
[9] C. Amatore, A. Jutand, *Acc. Chem. Res.* **2000**, *33*, 314 – 321.
[10] W. A. Herrmann, K. Öfele, D. von Preysing, S. K. Schneider, *J. Organomet. Chem.* **2003**, *687*, 229 – 248.
[11] I. P. Beletskaya, *Pure Appl. Chem.* **1997**, *69*, 471 – 476.
[12] M. Beller, *Angew. Chem.* **1995**, *107*, 1436 – 1437; *Angew. Chem. Int. Ed. Engl.* **1995**, *34*, 1316 – 1317.
[13] T. H. Riermeier, A. Zapf, M. Beller, *Top. Catal.* **1998**, *4*, 301 – 309.
[14] J. F. Hartwig, *Synlett* **1997**, 329 – 340.
[15] M. Miura, *Angew. Chem.* **2004**, *116*, 2251 – 2253; *Angew. Chem. Int. Ed.* **2004**, *43*, 2201 – 2203.
[16] A. C. Frisch, A. Zapf, O. Briel, B. Kayser, N. Shaikh, M. Beller, *J. Mol. Catal. A* **2004**, *214*, 231 – 239.
[17] *Metal-Catalyzed Cross-Coupling Reactions* (Eds.: F. Diederich, P. Stang), Wiley-VCH, Weinheim, **1998**.
[18] T. Hiyama, E. Shirakawa in *Handbook of Organopalladium Chemistry for Organic Synthesis*, *Vol. 1* (Eds.: E. Negishi, A. de Meijere), Wiley, New York, **2002**, pp. 285 – 309.
[19] T. Yamamoto, M. Nishiyama, Y. Koie, *Tetrahedron Lett.* **1998**, *39*, 2367 – 2370.
[20] A. F. Littke, G. C. Fu, *Angew. Chem.* **1998**, *110*, 3586 – 3587; *Angew. Chem. Int. Ed.* **1998**, *37*, 3387 – 3388.
[21] A. F. Littke, C. Dai, G. C. Fu, *J. Am. Chem. Soc.* **2000**, *122*, 4020 – 4028.
[22] A. F. Littke, G. C. Fu, *Angew. Chem.* **1999**, *111*, 2568 – 2570; *Angew. Chem. Int. Ed.* **1999**, *38*, 2411 – 2413.
[23] A. F. Littke, G. C. Fu, *J. Org. Chem.* **1999**, *64*, 10 – 11.
[24] M. Kawatsura, J. F. Hartwig, *J. Am. Chem. Soc.* **1999**, *121*, 1473 – 1478.
[25] N. A. Beare, J. F. Hartwig, *J. Org. Chem.* **2002**, *67*, 541 – 555.
[26] R. Kuwano, M. Utsunomiya, J. F. Hartwig, *J. Org. Chem.* **2002**, *67*, 6479 – 6486.
[27] M. W. Hooper, J. F. Hartwig, *Organometallics* **2003**, *22*, 3394 – 3403.
[28] M. W. Hooper, M. Utsunomiya, J. F. Hartwig, *J. Org. Chem.* **2003**, *68*, 2861 – 2873.
[29] R. Vilar, D. M. P. Mingos, C. J. Cardin, *J. Chem. Soc. Dalton Trans.* **1996**, 4313 – 4314.
[30] V. Dura-Vila, D. M. P. Mingos, R. Vilar, A. J. P. White, D. J. Williams, *J. Organomet. Chem.* **2000**, *600*, 198 – 205.
[31] J. P. Stambuli, R. Kuwano, J. F. Hartwig, *Angew. Chem.* **2002**, *114*, 4940 – 4942; *Angew. Chem. Int. Ed.* **2002**, *41*, 4746 – 4748.
[32] A. Zapf, A. Ehrentraut, M. Beller, *Angew. Chem.* **2000**, *112*, 4315 – 4317; *Angew. Chem. Int. Ed.* **2000**, *39*, 4153 – 4155.
[33] M. G. Andreu, A. Zapf, M. Beller, *Chem. Commun.* **2000**, 2475 – 2476.
[34] A. Aranyos, D. W. Old, A. Kiyomori, J. P. Wolfe, J. P. Sadighi, S. L. Buchwald, *J. Am. Chem. Soc.* **1999**, *121*, 4369 – 4378.
[35] J. P. Wolfe, R. A. Singer, B. H. Yang, S. L. Buchwald, *J. Am. Chem. Soc.* **1999**, *121*, 9550 – 9561.
[36] J. P. Wolfe, S. L. Buchwald, *Angew. Chem.* **1999**, *111*, 2570 – 2573; *Angew. Chem. Int. Ed.* **1999**, *38*, 2413 – 2416.
[37] a) J. P. Wolfe, H. Tomori, J. P. Sadighi, J. Yin, S. L. Buchwald, *J. Org. Chem.* **2000**, *65*, 1158 – 1174; b) X. Huang, K. W. Anderson, D. Zim, L. Jiang, A. Klapars, S. L. Buchwald, *J. Am. Chem. Soc.* **2003**, *125*, 6653 – 6655.
[38] D. Zim, S. L. Buchwald, *Org. Lett.* **2003**, *5*, 2413 – 2415.
[39] J. Yin, M. P. Rainka, X.-X. Zhang, S. L. Buchwald, *J. Am. Chem. Soc.* **2002**, *124*, 1162 – 1163.
[40] S. D. Walker, T. E. Barder, J. R. Martinelli, S. L. Buchwald, *Angew. Chem.* **2004**, *116*, 1907 – 1912; *Angew. Chem. Int. Ed.* **2004**, *43*, 1871 – 1876.
[41] U. Christmann, R. Vilar, A. J. P. White, D. J. Williams, *Chem. Commun.* **2004**, 1294 – 1295.
[42] W. A. Herrmann, C.-P. Reisinger, M. Spiegler, *J. Organomet. Chem.* **1998**, *557*, 93 – 96.
[43] K. Selvakumar, A. Zapf, M. Beller, *Org. Lett.* **2002**, *4*, 3031 – 3033.
[44] M. S. Viciu, R. A. Kelly III, E. D. Stevens, F. Naud, M. Studer, S. P. Nolan, *Org. Lett.* **2003**, *5*, 1479 – 1482.
[45] M. S. Viciu, R. M. Kissling, E. D. Stevens, S. P. Nolan, *Org. Lett.* **2002**, *4*, 2229 – 2231.
[46] G. A. Grasa, M. S. Viciu, J. Huang, S. P. Nolan, *J. Org. Chem.* **2001**, *66*, 7729 – 7737.
[47] G. Altenhoff, R. Goddard, C. W. Lehmann, F. Glorius, *Angew. Chem.* **2003**, *115*, 3818 – 3821; *Angew. Chem. Int. Ed.* **2003**, *42*, 3690 – 3693.
[48] A. K. De Lewis, S. Caddick, F. G. N. Cloke, N. C. Billingham, P. B. Hitchcock, J. Leonard, *J. Am. Chem. Soc.* **2003**, *125*, 10066 – 10073.
[49] C. W. K. Gstöttmayr, V. P. W. Bohm, E. Herdtweck, M. Grosche, W. A. Herrmann, *Angew. Chem.* **2002**, *114*, 1421 – 1423; *Angew. Chem. Int. Ed.* **2002**, *41*, 1363 – 1365.
[50] R. Jackstell, A. Frisch, M. Beller, D. Röttger, M. Malaun, B. Bildstein, *J. Mol. Catal. A* **2002**, *185*, 105 – 112.
[51] R. Jackstell, G. A. Andreu, A. Frisch, K. Selvakumar, A. Zapf, H. Klein, A. Spannenberg, D. Röttger, O. Briel, R. Karch, M. Beller, *Angew. Chem.* **2002**, *114*, 1028 – 1031; *Angew. Chem. Int. Ed.* **2002**, *41*, 986 – 989.
[52] O. Navarro, R. A. Kelly III, S. P. Nolan, *J. Am. Chem. Soc.* **2003**, *125*, 16194 – 16195.
[53] E. R. Strieter, D. G. Blackmond, S. L. Buchwald, *J. Am. Chem. Soc.* **2003**, *125*, 13978 – 13980.
[54] H. N. Nguyen, X. Huang, S. L. Buchwald, *J. Am. Chem. Soc.* **2003**, *125*, 11818 – 11819.
[55] J. F. Hartwig, *Angew. Chem.* **1998**, *110*, 2154 – 2177; *Angew. Chem. Int. Ed.* **1998**, *37*, 2046 – 2067.
[56] F. Paul, J. Patt, J. F. Hartwig, *J. Am. Chem. Soc.* **1994**, *116*, 5969 – 5970.
[57] J. Louie, J. F. Hartwig, *J. Am. Chem. Soc.* **1995**, *117*, 11598 – 11599.
[58] F. Paul, J. Patt, J. F. Hartwig, *Organometallics* **1995**, *14*, 3030 – 3039.
[59] E. Galardon, S. Ramdeehul, J. M. Brown, A. Cowley, K. K. Hii, A. Jutand, *Angew. Chem.* **2002**, *114*, 1838 – 1841; *Angew. Chem. Int. Ed.* **2002**, *41*, 1760 – 1763.
[60] J. P. Stambuli, M. Buehl, J. F. Hartwig, *J. Am. Chem. Soc.* **2002**, *124*, 9346 – 9347.
[61] J. P. Stambuli, C. D. Incarvito, M. Buehl, J. F. Hartwig, *J. Am. Chem. Soc.* **2004**, *126*, 1184 – 1194.
[62] M. Yamashita, J. F. Hartwig, *J. Am. Chem. Soc.* **2004**, *126*, 5344 – 5345.
[63] The existence of 14-electron T-shaped palladium complexes as intermediates in cross-coupling reactions has been previously questioned (see reference [70]). It was initially believed that

 © 2005 Wiley-VCH Verlag GmbH & Co. KGaA, Weinheim

such species would be too unstable to be detected or isolated under cross-coupling reaction conditions. In several of the T-shaped structures recently reported by Hartwig and co-workers, there is a stabilizing agostic interaction; however, in the more recent examples, such an interaction is not observed which indicates that that 14-electron T-shaped palladium(II) complexes can indeed be isolated.

[64] L. M. Alcazar-Roman, J. F. Hartwig, *J. Am. Chem. Soc.* **2001**, *123*, 12905 – 12906.

[65] Amatore, Jutand et al. have proposed that similar species are the active catalysts for cross-coupling and Heck reactions when using different palladium sources/PPh_3 mixtures as the catalyst system. See references [9] and [71] for details.

[66] A. Moravskiy, J. K. Stille, *J. Am. Chem. Soc.* **1981**, *103*, 4182 – 4186.

[67] M. K. Loar, J. K. Stille, *J. Am. Chem. Soc.* **1981**, *103*, 4174 – 4181.

[68] P. J. Stang, M. H. Kowalski, M. D. Schiavelli, D. Longford, *J. Am. Chem. Soc.* **1989**, *111*, 3347 – 3356.

[69] R. A. Widenhoefer, S. L. Buchwald, *J. Am. Chem. Soc.* **1998**, *120*, 6504 – 6511.

[70] J. A. Casares, P. Espinet, G. Salas, *Chem. Eur. J.* **2002**, *8*, 4843 – 4853.

[71] C. Amatore, A. A. Bahsoun, A. Jutand, G. Meyer, A. N. Ntepe, L. Ricard, *J. Am. Chem. Soc.* **2003**, *125*, 4212 – 4222.

[72] A. H. Roy, J. F. Hartwig, *J. Am. Chem. Soc.* **2004**, *126*, 1533 – 1541.

E. Heilbronner / F. A. Miller

A Philatelic Ramble through Chemistry

278 pages with 1025 color reproductions.
Softcover. € 79.00/ sFr 116.00.
ISBN 3-906390-31-4

A Philatelic Ramble through Chemistry is a light-hearted, historically based survey of chemistry and some related topics in physics. It is illustrated with more than 1000 beautiful color reproductions of postage stamps and covers. Many stories and anecdotes have been included. The book provides delightful personal reading and may be useful for courses on the history of chemistry. It is a source of numerous anecdotes which instructors can use to enliven their lectures.

€ -price is available only for Germany.

Wiley-VCH, Postfach 10 11 61, 69451 Weinheim, Germany
Fax: +49 (0) 6201 606-184, e-Mail: service@wiley-vch.de,
www.wiley-vch.de



Softcover edition!

Praise for the Hardcover Edition

'This is a gem of a book. [...] I recommend it to all those to whom chemistry means more than an academic discipline, but a multi-faceted part of human culture, as Heilbronner and Miller so beautifully demonstrated.'
Interdisciplinary Science Reviews

'The creation of an exceptional book must be driven not only by knowledge but also by passion. This book by two chemists, Heilbronner and Miller, is clearly the product of a love for the world of postage stamps as well for chemistry in its widest sense.'
Advanced Materials



14170409_vo

WILEY-VCH

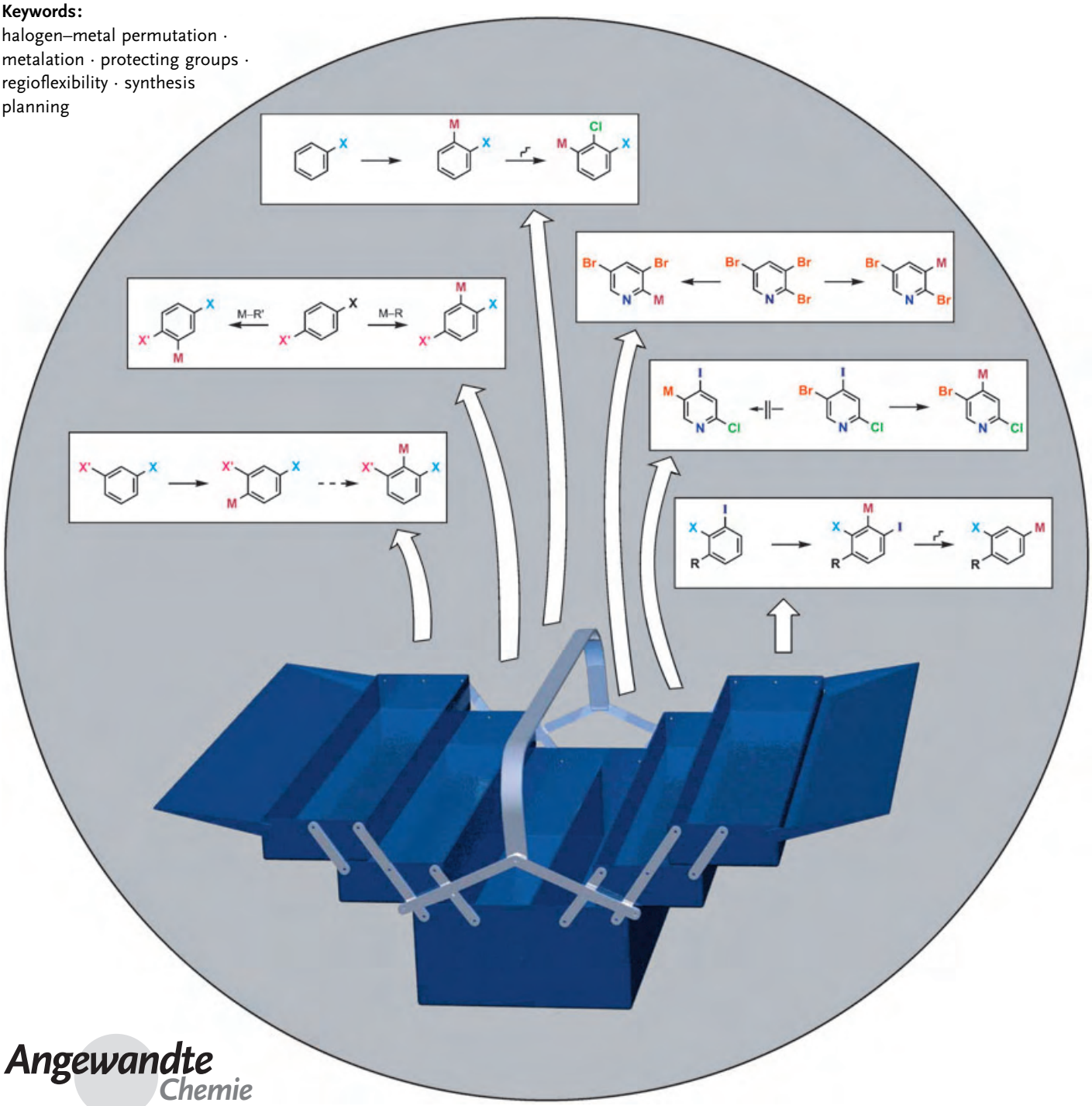
© 2005 Wiley-VCH Verlag GmbH & Co. KGaA, Weinheim

Synthesis Strategies

The 2 × 3 Toolbox of Organometallic Methods for Regiochemically Exhaustive Functionalization

*Manfred Schlosser**

Keywords:
halogen–metal permutation · metalation · protecting groups · regioflexibility · synthesis planning



© 2005 Wiley-VCH Verlag GmbH & Co. KGaA, Weinheim
DOI: 10.1002/anie.200300645

This Review describes a concept aimed at rational and maximal structure proliferation. To this end, simple aromatic or heterocyclic starting materials, often bulk chemicals, are converted into all regionisomerically possible polar organometallic intermediates (mostly lithiated species), which then may be combined with any of the countless electrophiles to provide attractive new building blocks, particularly functionalized derivatives. The practical implementation relies on a set ("toolbox") of sophisticated recipes developed by mechanistically guided modification of the two most prominent exchange methods used for the generation of polar organometallic compounds: hydrogen–metal and halogen–metal interconversion. These mutant methods ("old methods in a new outfit") amplify the existing options for organic synthesis by ensuring maximum regioflexibility. At the same time they offer new insight into factors that govern organometallic reactivity and provide hints on how to alter or finetune this reactivity judiciously.

From the Contents

1. Introduction 377

2. Regioflexibility in Hydrogen–Metal Exchange 377

3. Regioflexibility in Halogen–Metal Exchange 385

4. Synopsis, Perspectives, and Outlook 390

1. Introduction

"There remains no fundamentally new synthetic method to be discovered, at least not in main group chemistry."[1] This sentence gives the general sense of a statement written more than a decade ago which was widely regarded as provocative, although its truth is evident. The knowledge of organic reactions has attained a level of completeness and sophistication that makes it inconceivable that a major mode of reactivity has remained unidentified. This should by no means discourage us from exploring novel modifications and applications of known methods or to test new combinations of methods. The situation resembles cartography at the beginning of the 20th century. After the expeditions of Livingstone, Stanley, Hedin and many other heroic explorers, there was no empty space left on the globe. Nevertheless, one had to wait for the survey by satellites before all the missing details could be filled in. Furthermore, even nowadays one must keep track of the continuous changes in the terrestrial profile caused by climatic effects or by human activities such as diking polders or building dams.

Any synthetic method is characterized by its scope and limitations. Thus, an extension of its application will inevitably alter its track record and, as a corollary, its perceived potential. Moreover, when exposed to a new scenario, methods are rarely reproduced exactly but are generally adapted to the task by appropriate modifications. In this respect, synthetic methods can be compared to living organisms subject to evolutionary pressure, which manifests itself in mutations and metamorphosis if not reincarnation.

The choice of a method, no matter whether in its original or in an adapted version, must clearly be subordinated to the purpose. The endeavors summarized in the present Review were aimed at the elaboration of procedures that enable the substitution and, in particular, the functionalization of simple and inexpensive starting materials, so-called bulk chemicals, at any vacant position. On this basis, we suggest *regiochemically exhaustive functionalization* as a new benchmark for structural proliferation. The practical realization of the concept relies on a set ("toolbox") of tailormade organometallic methods ("mutant methods") which have been developed by adjusting the *two* most widespread modes for the generation of polar organometallic intermediates, the hydrogen–metal and halogen–metal interconversion reactions, each in *three* directions ("2×3").[2] The accomplishments underscore once again the virtues of the organometallic approach, in particular its simplicity and versatility.

2. Regioflexibility in Hydrogen–Metal Exchange

The permutational hydrogen–metal interconversion belongs to the family of acid–base reactions and one might thus expect the least-basic organometallic product to form preferentially or exclusively. Fortunately, however, the real outcome depends on several factors such as inductive electron withdrawal, metal coordination, and steric hindrance, the interplay of which can be modulated by the reaction conditions. This offers the opportunity to discriminate between competing pathways and, under favorable conditions, to control the outcome of a reaction by orienting it at will in any one of two or three possible directions.

[*] Prof. M. Schlosser
Institute of Chemical Sciences (ISIS)
École Polytechnique Fédérale, BCh
CH-1015 Lausanne (Switzerland)
Fax: (+41) 21-693-9365
E-mail: manfred.schlosser@epfl.ch
and
Faculté des Sciences
Université, BCh
CH-1015 Lausanne (Switzerland)

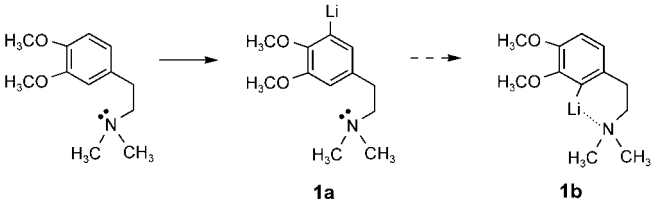
 DOI: 10.1002/anie.200300645 © 2005 Wiley-VCH Verlag GmbH & Co. KGaA, Weinheim

2.1. The Second-Chance Bonus: Thermodynamics versus Kinetics

Transition states and ground states do not necessarily reflect the influence of structural parameters to the same or to a proportional degree. For example, steric hindrance or coordinative assistance may, but need not, affect rates differently than equilibrium positions.

2.1.1. Steric Hindrance versus Electronic Stabilization

The first documented example of a conflict between steric accessibility and coordinative binding featured 2-(3,4-dimethoxyphenyl)ethyl-*N*,*N*-dimethylamine ("tetramethyldopamine") as the substrate.[3] When this reagent was treated with butyllithium at −75 °C in a 97:3 mixture of diethyl ether and *N*,*N*,*N*′,*N*′-tetramethylethylenediamine (TMEDA), metalation occurred at the unhindered 5-position. However, at +25 °C the initially produced intermediate **1a** slowly (in the course of 15 h; incomplete experimental details) displaced the metal by transmetalation to the 2-position (isomer **1b**) where coordination with the nitrogen-bearing side chain provides extra stability (Scheme 1).

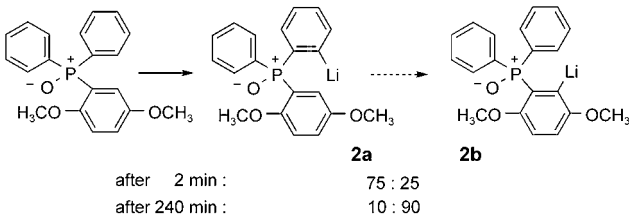


Scheme 1. Basicity-lowering isomerization of intermediate **1a** by transmetalation [Tool 2.1].

As the regioisomeric composition of the crude mixtures has never been rigorously established, a mutual contamination of the isomeric species **1a** and **1b**, one dominant at −75 °C and the other at +25 °C, cannot be ruled out. A careful investigation[4] of the reaction between (2,5-dimethoxyphenyl)diphenylphosphine oxide and *tert*-butyllithium did, indeed, reveal imperfect regioselectivity after short and long metalation times. The more-basic and the less-basic intermediate **2a** and **2b** were present in 75:25 and 10:90 ratios when quenched after 2 and 240 min, respectively (Scheme 2).[4]

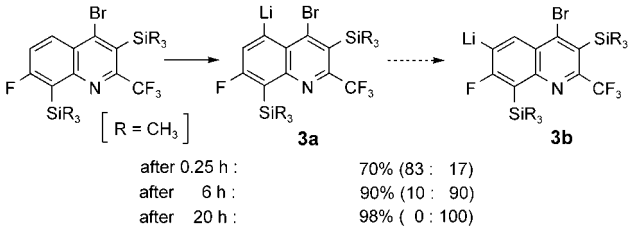


Manfred Schlosser was born in Ludwigshafen (Germany). He studied chemistry (and, to a lesser extent, medicine) at the University of Heidelberg (PhD 1960, Prof. Georg Wittig). After his habilitation in Heidelberg (1966), he became Senior Physician at the German Cancer Center in Heidelberg. In 1971 he succeeded Prof. Jiři Sicher at the University of Lausanne, from where his laboratory was later transferred to the Federal Institute of Technology. A significant part of his research is aimed at a deeper understanding of chemical reactivity in general and the behavior of organometallic species in particular.



Scheme 2. Basicity-lowering incomplete isomerization of intermediate **2a** by transmetalation [Tool 2.1].

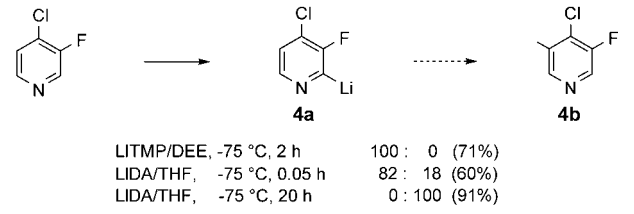
When 4-bromo-7-fluoro-2-trifluoromethyl-3,8-bis(trimethylsilyl)quinoline was treated with lithium diisopropylamide (LIDA) in tetrahydrofuran at −75 °C, deprotonation occurred concomitantly at the 5- and 6-positions in a 5:1 ratio.[5] The major intermediate **3a** then isomerized slowly, but ultimately completely to the less-basic component **3b**[5] (Scheme 3). The



Scheme 3. Basicity-lowering isomerization of intermediate **3a** by transmetalation [Tool 2.1].

initial preference for the 5-lithio species can be tentatively attributed to inductive neighboring-group assistance provided by the bromine atom and to a buttressing effect[6–9] exerted by the 8-trimethylsilyl substituent discriminating against attack at the 6-position.

Perfect optional site selectivity was achieved when 4-chloro-3-fluoropyridine served as the substrate.[10] With LIDA in tetrahydrofuran at −75 °C virtually the same scenario as described in the preceding paragraph was encountered. After 3 min, two metalated species **4a** and **4b** were present (82:18 ratio) and it took again 20 h until regioisomeric homogeneity in favor of the more-stable isomer **4b** was reached (Scheme 4). The more-basic isomer **4a** can be generated



Scheme 4. Basicity-lowering isomerization of intermediate **4a** by transmetalation [Tool 2.1].

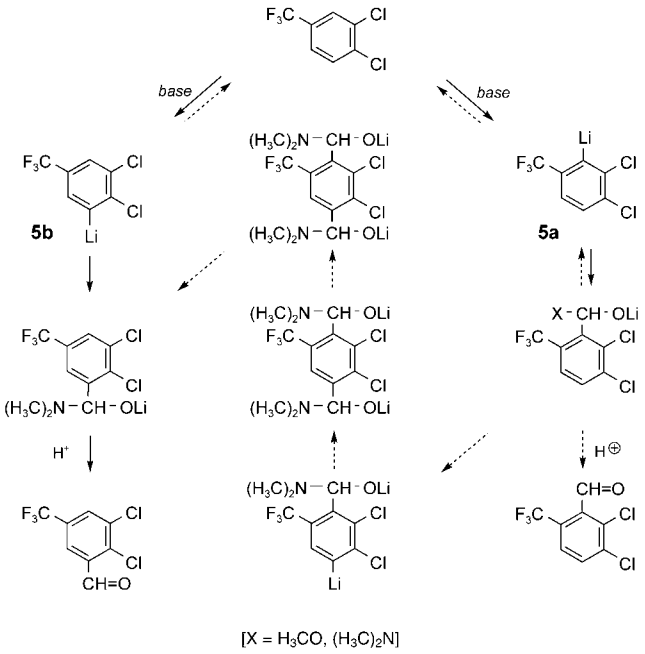
with lithium 2,2,6,6-tetramethylpiperidide (LITMP) in diethyl ether at −75 °C exclusively, under conditions in which transmetalation and consequently equilibration are negligible. The kinetic preference for the 2-position is dictated by the

 © 2005 Wiley-VCH Verlag GmbH & Co. KGaA, Weinheim

tendency of the metal-bearing base to dock at the nitrogen atom of the heterocyclic ring, an interaction that is particularly effective in solvents of low polarity.

2.1.2. Coupled Equilibria

A spontaneous "uphill equilibration" of an organometallic species into a more-basic isomer would, of course, violate the laws of thermodynamics. It can nevertheless be realized if the equilibration is coupled to trapping steps, one of which is reversible and the other not. As disclosed in patents of the Nippon Soda Company,[11,12] butyllithium in tetrahydrofuran at −75 °C promotes the metalation of 3,4-dichlorobenzotrifluoride at the 2-position. The subsequent addition of methyl formate afforded a transient *O*-lithiated hemiacetal which spontaneously eliminated lithium methoxide to release the 2,3-dichloro-6-(trifluoromethyl)benzaldehyde.[11] In contrast, when the intermediate **5a** was intercepted with *N*,*N*-dimethylformamide instead and the reaction mixture kept at +25 °C for several hours before being neutralized, the former aldehyde and the isomeric 2,3-dichloro-5-(trifluoromethyl)-benzaldehyde were obtained in a 1:7 ratio (Scheme 5).[12] Recently, the temperature-controlled regiodivergence of aryllithium formylations has been successfully extended to 1,2,4-trichlorobenzene.[13]

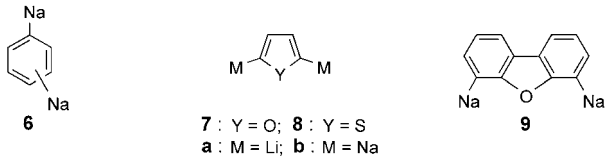


Scheme 5. Acid–base equilibria promoting the spontaneous, though slow conversion of an initially formed *O*-lithiated hemiaminal into a sterically less-congested isomer, each of them being the precursor to a different aldehyde [Tool 2.1].

The mechanistic implications are not yet elucidated. The direct interconversion of two *O*-lithio hemiaminals formed by addition of the species **5a** and **5b** to *N*,*N*-dimethylformamide through reversible decomposition to the precursor components appears feasible. Based on experimental and computational gas-phase acidities in this series,[14,15] the free energies of the competing organolithium reagents **5a** and **5b** can be estimated to differ by not much more than 1 kcal mol^{-1}. Alternatively, the more congested *O*-lithio hemiaminal (derived from **5a**) could isomerize to the less-hindered one (derived from **5b**) via an *O*,*O*′-dilithiated bishemiaminal. In either case, accidentally formed dimethylamine and lithium dimethylamide would have to mediate the protonation and deprotonation steps.

2.1.3. Mono- versus Dimetalation

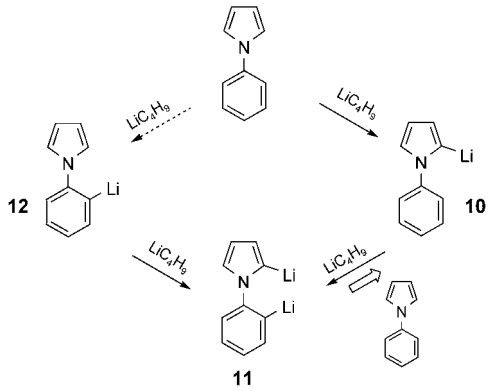
Dimetalated compounds such as phenylenedisodium (**6**; as a mixture of *meta* and *para* isomers),[16,17] furan-2,5-diyldisodium (**7a**),[18] furan-2,5-diyldilithium (**7b**),[19] thiophene-2,5-disodium (**8a**),[20] thiophene-2,5-diyldilithium (**8b**),[19] and dibenzofuran-4,6-diyldisodium (**9**)[21,22] have been known for a long while (Scheme 6). Their synthetic value is quite limited as they can only lead to symmetrically



Scheme 6. A few typical (het)arenediyldimetal reagents.

substituted derivatives. One can generally preclude the generation of dimetalated species by avoiding any excess of the metalating reagent and by working in a solvent of sufficient polarity such as tetrahydrofuran.

Despite such precautions, organodimetallic reagents may nevertheless emerge along with the monometalated species. This happens to be the case with *N*-phenylpyrrole (Scheme 7).[23] Upon treatment with butyllithium in neat diethyl ether and in the presence of TMEDA mainly the α,*o*-dilithio species **11** is produced via the α-lithio intermediate **10** (not the *o*-lithio intermediate **12**).[23] Evidently, neighboring-group assistance[24] provided by the C$^{\alpha}$–Li bond that is formed first confers a kinetic advantage on the second metalation step. However, the *N*-*o*-phenylene-α-pyrryldilithium is ther-



Scheme 7. Removing the undesired dimetalated species **11** by its "incubation" with the metal-free precursor *N*-phenylpyrrole [Tool 2.1].

 © 2005 Wiley-VCH Verlag GmbH & Co. KGaA, Weinheim

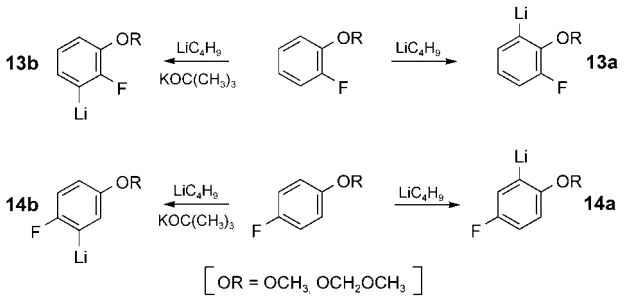
modynamically less stable and therefore slowly reverts to the monometal species **10** by reaction with the unconsumed *N*-phenylpyrrole[23] (Scheme 7).

2.2. Reagent-Modulated Optional Site Selectivity

The mechanism-based matching of neighboring groups and reagents is the easiest way to implement regioflexibility. The concept and its application have already been extensively reviewed.[2b,25,26] Hence only a few highlights will be revisited below and a few recent results added.

2.2.1. Arenes as Substrates

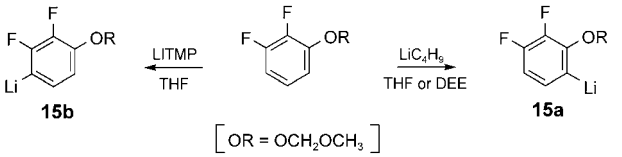
The first authentic case of an optionally site-selective metalation is still a prototypical example. In the presence of butyllithium, both 2- and 4-fluoroanisole were found to undergo clean deprotonation at the position adjacent to the oxygen atom,[27] thus generating the intermediates **13a** and **14a**. Clearly, when entering the transition state as a monomer or dimer rather than as a tetrameric aggregate, the required extra coordination can be easily supplied by the nearby methoxy group. In contrast, when the butyllithium was first complexed with potassium *tert*-butoxide or *N*,*N*,*N*′,*N*″,*N*″-pentamethyldiethylenetriamine (PMDTA) the metalation occurred at the position adjacent to the fluorine atom to give intermediates **13b** and **14b**, again exclusively.[27] As the reagent is optimally coordinated from the beginning in this case, the relative basicities of the organometallic intermediates now become the crucial factor. The superior inductive effect of fluorine relative to oxygen secures a more-efficient stabilization and hence a bigger driving force. As demonstrated recently,[28] the *O*-methoxymethyl-protected 2- and 4-fluorophenols exhibit the same regioselectivity divergence towards free and complexed organolithium bases (Scheme 8).



Scheme 8. Perfectly site-selective metalation of 2- and 4-fluoroanisole at a position either adjacent to the halogen or the oxygen atom [Tool 2.2].

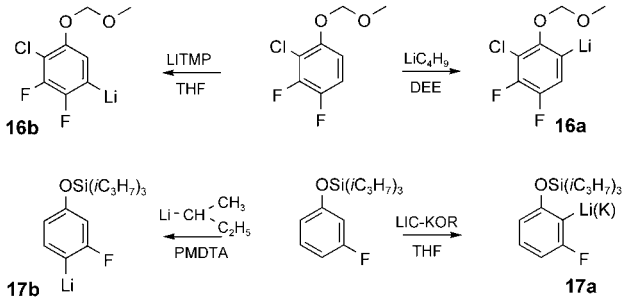
Similar principles apparently govern the case of the *O*-methoxymethyl protected 2,3-difluorophenol. It was found to react with butyllithium at C6 and with LITMP at C4 to afford intermediates **15a** and **15b**, respectively (Scheme 9).[29]

Phenols in general are ideal reagents for tracking optional site selectivities. Butyllithium in diethyl ether at −75 °C



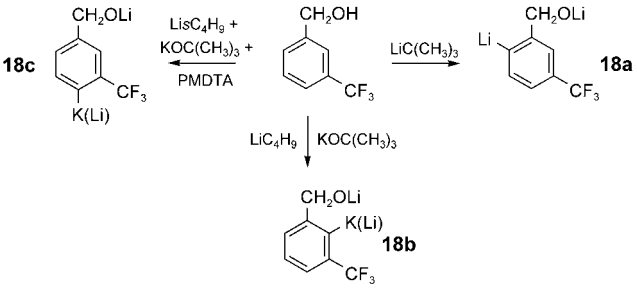
Scheme 9. Optional site selectivity in the metalation of *O*-methoxymethyl-protected 2,3-difluorophenol [Tool 2.2].

abstracts a proton from 3-chloro-1,2-difluoro-4-(methoxymethoxy)benzene at the position adjacent to the oxygen atom, whereas LITMP in tetrahydrofuran (again at −75 °C) metalates the 6-position next to the fluorine atom (intermediates **16a** and **16b**, respectively.[30] The superbasic mixture (LIC-KOR) of butyllithium and potassium *tert*-butoxide attacks 1-fluoro-3-(triisopropylsilyloxy)benzene exclusively at C2 whereas *sec*-butyllithium in the presence of PMDTA reacts preferentially (with a regioselectivity of >90 %) at C4, adjacent to the fluorine atom, giving rise to intermediates **17a** and **17b**, respectively (Scheme 10).[30]



Scheme 10. Optional site selectivity in the metalation of *O*-methoxymethyl-protected 2-chloro-3,4-difluorophenol and *O*-triisopropylsilyl-protected 3-fluorophenol [Tool 2.2].

3-(Trifluoromethyl)benzyl alcohol offers a triple choice of regioselectivity depending on the nature of the metalating reagent employed.[31] Treatment in tetrahydrofuran with *tert*-butyllithium generated the intermediate **18a**, with LIC-KOR the intermediate **18b**, and with *sec*-butyllithium in the presence of PMDTA and potassium *tert*-butoxide the intermediate **18c** (Scheme 11), thus providing 5-trifluoromethyl-2-

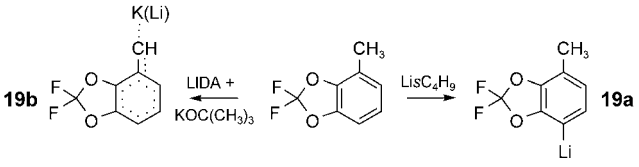


Scheme 11. Optional site-selective generation of three isomeric organometallic reagents starting from the same precursor, 3-(trifluoromethyl)-phenol [Tool 2.2].

 © 2005 Wiley-VCH Verlag GmbH & Co. KGaA, Weinheim

benzofuran-1(3*H*)-one or 7-trifluoromethyl-2-benzofuran-1(3*H*)-one or 4-hydroxymethyl-2-(trifluoromethyl)benzoic acid after trapping with carbon dioxide and subsequent acidification.[31] Although the yields are admittedly poor (12%, 47%, and 25%, respectively), they refer to regioisomerically uncontaminated, isolated products.[31]

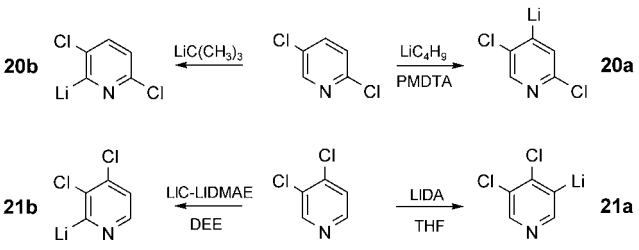
One new example can be added to the impressive list of optional site selectivities discriminating between aromatic and benzylic positions.[26] 2,2-Difluoro-4-methyl-1,3-benzodioxole was deprotonated by *sec*-butyllithium exclusively at C7, thus giving intermediate **19a**, whereas only derivatives of the benzyl metal species **19b** were isolated after treatment with LIDA in the presence of potassium *tert*-butoxide (Scheme 12).[32]



Scheme 12. Optional site-selective deprotonation of 2,2-difluoro-4-methyl-1,3-benzodioxole at either the benzylic or the aromatic 7-position [Tool 2.2].

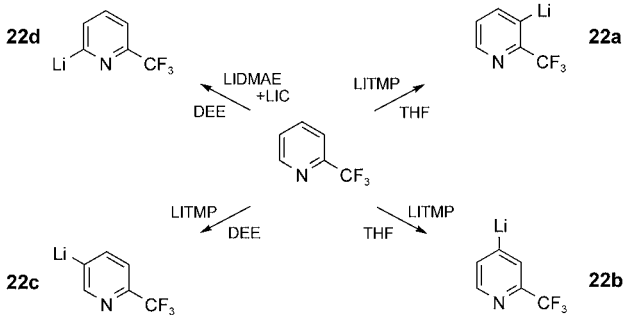
2.2.2. *Heterocycles as Substrates*

2,5-Dichloropyridine reacted with PMDTA-activated butyllithium at the 4-position and with *tert*-butyllithium at the 6-position, thus setting free the intermediates **20a** and **20b**, respectively.[33] The 3,4-isomer underwent deprotonation at the 5-position (intermediate **21a**) when LIDA was used and at the 2-position (intermediate **21b**) when LITMP was used (Scheme 13).[33] The regioselectivity of the latter transformation did not exceed 90%[33] but became quantitative when LITMP was replaced by the Caubère base[34] (i.e., butyllithium in the presence of lithium 2-dimethylaminoethoxide, LIC-LIDMAE).[35]



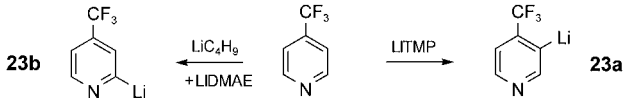
Scheme 13. Optional site selectivity in the metalation of 2,5- and 3,4-dichloropyridine [Tool 2.2].

2-(Trifluoromethyl)pyridine exhibits reagent-dependent selectivity at any of the four vacant positions.[36] When treated with LITMP in tetrahydrofuran at −75 °C for 6 h, selective metalation at C3 gave intermediate **22a**. However, when the reaction was quenched after only 15 min, 3- and 4-substituted derivatives resulting from intermediates **22a** and **22b**, respectively (2:3 ratio).[36] Again, the use of LITMP, but in diethyl ether as the solvent at −75 °C, allowed the preferential metalation of 2-(trifluoromethyl)pyridine at C5 (intermediate **22c**). Finally, deprotonation took place solely at the 6-position (producing intermediate **22d**) when the Caubère base was employed in diethyl ether at −75 °C (Scheme 14).[36]



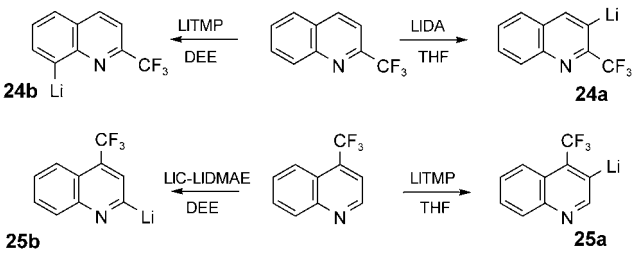
Scheme 14. Optional site selectivity in the metalation of 2-(trifluoromethyl)pyridine [Tool 2.2].

4-(Trifluoromethyl)pyridine has only two different positions. LITMP in tetrahydrofuran abstracted a proton selectively from the 3-position (intermediate **23a**), whereas the Caubère base promoted deprotonation neatly at the 2-position (intermediate **23b**) (Scheme 15).[36]



Scheme 15. Optional site selectivity in the metalation of 4-(trifluoromethyl)pyridine [Tool 2.2].

2-(Trifluoromethyl)quinoline[36] underwent clean metalation in the presence of LIDA at the 3-position to produce intermediate **24a**, whereas LITMP, again in tetrahydrofuran at −75 °C, abstracted protons concomitantly from the 3- and 4-positions (3:2 ratio). However, the latter reagent in diethyl ether (at −75 °C) attacked the 8-position exclusively (intermediate **24b**). 4-(Trifluoromethyl)quinoline[36] reacted with LITMP in tetrahydrofuran at the 3-position and with the Caubère base at the 2-position, thus giving rise to intermediates **25a** and **25b**, respectively (Scheme 16).



Scheme 16. Optional site selectivity in the metalation of 2- and 4-(trifluoromethyl)quinoline [Tool 2.2].

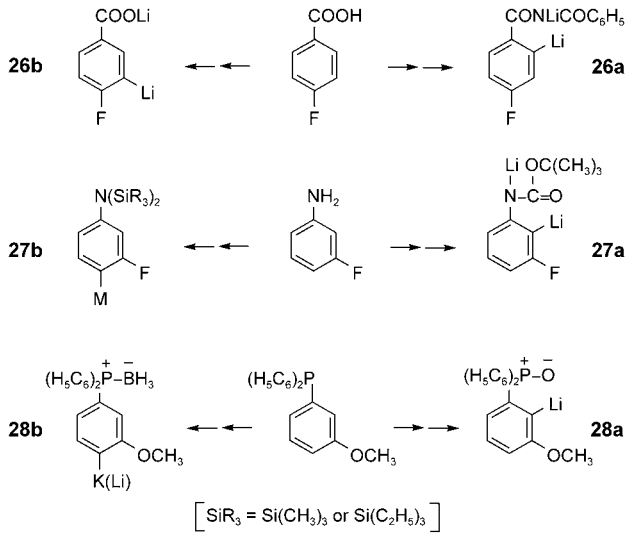
 © 2005 Wiley-VCH Verlag GmbH & Co. KGaA, Weinheim

2.3. Deploying Protecting Groups

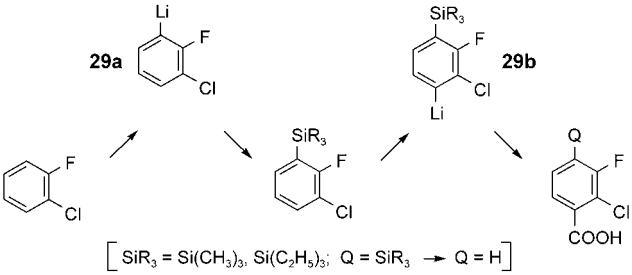
One has to differentiate between a protecting group located directly at a (hetero)aromatic ring or at its periphery. In the latter case, the group is attached to a heteroatom such as oxygen, sulfur, nitrogen, or phosphorus.

2.3.1. Switching Functional Groups On and Off

Although *O*-lithiated carboxy groups do activate neighboring positions towards metalation,[37–39] their effect remains fairly weak unless amplified by an additional electronegative substituent at C3. This enables regioflexibility as most other heterosubstituents outperform a competing lithiooxycarbonyl group by their superior *ortho*-directing power. The lithium salt of 4-fluorobenzoic acid is concomitantly attacked by *sec*- or *tert*-butyllithium at the 2- and 3-positions, whereas excess LITMP exclusively deprotonates the 3-position (up to 86% of trapping product derived from a lithium benzoate **26b**).[38,40] In contrast, the carbonyl group displays a very strong activating effect on its proximal positions when integrated into an *N*-alkyl-, *N*-aryl- or *N*,*N*-dialkylcarbamoyl unit. Thus, 4-fluorobenzanilide is cleanly deprotonated at the C2 (intermediate **26a**).[41] An amino group can be deactivated by replacing the N-bound hydrogen atoms with trialkylsilyl or, alternatively, activated by combining it with an acyl group, for example, *tert*-butoxycarbonyl (Boc).[42] In this way, either the 2- or the 4-position of 3-fluoroaniline can be metalated, generating the species **27a** or **27b**. Finally, oxidation or complexation at the phosphorus center with borane renders triarylphosphines more reactive or less reactive towards organometallic bases, respectively. For example, 3-anisyldiphenylphosphine oxide was smoothly deprotonated by LIDA at the 2-position (intermediate **28a**),[43] whereas the corresponding phosphine–borane adduct reacted solely at the 4-position, remote from the P atom (intermediate **28b**)[43] and this quite sluggishly even when the superbasic LIC-KOR mixture was used. Although the (phosphonio)boronate has a zwitterionic structure like the phosphine oxide, it lacks lone-pair electrons and is hence unable to coordinate organometallic reagents (Scheme 17).



Scheme 17. Selective introduction of a metal at the 2- or 3-position of *p*-fluorobenzoic acid, at the 2- or 4-position of *m*-fluoroaniline, and at the 2- or 4-position of *m*-anisyldiphenylphosphine, depending on the choice of the functionality-protecting group [Tool 2.3].

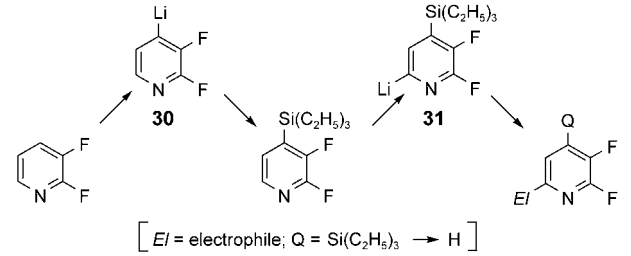


Scheme 18. Deactivation of the more-reactive position adjacent to the fluorine atom in 1-chloro-2-fluorobenzene by the introduction of a trialkylsilyl protecting group [Tool 2.3].

2.3.2. Steric Screening

1-Chloro-2-fluorobenzene undergoes metalation selectively at the position next to the lighter halogen atom (intermediate **29a**).[44] To favor the opposite regioselectivity, in other words, to realize an *o*→*o′ deflection*, one has to block the site adjacent to the fluorine atom by introducing a trialkylsilyl substituent, lithiating again (generating intermediate **29b**), delivering the electrophile, and removing the protecting group (Scheme 18).[9] The latter step can be brought about as a protodesilylation (with acids, bases, or fluoride ions in the presence of proton sources), as a halodesilylation (with molecular bromine or iodine), or even as a nitrodesilylation.

The introduction of a trialkylsilyl group at the 4-position of a pyridine ring shields the neighboring 3- and 5-positions. The reagent can only attack the intrinsically least acidic sites surrounding the nitrogen atom. In this way, 6-substituted derivatives of 2,3-difluoropyridine were prepared via intermediates **30** and **31** (Scheme 19).

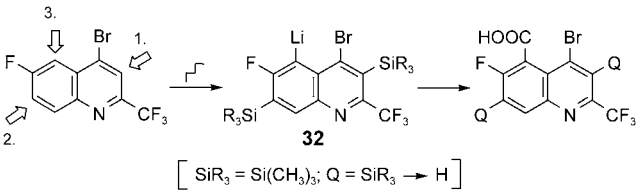


Scheme 19. Blocking the deprotonation of 2,3-difluoropyridine at both the 4- and 5-positions with a bulky 4-triethylsilyl group [Tool 2.3].

Multiple silylation allows one to inactivate progressively the most-reactive sites in a complex substrate and even to open a second battlefield by moving from one ring of an annulated system to the next. Thus, after a first and second

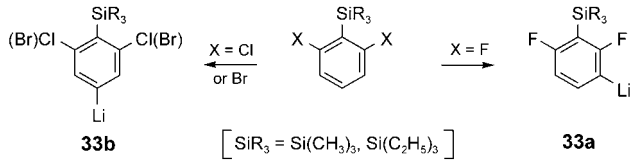
 © 2005 Wiley-VCH Verlag GmbH & Co. KGaA, Weinheim

LIDA-promoted metalation, two trimethylsilyl groups could be successively introduced at the 3- and 7-positions of 4-bromo-6-fluoro-2-(trifluoromethyl)quinoline before the third lithiation at the 5-position (Scheme 20). Carboxylation of the intermediate **32** and subsequent deprotection afforded the 4-bromo-6-fluoro-2-(trifluoromethyl)quinoline-5-carboxylic acid (Q = H) as the final product.[5]



Scheme 20. Blocking the deprotonation of 4-bromo-6-fluoro-2-(trifluoromethyl)quinoline at the 3-, 7-, and 8-positions with two 3,7-trimethylsilyl groups [Tool 2.3].

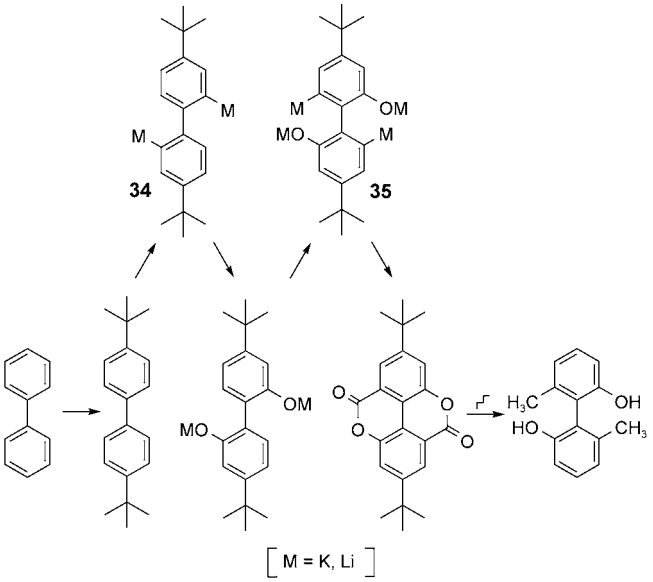
Possible complications may originate from the bulkiness of the trialkylsilyl groups and may distort the regular substrate behavior. Alkyl lithium reagents and lithium dialkyl amides abstract a proton exclusively from the halogen-neighboring 4-position of 1,3-difluoro-2-(trialkylsilyl)benzene derivatives to generate intermediates **33a**, whereas the corresponding 1,3-dichloro-2-(trialkylsilyl)benzene compounds react with alkyl lithium reagents or lithium dialkyl amides and the 1,3-dibromo congeners react with LIDA or LITMP preferentially or exclusively at the 5-position (remote to the halogen atom), thus giving rise to the intermediates **33b** (Scheme 21).[45,46] Details of how this untypical *buttressing effect* operates are not yet clear.[48–50]



Scheme 21. Deprotonation of (2,6-dihalophenyl)trialkylsilanes deflected from the 4- to the 5-position when the halogen is chlorine or bromine.

Trimethylsilyl groups have been sporadically used in earlier work to deactivate otherwise more-acidic sites. However, as they may undergo deprotonation themselves,[51,52] it is often deemed advisable to replace them with triethylsilyl[46,47,53] or, occasionally, even with triisopropylsilyl[17] groups.

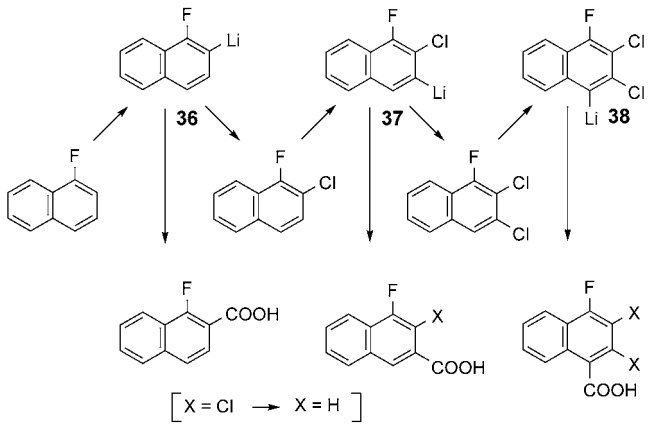
Any bulky substituent, in particular tertiary alkyl groups, can fulfill the same task. 1,3-Di(*tert*-butyl)benzene was metalated by the LIC-KOR superbase exclusively at the 5-position.[54] Two *tert*-butyl groups were readily introduced at the 4,4′-positions of biphenyl.[55] Subsequent treatment with 2 equivalents of LIC-KOR followed by fluorodimethoxyborane and hydrogen peroxide gave, via intermediate **34**, the 4,4′-di(*tert*-butyl)biphenyldiyl-2,2′-diol (OM = OH).[56] A second double metalation generates intermediate **35**, and trapping with carbon dioxide converts it into a bislactone, the carbonyl units of which could be reduced to methyl groups. The final *tert*-butyl deprotection was accomplished with aluminum trichloride as the catalyst and provided the final product 6,6′-dimethylbiphenyl-2,2′-diol (Scheme 22).[56]



Scheme 22. Blocking the base attack at the 3,3′,5,5′-positions of biphenyl by two 4,4′-*tert*-butyl groups [Tool 2.3].

2.3.3. *Blocking the Most Reactive Site and Simultaneous Activation of the Neighboring Position*

When, after metalation, trialkylsilyl groups are introduced into aromatic or heterocyclic substrates, they wipe out the reactivity potential of the formerly most-acidic site and at the time they sterically screen the immediate vicinity against any further attack. As a consequence, *ortho*-protected substrates such as 1-fluoro-2-(triethylsilyl)naphthalene[57] (Scheme 23) prove to be completely inert towards organometallic reagents,



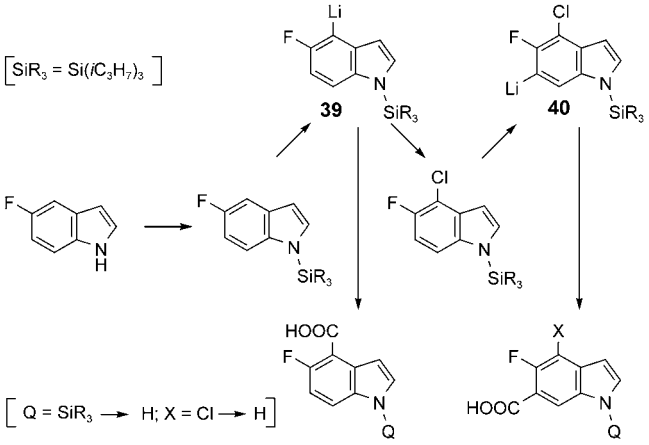
Scheme 23. Deflection of the base attack from the 2- to the 3- and 4-positions of 1-fluoronaphthalene by site-protecting chlorine atoms [Tool 2.3].

 © 2005 Wiley-VCH Verlag GmbH & Co. KGaA, Weinheim

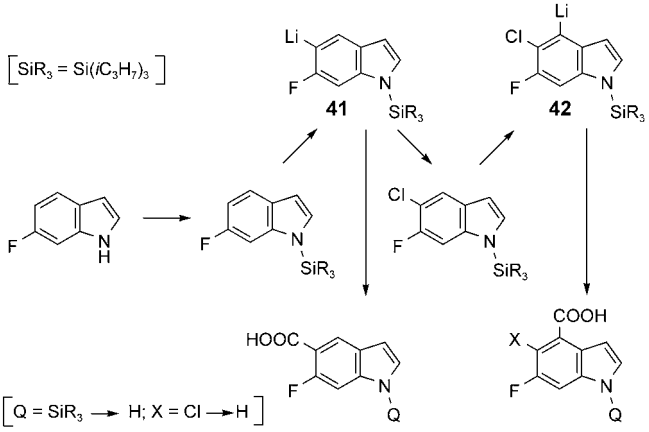
including superbases. In contrast, 2-chloro-1-fluoronaphthalene (prepared via intermediate **36**) readily underwent metalation at the 3-position now activated by the neighboring halogen (intermediate **37**; Scheme 23).

When another chlorine atom was introduced at this site, the resulting 2,3-dichloro-1-fluoronaphthalene (98%) was functionalized after a further deprotonation (intermediate **38**), at the 4-position this time. The heavier chlorine atom could be selectively removed by catalytic hydrogenation or reduction with zinc[58] to afford the 4-fluoronaphthalene-1-carboxylic acid (87%).[57].

The potential of chlorine to act simultaneously as a protecting and activating substituent in organometallic synthesis is immense. For reasons of space, the present survey will confine itself to two further examples. Triisopropylsilyl-protected 5-fluoroindole could be readily metalated at the 4- or, after chlorination, 6-positions (intermediates **39** and **40**, respectively) before being trapped with carbon dioxide and deprotected (Scheme 24).[59] In the same way, 6-fluoroindole could be functionalized via the intermediates **41** and **42** to afford the 6-fluoroindole-5-carboxylic acid and 6-fluoroindole-4-carboxylic acid, respectively (Scheme 25).[59]

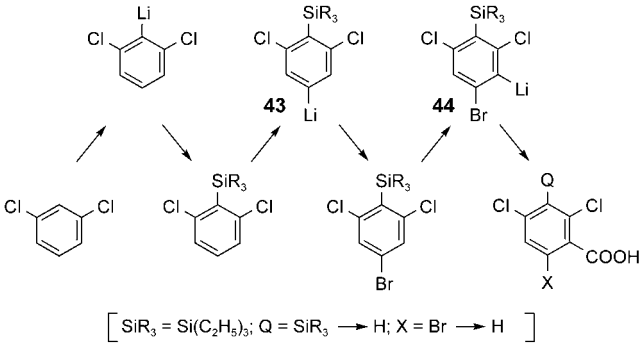


Scheme 24. Deflection of the base attack from the 4- to the 6- position of 5-fluoroindole by a 4-chloro substituent [Tool 2.3].



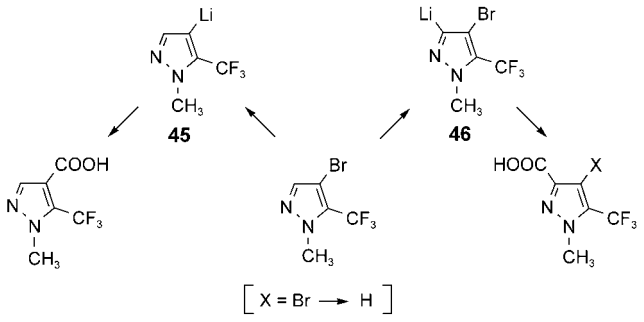
Scheme 25. Deflection of the base attack from the 5- to the 4- position of 6-fluoroindole by a 5-chloro substituent [Tool 2.3].

Bromine has a more restricted area of application as a protecting group than chlorine. It can, nevertheless, be most valuable when chlorine cannot be considered, for example, when the chlorine substituent must be present during the synthesis as it is part of the target molecule. Such a situation is encountered with the conversion of 1,3-dichlorobenzene into 2,4-dichlorobenzoic acid.[46] After silyl protection of the most acidic 2-position, the next metalation occurred preferentially at the remote 5-position. Interception of the resulting intermediate **43** with 1,2-dibromoethane provided a new substrate which could only undergo deprotonation of the 4-position when treated with LIDA, thus generating intermediate **44**. Carboxylation and removal of the bromo and triethylsilyl makeup afforded the desired product (Scheme 26).



Scheme 26. Protection of the 4-position of (2,6-dichlorophenyl)triethylsilane and activation of its 3-position by the introduction of a 4-bromo substituent [Tool 2.3].

Bromine offers the additional advantage that it can be introduced to electron-rich aromatic and heterocyclic rings under mild conditions. Thus, iron salt catalyzed bromination of 1-methyl-5-(trifluoromethyl)pyrazole gave the 4-bromo derivative in satisfactory yield (67%). The organolithium species **45**, which results from the halogen–metal permutation accomplished with *tert*-butyllithium, could be trapped as the carboxylic acid (88%).[60] LIDA-promoted deprotonation of the same 4-bromo derivative followed by carboxylation of the resulting species **46** and eventual reduction made the 1-methyl-5-(trifluoromethyl)pyrazole-3-carboxylic acid accessible in 65% overall yield (Scheme 27).[60] When the starting material 1-methyl-5-(trifluoromethyl)pyrazole was treated



Scheme 27. Protection of the 4-position of 1-methyl-5-(trichloromethyl)-pyrazole and activation of its 3-position by the introduction of a 4-bromo substituent [Tool 2.3].

 © 2005 Wiley-VCH Verlag GmbH & Co. KGaA, Weinheim

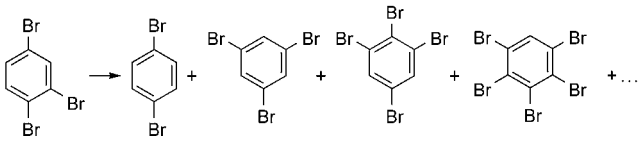
directly with LIDA and carbon dioxide, a mixture of the 4- and -3-carboxylic acids was formed in poor yield (25–33% and 2–6%, respectively).[60]

3. Regioflexibility in Halogen–Metal Exchange

The bromine–lithium and iodine–lithium permutation, discovered almost simultaneously by Wittig,[61] Gilman,[62] and their respective collaborators, was for a long while considered a mature method lacking both appeal and surprise. However, the last years marked a revival. Owing to new insight and techniques, the halogen–metal permutation has recaptured its former role as one of the most important and versatile methods in organic synthesis. From a methodological point of view, new exchange reagents such as the commercial isopropylmagnesium chloride and lithium tributylmagnesate[63,64] opened new avenues. At the same time the strategic options have been enlarged by devising new routes to difficultly accessible haloarene precursors. Moreover, methods have been developed to address a single halogen atom selectively, even when the substrate contained one or two other halogen substituents.

3.1 Deprotonation-Triggered Heavy-Halogen Migration

When polybromoarenes, for example, 1,2,4-tribromobenzene, are exposed to the action of strong bases such as sodium amide in liquid ammonia, a manifold of isomerization and dismutation products are obtained (Scheme 28).[65,66] Bunnett[67] coined the euphemistic term "halogen dance" for this randomization process although "halogen muddle" may be a more appropriate label.

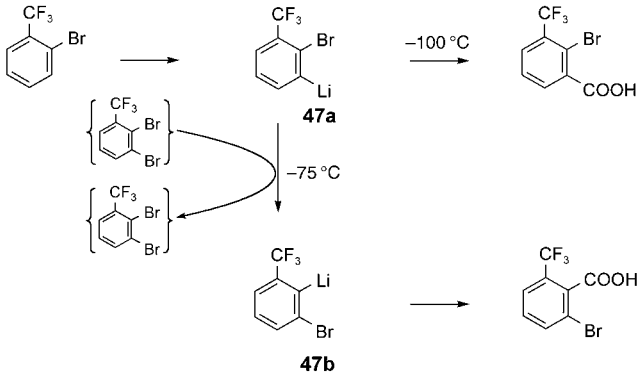


Scheme 28. Halogen scrambling upon treatment of 1,2,4-tribromobenzene with sodium amide.

The seemingly messy outcome of such experiments nevertheless conveys the message that the isomerization of readily available halogenated compounds into less-accessible ones is feasible and that one only has to find ways to make such reactions selective. Several conditions must be met if one wishes to achieve a unidirectional transformation. The base must be employed in stoichiometric amounts and it must be powerful enough to deprotonate the substrate irreversibly. Finally, a basicity gradient must exist that makes the conversion of the initially produced intermediate into an isomer energetically attractive. On the other hand, one does not need to worry about how the isomerization might be brought about. Accidentally produced polyhaloarenes are always present in trace amounts and can act as catalytic turntables, promoting a permanently ongoing halogen–metal permutation.

3.1.1. Halogen Migration in the Arene Series

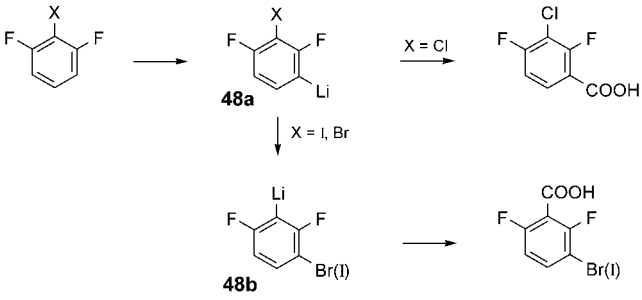
The first synthetically useful example of this kind still gains the beauty contest. When 2-bromobenzotrifluoride is treated with LITMP in tetrahydrofuran at −100 °C, a proton was abstracted from the position adjacent to the bromine atom. The resulting 2-bromo-3-(trifluoromethyl)phenyllithium (**47a**) could be trapped with an electrophile.[68] However, at −75 °C it isomerized quantitatively to 2-bromo-6-(trifluoromethyl)phenyllithium (**47b**), for which 2,3-dibromobenzotrifluoride acts as the exchange catalyst (Scheme 29).[68]



Scheme 29. Basicity-lowering heavy-halogen migration converting 2-bromo-3-(trifluoromethyl)phenyllithium into its 2,6-isomer [Tool 3.1].

This stop-and-go isomerization ("stop" at −100 °C, "go" at −75 °C) is only possible when the first lithiation is fast and the halogen–metal exchange only slightly exothermal, in other words, the driving force for swapping places between bromine and lithium atoms is moderate. If these conditions are not fulfilled, the first intermediate cannot be intercepted at all or only along with the isomerization product.

Initiated by the deprotonation of a position adjacent to a halogen atom, the basicity-gradient-driven halogen migration implies that a halogen–metal permutation is the final key step. Therefore it is restricted to bromo- or iodoarenes; chlorine atoms are unable to change places under such conditions. Whereas 1,3-difluoro-2-iodobenzene and 2-bromo-1,3-difluorobenzene (Scheme 30) experience both deprotonation (intermediate **48a**) and isomerization (intermediate **48b**)

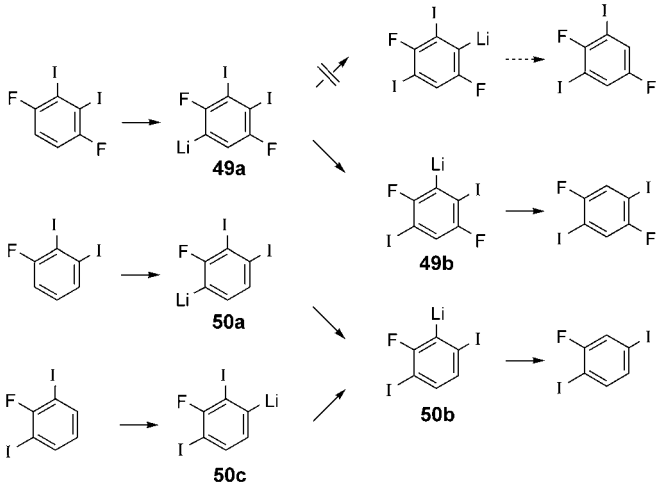


Scheme 30. Basicity-lowering isomerization of 3-bromo-2,4-difluorophenyllithium and 2,4-difluoro-3-iodophenyllithium by heavy-halogen migration [Tool 3.1].

 © 2005 Wiley-VCH Verlag GmbH & Co. KGaA, Weinheim

already at temperatures as low as −125 °C, the *ortho*-lithiated 2-chloro-1,3-difluorobenzene remains intact up to −50 °C (when β elimination of lithium fluoride sets in).[9]

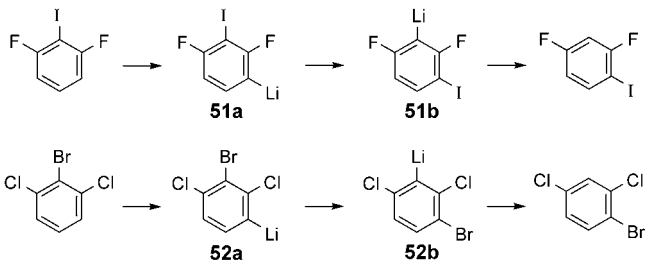
Iodine migrates with particular ease. Typical examples are the regioselective conversion of 1,4-difluoro-2,3-diiodobenzene into 1,4-difluoro-2,5-diiodobenzene (via intermediates **49a** and **49b**) and the product-convergent isomerizations of 1-fluoro-2,3-diiodobenzene and 2-fluoro-1,3-diiodobenzene (via intermediates **50a**, **50b**, and **50c**; Scheme 31). The latter substrate requires the use of LITMP, whereas all reactions triggered by deprotonation at a position adjacent to a fluorine atom can be accomplished with LIDA.[69]



Scheme 31. More examples of basicity-gradient-driven isomerizations of haloaryllithium reagents (intermediates **49a**, **50a**, and **50c**) by iodine migration [Tool 3.1].

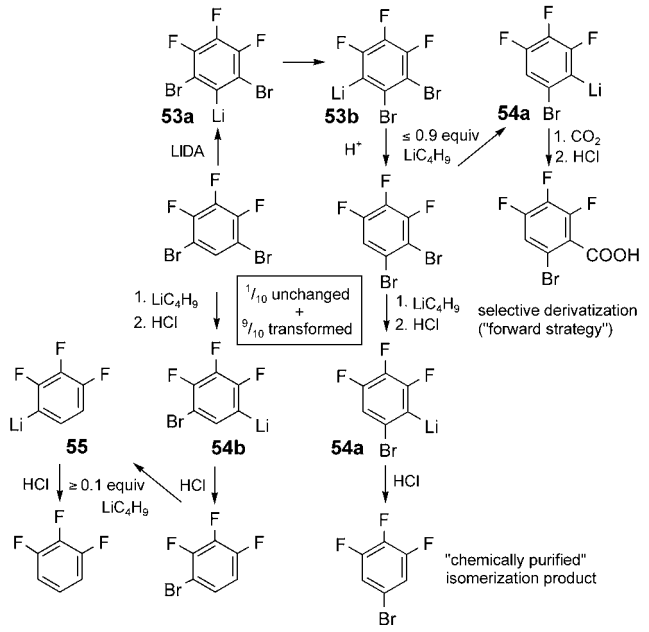
The isomerization does often not go to completion unless the reaction time is prolonged or an excess of the base is added. Thus, one frequently obtains the migration product as the major component contaminated with 10–20 % of starting material. Sometimes the two compounds can be readily separated by column chromatography. In general, however, it is more convenient to destroy the remaining starting material by addition of the stoichiometrically required quantity of butyllithium. In this way, pure 2,4-difluoro-1-iodo-benzene and 1-bromo-2,4-dichlorobenzene were isolated after isomerization starting from 1,3-difluoro-2-iodobenzene[69] and 2-bromo-1,3-dichlorobenzene[9] via intermediates **51a** and **51b** and **52a** and **52b**, respectively, and followed by a "kinetic cleanup" (Scheme 32).

The chemical purification step can be executed at two different levels if the substrate subjected to isomerization by halogen migration contains two heavy halogen atoms, one of which has to be sacrificed. To illustrate the existing options, let us assume the LIDA-promoted conversion of 1,5-dibromo-2,3,4-trifluorobenzene via intermediates **53a** and **53b** into 1,2-dibromo-3,4,5-trifluorobenzene loses momentum when a 1:9 product distribution is attained. After neutralization one bromine atom in the main component is flanked by two halogen neighbors. It represents the most activated center and is hence displaced first. If a properly dosed amount of



Scheme 32. Still more examples of basicity-gradient-driven heavy-halogen migrations, this time requiring "kinetic cleanup" [Tool 3.1].

butyllithium (0.8–0.9 equiv) is employed, it can be selectively transformed (via intermediate **54a**) and, after functionalization, the product readily separated[70] (Scheme 33). Alternatively, one may entirely reduce the isomeric products *via* the



Scheme 33. Two complementary options for the kinetic purification of incompletely isomerized haloarenes as exemplified with a 1:9 mixture of 1,5-dibromo-2,3,4-trifluorobenzene and 1,2-dibromo-3,4,5-trifluorobenzene [Tool 3.1].

lithiated species **54a** and **54b** to a 1:9 mixture of monobromo compounds, destroy the contaminating 1-bromo-2,3,4-trifluorobenzene (the heavy halogen of which is activated by the neighboring fluorine atom) selectively by adding the required quantity of butyllithium (0.1–0.2 equiv) and to remove, after neutralization, the trifluorobenzene by evaporation (Scheme 33).[70]

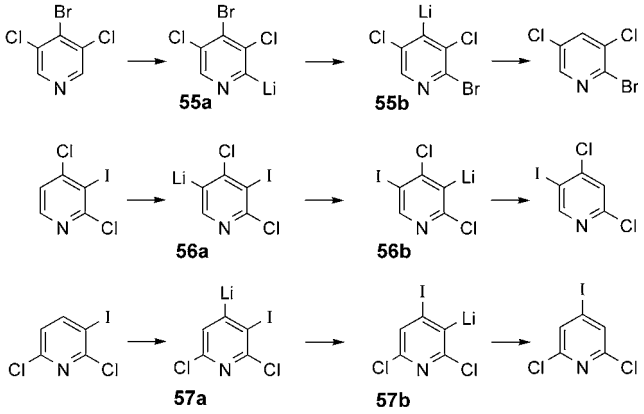
The principles outlined above are generally applicable. This has been demonstrated by numerous examples of deprotonation-triggered halogen migrations including those starting from 1,5-dibromo-2,4-difluoro-3-(triethylsilyl)benzene,[45] 1,5-dibromo-2,3,4-trichlorobenzene,[9] 1,5-dibromo-2,4-dichloro-3-fluorobenzene,[7] 1-bromo-2,3,4-trifluoro-5-iodobenzene,[70] and 1-bromo-2,4-difluoro-5-iodo-3-(triethylsilyl)benzene.[45]

 © 2005 Wiley-VCH Verlag GmbH & Co. KGaA, Weinheim

3.1.2. Halogen Migration in the Heterocyclic Series

Five- and six-membered heterocycles are more acidic than benzene; therefore even moderately strong bases such as lithium amide in liquid ammonia suffice to effect rapid deprotonation. If a suitably located bromine or iodine atom is present, heavy-halogen migrations can be observed. Such processes have been investigated more or less extensively by the groups of Gronowitz (thiophenes),[71,72] van der Plas (isothiazoles,[73] pyrazoles,[74] thiophenes[75]), Reinecke (thiophenes),[76,77] Shibuya (thiophenes),[78] Taylor (thiophenes),[79] Fröhlich (furans,[80,81] thiophenes[82,83]), and Quéguiner (pyridines,[84,85] quinolines[86]).

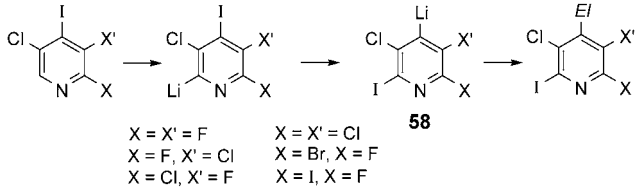
An indepth investigation of polyhalopyridines revealed an unexpectedly large synthetic potential for the method. Thus, 4-bromo-3,5-dichloropyridine, 2,4-dichloro-3-iodopyridine, and 2,6-dichloro-3-iodopyridine could be isomerized by LIDA-promoted heavy-halogen migration via intermediates **55a**,**b**, **56a**,**b**, and **57a**,**b** to afford 2-bromo-3,5-dichloropyridine, 2,4-dichloro-5-iodopyridine, and 2,6-dichloro-4-iodopyridine, respectively. The final products were purified by chromatography or crystallization (Scheme 34).[33]



Scheme 34. Basicity-lowering isomerization of lithiated halopyridines by bromine or iodine migration [Tool 3.1].

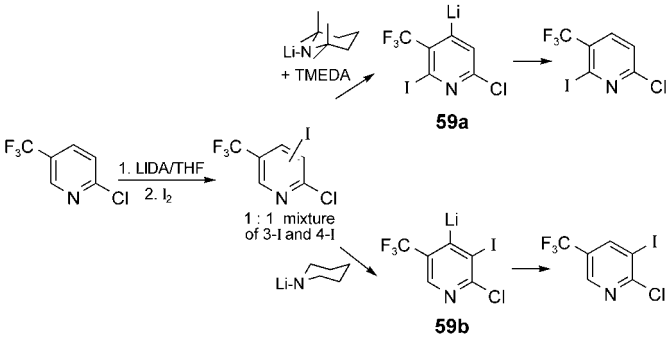
Analogously, but with LITMP as the base, an iodine migration was accomplished by using 5-chloro-2,3-dihalo-4-iodopyridines as the substrates. The isomerized organolithium species **58** were either quenched with water (*El* = H) or dry ice (*El* = COOH) (Scheme 35).[87,88]

An intriguing optional site selectivity was discovered when a 1:1 mixture of 2-chloro-3-iodo- and 2-chloro-4-iodo-5-(trifluoromethyl)pyridine, easily accessible by consecutive



Scheme 35. Further examples of halopyridine isomerizations by deprotonation-triggered iodine migration [Tool 3.1].

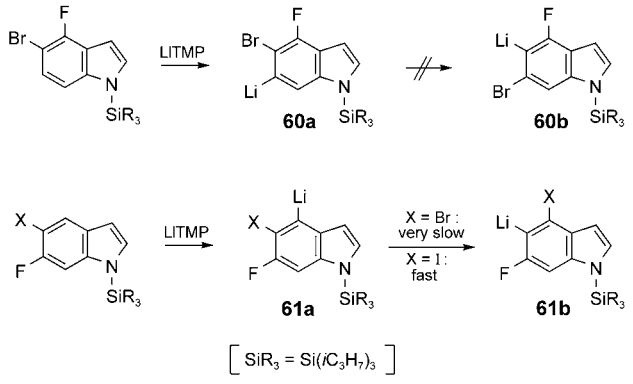
treatment of the commercially available 2-chloro-5-(trifluoromethyl)pyridine with LIDA in tetrahydrofuran for 2 h at −75 °C and elemental iodine, was treated with a variety of amide-type bases. After exposure to the bulky LITMP–TMEDA adduct in tetrahydrofuran for 2 h at −75 °C, 6-chloro-2-iodo-3-(trifluoromethyl)pyridine was obtained in 62 % yield (via intermediate **59a**) and was separated from the dismutation products 2-chloro-5-(trifluoromethyl)pyridine (10 %) and 6-chloro-2,4-diiodo-3-(trifluoromethyl)pyridine (8 %) by simple distillation (Scheme 36). Conversely,



Scheme 36. Regiodivergent isomerization of 2-chloro-4-iodo-5-(trifluoromethyl)pyridine by iodine migration to the 3- or 6-position, depending on the choice of base [Tool 3.1].

virtually pure 2-chloro-3-iodo-5-(trifluoromethyl)pyridine was isolated, though in moderate yield (33 %), when lithium piperidide was allowed to interact with the mixture of 3- and 4-iodo regioisomers for 24 h in tetrahydrofuran at −75 °C, thus generating intermediate **59b** (Scheme 36).[89]

Another surprise was encountered in the indole series. When 5-bromo-4-fluoro-1-(triisopropylsilyl)indole was treated with LIDA or LITMP, clean deprotonation occurred at the 6-position, but the lithiated intermediate **60a** (characterized by carboxylation) did not isomerize at all to the more stable species **60b** (Scheme 37).[59] Likewise, halogen migration did not occur with the 4-lithiated 5-bromo-6-fluoro-1-(triisopropylsilyl)indole (**61a**, X = Br).[59] On the other hand, the analogous 5-iodo compound reacted rapidly with PMDTA-activated LITMP to give directly and quantitatively (via **61a**, X = I) the isomerized species **61b** (Scheme 37).[59]

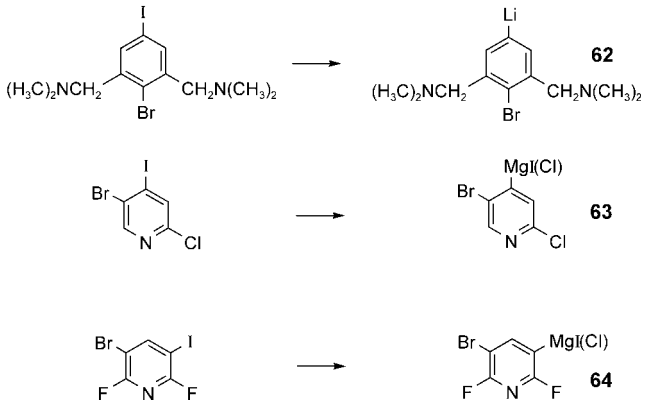


Scheme 37. Rapid isomerization of *N*-protected and 6-lithiated 6-fluoro-5-iodoindole, but no analogous bromine migration [Tool 3.1].

 © 2005 Wiley-VCH Verlag GmbH & Co. KGaA, Weinheim

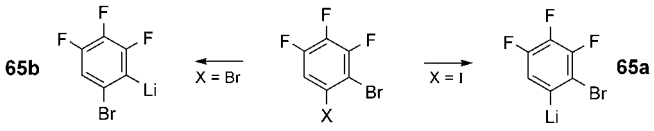
3.2. Discriminating between Different Halogen Substituents

Regardless of whether one has the reductive insertion of metals into halo compounds in mind or permutational halogen–metal interconversion, the well-known order of reactivity is the same. Iodine is displaced faster than bromine (by several powers of ten)[90] and chlorine is exchange-resistant, except in unusual situations. Thus, bromoiodobenzenes can be converted selectively into the corresponding bromophenyllithium reagents.[91–94] 2-Bromo-1,3-bis(dimethylamino)-5-iodobenzene reacts with *tert*-butyllithium to produce the 5-lithio species **62**.[95] Similarly, 5-bromo-2-chloro-4-iodopyridine[89] and 3-bromo-2,6-difluoro-5-iodopyridine[96] smoothly react with isopropylmagnesium chloride to afford the intermediates **63** and **64**, respectively (Scheme 38).



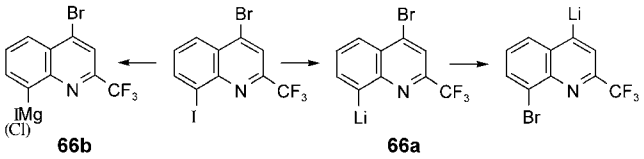
Scheme 38. Iodine participates in halogen–metal permutations much more readily than does bromine; chlorine does not compete at all [Tool 3.2].

Treatment of 2-bromo-3,4,5-trifluoro-1-iodobenzene with butyllithium in tetrahydrofuran at −100 °C afforded cleanly the intermediate **65a**.[70] In contrast, the 1,2-dibromo-3,4,5-trifluorobenzene gave rise to intermediate **65b** under the same conditions,[70] as the displacement of the bromine atom at the 2-position (which is now flanked by two other halogens) is now the energetically favored route (Scheme 39).



Scheme 39. Generating two different organometallic species (**65a** or **65b**), depending on whether 2-bromo-3,4,5-trifluoro-1-iodobenzene or 1,2-dibromo-3,4,5-trifluorobenzene serves as the substrate of a halogen–metal permutation [Tool 3.2].

At this stage a word of warning may be appropriate. A subsequent positional scrambling may compromise an initially perfect discrimination between iodine and bromine. Although 4-bromo-8-iodo-2-(trifluoromethyl)quinoline reacted with both isopropylmagnesium chloride and butyllithium under selective iodine–metal displacement, only the organomagnesium intermediate **66b** persisted as such, whereas the lithium species **66a** isomerized by positional permutation of the bromine and lithium atoms (Scheme 40).[97]

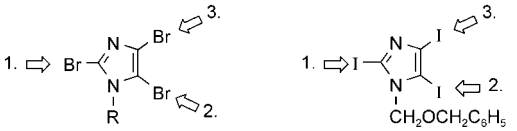


Scheme 40. Alternative conversion of 4-bromo-8-iodo-2-(trifluoromethyl)quinoline into a 4- and an 8-metal-bearing species [Tool 3.2].

3.3. Discriminating between Seemingly Equal Halogen Atoms

Modern synthesis has to cope more and more with structural complexity. For reasons of logistic simplicity, it would be advantageous to allow the presence of just one kind of halogen substituent, preferably bromine, and then to replace them successively by metal atoms and ultimately by various functional groups or other substituents. This raises the question of how to discriminate chemically between formally identical halogen atoms.

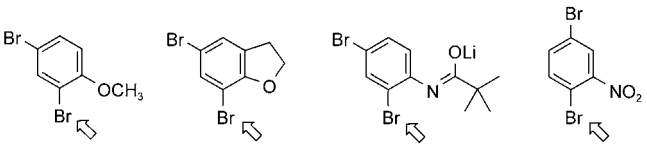
A spectacular case of sequentially controlled regioselectivity was reported which featured 1-alkyl-protected 2,4,5-tribromoimidazole[98–100] and 2,4,5-triiodoimidazole.[101,102] When butyllithium was employed as the exchange reagent, first the halogen at the 2-position, then that at the 5-position, and eventually that at the 4-position was replaced by the metal (Scheme 41).



Scheme 41. Controlled replacement of three heavy-halogen atoms from 2,4,5-trihaloimidazoles by sequential halogen–metal permutations.

3.3.1. Activation by Neighboring Heteroatoms

If there is only one heteroatom besides the halogen, the outcome of the permutation experiment is, in general, safely predictable. It is always the halogen atom adjacent to the electronegative substituent that has the highest exchange priority (Scheme 42). When 2,4-dibromoanisole is exposed to isopropylmagnesium chloride, first the bromine atom next to the methoxy group is exchanged;[103] 5,7-dibromo-2,3-dihydro-1-benzofuran[104] reacts exclusively at the position adja-



Scheme 42. Discrimination between two formally equal halogen atoms through neighboring-group assistance [Tool 3.3].

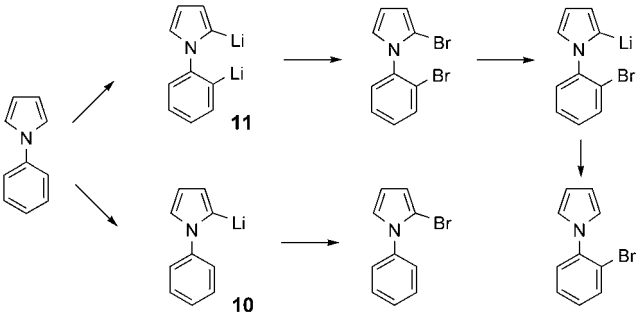
 © 2005 Wiley-VCH Verlag GmbH & Co. KGaA, Weinheim

cent to the oxygen atom. In the same way, 2,4-dibromo-*N*-pivaloylaniline[105] (after deprotonation of the NH center) and 1,4-dibromo-2-nitrobenzene[106] exhibit an absolute selectivity in favor of the bromine atom adjacent to the nitrogen atom (Scheme 42).

The "kinetic cleanup" described in the Section 3.1.1 also depends on the activation provided by neighboring heteroatoms. It was shown that fluorine or chlorine atoms are most effective in this context.

The activation provided by the neighboring heteroatom can be exploited in a different way too. The approach may be termed the Echternach procedure, as it boils down to a two-steps-forward-one-step-back strategy. Although historically unproven,[107] it has become a stereotyped description of the Echternach dancing procession as a forward and backward hopping of pilgrims, a choreography of locomotion that is nowadays regarded as an allegory of human behavior in general and political practice in particular.

As mentioned in Section 2.1, 1-phenylpyrrole can be easily subjected to a double metalation at an α- and an *o*-position (intermediate **11**). Trapping with 1,2-dibromoethane gives α,*o*-dibromo-*N*-phenylpyrrole in high yield. When this compound was treated with 1 equivalent of butyllithium, only the halogen atom attached to the heterocyclic ring was removed.[23] The 1-(2-bromophenyl)pyrrole isolated after neutralization is an isomer of α-bromo-*N*-phenylpyrrole, which can be readily prepared from 1-phenylpyrrole by consecutive monometalation (intermediate **10**) and bromination (Scheme 43).

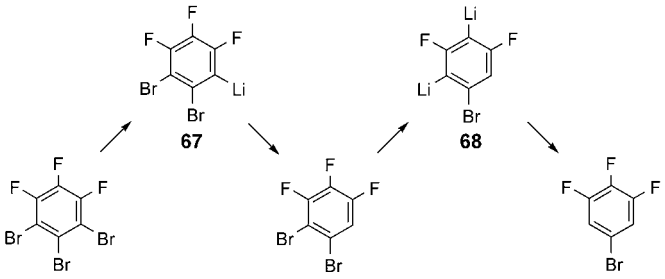


Scheme 43. The Echternach route to 1-(2-bromophenyl)pyrrole [Tool 3.3].

It may sometimes even be worthwhile to opt for a three-steps-forward-two-steps-back bargain. 1,2,3-Trifluorobenzene was readily converted into 1,2,3-tribromo-4,5,6-trifluorobenzene by repetitive alternating treatments with LIDA and bromine. Subsequent reactions with butyllithium at −100 °C and methanol (via intermediates **67** and **68**) eliminate the bromine atoms located next to a fluorine site one after the other, thus leading to 5-bromo-1,2,3-trifluorobenzene, which is difficult to make directly (Scheme 44).[70]

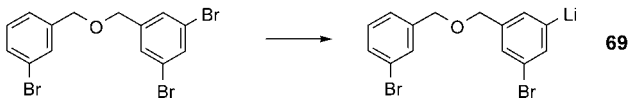
3.3.2. *Activation by Remote Heterosubstituents*

Systematic investigations by Leroux[90] have revealed striking differences in the rates of butyllithium-promoted



Scheme 44. Three steps forward two steps back: conversion of 1,2,3-trifluorobenzene into its 5-bromo derivative [Tool 3.3].

halogen–metal permutation processes with bromobenzene and heterosubstituted congeners. Thus, 1,3-dibromobenzene and 1-bromo-3,5-difluorobenzene were found to react faster (by several powers of ten) than the parent compound. The activating effect of the additional halogen substituent was also demonstrated in another way by an intramolecular competition experiment. In the presence of butyllithium, 1,3-dibromo-5-{[(3-bromobenzyl)oxy]methyl}benzene exclusively underwent halogen–metal permutation at the multiply substituted ring, affording the intermediate **69** and, after quenching with dry ice, a carboxylic acid with two halogen-bearing rings (Scheme 45).[108]



Scheme 45. Site-selective halogen–metal exchange owing to remote activation: 3,3′,5-tribromodibenzyl ether as the substrate [Tool 3.3].

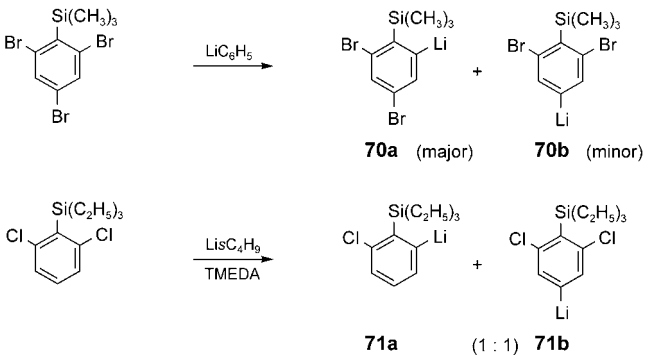
3.3.3. *Steric Acceleration*

As trialkylsilyl groups shield *ortho* hydrogen atoms against the deprotonating attack of organometallic reagents, one might expect them to exert a similar retarding or suppressing effect on halogen–metal permutations. The contrary proves to be true. Apparently, steric pressure overrides steric hindrance. The departure of a voluminous heavy-halogen atom from the immediate vicinity of a bulky silyl substituent means relief of strain. This must be the reason why (2,4,6-tribromophenyl)trimethylsilane produced mainly the 2-lithio species **70a** (rather than its 4-isomer **70b**) when treated with ethereal phenyllithium[9] and why (2,6-dichlorophenyl)triethylsilane underwent a totally unexpected chlorine–lithium displacement in the presence of *sec*-butyllithium along with metalation at the 5-position, as reflected by the 1:1 ratio of the intermediates **71a** and **71b** (Scheme 46).[9]

3.3.4. *Solvent-Modulated Optional Site Selectivity*

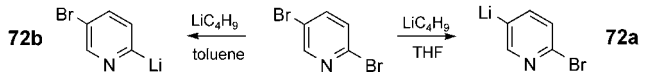
In 1977 Parham et al.[109] reported the halogen–metal permutation between 2,5-dibromopyridine and butyllithium in tetrahydrofuran to take place at the 5-position (remote

 © 2005 Wiley-VCH Verlag GmbH & Co. KGaA, Weinheim



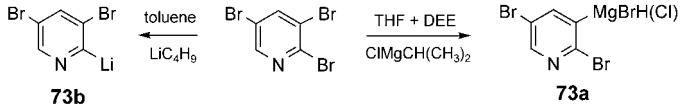
Scheme 46. Facilitated halogen–metal permutation at sites adjacent to silyl groups owing to relief of steric strain [Tool 3.3].

from the nitrogen atom) to afford intermediate **72a**. However, the same reaction performed again at −75 °C, but in toluene this time, replaces the halogen atom at the 2-position (intermediate **72b**; Scheme 47).[110] Evidently, the coordinating capacity of the nitrogen atom dictates the course of the reaction in apolar solvents such as toluene, whereas in ethereal media simply the least-basic species (in other words, metal compounds of the 4- rather than of the 3- not to speak of the 2-pyridyl anion[111]) is generated (Scheme 47).



Scheme 47. Solvent-dependent, optional site-selective halogen–metal permutation of 2,5-dibromopyridine as substrate [Tool 3.3].

This solvent dependence of the reaction is a most fascinating, if rare, phenomenon. Up to now only one further example has been discovered. When treated with isopropylmagnesium chloride in tetrahydrofuran at 0 °C or butyllithium in toluene at −75 °C, 2,3,5-tribromopyridine accommodates the metal at the 3- or 2-position, producing intermediates **73a** or **73b** and, after iodination, 2,5-dibromo-3-iodopyridine (77 %) and 3,5-dibromo-2-iodopyridine (75 %), respectively (Scheme 48).[89]



Scheme 48. Solvent-controlled halogen–metal permutation at the 2- or 3-position of 2,3,5-tribromopyridine [Tool 3.3].

4. Synopsis, Perspectives, and Outlook

In the preceding two Sections of this Review various possibilities were considered as to how regioselectivity can be secured in the derivatization of aromatic and heterocyclic substrates. Having thus examined the individual parts of a kit of methods separately, we now have to find how they fit together, what they have in common, and where they are complementary.

Although it may be clear, attention should be paid to a unique virtue of the organometallic approach to structure proliferation. A metal can be compared to a joker in a card game: it can be replaced by any known electrophile. This means that the same intermediate can potentially be converted into hundreds of new compounds, even if only a handful of trapping reagents are used to play a role in systematic investigations as those described above. Moreover, the choice of the electrophile and, as a corollary, of the target structure can be deferred until the last step of the reaction sequence. Such features hold the promise of unmatched synthetic flexibility and of access to an immense molecular diversity whenever organometallic species act as the turntables.

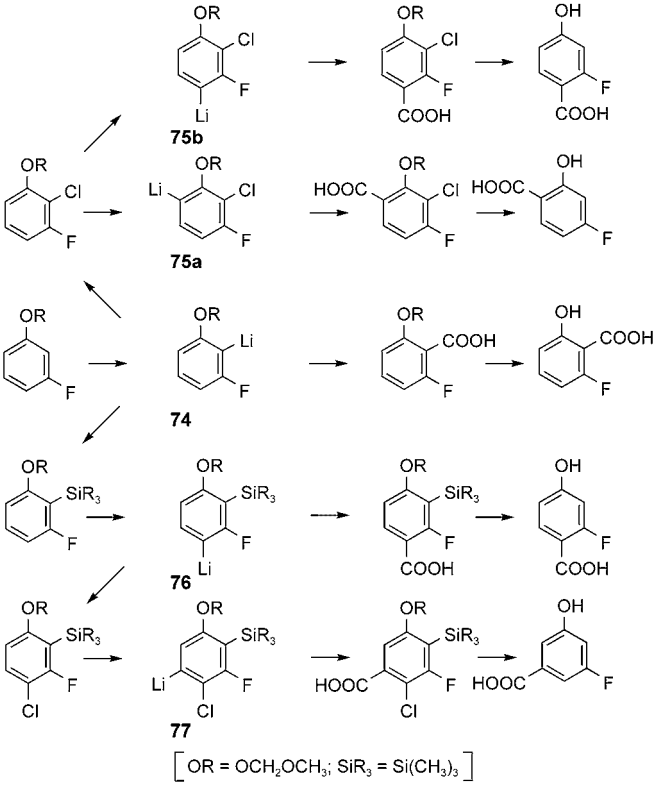
4.1. The Holy Grail: Regiochemically Exhaustive Functionalization

The goal defined in the Introduction was to make any vacant position of a given aromatic or heterocyclic substrate amenable to selective substitution. It cannot be tested mathematically but only empirically whether or not this challenge can be met by a suitable combination of the organometallic methods described above. Exhaustive regiochemical substitution has been successfully demonstrated in numerous model studies; three more-elaborate, though still typical, examples are presented below.

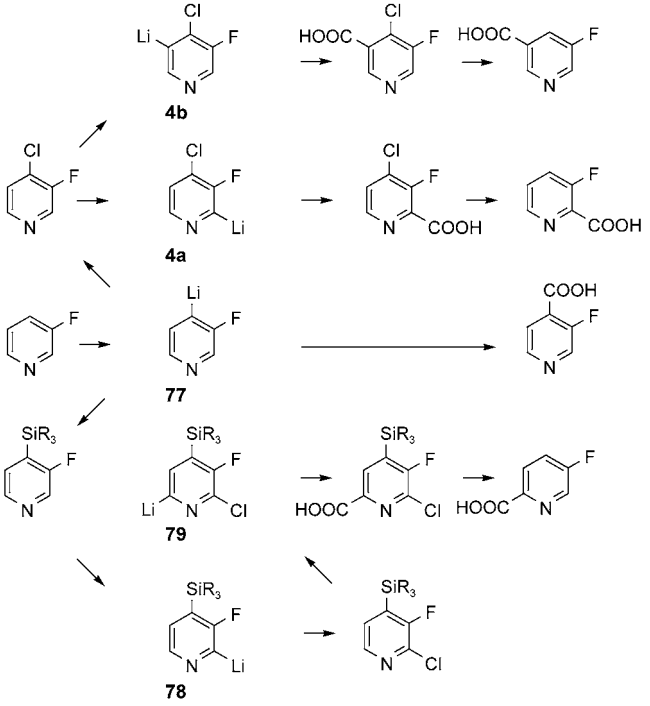
O-Methoxymethyl-protected 3-fluorophenol was rapidly metalated by butyllithium or *sec*-butyllithium at C2, and the intermediate **74** was trapped with dry ice to afford 2-fluoro-6-hydroxybenzoic acid. The use of chlorotrimethylsilane or 1,1,2-trichloro-1,2,2-trifluoroethane as the electrophile led to [(2-fluoro-6-methoxymethoxy)phenyl]trimethylsilane and 2-chloro-1-fluoro-3-(methoxymethoxy)benzene, respectively. The latter compound reacted with butyllithium exclusively at the 4-position, adjacent to the oxygen atom (thus generating intermediate **75a**), to give 4-fluoro-2-hydroxybenzoic acid upon consecutive carboxylation, acid hydrolysis, and reduction. However, when LITMP was employed, the deprotonation occurred at the 6-position, adjacent to the fluorine atom (intermediate **75b**), and ultimately led to the isomeric 2-fluoro-4-hydroxybenzoic acid. [(2-Fluoro-6-methoxymethoxy)phenyl]trimethylsilane, the other interception product, underwent metalation also solely at the position adjacent to the fluorine atom (producing intermediate **76**). The [(3-chloro-2-fluoro-6-methoxymethoxy)phenyl]trimethylsilane obtained upon chlorination was converted into 3-fluoro-5-hydroxybenzoic acid by consecutive metalation (intermediate **77**), carboxylation, fluoride-mediated protodesilylation, acid hydrolysis, and reduction (Scheme 49).[22]

3-Fluoropyridine, another fairly inexpensive starting material, is deprotonated by LIDA at C4. In this way, 3-fluoropyridine-4-carboxylic acid became immediately accessible. 4-Chloro-3-fluoropyridine, prepared by chlorination of the organometallic intermediate **78**, provided 3-fluoropyridine-2-carboxylic acid in a short sequence consisting of

 © 2005 Wiley-VCH Verlag GmbH & Co. KGaA, Weinheim



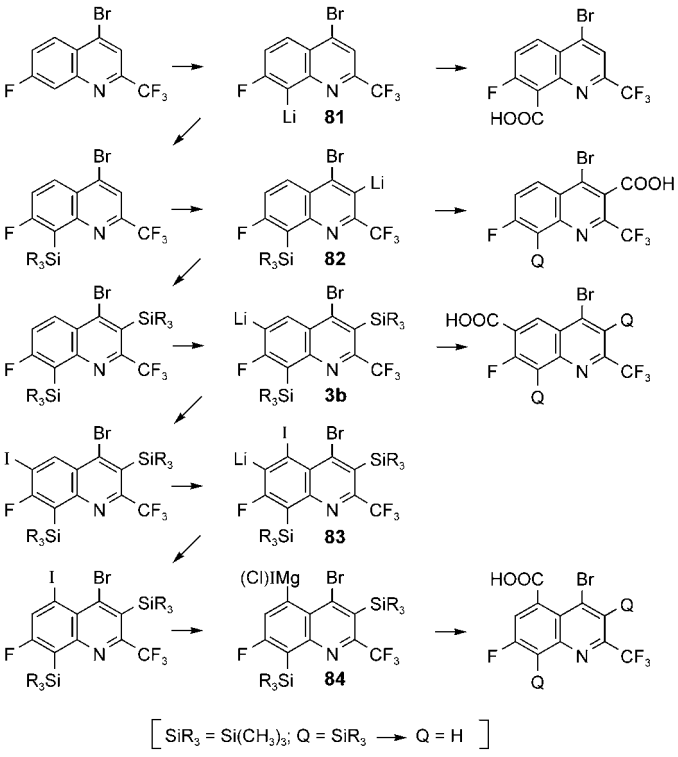
Scheme 49. The regiochemically exhaustive conversion of 3-fluorophenol into all four possible fluorohydroxybenzoic acids.



Scheme 50. The regiochemically exhaustive conversion of 3-fluoropyridine into all four possible fluoropyridinecarboxylic acids.

metalation (intermediate **4a**) with LITMP in diethyl ether, carboxylation, and reduction. However, it sufficed to replace the metalating reagent LITMP in diethyl ether with LIDA in tetrahydrofuran to revert the site selectivity completely. This time a proton was abstracted from the 5-position (neighboring the chlorine atom; intermediate **4b**) and ultimately 5-fluoropyridine-3-carboxylic acid was isolated. Finally, 5-fluoropyridine-2-carboxylic acid was made in seven steps involving intermediates **78**, **79**, and **80** by successive metalation and silylation, metalation and chlorination, metalation and carboxylation terminated eventually by deprotection (Scheme 50).[10]

The LIDA-promoted deprotonation of 4-bromo-7-fluoro-2-(trifluoromethyl)quinoline occurred first at the 8-position (intermediate **81**; Scheme 51). This opened the entry, by carboxylation, to 4-bromo-7-fluoro-2-(trifluoromethyl)quinoline-8-carboxylic acid or, by trimethylsilylation, to a silane that underwent the next deprotonation at the 3-position (generating intermediate **82**). Carboxylation and protodesilylation afforded 4-bromo-7-fluoro-2-(trifluoromethyl)quinoline-3-carboxylic acid or, after another trimethylsilylation, a 3,8-bissilane that, when treated with LIDA, generated a mixture of 5- and 6-lithiated species, which fortunately equilibrated completely in favor of the latter component (**3b**; see Section 2.1.).[5] Carboxylation and subsequent deprotection gave 4-bromo-7-fluoro-2-(trifluoromethyl)quinoline-6-carboxylic acid (Scheme 51). Iodination followed by deprotonation-triggered halogen migration and neutralization of intermediate **83** afforded a 5-iodo derivative that, when



Scheme 51. The regiochemical exhaustive conversion of 4-bromo-7-fluoro-2-(trifluoromethyl)quinoline into the four possible 4-bromo-7-fluoro-2-(trifluoromethyl)quinolinecarboxylic acids.

 © 2005 Wiley-VCH Verlag GmbH & Co. KGaA, Weinheim

subjected to a halogen–metal permutation with isopropylmagnesium chloride followed by carboxylation of the resulting Grignard compound **84** and protodesilylation, provided 4-bromo-7-fluoro-2-(trifluoromethyl)quinoline-5-carboxylic acid (Scheme 51).[5]

Further examples of regiochemically exhaustive functionalizations of bulk chemicals will be published periodically. The toolbox methods were, for instance, recently applied to prepare numerous chloro(trifluoromethyl)pyridine carboxylic acids, which are attractive building blocks for medicinal and agrochemical research.[89]

4.2. The Mechanistic Basis

According to widespread prejudice, organometallic reactions are unpredictable. This belief reflects a regrettable scarcity of valid information. Mechanistic and, in particular, kinetic studies of reactions involving metal derivatives in apolar media are complicated and hence have been largely neglected. On the other hand, it would be simpleminded to believe that one could have designed and elaborated the *toolbox methods* randomly or in a trial-and-error approach. To accumulate the required knowledge and insight, we have invested much time and effort in the assessment of gas-phase acidities, exchange equilibria of organolithium species, organometallic reaction rates, and related phenomena. Even a short survey of this work would go beyond the scope of the present article. Therefore, the reader is referred to a forthcoming review.[112]

The author is indebted to a marvelous team of competent collaborators. Major contributions to the present subject are credited to Carla Bobbio, Fabrice Cottet (now at AMCIS, Bubendorf), Assunta Ginanneschi, Joanna Gorecka, Christophe Heiss, Olivier Lefebvre, Frédéric Leroux (now at the University of Strasbourg), Giuseppe Mangano, Marc Marull, Elena Marzi, Florence Mongin (now at the University of Rennes, Thierry Rausis, and Jean-Noël Volle. Financial support was provided by the University of Lausanne, the Federal Institute of Technology at Lausanne, the Swiss National Science Foundation, Bern (grant 20-100′336-02), and the Federal Office for Education and Science, Bern (grant 97.0083 linked to the TMR project FMRXCT-970129 and grant C02.0060 linked to the COST-D24 project WG0006-02).

Received: December 22, 2003
Revised: May 17, 2004
Published Online: November 19, 2004

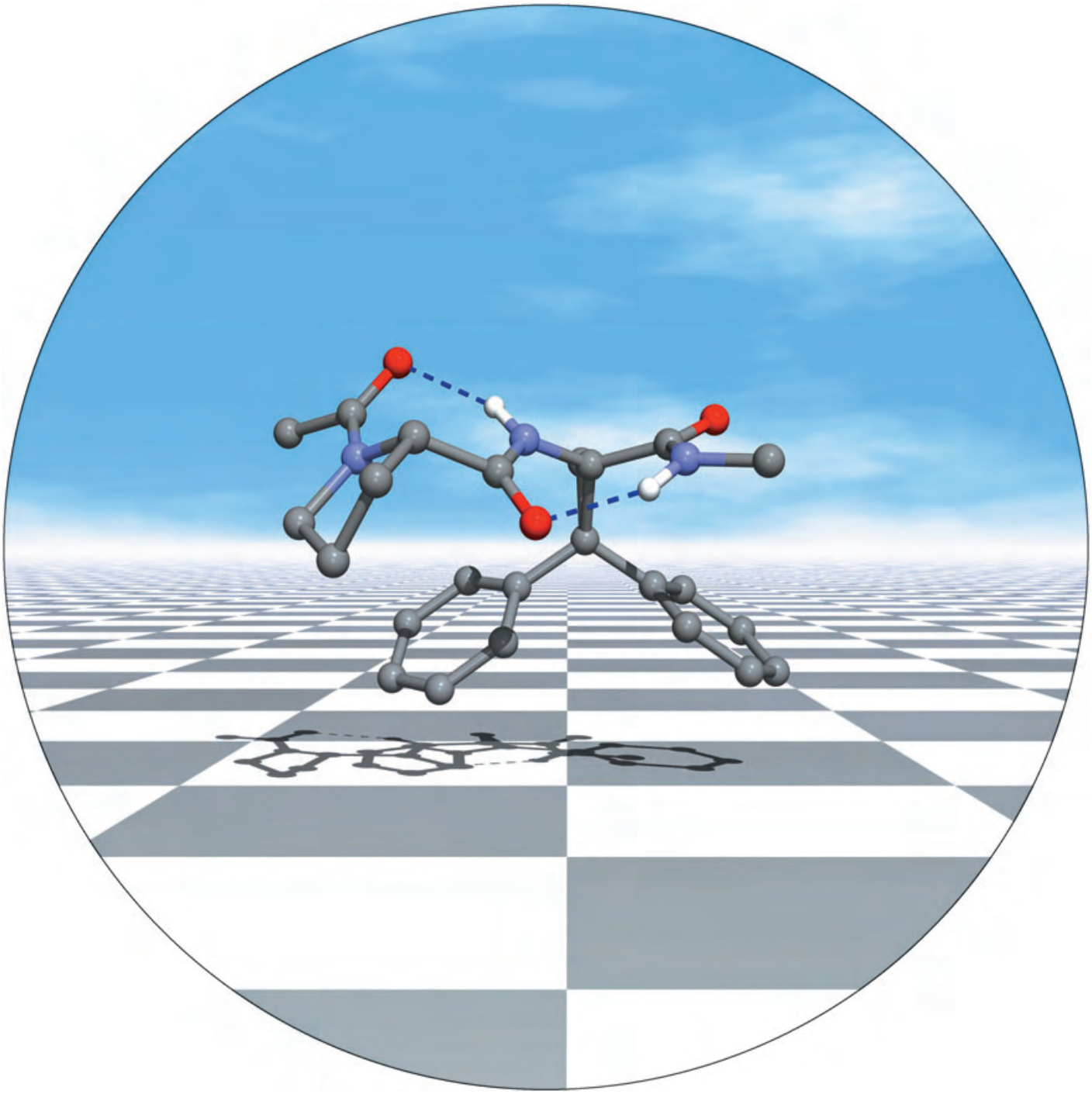
[1] D. Seebach, *Angew. Chem.* **1990**, *102*, 1363 – 1409; *Angew. Chem. Int. Ed. Engl.* **1990**, *29*, 1320 – 1367.
[2] M. Schlosser in *Organometallics in Synthesis: A Manual* (Ed.: M. Schlosser), Wiley, Chichester, **2002**, pp. 1 – 352; a) M. Schlosser in *Organometallics in Synthesis: A Manual* (Ed.: M. Schlosser), Wiley, Chichester, **2002**, pp. 85, 101 – 137, 185 – 284; b) M. Schlosser in *Organometallics in Synthesis: A Manual* (Ed.: M. Schlosser), Wiley, Chichester, **2002**, pp. 253 – 257.
[3] C. D. Liang, *Tetrahedron Lett.* **1986**, *27*, 1971 – 1974.
[4] J. M. Brown, S. Woodward, *J. Org. Chem.* **1991**, *56*, 6803 – 6809.
[5] M. Marull, M. Schlosser, *Eur. J. Org. Chem.* **2004**, 1008 – 1013.
[6] M. Schlosser, *Eur. J. Org. Chem.* **2001**, 3975 – 3984.
[7] F. Mongin, E. Marzi, M. Schlosser, *Eur. J. Org. Chem.* **2001**, 2771 – 2777.
[8] J. Gorecka, C. Heiss, R. Scopelliti, M. Schlosser, *Org. Lett.*, in press.
[9] C. Heiss, M. Schlosser, unpublished results, **2003**.
[10] C. Bobbio, M. Schlosser, unpublished results, **2003**.
[11] I. Kasahara, T. Sugiura, T. Inoue (Nippon Soda Co.), PCT Int. Appl. W09700845, filed Jan. 9, 1997 [*Chem. Abstr.* **1997**, *126*, 143985 f].
[12] T. Okabe, I. Kasahara, T. Suzuki (Nippon Soda Co.), PCT Int. Appl. W09804509, filed Feb. 5, 1998 [*Chem. Abstr.* **1998**, *128*, 127821 k].
[13] A. J. Burton, K. S. Cardwell, M. J. Fuchter, M. K. Lindvall, R. Patel, T. W. Packham, J. C. Prodger, M. B. Schilling, M. D. Walker, *Tetrahedron Lett.* **2003**, *44*, 5653 – 5656.
[14] M. Schlosser, F. Mongin, J. Porwisiak, W. Dmowski, H. H. Büker, N. M. M. Nibbering, *Chem. Eur. J.* **1998**, *4*, 1281 – 1286.
[15] M. Schlosser, E. Marzi, F. Cottet, H. H. Büker, N. M. M. Nibbering, *Chem. Eur. J.* **2001**, *7*, 3511 – 3516.
[16] A. A. Morton, I. Hechenbleikner, *J. Am. Chem. Soc.* **1936**, *58*, 1024 – 1027.
[17] M. Schlosser, J. H. Choi, S. Takagishi, *Tetrahedron* **1990**, *46*, 5633 – 5648.
[18] A. A. Morton, G. H. Patterson, *J. Am. Chem. Soc.* **1943**, *65*, 1346 – 1348.
[19] D. J. Chadwick, C. Willbe, *J. Chem. Soc. Perkin Trans. 1* **1977**, 887 – 893.
[20] A. A. Morton, C. E. Claff, *J. Am. Chem. Soc.* **1954**, *76*, 4935 – 4938.
[21] H. Gilman, R. V. Young, *J. Am. Chem. Soc.* **1935**, *57*, 1121 – 1123.
[22] H. Gilman, F. W. Moore, O. Baine, *J. Am. Chem. Soc.* **1941**, *63*, 2479 – 2482.
[23] F. Faigl, M. Schlosser, *Tetrahedron* **1993**, *49*, 10271 – 10278.
[24] J. E. Mulvaney, Z. G. Garlund, S. L. Garlund, D. J. Newton, *J. Am. Chem. Soc.* **1966**, *88*, 476 – 480.
[25] F. Mongin, R. Maggi, M. Schlosser, *Chimia* **1996**, *50*, 650 – 652.
[26] R. Maggi, M. Schlosser, *J. Org. Chem.* **1996**, *61*, 5430 – 5434.
[27] G. Katsoulos, S. Takagishi, M. Schlosser, *Synlett* **1991**, 731 – 732.
[28] E. Marzi, F. Mongin, A. Spitaleri, M. Schlosser, *Eur. J. Org. Chem.* **2001**, 2911 – 2915.
[29] J. Gorecka, M. Schlosser, unpublished results, **2003**.
[30] E. Marzi, J. Gorecka, M. Schlosser, *Synthesis* **2004**, 1609 – 1614.
[31] E. Marzi, A. Spitaleri, F. Mongin, M. Schlosser, *Eur. J. Org. Chem.* **2002**, 2508 – 2517.
[32] M. Schlosser, J. Gorecka, E. Castagnetti, *Eur. J. Org. Chem.* **2003**, 452 – 462.
[33] E. Marzi, A. Bigi, M. Schlosser, *Eur. J. Org. Chem.* **2001**, 1371 – 1376.
[34] P. Gros, Y. Fort, P. Caubère, *J. Chem. Soc. Perkin Trans. 1* **1998**, 1685 – 1689.
[35] E. Marzi, unpublished results, **2002**.
[36] M. Schlosser, M. Marull, *Eur. J. Org. Chem.* **2003**, 1569 – 1575.
[37] J. Mortier, J. Moyroud, B. Bennetau, P. A. Cain, *J. Org. Chem.* **1994**, *59*, 4042 – 4044.
[38] B. Bennetau, J. Mortier, J. Moyroud, K.-L. Guesnet, *J. Chem. Soc. Perkin Trans. 1* **1995**, 1265 – 1271.
[39] F. Gohier, A.-S. Castanet, J. Mortier, *Org. Lett.* **2003**, *5*, 1919 – 1922.
[40] J. Mortier, F. Gohier, unpublished results, **2003** (see also: F. Gohier, Ph.D. Thesis, Université du Maine, Le Mans, **2003**).
[41] A. Marxer, H. R. Rodriguez, J. M. McKenna, H. M. Tsai, *J. Org. Chem.* **1975**, *40*, 1427 – 1433.
[42] S. Takagishi, G. Katsoulos, M. Schlosser, *Synlett* **1992**, 360 – 362.

 © 2005 Wiley-VCH Verlag GmbH & Co. KGaA, Weinheim

[43] O. Desponds, C. Huynh, M. Schlosser, *Synthesis* **1998**, 983 – 985.
[44] F. Mongin, M. Schlosser, *Tetrahedron Lett.* **1996**, *37*, 6551 – 6554.
[45] M. Schlosser, C. Heiss, *Eur. J. Org. Chem.* **2003**, 4618 – 4624.
[46] C. Heiss, E. Marzi, M. Schlosser, *Eur. J. Org. Chem.* **2003**, 4625 – 4629.
[47] R. J. Mills, V. Snieckus, *J. Org. Chem.* **1989**, *54*, 4372 – 4385.
[48] S. L. Chien, R. Adams, *J. Am. Chem. Soc.* **1934**, *56*, 1787 – 1792.
[49] F. H. Westheimer in *Steric Effects in Organic Chemistry* (Ed.: M. S. Newman), Wiley, New York, **1956**, pp. 523 – 555.
[50] L. A. Paquette, J. M. Gardlik, *J. Am. Chem. Soc.* **1980**, *102*, 5033 – 5035.
[51] A. Mordini, M. Schlosser, *Chimia* **1986**, *40*, 309 – 310.
[52] J. E. Macdonald, G. S. Poindexter, *Tetrahedron Lett.* **1987**, *28*, 1851 – 1852.
[53] J. Gorecka, F. Leroux, M. Schlosser, *Eur. J. Org. Chem.* **2004**, 64 – 68.
[54] E. Baston, Q. Wang, M. Schlosser, *Tetrahedron Lett.* **2000**, *41*, 667 – 670.
[55] G. Häflinger, M. Beyer, *Liebigs Ann. Chem.* **1980**, 2012 – 2020.
[56] M. Schlosser, G. Mangano, F. Leroux, *Eur. J. Org. Chem.* **2004**, 1014 – 1017.
[57] G. Mangano, M. Schlosser, unpublished results, **2002**; G. Mangano, Ph.D. Thesis, École Polytechnique Fédérale, Lausanne, **2003**.
[58] M. Tashiro, G. Fukata, *J. Org. Chem.* **1977**, *42*, 835 – 838.
[59] A. Ginanneschi, M. Schlosser, unpublished results, **2002**.
[60] M. Schlosser, J.-N. Volle, F. Leroux, K. Schenk, *Eur. J. Org. Chem.* **2002**, 2913 – 2920.
[61] G. Wittig, U. Pockels, H. Dröge, *Ber. Dtsch. Chem. Ges.* **1938**, *71*, 1903 – 1912.
[62] H. Gilman, W. Langham, A. L. Jacoby, *J. Am. Chem. Soc.* **1939**, *61*, 106 – 109.
[63] T. Iida, T. Wada, K. Tomimoto, T. Mase, *Tetrahedron Lett.* **2001**, *42*, 4841 – 4844.
[64] J. Kondo, A. Inoue, H. Shinokubo, K. Oshima, *Angew. Chem.* **2001**, *113*, 2146 – 2148; *Angew. Chem. Int. Ed.* **2001**, *40*, 2085 – 2087.
[65] A. Vaitiekunas, F. F. Nord, *J. Am. Chem. Soc.* **1953**, *75*, 1764 – 1768.
[66] J. H. Wotiz, F. Huba, *J. Org. Chem.* **1959**, *24*, 595 – 598.
[67] J. F. Bunnett, *Acc. Chem. Res.* **1972**, *5*, 139 – 147.
[68] F. Mongin, O. Desponds, M. Schlosser, *Tetrahedron Lett.* **1996**, *37*, 2767 – 2770.
[69] T. Rausis, M. Schlosser, *Eur. J. Org. Chem.* **2002**, 3351 – 4458.
[70] C. Heiss, M. Schlosser, *Eur. J. Org. Chem.* **2003**, 447 – 451.
[71] P. Moses, S. Gronowitz, *Ark. Kemi* **1961**, *118*, 119 – 132 [*Chem. Abstr.* **1962**, *56*, 10173 c].
[72] S. Gronowitz, B. Holm, *Acta Chem. Scand.* **1969**, *23*, 2207 – 2208.
[73] D. A. de Bie, H. C. van der Plas, *Tetrahedron Lett.* **1968**, *9*, 3905 – 3908.
[74] D. A. de Bie, H. C. van der Plas, G. Geurtsen, K. Nijdam, *Recl. Trav. Chim. Pays-Bas* **1973**, *92*, 245 – 252.
[75] H. C. van der Plas, D. A. de Bie, G. Geurtsen, M. G. Reinecke, H. W. Adickes, *Recl. Trav. Chim. Pays-Bas* **1974**, *93*, 33 – 36.
[76] M. G. Reinecke, H. W. Adickes, *J. Am. Chem. Soc.* **1968**, *90*, 511 – 513.
[77] M. G. Reinecke, H. W. Adickes, C. Pyun, *J. Org. Chem.* **1971**, *36*, 2690 – 2692; M. G. Reinecke, H. W. Adickes, C. Pyun, *J. Org. Chem.* **1971**, *36*, 3820 – 3821.
[78] S. Kano, Y. Yuasa, T. Yokomatsu, S. Shibuya, *Heterocycles* **1983**, *20*, 2035 – 2037 [*Chem. Abstr.* **1984**, *100*, 6238 p].
[79] E. C. Taylor, D. E. Vogel, *J. Org. Chem.* **1985**, *50*, 1002 – 1004.
[80] J. Fröhlich, C. Hametner, W. Kalt, *Monatsh. Chem.* **1996**, *127*, 325 – 330.
[81] J. Fröhlich, C. Hametner, *Monatsh. Chem.* **1996**, *127*, 435 – 443.
[82] F. Sauter, H. Fröhlich, W. Kalt, *Synthesis* **1989**, 771 – 773.
[83] J. Fröhlich, *Prog. Heterocycl. Chem.* **1994**, *6*, 1 – 35 [*Chem. Abstr.* **1995**, *122*, 187273 u].
[84] M. Mallet, G. Branger, F. Marsais, G. Quéguiner, *J. Organomet. Chem.* **1990**, *382*, 319 – 332.
[85] P. Rocca, C. Cochennec, F. Marsais, L. Thomas-dit-Dumont, M. Mallet, A. Godard, G. Quéguiner, *J. Org. Chem.* **1993**, *58*, 7832 – 7838.
[86] E. Arzel, P. Rocca, F. Marsais, A. Godard, G. Quéguiner, *Tetrahedron* **1999**, *55*, 12149 – 12156.
[87] C. Bobbio, M. Schlosser, *Eur. J. Org. Chem.* **2001**, 4533 – 4536.
[88] M. Schlosser, C. Bobbio, *Eur. J. Org. Chem.* **2002**, 4174 – 4180.
[89] F. Cottet, M. Schlosser, unpublished results, **2002–2003** (see also: F. Cottet, Ph.D. Thesis, École Polytechnique Fédérale, Lausanne, **2003**).
[90] F. Leroux, unpublished results, **2003**.
[91] R. A. Benkeser, R. A. Hickner, D. I. Hoke, O. H. Thomas, *J. Am. Chem. Soc.* **1958**, *80*, 5289 – 5294.
[92] H. E. Katz, *Organometallics* **1986**, *5*, 2308 – 2311.
[93] P. Cali, M. Begtrup, *Synthesis* **2002**, 63 – 66.
[94] A. Inoue, K. Kitagawa, H. Shinokubo, K. Oshima, *J. Org. Chem.* **2001**, *66*, 4333 – 4339.
[95] M. Q. Slagt, R. J. M. Klein Gebbink, M. Lutz, A. L. Spek, G. van Koten, *J. Chem. Soc. Dalton Trans.* **2002**, 2591 – 2592.
[96] M. Schlosser, T. Rausis, *Eur. J. Org. Chem.* **2004**, 1018 – 1024.
[97] F. Cottet, M. Marull, O. Lefebvre, M. Schlosser, *Eur. J. Org. Chem.* **2003**, 1559 – 1568.
[98] B. Iddon, N. Khan, *J. Chem. Soc. Perkin Trans. 1* **1987**, 1445 – 1453.
[99] B. Iddon, A. K. Petersen, J. Becher, N. J. Christensen, *J. Chem. Soc. Perkin Trans. 1* **1995**, 1475 – 1481.
[100] B. H. Lipshutz, W. Hagen, *Tetrahedron Lett.* **1992**, *33*, 5865 – 5868.
[101] P. Groziak, L. Wei, *J. Org. Chem.* **1991**, *56*, 4296 – 4300.
[102] P. Groziak, L. Wei, *J. Org. Chem.* **1992**, *57*, 3776 – 3780.
[103] S. V. Sunthankar, H. Gilman, *J. Org. Chem.* **1951**, *16*, 8 – 16.
[104] R. A. Murphy, H. F. Kung, M.-P. Kung, J. Billings, *J. Med. Chem.* **1990**, *33*, 171 – 178.
[105] P. Stanetty, B. Krumpak, I. K. Rodler, *J. Chem. Res. Synop.* **1995**, 342 – 343.
[106] G. Voß, H. Gerlach, *Chem. Ber.* **1989**, *122*, 1199 – 1201.
[107] "La procession dansante d'Echternacht et ses descriptions au 19e siècle": P. Kauthen in *Echternacher Studien*, *Vol. 1* (Ed.: P. Margue), St-Paul, Luxemburg, **1979**, pp. 405 – 438, spec. 416 – 423; first published in: *Hémecht*, **1979**, *issue 3*, St-Paul, Luxembourg.
[108] F. Leroux, M. Schlosser, I. Marek, E. Zohar in *The Preparation of Organolithium Reagents and Intermediates* (Eds.: Z. Rappoport, I. Marek), Wiley, Chichester, **2004**.
[109] W. E. Parham, R. M. Piccirilli, *J. Org. Chem.* **1977**, *42*, 257 – 260.
[110] X. Wang, P. Rabbat, P. O'Shea, R. Tillyer, E. J. J. Grabowski, P. J. Reider, *Tetrahedron Lett.* **2000**, *41*, 4335 – 4388.
[111] I. F. Tupitsyn, N. N. Zatspeina, A. V. Kirova, Y. L. Kaminsky, A. G. Ivanenko, *Reakts. Sposobn. Org. Soedin.* **1973**, *10*, 143 – 162 [*Chem. Abstr.* **1973**, *79*, 114928 v; quoted according to: O. A. Reutov, I. P. Beletskaya, K. P. Butin, *CH-Acids*, Pergamon, Oxford, **1978**.
[112] M. Schlosser, *Correlating Organometallic Reactivity with Carbanion Basicity*, in preparation.

 © 2005 Wiley-VCH Verlag GmbH & Co. KGaA, Weinheim

Communications



The dipeptide Ac-L-Pro-D-c_3Dip-NHMe, which incorporates a cyclopropane amino acid, adopts two consecutive γ turns that are stabilized by intramolecular hydrogen bonds. For more details on this conformation, which has not been seen before in crystalline short linear peptides, see the Communication by A. I. Jiménez et al. on the following pages.

© 2005 Wiley-VCH Verlag GmbH & Co. KGaA, Weinheim
DOI: 10.1002/anie.200461230

Peptide Structures

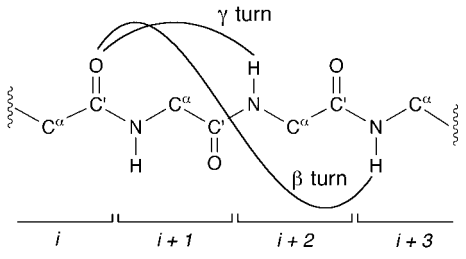
First Observation of Two Consecutive γ Turns in a Crystalline Linear Dipeptide**

Ana I. Jiménez, Gema Ballano, and Carlos Cativiela*

Dedicated to Dr. Michel Marraud

Reverse turns (or bends) are elements of primary importance both in the structure and function of peptides and proteins.[1] They give rise to a sharp reversal in the polypeptide chain, thus conferring on proteins their globular character. Turns have been suggested to play a role in the initial stages of protein folding and to be propitious sites for molecular recognition and receptor binding. Many naturally occurring oligopeptides have been proposed to adopt turns in their bioactive conformation.[1,2]

Different types of bends have been recognized according to the number and spatial arrangement of the residues involved. The most common is the β turn,[1,3] which involves four consecutive amino acids (*i* to *i*+3, Figure 1) and is generally stabilized by an intramolecular hydrogen bond between the CO group at position *i* and the NH group at *i*+3. Several subclasses of β turns are further distinguished on the basis of the backbone dihedral angles (φ,ψ) associated with the central *i*+1 and *i*+2 positions. Types I and II (Figure 1) are the most widely distributed and differ essentially in the orientation of the middle peptide group. The other main category of chain reversal is the so-called γ turn,[1,4] which is tighter and less common than the β bend. The γ turn is centered at a single residue (*i*+1, Figure 1), usually with a hydrogen bond between the CO and NH groups at positions *i* and *i*+2, respectively.

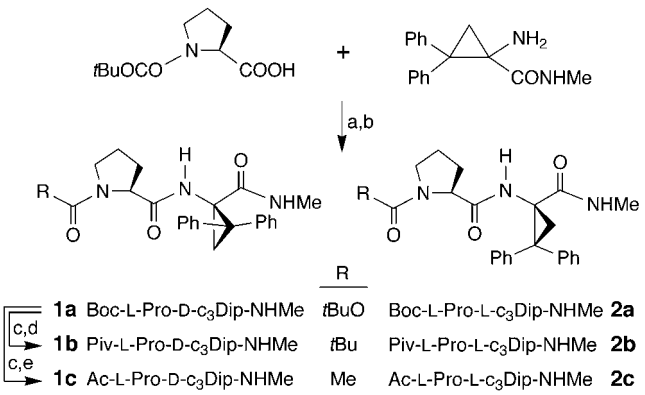


	ϕ	ψ	ϕ	ψ
βI turn	–60	–30	–90	0
βII turn	–60	120	80	0
γ turn	–75	60		

Figure 1. Schematic representation of the intramolecular hydrogen bond that stabilizes the β turn (*i*+3→*i*) and the γ turn (*i*+2→*i*) in a peptide chain. The ideal torsion angles of the central residues for the γ turn and the most common types of β turn are indicated.

We are involved in a research project aimed at evaluating the relative stability of the βI and βII turns in model peptides RCO-L-Pro-Xaa-NHR′ that incorporate different constrained α-amino acids at the *i*+2 position (Xaa).[5] Such terminally protected dipeptides constitute the smallest systems able to accommodate the β-turn conformation. As part of these investigations we undertook the study of the L-Pro-c_3Dip sequence, where c_3Dip denotes each enantiomer of α,β-methanodiphenylalanine,[6] a cyclopropane analogue of phenylalanine. The results of the solid-state conformational analysis, of high structural relevance, are reported herein.

Racemic *N*′-methyl-2,2-diphenyl-1-aminocyclopropanecarboxamide[7] (H-c_3Dip-NHMe) was coupled to *N*-*tert*-butoxycarbonyl-L-proline by the mixed-anhydride method (Scheme 1). Column chromatography allowed the separation of the resulting diastereomeric dipeptides (**1a**, **2a**), which were isolated in optically pure form. The difficulties encountered in growing single crystals from these compounds prompted us to replace the N-terminal urethane protecting group with different amide groups. Single crystals suitable for X-ray diffraction analysis were finally obtained from the pivaloyl derivative **2b** and the acetyl derivative **1c**.



Scheme 1. Synthesis of L-Pro-c_3Dip dipeptides. Reagents and conditions: a) *i*BuOCOCl, NMM, THF, −15 °C; b) column chromatography (CH_2Cl_2/*i*PrOH 93/7); c) 3 N HCl/EtOAc, RT; d) *t*BuCOCl, NMM, $CHCl_3$, 0 °C; e) Ac_2O, NMM, $CHCl_3$, RT. NMM = *N*-methylmorpholine.

The crystalline structure of dipeptide **2b** (Figure 2) revealed an L (or *S*) configuration for the c_3Dip residue. The molecule adopts a β-turn conformation with the terminal pivaloyl CO and methylamide NH groups intramolecularly hydrogen bonded (N···O: 2.97 Å; N–H···O: 156°). The (φ,ψ) torsion angles of the L-Pro (−63,133) and L-c_3Dip (69,−2) residues correspond to a β bend of type II (Figure 1). It should be noted that the βI turn is energetically more favorable for L-Pro-L-Xaa dipeptides in low-polarity solvents[5a,8] but, in general, this conformation is not retained in

[*] Dr. A. I. Jiménez, G. Ballano, Dr. C. Cativiela
Departamento de Química Orgánica, ICMA
Universidad de Zaragoza-CSIC
50009 Zaragoza (Spain)
Fax: (+34) 976-761-210
E-mail: anisjim@unizar.es

[**] The authors thank Dr. M. M. Zurbano for collection of the X-ray diffraction data. Financial support from the Ministerio de Educación y Ciencia (project PPQ2001–1834 and predoctoral fellowship for G.B.) and the Diputación General de Aragón is gratefully acknowledged.

 © 2005 Wiley-VCH Verlag GmbH & Co. KGaA, Weinheim

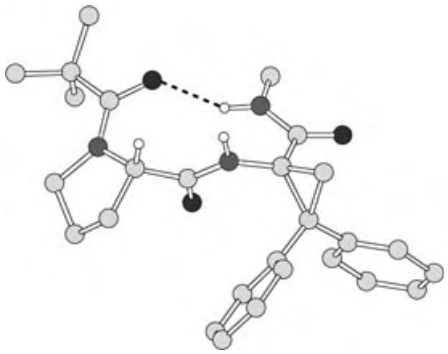


Figure 2. X-ray diffraction structure of Piv-L-Pro-L-c_3Dip-NHMe (**2b**) accommodating a βII turn. The intramolecular $i+3\rightarrow i$ hydrogen bond is indicated by a dashed line. Only the proline C^α and the amide hydrogen atoms are shown.

the solid state, where the βII turn becomes preferred because it allows the Xaa NH group to participate in intermolecular contacts.[5a,d,8] The L-c_3Dip NH site in **2b** is actually hydrogen bonded to a carbonyl group of a neighboring molecule. In comparison, RCO-L-Pro-D-Xaa-NHR′ dipeptides are more prone to βII folding under all environmental conditions and have been found to invariably crystallize in the βII form.[5,8]

On the basis of the above discussion, Ac-L-Pro-D-c_3Dip-NHMe (**1c**) was expected to accommodate a βII turn in the solid state. Surprisingly, a conformation consisting of two consecutive γ turns was found (Figure 3). The (φ,ψ) torsion

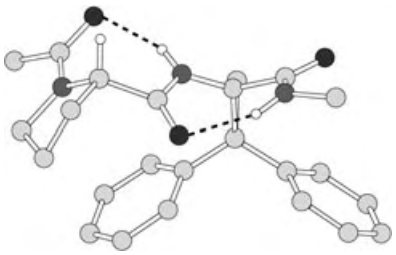


Figure 3. X-ray diffraction structure of Ac-L-Pro-D-c_3Dip-NHMe (**1c**) exhibiting two consecutive γ turns, each stabilized by an intramolecular $i+2\rightarrow i$ hydrogen bond (dashed lines). Only the proline C^α and the amide hydrogen atoms are shown.

angles for both L-Pro (−82,61) and D-c_3Dip (−72,47) lie close to the typical values (−75,60),[1] with the larger deviation being observed for the ψ angle of the D-c_3Dip residue. However, the excellent agreement between the observed ψ value and that predicted from theoretical calculations[9] for the γ-turn minimum energy conformation of cyclopropane residues bearing a phenyl substituent *cis* to the CO terminus ($\psi=47°$) is remarkable, and appears to reflect a balance between steric and hyperconjugative effects. Whatever the origin of this deviation, it does not seem to impede the appropriate alignment of the L-Pro CO and methylamide NH sites, which form a strong intramolecular hydrogen bond (N···O: 2.81 Å, N–H···O: 147°), as do the acetyl CO and D-c_3Dip NH groups (N···O: 2.78 Å, N–H···O: 152°).

The solid-state conformation exhibited by compound **1c** is of extraordinary structural significance. Although much less frequent than β bends, γ turns are found to be abundant in crystallized proteins,[10] where they are stabilized or induced by long-range interactions. Such a source of stabilization is not possible in small peptides and γ turns are observed almost exclusively in poor-solvating media,[1] that is, in the absence of competing intermolecular hydrogen-bonding interactions either with the solvent or with other peptide molecules in the crystal. A few examples of X-ray diffraction structures exhibiting a γ turn have been reported for cyclic oligopeptides—mostly pentapeptides with proline at the turn center—while this conformation is extremely uncommon in acyclic sequences.[1,8b,11] The double γ turn encountered in **1c** is, therefore, unique among crystalline short linear peptides. Moreover, a survey of the Cambridge Structural Database[12] indicates[13] that this is the first report in which proline accommodates a γ-turn conformation in the solid state in the absence of the constraints imposed by backbone cyclization. Proline is, in fact, the proteinogenic amino acid with the highest folding propensity[10b,14] and has been shown to adopt the γ-turn conformation in low-polarity solvents,[1b,c,15] a capacity that is not maintained in the solid state, where proline is overwhelmingly found in the (−60,−30) or (−60,140) region of the (φ,ψ) map.[1b,5,8,10b,14,16]

Accordingly, the γ-turn disposition accommodated by proline in **1c** can be ascribed to the presence of the contiguous D-c_3Dip residue, whose conformational tendencies appear to prevail over those of proline. The latter consideration is of special relevance given that proline is the proteinogenic amino acid with the strongest conformational preferences.[10b,14] Cyclopropane α-amino acids have been suggested as promising candidates for γ-turn stabilization on the basis of theoretical and experimental studies.[5c,d,9,17] However, the fact that theoretical calculations on small peptides generally overestimate the stability of γ-folded conformers,[18] together with the limited experimental evidence available to date, made it premature to proclaim the capacity of such residues to promote γ-turn conformations.

The result reported here constitutes the first unequivocal evidence of the ability of a cyclopropane α-amino acid to adopt a γ-turn disposition in a nonpropitious environment and to influence the overall folding of the peptide chain. Clearly, much work remains to be done to determine the precise conditions under which c_3Dip is able to nucleate γ turns and, thereafter, to establish its scope as a γ-turn inductor. The finding of an α-amino acid with a clear preference for the γ-turn conformation would be of enormous help in the stabilization of this structural motif in bioactive peptides, as well as in the construction of appropriate models to study the factors that govern γ folding.

Experimental Section

2b: m.p. 228 °C (iPr$_2$O/CH$_2$Cl$_2$); $[\alpha]_D^{26}=+56.1$ ($c=0.42$ in MeOH); IR (Nujol): $\tilde{\nu}=3377$, 3317, 1691, 1641, 1608 cm^{-1}; ^{1}H NMR ($CDCl_3$, 400 MHz): $\delta=1.18$–1.29 (m, 1H), 1.31 (s, 9H), 1.39–1.52 (m, 1H), 1.63–1.74 (m, 2H), 2.00 (d, $J=5.6$ Hz, 1H), 2.62 (d, $J=5.6$ Hz, 1H), 2.78 (d, $J=4.8$ Hz, 3H), 3.42 (m, 1H), 3.57 (m, 1H), 4.09 (dd, $J=8.3$, 5.0 Hz, 1H), 6.01 (brs, 1H), 7.16–7.29 (m, 6H), 7.37–7.43 (m, 4H), 7.45 ppm (brq, $J=4.8$ Hz, 1H); ^{13}C NMR ($CDCl_3$, 100 MHz): $\delta=$ 24.71, 25.73, 26.93, 27.10, 27.31, 39.10, 44.05, 45.44, 48.64, 63.20,

 © 2005 Wiley-VCH Verlag GmbH & Co. KGaA, Weinheim

126.74, 126.77, 128.12, 128.31, 128.93, 129.38, 140.42, 140.84, 168.94, 172.62, 178.20 ppm; elemental analysis (%) calcd for $C_{27}H_{33}N_3O_3$: C 72.46, H 7.43, N 9.39; found: C 72.61, H 7.37, N 9.47.

1c: m.p. 180 °C (Et_2O); $[\alpha]_D^{21} = -218.3$ ($c = 0.27$ in MeOH); IR (Nujol): $\tilde{\nu} = 3369$, 3347, 1676, 1660, 1629 cm^{-1}; ^1H NMR ($CDCl_3$, 400 MHz): $\delta = 1.51$–1.59 (m, 1H), 1.64–1.80 (m, 3H), 1.76 (s, 3H), 2.21 (m, 1H), 2.56 (d, $J = 5.6$ Hz, 1H), 2.64 (d, $J = 4.8$ Hz, 3H), 2.87 (m, 1H), 3.03 (m, 1H), 4.25 (dd, $J = 7.8$, 1.3, 1H), 7.04–7.18 (m, 6H), 7.34–7.39 (m, 4H), 7.86 (br s, 1H), 7.90 ppm (br q, $J = 4.8$ Hz, 1H); ^{13}C NMR ($CDCl_3$, 100 MHz): $\delta = 22.38$, 23.38, 24.72, 26.55, 26.75, 46.28, 46.31, 48.09, 59.26, 126.67, 126.94, 128.00, 128.27, 129.16, 129.44, 140.22, 140.96, 169.10, 171.21, 173.43 ppm; elemental analysis (%) calcd for $C_{24}H_{27}N_3O_3$: C 71.09, H 6.71, N 10.36; found: C 70.89, H 6.66, N 10.39.

The X-ray crystal structures of **2b** and **1c** were solved by direct methods using SHELXS-97.[19a] Refinement was performed using SHELXL-97[19b] by the full-matrix least-squares technique. Hydrogen atoms were located by calculation, with the exception of the cyclopropane and NH protons, which were found on the E map. CCDC-243527 (**2b**) and -243526 (**1c**) contain the supplementary crystallographic data for this paper. These data can be obtained free of charge via www.ccdc.cam.ac.uk/conts/retrieving.html (or from the Cambridge Crystallographic Data Centre, 12 Union Road, Cambridge CB2 1EZ, UK; fax: (+44) 1223-336-033; or deposit@ccdc.cam.ac.uk).

X-ray data for **2b** ($C_{27}H_{33}N_3O_3 \cdot 3/2\,H_2O$): $M_r = 474.59$, orthorhombic, space group $P2_12_12$, $a = 11.0690(10)$, $b = 23.498(2)$, $c = 10.1750(10)$ Å, $V = 2646.5(4)$ Å^3, $Z = 4$; $\rho_{calcd} = 1.191$ g cm^{-3}, $\mu(Mo_{K\alpha}) = 0.081$ mm^{-1}, $T = 293(2)$ K, $F(000) = 1020$, $2\theta_{max} = 50.1°$; 3449 reflections collected, of which 3241 unique ($R_{int} = 0.0308$). Final R indices (2380 observed reflections, $I > 2\sigma I$): $R_1 = 0.0529$, $wR_2 = 0.1257$; final R indices (all data): $R_1 = 0.0784$, $wR_2 = 0.1409$. Highest residual electron density 0.19 e Å^{-3}.

X-ray data for **1c** ($C_{24}H_{27}N_3O_3$): $M_r = 405.49$, orthorhombic, space group $P2_12_12_1$, $a = 10.4010(2)$, $b = 12.6760(2)$, $c = 15.8660(3)$ Å, $V = 2091.82(7)$ Å^3, $Z = 4$; $\rho_{calcd} = 1.288$ g cm^{-3}, $\mu(Mo_{K\alpha}) = 0.086$ mm^{-1}, $T = 173(2)$ K, $F(000) = 864$, $2\theta_{max} = 53°$; 13835 reflections collected, of which 4276 unique ($R_{int} = 0.0559$). Final R indices (3738 observed reflections, $I > 2\sigma I$): $R_1 = 0.0409$, $wR_2 = 0.0855$; final R indices (all data): $R_1 = 0.0501$, $wR_2 = 0.0892$. Highest residual electron density 0.15 e Å^{-3}.

Received: July 8, 2004

Keywords: β turn · conformation analysis · hydrogen bonds · peptide folding · structure elucidation

[1] a) C. Toniolo, *Crit. Rev. Biochem.* **1980**, *9*, 1; b) G. D. Rose, L. M. Gierasch, J. A. Smith, *Adv. Protein Chem.* **1985**, *37*, 1; c) E. Vass, M. Hollósi, F. Besson, R. Buchet, *Chem. Rev.* **2003**, *103*, 1917.

[2] A. F. Spatola in *Bioorganic Chemistry: Peptides and Proteins* (Ed.: S. M. Hecht), Oxford University Press, New York, **1998**, pp. 367–394.

[3] C. M. Venkatachalam, *Biopolymers* **1968**, *6*, 1425.

[4] G. Némethy, M. P. Printz, *Macromolecules* **1972**, *5*, 755.

[5] a) A. I. Jiménez, C. Cativiela, A. Aubry, M. Marraud, *J. Am. Chem. Soc.* **1998**, *120*, 9452; b) A. I. Jiménez, C. Cativiela, J. Gómez-Catalán, J. J. Pérez, A. Aubry, M. París, M. Marraud, *J. Am. Chem. Soc.* **2000**, *122*, 5811; c) A. I. Jiménez, C. Cativiela, M. Marraud, *Tetrahedron Lett.* **2000**, *41*, 5353; d) A. I. Jiménez, M. Marraud, C. Cativiela, *Tetrahedron Lett.* **2003**, *44*, 3147.

[6] For a given α-amino acid Xaa, we designate its cyclopropane analogue, obtained by linking the α and β carbon atoms with a methylene group, as c_3Xaa. β,β-Diphenylalanine is a phenylalanine derivative known in the abbreviated form as Dip and, accordingly, we have named its cyclopropane analogue as c_3Dip.

[7] This compound was obtained as a racemate by reaction of diphenyldiazomethane with an α,β-dehydroalanine derivative and subsequent elaboration of the protecting groups. G. Ballano, A. I. Jiménez, C. Cativiela, unpublished results.

[8] a) A. Aubry, M. T. Cung, M. Marraud, *J. Am. Chem. Soc.* **1985**, *107*, 7640; b) M. Marraud, A. Aubry, *Biopolymers* **1996**, *40*, 45.

[9] a) C. Alemán, A. I. Jiménez, C. Cativiela, J. J. Perez, J. Casanovas, *J. Phys. Chem. B* **2002**, *106*, 11849; b) J. Casanovas, A. I. Jiménez, C. Cativiela, J. J. Pérez, C. Alemán, *J. Org. Chem.* **2003**, *68*, 7088.

[10] a) K. Guruprasad, S. Rajkumar, *J. Biosci.* **2000**, *25*, 143; b) P. Chakrabarti, D. Pal, *Prog. Biophys. Mol. Biol.* **2001**, *76*, 1.

[11] a) E. Benedetti, *Biopolymers* **1996**, *40*, 3; b) C. Toniolo, M. Crisma, F. Formaggio, C. Peggion, *Biopolymers* **2001**, *60*, 396.

[12] The CSD covers peptides of up to 24 residues. a) F. H. Allen, *Acta Crystallogr. Sect. B* **2002**, *58*, 380; b) I. J. Bruno, J. C. Cole, P. R. Edington, M. Kessler, C. F. Macrae, P. McCabe, J. Pearson, R. Taylor, *Acta Crystallogr. Sect. B* **2002**, *58*, 389.

[13] The November 2003 version (2 updates) of the CSD was reviewed. The proline -CO-Pro-NH- fragment was searched, considering both L and D configurations and torsion angles within the ranges $(\varphi,\psi) = (-75 \pm 30, 60 \pm 30)$ (or their enantiomeric values). Only proline residues included in cyclic peptides were found to fulfill these requirements (refcodes: CGPGAP10, ICOGAI, PAPGAP, SIKMUU10, WAWQOA, DHCMYD10, HEBLIJ).

[14] M. W. MacArthur, J. M. Thornton, *J. Mol. Biol.* **1991**, *218*, 397.

[15] a) G. Boussard, M. Marraud, A. Aubry, *Biopolymers* **1979**, *18*, 1297; b) V. Madison, K. D. Kopple, *J. Am. Chem. Soc.* **1980**, *102*, 4855; c) G. B. Liang, C. J. Rito, S. H. Gellman, *Biopolymers* **1992**, *32*, 293; d) E. Beausoleil, W. D. Lubell, *J. Am. Chem. Soc.* **1996**, *118*, 12902; e) M. Miyazawa, K. Inouye, T. Hayakawa, Y. Kyogoku, H. Sugeta, *Appl. Spectrosc.* **1996**, *50*, 644.

[16] Note that these regions correspond to the $i+1$ position of a βI or a βII turn, respectively (Figure 1).

[17] a) K. Burgess, K.-K. Ho, B. M. Pettitt, *J. Am. Chem. Soc.* **1994**, *116*, 799; b) V. N. Balaji, K. Ramnarayan, M. F. Chan, S. N. Rao, *Pept. Res.* **1994**, *7*, 60; c) K. Burgess, C.-Y. Ke, *J. Org. Chem.* **1996**, *61*, 8627; d) C. Alemán, J. Casanovas, S. E. Galembeck, *J. Comput.-Aided Mol. Des.* **1998**, *12*, 259; e) D. Moye-Sherman, S. Jin, S. Li, M. B. Welch, J. Reibenspies, K. Burgess, *Chem. Eur. J.* **1999**, *5*, 2730; f) C. Peggion, F. Formaggio, M. Crisma, C. Toniolo, A. I. Jiménez, C. Cativiela, B. Kaptein, Q. B. Broxterman, M. Saviano, E. Benedetti, *Biopolymers* **2003**, *68*, 178.

[18] a) H.-J. Böhm, S. Brode, *J. Am. Chem. Soc.* **1991**, *113*, 7129; b) H. S. Shang, T. Head-Gordon, *J. Am. Chem. Soc.* **1994**, *116*, 1528.

[19] a) G. M. Sheldrick, SHELXS-97, Program for the Solution of Crystal Structures, University of Göttingen, Göttingen (Germany), **1997**; b) G. M. Sheldrick, SHELXL-97, Program for the Refinement of Crystal Structures, University of Göttingen, Göttingen (Germany), **1997**.

 © 2005 Wiley-VCH Verlag GmbH & Co. KGaA, Weinheim

Molecular Separations

Rotational Entropy Driven Separation of Alkane/Isoalkane Mixtures in Zeolite Cages**

Joeri F. M. Denayer, Refik A. Ocakoglu, Ilbige C. Arik, Christine E. A. Kirschhock, Johan A. Martens, and Gino V. Baron*

Molecular separation and purification processes are key operations in chemical industry.[1] High separation power is obtained in separation processes that are based on adsorption in zeolite micropores.[2] Molecular separation on zeolites can originate from several types of interactions. Electrostatic interactions are responsible for the selective adsorption of nitrogen from air, in the drying of gases, and the removal of polar impurities such as carbon monoxide, mercaptans, or organic chlorides from gases and liquids.[3,4] Shape-selectivity separation arises from the subtle matching of the size and shape of guest molecules and zeolite micropores.[5] Generally, adsorption and diffusion of more-bulky molecules is restricted by the small pore size. To boost octane ratings in gasoline, linear alkanes are sieved from the more-bulky branched alkanes by using narrow-pore molecular sieves.[5,6] Herein we take advantage of cage structures offered by special zeolite adsorbents such as MCM-22. The retention of alkane molecules in MCM-22 is governed by rotational freedom in its cages. The preferential adsorption of isopentane over *n*-pentane in MCM-22 zeolite is a first example of such rotational entropy driven separation.

The adsorptive separation power of a solid is determined by the equilibrium constants of adsorption of the molecules of interest. These equilibrium constants in turn relate to the adsorption enthalpy (the energetic interaction between the molecule and the host environment of the zeolite pore) and the adsorption entropy (the loss of freedom that a molecule experiences in the transition from the gaseous state to the adsorbed state). Depending on the strength of interaction and the pore type, molecules that are confined in zeolite pores lose rotational and translational freedom.[7] In large tubular pores, at least one degree of translational freedom is retained along the axis of the pore. However, in zeolite cages, translational freedom is severely reduced, hence the contribution of molecular rotation to the entropy becomes an essential factor in the relative adsorption equilibria of molecules of different sizes and shapes.[8]

The ability of a molecule to rotate in a cage can be estimated by comparing the radius of gyration of its van der Waals volume R_g, which assumes rotation around the centre of mass, to the radius R_c of the largest sphere that fits into the van der Waals contour of the cage or pore. Minimal loss of rotational entropy is combined with maximal energetic interactions when the sphere that circumscribes the rotational motion of the molecule matches the internal surface of the cage; that is, when the radius ratio R_g/R_c equals unity. The equilibrium adsorption properties of linear and branched alkanes on zeolites that comprise cages or tubular pores were determined to investigate this effect. Isoalkanes, with their shorter carbon backbone, have a smaller radius of gyration and a more spherical shape than their linear counterparts, thus they might rotate more easily in zeolite cages which could lead to their preferential adsorption.

Mordenite and ZSM-22 have one-dimensional pores with dimensions of $0.70 \times 0.65\ nm^2$ and $0.45 \times 0.55\ nm^2$, respectively (Figure 1). NaY contains spherical supercages with a diameter of 1.23 nm that are connected by windows of 0.73 nm (Figure 1). MCM-22 contains large nonspherical supercages of 1.82-nm height that are accessible through 10-ring apertures of $0.40 \times 0.54\ nm^2$ (Figure 1).[9] The top and bottom part of the MCM-22 supercages are pockets of 0.7–

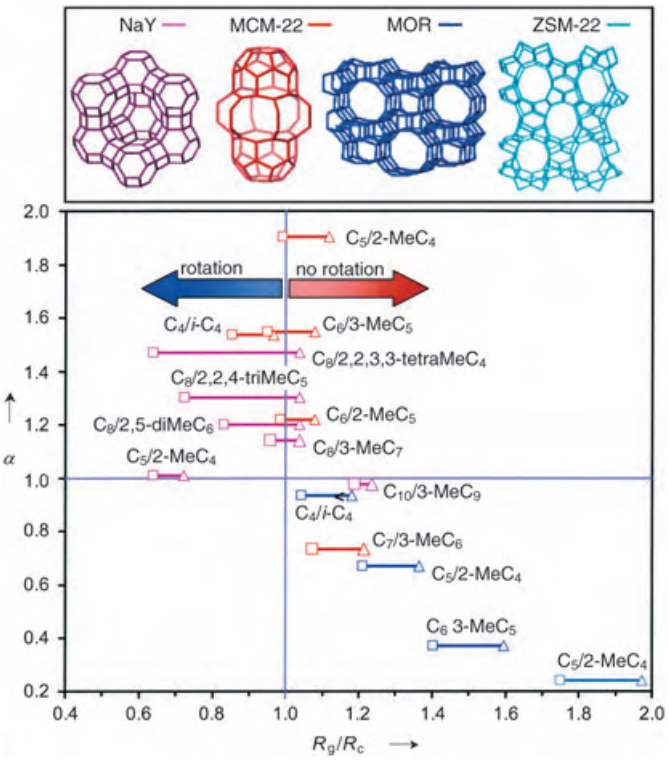


Figure 1. Ratio (α) of low coverage adsorption constants of branched and linear alkanes on MCM-22, NaY, Mordenite (MOR), and ZSM-22 plotted against the radius ratio R_g/R_c. $R_{g(i)}$ and $R_{g(n)}$ represent the radii of gyration of the iso- and *n*-alkanes, respectively, and R_c represents the radius of the largest sphere that fits in the zeolite cage. △ corresponds to $R_{g(n)}/R_c$ and □ corresponds to $R_{g(i)}/R_c$.

[*] Dr. J. F. M. Denayer, Dr. R. A. Ocakoglu, I. C. Arik, Prof. Dr. G. V. Baron
Department of Chemical Engineering
Vrije Universiteit Brussel
Pleinlaan 2, 1050 Brussel (Belgium)
Fax: (+32) 2-629-3248
E-mail: joeri.denayer@vub.ac.be
Dr. C. E. A. Kirschhock, Prof. Dr. J. A. Martens
Center for Surface Chemistry and Catalysis
Katholieke Universiteit Leuven
Kasteelpark Arenberg 23, 3001 Leuven (Belgium)

[**] J.F.M.D. and C.E.A.K. are grateful to FWO Vlaanderen for post-doctoral research fellowships. J.A.M. acknowledges the Flemish Government for supporting a Concerted Research Action on the understanding of the active site in catalysis.

 © 2005 Wiley-VCH Verlag GmbH & Co. KGaA, Weinheim DOI: 10.1002/anie.200454058

0.8 nm in diameter, whereas the broadened central part of this supercage, which resembles a squeezed ellipsoidal cage, is capable of hosting larger molecules. MCM-22 and related materials show interesting adsorption, diffusion, and catalytic properties.[10–15]

Separation factors (α), which are computed as the ratios of the Henry adsorption constants for branched over linear alkanes, are plotted against radius ratios R_g/R_c in Figure 1. For Mordenite and ZSM-22, separation factors of less than 1 are observed which indicates that the linear alkanes are adsorbed preferentially. *n*-Alkanes and isoalkanes have a radius of gyration which is larger than the largest sphere that fits in the tubular pores of Mordenite and ZSM-22, so rotational freedom is severely restricted for both types of molecules. For *n*-butane/isobutane on Mordenite, the preference for the linear alkane is the least pronounced. The radius of gyration of isobutane is only slightly larger than R_c for this zeolite.

With MCM-22 and NaY, a reversal of the normal order of selectivity is observed for several *n*-alkane/isoalkane couples. A selective adsorption of the isoalkane is observed for isobutane, 2-methylbutane, and 2- and 3-methylpentane on MCM-22. The largest separation factor (1.9) is obtained for the *n*-pentane/2-methylbutane couple. The sphere circumscribing the rotation of 2-methylbutane neatly fits into the pocket of the upper and lower parts of the MCM-22 supercage (Figure 2a), whereas *n*-pentane is unable to rotate in that volume. 2-Methylpentane and 3-methylpentane are too large to enable rotation in the pockets of MCM-22, but their gyration spheres fit into the central part of the MCM-22 supercage (Figure 2b).

A pronounced selectivity in favor of the isoalkane is also observed with 2,2,3,3-tetramethylbutane, 2,2,4-trimethylpentane, 2,5-dimethylhexane, and 3-methylheptane on NaY (Figure 1). *n*-Octane is a little too large to rotate freely in the NaY supercages, whereas its isomers retain rotational freedom. The selectivity becomes more pronounced when the difference in R_g between the branched and linear alkanes increases (Figure 1).

With smaller alkanes (e.g. *n*-pentane/2-methylbutane on NaY), the rotation of the *n*-alkane is barely hampered and the differences in rotational freedom between linear and branched alkanes are minor (Figure 1). Consequently, only a low selectivity for the branched alkane is observed. Similarly, when the isoalkane becomes too large to rotate in the zeolite cage, it loses its advantage in rotational freedom and selectivity in favor of the linear chain is observed (e.g. *n*-decane/3-methylnonane on NaY and *n*-heptane/3-methylhexane on MCM-22).

Differences in rotational freedom between molecules are reflected in the adsorption entropy. In Figure 3, the adsorption entropy is plotted as a function of adsorption enthalpy for

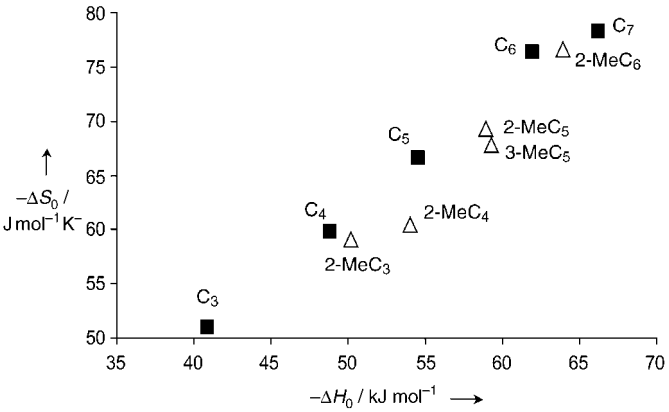


Figure 3. Compensation plot between the adsorption entropy and enthalpy for C_3–C_7 *n*-alkanes (■) and their methyl-branched isomers (△) on zeolite MCM-22.

MCM-22. For a branched molecule to have a higher Henry adsorption constant than its linear isomer, it needs to have a combination of adsorption enthalpy and entropy that results in a lower Gibbs free energy of adsorption. 2-Methylbutane, 2-methylpentane, and 3-methylpentane obviously lose much less entropy in the adsorbed state relative to their linear isomers. For example, the entropy loss of 3-methylpentane is lower than that of *n*-hexane by 9.0 J mol^{-1} K^{-1}. Consequently, these isoalkanes are adsorbed preferentially over their linear isomers despite their less favorable adsorption enthalpy. For the *n*-heptane/2-methylhexane couple, the difference in adsorption entropy is only 1.7 J mol^{-1} K^{-1} as a result of the restricted rotation of 2-methylhexane. Compared to *n*-butane, isobutane has a slightly higher adsorption enthalpy (*n*-butane: 48.8 kJ mol^{-1}; isobutane: 50.1 kJ mol^{-1}) which is explained by a better agreement between the shape of isobutane and the pockets of MCM-22. Moreover, isobutane has a less-negative adsorption entropy, which indicates that this molecule loses less freedom in the adsorbed state than its linear isomer although it is more strongly interacting.

By exploiting rotational entropy effects, separation patterns that are different from those found typically

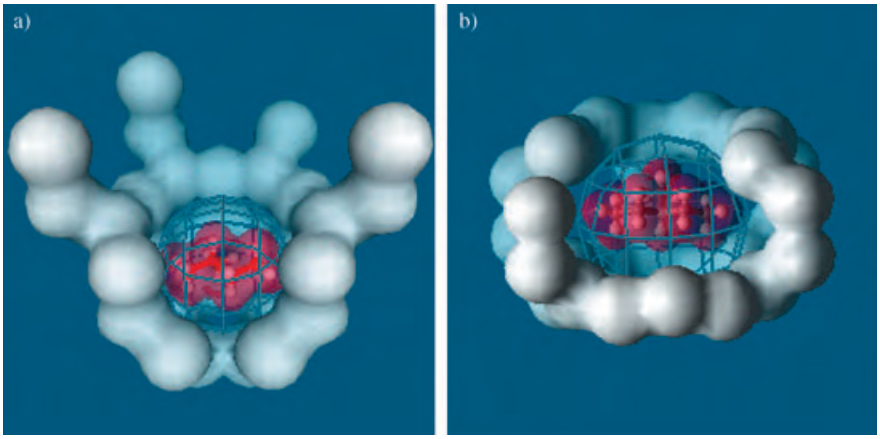


Figure 2. a) A molecule of 2-methylbutane with its radius of gyration in the lobe of the MCM-22 supercage and b) 3-methylpentane in the central part of the MCM-22 supercage.

 © 2005 Wiley-VCH Verlag GmbH & Co. KGaA, Weinheim

can be obtained. Figure 4, a–c, show the chromatograms obtained after injection of mixtures of linear and branched alkanes on zeolite columns. With Mordenite, 2-methylbutane elutes first from the column followed by *n*-pentane (Figure 4a). This order of affinity is common to zeolite types studied previously.[16–18] On an MCM-22 column, the retention order is reversed as a result of the higher adsorption equilibrium constant of the branched alkane (Figure 4b). Even more remarkable is the separation of a ternary mixture of differently branched alkanes on MCM-22 (Figure 4c). *n*-Hexane elutes between 2-methylpentane and 2,2-dimethylbutane; the bulkiest dibranched isomer is too large to enter the MCM-22 supercages and therefore elutes first.[10–12] Figure 4, d and e, show breakthrough profiles for *n*-pentane/2-methylbutane and *n*-butane/isobutane mixtures separated on an MCM-22 column. The branched alkanes are selectively trapped inside the MCM-22 pores and displace the adsorbed linear alkanes along the column profile until the composition inside the pores reaches thermodynamical equilibrium. Also under these conditions whereby the MCM-22 pores are saturated with molecules, a good separation with selectivity for the branched alkanes is found.

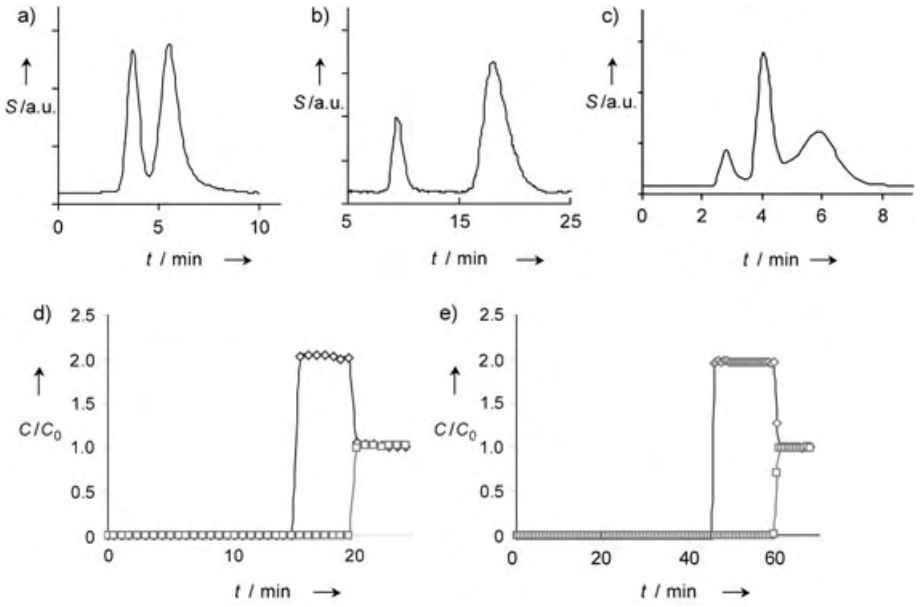


Figure 4. a–c) Chromatograms of *n*-alkane/isoalkane mixtures obtained on zeolite columns at 200 °C (*S* = detector signal): a) separation of *n*-pentane and 2-methylbutane on Mordenite, b) separation of *n*-pentane and 2-methylbutane on MCM-22, and c) separation of *n*-hexane, 3-methylpentane, and 2,2-dimethylbutane on MCM-22. d) and e) Breakthrough profiles obtained on an MCM-22 column at 130 °C with a total hydrocarbon pressure of 0.2 bar (*C* = concentration): d) equimolar *n*-pentane (◇)/2-methylbutane (□) mixture, e) equimolar *n*-butane (◇)/isobutane (□) mixture.

Recent molecular modeling studies demonstrated that a selective uptake of isoalkanes from *n*-/isoalkane mixtures might occur at high pressures and high zeolite loadings in zeolites with tubular pores of 0.6–0.75 nm because more of these shorter isoalkanes can be packed into a single file relative to the linear chains.[19,20] The effect observed in the present work already occurs at low pressure with isolated molecules adsorbed in zeolite cages rather than in tubular pores and does not invoke molecular packing phenomena. To investigate whether the preference of MCM-22 for monobranched alkanes extends beyond the low-coverage domain, where adsorbed molecules are isolated from each other, the adsorption selectivity for a *n*-pentane/2-methylbutane mixture was determined in the liquid phase at complete saturation of the pores of MCM-22. Also under these conditions, 2-methylbutane was selectively adsorbed with a separation factor between 2-methylbutane and *n*-pentane of 1.4.

In summary, a new principle for molecular separation based on differences in molecular rotation in zeolite cages has been introduced. Rotational entropy driven separation could be useful in the separation of structural isomers, such as *n*- and isoalkanes, aromatic compounds, or possibly other mixtures of differently shaped molecules. The recent development of new porous materials with much larger cavities than the ones investigated here opens perspectives for new, entropic-based separations with larger molecules.[21]

Experimental Section

MCM-22 (Si:Al 30) was synthesized according to the method described in US Patent 5146029.[22] ZSM-22 (Si:Al 30) was prepared according to the procedure reported by Ernst et al.[23] NaY (CBV100, Si:Al 2.5) and Mordenite (CP-500C-11, Si:Al 5.5) were purchased from Zeolyst. Chromatographic and breakthrough experiments were performed to study the adsorption properties of these adsorbents.[2] Adsorption equilibrium Henry constants were calculated from the first moment of the chromatographic response curves. Linearity of the experiments and absence of diffusion limitations was confirmed with different amounts of injection and by using different carrier flow rates. A detailed explanation of the experimental setup and procedure can be found elsewhere.[24] From the temperature dependence of the Henry coefficients (K'), the adsorption enthalpy (ΔH_0) is calculated according to Equation (1). The adsorption entropy (ΔS_0) is calculated by using Equation (2)[20] and Equation (3), wherein ρ_c is the crystal density of the zeolite, T corresponds to the temperature (K), and R is the universal gas constant.

$$K' = K'_0 e^{\frac{-\Delta H_0}{RT}} \quad (1)$$

$$\Delta G_0 = -R\,T \ln(K' \rho_c\, R\,T) \quad (2)$$

$$\Delta S_0 = \frac{\Delta H_0 - \Delta G_0}{T} \quad (3)$$

The adsorption selectivity in the liquid phase was determined by using a static method at room temperature.[25]

Received: February 19, 2004
Revised: October 4, 2004 [Z54058]

Keywords: adsorption · alkanes · isomers · thermodynamics · zeolites

 © 2005 Wiley-VCH Verlag GmbH & Co. KGaA, Weinheim

[1] J. M. Coulson, J. F. Richardson, J. R. Backhurst, J. H. Harker, *Chemical Engineering*, *Vol. 2*, Pergamon, Oxford, **1991**, pp. 735.
[2] D. M. Ruthven, *Principles of Adsorption and Adsorption Processes*, Wiley, New York, **1984**.
[3] J. D. Sherman, *Proc. Natl. Acad. Sci. USA* **1999**, *96*, 3471 – 3478.
[4] R. A. Meyers, *Handbook of Petroleum Refining Processes*, *2nd ed.*, McGraw-Hill, New York, **1996**, Chapter 10.6.
[5] N. Y. Chen, W. E. Garwood, F. G. Dwyer, *Shape-Selective Catalysis in Industrial Applications*, Marcel Dekker, New York, **1989**.
[6] S. Kulprathipanja, R. W. Neuzil, US Patent 4 445 444, **1984**, UOP.
[7] P. S. Rallabandi, D. M. Ford, *AIChE J.* **2000**, *46*, 99 – 109.
[8] R. Mukhopadhay, A. Sayeed, M. N. Rao, A. V. Anilkumar, S. Mitra, S. Yashonath, S. L. Chaplot, *Chem. Phys.* **2003**, *292*, 217 – 222.
[9] S. L Lawton, M. E. Leonowicz, R. D. Partridge, P. Chu, M. K. Rubin, *Microporous Mesoporous Mater.* **1998**, *23*, 109 – 117.
[10] H. Du, M. Kalyanaraman, M. A. Camblor, D. H. Olson, *Microporous Mesoporous Mater.* **2000**, *40*, 305 – 312.
[11] W. J. Roth, C. T. Kresge, J. C. Vartuli, M. E. Leonowicz, A. S. Fung, S. B. Mcullen, *Stud. Surf. Sci. Catal.* **1995**, *94*, 301 – 308.
[12] A. Corma, C. R. Catlow, G. Sastre, *J. Phys. Chem. B* **1998**, *102*, 7085 – 7090.
[13] R. Ravishankar, D. Bhattacharya, N. E. Jacob, S. Sivasanker, *Microporous Mater.* **1995**, *4*, 83 – 93.
[14] F. Eder, Y. He, G. Nivarthy, J. A. Lercher, *Recl. Trav. Chim. Pays-Bas* **1996**, *115*, 531 – 593.
[15] A. Corma, V. Fornes, S. B. Pergher, T. L. M. Maesen, J. G. Buglas, *Nature* **1998**, *396*, 353 – 356.
[16] K. Huddersman, M. Klimczyk, *J. Chem. Soc. Faraday Trans.* **1996**, *92*, 143 – 147.
[17] L. Boulicaut, S. Brandani, D. M. Ruthven, *Microporous Mesoporous Mater.* **1998**, *25*, 81 – 93.
[18] J. F. M. Denayer, G. V. Baron, P. A. Jacobs, J. A. Martens, *J. Phys. Chem. B* **1998**, *102*, 3077 – 3081.
[19] M. Schenk, S. Calero, T. L. M. Maesen, L. L. van Benthem, M. G. Verbeek, B. Smit, *Angew. Chem.* **2002**, *114*, 2609 – 2612; *Angew. Chem. Int. Ed.* **2002**, *41*, 2499 – 2502.
[20] M. Schenk, S. Calero, T. L. M. Maesen, T. J. H. Vlugt, L. L. van Benthem, M. G. Verbeek, B. Schnell, B. Smit, *J. Catal.* **2003**, *214*, 88 – 99.
[21] J. L. C. Roswell, O. M. Yaghi, *Microporous Mesoporous Mater.* **2004**, *73*, 3 – 14.
[22] J. R. A. Huss, C. Chu, A. Husain, R. G. Bundens, K. M. Keville (Mobil Oil Corp., US), US Patent 5 146 029.
[23] S. Ernst, J. Weitkamp, J. A. Martens, P. A. Jacobs, *Appl. Catal.* **1989**, *48*, 137 – 148.
[24] A. R. Ocakoglu, J. F. M. Denayer, G. B. Marin, J. A. Martens, G. V. Baron, *J. Phys. Chem. B* **2003**, *107*, 398 – 406.
[25] J. F. M. Denayer, K. De Meyer, J. A. Martens, G. V. Baron, *Angew. Chem.* **2003**, *115*, 2880 – 2883; *Angew. Chem. Int. Ed.* **2003**, *42*, 2774 – 2777.

 © 2005 Wiley-VCH Verlag GmbH & Co. KGaA, Weinheim

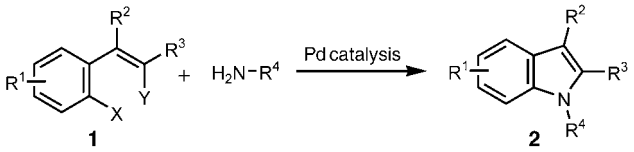
Nitrogen Heterocycles

Palladium-Catalyzed Tandem Alkenyl and Aryl C–N Bond Formation: A Cascade N-Annulation Route to 1-Functionalized Indoles**

Michael C. Willis, Gareth N. Brace, and Ian P. Holmes*

Indoles are preeminent amongst the heterocyclic motifs found in both designed medicinal agents and in natural products, and accordingly there exists a large and varied selection of methods for their preparation.[1] The majority of syntheses incorporate the key nitrogen atom of the indole nucleus early in the synthetic route. This can be problematic if systematic variation of the *N*-substituent is required without recourse to functionalization of the relatively non-nucleophilic indole N–H group. Herein we describe a tandem palladium-catalyzed process that allows installation of a diverse range of functionalized N units in a cascade indole-forming event that combines the introduction of the nitrogen atom with cyclization.

Palladium catalysis has had a major impact on indole synthesis;[2] arguably, the most important of the many reported methods are those based on Pd-catalyzed coupling of *o*-haloanilines with unsaturated carbon units.[3] Syntheses based on intra- and intermolecular Pd-catalyzed aryl–C–N bond formation,[4] the preparation of intermediates used in Fischer indole syntheses,[5] together with the use of Pd catalysis to functionalize intact indole rings[6] have all been the subjects of recent interest. To effect the desired cascade process, we focused on the introduction of functionalized nitrogen derivatives to an acyclic carbon framework **1** under the action of Pd catalysis; tandem alkenyl C–N and aryl C–N formation would then provide the indole structure (Scheme 1). Palladium-catalyzed aryl C–N bond formation



Scheme 1. A cascade *N*-annulation route to indoles.

[*] Dr. M. C. Willis, G. N. Brace
Department of Chemistry, University of Bath
Bath, BA2 7AY (UK)
Fax: (+44) 1225-386231
E-mail: m.c.willis@bath.ac.uk
I. P. Holmes
Discovery Research, GlaxoSmithKline
Medicines Research Centre, Gunnels Wood Road
Stevenage, Hertfordshire, SG1 2NY (UK)

[**] This work was supported by the EPSRC and GlaxoSmithKline. We thank Miss Dawn Taylor for helpful discussions. The EPSRC Mass Spectrometry Service at the University of Wales, Swansea, is also thanked for their assistance.

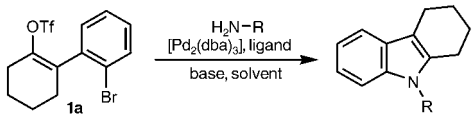
Supporting information for this article is available on the WWW under http://www.angewandte.org or from the author.

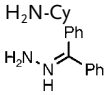
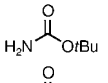
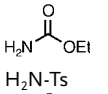
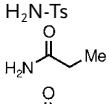
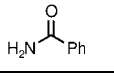
 DOI: 10.1002/anie.200461598 © 2005 Wiley-VCH Verlag GmbH & Co. KGaA, Weinheim

is now a well-established synthetic tool[7] and alkenyl C–N systems are also beginning to appear.[8] However, to the best of our knowledge, no examples of such a tandem process have been reported.[9]

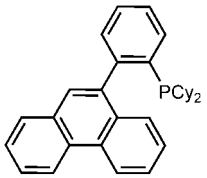
The biological relevance of *N*-arylated indoles,[10] together with the steric and electronic challenges associated with aniline nucleophiles, prompted us to select the union of triflate **1a**[11] with aniline as a platform to evaluate our proposed synthesis. Literature precedents suggested that for Pd-catalyzed C–N bond-forming processes, ligand choice is highly dependent on the electronic and steric properties of both the nucleophilic and electrophilic reaction components,[7] suggesting that identification of a catalyst capable of mediating both aryl and alkenyl C–N bond formation would present a challenge; in the event, phenanthrene ligand **3**[12] and dpephos (**4**)[13] were the most successful.[14] Dpephos has the advantage that it is commercially available

Table 1: Synthesis of *N*-substituted indoles.[a]

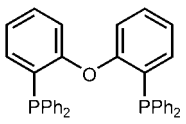


Entry	H_2N-R	Ligand	Base	Solvent	*T* [°C]	*t* [h]	Yield [%]
1	H_2N-Ph	**4**	Cs_2CO_3	toluene	100	20	83
2	H_2N-4-$MeOC_6H_4$	**4**	Cs_2CO_3	toluene	100	20	86
3	H_2N-4-ClC_6H_4	**4**	Cs_2CO_3	toluene	100	20	51
4	H_2N-2-ClC_6H_4	**4**	Cs_2CO_3	toluene	100	40	75
5	H_2N-Bu	**4**	NaO*t*Bu	toluene	100	16	62
6	H_2N-Bn	**4**	Cs_2CO_3	toluene	100	24	70
7	H_2N-Cy	**4**	NaO*t*Bu	toluene	100	24	46
8		**5**	Cs_2CO_3	toluene	115	21	82
9		**5**	Cs_2CO_3	dioxane	115	24	61
10		**5**	Cs_2CO_3	dioxane	115	25	70
11	H_2N-Ts	**5**	Cs_2CO_3	toluene	120	23	63
12		**5**	Cs_2CO_3	dioxane	115	24	79
13[c]		**5**	Cs_2CO_3	dioxane	115	24	80[c]
14		**5**	Cs_2CO_3	dioxane	115	26	66

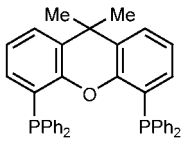
[a] Conditions: triflate (1.0 equiv), amine (1.2 equiv), $[Pd_2(dba)_3]$ (2.5 mol%); dpephos (6 mol%) or xantphos (7.5 mol%), base (2.5 equiv). [b] Yields of isolated products. [c] Free indole isolated following addition of KOH, H_2O, EtOH for 2 h. Ts = *p*-toluenesulfonyl, Tf = trifluoromethanesulfonyl, Cy = cyclohexyl, dba = dibenzylideneacetone.



3



4 dpephos

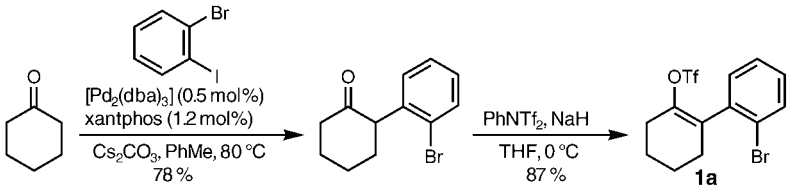


5 xantphos

and was selected for further application. Under optimized conditions ($[Pd_2(dba)_3]$, dpephos, Cs_2CO_3, PhMe, 100 °C, 20 h) the coupling of triflate **1a** with aniline delivered the required indole in 83% yield (Table 1, entry 1).

The scope of the process with respect to the N fragment was found to be broad and allowed good yields of indoles for a varied range of coupling partners (Table 1). Substituted aryl, alkyl, and benzyl amines all performed well, although the steric hindrance associated with the cyclohexyl group resulted in a lower reactivity (Table 1, entries 1–7). The use of 4- and 2-chloroanilines is notable as it allows the potential for product functionalization by subsequent palladium catalysis.[15] Hydrazine functionality could be readily incorporated, with the resultant protected 1-aminoindole being produced in high yield (Table 1, entry 8). For electron-poor nucleophiles, the use of xantphos (**5**)[13] as ligand was optimal. Under these modified conditions carbamate, sulfonamide, and amide functionalities were all incorporated in good yields (Table 1, entries 9–14). The use of propionamide has the benefit of also allowing efficient access to the free indole NH function; addition of ethanolic KOH prior to workup delivers the deprotected indole in 80% yield (Table 1, entry 13).

The required bis-activated carbon frameworks **1** could be conveniently prepared by triflate formation on the corresponding arylated ketones,[14] which in turn were readily available by Pd-catalyzed arylation of the parent ketone with a 1,2-dihaloarene.[16,17] For example, triflate **1a** was prepared from the arylation of cyclohexanone with 2-bromo-iodobenzene in the presence of a $[Pd_2(dba)_3]$/xantphos catalyst system followed by triflate formation with $PhNTf_2$ (Scheme 2).

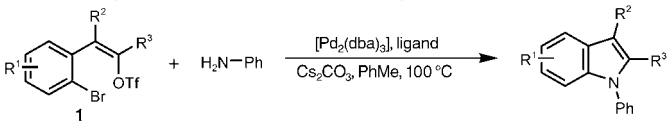


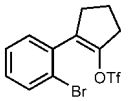
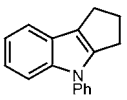
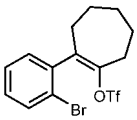
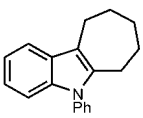
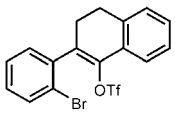
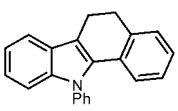
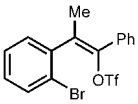
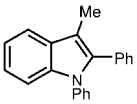
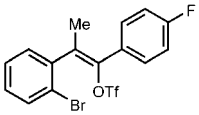
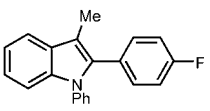
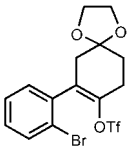
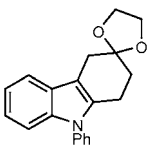
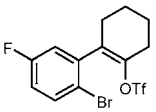
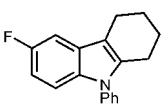
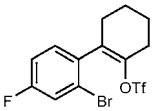
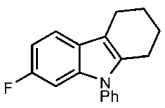
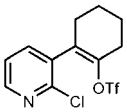
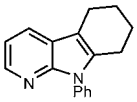
Scheme 2. Preparation of triflate **1a**.

Variations in the ketone and aryl halide components were explored with aniline as the nitrogen unit (Table 2). Indole formation was effective for a variety of architectures; five-, six-, and seven-membered cyclic ketones, simple acyclic, and aryl- and ketal-functionalized[18] ketones were all incorpo-

 © 2005 Wiley-VCH Verlag GmbH & Co. KGaA, Weinheim

Table 2: Scope of the ketone and arene components.[a]



Entry	Substrate	Ligand	Product	Yield (%)[b]
1		4		71
2		4		82
3[c]		4		90
4[c]		4		74
5[c]		4		65
6[c]		4		80
7		4		81
8		4		88
9		5		84

[a] Conditions: triflate (1.0 equiv), aniline (1.2 equiv), $[Pd_2(dba)_3]$ (2.5 mol%), dpephos (6 mol%) or xantphos (7.5 mol%), base (2.5 equiv), PhMe, 100°C. [b] Yields of isolated products. [c] NaO*t*Bu used as base.

rated efficiently. Medicinally attractive fluorine-substituted arenes together with simple heterocycles could also be readily introduced.

In summary, we have developed a new palladium-catalyzed route to *N*-functionalized indoles in which the N fragments are introduced in a single-step cascade sequence onto an acyclic carbon framework. A wide range of electronically and structurally varied N fragments can be introduced through a tandem C–N bond-forming process that employs commercially available catalyst components. This new synthesis allows the nitrogen atom of the indole core to be introduced as the final synthetic operation. The cyclization precursors are assembled from the union of a ketone and a 1,2-dihaloarene; variations in both components is well tolerated and allows the efficient synthesis of structurally varied indole systems. Studies to apply similar tandem processes to alternative heterocyclic motifs are underway.

Experimental Section

General procedure (Table 1, entry 1): Cesium carbonate (420 mg, 1.30 mmol) was added to an oven-dried flask charged with $[Pd_2(dba)_3]$ (12 mg, 0.01298 mmol) and dpephos (17 mg, 0.0312 mmol) under nitrogen. The flask was evacuated and back-filled with nitrogen three times. The reagents were suspended in anhydrous toluene (1.10 mL) and 2-(2-bromophenyl)cyclohexen-1-yl triflate (200 mg, 0.519 mmol) and aniline (58 mg, 0.057 mL, 0.623 mmol) were added under nitrogen. The reaction was heated at 100°C for 20 h. After cooling, the reaction mixture was diluted with diethyl ether (≈5 mL) and water (25 mL). The product was extracted with diethyl ether (3×25 mL). The combined organic extracts were washed with HCl (1M; 2× 25 mL) and brine (20 mL) and then dried over $MgSO_4$, filtered, and concentrated in vacuo. The product was purified by flash chromatography (1% diethyl ether/petroleum ether) to yield the title compound (106 mg, 83%) as an off-white solid.

Received: August 10, 2004

Keywords: amination · cascade reactions · indoles · nitrogen heterocycles · palladium

[1] For reviews on indoles, see: a) R. J. Sundberg, *Indoles*, Academic Press, London, **1996**; b) G. W. Gribble, *J. Chem. Soc. Perkin Trans. 1* **2000**, 1045.

[2] a) J. J. Li, G. W. Gribble, *Palladium in Heterocyclic Chemistry*, Pergamon, Amsterdam, **2000**; b) I. Nakamura, Y. Yamamoto, *Chem. Rev.* **2004**, *104*, 2127.

[3] For reviews, see: a) S. Cacchi, F. Marinelli in *Handbook of Organopalladium Chemistry for Organic Synthesis*, *Vol. 2* (Ed.: E.-I. Negishi), Wiley, New York, **2002**, p 2227; b) G. Zeni, R. C. Larock, *Chem. Rev.* **2004**, *104*, 2285.

[4] For selected recent examples, see: a) K. Aoki, A. J. Peat, S. L. Buchwald, *J. Am. Chem. Soc.* **1998**, *120*, 3068; b) J. A. Brown, *Tetrahedron Lett.* **2000**, *41*, 1623; c) K. Yamazaki, Y. Nakamura, Y. Kondo, *J. Org. Chem.* **2003**, *68*, 6011; d) H. Siebeneicher, I. Bytschkov, S. Doye, *Angew. Chem.* **2003**, *115*, 3151; *Angew. Chem. Int. Ed.* **2003**, *42*, 3042.

[5] S. Wagaw, B. H. Yang, S. L. Buchwald, *J. Am. Chem. Soc.* **1999**, *121*, 10251.

[6] For examples, see: a) J. F. Hartwig, M. Kawatsura, S. I. Hauck, K. H. Shaughnessy, L. M. Alcazar-Roman, *J. Org. Chem.* **1999**, *64*, 5575; b) D. W. Old, M. C. Harris, S. L. Buchwald, *Org. Lett.* **2000**, *2*, 1403; c) E. M. Beccalli, G. Broggini, *Tetrahedron Lett.* **2003**, *44*, 1919; d) E. M. Ferreira, B. M. Stoltz, *J. Am. Chem. Soc.* **2003**, *125*, 9578.

[7] For recent reviews on Pd-catalyzed C–O and C–N bond formation, see: a) J. F. Hartwig *in Modern Amination Methods* (Ed.: A. Ricci), Wiley-VCH, Weinheim, **2000**; b) A. R. Muci, S. L. Buchwald, *Top. Curr. Chem.* **2002**, *219*, 131; c) D. Prim, J.-M. Campagne, D. Joseph, B. Andrioletti, *Tetrahedron* **2002**, *58*, 2041.

[8] a) M. C. Willis, G. N. Brace, *Tetrahedron Lett.* **2002**, *43*, 9085; b) J. Barluenga, M. A. Fernández, F. Aznar, C. Valdés, *Chem. Commun.* **2002**, 2362; c) D. B. Wallace, D. J. Klauber, C.-y. Chen, R. P. Volante, *Org. Lett.* **2003**, *5*, 4749.

[9] For a carbazole synthesis that involves tandem palladium-catalyzed aryl C–N bond formation, see: K. Nozaki, K. Takahashi, K. Nakano, T. Hiyama, H.-Z. Tang, M. Fujiki, S.

 © 2005 Wiley-VCH Verlag GmbH & Co. KGaA, Weinheim

Yamaguchi, K. Tamao, *Angew. Chem.* **2003**, *115*, 2097; *Angew. Chem. Int. Ed.* **2003**, *42*, 2051.
[10] For *N*-arylated indoles, see: a) G. Spadoni, C. Balsamini, A. Bedini, G. Diamantini, B. Di Giacomo, A. Tontini, G. Tarzia, M. Mor, P. V. Plazzi, S. Rivara, R. Nonno, M. Pannacci, V. Lucini, F. Frachini, B. M. Stankov, *J. Med. Chem.* **1998**, *41*, 3624; b) K. Andersen, T. Liljefors, J. Hyttel, J. Perregaard, *J. Med. Chem.* **1996**, *39*, 3723; c) C. A. Harbert, J. J. Plattner, W. M. Welch, *J. Med. Chem.* **1980**, *23*, 635.
[11] Triflate **1** was prepared in 64% yield by the arylation of cyclohexanone with 1-bromo-2-iodobenzene, in the presence of a catalyst generated from $[Pd_2(dba)_3]$ and xantphos, followed by triflate formation (NaH, Tf_2NPh, Scheme 2). See Supporting Information for details.
[12] J. Yin, M. P. Rainka, X.-X. Zhang, S. L. Buchwald, *J. Am. Chem. Soc.* **2002**, *124*, 1162.
[13] M. Kranenburg, Y. E. M. van der Burgt, P. C. J. Kamer, P. W. N. M. van Leeuwen, K. Goubitz, J. Fraanje, *Organometallics* **1995**, *14*, 3081.
[14] See Supporting Information for details.
[15] A. F. Littke, G. C. Fu, *Angew. Chem.* **2002**, *114*, 4350; *Angew. Chem. Int. Ed.* **2002**, *41*, 4176.
[16] a) J. M. Fox, X. Huang, A. Chieffi, S. L. Buchwald, *J. Am. Chem. Soc.* **2000**, *122*, 1360; b) D. A. Culkin, J. F. Hartwig, *Acc. Chem. Res.* **2003**, *36*, 234; c) M. S. Viciu, R. F. Germaneau, S. P. Nolan, *Org. Lett.* **2002**, *4*, 4053.
[17] For an indole synthesis that commences with the arylation of ketones with *o*-halonitroarenes, see: J. L. Rutherford, M. P. Rainka, S. L. Buchwald, *J. Am. Chem. Soc.* **2002**, *124*, 15168.
[18] The ketal-functionalized indole could be deprotected to provide the corresponding ketone in 78% yield (PPTS, acetone, H_2O).

 © 2005 Wiley-VCH Verlag GmbH & Co. KGaA, Weinheim

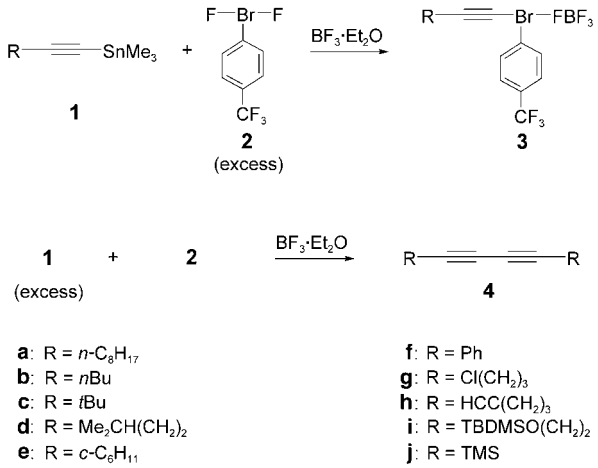
Synthetic Methods

1-Alkynyl(aryl)(tetrafluoroborato)-λ³-bromanes as Highly Efficient Michael Acceptors: Uncatalyzed Conjugate Addition of 1-Alkynyl(trialkyl)stannanes To Yield Symmetrical and Unsymmetrical 1,3-Butadiynes**

Masahito Ochiai, Yoshio Nishi, Satoru Goto, and Hermann J. Frohn*

In contrast to alkynylboron, -aluminium, and -nickel reagents, alkynylcopper species do not efficiently transfer the alkynyl group to electron-deficient olefins and alkynes in a conjugate fashion owing to the strength of the alkynyl–copper(I) bond.[1,2] Michael addition of alkynylstannanes appears to be a very difficult process, probably owing to the low polarity of a C–Sn bond, and there are no well-established precedents for the direct reaction. Specially designed alkynylstannanes with enhanced reactivity such as ynaminostannanes ($R_2NCCSnMe_3$) undergo conjugated addition toward acetylenedicarboxylates in MeCN under heating at reflux.[3] Palladium(0)-catalyzed Michael-type addition of alkynylstannanes to conjugated ynones and alkynoates by using an iminophosphine ligand was recently reported.[4] Herein we report bromine(III)-mediated homocoupling of alkynylstannanes to yield symmetrical 1,3-butadiynes that involves uncatalyzed Michael addition reactions of alkynylstannanes to highly electron-deficient alkynyl-λ³-bromanes.

Despite extensive studies on the chemistry of 1-alkynyl(phenyl)-λ³-iodanes,[5] little is known about the closely related group 17 1-alkynyl(aryl)-λ³-bromanes **3**, mostly because of the considerable difficulty of their synthesis. Recently, we reported the synthesis and characterization of 1-alkynyl(aryl)(tetrafluoroborato)-λ³-bromanes **3** through ligand exchange of a difluoro-λ³-bromane with alkynylstannanes.[6] Thus, exposure of 1-(trimethylstannyl)-1-alkyne **1** to an excess of *para*-trifluoromethylphenyl(difluoro)-λ³-bromane (**2**; 1.5 equiv; prepared from *para*-trifluoromethylphenyl(trimethyl)silane by ligand exchange with bromine trifluoride at −78 to −25 °C in dichloromethane) in the presence of $BF_3{\cdot}Et_2O$ at −78 °C in dichloromethane afforded 1-alkynyl(aryl)-λ³-bromane **3** in high yields (Scheme 1). Use of excess amounts of the 1-alkynylstannanes **1** (>2 equiv) relative to difluoro(aryl)-λ³-bromane **2** dramatically changed the reaction course and afforded the homocoupling products 1,3-butadiynes **4** in good yields.



Scheme 1. TBDMS = *tert*-butyldimethylsilyl, TMS = trimethylsilyl.

Rigid and sterically undemanding diacetylene moieties are frequently embodied in many natural products and find increasing application as key structural elements in synthetic receptors for molecular recognition.[7] Reaction of difluoro-λ³-bromane **2** with 2.2 equivalents of 1-decynylstannane **1a** in the presence of $BF_3{\cdot}Et_2O$ (1.2 equiv) from −78 °C to room

[*] Prof. M. Ochiai, Y. Nishi, Dr. S. Goto
Faculty of Pharmaceutical Sciences
University of Tokushima
1-78 Shomachi, Tokushima 770-8505 (Japan)
Fax: (+81) 88-633-9504
E-mail: mochiai@ph.tokushima-u.ac.jp
Prof. H. J. Frohn
Anorganische Chemie
Universitat Duisburg-Essen
Latharstrasse 1, 47048 Duisburg (Germany)

[**] We thank Central Glass Co., Japan, for a generous gift of BrF_3.

 © 2005 Wiley-VCH Verlag GmbH & Co. KGaA, Weinheim DOI: 10.1002/anie.200461985

temperature in dichloromethane under argon resulted in oxidative homocoupling with the formation of icosa-9,11-diyne (**4a**) in 69% yield (Table 1, Entry 3). The use of 2 equivalents of $BF_3{\cdot}Et_2O$ led to a slight improvement in the yield (72%), whereas in the absence of $BF_3{\cdot}Et_2O$ no formation of the diyne **4a** was observed. 1-Decynyl(tributyl)-stannane also afforded the diyne **4a** in 78% yield. However, the attempted dimerization of 1-decynyl(trimethyl)silane and -germane gave poor results and large amounts of the reactants were recovered (Table 1, Entries 6 and 7).

Table 1: Reaction of substituted 1-alkynes with difluoro-λ^3-bromane **2**.[a]

Entry	1-Alkynes	$BF_3{\cdot}Et_2O$ [equiv]	4	Yield [%][b]
1	**1a**	0	**4a**	0
2	**1a**	1[c]	**4a**	49
3	**1a**	1.2	**4a**	69
4	**1a**	2	**4a**	72
5	n-C_8H_{17}—≡—$SnBu_3$	1.2	**4a**	78
6	n-C_8H_{17}—≡—$GeMe_3$	1.2	**4a**	17
7	n-C_8H_{17}—≡—$SiMe_3$	1.2	**4a**	0

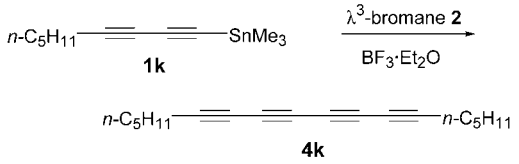
[a] Unless otherwise noted, reactions were carried out by using 2.2 equivalents of an alkyne in dichloromethane in the presence of $BF_3{\cdot}Et_2O$ from −78°C to room temperature during 5 h under argon. [b] Isolated yields. [c] Reaction conditions: −78°C, 2.5 h.

Our initial examination of the substrate generality for oxidative homocoupling of 1-alkynylstannanes **1** is shown in Table 2. Dimerization of simple primary, secondary, and tertiary alkylethynyl(trimethyl)stannanes afforded the 1,3-butadiynes **4b–e** in good yields (74–83%). 1,10-Dichlorodecadiyne **4g** was obtained in 69% yield from 5-chloropentynylstannane **1g**. However, phenylethynyl(trimethyl)stannane (**1f**) gave 1,4-diphenyl-1,3-butadiyne (**4f**) in only 33% yield. Ethynyl- and siloxy-substituted alkynyl(trimethyl)stannanes **1h** and **1i** gave 1,3-diynes in moderate yields. Selective coupling of trimethyl(trimethylsilylethynyl)stannane (**1j**) resulted in the formation of bis(trimethylsilyl)-1,3-diyne **4j**, although in a low yield (27%). The use of trimethylstannyl-1,3-diyne **1k** provided directly the conjugated octatetrayne **4k** (40%; Scheme 2). Both tetrabutylstannane and phenyltrimethylstannane do not undergo oxidative homocoupling.

Table 2: Oxidative homocoupling of alkynylstannanes **1** by reaction with difluoro-λ^3-bromane **2**.[a]

Entry	1	4	Yield [%][b]
1	**1b**	**4b**	74
2	**1c**	**4c**	83
3	**1d**	**4d**	76 (87)
4	**1e**	**4e**	80
5	**1f**	**4f**	33
6	**1g**	**4g**	69 (84)
7	**1h**	**4h**	45
8	**1i**	**4i**	47
9	**1j**	**4j**	27

[a] Reactions were carried out by using 2.2 equivalents of an alkyne **1** in dichloromethane in the presence of $BF_3{\cdot}Et_2O$ (1.2 equiv) from −78°C to room temperature during 5 h under argon. [b] Isolated yields. Yields obtained after GC are quoted in parentheses.



Scheme 2.

On the basis of our previous report[6] as well as the observation that the oxidative homocoupling of 1-alkynylstannane **1a** to yield the diyne **4a** does not take place in the absence of $BF_3{\cdot}Et_2O$ (Table 1, Entry 1),[8] it seems reasonable to assume that the bromine(III)-mediated homocoupling of 1-alkynylstannane **1** probably involves the initial formation of 1-alkynyl(aryl)(tetrafluoroborato)-λ^3-bromane **3** through ligand exchange and its further reaction with excess 1-alkynylstannane **1**. In fact, treatment of 1-decynyl-λ^3-bromane **3a** with 1-alkynylstannane **1a** at room temperature under argon afforded the 1,3-diyne **4a** in 59% yield. The reaction does not require activation with Lewis acids. Interestingly, in this reaction a 4% yield of the cyclopentene **5** was also produced.[9] The reaction with 1-decynyl(trimethyl)germane provided a comparable result with formation of a small amount of **5** (Table 3, Entry 2).

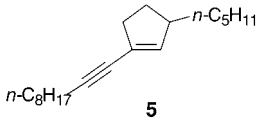


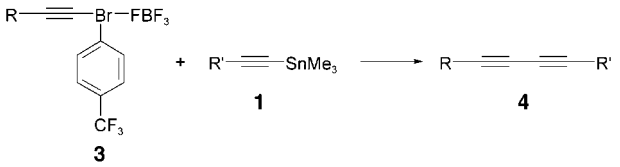
Table 3: Uncatalyzed cross-coupling of alkynyl-λ^3-bromanes **3** with alkynylstannanes **1** and -germanes.[a]

Entry	3	Alkyne	4	Yield [%][b]
1	**3a**	**1a**	**4a**	59
2	**3a**	n-C_8H_{17}—≡—$GeMe_3$	**4a**	64
3	**3a**	**1c**	**4l**	76
4	**3a**	**1e**	**4m**	71
5	**3a**	**1f**	**4n**	66
6	**3c**	**1a**	**4l**	76
7	**3c**	**1e**	**4o**	74
8	**3e**	**1a**	**4m**	71

[a] Reactions were carried out by using 2.2 equivalents of an alkyne in dichloromethane at room temperature for 5 h under argon. [b] Isolated yields.

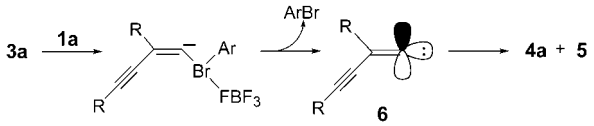
The cross-coupling reaction makes it possible to synthesize unsymmetrically substituted 1,3-butadiynes **4l–o** (Scheme 3, Table 3). For instance, reaction of **3a** with alkynylstannanes **1c** and **1e** afforded the unsymmetrical butadiynes **4l** (76%) and **4m** (71%; Table 3, Entries 3 and 4), which were also produced by the reaction of the inverse combinations (reaction of **1a** with **3c** and **3e**, respectively).

 © 2005 Wiley-VCH Verlag GmbH & Co. KGaA, Weinheim



Scheme 3.

Isolation of the byproduct cyclopentene **5** clearly indicates that the reaction of **3a** with **1a** involves the intermediacy of alkylidene carbene **6**, which is produced by Michael addition of 1-alkynylstannane **1a** and the subsequent reductive elimination of the aryl-λ^3-bromanyl group (Scheme 4). A



Scheme 4. R = *n*-C_8H_{17}, Ar = *p*-$CF_3C_6H_4$.

1,2-shift of the alkynyl group in **6** produces **4a**, while competing intramolecular 1,5 carbon–hydrogen insertion affords **5**.[5,10] High migratory aptitude of alkynyl groups in alkylidene carbenes and carbenoids are well established.[11]

The most important step in this mechanism should be an uncatalyzed Michael addition of 1-alkynyl(trimethyl)stannane **1** with rather low nucleophilicity to 1-alkynyl-λ^3-bromane **3**. Entry 2 in Table 3 shows that the less nucleophilic 1-decynyl(trimethyl)germane also serves as an efficient Michael donor toward **3**. The question arises why simple alkynylstannanes and -germanes undergo uncatalyzed conjugate addition toward **3**. We believe that the highly electron-deficient nature of 1-alkynyl-λ^3-bromanes **3**, evoked by a large electron-withdrawing inductive effect of an aryl(tetrafluoroborato)-λ^3-bromanyl group with a substituent constant σ_I of 1.63 (for PhBr(BF_4)),[12] will be responsible for this unusual addition reaction. Actually, 1-alkynyl(aryl)-λ^3-iodanes associated with a reduced inductive effect ($\sigma_I = 1.35$ for PhI(BF_4)) do not function as Michael acceptors, and no formation of 1,3-butadiyne **4a** was observed in the attempted reaction of 1-decynyl(*para*-trifluoromethylphenyl)(tetrafluoroborato)-λ^3-iodane with 1-alkynylstannane **1a** under the conditions described.

To better understand these differences in reactivity in λ^3-bromanes and λ^3-iodanes, density functional theory (DFT) calculations on the simplified 1-propynyl derivatives **7** were carried out (Figure 1). The acetylenic π^* orbital (LUMO+4) of 1-propynyl(phenyl)(fluoro)-λ^3-bromane **7a** is lower in energy than that for the λ^3-iodane **7b** (LUMO+4; 0.04672 eV for **7a**, 0.04778 eV for **7b**). Mulliken atomic charges show that the Cβ carbon atom in **7a** is apparently more positive than that in **7b**.

In summary, we have presented the first example of uncatalyzed Michael addition reactions of simple 1-alkynyl-(trimethyl)stannanes, a reaction which is involved in difluoro-λ^3-bromane-mediated coupling of 1-alkynylstannanes to yield

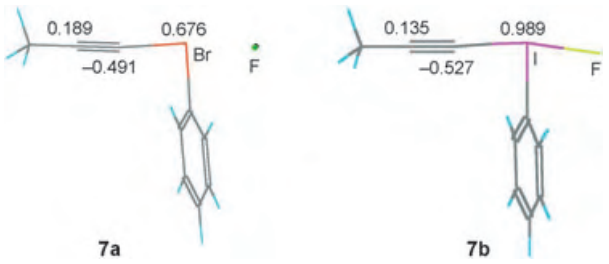


Figure 1. Mulliken atomic charges at Cα, Cβ, Br, and I calculated with the B3LYP/LanL2DZ method (Gaussian 03W).

symmetrical 1,3-butadiynes. Tandem Michael addition–carbene rearrangements of 1-alkynyl(aryl)-λ^3-bromanes with 1-alkynylstannanes provides a new route for the synthesis of unsymmetrical 1,3-butadiynes.[7]

Experimental Section

4a (Table 1, Entry 3): A solution of difluoro[4-(trifluoromethyl)-phenyl]-λ^3-bromane (**2**; 34 mg, 0.13 mmol) in dichloromethane (0.2 mL) followed by $BF_3{\cdot}Et_2O$ (22 mg, 0.16 mmol) were added dropwise to a stirred solution of 1-decynyl(trimethyl)stannane (**1a;** 86 mg, 0.29 mmol) in dichloromethane (0.8 mL) at −78 °C under argon. The mixture was gradually warmed to room temperature over 5 h. The reaction mixture was quenched with water and extracted with dichloromethane. The organic layer was dried over anhydrous sodium sulfate and concentrated under aspirator vacuum to give an oil, which was purified by preparative TLC (SiO_2, hexane/dichloromethane 4:1) to give a mixture (25.9 mg) of **4a** and **5** (95:5; 69% and 4%, respectively). **4a**: ^{1}H NMR (400 MHz, $CDCl_3$): $\delta = 2.25$ (t, $J =$ 7.4 Hz, 4H), 1.52 (quint, $J = 7.4$ Hz 4H), 1.41–1.33 (m, 4H), 1.33–1.21 (m, 16H), 0.88 ppm (t, $J = 6.3$ Hz, 6H); ^{13}C NMR (75 MHz, $CDCl_3$): $\delta = 77.5$, 65.3, 31.9, 29.2, 29.1, 28.9, 28.4, 22.7, 19.2, 14.1 ppm; IR (neat): $\tilde{\nu} = 2925$, 2855, 2233, 1465, 1377, 722 cm^{-1}; MS (70 eV): *m*/*z* (%): 274 (2) [M^+], 245 (3), 231 (3), 217 (9), 203 (8), 189 (4), 175 (10), 161 (19), 147 (22), 133 (31), 119 (43), 105 (56), 91 (100), 79 (65); HRMS: calcd for $C_{20}H_{34}$ [M^+]: 274.2661; found: 274.2663. A pure sample of **5** was obtained by preparative GC (20% silicon GE SF-96, 3 m). **5**: ^{1}H NMR (400 MHz, $CDCl_3$): $\delta = 5.89$ (br s, 1H), 2.69 (m, 1H), 2.46–2.34 (m, 2H), 2.31 (t, $J = 7.4$ Hz 2H), 2.12–2.02 (m, 1H), 1.53 (quint, $J = 7.4$ Hz 2H), 1.45–1.21 (m, 19H), 0.95–0.84 ppm (6H); IR ($CHCl_3$): $\tilde{\nu} = 2928$, 2856, 1465, 1265 cm^{-1}; MS (70 eV): *m*/*z* (%): 274 (22) [M^+], 203 (100) [M^+-C_5H_{11}]; HRMS: calcd for $C_{20}H_{34}$ [M^+]: 274.2661; found: 274.2651. **4l** (Table 3, Entry 7)**: 1a** (59 mg, 0.2 mmol) was added to a stirred solution of 3,3-dimethyl-1-butynyl-λ^3-bromane **3c** (35 mg, 0.09 mmol) in dichloromethane (2 mL) at room temperature under argon. The reaction mixture was stirred for 5 h, quenched with water, and extracted with dichloromethane. The organic layer was dried over anhydrous sodium sulfate and concentrated under aspirator vacuum to give an oil, which was purified by preparative TLC (SiO_2, hexane) to give **4l** as a colorless oil (15 mg, 76%). ^{1}H NMR (400 MHz, $CDCl_3$): $\delta = 2.25$ (t, $J = 7.2$ Hz, 2H), 1.51 (quint, $J = 7.2$ Hz, 2H), 1.42–1.33 (m, 2H), 1.32–1.25 (m, 8H), 1.24 (s, 9H), 0.88 ppm (t, $J = 6.7$ Hz, 3H); ^{13}C NMR (75 MHz, $CDCl_3$) $\delta = 85.0$, 78.8, 65.0, 63.9, 31.9, 30.6, 29.2, 29.1, 28.9, 28.4, 27.9, 22.7, 19.3, 14.1 ppm; IR ($CHCl_3$): $\tilde{\nu} = 2929$, 2858, 2147, 1457 cm^{-1}; MS (70 eV): *m*/*z* (%): 218 (9) [M^+], 203 (24), 189 (50), 175 (22), 161 (61), 147 (58), 133 (61), 119 (96), 105 (100), 91 (60); HRMS: calcd for $C_{16}H_{26}$ [M^+]: 218.2035; found: 218.2041.

Received: September 14, 2004

 © 2005 Wiley-VCH Verlag GmbH & Co. KGaA, Weinheim

Keywords: alkynes · carbenes · michael addition · stannanes · synthetic methods

[1] a) P. Perlmutter, *Conjugate Addition Reactions in Organic Synthesis*, Pergamon, Oxford, **1992**; b) S. Kim, J. H. Park, S. Y. Jon, *Bull. Korean Chem. Soc.* **1995**, *16*, 783.

[2] a) J. Hooz, R. B. Layton, *J. Am. Chem. Soc.* **1971**, *93*, 7320; b) R. T. Hansen, D. B. Carr, J. Schwartz, *J. Am. Chem. Soc.* **1978**, *100*, 2244; c) J. A. Sinclair, G. A. Molander, H. C. Brown, *J. Am. Chem. Soc.* **1977**, *99*, 954; d) R. Locher, D. Seebach, *Angew. Chem.* **1981**, *93*, 614; *Angew. Chem. Int. Ed. Engl.* **1981**, *20*, 569; e) J. M. Chong, L. Shen, N. J. Taylor, *J. Am. Chem. Soc.* **2000**, *122*, 1822; f) H. Fujishima, E. Takada, A. Suzuki, *Chem. Lett.* **1992**, 695.

[3] a) G. Himbert, *J. Chem. Res. Miniprint* **1978**, 1445; b) G. Himbert, *J. Chem. Res. Synop.* **1979**, 88.

[4] a) E. Shirakawa, H. Yoshida, T. Kurahashi, Y. Nakao, T. Hiyama, *J. Am. Chem. Soc.* **1998**, *120*, 2975; b) H. Yoshida, E. Shirakawa, T. Kurahashi, Y. Nakao, T. Hiyama, *Organometallics* **2000**, *19*, 5671.

[5] Reviews: a) M. Ochiai in *Topics in Current Chemistry*, *Vol. 224* (Ed.: T. Wirth), Springer, Berlin, **2003**, pp. 5 – 68; b) P. J. Stang, *J. Org. Chem.* **2003**, *68*, 2997; c) V. V. Zhdankin, P. J. Stang, *Tetrahedron* **1998**, *54*, 10927; d) G. F. Koser in *The Chemistry of Halides, Pseudo-halides, and Azides*, *Supplement D2* (Eds.: S. Patai, Z. Rappoport), Wiley, New York, **1995**, pp. 1173 – 1274; e) A. Varvoglis, *The Organic Chemistry of Polycoordinated Iodine*, VCH, Weinheim, **1992**.

[6] M. Ochiai, Y. Nishi, S. Goto, M. Shiro, H. J. Frohn, *J. Am. Chem. Soc.* **2003**, *125*, 15304.

[7] a) P. Siemsen, R. C. Livingston, F. Diederich, *Angew. Chem.* **2000**, *112*, 2740; *Angew. Chem. Int. Ed.* **2000**, *39*, 2632; b) L. Brandsma, *Preparative Acetylenic Chemistry*, Elsevier, Amsterdam, **1998**; c) K. Sonogashira in *Comprehensive Organic Synthesis*, *Vol. 3* (Eds.: B. M. Trost, I. Fleming), Pergamon, Oxford, **1991**, pp. 551 – 561.

[8] Ligand exchange of difluoro-λ^3-bromane **2** with alkynylstannanes **1** to yield 1-alkynyl-λ^3-bromanes **3** requires activation with $BF_3{\cdot}Et_2O$ with which hypervalent F-Br-F bonding in **2** is efficiently polarized by the coordination of BF_3 and the positive charge on the bromine(III) is increased.

[9] Cyclopentene **5** was also obtained as a byproduct (3–5%) in the bromine(III)-mediated homocoupling of **1a** (Table 1, Entries 2–4).

[10] An alternative ligand-coupling pathway on bromine(III) of (n-$C_8H_{17}CC)_2Br(p$-$CF_3C_6H_4$), produced by ligand exchange through the nucleophilic attack of alkynylstannane **1a** at the polarized bromine of **3a**, could account for the formation of 1,3-butadiyne **4a**. The observation that the diphenyls Ph-Ph and p-$CF_3C_6H_4Ph$ are not formed on the attempted dimerization of phenyl(trimethyl)stannane by the reaction with difluoro-λ^3-bromane **2** strongly suggests a tandem Michael addition–carbene rearrangement pathway. However, involvement of the ligand-coupling reaction as a competing minor process can not be rigorously ruled out. For ligand coupling in hypervalent compounds, see: a) S. Oae, Y. Uchida, *Acc. Chem. Res.* **1991**, *24*, 202; b) M. A. Carroll, S. Martin-Santamaria, V. W. Pike, H. S. Rzepa, D. A. Widdowson, *J. Chem. Soc. Perkin Trans. 2* **1999**, 2707; c) K. Akiba, T. Okinaka, M. Nakatani, Y. Yamamoto, *Tetrahedron Lett.* **1987**, *28*, 3367; d) J. P. Finet, *Ligand Coupling Reactions with Heteroatomic Compounds*, Pergamon, Oxford, **1998**.

[11] a) S. Eisler, R. R. Tykwinski, *J. Am. Chem. Soc.* **2000**, *122*, 10737; b) A. L. K. S. Shun, E. T. Chernick, S. Eisler, R. R. Tykwinski, *J. Org. Chem.* **2003**, *68*, 1339; c) Y. Tobe, N. Iwasa, R. Umeda, M. Sonoda, *Tetrahedron Lett.* **2001**, *42*, 5485.

[12] V. V. Grushin, I. I. Demkina, T. P. Tolstaya, M. V. Galakhov, V. I. Bakhmutov, *Organomet. Chem. USSR* **1989**, *2*, 373.

 © 2005 Wiley-VCH Verlag GmbH & Co. KGaA, Weinheim

Nanoparticles

Core/Shell Gold Nanoparticles by Self-Assembly and Crosslinking of Micellar, Block-Copolymer Shells**

*Youngjong Kang and T. Andrew Taton**

Core/shell nanoparticle architectures, in which a layer of inorganic or organic material surrounds an inorganic nanoparticle core, have been investigated both as a means to improve the stability and surface chemistry of the core nanoparticle and as a way of accessing unique physical properties that are not possible from one nanomaterial alone. As examples, silica shells isolate metal and semiconductor particle surfaces from interfacial chemistry;[1,2] gold shells allow covalent attachment of thiol ligands to particles[3] and generate unique optical signatures;[4] semiconductor shells increase the quantum yield of semiconductor nanoparticle cores;[5] and polymeric shells aid the compatibility of nanoparticles in polymer hosts.[6] Whereas inorganic shells are typically grown from the surface of the particle core, a number of methods have been described for generating organic polymer shells, including polymerization from particle-bound initiators,[7] direct attachment of functionalized polymers to surfaces,[8] layer-by-layer deposition,[9] and synthesis of the particle in the presence of polymeric ligand.[10,11] In all of these cases, the specific chemical interaction of the particle surface and the surface-bound polymer must be explicitly tailored in order to form the shell.

Diblock copolymer amphiphiles spontaneously form polymer monolayers on surfaces, and the thickness and composition of the assembled layer are determined by the lengths and properties of the component blocks.[12] Because this assembly can be driven by desolvation of one of the two polymer blocks and does not depend on any specific polymer–surface interaction, we hypothesized that block copolymers could be used to form shells around nanoparticle cores without chemical anchoring. Herein, we report the assembly of metal-core, block-copolymer-shell nanoparticles in which the structure and composition of the combined material are programmed in advance by the choice of particle and copolymer starting materials. Furthermore, we demonstrate that cross-linking the assembled shell leads to a permanent core/shell structure and physically isolates the core from its environment.

[*] Y. Kang, Prof. T. A. Taton
Department of Chemistry
University of Minnesota
207 Pleasant St SE, Minneapolis, MN 55455 (USA)
Fax: (+1) 612-626-7541
E-mail: taton@chem.umn.edu

[**] We thank the ACS Petroleum Research Fund for partial support of this research.

Supporting information for this article is available on the WWW under http://www.angewandte.org or from the author.

 DOI: 10.1002/anie.200461119 © 2005 Wiley-VCH Verlag GmbH & Co. KGaA, Weinheim

Our approach to the synthesis of copolymer-encapsulated nanoparticles (Scheme 1) employs block copolymers and cross-linking chemistry that were developed by Wooley and co-workers for shell-crosslinked micelles.[13] Briefly, poly(styrene-block-acrylic acid) (PS-b-PAA) and poly(methylmethacrylate-block-acrylic acid) (PMMA-b-PAA) copolymer surfactants with narrow molecular-weight polydispersities (PDI < 1.3) were synthesized through atom-transfer radical polymerization.[14,15] Amphiphilic copolymer was initially dissolved in DMF (*N*,*N*-dimethylformamide), which is a good solvent for both the hydrophobic (PS or PMMA) and the hydrophilic (PAA) polymer blocks. Citrate-capped Au nanoparticles[15,16] in aqueous solution were centrifuged and resuspended in DMF. The samples of polymer and nanoparticles in DMF were combined in the presence of a small amount of 1-dodecanethiol, which hydrophobically functionalizes the surfaces of the particles and directs them to the hydrophobic interior of a micellar shell.[17] Water was gradually added to this mixture to simultaneously desolvate both the particles and the hydrophobic polymer block from solution. In the absence of copolymer surfactant, the dodecanethiol-modified nanoparticles precipitated quickly from DMF as water was added. In the absence of dodecanethiol, the nanoparticles remained outside the assembled block-copolymer micelles. Transmission electron microscopy (TEM) images of these assemblies indicated that the external polyacrylate block of the micelles associated with the surfaces of the nanoparticles (Figure 1 a)[18] presumably by displacing bound citrate. However, for dodecanethiol-functionalized Au, the added water acted as a selective nonsolvent (that is, a solvent that does not solubilize a specific material) for both the hydrophobic polymer block and the hydrophobically modified nanoparticles and induced the formation of micelles around the nanoparticles (Figure 1 b). Micelle encapsulation was conducted with a substantial excess of polymer to limit the number of micelles that contained multiple particles. This process was successful for polymers with short PAA blocks (PS_{250}-b-PAA_{13}, PS_{160}-b-PAA_{13}, PS_{100}-b-PAA_{13}, and $PMMA_{240}$-b-PAA_{13}).[15]

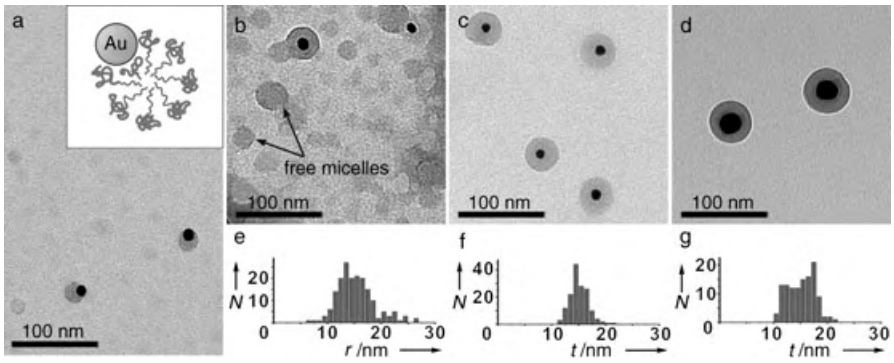
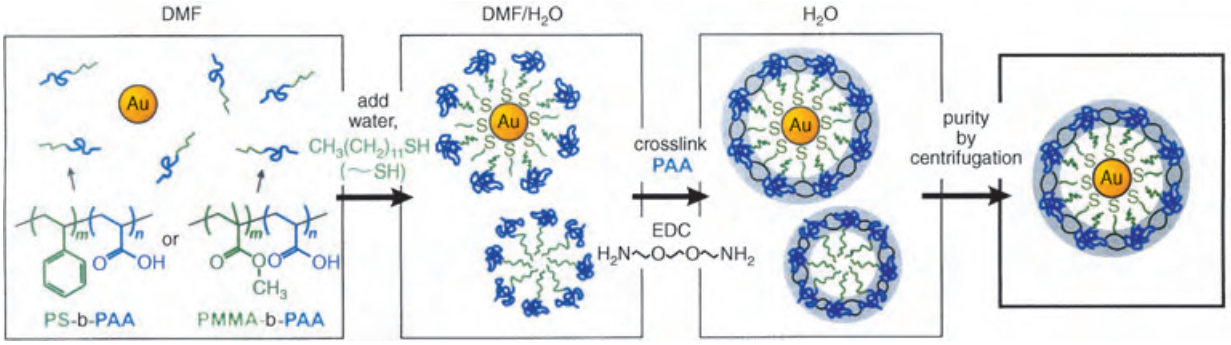


Figure 1. a–d) TEM images of Au nanoparticles encapsulated within PS_{250}-b-PAA_{13} micelles. a) Poorly encapsulated 12-nm Au nanoparticles exposed to PS_{250}-b-PAA_{13} in the absence of dodecanethiol. Empty copolymer micelles distort to maximize interactions between the polyacrylate corona and the surface of the Au nanoparticle. b) Encapsulated Au nanoparticles treated with dodecanethiol and PS_{250}-b-PAA_{13}, before purification. Nanoparticles are localized at the center of the micelles. c) Purified encapsulated 12-nm Au nanoparticles. d) Purified encapsulated 31-nm Au nanoparticles. e–g) Histograms of e) the radius (r) of empty micelles isolated from encapsulated 12-nm Au nanoparticle supernatant, f) the shell thickness (*t*) of encapsulated 12-nm Au nanoparticles, and g) the shell thickness of encapsulated 31-nm Au nanoparticles. *N* = number. See Supporting Information for the TEM images used to obtain the histograms.

The assembled copolymer was permanently fixed by cross-linking the polyacrylate block of the micelles with 2,2′-(ethylenedioxy)bis(ethylamine) and 1-(3-dimethylaminopropyl)-3-ethylcarbodiimide methiodide in water (see Scheme 1). After cross-linking, excess reagents were removed by dialysis of the suspension against H_2O. Fixed core/shell nanoparticles were separated from empty micelles by five or more consecutive cycles whereby the suspension was centrifuged, the supernatant was discarded, and the solid was resuspended in H_2O. After this treatment, the suspension consisted solely of micelles filled with Au nanoparticles (Figure 1, c and d). For Au nanoparticles larger than 10 nm in diameter, every micelle contained exactly one nanoparticle. Despite our presumption that a statistical distribution of particles might lead to a few micelles that contain two or more particles, no such structures were observed. For smaller (4-nm diameter) nanoparticles, however, multiple particles were sometimes encapsulated in each micelle.[15] Averaged over



Scheme 1. Preparation of core/shell gold nanoparticles. EDC = *N*-ethyl-*N*′-(3-dimethylaminopropyl)carbodiimide.

 © 2005 Wiley-VCH Verlag GmbH & Co. KGaA, Weinheim

more than 100 particles, the shell thicknesses for 12- and 31-nm Au nanoparticles encapsulated in PS_{250}-b-PAA_{13} ("Au@PS_{250}-b-PAA_{13}") were 15.1 ± 1.7 nm and 15.2 ± 2.5 nm, respectively, whereas the average radius of empty PS_{250}-b-PAA_{13} micelles isolated from the encapsulated 12-nm Au nanoparticle solution was 15.2 ± 3.5 nm. So, whereas the copolymer shell thickness could be predicted on the basis of the radius of empty copolymer micelles, the shells were consistently more uniform in size than the micelles. The fact that only single nanoparticles were found in each micelle as well as the uniformity of the micellar shells suggest that the encapsulated particles offer a spherical surface template for micelle assembly. Flat surfaces have been shown to template the formation of uniform surface layers of block copolymers.[12] Here we demonstrate that this phenomenon is observed even when the curvature of the surface is smaller in scale than the thickness of the polymer layer. This is surprising given that the micelles are much larger than the nanoparticles and could presumably accommodate multiple particle guests.

The optical properties of the Au nanoparticles can be controlled by variation of the composition of the copolymer shell which is consistent with the theoretical prediction that surface plasmon resonance energies decrease as the refractive index of the surrounding medium increases.[19] In water ($n = 1.33$), citrate-capped 31-nm-diameter Au particles show a characteristic absorbance maximum $\lambda_{max} = 529$ nm (Figure 2a). However, the higher refractive indices of PMMA

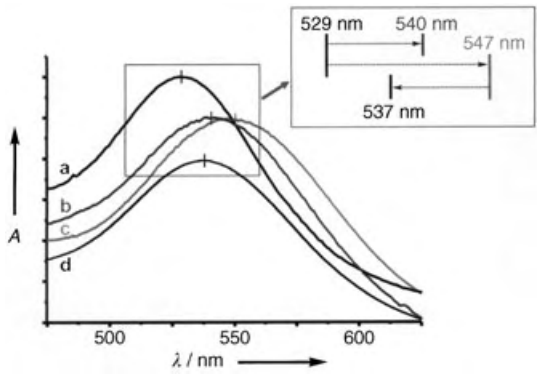


Figure 2. Shift of the surface plasmon resonance spectra upon encapsulation of Au nanoparticles (absorbance intensities are normalized). a) The absorbance spectrum of aqueous 31-nm-diameter gold nanoparticles. The spectrum is red-shifted by encapsulation within $PMMA_{240}$-b-PAA_{13} (b) or within PS_{250}-b-PAA_{13} (c). The spectrum is blue-shifted when the PS_{250}-b-PAA_{13} polymer shell is swollen with THF (d).

($n = 1.49$) and PS ($n = 1.59$) lead to red-shifted absorbance spectra for Au@$PMMA_{240}$-b-PAA_{13} ($\lambda_{max} = 540$ nm) and Au@PS_{250}-b-PAA_{13} ($\lambda_{max} = 547$ nm; see Figure 2, b and c). Similar plasmon shifts have been reported for Au nanoparticles within silica shells[1,20] in which the higher refractive index of SiO_2 ($n = 1.47$) results in higher values of λ_{max}.

In water, the glassy polystyrene block of the cross-linked copolymer shells provides a physical barrier that isolates and protects encapsulated nanoparticles from their chemical environment. When exposed to aqueous cyanide etching solution, citrate-capped gold nanoparticles are typically oxidized to $[Au(CN)_2]^-$ ions within seconds. Copolymer-encapsulated Au nanoparticles were stable indefinitely to much higher concentrations of etchant (Figure 3). By con-

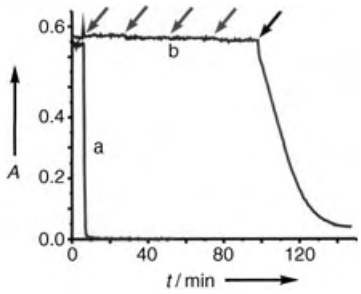


Figure 3. a) Cyanide-induced decomposition of citrate-stabilized, 12-nm Au nanoparticles in water. Similar, immediate decomposition was observed for dodecanethiol-stabilized nanoparticles.[15] b) Exposure of encapsulated 12-nm Au nanoparticles (within a PS_{250}-b-PAA_{13} shell) in water to a 25-fold molar excess of KCN (5-mM aqueous solution) every 20 min (gray arrows; total 100-fold molar excess), followed by the addition of 20 vol% THF after 100 min (black arrow). The absorbance was measured at the values of λ_{max} (519 nm and 529 nm for curves a and b, respectively). The initial 8% drop of absorbance upon addition of THF is attributed to a change in the refractive index of the solvent.[15]

trast, surface-bound molecular[21] and homopolymer[11] monolayers and silica shells[22] have been shown to be permeable with respect to cyanide corrosion. The permeability of the micellar shell could be modulated by addition of an organic cosolvent to the aqueous suspension of the particles to solvate the hydrophobic polymer block. For example, addition of 20 vol% THF to the suspension of encapsulated Au nanoparticles in a solution containing cyanide resulted in immediate etching (Figure 3). Variation of the degree of shell cross-linking had no effect on the extent or rate of etching which demonstrates that solvation of the shell, rather than the physical porosity of the polymer network, regulates exposure to etching. Further evidence of THF infiltration and swelling of the inner micelle block with THF was observed by a blue shift of the optical absorbance spectrum of the nanoparticles (in the absence of cyanide, Figure 2d). This shift reflects the contribution of the lower refractive index of THF ($n = 1.41$) to the PS environment around each nanoparticle.

Even though organic solvents solubilize the hydrophobic micelle block, chemical cross-links prevent the surfactant from dissolving away. As a result, micelle-encapsulated nanoparticles were found to be soluble in essentially any solvent that was compatible with either the hydrophobic or hydrophilic component polymers.[15] For example, nanoparticles encapsulated in PS-b-PAA were soluble in solvents in which PS can be dissolved, but notably not in acetone or 1:1 *i*PrOH/MEK (methyl ethyl ketone), which are both nonsolvents for PS. Also, nanoparticles encapsulated in PMMA-b-PAA were soluble in solvents in which PMMA can be dissolved, but not in cyclohexane, which is a nonsolvent for PMMA.

Because the shells were fixed, the solvated polymer cores could be desolvated again to regenerate the original glassy core/shell nanostructures. Au@PS_{250}-b-PAA_{13} particles dis-

 © 2005 Wiley-VCH Verlag GmbH & Co. KGaA, Weinheim

solved in an organic solvent such as THF could be returned to aqueous solution by exhaustive dialysis against H_2O. TEM images of these particles were indistinguishable from images of the originally synthesized, aqueous particles. On the basis of these results, we anticipate that copolymer micelle encapsulation could be used as a general aid to disperse nanoparticles in otherwise incompatible matrices. Along these lines, Au@PS_{250}-b-PAA_{13} was readily dispersed from solvent into bulk PS, and Au@$PMMA_{240}$-b-PAA_{13} into bulk PMMA, to form homogeneously pink-colored composite plastics.

In conclusion, we have demonstrated surface-templated self-assembly of copolymers around nanoparticles as a route to defined core/shell nanostructures. This approach yielded core/shell architectures in which the dimensions and properties of the nanostructures were determined by the characteristics of the component polymer blocks. We are currently applying this approach to other lyophilic nanoparticles such as TOPO-coated quantum dots[23] and oleic acid coated magnetic nanoparticles.[24] We anticipate that micelle encapsulation will allow shell functionalization, biomolecular conjugation, and polymer processing to be performed on nanomaterials that might otherwise show poor or no ligand chemistry.[25]

Received: June 29, 2004
Revised: August 26, 2004

Keywords: block copolymers · layered compounds · micelles · nanostructures · self-assembly

[1] L. M. Liz-Marzan, M. Giersig, P. Mulvaney, *Langmuir* **1996**, *12*, 4329 – 4335.
[2] a) K. Kamata, Y. Lu, Y. N. Xia, *J. Am. Chem. Soc.* **2003**, *125*, 2384 – 2385; b) D. Gerion, F. Pinaud, S. C. Williams, W. J. Parak, D. Zanchet, S. Weiss, A. P. Alivisatos, *J. Phys. Chem. B* **2001**, *105*, 8861 – 8871; c) S. P. Mulvaney, M. D. Musick, C. D. Keating, M. J. Natan, *Langmuir* **2003**, *19*, 4784 – 4790.
[3] a) Y. Cao, R. Jin, C. A. Mirkin, *J. Am. Chem. Soc.* **2001**, *123*, 7961 – 7962; b) J. L. Lyon, D. A. Fleming, M. B. Stone, P. Schiffer, M. E. Williams, *Nano Lett.* **2004**, *4*, 719 – 723.
[4] R. D. Averitt, D. Sarkar, N. J. Halas, *Phys. Rev. Lett.* **1997**, *78*, 4217 – 4220.
[5] M. A. Hines, P. Guyot-Sionnest, *J. Phys. Chem.* **1996**, *100*, 468 – 471.
[6] a) M. K. Corbierre, N. S. Cameron, M. Sutton, S. G. J. Mochrie, L. B. Lurio, A. Ruehm, R. B. Lennox, *J. Am. Chem. Soc.* **2001**, *123*, 10411 – 10412; b) S. Kim, M. G. Bawendi, *J. Am. Chem. Soc.* **2003**, *125*, 14652 – 14653.
[7] a) C. R. Vestal, Z. J. Zhang, *J. Am. Chem. Soc.* **2002**, *124*, 14312 – 14313; b) S. Nuss, H. Bottcher, H. Wurm, M. L. Hallensleben, *Angew. Chem.* **2001**, *113*, 4137 – 4139; *Angew. Chem. Int. Ed.* **2001**, *40*, 4016 – 4018; c) T. von Werne, T. E. Patten, *J. Am. Chem. Soc.* **2001**, *123*, 7497 – 7505; d) K. Sill, T. Emrick, *Chem. Mater.* **2004**, *16*, 1240 – 1243.
[8] a) M.-Q. Zhu, L.-Q. Wang, G. J. Exarhos, A. D. Q. Li, *J. Am. Chem. Soc.* **2004**, *126*, 2656 – 2657; b) M. K. Corbierre, N. S. Cameron, R. B. Lennox, *Langmuir* **2004**, *20*, 2867 – 2873.
[9] D. I. Gittins, F. Caruso, *J. Phys. Chem. B* **2001**, *105*, 6846 – 6852.
[10] a) A. B. Lowe, B. S. Sumerlin, M. S. Donovan, C. L. McCormick, *J. Am. Chem. Soc.* **2002**, *124*, 11562 – 11563; b) K. J. Watson, J. Zhu, S. T. Nguyen, C. A. Mirkin, *J. Am. Chem. Soc.* **1999**, *121*, 462 – 463.
[11] W. P. Wuelfing, S. M. Gross, D. T. Miles, R. W. Murray, *J. Am. Chem. Soc.* **1998**, *120*, 12696 – 12697.
[12] A. Halperin, M. Tirrell, T. P. Lodge, *Adv. Polym. Sci.* **1992**, *100*, 31 – 71.
[13] H. Y. Huang, T. Kowalewski, E. E. Remsen, R. Gertzmann, K. L. Wooley, *J. Am. Chem. Soc.* **1997**, *119*, 11653 – 11659.
[14] K. Matyjaszewski, J. Xia, *Chem. Rev.* **2001**, *101*, 2921 – 2990.
[15] See Supporting Information for further details of synthesis and characterization.
[16] a) G. Frens, *J. Nat. Phys. Sci.* **1973**, *241*, 20 – 22; b) K. R. Brown, D. G. Walter, M. J. Natan, *Chem. Mater.* **2000**, *12*, 306 – 313.
[17] A prerequisite of our encapsulation method is that the starting nanoparticles must be transiently stable in the encapsulation medium. Large (diameter > 5 nm), citrate-capped nanoparticles slowly precipitate from suspension in the presence of alkanethiol ligands, so the nanoparticles were functionalized with alkanethiol in situ. However, smaller alkanethiol-functionalized particles were prepared separately before encapsulation.
[18] I. Hussain, M. Brust, A. J. Papworth, A. I. Cooper, *Langmuir* **2003**, *19*, 4831 – 4835.
[19] a) T. R. Jensen, M. L. Duval, K. L. Kelly, A. A. Lazarides, G. C. Schatz, R. P. Van Duyne, *J. Phys. Chem. B* **1999**, *103*, 9846 – 9853; b) A. C. Templeton, J. J. Pietron, R. W. Murray, P. Mulvaney, *J. Phys. Chem. B* **2000**, *104*, 564 – 570.
[20] Y. Lu, Y. D. Yin, Z. Y. Li, Y. A. Xia, *Nano Lett.* **2002**, *2*, 785 – 788.
[21] a) T. Zhu, K. Vasilev, M. Kreiter, S. Mittler, W. Knoll, *Langmuir* **2003**, *19*, 9518 – 9525; b) R. Paulini, B. L. Frankamp, V. M. Rotello, *Langmuir* **2002**, *18*, 2368 – 2373.
[22] T. Ung, L. M. Liz-Marzan, P. Mulvaney, *Langmuir* **1998**, *14*, 3740 – 3748.
[23] D. V. Talapin, A. L. Rogach, A. Kornowski, M. Haase, H. Weller, *Nano Lett.* **2001**, *1*, 207 – 211.
[24] T. Hyeon, S. S. Lee, J. Park, Y. Chung, H. Bin Na, *J. Am. Chem. Soc.* **2001**, *123*, 12798 – 12801.
[25] Y. J. Kang, T. A. Taton, *J. Am. Chem. Soc.* **2003**, *125*, 5650 – 5651.

 © 2005 Wiley-VCH Verlag GmbH & Co. KGaA, Weinheim

Asymmetric Catalysis

Binol-Derived Monodentate Phosphites and Phosphoramidites with Phosphorus Stereogenic Centers: Novel Ligands for Transition-Metal Catalysis**

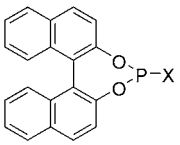
Manfred T. Reetz, Jun-An Ma, and Richard Goddard*

Recently three groups independently reported that binol-derived monodentate phosphites **1a**,[1] phosphonites **1b**,[2] and phosphoramidites **1c**[3] are efficient ligands in rhodium-catalyzed asymmetric olefin hydrogenation (*ee* values = 90–99%; binol = 2,2′-dihydroxy-1,1′-binaphthyl). A preliminary

[*] Prof. Dr. M. T. Reetz, Prof. Dr. J.-A. Ma, Dr. R. Goddard
Max-Planck-Institut für Kohlenforschung
Kaiser-Wilhelm-Platz 1
45470 Mülheim/Ruhr (Germany)
Fax: (+49) 208-306-2985
E-mail: reetz@mpi-muelheim.mpg.de

[**] Binol = 2,2′-dihydroxy-1,1′-binaphthyl.

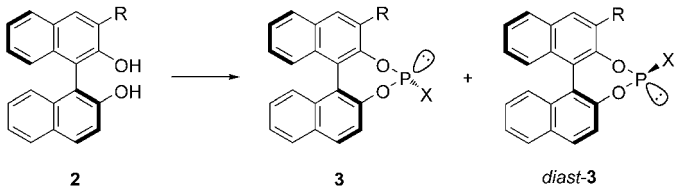
 © 2005 Wiley-VCH Verlag GmbH & Co. KGaA, Weinheim DOI: 10.1002/anie.200461624



1 a X = OR
b X = alkyl, aryl
c X = NR_2

mechanistic study by our group shows that two monodentate phosphorus compounds are bonded to rhodium in the hydrogenation transition state. In an extension of this work we demonstrated that mixtures of two different monodentate phosphorus ligands can be used in a combinatorial approach.[4] Since binol is one of the cheapest chiral auxiliaries currently available, chemical modification resulting in the formation of new modular ligands appears attractive.

We wondered whether binol derivatives bearing a single *ortho*-substituent as in (*S*)-**2** (Scheme 1) can serve as starting materials for structurally unusual monodentate phosphorus ligands. This modification would not only reduce C_2 to C_1 symmetry, it would also lead to the creation of a stereogenic center at phosphorus (R_P and S_P in diastereomers **3**; Scheme 1).[5] Herein we report the synthesis of this novel class of phosphorus ligands and their use in rhodium-catalyzed olefin hydrogenation.

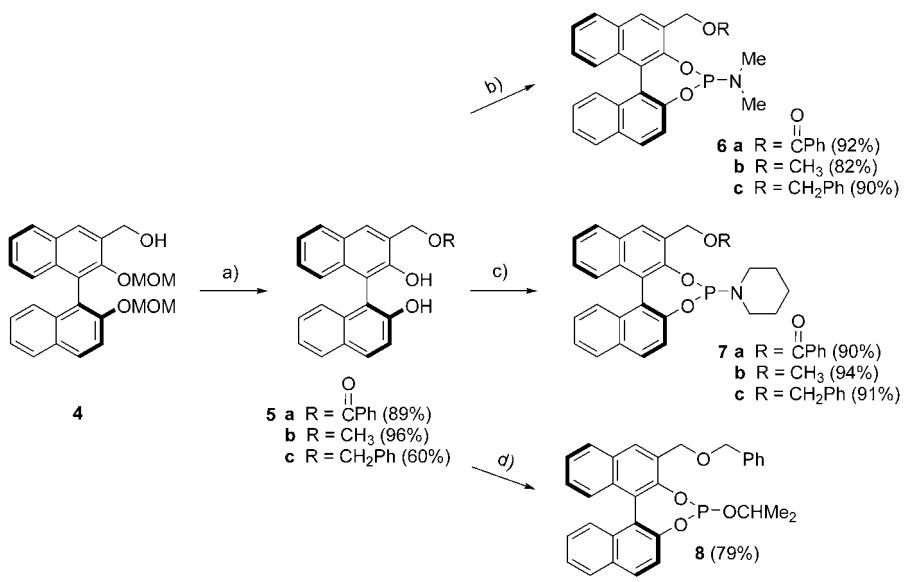


2 **3** *diast*-**3**

Scheme 1. Formation of diastereomeric ligands with stereogenic phosphorus centers.

Starting from the known methoxymethyl (MOM) protected (*S*)-binol-derivative **4**,[6] compounds **5a–c** were readily prepared which were then treated with $P(NMe_2)_3$ in boiling toluene. This reaction resulted in excellent yields of the phosphoramidites as diastereomeric mixtures or as pure compounds: **6a** (S,S_P:S,R_P = 2:1), **6b** (S,S_P pure), and **6c** (S,S_P:S,R_P = 10:1; Scheme 2). Reaction of **5a–c** with PCl_3/NEt_3 at −78 °C followed by treatment with piperidine provided phosphoramidites **7** (Scheme 2), the S,R_P compounds being the major diastereomers in these cases. The formation of the major diastereomers appears to be kinetically controlled under these conditions, because heating compound **7a** at 110 °C for 48 h changed the diastereomeric ratio S,R_P:S,S_P from 3:1 to 2.3:1. Treatment of compounds **5** with PCl_3/NEt_3 followed by reaction with an alcohol in the presence of NEt_3 provides the analogous phosphites, for example phosphite **8** (S,R_P:S,S_P = 3.8:1; Scheme 2).

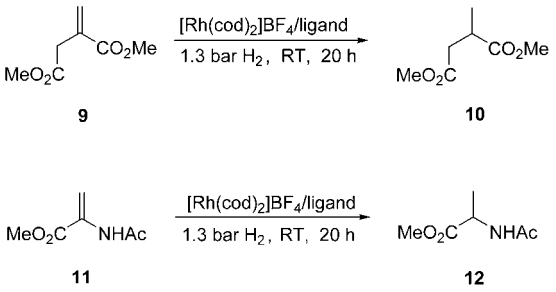
Some of the diastereomers were separated by crystallization, others by HPLC. The configuration assignments were



4
5 a R = CPh (89%)
b R = CH_3 (96%)
c R = CH_2Ph (60%)
6 a R = CPh (92%)
b R = CH_3 (82%)
c R = CH_2Ph (90%)
7 a R = CPh (90%)
b R = CH_3 (94%)
c R = CH_2Ph (91%)
8 (79%)

Scheme 2. Synthesis of phosphoramidites **6** and **7** and phosphite **8**. a) 1. RX/base, 2. CH_3OH/HCl; b) $P(NMe_2)_3$/toluene, 110 °C, 1–2 h; c) 1. PCl_3/Et_3N, Et_2O, −78→0 °C, 2. piperidine/Et_3N, Et_2O, RT, 24 h; d) 1. PCl_3/Et_3N, Et_2O, −78→0 °C, 2. *i*PrOH/Et_3N, Et_2O, RT, 24 h.

then made on the basis of an X-ray structural analysis of the major diastereomer of **6a**, which has the S,S_P configuration,[7] and in other cases by comparison of ^{31}P NMR spectroscopy data. In the ^{31}P NMR spectrum the signal of the S,S_P ligands appears at higher δ values than that of the S,R_P diastereomers, a conclusion that was corroborated by the X-ray data of another derivative (see below). Subsequently, the first rhodium-catalyzed hydrogenations were performed with olefins **9** and **11** (Scheme 3).



9 **10**
11 **12**

Scheme 3. Rhodium-catalyzed hydrogenation of olefins **9** and **11**; cod = cyclooctadiene.

Table 1 reveals that excellent enantioselectivities were achieved in some but not all cases and that the absolute configuration of the binol ligand dictates the direction of enantioselectivity. In the case of the hydrogenation of itaconic acid dimethyl ester (**9**) using ligand **6a** the configuration at the phosphorus center also plays a significant role. The pure S,S_P ligand leads to an *ee* value of 96.3 % (*S*; Table 1, entry 1), whereas the pure S,R_P diastereomer is less efficient (*ee* = 72.5 % *S*, entry 4). Thus, the S,S_P diastereomer represents the matched case. The mixtures of diastereomeric ligands give rise to intermediate *ee* values (entries 2 and 3). These

 © 2005 Wiley-VCH Verlag GmbH & Co. KGaA, Weinheim

Table 1: Rhodium-catalyzed hydrogenation of olefins **9** and **11** by using ligands **6**, **7**, and **8**.[a]

Entry	Olefin	Ligand	Major enantiomer of **10** or **12**	*ee* [%]
1	**9**	**6a** (S,S_P pure)	*S*	96.3
2	**9**	**6a** (S,S_P:S,R_P = 2:1)	*S*	93.0
3	**9**	**6a** (S,S_P:S,R_P = 1:2.3)	*S*	90.5
4	**9**	**6a** (S,R_P pure)	*S*	72.5
5	**9**	**6b** (S,S_P pure)	*S*	95.4
6	**9**	**6c** (S,S_P:S,R_P = 10:1)	*S*	96.1
7	**9**	**7a** (S,S_P:S,R_P = 1:3)	*S*	96.0
8	**9**	**7b** (S,S_P:S,R_P = 1:1.4)	*S*	96.3
9	**9**	**7c** (S,S_P:S,R_P = 1:2.2)	*S*	96.8
10	**9**	**8** (S,S_P:S,R_P = 1:3.8)	*S*	91.3
11	**11**	**6a** (S,S_P pure)	*R*	99.0
12	**11**	**6a** (S,S_P:S,R_P = 2:1)	*R*	98.7
13	**11**	**6a** (S,S_P:S,R_P = 1:2.3)	*R*	98.7
14	**11**	**6a** (S,R_P pure)	*R*	97.8
15	**11**	**6b** (S,S_P pure)	*R*	98.3
16	**11**	**6c** (S,S_P:S,R_P = 10:1)	*R*	98.4
17	**11**	**7a** (S,S_P:S,R_P = 1:3)	*R*	> 99.0
18	**11**	**7b** (S,S_P:S,R_P = 1:1.4)	*R*	93.8
19	**11**	**7c** (S,S_P:S,R_P = 1:2.2)	*R*	98.8
20	**11**	**8** (S,S_P:S,R_P = 1:3.8)	*R*	97.0

[a] All reactions in CH_2Cl_2; Rh:L = 1:2; Rh:olefin = 1:200; 1.3 bar; 20 h; 100% conversion in all cases.

mixtures constitute a more complex case because, as the rhodium center is coordinated by two binol ligands, three catalysts are actually involved, namely Rh(S,S_P/S,S_P), Rh(S,R_P/S,R_P), and Rh(S,S_P/S,R_P), each is present in a different amount and reacts with a different rate. Table 1 shows that with **9**, in five cases the *ee* values exceed 96%, which is distinctly better than the 87% *ee* resulting from the use of the parent C_2-symmetric phosphoramidite **1c** (R = CH_3).[3a] The mixture of diastereomeric phosphites **8** leads to a respectable 91.3% *ee* (entry 10), but at present we do not know how the pure diastereomers perform. In the hydrogenation of olefin **11**, ligand **6a** (S,S_P pure) also constitutes the matched case, but the cooperative effect is not as pronounced (entry 11 versus 14).

We phosphorylated the known (*S*)-binol derivatives **13**[8] which resulted in formation of phosphoramidites **14a–e**, and in two cases proceeded with complete diastereoselectivity (Scheme 4).

The X-ray structural analysis of the triphenylsilyl-derivative **14e** shows the free ligand to have the S,S_P configuration.[7] The precatalyst [Rh(**14e**)$_2$(cod)]BF_4 was also characterized by X-ray crystallography (Figure 1).[9] The metal cation has an almost ideal twofold axis of symmetry despite a highly unsymmetrical crystal environment caused by the

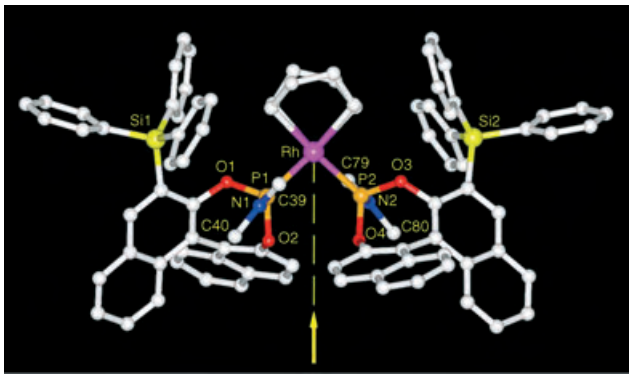
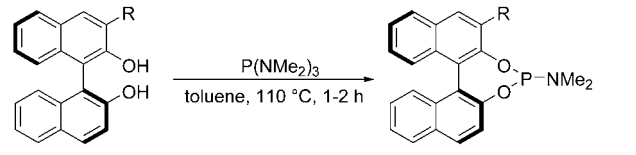


Figure 1. Structure of the cation of [Rh{(S,S_P)-**14e**}$_2$(cod)]BF_4 showing the almost exact twofold axis of symmetry passing through the Rh atom (arrow). Selected interatomic distances [Å], angles, and torsion angles [°]: Rh-P1 2.277(1), Rh-P2 2.275(1), P1-N1 1.640(2), P2-N2 1.633(3), C39···Rh 3.381(3), C79···Rh 3.377(3), P1-Rh-P2 94.89(2), C39-N1-P1-Rh 5(1), C79-N2-P2-Rh 3(1).[9]

$[BF_4]^-$ ion and CH_2Cl_2 solute of crystallization. This situation suggests that crystal-packing effects are not the cause of the high symmetry. An electron-donating effect of nitrogen onto phosphorus which is passed onto the positively charged rhodium center seems to be operating. Another feature is a weak C–H···Rh$^+$ interaction between one of the H atoms of a methyl group in the planar $N(CH_3)_2$ moiety and the metal.[10] Although the rhodium complexes of the other ligands which have less-bulky *ortho*-substituents could not be crystallized to date, they may have similar structures.

Upon employing the ligands **14** in the rhodium-catalyzed hydrogenation of olefins **9** and **11**, some remarkable observations were made (Table 2). The methyl derivative **14a** behaves much like the ligands **6**, **7**, and **8**, affecting *S* selectivity (91% *ee*, entry 1). In contrast, upon using the phenyl derivative **14b**, we were surprised to observe *R* selectivity (entries 2–5). This effect is opposite to what occurs when using the C_2-symmetric parent compounds (*S*)-**1** which also originates from (*S*)-binol; all of the parent ligands are known to be *S*-selective in the hydrogenation of **9** (**1a** (R = *i*Pr): 89.2% *ee*;[1] **1b** (X = CH_3): 90% *ee*;[2] **1c** (R = CH_3): 87% *ee*).[3a] Reversal of enantioselectivity on using ligand **14b** occurs both in the matched case S,R_P with 70% *ee* (entry 5) and in the non-cooperative combination S,S_P (20.6% *ee*, entry 2). This result means that breaking the symmetry of the ligands from C_2 to C_1 by introduction of an *ortho*-phenyl group induces a reversal of enantioselectivity which is independent of the configuration at the stereogenic phosphorus center. We also note that mixtures of diastereomers **14b** result in distinctly higher enantioselectivities than the use of the respective pure ligands themselves, *ee* values up to 90.3% being achieved (entries 3 and 4). The use of two diastereomers constitutes a novel extension of our concept of employing mixtures of two different monodentate ligands[4]



13 **a** R = CH_3
b R = Ph
c R = SPh
d R = $SiMe_3$
e R = $Si(Ph)_3$

14 **a** R = CH_3 [92%, (S,S_P):(S,R_P) = 7.8:1]
b R = Ph [85%, (S,S_P):(S,R_P) = 1:6]
c R = SPh [89%, (S,S_P):(S,R_P) = 1:1]
d R = $SiMe_3$ [97%, (S,S_P) pure]
e R = $Si(Ph)_3$ [96%, (S,S_P) pure]

Scheme 4. Synthesis of phosphoramidites **14**.

 © 2005 Wiley-VCH Verlag GmbH & Co. KGaA, Weinheim

Table 2: Rhodium-catalyzed hydrogenation of olefins **9** and **11** using ligands **14**.[a]

Entry	Olefin	Ligand	Major enantiomer of **10** or **12**	*ee* [%]
1	**9**	**14a** (S,S_P:S,R_P = 7.8:1)	*S*	91.0
2	**9**	**14b** (S,S_P pure)	*R*	20.6
3	**9**	**14b** (S,S_P:S,R_P = 1:1)	*R*	90.3
4	**9**	**14b** (S,S_P:S,R_P = 1:6)	*R*	79.6
5	**9**	**14b** (S,R_P pure)	*R*	70.0
6	**9**	**14c** (S,S_P:S,R_P = 1:1)	*S*	23.0
7	**9**	**14d** (S,S_P pure)	*rac*	0
8	**9**	**14d** (S,S_P pure)[b]	*R*	31.6
9	**9**	**14e** (S,S_P pure)	*R*	3.4
10	**9**	**14e** (S,S_P pure)[b]	*R*	17.0
11	**11**	**14a** (S,S_P:S,R_P = 7.8:1)	*R*	98.0
12	**11**	**14b** (S,S_P pure)	*S*	33.6
13	**11**	**14b** (S,R_P pure)	*R*	50.6
14	**11**	**14c** (S,S_P:S,R_P = 1:1)	*R*	97.2
15	**11**	**14d** (S,S_P pure)	*R*	87.2
16	**11**	**14e** (S,S_P pure)	*R*	34.0

[a] Same conditions as in Table 1; 100% conversion. [b] In this case a ligand:Rh ratio of 1:1 was chosen.

and raises fundamental theoretical questions. The fact that the triphenylsilyl-derivative **14e** is a poor ligand for catalysis can be rationalized on the basis of the crystal structure of [Rh{(S,S_P)-**14e**}$_2$(cod)]BF_4 (Figure 1). The silyl groups are so bulky that hydrogenation may actually be inhibited; the rhodium complex with only one phosphoramide ligand may function as the actual (pre)catalyst.

In summary, we have prepared and characterized a new class of binol-derived monodentate phosphorus ligands bearing phosphorus stereogenic centers. They are excellent ligands in rhodium-catalyzed olefin hydrogenation, a result which raises important mechanistic questions. On the practical side, this new class of modular phosphorus compounds enlarges the structural diversity of binol-derived monodentate phosphorus ligands, which means that they are also candidates for our combinatorial approach using mixtures[4] of chiral monodentate phosphorus ligands in hydrogenation and in other transition-metal-catalyzed reactions.

Received: August 12, 2004

Keywords: asymmetric catalysis · hydrogenation · P ligands · phosphites · rhodium

[1] a) M. T. Reetz, G. Mehler, *Angew. Chem.* **2000**, *112*, 4047 – 4049; *Angew. Chem. Int. Ed.* **2000**, *39*, 3889 – 3890; b) M. T. Reetz, *Chim. Oggi* **2003**, *21*(10/11), 5 – 8.

[2] a) M. T. Reetz, T. Sell, *Tetrahedron Lett.* **2000**, *41*, 6333 – 6336; b) C. Claver, E. Fernandez, A. Gillon, K. Heslop, D. J. Hyett, A. Martorell, A. G. Orpen, P. G. Pringle, *Chem. Commun.* **2000**, 961 – 962.

[3] a) M. van den Berg, A. J. Minnaard, E. P. Schudde, J. van Esch, A. H. M. de Vries, J. G. de Vries, B. L. Feringa, *J. Am. Chem. Soc.* **2000**, *122*, 11539 – 11540; b) D. Peña, A. J. Minnaard, A. H. M. de Vries, J. G. de Vries, B. L. Feringa, *Org. Lett.* **2003**, *5*, 475 – 478.

[4] a) M. T. Reetz, T. Sell, A. Meiswinkel, G. Mehler, *Angew. Chem.* **2003**, *115*, 814 – 817; *Angew. Chem. Int. Ed.* **2003**, *42*, 790 – 793; b) M. T. Reetz, G. Mehler, *Tetrahedron Lett.* **2003**, *44*, 4593 – 4596; c) M. T. Reetz, G. Mehler, A. Meiswinkel, *Tetrahedron: Asymmetry* **2004**, *15*, 2165 – 2167; see also: d) D. Peña, A. J. Minnaard, J. A. F. Boogers, A. H. M. de Vries, J. G. de Vries, B. L. Feringa, *Org. Biomol. Chem.* **2003**, *1*, 1087 – 1089; e) A. Duursma, R. Hoen, J. Schuppan, R. Hulst, A. J. Minnaard, B. L. Feringa, *Org. Lett.* **2003**, *5*, 3111 – 3113.

[5] Recent examples of P ligands with stereogenic centers at phosphorus for catalysis: a) W. Tang, X. Zhang, *Chem. Rev.* **2003**, *103*, 3029 – 3069; b) K. V. L. Crépy, T. Imamoto, *Adv. Synth. Catal.* **2003**, *345*, 79 – 101; c) P.-H. Leung, *Acc. Chem. Res.* **2004**, *37*, 169 – 177; d) W. Tang, W. Wang, Y. Chi, X. Zhang, *Angew. Chem.* **2003**, *115*, 3633 – 3635; *Angew. Chem. Int. Ed.* **2003**, *42*, 3509 – 3511; e) G. Hoge, *J. Am. Chem. Soc.* **2003**, *125*, 10219 – 10227; f) T. Imamoto, V. L. Crépy, K. Katagiri, *Tetrahedron: Asymmetry* **2004**, *15*, 2213 – 2218.

[6] S. Matsunaga, J. Das, J. Roels, E. M. Vogl, N. Yamamoto, T. Iida, K. Yamaguchi, M. Shibasaki, *J. Am. Chem. Soc.* **2000**, *122*, 2252 – 2260.

[7] The geometry of the phosphoramidito ligands is almost identical in the crystal structures of the (S,S_P)-3-benzoyloxymethyl-derivative **6a** and the (S,S_P)-3-triphenylsilyl-derivative **14e**.[9b]

[8] P. J. Cox, W. Wang, V. Snieckus, *Tetrahedron Lett.* **1992**, *33*, 2253 – 2256.

[9] a) Crystal data for [{(S,S_p)-**14e**}$_2$Rh(cod)]$^+$[BF_4]$^-$ ·CH_2Cl_2:[$C_{88}H_{76}N_2O_4P_2RhSi_2$]$^+$[$BF_4$]$^-$·$CH_2Cl_2$, crystals grown from dichloromethane/ethyl acetate/diethyl ether/pentane, M_r = 1618.27, crystal size: 0.04 × 0.08 × 0.18 mm^3; a = 9.9676(1), b = 24.3928(1), c = 31.6031(2) Å, V = 7683.9(1) Å^3, T = 100 K, orthorhombic, space group $P2_12_12_1$ (No. 19), Z = 4, ρ_{calcd} = 1.399 g cm^{-3}, $F(000)$ = 3344, Nonius KappaCCD diffractometer, $\lambda(Mo_{K\alpha})$ = 0.71073 Å, μ = 0.429 mm^{-1}, 75490 measured and 18928 independent reflections (R_{int} = 0.056), 17187 with $I > 2\sigma(I)$, θ_{max} = 28.28°, T_{min} = 0.968, T_{max} = 0.996, direct methods (SHELXS-97) and least-squares refinement (SHELXL-97) on F_o^2, both programs from G. Sheldrick, University of Göttingen, **1997**; 964 parameters, Flack parameter −0.03(1), H atoms riding, Chebyshev weights, R_1 = 0.0392 ($I > 2\sigma(I)$), wR_2 = 0.0898 (all data), $\Delta\rho_{max/min}$ = 0.868/−0.624 e Å^{-3}. b) CCDC-247341, CCDC-247342, CCDC-247343 contain the supplementary crystallographic data for this paper. These data can be obtained free of charge via www.ccdc.cam.ac.uk/conts/retrieving.html (or from the Cambridge Crystallographic Data Centre, 12 Union Road, Cambridge CB21EZ, UK; fax: (+44) 1223-336-033; or deposit@ccdc.cam.ac.uk).

[10] Examples of crystal structure of other rhodium phosphoramidite complexes: a) A.-G. Hu, Y. Fu, J.-H. Xie, H. Zhou, L.-X. Wang, Q.-L. Zhou, *Angew. Chem.* **2002**, *114*, 2454 – 2456; *Angew. Chem. Int. Ed.* **2002**, *41*, 2348 – 2350; b) M. van den Berg, A. J. Minnaard, R. M. Haak, M. Leeman, E. P. Schudde, A. Meetsma, B. L. Feringa, A. H. M. de Vries, C. E. P. Maljaars, C. E. Willans, D. Hyett, J. A. F. Boogers, H. J. W. Henderickx, J. G. de Vries, *Adv. Synth. Catal.* **2003**, *345*, 308 – 323.

 © 2005 Wiley-VCH Verlag GmbH & Co. KGaA, Weinheim

SAM Photochemistry

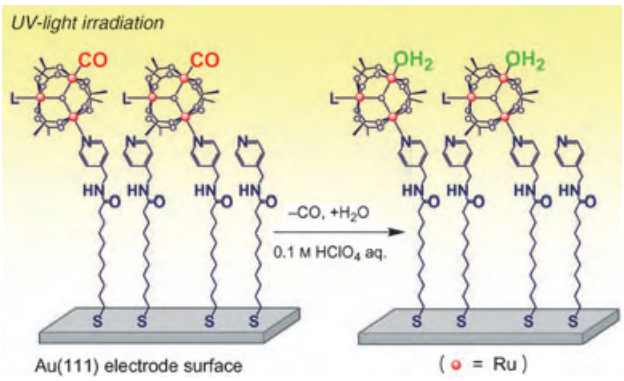
Photoconversion of a Redox-Active Self-Assembled Monolayer: In Situ Probing of Photoinduced CO Dissociation from a Triruthenium Cluster Center on Gold**

Masaaki Abe, Takuya Masuda, Toshihiro Kondo, Kohei Uosaki,* and Yoichi Sasaki**

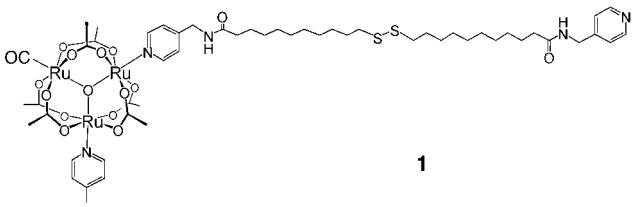
Investigations on the photoreactivity of molecular compounds assembled on solid surfaces or at solid/solution interfaces are a prerequisite for the photochemical design of functional molecular thin films.[1] Extensive studies have been made on the fabrication of photoresponsive molecular layers on electrode surfaces by using organic, inorganic, and biological building blocks, in which, for example, isomerization,[2] chemical bond formation and cleavage,[3] and directional electron transfer are observed.[4]

Photoinduced ligand substitution is an additional potential candidate for controlling surface properties of thin films that are constructed from transition-metal coordination compounds. Although significant progress has been made in solution-phase photoinduced substitution reactions,[5] their application to precise tuning of thin-film properties at solid surfaces have rarely been exploited to date.[6] Here we describe the in situ observation and analysis of photoinduced CO dissociation from a self-assembled monolayer (SAM) of a triruthenium cluster on Au(111), which is, to our knowledge, the first well-defined example of clean photoconversion of a redox-active SAM that leads to a significant shift of the redox potential. We also report on photocurrent generation by the present SAM, which is an unprecedented finding for this class of cluster molecules. This study thus provides a new route to photochemical design of redox-active molecular films on electrode surfaces, which should be of considerable use in molecular electronics and devices.

Scheme 1 illustrates the proposed photochemical reaction in the SAM. We employed disulfide-functionalized, CO-ligated triruthenium cluster **1** as photoresponsive molecule.[7] This compound was chosen because of its well-defined photoinduced CO dissociation in solution[8] and the availability of a methodology for preparing densely packed SAMs on the surface of a gold electrode.[7] Trinuclear clusters of this type[9] have been used to construct ligand-bridged extended molecular architectures by chemical synthesis[10–14] and layer-by-layer deposition on gold surfaces,[15] as well as to fabricate a ligand switching device.[16] Complex **1** is a mixed-valent $Ru_3^{II,III,III}$ complex in which the +II oxidation state is localized at the ruthenium site bound to CO[17,18] (here we designate the triruthenium redox moiety as $\{Ru^{II}\text{-}CO\}Ru^{III}Ru^{III}$). The CO ligand of **1** remains coordinated to the ruthenium center in the SAM as long as the $\{Ru^{II}\text{-}CO\}Ru^{III}Ru^{III}$ oxidation state is maintained, but it dissociates when the one-electron-oxidized $\{Ru^{III}\text{-}CO\}Ru^{III}Ru^{III}$ state is prepared electrochemically by holding the applied potential at +0.8 V (vs Ag/AgCl in 0.1 M $HClO_4$) to form an H_2O-terminated SAM as the result of interfacial ligand substitution.[7]



Scheme 1. Proposed photoinduced CO dissociation from a monolayer of **1** self-assembled on Au(111). L = 4-methylpyridine.



1

Cyclic voltammetry was used to probe photoinduced CO dissociation from the redox-active SAM on Au(111). A SAM-modified Au(111) disk ($A = 0.44\ cm^2$), together with a platinum-coil counterelectrode and an Ag/AgCl reference electrode, was placed in a photoelectrochemical cell filled with an Ar-purged aqueous solution of 0.1 M $HClO_4$. An Hg lamp (250 W; Ushio, USH-250D) was employed for irradiation through the 2 mm-thick quartz-plate window of the cell. To probe the photolytic reaction of the SAM, cyclic voltam-

[*] Dr. M. Abe, T. Masuda, Prof. Dr. T. Kondo,[+] Prof. Dr. K. Uosaki, Prof. Dr. Y. Sasaki
Division of Chemistry
Graduate School of Science
Hokkaido University
Kita-ku, Sapporo 060-0810 (Japan)
Fax: (+81) 11-706-3447
E-mail: mabe@sci.hokudai.ac.jp
uosaki@pcl.sci.hokudai.ac.jp
ysasaki@sci.hokudai.ac.jp

[+] Current address: Department of Chemistry
Faculty of Science, Ochanomizu University
2-1-1, Otsuka, Bunkyo-ku, Tokyo 112-8610 (Japan)

[**] This work was supported, in part, by Grant-in-Aids for Scientific Research on Priority Area of "Reaction Control of Dynamic Complexes" and "Electrochemistry of Ordered Interfaces" (Nos. 16033201 and 09237106, respectively) from the Ministry of Education, Science, Sports, and Culture of Japan, and Sasakawa Scientific Research Grant from the Japan Science Society. Experimental assistance by Dr. H. Noda (Hokkaido University) is acknowledged.

Supporting information for this article is available on the WWW under http://www.angewandte.org or from the authors.

© 2005 Wiley-VCH Verlag GmbH & Co. KGaA, Weinheim
DOI: 10.1002/anie.200460651

mograms (CVs) were recorded at constant time intervals of irradiation. During irradiation, the electrode potential was held at +0.3 V, a value that is more negative than $E_{1/2}$ of the SAM, to avoid electrochemical dissociation of CO from the cluster center.[7]

Figure 1 shows changes in CV on photolysis of an SAM of **1** on Au(111) in contact with 0.1 M $HClO_4$ aqueous solution at RT. Prior to irradiation (Figure 1a), the CV shows a redox

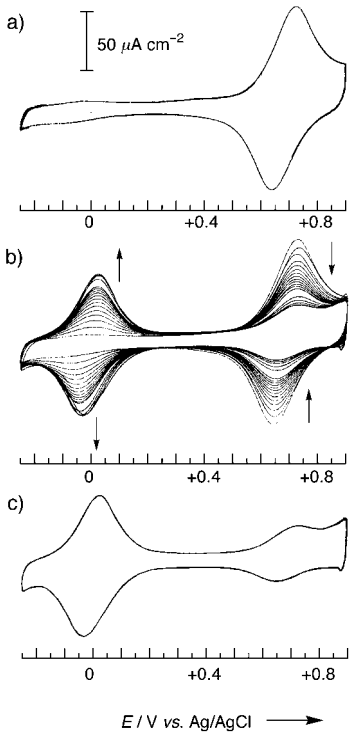


Figure 1. CVs of the SAM-modified Au(111) electrode. a) Prior to irradiation. b) Sequential variation in CV during UV irradiation ($0 < t < 520$ s). Upward and downward arrows represent the increase and decrease, respectively, in current of the redox waves. c) After 520 s irradiation. Electrolyte: 0.1 M aqueous $HClO_4$. Applied potential during irradiation: +0.3 V versus Ag/AgCl. Scan rate for CV: 500 $mV s^{-1}$.

wave which corresponds to the $\{Ru^{II}\text{-}CO\}Ru^{III}Ru^{III}/\{Ru^{III}\text{-}CO\}Ru^{III}Ru^{III}$ process[7] at +0.68 V versus Ag/AgCl with a surface coverage of $\Gamma = 2.5 \times 10^{-10}$ mol cm^{-2}. When the SAM-modified Au(111) electrode was exposed to UV light from the Hg lamp (Figure 1b), the redox wave at $E_{1/2} = +0.68$ V decreased in intensity, while a new redox wave appeared and increased in intensity at $E_{1/2} = 0.00$ V, a value that is very close to that of the H_2O-terminated SAM generated electrochemically.[7] This value is also close to that of CO-free solvento complex $[Ru_3(\mu_3\text{-}O)(\mu\text{-}CH_3COO)_6(4\text{-methylpyridine})_2(H_2O)]^+$ dissolved in acetonitrile containing 0.1 M nBu_4NPF_6 ($E_{1/2} = +0.04$ V vs Ag/AgCl).[19] After 520 s of UV exposure (Figure 1c), nearly complete transformation of the monolayer is observed. More direct evidence for photolytic dissociation of CO was obtained by IR spectroscopy.[20] The SAM of **1** assembled on Au(111) displays an intense absorption peak due to ν(CO) at $\tilde{\nu} = 1944$ cm^{-1}, which exhibits, as expected, a significant decrease in intensity after photolysis.

The photoinduced transformation was quantitatively analyzed by integrating charge density under the two redox waves presented in Figure 1. Figure 2a shows charge density profiles of surface-assembled **1**, H_2O-terminated photoproduct, and the sum of the two against irradiation time. As is visible from Figure 2b, the photoinduced dissociation of CO

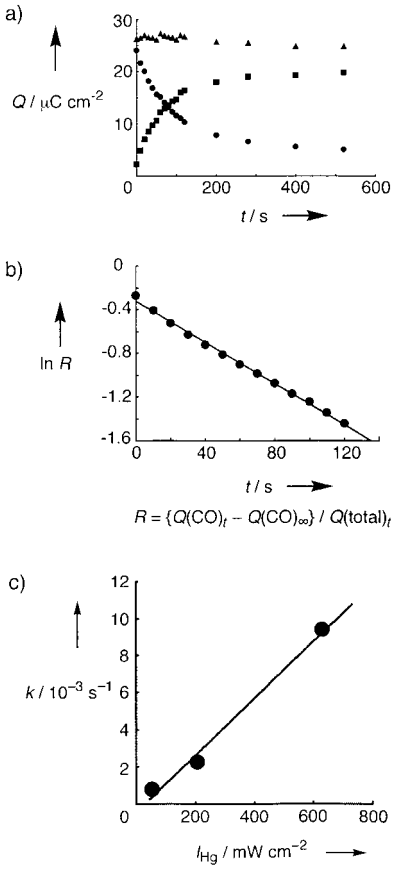


Figure 2. Analysis of photoinduced CO dissociation. a) Variation of charge Q of surface species obtained from CVs presented in Figure 1. ●: CO-terminated SAM; ■: H_2O-terminated SAM; ▲: sum of the two components. b) First-order plot of the decay of CO-terminated SAM as a function of irradiation time t. c) Linear dependence of the rate constant k for CO dissociation on light intensity I_{Hg}.

is well described by first-order kinetics with a rate constant of $(2.3 \pm 0.1) \times 10^{-3}$ s^{-1} at a light intensity of 210 mW cm^{-2}. The rate constant increases linearly with increasing light intensity (Figure 2c). Changing the electrolyte solution from 0.1 M $HClO_4$ to 0.05 M H_2SO_4 does not affect the rate constant of photodissociation; this suggests that the electrolyte anions do not participate in the photoexcited state of the cluster.

We emphasize that the photochemical transformation of the monolayer is clean: the two redox-active moieties remain undesorbed from the surface during irradiation (Figure 2a). The preservation of the monolayer on the electrode surface was also supported by a reductive desorption experiment (0.5 M aqueous KOH solution), which showed a well-defined Au–S desorption peak at −0.92 V for the photolytically

 © 2005 Wiley-VCH Verlag GmbH & Co. KGaA, Weinheim

generated H_2O-terminated SAM.[21] We speculate that the closely packed character of the photoactive cluster moieties, as well as the deaerated conditions employed for the measurement, minimize possible photodegradation of the SAM.[22]

We recently established photoinduced dissociation of CO from $[Ru_3(\mu_3\text{-}O)(\mu\text{-}CH_3COO)_6(pyridine)_2(CO)]$ in CH_3CN.[8] Photoexcitation at the cluster-to-CO ligand charge-transfer band at about 300 nm results in dissociation of CO to afford the corresponding CH_3CN complex $[Ru_3(\mu_3\text{-}O)(\mu\text{-}CH_3COO)_6(pyridine)_2(CH_3CN)]$ with a quantum yield of 0.012 at 298 K, while an intense absorption band at $\lambda_{max} = 585$ nm is not totally responsible for CO dissociation. In the present study, the importance of photoexcitation wavelength for triggering ligand substitution at the monolayer/solution interface was demonstrated by two experiments. First, when irradiation was performed with an Hg lamp through long-pass cutoff filters, the rate constant for CO dissociation ($k = 5.3 \times 10^{-4}\ s^{-1}$ for $\lambda > 340$ nm and $1.4 \times 10^{-4}\ s^{-1}$ for $\lambda > 380$ nm) became approximately one order of magnitude smaller than that obtained on unfiltered irradiation, that is, the photoactive band(s) lies in the UV region. Irradiation at 400 nm or longer wavelength does not cause any CO dissociation. Second, irradiation with visible light from an Xe lamp (630 mW cm^{-2}) also retarded the photoinduced substitution ($k = (8.1 \pm 0.1) \times 10^{-4}\ s^{-1}$).[23]

An additional interesting feature of the present SAM is the observation of photocurrent generation. Figure 3 shows the photocurrent action spectrum of the monolayer assembled on Au(111) and the UV/Vis absorption spectrum of **1** in acetonitrile. The anodic photocurrent response of the monolayer is shown in the inset. The photocurrent action spectrum shows a remarkable dependence on the irradiation wavelength. The maximum photocurrent was observed for excitation at 320 nm, while the photocurrent intensity was markedly decreased at shorter and longer wavelengths. Irradiation at 350 nm or longer wavelength did not lead to photocurrent generation, which clearly shows the inactivity of the absorption band in the visible region ($\lambda_{max} = 584$ nm) in the photocurrent response. The maximum peak of the action spectrum definitely corresponds to the location of the absorption shoulder in **1**, which has been tentatively assigned to cluster-to-ligand or cluster-to-CO charge-transfer transitions.[8] Since the intensity of the monochromated light employed here is fairly low (280 μW cm^{-2}), the action spectrum obtained indeed reflects the photocurrent response of the CO-terminated SAM. We note that the monolayer shows reproducible photocurrent data as long as the {Ru^{II}-CO} bond in **1** remains intact. Work to accurately determine the nature of the photocurrent and to fully address its mechanism is currently in progress. Our preliminary observation indicates that the aqua-terminated monolayer formed on intense irradiation of its CO-terminated counterpart also exhibits an anodic photocurrent but with much lower intensity. These observations indicate that photochemical ligand replacement can be used to tune not only the redox potential but also the photocurrent characteristics of our SAM on Au.

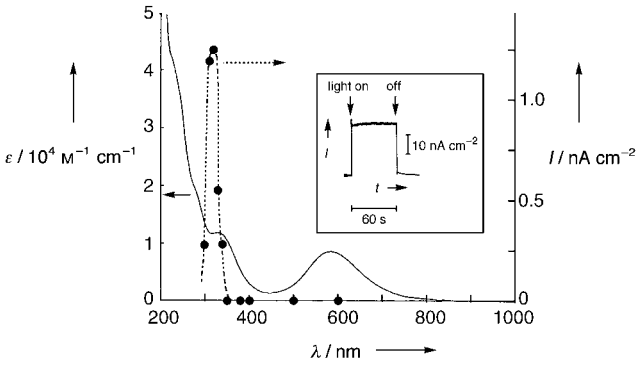


Figure 3. Absorption spectrum of **1** in acetonitrile (solid line) and photocurrent action spectrum (filled circles) of the monolayer of **1** on Au(111) in contact with 0.1 M $HClO_4$. Monochromated light intensity: 280 μW cm^{-2}. Applied potential: +0.3 V versus Ag/AgCl. Inset: anodic photocurrent response with irradiation from an Hg lamp (210 mW cm^{-2}).

In conclusion, we have described photochemical ligand substitution reaction of a redox-active SAM for the first time. We expect that suitable selection of photoresponsive coordination compounds, a CO-ligated triruthenium complex in our case, may offer a route to significant development in the fabrication of redoxactive and photoactive layers that can show device characteristics at an electrochemical interface.

Experimental Section

The Au(111) disk for SAM preparation was electrochemically etched and annealed as described in ref. [24]. The surface area was estimated from a cyclic voltammogram recorded in 0.1 M aqueous H_2SO_4, based on the charge under the cathodic wave due to gold oxide reduction.[25] The roughness factor of the Au(111) surface was 1.15. Prior to SAM formation, the Au(111) disk surface was flame-annealed with a hydrogen burner and slowly cooled in air. For SAM formation, the disk was immersed in an ethanol solution of **1** (50 μM) for 2 d at RT. The SAM-modified Au(111) was rinsed with ethanol and Milli-Q water, dried by blowing nitrogen gas over the surface, and it was subjected to photoelectrochemical measurements. The electrode potential was controlled by a Hokuto Denko HA-151 potentiostat, while the external potential was provided by a Hokuto Denko HB-111 function generator. The light intensity was determined by an optical power meter. For recording of the photocurrent action spectrum, monochromated light from the Hg lamp was used. The light intensity was adjusted to 280 μW cm^{-2} for each measurement.

Received: May 14, 2004
Revised: September 29, 2004

Keywords: electrochemistry · monolayers · photochemistry · surface chemistry

[1] For example: a) R. L. Carroll, C. B. Gorman, *Angew. Chem.* **2002**, *114*, 4556; *Angew. Chem. Int. Ed.* **2002**, *41*, 4378; b) A. N. Shipway, I. Willner, *Acc. Chem. Res.* **2001**, *34*, 421.

[2] a) D. G. Water, D. J. Campbell, C. A. Mirkin, *J. Phys. Chem. B* **1999**, *103*, 402; b) A. Doron, E. Katz, M. Portnoy, I. Willner, *Angew. Chem.* **1996**, *108*, 1626; *Angew. Chem. Int. Ed. Engl.* **1996**, *35*, 1535; c) I. Willner, S. Rubin, *Angew. Chem.* **1996**, *108*, 419; *Angew. Chem. Int. Ed. Engl.* **1996**, *35*, 367; d) M. Lion-Dagan, S. Marx-Tibbon, E. Katz, I. Willner, *Angew. Chem.* **1995**, *107*, 1730; *Angew. Chem. Int. Ed. Engl.* **1995**, *34*, 1604; e) I. Willner, V. Pardo-Yissar, E. Katz, K. T. Ranjit, *J. Electroanal. Chem.* **2001**, *497*, 172; f) K. T. Ranjit, S. Marx-Tibbon, I. Ben-

 © 2005 Wiley-VCH Verlag GmbH & Co. KGaA, Weinheim

Dov, I. Willner, *Angew. Chem.* **1997**, *109*, 90; *Angew. Chem. Int. Ed. Engl.* **1997**, *36*, 147; g) I. Willner, F. Patolsky, J. Wasserman, *Angew. Chem.* **2001**, *113*, 1913; *Angew. Chem. Int. Ed.* **2001**, *40*, 1861.

[3] a) S. Abbott, J. Ralston, G. Reynolds, R. Hayes, *Langmuir* **1999**, *15*, 8923; b) S. Sortino, S. Petralia, G. G. Condorelli, S. Conoci, G. Condorelli, *Langmuir* **2003**, *19*, 536.

[4] a) K. Uosaki, T. Kondo, X.-Q. Zhang, M. Yanagida, *J. Am. Chem. Soc.* **1997**, *119*, 8367; b) T. Kondo, T. Kanai, K. Uosaki, *Langmuir* **2001**, *17*, 6317; c) H. Yamada, H. Imahori, Y. Nishimura, I. Yamazaki, T. K. Ahn, S. K. Kim, D. Kim, S. Fukuzumi, *J. Am. Chem. Soc.* **2003**, *125*, 9129; d) D. Hirayama, K. Takimiya, Y. Aso, T. Otsubo, T. Hasobe, H. Yamada, H. Imahori, S. Fukuzumi, Y. Sakata, *J. Am. Chem. Soc.* **2002**, *124*, 532; e) Y. Kuwahara, T. Akiyama, S. Yamada, *Langmuir* **2001**, *17*, 5714.

[5] a) M. Wrighton, *Chem. Rev.* **1974**, *74*, 401; b) G. L. Geoffroy, M. Wrighton, *Organometallic Photochemistry*, Academic Press, New York, **1987**, p. 242; c) P. C. Ford, D. Wink, J. Dibenedetto, *Prog. Inorg. Chem.* **1983**, *30*, 213; d) J. G. Bentsen, M. S. Wrighton, *J. Am. Chem. Soc.* **1987**, *109*, 4530; e) M. F. Desrosiers, D. A. Wink, R. Trautman, A. E. Friedman, P. C. Ford, *J. Am. Chem. Soc.* **1986**, *108*, 1917; f) N. E. Leadbeater, J. Lewis, P. R. Raithby, G. N. Ward, *J. Chem. Soc. Dalton Trans.* **1997**, 2511; g) E. Eskelinen, M. Haukka, T. Venäläinen, T. A. Pakkanen, M. Wasberg, S. Chardon-Noblat, A. Deronzier, *Organometallics* **2000**, *19*, 163; h) K. Koike, J. Tanabe, S. Toyama, H. Tsubaki, K. Sakamoto, J. R. Westwell, F. P. A. Johnson, H. Hori, H. Saitoh, O. Ishitani, *Inorg. Chem.* **2000**, *39*, 2777; i) F.-W. Grevels, K. Kerpen, W. E. Klotzbücher, K. Schaffner, R. Goddard, B. Weimann, C. Kayran, S. Özkar, *Organometallics* **2001**, *20*, 4775; j) A. S. DelNegro, S. M. Woessner, B. P. Sullivan, D. M. Dattelbaum, J. R. Schoonover, *Inorg. Chem.* **2001**, *40*, 5056.

[6] a) E. W. Wollman, D. Kang, C. D. Frisbie, I. M. Lorkovic, M. S. Wrighton, *J. Am. Chem. Soc.* **1994**, *116*, 4395; b) D. Kang, M. S. Wrighton, *Langmuir* **1991**, *7*, 2169.

[7] A. Sato, M. Abe, T. Inomata, T. Kondo, S. Ye, K. Uosaki, Y. Sasaki, *Phys. Chem. Chem. Phys.* **2001**, *3*, 3420.

[8] D. Akashi, H. Kido, M. Abe, Y. Sasaki, T. Ito, *Dalton Trans.* **2004**, 2883.

[9] R. D. Cannon, R. P. White, *Prog. Inorg. Chem.* **1988**, *36*, 195.

[10] H. E. Toma, K. Araki, A. D. P. Alexiou, S. Nikolaou, S. Dovidauskas, *Coord. Chem. Rev.* **2001**, *219–221*, 187.

[11] a) J. A. Baumann, S. T. Wilson, D. J. Salmon, P. L. Hood, T. J. Meyer, *J. Am. Chem. Soc.* **1979**, *101*, 2916; b) J.-L. Chen, L.-Y. Zhang, Z.-N. Chen, L.-B. Gao, M. Abe, Y. Sasaki, *Inorg. Chem.* **2004**, *43*, 1481.

[12] H. Kido, H. Nagino, T. Ito, *Chem. Lett.* **1996**, 745.

[13] T. Ito, T. Hamaguchi, H. Nagino, T. Yamaguchi, H. Kido, I. S. Zavarine, T. Richmond, J. Washington, C. P. Kubiak, *J. Am. Chem. Soc.* **1999**, *121*, 4625.

[14] T. Ito, N. Imai, T. Yamaguchi, T. Hamaguchi, C. H. Londergan, C. P. Kubiak, *Angew. Chem.* **2004**, *116*, 1400; *Angew. Chem. Int. Ed.* **2004**, *43*, 1376.

[15] M. Abe, T. Michi, A. Sato, T. Kondo, W. Zhou, S. Ye, K. Uosaki, Y. Sasaki, *Angew. Chem.* **2003**, *115*, 3018; *Angew. Chem. Int. Ed.* **2003**, *42*, 2912.

[16] S. Ye, W. Zhou, M. Abe, T. Nishida, L. Cui, K. Uosaki, M. Osawa, Y. Sasaki, *J. Am. Chem. Soc.* **2004**, *126*, 7434.

[17] S. Ye, H. Akutagawa, K. Uosaki, Y. Sasaki, *Inorg. Chem.* **1995**, *34*, 4527.

[18] a) J. A. Baumann, D. J. Salmon, S. T. Wilson, T. J. Meyer, W. E. Hatfield, *Inorg. Chem.* **1978**, *17*, 3342; b) M. Abe, Y. Sasaki, Y. Yamada, K. Tsukahara, S. Yano, T. Yamaguchi, M. Tominaga, I. Taniguchi, T. Ito, *Inorg. Chem.* **1996**, *35*, 6724.

[19] M. Abe, A. Sato, T. Inomata, T. Kondo, K. Uosaki, Y. Sasaki, *J. Chem. Soc. Dalton Trans.* **2000**, 2693.

[20] IR spectra were recorded prior to and after photolysis of the SAM on a JASCO FT-IR 660Plus spectrophotometer (see Supporting Information).

[21] See Supporting Information.

[22] Selected references describing monolayer photodegradation: a) N. J. Brewer, R. E. Rawsterne, S. Kothari, G. J. Leggett, *J. Am. Chem. Soc.* **2001**, *123*, 4089; b) J. Huang, J. C. Hemminger, *J. Am. Chem. Soc.* **1993**, *115*, 3342.

[23] See Supporting Information. Unlike irradiation from the Hg lamp, the use of the Xe lamp at a prolonged exposure time ($>10^4$ s) resulted in a significant loss of redox-active moieties from the gold surface (ca. 24%, based on CV charge).

[24] T. Kondo, J. Morita, M. Okamura, T. Saito, K. Uosaki, *J. Electroanal. Chem.* **2002**, *532*, 201.

[25] R. Woods in *Electroanalytical Chemistry, A Series of Advances, Vol. 9* (Ed.: A. J. Bard), Marcel Dekker, New York, **1988**, p. 1.

 © 2005 Wiley-VCH Verlag GmbH & Co. KGaA, Weinheim

Drug Delivery

Supramolecular Nanocarrier of Anionic Dendrimer Porphyrins with Cationic Block Copolymers Modified with Polyethylene Glycol to Enhance Intracellular Photodynamic Efficacy**

*Woo-Dong Jang, Nobuhiro Nishiyama, Guo-Dong Zhang, Atsushi Harada, Dong-Lin Jiang, Satoko Kawauchi, Yuji Morimoto, Makoto Kikuchi, Hiroyuki Koyama, Takuzo Aida, and Kazunori Kataoka**

A great number of challenges have been overcome to create efficient photosensitizers (PSs) for photodynamic therapy (PDT) which have a high photocytotoxicity and selectivity for

[*] Dr. W.-D. Jang, Dr. N. Nishiyama, Dr. G.-D. Zhang, Dr. A. Harada, Prof. Dr. K. Kataoka
Department of Materials Science and Engineering
Graduate School of Engineering, The University of Tokyo
7-3-1 Hongo, Bunkyo-ku, Tokyo 113-8656 (Japan)
Fax: (+81) 3-5841-7139
E-mail: kataoka@bmw.t.u-tokyo.ac.jp

Dr. D.-L. Jiang, Prof. Dr. T. Aida
Department of Chemistry and Biotechnology
Graduate School of Engineering, The University of Tokyo
7-3-1 Hongo, Bunkyo-ku, Tokyo 113-8656 (Japan)

Dr. W.-D. Jang, Dr. G.-D. Zhang, Dr. A. Harada, Prof. Dr. K. Kataoka
CREST
Japan Science and Technology Corporation (Japan)

Dr. N. Nishiyama, Dr. H. Koyama
Department of Clinical Vascular Regeneration
Graduate School of Medicine, The University of Tokyo
7-3-1 Hongo, Bunkyo-ku, Tokyo 113-8655 (Japan)

Dr. S. Kawauchi, Dr. Y. Morimoto, Prof. Dr. M. Kikuchi
Department of Medical Engineering
National Defense Medical College
3-2 Namiki, Tokorozawa, Saitama, 359-8513 (Japan)

[**] This work was supported by Core Research for Evolutional Science and Technology (CREST), JST.

 DOI: 10.1002/anie.200461603 © 2005 Wiley-VCH Verlag GmbH & Co. KGaA, Weinheim

the diseased tissue.[1] To obtain high quantum yields and effective energy absorption, PSs generally need to have large π-conjugation domains such as a porphyrin structure. Therefore, most conventional PSs easily form aggregates, which produce a self-quenching effect of the excited state, in aqueous medium as a result of their π–π interactions and hydrophobic characteristics. These issues can be overcome, as we reported previously, by segregating PSs into the focal core of dendrimers (dendrimer porphyrins (DPs), Figure 1b).[2] DPs are attractive for biomedical purposes because of their predictable structures, that is, their monodisperse molecular weight and tunable three-dimensional structures, and their flexibility for a high density of tailored functional groups on the periphery.[3] Indeed, third-generation DPs with 32 cationic or anionic peripheral groups exhibit a high solubility in aqueous medium and have a high quantum yield for the generation of singlet oxygen, which leads to an appreciable photocytotoxicity.[2] These advantageous features of DPs are facilitated to an even greater extent by their inclusion into stealth nanocarriers, thus improving their longevity in blood circulation and results in their gradual accumulation in solid tumors through the enhanced permeation and retention (EPR) effect.[4] Furthermore, as demonstrated here, the inclusion of DPs into a novel type of nanocarrier, that is, polymeric micelles, has led to an unprecedented increase in the photocytotoxicity without compromising either the photophysical properties of DPs in regard to their efficient photochemical reactions or the physicochemical properties of the carriers necessary for tumor-selective delivery.

A novel polymeric micelle system[5] for PDT is based on an electrostatic assembly of an anionic DP,[6] which consists of zinc porphyrin at the focal core with a third generation of poly(benzyl ether) dendritic frameworks having 32 negative charges on the periphery, and poly(ethylene glycol)–poly(L-lysine) block copolymer (PEG-*b*-PLL) in aqueous media (polyion complex (PIC) micelles; Figure 1b).[7] The DP-incorporated micelles (DP/m), prepared with a stoichiometric ratio of negatively charged DP and positively charged PEG-*b*-PLL, were approximately 64 nm in diameter with an extremely narrow size distribution in physiological saline solution (Figure 2a). Our previous study using static light scattering (SLS) measurements demonstrated that an individual DP/m contains an average of 38 DP molecules and the micelles have a remarkable stability against salt concentrations,[7] which indicates the clear stabilization effect by the 32 negative charges of DP in the micellar structure. The dependency of the formation of DP/m on the pH value was investigated by dynamic and static light scattering (DLS and SLS) measurements. Figure 2b shows the pH-dependent changes in the translational diffusion coefficient (D_T) and normalized $(Kc/\Delta R(0))^{-1}$ (normalized to the micelle at pH 7.4) of DP/m, where D_T is related to the hydrodynamic size based on the Stokes–Einstein equation, and the normalized $(Kc/\Delta R(0))^{-1}$ value is related to the changes in the average apparent molecular weight of the micelles. Both the hydrodynamic size and normalized $(Kc/\Delta R(0))^{-1}$ value basically remained unchanged in the pH range from 6.4 to 8.5 (Figure 2b). However, the diameter of the micelles gradually

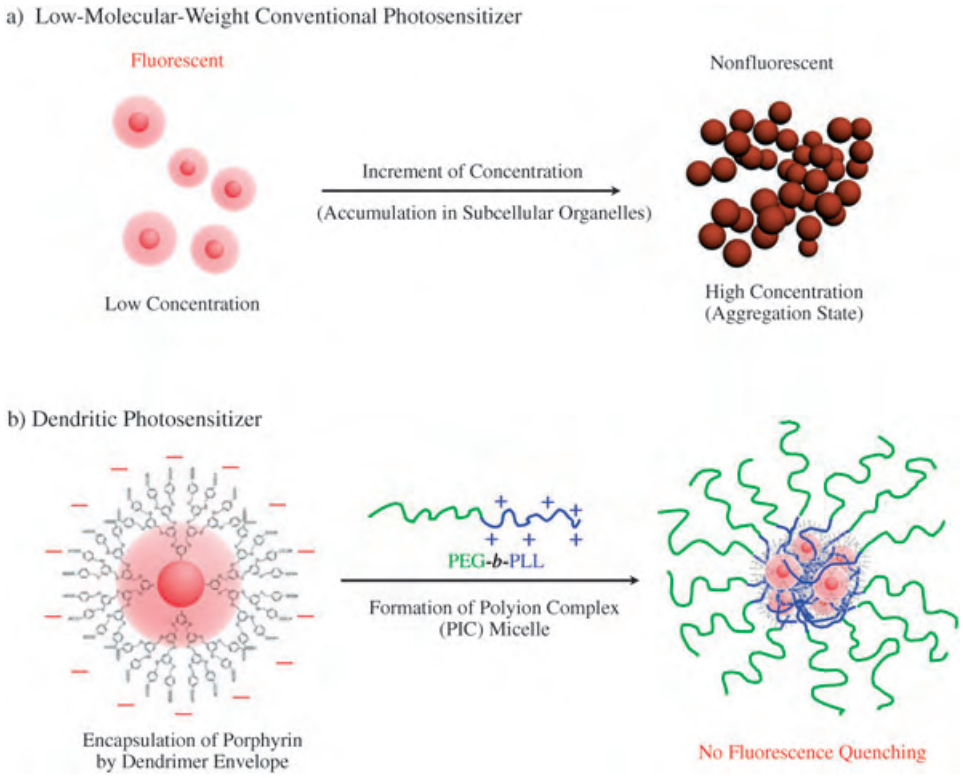


Figure 1. a) Conventional PS aggregate at a high concentration which results in quenching of PSs. b) Formation of polyion complex (PIC) micelles through electrostatic assembly of anionic dendrimer porphyrins (DPs) and PEG-*b*-PLL copolymers. The dendrimer envelope of DP can sterically prevent aggregation of the center porphyrin, thus there is no fluorescence quenching of the center porphyrin.

 © 2005 Wiley-VCH Verlag GmbH & Co. KGaA, Weinheim

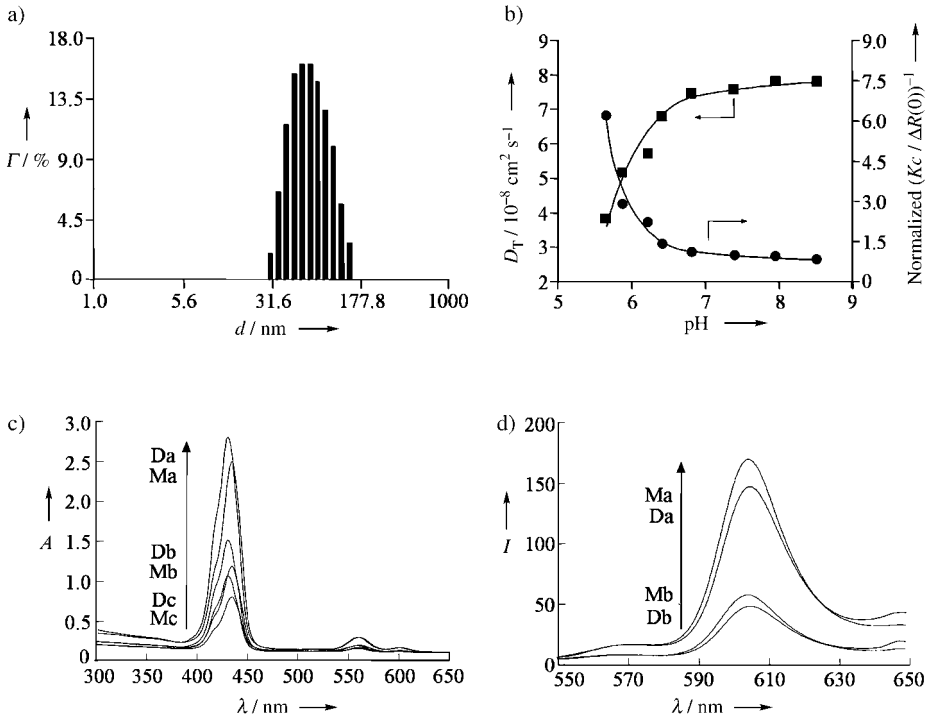


Figure 2. Physical properties of DP and DP/m. a) DLS histogram of DP/m in 150 mM NaCl at 25 °C; d = diameter. b) Dependency of the translational diffusion coefficients D_T (■) and normalized $(Kc/\Delta R(0))^{-1}$ (●) on the pH value for DP/m (1 mg mL^{-1}), measured by DLS and SLS, respectively, at 25 °C. c) Electronic absorption spectra of DP alone and DP/m in PBS (pH 7.4; a = 12 μM, b = 4 μM, c = 2 μM, D: DP, M: DP/m). d) Fluorescence emission spectra of DP alone and DP/m in PBS (pH 7.4; a = 12 μM, b = 4 μM, D: DP, M: DP/m).

increased with an increased apparent molecular weight below pH 6.4 (Figure 2b), and finally precipitated at pH 5.6, which indicates the acid-responsive feature of the micelles. Protonation of DP occurred under acidic pH conditions and resulted in the diminution of the electrostatic interaction between DP and PEG-*b*-PLL. Thus, the well-defined core–shell structure may become more diffuse and a merging of the micelles may take place. This pH-responsive behavior of the micelles allows their effective accumulation in solid tumors in response to the low pH value of the tumor tissue[8] or in an endosomal compartment in the tumor cells while achieving stable circulation in the bloodstream.

The electronic absorption and emission spectra of DP and DP/m are shown in Figure 2c and d, respectively. Unlike low-molecular-weight PSs,[9] DP clearly maintained its absorption and emission intensity in spite of the formation of micelles. The incorporation of DP into the micelles resulted in a 5-nm red-shift for the Soret band of the porphyrin core and a hypochromicity of about 5% (Figure 2c). Both of these effects are likely to be caused by the formation of an electrostatic assembly of charged porphyrins and oppositely charged compounds.[10] The shrinkage of the hydrophobic dendrimer frameworks, which arises from the relaxation of the charge repulsion of the negatively charged DP surface by the formation of an electrostatic assembly, may contribute to the hypochromicity.[11] Interestingly, although the local concentration of DP within each micelle is assumed to be extremely high, DP/m emitted a more intense fluorescence at 610 nm (Figure 2d). Unlike conventional PSs, the dendritic envelope of DP is able to prevent the porphyrin core from undergoing collisional quenching, even at an appreciably high concentration that induces self-quenching of the conventional PSs (Figure 1a).[12] Thus, encapsulation of the porphyrins by the dendritic envelope in the micellar structure is most likely to prevent fluorescence quenching (Figures 1b and 2d). Also, the high microviscosity in the micellar core could restrain the internal molecular motion of DP, which might lead to the inhibition of the nonradiative decay and is related to the increased fluorescence intensity of DP/m (Figure 2d).[13] In connection with this observation, the photoinduced oxygen consumption of DP and DP/m was measured in phosphate-buffered saline (PBS) containing 10% fetal bovine serum (FBS) as a singlet oxygen acceptor (Figure 3). Very interestingly, the result revealed that the oxygen consumption level of

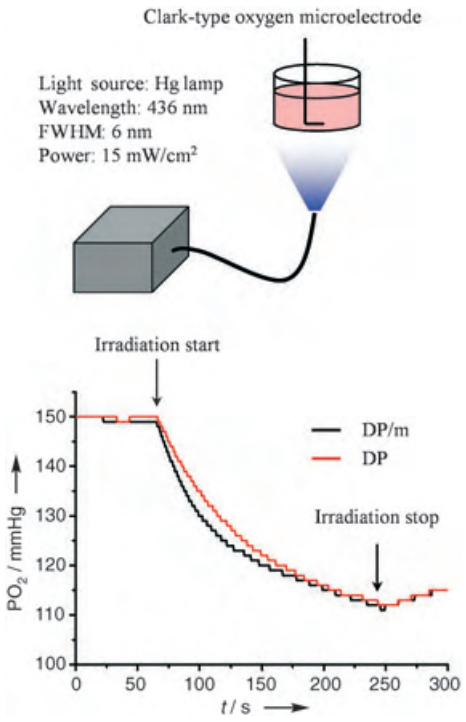


Figure 3. Experimental setup for the measurement of oxygen consumption and the results obtained. FWHM = full width of half maximum height.

 © 2005 Wiley-VCH Verlag GmbH & Co. KGaA, Weinheim

DP/m was almost identical to that of the free DP in PBS, which indicates that the singlet oxygen molecules can successfully escape the micellar structure. From the standpoint of the application to PDT, the DP ensures an effective photochemical reaction of the porphyrin core regardless of the local concentrations. It is possible that the DP/m attain an elevated concentration of local singlet oxygen, which cannot be achieved by other formulations containing conventional PSs.

However, the cellular uptake of free DP and DP/m increased with the incubation time, and DP/m showed six- to eightfold higher uptake levels than free DP (Figure 4a). In

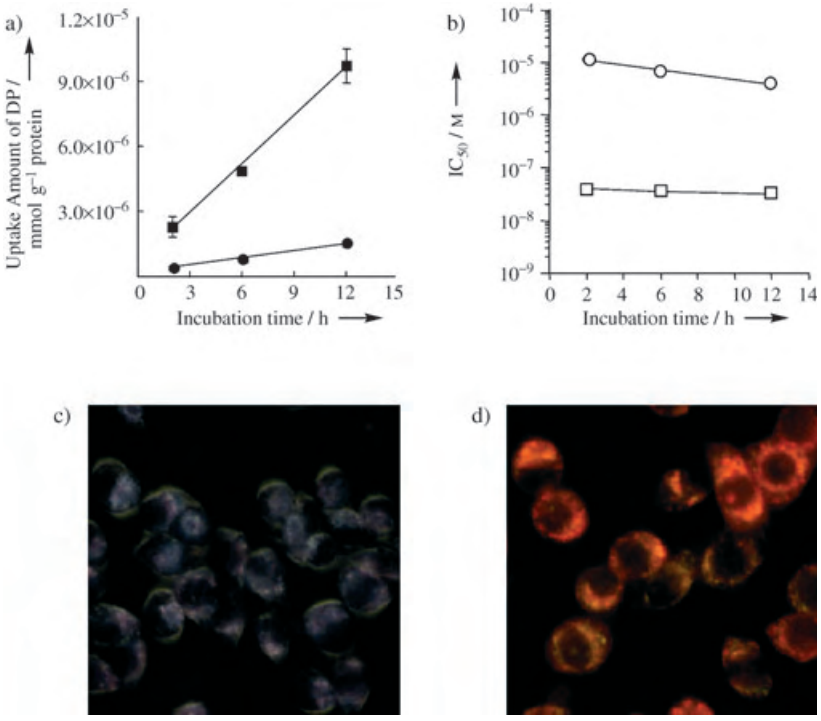


Figure 4. Results of in vitro evaluations of DP and DP/m. a) Cellular uptake level of DP (●) and DP/m (■) as a function of incubation time ($n=3$). LLC cells were incubated with dendrimers and the micelles at 12 μM of DP-equivalent concentration. b) Incubation time dependency of 50% growth inhibitory concentration (IC_{50}) of DP (○) and DP/m (□) after photoirradiation. c, d) Microscopy images of LLC cells incubated with 10 μM of DP (c) and DP/m (d) for 8 h. A Zeiss filter set (excitation: BP 395–440 nm; beam splitter: FT 460 nm; emission: LP 470 nm) was used.

view of the negatively charged surface of mammalian cells,[8] charge neutralization of DP by PEG-*b*-PLL could improve the cellular uptake of DP/m. The improved uptake of DP/m was also confirmed by microscopic observations (Figure 4c and d). No fluorescence quenching was observed for the cells incubated with DP/m, although the sensitizers are assumed to be extremely concentrated in the subcellular organelles such as the endosomes and lysosomes. This observation contrasts with the fact that the conventional mesochlorin e_6 conjugated *N*-(2-hydroxypropyl) methacrylamide (HPMA) copolymers exhibit fluorescence quenching when the cells are incubated with HPMA at an extremely high concentration.[14] The dendritic envelope of DP could prevent aggregation of the porphyrin in the subcellular loci, thus ensuring effective production of singlet oxygen for the photocytotoxicity.

Notably, the photocytotoxicity of DP/m was remarkably improved compared to that of free DP (Figure 4b). Incorporation of DP into the micelles resulted in an approximately 130–280-fold increased photocytotoxicity (Figure 4b). Such a distinctly enhanced photocytotoxicity of DP/m may not be fully explained by the six- to eightfold increase in their cellular uptake shown in Figure 4a; therefore, DP/m may have specific mechanisms to increase their photocytotoxicity. Recently, PEGylated chlorin e_6 and PEG-based polymeric micelles were reported to show an enhanced localization in several cytoplasmic organelles including the mitochondria.[15] Presumably the outer PEG layer of the DP/m and the microenvironment around DP, as mentioned above, may have a role in altering the intracellular mechanism of DP to increase the photocytotoxicity. Recently, several interesting observations concerning the intracellular mechanism have been reported. For example, Berg et al. proposed a photochemical internalization (PCI) in which the photodamage to endosomal membranes can burst the endocytic vesicles, which allows endosomal escape of macromolecules into the cytosol.[16] From this point of view, DP/m may localize in the cytoplasmic organelles susceptible to photodamage following endosomal escape of the micelles during photoirradiation. The DP/m are assumed to produce a significantly high concentration of singlet oxygen as a result of effective separation of the center porphyrin by the dendritic envelope. The mechanism for the efficient generation of singlet oxygen within the micellar structure remains to be explained. However, a dendritic structure that prevents aggregation of the center porphyrin should be essential for the enhanced photocytotoxicity of DP/m. Further investigation to address the detailed mechanisms of the enhanced photocytotoxicity of DP/m, together with dendrimer size and morphological effect, is now in progress.

In summary, the photodynamic efficacy of the DP was dramatically improved by inclusion into micelles. This process resulted in a more than two orders of magnitude increase in the photocytotoxicity compared with that of the free DP, as a result of the accumulated singlet oxygen in the intracellular compartment as well as the modulated intracellular localization related to the micellar structure. Furthermore, the DP/m system has a relevant size range (ca. 100 nm) and high stability for intravenous administration, with resultant EPR effect, and may have a high utility for in vivo PDT of cancer and macular degeneration, the study of which is now in progress.

Experimental Section

PEG-*b*-PLL was synthesized by the polymerization of the *N*-carboxy anhydride of N^{ε}-Z-L-lysine initiated by CH_3O-PEG-NH_2 (12000 g mol^{-1}) in DMF, followed by deprotection of the Z group according to a previously reported method.[17] The M_w/M_n ratio and degree of polymerization of PLL were determined to be 1.11:1 and 41 by gel-permeation chromatography and ^{1}H NMR spectroscopy,

 © 2005 Wiley-VCH Verlag GmbH & Co. KGaA, Weinheim

respectively. DP was synthesized as previously described,[6] and its purity was confirmed by a single peak in the MALDI-TOF mass spectrum (8030 g mol^{-1}). The DLS and SLS measurements of DP/m were performed using a Photal dynamic laser-scattering DLS-7000 spectrometer (Otsuka Electronics Co., Ltd., Osaka, Japan). The UV/Vis and fluorescence spectra were measured on a V-550 spectrophotometer and on an FP-777 spectrofluorometer (JASCO, Tokyo, Japan), respectively.

Lewis lung carcinoma (LLC) cells were used in the cell culture studies. In the quantitative analysis of the cellular uptake of DP, the cells incubated with free DP and DP/m were lyzed in 5% SDS solution, followed by measurement of the fluorescence intensity at 609 nm (excitation at 432 nm). In the cytotoxicity assay, the cells were photoirradiated for 10 minutes with broadband visible light using a xenon lamp (150 W) equipped with a filter passing light of 400–700 nm (fluence energy: 180 kJ cm^{-2}). The viability of the cells was evaluated by the 3-(4,5-dimethylthiazol-2-yl)-2,5-diphenyltetrazolium bromide (MTT) assay.

Oxygen consumption was measured by using a Clark-type oxygen microelectrode with a tip diameter of 200 μm (PO_2-100DW, Eikou Kagaku Co., Ltd., Tokyo, Japan). The microelectrode was inserted into the PBS, which contained 3.13 μM of DP or DP/m and 10% FBS as a singlet oxygen acceptor, so that the tip was 100 mm above the bottom of the solution. An Hg lamp (436 nm, FWHM: 6 nm, 15 mW cm^{-2}) was used for light irradiation. The solution was static and exposed to the atmosphere. Before each measurement, the system was calibrated in saline solution bubbled with air, in which the oxygen partial pressure was assumed to be 150 mm Hg.

Received: August 10, 2004

Keywords: block copolymers · dendrimers · drug delivery · micelles · porphyrinoids

[1] R. K. Pandey, G. Zhang in *Porphyrin Handbook*, *Vol. 6* (Eds.: K. M. Kadish, K. M. Smith, R. Guilard), Academic Press, **2000**, pp. 157–230.
[2] N. Nishiyama, H. R. Stapert, G. D. Zhang, D. Takasu, D. L. Jiang, T. Nagano, T. Aida, K. Kataoka, *Bioconjugate Chem.* **2003**, *14*, 58–66.
[3] a) A. W. Bosman, H. M. Jassen, E. W. Meijer, *Chem. Rev.* **1999**, *99*, 1665–1688; b) S. Hecht, J. M. J. Frechet, *Angew. Chem.* **2001**, *113*, 76–94; *Angew. Chem. Int. Ed.* **2001**, *40*, 74–91; c) M. Fischer, F. Vogtle, *Angew. Chem.* **1999**, *111*, 934–955; *Angew. Chem. Int. Ed.* **1999**, *38*, 884–905; d) H. R. Ihre, L. Gagne, J. M. J. Frechet, F. C. Szoka, Jr., *Bioconjugate Chem.* **2002**, *13*, 453–461; e) J. F. Kukowska-Latallo, A. U. Bielinska, J. Johnson, R. Spindler, D. A. Tomalia, J. R. Baker, *Proc. Natl. Acad. Sci. USA* **1996**, *93*, 4897–4902.
[4] a) Y. N. Konan, R. Gurny, E. Allemann, *J. Photochem. Photobiol. B* **2002**, *66*, 89–106; b) Y. Matsumura, H. Maeda, *Cancer Res.* **1986**, *46*, 6387–6392; c) M. Yokoyama, T. Okano, Y. Sakurai, S. Fukushima, K. Okamoto, K. Kataoka, *J. Drug Targeting* **1999**, *7*, 171–186.
[5] Y. Kakizawa, K. Kataoka, *Adv. Drug Delivery Rev.* **2002**, *54*, 203–222, and references therein.
[6] a) N. Tomioka, D. Takasu, T. Takahashi, T. Aida, *Angew. Chem.* **1998**, *110*, 1611–1614; *Angew. Chem. Int. Ed.* **1998**, *37*, 1531–1534; b) T. Aida, D.-L. Jiang in *The Porphyrin Handbook*, *Vol. 3* (Eds: K. M. Kadish, K. M. Smith, R. Guilard), Academic Press, **2003**, pp. 369–384.
[7] H. R. Stapert, N. Nishiyama, D. L. Jiang, T. Aida, K. Kataoka, *Langmuir* **2000**, *16*, 8182–8188.
[8] a) E. J. Ambros, D. M. Easty, P. C. T. Jones, *Br. J. Cancer* **1958**, *12*, 439–447; b) S. E. Kornguth, T. Kalinke, H. I. Robins, J. D. Cohen, P. Turski, *Cancer Res.* **1989**, *49*, 6390–6395.
[9] S. A. Gerhardt, J. W. Lewis, D. S. Kliger, J. Z. Zhang, U. Simonis, *J. Phys. Chem. A* **2003**, *107*, 2763–2767.
[10] a) N. C. Maiti, S. Mazumdar, N. Periasamy, *J. Phys. Chem. B* **1998**, *102*, 1528–1538; b) K. M. Kadish, G. B. Maiya, C. Araullo, R. Guilard, *Inorg. Chem.* **1989**, *28*, 2725–2731.
[11] R. Sadamoto, N. Tomioka, T. Aida, *J. Am. Chem. Soc.* **1996**, *118*, 3978–3979.
[12] T. Sato, D.-L. Jiang, T. Aida, *J. Am. Chem. Soc.* **1999**, *121*, 10658–10659.
[13] S. Basu, *J. Photochem. Photobiol. A: Chem.* **1991**, *56*, 339–347.
[14] N. Nishiyama, A. Nori, A. Malugin, Y. Kasuya, P. Kopeckova, J. Kopecek, *Cancer Res.* **2003**, *63*, 7876–7882.
[15] a) M. R. Hamblin, J. L. Miller, T. Hasan, *Cancer Res.* **2001**, *61*, 7155–7162; b) R. Savic, L. Luo, A. Eisenberg, D. Maysinger, *Science* **2003**, *300*, 615–618.
[16] a) K. Berg, P. K. Selbo, L. Prasmickaite, T. E. Tjelle, K. Sandvig, J. Moan, G. Gaudernack, O. Fodstad, S. Kjolsrud, H. Anholt, G. H. Rodal, S. K. Rodal, A. Hogest, *Cancer Res.* **1999**, *59*, 1180–1183; b) L. Prasmickaite, A. Høgset, P. K. Selbo, B. Ø. Engesæter, M. Hellum, K. Berg, *Br. J. Cancer* **2002**, *86*, 652–657.
[17] A. Harada, K. Kataoka, *Macromolecules* **1995**, *28*, 5294–5299.

 © 2005 Wiley-VCH Verlag GmbH & Co. KGaA, Weinheim

NMR Spectroscopic Methods (1)

Stretched Poly(vinyl acetate) Gels as NMR Alignment Media for the Measurement of Residual Dipolar Couplings in Polar Organic Solvents**

*J. Christoph Freudenberger, Sebastian Knör, Kyryl Kobzar, Dominik Heckmann, Thomas Paululat, Horst Kessler, and Burkhard Luy**

Residual dipolar couplings (RDCs) have revolutionized the NMR-based structure determination of large biomolecules[1–4] and lately demonstrated their potential in the field of small molecules.[5–12] The measurement of RDCs relies on the partial orientation of the molecule of interest, for which a so-called alignment medium is necessary. In aqueous solution a variety of alignment media are known, for example,

[*] Dr. J. C. Freudenberger, Dipl.-Chem. S. Knör, Dipl.-Chem. K. Kobzar, Dipl.-Chem. D. Heckmann, Prof. Dr. H. Kessler, Dr. B. Luy
Department Chemie, Lehrstuhl II für Organische Chemie
Technische Universität München
Lichtenbergstrasse 4, 85 747 Garching (Germany)
Fax: (+49) 89-289-13210
E-mail: horst.kessler@ch.tum.de
Burkhard.Luy@ch.tum.de

Dr. T. Paululat
Biofrontera Discovery GmbH
Waldhoferstrasse 104, 69123 Heidelberg (Germany)
Fax: (+49) 6221-820450

[**] B.L. and H.K. thank the Fond der Chemischen Industrie and the Deutsche Forschungsgemeinschaft (Emmy Noether fellowship LU 835/1-2; Ke 147/37-2) for financial support.

Supporting information for this article is available on the WWW under http://www.angewandte.org or from the author.

 DOI: 10.1002/anie.200461241 © 2005 Wiley-VCH Verlag GmbH & Co. KGaA, Weinheim

bicelles,[13] filamentous phage,[14] liquid-crystalline phases,[15] or stretched polyacrylamide-based gels.[16,17] For relatively apolar organic solvents, liquid crystals such as poly-γ-benzyl-L-glutamate (PBLG)[5–7,18] or deuterated 4-*n*-pentyl-4′-cyanobiphenyl (PCBP)[19] as well as stretched polystyrene (PS)[11] and polydimethylsiloxane (PDMS)[12] gels are used to obtain structural information from RDCs. For polar organic solvents such as methanol or DMSO, however, no alignment medium is available yet. Herein we propose the use of stretched poly(vinyl acetate) (PVAC) gels for partial orientation of molecules dissolved in polar organic solvents.

Crosslinked PVAC-polymer sticks were produced in a similar way to that described previously for PS.[11] Glass tubes with inner diameters of 2.4 mm, 3.4 mm, and 4.0 mm were sealed by melting one end and dried carefully. They were then treated with a 1:1 mixture of chlorotrimethylsilane and dichloromethylsilane for 18 h to ensure hydrophobic glass surfaces. After being washed with dichloromethane, the tubes were dried at 50 °C. Vinyl acetate (Fluka) and adipic acid divinyl ester (ABCR) were filtered with basic aluminum oxide (pH 10) and distilled under reduced pressure. The monomers then were degassed for 15 min under vacuum in an ultrasonic bath and ventilated with argon. Immediately afterwards, vinyl acetate, adipic acid divinyl ester, and azoisobutyronitrile were mixed in the desired concentrations and transferred to the glass tubes. The open end was sealed by melting, and polymerization was carried out for 5 days at 45 °C and for another 2 days at 60 °C.

As a first test, we put crosslinked PVAC sticks in various organic solvents and watched the swelling behavior. The sticks exhibited swelling in essentially all tested solvents, such as chloroform, THF, dioxane, benzene, ethyl acetate, acetone, acetonitrile, methanol, and dimethyl sulfoxide (DMSO). We repeated the swelling inside NMR tubes and added $CDCl_3$ (5% *v*/*v*) to the non-deuterated solvents to allow the monitoring of any induced anisotropy by the deuterium quadrupolar splitting ν_Q. In all cases, significant splittings with relatively sharp lines could be observed (Table 1) after allowing the gels to equilibrate for 13 days. Furthermore, we recorded the dependence of the quadrupolar splitting on the amount of crosslinker used for polymerization for four solvents (DMSO, MeOH, THF, and dioxane; Figure 1). The resulting curves are similar to that observed for PS gels,[11] corroborating the general trend that higher crosslinking concentrations lead to stronger induced anisotropies.[12]

In a next step we tested the alignment properties of norcamphor in PVAC gels swollen in the four deuterated solvents available in our laboratory. Norcamphor (Table 2) was chosen

Table 1: Quadrupolar deuterium splittings [Hz] of $CDCl_3$ (5% *v*/*v*) added to PVAC sticks (0.1% *v*/*v*) cross linker, 3.4 mm and 4.0 mm inner diameter) swollen in various non-deuterated solvents.

	MeCN	Acetone	EtOAc	Benzene	$CDCl_3$
3.4 mm	36.6	33.8	49.4	83.1	72.8
4.0 mm	47.5	54.7	67.7	–[a]	106.1
	DMSO	MeOH	THF	Dioxane	
4.0 mm	10.0	35.2	54.6	39.5	

[a] Gel disrupted during swelling.

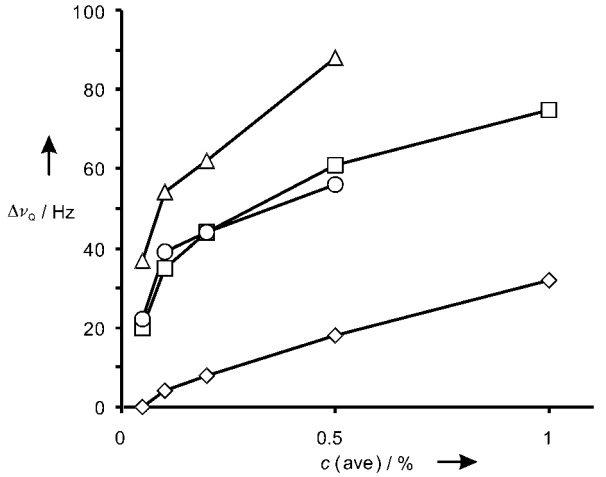
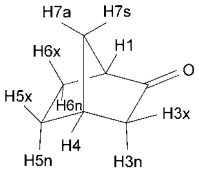


Figure 1. Dependence of the quadrupolar deuterium splitting ν_Q of $CDCl_3$ on the amount of crosslinker adipic acid divinyl ester (AVE). To obtain the splittings, $CDCl_3$ (5% *v*/*v*) was added to the PVAC sticks swollen in the otherwise non-deuterated solvents (◇: DMSO, □: MeOH, △: THF, ○: dioxane).

Table 2: RDCs and alignment-tensor parameters of norcamphor[a] dissolved in PVAC gels that are swollen in different deuterated solvents.



	[D$_6$]DMSO	CD_3OD	CD_3CN	$CDCl_3$
$\Delta\nu Q(CDCl_3)$	18.5 Hz[b]	70.4 Hz[b]	85.2 Hz[c]	21.7 Hz[d]
RDCs				
C_1–H_1	−2.37	−0.86	1.24	0.31
C_3–$H_{3,exo}$	−3.61	−12.61	−1.04	−0.44
C_3–$H_{3,endo}$	−15.51	−7.24	−8.51	−2.07
C_4–H_4	10.31	18.22	6.21	1.29
C_7–$H_{7,anti}$	15.71	−7.79	0.61	−3.70
C_7–$H_{7,syn}$	−10.83	8.22	−6.18	−3.97
A_{xx}	-1.6180×10^{-4}	4.1254×10^{-5}	-3.1161×10^{-5}	-8.9383×10^{-6}
A_{yy}	-3.6670×10^{-4}	9.2611×10^{-4}	-2.1580×10^{-4}	$-7.5429\times^{-5}$
A_{zz}	5.2850×10^{-4}	-9.6736×10^{-4}	$2.4696\times^{-4}$	$8.4368\times^{-5}$
D_a	2.6425×10^{-4}	-4.8368×10^{-4}	1.2348×10^{-4}	4.2184×10^{-5}
D_r	6.8302×10^{-5}	-2.9495×10^{-4}	6.1546×10^{-5}	2.2164×10^{-5}
R^2	0.992	0.990	1.000	0.854

[a] Norcamphor: ≈130 mg/sample. [b] PVAC: 0.5% crosslinker, stick diameter: 4.0 mm. [c] PVAC: 0.2% crosslinker, stick diameter: 4.0 mm. [d] PVAC: 0.1% crosslinker, stick diameter: 2.4 mm.

 © 2005 Wiley-VCH Verlag GmbH & Co. KGaA, Weinheim

as a sample for two reasons: it is highly soluble in almost every organic solvent and its protons all point in different directions. In [D_6]DMSO, CD_3OD, CD_3CN, and $CDCl_3$ we were able to measure at least six D_{CH} RDCs and derive the alignment tensors by using the program PALES with the *bestFit* option[20] (Table 2). Interestingly, the four alignment tensors differ significantly: D_a/D_r ratios differ for the four solvents and the axial component for methanol even has the opposite sign compared to the others. We can only speculate about this different behavior, but most probably specific interactions of the solvents with the polymer and/or the solute lead to this phenomenon. However, the most important result for the use of stretched PVAC gels as alignment media is that RDCs in the desired range of ± 20 Hz can be measured in all cases.

RDCs should be especially important for the structure determination of natural products. We therefore applied the method also to the well-characterized antibiotic sphaeropsidin A as a more realistic test sample.[21–23] After diffusion of ≈ 6 mg of sphaeropsidin A into an already swollen PVAC/DMSO gel with a quadrupolar $CDCl_3$ splitting of 10.1 Hz, two coupled HSQC spectra, optimized for aliphatic and olefinic nuclei, were acquired on a Bruker DMX900 spectrometer (Figure 2). Compared to sphaeropsidin A cross peaks, relatively strong PVAC and DMSO signals are present in both spectra, but D_{CH} RDCs can still be measured in most cases since sphaeropsidin A and PVAC signals do not overlap. Only the methylene protons attached to C_{11} show significant overlap and second-order effects so that a reliable RDC measurement was not possible. All couplings were carefully measured by extracting slices out of the 2D spectra and applying the phase correction approach described in detail elsewhere.[9] As a starting point we looked at the eight C–H vectors containing the atoms C1, C2, C3, C5, and C14. The diastereotopic protons of the methylene groups of C2 and C3 were easily derived by using the simple method to distinguish between axial and equatorial C–H vectors.[9] The initial alignment tensor calculated from six unambiguous D_{CH} couplings (also including C–H vectors from C5 and C14) then allowed the prochiral assignment of the methylene groups containing C1 and C12 (for methodology used, see references [6,7]). This is remarkable, because in both cases the difference in distance of axial/equatorial or *syn*/*anti* protons, respectively, to unambiguously identified neighboring protons such as 5-H or the methyl group containing C17 is only ≈ 0.1 Å, too small to be identified reliably by NOE studies. By deriving D_{CC} RDCs from the measured D_{CH} couplings with the formula given in reference [7], finally also the methyl groups at C4 could be assigned. RDCs of spin pairs containing C15, C16, and C17 could not be fitted to any reasonable structural model. This most probably is indicative for intrinsic dynamics that lead to averaged RDCs at this part of the molecule. Taking into account the significant changes in chemical shifts of C14–C16, and 14-H–16-H, it might even be concluded that the gel introduces a difference in population of the exchanging conformations in this region. However, this effect is not yet understood. The 12 remaining assigned RDCs were used to refine the alignment tensor that is shown together with the correspondence of experimentally determined and back-calculated RDCs in Figure 3b–d. The correlation factor R^2 of 0.966 in this case is a clear indication that the structural model is consistent with the experimental data, which also can be seen easily in Figure 3e.

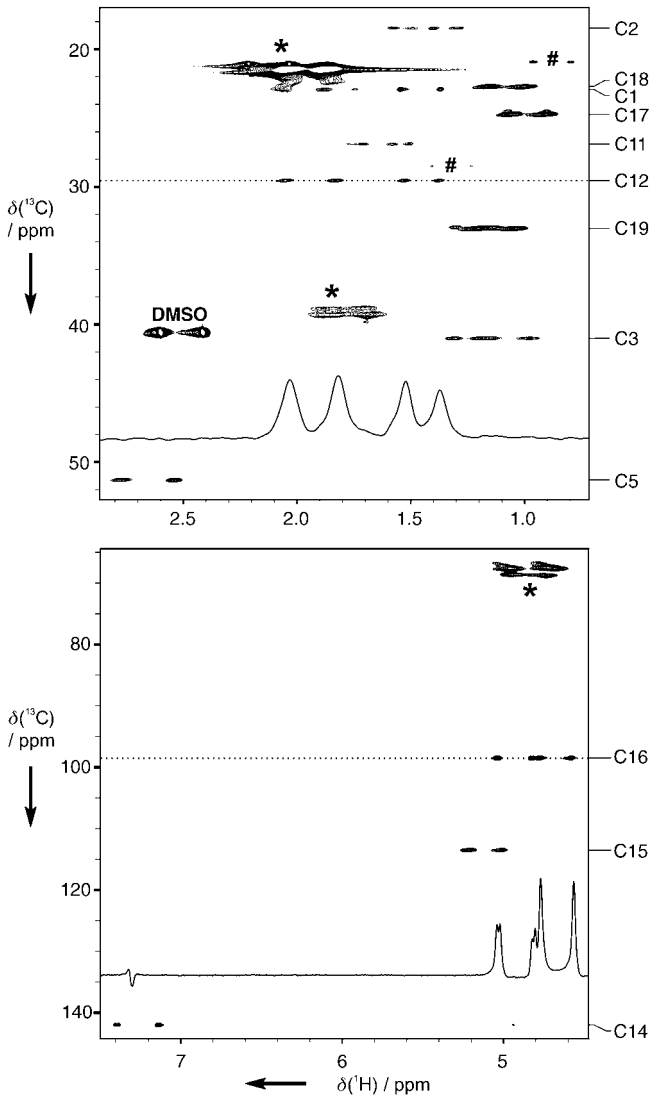


Figure 2. Aliphatic (top) and olefinic (bottom) coupled $^{13}C,^{1}H$-HSQC spectra acquired on ≈ 6 mg of sphaeropsidin A dissolved in a PVAC/DMSO gel. DMSO signals (DMSO), PVAC signals (*), and signals originating from unpolymerized monomers (#) are indicated in the spectra. Slices at the dotted lines are shown to give an impression on the overall quality of the cross peaks.

In summary, stretched PVAC gels can be used as scalable alignment media for polar organic solvents. With this possibility the gap between relatively apolar solvents such as dichloromethane or chloroform and aqueous solutions is closed and RDCs can now be measured in practically all common NMR solvents. The applicability of the new alignment method was demonstrated on norcamphor and the antibiotic sphaeropsidin A. Although PVAC signals did not pose a serious problem in heteronuclear correlation experiments, more sophisticated NMR spectroscopy methods such

 © 2005 Wiley-VCH Verlag GmbH & Co. KGaA, Weinheim

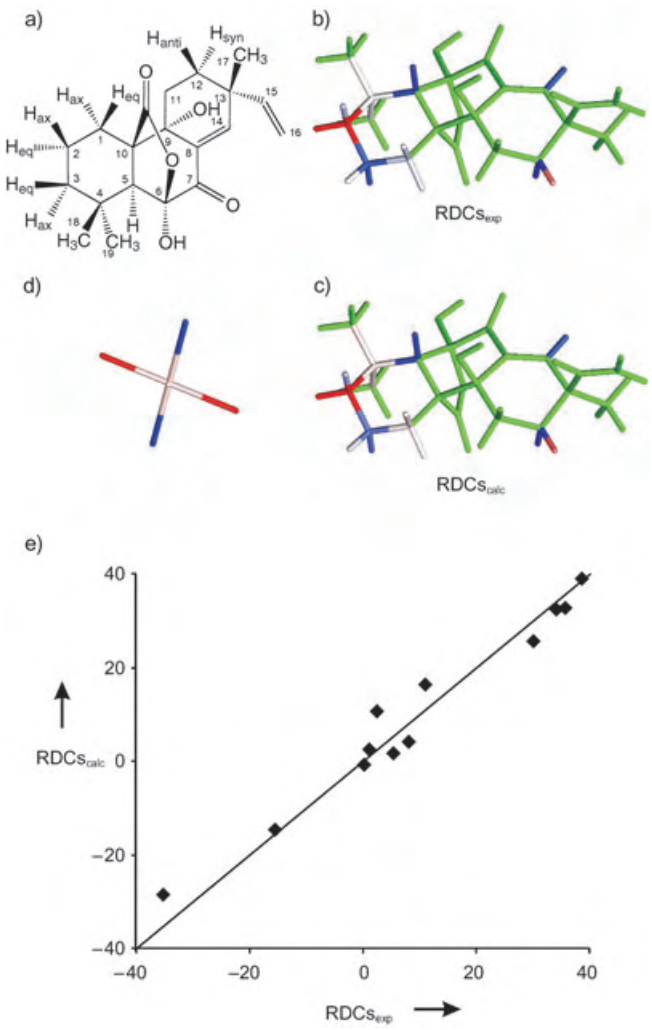


Figure 3. Correspondence between experimental and back-calculated RDCs of sphaeropsidin A dissolved in a PVAC/DMSO gel. a) Structure and numbering of sphaeropsidin A. b) and c) color representation of the experimental and back-calculated RDCs, respectively, onto sphaeropsidin A. Red corresponds to negative, blue to positive, white to intermediate, and green to no RDCs measured. d) Representation of the alignment tensor in the coordinate frame of sphaeropsidin A as shown in b, c) with red being negative and blue positive tensor axes. e) The plot of experimental versus back-calculated RDCs shows a good correlation.

as relaxation filters should be included in experiments to obtain spectra of higher quality.[24]

Received: July 8, 2004
Revised: August 9, 2004

Keywords: gels · NMR spectroscopy · partial alignment · residual dipolar coupling

[1] C. R. Sanders, B. J. Hare, K. P. Howard, J. H. Prestegard, *Prog. Nucl. Magn. Reson. Spectrosc.* **1994**, *30*, 421 – 444.
[2] J. R. Tolman, J. M. Flanagan, M. A. Kennedy, J. H. Prestegard, *Proc. Natl. Acad. Sci. USA* **1995**, *92*, 9279 – 9283.
[3] N. Tjandra, A. Bax, *Science* **1997**, *278*, 1111 – 1114.
[4] B. Simon, M. Sattler, *Angew. Chem.* **2002**, *114*, 453 – 456; *Angew. Chem. Int. Ed.* **2002**, *41*, 437 – 440.
[5] C. Aroulanda, V. Boucard, F. Guibé, J. Courtieu, D. Merlet, *Chem. Eur. J.* **2003**, *9*, 4536.
[6] C. M. Thiele, S. Berger, *Org. Lett.* **2003**, *5*, 705 – 708.
[7] L. Verdier, P. Sakhaii, M. Zweckstetter, C. Griesinger, *J. Magn. Reson.* **2003**, *163*, 353 – 359.
[8] A. Mangoni, V. Esposito, A. Randazzo, *Chem. Commun.* **2003**, 154 – 155.
[9] J. L. Yan, A. D. Kline, H. P. Mo, M. J. Shapiro, E. R. Zartler, *J. Org. Chem.* **2003**, *68*, 1786 – 1795.
[10] J. L. Yan, F. Delaglio, A. Kaerner, A. D. Kline, H. P. Mo, M. J. Shapiro, T. A. Smitka, G. A. Stephenson, E. R. Zartler, *J. Am. Chem. Soc.* **2004**, *126*, 5008 – 5017.
[11] B. Luy, K. Kobzar, H. Kessler, *Angew. Chem.* **2004**, *116*, 1112 – 1115; *Angew. Chem. Int. Ed.* **2004**, *43*, 1092 – 1094.
[12] J. C. Freudenberger, P. Spitteler, R. Bauer, H. Kessler, B. Luy, *J. Am. Chem. Soc.*, in press.
[13] J. H. Prestegard, *Nat. Struct. Biol.* **1998**, *5*, 517 – 522.
[14] M. R. Hansen, L. Mueller, A. Pardi, *Nat. Struct. Biol.* **1998**, *5*, 1065 – 1074.
[15] M. Rückert, G. Otting, *J. Am. Chem. Soc.* **2000**, *122*, 7793 – 7797.
[16] R. Tycko, F. J. Blanco, Y. Ishii, *J. Am. Chem. Soc.* **2000**, *122*, 9340 – 9341.
[17] H. J. Sass, G. Musco, S. J. Stahl, P. T. Wingfield, S. Grzesiek, *J. Biomol. NMR* **2000**, *18*, 303 – 309.
[18] A. Meddour, I. Canet, A. Loewenstein, J. M. Pechine, J. Courtieu, *J. Am. Chem. Soc.* **1994**, *116*, 9652 – 9956.
[19] B. Bendiak, *J. Am. Chem. Soc.* **2002**, *124*, 14862 – 14863.
[20] M. Zweckstetter, A. Bax, *J. Am. Chem. Soc.* **2000**, *122*, 3791 – 3792.
[21] G. A. Ellestad, M. P. Kunstmann, P. Mirando, G. O. Morton, *J. Am. Chem. Soc.* **1972**, *94*, 6206 – 6208.
[22] A. Evidente, L. Sparapano, A. Motta, F. Giordano, O. Fierro, S. Frisullo, *Phytochemistry* **1996**, *42*, 1541 – 1546.
[23] A. Evidente, L. Sparapano, O. Fierro, G. Bruno, F. Giordano, A. Motta, *Phytochemistry* **1998**, *48*, 1139 – 1143.
[24] For related work carried out simultaneously, but independently, see following Communication in this issue: P. Haberz, J. Farjon, C. Griesinger, *Angew. Chem.* **2005**, *117*, 431–433; *Angew. Chem. Int. Ed.* **2005**, *44*, 427–429.

 © 2005 Wiley-VCH Verlag GmbH & Co. KGaA, Weinheim

NMR Spectroscopic Methods (2)

A DMSO-Compatible Orienting Medium: Towards the Investigation of the Stereochemistry of Natural Products**

*Peter Haberz, Jonathan Farjon, and Christian Griesinger**

The elucidation of the relative stereochemistry of asymmetric centers of organic molecules is an important challenge in chemistry since it requires the simultaneous determination of conformation and configuration. Whereas conventional NMR spectroscopy parameters such as NOE and ^3J coupling constants, which provide internuclear distances and dihedral angles, yield the configuration of stereocenters in rigid compounds, this approach is difficult or impossible in cases in which the molecule is flexible or the stereocenters are remote in the bonding network. Residual dipolar couplings (RDCs) provide additional structural restraints, as has been abundantly shown in structural biology,[1] and might enhance the power of NMR spectroscopy in the determination of the conformation and configuration of small organic molecules at the same time. They rely on the weak alignment of molecules in solution and provide angular as well as distance information that are not contained in the NOE or J coupling values. RDCs have proven to be very efficient in the stereochemical assignment of moieties and hold promise as parameters for the determination of the stereochemistry, even in nonrigid molecules.[2]

Although a large variety of alignment media exist for aqueous solutions, such as filamentous phages,[3] phospholipid bicelles,[4] Otting phase,[5] and gels,[6] only few are currently available for organic molecules that cannot be dissolved in water. So far, only chiral liquid-crystalline media such as poly-γ-benzyl-L-glutamate (PBLG) or poly-γ-ethyl-L-glutamate (PELG),[2] which are compatible with $CHCl_3$, CH_2Cl_2, *N*,*N*-dimethylformamide (DMF), THF, and 1,4-dioxane and cross-linked polystyrene (PS),[7] which is compatible with $CHCl_3$ and THF, have been used. These media are limited to the mentioned solvents. Furthermore, PBLG aligns more-complex organic molecules so strongly that the resolution and sensitivity of ^{1}H spectra are dramatically lowered by line broadening. The PS orients weakly enough; however, it is incompatible with polar organic solvents. Therefore, additional alignment media are required.

Herein we introduce a copolymeric crosslinked polyacrylamide (PH gel), the first alignment medium compatible with dimethyl sulfoxide (DMSO), which has excellent solvent properties and is widely used in organic chemistry. The amount of alignment is much lower than that of PBLG, as can already be appreciated from the narrow ^{1}H-resonance lines observed for (+)-menthol in DMSO in PH-gel (Figure 1). Moreover, our results show that PH-gel is also compatible with DMF and D_2O.

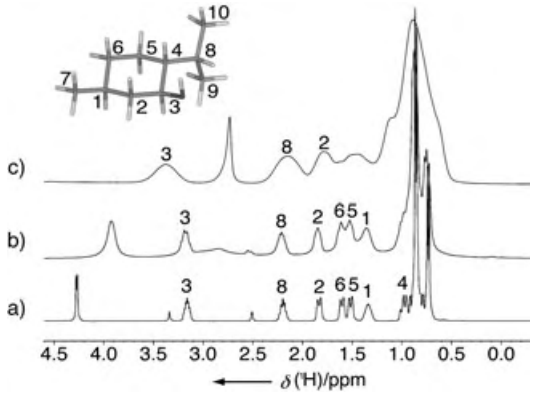


Figure 1. ^{1}H NMR spectra (400 MHz, 298 K) of (+)-menthol in a) DMSO, b) PH gel/DMSO, and c) PBLG/$CDCl_3$.

The PH gel can easily be obtained by the copolymerization of 2-(acrylamido)-2-methylpropanesulfonic acid (AMPS; ionizable monomer) with *N*,*N*-dimethylacrylamide (DMAA; comonomer) in the presence of *N*,*N*′-methylenebisacrylamide (BIS) as linker and ammonium persulphate (APS) as radical initiator.[8] The washed PH gel is dried on a glass capillary. It is then introduced into a 5-mm NMR tube, and the desired solvent is added (Figure 2). Within 1–2 days, the gel reswells and is compressed owing to the constraints of the glass wall.[7] The capillary allows the gel to be centered between the bottom of the tube and the surface of the solvent level within the NMR tube, which facilitates the reswelling of the gel. In contrast to the observations of Grzesiek et al.[6b] no significant stretching on the capillary could be determined. After 5 days, the deuterium spectra of the solvent show a quadrupolar splitting up to 4 Hz, indicating the alignment in the sample. The gel concentration of the NMR samples mentioned below needs to be adopted to obtain the described alignment.

The versatility of the PH gel is demonstrated on four different molecule/solvent-systems: (+)-menthol in DMSO and in DMF, the cyclic depsiheptapeptide hormaomycin[9] in DMSO, and a decasaccharide[10] in water (chemical formulas are shown in the Supporting Information). To measure the RDCs, t_2-coupled ^{1}H,^{13}C-HSQC[11] spectra were recorded in the presence (anisotropic solution) and in the absence (isotropic solution) of the orienting PH gel. The scalar $^1J_{CH}$

[*] Mag. P. Haberz, Dr. J. Farjon, Prof. Dr. C. Griesinger
Max Planck Institut for Biophysical Chemistry
Abt. 030: NMR-Based Structural Biology
Am Fassberg 11, 37077 Göttingen (Germany)
Fax: (+49) 551-201-2202
E-mail: cigr@nmr.mpibpc.mpg.de

[**] This work was supported by the DFG (SFB 472-Z-project), the Max Planck Gesellschaft, and the Fonds der Chemischen Industrie. J.F. is supported by a grant from the DAAD. We are grateful to Markus Radzom and Axel Zeeck for providing the hormaomycin, to Uwe Reinscheid for help with the hormaomycin spectra, to Hui Geng and Heike Neubauer for the preparation of the decasaccharide, to Christophe Farès and Jochen Junker for useful editorial advice, as well as to Markus Zweckstetter for very helpful discussions concerning the program PALES.

Supporting information for this article is available on the WWW under http://www.angewandte.org or from the author.

 DOI: 10.1002/anie.200461267 © 2005 Wiley-VCH Verlag GmbH & Co. KGaA, Weinheim

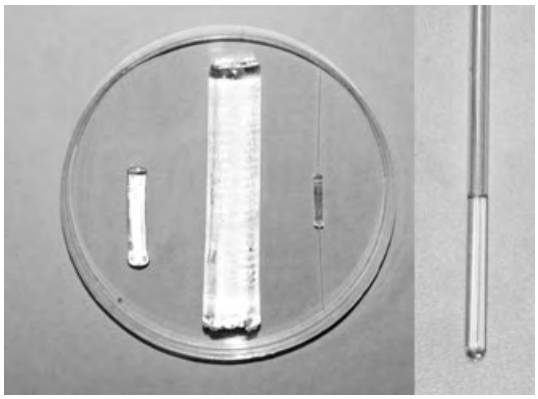


Figure 2. Photograph of the PH gel in the different states during preparation. From left to right : PH gel after polymerization, after washing in water, dried on a glass capillary, reswollen in the NMR tube with the desired solvent.

and total couplings $^1J_{CH}+{}^1D_{CH}$ can then be measured individually after extraction of the HSQC traces in the F2 dimension for all ^{13}C-bound protons of the studied molecule. The difference between the two coupling constants then results in the RDCs $^1D_{CH}$.[12] However, this method proved unreliable in cases in which the size of the RDC is small. To improve the precision of the RDCs, the corresponding traces from the isotropic and anisotropic HSQC spectra were superimposed and then fitted, based on the peak shapes (Figure 3). For the more difficult cases in which the spectral pattern of the isotropic and anisotropic traces were different, an exponential apodization function was applied to the spectra obtained from isotropic solution before the superimposition. This method determines the dipolar couplings directly and results in a significantly improved accuracy. The direct comparison of the upfield components of the anisotropic and isotropic spectra and similarly for the downfield components of the anisotropic and isotropic spectra as opposed to the extraction of the J value from the isotropic and the $J+D$ value from the anisotropic spectra is a small change in the extraction procedure, but is essential and beneficial owing to the strong coupling effects.

As a first test molecule, (+)-menthol was dissolved in [D$_6$]DMSO and the solution was introduced with a polyacrylamide gel stick (PH gel concentration 8 % *w*/*v*) into an NMR tube. The resulting quadrupolar splitting on the deuterium spectrum of the solvent was 4 Hz. The sign of the $^1J_{CH}$ couplings is always positive.[13] In weakly orienting media, $^1D_{CH}$ couplings are generally smaller than $^1J_{CH}$ couplings, and therefore the total coupling $^1J_{CH}+{}^1D_{CH}$ has a positive sign. All dipolar couplings are in the range 1.8–4.8 Hz. The single-value-decomposition module (SVD)[14] of the program PALES[15] was used to fit ten experimental dipolar couplings (excluding the $^1D_{CH}$ couplings of the isopropyl group because of its flexibility) to a reference structure. As there is no available crystal structure for (+)-menthol, we used the modified crystal structure of (−)-menthol, for which the chirality was inverted and the proton positions were optimized by conjugate-gradient energy minimization. The correlation factor R is 0.97. A similar fit ($R=0.96$) was obtained

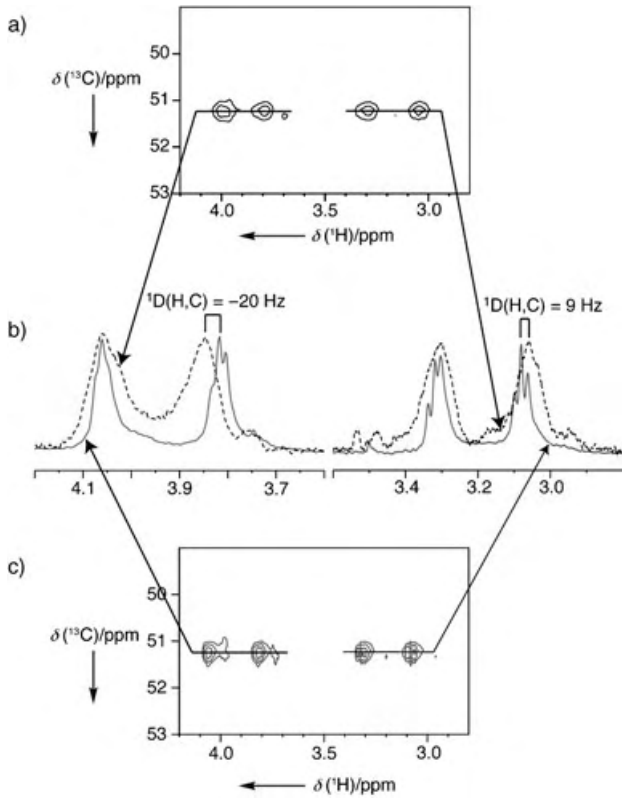


Figure 3. ^{1}H,^{13}C-HSQC spectra (t_2-coupled) of a sample of hormaomycin in DMSO (50 mM) recorded on a 600-MHz spectrometer equipped with a TXI cryoprobe at 298 K. a) Section of the anisotropic HSQC spectrum, b) superimposed traces through the anisotropic HSQC section (dotted line) and the isotropic HSQC section (solid line), c) section of the isotropic HSQC spectrum.

with a (+)-menthol/PH gel sample (PH gel concentration 12 % *w*/*v*) in DMF (see Supporting Information). The range of the dipolar couplings for this sample is 0.6–2.6 Hz. Menthol is a rather spherical molecule and it therefore orients more weakly than nonspherical molecules of similar size.

Finally, the following two experiments demonstrate the versatility of the PH gel. First, the cyclic depsiheptapeptide hormaomycin, which has a molecular weight of 1130 g mol^{-1}, was oriented in a PH gel/DMSO alignment medium resulting in a quadrupolar deuterium splitting for [D$_6$]DMSO of 2 Hz. Sections of the isotropic and anisotropic HSQC spectra show RDCs that range from −20 to 29 Hz, a range in which they can be evaluated easily and accurately. Experimental traces for two geminal methylene protons of the 4-[(*Z*)-propenyl]-proline residue are depicted in Figure 3. In the second application, we investigated a decasaccharide with a molecular weight of 1804 g mol^{-1}. It was dissolved in D$_2$O and aligned with the PH gel, causing a quadrupolar deuterium splitting for D$_2$O of 3 Hz. The measured $^1D_{CH}$ ranged from −22 to 28 Hz. The amount of alignment is scalable (see Experimental Section).

In summary, we have shown that a reliable alignment can be obtained by using PH gel with DMSO and other solvents for complex organic molecules of various sizes. The magnitude of the dipolar couplings is in a range in which they can be

 © 2005 Wiley-VCH Verlag GmbH & Co. KGaA, Weinheim

evaluated accurately since they are large enough to be measured with an acceptable spectral resolution since $^1H,^1H$ dipolar couplings do not cause extensive line broadening. Further research is underway in which this gel is being used to solve stereochemical problems in organic molecules that can neither be crystallized nor dissolved in water or chloroform.[16]

Experimental Section

PH-gel: AMPS, DMAA, and BIS (1:1:0.026) were dissolved in purified water to a total monomer concentration of 0.75 mol L^{-1}. The pre-gel solution was inserted into a gel cylinder with an inner diameter of 5.4 mm and polymerized for 2 h at 70 °C initiated by ammonium persulphate ($\approx$0.0015 g mL^{-1}). The gels were washed once with NaOH solution (0.02 M) and at least four times with water, each time for several hours. The swollen gels were dried on a glass capillary (diameter ~0.3–0.4 mm) under vacuum at 25–30 °C. The alignment is scalable by varying the diameter of the gel cylinder.

Received: July 11, 2004

Keywords: gels · NMR spectroscopy · partial alignment · residual dipolar coupling

[1] E. de Alba, N. Tjandra, *Prog. Nucl. Magn. Reson. Spectrosc.* **2002**, *40*, 175–197.
[2] a) C. Aroulanda, V. Boucard, F. Guibé, J. Courtieu, D. Merlet, *Chem. Eur. J.* **2003**, *9*, 4536–4539; b) L. Verdier, P. Sakhaii, M. Zweckstetter, C. Griesinger, *J. Magn. Reson.* **2003**, *163*, 353–359; c) C. Thiele. S. Berger, *Org. Lett.* **2003**, *5*, 705–708; d) C. M. Thiele, *J. Org. Chem.* **2004**, *69*, 7403–7413.
[3] M. R. Hansen, L. Mueller, A. Pardi, *Nat. Struct. Biol.* **1998**, *5*, 1065–1074.
[4] J. H. Prestegard, *Nat. Struct. Biol.* **1998**, *5*, 517–522.
[5] M. Rückert, G. Otting, *J. Am. Chem. Soc.* **2000**, *122*, 7793–7797.
[6] a) R. Tycko, F. J. Blanco, Y. Ishii, *J. Am. Chem. Soc.* **2000**, *122*, 9340–9341; b) S. Meier, D. Häussinger, S. Grzesiek, *J. Biomol. NMR* **2002**, *24*, 351–356.
[7] B. Luy, K. Kobzar, H. Kessler, *Angew. Chem.* **2004**, *116*, 1112–1115; *Angew. Chem. Int. Ed.* **2004**, *43*, 1092–1094.
[8] X. Liu, Z. Tong, F. Gao, *Polym. Int.* **1998**, *31*, 215–220.
[9] E. Rössner, A. Zeeck, W. A. König, *Angew. Chem.* **1990**, *102*, 84–85; *Angew. Chem. Int. Ed. Engl.* **1990**, *29*, 64–65.
[10] K. G. Rice, M. L. Corradi Da Silva, *J. Chromatogr. A* **1996**, *720*, 235–249.
[11] G. Bodenhausen, D. J. Ruben, *Chem. Phys. Lett.* **1980**, *69*, 185–189.
[12] L. E. Kay, D. S. Thomson, J. H. Prestegard, *Magn. Reson. Chem.* **1988**, *26*, 860–866.
[13] H. O. Kalinowski, S. Berger, S. Braun, *Carbon 13 NMR Spectroscopy*, Wiley, Chichester, **1984**.
[14] J. A. Losonczi, M. Andrec, M. W. F. Fischer, J. H. J. Prestegard, *J. Magn. Reson.* **1999**, *138*, 334–342.
[15] M. Zweckstetter, A. Bax, *J. Am. Chem. Soc.* **2000**, *122*, 3791.
[16] For related work carried out simultaneously, but independently, see previous Communication in this issue: J. C. Freudenberger, S. Knör, K. Kobzar, D. Heckmann, T. Paululat, H. Kessler, B. Luy, *Angew. Chem.* **2005**, *117*, 427–430; *Angew. Chem. Int. Ed.* **2005**, *44*, 423–426.

 © 2005 Wiley-VCH Verlag GmbH & Co. KGaA, Weinheim

Polymers

Aqueous Dispersions of Extraordinarily Small Polyethylene Nanoparticles**

*Ludmila Kolb, Vincent Monteil, Ralf Thomann, and Stefan Mecking**

Dedicated to Professor Wilhelm Keim on the occasion of his 70th birthday

Emulsion polymerization is among the most important polymerization processes.[1] As a product, polymer latices that are stable colloidal aqueous dispersions of polymer particles of about 50 nm to 1 μm in size are obtained. About ten million tons annually of polymer latices are used for a variety of applications, such as environmentally friendly coatings and paints.

To date, polymer latices are produced industrially by free-radical polymerization exclusively. Styrene–butadiene copolymers, acrylate homo- and copolymers, and vinyl acetate polymers are the major industrial products.[1,2] The range of polymer microstructures accessible by free-radical polymerization and corresponding materials properties is limited. For example, the synthesis of dispersions of saturated inert polymers, which do not bear hydrolyzable groups is a challenge.[1] It is desirable to synthesize dispersions from simple olefins obtained directly from cracking of hydrocarbon feedstocks. This process would avoid the need to convert the cracked products to monomers such as acrylates or vinyl esters, which consumes energy and raw materials.[3] We and the group of Claverie have recently reported the synthesis and properties of polyethylene dispersions by catalytic polymerization in emulsion.[4–6]

For traditional free-radical polymerization, the synthesis of very small particles is the subject of increasingly intense effort.[7,8] Microemulsion polymerization is a particularly suitable, albeit special, technique. Latices of, for example, polystyrene particles as small as 10 nm diameter have been prepared by microemulsion polymerization.[8] A strong limitation is that microemulsions only form under specific

[*] L. Kolb, Dr. V. Monteil, Prof. Dr. S. Mecking
Universität Konstanz
Lehrstuhl für Chemische Materialwissenschaft
Fachbereich Chemie
Universitätsstr. 10, 78457 Konstanz (Germany)
Fax: (+49) 7531-88-5152
E-mail: stefan.mecking@uni-konstanz.de
Dr. R. Thomann
Freiburger Materialforschungszentrum
Stefan-Meier-Str. 21, 79104 Freiburg (Germany)

[**] Financial support by BASF AG and the DFG (SFB 428) is gratefully acknowledged. S.M. is indebted to the Fonds der chemischen Industrie and the Hermann Schnell foundation for financial support.

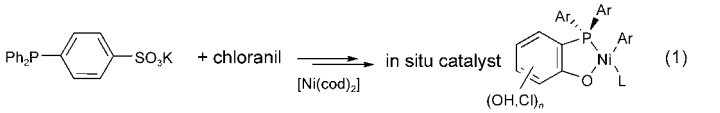
Supporting information for this article is available on the WWW under http://www.angewandte.org or from the author.

 DOI: 10.1002/anie.200460455 © 2005 Wiley-VCH Verlag GmbH & Co. KGaA, Weinheim

conditions that require large quantities of alcohols, or other organic solvents, and surfactants.

Concerning the aforementioned catalytic polymerization of ethylene in emulsion, a fine initial dispersion of the catalyst at the beginning of the reaction is a general prerequisite to obtain a large number of sub-micrometer polymer particles, that is, a polymer latex. This is usually achieved by using a miniemulsion technique. A solution of a liphophilic catalyst precursor (a nickel(II) complex) in a small amount of hydrocarbon solvent is dispersed in the continuous aqueous medium in the form of miniemulsion droplets.[9] Exposure to ethylene results in the formation of latices with the average sizes of polymer particle ranging from about 100 nm to 1 μm.[4,5] Although this technique enables the synthesis of polymer latices with lipophilic catalysts without the need for modifications to achieve water-solubility, a synthesis of much smaller particles would be desirable.[10] An aqueous solution of a hydrophilic catalyst clearly represents the highest possible initial degree of dispersion of the catalyst precursor, and therefore appears to be of interest for the synthesis of small particles.[11]

An active and easily accessible hydrophilic catalyst was obtained by the reaction of stoichiometic amounts of chloranil, potassium 4-(diphenylphosphino)benzene-sulfonate (TPPMS), and bis(1,5-cyclooctadiene)nickel ([Ni(cod)$_2$]).



possible structure of catalyst precursor
Ar = Ph, 4-$C_6H_4SO_3K$
L = solvent, monomer

As for a similar recently reported lipophilic catalyst,[4d] it can be speculated that a Ni^{II}-κ^2*P,O* phosphanylphenolate complex is the active species [Eq. (1)]. Catalyst preparation was performed in a small volume of 2-propanol (see the Supporting Information for experimental details). A careful choice of this solvent was found to be crucial to enable the reaction of the apolar chloranil with the polar TPPMS.



Figure 1. Optical appearance of a dispersion (2 wt% polyethylene).

Exposure of the catalyst in an aqueous solution that contained sodium dodecyl sulfate (SDS) as a surfactant to ethylene afforded clear or only slightly turbid products, despite an observed consumption of ethylene (Figure 1).

Apparently, latices consisting of extremely small particles with sizes far below the wavelength of visible light are formed. Dynamic light scattering (DLS) reveals volume average particle sizes < 20 nm (Table 1). Transmission electron microscopy (TEM) and atomic force microscopy (AFM) confirm these findings. TEM images of microtome cuts of latex particles embedded in a solid matrix[12] show very small particles (Figure 2) in accordance with AFM images of samples obtained by drying

Table 1: Polymerization results.[a]

Entry no.	Ethylene pressure [bar]	T [°C]	Solids content [%]	Average activity[b]	$\bar{M}_n$ [g mol^{-1}][c]	$\bar{M}_w/\bar{M}_n$	T_m [°C]	Average size of particles [nm][d]
1	40	25	0.4	70	6.0×10^3	5	139	n.d.
2	40	50	6.0	1070	2.0×10^3	7	n.d.	18
3	40	60	9.4	1675	2.6×10^3	5	130	n.d.
4	40	70	13.3	2370	1.9×10^3	5	129	28
5	40	80	6.8	1210	1.4×10^3	4	126	18
6	20	60	3.4	605	1.7×10^3	6	127	17
7	10	60	0.8	145	1.6×10^3	6	125	n.d.

[a] Reaction conditions: 90 mL of water, c(SDS) = 34.7 mmol L^{-1}, catalyst prepared in 10 mL of 2-propanol (100 μmol chloranil, 100 μmol TPPMS, 110 μmol [Ni(cod)$_2$]), polymerization time 2 h. [b] [mol(ethylene) mol(Ni)$^{-1}$ h^{-1}]. [c] Determined by GPC versus linear polyethylene (PE) standards. [d] Volume-average particle sizes determined by DLS. n.d. = not determined.

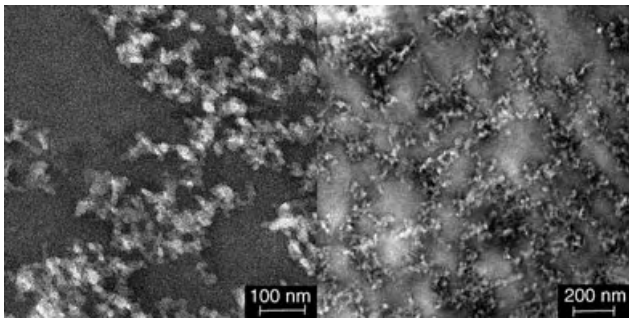


Figure 2. TEM micrographs of microtome cuts of latices.

the dispersions at room temperature (Supporting Information).

The course of the polymerization reaction was followed by using a mass flowmeter at a constant ethylene pressure of 40 bar at different polymerization temperatures (Table 1, entries 1–5; Figure 3). Although the reaction is sluggish at room temperature, satisfactory activities are observed at elevated temperatures of 50 to 70 °C, and the catalyst retains activity over the duration of the experiments (2 h).[13] Average catalyst activities over two hours range up to 2370 mol(ethylene) mol(Ni)$^{-1}$ h^{-1}. Further studies revealed that the polymerization continues for more than seven hours at 60 °C (see the Supporting Information). At 80 °C substantial catalyst deactivation within one hour is observed. Catalyst activities increase strongly with ethylene pressure in the range investigated (Table 1, entries 3, 6, and 7).

Incidentally, the results clearly demonstrate that efficient catalytic latex synthesis can be carried out without any water-immiscible liquid hydrocarbon phase. This offers some clear advantages for applications and for fundamental studies in comparison to the aforementioned miniemulsion technique. The simplification of the system, that is, the absence of

 © 2005 Wiley-VCH Verlag GmbH & Co. KGaA, Weinheim

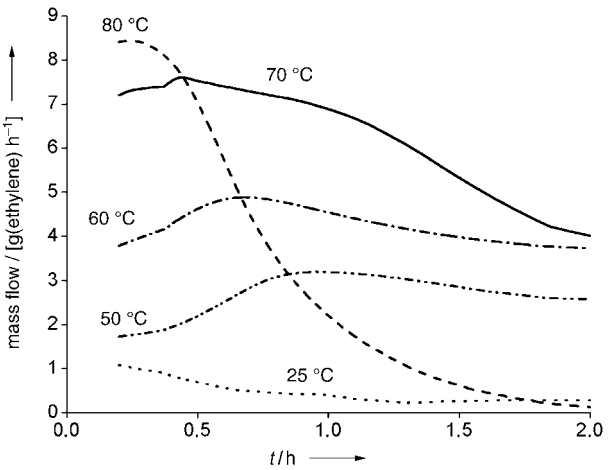


Figure 3. Temperature dependence of catalyst activity and stability over time (40 bars constant ethylene pressure, for the conditions see Table 1).

additional organic droplets, enables future studies of, for example, particle-formation processes.

Dispersions with a solids content of up to 15 wt% polymer were obtained without optimization. Up to about 6 wt%, the latices were transparent. The latices obtained were colloidally stable for more than six months. As for the amount of alcohol used in catalyst preparation, reduction from the usual 10 mL to 2 mL, which corresponds to only 2 vol% relative to the aqueous phase, had no significant effect on polymerization rate or otherwise. Increasing the scale of reaction from 0.1 L to 0.6 L did not result in a decrease in catalyst activity or dispersion stability (conditions of entry 3 in Table 1; 600 μmol Ni; dispersion obtained: 10.5% solids content).

A very simple picture of particle formation would involve initial chain growth on active sites dissolved in the aqueous phase and subsequent nucleation of one polymer particle per active catalyst molecule as continued chain growth results in increased hydrophobicity; the (surfactant-stabilized) particles thus formed continue to grow. However, further possibilities to be considered are, for example, the coalescence of already-existing particles (well-known from free-radical polymerization in general), the entry of a growing chain into an already-existing particle before nucleating a new particle, or the catalyst leaving an existing particle to nucleate a new one. In addition to the obvious possible complexity of particle-formation processes, it is not trivial to verify the number of active sites, particularly for the in situ catalyst system investigated. Nonetheless, it is interesting to know as a rough guideline the number of latex particles versus the number of metal centers to within an order of magnitude. From the number-average sizes of the latex particle, a ratio of Ni center:particle of only around 20 to 30 has been calculated. This high number of particles translates to a very efficient particle formation and stabilization in the polymerization investigated (particularly when keeping in mind that not all nickel added is necessarily present as an active site).

Concerning the microstructure of the dispersed polymer, ^{1}H and ^{13}C NMR spectroscopy demonstrate the formation of linear polyethylene as expected (see the Supporting Information). Number-average molecular weights ($\bar{M}_n$) of polyethylenes determined by high-temperature gel-permeation chromatography (GPC) are in the range of $\bar{M}_n = 1.4 \times 10^3$–$6 \times 10^3\ g\,mol^{-1}$. This is in accordance with $\bar{M}_n$ calculated from ^{1}H NMR spectra as well as T_m values.[14] As expected, molecular weights decrease with increasing reaction temperature due to an increase in β-hydride transfer. Interestingly, preliminary investigations by differential scanning calorimetry (DSC) on the polymer dispersions demonstrate stability of the colloids up to 140 °C and reveal high supercoolings of 55 °C due to an independent crystallization of individual droplets during the cooling cycle (cooling rate $10\ K\,min^{-1}$),[4e,15] which differs greatly from classical heterogeneous nucleation in bulk samples ($T_m - T_c = 18$ °C).

In summary, stable aqueous polyethylene dispersions consisting of extraordinarily small particles are reported. To our knowledge, such small stable polyethylene particles are not accessible by any other means. An easily prepared, robust catalyst is utilized for their synthesis.

Experimental data given in the Supporting Information: Catalyst preparation and polymerization procedure; ^{1}H and ^{13}C NMR spectra of polyethylene; DSC of latex and of bulk polymer; AFM images.

Received: April 26, 2004
Publication delayed at author's request.

Keywords: aqueous dispersions · homogeneous catalysis · nanostructures · polyethylene · polymerization

[1] a) *Wäßrige Polymerdispersionen* (Ed.: D. Distler), VCH, Weinheim, **1999**; b) *Emulsion Polymerization and Emulsion Polymers* (Eds.: P. A. Lovell, M. S. El-Aasser), Wiley, Chichester, **1997**.

[2] For syntheses of polymer latices by non-free-radical polymerization on a laboratory scale by polycondensation: a) K. Landfester, F. Tiarks, H.-P. Hentze, M. Antonietti, *Macromol. Chem. Phys.* **2000**, *201*, 1–5; By ionic polymerization: b) D. R. Weyenberg, D. E. Findlay, J. Cekada, A. E. Bey, *J. Polym. Sci. Part C* **1969**, *27*, 27–34; c) C. Maitre, F. Ganachaud, O. Ferreira, J. F. Lutz, Y. Paintoux, P. Hemery, *Macromolecules* **2000**, *33*, 7730–7736, and references therein.

[3] Petrochemical feedstocks versus renewable resources: S. Mecking, *Angew. Chem.* **2004**, *116*, 1096; *Angew. Chem. Int. Ed.* **2004**, *43*, 1078.

[4] a) A. Held, F. M. Bauers, S. Mecking, *Chem. Commun.* **2000**, 301; b) F. M. Bauers, S. Mecking, *Macromolecules* **2001**, *34*, 1165; c) F. M. Bauers, S. Mecking, *Angew. Chem.* **2001**, *113*, 3112; *Angew. Chem. Int. Ed.* **2001**, *40*, 3020; d) F. M. Bauers, M. M. Chowdhry, S. Mecking, *Macromolecules* **2003**, *36*, 6711; e) F. M. Bauers, R. Thomann, S. Mecking, *J. Am. Chem. Soc.* **2003**, *125*, 8838; f) M. A. Zuideveld, P. Wehrmann, C. Röhr, S. Mecking, *Angew. Chem.* **2004**, *116*, 887; *Angew. Chem. Int. Ed.* **2004**, *43*, 869; g) L. Kolb, R. Thomann, S. Mecking, *Macromol. Rapid Commun.* **2004**, *25*, 1824.

[5] a) A. Tomov, J.-P. Broyer, R. Spitz, *Macromol. Symp.* **2000**, *150*, 53; b) R. Soula, C. Novat, A. Tomov, R. Spitz, J. Claverie, X. Drujon, J. Malinge, T. Saudemont, *Macromolecules* **2001**, *34*, 2022; c) R. Soula, B. Saillard, R. Spitz, J. Claverie, M. F. Llaurro, C. Monnet, *Macromolecules* **2002**, *35*, 1513.

[6] Review: S. Mecking, A. Held, F. M. Bauers, *Angew. Chem.* **2002**, *114*, 564; *Angew. Chem. Int. Ed.* **2002**, *41*, 544.

 © 2005 Wiley-VCH Verlag GmbH & Co. KGaA, Weinheim

[7] a) Y. T. Choi, M. S. El-Aasser, E. D. Sudol, J. W. Vanderhoff, *J. Polym. Sci. Polym. Chem. Ed.* **1985**, *23*, 2973; b) K. Landfester, *Macromol. Rapid Commun.* **2001**, *22*, 896; c) J. M. Asua, *Prog. Polym. Sci.* **2002**, *27*, 1283.
[8] a) J. O. Stoffer, T. Bone, *J. Polym. Sci. Polym. Chem. Ed.* **1980**, *18*, 2641; b) S. S. Atik, K. J. Thomas, *J. Am. Chem. Soc.* **1981**, *103*, 4279; c) F. Candau, Y. S. Leong, G. Pouyet, S. J. Candau, *J. Colloid Interface Sci.* **1984**, *101*, 167; d) M. Antonietti, R. Basten, S. Lohmann, *Macromol. Chem. Phys.* **1995**, *196*, 441.
[9] Please note that the catalytic polymerization reactions of ethylene discussed differ from typical free-radical miniemulsion polymerization of a preformed miniemulsion of a liquid monomer. Gaseous ethylene monomer is fed continuously to the reaction mixture subsequently to miniemulsification of the catalyst solution.
[10] The water-immiscible hydrocarbon solvent introduced with the miniemulsion can be disadvantageous. Claverie and co-workers even suggested that swelling of the polymer by the added liquid hydrocarbon is mandatory to enable polyethylene formation at all; the amount of polymer attainable is limited to about 60% of the overall organics content, which would prohibit any commercial application.[5c] While we can not support this suggestion quantitatively from our experience,[4,11] the necessity of a certain amount of liquid hydrocarbon for any efficient ethylene polymerization remains questionable.
[11] Ethylene polymerization by water-soluble complexes has been demonstrated:see reference [4a] and F. M. Bauers, PhD thesis, University of Freiburg (Germany), **2003**. However, low polymer yields in combination with the synthetic effort for the catalyst precursors hampered any further studies.
[12] Microtome cuts were investigated, as in regular TEM aggregation of the sample during preparation hampered its analysis.
[13] Such elevated temperatures are beneficial to any technical-scale polymerization process to enable removal of the heat of reaction without the need of energy-consuming refrigeration of the coolant.
[14] H. Kraack, E. B. Sirota, M. Deutsch, *Polymer* **2001**, *42*, 8225.
[15] a) R. L. Cormia, F. P. Price, D. Turnbull, *J. Chem. Phys.* **1962**, *37*, 1333; b) G. S. Ross, L. J. Frolen, *J. Res. Natl. Bur. Stand. Sect. A* **1975**, *79*, 701.

 © 2005 Wiley-VCH Verlag GmbH & Co. KGaA, Weinheim

Fullerenes

Preparation and Structural Characterization of Two Kinetically Stable Chlorofullerenes, $C_{60}Cl_{28}$ and $C_{60}Cl_{30}$**

Sergey I. Troyanov, Natalia B. Shustova, Alexey A. Popov, Lev N. Sidorov, and Erhard Kemnitz*

Dedicated to Professor Arndt Simon on the occasion of his 65th birthday

Compared with bromo- and fluorofullerenes, fullerene chlorides have been studied to a lesser extent. However, they can find versatile application as synthons for valuable derivatives.[1] According to various sources, the reactions of [60]fullerene with different chlorinating agents yield $C_{60}Cl_n$ products with a bulk composition that varies from $C_{60}Cl_6$ to $C_{60}Cl_{40}$.[2] The most reliable data have been obtained for $C_{60}Cl_6$, which was prepared by treatment of C_{60} with ICl in solution in benzene. Its molecular structure was first suggested on the basis of ^{13}C NMR spectroscopy and was later confirmed in the structural study of related phenyl and methyl derivatives.[2b,3]

In our previous publication, higher chlorides of the variable-valency elements were suggested as effective chlorinating agents for fullerenes.[4] The use of $SbCl_5$ or VCl_4 resulted in the selective synthesis of T_h-$C_{60}Cl_{24}$ with high yields and isomeric purity. The structure was deduced by comparison of the experimental and theoretically calculated IR spectra. Very recently, a novel chlorofullerene, D_{3d}-$C_{60}Cl_{30}$, was synthesized and structurally characterized.[5] Here we report the preparation of two new chlorofullerenes, C_1-$C_{60}Cl_{28}$ and C_2-$C_{60}Cl_{30}$, which have been characterized by means of X-ray single-crystal diffraction studies, IR spectroscopy, and quantum chemical calculations.

Pure T_h-$C_{60}Cl_{24}$ can be prepared by reacting C_{60} (30 mg) with VCl_4 (2 g) in sealed ampoules at 160 °C for 14 days.[4] An increase in the reaction time was accompanied by the appearance of new bands in the IR spectra and the disappearance of the bands characteristic of T_h-$C_{60}Cl_{24}$. After 2 months heating, a new compound was formed with a ratio of Cl:C of 29 ± 1 according to elemental analysis data.

[*] Prof. Dr. S. I. Troyanov, N. B. Shustova, Dr. A. A. Popov, Prof. Dr. L. N. Sidorov
Chemistry Department
Moscow State University
119992 Moscow (Russia)
Fax: (+7) 095-939-1240
E-mail: troyanov@thermo.chem.msu.ru
Prof. Dr. E. Kemnitz
Institut für Chemie
Humboldt-Universität Berlin
12489 Berlin (Germany)

[**] This work was partially supported by the Deutsche Forschungsgemeinschaft (KE 489/20-1) and the Russian Foundation for Basic Research (03-03-04006 and 03-03-32179). We are grateful to A. P. Turnbull (BESSY (Germany)) for his help with the reduction of diffraction data for the crystal of **1**.

 © 2005 Wiley-VCH Verlag GmbH & Co. KGaA, Weinheim DOI: 10.1002/anie.200462139

The IR spectrum of the new compound is presented in Figure 1a.[6] Crystallization from bromine yielded a solvate whose composition $C_{60}Cl_{30}\cdot 1.5\,Br_2$ (**1**) was established by single-crystal X-ray crystallography.[7]

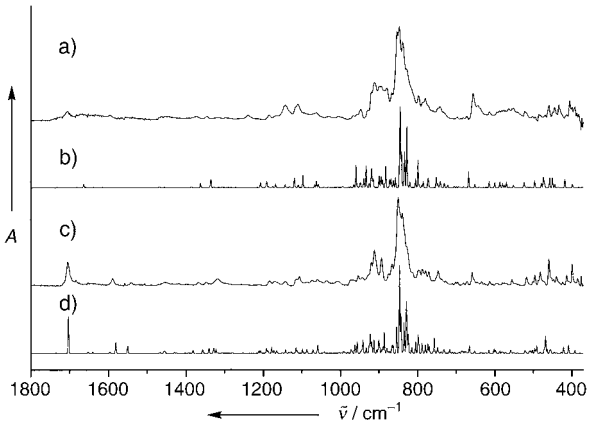


Figure 1. Experimental and calculated IR spectra of C_2-$C_{60}Cl_{30}$ (a and b) and C_1-$C_{60}Cl_{28}$ (c and d).

Chlorination of C_{60} with iodine monochloride at 120 °C for 30 days resulted in the formation of dark-brown crystals whose composition $C_{60}Cl_{28}\cdot ICl$ (**2**) was also determined by X-ray crystallography.[7] The IR spectrum of **2** is shown in Figure 1c. Some other experiments carried out at the same temperature for a shorter time revealed the presence of T_h-$C_{60}Cl_{24}$ in the reaction mixture according to IR spectra. Notably, the reaction of T_h-$C_{60}Cl_{24}$ with $SbCl_5$ at 300 °C for two days afforded pure D_{3d}-$C_{60}Cl_{30}$.

The formation of the chlorofullerenes $C_{60}Cl_{28}$ (**2**) and $C_{60}Cl_{30}$ (**1**) is quite remarkable. Their molecular structures are characterized by the presence of two planar aromatic rings (which are inclined to one another) and two long chains of sp^3-hybridized carbon atoms that bear chlorine atoms (Figure 2 and Figure 3). The $C_{60}Cl_{28}$ molecule has no symmetry elements (C_1), although the counterparts of most atoms (except C35 and C42) are located following 180° rotation around the pseudo-C_2 axis (parallel to the view directions on Figure 2 (left) and Figure 3 (left)). The addition of two Cl atoms to the $C_{60}Cl_{28}$ molecule at positions C35 and C42 produces the $C_{60}Cl_{30}$ molecule, which then possesses a (non-crystallographic) twofold axis (Figure 2b).

Quantum chemical DFT (density functional theory) calculations of the molecular structures of the chlorofullerenes[8a] revealed a comparatively good agreement between experimental and calculated C–C bond lengths. C–C bonds can be separated into five major groups according to their nature: isolated double bonds that connect nonaromatic sp^2-hybridized carbon atoms (average length, calcd for $C_{60}Cl_{28}$: 1.355; observed: 1.344 Å), aromatic bonds (calcd: 1.392; observed: 1.385 Å), $C(sp^2)$–$C(sp^2)$ bonds between two double

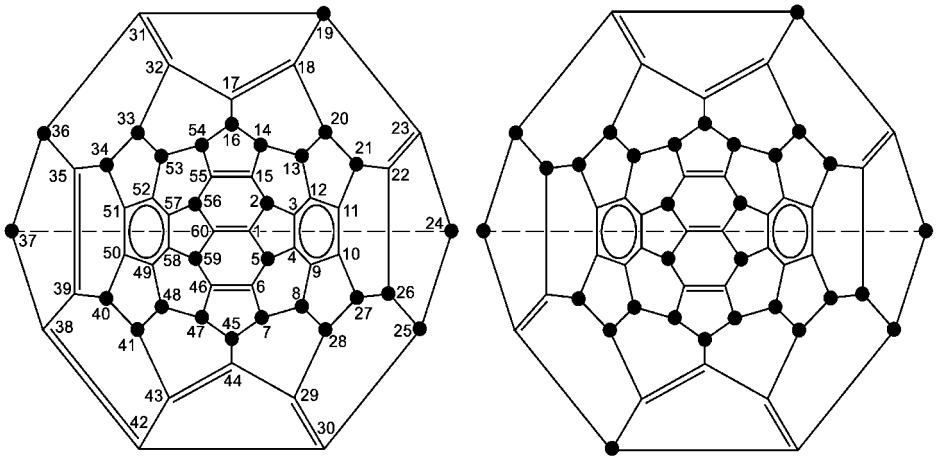


Figure 2. Schlegel diagrams of C_1-$C_{60}Cl_{28}$ and C_2-$C_{60}Cl_{30}$ with a numbering scheme for carbons that is identical for both molecules. For convenience, a nonstandard numbering scheme was used that fixed the sum of the numbers for equivalent positions in C_2-$C_{60}Cl_{30}$ to 61.

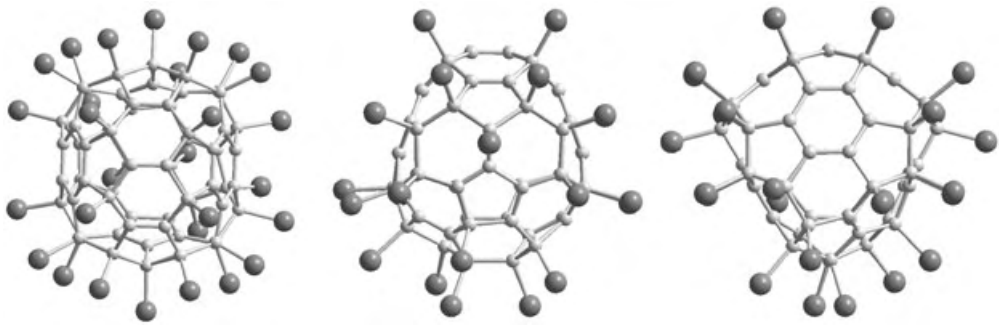


Figure 3. Top and side views of the C_1-$C_{60}Cl_{28}$ molecule.

 © 2005 Wiley-VCH Verlag GmbH & Co. KGaA, Weinheim

bonds (calcd: 1.439; observed: 1.443 Å), C(sp^2)–C(sp^3)bonds (calcd: 1.500; observed: 1.500 Å), and, finally, considerably elongated C(sp^3)–C(sp^3) bonds (calcd: 1.621; observed: 1.615 Å). Especially long C–C bond lengths (up to 1.65–1.66 Å) are observed for the 6/6 bonds of this latter type. A similar correspondence has been found for the $C_{60}Cl_{30}$ molecule. However, the addition of two Cl atoms to the $C_{60}Cl_{28}$ molecule results in local repositioning of the double bonds. Thus, bond lengths (Å) of 1.37–1.44–1.36 in the C35–C39–C38–C42 fragment in **2** become 1.53–1.33–1.44 in **1**.

IR spectra for C_1-$C_{60}Cl_{28}$ and C_2-$C_{60}Cl_{30}$ revealed their close similarity, especially in the range of the strongest absorptions between 700 and 1000 cm^{-1}. The most prominent differences in the spectra of **1** and **2** can be found for two bands at 1705 and 1589 cm^{-1} that are characteristic of $C_{60}Cl_{28}$ (Figure 1 d). According to DFT vibrational simulations, which give a very good match with the experimental spectrum (Figure 1 c) of $C_{60}Cl_{28}$ (**2**), these characteristic modes correspond, respectively, to the stretching vibration of the double bond between two pentagons (C38–C42) and the symmetric vibration of two double bonds in the "bare" pentagon (C29–C30 and C43–C44). In other words, these vibrations are located on the fragment which is subjected to further chlorination to yield C_2-$C_{60}Cl_{30}$ (**1**) and therefore these bands are absent in the calculated IR spectrum of the latter (Figure 1 b). At the same time, the experimental IR spectrum of **1** (Figure 1 a) showed weak absorptions near 1705 and 1589 cm^{-1} which indicates the presence of a small amount of $C_{60}Cl_{28}$ in the sample.

Chlorination of C_{60} with $SbCl_5$ or ICl carried out at higher temperature (above 250 °C) finally resulted in another chlorofullerene, namely, D_{3d}-$C_{60}Cl_{30}$.[5] DFT B3LYP computations of the relative energies[8b] show that C_2-$C_{60}Cl_{30}$ synthesized in this work is 78 kJ mol^{-1} less stable than the D_{3d} isomer. Moreover, the C_1-$C_{60}Cl_{28}$ isomer is 6 kJ mol^{-1} less stable than the hypothetical C_2-$C_{60}Cl_{28}$, which could be obtained by the removal of two chlorine atoms from D_{3d}-$C_{60}Cl_{30}$.[9] Hence, DFT computations favor the alternative addition patterns, especially for $C_{60}Cl_{30}$. Indeed, a sample of **1** heated with $SbCl_5$ at 300 °C for 2 days has been completely transformed into D_{3d}-$C_{60}Cl_{30}$ according to the IR spectra.

Experimental observations as well as theoretical calculations, therefore, unambiguously demonstrate that C_1-$C_{60}Cl_{28}$ and C_2-$C_{60}Cl_{30}$, which have been synthesized and investigated in this work, are kinetically stable chlorofullerenes. Owing to similarity in the addition patterns, C_2-$C_{60}Cl_{30}$ can be easily obtained from C_1-$C_{60}Cl_{28}$ by the addition of two chlorine atoms. Substantial differences in the addition patterns for T_h-$C_{60}Cl_{24}$ (no aromatic rings, only isolated double bonds), C_1-$C_{60}Cl_{28}$ or C_2-$C_{60}Cl_{30}$ (two nonparallel aromatic rings), and D_{3d}-$C_{60}Cl_{30}$ (two parallel aromatic rings along with equatorial 18-π trannulene belt) prevent transformation of less-chlorinated fullerenes into more-chlorinated ones by the simple addition of chlorine atoms (with an exception pointed out above). Therefore, such transformations should include the rearrangement of many chlorine atoms on the fullerene cage and can be regarded as a "chlorine dance".[10] Similar phenomena, "fluorine dance", were found to proceed in the course of fluorination of C_{60}.[11] If the chlorination of C_{60} occurs at temperatures lower than 200 °C, some intermediates of "chlorine dance" can be isolated in their pure form as shown in this work. At higher chlorination temperatures, only the thermodynamically stable D_{3d}-$C_{60}Cl_{30}$ should be obtainable.

In summary, the family of chlorofullerenes is growing. Besides $C_{60}Cl_6$, T_h-$C_{60}Cl_{24}$, and D_{3d}-$C_{60}Cl_{30}$, two new compounds have been isolated, C_1-$C_{60}Cl_{28}$ and C_2-$C_{60}Cl_{30}$, with the latter being the less stable isomer of $C_{60}Cl_{30}$. Their molecular structures contain two inclined aromatic rings and chains of "chlorinated" carbon atoms. C_1-$C_{60}Cl_{28}$ can be easily transformed into C_2-$C_{60}Cl_{30}$ by the addition of two chlorine atoms, a situation that is unique for known halogenated C_{60} structures. Finally, these molecules are kinetically stable intermediates in the process of "chlorine dance" on the way from $C_{60}Cl_{24}$ to the thermodynamically stable D_{3d}-$C_{60}Cl_{30}$.

Received: September 28, 2004

Keywords: density functional calculations · fullerenes · halogenation · IR spectroscopy · structure elucidation

[1] a) P. R. Birkett, A. G. Avent, A. D. Darwish, I. Hahn, H. W. Kroto, G. J. Langley, J. O'Loughlin, R. Taylor, D. R. M. Walton,, *J. Chem. Soc. Perkin. Trans. 2* **1997**, 1121; b) H. Jing, D. Chen, X. Ling, Q. Liu, X. Jing, Y. Zhang, *J. Appl. Polym. Sci.* **2002**, *86*, 3001.

[2] a) G. A. Olah, I. Bucsi, C. Lambert, R. Aniszfeld, N. J. Trivedy, D. K. Sensharma, G. K. S. Prakash, *J. Am. Chem. Soc.* **1991**, *113*, 9385; b) P. R. Birkett, A. G. Avent, A. D. Darwish, H. W. Kroto, R. Taylor, D. R. M. Walton, *J. Chem. Soc. Chem. Commun.* **1993**, 1230; c) D. Heymann, F. Cataldo, R. Fokkens, N. M. M. Nibbering, R. Vis, *Fullerene Sci. Technol.* **1999**, *7*, 159; d) P. A. Troshin, O. Popkov, R. N. Lyubovskaya, *Fullerenes Nanotubes Carbon Nanostruct.* **2003**, *11*, 163.

[3] a) P. R. Birkett, A. G. Avent, A. D. Darwish, H. W. Kroto, R. Taylor, D. R. M. Walton, *J. Chem. Soc. Perkin. Trans. 2* **1997**, 457; b) H. Al-Matar, Ala'a K. Abdul-Sada, A. G. Avent, P. W. Fowler, P. B. Hitchcock, K. M. Rogers, R. Taylor, *J. Chem. Soc. Perkin Trans. 2* **2002**, 53.

[4] S. I. Troyanov, N. B. Shustova, A. A. Popov, M. Feist, E. Kemnitz, *Zh. Neorg. Khim.* **2004**, *49*, 1413.

[5] P. A. Troshin, R. N. Lyubovskaya, I. N. Ioffe, N. B. Shustova, E. Kemnitz, S. I. Troyanov, *Angew. Chem.* **2005**, *117*, 238; *Angew. Chem. Int. Ed.* **2005**, *44*, 234.

[6] IR spectra were recorded on a NICOLET-200 FT spectrometer (KBr pellets, average of 128 scans, 0.5-cm^{-1} resolution).

[7] Data collection for a crystal of $C_{60}Cl_{30}{\cdot}1.5\,Br_2$ (**1**) was performed on a MAR345 image plate at 100 K by using synchrotron radiation at the BESSY storage ring ($\lambda = 0.9184$ Å, PSF BL14.2 of the Free University of Berlin, Germany). **1**: triclinic, $P\bar{1}$, $a = 13.023(1)$, $b = 13.226(1)$, $c = 20.523(2)$ Å, $\alpha = 87.692(5)$, $\beta = 73.942(5)$, $\gamma = 62.424(5)°$, $V = 2995.1(4)$ Å^3, $Z = 2$; 16913 reflections collected, 7888 independent. Structure solution with SHELXS-97. The final anisotropic LS refinement (SHELXL-97) with 839 parameters converged to $wR_2 = 0.162$ and $R_1 = 0.061$. The data for $C_{60}Cl_{28}{\cdot}ICl$ (**2**) were collected on an IPDS diffractometer (Stoe, $Mo_{K\alpha}$ radiation, $\lambda = 0.71073$ Å) at 150 K. **2**: monoclinic, $P2_1/c$, $a = 13.125(2)$, $b = 24.042(4)$, $c = 18.110(3)$ Å, $\beta = 100.58(1)°$, $V = 5618(1)$ Å^3, $Z = 4$; 41306 reflections collected, 11857 independent. The ICl molecule is disordered over three positions. Anisotropic LS refinement with 821 parameters gave the final values of $wR_2 = 0.102$ and $R_1 = 0.040$.

CCDC 247259 and CCDC 247260 contain the supplementary crystallographic data for this paper. These data can be obtained free of charge from the Cambridge Crystallographic Data Centre via www.ccdc.cam.ac.uk/data_request/cif.

[8] a) DFT calculations of molecular structures and IR spectra were performed with the PRIRODA package (see: D. N. Laikov, *Chem. Phys. Lett.* **1997**, *281*, 151) by using PBE functional (see: J. P. Perdew, K. Burke, M. Ernzerhof, *Phys. Rev. Lett.* **1996**, *77*, 3865) and TZ2P-quality basis set; b) Point-energy calculations at PBE/TZ2P geometry were also performed at B3LYP/cc-pVTZ (-f) level (see: A. D. Becke, *J. Chem. Phys.* **1993**, *98*, 5648) within PC GAMESS package, see: A. A. Granovsky, http://classic.chem.msu.su/gran/gamess/index.html.

[9] Relative energies for $C_{60}Cl_{30}$ and $C_{60}Cl_{28}$ computed at the PBE/TZ2P level of theory were 111 and 40 kJ mol^{-1}, respectively. Significant differences between PBE and B3LYP relative energies may be attributed partially to the approximate character of PBE/TZ2P values as computations with PRIRODA employed approximate expansion of the electron density in an auxiliary basis set to accelerate the evaluation of Coulomb- and exchange-correlation terms.

[10] M. H. Mach, J. F. Bunnett, *J. Org. Chem.* **1980**, *45*, 4660.

[11] a) A. A. Gakh, A. A. Tuinman, *Tetrahedron Lett.* **2001**, *42*, 7137; b) A. G. Avent, R. Taylor, *Chem. Commun.* **2002**, 2726.

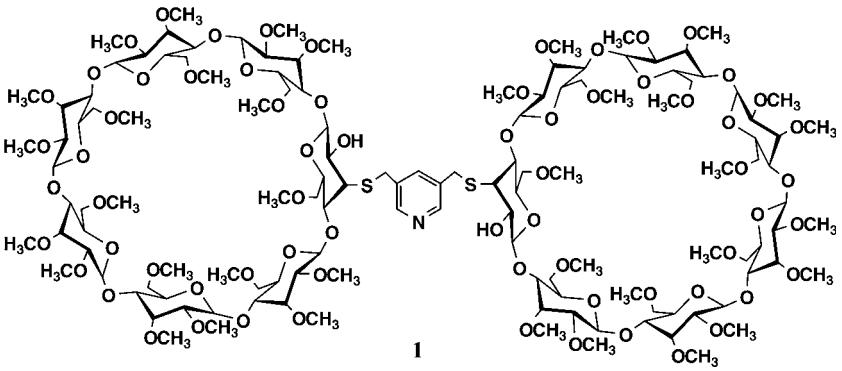
 © 2005 Wiley-VCH Verlag GmbH & Co. KGaA, Weinheim

Supramolecular Chemistry

Dioxygen Binding to a Simple Myoglobin Model in Aqueous Solution**

Koji Kano, Hiroaki Kitagishi, Masahito Kodera, and Shun Hirota*

Herein we report reversible dioxygen binding to a simple model system of myoglobin composed of a per-*O*-methylated β-cyclodextrin (CD) dimer having a pyridine linker (**1**) and [tetrakis(4-sulfonatophenyl)porphinato]iron(II) ([Fe^{II}(tpps)]) in aqueous solution. Myoglobin (Mb) and hemoglobin (Hb) form stable O_2 adducts in aqueous solution at a neutral pH value. Globin plays an essential role in stabilizing the O_2 adduct in biological systems. Without this protein, oxyheme is immediately oxidized to a Met form by the action of a proton or hydroxide ion.[1] Heme is protected from acid- or base-induced autoxidation by the globin that surrounds the iron porphyrin (FePor). Many model systems of Mb and Hb were examined after the development of the picket-fence porphyrin by Collman et al.[2,3] In most model systems O_2 binding was achieved in organic solvents, where a trace amount of water had to be removed from the system. The concept proposed by Collman's research group has been expanded into the binding of O_2 to hydrophobic picket-fence Fe^{II} porphyrins, which are included in vesicles[4] or albumin[5] in aqueous media. Although dendrimers with Fe^{II}Por cores were expected to mimic the function of Mb or Hb, no stable O_2 adducts were formed in these systems in aqueous solution.[6,7] Since the O_2 adduct of the dendrimers is efficiently formed in absolute toluene,[6] it is evident that construction of a hydrophobic pocket for placing the iron(II) center of an FePor is the essential factor for realizing O_2 binding in aqueous solution. In the present model system, we used the striking ability of per-*O*-methylated β-CD to include water-soluble tetraarylporphyrins and yield extremely stable 1:2 (Por:CD) inclusion complexes in aqueous solution.[8] Two per-*O*-methylated β-CD moieties were linked by a bridge involving a pyridine ligand. Such a CD dimer (**1**) worked well as a simple Mb model in aqueous solution.



1

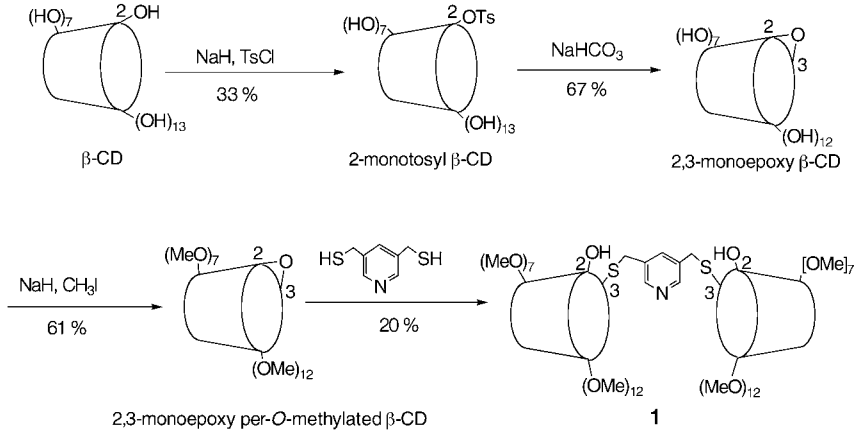
The synthesis of **1** (Scheme 1) was carried out by using the method reported by Lawrence et al.[9] The changes in the absorption spectrum of [Fe^{III}(tpps)] in phosphate buffer of pH 5.0 were measured as a function of the concentration of **1** (Figure 1) to examine whether **1** forms a suitable complex in which two CD moieties include the sulfonatophenyl groups at the 5 and 15 positions of [M(tpps)] (M = metal ion) and the pyridine ligand coordinates to the M^{II} or M^{III} site of the porphyrin. No μ-oxo dimer was formed at pH 5.0 and the predominant species involving [Fe^{III}(tpps)] was the diaqua complex [$Fe^{III}(H_2O)_2$(tpps)].[10] The Soret band of [$Fe^{III}(H_2O)_2$(tpps)] at 388 nm shifted to 421 nm upon addition of **1**. The spectral changes were sharply saturated after the addition of one equivalent of **1**, which indicated the formation of a very stable 1:1 complex between [$Fe^{III}(H_2O)_2$(tpps)] and **1**. Analysis of the titration curve provided a binding constant

[*] Prof. Dr. K. Kano, H. Kitagishi, Prof. Dr. M. Kodera
Department of Molecular Science and Technology
Doshisha University
Kyotanabe, Kyoto 610-0321 (Japan)
Fax: (+81) 774-65-6845
E-mail: kkano@mail.doshisha.ac.jp
Dr. S. Hirota
Kyoto Pharmaceutical University
Yamashina-ku, Kyoto 607-8414 (Japan)

[**] This study was supported by a Grant-in-Aid for Scientific Research B (KAKENHI 14340224) from the Ministry of Education, Culture, Sports, Science, and Technology, Japan, and the Sekisui Foundation. We thank Professor Teizo Kitagawa at the Institute for Molecular Science, Okazaki, for his helpful discussions.

Supporting information for this article is available on the WWW under http://www.angewandte.org or from the author.

 DOI: 10.1002/anie.200461609 © 2005 Wiley-VCH Verlag GmbH & Co. KGaA, Weinheim



Scheme 1. Synthetic route of **1**. Ts = toluene-4-sulfonyl.

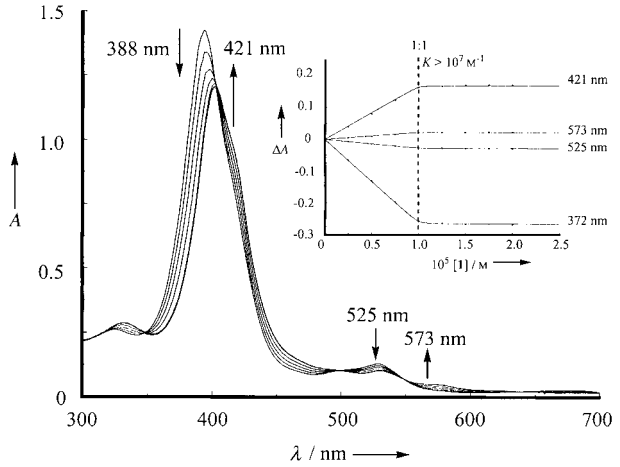


Figure 1. UV/Vis spectral changes of $[Fe^{III}(tpps)]$ (1×10^{-5} M) as a function of [**1**] in 0.05 M phosphate buffer at pH 5.0 and 25 °C. The titration curves were analyzed by the nonlinear least-squares method to estimate *K*.

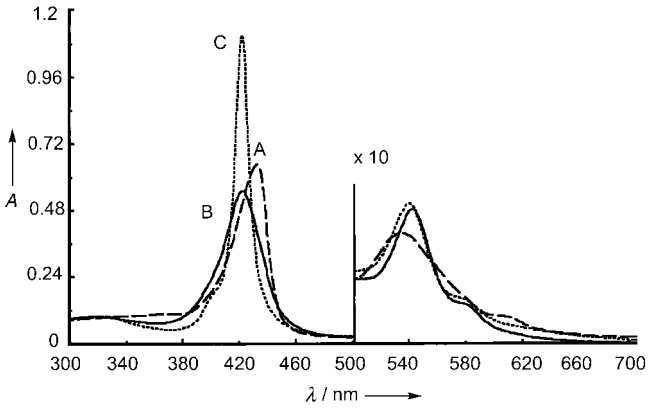
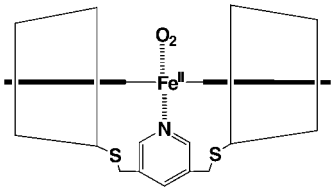


Figure 2. UV/Vis absorption spectra of $[Fe^{II}(tpps)(\mathbf{1})]$ (5×10^{-6} M) in the deoxy form (A) as well as the O_2-coordinated (B) and CO-coordinated forms (C) in 0.05 M phosphate buffer at pH 7.0 and 25 °C. The method of sample preparation is given in the text.

(K) for complexation of $[Fe^{III}(H_2O)_2(tpps)]$ with **1** of $> 10^7\,M^{-1}$, although the exact K value could not be determined. The ^1H NMR spectrum of the $[Fe^{III}(tpps)]$/**1** system in D_2O at pD 4.4 showed signals arising from the pyrrole β-protons at $\delta = 51$, 53, and 55 ppm (see the Supporting Information), which suggests the formation of a complex in a five-coordinate admixed intermediate spin state.[11] Such a complex should be pyridine-coordinated $[Fe^{III}(tpps)(\mathbf{1})]$ which has the desired structure. The pH-dependent UV/Vis absorption spectral changes suggest that the pyridine nitrogen–Fe^{III} coordination bond of the $[Fe^{III}(tpps)(\mathbf{1})]$ complex dissociates to give $[Fe^{III}(H_2O)_2(tpps)(\mathbf{1})]$ below pH 3 and $[Fe^{III}(OH)(tpps)(\mathbf{1})]$ above pH 7. The ^1H NMR signals resulting from the pyrrole β-protons at pD 0.5 appeared at $\delta = 71$ and 66 ppm as two singlets, which supports the formation of $[Fe^{III}(H_2O)_2(tpps)(\mathbf{1})]$ in a six-coordinate admixed intermediate spin state. Meanwhile, the pyrrole β-protons were observed at $\delta = 84$ ppm as a broad singlet at pD 8.7, which is ascribed to $[Fe^{III}(OH)(tpps)(\mathbf{1})]$ in a five-coordinate high-spin state. In addition, $[Zn^{II}(tpps)]$ was used as a divalent metalloporphyrin in place of $[Fe^{II}(tpps)]$. The structure of the complex of $[Zn^{II}(tpps)]$ and **1** was estimated by UV/Vis spectroscopy. As in the case of $[Fe^{III}(tpps)]$, an extremely stable 1:1 complex was formed and the pyridine moiety of **1** coordinated to the zinc ion above pH 3 (see the Supporting Information). From these findings, it can be expected that **1** forms a 1:1 complex with $[Fe^{II}(tpps)]$, in which the pyridine moiety of **1** can act as a proximal ligand.

Two equivalents of $Na_2S_2O_4$ were added to an aqueous solution of a mixture of $[Fe^{III}(tpps)]$ and **1** in an argon atmosphere to prepare a stock solution of $[Fe^{II}(tpps)]$ complexed with **1**, which was diluted by N_2-saturated phosphate buffer at pH 7.0 for measurement of the absorption spectrum (Figure 2). The Soret band of $[Fe^{II}(tpps)]$ included by **1** appeared at 433 nm ($\varepsilon_{max} = 129\,600$), which corresponds to the band from a five-coordinate high-spin Fe^{II}Por species.[12] Careful introduction of O_2 into a solution of $[Fe^{II}(tpps)(\mathbf{1})]$ caused a change in the absorption spectrum and a new Soret band appeared at 423 nm ($\varepsilon_{max} = 110\,400$). Replacing O_2 by CO resulted in a sharp Soret band appearing at 422 nm ($\varepsilon_{max} = 222\,600$) as a consequence of coordination of CO to $[Fe^{II}(tpps)]$. These spectral changes strongly suggest that the Soret band at 423 nm which appeared when the complex was formed in the O_2 atmosphere should be ascribed to $[Fe^{II}(O_2)(tpps)(\mathbf{1})]$.

The formation of the $[Fe^{II}(O_2)(tpps)(\mathbf{1})]$ complex was confirmed by ^1H NMR and resonance Raman spectroscopy. The ^1H NMR signals of the $[Fe^{II}(tpps)(\mathbf{1})]$ complex in anaerobic D_2O were broad because of the paramagnetic nature of the sample. These broad signals appeared at $\delta = 40$–



 © 2005 Wiley-VCH Verlag GmbH & Co. KGaA, Weinheim

60 ppm (with TSP as an external standard) and can be ascribed to a five-coordinate high-spin [Fe^{II}(tpps)] ($S=2$) complex.[13] This solution was charged with O_2, and all NMR signals between $\delta=0$ and 10 ppm were sharpened, which indicated the formation of a six-coordinate low-spin state ($S=0$). In other words, the ^{1}H NMR spectrum supports the formation of the [$Fe^{II}(O_2)$(tpps)(**1**)] complex. The sample obtained by replacing the O_2 atmosphere with CO was also diamagnetic.

The formation of the Fe^{II}–O bond was verified by resonance Raman spectroscopy (Figure 3). The sample was prepared by introducing $^{18}O_2$ into a phosphate buffer solution

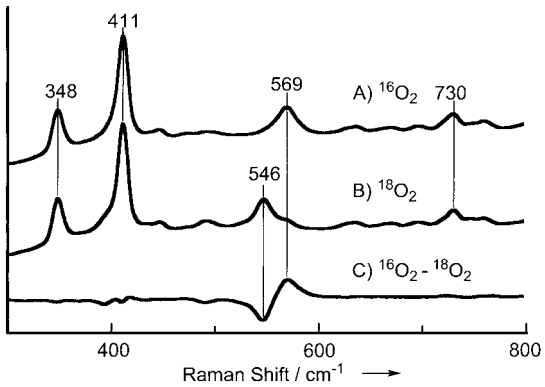


Figure 3. Resonance Raman spectra of the $^{16}O_2$ (A) and $^{18}O_2$ (B) adducts of the [Fe^{II}(tpps)(**1**)] complex (5×10^{-5} M) and the difference spectrum (C) between spectra A and B. Experimental conditions: 0.05 M phosphate buffer at pH 7.0; room temperature; 413.1 nm excitation; 12 mW power.

of the [Fe^{II}(tpps)(**1**)] complex at pH 7.0 and room temperature. A Raman signal was observed at 546 cm^{-1}, which was characterized as the stretching band of the Fe^{II}–^{18}O bond.[14] When the measurement was repeated after the sample had stood in air for a while, the band shifted to 569 cm^{-1}, which is ascribed to the Fe^{II}–^{16}O bond. On the basis of these data, it is concluded that a Fe^{II}–O bond is formed. In the case of horse heart Mb, the stretching bands of the Fe^{II}–^{18}O and Fe^{II}–^{16}O bonds appear at 545 and 571 cm^{-1}, respectively,[14] which is in good agreement with the bands measured in the present system.

The rates of autoxidation of the [$Fe^{II}(O_2)$(tpps)(**1**)] complex were determined by following the absorbance at the Soret band, and the results are summarized in Table 1. The [$Fe^{II}(O_2)$(tpps)(**1**)] ($\lambda_{max}=423$ nm) was gradually decomposed to [Fe^{III}(OH)(tpps)(**1**)] ($\lambda_{max}=418$ nm) and the half-life

Table 1: First-order rate constants (k) and half-lives ($t_{1/2}$) for the autoxidation of [$Fe^{II}(O_2)$(tpps)(**1**)] at 25 °C.

pH	k [h^{-1}]	$t_{1/2}$ [h]
4.0[a]	0.053	13.1
5.0[a]	0.055	12.6
6.0[a]	0.041	16.9
6.0[b]	0.020	34.7
7.0[b]	0.023	30.1
8.0[b]	0.024	28.9

[a] In 5 mM succinate buffer. [b] In 5 mM phosphate buffer.

($t_{1/2}$) of the [$Fe^{II}(O_2)$(tpps)(**1**)] complex was 30.1 h in phosphate buffer at pH 7.0. Interestingly, [$Fe^{II}(O_2)$(tpps)(**1**)] was still stable in aqueous acidic solution at pH 4.0 ($t_{1/2}=13.1$ h). The O_2 adduct of beef heart Mb is much more unstable in the lower pH region ($t_{1/2}=11$ h at pH 7 and 0.5 h at pH 5).[15] Such novel stabilization of the [$Fe^{II}(O_2)$(tpps)(**1**)] complex might be achieved by blocking the Fe^{II} center with two per-*O*-methylated β-CD moieties. Most water molecules seem to be excluded from the cleft of the [$Fe^{II}(O_2)$(tpps)(**1**)] complex, which was more stable in phosphate buffer at pH 6.0 than in succinate buffer at the same pH value. This observation might be ascribed to a slow anion-catalyzed autoxidation[1] caused by weak coordination of the CO_2^- group of the succinate anion to the iron center, since it is known that inorganic anions accelerate the autoxidation of oxyMb.[1]

The affinity of the present system for dioxygen was determined from the changes in the absorption spectrum of the [Fe^{II}(tpps)(**1**)] complex as a function of the partial pressure of O_2.[6b] The O_2 affinity ($P_{1/2}$) in 0.05 M phosphate buffer at pH 7.0 and 25 °C was 17.5 ± 1.7 Torr, which is larger than that of sperm whale Mb (0.29 Torr) and is somewhat smaller than the $P_{1/2}$ value of human Hb in the T state (26 Torr).[3]

The bound O_2 could be released from [$Fe^{II}(O_2)$(tpps)(**1**)] by introducing N_2 into the system. The present system showed good reversibility in the O_2 binding–releasing cycles, although gradual autoxidation occurred (see the Supporting Information).

In the present study, we found that **1** is an excellent model of Mb that binds O_2 reversibly in aqueous solution. Recently, a CD/Fe^{II}Por ensemble having a complex structure was prepared as a hemoprotein model which binds dioxygen, although no details of O_2 binding were investigated.[16] The present study introduced a new system to the family of metalloprotein models composed of CDs and metal complexes.[17]

Experimental Section

2,3-Monoepoxy-β-cyclodextrin,[18] 3,5-dimercaptomethylpyridine,[9a] and [Fe^{III}(tpps)][19] were synthesized according to the procedures reported in the literature.

2,3-Monoepoxy per-*O*-methylated β-cyclodextrin: 2,3-Monoepoxy-β-CD (2.00 g, 1.45 mmol) was added to a mixture of dry DMF (80 mL) and THF (30 mL) under an Ar atmosphere. After the mixture became translucent, the solution was cooled to 0 °C. NaH (1.39 g, 58.0 mmol) was added to the solution, and the mixture was stirred for 1 h at 0 °C. CH_3I (3.6 mL, 58.0 mmol) was added dropwise over a period of 20 min, and then the mixture was warmed to room temperature. After stirring the reaction mixture overnight, methanol (4 mL) was added to quench the reaction. The solvent was removed under reduced pressure, and the residue was extracted with $CHCl_3$ (100 mL) and H_2O (100 mL). The combined organic layer was separated and washed with aqueous $Na_2S_2O_3$ (100 mL) and then with H_2O (100 mL). The $CHCl_3$ layer was dried over Na_2SO_4 and concentrated. The residue was purified by column chromatography on silica gel with gradient elution from $CHCl_3$ to $CHCl_3$/acetone (5:2 (v/v)) to give 2,3-monoepoxy per-*O*-methylated β-CD as a colorless solid (1.50 g, 61 %). ^{1}H NMR (400 MHz, $CDCl_3$): $\delta=5.19$–5.00 (m, 7H), 3.92–3.19 ppm (m, 99H); MS (MALDI-TOF, α-cyano-4-hydroxycinnamic acid (α-CHCA)) m/z 1406.6 (calcd for $[M+Na]^+$: 1406.46). Elemental analysis (%) calcd for $C_{61}H_{106}O_{34}\cdot0.5\,CHCl_3$: C 51.18, H 7.44, O 37.69; found: C 51.15, H 7.42, O 38.26.

 © 2005 Wiley-VCH Verlag GmbH & Co. KGaA, Weinheim

1: A solution of 2,5-dimercaptomethylpyridine (50 mg, 0.29 mmol) in methanol (2 mL) was added to a solution of 2,3-monoepoxy per-*O*-methylated β-CD (1.0 g, 0.72 mmol) in aqueous 0.1M $NaHCO_3$ (25 mL). The mixture was refluxed under Ar for 24 h. After cooling the reaction mixture to room temperature, it was extracted with $CHCl_3$ (50 mL × 5) and the organic layer was dried over Na_2SO_4. The solvent was removed under reduced pressure, and the residue was purified by column chromatography on silica gel with gradient elution from $CHCl_3$/acetone (5:2 (v/v)) to $CHCl_3$, and then to $CHCl_3$/MeOH 10:1 (v/v) to give **1** as a colorless solid (0.21 g, 20%). ^{1}H NMR (400 MHz, $CDCl_3$): $\delta = 8.50$ (s, 2H, pyH^2), 7.81 (s, 1H, pyH^4), 5.28–5.00 (m, 12H, H^{1B-G}), 4.62 (d, 2H, $J = 7.6$ Hz, H^{1A}), 4.35 (m, 2H, H^{5A}), 4.10–3.14 (m, 200H, $-OCH_3$ and other H$^{2-6}$ protons), 3.03 ppm (dd, 2H, $J = 10.8$, 2.8 Hz, H^{3A}). The assignments of the ^{1}H NMR spectrum were performed by measuring the H–H COSY spectrum and by comparison with literature values.[9a,18b] MS (FAB, *m*-nitrobenzyl alcohol): *m*/*z* 2938 (calcd for M^+: 2938.23). Elemental analysis (%) calcd for $C_{129}H_{221}NO_{68}S_2$: C 52.73, H 7.58, N 0.48, O 37.03; found: C 51.96, H 7.31, N 0.62, O 36.89. The ^{1}H NMR and H–H COSY spectra of **1** are shown in the Supporting Information.

UV/Vis absorption spectra were measured on a Shimadzu UV-2100 spectrophotometer with a thermostatic cell holder. ^{1}H NMR spectra were recorded on a JEOL JNM-A400 spectrometer (400 MHz) in D_2O (CEA, 99.9%) using sodium 3-trimethylsilyl[2,2,3,3-$^2H_4$]propionate (TSP, Aldrich) as an external standard or in $CDCl_3$ (CEA, 99.8%) and tetramethylsilane as an internal standard. Mixed O_2–N_2 gases with various partial pressures of oxygen were prepared with a KOFLOC GM-4B gas-mixing apparatus (Kyoto, Japan). $P_{1/2}$ values were determined according to the procedure described in the literature.[6b,20] The average value of five repeated measurements was employed.

Received: August 11, 2004
Revised: September 24, 2004

Keywords: cyclodextrins · inclusion compounds · metalloproteins · porphyrinoids · supramolecular chemistry

[1] K. Shikama, *Chem. Rev.* **1998**, *98*, 1357–1373.
[2] J. P. Collman, R. Boulatov, C. J. Sunderland, L. Fu, *Chem. Rev.* **2004**, *104*, 561–588.
[3] M. Momenteau, C. A. Reed, *Chem. Rev.* **1994**, *94*, 659–698.
[4] a) E. Tsuchida, H. Nishide, M. Yuasa, E. Hasegawa, Y. Matsushita, *J. Chem. Soc. Dalton Trans.* **1984**, 1147–1151; b) T. Komatsu, M. Moritake, A. Nakagawa, E. Tsuchida, *Chem. Eur. J.* **2002**, *8*, 5469–5480; c) E. Tsuchida, *Artificial Red Cells*, Wiley, New York, **1995**.
[5] a) T. Komatsu, K. Hamamatsu, E. Tsuchida, *Macromolecules* **1999**, *32*, 8388–8391; b) T. Komatsu, T. Okada, M. Moritake, E. Tsuchida, *Bull. Chem. Soc. Jpn.* **2001**, *74*, 1695–1702; c) A. Nakagawa, T. Komatsu, N. Ohmichi, E. Tsuchida, *Chem. Lett.* **2003**, 504–505.
[6] a) P. J. Dandliker, F. Diederich, J.-P. Gisselbrecht, A. Louati, M. Gross, *Angew. Chem.* **1995**, *107*, 2906–2909; *Angew. Chem. Int. Ed. Engl.* **1995**, *34*, 2725–2728; b) A. Zingg, B. Felber, V. Gramlich, L. Fu, J. P. Collman, F. Diederich, *Helv. Chim. Acta* **2002**, *85*, 333–351.
[7] D.-L. Jiang, T. Aida, *Chem. Commun.* **1996**, 1523–1524.
[8] a) K. Kano, H. Tanaka, Y. Minamizono, Y. Kawakita, *Chem. Lett.* **1996**, 925–926; b) K. Kano, R. Nishiyabu, T. Asada, Y. Kuroda, *J. Am. Chem. Soc.* **2002**, *124*, 9937–9944.
[9] a) T. Jiang, D. K. Sukumaran, S.-D. Soni, D. S. Lawrence, *J. Org. Chem.* **1994**, *59*, 5149–5155; b) T. Jiang, D. S. Lawrence, *J. Am. Chem. Soc.* **1995**, *117*, 1857–1858.
[10] K. Kano, H. Kitagishi, S. Tamura, A. Yamada, *J. Am. Chem. Soc.* **2004**, *126*, 15202–15210.
[11] W. R. Sheidt, C. A. Reed, *Chem. Rev.* **1981**, *81*, 543–555.
[12] M. Momenteau, J. Mispelter, B. Loock, J.-M. Lhoste, *J. Chem. Soc. Perkin Trans. 1* **1985**, 221–231.
[13] J. P. Collman, P. C. Herrmann, L. Fu, T. A. Eberspacher, M. Eubanks, B. Boitrel, P. Hayoz, X. Zhang, J. I. Brauman, V. W. Day, *J. Am. Chem. Soc.* **1997**, *119*, 3481–3489.
[14] S. Hirota, T. Ogura, E. H. Appelman, K. Shinzawa-Itoh, S. Yoshikawa, T. Kitagawa, *J. Am. Chem. Soc.* **1994**, *116*, 10564–10570.
[15] Y. Sugawara, K. Shikama, *Eur. J. Biochem.* **1980**, *110*, 241–246.
[16] H. Zhou, J. T. Groves, *Biophys. Chem.* **2003**, *105*, 639–648.
[17] R. Breslow, S. D. Dong, *Chem. Rev.* **1998**, *98*, 1997–2011.
[18] a) D. Rong, V. T. D'Souza, *Tetrahedron Lett.* **1990**, *31*, 4275–4278; b) R. Breslow, A. W. Czarnik, M. Lauer, R. Leppkes, J. Winkler, S. Zimmerman, *J. Am. Chem. Soc.* **1986**, *108*, 1969–1979.
[19] E. B. Fleisher, J. M. Palmer, T. S. Srivastava, A. J. Chatterjee, *J. Am. Chem. Soc.* **1971**, *93*, 3162–3167.
[20] J. P. Collman, X. Zhang, K. Wong, J. I. Brauman, *J. Am. Chem. Soc.* **1994**, *116*, 6245–6251.

 © 2005 Wiley-VCH Verlag GmbH & Co. KGaA, Weinheim

Metal–Radical Complexes

An Unprecedented Bridging Phenoxyl Radical in Dicopper(II) Complexes: Evidence for an $S=\frac{3}{2}$ Spin State**

Fabien Michel, Stéphane Torelli, Fabrice Thomas, Carole Duboc, Christian Philouze, Catherine Belle, Sylvain Hamman, Eric Saint-Aman, and Jean-Louis Pierre*

The cooperativity between a radical and a transition-metal ion in a single molecular entity is demonstrated in highly sophisticated biocatalysts.[1] Galactose oxidase, which has an

[*] F. Michel, Dr. S. Torelli, Dr. F. Thomas, Dr. C. Philouze, Dr. C. Belle, Dr. S. Hamman, Pr. J.-L. Pierre
Laboratoire d'Etudes Dynamiques et Structurales de la Sélectivité
Equipe de Chimie Biomimétique
UMR CNRS 5616, ICMG FR CNRS 2607
Université J. Fourier
BP 53, 38041 Grenoble Cedex 9 (France)
Fax: (+33) 4-7651-4836
E-mail: fabrice.thomas@ujf-grenoble.fr

Dr. C. Duboc
High Magnetic Field Laboratory
CNRS-MPI UPR 5021
BP 166, 38042 Grenoble Cedex 9 (France)

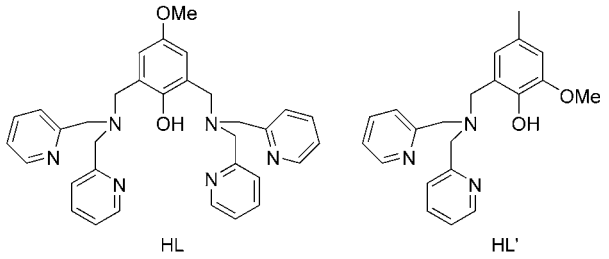
Pr. E. Saint-Aman
LEOPR, UMR CNRS 5630, ICMG FR CNRS 2607
Université J. Fourier
BP 53, 38041 Grenoble Cedex 9 (France)

[**] The authors thank the Institute of Metals in Biology of Grenoble, which provided facilities for the EPR studies, and Dr. Stephane Ménage for technical assistance with these experiments and fruitful discussions.

Supporting information for this article is available on the WWW under http://www.angewandte.org or from the author.

 © 2005 Wiley-VCH Verlag GmbH & Co. KGaA, Weinheim DOI: 10.1002/anie.200461462

active site composed of a tyrosyl radical magnetically coupled to a cupric ion, nicely exemplifies this synergy. In this example the two redox centers work together to promote the two-electron oxidation of primary alcohols to give aldehydes.[2] For a better understanding of the metal–radical interaction (and its biological relevance), transition-metal complexes involving one or two coordinating radicals have been characterized recently.[3] So far no complexes with a bridging radical have been reported. We describe herein an unprecedented metal–radical system, a dicopper(II) μ-phenoxyl complex. This was achieved using the dicopper(II) complexes of the dinucleating ligand HL. Its oxidative chemistry is compared to that of the copper(II) complex of the mononucleating analogue HL′.



When two equivalents of $Cu(ClO_4)_2{\cdot}6H_2O$ and HL were mixed in acetonitrile in the presence of one equivalent of NEt_3, complex $[L(CH_3CN)_2Cu_2]^{3+}$ (**1**) was obtained as its ClO_4^- salt.[4] Its crystal structure (Figure 1) shows that the ligand binds two copper(II) atoms having square-pyramidal geometry through coordination to three nitrogen atoms from the ligand (two pyridyl N atoms and one tertiary amino group) and one from an exogenous acetonitrile molecule. The coordination sphere is completed by an oxygen atom of a μ-phenolato group, which bridges the two metal centers having a separation of 4.06 Å. The use of HL and two equivalents of both $Cu(ClO_4)_2{\cdot}6H_2O$ and NEt_3 affords complex $[L(\mu OH)Cu_2]^{2+}$ (**2**) as its ClO_4^- salt.[5,6] Its crystal structure (Figure 1) has been previously reported:[5] the coordination sphere of the copper atoms contains three nitrogen atoms from the ligand (two pyridyl and one tertiary amino group) completed by two oxygen atoms (from one phenolato and one hydroxo groups) which bridge the metal centers. The two copper ions have trigonal-bipyramidal coordination geometry, with a Cu–Cu distance of 2.98 Å. Addition of one equivalent of $Cu(CF_3SO_3)_2$ or $Cu(ClO_4)_2{\cdot}6H_2O$ to HL′ in acetonitrile in the presence of one equivalent of NEt_3 affords the dimer $[L'Cu]_2^{2+}$ (**3**) as its $CF_3SO_3^-$ or ClO_4^- salt (Figure 1).[4] In **3** each copper atom is coordinated by two pyridyl nitrogens, one amino nitrogen, and two μ-phenolato oxygens (one from each ligand), and the intermetallic distance is 3.12 Å. This dimer is relatively stable, as reflected by its K_{py} value of 0.297 M^{-1}.[7] All the ligands thus afford copper(II) complexes involving at least one coordinating μ-phenolato unit.

The UV/Vis spectra of **1** (Figure 2), **2**, and **3** exhibit a μ-phenolato-to-copper charge-transfer (CT) transition in the region between 450 and 550 nm, and a broad absorption at

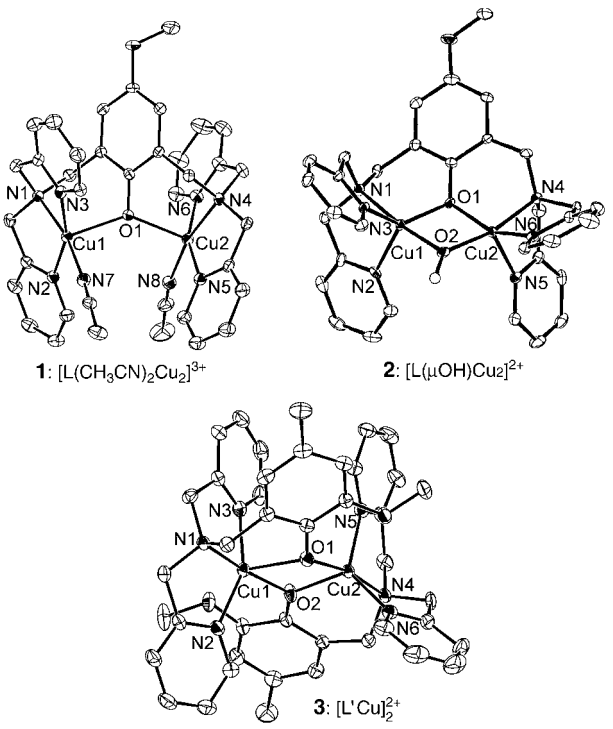


Figure 1. X-ray crystal structures of **1**–**3** (ORTEP diagrams, thermal ellipsoids at the 30% probability level). Selected bond lengths [Å] and angles [°]: $[L(CH_3CN)_2Cu_2]^{3+}$ (**1**): Cu1-O1 2.170(2), Cu2-O1 2.150(2), Cu1-Cu2 4.059(5), Cu1-O1-Cu2 140.0(1); $[L(\mu OH)Cu_2]^{2+}$ (**2**):[5] Cu1-O1 1.997(3), Cu2-O1 2.039(3), Cu1-Cu2 2.980(9), Cu1-O-Cu2 95.2(2); $[L'Cu]_2^{2+}$ (**3**): Cu1-O1 2.077(2), Cu1-O2 1.923(2), Cu2-O1 1.917(2), Cu2-O2 2.303(2), Cu1-Cu2 3.123(5), O1-Cu1-O2 82.72(7), O1-Cu2-O2 77.05(7).

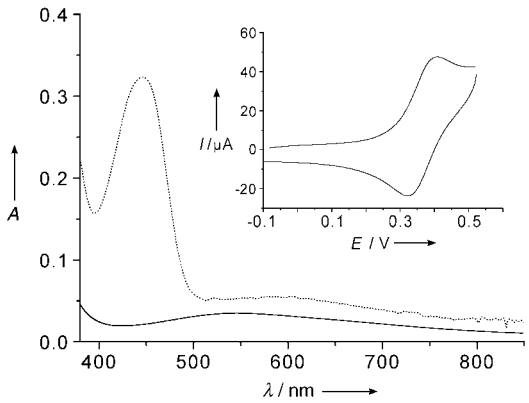


Figure 2. Electronic spectra of 0.1 mM solutions of **1** (solid lines) and electrochemically generated $\mathbf{1}^{\bullet+}$ (dotted lines) recorded in CH_3CN (0.01 M TBAP) at 233 K ($l = 1$ cm). Inset: Cyclic voltamogram (under Ar atmosphere) of **1** (1 mM in CH_3CN, 0.1 M TBAP) at 298 K; scan rate: 0.1 Vs^{-1}.

higher wavelengths attributed to d–d transitions.[8] The X-band EPR spectrum of **1** in CH_3CN exhibits a $\Delta M_S = \pm 2$ transition at $g = 4.3$, associated with spin triplet resonances at $g = 2.24$ and 1.99, indicating that the two copper(II) atoms are weakly ferromagnetically exchange-coupled. The zero-field splitting (zfs) parameters ($D = 0.036\ cm^{-1}$, $E = 0\ cm^{-1}$) and

 © 2005 Wiley-VCH Verlag GmbH & Co. KGaA, Weinheim

$g_{\parallel} = 2.30$, $g_{\perp} = 2.07$ were obtained from simulation. Using the point dipole approximation,[9] we calculated a 4.5-Å separation between the two copper(II) atoms, a value in reasonable agreement with the X-ray structure analysis. Complex **2** is EPR-silent, indicating that the two copper(II) atoms are strongly antiferromagnetically exchange-coupled, due to optimal magnetic orbital overlap.[5] Complex **3** exhibits a ferromagnetic coupling between the two copper atoms similar to that in **1** but with larger zfs parameters ($D = 0.080\ cm^{-1}$, $E = 0.027\ cm^{-1}$, $g_1 = 2.04$, $g_2 = 2.06$, $g_3 = 2.12$), as is expected for a complex with a shorter intermetallic separation. (The complex $[L'(py)Cu]^+$ exhibits a $S_{Cu} = \frac{1}{2}$ signal typical for a mononuclear copper(II) complex).

The cyclic voltammograms of **1** (Figure 2 inset) and **2** in CH_3CN (0.1 M tetrabutylammonium perchlorate (TBAP)) display a reversible one-electron wave in the positive region of potentials ($E_{1/2} = 0.36$ V vs Fc^+/Fc, $\Delta E_p = 0.09$ V and $E_{1/2} = 0.45$ V, $\Delta E_p = 0.09$ V for **1** and **2**, respectively), attributed to the oxidation of the μ-phenolato moiety into a μ-phenoxyl radical.[10] This signal is irreversible both for **3** (at $E_p^a = 0.45$ V) and $[L'(py)Cu]^+$ (at $E_p^a = 0.14$ V), showing that the radical evolves on the experiment timescale. Complexes **1**–**3** are thus oxidized in the same potential range, highlighting that the structure of the complex affects weakly the oxidation potential of the μ-phenolato ligand. However, $[L'(py)Cu]^+$ is oxidized at a potential 0.3 V lower, which can be explained by the lower electron density at the oxygen atom of a μ-phenolato ligand compared to that of a phenolate group. In addition, we have previously shown that species such as **3** do not retain their dimeric structure upon oxidation: if they are stable enough to be generated, the phenoxyl radical species evolve towards the corresponding monomers.[11] Thus, only **1** and **2** could be oxidized to give complexes with bridging phenoxyl radicals.

The one-electron-oxidized complexes $\mathbf{1}^{\bullet+}$ and $\mathbf{2}^{\bullet+}$ exhibit similar UV/Vis features: π–π* transitions typical of phenoxyl radicals[12] are observed at 440 nm ($3330\ M^{-1}cm^{-1}$) and 600 nm ($560\ M^{-1}cm^{-1}$) for $\mathbf{1}^{\bullet+}$ (Figure 2), and at 445 nm ($4730\ M^{-1}cm^{-1}$)[13] and 600 nm ($1000\ M^{-1}cm^{-1}$)[13] for $\mathbf{2}^{\bullet+}$. From the decay of the former band, a half-life of 22.3 min was obtained for $\mathbf{1}^{\bullet+}$ at 298 K, and of less than 20 s for $\mathbf{2}^{\bullet+}$ at 290 K.

The 9.4-GHz EPR spectrum of the electrochemically generated $\mathbf{1}^{\bullet+}$ recorded at 4 K (Figure 3) exhibits a $\Delta M_S = \pm 3$ transition at $g = 8$, typical of an $S = \frac{3}{2}$ spin state, whose intensity is proportional to the reciprocal of the absolute temperature (T^{-1}). This quartet thus corresponds to the ground state.[14] The zfs parameters $D = -0.056\ cm^{-1}$ and $E = 0.015\ cm^{-1}$ ($g_{\parallel} = 2.142$, $g_{\perp} = 2.039$) were obtained from simulation of both the 9.4-GHz and 115-GHz EPR spectra (Figure 3). The D value is close to that reported for an excited $S = \frac{3}{2}$ spin state in a triangular tricopper(II) complex (−53.5 mT),[15] but significantly different from those reported for organic triradicals ($|0.003–0.008|\ cm^{-1}$)[16] and mononuclear bis(phenoxyl) radical copper(II) complexes ($|0.4|\ cm^{-1}$).[17] The 9.4-GHz EPR spectrum of $\mathbf{2}^{\bullet+}$ exhibits two sets of signals, a weak $\Delta M_S = \pm 3$ transition at $g = 8$ and a dominating $S_{Cu} = \frac{1}{2}$ signal (attributed to a degraded complex containing noninteracting copper(II) nuclei) at $g = 2$.

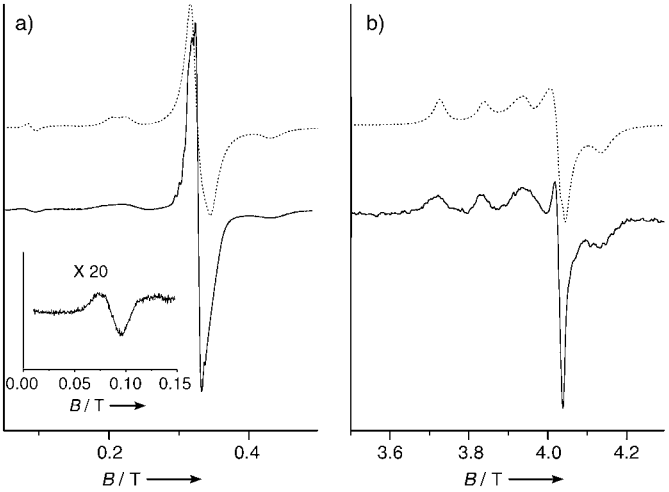


Figure 3. a) X-Band EPR spectrum of electrochemically generated $\mathbf{1}^{\bullet+}$ (1 mM in CH_3CN, 0.1 M TBAP): $T = 4$ K, modulation 0.393 mT/100 kHz, frequency 9.44 GHz, power 1 mW. Solid lines: experimental, dotted lines: simulation. b) 115-GHz EPR spectrum $\mathbf{1}^{\bullet+}$ (5 mM in CH_3CN, 0.1 M TBAP) at $T = 5$ K. Solid lines: experimental, dotted lines: simulation (parameters are given in the text).

Although the $\Delta M_S = \pm 3$ transition is weak (its intensity decreases as the temperature increases), these results demonstrate that $\mathbf{2}^{\bullet+}$ also exhibits a quartet ground state.

In summary, μ-phenoxyl dicopper(II) complexes in which the two copper(II) and the radical spins are ferromagnetically exchange-coupled could be obtained. Their stability, and thus their reactivity, is finely tuned by both the nuclearity of the complex and the nature of coordinating solvent. Since tyrosyl residues are ubiquitous in metalloenzymes, such species could be biologically relevant. On the other hand, the chemical reactivity of these μ-phenoxyl dicopper(II) species which formally contain "three oxidizing equivalents" constitute a promising and fascinating area for the studies of new chemical properties.

Received: July 28, 2004

Keywords: bridging ligands · copper · EPR spectroscopy · magnetic properties · radicals

[1] J. Stubbe, W. A. van der Donk, *Chem. Rev.* **1998**, *98*, 705; W. Kaim, *Dalton Trans.* **2003**, 761.

[2] N. Ito, S. E. V. Phillips, C. Stevens, Z. B. Ogel, M. J. McPherson, J. N. Keen, K. D. S. Yadav, P. J. Knowles, *Nature* **1991**, *350*, 87; J. W. Whittaker in *Advances in Protein Chemistry*, *Vol. 60* (Eds.: F. M. Richards, D. S. Eisenberg, J. Kuriyan), Academic Press, Elsevier, **2002**, p. 1–49.

[3] For reviews see: B. A. Jazdzewski, W. B. Tolman, *Coord. Chem. Rev.* **2000**, *200–202*, 633; S. Itoh, M. Taki, S. Fukuzumi, *Coord. Chem. Rev.* **2000**, *198*, 3; P. Chaudhuri, K. Wieghardt, *Prog. Inorg. Chem.* **2001**, *50*, 151.

[4] Crystal data: for $\mathbf{1}(ClO_4^-)_3 \cdot 0.33\,H_2O \cdot 0.66\,EtOH$: $C_{40.33}H_{46.67}Cl_3Cu_2N_9O_{15}$, purple–blue prisms, monoclinic, space group $P21/c$, $a = 21.322(2)$, $b = 10.920(3)$, $c = 23.131(5)$ Å, $\alpha = 90$, $\beta = 115.41(1)$, $\gamma = 90°$, $V = 4864.5(6)$ Å^3, $Z = 4$, $D = 1.544\ g\,cm^{-3}$, $T = 294$ K, $F(000) = 2322.60$, $\mu = 1.114\ mm^{-1}$,

$\lambda(Mo_{K\alpha}) = 0.71073$ Å, 55223 reflections collected, 13287 unique, 8321 reflections ($I > 2\sigma$), $R_{int} = 0.07971$. The final agreement factors are $R_1 = 0.0609$ for data with $F_0 > 2\sigma(F_0)$ and $wR_2 = 0.1006$ for all data. CCDC 244865 contains the supplementary crystallographic data for this paper. These data can be obtained free of charge via www.ccdc.cam.ac.uk/conts/retrieving.html (or from the Cambridge Crystallographic Data Centre, 12, Union Road, Cambridge CB21EZ, UK; fax: (+44) 1223-336-033; or deposit@ccdc.cam.ac.uk); for $\mathbf{3}_{1.5}(ClO_4^-)_3$: $C_{63}H_{66}Cl_3Cu_3N_9O_{18}$, brown needles, triclinic, space group $P-1$, $a = 12.605(1)$, $b = 13.213(1)$, $c = 21.692(2)$ Å, $\alpha = 74.5(3)$, $\beta = 86.8(3)$, $\gamma = 67.6(3)°$, $V = 3214(6)$ Å^3, $Z = 2$, $D = 1.585$ g.cm^{-3}, $T = 150$ K, $F(000) = 1578$, $\mu = 1.188$ mm^{-1}, $\lambda(Mo_{K\alpha}) = 0.71073$ Å, 43303 reflections collected, 21243 unique, 16811 reflections ($I > 2\sigma$), $R_{int} = 0.06431$. The final agreement factors are $R_1 = 0.0547$ for data with $F_0 > 2\sigma(F_0)$ and $wR_2 = 0.0763$ for all data. CCDC 245087 contains the supplementary crystallographic data for this paper. These data can be obtained free of charge via www.ccdc.cam.ac.uk/conts/retrieving.html (or from the Cambridge Crystallographic Data Centre, 12, Union Road, Cambridge CB21EZ, UK; fax: (+44) 1223-336-033; or deposit@ccdc.cam.ac.uk).

[5] C. Belle, C. Béguin, I. Gautier-Luneau, S. Hamman, C. Philouze, J.-L. Pierre, F. Thomas, S. Torelli, E. Saint-Aman, M. Bonin, *Inorg. Chem.* **2002**, *41*, 479.

[6] Mixing only one equivalent of $Cu(ClO_4)_2 \cdot 6H_2O$ and HL in acetonitrile in the presence of one equivalent of NEt_3 did not afford the expected mononuclear copper(II) complex of HL. Instead, **2** was isolated in 40% yield.

[7] Addition of pyridine (py) to **3** induces a dimmer-to-monomer conversion yielding $[L'(py)Cu]^+$. The exogenous pyridine coordinates to the copper instead of one μ-phenolato oxygen. $K_{py} = ([L'(py)Cu]^{+2}/([pyridine]^2[[L'Cu]_2^{2+}])$ was determined by UV/Vis titration from the equilibrium: $[L'Cu]_2^{2+} + 2\,pyridine \rightleftarrows 2\,[L'(py)Cu]^+$.

[8] UV/Vis data (λ_{max} (nm), ε ($M^{-1}cm^{-1}$) in CH_3CN: **1**: 547 (350), d–d transitions appear as a broad shoulder; **2**: 447 (330), 805 (190); **3**: 463 (340), 880 (250); $[L'(py)Cu]^+$: 531 (330), 880 (210).

[9] R. Srinivasan, I. Sougandi, K. Velavan, R. Venkatesan, B. Verghese, P. Sambasiva Rao, *Polyhedron* **2004**, *23*, 1115.

[10] A linear dependence of $E_{1/2}$ as a function of the μ-phenolate σ^+ Hammet constant is observed for related compounds (Figure S8 in the Supporting Information). Moreover, the UV/Vis feature of the oxidized species matches well that reported for methoxyphenoxyl–copper(II) complexes (D. Zurita, I. Gautier-Luneau, S. Ménage, J.-L. Pierre, *J. Biol. Inorg. Chem.* **1997**, *2*, 46; Y. Shimazaki, S. Huth, S. Hirota, O. Yamauchi, *Inorg. Chim. Acta* **2002**, *331*, 168). This further confirms that the one-electron electrochemical process is ligand-based rather than metal-based.

[11] This is evident in the CV curve from an irreversible anodic signal (corresponding to the oxidation of the bridging phenolato moiety) associated, in the reverse scan, with a cathodic peak which is observed ca. 0.3 V lower, that is, at a potential value similar to that of the nonbridging phenoxyl/phenolato couple: See F. Michel, F. Thomas, S. Hamman, E. Saint-Aman, C. Bucher, J.-L. Pierre, *Chem. Eur. J.* **2004**, *10*, 4115.

[12] J. G. Radziszewski, M. Gil, A. Gorski, J. Spanget-Larsen, J. Waluk, B. J. Mroz, *J. Chem. Phys.* **2001**, *115*, 9733.

[13] The ε values are probably under estimated for $\mathbf{2}^{\cdot+}$ due to its low stability.

[14] The 9.4-GHz EPR spectrum of $\mathbf{1}^{\cdot+}$ measured at 215 K lacks most of the transitions associated with the quartet. It still exhibits a signal at $g = 2.06$ that could be attributed to an excited ($S = \frac{1}{2}$) state, indicating that the exchange constant J is weak.

[15] B. Cage, F. A. Cotton, N. S. Dalal, E. A. Hillard, B. Rakvin, C. M. Ramsey, *C. R. Chim.* **2003**, *6*, 39.

[16] E. Beer, J. Daub, C. Palivan, G. Gescheidt, *J. Chem. Soc. Perkin Trans. 2* **2002**, 1605; D. A. Schultz, R. K. Kumar, *J. Am. Chem. Soc.* **2001**, *123*, 6431.

[17] E. Bill, J. Müller, T. Weyhermüller, K. Wieghardt, *Inorg. Chem.* **1999**, *121*, 5795; F. Thomas, O. Jarjayes, C. Duboc, C. Philouze, E. Saint-Aman, J.-L. Pierre, *Dalton Trans.* **2004**, 2662.

 © 2005 Wiley-VCH Verlag GmbH & Co. KGaA, Weinheim

Nanostructures

Inversion of Emulsions Stabilized Solely by Ionizable Nanoparticles**

Bernard P. Binks and Jhonny A. Rodrigues*

Emulsions occur as end products in a wide range of areas including the pharmaceutical, food, and cosmetic industries. They are mixtures of immiscible liquids where one liquid is dispersed as micrometer-sized drops in the continuous phase of the other.[1] To prevent separation, surfactants are usually added whose molecules cover the liquid–liquid interfaces. Recently,[2–5] it has been shown that certain solid nanoparticles act as excellent emulsifiers alone and, since particles are more strongly attached to interfaces, coalescence is absent. However, different types of particles are needed to prepare either oil-in-water (o/w) or water-in-oil (w/o) emulsions in mixtures containing equal volumes of the two liquids.[3,5–8] Herein we describe a new class of solid particle emulsifier capable of stabilizing both emulsion types efficiently. The spherical nanoparticles are those of polystyrene whose surfaces are coated with ionizable carboxylic acid groups. Inversion of the emulsion type is simply effected by either a change in the pH value or salt concentration. It should be possible to prepare a new range of stable simple and multiple emulsions by tuning the type and charge of such responsive emulsifiers.

Certain small solid particles act in many ways like surfactant molecules that adsorb at fluid–fluid interfaces and stabilize drops in emulsions and bubbles in foams.[3] It is only recently, however, that their precise role has been elucidated in surfactant-free systems. Particles stabilize emulsions in two ways:[2] In the first, they adsorb at the oil–water interface and remain there forming a film around dispersed drops and impede coalescence, and in the second, additional stabilization arises when the particle–particle interactions are such that a three-dimensional network of particles develops in the continuous phase. The enhanced

[*] Prof. B. P. Binks, J. A. Rodrigues
Surfactant & Colloid Group
Department of Chemistry
University of Hull
Hull HU6 7RX (UK)
Fax: (+44) 1482-466-410
E-mail: b.p.binks@hull.ac.uk

[**] This work was funded by GlaxoSmithKline, Weybridge (UK).

 DOI: 10.1002/anie.200461846 © 2005 Wiley-VCH Verlag GmbH & Co. KGaA, Weinheim

viscosity reduces the extent of gravity-induced separation. Hydrophilic particles, for example, metal oxides, tend to stabilize o/w emulsions whereas hydrophobic particles, for example, carbon, tend to stabilize w/o emulsions.[6–8] The different tendency is linked to the contact angle θ (measured through water) that particles exhibit at the interface. Inversion of emulsions from w/o to o/w is predicted to occur as the value of θ falls below 90°. If the particles are small enough (less than a few μm), the energy ΔG required to remove a spherical particle of radius r from an oil–water interface of tension γ_{ow} is given by Equation (1).[8,9]

$$\Delta G = \pi r^2 \gamma_{ow}(1 \pm \cos\theta)^2 \quad (1)$$

The sign inside the bracket is negative for removal into water and positive for removal into oil. When $r = 10^{-7}$ m (the size of the particles used here) and $\gamma_{ow} = 0.0533\ \mathrm{N\,m^{-1}}$ (hexadecane–water, 298 K), Equation (1) shows that the particle is most strongly held in the interface for $\theta = 90°$, with ΔG being $4.07 \times 10^5\ k_B T$. One consequence of this very high energy for the attachment of particles to fluid interfaces is that they can be thought of as irreversibly adsorbed, which is in marked contrast to surfactant molecules which adsorb and desorb. The absence of coalescence and the large range of particle types and shapes makes particle-stabilized emulsions attractive.

Control of the type of emulsion is important, as is the ability to invert from one to the other. Until now, obtaining both types of emulsion in a particular oil–water system was only possible by utilizing particles of different wettability,[5,8] by changing the oil:water ratio,[10] or by adding surfactant which adsorbs on particle surfaces and modifies their wettability in situ.[2] These routes may not be suitable in many cases. We describe here a simple strategy to invert these emulsions by using polystyrene nanoparticles whose surfaces contain carboxylic acid groups. Particles can be made sufficiently more or less hydrophilic for them to stabilize both types of emulsion in the same system by controlling the degree of charge on the particle surfaces (by changing the pH value or addition of salt). It was not possible to achieve this degree of control previously. Polystyrene particles containing surface sulfate groups preferentially formed w/o emulsions,[11] that is, these particles are relatively hydrophobic. In contrast, polystyrene particles with grafted copolymer molecules containing amine groups stabilized only o/w emulsions[12] since the particles were rendered more hydrophilic.

Spherical, monodisperse, surfactant-free polystyrene particles can be synthesized with different densities of carboxylic acid groups on their surfaces. Under conditions where these groups are predominantly un-ionized (COOH), the particles are expected to be more hydrophobic and stabilize water drops in oil relative to ionizing conditions (COO^-) in which the particles are more hydrophilic and should stabilize oil drops in water. Hexadecane–water emulsions (1:1 by volume) with particles of 200-nm diameter and high surface charge density (101 $\mu C\,cm^{-2}$) were o/w at all pH values between 2 and 11 and salt (NaCl) concentrations between 0 and 2 M. The same sized particles act as excellent emulsifiers for both emulsion types, however, when the charge density is reduced (12.7 $\mu C\,cm^{-2}$). Figure 1 shows the variation of the emulsion conductivity (immediately after preparation) with the pH value of the aqueous phase in systems containing 1 M

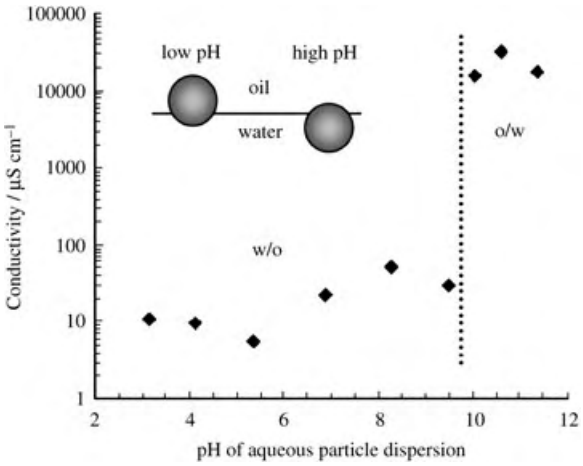


Figure 1. Inversion of particle-stabilized emulsions by changing the pH value. The plot shows the conductivity of emulsions of hexadecane and 1 M aqueous NaCl (1:1) stabilized by 2 wt% of carboxy-coated polystyrene latex particles (200 nm diameter) at different pH values. Emulsions are w/o below pH 9.5 and o/w at pH ≥ 10.0. The inset depicts the change in the position of a particle at the interface; low pH: $\theta > 90°$ and high pH: $\theta < 90°$.

NaCl. Up to pH 9.5, emulsions are of low conductivity (similar to pure oil), disperse in oil and not water, and are therefore w/o. Inversion (dotted line) to highly conducting (similar to aqueous NaCl) o/w emulsions, which disperse in water and not oil, occurs just below pH 10.0. The inset illustrates the effect of the pH value on the position of these particles at an interface. We note that emulsions were w/o at all pH values in the presence of 0.01 M NaCl and could not be inverted in this way.

The appearance of the emulsions at high salt concentration is shown in Figure 2 for different pH values, one year after preparation. All emulsions were completely stable to coalescence, as shown by no visible separation of the dispersed phase occurring and the drop-size distributions determined by light diffraction studies remaining unchanged. Since the density of hexadecane is less than that of water, sedimentation of the w/o emulsions occurs over time, with a clear oil phase separating above (3 vials on left), whereas o/w emulsions cream to the top of the vessel as a clear water phase drains below (3 vials on right). Although the dispersed phase volume fraction in both the sedimented and creamed emulsions increases from 0.5 to over 0.75, the emulsion drops remain stable to coalescence because the adsorbed layers of polystyrene particles act as a mechanical barrier to fusion. To visualize the particles around drops emulsions were prepared at low and high pH values using larger particles (3.2 μm diameter) of approximately the same surface charge density (11.8 $\mu C\,cm^{-2}$). Optical micrographs of similar-sized emulsion drops are shown in Figure 3. The left image is that of a water drop in oil formed at a low pH value. The particles

 © 2005 Wiley-VCH Verlag GmbH & Co. KGaA, Weinheim

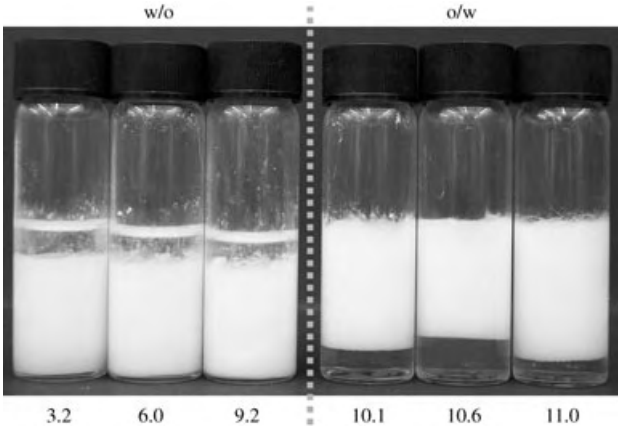


Figure 2. Appearance of vials at 25 °C of systems containing hexadecane and 1 M aqueous NaCl (1:1) and 2 wt% carboxy-coated polystyrene latex particles of 200 nm diameter as a function of the pH value (given). Emulsions (white) are w/o at pH $\leq$ 9.5 (left) and undergo sedimentation to liberate a clear oil phase above, and are o/w at pH $\geq$ 10.0 (right) which cream with a clear aqueous phase separating below. All emulsions are completely stable to coalescence.

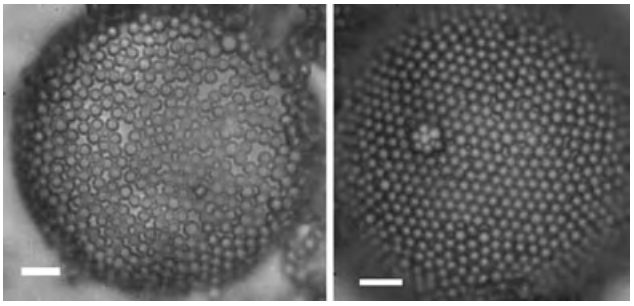


Figure 3. Optical micrographs of single w/o (left) and o/w (right) emulsion drops in hexadecane:1 M aqueous NaCl mixtures (1:1) stabilized by 3.2-μm diameter carboxy-coated polystyrene latex particles. The water drops are favored at low pH values (< 9.5) and particles are less than close-packed at their interfaces. The oil drops are favored at high pH values ($\geq$ 10.0) and particles are hexagonally close-packed. Scale bars are 10 μm.

cover most of the oil–water interface, but arrange themselves in a liquidlike order with parts of the interface devoid of particles. We observed that particles in the aqueous dispersions before emulsification were strongly flocculated at low pH values because of the absence of repulsion between uncharged COOH groups on the surface. It appears that some of the flocs adsorb intact to interfaces of the drop leaving voids between them. In contrast, the image on the right is that of an oil drop in water formed at a high pH value in which particles appear hexagonally close-packed over the entire interface. Dissociation of the acid groups occurs at these high pH values, and repulsion between like-charged particle surfaces in the bulk phase causes breakup of the flocs and results in a dispersion of discrete particles to be stabilized.

It is difficult to test our hypothesis that raising the pH value results in hydrophobic particles becoming increasingly hydrophilic, since a reliable method for determining the contact angles of submicron-sized particles at oil–water interfaces does not exist. However, the idea is given some credence from the contact angle data of water drops under oil on monolayers of a long-chain carboxylic acid adsorbed through a terminal thiol group on to gold.[13] The value of θ (through water) for a dilute layer of surface COOH groups decreases from 104° at pH 2 through 90° to 67° at pH 13 as the acid groups ionize and become more wettable by water. This decrease is in line with emulsion inversion from w/o to o/w with increasing pH value.

Charged particles are also sensitive to the presence of electrolyte.[14,15] A second way to effect emulsion inversion is to start with a hydrophilic system that forms an o/w emulsion and reduce the salt concentration, thus rendering the system more hydrophobic. Table 1 summarizes the influence of NaCl

Table 1: Effect of salt concentration on the conductivity (κ) and type of emulsions prepared.[a]

NaCl [M]	κ [μS cm^{-1}]	Type
0.30	20.5	w/o
0.42	26.8	w/o
0.47	33.4	w/o
0.54	34.2	w/o
0.66	17720	o/w
0.79	21200	o/w
1.15	31500	o/w
2.15	49500	o/w

[a] From hexadecane and aqueous NaCl (1:1) containing 2 wt% of carboxy-coated polystyrene latex particles (200 nm diameter) at pH 10.6 at 25 °C.

concentration on the conductivity and type of 1:1 emulsions stabilized by the same particles above: at high pH value, they invert from o/w to w/o on lowering the salt concentration to 0.6 M, as predicted. All emulsions were stable to coalescence. In summary, emulsions stabilized by ionizable carboxy-coated polystyrene nanoparticles invert from w/o to o/w upon increasing either the pH value or salt concentration as the particles become more hydrophilic. The reason for this change is that the degree of ionization of the surface acid groups increases not only with pH value but also with salt concentration.[14–16] A relatively high pH value (10) is required for inversion compared with the pH value for 50% ionization (pK_a) of a short-chain carboxylic acid in bulk water (4.8). Acid dissociation is more energetically unfavorable when such groups are at an interface (particle or drop) compared with isolated groups in the bulk phase because of the proximity of other similarly charged groups, which generate a surface potential ψ. For the particles used here, the area per charged group is approximately 1.25 nm^2. Protons are held more strongly at the surface and the surface pH value is lower than that in the bulk phase because of the existence of an electrostatic field around a negatively charged particle. Dissociation of weak acid groups on a surface will therefore only be complete at higher pH values in solution relative to that of a weak acid in the bulk phase. The addition of salt causes a reduction in the value of ψ and promotes further dissociation.

 © 2005 Wiley-VCH Verlag GmbH & Co. KGaA, Weinheim

Nanoparticles are effective emulsifiers of oil and water and, by controlling the extent of charge on their surfaces, ultrastable emulsions of both o/w and w/o can be prepared. Emulsion inversion is simply achieved by changing the pH value or salt concentration if the surface groups are ionizable. Manipulating the behavior of particles adsorbed at fluid interfaces in this way enables the development of a novel range of simple and multiple emulsions for use in food, drug, and cosmetic formulations.

Experimental Section

Methods: The pH value of aqueous dispersions of carboxy-coated, spherical, monodisperse polystyrene latex particles (IDC, Oregon) was adjusted with HCl or NaOH after addition of NaCl electrolyte. Batch emulsions of equal volumes of hexadecane and an aqueous dispersion of the particles were prepared by using an Ultra Turrax T25 homogenizer (1 cm head) operating at 11 000 rpm for 2 min. Their type was determined by measuring the conductivity and by the drop test. Their stabilities at 25 °C were measured by monitoring the movement of the oil–emulsion and water–emulsion interfaces. Drop-size distributions were measured by using a Malvern Master-Sizer 2000 instrument. For microscopy studies, a dilute sample of emulsion was placed in a haemocytometer cell (Weber Scientific) and viewed with a Nikon Labophot microscope fitted with a DIC-U camera (World Precision Instruments). Images were processed by using Adobe Photoshop 5.0 software.

Received: August 31, 2004

Keywords: carboxylic acids · emulsions · interfaces · ionization · nanostructures

[1] *Modern Aspects of Emulsion Science* (Ed.: B. P. Binks), Royal Society of Chemistry, Cambridge, **1998**.
[2] D. E. Tambe, M. M. Sharma, *Adv. Colloid Interface Sci.* **1994**, *52*, 1 – 63.
[3] B. P. Binks, *Curr. Opin. Colloid Interface Sci.* **2002**, *7*, 21 – 41.
[4] E. Vignati, R. Piazza, T. P. Lockhart, *Langmuir* **2003**, *19*, 6650 – 6656.
[5] S. Stiller, H. Gers-Barlag, M. Lergenmueller, F. Pflücker, J. Schulz, K. P. Wittern, R. Daniels, *Colloids Surf. A* **2004**, *232*, 261 – 267.
[6] N. X. Yan, M. R. Gray, J. H. Masliyah, *Colloids Surf. A* **2001**, *193*, 97 – 107.
[7] A. P. Sullivan, P. K. Kilpatrick, *Ind. Eng. Chem. Res.* **2002**, *41*, 3389 – 3404.
[8] B. P. Binks, S. O. Lumsdon, *Langmuir* **2000**, *16*, 8622 – 8631.
[9] S. Levine, B. D. Bowen, S. J. Partridge, *Colloids Surf.* **1989**, *38*, 325 – 343.
[10] B. P. Binks, S. O. Lumsdon, *Langmuir* **2000**, *16*, 2539 – 2547.
[11] B. P. Binks, S. O. Lumsdon, *Langmuir* **2001**, *17*, 4540 – 4547.
[12] J. I. Amalvy, S. P. Armes, B. P. Binks, J. A. Rodrigues, G.-F. Unali, *Chem. Commun.* **2003**, 1826 – 1827.
[13] C. D. Bain, G. M. Whitesides, *Langmuir* **1989**, *5*, 1370 – 1378.
[14] J. Stone-Masui, A. Watillon, *J. Colloid Interface Sci.* **1975**, *52*, 479 – 503.
[15] S. F. Schulz, T. Gisler, M. Borkovec, H. Sticher, *J. Colloid Interface Sci.* **1994**, *164*, 88 – 98.
[16] R. Aveyard, B. P. Binks, N. Carr, A. W. Cross, *Thin Solid Films* **1990**, *188*, 361 – 373.

 © 2005 Wiley-VCH Verlag GmbH & Co. KGaA, Weinheim

Carbene Ligands

An N-Heterocyclic Carbene/Iridium Hydride Complex from the Oxidative Addition of a Ferrocenyl–Bisimidazolium Salt: Implications for Synthesis**

*Mónica Viciano, Elena Mas-Marzá, Macarena Poyatos, Mercedes Sanaú, Robert H. Crabtree, and Eduardo Peris**

Despite the increasing recent use of N-heterocyclic carbenes (NHCs) in the preparation of new homogeneous catalysts, catalytic applications of NHC-based complexes have already been extended to a surprisingly wide range of synthetic organic reactions. The large number of reviews published in the last five years[1–5] shows the rapid development of NHC ligands in catalyst design.

Unlike phosphines, the coordination of NHCs to metal centers requires the activation or deprotonation of a precursor, which makes NHC-based complexes relatively less accessible than the analogous phosphine compounds. Several activation strategies have been used to prepare NHC–metal complexes: 1) insertion of a metal into the C=C bond of bis(imidazolidin-2-ylidene)-containing olefins (Lappert method);[6–8] 2) generation of a free carbene by deprotonation of the corresponding imidazolium precursor with a strong base (for example, NaH, *t*BuOK, *n*ButLi) and addition to the metal fragment;[9–13] 3) transmetalation from a silver–NHC complex prepared by direct reaction of an imidazolium precursor and Ag_2O;[14–17] 4) in situ deprotonation of an imidazolium salt with a weak base (for example, NEt_3, NaOAc, Cs_2CO_3),[18–24] and 5) oxidative addition by activation of the C2–X (X = Me, I, H) bond of an imidazolium cation.[25–31] We have found that methods 3 and 4 afford good results in the preparation of several Rh, Ir, Ru, and Pd complexes under very mild reaction conditions. Methods 2–5 all use imidazolium cations as precursors to the NHC ligands.

[*] M. Viciano, E. Mas-Marzá, M. Poyatos, Dr. E. Peris
Departamento de Química Inorgánica y Orgánica
Universitat Jaume I
12071 Castellón (Spain)
Fax: (+34) 964-728-214
E-mail: eperis@qio.uji.es

Dr. M. Sanaú
Departamento de Química Inorgánica
Universitat de València
46100 Burjassot (Spain)

Prof. R. H. Crabtree
Chemistry Department, Yale University
225 Prospect Street, New Haven
CT 06520-8127 (USA)

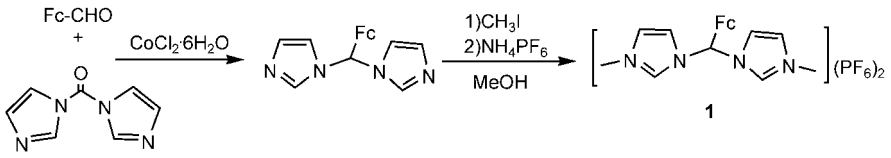
[**] We gratefully acknowledge financial support from the DGESIC (MAT2002-04421-C02-01) and Bancaixa (P1.1B2001-03). We would also like to thank the Spanish MEC for a fellowship (E.M.-M.).

Supporting information for this article is available on the WWW under http://www.angewandte.org or from the author.

 © 2005 Wiley-VCH Verlag GmbH & Co. KGaA, Weinheim DOI: 10.1002/anie.200461918

Experimental and theoretical studies have shown that a σ interaction is the main contribution to the NHC–M bond, with limited π backdonation. As regards the mechanistic aspects of the metalation, most experimental results seem to point to the direct formation of a M–C bond from free carbenes in those cases when an imidazolium precursor and a base are used (strategies 2 and 4), but deprotonation of an agostic CH group cannot be excluded in some cases. Some mechanistic aspects of the oxidative addition of C2–X bonds (X = Me, I, H; method 5) have been studied experimentally[25–29,31] and theoretically,[30] but this reaction has so far been limited to low-valent electron-rich coordinatively unsaturated Group 10 metal complexes. We now report the synthesis of a stable [Ir^{III}(H)(biscarbene)] complex by C2–H oxidative addition of a ferrocenyl–bisimidazolium precursor.

The reaction of bis(imidazolyl)ketone and ferrocene carboxaldehyde at 80 °C in the presence of $CoCl_2 \cdot 6H_2O$ affords bisimidazolylferrocenylmethane (Scheme 1). This compound can be methylated with CH_3I in the presence of NH_4PF_6 to yield the corresponding bis(methylimidazolium) salt **1**. We thought that the introduction of the ferrocenyl moiety could significantly modify the electronic and steric properties of the resulting biscarbene complexes.



Scheme 1. Preparation of bis(imidazolylferrocenylmethane) **1**. Fc = ferrocenyl.

The reaction of **1** with [{M(cod)Cl}$_2$] (cod = 1,5-cyclooctadiene; M = Rh, Ir) in the presence of NEt_3 at room temperature yields two different types of ligand coordination depending on the metal used (Scheme 2). For rhodium, the reaction gives the monometalated complex **2b**, where the ligand adopts a monodentate coordination mode. Compound **2b** was unambiguously characterized by NMR spectroscopic and mass spectrometric analysis. The ^{1}H NMR spectrum reveals that the twofold symmetry of the ligand is lost upon coordination. The downfield shift of the proton in the 2′-position of the imidazolium functionality ($\delta = 8.8$ ppm) shows that one of the rings remains unbound. The signals of the protons of the bound imidazolylidene ring appear at higher field than those of the unbound ring, thus indicating its coordination, as we have previously described for other similar systems.[18,20,23,32] A doublet at $\delta = 185$ ppm ($^1J_{Rh,C} = 49$ Hz) in the ^{13}C NMR spectrum confirms that metalation has occurred. Similar NMR patterns have been observed for related ligands in the monometalated form.[23]

The reaction of **1** with [{Ir(cod)Cl}$_2$] under the same conditions affords the compound **3a**. The NMR spectra confirm that the twofold symmetry of the ligand is maintained upon coordination. The ^{1}H NMR spectrum shows a hydride signal at $\delta = -14.7$ ppm. The two metalated carbon atoms appear as a singlet at $\delta = 145$ ppm. This compound represents the first example of a (NHC)-Ir-hydride complex. Compound **3a** is indefinitely stable in solution at room temperature. The failure of **3a** to reductively eliminate may be related to the chelating character of the bis-NHC, as it keeps the imidazole ring from achieving the rotameric conformation required for reductive elimination with Ir–H normal to the ring plane.

The molecular structure of **3a** was confirmed by single-crystal X-ray diffraction analysis. Figure 1 shows the ORTEP diagram and the more relevant bond lengths and angles. The Ir atom adopts a distorted octahedral geometry with a biscarbene bite angle C-Ir-C of 83.5°. The Ir–C bond lengths of 2.056 and 2.043 Å lie in the range of previously reported Ir–C bond

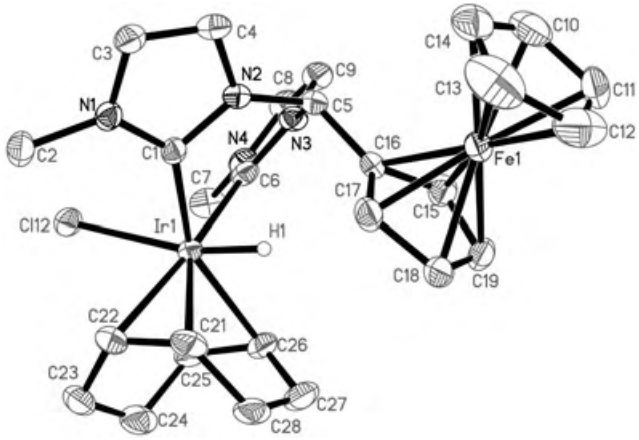
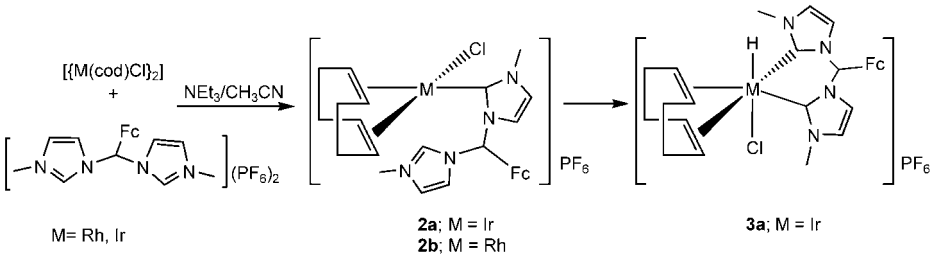


Figure 1. Molecular diagram of **3a**. Hydrogen atoms and the PF_6 anion have been omitted for clarity. Selected bond lengths [Å] and angles [°]: Ir1-C1 2.056(5), Ir1-C6 2.043(5), Ir1-H1 1.35 (6), H1-Cp_c 2.83(7), C6-Ir1-C1 83.4(2), H1-Ir1-Cl12 166(3), H1-Ir1-C1 81(3), H1-Ir1-C6 78(3).



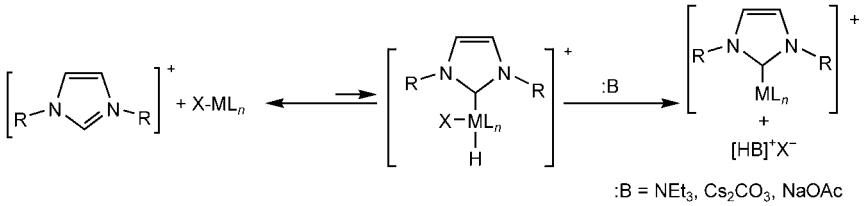
Scheme 2. Different ligand coordination modes produced after reaction of bisimidazolylferrocenylmethane **1** with [{M(cod)Cl}$_2$].

 © 2005 Wiley-VCH Verlag GmbH & Co. KGaA, Weinheim

lengths for NHC ligands.[17,32–34] The Ir–H bond length is 1.35 Å. Interestingly, the ferrocenyl group points towards at the hydride ligand, and so provides a high steric hindrance, which may partially explain the stability of this metal hydride. This steric hindrance is illustrated by the short IrH···Cp_c (Cp_c = centroid of the Cp (C_5H_5) ring) distance of 2.83 Å. This short distance can also be detected in solution by NOE experiments.

To elucidate the mechanism of the metalation process, we performed several reactions to test the reversibility of the last step in the formation of **3a**. We thought that the reaction of **3a** with CO to substitute the cod ligand would likely promote reductive elimination of the carbene and hydride to yield the carbonyl analogue of **2a**. However, the chelate carbene hydride in **3a** was extremely stable and resisted conversion under all the reaction conditions tried. Addition of a weak base (NEt_3, NaOAc) also failed to give the deprotonated compound by reductive elimination of HCl. On the other hand, attempts to metalate **2b** to obtain the rhodium analogue of **3a** failed under a variety of reaction conditions, such as refluxing in CH_3CN, addition of a weak base (NEt_3, NaOAc), or addition of phosphine. However, we were able to obtain the monodentate compound **2a** by treating **1** with [{Ir(cod)Cl}$_2$] in the presence of NEt_3 in CH_3CN for 10 minutes at room temperature. Unfortunately, **2a** could not be quantitatively separated from **3**-Ir, and only 70:30 mixtures of **2a**/**3a** could be isolated. The identification of **2a** was made by NMR spectroscopic and mass spectrometric analysis. The NMR spectrum of **2a** is virtually identical to that of **2b**.

Complex **2a** evolves to give **3a** quantitatively on standing for two hours at room temperature in an NMR tube ($CDCl_3$, [D_6]acetone, [D_6]DMSO) in the absence of an external base. This result now explains why we could not obtain **2a** in a quantitative form, since it spontaneously evolves to give **3a**. This result suggests that the metalation of the imidazolium ring proceeds through oxidative addition of the C2–H bond. If the metalation of the imidazolium precursor takes place in the absence of a base, could the overall reaction proceed without a base? To verify this point we performed the reaction of **1** and [{Ir(cod)Cl}$_2$] in CH_3CN at a range of temperatures (from room temperature to reflux). The reaction mixtures did not show any metalated species even after three days, so the base seems to be a key factor in the formation of the metalated products. Given this result, why should the base be important for the first step of the metalation (formation of compounds **2a** and **2b**) and not for the second one (formation of **3a**)? Previously, we have shown that the addition of a weak base facilitates the activation of the imidazolium precursor to yield the corresponding NHC compounds.[18–23] The p*K* values of the species involved make us think that NEt_3 is not strong enough to deprotonate the bisimidazolium salt. We originally rationalized this result on the grounds that the addition of an excess of the base (10:1), together with the rapid coordination of the carbene to the metal center, may displace the equilibrium towards the desired species.[20] We now see that smaller amounts of base (2:1) and milder reaction conditions (room temperature) yield the same desired product, so the role of the base needs to be reconsidered. We now believe that the role of the base can be explained by the reaction mechanism shown in Scheme 3.



Scheme 3. Proposed reaction mechanism explaining the role of the base.

The reaction of the imidazolium precursor with the metal complex may lead to an oxidative addition/reductive elimination equilibrium in which the starting materials are clearly favored over the oxidative addition product. In the absence of a base, only the starting compounds are detectable. In fact, this could also explain why NHC-metal-hydrides are so scarce, since reductive elimination to the imidazolium ions should be very favorable. If a base is now added to the reaction medium, the oxidative addition product can eliminate HX (X = halide) by reaction with the base. The overall process has the same effect as if the imidazolium salt had first been deprotonated and the resulting carbene had then replaced the halide in the coordination sphere of the metal. The result is the same, but the pathway is different, and has important implications in the design of synthetic procedures to NHC–metal compounds. In any case, while Scheme 3 is applicable to 16e d^8 complexes (Rh^I, Ir^I), further work is needed to see how far it applies to 18e d^6 complexes (for example, Ru^{II}/Ru^{IV}).

The ferrocenyl group may be a key factor in the stability of **3a**. We believe that the ferrocene group may be sterically protecting the hydride in the molecular structure of **3a**. Another key point in the preparation of **3a** is the use of a PF_6 salt of the imidazolium precursor instead of the corresponding halide salt. The reaction of the dichloride analogue of **1** with [{Ir(cod)Cl}$_2$] yields a mixture of compounds that we could not characterize, but no hydrides were detected. We believe that the introduction of the chloride into the reaction medium may favor other pathways.

We believe that our results may have important implications for NHC chemistry, in that oxidative addition may be a more useful general method to synthesize NHC–metal complexes than previously thought. Even if the process is endothermic, it can be driven by base and the overall reaction may be mistaken for a simple deprotonation of the azolium precursor. Although more detailed study is needed, we believe that our observations may modify current mechanistic concepts in the formation of an NHC–M bond, especially when a weak base is used to promote the metalation. Our synthetic procedure provides a method to obtain a highly stable NHC–Ir–H complex, thus challenging the idea that

 © 2005 Wiley-VCH Verlag GmbH & Co. KGaA, Weinheim

such complexes are usually unstable. It has also been pointed out that ionic liquids may not be "innocent" solvents with low-valent Group 10 metal complexes because of their capability to undergo oxidation addition.[27]

Received: September 8, 2004

Keywords: C–H activation · carbene ligands · hydrides · iridium · rhodium

[1] D. Bourissou, O. Guerret, F. P. Gabbai, G. Bertrand, *Chem. Rev.* **2000**, *100*, 39.
[2] K. J. Cavell, D. S. McGuinness, *Coord. Chem. Rev.* **2004**, *248*, 671.
[3] E. Peris, R. H. Crabtree, *C. R. Chim.* **2003**, *6*, 33.
[4] W. A. Herrmann, *Angew. Chem.* **2002**, *114*, 1342; *Angew. Chem. Int. Ed.* **2002**, *41*, 1291.
[5] A. J. Arduengo, *Acc. Chem. Res.* **1999**, *32*, 913.
[6] P. B. Hitchcock, M. F. Lappert, P. Terreros, *J. Organomet. Chem.* **1982**, *239*, C26.
[7] M. J. Doyle, M. F. Lappert, P. L. Pye, P. Terreros, *J. Chem. Soc. Dalton Trans.* **1984**, 2355.
[8] P. B. Hitchcock, M. F. Lappert, P. Terreros, K. P. Wainwright, *J. Chem. Soc. Chem. Commun.* **1980**, 1180.
[9] A. A. Danopoulos, S. Winston, W. B. Motherwell, *Chem. Commun.* **2002**, 1376.
[10] S. Burling, L. D. Field, H. L. Li, B. A. Messerle, P. Turner, *Eur. J. Inorg. Chem.* **2003**, 3179.
[11] W. A. Herrmann, L. J. Goossen, M. Spiegler, *J. Organomet. Chem.* **1997**, *547*, 357.
[12] U. Kernbach, M. Ramm, P. Luger, W. P. Fehlhammer, *Angew. Chem.* **1996**, *108*, 333; *Angew. Chem. Int. Ed. Engl.* **1996**, *35*, 310.
[13] R. E. Douthwaite, M. L. H. Green, P. J. Silcock, P. T. Gomes, *J. Chem. Soc. Dalton Trans.* **2002**, 1386.
[14] K. M. Lee, H. M. J. Wang, I. J. B. Lin, *J. Chem. Soc. Dalton Trans.* **2002**, 2852.
[15] H. M. J. Wang, I. J. B. Lin, *Organometallics* **1998**, *17*, 972.
[16] R. S. Simons, P. Custer, C. A. Tessier, W. J. Youngs, *Organometallics* **2003**, *22*, 1979.
[17] A. R. Chianese, X. W. Li, M. C. Janzen, J. W. Faller, R. H. Crabtree, *Organometallics* **2003**, *22*, 1663.
[18] M. Poyatos, E. Mas-Marza, J. A. Mata, M. Sanau, E. Peris, *Eur. J. Inorg. Chem.* **2003**, 1215.
[19] M. Poyatos, J. A. Mata, E. Falomir, R. H. Crabtree, E. Peris, *Organometallics* **2003**, *22*, 1110.
[20] M. Poyatos, M. Sanau, E. Peris, *Inorg. Chem.* **2003**, *42*, 2572.
[21] E. Mas-Marza, M. Poyatos, M. Sanau, E. Peris, *Organometallics* **2004**, *23*, 323.
[22] E. Mas-Marza, M. Poyatos, M. Sanau, E. Peris, *Inorg. Chem.* **2004**, *43*, 2213.
[23] M. Poyatos, E. Mas-Marza, M. Sanau, E. Peris, *Inorg. Chem.* **2004**, *43*, 1793.
[24] B. Cetinkaya, S. Demir, I. Ozdemir, L. Toupet, D. Semeril, C. Bruneau, P. H. Dixneuf, *Chem. Eur. J.* **2003**, *9*, 2323.
[25] D. S. McGuinness, K. J. Cavell, B. F. Yates, B. W. Skelton, A. H. White, *J. Am. Chem. Soc.* **2001**, *123*, 8317.
[26] M. A. Duin, N. D. Clement, K. J. Cavell, C. J. Elsevier, *Chem. Commun.* **2003**, 400.
[27] N. D. Clement, K. J. Cavell, C. Jones, C. J. Elsevier, *Angew. Chem.* **2004**, *116*, 1297; *Angew. Chem. Int. Ed.* **2004**, *43*, 1277.
[28] A. Furstner, G. Seidel, D. Kremzow, C. W. Lehmann, *Organometallics* **2003**, *22*, 907.
[29] M. S. Viciu, G. A. Grasa, S. P. Nolan, *Organometallics* **2001**, *20*, 3607.
[30] D. S. McGuinness, K. J. Cavell, B. F. Yates, *Chem. Commun.* **2001**, 355.
[31] S. Grundemann, M. Albrecht, A. Kovacevic, J. W. Faller, R. H. Crabtree, *J. Chem. Soc. Dalton Trans.* **2002**, 2163.
[32] M. Albrecht, J. R. Miecznikowski, A. Samuel, J. W. Faller, R. H. Crabtree, *Organometallics* **2002**, *21*, 3596.
[33] J. R. Miecznikowski, R. H. Crabtree, *Organometallics* **2004**, *23*, 629.
[34] A. R. Chianese, A. Kovacevic, B. M. Zeglis, J. W. Faller, R. H. Crabtree, *Organometallics* **2004**, *23*, 2461.

 © 2005 Wiley-VCH Verlag GmbH & Co. KGaA, Weinheim

Aminoglycosides

Dual Effect of Synthetic Aminoglycosides: Antibacterial Activity against *Bacillus anthracis* and Inhibition of Anthrax Lethal Factor**

Micha Fridman, Valery Belakhov, Lac V. Lee, Fu-Sen Liang, Chi-Huey Wong, and Timor Baasov**

Anthrax is an infectious disease caused by toxigenic strains of the Gram-positive *Bacillus anthracis*.[1] If inhaled, *B. anthracis* spores rapidly reach the regional lymphonodes of the lungs, where they germinate and release anthrax toxins.[2] These toxins inhibit the adaptive immune response, thereby enabling the bacteria to reach the blood system, where they cause bacteremia and toxemia, which rapidly kill the host. Non-toxigenic strains of *B. anthracis* are poorly pathogenic, thus indicating that the anthrax toxins play a major role from the

[*] Dr. L. V. Lee, Dr. F.-S. Liang, Prof. Dr. C.-H. Wong
Department of Chemistry and
The Skaggs Institute for Chemical Biology
The Scripps Research Institute
10550 Torrey Pines Road, La Jolla, CA 92037 (USA)
Fax: (+1) 858-784-2409
E-mail: wong@scripps.edu

M. Fridman, Dr. V. Belakhov, Prof. Dr. T. Baasov
Department of Chemistry and
Institute of Catalysis Science and Technology
Technion—Israel Institute of Technology
Haifa 32000 (Israel)
Fax: (+972) 4-829-5703
E-mail: chtimor@tx.technion.ac.il

[**] We thank Dr. Abed Atmana (The Triangle Research and Development Center, Kfar-Qaraa) for antibacterial tests and insightful discussions. This research was supported by the Israel Science Foundation founded by the Israel Academy of Sciences and Humanities (Grant no.: 766/04), and in part by the L. and L. Richmond Fund for Promotion of Research at the Technion and by the National Institutes of Health (C.H.W.). V.B. acknowledges the financial support of the Center of Absorption in Science, the Ministry of Immigration Absorption, and the Ministry of Science and Arts, Israel (Kamea Program).

Supporting information for this article (selected procedures and complete analytical data for compounds **14**–**15**, **17**, **18**, and **22a**–**e**, selected data for compounds **5**–**12**) is available on the WWW under http://www.angewandte.org or from the author.

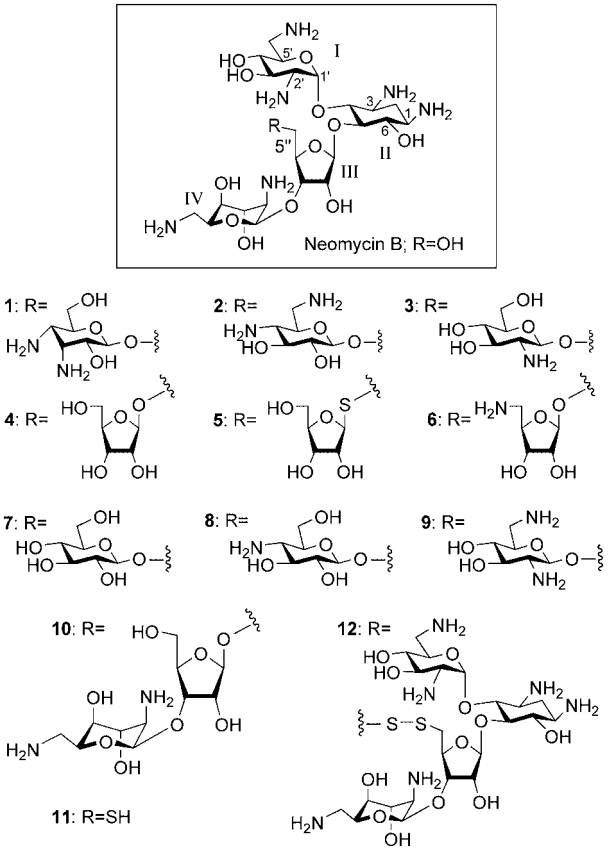
 DOI: 10.1002/anie.200462003 © 2005 Wiley-VCH Verlag GmbH & Co. KGaA, Weinheim

very beginning of infection to death. Since anthrax is asymptomatic until the bacterium reaches the blood,[1,2] the development of antitoxin therapeutic compounds for preventive use or for use in combination with antibiotics is of high urgency.[3] Alternatively, it would be highly beneficial if the developed material were bifunctional, with the ability to inactivate the released toxins and, in parallel, to function as an antibiotic.

The anthrax toxins consist of three proteins: protective antigen (PA), edema factor (EF), and lethal factor (LF).[4] Individually these proteins are nontoxic, so their toxic effects during anthrax infection require cooperation: PA binds to a cell-surface receptor and forms an oligomeric pore that translocates both EF and LF into the cytosol of target cells. Once inside the cell, EF causes edema by Ca^{2+}/calmodulin-dependent adenylate cyclase activity. LF is a zinc-dependent endopeptidase that specifically cleaves most isoforms of mitogen-activated protein kinase kinases, thereby inhibiting one or more signaling pathways of the host macrophage.[5] Although the precise mechanism is not yet well understood, this process results in the death of the host. Strains of *B. anthracis* deficient in EF remain pathogenic, whereas those that lack LF become attenuated. LF is therefore considered the dominant virulence factor of anthrax.[6] Consequently, an intensive search for specific inhibitors of LF has been performed during the last few years.[3,7,8]

To find novel inhibitors of LF, we recently tested a library of approximately 3000 compounds, over 60 of which were synthetic and commercial aminoglycosides.[9] Although a number of the compounds tested demonstrated some level of inhibitory activity, neomycin B, a commonly utilized aminoglycoside antibiotic, was found to be the most potent inhibitor of LF with an apparent inhibition constant (K_i) value in the low nanomolar concentration range.

To improve the inhibitory effect of neomycin B derivatives, we focused on the following points. First, aminoglycoside antibiotics such as neomycin B exert their antibacterial activity by selectively recognizing and binding to the decoding A site on the 16S subunit of the bacterial ribosomal RNA (rRNA), thereby causing deleterious misreading of the genetic code.[10] At physiological pH values, aminoglycosides are highly charged and their RNA binding relies on electrostatic interactions.[11,12] Second, examination of the recently determined X-ray crystal structure of LF shows that the active site of the protease consists of a broad, 40 Å groove with a highly negative electrostatic potential.[13] We performed docking experiments and found that neomycin B could reside within the vicinity of the catalytic zinc center and that multiple potential contacts could occur between the negatively charged residues of LF and neomycin B.[9] Based on these data we hypothesized that, since the interaction of neomycin B with both rRNA and LF is mainly determined by electrostatic interactions, it is likely that superior binding to both rRNA and LF, and probably better dual-effect antianthrax performance, would result from maintaining the whole antibiotic constitution intact but adding additional recognition/binding elements. The improved antibacterial activity of the first generation of pseudopentasaccharide derivatives of neomycin B (Scheme 1, compounds **1**–**4**),[14] along with the inhibition of various nucleic acid metabolizing enzymes by aminoglycosides,[15] support this hypothesis.

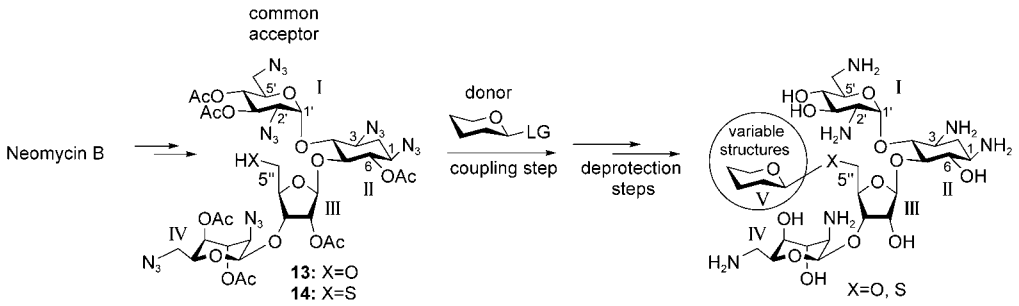


Scheme 1. Structures of neomycin B and the synthetic analogues.

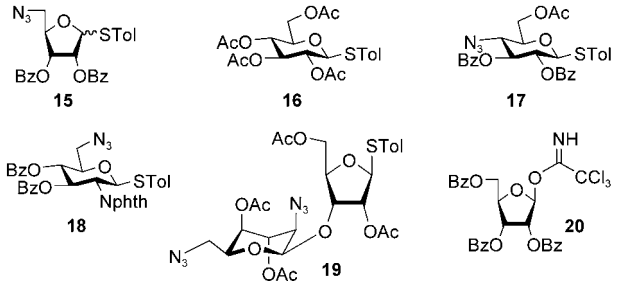
Taking into consideration the relative ease of derivatizing a primary alcohol, we selected position C5″ in neomycin B as a modification site and prepared a series of new derivatives, **5**–**12** (Scheme 1). These structures, along with the previously reported pseudopentasaccharides **1**–**4**, preserve the entire antibiotic domain as a recognition element for both the rRNA and LF. The extended sugar ring systems of each structure were designed in a manner that incorporates different combinations of hydroxy and amino groups as potential functionalities for recognition of the phosphodiester bond of rRNA[16] and, in parallel, the Asp/Glu and Asn/Gln clusters in the active site of LF.[9]

All the new derivatives of neomycin B were synthesized according to the general strategy illustrated in Scheme 2. This strategy involves conversion of neomycin B into the common acceptors **13** and **14**, to which various donor molecules can be attached, followed by a two-step deprotection to yield the target C5″-branched derivatives. The protecting groups used in this study were chosen based on their ease of attachment and removal, and their stability under the reaction conditions. The thioglycoside/*N*-iodosuccinimide (NIS)[17] and trichloroacetimidate/BF_3[18] glycosidation methods proved to be both rapid and efficient. Phthalimido and ester groups at C2 of the donors **15**–**20** (Scheme 3) were designed to allow, through neighboring-group participation, selective β-glycoside bond formation between rings V and III.

 © 2005 Wiley-VCH Verlag GmbH & Co. KGaA, Weinheim



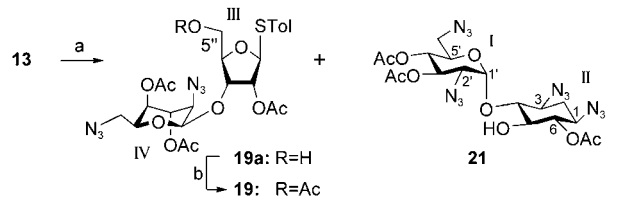
Scheme 2. General synthetic scheme for the assembly of C5″-branched derivatives of neomycin B. LG = leaving group.



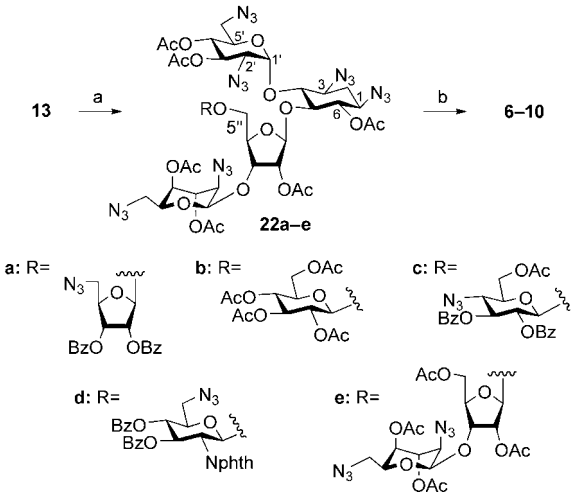
Scheme 3. Structures of the donors **15**–**20**. Bz = benzoyl, Nphth = phthalimido, Tol = tolyl.

The monosaccharide donors **15**–**18** and **20** were prepared by standard methods (see the Supporting Information for experimental details). The disaccharide donor **19** consists of derivatives of rings III and IV of neomycin B and was prepared by direct Lewis acid promoted cleavage of appropriately protected neomycin B according to the procedure of Swayze and co-workers[19] with some modification. As a starting material, instead of the perazidoperacetylneomycin B used in that work, we employed the acceptor **13** (readily accessible in four steps from neomycin B in 57% overall yield).[14] Treatment of **13** with $BF_3{\cdot}Et_2O$ in the presence of TolSH gave a mixture of two fragments, **19a** and **21**, which could be separated easily by chromatography on silica gel. Fragment **19a** was then readily converted into the desired donor **19** by acetylation (Scheme 4).

NIS-promoted coupling of the neomycin acceptor **13** with thioglycoside donors **15**–**19** furnished the designed protected derivatives **22a**–**e** in 47–91% yield (Scheme 5). The structures of **22a**–**e** were confirmed by a combination of various spectroscopic techniques, including HMQC, HMBC, 2D COSY, and 1D TOCSY NMR spectroscopy (see the Supporting Information). These protected compounds were then subjected to a two-step deprotection: removal of all the ester and phthalimido groups by treatment with methylamine (33% solution in EtOH) and reduction of all the azido groups by the Staudinger reaction, to furnish the final products **6**–**10**, which were isolated in excellent purity and yield.



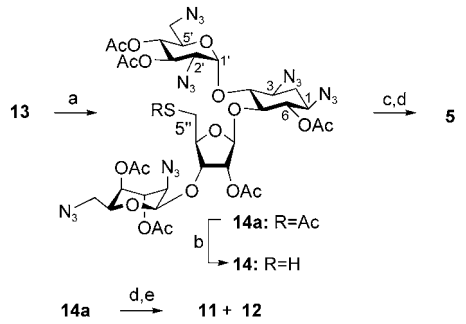
Scheme 4. Reagents and conditions: a) TolSH (1.1 equiv), $BF_3{\cdot}Et_2O$ (3 equiv), CH_2Cl_2, room temperature, 1 h, 32%; b) Ac_2O (1.5 equiv), pyridine, DMAP (cat.), room temperature, 97%. DMAP = 4-dimethylaminopyridine.



Scheme 5. Reagents and conditions: a) NIS, TfOH, CH_2Cl_2; **15**→**22a**: 57%, **16**→**22b**: 85%, **17**→**22c**: 64%, **18**→**22d**: 91%, **19**→**22e**: 47%; b) 1. $MeNH_2$ (33% in EtOH); 2. PMe_3, NaOH (0.1 M), THF/H_2O (3:1); **6**: 57%, **7**: 69%, **8**: 84%, **9**: 79%, **10**: 80%. NIS = *N*-iodosuccinimide, Tf = trifluoromethanesulfonyl.

Several methods[20,21] were examined in attempts to convert the primary hydroxy group in **13** into the corresponding thiol **14**. However, in most cases the yield for **14** was very low and the desired product was often accompanied by multiple by-products, which made the isolation of the target material difficult. The best result was obtained by utilizing the Mitsunobu reaction;[22] **13** was first converted into the corresponding thioacetate **14a** (84%), which after treatment with hydrazinium acetate provided the desired thiol **14** in 65% yield (Scheme 6). Lewis acid promoted coupling of the thiol acceptor **14** with the trichloroacetimidate donor **20** furnished the corresponding protected β-thioglycoside, which after a two-step deprotection as described above provided the designed thioglycoside **5** in 73% yield. When the chromatographically pure thioacetate **14a** was subjected directly to the same two-step deprotection procedure, treatment with methylamine followed by the Staudinger reaction, a mixture

 © 2005 Wiley-VCH Verlag GmbH & Co. KGaA, Weinheim



Scheme 6. Reagents and conditions: a) DIAD (3 equiv), PPh_3, $CH_3C(O)SH$ (3 equiv), THF, 0°C→RT, 84%; b) hydrazinium acetate (2 equiv), DMF, room temperature, 65%; c) **20** (4 equiv), $BF_3{\cdot}Et_2O$ (cat.), CH_2Cl_2, 4-Å molecular sieves, −10°C, 90%; d) 1. $MeNH_2$ (33% in EtOH); 2. PMe_3, NaOH (0.1 M), THF/H_2O (3:1); **5**: 73%, **11**+**12**: 88%; e) Biogel P-2 size-exclusion chromatography. DIAD = diisopropylazodicarboxylate, DMF = *N*,*N*-dimethylformamide.

(≈1:3) of **11** and the corresponding disulfide dimer **12** was obtained in an overall yield of 88%. This mixture was purified on a Biogel P-2 column to yield sufficiently pure **11** and **12** for biological tests.

By use of an in vitro fluorescence assay,[8,9] the analogues **1**–**12** were examined for their inhibition of LF protease activity (Table 1). All the compounds tested were found to be competitive inhibitors. From the measured apparent K_i values under low-ionic-strength assay conditions, it turns out that among the 12 analogues tested, 6 compounds (**2**, **6**, **9**–**12**), with K_i values in the range of 0.2–1.3 nM, are significantly better inhibitors than neomycin B itself ($K_i = 37$ nM). Interestingly, the binding affinity of the analogues in the gluco series (with a glucose substituent as ring V) increases gradually with an increasing number of amino groups on the ring: ($2NH_2$)glucose (**2**, **9**) > ($1NH_2$)glucose (**3**, **8**) > glucose (**7**). In this series of compounds, no particular influence of the position of the amino group(s) on the glucose ring is observed. The ring configuration, however, has a more significant effect: The ribosamino derivative **6** binds about 10-fold more strongly than the monoamino derivatives of glucose, **3** and **8**, and the diamino-D-allose derivative **1**, which contains an unusual *cis*-1,2-diamine substitution at ring V, binds about 20-fold more weakly than the diamino-D-glucose derivatives **2** and **9**. These data suggest that, although the number of amino groups on the ligand is in general critical for LF-binding affinity, structural features of the ligand play an important role in the proper recognition of LF.

Table 1: Apparent inhibition constant (K_i) values for commercial neomycin B and the synthetic derivatives **1**–**12** against the protease activity of LF under various assay conditions.

Aminoglycoside	K_i [nM] low salt concentration[a]	K_i [μM] high salt concentration[b]
neomycin B	37 ± 2 (34 ± 0.4)[c]	59 ± 6 (64 ± 8)[c]
1	11 ± 2	50 ± 7
2	0.5 ± 0.1 (17 ± 4)[c]	28 ± 6 (30 ± 5)[c]
3	13 ± 2	66 ± 9
4	28 ± 2	134 ± 17
5	52 ± 5	81 ± 21
6	1.3 ± 0.4	39 ± 6
7	23 ± 2	125 ± 25
8	15 ± 2 (36 ± 5)[c]	85 ± 11 (58 ± 8)[c]
9	0.6 ± 0.1 (15 ± 3)[c]	20 ± 3 (24 ± 3)[c]
10	0.4 ± 0.1	21 ± 4
11	0.2 ± 0.1 (0.3 ± 0.1)[c]	10 ± 2 (12 ± 3)[c]
12	0.7 ± 0.2 (33 ± 6)[c]	1.1 ± 0.2 (1.2 ± 0.2)[c]

[a] Low-salt conditions: potassium 2-[4-(2-hydroxyethyl)-1-piperazinyl]-ethanesulfonic acid (HEPES) buffer (10 mM) at pH 7.4, LF (≈33 nM), a fluorescent substrate (4, 6, 10, and 20 μM), and an inhibitor (the concentrations of **12** were 0, 16.2, 32.5, and 54.1 nM; the concentrations of all other compounds were 0, 165, 330, and 550 nM). The K_i values were estimated from double-reciprocal plots of initial velocities as a function of substrate concentration. [b] High-salt conditions: potassium HEPES buffer (10 mM) at pH 7.4, KCl (150 mM), LF (≈33 nM), a fluorescent substrate (10, 20, 40, and 100 μM), and an inhibitor (the concentrations of **12** were 0, 16.2, 32.5, and 54.1 μM; the concentrations of all other compounds were 0, 165, 330, and 550 μM). The K_i values were estimated as in [a]. [c] The data in parentheses were obtained under the same conditions as those of the parent experiments but with the additional presence of BSA (0.1 mg mL^{-1}). All assays were performed in triplicate and analogous results were obtained in at least two or three experiments.

Since the disulfide dimer **12** has twice as many amino groups as its parent "monomeric" **11**, its binding affinity to LF was expected to be significantly higher. The observed similar extent of inhibition of **12** and **11** was, however, very intriguing and suggested that in the case of dimer **12**, in addition to a "specific" active-site binding, an additional "nonspecific interaction" with the LF protein may occur. Various studies dealing with assorted protein–polyelectrolyte interactions[23] and with the interactions of aminoglycosides with ribozymes[12,21] support this presumption. To test this possibility, the analogues **2**, **8**, **9**, **11**, and **12**, along with neomycin B, were evaluated in the presence of 0.1 mg mL^{-1} of bovine serum albumin (BSA). Whereas the binding affinities of both neomycin B and **11** were not affected significantly, the binding of **12** decreased about 50-fold, which implies that nonspecific protein–ligand association may exist in the case of **12**. The data in the presence of BSA also indicate that this type of nonspecific protein–ligand association increases with an increasing number of amino groups on the ligand.

Although to date no direct structural data on the interaction of aminoglycosides with LF are available, our preliminary investigation of the binding mechanism showed that the inhibitory activity of aminoglycosides is ionic-strength dependent, thus indicating that the predominant interaction between LF and the aminoglycosides is electrostatic in origin.[21] An increase in the ionic strength from 0 to 150 mM KCl drastically shifts the K_i values of all aminoglycosides by a factor of ≈1500–53000 towards higher concentrations (Table 1). These data show that all of the synthetic analogues **1**–**12,** as well as the parent neomycin B, can be displaced from their LF-binding site even at a relatively low ionic strength. A possible reason for the observed different sensitivity of different aminoglycosides towards the ionic strength of the solution could be the different number of amino groups and their individual pK_a values. Furthermore, it is likely that the pK_a values of individual ammonium groups of neomycin B and of the dimer **12** are the same, which results in **12** behaving like a "monomer" and displaying the same sensitivity as neomycin B with respect to the ionic strength of

 © 2005 Wiley-VCH Verlag GmbH & Co. KGaA, Weinheim

the solution (≈1500-fold increase, Table 1).[24] Nevertheless, the observed 53-fold higher affinity of **12** relative to that of neomycin B, both at the low and high salt concentrations, indicates that the presence of twice the number of charged groups in **12** is probably responsible for the increased affinity. The high-ionic-strength conditions are also able to overcome the nonspecific LF–**12** association, as evidenced from the very similar K_i values observed for **12** in the presence and absence of BSA. Furthermore, since 150 mM KCl best resembles the physiological ionic strength in many cell types,[25] **12** can be considered the best aminoglycoside inhibitor of LF at putative physiological conditions.

When the new derivatives **1**–**12** were tested by means of surface plasmon resonance (SPR) techniques against an immobilized 27-mer RNA construct (AS-wt),[11] binding constant (K_d) values in the range of 0.4–2.9 μM were determined, with no obvious dependence of the K_d value on the modification type (Table 2). Several of these derivatives, including the dimer **12** ($K_d = 0.4$ μM), displayed a similar binding affinity to that of the parent neomycin B ($K_d = 0.3$ μM), thus showing no significant contribution of the number of amino groups on the ligand–RNA binding. These findings suggest that unlike the binding affinity to LF, whereby an increased number of amino groups on the natural drug leads to improved binding, a more subtle balance of interactions governs the binding affinity of these ligands to RNA. To compare the observed RNA-binding affinities to antibacterial activity, the analogues **1**–**12** were further investigated against *B. anthracis* (Sterne strain),[26] and the minimal inhibitory concentration (MIC) values were determined by using a microdilution assay with neomycin B as a control (Table 2). To our knowledge, no previous studies on the activity of aminoglycoside drugs against *B. anthracis* have been performed.

Table 2: Minimal inhibitory concentration (MIC) values against *B. anthracis* and binding constant (K_d) values with 16S A site RNA for commercial neomycin B and the synthetic derivatives **1**–**12**.

Aminoglycoside	MIC [μg mL^{-1}][a]	K_d [μM][b]
neomycin B	0.25	0.3 ± 0.1
1	8	2.0 ± 0.2
2	2	1.3 ± 0.3
3	2	0.9 ± 0.1
4	1	0.7 ± 0.1
5	2	1.0 ± 0.2
6	2	0.7 ± 0.1
7	8	1.1 ± 0.2
8	2	0.7 ± 0.1
9	1	0.6 ± 0.1
10	2	1.9 ± 0.3
11	8	2.9 ± 0.6
12	2	0.4 ± 0.1

[a] For the MIC value measurements, the concentrated stock solutions of aminoglycosides were prepared to known concentrations in distilled water. The solutions were then diluted twice with BHI (brain heart infusion) broth (100 μL) to concentrations in the range of 0.015–1024 mg L^{-1} and poured into the wells of microtiter plates (Nunc 96-well flat-bottomed microtiter plates; Nunc, Roskilde, Denmark). A 10-μL volume of culture containing *B. anthracis* (Sterne strain, 10^5 cfu mL^{-1}) was then added. Following incubation of the plates for 18 h at 37 °C in air, the MIC values were determined as the lowest concentration of an antibacterial agent that completely inhibited visible growth of the bacteria.[26] [b] The sequence of the 27-mer 16S A-site RNA construct used in this study was 5′-biotinyl-GGCGUCACACCUUCGGGUGAA-GUCGCC-3′. The binding assays were performed as previously described.[11]

From the MIC values, it can be seen that all of the synthetic derivatives possess significant antibacterial activity against *B. anthracis*, with some of them displaying activity levels comparable to that of neomycin B. In spite of the similar binding affinities of neomycin B and the dimer **12** to 16S A-site RNA, their antimicrobial activities differed by a factor of eight, thus suggesting that no direct correlation between rRNA binding and antibacterial activity can be made. Although this is in agreement with earlier reported data on other aminoglycoside analogues,[27] further structure–activity studies with more diverse structural analogues of neomycin B are clearly required to understand this issue in detail.

In conclusion, the neomycin B derivatives synthesized in this study represent a new class of C5″-branched aminoglycoside antibiotics that show a dual effect by inhibiting LF at seemingly physiological conditions and exhibiting activity against *B. anthracis* simultaneously. Thus, this study provides a new direction for the development of novel antibiotics that target both the toxigenic bacterium and its released lethal toxin; this progress may offer promise for the effective treatment of anthrax infections. Cytotoxicity assays to determine the ability of the designed structures to protect macrophages against LF and the rate at which *B. anthracis* is killed are currently underway.

Received: September 15, 2004

Keywords: aminoglycosides · anthrax · antibiotics · inhibitors

[1] T. C. Dixon, M. Meselson, J. Guillemin, P. C. Hanna, *N. Engl. J. Med.* **1999**, *341*, 815.
[2] N. S. Duesbery, G. F. Vande Woude, *Cell. Mol. Life Sci.* **1999**, *55*, 1599.
[3] C. Montecucco, F. Tonello, G. Zanotti, *Trends Biochem. Sci.* **2004**, *29*, 282.
[4] P. Ascenzi, P. Visca, G. Ippolito, A. Spallarossa, M. Bolognesi, C. Montecucco, *FEBS Lett.* **2002**, *531*, 384.
[5] N. S. Duesbery, C. P. Webb, S. H. Leppla, V. M. Gordon, K. R. Klimpel, T. D. Copeland, N. G. Ahn, M. K. Oskarsson, K. Fukasawa, K. D. Paull, G. F. Vande Woude, *Science* **1998**, *280*, 734; G. Vitale, L. Bernardi, G. Napolitani, M. Mock, C. Montecucco, *Biochem. J.* **2000**, *352*, 739; H. Enslen, R. J. Davis, *Biol. Cell* **2001**, *93*, 5.
[6] D. J. Maly, I. C. Choong, J. A. Ellman, *Proc. Natl. Acad. Sci. USA* **2000**, *97*, 2419; T. Bunyapaiboonsri, O. Ramstrom, S. Lohmann, J. M. Lehn, L. Peng, M. Goeldner, *ChemBioChem* **2001**, *2*, 438.
[7] F. Tonello, M. Seveso, O. Marin, M. Mock, C. Montecucco, *Nature* **2002**, *418*, 386; R. G. Panchal, A. R. Hermone, T. L. Nguyen, T. Y. Wong, R. Schwarzenbacher, J. Schmidt, D. Lane, C. McGrath, B. E. Turk, J. Burnett, M. J. Aman, S. Little, E. A. Sausville, D. W. Zaharevitz, L. C. Cantley, R. C. Liddington, R. Gussio, S. Bavari, *Nat. Struct. Mol. Biol.* **2004**, *11*, 67; I.

 © 2005 Wiley-VCH Verlag GmbH & Co. KGaA, Weinheim

Dell'Aica, M. Dona, F. Tonello, A. Piris, M. Mock, C. Montecucco, S. Garbisa, *EMBO Rep.* **2004**, *5*, 418.
[8] B. E. Turk, T. Y. Wong, R. Schwarzenbacher, E. T. Jarrell, S. H. Leppla, R. J. Collier, R. C. Liddington, L. C. Cantley, *Nat. Struct. Mol. Biol.* **2004**, *11*, 60.
[9] L. V. Lee, K. E. Bower, F. S. Liang, J. Shi, D. Wu, S. J. Sucheck, P. K. Vogt, C. H. Wong, *J. Am. Chem. Soc.* **2004**, *126*, 4774.
[10] D. Moazed, H. F. Noller, *Nature* **1987**, *327*, 389.
[11] M. Hendrix, E. S. Priestley, G. F. Joyce, C. H. Wong, *J. Am. Chem. Soc.* **1997**, *119*, 3641.
[12] Y. Tor, T. Hermann, E. Westhof, *Chem. Biol.* **1998**, *5*, R277; T. Hermann, E. Westhof, *J. Mol. Biol.* **1998**, *276*, 903.
[13] A. D. Pannifer, T. Y. Wong, R. Schwarzenbacher, M. Renatus, C. Petosa, J. Bienkowska, D. B. Lacy, R. J. Collier, S. Park, S. H. Leppla, P. Hanna, R. C. Liddington, *Nature* **2001**, *414*, 229.
[14] M. Fridman, V. Belakhov, S. Yaron, T. Baasov, *Org. Lett.* **2003**, *5*, 3575.
[15] Y. G. Ren, J. Martinez, L. A. Kirsebom, A. Virtanen, *RNA* **2002**, *8*, 1393.
[16] M. Hendrix, P. B. Alper, E. S. Priestley, C. H. Wong, *Angew. Chem.* **1997**, *109*, 119; *Angew. Chem. Int. Ed. Engl.* **1997**, *36*, 95.
[17] G. H. Veeneman, S. H. Vanleeuwen, J. H. Vanboom, *Tetrahedron Lett.* **1990**, *31*, 1331.
[18] R. R. Schmidt, *Angew. Chem.* **1986**, *98*, 213; *Angew. Chem. Int. Ed. Engl.* **1986**, *25*, 212.
[19] B. G. Wu, J. Yang, Y. He, E. E. Swayze, *Org. Lett.* **2002**, *4*, 3455.
[20] A. W. Snow, E. E. Foos, *Synthesis* **2003**, 509; B. P. Bandgar, V. S. Sadavarte, L. S. Uppalla, *Chem. Lett.* **2000**, 1304.
[21] K. Michael, H. Wang, Y. Tor, *Bioorg. Med. Chem.* **1999**, *7*, 1361.
[22] M.a.C. Merck Sharp and Dohme Research Laboratories, *Tetrahedron Lett.* **1981**, *22*, 119.
[23] Y. P. Wen, P. L. Dubin, *Macromolecules* **1997**, *30*, 7856.
[24] A similar effect of ionic strength on the interaction of tobramycin (Tob) and the Tob–Tob dimer with the *Tetrahymena* ribozyme has been reported: see reference [21].
[25] W. Hoppe, R. D. Bauer, *Biophysics*, Springer, Berlin, **1983**, p. 495.
[26] A. Athamna, M. Massalha, M. Athamna, A. Nura, B. Medlej, I. Ofek, D. Bast, E. Rubinstein, *J. Antimicrob. Chemother.* **2004**, *53*, 247.
[27] W. A. Greenberg, E. S. Priestley, P. S. Sears, P. B. Alper, C. Rosenbohm, M. Hendrix, S. C. Hung, C. H. Wong, *J. Am. Chem. Soc.* **1999**, *121*, 6527; S. J. Sucheck, A. L. Wong, K. M. Koeller, D. D. Boehr, K. Draker, P. Sears, G. D. Wright, C. H. Wong, *J. Am. Chem. Soc.* **2000**, *122*, 5230.

 © 2005 Wiley-VCH Verlag GmbH & Co. KGaA, Weinheim

Fluorous-Phase Synthesis

A Fluorous-Phase Pummerer Cyclative-Capture Strategy for the Synthesis of Nitrogen Heterocycles**

*Laura A. McAllister, Rosemary A. McCormick, Stephen Brand, and David J. Procter**

Nitrogen-containing heterocyclic organic compounds in the form of biologically active drugs or agents play an important role in the pharmaceutical and agrochemical industries.[1] The development of new strategies for the assembly of collections of heterocyclic compounds in a rapid and efficient high-throughput manner is therefore a key activity in synthetic chemistry.[2]

The Pummerer reaction[3] provides a useful tool for the synthesis of heterocyclic compounds.[4] We recently reported a solid-phase approach to oxindoles that utilizes the Pummerer cyclization of substrates attached to a resin by an "enabling" sulfur atom.[5] The approach is limited by the synthetic sequence required to access the immobilized heterocyclic framework (immobilization–oxidation–cyclization). A more general limitation, common to many solid-phase processes, arises from the considerable investment required to optimize solid-phase sequences because of difficulties in monitoring transformations.[6] Herein, we report our success in addressing these issues and describe a fluorous-phase[7,2b] Pummerer cyclative-capture strategy for the synthesis of a range of N heterocycles.

Our approach is based on the addition of thiols to glyoxamides **1** to form hemithioacetals at the correct oxidation level for activation and Pummerer cyclization. This constitutes a new, general strategy for triggering Pummerer cyclizations.[8] The use of a thiol-containing phase tag[9,10] leads to cyclative capture of the substrate. The choice of a fluorous phase tag both allows reactions to be monitored conveniently and allows phase-tag-assisted purification at each stage of the process. Our approach constitutes the first

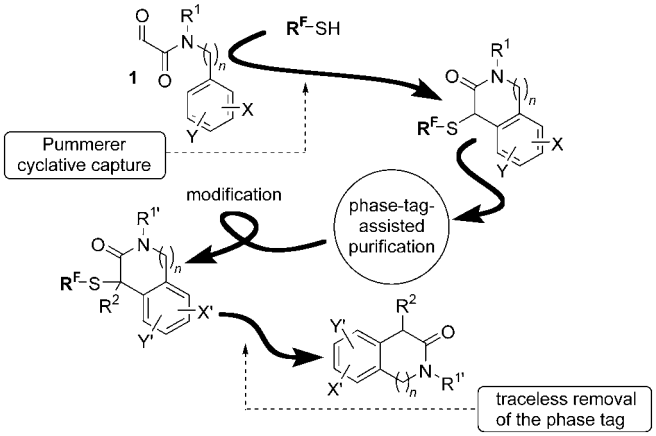
[*] L. A. McAllister, R. A. McCormick, Dr. D. J. Procter[+]
Department of Chemistry
The Joseph Black Building, University of Glasgow
Glasgow G12 8QQ (Scotland)
E-mail: david.j.procter@manchester.ac.uk
Dr. S. Brand
Celltech R&D Ltd
216 Bath Road, Slough, Berkshire SL1 4EN (UK)
[+] Current address:
School of Chemistry, University of Manchester
Oxford Road, Manchester M13 9PL (UK)
Fax: (+44) 161-275-4939

[**] We thank The Carnegie Trust for the Universities of Scotland (scholarship to L.A.M.), Celltech R&D (CASE award to L.A.M.), and the University of Glasgow (University Scholarship to R.A.M). Additional, unrestricted support was provided by AstraZeneca and Pfizer.

Supporting information for this article is available on the WWW under http://www.angewandte.org or from the author.

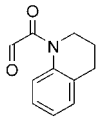
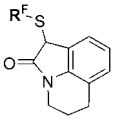
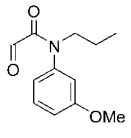
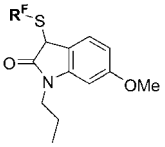
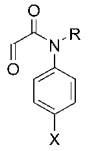
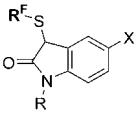
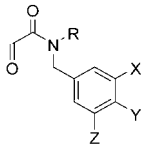
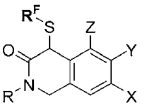
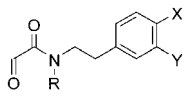
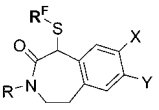
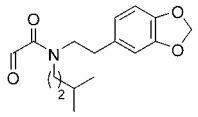
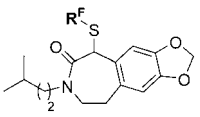
 © 2005 Wiley-VCH Verlag GmbH & Co. KGaA, Weinheim DOI: 10.1002/anie.200461930

example of fluorous-phase cyclative capture and utilizes a fluorous-phase scavenging reagent in a novel manner. Upon completion of the sequence, the fluorous phase tag can be removed under mild electron-transfer conditions[11] (Scheme 1). The treatment of readily accessible glyoxamide[12] starting materials with $C_8F_{17}CH_2CH_2SH$ results in rapid capture of the substrate and hemithioacetal formation. In the same reaction pot, activation with trifluoroacetic anhydride and treatment with $BF_3{\cdot}OEt_2$ then gave the product heterocycle in good yield after rapid purification by fluorous solid-phase extraction (FSPE).[7] The fluorous-phase Pummerer cyclative capture of a range of glyoxamides is summarized in Table 1.



Scheme 1. Fluorous-phase Pummerer cyclative-capture strategy ($\mathbf{R^F}$ = fluorous alkyl).

Table 1: Fluorous-phase Pummerer cyclative capture of glyoxamides.[a]

Entry	Glyoxamide	Tagged heterocycle[b]	Yield [%][c]
1			65
2			75[d]
3	X = Cl, R = Me			79
4	X = Br, R = *n*Pr			85
5	X = F, R = Me			80
6	X,Y,Z = H, R = Me			45
7	X = OMe, Y,Z = H, R = *n*Pr			51[e]
8	X,Y,Z = OMe, R = *n*-pentyl			60
9	X = H, Y = OMe, R = *n*Pr			76[f]
10	X = Y = OMe, R = *n*-pentyl			98
11			82

[a] Conditions: $C_8F_{17}CH_2CH_2SH$, CH_2Cl_2, 18 h, then trifluoroacetic anhydride, 1 h, then $BF_3{\cdot}OEt_2$, 1 h; see Supporting Information for details. [b] $\mathbf{R^F} = C_8F_{17}CH_2CH_2$. [c] Yield of isolated product. [d] Isomer ratio: 5:1. [e] Isomer ratio: ~1:1. [f] Isomer ratio: ~2:1. Major isomers shown.

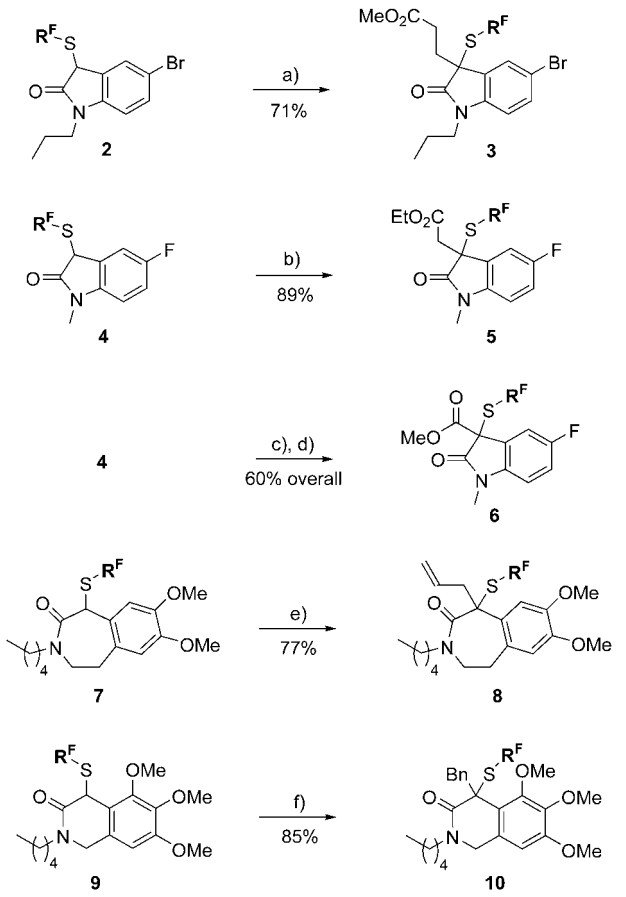
Oxindoles (Table 1, entries 1–5), tetrahydroisoquinolinones (Table 1, entries 6–8), and tetrahydrobenzazepinones (Table 1, entries 9–11) can be prepared by straightforward variation of the glyoxamide substrate. For the formation of six- and seven-membered heterocycles (Table 1, entries 6–11), electronic activation of the aromatic ring leads to higher yields of the product. In contrast, the formation of oxindoles (Table 1, entries 1–5) proceeds efficiently with neutral, electron-deficient, and electron-rich substrates.

The Pummerer cyclative-capture process allows convenient access to fluorous-tagged heterocyclic frameworks. These tagged heterocycles can be modified in a variety of ways. The sulfur-atom linkage to the fluorous phase tag can be used to facilitate elaboration by alkylation and acylation reactions (Scheme 2). For example, adducts **3** and **5** were prepared by Michael addition and alkylation, respectively, whereas the fluorous tetrahydrobenzazepinone and tetrahydroisoquinolinone derivatives **7** and **9** were alkylated in an analogous fashion. Ester **6** was prepared by O acylation followed by DMAP-catalyzed rearrangement.[13] Crucially, excess reagents can be used to drive reactions to completion, as purification after each modification step can be carried out conveniently by FSPE.

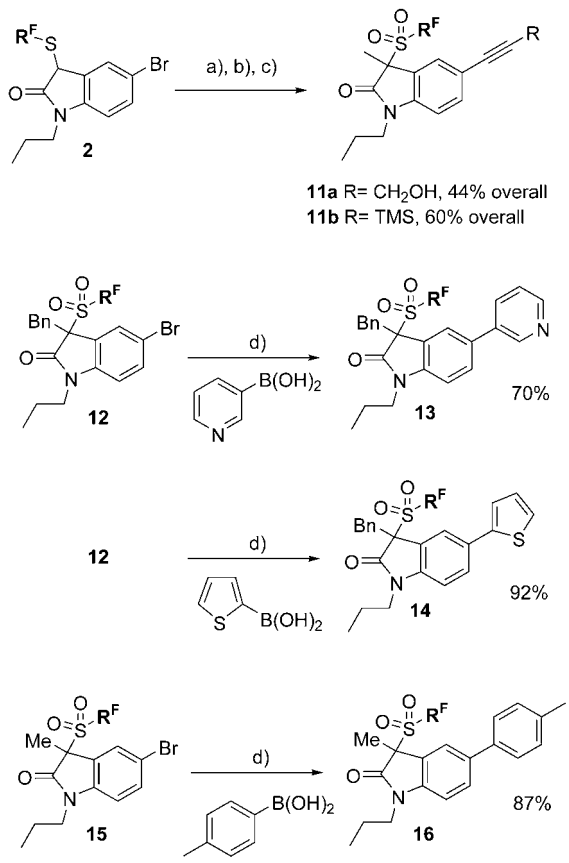
The transformations illustrated in Scheme 3 show the compatibility of the linker system with Pd-catalyzed cross-coupling technologies. Oxidation of the linking sulfur atom to the corresponding sulfone further facilitates elaboration of the tagged heterocyclic scaffolds. For example, sequences to prepare alkynes **11a** and **11b** include sulfone-assisted alkylation and Sonogashira cross-coupling. Tagged 5-bromooxindoles **12** and **15** readily undergo Suzuki cross-coupling with aryl and heteroaryl boronic acids to give **13**, **14**, and **16**. Again, purification after each modification step can be conveniently carried out by FSPE.

Traceless cleavage of the fluorous tag is possible with a range of electron-transfer reagents;[14] however, we have found that reduction with SmI_2[5,11a] results in the clean release of the heterocyclic product from the fluorous phase. No additives are required to activate SmI_2,[15] regardless of the oxidation state of the sulfur atom, because of the activated nature of the carbon–sulfur linkage to the phase tag. For the cleavage of fluorous sulfides, FSPE can again be used to assist

 © 2005 Wiley-VCH Verlag GmbH & Co. KGaA, Weinheim



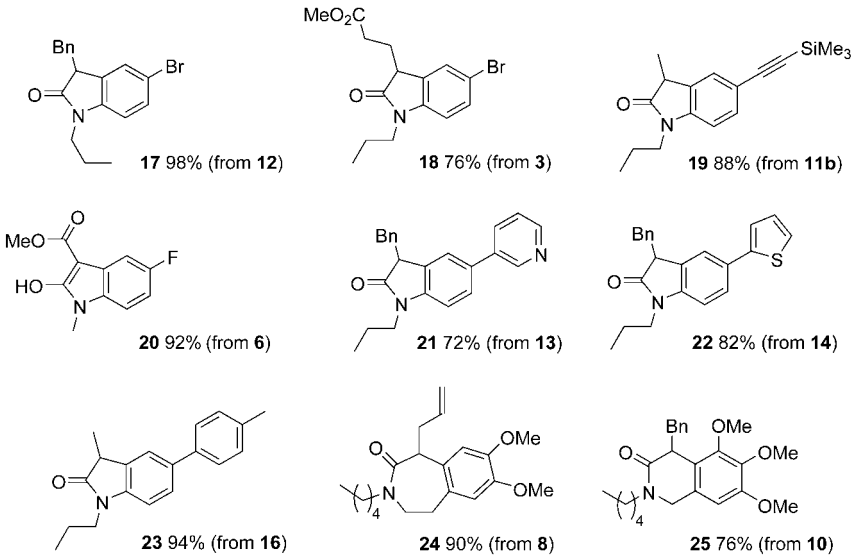
Scheme 2. Manipulation of fluorous-tagged heterocycles—modifications α to sulfur ($\mathbf{R^F} = C_8F_{17}CH_2CH_2$). Reagents and conditions: a) NaOMe, MeOH, methyl acrylate, 18 h; b) LDA, THF, −78 °C, 2.5 h, ethyl bromoacetate; c) methyl chloroformate, NEt_3, room temperature, 3 h; d) DMAP (30 mol%), toluene, 70 °C, 3 h; e) NaH, THF/DMF, 80 °C, 18 h, allyl bromide; f) LHMDS, THF, −78 °C, 7 h, BnBr. Bn = benzyl, DMAP = 4-dimethylaminopyridine, DMF = *N*,*N*-dimethylformamide, HMDS = hexamethyldisilazide, LDA = lithium diisopropylamide.



Scheme 3. Manipulation of fluorous-tagged heterocycles—Pd-catalyzed modifications ($\mathbf{R^F} = C_8F_{17}CH_2CH_2$). Reagents and conditions: a) *m*CPBA, CH_2Cl_2, room temperature, 2 h; b) K_2CO_3, MeI, DMF, 40 °C, 2 h; c) $[Pd(PPh_3)_4]$, NEt_3, 80 °C, 18 h, propargyl alcohol or trimethylsilylacetylene and CuI (20 mol%); d) $[Pd(PPh_3)_3]$, Na_2CO_3, H_2O, dioxane, 80 °C, 3.5 h, $ArB(OH)_2$. *m*CPBA = *m*-chloroperbenzoic acid, TMS = trimethylsilyl.

purification, the desired product now eluting in the non-fluorous fraction. For the cleavage of fluorous sulfones, the fluorous component is lost to the aqueous layer during work up, and no purification is required (Scheme 4).

In conclusion, we have developed a new strategy for the high-throughput, fluorous-phase synthesis of N-heterocycle libraries. The sequence involves several key features: a fluorous-phase Pummerer cyclative-capture strategy for rapid access to tagged, heterocyclic frameworks; modification of the fluorous heterocyclic scaffolds by a variety of approaches, including Pd-catalyzed cross-coupling reactions; traceless, reductive removal of the fluorous phase tag. Studies on the application of this



Scheme 4. Products of reductive, traceless cleavage of the fluorous phase tag. (Compound **20** was obtained as a 1:1 mixture of tautomers according to NMR spectroscopic analysis).

 © 2005 Wiley-VCH Verlag GmbH & Co. KGaA, Weinheim

strategy in solution-phase parallel and combinatorial library synthesis are currently underway.

Received: September 9, 2004

Keywords: fluorous phase · heterocycles · Pummerer reaction · samarium · synthetic methods

[1] a) J. K. Landquist in *Comprehensive Heterocyclic Chemistry* (Eds.: A. R. Katritzky, C. W. Rees), Pergamon, New York, **1984**, *Vol. 1*, p. 143; b) P. J. Crowley in *Comprehensive Heterocyclic Chemistry*, (Eds.: A. R. Katritzky, C. W. Rees), Pergamon, New York, **1984**, *Vol. 1*, p. 185.
[2] a) V. Krchnak, M. W. Holladay, *Chem. Rev.* **2002**, *102*, 61; b) For a review of fluorous-phase approaches in heterocycle synthesis, see: W. Zhang, *Chem. Rev.* **2004**, *104*, 2531.
[3] R. Pummerer, *Ber. Dtsch. Chem. Ges. B* **1909**, *42*, 2282.
[4] For recent reviews on the Pummerer reaction, see: a) S. K. Bur, A. Padwa, *Chem. Rev.* **2004**, *104*, 2401; b) A. Padwa, D. M. Danca, J. D. Ginn, S. M. Lynch, *J. Braz. Chem. Soc.* **2001**, *12*, 571; c) A. Padwa, A. G. Waterson, *Curr. Org. Chem.* **2000**, *4*, 175; d) A. Padwa, D. E. Gunn, Jr, M. H. Osterhout, *Synthesis* **1997**, 1353.
[5] L. A. McAllister, S. Brand, R. de Gentile, D. J. Procter, *Chem. Commun.* **2003**, 2380.
[6] F. Z. Dörwald, *Organic Synthesis on Solid Phase*, Wiley-VCH, Weinheim, **2000**.
[7] a) For a discussion of fluorous tagging, see: A. Studer, S. Hadida, R. Ferritto, S.-Y. Kim, P. Jeger, P. Wipf, D. P. Curran, *Science* **1997**, *275*, 823; for recent reviews, see: b) D. P. Curran in *The Handbook of Fluorous Chemistry* (Eds.: J. A. Gladysz, D. P. Curran, I. T. Horváth), Wiley-VCH, Weinheim, **2004**, p. 101; c) W. Zhang, *Tetrahedron* **2003**, *59*, 4475.
[8] For thiol addition to glyoxalates to prepare substrates for Pummerer cyclization, see: J. Milton, S. Brand, M. F. Jones, C. M. Rayner, *Tetrahedron Lett.* **1995**, *36*, 6961.
[9] For the use of fluorous thiols as nucleophilic scavenging reagents, see: a) C. W. Lindsley, Z. Zhao, W. H. Leister, *Tetrahedron Lett.* **2002**, *43*, 4225; b) W. Zhang, D. P. Curran, C. H.-T. Chen, *Tetrahedron* **2002**, *58*, 3871.
[10] For the use of fluorous thiols for the introduction of fluorous phase tags, see: a) W. Zhang, *Org. Lett.* **2003**, *5*, 1011; b) Y. Jing, X. Huang, *Tetrahedron Lett.* **2004**, *45*, 4615.
[11] a) F. McKerlie, D. J. Procter, G. Wynne, *Chem. Commun.* **2002**, 584; b) G. A. Molander, *Org. React.* **1994**, *46*, 211.
[12] Glyoxamide substrates were prepared from secondary amines in three steps; see: M. A. Marx, A.-L. Grillot, C. T. Louer, K. A. Beaver, P. A. Bartlett, *J. Am. Chem. Soc.* **1997**, *119*, 6153.
[13] For rearrangements to benzofuranones, see: a) T. H. Black, S. M. Arrivo, J. S. Schumm, J. M. Knobeloch, *J. Chem. Soc. Chem. Commun.* **1986**, 1524; b) T. H. Black, S. M. Arrivo, J. S. Schumm, J. M. Knobeloch, *J. Org. Chem.* **1987**, *52*, 5425; for the first studies on rearrangements to oxindoles, see: I. D. Hills, G. C. Fu, *Angew. Chem.* **2003**, *115*, 3969; *Angew. Chem. Int. Ed.* **2003**, *42*, 3921.
[14] Similar reductions with other electron-transfer reagents have been reported: a) J. M. Manthorpe, J. L. Gleason, *J. Am. Chem. Soc.* **2001**, *123*, 2091; b) J. M. Manthorpe, J. L. Gleason, *Angew. Chem.* **2002**, *114*, 2444; *Angew. Chem. Int. Ed.* **2002**, *41*, 2338; c) E. D. Burke, J. L. Gleason, *Org. Lett.* **2004**, *6*, 405.
[15] H. B. Kagan, J. L. Namy in *Lanthanides: Chemistry and Use in Organic Synthesis* (Ed.: S. Kobayashi), Springer, New York, **1999**, p. 155.

 © 2005 Wiley-VCH Verlag GmbH & Co. KGaA, Weinheim

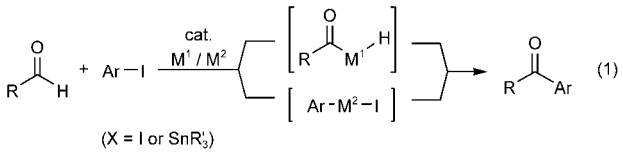
Homogeneous Catalysis

Cooperative Catalysis by Ru and Pd for the Direct Coupling of a Chelating Aldehyde with Iodoarenes or Organostannanes**

*Sangwon Ko, Byungman Kang, and Sukbok Chang**

Dedicated to Professor Yong Hae Kim

Transition-metal catalysts have been designed and utilized conventionally to mediate single-step transformations.[1] In addition to the traditional one catalyst/one reaction approach, however, some recent examples have revealed that the appropriate combination of suitable and compatible metal species is able to effect sequential or cooperative catalytic one-pot transformations that are unprecedented in single-metal systems.[2] The extensive efforts in this field have borne fruit recently, and have led to some significant examples in the area of chemical catalysis.[3] We describe herein a novel application of cooperative catalysis to the coupling of an aldehyde with iodoarenes or organostannanes, in which Ru and Pd collaborate, presumably through catalytic transmetalation pathways. As part of our interest in coordination-assisted organic transformations,[4] we envisaged the possibility that aldehydes could be directly coupled with aryl iodides to afford ketone products in the presence of the appropriate combination of two catalysts [Eq. (1), X = I].[5] In analogy, we anticipated that the coupling of aldehydes and organostannanes could also be possible (X = SnR_3). The synthetic utility of these transformations would be extremely high since multistep processes are generally required for the preparation of ketones in classical synthetic methods starting from the same compounds (aldehydes and aryl halides).[6]



We chose 8-quinolinecarboxaldehyde (**1**) as the coupling partner since it was initially anticipated that formation of a five-membered chelate intermediate would effectively sup-

[*] S. Ko, B. Kang, Prof. Dr. S. Chang
Center for Molecular Design and Synthesis (CMDS)
Department of Chemistry and School of Molecular Science (BK 21)
Korea Advanced Institute of Science and Technology (KAIST)
Daejeon 305-701 (Korea)
Fax: (+82) 42-869-2810
E-mail: sbchang@kaist.ac.kr

[**] This research was supported by KOSEF (R02-2003-000-10075-0) through the Basic Research Program.

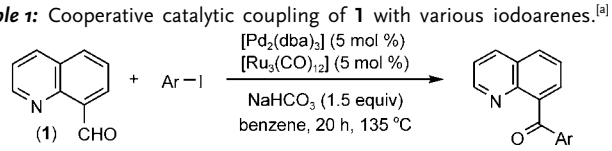
Supporting information for this article is available on the WWW under http://www.angewandte.org or from the author.

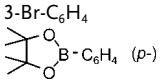
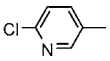
 DOI: 10.1002/anie.200462006 © 2005 Wiley-VCH Verlag GmbH & Co. KGaA, Weinheim

press any destructive decarbonylation pathway by catalytic activation of the formyl C–H bond. We found that treatment of iodobenzene with an acylrhodium hydride species,[7] obtained from the reaction of **1** with an equivalent amount of $[RhCl(PPh_3)_3]$, afforded the corresponding diaryl ketone in 60% yield in the presence of a catalytic amount of $[Pd_2(dba)_3]\cdot CHCl_3$ (5 mol%; dba = *trans*,*trans*-dibenzylideneacetone) at 135 °C after 5 h. We were further encouraged by the observation that a direct coupling between aldehyde **1** and iodobenzene took place even in systems containing both $[RhCl(PPh_3)_3]$ and $[Pd_2(dba)_3]\cdot CHCl_3$ (5 mol% each), albeit in lower yield (48%, 24 h), under otherwise identical conditions. The use of various other combinations of Rh and Pd catalysts proved to be far less efficient (< 5% yields), and no coupling was observed in the presence of any single-metal catalyst systems. A greatly improved efficiency was obtained when a Ru catalyst was employed instead of Rh in the presence of the Pd co-catalyst. Among all the Ru catalysts investigated, $[Ru_3(CO)_{12}]$ was found to be the most effective counterpart when combined with $[Pd_2(dba)_3]\cdot CHCl_3$. This combination afforded the ketone product in 83% yield (5 mol% of each catalyst) in the presence of $NaHCO_3$ (1.5 equiv) at 135 °C (20 h).

Under the optimized conditions, **1** was coupled with various iodoarenes to afford the corresponding aryl ketones in good yields (Table 1);[8] no noticeable electronic effects of the substituents on the iodoarenes were observed (Table 1, entries 1–5). The fact that a formyl group of the iodoarene substrate is tolerated suggests that the assumed coordination of the Ru center to the nitrogen atom of **1** is a driving force for the activation of the formyl C–H bond (Table 1, entry 6). An ester group also turned out to be compatible under these reaction conditions (Table 1, entry 7). Coupling of **1** with a bromoarene was much slower than with an iodoarene, as demonstrated in the reaction with 1-bromo-3-iodobenzene (Table 1, entry 8). The fact that a borate group is totally inert under these reaction conditions shows the highly selective nature of the present co-catalyst systems (Table 1, entry 9). The presence of heteroatoms such as nitrogen and sulfur does not affect the efficiency of the reactions (Table 1, entries 10 and 11). However, the coupling of **1** with vinyl iodides resulted in low yields (< 10%) with the present system.

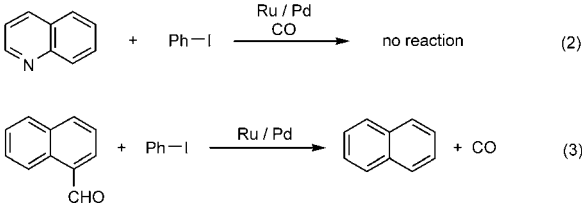
Table 1: Cooperative catalytic coupling of **1** with various iodoarenes.[a]



Entry	Ar	Yield [%][b]
1	C_6H_5	83
2	4-Me-C_6H_4	66
3	4-MeO-C_6H_4	62
4	4-Ac-C_6H_4	71
5	4-NO_2-C_6H_4	76
6	4-CHO-C_6H_4	80
7	4-EtO_2C-C_6H_4	79
8	3-Br-C_6H_4	73
9		63
10		89
11		90

[a] A mixture of **1** (0.5 mmol), iodoarene (1.0 mmol), $[Pd_2(dba)_3]\cdot CHCl_3$ and $[Ru_3(CO)_{12}]$ (5 mol% each), and $NaHCO_3$ (0.75 mmol) in benzene (1.0 mL) was stirred at 135 °C for 20 h. [b] Yield of isolated product.

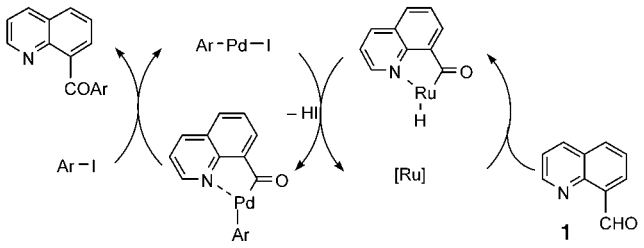
Control experiments were performed to verify the presumed cooperative catalytic pathways. No conversion was observed when quinoline was treated with iodobenzene under an atmosphere of CO under otherwise identical conditions [Eq. (2)]. This result may rule out the possibility that the reaction of aldehyde **1** and iodoarenes proceeds by Ru-catalyzed decarbonylation of **1** followed by Pd-catalyzed arylcarbonylation of iodobenzene.[9] In fact, there are several precedents for the $[Ru_3(CO)_{12}]$-catalyzed orthometalation of nitrogen-containing heteroaromatic compounds to provide *ortho*-carbonylated adducts.[10] Aldehydes devoid of a coordinating group were not coupled with iodobenzene, which implies that activation of a formyl C–H bond of **1** is coordination-directed [Eq. (3)].[11]



When **1** was treated with a stoichiometric amount of $[Ru_3(CO)_{12}]$ in 1,2-dichloroethane (120 °C, 30 min) the aldehydic proton signal disappeared gradually from the ^1H NMR spectrum, to be replaced by a signal for an acylruthenium hydride ($\delta = -15.9$ ppm; singlet in $CDCl_3$).[12] The IR spectrum of the isolated adduct shows an absorbance band at 1846 cm^{-1}, which is assignable to the stretching band of the speculative Ru–H bond.[13] It should be noted that a stoichiometric activation of **1** has previously been reported with Na_2PdCl_4 to afford a chloro-bridged Pd dimer.[14] However, no conversion was observed upon the treatment of **1** with aryl iodides in the presence of a range of Pd catalysts and in the absence of ruthenium co-catalysts. Moreover, the C–I bond of iodobenzene was inert to the Ru catalyst under the reaction conditions, even when one equivalent of $[Ru_3(CO)_{12}]$ was used, which strongly suggests that the activation of iodobenzenes is carried out selectively by Pd catalysts in the presence of ruthenium species. The above observation led us to propose a primitive mechanistic scenario for the cooperative catalysis (Scheme 1). Ruthenium may activate a formyl C–H bond of the chelating aldehyde **1** to afford a five-membered cycloacylruthenium hydride intermediate,[15] which is subsequently transferred into the Pd catalytic cycle with iodoarenes and eventually leads to coupled ketone products after a reductive-elimination step.

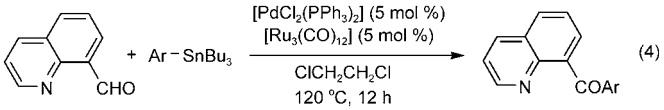
The concept of cooperative catalysis by Pd and Ru was further extended into coupling reactions of **1** with organostannanes [Eq. (4)]. Since it is known that organostannanes

 © 2005 Wiley-VCH Verlag GmbH & Co. KGaA, Weinheim



Scheme 1. Proposed pathway for the Ru/Pd co-catalytic coupling of aldehyde **1** with iodobenzenes.

are readily activated by certain Pd complexes,[16] their coupling with **1** was initially investigated in the presence of Ru and Pd co-catalysts. We were pleased to find that the corresponding ketone products were generated in acceptable yields from the reactions with a range of tin compounds (1.5 equiv relative to **1**). The reaction proceeds most effectively in 1,2-dichloroethane at 120 °C when $[PdCl_2(PPh_3)_2]$ and $[Ru_3(CO)_{12}]$ (5 mol % each) are used simultaneously. Various functional groups, including cyano, formyl, and heteroatoms, are tolerated under the present conditions. As anticipated, tributyltin hydride was generated as a side-product from the reactions (yields of over 60 %). It should be mentioned that, to the best of our knowledge, this represents the first example of a direct coupling between an aldehyde and organotin compounds.[17] As in the above coupling reactions between **1** and iodoarenes, the use of any single-catalyst systems of Ru, Pd, or Rh gave none of the desired products.



(4)

Ar = C_6H_5	60%
4-MeC_6H_4	56%
4-NCC_6H_4	61%
4-$CHOC_6H_4$	49%
thienyl	66%

In summary, we have demonstrated that the appropriate combination of two suitable and compatible metallic catalyst systems provides a new possibility for the development of novel synthetic methodologies that are difficult to carry out with any single-catalyst systems. More detailed mechanistic studies and further application of this cooperative catalysis are now in progress.

Received: September 16, 2004

Keywords: C–H activation · cooperative phenomena · homogeneous catalysis · palladium · ruthenium

[1] a) *Transition Metals for Organic Synthesis* (Eds.: M. Beller, C. Bolm), Wiley-VCH, Weinheim, **1998**; b) *Applied Homogeneous Catalysis with Organometallic Compounds* (Eds.: B. Cornils, W. A. Herrmann), Wiley-VCH, Weinheim, **2002**.

[2] a) E. K. van den Beuken, B. L. Feringa, *Tetrahedron* **1998**, *54*, 12985; b) E. Y.-X. Chen, T. J. Marks, *Chem. Rev.* **2000**, *100*, 1391.

[3] J. M. Lee, Y. Na, H. Han, S. Chang, *Chem. Soc. Rev.* **2004**, *33*, 302.

[4] a) S. Ko, Y. Na, S. Chang, *J. Am. Chem. Soc.* **2002**, *124*, 750; b) S. Ko, C. Lee, M.-G. Choi, Y. Na, S. Chang, *J. Org. Chem.* **2003**, *68*, 1607; c) S. Ko, H. Han, S. Chang, *Org. Lett.* **2003**, *5*, 2687; d) Y. Na, S. Ko, L. K. Hwang, S. Chang, *Tetrahedron Lett.* **2003**, *44*, 4475.

[5] a) G. Dyker, *Angew. Chem.* **1999**, *111*, 1808; *Angew. Chem. Int. Ed.* **1999**, *38*, 1698; b) V. Ritleng, C. Sirlin, M. Pfeffer, *Chem. Rev.* **2002**, *102*, 1731; c) F. Kakiuchi, N. Chatani, *Adv. Synth. Catal.* **2003**, *345*, 1077.

[6] For the metal-mediated synthesis of ketones from the reaction of aryl iodides with aldimines or aldehydes, albeit taking place by distinctively different mechanistic pathways compared to this study, see: a) T. Satoh, T. Itaya, M. Miura, M. Nomura, *Chem. Lett.* **1996**, 823; b) T. Ishiyama, J. Hartwig, *J. Am. Chem. Soc.* **2000**, *122*, 12043; c) Y.-C. Huang, K. K. Majumdar, C.-H. Cheng, *J. Org. Chem.* **2002**, *67*, 1682.

[7] J. W. Suggs, *J. Am. Chem. Soc.* **1978**, *100*, 640.

[8] All new compounds were fully characterized by ^{1}H NMR, ^{13}C NMR, and IR spectroscopy, as well as HRMS. See the Supporting Information for the spectral data.

[9] For the Pd-catalyzed alkoxycarbonylation of haloarenes, see: M. Mori, in *Handbook of Organopalladium Chemistry for Organic Synthesis*, *Vol. 2* (Ed.: E. Negishi), Wiley-Interscience, New York, **2002**, p. 2313.

[10] See, for example: N. Chatani, T. Fukuyama, F. Kakiuchi, S. Murai, *J. Am. Chem. Soc.* **1996**, *118*, 493.

[11] For selected examples of efficient C–C bond formation by catalytic C–H formyl activation, see: a) R. C. Larock, M. J. Dorty, S. Cacchi, *J. Org. Chem.* **1993**, *58*, 4579; b) K. Tanaka, G. C. Fu, *J. Am. Chem. Soc.* **2001**, *123*, 11492; c) M. C. Willis, S. J. McNally, P. J. Beswick, *Angew. Chem.* **2004**, *116*, 344; *Angew. Chem. Int. Ed.* **2004**, *43*, 340.

[12] a) J. A. Ayllon, S. F. Sayers, S. Sabo-Etienne, B. Donnadieu, B. Chaudret, E. Clot, *Organometallics* **1999**, *18*, 3981; b) S. G. Bott, H. Shen, R. A. Senter, M. G. Richmond, *Organometallics* **2003**, *22*, 1953; c) G. Albertin, S. Antoniutti, A. Bacchi, C. D'Este, G. Pelizzi, *Inorg. Chem.* **2004**, *43*, 1336.

[13] a) K. Abdur-Rashid, M. Faatz, A. J. Lough, R. H. Morris, *J. Am. Chem. Soc.* **2001**, *123*, 7473; b) S. Ogo, K. Uehara, T. Abura, Y. Watanabe, S. Fukuzumi, *Organometallics* **2004**, *23*, 3047.

[14] The catalytic activity of the thus-generated binuclear Pd complex was not reported: C. G. Anklin, P. S. Pregosin, *J. Organomet. Chem.* **1983**, *243*, 101.

[15] For a discussion of the preparation and characterization of a related acylplatinum hydride of **1**, see: J. J. Koh, W.-H. Lee, P. G. Williard, W. M. Risen, Jr., *J. Organomet. Chem.* **1985**, *284*, 409.

[16] E. Shirakawa, H. Yoshida, T. Kurahashi, Y. Nakao, T. Hiyama, *J. Am. Chem. Soc.* **1998**, *120*, 2975.

[17] It has been reported that Pd catalyzes the addition of organotin reagents to aldehydes to give alcohols rather than ketones: H. Nakamura, H. Iwama, Y. Yamamoto, *J. Am. Chem. Soc.* **1996**, *118*, 6641.

 © 2005 Wiley-VCH Verlag GmbH & Co. KGaA, Weinheim

Molecular Modeling

Asymmetric versus C_2-Symmetric Ligands: Origin of the Enantioselectivity in Ruthenium–Pybox-Catalyzed Cyclopropanation Reactions**

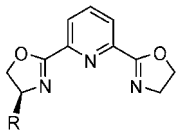
Alfonso Cornejo, José M. Fraile, José I. García, María J. Gil, Víctor Martínez-Merino, José A. Mayoral, and Luis Salvatella*

In memory of Juan Carlos del Amo

Enantioselective homogeneous catalysis is one of the most efficient ways of introducing chirality in a controlled manner in organic synthesis.[1] Although there are some exceptions,[2] C_2-symmetric ligands are usually preferred over asymmetric (C_1) ligands for enantioselective catalytic applications. Those ligands with C_1 symmetry that are successful for catalytic applications are generally both electronically and sterically asymmetric, such as salicylaldimines[2a] and phosphinooxazolines.[2b] Of course, there are evident advantages in using C_2-symmetric ligands. For example, fewer reaction channels are possible for the reaction, thus simplifying the induction of enantioselectivity. Furthermore, the synthesis of the ligands is often simpler.

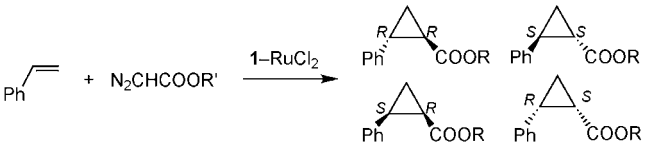
Oxazoline-based ligands, such as bis(oxazoline), azabis(oxazoline), and pyridinebis(oxazoline) (pybox) ligands, have attracted much attention because they have been used successfully in many different enantioselective organic reactions.[3] In the vast majority of cases, these ligands have C_2 symmetry.

In general, in cases in which the use of C_2-symmetric ligands leads to good enantioselectivities, the use of sterically asymmetric (but electronically symmetric, in the sense of a close similarity of the coordinating groups) analogues results in a dramatic worsening of the results. We recently found this behavior in the case of an asymmetric azabis(oxazoline) ligand used in the copper-catalyzed cyclopropanation of styrene with methyl diazoacetate.[4] However, there is at least one case in which the use of sterically asymmetric ligands results in enantioselectivities comparable to those obtained with the corresponding C_2-symmetric analogues, namely, the so-called "single-chiral" pybox ligands, described by Nishiyama et al. (Scheme 1).[5] When these ligands are used in the ruthenium-catalyzed cyclopropanation of styrene with alkyl diazoacetates (Scheme 2), very good enantioselectivities are observed for the *trans* cyclopropanes (up to 94% *ee*).[5] This result was explained by assuming that the carbene intermediate with the ester group *anti* to the bulky substituent of the ligand is the major intermediate, so that the carbene addition takes place mainly from the *Re* face (Figure 1).



1a: R = *i*Pr
1b: R = *t*Bu

Scheme 1. Structures of the asymmetric pyridinebis(oxazoline) (pybox) ligands of Nishiyama et al.



Scheme 2. A typical cyclopropanation reaction with styrene.

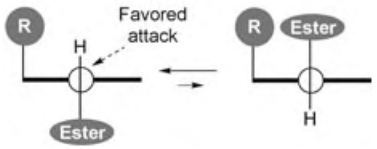


Figure 1. Schematic explanation given in the work of Nishiyama et al. for the good enantioselectivity observed with the asymmetric pybox ligands.

This is too simple an explanation, because the system is under Curtin–Hammett conditions at room temperature, as demonstrated by NMR spectroscopic experiments,[5] and hence the selectivity will only depend on the relative energies of the corresponding transition states (TSs) that result from the different ruthenium–carbene intermediates. The ester group can adopt, in principle, two different conformations with regard to the R substituent of the pybox ligand, so that four different carbene intermediates are possible. If only the *trans* addition to styrene from the *Re* and *Si* faces of the carbene is considered, eight different TSs are possible for this reaction, four of which lead to one cyclopropane enantiomer and the other four to the opposite enantiomer (Figure 2). The final enantioselectivity in the *trans*-cyclopropane products will then be determined by the relative energies of these TSs.

It is not evident at all, from an inspection of Figure 2, why high enantioselectivity should be expected for this system. In a first approach, if a mechanism for asymmetric induction similar to that described for copper–bis(oxazoline) complexes is assumed,[6] the steric interaction between the ester group and the R substituent of the chiral ligand should be responsible for the enantiodifferentiation. In the case of an

[*] Dr. J. M. Fraile, Dr. J. I. García, Dr. J. A. Mayoral, Dr. L. Salvatella
Instituto de Ciencia de Materiales de Aragón and
Instituto Universitario de Catálisis Homogénea
Dept. Química Orgánica
CSIC-Universidad de Zaragoza
Calle Pedro Cerbuna, 12, 50009 Zaragoza (Spain)
Fax: (+34) 976-76-2077
E-mail: jig@unizar.es
A. Cornejo, Dr. M. J. Gil, Dr. V. Martínez-Merino
Dept. Química Aplicada
Universidad Pública de Navarra
Edificio Los Acebos, 31006 Pamplona (Spain)

[**] In memory of Juan Carlos del Amo, who died in the 11-M Madrid terrorist attacks. This work was supported by the CICyT (Project no.: PPQ2002-04012) and the Navarra Government (Research no.: 5/2003). pybox = pyridinebis(oxazoline).

Supporting information for this article is available on the WWW under http://www.angewandte.org or from the author.

 © 2005 Wiley-VCH Verlag GmbH & Co. KGaA, Weinheim DOI: 10.1002/anie.200461418

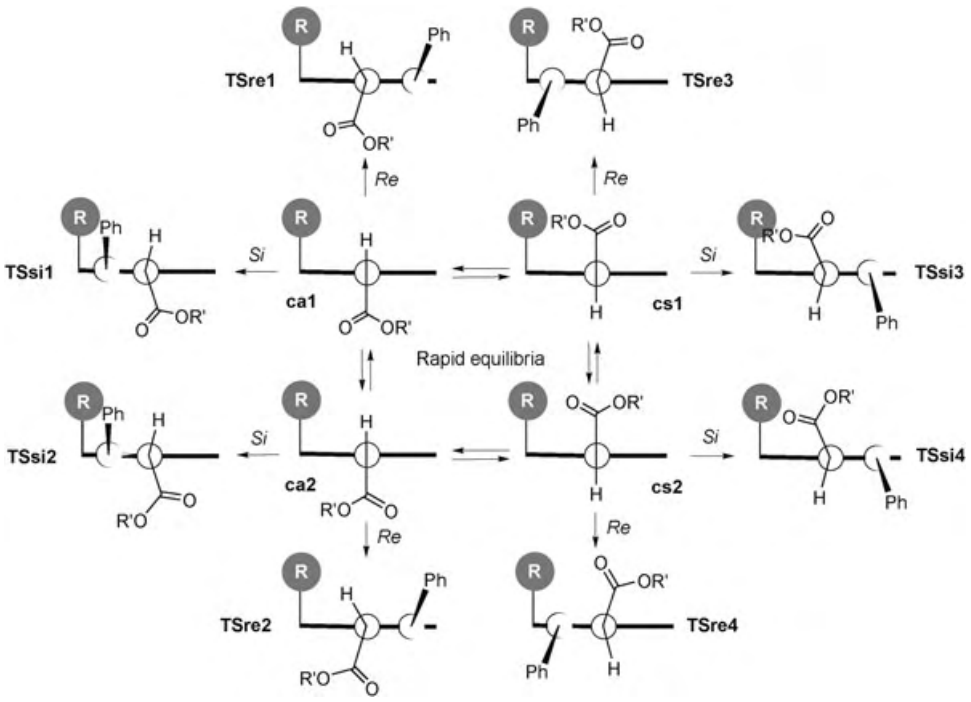


Figure 2. Schematic representation of the possible carbene intermediates and transition-state structures that lead to the *trans* cyclopropanes in the reaction of styrene with alkyl diazoacetates catalyzed by an asymmetric ruthenium–pybox complex.

asymmetric ligand, **TSsi1** and **TSsi2** would lack this interaction, so their energies should not differ very much from those, for example, of **TSre1** and **TSre2**, and there would be essentially no enantiodifferentiation. This situation is precisely that observed experimentally for asymmetric copper–azabis(oxazoline) complexes.[4] However, in the case of the asymmetric ruthenium–pybox complex this reasoning does not correspond with the experimental results, so it is clear that the enantiodifferentation mechanism must be different. Importantly, in the case of the copper–bis(oxazoline) catalysts, the approaching direction of the alkene to the carbon atom of the carbene avoids any steric interaction with the chiral ligand, since it takes place with the double bond in the plane of the complex and the phenyl group on the outside, far away from the R substituent of the chiral ligand, as would be the case for **TSsi1** and **TSsi2** if the same model were applicable.

We undertook the calculation of the critical points represented in Figure 2, with R = isopropyl (ligand **1a**), R′ = methyl (methyl diazoacetate as the diazo compound), and styrene as the alkene, with the aim of finding an explanation for the unexpectedly high enantioselectivity observed with these kinds of asymmetric ligands. All the calculations were carried out at the B3LYP/LANL2DZ level (see computational details in the Experimental Section), which has been proven to provide a good representation of the structures and energies of these systems.[7,8]

First, we calculated the energies of the four possible ruthenium–carbene intermediates shown in Figure 2. The relative energies of these intermediates are gathered in Table 1. Contrary to the assumption of Nishiyama et al., the four carbene intermediates have a very similar energy, and in fact the most stable structure, **cs1**, corresponds to a situation in which the R substituent and the ester group are in a *syn* arrangement. Questions can be raised concerning the accuracy of the B3LYP functional to describe steric interactions. Although it is known that this functional performs well in the calculation of conformer energy differences and conformational energy barriers of small molecules,[9] we decided to test this point further by carrying out some single-point energy calculations by using a two-layer ONIOM QM/MM scheme.[10] To this end, the isopropyl group of the pybox ligand was represented by the UFF force field[11] in the low layer, with the rest of the structure being calculated at the

Table 1: Calculated relative energies of the carbene intermediates and transition-state structures that lead to the *trans* cyclopropanes.

Structure	$\Delta\Delta E_{DFT}$ [kcal mol^{-1}][a]	$\Delta\Delta E_{ON}$ [kcal mol^{-1}][b]
ca1	0.4	0.0
ca2	0.5	0.6
cs1	0.0	0.2
cs2	0.4	1.4
TSre1	0.3	0.0
TSre2	1.1	0.6
TSre3	0.0	0.0
TSre4	0.3	0.5
TSsi1	3.2	3.4
TSsi2	2.7	2.8
TSsi3	0.9	1.0
TSsi4	1.3	3.7

[a] B3LYP/LANL2DZ level. [b] Single-point energy ONIOM B3LYP/LANL2DZ:UFF calculations; the isopropyl group is treated only at the MM level.

 © 2005 Wiley-VCH Verlag GmbH & Co. KGaA, Weinheim

B3LYP/LANL2DZ level in the high layer. In this way, any interaction between the isopropyl group and the ester group is never calculated at the DFT level, so that we have an independent estimation of the importance of this steric interaction. The results shown in Table 1 corroborate the theory that the origin of the enantioselectivity cannot be that a single carbene is favored energetically. As with the full DFT calculations, carbenes **cs1** and **ca1** have almost the same energy, although at this level the *anti* carbene is slightly favored.

Next, we calculated the eight possible transition-state structures that can result from the *Re* and *Si* approaches of styrene to the carbene carbon atom. The calculated relative energies of these TSs are also gathered in Table 1. There are three TSre states that are lower in energy than any of the TSsi states. The lowest energy TSsi state, **TSsi3**, is approximately 1 kcal mol^{-1} higher in energy than the lowest energy TSre state, **TSre3**. By considering a Boltzmann distribution of products based on the relative transition-state energies, the calculated *ee* value is approximately 74%, which is close to the experimental value of 71% *ee* described for the same system.[5] Of course, we do not claim that the theoretical level used is able to describe the relative energies to such a high accuracy, and the excellent numerical agreement is probably only coincidental, but it points to the origin of the behavior observed, as discussed below.

Independent estimations of the importance of steric effects were obtained by using the ONIOM QM/MM scheme. The phenyl group of styrene, the isopropyl group of the pybox ligand, and the methyl group of the ester were treated at the MM level. The corresponding results are gathered in Table 1, and they show essentially few differences with regard to the full DFT calculations. The stability of the TSre states relative to that of the TSsi states is somewhat enhanced and leads to a calculated value of 84% *ee*.

These results suggest that the origin of the enantioselectivity does not lie in one transition state being favored significantly over the others, but rather in the existence of more reaction channels that lead to *Re* than to *Si* products. The only TSsi states that contribute significantly to the reaction are **TSsi3** and **TSsi4**, and both are approximately 1 kcal mol^{-1} higher in energy than the corresponding **TSre3** and **TSre4** states. This energy difference can be explained by the steric interaction between the R and ester groups in the TSsi states. However, **TSsi1** and **TSsi2** represent the true critical points for explaining the high enantioselectivity observed experimentally.

A careful examination of the calculated geometries of the TSs (Figure 3) reveals some systematic differences with respect to the TSs from the copper–bis(oxazoline) complexes, with the most significant being the approaching direction of the alkene molecule. In the case of the ruthenium complexes, this approaching direction is out of the plane of the complex, with dihedral angles for the center of the double bond–$C_{carbene}$–Ru–$N_{oxazoline}$ of approximately 24–36° for the TSre states and approximately 30–73° for the TSsi states. This circumstance may result in close contacts between the alkene and the isopropyl group of the pybox ligand in some TSs, as discussed below.

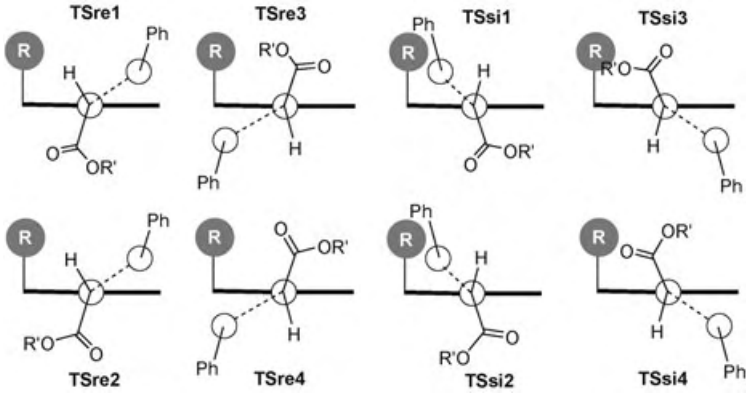


Figure 3. Calculated direction of approach of the styrene molecule to the pybox–ruthenium–carbene complex for the eight possible transition states.

TSsi1 and **TSsi2** are the only TSs for which the approach of the styrene molecule takes place in the same quadrant of the complex plane as that occupied by the isopropyl group. This direction of approach is a consequence of the general stereoelectronic requirements of the TS, as the pyramidalization of the carbene carbon atom results in dihedral angles for the center of the double bond–$C_{carbene}$–Ru–C_{ester} of approximately 120–130° in all cases (Figure 3). This fact leads to some geometrical differences in **TSsi1** and **TSsi2** with regard to the six other TSs (Figure 4). In the case of **TSsi1**, to avoid the steric interaction between the isopropyl group and one of

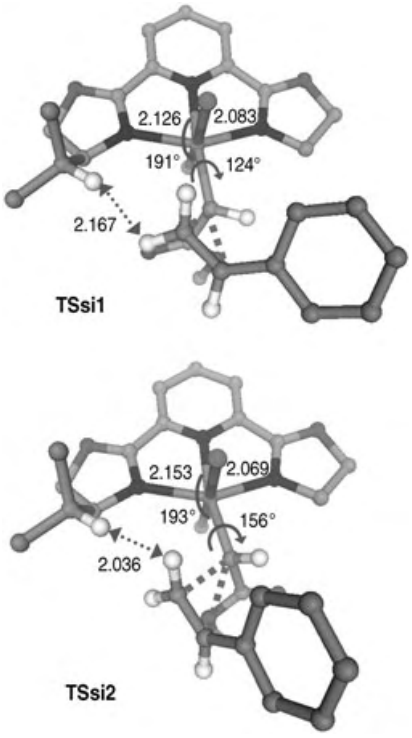


Figure 4. Some selected geometrical features of **TSsi1** and **TSsi2**. Most of the hydrogen atoms have been omitted for clarity.

 © 2005 Wiley-VCH Verlag GmbH & Co. KGaA, Weinheim

the hydrogen atoms of styrene, the carbene moiety is much more twisted relative to the complex plane (dihedral angle of 72.5° instead of the typical values of around 30° found in most of the other TSs). The $N_{pyridine}$–Ru–$C_{carbene}$ angle also deviates more from a straight line in **TSsi1** and **TSsi2** relative to the other TSs. In the case of **TSsi2**, this results in a more deformed complex, with one $N_{oxazoline}$–Ru distance significantly longer than the other. In spite of this deformation, there is a close contact between the isopropyl group and one of the hydrogen atoms of styrene.

It can therefore be concluded that the steric interaction between the incoming styrene and the isopropyl group of the chiral ligand is the origin of the high relative instability of **TSsi1** and **TSsi2**. On the other hand, the TSre states lack any steric interaction, either between the ester and the R group or between the styrene and the R group, which explains their closer relative energies.

As a corollary, it can be concluded that when the steric interaction between the ester group and the R group of the chiral ligand (an intramolecular interaction) dominates, as is the case for copper–bis(oxazoline) and copper–azabis(oxazoline) catalysts, the C_2 symmetry is mandatory to obtain good enantioselectivities. On the other hand, when the steric interaction between the R group and the incoming alkene (an intermolecular interaction) becomes dominant, as in the case described herein, a C_1 ligand can be enough to provide similar levels of enantioselectivity as a consequence of the subtle geometrical changes in the TS imposed by changes in the metal and the ligand, which modify the steric requirements of the reactions remarkably.

These conclusions contrast with the previously proposed explanation that both **TSsi1** and **TSsi2** present an *anti* arrangement of the R and ester groups, thereby suggesting that "chemically intuitive" stereochemical models may fail to explain the behavior of complex systems, such as enantioselective catalysts. These results also suggest that the establishment of a priori analogies to explain the behavior of different catalytic systems, even for the same reaction by the same mechanism, can give rise to misleading conclusions.

Experimental Section

All the theoretical calculations were carried out with the Gaussian 03 program.[12] The structures of the carbenes and TSs were optimized by using the B3LYP functional[13] and the LANL2DZ basis set, which consists of the valence double-zeta D95V basis set for first-row atoms[14] and the Los Alamos effective core potential[15] for Cl and Ru. In selected cases, the nature of the stationary points found was tested by the presence of the correct number of negative eigenvalues of the Hessian matrix by means of frequency calculations. Single-point energy calculations were carried out by following the ONIOM QM/MM scheme,[10] as implemented in Gaussian 03.

Received: July 23, 2004

Keywords: asymmetric catalysis · density functional calculations · enantioselectivity · N ligands · ruthenium

[1] *Comprehensive Asymmetric Catalysis* (Eds.: E. N. Jacobsen, A. Pfaltz, H. Yamamoto), Springer, Berlin, **1999**.

[2] a) For Aratani catalysts, industrially used in the production of chrisantemic acid derivatives, see: T. Aratani, *Pure Appl. Chem.* **1985**, *57*, 1839–1844; b) for phosphinooxazolines, see: O. Reiser, *Angew. Chem.* **1993**, *105*, 576–578; *Angew. Chem. Int. Ed. Engl.* **1993**, *32*, 547–549.

[3] See, for example: a) A. K. Ghosh, M. Packiarajan, J. Cappiello, *Tetrahedron: Asymmetry* **1998**, *9*, 1–45; b) J. S. Johnson, D. A. Evans, *Acc. Chem. Res.* **2002**, *33*, 325–335; c) G. Desimoni, G. Faita, P. Quadrelli, *Chem. Rev.* **2003**, *103*, 3119–3154; d) H. Lebel, J.-F. Marcoux, C. Molinaro, A. B. Charette, *Chem. Rev.* **2003**, *103*, 977–1050.

[4] A. Cornejo, J. M. Fraile, J. I. García, M. J. Gil, C. I. Herrerías, G. Legarreta, V. Martínez-Merino, J. A. Mayoral, unpublished results.

[5] H. Nishiyama, N. Soeda, T. Naito, Y. Motoyama, *Tetrahedron: Asymmetry* **1998**, *9*, 2865–2869.

[6] a) J. M. Fraile, J. I. García, V. Martínez-Merino, J. A. Mayoral, L. Salvatella, *J. Am. Chem. Soc.* **2001**, *123*, 7616–7625; b) T. Rasmussen, J. F. Jensen, N. Østergaard, D. Tanner, T. Ziegler, P.-O. Norrby, *Chem. Eur. J.* **2002**, *8*, 177–184; c) J. M. Fraile, J. I. García, M. J. Gil, V. Martínez-Merino, J. A. Mayoral, L. Salvatella, *Chem. Eur. J.* **2004**, *10*, 758–765.

[7] A. Cornejo, J. M. Fraile, J. I. García, M. J. Gil, V. Martínez-Merino, J. A. Mayoral, L. Salvatella, unpublished results.

[8] K. C. Zheng, Y. Shen, J. P. Wang, X. W. Liu, F. C. Yun, *Inorg. Chim. Acta* **2002**, *335*, 100–106.

[9] W. J. Hehre, *A Guide to Molecular Mechanics and Quantum Chemical Calculations*, Wavefunction, Irvine, **2003**.

[10] a) F. Maseras, K. Morokuma, *J. Comput. Chem.* **1995**, *16*, 1170–1179; b) F. Maseras, *Top. Organomet. Chem.* **1999**, *4*, 165–191.

[11] A. K. Rappé, C. J. Casewit, K. S. Colwell, W. A. Goddard III, W. M. Skiff, *J. Am. Chem. Soc.* **1992**, *114*, 10024–10035.

[12] Gaussian 03 (Revision B.04), M. J. Frisch, G. W. Trucks, H. B. Schlegel, G. E. Scuseria, M. A. Robb, J. R. Cheeseman, J. A. Montgomery, Jr., T. Vreven, K. N. Kudin, J. C. Burant, J. M. Millam, S. S. Iyengar, J. Tomasi, V. Barone, B. Mennucci, M. Cossi, G. Scalmani, N. Rega, G. A. Petersson, H. Nakatsuji, M. Hada, M. Ehara, K. Toyota, R. Fukuda, J. Hasegawa, M. Ishida, T. Nakajima, Y. Honda, O. Kitao, H. Nakai, M. Klene, X. Li, J. E. Knox, H. P. Hratchian, J. B. Cross, C. Adamo, J. Jaramillo, R. Gomperts, R. E. Stratmann, O. Yazyev, A. J. Austin, R. Cammi, C. Pomelli, J. W. Ochterski, P. Y. Ayala, K. Morokuma, G. A. Voth, P. Salvador, J. J. Dannenberg, V. G. Zakrzewski, S. Dapprich, A. D. Daniels, M. C. Strain, O. Farkas, D. K. Malick, A. D. Rabuck, K. Raghavachari, J. B. Foresman, J. V. Ortiz, Q. Cui, A. G. Baboul, S. Clifford, J. Cioslowski, B. B. Stefanov, G. Liu, A. Liashenko, P. Piskorz, I. Komaromi, R. L. Martin, D. J. Fox, T. Keith, M. A. Al-Laham, C. Y. Peng, A. Nanayakkara, M. Challacombe, P. M. W. Gill, B. Johnson, W. Chen, M. W. Wong, C. Gonzalez, J. A. Pople, Gaussian, Inc., Pittsburgh, PA, **2003**.

[13] a) C. Lee, W. Yang, R. Parr, *Phys. Rev. B* **1988**, *37*, 785–789; b) A. D. Becke, *J. Chem. Phys.* **1993**, *98*, 5648–5652.

[14] T. H. Dunning, Jr., P. J. Hay in *Modern Theoretical Chemistry* (Ed.: H. F. Schaeffer III), Plenum, New York, **1976**, pp. 1–28.

[15] P. J. Hay, W. R. Wadt, *J. Chem. Phys.* **1985**, *82*, 270–283.

 © 2005 Wiley-VCH Verlag GmbH & Co. KGaA, Weinheim

Metastable Molecules

Experimental Detection of Theoretically Predicted N_2CO**

Giulia de Petris, Fulvio Cacace, Romano Cipollini, Antonella Cartoni, Marzio Rosi, and Anna Troiani*

In memory of Fulvio Cacace

"Metastability" has drawn special attention as a means of energy storage, and much theoretical and experimental effort has been devoted to the study of the isoelectronic N_4, N_2CO, and C_2O_2 molecules.[1–3] The largest amounts of energy released per mass unit by dissociation of tetraazatetrahedrane N_4 (T_d; 200 kcal mol^{-1}), diazirinone N_2CO (100 kcal mol^{-1}), ethylenedione C_2O_2 (70 kcal mol^{-1}), and other theoretically predicted isomers prompted intense scrutiny of these 28-electron molecules as leading candidates for high-energy-density materials (HEDM). A renewed upsurge in interest springs from current missions to planetary atmospheres, where detection of reactive, even minor, species is one of the most attractive targets. After the recent experimental discovery of the open-chain N_4 molecule[4] and the ultimate answer to the long-standing challenge of synthesizing C_2O_2,[5] the question remains whether bound, high-energy N_2CO species can be experimentally observed.[6] Ab initio calculations at different levels of theory predict that three N_2CO species are potentially observable: the singlet C_{2v} diazirinone, which is the most stable N_2CO isomer, the triplet open-chain NNCO, and a strained tetrahedrane-like structure, whose "accumulated" energy (about 220 kcal mol^{-1}) would be higher than that of N_4 (T_d).[2] Despite the promising predictions, N_2CO has so far eluded experimental detection and defied all attempts at its characterization as a bound species.

Herein we report the preparation, positive detection, and characterization of N_2CO by the one-electron reduction of the N_2CO^+ cation, a result achieved by neutralization–reionization mass spectrometry (NRMS).[7] We have already utilized this approach for the detection of other metastable, elusive molecules[8] and for the detection of the related 28-electron molecule N_4,[4] which was recently extensively studied by the same technique with various pressure regimes and neutralizing target gases.[9]

The N_2CO^+ ion was formed by chemical ionization (CI) of a CO/N_2 mixture according to Equation (1).

$$CO^{(+/0)} + N_2{}^{(0/+)} \rightarrow N_2CO^+ \quad (1)$$

The interfering isobaric N_4^+ and $C_2O_2^+$ ions were separated by using ^{15}N-, ^{13}C-, and ^{18}O-labeled reagents. The remarkably high binding energy of the $(CO)_2^+$ ion[3c,10] required that CO and N_2 were introduced at a 1:20 pressure ratio, which typically ensures the $N_4^+/N_2CO^+/C_2O_2^+$ ratio displayed in the CI spectrum reported in Figure 1. Under such conditions the abundance of the N_2CO^+ species was appreciable, yet the intensity of the N_4^+ ion was far larger. To prevent any possible contamination from N_4^+ isotopomers, which are liable to neutralization, mixtures containing the following combinations of labeled reagents were examined: $N_2/C^{18}O$, $N_2/^{13}C^{18}O$, $^{15}N_2/CO$, $^{15}N_2/^{13}CO$, and $^{15}N_2/^{13}C^{18}O$.

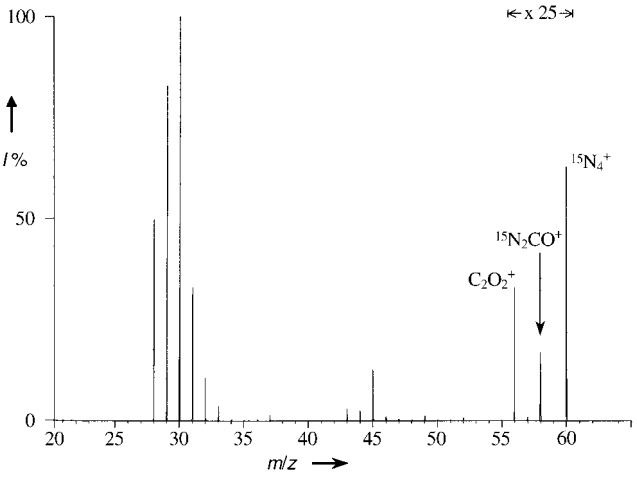


Figure 1. CI mass spectrum of the $^{15}N_2/CO$ mixture showing, in addition to the indicated adducts, peaks at m/z 28 = CO, m/z 29 = COH^+, m/z 30 = $^{15}N_2^+$, m/z 31 = $^{15}N_2H^+$, m/z 32 = O_2^+, m/z 43 = $^{15}NCO^+$, m/z 44 = CO_2^+, and m/z 45 = $^{15}N_3^+$.

The neutralization of the N_2CO^+ ions was accomplished by a one-electron redox sequence utilizing CH_4 (or Xe) and O_2 as neutralizing and reionizing gases, respectively [Eq. (2)].

$$N_2CO^+ \xrightarrow[CH_4,\ 1st\ cell]{+e} N_2CO \xrightarrow[O_2,\ 2nd\ cell]{-e} N_2CO^+ \quad (2)$$

The NR mass spectra of all the examined N_2CO^+ ions display significant recovery peaks at the same m/z value as that of the precursor ion (Figure 2). This result positively proves the existence of a neutral N_2CO species, which has survived at least for the time necessary to travel from the first cell, where it is generated, to the second cell, where it is reionized and detected. This time, which corresponds to the maximum "observation" time window available to the experi-

[*] Prof. Dr. G. de Petris, Prof. Dr. F. Cacace, Prof. Dr. R. Cipollini, Dr. A. Cartoni, Dr. A. Troiani
Dipartimento di Studi di Chimica e Tecnologia
delle Sostanze Biologicamente Attive
Università "La Sapienza"
P.le Aldo Moro 5, 00185 Roma (Italy)
Fax: (+39) 06-4991-3602
E-mail: giulia.depetris@uniroma1.it
Prof. Dr. M. Rosi
Dipartimento di Ingegneria Civile ed Ambientale
Sezione Tecnologie Chimiche e Materiali per l'Ingegneria
Università di Perugia
Via Duranti, 06131 Perugia (Italy)

[**] Financial support from the Italian Government (COFIN 2003), Rome University "La Sapienza", and the CNR-MIUR (Legge 16-10-2000 Fondo FISR) is gratefully acknowledged. This work was completed after Prof. Fulvio Cacace's death (deceased December 1, 2003).

Supporting information for this article is available on the WWW under http://www.angewandte.org or from the author.

 © 2005 Wiley-VCH Verlag GmbH & Co. KGaA, Weinheim DOI: 10.1002/anie.200460310

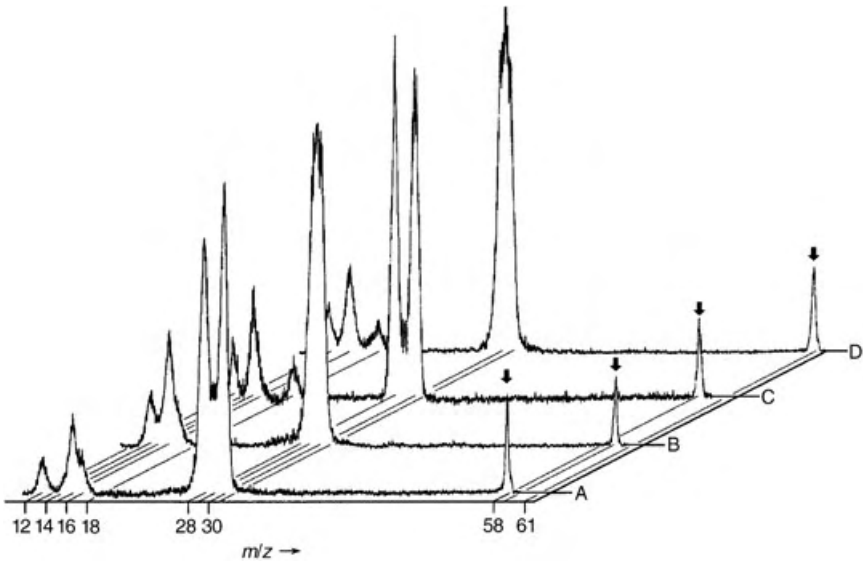


Figure 2. NR mass spectrum of N_2CO^+ ions from different mixtures: A) $^{15}N_2CO^+$ ions (m/z 58) from $^{15}N_2/CO$; B) $^{15}N_2{}^{13}CO^+$ ions (m/z 59) from $^{15}N_2/^{13}CO$; C) $N_2C^{18}O^+$ ions (m/z 58) from $N_2/C^{18}O$; and D) $^{15}N_2{}^{13}C^{18}O^+$ ions (m/z 61) from $^{15}N_2/^{13}C^{18}O$. Peaks at m/z 30 and 29 (trace B) and m/z 30 and 31 (trace D) are not resolved. The recovery peaks are indicated by arrows.

ment, marks the lower limit of the lifetime of the neutral species. The lifetime of N_2CO molecules having masses ranging from 56 to 61 Da and traveling with a kinetic energy of 4–6 keV is ≥ 0.8 μs. The successful detection of the neutral molecule hinges on the vertical character of the process, that is, the neutral species survives only if its geometry is not significantly different from that of the charged precursor. Such a constraint demands an accurate structural analysis of the parent ion.

The N_2CO^+ ions are seemingly formed by Equation (1) from both the CO^+ and N_2^+ reactant ions. In fact, as with many exothermic charge-transfer processes, the N_2^+/CO charge exchange is not very efficient ($k = 7.3 \times 10^{-11}$ cm^3 s^{-1}),[11] and the primary N_2^+ ions, largely supplied by the high N_2 pressure, are not totally depleted. Additional routes to N_2CO^+ ions can be envisaged from long-lived excited state reactants, such as N_2^+ ($A^2\Pi_u$) and N_2^+ ($a^4\Sigma_u^+$), acknowledged to be responsible for the formation of N_3^+,[12] which is indeed appreciably abundant under our experimental conditions. The population of the ionic N_2CO^+ species was probed by collisionally activated dissociation (CAD) and multistage mass spectrometry (MS^3) techniques. The CAD spectra (Figure 3) show CO^+ and N_2^+ as the major fragments, and minor peaks corresponding to the NCO^+ and CNN^+ fragments. The MS^3 spectra of all the daughter ions confirmed the isotopic assignments and the absence of any isobaric contamination.[13]

The fragmentation pattern clearly denotes an N–N–C–O connectivity and, on the basis of the absence of the N_2O^+ fragment among the dissociation products, one can exclude the tetrahedrane-like structure as a candidate for the detected neutral N_2CO species. Therefore, one is left with the singlet C_{2v} diazirinone and the triplet open-chain N_2CO, which both display the N–N–C–O connectivity. Previous experimental and theoretical studies identified only one N_2CO^+ stable ion, the open-chain transplanar N_2CO^+ ion ($X^2\Sigma_u^+$).[14] This would suggest the triplet open-chain N_2CO; however, its formation ($R_{N-C} = 1.234$ Å)[2] from N_2CO^+ ($R_{N-C} = 1.914$ Å)[14c] could be arguable because of an unfavorable Franck–Condon overlap.[15] The N_2CO^+ ($X^2\Sigma_u^+$) cluster ion is likely to prevail within the ionic N_2CO^+ population, yet formation of different ionic species cannot be excluded, especially from diatomic ions in long-lived electronically excited states, which are often conducive to formation of molecule-like ions rather than cluster ions. Although an extensive theoretical analysis was beyond the scope of this work, the results pictured by our NRMS experiments prompted us to make a theoretical study of the N_2CO^+ ion, with the study restricted to the open-chain and T-shaped geometries of the theoretically predicted N_2CO species.

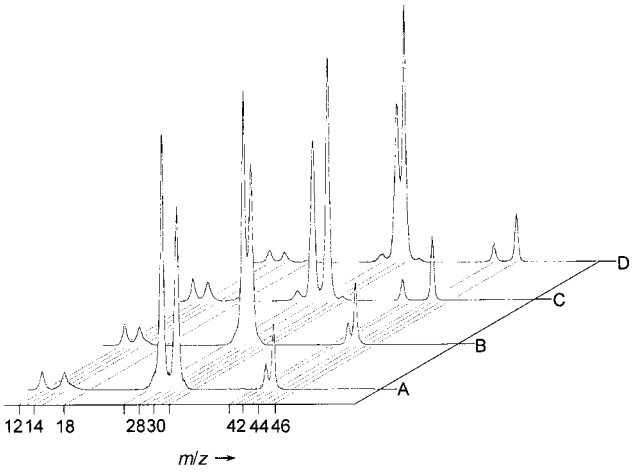


Figure 3. CAD spectra of N_2CO^+ ions from different mixtures: A) $^{15}N_2CO^+$ ions (m/z 58) from $^{15}N_2/CO$; B) $^{15}N_2{}^{13}CO^+$ ions (m/z 59) from $^{15}N_2/^{13}CO$; C) $N_2C^{18}O^+$ ions (m/z 58) from $N_2/C^{18}O$; D) $^{15}N_2{}^{13}C^{18}O^+$ ions (m/z 61) from $^{15}N_2/^{13}C^{18}O$.

Figure 4 illustrates the geometries and energies of the N_2CO^+ and N_2CO species identified. According to previous results, the only minimum found on the doublet surface of N_2CO^+ ions was the transplanar ion **1**. We were unable to find any stable T-shaped minimum on the doublet and quartet surfaces, since the doublet ion **2** is unstable toward dissociation once the zero-point energy correction is included. On the quartet surface we found the ions **3** and **4** of C_s symmetry, where the two diatoms are joined at a short distance. They are higher in energy than ion **1** by 97.3 and 106.8 kcal mol^{-1}, respectively, at the CCSD(T) level of theory. The known dissociation energy of the most stable N_2CO^+ ion (0.97 eV,[14b] 1.0 eV,[14c] 0.7 eV,[16]), and the difference between the ground state (CO^+ ($^2\Sigma^+$) and N_2 ($^1\Sigma_g^+$)) and the lowest spin-allowed

 © 2005 Wiley-VCH Verlag GmbH & Co. KGaA, Weinheim

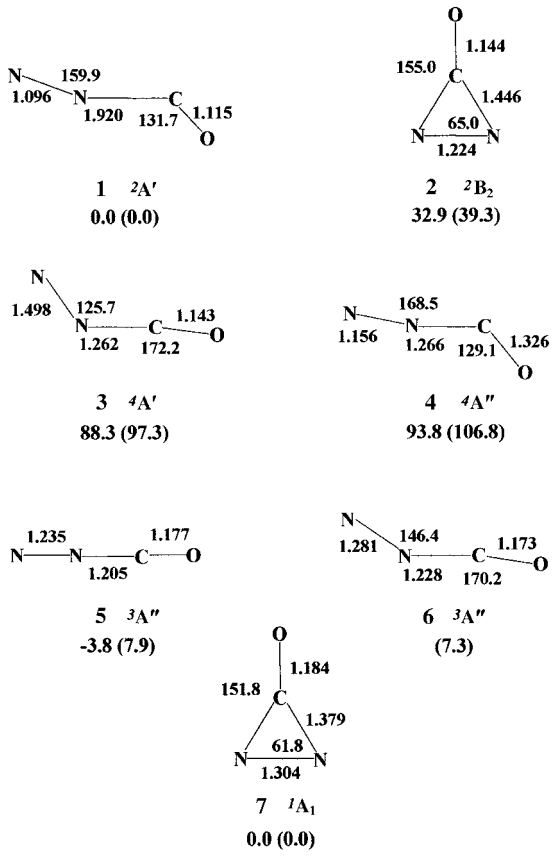


Figure 4. Optimized geometries of the stationary points localized on the potential energy surface of N_2CO^+ ions and N_2CO, at the B3LYP (**1**–**5**, **7**) and CCSD(T) (**6**) levels of theory. B3LYP (CCSD(T)) relative energies at 298 K are shown; bond lengths are in Å, angles in degrees, and energies in kcal mol^{-1}.

asymptotes,[17] allow one to evaluate that both the **3** and **4** quartet ions are stable with respect to dissociation. Since no T-shaped minima were found on either the doublet or quartet surfaces, one can reasonably exclude the diazirinone and assign the open-chain structure to the detected neutral species.

Geometry optimization of the triplet open-chain N_2CO led to the linear D_{2h} (^{3}A″) species **5** and to the bent C_s (^{3}A″) species **6**, which is consistent with previous results. Each is stable at only one level of theory—**5** at the B3LYP level and **6** at the MP2 level. However, their CCSD(T) energies only differ by 0.2 kcal mol^{-1}, and they are less stable by about 7 kcal mol^{-1} than singlet C_{2v} diazirinone **7**, which was identified as the most stable neutral N_2CO species. To settle the question, we resorted to the CCSD(T) geometry optimization, and found that the linear structure **5** is not a true minimum. To evaluate the internal energy excess of the neutral N_2CO C_s (^{3}A″) species **6** formed from ions **1**, **3**, and **4** we computed the CCSD(T) Franck–Condon energies of the vertical processes leading to **6**. The neutral N_2CO species **6** would be formed from the ground-state N_2CO^+ ion **1** with an energy excess of 46.1 kcal mol^{-1},[18] which is not unexpectedly above the dissociation threshold of 35 kcal mol^{-1}.[2] Conversely, species **6** is formed from **3** and **4** far below this limit, with an energy excess of 11.3 and 21.2 kcal mol^{-1}, respectively. It is clear that the bent N_2CO C_s (^{3}A″) species **6** is the most suitable candidate for the detected neutral species,[19] which could be formed with the least energy content from the ^{4}A′ ion **3**, which is the most probable precursor ion of strictly related structure, even if a possible role of ion **4** cannot be ruled out.

As to the formation of quartet states of N_2CO^+ ions, the N_4^+ ion is germane to the issue. It was recently confirmed[9] that the N_4^+ quartet ion is the most likely precursor of the N_4 ion detected by NRMS experiments, which is consistent with the effective clustering ability of diatomic reactant ions in long-lived electronically excited states. As a matter of fact, one of the advantages of the NRMS technique is the favorable access to elusive neutral species from nonthermalized or excited ionic species. A more advanced theoretical analysis would be required to ascertain the upper limit of the N_2CO lifetime, but the present result dictates that the kinetic stability of N_2CO is sufficient for observation within 1 μs, and provides the missing link in the family of open-chain N_4, N_2CO, and C_2O_2 molecules.

Experimental Section

The experiments were performed using a modified ZABSpec oa-TOF instrument (VG Micromass) of EBE-TOF configuration (E and B, electric and magnetic sectors; TOF, orthogonal time-of-flight mass spectrometer). Typical operating conditions of the CI source were: source temperature, 403 K; repeller voltage, 0 V; emission current, 1 mA; nominal electron energy, 50 eV; accelerating voltage, 4–8 kV. Helium was used as the collision gas in the CAD experiments, at such a pressure to achieve a 70% transmittance. In the NRMS experiments, CH_4 or Xe was used as the neutralizing gas and O_2 as the reionizing gas, admitted into the first and second cell, respectively, at such a pressure to achieve a beam transmittance of 80%. All ions were removed at the exit of the first cell by a pair of high-voltage (± 0.8 kV) deflecting electrodes, and the beam of fast neutral species entered the second cell. The NR mass spectra were averaged over 100 acquisitions to improve the signal-to-noise ratio. N_2 and CO were research-grade products with a stated purity in excess of 99.95 mol%. The MS/MS experiments were performed by admitting He into a cell located in the TOF sector, and recording the CAD spectra of the mass-selected daughter ion. The C^{18}O (98.8 ^{18}O atom%), ^{13}C^{18}O (99.9 ^{13}C atom%, 96.6 ^{18}O atom%), ^{13}CO (99.0 ^{13}C atom%), and $^{15}N_2$ (99.0 ^{15}N atom%) samples were obtained from Ikon Stable Isotopes, Inc.

Computational methods: Density functional theory, using the hybrid B3LYP functional,[20] was used to optimize the geometry of relevant species and evaluate their vibrational frequencies. Single-point energy calculations at the optimized geometries were performed using the coupled-cluster single and double excitation method with a perturbational estimate of the triple excitation (CCSD(T)) approach.[21] Selected states were also optimized at the CCSD(T) level. Transition states were located using the synchronous transit-guided quasi-Newton method of Schlegel and co-workers.[22] The 6-311+G(3d) basis set was used.[23] Zero-point energy corrections evaluated at the B3LYP/6-311+G(3d) level were added to CCSD(T) energies. The 0 K total energies of the species of interest were corrected to 298 K by adding translational, rotational, and vibrational contributions. The absolute entropies were calculated by standard statistical–mechanistic procedures from scaled harmonic frequencies and moments of inertia relative to B3LYP/6-311+G(3d) optimized geometries. All calculations were performed using Gaussian 03.[24] The Franck–Condon CCSD(T) energies were computed considering the CCSD(T) optimized geometry of the neutral species and the B3LYP optimized geometries of the ions.

Received: April 13, 2004
Revised: September 21, 2004

 © 2005 Wiley-VCH Verlag GmbH & Co. KGaA, Weinheim

Keywords: atmospheric chemistry · cations · mass spectrometry · nitrogen · reactive intermediates

[1] a) T. J. Lee, J. E. Rice, *J. Chem. Phys.* **1991**, *94*, 1215; b) M. N. Glukhovtsev, H. Jiao, P. von R. Schleyer, *Inorg. Chem.* **1996**, *35*, 7124; c) M. Bittererová, T. Brinck, H. Östmark, *J. Phys. Chem. A* **2000**, *104*, 11999; d) M. Bittererová, H. Östmark, T. Brinck, *Chem. Phys. Lett.* **2001**, *347*, 220.

[2] a) A. A. Korkin, P. von R. Schleyer, R. J. Boyd, *Chem. Phys. Lett.* **1994**, *227*, 312; b) A. A. Korkin, A. Balkova, R. J. Bartlett, R. J. Boyd, P. von R. Schleyer, *J. Phys. Chem.* **1996**, *100*, 5702.

[3] a) G. P. Raine, H. F. Schaefer III, R. C. Haddon, *J. Am. Chem. Soc.* **1983**, *105*, 194; b) H. Chen, J. L. Holmes, *Int. J. Mass Spectrom. Ion Processes* **1994**, *133*, 111; c) D. Schröder, H. Schwarz, *Int. J. Mass Spectrom. Ion Processes* **1995**, *146/147*, 183; d) D. Dawson, H. Chen, J. L. Holmes, *Eur. J. Mass Spectrom.* **1996**, *2*, 373.

[4] F. Cacace, G. de Petris, A. Troiani, *Science* **2002**, *295*, 480.

[5] D. Schröder, C. Heinemann, H. Schwarz, J. N. Harvey, S. Dua, S. J. Blanksby, J. H. Bowie, *Chem. Eur. J.* **1998**, *4*, 2550.

[6] The known nitrosyl cyanide NCNO is a stable compound synthesized in 1971: P. Horsewood, G. W. Kirby, *Chem. Commun.* **1971**, 1139; see also: G. Maier, H. P. Reisenauer, J. Eckwert, M. Naumann, M. De Marco, *Angew. Chem.* **1997**, *109*, 1785; *Angew. Chem. Int. Ed. Engl.* **1997**, *36*, 1707.

[7] a) G. I. Gellene, R. F. Porter, *Acc. Chem. Res.* **1983**, *16*, 200; b) J. K. Terlouw, H. Schwarz, *Angew. Chem.* **1987**, *99*, 829; *Angew. Chem. Int. Ed. Engl.* **1987**, *26*, 805; c) C. Wesdemiotis, F. W. McLafferty, *Chem. Rev.* **1987**, *87*, 485; d) J. L. Holmes, *Mass Spectrom. Rev.* **1989**, *8*, 513; e) C. A. Schalley, G. Hornung, D. Schröder, H. Schwarz, *Chem. Soc. Rev.* **1998**, *27*, 91.

[8] a) G. de Petris, *Acc. Chem. Res.* **2002**, *35*, 305; b) F. Cacace, G. de Petris, M. Rosi, A. Troiani, *Angew. Chem.* **2003**, *115*, 3093; *Angew. Chem. Int. Ed.* **2003**, *42*, 2985; d) G. de Petris, F. Cacace, A. Troiani, *Chem. Commun.* **2004**, *3*, 326.

[9] E. E. Rennie, P. M. Mayer, *J. Chem. Phys.* **2004**, *120*, 10561.

[10] K.-M. Weitzel, J. Mähnert, *Int. J. Mass Spectrom. Ion Processes* **2002**, *214*, 175.

[11] V. G. Anicich, *J. Phys. Chem. Ref. Data* **1993**, *22*, 1469.

[12] a) M. T. Bowers, P. R. Kemper, J. B. Laudenslager, *J. Chem. Phys.* **1974**, *61*, 4394; b) P. Tosi, W. Lu, D. Bassi, R. Tarroni, *J. Chem. Phys.* **2001**, *114*, 2149.

[13] For the consecutive dissociations leading to NO^+ and CN^+ ions and the accurate analysis of the elemental composition, see the Supporting Information.

[14] a) L. B. Knight, Jr., J. Steadman, P. K. Miller, J. A. Cleveland, Jr., *J. Chem. Phys.* **1988**, *88*, 2226; b) J. Baker, A. D. Buckingham, *J. Chem. Soc. Faraday Trans. 2* **1987**, *83*, 1609; c) M. Hochlaf, C. Léonard, E. E. Ferguson, P. Rosmus, E.-A. Reinsch, S. Carter, N. C. Handy, *J. Chem. Phys.* **1999**, *111*, 4948.

[15] N_2CO exists as a mere van der Waals complex, characterized by a long intermolecular distance of 4.025 Å, and bound with an energy of only 1.3 kJ mol^{-1}: a) Y. Kawashima, K. Nishizawa, *Chem. Phys. Lett.* **1996**, *249*, 87; b) C. Xia, A. R. W. McKellar, Y. Xu, *J. Chem. Phys.* **2000**, *113*, 525. Based on the available literature, such a binding energy value appears too low to ensure detection by NRMS. (The lowest value reported for a tetra-atomic molecule is 6 kcal mol^{-1}: D. Schröder, C. A. Schalley, N. Goldberg, J. Hrusák, H. Schwarz, *Chem. Eur. J.* **1996**, *2*, 1235.) Formation of the strictly related $(N_2)_2$ van der Waals dimer by NR was rigorously excluded in ref. [9].

[16] J. Glosík, G. Bánó, E. E. Ferguson, W. Lindinger, *Int. J. Mass Spectrom. Ion Processes* **1998**, *176*, 177.

[17] a) K. P. Huber, G. Herzberg, *Molecular spectra and molecular structure. IV. Constants of diatomic molecules.* Van Nostrand Reinhold, New York, **1978**; b) S. G. Lias, J. E. Bartmess, J. F. Liebman, J. L. Holmes, R. D. Levin, W. G. Mallard, *J. Phys. Chem. Ref. Data* **1988**, *17*, suppl. 1.

[18] The computed single-point energies indicate that formation of the ground-state triplet **6** from ion **1** would require an energy excess of 29.0 kcal mol^{-1}, which exceeds the dissociation limit of **1**.

[19] Isomerizations to [N_2, C, O] species of different connectivity, from either the N_2CO^+ precursor ion (within the source) or from N_2CO (in the time interval between the neutralization and reionization), were excluded on the basis of the following CCSD(T)/B3LYP calculations. Doublet $NCNO^+$ and $CNON^+$ ions are located 50–60 kcal mol^{-1} above the ground-state N_2CO^+ ion, whose binding energy is only 16–20 kcal mol^{-1} (see refs. [14] and [16]). On the quartet surface the $NCNO^+$ ion is located 25 kcal mol^{-1} above the quartet N_2CO^+ ion **3**. However, the latter has to overcome a barrier of $\approx$87 kcal mol^{-1} to isomerize to $NCNO^+$ (via a cyclic intermediate), that is some 40 kcal mol^{-1} above the lowest dissociation limit of **3**. As for the neutral species, the triplet CNNO is located 64 kcal mol^{-1} above the N_2CO species **6**, which is far above the barrierless dissociation limit of **6** (35 kcal mol^{-1}), whereas the triplet NCNO is located 22 kcal mol^{-1} above **6**. However, a large barrier, far exceeding the dissociation threshold, is expected for such an isomerization. The process requires a very extensive rearrangement involving the breaking of both the N–N and C–O bonds and, also consistent with the above, it is likely to proceed through the intermediacy of high-energy cyclic isomers (species of N–N–C–O and N–C–N–O connectivity on the singlet surface are connected by cyclic structures located 140 kcal mol^{-1} above the most stable diazirinone, see ref. [2]).

[20] a) A. D. Becke, *J. Phys. Chem.* **1993**, *97*, 5648; b) P. J. Stephens, F. J. Devlin, C. F. Chablowski, M. J. Frisch, *J. Phys. Chem.* **1994**, *98*, 11623.

[21] a) R. J. Bartlett, *Annu. Rev. Phys. Chem.* **1981**, *32*, 359; b) K. Raghavachari, G. W. Trucks, J. A. Pople, M. Head-Gordon, *Chem. Phys. Lett.* **1989**, *157*, 479.

[22] a) C. Peng, H. B. Schlegel, *Isr. J. Chem.* **1993**, *33*, 449; b) C. Peng, P. Y. Ayala, H. B. Schlegel, M. J. Frisch, *J. Comput. Chem.* **1996**, *17*, 49.

[23] a) R. Krishnan, J. S. Binkley, R. Seeger, J. A. Pople, *J. Chem. Phys.* **1980**, *72*, 650; b) A. D. McLean, G. S. Chandler, *J. Chem. Phys.* **1980**, *72*, 5639; c) T. Clark, J. Chandrasekhar, G. W. Spitznagel, P. v. R. Schleyer, *J. Comput. Chem.* **1983**, *4*, 294; d) M. J. Frisch, J. A. Pople, J. S. Binkley, *J. Chem. Phys.* **1984**, *80*, 3265.

[24] Gaussian 03 (Revision A.1), M. J. Frisch, G. W. Trucks, H. B. Schlegel, G. E. Scuseria, M. A. Robb, J. R. Cheeseman, J. A. Montgomery, Jr., T. Vreven, K. N. Kudin, J. C. Burant, J. M. Millam, S. S. Iyengar, J. Tomasi, V. Barone, B. Mennucci, M. Cossi, G. Scalmani, N. Rega, G. A. Petersson, H. Nakatsuji, M. Hada, M. Ehara, K. Toyota, R. Fukuda, J. Hasegawa, M. Ishida, T. Nakajima, Y. Honda, O. Kitao, H. Nakai, M. Klene, X. Li, J. E. Knox, H. P. Hratchian, J. B. Cross, C. Adamo, J. Jaramillo, R. Gomperts, R. E. Stratmann, O. Yazyev, A. J. Austin, R. Cammi, C. Pomelli, J. W. Ochterski, P. Y. Ayala, K. Morokuma, G. A. Voth, P. Salvador, J. J. Dannenberg, V. G. Zakrzewski, S. Dapprich, A. D. Daniels, M. C. Strain, O. Farkas, D. K. Malick, A. D. Rabuck, K. Raghavachari, J. B. Foresman, J. V. Ortiz, Q. Cui, A. G. Baboul, S. Clifford, J. Cioslowski, B. B. Stefanov, G. Liu, A. Liashenko, P. Piskorz, I. Komaromi, R. L. Martin, D. J. Fox, T. Keith, M. A. Al-Laham, C. Y. Peng, A. Nanayakkara, M. Challacombe, P. M. W. Gill, B. Johnson, W. Chen, M. W. Wong, C. Gonzalez, J. A. Pople, Gaussian, Inc., Pittsburgh, PA, **2003**.

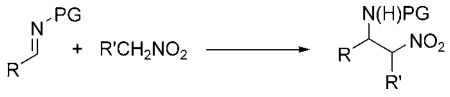
 © 2005 Wiley-VCH Verlag GmbH & Co. KGaA, Weinheim

Asymmetric Catalysis

Highly Enantioselective Thiourea-Catalyzed Nitro-Mannich Reactions**

*Tehshik P. Yoon and Eric N. Jacobsen**

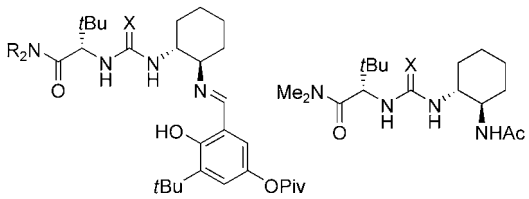
The addition of a nitroalkane across the C=N bond of an imine [Eq. (1), PG = protecting group], known as the nitro-



(1)

Mannich (or aza-Henry) reaction, is a carbon–carbon bond-forming process that can result in the generation of two contiguous nitrogen-bearing stereogenic centers. This reaction allows straightforward entry to a variety of nitrogen-containing chiral building blocks such as vicinal diamines by reduction of the nitro group [1,2] and α-amino carbonyl compounds by means of the Nef reaction.[3] As a result, considerable effort has been directed toward the development of catalytic asymmetric versions of the nitro-Mannich reaction over the past several years. Shibasaki et al. have described the enantioselective addition of nitroalkanes to *N*-phosphinoyl imines using chiral ytterbium[4] and aluminum[5] catalysts, while Jørgensen et al. have reported asymmetric copper-catalyzed additions to α-iminoesters.[6] Beyond these metal-catalyzed variants, two reports of enantioselective organocatalytic nitro-Mannich reactions have appeared recently. Takemoto et al. have reported a bifunctional thiourea catalyst that induces moderate enantioselectivity in the addition of nitromethane to a variety of aromatic *N*-phosphinoyl imines,[7] and Johnston et al. have developed a chiral bisamidine triflate salt that effects the diastereoselective addition of nitroethane to a range of electron-deficient *N*-Boc imines.[8]

Our laboratory has identified a family of chiral urea and thiourea catalysts (e.g. **1a** and **1b**, Figure 1) that catalyze a variety of enantioselective reactions with imines, including



1a X = O, NR_2 = NHBn
1b X = S, NR_2 = NMe_2
2a X = O
2b X = S

Figure 1. Urea and thiourea catalysts. Piv = pivaloyl.

hydrocyanation,[9] Mannich,[10] hydrophosphonylation,[11] and acyl-Pictet–Spengler[12] reactions. Intrigued by the possibility that these compounds might constitute an emerging class of "privileged"[13] enantioselective catalysts, we investigated their activity in the asymmetric nitro-Mannich reaction. Herein, we report the discovery that the new thiourea catalyst **2b** efficiently promotes the diastereoselective nitro-Mannich reaction of nitroalkanes with *N*-Boc imines with high levels of enantioselectivity.

Our initial exploratory efforts directed toward thiourea-catalyzed asymmetric nitro-Mannich reactions involved screening of catalysts **1a** and **1b**, which had been developed and optimized in the context of Strecker-type reactions.[9] Surprisingly, while the first-generation Strecker urea catalyst **1a** afforded promising activity in the model reaction of nitroethane with benzaldehyde-derived *N*-Boc imine **3a** [Eq. (2)] (20% conversion, 2.1:1 *syn*:*anti*, 50% *ee*; Table 1, entry 1), the improved thiourea Strecker catalyst **1b**[9b] failed to accelerate this transformation (entry 2). Systematic variation of catalyst structure revealed that the simplified acetamide catalyst **2a** provided excellent enantio- and diastereoselectivity at 0°C, although the poor solubility of the catalyst in ether resulted in poor activity (entry 3, 34% conversion, 7.5:1 *syn*:*anti*, 92% *ee*). On the other hand, catalyst **2a** displayed improved solubility in toluene, and the reaction proceeded to completion within 24 h with similar enantio- and diastereoselectivity (entry 4, >95% conversion, 8.4:1 *syn*:*anti*, 91% *ee*). However, the reaction under these conditions proved to be poorly reproducible and quite sensitive to the purity of the starting imine; high *ee* values were largely limited to the benzaldehyde-derived imine **3a**. After a screen of additives, it was discovered that the addition of powdered 4-Å molecular sieves improved the reproducibility of the process and provided a more diastereoselective

Table 1: Optimization of reaction conditions [Eq. (2), Ar = Ph].

Entry	Cat.	Solv.	Base (equiv)	Mol. sieves (4 Å)	*T* [°C]	*t* [h]	Conv. [%]	d.r. (*syn*:*anti*)	*ee* [%]
1	**1a**	ether	Et_3N (0.2)	–	23	4	20	2.1:1	50
2	**1b**	ether	Et_3N (0.2)	–	23	4	0	–	–
3	**2a**	ether	Et_3N (1)	–	0	18	34	7.5:1	92
4	**2a**	toluene	Et_3N (1)	–	0	24	>95	8.4:1	91
5	**2a**	toluene	Et_3N (1)	+	0	24	>95	10:1	92
6	**2a**	toluene	iPr_2NEt (1)	+	0	24	36	11:1	91
7	**2b**	toluene	iPr_2NEt (1)	+	0	18	>95	15:1	92

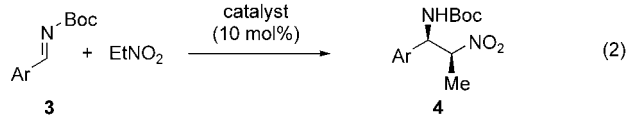
[*] T. P. Yoon, Prof. E. N. Jacobsen
Department of Chemistry and Chemical Biology
Harvard University
12 Oxford Street, Cambridge, MA 02138 (USA)
Fax: (+1) 617-496-1880
E-mail: jacobsen@chemistry.harvard.edu

[**] This work was supported by the NIH through GM-43214, P50 GM069721, and a postdoctoral fellowship to T.P.Y.

Supporting information for this article is available on the WWW under http://www.angewandte.org or from the author.

 © 2005 Wiley-VCH Verlag GmbH & Co. KGaA, Weinheim DOI: 10.1002/anie.200461814

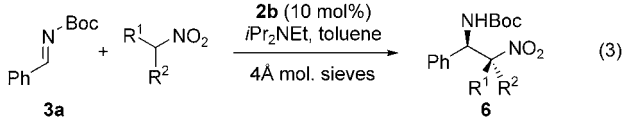
reaction (entry 5, 10:1 *syn*:*anti*). Variation of the tertiary amine base then led to the observation that the diastereoselectivity of the process could be improved further by the use of Hünig's base, albeit at the expense of reactivity (entry 6, 36% conversion, 11:1 *syn*:*anti*). Finally, a second screen of catalyst structures revealed that thiourea catalyst **2b** was significantly more reactive in the presence of molecular sieves than its urea analogue, allowing complete conversion to nitro-Mannich adduct **4** in 92% *ee* and 15:1 d.r. after 18 h (entry 7).[14]



(2)

Results obtained in the addition of nitroethane to a variety of *N*-Boc imines are summarized in Table 2. High enantioselectivities were obtained with a series substituted benzaldimine derivatives bearing both electron-donating and electron-withdrawing substitutents (entries 1–7, 92–96% *ee*).[15] These substrates also afforded good *syn* diastereoselectivity (7–16:1 *syn*:*anti*) in all cases examined, with the exception of *ortho*-chloro-substituted imine **3d** (entry 4, 2:1 *syn*:*anti*). This substrate proved to be less reactive than its *meta* and *para* isomers, and required slightly more forcing conditions for complete conversion (5 equiv nitroethane, 2 equiv Hünig's base). Aromatic heterocyclic *N*-imines (entries 8–9, 6–7:1 *syn*:*anti*, 93–97% *ee*) and 2-naphthaldehyde-derived imine **3j** (entry 10, 5:1 *syn*:*anti*, 97% *ee*) underwent reaction with excellent enantioselectivity and provided products with synthetically useful levels of diastereoselectivity.

As revealed in Table 3, useful results were obtained in nitro-Mannich reactions with a variety of nitroalkanes.[16] 1-Nitropropane underwent smooth reaction with *N*-Boc benzaldimine **3a** to provide adduct **6a** in 7:1 d.r. and 92% *ee* (entry 1: [Eq. (3)]). Nitromethane proved to be considerably less reactive and required longer reaction times (40 h) for complete conversion, but the adduct was obtained in 92% *ee* (entry 2). Reaction with the more sterically challenging 2-nitropropane did not proceed at all under the standard conditions, but when triethylamine was used as the tertiary base additive the desired product **5c** was obtained in 87% yield and 92% *ee* (entry 3). Finally, reaction of β-silyloxy nitroalkane **5** afforded the protected amino alcohol **6d** in 4:1 d.r. and 95% *ee* (entry 4). No desilylation or elimination of the silyloxy group was observed under the mild conditions of this catalytic process.



(3)

Table 3: Enantioselective nitro-Mannich reactions with representative nitroalkanes [Eq. (3)].[a]

Entry	Nitroalkane	Adduct	R^1	R^2	Yield [%][b]	d.r. (*syn*:*anti*)[c]	*ee* [%][c]
1	1-nitropropane	**6a**	Et	H	99	7:1	95
2	nitromethane	**6b**	H	H	87	–	92
3[d]	2-nitropropane	**6c**	Me	Me	87	–	92
4[e]	$TBSOCH_2CH_2NO_2$ (**5**)	**6d**	$TBSOCH_2$	H	85	4:1	95

[a] Unless otherwise noted, reactions were carried out with 1 equiv **3a** (0.25 mmol), 5 equiv nitroalkane, 10 mol% **2b**, 2 equiv DIPEA, and powdered 4-Å molecular sieves (150 mg) in toluene (1 mL) at 4°C. [b] Yield of product isolated after silica gel chromatography. [c] Determined by HPLC by using commercial chiral columns; see Supporting Information. [d] Reaction performed by using 2 equiv triethylamine. [e] Reaction performed by using 2.5 equiv **5** and 1 equiv DIPEA; TBS = *tert*-butyldimethylsilyl.

Table 2: Enantioselective catalytic addition of nitroethane to representative *N*-Boc imines [Eq. (2)].[a]

Entry	Ar	Adduct	Yield [%][b]	d.r. (*syn*:*anti*)[c]	*syn ee* [%][c]
1	Ph (**3a**)	**4a**	96	15:1	92
2	*p*-ClC_6H_4 (**3b**)	**4b**	98	7:1	95
3	*m*-ClC_6H_4 (**3c**)	**4c**	85	7:1	96
4[d]	*o*-ClC_6H_4 (**3d**)	**4d**	99	2:1	93
5	*p*-MeC_6H_4 (**3e**)	**4e**	90	12:1	96
6	*m*-MeC_6H_4 (**3e**)	**4f**	99	9:1	95
7	*p*-$(MeO)C_6H_4$ (**3g**)	**4g**	95	16:1	96
8[d]	3-pyridyl (**3h**)	**4h**	79	7:1	97
9	2-furyl (**3i**)	**4i**	95	6:1	93
10[d]	2-naphthyl (**3j**)	**4j**	91	5:1	97

[a] Unless noted otherwise, reactions were carried out with 1 equiv *N*-Boc imine (0.25 mmol), 2.5 equiv nitroethane, 10 mol% **2b**, 1 equiv diisopropylethylamine (DIPEA), and powdered 4-Å molecular sieves (150 mg) in 1 mL toluene at 4°C. [b] Yield of product isolated after silica gel chromatography. [c] Determined by HPLC using commercial chiral columns; see Supporting Information. [d] Reaction performed by using 5 equiv nitroethane and 2 equiv DIPEA.

In summary, the new thiourea catalyst **2b** was found to promote the stereoselective addition of a range of nitroalkanes to aromatic *N*-Boc imines. This new procedure represents an advance in the asymmetric nitro-Mannich reaction with regard to both enantioselectivity and substrate scope. A number of different mechanistic scenarios may be considered for this catalytic transformation. The sense of imine enantioface selectivity is the same as that observed in previously reported thiourea-catalyzed Strecker, Mannich, and hydrophosphonylation reactions, suggesting a common mechanism of imine activation. However, thiourea derivatives are also known to bind to and modulate the reactivity of nitronate anions;[17] therefore the role of **2b** in this transformation could be activation of the nitroalkane component[18] or dual activation of both reaction partners.[19] Further investigations into the mechanism and scope of this reaction are underway and will be reported in due course.

Received: August 27, 2004

 © 2005 Wiley-VCH Verlag GmbH & Co. KGaA, Weinheim

Keywords: amines · asymmetric catalysis · diastereoselectivity · enantioselectivity · Mannich reaction

[1] D. Lucet, T. Le Gall, C. Mioskowski, *Angew. Chem.* **1998**, *110*, 2724 – 2772; *Angew. Chem. Int. Ed. Engl.* **1998**, *37*, 2580 – 2627.
[2] H. Adams, J. C. Anderson, S. Peace, A. M. K. Pennell, *J. Org. Chem.* **1998**, *63*, 9932 – 9934.
[3] R. Ballini, M. Petrini, *Tetrahedron* **2004**, *60*, 1017 – 1047.
[4] K. Yamada, S. J. Harwood, H. Gröger, M. Shibasaki, *Angew. Chem.* **1999**, *111*, 3713 – 3715; *Angew. Chem. Int. Ed.* **1999**, *38*, 3504 – 3506.
[5] K. Yamada, G. Moll, M. Shibasaki, *Synlett* **2001**, 980 – 982.
[6] a) K. R. Knudsen, T. Risgaard, N. Nishiwaki, K. V. Gothelf, K. A. Jørgensen, *J. Am. Chem. Soc.* **2001**, *123*, 5843 – 5844; b) N. Nishiwaki, K. R. Knudsen, K. V. Gothelf, K. A. Jørgensen, *Angew. Chem.* **2001**, *113*, 3080 – 3083; *Angew. Chem. Int. Ed.* **2001**, *40*, 2992 – 2995.
[7] a) T. Okino, Y. Hoashi, Y. Takemoto, *J. Am. Chem. Soc.* **2003**, *125*, 12672 – 12673; b) T. Okino, S. Nakamura, T. Furukawa, Y. Takemoto, *Org. Lett.* **2004**, *6*, 625 – 627.
[8] B. M. Nugent, R. A. Yoder, J. N. Johnston, *J. Am. Chem. Soc.* **2004**, *126*, 3418 – 3419.
[9] a) M. S. Sigman, E. N. Jacobsen, *J. Am. Chem. Soc.* **1998**, *120*, 4901 – 4902; b) M. S. Sigman, P. Vachal, E. N. Jacobsen, *Angew. Chem.* **2000**, *112*, 1336 – 1338; *Angew. Chem. Int. Ed.* **2000**, *39*, 1279 – 1281; c) P. Vachal, E. N. Jacobsen, *Org. Lett.* **2000**, *2*, 867 – 870; d) P. Vachal, E. N. Jacobsen, *J. Am. Chem. Soc.* **2002**, *124*, 10012 – 10014.
[10] a) A. G. Wenzel, E. N. Jacobsen, *J. Am. Chem. Soc.* **2002**, *124*, 12964 – 12965; b) A. G. Wenzel, M. P. Lalonde, E. N. Jacobsen, *Synlett* **2003**, 1919 – 1922.
[11] G. D. Joly, E. N. Jacobsen, *J. Am. Chem. Soc.* **2004**, *126*, 4102 – 4103.
[12] M. S. Taylor, E. N. Jacobsen, *J. Am. Chem. Soc.* **2004**, *126*, 10558 – 10559.
[13] T. P. Yoon, E. N. Jacobsen, *Science* **2003**, *299*, 1691 – 1693.
[14] The role of powdered 4-Å molecular sieves in this process has not yet been established. Use of other desiccants, including 3-Å and 5-Å molecular sieves, had a detrimental effect on rate and enantioselectivity. This raises the intriguing possibility that the 4-Å sieves may play a more direct role in the reaction mechanism.
[15] Only aromatic imines were investigated because, as yet, no useful method exists for the synthesis of aliphatic *N*-Boc imine derivatives.
[16] α-Nitrotoluene was also observed to undergo rapid reaction under these conditions, but racemic product was obtained.
[17] B. R. Linton, M. S. Goodman, A. D. Hamilton, *Chem. Eur. J.* **2000**, *6*, 2449 – 2455.
[18] Takemoto et al. have postulated a mechanism for the nitro-Mannich reaction involving thiourea activation of the nitro-alkane. See ref. [7].
[19] For a recent example of dual-activation catalysis, see: G. M. Sammis, H. Danjo, E. N. Jacobsen, *J. Am. Chem. Soc.* **2004**, *126*, 9928 – 9929.

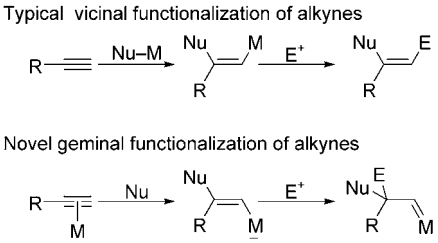
 © 2005 Wiley-VCH Verlag GmbH & Co. KGaA, Weinheim

Homogeneous Catalysis

Rhenium(I)-Catalyzed Intramolecular Geminal Carbofunctionalization of Alkynes: Tandem Cyclization of ω-Acetylenic Dienol Silyl Ethers**

*Hiroyuki Kusama, Hokuto Yamabe, Yuji Onizawa, Takahiko Hoshino, and Nobuharu Iwasawa**

1,2-Vicinal functionalization of alkynes can readily be carried out by carbometalation using various kinds of organometallic reagents, such as Cu, Al, Zr, etc., followed by reaction of the resulting alkenyl metallic species with electrophiles (Scheme 1).[1] However, geminal functionalization, and in particular geminal carbofunctionalization of alkynes, has remained unexplored despite its high potential as a synthetic method.[2,3]



Scheme 1. Vicinal- or geminal-functionalization of alkynes.

We have already reported that $[W(CO)_5(L)]$ can effectively activate terminal alkynes towards the intramolecular nucleophilic attack of enol silyl ethers to give various kinds of carbocycles catalytically.[4] The aim of these studies was to realize geminal carbofunctionalization of alkynes by using this strategy. Thus, by appropriate choice of the metallic reagent, the alkenyl metallic species produced by addition of carbo-nucleophiles to the electrophilically activated alkynes would react with carbo-electrophiles not at the α-position but at the β-position to the metal center to give carbene complex intermediates, in a similar way to the anions of Fischer-type carbene complexes[5] (Scheme 1). Further reaction of the

[*] Dr. H. Kusama, H. Yamabe, Y. Onizawa, T. Hoshino, Prof. Dr. N. Iwasawa
Department of Chemistry
Tokyo Institute of Technology
2-12-1, O-okayama, Meguro-ku, Tokyo 152-8551 (Japan)
Fax: (+81) 3-5734-2931
E-mail: niwasawa@chem.titech.ac.jp

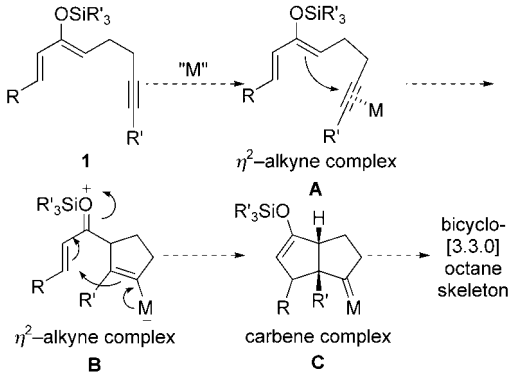
[**] This research was partly supported by the Novartis Science Foundation and a Grant-in-Aid for Scientific Research from the Ministry of Education, Culture, Sports, Science, and Technology of Japan. H.Y. was granted a Research Fellowship of the Japan Society for the Promotion of Science for Young Scientists. We also thank Central Glass Co., for their generous gift of trifluoromethanesulfonic acid.

Supporting information for this article is available on the WWW under http://www.angewandte.org or from the author.

 © 2005 Wiley-VCH Verlag GmbH & Co. KGaA, Weinheim DOI: 10.1002/anie.200461559

carbene moiety to release the reactive metallic species would constitute a catalytic method for the geminal carbofunctionalization of alkynes.

On the basis of the above considerations we designed the system shown in Scheme 2. Thus, treatment of acetylenic



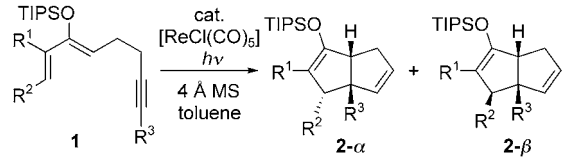
Scheme 2. Tandem cyclization of dienol silyl ethers.

dienol silyl ethers **1** with an appropriate metallic reagent should give zwitterionic intermediates **B** by 5-*endo* nucleophilic cyclization of the enol silyl ether to the electrophilically activated η^2-alkyne complexes **A**. The alkenyl metallic moiety produced should then undergo an intramolecular attack at the β-position of the metal center to the α,β-unsaturated silyloxonium moiety to generate bicyclic unstable carbene complexes **C**. Finally, the destabilized carbene complex moiety would undergo a typical carbene reaction, such as 1,2-hydrogen migration, to give the products with regeneration of the reactive metallic species.[6]

We first examined the reaction of ω-acetylenic dienol silyl ether **1a** with 10 mol% of $[W(CO)_6]$ under photoirradiation in toluene in the presence of molecular sieves (4 Å) (Table 1). Although the tungsten-catalyzed cyclization reaction of enol silyl ethers with an internal alkyne moiety has not been examined before,[7] the reaction proceeded as expected and the desired bicyclic enol silyl ether **2a** was obtained in high yield as a mixture of diastereomers accompanied by a small amount of tricyclic compound **3a**.[8] Since geminal carbofunctionalization was found to proceed as expected, we further examined the possibility of using other transition-metal complexes. $PtCl_2$[2b,c,e,f] (67% yield) and $AuBr_3$[2d,e] (79% yield) also showed moderate catalytic activity towards this transformation, and furthermore $[ReCl(CO)_5]$ was found to have an extremely high activity. The reaction proceeded even with 0.5 mol% of $[ReCl(CO)_5]$ to give the cyclized products **2a** and **3a** in 92% yield in a ratio of 86:14 by carrying out the reaction in toluene under photoirradiation.[9,10] Formation of the tricyclic compound **3a** explicitly implicates the presence of the intermediate carbene complex **C**, in which the carbene moiety inserts into the neighboring benzylic C–H bond.

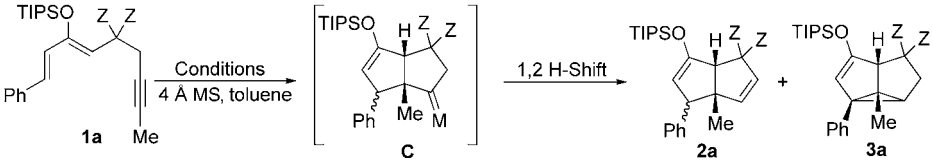
Once we established that $[ReCl(CO)_5]$ catalyzed the geminal carbofunctionalization reaction very efficiently, the reaction of several substrates was examined (Table 2). The trisubstituted dienes (**1b–e**)[11] with a methyl, primary, or secondary alkyl group as well as a phenyl group at the β-position (R^2) were cyclized to afford the corresponding bicyclic enol silyl ethers in high yield (Table 2, entries 1–4). Even the reaction of the tetrasubstituted dienes (**1f**, **1g**)[11] proceeded to afford the corresponding substituted bicyclic enol silyl ethers in high yield. The $[ReCl(CO)_5]$-catalyzed reaction gave superior results in most cases relative to that catalyzed by $[W(CO)_5(L)]$.[12] In particular, the rhenium-catalyzed reaction of dienyl silyl ethers **1h** and **1i** with no substituent at the β-position (R^2 = H) afforded the desired bicyclic enol silyl ethers in moderate to high yields. However, the corresponding tungsten-catalyzed reaction proceeded in very low yield (17%) even with a stoichiometric amount of $[W(CO)_5(L)]$ for **1i**. In addition, a substrate possessing a terminal alkyne moiety **1j**[11] could also be employed for this reaction (Table 2, entry 9). The use of low-valent rhenium complexes in catalytic synthetic reactions, in particular for C–C bond forming reactions, is quite limited.[13] The

Table 2: Rhenium-catalyzed reaction of dienol silyl ethers (**1b–j**).



Entry	R^1	R^2	R^3		[$ReCl(CO)_5$] [mol%]	Yield [%]	**2-α:2-β**
1	H	Me	Me	**1b**	0.5	92	67:33
2	H	Et	Me	**1c**	0.5	92	70:30
3	H	*i*Pr	Me	**1d**	1.0	86	70:30
4	H	Ph	Me	**1e**	1.0	73	50:50
5	Me	Me	Me	**1f**	3.0	68	22:78
6	Me	Ph	Me	**1g**	1.0	76	32:68
7	H	H	Me	**1h**	1.0	51	–
8	Me	H	Me	**1i**	1.0	81	–
9	H	Ph	H	**1j**	3.0	74	85:15

Table 1: Reaction of dienol silyl ether **1a**.



Conditions	*t* [h]	Yield (**2a**+**3a**) [%]	**2a**(α:β):**3a**
$[W(CO)_6]$ (10 mol%), *hν*	4	88	86(9:1):14
$[PtCl_2]$ (10 mol%), 70°C	48	67	59(1.3:1):41
$[AuBr_3]$ (10 mol%), RT	24	79	65(7.7:1):35
$[ReCl(CO)_5]$ (10 mol%), *hν*	3	98	91(12.5:1):9
$[ReCl(CO)_5]$ (0.5 mol%), *hν*	16	92	86(4.2:1):14

Z = CO_2Me, TIPS = triisopropylsilyl, MS = molecular sieves.

 © 2005 Wiley-VCH Verlag GmbH & Co. KGaA, Weinheim

extremely high activity of a rhenium(I)–carbonyl complex for the electrophilic activation of alkynes towards attack of carbo-nucleophiles observed here should be noted as a new potential use of rhenium complexes in organic synthesis.[14]

In summary, we have developed a geminal carbofunctionalization reaction of alkynes catalyzed by $[ReCl(CO)_4(L)]$. Utilization of this intermediate carbene moiety for further C–C bond formations will enable the construction of up to four C–C bonds onto an alkyne in a single operation.

Experimental Section

Cyclization of **1a**: Compound **1a** (292 mg, 0.60 mmol) was added to a mixture of $[ReCl(CO)_5]$ (1.1 mg, 0.0030 mmol, 0.5 mol%) and activated 4-Å molecular sieves in degassed toluene (1.0 mL). The mixture was photoirradiated (250 W super high-pressure Hg lamp) for 16 h, and then the reaction mixture was directly passed through silica gel deactivated with 5 wt% of water (10% ethyl acetate in hexane) to give the crude product, which was purified by preparative thin-layer chromatography (10% ethyl acetate in hexane) to give 269 mg (0.55 mmol, 92%) of **2a** and **3a** (**2a**-α:**2a**-β:**3a** = 69:17:14).

Received: August 6, 2004

Keywords: alkynes · cyclization · homogeneous catalysis · rhenium · silyl ethers

[1] For reviews on carbometalation, see: a) I. Marek, J. F. Normant in *Metal-catalyzed Cross-coupling Reactions* (Eds.: F. Diederich, P. J. Stang), Wiley-VCH, Weinheim, **1997**, p. 271; b) W. Oppolzer, *Angew. Chem.* **1989**, *101*, 39; *Angew. Chem. Int. Ed. Engl.* **1989**, *28*, 38; c) E. Negishi, *Chem. Eur. J.* **1999**, *5*, 411.

[2] To the best of our knowledge, the geminal carbofunctionalization reactions previously reported have been confined to cyclopropanations to generate cyclopropyl carbene complexes, see: a) N. Chatani, K. Kataoka, S. Murai, *J. Am. Chem. Soc.* **1998**, *120*, 9104; b) A. Fürstner, F. Stelzer, H. Szillat, *J. Am. Chem. Soc.* **2001**, *123*, 11863, and references therein; c) M. Méndez, M. P. Muñoz, C. Nevado, D. J. Cárdenas, A. M. Echavarren, *J. Am. Chem. Soc.* **2001**, *123*, 10511; d) C. Nieto-Oberhuber, M. P. Muñoz, E. Buñuel, C. Nevado, D. J. Cárdenas, A. M. Echavarren, *Angew. Chem.* **2004**, *116*, 2456; *Angew. Chem. Int. Ed.* **2004**, *43*, 2402; e) V. Mamane, T. Gress, H. Krause, A. Fürstner, *J. Am. Chem. Soc.* **2004**, *126*, 8654; f) Y. Harrak, C. Blaszykowski, M. Bernard, K. Cariou, E. Mainetti, V. Mouriès, A.-L. Dhimane, L. Fensterbank, M. Malacria, *J. Am. Chem. Soc.* **2004**, *126*, 8656; g) B. P. Peppers, S. T. Diver, *J. Am. Chem. Soc.* **2004**, *126*, 9524; h) M. R. Luzung, J. P. Markham, F. D. Toste, *J. Am. Chem. Soc.* **2004**, *126*, 10858.

[3] For examples of geminal functionalization of alkynes involving heteroatom–carbon bond formation, see: a) N. Iwasawa, M. Shido, H. Kusama, *J. Am. Chem. Soc.* **2001**, *123*, 5814; b) H. Kusama, J. Takaya, N. Iwasawa, *J. Am. Chem. Soc.* **2002**, *124*, 11592; c) J. Takaya, H. Kusama, N. Iwasawa, *Chem. Lett.* **2004**, *33*, 16; d) F. Nishino, K. Miki, Y. Kato, K. Ohe, S. Uemura, *Org. Lett.* **2003**, *5*, 2615; e) K. Miki, K. Ohe, S. Uemura, *J. Org. Chem.* **2003**, *68*, 8505; f) K. Miki, T. Yokoi, F. Nishino, Y. Kato, Y. Washitake, K. Ohe, S. Uemura, *J. Org. Chem.* **2004**, *69*, 1557.

[4] a) K. Maeyama, N. Iwasawa, *J. Am. Chem. Soc.* **1998**, *120*, 1928; b) N. Iwasawa, K. Maeyama, H. Kusama, *Org. Lett.* **2001**, *3*, 3871; c) H. Kusama, H. Yamabe, N. Iwasawa, *Org. Lett.* **2002**, *4*, 2569; d) N. Iwasawa, T. Miura, K. Kiyota, H. Kusama, K. Lee, P. H. Lee, *Org. Lett.* **2002**, *4*, 4463.

[5] For examples of the reaction of Group VI alkenyl metallic species with carbo-electrophiles, see; a) W. D. Wulff, S. R. Gilbertson, *J. Am. Chem. Soc.* **1985**, *107*, 503; b) Y.-C. Xu, W. D. Wulff, *J. Org. Chem.* **1987**, *52*, 3263; c) R. Aumann, H. Heinen, *Chem. Ber.* **1987**, *120*, 537; d) B. A. Anderson, W. D. Wulff, A. Rahm, *J. Am. Chem. Soc.* **1993**, *115*, 4602.

[6] Non-heteroatom-substituted alkyl carbene complexes, especially those having an α-hydrogen atom, are highly reactive to give 1,2-hydrogen migration products, see: a) C. P. Casey, L. D. Albin, T. J. Burkhardt, *J. Am. Chem. Soc.* **1977**, *99*, 2533; b) J. Barluenga, A. Ballesteros, R. de la R. Bernardo, J. Santamaría, E. Rubio, M. Tomás, *J. Am. Chem. Soc.* **2003**, *125*, 1834.

[7] The $[W(CO)_5(L)]$-catalyzed cyclizations are assumed to proceed through both a η^2-alkyne complex and a vinylidene complex as determined by deuterium experiments on the cyclization of an ω-acetylenic enol silyl ether.[4a]

[8] The tricyclic enol silyl ether **3** was not obtained when the substrates without a *gem*-diester (**1b–i**) were employed.

[9] The reaction of **1a** with 0.5 mol% of $[W(CO)_6]$ under photoirradiation in toluene proceeded to only a small extent after 16 h to give <5% of cyclized product **2a**.

[10] It has already been reported that coordinatively unsaturated species $[ReX(CO)_4(L)]$ was generated by thermal liberation of carbon monoxide from $[ReX(CO)_5]$ and acted as a Lewis acid for a Friedel–Crafts type acylation.[13a] The reactions of **1b** with 1.0 mol% $[ReCl(CO)_5]$ in refluxing toluene without photoirradiation also gave bicyclic product **2b** in 47% yield. On the basis of these results, we currently believe that $[ReCl(CO)_4(L)]$ is the active species in this reaction.

[11] The geometry of the major isomer is shown in the scheme; see the Supporting Information for details of the isomeric ratio of the starting materials.

[12] The reactions of **1a–g** and **1j** gave bicyclic silyl enol ethers in high yield (67–81% yield) with 5–20 mol% $[W(CO)_6]$ under photoirradiation in toluene. The $[W(CO)_5(L)]$-catalyzed reactions of **1e** and **1g** gave slightly better results than the corresponding rhenium-catalyzed reactions, but they required a larger amount of tungsten complex (for **1e**, 5 mol% of $[W(CO)_6]$ gave **2e** in 81% yield; for **1g**, 10 mol% of $[W(CO)_6]$ gave **2g** in 79% yield).

[13] For examples of $[ReX(CO)_5]$ (X = Cl, Br)-catalyzed C–C bond forming reactions, see: a) H. Kusama, K. Narasaka, *Bull. Chem. Soc. Jpn.* **1995**, *68*, 2379; b) Y. Nishiyama, F. Kakushou, N. Sonoda, *Bull. Chem. Soc. Jpn.* **2000**, *73*, 2779; See also, Ref. [2a]. For examples of $[ReCl(N_2)(PMe_2Ph)_4]$-catalyzed C–C bond-forming reactions, see: c) Y. Koga, H. Kusama, K. Narasaka, *Bull. Chem. Soc. Jpn.* **1998**, *71*, 475. For examples of $[ReOCl_3(dppm)]$-catalyzed C–C bond-forming reactions (dppm = bis(diphenylphosphanyl)methane), see: d) M. R. Luzung, F. D. Toste, *J. Am. Chem. Soc.* **2003**, *125*, 15760.

[14] For examples of $[ReBr(CO)_5]$-catalyzed additions of carboxylic acids to terminal alkynes, see; R. Hua, X. Tian, *J. Org. Chem.* **2004**, *69*, 5782.

 © 2005 Wiley-VCH Verlag GmbH & Co. KGaA, Weinheim

Bioorganic Chemistry

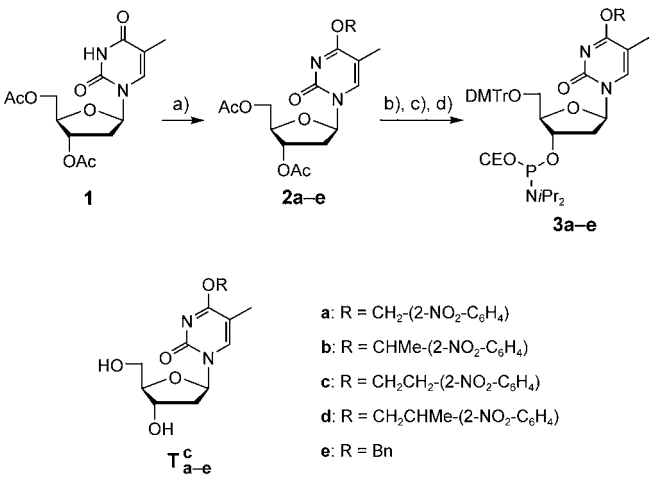
Photoinduced Transcription by Using Temporarily Mismatched Caged Oligonucleotides**

*Lenz Kröck and Alexander Heckel**

DNA and RNA are responsible for the storage and flow of information in nature. Additionally, and especially together with their analogues and derivatives, DNA and RNA can be used for a multitude of applications, such as regulation of gene expression (RNA interference,[1a] microRNA,[1b] riboswitches,[1c] antisense approach,[1d] DNAzymes[1e]), modulation of protein function (aptamers,[1f] DNA/RNA decoys[1g]), molecular diagnostics (microarrays[1h]), or as structural or functional building blocks for nanoscale material.[1i] In all of these applications the nucleobases play a central role. To develop a mechanism for the temporal and spatial control of the DNA or RNA function, we are investigating ways to temporarily block the recognition properties of the nucleobases. Since light has the advantage of being a highly orthogonal trigger signal we decided to use photolabile "protecting" groups for this purpose. The regulation of gene expression by light, for example, would be a valuable tool for the analysis of protein function. The strategy of masking the activity of a biological compound with a photolabile protecting group is called "caging" and, for example, caged neurotransmitters or Ca^{2+}-complexing agents have already been synthesized and investigated.[2] Likewise, in a pioneering investigation, adenosine triphosphate (ATP) caged with a photolabile 1-(2-nitrophenyl)ethyl group was used to study the Na/K-pump in human red blood cell ghosts.[3]

Herein, we report the synthesis of caged thymidine phosphoramidites and the use of caged oligonucleotides to control transcription by light. Photolabile protecting groups have been used before in oligonucleotide synthesis as temporary protecting groups[4] and photolabile protecting groups in the 2′-position in RNA can also inhibit ribozyme action[4b,5] but they do not prevent Watson–Crick base pairing. Also, nucleoside analogues and derivatives have been made which induce DNA strand breaks upon irradiation.[6]

The exocyclic O4 position of thymidine was chosen for the attachment of the photolabile group (caging group; Scheme 1). The O4-substituted derivatives of thymidine are conveniently accessible by the reaction of the suitably protected precursor **1** with triisopropylbenzenesulfonyl chloride and then with the respective alcohols of the caging groups (→**2a–e**). As photolabile protecting groups the commonly used 2-nitrobenzyl group and its faster deprotecting α-methyl-substituted derivative as well as the 2-nitrophenethyl group and its α-methyl-substituted derivative were chosen. The 2-nitrophenethyl group has been used by Pfleiderer et al.[7] and has the advantage of not forming a nitroso compound upon deprotection[8], a property that is important for cellular and in vivo studies. The benzylated derivative **2e** and its subsequent derivatives were also included in these studies as control compounds which are not deprotected by light. Deacetylation and DMTr-protection of the 5′-position afforded the protected 3′-OH-free intermediates which were converted under standard conditions into the phosphoramidites **3a–e**.



Scheme 1. Synthesis of the photoactivatable caged phosphoramidites **3a–e** as well the caged nucleosides $\mathbf{T^c_{a-e}}$. Reaction conditions: a) 1. *i*Pr$_3$C$_6$H$_2$SO$_2$Cl, DMAP, Et$_3$N; 2. respective alcohol, Et$_3$N; b) NH$_3$/MeOH (quant.); c) DMTrCl, pyridine; d) CEOP(Cl)N*i*Pr$_2$, DIEA. DMAP = N,N-dimethyl-aminopyridine, DMTr = dimethoxytrityl, DIEA = diisopropylethylamine, CE = (2-cyanoethyl), Bn = benzyl.

To investigate the duplex-destabilizing effect of the caged thymidine monomers $\mathbf{T^c_{a-e}}$ (Scheme 1; **c** = caged) they were included in 25-mer-oligodeoxynucleotides in the positions indicated in Table 1 and thermal denaturation experiments were performed using dA_{25} as the counter strand. As the results in Table 1 show, the introduction of just one caged nucleotide leads to a significant reduction in the melting temperature (up to 5 °C). This effect can be increased if more

Table 1: Results of thermal denaturation experiments of the given oligonucleotides with dA_{25} as counter strand.[a]

X	5′-T$_8$TTTTXTTTTT$_8$–3′	5′-T$_8$TTTXXXTTTT$_8$-3′	5′-T$_8$XTTTXTTTXT$_8$-3′
$\mathbf{T^c_a}$	50.3 (51.1)	47.3 (46.9)	41.2 (44.3)
$\mathbf{T^c_b}$	48.6 (53.2)	44.2 (51.1)	32.3 (51.9)
$\mathbf{T^c_c}$	48.9 (53.0)	44.9 (51.7)	34.7 (51.8)
$\mathbf{T^c_d}$	48.5 (54.0)	44.5 (52.7)	32.3 (53.2)
$\mathbf{T^c_e}$			33.8 (34.2)

[a] Melting temperatures in °C before and (in parenthesis) after irradiation of the sample at 366 nm for 30 min (error ca. 0.7 °C). With unmodified T_{25} a melting temperature of 53.8 (54.0) °C was obtained.

[*] L. Kröck, Dr. A. Heckel
Rheinische Friedrich-Wilhelms-Universität Bonn
Kekulé-Institut für Organische Chemie und Biochemie
Gerhard-Domagk-Strasse 1, 53121 Bonn (Germany)
Fax: (+49) 228-73-5388
E-mail: heckel@uni-bonn.de

[**] This work was funded by a Liebig-Fellowship of the "Verband der Chemischen Industrie" (VCI (Germany)) for A.H.

Supporting information for this article is available on the WWW under http://www.angewandte.org or from the author.

 DOI: 10.1002/anie.200461779 © 2005 Wiley-VCH Verlag GmbH & Co. KGaA, Weinheim

caged nucleotides are included, especially if they are not cumulated around one position within the oligonucleotide. Branched caging groups result in a slightly increased destabilization of the duplex compared to their nonbranched analogues (see for example the entries for the oligomers containing $\mathbf{T}^{c}_{a}$ und $\mathbf{T}^{c}_{b}$). With the incorporation of only three caged nucleotides a maximum decrease in melting temperature of 21.5 °C was obtained. In a second series of experiments the melting temperatures were determined after irradiation of the samples for 30 min at 366 nm. As can be seen in Table 1, only the oligonucleotides with the caged $\mathbf{T}^{c}_{d}$ showed the same melting temperature, after irradiation, as the unmodified T_{25} oligomer used as control compound. These findings suggest that the caged nucleotides can be thought of as being "temporary mismatches". Including the benzylated thymidine $\mathbf{T}^{c}_{e}$ in an oligonucleotide leads to a decrease in melting temperature which remained unchanged upon irradiation with light.

To study the deprotection kinetics 4 nmol of each of the oligonucleotides shown in Table 1 was irradiated at 366 nm and the formation of the resulting uncaged T_{25} was detected by HPLC (Figure 1). As can be seen, in the case of the

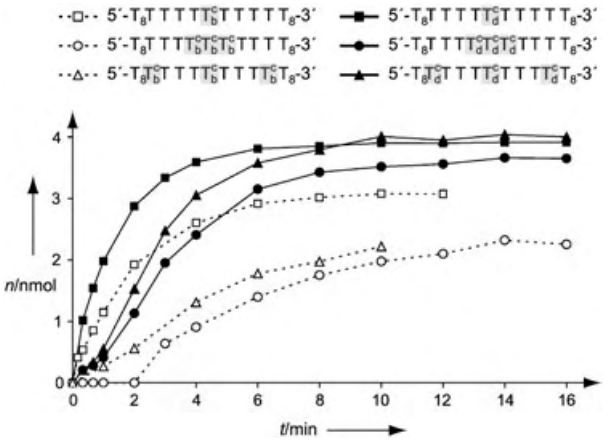


Figure 1. Amount of uncaged oligonucleotide during the photodeprotection (366 nm). In every experiment 4 nmol of the caged oligonucleotide was used and the product formation was detected by HPLC.

photodeprotection of the oligomers containing the caged $\mathbf{T}^{c}_{b}$ the reaction reached a stationary state in which, as well as the product, an as yet unidentified byproduct was present which did not react further upon irradiation. In the case of the oligomers with the caged $\mathbf{T}^{c}_{d}$ however, the deprotection was not only faster under the irradiation conditions used but the yield of resulting uncaged oligonucleotide was almost quantitative within error limits. The oligomers with the caged $\mathbf{T}^{c}_{a}$ and $\mathbf{T}^{c}_{c}$ were also subjected to this test. However, especially with several caged nucleotides in the same oligomer, the deprotection was very slow and the yields were poor. In conclusion, the caged $\mathbf{T}^{c}_{d}$ showed the best properties with regard to perturbation of duplex structure and ease of photodeprotection.

To studying the use of caged photoactivatable nucleotides in biological systems we tried to temporarily block transcription (Figure 2). An assay was used in which a 68-nucleotide (nt) antisense strand with a T7-promoter served as the template. The T7-promoter region was complemented with the shorter oligonucleotides $\mathbf{S_1}$–$\mathbf{S_6}$ to for a double strand

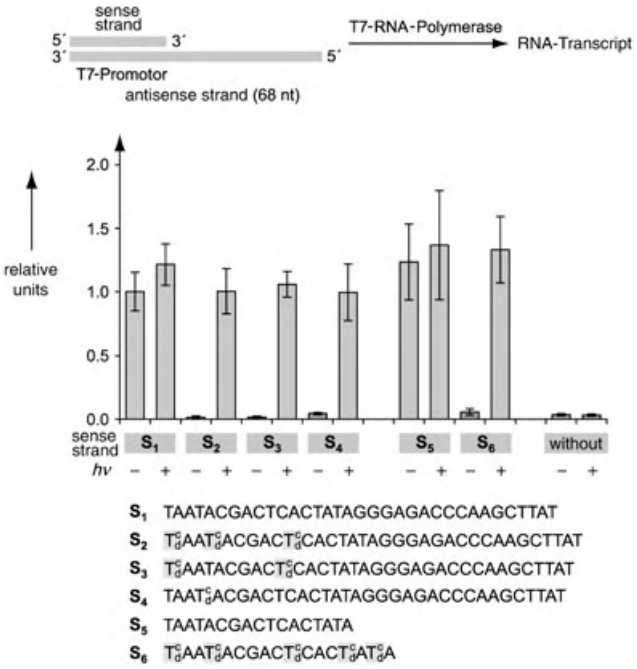


Figure 2. Relative amounts of transcription product formed after 1 h with or without initial irradiation (1 h, 366 nm) of the sample before starting the transcription by addition of the T7 RNA polymerase.

and allow the T7 RNA polymerase to recognize the promoter region. The amount of transcription product after 1 h of incubation was determined by phosphorimaging (α-^{32}P-guanosine triphosphate (GTP) was used for body labeling). The three oligonucleotides $\mathbf{S_2}$, $\mathbf{S_3}$, and $\mathbf{S_4}$ contain, respectively, three, two, and one caged nucleotide in the T7 promoter region. Unlike with the control oligonucleotide $\mathbf{S_1}$, in the presence of these unmodified oligonucleotides no transcription takes place. This result is not because the two DNA-strands in the experiment are not associated to one another since, for example, $\mathbf{S_4}$ and the antisense strand show a melting temperature of 72.0 °C in the transcription buffer. It must rather be due to a severe perturbation of the local duplex structure owing to the caging group which prevents the RNA polymerase from recognizing the promoter region.[9] After irradiation of the respective samples (before the addition of the T7 RNA polymerase) the same amount of transcription product was formed as in the control reaction with the uncaged oligomer $\mathbf{S_1}$. Transcription could also be triggered by irradiating the samples containing the intact caged sense strands after 1 h of incubation with T7 RNA polymerase in which no product had been formed. The shorter oligomers $\mathbf{S_5}$ and $\mathbf{S_6}$ behaved similarly.[10] However, the results shown in Figure 2 demonstrate that it is not necessary to heavily destabilize the entire duplex to prevent transcription and that the incorporation of one or two caged nucleotides is quite enough.

 © 2005 Wiley-VCH Verlag GmbH & Co. KGaA, Weinheim

Other groups have also studied the regulation of gene expression by light.[11] However in their approaches entire plasmids or mRNA strands were subjected to benzylating conditions in which the photolabile groups were attached presumably to backbone phosphates. In contrast to the strategy presented herein, this approach does not lead to a well-defined product but rather to a statistical distribution of caged positions and introduces more modifications than necessary. In the other investigations the full transcriptional activity could not be restored.

In conclusion we have demonstrated that caged thymidines can be used as temporary mismatches to inhibit a function, transcription in this case. They can be introduced in oligomers at any desired and well-defined position through their easily accessible phosphoramidites **3a**–**e**. With long-wavelength UV light (366 nm) the photodeprotection of the caged $\mathbf{T}^{\mathbf{c}}_{\mathbf{d}}$ occurs fast, with high yield, and without formation of nitroso compounds. One or two caged nucleotides at the right position can be enough to completely inhibit a function.

Received: August 25, 2004

Keywords: DNA · gene expression · oligonucleotides · photoactivation

[1] a) Y. Dorsett, T. Tuschl, *Nat. Rev. Drug Discovery* **2004**, *3*, 318–329; b) D. P. Bartel, *Cell* **2004**, *116*, 281–297; c) M. Mandal, R. R. Breaker, *Nat. Rev. Mol. Cell Biol.* **2004**, *5*, 451–463; d) S. T. Crooke, *Curr. Mol. Med.* **2004**, *4*, 465–487; e) C. R. Dass, *Trends Pharmacol. Sci.* **2004**, *8*, 395–397; f) D. S. Wilson, J. W. Szostak, *Annu. Rev. Biochem.* **1999**, *68*, 611–647; g) Y. S. Cho-Chung, Y. G. Park, Y. N. Lee, *Curr. Opin. Mol. Ther.* **1999**, *1*, 386–392; h) M. C. Pirrung, *Angew. Chem.* **2002**, *114*, 1326–1341; *Angew. Chem. Int. Ed.* **2002**, *41*, 1276–1289; i) N. C. Seeman, *Angew. Chem.* **1998**, *110*, 3408–3428; *Angew. Chem. Int. Ed.* **1998**, *37*, 3220–3238.

[2] a) "Caged Compounds": *Methods in Enzymology*, *Vol. 291* (Ed.: G. Mariott), Academic, London, **1998**; b) A. P. Pelliccioli, J. Wirz, *Photochem. Photobiol. Sci.* **2002**, *1*, 441–458.

[3] J. H. Kaplan, B. Forbush III, J. F. Hoffman, *Biochemistry* **1978**, *17*, 1929–1935.

[4] a) K. Alvarez, J. J. Vasseur, T. Beltran, J. L. Imbach, *J. Org. Chem.* **1999**, *64*, 6319–6328; b) S. Pitsch, P. A. Weiss, X. Wu, D. Ackermann, T. Honegger, *Helv. Chim. Acta* **1999**, *82*, 1753–1761.

[5] S. G. Chaulk, A. M. MacMillan, *Nucl. Acids Res.* **1998**, *26*, 3173–3178.

[6] a) A. Dussy, C. Meyer, E. Quennet, T. A. Bickle, B. Giese, A. Marx, *ChemBioChem* **2002**, *3*, 54–60; b) C. Crey-Desbiolles, J. Lhomme, P. Dumy, M. Kotera, *J. Am. Chem. Soc.* **2004**, *126*, 9532–9533; c) H. J. Lenox, C. P. McCoy, T. L. Sheppard, *Org. Lett.* **2001**, *3*, 2415–2418; d) M. C. Pirrung, X. Zhao, S. V. Harris, *J. Org. Chem.* **2001**, *66*, 2067–2071; e) P. Ordukhanian, J. S. Taylor, *Bioconjugate Chem.* **2000**, *11*, 94–103.

[7] a) A. Hasan, K. P. Stengele, H. Giegrich, P. Cornwell, K. R. Isham, R. A. Sachleben, W. Pfleiderer, R. S. Foote, *Tetrahedron* **1997**, *53*, 4247–4264; b) H. Giegrich, S. Eisele-Bühler, C. Hermann, E. Kvasyuk, R. Charubala, W. Pfleiderer, *Nucleosides Nucleotides* **1998**, *17*, 1987–1996; c) S. Bühler, H. Giegrich, W. Pfleiderer, *Nucleosides Nucleotides* **1999**, *18*, 1281–1283.

[8] S. Walbert, W. Pfleiderer, U. E. Steiner, *Helv. Chim. Acta* **2001**, *84*, 1601–1611.

[9] For a crystal structure of the T7 RNA polymerase with the T7-promoter region see: G. M. T. Cheetham, D. Jeruzalmi, T. A. Steitz, *Nature* **1999**, *399*, 80–83.

[10] It was confirmed experimentally, in all cases, that the oligonucleotides produced upon irradiation were indeed the expected ones.

[11] a) W. T. Monroe, M. M. McQuain, M. S. Chang, J. S. Alexander, F. R. Haselton, *J. Biol. Chem.* **1999**, *274*, 20895–20900; b) H. Ando, T. Furuta, R. Y. Tsien, H. Okamoto, *Nat. Genet.* **2001**, *28*, 317–325.

 © 2005 Wiley-VCH Verlag GmbH & Co. KGaA, Weinheim

Tin Complexes

Distannenes Turned Inside Out: Bis(stannylenes) with an Unusual Structural Motif**

Frank Breher and Heinz Rüegger*

Since the pioneering work of Lappert and West on distannenes[1] and disilenes,[2] multiple bonding between heavier main-group elements has attracted considerable attention, and led to the isolation of numerous homo- and heteroleptic heavier Group 14 element analogues of olefins.[3] The unusual *trans*-bent geometries of the E_2R_4 entities raised fundamental questions concerning the nature of the bonding mode within these systems. To clarify these E–E interactions, Trinquier performed comprehensive quantumchemical calculations for the model systems E_2H_4 in the early 1990s (structures **A**–**E** in Scheme 1; E = Group 14 element).[4]

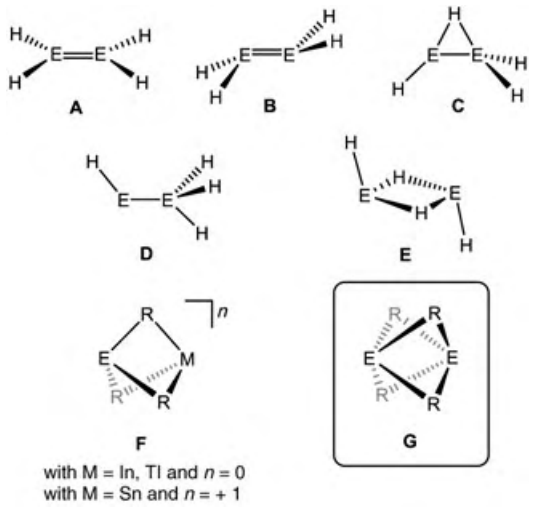
Among other important results within this series, the investigations concerning the tin derivatives revealed that all four isomers **B**–**E** correspond to minima on the Sn_2H_4 potential energy surface and differ by only 42 kJ mol^{-1}. However, this relatively low energy gap is not surprising because the potential energy surfaces for heavier congeners of main-group element compounds are much flatter than for comparable hydrocarbons. Thus a substituent-dependent control over their distribution and interconversion of the main-group element compounds might be possible. This concept was impressively elaborated by Power and co-workers. They were able to isolate diverse aryl-substituted tin

[*] Dr. F. Breher, Dr. H. Rüegger
Department of Chemistry and Applied Biosciences (D-CHAB)
ETH Hönggerberg
Wolfgang-Pauli Strasse, 8093 Zürich (Switzerland)
Fax: (+41) 1-633-1032
E-mail: breher@inorg.chem.ethz.ch

[**] This work was supported by the Swiss National Science Foundation (SNF) and the ETH Zürich. We thank Dr. I. Krossing for his help concerning the quantum chemical calculations. F.B. gratefully acknowledges a Liebig scholarship provided by the Fonds der Chemischen Industrie and thanks Prof. H. Grützmacher for valuable discussions and generous support.

Supporting information for this article is available on the WWW under http://www.angewandte.org or from the author.

 DOI: 10.1002/anie.200460910 © 2005 Wiley-VCH Verlag GmbH & Co. KGaA, Weinheim

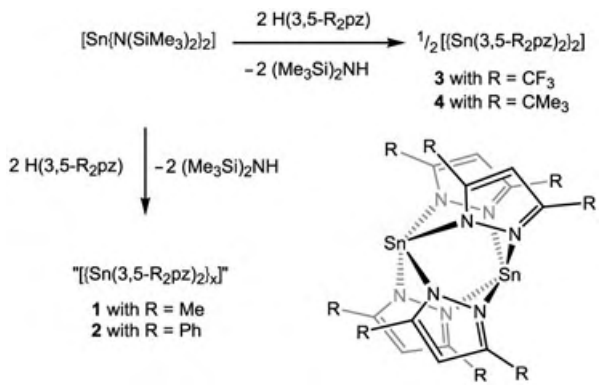


Scheme 1. Possible isomers **A**–**E** for the model compounds E_2H_4 (E = Group 14 element). Triply R-bridged derivatives (**F**) have been reported, and the conceivable quadruply R-bridged derivative (**G**).

derivatives comprising the asymmetric[5] and doubly H-bridged[6] structures **D** and **E**[7] as well as the monobridged alkene isomer **C**.[8] In addition, some neutral and cationic, triply R-bridged main-group element cage compounds of the general formula **F** have been obtained by the groups of Veith[9] and Stalke.[10] However, to our knowledge, the conceivable structural motif **G** has not been observed or discussed to date. Herein we show that an additional donor functionality within the substituent attached to tin yields two stable tin–nitrogen cage compounds, which are formally analogues of the quadruply bridged alkene isomer **G**.

Following the synthetic strategy of a well-established acid–base reaction,[11] $[Sn\{N(SiMe_3)_2\}_2]$ was treated with various 3,5-substituted pyrazoles, H(3,5-R_2pz), in aliphatic solvents (Scheme 2).

With R = Me (**1**) or Ph (**2**), this reaction leads to colorless solids $[\{Sn(3,5\text{-}R_2pz)_2\}_x]$, which are insoluble in organic solvents. By applying sterically more demanding pyrazoles in this reaction, we were able to isolate the first neutral, homoleptic tin(II) pyrazolyl compounds $[\{Sn(3,5\text{-}R_2pz)_2\}_2]$ (R = CF_3 (**3**); R = CMe_3(**4**)) in 70% (**3**) and 91% (**4**) yield.



Scheme 2. Synthesis of polymeric (**1**, **2**) and dimeric (**3**, **4**) pyrazolyl stannylenes.

Compounds **3** and **4** are colorless crystalline materials which are moderately soluble in aliphatic and aromatic solvents but highly soluble in ethereal solvents, such as THF. They are fairly air- and moisture-sensitive, but thermally stable with melting points of 182 °C (**3**) and 190 °C (**4**).

The X-ray crystal structure of **3** (Figure 1)[12] confirmed the proposed formation of a neutral, dimeric tin(II) compound with each tin atom pseudo square-pyramidally surrounded by

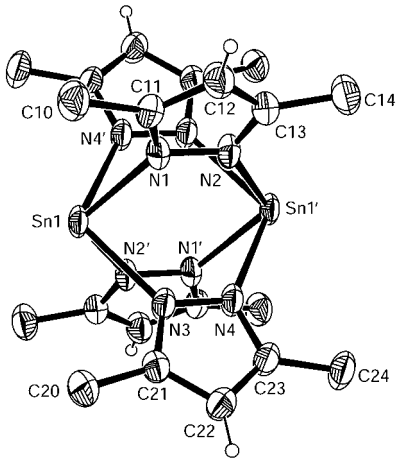


Figure 1. Molecular structure of **3**, thermal ellipsoids are set at 30% probability. Fluorine atoms have been omitted for clarity. Selected bond lengths [pm] and angles [°]: Sn···Sn′ 385.1, Sn1-N1 235.3(4), Sn1-N3 235.9(4), Sn1-N2′ 238.6(4), Sn1-N4′ 233.9(4), N1-N2 135.7(5), N3-N4 135.4(5); N1-Sn1-N3 74.0(1), N1-Sn1-N4′ 73.2(1), N3-Sn1-N2′ 74.1(1), N2′-Sn1-N4′ 73.7(1), Sn1-N1-N2 120.2(3), Sn1′-N1-N2 123.3(3), Sn1-N3-N4 121.9(3), Sn1′-N4-N3 122.2(3) (symmetry equivalent atoms generated by $-x+1$, $-y+2$, $-z$).

four pyrazole nitrogen atoms and one lone pair. Although the tin–nitrogen cage shows nearly local D_{4h} symmetry, the molecule does not have crystallographic fourfold symmetry but a center of inversion is located in the middle of the Sn···Sn′ vector. The intramolecular Sn···Sn′ separation of 385.1 pm is in the range of those found for other bridged Sn^{II} compounds.[7] Although the tin atoms are arranged in close spatial proximity and the Sn···Sn′ separation is much shorter than the double of the tin van der Waals radius the interaction seems to be of nonbonding type. The tin atoms reside approximately 125 pm above the plane of the four nitrogen atoms;[13] the Sn–N bond lengths fall in a narrow range of 233.9 to 238.6 pm, they are approximately 10 pm longer than the shortest Sn–N bonds in tin(II) polypyrazolylborate complexes[14] or the cationic moiety of the cage compound $[Sn(3,5\text{-}Me_2pz)_3Sn]^+[SnCl_3]^-$.[10] This slight elongation may be attributed to steric interactions between the trifluoromethyl substituents attached to the heteroaromatic ring. For the *tert*-butyl substituted derivative **4** this steric repulsion is even more pronounced so that the planes of the pyrazole rings are inclined at an angle of about 26° with respect to the Sn···Sn′ vector. Owing to this tilting, the tin–nitrogen cage is distorted towards a C_4 symmetric, screw-like entity. However, because of strongly disordered groups, the X-ray structure analysis of **4**

 © 2005 Wiley-VCH Verlag GmbH & Co. KGaA, Weinheim

is of inferior quality and therefore will not be discussed in detail.

The solid-state ^{119}Sn NMR spectrum of **3** (Figure 2) shows a single resonance at an isotropic chemical shift of $\delta_{iso} =$ -800 ppm together with a large anisotropy pattern which deviates only slightly from the expected axial symmetry. Number, chemical shift, span, and shape of the resonance are all in full agreement with the centrosymmetric structure determined by the X-ray structure analysis of the molecule. In solution, the ^{119}Sn NMR spectrum of **3** shows a resonance signal at around $\delta = -720$ ppm ($w_{1/2} \approx 480$ Hz) indicating a nucleus which is slightly less shielded compared to the solid-state but still in the region expected for an Sn^{II} center at higher connectivity sites. No sizeable coupling among tin isotopes was detected,[16] which suggests only weak Sn···Sn interactions if at all. One-dimensional ^{1}H, ^{13}C, and ^{19}F NMR spectroscopy show the expected resonance signals of intact and equivalent pyrazolyl groups with only single resonances for equivalent CF_3 (**3**) or CMe_3 (**4**) and CH_{pz} moieties being observed at room temperature. While these observations are in agreement with the expected symmetrical compound it cannot be ruled out that dynamic processes average less-symmetrical structures. The slight differences between the solid-state and solution ^{119}Sn NMR spectroscopy data might also be evidence of this situation.[17] Further support for this observation derives from a) the determination of the diffusion coefficient for **3** which suggests a hydrodynamic radius somewhat smaller than expected for the associated, that is, dimeric structure of **3**;[18] and b) low-temperature solution NMR spectroscopy investigations for **3** reveal marginally broadened ^{1}H and ^{19}F NMR signals and a ^{119}Sn NMR resonance signal shifted to slightly lower frequency. For the alkyl-substituted cage **4** a rather complicated ^{1}H NMR spectrum as well as two ^{119}Sn NMR resonance signals with chemical shifts of $\delta = -351$ ($w_{1/2} \approx 1100$ Hz) and -614 ppm ($w_{1/2} \approx 1100$ Hz) are detected at lower temperature.[19]

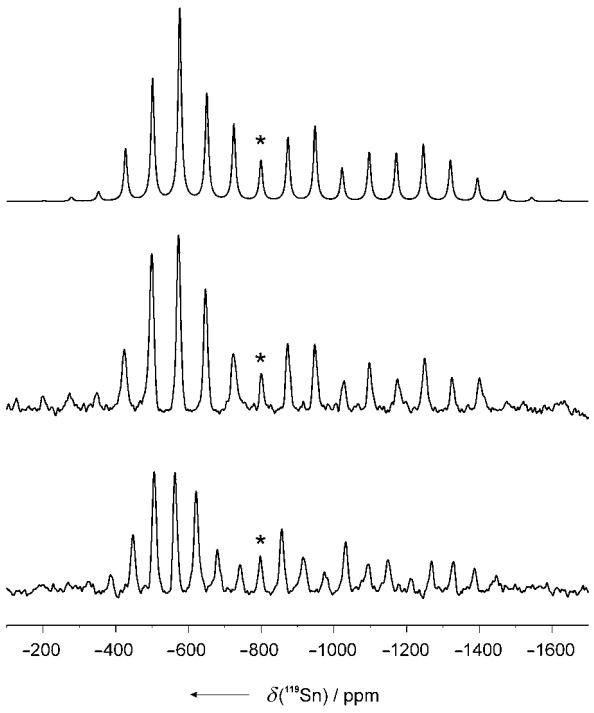


Figure 2. ^{119}Sn NMR spectra (186.5 MHz) of **3** recorded with magic angle spinning (MAS) with rotational frequencies of 11 (bottom) and 14 kHz (middle). The top trace is a spectrum simulated with SIMPSON[15] and the principal values $\delta_{11} = -430$, $\delta_{22} = -530$, and $\delta_{33} = -1450$ ppm. The asterisk marks the position of the isotropic chemical shift δ_{iso}.

Two possible dynamic processes in solution are shown in Equations (1) and (2) (with pz = 3,5-R_2pz). For the latter equilibrium product [Sn(μ^2-pz)$_3$Sn(pz)], two ^{119}Sn NMR resonances would be anticipated. Nevertheless, the true nature of the dynamic behavior in solution remains the subject of speculation.

$$[Sn(\mu^2\text{-pz})_4Sn] \rightleftharpoons [Sn(\mu^2\text{-pz})_3Sn]^+[pz]^- \quad (1)$$

$$[Sn(\mu^2\text{-pz})_4Sn] \rightleftharpoons [Sn(\mu^2\text{-pz})_3Sn(pz)] \quad (2)$$

The tin(II) pyrazolyl compounds presented herein are electronically related to stannocene[20] or triphospholyl tin(II) derivatives[21] that predominantly contain η^5-coordinating ligands. However, in our system the disk-shaped pyrazolyl ligands are solely σ bound and two stannylene entities are arranged in a head-to-tail fashion to form dimeric units. Preliminary theoretical investigations revealed that for the CF_3-substituted derivative this type of dimerization is energetically favored by about 100 kJ mol^{-1} (around 44 kJ mol^{-1} for R = H) with respect to the doubly bridged dimer which contains two terminal and two bridging ligands (see Supporting Information for details). As no covalent Sn–Sn bond is apparent, these compounds may formally be described as distannenes turned inside out, which represent the first structurally authenticated, quadruply R-bridged olefin isomer of a heavier Group 14 element.

Experimental Section

All procedures were carried out under argon. Solvents were freshly distilled from sodium/benzophenone (THF) or from sodium/tetraglyme/benzophenone (*n*-hexane). Starting materials were prepared according to literature methods;[22] H(3,5-Me_2pz) was purchased from Aldrich. The pyrazoles were dried in a desiccator in vacuo prior to use. NMR spectra were measured on Bruker Avance spectrometers and chemical shifts are given relative to tetramethylsilane (^{1}H, ^{13}C), NH_3 (^{15}N), $CFCl_3$ (^{19}F), and tetramethyl tin (^{119}Sn).

3 and **4**: A solution of [Sn{N(SiMe$_3$)$_2$}$_2$] (2.486 g, 5.656 mmol for **3**; 2.768 g, 6.298 mmol for **4**) in *n*-hexane (30 mL) was added dropwise to a solution of the corresponding pyrazole H(3,5-R_2pz) (R = CF_3: 2.309 g, 11.315 mmol for **3**; R = CMe_3: 2.271 g, 12.597 mmol for **4**) in *n*-hexane (30 mL) at room temperature. The intense orange color of Lappert's stannylene disappeared immediately upon addition to the pyrazole solution and in the course of the addition a colorless, crystalline solid precipitated. The reaction mixture was heated at approximately 50 °C until the precipitate was dissolved. The stirring was stopped and the clear solution was stepwise cooled to room temperature and 0 °C. Colorless, fairly moisture and air-sensitive crystals of the product were isolated and dried in vacuo. A second crop of the product could be isolated from the mother liquor after removal of all the volatile components under vacuum and crystallization from *n*-hexane at −30 °C. Yield: **3**: 2.070 g (70 %); **4**: 2.735 g

 © 2005 Wiley-VCH Verlag GmbH & Co. KGaA, Weinheim

(91%). Characterization of **3**: M.p. (argon, sealed capillary): 182°C (decomp); elemental analysis (%) calcd for $C_{20}H_4N_8F_{24}Sn_2$: C 22.9, H 0.4, N 10.7; found: C 21.8, H 0.4, N 10.7; ^{1}H NMR (500.2 MHz, [D$_8$]THF): $\delta = 7.12$ ppm (s, CH_{pz}); ^{13}C NMR (125.8 MHz, [D$_8$]THF): $\delta = 142.4$ (q, $^2J(^{19}F,^{13}C) = 37.7$ Hz, pz C_{quart}), 121.9 (q, $^1J(^{19}F,^{13}C) = 268.5$ Hz, CF_3), 104.7 ppm (sept, $^3J(^{19}F,^{13}C) = 2.3$ Hz, CH_{pz}); ^{15}N NMR (50.7 MHz, 203 K, [D$_8$]THF): $\delta = 300.5$ ppm. ^{19}F NMR (470.7 MHz, [D$_8$]THF): $\delta = -60.99$ ppm (s, CF_3); ^{119}Sn NMR (186.4 MHz, [D$_8$]THF): $\delta = -722$ ppm; IR (solid, attenuated total reflection (ATR)): $\tilde{\nu} = 1540$ m, 1502 m (ν(pyrazole ring)); 1346 m, 1253 vs, 1228 s, 1107 vs, 1082 (sh) vs, 1011 vs, 985 s (δ(CF_3), ν(CC)); 824 m, 815 (sh) m, 759 s, 735 m, 717 w, 605 vw, 556 s, 537 s (ν(CC), δ(CC), ν(SnN)) cm^{-1}. Characterization of **4**: M.p. (argon, sealed capillary): 190°C (decomp); elemental analysis (%) calcd for $C_{44}H_{76}N_8Sn_2$: C 55.4, H 8.0, N 11.7; found: C 55.4, H 8.1, N 11.6; ^{1}H NMR (500.2 MHz, [D$_8$]THF/[D$_8$]toluene): $\delta = 6.31$ (s, 4H, CH_{pz}), 1.39 ppm (s, 72H, CMe_3); ^{13}C NMR (125.8 MHz, [D$_8$]THF/[D$_8$]toluene): $\delta = 163.5$ (s, pz C_{quart}), 102.2 (s, CH_{pz}), 32.6 (s, CMe_3), 31.7 ppm (s, CMe_3); ^{119}Sn NMR (186.5 MHz, 213 K, [D$_8$]THF/[D$_8$]toluene): $\delta = -351$, -614 ppm; IR (solid, ATR): $\tilde{\nu} = 2951$ vs, 2901 (sh) m, 2863 (sh) m (ν (CH, CH_3)); 1516 m, 1496 w (ν(pyrazole ring)); 1461 m, 1435 m, 1358 s (δ (CH, CH_3)); 1306 s, 1248 s, 1218 m, 1200 m, 1091 s, 1033 s, 1021 m, 1005 s (δ(CH, CH_3), ν CC)); 928 w, 778 vs, 711 s, 632 w, 564 w, 530 vw (ν(CC), δ(CC), ν(SnN)) cm^{-1}.

Received: June 8, 2004

Keywords: cage compounds · carbene homologues · Group 14 elements · N ligands · tin

[1] a) P. J. Davidson, M. F. Lappert, *J. Chem. Soc. Chem. Commun.* **1973**, 317; b) D. E. Goldberg, D. H. Harris, M. F. Lappert, K. M. Thomas, *J. Chem. Soc. Chem. Commun.* **1976**, 261.

[2] R. West, M. J. Fink, J. Michl, *Science* **1981**, *214*, 1343.

[3] For reviews see a) M. Weidenbruch, *J. Organomet. Chem.* **2002**, *646*, 39; b) P. P. Power, *Chem. Rev.* **1999**, *99*, 3463; c) M. Driess, H. Grützmacher, *Angew. Chem.* **1996**, *108*, 900; *Angew. Chem. Int. Ed. Engl.* **1996**, *35*, 828; d) N. Tokitoh, R. Okasaki, *Coord. Chem. Rev.* **2000**, *210*, 251; e) M. F. Lappert, *Main Group Met. Chem.* **1994**, *17*, 183; f) M. Weidenbruch, *Organometallics* **2003**, *22*, 4348.

[4] a) G. Trinquier, *J. Am. Chem. Soc.* **1990**, *112*, 2130; b) G. Trinquier, *J. Am. Chem. Soc.* **1991**, *113*, 144; see also I. Ganzer, M. Hartmann, G. Frenking in *The Chemistry of Organic Germanium, Tin and Lead Compounds*, *Vol. 2* (Eds.: S. Patai, Z. Rappoport), Wiley, New York, **2002**, pp. 169–282; d) Y. Apeloig, T. Müller, *J. Am. Chem. Soc.* **1995**, *117*, 5363.

[5] a) A. D. Phillips, S. Hino, P. P. Power, *J. Am. Chem. Soc.* **2003**, *125*, 7520; b) for an example of an intramolecular donor-stabilized stannyl stannylene [RSnSnR$_3$], see C. J. Cardin, D. J. Cardin, S. P. Constantine, A. K. Todd, S. J. Teat, S. Coles, *Organometallics* **1998**, *17*, 2144.

[6] B. E. Eichler, P. P. Power, *J. Am. Chem. Soc.* **2000**, *122*, 8785.

[7] For doubly R-bridged isomers see, for example a) J. R. Babcock, C. Incarvito, A. L. Rheingold, J. C. Fettinger, L. R. Sita, *Organometallics* **1999**, *18*, 5729; b) R. S. Simons, L. Pu, M. M. Olmstead, P. P. Power, *Organometallics* **1997**, *16*, 1920; c) M. J. McGeary, K. Folting, K. G. Caulton, *Inorg. Chem.* **1989**, *28*, 4051; d) M. M. Olmstead, P. P. Power, *Inorg. Chem.* **1984**, *23*, 413. Doubly bridged E_2R_4 intermediates have been suggested to be involved in an alternative mechanism for the 1,2-diaryl rearrangement in tetraaryldisilenes: H. B. Yokelson, D. A. Siegel, A. J. Millevolte, J. Maxka, R. West, *Organometallics* **1990**, *9*, 1005.

[8] C. Stanciu, A. F. Richards, P. P. Power, *J. Am. Chem. Soc.* **2004**, *126*, 4106.

[9] a) M. Veith, J. Hans, *Angew. Chem.* **1991**, *103*, 845; *Angew. Chem. Int. Ed. Engl.* **1991**, *30*, 878; b) M. Veith, K. Kunze, *Angew. Chem.* **1991**, *103*, 92; *Angew. Chem. Int. Ed. Engl.* **1991**, *30*, 95; c) M. Veith, D. Käfer, J. Koch, P. May, L. Stahl, V. Huch, *Chem. Ber.* **1992**, *125*, 1033, and references therein.

[10] A. Steiner, D. Stalke, *Inorg. Chem.* **1995**, *34*, 4846.

[11] For instance, the reaction of tin(II) amido compounds with primary amines leads to imido tin(II) heterocubanes of the general formula [{Sn(NR)}$_4$]. Some selected examples and references therein: a) M. Veith, M. Opsölder, M. Zimmer, V. Huch, *Eur. J. Inorg. Chem.* **2000**, 1143; b) D. R. Armstrong, F. Benevelli, A. D. Bond, N. Feeder, E. A. Harron, A. D. Hopkins, M. McPartlin, D. Moncrieff, D. Sáez, E. A. Quadrelli, A. D. Woods, D. S. Wright, *Inorg. Chem.* **2002**, *41*, 1492.

[12] Crystal structure of **3**: single crystals were obtained from *n*-hexane at room temperature; $C_{20}H_4N_8F_{24}Sn_2$, monoclinic, space group $P2(1)/n$; $a = 10.552(3)$, $b = 9.282(3)$, $c = 16.194(5)$ Å, $\beta = 97.575(7)°$; $V = 1572.3(9)$ Å^3; $Z = 2$; $\rho_{calcd} = 2.217$ Mg m^{-3}; crystal dimensions $0.48 \times 0.50 \times 0.50$ mm; diffractometer Bruker SMART Apex; $Mo_{K\alpha}$ radiation, 298 K, $2\Theta_{max} = 49.40°$; 8382 reflections, 2637 independent ($R_{int} = 0.0212$), direct methods; empirical absorption correction SADABS (ver. 2.03); refinement against full matrix (versus F^2) with SHELXTL (ver. 6.12) and SHELXL-97, 272 parameters, $R1 = 0.0353$ and w$R2$ (all data) $= 0.0946$, max./min. residual electron density 0.569/-0.461 e Å^{-3}. The hydrogen atoms were placed in idealized positions and included as riding atoms. One CF_3 group of a SnR_2 moiety was disordered and had to be split over two positions, which were refined against each other (FVAR = 0.63). CCDC-241013 contains the supplementary crystallographic data for this paper. These data can be obtained free of charge via www.ccdc.cam.ac.uk/conts/retrieving.html (or from the Cambridge Crystallographic Data Centre, 12 Union Road, Cambridge CB2 1EZ, UK; fax: (+44) 1223-336-033; or deposit@ccdc.cam.ac.uk).

[13] Selected examples of tin(II) complexes of macrocyclic N_4 ligands in which the tin center is the apex of a square pyramid ($d_{Sn\text{-}N4}$ is the displacement of Sn from the macrocyclic N_4 plane) a) $d_{Sn\text{-}N4} = 112$ pm: M. C. Kuchta, G. Parkin, *J. Am. Chem. Soc.* **1994**, *116*, 8372; b) $d_{Sn\text{-}N4} = 115$ pm: D. A. Atwood, V. O. Atwood, A. H. Cowley, J. L. Atwood, E. Román, *Inorg. Chem.* **1992**, *31*, 3871; c) $d_{Sn\text{-}N4} = 113$ pm:R. Kubiak, J. Janczak, *J. Alloys Compd.* **1992**, *189*, 107; d) $d_{Sn\text{-}N4} = 102$ pm: J.-M. Barbe, C. Ratti, P. Richard, C. Lecomte, R. Gerardin, R. Guilard, *Inorg. Chem.* **1990**, *29*, 4126; e) $d_{Sn\text{-}N4} = 111$ pm: M. K. Friedel, B. F. Hoskins, R. L. Martin, S. A. Mason, *J. Chem. Soc. D* **1970**, 400.

[14] a) D. L. Reger, S. S. Mason, J. Takats, X. W. Zhang, A. L. Rheingold, B. S. Haggerty, *Inorg. Chem.* **1993**, *32*, 4345; b) A. H. Cowley, R. L. Geerts, C. M. Nunn, C. J. Carrano, *J. Organomet. Chem.* **1988**, *341*, C27; c) D. L. Reger, S. J. Knox, M. F. Huff, A. L. Rheingold, B. S. Haggerty, *Inorg. Chem.* **1991**, *30*, 1754.

[15] M. Bak, J. T. Rasmussen, N. C. Nielsen, *J. Magn. Reson.* **2000**, *147*, 296.

[16] A modest $^1J(^{119}Sn,^{117}Sn)$ coupling constant of 1340 Hz was reported for the dimer [R_2SnSnR_2] ($R = CH(SiMe_3)_2$) K. W. Zilm, G. A. Lawless, R. M. Merrill, J. M. Millar, G. G. Webb, *J. Am. Chem. Soc.* **1987**, *109*, 7236. Satellites arising from an interaction of this magnitude would be hidden in our case under the 2 kHz broad main line.

[17] For a discussion concerning the differences of ^{119}Sn NMR liquid- and solid-state isotropic shifts see B. E. Eichler, B. L. Phillips, P. P. Power, M. P. Augustine, *Inorg. Chem.* **2000**, *39*, 5450.

[18] Diffusion coefficient $D = 8.76 \times 10^{-10}$ m^2 s^{-1} in THF at room temperature; hydrodynamic radius determined by ^{1}H-PGSE NMR experiments: r_H (exp) = 4.9 Å; expected for the dimer (X-ray data): r_H (dimer) = 5.7 Å (see Supporting Information for

further information). For an overview concerning PGSE methods in coordination chemistry see P. S. Pregosin, E. Martínez-Viviente, P. G. A. Kumar, *Dalton Trans.* **2003**, 4007.

[19] No detectable ^{119}Sn NMR resonance for **4** in solution at room temperature.

[20] a) E. O. Fischer, H. Grubert, *Z. Naturforsch. B* **1956**, *11*, 423; b) J. L. Atwood, W. E. Hunter, A. H. Cowley, R. A. Jones, C. A. Stewart, *J. Chem. Soc. Chem. Commun.* **1981**, 925.

[21] Although no single crystals of bis(triphospholyl)tin(II) of sufficient quality have been obtained yet, some NMR spectroscopic investigations and related Group 14 element complexes have been published. a) A. Elvers, F. H. Heinemann, B. Wrackmeyer, U. Zenneck, *Chem. Eur. J.* **1999**, *5*, 3143; b) J. J. Durkin, M. D. Francis, P. B. Hitchcock, C. Jones, J. F. Nixon, *J. Chem. Soc. Dalton Trans.* **1999**, 4057

[22] a) H[3,5-$(CMe_3)_2$pz]: A. Beck, A. Barth, E. Hübner, N. Burzlaff, *Inorg. Chem.* **2003**, *42*, 7182; b) H[3,5-$(CF_3)_2$pz]: P. P. K. Claire, P. L. Coe, C. J. Jones, J. A. McCleverty, *J. Fluorine Chem.* **1991**, *51*, 283; c) H(3,5-Ph_2pz): N. Kitajima, K. Fujisawa, C. Fujimoto, Y. Morooka, S. Hashimoto, T. Kitagawa, K. Toriumi, K. Tatsumi, A. Nakamura, *J. Am. Chem. Soc.* **1992**, *114*, 1277; d) [Sn{$N(SiMe_3)_2$}$_2$]: D. H. Harris, M. F. Lappert, *J. Chem. Soc. Chem. Commun.* **1974**, 895.

 © 2005 Wiley-VCH Verlag GmbH & Co. KGaA, Weinheim

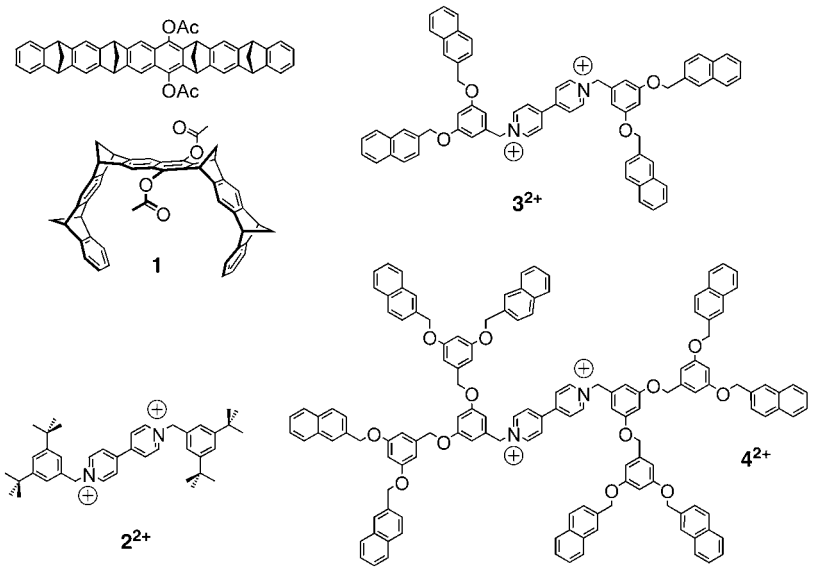
Dendritic Effects

Gas-Phase Host–Guest Chemistry of Dendritic Viologens and Molecular Tweezers: A Remarkably Strong Effect on Dication Stability**

Christoph A. Schalley, Carla Verhaelen, Frank-Gerrit Klärner, Uwe Hahn, and Fritz Vögtle*

Gas-phase chemistry in the ultrahigh vacuum of a mass spectrometer provides insight into intrinsic features of the species under study. Comparison of gas-phase and solution properties thus permits a detailed analysis of the influence of the solvents and counterions in the solution phase that are absent in the gas phase. This advantage of the gas phase is particularly beneficial for the analysis of weakly bound complexes, in which the noncovalent bonds have bond energies not much larger than the interactions with their environment in the condensed phase.[1] Although mass spectrometry has often been used as a powerful tool for the analytical characterization of dendrimers,[2] their gas-phase fragmentations have only rarely been studied,[3] and their host–guest chemistry in the gas-phase is to date almost completely unexplored.[4]

Viologens substituted with Fréchet dendrons[5,6] (Scheme 1) have a highly electron-deficient, dicationic core.



Scheme 1. Viologens $\mathbf{2}^{2+}$–$\mathbf{4}^{2+}$ and the molecular tweezers **1**.

They are excellent guests for the molecular tweezers **1**[7] with its extended aromatic systems.[8] A rather negative electrostatic potential is generated on the concave interior of **1** owing to overlapping π-systems.[9] The positively charged viologens form highly stable complexes with **1** ($K_a \geq 9000\,M^{-1}$ in dichloromethane).[10] The stability of the viologen–tweezers complexes is, however, highly solvent-dependent.[11] Herein, we report the intrinsic properties of the host–guest complexes between tweezers **1** and the viologen derivatives $\mathbf{2}^{2+}$, $\mathbf{3}^{2+}$, and $\mathbf{4}^{2+}$. In view of the positively charged guests, insight into these properties should be gained easily in the gas phase by electrospray ionization Fourier-transform ion-cyclotron-resonance (ESI-FT-ICR) mass spectrometry.

Electrospray ionization of 50 μM methanol solutions of viologen $\mathbf{2}^{2+}(PF_6^-)_2$ gives the mass spectrum shown in Figure 1a. Irrespective of the ionization conditions, no naked $\mathbf{2}^{2+}$ dications were detected in the spectrum. This situation is in line with preliminary BHLYP/TZP density functional (DFT) calculations for the model compound in Scheme 2, which predict the viologen dication to be intrinsically unstable. Upon its transfer into the gas phase, $\mathbf{2}^{2+}$ tends to stabilize itself by 1) formation of singly charged $(\mathbf{2}^{2+})_n(PF_6^-)_{2n-1}$ $(n=1)$ and doubly charged $(\mathbf{2}^{2+})_n(PF_6^-)_{2n-2}$ $(n>1)$ clusters in which the anions counterbalance the

[*] Priv.-Doz. Dr. C. A. Schalley, Dr. U. Hahn, Prof. Dr. F. Vögtle
Kekulé-Institut für Organische Chemie und Biochemie
Universität Bonn
Gerhard-Domagk-Strasse 1, 53121 Bonn (Germany)
Fax: (+49) 228-735-662
E-mail: c.schalley@uni-bonn.de
Dipl.-Chem. C. Verhaelen, Prof. Dr. F.-G. Klärner
Institut für Organische Chemie
Universität Duisburg-Essen
Campus Essen, Universitätsstrasse 5, 45117 Essen (Germany)

[**] We are grateful to Dipl.-Chem. W. Reckien and Prof. Dr. S. Peyerimhoff for support with density functional calculations and to W. M. Müller and U. Müller for synthetic assistance. This work was funded by the Deutsche Forschungsgemeinschaft (DFG) and the Fonds der Chemischen Industrie (FCI). C.A.S. thanks the DFG for a Heisenberg fellowship and the FCI for a Dozentenstipendium.

Supporting information for this article is available on the WWW under http://www.angewandte.org or from the author.

 DOI: 10.1002/anie.200461872 © 2005 Wiley-VCH Verlag GmbH & Co. KGaA, Weinheim

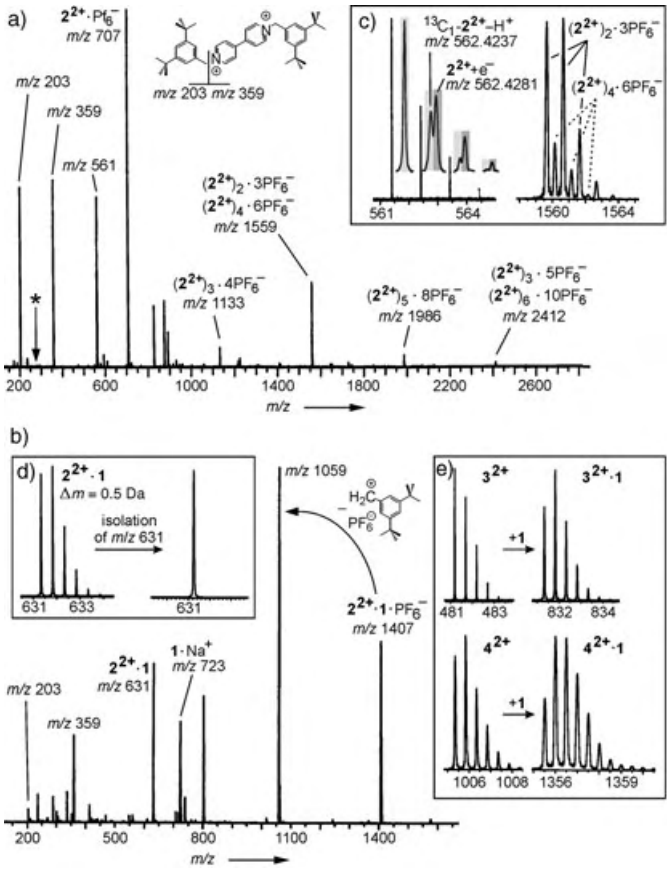
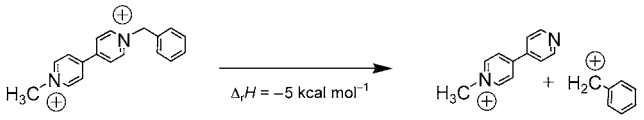


Figure 1. ESI-FT-ICR mass spectra of 50 μM solutions of a) viologen $\mathbf{2}^{2+}(PF_6^-)_2$ in methanol (asterisk: position of absent, naked $\mathbf{2}^{2+}$ dications) and b) $\mathbf{2}^{2+}(PF_6^-)_2$ with one equivalent of tweezers **1**. Inset: c) high-resolution isotope pattern for monocationic $[\mathbf{2}^{2+}-H^+]$ and $[\mathbf{2}^{2+}+e^-]$ ions at *m*/*z* 561 and 562 and the isotope pattern of the signal at *m*/*z* 1559 confirming the presence of a singly and a doubly charged cluster with peak spacings of 1 and 0.5 Da, respectively. Inset: d) isotope pattern ($\Delta m = 0.5$ Da) of the $\mathbf{2}^{2+}\cdot\mathbf{1}$ tweezers–guest complex before and after isolation of the monoisotopic peak for MS/MS experiments. Inset: e) The isotope patterns corresponding to the dications of dendritic substituted viologens $\mathbf{3}^{2+}$ and $\mathbf{4}^{2+}$ and the corresponding tweezers complexes.



Scheme 2. Results of BHLYP/TPZ DFT calculations on the stability of a model viologen cation.

repulsion of the positive charges, 2) by separation of the two charges through dissociation into the two singly charged fragment ions with *m*/*z* 359 and 203, 3) by proton loss giving rise to singly charged $[\mathbf{2}^{2+}-H^+]$ ions with *m*/*z* 561, and 4) by a one-electron reduction during the ionization process leading to monocationic $[\mathbf{2}^{2+}+e^-]$ with *m*/*z* 562. The processes (3) and (4) lead to overlapping isotope patterns which can easily be separated by the high resolving power of the FT-ICR instrument (Figure 1c, left). These results already point to the importance of the environment: Owing to the presence of counterions, $\mathbf{2}^{2+}$ is stable in solution, but is not observed as a naked dication in the gas phase because of strong intramolecular charge-repulsion effects.

Upon addition of one equivalent of tweezers **1** to the solution of $\mathbf{2}^{2+}(PF_6^-)_2$, the spectrum changes dramatically (Figure 1b):[12] Instead of any cluster ions, a tweezers–viologen complex is detected at *m*/*z* 1407 confirming the 1:1 stoichiometry in solution. Loss of a $[C_6H_5CH_2]^+$–$[PF_6]^-$ ion pair gives rise to a signal at *m*/*z* 1059. In addition, a rather intense signal for doubly charged $\mathbf{2}^{2+}\cdot\mathbf{1}$ with an isotope pattern spacing of $\Delta m = 0.5$ Da is observed at *m*/*z* 631. Complex formation with the tweezers significantly stabilizes the dication through charge-transfer interactions that dissipate the charge and diminish charge repulsion sufficiently to prevent the fragmentation of $\mathbf{2}^{2+}$.

Significantly different behavior was encountered for the dendritic viologens $\mathbf{3}^{2+}(PF_6^-)_2$ and $\mathbf{4}^{2+}(PF_6^-)_2$: Under the mildest possible ionization conditions the naked dication of the first generation (G1) viologen $\mathbf{3}^{2+}$ could be generated with some difficulties; the formation of naked $\mathbf{4}^{2+}$ was achieved easily even under somewhat harder conditions (Figure 1e, left). Evidently, a trend towards higher dication stability with increasing dendron size exists. Both compounds formed abundant doubly charged complexes with tweezers **1** (Figure 1e, right).

For an analysis of its fragmentation behavior, monoisotopic $\mathbf{2}^{2+}\cdot\mathbf{1}$ was isolated in the FT-ICR cell and subjected to collisions with argon as the collision gas (Figure 2a).[13] Owing to the intrinsic instability of $\mathbf{2}^{2+}$, this dication is not observed as fragmentation product. Instead, one zero generation (G0)-benzyl ion (*m*/*z* 203) is expelled giving rise to a singly charged tweezers–bipyridinium ion complex with *m*/*z* 1059 which subsequently fragments through loss of the tweezers to yield the bipyridinium ion with *m*/*z* 359 (for the structural formula of this ion, see Figure 1a). As a mechanistic alternative, the two ions with *m*/*z* 203 and 359 could be formed by tweezers loss, immediately followed by decomposition of the resulting instable $\mathbf{2}^{2+}$ ion. However, a double-resonance experiment (Figure 2b), in which the intermediate with *m*/*z* 1059—and with it, all the subsequent fragments—is constantly expelled from the FT-ICR cell during the whole experiment, provides evidence that the latter fragmentation pathway does not play a major role. The intensity of the signal at *m*/*z* 359 almost vanishes in this experiment, which indicates that the corresponding ion is thus formed predominantly from $\mathbf{2}^{2+}\cdot\mathbf{1}$ through the upper pathway in Scheme 3. The same behavior is observed for G1-substituted $\mathbf{3}^{2+}\cdot\mathbf{1}$. The only difference is that the G1-benzyl cation undergoes further consecutive fragmentations giving rise to the 2-naphthylmethyl ion (*m*/*z* 141). This type of fragmentation pattern is observed as well for naked $\mathbf{3}^{2+}$.

This reactivity pattern—first loss of a benzyl cation followed by dissociation of the remaining complex—is completely reversed for $\mathbf{4}^{2+}\cdot\mathbf{1}$ to a tweezers loss with subsequent decomposition of the dicationic viologen. Upon collisional activation of $\mathbf{4}^{2+}\cdot\mathbf{1}$, an intense signal for the naked $\mathbf{4}^{2+}$ dication is observed at *m*/*z* 1005, while the product of the loss of a second generation (G2) benzyl cation (signal

 © 2005 Wiley-VCH Verlag GmbH & Co. KGaA, Weinheim

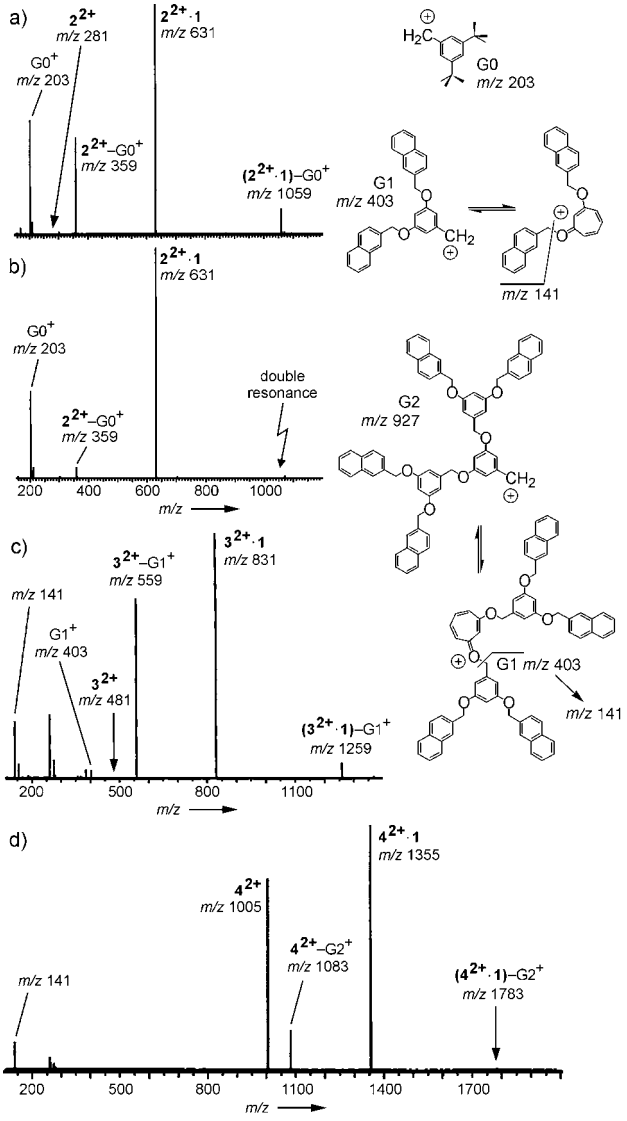
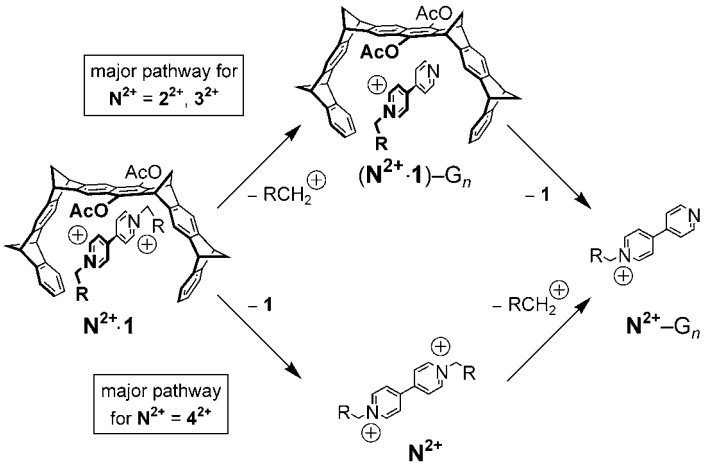


Figure 2. a) Collision-induced decomposition (CID) of mass selected 2^{2+}·**1** ions. b) Double resonance experiment with mass selected 2^{2+}·**1**, in which the fragment at *m*/*z* 1059 was ejected from the reaction cell during the whole experiment. c) CID experiment with 3^{2+}·**1**. d) CID experiment with 4^{2+}·**1** revealing a complete change in reactivity. Tweezers loss is the major fragmentation pathway giving rise to dicationic 4^{2+} at *m*/*z* 1005. The structures on the right show the fragments by which dendritic benzyl cations can give 2-naphthylmethyl ions at *m*/*z* 141 without the formation of the benzyl cation itself rather than the complete G1 and G2 dendritic wedges.

expected at *m*/*z* 1783) is not seen at all. Consecutive fragmentations of 4^{2+} can be identified at *m*/*z* 1083 and 141 and are in agreement with those found in the same experiment with independently generated naked 4^{2+}. This remarkable change in reactivity can be traced back to the stabilizing effect of the larger dendrons on the dication. While the dication becomes more stable with larger dendritic substituents, its binding energy to tweezers **1** is reduced. Consequently, these experiments nicely uncover a remarkable effect of the dendritic substituents on the host–guest chemistry of the viologen–tweezers complexes studied.



Scheme 3. Main fragmentation pathways for 2^{2+}–4^{2+} in the gas phase.

In conclusion, we have shown 1) tweezers **1** forms stable 1:1 complexes with dendritic viologens 2^{2+}–4^{2+} in the gas phase. 2) Tweezers **1** significantly stabilizes dicationic guests, which are unstable (2^{2+}) or hardly stable (3^{2+}) as isolated dications in the gas phase, most likely through charge-transfer interactions. 3) The dendritic substituents have a surprisingly large influence on the fragmentation pattern of the tweezers complexes of viologen dications 2^{2+}–4^{2+}. The fragmentation pattern changes completely from the G0 and G1 to the G2 dendrimers. Evidently, dendritic substituents of increasing size at the viologen core provide increasing stability of the naked dication. This finding can be explained by force-field calculations (Figure 3). The G2 dendron is calculated to completely embrace the viologen dication by back folding[14] of the dendritic "arms" leading to an "intramolecular solvation" and hence to a stabilization of the viologen core. The viologen core is, however, calculated to be less efficiently or entirely not embraced by folding of the G1 and G0 dendrons, respectively, which results in the instability observed for 2^{2+} and 3^{2+}.

These studies not only provide insight into the host–guest chemistry of dendrimers and the influences of dendron size as

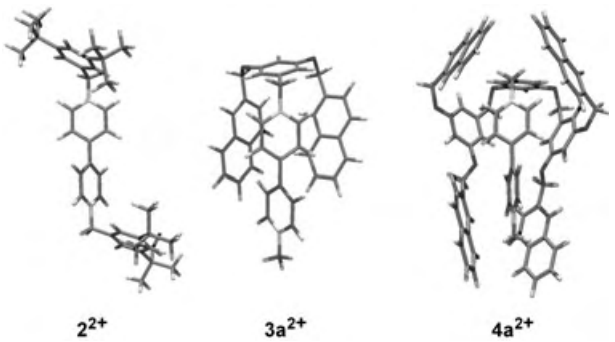


Figure 3. Lowest energy conformations of the viologen derivatives substituted by two 3,5-di-*tert*-butylbenzyl groups (2^{2+}), by model complexes with methyl and G1 dendron ($3a^{2+}$), and by methyl and G2 dendron ($4a^{2+}$) calculated by Monte Carlo conformer search using the MMFF force field implemented in SPARTAN 04.

 © 2005 Wiley-VCH Verlag GmbH & Co. KGaA, Weinheim

it increases with the generation number. They also underline the importance of gas-phase studies of such systems which significantly contribute to our understanding of the effects of the environment on noncovalent compounds.

Received: September 2, 2004

Keywords: dendrimers · gas-phase chemistry · host–guest chemistry · mass spectrometry · supramolecular chemistry

[1] Recent reviews: a) C. A. Schalley, *Int. J. Mass Spectrom.* **2000**, *194*, 11–39; b) C. A. Schalley, *Mass Spectrom. Rev.* **2001**, *20*, 253–309; crown ether–cation complexes are a particularly well studied: c) P. B. Armentrout, *Int. J. Mass Spectrom.* **1999**, *193*, 227–240, and references therein.

[2] Selected examples: a) J. C. Hummelen, J. L. J. van Dongen, E. W. Meijer, *Chem. Eur. J.* **1997**, *3*, 1489–1493; b) M. S. Wendland, S. C. Zimmerman, *J. Am. Chem. Soc.* **1999**, *121*, 1389–1390; c) J.-C. Blais, C.-O. Turrin, A.-M. Caminade, J.-P. Majoral, *Anal. Chem.* **2000**, *72*, 5097–5105; d) L. Bu, W. K. Nonidez, J. W. Mays, N. B. Tan, *Macromolecules* **2000**, *33*, 4445–4452; e) S. M. Cohen, S. Petoud, K. N. Raymond, *Chem. Eur. J.* **2001**, *7*, 272–279; f) Y. Rio, G. Accorsi, H. Nierengarten, J.-L. Rehspringer, B. Hönerlage, G. Kopitkovas, A. Chugreev, A. Van Dorsselaer, N. Armaroli, J.-F. Nierengarten, *New J. Chem.* **2002**, *26*, 1146–1154.

[3] See, for example: a) J.-W. Weener, J. L. J. van Dongen, E. W. Meijer, *J. Am. Chem. Soc.* **1999**, *121*, 10346–10355; b) U. Puapaiboon, R. T. Taylor, J. Jai-nhuknan, *Rapid Commun. Mass Spectrom.* **1999**, *13*, 516–520; c) S. Koster, M. C. Duursma, X. Guo, R. A. T. M. Benthem, C. G. de Koster, J. J. Boon, R. M. A. Heeren, *J. Mass Spectrom.* **2002**, *37*, 792–802; d) A. Adhiya, C. Wesdemiotis, *Int. J. Mass Spectrom.* **2002**, *214*, 75–88; e) H. Neubert, K. A. Knights, Y. R. de Miguel, D. A. Cowan, *Macromolecules* **2003**, *36*, 8297–8303; f) S. Koster, M. C. Duursma, J. J. Boon, R. M. A. Heeren, S. Ingemann, R. A. T. M. van Benthem, C. G. de Koster, *J. Am. Soc. Mass Spectrom.* **2003**, *14*, 332–341; f) M. He, S. A. McLuckey, *Rapid Commun. Mass Spectrom.* **2004**, *18*, 960–972.

[4] a) L. Zhou, D. H. Russell, M. Zhao, R. M. Crooks, *Macromolecules* **2001**, *34*, 3567–3573; b) M. A. C. Broeren, J. L. J. van Dongen, M. Pittelkow, J. B. Christensen, M. H. P. van Genderen, E. W. Meijer, *Angew. Chem.* **2004**, *116*, 3541–3646; *Angew. Chem. Int. Ed.* **2004**, *43*, 3557–3562.

[5] a) C. J. Hawker, J. M. J. Fréchet, *J. Am. Chem. Soc.* **1990**, *112*, 7638–7647; b) C. J. Hawker, J. M. J. Fréchet, *J. Chem. Soc. Chem. Commun.* **1990**, 1010–1013; reviews: c) S. K. Grayson, J. M. J. Fréchet, *Chem. Rev.* **2001**, *101*, 3819–3867; d) S. Hecht, J. M. J. Fréchet, *Angew. Chem.* **2001**, *113*, 76–94; *Angew. Chem. Int. Ed.* **2001**, *40*, 74–91; e) G. R. Newkome, C. N. Moorefield, F. Vögtle, *Dendrimers and Dendrons: Concepts, Syntheses, Applications*, Wiley-VCH, Weinheim, **2001**.

[6] a) G. M. Stewart, M. A. Fox, *J. Am. Chem. Soc.* **1996**, *118*, 4354–4360; b) M. Plevoets, F. Vögtle, L. De Cola, V. Balzani, *New J. Chem.* **1999**, *23*, 63–69; c) T. H. Ghaddar, J. F. Wishart, D. W. Thompson, J. K. Whitesell, M. A. Fox, *J. Am. Chem. Soc.* **2002**, *124*, 8285–8289.

[7] a) F.-G. Klärner, U. Burkert, M. Kamieth, R. Boese, J. Benet-Buchholz, *Chem. Eur. J.* **1999**, *5*, 1700–1707; b) F.-G. Klärner, U. Burkert, M. Kamieth, R. Boese, *J. Phys. Org. Chem.* **2000**, *13*, 604–611; c) F.-G. Klärner, J. Polkowska, J. Panitzky, U. P. Seelbach, U. Burkert, M. Kamieth, M. Baumann, A. E. Wigger, R. Boese, D. Bläser, *Eur. J. Org. Chem.* **2004**, *7*, 1405–1423.

[8] F.-G. Klärner, B. Kahlert, *Acc. Chem. Res.* **2003**, *36*, 919–935.

[9] a) M. Kamieth, F.-G. Klärner, F. Diederich, *Angew. Chem.* **1998**, *110*, 3497–3500; *Angew. Chem. Int. Ed.* **1998**, *37*, 3303–3306; b) F.-G. Klärner, J. Panitzky, D. Preda, L. T. Scott, *J. Mol. Model.* **2000**, *6*, 318–327.

[10] V. Vicinelli, V. Balzani, C. Verhaelen, F.-G. Klärner, unpublished results.

[11] a) M. Kamieth, F.-G. Klärner, *J. Prakt. Chem.* **1999**, *341*, 245–251; b) M. Kamieth, U. Burkert, P. S. Corbin, S. J. Dell, S. C. Zimmerman, F.-G. Klärner, *Eur. J. Org. Chem.* **1999**, 2741–2749.

[12] For complex formation of dendritic viologens with cucurbit[7]uril, see: W. Ong, A. E. Kaifer, *Angew. Chem.* **2003**, *115*, 2214–2217; *Angew. Chem. Int. Ed.* **2003**, *42*, 2164–2167. These complexes were detected by MALDI-TOF mass spectrometry, but their gas-phase chemistry was not examined. The two substituents at the viologen are aliphatic and consequently more stable than $\mathbf{2}^{2+}$–$\mathbf{4}^{2+}$.

[13] Note that a precise collision energy cannot be determined in this experimental setup owing to broad non-Boltzmann energy distributions.

[14] a) D. Pötschke, M. Ballauff, P. Lindner, M. Fischer, F. Vögtle, *Macromolecules* **1999**, *32*, 4079–4087; b) D. Pötschke, M. Ballauff, P. Lindner, M. Fischer, F. Vögtle, *Macromol. Chem. Phys.* **2000**, *201*, 330–339; review: M. Ballauf, C. N. Likos, *Angew. Chem.* **2004**, *116*, 3060–3082; *Angew. Chem. Int. Ed.* **2004**, *43*, 2998–3020

 © 2005 Wiley-VCH Verlag GmbH & Co. KGaA, Weinheim

Cage Compounds

Rational Design of Tightly Closed Coordination Tetrahedra that are Stable in the Solid State, in Solution, and in the Gas Phase**

Iris M. Müller, Daniela Möller, and Christoph A. Schalley*

Molecular "Lego" utilizing simple building blocks with a rationally programmed arrangement of binding sites permits the construction of complex coordination cages by self-assembly,[1] among them different types of coordination

[*] Dr. I. M. Müller, Dipl.-Chem. D. Möller
Lehrstuhl für Analytische Chemie, NC 4/27
Ruhr-Universität Bochum
44780 Bochum (Germany)
Fax: (+49) 234-321-4420
E-mail: iris.m.mueller@rub.de

Priv.-Doz. Dr. C. A. Schalley
Kekulé-Institut für Organische Chemie und Biochemie
Universität Bonn, 53121 Bonn (Germany)

[**] The authors thank Heike Schucht (Max Planck Institut für Bioanorganische Chemie, Mülheim) for the data collection of **1a**, **2**, **3**,and **4** and Manuela Winter (Anorganische Chemie II, Ruhr-Universität Bochum) for the data collection of **1b**. We are grateful to the Deutsche Forschungsgemeinschaft and the Fonds der Chemischen Industrie for financial support. C.A.S. thanks the DFG for a Heisenberg fellowship and the F.C.I. for a Dozentenstipendium.

Supporting information for this article is available on the WWW under http://www.angewandte.org or from the author.

 © 2005 Wiley-VCH Verlag GmbH & Co. KGaA, Weinheim DOI: 10.1002/anie.200461800

tetrahedra (Figure 1). The oldest and most common $[M_4L_6]$ systems combine four metal centers at the corners with six bridging ligands as edges (Figure 1a).[2] $[M_4L_4]$ tetrahedral cages, whose faces are covered by ligands with threefold

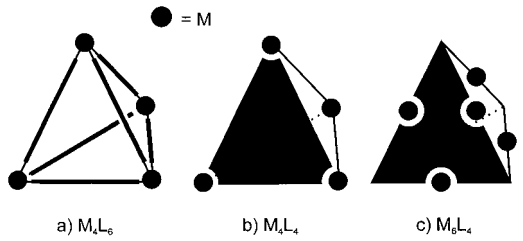
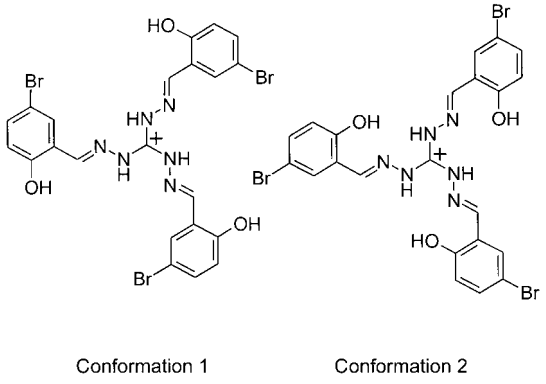


Figure 1. Tetrahedral cage molecules with different topologies.

symmetry (Figure 1b) have been reported more rarely.[3] Nearly all $[M_6L_4]$ systems are truncated tetrahedra or adamantanoid cages (Figure 1c) with rather wide openings at their corners allowing encapsulated guest molecules to be exchanged.[4] To our knowledge, only one $[M_6L_4]$ tetrahedron with an almost completely closed surface has been reported.[5] In this case, M is a $(CdO)_2$ four-membered ring and an $[Et_4N]^+$ ion is securely trapped within the octaanionic capsule.

The structural characterization of such large cage compounds by X-ray crystallography is often difficult owing to rapid solvent loss and severe disorder of counterions and solvent molecules. The introduction of heavy atoms with their higher scattering power into the ligands should help to improve the resolution and quality of the X-ray data. With tris[(5-bromo-2-hydroxybenzylidene)amino]guanidinium chloride ($[H_6Br_3L]Cl$ (**1**)), we herein present a new ligand suitable for the formation of chiral (although racemic), tightly closed tetrahedral cages with the formal $[M_6L_4]$ topology.

Compound **1** is easily obtained by a Schiff base reaction of 5-bromosalicylaldehyde and triaminoguanidinium chloride.[6] Diffusion of HCl into an acetonitrile solution of **1** leads to orthorhombic pale yellow crystals of $[H_6Br_3L]Cl{\cdot}3\,CH_3CN{\cdot}H_2O$ (**1a**).[7] In the solid state **1a** adopts conformation 1 (Scheme 1) which is unfavorable for the coordination of metal centers and which is stabilized through hydrogen bonding with the Cl^- counterions and solvent molecules (see Supporting Information). In slightly



Scheme 1. Unfavorable and favorable conformation for the coordination of metal centers to **1**.

basic solution, a change to conformation 2 is observed.[6] To examine whether metalation of **1** has the same effect, we allowed a mixture of $CdCl_2$ and **1** to react in acetone at 88 °C. The solid-state structure of the pale yellow crystals of the resulting complex $[H_6Br_3L]_2[CdCl_4]{\cdot}6(CH_3)_2CO{\cdot}H_2O$ (**1b**) showed no change in conformation of **1**.[8] In **1b** there are two $[H_6Br_3L]^+$ ligands together with a $[CdCl_4]^{2-}$ counterion in the asymmetric unit.

A similar reaction of $CdCl_2$ and **1** in methanol in the presence of Et_4NCl (as a tetrahedral counterion) and Et_3N as base leads to the formation of bright yellow crystals.[9] This time, the ligand is fully deprotonated and binds three CdCl units. All observed bond lengths and angles at the square pyramidal cadmium centers fall in the expected ranges (see Supporting Information) with three coordination sites taken by the ligand $[Br_3L]^{5-}$ and one by a Cl^- ligand. The fifth site is occupied by a phenolate oxygen atom of a neighboring $[(CdCl)_3Br_3L]$ building block so that a chiral cage with the formula $(Et_4N)_5(Et_3NH)_3[\{(CdCl)_3Br_3L\}_4]$ (**2**), is formed as shown in Figure 2 with each $[(CdCl)_3Br_3L]^{2-}$ unit color coded

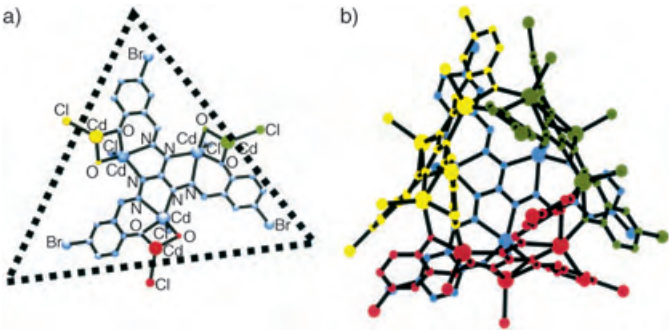


Figure 2. a) Connectivity of one $[(CdCl)_3Br_3L]$ unit. b) Crystal structure of $[\{(CdCl)_3Br_3L\}_4]^{8-}$, hydrogen atoms and counterions are omitted for clarity.

differently. Although the ligand $[H_6Br_3L]^+$ is fully deprotonated and coordinating three Cd^{2+} centers in **2** the observed bond lengths and angles remain at the 3σ level the same as those found in **1a** and **1b**. Only the propeller-like distortion becomes more distinct, with dihedral angles of 16.9–36.4°. Not unexpectedly, this avoids close Br···Br contacts at the tightly packed tetrahedron corners with their already short Br···Br separations of 3.72(2)–4.89(2) Å (Figure 3). The cage dimensions can be determined by an imaginary inner sphere that is defined by the four central carbon atoms ($r = 4.31(8)$ Å). The theoretical edge length (a) is calculated to be 21.1(4) Å, the height (h) to be 17.2(3) Å (Scheme 2, Table 1). The observed edge length can be gauged by the H···Br separation (d) which has values of 15.46(3)–15.99(3) Å, so that only the ends of the corners remain uncovered. This situation also confirms that the $[(CdCl)_3Br_3L]$ units are triangular building blocks, each of which covers almost completely one face of the tetrahedron leaving effectively no opening at the cage corners. In the asymmetric unit of **2**, two cages and 16 counterions can be found, two of the $[Et_4N]^+$ ions are located in the cavities of the two cage anions. The remaining 14 cations (six $[Et_3NH]^+$, eight $[Et_4N]^+$) are located outside the cages with the $[Et_3NH]^+$

 © 2005 Wiley-VCH Verlag GmbH & Co. KGaA, Weinheim

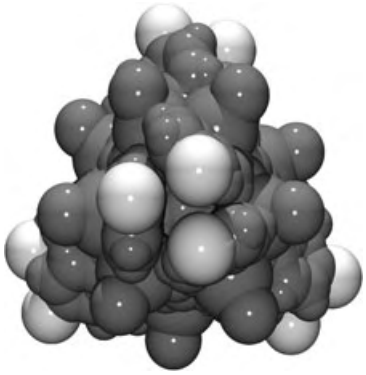
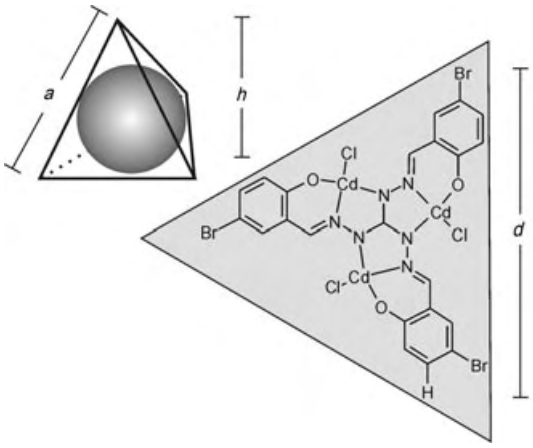


Figure 3. Space-filling model of $[\{(CdCl)_3Br_3L\}_4]^{8-}$ in **2**, view towards the corner of the cage (counterions not shown).



Scheme 2. Definition of the cage dimensions in **2**.

Table 1: Theoretical and observed dimensions [Å] of the tetrahedral cages **2**–**4**.

Dimension[a]	2	3	4
r	4.31(8)	4.36(8)	4.36(5)
a	21.1(4)	21.3(4)	21.3(3)
h	17.2(3)	17.5(3)	17.4(2)
Br···Br	3.72(2)–4.89(2)	3.77(2)–4.72(2)	3.85(2)–4.56(2)
d	15.46(3)–15.99(3)	15.60(3)–16.02(3)	15.68(3)–15.96(3)

[a] See Scheme 2.

ions forming hydrogen bridges to the Cl ligands of the tetrahedra (N···Cl = 3.13(2) Å).

To learn more about the influence of the size and geometry of the counterion, $[Et_4N]^+$ was replaced by larger $[Ph_4P]^+$ ions in a second reaction of $CdCl_2$ and $[H_6Br_3L]Cl$ with Et_3N performed under identical conditions. Again bright yellow crystals were obtained which according to the crystal-structure analysis correspond to a tetrahedral cage with the formula $(PPh_4)_{1.33}(Et_3NH)_{6.67}[\{(CdCl)_3Br_3L\}_4]$ (**3**)[10] and of the same size as **2**. An $[Et_3NH]^+$ ion is located inside the cage. Encouraged by these results, the experiment was repeated without the addition of any tetrahedral cations. Again, bright yellow crystals suitable for crystal-structure analysis were obtained corresponding to $(Et_3NH)_8[\{(CdCl)_3Br_3L\}_4]\cdot x\,H_2O$ (**4**).[11] Again, all crystallographically observed bond lengths and angles fall in the expected ranges and show no additional distortion compared with **2** or **3**. An $[Et_3NH]^+$ ion is captured inside tetrahedron **4**, together with a water molecule, which is hydrogen bonded to the cation (N···O 2.66(9) Å). Apparently, the size of the guest is more important than its symmetry for efficiently templating the tetrahedron formation.

Cage **4** is quite stable in solution. The ^1H NMR spectrum of **4** in $[D_6]$acetone shows different signals for the $[Et_3NH]^+$ ions inside (methyl groups, $\delta_H = 0.95$ ppm) and outside (methyl groups, $\delta_H = 1.27$ ppm) the cage, which indicates that their exchange is slow on the NMR timescale.

Electrospray ionization Fourier-transform ion-cyclotron-resonance (ESI-FT-ICR) mass spectrometry provides a soft method for the ionization of intact tetrahedra **4** and other metallosupramolecular assemblies.[12] When sprayed from acetonitrile or acetone, doubly, triply, and quadruply charged anions are generated by successively stripping off $[Et_3NH]^+$ counterions (Figure 4a). Although the spectra are complex, they can be analyzed in detail. In addition to the $[M-nEt_3NH]^{n-}$ ions, losses of Et_3N and Et_3NHCl are observed (Figure 4b). An exact comparison of the experimental spectrum with that simulated on the basis of natural isotope abundances reveals that each of these ions is accompanied by an ion bearing exactly one water molecule although dry acetonitrile was used as the spray solvent. In marked contrast, no such ions bearing water molecules are observed in the mass spectrum of **2** obtained under the same conditions (Figure 4c). This finding rules out incomplete desolvation as the reason for the presence of a water molecule in the spectra of **4** and points to its presence as a guest inside the cage, thus providing evidence for the intact structure of the tetrahedron even in the gas phase. Consequently, it can safely be assumed that the much larger $[Et_3NH]^+$ guest is also still inside the cage in these ions.

In conclusion, a tightly closed tetrahedral cage successfully self-assembles around templating cations as long as these cations have a suitable size. While $[Et_4N]^+$ almost exactly fills the space inside, $[Et_3NH]^+$ leaves enough space for an additional water molecule, which is co-encapsulated in the cavity of the tetrahedron. The crystal structures of several tetrahedra are in excellent agreement with data from solution and the gas phase which provide evidence for their existence as stable, discrete entities. It is particularly surprising, that ESI mass spectrometry is capable of identifying the encapsulated water molecule, which may also be interpreted as an effect of the tightly closed surfaces of the tetrahedra, which impose a considerable barrier for the water expulsion from the interior. The tetrahedra are chiral, although they form as a racemic mixture. As cations template their formation, a diastereoselective formation of one tetrahedron enantiomer around an enantiopure guest cation might be possible.

Received: August 26, 2004

 © 2005 Wiley-VCH Verlag GmbH & Co. KGaA, Weinheim

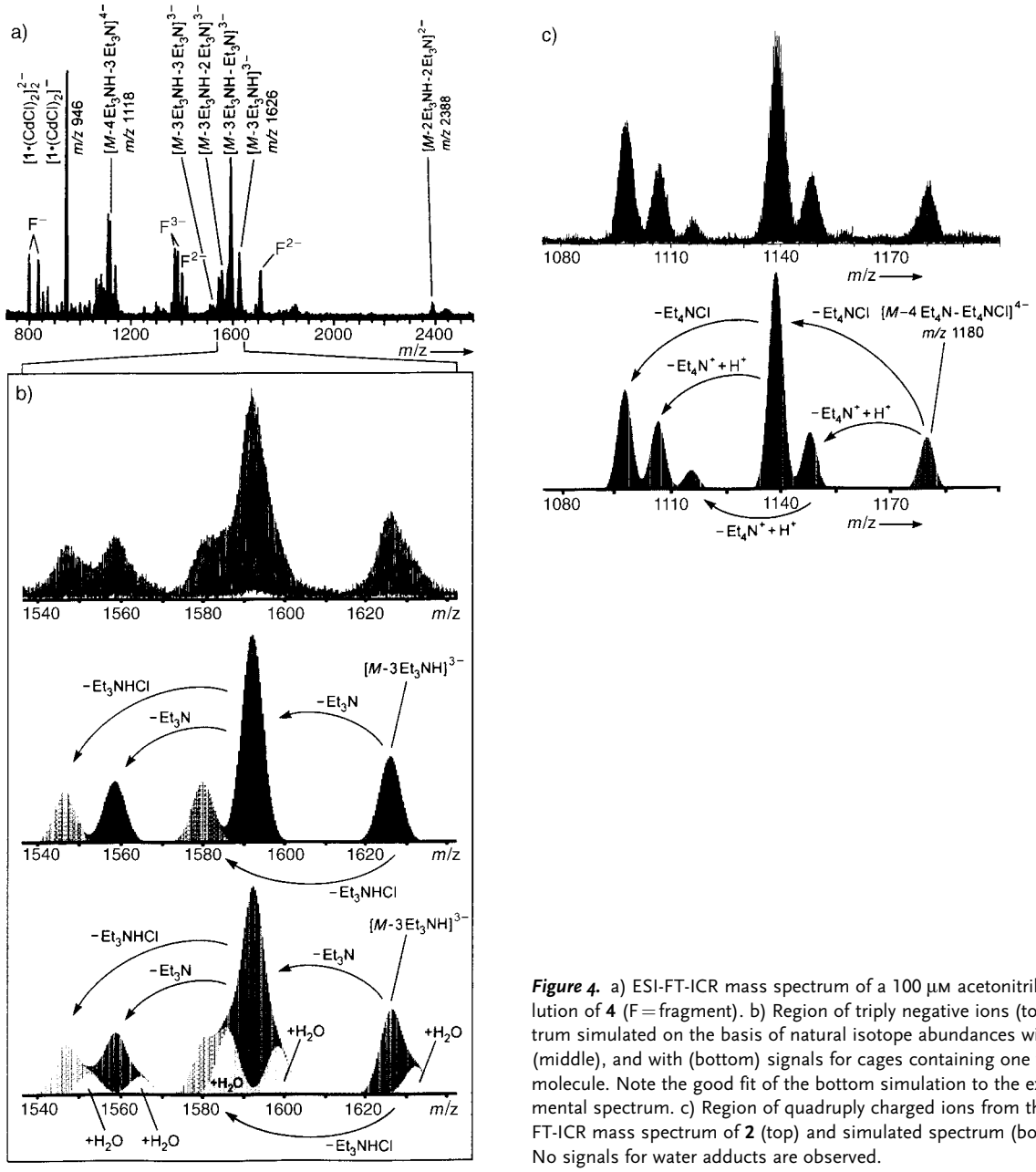


Figure 4. a) ESI-FT-ICR mass spectrum of a 100 μM acetonitrile solution of **4** (F = fragment). b) Region of triply negative ions (top), spectrum simulated on the basis of natural isotope abundances without (middle), and with (bottom) signals for cages containing one water molecule. Note the good fit of the bottom simulation to the experimental spectrum. c) Region of quadruply charged ions from the ESI-FT-ICR mass spectrum of **2** (top) and simulated spectrum (bottom). No signals for water adducts are observed.

Keywords: cadmium · cage compounds · mass spectrometry · self-assembly · structure elucidation

[1] For reviews see: a) T. D. Hamilton, L. R. MacGillivray, *Cryst. Growth Des.* **2004**, *4*, 419; b) R. W. Saalfrank, B. Demleitner, H. Glaser, H. Maid, S. Reihs, W. Bauer, M. Maluenga, F. Hampel, M. Teichert, H. Krautscheid, *Eur. J. Inorg. Chem.* **2003**, 822; c) G. F. Swieger, T. J. Malefetse, *Coord. Chem. Rev.* **2002**, *225*, 91; d) S. Leininger, B. Olenyuk, P. J. Stang, *Chem. Rev.* **2000**, *100*, 853; e) J. A. R. Navarro, B. Lippert, *Coord. Chem. Rev.* **1999**, *185–186*, 653.

[2] First example: a) R. W. Saalfrank, A. Stark, K. Peters, H. G. von Schnering, *Angew. Chem.* **1988**, *100*, 878; *Angew. Chem. Int. Ed. Engl.* **1988**, *27*, 851; recent articles: b) D. H. Leung, D. Fiedler, R. G. Bergman, K. N. Raymond, *Angew. Chem.* **2004**, *116*, 981; *Angew. Chem. Int. Ed.* **2004**, *43*, 963; c) Y. Bai, D. Guo, C. Duan, D. Dang, K. Pang, Q. Meng, *Chem. Commun.* **2004**, 186; d) D. Fiedler, D. Pagliero, J. L. Brumaghim, R. G. Bergman, K. N. Raymond, *Inorg. Chem.* **2004**, *43*, 846; e) D. Fiedler, D. H. Leung, R. G. Bergman, K. N. Raymond, *J. Am. Chem. Soc.* **2004**, *126*, 3674.

[3] Recent articles: a) M. Albrecht, I. Janser, S. Meyer, P. Weis, R. Fröhlich, *Chem. Commun.* **2003**, 2854; b) R. W. Saalfrank, H. Glaser, B. Demleitner, F. Hampel, M. M. Chowdhry, V. Schünemann, A. X. Trautwein, G. B. M. Vaughan, R. Yeh, A. V. Davis, K. N. Raymond, *Chem. Eur. J.* **2002**, *8*, 493.

[4] Recent articles: a) M. Yoshizawa, M. Tamura, M. Fujita, *J. Am. Chem. Soc.* **2004**, *126*, 6846; b) M. Yoshizawa, Y. Takeyama, T. Okano, M. Fujita, *J. Am. Chem. Soc.* **2003**, *125*, 3243; c) T. Kusukawa, T. Nakai, T. Okano, M. Fujita, *Chem. Lett.* **2003**, *32*, 284.

[5] I. M. Müller, R. Robson, F. Separovic, *Angew. Chem.* **2001**, *113*, 4519; *Angew. Chem. Int. Ed.* **2001**, *40*, 4385.

[6] I. M. Müller, D. Möller, *Eur. J. Inorg. Chem.* **2004**, in press.

 © 2005 Wiley-VCH Verlag GmbH & Co. KGaA, Weinheim

[7] Experimental details are given in the Supporting Information. $0.16\times0.19\times0.25\ mm^3$, orthorhombic, *Pbcn*, $a=28.649(6)$, $b=15.133(3)$, $c=15.739(3)$ Å, $V=6823(2)$ Å^3, $\rho_{calcd}=1.617\ g\,cm^{-3}$, $2\theta_{max}=62.08°$, $\lambda=0.71073$ Å, $T=100$ K, 63876 measured reflections, 10825 independent reflections ($R_{int}=0.0701$), 7685 observed reflections ($I>2\sigma(I)$), $\mu=3.673\ mm^{-1}$, numerical absorption correction, $T_{min}=0.460$, $T_{max}=0.591$, 406 parameters, $R_1(I>2\sigma(I))=0.0492$, wR_2(all data) $=0.0856$, max./min. residual electron density 0.63/−0.48 e Å^{-3}.[13]

[8] Experimental details are given in the Supporting Information. $0.24\times0.18\times0.14\ mm^3$, triclinic, $P\bar{1}$, $a=16.437(7)$, $b=16.746(6)$, $c=16.889(7)$ Å, $\alpha=80.529(9)$, $\beta=74.212(5)$, $\gamma=61.36(1)°$, $V=3923(3)$ Å^3, $\rho_{calcd}=1.633\ g\,cm^{-3}$, $2\theta_{max=}47.50°$, $\lambda=0.71073$ Å, $T=213$ K, 18324 measured reflections, 11762 independent reflections ($R_{int}=0.0805$), 5118 observed reflections ($I>2\sigma(I)$), $\mu=3.534\ mm^{-1}$, empirical absorption correction, $T_{min}=0.472$, $T_{max}=0.608$, 560 parameters, $R_1(I>2\sigma(I))=0.0767$, wR_2(all data) $=0.1947$, max./min. residual electron density 0.76/−0.97 e Å^{-3}.[13] Owing to the weak scattering power of **1b**, the large number of solvent molecules and the poor reflection to parameter ratio, all solvent molecules as well as the phenyl groups were refined isotropically. The bond lengths in the solvent molecules were fixed to literature values.

[9] Experimental details are given in the Supporting Information. $0.08\times0.14\times0.14\ mm^3$, triclinic, $P\bar{1}$, $a=19.7629(1)$, $b=31.7856(1)$, $c=34.1879(2)$ Å, $\alpha=107.491(2)$, $\beta=94.548(2)$, $\gamma=96.091(2)°$, $V=20227.0(2)$ Å^3, $\rho_{calcd}=1.748\ g\,cm^{-3}$, $2\theta_{max}=50.50°$, $\lambda=0.71073$ Å, $T=100$ K, 248756 measured reflections, 73078 independent reflections ($R_{int}=0.0697$), 50612 observed reflections ($I>2\sigma(I)$), $\mu=3.819\ mm^{-1}$, empirical absorption correction, $T_{min}=0.597$, $T_{max}=0.732$, 3026 parameters, $R_1(I>2\sigma(I))=0.0634$, wR_2(all data) $=0.1984$, max./min. residual electron density 1.07/−1.14 e Å^{-3}.[13]

[10] Experimental details are given in the Supporting Information. $0.15\times0.19\times0.19\ mm^3$, trigonal, *R*3*c*, $a=34.764(1)$, $c=94.689(1)$ Å, $V=99102(1)$ Å^3, $\rho_{calcd}=1.664\ g\,cm^{-3}$, $2\theta_{max}=47.74°$, $\lambda=0.71073$ Å, $T=100$ K, 140050 measured reflections, 28466 independent reflections ($R_{int}=0.0517$), 26602 observed reflections ($I>2\sigma(I)$), $\mu=3.520\ mm^{-1}$, numerical absorption correction, $T_{min}=0.476$, $T_{max}=0.571$, 1476 parameters, $R_1(I>2\sigma(I))=0.0585$, wR_2(all data) $=0.1553$, max./min. residual electron density 1.38/−1.00 e Å^{-3}.[13]

[11] Experimental details are given in the Supporting Information. $0.10\times0.19\times0.22\ mm^3$, monoclinic, *C*2/*c*, $a=65.484(1)$, $b=20.4154(4)$, $c=33.0347(6)$ Å, $\beta=113.215(1)°$, $V=40588(1)$ Å^3, $\rho_{calcd}=1.703\ g\,cm^{-3}$, $2\theta_{max}=50.50°$, $\lambda=0.71073$ Å, $T=100$ K, 128167 measured reflections, 36682 independent reflections ($R_{int}=0.0381$), 27665 observed reflections ($I>2\sigma(I)$), $\mu=3.805\ mm^{-1}$, numerical absorption correction, $T_{min}=0.470$, $T_{max}=0.683$, 1499 parameters, $R_1(I>2\sigma(I))=0.0510$, wR_2(all data) $=0.1630$, max./min. residual electron density 0.94/−1.10 e Å^{-3}.[13]

[12] a) S. Sakamoto, M. Fujita, K. Kim, K. Yamaguchi, *Tetrahedron* **2000**, *56*, 955; b) C. A. Schalley, T. Müller, P. Linnartz, M. Witt, M. Schäfer, A. Lützen, *Chem. Eur. J.* **2002**, *8*, 3538; reviews: c) C. A. Schalley, *Int. J. Mass Spectrom.* **2000**, *194*, 11; d) C. A. Schalley, *Mass Spectrom. Rev.* **2001**, *20*, 253.

[13] CCDC-248614–248618 contain the supplementary crystallographic data for this paper. These data can be obtained free of charge via www.ccdc.cam.ac.uk/conts/retrieving.html (or from the Cambridge Crystallographic Data Centre, 12 Union Road, Cambridge CB2 1EZ, UK; fax: (+44) 1223-336-033; or deposit@ccdc.cam.ac.uk).

 © 2005 Wiley-VCH Verlag GmbH & Co. KGaA, Weinheim

Single-Molecule Studies

Supramolecular Chemistry at the Single-Molecule Level**

Rainer Eckel, Robert Ros, Björn Decker, Jochen Mattay, and Dario Anselmetti**

In supramolecular chemistry[1] synthetically designed organic constituents interact noncovalently, in a directed and specific way to form host–guest complexes of higher complexity. The ability to tailor the molecular interplay with respect of chemical design, specificity, and molecular switching opens up the development of new molecular materials for artificial molecular recognition, molecular organization, and self-assembly. We have used mechanical single-molecule force spectroscopy to investigate the binding of individual resorc-[4]arene–ligand host–guest complexes. By using diluted samples of the host and guest molecules that are modified with a long linker which is attached to an atomic force microscope (AFM) tip, we were able to prevent multiple binding and to observe single host–guest unbinding events in a supramolecular system for the first time. The molecular binding forces, their dependence on external loading rates, the rate of dissociation, and the molecular cavity length directly relate to the molecular properties of the supramolecular species and are consistent with an activated decay of a metastable bound state, a finding already established for biological receptor–ligand complexes. This result allows new insights into the mechanisms, kinetics, and thermodynamics of intermolecular association in chemistry and biology, and opens new possibilities in the investigation, design, and development of synthetic receptor systems.

Calixarenes are model receptor systems providing synthetic receptor cavities for the inclusion of small cationic guests, such as alkali-metal or ammonium ions.[2–5] Organic cations, such as ammonium ions, play a significant role in molecular recognition processes in nature (e.g. in protein side chains). Calix[*n*]arenes, generally, are a class of macrocyclic compounds formed by the base-catalyzed condensation of *n*-phenol derivatives and formaldehyde.[2,3] The resorc[4]arenes[6,7] considered herein are calixarenes formed from four

[*] Dipl.-Chem. R. Eckel, Priv.-Doz. Dr. R. Ros, Prof. Dr. D. Anselmetti
Experimental Biophysics and Applied Nanoscience
Bielefeld University
Universitätsstrasse 25, 33615 Bielefeld (Germany)
Fax: (+49) 521-106-2959
E-mail: dario.anselmetti@physik.uni-bielefeld.de

Dipl.-Chem. B. Decker, Prof. Dr. J. Mattay
Organic Chemistry
Bielefeld University
Universitätsstrasse 25, 33615 Bielefeld (Germany)
Fax: (+49) 521-106-6417
E-mail: mattay@uni-bielefeld.de

[**] Financial support from the Deutsche Forschungsgemeinschaft (SFB 613) is gratefully acknowledged.

Supporting information for this article is available on the WWW under http://www.angewandte.org or from the author.

 © 2005 Wiley-VCH Verlag GmbH & Co. KGaA, Weinheim DOI: 10.1002/anie.200461382

resorcinol building blocks linked by methine groups. This structure leaves degrees of freedom for rotation around the methine C–C bonds, which results in five discernible conformations: crown (C_{4v}), boat (C_{2v}), chair (C_{2h}), diamond (C_s), and saddle (D_{2d}). A means to constrain this conformational flexibility in resorc[4]arenes is to link the hydroxy groups at the upper rim of the molecule, to form ether bridges. In this way, the molecule is fixed in the crown conformation, a so-called cavitand,[8] and the rigid cavity of this host serves as a template for the inclusion of small guest ions. The binding of cations to the resorc[4]arene cavitand is facilitated by ion–dipole interactions, although hydrogen bonds and cation–π interactions between the positive charge of the ion and the cavitand with the aromatic rings also have considerable influence.[9] The specificity of the binding is governed by the steric complementarity of the host and guest: only cations small enough to fit into the tailored cavity are recognized by the resorc[4]arene cavitand receptor. In our experiments the 2,8,14,20-tetra-(10-(decylthio)decyl) cavitand, which has a calculated cavity width of 0.7 nm, serves as a host and its specific recognition of ammonium ions and ammonium-ion derivatives is tested (Figure 1).[9]

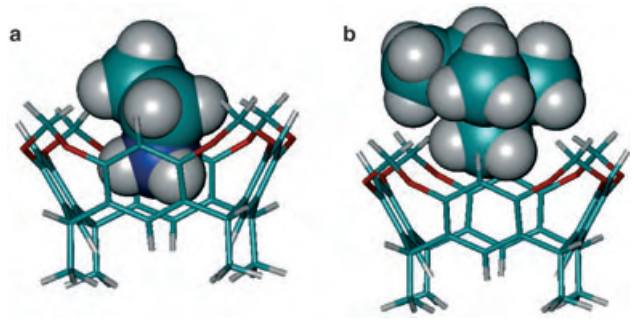


Figure 1. Gas-phase structure for the complex formed by the cavitand with a) an ethyl ammonium ion and b) an ethyl trimethyl ammonium ion. Structure optimized at the B3LPY/3-21G* level.

To investigate these interactions we applied single-molecule force spectroscopy, a method which uses the deflection of an AFM cantilever to measure minute forces in the pico-Newton (pN) range under physiological conditions. In combination with its sub-nanometer spatial resolution, single-molecule force spectroscopy provides, in contrast to standard ensemble experiments, a potent tool to address and manipulate single molecules and investigate forces within and between individual molecules, to yield information about the molecular energy landscape. During the last fifteen years, AFM spectroscopy and related single-molecule techniques based on ultra-sensitive force probes have found applications in the study of molecular recognition and of the specific bond formation in a variety of systems, such as biotin–streptavidin/avidin,[10,11] antibody–antigen,[12–15] selectin–ligand,[16] DNA–protein,[17] between individual strands of DNA,[18,19] and cell-adhesion proteoglycans.[20]

Similarly, host–guest interactions in supramolecular systems have been investigated on β-cyclodextrin–ferrocene[21–23] and [18]crown-6–ammonium systems.[24,25] In both cases single-molecule host–guest interaction could only be identified by a statistical analysis of the measured force distribution histograms, however, with no evidence of a loading-rate-dependent force spectrum, which could account for a thermally driven unbinding and give access to the energy landscape of this interaction. In contrast to these experiments, we used diluted cavitand monolayers on a gold surface in a 1:40 mixture with didecylsulfide. The guest ions (ammonium, trimethyl ammonium, and triethyl ammonium, each carrying one additional functional group) were covalently attached to the AFM tip with a flexible poly(ethylene glycol) (PEG) linker (Figure 2). This method introduces more steric flexibility which facilitates complex formation and supports binding of a single host–guest pair and its proper identification. The functionalized AFM tip was repetitively approached to and retracted from the cavitand surface (in ethanol) at an adjustable but constant velocity.

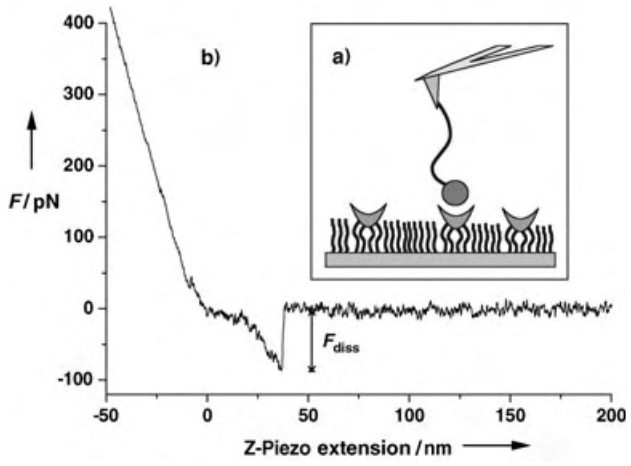


Figure 2. Force spectroscopy: a) schematic setup. The cavitand is immobilized together with didecylsulfide in a 1:40 mixture on a gold substrate. The (tetraorganyl) ammonium residue (shaded circle), is attached to an Si_3N_4 AFM tip by a flexible polymer linker. b) Typical force–distance curve (only retractive trace shown). The stretching of the PEG linker over a certain distance prior to bond rupture (tip detachment and relaxation of the cantilever) indicates an unbinding event.

Molecular unbinding events could be identified by plotting the force response of the AFM cantilever against the z-position of the piezo actuator (of the cavitand surface; Figure 2). The elastic stretching of the PEG spacer before the point of detachment, which shows an elasticity curve in accordance with the wormlike-chain polymer-elasticity model, served as the criterion to discriminate real single-binding events from unspecific adhesion. Since the molecular unbinding process is of stochastic nature, rupture forces from many rupture events (typically 200) were compiled in a force histogram. The mean value resulting from a single-nodal Gaussian fit to the histogram distribution is the most probable unbinding force. The experimental error is based on the statistical error (standard variation) and the uncertainty in the effective spring constant of the cantilever; the errors given

 © 2005 Wiley-VCH Verlag GmbH & Co. KGaA, Weinheim

below for the thermal dissociation (off rate) at zero force and the width of the binding pocket are derived from these values by error propagation.

Figure 3 shows three force histograms for the binding of the cavitand to ammonium, trimethyl ammonium, and triethyl ammonium residues and the corresponding competition experiments. The total unbinding probability (that is, the total number of identified rupture events divided by the number of approach–retract cycles) for the ammonium and trimethyl ammonium residues both amount to approximately 25%. As a control experiment for validating the specificity of the host–guest interaction, free ammonium or tetramethyl ammonium ions were added to the solvent as competing ligands. In both cases the total (integrated) unbinding probability was significantly reduced. The effect was stronger for solvent saturated with the tetramethyl ammonium ion (Figure 3b,e). After washing tip and sample again with the original solvent (ethanol without competitor), the systems could be reactivated to their full former unbinding functionality (Figure 3c,f). This effect of the free ions competing with the modified ions linked to the AFM tip demonstrates the specificity of the molecular recognition between the host and guest.

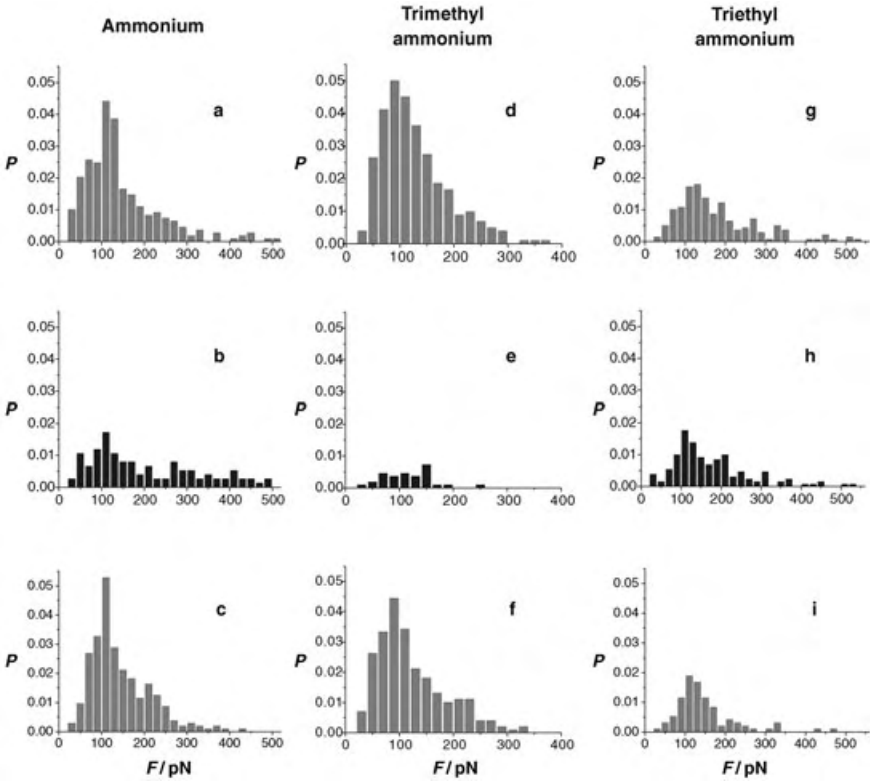


Figure 3. Force spectroscopy experiments in ethanol (a,d,g), in ethanol saturated with the respective free ions (b,e,h), washing with ethanol restored the original unbinding probability *P* (c,f,i).

For the triethyl ammonium residue, the results are different. From Figure 3, it can be seen that the integrated unbinding probability is much lower for this system than for the ammonium or tetramethyl ammonium ions, whereas the rupture force was comparable. Moreover, changing the solvent to ethanol saturated with competitor ion did not lead to a significant reduction of the total unbinding probability (Figure 3h), and also washing with pure ethanol again did not lead to a change (Figure 3i). These findings correlate with the fact that the triethyl ammonium residue, which has a calculated diameter of 0.8 nm, clearly exceeds the receptor cavity diameter of the resorc[4]arene cavitand: Our single-molecule experiments strongly indicate the specific and selective nature of this host–guest interaction.

According to the thermally driven unbinding theory of an activated decay of a metastable bound state[26,27] the measured forces are not constant and depend on the temporal force evolution on the molecular complex, which is referred to as the loading rate, and can be calculated from the experimental velocity multiplied by the molecular elasticity. The elasticity of the molecular system was obtained from the slope of the force–distance curves (corrected for molecular extension) for the last 20 data points prior to detachment of the cantilever. The loading rate then was given by the system elasticity multiplied by the retract velocity.

With dynamic force spectroscopy (force-loading-rate plots) details about the kinetics of the binding and information concerning the length scale of the interaction can be extracted. The results for the natural thermal off-rates are presented in Figure 4, yielding $k_{off} = (0.99 \pm 0.81)\ s^{-1}$ for the ammonium and $k_{off} = (1.87 \pm 0.75) \times 10^{-2}\ s^{-1}$ for the trimethyl ammonium residue, resulting in a bond lifetime of $\tau = 1.01$ s (for the ammonium residue) and $\tau = 53.5$ s (trimethyl ammonium residue). This finding, together with the results of the competition experiments, indicate that the trimethyl ammonium residue fits more

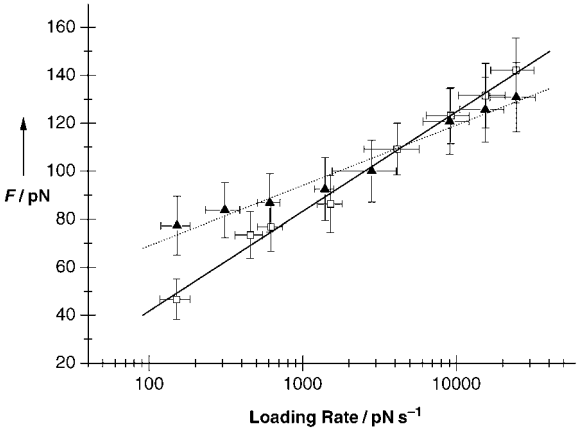


Figure 4. The unbinding forces, plotted logarithmically against the corresponding loading rates, for the binding of the ammonium (□) and trimethyl ammonium (▲) residues to the resorc[4]arene cavitand. For details see text.

 © 2005 Wiley-VCH Verlag GmbH & Co. KGaA, Weinheim

tightly into the receptor cavity, that is, its complexation is accompanied by a greater rise in binding affinity than for ammonium. In receptor–ligand interactions, the interaction affinity (equilibrium constant of dissociation $K_{diss} = k_{off}/k_{on}$) is mostly dominated (and varied) by the reaction off-rate k_{off}, whereas the values for the reaction on-rate k_{on} do not exhibit such a drastic variation.[13] Assuming a diffusion-limited association with a typical on-rate for a ligand binding to a receptor pocket of $k_{on} = 10^5\,\text{M}^{-1}\,\text{s}^{-1}$,[13,28] we can deduce equilibrium constants of $K_{diss} = 0.99\ \text{s}^{-1}/10^5\,\text{M}^{-1}\,\text{s}^{-1} \approx 10^{-5}\,\text{M}$ for ammonium ions and $K_{diss} = 2\times10^{-2}\ \text{s}^{-1}/10^5\,\text{M}^{-1}\,\text{s}^{-1} = 2\times10^{-7}\,\text{M}$ for trimethyl ammonium ions. From the equilibrium constants for these host–guest systems the Gibbs' free energy difference $\Delta G = RT\ln K_{diss}$ can be derived, which gives a rough estimate of the related binding energies of $\Delta G \approx -28\ \text{kJ mol}^{-1}$ (ammonium) and $\Delta G \approx -38\ \text{kJ mol}^{-1}$ (trimethyl ammonium). These values for ΔG correspond well with calorimetric or NMR spectroscopic data obtained for related supramolecular systems, such as cyclodextrins[23,29] and water-soluble cavitands.[30] This aspect is important for two reasons: 1) it shows that AFM force spectroscopy can be used to investigate single-molecule affinity interactions in a broad affinity range of ten orders of magnitude ($10^{-15}\,\text{M}$ (biotin–streptavidin) to $10^{-5}\,\text{M}$ (this work)), and 2) that this technique allows the estimation of equilibration constants and related binding energies of single (supra)molecular complexes. This factor is of broad interest, since a determination of reaction equilibrium constants and associated binding energies of ionic binding partners with a wide variation in solubility, for example, by NMR spectroscopic titration experiments, is extremely difficult to accomplish, and no corresponding values for our system are known to us.

From the inverse slope of the loading-rate dependency the molecular reaction lengths (width of binding pocket) can be extracted yielding $x_\beta = (0.22 \pm 0.04)$ nm for ammonium, and $x_\beta = (0.38 \pm 0.06)$ nm for the trimethyl ammonium ions. These values are qualitatively comparable with calculated van der Waals diameters of 0.3 nm for ammonium and 0.6 nm for trimethyl ammonium.[9] Therefore we can conclude that the steric complementarity of the host and guest plays an important role in the interaction, with cation–π interactions contributing considerably to the molecular binding mechanism. This finding is also consistent for the interaction of the trimethyl ammonium residue with the cavitand because a the positive-charge distribution has been shown to reside on the hydrogen atoms of the methyl groups.[31,31]

In summary, we could show that the specific interaction and dissociation of single guest molecules and their host receptors in supramolecular systems are consistent with an activated decay of a metastable bound state and obey the laws of thermally driven unbinding, as predicted theoretically and verified in biological ligand–receptor systems. The measured reaction lengths were compatible with the calculated van der Waals diameters of the corresponding guest ligands, and give a rough estimate of how deep a ligand enters the receptor site of a calixarene cavitand. The measured single-molecule kinetic reaction rates are consistent with the expected nature of a moderate-affinity host–guest interaction, whereas a clear affinity ranking between the probed host ligands by single-molecule force spectroscopy was possible for the first time.

Received: July 21, 2004

Keywords: atomic force microscopy · calixarenes · host–guest systems · single molecules · supramolecular chemistry

[1] a) J.-M. Lehn, *Supramolecular Chemistry*, VCH, Weinheim, **1995**; b) F. Vögtle, *Supramolecular Chemistry*, Wiley, Chichester, **1991**; c) J. L. Atwood, J. E. D. Davies, D. D. Macnicol, F. Vögtle, J.-M. Lehn, *Comprehensive Supramolecular Chemistry*, Pergamon, New York, **1996**; d) J. W. Steed, J. L. Atwood, *Supramolecular Chemistry*, Wiley, Chichester, **2000**; e) E. Fischer, *Ber. Dtsch. Chem. Ges.* **1894**, *27*, 2985–2993; f) P. Ehrlich, *Klin. Jahrb.* **1897**, *6*, 299–326; g) A. Werner, *Ber. Dtsch. Chem. Ges.* **1907**, *40*, 15–69.

[2] C. D. Gutsche, *Calixarenes*, Royal Society of Chemistry, Cambridge, **1989**.

[3] C. D. Gutsche, *Calixarenes Revisited*, Royal Society of Chemistry, Cambridge, **1998**.

[4] J. Vicens, V. Böhmer, *Calixarenes. A Versatile Class of Macrocyclic Compounds*, Kluwer, Dordrecht, **1991**.

[5] L. Mandolini, R. Ungaro, *Calixarenes in Action*, Imperial College Press, London, **2000**.

[6] V. Böhmer, *Angew. Chem.* **1995**, *107*, 785–818; *Angew. Chem. Int. Ed. Engl.* **1995**, *34*, 713-745.

[7] P. Timmerman, W. Verboom, D. N. Reinhoudt, *Tetrahedron* **1996**, *52*, 2663–2704.

[8] D. J. Cram, S. Karbach, H. E. Kim, C. B. Knobler, E. F. Maverick, J. L. Ericson, R. C. Helgeson, *J. Am. Chem. Soc.* **1988**, *110*, 2229–2237.

[9] A. B. Rozhenko, W. W. Schoeller, M. C. Letzel, B. Decker, C. Agena, J. Mattay, unpublished results.

[10] G. U. Lee, D. A. Kidwell, R. J. Colton, *Langmuir* **1994**, *10*, 354–357.

[11] E.-L. Florin, V. T. Moy, H. E. Gaub, *Science* **1994**, *264*, 415–417.

[12] P. Hinterdorfer, W. Baumgartner, H. Gruber, K. Schilcher, H. Schindler, *Proc. Natl. Acad. Sci. USA* **1996**, *93*, 3477–3481.

[13] F. Schwesinger, R. Ros, T. Strunz, D. Anselmetti, H.-J. Güntherodt, A. Honegger, L. Jermutus, L. Tiefenauer, A. Plückthun, *Proc. Natl. Acad. Sci. USA* **2000**, *97*, 9972–9977.

[14] U. Dammer, M. Hegner, D. Anselmetti, P. Wagner, M. Dreier, W. Huber, H.-J. Güntherodt, *Biophys. J.* **1996**, *70*, 2437–2441.

[15] R. Ros, F. Schwesinger, D. Anselmetti, M. Kubon, R. Schäfer, A. Plückthun, L. Tiefenauer, *Proc. Natl. Acad. Sci. USA* **1998**, *95*, 7402–7405.

[16] J. Fritz, A. G. Katopodis, F. Kolbinger, D. Anselmetti, *Proc. Natl. Acad. Sci. USA* **1998**, *95*, 12283–12288.

[17] F. W. Bartels, B. Baumgarth, D. Anselmetti, R. Ros, A. Becker, *J. Struct. Biol.* **2003**, *143*, 145–152.

[18] G. U. Lee, L. A. Chrisey, R. J. Colton, *Science* **1994**, *266*, 771–773.

[19] T. Strunz, K. Oroszlan, R. Schäfer, H.-J. Güntherodt, *Proc. Natl. Acad. Sci. USA* **1999**, *96*, 11277–11282.

[20] U. Dammer, O. Popescu, P. Wagner, D. Anselmetti, H.-J. Güntherodt, G. N. Misevic, *Science* **1995**, *267*, 1173–1175.

[21] H. Schönherr, M. W. J. Beulen, J. Bügler, J. Huskens, F. C. J. M. van Veggel, D. N. Reinhoudt, G. J. Vancso, *J. Am. Chem. Soc.* **2000**, *122*, 4963–4967.

[22] S. Zapotoczny, T. Auletta, M. R. de Jong, H. Schönherr, J. Huskens, F. C. J. M. van Veggel, D. N. Reinhoudt, G. J. Vancso, *Langmuir* **2002**, *18*, 6988–6994.

[23] T. Auletta, M. R. de Jong, A. Mulder, F. C. J. M. van Veggel, J. Huskens, D. N. Reinhoudt, S. Zou, S. Zapotoczny, H. Schönherr,

 © 2005 Wiley-VCH Verlag GmbH & Co. KGaA, Weinheim

G. J. Vancso, L. Kuipers, *J. Am. Chem. Soc.* **2004**, *126*, 1577 – 1584.
[24] S. Kado, K. Kimura, *J. Am. Chem. Soc.* **2003**, *125*, 4560 – 4564.
[25] S. Kado, K. Yamada, K. Kimura, *Langmuir* **2004**, *20*, 3259 – 3263.
[26] G. I. Bell, *Science* **1978**, *200*, 618 – 627.
[27] E. Evans, K. Ritchie, *Biophys. J.* **1997**, *72*, 1541 – 1555.
[28] M. Schlosshauer, D. Baker, *Protein Sci.* **2004**, *13*, 1660 – 1669.
[29] L. A. Godínez, L. Schwartz, C. M. Criss, A. E. Kaifer, *J. Phys. Chem. B* **1997**, *101*, 3376 – 3380.
[30] T. Haino, D. M. Rudkevich, A. Shivanyuk, K. Rissanen, J. Rebek, Jr., *Chem. Eur. J.* **2000**, *6*, 3797 – 3805.
[31] C. A. Deakyne, M. Meot-Ner (Mautner), *J. Am. Chem. Soc.* **1985**, *107*, 474 – 479.
[32] H. J. Schneider, T. Schiestel, P. Zimmermann, *J. Am. Chem. Soc.* **1992**, *114*, 7698 – 7703.

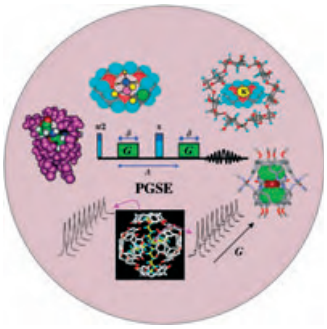
 © 2005 Wiley-VCH Verlag GmbH & Co. KGaA, Weinheim

Cover Picture

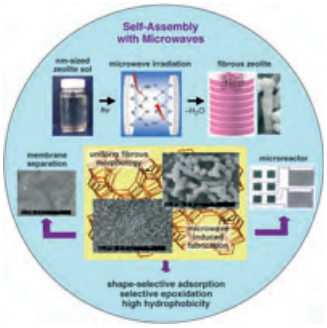


Kelly Velonia,* Ophir Flomenbom, Davey Loos, Sadahiro Masuo, Mircea Cotlet, Yves Engelborghs, Johan Hofkens,* Alan E. Rowan,* Joseph Klafter, Roeland J. M. Nolte, and Frans C. de Schryver

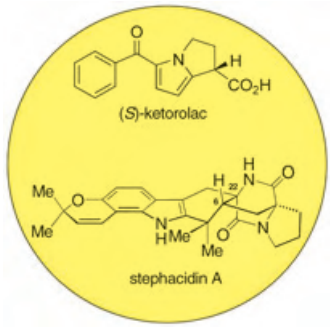
Direct observation of the real-time kinetics at a single enzyme level is possible. The cover picture background shows a confocal fluorescent microscope image obtained after addition of a profluorescent substrate to a CALB-enzyme-decorated surface. The fluorescence emission of a single enzyme molecule as a function of time is shown in red. As described by K. Velonia, J. Hofkens, A. E. Rowan et al. in their Communication on page 560 ff., this method reveals aspects of the catalytic behavior which are hidden in ensemble measurements.



NMR Spectroscopy
Diffusion NMR spectroscopy is a simple method for the simultaneous investigation of several substances in supramolecular and combinatorial chemistry. Y. Cohen, L. Avram, and L. Frish describe more about this in their Review on page 520 ff.



Microporous Materials
MFI Zeolites fabricated with microwave irradiation form a fibrous structure with interesting properties, as described by J.-S. Chang, S.-E. Park et al. in their Communication on page 556 ff.



Asymmetric Syntheses
P. S. Baran and co-workers have developed short enantioselective syntheses for the antiinflammatory drug (*S*)-ketorolac and the natural product stephacidin A. In their Communications on page 606 ff. and page 609 ff., the advantages of the new routes are discussed.

Contents

VIP ***The following Communications have been judged by at least two referees to be "very important papers" and will be published online at www.angewandte.org soon:***

D. Enders, C. Grondal*
Direct Organocatalytic de novo Synthesis of Carbohydrates

*T. Fink, H. Bruggesser, J.-L. Reymond**
Virtual Exploration of the Small-Molecule Chemical Universe Below 160 Daltons

S. Kobayashi, K. Arai, H. Shimizu, Y. Ihori, H. Ishitani, Y. Yamashita*
A Bimetallic Chiral Niobium Complex for Lewis Acid Catalyzed Enantioselective Reactions: Design of a Tridentate Ligand and Elucidation of the Catalyst Structure

H. Braunschweig, K. Radacki, D. Rais, G. R. Whittell*
The First Boryl-Bridged Complex: An Unprecedented Coordination Mode of the BR_2 Ligand

C. Whitehouse, J. Fang, A. Aggeli, M. Bell, R. Brydson, C. W. G. Fishwick, J. Henderson, C. M. Knobler, R. W. Owens, N. H. Thomson, D. A. Smith, N. Boden**
Adsorption and Self-Assembly of Peptides on Mica Substrates

*You Seok Seo, C. Lee, K. H. Lee, K. B. Yoon**
1:1 and 2:1 Charge-Transfer Interactions between Aromatic Hydrocarbons and Dry Titanium Dioxide

News

R. Zare Receives Teaching Award — **510**

Distinction for G. Höfle — **510**

Franco-Spanish Prize to E. Carmona — ***510***

Books

Chemoinformatics — Jürgen Bajorath — *reviewed by G. Schneider* — ***511***

Chemical Biology — Herbert Waldmann, Petra Janning — *reviewed by H. Breyhan, T. Kolter* — ***511***

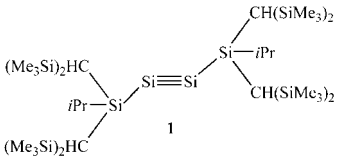
Highlights

Silicon Compounds

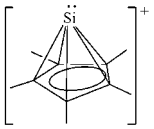
M. Weidenbruch* — **514–516**

Molecules with a Genuine Si–Si Triple Bond and a Stable Derivative of $[SiH]^+$

Bye bye multiple-bond rule: Recent successes in silicon chemistry are the silicon-containing compounds **1**, which has a Si–Si triple bond, and the $[(Me_5C_5)Si]^+$ ion **2**, which is a stable derivative of the $[HSi]^+$ ion. Both species are also notable from a bond-theory point of view and can be regarded as valuable starting materials for synthetic organosilicon chemistry.



1



2

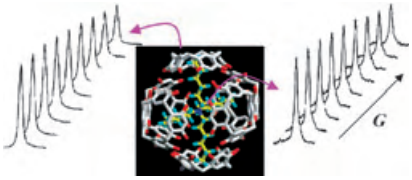
Reviews

Analytical Methods

Y. Cohen,* L. Avram, L. Frish — **520–554**

Diffusion NMR Spectroscopy in Supramolecular and Combinatorial Chemistry: An Old Parameter—New Insights

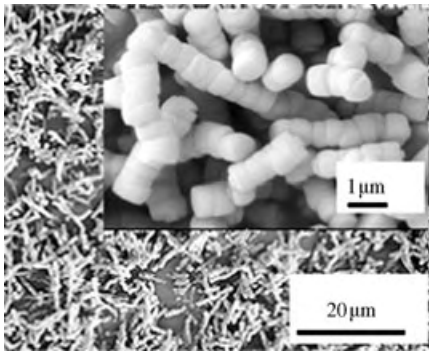
Finger on the pulse: Diffusion NMR spectroscopy, based on pulse gradient spin echo NMR experiments, is a valuable method for mapping molecular interactions at the molecular level in supramolecular and combinatorial chemistry. The decay of the NMR signals also enables, for example, information on the intermolecular interactions in host–guest systems to be obtained (see picture; G is the pulsed gradient strength).



© 2005 Wiley-VCH Verlag GmbH & Co. KGaA, Weinheim

Communications

Metal incorporation and synthesis of MFI zeolites with microwave irradiation result in crystal stacking in one direction to form a fibrous morphology (see images of the Ti-MFI zeolite). These materials display several interesting physicochemical properties including lower packing density and higher hydrophobicity than their non-fibrous counterparts, and as a result, enhanced catalytic properties and increased shape-selective adsorption.

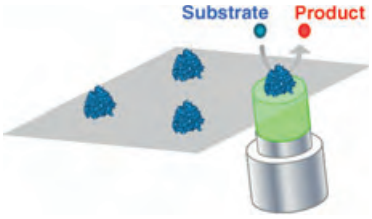


Zeolite Synthesis

Y. K. Hwang, J.-S. Chang,* S.-E. Park,* D. S. Kim, Y.-U. Kwon, S. H. Jhung, J.-S. Hwang, M. S. Park ——— **556 – 560**

Microwave Fabrication of MFI Zeolite Crystals with a Fibrous Morphology and Their Applications

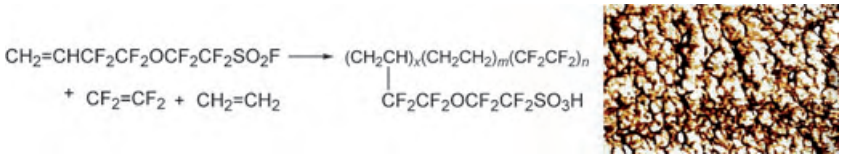
Real-time measurement of the catalysis and substrate kinetics of a single-enzyme hydrolysis reaction is demonstrated with confocal fluorescence microscopy (CFM; see picture, green = CFM beam). A single lipase is shown to have a broad range of conformations; each conformation contributes to the overall enzymatic activity, an observation that is often masked by ensemble measurements.



Single-Molecule Studies

K. Velonia,* O. Flomenbom, D. Loos, S. Masuo, M. Cotlet, Y. Engelborghs, J. Hofkens,* A. E. Rowan,* J. Klafter, R. J. M. Nolte, F. C. de Schryver ——— **560 – 564**

Single-Enzyme Kinetics of CALB-Catalyzed Hydrolysis



Excellent thermal stability and mechanical properties are exhibited by high-proton-conductive membranes synthesized by a facile copolymerization of tetrafluoroethylene, ethylene, and $CH_2{=}CHCF_2CF_2O$-$CF_2CF_2SO_2F$ (see scheme and AFM image). These membranes have been successfully used in a direct MeOH fuel cell.

Membranes

Z.-Y. Yang,* R. G. Rajendran ___ **564 – 567**

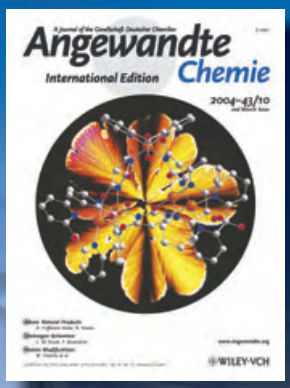
Copolymerization of Ethylene, Tetrafluoroethylene, and an Olefin-Containing Fluorosulfonyl Fluoride: Synthesis of High-Proton-Conductive Membranes for Fuel-Cell Applications

For the USA and Canada:
ANGEWANDTE CHEMIE International Edition (ISSN 1433-7851) is published weekly by Wiley-VCH PO Box 191161, D 69451 Weinheim, Germany. Air freight and mailing in the USA by Publications Expediting Inc. 200 Meacham Ave., Elmont, NY 11003. Periodicals postage paid at Jamaica NY 11431. US POSTMASTER: send address changes to *Angewandte Chemie*, Wiley-VCH, 111 River Street, Hoboken, NJ 07030. Annual subscription price for institutions: US$ 4948.00/4498.00 (valid for print and electronic / print or electronic delivery); for individuals who are personal members of a national chemical society, or whose institution already subscribes, or who are retired or self-employed consultants, print only: US$ 394.00. Postage and handling charges included. All Wiley-VCH prices are exclusive VAT.

 © 2005 Wiley-VCH Verlag GmbH & Co. KGaA, Weinheim

The best in chemistry –

for more than a hundred years



A Journal of the Gesellschaft Deutscher Chemiker

Angewandte International Edition **Chemie**

www.angewandte.org

1888: ***The beginning of a success story***

Constant Innovations

1962: *First issue of the International Edition*
1976: *Graphical abstracts*
1979: *Cover pictures*
1988: *Centenary of Angewandte*
1989: *Routine use of color*
1991: *New section: Highlights*
1992: *Computerized editorial tracking system*
1995: *Internet service for readers*
1998: *Regular press service; full-text online*
2000: *New section: Essays; EarlyView: Communications available online ahead of the printed version*
2001: *New section: Minireviews*
2002: *Online submission of manuscripts*
2003: *Weekly publication; new section: News; new layout*
2004: *Backfiles (1962-1997); ManuscriptXpress: Online system for authors and referees*



Angewandte's advisors...

Ulrich Stilz
Aventis, Frankfurt/Main

» With its interdisciplinary and international orientation ***Angewandte Chemie*** *has set the benchmark for publishing innovative results. The editorial team is acknowledged for the success of this renowned journal, that provides scientists with a unique forum, in which to discuss their discoveries. «*

Angewandte Chemie International Edition *is a journal of the German Chemical Society (GDCh)*

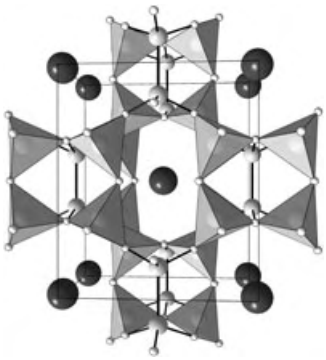
GDCh

WILEY InterScience® DISCOVER SOMETHING GREAT

WILEY-VCH

1198140_4_gu

Unlike any other known crystalline silicate, the reduced nitridosilicate $SrSi_6N_8$ contains Si—Si single bonds (see picture). The Si—Si distance is 235 pm, which precisely matches that in diamond-type silicon. The Si—Si unit is embedded in a framework of corner-sharing SiN_4 tetrahedra. Thus, Si^{4+} and Si^{3+} coexist within the same framework structure.

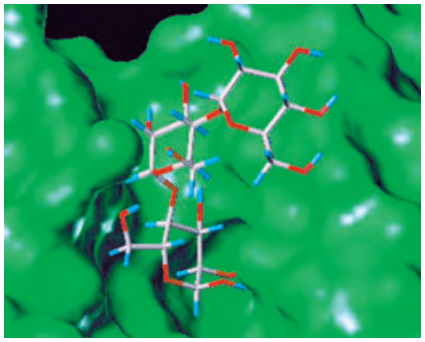


Silicates

F. Stadler, O. Oeckler, J. Senker, H. A. Höppe, P. Kroll, W. Schnick* _____ 567 – 570

$SrSi_6N_8$—A Reduced Nitridosilicate with a Si—Si Bond

Specificity in weak biomolecular interactions: A novel technique, cold-spray ionization, can detect the weak but specific noncovalent binding of carbohydrates to proteins, water, and to other carbohydrate molecules. It allows the determination of dissociation constants and can assist in computer simulations of putative receptor–ligand binding environments (see picture).

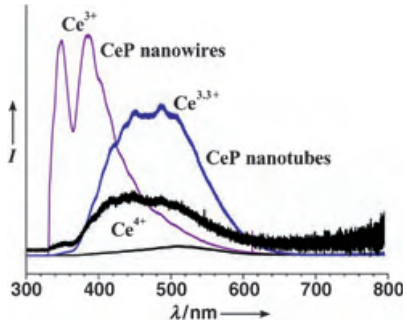


Biomolecular Interactions

S.-I. Nishimura,* N. Nagahori, K. Takaya, Y. Tachibana, N. Miura, K. Monde _____ 571 – 575

Direct Observation of Sugar–Protein, Sugar–Sugar, and Sugar–Water Complexes by Cold-Spray Ionization Time-of-Flight Mass Spectrometry

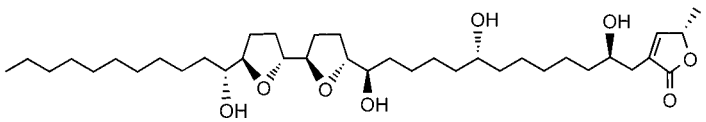
A strong blue emission is observed for hybrid Ce^{3+}/Ce^{4+} cerium phosphate nanotubes, whereas Ce^{3+} phosphate nanowires exhibit a characteristic double-peak UV luminescence (see picture). These cerium phosphate systems were obtained by annealing novel cerium(IV) phosphate nanotubes at different temperatures.



Nanomaterials

C. Tang,* Y. Bando, D. Golberg, R. Ma _____ 576 – 579

Cerium Phosphate Nanotubes: Synthesis, Valence State, and Optical Properties



1

Orthogonal and modular templating is an effective basis for the preparation of the biologically active annonaceous acetogenin 10-hydroxyasimicin (**1**). The versatile tartrate-derived 2,3-butanediacetal building block together with a highly diastereoselective hetero-Diels–Alder approach to the butenolide unit were usefully employed in this novel synthetic route.

Natural Products Synthesis

G. L. Nattrass, E. Díez, M. M. McLachlan, D. J. Dixon, S. V. Ley* _____ 580 – 584

The Total Synthesis of the Annonaceous Acetogenin 10-Hydroxyasimicin

 © 2005 Wiley-VCH Verlag GmbH & Co. KGaA, Weinheim

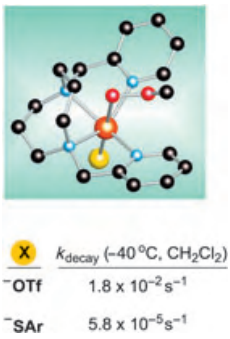
Contents

Bioinorganic Chemistry

M. R. Bukowski, H. L. Halfen, T. A. van den Berg, J. A. Halfen,* L. Que, Jr.* ——— **584 – 587**

Spin-State Rationale for the Peroxo-Stabilizing Role of the Thiolate Ligand in Superoxide Reductase

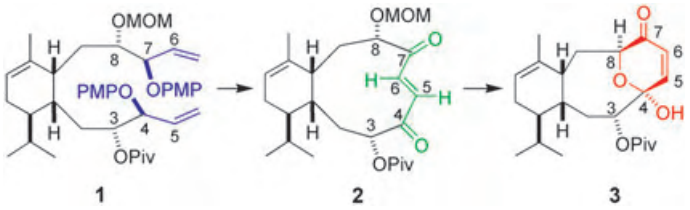
Anti-push: The axial thiolate ligand stabilizes high-spin Fe^{III}-OOR species (see picture) such as those found in superoxide reductase. This situation is in contrast to the "push effect" observed in structurally similar low-spin Fe^{III}-OOR systems, including cytochrome P450, which promote O–O bond cleavage. These results show how very similar enzyme-active sites can carry out two very different functions.



Antitumor Agents

D. Castoldi, L. Caggiano, L. Panigada, O. Sharon, A. M. Costa, C. Gennari* ——— **588 – 591**

A Formal Total Synthesis of Eleutherobin Through an Unprecedented Kinetically Controlled Ring-Closing-Metathesis Reaction of a Densely Functionalized Diene

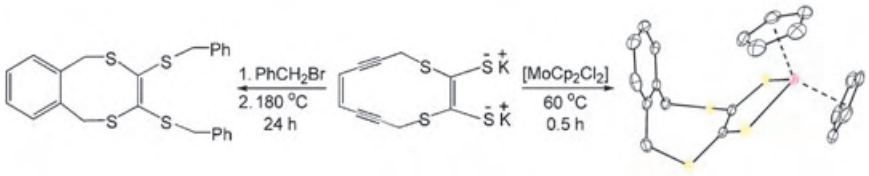


The key step in a formal total synthesis of eleutherobin was an unprecedented kinetically controlled RCM reaction of a densely functionalized diene **1** bearing two PMP-protected allylic alcohols in the presence of a second-generation Grubbs catalyst. Subsequent isomerization of the *E* 10-membered enedione **2** to the more stable *Z* isomer and cleavage of the MOM protecting group led to the known precursor **3**. MOM = methoxymethyl; PMP = *p*-methoxyphenyl.

Metal-Induced Cyclization

S. Bhattacharyya, M. Pink, M.-H. Baik,* J. M. Zaleski* ——— **592 – 595**

A Unique Approach to Metal-Induced Bergman Cyclization: Long-Range Enediyne Activation by Ligand-to-Metal Charge Transfer

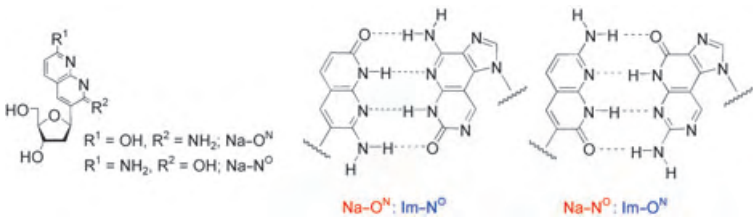


Dramatic differences are found in the temperatures at which Bergman cyclizations occur when Mo^{IV}–enedithiolate–enediyne complexes are used (see scheme; S: yellow, Mo: red), and this can be directly attributed to a long-range electronic polarization effect of the metal center. Ligand-to-metal charge transfer within the C_2S_4 substructure and differential charge repulsion in the transition state lead to a lowering of the barrier to cyclization.

Nonnatural Nucleotides

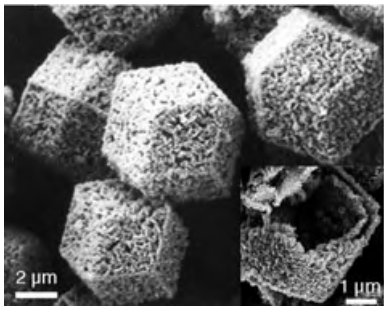
S. Hikishima, N. Minakawa,* K. Kuramoto, Y. Fujisawa, M. Ogawa, A. Matsuda* ——— **596 – 598**

Synthesis of 1,8-Naphthyridine C-Nucleosides and Their Base-Pairing Properties in Oligodeoxynucleotides: Thermally Stable Naphthyridine:Imidazopyridopyrimidine Base-Pairing Motifs



Out with the old, in with the new: Novel 1,8-naphthyridine C-nucleosides, Na-N^O and Na-O^N (see formulae), were synthesized through Heck coupling reactions. Oligodeoxynucleotides containing the Na-N^O and Na-O^N nucleosides formed extremely stable duplexes by the base-pairing motifs Na-N^O:Im-O^N and Na-O^N:Im-N^O.

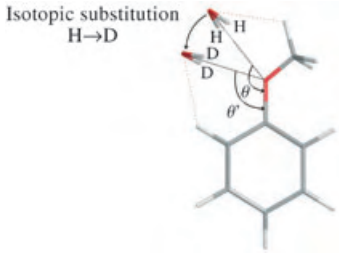
Through the reduction of micrometer-sized silver phosphate crystals with a perfect rhombododecahedral shape by a reaction/diffusion process to hierarchical, rhombododecahedral silver cages (see picture): The controlled self-assembly of silver particles around the precursor crystal surfaces leads to the formation of morphology-preserved single- or double-walled silver cages constructed from different building units.



Crystal Engineering

J. Yang, L. Qi,* C. Lu, J. Ma, H. Cheng ——— **598 – 603**

Morphosynthesis of Rhombododecahedral Silver Cages by Self-Assembly Coupled with Precursor Crystal Templating

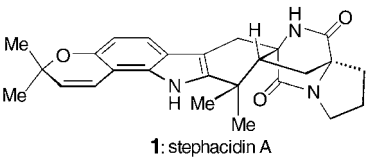


The deuteration of water produces the conformational change shown in the figure in the anisole···water complex. The value of the θ angle decreases from 138 to 128°, and the secondary interaction O···H_{Me} is replaced by O···H_{Ph}.

Molecular Dynamics

B. M. Giuliano, W. Caminati* ... **603 – 606**

Isotopomeric Conformational Change in Anisole–Water



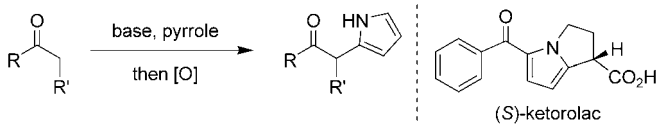
1: stephacidin A

A concise route to the heptacyclic indole alkaloid stephacidin A (**1**) includes a simple method for the gram-scale synthesis of substituted tryptophans, a remarkable indole annulation, and the first enolate coupling of an amide to an ester. This synthesis secures the relative configuration of the natural product and paves a potential path to several of its congeners.

Natural Products Synthesis

P. S. Baran,* C. A. Guerrero, N. B. Ambhaikar, B. D. Hafensteiner ——— **606 – 609**

Short, Enantioselective Total Synthesis of Stephacidin A



(*S*)-ketorolac

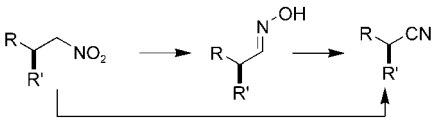
An odd couple: The union of pyrroles and carbonyl compounds (ketones, amides, esters, lactones, lactams, see scheme) is described, and by the use of an intramolecular variant of this new method, the nonsteroidal, anti-inflammatory drug (*S*)-ketorolac has been prepared in a short enantioselective synthesis. Mechanistic underpinnings of this reaction, which couples unfunctionalized C(sp^2) and C(sp^3) atoms, are also discussed.

Synthetic Methods

P. S. Baran,* J. M. Richter, D. W. Lin ——— **609 – 612**

Direct Coupling of Pyrroles with Carbonyl Compounds: Short Enantioselective Synthesis of (*S*)-Ketorolac

An environmentally friendly reaction that excludes the potential contamination of the products by metal impurities is reported. In this reaction, optically active aldoximes and nitriles are prepared from chiral nitroalkanes (see scheme). The methodology described expands the possibilities available for the conversion of nitroalkanes into valuable targets.



Organic Synthesis

C. Czekelius, E. M. Carreira* ... **612 – 615**

Convenient Transformation of Optically Active Nitroalkanes into Chiral Aldoximes and Nitriles

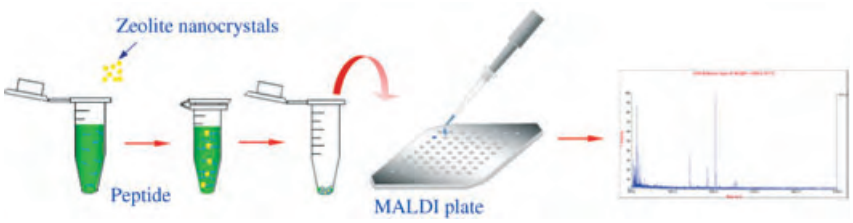
 © 2005 Wiley-VCH Verlag GmbH & Co. KGaA, Weinheim

Contents

Peptide Enrichment

Y. Zhang, X. Wang, W. Shan, B. Wu, H. Fan, X. Yu, Y. Tang,* P. Yang* ____ **615 – 617**

Enrichment of Low-Abundance Peptides and Proteins on Zeolite Nanocrystals for Direct MALDI-TOF MS Analysis

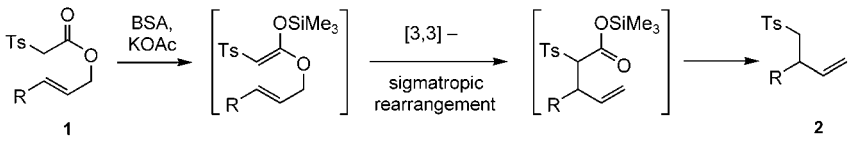


Concentrated efforts: A zeolite-nanocrystal-mediated enrichment procedure that doubles as a desalting step allows low-abundance proteins to be readily detected with MALDI-TOF MS (see picture). Mass spectral signal-to-noise ratios are greatly improved for a wide range of peptides, which underscores the potential of this procedure to boost proteomics research.

Homoallylic Sulfones

D. Bourgeois, D. Craig,* N. P. King, D. M. Mountford ____ **618 – 621**

Synthesis of Homoallylic Sulfones through a Decarboxylative Claisen Rearrangement Reaction

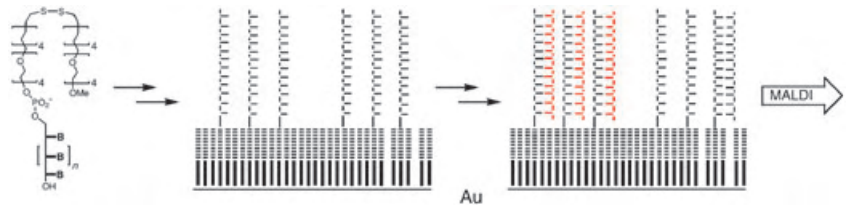


A high-yielding preparation of homoallylic sulfones **2** entails the treatment of allylic tosylacetate esters **1** with stoichiometric or substoichiometric quantities of BSA and substoichiometric quantities of KOAc under conventional thermal or microwave conditions. A possible mechanism involves silyl ketene acetal formation, [3,3]-sigmatropic rearrangement, and desilylation-decarboxylation. BSA = *N*,*O*-bis(trimethylsilyl)acetamide; Ts = *p*-toluenesulfonyl.

DNA Assays

U. Plutowski, C. Richert* ____ **621 – 625**

A Direct Glimpse of Cross-Hybridization: Background-Passified Microarrays That Allow Mass-Spectrometric Detection of Captured Oligonucleotides

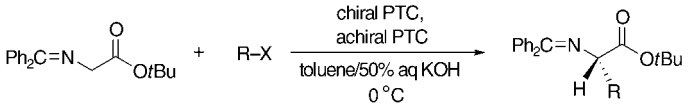


Oligonucleotides immobilized in SAMs (self-assembled monolayers) with a passifying surface layer, prepared from thermally smoothed gold surfaces and disulfides, allow the direct detection of bound strands by MALDI-TOF mass spectrometry. The binding of perfectly matched (PM) and mismatched (MM) DNA targets is observed (see picture). The extent to which cross-hybridization occurs depends on the type and position of the mismatch.

Phase-Transfer Catalysis

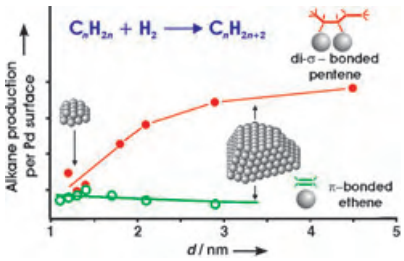
S. Shirakawa, K. Yamamoto, M. Kitamura, T. Ooi, K. Maruoka* ____ **625 – 628**

Dramatic Rate Enhancement of Asymmetric Phase-Transfer-Catalyzed Alkylations



The intervention of crown ethers or achiral quaternary ammonium salts as achiral phase-transfer catalysts (PTCs, see scheme) in a chiral PTC system leads to dramatic rate enhancements in the asymmetric alkylation of glycine derivatives.

 © 2005 Wiley-VCH Verlag GmbH & Co. KGaA, Weinheim



Size matters: The adsorption of *trans*-2-pentene on Pd/Al_2O_3 model catalysts exhibits site-specific behavior, which results in a strong increase in hydrogenation activity within the 1–5-nm particle size range, in contrast to ethene hydrogenation (see figure). The size effects are explained by the reactions proceeding via di-σ-bonded pentene, which is favored on the terrace sites of large particles, and π-bonded ethene.

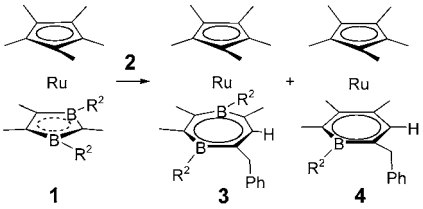
Hydrogenation

A. M. Doyle, S. K. Shaikhutdinov,* H.-J. Freund ——— **629 – 631**

Surface-Bonded Precursor Determines Particle Size Effects for Alkene Hydrogenation on Palladium

---

Away from the fold: Insertion of the terminal alkyne $PhCH_2C_2H$ (**2**) into the folded C_3B_2 heterocycle ($R^2 = CH_2SiMe_3$, Me) of the formal 16-valence-electron complexes **1** gives the 18-valence-electron boron-containing ruthenocene analogues **3** with a 4-borataborepine as 6π-electron ligand. Side products **4** and $C_6H_3(CH_2Ph)_3$ are detected by mass spectrometry. Compound **4** is formed directly as the only product when **1** is treated with R_2C_2 (R = Et, *p*-tolyl).



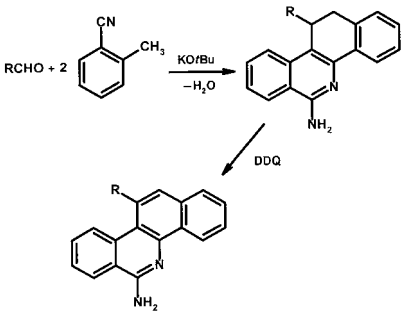
Metallocenes

Y. Nie, H. Pritzkow, C. Hu, T. Oeser, B. Bach, T. Müller, W. Siebert* **632 – 634**

Ruthenocene Analogues with a Novel C_5B_2 Ligand: (η^7-4-Borataborepine)(η^5-pentamethylcyclopentadienyl)ruthenium Complexes

---

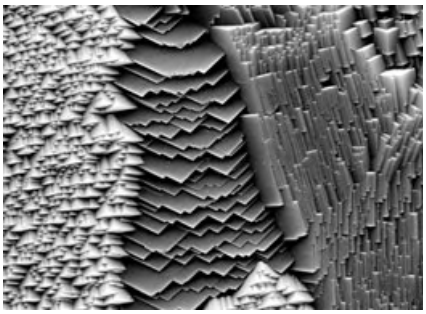
Lots, fast: Benzo[*c*]phenanthridine derivatives are prepared efficiently by the reaction of aldehydes and 2-methylbenzonitrile in the presence of potassium *tert*-butanolate, followed by dehydration (see scheme). Some of these compounds demonstrate excellent cytostatic activity, and it is possible to introduce substituents directly into the basic molecular ring system.



B. Clement,* M. Weide, U. Wolschendorf, I. Kock ——— **635 – 638**

A Two-Step Synthesis of Cytostatically Active Benzo[*c*]phenanthridine Derivatives

---



A striking similarity to the structure of mother-of-pearl (nacre) is displayed by the crystal architecture of highly oriented laminated $CaCO_3$ coatings (see scanning electron microscope image), which were prepared by a multistep procedure. A novel retardance imaging system (LC-PolScope) was employed to characterize the crystal texture of the polycrystalline thin films.

Biomineralization

D. Volkmer,* M. Harms, L. Gower, A. Ziegler ——— **639 – 644**

Morphosynthesis of Nacre-Type Laminated $CaCO_3$ Thin Films and Coatings

 © 2005 Wiley-VCH Verlag GmbH & Co. KGaA, Weinheim

Contents

"Hot Papers" are chosen by the Editors for their importance in a rapidly evolving field of high current interest. A preview with the graphical abstracts of these articles can be found on the *Angewandte Chemie* homepage in Wiley InterScience at www.angewandte.org.

All articles in *Angewandte Chemie* are published online up to several weeks ahead of print. They are found under the "EarlyView" link on the journal's homepage in Wiley InterScience.

Service

Keywords 646

Authors 647

Angewandte's Sister Journals 648 – 649

Preview 651

Corrigendum

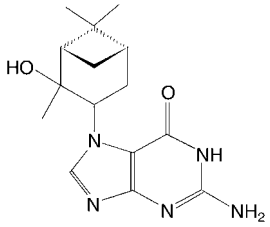
Mass Spectrometric Studies of DNA Adducts from a Reaction with Terpenoids**

W. Schrader,* S. Döring, W. Joppek — **6657–6660**

Angew. Chem. Int. Ed. **2004**, *43*

DOI 10.1002/anie.200461022

The structural formula of the N7-guanine adduct in the Table of Contents for this Communication contains an error. The correct structral formula is given below.



An Unusual Cyclization in a Bis(cysteinyl-*S*) Diiron Complex Related to the Active Site of Fe-Only Hydrogenases**

C. He, M. Wang,* X. Zhang, Z. Wang, C. Chen, J. Liu, B. Åkermark, L. Sun* — **3571–3574**

Angew. Chem. Int. Ed. **2004**, *43*

DOI 10.1002/anie.200453961

The authors wish to add the following sentence to the Acknowledgements: B. Å. and L. S. thank the Swedish Energy Agency and the Swedish Research Council for financial support.

 © 2005 Wiley-VCH Verlag GmbH & Co. KGaA, Weinheim



R. Zare Receives Teaching Award

Richard N. Zare, Professor in Natural Science at Stanford University (USA), received the 2004 James Flack Norris Award of the Northeastern Section of the American Chemical Society for outstanding achievement in teaching. His award speech was entitled "Chemical Fizzics: Seeing Chemistry in Action". Zare's research on laser chemistry has led to a better understanding of chemical reactions at the molecular level. His important experimental and theoretical contributions to our knowledge of molecular collision processes and to chemical analysis include the development of laser-induced fluorescence as a means to investigate reaction dynamics. He recently co-authored a Communication in *Angewandte Chemie* entitled "Continuous Two-Channel Time-of-Flight Mass Spectrometric Detection of Electrosprayed Ions" and an article in *ChemPhysChem* on the photon-counting histogram and one-photon excitation.[1] Zare is a member of the editorial advisory boards of these two journals and the author of a textbook on angular momentum in chemistry and physics.[1c]



R. N. Zare

Zare completed his PhD in chemical physics in 1964 at Harvard University (USA) under the guidance of D. Herschbach (Nobel Prize 1986) and then became assistant professor at the Massachusetts Institute of Technology (MIT, USA). From 1966 to 1969 he held joint appointments at the University of Colorado at Boulder in the departments of chemistry, physics, and astrophysics. He was appointed full professor at Columbia University in 1969 and moved to Stanford University in 1977.

Distinction for G. Höfle

Gerhard Höfle has been recognized with a Karl Heinz Beckurts Award for his work in the field of natural products synthesis along with Hans Reichenbach. The award is presented in memory of the physicist Karl Heinz Beckurts by the foundation of the same name of the Helmholtz Association of National Research Centers (in Germany). Beckurts worked at the nuclear research facilities in Karlsruhe und Jülich (Germany). From 1980 he was a member of the board of directors of Siemens AG. His commitment to nuclear energy made him a target for terrorism, and he died as a victim of a terrorist attack in 1986.



G. Höfle

Höfle completed his PhD in 1968 with W. Steglich at the Technische Hochschule München (Germany), undertook postdoctoral research with J. E. Baldwin at MIT, and completed his habilitation in 1975 at the Technische Universität Berlin (Germany) with F. Bohlmann. He has been director of the natural products chemistry section of the Gesellschaft für Biotechnologische Forschung in Braunschweig (Germany) since 1978 and extraordinary professor at the technical university there since 1983. The work of Höfle and Reichenbach on secondary metabolites from myxobacteria have enabled access to novel classes of natural products. Höfle discovered the epothilones: a class of natural products which are active against tumor cells that are resistant to other cytostatic drugs. An epothilone drug is currently in the final phase of clinical trials. Recently both prize winners reported in *Angewandte Chemie* on tubulysins from myxobacteria.[2] A Highlight by Höfle entitled "Long Sought The Bioactive Conformation of Epothilone and Its Binding in Tubulin" will appear soon in *Angewandte Chemie*.

Franco-Spanish Prize to E. Carmona

Ernesto Carmona has been awarded the Franco-Spanish Prize of the Société Française de Chimie for his internationally recognized work in organometallic chemistry. Carmona completed his PhD in 1974 at the University of Seville (Spain) under the guidance of F. Gonzalez. After a postdoctoral period from 1974 to 1977 with the Nobel laureate Sir Geoffrey Wilkinson at Imperial College London (UK), he returned as assistant professor to Seville, where he has been professor since 1983. He has been a visiting professor in Alabama (USA), Oxford (UK), and Toulouse (France).



E. Carmona

Carmona's research on organometallic chemistry and homogeneous catalysis is focused in particular on C–H activation, C–C bond-forming reactions, transition-metal–alkyl compounds and similar species in insertion and polymerization reactions, and the activation of small molecules, such as N_2, CO, CO_2, and ethene. He recently described in *Angewandte Chemie* an equilibrium between iridium hydride alkylidene and iridium hydride alkene isomers.[3] Carmona is a member of the Editorial Board of *Chemistry – A European Journal*, which is celebrating its 10th anniversary this year.

[1] a) O. Trapp, J. R. Kimmel, O. K. Yoon, I. A. Zuleta, F. M. Fernandez, R. N. Zare, *Angew. Chem.* **2004**, *116*, 6703; *Angew. Chem. Int. Ed.* **2004**, *43*, 6541; b) B. Huang, T. D. Perroud, R. N. Zare, *ChemPhysChem* **2004**, *5*, 1523; c) R. N. Zare, *Angular Momentum: Understanding Spatial Aspects in Chemistry and Physics*, Wiley, New York, **1988**.

[2] H. Steinmetz, N. Glaser, E. Herdtweck, F. Sasse, H. Reichenbach, G. Höfle, *Angew. Chem.* **2004**, *116*, 4996; *Angew. Chem. Int. Ed.* **2004**, *43*, 4888.

[3] M. Paneque, M. L. Poveda, L. L. Santos, E. Carmona, A. Lledós, G. Ujaque, K. Mereiter, *Angew. Chem.* **2004**, *116*, 3794; *Angew. Chem. Int. Ed.* **2004**, *43*, 3708.

© 2005 Wiley-VCH Verlag GmbH & Co. KGaA, Weinheim
DOI: 10.1002/anie.200462973

Silicon Compounds

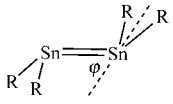
Molecules with a Genuine Si–Si Triple Bond and a Stable Derivative of $[SiH]^+$

*Manfred Weidenbruch**

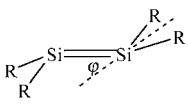
Keywords:
cations · half-sandwich compounds · multiple bonds · silicon

The multiple-bond rule, often simply named as the double-bond rule was considered to be valid for the molecular chemistry of the main-group elements. According to this rule, the elements of the first eight-element period, but not those of the following periods, are capable of forming multiple bonds. Although the origins of this are obscure, it probably arose from the work of Pitzer[1] and Mulliken[2] who, more than 50 years ago, posed the question as to why nitrogen, for example, has such a high bond-dissociation energy whereas the homologous P_2 molecule only exists as a species at high temperature and on cooling reverts to the P_4 molecule with P–P single bonds. The repulsive forces between the fully occupied inner electron shells were postulated as a reason for the highly different stabilities of the triple bonds in N_2 and P_2. In the case of N_2 there are only repulsive forces between the first shells, each occupied by merely two electrons, whereas in the P_2 molecule there are the additional eight electrons of the second shells, making the P–P triple bond unstable at room temperature.

This rule—that had almost acquired dogma status—came under attack with, among others, the synthesis and structural characterization of the distannene **1**, the first molecule with a homonuclear double bond between two of the heavier



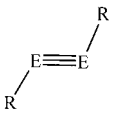
1, R = $CH(SiMe_3)_2$



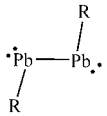
2, R = 2,4,6-$Me_3C_6H_2$

Group 14 elements.[3] The preparation of the disilene **2** followed five years later,[4] and aroused particular interest because carbon and silicon are direct neighbors in Group 14. In the mean time more than 50 compounds with Si–Si double bonds are known and homonuclear double bonds have also been demonstrated for the heavier homologues.[5] Characteristic for these compounds is the observation, with increasing atomic number, of an increased *trans*-bending angle φ of the substituents and the highly varying lengths of the E–E double bonds which, in the case of lead, are even longer than comparable single bonds.[5]

Until recently the isolation of a stable molecule with an Si–Si triple bond remained a challenge. This situation was rather surprising because alkyne analogues of germanium **3**,[6] tin **4**,[7] and lead **5**[8] had been synthesized and structurally characterized. However, the structural data indicate that the bond orders in the molecules **3** and **4** are about two. On the basis of the large Pb–Pb bond length—markedly longer then a lead–lead single bond—and the *trans*-bending of the substituents of 94.26° the corresponding dilead compound **5** must rather be considered as a diplumbylene with a Pb–Pb single bond and a free electron pair on each of the lead atoms.[9] The experimental observations are supported by quantum chemical calculations that unequivocally confirm the diplumbylene form **5** as the energy minimum.



3, E = Ge, **4**, E = Sn

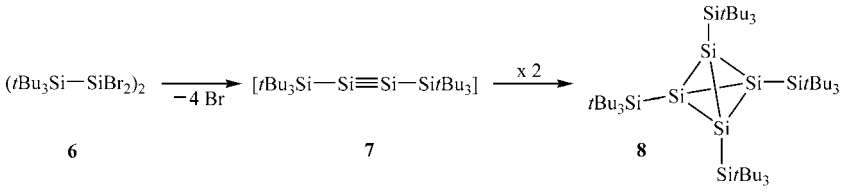


5

R = 2,6-(2,6-*i*$Pr_2C_6H_3)_2C_6H_3$

Earlier attempts to prepare a disilyne analogue of acetylene showed, in agreement with the calculations,[10–12] that Si_2H_2 does not possess a triple bond but exists as a doubly[13] or singly[14] H-bridged molecule. This and similar attempts to form disilynes with sterically undemanding substituents have been surveyed in a Highlight[15] as well as a Review article.[16]

The first indications for the intermediate occurrence of a disilyne emerged from the dehalogenation of



6 → (−4 Br) → **7** → (x 2) → **8**

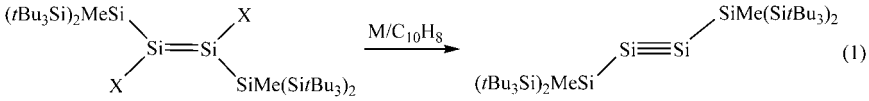
Scheme 1. Postulated formation of disilyne **7** and its spontaneous reaction to afford *tetrahedro*-tetrasilane **8**.

[*] Prof. Dr. M. Weidenbruch
Institut für Reine und Angewandte Chemie
Universität Oldenburg
Postfach 25 03, 26111 Oldenburg
(Germany)
Fax: (+49) 441-798-3352
E-mail:
manfred.weidenbruch@uni-oldenburg.de

 © 2005 Wiley-VCH Verlag GmbH & Co. KGaA, Weinheim DOI: 10.1002/anie.200462273

the tetrasilane **6** (Scheme 1), that presumably proceeds via the disilyne **7** which, in analogy to the "perpendicular" acetylene complexes[17] spontaneously reacts further to afford the first *tetrahedro*-tetrasilane **8**.[18]

Apparently, the bulkiness of the spatially demanding tBu$_3$Si group is not sufficient to protect the postulated disilyne **7** from further reactions. By using the even more sterically overcrowded (tBu$_3$Si)$_2$MeSi group as a substituent and starting from the dihalodisilenes **9**, Wiberg et al. successfully constructed the mustard-yellow disilyne **10** [Eq. (1)] that was characterized by NMR spectroscopy data and trapping reactions.[19]



(1)

9, X = Cl, Br

10

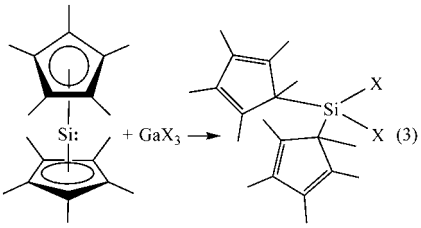
M = Li, Na, K

These experimental observations are supported by DFT calculations showing that **10** should be very stable against both isomerization and dimerization processes. The calculations reveal a very short Si–Si bond length of 207.2 pm and a *trans*-bending angle Si–Si≡Si of 148.0°.[20] Final doubts about the existence of Si–Si triple bonds were resolved by the synthesis and structural characterization of the emerald-green disilyne **12** [Eq. (2)] that was prepared by Sekiguchi et al. by dehalogenations of the tetrasilane **11**.[21]

In spite of the different substitution patterns, the observed Si–Si bond length of 206.22(9) pm in **12** is in good agreement with the value calculated for the molecule **10**. However, the *trans*-bending angle Si–Si≡Si of 137.44(4)° is markedly smaller than the calculated value for **10**. In a commentary on the formation of the stable compound **12** West concluded with the statement that "The synthesis of a stable disilyne is a milestone both for silicon chemistry and for multiple-bond chemistry in general."[22]

Last but not least, the bond orders in these formal alkyne analogues of Group 14 elements are of interest. While for **12** a natural bond order (NBO) analysis gives a value of 2.62 indicating a genuine triple bond, the bond orders decrease to about 2 in **3** and **4** and to a value of only 1 for the formal diplumbyne **5**, reflecting the decreasing tendency for hybridization between the heavier elements of Group 14.

In spite of all the advances achieved in the past decades, with regard to the lower coordination numbers, carbon is still far ahead of silicon. However, this position is reversed when we consider higher coordination numbers, that is, those over four. Whereas carbon typically achieves the coordination numbers five, six, or seven in electron-deficient compounds in combination with metals of Groups 1, 2, or 13, in silicon chemistry higher coordination numbers are also known in directed bonds. An extreme case is the decamethylsilicocene **13** isolated by Jutzi et al. as early as 1986 which contains a tenfold coordinated silicon atom in oxidation state +2.[23] Compound **13** exhibits the expected reactivity for a nucleophilic silylene which is usually accompanied by a ready change from η^5-Cp* to η^1-Cp* (Cp* = C_5Me_5) coordination. For example, **13** reacts with the gallium trihalides $GaCl_3$ and $GaBr_3$ to give products **14** in which a rearrangement of the η^5-Cp* groups has occurred [Eq. (3)].[24]

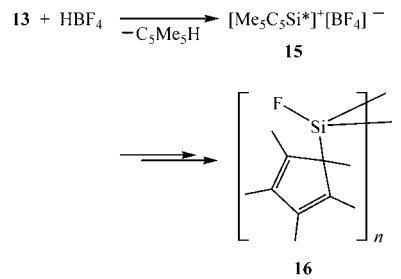


(3)

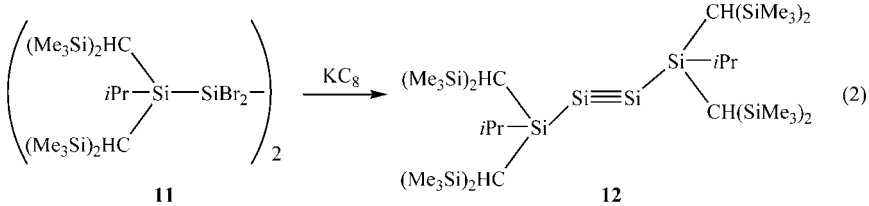
13

14, X = Cl, Br

Attempts to generate the cationic species [(Me_5C_5)Si$^+$] by protonation of **13** and cleavage of an Me_5C_5H ring proved to be more difficult. The reaction of **13** with HBF_4 in diethyl ether presumably proceeds through the ionic compound **15** that decomposes even at low temperature by fluoride transfer to give BF_3 and a short-lived silylene and then the oligomeric end product **16** (Scheme 2).[25] The salt **17** finally proved to be the protonating agent of choice: its reaction with **13** gave exclusively the colorless salt **18** with the long sought after [C_5Me_5Si]$^+$ ion [Eq. (4)].[26]



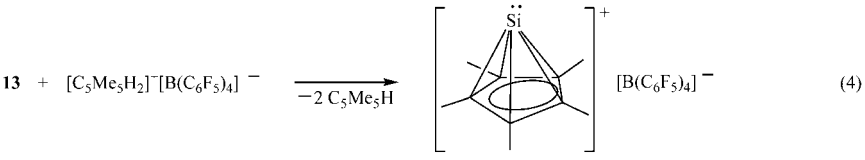
Scheme 2. Attempts to form [(Me_5C_5)Si]$^+$ through the protonation of **13** with HBF_4 gives oligomeric products.



(2)

11

12



(4)

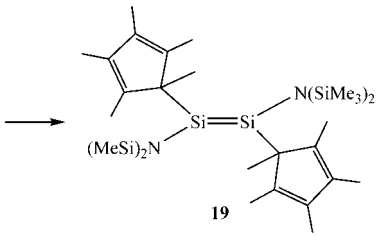
17

18

 © 2005 Wiley-VCH Verlag GmbH & Co. KGaA, Weinheim

The cation of **18** forms an almost ideal pentagonal pyramid with only weak interactions to the fluorine atoms of the anion. It can be considered as a derivative of the silyliumylidene cation $[SiH]^+$, the smallest polyatomic molecule in the chemistry of silicon. The X-ray crystal-structure analysis of **18** and the occurrence in the ^{29}Si NMR spectrum of a signal at very high field ($\delta = -400.2$ ppm) clearly indicate that the silicon atom is fivefold coordinated by the ring carbon atoms. That a change of hapticity from η^5 to η^1 in the cation of **18** is possible is impressively demonstrated by the reaction with lithium bis(trimethylsilyl)amide, which proceeds through a reactive silylene intermediate to finally afford the disilene **19** that has an Si=Si double bond length 216.83(5) pm, that is, in the expected range [Eq. (5)].[26]

18 + $Li[N(SiMe_3)_2]$



19 (5)

The molecule **13** and the salt **18** once again illustrate the ability of silicon to form compounds with high coordination numbers. In a commentary to the work of Jutzi et al. Bertrand comes to the conclusion that "…, it is difficult to imagine that Cp^*C^+ would be stable because of the reluctance of carbon to be hypercoordinate: The carbon would be almost totally and not modestly naked, as the silicon is in Cp^*Si^+".[27]

Published online: December 21, 2004

[1] K. S. Pitzer, *J. Am. Chem. Soc.* **1948**, *70*, 2140.
[2] R. S. Mulliken, *J. Am. Chem. Soc.* **1950**, *72*, 4493.
[3] D. E. Goldberg, D. H. Harris, M. F. Lappert, K. M. Thomas, *J. Chem. Soc. Chem. Commun.* **1976**, 261.
[4] R. West, M. J. Fink, J. Michl, *Science* **1981**, *214*, 1341.
[5] Selected recent reviews: a) P. P. Power, *Chem. Rev.* **1999**, *99*, 3463; b) M. Weidenbruch, *J. Organomet. Chem.* **2002**, *646*, 39; c) M. Weidenbruch, *Organometallics* **2003**, *22*, 4348.
[6] M. Stender, A. D. Phillips, R. J. Wright, P. P. Power, *Angew. Chem.* **2002**, *114*, 1863; *Angew. Chem. Int. Ed.* **2002**, *41*, 1785.
[7] A. D. Phillips, R. J. Wright, M. M. Olmstead, P. P. Power, *J. Am. Chem. Soc.* **2002**, *124*, 5930.
[8] L. Pu, B. Twamley, P. P. Power, *J. Am. Chem. Soc.* **2000**, *122*, 3524.
[9] Y. Chen, M. Hartmann, M. Diedenhofen, G. Frenking, *Angew. Chem.* **2001**, *113*, 2108; *Angew. Chem. Int. Ed.* **2001**, *40*, 2052.
[10] H. Lischka, H. Köhler, *J. Am. Chem. Soc.* **1983**, *105*, 6646.
[11] B. T. Colegrove, H. F. Schaefer, *J. Phys. Chem.* **1990**, *94*, 5597.
[12] R. S. Grev, H. F. Schaefer, *J. Chem. Phys.* **1992**, *97*, 7990.
[13] M. Bogey, H. Bolvin, C. Demuynck, J. L. Destombes, *Phys. Rev. Lett.* **1991**, *66*, 413.
[14] M. Cordonnier, M. Bogey, C. Demuynck, J. L. Destombes, *J. Chem. Phys.* **1992**, *97*, 7984.
[15] P. Jutzi, *Angew. Chem.* **2000**, *112*, 3953; *Angew. Chem. Int. Ed.* **2000**, *39*, 3797.
[16] M. Weidenbruch in *The Chemistry of Organic Silicon Compounds, Vol. 3* (Eds.: Z. Rappoport, Y. Apeloig), Wiley, Chichester, **2001**, chap. 5, p. 391.
[17] D. M. Hoffmann, R. Hoffmann, C. R. Fisel, *J. Am. Chem. Soc.* **1982**, *104*, 3858.
[18] N. Wiberg, C. M. M. Finger, K. Polborn, *Angew. Chem.* **1993**, *105*, 1140; *Angew. Chem. Int. Ed. Engl.* **1993**, *32*, 923.
[19] a) N. Wiberg, W. Niedermayer, G. Fischer, H. Nöth, M. Suter, *Eur. J. Inorg. Chem.* **2002**, 1066; b) N. Wiberg, S. K. Vasisht, G. Fischer, P. Mayer, *Z. Anorg. Allg. Chem.* **2004**, *630*, 1823.
[20] N. Takagi, S. Nagase, *Eur. J. Inorg. Chem.* **2002**, 2775.
[21] A. Sekiguchi, R. Kinjo, M. Ichinohe, *Science* **2004**, *305*, 1755.
[22] R. West, *Science* **2004**, *305*, 1724.
[23] P. Jutzi, D. Kanne, C. Krüger, *Angew. Chem.* **1986**, *98*, 163; *Angew. Chem. Int. Ed. Engl.* **1986**, *25*, 164.
[24] U. Holtmann, P. Jutzi, T. Kühle, B. Neumann, H.-G. Stammler, *Organometallics* **1999**, *18*, 5531.
[25] P. Jutzi, U. Holtmann, H. Bögge, A. Müller, *J. Chem. Soc. Chem. Commun.* **1988**, 305.
[26] P. Jutzi, A. Mix, B. Rummel, W. W. Schoeller, B. Neumann, H.-G. Stammler, *Science* **2004**, *305*, 849.
[27] G. Bertrand, *Science* **2004**, *305*, 783.

 © 2005 Wiley-VCH Verlag GmbH & Co. KGaA, Weinheim

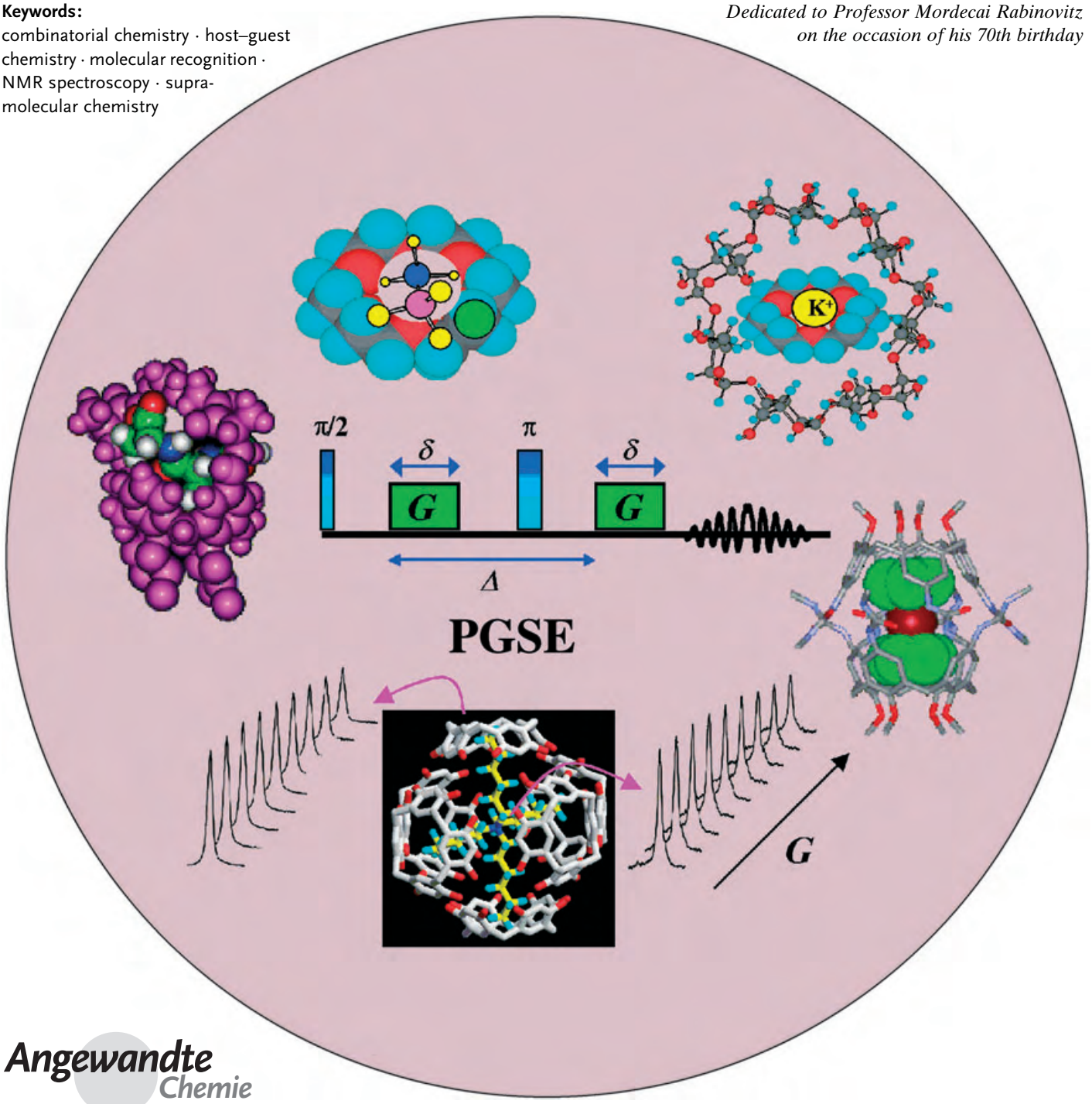
Analytical Methods

Diffusion NMR Spectroscopy in Supramolecular and Combinatorial Chemistry: An Old Parameter—New Insights

Yoram Cohen, Liat Avram, and Limor Frish*

Keywords:
combinatorial chemistry · host–guest chemistry · molecular recognition · NMR spectroscopy · supramolecular chemistry

Dedicated to Professor Mordecai Rabinovitz on the occasion of his 70th birthday



© 2005 Wiley-VCH Verlag GmbH & Co. KGaA, Weinheim
DOI: 10.1002/anie.200300637

Intermolecular interactions in solution play an important role in molecular recognition, which lies at the heart of supramolecular and combinatorial chemistry. Diffusion NMR spectroscopy gives information over such interactions and has become the method of choice for simultaneously measuring diffusion coefficients of multicomponent systems. The diffusion coefficient reflects the effective size and shape of a molecular species. Applications of this technique include the estimation of association constants and mapping the intermolecular interactions in multicomponent systems as well as investigating aggregation, ion pairing, encapsulation, and the size and structure of labile systems. Diffusion NMR spectroscopy can also be used to virtually separate mixtures and screen for specific ligands of different receptors, and may assist in finding lead compounds.

From the Contents

1. Introduction 521
2. Concepts of Molecular Diffusion 522
3. NMR Methods for Measuring Diffusion 524
4. Applications of NMR Diffusion Measurements in Supramolecular Chemistry 528
5. Applications of Diffusion NMR Measurements in Combinatorial Chemistry 546
6. Summary and Outlook 550

1. Introduction

1.1. Measuring High-Resolution Diffusion by NMR Spectroscopy

Over the last decade, pulsed field-gradient (PFG) NMR spectroscopy has become the method of choice for measuring diffusion in solutions in both chemical and biological systems. In principle, the diffusion coefficient of a certain molecular species under given conditions (for example, solvent and temperature) depends on its "effective" molecular weight, size, and shape. Therefore, it is evident that diffusion can be used to map intermolecular interactions that play an important role in both chemistry and biology in solution and which lie at the heart of molecular recognition, a process which is essential to supramolecular and combinatorial chemistry.[1–3] Nevertheless, chemists working in these fields have only recently started to use diffusion NMR spectroscopy to study their systems.

The fact that molecular diffusion can be measured by NMR methods was realised in the early days of NMR spectroscopy.[4] The most practical pulse sequence for measuring diffusion coefficients by NMR spectroscopy was introduced by Stejskal and Tanner in 1965,[5a] long before the advent of 2D NMR spectroscopy,[6–8] which is currently routinely used by chemists worldwide. Indeed, diffusion NMR measurements have increasingly been used since 1965, and most of these applications in solution up until 1987 were reviewed by Stilbs and Kärger et al.[9,10a]

The last decade has witnessed an explosion in the utilization of gradients in all areas of NMR spectroscopy, ranging from coherence selection in high-resolution NMR spectroscopy[11] to magnetic resonance imaging (MRI).[12] Indeed, the use of diffusion MRI of the central nervous systems (CNS) has, in particular, increased considerably over the last decade.[13] This is partially a result of the surprising efficacy of diffusion-weighted MRI in the early diagnosis of a stroke[14] and the opportunities that diffusion tensor imaging (DTI) provides in mapping the fiber tracts in the CNS.[15]

In view of the above, it may seem quite surprising that the application of diffusion NMR spectroscopy as a tool for studying molecular interactions in the context of supramolecular and combinatorial chemistry only began being implemented over the last few years. One reason for this is probably the fact that gradient sets, which are needed for the pulsed gradient spin echo (PGSE) experiment used to measure diffusion by NMR spectroscopy, were not commercially available until recently. However, with the advent of high-resolution gradient-enhanced spectroscopy[11] and the technological improvement in gradient performance, mainly because of the development of MRI, such gradient sets became commercially available and are currently conventional accessories of standard modern high-resolution NMR spectrometers. These gradient-containing high-resolution probes provide a means to simultaneously determine the diffusion coefficient for the entire set of signals in a high-resolution spectrum with high sensitivity and accuracy. It should be noted that diffusion NMR spectroscopy, as will be demonstrated herein, provides a means for studying diffusion in systems in equilibrium where no concentration gradients exist. In addition, new pulse sequences and methodologies, some of which will be briefly discussed herein, were developed, thus enabling modern NMR spectrometers to routinely perform simple and complex NMR diffusion experiments.

1.2. Applications of Diffusion NMR Spectroscopy

Diffusion NMR measurements are used in many different fields ranging from the medical sciences[12–15] to material sciences.[16–18] Recently, with the advent of high-resolution

[*] Prof. Y. Cohen, L. Avram, Dr. L. Frish
School of Chemistry
Tel Aviv University
Ramat Aviv, Tel Aviv 69978 (Israel)
Fax: (+972) 3-6409-293
E-mail: ycohen@post.tau.ac.il

 DOI: 10.1002/anie.200300637 © 2005 Wiley-VCH Verlag GmbH & Co. KGaA, Weinheim

gradient enhanced spectroscopy, some general reviews dealing with the theoretical and practical aspects of gradient NMR specroscopy have been published.[11,17] In addition, more-specific reviews on diffusion in polymers,[16b] zeolites and porous systems,[16a,18] surfactants,[19] and liquid crystals and membranes[20] have also been published. Since diffusion NMR spectroscopy is a totally non-invasive technique it is particularly suited to studying molecular dynamics and translational diffusion, and hence structural details in biological and physiological systems. Indeed, the application of diffusion NMR spectroscopy to membrane transport was recently reviewed,[21] and several reviews dealt with diffusion in restricted geometries.[17] q-Space diffusion NMR spectroscopy[22] laid the foundations for the utilization of such experiments to obtain structural information and compartment size. In addition, because of the non-invasiveness of the technique and the fact that the current technology is suitable for studying compartments of only a few microns in size, q-space diffusion MR was recently used to study biological systems.[23–25] Very recently, we expanded this approach to q-space MRI of the CNS.[26,27] Callaghan and others have used diffusion NMR spectroscopy and MRI to study complex fluids.[28] Van As and co-workers, for example, used these techniques to study flow in porous materials used for chromatography.[29]

In this Review the applications of high-resolution diffusion NMR spectroscopy in solution will be discussed, with special emphasis on applications in the fields of supramolecular and combinatorial chemistry. The Review will concentrate on the applications in these fields of chemistry rather than on an extensive description of the theory of diffusion NMR experiments which can be found in many of the recently published reviews.[9–11,16–21,28] We shall include a brief description of diffusion in the context of NMR measurements (Section 2) and a basic description of the NMR methods used to measure diffusion, with emphasis mainly on the most simple and commonly ones used to study diffusion in isotropic solutions (Section 3). In the main body of this Review (Sections 4 and 5) we shall describe different applications of diffusion NMR spectroscopy to demonstrate, through selected literature examples, the potential of simple diffusion NMR measurements in supramolecular and combinatorial chemistry. The final section gives future prospects for diffusion NMR spectroscopy (Section 6).

2. Concepts of Molecular Diffusion

2.1. Translational Diffusion in Isotropic Systems—"Free Diffusion"

Translational diffusion is one of the most important modes of molecular transport.[30] Self-diffusion is the random translational motion of ensembles of particles (molecules or ions) as a consequence of their thermal energy. In the case of self-diffusion, no (net) force acts on the molecular particles and, consequently, no net displacement is observed. In an isotropic homogeneous system the conditional probability $P(r_0,r,t_d)$ of finding a molecule, which was initially at position r_0, at position r after a time t_d is given by Equation (1), where D is

$$P(r_0,r,t_d) = (4\pi D t_d)^{-3/2} \exp\left(-\frac{(r-r_0)^2}{4 D t_d}\right) \quad (1)$$

the self-diffusion coefficient. This equation shows that the volume occupied by a molecule, originally at position r_0 relative to an arbitrary reference position, in a nonrestricted system is a Gaussian distribution that broadens with the increase in the diffusion time t_d (Figure 1). Therefore, the mean displacement of a particle under these conditions in all three directions by random walk is zero. However, the self-diffusion root-mean-square displacement $(\langle X^2\rangle)^{1/2}$ in such systems is given by the Einstein equation [Eq. (2)], where n is

$$(\langle X^2\rangle)^{1/2} = (n D t_d)^{1/2} \quad (2)$$

2, 4, or 6 for the cases of one-, two- and three-dimensional diffusion. From this equation it follows that the mean displacement for free diffusion increases linearly with the square root of the diffusion time.[31]

In addition, it is well known that diffusion is closely related to molecular size, as seen from the Einstein–Smoluchowski equation [Eq. (3)],[21,30] where k_b is the Boltzmann

$$D = \frac{k_b T}{f} = \frac{R T}{N f} \quad (3)$$

constant, T is the absolute temperature, f is the so-called hydrodynamic frictional coefficient, N is Avogadro's number, and R is the gas constant. For a sphere in a continuous



Yoram Cohen was born in 1956 in Israel and received his BSc (1981) and a PhD (1987) from the Hebrew University of Jerusalem under the supervision of Professors M. Rabinovitz and J. Klein. He then spent three years with Professor Tom James at the University of California at San Francisco (UCSF) as a Fulbright postdoctoral fellow. He joined the faculty of the School of Chemistry at Tel Aviv University in 1992 as a lecturer and was appointed senior lecturer in 1996 and associate professor in 2000. His research interests encompass NMR spectroscopy of supramolecular systems and MRS/MRI of the CNS with an emphasis on diffusion MR.



Limor Frish was born in Ramat Gan, Israel, in 1973 and received her BSc in chemistry from the School at Chemistry of Tel Aviv University in 1997. She has just received her PhD, which was carried out under the supervision of Prof. Yoram Cohen. Her main interest is the applications of diffusion NMR spectroscopy in supramolecular chemistry.

© 2005 Wiley-VCH Verlag GmbH & Co. KGaA, Weinheim

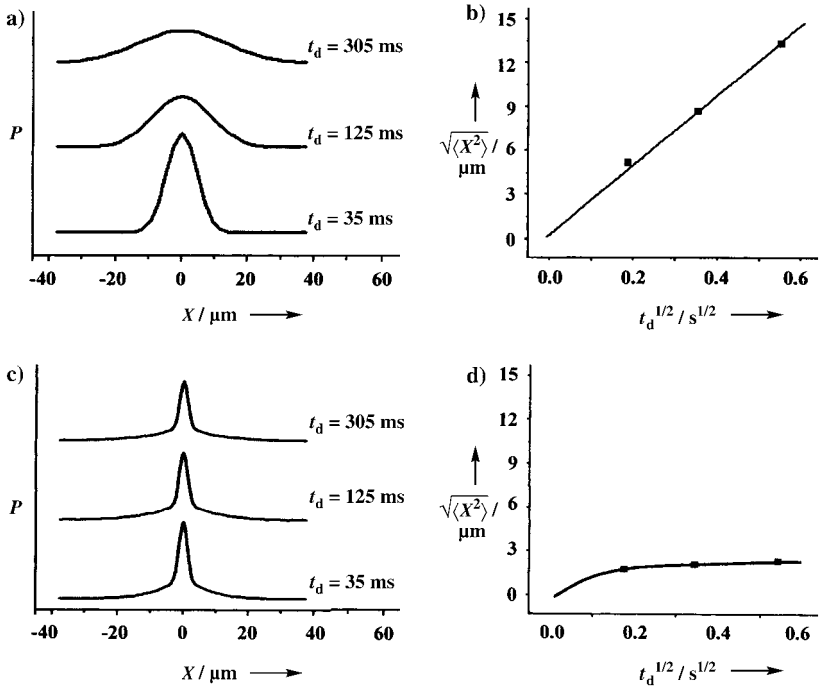


Figure 1. a), b) Free diffusion in a solution of *tert*-butanol; c), d) restricted diffusion (water in optic nerve). a), c) displacement distribution profiles; b), d) root-mean-square of the displacement *X* calculated from the full width at half height of the displacement distribution profiles shown in (a) and (c), respectively, against the square root of the diffusion time The slope of the straight line in (b) provides the self-diffusion coefficient of *tert*-butanol (2.7×10^{-6} $cm^2 s^{-1}$).[26c].

medium of viscosity η, f is given by the Stokes Equation [Eq. (4)].[30] In this equation, r_s is the hydrodynamic radius,

$$f = 6\pi\eta r_s \tag{4}$$

often called the Stokes' radius. Combining Equations (3) and (4) leads to the familiar Stokes–Einstein equation [Eq. (5)]. It

$$D = \frac{k_b T}{6\pi\eta r_s} \tag{5}$$

should be noted, however, that, different theories are needed to describe the hydrodynamic frictional coefficient f for molecular species of different geometries.[30]



Liat Avram was born in Tel Aviv, Israel, in 1977 and received her BSc and MSc in 1999 and 2001, respectively, from the School of Chemistry at Tel Aviv University. Since October 2001 she has been pursuing a PhD under the supervision of Prof. Yoram Cohen. She is a Charles Clore PhD Scholar.

Equation (5) indicates that, by measuring the self-diffusion coefficient of a given molecular species under controlled conditions, one may obtain information on its effective size or weight and, therefore, on the specific interactions of the species with its molecular environment. Thus, the diffusion coefficients are sensitive to structural properties of the observed molecular species such as weight, size, and shape, as well as binding phenomena, aggregation, and molecular interactions. In addition, there is no need for further interpretation of the diffusion coefficients, the values of which are directly related to the translational molecular displacement in the laboratory frame when diffusion occurs in a homogeneous medium that allows free and isotropic diffusion. However, in nonhomogeneous samples, where different modes of diffusion prevail, the extraction of diffusion coefficients from diffusion NMR experiments is a much more difficult task.

2.2. Other Modes of Diffusion: Restricted and Anisotropic Diffusion

As will be shown in Section 3, the spins are tagged at at least two time points in the different NMR methods used to study diffusion.[5,9–10,13–29] Therefore, the signal decay in a diffusion NMR experiment depends on the mean displacement of the particles during a certain time, called the diffusion time. Figure 1 shows the displacement distribution profiles for different diffusion times for free and restricted diffusion (Figure 1 a and c), as well as the mean displacement as a function of the square root of the diffusion time for free isotropic diffusion and restricted diffusion (Figure 1 b and d). For the case of free diffusion, the mean displacement experienced by the diffusing molecular species increases linearly with the square root of the diffusion time, as expected from Equation (2). By plotting the mean displacement as a function of the square root of the diffusion time, a linear graph is obtained, the slope of which reflects the diffusion coefficient (Figure 1 b). In a system where there are barriers which prohibit free diffusion, a situation may be envisaged in which an increase in the diffusion time does not translate into an increase in the mean displacement of the diffusing species. In such a situation there is no longer a linear relationship between the mean displacement and the square root of the diffusion time as shown in Figure 1 d. Restricted diffusion prevails in this situation and only an apparent diffusion coefficient can be obtained.[14,15] It is clear that such a restriction will occur when the diffusion time t_d is larger than $l^2/2D$, where l is the length of the compartment and D the diffusion coefficient of the diffusing molecular species. This means that the extracted apparent diffusion coefficients in such systems may be affected by the diffusion time t_d of the diffusion NMR experiment. Anisotropic diffusion may be

 © 2005 Wiley-VCH Verlag GmbH & Co. KGaA, Weinheim

found in cases where the barriers which impose restriction are not uniformly distributed.[15] Both restricted and anisotropic diffusion are extremely important phenomena in heterogeneous systems such as porous materials and biological systems and provide, under certain experimental conditions, a means for obtaining structural information on the investigated system.[22–29] Since these phenomena are much less important in homogeneous solutions, we shall not elaborate any further on these modes of diffusion.

3. NMR Methods for Measuring Diffusion

In recent years diffusion NMR methods have replaced the traditional way of measuring self-diffusion coefficients with radioactive tracers, since NMR methods are easier to perform, are totally non-invasive, and allow simultaneous determination of diffusion coefficients in multicomponent systems. In the next section we shall outline the effect of magnetic field gradients on the measured NMR signal.[5a,9–11,16–18] Thereafter, we shall outline some of the most useful NMR methods for measuring diffusion in solution.

3.1. The Modified Spin-Echo Experiment: The Pulse Gradients Spin Echo Experiment

The basis for diffusion measurements is the fact that magnetic field gradients can be used indirectly to label the position of NMR-active nuclei through their Larmor frequency. This is done by applying an external gradient of the magnetic field, which is described by Equation (6), where $\hat{i}$, $\hat{j}$,

$$G = \frac{\partial Bz}{\partial x}\hat{i} + \frac{\partial Bz}{\partial y}\hat{j} + \frac{\partial Bz}{\partial z}\hat{k} \tag{6}$$

and $\hat{k}$ are the unit vectors in the x, y, and z directions, respectively. Thus, the total external magnetic field at position r is given by Equation (7). Spins precess with an angular

$$B(r) = B_0 + G\,r \tag{7}$$

frequency according to Equation (8). The acquired phase angle depends linearly on both $B(r)$ and the duration of the

$$\omega(r) = -\gamma B(r) \tag{8}$$

gradient δ. In the following, we assume that only a z gradient is present; hence, the gradient produces the position-dependent phase angle $\Phi(z)$ [Eq. (9)]. From these equations it is

$$\Phi(z) = -\gamma B(z)\delta \tag{9}$$

clear that the magnetic field gradient can be used to label the z position of the spins.

The most common approach to measuring diffusion is to use the pulsed gradient spin echo (PGSE) NMR technique,[5a] which is a modification of the Hahn spin echo pulse sequence.[4] In this sequence, two identical gradient pulses are inserted, one into each period τ of the spin-echo sequence (Figure 2).[5a,17a] The PGSE sequence and a schematic representation of its effect on the magnetization of an ensemble of spins are shown in Figure 2. The net magnetization at the beginning of the experiment is oriented along the z-axis,

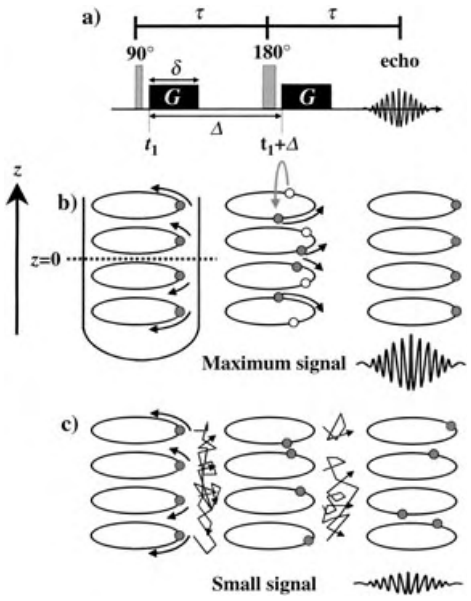


Figure 2. a) The PGSE pulse sequence.[5a] G is the amplitude of the pulsed gradient, δ its duration, and Δ the separation between the leading edges of the pulsed gradients. Also shown is the effect of the absence (b) and presence (c) of diffusion on the phase shift and signal intensity in a PGSE experiment. In the sequence shown in (a), the term $(\Delta-\delta/3)$ is the diffusion time. Adapted with permission from Ref. [17a].

which means that the ensemble of spins are in thermal equilibrium. A 90° radiofrequency (RF) pulse is then applied and, as a consequence, the magnetization rotates from the z-axis to the x-y plane. A pulse gradient of duration δ and magnitude G is then applied at a time point t_1. As a result, each spin experiences a phase shift according to Equation (10) at the end of the first period τ, just before

$$\Phi i(\tau) = \gamma B_0 \tau + \gamma G \int_{t_1}^{t_1+\delta} z_i(t)\mathrm{d}t \tag{10}$$

application of the 180° RF pulse. The left term is the phase shift arising from the static magnetic field, and the term on the right is the phase shift arising from the applied magnetic gradient pulse.

The next step is the application of a 180° RF pulse, which causes the reversal of the sign of the processing and the sign of the phase angle as depicted in Figure 2 (hollow circles become filled circles). A second gradient, equal in magnitude and duration to the first, is applied at time $t_1+\Delta$. At this point, two different scenarios can be considered. In the first scenario (Figure 2b) the spins do not undergo any translational motion along the z-axis, that is, there is no diffusion during the time interval. In this case, the phase shift of each spin after the first period τ is equal in magnitude to the phase shift of each spin

 © 2005 Wiley-VCH Verlag GmbH & Co. KGaA, Weinheim

after the second period τ. Hence, the effects of the two pulsed gradients cancel out and all the spins refocus. In this case, a maximum echo signal is obtained. In the presence of diffusion (the second scenario, Figure 2c), however, the phase shift of each spin after the first period τ is different in magnitude from the phase shift of each spin after the second period τ. This effect occurs since, in the presence of diffusion, each species is located in a different position along the z-axis at times t_1 and $t_1+\Delta$, and hence each species is situated in a different magnetic field [Eq. (7)]. Therefore, the spins precess with altered angular frequencies in these different periods of time [Eq. (8)]. Thus, the phase angle fans out (at least partially) in the presence of diffusion, and the echo signal is consequently smaller. It can be intuitively deduced that larger diffusion is reflected by poorer refocusing of the spins and, consequently, by a smaller echo signal.

From these equations, it is apparent that the stronger and longer the phase of the pulsed gradients are, the poorer the refocusing of the spins and the smaller the recovered echo signal for diffusing spins. In addition, it is clear that the larger the Δ value is (the duration between the pulsed gradients) the smaller the echo intensity will be. Thus, without presenting the complete mathematical manipulations, it is clear that the signal intensity should be described by Equation (11), where

$$I_{(2\tau,G)} = I_{(0,0)}\exp\left(-\frac{2\tau}{T_2}\right)f(\delta,G,\Delta,D) = I_{(2\tau,0)}f(\delta,G,\Delta,D) \tag{11}$$

$I_{(0,0)}$ and $I_{(2\tau,0)}$ are the signal and echo intensity that would be observed immediately after the first 90° RF pulse and at 2τ, respectively, and $f(\delta,G,\Delta,D)$ is a function that represents the signal attenuation as a result of diffusion.

If the PGSE experiment is preformed such that τ is kept constant, then it is possible to separate the T_2 relaxation time and the diffusion contributions. Hence, after normalizing out the attenuation arising from T_2 relaxation, only the attenuation arising from the diffusion remains [Eq. (12)]. Stejskal

$$\frac{I_{(2\tau,G)}}{I_{(2\tau,0)}} = f(\delta,G,\Delta,D) \tag{12}$$

and Tanner have shown that the signal intensity for a single free-diffusing component is described in the case of rectangular pulse gradients by Equation (13),[5] and gives Equation (14), where γ is the gyromagnetic ratio, G is the pulsed

$$\begin{aligned} I_{(2\tau,G)} &= I_{(0,0)}\exp\left(\frac{-2\tau}{T_2}\right)\exp(-\gamma^2 G^2\delta^2(\Delta-\delta/3)D) \\ &= I_{(2\tau,0)}\exp(-\gamma^2 G^2\delta^2(\Delta-\delta/3)D) \end{aligned} \tag{13}$$

$$\ln\left(\frac{I_{(2\tau,G)}}{I_{(2\tau,0)}}\right) = -\gamma^2 G^2\delta^2(\Delta-\delta/3)D = -b\,D \tag{14}$$

gradient strength, Δ is the time separation between the pulsed-gradients, δ is the duration of the pulse, and D is the diffusion coefficient. The product $\gamma^2G^2\delta^2(\Delta-\delta/3)$ is termed the b value. Thus, a plot of $\ln(I_{(2\tau,G)}/I_{(2\tau,0)})$ versus the b values for an isotropic solution should give a straight line, the slope of which is equal to $-D$. In principle, any of the parameters δ, Δ, and G can be increased during the experiment to obtain increased signal attenuation. However, technical factors and the relaxation charactarictics of the sample may limit the choice. The term $(\Delta-\delta/3)$ is generally refered to as the diffusion time.[5b]

Figure 3 shows the results for a PGSE experiment in which the strength of the gradient pulse was incremented

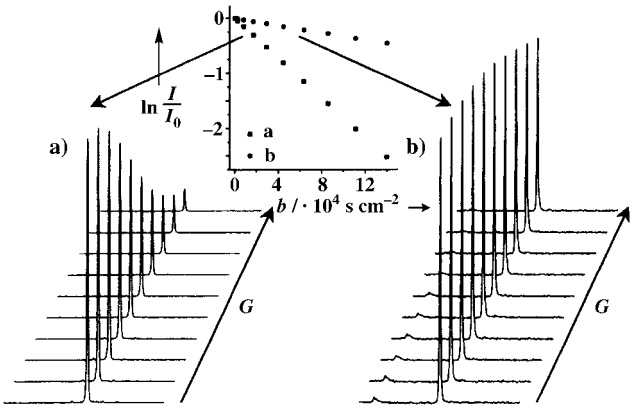


Figure 3. Signal decays as a function of G of the following diffusion coefficients: a) $D=1.81\times10^{-5}$ cm^{2}s^{-1} and b) $D=0.33\times10^{-5}$ cm^{2}s^{-1} together with the corresponding graphical analysis of the data; $\ln(I/I_0)\equiv\ln(I_{(2\tau,G)}/I_{(2\tau,0)})$.

from 0 to approximately 30 G cm^{-1} in ten steps while δ and Δ were kept constant. Figure 3a shows the signal attenuation of a small molecule, the diffusion coefficient of which is 1.81×10^{-5} cm^{2}s^{-1}, while Figure 3b shows the signal attenuation of another molecule having a diffusion coefficient of 0.33×10^{-5} cm^{2}s^{-1}. This figure shows that there is a more prononced attenuation of the signal intensity for the fast diffusing species as reflected by the steeper slope of the graph of $\ln(I_{(2\tau,G)}/I_{(2\tau,0)})$ versus the b values. It should be noted that $\ln(I_{(2\tau,G)}/I_{(2\tau,0)})$ is generally abreviated as $\ln(I/I_0)$.

3.2. The Stimulated Echo Diffusion Sequence

The standard stimulated echo (STE) diffusion experiment is shown in Figure 4a.[32] This sequence contains three 90° pulses; the echo after the third RF pulse was named by Hahn[4] as the "stimulated echo". The signal intensity of the STE diffusion experiment with rectangular pulse gradients is thus given by Equation (15).[32] From this equation it is clear

$$\begin{aligned} I_{(T_M+2\tau,G)} &= (I_{(0,0)}/2)\exp\left[\left(\frac{-2\tau}{T_2}\right)-\left(\frac{T_M}{T_1}\right)\right] \\ \exp(-\gamma^2 G^2\delta^2(\Delta-\delta/3)D) &= I_{(T_M+2\tau,0)}\exp(-\gamma^2 G^2\delta^2(\Delta-\delta/3)D) \end{aligned} \tag{15}$$

that the effects of relaxation and diffusion can again be separated in the signal decay. It was shown by performing the diffusion experiments with constant time intervals that the normalized signal decay in the STE diffusion experiments has the same dependency as the PGSE experiment.[5a,32] Comparison of Equation (15) with the expression for the signal

 © 2005 Wiley-VCH Verlag GmbH & Co. KGaA, Weinheim

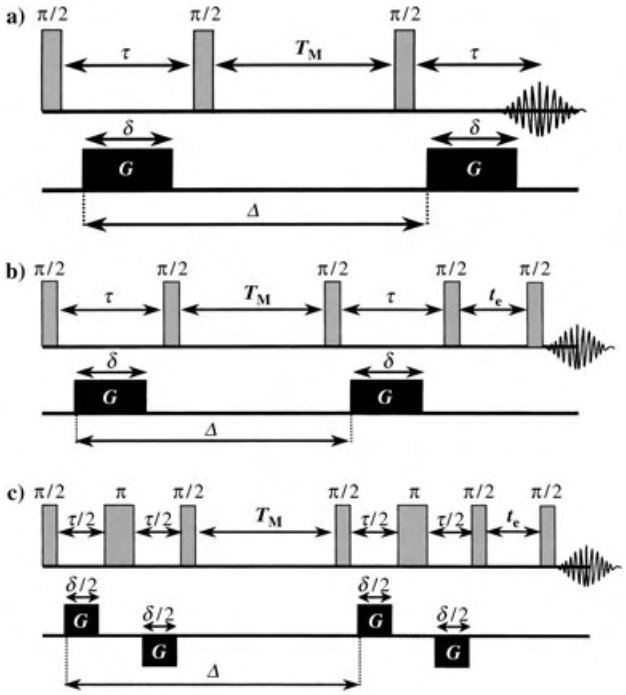


Figure 4. a) The STE diffusion pulse sequence,[32] b) the LED pulse sequence,[33] and c) the bipolar LED (BPLED) pulse sequence.[35a]

intensity of the PGSE [Eq. (13)] reveals two differences between the two equations: the reduction of the amplitude by a factor of two and—more importantly in the context of diffusion—the relaxation attenuation of the stimulated echo is dependent on T_1 during most of the diffusion interval (that is, during the time interval between the second and the third 90° pulses). This observation implies that one can use a STE diffusion sequence to obtain diffusion spectra of systems characterized by short T_2 times. This is an advantage since, in many systems, T_1 is significantly longer than T_2. The STE diffusion sequence allows an increase of the diffusion weighting by "paying" in the T_1 and not the T_2 relaxation time. The use of longer diffusion times is required for increasing the b values when measuring low diffusion coefficients and in situations where the diffusion coefficients may be dependent on the diffusion times (that is, in the cases of chemical exchange or restricted diffusion). In addition, the stimulated echo diffusion sequence is more suitable for measuring diffusion of spin–spin coupled systems.

The PGSE and STE diffusion sequences were introduced long before the advent of 2D NMR spectroscopy, but an important technical development at the beginning of the 1990s was that of diffusion ordered spectroscopy (DOSY), which was introduced by Johnson, Jr. and co-workers.[33–35]

3.3. The DOSY Technique

DOSY provides a means for "virtual separation" of compounds, by providing a 2D map in which one axis is the chemical shift while the other is that of the diffusion coefficient.[34–35] It is based on the longitudinal eddy-current delay (LED) and bipolar LED sequences and, more recently, 3D DOSY experiments have also been presented. We shall provide only a brief introduction to DOSY and the interested reader should refer to the comprehensive review recently published.[34]

3.3.1. The Basic LED and BPLED Experiments

An important requirement of the DOSY technique is the ability to discriminate between diffusion coefficients even when signals for similar-sized molecules overlap. To accomplish this goal it is essential to minimize spectral distortions that may result from eddy currents, which are induced from the gradient pulses and may, consequently, generate spectral distortions. The best way to avoid the effects of eddy currents is to prevent their formation in the first place. However, in spite of the best efforts, they may still be significant, especially when strong gradient pulses are used with short delays. Therefore, the LED sequence,[33] which is a modification of the stimulated echo sequence shown in Figure 4a, was introduced (Figure 4b).

As shown in Figure 4, the difference between these two sequences is the addition of two 90° pulses and a delay t_e at the end of the stimulated echo sequence. As a result of the fourth 90° pulse, the magnetization is stored in the longitudinal direction while the eddy currents decay. After the eddy current settling period t_e, the magnetization is recalled with an additional 90° pulse and an acquisition takes place (Figure 4b).

The bipolar LED (BPLED) sequence,[35a] which is a modification of the LED sequence, is shown in Figure 4c. In this sequence, each gradient pulse in the LED sequence is replaced by two pulses of different polarity separated by a 180° pulse. There are two advantages to using the BPLED over the LED experiment: Firstly, eddy currents are reduced to a minimum and, secondly,[35b] the effective gradient output is doubled. Thus, this sequence is useful in cases where large gradients are required to measure relatively low diffusion coefficients. For these reasons BPLED is the sequence of choice at present for many DOSY experiments. The DOSY sequence was also coupled into other methods such as INEPT and DEPT.[36]

3.3.2. The 2D DOSY Technique

The diffusion experiments presented above can be processed and displayed as a 2D matrix with chemical shifts plotted along one axis and diffusion coefficients plotted along the perpendicular axis (Figure 5). While the chemical shift information is obtained by fast Fourier transformation (FFT) of the time domain data, the diffusion information is obtained by an inverse Laplace transformation (ILT) of the signal decay data (Figure 6). The goal of the DOSY experiment is to separate species spectroscopically (not physically) present in a mixture of compounds. In this sense, the use of the DOSY experiment is reminiscent of the physical separation of compounds by chromatography. Thus, DOSY is also termed "NMR chromatography".[37] Figure 5 illustrates this concept. Each horizontal line represents a distinct diffusion coefficient

 © 2005 Wiley-VCH Verlag GmbH & Co. KGaA, Weinheim

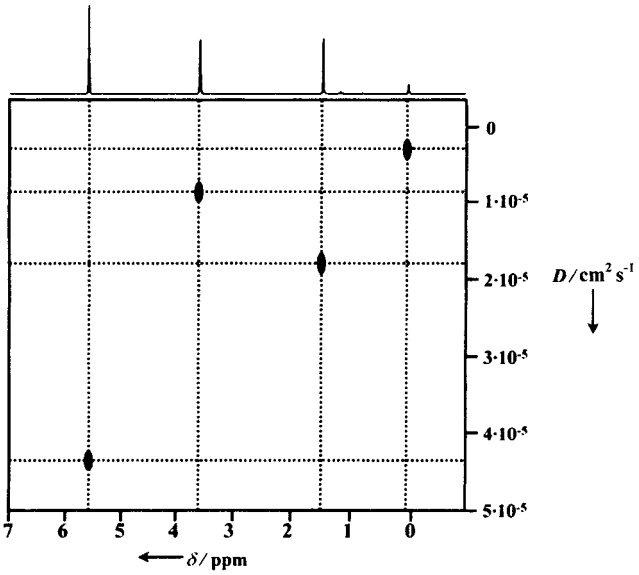


Figure 5. 2D DOSY spectrum showing four different species characterized by four different diffusion coefficients.

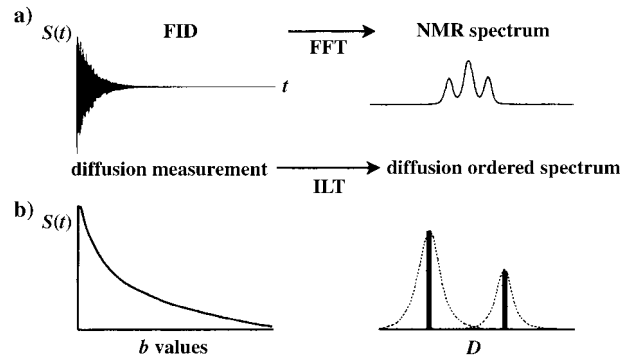


Figure 6. Comparison of FFT and ILT transformations. In contrast to the FT for the inverse laplace transform (ILT), there is not a single solution. Adapted with permission from Ref. [34].

and, hence, all the peaks on this horizontal line correlate with signals in the chemical shifts dimension, and should be attributed to a specific molecular species.

At a certain frequency, where a continuum of diffusion coefficients should be considered, the data sets $I(s)$, which describe the attenuation of this signal, should be described as Equation (16) ($\lambda = D(\Delta - \delta/3)$ and $s = \gamma^2\delta^2 G^2$). From Equation (16) it can be seen that $I(s)$ is the Laplace transform of $a(\lambda)$ and that $a(\lambda)$ is the Laplace spectrum of the diffusion coefficients. Thus, the desired spectrum $a(\lambda)$ is the inverse Laplace transform (ILT) of the decay function $I(s)$.

$$I(s) = \int_0^\infty a(\lambda)\exp(-\lambda s)\mathrm{d}\lambda \qquad (16)$$

It should be noted that a perfect transform produces the Laplace transform of delta functions and the inverse transformation should therefore exist. The required situation is that a unique transformation will exist as in the case of the FT shown in Figure 6a. However, there is no perfect transformation and the dotted lines in Figure 6b are the practical results which depict this statement. Hence, when running a DOSY experiment it is preferable that the diffusion coefficients differ as much as possible from one another and the standard errors in the diffusion coefficients be as marginal as possible.

3.3.3. *The 3D DOSY Technique*

In 3D DOSY experiments a diffusion coordinate is added to the conventional 2D map. Like the conventional 2D applications, these experiments reduce the probability of spectral overlap by spreading the NMR signals of the same species over an entire 2D plane[6–8] rather than along a single axis, while spreading the different species on a third axis on the basis of their diffusion coefficients. Indeed, in the first 3D DOSY experiment,[38] which was a DOSY-NOESY sequence, the overlapping peaks from a DNA duplex and a dinucleotide were resolved.

Figure 7a shows the pulse sequence for a DOSY-COSY experiment.[39a] This pulse sequence is constructed by linking the BPLED and the COSY sequences, with an eddy current delay t_e introduced between the BPLED and COSY sequences. Other 3D DOSY sequences, for example, DOSY-TOCSY[39b] and DOSY-HMQC,[39c] have been reported following the same rationale. Figure 7b shows a schematic representation of the results of a 3D DOSY sequence, and depicts the ability of this sequence to "virtually separate"

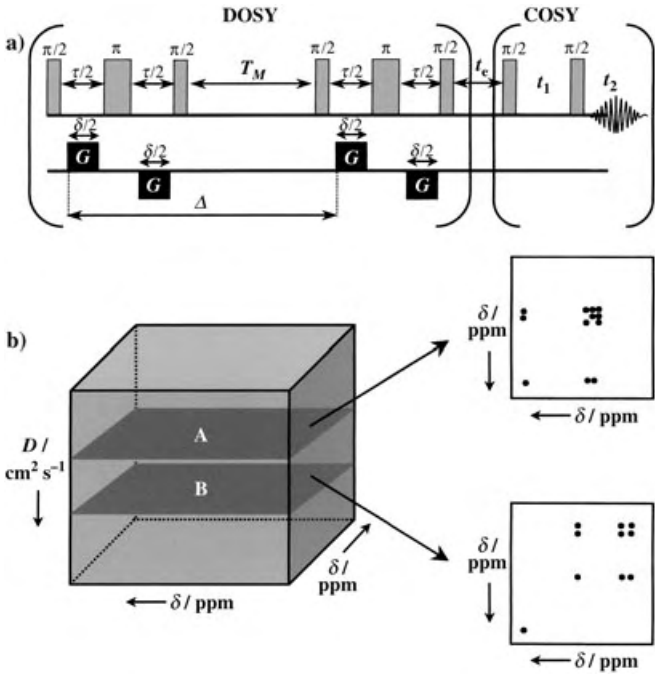


Figure 7. a) The DOSY-COSY pulse sequence[38] and b) a schematic representation of a 3D DOSY data obtained from a pulse sequence such as the one shown in (a). The DOSY-COSY experiment gives, after 3D transformation, a 2D COSY spectrum in each plane of the cube. Each plane in the cube represents a different diffusion coefficient. Adapted with permission from Ref. [34].

 © 2005 Wiley-VCH Verlag GmbH & Co. KGaA, Weinheim

different components. The various compounds are spectroscopically separated according to their different diffusion coefficients. Thus, the planes at different altitudes on the diffusion axis of the cube represents the 2D spectrum of a different species. Figure 7b shows two schematic COSY spectra of compounds A and B, which clearly differ in their diffusion coefficients. It should be kept in mind that a 3D DOSY experiment is a time-consuming method, as are all 3D NMR methods. Indeed this is one of the major disadvantages of the 3D DOSY method.

4. Applications of NMR Diffusion Measurements in Supramolecular Chemistry

4.1. Molecular Interactions

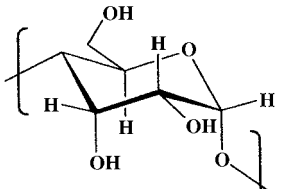
Molecular interactions, which are so essential in supramolecular and combinatorial chemistry, have been studied by many different spectroscopic methods.[40] Despite the major role played by NMR spectroscopy in these fields, diffusion NMR spectroscopy, which we believe has great potential in assisting the characterization of such systems, is still not fully exploited. However, an increasing number of applications have demonstrated this potential in recent years. Some of these applications will be outlined below in a way that emphasizes the chemical information that can be obtained from such measurements.

4.1.1 Binding and Association Constants

The association constant K_a is a valuable measure that quantifies molecular interactions. In recent decades, tens of thousands of such constants have been determined by many different methods.[40,41] Despite the fact that NMR spectroscopy has become an important tool for studying association constants over the last two decades, diffusion NMR spectroscopy was not even mentioned as a possible option for studying host–guest systems in many of these reviews.[40a,42] Only a few very recent reviews devoted a short paragraph to the use of diffusion NMR spectroscopy for determining association constants.[43]

It was suggested many years ago that diffusion can be used to determine association constants.[44] The first example of such an application on a system that can be classified as an organic host–guest system was reported by Stilbs et al., who pioneered diffusion NMR spectroscopy of chemical systems by using a home-built gradient system.[45] In 1983 they measured the K_a values of different alcohols with α- and β-cyclodextrins (α-CD (**1**) and β-CD (**2**)) in D_2O.[46] The experimental errors for the determined association constants were relatively high in some cases.[46] However, the advancement of gradient technology has made such measurements much more accurate and reliable today.

In fact, since NMR diffusion coefficients can be directly observed by NMR spectroscopy, it can be used in a very similar way as chemical shifts to determine the stoichiometry and association constants of complexes.[43,44,46,47] For the simple case of a 1:1 stoichiometric host–guest complex



1 $n = 6$
2 $n = 7$
3 $n = 8$

(HG) formed between a host (H) and a guest (G), K_a is determined by Equation (17), where [H], [G], and [HG] are

$$K_a = \frac{[HG]}{[H]\,[G]} \tag{17}$$

the concentrations of the host, guest, and host–guest complex formed at equilibrium, respectively. In the case of slow exchange on the NMR time scale, the association constant can be determined by simple integration of the peaks of a solution of known concentrations. In these cases, diffusion measurements can only be used to probe the association between the different molecular species, however, numerical values of K_a cannot be obtained. However, in the case of fast exchange, the numerical value of the association constant can be determined.

The rationale behind the extraction of the bound fraction from diffusion NMR measurement is simple:[43,44,46,47] The host and guest have their own diffusion coefficients in the free state that reflect their molecular weight and shape. However, when a complex is formed and the host and guest are tightly bound, they should have the same diffusion coefficient since they diffuse as a single molecular entity.[44,46,47] In the case of a weak or negligible association, the diffusion coefficients of the host and the guest will remain unchanged. For any other case, assuming fast exchange on the NMR time scale, the observed (measured) diffusion coefficient (D_{obs}) is a weighted average of the free and bound diffusion coefficients (D_{free} and D_{bound}, respectively) and can, therefore, be used to calculate the bound fraction X, as shown in Equation (18), in the same

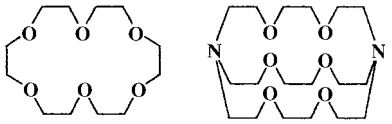
$$D_{obs} = X\,D_{bound} + (1-X)\,D_{free} \tag{18}$$

way that chemical shifts are used. Therefore, in principle, the same graphical and curve-fitting methodologies used to obtain K_a values from changes in chemical shifts in titration experiments[43] can be used to obtain association constants from diffusion NMR measurements. The most important difference between the two methods is that in many cases a complete titration to find D_{bound} for the guest is not a necessity with the former method. This is true in cases where there is a large difference between the molecular weight of the host and the guest (usually the guest has a significantly lower molecular weight) and, hence, one can predict, a priori, that the D_{bound} value of the guest will be very similar to the D_{free} value of the much larger host.[47]

One of the first examples of the determination of an association constant in the context of supramolecular chemis-

 © 2005 Wiley-VCH Verlag GmbH & Co. KGaA, Weinheim

try by diffusion NMR spectroscopy using a conventional high-resolution NMR probe on a commercial instrument was the determination of the association constants of methylammonium chloride with [18]crown-6 (**4**) and [2.2.2]cryptand (**5**) in



4 **5**

water and methanol.[47] Figure 8 shows the signal decay of **4** and methylammonium chloride in the absence and presence of **4** in methanol as a function of the gradient strength (G).

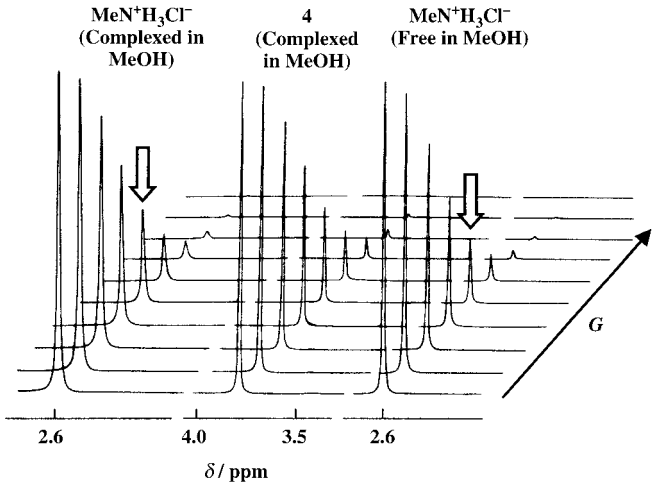


Figure 8. The signal decays in the Stejskal–Tanner diffusion experiments performed on a 50 mM solution of **4** and $MeNH_3^+Cl^-$ (1:1) in CD_3OD (middle and left) and on a 50 mM solution of free $MeNH_3^+Cl^-$ in CD_3OD (right). The arrows point to the difference in the intensities of the tetramethylammonium signal in the presence and absence of **4**. Reprinted with permission from Ref. [47].

This plot demonstrates that the signal attenuation of methylammonium chloride as a function of G in the presence of **4** is significantly smaller because of the formation of a complex with **4**. Here, the diffusion coefficients were extracted using the Stejskal–Tanner equation [Eq. (14)]. Figure 9 shows the normalized signal decays of **4**, methylammonium chloride, and their 1:1 mixture in CD_3OD as a function of G^2. The diffusion coefficients of these species and their 1:1 mixture, as well as the extracted association constants determined from the changes in the diffusion coefficients, are given in Table 1. The changes in the chemical shifts in the complexation of methylammonium chloride with **4** were small, thus making diffusion NMR spectroscopy an attractive alternative for determining the association constant.[47]

In principle, the determination of association constants using diffusion NMR measurements has advantages and limitations arising from the fact that this is an NMR-based

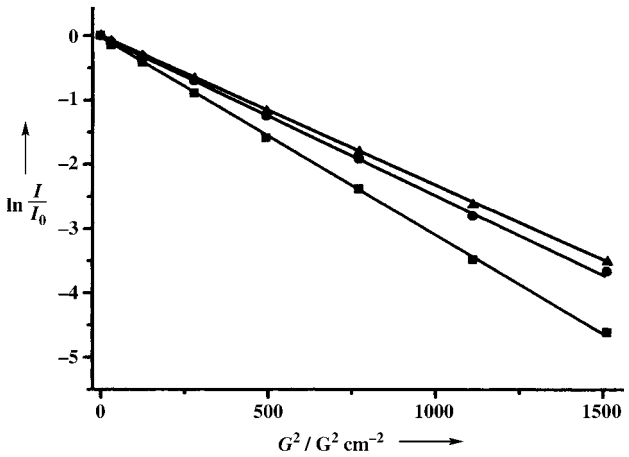


Figure 9. Normalized signal decay as a function of G^2 for methylammonium chloride in CD_3OD and methylammonium chloride and **4** (1:1) in 50 mM CD_3OD solution. ■: $MeNH_3^+Cl^-$ (free), ●: $MeNH_3^+Cl^-$ (complexed), ▲: **4**.

Table 1: Diffusion coefficients D and logarithm of the association constants K_a for the methylammonium chloride complex of [18]crown-6 (**4**) and [2.2.2]cryptand (**5**)[a] in D_2O and CD_3OD at various temperatures.[47]

Substance	Solvent	T/K	D_m [10^{-5} cm^2 s^{-1}]	$D_{MeNH_3^+}$ [10^{-5} cm^2 s^{-1}]	lg K_a [M^{-1}]
4 + $MeNH_3^+$	D_2O	298	0.55 ± 0.01	1.23 ± 0.02	0.67
4	D_2O	298	0.56 ± 0.01	–	
$MeNH_3^+$	D_2O	298	–	1.36 ± 0.01	
4 + $MeNH_3^+$	CD_3OD	298	1.34 ± 0.01	1.37 ± 0.02	3.69
4	CD_3OD	298	1.35 ± 0.02	–	
$MeNH_3^+$	CD_3OD	298	–	1.70 ± 0.01	
5 + $MeNH_3^+$	D_2O	298	0.46 ± 0.02	0.95 ± 0.04	1.53
5	D_2O	298	0.45 ± 0.04	–	
$MeNH_3^+$	D_2O	298	–	1.38 ± 0.01	
5 + $MeNH_3^+$	D_2O	277	0.21 ± 0.01	0.59 ± 0.01	1.67
5	D_2O	277	0.20 ± 0.01	–	
$MeNH_3^+$	D_2O	277	–	0.72 ± 0.01	
5 + $MeNH_3^+$	CD_3OD	298	1.14 ± 0.03	1.14 ± 0.03	> 4
$MeNH_3^+$	CD_3OD	298	–	1.64 ± 0.01	
5 + $MeNH_3^+$	CD_3OD	213	0.28 ± 0.01	0.29 ± 0.01	> 4
$MeNH_3^+$	CD_3OD	213	–	0.42 ± 0.06	

[a] All experiments were performed three times and the reported values are means ± standard deviation. m = macrocycle.

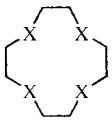
method.[43] Therefore, on the one hand, this method is less prone to misinterpretation because of minor impurities than methods based on UV and fluorescence, for example.[48] On the other hand, diffusion NMR spectroscopy is only suitable for measuring, in a direct way, association constants in the range of 10–10^5 M^{-1}. However, one of the main advantages of using diffusion NMR measurements to extract association constants, as compared with other NMR-based techniques such as chemical-shift titrations, is the elimination of one of the main possible sources of error in such techniques, namely, confusing acid–base chemistry with binding processes.[47] It should be noted, however, that in contrast to chemical shifts, proton transfer has only a marginal effect on the measured

 © 2005 Wiley-VCH Verlag GmbH & Co. KGaA, Weinheim

diffusion coefficient.[47] This property enabled simple extraction of the association constant between methylammonium chloride and **5**, where partial protonation of **5** occurred as expected.

Since the diffusion of a certain molecular species depends on its effective molecular size, which should change with any intermolecular interaction, it is clear that diffusion coefficients are intuitively related to aggregation and intermolecular interactions. This means that only in diffusion measurements can the observable parameters of the bound guest be predicted a priori, thus reducing the need for a complete titration. The main limitation of the diffusion coefficient D as a parameter for the determination of the association constant is in systems where the interacting species happen to have similar diffusion coefficients in the free state, thus making the method much less sensitive or even impractical.

Particularly interesting host–guest systems are those in which the guest itself can act as the host for yet another smaller guest. Early examples of such systems are the macrocycle complexes with γ-CD (**3**) introduced by Vögtle and Muller as early as 1979.[49] These systems, subsequently analyzed by X-ray crystallography,[50,51] were recently studied in solution by diffusion NMR measurements.[52] In this study, complexation of [12]crown-4 (**6**), cyclen (**7**), and 1,4,7,10-tetrathiacyclododecane (**8**) with γ-CD were studied in the presence and absence of salts in various solvents and in D_2O at various pH values.[52] Although the ^{1}H NMR chemical shift changes were found to be very small in these systems, the difference in the molecular weight of the different macrocycles and that of γ-CD (**3**) enabled accurate determination of these relatively weak and modest association constants.[52] Figure 10 shows the normalized signal decay of **6** in the absence and presence of γ-CD before and after addition of lithium acetate (LiOAc) as an example. The diffusion coefficients of these systems, along with the extracted association constants, are given in Table 2. Interestingly, it was found that the presence of alkali metal salts decreased the association between the macrocycles and the γ-CD and that the pH value had practically no effect on the extracted association constants, thus suggesting that hydrogen bonding is not a dominant factor governing the association constant in these host–guest systems.[52] It was also found in these complexes that hydrophobic interactions, which are the major driving force of many of the complexes formed from cyclodextrins and organic systems in water, are not the major factor responsible for complexation.[52,53] In these systems, the changes in the chemical shifts were rather small and both the cation and the γ-CD had some effect on the chemical shift of the macrocycles, which made the extraction of association constants from this parameter very difficult and problematic. This example emphasizes the advantage of using diffusion coefficients to map the interaction of many molecular species simultaneously.



6 X = O
7 X = N
8 X = S

Table 2: Diffusion coefficients D and calculated association constants K_a of the γ-CD:macrocycle, macrocycle:salt, and the three-component systems at 298 K.[a],[b][52]

System	D_3 [10^{-5} cm^2 s^{-1}]	D_m [10^{-5} cm^2 s^{-1}]	D_{OAc^-} [10^{-5} cm^2 s^{-1}]	K_a [M^{-1}]
6 + **3** + LiOAc	0.27 ± 0.01	0.56 ± 0.01	0.86 ± 0.02	11
6 + **3**	0.27 ± 0.01	0.48 ± 0.01	–	187
6	–	0.68 ± 0.02	–	
3	0.32 ± 0.02	–	–	
LiOAc	–	–	1.02 ± 0.01	
6 + LiOAc	–	0.60 ± 0.01	0.90 ± 0.01	40
7 + **3** + LiOAc	0.30 ± 0.01	0.53 ± 0.01	0.96 ± 0.01	19
7 + **3**	0.29 ± 0.01	0.42 ± 0.01	–	165
7	–	0.60 ± 0.01	–	
3	0.32 ± 0.02	–	–	
LiOAc	–	–	1.09 ± 0.01	
7 + LiOAc	–	0.58 ± 0.01	0.96 ± 0.01	29
8 + **3** + LiOAc	0.19 ± 0.02	0.36 ± 0.02	0.82 ± 0.01	21
8 + **3**	0.19 ± 0.01	0.34 ± 0.02	–	69
8	–	0.41 ± 0.02	–	
3	0.24 ± 0.02	–	–	
LiOAc	–	–	0.87 ± 0.02	
8 + LiOAc	–	0.39 ± 0.01	0.84 ± 0.01	10

[a] All experiments were performed three times and the reported values are averages ± standard deviation. [b] Systems with **6** and **7** were measured in a D_2O solution at pD = 7.6 while the system with **8** was measured in [D_6]DMSO. m = macrocycle.

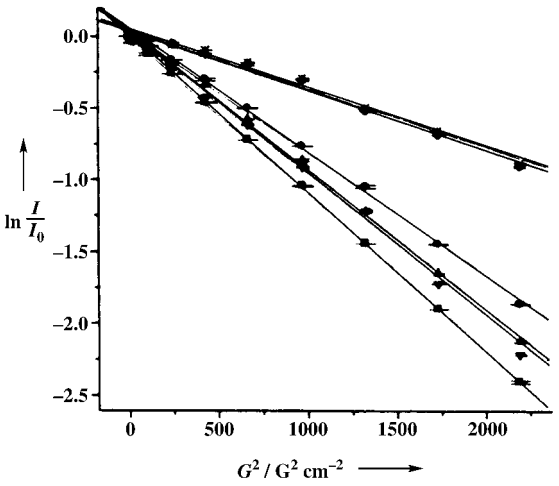
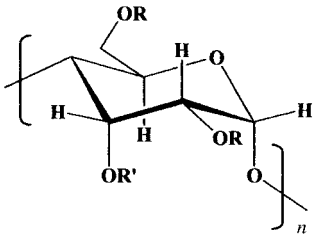


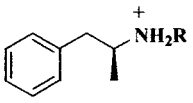
Figure 10. Normalized signal decay as a function of the gradient strength squared (G^2) in D_2O,; ■: **6**, ●: **6** (+ **3**), ▲: **6** (+ LiOAc + **3**), ▼: **6** (+ LiOAc), ◆: **3** (+ LiOAc + **6**), ⋆: **3** (+ **6**). All measurements were performed at 298 K and pD = 7.6. Adapted with permission from Ref. [52].

Gafni et al. demonstrated for the first time that diffusion NMR measurements provide a means to probe enantiomer discrimination by lipophilic cyclodextrins.[54] It was found that the α-cyclodextrin derivative **9** and its β analogue (**10**) show some chiral discrimination when complexed with amphetamine (**12**), ephedrine (**13**), and propranolol (**14**). The highest $K_{(+)}/K_{(-)}$ value was found for propranolol (**14**) with **10**. Interestingly, when the 3-position of **9** and **10** were blocked, as in **11**, no enantiomeric preference could be found.[54] Both the changes in the chemical shifts and the T_1 relaxation times were also measured in these systems. Complex formation resulted in these parameters changing in different directions,

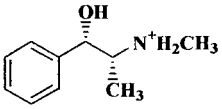
 © 2005 Wiley-VCH Verlag GmbH & Co. KGaA, Weinheim



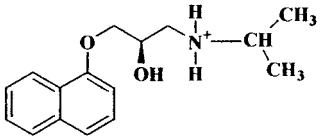
9: R = $C_{12}H_{25}$ R′ = H $n = 6$
10: R = $C_{12}H_{25}$ R′ = H $n = 7$
11: R = $C_{12}H_{25}$ R′ = CH_3 or C_8H_{17} $n = 7$



(*S*) - (+) - **12**
R = H



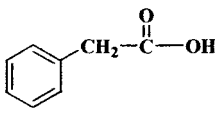
(1*S*,2*R*) - (+) - **13**



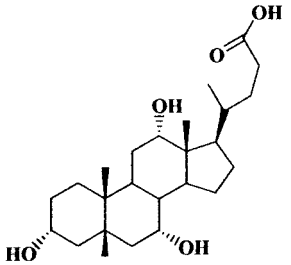
(*R*) - (+) - **14**

and the diffusion coefficient, which changed uniformly for all signals, was found to be the most robust parameter for characterization of the association constant for these systems.

As previously stated, one of the main advantages of using diffusion coefficients to extract the association constants of host–guest systems, as compared with chemical shifts for example, is the fact that D_{bound} for the guest is usually not very different from that of D_{free} of the host since the host is much larger than the guest in most host–guest systems. This may, in some cases (but not all), eliminate the need for a complete titration to describe the binding curve. It is clear that the larger the difference in the size of the interacting molecules, the better this approximation, and Cameron and Fielding recently tested this assumption both theoretically and experimentally.[55] It was found that when β-CD ($M_r = 1135$) forms a complex with cyclohexylacetic acid (**15**, $M_r = 136$) with $K_a = 1800 \pm 100$ there is a small gradual reduction in the diffusion



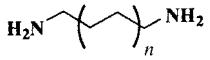
15



16

coefficient of β-CD upon addition of **15**, but these changes were on the order of the error bars of the diffusion measurements. However, much more significant changes in the value of D_{host} were found following the addition of cholic acid (**16**, $M_r = 420$) as the guest, which implies that $D_{complex}$ differs from D_{host} and thus emphasizing the need for a complete titration, or at least measurement at several different mixing ratios, to obtain the binding curve in this complex. These results clearly indicate that a single binding experiment using diffusion NMR spectroscopy needs to be viewed with caution in cases where the different partners of the host–guest systems are similar in size.[43,51,55]

Diffusion measurements were used recently to probe the interactions of α-CD-based pseudorotaxanes with diaminoalkanes (**17**).[56a] The motivation of this study included the



17a: $n = 1$ **17f:** **17a** · 2HCl
17b: $n = 2$ **17g:** **17b** · 2HCl
17c: $n = 3$ **17h:** **17c** · 2HCl
17d: $n = 4$ **17i:** **17d** · 2HCl
17e: $n = 5$ **17j:** **17e** · 2HCl

verification of whether protonation could convert these pseudorotaxanes into rotaxanes,[57] and hence there was a need to determine the association constants of the different diaminoalkanes before and after protonation.[56a] Since the changes in chemical shifts upon the formation of these pseudorotaxanes are small, and to avoid attributing chemical shift changes arising from protonation to binding phenomena (in the case of the protonated amines), diffusion measurements rather than NMR chemical shift titrations were used. Representative diffusion coefficients in these systems along with the $\lg K_a$ values extracted for these systems are shown in Table 3. Only in the last entry, which describes the formation of the pseudorotaxanes from α-CD and **17e**, was a small effect on the diffusion coefficient of **1** observed. A dependency was found between the length of the diaminoalkanes and the association constants to **1** (Figure 11).[56a] It was found that protonation considerably reduced the stability of the pseudorotaxanes formed with the shorter diaminoalkanes. Only with the longest diaminoalkane studied, that is, diaminododecane (**17e**), were the same association constants found for the diaminoalkane and its corresponding disalt.

The simple PGSE technique was also used to study the binding affinity of the peptidocalixarene **18**,[58] a vancomycin mimic prepared by Ungaro and co-workers.[59] Vancomycin is an important antibiotic that acts by binding to the mucopeptide precursors of the cell wall through the terminal D-alanyl-D-alanine sequence.[60] Recently, however, resistance toward this class of antibiotics has been reported and the need for synthetic analogues of vancomycin has emerged.[61] Since **18**, like vancomycin, contains several functional groups of different types, its interaction with the D-alanyl-D-alanine residue may be a superposition of electrostatic and/or hydrophobic interaction and may also involve π–hydrogen and dipole–dipole interactions or hydrogen bonds. Therefore, the association constant had to be determind in different solvents with guests having or lacking the D-alanyl-D-alanine residue (**19**–**24**). Diffusion NMR spectroscopy was used since NMR titration was difficult to apply and gave inconsistant results with relatively large errors. From the changes in the diffusion coefficients of a series of guests, some of which contain one or two alanine residues, upon addition of **18** in different solvents it was concluded that[58] in $CDCl_3$ **18** forms a complex of

 © 2005 Wiley-VCH Verlag GmbH & Co. KGaA, Weinheim

Table 3: Diffusion coefficients D and the computed $\lg K_a$ values of host α-CD and guests **17a**, **17b**, **17c**, **17d**, **17e** in D_2O at 298 K.[56a]

System	D_{amine} [$\times 10^{-5}$ cm^{2}s^{-1}]	D_{CD} [$\times 10^{-5}$ cm^{2}s^{-1}]	D_{water} [$\times 10^{-5}$ cm^{2}s^{-1}]	X[a]	$\lg K_a$ [M^{-1}]
α-CD [2.8 mM]		0.30 ± 0.01	1.96 ± 0.01	–	–
17a	0.76 ± 0.01	–	1.97 ± 0.01	–	–
17a:α-CD (1:2.9)	0.71 ± 0.01	0.29 ± 0.01	1.97 ± 0.01	0.11 ± 0.03	1.18 ± 0.14
17b	0.65 ± 0.01	–	1.96 ± 0.01	–	–
17b:α-CD (1:5.1)	0.49 ± 0.02	0.30 ± 0.01	1.96 ± 0.01	0.46 ± 0.04	1.81 ± 0.07
17c	0.60 ± 0.01	–	1.96 ± 0.01	–	–
17c:α-CD (1:0.8)	0.47 ± 0.01	0.29 ± 0.01	1.95 ± 0.01	0.42 ± 0.05	2.83 ± 0.21
17d	0.55 ± 0.01	–	1.96 ± 0.01	–	–
17d:α-CD (1:0.7)	0.38 ± 0.01	0.29 ± 0.01	1.96 ± 0.01	0.65 ± 0.06	4.13 ± 0.30
17e	0.50 ± 0.01	–	1.94 ± 0.01	–	–
17e:α-CD (1:0.9)	0.32 ± 0.01	0.26 ± 0.01	1.94 ± 0.01	0.75 ± 0.10	3.85 ± 0.27

[a] The bound molar fraction.

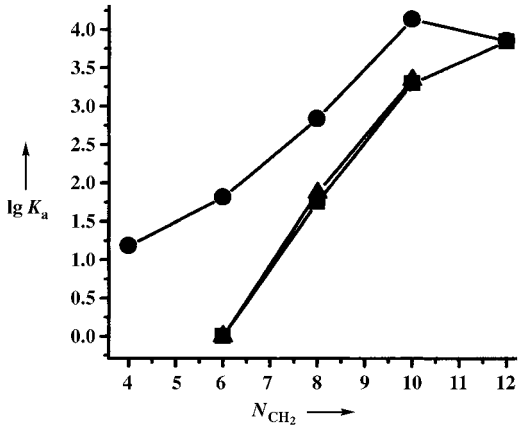
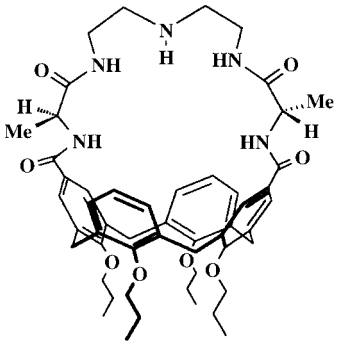
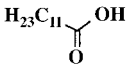


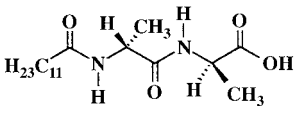
Figure 11. $\lg K_a$ values determined from diffusion data as a function of the number of CH_2 groups N_{CH_2} in the α-CD pseudorotaxanes of α,ω-diaminoalkanes (**17a**–**e**; ●) as well as their respective disalts before (▲) and after the addition of DCl (■). These experiments were performed on approximately 3 mM samples with an acquisition time of 20 minutes. Reproduced with permission from Ref. [56a].



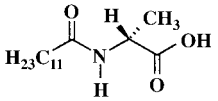
18



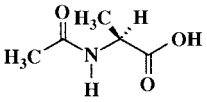
19



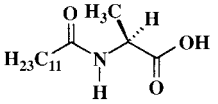
22



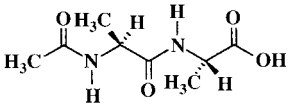
20



23



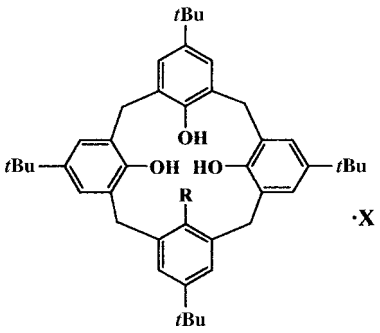
21



24

moderate stability with lauric acid (**19**; $\lg K_a = 2.7 \pm 0.2$) and stronger complexes with guests containing alanine residues ($\lg K_a \sim 4.0$). Hydrogen-bond-competing solvents resulted in a decrease in the K_a values, with this decrease being more pronounced in complexes formed between **18** and guests **20**, **23**, and **24**, which contain the alanine group, than in the complex of **18** with **19**. The K_a values determined by diffusion NMR spectroscopy for the various guests in the different solvents are consistant with the fact that hydrogen bonds (amongst other factors) play a significant role in these complexes in chloroform. This study was the first direct quantitative evaluation of the binding constant of **18** with dipeptides, since it was not possible to determine the K_a values of these complexes by classical ^{1}H NMR experiments. This result demonstrates that diffusion measurements may be superior to standard NMR techniques for determination of the association constants when complexation is associated with proton exchange.

A demonstration of the ability of a quick qualitative measurement of diffusion coefficients in determining the mutual interaction between different molecular species in solution is the study of the *p-tert*-butylcalix[4]arene–Cs–CH_3CN complex **25** in $CDCl_3$.[62] The solid-state structure of this complex, in which a CH_3CN molecule was found to be coordinated to the cesium ion, was said to maintain its structure in solution based on its cesium NMR spectrum.[63] The ^{1}H NMR spectrum of the isolated crystals and a side view of the crystal structure of **25** are shown in Figure 12a and Figure 12b, respectively. Figure 12c shows the signal decays for the signals of the *tert*-butyl group of **25**, the CH_3CN molecules originating from the dissolved crystals of complex **25**, and the signal decay of the solvent ($CHCl_3$). This figure clearly demonstrates that the CH_3CN molecules have a much higher diffusion coefficient than the complex, which is the



25 R : O^- X : Cs^+ ···· N≡C–CH_3

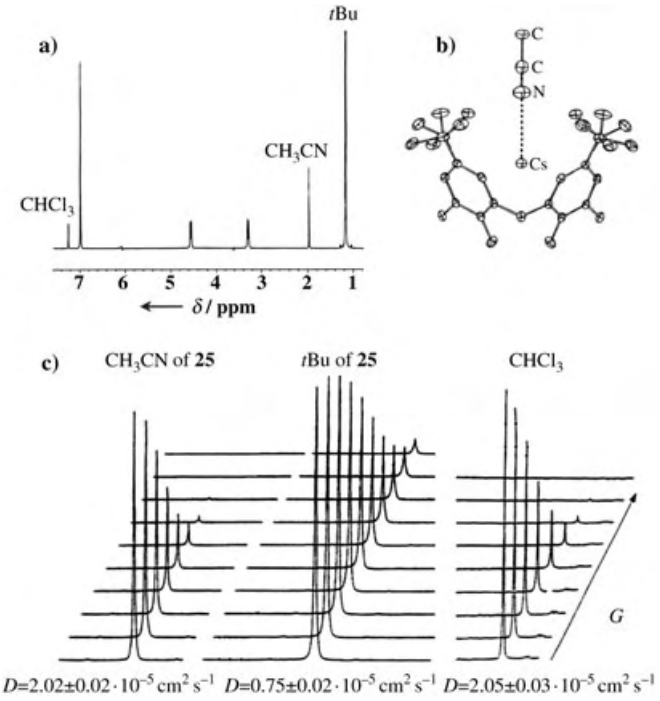


Figure 12. a) Section of the ^{1}H NMR spectrum (500 MHz) of **25** (crystallized from CH_3CN) in a $CDCl_3$ solution; b) side view of the crystal structure of **25**;[63] and c) the signal decay in a PGSE experiment of the *tert*-butyl signal of **25**, the CH_3CN originating from complex **25**, and $CHCl_3$ as a function of the gradient strength (*G*). The diffusion coefficient extracted for each signal is indicated.[62]

expected result if there is no interaction between the small CH_3CN molecule and the much larger complex. Comparison of the diffusion coefficient of the CH_3CN signal originating from the crystals of **25** with the diffusion coefficient of CH_3CN in $CDCl_3$ ($2.01 \pm 0.02 \times 10^{-5}$ $cm^2 s^{-1}$) led to the conclusion that, as expected, there is practically no interaction between the CH_3CN molecules and the complex in $CDCl_3$.[62] In fact, a clear visualization of the lack of interaction is obtained conclusively from Figure 12c. It should be noted that the entire diffusion experiment shown in Figure 12c, which proves unequivocally that there is no interaction between CH_3CN and the other part of complex **25**, was acquired in 10 minutes, thus demonstrating the robustness of this approach for determining molecular interactions in solution. In contrast, the acquisition of only a single ^{133}Cs NMR spectrum of the same sample, just to ascertain that complex **25** was indeed obtained, required several hours.

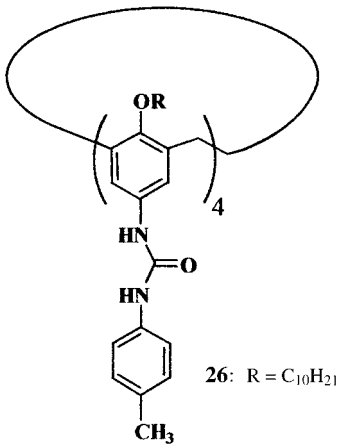
The determination of association constants by using diffusion NMR spectroscopy is based on the fact that there is a fast exchange between the free and bound states of the guest. However, there are important applications of diffusion measurements, even in the case of slow exchange—such as for the study of molecular capsules and the encapsulation phenomenon outlined in the next section.

4.1.2. Encapsulation and Molecular Capsules

Molecular capsules in general,[64,65] and those obtained by self-assembly in particular, are intriguing molecular systems that have attracted considerable attention over the last decade.[64–66] Molecular capsules are molecules that can accommodate smaller molecules in their cavity, thus isolating them from the immediate bulk, and can therefore, be regarded as microreactors.[67] Indeed, in recent years, such systems have been used to stabilize reactive intermediates[67a] and enhance the rate of some reactions.[67b,c]

The diffusion coefficient should be a powerful tool for detecting and probing encapsulation,[68] since the encapsulated guests are generally much smaller molecular species than the capsule itself and, therefore, should have a much higher diffusion coefficient in its free state. Moreover, the encapsulated molecules, which are in slow exchange with the bulk, should have the same diffusion coefficient as the capsule itself since the capsule and the encapsulated molecules diffuse as a single molecular entity.[68]

Such a diffusion-based argument was used recently to probe benzene encapsulation in the tetraureacalix[4]arene dimer (**26**·**26**).[68] Figure 13a shows part of the ^{1}H NMR



26: R = $C_{10}H_{21}$

spectrum of dimer **26**·**26** prepared in a 80:20 mixture of C_6H_6 and C_6D_6. The signal at about $\delta = 4.4$ ppm was suspected to be that of the encapsulated benzene. Figure 13b shows the decay of this signal, the signal of "free" benzene (at $\delta = 7.15$ ppm), and one representative signal of the dimer (at $\delta = 1.95$ ppm) as a function of the diffusion gradient strength *G*. This figure

 © 2005 Wiley-VCH Verlag GmbH & Co. KGaA, Weinheim

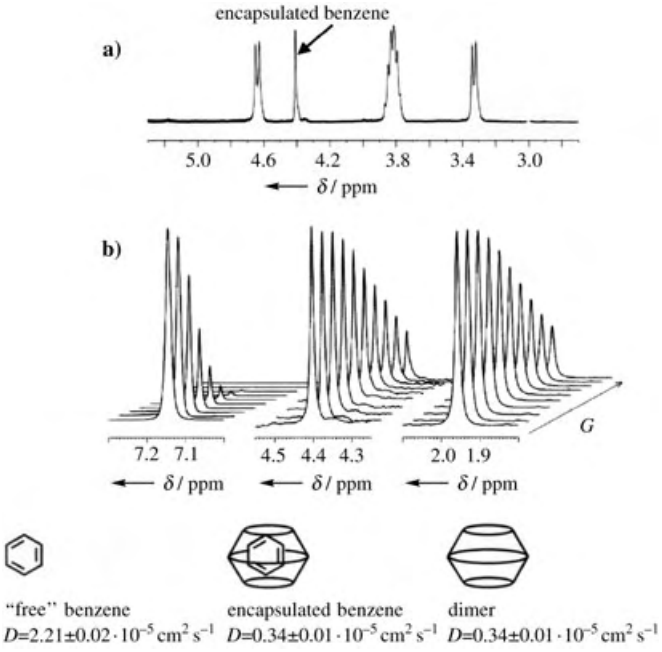


Figure 13. a) Section of the ^{1}H NMR spectrum (500 MHz) of **26** in an 80/20 (v/v) solution of benzene and C_6D_6. b) ^{1}H NMR spectra (500 MHz) of the same sample (recorded with a Stejskal–Tanner diffusion experiment). The figure shows the decay of the signal intensity as a function of *G*. For clarity, only the signal of **26** at $\delta = 1.95$ ppm and the signals attributed to the "free" and encapsulated benzene at $\delta = 7.15$ and 4.4 ppm, respectively, are shown.[68]

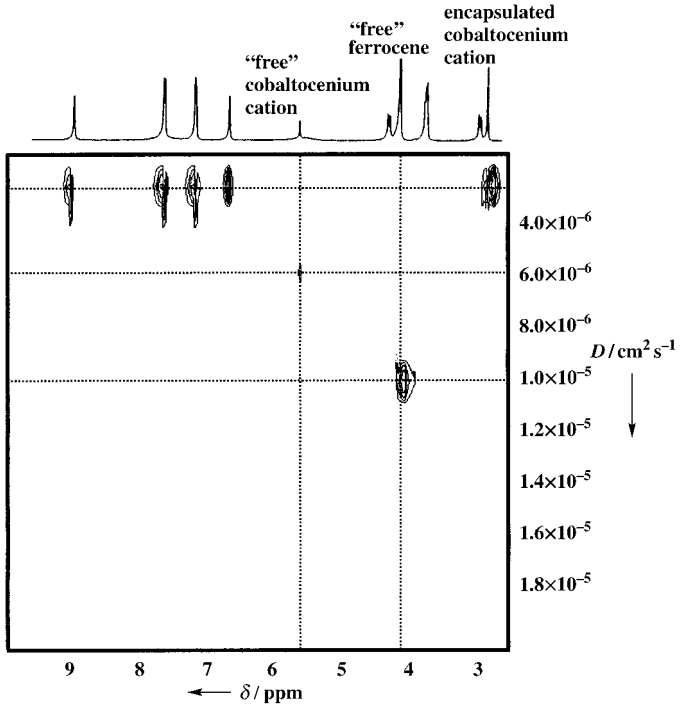


Figure 14. The DOSY spectrum (400 MHz, 298 K) of a solution containing **26**, ferrocene, and cobaltocenium cation in $C_2D_4Cl_2$. The signal at $\delta = 2.72$ ppm, suspected to be the encapsulated cobaltocenium cation, has the same diffusion coefficient as all the signals of **26**·**26**. The signals of the free ferrocene and cobaltocenium cation at $\delta = 4.06$ and 5.61 ppm, respectively, were found to have much higher diffusion coefficients, as expected.

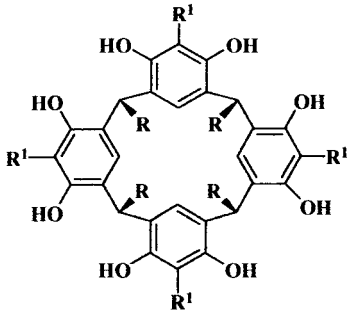
demonstrates that the signal at $\delta = 4.4$ ppm has a much lower diffusion coefficient than that of the free benzene, and that the extracted diffusion coefficient for this signal ($0.34 \pm 0.01 \times 10^{-5}$ cm^{2}s^{-1}) was exactly the same as the one determined for the dimer[68] and illustrates that, as expected, the encapsulated benzene and the dimer diffuse as a single molecular entity. A titration experiment in which the diffusion coefficients of the dimer and the DMSO molecules added to the benzene solution of **26**·**26** were followed demonstrated that it was possible to determine by diffusion NMR spectroscopy that about four DMSO molecules per molecule of **26** are required to disrupt the dimer.[68]

Frish et al. subsequently used a similar approach to probe the encapsulation of a tropylium cation by **26**·**26** in an attempt to evaluate the relative importance of electronic effects, namely, the importance of π–cation interactions[69], in determining the guest affinity for the cavity of the dimer. It was found that π–cation interactions indeed play an important role in determining the relative affinity toward the dimer cavity, as it was found that the tropylium cation affinity is about four orders of magnitude larger than that of benzene, which happens to have a very similar size.[70a] The same approach was recently used to demonstrate that the affinity of the cobaltocenium cation is at least five orders of magnitude larger than that of ferrocene.[70b] The DOSY spectrum shown in Figure 14 demonstrates how easy and simple the analysis and mapping of the mutual interactions was between the different molecular species that prevail in the solution, that is, between ferrocene, the cobaltocenium cation (bound and free), and the dimer **26**·**26**.

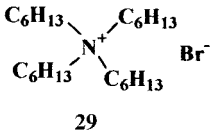
These small complexes are relatively simple systems that are assembled, in most cases, from only three molecular species. However, as will be demonstrated, the advantage of using diffusion NMR spectroscopy to map the interactions between different molecular species may be even more important in systems that contain multiple molecular species and interactions.

Recently, the potential of simple diffusion NMR experiments in mapping the different molecular interactions in the spectacular resorcinarene hexamer capsule,[71] first characterized by Atwood and co-workers,[72] was demonstrated. Atwood's group showed that **27a** forms a hexamer of the type $[(\mathbf{27a})_6(H_2O)_8]$ in the solid state.[72] It was shown subsequently by Shivanyuk and Rebek that **27b** forms such a hexamer in the presence of suitable guests in water-saturated $CDCl_3$.[73] It was found that the cation of tetrahexylammonium bromide (THABr, **29**) is encapsulated in the large cavity of the hexamer.[73] The addition of THABr to **27b** resulted in a change in the chemical shifts of **27b** and the appearance of very high field signals at $\delta \sim -1.00$ ppm. On the basis of chemical shifts arguments, it was logically assumed that guest **29** induces the formation of the hexameric capsule. However, simple diffusion measurements demonstrated that this is not the case in these systems. Diffusion measurements of **27b**, before and after the addition of **29**, showed that the

 © 2005 Wiley-VCH Verlag GmbH & Co. KGaA, Weinheim



27a: R = CH_3 R^1 = H
27b: R = $C_{11}H_{23}$ R^1 = H
28: R = $C_{11}H_{23}$ R^1 = OH



29

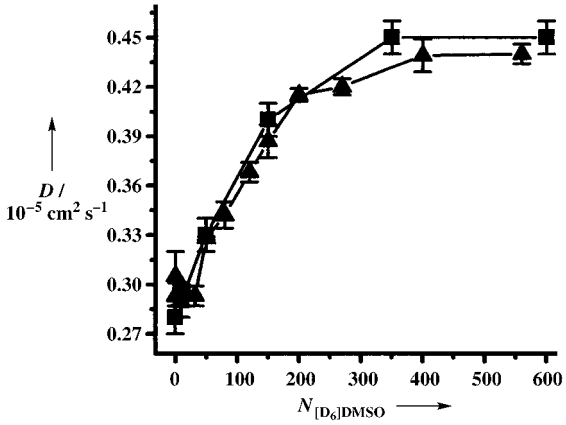


Figure 15. Changes in the diffusion coefficients *D* for the water-saturated $CDCl_3$ solutions of **27b** (■) and **27b** in the presence of **29** (▲) as a function of the addition of [D_6]DMSO ($N_{[D_6]DMSO}$: number of equivalents of added [D_6]DMSO). Adapted with permission from Ref. [71].

same diffusion coefficients (that is, $0.28 \pm 0.01 \cdot 10^{-5}$ $cm^2 s^{-1}$ for a 3 mM solution at 298 K) are obtained, within experimental error, for the two systems. This result clearly contradicted the notion that **27b** is a monomer that self-assembles into a hexamer in the presence of **29** in $CDCl_3$. Therefore, it was suggested that **27b** self-assembles spontaneously into a hexameric capsule in water-saturated $CDCl_3$.[71] Indeed, when **27b** was subsequently dissolved in water-saturated $CHCl_3$, new high-field singlets appeared at about 4.8–5.1 ppm. The peaks were tentatively assigned to encapsulated $CHCl_3$ molecules. These singlets were found to have the same diffusion coefficient as that of the resorcinarene moiety, thus further supporting the assignment of these singlets to encapsulated chloroform molecules. Moreover, addition of **29** to this chloroform solution resulted in the immediate disappearance of these signals, thus corroborating the conclusion that **27b** spontaneously self-assembles into a hexameric capsule in water-satuated $CDCl_3$. Very recently Shivanyuk and Rebek came to the same conclusion by using a different methodology.[74]

The results of titration experiments in which the diffusion coefficient of the resorcinarene moiety was measured as a function of the amount of DMSO added to the $CDCl_3$ solution are shown in Figure 15.[71] This study demonstrated that there is an increase in the diffusion coefficient of **27b** with the addition of DMSO. Very similar titration curves were found for the hexamer in the presence and absence of **29**.[71] The fact that the minor changes in the chemical shifts observed upon addition of DMSO is accompanied by an increase in the diffusion coefficient of **27b** (an increase in the viscosity of the solution is expected because of this addition) strongly supports the interpretation that the process followed is the disruption of the hexamer into its monomer.

The role of water in the formation of the hexameric capsule of **27b** and **28** in water-saturated chloroform was also studied by measuring the diffusion coefficient of the water signal and the hexamer signals in solutions with different **27b**,**28**/H_2O ratios. Only a single water signal was observed in these samples, thus indicating that the different observable water pools are in fast exchange on the NMR time scale.[75a,c] However, since the chemical shift and width of the water signal were found to be very sensitive to different parameters and to conditions other than the **27b**/H_2O ratio (Figure 16a), the measurement of diffusion coefficients was selected as an alternative method to evaluate the role of water molecules in these hexameric capsules. Figure 16b shows the effect of the **27b**/H_2O ratios on the diffusion coefficients of water and of **27b** in the presence and absence of THABr.[75a] It was found that there was a decrease in the diffusion coefficient of the water signal as the relative amount of H_2O decreased. Interestingly, the diffusion coefficient for the water signal was nearly twice that of the hexamer even when the **27b**/H_2O ratio was 6:8.4. However, the diffusion coefficient of the water signal was found to be equal to that of the hexamer when that ratio was less than 6:8 (for example, 6:7.2). It was found for the **29**@$\mathbf{27b}_6$ system that the diffusion coefficient of the water signal is still several times that of the hexamer, even when the **27b**/H_2O ratio was less than 6:8 (Figure 16b).[75b] The diffusion NMR measurements seem to indicate that the water molecules play a different role in the two capsules. In $CDCl_3$ solution and in the absence of THABr the water molecules seem to be part of the supramolecular structure of the capsule. Indeed, it was found that about eight water molecules per six molecules of **27b** have the same diffusion coefficient as **27b** in the hexamer. It should be noted, however, that diffusion measurements cannot distinguish between encapsulated water molecules and water molecules which are part of the hexamer since the water diffusion coefficient in both situations should be equal to the diffusion coefficient of the hexamer when slow exchange occurs. However, because of the fast exchange of H_2O with bulk water and the fact that $[(\mathbf{27b})_6(H_2O)_8]$-type capsules were observed in the solid state,[72] the more plausible explanation seems to be that the eight water molecules which have the same diffusion coefficient as the hexamer are part of the supramolecular structure in the solution. However, it seems that in the presence of THABr there is no need for water molecules for the construction of the supramolecular capsule.[75b] By using the same methodology (Figure 16c) it was found that water has no role in the construction of the hexameric capsule of **28** in $CDCl_3$ solutions,[75c] an observation in line with the results of X-ray crystallographic analysis of

 © 2005 Wiley-VCH Verlag GmbH & Co. KGaA, Weinheim

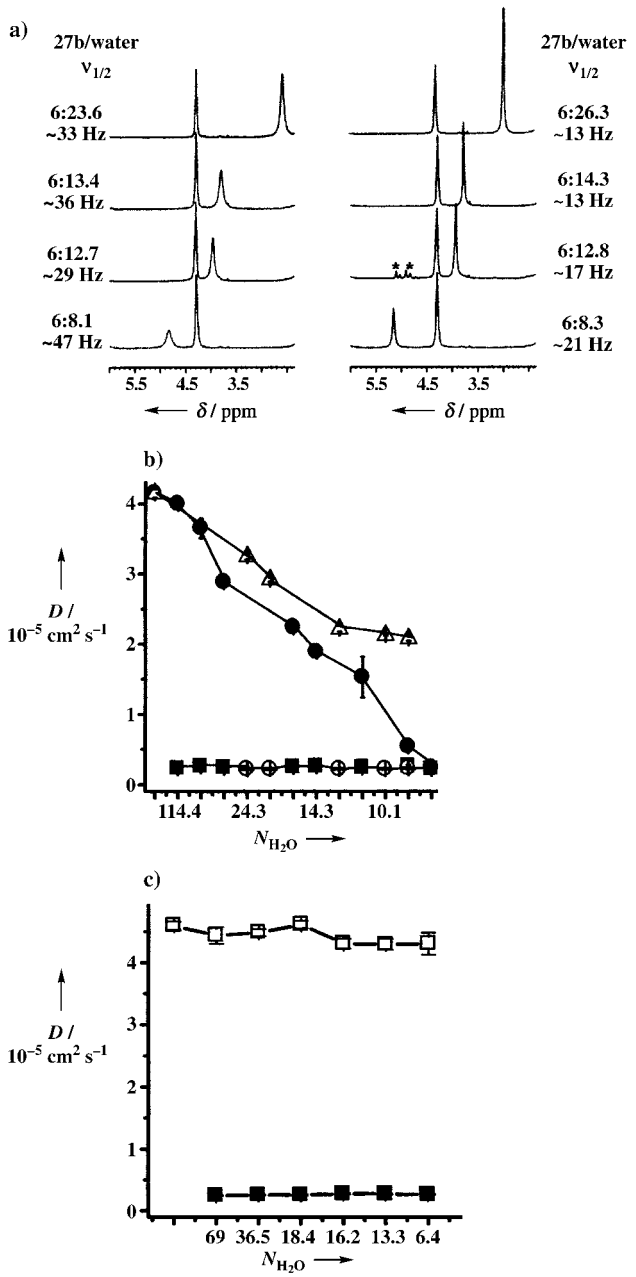


Figure 16. a) Sections of the ^{1}H NMR spectra from different studies of **27b** as a function of the **27b**/H_2O ratios for $CDCl_3$ solutions. Both the line shape and chemical shift may be very different even when the **27b**/H_2O ratio is very similar. b) Diffusion coefficients of **27b** and the water signal in the presence of **29** (○ and △, respectively) and absence of **29** (■ and ●, respectively) as a function of the number of water equivalents (N_{H_2O}) per six equivalents of **27b**.[75b] c) Diffusion coefficients of **28** and the water signal (■ and □, respectively) as a function of the number of water equivalents (N_{H_2O}) per six equivalents of **28**. Figure 16b and c are adapted with permission from Ref. [75b,c].

this system.[75d,e] In addition, it was found by combining the results from chemical shift experiments and diffusion NMR spectroscopy that **27b** encapsulates trialkylamines and tetraalkylammonium salts. However, **28** was shown to encapsulate only trialkylamines which are ejected from the cavity of the hexamer of **28** following addition of DCl and the in situ formation of ammonium salts.[75f] These examples demonstrate the ability of diffusion NMR spectroscopy to provide a simple means to map the molecular interactions in such multicomponent systems. The maps of some of the molecular interactions that prevail in these systems are summarized graphically in Figure 17.[71,75a–c]

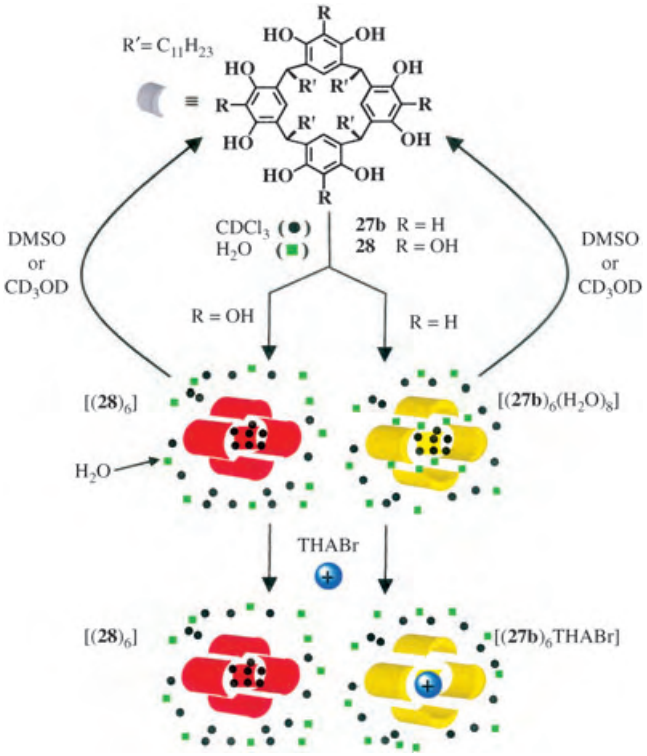


Figure 17. Schematic representation of some of the different molecular interactions and aggregation modes identified in these capsules by diffusion NMR spectroscopy.[71,75a–c]

The evaluation of the interaction of the water molecules with the organic systems in this section indicates that the interaction of water molecules with organic systems in nonaqueous solutions could, in principle, be approached by diffusion NMR measurements—this is briefly outlined in the next section.

4.1.3. Hydrogen Bonds and Water Hydration in Organic Solutions

Many NMR methods have been used to study the interaction of water molecules with biomolecules, since such interactions are of prime importance.[76] Hydration of biomolecules has been approached by NMR methods based on the nuclear Overhauser effect (NOE) and magnetic relaxation dispersion (MRD).[77,78] In principle, the interaction of water molecules with a biomolecule should be easy to probe by diffusion NMR spectroscopy because of the large difference in the sizes and molecular weights of the small water

© 2005 Wiley-VCH Verlag GmbH & Co. KGaA, Weinheim

molecules and the large biomolecule. Interactions between water molecules and biomolecules in an aqueous solution is beyond the scope of the present review, and we shall restrict ourselves to the few studies that measured the interaction of water with organic species in non-aqueous media.[76–78]

In addition to the studies described in Section 4.1.2 regarding the role of water molecules in the hydrogen-bonded capsule,[75a–c] an early report dealt with the hydration, or more accurately the interaction of water molecules with [18]crown-6 (**4**) and its KI complex ($\mathbf{4}_{KI}$) in water-saturated $CDCl_3$ solutions.[79] In this study, the process was followed by comparing the changes observed in the chemical shift and the diffusion coefficient of the water signal upon changing the H_2O:**4** and the H_2O:$\mathbf{4}_{KI}$ ratios. It was found that the average fraction of bound water molecules was independent of the H_2O:$\mathbf{4}_{KI}$ ratio but increased considerably when the H_2O:**4** ratio was increased. In this study, similar conclusions were obtained from the chemical shift titrations and the diffusion NMR measurements.[79] The results of this study (Figure 18)

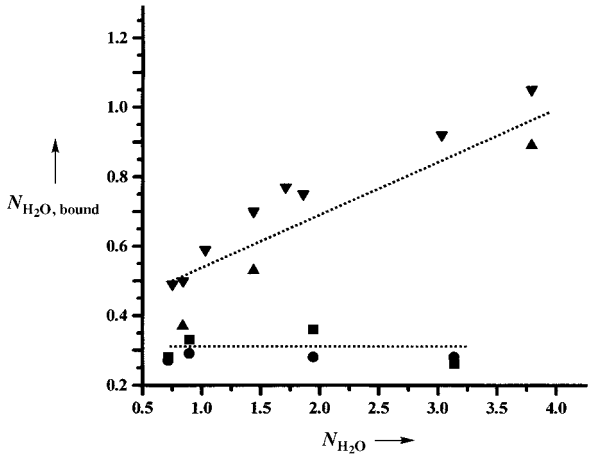


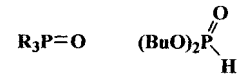
Figure 18. Average number of water molecules ($N_{H_2O,\,bound}$) interacting with **4** and $\mathbf{4}_{KI}$ in $CDCl_3$ solutions. The numbers were calculated from the changes in the chemical shift (δ) and diffusion coefficients (D) of the water signal as a function of the number of water equivalents present N_{H_2O} in $CDCl_3$. ■: $\mathbf{4}_{KI}$ (from D), ●: $\mathbf{4}_{KI}$ (from δ), ▲: **4** (from D), ▼: **4** (from δ).[79]

show that the bound fraction of water molecules was higher in the case of the noncomplexed crown ether. An average of about 0.3 water molecules per complex molecule were obtained for the $\mathbf{4}_{KI}$ system, which was consistent with the finding of Iwachido et al. who found that the potassium complex of **4** can extract on average 0.3 water molecules per complex molecule into nitromethane while **4** can extract up to 1.6 water molecule per molecule.[80] These results imply that **4** acts as an efficient solvation shell for the potassium ion. In the case of **4**, the fraction of bound H_2O was found to depend on the H_2O:**4** ratio. In this case, it was suggested that complexation of the water molecules into the empty cavity of **4** cannot be ruled out.

The hydration of macromolecules in aqueous media is very complex and different types of hydration spheres have been evoked on the basis of their average lifetime in the bound state.[76–78] One of the main problems in aqueous media is to avoid the large signal of the bulk water, which is in most cases in fast exchange with the water molecules that do interact with the (bio)molecules. This problem is much less severe in organic solvents, however. Nevertheless, it should be noted that diffusion measurements give only an average picture. A bound fraction of 0.3 may well be one molecule that spends 30% of its lifetime in the bound state or two molecules that each spend only 15% of their lifetimes in the bound state and so on.[79]

Hydrogen bonds have well-established effects in NMR spectroscopy,[81] such as downfield shifts,[82a] an intermolecular NOE effect,[82b] and spin–spin coupling which may be observed through such hydrogen bonds in some cases.[82c] Recently, Berger and co-workers demonstrated how DOSY could be used to qualitatively study the strength of hydrogen bonds between different species in solutions.[83] The principle behind the measurement is clear: The formation of a hydrogen bond will decrease the diffusion coefficient of a certain molecule from that expected from its molecular weight and shape in a given medium at a given temperature. DOSY was used for this purpose because it has the advantage of visualizing the effect very clearly even in complex mixtures.[83a]

It was shown that the addition of DMSO (a known H-bond acceptor) results in a more pronounced decrease in the diffusion coefficient of phenol than that of cyclohexanol. These different responses were attributed to the higher tendency of phenol, which is the more acidic compound, to form hydrogen bonds with the added DMSO molecules.[83a] A similar phenomenon was observed for a mixture of phosphorus-containing compounds: The four compounds studied by using the ^{31}P DOSY technique were trimethyl phosphate (**30a**), triphenylphosphine oxide (**30b**), triethylphosphine oxide (**32**), and dibutylphosphite (**31**). The results of the DOSY spectra of these systems obtained before and after the addition of triethanolamine are shown in Figure 19a and b, respectively. It can be seen that the largest change in the diffusion coefficients were observed for **32**, which is expected to form the strongest hydrogen bonds. However, a closer look at the data shows that the addition of triethanolamine caused a decrease in the diffusion coefficients of all the solutes in both samples thus suggesting that the addition of the H-bond acceptor affected the solutions viscosity. More recently, the same research group suggested the use of tetramethylsilane (TMS) as a reference for studying this effect in a more quantitative manner by using the ratios of the diffusion coefficients relative to the diffusion coefficients of TMS before and after addition of an H-bond acceptor. This was done since TMS is considered to be unaffected by hydrogen bonds and can therefore be used to report on the effect of the change in viscosity on the measured diffusion coefficients.[83b]



30a: R = OCH_3 **31**
30b: R = Ph
32: R = Et

© 2005 Wiley-VCH Verlag GmbH & Co. KGaA, Weinheim

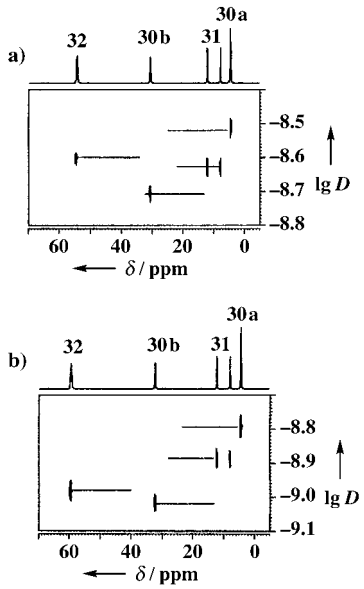
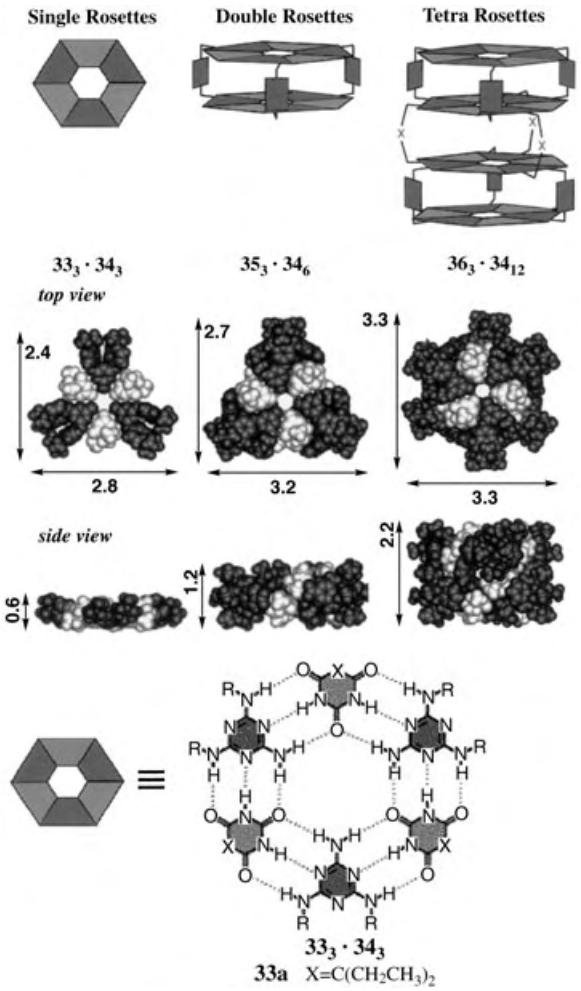


Figure 19. a) The ^{31}P DOSY spectrum of a mixture of trimethyl phosphate (**30a**), triphenylphosphine oxide (**30b**), triethylphosphine oxide (**32**), and dibutyl phosphite (**31**); b) the ^{31}P DOSY spectrum of the same mixture containing triethanolamine as an additional component. The spectrum was recorded using the BPLED sequence with gradient strengths of 2 ms in 32 steps. Reproduced with permission from Ref. [83a].

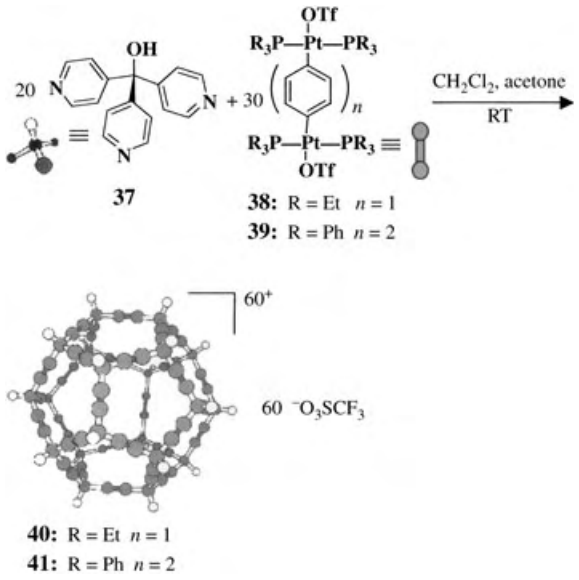
4.2. Molecular Size and Shape

Diffusion coefficients, being intuitively related to the effective radius of the molecular species through the Stokes–Einstein equation [see Eq. (5)], have also been used to determine the size and shape of different supramolecular entities called rosettes.[84,85] The pulsed gradient spin echo (PGSE) sequence was used to characterize several rosettes prepared by the research group of Reinhoudt.[86] In this study, single, double, and tetrarosettes of the type shown in Scheme 1 were classified on the basis of their diffusion coefficients.[86] Relatively good agreement was found between the hydrodynamic diameter extracted from diffusion NMR measurements and those obtained from gas-phase-minimized structures.[86] More importantly, by measuring the diffusion coefficient of the single rosette (**33a**$_3$·**34**$_3$) to which **33a** was added, it was possible to show that these rosettes are kinetically labile and in fast exchange with their components on the NMR time scale under the given conditions (2 mM sample in $CDCl_3$, 298 K, 500 MHz). In addition, it was also possible to determine by using this approach which of the double rosettes were in fast exchange with their components and which were kinetically less labile. This information was difficult to obtain from conventional NMR spectroscopic analysis of these systems.

In another recent application, Stang and co-workers[87a] used the PGSE sequence to corroborate the formation of their spectacular dodecahedra constructed from 50 predesigned components (Scheme 2). The diffusion coefficients of the two dodecahedra **40** and **41**, the molecular weights of



Scheme 1. Single (**33**$_3$·**34**$_3$), double (**35**$_3$·**34**$_6$), and tetrarosettes (**36**$_3$·**34**$_{12}$), which could be characterized by their diffusion coefficients.

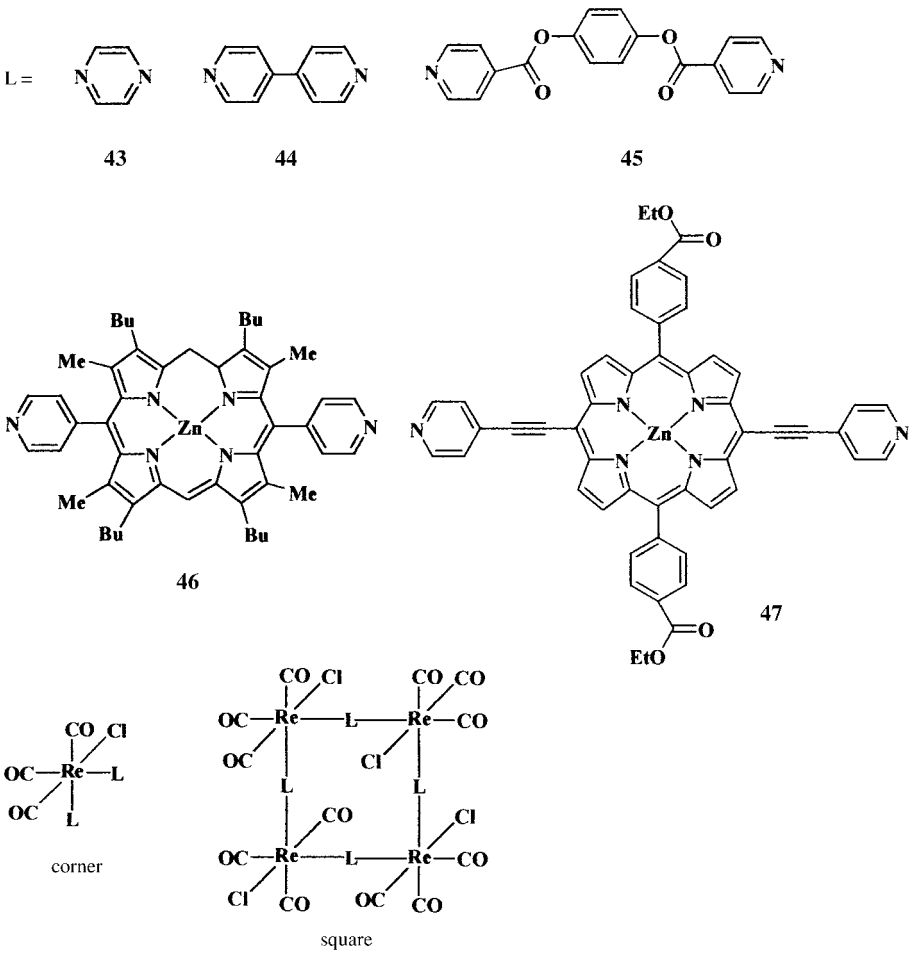


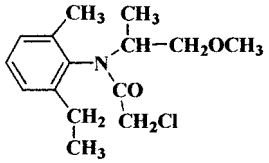
Scheme 2. Synthesis of the dodecahedra **40** (R = Et, n = 1, M_r = 41 656 Da) and **41** (R = Ph, n = 2, M_r = 61 955 Da) from 20 monomers of **37** with 30 monomers of **38** (R = Et, n = 1) and **39** (R = Ph, n = 2), respectively.[87a]

© 2005 Wiley-VCH Verlag GmbH & Co. KGaA, Weinheim

which were calculated to be 41656 and 61955 Da, were found to be $0.18 \pm 0.005 \times 10^{-5}$ and $0.13 \pm 0.006 \times 10^{-5}$ $cm^2 s^{-1}$, respectively, in a mixture of acetone and dichloromethane.[87a] Simulation of the motion with such diffusion coefficients through that medium (taking into account its viscosity) enabled them to extract diameters of 5.2 and 7.5 nm, which are in good agreement with the estimated calculated diameters of 5.5 and 7.5 nm, respectively. Recently, Viel et al. demonstrated by using DOSY that π–π stacking interactions occurred in the hydrophobic compound metolachlor (**42**) in concentrated aqueous solutions.[87b] These authors reached the conclusion that the polymer formed was held together by π–π interactions from the much lower diffusion coefficient of the extra signals observed at high concentration.[87b] Comparison of the surprising DOSY data with other NMR methods (such as 2D NOESY) led to the conclusion that, indeed, the formed aggregate is not a dimer or a trimer but a polymer.[87b]

Diffusion NMR spectroscopy was used to corroborate the formation of double-stranded helicates in solutions in several cases.[88a,b] Larive and co-workers recently used diffusion NMR measurements to characterize a series of ligands (**43**–**47**) and rhenium complexes that were used as





building units for the construction of molecular squares, which could not be characterized by mass spectrometry.[88c] In this case, a good correlation was found between the diffusion coefficient and the reciprocal of the estimated stokes radii ($1/r_s$), as shown in Figure 20. The authors also concluded on the basis of the diffusion NMR measurements that the complexity of some of the spectra are intrinsic characteristics of the supramolecular systems prepared rather than contamination from species of low-molecular weight.[88c] The data extracted from these diffusion NMR experiments are presented in Table 4.

A specific field where size determination by diffusion NMR spectroscopy can assist the characterization of the obtained system in solution is dendrimer chemistry, in which generations can be probed easily by using diffusion NMR spectroscopy, as demonstrated briefly in the next section.

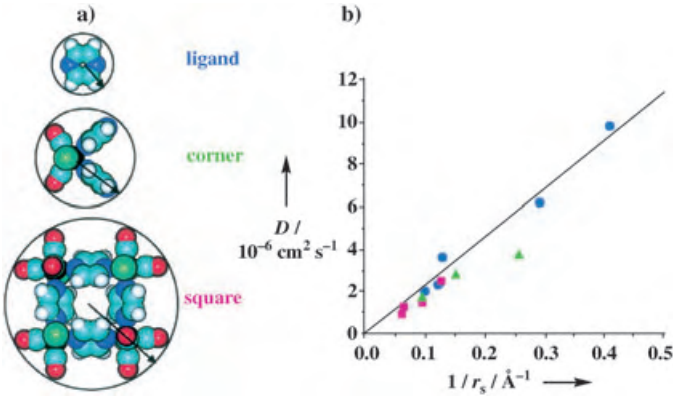


Figure 20. a) Approximated molecular radii of ligands **43**–**47** as well as their respective monomers (corners) and square complexes; b) the correlation between their diffusion coefficients and the reciprocal of the estimated Stokes radii ($1/r_s$) for ligands (●), corners (▲), and squares (■). Reproduced with permission from Ref. [88c].

4.3. Dendrimers and Dendrons: Size, Shape, and Function

Diffusion NMR measurements may assist in characterizing dendrimers[89] and it is surprising that, until recently, relatively few studies have used this technique to characterize

 © 2005 Wiley-VCH Verlag GmbH & Co. KGaA, Weinheim

Table 4: Molecular diffusion coefficients D of the ligands **43**–**47** and their rhenium complexes.[88c]

Molecule	D_{43} [$\times 10^{-6}$ cm^2 s^{-1}]	D_{44} [$\times 10^{-6}$ cm^2 s^{-1}]	D_{45} [$\times 10^{-6}$ cm^2 s^{-1}]	D_{46} [$\times 10^{-6}$ cm^2 s^{-1}]	D_{47} [$\times 10^{-6}$ cm^2 s^{-1}]
ligand	9.68 ± 0.09	6.03 ± 0.04	3.53 ± 0.04	2.24 ± 0.02	1.94 ± 0.06
corner	3.62 ± 0.08	2.69 ± 0.02		1.61 ± 0.03	
square	2.37 ± 0.11	1.42 ± 0.05	0.87 ± 0.02	1.20 ± 0.04	1.04 ± 0.03

dendrimers.[90–94] One of the early applications of diffusion NMR spectroscopy in the field of dendrimers was reported on the first, second, third, and fourth generations of dentritic aliphatic polyesters based on 2,2-bis(hydroxymethyl)propionic acid and 1,1,1-tris(hydroxyphenyl)ethane.[91] The signal decays for these dendrimers were fitted to a modified Stejskal–Tanner equation as shown in Equation (19), where

$$I_{(2\tau,G)} = I_{(2\tau,0)} \exp(-\gamma^2 G^2 \delta^2 (\Delta - \delta/3) D_{app})^{\beta} \quad (19)$$

D_{app} represents the apparent diffusion coefficient and β is a measure of the width of the distribution ($0 < \beta < 1$). In the fitting procedure, β was found to be 1, thus indicating that the dendrimers are nearly monodisperse. By assuming that the dendrimers had a spherical shape, these authors were able to compute the hydrodynamic radii r_s of the dendrimers by using the Stokes–Einstein equation. The values estimated were 7.8, 10.3, 12.6, and 17.1 Å for the first, second, third, and fourth generation dendrimers, respectively, and were said to be in good agreement with those obtained from molecular modeling studies.[91]

One of the earliest applications of DOSY demonstrated that diffusion NMR measurements are sensitive to the structural changes induced by the external stimulation of dendrimers.[90b] Indeed, it was shown that the diffusion coefficients, and hence the hydrodynamic radii, can give information on the structural changes induced in these materials by a pH change. It was shown that the dendrimers with terminal CO_2H groups swell at neutral pH values and shrink in acidic conditions. The dendrimers with terminal CH_2NH_2 groups shrank in basic pH conditions, while those with terminal CH_2OH groups were practically insensitive to pH changes.[90b] Interestingly, the changes in the chemical shifts in these systems as a result of the pH changes were marginal. These findings imply that diffusion NMR spectroscopy has the potential to relate structural changes and the packing mode of dendrimers with their functional performances.

Gorman et al. combined diffusion NMR measurements with the determination of electron-transfer rate constants and molecular modeling studies in an attempt to determine the relationships between molecular structure and electron transfer in dendritic systems.[92] Interestingly, these diffusion NMR measurements carried out on the flexible and inflexible electroactive dendrimers **48**–**52** (Scheme 3) and **53**–**57** (Scheme 4), respectively, showed a dramatic effect of the solvent on the hydrodynamic radii of only the flexible dendrimers. For the flexible dendrimers **48**–**52**, a better correlation between the hydrodynamic radii and the radii of gyration, calculated using molecular dynamics simulation, was obtained for the diffusion measurements performed on the DMF solutions, where the dendrimers have compact hard-sphere-like structures, and not in THF, where some swelling seems to occur.[92] Moreover, the correlation between these two parameters for the inflexible dendrimers was less significant, thus implying that these electroactive rigid dendrimers **53**–**57** have a nonspherical/noncompact shape. A comparison of the structural features of these two classes of dendrimers in the different solvents with the electron-transfer rates in these systems led the authors to evoke a molecular structure/property relationship for the attenuation of the electron transfer in these systems.[92]

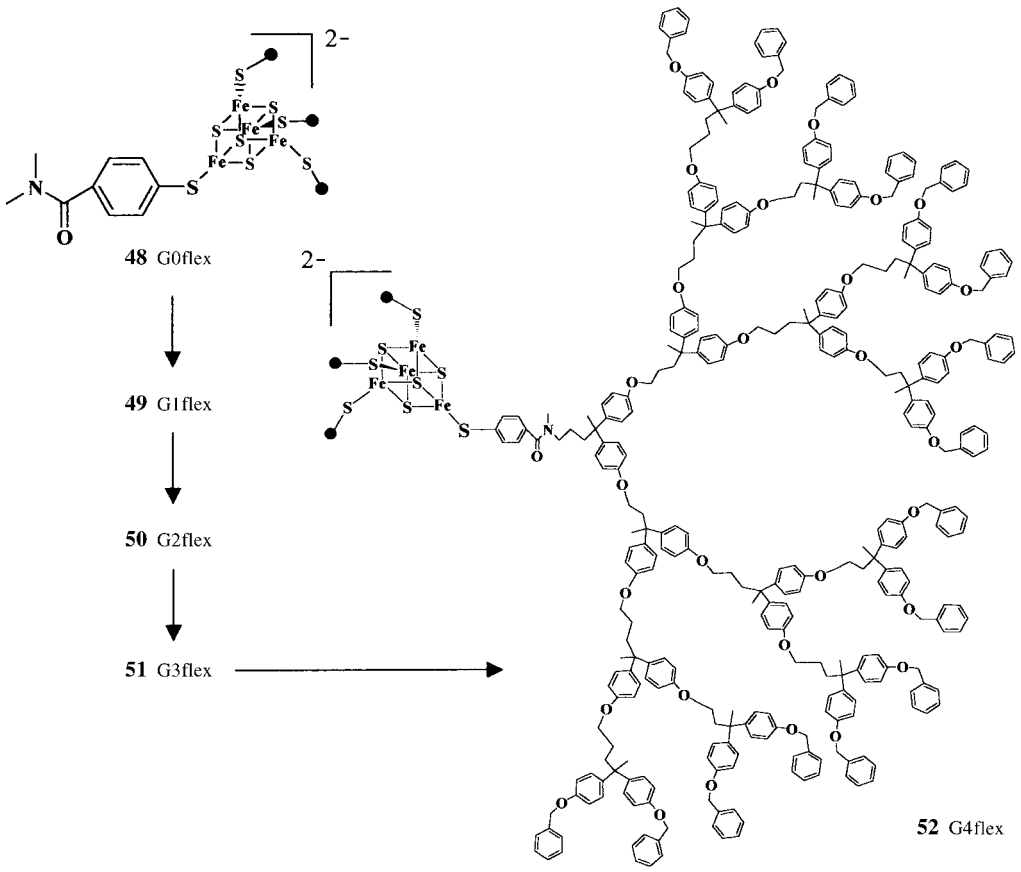
Riley et al. studied the relationship between the diffusion characteristics of pyrene-labeled poly(aryl ether) monodendrons[93] (Scheme 5) and their photophysical performance. Interestingly, it was found that the increase in the Stokes radii with the increase in dendron generation is much more pronounced in THF than in CH_3CN (Table 5). However, comparison of the experimental data with theoretical values showed that the dendrons are not fully extended ($r_s < R_{theory}$), even in THF, and that the smaller dendrons are more open and flexible than the larger ones. The structures are much more collapsed in CH_3CN, and there is a structural change between G2 (**60**) and G3 (**61**), with G3 (**61**) apparently having the more compact structure. Comparison of the structural information obtained from the diffusion NMR measurements and the quenching experiments revealed that G0–G3 (**58**–**61**) in THF and G0–G2 (**58**–**60**) in acetonitrile have a minimal barrier to the passage of the dioxygen-quenching molecules, while the larger dendrons G4 (**62**) in THF as well as G3 and G4 in CH_3CN are more dense and less permeable. The structure is even more collapsed in cyclohexane.[93] The change in the diffusion behavior in THF occurs between G2 and G3, while the quenching data shows the change in behavior occurs between G3 and G4. The authors pointed out that the different breaking points arise from the different probes used in both processes (THF or dioxygen).[93]

The last two examples demonstrate how diffusion NMR spectroscopy gives a better insight into the solution structure of dendritic materials, which, in turn, may affect their properties, and demonstrate the potential of such measurements to establish the structure/functional activity of such complex systems.[93]

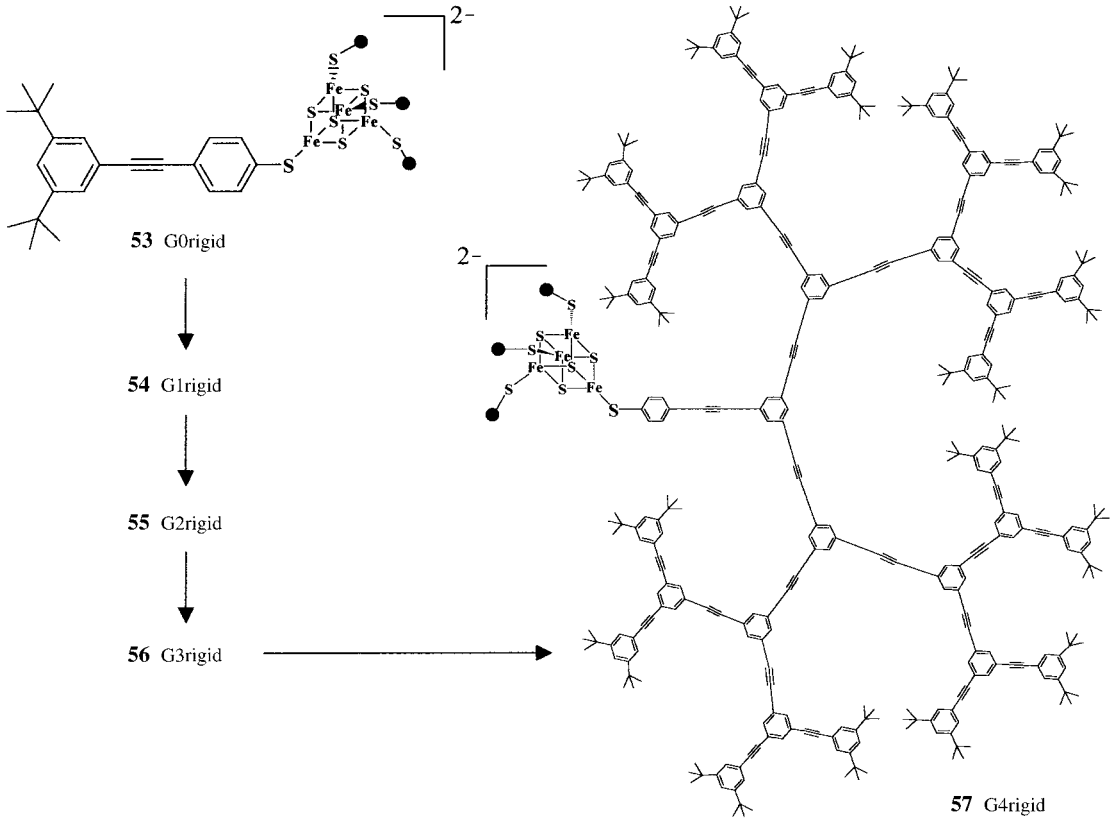
4.4. Reactive Intermediates, Ion Pairing, and Organometallic Systems

The interactions of different ions with different systems and polyelectrolytes, their binding to micelles, and their involvement in the formation of microemulsions have been studied extensively by diffusion NMR spectroscopy and are

 © 2005 Wiley-VCH Verlag GmbH & Co. KGaA, Weinheim

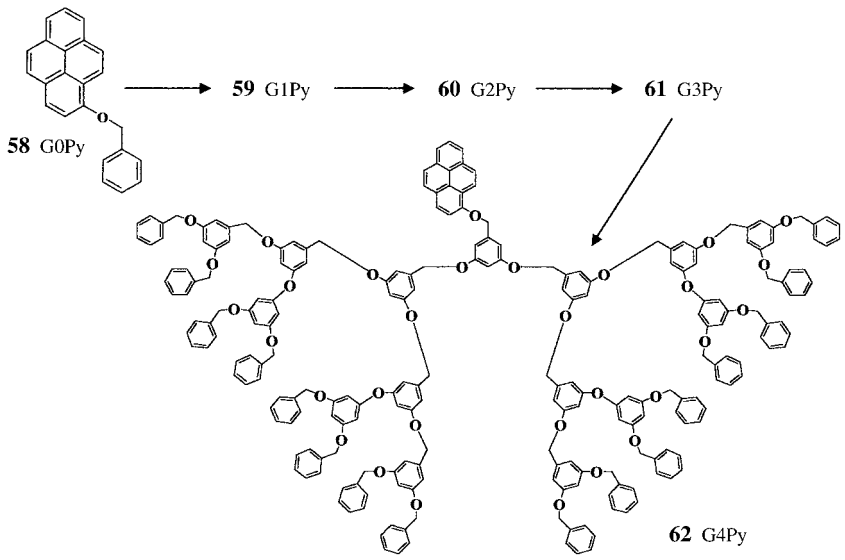


Scheme 3. A strong influence of the solvent on the hydrodynamic radii was found for the flexible electroactive dendrimers **48**–**52** (compact structure in DMF, slightly swollen structure in THF).



Scheme 4. The rigid electroactive dendrimers **53**–**57** probably have a nonspherical and noncompact structure.

 © 2005 Wiley-VCH Verlag GmbH & Co. KGaA, Weinheim



Scheme 5. Pyrene-labeled poly(aryl ether) monodendrons **58**–**62**.

Table 5: Diffusion coefficients D, radii r, volumes V, and densities ρ from pulsed-field-gradient NMR experiments.[93]

Compound	M_r	D_{py} [$cm^2 s^{-1}$][a]	r_s [Å][b]	V_{stokes} [$Å^3$][c]	ρ_{stokes} [$Da Å^{-3}$][d]	R_{theory} [Å][e]	V_{theory} [$Å^3$][f]
			tetrahydrofuran				
pyrene	82	1.7×10^{-5}	2.8	92	2.19	(3.5)	180
58	308	1.3×10^{-5}	3.7	210	1.47	7.2	1560
59	521	0.97×10^{-5}	4.9	490	1.06	10.1	4320
60	932	0.78×10^{-5}	6.1	950	0.99	13.0	9200
61	1822	0.48×10^{-5}	10	4200	0.43	15.9	16800
62	3495	0.34×10^{-5}	14	11500	0.30	18.8	27800
			acetonitrile				
pyrene	82	2.3×10^{-5}	2.6	74	2.72	(3.5)	180
58	308	1.8×10^{-5}	3.3	150	2.06	7.2	1560
59	521	1.4×10^{-5}	4.1	289	1.80	10.1	4320
60	932	1.2×10^{-5}	4.9	490	1.92	13.0	9200
61	1822	1.1×10^{-5}	5.4	660	2.72	15.9	16800
			cyclohexane				
pyrene	82	9.4×10^{-6}	2.6	74	2.73	(3.5)	180
58	308	8.7×10^{-6}	2.8	92	2.52	7.2	1560

[a] Calculated from NMR diffusion data. [b] Calculated from Equation (4) using, $\eta = 4.56\times10^{-4}$ Pa s for THF. [c] Calculated from R_{Stokes} given above, $V_{Stokes} = {}^4/_3\pi(R_{Stokes})^3$. [d] Calculated from V_{Stokes} given above and M_r, $\rho_{Stokes} = M_r/V_{Stokes}$. [e] Radii of fully extended structures calculated from models. [f] Volume of fully extended structures, from radii given above, $V_{theory} = {}^4/_3\pi(R_{theory})^3$. Measurements were performed at 298 K.

beyond the scope of the present Review.[9,10,19,20,95] Some selected examples of the applications of diffusion NMR spectroscopy in the field of organic reactive intermediates, ion pairs, and organometallic systems which bear some relevance to supramolecular chemistry are outlined below. In fact, diffusion NMR spectroscopy should make an important contribution in the field of reactive intermediates since most of these species are unstable and therefore classical methods for measuring diffusion, such as Rayleiigh interferometry[96] or radioactive tracer techniques,[97] are impractical. Diffusion NMR spectroscopy, which provides a means for studying diffusion without perturbating the systems or the need for any chemical modification, is much more suitable for measuring the diffusion characteristics of such unstable species. In addition, many ions and organometallic systems tend to dimerize and self-aggregate, thus making diffusion an intuitively important parameter for such systems. Therefore, it seems surprising that diffusion NMR spectroscopy of such systems only became popular over the last few years.

One of the first applications of high-resolution diffusion NMR spectroscopy in the study of reactive intermediates was the determination of the diffusion coefficients of a series of polycyclic systems, such as compounds **63**–**69**, and their respective doubly and quadruply charged derivatives.[98] In this study, both external and internal references were used since it was anticipated that the reduction of the polycyclic systems into their respective charged derivatives would affect the solution viscosity and hence the diffusion coefficient, and would limit the utility of the diffusion coefficient as a characterizing parameter of the systems. Indeed, a pronounced decrease in the diffusion coefficients of the polycycles was observed upon reduction (Table 6), with only a small change in the viscosity seen. Since the two-electron reduction has no effect on the molecular weight of the systems, it is clear that the decrease in the diffusion coefficients should be attributed to a superposition of the higher solvation and the probable partial self-aggregation of the charged systems.[98] The dilithium, disodium, and dipotassium salts of the tetracene dianion ($\mathbf{65}^{2-}$), for example, were found to have very similar diffusion coefficients, thus implying that the ion-pair phenomenon had only a marginal effect on these systems under the experimental conditions used.[98] An interesting point that emerged from the comparison of the diffusion coefficients of the charged systems with their respective noncharged parent systems was that a larger decrease in the diffusion coefficients was observed for systems that are more suited to self-aggregation. A decrease in the diffusion coefficients to nearly 50% of their initial values was found and attributed to partial self-aggregation in these systems.[98] Indeed, the corannulene tetranion $G3^{4-}$, which showed a pronounced decrease in the diffusion coefficient, was previously shown to form dimers.[99] The conclusion of this study was that self-aggregation and dimerization in these systems might be more important than previously thought.[98]

Rabinovitz and co-workers subsequently showed through the use of diffusion NMR spectroscopy that there is a fair to good correlation between $1/D$ and the van der Waals radii of neutral polycyclic compounds.[100a] A somewhat weaker correlation was found between the Stokes–Einstein radii

 © 2005 Wiley-VCH Verlag GmbH & Co. KGaA, Weinheim

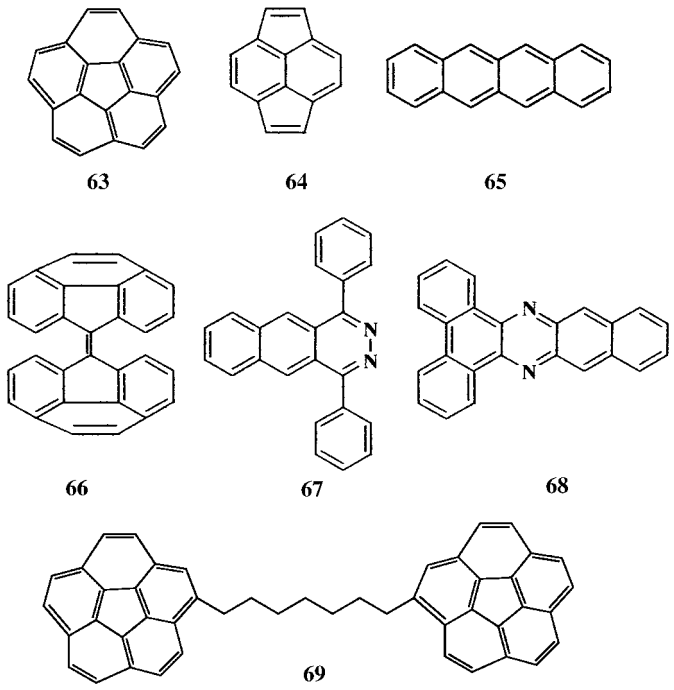


Table 6: Diffusion coefficients *D* of polycyclic systems and their anions in [D_8]THF at 298 K.[98]

System	*D* (CH_2Cl_2; ext. stand.) [10^{-5} cm^2s^{-1}]	*D* (benzene; int. stand.) [10^{-5} cm^2s^{-1}]	*D* (polycyclic system) [10^{-5} cm^2s^{-1}]
63	3.73 ± 0.002	2.87 ± 0.017	1.57 ± 0.017
$\mathbf{63}^{4-}$/4 Li^+	3.73 ± 0.002	2.90 ± 0.041	0.84 ± 0.017
65	3.83 ± 0.031	2.96 ± 0.027	1.83 ± 0.032
$\mathbf{65}^{2-}$/2 Li^+ (2 mg)	3.79 ± 0.006	2.86 ± 0.039	0.96 ± 0.038
$\mathbf{65}^{2-}$/2 Li^+ (20 mg)	3.78 ± 0.000	2.39 ± 0.043	0.71 ± 0.020
		2.86 ± 0.039	0.86 ± 0.017[a]
$\mathbf{65}^{2-}$/2 Na^+	3.80 ± 0.003	2.74 ± 0.014	0.94 ± 0.015
$\mathbf{65}^{2-}$/2 K^+	3.79 ± 0.004	[b]	0.94 ± 0.014
64	3.82 ± 0.017	2.86 ± 0.025	1.90 ± 0.011
$\mathbf{64}^{2-}$/2 Li^+	3.78 ± 0.015	2.82 ± 0.048	1.06 ± 0.057
66	3.80 ± 0.002	2.97 ± 0.014	1.38 ± 0.021
$\mathbf{66}^{2-}$/2 Na^+	3.82 ± 0.002	2.99 ± 0.003	1.05 ± 0.014
67	3.79 ± 0.000	2.85 ± 0.041	1.17 ± 0.008
$\mathbf{67}^{2-}$/2 Na^+	3.72 ± 0.030	2.84 ± 0.003	0.93 ± 0.030
68	3.79 ± 0.002	2.90 ± 0.015	1.38 ± 0.010
$\mathbf{68}^{2-}$/2 Na^+	3.80 ± 0.002	2.97 ± 0.032	1.10 ± 0.026

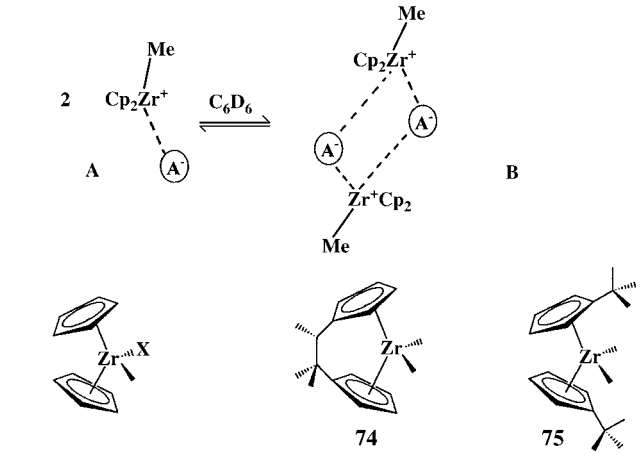
[a] After correcting for viscosity changes. [b] Very broad signal for benzene, undetectable in the spin echo.

obtained from the diffusion coefficients and the van der Waals radii for the neutral polycyclic systems. The authors suggested that this is partially a result of the fact that the Stokes–Einstein equation does not hold very well when the diffusing particles are less than about five times the radius of the solvent molecules in which the diffusion takes place. There was practically no correlation between $1/D$ and the extracted Stokes–Einstein radii for the charged systems.[100a] This may be a consequence of the different solvation of the anions studied, which also differed in their number of charges. In a different study,[100b] the same research group used diffusion NMR spectroscopy to try to verify whether or not the octaanion of **69** forms dimers. They found that the diffusion coefficient of $\mathbf{69}^{8-}$ is 0.55×10^{-5} cm^2s^{-1} while that of the dimer of $\mathbf{63}^{4-}$ is 0.76×10^{-5} cm^2s^{-1} in [D_8]THF solutions, and concluded that $\mathbf{69}^{8-}$ forms an intermolecular sandwich.[100b]

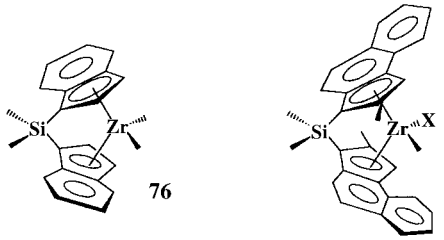
Pochapsky et al., who studied the phenomenon of ion pairing by NMR spectroscopy quite extensively,[101] recently used diffusion NMR spectroscopy to study the aggregation of tetrabutylammonium chloride (**70**).[102a] In this study the diffusion coefficient ratios of **70** were compared with that of tetrabutylsilane (**71**), a non-aggregating standard with a similar molecular weight and shape, as a function of the concentration. Pochapsky et al. found that this ratio decreased when the concentration was decreased, and achieved a value of nearly 1.0 in very dilute solutions ($\sim 10^{-4}$ M). The aggregation number for **70** was estimated to be 3 at a concentration of about 30 mM in $CDCl_3$.[102a] Subsequently, Pochapsky et al. used the same rationale to study the ion pairs of tetrabutylammonium tetrahydrobrate (**72**) by simultaneously monitoring the diffusion coefficients of the cation and the anion.[102b] They showed that the diffusion coefficients of the cation and anion in $CDCl_3$ are not very different and are much lower than that of tetrabutylsilane (**71**). The interpretation was that, indeed, a tight ion pair is formed. The fact that the diffusion coefficient ratio was found to be concentration-dependent clearly indicated that this ion pair forms aggregates in $CDCl_3$, which is to be expected because of the low solvating power of the solvent.[102b] Recently, Keresztes and Williard demonstrated by diffusion NMR experiments that the tetramer and dimer of *n*-butyllithium can be identified in [D_8]THF.[103] This was accomplished by comparing the diffusion coefficients obtained experimentally from diffusion NMR measurements with the those expected from known X-ray parameters of these species. The data was also presented in a DOSY form.[103]

Organometallic chemistry, where ligand insertion and/or dissociation and aggregation may play an important role, is an additional field in which diffusion NMR spectroscopy may complement other NMR methods for the characterization of species in solution. Since this field was recently reviewed by Pregosin and co-workers,[104] we shall only outline a few examples here. Beck et al. have claimed on the basis of diffusion NMR experiments that the formation of ion quadruples (B) from simple ion pairs (A), as shown in Scheme 6, is probably more important than previously thought in zirconocene-based catalytic systems.[105] This was concluded by measuring the diffusion coefficient of the zirconocenes **73–77** (Scheme 6), and by comparing the findings with the diffusion coefficient obtained for a series of ion pairs such as **73a/b** and **77a/b** with the diffusion coefficient of **73c**, for which the binuclear structure was previously established by X-ray crystallogra-

 © 2005 Wiley-VCH Verlag GmbH & Co. KGaA, Weinheim

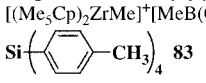


73 X = Me
73a X = $MeB(C_6F_5)_3^-$
73b X = $B(C_6F_5)_4^-$
73c X = (μ–Me)[$(C_2H_5)_2ZrMe^+$][$B(C_6F_5)_4$]$^-$



77 X = Me
77a X = $MeB(C_6F_5)_3^-$
77b X = $B(C_6F_5)_4^-$

[$Me_2Si(Me_4Cp)(tBuN)TiMe$]$^+$[$MeB(C_6F_5)_3$]$^-$ **78**
[Me_2C(fluorenyl)(Cp)ZrMe]$^+$[$MeB(C_6F_5)_3$]$^-$ **79**
[$(Me_5Cp)_2ThMe$]$^+$[$B(C_6F_5)_4$]$^-$ **80**
[$(Me_2SiCp)_2ZrMe$]$^+$[$MeB(C_6F_5)_3$]$^-$ **81**
[Cp_2ZrMe]$^+$[$MeB(C_6F_5)_3$]$^-$ **82a**
[$(Me_5Cp)_2ZrMe$]$^+$[$MeB(C_6F_5)_3$]$^-$ **82b**



Scheme 6. Possible formation of ion quadruples (B) from simple ion pairs (A).

phy.[106a] Since the diffusion coefficient of **73b** deviated from that of **73** and **74**, and was similar to that of the dinuclear complex of **73c**, it was concluded that **73b** is an ion quadruple (structure **8** in Scheme 6). These measurements were performed in benzene in the 1.6–4.7 mM concentration range. However, a very recent study on very similar complexes (**78**–**82**) and with (*p*-tolyl)$_4$Si (**83**) as a reference (Scheme 6) demonstrated that there is a good correlation between the hydrodynamic volumes of these complexes, as obtained from the PGSE diffusion data, and the van der Waals volumes computed for 1:1 ion pairs from the crystal structures of these complexes (Figure 21).[106b] The concentrations of the studied metalocenes were well above the 10^{-4}–10^{-5} M range generally used in polymerizations and it was therefore concluded that aggregation of the metallocenium catalysts is unlikely to be of major importance for chain growth in olefin polymerization.[106b]

Zuccaccia et al. measured the diffusion coefficients of the cationic complex **84** and its neutral analogue **85** in different solvents at various concentrations.[107] In this study, the simple STE pulsed gradient sequence was used for the diffusion

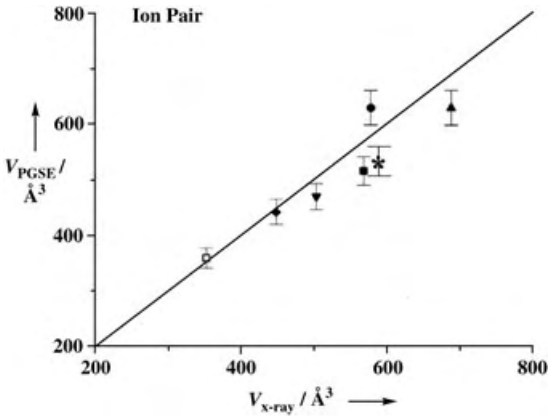
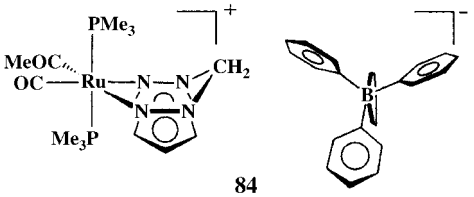
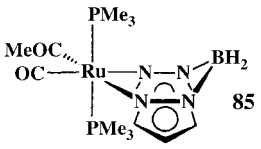


Figure 21. Plot of PGSE-derived hydrodynamic volumes V_{PGSE} for the metallocenium ion pairs versus van der Waals volumes $V_{X\text{-}ray}$ computed for 1:1 ion pairs from the corresponding crystal structures. The straight line represents the equation $V_{PGSE} = V_{X\text{-}ray}$. ■: **78**, ●: **79**, ▲: **80**, ▼: **81**, ◆: **82a**, ⋆: **82b**, □: (*p*-tolyl)$_4$Si (**83**). Adapted with permission from Ref. [106b].

measurements. The results clearly indicated that compound **84** exists as a tight ion pair in $CDCl_3$. It seems that the equilibrium is shifted to a looser ion pair in CD_3NO_2, as witnessed by the higher diffusion coefficient of BPh_4^- relative to the cation. In this solvent, there was only about a 10% difference between the diffusion coefficient of **84** and **85**;[107] in the $CDCl_3$ and CD_2Cl_2 solutions, however, the difference between these diffusion coefficients was much more pronounced and found to be concentration-dependent.[107] The authors suggested on the basis of these results that higher aggregates were involved in these solutions. It should be noted that reference **85** has a lower molecular weight than **84**, for which the molecular weight of the ion pair (cation and





anion) should be taken into account. In addition, compound **85** is probably less solvated than **84** since **85** is an uncharged molecule and therefore should have a somewhat higher diffusion coefficient. However, the fact that the changes in the diffusion coefficients are smaller in solvents with higher solvating power and the fact that the difference in diffusion coefficients are concentration-dependent favors the explanation of higher aggregates in the case of **84** in the chlorinated solvents under the experimental conditions used.[107]

 © 2005 Wiley-VCH Verlag GmbH & Co. KGaA, Weinheim

In a recent application Pregosin and co-workers reported the diffusion coefficients of a series of Pd^{II}–arsine complexes of the type $[PdCl_2L_2]$ (**86–89**; $L = AsMe_xPh_{3-x}$ ($x = 3$–0)) and some other organometallic complexes of different sizes (**90–93**; Tp′ = hydrotris(3,5-dimethylpyrazolyl)borate, Ar = *p*-tolyl, dba = *trans,trans*-dibenzylideneacetone), from which they calculated their hydrodynamic radii r_s by using the

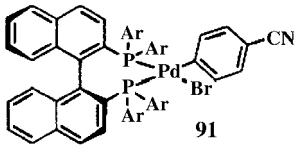
$[PdCl_2(AsMe_2Ph)_2]$ **86**

$[PdCl_2(AsMePh_2)_2]$ **87**

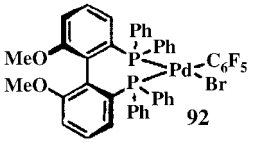
$PdCl_2(AsMe_3)_2$ **88**

$PdCl_2(AsPh_3)_2$ **89**

$[Tp'W(CO)_3H]$ **90**



91



92

$Pd_2(dba)_3$ **93**

Stokes–Einstein equation [see Eq. (5)].[108a] They found a good correlation between the r_s values and the estimated radii compiled from the X-ray structures of these systems (Figure 22).[108a] This approach was further extended to ruthenium(II) complexes through the use of ^{19}F and ^{1}H PGSE measurements.[108b]

A recent demonstration of how diffusion NMR spectroscopy could be used to characterize organometallic reactive intermediates in solution was recently given by Berger and coworkers, who provided a snapshot of the reaction of $^{13}CO_2$ with $[Cp_2Zr(Cl)H]$ (**94**) by using ^{13}C diffusion NMR spectroscopy (Scheme 7).[109] The authors used $^{13}CO_2$ to increase the sensitivity, and combined the DOSY sequence with the INEPT sequence to enhance the signal of the protonated

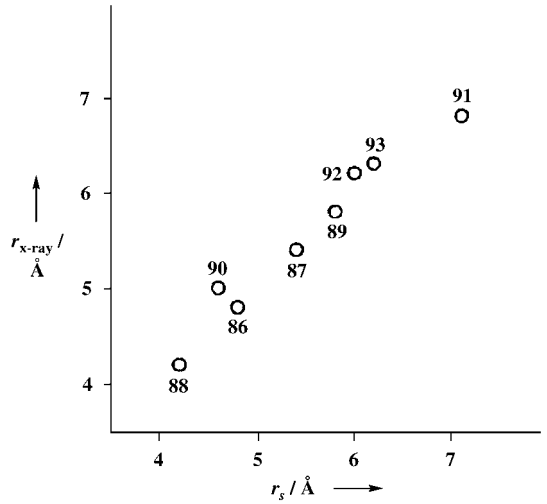


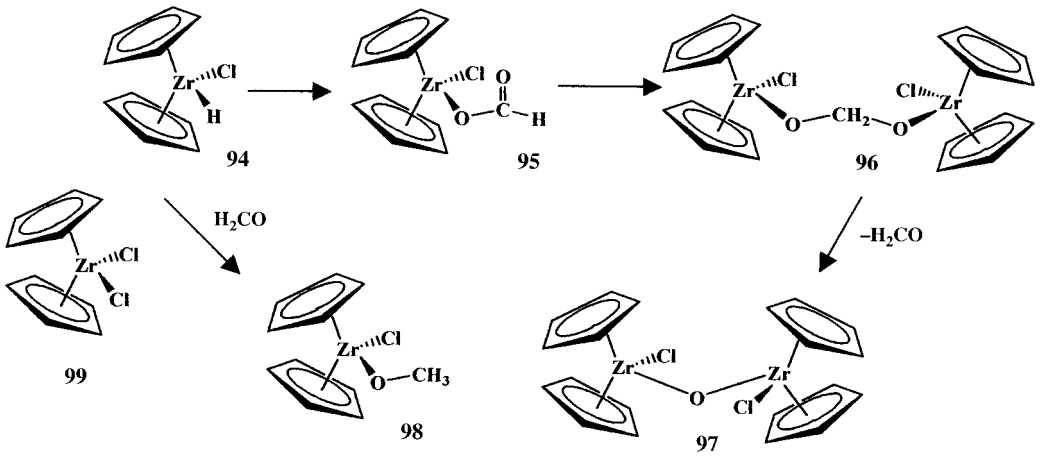
Figure 22. Plot of the hydrodynamic radii (r_s) versus the radii $r_{X\text{-ray}}$ calculated from the crystallographic data for **86–93**. The radii of **86–89** in the solid state were estimated from reported structures for the analogous phosphine, instead of arsine. Adapted with permission from Ref. [108a].

carbon atoms formed during the course of the reaction.[110] The dimeric nature of intermediate **96** was elucidated by comparing the diffusion coefficients, and hence the hydrodynamic radii, of the formed intermediates with those of a series of known zirconocenes, such as **97–99** (see Table 7).

Table 7: Experimental and calculated diffusion coefficients *D* and hydrodynamic radii r_s of the studied zirconium complexes.[109]

	Experimental		Calculated	
	r_s [Å][a]	D [$cm^2 s^{-1}$]	r_s [Å]	D [$cm^2 s^{-1}$][a]
99	3.0	1.61×10^{-5}	3.1[b]	1.55×10^{-5}
97	3.7	1.31×10^{-5}	3.9[b]	1.30×10^{-5}
98	4.2	1.55×10^{-6}	3.6[c]	1.81×10^{-6}
96	6.3	1.05×10^{-6}	6.1[c]	1.07×10^{-6}

[a] Calculated from the Stokes–Einstein equation. [b] Calculated from X-ray structure data under the assumption of a spherical shape. [c] Calculated from the minimized gas-phase structure (PM3).



Scheme 7. The combination of DOSY and INEPT sequences enabled the structure of the dimeric intermediate **96** in the reaction of CO_2 with $[Cp_2Zr(Cl)H]$ to be elucidated.

 © 2005 Wiley-VCH Verlag GmbH & Co. KGaA, Weinheim

This study demonstrates the tremendous utility of diffusion NMR spectroscopy in probing the structure of organometallic complexes where aggregation, dimerization, and ligand insertion may occur.

5. Applications of Diffusion NMR Measurements in Combinatorial Chemistry

Combinatorial chemistry has become an important tool in organic and pharmaceutical research in recent years.[3,110,111] One of the main consequences of combinatorial chemistry is the generation of mixtures of a large number of products in minute concentrations that require high-throughput NMR methods. Therefore, methods that can be used to assign mixtures of compounds, preferably without their isolation, are needed. In addition, as one of the main concerns of combinatorial chemistry is finding new lead compounds and specific ligands for different receptors, efficient screening methods for the identification of the interaction of tentative ligands with their specific receptors are required. In addition, the kinetics of solid-phase reactions may depend on the ability of the solid support to swell and the ability of reagents to reach the interface of the solid support. Therefore, it seems only logical to use diffusion NMR spectroscopy in the context of combinatorial chemistry where mixture characterization and screening for potential new ligands are central issues. Herein, we outline some of these applications, emphasizing DOSY applications that were originally developed by the group of Johnson[33–36] and applied by Shapiro and co-workers[37,112] and several other research groups.[113] The next section emphasizes the potential and limitations of diffusion NMR techniques in the context of combinatorial chemistry by focusing on only two issues, mixture characterization and ligand screening.

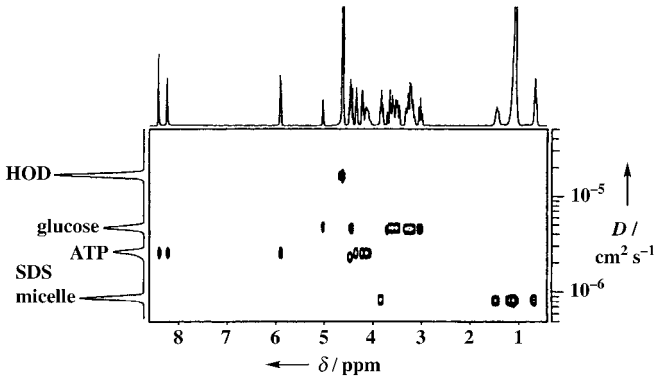


Figure 23. 2D DOSY spectrum of a mixture containing HOD, glucose, ATP, and SDS micelles. Reproduced with permission from Ref. [36a].

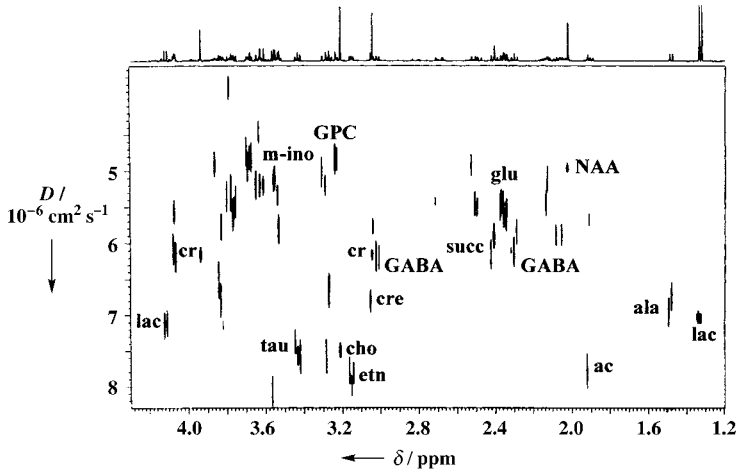


Figure 24. 2D DOSY spectrum (500 MHz) of the perchloric acid extract of a gerbil brain in D_2O. The assignments are as follows: ac = acetate, ala = alanine, cho = choline, cr = creatinine, etn = ethanolamine, GABA = γ-aminobutyric acid, glu = glutamine, GPC = glycerophosphocholine, lac = lactate, *m*-ino = myo-inositol, NAA = *N*-acetylaspartate, succ = succinate, and tau = taurine. Reproduced with permission from Ref. [115].

5.1. DOSY for Mixture Evaluation

DOSY provides an efficient means for the "virtual separation" of compounds.[34,35,37,113] As already shown in Section 3.3, DOSY provides 2D maps in which one axis corresponds to the chemical shifts and the other the diffusion coefficients. In fact, the validation of the DOSY approach was first demonstrated on different mixtures.[34,37,112–115] Figure 23 shows one of the first applications of DOSY, where it was demonstrated that one could indeed "virtually separate" compounds on the basis of their molecular weights. In this study, compounds of significantly different sizes, such as water, glucose, ATP, and sodium dodecylsulfate SDS micelles, were identified.[36a] Subsequently, with the advance in gradient hardware as well as DOSY acquisition and processing schemes, more demanding mixtures were characterized[115–117] (Figure 24) by using high-resolution DOSY (HR-DOSY).[115] In this study, a handful of different metabolites, some of which are not very different in their molecular weights, were resolved.[115]

Diffusion coefficients that differ by only few percent can be resolved with the current conventional technology for non-overlapping peaks (in the same sample). However, it should be noted that, for overlapping peaks, one needs at least a factor of 2–3 in the diffusion coefficients to render them resolvable in a conventional DOSY spectrum.[34,112] The DOSY approach requires the acquisition of a number of 1D spectra with relatively good signal-to-noise ratios (SNR) and are therefore more easily performed by using proton NMR spectroscopy. Overlapping signals may present a real problem when mixtures of large numbers of compounds or complex compounds having many types of protons are present in the mixture. One way to alleviate this problem is to couple the DOSY approach with a 2D NMR sequence where overlapping signals are less of a problem; this affords a 3D sequence, referred to as 3D DOSY. Since diffusion can easily

 © 2005 Wiley-VCH Verlag GmbH & Co. KGaA, Weinheim

be coupled to a 2D sequence, many 3D DOSY sequences were developed with relative ease.[34,38,39,112]

However, there are only limited applications of these techniques in real chemical or combinatorial systems besides those of the systems used to demonstrate that these sequences are indeed operable. One of the main reasons for this might be the fact that these 3D DOSY sequences require long acquisition times and larger data storages, with the former being the much more important. Figure 25 shows a 3D

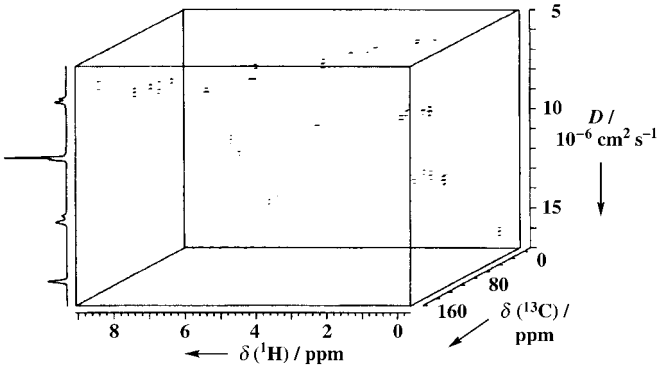
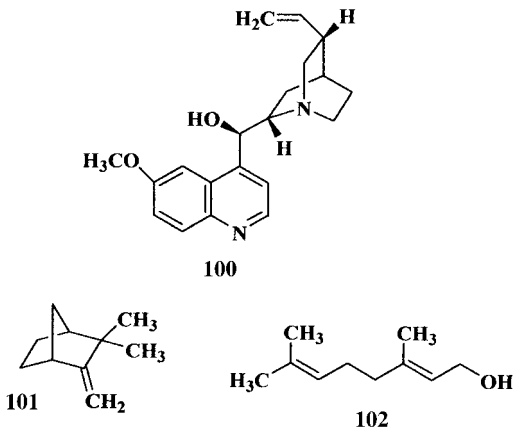


Figure 25. 3D DOSY-HMQC spectrum of quinine, camphene, and geraniol in CD_3OD. Left: projection of the integral onto the diffusion axis. Reproduced with permission from Ref. [39c].

DOSY-HMQC spectrum obtained on a simple mixture consisting of quinine (**100**), camphene (**101**), and geraniol (**102**) in CD_3OD as an example.[39c] This 3D DOSY spectrum



shows no overlap, and it is therefore much easier to extract the structural information from these maps and assign the different signals to the actual compounds present in the mixture. Although there is considerable potential for this type of spectrum, the acquisition schemes are only practical for relatively concentrated samples. A better solution is to use hybrid sequences, which introduce diffusion weighting into the 2D NMR spectrum without elongation of the acquisition time.[116b] Another way to overcome this problem is to use different nuclei whose chemical shifts extend over a larger range. An example was recently provided by the research group of Morris, who demonstrated that a mixture of silicon compounds can indeed be identified and assigned by performing a ^{29}Si DOSY experiment.[117] There was clear resolution of the four principle species in the system, namely, the monomeric silicate **103**, the cyclic trimer **105**, the prismatic hexamer **107**, and the cubic octamer **108** (Figure 26). It also seems that the dimer **104** and the cyclic tetramer **106** are also resolved. A good resolution of compounds was achieved in this study, but it should be noted that it was performed on a concentrated sample using enriched silicates (99.35 % $^{29}SiO_2$) and required several hours.

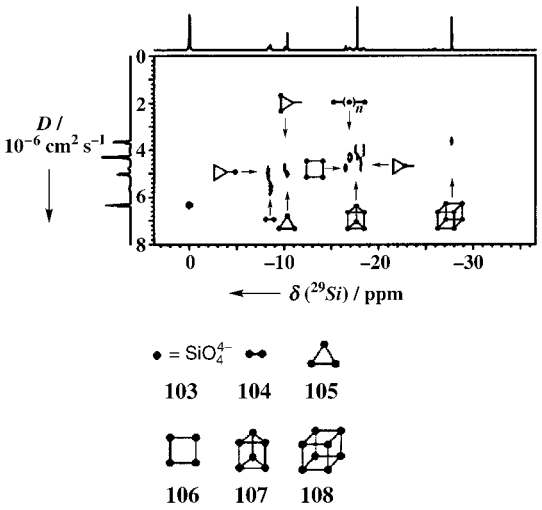


Figure 26. ^{29}Si DOSY spectrum (99.34 MHz) of silicates (0.5 M (99.35 % with 99.35 % ^{29}Si); top: ^{29}Si spectrum, side: projection of the integral onto the diffusion axis. The ten bipolar STE spectra acquired with 320 transients each were measured in a total time of 7 h. Reproduced with permission from Ref. [117].

These recent examples, which were obtained by using conventional instruments, demonstrate that the current technology is already suitable for identifying relatively subtle differences in molecular weights as a means to virtually separate different compounds spectroscopally.

5.2. Ligand Screening by Diffusion and Affinity NMR Spectroscopy

A number of NMR parameters that change upon complex formation, such as chemical shift, transferred nuclear Overhauser effect (NOE), relaxation, and diffusion, were suggested as a screening method.[118] The most widely used NMR screening method is the structure/activity relationships (SARs) introduced by Fesik and co-workers.[119] Diffusion coefficients can be used to screen for the interaction between small molecules and specific receptors, thus separating the spectra of different compounds without really physically separating the compounds in the mixture. As already demonstrated in Section 4.1.1, one can translate the fast change in the diffusion coefficient into an association constant. The calculation of the association constant requires

 © 2005 Wiley-VCH Verlag GmbH & Co. KGaA, Weinheim

quantitative determination of the diffusion coefficients, and hence requires the full characterization of the signal decay as a function of the diffusion weighting. However, for screening purposes, where the indication of binding or relative binding is the required information, one can use only a few gradient points to screen for the possible binding of a certain ligand to a given receptor.[120a,b]

An approach where only one gradient point is measured was provided by Shapiro and co-workers and is depicted in Figure 27.[120b] These researchers first measured the 1D ^{1}H spectrum of the mixture of the eight potential ligands (**109**–**116**) and hydroquinine 9-phenanthryl ether (**117**) as the receptor (Figure 27a). They then found the experimental PFG conditions (gradient strength and duration) needed to eliminate the spectrum of the mixture of the eight tentative ligands in the absence of **117** (Figure 27b). They then repeated the same PFG 1D ^{1}H NMR spectrum after addition of **117** to the mixture and indeed observed, in addition to the signals of **117**, signals originating from compounds **109** and **110** that interact with the receptor molecule **117** (Figure 27c). Only the compounds which interact with the receptor experience a decrease in their diffusion coefficients and, hence, their signals reappear under the previously selected PFG conditions.

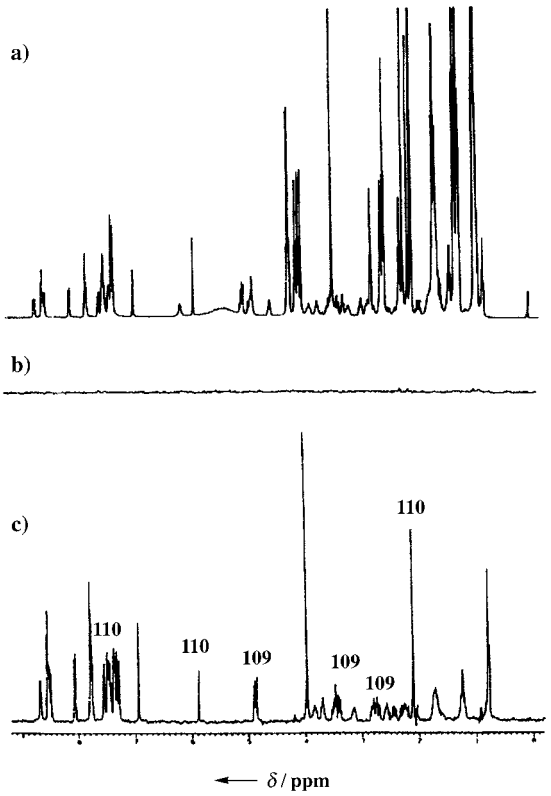
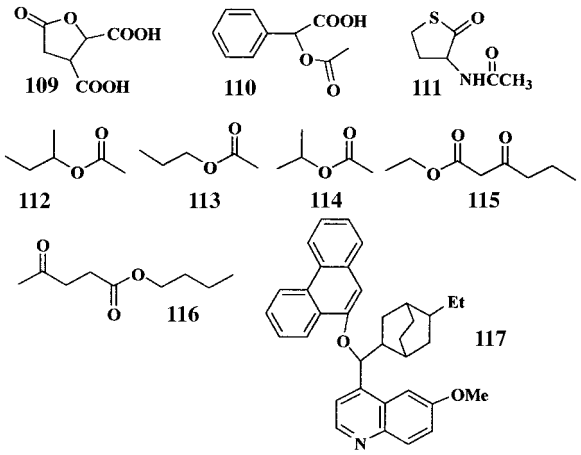


Figure 27. Screening by NMR methods: a) 1D ^{1}H NMR spectrum (400 MHz) of the nine-component mixture (**109**–**117**) in $CDCl_3$ at concentrations of 10 mM; b) 1D pulse gradient ^{1}H NMR spectrum of the mixture without **117** using the LED sequence; and c) 1D pulse gradient ^{1}H NMR spectrum of the eight-component mixture after addition of **117** using the same experimental conditions as (b). Signals arising from compounds **109** and **110** are labeled. All other signals are from compound **117**. Reproduced with permission from Ref. [120b].

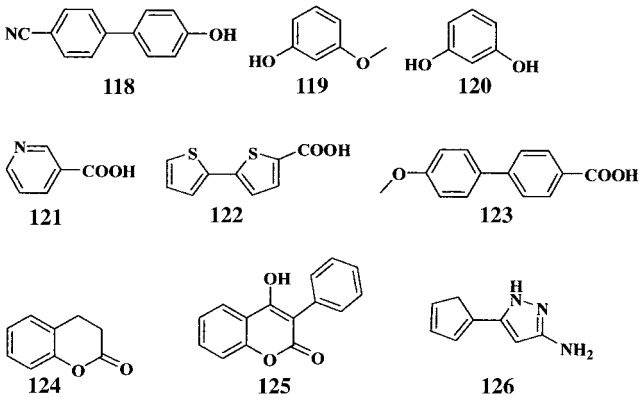


This simple method for screening potential ligands and receptors has the following advantages: The measured parameter, that is, the diffusion coefficient, is intuitively related to the followed phenomenon; the expected decrease in the diffusion coefficient for the compounds that interact with the receptor is indeed observed. This is in contrast to other (non-NMR) parameters and NMR chemical shifts and relaxation times, where the sign of the changes can be both positive or negative. Additionally, this quantitative result can be obtained in a matter of a few minutes from a mixture of several ligands. An important advantage of screening by diffusion NMR spectroscopy is the fact that the method is applicable to all receptors, even to systems of unknown ligands and receptors. This is in clear contrast to the main competing NMR approach for ligand screening, namely, SAR-NMR spectroscopy,[118–119] which is based on monitoring the changes in the ^{15}N/^{1}H hetreonuclear single quantum coherence (HSQC) of a uniformly ^{15}N-labeled receptor after the addition of a mixture of potential ligands. This method is, therefore, only applicable to known receptors for which a large quantity (about 200 mg) of labeled compounds is available. The receptor should have a relatively high solubility, with a molecular weight not more that about 20000–30000 Da.[121] Diffusion NMR spectroscopy, on the other hand, is a nonspecific method and, as such, can be used for the screening of possible ligands for possible receptors with practically no limitation in the size of the receptor. This technique can, in principle, also be applied in combination with other NMR sequences and using all NMR-active nuclei. As in all NMR methods, screening by diffusion NMR spectroscopy is less prone to complications arising from impurities as compared with non-NMR methods. In addition, it should be noted that the larger the difference in the size of the screened ligands and receptors, the higher the sensitivity of the method and, in fact, it may even be easier to monitor ligand association to larger receptors which are NMR silent. The major drawback of the simple approach for ligand screening by diffusion NMR spectroscopy, as outlined in Figure 27, is the fact that both the signals of the ligands interacting with the receptor and the receptor signals are all observed in the final spectrum.[120a] This implies that there is a good chance for signal overlap that will preclude the identification of the interacting ligand(s). However, the

 © 2005 Wiley-VCH Verlag GmbH & Co. KGaA, Weinheim

identification of interacting ligands may be even simpler in cases where relatively large receptors, which have a short T_2 value that renders them NMR silent under the conditions used, are screened by this diffusion NMR screening method.[121] In such systems only the signals of the interacting ligand(s) will appear in the final spectrum.

Several approaches to increase the assignment capability of the diffusion NMR screening method were proposed to identify the interacting ligand(s). Fesik and co-workers suggested using diffusion editing to simplify the spectrum of the interacting ligand by eliminating the signals of the receptor, thus leaving only the signals of the interacting ligands after few spectra subtractions.[122] They demonstrated this approach for ligands of the FK506 binding protein and the catalytic domain of stromelysin. For the stromelysin system, the ligand **118** and an additional eight small molecules



119–126 that were not expected to interact with FK506 were examained (Figure 28). First, they measured the ^{1}H NMR spectra at low gradient strengths of compounds **118–126** in the absence (Figure 28a) and presence of stromelysin. The signal of the protein was then eliminated by subtracting the spectrum of the mixture of the ligands in the presence of stromelysin, obtained at high gradient strengths (data not shown), from the spectrum of the same mixture obtained at low gradient strengths (Figure 28b). Then by subtracting the spectra shown in Figure 28a and Figure 28b, they could identify the peaks of the interacting ligand, namely, compound **118** as shown in Figure 28c. This approach is likely to be operational only in cases in which there are no dramatic changes in the chemical shifts of the compounds involved in the complexation, and it is likely to be more efficient for systems in which the ligands and the receptors differ greatly in size. In fact, Shapiro and co-workers reported that the Fesik approach did not work well in the screening of a mixture of ten different tetrapeptides (two ligands and eight nonbonding tetrapaptides) for their affinity with respect to vancomycin.[123a] They suggested another approach to identify the interacting ligands, namely, to couple the diffusion weighting with a 2D TOCSY sequence (TOCSY = total correlation spectroscopy) which they named DECODES (diffusion encoded spectroscopy).[123b] They showed by comparing the DECODES and TOCSY spectra of the series of ten

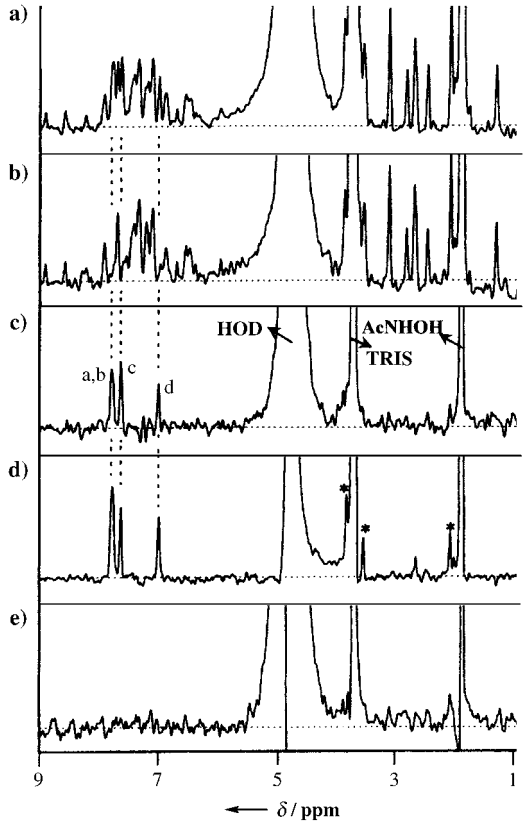


Figure 28. Analysis of ligand binding to the catalytic domain of stromelysin by using a diffusion-edited approach.[122] a) PFG-STE spectrum of a mixture of **118–126** in the absence of stromelysin using pulse gradients of low strength. b) The same spectrum as (a) after removal of protein signals by subtracting a spectrum obtained with strong pulse gradients of the same sample. c) Difference spectrum (a) − (b). The signals of **118** at $\delta = 7.84$, 7.70, and 7.06 ppm in the absence of the protein are indicated by the vertical dashed lines. The signals from 2-amino-2-(hydroxymethyl)propan-1,3-diol) (tris; $\delta = 3.74$ ppm) and acetohydroxamic acid (AcNHOH, $\delta = 1.94$ ppm) were significantly attenuated in the difference spectrum, but not eliminated. d) Reference spectrum of **118** alone. Asterisks (*) indicate impurities in the buffer. e) Difference spectrum obtained in an analogous fashion to the spectrum shown in (c), but on a mixture of eight compounds (**119–126**) which do not bind to stromelysin. Reproduced with permission from Ref. [122].

tetrapaptides in the presence of vancomycin that only signals from amino acids D, F, S, and A remain in the spectrum, thus indicating that only the two peptides DDFA and DDFS bind to vancomycin (see Figure 29). This system, in which there is relatively weak binding and in which the different ligands are of very similar size and not always very different from that of the small receptor of the vancomycin, clearly demonstrates the potential of this simple approach.[123b] Recently, such an approach was used to decode the binding affinity to a DNA dodecamer.[123c]

In fact, few DOSY spectra can, in principle, be used to screen for potential ligands for known or unknown receptors.[34] All that has to be done is obtain the DOSY spectra of a mixture of the potential ligands in the absence and presence of the alleged receptor—it must, however, be ensured that the addition of the receptor has no effect on the viscosity of the

 © 2005 Wiley-VCH Verlag GmbH & Co. KGaA, Weinheim

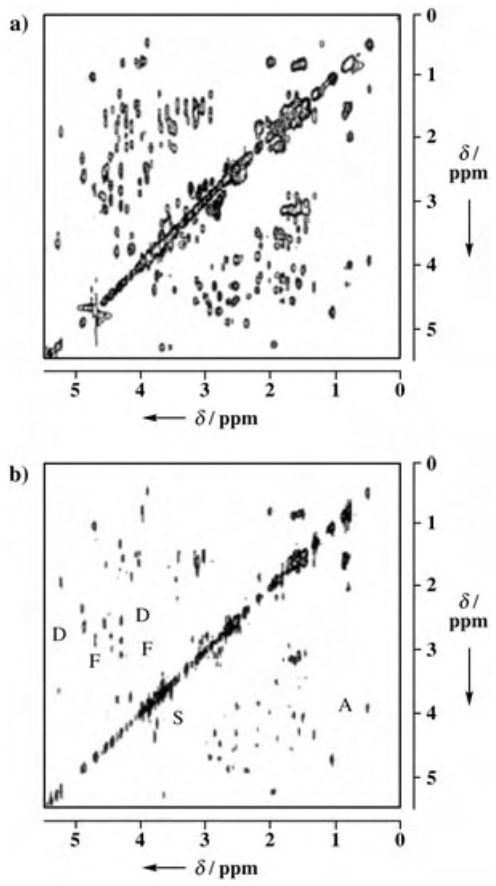


Figure 29. a) TOCSY NMR spectrum for the tetrapeptide mixture containing DDFA, YPFV, GLGG, GPRP, RGDS, GRGD, RGFF, KDEL, DASV, and DDFS in the presence of vancomycin. b) The corresponding DECODES spectrum highlighting the amino acids that remain: D, F, S, and A. Adapted with permission from Ref. [123b].

sample. It should then be possible to identify the interacting ligands by comparing the change in the DOSY spectra. In this approach, the signal separation should be significantly increased since the information is now spread in two dimensions and one has to compare the two 2D spectra of the DOSY experiment. If signal overlap does occur, one can resort to any of the 3D DOSY sequences to try to alleviate the signal overlap at the cost of a longer acquisition time.

6. Summary and Outlook

High-resolution diffusion NMR spectroscopy is a very simple, flexible, and accurate method to obtain diffusion coefficients in solution. With this method it is possible to analyze ensembles of signals simultaneously by using standard NMR spectroscopic technology, thus allowing the addition of the diffusion coefficient into the set of parameters used to characterize systems in solution. In this Review we attempted to describe, through the use of examples, the range of chemical problems that can be addressed with diffusion NMR spectroscopy, including determination of association constants, aggregation, encapsulation, solvation, hydration, ion pairing, estimation of mutual interaction in multicomponent systems, determination of effective size and structures of reactive intermediates, organometallic systems, and other supramolecular systems such as rotaxanes, catenanes, and molecular capsules. The combination of diffusion NMR spectroscopy with other NMR methods provides an improved tool for mapping the different interactions between the different components of the multicomponent systems in solution. Diffusion coefficients can also be used to probe the kinetic stability of multicomponent systems by merely monitoring the effect of a small excess of one of the components on the diffusion coefficient of the supramolecular system. In addition, diffusion NMR spectroscopy can be used for "virtual separation" of mixtures or libraries of compounds of modest size, and provides an efficient and general means, which imposes no requirement on the investigated system, to screen for lead compounds and also potential ligands for unknown receptors. An important feature of diffusion NMR spectroscopy is that the measured parameter, that is, the diffusion coefficient, is intuitively related to many of the phenomena that are studied in a much more direct way than many of the more conventional and heavily used NMR parameters, such as chemical shifts and relaxation times. Diffusion is also a filter, which can be obtained relatively easy and can easily be coupled to nearly any known NMR sequence.

In this Review we have not elaborated on technical issues and the theory of diffusion, which can be found in the many extensive technical reviews recently written on the subject (some of which were cited), since we have focused on applications relevant to supramolecular and combinatorial chemistry. Although we avoided technical issues, it is clear that current technology (conventional instruments and programs) allows easy, simple, and accurate determination of diffusion coefficients in high-resolution probes. In fact, the systems studied, which are characterized by a relatively long T_2 relaxation time and large diffusion coefficients, are simple cases for the current technology. We foresee continuous improvement in gradient technology, mainly arising from its important role in other MR applications. Current gradient technology with conventional PGSE and STE diffusion sequences already gives very good results on not very demanding systems that do not have very short T_2 relaxation times. Therefore, there is much less need for the LED and BPLED sequences, which were so important in the early days of DOSY when much less developed gradient technology was available in many laboratories. Currently, commercial instruments already have DOSY packages and there are ample sequences which can be installed that incorporate diffusion weighting. It therefore seems plausible to speculate that the application of diffusion NMR spectroscopy in the context of supramolecular and combinatorial chemistry will flourish in the coming years.

The main problem of diffusion NMR spectroscopy, like all NMR spectroscopic techniques in general, is its relative low sensitivity, which requires relatively concentrated samples and a long acquisition time. In addition, diffusion weighting means that a filtering out of the signal occurs. Moreover, in conventional DOSY sequences 1D and 2D NMR sequences are transformed into 2D and 3D NMR experiments, respec-

 © 2005 Wiley-VCH Verlag GmbH & Co. KGaA, Weinheim

tively. This implies that relatively long acquisition times are required, but this will probably be partially alleviated in the future by using gradient systems on high-field magnets (more than 600 MHz) in combination with cryoprobes. This limitation is not very severe, however, and with current technology the PGSE or the STE diffusion experiments can be performed on host–guest or supramolecular systems having molecular weights of a few kilodaltons and a reasonable lineshape (that is, $\Delta\tilde{\nu}_{1/2} = 10$ Hz) within one hour on a conventional 400 or 500 MHz spectrometer when the concentration is in the range of about 5 mM.

Two additional areas of application of diffusion NMR spectroscopy, not dealt within the present Review because of space limitations, that deserve mentioning are: biochemistry and protein research,[124] as well as the newly emerging field of semisolid samples, where diffusion NMR spectroscopy is used in combination with magic angle spinning (MAS).[125] Diffusion measurements have been used in the context of biochemistry and protein research to study self-aggregation, the association of different ligands and DNA, as well as protein folding.[124,126] However, a very exciting recent development is the use of diffusion NMR spectroscopy to study protein folding in real time.[127] Buevich and Baum used the much more sophisticated ^{1}H-^{15}N LED-HSQC diffusion sequence to measure the protein-folding process in real time for residue-specific ^{15}N-labeled T1-892. They followed the disappearance of the monomer, the appearance of the trimer, and other kinetic intermediates by using diffusion NMR spectroscopy. This exciting demonstration was performed on a relatively slow folding process, but with the advent of high-sensitivity cryoprobes in combination with high-field magnets and fast 2D sequences, one may anticipate the study of much faster processes in the future.

The other field which is currently emerging is the measurement of diffusion by MAS probes on semisolid samples.[125] These probes, which only recently became available, have been used to distinguish between trapped or covalently bonded small molecules in swollen Wang resin beads. The combination of the bipolar LED and CPMG sequences (CPMG = Carr–Purcell–Meiboom–Gill) is useful for studying the interaction of different molecules with resins—an area vital to combinatorial chemistry.[125a,b]

With the above applications already published in the literature and in view of the rapid advancement of instruments and software, which will make diffusion NMR spectroscopy more accurate and efficient, it is possible to speculate that diffusion NMR spectroscopy will, in the near future, become a popular tool in the hands of chemists interested in molecular interactions in solution. The triumph of diffusion NMR spectroscopy will be when it becomes as commonplace as other NMR methods. Our aim in this Review was to convince organic, inorganic, organometallic and supramolecular chemists to add diffusion NMR spectroscopy to their arsenal of analytical tools used to study molecular interactions in solution.

We thank the Israel Science Foundation administered by the Israel Academy of Science and Humanities, Jerusalem, Israel, for supporting the early stage of this research. We also wish to thank Professors S. E. Biali, V. Böhmer, R. Ungaro, and D. N. Reinhoudt for collaborative efforts and Professor S. E. Biali for reading and commenting on the manuscript.

Received: October 23, 2003

[1] a) J.-M. Lehn, *Supramolecular Chemistry Concepts and Perspectives*, VCH, Weinheim, **1995**; b) J. W. Steed, J. L. Atwood, *Supramolecular Chemistry*, Wiley, New York, **2000**.

[2] a) *Comprehensive Supramolecular Chemistry*, *Vols. 1–10* (Eds.: J. L. Atwood, J. E. D. Davis, D. D. MacNicol, F. Vögtle, J.-M. Lehn), Pergamon, Oxford, **1996**; b) *Proc. Natl. Acad. Sci. USA* **2002**, *99*, 4755–5750, (special issue on supramolecular chemistry and self-assembly (Ed.: J. Halpern).

[3] *Combinatorial Chemistry: a Practical Approach* (Eds.: W. Bannwarth, E. Felder), Wiley-VCH, Weinheim, **2000**.

[4] E. L. Hahn, *Phys. Rev.* **1950**, *80*, 580–594.

[5] a) O. E. Stejskal, J. E. Tanner, *J. Chem. Phys.* **1965**, *42*, 288–292; b) it should be noted that the diffusion time depends on the shape of the pulse gradients used, as expected from Equation (9). For example, for the PGSE or the STE diffusion sequence with sine-shape gradient pulses, the effective diffusion time is $\Delta - \delta/4$. When $\Delta \gg \delta$ the diffusion time is $\approx \Delta$.

[6] a) J. Jeener, Ampére International Summer School, Basko Polje, Yugoslavia, **1971**; b) W. P. Aue, E. Bartholdi, R. R. Ernst, *J. Chem. Phys.* **1976**, *64*, 2229–2246.

[7] A. Bax, *Two-Dimensional Magnetic Resonance in Liquids*, Delft University Press, D. Reidel Publishing Company, **1982**.

[8] R. R. Ernst, G. Bodenhausen, A. Wokaun, *Principles of Nuclear Magnetic Resonance in One and Two Dimensions*, Oxford University Press, Oxford, **1987**; b) T. D. W. Claridge, *High-Resolution NMR Techniques in Organic Chemistry*, Pergamon, Amsterdam, **1999**.

[9] P. Stilbs, *Prog. Nucl. Magn. Reson. Spectrosc.* **1987**, *17*, 1–45, and references therein.

[10] a) J. Kärger, H. Pfeifer, W. Heink, *Adv. Magn. Reson.* **1988**, *12*, 1–88; b) for a recent volume concerning the use of diffusion NMR spectroscopy in chemical systems see: *Magn. Reson. Chem.* **2002**, *40*, S15–S152; c) for a recent volume regarding the use of diffusion NMR spectroscopy in chemical and biological systems see: *Diffusion NMR and MRI: Basic Concepts and Applications* (Eds.: Y. Cohen, M. Neeman), *Israel. J. Chem.* **2003**, *43*, 1–163.

[11] W. S. Price in *Annual Reports on NMR spectroscopy* (Ed.: G. A. Webb), Academic, London, **1996**, pp. 51–142; b) T. Parella, *Magn. Reson. Chem.* **1996**, *34*, 329–347; c) T. Parella, *Magn. Reson. Chem.* **1998**, *36*, 467–495.

[12] a) P. C. Lauterbur, *Nature* **1973**, *242*, 190–191; b) D. D. Stark, W. G. Bardley, *Magnetic Resonance Imaging*, 2nd ed., Mosby Company, St. Louis, **1992**; c) *Methods of Magnetic Resonance Imaging and Spectroscopy* (Ed.: I. R. Young), Wiley, Chichester, **2000**.

[13] *Perfusion and Diffusion Magnetic Resonance Imaging: Applications to functional MRI* (Ed.: D. Le Bihan), Raven Press, New York, **1995**.

[14] M. E. Moseley, Y. Cohen, J. Mintorovitch, L. Chileuitt, H. Shimizu, J. Kucharczyk, M. F. Wendland, P. R. Weinstein, *Magn. Reson. Med.* **1990**, *16*, 330–346.

[15] P. J. Basser, *NMR Biomed.* **1995**, *8*, 333–344; P. J. Basser, J. Mattiello, D. Le Bihan, *Biophys. J.* **1994**, *66*, 259–267; for a recent special volume on DTI see: *NMR Biomed.* **2002**, *15*, 431–593.

[16] a) J. Kärger, D. M. Ruthven, *Diffusion in Zeolites and Other Microporous Solids*, Wiley, New York, **1992**; b) T. Nose, *Annu. Rep. NMR Spectrosc.* **1993**, *27*, 218–253.

 © 2005 Wiley-VCH Verlag GmbH & Co. KGaA, Weinheim

[17] a) W. S. Price, *Concepts Magn. Reson.* **1997**, *9*, 299 – 336; b) P. T. Callaghan, S. L. Codd, J. D. Seymour, *Concepts Magn. Reson.* **1999**, *11*, 181 – 202; c) W. S. Price, *Concepts Magn. Reson.* **1998**, *10*, 197 – 237.

[18] a) J. Kärger, H. Pfeifer, *NMR and Catalysis*, (Eds.: A. Pines, A. Bell), Dekker, New York, **1994**; b) P. T. Callaghan, A. Coy in *NMR Probes and Molecular Dynamics* (Ed.: R. Tycko), Kluwer, Dordrecht, **1993**, pp. 490 – 523.

[19] O. Söderman, P. Stilbs, *Prog. Nucl. Magn. Reson. Spectrosc.* **1994**, *26*, 445 – 482.

[20] G. Lindblom, G. Oradd, *Prog. Nucl. Magn. Reson. Spectrosc.* **1994**, *26*, 483 – 515.

[21] A. R. Waldeck, P. W. Kuchel, A. J. Lennon, B. E. Chapman, *Prog. Nucl. Magn. Reson. Spectrosc.* **1997**, *30*, 39 – 68.

[22] a) D. G. Corry, D. N. Garroway, *Magn. Reson. Med.* **1990**,*14*, 435 – 444; b) P. T. Callaghan, D. MacGowan, K. J. Packer, F. O. Zelaya, *J. Magn. Reson.* **1990**, *90*, 177 – 182; c) P. T. Callaghan, A. Coy, D. MacGowan, K. J. Packer, F. O. Zelaya, *Nature* **1991**, *351*, 467 – 469.

[23] P. W. Kuchel, A. Coy, P. Stilbs, *Magn. Reson. Med.* **1997**, *37*, 637 – 643.

[24] A. M. Torres, A. T. Taurins, D. G. Regan, B. E. Chapman, P. W. Kuchel, *J. Magn. Reson.* **1999**, *138*, 135 – 143.

[25] P. W. Kuchel, C. J. Durrant, *J. Magn. Reson.* **1999**, *139*, 258 – 272.

[26] a) Y. Assaf, A. Mayk, Y. Cohen, *Magn. Reson. Med.* **2000**, *44*, 713 – 722; b) Y. Assaf, D. Ben-Bashat, J. Chapman, S. Peled, I. E. Biton, M. Kafri, Y. Segev, T. Hendler, A. D. Korczyn, M. Graif, Y. Cohen, *Magn. Reson. Med.* **2002**, *47*, 115 – 126; c) Y. Assaf, Ph.D. Thesis, Tel Aviv University, **2001**.

[27] Y. Cohen, Y. Assaf, *NMR Biomed.* **2002**, *15*, 516 – 542.

[28] P. T. Callaghan, *Rep. Prog. Phys.* **1999**, *62*, 599 – 670, and references therein.

[29] a) U. Tallarek, D. van Dusschoten, H. Van As, E. Bayer, G. Guiochon, *J. Phys. Chem. B* **1998**, *102*, 3486 – 3497; b) U. Tallarek, F. J. Vergeldt, H. Van As, *J. Phys. Chem. B* **1999**, *103*, 7654 – 7664; c) U. Tallarek, E. Rapp, A. Seidel-Morgenstern, H. Van As, E. Bayer, G. Guiochon, *J. Phys. Chem. B* **2002**, *106*, 12709 – 12721.

[30] The theory of molecular diffusion and transport is highly developed and details can be found in the following excellent monograph: a) J. Crank, *The Mathematics of Diffusion*, 2nd ed., Claxendon Press, Oxford, **1975**; b) E. L. Cussler, *Diffusion: Mass Transfer in Fluid Systems*, Cambridge University Press, Cambridge, **1984**.

[31] A. Einstein, *Ann. Phys.* **1906**, *19*, 289 – 306.

[32] J. E. Tanner, *J. Chem. Phys.* **1970**, *52*, 2523 – 2526.

[33] S. J. Gibbs, C. S. Johnson, Jr., *J. Magn. Reson.* **1991**, *93*, 395 – 402.

[34] C. S. Johnson, Jr., *Prog. Nucl. Magn. Reson. Spectrosc.* **1999**, *34*, 203 – 256, and references therein.

[35] a) D. Wu, A. Chen, C. S. Johnson, Jr., *J. Magn. Reson. Ser. A* **1995**, *115*, 123 – 126; b) to further reduce the eddy currents sine-shaped gradient pulses rather than the classical rectangular gradient pulses can be used.

[36] a) D. Wu, A. Chen, C. S. Johnson, Jr., *J. Am. Chem. Soc.* **1993**, *115*, 4291 – 4299; b) D. Wu, A. Chen, C. S. Johnson, Jr., *J. Magn. Reson. Ser. A* **1996**, *123*, 215 – 218.

[37] J. S. Gounarides, A. Chen, M. J. Shapiro, *J. Chromatogr. B* **1999**, *725*, 79 – 90, and references therein.

[38] E. Gozansky and D. G. Gorenstein, *J. Magn. Reson. Ser. B* **1996**, *111*, 94 – 96.

[39] a) D. Wu, A. Chen, C. S. Johnson, Jr., *J. Magn. Reson. Ser. A* **1996**, *121*, 88 – 91. These authors have not inverted the third dimension to obtain the diffusion coefficients. b) A. Jerschow and N. Müller, *J. Magn. Reson. Ser. A* **1996**, *123*, 222 – 225; c) H. Barjat, G. A. Morris, A. G. Swanson, *J. Magn. Reson.* **1998**, *131*, 131 – 138.

[40] a) K. A. Connors, *Binding Constants*, Wiley, New York, **1987**; b) H. Tsukube, H. Furuta, A. Odani, Y. Takeda, Y. Kudo, Y. Inoue, Y. Liu, H. Sakamoto, K. Kimura in *Comprehensive Supramolecular Chemistry*, *Vol. 3* (Eds.: J. L. Atwood, J. E. D. Davis, D. D. MacNicol, F. Vögtle), Pergamon, Oxford, **1996**, chap. 10; c) H.-J. Schneider, A. Yatsimirsky, *Principle and Methods in Supramolecular Chemistry*, Wiley, New York, **2000**, pp. 137 – 226.

[41] For some selected examples and the compilation of association constants, see: a) J. J. Christensen, D. J. Eatough, R. M. Izatt, *Chem. Rev.* **1974**, *74*, 351 – 384; b) R. M. Izatt, J. S. Bradshaw, S. A. Nielsen, J. D. Lamb, J. J. Christensen, *Chem. Rev.* **1985**, *85*, 271 – 339; c) K. E. Krakowiak, J. S. Bradshaw, D. J. Zamecka-Krakowiak, *Chem. Rev.* **1989**, *89*, 929 – 972; d) R. M. Izatt, K. Pawlak, J. S. Bradshaw, *Chem. Rev.* **1991**, *91*, 1721 – 2085; e) H. An, J. S. Bradshaw, R. M. Izatt, *Chem. Rev.* **1992**, *92*, 543 – 572.

[42] a) T. Wang, J. S. Bradshaw, R. M. Izatt, *J. Heterocycl. Chem.* **1994**, *31*, 1097 – 1114; b) Y. Inoue, *Annu. Rep. NMR Spectrosc.* **1993**, *31*, 59 – 101; c) K. A. Connors, *Chem. Rev.* **1997**, *97*, 1325 – 1357; d) C. S. Wilcox in *Frontiers of Supramolecular Chemistry and Photochemistry* (Eds.: H.-J. Schneider, H. Durr) Weinheim, **1991**, pp. 123 – 143.

[43] a) L. Fielding, *Tetrahedron* **2000**, *56*, 6151 – 6170; b) L. Fielding, *Curr. Top. Med. Chem.* **2003**, *3*, 39 – 53.

[44] B. Lévay, *J. Chem. Phys.* **1973**, *77*, 2118 – 2121.

[45] For some early diffusion measurements by the Stilbs research group, see: P. Stilbs, M. E. Moseley, *Chem. Scr.* **1979**, *13*, 26 – 30; P. Stilbs, M. E. Moseley, *Chem. Scr.* **1980**, *15*, 215 – 217; P. Stilbs, B. Lindman, *J. Phys. Chem.* **1981**, *85*, 2587 – 2589; W. Brown, R. M. Johnsen, P. Stilbs, B. Lindman, *J. Phys. Chem.* **1983**, *87*, 4548 – 4553; M. Jansson, P. Stilbs, *J. Phys. Chem.* **1985**, *89*, 4868 – 4873.

[46] R. Rydén, J. Carlfors, P. Stilbs, *J. Inclusion Phenom.* **1983**, *1*, 159 – 167.

[47] O. Mayzel, Y. Cohen, *J. Chem. Soc. Chem. Commun.* **1994**, 1901 – 1902.

[48] For example, fluorescence was used to calculate the association constant of 5,10,15,20 tetrakis(4-carboxyphenyl) porphyrin with β-CD. The discrepancy was not only in the values obtained but also in the sign of the changes in the fluorescence observed upon complex formation: in one report, S. S. Zhao, J. H. T. Luong, *J. Chem. Soc. Chem. Commun.* **1994**, 2307 – 2308, an increase in the fluorescence is reported, while in another, F. Venema, A. E. Rowan, R. Nolte, *J. Am. Chem. Soc.* **1996**, *118*, 257 – 258, a decrease in fluorescence was reported.

[49] F. Vögtle, W. M. Muller, *Angew. Chem.* **1979**, *91*, 676 – 677; *Angew. Chem. Int. Ed. Engl.* **1979**, *18*, 623 – 624.

[50] S. Kamitori, K. Hirotsu, T. Higuchi, *J. Chem. Soc. Chem. Commun.* **1986**, 690 – 691.

[51] a) S. Kamitori, K. Hirotsu, T. Higuchi, *J. Am. Chem. Soc.* **1987**, *109*, 2409 – 2414; b) S. Kamitori, K. Hirotsu, T. Higuchi, *Bull. Chem. Soc. Jpn.* **1988**, *61*, 3825 – 3830.

[52] A. Gafni, Y. Cohen, *J. Org. Chem.* **1997**, *62*, 120 – 125.

[53] The hydrophobic interaction is the major driving force for most organic molecule complexes containing cyclodextrins in aqueous solutions. Only a few cases are known in which the addition of alcohol brings about an increase in the association constant of CD complexes in water and, even there, a decrease in the K_a value was observed for high alcohol concentrations; see, for example: G. Nelson, G. Patonay, I. M. Warner, *J. Inclusion Phenom.* **1988**, *6*, 277 – 289; K. A. Connors, M. J. Mulski, A. Paulson, *J. Org. Chem.* **1992**, *57*, 1794 – 1798.

[54] A. Gafni, Y. Cohen, R. Kataky, S. Palmer, D. Parker, *J. Chem. Soc. Perkin Trans. 2* **1998**, *19*–23.

[55] K. S. Cameron, L. Fielding, *J. Org. Chem.* **2001**, *66*, 6891 – 6895.

 © 2005 Wiley-VCH Verlag GmbH & Co. KGaA, Weinheim

[56] a) L. Avram, Y. Cohen, *J. Org. Chem.* **2002**, *67*, 2639 – 2644; b) for an additional paper in which diffusion NMR spectroscopy was used to corroborate the formation of rotaxanes, see: P. J. Skinner, S. Blair, R. Kataky, D. Parker, *New J. Chem.* **2000**, *24*, 265 – 268.

[57] It was suggested that protonation of nitrogen atoms in nitrogen-containing pseudorotaxanes might convert them into rotaxanes: Y. Kawaguchi, A. Harada, *J. Am. Chem. Soc.* **2000**, *122*, 3797 – 3798.

[58] L. Frish, F. Sansone, A. Casnati, R. Ungaro, Y. Cohen, *J. Org. Chem.* **2000**, *65*, 5026 – 5030.

[59] a) A. Casnati, M. Fabbi, N. Pelizzi, A. Pochini, F. Sansone, R. Ungaro, *Bioorg. Med. Chem. Lett.* **1996**, *6*, 2699 – 2704; b) A. Casnati, F. Sansone, R. Ungaro, *Acc. Chem. Res.* **2003**, *36*, 246 – 254.

[60] a) B. K. Hubbard, C. T. Walsh, *Angew. Chem.* **2003**, *115*, 752 – 789; *Angew. Chem. Int. Ed.* **2003**, *42*, 730 – 765; b) D. H. Williams, B. Bardsley, *Angew. Chem.* **1999**, *111*, 1264 – 1286; *Angew. Chem. Int. Ed.* **1999**, *38*, 1172 – 1193, and references therein.

[61] C. T. Walsh, S. L. Fisher, I. S. Park, M. Prahaland, Z. Wu, *Chem. Biol.*, **1996**, *3*, 21 – 28.

[62] O. Mayzel, O. Aleksiuk, F. Grynszpan, S. E. Biali, Y. Cohen, *J. Chem. Soc. Chem. Commun.* **1995**, 1183 – 1184.

[63] J. M. Harrowfield, M. I. Odgen, W. R. Richmond, A. H. White, *J. Chem. Soc. Chem. Commun.* **1991**, 1159 – 1160.

[64] a) D. J. Cram, *Nature* **1992**, *356*, 29 – 36; b) R. G. Chapman, J. C. Sherman, *Tetrahedron* **1997**, *53*, 15911 – 15945; c) A. Jasat, J. C. Sherman, *Chem. Rev.* **1999**, *99*, 931 – 967.

[65] a) M. M. Conn, J. Rebek, Jr., *Chem. Rev.* **1997**, *97*, 1647 – 1668; b) M. Fujita, K. Umemoto, M. Yoshizawa, N. Fujita, T. Kusukawa, K. Biradha, *Chem. Commun.* **2001**, 509 – 518; c) F. Hof, S. L. Craig, C. Nuckolls, J. Rebek, Jr., *Angew. Chem.* **2002**, *114*, 1556 – 1578; *Angew. Chem. Int. Ed.* **2002**, *41*, 1488 – 1508.

[66] a) K. D. Shimizu, J. Rebek, Jr., *Proc. Natl. Acad. Sci. USA* **1995**, *92*, 12403 – 12407; b) V. Böhmer, O. Mogck, M. Pons, E. F. Paulus in *NMR in Supramolecular Chemistry* (Ed.: M. Pons), Kluwer Academic Publishers, Dordrecht, **1999**, pp. 45 – 60; c) J. Rebek, Jr., *Acc. Chem. Res.* **1999**, *32*, 278 – 286; d) J. Rebek, Jr., *Chem. Commun.* **2000**, 637 – 643; e) V. Böhmer, M. O. Vysotsky, *Aust. J. Chem.* **2001**, *54*, 671 – 677.

[67] a) R. Warmuth, *J. Inclusion Phenom. Macrocyclic Chem.* **2000**, *37*, 1 – 38; b) J. Chen, S. Körner, S. L. Craig, D. M. Rudkevich, J. Rebek, Jr., *Nature* **2002**, *414*, 385 – 386; c) J. Chen, S. Körner, S. L. Craig, S. Lin, D. M. Rudkevich, J. Rebek, Jr., *Proc. Natl. Acad. Sci. USA* **2002**, *99*, 2593 – 2596.

[68] L. Frish, S. E. Matthews, V. Böhmer, Y. Cohen, *J. Chem. Soc. Perkin Trans. 2* **1999**, 669 – 671.

[69] a) D. A. Dougherty, D. A. Stauffer, *Science* **1990**, *250*, 1558 – 1560; b) J. C. Ma, D. A. Dougherty, *Chem. Rev.* **1997**, *97*, 1303 – 1324.

[70] a) L. Frish, M. O. Vysotsky, S. E. Matthews, V. Böhmer, Y. Cohen, *J. Chem. Soc. Perkin Trans. 2* **2002**, 88 – 93; b) L. Frish, M. O. Vysotsky, V. Böhmer, Y. Cohen, *Org. Biomol. Chem.* **2003**, *1*, 2011 – 2014.

[71] L. Avram, Y. Cohen, *J. Am. Chem. Soc.* **2002**, *124*, 15148 – 15149.

[72] L. R. MacGillivray, J. L. Atwood, *Nature* **1997**, *389*, 469 – 472.

[73] a) A. Shivanyuk, J. Rebek, Jr., *Proc. Natl. Acad. Sci. USA* **2001**, *98*, 7662 – 7665; b) A. Shivanyuk, J. Rebek, Jr., *Chem. Commun.* **2001**, 2424 – 2425.

[74] A. Shivanyuk, J. Rebek, Jr., *J. Am. Chem. Soc.* **2003**, *125*, 3432 – 3433.

[75] a) L. Avram, Y. Cohen, *Org. Lett.* **2002**, *4*, 4365 – 4368; b) L. Avram, Y. Cohen, *Org. Lett.* **2003**, *5*, 1099 – 1102; c) L. Avram, Y. Cohen, *Org. Lett.* **2003**, *5*, 3329 – 3332; d) T. Gerkensmeier, W. Iwanek, C. Agena, R. Fröhlich, S. Kotila, C. Näther, J. Mattay, *Eur. J. Org. Chem.* **1999**, 2257 – 2262; e) J. L. Atwood, L. J. Barbour, A. Jerga, *Chem. Commun.* **2001**, 2376 – 2377; f) L. Avram, Y. Cohen, *J. Am. Chem. Soc.* **2003**, *125*, 16180 – 16181.

[76] I. P. Gerothanassis, *Prog. Nucl. Magn. Reson. Spectrosc.* **1994**, *26*, 171 – 237, and references therein.

[77] G. Otting, *Prog. Nucl. Magn. Reson. Spectrosc.* **1997**, *31*, 259 – 285, and references therein.

[78] B. Halle, V. P. Denisov, *Methods Enzymol.* **2001**, *338*, 178 – 201.

[79] O. Mayzel, A. Gafni, Y. Cohen, *Chem. Commun.* **1996**, 911 – 912.

[80] T. Iwachido, M. Minami, M. Kimura, A. Sadakane, M. Kawasaki, K. Toei, *Bull. Chem. Soc. Jpn.* **1980**, *53*, 703 – 708.

[81] For a recent volume regarding NMR spectroscopy of H-bonded systems, see: *Magn. Reson. Chem.* **2001**, *39*, S5–S213.

[82] a) R. Konrat, M. Tollinger, G. Kontaxis, B. Kräutler, *Monatsh. Chem.* **1990**, *130*, 961 – 967; b) H. B. Seba, B. Ancian, *J. Chem. Soc. Chem. Commun.* **1990**, 996 – 997; c) F. Cordier, S. Grzesiek, *J. Am. Chem. Soc.* **1999**, *121*, 1601 – 1602.

[83] a) G. S. Kapur, E. J. Cabrita, S. Berger, *Tetrahedron Lett.* **2000**, *41*, 7181 – 7185; b) E. J. Cabrita, S. Berger, *Magn. Reson. Chem.* **2001**, *39*, S142 – S148.

[84] G. M. Whitesides, E. E. Simanek, J. P. Mathias, C. T. Seto, D. N. Chin, M. Mammen, D. M. Gorden, *Acc. Chem. Res.* **1995**, *28*, 37 – 44.

[85] a) R. H. Vreekamp, J. P. M. van Duynhoven, M. Hubert, W. Verboom, D. N. Reinhoudt, *Angew. Chem.* **1996**, *108*, 1306 – 1309; *Angew. Chem. Int. Ed. Engl.* **1996**, *35*, 1215 – 1218; b) P. Timmerman, R. H. Vreekamp, R. Hulst, W. Verboom, D. N. Reinhoudt, K. Rissanen, K. A. Udachin, J. Ripmeester, *Chem. Eur. J.* **1997**, *3*, 1823 – 1832; c) K. A. Jolliffe, P. Timmerman, D. N. Reinhoudt, *Angew. Chem.* **1999**, *111*, 983 – 986; *Angew. Chem. Int. Ed.* **1999**, *38*, 933 – 937.

[86] P. Timmerman, J. L. Weidmann, K. A. Jolliffe, L. J. Prins, D. N. Reinhoudt, S. Shinkai, L. Frish, Y. Cohen, *J. Chem. Soc. Perkin Trans. 2* **2000**, 2077 – 2089.

[87] a) B. Olenyuk, M. D. Levin, J. A. Whiteford, J. E. Shield, P. J. Stang, *J. Am. Chem. Soc.* **1999**, *121*, 10434 – 10435; b) S. Viel, L. Mannina, A. Segre, *Tetrahedron Lett.* **2002**, *43*, 2515 – 2519.

[88] a) M. Greenwald, D. Wessely, I. Goldberg, Y. Cohen, *New J. Chem.* **1999**, *23*, 337 – 344; b) M. Shaul, Y. Cohen, *J. Org. Chem.* **1999**, *64*, 9358 – 9364; c) W. H. Otto, M. H. Keefe, K. E. Splan, J. T. Hupp, C. K. Larive, *Inorg. Chem.* **2002**, *41*, 6172 – 6174.

[89] G. R. Neukome, C. N. Morefield, F. Vogtle, Dendritic Macromolecules, 2nd ed., VCH, New York, **2001**.

[90] a) G. R. Newkome, J. K. Young, G. R. Baker, R. L. Potter, L. Audoly, D. Cooper, C. D. Weis, K. Morris, C. S. Johnson, Jr., *Macromolecules* **1993**, *26*, 2394 – 2396; b) J. K. Young, G. R. Baker, G. R. Newkome, K. F. Morris, C. S. Johnson, Jr., *Macromolecules* **1994**, *27*, 3464 – 3471.

[91] H. Ihre, A. Hult, E. Söderlind, *J. Am. Chem. Soc.* **1996**, *118*, 6388 – 6395.

[92] C. B. Gorman, J. C. Smith, M. W. Hager, B. L. Parkhurst, H. Sierzputowska-Gracz, C. A. Haney, *J. Am. Chem. Soc.* **1999**, *121*, 9958 – 9966.

[93] J. M. Riley, S. Alkan, A. Chen, M. Shapiro, W. A. Khan, W. R. Murphy, Jr., J. E. Hanson, *Macromolecules* **2001**, *34*, 1797 – 1809.

[94] a) S. Hecht, N. Vladimirov, J. M. J. Fréchet, *J. Am. Chem. Soc.* **2001**, *123*, 18 – 25; b) A. I. Sagidullin, A. M. Muzafarov, M. A. Krykin, A. N. Ozerin, V. D. Skirda, G. M. Ignat'eva, *Macromolecules* **2002**, *35*, 9472 – 9479; c) S. W. Jeong, D. F. O'Brien, G. Orädd, G. Lindblom, *Langmuir* **2002**, *18*, 1073 – 1076.

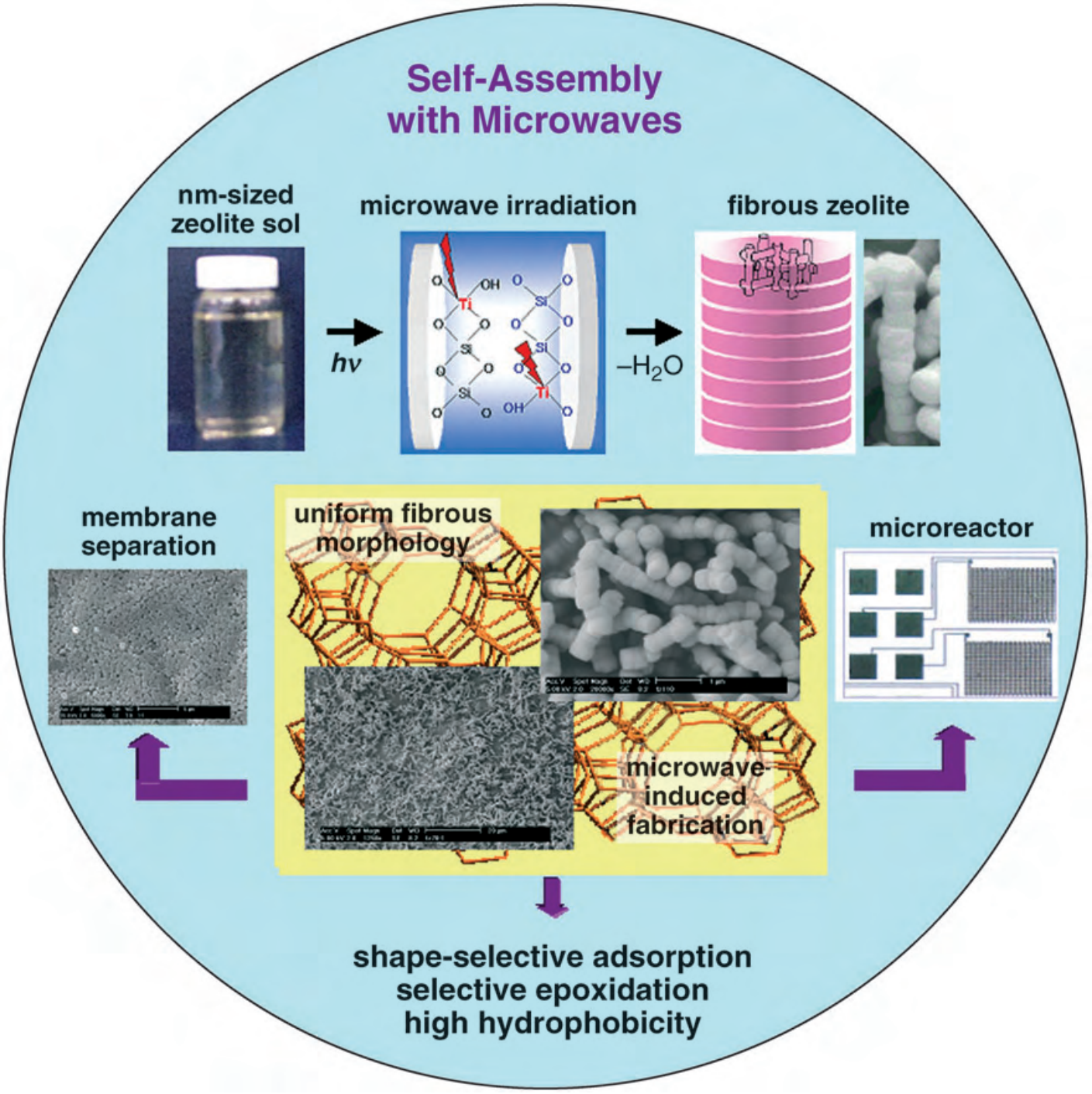
[95] a) D. Bratko, P. Stilbs, M. Bester, *Macromol. Rapid Commun.* **1985**, *6*, 163 – 168; b) R. Rymden, P. Stilbs, *J. Phys. Chem.* **1985**, *89*, 3502 – 3505.

 © 2005 Wiley-VCH Verlag GmbH & Co. KGaA, Weinheim

[96] a) L. G. Longsworth, *J. Am. Chem. Soc.* **1952**, *74*, 4155 – 4159; b) L. G. Longsworth, *J. Phys. Chem.* **1960**, *64*, 1914 – 1917.
[97] H. J. Tyrell, K. R. Harris, *Diffusion in Liquids*, Butterworth, London, **1984**.
[98] Y. Cohen, A. Ayalon, *Angew. Chem.* **1995**, *107*, 888 – 890; *Angew. Chem. Int. Ed. Engl.* **1995**, *34*, 816 – 818.
[99] A. Ayalon, A. Sygula, P.-C. Cheng, M. Rabinovitz, P. W. Rabideau, L. T. Scott, *Science* **1994**, *265*, 1065 – 1067.
[100] a) R. E. Hoffman, E. Shabtai, M. Rabinovitz, V. S. Iyer, K. Müllen, A. K. Rai, E. Bayrd, L. T. Scott, *J. Chem. Soc. Perkin Trans. 2* **1998**, 1659 – 1664; b) E. Shabtai, R. E. Hoffman, P. Cheng, E. Bayrd, D. V. Preda, L. T. Scott, M. Rabinovitz, *J. Chem. Soc. Perkin Trans. 2* **2000**, 129 – 133.
[101] a) T. C. Pochapsky, P. M. Stone, *J. Am. Chem. Soc.* **1990**, *112*, 6714 – 6715; b) T. C. Pochapsky, A. P. Wang, P. M. Stone, *J. Am. Chem. Soc.* **1993**, *115*, 11 084 – 11 091.
[102] a) S. S. Pochapsky, H. Mo, T. C. Pochapsky, *J. Chem. Soc. Chem. Commun.* **1995**, 2513 – 2514; b) H. Mo, T. C. Pochapsky, *J. Phys. Chem. B* **1997**, *101*, 4485 – 4486.
[103] I. Keresztes, P. G. Williard, *J. Am. Chem. Soc.* **2000**, *122*, 10 228 – 10 229.
[104] M. Valentini, H. Rüegger, P. S. Pregosin, *Helv. Chim. Acta* **2001**, *84*, 2833 – 2853.
[105] S. Beck, A. Geyer, H.-H. Brintzinger, *Chem. Commun.* **1999**, 2477 – 2478.
[106] a) S. Beck, M. H. Prosenc, H. H. Brintzinger, R. Goretzki, N. Herfert, G. Fink, *J. Mol. Catal.* **1996**, *11*, 67 – 79; b) N. G. Stahl, C. Zuccaccia, T. R. Jensen, T. J. Marks, *J. Am. Chem. Soc.* **2003**, *125*, 5256 – 5257.
[107] C. Zuccaccia, G. Bellachioma, G. Cardaci, A. Macchioni, *Organometallics* **2000**, *19*, 4663 – 4665.
[108] a) M. Valentini, P. S. Pregosin, H. Rüegger, *Organometallics* **2000**, *19*, 2551 – 2555; b) M. Valentini, P. S. Pregosin, H. Rüegger, *J. Chem. Soc. Dalton Trans.* **2000**, 4507 – 4510.
[109] N. E. Schöler, E. J. Cabrita, S. Berger, *Angew. Chem.* **2002**, *114*, 114 – 116; *Angew. Chem. Int. Ed.* **2002**, *41*, 107 – 109.
[110] R. A. Fecik, K. E. Frank, E. J. Gentry, S. R. Menon, L. A. Mitscher, H. Telikepalli, *Res. Lab.* **1998**, *18*, 149 – 185.
[111] *Combinatorial Chemistry: Synthesis, Analysis, Screening* (Ed.: G. Jung), Wiley-VCH, Weinheim, **1999**.
[112] M. J. Shapiro, J. S. Gounarides, *Prog. Nucl. Magn. Reson. Spectrosc.* **1999**, *35*, 153 – 200, and references therein.
[113] H. Barjat, G. A. Morris, S. C. Smart, A. G. Swanson, S. C. R. Williams, *J. Magn. Reson. Ser. B* **1995**, *108*, 170 – 172; b) M. D. Palta, H. Barjat, G. A. Morris, A. L. Davis, S. J. Hammond, *Magn. Reson. Chem.* **1998**, *36*, 706 – 714; c) A. M. Dixon, C. K. Larive, *Anal. Chem.* **1997**, *69*, 2122 – 2128.
[114] For an early example of mixture evaluation by using DOSY see: K. F. Morris, P. Stilbs, C. S. Johnson, Jr., *Anal. Chem.* **1994**, *66*, 211 – 215.
[115] For high-resolution DOSY applications see: G. A. Morris, H. Barjat in *Methods for Structure Elucidation by High-Resolution NMR* (Eds.: Gy. Batta, K. E. Köveŕ, Cs. Szántay, Jr.), Elsevier, Amsterdam, **1997**, pp. 209 – 226.
[116] a) H. Barjat, G. A. Morris, A. G. Swanson, *J. Magn. Reson.* **1998**, *131*, 131 – 138; b) for hybrid sequences, see: N. Birlirakis, E. Guittet, *J. Am. Chem. Soc.* **1996**, *118*, 13 083 – 13 084.
[117] R. K. Harris, K. A. Kinnear, G. A. Morris, M. J. Stchedroff, A. Samadi-Maybodi, N. Azizi, *Chem. Commun.* **2001**, 2422 – 2423.
[118] a) P. J. Hajduk, R. P. Meadows, S. W. Fesik, *Q. Rev. Biophys.* **1999**, *32*, 211 – 240; b) M. van Dongen, J. Weight, J. Uppenberg, J. Schultz, M. Wikström, *Drug Discovery Today* **2002**, *7*, 471 – 478c) B. Meyer, T. Peters, *Angew. Chem.* **2003**, *115*, 890 – 918; *Angew. Chem. Int. Ed.* **2003**, *42*, 864 – 890.
[119] a) S. B. Shuker, P. J. Hajduk, R. P. Meadows, S. W. Fesik, *Science* **1996**, *274*, 1531 – 1534; b) P. J. Hajduk, R. P. Meadows, S. W. Fesik, *Science* **1997**, *278*, 497 – 499.
[120] a) M. Lin, M. J. Shapiro, *J. Org. Chem.* **1996**, *61*, 7617 – 7619; b) M. Lin, M. J. Shapiro, J. R. Wareing, *J. Am. Chem. Soc.* **1997**, *119*, 5249 – 5250; c) A. Chen, M. J. Shapiro, *Anal. Chem.* **1999**, *71*, 669A – 675A; d) the research groups of Lindon and Nicholson suggested in parallel a similar approach to study complex biofluids, see: M. Liu, J. K. Nicholson, J. A. Parkinson, J. C. Lindon, *Anal. Chem.* **1997**, *69*, 1504 – 1509; for a recent review from these research groups concerning the use of diffusion NMR spectroscopy in biochemicals and pharmacological applications, see: J. C. Lindon, M. Liu, J. K. Nicholson, *Rev. Anal. Chem.* **1999**, *18*, 23 – 66.
[121] The determination of SARs by NMR spectroscopy is currently applicable for proteins having a molecular weight of 20–30 kDa although transverse relaxation-optimized spectroscopy (TROSY) can extend the molecular weights amenable to NMR investigation beyond 100 kDa, see: K. Pervushin, R. Riek, G. Wider, K. Wüthrich, *Proc. Natl. Acad. Sci. USA* **1997**, *94*, 12 336 – 12 371. In contrast, this size limitation does not exist for NMR screening methods based on diffusion filtering (see the text).
[122] P. J. Hajduk, E. T. Olejniczak, S. W. Fesik, *J. Am. Chem. Soc.* **1997**, *119*, 12 257 – 12 261.
[123] a) M. Lin, M. J. Shapiro, J. R. Wareing, *J. Org. Chem.* **1997**, *62*, 8930 – 8931; b) K. Bleicher, M. Lin, M. J. Shapiro, J. R. Wareing, *J. Org. Chem.* **1998**, *63*, 8486 – 8490; c) R. C. Anderson, M. Lin, M. J. Shapiro, *J. Comb. Chem.* **1999**, *1*, 69 – 72.
[124] a) J. A. Jones, D. K. Wilkins, L. J. Smith, C. M. Dobson, *J. Biomol. NMR* **1997**, *10*, 199 – 203; b) S. L. Mansfield, D. A. Jayawickrama, J. S. Timmons, C. K. Larive, *Biochim. Biophys. Acta* **1998**, *1382*, 257 – 265; c) X. Gao, T. C. Wong, *Biophys. J.* **1998**, *74*, 1817 – 1888; d) W. Zhang, T. E. Smithgall, W. H. Gmeiner, *Biochemistry* **1998**, *37*, 7119 – 7126; e) M. L. Tillett, M. A. Horsfield, L.-Y. Lian, T. J. Norwood, *J. Biomol. NMR* **1999**, *13*, 223 – 232; f) W. S. Price, F. Tsuchiya, Y. Arata, *J. Am. Chem. Soc.* **1999**, *121*, 11 503 – 11 511; g) W. S. Price, F. Tsuchiya, C. Suzuki, Y. Arata, *J. Biomol. NMR* **1999**, *13*, 113 – 117; h) X. Gao, T. C. Wong, *Biopolymers* **1999**, *50*, 555 – 568; i) S. Yao, G. J. Howlett, R. S. Norton, *J. Biomol. NMR* **2000**, *16*, 109 – 119; j) X. Chang, D. Keller, S. I. O'Donoghue, J. J. Led, *FEBS. Lett.* **2002**, *515*, 165 – 170; k) T. S. Derrick, E. F. McCord, C. K. Larive, *J. Magn. Reson.* **2002**, *155*, 217 – 225; l) A. M. Weljie, A. P. Yamniuk, H. Yoshino, Y. Izumi, H. J. Vogel, *Protein Sci.* **2003**, *12*, 228 – 236.
[125] a) M. J. Shapiro, J. Chin, A. Chen, J. R. Wareing, Q. Tang, R. A. Tommasi, H. R. Marepalli, *Tetrahedron Lett.* **1999**, *40*, 6141 – 6143; b) J. A. Chin, A. Chen, M. J. Shapiro, *J. Comb. Chem.* **2000**, *2*, 293 – 296; c) J. Chin, A. Chen, M. J. Shapiro, *Magn. Reson. Chem.* **2000**, *38*, 782 – 784.
[126] a) J. Lapham, J. P. Rife, P. B. Moore, D. M. Crothers, *J. Biomol. NMR* **1997**, *10*, 255 – 262; b) W. H. Gmeiner, C. J. Hudalla, A. M. Soto, L. Marky, *FEBS. Lett.* **2000**, *465*, 148 – 152; c) X. Yang, Y. S. Sanghvi, X. Gao, *J. Biomol. NMR* **1997**, *10*, 383 – 388.
[127] a) J. Balbach, *J. Am. Chem. Soc.* **2000**, *122*, 5887 – 5888; b) A. V. Buevich, J. Baum, *J. Am. Chem. Soc.* **2002**, *124*, 7156 – 7162.

 © 2005 Wiley-VCH Verlag GmbH & Co. KGaA, Weinheim

Communications



Metal-containing zeolites synthesized under microwave conditions stack in one direction to form a fibrous morphology. The resulting materials show enhanced shape-selective adsorption of xylene isomers and have potential applications in microreactors and separation technology. For more information see the Communication by J.-S. Chang, S.-E. Park et al. on the following pages.

© 2005 Wiley-VCH Verlag GmbH & Co. KGaA, Weinheim
DOI: 10.1002/anie.200461403

Zeolite Synthesis

Microwave Fabrication of MFI Zeolite Crystals with a Fibrous Morphology and Their Applications**

Young Kyu Hwang, Jong-San Chang, Sang-Eon Park,* Dae Sung Kim, Young-Uk Kwon, Sung Hwa Jhung, Jin-Soo Hwang, and Min Seok Park*

Zeolite molecular sieves are good candidates for designed microscopically and nanoscopically engineered materials due to their well-defined pore structures.[1,2] Among them, silicalites, zeolites having the MFI framework topology, have been studied extensively with regards to the selective separation of hydrocarbons[3] and the development of electrode materials,[4] membranes,[5] and catalysts.[6] Because many emerging applications of porous materials require precise control of crystal size, shape, and orientation,[7,8] the development of new synthesis strategies is increasingly important. For example, the properties of spherical mesoporous silica particles with a narrow particle size distribution as a material for column chromatography are superior to those of curved hexagonal rods with the same structure.[7]

Recently, it has been reported that the microwave synthesis method could provide an efficient way to control particle size distribution,[9] phase selectivity,[10] and macroscopic morphology[11] in the synthesis of porous materials as well as result in fast crystallization.[12] However, to our knowledge, there are few reports of microwave techniques being utilized to control the morphology of porous materials.[11,13] Here, we report on new applications of the microwave method for the fabrication of MFI-type zeolite crystals incorporating Ti and other metal species. By using the method, we prepared fibrous MFI zeolites that exhibited useful physicochemical properties due to their self-stacking.

Pure and metal-incorporated MFI crystals were synthesized by microwave-heating precursor solutions at 438 K. These samples will be denoted as M-MFI-MW, where M stands for the incorporated metal (Ti, Fe, Zr, and Sn) and MW for the microwave conditions; metal-free MFI from a microwave reaction will be denoted as Si-MFI-MW.

The powder X-ray diffraction (XRD) patterns of Ti-MFI-MW samples show the characteristic peaks for the MFI structure without any impurities. The IR spectra of the calcined Ti-MFI-MW samples exhibit an absorption band at 960 cm^{-1} for the stretching mode of a [SiO_4] unit bonded to a Ti^{4+} ion (O_3SiOTi). UV/Vis diffuse reflectance spectra, collected in vacuo after evacuation ($\leq 10^{-5}$ torr) at 627 K, revealed a strong peak around 210–240 nm, assignable to the ligand-to-metal charge-transfer absorption band from the oxygen to tetrahedral titanium(IV) atom in the zeolite framework.[14] The Ti-MFI-CH from the hydrothermal syntheses also showed practically the same XRD and IR data, indicating that the difference in the synthesis methods did not influence the identity of the final products.

However, we observed that the microwave synthesis induces a dramatic change in the morphology depending on the composition. Si-MFI-MW and Ti-MFI-CH show the characteristic pucklike crystals of submicrometer sizes with well-developed large (010) faces (Figure 1a and b). The aggregated morphology of individual particles appears to be attributed to superfast crystallization (Figure 1b).[9] The microwave reactions of incorporated metal systems produced similar primary crystals, but this time the crystals are all

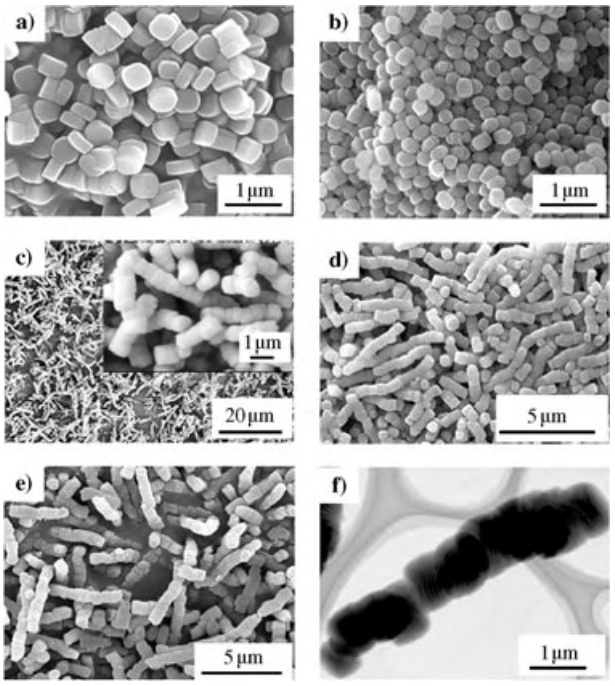


Figure 1. SEM images of a) Si-MFI-MW, b) Ti-MFI-CH (Si/Ti = 70), c) Ti-MFI-MW (Si/Ti = 120), d) Ti-MFI-MW (Si/Ti = 70), and e) Sn-MFI-MW, and f) TEM image of Sn-MFI-MW. Inset is a large-scale image of (c).

[*] Dr. Y. K. Hwang, Dr. J.-S. Chang, Dr. D. S. Kim, Dr. S. H. Jhung, Dr. J.-S. Hwang, Dr. M. S. Park
Research Center for Nanocatalysis
Korea Research Institute of Chemical Technology (KRICT)
P.O. Box 107, Yusung, Taejon 305-600 (Korea)
Fax: (+82) 42-860-7676
E-mail: jschang@krict.re.kr
Prof. S.-E. Park
Department of Chemistry, Inha University
Incheon 402-751 (Korea)
Fax: (+82) 32-874-7674
E-mail: separk@inha.ac.kr
Prof. Y.-U. Kwon
Department of Chemistry and BK-21
School of Molecular Science, Sungkyunkwan University
Suwon 440-746 (Korea)

[**] This work was supported by the Korean Ministry of Science and Technology through the National Science Programs for Key Nanotechnology and Institutional Research Program. The authors thank especially Prof. J. M. Kim for helpful collaboration, Dr. C. H. Xue and T. H. Jin for experimental assistance, and Dr. J. S. Yoo and P. M. Forster for useful discussions.

Supporting information for this article is available on the WWW under http://www.angewandte.org or from the author.

 © 2005 Wiley-VCH Verlag GmbH & Co. KGaA, Weinheim

stacked on top of one another along their [010] direction to form a wormlike or fibrous morphology (Figure 1 c–f). This stacking is sufficiently robust that it is not destroyed by sonication for 1 h or more, indicating that this morphology is not a result of simple aggregation but of strong chemical bonds between the crystals. This fibrous morphology persists as long as there is incorporated Ti and its concentration is kept in the range of Si/Ti = 70–230. When the concentration of Ti is increased (Si/Ti ≤ 50), the product is composed of isolated ellipsoidal crystals (not shown). This is probably because the high concentration of Ti interferes with the mechanism of crystal growth, and the lack of flat surfaces does not allow crystal stacking. The crystals with other incorporated metals (Fe, Zr, Sn) also show the fibrous morphology, and we show the images of Sn-MFI-MW in Figure 1 e and f.

We also have monitored the reaction progress in the Ti-MFI-MW system by XRD and scanning electron microscopy (SEM). The XRD patterns show that the crystals are starting to grow out of embryos after about 10 min, grow rapidly during the next 30 min, and reach the full crystallization at about 60 min. The SEM images show that the stacking of crystals begins at 20 min and culminates after 60 min. These observations suggest that the fibrous morphology is achieved through interactions between already present crystals (see the Supporting Information).

Although it is not clear how the incorporated metals induce the stacking of crystals under the microwave conditions, it appears to be related with the magnitude of the local dipole moment of the M–O bonds. Electrically insulating materials absorb microwave energy through the oscillation of dipoles, and the magnitude of absorption increases with an increase in the dipole moment. The magnitude of the dipole moment is determined mainly by the difference in the electronegativities ($\Delta\chi$) of the two bonded atoms. Therefore, the Ti–O bond ($\Delta\chi = 2.18$ according to the Allred–Rochow scheme)[15] is a better microwave absorber than the Si–O bond ($\Delta\chi = 1.76$). The Ti–O bonds on the surfaces are strongly activated by microwave absorption and can undergo condensation reactions to form Ti-O-Ti and/or Ti-O-Si bonds between crystals. The same explanation applies to the Fe-MFI-MW and Zr-MFI-MW zeolites because of the large $\Delta\chi$ values for Fe–O and Zr–O bonds. In the case of Sn-MFI-MW, the $\Delta\chi$ value of the Sn–O bond (1.78) is rather small, close to that of Si–O bond. However, because Sn is a large atom, the valence electron density of the Sn–O bond is shifted to the O side, making this bond more polar than would be estimated by the $\Delta\xi$ value alone. In other words, the homopolar contribution to the dipole moment[16] and the above explanation of microwave absorption by polar bonds can be applied to the Sn-MFI-MW case. Further work is needed to fully understand the role of the incorporated metals in the stacking of crystals under microwave conditions.

The concentration of the reagent also influences the stacking behavior of crystals. When the concentration is too low ($H_2O/SiO_2 = 50$ and 100), the crystals become larger than those mentioned above ($H_2O/SiO_2 = 22$) and the stacking occurs to a much lesser extent. Probably, the large crystal sizes and the dilute conditions provide fewer chances for the crystals to meet with the correct relative orientation for stacking. When the concentration is too high ($H_2O/SiO_2 = 10$), the product is composed of granules of much smaller sizes because the reaction occurs too quickly for the crystals to attain the pucklike morphology, and the lack of large and flat surfaces prohibits the crystal stacking.

The fibrous morphology of Ti-MFI-MW crystals leads to several unique properties that may be advantageous for applications. To show this, we chose a fibrous Ti-MFI-MW synthesized from a Si/Ti = 70 solution and compared its properties with those of nonfibrous MFI zeolites such as Si-MFI-MW, Ti-MFI-CH, and Ti-MFI-MW (hereafter, NF-Ti-MFI-MW) synthesized from a solution with $H_2O/SiO_2 = 100$. The packing density of fibrous Ti-MFI-MW powder is 1.9 times lower than that of the Si-MFI-MW and Ti-MFI-CH powders. However, the BET surface areas and micropore volumes from N_2-adsorption experiments (Table 1) show that all three Ti-MFIs (Ti-MFI-MW, Ti-MFI-CH, and NF-Ti-MFI-MW) have comparable pore characteristics, suggesting that the crystal stacking hardly affects the intracrystalline pore structure and that the reduced density of Ti-MFI-MW is a result of the fibrous morphology. The hydrophobicity index data from the adsorption mass ratio of toluene and water show that the hydrophobicity of fibrous Ti-MFI-MW is 36% higher than that of Ti-MFI-CH (Supporting Information). It can be rationalized in terms of the consumption of terminal hydroxyl groups by stacking crystals in Ti-MFI-MW. According to IR spectra of Ti-MFI-MW dehydrated at 673 K under vacuum, the intensity of surface hydroxyl band (ca. 3740 cm^{-1}) of the Ti-MFI-MW is much smaller than those of

Table 1: Physicochemical and catalytic properties of Ti-MFI zeolites according to the morphology and preparation method.

Catalyst[a]	S_{BET} [$m^2 g^{-1}$]	Pore volume [$mL g^{-1}$]	Hydrophob. index[b]	Reaction time [h]	Styrene epoxidation[c] Conv. [%][d]	Sel. [%][e]
Ti-MFI-MW (fibrous)	423	0.21	8.2	4	55.6	63.1
				8	70.5	65.2
NF-Ti-MFI-MW (nonfibrous)	432	0.22	6.3	4	39.5	54.5
				8	48.7	51.9
Ti-MFI-CH (nonfibrous)	453	0.25	6.0	4	39.5	52.5
				8	48.0	44.2

[a] Ti-MFI-MW (fibrous): prepared by microwave irradiation for 60 min with a H_2O/SiO_2 ratio of 22; NF-Ti-MFI-MW (nonfibrous): prepared by microwave irradiation for 60 min with a H_2O/SiO_2 ratio of 100; Ti-MFI-CH (nonfibrous): prepared by the conventional hydrothermal method at 438 K for 24 h in a Si/Ti ratio of 70. [b] The hydrophobicity index was calculated from the amount of adsorbed water and toluene. [c] Reaction conditions: 343 K, 5 mL styrene, 1.3 mL H_2O_2 (30%), 18 mL acetone (solvent), 0.35 g catalyst. [d] (Styrene conversion/maximum expected conversion) × 100. [e] Other products: benzaldehyde and phenylacetaldehyde.

 © 2005 Wiley-VCH Verlag GmbH & Co. KGaA, Weinheim

Ti-MFI-CH and even NF-Ti-MFI-MW. (Supporting Information). The enhanced surface hydrophobicity affects the catalytic properties of Ti-MFI-MW. As summarized in Table 1, Ti-MFI-MW is more reactive and selective than nonfibrous Ti-MFI-CH and NF-Ti-MFI-MW for the epoxidation of styrene with H_2O_2 to produce styrene oxide. Although the fibrous structure of Ti-MFI-MW may limit the diffusion of reactants and products, this drawback is more than offset by the positive effect of the increased hydrophobicity for this reaction.[17]

Even more importantly, the fibrous Ti-MFI-MW zeolite presents significantly enhanced shape selectivity in adsorption. Figure 2 shows the temperature-programmed desorption

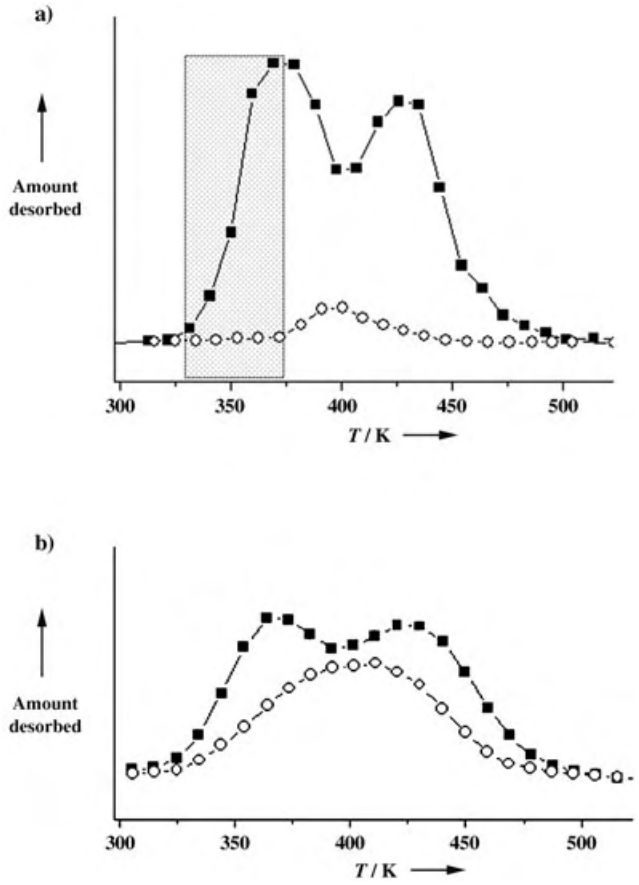


Figure 2. Xylene TPD profiles of a) fibrous Ti-MFI-MW and b) nonfibrous Ti-MFI-CH after vapor-phase competitive adsorption of an equimolar mixture of *p*-xylene (■) and *o*-xylene (○) at 323 K. Adsorbent weight: 0. 25 g; carrier gas: nitrogen (flow rate = 30 mL min^{-1}); ramp rate = 5 K min^{-1}; mL xylenes per gram of adsorbent = 0.168 for plot a and 0.175 for plot b.

(TPD) profiles of xylene isomers after vapor-phase adsorption of an equimolar mixture of *p*-xylene and *o*-xylene over Ti-MFI-MW and Ti-MFI-CH at 323 K.[3,8] The xylene TPD patterns are similar over the two adsorbents, that is, two peaks for *p*-xylene and one peak for *o*-xylene, while the fibrous Ti-MFI-MW reveals a remarkably enhanced adsorption selectivity to *p*-xylene (*p*-xylene/*o*-xylene = 10.7), which is 6.7 times higher than that of the nonfibrous Ti-MFI-CH. Moreover, it is notable that Ti-MFI-MW selectively desorbs only *p*-xylene in the low-temperature range 323–373 K (shaded area of Figure 2 a), implying that this material can be applied in producing highly pure *p*-xylene from a xylene mixture when combined with temperature swing desorption. The preferential adsorption of *p*-xylene (*p*-xylene/*o*-xylene = 9.9) in the fibrous Ti-MFI-MW has also been confirmed in competitive liquid-phase adsorption of a *p*-xylene/*o*-xylene mixture at 293 K (see the Supporting Information).

The MFI structure has three different sites for adsorption: straight and sinusoidal channels along the [010] and [100] directions, respectively, and their intersections. The diffusivity in the straight channel is reportedly much higher than in the sinusoidal channel.[18] Because of the crystal stacking along the [010] direction, the straight channels of Ti-MFI-MW are longer and their openings are much fewer than those of the nonfibrous Ti-MFI-CH crystals. Therefore, the difference between the diffusivities of *p*- and *o*-xylene would be amplified, resulting in the enhanced adsorption selectivity of Ti-MFI-MW. Further work is needed to fully understand the present adsorption behaviors.

In summary, we have demonstrated that the coupled effect of metal incorporation at a suitable concentration level and microwave irradiation during the synthesis of MFI zeolites produces fibrous MFI crystals. This effect appears to be related to the dipole moment strength of the surface M–O bonds. The fibrous Ti-MFI-MW zeolites show several interesting properties such as lower packing density, higher hydrophobicity, enhanced catalytic properties, and higher shape-selectivity in adsorption as compared to nonfibrous MFI zeolites.

Experimental Section

Ti-MFI-MW and Fe-MFI-MW were synthesized at 438 K for 60 min under microwave (MW) irradiation at 600 W. Tetraethyl orthosilicate (TEOS, Aldrich, 98%), tetrapropyl orthotitanate (TPOT, Aldrich, 96%) and tetrapropylammonium hydroxide (TPAOH, Aldrich, 25%) were used. The molar composition of the reaction mixture was 1 TEOS:0.2 TPAOH:0–0.05 TPOT or 0–0.05 $FeCl_3$:1 isopropyl alcohol:22.2 H_2O. The precursor gel of 30–60 g was loaded in a 100-mL Teflon autoclave, which was sealed and placed in a microwave oven (Mars-5, CEM). Ti-MFI-CH was prepared under conventional hydrothermal conditions at 438 K for 24 h with the same precursor-gel composition as Ti-MFI-MW. Sn- and Zr-MFI zeolites were synthesized with the same precursor compositions as Ti-MFI-MW at 438 K except for the modification of metal alkoxides using acetylacetone as a chelating agent to reduce the rate of alkoxide hydrolysis. Further details are given in Supporting Information.

Vapor-phase adsorption and TPD measurements of xylene isomers were conducted in a plug-flow glass reactor with an internal diameter of 6 mm at 323 K. The xylene mixture that passed through the reactor was analyzed using an on-line gas chromatograph (Donam model DS-6200) that was equipped with a capillary column (Bentone-34) and a flame ionization detector. TPD profiles of the adsorbed xylenes were obtained by temperature-programmed heating (ramp rate: 5 K min^{-1}) from 323 K to 573 K after sufficient desorption of physisorbed xylenes at 323 K. Detailed methods for the adsorption and TPD analysis of xylene isomers are described in the Supporting Information.

Received: July 23, 2004
Published online: November 11, 2004

 © 2005 Wiley-VCH Verlag GmbH & Co. KGaA, Weinheim

Keywords: crystal growth · microporous materials · zeolites

[1] a) G. A. Ozin, *Adv. Mater.* **1992**, *4*, 612; b) T. Bein, *Chem. Mater.* **1996**, *8*, 1636.
[2] M. E. Davis, *Nature* **2002**, *417*, 813.
[3] a) W. Yuan, Y. S. Lin, W. Yang, *J. Am. Chem. Soc.* **2004**, *126*, 4776; b) .S. Li, C. Demmelmaier, M. Itkis, Z. Liu, R. C. Haddon, Y. Yan, *Chem. Mater.* **2003**, *15*, 2687.
[4] S. Li, X. Wang, D. Beving, Z. Chen, Y. Yan, *J. Am. Chem. Soc.* **2004**, *126*, 4122.
[5] G. Xomeritakis, Z. Lai, M. Tsapatsis, *Ind. Eng. Chem. Res.* **2001**, *40*, 544.
[6] a) B. Notari, *Adv. Catal.* **1996**, *41*, 253; b) V. Ramaswamy, B. Tripathi, D. Srinivas, A. V. Ramaswamy, R. Cattaneo, R. Prins, *J. Catal.* **2001**, *200*, 250.
[7] C. Thoelen, J. Paul, I. F. J. Vankelecom, P. A. Jacobs, *Tetrahedron: Asymmetry* **2000**, *11*, 4819.
[8] Z. Lai, G. Bonilla, S. Diaz, J. G. Nery, K. Sujaoti, M. A. Amat, E. Kokkoli, O. Terasaki, R. W. Thompson, M. Tsapatsis, D. G. Vlachos, *Science* **2003**, *300*, 456.
[9] a) S. Komarneni, R. Roy, Q. H. Li, *Mater. Res. Bull.* **1992**, *27*, 1393; b) C. S. Cundy, *Collect. Czech. Chem. Commun.* **1998**, *63*, 1699; c) C. Gabriel, S. Gabriel, E. H. Grant, B. S. J. Halstead, D. M. P. Mingos, *Chem. Soc. Rev.* **1998**, *27*, 213; d) S.-E. Park, D. S. Kim, J.-S. Chang, W. Y. Kim, *Catal. Today* **1998**, *44*, 301; e) X. Xu, W. Yang, J. Liu, L. Lin, *Adv. Mater.* **2000**, *12*, 195; f) D. P. Serrano, M. A. Uguina, R. Sanz, E. Castillo, A. Rodriguez, P. Sanchez, *Microporous Mesoporous Mater.* **2004**, *69*, 197; g) C. S. Cundy, J. O. Forrest, *Microporous Mesoporous Mater.* **2004**, *72*, 67.
[10] a) S. H. Jhung, J.-S. Chang, J.-S. Hwang, S.-E. Park, *Microporous Mesoporous Mater.* **2003**, *64*, 33; b) S.-E. Park, J.-S. Chang, Y. K. Hwang, S. H. Jhung, D. S. Kim, J. S. Hwang, J.-S. Hwang, *Catal. Surv. Asia* **2004**, *8*, 91.
[11] a) S. H. Jhung, J.-S. Chang, Y. K. Hwang, S.-E. Park, *J. Mater. Chem.* **2004**, *14*, 280; b) Y. K. Hwang, J.-S. Chang, Y.-U. Kwon, S.-E. Park, *Microporous Mesoporous Mater.* **2004**, *68*, 280; c) J.-C. Lin, J. T. Dipre, M. Z. Yates, *Langmuir* **2004**, *20*, 1039.
[12] a) B. L. Newalkar, S. Komarneni, H. Katsuki, *Chem. Commun.* **2000**, 2389; b) C. S. Cundy, R. J. Plaisted, J. P. Zhao, *Chem. Commun.* **1998**, 1465; c) S. Mintova, S. Mo, T. Bein, *Chem. Mater.* **1998**, *10*, 4030; d) P. Chu, F. G. Dwyer, Patent US 4778666, **1988**; e) D. S. Kim, J.-S. Chang, J. S. Hwang, S.-E. Park, J. M. Kim, *Microporous Mesoporous Mater.* **2004**, *68*, 77.
[13] a) S. H. Jhung, J.-S. Chang, S.-E. Park, P. M. Forster, G. Férey, A. K. Cheetham, *Chem. Mater.* **2004**, *16*, 1394; b) M. Ganschow, G. Schulz-Eldoff, M. Mark, M. Wendschuh-Josties, D. Wöhrle, *J. Mater. Chem.* **2001**, *11*, 1823.
[14] E. Duprey, P. Beaunier, M.-A. Springuel-Huet, F. Bozon-Verduraz, J.-M. Manoli, J.-M. Bregeault, *J. Catal.* **1997**, *165*, 22.
[15] A. L. Allred, E. G. Rochow, *J. Inorg. Nucl. Chem.* **1958**, *5*, 264.
[16] P. W. Atkins, *Physical Chemistry*, 6th ed., Oxford University Press, Oxford, **1999**, p. 651.
[17] a) M. Ogura, S.-I. Nakata, E. Kikuchi, M. Matsukata, *J. Catal.* **2001**, *199*, 41; b) S. Klein, W. F. Maier, *Angew. Chem.* **1996**, *108*, 2376; *Angew. Chem. Int. Ed. Engl.* **1996**, *35*, 2230.
[18] a) P. Szabelski, J. Narkiewicz-Michalek, W. Rudziński, *Appl. Surf. Sci.* **2002**, *196*, 191; b) S. Nair, M. Tsapatsis, *J. Phys. Chem.* B **2000**, *104*, 8982; c) S. Mohanty, H. T. Davis, A. V. McCormick, *Chem. Eng. Sci.* **2000**, *55*, 2779; d) P. Szabelski, J. Narkiewicz-Michalk, *Langmuir* **2001**, *17*, 61.

 © 2005 Wiley-VCH Verlag GmbH & Co. KGaA, Weinheim

Single-Molecule Studies

Single-Enzyme Kinetics of CALB-Catalyzed Hydrolysis**

Kelly Velonia, Ophir Flomenbom, Davey Loos, Sadahiro Masuo, Mircea Cotlet, Yves Engelborghs, Johan Hofkens,* Alan E. Rowan,* Joseph Klafter, Roeland J. M. Nolte, and Frans C. de Schryver*

Insight into the dynamic behavior of chemical processes is typically derived from ensemble measurements. Direct experimental information about the dynamics at the single-molecular level, however, is sparse and has until recently been primarily deduced from molecular-dynamics simulations. Current advances in single-molecule spectroscopy have paved the way for exploring the behavior of individual molecules in the course of a chemical reaction. Thus far it has proven possible to monitor in real time the dynamic behavior of single-biomolecular processes and observe the enzymatic turnovers of a few motor proteins,[1–5] an oxidase,[6] horseradish peroxidase,[7] and a nuclease.[8] More recently, structural fluctuations of a single flavin reductase[9] and of T4 lysozyme during the course of a reaction[10] have been detected. These few examples clearly demonstrate the tremendous potential of studying an enzymatic process at the single-molecular level.

Herein we report the direct observation of the real-time catalysis and substrate kinetics of a single-enzyme-catalyzed

[*] Dr. K. Velonia, Dr. A. E. Rowan, Prof. Dr. R. J. M. Nolte
Institute of Molecules and Materials
Department of Organic Chemistry
Raboud University of Nijmegen
6525 ED Nijmegen (The Netherlands)
Fax: (+31) 24-365-2929
E-mail: Kelly.velonia@chiorg.unige.ch
a.rowan@science.ru.nl

D. Loos, S. Masuo, Dr. M. Cotlet, Prof. Dr. J. Hofkens, Prof. Dr. F. C. de Schryver
Department of Chemistry
Katholieke Universiteit Leuven
Celestijnenlaan 200 F, 3001 Heverlee (Belgium)
Fax: (+32) 16-327989
E-mail: johan.hofkens@chem.kuleuven.ac.be

O. Flomenbom, Prof. Dr. J. Klafter
School of Chemistry, Sackler Faculty of Exact Sciences
Tel Aviv University, Ramat Aviv, Tel Aviv 69978 (Israel)

Prof. Dr. Y. Engelborghs
Department of Biochemistry
Laboratory of Chemical and Biological dynamics
Celestijnenlaan 200D, 3001 Heverlee (Belgium)

[**] This research was supported by the SISITOMAS European network and an EC Marie Curie fellowship (K.V.). The FWO-vlaanderen, the federal science policy through IAP/V/03 and the KULeuven through GOA 01/2 are thanked. O.F. thanks fruitful discussions with Attila Szabo and Irina Gopich. D.L. thanks the IWT for financial support. CALB = Lipase B from *Candida antarctica*.

Supporting information for this article is available on the WWW under http://www.angewandte.org or from the author.

 © 2005 Wiley-VCH Verlag GmbH & Co. KGaA, Weinheim DOI: 10.1002/anie.200460625

reaction, using a simple method, a robust enzyme, and confocal fluorescence microscopy (CFM). With the method described herein, we were able to monitor single enzyme turnovers for extended periods of time (hours) and use these measurements to unravel hidden characteristics in the catalytic behavior of individual enzymes. The lipase B from *Candida antarctica* (CALB) proved to be an excellent candidate for the present studies.[11,12] This 33 kDa workhorse enzyme catalyzes the hydrolysis of esters in aqueous solutions following the same reaction mechanism as a serine protease.[13]

A prerequisite for the imaging of single CALB molecules with CFM is that they are fluorescent and fixed onto a surface. To make it fluorescent the native lipase B from CALB was non-specifically labeled with Alexa Fluor^{488} dye molecules.[14,15] To fix the CALB molecules to a surface, a variety of immobilization techniques were examined. A commonly used protein-immobilization method is the trapping of enzyme molecules in agarose or polyacrylamide gels.[6] However, in the case of the CALB, this trapping method proved inadequate as it led to either inactivation of the protein, or cleavage of the Alexa Fluor^{488} markers, or to substrate-diffusion limitations. An alternative immobilization technique involves the deposition of enzymes on hydrophilic glass surfaces. Using this procedure, deposition of the protein in single-molecule concentrations again led to inactivation of CALB. The only solid support that allowed the study of the enzymatic conversion without inactivation or free movement (translational diffusion) of the protein, was a simple hydrophobic glass surface derivatized with dichlorodimethylsilane.

A scanning confocal microscope (CFM) with a focused laser spot was used to image the surface-immobilized CALB molecules and measure their individual emission time trajectories. At an optimum concentration of 3 nM Alexa^{488}–CALB, the enzymes were adsorbed onto the hydrophobic glass surface with a density sufficiently low that the fluorescence emission from a single labeled enzyme as a function of time could be observed. Blank experiments involving the imaging of the samples before and after the addition of water revealed that the enzymes remained immobilized and that the background emission level was negligible.

When a single Alexa^{488}–CALB molecule was positioned under the laser excitation spot ($\lambda_{ex} = 488$ nm, $\lambda_{em} = 520$ nm), a strong emission, followed by an abrupt photobleaching was observed (see Supporting Information). The emission traces of different Alexa^{488}–CALB molecules showed a variation in the time scale of photobleaching of 0 to 15 s, which reflects the different orientations of the fluorophores and the differing degrees of labeling (1 to 11 dye molecules can be attached to the lysine residues on the protein surface).[16] To study the catalysis by the single Alexa^{488}–CALB, we used as the fluorogenic substrate the non-fluorescent ester BCECF, AM (Figure 1 A)[17,18] which upon hydrolysis forms a highly fluorescent product.

Adsorption of the labeled enzymes onto the hydrophobic surface and initial scanning with the confocal microscope revealed spots of fluorescence attributable to the Alexa-labeled single enzymes. Onto this lipase functionalized surface a solution of the substrate was added and the fluorescence emission was monitored. Sequential fluorescence images of the surface revealed an increase in fluorescence emission, originating at the single enzymes and a gradual small increase in the background fluorescence. We attribute this increase in fluorescence emission to the formation and subsequent accumulation of the fluorescent product generated from BCECF, AM. Confirmation that the observed fluorescent product is formed by enzymatic hydrolysis was obtained by studies on the non-fluorescent native CALB (Figure 1 B). In these experiments the enzymes deposited on the surface could not be visualized until the addition of the substrate solution, at which time, points of fluorescence appeared and increased in intensity in a manner similar to that seen for the Alexa^{488}-labeled CALB. In addition these points of fluorescence were observed to blink on and off, a behavior, which we attributed to product formation followed by product diffusion. Each of these blinking (on-off) events is considered to be a single enzymatic turnover cycle (ETOC, see below). Several blank experiments with the enzyme in the absence of substrate and with the substrate in the absence of enzyme confirmed that these blinking phenomena only arise from enzyme-catalyzed hydrolysis (see Supporting Information). The observed enzyme blinking is a direct measure of the enzymatic catalysis and was thus studied in more detail. To be able to monitor the reaction immediately after the addition of substrate, individual Alexa^{488}-labeled CALB molecules were first positioned under the focus point of the laser and then the fluorophores were photobleached prior to the addition of the substrate. Subsequently the substrate solution was added and the fluorescence emission of this specific enzyme was recorded for long periods of time (up to 2 h, Figure 1 C, D).[19] In contrast to previous experiments,[6] where the length of the trajectories was curtailed either because of photobleaching or photooxidation, in our study the length of the trajectories had no limiting factors except the depletion of the substrate.

To analyze the recorded trajectories of the photon counts, we view the ETOC as a two-state process. The two distinct states are defined by the absence (off-state) and the presence (on-state) of fluorescence emission. Accordingly, the ETOC dynamics can be described by the waiting-time probability density function (pdf) of the off-state, $\phi_{off}(t)$, and of the on-state, $\phi_{on}(t)$. Thus, $\phi_{off}(t)dt$ (or $\phi_{on}(t)dt$) is the probability that a given off (or on) event along the trajectory lasts the time between t and $t + dt$. The waiting-time pdfs (which have units of one over time) are the main basic outcome of the trajectory analysis obtained from single-molecule measurements. This result differs from ensemble measurements which provide only a survival probability which is dimensionless.[20] If we denote by $a(t)$ the photon count value at time $t \equiv t_i = i\Delta t$ ($\Delta t =$ 1 ms), then, by setting a threshold value, the two states are separated, so that each $a(t)$ can be attributed either to the off-state, $a_{off}(t)$, or the on-state, $a_{on}(t)$ (Figure 1 D).[21,22] (The full local treatment and theoretical analysis will be described elsewhere).[23] As a result of this treatment, the trajectory is now characterized by the binary random process, $\xi(t)$, with values $\xi = 1$ for on events, and $\xi = 0$ for off events. The off and on waiting-time pdfs, $\phi_{off}(t)$ and $\phi_{on}(t)$ can then be constructed by building a histogram from the time durations of the

 © 2005 Wiley-VCH Verlag GmbH & Co. KGaA, Weinheim

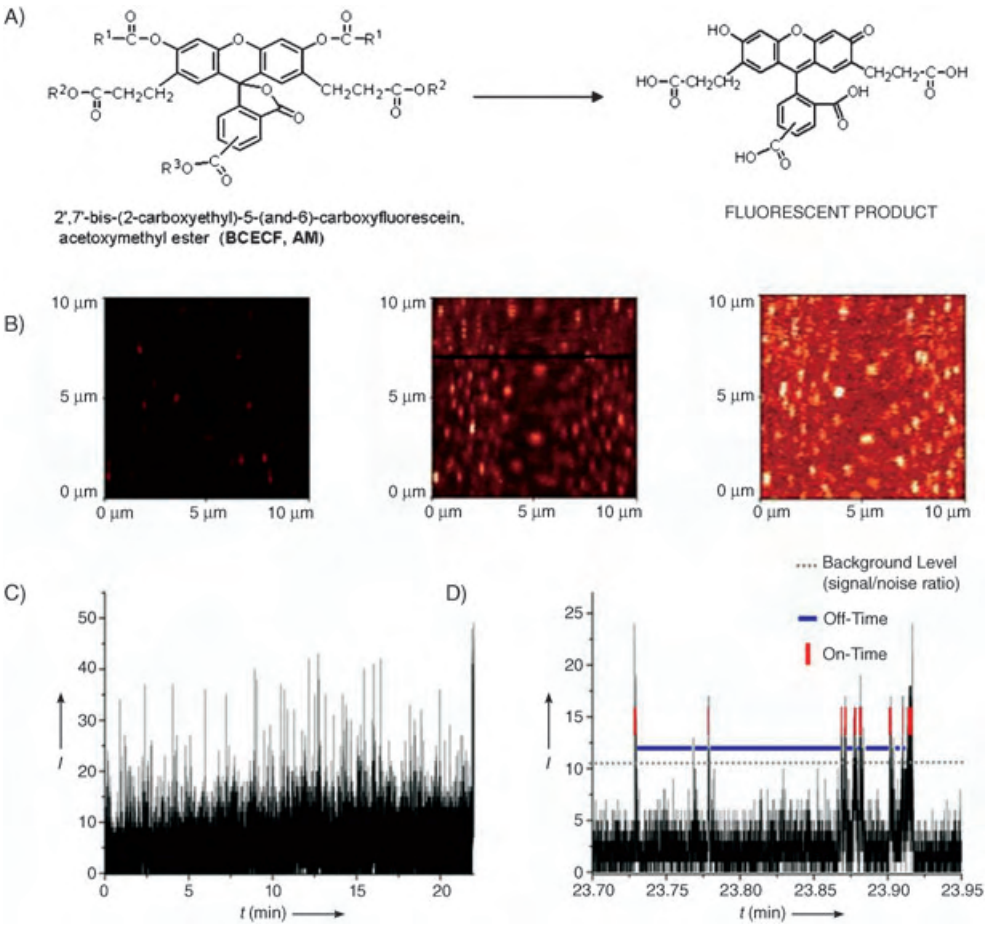


Figure 1. Fluorescence emission studies on the catalytic activity of single CALB molecules. A) Structure of the fluorogenic substrate BCECF, AM. B) Sequential CFM images (10 μm × 10 μm, $t = 0$ (left), 15 (middle), 30 min (right)) of a native CALB-coated surface during the enzymatic hydrolysis of BCECF, AM. C) Fluorescence emission as a function of time of a single Alexa^{488}-labeled CALB molecule during catalysis over 22 min. D) Expansion revealing the signal to noise ratio. By setting a threshold value the photon-count trajectory is transformed into a dichotomous trajectory containing a time series of on and off events.[23]

corresponding events along the trajectory, which allows the analysis of the data accumulated during the single-enzyme-catalyzed reaction.

To investigate the substrate kinetics of an individual enzyme, the behavior of a single lipase molecule was followed at different substrate concentrations. In contrast to other experiments,[6,7] all the experiments described herein were performed using the same single enzyme, since each single enzyme was anticipated to exhibit different activity owing to the non-specific adsorption on the hydrophobic support. To this end, the substrate concentration was gradually increased by sequentially adding a fresh substrate solution onto the same area under the laser excitation spot while the same single CALB molecule was studied. The off-state waiting-time pdf $\phi_{off}(t)$ for three different substrate concentrations [S], [S] = 0.6, 0.9, 1.4 μM, revealed that for all substrate concentrations, the relaxation patterns are non-exponential (Figure 2). The best fit for these curves is found to be a normalized stretched exponential function [Eq. (1)][24] where $\Gamma(-)$ is the gamma function.[25] The exponent parameter α and the parameter τ are independent of [S] within the investigated range, $\alpha = 0.15$ and $\tau = 1.15$ μs. Note that the pair

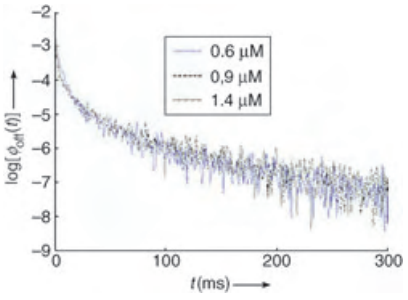


Figure 2. A log-linear scale plot of the off-state waiting-time pdf, $\phi_{off}(t)$, which highlights the non-exponential relaxation pattern. (The normalization used is such that $\phi_{off}(t = 0) = 1$).

of parameters (α,τ), and not each of these parameters by itself, is the relevant kinetic information obtained on the system, which can be realized by calculating, for example, the average time the process occupies the off state.

$$\phi_{off}(t) = \frac{\alpha/\tau}{\Gamma(1/\alpha)} e^{-(t/\tau)^{\alpha}} \quad (1)$$

 © 2005 Wiley-VCH Verlag GmbH & Co. KGaA, Weinheim

As observed for other systems (such as glassy materials)[26,27] a stretched exponential decaying pattern can arise from the combined contributions of a large number of weighted exponentials owing to an inhomogeneous environment. In the current case of single-enzyme catalysis measurements, the stretched exponential decay pattern of $\phi_{off}(t)$ serves as an indication that an individual enzyme exhibits dynamic disorder. The origin of this dynamic disorder does not stem from different diffusion times of the substrate to the vicinity of the enzyme, since the log linear plots of the off-state waiting-time pdfs at three different substrate concentrations, [S] = 0.6, 0.9, 1.4 μM, all have the same values for α and τ (Figure 2). This conclusion is further supported when plotting the number of ETOCs as a function of time (per time interval of 20 min; Figure 3), which was collected from the same single enzyme at different substrate concentrations (201 nM to 1.4 μM). Figure 3 reveals a saturation profile for a single enzyme which is similar to that observed for enzymes in solution. This is the first time that such a kinetic experiment has been performed on the same single enzyme revealing saturation behavior. Thus, the dynamic disorder shown, which leads to a stretched exponential waiting-time pdf, is apparently an inherent property of the enzyme, and can be interpreted as originating from different enzymatic conformations, each of which contributes an exponential to the overall decay of the off-state pdf. This concept of a multiple sub-state enzyme can be compared to the general model [Eq. (2)], which is often applied to enzyme activity.[7,28]

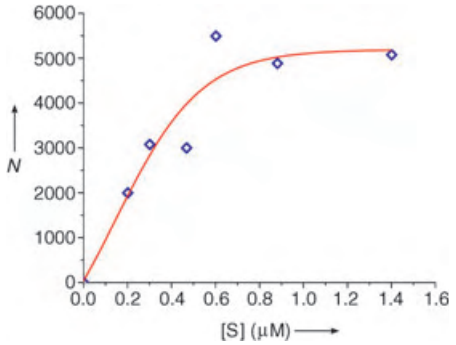


Figure 3. Plot of the number of ETOCs in 20 min (*N*), as a function of the effective total substrate concentration [S]. The plot reveals a saturation profile, similar to that observed for enzymes in solution, reached at approximately 600 nM.

$$\{E + S \leftrightarrow ES \rightarrow\}_{off}\ \{EP \rightarrow E + P\}_{on} \qquad (2)$$

In Equation (2) the symbols E, S, and P stand for the enzyme, substrate, and product molecules, respectively, and the ES stands for the enzyme–substrate complex and EP for the enzyme–product complex. In this model the fluorescent properties of each of the stages are also indicated. More precisely, the symbols represent the species concentrations in bulk experiments and should be replaced by the species probability densities in single-molecule measurements. Given a set of reaction rates and appropriate initial conditions, it is found that the decaying pattern of the off state predicted by the standard scheme in Equation (2) is bi-exponential given a high enough substrate concentration. It is therefore necessary to extend this general model, so that the proposed enzymatic mechanism can account for the functional form of $\phi_{off}(t)$. For this reason we considered a model that involves simultaneously enzymatic activity and conformational changes (Figure 4). The new model describes an off state that consists of a broad spectrum of conformational sub-states, which are coupled. Recently a distribution of reaction rates was extracted from single T4 Lysozyme TOC trajectories (approximately 50), lasting only about 20 s.[10] In our studies, each of the trajectories is considerably long lasting (about 30 min) and contains contributions from the entire distribution, which leads to a non-exponential decay pattern.

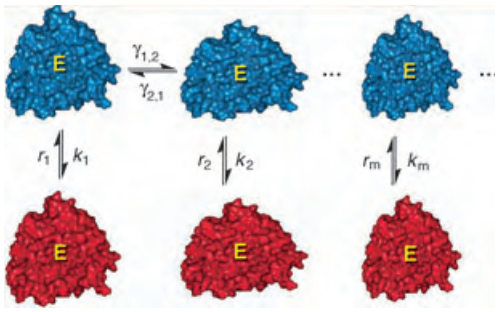


Figure 4. The model for the enzyme (E) conformational–reactivity behavior. The off-stage (blue) consists of a variety of coupled sub-states that interconvert. Each of the off sub-states reacts at a (possible) different reaction rate. Once the enzyme has transformed the substrate into the fluorescent product the on state is seen (red). The product then diffuses away from the enzyme and the process returns to the relevant off sub-state.

The chronologically ordered time duration of the off-state events revealed local trends. Events of similar time duration were observed to follow each other and, noticeable were clusters of "fast" events, with an average of three events per event cluster and an average of 12 ms per event. Considering the average of approximately 5000 events/20 min (5 events/1200 ms) calculated for 1.4 μM BCECF, AM (Figure 3), it is apparent that the enzyme is catalytically less active for long periods of time before it acquires a more reactive conformation.

In summary we have demonstrated that the direct observation of the real-time catalysis and substrate kinetics of a single-enzyme-catalyzed reaction, is possible for a commonly used, robust enzyme by using confocal fluorescence microscopy and a simple method. Furthermore, we have observed a stretched exponential waiting-time pdf in the enzymatic catalytic activity of the single lipase B enzymes from *Candida antarctica* studied that has not been observed earlier. Previous experiments have, however, revealed a non-exponential behavior of the biomolecules in several systems.[9,26] A possible explanation regarding the origin of the non-exponential behavior of the $\phi_{off}(t)$ is that the enzymatic kinetics involves a broad conformational spectrum, of which only certain conformations are catalytically active. Each conformation contributes a specific exponential factor to the

 © 2005 Wiley-VCH Verlag GmbH & Co. KGaA, Weinheim

overall ETOC, an observation, which is often masked by ensemble measurements. The ability to measure the activity of a single enzyme for a long time offers a powerful tool for the investigation of numerous other enzymes and a more complete understanding of their complex behavior.

Received: May 11, 2004
Revised: July 7, 2004
Published online: December 23, 2004

Keywords: analytical methods · enzymes · fluorescence microscopy · kinetics · single-molecule studies

[1] R. D. Vale, T. Funantsu, D. W. Pierce, L. Romberg, Y. Harada, T. Yanagida, *Nature* **1996**, *380*, 451 – 453.
[2] T. Funantsu, Y. Harada, M. Tokunaga, K. Saito, T. Yanagida, *Nature* **1995**, *374*, 555 – 559.
[3] A. Ishijima, H. Kojima, T. Funantsu, M. Tokunaga, H. Higucki, H. Tanaka, T. Yanagida, *Cell* **1998**, *92*, 161 – 171.
[4] H. Noji, R. Yasuda, M. Yoshida, K. Kinosita, *Nature* **1997**, *386*, 299 – 302.
[5] R. Yasuda, H. Moji, K. Kinoshita, M. Yoshida, *Cell* **1998**, *93*, 1117 – 1124.
[6] H. Lu, L. Xun, X. S. Xie, *Science* **1998**, *282*, 1877 – 1882.
[7] a) L. Edman, Z. Földes-Papp, S. Wennmalm, R. Rigler, *Chem. Phys.* **1999**, *247*, 11 – 22; b) L. Edman, R. Rigler, *Proc. Natl. Acad. Sci. USA* **2000**, *97*, 8266 – 8271.
[8] T. Ha, A. Y. Ting, J. Liang, W. B. Caldwell, A. A. Deniz, D. S. Chemla, P. G. Schultz, S. Weiss, *Proc. Natl. Acad. Sci. USA* **1999**, *96*, 893 – 898.
[9] H. Yang, G. Luo, P. Karnchanaphanurach, T.-M. Louie, I. Rech, S. Cova, L. Xun, X. S. Xie, *Science* **2003**, *302*, 262 – 266.
[10] Y. Chen, D. Hu, E. R. Vorpagel, H. P. Lu, *J. Phys. Chem. B* **2003**, *107*, 7947 – 7956.
[11] J. Uppenberg, M. T. Hansen, S. Patkar, T. A. Jones, *Structure* **1994**, *2*, 293 – 307.
[12] J. Uppenberg, N. Öhrner, M. Norin, K. Hult, G. J. Kleywegt, S. Patkar, V. Waagen, T. Anthinsen, A. Jones, *Biochemistry* **1995**, *34*, 16838 – 16851.
[13] E. M. Anderson, K. M. Larsoon, O. Kirk, *Biocatal. Biotransform.* **1998**, *16*, 181 – 204.
[14] N. Panchuk-Voloshina, R. P. Haugland, J. Bishop-Stewart, M. K. Bhalgat, P. J. Millard, F. Mao, W. Y. Leung, R. P. Haugland, *J. Histochem. Cytochem.* **1999**, *47*, 1179 – 1188.
[15] R. K. Kumar, C. C. Chapple, N. Hunter, *J. Histochem. Cytochem.* **1999**, *47*, 1213 – 1218.
[16] J. Hofkens, M. Maus, T. Gensch, T. Vosch, M. Cotlet, F. Köhn, A. Herrmann, K. Müllen, F. De Schryver, *J. Am. Chem. Soc.* **2000**, *122*, 9278 – 9288.
[17] R. Marches, E. S. Vitetta, J. W. Uhr, *Proc. Natl. Acad. Sci. USA* **2001**, *98*, 3434 – 3439.
[18] J. Heo, K. J. Thomas, G. H. Seong, R. M. Crooks, *Anal. Chem.* **2003**, *75*, 22 – 26.
[19] We were able to record fluorescence emission with 10000 turnovers and 10^7 emitted photons (detection efficiency 5% approximately 30 min reaction time).
[20] G. H. Weiss, *Aspects and Application of the Random Walk*, North-Holland, New York, **1994**.
[21] The histogram of the recorded photon counts, $P(a)$, allowed the translation of the trajectory to a dichotomous process and expressed both the noise off state and the on state.
[22] To reduce the effect of the background fluorescence, which we attribute to product accumulation, a separate local treatment was performed.[23]
[23] O. Flomenbom, K. Velonia, D. Loos, S. Masuo, M. Cotler, Y. Engelborghs, J. Hofkens, A. E. Rowan, R. J. M. Nolte, F. C. de Schryver, J. Klafter, *Proc. Natl. Acad. Sci. USA* in press.
[24] J. Klafter, M. F. Shlesinger, *Proc. Natl. Acad. Sci. USA* **1986**, *83*, 848 – 851.
[25] M. Abramowitz, I. A. Stegun, *Handbook of Mathematical Functions with Formulas, Graphs, and Mathematical Table*, Government Printing office, Washington, D.C., **1964**.
[26] a) R. Metzler, J. Klafter, J. Jortner, *Proc. Natl. Acad. Sci. USA* **2003**, *100*, 11085 – 11089; b) Y. Chen, D. Hu, E. R. Vorpagel, H. P. Lu, *J. Phys. Chem. B* **2003**, *107*, 7947 – 7956.
[27] a) H. Frauenfelder, B. H. McMahon, R. H. Austin, K. Chu, J. T. Groves, *Proc. Natl. Acad. Sci. USA* **2001**, *98*, 2370 – 2374; b) H. Frauenfelder, P. G. Wolynes, R. H. Austin, *Rev. Mod. Phys.* **1999**, *71*, S419-S430.
[28] N. Richter-Dyn, N. S. Goel, *Stochastic Models in Biology*, Academic Press, New York, **1974**.

 © 2005 Wiley-VCH Verlag GmbH & Co. KGaA, Weinheim

Membranes

Copolymerization of Ethylene, Tetrafluoroethylene, and an Olefin-Containing Fluorosulfonyl Fluoride: Synthesis of High-Proton-Conductive Membranes for Fuel-Cell Applications**

Zhen-Yu Yang and Raj G. Rajendran*

Fuel cells, which are devices that convert the chemical energy stored in the fuel directly into electricity, are one of the most important technologies in the 21st century. They not only provide pollution-free clean energy, but also give high-quality and more-reliable power.[1] Of all the types known today, the technology based on proton-exchange membrane fuel cells (PEMFC) is the most attractive for various applications, especially transportation and for stationary and portable devices.[2] The most important component of the PEMFC is the membrane electrode assembly (MEA), at the heart of which is the proton-conductive membrane. The key functions of the membrane are to transport protons from the anode to the cathode of the cell and to separate the fuel and the oxidant.

Significant resources have been devoted worldwide to the development of high-performance and reliable membranes.

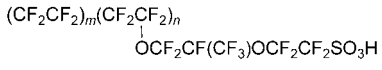
[*] Dr. Z.-Y. Yang, Dr. R. G. Rajendran
DuPont Central Research and Development
Experimental Station, Wilmington, DE 19880-0328 (USA)
Fax: (+1) 302-695-9799
E-mail: Zhenyu.yang-1@usa.dupont.com

[**] Publication no.: 8560. The authors thank Mr. D. Irino for technical assistance, the Pressure Lab of DuPont for running all polymerization reactions, Prof. S. Zhu at the Shanghai Institute of Organic Chemistry, China, for providing compound **1**, and Dr. A. E. Feiring and Dr. M. Hofmann for their comments on this manuscript.

Supporting information for this article is available on the WWW under http://www.angewandte.org or from the author.

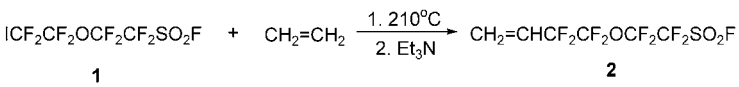
 © 2005 Wiley-VCH Verlag GmbH & Co. KGaA, Weinheim DOI: 10.1002/anie.200461104

Academic researchers are working on the development of new membrane materials, while government and industry are driving the commercialization of fuel-cell technology.[3] Although many proton-exchange membranes have been developed, the perfluorinated-ionomer membrane nafion is still the best known today.[4] Nafion, which was invented and introduced by DuPont in the early 1960s, revolutionized fuel-cell technology, and is synthesized by copolymerization of tetrafluoroethylene (TFE) and a perfluorovinyl ether (PSEPVE) containing a sulfonyl fluoride.[5] Although nafion is the most widely used membrane in fuel cells and provides the best overall performance at temperatures below 100 °C, it is relatively expensive. The high cost of nafion is primarily attributed to the difficult polymerization and the need for an expensive monomer (PSEPVE). In addition, perfluorinated nafion is difficult to further modify to improve its desired properties. We report here a new, potentially lower cost and high-performance proton-conductive membrane for fuel-cell applications.

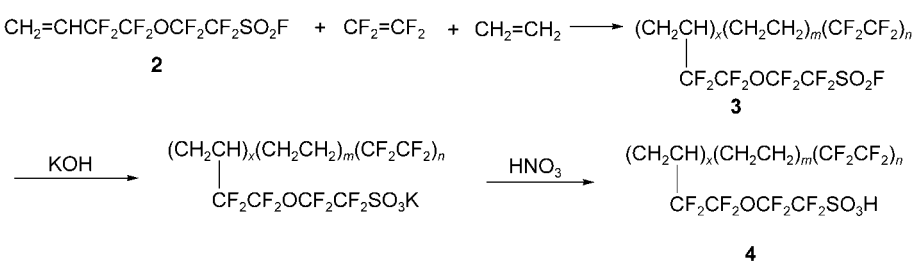


TFE/PSEPVE, nafion

Although perfluorinated polymers provide the best combination of both thermal and chemical properties, selective introduction of H atoms into polymers does not affect the stability dramatically.[6] In fact, a copolymer of ethylene and tetrafluoroethylene (ETFE), tefzel®, made by DuPont, still has excellent thermal and chemical stability and has better mechanical properties than perfluorinated polymers.[7] In addition, the ETFE portion can be cross-linked readily to further improve its properties, whereas perfluorinated polymers are extremely difficult to modify.[8] More importantly, TFE and ethylene copolymerize mostly alternately, which may help in the incorporation of olefins other than expensive perfluorovinyl ethers.[9] If this is the case, we might be able to design a low-cost, fluorinated monomer containing a sulfonyl fluoride group. Monomer **2** was readily synthesized from ethylene and **1**, which is commercially available, or by reaction of TFE, FSO_2CF_2COF, and I–Cl in one step.[10]



Although copolymerization of **2** and TFE was unsuccessful, and only a small amount of **2** was incorporated into the polymers, we found that copolymerization of TFE, ethylene, and **2** was more effective. Copolymerization in the presence of an organic peroxide, such as lupersol 11, as an initiator in 100 mL of 1,1,2-trichloro-1,2,2-trifluoroethane (CFC113) in a 240-mL shaker tube at 60 °C for seven hours provided the terpolymers shown in Table 1.



All polymerizations proceeded smoothly to give polymers in good yields. The remarkably high conversion of termonomer **2** makes this polymerization system particularly attractive for practical applications. In most cases, conversions of **2** were up to 90%. The polymerization pressure drops with polymerization time, while the rate of polymerization decreases with an increase of monomer **2** in the presence of given amounts of TFE and ethylene. Incorporation of termonomer **2** increases in the polymers with an increase of the pre-charged amount of **2**. It is interesting to note that the ratio

Table 1: Coolymerization of TFE, ethylene (E), and **2**.

Entry	Monomers [g, mol]	(TFE + E)/**2** [mol]	ΔP[a] [psi/7 h]	Yield [g]	Analysis[b] (TFE + E)/**2**	EW	Conductivity[c] [mS cm^{-1}]
1	TFE (22, 0.22) E (7, 0.25) **2** (10, 0.031)	15.2	316	35.7	$(E)_{7.7}(TFE)_{6.5}$(**2**) 14.2/1	1192	40
2	TFE (22, 0.22) E (7, 0.25) **2** (13, 0.040)	11.8	247	33.5	$(E)_{7.3}(TFE)_{5.5}$(**2**) 12.8/1	1080	75.7
3	TFE (22, 0.22) E (7, 0.25) **2** (14, 0.043)	10.9	282	35.8	$(E)_{6.4}(TFE)_{5.5}$(**2**) 11.9/1	1055	77.8
4	TFE (22, 0.22) E (7, 0.25) **2** (15, 0.046)	10.2	222	30.2	$(E)_{6.2}(TFE)_{3.7}$(**2**) 9.9/1	870	94.6
5	TFE (22, 0.22) E (7, 0.25) **2** (16, 0.049)	9.6	244	35.5	$(E)_{5.7}(TFE)_{4.0}$(**2**) 9.7/1	886	99.6
6	TFE (22, 0.22) E (7, 0.25) **2** (20, 0.061)	7.7	186	35.6	$(E)_{5.4}(TFE)_{3.3}$(**2**) 8.7/1	807	102
7	TFE (22, 0.22) E (7, 0.25) **2** (25, 0.077)	6.1	152	30.6	$(E)_{3.6}(TFE)_{3.0}$(**2**) 6.6/1	727	122

[a] Pressure change between beginning and end of polymerization in 7 h. [b] Based on elemental analysis. [c] At room temperature.

 © 2005 Wiley-VCH Verlag GmbH & Co. KGaA, Weinheim

of TFE plus ethylene to **2**, (TFE + E)/**2**, in the polymers is similar to that of the precharged monomers.

Terpolymers **3** show excellent thermal stability. As observed in the TGA studies, the polymers start to decompose at about 370 °C and a 10 % weight loss occurs up to 425 °C. DSC analysis indicated that the polymers have no melting points, except for the polymer of entry 1, which has a broad melting point at 210 °C, although X-ray diffraction studies showed that the polymers have some degree of crystallinity. The degree of crystallinity decreases with increasing amounts of incorporated **2** in the polymers. These polymers are insoluble in common organic solvents at room temperature, so it is difficult to obtain their molecular weights.

All terpolymers **3** were readily pressed to transparent, strong and tough films at 220–250 °C, thus indicating their high molecular weight. The films were hydrolyzed with 10 % KOH in MeOH/H_2O/DMSO (4:5:1, *v*/*v*/*v*) at 60 °C to give the potassium salt of the ionomer membrane. The films became light yellow in color when hydrolysis was carried out above 100 °C. This is probably a consequence of the attack of the hydroxy anion on the backbone of the polymers. The potassium ionomers were immersed in 10 % HNO_3 at 60 °C for two hours twice, and then washed and boiled with deionized water several times to obtain membranes **4**.

The proton conductivity of **4** is, in general, similar to, or higher than that of nafion, and depends on the amount of incorporated termonomer **1**. It was found that the conductivity follows a linear relationship with the ratio of units of (TFE + ethylene)/**2**, or with equivalent weight (EW), as indicated in Table 1. Interestingly, the conductivity of the new membranes is higher than that of nafion samples containing the same mol percent of PSEPVE. For example, membranes containing less than 10 mol % of **2** (entries 4 or 5 of Table 1) have the same conductivity as nafion 117, which contains 15 mol % PSEPVE. Membranes containing 15 mol % of **1** (entry 7) have a conductivity of 122 mS cm^{-1}, which is 22 % higher than that of nafion 117.

Although the exact reason for the high conductivity of membrane **4** is not fully understood, the more-polar and flexible backbones of the polymer and lower equivalent weight may, in part, be responsible for the proton conduction, as a result of higher water uptake.[11] In fact, the membrane in entry 5 takes-up 49 % (by weight) water compared with 39 % water for nafion under the same conditions. A clear phase-separation in **4** (entry 5) between the hydrophilic sulfonic acid and the hydrophobic hydrofluorocarbon backbone was observed by atomic-force microscopy (AFM; Figure 1), which is very similar to the images generated from nafion.[12]

The experimental membrane **4** from entry 5 in Table 1 without any optimization was tested in a direct MeOH fuel-cell. The membrane and electrode assembly required for the fuel-cell evaluation was fabricated using a standard method.[13] The anode and cathode catalysts were Pt–Ru and Pt black, respectively, and the loadings were kept close to 4 mg cm^{-2}. Commercial carbon cloths—E-Tek's ELAT and Zoltek's plain carbon cloth—were used as the cathode and anode gas diffusion backing, respectively. The anode was fed with a 1 M methanol/water mixture at a rate of 25 mL min^{-1},

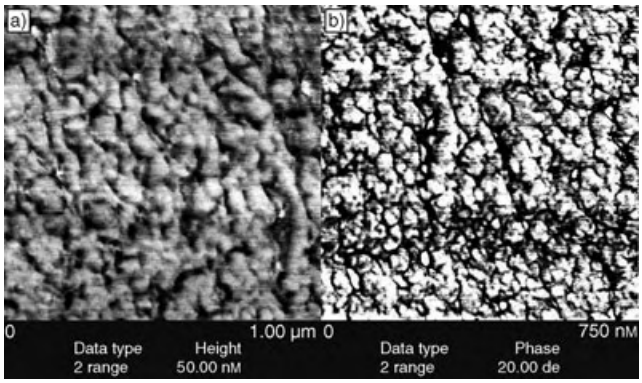


Figure 1. AFM images: a) Tapping-force height: 50 nm scale; b) phase: 750 nm scale.

and the cathode with oxygen (3 L min^{-1}). The cell was heated to 80 °C, and the fuel-cell performance data were recorded. The fuel-cell performance of the membrane **4** is compared with the performance of commercial nafion 115 under the same conditions in Figure 2. The new 5-mil (127 µm) membrane exhibits a similar power output to a 5-mil commercial nafion membrane, although it has 9 % higher methanol crossover (10.9×10^{-4} g min^{-1} cm^{-2} for membrane **4** and 9.9×10^{-4} g min^{-1} cm^{-2} for 5-mil nafion). This difference is partly a consequence of the variation in the thickness of the new membrane. We anticipate that higher EW samples may reduce the methanol crossover significantly. Of course, the high EW also affects the fuel-cell performance, although cross-linking may reduce MeOH crossover and further improve the fuel-cell performance.

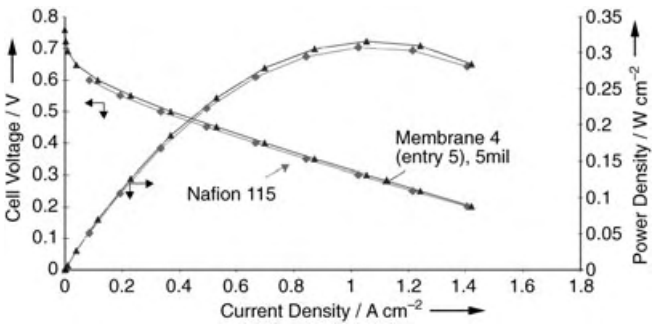


Figure 2. MeOH/O_2 fuel-cell performance with membrane **4** (entry 5) at 80 °C by monitoring cell voltage and power density versus current density. The anode was fed with 1 M methanol at a rate of 25 mL min^{-1} and the cathode was fed with oxygen at a rate of 3 L min^{-1}.

In conclusion, we have discovered an effective copolymerization of tetrafluoroethylene and ethylene with **2** to give melt-processable terpolymers, which can be readily hydrolyzed and acidified to give membranes. The new membranes exhibit excellent conductivity and stability. The fuel-cell performance is comparable to, or slightly better than, that of nafion, although it is still to be optimized. Their polymeric lithium salts also exhibit excellent lithium-ion conductivity and are attractive candidates for lithium-battery applications. The new membranes could be produced more cheaply

 © 2005 Wiley-VCH Verlag GmbH & Co. KGaA, Weinheim

because of the simple polymerization process and the low monomer cost.

Experimental Section

General preparation of membranes: A 210-mL, stainless-steel tube was charged with F113 (100 mL), **2** (15 g), and lupersol 11 (0.5 g), and attached to a gas manifold. The tube was cooled in dry ice and the contents degassed by several cycles of evacuation and repressurization with nitrogen gas. After the final evacuation step, the tube was pressurized with ethylene (7 g) and TFE (22 g). The tube was then sealed and heated to 60 °C and held for 7 h to effect the polymerization. After completion of the polymerization, any remaining ethylene and TFE were removed by venting, and the remaining white solid was washed with MeOH and dried in a partial vacuum oven at 100 °C to give 30.2 g of polymer. IR(KBr): $\tilde{\nu} = 1464\ cm^{-1}$ (SO_2F). Elemental analysis of the polymer indicated that its composition was $(CF_2CF_2)_{3.7}(CH_2CH_2)_{6.2}(CH_2CHCF_2CF_2OCF_2CF_2SO_2F)$ on a molar basis, based on C 34.68 %, H 2.64 %, F 50.65 %, and S 3.72 %. DSC showed that the polymer had no melting point. A 10 % weight loss was noted up to 430 °C under N_2 by TGA. A colorless, transparent, and tough film was pressed by placing a sample of the polymer between the platens of a hydraulic press and heated to 225 °C with a ram force 20000 lbs. This film was then immersed in a suspension of 10 % KOH in H_2O/MeOH/DMSO (5:4:1 *v*/*v*/*v*) at 60 °C for 6 h. The film was removed from the solution, washed with water many times, and then treated with 10 % HNO_3 at 60 °C for 2 h twice. It was then washed with deionized water until neutral, and then boiled in deionized water for 1 h.

Received: June 28, 2004
Revised: September 1, 2004
Published online: December 13, 2004

Keywords: fluorine · fuel cells · membranes · polymerization

[1] a) M. S. Dresselhaus, I. L. Thomas, *Nature* **2001**, *414*, 337; b) G. J. Schaeffer, R. Uyterlinde, *J. Power Sources* **1998**, *71*, 256; c) K. D. William, W. K. D. Borthwick, *J. Power Sources* **2000**, *86*, 52.

[2] a) B. D. McNicol, D. A. J. Rand, K. R. Williams, *J. Power Sources* **2001**, *100*, 47; b) S. Kawatsu, *J. Power Sources* **1998**, *71*, 150; c) R. Nolt, *J. Power Sources* **2001**, *4573*, 1; d) N. M. Smammes, R. Boersma, *J. Power Sources* **2000**, *86*, 98; e) D. Chu, R. Jiang, K. Gardner, R. Jacobs, J. Schmidt, T. Quakenbush, J. R. Stephens, *J. Power Sources* **2001**, *96*,174.

[3] a) B. C. H. Steele, A. Heinzel, *Nature* **2001**, *414*, 345; b) G. J. K. R. Acres, *J. Power Sources* **2001**, *100*, 60; c) M. Conte, A. Iacobazzi, M. Ronchetti, R. R. Vellone, *J. Power Sources* **2001**, *100*, 171; d) P. Costamagna, S. Srinivasan, *J. Power Sources* **2001**, *102*, 242; e) H. L. Maynard, J. P. Meyers, *J. Vac. Sci. Technol. B.* **2002**, *20*, 1287; f) X. Ren, P. Zelenay, S. Thomas, J. Davey, S. Gottesfeld, *J. Power Sources* **2000**, *86*, 111.

[4] a) S. M. Haile, D. A. Boysen, C. R. I. Chisholm, R. Merle, *Nature* **2001**, *410*, 910; b) G. Alberti, M. Casciola, *Solid State Ionics* **2001**, *145*, 3; c) J. A. Kerres, *J. Membr. Sci.* **2001**, *185*, 3; d) K. D. Kreuer, *J. Membr. Sci.* **2001**, *185*, 29; e) D. J. Jones, J. Roziere, *J. Membr. Sci.* **2001**, *185*, 41; f) C. Heitner-Wirguin, *J. Membr. Sci.* **1996**, *120*, 1.

[5] a) W. G. Grot, *Macromol. Symp.* **1994**, *77–88*, 161; b) A. Eisenberg, F. Bailey, *ACS Symp. Ser.* **1986**, 302; c) A. Eisenberg, M. King, *Ion-Containing Polymers*, Academic Press, New York, **1977**; d) A. Eisenberg, H. Yeager, *ACS Symp. Ser.* **1982**, 180; e) D. Lloyd, *ACS Symp. Ser.* **1985**, 269.

[6] a) *Fluoropolymers, Vol. XXV* (Ed.: L. A. Wall), John Wiley & Sons, New York, **1972**; b) *Modern Fluoropolymers* (Ed.: J. Scheirs); John Wiley & Sons, New York, **1997**.

[7] *Ullmann's Encyclopedia of Industrial Chemistry*, *Vol A11* (Eds.: D. P. Carlson, W. Schmiegel), VCH, Weinheim, **1988**, p. 395.

[8] J. S. Forsythe, D. J. T. Hill, *Prog. Polym. Sci.* **2000**, *25*, 101.

[9] TFE copolymerizes poorly with perfluoroalkenes such as $CF_2=CFR_FSO_2F$ or perfluoroalkylethylenes. Only small amounts of co-monomers can be incorporated into the polymers; see: a) C. G. Krespan, *US Patent* 4275255; b) A. W. Anderson, S. J. Fritschel, H. E. Holmquist, *US Patent* 4522995.

[10] a) Z. Zhang, J. Lu, P. Song, C. Xu, N. Chen, *Huaxue Shijie* **1990**, *31*, 272; b) G. A. Bargigia, G. Caporiccio, M. Pianca, *J. Fluorine Chem.* **1982**, *19*, 403.

[11] a) W. Y. Hsu, T. D. Gierke, *J. Membr. Sci.* **1983**, *13*, 307; b) C. A. Edmondson, P. E. Stallworth, M. C. Wintersgill, J. J. Fontanella, Y. Dai, S. G. Greenbaum, *Electrochim. Acta* **1998**, *43*, 1295.

[12] P. J. James, J. A. Elliott, T. J. McMaster, J. M. Newton, A. M. S. Elliott, S. Hanna, M. J. Miles, *J. Mater. Sci.* **2000**, *35*, 5111; b) R. S. McLean, M. Doyle, B. B. Sauer, *Macromolecules* **2000**, *33*, 6541; c) K. D. Kreuer, *Solid State Ionics* **2000**, *136–137*, 149.

[13] a) X. Ren, M. S. Wilson, S. Gottesfeld, *J. Electrochem. Soc.* **1996**, *143*, L12; b) X. Ren, T. E. Springer, S. Gottesfeld, *J. Electrochem. Soc.* **2000**, *147*, 92.

 © 2005 Wiley-VCH Verlag GmbH & Co. KGaA, Weinheim

Silicates

$SrSi_6N_8$—A Reduced Nitridosilicate with a Si–Si Bond**

*Florian Stadler, Oliver Oeckler, Jürgen Senker, Henning A. Höppe, Peter Kroll, and Wolfgang Schnick**

Dedicated to Professor Arndt Simon on the occasion of his 65th birthday

Silicates are a very important class of minerals that form about 80 wt% of the earth's crust. Nearly all naturally occurring silicates are oxosilicates. However, sinoite (Si_2N_2O), a mineral that occurs in meteorites, contains a framework of corner-sharing $Si(O,N)_4$ tetrahedrons.[1,2] In the

[*] Dipl.-Chem. F. Stadler, Dr. O. Oeckler, Dr. J. Senker, Prof. Dr. W. Schnick
Department Chemie und Biochemie
Ludwig-Maximilians-Universität
Lehrstuhl für Anorganische Festkörperchemie
Butenandtstrasse 5–13(D), 81377 München (Germany)
Fax: (+49) 89-2180-77440
E-mail: wolfgang.schnick@uni-muenchen.de
Dr. H. A. Höppe
New address: Institut für Anorganische Chemie
Albert-Ludwigs-Universität
Albertstrasse 21, 79104 Freiburg (Germany)
Dr. P. Kroll
Institut für Anorganische Chemie
RWTH Aachen
Professor-Pirlet-Strasse 1, 52056 Aachen (Germany)

[**] This work was supported by the Fonds der Chemischen Industrie and the Deutsche Forschungsgemeinschaft.

 DOI: 10.1002/anie.200461633 © 2005 Wiley-VCH Verlag GmbH & Co. KGaA, Weinheim

past few years an increasing number of nitridosilicates has been synthesized. The characteristic structural entities in oxo- and nitridosilicates as well as in oxonitridosilicates (sions) are SiX_4 tetrahedrons (X = O, N), which are typically connected through common corners (X = O, N)[3a] or edges (X = N).[3b] Higher coordination numbers of silicon (CN > 4) mainly occur in high-pressure phases (e.g. the SiO_2 polymorph stishovite or perovskite-type $(Mg,Fe)SiO_3$).[4]

All known crystalline silicates exhibit Si–X substructures, in which Si and X atoms (X = O, N) alternate in a strictly regular fashion. According to IUPAC nomenclature, the term "silicate" indicates a compound with silicon in the oxidation state +IV. Very few reduced silicon oxides and nitrides have been reported that contain silicon in oxidation states < +IV. For example, Hengge synthesized an amorphous subnitride with the postulated formula Si_6N_2 starting from $CaSi_2$ and NH_4Br at 550 °C. He assumed that this compound contained Si–Si bonds (230 pm) although no comprehensive structural model could be ascertained.[10] Based on this work Kniep et al. described another subnitride with the formula Si_2N. It was obtained as an amorphous product, too, by the topochemical reaction of $CaSi_2$ with NH_4X (X = F, Cl, Br, I) at 330–370 °C.[11] A structural model with sphalerite- or wurtzite-analogous layers was proposed and a Si–Si distance of 230 pm was assumed, which has not yet been proven by experimental methods. Furthermore, Jansen et al. reported on the amorphous suboxide Si_2O_3.[12] The product was obtained by a sol–gel process from Si_2Cl_6 and H_2O at −75 °C. A Si–Si bond length of 230 pm was derived from pair correlation functions.

In the past couple of years we have been focussing on the preparation and characterization of new nitrido- and oxonitridosilicates as well as oxonitridoaluminosilicates (sialons).[13] We have now obtained the first crystalline reduced nitridosilicate $SrSi_6N_8$ by reaction of strontium with silicon diimide at 1630 °C in a radio-frequency furnace (see Experimental Section).

The structure of $SrSi_6N_8$ was determined by a single-crystal X-ray structure analysis.[14] Considering the stoichiometric formula of the colorless compound, the charge balance does not allow us to assume the presence of exclusively tetravalent silicon. Actually, SiN_4 tetrahedrons as well as $N_3Si–SiN_3$ entities, in which each nitrogen atom bridges three silicon atoms, occur in $SrSi_6N_8$ (Figure 1, left). Such N[3] connections are frequently observed in the class of nitridosilicates.[3b] The Si–N bond lengths (166–176 pm) correspond well with those in other nitridosilicates.[13] The framework structure of $SrSi_6N_8$ significantly differs from any other known silicate structure as it does not comprise a strictly alternating sequence of Si and X atoms (X = O, N). In contrast, it contains additional Si–Si single bonds (235.2(2) pm), the length of which precisely matches (within less than 0.1 %) that of the archetypical covalent Si–Si single bond in diamond-type silicon. It also resembles Si–Si bond lengths of the molecular compounds Si_2H_6, Si_2F_6, or Si_2Me_6, which range between 213 and 234 pm.[15]

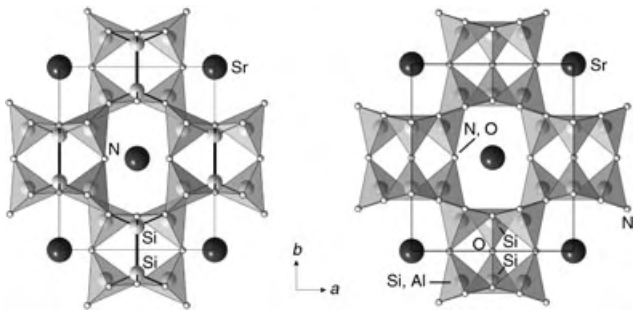


Figure 1. Left: Crystal structure of $SrSi_6N_8$ (view along [001]). In addition to SiN_4 tetrahedrons there are $N_3Si–SiN_3$ units with formally trivalent silicon. Right: Crystal structure of $Sr_2Al_xSi_{12-x}N_{16-x}O_{2+x}$ ($x \approx 2$)[16] (view along [001]).

The Sr^{2+} ions in $SrSi_6N_8$ are ten-coordinate, surrounded by nitrogen at distances of 269–316 pm. A quite similar crystal structure occurs in the sialon $Sr_2Al_xSi_{12-x}N_{16-x}O_{2+x}$ ($x \approx 2$; Figure 1, right), which also crystallizes in the space group *Imm*2.[16] Comparing the tetrahedron frameworks of the two structures (Figure 2), it is evident that in the sialon an oxygen

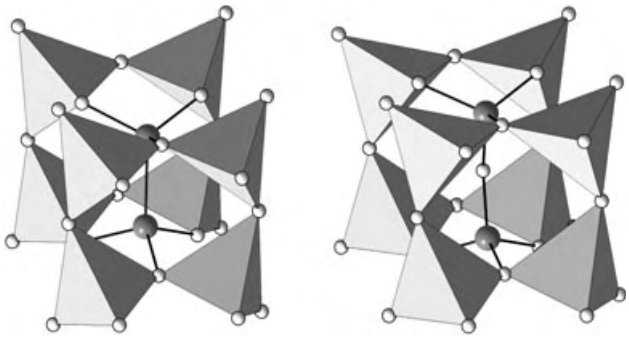


Figure 2. Tetrahedron frameworks in $SrSi_6N_8$ (left) and in $Sr_2Al_xSi_{12-x}N_{16-x}O_{2+x}$ ($x \approx 2$)[16] (right).

atom is formally inserted into the Si–Si bond, thus leading to two corner-sharing tetrahedrons. The Si–Si distance for these oxygen-linked Si atoms are 310.1(4) pm, the Si-O-Si angle is 152.3(2)°.[16] In the meantime we have also obtained $BaSi_6N_8O$, which is isotypic with the sialon $Sr_2Al_xSi_{12-x}N_{16-x}O_{2+x}$ ($x \approx 2$).[17]

A first validation of the crystal structure of $SrSi_6N_8$ was performed computationally by using standard density functional theory methods (see Experimental Section). After complete geometry optimization of the crystal structure of $SrSi_6N_8$, we obtained lattice parameters that agree perfectly with the experimental findings. Our results, which were calculated within both the local density approximation (LDA) and the generalized gradient approximation (GGA), reflect the usual trend of these functionals to provide lower and upper boundaries for *a*, *b*, and *c* within 1 % of the experimentally determined values.

We obtained values of 233.3 pm (LDA) and 237.7 pm (GGA) for the Si–Si bond length. These values nicely enclose the experimental value of 235.2(2) pm. The nature of the covalent Si–Si bond was analyzed further by the electron localization function (ELF). The ELF isosurface plot of the central $N_3Si–SiN_3$ fragment within the crystal structure of $SrSi_6N_8$, accessed at a value of 0.88, is shown in Figure 3. In the center of the Si–Si bond we found a maximum ELF value of

 © 2005 Wiley-VCH Verlag GmbH & Co. KGaA, Weinheim

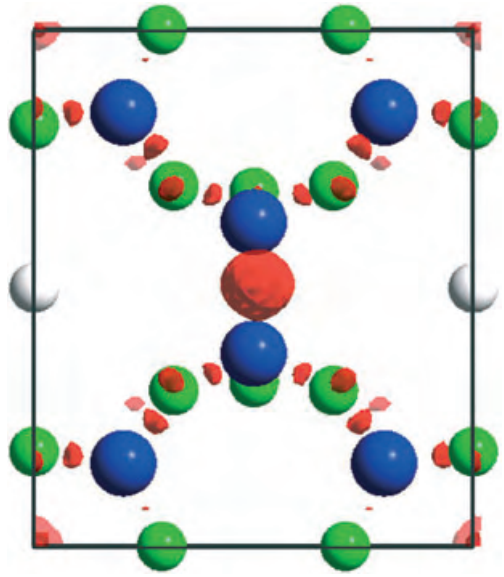


Figure 3. ELF of valence electrons in $SrSi_6N_8$ (Sr white, Si blue, and N green), view along [00$\bar{1}$]. To enhance the clarity, the figure shows the ELF around the central $N_3Si{-}SiN_3$ unit only ($-0.2 \le z \le 0.3$). The isosurface is shown for ELF = 0.88, which is approximately the maximum of the ELF found within the Si–N bonds. Compared to the view in Figure 2, in this case the unit cell has been translated by the vector [$^1/_2$00].

nearly 1.0, which indicates an almost ideal pairing of two electrons of opposite spin in a bonding crystal orbital.

One of the strengths of the computational approach is the ability to test the properties of a hypothetical "$SrSi_6N_8O$" by inserting an oxygen atom into the Si–Si bond. After complete optimization of the structure ($SrSi_6N_8O$: $a = 810.3/820.6$, $b = 962.3/972.1$, and $c = 480.0/486.5$ pm calculated by LDA/GGA, respectively), we obtained unit cell parameters a and b, which differ significantly from the experimentally determined lattice parameters of $SrSi_6N_8$.[14] Insertion of the oxygen atom extends b by more than 3%, mainly due to the increased spacing between the two Si atoms bound to O. Furthermore, this causes a rotation of the SiN_4 tetrahedrons of the SiN-framework structure, which becomes visible by comparing the left- and right-hand side of Figures 1 and 2. As a net effect, the cell parameter a increases by more than 4%. Moreover, although the computed atomic positions of $SrSi_6N_8$ match those obtained from the refinement procedure within 2 pm, atomic positions of the hypothetical oxygen-containing compound $SrSi_6N_8O$ are shifted by up to 50 pm. The computational results, therefore, corroborate the structure and bonding of the reduced silicate $SrSi_6N_8$. In particular, they unequivocally establish the single bond between the two Si atoms. However, given the existence of $BaSi_6N_8O$,[17] it would appear that it should be possible to find a synthetic pathway to $SrSi_6N_8O$ as well, for instance by a topotactic diffusion of oxygen into $SrSi_6N_8$. Conversely, one can envisage transforming $BaSi_6N_8O$ into $BaSi_6N_8$ topotactically by elimination of oxygen. Currently, we are investigating the compounds $AESi_6N_8(O)$ with AE = Ca, Sr, or Ba by both theoretical and experimental methods.

To obtain further proof for the existence of a Si–Si bond in $SrSi_6N_8$, we conducted ^{29}Si solid-state NMR investigations. The NMR spectrum in Figure 4 clearly confirms the results from the single-crystal structure analysis. The two ^{29}Si

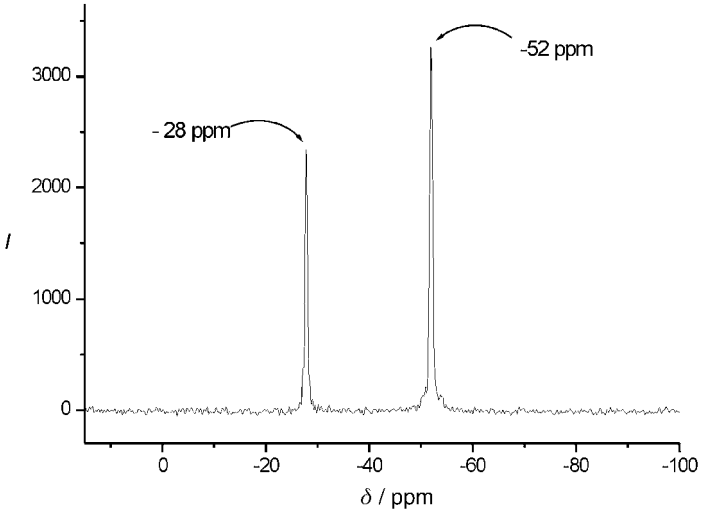


Figure 4. ^{29}Si NMR spectrum of $SrSi_6N_8$. The two signals derive from SiN_4 ($\delta = -52$ ppm) and from $N_3Si{-}SiN_3$ ($\delta = -28$ ppm), respectively.

resonances show an intensity ratio of 1:2 corresponding to the multiplicity of the Wyckoff sites 4*d* ($(SiN_3)_2$) and 8*e* (SiN_4). The chemical shift of $\delta = -52$ ppm is assigned to SiN_4 tetrahedrons (cf. $\delta(SiN_4) = -50$ ppm in c-Si_3N_4[18] or $\delta(SiN_4) = -64.5/-56.5$ ppm in $LaSi_3N_5$[19]). In contrast, the signal at $\delta = -28$ ppm corresponds to the $(SiN_3)_2$ group. The strong low-field shift could also be caused by carbon-containing SiX_4 tetrahedrons (X = N, C), cf. $\delta(SiC_4) \approx -20$ ppm in SiC[20] or $\delta(SiCN_3) \approx 37$ ppm in $Y_2Si_4N_6C$.[21] However, the presence of carbon has been unequivocally ruled out by chemical analyses. Furthermore, oxygen within the coordination sphere of Si would rather lead to a high-field shift (e.g. $\delta(SiON_3) = -61.2$ ppm in Si_2N_2O (sinoite) or $\delta(SiO_2N_2) = -75.3$ ppm in SiON glasses[22]).[23]

$SrSi_6N_8$ thus represents the first crystalline ternary silicate with a partially reduced silicate substructure in which Si is present in the oxidation states +III and +IV. Recently, another silicate with Si in two oxidation states (+IV and −I) was reported, namely $Cs_{10}Si_7O_9$. However, according to the formula $Cs_{10}[Si_4][Si_3O_9]$, this mixed silicide silicate contains isolated $[Si_4]^{4-}$ Zintl anions and $[Si_3O_9]^{6-}$ Dreier rings, which are not directly bound to each other.[24]

Experimental Section

In a typical experiment Sr (43.8 mg; dendritic, ABCR GmbH & Co. KG, Karlsruhe, 99.95%) and silicon diimide (156.3 mg; synthesized according to reference [13b]) were placed in a tungsten crucible under argon atmosphere inside a glove box (Unilab, Fa. Mbraun, Garching, $O_2 < 1$ ppm, $H_2O < 1$ ppm). Subsequently, the crucible was heated inductively in the reactor of a r.f. furnace[13b] under N_2 atmosphere (dried over silica gel/KOH/molecular sieve (pore width 4 Å)/P_2O_5 and activated BTS catalyst) to 1630 °C at a rate of 8.9 °C min^{-1} and then kept at this temperature for 6.5 h. The reaction product was then

 © 2005 Wiley-VCH Verlag GmbH & Co. KGaA, Weinheim

cooled down to 900 °C at a rate of about 1 °C min^{-1} and then quenched to room temperature by switching off the furnace. A colorless, coarsely crystalline product was obtained, which according to the X-ray powder pattern is single-phase $SrSi_6N_8$. Elemental analysis (double determinations by the Mikroanalytisches Labor Pascher, Remagen) calcd for $SrSi_6N_8$ (368.24): Sr 23.8, Si 45.8, N 30.4, O 0.0; found: Sr 23.1, Si 45.9, N 30.7, O < 1.0. The single crystals obtained were suitable for X-ray structure analysis. A theoretical powder diffraction pattern calculated on the basis of the single-crystal data showed excellent agreement with a measured powder diffraction pattern for $SrSi_6N_8$ with respect to the positions and intensities of all the observed reflections.

Calculations: For density functional[25] calculations, we applied the VASP software package.[26] The pseudopotentials employed are based on the projector-augmented-wave (PAW) method.[27] We used both the local density approximation (LDA) and the generalized-gradient approximation (GGA) to treat the exchange-correlation energy of the electrons. All the results rely on well-converged calculations with respect to cut-off energy (500 eV) and *k*-point sampling ($2\times2\times4$ mesh). Residual forces and stresses in the optimized structures are less than 0.005 eV Å^{-1} and 1 kbar, respectively. The electron localization function (ELF) is a local descriptor of the probability of electron pairing.[28] By definition the ELF takes values within the interval [−1,1]. ELF tends to zero in regions of space, where the average distances between spin-like and spin-unlike electrons are similar, hence, electrons are unpaired. When spin-unlike electrons are paired, ELF tends to +1; when spin-like electrons are paired, ELF tends to −1. Regions corresponding to electron pairing exhibit a maximum, and all the regions corresponding to a lack of electron pairing exhibit a minimum. Since we are interested in the bonding between the two Si atoms, we focussed on pairing maxima.

Received: August 13, 2004
Published online: December 13, 2004

Keywords: NMR spectroscopy · Si—Si bonds · silicates · structure elucidation

[1] K. Keil, C. A. Andersen, *Nature* **1965**, *207*, 745.
[2] W. R. Ryall, A. Muan, *Science* **1969**, *165*, 1363.
[3] a) F. Liebau, *Structural Chemistry of Silicates*, Springer, Berlin, **1985**; b) H. Huppertz, W. Schnick, *Chem. Eur. J.* **1997**, *3*, 679.
[4] In silicates, higher coordination numbers of Si (CN > 4) are found only in a few cases, mostly high-pressure phases,[3,5,6] for example, rutile-type SiO_2 (high-pressure polymorph stishovite), perovskite-type (Mg,Fe)SiO_3 occurring in the deeper mantle of the earth, or hollandite-analogous $CaAl_2Si_2O_8$.[5] At lower pressures a few silicates can be obtained that contain both SiO_6 octahedrons and SiO_4 tetrahedrons (e.g. $K_2Si_4O_9$,[7] $BaSi_4O_9$,[8] and $Na_{1.8}Ca_{1.1}Si_6O_{14}$[9]).
[5] L. W. Finger, R. M. Hazen, *Acta Crystallogr. Sect. B* **1991**, *47*, 561.
[6] R. M. Hazen, R. T. Downs, L. W. Finger, *Science* **1996**, *272*, 1769.
[7] D. K. Swanson, C. T. Prewitt, *Am. Mineral.* **1983**, *68*, 581.
[8] L. W. Finger, R. M. Hazen, B. A. Fursenko, *J. Phys. Chem. Solids* **1995**, *56*, 1389.
[9] T. Gasparik, J. B. Parise, B. A. Eiben, J. A. Hriljac, *Am. Mineral.* **1995**, *80*, 1269.
[10] E. Hengge, *Z. Anorg. Allg. Chem.* **1962**, *315*, 298.
[11] a) R. Kniep, J. Haberecht, PCT Int. Appl. WO 02/096799A2, **2002**; b) J. Haberecht, PhD Thesis, TU Dresden, **2001**.
[12] R. M. Hagenmeyer, B. Friede, M. Jansen, *J. Non-Cryst. Solids* **1998**, *226*, 225.
[13] a) R. Lauterbach, W. Schnick, *Z. Anorg. Allg. Chem.* **1998**, *624*, 1154; b) W. Schnick, H. Huppertz, R. Lauterbach, *J. Mater. Chem.* **1999**, *9*, 289; c) K. Köllisch, W. Schnick, *Angew. Chem.* **1999**, *111*, 368; *Angew. Chem. Int. Ed.* **1999**, *38*, 357; d) R. Lauterbach, W. Schnick, *Z. Anorg. Allg. Chem.* **2000**, *626*, 56; e) E. Irran, K. Köllisch, S. Leoni, R. Nesper, P. F. Henry, M. T. Weller, W. Schnick, *Chem. Eur. J.* **2000**, *6*, 2714; f) R. Lauterbach, E. Irran, P. F. Henry, M. T. Weller, W. Schnick, *J. Mater. Chem.* **2000**, *10*, 1357; g) R. Lauterbach, W. Schnick, *Solid State Sci.* **2000**, *2*, 463; h) H. A. Höppe, G. Kotzyba, R. Pöttgen, W. Schnick, *J. Solid State Chem.* **2002**, *167*, 393.
[14] Crystal structure data of $SrSi_6N_8$: STOE IPDS, $Mo_{K\alpha}$ (71.073 pm), $2\theta_{max} = 65°$, crystal size $0.11\times0.09\times0.04$ mm^3, orthorhombic, space group *Imm*2 (no. 44), $a = 785.5(2)$, $b = 925.9(2)$, $c = 480.1(1)$ pm, $V = 0.3492(2)$ nm^3, $Z = 2$, $\rho_{calcd} = 3.507$ g cm^{-3}, $\mu Mo_{K\alpha} = 8.717$ mm^{-1}, 2242 measured reflections, 694 of which are independent, $R_{int} = 0.030$, least-squares refinement (all atoms anisotropic) on F^2 (G. M. Sheldrick, SHELXL-97, program for the refinement of crystal structures, Universität Göttingen, Göttingen (Deutschland), **1997**); semiempirical absorption correction (min./max. transmission factor 0.249/0.292), Flack parameter $\eta = 0.565(9)$, refined as an inversion twin, *R* values (all data/$F_o^2 \geq 2\sigma(F_o^2)$) $R_1 = 0.0239/0.0218$, $wR_2 = 0.0487/0.0482$, GooF = 0.978 for 657 observed reflections ($F_o^2 \geq 2\sigma(F_o^2)$) and 43 refined parameters. Further details on the crystal structure investigations may be obtained from the Fachinformationszentrum Karlsruhe, 76344 Eggenstein-Leopoldshafen, Germany (fax: (+49) 7247-808-666; e-mail: crysdata@fiz-karlsruhe.de), on quoting the depository number CSD-391265.
[15] S. G. Cho, O. K. Rim, G. Park, *J. Comput. Chem.* **1997**, *18*, 1523.
[16] Z. Shen, J. Grins, S. Esmaeilzadeh, H. Ehrenberg, *J. Mater. Chem.* **1999**, *9*, 1019.
[17] Crystal data of $BaSi_6N_8O$: space group *Imm*2 (no. 44), $a = 808.5(2)$, $b = 967.2(2)$, $c = 483.4(1)$ pm, $V = 0.378$ nm^3, $Z = 2$, F. Stadler, S. Schmid, W. Schnick, unpublished results.
[18] T. Sekine, M. Tansho, M. Kanzaki, *Appl. Phys. Lett.* **2001**, *78*, 3050.
[19] G. R. Hatfield, B. Li, W. B. Hammond, F. Reidinger, J. Yamanis, *J. Mater. Sci.* **1990**, *25*, 4032.
[20] J. S. Hartman, M. F. Richardson, B. L. Sherriff, B. G. Winsborrow, *J. Am. Chem. Soc.* **1987**, *109*, 6059.
[21] C. Schmolke, J. Senker, W. Schnick, unpublished results.
[22] S. Kohn, W. Hoffbauer, M. Jansen, R. Franke, S. Bender, *J. Non-Cryst. Solids* **1998**, *224*, 232.
[23] Double-quantum ^{29}Si solid-state NMR experiments with ^{29}Si-enriched samples (natural abundance of ^{29}Si is only 4.70%) confirm the obtained results: F. Stadler, J. Senker, W. Schnick, unpublished results.
[24] S. Hoffmann, T. F. Fässler, C. Hoch, C. Röhr, *Angew. Chem.* **2001**, *113*, 4527; *Angew. Chem. Int. Ed.* **2001**, *40*, 4398.
[25] P. Hohenberg, W. Kohn, *Phys. Rev. A* **1964**, *136*, 864.
[26] a) G. Kresse, J. Hafner, *Phys. Rev. B* **1993**, *47*, 558; b) G. Kresse, J. Hafner, *Phys. Rev. B* **1994**, *49*, 14251; c) G. Kresse, J. Furthmüller, *Comput. Mater. Sci.* **1996**, *6*, 15; d) G. Kresse, J. Furthmüller, *Phys. Rev. B* **1996**, *54*, 11169.
[27] a) P. E. Blöchl, *Phys. Rev. B* **1994**, *50*, 7953; b) G. Kresse, D. Joubert, *Phys. Rev. B* **1999**, *59*, 1758.
[28] a) A. D. Becke, K. E. Edgcombe, *J. Chem. Phys.* **1990**, *92*, 5397; b) A. Savin, A. D. Becke, J. Flad, R. Nesper, H. Preuß, H. G. von Schnering, *Angew. Chem.* **1991**, *103*, 421; *Angew. Chem. Int. Ed. Engl.* **1991**, *30*, 409.

Biomolecular Interactions

Direct Observation of Sugar–Protein, Sugar–Sugar, and Sugar–Water Complexes by Cold-Spray Ionization Time-of-Flight Mass Spectrometry**

Shin-Ichiro Nishimura, Noriko Nagahori, Kenji Takaya, Yuki Tachibana, Nobuaki Miura, and Kenji Monde*

The direct observation of noncovalent and specific intermolecular-recognition events such as enzyme–substrate, antigen–antibody, receptor–ligand, carbohydrate–protein, and carbohydrate–carbohydrate interactions is important for understanding the mechanisms behind these biological processes. Electrospray ionization mass spectrometry (ESI MS) is an important tool for investigations of the sensitivity, specificity, and speed of noncovalent complex formation.[1] The advantages of MS over traditional methods such as UV/Vis spectroscopy, fluorescence spectroscopy, surface plasmon resonance (SPR), isothermal titration microcalorimetry, NMR spectroscopy, and X ray crystallographic analysis include the accuracy of mass measurement, speed of analysis, and small sample quantities. However, the harsh conditions of the ionization process in MS are often detrimental to the survival of noncovalent and unstable biomolecular interactions such as those of sugar–protein, sugar–sugar, and sugar–water complexes. Recently, Yamaguchi and co-workers developed cold-spray ionization mass spectrometry (CSI MS), which allows facile and precise characterization of labile self-assembling nanostructures and unstable organometallic complexes in solution.[2] CSI MS may become one of the most promising and versatile tools for characterizing a variety of weak but specific biomolecular interactions, as the ionization at low temperature (−20 °C) allows direct observation of unstable large-scale aggregates of amino acids or nucleosides in organic solvents with magnetic-sector-equipped instruments.[2d,e] It was suggested that a cooled ion spray promotes stable solvation–ionization processes through increased compound polarizability caused by higher dielectric constants at low temperature. Moreover, CSI MS combined with an orthogonal acceleration time-of-flight (oa-TOF) mass analyzer extends the applicability of this method to the characterization of dynamic interactions of biomacromolecules. This is possible through a number of attractive features of TOF MS analyzers, such as their theoretically unlimited mass range, very high spectrum acquisition rates, high ion transmission, high sensitivity, multiplex detection capacity, reasonable mass resolution, and simplicity in instrument design. Our interest is focused on the potential of CSI-TOF MS, with particular respect to specific and weak biomolecular interactions in water at low temperature. Herein we report the feasibility of the CSI-TOF MS method to monitor directly the formation of noncovalent protein–carbohydrate, carbohydrate–carbohydrate, and carbohydrate–water complexes in aqueous solution at 4 °C.

Figure 1a shows the effect of temperature on complex formation between hen egg lysozyme and the chitooligosaccharide, chitotetraose. As anticipated, the intensity of the signal that corresponds to the lysozyme–chitotetraose complex as the major hydrolytic product was gradually enhanced by lowering the ion spray temperature of the reaction mixture from 200 to 4 °C. As shown in Figure 1b, CSI-TOF MS is quite an efficient and simple method for the determination of dissociation constants of protein–ligand interactions, as it does not require the use of molecular probes. Indeed, the dissociation constant K_d of lysozyme with chitotetraose was determined to be 1.6×10^{-5} M, which is in good agreement with data reported previously.[3] Furthermore, CSI-TOF MS can be used to search for a compound that shows the highest affinity for the target protein in a mixture of several oligosaccharides by making a simple "snapshot assay".[4] As illustrated in Figure 2a, lysozyme interacted selectively with chitooligosaccharides $(GlcNAc)_3$, $(GlcNAc)_4$, and $(GlcNAc)_5$ at 4 °C in a compound library containing 23 different oligosaccharide types. Such valuable information could not be obtained by common ESI-TOF MS techniques carried out at 200 °C as shown in Figure 2b. Moreover, when a compound library void of chitooligosaccharides was assayed at 4 °C, lysozyme showed significant affinity toward the maltooligosaccharides $(D\text{-glucose})_{3-7}$ and γ-cyclodextrin. These interactions cannot be detected by general spectroscopic analyses such as UV/Vis, fluorometric, and SPR methods.[5] Figure 3a shows binding between lysozyme and maltotriose $((Glc)_3)$ (m/z 1646.3 $[M+9A]^{9+}$ and m/z 1851.9 $[M+8A]^{8+}$; 'A' = ion adduct). Although the interaction is weak and is considered nonspecific,[5] the CSI-TOF MS data instead indicate specific binding. The results of a competition experiment (Figure 3a and b) suggest that maltotriose binding involves the same lysozyme cavity as for the chitotriose $(GlcNAc)_3$. This is supported by computer-assisted docking simulations carried out in our laboratory (Figure 3c). Notably, CSI-TOF MS can be employed to search for unexpected ligand candidates with "specific and low affinity" for a target protein. Identified ligands could then be applied as scaffold molecules for the design of new drugs (inhibitors) with high potential for success.

[*] Prof. S.-I. Nishimura, Dr. N. Nagahori, K. Takaya, Dr. Y. Tachibana, Dr. N. Miura, Dr. K. Monde
Division of Biological Sciences, Graduate School of Science
Frontier Research Center for Post-Genome Science and Technology
Hokkaido University
N21, W11, Sapporo 001-0021 (Japan)
Fax: (+81) 11-706-9042
E-mail: shin@glyco.sci.hokudai.ac.jp

[**] This work was supported in part by a grant from the National Project on Functional Glycoconjugate Research Aimed at Developing for New Industry by the Ministry of Education, Science, and Culture of Japan. A portion of this study was presented at the 84th Annual Meeting of the Chemical Society of Japan on March 29, 2004 in Nishinomiya, Japan. We acknowledge Prof. K. Yamaguchi of Tokushima Bunri University for valuable suggestions and comments on CSI mass spectrometry.

Supporting information for this article is available on the WWW under http://www.angewandte.org or from the author.

 DOI: 10.1002/anie.200461867 © 2005 Wiley-VCH Verlag GmbH & Co. KGaA, Weinheim

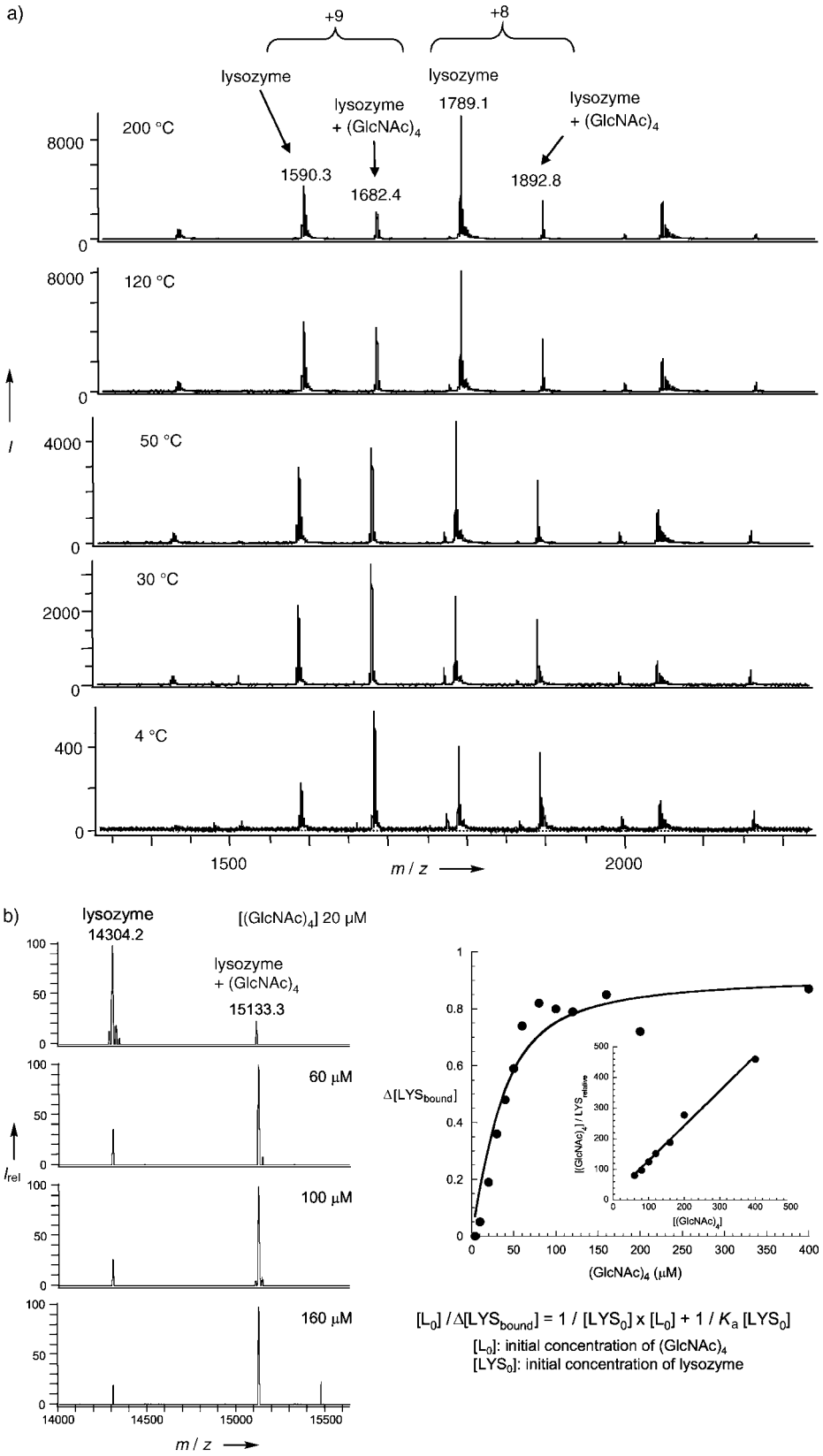


Figure 1. Interaction of hen egg lysozyme with chitooligosaccharides. a) Temperature dependence of signal intensities of the lysozyme–chitotetraose ($(GlcNAc)_4$) complex in ESI (CSI) MS. Spray temperatures are indicated. [Lysozyme] = 35 µM, $[(GlcNAc)_4]$ = 200 µM. b) The binding of lysozyme with $(GlcNAc)_4$ at 4 °C. [Lysozyme] = 35 µM; the $(GlcNAc)_4$ concentrations are indicated. The peak intensities from mass spectra were used to determine the relative amount of bound lysozyme as a function of $[(GlcNAc)_4]$, and a sample K_d determination is shown at the bottom. GlcNAc = *N*-acetyl-D-glucosamine.

 © 2005 Wiley-VCH Verlag GmbH & Co. KGaA, Weinheim

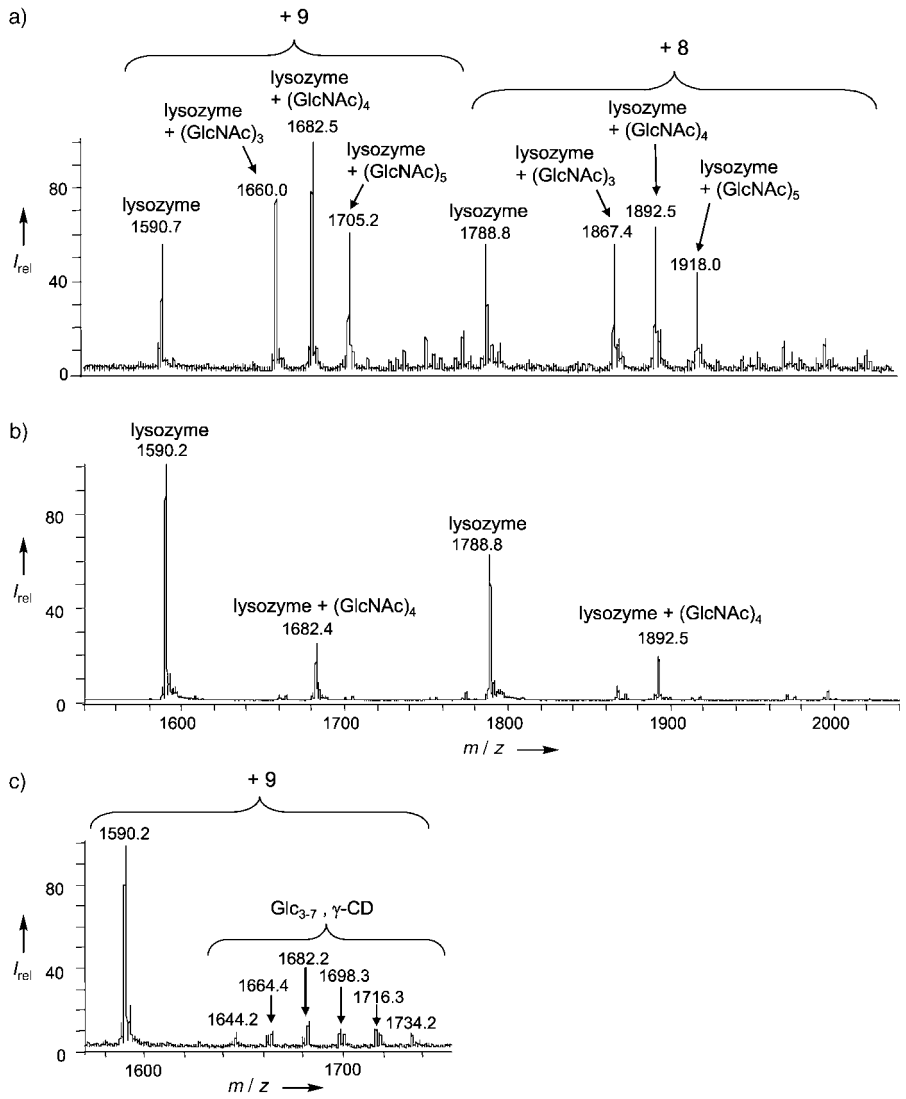


Figure 2. Oligosaccharide–protein complex screening. The interaction of lysozyme with an oligosaccharide library containing GlcNAc, $(GlcNAc)_2$, $(GlcNAc)_3$, $(GlcNAc)_4$, $(GlcNAc)_5$, Glc, $(Glc)_3$, $(Glc)_4$, $(Glc)_5$, $(Glc)_6$, $(Glc)_7$, cellobiose (β-Glc-[1→4]-Glc), lactose (β-Gal-1[→4]-Glc), methyl α-mannoside, $(Man)_5$, D-glucosamine, L-arabinose, lactose, xylose, L-gluconolactone, α-CD, β-CD, and γ-CD (all at 35 μM) was monitored by a) CSI-TOF MS at 4 °C and b) ESI-TOF MS at 200 °C. c) CSI-TOF MS analysis (4 °C) of lysozyme with an oligosaccharide library lacking chitooligosaccharides $(GlcNAc)_2$, $(GlcNAc)_3$, $(GlcNAc)_4$, and $(GlcNAc)_5$. [Lysozyme] = 35 μM. Glc = D-glucose; Gal = D-galactose; Man = D-mannose; CD = cyclodextrin.

Our attention was next directed toward monitoring the weak but specific noncovalent interactions of glycoconjugates in nature. Carbohydrate–carbohydrate interactions may be crucial to intercellular interactions that lead to cellular differentiation, growth, and malignancy. Lewis^X trisaccharide (Le^X) has been reported to self-assemble through carbohydrate–carbohydrate interactions in the presence of Ca^{2+} ions.[6] As shown in Figure 4, CSI-TOF MS spectra measured at 4 °C clearly demonstrate that Le^X trisaccharides preferentially dimerize by binding to Ca^{2+} ions, and that in the absence of Ca^{2+}, Le^X trisaccharides form a range of larger aggregates of up to 10 trisaccharide units (*m*/*z* 2670.0 $[10\,Le^X + 2\,Na]^{2+}$) (Figure 4b). Several ion peaks shown in Figure 4a are evidence for the preferential Le^X–Ca^{2+} complex formation such as $[Le^X + Ca - H]^+$, $[Le^X + Ca - H + H_2O]^+$, and $[Le^X + CaCl]^+$. The ion peaks of $[2\,Le^X + Ca]^{2+}$, $[2\,Le^X + 2\,Ca - 2\,H + 2\,H_2O]^{2+}$, and $[2\,Le^X + 2\,CaCl]^{2+}$ provide valuable information that reveals the mechanism of Le^X–Le^X dimerization in the presence of Ca^{2+} ions.

Surprisingly, it also appears that the minimal active structure of the antifreeze glycopeptide (*sy*$AFGP_3$)[7] forms specific complexes with three water molecules as shown in Figure 5, whereas the inactive monomeric AFGP (*sy*$AFGP_1$) produced neither the complex with water nor the self-aggregation behavior found with the Le^X trisaccharide. Hydration of *sy*$AFGP_3$ at 4 °C (*m*/*z* 949.4 $[M + 3\,H_2O + 2\,H]^{2+}$, *m*/*z* 960.4 $[M + 3\,H_2O + H + Na]^{2+}$, and *m*/*z* 968.4 $[M + 3\,H_2O + H + K]^{2+}$) by CSI-TOF MS may become an important way to investigate AFGP binding with the ice (water) lattice, and hence the mechanism of its antifreeze

 © 2005 Wiley-VCH Verlag GmbH & Co. KGaA, Weinheim

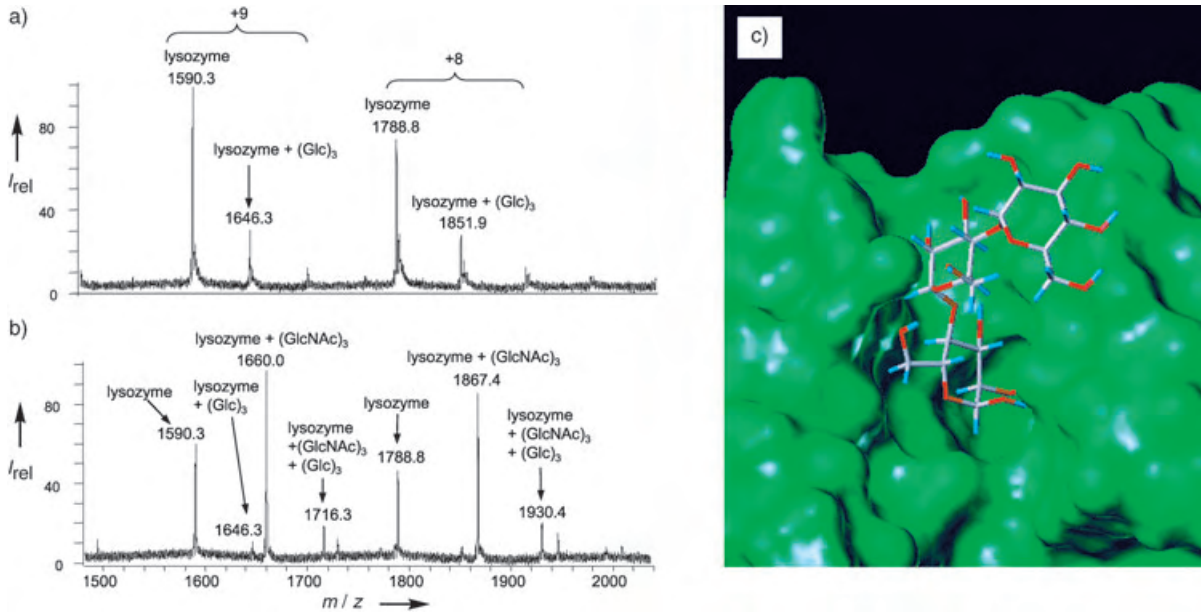


Figure 3. CSI-TOF MS (4 °C) evaluation and computer simulation of "nonspecific" interactions. a) The interaction between lysozyme (35 μM) and $(Glc)_3$ (100 μM). b) Competitive assay between lysozyme (35 μM) and $(GlcNAc)_3$ (100 μM). (c) Docking simulation of maltotriose ($(Glc)_3$) with the subsite of lysozyme calculated with the SYBYL FlexX module.[8]

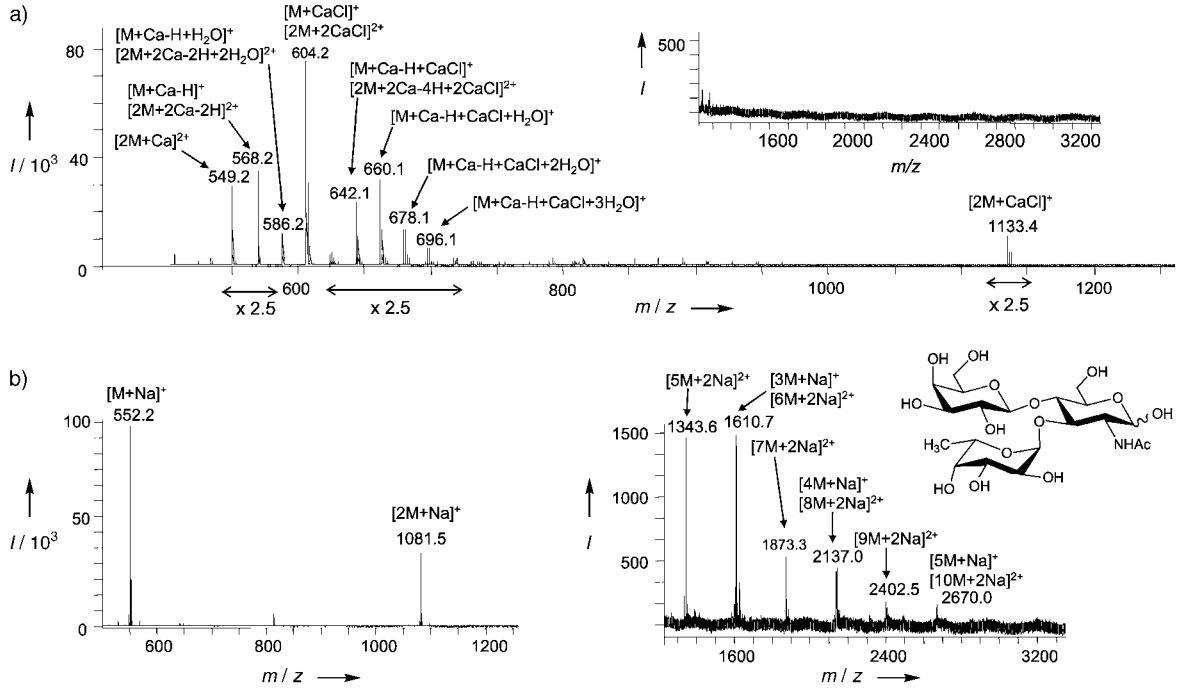


Figure 4. CSI-TOF mass spectra of Le^X self-assembly at 4 °C a) in the presence and b) in the absence of Ca^{2+}. The experiments were performed by injecting 20 μL $Le^X/CaCl_2$ stock solution ($[Le^X] = 190$ μM (3.8 nmol Le^X) and $[CaCl_2] = 1.0$ mM). Le^X = Lewis^X trisaccharide, with structure shown.

activity.[9] As illustrated in Figure 5c, when fully deuterated *sy*AFGP$_3$ with D_2O as solvent were observed, an analogous spectrum with the "water signals" shifted by 20 Da instead of 18 Da was obtained. This is evidence that the binding of three water molecules is favored over the binding of just one or two.

In conclusion, we found that CSI-TOF MS is a highly sensitive and reliable method for analyzing specific non-covalent complexes of glycoconjugates under nondisruptive conditions. The results reported herein demonstrate the ability and versatility of CSI-TOF MS as a means of direct observation and characterization of weak and specific carbohydrate-related interactions in aqueous solution at low temperature. The merits of this novel technique are evident as it will provide not only fundamental insight into the

 © 2005 Wiley-VCH Verlag GmbH & Co. KGaA, Weinheim

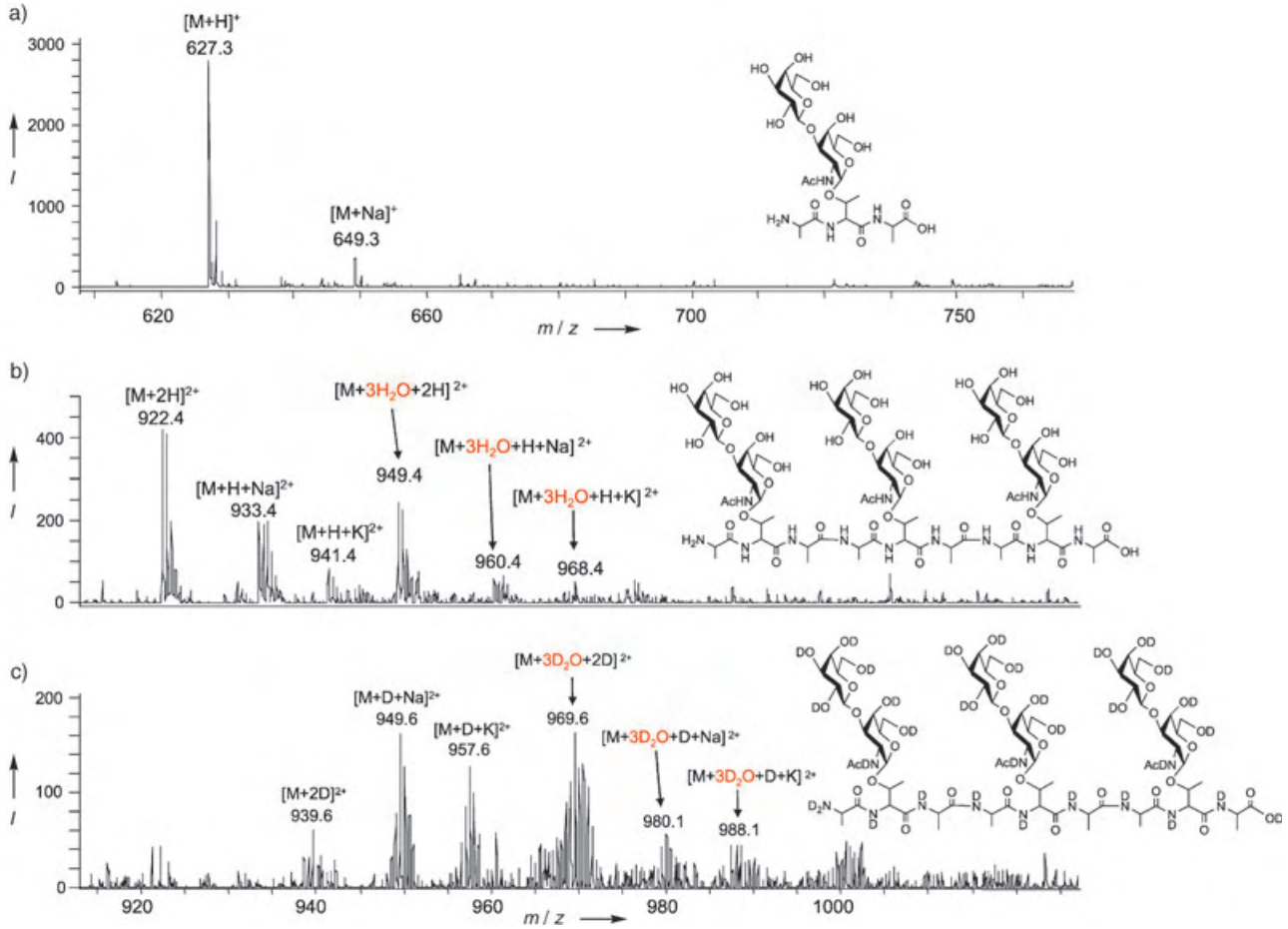


Figure 5. Direct observation of the specific interaction between *sy*AFGP$_3$ and water (D_2O) at 4 °C. CSI-TOF MS of a) monomeric AFGP (*sy*AFGP$_1$) and b) trimeric AFGP (*sy*AFGP$_3$) in water, and c) *sy*AFGP$_3$ in D_2O. AFGP injection volumes (20 μL) contained 320 pmol AFGP. [AFGP] = 16 μM.

mechanisms of biomolecular recognition, but also valuable information for high-throughput molecular screening for bioactive compounds.

Received: September 2, 2004
Revised: October 23, 2004
Published online: December 13, 2004

Keywords: aggregation · carbohydrates · enzymes · glycoproteins · mass spectrometry

[1] a) J. B. Fenn, *Angew. Chem.* **2003**, *115*, 3999 – 4024; *Angew. Chem. Int. Ed.* **2003**, *42*, 3871 – 3894; b) J. B. Fenn, M. Mann, K. Meng, S. F. Wong, C. M. Whitehouse, *Science* **1989**, *246*, 64 – 70; c) B. Ganem, Y. T. Li, J. D. Henion, *J. Am. Chem. Soc.* **1991**, *113*, 6294 – 6296; d) V. Katta, B. T. Chait, *J. Am. Chem. Soc.* **1991**, *113*, 8534 – 8535; e) M. Baca, S. B. H. Kent, *J. Am. Chem. Soc.* **1992**, *114*, 3992 – 3993; f) P. Kebarle, L. Tang, *Anal. Chem.* **1993**, *65*, 972A – 986A.

[2] a) S. Sakamoto, M. Fujita, K. Kim, K. Yamaguchi, *Tetrahedron* **2000**, *56*, 955 – 964; b) Y. Yamanoi, Y. Sakamoto, T. Kusukawa, M. Fujita, S. Sakamoto, K. Yamaguchi, *J. Am. Chem. Soc.* **2001**, *123*, 980 – 981; c) S. Sakamoto, T. Imamoto, K. Yamaguchi, *Org. Lett.* **2001**, *3*, 1793 – 1795; d) M. Kunimura, S. Sakamoto, K. Yamaguchi, *Org. Lett.* **2002**, *4*, 347 – 350; e) S. Sakamoto, K. Nakatani, I. Saito, K. Yamaguchi, *Chem. Commun.* **2003**, 788 – 789; f) S. Sakamoto, K. Yamaguchi, *Angew. Chem.* **2003**, *115*, 933 – 936; *Angew. Chem. Int. Ed.* **2003**, *42*, 905 – 908; g) K. Yamaguchi, *J. Mass Spectrom.* **2003**, *38*, 473 – 490.

[3] For more information regarding K_d for the interaction between lysozyme and chitotetraose ($K_d = 5.6 \times 10^{-6}$ M), see: M. Schindler, Y. Assaf, N. Sharon, D. M. Chipman, *Biochemistry* **1977**, *16*, 423 – 431.

[4] An ESI MS based diffusion measurement can also be used to screen for noncovalent complexes of lysozyme and maltotriose: S. M. Clark, L. Konermann, *Anal. Chem.* **2004**, *76*, 1257 – 1263.

[5] Excellent methods and applications of nanoelectrospray fourier transform ion cyclotron resonance (FT-ICR) mass spectrometry have recently been reported: a) W. Wang, E. N. Kitova, J. S. Klassen, *Anal. Chem.* **2003**, *75*, 4945 – 4955; b) R. Daneshfar, E. N. Kitova, J. S. Klassen, *J. Am. Chem. Soc.* **2004**, *126*, 4786 – 4787.

[6] a) I. Eggens, B. Fenderson, T. Toyokuni, B. Dean, M. Stroud, S. Hakomori, *J. Biol. Chem.* **1989**, *264*, 9476 – 9484; b) G. Siuzdak, Y. Ichikawa, T. J. Caulfield, B. Munoz, C.-H. Wong, K. C. Nicolaou, *J. Am. Chem. Soc.* **1993**, *115*, 2877 – 2881.

[7] Y. Tachibana, G. L. Fletcher, N. Fujitani, S. Tsuda, K. Monde, S.-I. Nishimura, *Angew. Chem.* **2004**, *116*, 874 – 880; *Angew. Chem. Int. Ed.* **2004**, *43*, 856 – 862.

[8] T. Ohta, N. Miura, N. Fujitani, F. Nakajima, K. Niikura, R. Sadamoto, C.-T. Guo, T. Suzuki, Y. Suzuki, K. Monde, S.-I. Nishimura, *Angew. Chem.* **2003**, *115*, 5344 – 5347; *Angew. Chem. Int. Ed.* **2003**, *42*, 5186 – 5189.

[9] M. Matsumoto, S. Saito, I. Ohmine, *Nature* **2002**, *416*, 409 – 413.

 © 2005 Wiley-VCH Verlag GmbH & Co. KGaA, Weinheim

Nanomaterials

Cerium Phosphate Nanotubes: Synthesis, Valence State, and Optical Properties**

Chengchun Tang, Yoshio Bando, Dmitri Golberg, and Renzhi Ma*

Metal phosphates are widely utilized in nonlinear optical materials, phosphors, sensors, heat-resistant, and biocompatible materials. A particular emphasis has been placed on the study of rare-earth or rare-earth-doped phosphate materials for applications in photonic devices.[1] This interest is primarily attributed to the position of the 4f electrons, which are well shielded from the effects of the neighboring ions. Such shielding leads to discrete and well-defined energy level schemes, as well as to rather weak coupling between the electronic and vibrational wave functions. The specific luminescence with a characteristic long lifetime originates from the f–f emissions. However, at present, the progress with regard to new luminescent materials is chiefly focussed on short emission wavelengths, which are useful for imaging, lithography, and optical data recording.[2] The rare-earth ions Ce^{3+} and Sm^{2+} exhibit a 5d–4f emission with a larger absorption in the UV region and a shorter luminescence lifetime due to allowed electric dipole transitions; thus, they display excellent properties for applications in these fields.[3] On the other hand, although the doping of transparent Ce^{4+} ions in luminescence materials has been prohibited due to the competitive absorption in UV region, some Ce^{3+}/Ce^{4+} hybrid systems in glass hosts exhibit a strong blue emission, which possibly results from electron transfer from a donor level to the neighboring Ce^{4+} ions, consequently forming excited states of Ce^{3+} ions.[4] Taking into account the strong UV absorption of Ce^{4+} ions, such hybrid structures are good candidates for materials that display blue emission with high absorption and fast emissive rates.[5]

One-dimensional nanomaterials, that is, nanotubes made of, for example, C, BN, WS_2, VO_x, TiO_2, and InP[6] have been synthesized and display novel properties that are frequently different from those of the bulk forms. However, the synthesis and emission behaviour of nanotube-like hybrid materials containing Ce^{4+}/Ce^{3+} ions has received much less attention.

Herein, we report on a reproducible and controllable route for the production of cerium phosphate nanotubes, the first rare-earth phosphate nanotubes. Tetravalent cerium phosphate (CeP, $Ce(HPO_4)_2{\cdot}nH_2O$) nanotubes were first synthesized after improving the traditional synthetic route toward a CeP fiber.[7] Subsequent annealing of the as-synthesized nanotubes led to a mixture of valence states, and the desired Ce^{3+}/Ce^{4+} hybrid phosphate nanotubes were obtained for the first time. The nanotubes display novel optical properties; that is, the Ce^{4+} ions effectively absorb the UV light, whereas the Ce^{3+} ions exhibit strong emission in the blue region of a photoluminescence spectrum.

It has been reported that a high PO_4/Ce ratio (20:1–120:1) in the initial solution and a high reaction temperature (up to 95 °C) are needed to form a CeP fiber.[7,8] In this study, we have increased the PO_4/Ce ratio to 300:1 and increased the reaction temperature to above 95 °C. Figures 1 a–d show the scanning electron microscope (SEM) images of a CeP material synthesized at 70, 90, and 105 °C, respectively. A fibrous structure can be found for all the samples examined, although an amorphous phase may exist in a lower temperature product (ca. 50–80 °C), and some microcrystalline particles are visible in a higher temperature product (> 95 °C). X-ray diffraction (XRD) measurements indicate that the CeP material displays different crystalline structures, depending on the reaction temperature (Figure 1 e). The XRD patterns of a CeP sample synthesized at temperatures lower than 70 °C show broad peaks and a peak at about 7.8°

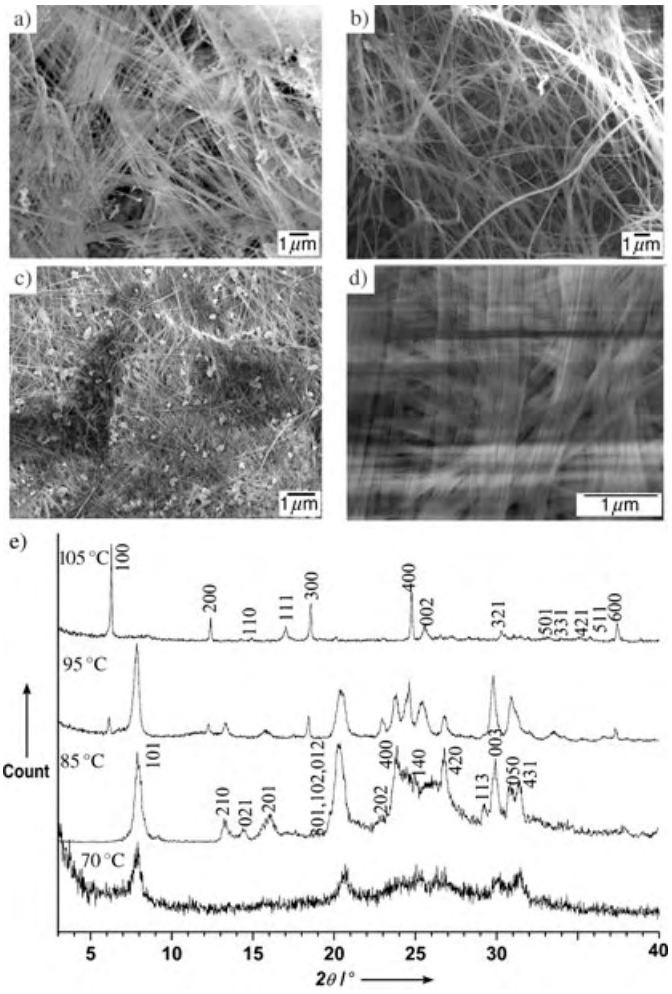


Figure 1. SEM images of a CeP nanomaterial synthesized at 70 (a), 90 (b), and 105 °C (c, d). e) The representative XRD patterns recorded for the products synthesized at different temperatures.

[*] Dr. C. Tang, Prof. Y. Bando, Dr. D. Golberg, Dr. R. Ma
Advanced Materials Laboratory
National Institute for Materials Science (NIMS)
1-1 Namiki, Tsukuba, Ibaraki 305-0044 (Japan)
Fax: (+81) 29-851-6280
E-mail: tang.chengchun@nims.go.jp

[**] We thank Y. Uemura and R. Xie for their help in the measurement of the absorption spectra.

 © 2005 Wiley-VCH Verlag GmbH & Co. KGaA, Weinheim DOI: 10.1002/anie.200461171

(2θ), $d = 1.12$ nm, indicating a layered structure. Thermogravimetric analyses indicate that the water content in CeP varies from $n = \approx 2$ to ≈ 3, depending on the temperature at which the synthesis was carried out. The comparison of the d spacing and the relative intensities measured for the XRD patterns with those of a CeP ($Ce(HPO_4)_2 \cdot H_2O$) fiber,[8] reveal a fairly good agreement, except for a slightly expanded layer-to-layer distance ($d = 1.10$ nm, the difference may result from the variations in the water content in CeP). Though the detailed crystal structure is still unknown, the present pattern can be readily indexed to an orthorhombic structure ($a = 1.494$, $b = 1.436$, $c = 0.906$ nm). On increasing the temperature, the CeP nanomaterial gradually changes its morphology (Figure 1). An XRD pattern of CeP synthesized at 105 °C can be indexed to a hexagonal structure with the lattice parameters ($a = 1.668$, $c = 0.678$ nm). Thermogravimetric analysis suggested that the formula of the novel phase was $Ce(HPO_4)_2 \cdot H_2O$. The two phases coexist from 90 to 100 °C, but the orthorhombic phase is rarely observed when the synthesis temperature is higher than 100 °C.

An important consequence of the temperature-dependent transformation is the appearance of a nanotube-like morphology. The CeP material synthesized below 90 °C usually comprises solid fibers with diameters ranging from several tens of nanometers up to about 500 nm (Figure 1a and b). However, the diameters of the nanofibers of the CeP material synthesized at 105 °C are smaller and more unified in size (20 to 100 nm; see the transmission electron microscope (TEM) image in Figure 2a). The nanotubes become the dominant morphology, though some nanofibers with a diameter of several tens of nanometers can be occasionally observed. Figure 2b shows the magnified image of an individual nanotube. The nanotubes are usually open at their tips. The tubular morphology was verified by tilting the sample in the transmission electron microscope, while recording the corresponding selected-area electron diffraction (SAED) pattern (inset, Figure 2b). The pattern recorded along the [110] zone axis clearly exhibits the "zigzag"-type chirality of a tubular shell.[9] Although the CeP nanotubes were unstable under irradiation with an electron beam, we were able to obtain high-resolution TEM images that confirmed the nanotube-like morphology (Figure 2c).

X-ray photoelectron spectroscopy (XPS) can usually provide clear information about the valence state of Ce; however, in this study it was not applied because minor amorphous and/or microcrystal impurities exist in the products. Therefore, the chemical valence of the cerium ions within an individual CeP nanotube was determined by using a parallel electron energy loss spectrometer (EELS), taking into consideration that the occupancy of the 4f shell of light lanthanides is sensitive to the ratio of the $3d_{3/2} \rightarrow 4f_{5/2}$ (M_4) to $3d_{5/2} \rightarrow 4f_{7/2}$ (M_5) peak areas.[10] The EEL spectrum of the CeP nanotubes (Figure 2d) contains the features consistent with the multiplet structure of the $3d^9 4f^2$ final states (M_5 at ca. 884 eV and M_4 at ca. 901 eV).[11] The extra peaks, about 7 eV higher in energy than the M_4 and M_5 lines, respectively, are clearly detected, indicating the existence of Ce^{4+}.[12] The fitted M_4/M_5 ratio for the EEL spectrum is about 1.20:1; thus, in accord with the reference M_4/M_5 values of 0.78:1 for trivalent cerium orthophosphate and 1.1:1 for CeO_2,[10] the Ce^{4+} states should be present, although there has been much debate concerning the existence of pure Ce^{4+}.

The temperature-dependent stability of Ce valences in CeP nanotubes was analyzed by using a temperature-controlled annealing procedure under a reduced atmosphere. Such an atmosphere can maintain the one-dimensional morphology up to about 900 °C (Figure 3a), although the formation of glass-phase particles is visible in the SEM images (dark contrast areas within the fibers). The TEM images indicate that no nanotubes were present in the sample heat-treated at 900 °C. The initial nanotubes are thus completely transformed into solid fibers. Figure 3b displays a high-resolution TEM image of a polycrystalline nanowire with diameters similar to those of the starting nanotubes. However,

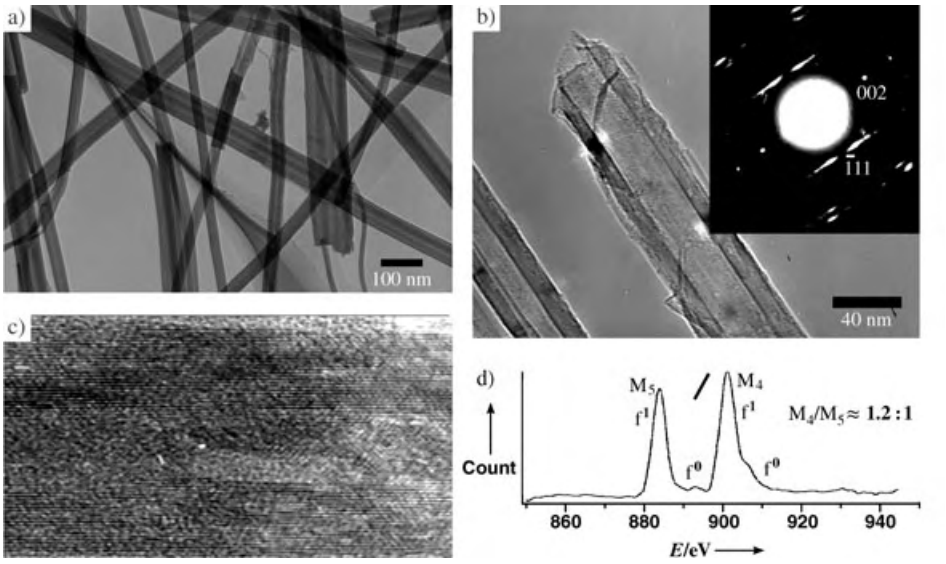


Figure 2. CeP nanotubes synthesized at 105 °C: a) Low-magnification TEM image revealing a tube-like morphology; b) TEM image of a nanotube and its corresponding SAED pattern; c) high-resolution TEM image of a nanotube with a diameter of about 20 nm; d) EEL spectrum displaying the characteristics for a tetravalent cerium ion.

 © 2005 Wiley-VCH Verlag GmbH & Co. KGaA, Weinheim

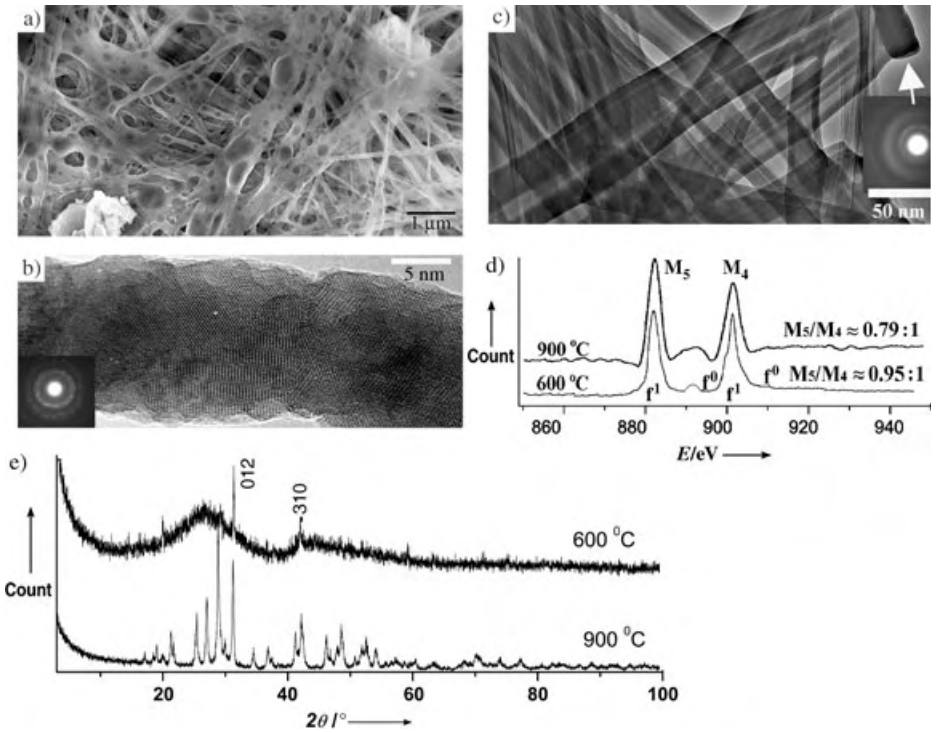


Figure 3. a) SEM image of CeP nanowires synthesized by annealing CeP nanotubes at 900 °C, b) the corresponding high-resolution TEM image; the inset in b) is the SAED pattern recorded for an individual nanowire; c) TEM image of CeP nanotubes annealed at 600 °C; d) EEL spectra, and e) XRD patterns for the annealed samples.

the nanotubes represent a dominant morphology in the CeP products prepared at a relatively low temperature. The CeP nanotubes post-treated at 600 °C are shown in Figure 3c; the SAED pattern taken from the arrowed tip area clearly indicates a glass-like structure at the tip (inset).

The EEL spectra recorded for an individual nanotube (600 °C) and a nanowire (900 °C) are shown in Figure 3d. The measured M_4/M_5 ratio decreases from about 0.95:1 (600 °C) to about 0.79:1 (900 °C). Given that the ratio of about 0.79:1 is in a good agreement with the previously reported value for cerium(III) orthophosphate,[10] we assume that the CeP material produced during the heat treatment at 900 °C mainly contains trivalent cerium. By assuming a linear interpolation between the M_4/M_5 values for Ce^{4+} (1.20:1) and Ce^{3+} (0.79:1), a nominal valence of +3.34 was calculated for the cerium in CeP heated at 600 °C.

The XRD pattern recorded for CeP nanowires (Figure 3e) can be indexed to a monoclinic structure for which the peak positions and intensities are similar to those of trivalent monazite $CePO_4$ (JCPDS 32-0199). Analysis of the patterns obtained from CeP nanotubes post-treated at 600 °C seems to indicate that the trivalent phase is also present here, but there are only traces of it in an amorphous matrix.

Figure 4a displays the UV/Vis spectra of the CeP nanotubes and their post-treated products. Tetravalent CeP nanotubes that have not been heat-treated can absorb UV light, almost completely, with the cutoff wavelength of about 450 nm. The cutoff wavelength shifts to about 420 nm, when the CeP nanotubes are treated at 300 °C. The nonlinear spectrum with an absorption extension of 300–450 nm is caused by the Ce^{4+} ions, since their d-electron exited states exhibit strong electron–phonon coupling.[13] It is noteworthy that the absorption peaks attributed to the f–d electron transitions of Ce^{3+} (200–320 nm), can be observed in the samples heat-treated at a temperature higher than 300 °C. The absorption spectrum of a sample annealed at 600 °C consists of two overlapping patterns originating from Ce^{4+} bands (cutoff wavelength ca. 420 nm) and Ce^{3+} lines (visible absorptions at 210 and 235 nm). The absorption spectrum of CeP nanowires produced by heat treatment at 900 °C contains the characteristic peaks of Ce^{3+} with maxima at 208, 216, 227, 261, and 275 nm within an f–d transition absorption band. These peaks correspond to the theoretical values (203–276 nm) of Ce^{3+} f–d transitions from a $4f^1$ ground state to the five $5d^1$ levels split within a monoclinic crystal field.[14] The absorption characteristics are in good agreement with the mixed-valence state mentioned above.

Figure 4b displays the photoluminescence (PL) spectra. No luminescence was

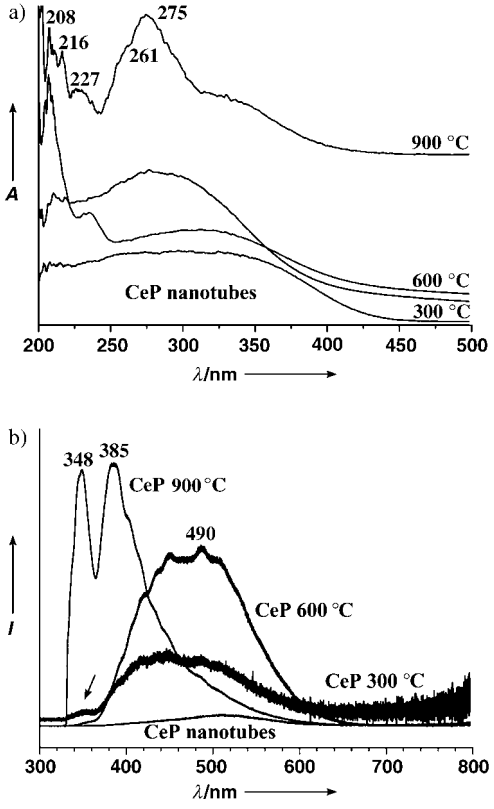


Figure 4. Absorption (a) and photoluminescence (b) spectra of CeP nanotubes and their products post-heat-treated at 300, 600, and 900 °C.

 © 2005 Wiley-VCH Verlag GmbH & Co. KGaA, Weinheim

observed for the as-synthesized CeP nanotubes due to the absence of Ce^{3+}. The pure trivalent CeP nanowires exhibit strong UV luminescence; the two sharp peaks are centered at about 348 nm and about 385 nm with a full-width at half maximum (FWHM) of about 12 nm and about 30 nm, respectively. The double-peak luminescence corresponds to the direct emission from the $^2D(5d^1)$ state to the two split $4f^1$ ground states of $^2F_{5/2}$ and $^2F_{7/2}$ caused by spin-orbit coupling. The small FWHM values also imply that the exited state of Ce^{3+} is scarcely affected by the charge transfer transitions from the host ligands. In contrast to pure Ce^{3+} nanowires and Ce^{4+} nanotubes, the PL spectra of the Ce^{3+}/Ce^{4+} hybrid CeP nanotubes exhibit a strong blue luminescence. A broad and prominent blue emission at about 490 nm is visible for the $Ce^{+3.34}P$ nanotubes (heated at 600 °C; Figure 4b). Such a broad, blue emission for Ce^{3+} ions has been observed and attributed to a charge transfer.[4,15] The charge transfer between Ce^{4+} electron donation centers and Ce^{3+} luminescence centers in the present nanotubes may occur due to the electron–photon interaction. It has been reported that the 4f–5d bands of Ce^{3+} and the charge-transfer transition bands of Ce^{4+} ions appear in the same wavelength range and overlap.[16] Therefore, Ce^{4+} bands form the exited state and cause the blue emission. We also noticed that the intensity of the blue emission depends on the concentration of Ce^{3+} in a Ce^{4+} phosphate host. The hybrid CeP nanotubes heat-treated at 300 °C exhibit a weak blue emission. The direct emission of Ce^{3+} ions can be observed as an additional broad peak between 330 and 380 nm (see arrow in Figure 4b).

In summary, the first rare-earth metal phosphate nanotubes made of CeP have been synthesized by careful control of the composition of the reactants and the reaction temperature. Under post-heat treatments in a reduced atmosphere, the tubular morphology was maintained up to about 900 °C. Further increase in the temperature results in the formation of nanowires, and leads to valence change from +4 to +3 for the cerium ion. Strong blue and UV luminescence was observed for the Ce^{3+}/Ce^{4+} hybrid nanotubes and pure Ce^{3+} nanowires, respectively. Taking into account the short emission lifetime (a few ns) of Ce^{3+}, CeP one-dimensional nanostructures and, in particular, valence-hybrid nanotubes developed in the present work are promising candidates for light-emission-diode lamps, electroluminescence devices, non-mercury-fluorescent lamps, and plasma display panels.

Experimental Section

CeP nanotubes were prepared according to the procedure reported by Alberti et al,[7,8] though a higher reaction temperature range and reactant PO_4/Ce concentration ratio were used in the present work. The apparatus utilized was similar to that employed by Ali et al[17] to prepare phosphate salts. In our experiments, a 6 M aqueous phosphoric acid solution was first heated to a temperature ranging from 50 to 110 °C, and stirred for 4 h to form a condensed linear polyphosphate $(P_nO_{3n+1})^{(n+2)-}$. A 0.02 M aqueous solution of diammonium cerium(IV) nitrate was added dropwise to the phosphoric acid solution (care was taken during the addition to keep the temperature fluctuations to less than 2 °C), and the mixture was allowed to react for 2 h. After washing with water, a flexible, cellulose paperlike material was obtained, suggesting a fibrous morphology.

CeP nanotubes can be synthesized at 105 °C. Although we have not fully clarified the growth mechanism, we believe that the appearance of nanotubes is related to the morphology of the initial condensed linear polyphosphate at the different temperatures. The as-synthesized CeP nanotubes were further heated in a flowing mixture of argon and ammonia (volume ratio of 20:1). A heating rate of 50 $K\,h^{-1}$ was used to allow a smooth structure modification.

The products were analyzed by using an X-ray diffractometer with $Cu_{K\alpha}$ radiation, a differential thermal and thermogravimetric apparatus, a UV/Vis spectrometer, a photoluminescence spectrometer (He-Cd laser, $\lambda_{exc} = 325$ nm), a scanning electron microscope, and a transmission electron microscope (TEM, JEOL 3000F). A Gatan DigiPEELS 766 parallel detection spectrometer attached to the latter microscope was used to collect electron energy loss spectra from an individual nanotube.

Received: July 3, 2004
Published online: December 21, 2004

Keywords: hybrid materials · luminescence · nanostructures · nanotubes · scanning probe microscopy

[1] M. Z. Yates, K. C. Ott, E. R. Birnbaum, T. M. McCleskey, *Angew. Chem.* **2002**, *114*, 494–496; *Angew. Chem. Int. Ed.* **2002**, *41*, 476–478.
[2] a) K. Riwotzki, H. Meyssamy, H. Schnablegger, A. Kornowski, H. Markus, *Angew. Chem.* **2001**, *113*, 574–578; *Angew. Chem. Int. Ed.* **2001**, *40*, 573–576; b) M. Nikl, E. Mihokova, Z. Malkova, A. Vedda, M. Martini, K. Shimmamura, T. Sukuda, *Phys. Rev. B* **2002**, *66*, 184101; c) P. Schlotter, R. Schmidt, J. Schneider, *Appl. Phys. A* **1997**, *64*, 417–418.
[3] R. Francini, U. M. Grassano, L. Landi, A. Scacco, M. D. Elena, M. Nikl, N. Cechova, N. Zema, *Phys. Rev. B* **1997**, *56*, 15109–15114.
[4] a) K. Annapurna, R. N. Dwivedi, P. Kundu, S. Buddhudu, *Mater. Lett.* **2004**, *58*, 7–789; b) Y. X. Pan, M. M. Wu, Q. Su, *Mater. Sci. Eng. B* **2004**, *106*, 251–256.
[5] T. Masui, M. Yamamoto, T. Sakata, H. Mori, G. Adachi, *J. Mater. Chem.* **2000**, *10*, 353–357.
[6] a) S. Iijima, *Nature* **1991**, *354*, 56–58; b) N. G. Chopra, R. J. Cherrey, V. H. Crespi, M. L. Cohen, S. G. Louie, A. Zettl, *Science* **1995**, *269*, 966–967; c) R. Tenne, L. Margulis, M. Genut, G. Hodes, *Nature* **1992**, *360*, 444–446; d) M. Niederberger, H. J. Muhr, F. Krumeich, F. Bieri, D. Gunther, R. Nesper, *Chem. Mater.* **2000**, *12*, 1995–2000; e) P. Hoyer, *Langmuir* **1996**, *12*, 1411–1413; P. Hoyer, *Adv. Mater.* **1996**, *12*, 857; f) C. C. Tang, Y. Bando, Z. W. Liu, D. Golberg, *Chem. Phys. Lett.* **2003**, *376*, 676–682; g) C. N. R. Rao, M. Nath, *Dalton Trans.* **2003**, 1–24.
[7] G. Alberti, U. Constantino, *J. Mol. Catal.* **1984**, *27*, 235–250.
[8] G. Alberti, U. Constantino, F. Di Gregorio, P. Galli, E. Torracca, *J. Inorg. Nucl. Chem.* **1968**, *30*, 295–304.
[9] X. F. Zhang, X. B. Zhang, G. Van Tendeloo, S. Amelinckx, M. Op de Beeck, J. Van Landuyt, *J. Cryst. Growth* **1993**, *130*, 368–382.
[10] J. A. Fortner, E. C. Buck, A. J. G. Ellison, J. K. Bates, *Ultramicroscopy* **1997**, *67*, 77–81.
[11] F. F. Xu, Y. Bando, *J. Appl. Phys.* **2001**, *89*,5469–5472.
[12] A. Fujimori, *Phys. Rev. B* **1983**, *28*, 4489–4493.
[13] a) W. Vanschaik, S. Lizzo, W. Smit, G. Blasse, *J. Electrochem. Soc.* **1993**, *140*, 216–222; b) N. Imanaka, T. Masui, H. Hirai, G. Adachi, *Chem. Mater.* **2003**, *15*, 2289–2291.
[14] E. Nakazawa, F. Shiga, *Jpn. J. Appl. Phys. Part 1* **2003**, *42*, 1642–1647.
[15] N. El Jouhari, C. Parent, G. L. Flem, *J. Solid State Chem.* **1996**, *123*, 398–407.
[16] H. Ebendorff-Heidepriem, D. Ehrt, *Opt. Mater.* **2000**, *15*, 7–25.
[17] A. F. Ali, P. Mustarelli, A. Magistris, *Mater. Res. Bull.* **1998**, *33*, 697–710.

 © 2005 Wiley-VCH Verlag GmbH & Co. KGaA, Weinheim

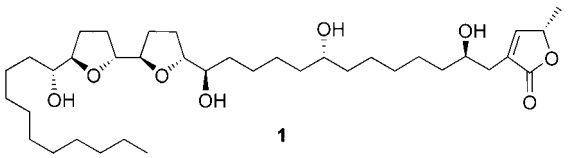
Natural Products Synthesis

The Total Synthesis of the Annonaceous Acetogenin 10-Hydroxyasimicin**

*Gillian L. Nattrass, Elena Díez, Matthew M. McLachlan, Darren J. Dixon, and Steven V. Ley**

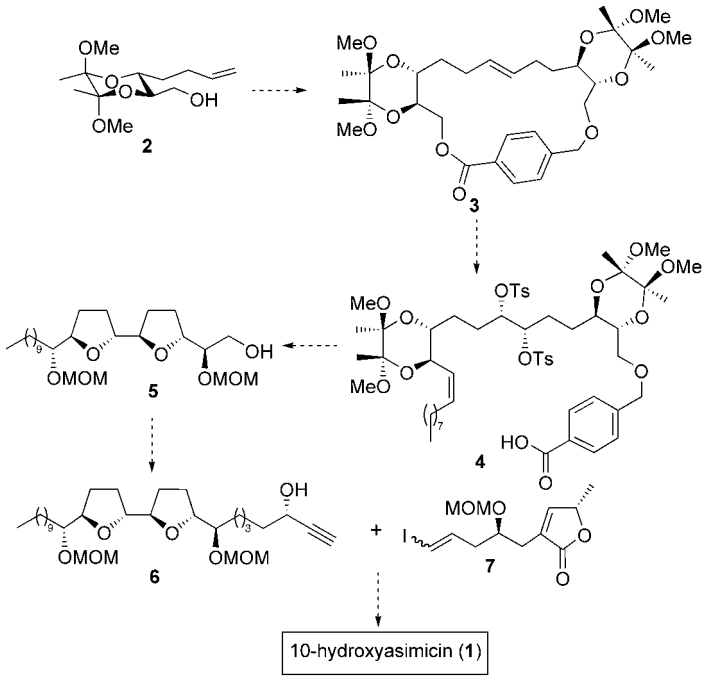
The annonaceous acetogenins comprise a class of almost 400 natural products that exhibit a remarkably broad spectrum of biological activity. They function as insecticides, fungicides, herbicides, and, perhaps most importantly, in vivo antitumor agents and have been shown to overcome resistance in multidrug-resistant tumors.[1] Structurally, the acetogenins are characterized by a long lipophilic tail, a central polyoxygenated core, and a terminal α,β-unsaturated γ-lactone. The structural diversity in this family arises principally from variations in the stereochemistry and connectivity of the polyoxygenated central core, which can consist of one or more tetrahydrofuranyl (THF) rings or, occasionally, a tetrahydropyranyl (THP) ring with various patterns of hydroxylation. These variations and the stereochemical consequences give rise to an impressive molecular diversity within the family. Owing to their biological activity and limited availability from natural sources, these compounds have attracted worldwide attention and have become the targets for total synthesis for a number of research groups,[2–9] including our own.[10] The majority of publications to date have focused on the synthesis of individual members of the family that suit a particular reaction type or stereochemical outcome. Motivated by the bioactivity of the annonaceous acetogenins, we embarked on a project to develop a more general route that utilizes an orthogonal and modular templating approach to provide access to many members in the series. Herein we describe the first successful synthesis of 10-hydroxyasimicin (**1**),[11] which contains a bis-THF motif in the central core.

The crucial component in the synthesis of any of these natural products is the stereoselective preparation of the polyoxygenated central fragment. 10-Hydroxyasimicin bears adjacent bis-THF rings flanked by two hydroxy groups with a *threo,trans,threo,trans,threo* stereochemistry. Our synthetic strategy to this oxygenated arrangements (Scheme 1) hinged upon the design of a



1

tether that could temporarily link two BDA-protected alkenol building blocks **2** (BDA = 2,3-butanediacetal) of, in principle, any desired stereochemical arrangement.[12] The tether could then induce stereocontrol during the critical ring-closing metathesis (RCM) to give compound **3**.[13] Subsequent Sharpless asymmetric dihydroxylation and chemoselective cleavage of the tether would afford **4**.[14] Intramolecular displacement by the unmasked hydroxy groups of the desymmetrized bistosylate **4** would yield the bis-THF unit **5**. Late-stage Sonogashira coupling of the terminal alkyne **6** and the butenolide **7** (constructed through a hetero-Diels–Alder (HDA) reaction to install the 1,5-stereochemical relationship and mask the butenolide double bond simultaneously, as reported in our synthesis of muricatetrocin C)[10] would



Scheme 1. Proposed synthetic route to 10-hydroxyasimicin (**1**). Ts = *p*-toluenesulfonyl, MOM = methoxymethyl.

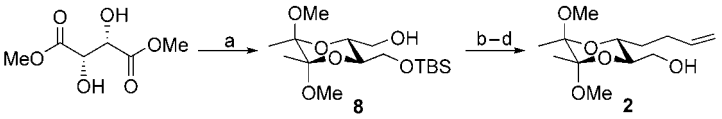
complete the carbon skeleton. Finally, selective hydrogenation and global deprotection would furnish the natural product **1** (Scheme 1).

Synthesis of fragment **2** began from (*S*,*S*)-dimethyl-D-tartrate, which was readily converted into the monoprotected diol **8** in three steps according to a previously established procedure (Scheme 2).[12] Subsequent tosylation of **8** and treatment of the corresponding tosyl derivative with allylmagnesium bromide in the presence of CuBr afforded **2** in multigram quantities after deprotection with TBAF.

[*] G. L. Nattrass, E. Díez, M. M. McLachlan, D. J. Dixon, Prof. Dr. S. V. Ley
Department of Chemistry
University of Cambridge
Lensfield Road, Cambridge, CB2 1EW (UK)
Fax: (+44) 1223-336-442
E-mail: svl1000@cam.ac.uk

[**] We thank the Commonwealth Scholarship Commission in the United Kingdom for funding (G.L.N.), the EU for a Marie Curie Fellowship (E.D.), GlaxoSmithKline (M.M.M.), Novartis for a research fellowship (S.V.L.), and Pfizer Global Research and Development for unrestricted funding towards the work.

 © 2005 Wiley-VCH Verlag GmbH & Co. KGaA, Weinheim DOI: 10.1002/anie.200462264



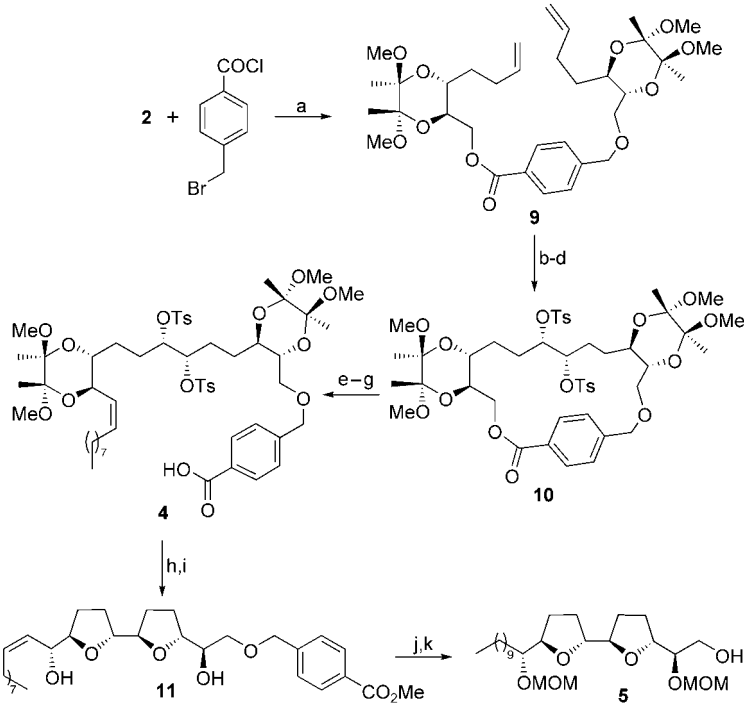
Scheme 2. Synthesis of alkenol **2**. a) Reference [12]; b) NEt_3, TsCl, DMAP, CH_2Cl_2, 1.5 h, room temperature, 99%; c) allylMgBr, CuBr, Et_2O, 8 h, 0°C, 84%; d) TBAF, THF, 5 h, 0°C, 100%. DMAP = 4-(dimethylamino)pyridine, TBAF = tetrabutylammonium fluoride.

The next step in the synthesis involved the development of a suitable template to link the two alkenol molecules together in order to proceed with an intramolecular metathesis reaction. As mentioned earlier, we required a tethering unit that could adjust the conformation of the macrocycle to control the stereoselectivity during the RCM reaction.[13] The chosen tethering template should behave as a "molecular workbench" and help orientate the olefin so that one face is preferentially available for attack during a *syn*-stereoselective dihydroxylation reaction.[14] Furthermore, the tether would play the role of a protecting group upon cleavage of the macrocycle to enable desymmetrization of the core. Hence the unit had to be dissymmetric to allow orthogonal cleavage upon completion of the dihydroxylation. On top of this, a dissymmetric tethering unit would enable us to attach different BDA-protected alkenol units sequentially to produce acetogenins with alternative stereochemistries at the core.[15] To put these concepts into effect, a differentiated arene with orthogonal substituents was chosen, as we could fine-tune the macrocycle ring size simply by varying the substitution pattern of the aryl system. 4-Bromomethylbenzoyl chloride was found to give the best results and was used in all subsequent investigations.[16]

Coupling of alkenol **2** with 4-bromomethylbenzoyl chloride in the presence of KHMDS gave the doubly loaded *para*-linked diene **9** in 69% yield. Subsequent treatment of **9** with a second-generation Grubbs catalyst[17] in dichloromethane at reflux delivered the intramolecular metathesis product in excellent yield, exclusively as the *E* adduct. Sharpless asymmetric dihydroxylation of the olefin with AD-mix-α afforded the diol in a diastereomeric ratio of 16:1 favoring the desired *S*,*S* product (Scheme 3).[18] Treatment of the diol with TsCl in pyridine afforded the ditosylated compound **10** in 90% yield.

The macrocycle was opened by treatment of **10** with sodium methoxide in methanol at room temperature to afford the primary alcohol.[19] Swern oxidation and a subsequent Wittig reaction installed the nine-membered carbon side-chain terminus as the *Z* olefin **4**. Removal of the BDA groups followed by an intramolecular Williamson cyclization with potassium carbonate as the base led to the formation of the bis-THF core **11** in 80% yield over the two steps. Finally, protection of the free secondary alcohols with MOMCl, followed by parallel reduction of the double bond and debenzylation under transfer-hydrogenation conditions completed the synthesis of fragment **5** (Scheme 3).

Fragment **5** was further elaborated by Dess–Martin oxidation, followed by Horner–Wadsworth–Emmons olefination with phosphonate **15**, which afforded an *E*,*E* diene exclusively.[20] Exhaustive reduction of the *E*,*E* diene with the Pearlman catalyst then afforded saturated ester **12** in 94% yield (Scheme 4). To generate the last stereocenter, further chain extension to propargylic ketone **13** was required. To this end ketone **13** was obtained by conversion of the saturated ester into the Weinreb amide,[21] which was then

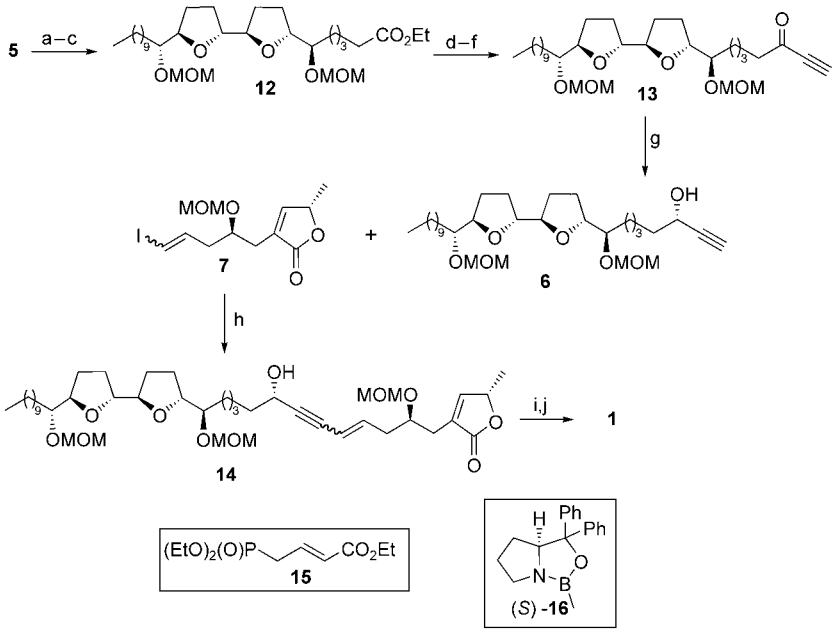


Scheme 3. Synthesis of bis-THF framework **5**. a) KHMDS, THF, 5 h, −78→0°C, 69%; b) second-generation Grubbs catalyst, CH_2Cl_2, 1 h, reflux, 99%; c) AD-mix-α, $MeSO_2NH_2$, $NaHCO_3$, *t*BuOH/H_2O (1/1), 96 h, 0°C→RT, 96% (*S*,*S*/*R*,*R* 16:1); d) TsCl, pyridine, 20 h, 0°C→RT, 90%; e) NaOMe, MeOH, 44 h, room temperature, 93%; f) DMSO, $(COCl)_2$, CH_2Cl_2, −78°C; NEt_3, −78°C→RT, 98%; g) $CH_3(CH_2)_8PPh_3Br$, *n*BuLi, THF, 7 h, −78→0°C, 69%; h) TFA/H_2O (2:1), 5 min (repeat twice), room temperature; i) K_2CO_3, MeOH, 3.5 h, reflux, 80% over two steps; j) MOMCl, Hünig base, DMAP, CH_2Cl_2, 18 h, 0°C→RT, 78%; k) Pd/C, $HCO_2^-NH_4^+$, MeOH, 2 h, reflux, 79%. HMDS = hexamethyldisilazide, DMSO = dimethyl sulfoxide, TFA = trifluoroacetic acid.

treated with the lithium derivative of trimethylsilylacetylene followed by desilylation with TBAF to give **13** in 60% yield over the two steps.[22] Diastereoselective oxazaborolidine-catalyzed (CBS)[23] reduction gave **6** in 78% yield, with an excellent ratio favoring the desired isomer (44:1).

With the synthesis of fragment **6** completed, we now turned our attention to the synthesis of butenolide **7** in preparation for the final coupling reaction. Diene **17** was synthesized in seven steps from 1,4-butanediol according to a previously established procedure (Scheme 5).[10] As in our synthesis of muricatetrocin C, the 1,5-stereochemical relationship in the butenolide moiety was installed through the HDA reaction with nitrosobenzene at 0°C which afforded an inseparable 7:3 mixture of regioisomers favoring the desired adduct **18**.[24] The N–O bond was cleaved by using freshly

 © 2005 Wiley-VCH Verlag GmbH & Co. KGaA, Weinheim

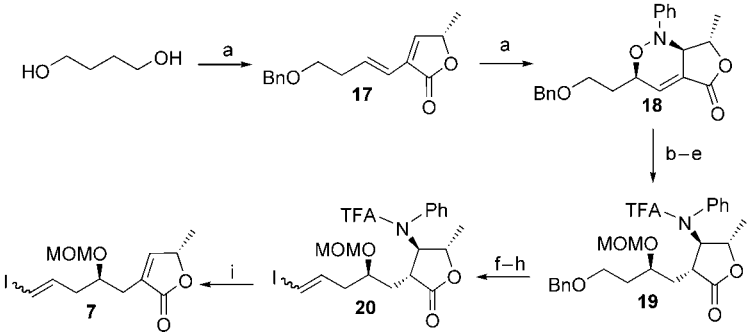


Scheme 4. Synthesis of 10-hydroxyasimicin (**1**). a) DMP, $NaHCO_3$, CH_2Cl_2, 1 h, 0 °C→RT, 95 %; b) **15**, NaHMDS, THF, 18 h, −78 °C→RT, 81 %; c) $Pd(OH)_2/C$, H_2, THF, 1 h, room temperature, 94 %; d) Me(MeO)NH·HCl, *i*PrMgCl, THF, 1.5 h, −10 °C, 82 %; e) trimethylsilylacetylene, *n*BuLi, THF, 1 h, −78→0 °C; f) TBAF, THF, 20 min, −20 °C, 60 % over two steps; g) (*S*)-**16**, $BH_3{\cdot}Me_2S$, THF, 1 h, −35 °C, 78 % (*S*/*R* 44:1); h) $[Pd(PPh_3)_2Cl_2]$, CuI, NEt_3, 45 min, room temperature, 86 %; i) $[Rh(PPh_3)_3Cl]$, H_2, benzene/EtOH (1:1), 23 h, room temperature, 74 %; j) $BF_3{\cdot}OEt_2$, Me_2S, 20 min, room temperature, 68 %. DMP = Dess–Martin periodinane.

prepared $[Mo(CO)_3(MeCN)_3]$ in the presence of water at room temperature.[25] Protection of the resultant secondary hydroxy group as a MOM ether enabled the separation of the regio- and stereoisomers through flash-column chromatography, thus avoiding the need for the laborious preparative HPLC separation required in the previous synthesis of muricatetrocin C. Subsequent hydrogenation over catalytic palladium and protection of the amine as the trifluoroacetamide afforded compound **19**. Debenzylation with the Pearlman catalyst afforded the free alcohol. Oxidation of the released primary alcohol with TPAP,[26] followed by one-carbon homologation, according to the Takai procedure,[27] provided the vinyl iodide **20** as a mixture of isomers (3.7:1 ratio favoring the *E* geometry) in 59 % yield over two steps. Subsequent elimination of the trifluoroacetamide group in the presence of DBU in acetonitrile at 0 °C afforded fragment **7** without epimerization of the butenolide methyl substituent (Scheme 5).

Sonogashira cross-coupling of vinyl iodide **7** with the propargylic alcohol **6** proceeded smoothly to produce the skeleton **14** in 86 % yield (Scheme 4).[28] The enyne functional group was reduced selectively over the butenolide double bond by using the Wilkinson catalyst to afford the protected acetogenin in 74 % yield. Final global deprotection with $BF_3{\cdot}Et_2O$ in methyl sulfide afforded **1** as a colorless wax in 68 % yield. The spectroscopic data for synthetic **1** (^{1}H NMR, ^{13}C NMR, IR, MS, and specific rotation)[29] were in excellent agreement with those reported for naturally occurring 10-hydroxyasimicin (**1**).[11]

In conclusion, the successful synthesis of 10-hydroxyasimicin (**1**) demonstrates the potential of the template approach to the oxygenated core of the acetogenins in an efficient and easily adapted manner. This route provides an efficient method for the construction of the bis-THF moiety incorporating a tether that enhances the stereochemical outcome of the RCM step and enables desymmetrization of the central fragment for further chain extension. The TBS-protected diol building block **8**, arising from (*R*,*R*,*S*,*S*)-2,3-BDA-protected (*S*,*S*)-dimethyl-D-tartrate, and the highly diastereoselective HDA approach to the butenolide unit are usefully employed in this new synthesis of an acetogenin natural product. Further applications of these general approaches will be employed in the preparation of other members of the acetogenin series in due course.



Scheme 5. Synthesis of butenolide **7**. a) Reference [10]; b) $[Mo(CO)_6]$, MeCN, 4 h, reflux; then **18**, H_2O, 15 min, room temperature; c) MOMCl, Hünig base, DMAP, CH_2Cl_2, 16 h, 0 °C→RT, 20 % over three steps, including HDA; d) Pd/C, H_2, THF, 2 h, room temperature, 100 %; e) TFAA, Hünig base, CH_2Cl_2, 30 min, 0 °C, 74 %; f) $Pd(OH)_2/C$, H_2, MeOH, 30 min, room temperature, 99 %; g) TPAP, NMO, NEt_3, CH_2Cl_2, 2 h, room temperature, 84 %; h) $CrCl_2$, CHI_3, THF, 17 h, 0 °C→RT, 70 % (*E*/*Z* 3.7:1); i) DBU, CH_3CN, 6 h, −15→−5 °C (60 %). TFAA = trifluoroacetic anhydride, TPAP = tetrapropylammonium perruthenate, DBU = 1,8-diazobicyclo[5.4.0]undec-7-ene.

Received: October 11, 2004
Published online: December 13, 2004

Keywords: metathesis · natural products · templating effect · total synthesis

[1] a) F. Q. Alali, X.-X. Liu, J. L. McLaughlin, *J. Nat. Prod.* **1999**, *62*, 504; b) N. H. Oberlies, V. L. Croy, M. L. Harrison, J. L. McLaughlin, *Cancer Lett.* **1997**, *15*, 73; c) L. Zeng, Q. Ye, N. H. Oberlies, G. Shi, Z. Gu, K. He, J. L. McLaughlin, *Nat. Prod. Rep.* **1996**, *13*, 275, and references therein.

[2] For recent reviews, see: a) G. Cassiraghi, F. Zanardi, L. Battistini, G. Rassu, G. Appendino, *Chemtracts: Org. Chem.* **1998**, *11*, 803; b) J. A. Marshall, K. W. Hinkle, C. E. Hagedorn, *Isr. J. Chem.* **1997**, *37*, 97; c) R. Hoppe, H. D. Scharf, *Synthesis* **1995**, 1447; d) B. Figadère, *Acc. Chem. Res.* **1995**, *28*, 359, and references therein.

[3] For syntheses from 1998, see: a) P. Neogi, T. Doundoulakis, A. Yazbak, S. C. Sinha, E. Keinan, *J. Am. Chem. Soc.* **1998**, *120*, 11279; b) S. C. Sinha, A. Sinha, E. Keinan, *J. Am. Chem. Soc.*

 © 2005 Wiley-VCH Verlag GmbH & Co. KGaA, Weinheim

1998, *120*, 4017; c) S. Sasaki, K. Maruta, H. Naito, R. Maemura, E. Kawahara, M. Maeda, *Chem. Pharm. Bull.* **1998**, *46*, 154; d) J. A. Marshall, H. J. Jiang, *J. Org. Chem.* **1998**, *63*, 7066; e) A. Yazbak, S. C. Sinha, E. Keinan, *J. Org. Chem.* **1998**, *63*, 5863; f) S. E. Schaus, J. Branalt, E. N. Jacobsen, *J. Org. Chem.* **1998**, *63*, 4876; g) S. Hanessian, T. A. Grillo, *J. Org. Chem.* **1998**, *63*, 1049; h) H. Makabe, A. Tanaka, T. Oritani, *Tetrahedron* **1998**, *54*, 6329; i) J. A. Marshall, H. J. Jiang, *Tetrahedron Lett.* **1998**, *39*, 1493; j) J. A. Marshall, K. W. Hinkle, *Tetrahedron Lett.* **1998**, *39*, 1303.

[4] For syntheses from 1999, see: a) S. Bäurle, S. Hoppen, U. Koert, *Angew. Chem.* **1999**, *111*, 1341; *Angew. Chem. Int. Ed.* **1999**, *38*, 1263; b) W. Kuruyama, K. Ishigami, T. Kitahara, *Heterocycles* **1999**, *50*, 981; c) J. A. Marshall, H. J. Jiang, *J. Nat. Prod.* **1999**, *62*, 1123; d) S. C. Sinha, E. Keinan, *J. Org. Chem.* **1999**, *64*, 7067; e) Q. Yu, Z. J. Yao, X. G. Chen, Y. L. Wu, *J. Org. Chem.* **1999**, *64*, 2440; f) A. Sinha, S. C. Sinha, E. Keinan, *J. Org. Chem.* **1999**, *64*, 2381; g) J. A. Marshall, H. J. Jiang, *J. Org. Chem.* **1999**, *64*, 971; h) S. Takahashi, K. Maeda, S. Hirota, T. Nakata, *Org. Lett.* **1999**, *1*, 2025; i) T. S. Hu, Q. Lin, Y. L. Wu, Y. K. Wu, *Org. Lett.* **1999**, *1*, 399; j) Q. Yu, Y. K. Wu, H. Ding, Y. L. Wu, *J. Chem. Soc. Perkin Trans. 1* **1999**, 1183; k) Z. M. Wang, S. K. Tian, M. Shi, *Tetrahedron: Asymmetry* **1999**, *10*, 667; l) W. Q. Yang, T. Kitahara, *Tetrahedron Lett.* **1999**, *40*, 7827; m) U. Emde, U. Koert, *Tetrahedron Lett.* **1999**, *40*, 5979; n) Z. M. Wang, S. K. Tian, M. Shi, *Tetrahedron Lett.* **1999**, *40*, 977; o) S. Takahashi, T. Nakata, *Tetrahedron Lett.* **1999**, *40*, 727; p) Z. M. Ruan, D. R. Mootoo, *Tetrahedron Lett.* **1999**, *40*, 49.

[5] For syntheses from 2000, see: a) S. Hoppen, S. Bäurle, U. Koert, *Chem. Eur. J.* **2000**, *6*, 2382; b) S. Bäurle, U. Peters, T. Friedrich, U. Koert, *Eur. J. Org. Chem.* **2000**, 2207; c) U. Emde, U. Koert, *Eur. J. Org. Chem.* **2000**, 1889; d) Z. M. Wang, S. K. Tian, M. Shi, *Eur. J. Org. Chem.* **2000**, 349; e) Z. M. Wang, S. K. Tian, M. Shi, *Chirality* **2000**, *12*, 581; f) M. Szlosek, J. F. Peyrat, C. Chaboche, X. Franck, R. Hocquemiller, B. Figadère, *New J. Chem.* **2000**, *24*, 337; g) W. Q. Yang, T. Kitahara, *Tetrahedron* **2000**, *56*, 1451; h) T.-S. Hu, Y.-L. Wu, Y. Wu, *Org. Lett.* **2000**, *2*, 887.

[6] For syntheses from 2001, see: a) C. Harken, R. Bruckner, *New J. Chem.* **2001**, *25*, 40; b) T.-S. Hu, Q. Yu, Y.-L. Wu, Y. Wu, *J. Org. Chem.* **2001**, *66*, 853; c) N. Maezaki, N. Kojima, A. Sakamoto, C. Iwata, T. Tanaka, *Org. Lett.* **2001**, *3*, 429; d) S. D. Burke, L. Jiang, *Org. Lett.* **2001**, *3*, 1953.

[7] For syntheses from 2002, see: a) S. Takahashi, A. Kubota, T. Nakata, *Angew. Chem.* **2002**, *114*, 4945; *Angew. Chem. Int. Ed.* **2002**, *41*, 4751; b) S. Takahashi, T. Nakata, *J. Org. Chem.* **2002**, *67*, 5739; c) S. Jiang, Z.-H. Liu, G. Sheng, B.-B. Zeng, X.-G. Cheng, Y.-L. Wu, Z.-J. Yao, *J. Org. Chem.* **2002**, *67*, 3404; d) A. R. L. Cecil, R. C. D. Brown, *Org. Lett.* **2002**, *4*, 3715; e) H. Makabe, Y. Hattori, A. Tanoka, T. Oritani, *Org. Lett.* **2002**, *4*, 1083; f) E. Keinan, S. C. Sinha, *Pure Appl. Chem.* **2002**, *74*, 93; g) S. Takahashi, A. Kubota, T. Nakata, *Tetrahedron Lett.* **2002**, *43*, 8661.

[8] For syntheses from 2003, see: a) N. Maezaki, N. Kojima, A. Sakamoto, H. Tominaga, C. Iwata, T. Tanaka, M. Monden, B. Damdinswen, S. Nakamori, *Chem. Eur. J.* **2003**, *9*, 390; b) B.-B. Zeng, Y. Wu, S. Jiang, Q. Yu, Z.-J. Yao, Z.-H. Liu, H.-Y. Li, Y. Li, X.-G. Chen, Y.-L. Wu, *Chem. Eur. J.* **2003**, *9*, 282; c) P. A. Evans, J. Cui, S. J. Gharpure, A. Polosukhi, H. R. Zhang, *J. Am. Chem. Soc.* **2003**, *125*, 14072; d) J. A. Marshall, A. Piettre, M. A. Paige, F. Valeriate, *J. Org. Chem.* **2003**, *68*, 8290; e) J. A. Marshall, A. Piettre, M. A. Paige, F. Valeriate, *J. Org. Chem.* **2003**, *68*, 1780; f) J. A. Marshall, A. Piettre, M. A. Paige, F. Valeriate, *J. Org. Chem.* **2003**, *68*, 1771; g) L. Zhu, D. R. Mootoo, *Org. Lett.* **2003**, *5*, 3475; h) S. Takahashi, A. Kubota, T. Nakata, *Org. Lett.* **2003**, *5*, 1353; i) R. V. A. Orru, B. Groenendaal, J. van Heyst, M. Hunting, C. Wesseling, R. F. Schmitz, S. F. Mayer, K. Faber, *Pure Appl. Chem.* **2003**, *75*, 259; j) S. Takahashi, A. Kubota, T. Nakata, *Tetrahedron* **2003**, *59*, 1627; k) J. L. Lee, C. F. Lin, L. Y. Hsieh, W. R. Lin, H. F. Chiu, Y. C. Wu, K. S. Wang, M. J. Wu, *Tetrahedron Lett.* **2003**, *44*, 7833; l) S. R. V. Kandula, P. Kumar, *Tetrahedron Lett.* **2003**, *44*, 6149.

[9] For syntheses from 2004, see: a) N. Maezaki, H. Tominaga, N. Kojima, M. Yanai, D. Urabe, T. Tanaka, *Chem. Commun.* **2004**, 406; b) H. N. Han, M. K. Sinha, L. J. D'Souza, E. Keinan, S. C. Sinha, *Chem. Eur. J.* **2004**, *10*, 2149; c) Q. S. Zhang, H. J. Lu, C. Richard, D. P. Curran, *J. Am. Chem. Soc.* **2004**, *126*, 36; d) A. R. Cecil, Y. L. Hu, M. J. Vicent, R. Duncan, R. C. D. Brown, *J. Org. Chem.* **2004**, *69*, 3368; e) L. Zhu, D. R. Mootoo, *J. Org. Chem.* **2004**, *69*, 3154; f) T. Yoshimitsu, T. Makino, H. Nagaoka, *J. Org. Chem.* **2004**, *69*, 1993; g) H. Makabe, A. Miyawaki, R. Takahashi, Y. Hattori, M. Abe, H. Miyoshi, *Tetrahedron Lett.* **2004**, *45*, 973.

[10] a) D. J. Dixon, S. V. Ley, D. J. Reynolds, *Angew. Chem.* **2000**, *112*, 3768; *Angew. Chem. Int. Ed.* **2000**, *39*, 3622; b) D. J. Dixon, S. V. Ley, D. J. Reynolds, *Chem. Eur. J.* **2002**, *8*, 1621.

[11] K. He, G. Shi, G.-X. Zhao, L. Zeng, Q. Ye, J. T. Schwedler, K. V. Wood, J. L. McLaughlin, *J. Nat. Prod.* **1996**, *59*, 1029.

[12] S. V. Ley, D. K. Baeschlin, D. J. Dixon, A. C. Foster, S. J. Ince, H. W. M. Priepke, D. J. Reynolds, *Chem. Rev.* **2001**, *101*, 53; and references therein.

[13] a) Y. Sakamoto, M. Okazaki, K. Miyamoto, T. Nakata, *Tetrahedron Lett.* **2001**, *42*, 7633; b) E. C. Hansen, D. Lee, *J. Am. Chem. Soc.* **2003**, *125*, 9582; c) P. A. Evans, J. Cui, G. P. Buffone, *Angew. Chem.* **2003**, *115*, 1776–1779; *Angew. Chem. Int. Ed.* **2003**, *42*, 1734, and references therein.

[14] a) J. Mulzer, K. Schein, J. W. Bats, J. Buschmann, P. Luger, *Angew. Chem.* **1998**, *110*, 1625; *Angew. Chem. Int. Ed.* **1998**, *37*, 1566; b) J. Mulzer, I. Böhm, J. W. Bats, *Tetrahedron Lett.* **1998**, *39*, 9643.

[15] In this particular synthesis, the two alkenol units are the same, but any absolute configurational arrangement can, in principle, be loaded onto the orthogonal 4-bromomethylbenzyl chloride template by making use of the greater reactivity of the acyl chloride relative to the alkyl bromide substituent.

[16] A noticeable improvement in stereocontrol was observed in going from *ortho* to *meta* and finally to *para* substitution. The results of these investigations will be published in a full paper at a later date.

[17] M. Scholl, S. Ding, C. W. Lee, R. H. Grubbs, *Org. Lett.* **1999**, *1*, 953.

[18] Comparable diastereoselectivity was obtained in the Sharpless asymmetric dihydroxylation reaction when performed on the open chain hydroxy ester, obtained from the transesterfiction reaction on the alkene formed immediately after the RCM reaction.

[19] Orthogonal macrocycle opening was achieved under transfer-hydrogenation conditions and will be communicated in a full paper at a later date.

[20] a) D. B. Dess, J. C. Martin, *J. Org. Chem.* **1983**, *48*, 4155; b) D. B. Dess, J. C. Martin, *J. Am. Chem. Soc.* **1991**, *113*, 7277.

[21] J. M. Williams, R. B. Jobson, N. Yasuda, G. Marchesini, U.-H. Dolling, E. J. J. Grabowski, *Tetrahedron Lett.* **1995**, *36*, 5461.

[22] M. Muller, A. Mann, M. Taddei, *Tetrahedron Lett.* **1993**, *34*, 3289.

[23] E. J. Corey, R. K. Bakshi, S. J. Shibata, *J. Am. Chem. Soc.* **1987**, *109*, 5551.

[24] Investigations into using alternative nitrosodienophiles to improve the regioselectivity of the desired HDA reaction indicated that nitrosobenzene gives the most favorable results and could not be improved on. These results will be communicated in a full paper at a later date.

[25] a) M. Nitta, T. Kobayashi, *J. Chem. Soc. Perkin Trans. 1* **1985**, 1401; b) S. Cicchi, A. Goti, A. Brondi, A. Guarna, F. De Sarlo, *Tetrahedron Lett.* **1990**, *31*, 3351.

[26] S. V. Ley, J. Norman, W. P. Griffith, S. P. Marsden, *Synthesis* **1994**, 639.

 © 2005 Wiley-VCH Verlag GmbH & Co. KGaA, Weinheim

[27] K. Takai, K. Nitta, K. Utimoto, *J. Am. Chem. Soc.* **1986**, *108*, 7408.
[28] a) T. R. Hoye, P. R. Hanson, A. C. Kovelesky, T. D. Ocain, Z. P. Zhuang, *J. Am. Chem. Soc.* **1991**, *113*, 9369; b) K. Sonogashira, Y. Thoda, N. Magihara, *Tetrahedron Lett.* **1975**, 4467.
[29] Spectroscopic data for synthetic **1**, a colorless wax: $[\alpha]_D^{25} = +16$ ($c = 0.25$ in $CHCl_3$, lit. [11] $[\alpha]_D^{22} = +17.3$ in $CHCl_3$); ^{1}H NMR (400 MHz; $CDCl_3$): $\delta = 7.18$ (d, $J = 1.3$ Hz, 1H; 35-H), 5.05 (qd, $J = 6.8$, 1.4 Hz, 1H; 36-H), 3.86 (m, 5H; 16-H, 19-H, 20-H, 23-H), 3.60 (m, 1H; 10-H), 3.41–3.38 (m, 2H; 15-H, 24-H), 2.53 (dddd, $J = 15.2$, 3.2, 1.5, 1.5 Hz, 1H; 3a-H), 2.40 (dddd, $J = 15.1$, 8.3, 1.2, 1.2 Hz, 1H; H-3b), 1.97 (m, 8H; 17-H, 18-H, 21-H, 22-H), 1.70–1.26 (m, 36H; 5–9-H, 1–14-H, 25–33-H), 1.43 (d, $J = 6.7$ Hz, 3H; 37-H), 0.88 ppm (t, $J = 6.7$ Hz, 3H; 34-H); ^{13}C NMR (125 MHz; $CDCl_3$): $\delta = 174.6$ (C1), 151.8 (C35), 131.2 (C2), 83.2, 83.1 (C16, C23), 81.81, 81.75 (C19, C20), 78.0 (C36), 74.1, 74.0 (C15, C24), 71.7 (C10), 69.9 (C4), 37.34 (C5), 37.3 (C11), 37.2 (C9), 33.41, 33.36, 33.32 (C3, C14, C25), 31.9 (C32), 29.71, 29.61, 29.60, 29.59, 29.47, 29.32 (C6–C8, C12, C13, C26–C31), 29.0 (C21, C18), 28.3 (C17, C22), 25.64, 25.62, 25.5 (C6–C8, C12, C13, C26–C31), 22.7 (C33), 19.1 (C37), 14.1 ppm (C34); IR (thin film): $\tilde{\nu}_{max} = 3404$ br (OH), 2924, 2853 (CH), 1753 (C=O) cm^{-1}; HRMS: calcd for $C_{37}H_{66}O_8Na$ $[M+Na]^+$: 661.4650; found: 661.4651.

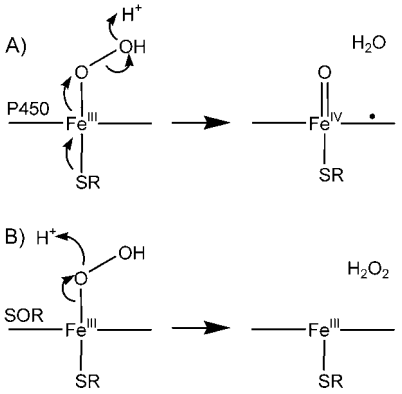
 © 2005 Wiley-VCH Verlag GmbH & Co. KGaA, Weinheim

Bioinorganic Chemistry

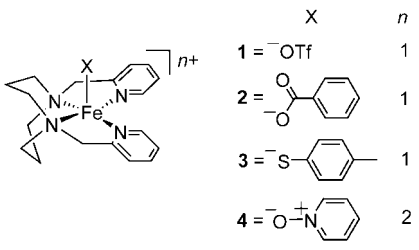
Spin-State Rationale for the Peroxo-Stabilizing Role of the Thiolate Ligand in Superoxide Reductase**

Michael R. Bukowski, Heather L. Halfen, Tieme A. van den Berg, Jason A. Halfen, and Lawrence Que, Jr.**

Nature uses cysteine to modulate the electronic properties of the metal centers in metalloproteins.[1] Particularly interesting is the contrast in function between two mononuclear iron enzymes with similar square pyramidal $\{Fe^{II}(N)_4(Cys_{apical})\}$ active sites: cytochrome P450[2] and superoxide reductase (SOR).[3,4] The well-studied cytochrome P450 has an $\{Fe^{II}$-(porphyrin dianion)(Cys)$\}$ site that activates dioxygen to oxidize hydrocarbon substrates.[5] Dioxygen activation is proposed to occur via a low-spin Fe^{III}-OOH intermediate that converts into a high-valent iron-oxo oxidizing species[6,7] with the heterolytic O–O bond-cleavage step assisted by a "push" of electron density from the *trans* thiolate ligand (Scheme 1 A).[8] In contrast, superoxide reductase (SOR) uses a similar $\{Fe^{II}(His)_4(Cys)\}$ site to convert superoxide into hydrogen peroxide as a means of protecting anaerobes and microaerophiles from the inimical effects of superoxide that may be formed from occasional intrusion of O_2 into the cell.[9] The superoxide reduction mechanism is proposed to go through an iron(III)-peroxo intermediate that undergoes protonation at both oxygen centers to release H_2O_2 (Scheme 1 B).[10–12] It has been suggested that the difference in function between P450 and SOR arises from the different spin states of the intermediates.[9,11,13] To understand nature's rationale for using such similar active sites for apparently opposite functions, we have carried out a systematic study of a series of square pyramidal $[Fe^{II}(L^8py_2)(X_{apical})]$ precursor complexes, where L^8py_2 is a tetradentate nonheme ligand *N*,*N*′-bis(2-pyridylmethyl)-1,5-diazacyclooctane that is constrained to adopt a near planar arrangement of four nitrogen atoms[14] and X_{apical} can be triflate (**1**), benzoate (**2**), or 4-methylbenzenethiolate (**3**; Scheme 2). These complexes react with *t*BuOOH to afford high-spin alkylperoxoiron(III) intermediates. We find that the more basic apical ligand enhances



Scheme 1.



Scheme 2.

[*] M. R. Bukowski, T. A. van den Berg, Prof. Dr. L. Que, Jr.
Center for Metals in Biocatalysis and
Department of Chemistry
University of Minnesota
207 Pleasant Street SE, Minneapolis, MN 55455 (USA)
Fax: (+1) 612-624-7029
E-mail: que@chem.umn.edu
H. L. Halfen, Prof. Dr. J. A. Halfen
Deparment of Chemistry
University of Wisconsin-Eau Claire
105 Garfield Avenue, Eau Claire, WI 54702 (USA)
Fax: (+1) 715-836-4979
E-mail: halfenja@uwec.edu

[**] This work was supported by grants from the National Science Foundation (CHE-0234951 to J.A.H.) and the National Institutes of Health (GM-33162 to L.Q.). J.A.H. acknowledges sabbatical support from the University of Minnesota NSF/RSEC program (CHE-0113894) and the University of Wisconsin-Eau Claire. The authors would like to acknowledge Dr. Neil R. Brooks, Dr. Victor G. Young, Jr., and the X-Ray Crystallographic Laboratory, Department of Chemistry, University of Minnesota.

 © 2005 Wiley-VCH Verlag GmbH & Co. KGaA, Weinheim DOI: 10.1002/anie.200461527

the stability of the high-spin Fe^{III}-OOR intermediate, an effect opposite to that deduced for corresponding low-spin centers,[15] which provides a rationale for the presence of an apical thiolate in SOR.

Complexes **1**–**3** (Scheme 2) can be readily obtained in high yield by combining the components in the appropriate solvent. The crystal structures of **1** and **2** shown in Figure 1

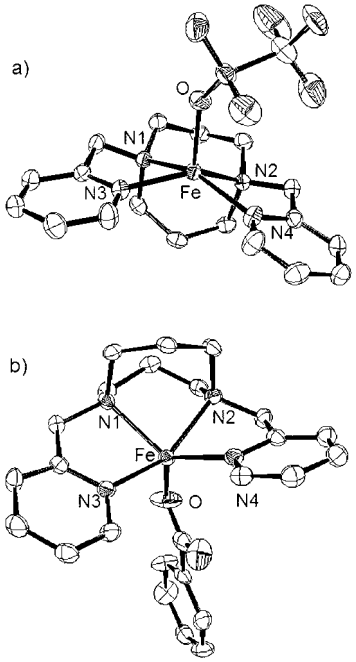


Figure 1. ORTEP plots for a) $[(L^8py_2)Fe(OTf)]^+$ (**1**) and b) $[(L^8py_2)Fe(O_2CPh)]^+$ (**2**) with thermal ellipsoids set at 50% probability. Selected interatomic distances [Å] and angles [°]: a) Fe-N1 2.176(3), Fe-N2 2.216(2), Fe-N3 2.164(3), Fe-N4 2.137(3), Fe-O 2.011(2); N3-Fe-N2 148.60(10), N4-Fe-N1 149.49(11). b) Fe-N1 2.198(3), Fe-N2 2.208(3), Fe-N3 2.164(3), Fe-N4 2.106(3), Fe-O 1.999(3); N3-Fe-N2 129.43(12), N4-Fe-N1 152.60(12).

reveal square pyramidal ($\tau = 0.02$ (**1**) and 0.38 (**2**)) iron(II) centers with the L^8py_2 nitrogen atoms occupying the basal plane and an anionic ligand in the apical site, similar to that reported for **3**.[14] The average Fe–N separation ranges from 2.17 and 2.21 Å, typical of high-spin Fe^{II} complexes with neutral nitrogen-ligand sets[16] and increases in the order of **1**, **2**, **3** in response to the basicity of the apical ligand. In UV/Vis spectra obtained in CH_2Cl_2 solution, **1**–**3** exhibit absorption shoulders at 350, 380, and 400 nm ($\varepsilon \approx$ 500–600 $M^{-1}cm^{-1}$), respectively; the progressive red shift observed correlates with the increased basicity of the apical ligand, so the features can be assigned to iron(II)-to-pyridine charge-transfer transitions.

The reaction of **1** with excess *t*BuOOH in CH_2Cl_2 at −80 °C affords a deep purple chromophore, **1a**, with λ_{max} at 580 nm ($\varepsilon =$ 2500 $M^{-1}cm^{-1}$; Figure 2 and Table 1), parameters comparable to those associated with

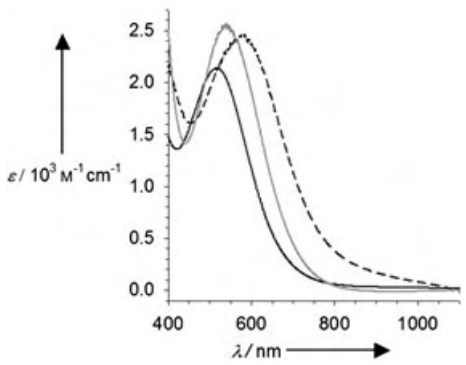


Figure 2. Intermediates **1a** (– – –), **2a** (——), and **3a** (——) generated at −80 °C in CH_2Cl_2.

the reported alkylperoxoiron(III) intermediates.[16–18] Species **1a** exhibits an EPR spectrum with signals at $g = 8.8$, 5.2, and 3.2 that correspond to a high-spin iron(III) ($S = 5/2$) center with $E/D = 0.17$ and a resonance Raman spectrum with four resonance-enhanced vibrations at 463, 627, 833, and 870 cm^{-1} that arise from coordinated alkylperoxide (Figure 3 and Table 1).This pattern of Raman vibrations has been observed for high-spin alkylperoxoiron(III) intermediates and is distinct from that associated with their low-spin counterparts.[16] Thus **1a** can be characterized as the high-spin $[Fe^{III}(L^8py_2)(OOt\text{-}Bu)(OTf)]^+$ ion.

Parallel reactions using either **2** or **3** yield intermediates **2a** or **3a**, respectively, with absorbance maxima that are blue-shifted relative to that of **1a** (Figure 2, Table 1). The progressive blue shift observed from **1a** to **2a** to **3a** can be rationalized by the substitution of the axial triflate ligand in **1a** with more Lewis basic benzoate and thiolate ligands in **2a** and **3a**, respectively, and confirms the assignment of the chromophore as an alkylperoxo-to-iron(III) charge-transfer transition. Like **1a**, compounds **2a** and **3a** exhibit $S = 5/2$ EPR signals and the same pattern of Raman vibrations (Table 1; Figure 3). These three species thus constitute a series of high-spin Fe^{III}-OO*t*Bu intermediates.

Intermediates **1a**–**3a** are stable for hours at −80 °C but exhibit differing lifetimes at −40 °C. Intermediate **1a** formed with 3 equivalents *t*BuOOH at −40 °C decays completely

Table 1: Properties of $[Fe^{III}(L)(OOtBu)(X)]$ Intermediates.

	Solvent	Spin-State (E/D)	λ_{max} [nm]	ε [$M^{-1}cm^{-1}$]	δ_{tBu} [cm^{-1}]	ν_{Fe-O} [cm^{-1}]	ν_{O-O} [cm^{-1}]	k_{dec}[a] [s^{-1}]
$L = L^8py_2$								
1a (X = OTf)	CH_2Cl_2	5/2 (0.17)	580	2500	463	627	833, 870	1.8×10^{-2}
2a (X = OBz)	CH_2Cl_2	5/2 (0.17)	545	2700	463	623	832, 873	5.4×10^{-4}
3a (X = SAr)	CH_2Cl_2	5/2 (0.20)	510	2200	461	623	830, 874	5.8×10^{-5}
4a (X = pyO)	CH_2Cl_2	5/2 (0.18)	550	2450	463	623	831, 878	8.2×10^{-4}
6-Me_3-TPA[b]	CH_3CN	5/2 (0.33)	562	2200	468	637	842, 877	
TPA[b]	CH_3CN	1/2	600	2000	490	696	796	

[a] 1 mM Fe, 3 equiv *t*BuOOH, −40 °C in CH_2Cl_2. [b] From Ref. [16].

 © 2005 Wiley-VCH Verlag GmbH & Co. KGaA, Weinheim

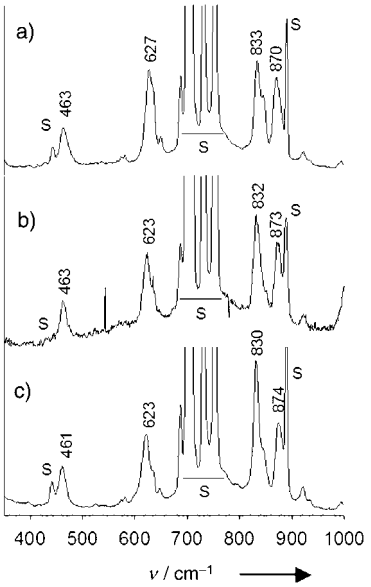
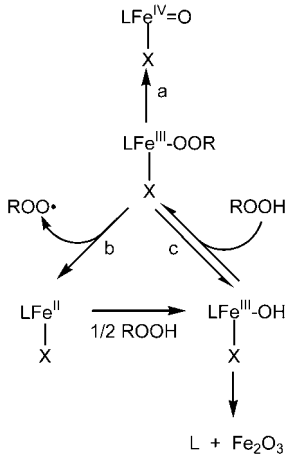


Figure 3. Resonance Raman spectra of a) **1a**, b) **2a**, and c) **3a** in CH_2Cl_2 at 77 K (λ_{ex} = 514.5 nm, power = 100 mW).



Scheme 3.

within 7 minutes in a first order process ($k = 1.8(1) \times 10^{-2}\ s^{-1}$). In contrast, **2a** and **3a** formed under these conditions are more stable by approximately two orders of magnitude, requiring 5 and 14 h, respectively, for complete decay. Thus a more basic axial ligand appears to stabilize the Fe^{III}-OO*t*Bu unit.

The stabilizing effect of a Lewis basic sixth ligand observed for the $[Fe^{III}(L^8py_2)(OOtBu)(X)]^{n+}$ series is opposite to that recently demonstrated for the mononuclear $[Fe^{III}$-(TPA)(OO*t*Bu)] complex (TPA = tris(2-pyridylmethyl)amine).[15] In the $[Fe^{III}(TPA)(OOtBu)]^{2+}$ complex, decomposition of the TPA intermediate to form $[Fe^{IV}(O)(TPA)]^{2+}$ at −40 °C is greatly accelerated by pyridine N-oxide (PyO). In contrast, the addition of PyO to **1a** significantly retards its decay ($k = 8.2 \times 10^{-4}\ s^{-1}$) and results in a blue shift in the alkylperoxo-to-iron(III) charge-transfer band (λ_{max} = 550 nm). This new species, designated **4a**, is characterized as a high-spin Fe^{III}-OO*t*Bu intermediate with PyO as the sixth ligand on the basis of the similarity of its UV/Vis, EPR, and resonance Raman spectroscopic features to those of **1a**–**3a** (Table 1). The effect of PyO on the λ_{max} and the stability of the Fe^{III}-OO*t*Bu unit is consistent with its expected Lewis basicity, which lies between those of triflate and benzoate.

The stabilizing effect of Lewis bases observed for the L^8py_2 series of iron peroxo complexes clearly contrasts the destabilizing effect observed for $[Fe^{III}(TPA)(OOR)]^{2+}$ intermediates[15,19] and the "push" effect that promotes O–O bond cleavage in heme systems.[5] We attribute these opposing effects to the difference in the spin states of the peroxoiron(III) species: high spin for the L^8py_2 series and low spin for TPA and heme complexes. Earlier Raman studies of end-on bound hydroperoxo- and alkylperoxoiron(III) species have shown that low-spin centers give rise to stronger Fe–O and weaker O–O bonds, thereby setting the stage for O–O bond cleavage (Scheme 3, pathway a); electron donation to the metal center would then facilitate access to the iron(IV) oxidation state.[18,20,21] High-spin centers, on the other hand, give rise to the opposite effect, affording weaker Fe–O and stronger O–O bonds that favor Fe–O bond homolysis instead as a decomposition pathway for the peroxoiron(III) species to form iron(II) and peroxyl radicals (Scheme 3, pathway b).[17] In this case, electron donation to the metal center would lower the $Fe^{III/II}$ potential and be expected to retard the decay. This outcome has been observed for a series of high-spin $[Fe^{III}(6$-Me_3-TPA)(OO*t*Bu)$(O_2CC_6H_4$-X)$]^+$ complexes, where decay by Fe–O bond homolysis is promoted by electron-withdrawing substituents and the lifetime of the intermediate is prolonged by electron-donating groups.[22] The L^8py_2 series reported herein further illustrates this notion by expanding the range of sixth ligands and including the thiolate relevant to SOR chemistry. Indeed the thiolate ligand provides the longest lived peroxoiron(III) species in the L^8py_2 series.

Intermediates **1a**–**3a** decay to yield an Fe_2O_3 precipitate and free ligand. We speculate that these products are obtained because of the instability of the $[Fe^{III}(L^8py_2)OH]^{2+}$ intermediate proposed in Scheme 3, which is consistent with the fact that we have been unable to obtain $\{Fe^{III}(L^8py_2)\}$ complexes by direct synthesis from iron(III) salts. The putative $[Fe^{III}(L^8py_2)OH]^{2+}$ intermediate may be formed in two steps by pathway b in Scheme 3 and subsequent oxidation of the resulting iron(II) precursor by residual *t*BuOOH or in one step by hydrolysis (pathway c). Indeed pathway c may be expected to become more important with a more electron-donating sixth ligand.

The current data allow us to speculate on the function of the high-spin $\{Fe(His)_4(Cys)\}$ active site of SOR. The electron-rich thiolate would be expected to lower the $Fe^{III/II}$ potential and promote the reduction of superoxide to form a high-spin peroxoiron(III) intermediate. The O–O bond cleavage to produce undesired high-valent oxoiron species is prevented by the high-spin iron(III) center and the presence of the axial thiolate ligand. These features may also function to prolong the lifetime of the peroxoiron(III) species to allow its protonation by a second-sphere residue and subsequent

 © 2005 Wiley-VCH Verlag GmbH & Co. KGaA, Weinheim

release of H_2O_2. The contrasting effects of Lewis bases on the stability of low-spin and high-spin peroxoiron(III) species thus provide a rationale for nature's use of an axial thiolate in cytochrome P450 and SOR for two apparently distinct roles.

Experimental Section

1: Solutions of L^8py_2 (68.0 mg, 0.229 mmol) in anhydrous, inhibitor-free THF (5 mL) and $[Fe(MeCN)_2(OTf)_2]$ (105 mg, 0.240 mmol) in a minimum of acetonitrile were combined and stirred for 20 min at ambient temperature then left to stand at −30 °C. Large, colorless crystals suitable for X-ray diffraction formed after 5 h: yield 116 mg (78%) Alternatively, diethyl ether can be layered on the THF solution after stirring, which results in immediate formation of fine white crystals: 120 mg (80% yield); elemental analysis (%) calcd for $C_{20}H_{24}F_6FeN_4O_6S_2$: C 36.93, H 3.72, F 17.53, N 8.61; found: C 37.19, H 3.96, F 17.35, N 8.61

2: A light yellow solution of L^8py_2 (41.1 mg, 0.139 mmol) and $[Fe(H_2O)_6](BF_4)_2$ (47.0 mg, 0.139 mmol) in CH_3OH (3 mL) was treated with NaO_2CPh (30.0 mg, 0.209 mmol). After stirring for 1 h, the yellow solution was treated with a solution of $NaBPh_4$ (95 mg, 0.28 mmol) in CH_3OH (2 mL), resulting in the immediate deposition of a bright yellow crystalline solid. The solid was collected by vacuum filtration, washed with CH_3OH and Et_2O, and dried under vacuum: 95 mg (86%). Crystals suitable for X-ray crystallography were grown from CH_3CN/Et_2O. Elemental analysis (%) calcd for $C_{49}H_{49}BFeN_4O_2$: C 74.25, H 6.23, N 7.07; found: C 74.69, H 6.11, N 7.21; UV/Vis (CH_3CN) λ_{max} (ε, $M^{-1}\,cm^{-1}$) 375 nm (450).

Crystal structure determination for **1**: Colorless plates from THF; $C_{20}H_{24}F_6FeN_4O_6S_2$, monoclinic, space group $P2_1/c$, $a = 11.352(2)$, $b = 14.333(3)$, $c = 16.013(3)$ Å, $\beta = 100.469(4)°$, $V = 2562.1(8)$ Å^3, $Z = 4$, $\rho_{calcd} = 1.686\,g\,cm^{-3}$, crystal dimensions: $0.36 \times 0.32 \times 0.08$ mm; diffractometer: Bruker CCD; $Mo_{K\alpha}$ radiation, 173(2) K; $2\theta_{max} = 50.1°$, 13032 reflections, 4540 independent ($R_{int} = 0.039$), direct methods; absorption correction semi-empirical from equivalents ($\mu = 0.840\,mm^{-1}$); Refinement (on F^2) with SHELXTL-Plus (version 5.10) and, 364 parameters, 75 restraints, $R_1 = 0.0421$ ($I > 2\sigma$) and wR_2 (all data) = 0.1094, Goof = 1.025, max/min residual electron density: 0.576/−0.602 e Å^{-3}.

Crystal structure determination for **2**: Yellow prisms from CH_3CN/Et_2O; $C_{51}H_{52}BFeN_5O_2$, monoclinic, space group $P2_1/c$, $a = 19.360(3)$, $b = 12.174(2)$, $c = 19.844(2)$ Å, $\beta = 112.64(1)°$, $V = 4316.6(11)$ Å^3, $Z = 4$, $\rho_{calcd} = 1.283\,g\,cm^{-3}$, crystal dimensions: $0.30 \times 0.25 \times 0.18$ mm; diffractometer: Bruker-Nonius MACH3S; $Mo_{K\alpha}$ radiation, 173(2) K; $2\theta_{max} = 51.96°$, 8446 reflections, 5092 independent ($R_{int} = 0.0391$), direct methods; no absorption correction required ($\mu = 0.396\,mm^{-1}$); Refinement (on F^2) with SHELXTL-Plus (version 5.10) and, 542 parameters, 0 restraints, $R_1 = 0.0661$ ($I > 2\sigma$) and wR_2 (all data) = 0.1317, Goof = 1.035, max/min residual electron density: 0.411/−0.463 e Å^{-3}.

CCDC 241381 and CCDC 241382 contain the supplementary crystallographic data for this paper. These data can be obtained free of charge via www.ccdc.cam.ac.uk/conts/retrieving.html (or from the Cambridge Crystallographic Data Centre, 12 Union Road, Cambridge CB2 1EZ, UK; fax: (+44) 1223-336-033; or deposit@ccdc.cam.ac.uk).

Received: August 3, 2004
Published online: December 15, 2004

Keywords: bioinorganic chemistry · coordination compounds · iron · peroxides · S ligands

[1] S. J. Lippard, J. M. Berg, *Principles of Bioinorganic Chemistry*, University Science Books, Mill Valley, **1994**.
[2] T. L. Poulos, B. C. Finzel, A. J. Howard, *J. Mol. Biol.* **1987**, *195*, 687.
[3] A. P. Yeh, Y. Hu, F. E. J. Jenney, M. W. W. Adams, D. C. Rees, *Biochemistry* **2000**, *39*, 2499.
[4] A. V. Coelho, P. Matias, V. Fülöp, A. Thompson, A. Gonzalez, M. A. Carrondo, *J. Biol. Inorg. Chem.* **1997**, *2*, 680.
[5] M. Sono, M. P. Roach, E. D. Coulter, J. H. Dawson, *Chem. Rev.* **1996**, *96*, 2841.
[6] R. Davydov, T. M. Makris, V. Kofman, D. E. Werst, S. G. Sligar, B. M. Hoffman, *J. Am. Chem. Soc.* **2001**, *123*, 1403.
[7] I. Schlichting, J. Berendzen, K. Chu, A. M. Stock, S. A. Maves, D. E. Benson, R. M. Sweet, D. Ringe, G. A. Petsko, S. G. Sligar, *Science* **2000**, *287*, 1615.
[8] D. L. Harris, G. H. Loew, *J. Am. Chem. Soc.* **1998**, *120*, 8941.
[9] J. A. Kovacs, *Chem. Rev.* **2004**, *104*, 825.
[10] C. Mathé, T. A. Mattioli, O. Horner, M. Lombard, J.-M. Latour, M. Fontecave, V. Nivière, *J. Am. Chem. Soc.* **2002**, *124*, 4966.
[11] M. D. Clay, F. E. Jenney, Jr., P. L. Hagedoorn, G. N. George, M. W. W. Adams, M. K. Johnson, *J. Am. Chem. Soc.* **2002**, *124*, 788.
[12] J. P. Emerson, E. D. Coulter, R. S. Phillips, D. M. Kurtz, Jr., *J. Biol. Chem.* **2003**, *278*, 39662.
[13] R. Silaghi-Dumitrescu, I. Silaghi-Dumitrescu, E. D. Coulter, D. M. Kurtz, Jr., *Inorg. Chem.* **2003**, *42*, 446.
[14] J. A. Halfen, H. L. Moore, D. C. Fox, *Inorg. Chem.* **2002**, *41*, 3935.
[15] J. Kaizer, M. Costas, L. Que, Jr., *Angew. Chem.* **2003**, *115*, 3799; Angew. *Chem. Int. Ed.* **2003**, *42*, 3671.
[16] Y. Zang, J. Kim, Y. Dong, E. C. Wilkinson, E. H. Appelman, L. Que, Jr., *J. Am. Chem. Soc.* **1997**, *119*, 4197.
[17] N. Lehnert, R. Y. N. Ho, L. Que, Jr., E. I. Solomon, *J. Am. Chem. Soc.* **2001**, *123*, 12802.
[18] N. Lehnert, R. Y. N. Ho, L. Que, Jr., E. I. Solomon, *J. Am. Chem. Soc.* **2001**, *123*, 8271.
[19] A. Mairata I Payeras, R. Y. N. Ho, M. Fujita, L. Que, Jr., *Chem. Eur. J.* **2004**, *10*, 4944.
[20] R. Y. N. Ho, G. Roelfes, B. L. Feringa, L. Que, Jr., *J. Am. Chem. Soc.* **1999**, *121*, 264.
[21] N. Lehnert, F. Neese, R. Y. N. Ho, L. Que, Jr., E. I. Solomon, *J. Am. Chem. Soc.* **2002**, *124*, 10810.
[22] J. Kim, Y. Zang, M. Costas, R. G. Harrison, E. C. Wilkinson, L. Que, Jr., *J. Biol. Inorg. Chem.* **2001**, *6*, 276.

 © 2005 Wiley-VCH Verlag GmbH & Co. KGaA, Weinheim

Antitumor Agents

A Formal Total Synthesis of Eleutherobin Through an Unprecedented Kinetically Controlled Ring-Closing-Metathesis Reaction of a Densely Functionalized Diene**

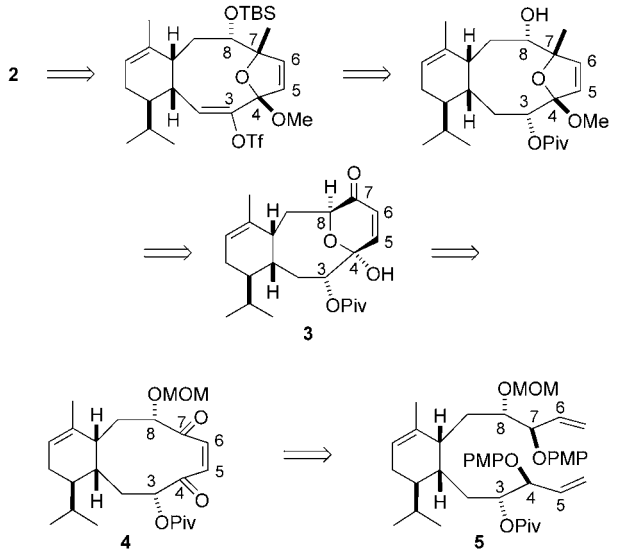
*Damiano Castoldi, Lorenzo Caggiano, Laura Panigada, Ofer Sharon, Anna M. Costa, and Cesare Gennari**

Sarcodictyins A (**1a**) and B (**1b**) were isolated in 1987 by Pietra and co-workers from the Mediterranean stoloniferan coral *Sarcodictyon roseum*.[1] Their antitumor activity was recognized about a decade later, and their taxol-like mechanism of action was discovered in 1996.[2] In the meantime, the diterpene glycoside eleutherobin (**2**) was reported by Fenical et al. from an *Eleutherobia* species of Australian soft coral, accompanied by disclosure of its potent cytotoxicity in 1995.[3] Two years later, eleutherobin was shown to act similarly to the sarcodictyins, effecting mitotic arrest through tubulin polymerization.[4] Both sarcodictyins and eleutherobin (the "eleutheside" family of microtubule-stabilizing drugs) are characterized by an activity profile different from that of taxol; they are active against taxol-resistant tumor cell lines and therefore hold potential as second-generation microtubule-stabilizing anticancer agents.[4,5] The scarce availability of **1** and **2** from natural sources makes their total syntheses vital for further biological investigations.[5] To date, sarcodictyin A and B have been synthesized successfully by Nicolaou et al.,[6] who have also exploited a similar route to eleutherobin.[7] A subsequent report by Danishefsky and co-workers details an elegant alternative access to eleutherobin.[8] A number of synthetic approaches to the eleutheside natural products and syntheses of simplified analogues have also been described.[9]

1a: R = Me
1b: R = Et

2

Herein we report the preparation of **3**, a key intermediate in the synthesis reported by Danishefsky and co-workers,[8] and thus a formal total synthesis of eleutherobin (**2**) (Scheme 1). The main step of our strategy, used for obtaining the [8.4.0] fused bicyclic ring system **4**, is a ring-closing metathesis (RCM)[10] reaction of the densely functionalized diene **5**.



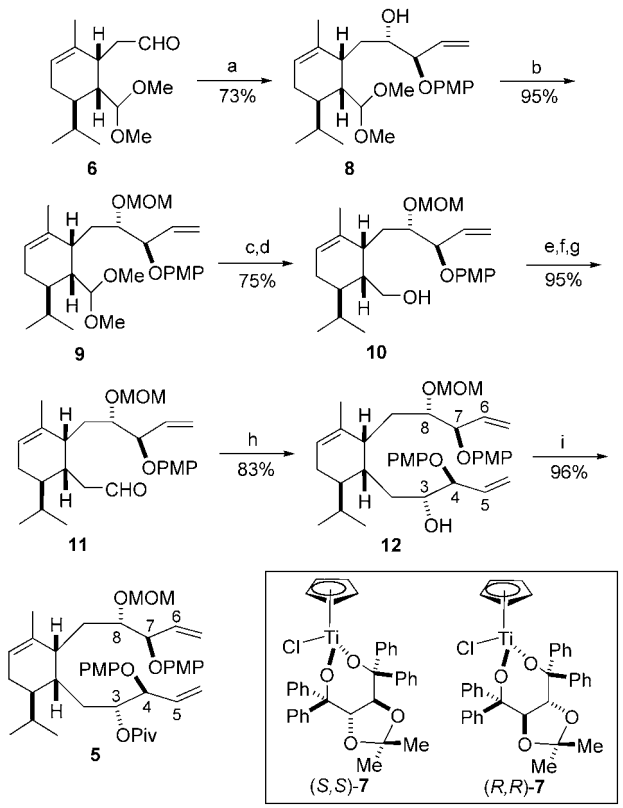
Scheme 1. Retrosynthetic analysis of eleutherobin (**2**).

Diene **5** was synthesized from aldehyde **6** (prepared in six steps on a multigram scale from *R*-(−)-carvone in 30% overall yield)[9a,g] through multiple stereoselective Hafner–Duthaler oxyallylations (Scheme 2).[11] The first oxyallylation, in the presence of the [(*S*,*S*)-taddolCpTiCl] complex **7**, proceeded with complete stereocontrol to give the desired stereoisomer **8** in 73% yield. After standard protection of the alcohol as the methoxymethyl ether **9** in 95% yield, cleavage of the dimethylacetal group and reduction with $NaBH_4$ to give **10** in 75% yield, an efficient and well-established sequence of steps[8c,9n] led to the homologated aldehyde **11** (95%). The same oxyallylation procedure described above was applied, this time in the presence of the [(*R*,*R*)-taddolCpTiCl] complex **7**, to give the desired alcohol **12** in 83% yield with

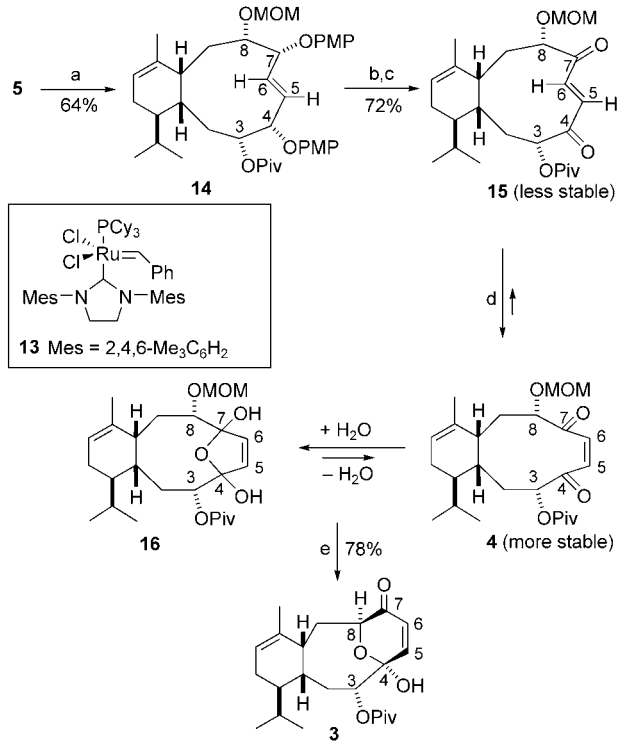
[*] D. Castoldi, Dr. L. Caggiano,[+] L. Panigada, Dr. O. Sharon, Prof. Dr. C. Gennari
Dipartimento di Chimica Organica e Industriale
Centro di Eccellenza C.I.S.I., Università degli Studi di Milano
Istituto di Scienze e Tecnologie Molecolari (ISTM) del CNR
Via G. Venezian 21, 20133 Milano (Italy)
Fax: (+39) 02-5031-4072
E-mail: cesare.gennari@unimi.it
Dr. A. M. Costa
Departamento de Química Orgànica
Universitat de Barcelona
Av. Diagonal 647, 08028 Barcelona (Spain)
[+] Current address: Department of Chemistry
University of Sheffield
Dainton Building, Brook Hill, Sheffield, S3 7HF (UK)

[**] We thank the European Commission for financial support (IHP Network grant "Design and synthesis of microtubule stabilizing anticancer agents" HPRN-CT-2000-00018) and for postdoctoral fellowships to L. C. (HPRN-CT-2000-00018) and O. S. ("Marie Curie" MEIF-CT-2003-500880). We also thank "Merck Research Laboratories" (Merck's Academic Development Program Award to C. G.) and Università degli Studi di Milano for financial support and for a graduate fellowship (to D. Castoldi). We thank Dr. Raphael Beumer, Dr. Pau Bayón, Dr. Joachim Telser, and Dr. Fabienne Pradaux for preliminary experiments related to this work, as well as Dr. Nicola Mongelli (Nerviano Medical Science) and Prof. Jaume Vilarrasa (University of Barcelona) for inspiring discussions.

 © 2005 Wiley-VCH Verlag GmbH & Co. KGaA, Weinheim DOI: 10.1002/anie.200461767



Scheme 2. Reagents and conditions: a) *s*-BuLi (1.3 M in cyclohexane), PMPOAllyl, [(*S*,*S*)-taddolCpTiCl] **7**, THF/Et_2O (57:43), −78→0 °C, 73 %; b) DIPEA, TBAI, MOMCl, CH_2Cl_2, 25 °C, 95 %; c) $LiBF_4$, CH_3CN/H_2O (98:2), 25 °C; d) $NaBH_4$, EtOH, 25 °C, 75 % over two steps; e) MsCl, TEA, CH_2Cl_2, 0→25 °C, 95 %; f) KCN, [18]crown-6, CH_3CN, 80 °C, quant.; g) DIBAL-H, toluene/hexane (1:2), −78 °C, quant.; h) *s*-BuLi (1.4 M in cyclohexane), PMPOAllyl, [(*R*,*R*)-taddolCpTiCl] **7**, Et_2O/THF (81:19), −78→25 °C, 83 %; i) PivCl, DMAP, DIPEA, CH_2Cl_2, 25 °C, 96 %. PMP = *p*-methoxyphenyl; DIPEA = diisopropylethylamine; TBAI = tetrabutylammonium iodide; MOM = methoxymethyl; Ms = methanesulfonyl; TEA = triethylamine; DIBAL-H = diisobutylaluminum hydride; Piv = *tert*-BuCO; DMAP = 4-(dimethylamino)pyridine; taddol = 1,1,4,4-tetraphenyl-2,3-O-isopropylidene-threitol.



Scheme 3. Reagents and conditions: a) cat. **13** (30 mol %), toluene, 110 °C, 6.5 h, 64 %; b) CAN, CH_3CN/H_2O (4:1), 0 °C, 80 %; c) DMP, CH_2Cl_2, 25 °C, 90 %; d) $CDCl_3$, 25 °C; e) $BF_3{\cdot}Et_2O$, Me_2S, CH_2Cl_2, −78→−20 °C, 78 %. CAN = ceric ammonium nitrate; DMP = Dess–Martin periodinane.

complete stereocontrol. Homoallylic alcohol **12** was then transformed into the pivalate **5** (96 %), and this diene was subjected to ring-closing metathesis.

The RCM reaction of a number of densely functionalized diene cyclization precursors of type **5** (bearing protected and/or free alcohol functionalities at both the allylic and the homoallylic positions) had previously been investigated with a variety of catalysts, but no desired cyclized frameworks were obtained.[9o] However, none of the previously examined diene precursors had the allylic alcohols protected as *p*-methoxyphenyl (PMP) ethers, which were discovered to facilitate the RCM reaction in comparison with other protective groups and with the free alcohols.[9o]

Based on these premises, diene **5** was treated with the second-generation Grubbs RCM catalyst[12] **13** (Scheme 3). Under forcing conditions[13] (slow addition by syringe pump (over 2.5 h) of a solution of RCM catalyst **13** (30 mol %) in toluene to a boiling solution of **5** in toluene, and additional stirring for 4 h at 110 °C), the *E* stereoisomer **14**[14] was formed and isolated in 64 % yield. This result contrasts sharply with many other *Z*-selective RCM reactions of diene cyclization precursors less-densely functionalized than diene **5**, that is, bearing protected and/or free alcohol functionalities at both the homoallylic positions and at only one allylic position.[9-h,m,n,o] In the presence of a second-generation Grubbs catalyst, these dienes lead to the more stable *Z*-cyclized products under thermodynamic control.[15] Preliminary molecular-mechanics calculations[16] show that the *E* stereoisomer **A** (corresponding to **14**) is less stable than the *Z* stereoisomer **B** by ≈ 6.6 kJ mol^{-1} (Figure 1). This energy difference increases to approximately 15.0 kJ mol^{-1} when the lowest-energy conformers are optimized at the PM3 level.[17] The reasons why the less stable *E* stereoisomer **14** was formed on this occasion (under kinetic control) and no trace of the more stable *Z* stereoisomer could be identified in the reaction mixture are not completely clear and will be investigated in detail. At the moment we can offer a tentative explanation as follows: the *trans* ruthenium-cyclobutane intermediate might be more stable than the *cis* species, leading to the *E* stereoisomer under kinetic control. Once formed, the *E* double bond of **14**, flanked by two bulky OPMP groups, might be too sterically hindered to react again with the ruthenium methylidene via cycloaddition and cycloreversion, thus arresting the equilibrium between the ring-closed and ring-opened products and inhibiting thermodynamic control.[18]

Confident that the greater stability of the *Z* 10-membered carbocycle would eventually prevail, we continued our

 © 2005 Wiley-VCH Verlag GmbH & Co. KGaA, Weinheim

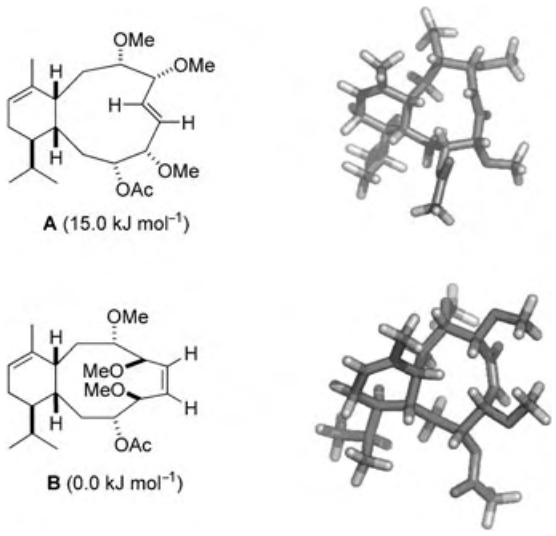


Figure 1. Lowest energy conformers and relative energies of the *E* stereoisomer **A** (corresponding to **14**) and of the *Z* stereoisomer **B**, obtained at the PM3 level.[16,17]

planned synthesis by removal of the PMP groups (CAN, 80%) and oxidation of the allylic diol (DMP, 90%). Enedione **15** (5-H, 6-H: $\delta = 7.02$, 6.64 ppm; $^3J_{5,6\text{-H}} = 17.3$ Hz) showed remarkable properties: while recording its ^{1}H NMR spectrum in $CDCl_3$ it cleanly isomerized to the more stable *Z* stereoisomer **4** (5-H, 6-H: $\delta = 7.20$, 6.13 ppm; $^3J_{5,6\text{-H}} = 14.0$ Hz; $t_{1/2} =$ 63 h). Bis-hemiacetal **16** (5-H, 6-H: $\delta = 6.29$, 6.18 ppm; $^3J_{5,6\text{-H}} = 5.8$ Hz) was obtained as the only product after flash chromatography of the *Z* enedione **4**, showing the propensity of **4** to add water and equilibrate with its hydrated form.[19] Finally, the MOM protecting group of the **15**/**4**/**16** mixture was removed ($BF_3{\cdot}Et_2O$, Me_2S)[20] to give compound **3** (78%), which produced analytical data identical to those previously reported by Danishefsky and co-workers (^{1}H NMR, ^{13}C NMR, IR spectroscopy, HRMS, R_f, $[\alpha]_D$).[8c]

In summary, we have completed a formal total synthesis of eleutherobin (**2**) through: 1) multiple stereoselective titanium-mediated oxyallylations, 2) an unprecedented kinetically controlled RCM reaction of a densely functionalized diene bearing two allylic alcohols protected as PMP ethers in the presence of a second-generation Grubbs catalyst, and 3) the isomerization of an *E* 10-membered enedione to the more stable *Z* 10-membered enedione.

Received: August 23, 2004
Published online: December 13, 2004

Keywords: antitumor agents · asymmetric synthesis · metathesis · natural products · total synthesis

[1] a) M. D'Ambrosio, A. Guerriero, F. Pietra, *Helv. Chim. Acta* **1987**, *70*, 2019–2027; b) M. D'Ambrosio, A. Guerriero, F. Pietra, *Helv. Chim. Acta* **1988**, *71*, 964–976.

[2] a) M. Ciomei, C. Albanese, W. Pastori, M. Grandi, F. Pietra, M. D'Ambrosio, A. Guerriero, C. Battistini, *Proc. Am. Assoc. Cancer Res.* **1997**, *38*, 5 ; b) C. Battistini, M. Ciomei, F. Pietra, M. D'Ambrosio, A. Guerriero (Pharmacia S.p.A.), PCT Int. Appl. WO 9636335, **1996** [*Chem. Abstr.* **1997**, *126*, P54863x].

[3] W. Fenical, P. R. Jensen, T. Lindel (University of California), US 5473057, **1995** [*Chem. Abstr.* **1996**, *124*, P194297z].

[4] a) T. Lindel, P. R. Jensen, W. Fenical, B. H. Long, A. M. Casazza, J. Carboni, C. R. Fairchild, *J. Am. Chem. Soc.* **1997**, *119*, 8744–8745; b) B. H. Long, J. M. Carboni, A. J. Wasserman, L. A. Cornell, A. M. Casazza, P. R. Jensen, T. Lindel, W. Fenical, C. R. Fairchild, *Cancer Res.* **1998**, *58*, 1111–1115.

[5] For a comprehensive review on the chemistry and biology of the eleuthesides, see: K. C. Nicolaou, J. Pfefferkorn, J. Y. Xu, N. Winssinger, T. Ohshima, S. Kim, S. Hosokawa, D. Vourloumis, F. van Delft, T. Li, *Chem. Pharm. Bull.* **1999**, *47*, 1199–1213. See also: a) K. C. Nicolaou, N. Winssinger, D. Vourloumis, T. Ohshima, S. Kim, J. Pfefferkorn, J. Y. Xu, T. Li, *J. Am. Chem. Soc.* **1998**, *120*, 10814–10826; b) R. Britton, E. D. de Silva, C. M. Bigg, L. M. McHardy, M. Roberge, R. J. Andersen, *J. Am. Chem. Soc.* **2001**, *123*, 8632–8633, and references therein.

[6] a) K. C. Nicolaou, J. Y. Xu, S. Kim, T. Ohshima, S. Hosokawa, J. Pfefferkorn, *J. Am. Chem. Soc.* **1997**, *119*, 11353–11354; b) K. C. Nicolaou, J. Y. Xu, S. Kim, J. Pfefferkorn, T. Ohshima, D. Vourloumis, S. Hosokawa, *J. Am. Chem. Soc.* **1998**, *120*, 8661–8673; c) K. C. Nicolaou, S. Kim, J. Pfefferkorn, J. Y. Xu, T. Ohshima, S. Hosokawa, D. Vourloumis, T. Li, *Angew. Chem.* **1998**, *110*, 1484–1487; *Angew. Chem. Int. Ed.* **1998**, *37*, 1418–1421.

[7] a) K. C. Nicolaou, F. van Delft, T. Ohshima, D. Vourloumis, J. Y. Xu, S. Hosokawa, J. Pfefferkorn, S. Kim, T. Li, *Angew. Chem.* **1997**, *109*, 2631–2634; *Angew. Chem. Int. Ed. Engl.* **1997**, *36*, 2520–2524; b) K. C. Nicolaou, T. Ohshima, S. Hosokawa, F. L. van Delft, D. Vourloumis, J. Y. Xu, J. Pfefferkorn, S. Kim, *J. Am. Chem. Soc.* **1998**, *120*, 8674–8680.

[8] a) X.-T. Chen, C. E. Gutteridge, S. K. Bhattacharya, B. Zhou, T. R. R. Pettus, T. Hascall, S. J. Danishefsky, *Angew. Chem.* **1998**, *110*, 195–197; *Angew. Chem. Int. Ed.* **1998**, *37*, 185–187; b) X.-T. Chen, B. Zhou, S. K. Bhattacharya, C. E. Gutteridge, T. R. R. Pettus, S. J. Danishefsky, *Angew. Chem.* **1998**, *110*, 835–838; *Angew. Chem. Int. Ed.* **1998**, *37*, 789–792; c) X.-T. Chen, S. K. Bhattacharya, B. Zhou, C. E. Gutteridge, T. R. R. Pettus, S. J. Danishefsky, *J. Am. Chem. Soc.* **1999**, *121*, 6563–6579.

[9] a) S. Ceccarelli, U. Piarulli, C. Gennari, *Tetrahedron Lett.* **1999**, *40*, 153–156; b) A. Baron, V. Caprio, J. Mann, *Tetrahedron Lett.* **1999**, *40*, 9321–9324; c) R. Carter, K. Hodgetts, J. McKenna, P. Magnus, S. Wren, *Tetrahedron* **2000**, *56*, 4367–4382; d) S. Ceccarelli, U. Piarulli, C. Gennari, *J. Org. Chem.* **2000**, *65*, 6254–6256; e) Q. Xu, M. Weeresakare, J. D. Rainier, *Tetrahedron* **2001**, *57*, 8029–8037; f) S. Ceccarelli, U. Piarulli, J. Telser, C. Gennari, *Tetrahedron Lett.* **2001**, *42*, 7421–7425; g) S. Ceccarelli, U. Piarulli, C. Gennari, *Tetrahedron* **2001**, *57*, 8531–8542; h) J. Telser, R. Beumer, A. A. Bell, S. M. Ceccarelli, D. Monti, C. Gennari, *Tetrahedron Lett.* **2001**, *42*, 9187–9190; i) C. Sandoval, E. Redero, M. A. Mateos-Timoneda, F. A. Bermejo, *Tetrahedron Lett.* **2002**, *43*, 6521–6524; j) K. P. Kaliappan, N. Kumar, *Tetrahedron Lett.* **2003**, *44*, 379–381; k) J. D. Winkler, K. J. Quinn, C. H. MacKinnon, S. D. Hiscock, E. C. McLaughlin, *Org. Lett.* **2003**, *5*, 1805–1808; l) G. Scalabrino, X.-W. Sun, J. Mann, A. Baron, *Org. Biomol. Chem.* **2003**, *1*, 318–327; m) R. Beumer, P. Bayón, P. Bugada, S. Ducki, N. Mongelli, F. Riccardi Sirtori, J. Telser, C. Gennari, *Tetrahedron Lett.* **2003**, *44*, 681–684; n) R. Beumer, P. Bayón, P. Bugada, S. Ducki, N. Mongelli, F. Riccardi Sirtori, J. Telser, C. Gennari, *Tetrahedron* **2003**, *59*, 8803–8820; o) L. Caggiano, D. Castoldi, R. Beumer, P. Bayón, J. Telser, C. Gennari, *Tetrahedron Lett.* **2003**, *44*, 7913–7919; p) N. Ritter, P. Metz, *Synlett* **2003**, 2422–2424.

[10] For reviews, see: a) R. H. Grubbs, S. Chang, *Tetrahedron* **1998**, *54*, 4413–4450; b) S. K. Armstrong, *J. Chem. Soc. Perkin Trans. 1* **1998**, 371–388; c) M. E. Maier, *Angew. Chem.* **2000**, *112*, 2153–

 © 2005 Wiley-VCH Verlag GmbH & Co. KGaA, Weinheim

2157; *Angew. Chem. Int. Ed.* **2000**, *39*, 2073 – 2077; d) A. Fürstner, *Angew. Chem.* **2000**, *112*, 3140 – 3172; *Angew. Chem. Int. Ed.* **2000**, *39*, 3012 – 3043.

[11] A. Hafner, R. O. Duthaler, R. Marti, G. Rhis, P. Rothe-Streit, F. Schwarzenbach, *J. Am. Chem. Soc.* **1992**, *114*, 2321 – 2336, and references therein.

[12] a) J. Huang, E. D. Stevens, S. P. Nolan, J. L. Petersen, *J. Am. Chem. Soc.* **1999**, *121*, 2674 – 2678; b) M. Scholl, T. M. Trnka, J. P. Morgan, R. H. Grubbs, *Tetrahedron Lett.* **1999**, *40*, 2247 – 2250; c) J. Huang, H.-J. Schanz, E. D. Stevens, S. P. Nolan, *Organometallics* **1999**, *18*, 5375 – 5380; d) M. Scholl, S. Ding, C. W. Lee, R. H. Grubbs, *Org. Lett.* **1999**, *1*, 953 – 956; e) T. M. Trnka, R. H. Grubbs, *Acc. Chem. Res.* **2001**, *34*, 18 – 29.

[13] For a discussion of these optimized RCM conditions, see: K. Yamamoto, K. Biswas, C. Gaul, S. J. Danishefsky, *Tetrahedron Lett.* **2003**, *44*, 3297 – 3299.

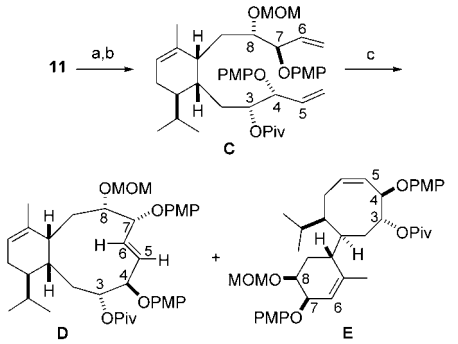
[14] The 5-H/6-H coupling constant was determined from a decoupled ^{1}H NMR spectrum acquired by irradiation at $\delta = 5.04$ ppm, which corresponds to the frequency of protons 4-H and 7-H. The signals of the olefinic protons (at $\delta = 5.96$ and 5.71 ppm, assigned to protons 5-H and 6-H) became two doublets whose coupling constant, typical of an *E* double bond, was easily determined: $^3J_{5,6\text{-H}} = 16.5$ Hz. The NOESY spectrum showed two positive cross peaks due to scalar coupling (*E* double bond), instead of two negative cross peaks due to NOE (*Z* double bond).

[15] The use of second-generation metathesis catalysts usually results in the selective formation of the thermodynamically favored stereoisomeric products in RCM reactions, which furnish medium-sized rings: a) C. W. Lee, R. H. Grubbs, *Org. Lett.* **2000**, *2*, 2145 – 2147; b) A. Fürstner, K. Radkowski, C. Wirtz, R. Goddard, C. W. Lehmann, R. Mynott, *J. Am. Chem. Soc.* **2002**, *124*, 7061 – 7069; c) J. Murga, E. Falomir, J. Garcìa-Fortanet, M. Carda, J. A. Marco, *Org. Lett.* **2002**, *4*, 3447 – 3449; d) J. Prunet, *Angew. Chem.* **2003**, *115*, 2932 – 2936; *Angew. Chem. Int. Ed.* **2003**, *42*, 2826 – 2830.

[16] The calculations were performed at the University of Barcelona. Lowest-energy conformers of structures **A** and **B** were calculated by performing Monte Carlo conformational searches (50000 steps for each isomer) with MacroModel 8.5 (MM2*, $CHCl_3$ GB/SA): a) F. Mohamadi, N. G. J. Richards, W. C. Guida, R. Liskamp, M. Lipton, C. Caufield, G. Chang, T. Hendrickson, W. C. Still, *J. Comput. Chem.* **1990**, *11*, 440 – 467; b) G. Chang, W. C. Guida, W. C. Still, *J. Am. Chem. Soc.* **1989**, *111*, 4379 – 4386; c) W. C. Still, A. Tempczyk, R. C. Hawley, T. Hendrickson, *J. Am. Chem. Soc.* **1990**, *112*, 6127 – 6129.

[17] The lowest-energy conformers obtained with MacroModel for isomers **A** and **B** (180 and 97 conformers respectively, using a 20.0 kJ mol^{-1} energy window from the global minima) were optimized at the PM3 level using the Gaussian 03 package (Gaussian 03 (Revision B.04), M. J. Frisch, G. W. Trucks, H. B. Schlegel, G. E. Scuseria, M. A. Robb, J. R. Cheeseman, J. A. Montgomery, Jr., T. Vreven, K. N. Kudin, J. C. Burant, J. M. Millam, S. S. Iyengar, J. Tomasi, V. Barone, B. Mennucci, M. Cossi, G. Scalmani, N. Rega, G. A. Petersson, H. Nakatsuji, M. Hada, M. Ehara, K. Toyota, R. Fukuda, J. Hasegawa, M. Ishida, T. Nakajima, Y. Honda, O. Kitao, H. Nakai, M. Klene, X. Li, J. E. Knox, H. P. Hratchian, J. B. Cross, C. Adamo, J. Jaramillo, R. Gomperts, R. E. Stratmann, O. Yazyev, A. J. Austin, R. Cammi, C. Pomelli, J. W. Ochterski, P. Y. Ayala, K. Morokuma, G. A. Voth, P. Salvador, J. J. Dannenberg, V. G. Zakrzewski, S. Dapprich, A. D. Daniels, M. C. Strain, O. Farkas, D. K. Malick, A. D. Rabuck, K. Raghavachari, J. B. Foresman, J. V. Ortiz, Q. Cui, A. G. Baboul, S. Clifford, J. Cioslowski, B. B. Stefanov, G. Liu, A. Liashenko, P. Piskorz, I. Komaromi, R. L. Martin, D. J. Fox, T. Keith, M. A. Al-Laham, C. Y. Peng, A. Nanayakkara, M. Challacombe, P. M. W. Gill, B. Johnson, W. Chen, M. W. Wong, C. Gonzalez, J. A. Pople, Gaussian, Inc., Pittsburgh, PA, **2003**).

[18] The RCM reaction of a diastereoisomer of **5** (**C**) was also investigated. The *E* stereoisomer **D** ($^3J_{5,6\text{-H}} = 17.0$ Hz) was obtained (27%) together with the rearranged product **E** (15%), which originates from a ring-opening metathesis/ring-closing metathesis (ROM/RCM) process involving the trisubstituted double bond of the cyclohexene ring and the two terminal alkenes. Compound **D** was transformed into the target molecule **3** through the same sequence of reactions described in Scheme 3. Reagents and conditions: a) PMPOAllyl, *s*-BuLi (1.4 M in cyclohexane), (+)-Ipc_2BOMe, $BF_3{\cdot}Et_2O$, THF, −78 °C → 25 °C, 40%; b) PivCl, DMAP, DIPEA, CH_2Cl_2, 25 °C, 83%; c) cat. **13** (30 mol%), toluene, 110 °C, 6.5 h, 27% **D**, 15% **E**. PMP = *p*-methoxyphenyl; Piv = *tert*-BuCO; DMAP = 4-(dimethylamino)pyridine; DIPEA = diisopropylethylamine; (+)-Ipc_2BOMe = (+)-*B*-methoxydiisopinocampheylborane. For *syn*-selective boron-mediated oxyallylation reactions, see: H. C. Brown, P. K. Jadhav, K. S. Bhat, *J. Am. Chem. Soc.* **1988**, *110*, 1535 – 1538.



[19] ESI HRMS (resolution: 25800) of the *Z* enedione **4**, from a MeOH/H_2O (98:2) solution, gave the exact molecular ions $[M+Na]^+$ for **4** (calcd for $C_{25}H_{38}NaO_6$: 457.25606; found: 457.25582; error = 0.52 ppm), the hydrated form **16** (calculated for $C_{25}H_{40}NaO_7$: 475.26662; found: 475.26681; error = 0.40 ppm), and the hemiacetal-methylacetal corresponding to the addition of MeOH (calcd for $C_{26}H_{42}NaO_7$: 489.28227; found: 489.28031; error = 4.00 ppm).

[20] a) K. Fuji, T. Kawabata, E. Kujita, *Chem. Pharm. Bull.* **1980**, *28*, 3662 – 3664; b) M. Sasaki, T. Noguchi, K. Tachibana, *J. Org. Chem.* **2002**, *67*, 3301 – 3310.

 © 2005 Wiley-VCH Verlag GmbH & Co. KGaA, Weinheim

Metal-Induced Cyclization

A Unique Approach to Metal-Induced Bergman Cyclization: Long-Range Enediyne Activation by Ligand-to-Metal Charge Transfer**

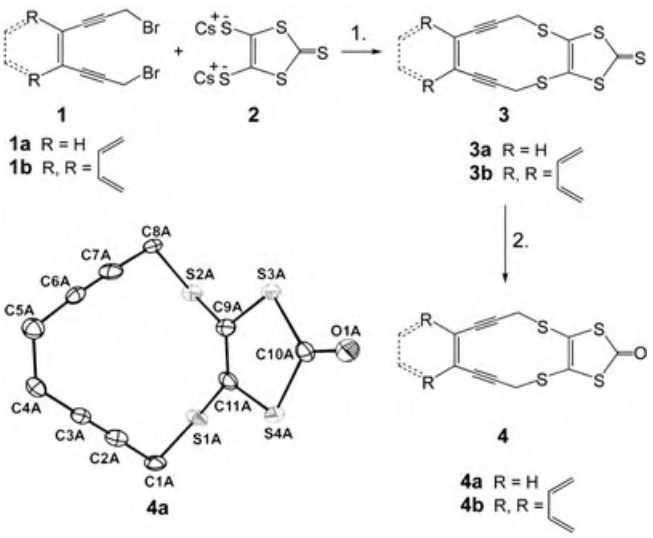
Sibaprasad Bhattacharyya, Maren Pink, Mu-Hyun Baik, and Jeffrey M. Zaleski**

The development of stable enediyne constructs and subsequent low-temperature routes to Bergman-cyclized diradical formation are paramount for this class of molecule to realize its potential in biological applications. Metals have been shown to thermally activate stable enediynes by both σ-donor coordination[1–5] and π complexation,[6,7] which induce a marked reduction in the thermal barrier to Bergman cyclization. Despite these advances, the scope of the metal-activated Bergman cyclization remains poorly defined.

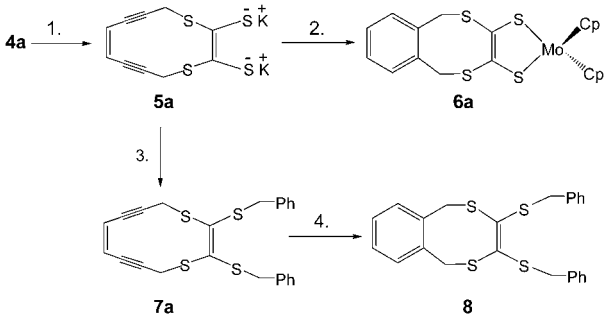
Electronic factors[8] that contribute to metal-centered enediyne activation are more elusive than the established influences of the geometry around the metal center.[1–5] Computational[9,10] and experimental[11] evaluations of the Bergman cyclization reaction coordinate show that σ acceptor/π donor functionalities at the alkyne termini reduce the activation barrier to diradical formation. In an effort to extend this model, we questioned whether binding of a strong Lewis acid in the vicinity of the alkyne termini would induce sufficient electron polarization to promote enediyne cyclization in an analogous manner. Herein, we report the preparation of Mo^{IV}–enedithiolate–enediyne complexes that show considerable differences in reactivity, which can be directly attributed to electron polarization rather than geometric effects of the metal center.

Reaction of 1,8-dibromooct-4-ene-2,6-diyne (**1a**) with the dicesium salt of 1,3-dithiole-2-thione-4,5-dithiolate (DMIT; **2**) generates **3a** in low (ca. 20%) yield (Scheme 1). Addition of **3a** to a stirred slurry of mercury(II) acetate in chloroform/acetic acid (3:1) affords the dithiol-2-one **4a** in 60% yield. The benzannulated counterpart **4b** was prepared analogously using 1,2-bis(3-bromopropynyl)benzene (**1b**) as the starting material. Compounds **4a** and **4b** are stable in solution and do not cyclize upon heating at 180°C in DMSO/1,4-cyclohexadiene (CHD; 1:100) over 12 h.

The dipotassium salt of enediyne ligand 3,10-dialkylthiacyclododec-1,6-ene-4,8-diyne-1,2-dithiolate (**5a**) was prepared by addition of two equivalents of EtOK to a slurry of **4a** in methanol to yield **5a** in situ as a light yellow solution (Scheme 2). The benzannulated dipotassium salt **5b** was prepared in the same manner from **4b**. Both **5a** and **5b** are stable at ambient temperature in methanol under nitrogen for 3 hours, and at 80°C for 1.5 hours, prior to slow decomposition to non-Bergman side products.



Scheme 1. Synthesis and X-ray structure of **4** (40% probability). 1) MeOH, 0°C, 12 h, 20%; 2) $CHCl_3$/AcOH (3:1), $Hg(OAc)_2$, RT, 12 h, 60%.



Scheme 2. Bergman cyclization of **5a** and thermal reactivity of **7a**. 1) MeOH, KOEt (2 equiv), RT, 15 min; 2) $[MoCp_2Cl_2]$, CHD, 60°C, 30 min, 40%; 3) $PhCH_2Br$, 25°C, 80%; 4) DMSO, CHD, 180°C, 24 h, 60%.

Heating of **5a** in the presence of dichlorobis(η⁵-cyclopentadienyl)molybdenum(IV) in methanol/CHD (1:100) at 60°C for 0.5 h affords the Bergman-cyclized product **6a** in approximately 40% yield, with the remaining mass balance consisting of insoluble polymeric materials common to Bergman cyclization reactions. No metal complexation or product formation are observed at lower temperatures, while decomposition occurs without an increase in product yield at higher temperatures. The X-ray structure of **6a** (Figure 1) exhibits a pseudo-tetrahedrally coordinated Mo^{IV} center with two thiolate ligands from the enediyne chelate and two η⁵-cyclopentadienyl (Cp) rings bound in the plane perpendicular to the enedithiolate core. The newly formed aromatic ring is

[*] S. Bhattacharyya, M. Pink, Prof. M.-H. Baik, Prof. J. M. Zaleski
Department of Chemistry
Indiana University
800 E. Kirkwood Avenue, Bloomington, IN 47405 (USA)
Fax: (+1) 812-855-8300
E-mail: mbaik@indiana.edu
zaleski@indiana.edu

[**] The support of the National Institutes of Health (R01 GM62541-01) and the National Science Foundation (0116050) is gratefully acknowledged.

Supporting information for this article is available on the WWW under http://www.angewandte.org or from the author.

 © 2005 Wiley-VCH Verlag GmbH & Co. KGaA, Weinheim DOI: 10.1002/anie.200461825

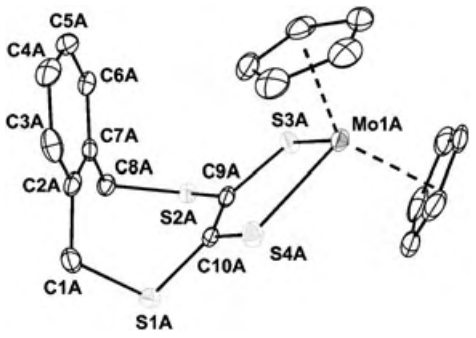
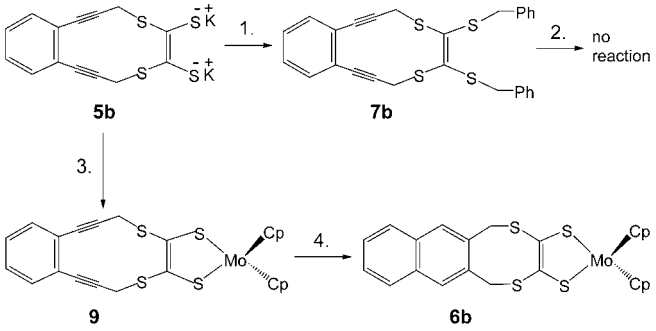


Figure 1. X-ray structure of **6a**. Thermal ellipsoids are illustrated at 40% probability.



Scheme 3. Contrasting reactivities of **7b** and **9**. 1) $PhCH_2Br$, 25 °C, 80%; 2) DMSO, CHD, 180 °C, 24 h; 3) MeOH, $[MoCp_2Cl_2]$, 60 °C, 30 min, 42%; 4) DMSO, CHD, 120 °C, 5 h, 15%.

poised above the Mo–S_2C_2 plane as a consequence of the two pairs of sp^3 sulfur and carbon atoms between the metal–enedithiolate and aromatic substructures.

To evaluate whether σ coordination or π complexation promoted the cyclization reaction, **5a** was benzylated to **7a** by reaction with benzyl bromide (Scheme 2). Compound **7a** is highly stable, but can be cyclized to **8** in 60% yield by heating in solution (DMSO/CHD, 1:100) for 24 h at 180 °C. In contrast, the refluxing of **7a** with $[MoCp_2Cl_2]$ in methanol/THF solution at 60 °C in the presence of excess CHD results in no reaction, thereby disqualifying a π interaction between the enediyne fragment and molybdenum as the origin of enediyne activation. DFT calculations[12] confirm the enhancement in reactivity by molybdenum complexation, and predict an activation enthalpy of 17.7 kcal mol^{-1} to give the transition state **7c-TS**, whereas the transition state **7a-TS** for the benzylated analogue **7a** has an activation enthalpy of 21.9 kcal mol^{-1}. The structures of the transition states are analogous to that previously described elsewhere for a prototype reaction.[13] These activation parameters are in excellent agreement with the kinetics for conversion of **5a**→**6a** ($\Delta H^{\neq} = 14.25$ kcal mol^{-1}; $\Delta S^{\neq} = -31.52$ eu). Since cyclization of **7a**→**8** requires heating between 150 °C (no reaction) and 180 °C (24 h, 60%), the reaction barrier is estimated from a simple Arrhenius proportion to be 3–5 kcal mol^{-1} higher than that for formation of **6a**, which is also in good agreement with the trend of the calculated enthalpies of activation for these compounds.

Parallel reactions were performed with the benzannulated ligand **5b**, which is thermally more stable toward Bergman cyclization than **5a** as a result of the higher endothermicity of the Bergman reaction, which makes the retrocyclization competitive with H-atom abstraction.[14,15] Within this theme, heating of benzylated derivative **7b** (prepared in an analogous manner to **7a**) at 180 °C for 24 h in DMSO/CHD (1:100) results in no reaction, which reflects the added enediyne stability introduced by benzannulation (Scheme 3). As a consequence of the enhanced stability and in contrast to the reactivity of **5a**, reaction of **5b** with $[MoCp_2Cl_2]$ at 60 °C for 0.5 h gives the uncyclized enediyne complex **9** in 42% yield. Subsequent heating of **9** at 120 °C for 5 h activates the ligand and generates Bergman-cyclized product **6b** in 15% yield, with considerable recovery of starting material (60%). Heating at higher temperatures leads to gradual decomposition of both starting material and cyclized product. The X-ray structures of metalloenediyne **9** and cyclized product **6b** (Figure 2) reveal similar pseudo-tetrahedral structures to that of **6a**. The separations of the alkyne termini (C2···C7) in **4a** and **9** are identical (4.05 Å), which suggests an electronic rather than a geometric origin for the observed cyclization temperatures. Consistent with this premise, Mo^{IV} complexes **6a**, **6b**, and **9** show characteristic $S \rightarrow Mo^{IV}$ ligand-to-metal charge-transfer transitions between 500 and 535 nm with significant molar extinction coefficients of $\varepsilon \approx 1300$–1700 M^{-1} cm^{-1} (Figure 3).

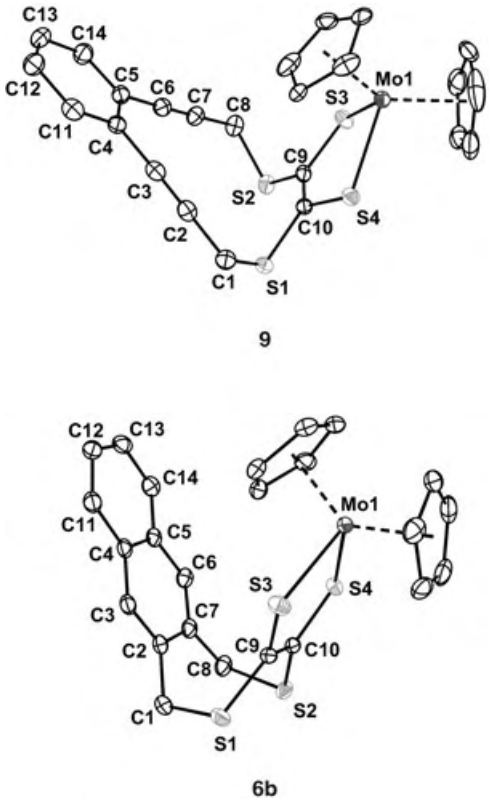


Figure 2. X-ray structures of metalloenediyne **9** and subsequent cyclized product **6b**. Thermal ellipsoids are illustrated at 40% probability.

 © 2005 Wiley-VCH Verlag GmbH & Co. KGaA, Weinheim

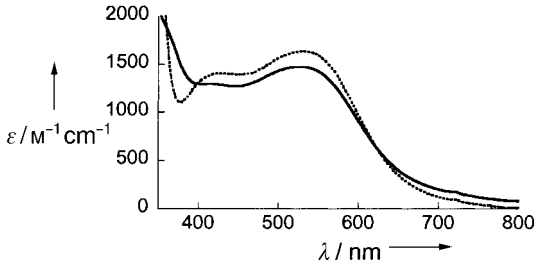


Figure 3. Electronic spectra of **9** (——) and **6b** (-----) in CH_2Cl_2.

To quantify the polarization effect, we examined the partial charges derived from our DFT-computed total densities (Figure 4) for cyclization of benzylated ligand **7a**→**7a-TS** and Mo complex **7c**→**7c-TS**. For the **7a**→**7a-TS** transformation, the enediyne carbon atoms C2 and C7 which form the developing σ bond become positively polarized by as much as 0.3–0.4 electron units as a result of the change in hybridization from sp^1 to sp^2, while C3 and C6 become the centers of the diradical electrons and are consequently negatively polarized. Complexation of the $\{MoCp_2\}$ fragment reduces the amplitudes of these differential charges at C2,C7 and C3,C6 notably for progression from **7c** to **7c-TS** (for example, the differential charges at C2 for **7a**→**7a-TS** and **7c**→**7c-TS** are 0.29 and 0.08, respectively), thus indicating a net delocalization of charge upon metal complexation, which lowers the energy of the cyclization transition state by reducing charge repulsion. This concept is a logical extension of a previously suggested mechanism that considered delocalization through hyperconjugation and electron repulsion as key contributions to the energy barriers for Bergman cyclization.[16–18]

In addition to the metal-induced electrostatic contribution to the disparate reactivities of **7a** and **7c**, there is superimposed a more complex ensemble of orbital effects that also supports a decrease in the activation barrier upon Lewis acid (for example, Mo^{IV}) complexation. The first consequence of metal binding is a lowering of the symmetric and antisymmetric enedithiolate orbitals by bonding interactions with the effective d_{z^2} and d_{xy} orbitals, respectively (see Supporting Information). Second, the molecular orbitals (MOs) involved in the formation of the developing C2–C7 σ bond, the in-phase and out-of-phase combinations of the in-plane π orbitals of the diyne (MO-104/MO-107 and MO-99/MO-101 of **7a** and **7c**, respectively; Figures 5 and 6), display no direct electronic interaction of the Mo center with the π orbitals, which suggests that the function of the metal center reported here may be general and valid for any Lewis acid. Third, comparison of the shapes of the two π MOs of **7a** and **7c** reveals that the disposition of the S-based lone-pair orbitals to

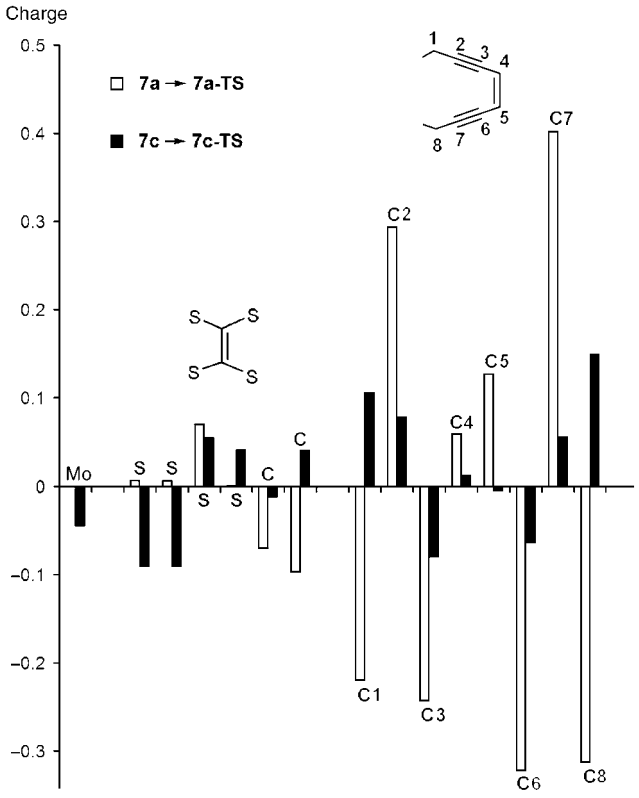


Figure 4. Partial charge changes accompanying the formation of the respective transition states. Charges are derived from fits of the electrostatic potential generated by the DFT-computed total electron densities.

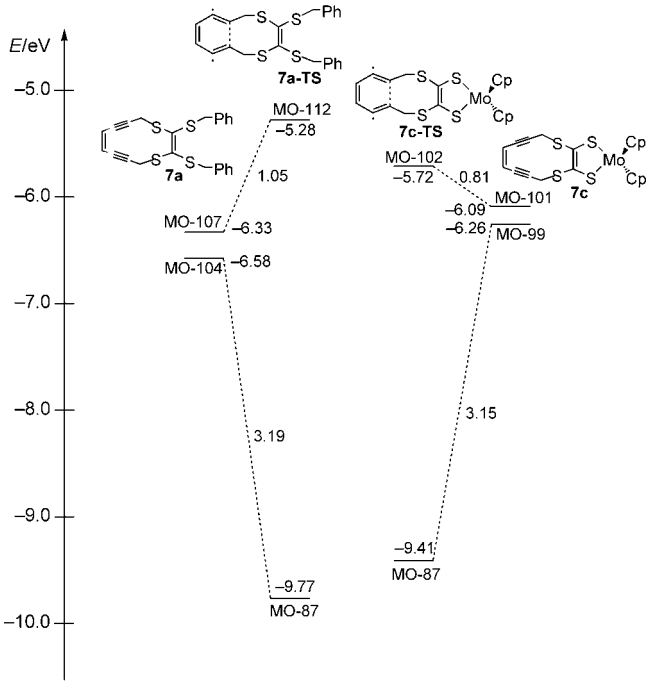


Figure 5. MO diagram illustrating the relative energy changes of the two most important MOs that promote C–C bond formation between the ground and transition states for the benzylated and metal-substituted enediynes, respectively. Orbital energies are indicated in eV.

 © 2005 Wiley-VCH Verlag GmbH & Co. KGaA, Weinheim

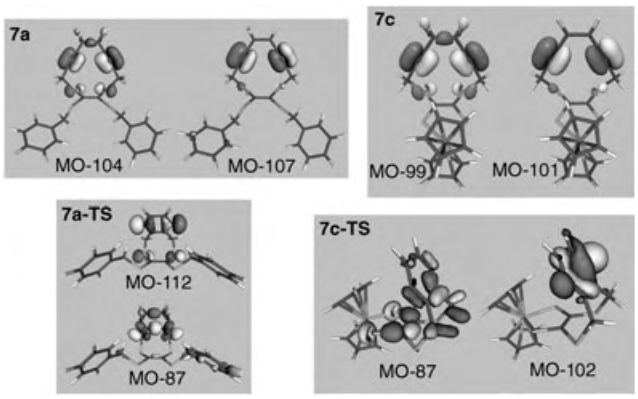


Figure 6. Isosurface plots (0.05 a.u.) of the most important MOs that are also illustrated in Figure 5.

lower energies by Mo complexation allows them to more efficiently mix with the diyne-based π orbitals. This differential polarization effect is strongly pronounced in the transition states; MO-87 of the metal complex (**7c**-**TS**) shows substantially more S character than the corresponding MO-87 of the benzylated ligand (**7a**-**TS**). Interestingly, this mixing has only a modest influence on the energy change of these MOs (Figure 5). Upon formation of **7a**-**TS**, MO-104 of **7a** becomes stabilized by 3.19 eV to give MO-87 of **7a**-**TS**, compared to the essentially identical stabilization of MO-99 in **7c** (3.15 eV) to give MO-87 in **7c**-**TS**. Thus, binding of the Lewis acid has only a minor impact on the energetics of σ-bond formation. However, the Mo center stabilizes the diradicaloid transition state by lowering the energy of MO-102 in **7c**-**TS** by 0.44 eV relative to its analogue MO-112 in **7a**-**TS**. This effect derives from the fact that MO-102 of **7c**-**TS** is characterized by a localized diradical, where electron density arising from a lone pair of electrons on the sulfur atom that could contribute to electron–electron repulsion in the transition state has been energetically removed by metal complexation. In contrast, MO-112 of **7a**-**TS** reveals participation of the electron density from the lone pair of electrons on the sulfur atom in the diradicaloid orbital of the transition state, which causes a net destabilization and concomitant decrease in thermal reactivity.

Summarizing the electronic structure origin of the differential reactivity of **7a** and **7c**: 1) many orbitals show σ-bond polarization upon metal complexation without a single dominant contribution; 2) net polarization caused by Mo^{IV} complexation delocalizes enediyne electron density and simultaneously removes charge repulsion in the 1,4-diradical orbital of the transition state; and 3) the net polarization effect on enediyne reactivity is likely transferable to other metal–enediyne motifs. More generally, we have demonstrated that high-valent metals can be effective cofactors for enediyne activation through electronic rather than geometric influences.

Received: August 30, 2004
Published online: December 7, 2004

Keywords: charge transfer · cyclization · enediynes · molybdenum · radicals

[1] B. P. Warner, S. P. Millar, R. D. Broene, S. L. Buchwald, *Science* **1995**, *269*, 814 – 816.
[2] B. Konig, W. Pitsch, I. Thondorf, *J. Org. Chem.* **1996**, *61*, 4258 – 4261.
[3] A. Basak, J. C. Shain, *Tetrahedron Lett.* **1998**, *39*, 3029 – 3030.
[4] P. J. Benites, D. S. Rawat, J. M. Zaleski, *J. Am. Chem. Soc.* **2000**, *122*, 7208 – 7217.
[5] D. S. Rawat, J. M. Zaleski, *J. Am. Chem. Soc.* **2001**, *123*, 9675 – 9676.
[6] J. M. O'Connor, L. I. Lee, P. Gantzel, A. L. Rheingold, K.-C. Lam, *J. Am. Chem. Soc.* **2000**, *122*, 12057 – 12058.
[7] J. M. O'Connor, S. J. Friese, M. Tichenor, *J. Am. Chem. Soc.* **2002**, *124*, 3506 – 3507.
[8] S. Bhattacharyya, A. E. Clark, M. Pink, J. M. Zaleski, *Chem. Commun.* **2003**, 1156 – 1157.
[9] N. Koga, K. Morokuma, *J. Am. Chem. Soc.* **1991**, *113*, 1907 – 1911.
[10] M. Prall, A. Wittkopp, A. A. Fokin, P. R. Schreiner, *J. Comput. Chem.* **2001**, *22*, 1605 – 1614.
[11] M. Nath, J. C. Huffman, J. M. Zaleski, *J. Am. Chem. Soc.* **2003**, *125*, 11484 – 11485.
[12] Calculations were carried out using Jaguar 5.5 (Schrödinger, Inc.) at the BPW91/6-31G**++ level of theory; the LACVP**++ basis set was utilized for Mo. Transition states were confirmed by vibrational frequency calculations.
[13] C. J. Cramer, *J. Am. Chem. Soc.* **1998**, *120*, 6261 – 6269.
[14] S. Koseki, Y. Fujimura, M. Hirama, *J. Phys. Chem. A* **1999**, *103*, 7672 – 7675.
[15] T. Kaneko, M. Takahashi, M. Hirama, *Tetrahedron Lett.* **1999**, *40*, 2015 – 2018.
[16] I. V. Alabugin, M. Manoharan, *J. Phys. Chem. A* **2003**, *107*, 3363 – 3371.
[17] I. V. Alabugin, M. Manoharan, S. V. Kovalenko, *Org. Lett.* **2002**, *4*, 1119 – 1122.
[18] I. V. Alabugin, T. A. Zeidan, *J. Am. Chem. Soc.* **2002**, *124*, 3175 – 3185.

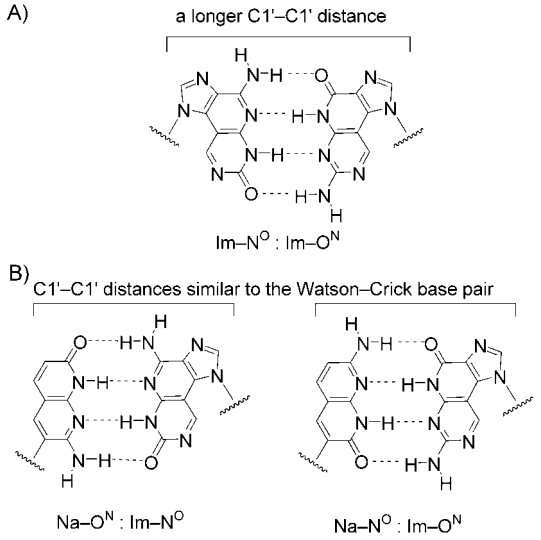
 © 2005 Wiley-VCH Verlag GmbH & Co. KGaA, Weinheim

Nonnatural Nucleotides

Synthesis of 1,8-Naphthyridine C-Nucleosides and Their Base-Pairing Properties in Oligodeoxynucleotides: Thermally Stable Naphthyridine:Imidazopyridopyrimidine Base-Pairing Motifs**

Sadao Hikishima, Noriaki Minakawa, Kazuyuki Kuramoto, Yuki Fujisawa, Maki Ogawa, and Akira Matsuda**

A number of nucleoside analogues that contain non-natural nucleobases have been synthesized and incorporated into oligodeoxynucleotides (ODNs) with the aim of biological, bioengineering, and therapeutic applications.[1,2] The development of new base-pairing motifs beyond the Watson–Crick hydrogen bonding (H bonding) model for thermal stability and specificity is therefore still an area of active research.[3,4] We recently reported the synthesis of imidazo[5′,4′:4,5]pyrido[2,3-*d*]pyrimidine nucleosides with the ability to form four H bonds and discussed their hybridization properties in ODNs (Scheme 1 A).[5,6] Accordingly, the Im-N^O:Im-O^N base pair markedly stabilized a duplex when three of the pairs were consecutively incorporated into ODNs. However, incorporation of one pair into ODNs resulted in destabilization of the duplex relative to those containing A:T and G:C base pairs. These results were explained by the conflicting effects of the Im-N^O:Im-O^N pair in ODNs, that is, the pair stabilizes the duplex with four H bonds, but it widens of the helix because the C1′–C1′ distance is longer than that in the Watson–Crick base pair—a destabilizing factor for the duplex that contains the pair. Since the goal of our continuing study is to develop base-pairing motifs that stabilize and regulate DNA structures, including a double-helix-independent mode of incorporation of the new base pair(s) (i.e., one pair, three nonconsecutive pairs, and three consecutive pairs in this study), the novel 1,8-naphthyridine C-nucleosides **7** (which bears an Na-N^O base) and **9** (which bears an Na-O^N base) were designed.[6] These C-nucleosides are expected to form two sets of naphthyridine:imidazopyridopyrimidine base-pairing motifs (Na-O^N:Im-N^O and Na-N^O:Im-O^N) with four hydrogen bonds when these are incorporated into ODNs



Scheme 1. A) Im-N^O:Im-O^N base-pairing motif. B) Newly designed naphthyridine:imidazopyridopyrimidine base-pairing motifs.

(Scheme 1 B). Furthermore, the new motifs can be regarded as an expanded pyrimidine:purine-type base pair (with C1′–C1′ distances similar to the Watson–Crick base pair), which, unlike the Im-N^O:Im-O^N pair, would not distort the helical structure.[5] Herein we describe the synthesis of the 1,8-naphthyridine C-nucleosides **7** and **9**, and the effects on the thermal stabilities of the ODNs containing the naphthyridine:imidazopyridopyrimidine base-pairing motifs.[7]

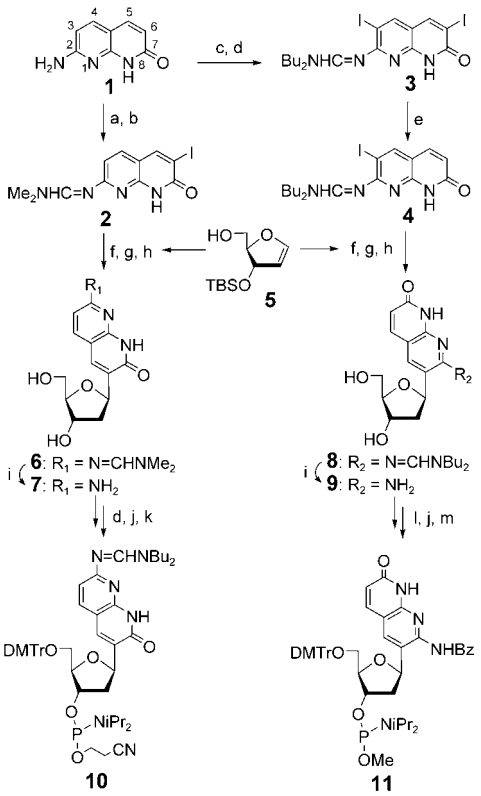
The synthetic route to the target compounds is illustrated in Scheme 2. The synthesis started from 2-amino-7-hydroxy-1,8-naphthyridine (**1**).[8] Iodination of **1** with *N*-iodosuccinimide (NIS) was followed by protection of the exocyclic amino group to give the 6-iodo-1,8-naphthyridine derivative **2**, a substrate for the synthesis of **7**. On the other hand, the synthesis of **9** requires the 3-iodo-1,8-naphthyridine derivative. Treatment of **1** with excess NIS, followed by protection of the exocyclic amino group gave the 3,6-diiodo derivative **3**, which was converted into the 3-iodo derivative **4** by treatment with a stoichiometric amount of tributyltin hydride in the presence of [$Pd(PPh_3)_4$]. This regioselective reduction of the 6-iodo group in **3** can be explained by the electron densities at C3 and C6, which were estimated from the ^{13}C NMR spectrum (C3: $\delta = 84.7$ ppm and C6: $\delta = 91.0$ ppm).[9] Heck coupling of the 6-iodo derivative **2** with the glycal **5**[10] was followed by deprotection and reduction[11] to afford the desired **6** in 78% overall yield (from **2**). In the same manner, the reaction of **4** with **5** afforded **8** in 76% yield. Treatment of **6** and **8** with methanolic ammonia gave the free nucleosides **7** and **9**, respectively. To incorporate both C-nucleosides **7** and **9** into ODNs, they were converted into the corresponding phosphoramidites **10** and **11**, respectively. For the conversion of **9**, the *N*-benzoyl group was the best choice as a protecting group for the exocyclic amino function,[12] and methyl *N*,*N*-diisopropylchlorophosphoramidite was used to give **11** because of purification problems that arose when 2-cyanoethyl *N*,*N*-diisopropylchlorophosphoramidite was used.

[*] S. Hikishima, Prof. N. Minakawa, K. Kuramoto, Y. Fujisawa, M. Ogawa, Prof. A. Matsuda
Graduate School of Pharmaceutical Sciences
Hokkaido University
Kita-12, Nishi-6, Kita-ku, Sapporo 060-0812 (Japan)
Fax: (+81) 11-706-4980
E-mail: noriaki@pharm.hokudai.ac.jp
matuda@pharm.hokudai.ac.jp

[**] This work was supported in part by a Grant-in-Aid for Scientific Research on Priority Areas and Encouragement of Young Scientists from the Ministry of Education, Science, Sports, and Culture of Japan. This paper constitutes Part 229 of Nucleosides and Nucleotides. Part 228 is reference [15].

Supporting information for this article is available on the WWW under http://www.angewandte.org or from the author.

 © 2005 Wiley-VCH Verlag GmbH & Co. KGaA, Weinheim DOI: 10.1002/anie.200461857



Scheme 2. Reagents and conditions: a) NIS (1.1 equiv), DMF; b) dimethylformamide dimethylacetal, DMF, 80 °C; c) NIS (2.9 equiv), DMF, 80 °C; d) dibutylformamide dimethylacetal, DMF; e) Bu_3SnH, $[Pd_2dba_3]\cdot CHCl_3$, PPh_3, DMF, 60 °C; f) **5**, $Pd(OAc)_2$, $AsPh_3$, Bu_3N, DMF, 60 °C; g) TBAF, THF; h) $NaBH(OAc)_3$, AcOH, CH_3CN; i) NH_3/MeOH, 80 °C; j) DMTrCl, pyridine; k) 2-cyanoethyl *N*,*N*-diisopropylchlorophosphoroamidite, iPr_2NEt, CH_2Cl_2; l) 1) TMSCl, pyridine then BzCl, 2) NH_4OH; m) methyl *N*,*N*-diisopropylchlorophosphoroamidite, iPr_2NEt, DMAP, CH_2Cl_2. NIS = *N*-iodosuccinimide; DMF = *N*,*N*-dimethylformamide; dba = dibenzylideneacetone; TBAF = tetrabutylammonium fluoride; DMTr = 4,4′-dimethoxytrityl; TMS = trimethylsilyl; DMAP = 4-(dimethylamino)pyridine.

To investigate the base-pairing properties of Na-N^O and Na-O^N, three classes of complementary duplexes were synthesized. As shown in Table 1, the first class consists of duplexes (a series of ODN I:ODN II) that contain one X:Y pair in the center of the duplexes (containing Na-N^O, Na-O^N, Im-N^O, Im-O^N, or natural bases in their X or Y positions). The second class is made up of duplexes (a series of ODN III:ODN IV) that contain three nonconsecutive X:Y pairs, and the last class (a series of ODN V:ODN VI) is made up of three consecutive X:Y pairs. The thermal stability of all duplexes was measured by thermal denaturation in a buffer of 10 mM sodium cacodylate (pH 7.0) containing 1 mM NaCl.[13] The resulting melting temperatures T_ms and the ΔT_ms values calculated based on the T_m of the duplex (X:Y = A:T, common to ODN I:ODN II, ODN III:ODN IV, and ODN V:ODN VI) are listed in Table 1. As we expected, the Im-O^N:Na-N^O and Im-N^O:Na-O^N pairs stabilized the duplex by +9.4 °C and +8.6 °C, respectively, relative to that containing the A:T pair. In contrast, the Im-O^N:Im-N^O pair destabilized the duplex by −3.8 °C, which agreed with our previous

Table 1: Sequences of ODNs and hybridization data.

Duplex	X	Y	T_m [°C][a]	ΔT_m [°C][b]
ODN I:ODN II	Im-O^N	Na-N^O	57.2	+9.4
	Im-N^O	Na-O^N	56.4	+8.6
5′-GCACCGAAXAAACCACG-3′	Im-O^N	Im-N^O	44.0	−3.8
3′-CGTGGCTTYTTTGGTGC-5′	Na-N^O	Na-O^N	50.1	+2.3
	G	C	49.1	+1.3
	A	T	47.8	
ODN III:ODN IV	Im-O^N	Na-N^O	82.2	+34.4
	Im-N^O	Na-O^N	80.9	+33.1
5′-GCXCCGAAXAAACCXCG-3′	Im-O^N	Im-N^O	53.3	+5.5
3′-CGYGGCTTYTTTGGYGC-5′	Na-N^O	Na-O^N	48.9	+1.1
	G	C	56.7	+8.9
ODN V:ODN VI	Im-O^N	Na-N^O	80.2	+32.4
	Im-N^O	Na-O^N	81.0	+33.2
5′-GCACCGAXXXAACCACG-3′	Im-O^N	Im-N^O	70.4	+22.6
3′-CGTGGCTYYYTTGGTGC-5′	Na-N^O	Na-O^N	68.1	+20.3
	G	C	55.2	+7.4

[a] Experimental conditions are described in the Supporting Information. The data presented are averages of triplicates. [b] The ΔT_m values were obtained by subtracting data for the T_m possessing X:Y = A:T from that for each duplex.

results.[5] Although the Na-N^O:Na-O^N pair stabilized the duplex by +2.3 °C, the value was much less than those of Im-O^N:Na-N^O and Im-N^O:Na-O^N, and similar to that of the G:C pair. The preferable base-pairing motifs by Im-O^N:Na-N^O and Im-N^O:Na-O^N were emphasized in a series of ODN III:ODN IV. Both pairs stabilized the duplexes by more than +30 °C, and the effects of Im-O^N:Im-N^O and Na-N^O:Na-O^N were insufficient, despite the expected base-pairing motifs with four H bonds. In the series ODN V:ODN VI, not only the Im-O^N:Na-N^O and Im-N^O:Na-O^N pairs but also the Im-O^N:Im-N^O and Na-N^O:Na-O^N pairs stabilized the duplexes much more than G:C and A:T pairs, although the first pairs are generally considered more effective for thermal stability. From these results, it can be concluded that the newly designed base pairing motifs Im-O^N:Na-N^O and Im-N^O:Na-O^N thermally stabilized the duplex by nearly 10 °C more per pair than the A:T pair and 8 °C more than the G:C pair independent of the mode of incorporation of the new base pair(s) into the ODNs. This effect is presumably caused by the noncanonical base pairs consisting of four H bonds and the stacking effect of the expanded aromatic surfaces.[14] Furthermore, the fact that the shape of the pairs resembles a pyrimidine:purine base pair (i.e., shape complementarity) would also be critical for their effect because of the sequence-dependent thermal stabilizing effect of the Im-O^N:Im-N^O and Na-N^O:Na-O^N pairs. As we expected, the Im-O^N:Na-N^O and Im-N^O:Na-O^N pairs did not cause the disruption of the helical structure, unlike the Im-O^N:Im-N^O pair. Although some shift in the base-pairing phase from the usual pyrimidine:purine base pairing could occur to complete the base pairing of Im-O^N:Na-N^O and Im-N^O:Na-O^N (see Scheme 1B), the effect of this shift should be negligible for the thermally stable duplex formation, since

 © 2005 Wiley-VCH Verlag GmbH & Co. KGaA, Weinheim

both pairs stabilized the duplex, irrespective of the mode of incorporation.

To clarify the specificity of the naphthyridine:imidazopyridopyrimidine base pairs, the base-pairing properties of Na-N^O with natural bases, as an example, were examined in a series of ODN I:ODN II and ODN V:ODN VI. As can be seen in Table 2, the resulting T_ms were all lower than that of A:T

Table 2: Sequences of ODNs and hybridization data of Na-N^O with natural bases.

duplex	X	Y	T_m [°C][a]	ΔT_m [°C][b]
ODN I:ODN II	Na-N^O	A	61.0	−2.6
	Na-N^O	G	58.4	−5.2
5′-GCACCGAAXAAACCACG-3′	Na-N^O	C	54.3	−9.3
3′-CGTGGCTTYTTTGGTGC-5′	Na-N^O	T	59.0	−4.6
	G	C	64.8	+1.2
	A	T	63.6	
ODN V:ODN VI	Na-N^O	A	60.3	−3.3
	Na-N^O	G	55.6	−8.0
5′-GCACCGAXXXAACCACG-3′	Na-N^O	C	45.2	−18.4
3′-CGTGGCTYYYTTGGTGC-5′	Na-N^O	T	60.0	−3.6
	G	C	69.0	+5.4

[a] Experimental conditions are described in the Supporting Information. The data presented are averages of triplicates. [b] The ΔT_m values were obtained by subtracting data for the T_m possessing X:Y = A:T from that for each duplex.

pair. Although the adenine base is expected to form a base pair with Na-N^O like the A:T pair, Na-N^O:A pair also destabilized the duplex.

In conclusion, the novel 1,8-naphthyridine C-nucleosides **7** and **9** with the ability to form four H bonds were synthesized through Heck coupling. The ODNs containing **7** and **9** formed extremely stable duplexes by the base-pairing motifs Im-O^N:Na-N^O and Im-N^O:Na-O^N. Furthermore, these motifs are specific, so that these would be versatile in stabilizing and regulating a variety of DNA structures.

Received: September 1, 2004
Published online: December 21, 2004

Keywords: DNA recognition · hydrogen bonds · nucleobases · nucleosides · oligonucleotides

[1] For recent reviews, see: a) E. T. Kool, *Acc. Chem. Res.* **2002**, *35*, 936–943; b) A. A. Henry, F. E. Romesberg, *Curr. Opin. Chem. Biol.* **2003**, *7*, 727–733; and references therein.
[2] W. M. Flanagan, J. J. Wolf, P. Olson, D. Grant, K.-Y. Lin, R. W. Wagner, M. D. Matteucci, *Proc. Natl. Acad. Sci. USA* **1999**, *96*, 3513–3518.
[3] For a recent review, see: C. R. Geyer, T. R. Battersby, S. A. Benner, *Structure* **2003**, *11*, 1485–1498, and references therein
[4] H. Liu, J. Gao, S. R. Lynch, Y. D. Saito, L. Maynard, E. T. Kool, *Science* **2003**, *302*, 868–871.
[5] N. Minakawa, N. Kojima, S. Hikishima, T. Sasaki, A. Kiyosue, N. Atsumi, Y. Ueno, A. Matsuda, *J. Am. Chem. Soc.* **2003**, *125*, 9970–9982.
[6] For the sake of simplicity, the imidazopyridopyrimidine nucleobases shown in Scheme 1 A are referred to as Im-N^O and Im-O^N. The aglycons of **7** and **9**, which contain naphthyridine nucleobases, are referred to as Na-N^O and Na-O^N, respectively.
[7] Recently, the synthesis and properties of peptide nucleic acids that contain 1,8-naphthyridine bases were reported: A. B. Eldrup, C. Christensen, G. Haaima, P. E. Nielsen, *J. Am. Chem. Soc.* **2002**, *124*, 3254–3262.
[8] G. R. Newkome, S. J. Garbis, V. K. Majestic, F. R. Fronczek, G. Chiari, *J. Org. Chem.* **1981**, *46*, 833–839.
[9] W.-S. Kim, H.-J. Kim, C.-G. Cho, *J. Am. Chem. Soc.* **2003**, *125*, 14288–14289.
[10] R. S. Coleman, M. L. Madaras, *J. Org. Chem.* **1998**, *63*, 5700–5703.
[11] H.-C. Zhang, G. Doyle Daves, Jr., *J. Org. Chem.* **1992**, *57*, 4690–4696.
[12] As the reaction of **8** with DMTrCl gave the desired product in poor yield, a protecting group for the exocyclic amino function was examined.
[13] In a buffer containing 100 mM NaCl (conditions used in the previous paper[5]), some duplexes showed T_ms higher than 95 °C. Therefore, 1 mM NaCl was used in this study.
[14] For example, the stacking ability of Na-N^O was higher than those of purine bases and similar to those of the imidazopyridopyrimidine bases (Im-N^O and Im-O^N).
[15] S. Hoshika, N. Minakawa, A. Matsuda, *Nucleic Acids Res.* **2004**, *32*, 3815–3825.

 © 2005 Wiley-VCH Verlag GmbH & Co. KGaA, Weinheim

Crystal Engineering

Morphosynthesis of Rhombododecahedral Silver Cages by Self-Assembly Coupled with Precursor Crystal Templating**

Jinhu Yang, Limin Qi, Conghua Lu, Jiming Ma, and Humin Cheng*

The self-assembly and higher-order organization of micro- and nanostructured building blocks into complex architectures with hierarchy across extended length scales is a key challenge in current materials synthesis and device fabrication.[1–8] In particular, many recent efforts have been devoted to the controlled organization of primary building blocks into hollow spheres or cages,[9–14] as these hollow structures with nanometer-to-micrometer dimensions have widespread potential applications, including in catalysis, in drug delivery,

[*] J. Yang, Prof. L. Qi, Dr. C. Lu, Prof. J. Ma, Prof. H. Cheng
State Key Laboratory for Structural Chemistry
of Unstable and Stable Species
College of Chemistry, Peking University
Beijing 100871 (China)
Fax: (+86) 10-6275-1708
E-mail: liminqi@chem.pku.edu.cn

[**] This work was supported by NSFC (20325312, 20473003, 20233010), and FANEDD (200020).

Supporting information for this article is available on the WWW under http://www.angewandte.org or from the author.

 © 2005 Wiley-VCH Verlag GmbH & Co. KGaA, Weinheim DOI: 10.1002/anie.200461859

as artificial cells, as light fillers, and as photonic crystals.[15] In most cases, however, only spherical hollow structures have been obtained either by using colloidal particles[9] or emulsion droplets[10] as templates, or by direct self-assembly of the primary particles without using external templates.[11–13] It is expected that tailoring the external morphology of hollow structures would endow them with unique properties as a consequence of the importance of shape and texture in determining the properties of the materials.[16] It is noteworthy that hexagon-based drums formed by textured self-assembly of ZnO nanocrystals were recently produced in a solid–vapor deposition process involving epitaxial surface oxidation;[14] however, the geometrical shapes of the polyhedral cages are, in general, not well-defined, and such a process could be largely limited to specific oxide systems. Thus, it is desirable to explore feasible methods to organize primary building blocks into hollow cages with well-defined, novel geometrical morphologies.

The controlled synthesis of metal particles has attracted much attention because of their important roles in many areas of modern science and technology.[17–23] Considerable progress has been made in recent years in the shape-controlled synthesis of metal nanoparticles; examples include silver nanorods,[17] nanoprisms,[18] and nanocubes.[19] Hollow spheres of a variety of metals, such as Pd,[20] Pt,[21] and Ag,[22] have also been successfully produced by employing hard or soft sacrificial templates. Interestingly, unique polyhedral Au–Ag alloy nanoboxes have been synthesized by the replacement reaction between silver nanocubes and chloroauric acid in a refluxing aqueous medium.[19,23] However, to the best of our knowledge, there have been no reports on the hierarchical assembly of hollow structures from nonspherical metal particles. Inspired by a promising recent study on the formation of hollow nanocrystals of cobalt oxide and chalcogenides by cobalt nanocrystal templating through a nanoscale Kirkendall effect,[24] we extend this strategy here to the facile synthesis of well-defined, rhombododecahedral silver cages by the reduction of micrometer-sized silver phosphate crystals with a perfect rhombododecahedral shape through a microscale Kirkendall effect. We demonstrate that the controlled self-assembly of silver particles produced in situ around the precursor crystal surfaces leads to the formation of morphology-preserved, single- or double-walled silver cages constructed from different building units, such as particles, nanoplates, and quasispherical assemblies of nanoplates. This method of self-assembly coupled with templating of the precursor crystals has been further used for the synthesis of unique hollow silver cones consisting of silver nanoplate assemblies.

Our synthesis of hierarchical silver hollow structures involves the sulfated dextran-directed crystallization of Ag_3PO_4 with specific morphologies in mixed solvents, followed by reduction of the Ag_3PO_4 precursor crystals with different reducing agents in aqueous solution. It is well known that soluble macromolecules can considerably influence the form and appearance (crystal habit) by specific interactions with inorganic crystal surfaces in solution, and the effect of macromolecular additives can be further modified by varying the solvent composition.[2] Here we chose the anionic derivative of dextran (dextran sulfate) as an effective crystal-growth modifier for the crystallization of Ag_3PO_4 in a water/formamide mixture, as our preliminary experiments suggested that usually only irregular Ag_3PO_4 polyhedrons are obtained in pure water. Figure 1a presents a typical scanning

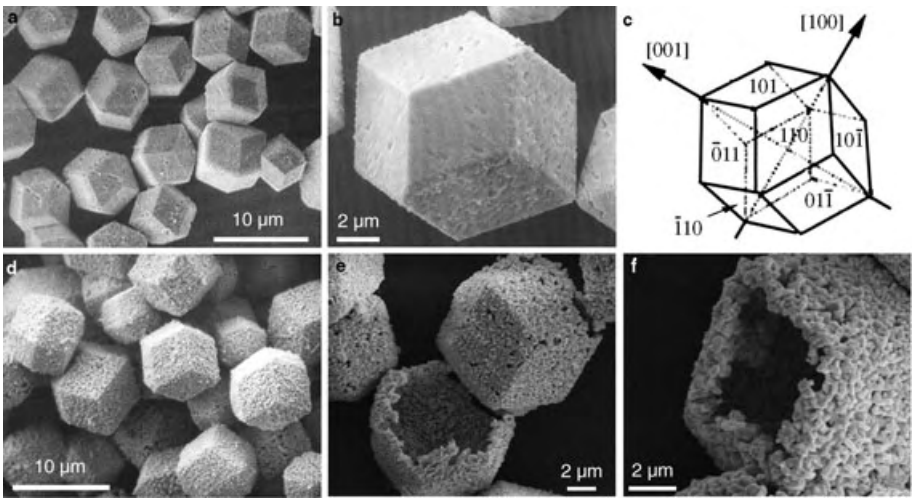


Figure 1. a, b) SEM images of Ag_3PO_4 rhombododecahedral crystals formed in a mixed water/formamide solvent, and c) index of a rhombododecahedral crystal model. SEM images of single-walled Ag rhombododecahedral cages: d) before and e, f) after sonication. The Ag cages were produced by reducing the Ag_3PO_4 precursor crystals shown in (a) with ascorbic acid at 20°C.

electron microscopy (SEM) image of the Ag_3PO_4 crystals obtained in the presence of 10 gL^{-1} dextran sulfate, and shows that all of the obtained Ag_3PO_4 crystals exhibit a uniform rhombododecahedral morphology. The size of the rhombododecahedra, as estimated from the distance between the two parallel surfaces, typically ranges from 4 to 8 μm, with an average size of about 6 μm. The related X-ray diffraction (XRD) pattern (see the Supporting Information) shows sharp reflections characteristic of simple cubic Ag_3PO_4 (JCPDS No. 6-0505), thus suggesting that the rhombododecahedra are pure Ag_3PO_4 crystals. An enlarged SEM image (Figure 1b) clearly shows that the ideal rhombododecahedron consists of 12 well-defined crystal faces and exhibits cubic symmetry, thus confirming that each rhombododecahedron is a single crystal of cubic Ag_3PO_4. The 12 faces can be indexed to the {110} planes (Figure 1c).

As Ag_3PO_4 can be readily reduced by a variety of reductants to metallic Ag, Ag_3PO_4 crystals with well-defined morphologies may be used as precursors for the morphology-preserved synthesis of silver particles. Ascorbic acid, hydrazine, and $NaBH_4$ are three widely used reducing agents with an increasing reducing ability; moreover, they are expected to show increasing diffusion ability in water, as their molecular

 © 2005 Wiley-VCH Verlag GmbH & Co. KGaA, Weinheim

volume decreases from ascorbic acid through hydrazine hydrate to the BH_4^- ion. It was therefore interesting to explore the synthesis of silver particles by reduction of the rhombododecahedral Ag_3PO_4 precursor crystals with these three reductants. Figure 1 d shows a typical SEM image of the silver product obtained by the reduction of the precursor crystals in 0.02 M ascorbic acid solution at 20 °C; it suggests the formation of silver particles with a well-preserved rhombododecahedral morphology. The rhombododecahedra have an average size of about 7 μm, which is slightly larger than the precursor rhombododecahedra (ca. 6 μm), and exhibit rather rough surfaces, in contrast to the smooth surfaces of the precursor rhombododecahedra. The corresponding XRD pattern (see the Supporting Information) exhibits sharp reflections attributed to fcc silver (JCPDS No. 04-0783), thus confirming a complete transformation of the Ag_3PO_4 precursor crystals to silver crystals. After 10 min of ultrasonic treatment in water, the rhombododecahedral particles can be broken and the hollow structure of the rhombododecahedra is clearly revealed by the SEM images (Figure 1 e, f). It can be seen that the rhombododecahedral cages have a shell consisting of interconnected, irregularly shaped, primary particles about 200–400 nm in size, which results in an average shell thickness of about 300–400 nm. Although there is a clear difference in the length scale, this formation of micrometer-sized, rhombododecahedral cages around rhombododecahedral precursor crystals is analogous to the reported formation of hollow nanospheres around spherical precursor nanoparticles,[24] which was attributed to a fundamental solid-state phenomenon, known as the Kirkendall effect[25] that deals with the movement of the interface between a diffusion couple. In the present case, ascorbic acid and Ag_3PO_4 can react with each other and form a diffusion pair. The coupled reaction/diffusion at the crystal/solution interface could lead to the quick formation of an interconnected silver shell around the external surfaces of the Ag_3PO_4 crystals. This process is followed by a continuous outward flow of Ag_3PO_4 from the solution to and through the porous silver shell to form a hollow interior and a relatively compact shell, as well as some small, individual silver particles precipitated outside the shell. This result demonstrates that, similar to the nanoscale Kirkendall effect used for the fabrication of hollow nanoparticles, a microscale Kirkendall effect can be used for the fabrication of micrometer-sized hollow cages with well-preserved morphologies if a suitable reaction-diffusion process exists at the solid/liquid interface. It may be argued that the polymer could play a role in the self-assembly process, for example, by gluing together the primary particles; however, this role is likely to be negligible, as a preliminary thermogravimetric analysis (TGA) suggested that the Ag_3PO_4 crystals do not contain significant amounts of polymer after being washed thoroughly with water.

The formation of single-walled silver cages when using ascorbic acid as the reductant indicates that the outward diffusion of Ag_3PO_4 is most likely faster than the inward diffusion of ascorbic acid. Hydrazine is a stronger reductant than ascorbic acid, and has a higher diffusion ability. As shown in Figure 2 a, well-defined, rhombododecahedral silver particles of about 6–7 μm were again obtained when hydrazine was used to reduce the rhombododecahedral Ag_3PO_4 crystals at 20 °C instead of ascorbic acid. A high-magnification image (Figure 2 b) reveals that the shell mainly consists of nanoplates ranging from 200 to 400 nm in size and less than 100 nm in thickness. The TEM image and electron diffraction (ED) pattern of separated silver nanoplates obtained by ultrasonically breaking the rhombododecahedral particles suggest that the nanoplates normally exhibit a hexagonal shape and that they are single crystals of fcc silver with the top face bounded by the {111} planes (see the Supporting Information); this arrangement is typical for platelike silver nanocrystals.[18] The representative SEM images of the broken rhombododecahedral particles shown in Figure 2 c suggest that most of the rhombododecahedra are actually double-walled hollow cages. It should be noted that single- and triple-walled cages can be occasionally observed in the product, although the double-walled cages form the overwhelming majority. The primary platelike particles and the double-walled structure are unique for the rhombododecahedral cages synthesized under these conditions. Platelike silver nanocrystals with a (111) top face are usually obtained in the presence of an appropriate surface-capping reagent;[18] therefore, it can be reasonably assumed that the reductant (hydrazine) may also act as an effective stabilizer for the silver nanoplates here. The formation of the double-walled

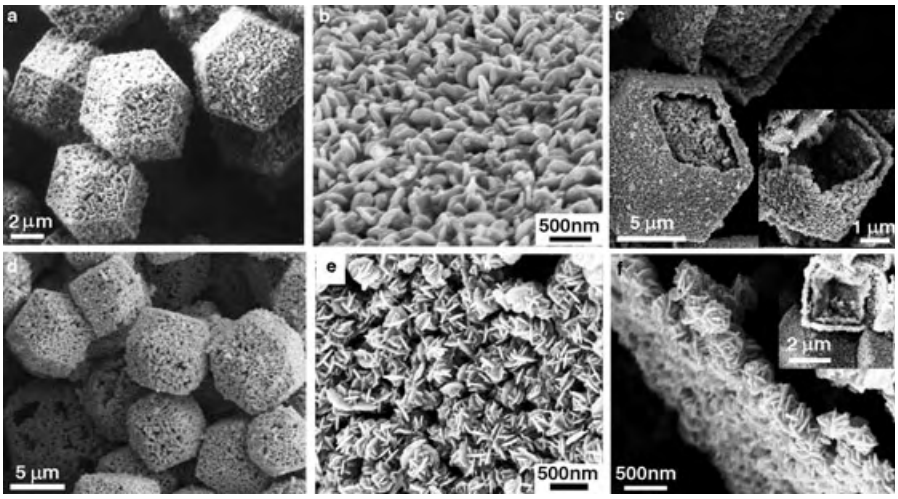


Figure 2. SEM images of double-walled Ag rhombododecahedral cages produced by reducing the Ag_3PO_4 precursor crystals shown in Figure 1 a with hydrazine at: a–c) 20 °C and d–f) 4 °C. The images shown in (c) and (f) correspond to the broken cages after sonication. The insets show the double-walled structures of the broken rhombododecahedral cages.

 © 2005 Wiley-VCH Verlag GmbH & Co. KGaA, Weinheim

structure is surprising. However, it is still in accordance with the Kirkendall effect because significant inward hydrazine transport could occur after the initial formation of the shell around the rhombododecahedral precursor crystals, as hydrazine diffuses considerably faster than ascorbic acid. This leads to the formation of a second shell inside the first as a result of the coupled reaction/diffusion process. The double-walled pattern is reminiscent of the well-known Liesegang patterns[26] that typically form by a periodic precipitation through the moving reaction front when two coprecipitating reactants interdiffuse in a gel medium. The Liesegang phenomenon observed in reaction/diffusion systems has been studied for a long time because of its similarities with natural, pattern-forming systems and potential applications in materials patterning; however, the mechanisms responsible for the patterns are still under discussion because of the rich, nonequilibrium dynamics involved.[27] Nevertheless, the formation of multiwalled hollow cages in a coupled reaction/diffusion process is unprecedented, and the exact mechanism is worthy of further study.

When the reduction reaction was conducted at a lower temperature (ca. 4 °C), the reaction rate and the reactant diffusion decreased considerably, which led to the formation of double-walled, rhombododecahedral cages with relatively loose shells (Figure 2 d–f). It is worth noting that the shell is composed of quasispherical assemblies of interconnected silver nanoplates about 50 nm thick and 200–300 nm wide. We propose that a lower reaction and diffusion rate would favor the formation of loosely packed nanoplate self-assemblies rather than densely packed nanoplate aggregates, which results in a change of the building units of the rhombododecahedral shells at different temperatures. The unique silver product shows a multilevel structure: nanoplates→quasispherical assemblies→rhombododecahedral shell→double-walled rhombododecahedral cage, which is similar to the complex, hierarchical structures adopted by biological minerals, such as the shells of single-celled organisms.[16] This one-pot, organic-free method based on self-assembly coupled with templating of the precursor crystals may form the basis of a new route to hierarchical inorganic hollow structures.

If $NaBH_4$, which has an even higher reducing ability and diffusion ability, is used as the reducing agent, novel core–shell-structured silver rhombododecahedra can be produced. As shown in Figure 3 a, the silver product consists of rhombododecahedral particles (ca. 7 μm) with some small particles attached to the exterior surfaces. The rhombododecahedra show a core–shell structure with a dense shell and a loose core after having been broken by sonication (Figure 3 b). A high-magnification image of the core (Figure 3 c) suggests that it consists of entangled nanowires ranging in diameter from 60 to 100 nm. The formation of the core–shell structure can be rationalized by considering that the very fast inward diffusion of BH_4^- ions could bring about a quick reduction of the Ag_3PO_4 inside the silver shell that is formed immediately after mixing the Ag_3PO_4 rhombododecahedra and $NaBH_4$ in solution. The formation of the clewlike core could be related to the specific reduction reaction between Ag_3PO_4 and $NaBH_4$, although the mechanism is still unclear.

All three reducing agents can therefore be used successfully for the synthesis of well-defined silver rhombododecahedra by reducing Ag_3PO_4 crystals. Our preliminary experiments have shown that a minimum reductant concentration is necessary for the morphology-preserved transformation from Ag_3PO_4 to silver. For example, only rhombododecahedral Ag_3PO_4 skeletons along with small separated silver particles were produced at a low $NaBH_4$ concentration (see the Supporting Information), which indicates that a quick formation of extended silver networks is essential to preserve the morphology. Accordingly, a tentative mechanism for the formation of the three different types of silver rhombododecahedra can be proposed (see the Supporting Information). Briefly, a layer of interconnected silver networks forms around the exterior surface of the Ag_3PO_4 rhombododecahedra as long as they are surrounded by a sufficient concentration of the reductant. Then, the network layer develops into a denser shell, which is accompanied by the formation of a depletion layer near the shell as a result of the coupled reaction/diffusion process. The final silver structure depends on the inward diffusion rate of the reductant relative to the outward diffusion rate of the Ag^+ ions, namely, single-walled rhombododecahedra form with ascorbic acid, which has a low diffusion rate, whereas double-walled rhombododecahedra form with hydrazine, which has a medium diffusion rate, and core–shell structured rhombododecahedra form with $NaBH_4$, which has a high diffusion rate. Such a morphology-preserved transformation process is not limited to the Ag_3PO_4/Ag system. For example, hollow Ag octahedra have been readily fabricated by reducing octahedral Ag_2O crystals with ascorbic acid following a similar strategy (see the Supporting Information).

This method of self-assembly coupled with templating of the precursor crystals can be extended to the morphology-preserved synthesis of hierarchical silver structures with morphologies other than polyhedra. As shown in Figure 4 a and b, hollow Ag_3PO_4 cones consisting of parallel fibers (longer than 100 μm) were formed in a solution of dextran sulfate in mixed water/acetamide solvent. It should be noted that similar hollow-cone structures have been obtained in the polymer-controlled morphogenesis of $BaSO_4$[28] and bundles of $BaCrO_4$[29] nanofibers. The hollow Ag_3PO_4 cones

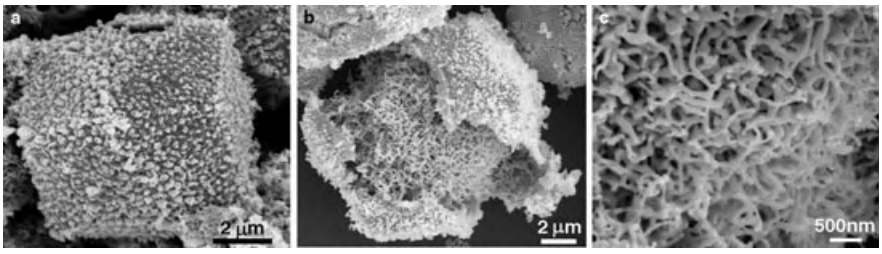


Figure 3. SEM images of: a) intact and b, c) broken Ag rhombododecahedral particles with a core–shell structure that were produced by reducing the Ag_3PO_4 precursor crystals shown in Figure 1 a with $NaBH_4$ at 20 °C.

 © 2005 Wiley-VCH Verlag GmbH & Co. KGaA, Weinheim

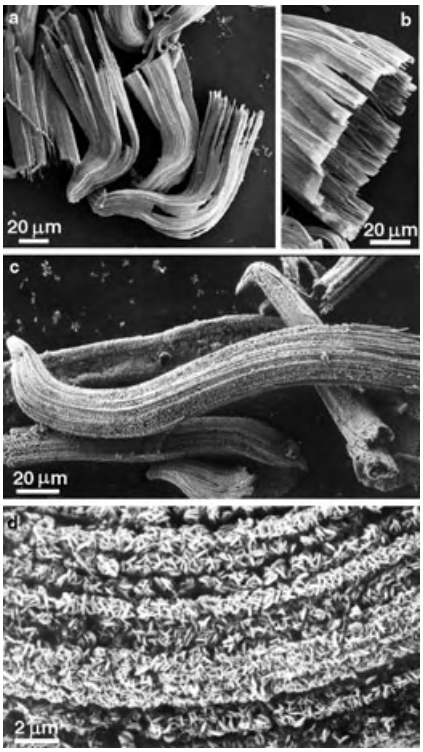


Figure 4. a, b) SEM images of Ag_3PO_4 hollow cones formed in a mixed water-acetamide solvent and c, d) hierarchical Ag hollow cones produced by reducing the Ag_3PO_4 precursor crystals shown in (a) with ascorbic acid at 20 °C.

were converted into hierarchical, hollow silver cones that consist of parallel fibers constructed from nanoplate assemblies (Figure 4c, d) after reduction by ascorbic acid.

In summary, a variety of silver microstructures exhibiting a well-defined, rhombododecahedral exterior morphology and a remarkably complex hierarchy have been readily fabricated in solution by self-assembly coupled with templating of the precursor crystals. The rhombododecahedral silver cages showing faceted shells consisting of tailored, nanostructured building units could find applications in various areas, including catalysis[20] and surface-enhanced Raman scattering (SERS) detection.[30] The synthesis based on a coupled reaction/diffusion process is related to the Kirkendall effect and the Liesegang phenomenon, which suggests that it could provide a useful model for the re-examination of these well-established physical phenomena. The process provides a general route to the synthesis of silver superstructures with unique morphologies and complex hierarchies. Furthermore, the synthesis may be extended to other metal systems and could possibly be used for device fabrication with appropriate metal/precursor/reductant combinations.

Experimental Section

In a typical synthesis of Ag_3PO_4 rhombododecahedra, Na_3PO_4 (0.005 mmol) and dextran sulfate (0.05 g, Fluka, M_W 500000) were dissolved in a solvent mixture containing water (3 mL) and formamide (1.5 mL), followed by addition of 0.2 M aqueous $AgNO_3$ solution (0.5 mL), with vigorous stirring, to give a final phosphate ion concentration of 1 mM and an excess of Ag^+ ions. After stirring the mixture for 1 min the slightly yellow, cloudy solution was aged for 1 day to give a yellow precipitate, which was collected, washed with water thoroughly, and dried in air. A similar process was employed for the synthesis of Ag_3PO_4 hollow cones, except that the solvent was a mixture of water (4.5 mL) and acetamide (0.74 g) instead of the mixed water/formamide solvent, and a longer aging time (4–5 days) was adopted. The obtained Ag_3PO_4 crystals were subsequently used as templates for the precursor crystals for the fabrication of the corresponding silver hollow structures. In a typical synthesis procedure, 0.004 g of the Ag_3PO_4 precursor crystals (ca. 0.01 mmol) was dispersed in water (9 mL) and a 0.2 M aqueous solution (1 mL) of the reducing agent (ascorbic acid, hydrazine, or sodium brorohydride) was added at room temperature (ca. 20 °C) to give a final reducing-agent concentration of 20 mM. After aging the mixture for 10 h in the solution, the resultant gray precipitate was collected by centrifugation at 3000 rpm and washed with water repeatedly to remove any separately precipitated small particles.

Received: September 1, 2004
Published online: December 15, 2004

Keywords: crystal engineering · nanostructures · polyhedral cages · self-assembly · silver

[1] G. M. Whitesides, B. Grzybowski, *Science* **2002**, *295*, 2418.
[2] H. Cölfen, S. Mann, *Angew. Chem.* **2003**, *115*, 2452; *Angew. Chem. Int. Ed.* **2003**, *42*, 2350.
[3] J. M. Garcia-Ruiz, S. T. Hyde, A. M. Carnerup, A. G. Christy, M. J. Van Kranendonk, N. J. Welham, *Science* **2003**, *302*, 1194.
[4] D. Whang, S. Jin, Y. Wu, C. M. Lieber, *Nano Lett.* **2003**, *3*, 1255.
[5] Z. R. Tian, J. Liu, J. A. Voigt, B. Mckenzie, H. Xu, *Angew. Chem.* **2003**, *115*, 429; *Angew. Chem. Int. Ed.* **2003**, *42*, 413.
[6] H. Shi, L. Qi, J. Ma, H. Cheng, *J. Am. Chem. Soc.* **2003**, *125*, 3450.
[7] S. Park, J.-H. Lim, S.-W. Chung, C. A. Mirkin, *Science* **2004**, *303*, 348.
[8] H. Fan, K. Yang, D. M. Boye, T. Sigmon, K. J. Malloy, H. Xu, G. P. Lopez, C. J. Brinker, *Science* **2004**, *304*, 567.
[9] F. Caruso, R. A. Caruso, H. Möhwald, *Science* **1998**, *282*, 1111.
[10] A. D. Dinsmore, M. F. Hsu, M. G. Nikolaides, M. Marquez, A. R. Bausch, D. A. Weitz, *Science* **2002**, *298*, 1006.
[11] A. Bigi, E. Boanini, D. Walsh, S. Mann, *Angew. Chem.* **2002**, *114*, 2267; *Angew. Chem. Int. Ed.* **2002**, *41*, 2163.
[12] J. Yuan, K. Laubernds, Q. Zhang, S. L. Suib, *J. Am. Chem. Soc.* **2003**, *125*, 4966.
[13] B. Liu, H. C. Zeng, *J. Am. Chem. Soc.* **2004**, *126*, 8124.
[14] P. X. Gao, Z. L. Wang, *J. Am. Chem. Soc.* **2003**, *125*, 11299.
[15] F. Caruso, *Chem. Eur. J.* **2000**, *6*, 413.
[16] S. Mann, *Angew. Chem.* **2000**, *112*, 3532; *Angew. Chem. Int. Ed.* **2000**, *39*, 3392.
[17] N. R. Jana, L. Gearheart, C. J. Murphy, *Chem. Commun.* **2001**, 617.
[18] R. Jin, Y. Cao, C. A. Mirkin, K. L. Kelly, G. C. Schatz, J. G. Zheng, *Science* **2001**, *294*, 1901.
[19] Y. Sun, Y. Xia, *Science* **2002**, *298*, 2176.
[20] S.-W. Kim, M. Kim, W. Y. Lee, T. Hyeon, *J. Am. Chem. Soc.* **2002**, *124*, 7642.
[21] H.-P. Liang, H.-M. Zhang, J.-S. Hu, Y.-G. Guo, L.-J. Wan, C.-L. Bai, *Angew. Chem.* **2004**, *116*, 1566; *Angew. Chem. Int. Ed.* **2004**, *43*, 1540.
[22] D. Zhang, L. Qi, J. Ma, H. Cheng, *Adv. Mater.* **2002**, *14*, 1499.
[23] Y. Sun, Y. Xia, *J. Am. Chem. Soc.* **2004**, *126*, 3892.
[24] Y. Yin, R. M. Rioux, C. K. Erdonmez, S. Hughes, G. A. Somorjai, A. P. Alivisatos, *Science* **2004**, *304*, 711.

 © 2005 Wiley-VCH Verlag GmbH & Co. KGaA, Weinheim

[25] A. D. Smigelskas, E. O. Kirkendall, *Trans. Am. Inst. Min., Metall. Pet. Eng.* **1947**, *171*, 130.
[26] R. E. Liesegang, *Naturwissenschaften* **1896**, *11*, 353.
[27] M. I. Lebedeva, D. G. Vlachos, M. Tsapatsis, *Phys. Rev. Lett.* **2004**, *92*, 088301.
[28] L. Qi, H. Cölfen, M. Antonietti, M. Li, J. D. Hopwood, A. J. Ashley, S. Mann, *Chem. Eur. J.* **2001**, *7*, 3526.
[29] S.-H. Yu, H. Cölfen, M. Antonietti, *Chem. Eur. J.* **2002**, *8*, 2937.
[30] S. Chan, S. Kwon, T.-W. Koo, L. P. Lee, A. A. Berlin, *Adv. Mater.* **2003**, *15*, 1595.

 © 2005 Wiley-VCH Verlag GmbH & Co. KGaA, Weinheim

Molecular Dynamics

Isotopomeric Conformational Change in Anisole–Water**

*Barbara M. Giuliano and Walther Caminati**

Isotopic substitution is generally considered not to perturb the structure of a molecular system. It affects, however, the molecular spectroscopy of the system, especially the frequencies of rotational transitions, which depend on moments of inertia. Differences in moments of inertia among isotopomers represent, in turn, the best tool for the determination of molecular structure.[1] Furthermore, changes in chemical properties, such as kinetics[2] and equilibrium constants,[3] are well known, and it has been observed that the temperature of spontaneous phase transitions can vary,[4] sometimes by as much as 25 K.[5] A smaller modification (relative to that described herein) of the structure of a system through the so-called geometric isotope effect was outlined by Ichikawa.[6] However, when isotopically labeled substances are used, the usually justified assumption is made that they do not alter the fundamental nature of the material under study. Reasonable information on the geometry of molecular complexes, for example of complexes of water with ethers, has been obtained upon deuteration of the water moiety. Limitations to this assumption are due to a remarkable shrinking (Ubbelohde effect[7]) of the distance between the two heavy atoms involved in the hydrogen bond upon deuteration. Such an effect has been observed both in crystals[7] and in the gas phase.[8] Zhou et al. showed very recently that this assumption is unjustified for the complex of pentachlorophenol with 4-methylpyridine, because the substitution of a single hydrogen atom for a deuterium atom leads to the thermodynamic stability of an entirely different crystal polymorph. [9] We show herein that a similar large effect is observed for the gas-phase configuration of the molecular complex anisole–water (ANI···water; see Figure 1).

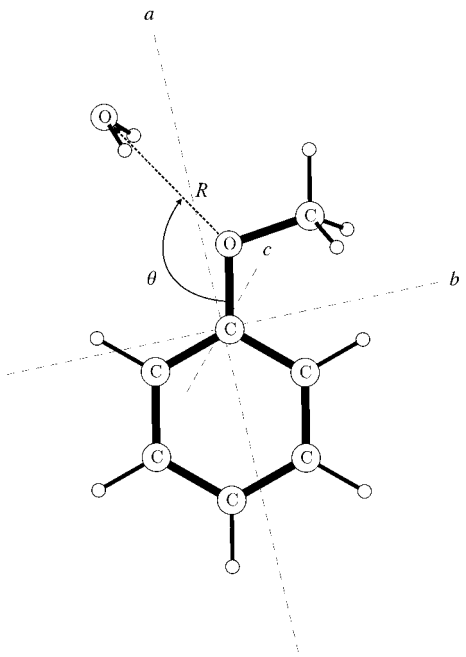


Figure 1. Conformation, relevant structural parameters, and principal axes of ANI···water.

Two recent publications have appeared on spectroscopic and quantum-chemical investigations of ANI···water. The first, based on resonant two-photon ionization and IR–UV double-resonance vibrational spectroscopy in the region of the OH stretches, and on MP2/6-31G* ab initio calculations, suggests that the minimum conformation includes an OH−O H bond and a "free" water hydrogen atom.[10] In the second the authors suggest a conformation of the complex with the water oxygen atom coplanar to the ring based on the results of vibronically and rotationally resolved spectroscopy and molecular-mechanics calculations.[11]

We measured the molecular-beam Fourier transform microwave spectra of six isotopomers of ANI···water, namely, ANI···H_2O, ANI···D_2O, ANI···DOH, ANI···$H_2{}^{18}O$, ANI···$D_2{}^{18}O$, and ANI···$D^{18}OH$. We first assigned the rotational spectrum of the normal species, ANI···H_2O. Each rotational transition was split into two component lines with an intensity ratio of 1:3, as expected for the tunneling states of a vibrational motion inverting two equivalent hydrogen atoms, and with two equivalent minima describing the potential-energy surface. Similar spectra were observed for phenol–water[12] and indole–water.[13] In these molecular complexes the water moiety acts as a proton acceptor, and the two hydrogen atoms of the water molecule are therefore equivalent to each other, located one above and one below the plane of symmetry of the partner molecule. After measuring the spectrum of ANI···H_2O and performing a partial fitting (based on the spectroscopic constants of the

[*] B. M. Giuliano, Prof. Dr. W. Caminati
Dipartimento di Chimica "G. Ciamician" dell'Università
Via Selmi 2, 40126 Bologna (Italy)
Fax: (+39) 051-209-9456
E-mail: walther.caminati@unibo.it

[**] We thank the University of Bologna and the MIUR for financial support.

Supporting information for this article is available on the WWW under http://www.angewandte.org or from the author.

 DOI: 10.1002/anie.200461860 © 2005 Wiley-VCH Verlag GmbH & Co. KGaA, Weinheim

normal species) of the r_0 structure, limited to the R and θ parameters of the H bond in Figure 1, we planned to measure the spectrum of ANI···D_2O. However, we were unable to locate the rotational lines for this isotopomer based on the hypothesis made about the conformation of the two water hydrogen atoms in the normal species. In contrast, the assignment of the lines in the spectrum of ANI···$H_2{}^{18}O$ after the above-mentioned structural adjustment was straightforward. We then returned to the search for the dideuterated species, and were finally able to assign a spectrum that was not in agreement with the geometry of the normal species. We also assigned the spectrum of the complex with partially deuterated water, with features intermediate between those of the H_2O and D_2O adducts. The spectrum of this isotopomer displayed only one set of lines, doubly intense with respect to the overall intensity of the H_2O or D_2O doublets, thus confirming that the two water hydrogen atoms are quantum-mechanically equivalent in the complex. Finally, we measured the spectra of the ANI···$D_2{}^{18}O$ and ANI···$D^{18}OH$ isotopomers in a mixture containing all six (H/D, $^{16}O/^{18}O$) isotopic species. The line frequencies (μ_a- and μ_b-type rotational transitions) for all isotopomers (available as Supporting Information) were fitted with a standard "S"-reduced Watson semirigid-rotor Hamiltonian[14] to yield the spectroscopic parameters given in Table 1. The two tunneling states of the ANI···H_2O and ANI···D_2O species were fitted separately.

It is well known that rotational constants, which are proportional to the reciprocal of the moments of inertia, should decrease upon substitution with heavier isotopes. In the case of ANI···water, the rotational constants decrease when ^{16}O is substituted for ^{18}O, but not when H is substituted for D. The rotational constant B increases in going from ANI···H_2O to ANI···HOD to ANI···D_2O (Table 1). The increase in B corresponds to a decrease, rather than an increase, in the mass extensions along the direction of the a axis, as indicated by the related changes in the M_{aa} planar moments of inertia, also reported in Table 1. This effect can be explained only if the $O_{water}\cdots O{-}C_{Ph}$ angle (θ in Figure 1) decreases by about 10° in going from ANI···H_2O to ANI···D_2O. This argument is shown graphically in Figure 2.

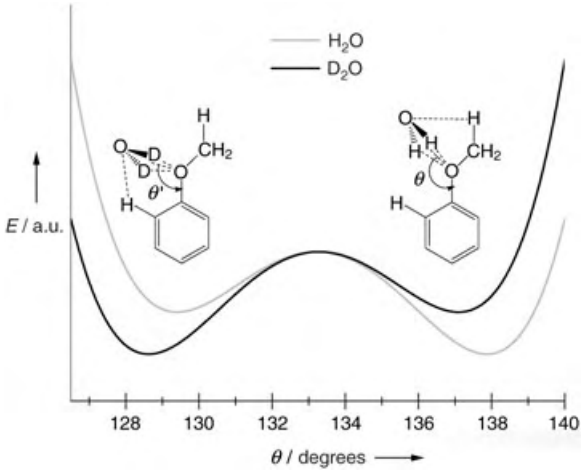


Figure 2. A qualitative hypothesis to explain the change in conformation of ANI···water upon H→D isotopic substitution: a slight variation in the potential-energy function, $E(\theta)$.

It was also possible, for each of the pairs ANI···H_2O/ANI···$H_2{}^{18}O$, ANI···HOD/ANI···$H^{18}OD$ and ANI···D_2O/ANI···$D_2{}^{18}O$, to obtain the substitution coordinates[15] of the oxygen atom of the water molecule. We believe the data are reliable because for each pair the hydrogen-bonding interactions and the molecular vibrations are the same. Based on the assumption that the geometries of isolated anisole[16] and water[17] remain unaltered in the adduct, we could estimate the local r_0 structure at the H bond, that is, the parameters R and θ in Figure 1. To estimate these values we needed to

Table 1: Spectroscopic constants for the isotopomers of the anisole–water complex.

	ANI···H_2O[a]		ANI···D_2O		ANI···HOD	ANI···$H_2{}^{18}O$		ANI···$D_2{}^{18}O$		ANI···$H^{18}OD$
	v=0	v=1	v=0	v=1		v=0	v=1	v=0	v=1	
A[b]	2943.058(2)[c]	2943.578(2)	2660.639(1)	2660.657(2)	2847.47(1)	2912.223(8)	2912.769(6)	2621.694(9)	2621.80(3)	2813.57(1)
B[b]	900.1885(9)	900.0276(8)	914.1605(5)	914.1581(6)	907.4638(6)	857.1386(9)	856.9846(7)	876.3307(6)	876.3222(6)	866.2243(2)
C[b]	694.1488(9)	694.1155(8)	687.0905(3)	687.0900(4)	692.5413(8)	666.5972(7)	666.5624(5)	662.9146(2)	662.9170(9)	666.2012(1)
D_J[d]	4.25(2)	4.22(2)	4.509(3)	4.510(4)	5.73(1)	4.054(5)	4.029(4)	4.419(7)	4.39(2)	5.789(2)
D_{JK}[d]	−54.0(1)	−53.8(1)	−54.4(6)	−54.36(5)	−72.3(2)	−52.4(2)	−52.3(1)	−54.6(2)	−56.(1)	−75.5(2)
D_K[d]	219.0(2)	218.3(2)	202.3(2)	203.5(2)	200(10)	218(1)	218(1)	271(5)	317(9)	196(3)
d_1[d]	−1.760(2)	−1.751(2)	−1.843(2)	−1.845(3)	−2.394(3)	−1.644(4)	−1.638(3)	−1.802(4)	[−1.845][e]	[−2.394]
d_2[d]	−0.108(2)	−0.106(1)	−0.065(2)	−0.064(2)	−0.086(6)	−0.105(3)	−0.106(2)	[−0.065]	[−0.064]	[−0.086]
H_J[f]	0.7(2)	0.6(1)			0.14(4)	[0.7]	[0.6]			[0.14]
H_{JK}[f]	−15.0(1)	−14.0(9)				−12(2)	−13(2)			
H_{KJ}[f]	85(10)	83(9)				80(10)	78(10)			
M_{aa}[g]	558.8757(8)	558.9585(7)	549.2111(5)	549.2128(5)	554.5879(9)	587.1110(9)	587.2001(7)	573.1450(6)	573.150(2)	581.2018(4)
M_{bb}[g]	169.1800(8)	169.1322(7)	186.3237(5)	186.3226(5)	175.1577(9)	171.0365(9)	170.9870(7)	189.2141(6)	189.206(2)	177.3964(4)
M_{cc}[g]	2.5390(8)	2.5565(7)	3.6228(5)	3.6226(5)	2.3258(9)	2.5007(9)	2.5176(7)	3.5540(6)	3.554(2)	2.2256(4)
σ[f]	5	5	6	6	5	5	5	1	4	3
N[h]	42	42	40	42	35	30	31	12	10	13

[a] The rotational constants for the normal species from reference [11] are $A=2941.4(2)$, $B=899.65(6)$, $C=693.93(4)$ MHz. [b] MHz. [c] Standard errors in units of the last digit are given in parentheses. [d] kHz. [e] Parameters in square brackets were fixed to those of the corresponding $H_2{}^{16}O$ species. [f] Hz. [g] uÅ^2. [h] Number of fitted transitions.

 © 2005 Wiley-VCH Verlag GmbH & Co. KGaA, Weinheim

predict the positions of the hydrogen atoms of the water molecule. Since the statistical weight indicates that they are equivalent to one other, we assumed that they point towards the oxygen atom of anisole, thus forming a bifurcated H bond. All these structural data are reported in Table 2. The

Table 2: Changes in the local structural features of the H bond upon H→D isotopic substitution.

r_0 distances [Å] and angles [°]; see Figure 1.			
	ANI···H_2O	ANI···HOD	ANI···D_2O
R	2.90(1)	2.87(1)	2.92(1)
θ	137.4(2)	134.2(2)	128.7(2)
O···H_{Me}	2.73(3)	3.22(3)	3.43(3)
O···H_{Ph}	3.74(3)	3.34(3)	3.17(3)

r_s coordinates [Å] for the oxygen atom of the water molecule						
	ANI···H_2O		ANI···HOD		ANI···D_2O	
	Exptl[a]	Calcd[b]	Exptl	Calcd	Exptl	Calcd
$\lvert a \rvert$	3.774	3.714	3.662	3.610	3.469	3.542
$\lvert b \rvert$	1.005	1.162	1.102	1.182	1.250	1.227
$\lvert c \rvert$	0.0	0.0	0.0	0.0	0.0	0.0

[a] The experimental errors in the substitution coordinates are not given because they are unrealistically small (in the fourth decimal digit): They do not take into account the vibrational contributions. [b] Calculated from the r_0 structure reported above.

discrepancies between the experimental and calculated values of the $|b|$ coordinates might result from the fact that the hydrogen atoms of the water molecule do not point, as we assumed, exactly towards the ether oxygen atom for the three isotopomers. We also calculated the $O_{water}\cdots H_{Me}$ and $O_{water}\cdots H_{Ph}$ distances (Table 2), which are relevant for secondary interactions (weak H bonds[18]). These distances change from 2.73 and 3.74 Å, respectively, in ANI···H_2O to 3.43 and 3.17 Å in ANI···D_2O. The H→D substitution destroys the weak H bond $O_{water}\cdots H_{Me}$ and seems to lead to the formation of the weak H bond $O_{water}\cdots H_{Ph}$.

It is likely that the water molecule forms a strong hydrogen bridge—probably bifurcated (or effectively bifurcated)—with the ether oxygen atom, and that the hydrogen-bonding interaction of the oxygen atom of the water molecule can oscillate between the methyl and the phenyl hydrogen atoms: The shrinking of the O–H/D distances within the water molecule upon deuteration alters this equilibrium. Two qualitative hypotheses are plausible: 1) a small change, upon deuteration, in the potential-energy surface, as shown qualitatively in Figure 2; 2) a substantial change, upon deuteration, in some of the frequencies of the six low-frequency normal vibrational modes of water with respect to anisole, and therefore in the relative r_0 energies of the two $O_{water}\cdots H_{Me}$ and $O_{water}\cdots H_{Ph}$ conformations, even in the case of two nearly equivalent wells in the potential-energy surface. Quantitative data on this potential-energy surface are difficult to obtain as a result of the complexity and flexibility of the problem, and the scarcity of experimental data.

In summary, we have described a novel isotopic effect: the conformational change of a hydrogen-bonded adduct upon deuteration of the hydrogen atoms involved in the H bond. Rotational resolved spectroscopy again proved to be a powerful tool for obtaining detailed chemical information that would be difficult to obtain by other techniques. However, we have also shown that structural information should only be derived with caution from shifts of moments of inertia in cases of H→D isotopic substitution of a hydrogen atom involved in hydrogen bonding. The results presented herein may also serve as a stimulus for new developments in theoretical calculations, which at present, to our knowledge, can not take into account such isotopomeric effects.

Experimental Section

A commercial sample of anisole (Aldrich) was used without further purification. D_2O (99%) and $H_2{}^{18}O$ (90%) were supplied by Promochem GmbH (Germany).

The MB-FTMW spectrum in the 6–18.5-GHz frequency region was measured by using a COBRA-type[19] molecular-beam Fourier transform microwave (MB-FTMW) spectrometer described elsewhere.[20] He at a pressure of ≈2 bar was blown over a 1:1 (*v*/*v*) mixture of water and anisole, and out through the solenoid valve (general valve, series 9, nozzle diameter 0.5 mm) into the Fabry–Pérot cavity, where the mixture reached an estimated rotational temperature of 1–2 K. The frequencies were determined after Fourier transformation of the 8k-data-point time-domain signal, recorded with 100-ns sample intervals. Each rotational transition was split by the Doppler effect as a result of the coaxial arrangement of the supersonic jet and resonator axes. The rest frequency was calculated as the arithmetic mean of the frequencies of the Doppler components. The estimated accuracy of the frequency measurements is better than 3 kHz. Lines separated by more than 7 kHz are resolvable.

Received: September 1, 2004
Published online: December 13, 2004

Keywords: hydrogen bonds · isotope effects · molecular beams · molecular complexes · molecular dynamics

[1] W. Gordy, R. L. Cook, *Microwave Molecular Spectra*, 3rd ed., Wiley, New York, **1984**, chap. 13, p. 576.
[2] J. P. Klinman, *Pure Appl. Chem.* **2003**, *75*, 601.
[3] J. Bigeleisen, M. W. Lee, F. Mandel, *Annu. Rev. Phys. Chem.* **1973**, *24*, 31.
[4] J. Szydlowski, *J. Mol. Struct.* **1994**, *321*, 101.
[5] R. E. Wasylishen, S. Peiris, D. R. Arnold, *Chem. Phys. Lett.* **1985**, *114*, 31.
[6] M. Ichikawa, *J. Mol. Struct.* **2000**, *552*, 63.
[7] A. R. Ubbelohde, K. J. Gallagher, *Acta Crystallogr.* **1955**, *11*, 71–83.
[8] R. E. Penn, R. J. Olsen, *J. Mol. Spectrosc.* **1976**, *62*, 423; J. L. Alonso, E. B. Wilson, *J. Am. Chem. Soc.* **1980**, *102*, 1248.
[9] J. Zhou, Y.-S. Kye, G. S. Harbison, *J. Am. Chem. Soc.* **2004**, *126*, 8392.
[10] B. Reimann, K. Buchhold, H.-D. Barth, B. Brutschy, *J. Chem. Phys.* **2002**, *117*, 8805.
[11] M. Becucci, G. Pietraperzia, M. Pasquini, G. Piani, A. Zoppi, R. Chelli, E. Castellucci, W. Demtroeder, *J. Chem. Phys.* **2004**, *120*, 5601.
[12] S. Melandri, A. Maris, P. G. Favero, W. Caminati, *Chem. Phys.* **2002**, *283*, 185–192.
[13] S. Blanco, J. C. Lopez, J. L. Alonso, P. Ottaviani, W. Caminati, *J. Chem. Phys.* **2003**, *119*, 880–886.
[14] J. K. G. Watson in *Vibrational Spectra and Structure*, *Vol. 6* (Ed.: J. R. Durig), Elsevier, Amsterdam, **1977**, pp. 1–89.
[15] J. Kraitchman, *Am. J. Phys.* **1953**, *21*, 17.

 © 2005 Wiley-VCH Verlag GmbH & Co. KGaA, Weinheim

[16] M. Onda, A. Toda, S. Mori, I. Yamaguchi, *J. Mol. Struct.* **1986**, *144*, 47.
[17] F. C. de Lucia, P. Helminger, R. L. Cook, W. Gordy, *Phys. Rev.* A **1972**, *5*, 487.
[18] For a detailed description of these weak H bonds, see, for example: J. L. Alonso, S. Antolínez, S. Blanco, A. Lesarri, J. C. López, W. Caminati, *J. Am. Chem. Soc.* **2004**, *126*, 3244.
[19] J.-U. Grabow, W. Stahl, *Z. Naturforsch. A* **1990**, *45*, 1043; J.-U. Grabow, PhD thesis, Kiel University (Germany), **1992**.
[20] W. Caminati, A. Millemaggi, J. L. Alonso, A. Lesarri, J. C. Lopez, S. Mata, *Chem. Phys. Lett.* **2004**, *392*, 1.

 © 2005 Wiley-VCH Verlag GmbH & Co. KGaA, Weinheim

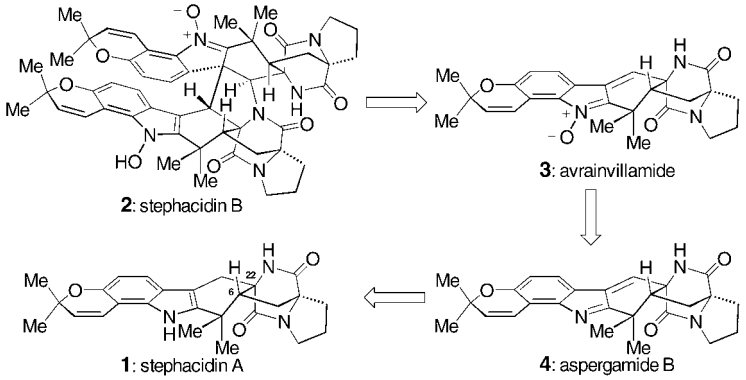
Natural Products Synthesis

Short, Enantioselective Total Synthesis of Stephacidin A**

Phil S. Baran, Carlos A. Guerrero, Narendra B. Ambhaikar, and Benjamin D. Hafensteiner*

Prenylated indole alkaloids have been a vibrant source of inspiration for synthetic chemists for over half a century.[1] Representative members of this natural product family include the spirotryprostatins,[2] brevianamides,[3] austamides,[4] and okaramines.[5] Stephacidin A and B (**1** and **2**, respectively in Scheme 1), recently disclosed by scientists at Bristol-Myers Squibb, signify a new peak of structural complexity within this family.[6,7] Isolated from the fungus *Aspergillus ochraceus* WC76466, stephacidin B (**2**) "represents one of the most structurally complex and novel alkaloids occurring in Nature"[6] and contains 15 rings, nine stereogenic centers, and the ubiquitous 6-oxyindole substructure. Furthermore, compounds **1** and **2** exhibit potent in vitro cytotoxic activity against a variety of human tumor cell lines. The bioactivity of the stephacidins is not mediated by p53, mdr, bcl2, tubulin, or topoisomerase II, which suggests a novel mechanism of action.[6] Taken together, these facts provided a strong impetus for the design of a concise total synthesis that employs **1** en route to **2** (Scheme 1) and that proceeds through the intermediacy of avrainvillamide[7] (**3**) and aspergamide B (**4**).[8]

The heptacyclic alkaloid stephacidin A (**1**) poses a number of challenges for synthesis. Pioneering work from the Williams laboratory[9] has verified the proposals of Birch[3] and Sammes[10] that the bicyclo[2.2.2]diazaoctane core of these alkaloids are likely formed by a Diels–Alder reaction in Nature. However, this elegant biomimetic approach would be difficult to employ in an enantioselective laboratory synthesis of **1**, especially as a proposed intermediate in the cascade sequence is achiral.[11] Furthermore, there is a clear gap in indole synthesis methodology, as published methods[12,13] for the preparation of the 6-hydroxytryptophan core require multistep, tedious procedures. Herein we report a concise, enantioselective total synthesis of stephacidin A (**1**) that establishes its relative configuration and addresses its inherent chemical challenges in a unique way.



Scheme 1. Stephacidins and their proposed[6,7] biogenetic relationships.

The challenge of a practical and rapid synthesis of the 6-hydroxytryptophan core of **1** was met by modifying a palladium-catalyzed indole synthesis developed at Merck (Scheme 2).[14] Thus, after extensive optimization, readily available pyroglutamate **5** was chemoselectively reduced with Super Hydride[15] and the crude lactol was immediately converted into tryptophan **8** in 75% overall yield through the intermediacy of enamine **7**. This enamine could be isolated, characterized, and converted into **8**. The high yield of this simple process is not diminished even on a multigram scale. Tetrabutylammonium iodide (3.0 equiv) was vital as the yield ranged from 10–35% in its absence. The benzopyran subunit was then installed and subsequently modified for coupling to the proline subunit through the sequence shown in Scheme 2. Protection with Boc_2O was followed by removal of the tosylate group.[16] Propargylation of the resulting phenol under standard Cu-catalyzed conditions with **9** [17] furnished **10** in 75% yield over two steps. Allenyl Claisen rearrangement[18] followed by reprotection of the indole NH group and subsequent hydrolysis led to the formation of acid **12**.

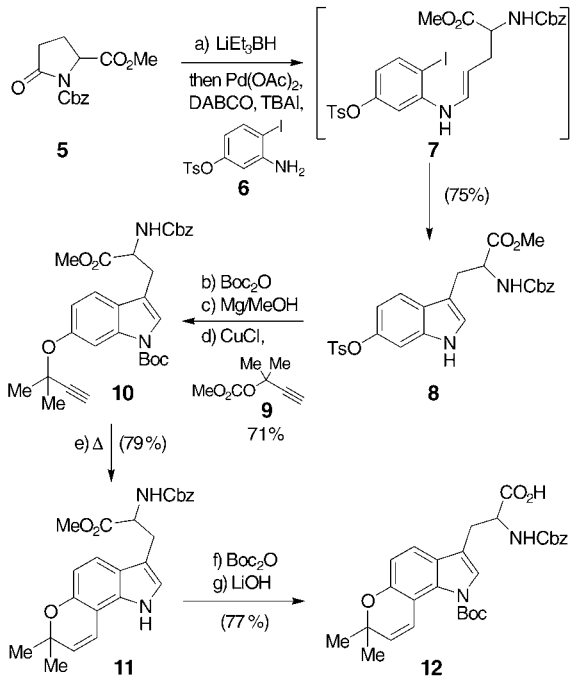
Racemic tryptophan derivative **12** was then coupled with the enantiomerically pure proline derivative **13**[19] to afford an

[*] Prof. Dr. P. S. Baran, C. A. Guerrero, Dr. N. B. Ambhaikar, B. D. Hafensteiner
Department of Chemistry
The Scripps Research Institute
10650 North Torrey Pines Road, La Jolla, CA 92037 (USA)
Fax: (+1) 858-784-7375
E-mail: pbaran@scripps.edu

[**] We thank Dr. D. H. Huang and Dr. L. Pasternack for NMR spectroscopic assistance, and Dr. G. Siuzdak and Dr. R. Chadha for mass-spectrometric and X-ray crystallographic assistance, respectively. We are grateful to Biotage for a generous donation of process vials used extensively during these studies. Financial support for this work was provided by The Scripps Research Institute, Eli Lilly & Co, and the NIH (predoctoral fellowship to C.A.G.).

Supporting information for this article is available on the WWW under http://www.angewandte.org or from the author.

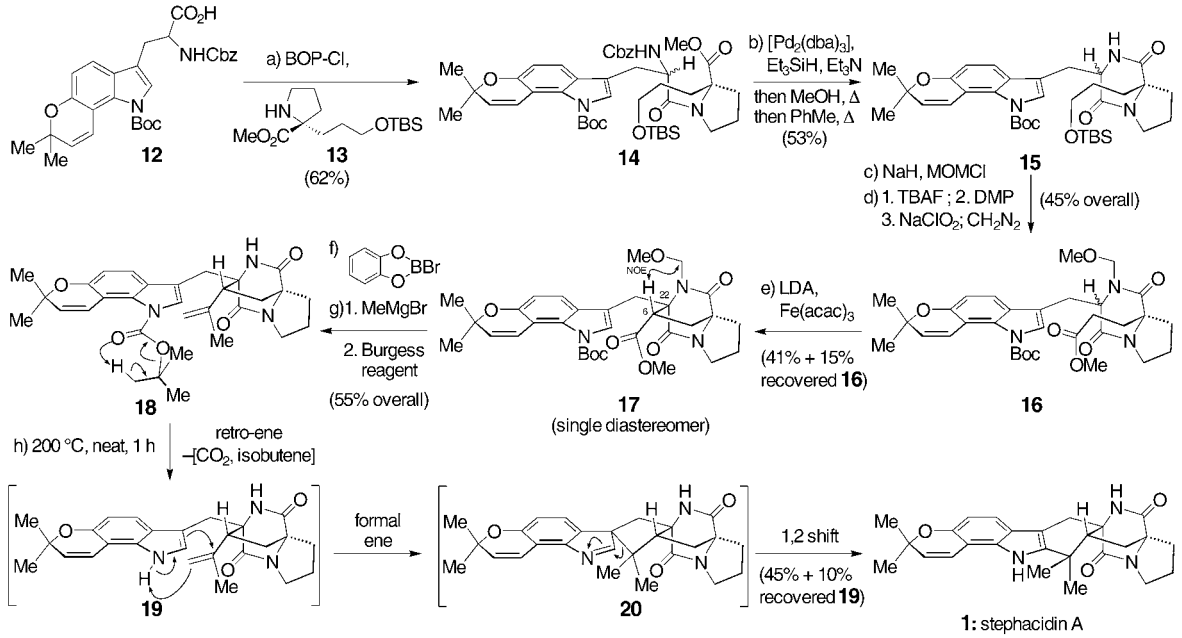
 © 2005 Wiley-VCH Verlag GmbH & Co. KGaA, Weinheim DOI: 10.1002/anie.200461864



Scheme 2. Synthesis of the benzopyran-tryptophan subunit **12**. Reagents and conditions: a) 1. $LiEt_3BH$ (1.1 equiv), THF, −78 °C, 10 min; 2. $Pd(OAc)_2$ (0.05 equiv), DABCO (3.0 equiv), **6** (1.1 equiv), TBAI (3.0 equiv), DMF, 105 °C, 4 h, 75% overall; b) Boc_2O (1.0 equiv), DMAP (0.01 equiv), CH_2Cl_2/CH_3CN (1:1), 25 °C, 30 min, 95%; c) Mg (10.0 equiv), MeOH, 0→25 °C, 2.5 h; d) **9** (3.0 equiv), $CuCl_2$ (0.001 equiv), DBU (3.0 equiv), CH_3CN, 0 °C, 24 h, 75% over two steps; e) AcOH, 120 °C, 80 min, 79%; f) Boc_2O (1.0 equiv), DMAP (0.01 equiv), CH_2Cl_2/CH_3CN (1:1), 25 °C, 30 min, 77%; g) LiOH (15.0 equiv), THF/H_2O (1:1), 0 °C, 3 h, 100%. DABCO = 1,4-diazabicyclo[2.2.2]octane; TBAI = tetra-*n*-butylammonium iodide; DMF = *N*,*N*-dimethylformamide; Boc = *tert*-butoxycarbonyl; DMAP = 4-dimethylaminopyridine; DBU = 1,8-diazabicyclo[5.4.0]undec-7-ene.

inconsequential mixture of diastereomeric amides **14** in 62% yield (Scheme 3). The Cbz group was chemoselectively excised and the diketopiperazine was formed in a single operation[20] without harm to the benzopyran or to either the *N*-Boc or silyl ether functionalities to provide diketopiperazine **15** in 53% yield. Protection of the diketopiperazine NH function followed by TBAF-mediated removal of the TBS group and sequential oxidation to the corresponding ester **16** set the stage for a remarkable C–C bond-forming event.

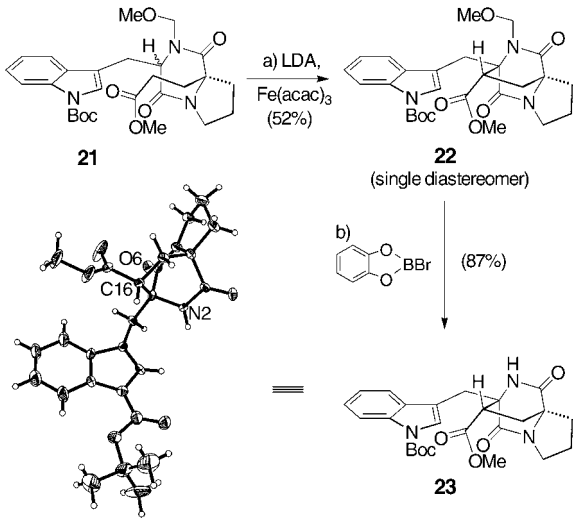
Although the metal-mediated oxidative coupling of enolates has immense potential for synthesis, it has been employed only sporadically since the seminal reports from the groups of Mislow and Saegusa.[21,22] Our objective was to effect the conversion of **16** into **17** by forming the key C6–C22 bond (stephacidin A numbering,[6] see Scheme 3, **17**) with complete stereocontrol through an oxidative coupling. Mechanistically, it is believed that such reactions proceed via radical species, despite a lack of evidence to rule out metal-bound intermediates. Recent findings in our laboratory[23]



Scheme 3. Enantioselective total synthesis of stephacidin A (**1**). Reagents and conditions: a) **13** (1.5 equiv), BOPCl (1.1 equiv), iPr_2EtN (1.1 equiv), CH_2Cl_2, 0→25 °C, 10 h, 62%; b) $[Pd_2(dba)_3]$ (0.2 equiv), Et_3SiH (40 equiv), Et_3N (2.0 equiv), CH_2Cl_2, 25 °C, 4 h; then MeOH, reflux, 30 min; then toluene, reflux, 2 h, 53% overall; c) NaH (1.2 equiv), MOMCl (1.1 equiv), DMF, 0 °C, 1 h, 65%; d) TBAF (3.0 equiv), THF, 25 °C, 1 h; then DMP (1.5 equiv), CH_2Cl_2, 25 °C, 2 h; then 2-methyl-2-butene (20 equiv), $NaH_2PO_4{\cdot}H_2O$ (3.0 equiv), $NaClO_2$ (2.8 equiv), THF, H_2O, 20 min; then CH_2N_2 in Et_2O, MeOH, 5 min, 69% overall; e) LDA (2.2 equiv), THF, −78 °C, 5 min then $[Fe(acac)_3]$ (2.2 equiv), THF, −78→25 °C, 1 h, 41% **17** with 15% recovered **16**; f) *B*-bromocatecholborane (1.5 equiv), CH_2Cl_2, 0 °C, 1.5 h, 63%; g) MeMgBr (6.0 equiv), toluene, 25 °C, 1 h, then Burgess reagent (2.0 equiv), benzene, 50 °C, 30 min, 88% overall; h) 200 °C, 1 h, 45% **1** with 10% recovered **19**. BOP = bis(2-oxo-3-oxazlidinyl)phosphinic chloride; dba = *trans*,*trans*-dibenzylideneacetone; MOM = methoxymethyl; TBAF = tetra-*n*-butylammonium fluoride; DMP = Dess–Martin periodinane; LDA = lithium diisopropylamide; acac = acetylacetonate.

 © 2005 Wiley-VCH Verlag GmbH & Co. KGaA, Weinheim

suggest that some of the metallic oxidants employed (Fe^{III}- and Cu^{II}-based) may play a more intimate role in these reactions. We imagined that the reaction of **16** would proceed with the desired stereochemical outcome to furnish **17** through a metal-chelated transition state. To probe this possibility, the model ester **21** (Scheme 4) was synthesized



Scheme 4. Stereocontrolled intramolecular oxidative coupling of the model ester **21**. Reagents and conditions: a) LDA (2.5 equiv), THF, −78 °C, 30 min then [Fe(acac)$_3$] (2.5 equiv), THF, −78 → 25 °C, 1 h, 52 % b) *B*-bromocatecholborane (2.0 equiv), CH_2Cl_2, 0 °C, 1 h, 87 %.

and subjected to modified oxidative coupling conditions, which furnished the desired cyclized product **22** in 52 % yield. The stereochemistry was secured upon removal of the MOM group in 87 % yield with *B*-bromocatecholborane[24] and X-ray crystallographic analysis of the resulting crystalline pentacycle **23**[25] (colorless needles, m.p. 125–128 °C (EtOAc), see Scheme 4 for ORTEP illustration). Notably, this reaction fails when using silver salts, iodine, and ferricinium hexafluorophosphate (an oxidant known to give radicals from enolates).[26] Participation of the MOM group in this reaction was ruled out as a PMB group could be used interchangeably with the same stereochemical outcome and yield.

With the encouraging reconnaissance gained in the model study, addition of LDA (2.2 equiv) to a solution of substrate **16** in THF at −78 °C followed by [Fe(acac)$_3$] after 5 minutes of enolization and warming to room temperature led to **17** in 41 % yield as a single diastereomer (along with 15 % recovery of **16**, Scheme 3). The extremely brief enolization time (5 min) was essential for the success of this reaction. With the exception of the benzopyran resonances, the NMR spectral properties of **17** were nearly identical to the model compound **22** (Scheme 3); the stereochemistry of the newly formed C6–C22 bond of **17** was further verified by the observed NOE (see **17** in Scheme 3 and Supporting Information).

To complete the synthesis of **1**, only one ring remained to be stitched onto **17**. The challenge of installing this ring led to the discovery of a new method for indole annulation. Thus, following removal of the MOM group in 63 % yield with *B*-bromocatecholborane, reaction with MeMgBr cleanly furnished a tertiary alcohol, which was directly dehydrated with Burgess reagent[27] to afford olefin **18** in 88 % overall yield. Although a variety of acidic conditions are known to effect ring closure in closely related systems,[28] our efforts to convert **18** or its hydrated precursor into **1** were all thwarted by the acid-labile nature of the substrate. Remarkably, when **18** was simply heated at 200 °C, in the absence of solvent, for 1 h, **1** was obtained in 45 % yield. We believe that thermolytic removal of the Boc group (through a retro-ene reaction) of **18** occurs first to afford **19** followed by a formal ene reaction leading to a fleeting spirocyclic intermediate **20** reminiscent of the venerable Pictet–Spengler reaction. A 1,2-shift then terminates the cascade and furnishes **1** (Scheme 3). The exact nature of the latter transformation has not been fully elucidated. However, this thermal reaction appears to be general for these types of systems and will be detailed in the full account. Synthetic **1** has identical spectral properties (both in [D$_6$]DMSO and $CDCl_3/CD_3OD$ 4:1) to that reported by Cutrone et al., thus establishing the relative configuration as shown in Scheme 1. The absolute configuration could not be secured as the optical rotation of natural **1** was not recorded and little or no material remains.[29] Incidentally, **23** could be converted into epibrevianamide by following a similar pathway, further confirming our assignment of the relative configuration.[30]

In summary, the first total synthesis of **1** from the commodity chemicals pyroglutamate and L-proline was completed in 15 operations. Efforts are now underway to access the highly oxidized congeners of stephacidin A (Scheme 1). The journey to stephacidin A was accompanied by some interesting discoveries and inventions, including: 1) a general methodology for the rapid and practical synthesis of tryptophan derivatives from pyroglutamate, 2) a remarkable deprotection/annulation cascade which occurs simply with heat to forge the final ring (**18**→**1**), and 3) simple, stereocontrolled assembly of two of the three stereocenters of **1** by a rare intramolecular oxidative coupling (**16**→**17** and **21**→**22**). The latter set of transformations proceeds cleanly and represents the first such couplings of esters to amides. The counterintuitive strategy employed in this total synthesis points to an attractive direction for further study in the general areas of oxidative C–C bond formation and synthetic design.[31]

Received: September 2, 2004
Published online: December 7, 2004

Keywords: alkaloids · cascade reactions · indoles · natural products · total synthesis

[1] M. Hesse, *Alkaloids: Nature's Curse or Blessing*, Wiley-VCH, Weinheim, **2002**, chap. 6.
[2] C.-B. Cui, H. Kakeya, H. Osada, *Tetrahedron* **1997**, *53*, 59–72.
[3] A. J. Birch, J. J. Wright, *Tetrahedron* **1970**, *26*, 2329–2344.
[4] P. S. Steyn, *Tetrahedron Lett.* **1971**, *12*, 3331–3334.

 © 2005 Wiley-VCH Verlag GmbH & Co. KGaA, Weinheim

[5] Y. Shiono, K. Akiyama, H. Hayashi, *Biosci. Biotechnol. Biochem.* **2000**, *64*, 103 – 110; Y. Shiono, K. Akiyama, H. Hayashi, *Biosci. Biotechnol. Biochem.* **2000**, *64*, 1519 – 1521.
[6] a) J. Qian-Cutrone, S. Huang, Y.-Z. Shu, D. Vyas, C. Fairchild, A. Menendez, K. Krampitz, R. Dalterio, S. E. Klohr, Q. Gao, *J. Am. Chem. Soc.* **2002**, *124*, 14556 – 14557; b) J. Qian-Cutrone, K. D. Krampitz, Y.-Z. Shu, L.-P. Chang, S. E. Lowe, U. S. Patent 6,291,461, **2001** [*Chem. Abstr.* **2001**, *135*, 236411]; c) isolation of avrainvillamide: W. Fenical, P. R. Jensen, X. C. Cheng U.S. Patent 6066635, **2000** [*Chem. Abstr.* **2000**, *132*, 346709].
[7] F. von Nussbaum, *Angew. Chem.* **2003**, *115*, 3176 – 3179; *Angew. Chem. Int. Ed.* **2003**, *42*, 3068 – 3071.
[8] For studies towards the total synthesis of the stephacidins or avrainvillamide, see: A. G. Myers, S. B. Herzon, *J. Am. Chem. Soc.* **2003**, *125*, 12080 – 12081; L. A. Adams, C. R. Gray, R. M. Williams, *Tetrahedron Lett.* **2004**, *45*, 4489 – 4493.
[9] a) E. M. Stocking, R. M. Williams, *Angew. Chem.* **2003**, *115*, 3186 – 3223; *Angew. Chem. Int. Ed.* **2003**, *42*, 3078 – 3115; b) R. M. Williams, R. J. Cox, *Acc. Chem. Res.* **2003**, *36*, 127 – 139.
[10] A. E. A. Porter, P. G. Sammes, *Chem. Commun.* **1970**, 1103.
[11] R. M. Williams, E. M. Stocking, J. F. Sanz-Cervera, *Top. Curr. Chem.* **2000**, *209*, 97 – 173.
[12] M. S. Allen, L. K. Hamaker, A. J. La Loggia, J. M. Cook, *Synth. Comm.* **1992**, *22*, 2077 – 2102.
[13] a) T. Hino, M. Taniguchi, *J. Am. Chem. Soc.* **1978**, *100*, 5564 – 5565; b) M. Taniguchi, T. Anjiki, M. Nakagawa, T. Hino, *Chem. Pharm. Bull.* **1984**, *32*, 2544 – 2554.
[14] C.-Y. Chen, D. R. Lieberman, R. D. Larsen, T. R. Verhoeven, P. J. Reider, *J. Org. Chem.* **1997**, *62*, 2676 – 2677.
[15] C. Pedregal, J. Ezquerra, A. Escribano, M. C. Carreño, J. L. García Ruano, *Tetrahedron Lett.* **1994**, *35*, 2053 – 2056.
[16] M. Sridhar, B. A. Kumar, R. Narender, *Tetrahedron Lett.* **1998**, *39*, 2847 – 2850.
[17] E. J. Tisdale, B. G. Vong, H. Li, S. H. Kim, C. Chowdhury, E. A. Theodorakis, *Tetrahedron* **2003**, *59*, 6873 – 6887.
[18] R. J. Cox, R. M. Williams, *Tetrahedron Lett.* **2002**, *43*, 2149 – 2152.
[19] Proline **13** was synthesized by hydroboration and protection (TBSCl) of the corresponding enantiopure allylated proline: D. Seebach, M. Boes, R. Naef, W. B. Schweizer, *J. Am. Chem. Soc.* **1983**, *105*, 5390 – 5398; M. G. Hinds, J. H. Welsh, D. M. Brennand, J. Fischer, M. J. Glennie, N. G. J. Richards, D. L. Turner, J. A. Robinson, *J. Med. Chem.* **1991**, *34*, 1777 – 1789; for further details, see Supporting Information.
[20] M. Sakaitani, Y. Ohfune, *J. Org. Chem.* **1990**, *55*, 870 – 876.
[21] C. A. Maryanoff, B. E. Maryanoff, R. Tang, K. Mislow, *J. Am. Chem. Soc.* **1973**, *95*, 5839 – 5840.
[22] Y. Ito, T. Konoike, T. Harada, T. Saegusa, *J. Am. Chem. Soc.* **1977**, *99*, 1487 – 1493.
[23] P. S. Baran, J. M. Richter, *J. Am. Chem. Soc.* **2004**, *126*, 7450 – 7451; P. S. Baran, J. M. Richter, D. W. Lin, *Angew. Chem.* **2005**, *117*, 615 – 618; *Angew. Chem. Int. Ed.* **2005**, *44*, 609 – 612.
[24] R. K. Boeckman, Jr., J. C. Potenza, *Tetrahedron Lett.* **1985**, *26*, 1411 – 1414.
[25] CCDC-248573 (**23**) contains the supplementary crystallographic data for this paper. These data can be obtained free of charge via www.ccdc.cam.ac.uk/retrieving.html (or from the Cambridge Crystallographic Data Centre, 12, Union Road, Cambridge CB21EZ, UK; fax: (+44)1223-336-033; or deposit@ccdc.cam.ac.uk).
[26] U. Jahn, P. Hartmann, *Chem. Commun.* **1998**, 209 – 210.
[27] E. M. Burgess, H. R. Penton, Jr., E. A. Taylor, *J. Org. Chem.* **1973**, *38*, 26 – 31.
[28] a) C. Mirand, G. Massiot, J. Levy, *J. Org. Chem.* **1982**, *47*, 4169 – 4170; b) H. J. Borschberg, *Helv. Chim. Acta* **1984**, *67*, 1878 – 1882; c) T. Darbre, C. Nossbaumer, H. J. Borschberg, *Helv. Chim. Acta* **1984**, *67*, 1040 – 1052; c) D. Stoermer, C. H. Heathcock, *J. Org. Chem.* **1993**, *58*, 564 – 568.
[29] J. Qian-Cutrone, personal communication. We are grateful to J. Qian-Cutrone for copies of NMR spectra in $CDCl_3/CD_3OD$ (4:1) and DMSO.
[30] R. M. Williams, T. Glinka, E. Kwast, H. Coffman, J. K. Stille, *J. Am. Chem. Soc.* **1990**, *112*, 808 – 821.
[31] Detailed experimental procedures, copies of spectral data and full characterization are contained in the Supporting Information.

 © 2005 Wiley-VCH Verlag GmbH & Co. KGaA, Weinheim

Synthetic Methods

Direct Coupling of Pyrroles with Carbonyl Compounds: Short Enantioselective Synthesis of (*S*)-Ketorolac**

Phil S. Baran, Jeremy M. Richter, and David W. Lin*

Pyrroles and indoles are the foundation of innumerable medicines, natural products, and synthetic materials.[1] Alkylations, acylations, and transition-metal-mediated couplings are the staple reactions for intermolecular C–C bond formation between these heterocycles and other organic substrates.[1–3] Typically, organometallic couplings require that one[3] or both entities are prefunctionalized (i.e. halogenation or any other disposable functionality).[2] Simple and practical methods that eliminate this prerequisite in synthetic design are rare.[4]

Inspired by a family of naturally occurring indole alkaloids, we recently reported a remarkably simple method for the direct coupling of the C-3 carbon of indoles with the α-carbon of carbonyl compounds as shown in Figure 1.[5] We imagined that these results could be extended to the analogous coupling of pyrroles (at C-2) with carbonyl compounds. Herein, we demonstrate the coupling of pyrroles with ketones, esters, amides, lactones, and lactams. An intramolecular variant of this methodology has also been

[*] Prof. Dr. P. S. Baran, J. M. Richter, D. W. Lin
Department of Chemistry
The Scripps Research Institute
10650 North Torrey Pines Road
La Jolla, CA 92037 (USA)
Fax: (+1) 858-784-7375
E-mail: pbaran@scripps.edu

[**] We thank Dr. D. H. Huang and Dr. L. Pasternack for assistance with NMR spectroscopic measurements, Dr. G. Siuzdak for help with mass spectrometric analyses, and Dr. R. Chadha for assistance with X-ray crystallographic studies. We are grateful to Professor Dennis Liotta for helpful suggestions regarding a mechanism involving chelated Cu^{II}. Financial support for this work was provided by The Scripps Research Institute, Eli Lilly & Co, and the National Science Foundation (predoctoral fellowships to J.M.R. and D.W.L.).

Supporting information for this article is available on the WWW under http://www.angewandte.org or from the author.

 DOI: 10.1002/anie.200462048 © 2005 Wiley-VCH Verlag GmbH & Co. KGaA, Weinheim

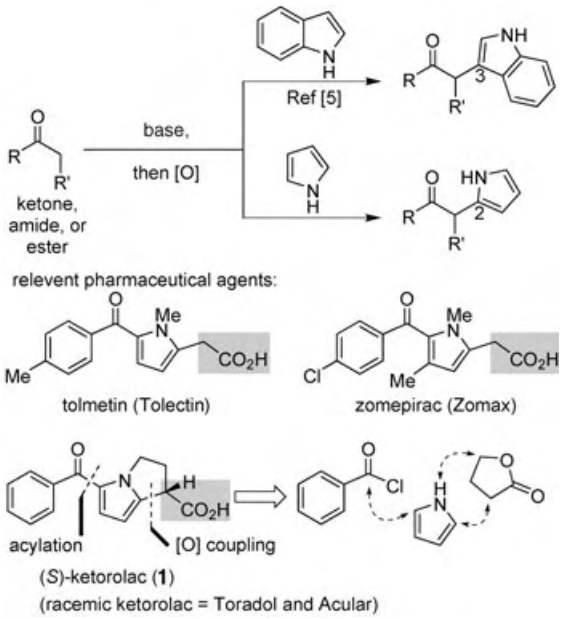
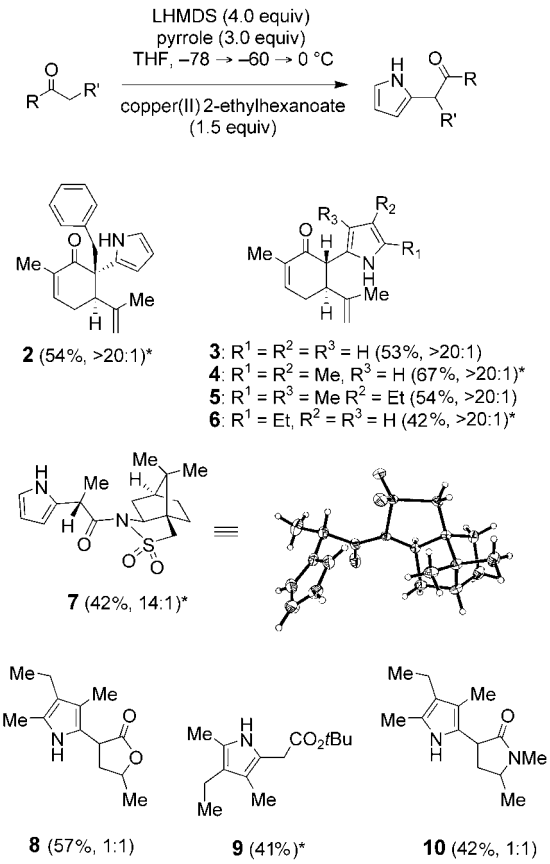


Figure 1. Direct coupling of indoles and pyrroles to carbonyl compounds and retrosynthetic analysis of (*S*)-ketorolac.

developed and applied to a concise, enantioselective synthesis of the nonsteroidal anti-inflammatory drug (*S*)-ketorolac (**1**) that can be performed without the need for protecting groups. The underlying mechanisms of these processes are also discussed.

Whereas the locus of nucleophilicity of the indole anion is at C-3, it resides at C-2 for the pyrrole anion,[1] and it was expected that direct coupling would link pyrroles to carbonyl compounds at that site. By slight modification of our previously reported conditions,[5] this proved to be the case as shown in Scheme 1. As with most electron-rich pyrroles, the products shown in Scheme 1 are quite sensitive to air and light. Nevertheless, both the pyrrole and indole[5] couplings can be performed on a multigram scale (>100 mmol). Further, complex pyrrolidines, pyrrolidinones, and pyridines are accessible from the pyrrole adducts.[1] A range of substitution patterns are tolerated on the pyrrole subunit (**3**–**6**) and, as with indoles,[5] highly congested pyrroles fused at a quaternary center are easily prepared with complete diastereocontrol (**2**). Sultam **7** was prepared as a 14:1 mixture of diastereomers, and the structure was confirmed by X-ray crystallographic analysis (colorless needles (1:1 cyclohexane/Et_2O), mp 131–133 °C). Although lactones (**8**) and lactams (**10**) are easily joined with pyrroles, esters (**9**) generally couple in lower yield (see Supporting Information for details), and pyrroles that bear electron-withdrawing groups either do not couple or do so in low yield. However, efforts to overcome these limitations are underway.

As shown in Figure 1, the pyrroleacetic acid scaffold is found in the widely marketed pharmaceutical agents tolmetin and ketorolac and the previously marketed agent zomepirac. Our retrosynthetic analysis of ketorolac (**1**, Toradol and Acular) was influenced strategically by the pioneering syntheses patented in the literature[6,7] and by the fact that the *S* antipode of ketorolac is more potent and causes fewer

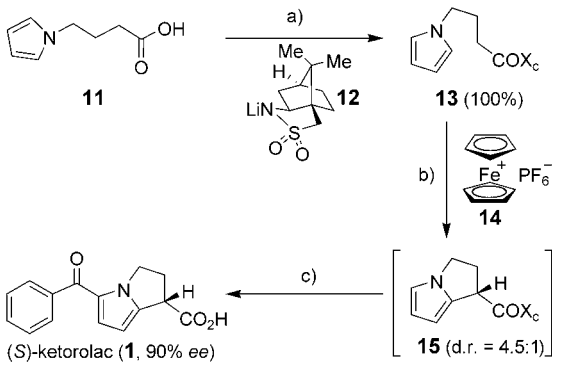


Scheme 1. Preparation of pyrrole–carbonyl compounds (LHMDS = lithium hexamethyldisilazide). Yields (%, isolated after chromatography unless otherwise stated) and d.r. values of the products are indicated in parentheses. [*] Yield based on recovered starting material.

side effects.[8] Our aim was not to improve upon the extremely efficient and practical five-step Syntex route[7] ($\approx 45\%$ yield from pyrrole, racemic); an enantioselective synthesis[9] of **1** would merely serve as an ideal proving ground for the versatility of the current method.

Our synthesis (Scheme 2) commences with pyrrole acid **11**, which results from the near-quantitative union of pyrrole with butyrolactone on a multigram scale.[10] The stage was set for an intramolecular pyrrole–carbonyl coupling after installing the chiral auxiliary to afford **13** (Et_3N, MeOCOCl, then **12**, 100%).[11] In the event, we were unable to achieve the oxidative annulation of **13** with many standard oxidants (Cu^{II}, Fe^{III}, Ag^{I}, Ag^{II}, Ti^{IV}, Mn^{III}, Ce^{IV}). After considerable exploration, ferrocenium hexafluorophosphate (**14**, a practical, recyclable, and commercially available oxidant)[12] was found to elicit the cyclization of **13** to **15** in 65% yield (based on recovered starting material and determined by ^1H NMR spectroscopy) as a 4.5:1 mixture of diastereomers. The isolated yield of **15** was about 35%, however, as **15** was quite sensitive to air and moisture, so the crude reaction mixture that contained **13**, **15**, and ferrocene was carried forward without purification (benzoyl chloride, 70 °C, remaining **13** and ferrocene easily separable).[13] Hydrolysis of the resulting benzoylated pyrrole by using tetrabutylammonium

 © 2005 Wiley-VCH Verlag GmbH & Co. KGaA, Weinheim



Scheme 2. Short, enantioselective synthesis of (*S*)-ketorolac. Reagents and conditions: a) Et_3N (1.1 equiv), MeOCOCl (1.0 equiv), THF (0.1 M), 0 °C, 1 h; then **12**, 100%; b) LHMDS (1.2 equiv), Et_3N (2.0 equiv), THF (0.01 M), −78 °C, 30 min; then 12 °C, **14** (0.75 equiv), 5 min, 65% bsm; (c) BzCl, 70 °C, 4 h; then TBAH (2.0 equiv), H_2O_2 (2.0 equiv), 2-methylbut-2-ene (3.0 equiv), DME (0.25 M), −10 °C, 3 h, 38%. X_c = camphor sultam auxiliary, bsm = based on recovered starting materials, Bz = benzoyl, TBAH = tetra-*n*-butylammonium hydroperoxide, DME = 1,2-dimethoxyethane.

hydroperoxide[14] furnished *S*-ketorolac (**1**, 90% *ee* determined by chiral HPLC, 38% isolated yield over 2 steps) along with recovered auxiliary. From the vantage point of synthetic design, certain details are worth noting: 1) the oxidation state of **11** is conserved (reduction, decarboxylation, and halogenation processes avoided),[15] 2) protecting groups are absent, 3) decent stereocontrol is observed in the ring closure despite the readily enolizable[9] nature of the newly formed stereocenter, and 4) overall brevity of the sequence (≈25% overall unoptimized yield from pyrrole in four operations).

Although conceptually similar, the direct coupling of carbonyl compounds with pyrroles (Scheme 1) by using a Cu^{II} oxidant probably differs mechanistically from the intramolecular cyclization (**13**→**15**) by using Fe^{III}-based **14**. As shown in Figure 2, we believe that in the former case an intermediate

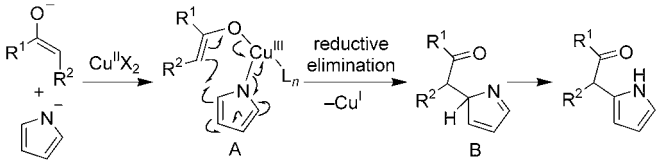


Figure 2. Proposed mechanism for the direct coupling of pyrroles with carbonyl compounds by using Cu^{II}.

Cu^{III}-chelated species (A) may be involved.[16] Reductive elimination and loss of Cu^{I} should lead to B, followed by tautomerization to yield the product. Several observations support this tentative mechanistic model: 1) dimerization of the pyrrole is never observed, as expected from geometrical constraints, 2) N-protected pyrroles do not react, 3) only 1 equivalent of oxidant is necessary, although the use of 1.5 equivalents gives a slight improvement in yield, and 4) the characteristic red-brown color of copper(I) salts is often observed at the end of the reaction. The same trends are seen for the analogous coupling with indoles and implies that a similar mechanism may be active.[5] To effect the conversion of **13** into **15**, oxidant **14** was employed because it has been firmly established by the scholarly studies of Jahn et al. to convert enolates into radical species by an outer-sphere single-electron-transfer pathway.[12] Remarkably, Fe^{III}-based oxidant **14** is ineffective for the couplings in Scheme 1 as are Cu^{II}-based oxidants for the annulation (**13**→**15**).

In summary, we have developed a new method for the one-step construction of a variety of pyrroles that would ordinarily require multistep sequences to synthesize. The method is scalable, practical, and reliable. The intermolecular heteroarylation of enolates (Scheme 1) uses a Cu^{II}-based oxidant, whereas the intramolecular variant proceeds by a different mechanism that functions using the Fe^{III}-based oxidant **14** (Scheme 2). The waste associated with protecting groups, prior modification of the substrates (such as halogenation or any other disposable functionalities), and expensive metals is eliminated. These studies point to a unique approach for the synthesis of π-electron-rich heterocyclic systems through coupling of unfunctionalized $C(sp^2)$ and $C(sp^3)$ atoms.[17]

Experimental Section

General Procedure for Direct Pyrrole Coupling: The carbonyl compound (0.25 mmol) was dissolved in benzene (1.0 mL) and the solvent was removed in vacuo. Pyrrole (0.75 mmol) was then added and the starting materials were dissolved in THF (8.0 mL). The solution was cooled to −78 °C and a solution of LHMDS (0.50 M, 2.0 mL) was added. The reaction mixture was allowed to stir for 30 min, after which time the septum was removed and copper(II)-2-ethylhexanoate (131 mg, 0.38 mmol) was rapidly added as a solid and then the septum was replaced. The reaction was allowed to warm to −60 °C and stirred for 3 h. The reaction was subsequently warmed slowly to ambient temperature and quenched by pouring into 5% aqueous NH_4OH (15 mL). The aqueous layer was partitioned with EtOAc (20 mL). The organic layer was separated and washed successively with water (15 mL) and then brine (15 mL), dried ($MgSO_4$), and filtered, and the solvent was removed in vacuo. Flash chromatography (silica gel) of the crude reaction mixture afforded pure coupled product. With the exception of compound **2**, all the pyrroles began to darken in color immediately after concentration, but NMR spectroscopic analysis showed no loss in purity. In general it was found that the couplings of ketones, amides, lactones, and lactams worked well with the exception of esters, which proved to be more unpredictable.

Received: September 21, 2004
Published online: December 6, 2004

Keywords: C–C coupling · copper · enantioselectivity · heterocycles · total synthesis

[1] J. A. Joule, K. Mills, *Heterocyclic Chemistry*, Blackwell, Oxford, **2000**, p. 589.
[2] a) J. J. Li, G. W. Gribble, *Palladium in Heterocyclic Chemistry*, Pergamon, Amsterdam, **2000**, p. 413; b) A. F. Littke, G. C. Fu, *Angew. Chem.* **2002**, *114*, 4350–4386; *Angew. Chem. Int. Ed.* **2002**, *41*, 4176–4211, and references therein.
[3] a) For a review of metal-mediated couplings of this type, see: M. Miura, M. Nomura, *Top. Curr. Chem.* **2002**, *219*, 211–241; b) For recent advances in this area, see: B. Sezen, D. Sames, *J. Am.*

 © 2005 Wiley-VCH Verlag GmbH & Co. KGaA, Weinheim

Chem. Soc. **2003**, *125*, 10580 – 10585, and references therein; c) For a review of palladium-mediated α-arylation of enolates, see: D. A. Culkin, J. F. Hartwig, *Acc. Chem. Res.* **2003**, *36*, 234 – 245.
[4] T. Tsuchimoto, Y. Ozawa, R. Negoro, E. Shirakawa, Y. Kawakami, *Angew. Chem.* **2004**, *116*, 4327 – 4329; *Angew. Chem. Int. Ed.* **2004**, *43*, 4231 – 4233, and references therein.
[5] P. S. Baran, J. M. Richter, *J. Am. Chem. Soc.* **2004**, *126*, 7450 – 7451.
[6] For an authoritative review of Syntex's landmark discovery and the development of ketorolac, see: J. M. Muchowski, *Adv. Med. Chem.* **1992**, *1*, 109 – 135.
[7] P. J. Harrington, H. N. Khatri, G. C. Schloemer, Patent 6197976, **2001**, and references therein.
[8] A. Guzmán, F. Yuste, R. A. Toscano, J. M. Young, A. R. Van Horn, J. M. Muchowski, *J. Med. Chem.* **1986**, *29*, 589 – 591.
[9] a) One practical path to enantiopure (*S*)-**1** uses enzymatic kinetic resolution (92% yield, 85% *ee*), see: G. Fulling, C. J. Sih, *J. Am. Chem. Soc.* **1987**, *109*, 2845 – 2846; b) For an approach to (*S*)-**1**, see: R. L. Pederson, I. M. Fellows, T. A. Ung, H. Ishihara, S. P. Hajela, *Adv. Synth. Catal.* **2002**, *344*, 728 – 735.
[10] J.-H. Li, J. K. Snyder, *J. Org. Chem.* **1993**, *58*, 516 – 519.
[11] W. Oppolzer in *Comprehensive Organic Synthesis*, *Vol. 5* (Eds.: B. M. Trost, I. Flemming), Pergamon, Oxford, **1991**, pp. 315 – 399.
[12] a) U. Jahn, P. Harmann, *Chem. Commun.* **1998**, 209 – 210; b) U. Jahn, *J. Org. Chem.* **1998**, *63*, 7130 – 7131; c) U. Jahn, P. Hartmann, S. Aussieker, *J. Am. Chem. Soc.* **2000**, *122*, 5212 – 5213; d) U. Jahn, P. Hartmann, *J. Chem. Soc. Perkin Trans. 1* **2001**, 2277 – 2282; e) U. Jahn, P. Hartmann, I. Dix, P. G. Jones, *Eur. J. Org. Chem.* **2001**, 3333 – 3355; f) U. Jahn, P. Hartmann, I. Dix, P. G. Jones, *Eur. J. Org. Chem.* **2002**, 718 – 735.
[13] J. M. Muchowski, S. H. Unger, J. Ackrell, P. Cheung, G. F. Cooper, J. Cook, P. Gallegra, O. Halpern, R. Koehler, A. F. Kluge, A. R. Van Horn, Y. Antonio, H. Carpio, F. Franco, E. Galeazzi, I. Garcia, R. Greenhouse, A. Guzmán, J. Iriarte, A. Leon, A. Peña, V. Peréz, D. Valdéz, N. Ackerman, S. A. Ballaron, D. V. Krishna Murthy, J. R. Rovito, A. J. Tomolonis, J. M. Young, W. H. Rooks II, *J. Med. Chem.* **1985**, *28*, 1037 – 1049.
[14] T. Hasegawa, H. Yamamoto, *Synlett* **1998**, 882 – 884.
[15] D. R. Artis, I.-S. Cho, J. M. Muchowski, *Can. J. Chem.* **1992**, *70*, 1838 – 1842. This paper reports the oxidative cyclization of a malonate onto a pyrrole. Such a strategy would obviously not be amenable to an enantioselective variant and it requires decarboxylation of the extraneous carboxyl group. For a related approach using a carbenoid generated from a diazoketone, see: P. Müller, P. Pholleux, *Helv. Chim. Acta* **1998**, *81*, 317 – 323.
[16] Intermediate **A** may be oxidized by another equivalent of Cu^{II} or by O_2. For related mechanistic scenarios, see: a) T. Arnauld, D. H. R. Barton, E. Doris, *Tetrahedron* **1997**, *53*, 4137 – 4144; b) D. A. Evans, J. L. Katz, T. R. West, *Tetrahedron Lett.* **1998**, *39*, 2937 – 2940.
[17] Detailed experimental procedures, copies of all spectral data and full characterization are contained in the Supporting Information. CCDC 251395 contains the supplementary crystallographic data for this paper. These data can be obtained free of charge from the Cambridge Crystallographic Data Centre via www.ccdc.cam.ac.uk/data_request/cif..

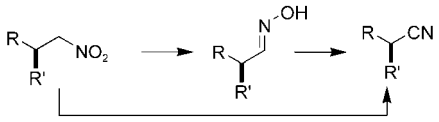
 © 2005 Wiley-VCH Verlag GmbH & Co. KGaA, Weinheim

Organic Synthesis

Convenient Transformation of Optically Active Nitroalkanes into Chiral Aldoximes and Nitriles**

*Constantin Czekelius and Erick M. Carreira**

The chemistry of nitro compounds forms the basis of a number of well-known processes, such as the Henry or the Nef reactions.[1] Transformations such as the latter permit the interconversion between nitro and other functional groups and are therefore of prime importance. They make possible the application of nitroalkanes as useful intermediates in synthesis. There has been intense activity in the development of catalytic, enantioselective methods for the preparation of chiral nitroalkanes.[2,3] The use of optically active organonitro compounds would significantly benefit from the availability of methods for their conversion under mild conditions into other chiral compound classes. Herein we report a convenient heavy-metal-free transformation of optically active nitroalkanes into chiral aldoximes at room temperature by employing inexpensive reagents: benzyl bromide, KOH, and 5 mol% nBu$_4$NI (Scheme 1). This also makes possible a one-pot conversion of nitroalkanes into optically active nitriles.



Scheme 1. Transformation of optically active nitroalkanes into chiral aldoximes and nitriles in the absence of heavy metals.

The most commonly employed methods for the reduction of primary nitroalkanes to oximes involve the use of Bu_3SnH, $Se/NaBH_4$, CS_2, or $SnCl_2$ (often in combination with thiophenol).[4,5] Our interest in the synthesis and use of optically active nitroalkanes as chiral building blocks has led us to focus on the development of milder, more convenient alternatives.

In analogy to the Kornblum oxidation that uses DMSO, 2-nitropropane has been employed for the conversion of benzyl halides into benzaldehydes.[6] The applications of this transformation have been solely focused on the halide partners and their oxidation to aldehydes. No study has appeared that addresses the scope of the nitroalkanes that may be successfully employed.[7] This leaves a number of critical issues

[*] C. Czekelius, Prof. Dr. E. M. Carreira
Laboratorium für Organische Chemie
ETH Hönggerberg, HCI H335
8093 Zürich (Switzerland)
Fax: (+41) 1-632-1328
E-mail: carreira@org.chem.ethz.ch

[**] This work was generously supported by Sumika Fine Chemicals, Japan (currently Sumitomo Chemical Co.).

Supporting information for this article is available on the WWW under http://www.angewandte.org or from the author.

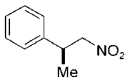
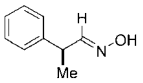
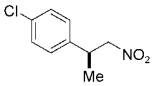
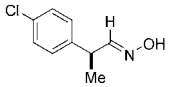
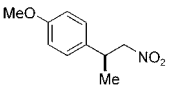
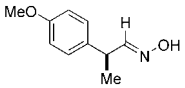
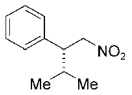
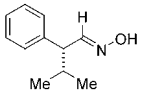
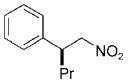
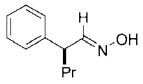
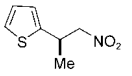
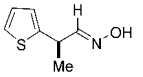
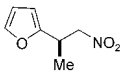
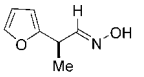
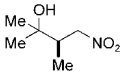
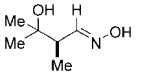
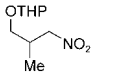
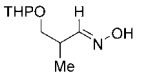
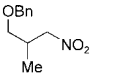
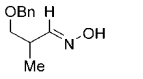
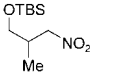
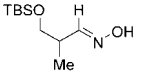
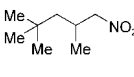
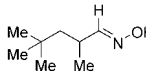
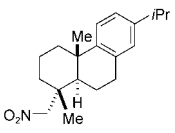
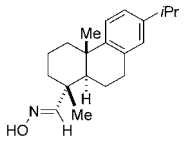
 © 2005 Wiley-VCH Verlag GmbH & Co. KGaA, Weinheim DOI: 10.1002/anie.200461879

unresolved that would be important for the successful implementation of such methodology for the reduction of a range of synthetically useful chiral nitroalkanes. In this respect, first, it was not clear whether the process would be generally applicable for non-benzylic primary nitroalkanes. Second, a chief concern when using optically active β-substituted nitroalkanes was whether the stereochemical integrity of the compound would be preserved.

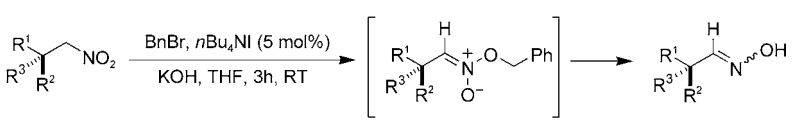
In initial investigations, treatment of 2-phenyl-1-nitropropane with benzyl bromide and KOH in THF in the presence of 5 mol% nBu$_4$NI at room temperature led to the formation of the corresponding aldoxime in 3 h and with 72% yield. The use of soluble amine bases failed to give product, whereas the heterogeneous conditions KOH/THF proved optimal in promoting aldoxime formation for a broad range of substrates. As shown in Table 1, optically active nitroalkanes including aromatic (electron-rich and electron-deficient), heteroaromatic, branched and unbranched aliphatic substrates, as well as substrates that incorporate unprotected alcohol functionalities were successfully reduced. Furthermore, it was demonstrated (Table 1, entry 13) that a nitroalkane which bears a quaternary center in the β-position was successfully reduced under these conditions, despite the longer reaction times needed (24 h compared to 3 h). Importantly, by means of a chiral HPLC assay, we determined that no racemization occurred during the process. This is particularly important for entries 1–7 (Table 1) as they involve intermediates in which an acidic C–H bond is rendered labile by both the *O*-alkylnitronate [Eq. (1), R^3 = H] and aryl groups. Also, nitroarenes are unreactive under these conditions.[8] Consequently, the method we describe provides a chemoselective reduction of nitroalkanes, which in effect reverses the reactivity pattern seen with traditional reductants.

Chiral oxime products serve as a source of aldehydes and chiral nitrile oxides [Eq. (2)].[9,10] Chiral nitrile oxides have been shown to be convenient starting materials for the synthesis of ketides in highly diastereoselective [3+2] dipolar cycloadditions with allylic alcohols. The ability to access a range of optically active oximes through a sequence that involves catalytic enantioselective reduction of nitroalkenes followed by their conversion into oximes as described above considerably expands the scope of such approaches to the synthesis of polyketides.

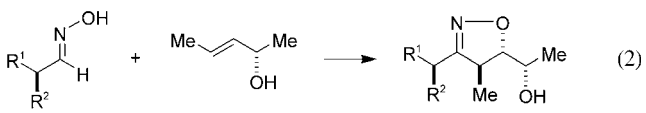
Table 1: Conversion of nitroalkanes into oximes [Eq. (1)].[a]

Entry	Substrate	Product	Yield [%]
1			72
2			80
3			69
4			81
5			80
6			76
7			75
8			60
9			78
10			65
11			70
12			73
13			56

[a] Typical reaction conditions: BnBr (1.1 equiv), KOH (1.05 equiv), and nBu$_4$NI (5 mol%) in THF at room temperature. THP = tetrahydropyran, Bn = benzyl, TBS = *t*-butyldimethylsilyl.



(1)

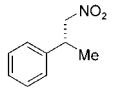
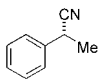
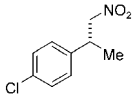
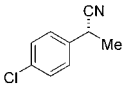
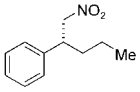
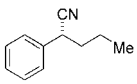


(2)

To further expand the application of the reduction protocol described above, we examined the possibility of carrying out a one-pot transformation of nitroalkanes into nitriles through the oxime. Of particular concern again was whether the desired nitrile could be isolated without loss of optical purity. The screening of a variety of dehydrating reagents revealed that by using trifluoroacetic anhydride (TFAA) or thionyl chloride and base (e.g. NEt_3), efficient formation of nitriles through the dehydration of the aldoximes occurs.[11] Thus, following treatment of the starting organonitro compound with benzyl bromide, KOH, and nBu$_4$NI in THF (3 h at room temperature) and when the consumption of the nitroalkane was judged to be complete, the simple addition of $SOCl_2$ or TFAA [Eq. (3) and Table 2] leads directly to nitriles in preparatively useful yields without loss of optical activity as

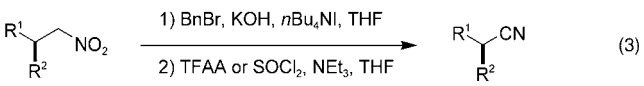
 © 2005 Wiley-VCH Verlag GmbH & Co. KGaA, Weinheim

Table 2: One-pot transformation of chiral nitroalkanes into nitriles.[a]

Entry	Substrate	Reagent	Product	Yield [%]
1		TFAA		62
2		$SOCl_2$		66
3		TFAA		63
4		$SOCl_2$		69
5		TFAA		73
6		$SOCl_2$		72

[a] Typical reaction conditions: BnBr (1.1 equiv), KOH (1.05 equiv), nBu$_4$NI (5 mol%) in THF, room temperature, 3 h; then TFAA (trifluoroacetic anhydride) or $SOCl_2$ (4.5 equiv), NEt_3 (9 equiv), −20 °C, 12 h.

verified by chiral HPLC assays. The overall protocol provides access to a class of compounds that are otherwise not easily accessed by known methods in catalytic asymmetric synthesis.[12]



(3)

In summary, we have documented a convenient protocol for the synthesis of optically active aldoximes and nitriles starting from chiral nitroalkanes. The salient features of the method include: 1) the reaction can be performed at room temperature under ambient atmosphere, 2) inexpensive reagents are employed (BnBr, KOH, nBu$_4$NI), and 3) the use of heavy metals is precluded. This provides an environmentally friendly reaction that excludes the potential contamination of the products by metal impurities. Given the ongoing advances in catalytic asymmetric synthesis that involve nitro compounds, the methodology described herein expands their possibilities for conversion into valuable synthetic targets.

Received: September 3, 2004
Published online: December 21, 2004

Keywords: chirality · nitro compounds · oximes · reduction · synthetic methods

[1] a) N. Ono, *The Nitro Group in Organic Synthesis*, Wiley-VCH, New York, **2001**; b) V. V. Perekalin, E. S. Lipina, V. M. Berestovitskaya, D. A. Efremov, *Nitroalkenes*, Wiley, Chichester, **1994**; c) *Nitro Compounds—Recent Advances in Synthesis and Chemistry: Organic Nitro Chemistry Series* (Eds.: H. Feuer, A. T. Nielsen), VCH, Weinheim, **1990**; d) D. Seebach, E. W. Colvin, F. Lehr, T. Weller, *Chimia* **1979**, *33*, 1.

[2] a) For an excellent review, see: O. M. Berner, L. Tedeschi, D. Enders, *Eur. J. Org. Chem.* **2002**, 1877; b) H. Schäfer, D. Seebach, *Tetrahedron* **1995**, *51*, 2305; c) N. Sewald, V. Wendisch, *Tetrahedron: Asymmetry* **1998**, *9*, 1341; d) C. Luchaco-Cullis, A. H. Hoveyda, *J. Am. Chem. Soc.* **2002**, *124*, 8192; e) D. M. Mampreian, A. H. Hoveyda, *Org. Lett.* **2004**, *6*, 2829; f) A. Alexakis, C. Benhaim, S. Rosset, M. Humam, *J. Am. Chem. Soc.* **2002**, *124*, 5262; g) A. Duursma, A. J. Minnaard, B. L. Feringa, *J. Am. Chem. Soc.* **2003**, *125*, 3700; h) H. Li, Y. Wang, L. Tang, L. Deng, *J. Am. Chem. Soc.* **2004**, *126*, 9906; i) H. Choi, Z. Hua, I. Ojima, *Org. Lett.* **2004**, *6*, 2689; j) T. Ishii, S. Fujioka, Y. Sekiguchi, H. Kotsuki, *J. Am. Chem. Soc.* **2004**, *126*, 9558; k) J. M. Betancourt, C. F. Barbas III, *Org. Lett.* **2001**, *3*, 3737; l) C. Czekelius, E. M. Carreira, *Angew. Chem. Int. Ed.* **2003**, *42*, 4793; *Angew. Chem.* **2003**, *115*, 4941.

[3] a) H. Sasai, T. Suzuki, S. Arai, T. Arai, M. Shibasaki, *J. Am. Chem. Soc.* **1992**, *114*, 4418; b) H. Sasai, T. Tokunaga, S. Watanabe, T. Suzuki, N. Itoh, M. Shibasaki, *J. Org. Chem.* **1995**, *60*, 7388; c) M. Shibasaki, H. Sasai, T. Arai, *Angew. Chem.* **1997**, *109*, 1290; *Angew. Chem. Int. Ed. Engl.* **1997**, *36*, 1236; d) T. Arai, Y. M. A. Yamada, N. Yamamoto, H. Sasai, M. Shibasaki, *Chem. Eur. J.* **1996**, *2*, 1368; e) H. Sasai, N. Itoh, T. Suzuki, M. Shibasaki, *Tetrahedron Lett.* **1993**, *34*, 855; f) H. Sasai, Y. M. Yamada, T. Suzuki, M. Shibasaki, *Tetrahedron* **1994**, *50*, 12313; g) H. Sasai, T. Suzuki, N. Itoh, S. Arai, M. Shibasaki, *Tetrahedron Lett.* **1993**, *34*, 2657; h) B. M. Trost, V. S. C. Yeh, *Angew. Chem.* **2002**, *114*, 889; *Angew. Chem. Int. Ed.* **2002**, *41*, 861; i) B. M. Trost, V. S. C. Yeh, H. Ito, N. Bremeyer, *Org. Lett.* **2002**, *4*, 2621; j) D. A. Evans, D. Seidel, M. Rueping, H. W. Lam, J. T. Shaw, C. W. Downey, *J. Am. Chem. Soc.* **2003**, *125*, 12962.

[4] a) J. von Braun, W. Sobecki, *Ber. Dtsch. Chem. Ges.* **1911**, *44*, 2526; b) J. von Braun, E. Danziger, *Ber. Dtsch. Chem. Ges.* **1913**, *46*, 103; c) M. Bartra, P. Romea, F. Urpí, J. Vilarasa, *Tetrahedron* **1990**, *46*, 587; d) D. Edmont, D. M. Williams, *Tetrahedron Lett.* **2000**, *41*, 8581; e) C. C. Hughes, D. Trauner, *Angew. Chem.* **2002**, *114*, 4738; *Angew. Chem. Int. Ed.* **2002**, *41*, 4556; f) D. H. R. Barton, I. Fernandez, C. S. Richard, S. Z. Zard, *Tetrahedron* **1987**, *43*, 551; g) D. Albanese, D. Landini, M. Peno, G. Pozzi, *Synth. Commun.* **1990**, *20*, 965; h) D. Albanese, D. Landini, M. Penseo, *Synthesis* **1990**, 333.

[5] For other metal-mediated reductions of nitroalkanes to oximes, see: a) M. Hudlický, *Reductions in Organic Chemistry*, Ellis Horwood, Chichester, **1984**; b) K. Johnson, E. F. Degering, *J. Am. Chem. Soc.* **1939**, *61*, 3194; c) J. E. McMurry, J. Melton, *J. Org. Chem.* **1973**, *38*, 4367; d) Y. Akita, M. Inaba, H. Uchida, A. Ohta, *Synthesis* **1977**, 792.

[6] a) H. B. Hass, M. L. Bender, *J. Am. Chem. Soc.* **1949**, *71*, 1767; b) H. B. Hass, M. L. Bender, *J. Am. Chem. Soc.* **1949**, *71*, 3482; c) C. D. Nenitzescu, D. A. Isacescu, *Ber. Dtsch. Chem. Ges. B.* **1930**, *63*, 2484; d) R. Filler, H. Novar, *J. Org. Chem.* **1960**, *25*, 733; e) C. F. Bigge, J. T. Drummond, G. Johnson, T. Malone, A. W. Probert, Jr., F. W. Marcoux, L. L. Coughenour, L. J. Brahce, *J. Mol. Chem.* **1989**, *32*, 1580; f) T. C. Bedard, J. Y. Corey, L. D. Lange, N. P. Rath, *J. Organomet. Chem.* **1991**, *401*, 261; g) W. Kirmse, W. Konrad, D. Schnitzler, *J. Org. Chem.* **1994**, *59*, 3821.

[7] For the transformation of phenylnitromethane into benzaldehyde oxime, see: L. Weisler, R. W. Helmkamp, *J. Am. Chem. Soc.* **1945**, *67*, 1167.

[8] No reaction was observed by ^{1}H NMR spectroscopy when nitrobenzene was treated with benzyl bromide (1.1 equiv), KOH (1.05 equiv), and nBu$_4$NI (5 mol%) in THF at room temperature for 6 h.

[9] a) C. Schöpf, G. Lehmann, *Justus Liebigs Ann. Chem.* **1935**, *518*, 1; b) J. Tadanier, C.-M. Lee, D. Whittern, N. Wideburg, *Carbohydr. Res.* **1990**, *201*, 185.

[10] a) J. W. Bode, N. Fraefel, D. Muri, E. M. Carreira, *Angew. Chem.* **2001**, *113*, 2128; *Angew. Chem. Int. Ed.* **2001**, *40*, 2082; b) L. D. Fader, E. M. Carreira, *Org. Lett.* **2004**, *6*, 2485; c) For a review of asymmetric 1,3-dipolar cycloaddition reactions, see: K. V. Gothelf, K. A. Jørgensen, *Chem. Rev.* **1998**, *98*, 863.

[11] a) W. Steinkopf, L. Bohrmann, *Ber. Dtsch. Chem. Ges.* **1908**, *41*, 1044; b) L. Hellerman, R. L. Garner, *J. Am. Chem. Soc.* **1946**, *68*,

 © 2005 Wiley-VCH Verlag GmbH & Co. KGaA, Weinheim

819; c) A. B. Charette, A. Gagnon, M. Janes, C. Mellon, *Tetrahedron Lett.* **1998**, *39*, 5147; d) R. Tsang, B. Fraser-Reid, *J. Am. Chem. Soc.* **1986**, *108*, 2116; e) J. Marco-Contelles, P. Gallego, M. Rodríguez-Fernández, N. Khiar, C. Destabel, M. Bernabé, A. Martínez-Grau, J. L. Chiara, *J. Org. Chem.* **1997**, *62*, 7397.

[12] For the hydrocyanation of monosubstituted vinylarenes, see: T. V. Rajanbabu, A. L. Casalnuovo, *J. Am. Chem. Soc.* **1996**, *118*, 6325.

 © 2005 Wiley-VCH Verlag GmbH & Co. KGaA, Weinheim

Peptide Enrichment

Enrichment of Low-Abundance Peptides and Proteins on Zeolite Nanocrystals for Direct MALDI-TOF MS Analysis**

Yahong Zhang, Xiaoyan Wang, Wei Shan, Biyun Wu, Huizhi Fan, Xijuan Yu, Yi Tang, and Pengyuan Yang**

Proteomics, one of the most important research areas in the post genomics era, is arousing considerable attention because of its pertinence to functional genomics.[1] Its premise is the high-throughput separation and identification of proteins and peptides. Peptide mapping by MALDI-TOF MS has become a major tool for protein identification in proteome analysis.[2] However, many proteins are quite scarce owing to the difficulties of sample isolation. This is especially true for proteins that are expressed in low abundance, such as disease-associated proteins.[3] Moreover, a further decrease in sample yield may occur during the preparation of a peptide digest prior to MALDI-TOF MS analysis which therefore requires that peptide preparations undergo an enrichment step beforehand. However, conventional methods for concentrating peptides by simple evaporation result in sample loss through protein adsorption onto the surface of the container. An additional problem with evaporation is the simultaneous concentration of buffer components (e.g. salts) and other contaminants. Alternative methods for peptide enrichment by reversed-phase resin are complex and are typically suitable only for hydrophobic peptides.[4] Therefore a universal and simple peptide enrichment method is in high demand.

Zeolite has attracted considerable attention as a novel chromatographic carrier in the adsorption and purification of proteins.[5] Zeolite particles at the nanometer scale (nanozeolites) show a number of distinct characteristics: large external surface area, high dispersibility in both aqueous and organic solutions, and a variety of tunable surface properties, such as adjustable surface charge and hydrophilicity/hydrophobicity.[6] These properties make them promising candidates for the concentration of trace biomolecules in large solution volumes through various protein–zeolite-surface interactions.

Very recently, our group has successfully separated the selenoprotein-P (Se-P) proteins in mouse plasma through their chelation with Co^{2+}-exchanged nanozeolite/diatomite composites.[7] Herein, we report a remarkable enrichment of low-abundance peptides on zeolite nanocrystals based on their strong adsorption ability[8] and high dispersibility. Meanwhile, nanozeolites exhibited universality toward the peptides tested, and resisted the co-concentration of salts during the enrichment process. More importantly, the peptides adsorbed on the nanozeolites can be directly analyzed by MALDI-TOF MS. Hence, the risk of sample loss from any elution steps is avoided and the concentration procedure is simplified.

All nanozeolite particles were hydrothermally synthesized according to literature procedures.[9] Scanning electron microscopy and dynamic light scattering (DLS) analysis show that the size of zeolite particles is less than 100 nm (Table 1), which endows them with both high dispersibility in peptide solutions and large active surface areas for peptide adsorption. The X-ray diffraction (XRD) patterns confirm their corresponding crystal structures. To study the enrichment effect of nanozeolites on peptide analysis, the nanozeolites were dispersed in a dilute aqueous solution containing three standard peptides (0.04–1 $pg\,\mu L^{-1}$ for each peptide) (peptide I: KHHDKHGH, M_w 995.07, isoelectric point (pI) 8.62; peptide II: CYIQNCPRG, M_w 1050.22, pI 8.06; and peptide III: DRVYIHPFHL, M_w 1296.49, pI 6.92). After centrifugation and redispersion, the suspension of peptide-adsorbed nanozeolites (peptides/nanozeolites) was mixed with a MALDI matrix (α-cyano-4-hydroxycinnamic acid). The mixture was then spotted onto a MALDI plate for MS analysis. For comparison, peptide solutions of 20 and 50 $pg\,\mu L^{-1}$ were prepared without enrichment and also analyzed by MALDI-TOF MS.[4]

Figure 1 displays MALDI-TOF mass spectra of the three peptides with or without nanozeolite-mediated enrichment. The peptides at concentrations lower than 20 $pg\,\mu L^{-1}$ were scarcely detected by MS without the nanozeolite-enrichment step (Figure 1b). However, after enrichment, peaks of all peptides became clearly apparent (Figure 1c), even at a peptide concentration as low as 1 $pg\,\mu L^{-1}$. The intensities and signal-to-noise ratios (S/N) of peptides I and II were even higher than those of the peptides at 50 $pg\,\mu L^{-1}$ that were

[*] Dr. Y. Zhang,[+] W. Shan, B. Wu, Prof. Y. Tang
Department of Chemistry and
Shanghai Key Laboratory of Molecular Catalysis and Innovative Materials
Fudan University
Shanghai 200433 (P. R. China)
Fax: (+86) 21-6564-1740
E-mail: yitang@fudan.edu.cn
Dr. X. Wang,[+] Dr. H. Fan, Dr. X. Yu, Prof. P. Yang
Department of Chemistry, Fudan University
Shanghai 200433 (P. R. China)
Fax: (+86) 21-6564-1740
E-mail: pyyang@fudan.edu.cn
[+] These authors contributed equally to this communication.

[**] This work was supported by the NSFC (20273016, 20303003, 20325313, 20205002), the SNPC (0249m028), and the Major State Basic Research Development Program (2001CB5102).
Supporting information for this article is available on the WWW under http://www.angewandte.org or from the author.

 DOI: 10.1002/anie.200460741 © 2005 Wiley-VCH Verlag GmbH & Co. KGaA, Weinheim

Table 1: Particle sizes and Si/Al ratios of the synthesized zeolite nanocrystals, and the MS data and S/N of peptides/nanozeolite samples after enrichment in the absence or presence of $CaCl_2$.

Nanozeolite		Si/Al[a]	Size[a] [nm]	Intensity and S/N (in parentheses) of MS signal					
				Peptide I[b]	Peptide II[b]	Peptide III[b]	Peptide I[c]	Peptide II[c]	Peptide III[c]
	β-15	15	95	~0 (~0)	6637 (1540)	116 (27)			
BEA	β-25	25	68	898 (149)	4435 (797)	535 (109)	8959 (845)	6347 (672)	4682 (699)
	β-37	37	81	311 (34)	1876 (448)	157 (163)	2432 (450)	3085 (629)	352 (98)
MFI	S-1	∞	70	707 (128)	1028 (204)	2340 (557)	5920 (638)	207 (118)	2111 (341)

[a] The Si/Al ratio and size of zeolite nanocrystals were determined by energy dispersive X-ray (EDX) analysis and dynamic light scattering (DLS), respectively. [b] The concentration of peptide solutions for enrichment was 1 $pg\,\mu L^{-1}$ for each peptide. [c] The concentration of peptide solutions for enrichment was 1 $pg\,\mu L^{-1}$ for each peptide, in the presence of 1 M $CaCl_2$.

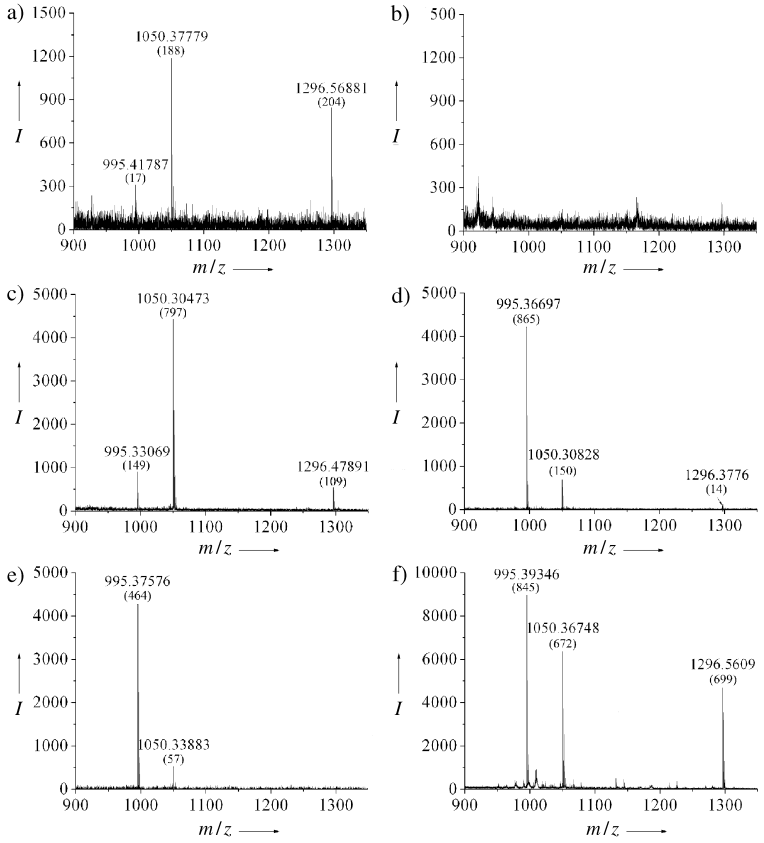


Figure 1. MALDI-TOF mass spectra of the peptide mixtures prepared without enrichment: a) 50 $pg\,\mu L^{-1}$ and b) 20 $pg\,\mu L^{-1}$, and the peptides/nanozeolite (β-25) samples after enrichment in peptide mixture solutions of c) 1 $pg\,\mu L^{-1}$, d) 0.4 $pg\,\mu L^{-1}$, e) 0.04 $pg\,\mu L^{-1}$, and f) 1 $pg\,\mu L^{-1}$ containing 1 M $CaCl_2$. The data in parentheses are S/N of the corresponding peptides. MALDI-TOF MS experiments were performed on a 4700 Proteomics Analyzer (Applied Biosystems, USA). Samples were desorbed with an Nd-YAG laser (355 nm) operated at a repetition rate of 200 Hz and an acceleration voltage of 20 kV. Measurements were performed in the reflector TOF detection mode.

prepared without the enrichment step (Figure 1a). Furthermore, the presence of nanozeolites neither interfered with the MS signals of the three peptides nor introduced impurities. Notably, when the peptide solution was diluted to 0.4 $pg\,\mu L^{-1}$, the three peptides could still be detected after enrichment (Figure 1d); even when the concentration was decreased to 0.04 $pg\,\mu L^{-1}$, peptides I and II remained detectable (Figure 1e). In this case, a concentration factor of 10^2–10^3 could be estimated.

The application of nanozeolites to enrichment and subsequent MS detection of the peptides was studied by using zeolite beta (β-X, X = Si/Al ratio) and silicalite-1 (S-1) nanocrystals in a 1-$pg\,\mu L^{-1}$ three-peptide mixture (Table 1). It was found that, except for the case of zeolite β-15 (the lowest Si/Al ratio), peptides enriched on all nanozeolites exhibited strong MS signals and high S/N, indicating that these nanozeolites are good candidates for peptide enrichment. The discrimination of β-15 against peptide I could be attributed to too strong an adsorption as a result of strong hydrophilic and coulombic interactions[10,5e] which prevents desorption/ionization in MALDI-TOF MS.

During extraction and/or proteolysis procedures, some inorganic salts are normally added to promote dissolution of proteins and peptides, and to maintain an appropriate ionic strength. However, the presence of salts can severely upset the MALDI process and result in poor mass spectra.[11] Therefore, a desalting step necessarily follows conventional protein concentration processes in order to obtain a satisfactory analysis. The influence of salt on the nanozeolite-mediated enrichment process was investigated in peptide solutions containing 1 M $CaCl_2$ (Table 1). In most cases, the three peptides enriched on the nanozeolites in the presence of $CaCl_2$ presented even stronger MS signals with higher S/N (Table 1 and Figure 1f) than those enriched in the absence of $CaCl_2$ (Figure 1c and Table 1). This could be ascribed to the shielding effect of Ca^{2+} ions toward the surface charge of nanozeolites[10] which may facilitate the ionization of adsorbed peptides. The results show that these nanozeolites exhibit an excellent means by which to avoid the problems of high salt levels in protein preparations and to obviate the need for a desalting step.

To evaluate the universality of this approach, β-25 and S-1 nanocrystals were applied to a typical myoglobin tryptic digest. A database search (Protein Prospector)[12] identified about 10 peptides that represent 60–70% coverage of the myoglobin sequence. Figure 2a displays the MS result of a myoglobin (50 $pg\,\mu L^{-1}$) digest enriched by β-25. In comparison with the MS data from the high-myoglobin-concentration (5000 $pg\,\mu L^{-1}$) digest without the enrichment step (Figure 2b), the advantage of zeolite-mediated enrichment is clear: a similar tryptic fragment profile is present, and

 © 2005 Wiley-VCH Verlag GmbH & Co. KGaA, Weinheim

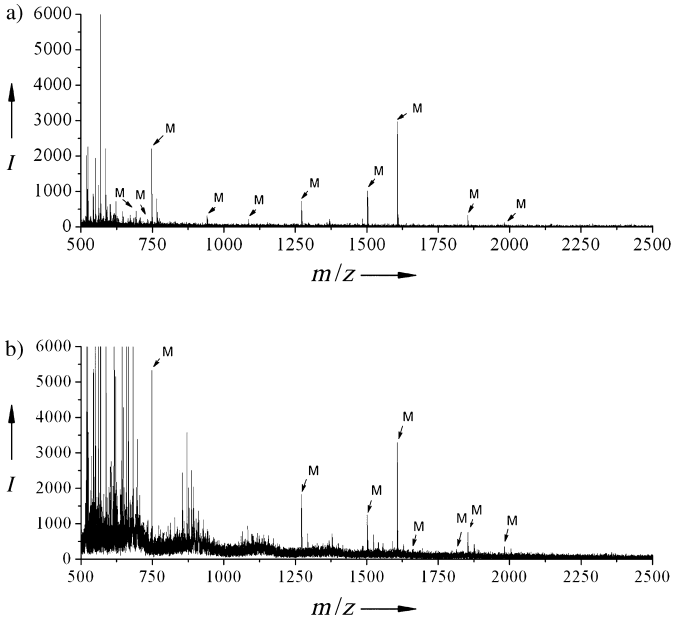


Figure 2. MALDI-TOF mass spectra of myoglobin tryptic digests: a) sample at 50 pg μL^{-1} enriched with β-25 nanocrystals, and b) sample at 5000 pg μL^{-1} without enrichment. The peaks marked with M represent the myoglobin fragments.

the S/N is much higher even for a preparation containing 100-fold less protein (Figure 2a). This indicates that nanozeolites appear not to discriminate against the various peptides.

In summary, nanozeolite particles were applied for the first time in the enrichment and identification of trace peptides and proteins. The direct MALDI-TOF MS analysis protocol eliminates the peptide-elution step and therefore circumvents the risk of sample loss. It was found that nanozeolites with medium and high Si/Al ratios exhibited excellent enrichment and desalting qualities for MALDI-TOF MS analysis of peptides. This technique is expected to open up new horizons for the preconcentration and identification of low-abundance peptides and proteins, as well as a new application of nanozeolites.

Experimental Section

Nanozeolite suspensions (10 μL of 10 mg mL^{-1}) were added to standard peptide or peptide digest solutions (1 mL) at varied concentrations. The resulting mixtures were agitated for 90 min at 37 °C, and centrifuged at 16000 rpm for 20 min. After decanting the supernatant, the residual peptides/nanozeolite pellets were rinsed with water three times and resuspended in acetonitrile (50%; 2.5 μL) for subsequent MALDI sample preparation. A volume of the above slurry (0.5 μL) was mixed with α-cyano-4-hydroxycinnamic acid (0.25 μL, a saturated solution in 50% aqueous acetonitrile containing 0.1% trifluoroacetic acid) on the MALDI plate and applied for MALDI-TOF MS analysis.

Received: May 21, 2004
Revised: October 29, 2004
Published online: December 13, 2004

Keywords: mass spectrometry · peptides · proteins · zeolites

[1] a) V. C. Wasinger, S. J. Cordwell, A. Cerpapoljak, J. X. Yan, A. A. Gooley, M. R. Wilkins, M. W. Duncan, R. Harris, K. L. Williams, I. Humpherysmith, *Electrophoresis* **1995**, *16*, 1090; b) A. Abbott, *Nature* **2001**, *409*, 747; c) S. Fields, *Science* **2001**, *291*, 1221.
[2] a) M. Mann, P. Hojrup, P. Roepstorff, *Biol. Mass Spectrom.* **1993**, *22*, 338; b) J. R. Yates, S. Speicher, P. R. Griffin, T. Hunkapiller, *Anal. Biochem.* **1993**, *214*, 397.
[3] K. Karlsson, N. Cairns, G. Lubec, M. Fountoulakis, *Electrophoresis* **1999**, *20*, 2970.
[4] M. Kussmann, E. Nordho, H. Rahbek-Nielsen, S. Haebel, M. Rossel-Larsen, L. Jakobsen, J. Gobom, E. Mirgorodskaya, A. Kroll-Kristensen, L. Palmp, P. Roepstor, *J. Mass Spectrom.* **1997**, *32*, 593.
[5] a) S. Ghose, B. Mattiasson, *Biotechnol. Appl. Biochem.* **1993**, *18*, 311; b) D. Klint, H. Eriksson, *Protein Expression Purif.* **1997**, *10*, 247; c) Y. C. Yu, Y. C. Huang, T. Y. Lee, *Biotechnol. Prog.* **1998**, *8*, 332; d) D. Klint, G. Karlsson, J. O. Bovin, *Angew. Chem.* **1999**, *111*, 2736; *Angew. Chem. Int. Ed.* **1999**, *38*, 2560; e) M. Matsui, Y. Kiyozumi, T. Yamamoto, Y. Mizushina, F. Mizukami, K. Sakaguchi, *Chem. Eur. J.* **2001**, *7*, 1555; f) H. Chiku, M. Matsui, S. Murakami, Y. Kiyozumi, F. Mizukami, K. Sakaguchia, *Anal. Biochem.* **2003**, *318*, 80.
[6] W. Shan, Y. H. Zhang, W. L. Yang, C. Ke, Z. Gao, Y. F. Ye, Y. Tang, *Microporous Mesoporous Mater.* **2004**, *69*, 35.
[7] F. Xu, Y. J. Wang, X. D. Wang, Y. H. Zhang, Y. Tang, P. Y. Yang, *Adv. Mater.* **2003**, *15*, 1751.
[8] We have studied the adsorption of three standard proteins (egg albumin, myoglobin, and cytochrome *c*) onto these nanozeolites through the Bradford protein-concentration method, and the results showed that their surface concentration could reach 100–300 mg g^{-1}. For a description of the Bradford method, see: M. M. Bradford, *Anal. Biochem.* **1976**, *72*, 248.
[9] a) M. A. Camblor, A. Corma, A. Mifsud, J. Perez-Pariente, S. Valencia, *Stud. Surf. Sci. Catal.* **1997**, *105*, 341; b) A. E. Persson, B. J. Schoeman, J. Sterte, J.-E. Ottesstedt, *Zeolites* **1994**, *14*, 557.
[10] X. D. Wang, Y. J. Wang, W. L. Yang, A. G. Dong, N. Ren, Z. K. Xie, Y. Tang, *Acta Chim. Sin. (Chin. Ed.)* **2003**, *61*, 354.
[11] R. Westermeier, T. Naven, *Proteomics in Practice: A Laboratory Manual of Proteome Analysis*, Wiley-VCH, Weinheim, 2002, p. 263.
[12] http://prospector.ucsf.edu/ucsfhtml4.0/msfit.htm.

 © 2005 Wiley-VCH Verlag GmbH & Co. KGaA, Weinheim

Homoallylic Sulfones

Synthesis of Homoallylic Sulfones through a Decarboxylative Claisen Rearrangement Reaction**

Damien Bourgeois, Donald Craig, N. Paul King, and David M. Mountford*

The Claisen rearrangement continues to enjoy widespread use as one of the premier carbon–carbon bond-forming reactions in organic synthesis. Contributing to its longstanding preeminence are ease of synthesis of substrates, reliable stereoselectivity based on well-established empirical trends, and adaptability to deliver a range of carbonyl-based functionalities according to the reaction mode selected.[1] We recently began a new research programme aimed towards developing an understanding of the effect on Ireland–Claisen rearrangement[2] stereoselectivity of stereocenters positioned outside but adjacent to the pericyclic array. To this end, we were keen to probe the effect on selectivity of introducing disposable, bulky groups at the α-position of the ketene acetal. Tolylsulfonyl appeared to be a promising choice of group because of its ready incorporation into substrates (by using as starting material commercially available tosylacetic acid), steric bulk, electron-withdrawing nature (in principle thereby facilitating ketene acetal formation), and ease of removal after rearrangement. Prior to commencement of our work there existed a single instance of Ireland–Claisen rearrangement of a ketene acetal derived from an allylic arylsulfonylacetate substrate.[3] In this work Davidson and coworkers generated the ketene acetal under standard conditions, which involves the low-temperature reaction of the ester substrate with LDA followed by chlorotrimethylsilane prior to warming to ambient temperature; sigmatropic rearrangement reached completion in 10 h. Decarboxylation of the derived α-phenylsulfonyl carboxylic acid subsequently took place in a separate step upon heating with weak base. After repeated failures to apply successfully this ketene acetal generation–rearrangement method to structurally simpler substrates, we investigated alternative reaction conditions for the generation of these intermediates. We now report a novel, decarboxylative Claisen rearrangement (DCR) reaction of allyl tosylacetates which yields homoallylic sulfones stereoselectively and in high yields.

The tosylacetate esters **1** required for this study were simply prepared from allylic alcohols and commercially available[4] tosylacetic acid by using standard DCC/DMAP-mediated condensation reactions.[5] Following the failure of conventional ketene acetal forming conditions with lithium diisopropylamide and chlorosilanes, attention was turned to milder methods based on *N*,*O*-bis(trimethylsilyl)acetamide (BSA) and potassium acetate, which we anticipated might provide an effective silylating reagent combination given the acidity of the methylene protons in **1**.[6,7] In the initial phase of the work, solutions of **1** and BSA[8] (1.0 equiv) in toluene together with potassium acetate (0.1 equiv)[9] were heated at reflux for 15 h. Homoallylic sulfones **2** were obtained cleanly and in good to excellent yields upon simple reduced-pressure concentration of the reaction mixtures followed by column chromatography on silica gel. We subsequently found that the same transformations could be carried out on **1** by brief exposure to microwave irradiation in the *presence or absence* of solvent, and that these modified procedures gave similar yields of **2** in most cases where comparison was made. The results of the reactions are collected in Table 1.

Several features of the DCR reactions of **1** are worthy of comment. First, the reaction is tolerant of oxygen and nitrogen substitution (Table 1, entries **4**, **12**, **13**), provided that the heteroatom is fully masked; the nonbenzylated analogue of substrate **1m** failed to undergo DCR reaction. Second, the transformations take place regardless of whether the substrates **1** are derived from primary or secondary (Table 1, entry 11) alcohols, and irrespective of the substitution level of the olefinic carbon atom distal to the oxygen atom within the allylic portion of the substrate (compounds **1g**, **1h**,[10] and **1k** give rise to products **2** that bear quaternary centres). Third, the reactions of **1i** and **1j** are completely stereoselective, and delivery of the (tolylsulfonyl)methyl moiety takes place in an *anti* sense with respect to the more hindered face of the allylic double bond.[11] Finally, in one example (Table 1, entry **12**) a striking level of *acyclic* stereoselectivity was observed in which sulfone **2l** was formed as a 7:1 mixture of diastereoisomers; substrates **1m** and **1n** rearranged with virtually zero selectivity. We have not yet assigned the major diastereomer of **2l**.

During the course of these investigations we became aware of a report of a single instance of a related transformation in which tosylacetic ester **3** was converted into the rearranged, decarboxylated homoallylic sulfone **4** in high yield under strongly basic conditions.[12] It was reasonably postulated that this transformation proceeded via an enolate intermediate, which subsequently rearranged with loss of carbon dioxide in a Carroll-type process.[13] In our hands, treatment of substrate **1a** with NaH in xylenes at reflux resulted in extensive decomposition after 2 h, and at lower temperatures in toluene **2a** was isolated only in low yield (< 10%). In contrast, the more hindered, secondary alcohol-derived substrate **1o** was gradually converted into **2o** in good yield after prolonged exposure to the NaH–toluene conditions (Scheme 1). These findings prompted a more thorough

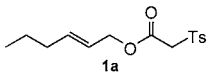
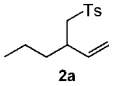
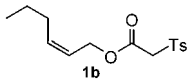
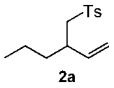
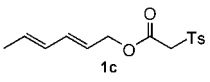
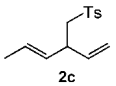
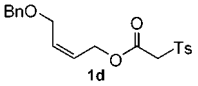
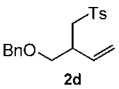
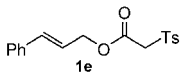
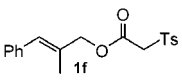
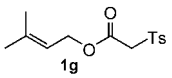
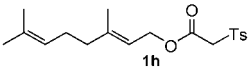
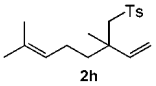
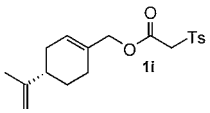
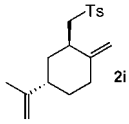
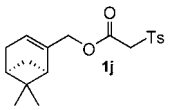
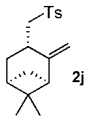
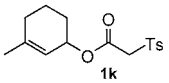
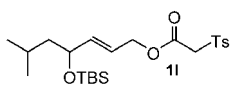
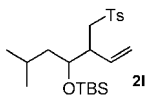
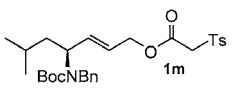
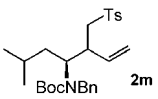
[*] Dr. D. Bourgeois, Prof. Dr. D. Craig, D. M. Mountford
Department of Chemistry
Imperial College London
South Kensington Campus, London SW7 2AZ (U.K.)
Fax: (+44) 20-7594-5868
E-mail: d.craig@imperial.ac.uk
Dr. N. P. King
Neurology and GI Centre of Excellence for Drug Discovery
GlaxoSmithKline Research Limited
New Frontiers Science Park
Third Avenue, Harlow, Essex CM19 5AW (U.K.)

[**] We thank the EPSRC (grant GR/N31412: postdoctoral research associateship to D.B.) and EPSRC/GlaxoSmithKline (supported DTA studentship to D.M.M.) for financial support of this research.

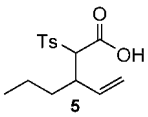
Supporting information for this article is available on the WWW under http://www.angewandte.org or from the author.

 © 2005 Wiley-VCH Verlag GmbH & Co. KGaA, Weinheim DOI: 10.1002/anie.200462023

Table 1: Decarboxylative Claisen rearrangement reactions of tosylacetates **1**.

Entry	Substrate	Product	Yield [%] A[a]	B[a]	C[a,b]
1	 **1a**	 **2a**	80	81	92
2	 **1b**	 **2a**	92	–	59
3	 **1c**	 **2c**	90	81	
4	 **1d**	 **2d**	77	–	58
5	 **1e**	 **2e**	74	–	
6	 **1f**	 **2f**	88	–	72
7	 **1g**	 **2g**	88	–	
8	 **1h**	 **2h**	83	89	83
9	 **1i**	 **2i**	89	67	80
10	 **1j**	 **2j**	81	–	80
11[c]	 **1k**	 **2k**	86	–	74
12[c,d]	 **1l**	 **2l**	62	–	
13[e]	 **1m**	 **2m**	74	18	67

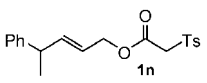
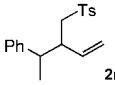
examination of the components necessary for the DCR reaction to proceed. Heating of toluene solutions of **1a** in the presence of potassium acetate alone (0.1, 0.5, 1.0 equiv) returned starting material quantitatively. Substitution of BSA with either Me_3SiOAc, $Me_3SiOSiMe_3$, or $(Me_3Si)_2NH$ resulted in complete suppression of the reaction, as did the use of *N*-trimethylsilylacetamide in place of BSA. In contrast, substitution of KOAc with Et_3N, 1,8-diazabicyclo[5.4.0]undec-7-ene (DBU), or pyrrolidine resulted in the formation of the rearranged but not decarboxylated carboxylic acid product **5** in yields of 70, 56, and 63%, respectively. We propose that **5** was formed by hydrolysis during workup of the corresponding silyl ester presumably formed in the [3,3]-sigmatropic rearrangement step. Exposure of **1a** to BSA alone (1.1 equiv) in toluene at reflux gave **5** in 49% yield. Use of Me_3SiOTf or *t*$BuMe_2SiOTf$ in conjunction with DBU gave **2a** in 15 and 28% yield, respectively, whilst Me_3SiCl–DBU combinations again gave **5**. Finally, exposure of **1a** to a mixture of *N*-trimethylsilylacetamide, *t*BuLi, and Me_3SiOAc gave **2a** in 67% yield; replacing *t*BuLi with KH in this modified reaction returned **2a** in 51% yield.


5

We interpret the results described above in terms of a mechanism involving the initial, reversible combination of KOAc and BSA to generate the conjugate base of *N*-trimethylsilylacetamide and Me_3SiOAc. The former species deprotonates **1** and the resultant enolate is silylated by Me_3SiOAc to generate the silyl ketene acetal **A** and regenerate acetate. Following [3,3]-sigmatropic rearrangement of **A** the γ,δ-unsaturated silyl ester **B** is reversibly desilylated by acetate ion, regenerating Me_3SiOAc and giving a carboxylate species; this spontaneously fragments to give CO_2 and the conjugate base of **2**. Finally, this strongly basic intermediate abstracts a proton from *N*-

 © 2005 Wiley-VCH Verlag GmbH & Co. KGaA, Weinheim

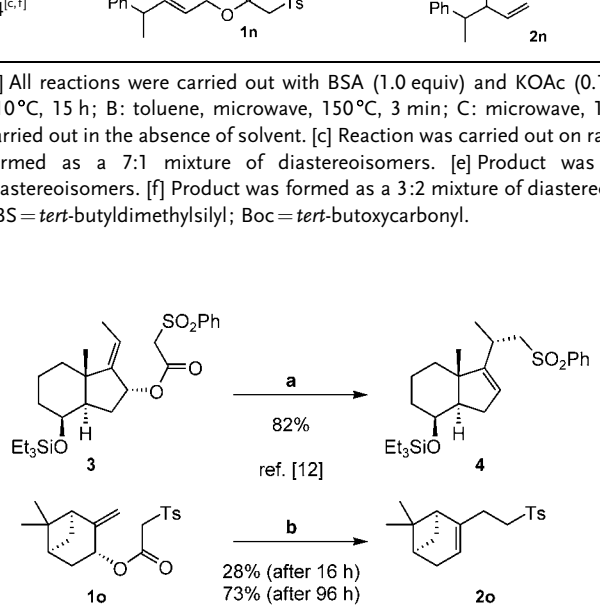
Table 1: (Continued)

Entry	Substrate	Product	Yield [%] A[a]	B[a]	C[a,b]
14[c,f]	 1n	 2n	63	–	

[a] All reactions were carried out with BSA (1.0 equiv) and KOAc (0.1 equiv). Conditions: A: toluene, 110 °C, 15 h; B: toluene, microwave, 150 °C, 3 min; C: microwave, 150 °C, 3 min. [b] Reactions were carried out in the absence of solvent. [c] Reaction was carried out on racemic substrate. [d] Product was formed as a 7:1 mixture of diastereoisomers. [e] Product was formed as a 1:1 mixture of diastereoisomers. [f] Product was formed as a 3:2 mixture of diastereoisomers. Ts = *p*-toluenesulfonyl; TBS = *tert*-butyldimethylsilyl; Boc = *tert*-butoxycarbonyl.

yielding DCR reactions conducted in the presence of substoichiometric amounts of BSA. In the event, substrates **1a**, **1e**, **1h**, **1j**, and **1o** underwent efficient DCR reaction in the presence of only 10 mol % of BSA and potassium acetate. Again, yields of the conventionally and microwave-heated reactions were comparable in all cases studied (Table 2).

In summary, we have uncovered a novel variant of the Ireland–Claisen rearrangement reaction in which the silyl ketene acetals formed in situ undergo sigmatropic rearrangement followed by acetate-induced decarboxylation. To our knowledge, this is the first example of a ketene acetal formation–Claisen rearrangement sequence that utilizes substoichiometric amounts of base and silylating agent.[14] We note that the mildness of the reaction conditions, especially in the catalytic mode, and the apparent compatibility of the transformation with a number of different substrate substitution patterns augur well for its general applicability. Planned future work in this area includes 1) evaluation of the efficiency of DCR reactions of substrates substituted α to the tosyl group, 2) assessment of the sense and level of diastereoselectivity of DCR reactions of chiral tosylacetates such as **1l**, and of analogous sulfoximine-containing substrates; 3) exploration of tandem DCR reactions of the related allylic tosylmalonates; and 4) application of the DCR reaction as a key process in target-oriented natural product synthesis.



Scheme 1. Carroll-type reactions of tosylacetates. a) NaH, xylenes, 140 °C; b) NaH, toluene, 110 °C.

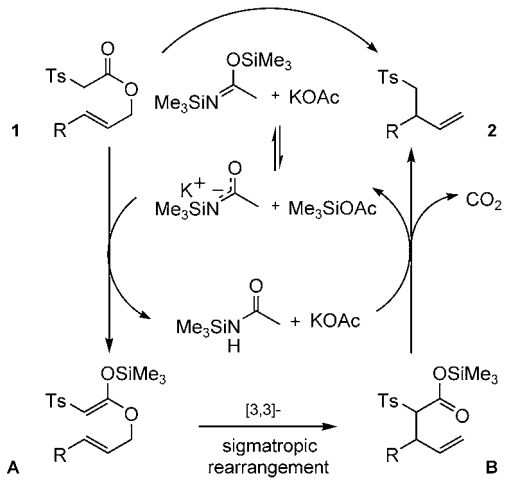
Table 2: Catalytic decarboxylative Claisen rearrangement reactions of tosylacetates **1**.

Entry	Substrate	Product	Yield [%] A[a]	B[a]
1	**1a**	**2a**	88	94
2	**1e**	**2e**	92	85
3	**1h**	**2h**	75	87
4	**1j**	**2j**	98	93
5	**1o**	**2o**	91	87

[a] All reactions were carried out with BSA (0.1 equiv) and KOAc (0.1 equiv). Conditions: A: toluene, 110 °C, 15 h; B: toluene, microwave, 150 °C, 3 min.

trimethylsilylacetamide formed in the initial deprotonation event, giving **2** and regenerating the conjugate base of *N*-trimethylsilylacetamide, which enters a subsequent cycle; alternatively, the conjugate base of **2** abstracts a proton *directly* from **1** to generate further nucleophilic enolate. This model is consistent with the results obtained in the reactions carried out with *N*-trimethylsilylacetamide, *t*BuLi or KH, and Me_3SiOAc, which differ only with respect to the mode of generation of the conjugate base of *N*-trimethylsilylacetamide. The proposed mechanism is depicted in Scheme 2.

It was felt that more-conclusive evidence for the proposed catalytic cycle would come from the observation of high-



Scheme 2. Proposed catalytic cycle for DCR reactions of **1**.

Received: September 17, 2004
Published online: December 21, 2004

Keywords: C–C coupling · Claisen rearrangement · homogeneous catalysis · microwave-assisted synthesis · synthetic methods

[1] For a recent, comprehensive review of the Claisen rearrangement, see: A. M. M. Castro, *Chem. Rev.* **2004**, *104*, 2939.
[2] For a recent review of the Ireland–Claisen rearrangement, and leading references, see: M. C. McIntosh, *Tetrahedron* **2002**, *58*, 2905.

 © 2005 Wiley-VCH Verlag GmbH & Co. KGaA, Weinheim

[3] A. H. Davidson, N. Eggleton, I. H. Wallace, *J. Chem. Soc. Chem. Commun.* **1991**, 378.
[4] Purchased from Aldrich Chemical Co.
[5] U. Kazmaier, C. Schneider, *Synthesis* **1998**, 1321. DCC = dicyclohexylcarbodiimide; DMAP = 4-(dimethylamino)pyridine.
[6] G. Giambastiani, B. Pacini, M. Porcelloni, G. Poli, *J. Org. Chem.* **1998**, *63*, 804.
[7] B. M. Trost, D. J. Murphy, *Organometallics* **1985**, *4*, 1143.
[8] BSA was purchased from Aldrich Chemical Co. and distilled prior to use.
[9] Reagent-grade potassium acetate used in this study was dried prior to use by heating overnight at 100 °C.
[10] Compound **1h** has been described previously: K. Sato, S. Inoue, T. Sakamoto, *Synthesis* **1981**, 796.
[11] The structure of **2i** was assigned based on the ^{1}H NMR signal corresponding to the allylic methine group. This appeared as a broad multiplet, indicating its equatorial disposition, and therefore the *anti* relationship of the (tolylsulfonyl)methyl and isopropenyl groups. The structure of **2j** was assigned unambiguously by X-ray crystallographic analysis. We thank Dr. Andrew J. P. White (Imperial College) for this determination; full details will be published elsewhere.
[12] M. A. Hatcher, G. H. Posner, *Tetrahedron Lett.* **2002**, *43*, 5009.
[13] For recent reports of highly regioselective, nonregiospecific metal-catalyzed formal Carroll rearrangements, see: E. C. Burger, J. A. Tunge, *Org. Lett.* **2004**, *6*, 2603; for recent applications of the Carroll rearrangement in synthesis, see: M. Defosseux, N. Blanchard, C. Meyer, J. Cossy, *Org. Lett.* **2003**, *5*, 4037; M. E. Jung, B. A. Duclos, *Tetrahedron Lett.* **2004**, *45*, 107; for a review, including an account of asymmetric Carroll rearrangements, see: A. Job, C. F. Janeck, W. Bettray, R. Peters, D. Enders, *Tetrahedron* **2002**, *58*, 2253.
[14] Typical procedure for the DCR of **1**. Conventional thermal conditions: BSA (16.6 μL, 0.07 mmol, 0.1 equiv) and KOAc (6.6 mg, 0.07 mmol, 0.1 equiv) were added to a solution of ester **1a** (200 mg, 0.68 mmol, 1 equiv) in dry toluene (5 mL), and the resulting mixture was heated at 110 °C for 15 h. Concentration under reduced pressure and chromatography (10% EtOAc/petroleum ether) gave sulfone **2a** (150 mg, 88%) as a colorless oil. Microwave conditions: KOAc (3.3 mg, 0.03 mmol, 0.1 equiv) was added to a microwave vial followed by ester **1a** (100 mg, 0.34 mmol, 1 equiv), BSA (8.3 μL, 0.03 mmol, 0.1 equiv) and toluene (1 mL). The mixture was heated at 150 °C (250 W) for 3 min. Concentration under reduced pressure and chromatography (10% EtOAc/petroleum ether) gave **2a** (79 mg, 94%) as a colorless oil.

 © 2005 Wiley-VCH Verlag GmbH & Co. KGaA, Weinheim

DNA Assays

A Direct Glimpse of Cross-Hybridization: Background-Passified Microarrays That Allow Mass-Spectrometric Detection of Captured Oligonucleotides**

*Ulrich Plutowski and Clemens Richert**

The generation of DNA microarrays or DNA chips[1,2] has made possible the massively parallel detection of DNA and RNA sequences. The ability to detect DNA or RNA sequence selectivity with DNA chips relies on the formation of Watson–Crick duplexes between immobilized strands (probes) and the target strands in solution. High-density DNA chips feature up to 250 000 spots and allow gene expression to be monitored on the level of entire genomes.[3,4] Duplex formation between DNA strands with only partial complementarity (cross-hybridization) is difficult to suppress at this level of complexity. As conventional DNA chip experiments use the same fluorophore for labeling all sequences from one biological sample, cross-hybridization can lead to false positive results, threatening the reliability of chip experiments. This is particularly true when single-base resolution is required, either because single-nucleotide polymorphisms have to be detected or because the expression of closely related genes has to be monitored.[5] Single-mismatch resolution is also important for control sequences employed on some chips for background correction,[6] an approach that has been challenged.[7]

Several approaches for simulating cross-hybridization computationally have been reported.[8,9] Accurate prediction of duplex stability remains difficult, however,[10] making it desirable to determine cross-hybridization experimentally. MALDI-TOF mass spectrometry[11] offers detection capabilities for short DNA strands that differ in base composition. The tiny amounts of DNA bound to micrometer-sized spots on flat surfaces make it difficult, however, to obtain sufficient signal to evaluate hybridization events. The direct ablation of oligonucleotides captured by complementary strands covalently bound to silicon surfaces has been reported.[12] The method reported in the literature involves a single genotyping target and a polymerase-catalyzed step. It provides sufficient resolution to distinguish between DNA strands of different lengths.

[*] Dipl.-Chem. U. Plutowski, Prof. C. Richert
Institut für Organische Chemie, Universität Karlsruhe (TH)
76131 Karlsruhe (Germany)
Fax: (+49) 721-608-4825
E-mail: cr@rrg.uka.de

[**] The authors are grateful to S. Jester for flame-smoothed gold surfaces, K. Dombi for oligonucleotides used in exploratory work, and R. Paulini for helpful discussions. This work was supported by DFG (RI 1063/1-3 and CFN, project C4.5) and the Fonds der Chemischen Industrie (No. 164431).

Supporting information for this article is available on the WWW under http://www.angewandte.org or from the author.

 DOI: 10.1002/anie.200461212 © 2005 Wiley-VCH Verlag GmbH & Co. KGaA, Weinheim

We reasoned that metal surfaces would be most useful because they are electrically conductive, as required for the desorption process in MALDI mass spectrometers. Our initial attempts to detect directly from gold surfaces were unsuccessful,[13] but the refined approach reported herein allows the direct mass spectrometric detection of cross-hybridization. The approach uses background-passified surfaces[14] to prevent nonspecific adsorption of DNA on gold surfaces.[15]

Our method involves the capture of DNA strands on the surface by hybridization to immobilized probes, a washing step to remove unbound strands, the addition of the matrix 2,4,6-trihydroxyacetophenone in an ethanolic solution to favor dissociation of duplexes and desorption, and mass-spectrometric detection of the captured target strands. Several factors were found to be critical for obtaining DNA signals. One such factor is a smooth surface. For this, gold layers (250-nm thickness) on quartz substrates were smoothed by heating in an H_2 flame. Another factor is the generation of a surface that prevents nonspecific adsorption of probe and target strands. To this end, we generated self-assembled monolayers (SAMs)[16] on smoothed gold surfaces in which the solvent-exposed portions of the assembly chains consisted of tetraethylene glycol units. The ethylene glycol moieties suppress nonspecific adsorption. Similar constructs have previously been employed in studies on cell adhesion.[17] Unlike typical oligoethylene glycol SAMs, our tetraethylene glycol chains terminate in a methyl ether, not a free hydroxy group. This renders the surface less sticky and allows the detection of DNA-bearing spots by their ability to retain water drops on a surface that is moderately hydrophobic (Figure 1). Fluorinated compounds are also known to generate hydrophobic surfaces on DNA chips.[18] The current spot diameter is 2 mm, but spot sizes as small as the laser beam diameter in the MALDI mass spectrometer are conceivable.

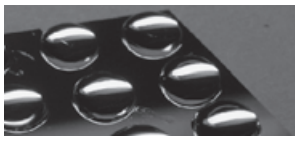
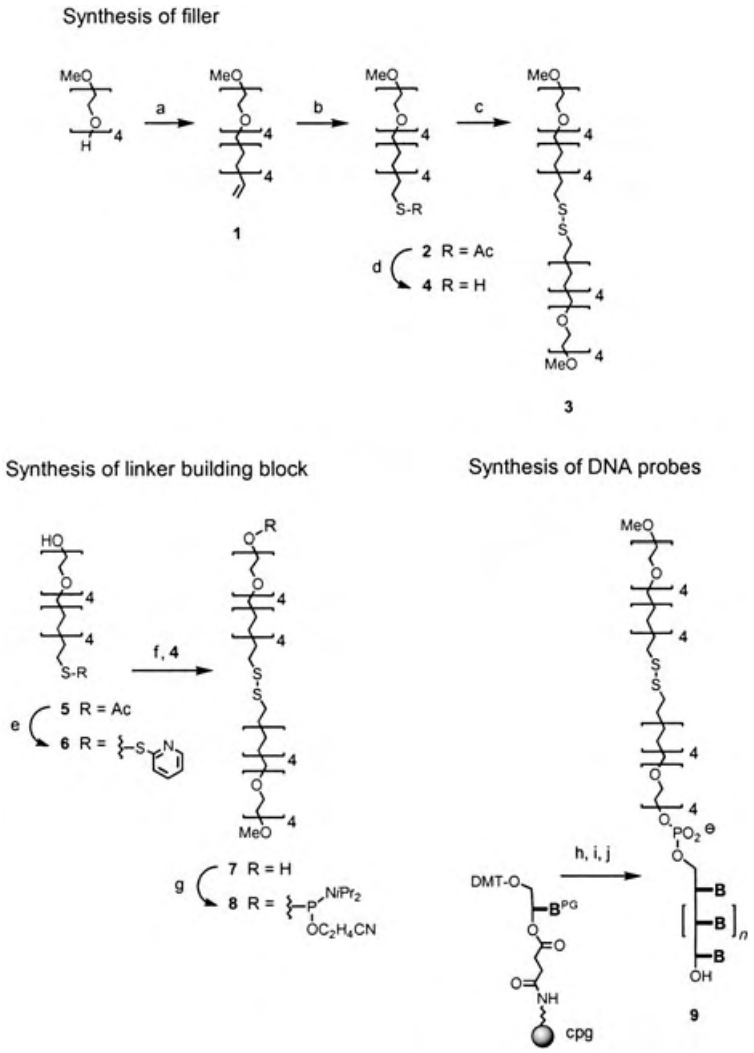


Figure 1. Photograph of a chip with immobilized DNA and filler after washing and inverting the chip. DNA-bearing spots retain the aqueous solution preferentially over the surrounding areas. During hybridization, a cover slip may be used to ensure contact between all spots and the solution.

We decided to favor the formation of as tight a SAM as possible by employing the same chains for DNA immobilization that were used for passifying the background surface. This was done by preparing oligonucleotides of general structure **9** (Scheme 1). These feature DNA linked to a tetraethylene glycol unit, which in turn is linked to the alkylthiol that forms the bottom portion of the SAM. Key to the successful generation of highly DNA-sensitive surfaces was the protecting-group scheme used to generate the oligonucleotide probes. Our immobilization method uses disulfides instead of thiols. The very filler for passifying the surface is also used as a disulfide-forming protecting group. As the removal of these protecting groups produces additional filler molecules without the generation of disruptive protecting group fragments, it favors particularly homogeneous surfaces. The absence of protecting and deprotecting steps also leads to a shorter route than those employing trityl-protected thiols.

The passifier or filler molecules were prepared as shown in Scheme 1. Starting from **1**, thioacetate **2** was prepared in a thermal addition of AcSH[19] and either converted into symmetrical disulfide **3** or deprotected to thiol **4**, whose reaction with 1 equivalent of activated disulfide **6** gave



Scheme 1. a) NaH, THF, 11-bromo-1-undecene (52%); b) AcSH, toluene, AIBN, Δ (79%); c) NH_4OH (quant.); d) HCl in MeOH (quant.); e) dithiodipyridine; NH_4OH, MeOH (84%); f) **4**, THF (78%); g) DIEA, chloro-*N*-(diisopropylamino)-2-cyanoethoxyphosporamidite, CH_2Cl_2 (75%); h) standard DNA synthesis, including extension cycle with **8**; i) I_2, py, THF, H_2O; j) NH_4OH; B = nucleobase, PG = protecting group, cpg = controlled pore glass, AIBN = azobisisobutyronitrile, DIEA = diisopropylethylamine.

 © 2005 Wiley-VCH Verlag GmbH & Co. KGaA, Weinheim

alcohol **7**. The alcohol was phosphitylated to **8**, which was directly coupled to DNA oligomers conventionally prepared on controlled pore glass. Disulfides **9**, obtained upon treatment with aqueous ammonia, are more readily purified by HPLC than symmetrical disulfides featuring two DNA strands or oxygen-sensitive free thiols. Their separation from failure sequences of DNA syntheses is quite facile, because the disulfide tail increases the elution time from reversed phases. Furthermore, removal of the thiol protecting group, another step often found to give low yields in our hands, is not required with oligonucleotides of general structure **9**, as they can be directly added to gold surfaces. After spotting the oligonucleotide probes for surface attachment, remaining exposed gold surface regions were filled by treating with a solution of the passifier disulfide **3** (Scheme 2).

When layering gold surfaces thus prepared with a MALDI matrix, we were able to detect traces of disulfide **3** upon irradiation with the MALDI laser.[20] This signal disappeared, however, after washing with THF, suggesting that the disulfides desorbable by the MALDI process had not been covalently linked to the surface, but were noncovalently incorporated in the SAM. Brief exposure of SAMs to THF is known to lead to minimal loss of covalently held chains.[21] When surfaces of general structure **10** (Scheme 2) were incubated with mixtures of strands with full or partial complementarity, and washed with ammonium acetate solution, spectra such as those shown in Figure 2 were obtained. At high laser power, each spot gave signal for the target strands both in linear and in reflectron mode, when analyzed with an unmodified commercial spectrometer. No signal for the immobilized strands or their disulfides were detected, suggesting that they were stably immobilized.

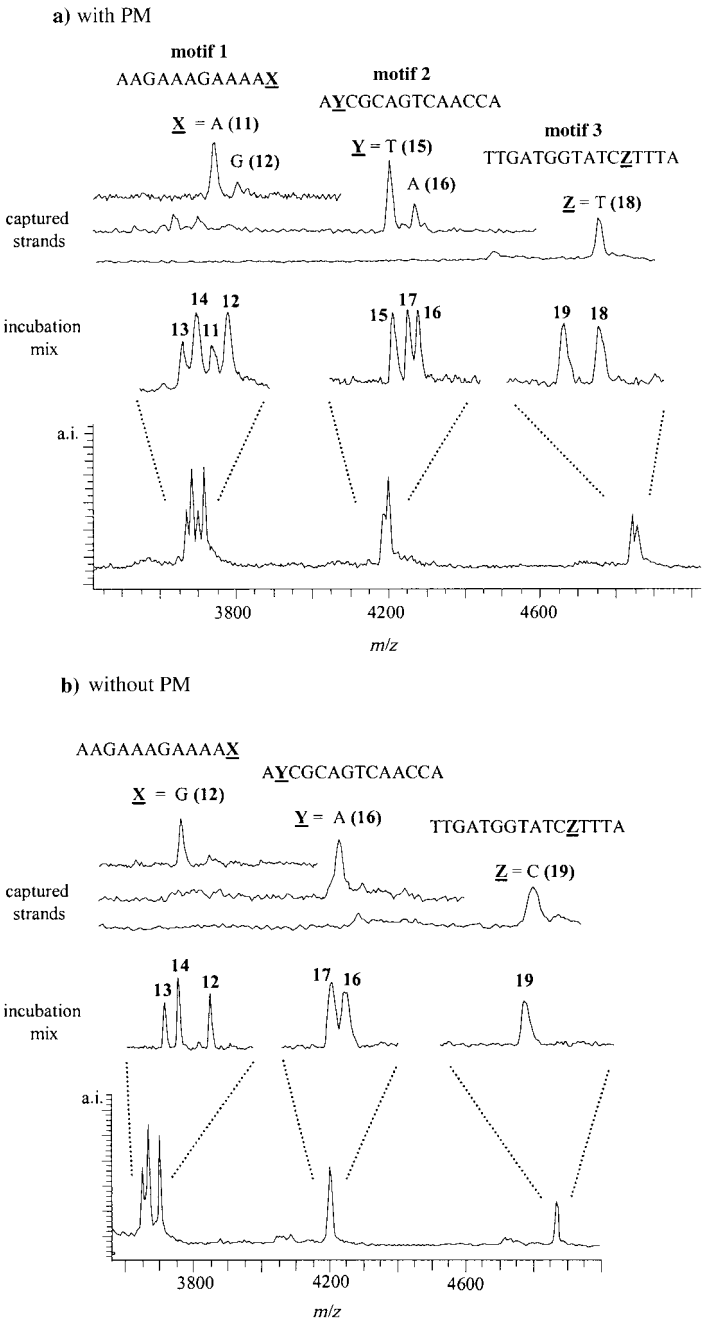
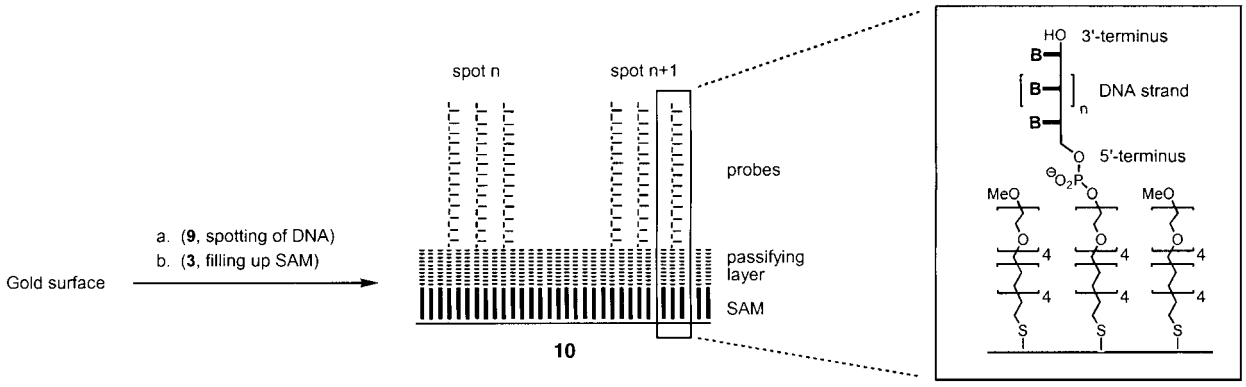


Figure 2. MALDI-TOF mass spectra of oligonucleotides prior to (bottom spectra labeled 'incubation mix') or after capture by surface-bound probes (upper spectra labeled 'captured strands'). The spectra at the very bottom were acquired in linear mode; expansions immediately above are from spectra in reflectron mode. Spectra of captured strands are from the individual spots of the chip. The probe on each spot was complementary to the motif indicated above the spectra, with positions of the variable bases indicated. a) Hybridization experiment with all DNA strands (**11**–**19**), including the perfectly matched (PM) targets. b) Hybridization experiments with DNA strands **12**, **13**, **14**, **16**, **17**, and **19**, that is, without the PM targets.



Scheme 2. a) Spotting of 2 μM solutions of DNA probes of general structure **9** in 1 M KH_2PO_4 (pH 7) at individual locations; b) incubation of entire surface with 1 mM solution of disulfide filler (**3**) in EtOH/H_2O (1:1).

 © 2005 Wiley-VCH Verlag GmbH & Co. KGaA, Weinheim

For all three DNA sequence motifs, the signal for the fully complementary DNA strand was the strongest when employing equimolar mixtures of all strands. The extent to which strands with a single mismatch were captured differed for the different sequences. Whereas **motif 3** gave little binding of the mismatched (MM) strand, **motifs 1** and **2** showed a substantial degree. Furthermore, in the absence of perfectly matched (PM) targets, all spots gave strong false-positive signals (Figure 2b). When PM targets were added to hybridization mixtures preincubated with MM strands only, the PM targets appeared in the MALDI-detectable signals, indicating that strand exchange can be induced. Exchange kinetics can also be studied. For example, a 15 h incubation of a mixture that contains only MM strands followed by a 9 h incubation with a solution containing both MM and PM sequences results in 40% cross-hybridization for **motif 3**.

Previous studies involving DNA strands with single and double mismatches had to be carried out with separate solutions, and showed strong binding of each in the absence of fully complementary target.[22] Our directly monitored competition experiments now show that the presence of the fully matched strand partially suppresses the binding of the mismatched strands, and that the extent of the suppression depends on the individual binding constants. Table 1 gives UV melting data for DNA duplexes formed in solution. Table 2 compiles the results from the on-chip hybridization experiments involving MALDI detection, and the expected distributions based on simulation with the computer program ChipCheck.[9] Target strand distributions on the spots calculated by ChipCheck with thermodynamic values determined from UV melting curves in solution are in good agreement with the experimental values for binding of mismatched target **16** for **motif 2** (Table 1 and Table 2). For **motif 1**, however, the cross-hybridization predicted based on database[24] thermodynamic values is closer to that calculated with thermodynamic values determined experimentally for the strands in solution. Furthermore, the mismatch in the hexadecamer of **motif 3** did not lead to as stable a duplex as

Table 1: UV Melting data for DNA duplexes studied in solution.

Probe	Target sequence[a]	No.	T_m [°C][b]	ΔT_m	Hyperchromicity [%][c]	$\Delta G°$ [kcal mol^{-1}][d]
motif 1						
TTTTTCTTTCTT (**9a**)	AAGAAAGAAAAA	**11**	33.7 ± 0.4		22.1 ± 1.2	−11.1
	AAGAAAGAAAA**G**	**12**	29.9 ± 0.7	−3.8	21.1 ± 0.5	−10.1
	A**C**GAAAGAAAT**A**	**13**	22.9 ± 1.3	−10.8	22.9 ± 1.5	−8.6
	TTGAAAGAAAA	**14**	27.1 ± 0.5	−6.6	16.9 ± 0.5	−9.5
motif 2						
TGGTTGACTGCGAT (**9b**)	ATCGCAGTCAACCA	**15**	58.7 ± 0.3		21.7 ± 0.9	−16.8
	A**A**CGCAGTCAACCA	**16**	56.4 ± 0.8	−2.3	16.1 ± 0.3	−16.1
	ATCGCAGTCAAC**T**A	**17**	53.2 ± 0.4	−5.5	18.6 ± 1.1	−15.8
motif 3						
TAAAAGATACCATCAA (**9c**)	TTGATGGTATCTTTTA	**18**	49.4 ± 0.3		29.7 ± 3.3	−17.2
	TTGATGGTATC**C**TTTA	**19**	37.6 ± 0.8	−11.8	25.8 ± 2.7	−12.3

[a] Bases underlined and bold indicate mismatches with probe sequences. [b] Average of four melting points ± SD (standard deviation) at 1.1 μM strand concentration and 0.25 M NH_4OAc buffer. [c] Hyperchromicity accompanying duplex dissociation. [d] At 298 K.

Table 2: Target strands captured on chip surfaces.[a] (For sequences **11**–**19**, see Table 1.)

	11	**12**	**13**	**14**	**15**	**16**	**17**	**18**	**19**
Spot 1: TTTTTCTTTCTT **9a** (**motif 1**)									
MALDI[b]	86	14 ± 5	< 1	< 1	< 1	< 1	< 1	< 1	< 1
calcd (td data)[c]	92.1	4.2	3.3	< 1	< 1	< 1	< 1	< 1	< 1
calcd (Mfold)[d]	88.9	11.1	< 1	< 1	< 1	< 1	< 1	< 1	< 1
Spot 2: TGGTTGACTGCGAT **9b** (**motif 2**)									
MALDI[b]	< 1	< 1	< 1	< 1	81	19 ± 11	< 1	< 1	< 1
calcd (td data)[c]	< 1	< 1	< 1	< 1	62.5	19.6	17.9	< 1	< 1
calcd (Mfold)[d]	< 1	< 1	< 1	< 1	98.6	< 1	< 1	< 1	< 1
Spot 3: TAAAAGATACCATCAA **9c** (**motif 3**)									
MALDI[b]	< 1	< 1	< 1	< 1	< 1	< 1	< 1	> 99	< 1
calcd (td data)[c]	< 1	< 1	< 1	< 1	< 1	< 1	< 1	> 99	< 1
calcd (Mfold)[d]	< 1	< 1	< 1	< 1	< 1	< 1	< 1	> 99	< 1
Spot 4: ATCGCAGTCAACCA **9d** (negative control)									
MALDI[b]	< 1	< 1	< 1	< 1	< 1	< 1	< 1	< 1	< 1
calcd (Mfold)[d]	< 1	< 1	< 1	< 1	< 1	< 1	< 1	< 1	< 1

[a] Values in percent of the sum of MALDI peak heights for all targets. [b] Mean of different hybridization experiments with incubation times between 5 h and 144 h. [c] Calculated by ChipCheck with thermodynamic (td) data from UV-melting curves analyzed with MeltWin[23] (compare Table 1). [d] Calculated by ChipCheck with theoretical thermodynamic data obtained from Mfold.[24]

 © 2005 Wiley-VCH Verlag GmbH & Co. KGaA, Weinheim

one might have expected.[10] Still, it gives strong cross hybridization when there is no PM target strand (Figure 2b). An example of cross-hybridization between strands with internal mismatches is provided in the appendix to the Supporting Information.

These results illustrate how difficult it is to predict cross-hybridization, and underscore the need for directly measuring this process experimentally with methods that provide strand-specific signals. We are currently developing methods that provide increased dynamic range and increased sensitivity for the detection of longer DNA sequences. Longer sequences are more likely to cross-hybridize, as partial annealing to capture probes may suffice to form a stable duplex. We also plan to employ internal standards in our work to allow absolute quantitation of the strands captured.[25] It has not escaped our attention that even with the current level of our technique, it should be possible to select oligonucleotides with chemical modifications that increase target affinity or base pairing fidelity[26] from small chemical libraries. Thus, this technique should offer a valuable alternative to spectrometrically monitored selection experiments (SMOSE).[27] Furthermore, directly monitoring DNA captured on surfaces could be useful in the context of DNA computing[28] and the generation of arrays for nanotechnology.[29]

Received: July 6, 2004
Revised: October 17, 2004
Published online: December 13, 2004

Keywords: cross-hybridization · DNA recognition · mass spectrometry · oligonucleotides · self-assembled monolayers

[1] S. P. A. Fodor, J. L. Read, M. C. Pirrung, L. Stryer, A. T. Lu, D. Solas, *Science* **1991**, *251*, 767 – 773.
[2] M. C. Pirrung, *Angew. Chem.* **2002**, *114*, 1326 – 1341; *Angew. Chem. Int. Ed.* **2002**, *41*, 1276 – 1289.
[3] J. L. DeRisi, V. R. Iyer, P. O. Brown, *Science* **1997**, *278*, 680 – 686.
[4] E. Pennisi, *Science* **2003**, *302*, 211.
[5] E. M. Evertsz, J. Au-Young, M. V. Ruvolo, A. C. Lim, M. A. Reynolds, *Biotechniques* **2001**, *31*, 1182 – 1186.
[6] R. J. Lipshutz, S. P. A. Fodor, T. R. Gingeras, D. J. Lockhart, *Nat. Genet.* **1999**, *21*, 20 – 24.
[7] R. A. Irizarry, B. M. Bolstad, F. Collin, L. M. Cope, B. Hobbs, T. P. Speed, *Nucleic Acids Res.* **2003**, *31*, e15.
[8] L. Zhang, M. F. Miles, K. D. Aldape, *Nat. Biotechnol.* **2003**, *21*, 818 – 821.
[9] K. Siegmund, U. E. Steiner, C. Richert, *J. Chem. Inf. Comput. Sci.* **2003**, *43*, 2153 – 2162.
[10] T. S. Hall, P. Pancoska, P. V. Riccelli, K. Mandell, A. S. Benight, *J. Am. Chem. Soc.* **2001**, *123*, 11811 – 11812.
[11] M. Karas, F. Hillenkamp, *Anal. Chem.* **1988**, *60*, 2299 – 2301.
[12] a) M. J. O'Donnell, K. Tang, H. Köster, C. L. Smith, C. R. Cantor, *Anal. Chem.* **1997**, *69*, 2438 – 2443; b) K. Tang, D.-J. Fu, D. Julien, A. Braun, C. R. Cantor, H. Köster, *Proc. Natl. Acad. Sci. USA* **1999**, *96*, 10016 – 10020.
[13] U. Plutowski, Diploma thesis, University of Karlsruhe, Germany, 2002.
[14] K. L. Dombi, N. Griesang, C. Richert, *Synthesis* **2002**, 816 – 824.
[15] D. Y. Petrovykh, H. Kimura-Suda, L. J. Whitman, M. J. Tarlov, *J. Am. Chem. Soc.* **2003**, *125*, 5219 – 5226.
[16] C. Pale-Grosdemange, E. S. Simon, K. L. Prime, G. M. Whitesides, *J. Am. Chem. Soc.* **1991**, *113*, 12 – 20.
[17] X. Jiang, R. Ferrigno, M. Mrksich, G. M. Whitesides, *J. Am. Chem. Soc.* **2003**, *125*, 2366 – 2367.
[18] J. H. Butler, M. Cronin, K. M. Anderson, G. M. Biddison, F. Chatelain, M. Cummer, D. J. Davi, L. Fisher, A. W. Frauendorf, F. W. Frueh, C. Gjerstad, T. F. Harper, S. D. Kernahan, D. Q. Long, M. Pho, J. A. Walker, T. W. Brennan, *J. Am. Chem. Soc.* **2001**, *123*, 8887 – 8894.
[19] R. Hong, N. O. Fischer, A. Verma, C. M. Goodman, T. Emrick, V. M. Rotello, *J. Am. Chem. Soc.* **2004**, *126*, 739 – 743.
[20] J. Su, M. Mrksich, *Angew. Chem.* **2002**, *114*, 4909 – 4912; *Angew. Chem. Int. Ed.* **2002**, *41*, 4715 – 4718.
[21] J. B. Schlenoff, M. Li, H. Ly, *J. Am. Chem. Soc.* **1995**, *117*, 12528 – 12536.
[22] A. W. Peterson, L. K. Wolf, R. M. Georgiadis, *J. Am. Chem. Soc.* **2002**, *124*, 14601 – 14607.
[23] J. A. McDowell, D. H. Turner, *Biochemistry* **1996**, *35*, 14077 – 14089.
[24] J.-M. Rouillard, M. Zuker, E. Gulari, *Nucleic Acids Res.* **2003**, *31*, 3057 – 3062.
[25] D. Sarracino, C. Richert, *Bioorg. Med. Chem. Lett.* **1996**, *6*, 2543 – 2548.
[26] Z. Dogan, R. Paulini, J. A. Rojas Stütz, S. Narayanan, C. Richert, *J. Am. Chem. Soc.* **2004**, *126*, 4762 – 4763.
[27] A. A. Mokhir, C. N. Tetzlaff, S. Herzberger, A. Mosbacher, C. Richert, *J. Comb. Chem.* **2001**, *3*, 374 – 386.
[28] Q. Liu, L. Wang, A. G. Frutos, A. E. Condon, R. M. Corn, L. M. Smith, *Nature* **2000**, *403*, 175 – 179.
[29] C. M. Niemeyer, B. Ceyhan, P. Hazarika, *Angew. Chem.* **2003**, *115*, 5944 – 5948; *Angew. Chem. Int. Ed.* **2003**, *42*, 5766 – 5770.

 © 2005 Wiley-VCH Verlag GmbH & Co. KGaA, Weinheim

Phase-Transfer Catalysis

Dramatic Rate Enhancement of Asymmetric Phase-Transfer-Catalyzed Alkylations**

*Seiji Shirakawa, Kenichiro Yamamoto, Masanori Kitamura, Takashi Ooi, and Keiji Maruoka**

The synthesis of optically active organic molecules from prochiral substrates by using chiral catalysts under phase-transfer conditions is one of the most exciting topics in practical organic synthesis because of its operational simplicity, mild reaction conditions, and environmental consciousness.[1] Hence, numerous efforts have been devoted to the elaboration of effective chiral quaternary ammonium salts,

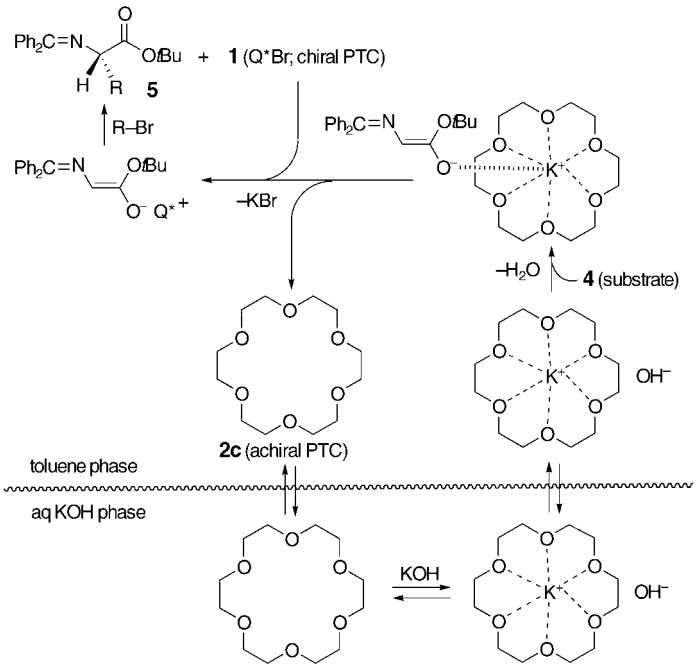
[*] Dr. S. Shirakawa, K. Yamamoto, Dr. M. Kitamura, Dr. T. Ooi, Prof. K. Maruoka
Department of Chemistry
Graduate School of Science
Kyoto University
Sakyo, Kyoto, 606-8502 (Japan)
Fax: (+81) 75-753-4041
E-mail: maruoka@kuchem.kyoto-u.ac.jp

[**] This work was partially supported by a grant-in-aid for scientific research from the Ministry of Education, Culture, Sports, Science, and Technology, Japan. S.S. and M.K. are grateful to the Japanese Society for the Promotion of Science for Young Scientists for research fellowships.

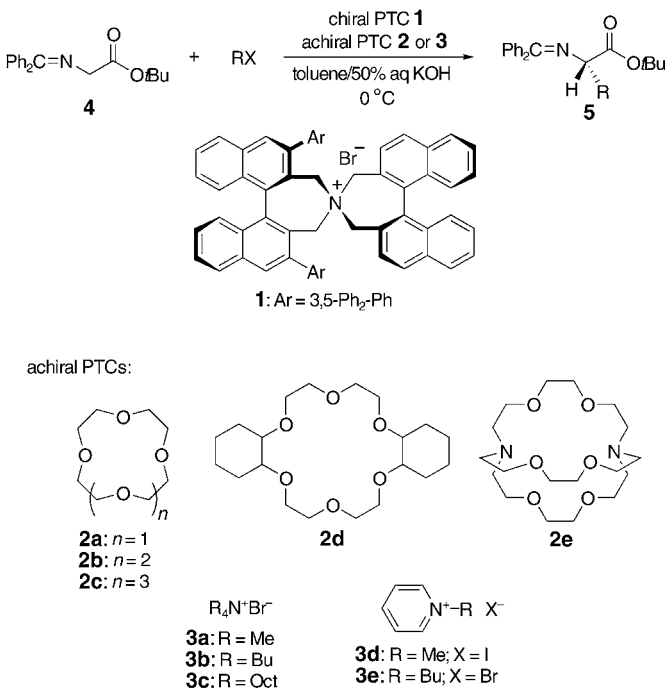
 DOI: 10.1002/anie.200462035 © 2005 Wiley-VCH Verlag GmbH & Co. KGaA, Weinheim

and considerable progress has recently made it possible to successfully perform various asymmetric bond-forming reactions under mild phase-transfer conditions.[2] However, one intrinsic yet critical problem associated with this type of reaction is insufficient catalytic efficiency, which often necessitates the use of a relatively large amount of catalyst (1–10 mol%). As part of our program for the truly practical asymmetric synthesis of α-amino acids utilizing designed C_2-symmetric chiral quaternary ammonium bromide **1**,[3] we required a new approach to fully induce its potential catalytic activity in the asymmetric phase-transfer alkylation of the *tert*-butyl glycinate Schiff base **4** to adequately reduce the catalyst loading. Our strategy to this end is the development of a dual mode of phase-transfer catalysis (Scheme 1).

Owing to the highly lipophilic nature of **1**, the reaction would proceed through the interfacial mechanism initiated by the direct interfacial deprotonation of **4** by an alkaline metal hydroxide such as potassium hydroxide.[4] On the basis of this plausible mechanistic profile, we envisioned that the addition of an achiral cocatalyst which is capable of extracting KOH into the organic phase would substantially accelerate the otherwise slow deprotonation process. This process should result in a significant rate enhancement without diminishing the enantioselectivity if the subsequent enolate exchange with **1** is extremely fast. Verification of this hypothesis is illustrated by the novel binary phase-transfer catalyst systems with the chiral phase-transfer catalyst **1** and the crown ether **2** as an ideal achiral cocatalyst, taking advantage of its well-known ability of extracting metal cations (Scheme 2). This conceptually new approach allowed the reaction to be implemented with as low as 0.05 mol% each of **1** and **2** to give the corresponding alkylation product **5** in excellent yield and enantioselectivity.



Scheme 2. Proposed mechanism of the binary phase-transfer system. Q*Br = chiral PTC **1**.



Scheme 1. Catalytic asymmetric alkylation of **4** with binary phase-transfer system. PTC = phase-transfer catalyst.

First, we investigated the effect of achiral phase-transfer catalysts as additives on the chemical yield and enantioselectivity in the phase-transfer benzylation of benzophenone derivative **4** under the influence of the chiral phase-transfer catalyst **1**. Thus, treatment of the protected glycine derivative **4** with benzyl bromide (1.2 equiv) and 50% aqueous KOH/toluene (volume ratio 2:3) with 0.10 mol% of chiral catalyst **1** at 0°C for 3 h resulted in the formation of phenylalanine derivative **5** ($R = CH_2Ph$) in only 8% yield with 94% *ee* (entry 1 in Table 1). In marked contrast, however, addition of 18-crown-6 **2c** (0.10 mol%) as the achiral phase-transfer catalyst under similar conditions gave rise to **5** in 98% yield with 98% *ee* (entry 4 in Table 1). Without the chiral phase-transfer catalyst **1**, 18-crown-6 (0.10 mol%) did not show any acceleration effect (entry 5 in Table 1) which suggests a low reactivity of the potassium enolate/18-crown-6 complex. Analogues of 18-crown-6, **2d** and **2e**, showed similar reactivity and enantioselectivity (entries 6 and 7 in Table 1).

Other examples including various achiral phase-transfer catalysts are also included in Table 1. Several characteristic features of the present benzylation follow: 1) 18-Crown-6 and its analogues **2c–e** as additives led to high chemical yields with high enantioselectivities compared to when other crown ethers **2a–b** of smaller cavity sizes were used (entries 2–3 in Table 1).[5] 2) Tetrabutyl- and tetraoctylammonium bromide **3b–c** as achiral phase-transfer catalysts gave relatively high yields with high enantioselectivities (entries 9 and 11 in Table 1). As tetrabutylammonium bromide itself gave a similarly high chemical yield (84%) in the phase-transfer-catalyzed benzylation of **4** (entry 10 in Table 1), the chiral

 © 2005 Wiley-VCH Verlag GmbH & Co. KGaA, Weinheim

Table 1: Catalytic enantioselective phase-transfer benzylation of **4** with chiral and achiral phase-transfer catalysts (PTCs).[a]

Entry	Chiral PTC	Achiral PTC	Yield[b] [%]	*ee*[c] [%] (config)[d]
1	**1**	none	8	94 (*S*)
2	**1**	**2a**	16	96 (*S*)
3	**1**	**2b**	29	96 (*S*)
4	**1**	**2c**	98	98 (*S*)
5	none	**2c**	3	
6	**1**	**2d**	92	97 (*S*)
7	**1**	**2e**	96	96 (*S*)
8	**1**	**3a**	17	97 (*S*)
9	**1**	**3b**	80	96 (*S*)
10	none	**3b**	84	
11	**1**	**3c**	90	96 (*S*)
12	**1**	**3d**	9	91 (*S*)
13	**1**	**3e**	13	91 (*S*)

[a] Unless otherwise specified, the reaction was carried out with 1.2 equiv of $PhCH_2Br$ in the presence of 0.1 mol% of **1** and 0.1 mol% of **2** or **3** in 50% aq KOH/toluene (v/v 2:3) at 0°C for 3 h under argon atmosphere. [b] Isolated yield. [c] Enatiopurity of **5** was determined by HPLC analysis of the alkylated imine by using a chiral column (DAICEL Chiralcel OD or OD-H) with hexane/propan-2-ol (v/v 100:1) as solvent. [d] The absolute configuration of **5** was determined by comparison of the HPLC retention time with that of the authentic sample independently synthesized by the reported procedure.[3a]

Table 2: Catalytic enantioselective phase-transfer alkylation of **4** with chiral PTC **1** and achiral 18-crown-6 **2c**.[a]

Entry	RX	**1** [mol%]	**2c** [mol%]	*t* [h]	Yield[b] [%]	*ee* [%][c] (config)[d]
1	$PhCH_2Br$	0.1	none	3	8	94 (*S*)
2		0.1	0.1	3	98	98 (*S*)
3		0.05	none	3	4	92 (*S*)
4		0.05	0.05	3	90	98 (*S*)
5		0.05	none	5	2	93 (*S*)
6		0.05	0.05	5	97	91 (*S*)
7		0.2	0.1	1.5	93	91 (*S*)
8		0.1	none	2	13	86 (*S*)
9		0.1	0.1	2	87	85 (*S*)
10	EtI	1.0	none	5	9	96 (*S*)[e]
11		1.0	0.5	5	70	95 (*S*)[e]
12		0.5	0.5	20	63	94 (*S*)[e]
13		0.5	0.5	3	86	91 (*S*)[e,f]

[a] Unless otherwise specified, the reaction was carried out with 1.2 equiv of RX in 50% aq KOH/toluene (v/v 2:3) under the given reaction conditions under argon. [b] Isolated yield. [c] The enantiopurity of **5** was determined by HPLC analysis of the alkylated imine by using a chiral column (DAICEL Chiralcel OD or OD-H) with hexane/propan-2-ol as solvent. [d] The absolute configuration of **5** was determined by comparison of the HPLC retention time with that of the authentic sample independently synthesized by the reported procedure.[3a] [e] 5.0 equiv of EtI employed. [f] Reaction under ultrasonic irradiation.

catalyst **1** must induce extremely facile enolate exchange with tetrabutylammonium enolate.[6] However, polar tetramethylammonium bromide **3a** and pyridinium salts **3d–e** were not effective for the system (entries 8, 12, and 13 in Table 1). 3) The enantioselectivity of **5** was lowered by increasing or decreasing the amount of achiral catalyst **2** or **3**.

We further found that the amounts of chiral catalyst **1** and 18-crown-6 **2c** as achiral catalyst could both be reduced to 0.05 mol% without losses in yields or enantioselectivity of the products as shown in Table 2 (entry 4). The present catalytic system is also applicable to other alkyl halides, and some selected results are summarized in Table 2. By the addition of a catalytic amount of 18-crown-6 **2c**, the reaction rate is dramatically accelerated (6.7–49-times faster than in the absence of **2c** under the same reaction conditions). The satisfactory yield and enantioselectivity of product **5** results by the use of only 0.05–0.10 mol% of chiral catalyst **1** and **2c**, except when less-reactive alkyl halides such as EtI are used. Combination of ultrasonic irradiation with this catalytic system further accelerated the rate of the alkylation (entry 13 in Table 2).[7]

In conclusion, we have demonstrated a dramatic rate enhancement by combination of an achiral phase-transfer catalyst with a chiral phase-transfer catalyst. The present catalyst system provides powerful options in asymmetric reactions for practical organic synthesis.

Experimental Section

General procedure for catalytic enantioselective alkylation of **4** with catalyst **1** and **2c**: Benzyl bromide (0.36 mmol) was added dropwise to a mixture of **4** (0.30 mmol), chiral catalyst **1** (0.15 μmol, 0.05 mol%), and 18-crown-6 **2c** (0.15 μmol, 0.05 mol%) in toluene (3.0 mL) and 50% aqueous KOH solution (2.0 mL) at 0°C. The reaction mixture was then stirred vigorously at 0°C for 3 h and then poured into water and extracted with ether. The organic extracts were washed with brine and dried over Na_2SO_4. Evaporation of solvents and purification of the residual oil by column chromatography on silica gel (1:10 ether/hexane) gave the corresponding benzylation product **5** (104 mg, 0.27 mmol, 90% yield, 98% *ee*). The enantiomeric excess was determined by HPLC analysis (Daicel Chiralcel OD, 100:1 hexane/propan-2-ol, flow rate: 0.5 mL min^{-1}, retention times: 14.8 min (*R*) and 28.2 min (*S*)). The absolute configuration was determined by comparison of the HPLC retention time with that of the authentic sample independently synthesized by the reported procedure.[3a]

Received: September 18, 2004
Published online: December 13, 2004

Keywords: alkylation · amino acids · crown compounds · enantioselectivity · phase-transfer catalysis

[1] Reviews: a) M. J. O'Donnell in *Catalytic Asymmetric Synthesis, 2nd ed.*, (Ed.: I. Ojima), Wiley-VCH, New York, **2000**, chap. 10; b) T. Shioiri in *Handbook of Phase-Transfer Catalysis* (Eds.: Y. Sasson, R. Neumann), Blackie Academic & Professional, London, **1997**, chap. 14; c) M. J. O'Donnell in *Phases—The Sachem Phase-Transfer Catalysis Review* **1998**, *4*, 5; M. J. O'Donnell in *Phases—The Sachem Phase-Transfer Catalysis Review* **1999**, *5*, 5; d) T. Shioiri, S. Arai in *Stimulating Concepts in Chemistry* (Eds.: F. Vogtle, J. F. Stoddart, M. Shibasaki), Wiley-VCH, Weinheim, **2000**, p. 123; e) M. J. O'Donnell, *Aldrichimica Acta* **2001**, *34*, 3; f) K. Maruoka, T. Ooi, *Chem. Rev.* **2003**, *103*, 3013; g) M. J. O'Donnell, *Acc. Chem. Res.* **2004**, *37*, 506; h) B. Lygo, B. I. Andrews, *Acc. Chem. Res.* **2004**, *37*, 518; i) T. Ooi, K. Maruoka, *Acc. Chem. Res.* **2004**, *37*, 526.

 © 2005 Wiley-VCH Verlag GmbH & Co. KGaA, Weinheim

[2] Representative examples: a) M. J. O'Donnell, W. D. Bennett, S. Wu, *J. Am. Chem. Soc.* **1989**, *111*, 2353; b) E. J. Corey, F. Xu, M. C. Noe, *J. Am. Chem. Soc.* **1997**, *119*, 12414; c) B. Lygo, P. G. Wainwright, *Tetrahedron Lett.* **1997**, *38*, 8595; d) M. Nakoji, T. Kanayama, T. Okino, Y. Takemoto, *Org. Lett.* **2001**, *3*, 3329; e) H.-G. Park, B.-S. Jeong, M.-S. Yoo, J.-H. Lee, M.-K. Park, Y.-J. Lee, M.-J. Kim, S.-S. Jew, *Angew. Chem.* **2002**, *114*, 3162; *Angew. Chem. Int. Ed.* **2002**, *41*, 3036; f) T. Kita, A. Georgieva, Y. Hashimoto, T. Nakata, K. Nagasawa, *Angew. Chem.* **2002**, *114*, 2956; *Angew. Chem. Int. Ed.* **2002**, *41*, 2832; g) T. Shibuguchi, Y. Fukuta, Y. Akachi, A. Sekine, T. Oshima, M. Shibasaki, *Tetrahedron Lett.* **2002**, *43*, 9539; h) S. Arai, R. Tsuji, A. Nisida, *Tetrahedron Lett.* **2002**, *43*, 9535; i) S.-S. Jew, M.-S. Yoo, B.-S. Jeong, I. Y. Park, H.-G. Park, *Org. Lett.* **2002**, *4*, 4245; j) N. Mase, T. Ohno, N. Hoshikawa, K. Ohishi, H. Morimoto, H. Yoda, K. Takabe, *Tetrahedron Lett.* **2003**, *44*, 4073; k) B. Lygo, B. Allbutt, S. R. James, *Tetrahedron Lett.* **2003**, *44*, 5629.

[3] a) T. Ooi, M. Kameda, K. Maruoka, *J. Am. Chem. Soc.* **1999**, *121*, 6519; b) T. Ooi, M. Takeuchi, M. Kameda, K. Maruoka, *J. Am. Chem. Soc.* **2000**, *122*, 5228; c) T. Ooi, M. Takeuchi, D. Ohara, K. Maruoka, *Synlett* **2001**, 1185; d) T. Ooi, M. Takeuchi, K. Maruoka, *Synthesis* **2001**, 1716; e) K. Maruoka, *J. Fluorine Chem.* **2001**, *112*, 95; f) T. Ooi, Y. Uematsu, M. Kameda, K. Maruoka, *Angew. Chem.* **2002**, *114*, 1621; *Angew. Chem. Int. Ed.* **2002**, *41*, 1551; g) T. Ooi, Y. Uematsu, K. Maruoka. *Adv. Synth. Catal.* **2002**, *344*, 288; h) T. Ooi, M. Taniguchi, M. Kameda, K. Maruoka, *Angew. Chem.* **2002**, *114*, 4724; *Angew. Chem. Int. Ed.* **2002**, *41*, 4542; i) T. Ooi, E. Tayama, K. Maruoka, *Angew. Chem.* **2003**, *115*, 599; *Angew. Chem. Int. Ed.* **2003**, *42*, 579; j) T. Ooi, M. Kameda, K. Maruoka, *J. Am. Chem. Soc.* **2003**, *125*, 5139; k) T. Ooi, M. Kameda, M. Taniguchi, K. Maruoka, *J. Am. Chem. Soc.* **2004**, *126*, 9685; l) K. Maruoka, E. Tayama, T. Ooi, *Proc. Natl. Acad. Sci. USA* **2004**, *101*, 5824.

[4] For a discussion of mechanisms in normal chiral phase-transfer catalyst systems, see: a) K. B. Lipkowitz, M. W. Cavanaugh, B. Baker, M. J. O'Donnell, *J. Org. Chem.* **1991**, *56*, 5181; b) M. J. O'Donnell, S. Wu, J. C. Huffman, *Tetrahedron* **1994**, *50*, 4507.

[5] 18-Crown-6 derivatives are known to make the most-stable host–guest complex with potassium ions and hence they accelerate the phase-transfer reaction with potassium hydroxide compared with other crown ethers that have a different ring size. For reviews, see: a) E. V. Dehmlow, S. S. Dehmlow, *Phase Transfer Catalysis, 3rd ed.*, VCH, Weinheim, **1993**; b) C. M. Starks, C. L. Liotta, M. Halpern, *Phase-Transfer Catalysis*, Chapman & Hall, New York, **1994**; c) *Handbook of Phase-Transfer Catalysis* (Eds.: Y. Sasson, R. Neumann), Blackie Academic & Professional, London, **1997**; d) *Phase-Transfer Catalysis, ACS Symposium Series 659* (Ed.: M. E. Halpern), American Chemical Society, Washington DC, **1997**.

[6] A similar acceleration effect with some loss of enantioselectivity was observed by adding tetrahexylammonium bromide (1 mol%) in the phase-transfer catalyzed asymmetric cyclopropanation reaction. See: S. Arai, K. Nakayama, T. Ishida, T. Shioiri, *Tetrahedron Lett.* **1999**, *40*, 4215.

[7] T. Ooi, E. Tayama, K. Doda, M. Takeuchi, K. Maruoka, *Synlett* **2002**, 1500.

 © 2005 Wiley-VCH Verlag GmbH & Co. KGaA, Weinheim

Hydrogenation

Surface-Bonded Precursor Determines Particle Size Effects for Alkene Hydrogenation on Palladium**

Aidan M. Doyle, Shamil K. Shaikhutdinov, and Hans-Joachim Freund*

Reactions of linear alkenes with metal surfaces have been previously studied on model catalyst systems with varying degrees of complexity, from single crystals to metal particles deposited on well-ordered oxide films.[1–15] Based on these studies, the majority of which were conducted with ethene, it has been suggested that alkene hydrogenation is structure insensitive. This means that the reaction only depends on the number of metal atoms on the surface and is independent of the crystallographic orientation of the particle facets and particle size. These size effects are difficult to study in real catalytic systems because the mean particle size and distribution cannot be controlled accurately. Herein, we report the particle size effects on alkene reactivity (ethene and *trans*-2-pentene) using well-defined Pd/Al_2O_3 model catalysts, where the particle size can be varied in a controllable manner. Temperature-programmed desorption (TPD) indicated that alkene adsorption exhibits site-specific behavior, which is assigned to the reactions occurring separately on facets and on low-coordination-number atoms such as edge and corner atoms. A strong particle size effect (within the 1–5-nm range) is observed for the hydrogenation of pentene over a hydrogen-precovered surface, whereas the reaction for ethene is independent of size. These effects are explained by the reactions proceeding via di-σ-bonded pentene, which is favored on the terrace sites of large particles, and π-bonded ethene.

The morphology of the Pd model system has been studied intensively in our laboratory by scanning tunneling microscopy.[9,16] Thin alumina films were grown on a clean NiAl(110) single crystal, and subsequently Pd was vapor-deposited onto the films (see the Experimental Section for details). An average particle size was determined from the amount of Pd deposited and could be varied within the range 1–5 nm with a narrow particle-size distribution (20%);[16] the corresponding relationship is presented in reference [9]. To exclude any effects of morphology changes on Pd particles during TPD measurements, the samples were preannealed at 500 K before the adsorption experiments.

[*] Dr. A. M. Doyle, Dr. S. K. Shaikhutdinov, Prof. H.-J. Freund
Fritz-Haber-Institut der Max-Planck-Gesellschaft
Faradayweg 4–6
14195 Berlin (Germany)
Fax: (+49) 30-8413-4105
E-mail: shaikhutdinov@fhi-berlin.mpg.de

[**] We acknowledge support by the Athena project funded by the Engineering & Physical Sciences Research Council (EPSRC) of the U.K. and Johnson Matthey plc. We also thank Prof. S. D. Jackson for fruitful discussions.

The TPD spectra showed that ethene desorption occurs from at least two distinct states.[9,10] Weakly bonded ethene in a π configuration desorbs at temperatures below 200 K, while the high-temperature (HT) state at about 300 K is associated with di-σ-bonded molecules, which is in agreement with calculations showing that di-σ-bonded alkenes (e.g., ethene, various butene isomers) are more strongly bound on the Pd(111) surface.[8,15,17] A similar desorption behavior is observed for various pentene isomers.[18,19] Weakly bound pentene in a π-bonded geometry desorbs at about 170 K. Accordingly, the HT state at about 230 K is associated with di-σ-bonded molecules. At elevated temperature, alkene molecules undergo stepwise dehydrogenation as evidenced by multiple hydrogen peaks in the TPD spectra.

Deuterium presaturation on the Pd surface suppresses alkene adsorption in the di-σ state and favors π bonding.[9,12,15] A H–D exchange reaction is clearly observed by detecting the desorption of $C_2H_{4-x}D_x$ and $C_5H_{10-x}D_x$ molecules for ethene and *trans*-2-pentene, respectively, on Pd particles as well as Pd(111). The D-substituted molecules desorb in the same temperature range as the HT state observed on D-free Pd surfaces.[19] This observation implies that the di-σ-bonded alkenes rapidly exchange H atoms with D atoms present on the surface via half-hydrogenated ethyl and pentyl species from which alkenes desorb, thus resulting in the HT peak in the TPD spectra. This finding is in line with results previously reported by Vasquez Jr. and Madix[20] for 1-hexene on Pd(111) and by Sekitani et al.[21] for ethene on Pd(110), and can explain the H–D exchange reaction observed. Stacchiola et al.[13] have recently proposed the formation of an η^1-allyl species for propene on Pd(111), based on infrared spectroscopic measurements. In principle, the adsorbed allyl groups (in particular π-allyl species), which are in a dynamic equilibrium with di-σ-bonded species, could also result in a H–D exchange reaction. However, Zaera and Chrysostomou[22] provided evidence against this mechanism, at least for Pt(111), and further supported the proposal that the half-hydrogenated (2-propyl) species is an intermediate in both the exchange and hydrogenation reactions.

Figure 1 shows a series of TPD spectra recorded for *trans*-2-pentene adsorbed on D_2-presaturated particles as a function of the nominal thickness of a Pd overlayer. The H–D exchange and hydrogenation reactions clearly occur under these conditions, as seen by the formation of $[D_1]$pentene ($C_5H_9D_1$) and $[D_2]$pentane ($C_5H_{10}D_2$) which desorb at 200–250 K (Figure 1 a,b). As pentane desorbs from Pd at a much lower temperature, the desorption of $[D_x]$pentane during the TPD experiment is reaction limited. Again, this is the temperature range where the pentene desorbs from the di-σ-bonded state. Therefore, the results indicate that the hydrogenation reaction proceeds by the addition of H/D to di-σ-bonded pentene to form a pentyl species, which may transform back to D-substituted di-σ-bonded pentene, or react by further H/D addition to form pentane.

Figure 1 a,b shows that the desorption temperatures for both $[D_1]$pentene and $[D_2]$pentane continuously shift as the Pd coverage increases from 0.4 to 14 Å, which indicates a particle size effect for the reaction. The size effect is more clearly seen by monitoring the H_2 and D_2 signals (see

 DOI: 10.1002/anie.200461614 © 2005 Wiley-VCH Verlag GmbH & Co. KGaA, Weinheim

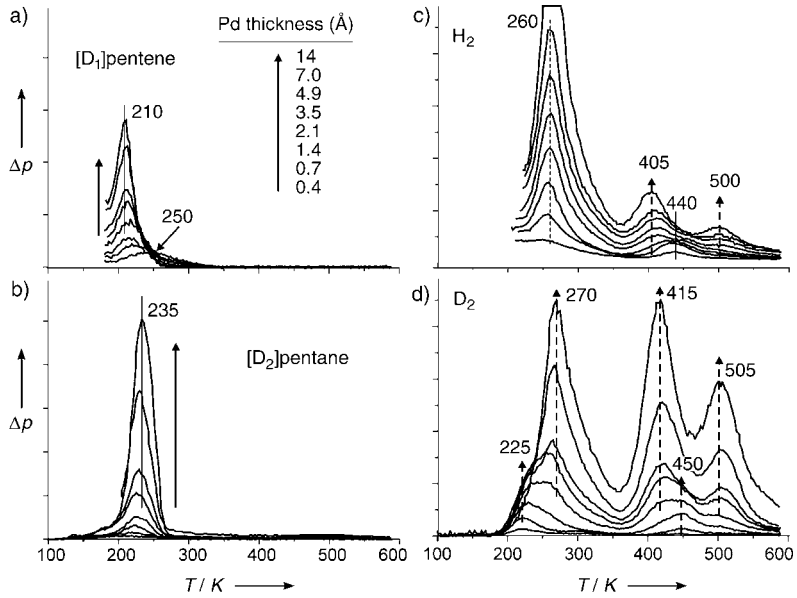


Figure 1. TPD spectra of 1 L of *trans*-2-pentene adsorbed at 100 K on Pd/Al_2O_3/NiAl(110) presaturated with D_2 at 200 K as a function of nominal thickness of the Pd overlayer. $[D_1]$pentene (a), $[D_2]$pentane (b), H_2 (c), and D_2 (d) desorption signals are shown.

Figure 1c,d). For the lowest Pd coverage, a small quantity of desorption-limited D_2 is detected at 225 K, and a single, reaction-limited D_2 peak at 450 K is observed. As the particle size is increased, additional D_2 peaks emerge at 415 and 505 K, which prevail for the largest Pd coverage such that the signal at 450 K is only seen as a shoulder at intermediate Pd coverage. Similar trends are found for the H_2 signal. For the smallest particles, peaks at 260 and 440 K are detected. Peaks at 260, 405, and 500 K are prominent at the highest Pd coverage. At intermediate Pd coverage, both groups of peaks are present with corresponding weighting factors. In other words, *de*hydrogenation of D-exchanged pentenes proceeds separately on two types of sites.

It is known that particles expose both low-coordination sites, such as edges and corners, and regular terrace sites on facets. Clearly, the small particles are composed mainly of low-coordination atoms while terrace sites dominate the larger particles. Therefore, the H_2 peaks at 260 and 440 K, as well as the D_2 peaks at 225 and 450 K, recorded for the smaller particles may correspond to dehydrogenation reactions of H(D)-containing molecules that occur on low-coordination atoms. Consequently, the signals at 260 K (270 K for D_2), 405 (415) K, and 500 (505) K, which prevail for higher Pd coverage, may result from dehydrogenation on the (111) facets dominating the large Pd particles.

Such a site specificity of the pentene reactions on Pd particles is further supported by the correlation between hydrogenation activity and Pd particle size (Figure 2a). The activity was measured by the TPD areas of the $[D_2]$pentane desorption signal per Pd surface area as determined from STM studies.[9] The diagram clearly shows that the activity increases by a factor of 4 over the range 1.5 to 4.5 nm. The increase in hydrogenation activity correlates well with the ratio of terrace sites to total surface Pd atoms shown on the same diagram in Figure 2a. This correlation strongly indicates that the terrace sites favor *trans*-2-pentene hydrogenation. This result also supports the conclusion that pentene hydrogenation proceeds via the di-σ-bonded species as the precursor. Indeed, adsorption in a di-σ-bonded geometry occurs preferentially on flat surfaces, which are characteristic for the larger particles.[9] As a result, the activity increases with particle size, which indicates that *trans*-2-pentene hydrogenation is structure sensitive.

In comparison, Figure 2b shows the $[D_6]$ethane production for ethene (C_2D_4) hydrogenation determined in a similar manner. We only observed a slight decrease in activity over the 1–3.5-nm range. This means that this reaction is essentially structure insensitive. This difference in the size dependence observed for ethene and pentene is considerable, even though the di-σ state is more favorable on terraces for both molecules and, therefore, one would expect similar behavior for both alkenes. However, Neurock and van Santen,[8] using cluster and DFT calculations, showed that it is π-bonded ethene, rather than di-σ-bonded ethene, that converts to an ethyl group (and subsequently to ethane) when adsorbed at high coverage on the H-precovered Pd(111) surface. This finding is consistent with experimental data showing that π-bonded ethene is the active species in ethene hydrogenation,[1,6,14,22] and may explain its structure insensitivity.

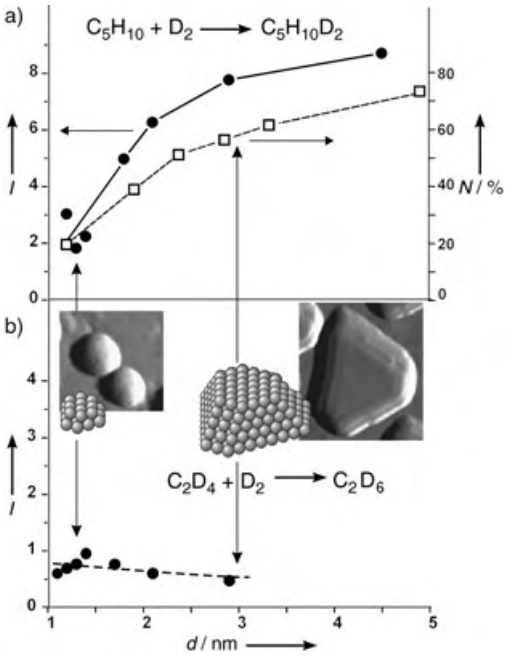


Figure 2. a, b) Integral $[D_2]$alkane desorption signals per Pd surface area as a function of particle size (●). The ratio of terrace sites (□) to the total number of surface atoms on the particles (*N*) of the same aspect (height/diameter) ratio is shown for comparison. The insets in (b) show typical STM images of the Pd nanoparticles[9] (presented in differentiated contrast as if they are illuminated from the right-hand side) and schematic representations of their structures.

 © 2005 Wiley-VCH Verlag GmbH & Co. KGaA, Weinheim

To our knowledge, there are no similar calculations for pentene. However, it is expected that hydrocarbons, beginning with propene, adsorb in a less distorted geometry (π bonded) in a *second* layer[13,22] on top of the most strongly bound di-σ species. In other words, π-bonded species may not be in direct contact with the Pd surface. Therefore, it seems plausible that π-bonded pentene on the H(D)-precovered Pd surface desorbs intact, and the hydrogenation proceeds only via di-σ-bonded pentene, in contrast to π- and di-σ-bonded ethene, which transform into ethyl intermediates.

In summary, we have shown that reactions of *trans*-2-pentene exhibit site-specific behavior, assigned to the reactions occurring separately on facets, and on low-coordination sites such as edge and corner atoms. Under the conditions studied, a strong particle size effect is observed for pentene hydrogenation, while ethene hydrogenation is structure insensitive. The results are explained by hydrogenation proceeding via di-σ-bonded pentene, which is favored on the terrace sites of large particles, and π-bonded ethene. Certainly, the question remains as to what extent these results can be extrapolated to high-pressure conditions. However, our previous experiments with ethene at nearly atmospheric pressure showed a good match with the results obtained by TPD.[23]

Experimental Section

The experiments were performed in an ultrahigh-vacuum chamber (base pressure $< 10^{-10}$ mbar) equipped for low-energy electron diffraction and Auger electron spectroscopy, and with a differentially pumped quadrupole mass spectrometer for TPD experiments. Thin alumina films were grown on a clean NiAl(110) single crystal as described elsewhere.[16] Palladium (99.99%) was deposited onto the alumina films using a commercial evaporator (Focus EM3). The sample was biased with a retarding voltage to prevent metal ions from being accelerated toward the sample and creating nucleation centers on the surface. A deposition rate of 1 Å min^{-1} was used, calibrated with a quartz microbalance. The amount of Pd deposited is presented in the text as a nominal thickness.

All gas exposures (measured in Langmuirs, $1\,L = 10^{-6}$ Torr s) were performed with a calibrated directional gas doser. Deuterium (99.9%, isotopic content 99.5%) and C_2H_4 (99.5%) were supplied by AGA Gas, and *trans*-2-pentene (99%) by Fluka. C_2D_4 (isotopic content 99%) was supplied by Isotec Inc. *trans*-2-pentene was purified by a number of freeze–thaw cycles before adsorption. To increase sensitivity, the signals for fragmented masses[24] were used to analyze the hydrocarbon molecules: 56 amu for $C_5H_9D_1$ and 45 amu for $C_5H_{10}D_2$. We checked that these signals fully described the desorption of the corresponding molecules. The full mass signals were used for the reactions of deuterated ethene.

The TPD spectra presented here were not corrected for ionization gauge sensitivities. In all TPD experiments, deuterium was adsorbed at 200 K and pentene at 100 K. A linear temperature ramp with a heating rate of 5 K s^{-1} was generated using a feedback control system. A new alumina film was grown for each Pd sample. Clean alumina films did not show any reactivity toward ethene or pentene.

Pd was deposited at 90 K and subsequently oxidized in O_2 at 500 K for 30 min and reduced with CO at 300 K until no CO_2 was produced. The individual alkene and hydrogen adsorptions on these Pd/Al_2O_3 samples were essentially similar to those obtained for the nontreated system. In addition, both systems were previously shown to exhibit identical behavior in CO adsorption and oxidation reactions.[25]

Received: August 11, 2004
Published online: December 13, 2004

Keywords: alkenes · heterogeneous catalysis · hydrogenation · palladium

[1] G. A. Somorjai, *Introduction to Surface Chemistry and Catalysis*, Wiley, New York, **1994**.
[2] D. R. Rainer, D. W. Goodman, *J. Mol. Catal. A* **1998**, *131*, 259.
[3] M. Frank, M. Bäumer, *Phys. Chem. Chem. Phys.* **2000**, *2*, 3723.
[4] F. Zaera, *Prog. Surf. Sci.* **2001**, *69*, 1.
[5] S. T. Ceyer, *Acc. Chem. Res.* **2001**, *34*, 737.
[6] N. Sheppard, C. De La Cruz, *Adv. Catal.* **1996**, *41*, 1; N. Sheppard, C. De La Cruz, *Adv. Catal.* **1998**, *42*, 181.
[7] J. A. Gates, L. L. Kesmodel, *Surf. Sci.* **1983**, *124*, 68.
[8] M. Neurock, R. A. van Santen, *J. Phys. Chem. B* **2000**, *104*, 11127.
[9] S. K. Shaikhutdinov, M. Heemeier, M. Bäumer, T. Lear, D. Lennon, R. J. Oldman, S. D. Jackson, H.-J. Freund, *J. Catal.* **2001**, *200*, 350.
[10] S. K. Shaikhutdinov, M. Frank, M. Bäumer, S. D. Jackson, R. J. Oldman, J. C. Hemminger, H.-J. Freund, *Catal. Lett.* **2002**, *80*, 115.
[11] D. Stacchiola, S. Azad, L. Burkholder, W. T. Tysoe, *J. Phys. Chem. B* **2001**, *105*, 11233.
[12] D. Stacchiola, W. T. Tysoe, *Surf. Sci.* **2003**, *540*, L600.
[13] D. Stacchiola, L. Burkholder, W. T. Tysoe, *Surf. Sci.* **2003**, *542*, 129.
[14] P. S. Cremer, G. A. Somorjai, *J. Chem. Soc. Faraday Trans.* **1995**, *91*, 3671.
[15] M. Sock, A. Eicher, S. Surnev, J. N. Andersen, B. Klötzer, K. Hayek, M. G. Ramsey, F. P. Netzer, *Surf. Sci.* **2003**, *545*, 122.
[16] M. Bäumer, H.-J. Freund, *Prog. Surf. Sci.* **1999**, *61*, 127.
[17] A. Valcarcel, A. Clotet, J. M. Ricart, F. Delbecq, P. Sautet, *Surf. Sci.* **2004**, *549*, 121.
[18] A. M. Doyle, S. K. Shaikhutdinov, S. D. Jackson, H.-J. Freund, *Angew. Chem.* **2003**, *115*, 5398; *Angew. Chem. Int. Ed.* **2003**, *42*, 5240.
[19] A. M. Doyle, S. K. Shaikhutdinov, H.-J. Freund, *J. Catal.* **2004**, *123*, 444.
[20] N. Vasquez, Jr., R. J. Madix, *J. Catal.* **1998**, *178*, 234.
[21] T. Sekitani, T. Takaoka, M. Fujisawa, M. Nishijima, *J. Phys. Chem.* **1992**, *96*, 8462.
[22] F. Zaera, D. Chrysostomou, *Surf. Sci.* **2000**, *457*, 89.
[23] H.-J. Freund, M. Bäumer, J. Libuda, T. Risse, G. Rupprechter, S. Shaikhutdinov, *J. Catal.* **2003**, *216*, 223.
[24] http://webbook.nist.gov.
[25] S. K. Shaikhutdinov, M. Heemeier, J. Hoffman, I. Meusel, B. Richter, M. Bäumer, H. Kuhleneck, J. Libuda, H.-J. Freund, R. J. Oldman, S. D. Jackson, C. Konvicka, M. Schmid, P. Varga, *Surf. Sci.* **2002**, *501*, 270.

 © 2005 Wiley-VCH Verlag GmbH & Co. KGaA, Weinheim

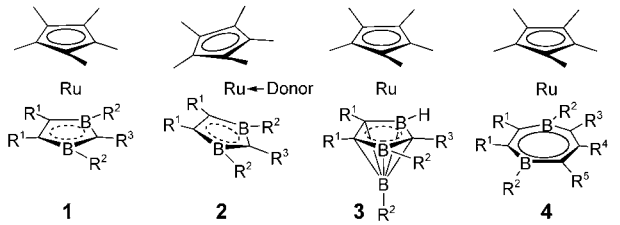
Metallocenes

Ruthenocene Analogues with a Novel C_5B_2 Ligand: (η^7-4-Borataborepine)(η^5-pentamethylcyclopentadienyl)ruthenium Complexes**

*Yong Nie, Hans Pritzkow, Chunhua Hu, Thomas Oeser, Bettina Bach, Thomas Müller, and Walter Siebert**

Dedicated to Professor Michael Veith on the occasion of his 60th birthday

The violet, formally 16 valence electron (VE) sandwich complexes **1**[1] are folded along the B···B vector of the heterocycle, as are the corresponding green iron complexes (folding angle $\alpha = 41.3°$).[2] This effect causes a unique reactivity leading to classic 18 VE complexes. Coordination of the donor ligands :CO and :CN-R at the ruthenium center yields yellow **2** with decreased folding angles ($< 20°$).[1a] The



incorporation of boranediyl ([:BH] from BH_3·THF) results in the formation of ruthenacarboranes **3** and likewise the incorporation of sulfur (from H_2S) gives ruthenathiacarboranes.

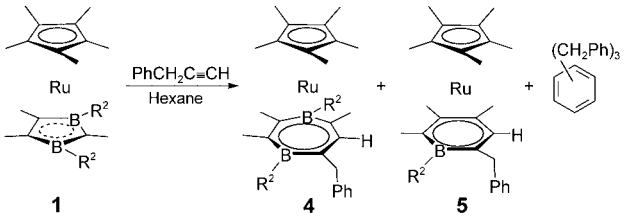
With phosphines, **1** forms donor–acceptor complexes **1**-PH_2R (R = H, Ph), however, the triorganylphosphine adducts **1**-PR_3 (R = Me, Ph) are unstable. With *tert*-butylphosphaalkyne :P≡C-CMe_3, no adduct but its incorporation into **1** is observed, however, it is not yet known which of the possible isomers of the resulting ruthenaphosphacarborane is formed.[1b]

[*] Y. Nie, Dr. H. Pritzkow, Dr. B. Bach, Dr. T. Müller, Prof. W. Siebert
Anorganisch-Chemisches Institut
Universität Heidelberg
Im Neuenheimer Feld 270, 69120 Heidelberg (Germany)
Fax: (+49) 6221-545-609
E-mail: walter.siebert@urz.uni-heidelberg.de
Dr. C. Hu
Institut für Anorganische Chemie, RWTH Aachen
Professor Pirlet Strasse 1, 52056 Aachen (Germany)
Dr. T. Oeser
Organisch-Chemisches Institut
Universität Heidelberg
Im Neuenheimer Feld 270, 69120 Heidelberg (Germany)

[**] This work was supported by the Deutsche Forschungsgemeinschaft. We thank Prof. Dr. U. Englert (Aachen) for arranging the X-ray analyses.

Herein we report the insertion of terminal alkynes into the heterocycle of **1**, which leads to the 18 VE complexes **4** with the novel η^7-4-borataborepine as a six-electron (6e) ligand, whereas with diorganylacetylenes the formation of boratabenzene complexes **5** occurs.

Treatment of **1a** with 3-phenyl-1-propyne (Scheme 1) in hexane yields the yellow, relatively air-stable solid **4a**, which exhibits one broad signal at $\delta = 29$ ppm in the ^{11}B NMR



Scheme 1. Insertion of a terminal alkyne into **1** to give the 4-borataborepine complexes **4**; $R^2 = CH_2SiMe_3$ (**4a**), $R^2 = Me$ (**4b**).

spectrum (downfield compared to that of **1a**, $\delta = 21.7$ ppm). The absence of a second ^{11}B NMR signal in the upfield region indicates that the uptake of the alkyne did not give a ruthenacarborane with an apical boron atom, such as **3**. In the EI-MS spectra, a cutoff peak at *m*/*z* 630 [M^+] shows that the 1:1 product does not lose the alkyne (which would occur an adduct of **2**). A weak signal at *m*/*z* 532 [**4a**−BCH_2SiMe_3]$^+$ was tentatively assigned to the complex [Cp*Ru(boratabenzene)] (**5a**; Cp* = C_5Me_5). In addition, tribenzylbenzene was identified by MS as a side product. The structure of **4a** (Figure 1), established by a single-crystal X-ray diffraction,[3] demonstrates the formation of a novel sandwich complex with the 4-borataborepine ligand, as a result of the insertion of the C≡C unit of the alkyne into a B–C bond of **1a**.[5] As the B1–C2 and B3–C2 bonds in **1a** are equivalent, both bonds react with the alkyne yielding enantiomers, which are found in the crystal structure.[3]

The seven-membered ring in **4a** is less folded along the B···B vector ($\alpha = 26°$), and the Ru–B separations (2.527 and 2.542 Å) are significantly elongated compared to those in **1a**.[5] The Ru–C bond lengths of the C_5B_2 ring vary between 2.203 (Ru–C4) and 2.345 Å (Ru–C2). Because of the bonding between the ruthenium center and the larger ring, the bonds to the exocyclic α-atoms are tilted towards the ruthenium, with the exception of those to C16 and C20, which are bound to the boron atoms, which tilt in the opposite direction.

The influence of the bulky silyl groups in **4a** is evident when compared with **4b**, obtained from the reaction of violet **1b** and 3-phenyl-1-propyne in hexane (Scheme 1). The yellow product was identified as a mixture of the expected 4-borataborepine complex **4b** and the boratabenzene compound **5b** by MS. While most of the bond lengths and angles are similar to those in **4a**, some differences arise in **4b** (Figure 1)[3] owing to the absence of the silyl groups: the Ru–B bond lengths of 2.429 and 2.443 Å are significantly shorter than those in **4a**, and the folding along the B···B vector ($\alpha = 12.5°$) is only half the value of that in **4a**. The seven-

 © 2005 Wiley-VCH Verlag GmbH & Co. KGaA, Weinheim DOI: 10.1002/anie.200461719

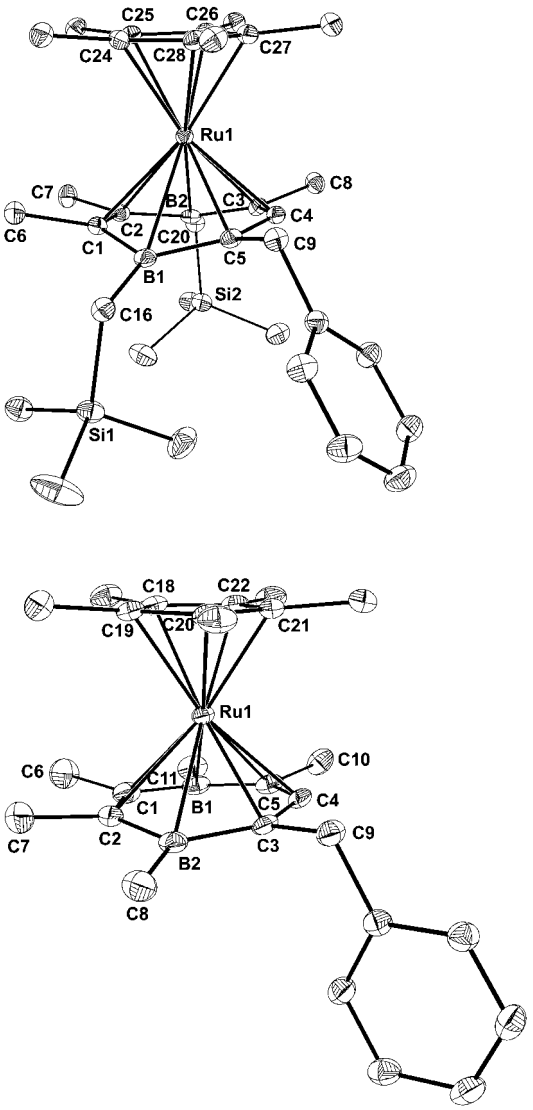
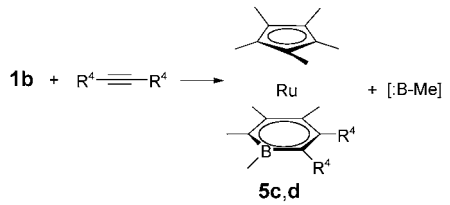


Figure 1. Molecular structures of **4a** (top) and **4b** (bottom). Hydrogen atoms are omitted for clarity. Selected bond lengths [Å]: **4a**: Ru-C_{Cp^*} 2.172(3)–2.205(3), Ru-C1 2.287(3), Ru-C2 2.345(3), Ru-B2 2.542(3), Ru-C3 2.311(3), Ru-C4 2.203(3), Ru-C5 2.303(3), Ru-B1 2.527(3), B1-C5 1.531(4), C5–C4 1.409(4), C4-C3 1.412(4), C3-B2 1.524(4), B2-C2 1.540(4), C2-C1 1.413(4), C1-B1 1.545(4). **4b**: R–C_{Cp^*} 2.178(3)-2.201(3), Ru-C2 2.332(3), Ru-B2 2.443(3), Ru-C3 2.299(3), Ru-C4 2.234(3), Ru-C5 2.315(3), Ru-B1 2.429(4), Ru-C1 2.330(3), B2-C3 1.520(5), C3-C4 1.415(4), C4-C5 1.400(4), C5-B1 1.528(5), B1-C1 1.531(5), C1-C2 1.415(5), C2-B2 1.542(5).

membered C_5B_2 ring is almost parallel to the Cp* ring, the dihedral angle between the two best planes is 6.6°.

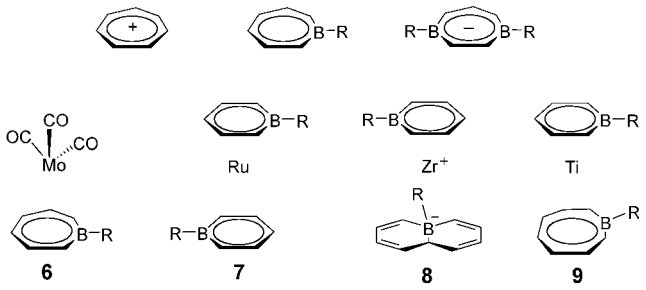
To elucidate the unexpected formation of boratabenzene complexes **5a**,**b**, the stability of **4a** in solution was monitored by ^{11}B NMR spectroscopy. Over several weeks a weak signal at $\delta = 16$ ppm increased, which indicates that the boratabenzene complex **5a** was formed from **4a**. In addition, the reactions of **1b** and 3-hexyne and di-*p*-tolylacetylene, respectively, were carried out (Scheme 2), which led to the boratabenzene complexes **5c**,**d**, identified by MS and confirmed by an X-ray crystallographic study of **5c**.[6] Clearly steric requirements in the anticipated peralkylated complexes



Scheme 2. Insertion of disubstituted alkynes into **1b** to give the boratabenzene complexes **5**; R^4 = Et (**5c**), R^4 = *p*-tolyl (**5d**).

4c,**d** cause the complete elimination of one methylboranediyl moiety [:B-Me] to give **5c**,**d** directly, whereas **4a**,**b** eliminate [:B-R^2] only slowly in solution (Scheme 2).

As with boratabenzenes,[7a] the 4-borataborepines in **4** function as 6e ligands, their 2e ene and the 4e allylic groups are separated by two boron atoms, but are electronically connected by their p_z orbitals, as indicated by the short boron–carbon bond lengths. The 4-borataborepine is formally derived from the tropylium ion $[C_7H_7]^+$ and the neutral borepine C_6H_6BR[8a] (a 6e ligand in **6** with R = Cl[8b]) by replacing two CH in $[C_7H_7]^+$ by two BR^- units and one CH in C_6H_6BR by one BR^- unit. Thus **4** is an isomer of **7**[7b] and a structural analogue of (η^5-cyclopentadienyl)(η^7-cycloheptatrienyl)chromium.[9]



The driving force for the alkyne insertion into the electron-poor complex **1** is the formation of the 6π-electron ligand 4-borataborepine in the 18 VE complexes **4**. The first insertion reactions of ethyne into one of the boratabenzene rings of bis(boratabenzene)-zirconium and -titanium complexes were reported by Ashe et al.[10] and Bazan et al.,[11] who obtained complexes **8** and **9** containing 8a*H*-4-boratanaphthalene (R = Ph)[10] and boratacyclooctatetraene (R = Me)[11] ligands, respectively.

In conclusion, we have demonstrated that the insertion of terminal alkynes into the C_3B_2 heterocycle of the complexes **1** results in 18 VE boron-containing ruthenocene analogues **4**, which contain 4-borataborepine as a 6e ligand with classical π bonding,[12] as the main products, together with the formation (from **4**) of boratabenzene complexes **5**, which are formed as the only products in the reactions of **1** with disubstituted alkynes.

Experimental Section

4a: 3-Phenyl-1-propyne (82 mg, 0.7 mmol) in hexane (5 mL) was added to a violet solution of **1a**[1a] (244 mg, 0.47 mmol) in hexane

 © 2005 Wiley-VCH Verlag GmbH & Co. KGaA, Weinheim

(10 mL) at −45 °C. After 30 min the cooling bath was removed and the reaction mixture warmed to room temperature, during which the solution turned yellow. After filtration, the filtrate was dried in vacuo, and the resultant oily residue purified by column chromatography on silica gel. Eluting with hexane and then with hexane/CH_2Cl_2 (4:1) gave a yellow elute, which was dried in vacuo and gave **4a** as a yellow solid (100 mg, 34 %). Crystals suitable for X-ray analysis were grown from a CH_2Cl_2 solution of **4a** at room temperature, m.p. 175 °C; ^{1}H NMR (200 MHz, $CDCl_3$): $\delta = 7.39$–7.17 (m, 5H; Ph), 5.41 (s, 1H; CH), 3.86 (d, 1H; ^2J(H,H) = 14.3 Hz, CH_2Ph), 3.07 (d, 1H; ^2J(H,H) = 14.3 Hz, CH_2Ph), 1.94 (s, 3H; BCCH_3CH), 1.85 (s, 3H; =CCH_3), 1.80 (s, 3H; =CCH_3), 1.57 (s, 15H; C_5(CH_3)$_5$), 0.15 (s, 18H; $SiMe_3$), −0.28 (s, 2H; BCH_2), −0.51 ppm (s, 2H; BCH_2); ^{11}B NMR (64 MHz, $CDCl_3$): $\delta = 34$ ppm (br.); ^{11}B NMR (64 MHz, CD_2Cl_2): $\delta = 29$ ppm (br.); ^{13}C NMR (53 MHz, $CDCl_3$): $\delta = 143.3$, 128.8, 128.0, 125.4 (Ph), 117.4 (allyl moiety, central carbon), 86.1 (C_5(CH$_3$)$_5$), 47.7 (CH$_2$Ph), 28.7 (BCCH$_3$CH), 19.8, 18.3 (BC=CCH$_3$), 9.7 (C_5(CH$_3$)$_5$), 1.02 ppm ($SiMe_3$). The signals for the boron-bound carbon atoms of the allyl moiety, for BCH$_2$SiMe$_3$, and for the two =CMe moieties were not observed; EI-MS: m/z (%) = 630 [M^+] (57), 615 [M^+−CH$_3$] (11), 557 [M^+−SiMe$_3$] (32), 532 [M^+−SiMe$_3$−BCH$_2$] (66), 446 [M^+−2 SiMe$_3$−BCH$_2$−CH] (100). HR-MS: m/z calcd for $^{12}C_{33}{}^1H_{54}{}^{28}Si_2{}^{11}B_2{}^{102}Ru$: 630.2993, found: 630.2996, $\Delta = 0.3$ mmu.

4b: obtained analogously to **4a**. 3-phenyl-1-propyne (58 mg, 0.5 mmol) in hexane, **1b**[1a] (140 mg, 0.38 mmol) in hexane (20 mL) gave a yellow reaction mixture. After filtration a yellow residue was obtained (40 mg), which is a mixture of **4b**, **5b** and tribenzylbenzene (detected by MS). The filtrate resulted in a yellow solid (150 mg), a mixture of **4b** and **5b** (detected by MS), which was recrystallized in CH_2Cl_2 at room temperature to give **4b** (81 %), m.p. 203–205 °C; ^{1}H NMR (200 MHz, $CDCl_3$): $\delta = 7.09$–7.36 (m, 5H; Ph), 5.54 (s, 1H; CH), 3.97 (d, 1H; ^2J(H,H) = 14.7 Hz, CH_2Ph), 3.02 (d, 1H; ^2J(H,H) = 14.7 Hz, CH_2Ph), 1.97 (s, 3H; BCCH_3CH), 1.92 (s, 3H; =CCH_3), 1.88 (s, 3H; =CCH_3),1.57 (s, 15H; C_5(CH$_3$)$_5$), 0.68 (s, 3H; BCH$_3$), 0.61 ppm (s, 3H; BCH$_3$); ^{11}B NMR (64 MHz, $CDCl_3$): $\delta = 26$ ppm (br.); ^{13}C NMR (53 MHz, $CDCl_3$): $\delta = 142.9$, 128.7, 127.9, 125.3 (Ph), 118.5, (allyl moiety, central carbon), 86.3 (C_5(CH$_3$)$_5$), 46.5 (CH$_2$Ph), 27.9 (BCCH$_3$CH), 22.2, 22.1 (BC=CCH$_3$), 9.5 ppm (C_5(CH$_3$)$_5$). The signals for the boron-bound carbon atoms of the allyl moiety, for BCH$_3$, and for the two =CMe moieties were not observed. EI-MS: m/z (%) = 486 [M^+] (54), 444 [M^+−BCH$_3$−CH$_4$] (41), [M^+−CH$_2$Ph] (100). HR-MS: m/z calcd. for $^{12}C_{27}{}^1H_{38}{}^{11}B_2{}^{102}Ru$: 486.2203, found: 486.2218, $\Delta = 1.5$ mmu.

Received: August 19, 2004
Published online: December 23, 2004

Keywords: boron · heterocycles · ring expansion · ruthenium · sandwich complexes

[1] a) T. Müller, M. Kaschke, M. Strauch, A. Ginsberg, H. Pritzkow, W. Siebert, *Eur. J. Inorg. Chem.* **1999**, 1685–1692; b) B. Bach, Y. Nie, H. Pritzkow, W. Siebert, *J. Organomet. Chem.* **2004**, *689*, 429–437.

[2] a) W. Siebert, R. Hettrich, H. Pritzkow, *Angew. Chem.* **1994**, *106*, 215–217; *Angew. Chem. Int. Ed. Engl.* **1994**, *33*, 203–204; b) R. Hettrich, M. Kaschke, H. Wadepohl, W. Weinmann, M. Stephan, H. Pritzkow, W. Siebert, I. Hyla-Kryspin, R. Gleiter, *Chem. Eur. J.* **1996**, *2*, 487–494.

[3] Crystal structure analyses for **1a**, **4a**, and **4b**: intensity data for **1a** were collected on a Bruker AXS SMART CCD diffractometer at $T = 103$ (2) K, for **4a** and **4b** on a Bruker Apex CCD diffractometer at $T = 120(2)$ K. $Mo_{K\alpha}$ radiation, $\lambda = 0.71073$ Å, graphite monochromator, ω-scans. The structures were solved by direct methods and refined by least-squares methods based on F^2 with all measured reflections, all non-hydrogen atoms are refined anisotropically.[4] **1a**: Monoclinic, space group $P2_1/c$, $C_{24}H_{46}B_2RuSi_2$, $a = 18.7559(8)$, $b = 8.9859(4)$, $c = 18.0098(8)$ Å, $\beta = 114.131(1)°$, $V = 2770.1(2)$ Å^3, $Z = 4$, $\rho_{calcd} = 1.231$ g cm^{-3}; 38020 reflections ($\theta_{max} = 32°$) collected, 9545 independent reflections [R(int) = 0.0539]. $R1 = 0.0338$ ($I > 2\sigma$(I)), $wR2 = 0.0823$ (all data). **4a**: Monoclinic, space group $P2_1/n$, $C_{33}H_{54}B_2RuSi_2$, $a = 11.2417(7)$, $b = 19.6225(13)$, $c = 15.6347(10)$ Å, $\beta = 102.466(3)°$, $V = 3367.6(3)$ Å^3, $Z = 4$, $\rho_{calcd} = 1.242$ g cm^{-3}; 53110 reflections ($\theta_{max} = 28.4°$) collected, 8451 unique reflections [R(int) = 0.0820]. $R1 = 0.0477$ ($I > 2\sigma$(I)), $wR2 = 0.0956$ (all data). **4b**: Triclinic, space group $P\bar{1}$, $C_{27}H_{38}B_2Ru$, $a = 7.5443(6)$, $b = 8.8867(7)$, $c = 18.6554(15)$ Å, $\alpha = 87.062(4)$, $\beta = 88.683(4)$, $\gamma = 69.228(4)°$, $V = 1167.88(16)$ Å^3, $Z = 2$, $\rho_{calcd} = 1.380$ g cm^{-3}; 18121 reflections ($\theta_{max} = 28.3°$) collected, 5778 unique reflections [R(int) = 0.0391]. $R1 = 0.0401$ ($I > 2\sigma$(I)), $wR2 = 0.0926$ (all data). CCDC-244072 (**1a**), CCDC-244073 (**4a**), CCDC-244074 (**4b**) contains the supplementary crystallographic data for this paper. These data can be obtained free of charge via www.ccdc.cam.ac.uk/conts/retrieving.html (or from the Cambridge Crystallographic Data Centre, 12 Union Road, Cambridge CB21EZ, UK; fax: (+44) 1223-336-033; or deposit@ccdc.cam.ac.uk).

[4] a) G. M. Sheldrick, SHELXS86, Univ. Göttingen, **1986**; b) G. M. Sheldrick, SHELXL97, Univ. Göttingen, **1997**; c) G. M. Sheldrick, SHELXTL, Version 5.1, Program Package for Structure Solution and Refinement, Bruker Analytical X-ray Systems, Inc., Madison, WI, **1998**.

[5] **1a**,[1a] a dark violet oil, on cooling in hexane finally yielded suitable crystals for an X-ray structural analysis,[3] which confirms that the 1,3-diborolyl ring C_3B_2 is folded by 40.7° along the B···B vector, very similar to its green iron analogue.[2] The Ru–C2 bond length [2.029, cf. Fe-C 1.899 Å] is markedly shorter than the other Ru–C bond lengths of the heterocycle.

[6] Crystal data for **5c**: data were collected on a Bruker Apex CCD diffractometer at 200 K, triclinic, space group $P\bar{1}$, $C_{23}H_{37}BRu$, $a = 7.6562(9)$, $b = 8.928(1)$, $c = 16.051(2)$ Å, $\alpha = 92.905(2)$, $\beta = 93.060(2)$, $\gamma = 104.370(2)°$, $V = 1061.6(2)$ Å^3, $Z = 2$, $\rho_{calcd} = 1.33$ g cm^{-3}; 6546 reflections ($\theta_{max} = 26.4°$) collected, 4077 independent reflections [R(int) = 0.0193]. $R1 = 0.031$ ($I > 2\sigma$(I)), $wR2 = 0.0823$. CCDC number: CCDC-256654. **5c**: HR-MS: m/z calcd. for $^{12}C_{23}{}^1H_{37}{}^{11}B^{102}Ru$: 426.2031, found: 426.2023, $\Delta = -0.8$ mmu. **5d**: HR-MS: m/z calcd. for $^{12}C_{33}{}^1H_{41}{}^{11}B^{102}Ru$: 550.2344, found: 550.2338, $\Delta = -0.7$ mmu.

[7] a) G. E. Herberich, H. Ohst, *Adv. Organomet. Chem.* **1986**, *25*, 199–236; b) G. E. Herberich, H. J. Becker, K. Carsten, C. Engelke, W. Koch, *Chem. Ber.* **1976**, *109*, 2382–2388.

[8] a) A. J. Ashe III, F. J. Drone, C. M. Kausch, J. Kroker, S. M. Al-Taween, *Pure Appl. Chem.* **1990**, *62*, 513–517; b) A. J. Ashe III, J. W. Kamp, W. Klein, R. Rousseau, *Angew. Chem.* **1993**, *105*, 1112; *Angew. Chem. Int. Ed. Engl.* **1993**, *32*, 1065–1066, and references therein.

[9] E. O. Fischer, S. Breitschaft, *Angew. Chem.* **1963**, *75*, 94–95; *Angew. Chem. Int. Ed. Engl.* **1963**, *2*, 44.

[10] A. J. Ashe III, S. Al-Ahmad, J. W. Kamp, V. G. Young, Jr., *Angew. Chem.* **1997**, *109*, 2104–2106; *Angew. Chem. Int. Ed. Engl.* **1997**, *36*, 2014–2016.

[11] X. Fang, D. Woodmansee, X. Bu, G. C. Bazan, *Angew. Chem.* **2003**, *115*, 4648–4652; *Angew. Chem. Int. Ed.* **2003**, *42*, 4510–4514.

[12] MO calculations for **1** and **4** are in progress (Dr. I. Hyla-Kryspin, University of Münster, Germany).

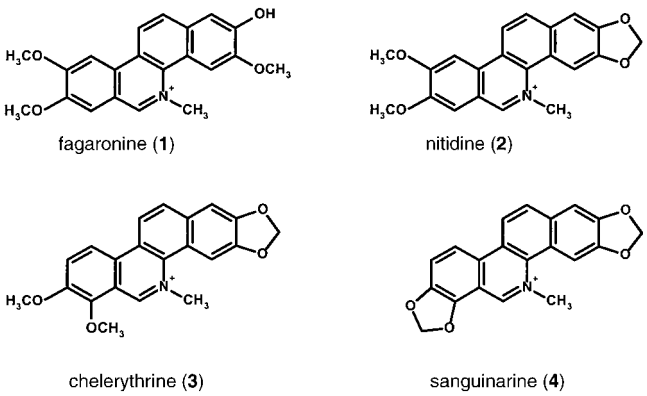
 © 2005 Wiley-VCH Verlag GmbH & Co. KGaA, Weinheim

Synthetic Methods

A Two-Step Synthesis of Cytostatically Active Benzo[*c*]phenanthridine Derivatives**

Bernd Clement, Matthias Weide, Ulrich Wolschendorf, and Ilka Kock*

The benzo[*c*]phenanthridine class of substances display a variety of pharmacological properties. A large number of naturally occurring alkaloids that contain a benzo[*c*]phenanthridine ring system and have a known spectrum of activity are mentioned in the literature.[1,2] Aside from fagaronine (**1**), the most important representative of this group of natural products, other alkaloids with extensive pharmacological potential are nitidine (**2**), chelerythrine (**3**), and sanguinarine (**4**; Scheme 1).[3–5] The synthesis of these natural products is of great interest, because they can be isolated from plant materials only in very small amounts. Cushman et al.[6] describe yields in the 0.003 to 0.07% range for the isolation of **2** from a series of zanthoxylum and fagara varieties. Compound **1** was first isolated from the root of *Fagara zanthoxyloides* in 1972.[7]



Scheme 1. Structural formulas of known benzo[*c*]phenanthridine alkaloids.

The first total synthesis of **1** was described by Gillespie et al. in 1974.[8] This synthetic route gave **1** in 0.7% yield starting from 2,3-dimethoxy-5-nitronaphthalene. Other synthetic routes to **1** have been described by Ishii et al.,[9] Treus et al.,[4] Lunch et al.,[5]and Šmidrkal[10], the latter being only a slight variation on the synthetic sequence reported by Gillespie et al.[8].

Messmer et al.[7] demonstrated the pronounced in vivo antileukemia activity of **1**, which was then verified by Stermitz et al.[11] and in preclinical studies at the National Cancer Institute[12]. The pharmacological and toxicological effects of **1** and other alkaloids in this group have since been tested in many investigations. Sethi[13] and Kakiuchi et al.[14] have thus reported the inhibition of reverse transcriptases, which, as enzymes specific to tumor viruses, are responsible for the transcription of viral RNA into the complementary DNA. This DNA version of the viral genome is incorporated into the DNA of the host and is replicated in the cell-division process. Compound **1** additionally demonstrates DNA-polymerase-inhibiting properties, presumably a result of interaction with adenosine/thymine base pairs.[15]

In 1983 Pezzuto et al.[16] reported that the primary mechanism of the interaction of fagaronine with deoxyribonucleic acid is DNA intercalation. It was additionally demonstrated that binding of **1** is not—as described by Sethi[15]—limited to adenine- and thymine-containing polynucleotides. Furthermore, **1** has the ability to act as an inhibitor of topoisomerase I and II. In addition to restraining topomerase activity, this leads to a stabilization of the DNA–enzyme complex.[17]

Compound **2** exhibits a spectrum of activity similar to that of **1**.[18] As a result of the acute toxicity demonstrated by **2** in preclinical trials, its development as a pharmaceutical was not pursued.[19] Because the structures of **1** and **2** differ only by one methylenedioxy group, this is thought to be linked to the toxicity of **2**.[20]

Because of the great interest in the biological activity of these natural substances, the synthesis of benzo[*c*]phenanthridine derivatives and alkaloids in this family is an important area of heterocyclic chemistry. The toxicological problems that accompany some of the naturally occurring alkaloids have led to the development of new synthetic pathways for benzo[*c*]phenanthridine derivatives.[2,21,22] A variety of benzo[*c*]phenanthridine derivatives have thus become synthetically accessible.[23–26] However, these syntheses are very unwieldy and require many steps. In particular, compounds with substituents directly flanking the endocyclic nitrogen atom have thus far been very inconvenient to produce.[27,28]

By raising the reaction temperature when we attempted the synthesis of *E*-2-[2-(4-dimethylaminophenyl)vinyl]benzonitrile (**8**; Scheme 3) from 4-dimethylaminobenzaldehyde (**5**) and 2-methylbenzonitrile (**6**) as given in ref. [29], we surprisingly obtained **7a** as the main product (Scheme 2). Doubling the concentration of **6** used in the reaction increased the yield of **7a**, which is formed as a racemic mixture.

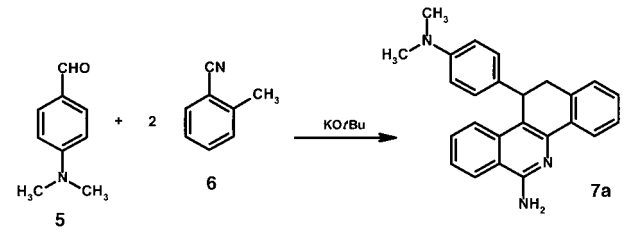
No synthesis of benzo[*c*]phenanthridines with phenyl substituents at C11 have thus far been described. In 1968 Devanathan et al.[30] reported attempting the synthesis of 4*b*,10*b*,11,12-tetrahydro-11-phenylbenzo[*c*]phenanthridine. The synthesis failed in the cyclization of the acetamido or benzamido derivative of 2,3-diphenyl-1,2,3,4-tetrahydrobenzo-1-naphthylamine mediated by phosphorus oxychloride or polyphosphoric acid to form the corresponding benzo[*c*]-

[*] Prof. Dr. B. Clement, Dr. M. Weide, Dr. U. Wolschendorf, Dr. I. Kock
Pharmazeutisches Institut
Lehrstuhl für Pharmazeutische Chemie
Universität Kiel
Gutenbergstrasse 76, 24118 Kiel (Germany)
Fax: (+49) 431-880-1352
E-mail: bclement@pharmazie.uni-kiel.de

[**] We thank the Fonds der chemischen Industrie for financial support.

Supporting information for this article (analytical data of the compounds synthesized) is available on the WWW under http://www.angewandte.de or from the author.

 DOI: 10.1002/anie.200461969 © 2005 Wiley-VCH Verlag GmbH & Co. KGaA, Weinheim



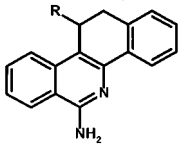
Scheme 2. Synthesis of **7a**.

phenanthridine. The synthesis of **7a** from **5** and **6** reveals a new and surprisingly simple synthetic route for the production of benzo[*c*]phenanthridine derivatives. The direct reaction of **8** with **6** under the conditions described above also leads to **7a**. We can thus assume that the formation of **7a** proceeds by formation of intermediate **8** (Scheme 3).

We view the following to be a probable reaction pathway. In analogy to a vinylogous Michael reaction, a further equivalent of **6** adds to the double bond in **8**. The negative mesomeric and inductive effect of the nitrile group facilitates the nucleophilic addition. Protonation could lead to **9**; however, in the presence of potassium *tert*-butanolate the carbanion **10** is very likely to be present. The intramolecular nucleophilic addition of this carbanion to the nitrile group in the manner of a Thorpe–Ziegler reaction then leads to the tautomeric phenylogous enaminonitrile **12** by way of the iminonitrile **11**. According to investigations carried out by Baldwin,[31] the enaminonitrile **12** should be favored over iminonitrile **11**. Nitrile functionalities in enaminonitriles are activated toward nucleophilic attack by the formation of mesomeric structures.[31,32] In this way, and also supported by the steric arrangement, the amino group of **12** adds intramolecularly to the nitrile group, resulting in **13**. Subsequent tautomerization finally leads to **7a**.

The route used for the formation of **7a** was also used to obtain other benzo[*c*]phenanthridine derivatives (Table 1).

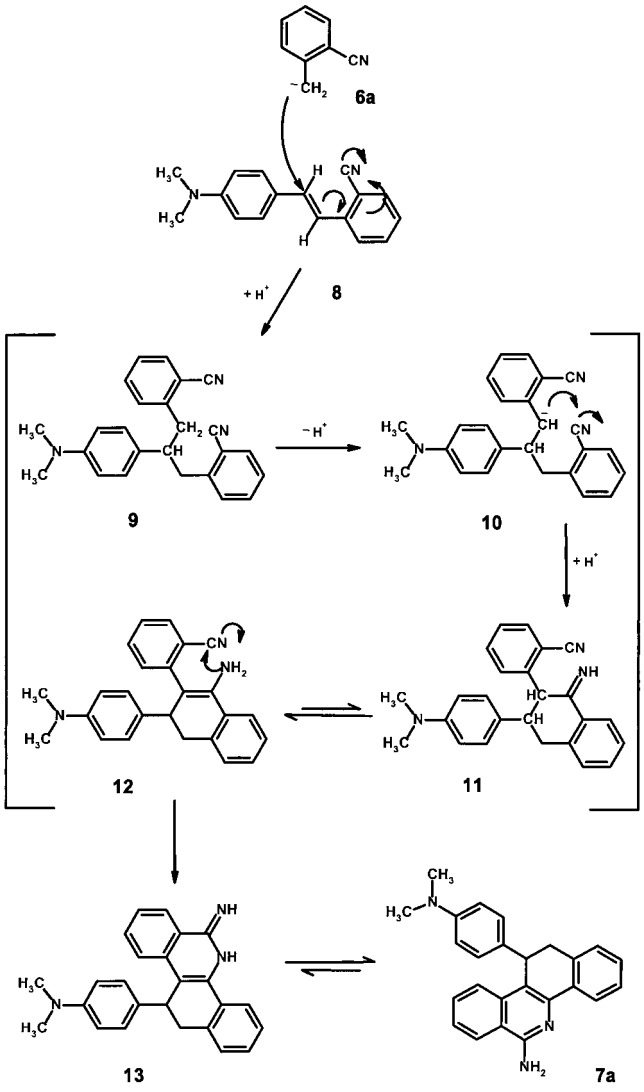
Table 1: Synthesis of 6-amino-11,12-dihydrobenzo[*c*]phenanthridines.



R	Product	Yield [%]
4-$Me_2NC_6H_4$	**7a**	40
Ph	**7b**	37
4-$MeOC_6H_4$	**7c**	53
2,4-$(MeO)_2C_6H_3$	**7d**	37
3,4-$(MeO)_2C_6H_3$	**7e**	57
H	**7f**	11

As demonstrated by the successful use of benzaldehyde, an electron-donating group is not necessary for sufficient polarization of the double bond. The phenyl derivative **7b** was obtained in similar yields to **7a**. Replacement of the dimethylamino group by a methoxy group led to higher product yields (**7c**). The dimethoxy derivative **7d** was obtained in lower yields, probably because of steric hindrance. In contrast, the dimethoxy derivative **7e** was obtained in yields similar to those of **7c**. The use of formaldehyde as the aldehyde component resulted in a lower yield (**7f**); the reasons for this are unclear.

Dehydration with 2,3-dichloro-5,6-dicyano-*p*-benzoquinone (DDQ)[33] converted the dihydro compounds into the corresponding 6-aminobenzo[*c*]phenanthridines in yields ranging from 14 to 38% (Scheme 4). These results contradict previous findings,[24] in which 11,12-dihydrobenzo[*c*]phenanthridine and a series of substituted 11,12-dihydrobenzo[*c*]-phenanthridines could be dehydrated only by heating in the presence of 30% palladium over activated carbon. Heating



Scheme 3. Postulated mechanism for the formation of **7a**.

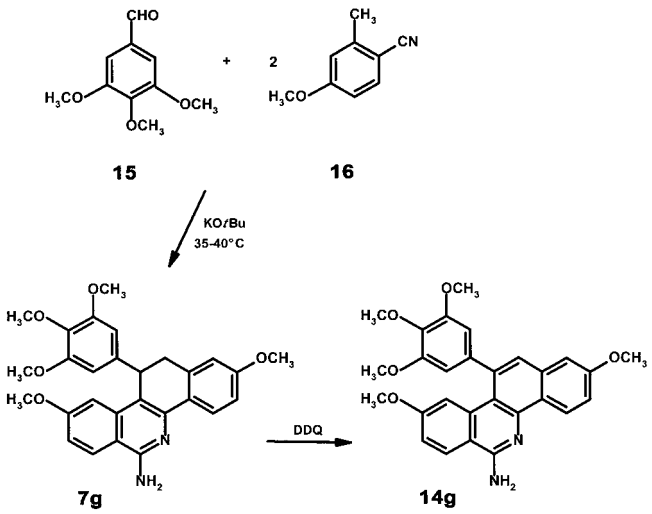


Scheme 4. Dehydration of **7** to form **14**.

 © 2005 Wiley-VCH Verlag GmbH & Co. KGaA, Weinheim

with DDQ in various solvents or heating with 10% palladium over activated carbon did not lead to the desired products. In preliminary experiments, the hydrochlorides of **7** could also be dehydrated by heating with sulfur.[34] However, this method demonstrated no advantages over dehydration with DDQ, as the yields were lower. As described above,[24] attempts at dehydration with 10% palladium over activated carbon were not successful.

Since many natural products have substituents in positions 2 and 3, or 8 and 9, we were interested determining whether the method described above could be used to prepare derivatives having substituents in these positions directly. For this, substituted 2-methylbenzonitriles are necessary. Whereas electron-withdrawing groups should not be problematic, electron-donating groups could have an adverse effect on both the deprotonation of the methyl groups in the *ortho* position and on the nucleophilic addition. The example of easily accessible 4-methoxy-2-methylbenzonitrile[35] and its conversion with 3,4,5-trimethoxybenzaldehyde to **7g** demonstrates the broad applicability of this synthetic route (Scheme 5). At 71%, the yield was even surprisingly high. The 24% overall yield obtained after dehydration of **14g** was within the same range as the other conversions.



Scheme 5. Synthesis of **7g** and **14g**.

The products obtained can be converted into other benzo[*c*]phenanthridine derivatives, especially by substitution in the 6-position. In particular, removal of the amino group from **14f** should make the basic ring system of this class of compounds easily accessible. The use of 4,5-dimethoxy-2-methylbenzonitrile and paraformaldehyde should allow for the straightforward formation of a fagaronine precursor.

The yields of **7** and **14** are not outstanding; however, the substances can be prepared in large amounts and with analytical purity (for pharmacological studies, for example), without chromatographic purification. Initial investigations of compounds of type **14** and to some extent type **7** demonstrated a very high cytotoxic potential. Studies of **7g** and **14g** by the U.S. National Cancer Institute (NCI) serve to illustrate this. NCI uses in vitro cell line screening to test compounds for activity against 60 human tumor cell lines from nine different types of cancer.[36] For each compound tested, 60 dose–activity curves, corresponding to the number of tumor cell lines, with five test concentrations each are obtained. This makes it possible to obtain information about the cytotoxicity as well as the selectivity of each compound against one or more forms of cancer. In order to characterize the antitumor activity of a tested compound, the dose-dependent parameters GI_{50} (growth inhibition 50%), TGI (total growth inhibition), and LC_{50} (lethal concentration 50%) are calculated. For each of these three parameters, the meangraph midpoint (MG_MID) is also calculated; this is the mean of the logarithms of the GI_{50} values and corresponds to an average response characteristic of all 60 cell lines to the test substance. This factor allows for the characterization of the activity of a compound in the test system and for its quantitative comparison with other compounds. Taking the antilogarithm of this value gives the mean of the GI_{50} values over all cell lines.[37]

According to these studies, a 3.39 μM concentration of **7g** and a 0.18 μM concentration of **7e** halve the growth rate of the tumor cells. Both compounds thus demonstrate a higher activity than fagaronine (**1;** 9.48 μM). In addition to these data, Table 2 contains data for other cytostatically active compounds. With the exception of paclitaxel, **7e** and **7g** demonstrate better cytostatic activity than established cystostatics such as cyclophosphamide in the in vitro cell line testing of the NCI. Further benzo[*c*]phenanthridine derivatives (not presented here) demonstrated similar cytostatic activities. These results will thus initiate the further development of new potential cancer drugs.

Table 2: Cytotoxic activity of benzo[*c*]phenanthridine derivatives and selected cytostatics from in vitro cell line screening by the NCI.[12]

Name	MG_MID (GI_{50})	$\frac{\sum GI_{50}}{60}$ [μM]
7g	−5.47	3.39
7e	−6.74	0.18
fagaronine	−5.00	9.48
cyclophosphamide	−3.68	210
5-fluorouracil	−4.75	17.6
6-sulfanylpurine	−5.13	7.36
paclitaxel	−7.65	0.02

Experimental Section

7a–d: General synthetic protocol: A solution of the appropriate aldehyde (10 mmol) and 2-methylbenzonitrile (2.34 g, 20 mmol) in 5 mL 1,3-dimethyltetrahydro-2-pyrimidone (DMPU) was added dropwise under nitrogen to a solution of potassium *tert*-butanolate (2.47 g, 22 mmol) in 20 mL DMPU. The reaction mixture was stirred under nitrogen for 5 h at 35°C, then poured into a solution of ammonium chloride (2.2 g, 40 mmol) in 100 mL ice water, and extracted three times with 100 mL dichloromethane. The organic phase was filtered through cotton if necessary and concentrated to a volume of about 100 mL on a rotary evaporator. The organic phase was vigorously shaken with 3N hydrochloric acid; the resulting precipitate was filtered, washed with dichloromethane, and dried. The corresponding 11-substituted 6-amino-11,12-dihydro-benzo[*c*]phe-

 © 2005 Wiley-VCH Verlag GmbH & Co. KGaA, Weinheim

nanthridinium chlorides were obtained after recrystallization. The free amines were released in diethyl ether with dilute ammonia. Addition of petroleum ether and removal of the diethyl ether on a rotary evaporator provided the solid products.

7e: As described above, with the following changes: 9.86 g (88 mmol) potassium *tert*-butanolate in 90 mL DMPU; 6.65 g (40 mmol) 3,4-dimethoxybenzaldehyde, 9.36 g (80 mmol) 2-methylbenzonitrile in 40 mL DMPU; dropwise addition at 40 °C; stirring for 4 h at 35–40 °C; 8.8 g (80 mmol) ammonium chloride in 400 mL ice water; extracted three time with 150 mL dichlormethane; vigorously stirred overnight with 20 mL 5 N hydrochloric acid.

7f: As described above, with the following changes: 2.47 g (22 mmol) potassium *tert*-butanolate in 20 mL DMPU; 0.3 g (10 mmol) paraformaldehyde; 2.34 g (20 mmol) 2-methylbenzonitrile in 12 mL DMPU; dropwise addition in 2 mL portions every 15 minutes; stirring for 6 h at 35 °C. The organic phase was concentrated on a rotary evaporator until vigorous precipitation occurred and was then stored overnight in a refrigerator; recrystallization from methanol/dichloromethane.

7g: A solution of 4-methoxy-2-methylbenzonitrile (8.83 g, 60 mmol) and 3,4,5-trimethoxybenzaldehyde (5.89 g, 30 mmol) in 30 mL DMPU was added dropwise under nitrogen to a solution of potassium *tert*-butanolate (7.41 g, 66 mmol) in 70 mL DMPU at 30 °C. The reaction mixture was subsequently stirred for 4 h at 35–40 °C and then carefully hydrolyzed in a solution of ammonium chloride (6.54 g, 120 mmol) in 300 mL ice water. The aqueous phase was extracted three times with 150 mL dichloromethane, and the combined organic phases were then dried over sodium sulfate and concentrated on a rotary evaporator. Precipitation of **7g** occurred after the organic phase had been stirred vigorously overnight with 10 mL concentrated hydrochloric acid and 10 mL water. The precipitate was filtered out, washed with a small amount of dichloromethane, recrystallized from methanol, and dried for 24 h under vacuum (oil pump).

14b–g: General synthetic protocol: A solution of DDQ in dioxane was added to a solution of **7a–g** in dioxane and heated to reflux. The cooled reaction mixture was hydrolyzed by pouring it into a saturated sodium hydrogen carbonate solution, and the reaction mixture was then extracted with diethyl ether. The ether phase was washed once with dilute sodium hydrogen carbonate solution and three times with water. The organic phase was dried over sodium sulfate and concentrated on a rotary evaporator. The 6-aminobenzo[*c*]phenanthridiniumperchlorate was precipitated by vigorous stirring of the organic phase overnight with 70% perchloric acid. The precipitate was filtered out and recrystallized from methanol. **14b**: 0.5 g (1.6 mmol) **7b** in 25 mL dioxane, 0.63 (2.8 mmol) DDQ in 25 mL dioxane, 4 h reflux; **14c**: 1.5 g (4.3 mmol) **7c** in 100 mL dioxane, 3.8 g (16.7 mmol) DDQ in 100 mL dioxane, 8 h reflux; **14d**: 0.5 g (1.3 mmol) **7d** in 10 mL dioxane, 0.54 g (2.3 mmol) DDQ in 35 mL dioxane, 4 h reflux; **14e**: 2.0 g (5.2 mmol) **7e** in 50 mL dioxane, 4.4 g (21.0 mmol) DDQ in 100 mL dioxane, 16 h reflux; **14f**: 0.25 g (1.0 mmol) **7f** in 15 mL dioxane, 0.40 (1.7 mmol) DDQ in 35 mL dioxane, 4 h reflux; **14g**: 1.62 g (3.4 mmol) **7g** in 90 mL dioxane, 3.11 g (13.7 mmol) DDQ in 70 mL dioxane, 9 h reflux.

Received: September 13, 2004
Published online: December 13, 2004

Keywords: alkaloids · antitumor agents · benzophenanthridines · synthetic methods

[1] S. Simeon, J. L. Rios, A. Villar, *Pharmazie* **1989**, *44*, 593–597.
[2] T. Ishikawa, H. Ishii, *Heterocycles* **1999**, *50*, 627–639.
[3] S. D. Phillips, R. N. Castle, *J. Heterocycl. Chem.* **1981**, *18*, 223–232.
[4] M. Treus, J. C. Estevez, L. Castedo, R. J. Esteves, *Tetrahedron Lett.* **2002**, *43*, 5323–5325.
[5] M. A. Lunch, O. Duval, P. Pochet, R. D. Waigh, *Bull. Soc. Chim. Fr.* **1994**, *131*, 718–722.
[6] M. Cushman, L. Cheng, *J. Org. Chem.* **1978**, *43*, 286–288.
[7] W. M. Messmer, M. Tin-Wa, H. H. S. Fong, C. Bevelle, N. R. Farnsworth, D. J. Abraham, J. Trojanek, *J. Pharm. Sci.* **1972**, *61*, 1858–1859.
[8] J. P. Gillespie, L. G. Amoros, F. R. Stermiz, *J. Org. Chem.* **1974**, *39*, 3239–3241.
[9] H. Ishii, I. S. Cheng, T. Ishikawa, *J. Chem. Soc. Perkin Trans. 1* **1987**, 671–676.
[10] J. Šmidrkal, *Collect. Czech. Chem. Commun.* **1988**, *53*, 1384–1392.
[11] F. R. Stermiz, J. P. Gillespie, L. G. Amoros, R. Romero, T. A. Stermiz, *J. Med. Chem.* **1975**, *18*, 708–713.
[12] National Cancer Institute, Cancer Screen 10/**2002** Data; http://dtp.nci.nih.gov.
[13] M. L. Sethi, *J. Nat. Prod.* **1979**, *42*, 187–196.
[14] N. Kakiuchi, M. Hattori, H. Ischi, T. Namba, *Planta Med.* **1987**, 22–27.
[15] V. S. Sethi, *Cancer Res.* **1976**, *36*, 2390–2395.
[16] J. N. Pezzuto, S. K. Antosiak, W. M. Messmer, M. B. Salytor, G. R. Honig, *Chem.-Biol. Interact.* **1983**, *43*, 323–339.
[17] A. K. Larsen, L. Gronard, J. Couprie, B. Desoize, L. Comoe, J.-C. Jardillier, J.-F. Riou, *Biochem. Pharmacol.* **1993**, *46*, 1403–1412.
[18] S. D. Phillips, R. N. Castle, *J. Heterocycl. Chem.* **1981**, *18*, 223–232.
[19] Y. L. Janin, E. Bisagni, *Tetrahedron* **1993**, *49*, 10305–10316.
[20] H. Ishii, J.-I. Ichikawa, E. Kawabane, M. Ishikawa, T. Ishikawa, K. Kuretani, M. Inomata, A. Hoshi, *Chem. Pharm. Bull.* **1995**, *33*, 4139–4151.
[21] I. Ninomiya, T. Naito, *Rec. Dev. Chem. Nat. Carbon Compd.* **1984**, *10*, 11–90.
[22] S. P. Mackay, O. Meth-Cohn, R. D. Waigh, *Adv. Heterocycl. Chem.* **1987**, *25*, 345–389.
[23] R. K.-Y. Zee-Cheng, C. C. Cheng, *J. Med. Chem.* **1975**, *18*, 66–71.
[24] R. Beugelmans, J. Chastanet, H. Ginsburg, L. Quintero-Cortez, G. Roussi, *J. Org. Chem.* **1985**, *50*, 4933–4938.
[25] S. P. Mackay, L. Comoe, B. Desoize, O. Duvall, J.-C. Jardellier, R. D. Waigh, *Anticancer Drug Des.* **1998**, *13*, 797–813.
[26] T. Ishikawa, *Med. Res. Rev.* **2001**, *21*, 61–72.
[27] S. V. Kessar, Y. P. Gupta, P. Balakrishnan, K. K. Sawal, T. Mohammed, M. Dutt, *J. Org. Chem.* **1988**, *53*, 1708–1713.
[28] Y. L. Janin, A. Croisy, J.-F. Riu, E. Bisagni, *J. Med. Chem.* **1993**, *36*, 3686–3692.
[29] K. Takhaschi, T. Okamoto, K. Yamada, H. Iida, *Synthesis* **1977**, 58–59.
[30] V. C. Devanathan, V. Kesavan, N. Arumugam, *Indian J. Chem.* **1968**, *7*, 124–126.
[31] S. Baldwin, *J. Org. Chem.* **1961**, *26*, 3288–3295.
[32] I. F. Barnard, J. A. Elvidge, *J. Chem. Soc. Perkin Trans. 1* **1983**, 1137–1140.
[33] D. Walker, J. D. Hiebert, *J. Org. Chem.* **1967**, *32*, 153–196.
[34] P. A. Plattner, *Angew. Chem.* **1942**, *55*, 131–146; P. A. Plattner, *Angew. Chem.* **1942**, *55*, 154–158.
[35] J. L. Neumeyer, K. K. Weinhardt, *J. Med. Chem.* **1970**, *13*, 613–616.
[36] A. Monks, D. Scudiero, P. Skehan, R. Shoemaker, K. Paull, D. Vistica, C. Hose, J. Langley, P. Cronise, A. Vaigro-Wolff, M. Gray-Goodric, H. Campell, J. Mayo, M. Boyd, *J. Natl. Cancer Inst.* **1991**, *83*, 757–766.
[37] M. R. Boyd, K. D. Paull, *Drug Dev. Res.* **1995**, *34*, 91–109.

 © 2005 Wiley-VCH Verlag GmbH & Co. KGaA, Weinheim

Biomineralization

Morphosynthesis of Nacre-Type Laminated $CaCO_3$ Thin Films and Coatings**

Dirk Volkmer, Marc Harms, Laurie Gower, and Andreas Ziegler*

$CaCO_3$ is one of the most abundant biogenic minerals. Biological organisms utilize mainly the thermodynamically most stable crystal polymorphs of $CaCO_3$, that is, calcite or aragonite, for the construction of protective shells and casings.[1] Among the many intricate shapes and architectures of naturally occurring biominerals, the structure and properties of nacre ("mother-of-pearl"), the iridescent inner layer of mollusc shells, has had a special attraction for scientists. Nacre consists of stacked layers of tabular aragonite crystals that are interspersed with a thin organic matrix. Investigations on the ultrastructure of nacre suggest that mineral bridges exist between adjacent layers of aragonite crystals and, therefore, the highly uniform coorientation of the crystals is maintained over long distances.[2] The unique crystal texture of nacre gives rise to unusual material properties such as toughness, corrosion resistance, and its characteristic luster.[3] Noteworthy, this laminated crystal texture sometimes is found in (fossil) brachiopods, which, however, are made up of thin layers of calcite instead of aragonite crystals.[4,5]

Many investigations have focussed on the biosynthesis of nacre to elucidate the mechanisms by which the mollusc gains control over the selection of the $CaCO_3$ polymorph, the shape and the size of individual crystals, and their integration into a brickwork-like pattern. It has been proposed that the organic matrix acts as a template for the nucleation of a first layer of aragonite crystals.[6] Reconstitution experiments[7] employing macromolecules extracted from different sites of de-mineralized mollusc shells indicate that the selection of $CaCO_3$ polymorph might be triggered by specific soluble peptides that have an unusually high content of acidic amino acid side chains.[8] Moreover, model systems employing self-assembled monolayers (SAMs) of carboxy-terminated alkylthiols bound to Au or Ag surfaces have impressively demonstrated that the growth orientation of calcite crystals might be well controlled by virtue of a geometrical or stereochemical match between the carboxylate moieties of the immobilized SAM and the juxtaposed calcite crystal face.[9] However, this approach as yet has not proven to be applicable for the construction of nacre-type materials, in which both the laminated structure can be achieved, as well as control over crystal orientation and phase. Complementary investigations by our group,[10] among others,[11] in which non-immobilized monolayers of amphiphilic macrocycles were employed, on the other hand have shown that the average charge distribution at the template surface is the predominant factor that governs the selection of crystal polymorphs and the orientation of crystals.

We present here an alternative process for synthesizing a highly organized nacre-type material (Figure 1). This novel morphosynthetic approach[12] rests on the deposition of a polycrystalline calcite thin film starting from a metastable amorphous precursor phase. The polycrystalline thin film, in turn, serves as a template upon which highly oriented layers of calcite crystals are deposited under nonequilibrium conditions.

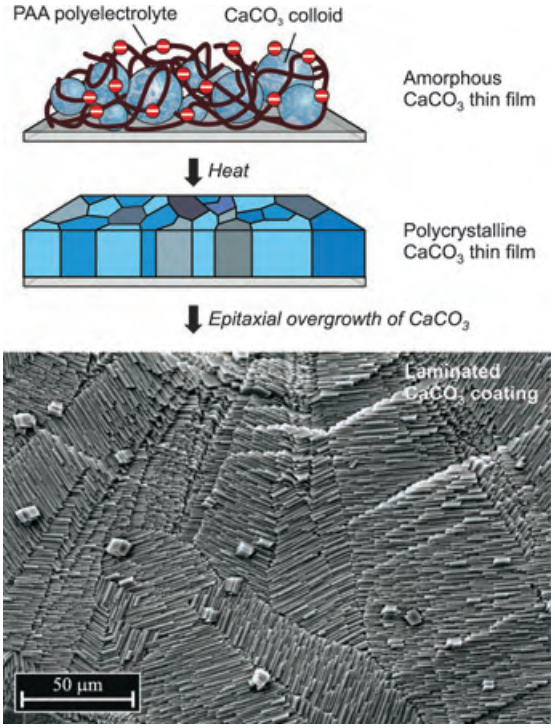


Figure 1. Scheme of a three-step procedure for the morphosynthesis of nacre-type laminated $CaCO_3$ coatings. In the first step an amorphous highly hydrated $CaCO_3$ thin film is deposited on a glass substrate. Upon heating this precursor film is transformed into a polycrystalline thin film consisting of a mosaic of flat single-crystalline calcite domains. In the last step highly oriented single and multiple layers of calcite crystals are grown epitaxially on the underlying polycrystalline thin film.

[*] Prof. Dr. D. Volkmer, M. Harms
Inorganic Chemistry II
University of Ulm
Albert-Einstein-Allee 11, 89081 Ulm (Germany)
Fax: (+49) 731-50-23039
E-mail: dirk.volkmer@chemie.uni-ulm.de
Prof. Dr. L. Gower
Department of Materials Science & Engineering
University of Florida
P.O. Box 116400, Gainesville (USA)
Priv.-Doz. Dr. A. Ziegler
Central Faculty of Electron Microscopy
University of Ulm
Albert-Einstein-Allee 11, 89069 Ulm (Germany)

[**] This work was financially supported by the Deutsche Forschungsgemeinschaft (DFG Schwerpunktprogramm 1117, "Prinzipien der Biomineralisation"; DFG grant Vo829/2-1). The authors are grateful to R. Oldenbourg (Marine Biological Laboratory, Woods Hole, USA) for helpful comments on LC-PolScope data analysis.

Supporting information for this article is available on the WWW under http://www.angewandte.org or from the author.

 DOI: 10.1002/anie.200461386 © 2005 Wiley-VCH Verlag GmbH & Co. KGaA, Weinheim

In a typical experiment, a supersaturated solution of $CaCO_3$ continuously flows through a perfusion cell mounted on a microscope stage. A constant supersaturation level is maintained by feeding a 10 mM solution of $CaCl_2$ and Na_2CO_3 into a mixing chamber that is connected to the inlet port of a perfusion cell. (A complete description of the experimental set-up is given in the Supporting Information). In the first step an amorphous $CaCO_3$ precursor film is deposited on the surface of the glass slides that are at the top and the base of the perfusion cell. An anionic polymer is added to the Na_2CO_3 solution that serves as a process-directing agent which induces liquid–liquid phase separation and ultimately deposition of an amorphous precursor film.[13] Preliminary investigations on the influence of the polyelectrolytes's molecular weight, its concentration, and its chemical nature showed us that low-molecular-weight atactic poly(acrylic acid) (PAA, av $M_w = 2100\ g\,mol^{-1}$; 8.0×10^{-3} wt%) is most suitable for stabilizing amorphous $CaCO_3$ precursor films on glass substrates. The amorphous thin film displays characteristic alterations of its optical density ("meander texture", Figure 2a). Scanning electron micrographs (Figure 2b–d) taken from different film regions indicate that the meander texture is due to an irregular distribution of granular matter, which is presumably caused by a turbulent flow of solution in the perfusion cell. At higher magnifications it is clearly seen that the amorphous thin film consists of aggregated colloid particles with a narrow size dispersion between 20–30 nm. The IR spectrum of the amorphous thin film shows a broad split peak at 1479 and 1419 cm^{-1} and a weak band appearing at around 675 cm^{-1}, which demonstrates that the colloid particles mainly consist of amorphous $CaCO_3$.[14]

If the mother liquor is removed and the coated substrate is subjected to drying at room temperature for several days, the amorphous $CaCO_3$ thin film partially transforms into the crystalline state. However, a complete transition is readily achieved if the amorphous precursor thin film is heated at 400 °C for about 2 h. This yields an optically birefringent thin film of constant thickness (typically 500–700 nm), the polarization optical micrograph of which reveals a characteristic mosaic structure (Figure 3a). Domains appearing homogeneous in the polarization optical micrograph are separated by cracks that develop during the drying/heating procedure. Scanning electron micrographs (Figure 3b,c) reveal that the amorphous $CaCO_3$ colloid particles have coalesced to form an almost homogeneous crystalline thin film. These results are complemented by atomic force microscopy (AFM) surface topography images (see Supporting Information), which demonstrate that the film surface is not atomically flat, but retains a rough surface (rms surface roughness $R_q = 16.90\ nm^{-1}$) that is commensurate to the size of the $CaCO_3$ colloid particles found in the precursor film.

The mineral phase was characterized by IR spectroscopy and X-ray diffraction. The three bands observed in the IR spectrum at $\tilde{\nu} = 1415$, 875, and 711 cm^{-1} are characteristic of crystalline calcite.[14] X-ray diffraction yields sharp peaks that can be assigned to the XRD pattern of calcite (see Supporting Information).[15] There is no indication of other $CaCO_3$ polymorphs (aragonite, vaterite) being formed upon heating the sample. The relative intensities of the observed XRD peaks, however, differ only slightly from those of a calcite powder reference sample, the most notable deviation being

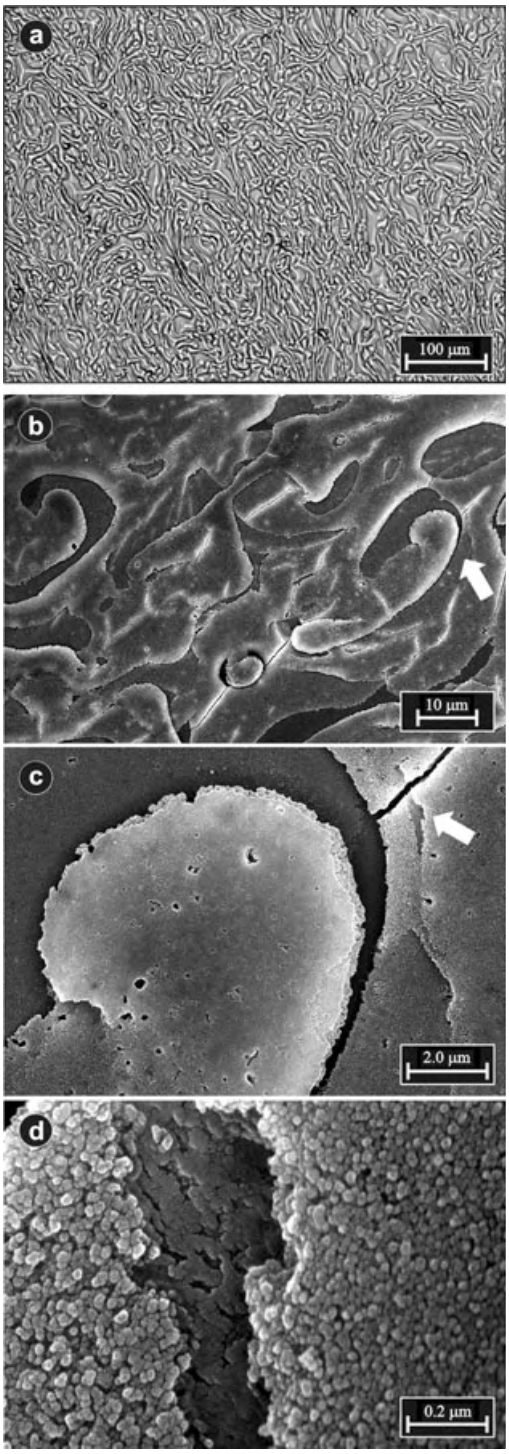


Figure 2. a) Optical texture of an amorphous $CaCO_3$ precursor thin film grown after 45 min on a glass cover slide under constant perfusion (0.75 mL min^{-1}) of a supersaturated solution of $CaCO_3$ (10 mM $CaCl_2$, 10 mM Na_2CO_3, 8.0×10^{-3} wt% PAA ($M_w = 2100\ g\,mol^{-1}$, $T = 295$ K). (Bright field optical micrograph, digital contrast enhancement). b–d) Scanning electron micrographs of the film at different magnifications showing a meander texture of aggregated amorphous $CaCO_3$ colloid particles. (White arrows point to the approximate image area shown at the next higher magnification level).

 © 2005 Wiley-VCH Verlag GmbH & Co. KGaA, Weinheim

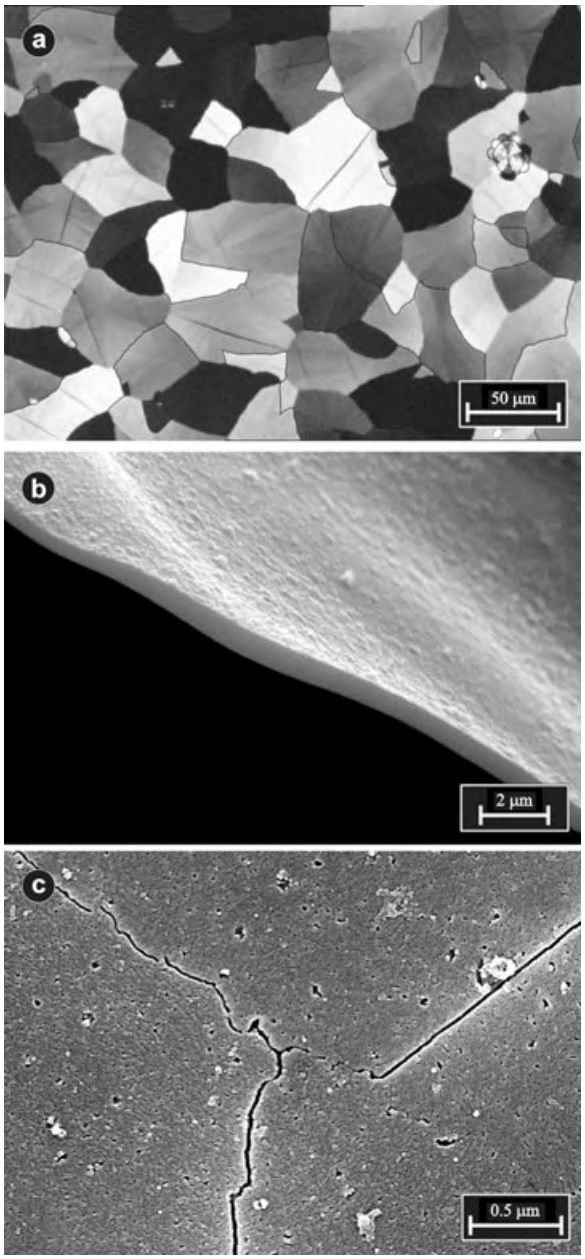


Figure 3. a) Polarization optical micrograph of a polycrystalline $CaCO_3$ thin film obtained from an amorphous precursor film after heating at 400 °C for 2 h. The observed mosaic structure of the thin film is due to the presence of discrete domains each consisting of a flat calcite single crystal. The typical domain sizes range from 50–200 μm in diameter. b,c) Scanning electron micrographs of a polycrystalline $CaCO_3$ thin film obtained from an amorphous precursor film after heating at 400 °C for 2 h. The film thickness was measured at the edge of films where pieces occasionally lifted off the substrate surface. The average film thickness is 600 nm (±100 nm).

the slightly weakened intensity of the calcite (10.4) peak. However, the XRD pattern of the polycrystalline calcite thin film does not show any exceptional preference in favor of a single crystal orientation.

Digital image analysis of the polarization optical micrographs taken from a polycrystalline calcite thin film mounted between crossed polarizers shows that for each individual domain an almost constant gray level can be assigned. This behavior can be easily understood if we assume that each domain constitutes a calcite single crystal that arises from a singular nucleation event occurring within the amorphous precursor film, the orientation of which differs from that of its neighbor(s). To demonstrate the single-crystalline nature of the domains, $CaCO_3$ overgrowth experiments were performed, by using the polycrystalline thin film as an isoepitaxial substrate.[16] Thus, a glass slide carrying the polycrystalline thin film was subjected once again to a continuous flow of supersaturated $CaCO_3$ solution, which at this time was lacking the PAA inhibitor. To our delight, single and multiple layers of highly oriented calcite crystals grew on top of the polycrystalline thin film, thus leading to a notable iridescence. Marked areas of the polycrystalline thin films were examined by polarization optical microscopy as well as by scanning electron microscopy before and after calcite overgrowth had taken place (Figure 4). The micrographs clearly show that the underlying flat calcite domains direct the orientation of the overgrowing polycrystalline calcite layer. The crystal texture changes abruptly at the borderline between different domains but stays constant within each individual domain area. Within many domains calcite crystals are grown together forming stacks of perfectly co-aligned platelets. Determining the crystal growth orientation in different domains is straightforward since the rhombohedral calcite morphology is preserved in all cases.[17] Figure 4 c,d shows the representative details of oriented calcite layers thus obtained. When the growth of the calcite layer onto the polycrystalline film is interrupted after 45 min, the crystals have a narrow thickness distribution typically ranging from 700 to 1200 nm. (The maximum film thickness thus achievable is about 4.5–5.8 μm after 12 h.). We currently anticipate that the combination of mesoscopic size and parallel periodic arrangement of the crystals leads to the glistening appearance of the samples.

To gain deeper insights into the structure-directing role of the polycrystalline $CaCO_3$ thin film obtained from the amorphous precursor film, we employed a novel optical birefringence imaging system (LC-PolScope).[18] This system provides a means to visualize and measure retardance magnitude and slow-axis orientation at every pixel of a charge-coupled device (CCD) image within seconds. Since calcite is a uniaxial birefringent material, a thin calcite platelet will lead to an optical retardance value that depends on the sample thickness and the orientation of the crystallographic c axis (= optical axis) with respect to the direction of the polarized light beam propagating through the sample. The retardance δ (in nm) of a uniformly thin calcite platelet is given by Equation (1)[19], where ϑ is the angle between the

$$\delta = \rho(n_e - n_o)\sin^2\theta \qquad (1)$$

optical axis and the propagation direction of the beam, ρ (in nm) is the thickness of the crystal sheet and $(n_e - n_o)$ the birefringence of calcite (ca. −0.174 at $\lambda = 546.5$ nm).[20] Thus, measuring the optical retardance of many different calcite domains simultaneously yields information about the frequency by which different crystal orientations occur in the polycrystalline thin film obtained from the amorphous

 © 2005 Wiley-VCH Verlag GmbH & Co. KGaA, Weinheim

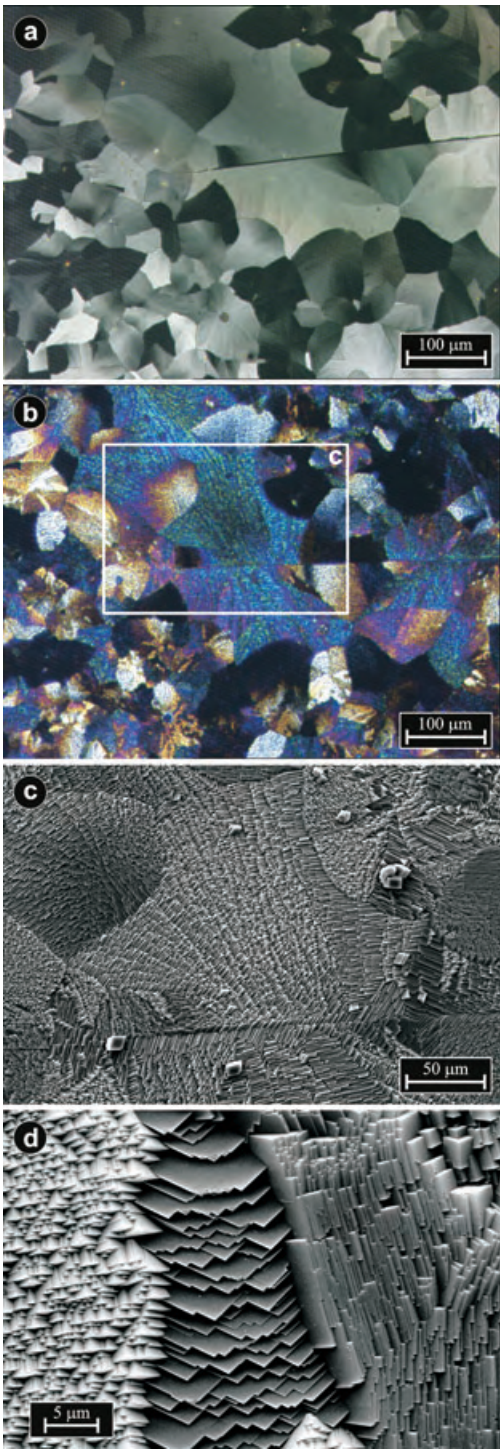


Figure 4. Highly oriented laminated calcite layers grown on a flat calcite thin film. Optical micrographs of a polycrystalline calcite thin film mounted between crossed polarizers before (a) and after calcite overgrowth (b). Scanning electron micrographs showing details of the crystal texture (c, d). d) Detail of a calcite layer showing abrupt changes of crystal orientations at the domain boundaries. Growth directions were tentatively assigned by measuring the projected interfacial angles of the calcite rhombohedra in the micrograph and comparing these to calculated values. (Left: $<00.1>$, middle: $<01.8>$, right $<11.0>$)

precursor. Unfortunately, for materials possessing uniaxial birefringence, the ϑ value cannot be assigned to a unique crystallographic direction. However, it is possible to calculate retardance values for characteristic calcite crystal orientations that are frequently observed in calcite overgrowth experiments. Figure 5a shows an LC-PolScope pseudo-color repre-

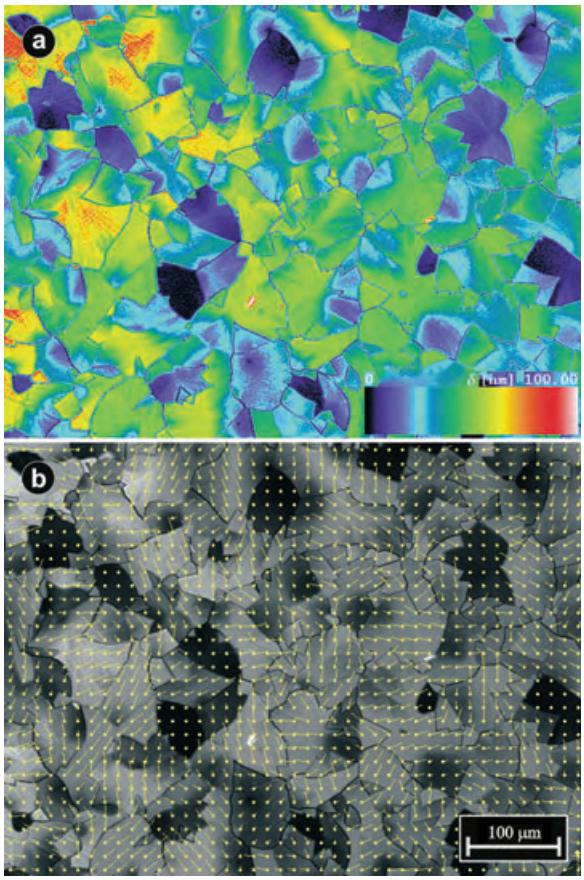


Figure 5. a) LC-PolScope image of a polycrystalline calcite thin film (retardance given as pseudo-color). b) Retardance grayscale image overlaid by short lines indicating the orientations of the slow birefringence axis measured in each location. (Slow axis orientations are typically shown for every 15 pixel in the horizontal and vertical direction of the original video frame).

sentation of optical retardance values δ of a polycrystalline thin film measured for each point of the image. Note that experimental δ values differ from domain to domain, but stay nearly constant within each individual domain. (Some calcite domains show a biaxial birefringence pattern that might be stress-induced, presumably caused by the shrinkage occurring during the drying process which is necessary to transform the highly hydrated amorphous precursor into an anhydrous polycrystalline thin film.) The most frequent retardance values cluster around $80(\pm 5)$, $49(\pm 4)$, $20(\pm 3)$, $15(\pm 2)$, and $0(\pm 2)$ nm. The best matching calculated retardance values are 82.1 {01.2}, 50.9 {01.4}, 20.2 {10.10}, 13.6 {01.8}, and 0 nm {00.1} for a sample thickness of 600 nm, (the crystal face which is parallel to the glass substrate, or perpendicular to the light direction, respectively, is given in braces).[21] Figure 5b displays the same film area with the direction of the slow birefringence axis indicated as small vectors at different points. Note that most domains within the mosaic thin film are

 © 2005 Wiley-VCH Verlag GmbH & Co. KGaA, Weinheim

uniformly oriented.

LC-PolScope imaging of polycrystalline calcite thin films yields two important features: First, there is strong evidence that the polycrystalline calcite thin films in fact consist of flat single crystals. The crystal orientation switches at the domain boundaries, but there is no preference for a particular orientation, which is in agreement with the results of XRD measurements. Second, experimental retardance values are fully consistent with theoretical ones, based on crystal orientations that we have observed in crystal overgrowth experiments (Figure 4d). These findings lead us to conclude that calcite overgrowth most likely occurs by isoepitaxy, which is, however, somewhat unexpected, considering the mesoscopic surface roughness of the underlying polycrystalline thin film (Figure 3c).

The preparation of biologically inspired laminates mimicking the architectural concept of nacre, albeit at a somewhat smaller length scale, has been described previously.[22] Amorphous $CaCO_3$ thin films have been grown underneath Langmuir monolayers in the presence of PAA,[23] and their formation has been monitored in situ by synchrotron reflectivity studies.[23b] The effects of functional groups of insoluble biopolymers on $CaCO_3$ thin film formation have been investigated,[24] and the formation of aragonite thin films on chitosan matrices in the presence of Mg^{2+} ions and poly-Asp (Asp = aspartic acid) has been demonstrated.[25] However, as yet none of these approaches has led to highly oriented laminated crystal architectures similar to those reported here. Our investigations show that nacre-type $CaCO_3$ thin films and coatings can be obtained by a morphosynthetic approach[26] that requires *no* structurally preorganized organic matrix. The key steps involve the transformation of an amorphous $CaCO_3$ precursor thin film into a polycrystalline calcite thin film, which, in turn, serves as a template for epitaxial overgrowth of highly oriented layers of uniform calcite platelets. This strategy leads to a general, technically feasible approach towards highly ordered materials consisting of microcrystals with typical sizes ranging from a few tens to a few hundreds of nm, which could be technologically interesting for photonic applications, for example for diffraction gratings,[27] photonic band gap materials,[28] and coatings based on structural colours instead of pigments.[29]

In terms of rationalizing the formation of highly organized crystal textures in biological organisms, our investigations might provide an alternative concept as opposed to the commonly believed structure-directing role of organic templates in biomineralization. It is thus imaginable that highly organized crystal architectures such as nacre or the foliated and prismatic layers, may grow spontaneously and continuously once a first crystal layer has been deposited, requiring no further elaborate control mechanisms.[30] However, the transition of an amorphous precursor into crystalline polymorphs is a key step involved in many biomineralization processes, and the mechanism(s) by which organisms trigger this particular transformation are largely unknown.[31]

The availability of a nondestructive, real-time retardance imaging system such as the LC-PolScope used here represents a significant addition to analytical tools available for characterizing the amorphous–solid state transition of (inorganic) materials in situ. Investigations are underway to find the appropriate experimental conditions under which regular biomimetic $CaCO_3$ architectures constructed from aragonite instead of calcite can be produced.

Received: July 22, 2004
Published online: December 15, 2004

Keywords: amorphous materials · bioinorganic chemistry · biomineralization · crystal growth · scanning probe microscopy

[1] H. A. Lowenstam, S. Weiner, *On Biomineralization*, Oxford University Press, New York, **1989**.
[2] a) S. W. Wise, *Science* **1970**, *167*, 1486–1488; b) H. K. Erben, N. Watabe, *Nature* **1974**, *248*, 128–130; c) T. E. Schaffer, C. Ionescu-Zanetti, R. Proksch, M. Fritz, D. A. Walters, N. Almqvist, C. M. Zaremba, A. M. Belcher, B. L. Smith, G. D. Stucky, D. E. Morse, P. K. Hansma, *Chem. Mater.* **1997**, *9*, 1731–1740; d) X. Su, A. M. Belcher, C. M. Zaremba, D. E. Morse, G. D. Stucky, A. H. Heuer, *Chem. Mater.* **2002**, *14*, 3106–3117.
[3] a) J. D. Currey, *Proc. R. Soc. London* B **1977**, *196*, 443–463; b) A. P. Jackson, J. F. V. Vincent, R. M. Turner, *Proc. R. Soc. London* B **1988**, *234*, 415–440; c) A. G. Evans, Z. Suo, R. Z. Wang, I. A. Aksay, M. Y. He, J. W. Hutchinson, *J. Mater. Res.* **2001**, *16*, 2475–2484.
[4] K. M. Towe, C. W. Harper, *Science* **1966**, *154*, 153–155.
[5] A comparable architecture is found in non-molluscan species such as bryozoan lophophorates, in which laminated calcite tablets are referred to as seminacre since they are less organized than the nacre of molluscs. M. J. Weedon, P. D. Taylor, *Biol. Bull.* **1995**, *188*, 281–292.
[6] a) S. Weiner, W. Traub, *Phil. Trans. R. Soc. Lond.* B **1984**, *304*, 425–433; b) S. Mann, *Nature* **1988**, *332*, 119–124; c) Y. Levi-Kalisman, G. Falini, L. Addadi, S. Weiner, *J. Struct. Biol.* **2001**, *135*, 8–17.
[7] a) G. Falini, S. Albeck, S. Weiner, L. Addadi, *Science* **1996**, *271*, 67–69; b) Y. Levi, S. Albeck, A. Brack, S. Weiner, L. Addadi, *Chem. Eur. J.* **1998**, *4*,389–396.
[8] a) P. E. Hare, *Science* **1963**, *139*, 216–217; b) B. A. Gotliv, L. Addadi, S. Weiner, *ChemBioChem* **2003**, *4*, 522–529.
[9] a) J. Aizenberg, J. A. Black, G. M. Whitesides, *J. Am. Chem. Soc.* **1999**, *121*, 4500–4509; b) A. M. Travaille, L. Kaptijn, P. Verwer, B. Hulsken, J. A. A. W. Elemans, R. J. M. Nolte, H. van Kempen, *J. Am. Chem. Soc.* **2003**, *125*, 11571–11577.
[10] a) D. Volkmer, M. Fricke, D. Vollhardt, S. Siegel, *J. Chem. Soc. Dalton Trans.* **2002**, 4547–4554; b) D. Volkmer, M. Fricke, C. Agena, J. Mattay, *J. Mater. Chem.* **2004**, *14*, 2249–2259.
[11] a) M. J. Lochhead, S. R. Letellier, V. Vogel, *J. Phys. Chem. B* **1997**, *101*, 10821–10827; b) P. Calvert, S. Mann, *Nature* **1997**, *386*, 127–129.
[12] D. Volkmer, S. Tugulu, M. Fricke, T. Nielsen, *Angew. Chem.* **2003**, *115*, 60–64; *Angew. Chem. Int. Ed.* **2003**, *42*, 58–61.
[13] L. B. Gower, D. J. Odom, *J. Cryst. Growth* **2000**, *210*, 719–734.
[14] The strong band at $\tilde{\nu}_3 = 1415\ cm^{-1}$ can be assigned to the asymmetric C–O stretching mode of CO_3^{2-} in calcite while those centred at $\tilde{\nu}_2 = 875\ cm^{-1}$ corresponds to the CO_3^{2-} out-of-plane deformation mode. The band at $\tilde{\nu}_4 = 711\ cm^{-1}$ corresponds to the O-C-O bending mode of crystalline calcite. F. A. Andersen, L. Brecevic, *Acta Chem. Scand.* **1991**, 1018–1024.
[15] Crystallographic indices are presented in three-index (*hk.l*) notation, based on the hexagonal setting of the calcite unit cell ($R\bar{3}c$, $a = 4.96$, $c = 17.002$ Å).
[16] This technique has been used by others to determine the crystal orientation of underlying biogenic crystals that lack facets due to their nonequilibrium morphologies: a) K. Okazaki, R. M. Dilla-

 © 2005 Wiley-VCH Verlag GmbH & Co. KGaA, Weinheim

man, K. M. Wilbur, *Biol. Bull.* **1981**, *161*, 402 – 415; b) J. Aizenberg, S. Albeck, S. Weiner, L. Addadi, *J. Cryst. Growth* **1994**, *142*, 156 – 164.

[17] D. D. Archibald, S. B. Qadri, B. P. Gaber, *Langmuir* **1996**, *12*, 538 – 546. A projection of rhombohedral faces onto the image plane of the micrograph yields characteristic interfacial angles, based on which the crystal's orientations can be assigned in many cases. Note, however, that this procedure strictly necessitates that the sample is aligned perpendicular to the viewing direction while at the same time perspective aberrations of the optical system have to be kept at a minimum.

[18] a) R. Oldenbourg, G. Mei, *J. Microsc.* **1995**, *180*, 140 – 147; b) R. Oldenbourg, *Nature* **1996**, *381*, 811 – 812.

[19] M. Born, E. Wolf, *Principles of Optics*, *6th ed.*, Pergamon, Oxford, **1986**, p. 699. Compared to Equation (36) given in the textbook, the formula presented here omits the factor $(2\pi/\lambda)$ to obtain δ directly in nm, after entering ρ in nm.

[20] G. Gosh, *Opt. Commun.* **1999**, *163*, 95 – 102.

[21] Since the optical axis of calcite coincides with its crystallographic *c* axis, the angle parameter ϑ is obtained from calculating angles between pairs of (00.1) and (*hk.l*) crystal planes represented by Miller indexes. Calculations were conveniently performed with two public domain software tools located at http://www.public.asu.edu/~bdegreg/Xtalplanes.html, and http://www.jcrystal.com/steffenweber/JAVA/juvw/JCELL.html. (Calcite unit cell parameters: $a = b = 4.988$, $c = 17.068$ Å, $\alpha = \beta = 90°$, $\gamma = 120°$). Full analytical expressions are given in the *International Tables for X-Ray Crystallography*, *Vol. II*, IUCr, Kynoch, Birmingham, **1972**, p. 168. Computed ϑ values are as follows: 63.2° {01.2}, 44.7° {10.4}, 90.0° {11.0}, 66.3° {11.3}, 75.8° {20.2}, 48.8° {11.6}, 21.6 {10.10}, 26.3° {11.8}.

[22] a) A. Sellinger, P. M. Weiss, A. Nguyen, Y. F. Lu, R. A. Assink, W. L. Gong, J. C. Brinker, *Nature* **1998**, *394*, 256 – 260; b) Z. Tang, N. A. Kotov, S. Magonov, B. Ozturk, *Nat. Mater.* **2003**, *2*, 413 – 418.

[23] a) G. Xu, N. Yao, I. A. Aksay, J. T. Groves, *J. Am. Chem. Soc.* **1998**, *120*, 11977 – 11985; b) E. DiMasi, V. M. Patel, M. Sivakumar, M. J. Olszta, Y. P. Yang, L. B. Gower, *Langmuir* **2002**, *18*, 8902 – 8909.

[24] N. Hosoda, T. Kato, *Chem. Mater.* **2001**, *13*, 688 – 693.

[25] A. Sugawara, T. Kato, *Chem. Commun.* **2000**, 487 – 488.

[26] S. Mann, G. A. Ozin, *Nature* **1996**, *382*, 313 – 318.

[27] J. Aizenberg, D. A. Muller, J. L. Grazul, D. R. Hamann, *Science* **2003**, *299*, 1205 – 1208.

[28] A. A. Zakhidov, R. H. Baughman, Z. Iqbal, C. X. Cui, I. Khayrullin, S. O. Dantas, I. Marti, V. G. Ralchenko, *Science* **1998**, *282*, 897 – 901.

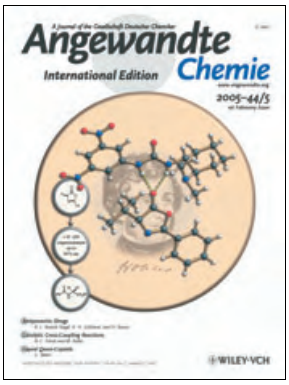
[29] a) A. R. Parker, R. C. McPhedran, D. R. McKenzie, L. C. Botten, N. A. P. Nicorovici, *Nature* **2001**, *409*, 36; b) S. Kinoshita, S. Yoshioka, K. Kawagoe, *Proc. R. Soc. London Ser. B* **2002**, *269*, 1417 – 1421.

[30] R. Giles, S. Manne, S. Mann, D. E. Morse, G. D. Stucky, P. K. Hansma, *Biol. Bull.* **1995**, *188*, 1 – 15.

[31] L. Addadi, S. Raz, S. Weiner, *Adv. Mater.* **2003**, *15*, 959 – 970.

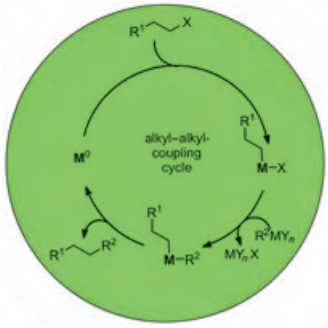
 © 2005 Wiley-VCH Verlag GmbH & Co. KGaA, Weinheim

Cover Picture

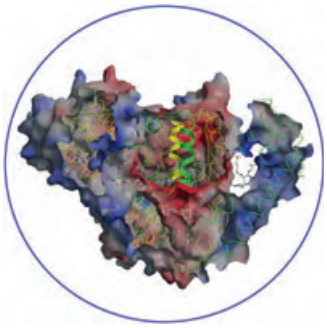


Albrecht Berkessel,* Felix Cleemann, Santanu Mukherjee, Thomas N. Müller, and Johann Lex

Ureas have come a long way from Wöhler's preparation of urea from ammonium cyanate in 1828 to the chiral ureas that play an important role in asymmetric organocatalysis today. In their Communication on page 807 ff. Berkessel et al. report the use of bifunctional urea-based organocatalysts for the highly enantioselective dynamic kinetic resolution of azlactones. The cover picture shows the hydrogen-bonded supramolecular aggregate formed from the urea catalyst and an azlactone substrate (graphic: K. Etzenbach-Effers).



Cross-Coupling Reactions
A. C. Frisch and M. Beller give an account of C–C bond-forming reactions that involve non-activated alkyl halides in their Minireview on page 674 ff.



Drug Research
New approaches in the search for antiparasitic drugs are based on enzyme inhibitors that suppress the antioxidative systems in the parasite. In their Review on page 690 ff., R. L. Krauth-Siegel, H. Bauer, and R. H. Schirmer describe the current trends in this field of research.



Prodrug Dendrimers
In their Communication on page 716 ff. D. Shabat et al. present the advantages of incorporating three drug molecules in the same prodrug platform to effectively allow triple drug therapy in a single molecule.

Contents

VIP ***The following Communications have been judged by at least two referees to be "very important papers" and will be published online at www.angewandte.org soon:***

Xuejun Liu, Gaosheng Chu, Robert A. Moss, Ronald R. Sauers,* Ralf Warmut*:*
Fluorophenoxycarbene Inside a Hemicarcerand: A Bottled Singlet Carbene

Silvio Aime, Carla Carrera, Daniela Delli Castelli, Simonetta Geninatti Crich, Enzo Terreno:*
Light-On/Light-Off of Cells Labeled with MRI-PARACEST Agents

Zulfiya Orynbayeva, Sofiya Kolusheva, Etta Livneh, Alexandra Lichtenshtein, Ilana Nathan, Raz Jelinek:*
Visualization of Membrane Processes in Living Cells by Surface-Attached Chromatic Polymer Patches

Gábor Bunkóczi, László Vértesy, George M. Sheldrick:*
The Antiviral Antibiotic Feglymycin: First Direct Methods Solution of a 1000+ Equal-Atom Structure

Dieter Enders, Christoph Grondal:*
Direct Organocatalytic de novo Synthesis of Carbohydrates

Tobias Fink, Heinz Bruggesser, Jean-Louis Reymond:*
Virtual Exploration of the Small-Molecule Chemical Universe Below 160 Daltons

News

Organometallic Chemistry: Le Bel Award to J.-P. Genêt ——— **668**

Supramolecular Chemistry: Süe Award to J.-P. Sauvage ——— **668**

Inorganic Chemistry: Franco-German Award to H. W. Roesky ——— **668**

Books

Chemical Structure, Spatial Arrangement — Peter J. Ramberg — *reviewed by M. Reggelin* ——— ***669***

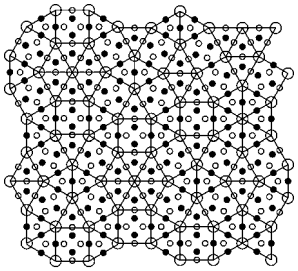
Highlights

Liquid Crystals

G. H. Mehl* ——— **672–673**

Quasi-Periodic Organization in Soft Self-Assembling Matter

Micelles made up of dendritic molecules can form a liquid quasi-crystalline phase. The phase structure (see picture) is characterized by a 12-fold symmetry, defying the rules of classical crystallography. The phase structure is assembled from only one set of building blocks, differentiating this system from metal alloys, in which at least two different types of atoms are required.

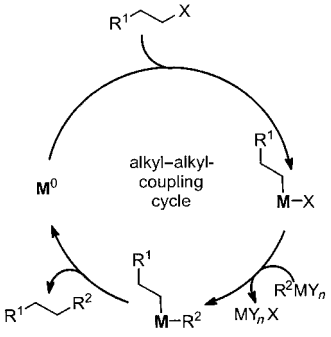


Minireviews

Cross-Coupling Reactions

A. C. Frisch, M. Beller* ——— **674–688**

Catalysts for Cross-Coupling Reactions with Non-activated Alkyl Halides

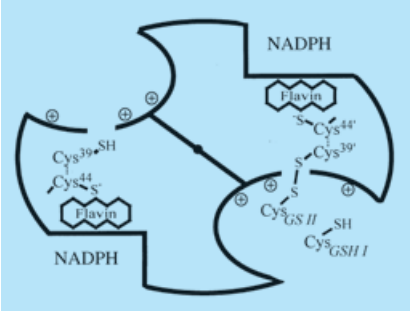


The trends and latest developments in metal-catalyzed cross-coupling reactions of alkyl halides are examined in an overview of this highly topical area of research. Mechanistic investigations have led to a variety of procedures for the selective cross-coupling of non-activated alkyl halides with a variety of organometallic nucleophiles under mild reaction conditions (see scheme).

© 2005 Wiley-VCH Verlag GmbH & Co. KGaA, Weinheim

Reviews

Parasitic diseases such as sleeping sickness, Chagas' disease, and malaria are widespread throughout the world, and there is an urgent need for affordable antiparasitic medication. An approach in the search for new drugs is based on the use of enzyme inhibitors that block the antioxidative pathways in the pathogens. The picture shows glutathione reductase from the malaria parasite *Plasmodium falciparum*.

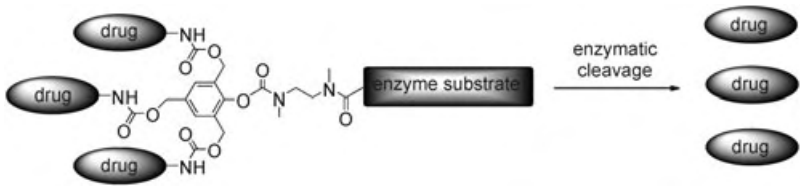


Drug Design

R. L. Krauth-Siegel,* H. Bauer, R. H. Schirmer* ——— 690 – 715

Dithiol Proteins as Guardians of the Intracellular Redox Milieu in Parasites: Old and New Drug Targets in Trypanosomes and Malaria-Causing Plasmodia

Communications

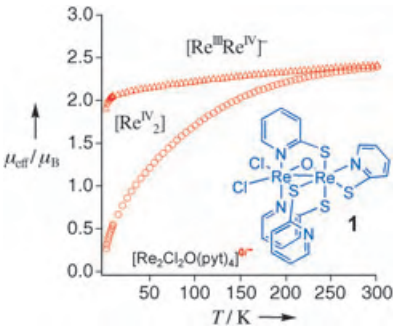


The knock-on effect of a single catalytic reaction by a specific enzyme on a prodrug platform initiates the sequential collapse of the whole array to release the active drug units (see scheme). Such a dendritic system may provide a means to improve selective chemotherapeutic approaches in cancer therapy.

Prodrug Dendrimers

K. Haba, M. Popkov, M. Shamis, R. A. Lerner, C. F. Barbas III, D. Shabat* ——— 716 – 720

Single-Triggered Trimeric Prodrugs



A thermally accessible triplet excited state: The dirhenium(IV) complex $[Re_2Cl_2O(pyt)_4]$ (**1**; Hpyt = pyridine-2-thiol) and its one-electron-reduced species were prepared and structurally characterized. Unique temperature-dependent magnetic behavior was observed for the Re^{IV}_2 species (see picture).

Temperature-Dependent Magnetism

K. Umakoshi,* N. Misasa, C. Ohtsu, T. Kojima, M. Sokolov, M. Wakeshima, Y. Hinatsu, M. Onishi* ——— 720 – 724

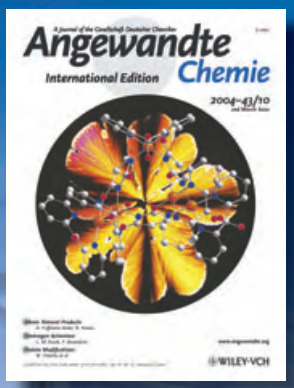
Unusual Magnetic Properties of the Edge-Sharing Bioctahedral Dirhenium(IV) Complex of Pyridine-2-thiolate

For the USA and Canada:
ANGEWANDTE CHEMIE International Edition (ISSN 1433-7851) is published weekly by Wiley-VCH PO Box 191161, D 69451 Weinheim, Germany. Air freight and mailing in the USA by Publications Expediting Inc. 200 Meacham Ave., Elmont, NY 11003. Periodicals postage paid at Jamaica NY 11431. US POSTMASTER: send address changes to *Angewandte Chemie*, Wiley-VCH, 111 River Street, Hoboken, NJ 07030. Annual subscription price for institutions: US$ 4948.00/4498.00 (valid for print and electronic / print or electronic delivery); for individuals who are personal members of a national chemical society, or whose institution already subscribes, or who are retired or self-employed consultants, print only: US$ 394.00. Postage and handling charges included. All Wiley-VCH prices are exclusive VAT.

 © 2005 Wiley-VCH Verlag GmbH & Co. KGaA, Weinheim

The best in chemistry –

for more than a hundred years



A Journal of the Gesellschaft Deutscher Chemiker

Angewandte International Edition Chemie

www.angewandte.org

1888: ***The beginning of a success story***

Constant Innovations

- **1962:** *First issue of the International Edition*
- **1976:** *Graphical abstracts*
- **1979:** *Cover pictures*
- **1988:** *Centenary of Angewandte*
- **1989:** *Routine use of color*
- **1991:** *New section: Highlights*
- **1992:** *Computerized editorial tracking system*
- **1995:** *Internet service for readers*
- **1998:** *Regular press service; full-text online*
- **2000:** *New section: Essays; EarlyView: Communications available online ahead of the printed version*
- **2001:** *New section: Minireviews*
- **2002:** *Online submission of manuscripts*
- **2003:** *Weekly publication; new section: News; new layout*
- **2004:** *Backfiles (1962-1997); ManuscriptXpress: Online system for authors and referees*



Angewandte's advisors...

J. Fraser Stoddart
University of California, Los Angeles

» *When it comes to informing myself, I have two weekly fixations. The Economist and* ***Angewandte Chemie****. Both are compulsive browsing and there are many articles in each that are essential reading. I simply cannot afford not to know what's in every issue of* ***Angewandte****. Being on the board of* ***Angewandte Chemie*** *has been a real pleasure. Whether or not it's true, I have the feeling that I have really been able to influence how some of the most creative chemistry in my time has been presented to the scientific community at large.* «

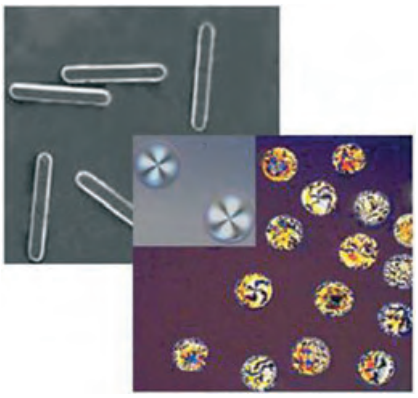
Angewandte Chemie International Edition *is a journal of the German Chemical Society (GDCh)*

GDCh

WILEY InterScience® DISCOVER SOMETHING GREAT

WILEY-VCH

1193140_gu

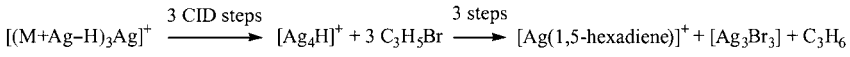


Small-scale engineering: A new strategy for the production of monodisperse colloid particles with precise control of their size, shape, and composition has been developed. Highly monodisperse liquid droplets are formed by using a microfluidic device. The droplets are shaped in a microchannel (spheres, disks, and rods; see images) and solidified in situ by either polymerization or thermal setting.

Particle Design

S. Xu, Z. Nie, M. Seo, P. Lewis, E. Kumacheva,* H. A. Stone, P. Garstecki, D. B. Weibel, I. Gitlin, G. M. Whitesides* ——— **724 – 728**

Generation of Monodisperse Particles by Using Microfluidics: Control over Size, Shape, and Composition

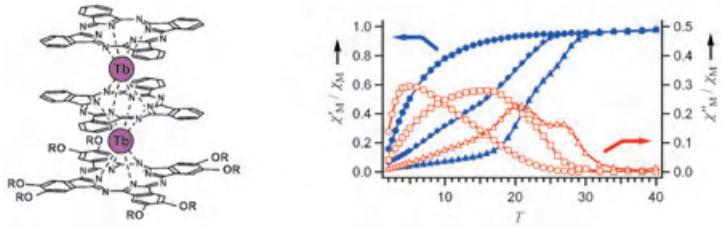


Collision-induced dissociation (CID) of silver–amino acid clusters results in the formation of the silver hydride cluster $[Ag_4H]^+$, which mediates C–C bond coupling of allyl bromide (see scheme). Energy-resolved CID experiments reveal that the product is 1,5-hexadiene and suggest analogies between the chemistry of the clusters and that of silver surfaces and nanoparticles.

Reactive Intermediates

G. N. Khairallah, R. A. J. O'Hair* ——— **728 – 731**

Gas-Phase Synthesis of $[Ag_4H]^+$ and Its Mediation of the C–C Coupling of Allyl Bromide

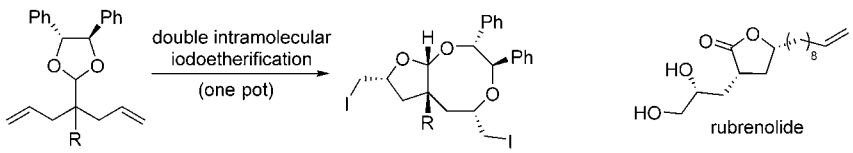


The sandwich complex tris(phthalocyaninato)diterbium with a coupled $4f^8$ system exhibits dynamic magnetic properties, which were clarified by means of alternating current magnetic susceptibility measurements on the bis-terbium and isostructural Tb–Y complexes (see picture, R = C_4H_9).

Single-Molecule Magnets

N. Ishikawa,* S. Otsuka, Y. Kaizu* ——— **731 – 733**

The Effect of the f–f Interaction on the Dynamic Magnetism of a Coupled $4f^8$ System in a Dinuclear Terbium Complex with Phthalocyanines



Tetrahydrofuran units with multiple chiral centers are formed in a highly diastereoselective manner through the one-pot double intramolecular haloetherification of σ-symmetric diene acetals (see scheme). The utility of the method was demonstrated by the short asymmetric synthesis of (+)-rubrenolide.

Asymmetric Synthesis

H. Fujioka,* Y. Ohba, H. Hirose, K. Murai, Y. Kita* ——— **734 – 737**

A Double Iodoetherification of σ-Symmetric Diene Acetals for Installing Four Stereogenic Centers in a Single Operation: Short Asymmetric Total Synthesis of Rubrenolide

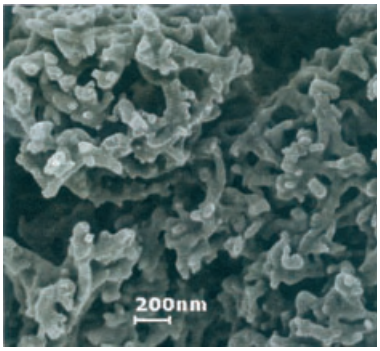
 © 2005 Wiley-VCH Verlag GmbH & Co. KGaA, Weinheim

Contents

Carbon Nitrides

M. H. V. Huynh,* M. A. Hiskey,*
J. G. Archuleta, E. L. Roemer ... 737 – 739

Preparation of Nitrogen-Rich Nanolayered, Nanoclustered, and Nanodendritic Carbon Nitrides



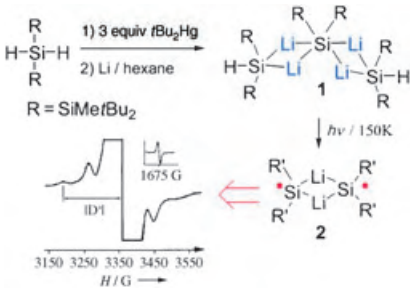
Only C and N atoms are present in the high-nitrogen compound 4,4′,6,6′-tetra-(azido)azo-1,3,5-triazine (TAAT), which is thus an ideal precursor for carbon nitrides. Controlled pyrolysis of TAAT afforded novel nitrogen-rich carbon nitrides in the form of nanolayers (C_2N_3), nanoclusters (C_3N_5), and nanodendrites (C_3N_5, see SEM image). The pyrolyses occur at low temperature and without applied pressure and require no vacuum systems, extraction, carbonization, or purification.

Radicals

D. Bravo-Zhivotovskii,* I. Ruderfer, S. Melamed, M. Botoshansky, B. Tumanskii, Y. Apeloig* ... 739 – 743

Nonsolvated, Aggregated 1,1-Dilithiosilane and the Derived Silyl Radicals

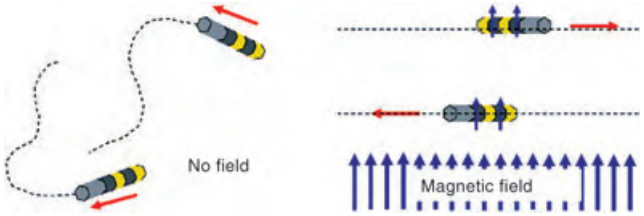
A triplet-state silyl biradical 2 and a family of silyl radicals, in which the silyl radical center is part of a silyllithium aggregate, are generated photochemically from the *gem*-dilithiosilane [$(R_2SiLi_2)(R_2HSiLi)_2$] (**1**, see scheme; R′: unknown). The EPR spectrum of **2** consists of four side lines from $\Delta M = 1$ transitions and a signal at half-field resulting from the forbidden $\Delta M = 2$ transitions.



Molecular Devices

T. R. Kline, W. F. Paxton, T. E. Mallouk, A. Sen* ... 744 – 746

Catalytic Nanomotors: Remote-Controlled Autonomous Movement of Striped Metallic Nanorods

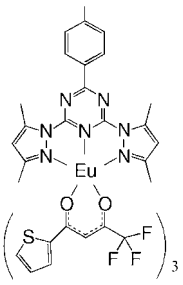


A move in the right direction: Micrometer-sized rods with Pt/Ni/Au/Ni/Au segments move autonomously with good directionality in the presence of a magnetic field when placed in aqueous hydrogen peroxide (see picture). The propulsive force results from an interfacial tension gradient generated by the catalytic decomposition of H_2O_2 at the Pt end while the orientation stems from the interaction of the magnetic field with the magnetized Ni segments.

Lanthanide Luminescence

L.-M. Fu, X.-F. Wen, X.-C. Ai, Y. Sun, Y.-S. Wu, J.-P. Zhang,* Y. Wang* ... 747 – 750

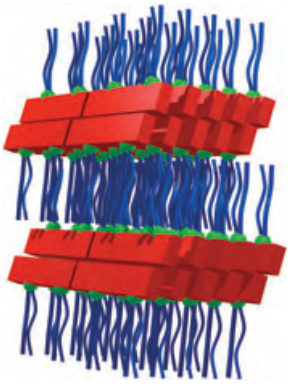
Efficient Two-Photon-Sensitized Luminescence of a Europium(III) Complex



1

Red emission ($\lambda_{em} = 614$ nm) from Eu^{III}, sensitized by two-photon absorption, has been demonstrated for the europium(III) complex [$Eu(tta)_3dpbt$] (**1**). A large two-photon-absorption cross section and a high luminescence efficiency of the europium complex ensure a high efficiency of two-photon sensitization.

© 2005 Wiley-VCH Verlag GmbH & Co. KGaA, Weinheim

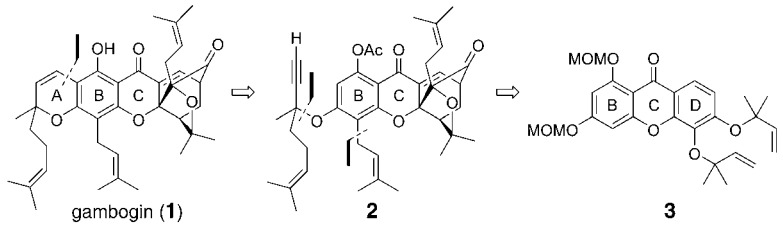


Functional and externally controllable electroactive nanostructures are obtained by an ionic self-assembly process. 2D rectangular columnar structures (see picture) comprising oligoanilines were prepared by complexation with double-tail phosphate surfactants. Upon heating, tetraaniline complexes show an order–disorder transition from this 2D phase structure to a disordered state as a reversible change in the electrical conductivity.

Oligoaniline Complexes

Z. Wei, T. Laitinen, B. Smarsly, O. Ikkala, C. F. J. Faul* ——— **751 – 756**

Self-Assembly and Electrical Conductivity Transitions in Conjugated Oligoaniline–Surfactant Complexes

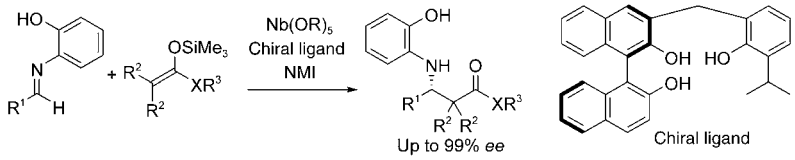


A significant rate acceleration of a Claisen rearrangement and of a Claisen/Diels–Alder reaction cascade sequence was observed in the presence of water. This reaction sequence was used in a total synthesis of gambogin (**1**) from a tricyclic dialkene **3** via **2**.

Natural Products Synthesis

K. C. Nicolaou,* H. Xu, M. Wartmann ——— **756 – 761**

Biomimetic Total Synthesis of Gambogin and Rate Acceleration of Pericyclic Reactions in Aqueous Media

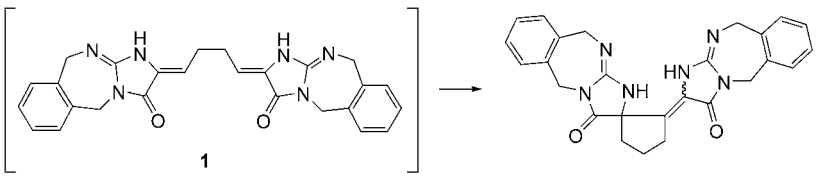


Two's company: By using a novel chiral ligand a dinuclear chiral niobium catalyst for highly enantioselective Mannich-type reactions was developed. Tridentate binol derivatives provide excellent asymmetric environments around the niobium atom, and the Mannich-type reactions proceeded smoothly in high yields with high enantioselectivities (see scheme; NMI = *N*-methylimidazole).

Asymmetric Catalysis

S. Kobayashi,* K. Arai, H. Shimizu, Y. Ihori, H. Ishitani, Y. Yamashita ——— **761 – 764**

A Novel Dinuclear Chiral Niobium Complex for Lewis Acid Catalyzed Enantioselective Reactions: Design of a Tridentate Ligand and Elucidation of the Catalyst Structure



The facile spirocyclization of tethered bisalkylidene **1** suggests a general synthetic strategy for preparing alkaloids of the palau'amine family. The development and characteristics of this core model system are discussed.

Natural Product Synthesis

H. Garrido-Hernandez, M. Nakadai, M. Vimolratana, Q. Li, T. Doundoulakis, P. G. Harran* ——— **765 – 769**

Spirocycloisomerization of Tethered Alkylidene Glycocyamidines: Synthesis of a Base Template Common to the Palau'amine Family of Alkaloids

 © 2005 Wiley-VCH Verlag GmbH & Co. KGaA, Weinheim

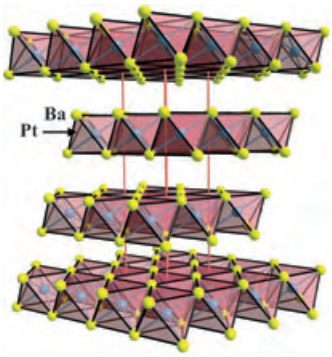
Contents

Platinum Anions

A. Karpov, U. Wedig, R. E. Dinnebier, M. Jansen* ——— **770 – 773**

Dibariumplatinide: $(Ba^{2+})_2Pt^{2-}\cdot 2e^-$ and Its Relation to the Alkaline-Earth-Metal Subnitrides

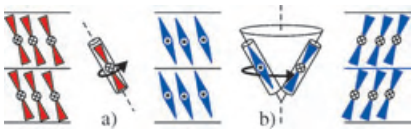
Solitary confinement: Ba_2Pt (see structure) which contains isolated platinide ions (Pt^{2-}) was synthesized from the elements, sealed in tantalum ampoules, at 1223 K in argon. In contrast to the related Cs_2Pt, the Ba compound contains excess electrons, which are responsible for its metallic behavior. The presence of isolated Pt^{2-} ions was confirmed by high resolution X-ray diffraction and by theoretical calculations.



Chirality Switching

R. Amaranatha Reddy, M. W. Schröder, M. Bodyagin, H. Kresse, S. Diele, G. Pelzl,* W. Weissflog ——— **774 – 778**

Field-Induced Switching of Chirality in Undulated Ferroelectric and Antiferroelectric SmCP Phases Formed by Bent-Core Mesogens



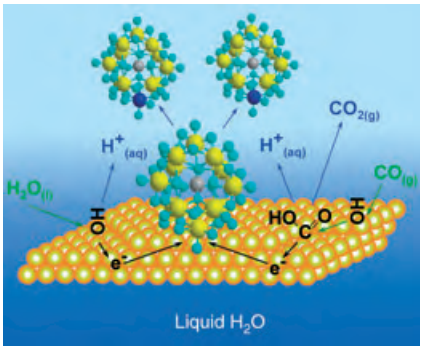
Switching signs: The polar structure of a tilted smectic C phase formed by a homologous series of bent-core mesogens changes from antiferroelectric to ferroelectric with increasing chain length. The polar switching of the banana-shaped molecules occurs by collective rotation around their long molecular axes (a) or by rotation of the director around the tilt cone (b). Red and blue designate layers of opposite chirality.

Heterogeneous Catalysis

W. B. Kim, T. Voitl, G. J. Rodriguez-Rivera, S. T. Evans, J. A. Dumesic* ——— **778 – 782**

Preferential Oxidation of CO in H_2 by Aqueous Polyoxometalates over Metal Catalysts

Stream cleaning: CO in CO/H_2 mixtures is oxidized preferentially at room temperature with an aqueous polyoxometalate (POM) solution over gold catalysts (see scheme). The rate of H_2 oxidation is slow and is inhibited by CO. This process can be used to remove CO efficiently from H_2 gas streams. The solution containing protons and reduced POM can be used to produce electrical energy at a fuel-cell anode through re-oxidation of the reduced POM.



Surface Chemistry

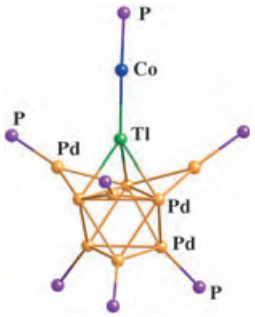
R. M. Jisr, H. H. Rmaile, J. B. Schlenoff* ——— **782 – 785**

Hydrophobic and Ultrahydrophobic Multilayer Thin Films from Perfluorinated Polyelectrolytes

Making contact: The hydrophobicity of the top layer of a multilayer thin film composed of polyelectrolytes and clay nanorods determines the contact angle of a water drop on the surface (see picture). The film is built up layer-by-layer on a silicon surface, thus enabling the surface properties to be readily modified by changing the polyelectrolyte used.



© 2005 Wiley-VCH Verlag GmbH & Co. KGaA, Weinheim

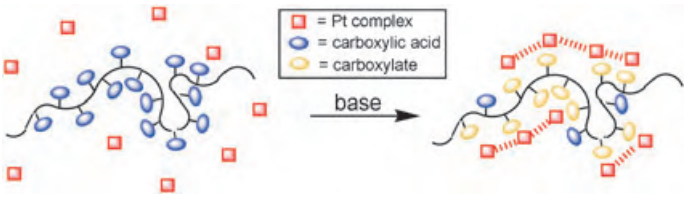


Easy come, easy go: The reaction of $[Pd_4(CO)_5L_4]$ and/or $[Pd_{10}(CO)_{12}L_6]$ ($L = PEt_3$) with $[TlCo(CO)_4]$ gives the title compound (see structure, CO and ethyl groups removed), in which the $[TlCo(CO)_4]$ reactant serves as a ligand (in its monosubstituted $[TlCo(CO)_3L]$ form). Temperature-dependent NMR spectroscopy indicates dynamic behavior involving the rapid reversible dissociation/association of the entire $[TlCo(CO)_3L]$ ligand.

Cluster Chemistry

E. G. Mednikov, C. G. Fry, L. F. Dahl* ——— 786 – 790

The First Trimetallic Pd/Tl/Co Carbonyl Cluster, Trigonal $[Pd_9\{\mu_3\text{-}TlCo(CO)_3L\}(\mu_2\text{-}CO)_6(\mu_3\text{-}CO)_3L_6]$: Ligand-Stabilization of the Trigonal-Bipyramidal $[TlCo(CO)_3L]$ Entity

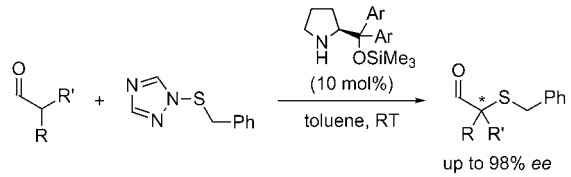


Deprotonation of polycarboxylic acids induces the self-assembly of terpyridylplatinum(II) complexes (see picture) and triggers remarkable changes in the UV/Vis spectra and emission intensities. The changes in the electronic spectra arise from metal-metal-to-ligand charge transfer transitions resulting from the aggregation of the complexes.

Noncovalent Interactions

C. Yu, K. M.-C. Wong, K. H.-Y. Chan, V. W.-W. Yam* ——— 791 – 794

Polymer-Induced Self-Assembly of Alkynylplatinum(II) Terpyridyl Complexes by Metal···Metal/π···π Interactions



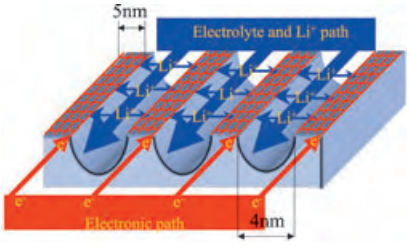
The facile elaboration of optically active α-sulfanyl-substituted aldehydes makes their direct preparation from unmodified aldehydes and 1-benzylsulfanyl-1,2,4-triazole particularly valuable. The substituted aldehydes are formed with excellent enantioselectivities in the presence of sterically demanding chiral pyrrolidine derivatives as organocatalysts (see scheme). R, R′ = H, alkyl, allyl, benzyl, Ph.

Asymmetric Catalysis

M. Marigo, T. C. Wabnitz, D. Fielenbach, K. A. Jørgensen* ——— 794 – 797

Enantioselective Organocatalyzed α Sulfenylation of Aldehydes

Current technology: A lithium-based storage device with both high power and high energy densities is formed by a nanocomposite composed of a framework of three-dimensional glass networks with uniform channels. The channels are filled by electrolyte solution and act as a lithium-ion path and the framework contains an electronic conductive oxide and therefore act as an electronic path (see picture).



Nanoporous Materials

H. Zhou,* D. Li, M. Hibino, I. Honma ——— 797 – 802

A Self-Ordered, Crystalline–Glass, Mesoporous Nanocomposite for Use as a Lithium-Based Storage Device with Both High Power and High Energy Densities

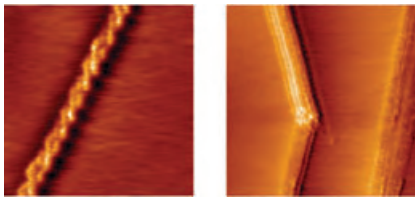
 © 2005 Wiley-VCH Verlag GmbH & Co. KGaA, Weinheim

Contents

Coordination Polymers

S. Novokmet, M. S. Alam, V. Dremov, F. W. Heinemann, P. Müller,* R. Alsfasser* ——— **803 – 806**

The Deposition of Metallopeptide-Based Coordination Polymers on Graphite Substrates: Effects of Side-Chain Functional Groups and Local Surface Structure

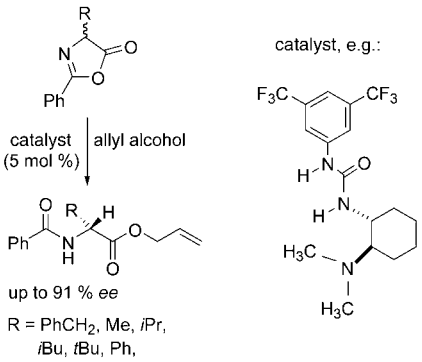


The surface dictates: The metallodipeptide complex $[\{Zn(Dpg\text{-}Tyr\text{-}O)\}_n]^{n+}$ (Dpg = dipicolylglycyl, Tyr = tyrosine) is a right-handed homochiral helical coordination polymer. Depending on the local structure of a pyrolytic graphite surface, it aggregates to form double-helical plaits (left) or two-dimensional assemblies of linearly stretched strands (right). The strands represent the first step in the formation of a three-dimensional crystal.

Asymmetric Organocatalysis

A. Berkessel,* F. Cleemann, S. Mukherjee, T. N. Müller, J. Lex ——— **807 – 811**

Highly Efficient Dynamic Kinetic Resolution of Azlactones by Urea-Based Bifunctional Organocatalysts



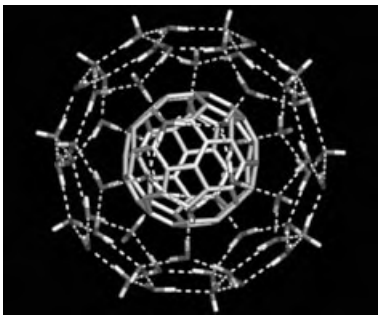
Novel tasks for a venerable molecule: Bifunctional organocatalysts of the type shown, with a quasi Lewis acidic urea or thiourea unit and a Brønsted basic amine functionality, effect the dynamic kinetic resolution of azlactones with high enantioselectivity. *N*-Benzoyl amino acid esters were obtained with up to 91 % *ee* in high yields from racemic azlactones.

Water Structures

R. Ludwig,* A. Appelhagen* ——— **811 – 815**

Calculation of Clathrate-Like Water Clusters Including H_2O-Buckminsterfullerene

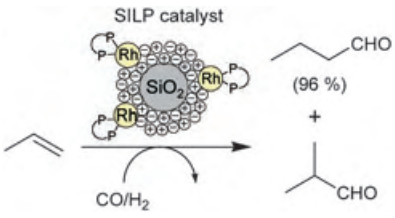
A true minimum structure, the buckminsterfullerene of water, $(H_2O)_{60}$, was studied by ab initio and density functional calculations of a total of seven water clusters. The water buckyball can be stabilized further by contact with large hydrophobic molecules such as the famous carbon analogue C_{60} (see picture).



Catalyst Development

A. Riisager,* R. Fehrmann, S. Flicker, R. van Hal, M. Haumann, P. Wasserscheid* ——— **815 – 819**

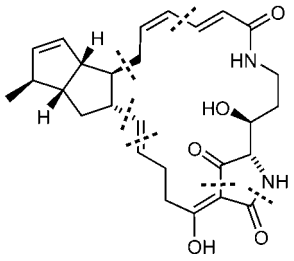
Very Stable and Highly Regioselective Supported Ionic-Liquid-Phase (SILP) Catalysis: Continuous-Flow Fixed-Bed Hydroformylation of Propene



The advantages of heterogeneous catalysis and transition-metal catalysis in ionic liquids are combined in rhodium bisphosphine catalysts in an ionic-liquid phase on a silica support. These active, regioselective, and highly stable catalysts were applied in a fixed-bed reactor for the continuous-flow gas-phase hydroformylation of propene.

© 2005 Wiley-VCH Verlag GmbH & Co. KGaA, Weinheim

Key steps in the convergent enantioselective synthesis of the cytotoxic natural product (see structural formula) are tandem Michael addition/electrophilic trapping reactions, Sonogashira coupling, Julia–Kocienski olefination, and macrocyclization. Formation of the tetramic acid completed the synthesis.



Natural Product Synthesis

N. Cramer, S. Laschat,* A. Baro, H. Schwalbe, C. Richter ——— **820 – 822**

Enantioselective Total Synthesis of Cylindramide

The issues for January 2005 appeared online on the following dates
Issue 1: December 15 · Issue 2: December 21 · Issue 3: December 29 · Issue 4: January 11

Sources

Product and Company Directory

You can start the entry for your company in "Sources" in any issue of *Angewandte Chemie*.

If you would like more information, please do not hesitate to contact us.

Wiley-VCH Verlag – Advertising Department
Tel.: 0 62 01 - 60 65 65
Fax: 0 62 01 - 60 65 50
E-Mail: MSchulz@wiley-vch.de

Service

Keywords ——— *824*

Authors ——— *825*

Angewandte's Sister Journals ——— *826*

Sources ——— *A5*

Preview ——— *827*

 © 2005 Wiley-VCH Verlag GmbH & Co. KGaA, Weinheim



J.-P. Genêt Receives Le Bel Award

Jean-Pierre Genêt of the Ecole Nationale Supérieure de Chimie de Paris (ENSCP) has been awarded the Prix Le Bel of the French Chemical Society (Société Française de Chimie, SFC) in recognition of his work on catalytic asymmetric hydrogenation. The results of his research have been implemented in the pharmaceutical and cosmetic industries. Genêt's research covers organometallic chemistry in general with a particular emphasis on homogeneous catalysis. Focal points are the design and application in organic synthesis of water-soluble organometallic complexes, the synthesis of chiral phosphines, and asymmetric catalysis, as well as the development of new reactions in organic synthesis, and the asymmetric synthesis of biomolecules. He recently reported in *Angewandte Chemie* on a tandem reaction consisting of a 1,4-addition and enantioselective protonation under rhodium catalysis as an efficient route to α-amino acids.[1]



J.-P. Genêt

Genêt studied chemistry at the Université Pierre et Marie Curie in Paris and completed his PhD in 1972 under the guidance of J. Ficini on the reactivity of ynamines. After postdoctoral studies on the synthesis of ibogamine at the University of Wisconsin (USA) in the research group of B. M. Trost, he returned to the Université Pierre et Marie Curie, at first as assistant professor, and from 1980 as Professor of Organic Chemistry. In 1988 he additionally became professor at the ENSCP, and since 1989 has also been CNRS (Centre national de la recherche scientifique) Director of Research. Since 1992 he has directed the Department of Organic and Bioorganic Chemistry of the ENSCP. From 1994 to 1998 he was a member of the council of the French Ministry of Education and president of the organic division of the SFC.

Süe Award to J.-P. Sauvage

Jean-Pierre Sauvage (Université Louis Pasteur, Strasbourg) has been recognized by the SFC with the Prix Süe for his work on chemical topology and supramolecular chemistry. Sauvage studied at the Ecole Nationale Supérieure de Chimie de Strasbourg (France) and completed his PhD in 1971 under the direction of the Nobel laureate J.-M. Lehn. He then joined the CNRS and from 1973 to 1974 carried out postdoctoral research with M. L. H. Green in Oxford (UK). In 1981 he became professor at the Université Louis Pasteur in Strasbourg, and since 1988 has simultaneously been CNRS director of research. He has received many awards, including the Prelog Medal in Gold of the ETH Zürich (Switzerland) and the Centenary Lectureship of the Royal Society of Chemistry (UK). Sauvage is a member of the French Academy of Sciences.



J.-P. Sauvage

Sauvage's research focuses on chemical topology with transition metals as templates, electron and energy transfer in supramolecular multicomponent systems that incorporate transition metals and porphyrins, and the development of molecular motors from transition-metal-containing catenanes and rotaxanes. In his most recent Communication in *Angewandte Chemie* he reported on the synthesis of a topologically chiral molecule in the form of a trefoil knot.[2]

Franco-German Award to H. Roesky

Herbert W. Roesky (Universität Göttingen) has been awarded the Franco-German Award of the SFC. The award recognizes not only Roesky's research on a broad range of topics in inorganic chemistry, including organometallic chemistry,[3a,b] catalysis, and the development of precursors for vapor deposition, but also his commitment to science education. Roesky is well known for his extraordinary lectures in which he performs spectacular chemistry experiments.[3c,d]

Roesky completed his PhD in 1963 in the research group of O. Glemser in Göttingen (Germany) and then undertook postdoctoral research with E. L. Mutterties in Delaware (USA). He completed his habilitation in 1967 in Göttingen and accepted a position in 1971 at the Universität Frankfurt am Main (Germany). In 1980 he returned as Professor of Inorganic Chemistry to the Universität Göttingen. Roesky has received numerous distinctions. He is a foreign member of the French Academy of Sciences and recipient of the Literature Prize of the Fonds der Chemischen Industrie and the Alfred Stock Memorial Prize of the German Chemical Society (Gesellschaft Deutscher Chemiker).



H. Roesky

[1] L. Navarre, S. Darses, J.-P. Genêt, *Angew. Chem.* **2004**, *116*, 737; *Angew. Chem. Int. Ed.* **2004**, *43*, 719.

[2] L.-E. Perret-Aebi, A. von Zelewsky, C. Dietrich-Buchecker, J.-P. Sauvage, *Angew. Chem.* **2004**, *116*, 4582; *Angew. Chem. Int. Ed.* **2004**, *43*, 4482.

[3] a) Y. Peng, H. Fan, V. Jancik, H. W. Roesky, R. Herbst-Irmer, *Angew. Chem.* **2004**, *116*, 6316; *Angew. Chem. Int. Ed.* **2004**, *43*, 6190; b) V. Jancik, H. W. Roesky, D. Neculai, A. M. Neculai, R. Herbst-Irmer, *Angew. Chem.* **2004**, *116*, 6318; *Angew. Chem. Int. Ed.* **2004**, *43*, 6192; c) H. W. Roesky, K. Möckel, *Chemical Curiosities*, VCH, Weinheim, **1996**; d) H. W. Roesky, *Chemie en Miniature*, Wiley-VCH, Weinheim, **2001**.

 © 2005 Wiley-VCH Verlag GmbH & Co. KGaA, Weinheim DOI: 10.1002/anie.200463011

Liquid Crystals

Quasi-Periodic Organization in Soft Self-Assembling Matter

*Georg H. Mehl**

Keywords:
dendrimer · liquid crystals · micelles · quasi-crystals · self assembly

The correlation between chemical structure and physical properties in the condensed state has been one of the main research themes of organic materials chemistry. Great success in the basic understanding and in the development of systems for technological applications has been achieved for soft self-assembling materials of which lyotropic compounds (e.g. lipid-water, soap-water), a range of block copolymers, and thermotropic liquid crystals are examples.[1,2]

Materials self-assemble into bulk phases with lattices having periodicities in the range of a few nanometers, typically found for thermotropic low-molar-mass liquid crystals, to hundreds of nanometers for block copolymers. The structures (owing to positional long-range order) of these systems can be one-dimensional (lamellar phases), two-dimensional (columnar phases), or three-dimensional (micellar or bicontinuous phases) and their symmetry can be described by one of the 17 plane groups or 230 space groups of classical crystallography.

This self-assembly behavior is a function of the anisotropy of molecular shape, the degree of the amphiphilic character, and often the presence of additional noncovalent interactions (e.g. hydrogen bonding, van der Waals interactions). For liquid crystals the hyperpolarizability of aromatic groups in either rod- (calamitic) or disc-shaped (discotic) molecules implies an attractive force that is important for the phase formation, whereas for block copolymers, in the absence of favorable interactions, nanosegregation of incompatible parts tends to be the dominant feature for the phase formation.[3]

The extension of the precision of organic synthetic methods previously associated with small molecules to polymers and dendrimers in recent years and the advances in analytical techniques (e.g. MALDI-TOF mass spectrometry, small angle X-ray diffraction) has advanced greatly the understanding of systems placed between polymers and low-molar-mass liquid crystals.[4] These improvements have allowed the investigation of a series of systems where the phase behavior typically associated for rod-shaped molecules has been observed for plate-containing molecules; perforated lamellar or bicontinuous (mesh) phase behavior which is usually found for copolymers or lyotropic systems has been detected in polyphilic thermotropic liquid-crystal systems.[5] The formation of micellar super structures in rod-shaped and a range of wedge-shaped dendrons (tapered molecules) has furthered considerably the understanding of the correlation between chemical structure and physical properties.[5,6]

In this context the report by Zeng et al. on the observation of the first liquid quasi-crystal structure formed by micellar systems which are made up of mesomorphic dendrons (Figure 1) constitutes a major step forward.[7]

The structure of the reported system is characterized by the periodic stacking of nonperiodic planes (nonperiodic plane: the plane is tiled without gaps by two sets of tiles in a nonperiodic manner; the classical crystallographic rules cannot be applied). The quasi-periodic ordering of the planes is determined by a 12-fold rotational symmetry. A diffraction pattern of a sample aligned parallel to the 12-fold rotational-symmetry axis and a model of the structure of the nonperiodic plane is shown in Figure 2.[8]

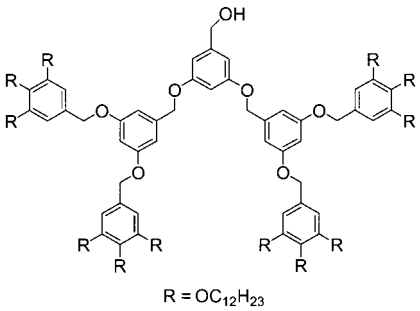


Figure 1. Structure of the mesomorphic dendron.

Arguably the most well known examples of models for the nonperiodic tiling of planes are based on the Penrose tiles of oblate and prolate rhombi with a tenfold symmetry.[9] Since the discovery of the first quasi-crystals in an aluminum–manganese phase twenty years ago, numerous systems have been discovered in metal alloys.[10,11]

The importance of the report of Zeng et al.[7] is on several levels. For metal systems quasi-crystalline behavior has to date only been observed for alloys containing two, and in most cases, three different types of metal atoms, of which at least one is a transition-metal atom. In the organic system, the micelles, which are the crystallographic equivalent of the atoms, though 10^3–10^4 larger in molecular mass than single atoms, are

[*] Dr. G. H. Mehl
Department of Chemistry
University of Hull
Hull HU6 7RX (UK)
Fax: (+44) 1482-466-411
E-mail: g.h.mehl@hull.ac.uk

 © 2005 Wiley-VCH Verlag GmbH & Co. KGaA, Weinheim DOI: 10.1002/anie.200461639

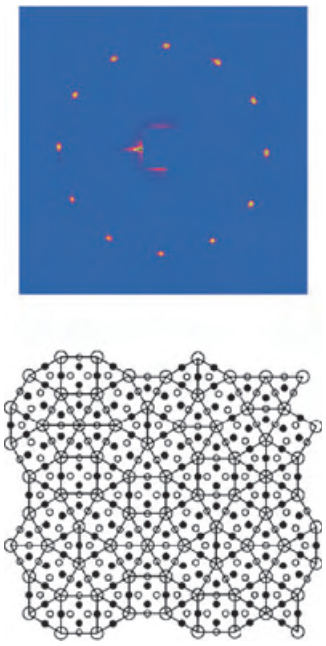


Figure 2. Top: diffraction pattern parallel to the 12-fold rotational axis; bottom: model of the nonperiodic tiling of a plane, each circle represents a micelle, different shading and size indicates a different crystallographic environment.

made up of one type of mesomorphic dendron. A variation in the self-assembly structure in the packing of the aromatic and aliphatic groups in the micelles allows for the quasi-periodic tiling. This situation means, that the particular mode of the soft self-assembly behavior of the system allows for a global minimization of the free energy of the whole system at a cost for some micelles.[12] The subtle interplay between the van der Waals interactions of the aromatic groups, the wedge structure of the dendrons, and the size of the alkyl chains is the basis for this self-assembly behavior.

Viewed in a wider context, the observed nonperiodic tiling of planes (2D nonperiodicity) is only one of the possibilities to tile space nonperiodically. Experimental evidence of one-dimensional and three-dimensional quasi-crystalline tiling has been reported and furthermore, for metal alloys nonperiodic planes with an eightfold and tenfold symmetry have been found.[11] From the results by Zeng et al. and the other work in this field, it can be estimated, that further investigations should yield more liquid quasi-crystal systems.

On heating, the reported liquid quasi-crystal (LQC) system shows the phase sequence, LQC$\rightarrow Pm\bar{3}n \rightarrow P4_2/mmm \rightarrow$ *bcc*$\rightarrow$isotropic, which suggests that the LQC phase is of lower energy than the $Pm\bar{3}n$ and the *bcc* (body centered cubic) phases.[7] As to date these two phase structures have been associated strongly with the optimal solutions for the Kelvin problem (the question of the minimum surface area per bubble in an ultimate equilibrium dry foam), the investigation of liquid quasi-crystals may have importance well beyond the limits of liquid crystal research.[12,13]

Published Online: December 21, 2004

[1] *Handbook of Liquid Crystals* (Eds.: D. Demus, J. W. Goodby, G. W. Gray, H.-W. Spiess, V. Vill), Wiley-VCH, Weinheim, **1998**.

[2] a) R. Stadler, C. Auschara, J. Beckmann, U. Krappe, I. Voigt-Martin, L. Leibler, *Macromolecules* **1995**, *28*, 3080; b) I. W. Hamley, *The Physics of Block Copolymers*, Oxford University Press, Oxford, **1998**.

[3] a) C. Tschierske, *J. Mater. Chem.* **1998**, *8*, 1485; b) Note: owing to the size of the polymers the entropy gain of mixing is small and cannot compensate for the concurrent enthalpy loss, hence the formation of segregated structures.

[4] G. R. Newkome, C. N. Moorefield, F. Vögtle, *Dendrimers and Dendrons*, Wiley-VCH, Winheim, **2001**.

[5] Examples: a) X. H. Cheng, M. Prehm, M. K. Das, L. Kain, U. Baumeister, S. Diele, D. Leine, A. Blume, C. Tschierske, *J. Am. Chem. Soc.* **2003**, *125*, 10977, and references therein; b) M. Marcos, R. Giménez, J. L. Serrano, B. Donnio, B. Heinrich, D. Guillon, *Chem. Eur. J.* **2001**, *7*, 1006, and references therein; c) P. H. J. Kouwer, G. H. Mehl, *Angew. Chem.* **2003**, *115*, 6197; *Angew. Chem. Int. Ed.* **2003**, *42*, 6015; d) review: M. Lee, B.-K. Cho, W.-C. Zin, *Chem. Rev.* **2001**, *101*, 2869; e) H.-A. Klok, S. Lecommendoux, *Adv. Mater.* **2001**, *13*, 1217.

[6] Examples: a) V. S. Belagurasamy, G. Ungar, V. Percec, G. Johansson, *J. Am. Chem. Soc.* **1997**, *119*, 1539; b) R. M. Richardson, S. A. Ponomarenko, N. I. Boiko, V. P. Shibaev, *Liq. Cryst.* **1999**, *26*, 101; c) T. Kato, T. Matsuoka, M. Nishii, Y. Kamikawa, K. Kamie, E. Yashima, S. Ujie, *Angew. Chem.* **2004**, *116*, 2003; *Angew. Chem. Int. Ed.* **2004**, *43*, 1969; d) M. R. Leduc, W. Hayes, J. M. J Frêchet, *J. Polym. Sci. Part A* **1998**, *36*, 1; e) M. Suarez, J. M. Lehn, S. C. Zimmermann, A. Skouilos, B. Heinrich, *J. Am. Chem. Soc.* **1998**, *120*, 9526; f) E. R. Zubarev, M. U. Pralle, E. D. Sone, S. I. Stupp, *J. Am. Chem. Soc.* **2001**, *123*, 4105.

[7] X. Zeng, G. Ungar, Y. Liu, V. Percec, A. E. Dulcey, J. K. Hobbs, *Nature* **2004**, *428*, 157.

[8] The diffractogram and the model of the aperiodic tiling of the plane in a 12-fold symmetry are courtesy of Prof. G. Ungar, Sheffield.

[9] a) B. Grünbaum, G. C. Shepard, *Tilings and Patterns*, Freeman, New York, **1987**; b) P. J. Steinhardt, H.-J. Jeong, K. Saitoh, M. Tanaka, E. Abe, A. P. Tsai, *Nature*, **1998**, 396, 55; c) R. Penrose, *Bull. Inst. Math. Appl.* **1974**, *10*, 266.

[10] D. Shechtman, I. Blech, D. Gratias, J. W. Cahn, *Phys. Rev. Lett.* **1984**, *53*, 1951.

[11] Recent review: E. Berlin-Ferre, V. Demange, J. M. Dubois, *Crystallogr. Rev.* **2004**, *10*, 111, and references therein.

[12] G. Ungar, Y. Liu, V. Percec, W.-K. Cho, *Science* **2003**, *299*, 1208.

[13] *The Kelvin Problem: Foam Structures of Minimal Surface Area* (Ed.: D. Weaire), Taylor & Francis, London, **1997**.

 © 2005 Wiley-VCH Verlag GmbH & Co. KGaA, Weinheim

Cross-Coupling Reactions

Catalysts for Cross-Coupling Reactions with Non-activated Alkyl Halides

*Anja C. Frisch and Matthias Beller**

Keywords:
alkyl halides · β-hydride elimination · cross-coupling · nickel · palladium

Despite the problems inherent to metal-catalyzed cross-coupling reactions with alkyl halides, these reactions have become increasingly important during the last few years. Detailed mechanistic investigations have led to a variety of novel procedures for the selective cross-coupling of non-activated alkyl halides bearing β hydrogen atoms with a variety of organometallic nucleophiles under mild reaction conditions. This Minireview highlights selected examples of metal-catalyzed coupling methods and is intended to encourage chemists to exploit the potential of these approaches in organic synthesis.

1. Introduction

C–C coupling reactions are among the most important transformations in organic synthesis, as they make it possible to build up complex structures from readily available components in diverse ways. As a result of the development of a large number of metal-catalyzed coupling reactions of various C–X-containing compounds (X = Cl, Br, I, OTf, OMs, N_2^+, etc.; Tf = trifluoromethanesulfonyl, Ms = methanesulfonyl) over the last three decades, efficient methods are now available for the direct formation of bonds between of sp^3-, sp^2-, and sp-hybridized carbon atoms.[1]

Not all C–C coupling reactions have been thoroughly examined and developed. The intensively used reactions with aryl and vinyl electrophiles play a prominent role in organic synthesis because of the ready availability of substrates, their general applicability, and their high selectivities (comparatively simple oxidative addition, no β-hydride elimination). The relatively mild reaction conditions of such processes, as well as the high tolerance of functional groups under palladium, nickel, and copper catalysis, contributed substantially to the advancement of these reactions and paved the way for their abundant use in natural product syntheses.[2]

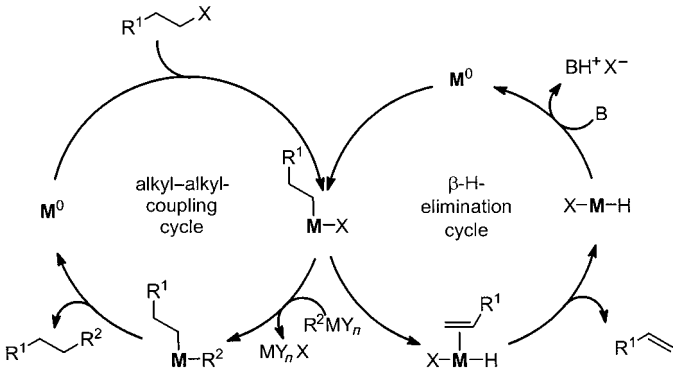
[*] Dr. A. C. Frisch, Prof. Dr. M. Beller
Leibniz-Institut für Organische Katalyse
Universität Rostock e.V.
Buchbinderstrasse 5–6, 18055 Rostock (Germany)
Fax: (+49) 381-466-9324
E-mail: matthias.beller@ifok.uni-rostock.de

Furthermore, numerous metal-catalyzed cross-coupling reactions are applied in the industrial synthesis of fine and agrochemicals, pharmaceuticals, and polymers.[3]

Alkyl halides R_{alkyl}–X, especially those with β hydrogen atoms, represent a more difficult class of electrophiles for cross-coupling reactions than the corresponding vinyl or aryl halides. Although industrial processes that involve the activation of methyl iodide or 2-chloroacetates are well known (e.g. acetic acid and malonic ester synthesis), until recently no efficient and general metal-catalyzed cross-coupling methodologies existed for non-activated alkyl electrophiles (i.e. compounds with β hydrogen atoms).[4] The reluctance of these compounds to undergo oxidative addition and their tendency to participate in competitive side reactions (elimination, hydrodehalogenation) were the largest hurdles in the development of selective cross-coupling reactions with alkyl halides. A new era of cross-coupling methodology dawned when pioneering work by Kochi and Tamura[5] in the 1970s and by Suzuki and co-workers[6] and Knochel and co-workers[7] in the 1990s proved the general feasibility of metal-catalyzed cross-coupling reactions with non-activated alkyl halides.

A simplified general catalytic cycle for metal-catalyzed cross-coupling reactions with alkyl halides is shown in Scheme 1. The underlying mechanism involves the usual sequence of oxidative addition to a coordinatively unsaturated metal complex, transmetalation of the organometallic nucleophile to the catalyst species, and reductive elimination of the functionalized alkane. As the C(sp^3)–X bond in alkyl halides is more electron rich than the C(sp^2)–X bond in aryl and vinyl halides, the propensity of alkyl halides to undergo oxidative addition to a low-valent transition-metal complex (i.e. formal reduction of C(sp^3)–X) is much lower than that of aryl and vinyl halides. The resulting alkyl–metal complex is

 © 2005 Wiley-VCH Verlag GmbH & Co. KGaA, Weinheim DOI: 10.1002/anie.200461432



Scheme 1. Postulated mechanism of the alkyl–alkyl cross-coupling and the β-H elimination as a side reaction.

highly reactive owing to the absence of stabilizing electronic interactions with the metal d orbitals. The fast and thermodynamically favored β-hydride elimination leads to the predominant formation of olefinic by-products with most catalyst systems. The relatively slow reductive elimination of the cross-coupling product from the catalyst (aryl–aryl > aryl–alkyl > alkyl–alkyl) makes side reactions even more likely. Therefore, the design of new, more active catalyst systems and the development of suitable reaction conditions for cross-coupling reactions of alkyl halides have generally been aimed at facilitating the oxidative-addition and reductive-elimination steps and preventing the competing β-hydride elimination.

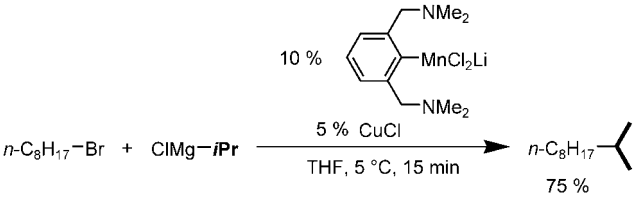
In the last three years, the development of cross-coupling reactions of alkyl halides with β hydrogen atoms has undergone remarkable progress. A variety of highly selective and practicable transition-metal-catalyzed methods have been introduced. Herein the most important recent developments in this area are summarized to provide the reader with a concise overview of the impressive scope of these methods. Emphasis is placed on direct cross-coupling reactions of organometallic nucleophiles with non-activated alkyl halides and related electrophiles in the presence of metal catalysts. Reactions of activated[4] alkyl halides, electrochemically initiated coupling reactions, and reactions with stoichiometric quantities of the metal reagent are not treated.[8] The reaction classes are organized by nucleophile type; in schemes and tables the nucleophilic component is shown in **bold**.

2. Cross-Coupling with Alkyl Nucleophiles

2.1. Alkyl–MgX (Kumada Coupling)

In the early 1970s, Kochi and Tamura reported on a series of kinetic and thermodynamic investigations into cross-coupling reactions with alkyl halides.[5] Subsequently, individual examples of metal-catalyzed coupling reactions with primary alkyl halides were published, although yields were modest and no general applications were demonstrated.[9] The first, if controversial, preparative work on the cross-coupling of alkyl iodides with alkyl Grignard reagents was reported by Castle and Widdowson in 1986.[10] Primary and secondary alkyl iodides were shown to react with alkyl magnesium bromides in the presence of [Pd(dppf)] (formed in situ from [$PdCl_2$(dppf)] and diisobutylaluminum hydride (DIBAL); dppf = 1,1′-bis(diphenylphosphanyl)ferrocene) in very good yields. Later these results were called into question by Scott and co-workers, who observed predominant reductive dehalogenation under identical conditions.[11]

In 1998, van Koten, Cahiez, and co-workers described the coupling of primary, secondary, and tertiary alkyl magnesium chlorides with *n*-alkyl bromides in the presence of a Mn/Cu catalyst mixture (Scheme 2). The reaction seems to involve



Scheme 2. Manganese-catalyzed coupling (van Koten and co-workers).

transmetalation to give a heteroleptic diorganomanganese compound, which undergoes efficient coupling at 5 °C within 15 min in the presence of copper catalysts. α-Branched alkyl bromides, which are not suitable substrates for purely manganese-[12] or copper-catalyzed[13] reactions, can be coupled by applying the Mn/Cu protocol.[14]

Cahiez et al. reported an improved copper-catalyzed Kumada protocol with alkyl halides in 2000 (Scheme 3). In the presence of Li_2CuCl_4 (3 mol %), functionalized alkyl

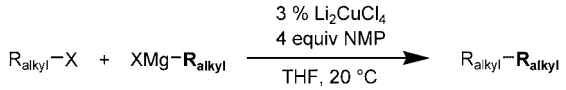


Anja C. Frisch was born in Fürth/Bayern (Germany) in 1972. She studied chemistry at the nearby Universität Erlangen-Nürnberg and completed her degree with a research project in the group of J. A. Gladysz at the University of Utah (USA) on complexes of transition-metal-capped carbon chains. After a six-month industrial placement at Merck in Darmstadt (Germany), she joined the research group of M. Beller in Rostock. She completed her PhD thesis on palladium catalysts for cross-coupling reactions in late 2003 and is currently undertaking postdoctoral research in Scotland.



Matthias Beller was born in Gudensberg (Germany) in 1962. He completed his PhD in 1989 at the Georg-August-Universität in Göttingen under the guidance of L.-F. Tietze, then carried out postdoctoral research with K. B. Sharpless at the Massachussetts Institute of Technology (USA). After working at Hoechst AG from 1991 to 1995, he moved to the Technische Universität München as Professor of Inorganic Chemistry. In 1998, he relocated to the University of Rostock to head the Leibniz Institute for Organic Catalysis (IfOK). He is head of the German Catalysis Competence Network ("Connecat").

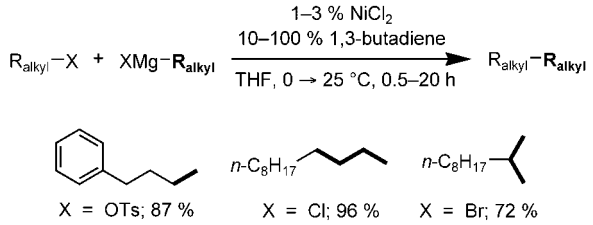
 © 2005 Wiley-VCH Verlag GmbH & Co. KGaA, Weinheim



Scheme 3. Copper-catalyzed cross-coupling (Cahiez and co-workers).

bromides react in good yields at room temperature. Key to success was the use of the solvent *N*-methylpyrrolidinone (NMP), which greatly accelerates the coupling reaction and thus prevents possible side reactions. However, secondary and tertiary halides, as well as the commercially more attractive alkyl chlorides, proved to be unreactive.[15]

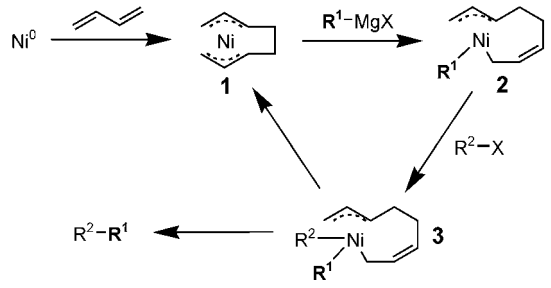
As an extension of the protocol developed by Kumada and co-workers[16] as well as Corriu and Masse[17] for nickel-catalyzed cross-coupling with Grignard reagents, Kambe and co-workers reported similar reactions of alkyl bromides, chlorides, and tosylates in 2002 (Scheme 4).[18] Interestingly,



Scheme 4. Nickel–butadiene catalyst in Kumada cross-coupling reactions (Kambe and co-workers). Ts = toluenesulfonyl.

the addition of 1,3-butadiene instead of phosphine ligands proved necessary to stabilize the active catalyst and accelerate the reductive elimination of the product. With alkyl bromides and tosylates, the products were obtained in almost quantitative yield at 0 °C in the presence of $NiCl_2$ (1–3 mol %) and butadiene (10–100 mol %). In the absence of a diene, reduction and/or elimination of the electrophile were mainly observed.

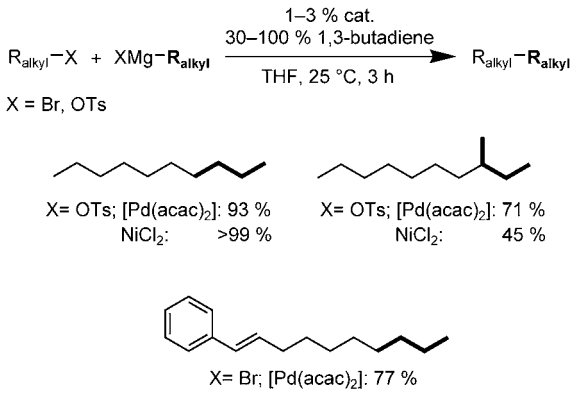
The postulated mechanism of the reaction is shown in Scheme 5. The actual catalyst **1** results from the reduction of $NiCl_2$ with R^1MgX and subsequent reaction of the Ni^0 formed with 2 equivalents of 1,3-butadiene. This catalyst is unreactive towards R^2X and undergoes transmetalation with R^1MgX to form the anionic alkyl nickel(II) complex **2**. Subsequent alkylation with R^2X and reductive elimination give the cross-coupled alkane product with regeneration of the active



Scheme 5. Mechanism postulated by Kambe and co-workers for the nickel-catalyzed Kumada coupling.

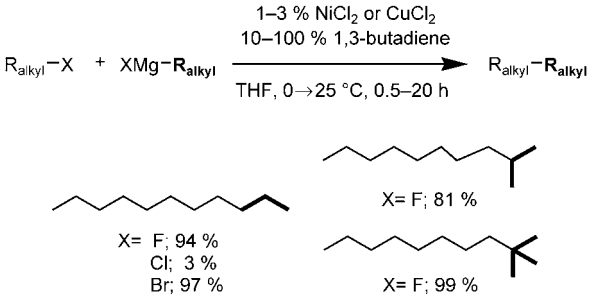
catalyst. The postulation of a Ni^{IV} intermediate, however, contradicts the mechanistic interpretations of similar nickel-catalyzed cross-coupling reactions with aryl or vinyl halides.

In 2003, Kambe and co-workers also reported the palladium-catalyzed coupling of alkyl tosylates and bromides with alkyl magnesium reagents in the presence of 1,3-butadiene and $[Pd(acac)_2]$ (Scheme 6).[19] The palladium catalyst[20] exhibited higher chemoselectivity for tosylates



Scheme 6. Palladium- or nickel-catalyzed variant of the Kumada coupling (Kambe and co-workers). acac = acetylacetonate.

and led to significantly improved yields with secondary alkyl magnesium compounds.[19] In the same year, nickel- and copper-catalyzed alkyl–alkyl coupling reactions with otherwise unreactive alkyl fluorides were reported to proceed under similar reaction conditions (Scheme 7). The best



Scheme 7. Alkyl fluorides in Kumada cross-coupling reactions.

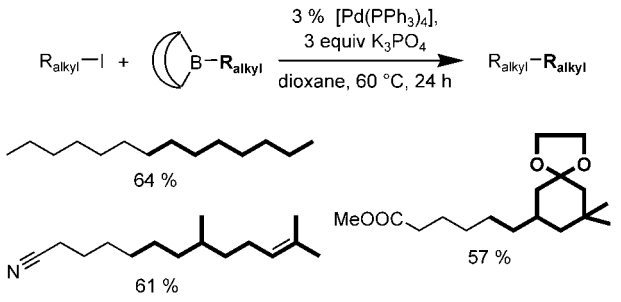
reactivities were found in the presence of $CuCl_x$ (3 mol %; $x = 1,2$) and 1,3-butadiene (20 mol %) additives. Surprisingly, the reactivities of the alkyl halides increased in the order Cl < F < Br, a trend that can not be explained by the bond energies of the alkyl halides and the magnesium salts formed.[21]

2.2. Alkyl–BX_2 (Suzuki–Miyaura Coupling)

In 1992, Suzuki and co-workers reported the first palladium-catalyzed alkyl–alkyl cross-coupling of primary alkyl iodides with alkyl boranes and thereby paved the way for the development of this general method.[6] In the presence of

 © 2005 Wiley-VCH Verlag GmbH & Co. KGaA, Weinheim

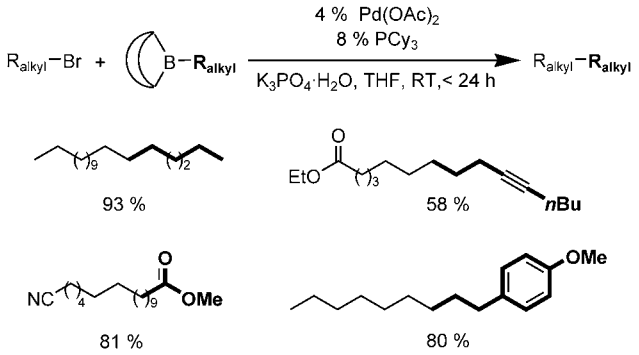
$[Pd(PPh_3)_4]$ (3 mol%) and K_3PO_4 (3 equiv) as a base, cross-coupling reactions of functionalized nucleophiles R_{alkyl}–9-BBN were effected in moderate yields (< 64%; 9-BBN = 9-borabicyclononane; Scheme 8). A variety of functional



Scheme 8. Suzuki coupling with alkyl iodides.

groups are tolerated, and β-hydride elimination is largely suppressed. However, significant hydrodehalogenation of the electrophile is observed, and neither alkyl bromides nor secondary alkyl iodides react under these conditions.

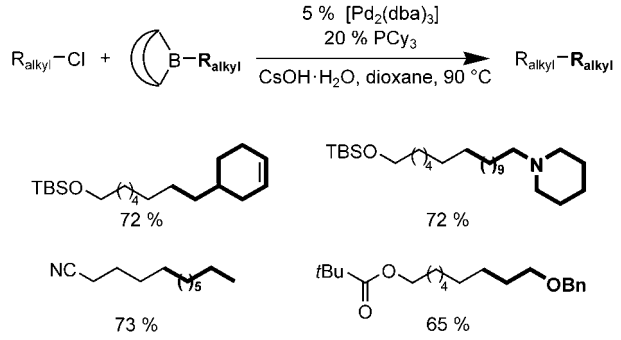
The most important general method for alkyl–alkyl cross-coupling reactions was developed by Fu and co-workers and is based on the Suzuki reaction. Over the last few years, numerous examples of the palladium-catalyzed cross-coupling of alkyl boranes with primary alkyl bromides, chlorides, and tosylates in the presence of catalysts with bulky electron-rich phosphane ligands have demonstrated the broad scope of the reaction.[22] Because of the mild reactivity of organoboron nucleophiles, many functional groups of particular importance for organic synthesis are tolerated (e.g. ester, nitrile, amide, and ether functionalities, as well as double and triple bonds; Scheme 9). Generally, individual fine-tuning of the



Scheme 9. Optimized palladium-catalyzed Suzuki coupling with alkyl bromides.

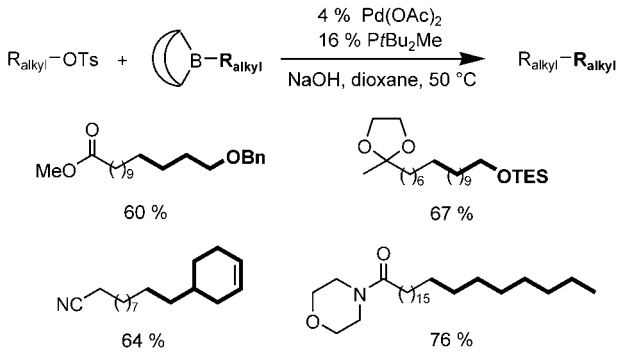
ligand and base employed is required to assure high selectivity in the cross-coupling reaction and suppression of competitive β-hydride elimination.

After extensive ligand screening, Fu and co-workers reported that the ligand PCy_3 (Cy = cyclohexyl) gave the highest selectivity and yield in the cross-coupling of primary alkyl bromides and chlorides with nucleophiles R_{alkyl}–9-BBN. Interestingly, the sterically and electronically similar ligands $P(c\text{-}C_5H_9)_3$ and $PiPr_3$ were significantly less effective. Furthermore, the choice of the precatalyst (RBr: $Pd(OAc)_2$;[22a] RCl: $[Pd_2(dba)_3]$[22b]) and the base is of special importance. The nature of the latter has a crucial influence on the nucleophilicity of the alkyl borane and on the tolerance of functional groups. Tripotassium phosphate monohydrate ($K_3PO_4 \cdot H_2O$) was demonstrated to be superior to various other inorganic bases for the cross-coupling of alkyl bromides at room temperature.[22a] Alkyl chlorides, however, require higher catalyst loadings and reaction temperatures, as well as the use of hydroxide bases, such as $CsOH \cdot H_2O$ and NaOH (Scheme 10).[22b]



Scheme 10. Alkyl chlorides in the Suzuki reaction (Fu and co-workers). Bn = benzyl, dba = dibenzylideneacetone, TBS = *tert*-butyldimethylsilyl.

In contrast to reactions with alkyl bromides and chlorides, $PtBu_2Me$ was found to be the best ligand for Suzuki reactions with alkyl tosylates (Scheme 11). The results of mechanistic

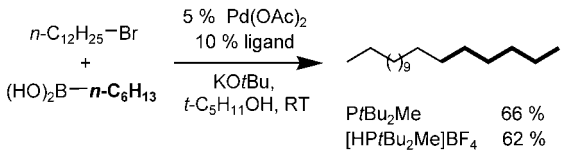


Scheme 11. Suzuki coupling with alkyl tosylates. TES = triethylsilyl.

investigations suggest that the oxidative addition of the alkyl tosylate and the reductive elimination proceed with inversion of the configuration at the α carbon atom.

The same catalyst system ($Pd(OAc)_2$/$PtBu_2Me$) was used successfully in Suzuki cross-coupling reactions of alkyl bromides with alkyl boronic acids (Scheme 12). The nearly quantitative oxidative addition of an alkyl bromide to $[PdL_2]$ (L = $PtBu_2Me$) at 0 °C demonstrates the high activity of this catalyst system. The resulting alkyl–palladium complex was shown to resist β-hydride elimination and was characterized crystallographically.

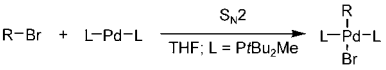
 © 2005 Wiley-VCH Verlag GmbH & Co. KGaA, Weinheim

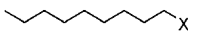
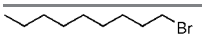
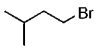


Scheme 12. Ligand-free Suzuki coupling with alkyl boronic acids.

Extensive mechanistic studies on the model reaction with *n*-nonylbromide in THF revealed the activation parameters for the oxidative addition to $[Pd(PtBu_2Me)_2]$: $\Delta G^* = 20.8\ kcal\,mol^{-1}$; $\Delta H^* = 2.4\ kcal\,mol^{-1}$; $\Delta S^* = -63$ eu. An increase in the solvent polarity (in the order THF < *t*-$C_5H_{11}OH$ < NMP < *N*,*N*-dimethylformamide (DMF)) was shown to lead to a decrease in the activation barrier, as expected for an S_N2-type nucleophilic attack of $[PdL_2]$ onto RX. Branching at the β or γ position in the electrophile resulted in significantly lower reactivities, and α-branched electrophiles are inert towards oxidative addition under the reaction conditions (Table 1).[23] The substantially lower reactivity of complexes $[PdL_2]$ with $L = PtBu_2Et$ or $PtBu_3$ is attributed to conformational restriction and resulting steric shielding of the palladium center.

Table 1: Kinetic investigations of oxidative addition to $[PdL_2]$.

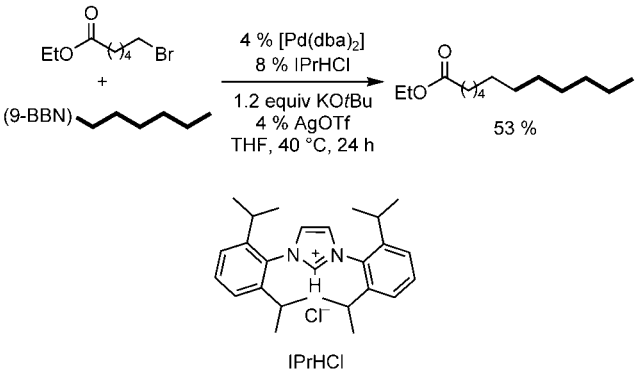


R–X	X	$t_{1/2}$ (*T*)
	I	2.2 h (−60 °C)
	Br	2.3 h (0 °C)
	Cl	2.0 days (60 °C)
	F	[a]
	OTs	10.4 h (40 °C)
R–Br		**k_{rel} at 0 °C**
		1.0
		0.19
		0.054
		< 0.0001

[a] Yield: < 2% after 43 h at 60 °C.

By virtue of the mildness of the reaction conditions and the broad functional-group tolerance, this palladium-catalyzed cross-coupling of alkyl bromides with alkyl boranes qualifies as a general method for selective C–C bond formation suitable for application in natural product synthesis. The required alkyl boranes can be accessed readily through the hydroboration of alkenes on a multigram scale. The restriction to primary alkyl halides has somewhat impeded a more general application of this reaction. Until very recently, no efficient catalyst system had been developed for the conversion of secondary and tertiary alkyl halides.

N-Heterocyclic carbene ligands have also been used successfully in alkyl–alkyl cross-coupling reactions with alkyl boranes (Scheme 13). However, Cloke and co-workers obtained the products of palladium-catalyzed reactions of primary alkyl bromides with alkyl–9-BBN derivatives in the presence of IPrHCl (IPr = 1,3-bis(2,6-diisopropylphenyl)imidazol-2-ylidene) as the ligand precursor in only moderate yields (28–56 %).[24]



Scheme 13. First alkyl–alkyl Suzuki coupling with carbene ligands.

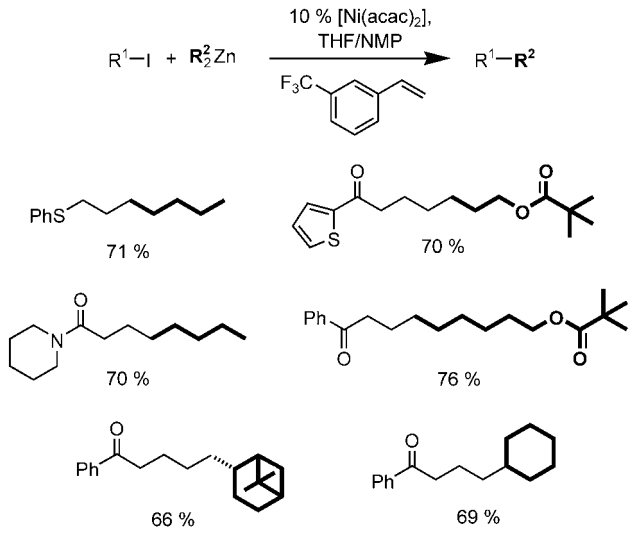
2.3. $Alkyl_x$–ZnX_y (Negishi Coupling)

Early investigations by Tucker and Knochel focused on reactions of alkyl iodides with dialkyl zinc reagents in the presence of stoichiometric quantities of $[Cu(CN)Me_2\text{-}(MgCl_2)]$.[25] Shortly afterwards, Knochel and co-workers reported a nickel-catalyzed cross-coupling between $C(sp^3)$ centers. The introduction of a double bond at the 4- or 5-position of the alkyl iodide made possible this first efficient purely nickel-catalyzed alkyl–alkyl cross-coupling reaction. The reductive elimination of the coupling product is facilitated by intramolecular coordination of the double bond and can be further enhanced by electron-withdrawing substituents on the double bond.[7] The reaction proceeds in the presence of $[Ni(acac)_2]$ (7 mol %) in a THF/NMP solvent mixture. However, the generality of this method is clearly limited by the structural requirements.

A few years later, Knochel and co-workers extended the scope of this methodology with a similar protocol that exploits intermolecular olefin coordination at the nickel catalyst (Scheme 14). In this case the $[Ni(acac)_2]$-catalyzed coupling of alkyl iodides, which now no longer require a pendant double bond for coordination to the metal center, could be effected by adding a π-acceptor ligand, such as acetophenone, benzophenone, or a styrene derivative. A screening of different ligands identified 3-trifluoromethylstyrene as the most effective cocatalyst.[26] The optimized reaction conditions tolerate ester and amide functionalities in the alkyl iodides. The presence of a thioether or thioacetal group leads to a significant increase in the reaction rate, presumably as a result of complexation by the sulfur atom to the metal center. The reaction is generally limited to primary alkyl iodides.

An extension of this method to secondary dialkyl zinc nucleophiles allowed the conversion of ω-functionalized alkyl iodides in good yields.[27] Knochel and co-workers also described the boron–zinc exchange as a selective route to

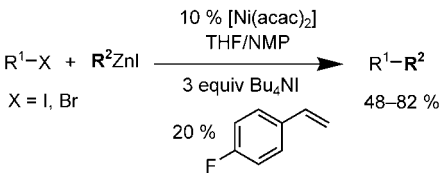
 © 2005 Wiley-VCH Verlag GmbH & Co. KGaA, Weinheim



Scheme 14. Nickel-catalyzed alkyl–alkyl Negishi coupling with diorganozinc nucleophiles (Knochel and co-workers).

secondary diorganozinc compounds through a hydroboration–transmetalation sequence.[28] Retention of configuration was observed for both the B–Zn transmetalation and the reductive elimination, thus permitting the synthesis of stereoisomerically pure coupling products. The required chiral boranes are readily accessible by the stereoselective hydroboration of olefins.

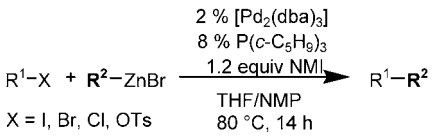
Under optimized conditions, the less reactive alkyl zinc iodides, which tolerate a wider variety of functional groups, can also be used in coupling reactions (Scheme 15). The



Scheme 15. Negishi coupling with secondary alkyl zinc iodides.

presence of tetrabutylammonium iodide (3 equiv) and 4-fluorostyrene (20 mol %) is required for the cross-coupling with primary alkyl iodides and bromides. By using this protocol, secondary alkyl zinc iodides could be used for the first time. Ether, keto, nitrile, and amide groups are compatible with the reaction conditions.[27]

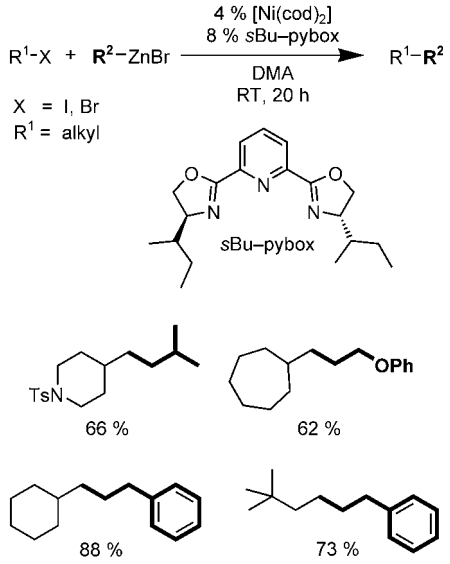
Zhou and Fu recently described a powerful catalyst system for alkyl–alkyl Negishi coupling reactions. A variety of non-activated primary alkyl iodides, bromides, chlorides, and tosylates underwent cross-coupling with alkyl zinc nucleophiles in the presence of the catalyst system $[Pd_2(dba)_3]$/P(*c*-$C_5H_9)_3$/NMI at 80 °C (Scheme 16). Alkene, ether, nitrile, amide, and ester functionalities are tolerated in both reactants, but the reaction is limited to primary alkyl halides and alkyl zinc iodides. The presence of NMI facilitates the transmetalation to palladium and leads to improved yields. In analogy with the results of Knochel and co-workers,



Scheme 16. Palladium/phosphine-catalyzed Negishi coupling by Zhou and Fu. NMI = *N*-methylimidazole.

an NMP/THF mixture proved to be the optimal solvent. Interestingly, the corresponding air- and moisture-stable phosphonium salt can be used instead of the trialkyl phosphine ligand.[29]

The first cross-coupling reaction of non-activated secondary alkyl bromides and iodides was possible with nickel catalysts in the presence of bis(oxazolinyl)pyridine (pybox) ligands (Scheme 17). The fine-tuning of the substituents on



Scheme 17. First nickel-catalyzed Negishi coupling with secondary alkyl bromides and iodides. DMA = *N*,*N*-dimethylacetamide.

the ligand revealed the best catalyst activities with *s*-butyl groups; significantly lower activities were observed with larger or smaller groups (*i*Pr, *t*Bu, Ph). However, many nickel–phosphine catalyst mixtures were shown to be inactive under the test conditions. The cross-coupling reaction proceeds at room temperature within 20 h in moderate to good yields, but requires an excess of the nucleophile (1.6 equiv).[30] This protocol constitutes a milestone in the development of efficient alkyl–alkyl cross-coupling methodology, as the use of secondary alkyl halides is an indispensable requirement for the development of stereoselective coupling reactions.

3. Cross-Coupling with Aryl Nucleophiles

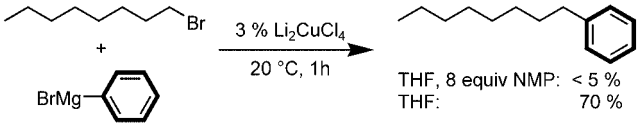
Aryl nucleophiles are generally less reactive in cross-coupling reactions with electrophiles R_{alkyl}–X because of the lower nucleophilicity of the sp^2-hybridized carbon atom. However, they also undergo fewer side reactions owing to the

 © 2005 Wiley-VCH Verlag GmbH & Co. KGaA, Weinheim

lack of β hydrogen atoms. The large number of known palladium- or nickel-catalyzed inverse cross-coupling reactions (alkyl–MX with aryl–X)[16,17,31] suggests that the oxidative addition of the electrophile in the first step, rather than the nature of the nucleophile, is crucial for good reactivity. Considerably fewer examples exist of cross-coupling reactions between an aryl metal species and an alkyl halide.

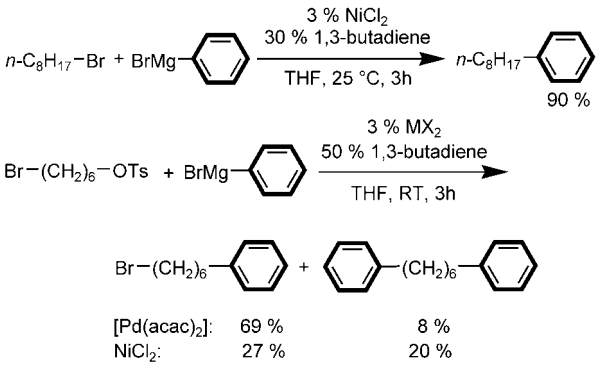
3.1. Alkyl–MgX (Kumada Coupling)

Fuchikami and co-workers reported copper-catalyzed cross-coupling reactions of β-perfluoroalkyl-substituted alkyl bromides with aryl magnesium compounds under mild conditions as early as 1996.[32] In 2000, Cahiez et al. documented a copper-catalyzed cross-coupling reaction of aryl magnesium compounds with alkyl bromides at room temperature (Scheme 18). Interestingly, the reaction is inhibited by NMP, which was added as an activator in the related alkyl–alkyl cross-coupling protocol.[15] A similar effect was also observed in reactions with aryl manganese compounds.[12]



Scheme 18. The Cahiez variant of the alkyl–aryl Kumada coupling.

Kambe and co-workers described the application of the $NiCl_2$/butadiene catalyst system they developed for cross-coupling reactions of R_{alkyl}–X with R_{alkyl}–MgX to two reactions with phenyl magnesium bromide (Scheme 19). With

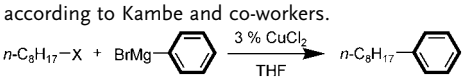


Scheme 19. Alkyl–aryl cross-coupling (Kambe and co-workers).

primary alkyl tosylates and bromides the products were obtained in moderate yields at 0–25 °C.[18] Similar yields and chemoselectivity were observed for alkyl tosylates with $[Pd(acac)_2]$ as the precatalyst.[19]

Kambe and co-workers also reported copper-catalyzed reactions analogous to their alkyl–alkyl cross-coupling protocol with various nucleophiles ArMgX. Interestingly, the reactivities of alkyl fluorides and bromides were similar or even higher in the absence of 1,3-butadiene than with the additive (Table 2).[21]

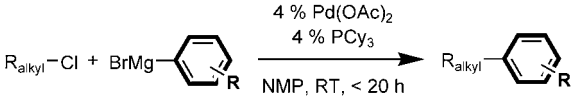
Table 2: Copper-catalyzed Kumada coupling according to Kambe and co-workers.



X	*T* [°C]	*t* [h]	Yield [%]
F	25	6	38[a]
F	25	6	53
F	67	1	99
Cl	67	1	42
Br	67	1	99

[a] In the presence of 1,3-butadiene (0.2 mmol).

In our laboratory, a general method was developed for the palladium-catalyzed Kumada cross-coupling of aryl magnesium halides with inexpensive alkyl chlorides at room temperature in the presence of a catalytic amount of $Pd(OAc)_2$ (Scheme 20).[33] The choice of the solvent (NMP)



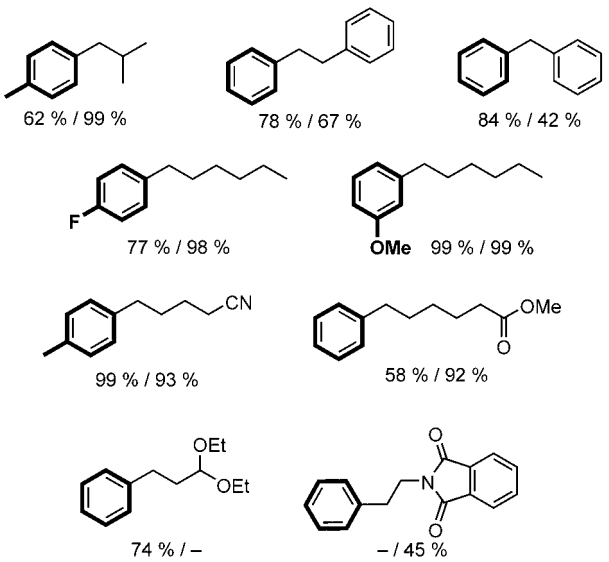
Scheme 20. Palladium-catalyzed Kumada coupling with alkyl chlorides at room temperature.

and ligand (PCy_3) proved to be crucial for high yields and selectivities to be attained. In the presence of PCy_3 or $PiPr_3$, the coupling products were obtained in good yields. However, secondary and tertiary alkyl chlorides do not react under these conditions. In contrast to reactions with alkyl bromides,[34] an optimal palladium/ligand ratio of 1:1 was established for reactions in NMP. It is assumed that the presence of a large excess of weakly coordinating NMP inhibits the competitive β-hydride elimination by coordinative saturation of the palladium atom. Reactions with the sterically more demanding $PtBu_3$ ligand or the aromatic phosphines PPh_3 and $P(o\text{-Tol})_3$ (Tol = tolyl) were found to be less strongly dependent on the Pd/L ratio, but gave the cross-coupling products in only moderate yields (< 30 %).

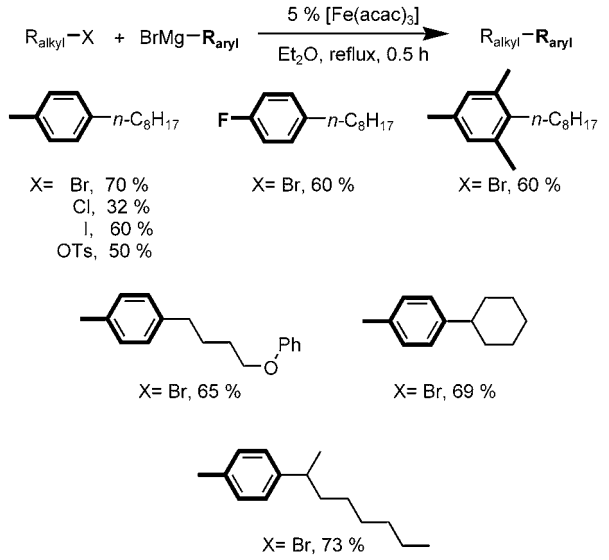
We also investigated similar cross-coupling reactions in the presence of N-heterocyclic carbene ligands.[35] A significant increase in selectivity and activity was observed with the monocarbene palladium dimer $[\{Pd(IMes)(NQ)\}_2]$ (IMes = 1,3-bis(2,4,6-trimethylphenyl)imidazol-2-ylidene; NQ = naphthoquinone). The generality of the new procedure was demonstrated in reactions of a variety of functionalized alkyl chlorides (Scheme 21). This Kumada cross-coupling of alkyl chlorides with aryl magnesium reagents at room temperature constitutes a robust method for practicable access to functionalized alkanes in good yields and under mild conditions.

Very recently, iron-catalyzed coupling reactions of secondary alkyl halides were described independently by the research groups of Hayashi and Nakamura (Schemes 22 and

 © 2005 Wiley-VCH Verlag GmbH & Co. KGaA, Weinheim



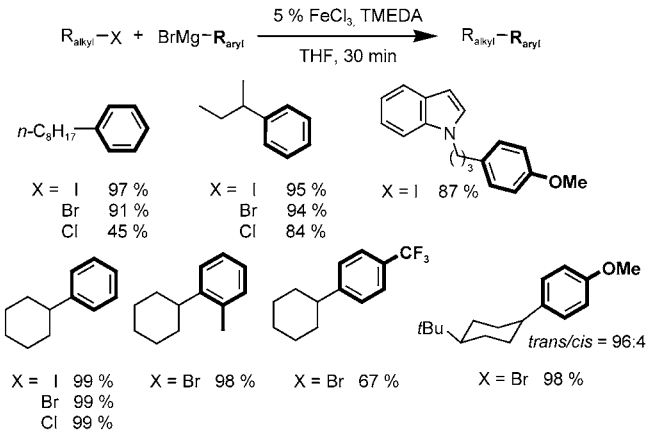
Scheme 21. Selected products of the Kumada coupling with alkyl chlorides. Left-hand yields: with $Pd(OAc)_2/PCy_3$; right-hand yields: with $[\{Pd(IMes)(NQ)\}_2]$.



Scheme 22. Iron-catalyzed coupling with secondary alkyl halides (Nagano and Hayashi).

23). Nagano and Hayashi reported the use of $[Fe(acac)_3]$ as an efficient catalyst for cross-coupling reactions of diversely substituted reagents ArMgBr (2 equiv).[36] The best results were obtained with secondary alkyl bromides under mild reaction conditions (Et_2O, 35 °C). When THF or solvent mixtures with NMP were used, significant quantities of elimination and homocoupling products were obtained.

Nakamura and co-workers reported a $FeCl_3$-catalyzed reaction with secondary alkyl bromides and iodides,[37] which were substantially more reactive than primary halides under these conditions. The addition of *N*,*N*,*N*′,*N*′-tetramethylethylenediamine (TMEDA) led to significantly higher selectivities

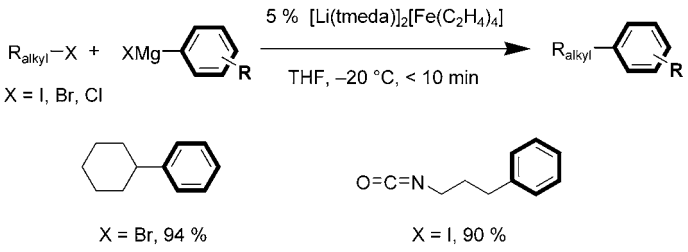


Scheme 23. Iron-catalyzed coupling (Nakamura and co-workers).

and largely suppressed competitive elimination and hydrodehalogenation. Tertiary alkyl halides are converted faster than secondary, but give predominantly undesired by-products. The reactivity of the electrophile follows the expected pattern and decreases from the alkyl iodide to the alkyl chloride.

Secondary alkyl chlorides generally require slightly higher temperatures (up to 40 °C) and an excess of the Grignard reagent (1.5 equiv) for successful coupling. Electron-rich aryl groups on the Grignard reagent accelerate the reaction. Cyclic and acyclic secondary alkyl halides gave similar results. The reactions seem to involve radical intermediates, as complete epimerization was observed with alkyl halides with α stereocenters.

A further contribution to the art of iron-catalyzed alkyl–aryl cross-coupling reactions was made by Martin and Fürstner. They postulated that the active catalysts were Fe/Mg clusters of the formal composition $[Fe(MgX)_2]_n$ formed in situ, and carried out iron-catalyzed Kumada-type reactions with the tetrakis(ethylene)ferrate(II) compound $[Li(tmeda)]_2[Fe(C_2H_4)_4]$ (5 mol %; Scheme 24).[38] In the presence of



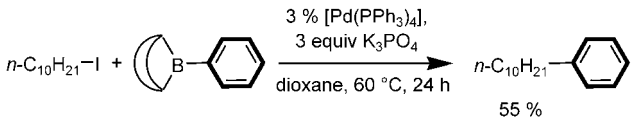
Scheme 24. Iron-catalyzed coupling (Martin and Fürstner).

this well-defined precatalyst, primary and secondary alkyl bromides and iodides as well as propargyl and allyl halides react smoothly to afford the desired arylated products in good to very good selectivity. The mechanism seems to involve radical species, as racemization has been observed with enantiomerically pure substrates and cyclization with 5-haloalkenes.

 © 2005 Wiley-VCH Verlag GmbH & Co. KGaA, Weinheim

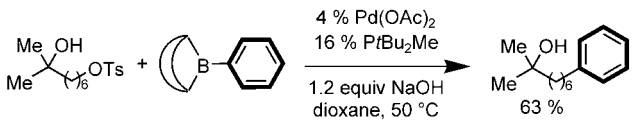
3.2. Aryl–BX_2 (Suzuki Coupling)

The first palladium-catalyzed coupling of an aryl borane with an alkyl iodide was reported by Suzuki and co-workers in 1992 (Scheme 25).[6] The reactions were carried out in the



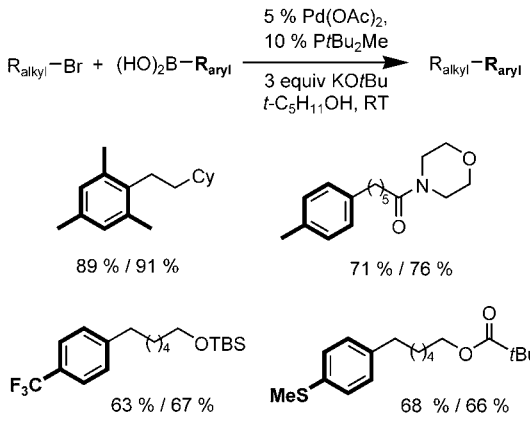
Scheme 25. First efficient alkyl–aryl Suzuki coupling.

presence of $[Pd(PPh_3)_4]$ (3 mol%) and K_3PO_4 (3 equiv) as a base in dioxane at 60°C. Ten years later, Fu and co-workers presented an optimized set of conditions for palladium-catalyzed coupling reactions of alkyl tosylates with 9-BBN derivatives (Scheme 26). The catalyst is formed in situ from $Pd(OAc)_2$ (4 mol%) and an excess of the basic and sterically demanding ligand $PtBu_2Me$.[22c]



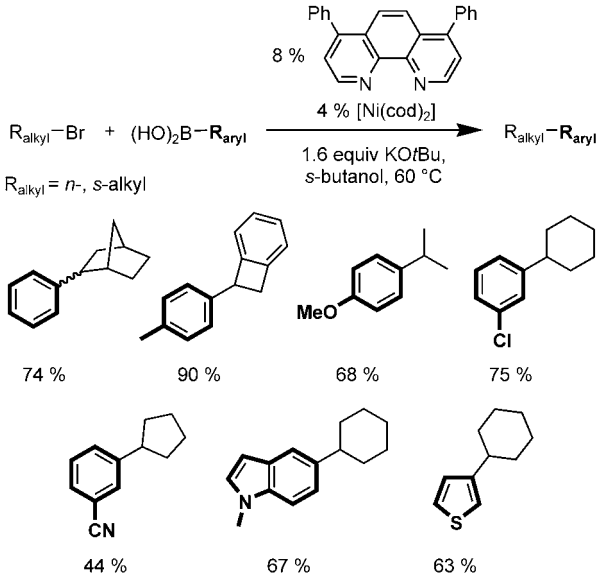
Scheme 26. Suzuki reaction of alkyl tosylates with aryl 9-BBN derivatives.

These reaction conditions for the coupling of alkyl tosylates with 9-BBN derivatives were shown to be ineffective for the more practical, commercially available aryl boronic acids. However, conditions were found for the cross-coupling of aryl boronic acids with alkyl bromides at room temperature with *t*-amyl alcohol as the solvent and KO*t*Bu as the base (Scheme 27). The catalyst system $Pd(OAc)_2/PtBu_2Me$ tolerates a large number of functional groups, such as ester, ether, thioether, amide, nitrile, and acetal functionalities. Deactivated $(4\text{-}CF_3C_6H_4\text{–}B(OH)_2)$ and sterically demanding (o-tolyl–$B(OH)_2$) aryl boronic acids can also be coupled in good to very good yields under these reaction conditions.[22d] The stable alkyl palladium(II) complex formed at 0°C through the oxidative addition of an alkyl bromide to $[Pd(PtBu_2Me)_2]$ was characterized crystallographically and identified as an intermediate in the catalytic cycle.



Scheme 27. Aryl boronic acids as coupling partners in the presence of palladium catalysts. Left-hand yields: with $PtBu_2Me$; right-hand yields: with $[HPtBu_2Me]BF_4$.

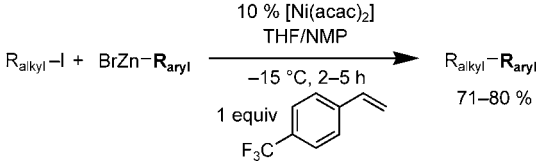
In 2004, Zhou and Fu described the first efficient protocol for the cross-coupling of non-activated secondary alkyl bromides and iodides with aryl boronic acids (Scheme 28). A similar catalyst system to that for the alkyl–alkyl Negishi reaction was used. Although in the presence of the *s*Bu–pybox ligand only marginal activity was observed, the coupling products were obtained in moderate to good yields with the chelating dinitrogen ligand bathophenanthroline. Interestingly, reasonable selectivities were observed only with $[Ni(cod)_2]$ as the precatalyst.[39]



Scheme 28. First nickel-catalyzed Suzuki coupling of secondary alkyl bromides with the ligand bathophenanthroline. cod = 1,5-cyclooctadiene.

3.3. $Aryl_x$–ZnX_{2-x} (Negishi Coupling)

In 1998, Giovannini and Knochel reported nickel-catalyzed Negishi reactions with aryl zinc derivatives and alkyl iodides (Scheme 29). As in the related alkyl–alkyl coupling protocol, an olefin is required as a coligand to accelerate the reductive elimination of the cross-coupling product from the

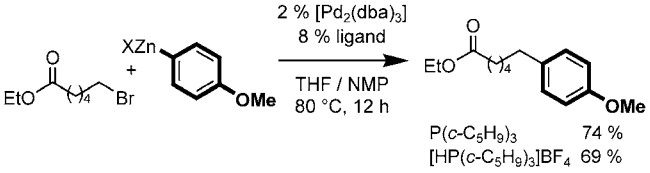


Scheme 29. Alkyl–aryl Negishi coupling (Giovannini and Knochel).

© 2005 Wiley-VCH Verlag GmbH & Co. KGaA, Weinheim

Ni^{II} intermediate. In the absence of the coligand 4-trifluoromethylstyrene, substantial quantities of homocoupling and iodine–zinc-exchange products were formed. With $[Ni(acac)_2]$ (10 mol%) and 1 equivalent of the activator in an NMP/THF mixture at −15 °C, primary alkyl iodides coupled with aryl zinc bromides in good yields (71–80%). These reaction conditions tolerate keto, ester, amide, nitrile, ether, and thioether substituents on both substrates, as well as chlorine substituents on the aryl zinc substrate.[40]

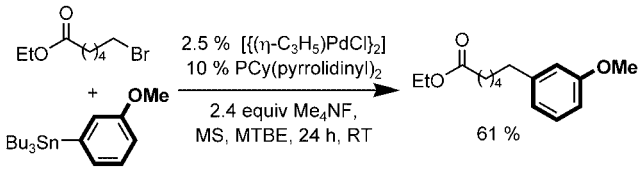
During their studies of the palladium-catalyzed alkyl–alkyl Negishi coupling, Zhou and Fu established $[Pd_2(dba)_3]$/$P(c\text{-}C_5H_9)_3$ as a suitable catalyst system for alkyl–aryl cross-coupling reactions of aryl zinc compounds with alkyl bromides and iodides.[29] As shown in Scheme 30, instead of the air-sensitive phosphine, the corresponding phosphonium salt $[HP(c\text{-}C_5H_9)_3]BF_4$ can be used advantageously as the ligand precursor.



Scheme 30. Palladium/phosphine-catalyzed Negishi coupling (Zhou and Fu).

3.4. Aryl–SnX_3 (Stille Coupling)

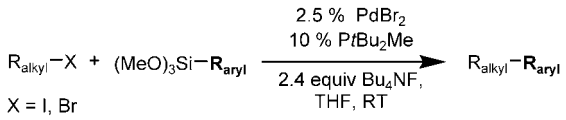
Arylations of β-perfluoroalkyl-substituted alkyl iodides with aryl tin reagents under $[PdCl_2(PPh_3)_2]$ catalysis have been reported. However, only moderate yields were observed and high catalyst loadings (up to 50 mol%) were required.[41] In contrast, Stille cross-coupling reactions of aryl stannanes can generally be effected in good yields with palladium/phosphine catalyst systems. A screening of ligands resulted in optimal yields for electron-rich alkyl diaminophosphines, whereas simple trialkyl phosphines, such as $PtBu_2Me$, showed only low activities. In the presence of tetramethylammonium fluoride, molecular sieves, and a large excess of cyclohexyldi(pyrrolidinyl)phosphane ($PCy(pyrr)_2$) as the ligand, ω-functionalized primary alkyl bromides reacted smoothly with electron-rich and, albeit in slightly lower yields, electron-deficient aryl tributylstannanes at room temperature (Scheme 31).[42]



Scheme 31. Palladium-catalyzed alkyl–aryl Stille reaction (Fu and coworkers). MS = molecular sieves, MTBE = *tert*-butyl methyl ether.

3.5. Aryl–SiX_3 (Hiyama Coupling)

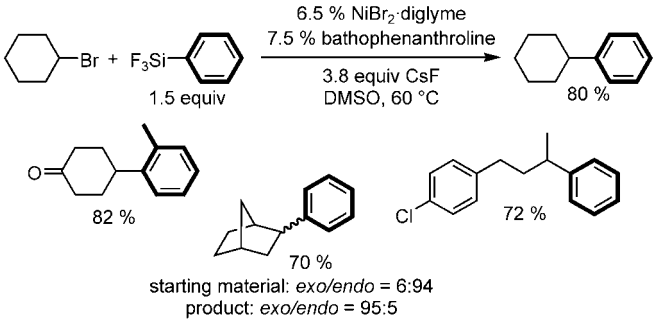
$PtBu_2Me$ is also a suitable ligand for palladium-catalyzed Hiyama cross-coupling reactions of primary alkyl iodides and bromides with aryl silanes. Under identical conditions to those for related Suzuki reactions, no conversion was observed with aryl silanes. However, the addition of Bu_4NF as an activator led to the in situ generation of a more nucleophilic hypervalent silicate species, which reacted cleanly with alkyl bromides, even at room temperature (Scheme 32). In the presence of $PdBr_2$ (4 mol%) and



Scheme 32. Palladium-catalyzed Hiyama reaction with aryl siloxanes.

$PtBu_2Me$ (10 mol%), coupling products were obtained in moderate to good yields with ω-functionalized alkyl bromides and iodides. Significantly lower activities were observed with electron-deficient aryl silanes and when the air-stable phosphonium salt $[HPtBu_2Me]BF_4$ was used in place of the phosphine ligand.[43]

Good yields were also described in the Hiyama coupling of secondary alkyl bromides in the presence of the convenient catalyst system $NiBr_2$·diglyme/bathophenanthroline (Scheme 33). Only slightly lower yields were observed with



Scheme 33. Nickel-catalyzed Hiyama coupling of secondary alkyl bromides with $ArSiF_3$. diglyme = diethyleneglycol dimethyl ether, DMSO = dimethyl sulfoxide.

$NiBr_2$ or $[Ni(cod)_2]$ as metal sources and the structurally related dinitrogen ligands 1,10-phenanthroline and 2,2′-bipyridine.[44] However, the reaction was limited to aryl trifluorosilanes and required a large excess of the promotor cesium fluoride (4 equiv). Again, the conditions for Suzuki and Negishi coupling reactions of secondary alkyl bromides proved to be rather inefficient for these cross-coupling reactions.

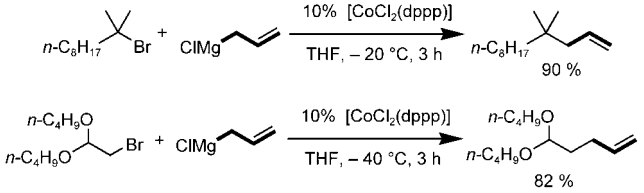
 © 2005 Wiley-VCH Verlag GmbH & Co. KGaA, Weinheim

4. Cross-Coupling with Other Nucleophiles

Besides the cross-coupling reactions of alkyl electrophiles with alkyl and aryl metal nucleophiles, a few protocols for similar reactions with allyl, vinyl, and alkynyl nucleophiles have been reported more recently. Furthermore, sparse examples of direct carbonylation reactions of non-activated alkyl halides are known.

4.1. Allyl–MX_n

Oshima and co-workers reported the first cobalt-catalyzed cross-coupling reactions of allyl magnesium compounds with alkyl iodides, bromides, and chlorides at low temperatures (−40 to 0 °C). Interestingly, tertiary alkyl halides also underwent successful cross-coupling (Scheme 34). A radical

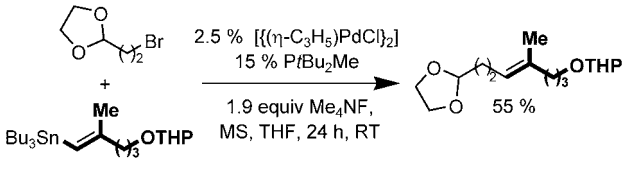


Scheme 34. Cobalt-catalyzed allylation of secondary and tertiary alkyl bromides. dppp = 1,3-bis(diphenylphosphanyl)propane.

mechanism was proposed for this reaction, with the oxidative addition involving single-electron transfer (SET) from the electron-rich allyl–cobalt complex to the alkyl halide. π-Allyl ligands can block free coordination sites at the cobalt center and thus enable the allylation of tertiary and secondary alkyl halides as well as alkyl halides with β-alkoxy substituents without significant β-hydride or β-alkoxy eliminination.[45]

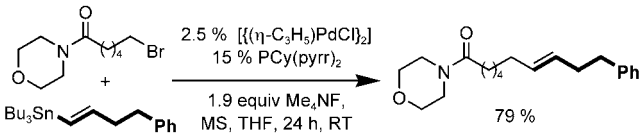
4.2. Vinyl–MX_n

Shimizu and Fuchikami reported palladium-catalyzed Stille reactions of β-perfluoroalkyl-substituted alkyl iodides with vinyl and alkynyl stannanes at elevated temperatures.[41] The palladium-catalyzed Stille coupling of primary alkyl bromides with alkenyl tin reagents is also known to proceed at room temperature (Scheme 35). With P*t*Bu_2Me as the ligand, substituted olefins were formed in good to very good yields in the presence of [{Pd(η-C_3H_5)Cl}$_2$] (2.5 mol %) and Me_4NF (1.9 equiv).[46]



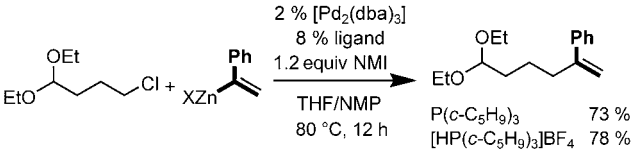
Scheme 35. Palladium-catalyzed alkyl–vinyl Stille reaction. THP = tetrahydropyranyl.

Furthermore, alkyl diaminophosphines were shown to be active ligands under similar reaction conditions (Scheme 36). Although the yields were comparable to those observed for the system with P*t*Bu_2Me, aryl stannanes can also be used as substrates with this modified catalyst system.[42]



Scheme 36. The diaminophosphine ligand PCy(pyrr)$_2$ in the Stille reaction (Fu and co-workers).

A general procedure for palladium-catalyzed Negishi cross-coupling reactions of alkyl electrophiles (RI, RBr, RCl, ROTs) with alkenyl zinc reagents in good yields (53–98 %) was described by Zhou and Fu.[29] In the presence of P(*c*-C_5H_9)$_3$ or its stable phosphonium salt, good reactivities were observed even with sterically hindered geminal or *cis*-substituted vinyl zinc halides (Scheme 37). A one-pot hydro-

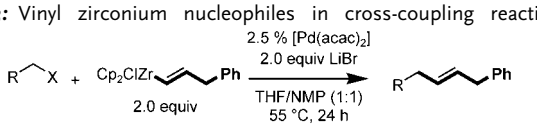


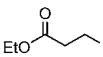
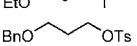
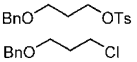
Scheme 37. Alkyl–vinyl Negishi coupling and domino hydrometalation–cross-coupling.

zincation–cross-coupling sequence constitutes an interesting extension of this methodology: Vinyl zinc halides formed in situ through the titanium-catalyzed reduction of alkynes react with primary alkyl electrophiles under palladium catalysis in moderate yields.

[Pd(acac)$_2$] was used as a catalyst for reactions of alkyl halides with alkenyl zirconium reagents under mild conditions (Table 3). With this ligand-free catalyst system, primary alkyl bromides, iodides, and tosylates react in good yields. However, β-branched alkyl bromides could only be coupled in moderate yields, and alkyl chlorides also exhibit lower reactivities.[47]

Table 3: Vinyl zirconium nucleophiles in cross-coupling reactions.

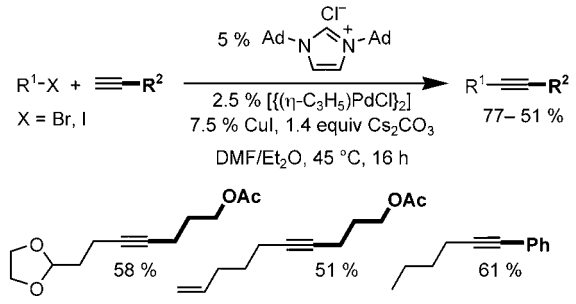


Alkyl halide	Yield [%]
	60
	82
	83
	46

© 2005 Wiley-VCH Verlag GmbH & Co. KGaA, Weinheim

4.3. Alkynyl–MX_n

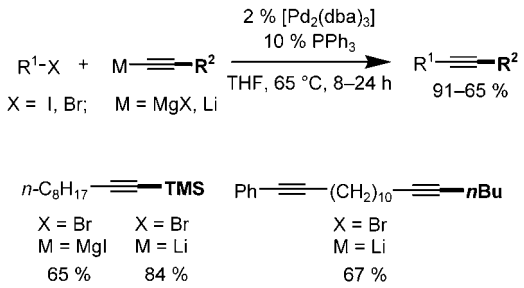
Surprisingly, to date no example of the palladium/copper-catalyzed Sonogashira coupling of primary alkyl bromides and iodides with terminal alkynes in the presence of phosphine ligands has been reported. However, in the presence of N-heterocyclic carbene ligands, the reaction proceeds in moderate yields (Scheme 38). A multitude of



Scheme 38. Palladium/carbene-catalyzed Sonogashira coupling (Eckhardt and Fu).

functional groups (ester, nitrile, and acetal functionalities, double bonds, and unprotected hydroxy groups) are tolerated in this process. Variations in the substitution pattern on the alkyne have a significant influence on the reactivity. Thus, the reaction conditions (temperature, catalyst loading) must be adjusted for each substrate. As alkyl chlorides do not react, chemoselective transformations with halochloroalkanes are possible.[48]

$[Pd_2(dba)_3]/PPh_3$ constitutes another viable catalyst system for alkyl–alkynyl coupling reactions. In this Kumada–Corriu-type reaction of primary alkyl bromides and iodides with alkynyl lithium compounds or the corresponding Grignard reagents, the coupling products were obtained in good yields (Scheme 39). In general, yields with the alkynyl



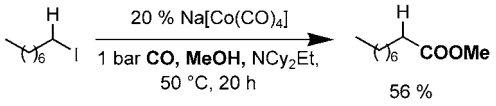
Scheme 39. Palladium-catalyzed alkynylation (Luh and co-workers).

lithium compounds were slightly better. PPh_3 proved to be a superior ligand to electron-rich trialkyl phosphines. This effect suggests that the reductive elimination may be rate determining. The choice of the palladium source was shown to influence the amount of homocoupling product formed.[49]

4.4. Carbonylations of Alkyl Electrophiles

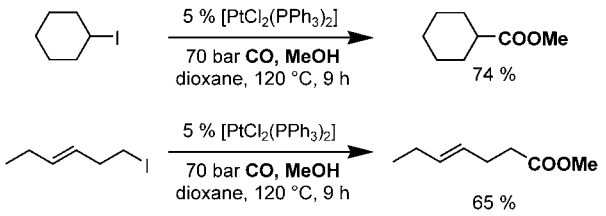
Beside cross-coupling reactions with organometallic nucleophiles, the carbonylation of alkyl halides ranks among the most important C–C coupling reactions on an industrial scale, and therefore deserves a brief discussion in the context of this Minireview. Radical carbonylations of alkyl iodides[50] will not be dealt with.

The carbonylation of alkyl halides enables the direct synthesis of aldehydes, ketones, esters, and amides. The industrial importance of such syntheses is underlined by the carbonylation of methanol to give acetic acid (Monsanto, Cativa processes),[51] which involves the rhodium- or iridium-catalyzed activation of methyl iodide. The efficient transition-metal-catalyzed carbonylation of alkyl halides is generally limited to activated substrates, such as methyl, benzyl, or allyl halides.[4] Thus, the carbonylation of alkyl halides with β hydrogen atoms at a $C(sp^3)$ center still presents a synthetic challenge, although Heck and Breslow reported a cobalt-catalyzed carbonylation of alkyl iodides under basic conditions as early as 1963 (Scheme 40).[52] Because of the formation of a stoichiometric quantity of HX as a by-product, the addition of a stoichiometric amount of a base is required.



Scheme 40. First cobalt-catalyzed carbonylation of alkyl iodides.

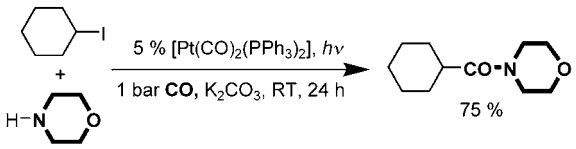
In the mid 1980s Alper and co-workers showed that $[Pd(PPh_3)_4]$[53] and the bimetallic mixture $[Pd(PPh_3)_4]/[\{RhCl(hd)\}_2]$ (hd = 1,5-hexadiene)[54] are active catalysts for the carbonylative synthesis of alkyl esters (Scheme 41). Later, platinum catalysts were used in the carbonylation of alkyl halides under thermal[55] as well as photochemical[56] conditions. For most thermal carbonylations, K_2CO_3 is the base of choice.



Scheme 41. Platinum-catalyzed thermal carbonylation of alkyl halides.

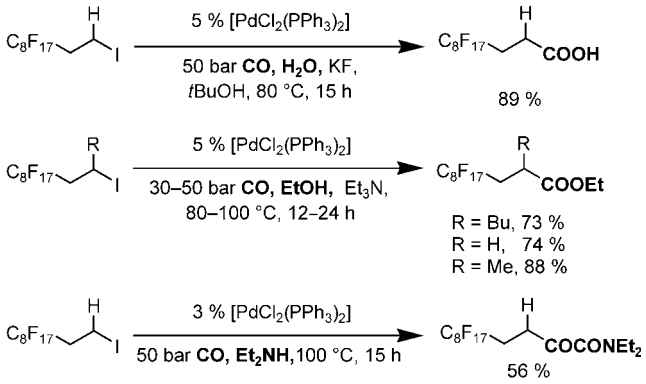
The carbonylation of alkyl iodides in the presence of 2–5 mol% of different metal carbonyl compounds ($[Mn_2(CO)_{10}]$, $[Co_2(CO)_8]$, $[Ru_3(CO)_{12}]$, $[Re_2(CO)_{10}]$, and $[Os_3(CO)_{12}]$) under UV irradiation is possible at room temperature and 1 bar CO (Scheme 42).[56] A radical mechanism was excluded, since reactions also proceed in the presence of radical inhibitors.

 © 2005 Wiley-VCH Verlag GmbH & Co. KGaA, Weinheim



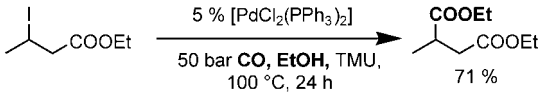
Scheme 42. Platinum-catalyzed photoinduced carbonylation.

Carboxylic acids and esters with perfluoroalkyl substituents were obtained by the thermal carbonylation of the corresponding iodides in the presence of KF or Et_3N as a base (Scheme 43).[57] Interestingly, double carbonylation to give α-ketoamides occurred when secondary amines were used as nucleophiles.[58]



Scheme 43. Palladium-catalyzed carbonylation of alkyl iodides.

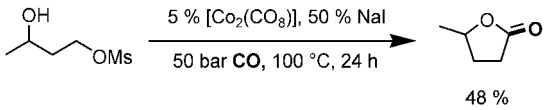
Unfortunately, the aforementioned carbonylation conditions are not suitable for the conversion of base-sensitive halides. In this context, the base-free carbonylations of Fuchikami and co-workers[59] in polar aprotic solvents[60] or with molecular sieves[61] as HX sponges are interesting (Scheme 44).



Scheme 44. Base-free carbonylation.

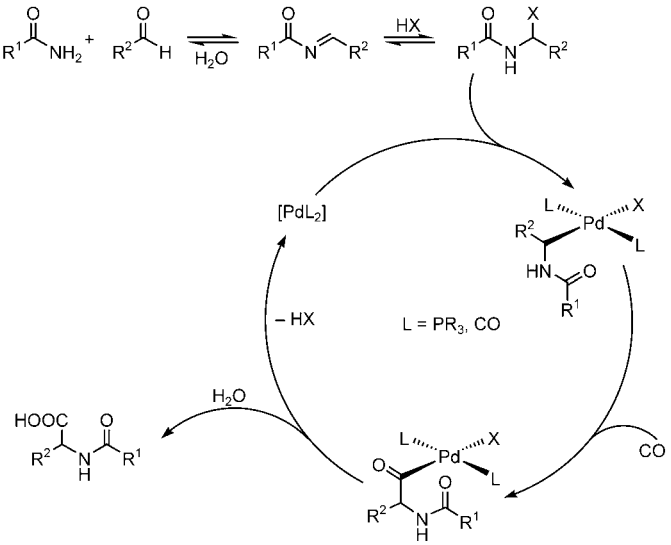
Alkyl sulfonates can be carbonylated in a similar manner.[62] As shown in Scheme 45, lactones are generated directly from alkyl sulfonates under cobalt catalysis.

Most industrial-scale syntheses of acetic acid derivatives involve the in situ generation of the more reactive methyl iodide from methanol. A related approach was utilized in the palladium-catalyzed amidocarbonylation of aldehydes, which



Scheme 45. Carbonylation of alkyl sulfonates.

constitutes an interesting three-component reaction for the synthesis of *N*-acyl α-amino acids (Scheme 46).[63] Model studies with *N*-(chloromethyl)phthalimides revealed the palladium-catalyzed activation of an intermediate α-halo *N*-acyl amine.[64] Subsequent carbonylation of the resulting alkyl palladium species leads directly to a wide range of amino acids, such as aryl glycines and hydantoins.[65]



Scheme 46. Amidocarbonylation of aldehydes.

5. Summary

Metal-catalyzed cross-coupling reactions of alkyl halides with organometallic compounds have been developed to an advanced stage and provide synthetic organic chemists with a versatile arsenal of C–C bond-forming methods. The most important synthetic variations are summarized in Table 4.

Combinations of palladium sources and phosphine ligands, which are the most prevalent type of catalyst system, allow for mild reaction conditions and a large range of applications owing to their functional-group tolerance. Thus, general protocols for Kumada, Suzuki, Negishi, Stille, and Hiyama cross-coupling reactions with alkyl, vinyl, and aryl metal nucleophiles in the presence of bulky, electron-rich trialkyl phosphines have been developed. However, the sluggishness of the reactions of secondary and β-branched electrophiles still prevents an even broader use of these palladium/phosphine-catalyzed methods in organic chemistry. Nickel and iron catalysts address this challenge and lead to excellent yields with secondary alkyl halides and a wide variety of organometallic nucleophiles.

Future research will certainly be aimed at the further optimization of reaction conditions to attain higher catalyst productivity (<1 mol% catalyst) and greater tolerance towards sensitive functional groups. Further mechanistic studies are required to establish the often unpredictable effects of specific solvents and additives. With regard to efficiency criteria, improvements in the atom economy of most processes are necessary, as most of the known procedures require nucleophiles (organometallic unit) of high

 © 2005 Wiley-VCH Verlag GmbH & Co. KGaA, Weinheim

Table 4: Important cross-coupling methods with alkyl electrophiles.

R	X	Nucleophile	Catalyst	Conditions	Ref.
n	Br, I	*n*-, *s*-, *t*-RMgX	Li_2CuCl_4	NMP, RT	[15]
n	Cl, Br, OTs	*n*-, *s*-, *t*-RMgX	$NiCl_2$, 1,3-butadiene	RT	[18]
n	Br, OTs	*n*-, *s*-RMgX	$[Pd(acac)_2]$, 1,3-butadiene	RT	[19]
n	F, Br	*n*-, *s*-RMgX	$NiCl_2$ or $CuCl_2$, 1,3-butadiene	below RT	[21]
n	Br	*n*-, *s*-RMgX	$Pd(OAc)_2/PCy_3$	$K_3PO_4 \cdot H_2O$, RT	[22a]
n	Cl	*n*-R-(9-BBN)	$[Pd_2(dba)_3]/PCy_3$	$CsOH \cdot H_2O$, 90 °C	[22b]
n	OTs	*n*-R-(9-BBN)	$Pd(OAc)_2/PtBu_2Me$	NaOH, 50 °C	[22c]
n	I	*n*-R_2Zn	$[Ni(acac)_2]$, 3-CF_3-styrene	THF/NMP, −35 °C	[26]
n	Br, I	*n*-, *s*-R_xZnX_{2-x}	$[Ni(acac)_2]$, 4-F-styrene	Bu_4NI	[27]
n	Cl, Br, I, OTs	*n*-RZnX	$[Pd_2(dba)_3]/P(c\text{-}C_5H_9)_3$	NMI, NMP/THF, 80 °C	[29]
s	Br, I	*n*-RZnX	$[Ni(cod)_2]$/sBu–pybox	RT	[30]
n	Cl	ArMgX	$Pd(OAc)_2/PCy_3$	RT	[33]
n	Cl	ArMgX	$[\{Pd(IMes)(NQ)\}_2]$	RT	[35]
n, *s*	Cl, Br, I	ArMgX	$FeCl_3$	TMEDA, below RT	[37]
n	Br	$ArB(OH)_2$	$Pd(OAc)_2/PtBu_2Me$	KO*t*Bu, RT	[22d]
n, *s*	Br, I	$ArB(OH)_2$	$[Ni(cod)_2]$/bathophenanthroline	KO*t*Bu, 60 °C	[39]
n	I	ArZnX	$[Ni(acac)_2]$, 4-CF_3-styrene	THF/NMP	[40]
n	Br, I	$ArSi(OMe)_3$	$PdBr_2/PtBu_2Me$	Bu_4NF, RT	[43]
n, *s*	Br, I	$ArSiF_3$	$NiBr_2$·diglyme/bathophenanthroline	CsF, 60 °C	[44]
n	Br	$ArSnBu_3$, vinyl–$SnBu_3$	$[\{Pd(\eta\text{-}C_3H_5)Cl\}_2]/PCy(pyrr)_2$	Me_4NF, MS, RT	[46]
n	Cl, Br, I, OTs	vinyl–Zn	$[Pd_2(dba)_3]/P(c\text{-}C_5H_9)_3$	NMI, THF/NMP, 80 °C	[29]
n	Cl, Br, I, OTs	vinyl–Zr	$[Pd(acac)_2]$	LiBr, THF/NMP, 55 °C	[47]
n	Br, I	alkynyl–Cu	$[\{Pd(\eta\text{-}C_3H_5)Cl\}_2]$/CuI/IAdHCl	Cs_2CO_3, DMF/Et_2O, 45 °C	[48]
s	Cl, Br	CO	$PdBr_2$ (or $Pd(OAc)_2$, $[Pd_2(dba)_3]$) /PPh_3	NMP, LiBr, 80–120 °C, 20–100 bar	[63]

[a] IAd = 1,3-bis(adamantyl)imidazol-2-ylidene.

molecular mass, an excess of one reaction partner, and several additives. The progress made in the last few years in metal-catalyzed cross-coupling reactions of alkyl electrophiles with β hydrogen atoms makes us optimistic that the development of more efficient catalysts and reaction conditions might be expected in the near future. Furthermore, if selective (and even stereospecific) reactions with sterically hindered secondary and tertiary alkyl halides become possible, these cross-coupling methods will undoubtedly become part of the standard repertoire of synthetic organic chemistry for use in the synthesis of more complex molecules.

Received: July 26, 2004

[1] *Metal-Catalyzed Cross-Coupling Reactions* (Eds.: A. de Meijere, P. J. Stang), 2nd ed., Wiley-VCH, Weinheim, **2004**; *Transition Metals for Organic Synthesis* (Eds.: M. Beller, C. Bolm), 2nd ed., Wiley-VCH, Weinheim, **2004**.

[2] K. C. Nicolaou, E. J. Sorensen, *Classics in Total Synthesis*, VCH, Weinheim, **1996**, chap. 31.

[3] a) A. Zapf, M. Beller, *Top. Catal.* **2002**, *19*, 101 – 109; b) A. Zapf, M. Beller in *Handbook of Organopalladium Chemistry for Organic Synthesis*, *Vol. 1* (Ed.: E. I. Negishi), Wiley, New York, **2002**, p. 1209.

[4] Herein non-activated alkyl electrophiles are considered to be those alkyl halides that are not functionalized with activating groups in the α position. Because of the special reactivity of benzyl, allyl, propargyl, cyclopropyl, α-alkoxy alkyl, and α-carbonyl alkyl halides, their reactions are generally not covered.

[5] a) J. K. Kochi, M. Tamura, *J. Am. Chem. Soc.* **1971**, *93*, 1483 – 1485; b) J. K. Kochi, M. Tamura, *J. Am. Chem. Soc.* **1971**, *93*, 1485 – 1487; c) M. Tamura, J. K. Kochi, *J. Organomet. Chem.* **1972**, *42*, 205 – 228.

[6] T. Ishiyama, S. Abe, N. Miyaura, A. Suzuki, *Chem. Lett.* **1992**, 691 – 694.

[7] A. Devasagayaraj, T. Stüdemann, P. Knochel, *Angew. Chem.* **1995**, *107*, 2952 – 2954; *Angew. Chem. Int. Ed. Engl.* **1995**, *34*, 2723 – 2725.

[8] For recent reviews, see: a) D. J. Cardenas, *Angew. Chem.* **2003**, *115*, 398 – 401; *Angew. Chem. Int. Ed.* **2003**, *42*, 384 – 387; b) D. J. Cardenas, *Angew. Chem.* **1999**, *111*, 3201 – 3203; *Angew. Chem. Int. Ed.* **1999**, *38*, 3018 – 3020; c) T.-Y. Luh, M.-K. Leung, K.-T. Wong, *Chem. Rev.* **2000**, *100*, 3187 – 3204.

[9] For selected examples, see: a) S. Nunomoto, Y. Kawakami, Y. Yamashita, *J. Org. Chem.* **1983**, *48*, 1912 – 1914; b) M. E. Wright, M.-J. Jin, *J. Organomet. Chem.* **1990**, *387*, 373 – 379.

[10] P. L. Castle, D. A. Widdowson, *Tetrahedron Lett.* **1986**, *27*, 6013 – 6016.

[11] a) K. Yuan, W. J. Scott, *Tetrahedron Lett.* **1989**, *30*, 4779 – 4782; b) K. Park, K. Yuan, W. J. Scott, *J. Org. Chem.* **1993**, *58*, 4866 – 4870.

[12] G. Cahiez, S. Marquais, *Synlett* **1993**, 45 – 47.

[13] M. Tamura, J. K. Kochi, *Synthesis* **1971**, 303.

[14] J. G. Donkervoort, J. L. Vicario, J. T. B. H. Jastrzebski, R. A. Gossage, G. Cahiez, G. van Koten, *J. Organomet. Chem.* **1998**, *558*, 61 – 69.

[15] G. Cahiez, C. Chaboche, M. Jezequel, *Tetrahedron* **2000**, *56*, 2733 – 2737.

[16] K. Tamao, K. Zumitani, M. Kumada, *J. Am. Chem. Soc.* **1972**, *94*, 4374 – 4376.

[17] R. J. P. Corriu, J. P. Masse, *J. Chem. Soc. Chem. Commun.* **1972**, 144 – 145.

[18] J. Terao, H. Watanabe, A. Ikumi, H. Kuniyasu, N. Kambe, *J. Am. Chem. Soc.* **2002**, *124*, 4222 – 4223.

[19] J. Terao, Y. Naitoh, H. Kuniyasu, N. Kambe, *Chem. Lett.* **2003**, *32*, 890 – 891.

[20] P. W. Jolly, *Angew. Chem.* **1985**, *97*, 279 – 291; *Angew. Chem. Int. Ed. Engl.* **1985**, *24*, 283 – 295.

[21] J. Terao, A. Ikumi, H. Kuniyasu, N. Kambe, *J. Am. Chem. Soc.* **2003**, *125*, 5646 – 5647.

 © 2005 Wiley-VCH Verlag GmbH & Co. KGaA, Weinheim

[22] a) M. R. Netherton, C. Dai, K. Neuschütz, G. C. Fu, *J. Am. Chem. Soc.* **2001**, *123*, 10099 – 10100; b) J. H. Kirchhoff, C. Dai, G. C. Fu, *Angew. Chem.* **2002**, *114*, 2025 – 2027; *Angew. Chem. Int. Ed.* **2002**, *41*, 1945 – 1947; c) M. R. Netherton, G. C. Fu, *Angew. Chem.* **2002**, *114*, 4066 – 4068; *Angew. Chem. Int. Ed.* **2002**, *41*, 3910 – 3912; d) J. H. Kirchhoff, M. R. Netherton, I. D. Hills, G. C. Fu, *J. Am. Chem. Soc.* **2002**, *124*, 13662 – 13663.

[23] I. D. Hills, M. R. Netherton, G. C. Fu, *Angew. Chem.* **2003**, *115*, 5927 – 5930; *Angew. Chem. Int. Ed.* **2003**, *42*, 5749 – 5752.

[24] K. Arentsen, S. Caddick, F. G. N. Cloke, A. P. Herring, P. B. Hitchcock, *Tetrahedron Lett.* **2004**, *45*, 3511 – 3515.

[25] C. E. Tucker, P. Knochel, *J. Org. Chem.* **1993**, *58*, 4781 – 4782.

[26] a) R. Giovannini, T. Stüdemann, G. Dussin, P. Knochel, *Angew. Chem.* **1998**, *110*, 2512 – 2515; *Angew. Chem. Int. Ed.* **1998**, *37*, 2387 – 2390; b) R. Giovannini, T. Stüdemann, A. Devasagayaraj, G. Dussin, P. Knochel, *J. Org. Chem.* **1999**, *64*, 3544 – 3553.

[27] A. E. Jensen, P. Knochel, *J. Org. Chem.* **2002**, *67*, 79 – 85.

[28] a) A. Boudier, C. Darcel, F. Flachsmann, L. Micouin, M. Oestreich, P. Knochel, *Chem. Eur. J.* **2000**, *6*, 2748 – 2761; b) A. Boudier, E. Hupe, P. Knochel, *Angew. Chem.* **2000**, *112*, 2396 – 2399; *Angew. Chem. Int. Ed.* **2000**, *39*, 2294 – 2297.

[29] J. Zhou, G. C. Fu, *J. Am. Chem. Soc.* **2003**, *125*, 12527 – 12530.

[30] J. Zhou, G. C. Fu, *J. Am. Chem. Soc.* **2003**, *125*, 14726 – 14727.

[31] a) A. Fürstner, A. Leitner, M. Mendez, H. Krause, *J. Am. Chem. Soc.* **2002**, *124*, 13856 – 13863; b) S. J. Danishefsky, S. R. Chemler, D. Trauner, *Angew. Chem.* **2001**, *113*, 4676 – 4701; *Angew. Chem. Int. Ed.* **2001**, *40*, 4544 – 4568; c) N. Kataoka, Q. Shelby, J. P. Stambuli, J. F. Hartwig, *J. Org. Chem.* **2002**, *67*, 5553 – 5566.

[32] R. Shimizu, E. Yoneda, T. Fuchikami, *Tetrahedron Lett.* **1996**, *37*, 5557 – 5560.

[33] A. C. Frisch, N. Shaikh, A. Zapf, M. Beller, *Angew. Chem.* **2002**, *114*, 4218 – 4221; *Angew. Chem. Int. Ed.* **2002**, *41*, 4056 – 4059.

[34] a) A. C. Frisch, M. Beller, unpublished results; b) see also: A. C. Frisch, Dissertation, University of Rostock, **2003**.

[35] A. C. Frisch, F. Rataboul, A. Zapf, M. Beller, *J. Organomet. Chem.* **2003**, *687*, 403 – 409.

[36] T. Nagano, T. Hayashi, *Org. Lett.* **2004**, *6*, 1297 – 1299.

[37] M. Nakamura, K. Matsuo, S. Ito, E. Nakamura, *J. Am. Chem. Soc.* **2004**, *126*, 3686 – 3687.

[38] R. Martin, A. Fürstner, *Angew. Chem.* **2004**, *116*, 4045 – 4047; *Angew. Chem. Int. Ed.* **2004**, *43*, 3955 – 3957.

[39] J. Zhou, G. C. Fu, *J. Am. Chem. Soc.* **2004**, *126*, 1340 – 1341.

[40] R. Giovannini, P. Knochel, *J. Am. Chem. Soc.* **1998**, *120*, 11186 – 11187.

[41] R. Shimizu, T. Fuchikami, *Tetrahedron Lett.* **1996**, *37*, 8405 – 8408.

[42] H. Tang, K. Menzel, G. C. Fu, *Angew. Chem.* **2003**, *115*, 5233 – 5236; *Angew. Chem. Int. Ed.* **2003**, *42*, 5079 – 5082.

[43] J.-Y. Lee, G. C. Fu, *J. Am. Chem. Soc.* **2003**, *125*, 5616 – 5617.

[44] D. A. Powell, G. C. Fu, *J. Am. Chem. Soc.* **2004**, *126*, 7788 – 7789.

[45] T. Tsuji, H. Yorimitsu, K. Oshima, *Angew. Chem.* **2002**, *114*, 4311 – 4313; *Angew. Chem. Int. Ed.* **2002**, *41*, 4137 – 4139.

[46] K. Menzel, G. C. Fu, *J. Am. Chem. Soc.* **2003**, *125*, 3718 – 3719.

[47] S. L. Wiskur, A. Korte, G. C. Fu, *J. Am. Chem. Soc.* **2004**, *126*, 82 – 83.

[48] M. Eckhardt, G. C. Fu, *J. Am. Chem. Soc.* **2003**, *125*, 13642 – 13643.

[49] L.-M. Yang, L.-F. Huang, T.-Y. Luh, *Org. Lett.* **2004**, *6*, 1461 – 1463.

[50] a) I. Ryu, K. Nagahara, H. Yamazaki, S. Tsunoi, N. Sonoda, *Synlett* **1994**, 643; b) I. Ryu, N. Sonoda, *Angew. Chem.* **1996**, *108*, 1140; *Angew. Chem. Int. Ed. Engl.* **1996**, *35*, 1050.

[51] *Industrial Organic Chemistry* (Eds.: K. Weissermel, H.-J. Arpe), Wiley-VCH, Weinheim, **1997**.

[52] R. F. Heck, R. S. Breslow, *J. Am. Chem. Soc.* **1963**, *85*, 2779 – 2782.

[53] J. B. Woell, S. B. Fergusson, H. Alper, *J. Org. Chem.* **1985**, *50*, 2134 – 2136.

[54] K. E. Hashem, J. B. Woell, H. Alper, *Tetrahedron Lett.* **1984**, *25*, 4879 – 4880.

[55] R. Takeuchi, Y. Tsuji, M. Fujita, T. Konda, Y. Watanabe, *J. Org. Chem.* **1989**, *54*, 1831 – 1836.

[56] T. Konda, Y. Tsuji, Y. Watanabe, *Tetrahedron Lett.* **1988**, *29*, 3833 – 3836.

[57] a) H. Urata, O. Kosukegawa, Y. Ishii, H. Yugari, T. Fuchikami, *Tetrahedron Lett.* **1989**, *30*, 4403 – 4406; b) H. Urata, Y. Kinoshita, T. Asanuma, O. Kosukegawa, T. Fuchikami, *J. Org. Chem.* **1991**, *56*, 4996 – 4999; c) M. Imbeaux, H. Mestdagh, K. Moughamir, C. Rolando, *J. Chem. Soc. Chem. Commun.* **1992**, 1678 – 1679.

[58] H. Urata, Y. Ishii, T. Fuchikami, *Tetrahedron Lett.* **1989**, *30*, 4407 – 4410.

[59] H. Urata, H. Maekawa, S. Takahashi, T. Fuchikami, *J. Org. Chem.* **1991**, *56*, 4320 – 4322.

[60] TMU = *N*,*N*,*N*′,*N*′-tetramethylurea; DMI = 1,3-dimethyl-2-imidazolidinone; DMPU = 1,3-dimethyl-3,4,5,6-tetrahydro-2(1*H*)-pyrimidinone.

[61] H. Urata, N.-Y. Hu, H. Maekawa, T. Fuchikami, *Tetrahedron Lett.* **1991**, *32*, 4733 – 4736.

[62] H. Urata, D. Goto, T. Fuchikami, *Tetrahedron Lett.* **1991**, *32*, 3091 – 3094.

[63] a) M. Beller, M. Eckert, *Angew. Chem.* **2000**, *112*, 1027 – 1044; *Angew. Chem. Int. Ed.* **2000**, *39*, 1010 – 1027; b) M. Beller, M. Eckert, F. Vollmüller, S. Bogdanovic, H. Geissler, *Angew. Chem.* **1997**, *109*, 1534 – 1536; *Angew. Chem. Int. Ed. Engl.* **1997**, *36*, 1494 – 1496.

[64] A. Enzmann, M. Eckert, W. Ponikwar, K. Polborn, S. Schneiderbauer, M. Beller, W. Beck, *Eur. J. Inorg. Chem.* **2004**, 1330 – 1340.

[65] a) D. Gördes, H. Neumann, A. Jacobi von Wangelin, C. Fischer, K.-H. Drauz, H.-P. Krimmer, M. Beller, *Adv. Synth. Catal.* **2003**, *345*, 510 – 516; b) D. A. Freed, M. C. Kozlowski, *Tetrahedron Lett.* **2001**, *42*, 3403 – 3406; c) M. Beller, M. Eckert, W. Moradi, H. Neumann, *Angew. Chem.* **1999**, *111*, 1562 – 1565, *Angew. Chem. Int. Ed.* **1999**, *38*, 1454 – 1457; d) M. Beller, M. Eckert, W. A. Moradi, *Synlett* **1999**, 108 – 111; e) M. Beller, W. A. Moradi, M. Eckert, H. Neumann, *Tetrahedron Lett.* **1999**, *40*, 4523 – 4526; f) M. Beller, M. Eckert, E. W. Holla, *J. Org. Chem.* **1998**, *63*, 5658 – 5661; e) M. Beller, M. Eckert, H. Geissler, B. Napierski, H.-P. Rebenstock, E. W. Holla, *Chem. Eur. J.* **1998**, *4*, 935 – 941.

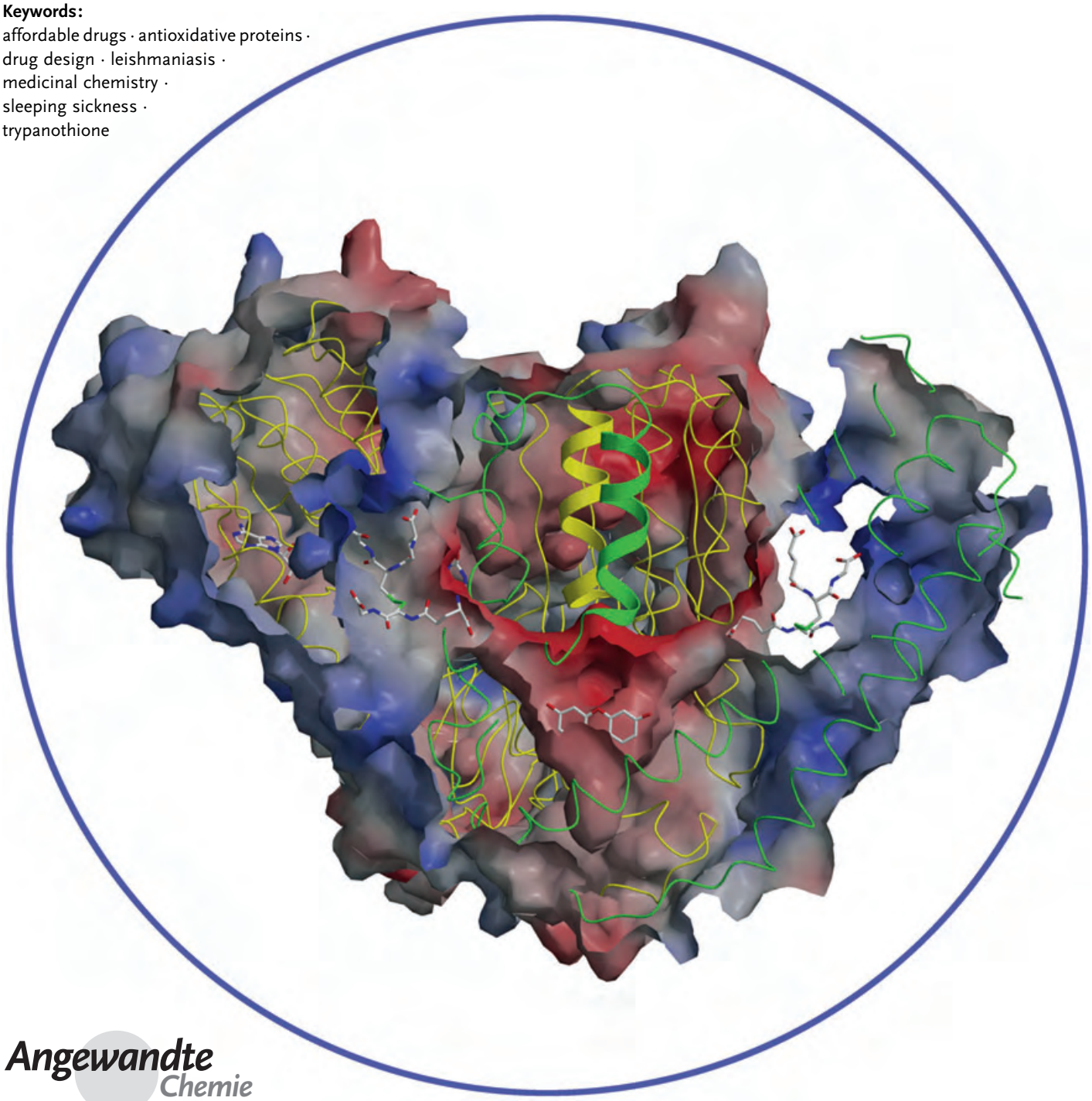
 © 2005 Wiley-VCH Verlag GmbH & Co. KGaA, Weinheim

Drug Design

Dithiol Proteins as Guardians of the Intracellular Redox Milieu in Parasites: Old and New Drug Targets in Trypanosomes and Malaria-Causing Plasmodia

R. Luise Krauth-Siegel, Holger Bauer, and R. Heiner Schirmer**

Keywords:
affordable drugs · antioxidative proteins · drug design · leishmaniasis · medicinal chemistry · sleeping sickness · trypanothione



Angewandte Chemie

© 2005 Wiley-VCH Verlag GmbH & Co. KGaA, Weinheim
DOI: 10.1002/anie.200300639

Parasitic diseases such as sleeping sickness, Chagas' heart disease, and malaria are major health problems in poverty-stricken areas. Antiparasitic drugs that are not only active but also affordable and readily available are urgently required. One approach to finding new drugs and rediscovering old ones is based on enzyme inhibitors that paralyze antioxidant systems in the pathogens. These antioxidant ensembles are essential to the parasites as they are attacked in the human host by strong oxidants such as peroxynitrite, hypochlorite, and H_2O_2. The pathogen-protecting system consists of some 20 thiol and dithiol proteins, which buffer the intraparasitic redox milieu at a potential of −250 mV. In trypanosomes and leishmania the network is centered around the unique dithiol trypanothione (N^1,N^8-bis(glutathionyl)spermidine). In contrast, malaria parasites have a more conservative dual antioxidative system based on glutathione and thioredoxin. Inhibitors of antioxidant enzymes such as trypanothione reductase are, indeed, parasiticidal but they can also delay or prevent resistance against a number of other antiparasitic drugs.

From the Contents

1. Present Chemotherapy of Trypanosomal Infections 691
2. New Strategies for the Development of Antitrypanosomal Drugs 693
3. The Thiol-Dependent Redox Metabolism of Trypanosomatids 693
4. Enzymes of the Trypanothione Metabolism as Potential Drug Targets 696
5. Drug Therapy and Prophylaxis of Malaria—Current Problems 701
6. The Thiol-Based Redox Network of Plasmodium falciparum 701
7. Enzymes of the Plasmodial Thiol Metabolism as Drug Targets 704
8. Outlook on Drug Development 708

1. Present Chemotherapy of Trypanosomal Infections

Trypanosomatids are parasitic protozoa within the order Kinetoplastida which comprise the causative agents of African sleeping sickness (*Trypanosoma brucei gambiense* and *T. b. rhodesiense*; see http://www.who.int/tdr/diseases/tryp), South American Chagas' disease (*T. cruzi*; see http://www.who.int/health-topics/chagas),[1] Nagana cattle disease (*T. congolense* and *T. b. brucei*), and the different forms of leishmaniasis (*Leishmania donovani*, *L. major*, and *L. tropica*).

Chemotherapy against all forms of trypanosomiasis is very limited and unsatisfactory (Table 1).[2] The current treatment of African sleeping sickness is based on four drugs of which two, suramin and pentamidine, are only active in the first stage of the disease when the parasites reside in the bloodstream and lymphatic system. The trivalent arsenic compound melarsoprol is used for the treatment of late-stage sleeping sickness when the parasites have established themselves in the central nervous system. Eflornithine (DFMO), the second drug capable of crossing the blood–brain barrier, is active against late-stage West African sleeping sickness caused by *T. brucei gambiense* but not against *T. brucei rhodesiense*, which is responsible for East African sleeping sickness. The only clinically available drugs for the chemotherapy of Chagas' disease are nifurtimox and benznidazole. Both compounds are active in the acute phase but their usefulness in the intermediate and late chronic stage of the infection is questionable. In addition, both drugs have serious side effects.

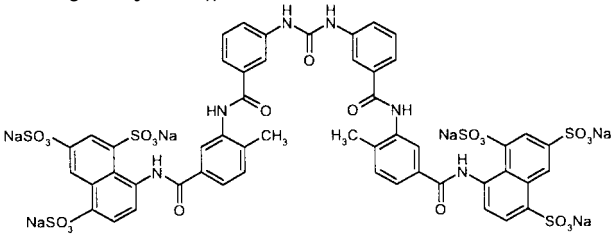
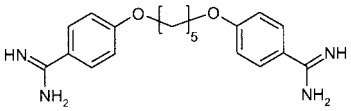
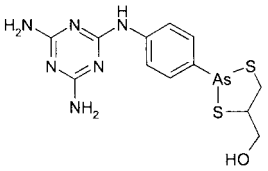
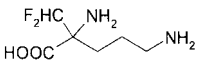
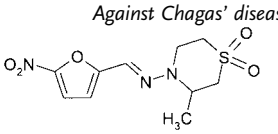
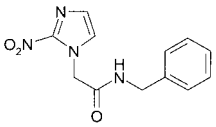
The mode of action is not fully understood for any of the current drugs, except eflornithine, and all of them appear to have multiple target sites. Arsenic compounds were the very first drugs against sleeping sickness, and the melaminophenyl derivative melarsoprol (MelB) is still the only effective drug against late-stage East African sleeping sickness. It is very toxic and about 5% of patients die of a reactive encephalopathy caused by the drug.[19] Melarsen oxide (MelOx), another melaminophenyl arsenical, is transported into *T. brucei* by the P2 adenosine/adenine transporter,[9] which is most probably identical to the transporter TbAT1.[20] The mechanisms for the uptake of arsenicals by the parasites and how they cross the blood–brain barrier have been reviewed recently.[3] Trypanosomes exposed to arsenicals rapidly undergo cell lysis but the underlying molecular mechanisms have yet to be established.

Trivalent arsenicals form stable complexes with numerous protein thiols and other (di)thiol compounds. In *T. brucei*, trypanothione as well as dihydrolipoate and dihydrolipoamide form adducts with melarsen oxide.[21] Besides many other enzymes, trypanothione reductase and lipoamide dehydrogenase (see below) are irreversibly inhibited by melarsen oxide owing to its interaction of their two vicinal active-site cysteine residues. Affinity chromatography with a melarsoprol analogue as a bait identified *T. brucei* glycerol-3-phosphate dehydrogenase as specifically binding to the column.[13]

[*] Prof. Dr. R. L. Krauth-Siegel, Dr. H. Bauer, Prof. Dr. R. H. Schirmer
Universität Heidelberg
Biochemie-Zentrum (BZH)
Im Neuenheimer Feld 504
D-69120 Heidelberg (Germany)
Fax: (+49) 6221-545-586
E-mail: krauth-siegel@urz.uni-heidelberg.de
heiner.schirmer@bzh.uni-heidelberg.de

 DOI: 10.1002/anie.200300639 © 2005 Wiley-VCH Verlag GmbH & Co. KGaA, Weinheim

Table 1: Current chemotherapy for African trypanosomiasis and Chagas' disease.

Drug	Structure	Uptake	Mode of action
	Against African trypanosomiasis		
suramin (introduced in 1922)		receptor-mediated endocytosis, for example, as a complex with LDL[a][3,4]; but see also reference [5]	unknown; the sulfonated naphthylamine interacts electrostatically with many enzymes[6,7]
pentamidine (1937)		multiple transporters[3,8,9], for example, the P2 adenine/adenosine transporter	the aromatic diamidine is enriched in the parasite to millimolar concentrations; thus there are many targets (proteins, lipids, minor groove of DNA[10–12])
melarsoprol (melB) (1949)		P2 (TbAT1) adenine/adenosine transporter[3,9]	unknown, the melaminophenyl-based organic arsenical form complexes with thiols and thiol proteins[13]
eflornithine (1990) (α-difluoromethylornithine)		probably a combination of passive and mediated diffusion[3]	suicide inhibitor of ornithine decarboxylase[14]
	Against Chagas' disease		
nifurtimox (lampit) (1970)		passive diffusion	induces increased oxygen consumption and the formation of hydrogen peroxide[15,16]
benznidazole (radanil) (1966)		has not been studied	covalent binding of reduced metabolites to macromolecules[17,18]

[a] LDL = low-density lipoprotein.

Eflornithine (DFMO, Table 1), originally developed as an anticancer drug, is the only modern chemotherapeutic agent against the West African sleeping sickness. It is a suicide inhibitor of ornithine decarboxylase, which in most organisms catalyzes the rate-limiting step in polyamine synthesis. Interestingly, the specificity of DFMO against *T. brucei gambiense* arises exclusively from the different half-lives of the host and parasite proteins.[14,22] Whereas the mammalian enzyme is turned over very rapidly within minutes, ornithine decarboxylase from *T. brucei gambiense* has an in vivo half-life of more than 18 h. It is susceptible to DFMO and the parasites stop proliferation after repeated treatment. The



Luise Krauth-Siegel studied chemistry in Heidelberg (1972–1979). After completing her PhD with Prof. Heinz A. Staab at the Max-Planck-Institut für Medizinische Forschung in 1982, she joined the Institut für Biochemie at Heidelberg University and earned her habilitation (1989). She was Visiting Professor at the University of Michigan (1995); subsequently she became professor and group leader at the newly founded BZH of Heidelberg University. Her current research focuses on enzymes of the parasite-specific trypanothione metabolism as targets for structure- and mechanism-based drug development.



Holger Bauer studied chemistry in Karlsruhe (1994–2000). He then conducted his PhD thesis work on the thioredoxin systems of the malaria mosquito and the fruit fly at the Biochemie-Zentrum of Heidelberg University (BZH). After pre- and postdoctoral studies on single-turnover kinetics of enzyme catalysis with Professor C. H. Williams and Professor V. Massey at the University of Michigan in Ann Arbor, he returned to the BZH to work on the design and synthesis of disulfide reductase inhibitors.

 © 2005 Wiley-VCH Verlag GmbH & Co. KGaA, Weinheim

failure to treat East African sleeping sickness with DFMO is probably due to the shorter half-life of the *T. brucei rhodesiense* enzyme together with its higher basal activity than that in *T. brucei gambiense*.[23] Although the primary target has clearly been established, the chain of events finally responsible for the cytostatic effect of DFMO is not fully understood. Treatment of *T. brucei* with DFMO increases the intracellular levels of ornithine, *S*-adenosylmethionine, and decarboxylated *S*-adenosylmethionine[24] and decreases the levels of putrescine, spermidine, and subsequently of the parasite-specific bis(glutathionyl)spermidine trypanothione (Figure 1a).[25,26] Furthermore, DFMO causes the arrest of the cell cycle.[27]

The two drugs used against Chagas' disease are the nitroaromatic compounds nifurtimox and benznidazole.[28] In *T. cruzi* cultures, nifurtimox induces increased O_2 consumption and the formation of hydrogen peroxide.[15] The reaction sequence starts with the single-electron reduction of the nitro group by a (flavo)enzyme to generate the nitro anion radical as revealed by electron spin resonance (ESR) measurements.[16] Subsequent reaction with molecular oxygen leads to superoxide anions, which then dismutate to give hydrogen peroxide. Benznidazole does not lead to superoxide and hydrogen peroxide production when applied at concentrations that inhibit *T. cruzi* growth.[29] The nitroimidazole is biotransformed into metabolites that covalently bind to DNA, lipids, and proteins of the parasite.[17,18]

It is most probably the lack of specificity of the old antitrypanosomal drugs that is the main reason for their long-lasting reliability and the overall slow development of resistance. Nevertheless, up to 20% of patients with secondary-stage sleeping sickness currently show resistance to melarsoprol.[19]

2. New Strategies for the Development of Antitrypanosomal Drugs

Only very few drugs are currently in clinical testing for the treatment of trypanosomal infections. One is megazol, a 5-nitroimidazole that was synthesized as early as 1968 but discarded because of a positive Ames test. When considering that many cancer drugs are licensed despite serious problems of toxicity and mutagenicity this constraint appears somehow bizarre. The ethical criteria concerning a drug for arsenical-refractory sleeping sickness are identical to those for untreatable cancer.[19]

Since the pharmaceutical industry has virtually ceased all activity in the development of drugs against tropical diseases, present efforts rely nearly exclusively on basic research in the public sector. One approach towards new antiparasitic drugs is aimed at the elucidation of the active principles of plants that were traditionally used against parasitic infections.[30] Another approach focuses on drugs that are in use for the treatment of other human diseases. Such compounds would have the advantage that they already passed several of the extremely expensive clinical trials necessary for the development of any new drug. Examples are aminobisphosphonates, which are administered for the treatment of osteoporosis and other bone diseases,[31,32] and imidazole or triazole derivatives that are used as antifungal agents.[33,34]

Trypanosomes diverged very early from the common eukaryotic lineage, and their biochemical composition differs in numerous aspects from that of mammalian cells. Thus parasite-specific processes may provide selective targets for drug development. Especially the genome projects will add a large number of species-specific pathways in the near future, as was impressively shown in the case of *P. falciparum*.[35] The complete genomes of *T. brucei*, *T. cruzi*, and *Leishmania major* will be available in 2005.

A simple difference between host and parasite, however, is not sufficient for an enzyme to be a drug-target molecule. Target validation is a prerequisite in the rational approach to chemotherapy. The oldest method to verify that the enzyme is essential for an organism is based on the use of a highly specific inhibitor, but such compounds are rarely available and genetic approaches such as knock-out mutants or the inducible depletion of the specific mRNA by RNA interference are now widely in use.[36,37] Even if an enzyme has been demonstrated to be essential for the parasite, it is not necessarily a drug target. In the case of a very abundant protein it will be difficult to maintain the required high drug concentrations of a reversibly binding inhibitor within the cell. Another important aspect is the in vivo half-life of the target because a rapid de novo synthesis of the protein will overcome the effect of an irreversible inhibitor.



Heiner Schirmer studied medicine and philosophy in Heidelberg and Basel and received his MD degree in 1966. After clinical internships in Germany and postdoctoral studies at Dartmouth Medical School, New Hampshire, he became group leader at the MPI für Medizinische Forschung in 1969. He completed his habilitation (1975) and was appointed professor of biochemistry at Heidelberg University (1980). Since 1976 he has been Bicentennial Lecturer in Boston and Philadelphia. In 2002 he won the Dream Action Award of the Dutch Chemistry Group DSM for his studies on the biochemistry and chemotherapy of malaria.

3. The Thiol-Dependent Redox Metabolism of Trypanosomatids

3.1. Occurrence and Biosynthesis of Trypanothione

Trypanosomatids differ from nearly all other eukaryotes and prokaryotes in their specific redox metabolism, which is based on the thiol–polyamine conjugate trypanothione and the flavoenzyme trypanothione reductase (Figures 1 and 2).[38] The trypanothione system [Eq. (1)] replaces the glutathione/glutathione reductase couple [Eq. (2)] and probably also the enzyme thioredoxin reductase (Figure 2b) in these parasites.[39]

$$TS_2 + NADPH + H^+ \rightarrow T(SH)_2 + NADP \quad (1)$$

 © 2005 Wiley-VCH Verlag GmbH & Co. KGaA, Weinheim

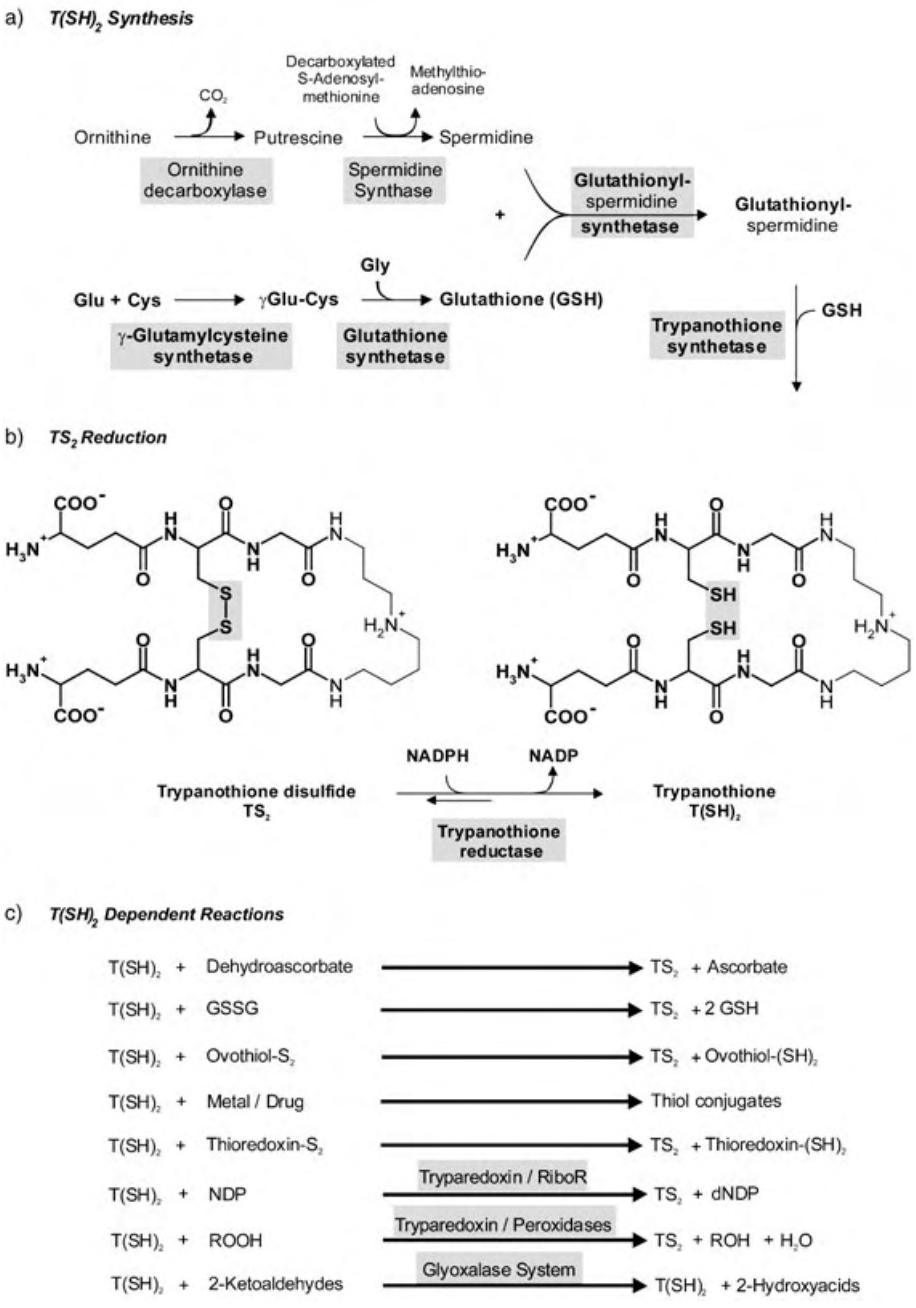


Figure 1. The trypanothione metabolism of trypanosomatids. a) Spermidine and glutathione (bold letters), the two components of trypanothione ($T(SH)_2$), are synthesized separately and then combined to the bis(glutathionyl)spermidine conjugate trypanothione. b) Trypanothione is kept in the reduced state by NADPH and the flavoenzyme trypanothione reductase. c) Trypanothione is a spontaneous reductant of dehydroascorbate as well as of the disulfides of glutathione, ovothiol A, and the parasitic thioredoxin. Trypanothione is involved in the synthesis of DNA precursors as well as in the detoxification of metals and drugs, hydroperoxides, peroxynitrite, and ketoaldehydes. The reaction sequence $T(SH)_2 + ONOO^- \rightarrow TS_2 + NO_2^- + H_2O$ is analogous to that shown for hydroperoxide reduction. NDP = nucleoside diphosphate, dNDP = deoxynucleoside diphosphate, RiboR = ribonucleotide reductase.

$$GSSG + NADPH + H^+ \rightarrow 2GSH + NADP \quad (2)$$

Other organisms reported to have a trypanothione metabolism are *Entamoeba histolytica*, the causative agent of amoebiasis (GenBank Acc. No AF503571),[40] as well as *Euglena gracilis*. The latter organism appears to have both trypanothione reductase and glutathione reductase at its disposal.[41]

Trypanothione is synthesized by conjugation of the polyamine spermidine and the tripeptide glutathione (Figure 1a). The first step in the biosynthesis of glutathione is catalyzed by γ-glutamylcysteine synthetase, an enzyme recently shown to be essential for *T. brucei*.[42] γ-Glutamylcysteine is then linked with glycine to form glutathione. A glutathione synthetase has not yet been characterized in any trypanosomatid organism, but a putative gene for it is localized on chromosome 14 of *L. major* (Acc. No AL356246). There is no uniform mechanism for the generation of spermidine in the different trypanosomatids. *T. cruzi* epimastigotes are unable to synthesize putrescine de novo, but take up polyamines from the medium and convert them into spermidine.[43,44] Although it is not known if this is also the case in the mammalian stage of the parasite, this is very likely. The intracellular amastigotes of *T. cruzi* multiply in the cytosol of the host cell and thus should have access to sufficient polyamines. In contrast, the extracellularly operating African trypanosomes synthesize spermidine endogenously from ornithine (Figure 1a).

The biosynthesis of trypanothione starts with the formation of monoglutathionylspermidine, which then reacts with a second glutathione molecule to give trypanothione. As depicted in Figure 1a, in the insect parasite *Crithidia fasciculata* distinct synthetases catalyze the two consecutive steps.[45] In contrast, a single polypeptide is responsible for both ATP-dependent reactions in *T. cruzi* as well as *T. brucei*.[46,47] The *T. cruzi* synthetase also accepts other polyamines as substrates which may be important under conditions in which spermidine becomes limiting.[47,48]

3.2. Comparison of Trypanothione and Glutathione

Trypanothione is an efficient spontaneous reductant of dehydroascorbate, glutathione disulfide, and of the disulfide form of ovothiol A (Figure 1c). (This mercaptohistidine, present in several trypanosomatids,[49–51] is a potent radical scavenger and catalyzes the decomposition of nitrosothiols such as nitrosoglutathione (GSNO) and bis(nitroso)trypanothione ($[T(SNO)_2]$.[52]) The redox potential of trypanothione (−242 mV)[53] is similar to that of glutathione (−230

 © 2005 Wiley-VCH Verlag GmbH & Co. KGaA, Weinheim

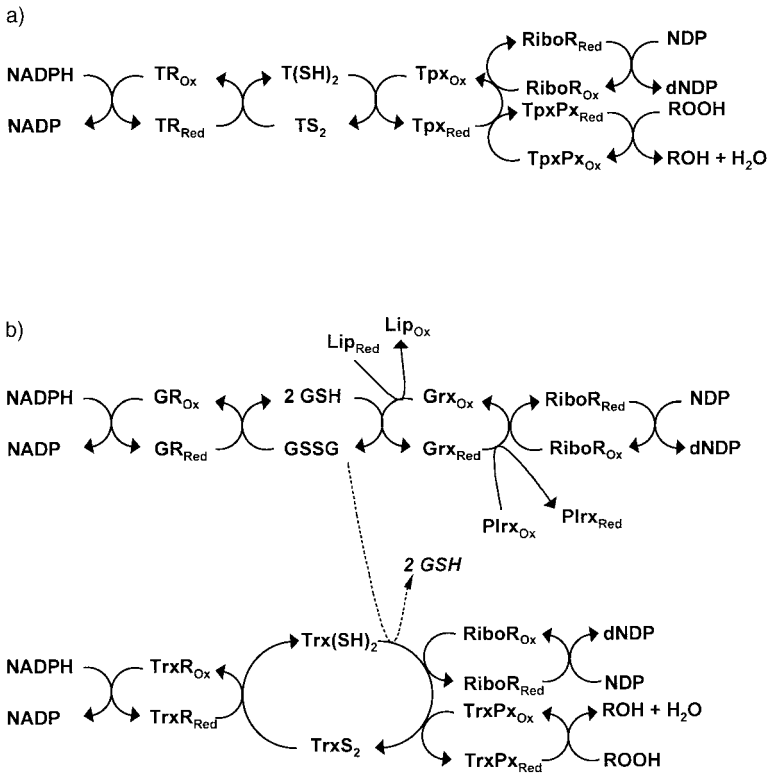


Figure 2. Dithiol-based redox systems of trypanosomes and *Plasmodia*. a) In trypanosomes, a cascade composed of trypanothione reductase (TR), trypanothione ($T(SH)_2$), and tryparedoxin (Tpx) transfers electrons from NADPH to ribonucleotide reductase (RiboR)—which catalyzes the reduction of nucleoside diphosphates (NDP) to deoxynucleoside diphosphates (dNDP), precursors of DNA synthesis—as well as to various tryparedoxin peroxidases (TpxPx) that catalyze the detoxification of hydroperoxides (ROOH). At high concentrations, trypanothione directly reduces ribonucleotide reductase as well as hydroperoxides. b) In *P. falciparum*, two different systems occur. The glutathione system, consisting of glutathione reductase (GR), glutathione (GSH), and glutaredoxin (Grx), transfers electrons to ribonucleotide reductase either directly or through plasmoredoxin (Plrx). Glutaredoxin can also be reduced by lipoamide (Lip). The second system is composed of thioredoxin reductase (TrxR) and thioredoxin (Trx); it delivers reducing equivalents for the synthesis of DNA precursors and is the electron donor for a thioredoxin-dependent peroxidase (TrxPx). The two systems are connected, as glutathione disulfide (GSSG) can be reduced by thioredoxin (dashed line). All three dithiol proteins (glutaredoxin, plasmoredoxin, and thioredoxin) can act as thiol transferases, which convert proteins from the oxidized into the reduced state. The subscript "Ox" stands for the disulfide and the subscript "Red" for the dithiol form of a protein.

to −250 mV) and is thus not responsible for the higher reactivity of the parasite compound. One crucial difference is that trypanothione is a dithiol and thus kinetically favored as a reductant of disulfides.[54] A second striking difference concerns the thiol pK_a values. The trypanothione thiols have a low pK_a value of 7.4,[55] probably as a result of the positively charged nitrogen atom in the spermidine bridge, whereas the pK_a value of glutathione is in the order of 8.7 to 9.2. The pK_a of trypanothione coincides with the intracellular pH of the parasites.[56] This certainly contributes to its reactivity, as the second-order rate constants for thiol–disulfide exchange reactions exhibit an optimum when the pK_a value of the thiol is equal to the pH value of the surrounding solution.[54]

The reducing capacity of trypanothione is strongly enhanced in the presence of tryparedoxin, a small dithiol protein of the parasites. The trypanothione/tryparedoxin couple plays a central part in parasite-specific cascades that catalyze the reduction of hydroperoxides[57–59] and ribonucleotides (Figure 2a).[60] In addition, trypanothione is probably the physiological reductant of *T. brucei* thioredoxin, as a specific thioredoxin reductase has not yet been identified in any kinetoplastid organism (Figure 1c).[39]

3.3. Trypanothione in Drug Resistance

Extrusion or sequestration of drug–thiol conjugates is an important mechanism in drug resistance. In *Leishmania* that are resistant to trivalent arsenic or antimony, the PGPA (P-glycoprotein-like protein A) gene is frequently found to be amplified.[61,62] This ATP-binding cassette (ABC) transporter has been shown to force out arsenite–glutathione conjugates.[63] Because trypanothione forms adducts with arsenite and antimonite in *L. tarentolae*[64,65] it is most likely the physiological thiol in conjugates transported by PGPA. In bloodstream *T. brucei*, overexpression of multidrug resistance-associated protein A, which is structurally closely related to the *L. tarentolae* PGPA, resulted in a tenfold increase in the IC_{50} value for the arsenical drug melarsoprol.[66]

3.4. Trypanothione-Dependent Detoxication of Hydroperoxides

Trypanosomes tolerate only low levels of hydroperoxides,[67] probably because they lack the enzymes catalase and selenocysteine-containing glutathione peroxidase. Three classes of peroxidases have been characterized in trypanosomatids so far, and in each case trypanothione is the electron donor. The first is a 2 Cys-peroxiredoxin-type enzyme (Figure 2a).[57,59,68] Members of the second class are structurally related to glutathione peroxidases but contain a catalytic cysteine instead of selenocysteine.[69,70] They show very low activity with glutathione as an electron donor but much higher activities with the trypanothione/tryparedoxin couple.[70] Both types of peroxidases, the cytosolic peroxiredoxin- and the glutathione peroxidase-type enzymes appear to be essential for *T. brucei* viability.[71] The third class of parasite peroxidases is a plantlike ascorbate-dependent heme enzyme found in the endoplasmic reticulum of *T. cruzi*.[72] Dehydroascorbate formed in the enzymatic reaction is then

 © 2005 Wiley-VCH Verlag GmbH & Co. KGaA, Weinheim

reduced by trypanothione (Figure 1c). None of the trypanosomal peroxidases has a catalytic efficiency comparable with that of classical selenocysteine-containing glutathione peroxidases. This may at least partially be compensated by their high cellular concentrations.[59] Another explanation for the relatively low catalytic efficiencies might be that these enzymes have additional physiological functions.[73]

3.5. Trypanothione-Dependent Reduction of Peroxynitrite

Peroxynitrite ($ONOO^-$), the reaction product between superoxide radical and nitric oxide radical, is not only a tyrosine-nitrating agent but also a powerful oxidant that contributes to human macrophage competence against pathogens. Trypanothione, $T(SH)_2$, is readily converted into trypanothione disulfide, TS_2, when *T. cruzi* cells are exposed to peroxynitrite.[74] In contrast, glutathione, which is present in *T. cruzi* at lower concentrations than trypanothione, mainly forms mixed disulfides with protein cysteines upon treatment with peroxynitrite.

Peroxynitrite can oxidize $T(SH)_2$ directly; alternatively, $T(SH)_2$ is consumed secondarily to the reactions of peroxynitrite with tryparedoxin peroxidase and tryparedoxin (Figures 1c and 2a). Peroxynitrite-derived carbonate and nitrogen dioxide radicals can be formed in the presence of CO_2 and promote one-electron oxidations. In the case of $T(SH)_2$, the thiyl radical yields a transient disulfide radical anion, which ultimately leads to the disulfide. For glutathione, the thiyl radical can either combine with protein thiols (proteinSH) to form mixed disulfides (PSSG; see Table 3 in Section 6) or react with molecular oxygen to yield products with higher oxidation states of sulfur. These findings support a protective key role of $T(SH)_2$ and the trypanothione-dependent antioxidative system in *T. cruzi* against peroxynitrite which may facilitate the survival of trypanosomes in the oxidative environment produced by activated macrophages.[74]

3.6. Detoxication of Ketoaldehydes

The ubiquitous glyoxylase system, composed of glyoxalase I and II, catalyzes the glutathione-dependent dismutation of ketoaldehydes into the respective hydroxyacids. Its main physiological substrate is methylglyoxal, which is formed as an inevitable by-product of glycolysis. *T. brucei* has a glyoxalase II that exerts high preference for trypanothione over glutathione thioesters.[75] This shows that glutathione is replaced by trypanothione in this pathway too (Figure 1c).

4. Enzymes of the Trypanothione Metabolism as Potential Drug Targets

The sensitivity of trypanosomatids towards oxidative stress and the absence of trypanothione in the mammalian host render the enzymes of the trypanothione metabolism attractive drug-target molecules.[2,76–79] The first report suggesting that interference with the redox metabolism of trypanosomes can be exploited for drug development dealt with buthionine sulfoximine (BSO), an inhibitor of γ-glutamylcysteine synthetase (Figure 1a). BSO cures mice infected with *T. brucei*[80] and decreases the infectivity of amastigote *L. donovani*.[81] As already described, difluoromethylornithine (DFMO; Table 1) is a suicide inhibitor of ornithine decarboxylase and leads to a decrease in cellular trypanothione levels.

Of the trypanothione synthesis enzymes, glutathionylspermidine synthetase and trypanothione synthetase may become attractive drug-target molecules because they have no counterparts in the mammalian host. As outlined above (Figure 1a), in *T. cruzi and T. brucei* a single polypeptide is responsible for both consecutive steps.[46,47,82] So far the glutathionylspermidine synthetase/amidase (GspS) species from *E. coli* and *C. fasciculata* are used in inhibitor design studies. A phosphinate substrate analogue proved to be an efficient slow-binding inhibitor of the *E. coli* enzyme with a K_i value of 3.2 μM and a K_i^* value of 7.8 nM.[83] γ-Glu-Leu-X derivatives (X = nucleophilic group) are mixed-type inhibitors of glutathionylspermidine synthetase from *C. fasciculata*, the most efficient compounds with K_i and K_i' values in the low micromolar range.[84] The fact that the synthesis of trypanothione is not identical in trypanosomes and *C. fasciculata* raises the question as to whether the enzymes from the insect parasite are appropriate models in drug design studies.

4.1. Inhibitors of Trypanothione Reductase

Trypanothione reductase is the most thoroughly studied enzyme of the trypanothione redox metabolism. It is a key enzyme of the parasite antioxidant defense, does not occur in the mammalian host, and is essential for all trypanosomatids studied so far.[85] Trypanothione reductase belongs to the protein family of FAD disulfide oxidoreductases, which comprise glutathione reductase, lipoamide dehydrogenase, thioredoxin reductase, etc. (Figure 3).[86] The catalytic mechanism of trypanothione reductase closely resembles that of glutathione reductase (Figure 3a and b and Section 7.3).[87,88] The main difference is the specificity for their respective disulfide substrates. Furthermore, with a dimension of approximately $22 \times 20 \times 28$ Å^3, the disulfide substrate binding site of trypanothione reductase is much wider than that of glutathione reductase. The three-dimensional structure of trypanothione reductase has been solved in free form,[92–94] in complex with the substrates NADPH,[94] glutathionylspermidine,[95] and trypanothione,[96] and with the competitive inhibitor mepacrine[91] (Figure 4, Table 2).

During the last 15 years, numerous studies have aimed at inhibitors of trypanothione reductase that are suited as lead compounds for the development of new antiparasitic drugs (for reviews, see references [76,85,116–118]). Most approaches were focused on compounds that inhibit the parasite enzyme but not human glutathione reductase, the closest related host enzyme. A drawback of high-throughput screenings for putative trypanothione reductase inhibitors is the high cost of trypanothione disulfide. A recently developed

 © 2005 Wiley-VCH Verlag GmbH & Co. KGaA, Weinheim

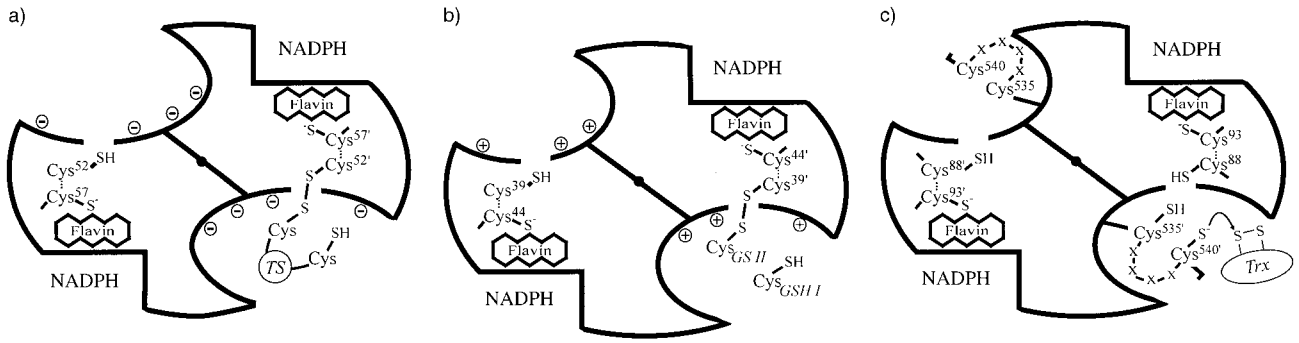


Figure 3. Schematic representation of *T. cruzi* trypanothione reductase, *P. falciparum* glutathione reductase, and thioredoxin reductase. There are two identical active sites per homodimeric enzyme. The dimer interface is shown as a diagonal line with a filled circle at the center, which represents the molecular twofold symmetry axis. In one subunit the residues are labeled with primed numbers. a) In trypanothione reductase, electrons flow from NADPH through the flavin ring to the active-site disulfide between Cys52 and Cys57. In the resulting dithiol form of the enzyme, the thiolate57 interacts with the flavin and Cys52 attacks trypanothione disulfide to form a mixed disulfide with one of the substrate thiol groups (shown here).The mixed disulfide is then attacked by Cys57, releasing trypanothione and regenerating the protein disulfide bridge. Trypanothione reductase only accepts positively charged glutathionylsperimidine conjugates as substrates, whereas glutathione reductase is specific for glutathione disulfide, which has an overall charge of −2. This specificity is mainly the result of an exchange of five residues, which makes the active center of the trypanosomal enzyme negatively charged and more hydrophobic than the GSSG-binding site in the glutathione reductase (Figures 3 a, b and 4).[90] Furthermore, the active site of trypanothione disulfide is much more spacious than that of glutathione reductase. *T. cruzi* trypanothione reductase and *P. falciparum* glutathione reductase do not have a C-terminal redox center as is the case in *P. falciparum* thioredoxin reductase (Figure 3 c). Rather, their disulfide substrates are bound at a position equivalent to Cys535′ and Cys540′ of thioredoxin reductase. b) In glutathione reductase, the electrons flow from NADPH to flavin and from there to the disulfide between Cys44 and Cys39. The resulting dithiol consists of thiolate 44 interacting with the flavin and the interchange thiol 39, which attacks the substrate GSSG. This leads to the release of one GSH, whereas the second is bound as a mixed disulfide to Cys39. This intermediate, the glutathionylated enzyme, is shown here. In a final step of the catalytic cycle, the mixed disulfide is attacked by the thiolate of Cys44, GSH is released, and the original disulfide bridge of the active site (Cys44/Cys39) forms again. c) The first catalytic cycle of thioredoxin reductase starts in a state of the active site, in which all cysteine residues are present as disulfides. When NADPH binds, its electrons flow through the flavin to the disulfide Cys93/Cys88. The resulting dithiol reduces the disulfide between Cys535′ and Cys540′, and hence the electrons are transferred to the disulfide bridge of the substrate thioredoxin. The figure shows the intermediate in which a mixed disulfide is formed between the enzyme and substrate. At this stage a second NADPH can again reduce the disulfide Cys93/Cys88. A nucleophilic attack of Cys535′ on the mixed disulfide leads to the release of the product $Trx(SH)_2$ and the regeneration of the disulfide bridge between the C-terminal residues Cys535′ and Cys540′. In subsequent catalytic cycles only one NADPH is consumed.[89]

assay with 5,5′-dithiobis-(2-nitrobenzoate) (DTNB) to maintain constant concentrations of the disulfide substrate should now allow kinetic studies at trypanothione concentrations as low as 1 μM.[119]

4.1.1. ***Polyamine-Based Inhibitors***

The largest group of inhibitors studied so far bind to trypanothione reductase reversibly (Table 2). Kukoamine A, a natural spermine derivative from the root bark of *Lycium chinensea*, is a mixed-type inhibitor of trypanothione reductase.[97] Several spermidine and spermine-based compounds have been synthesized. In many cases, the spermine derivatives were significantly more effective than the corresponding spermidines, and high-affinity ligands with K_i values in the submicromolar range have been obtained.[105] Screening of a library of spermidine–peptide conjugates revealed several highly efficient noncompetitive inhibitors. A structure–activity relationship study of *N*-(3-phenylpropyl)-substituted spermine and spermidines yielded N^1,N^1,N^4,N^8,N^{12}-penta(3-phenylpropyl)spermine (Table 2) as the most effective competitive inhibitor of *T. cruzi* trypanothione reductase.[99] The compounds of this series were strong trypanocides but a clear correlation between enzyme inhibition and antiparasitic activity was not observed.

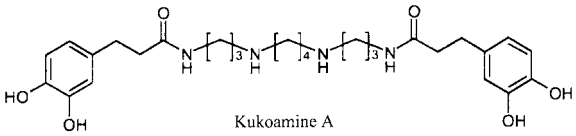
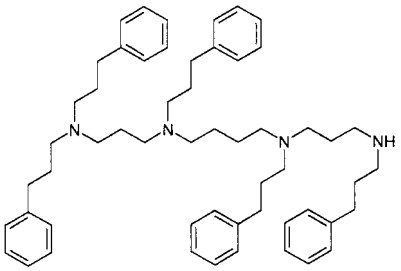
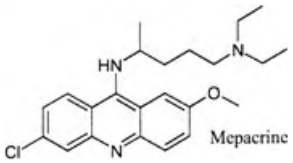
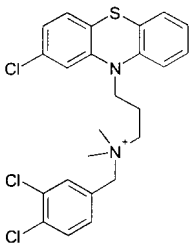
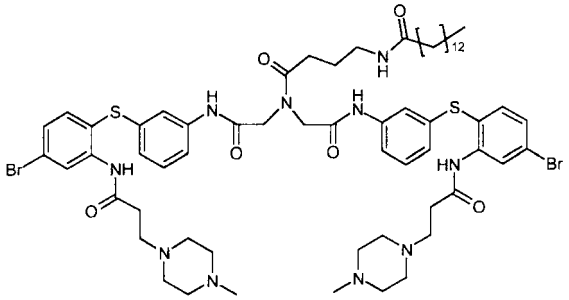
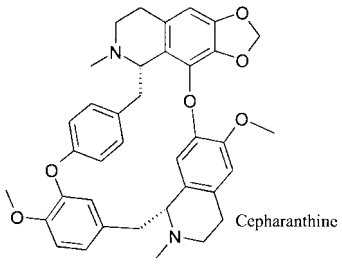
4.1.2. ***Tricyclic Compounds***

The acridine drug mepacrine (quinacrine) (Table 2 and Figure 4) has strong trypanocidal activity against *T. cruzi* and prevents the transmission of Chagas' disease by blood transfusion.[120] Mepacrine was the first tricyclic compound identified as a competitive inhibitor of *T. cruzi* trypanothione reductase but not of human glutathione reductase.[100] The acridine ring is fixed at the active site close to the hydrophobic wall formed by Trp21 and Met113, and the alkylamino side chain points towards the side chain of Glu18. Specific pairwise interactions between functional groups of the drug and the protein are with those residues that are not conserved in human glutathione reductase (Figure 4).[91] A subsequent kinetic analysis showed that trypanothione reductase can bind more than one molecule of the competitive 9-aminoacridine. In contrast, structurally related 9-thioacridines showed mixed-type inhibition.[100] Sulfonamide and urea derivatives of mepacrine with an aromatic group in the N9 side chain inhibit the enzyme with tenfold lower IC_{50} values than mepacrine and they are active against cultures of *L. donovani* and *T. brucei*.[121]

Phenothiazine, imipramine, and other tricyclic compounds used as antidepressant drugs are also competitive inhibitors of trypanothione reductase with low micromolar

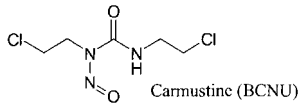
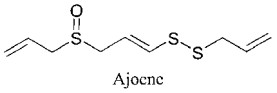
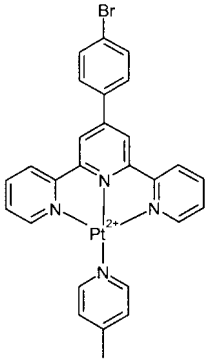
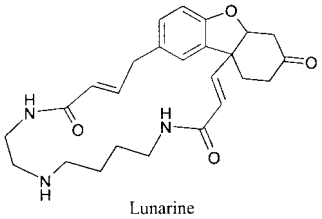
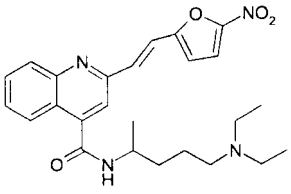
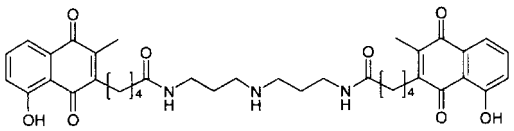
 © 2005 Wiley-VCH Verlag GmbH & Co. KGaA, Weinheim

Table 2: Inhibitors of trypanothione reductase studied as lead compounds for the development of antitrypanosomal drugs.

Inhibitor types	Examples	Mode of action
	reversible inhibitors	competitive, noncompetitive, uncompetitive and mixed-type inhibition
polyamines	 Kukoamine A	mixed-type, $K_i = 1.8\ \mu M$, $K_i' = 13\ \mu M$[97]
	H-Trp-Arg-Spermidine-Arg(Pmc)-Trp-H	noncompetitive, $K_i = 100\ nM$[98]
	 N^1,N^1,N^4,N^8,N^{12}-Penta-(3-phenylpropyl)spermine	competitive, $K_i = 151\ nM$[99]
tricyclic compounds	 Mepacrine	mepacrine and other 9-aminoacridines act competitively, $K_i = 5$–$45\ \mu M$, with more than one inhibitor molecule binding simultaneously; 9-thioacridines are mixed-type inhibitors, $K_i = 21$–$37\ \mu M$; $K_i' = 67$–$83\ \mu M$[91,100]
		competitive, $K_i = 120\ nM$;[101,102] other phenothiazines are competitive inhibitors with K_i values in the low micromolar range[101,102]
		mixed type, $IC_{50} = 200\ nM$;[103,104] other aminodiphenylsulfides (opened phenothiazines) are mixed-type or competitive inhibitors ($IC_{50} = 0.3$–$3\ \mu M$)[103–105]
	 Cepharanthine	mixed-type, $K_i = 7.6\ \mu M$, $K_i' = 51.6\ \mu M$[30]

© 2005 Wiley-VCH Verlag GmbH & Co. KGaA, Weinheim

Table 2: (Continued)

Inhibitor types	Examples	Mode of action
	irreversible inhibitors	time-dependent inactivation of the reduced enzyme
	 Carmustine (BCNU)	carbamoylation of Cys52[106,107]
	 Ajoene	modification of Cys52[108]
		complex formation with Cys52 after replacement of the fourth ligand[109]
	 Lunarine	$K_i = 144\ \mu M$; $k_{inact} = 0.116\ min^{-1}$[96,110]
	subversive substrates (turncoat inhibitors)	they inhibit the physiological reduction of trypanothione disulfide and are redox-cycling agents; that is they are reduced by the enzyme at the expense of NADPH and subsequently reoxidized by O_2
	 Chinifur	noncompetitive, $K_i = 4.5\ \mu M$; $k_{cat} = 3\ s^{-1}$; $k_{cat}/K_m = 3.2 \times 10^4\ M^{-1} s^{-1}$;[111] nitrofurans are reduced by the enzyme to the nitroanion radical, which reacts with molecular oxygen to give superoxide anion radical, the nitrofuran being recycled[111–114]
		$IC_{50} = 450\ nM$, $K_m = 28\ \mu M$, $k_{cat}/K_m = 1.1 \times 10^5\ M^{-1} s^{-1}$;[115] naphthoquinones are reduced to the semiquinone, which reacts with molecular oxygen to the superoxide anion radical and the quinone is thus regenerated[112,113,115]

inhibition constants.[101] The compounds have been modeled into the active site of trypanothione reductase with the ring moiety lodged against the hydrophobic wall formed by Trp21 and Met113 and the aminopropyl chain pointing towards Glu465′ and Glu466′; these two residues are provided by the other subunit of the homodimeric protein. A second hydrophobic region, which is named the Z-site and is mainly formed by Phe395′, Pro397′, and Leu398′, was later proposed also to accommodate hydrophobic ligands.[102,122] The most evident discrepancy between the docking studies on tricyclic antidepressants and the analysis of the trypanothione reductase–mepacrine structure is the binding mode of the aminoalkyl side chain of the inhibitors. Only the rigid-body docking approach used by Horvath (1997)[123] includes a possible interaction with Glu18, as was observed in the trypanothione reductase–mepacrine structure. In contrast to Glu18, Glu465′

 © 2005 Wiley-VCH Verlag GmbH & Co. KGaA, Weinheim

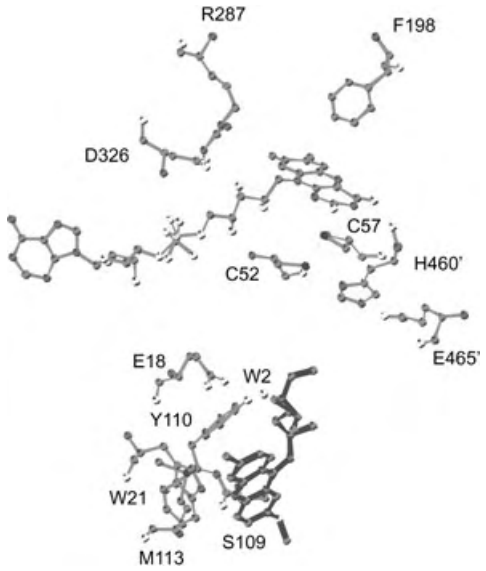


Figure 4. Active site of *T. cruzi* trypanothione reductase with bound mepacrine. The flavin ring of FAD forms the center of the active site. The dashed line marks the redox-active dithiol/disulfide. His460′ and Glu465′ are residues provided by the second subunit of the homodimeric protein. Mepacrine (bold lines) binds with the acridine ring close to the hydrophobic wall formed by Trp21 and Met113, and the alkylamino chain is fixed to Glu18 through a solvent molecule (W2). Residues at the trypanothione binding site, which differ in trypanothione reductase and human glutathione reductase, are: Glu18 (Ala34 in glutathione reductase), Trp21 (Arg37), Ser109 (Ile113), Met113 (Asn117), and Ala342 (Arg347).[91]

and Glu466′ are conserved in the host glutathione reductase and it is therefore not clear how an interaction with these residues accounts for the selective binding of positively charged ligands to the parasite enzyme. The finding that 9-aminoacridines are competitive inhibitors with more than one inhibitor molecule bound to the enzyme simultaneously offers the possibility that both binding sites are occupied.[100] Another possibility is that the second binding site is a cavity at the twofold axis of the homodimeric protein. This is exemplified by the binding of dinitrophenylglutathione in glutathione reductase crystals. The substrate analogue, showing the same type of inhibition kinetics as the 9-aminoacridines, causes high electron density at the GSSG binding site but also some density at the twofold axis.[124]

Substituted benzyl[3-(2-chloro-phenothiazine-10-yl)propyl]dimethylammonium salts (Table 2) were synthesized to introduce a permanent positive charge into inhibitor molecules. The quaternary arylalkylammonium chloropromazines were linear competitive inhibitors against trypanothione disulfide. The strongest inhibitor of this series yielded a K_i value of 120 nM, which is a 100-fold lower inhibitor constant than that of chloropromazine.[102]

4.1.3. *Aminodiphenylsulfides*

Opening of the central ring of phenothiazines generated 2-aminodiphenylsulfides that were nearly as powerful inhibitors as their conformationally restricted parent analogues. Linkage of two 2-aminodiphenylsulfide moieties by a spermine bridge resulted in a competitive inhibitor with a K_i value of 400 nM.[105] Bis(2-aminodiphenylsulfides) with a secondary amino group in the linker allowed the introduction of a third bulky side chain.[104] The most efficient derivative had an IC_{50} value of 200 nM in the presence of 57 μM trypanothione disulfide (Table 2). The further increase in binding strength shows that the active site of trypanothione reductase easily accommodates extremely bulky ligands.

4.1.4. *Irreversible Inhibitors*

Covalent inhibitors have the advantage that substrate accumulation cannot overcome inhibition. The nitrosourea drug carmustine (BCNU, Table 2) is an irreversible inhibitor of trypanothione reductase but also inactivates human glutathione reductase. BCNU acts syncatalytically by carbamoylating an active-site cysteine residue that becomes available only upon reduction of these enzymes by NADPH.[106,125] Ajoene (4,5,9-trithiadodeca-1,6,11-triene-9-oxide, Table 2), the spontaneous degradation product of allicin, the major sulfur component of garlic, is known for its antifungal, antiviral, antitrypanosomal, and antimalarial activity. Ajoene is a subversive substrate and a covalent inhibitor of both reductases, and the modified enzymes show increased NADPH oxidase activity.[108] (2,2′:6′,2″-Terpyridine)platinum(II) complexes (Table 2) are irreversible ligands of *T. cruzi* trypanothione reductase but not of human glutathione reductase.[109] The organometallic complexes are probably fixed in the active site through coordination of the platinum ion to Cys52 after replacement of the fourth ligand. Also in this case, inactivation of the enzyme is accompanied by an increase in NADPH oxidase activity. Blocking the redox-active cysteinyl residue (Cys52 in *T. cruzi* trypanothione reductase), which physiologically interacts with the disulfide substrate, clearly shifts the electron density in the reduced enzyme towards the flavin and thus promotes the direct reduction of molecular oxygen at the isoalloxazine ring. Unexpectedly, formation of chimeric ligands between a (2,2′:6′,2″-terpyridine)platinum(II) complex and 9-aminoacridine did not maintain the irreversible type of inhibition but resulted in strong mixed-type inhibitors.[126] These findings underscore once again the difficulties of structure–activity predictions for trypanothione reductase inhibitors: the extended active site evidently allows many different binding modes.

4.1.5. *Subversive Substrates*

A subversive agent (turncoat or sabotage inhibitor) is a molecule that converts an antioxidative disulfide reductase into a prooxidative enzyme.

Nitrofurans and naphthoquinones act as subversive substrates of trypanothione reductase and other flavoenzymes.[111–115] Typical subversive substrates (X) are reduced in single-electron steps to the respective radicals [Eq. (3)], which then react with molecular oxygen to yield superoxide anion radicals [Eq. (4)]:

 © 2005 Wiley-VCH Verlag GmbH & Co. KGaA, Weinheim

$$NADPH + 2X \rightarrow NADP + 2X^{\bullet -} + H^{+} \quad (3)$$

$$2X^{\bullet -} + 2O_2 \rightarrow 2X + 2O_2^{\bullet -} \quad (4)$$

In the case of trypanothione reductase, this process leads to an impaired physiological reduction of trypanothione disulfide, the waste of NADPH and O_2, and a lowered cellular thiol/disulfide ratio. As the reaction of the radical intermediate with molecular oxygen regenerates the subversive substrate, the compounds act as catalysts for oxidative stress; thus they are expected to have a strong impact on the redox metabolism of the parasite.[107] In a comparative study, antimicrobial nitrofuran drugs were investigated for their ability to inhibit and/or to serve as subversive substrates of *T. cruzi* trypanothione reductase and *T. cruzi* lipoamide dehydrogenase, as well as mammalian glutathione reductase and lipoamide dehydrogenase.[114] The compounds were moderate inhibitors of human glutathione reductase and *T. cruzi* trypanothione reductase but not at all of lipoamide dehydrogenase. In contrast, the parasite lipoamide dehydrogenase showed the highest rates of nitrofuran reduction. Chinifur, a nitrofuran derivative with an aminoalkyl side chain (Table 2), is an inhibitor and subversive substrate of trypanothione reductase,[111] but it interacts weakly with lipoamide dehydrogenase.[114] Trypanothione reductase seems not to be involved in nifurtimox resistance since sensitive and resistant *T. cruzi* strains show identical trypanothione reductase mRNA levels.[127] In contrast to nitrofurans, 5-nitroimidazoles such as megazol, currently being reevaluated as a drug against Chagas' disease, do not act as redox cyclers; rather they cause a depletion of trypanothione and thus also interfere with the thiol metabolism of the parasite.[128]

Naphthoquinones such as menadione, plumbagin, and lapachol, display notable trypanocidal activities and interact with trypanothione reductase, lipoamide dehydrogenase, as well as human glutathione reductase. Menadione, plumbagin, and other 1,4-naphthoquinones are inhibitors and subversive substrates for trypanothione reductase.[112–115] The ability of lipoamide dehydrogenase to reduce quinones is well known since the yeast enzyme was first described as a menadione reductase. In lipoamide dehydrogenase from *Mycobacterium tuberculosis,* quinone reduction occurs by the four-electron-reduced enzyme (EH_4) in which both the flavin and the redox-active cysteines are present in reduced states. EH_2, which contains flavin in the oxidized form, is the catalytic intermediate in disulfide substrate reduction but is ineffective in quinone reduction.[129] 1,4-Naphthoquinones are mainly reversible inhibitors[112–114] and weak subversive substrates[130] for glutathione reductase. To obtain trypanocidal 1,4-naphthoquinones with specificity for *T. cruzi* trypanothione reductase, series of menadione, plumbagin, and juglone derivatives have been synthesized. The most potent derivatives contained two 1,4-naphthoquinone moieties linked by a polyamine spacer (Table 2). The thorough study indicated that inhibition of trypanothione reductase is not sufficient for a strong trypanocidal activity but that the combination of both redox cycling and inhibition of TS_2 reduction is crucial.[115]

T. cruzi old yellow enzyme, another flavin-dependent oxidoreductase, also catalyzes the single-electron reduction of naphthoquinones to the semiquinone anion radicals[131] and has been suggested to play a key role in the activation of quinone drugs under anaerobic conditions. So far the binding mode of a turncoat inhibitor has not been elucidated for any of these flavoenzymes. The crystal structure of human glutathione reductase with bound menadione, an uncompetitive inhibitor[132] and weak subversive substrate,[115] showed the highest electron density at the twofold axis, with additional low occupancies at the NADPH- and glutathione-binding sites.[133] Therefore one may speculate that one binding site for the naphthoquinones is the large cavity at the twofold axis of trypanothione reductase. Modeling studies suggest that this site of the parasite enzyme also exerts preference for positively charged ligands.[115] Chimeric compounds containing a naphthoquinone and a dimerization inhibitor are of future interest. Denaturation-inducing agents that are directed against the helix pair at the twofold molecular axis (see Table 6) are discussed in Section 7.3.3.

5. Drug Therapy and Prophylaxis of Malaria—Current Problems

Tropical malaria constitutes one of the most impoverishing infectious diseases, annually affecting 200–500 million people worldwide and causing the death of a million children in Africa. Every 15 seconds, an African child dies or suffers permanent neurological damage as a result of malaria. About 40% of the world population is at risk of being infected.[134] The actual disease develops when the malarial parasite *Plasmodium falciparum* multiplies in human erythrocytes (see http://sites.huji.ac.il/malaria). Consequently most drugs are directed against this stage of the life cycle of the parasite.[107,135] Past achievements and new developments in antimalarial drug research have been reviewed recently.[136,137] Inexpensive drugs against uncomplicated malaria in children are urgently required. In many African countries, and elsewhere in the world, the 10-cent drugs chloroquine and sulfadoxin/pyrimethamine lose efficiency because resistance against these compounds spreads rapidly. There is no answer to the question as to what the standard therapy for malaria could be in a few years time.[138] Standard therapy implies that the medicine is available and affordable for those who need it.

6. The Thiol-Based Redox Network of Plasmodium falciparum

Parasitized red blood cells are exposed to high fluxes of reactive oxygen species and additional prooxidant agents or anti-antioxidants are effective inhibitors of parasite growth.[77,139–143] As is the case in trypanosomes, the canonical antioxidant enzymes catalase and selenocysteine-containing glutathione peroxidase do not occur in *P. falciparum* which might result in a particular susceptibility to oxidative stress. The thiol-based redox metabolism is involved in the pathology of malaria and plays a major role in parasite resistance to

 © 2005 Wiley-VCH Verlag GmbH & Co. KGaA, Weinheim

drugs. Thus the network of thiols and dithiol proteins (Figure 2b) is a promising target area for antimalarial drug development.[77,107,144,145] The key enzymes feeding reducing equivalents into the antioxidant network are thioredoxin reductase and glutathione reductase (Figure 3). As shown by biochemical tests and whole genome analyses, trypanothione reductase and its substrate trypanothione (Figure 1a and 3a) do not occur in *P. falciparum* and its hosts.[35] Thioredoxin reductase exhibits a broad substrate specificity; it does, however, not reduce glutathione disulfide (GSSG).[146] The major substrate is the 12-kDa protein thioredoxin disulfide ($TrxS_2$) [Eq. (5)]:

$$NADPH + TrxS_2 + H^+ \rightarrow NADP + Trx(SH)_2 \quad (5)$$

Cell biological reactions that are based on thioredoxin and glutathione are shown in Figure 2b and Table 3, respectively. The thioredoxin system[149–151] includes thioredoxin reductase, thioredoxin,[146,152–154] and thioredoxin-dependent peroxidases.[155–157] The glutathione system comprises two synthetases that make up the tripeptide glutathione from its constituent amino acids[158,159] as well as glutathione reductase,[160,161] glutathione itself, glutathione *S*-transferase,[162,163] and glutaredoxins.[164,165] The newly discovered redox protein plasmoredoxin is one of the links between the two systems.[141]

Most processes based on thioredoxin and glutathione can be summarized as defense reactions against reactive oxygen species and other forms of chemical stress (Tables 3 and 4). From a cell-pathological aspect, it is not justified to consider only direct chemical interception of a noxious agent as a defense reaction. Thus Table 3 also includes compounds and reactions that represent defense mobilization, prevention of further damage, and repair processes.[147] The majority of these spontaneous or enzyme-catalyzed reactions do not represent chemical equilibria; indeed, forward and reverse reactions can be separated in space and time. A case in point, when the parasite is challenged by a burst of oxidants, is the formation of disulfides between protein sulfenate and glutathione [Eq. (6)].

$$proteinSOH + GSH \rightarrow proteinSSG + H_2O \quad (6)$$

In this way, protein thiols are prevented from being oxidized beyond the sulfenate stage. Furthermore, this reaction blocks the loss of glutathione in the form of GSSG from the cell. When the oxidant stress situation is over, the mixed disulfides must be reduced in order to reconstitute the functional thiol proteins [Eq. (7)].

$$proteinSSG + GSH \rightarrow proteinSH + GSSG \quad (7)$$

Glutathione disulfide, as the final relict of oxidative stress, is then reduced by glutathione reductase [Eq. (2)].

Table 3: Thiol-based defense reactions in *Plasmodium falciparum* against chemical stress.

Defense category[a]	Reaction[b]	Enzymes involved[148]
DM	$TrxS_2 + H^+ + NADPH \rightarrow Trx(SH)_2 + NADP$	thioredoxin reductase
DM	$Glu + Cys + Gly + 2\,ATP \rightarrow GSH + 2\,AMP + 4\,P_i$	γ-glutamylcysteine synthetase plus glutathione synthetase plus pyrophosphatase
DM	$GSSG + H^+ + NADPH \rightarrow 2\,GSH + NADP$	glutathione reductase
P	$proteinSH + GSSG \rightarrow proteinSSG + GSH$	1-cysteine-glutaredoxin
P	$protein(SH)_2 + GSSG \rightarrow proteinS_2 + 2\,GSH$	glutaredoxins
P	$proteinSOH + GSH \rightarrow proteinSSG + H_2O$	
P	*CoenzymeA*-SOH + GSH → *CoenzymeA*-SSG + H_2O	
I	$Trx(SH)_2 + ROOH \rightarrow TrxS_2 + ROH + H_2O$	peroxiredoxins and glutathione peroxidase-like thioredoxin peroxidase
I	GSH + 2-ketoaldehyde → GSH + 2-hydroxy acid	glyoxalase I plus glyoxalase II
I	GSH + drug → drug conjugate of glutathione	glutathione *S*-transferase
I	GSH + rns → GSNO	
I	GSNO + R• → RSG + NO	
I	$R^\bullet + 2\,GSH + {}^1/_2O_2 \rightarrow RH + GSSG + {}^1/_2H_2O_2$ as the sum of the following reaction sequence: $R^\bullet + GSH \rightarrow RH + GS^\bullet$; $GS^\bullet + GS^- \rightarrow GSSG^{\bullet-}$; $GSSG^{\bullet-} + O_2 \rightarrow GSSG + O_2^{\bullet-}$; $O_2^{\bullet-} + H^+ \rightarrow {}^1/_2H_2O_2 + {}^1/_2O_2$	superoxide dismutase C followed by glutathione reductase and thioredoxin peroxidase to remove GSSG and H_2O_2, respectively
I	GSSG transport out of the parasite as *one* mechanism for keeping the GSH/GSSG ratio high	transport systems in the membranes
R	$proteinSSG + GSH \rightarrow proteinSH + GSSG$	1-cysteine-glutaredoxin
R	$proteinS_2 + 2\,GSH \rightarrow protein(SH)_2 + GSSG$	glutaredoxins
R	$proteinS_2 + Trx(SH)_2 \rightarrow protein(SH)_2 + TrxS_2$	

[a] The defense reactions are classified from a biological perspective: DM = defence mobilization of the parasite, P = prevention of primary or secondary damage to the parasite, I = interception of toxic agents, R = repair processes.[147] [b] A reaction postulated for peroxynitrite interception ($GSH + proteinSH + ONOO^- \rightarrow proteinSSG + NO_2^- + H_2O$[74]) remains to be verified for *P. falciparum*. Many of the shown reactions create a signal that may lead to responses in the parasite such as the synthesis of specific proteins or membrane lipids. R• = radical formed in a macromolecule, ros = reactive oxygen species, rns = reactive nitrogen species, ROOH = organic hydroperoxide or H_2O_2.

 © 2005 Wiley-VCH Verlag GmbH & Co. KGaA, Weinheim

Table 4: Chemical stress on the parasite cell.[a]

Cell-damaging processes	Comment
proteinSH + ONOOH + O_2 → proteinSO$_2$H + HNO$_2$ + H_2O	protein sulfinic acid formation is irreversible in parasite and host cells
proteinSH + ros → proteinSOH + H_2O	reversible sulfenic acid formation
protein(SH)$_2$ + ros → proteinS_2	reversible disulfide formation
proteinSOH + ros → proteinSO$_2$H + H_2O	irreversible sulfinic acid formation
protein-SCH$_3$ + ros → proteinSOCH$_3$	methionine sulfoxide and sulfone formation
proteinSH + rns → proteinSNO + H_2O	thiol nitrosylation
protein + rns → nitrated protein	irreversible nitrotyrosine formation
membrane lipid + ros → membrane lipid peroxide	(= ROOH) in Table 3
DNA + methylglyoxal → base mutations in DNA	
DNA + R$^{\bullet}$ → strand breakage, base mutation in DNA	

[a] Chemicals that can stress the parasite include reactive oxygen species (ros) such as H_2O_2, reactive nitrogen species (rns) such as nitrogen monoxide or peroxynitrite, heteroaromatic drugs, methylglyoxal resulting as a side product of glycolysis,[166] and organic radicals (R$^{\bullet}$) resulting from iron-catalyzed reactions.

6.1. *Glutathione Species in* Plasmodium falciparum

Most studies on malarial parasites have been conducted at the trophozoite stage in human red blood cells. Relevant glutathione species[148] in the parasite include the thiol GSH (≈2 mM), the thiolate anion GS^- (≈30 μM when assuming a pK_a of 9.2 for the SH group under physiological conditions), and glutathione disulfide (GSSG, present at 10 μM or less). A high GSH/GSSG ratio is essential for intracellular redox homeostasis (see Appendix and Reference [167]). *S*-glutathionylated proteins (proteinSSG, also called mixed disulfides) occur at a total concentration of 100 μM to 1 mM (Table 3). The thiyl radical GS$^{\bullet}$ and the glutathione disulfide radical $GSSG^{\bullet-}$ are intermediates in reaction sequences that terminate radical-based chain reactions.[168,169]

6.2. *Interactions between the Glutathione System and the Thioredoxin System*

Intracellular GSSG is reduced enzymatically by glutathione reductase [Eq. (2)] and non-enzymically by thioredoxin [Eq. (8)]:[146,148]

$$Trx(SH)_2 + GSSG \rightarrow TrxS_2 + 2\,GSH \quad (8)$$

A high steady-state concentration of $Trx(SH)_2$ and thus a high $Trx(SH)_2/TrxS_2$ ratio is maintained by thioredoxin reductase [Eq. (5)]. The second-order rate constant for the reaction [Eq. (8)] is $650\,M^{-1}s^{-1}$, which allows rates that can satisfy most metabolic needs. The rate of the reverse reaction is probably negligible under in vivo conditions.

Notably, at rapidly rising GSSG concentrations the chemical reaction [Eq. (8)] is more adaptable than the enzyme-catalyzed reaction [Eq. (2)]: Above a concentration of 250 μM GSSG, glutathione reductase can increase the rate of GSSG reduction by only 25%, as the enzyme is already largely saturated by the substrate. In contrast, $Trx(SH)_2$-mediated GSSG reduction remains proportional to the GSSG concentration, which can reach 3 mM under extreme oxidative conditions. This has been observed not only in parasites but also in yeast mutants and in lymphocytes of AIDS patients.[146]

The reduction of GSSG by $Trx(SH)_2$ might be particularly relevant for stages of *P. falciparum*, such as the merozoites, that contain glutathione but practically no glutathione reductase.[170] Chemical and functional interactions of the glutathione system with the thioredoxin system occur also on the level of glutaredoxins and thioredoxins (Figure 2b).[164] As GSSG reduction by the thioredoxin system plays a role in a variety of physiological and pathological conditions it would be of interest to develop a pharmacological agent that inhibits both thioredoxin reductase and glutathione reductase. These mechanistically and structurally closely related enzymes are discussed as drug targets in Section 7.

6.3. *Thioredoxin-Dependent Hydroperoxide Detoxication*

H_2O_2 is the major oxidant to which blood parasites are exposed. In *P. falciparum*, hydroperoxides are mainly reduced by thioredoxin [Eq. (9)]:

$$Trx(SH)_2 + H_2O_2 \rightarrow TrxS_2 + 2\,H_2O \quad (9)$$

This reaction is catalyzed in *P. falciparum* by a variety of thioredoxin peroxidases. In comparison to mammalian cells, there is little glutathione peroxidase activity in the parasite. As found by Flohé and co-workers, even an enzyme that structurally resembles mammalian glutathione peroxidase turned out to have a 1000-fold higher catalytic competence with $Trx(SH)_2$ than with GSH as a substrate.[148,171] An important aspect is that most thioredoxin peroxidases are inactivated at high peroxide concentrations or peroxide fluxes,[150,156] thus they act as floodgates for H_2O_2.[172]

Taking these factors into account, we propose the following working model for the two antioxidative systems of *P. falciparum*: The basal peroxide flux is dealt with by the thioredoxin system. Under these conditions the GSSG concentration would not rise. In situations of sudden transient H_2O_2 exposure, for instance during an oxidant attack exerted by human defense cells on the parasitized erythrocyte, the glutathione system takes over and produces GSSG, which in turn leads to protective glutathionylation of SH groups in

 © 2005 Wiley-VCH Verlag GmbH & Co. KGaA, Weinheim

coenzymes and proteins (Table 3). The contribution of the host erythrocyte to the detoxification of parasite-borne H_2O_2 must also be considered.[148] H_2O_2 diffuses through biological membranes, and the erythrocyte compartment of the host cell is well equipped with H_2O_2-degrading enzymes such as catalase and glutathione peroxidase. As reported by Ginsburg and Atamna, the parasite may even supply the erythrocyte with reduced GSH in order to stabilize its host cell against oxidant attack. The quantitative aspects of this remarkable process need to be confirmed.[167]

6.4. Consequences of Thioredoxin Reductase Inhibition In Vivo

The following considerations are relevant when dealing with enzymes and enzyme inhibitors as drugs in vivo.[149] As explained below, enzyme inhibition can upset cellular dynamics because the steady state substrate concentration rises while the enzyme still appears to fulfill its metabolic function. A basic aspect is that substrate turnover by an enzyme is determined by the rate at which this substrate is metabolically generated, that is, by the substrate flux. Let us consider *P. falciparum* thioredoxin reductase as an example: The cellular H_2O_2 production, the H_2O_2 flux, is in the order of 50 $\mu M\,min^{-1}$ in most cells.[54] This leads to the formation of 50 μM oxidized thioredoxin per minute. The $TrxS_2$ in turn must be dealt with by thioredoxin reductase [Eq. (5)]. The decisive question for the enzyme activity is: at what substrate concentration does the enzyme cope with a given rate of substrate production? To answer this question, we apply the Michaelis–Menten equation. Solving for the substrate concentration gives Equation (10):

$$[S] = K_M(V_{max}/v-1)^{-1} = K_M(k_{cat}\,[E_t]/v-1)^{-1} \quad (10)$$

A steady-state $TrxS_2$ concentration [S] of 2.0 μM was obtained when using the parameters $K_m = 10.4\ \mu M$, $k_{cat} = 3100\,min^{-1}$, $TrxS_2$ flux $v = 50\ \mu M\,min^{-1}$, and assuming an intracellular thioredoxin reductase concentration $[E_t]$ of 0.1 μM.[146] When the enzyme is inactivated by a drug such as carmustine or CDE4 (Table 5) the concentration of active enzyme drops below 0.02 μM. Assuming the same H_2O_2 flux as before, the $TrxS_2$ concentration rises above 40 μM, that is, practically all thioredoxin is present in the oxidized form and other $Trx(SH)_2$-dependent processes cannot take place. In addition, the high level of $TrxS_2$ will lead to the nonphysiological oxidation of protein or coenzyme thiols by dithiol/disulfide exchange reactions. These effects have also been described for glutathione reductase inhibition.[54,181]

7. Enzymes of the Plasmodial Thiol Metabolism as Drug Targets

7.1. Thioredoxin Reductase as a Validated Drug Target

Dimeric thioredoxin reductase (Figure 3c and [Eq. (5)]) is an exemplary target for modern antimalarial drug development. The gene was identified in the genome of *P. falciparum*, cloned, and expressed as a recombinant functional flavoenzyme.[152,182–184]

Subsequently, Müller and co-workers used gene-ablation and gene-substitution techniques to show that thioredoxin reductase is an essential enzyme for the blood stages of *P. falciparum*.[153,154] These studies validated thioredoxin reductase as a drug target. The catalytic mechanism of the enzyme has been elucidated by Williams and co-workers by using single turnover kinetics based on flavin absorption spectroscopy.[152] Catalysis by *P. falciparum* thioredoxin reductase involves, in addition to the flavin, two redox-active dithiols. One is made up of Cys88 (the interchange thiol) and Cys93 (the thiol that interacts with flavin). The second dithiol, close to the C terminus of the other subunit, is composed of Cys535′ and Cys540′ (Figure 3c). The two cysteine pairs are in redox communication with each other. A key intermediate in catalysis is a charge transfer complex (the thiolate of Cys93 is the donor and flavin is the acceptor) characterized by a long-wavelength absorbance around 540 nm.[183,184]

A high-throughput-screening program with 350000 compounds of the Pfizer library yielded about 30 compounds that inhibit thioredoxin reductase. The bewildering chemical diversity among these hits was resolved by Davioud-Charvet et al., who noted that most of them were Mannich bases. One of them, CDE4, is a promising lead compound (Table 5), whose inhibitory mechanism was elucidated: A complex series of protein-assisted reactions leads to bisalkylation of the vicinal thiols (Cys535′ and Cys540′) at the C-terminal redox center of thioredoxin reductase.[173]

7.1.1. C-Terminal Redox Centers of Thioredoxin Reductase as Targets

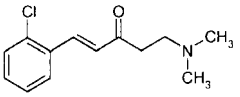
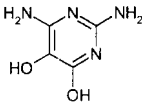
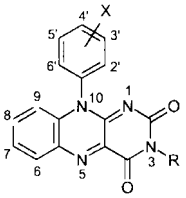
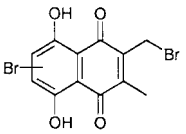
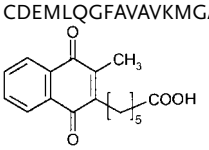
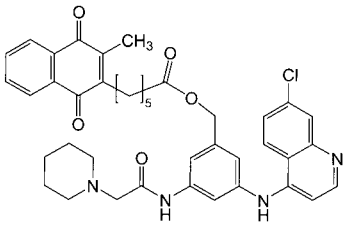
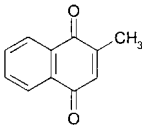
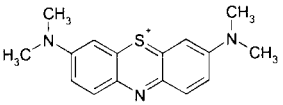
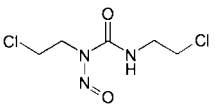
Structural and mechanistic comparisons among the thioredoxin reductases of the *P. falciparum* malaria system (malaria parasite, human host, and insect vector) showed that these orthologous enzymes have similar structures but they differ significantly in their C-terminal redox center which interacts directly with oxidized thioredoxin. This redox center is Gly-Cys-Sec-Gly in the human enzyme,[185] Thr-Cys-Cys-Ser in the mosquito *Anopheles gambiae* protein,[186] and Gly-Cys-Gly-Gly-Gly-Lys-Cys-Gly in the *P. falciparum* enzyme.[184] These chemical differences represent molecular targets for developing selective inhibitors of the respective thioredoxin reductase in human (cancer) cells, in the malarial parasite, and in disease-transmitting insects.

7.2. Drug Targets in the Glutathione Metabolism of the Parasite

Promising drug targets in the glutathione metabolism of the parasite include the two synthetases that build up the tripeptide glutathione from its constituent amino acids: γ-glutamyl-cysteine synthetase—the target of the inhibitor BSO[158]—and glutathione synthetase.[159] *P. falciparum* contains only one glutathione-*S*-transferase, an abundant protein that detoxifies endogenous compounds such as free heme and pathological membrane components but also xenobiotics

 © 2005 Wiley-VCH Verlag GmbH & Co. KGaA, Weinheim

Table 5: Inhibitors of disulfide reductases of *P. falciparum* as lead compounds.

Compounds		Mode of action[a]
CDE4, an unsaturated Mannich base		irreversible inhibition of thioredoxin reductase by covalent binding to the C-terminal redox-center[173]
Divicine (from *Vicia faba*), a redox-cycling agent		a divicine–glutathione adduct is substrate and competitive inhibitor of human GR[174]
isoalloxazines		noncompetitive inhibition of GR $K_i = 1.9\ \mu M$ for X = pentafluorophenyl and R = methyl[161,175]
JD145, a naphthazarine derivative		competitive inhibition of TrxR ($K_i = 500$ nM); the human orthologue is inhibited with a K_i of 5 nM[144]
K16	sequence CDEMLQGFAVAVKMGA	dimerization and folding inhibitor of PfGR and human GR ($IC_{50} = 100$ nM)[161]
M5, an acidic menadione derivative		reversible inhibition of GR[176]
M5Q ester, a double prodrug		the prodrug is hydrolyzed in vivo and releases M5 as a GR inhibitor as well as a parasitotoxic 4-anilinoquinoline derivative[176]
menadione		reversible inhibitor and subversive substrate of TrxR and GR (Eubel, Merkle, and Schirmer, unpublished results); uncompetitive inhibitor of human GR[114,132,219]
methylene blue		noncompetitive inhibitor and subversive substrate of GR and TrxR[160,161,177,178]
nitrosoureas e.g. carmustine		irreversible inactivation of GR, TrxR, and of trypanothione reductase; carmustine acts syncatalytically by carbamoylating one active-site cysteine residue in the NADPH-reduced enzymes.[106,125]
peroxynitrite	$ONOO^-$	inactivating nitration of Tyr86 and Tyr94 of GR; in addition $ONOO^-$ is a substrate of GR and bisnitro-GR[179]
pyrogenic compounds or fever		destabilization of NADPH-reduced GR[180]

[a] GR and TrxR refer to glutathione reductase and thioredoxin reductase of the parasite unless stated otherwise.

such as antimalarial drugs.[162,187] The structure of this pharmacologically important protein was determined recently.[163] The glyoxalases I and II, which scavenge methylglyoxal, a toxic byproduct of the intensive glucose catabolism of the parasite, are other interesting drug targets.[166] This is also true for glutathione reductase, the enzyme that is largely responsible for buffering the redox potential of cytosolic spaces by maintaining a high ratio of GSH/GSSG and, indirectly, a high GSH concentration. The reducing milieu of the cell interior, a well regulated biochemical quantity, is dealt with in the Appendix.

7.3. *Glutathione Reductase from* Plasmodium Falciparum *as a Target*

Glutathione reductase and thioredoxin reductase have similar overall structures and mechanisms but they are mutually exclusive with respect to their disulfide substrates. The main structural difference is the additional C-terminal redox center in thioredoxin reductase, which is not present in glutathione reductase (Figures 3b and 3c). The structure of *P. falciparum* glutathione reductase was solved recently and compared with human glutathione reductase.[161] Thus it will now be possible to design and improve specific inhibitors of the parasite enzyme as potential antimalarial drugs. These compounds will also be valuable for studying the role of the enzyme in parasite metabolism, drug action, and multidrug resistance.

The homodimeric flavoenzyme contains a 33 amino acid insertion in the central domain, the malaria-specific subdomain, which is present only in the enzyme from *Plasmodium* species.[188,189] Further target structures of inhibitors within the parasite enzyme are the active sites around Cys39 and Cys44, the par-

 © 2005 Wiley-VCH Verlag GmbH & Co. KGaA, Weinheim

allel helices H11 and H11′ at the subunit interface, and the intersubunit cavity (Figure 5). Inhibitors of *P. falciparum* glutathione reductase are listed in Table 5, which also includes natural defense mechanisms of the human host (e.g. peroxynitrite production and the fever reaction) that affect the parasite enzyme.

To understand inhibitor action, we first have to consider the enzyme mechanism and the redox forms of the enzyme that occur in the parasites. During catalysis, the electrons flow from NADPH to flavin and from the reduced flavin to the disulfide Cys39/Cys44. One cysteine of the resulting dithiol, Cys39, reacts with GSSG, to form glutathionylated glutathione reductase (the mixed disulfide enzymeSSG in Figure 3b) while GSH is released. The thiolate 44 then attacks the mixed disulfide, the second GSH is set free, and the active-site disulfide is reestablished.[191] This ground state of the enzyme is called E_{ox}. In the two-electron-reduced enzyme (EH_2) a charge transfer complex is formed between one of the nascent thiolates (Cys44) and the flavin.[160,188] A four-electron-reduced enzyme species (EH_4), which contains the active-site dithiol and reduced flavin, represents an unstable and catalytically inactive "standby" form of the enzyme. EH_4

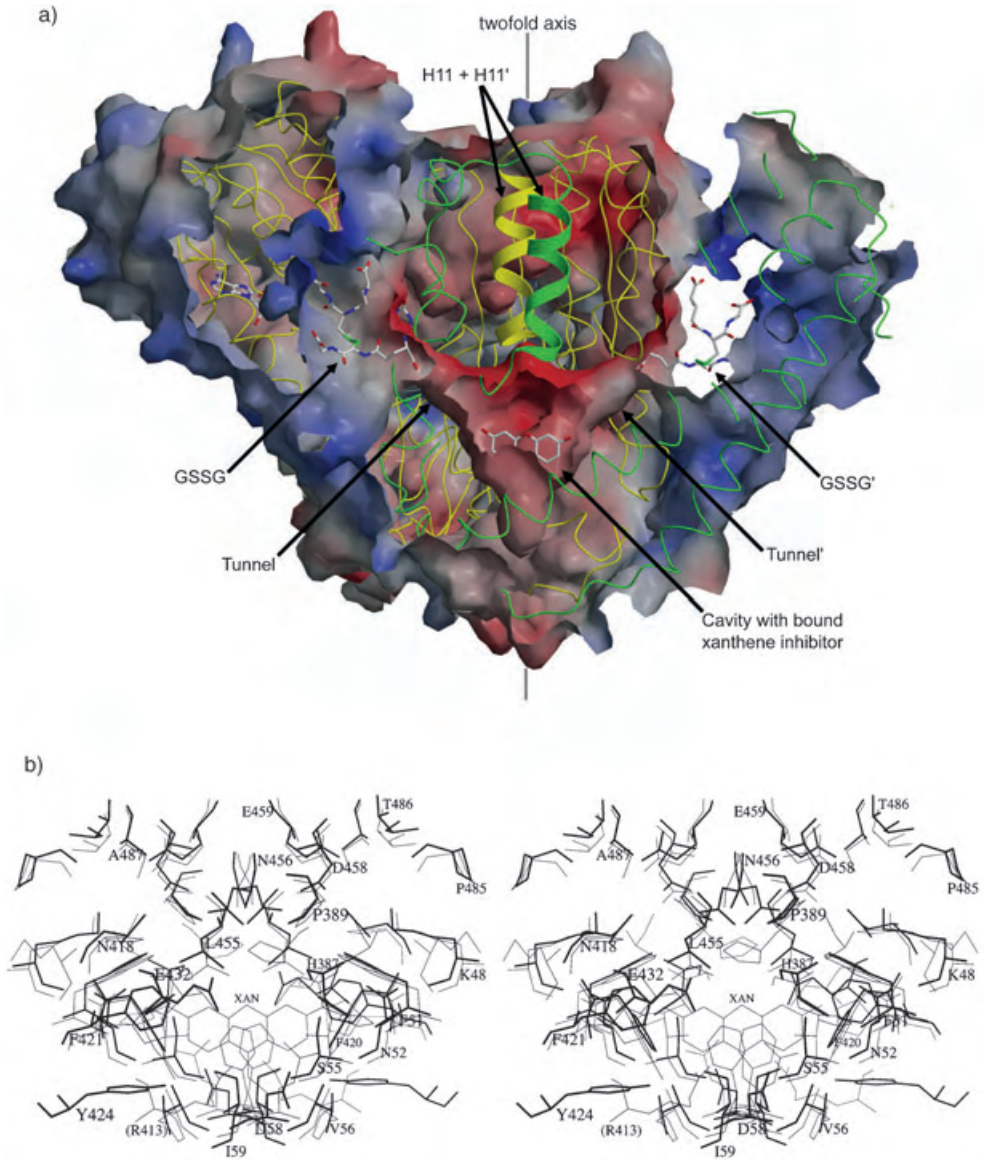


Figure 5. The dimer cavity and helices of human glutathione reductase. a) The solvent-accessible surface of human glutathione reductase is shown with the front portion clipped away to reveal the cavity at the dimer interface. The helices H11 and H11′ at the dimer interface, whose interaction is targeted by dimerization inhibitors, are highlighted by representation as ribbons. Stick models of the substrate GSSG and xanthene, a tricyclic noncompetitive inhibitor, are shown to indicate the binding positions. Note the tunnels connecting the central cavity to the two GSSG binding sites. The structure of *Plasmodium falciparum* glutathione reductase is similar; however, the structure of the enzyme–substrate complex has not yet been elucidated. b) The stereoview shows the residues that line the cavities. Residues of *P. falciparum* glutathione reductase (thick lines) are numbered with labels on only one of the symmetry partners. In human glutathione reductase (thin lines, Protein Data Bank entry 3GRS) only Arg413 carries a number. A bound inhibitor (XAN, taken from Protein Data Bank entry 1XAN) is shown for reference; the tricyclic xanthene ring is sandwiched between the two phenylalanine residues 78 and 78′ of human GR.[161,190]

 © 2005 Wiley-VCH Verlag GmbH & Co. KGaA, Weinheim

as well as glutathionylated enzyme are likely to occur in relevant concentrations only in the parasite but not in human cells and should thus be considered as targets of redox-state-specific inhibitors.[191]

The color of glutathione reductase solutions or crystals indicates the different redox forms: E_{ox} is bright yellow, EH_2 is orange, the EH_2·NADPH complex is red, and EH_4 is pale yellow. This is the basis for using microinjected glutathione reductase crystals as probes for determining the redox potential of subcellular compartments.[192]

The conspicuous symptom of malaria is the fever bout, and a large percentage of the parasites are killed during these fever episodes.[193] In culture, the parasites multiply by more than 1000% in 4 days at 37°C, but their number decreases to 20% when they are grown at 40°C. Our data suggest that the inactivation of thermolabile enzyme species such as the EH_2·NADPH of *P. falciparum* glutathione reductase contributes to the thermosensitivity of the malarial parasites.[180] In any case, labile EH_2·NADPH, rather than stable E_{ox} is the predominant form of the disulfide reductases in active cells and this ought to be accounted for in pharmacological and pathophysiological studies on the enzymes.[148,191]

7.3.1. *Inhibitors Target Different Redox Forms of Glutathione Reductase*

Peroxynitrite as a tyrosine-nitrating agent and bulky heteroarenes binding in the intersubunit cavity interact with all redox states of the enzyme described above (Table 5). In contrast, nitrosoureas as carbamoylating and alkylating agents attack only glutathione reductase forms with a free thiol at Cys39, that is, EH_2 and EH_4; they do not react with E_{ox} or with the glutathionylated enzyme. Dimer-dissociating agents such as the peptide K16 as well as a temperature increase from 37 to 40°C apparently affect only the labile forms EH_2·NADPH and EH_4. K16 also interferes with the folding process of the polypeptide chain.[161,180] Menadione, an uncompetitive inhibitor and a subversive substrate of *P. falciparum* glutathione reductase (Table 5), probably binds only to enzyme–substrate complexes, but not to the free enzyme.

7.3.2. *Peroxynitrite Binds at the GSSG Site*

The GSSG-binding site is positively charged and attracts peroxynitrite.[179] Peroxynitrite leads to specific nitration of two active-site tyrosine residues and thus to enzyme inactivation. On top of that, it oxidizes the active-site dithiol Cys39–Cys44 to the disulfide which in turn is re-reduced by NADPH. In balance, this leads to the enzyme-catalyzed reaction [Eq. (11)]:

$$\mathrm{NADPH + ONOO^- + H^+ \rightarrow NADP + nitrite + H_2O} \qquad (11)$$

Consequently *P. falciparum* glutathione reductase can act as a peroxynitrite reductase, and this is true even for the bisnitrated enzyme, which cannot reduce the natural substrate glutathione disulfide. Thus, in addition to being a covalent inhibitor (Table 5), peroxynitrite operates as a substrate.

The acidic naphthoquinone M5 inhibits glutathione reductase by binding to the GSSG site but probably also to another site.[176] As M5 carries a negative charge at pH 7, it is unlikely to reach its target in the interior of the parasite through the impermeable membrane. An elegant way to solve this problem was the introduction of double-headed prodrugs. M5 was linked to quinoline-based alcohols with known antimalarial activity through a metabolically labile ester (Table 5). The 4-aminoquinoline moiety directs the prodrugs to their primary destination, the food vacuole of the parasite, where the ester bond is cleaved so that two active drugs are generated on site. The antimalarial efficacy of the double-headed prodrugs was proven in parasite cultures and in a mouse model.[176]

7.3.3. *Helix 11 Analogues as Dimerization Inhibitors*

The pair of parallel helices (H11/H11′) at the core of the dimer interface (Figure 5a, Table 6) is regarded as a dimerization and folding nucleus of glutathione reductase.[161,194] Only dimeric glutathione reductase has enzyme activity as each active site uses residues from both subunits.

Table 6: Helix 11 and 11′ sequences in disulfide reductases from different organisms.[a]

Enzyme	Amino acid sequence	Organism
Thioredoxin reductase	NAGEVTQGMALALRLK	*Plasmodium falciparum*
	NAGEVTQGFAAALKCG	*Homo sapiens sapiens*
	AAGEVIQGFAAALKCGL	*Anopheles gambiae*
	NAGEVTQGFGIALKCG	*Caenorhabditis elegans*
Glutathione reductase	NADEIVQGFAVALKMN	*Plasmodium falciparum*
	GCDEMLQGFAVAVKMG	*Homo sapiens sapiens*
	NAAEVIQGYAVAFRVG	*Caenorhabditis elegans*
	GMDEMLQGFAVALKMG	*Escherichia coli*
	GCDEMIQGFAVAIKMG	*Haemophilus influenza*
	SSAEILQGFGVAIKMG	*Saccharomyces cerevisiae*
	DAAEIMQGIAIALKCG	*Arabidopsis thaliana*
Trypanothione reductase	GAPEIIQAVGVCLRLN	*Trypanosoma brucei brucei*
	SSPEIIQAVGICMKLN	*Trypanosoma congolese*
	NAPEIIQGVGICLKLN	*Trypanosoma cruzi*
	SAPEIIQSVGICMKMG	*Leishmania donovani*
	SSPEIIQSVAICLKMG	*Crithidia fasciculata*

[a] In *P. falciparum* thioredoxin reductase, this helix comprises residues 481 to 496, in *P. falciparum* glutathione reductase residues 456–471, and in *T. cruzi* trypanothione reductase the residues 431 to 446

Synthetic peptides representing helix 11 of human glutathione reductase were tested as inhibitors. Only the 16-mer peptide $K16_{hGR}$ (Table 6) strongly interfered with dimerization and folding of both human and *P. falciparum* glutathione reductase, with IC_{50} values of approximately 100 nM. The

 © 2005 Wiley-VCH Verlag GmbH & Co. KGaA, Weinheim

similarity of the IC_{50} values had been predicted on the basis of the enzyme structures. In contrast, human thioredoxin reductase, whose helix 11 sequence differs in 8 out of 16 positions from human glutathione reductase, was much less affected by $K16_{hGR}$, the IC_{50} value being 12 μM.[161]

These results suggest that peptide $K16_{hGR}$ could serve as a lead structure for studying the processes of folding and dimerization in FAD-dependent disulfide reductases (Table 6). Specificity for an individual enzyme of this huge family, for instance, *T. cruzi* trypanothione reductase or *P. falciparum* glutathione reductase, might be obtainable by systematic mutations of the peptide sequence. In addition, the structure of $K16_{hGR}$ recommends itself for developing peptidomimetic agents as folding inhibitors or as dimer-dissociating agents (G. Haberhauer, personal communication). Such inhibitors are expected to act in catalytic amounts since the resulting protein monomers are readily degraded, thereby releasing the dissociating agent.

The concept of denaturation-inducing inhibitors is supported by studies on the helix 11 mutants Gly446Glu/Phe447Pro of human glutathione reductase and Gly463Glu/Phe464Pro of *P. falciparum* glutathione reductase. These mutants that form full-length protein subunits but without detectable folding in any domain are extremely sensitive to proteolytic degradation.[161,194]

7.3.4. *Drug Binding in the Central Cavity*

An inviting site for drug design are the structures lining the wall of the cavity at the dimer interface; only 9 out of 21 residues are conserved when comparing *P. falciparum* and human glutathione reductase. This "drug" cavity (tricyclic center) is the binding site of numerous bulky heteroarenes such as xanthene and phenylisoalloxazine derivatives (for a literature review, see reference [161]). A physiologically occurring ligand for this site is unknown. These compounds act as noncompetitive, uncompetitive, or mixed type inhibitors. An attractive hypothesis is that they dislocate helix 37–62 and helix 37′–62′ which form part of the cavity wall but also carry the active-site cysteines in the two subunits. The X-ray crystal structure at 2 Å resolution, however, did not reveal a significant shift of these helices when comparing free enzyme and an enzyme–inhibitor complex.[133]

A comparison of the cavities in *P. falciparum* and human glutathione reductase is shown in Figure 5b. Although the cavities have similar volumes (≈450 Å^3), their shapes and chemical characteristics are at variance. Most conspicuously, the upper part of the cavity in the parasite enzyme is much smaller than the cavity in human glutathione reductase. The overall electrical charges on the cavity walls are also very different, negative in the human enzyme and neutral in *P. falciparum* glutathione reductase.[161]As a step towards understanding structure–activity relationships, we determined the K_i values of a series of 10-aryl isoalloxazines acting as noncompetitive inhibitors of glutathione reductases (Table 5). Crystallographic data are available for two water-soluble derivatives that were found to bind in the central cavity of the human enzyme.[175]. The 10-aryl isoalloxazines have favorable properties (effectivity against Plasmodia in vitro and in vivo, low toxicity, and low production costs) which recommend them as potential drug candidates against malaria.[144,175]

7.3.5. *Methylene Blue as an Inhibitor of* P. Falciparum *Glutathione Reductase*

The most promising tricyclic compound is the phenothiazine derivative methylene blue, which acts as a noncompetitive inhibitor of *P. falciparum* glutathione reductase but not of the human enzyme at therapeutically used concentrations.[160,161] Methylene blue, which was used against malaria in the past,[195,196] is today the standard medication against methemoglobinemia and against ifosfamid-associated neurotoxicity.[178]

Methylene blue has a number of desirable properties as an antimalarial drug. It has multiple targets in *P. falciparum* and of which two—methemoglobin and β-hematin—are not controllable by the genome of the parasite.[178,197,198] This makes resistance development against methylene blue unlikely. Furthermore, as a turncoat inhibitor of glutathione reductase and thioredoxin reductase it leads to glutathione depletion in the parasite (Eubel, Merkle, and Schirmer, unpublished results). This in turn sensitizes the parasite for chloroquine,[145] the most valuable of all antimalarial drugs. Thus the drug combination methylene blue–chloroquine (BlueCQ[178]) is expected to protect the efficacy of chloroquine and slow down the spread of chloroquine resistance.[199] Other clinically relevant properties of methylene blue, including the blue coloration of the urine, have been summarized elsewhere.[178] Clinical studies with BlueCQ for the treatment of malaria in children are currently being carried out in the Nouna district, Burkina Faso.[178]

8. Outlook on Drug Development

Differences between the redox metabolism of the host and parasite render interesting starting points for specific drug development.[107,148] Prominent examples include the trypanothione system of trypanosomes, the lack of catalase and glutathione peroxidase in trypanosomes and *P. falciparum*, as well as the presence of a unique protein such as plasmoredoxin in the latter parasite.[141] However, more subtle differences such as the structures of the redox-active C-terminal ends of human and *P. falciparum* thioredoxin reductase and the chemically distinct walls of the intersubunit cavities in human glutathione reductase, trypanosomal trypanothione reductase, and *P. falciparum* glutathione reductase will also guide future drug design.

At the same time, compelling arguments suggest that in the case of malaria we should not neglect human erythrocyte glutathione reductase as a potential drug target.[77,200] These arguments include clinical and epidemiological observations as well as pharmacological studies showing that a low level of human glutathione reductase activity—this low enzyme level is usually restricted to erythrocytes—does not significantly interfere with erythrocyte function but offers protection from malaria.[143,181,201] Another argument in favor of choosing a

 © 2005 Wiley-VCH Verlag GmbH & Co. KGaA, Weinheim

host cell enzyme as a target is the a priori prevention of drug resistance.[135–137] In conclusion, on a short term basis the structure-based development of *P. falciparum* glutathione reductase-specific inhibitors will have high priority; on a long term basis, however, compounds inactivating both *P. falciparum* and erythrocyte glutathione reductase might become equally important for the chemotherapy of malaria.

In the case of trypanosomal infections the most intensively studied drug target candidate is trypanothione reductase; however, the extremely spacious active site of the enzyme renders the establishment of quantitative structure–activity relationships difficult for any ligand. Several general aspects should be considered when selecting an enzyme as a potential drug target. With reversible ligands as drug candidates one has to take into account that often the enzyme activity has to be suppressed nearly completely in order to induce a lethal effect on the cell. In bloodstream *T. brucei*, for instance, trypanothione reductase has to be inhibited by $>$ 95% to induce growth arrest and increased sensitivity against oxidative stress.[202] For the development of a ligand that binds reversibly to the enzyme E the law of mass action ($K_{diss} = [E][I]/[EI] = k_{diss}/k_{ass}$) can serve as a guide to estimate the free-drug concentration needed to obtain the required degree of inhibition. An inhibition of 95% is achieved when $[I] = 20\,K_{diss}$. Drug design should therefore aim at inhibitors with a K_{diss} of less than 10 nM for the case of reversible inhibition; otherwise the drug concentration must be very high in order to sustain the inactive complex.[107]

Most irreversible inhibitors generally lead to covalent modifications of essential amino acid residues of a protein. Attractive drug candidates are irreversible inhibitors that switch off an enzyme permanently within the physiological time scale. Such compounds either covalently modify the enzyme or are slow-binding inhibitors. A rate constant of less than $10^{-5}\ s^{-1}$ means that the half-life of the complex is greater than 19 h. Ligands that induce a slow conformational change after binding, so-called tight-binding inhibitors, are also promising drug candidates.[203]

Another important aspect when regarding irreversible ligands as drug candidates is the in vivo half-life $t_{1/2}$ of the target enzyme. If $t_{1/2}$ is very short (few minutes), an irreversible inhibitor will not be able to switch off the enzyme activity under physiological conditions; a well-studied example is eflornithine (DFMO, see Section 1). The in vivo half-life is not known for any of the parasite flavoenzymes discussed herein, but because they are housekeeping enzymes, we can assume that their turnover is slow.

Very promising drug candidates are turncoat inhibitors. For a series of naphthoquinones a correlation between their potency to act as turncoat inhibitor of trypanothione reductase and their trypanocidal activity has been demonstrated.[115] Their multiple effects—inhibition of $T(SH)_2$ regeneration, lowering of the $T(SH)_2/TS_2$ ratio, waste of NADPH, and active production of reduced oxygen species—should have a great impact on the redox balance of the parasite. In addition, turncoat inhibitors function as catalysts and thus should be active in substoichiometric concentrations. The same is, incidentally, true for peptidomimetics when acting as folding inhibitors (Section 7.3.3).[107]

Appendix: Intracellular Redox Homeostasis

The Reducing Milieu as a Chemical Fossil. The reducing milieu of the cell interior is a well-regulated biochemical quantity. The high ratio of 2GSH/GSSG of about 100 is probably not different from dithiol/disulfide ratios within primordial cells that existed under a reducing atmosphere 2 billion years ago.[204] Thiol functions in proteins and coenzymes are crucial for cellular life and must be protected. In the absence of redox buffering mechanisms, atmospheric O_2 would lead to complete disappearance of intracellular thiols, and instead sulfates and sulfinates would become the predominant form of sulfur compounds in the presence of dioxygen.[54,204]

Redox Environment. Schafer and Buettner[205] define the redox environment in a cell compartment as [Eq. (12)] (E_i is the redox potential of a given redox system):

$$\text{Redox environment} = \sum E_i\,[\text{reducing species}]_i \qquad (12)$$

In the cytosolic spaces of many organisms, including *Plasmodium falciparum,* biologically relevant reducing species are NADPH, reduced thioredoxin, GSH, and ascorbate (Figure 6). The GSH concentration (1–10 mM) is much higher than that of NADPH (100 μM), and thioredoxin (≤ 50 μM) which implies that glutathione is the major redox buffer in the parasite (and most known organisms).

The contribution of GSH would be $(2.5\text{ mM}) \times (-240\text{ mV}) = -600\text{ mV mM}$ and thus orders of magnitude higher than for other redox systems to which it is linked. The

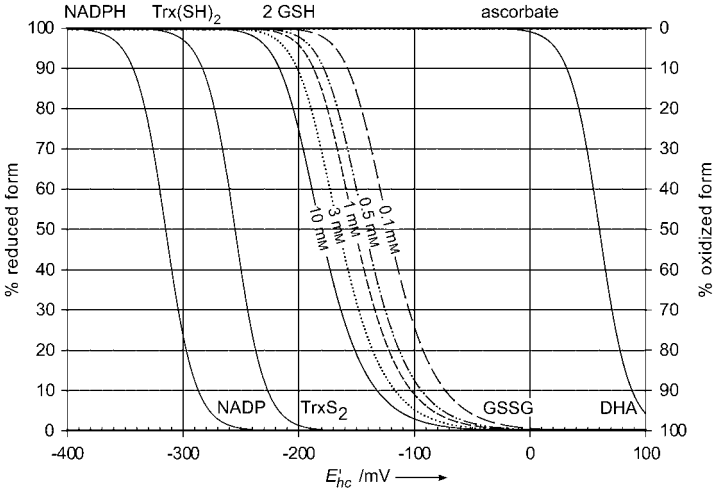


Figure 6. Redox systems in *P. falciparum* trophozoites. The diagram represents the Nernst equation for different redox systems. Except for the glutathione system, the curves are based on the equation $E'_{hc} = E^{\circ\prime} + 29.6\log([\text{oxidized form}]/[\text{reduced form}])$. $E^{\circ\prime}$ at 25 °C and pH 7.0 is −315 mV for NADP/NADPH, −255 mV for *P. falciparum* thioredoxin ($TrxS_2/Trx(SH)_2$)[146] and +80 mV for dehydroascorbate/ascorbate.[209] In the case of the glutathione redox system, the redox potential depends not only on the GSSG/GSH ratio but also on the concentration of GSH. The corresponding curves for different glutathione concentrations (10, 3, 1, 0.5, and 0.1 mM GSH) were calculated according to the equations $E'_{hc} = -240 - 29.6\log([GSH]/[GSSG]) - 29.6\log[GSH]$ mV and [total glutathione] $= [GS_t] = 2[GSSG] + [GSH]$. When applying these equations, [GSSG] and [GSH] must be expressed in molar (not millimolar!) units.

 © 2005 Wiley-VCH Verlag GmbH & Co. KGaA, Weinheim

glutathione system has the additional biological advantage that it readily receives electrons from NADPH in the glutathione reductase-catalysed reaction [Eq. (2)].[161,181] Under physiological conditions this reaction is irreversible. Its function is to maintain the required high ratio of 2[GSH]/[GSSG]; in the cytosol of *P. falciparum* trophozoites, for instance, this ratio is $\approx$120:1.[167] Indirectly, glutathione reductase promotes GSH-dependent reactions and inhibits processes in which GSSG is a substrate. The only proteins that receive electrons directly from NADPH are the thioredoxins—in a reaction catalyzed by thioredoxin reductase [Eq. (5)].[86,140,206]

Potential Electrical Energy of the Glutathione System. One might also consider the reducing environment in terms of potential electrical energy. The energy per unit volume is described by [Eq. (13)] and has the dimensions of JL^{-1} or $VC^{-1}L^{-1}$:

$$\Delta G/V = -\Delta E\,Q/V = -n\,\Delta E\,F/V \tag{13}$$

Since n is the number of moles of electrons that can be transferred from GSH, we replace nV^{-1} in Equation (13) by $2c$ [Eq. (14)]:

$$\Delta G/V = -n/V\,\Delta E\,F = -2\,c\,F\,\Delta E \tag{14}$$

(c = GSH concentration, F = Faraday constant (96500 $Cmol^{-1}$), ΔE = difference between the redox potential of the glutathione redox system and the potential of the redox systems linked to it). Thus Δ is the energy contribution of the glutathione system for stabilizing the reducing milieu. As a worked example, if there is an instantaneous increase in the redox potential of a linked system by 0.03 V, the reducing energy per volume would be $\Delta G/V^{-1} = -2 \times 2.5 \times 10^{-3}\,mol\,L^{-1} \times 96500\,C\,mol^{-1} \times 0.03\,V = -15\,J\,L^{-1}$. This corresponds to the hydrolysis energy of 0.5 mmol ATP L^{-1}.

The Nernst Equation for the GSSG/2GSH System. The intracellular redox potential E' that is established by the glutathione system can be estimated by using the Nernst equation. The standard redox potential $E^{\circ\prime}$ of the GSSG/2GSH system at pH 7.0, physiological ionic strength, and 25 °C has been determined as −240 mV.[86,205] The Nernst equation of the half-cell potential (E' in mV) for the GSSG/2GSH system is then [Eq. (15)]:

$$E' = -240 - 59.1/2\log([GSH]^2/[GSSG])\,mV \tag{15}$$

By applying logarithm rules, we obtain handier forms [Eq. (16)] and [Eq. (17)]:

$$E' = -240 - 29.6\log([GSH]/[GSSG]) - 29.6\log[GSH]\,mV \tag{16}$$

$$E' = -240 + 29.6\log[GSSG] - 59.1\log[GSH]\,mV \tag{17}$$

Let us apply values measured for the *P. falciparum* trophozoite (2.39 mM GSH; 8.4 μM GSSG).[167] For the redox potential of the glutathione system we obtain $E' = -240 + 29.6\log[8.4 \times 10^{-6}] - 59.1\log[2.39 \times 10^{-3}] = -235$ mV. Under more physiological conditions (pH 7.2 and 37 °C) the corresponding value can be estimated to be −265 mV.[207]

Equation (15) shows the square term $[GSH]^2$, which implies that the redox potential E' depends not only on the ratio [reduced form]/[oxidized form] as in the case of redox couples such as NADPH/NADP or $Trx(SH)_2/TrxS_2$, but also on the absolute concentration of GSH ([Eq. (16)], Figure 6). A decrease in [GSH] from 2 mM to 100 μM leads to an increase in E' by $\approx$40 mV, even when the [GSH]/[GSSG] ratio does not change. Such dramatic changes of the GSH concentrations occur when a cell renders itself to a dormant state or if the enzyme glutathione reductase becomes insufficient in cells stressed by oxidants or enzyme inhibitors, or if a glutathione reductase is absent.[146,170,208]

Protein Thiols as Nanoswitches. What are the biological implications of a redox environment with an adjustable redox potential? Let us consider a protein cysteine pair with a redox potential $E^{\circ\prime}$. It will be largely in the protein$(SH)_2$ state when the environmental redox potential E' is 30 mV lower than the $E^{\circ\prime}$ value and in the disulfide state proteinS_2 when the environmental redox potential E' is 30 mV higher than $E^{\circ\prime}$.[205] Protein$(SH)_2$ and proteinS_2 can be considered as redox-interconvertible forms of the protein or as two positions of a switch if we consider the protein as a "nanoswitch".

This is illustrated by the Henderson–Hasselbalch equation applied to the redox couple proteinS_2/protein$(SH)_2$ [Eq. (18)] ($E^{\circ\prime}$, E' in mV):

$$10^{(E'-E^{\circ\prime})/29.6} = [ProteinS_2]/[Protein(SH)_2] \tag{18}$$

The equivalent equations for H^+-controlled switches and Ca^{2+} controlled switches are [Eq. (19)] and [Eq. (20)], respectively:

$$10^{(pH-pK_a)} = [A^-]/[HA] \tag{19}$$

$$10^{(pCa-pK_d)} = [\text{free protein}]/[Ca^{2+}\text{–protein}] \tag{20}$$

In each case a biologically controlled quantity (redox environment, pH, pCa) determines the switch position, that is, protein$(SH)_2$ versus proteinS_2, A^- versus HA, and free protein versus Ca^{2+}–protein complex.

Two types of redox-form interconversions are common [Eq. (21)] and [Eq. (22)]:

$$\text{protein}(SH)_2 + GSSG = \text{protein}S_2 + 2GSH \tag{21}$$

$$\text{protein}SH + GSSG = \text{protein}SSG + GSH \tag{22}$$

Equation (21) applies to vicinal Cys residues, which can be located even on different subunits of a protein complex, Equation (22) concerns isolated thiol groups. The reactions appear to be selective so that only defined cysteine residues of selected proteins are affected; they are reversible but forward and reverse reactions can occur separately in time and space and are probably governed by different glutaredoxins.[148] Studies on in vivo protein glutathionylation have become possible only recently, for which two-dimensional protein gel electrophoresis and mass spectrometry are the major tools.

 © 2005 Wiley-VCH Verlag GmbH & Co. KGaA, Weinheim

It is hypothesized that the phases of parasite growth and differentiation as well as the relationship between host cell and parasite are under control of these nanoswitches and thus under control of the glutathione-based redox environment.[206,210] In mammalian cells, controlled changes of the reduction potential of the GSSG/2GSH couple appear to correspond to the biological status. Values around −240 mV, −210 mV, and −170 mV were found to correlate with cell growth, cell differentiation, and cell apoptosis, respectively; in necrotic cells the redox potential is less negative than −150 mV.[205]

In analogy to phosphorylatable protein-OH groups, one may regard redox-regulated protein cysteines as nanoswitches for biological processes.[211,212] Protein redox interconversions are likely to be influenced by the redox potential of the glutathione redox system. Furthermore, proteins containing a sulfenate group or a disulfide can also represent a hysteresis signal indicating that the cell has been under oxidative stress. This may be the case if a thiol or a dithiol of a transcription factor protein is oxidized. How long a given protein will be in the oxidized form after transient local or global oxidative stress depends on, among other factors, its being a good or bad substrate of glutaredoxins and thioredoxins (Figure 2b). Thus sulfenate formation followed by glutathionylation and deglutathionylation can modify the basic pattern of redox control and in addition introduce kinetic regulatory elements.[210,213]

Addendum (November 11, 2004)

While this review was in press, new developments corroborating the conclusions and extending the field of antioxidative networks have been published. Novel methods include a cell-biological procedure for monitoring disulfide formation and thus the dynamic determination of the 2[GSH]/[GSSG] ratio in eukaryotic cells (see Section 6.1).[214] Transcriptome analysis has been applied to the antioxidant protein network of *Plasmodium falciparum* (Section 6).[215] Among new observations, the discovery of reversible cysteine sulfinate formation as part of the floodgate function of peroxiredoxins represents an important discovery (see Section 6.3).[216,217] A template for drug design based on two interacting binding sites for quinacrine in trypanothione reductase (Section 4.1.2), [218] and the uncompetitive inhibition of *P. falciparum* glutathione reductase with naphthoquinone[219] present new paradigms for disulfide reductases as targets in parasites. Advances in the chemistry and function of disulfide reductases and their possible impact on drug development were reported in a comprehensive review by Argyrou and Blanchard (Sections 4.1 and 7).[220] First results of chemotherapeutic trials with methylene blue as a constituent of the antimalarial combination BlueCQ were published recently. [221] Dosage-optimization trials are currently being conducted in Burkina Faso.

Our work is supported by the Sonderforschungsbereich 544 "Control of Tropical Infectious Diseases" of the Deutsche Forschungsgemeinschaft (PrB3 to L.K.S. and PrB2 to R.H.S.). H.B. (Davioud-Charvet group) is a fellow of the CNRS-DFG joint program.

Received: October 24, 2003

[1] M. H. Gelb, W. G. Hol, *Science* **2002**, *297*, 343 – 344.
[2] J. Keiser, A. Stich, C. Burri, *Trends Parasitol.* **2001**, *17*, 42 – 49.
[3] H. P. de Koning, *Int. J. Parasitol.* **2001**, *31*, 512 – 522.
[4] E. L. Vansterkenburg, I. Coppens, J. Wilting, O. J. Bos, M. J. Fischer, L. H. Janssen, F. R. Opperdoes, *Acta Trop.* **1993**, *54*, 237 – 250.
[5] A. Pal, B. S. Hall, M. C. Field, *Mol. Biochem. Parasitol.* **2002**, *122*, 217 – 221.
[6] X. G. Gao, G. Garza-Ramos, E. Saavedra-Lira, N. Cabrera, M. T. De Gomez-Puyou, R. Perez-Montfort, A. Gomez-Puyou, *Biochem. J.* **1998**, *332*, 91 – 96.
[7] R. J. Burchmore, P. O. Ogbunude, B. Enanga, M. P. Barrett, *Curr. Pharm. Des.* **2002**, *8*, 256 – 267.
[8] H. P. de Koning, S. M. Jarvis, *Acta Trop.* **2001**, *80*, 245 – 250.
[9] N. S. Carter, A. H. Fairlamb, *Nature* **1993**, *361*, 173 – 176.
[10] M. P. Barrett, A. H. Fairlamb, *Parasitol. Today* **1999**, *15*, 136 – 140.
[11] A. C. Coelho, S. M. Beverley, P. C. Cotrim, *Mol. Biochem. Parasitol.* **2003**, *130*, 83 – 90.
[12] B. Nguyen, M. P. Lee, D. Hamelberg, A. Joubert, C. Bailly, R. Brun, S. Neidle, W. D. Wilson, *J. Am. Chem. Soc.* **2002**, *124*, 13680 – 13681.
[13] H. Denise, C. Giroud, M. P. Barrett, T. Baltz, *Eur. J. Biochem.* **1999**, *259*, 339 – 346.
[14] M. A. Phillips, P. Coffino, C. C. Wang, *J. Biol. Chem.* **1987**, *262*, 8721 – 8727.
[15] R. Docampo, A. O. Stoppani, *Arch. Biochem. Biophys.* **1979**, *197*, 317 – 321.
[16] L. J. Nunez-Vergara, M. E. Ortiz, S. Bollo, J. A. Squella, *Chem.-Biol. Interact.* **1997**, *106*, 1 – 14.
[17] M. Masana, E. G. de Toranzo, J. A. Castro, *Biochem. Pharmacol.* **1984**, *33*, 1041 – 1045.
[18] E. G. Diaz de Toranzo, J. A. Castro, B. M. Franke de Cazzulo, J. J. Cazzulo, *Experientia* **1988**, *44*, 880 – 881.
[19] M. P. Barrett, *Lancet* **1999**, *353*, 1113 – 1114.
[20] P. Mäser, C. Sütterlin, A. Kralli, R. Kaminsky, *Science* **1999**, *285*, 242 – 244.
[21] A. H. Fairlamb, N. S. Carter, M. Cunningham, K. Smith, *Mol. Biochem. Parasitol.* **1992**, *53*, 213 – 222.
[22] N. V. Grishin, A. L. Osterman, H. B. Brooks, M. A. Phillips, E. J. Goldsmith, *Biochemistry* **1999**, *38*, 15174 – 15184.
[23] M. Iten, H. Mett, A. Evans, J. C. Enyaru, R. Brun, R. Kaminsky, *Antimicrob. Agents Chemother.* **1997**, *41*, 1922 – 1925.
[24] T. L. Byers, T. L. Bush, P. P. McCann, A. J. Bitonti, *Biochem. J.* **1991**, *274*, 527 – 533.
[25] C. J. Bacchi, J. Garofalo, D. Mockenhaupt, P. P. McCann, K. A. Diekema, A. E. Pegg, H. C. Nathan, E. A. Mullaney, L. Chunosoff, A. Sjoerdsma, S. H. Hutner, *Mol. Biochem. Parasitol.* **1983**, *7*, 209 – 225.
[26] A. H. Fairlamb, G. B. Henderson, C. J. Bacchi, A. Cerami, *Mol. Biochem. Parasitol.* **1987**, *24*, 185 – 191.
[27] F. Li, S. B. Hua, C. C. Wang, K. M. Gottesdiener, *Mol. Biochem. Parasitol.* **1996**, *78*, 227 – 236.
[28] For a review, see: H. Cerecetto, M. Gonzalez, *Curr. Top. Med. Chem.* **2002**, *2*, 1187 – 1213.
[29] S. N. Moreno, R. Docampo, R. P. Mason, W. Leon, A. O. Stoppani, *Arch. Biochem. Biophys.* **1982**, *218*, 585 – 591.
[30] For a review, see: A. Fournet, V. Munoz, *Curr. Top. Med. Chem.* **2002**, *2*, 1215 – 1237.
[31] R. Docampo, S. N. Moreno, *Curr. Drug Targets Infect. Disord.* **2001**, *1*, 51 – 61.

 © 2005 Wiley-VCH Verlag GmbH & Co. KGaA, Weinheim

[32] M. B. Martin, J. S. Grimley, J. C. Lewis, H. T. Heath III, B. N. Bailey, H. Kendrick, V. Yardley, A. Caldera, R. Lira, J. A. Urbina, S. N. Moreno, R. Docampo, S. L. Croft, E. Oldfield, *J. Med. Chem.* **2001**, *44*, 909 – 916.
[33] R. Docampo, *Curr. Pharm. Des.* **2001**, *7*, 1157 – 1164.
[34] J. A. Urbina, *Curr. Pharm. Des.* **2002**, *8*, 287 – 295.
[35] M. J. Gardner, N. Hall, E. Fung, O. White, M. Berriman, R. W. Hyman, J. M. Carlton, A. Pain, K. E. Nelson, S. Bowman, I. T. Paulsen, K. James, J. A. Eisen, K. Rutherford, S. L. Salzberg, A. Craig, S. Kyes, M. S. Chan, V. Nene, S. J. Shallom, B. Suh, J. Peterson, S. Angiuoli, M. Pertea, J. Allen, J. Selengut, D. Haft, M. W. Mather, A. B. Vaidya, D. M. Martin, A. H. Fairlamb, M. J. Fraunholz, D. S. Roos, S. A. Ralph, G. I. McFadden, L. M. Cummings, G. M. Subramanian, C. Mungall, J. C. Venter, D. J. Carucci, S. L. Hoffman, C. Newbold, R. W. Davis, C. M. Fraser, B. Barrell, *Nature* **2002**, *419*, 498 – 511.
[36] G. J. Hannon, *Nature* **2002**, *418*, 244 – 251.
[37] A. M. Denli, G. J. Hannon, *Trends Biochem. Sci.* **2003**, *28*, 196 – 201.
[38] A. H. Fairlamb, P. Blackburn, P. Ulrich, B. T. Chait, A. Cerami, *Science* **1985**, *227*, 1485 – 1487.
[39] H. Schmidt, R. L. Krauth-Siegel, *J. Biol. Chem.* **2003**, *278*, 46329 – 46336.
[40] E. M. Tamayo, A. Iturbe, E. Hernández, G. Hurtado, M. L. Gutiérrez-X., J. L. Rosales, M. Woolery, R. N. Ondarza, *Biotechnol. Appl. Biochem.*, in press.
[41] F. Montrichard, F. Le Guen, D. L. Laval-Martin, E. Davioud-Charvet, *FEBS Lett.* **1999**, *442*, 29 – 33.
[42] T. T. Huynh, V. T. Huynh, M. A. Harmon, M. A. Phillips, *J. Biol. Chem.* **2003**, *278*, 39794 – 39800.
[43] M. R. Ariyanayagam, A. H. Fairlamb, *Mol. Biochem. Parasitol.* **1997**, *84*, 111 – 121.
[44] K. J. Hunter, S. A. Le Quesne, A. H. Fairlamb, *Eur. J. Biochem.* **1994**, *226*, 1019 – 1027.
[45] S. L. Oza, M. R. Ariyanayagam, A. H. Fairlamb, *Biochem. J.* **2002**, *364*, 679 – 686.
[46] M. Comini, U. Menge, L. Flohé, *Biol. Chem.* **2003**, *384*, 653 – 656.
[47] S. L. Oza, E. Tetaud, M. R. Ariyanayagam, S. S. Warnon, A. H. Fairlamb, *J. Biol. Chem.* **2002**, *277*, 35853 – 35861.
[48] M. R. Ariyanayagam, S. L. Oza, A. Mehlert, A. H. Fairlamb, *J. Biol. Chem.* **2003**, *278*, 27612 – 27619.
[49] H. S. Spies, D. J. Steenkamp, *Eur. J. Biochem.* **1994**, *224*, 203 – 213.
[50] D. J. Steenkamp, H. S. Spies, *Eur. J. Biochem.* **1994**, *223*, 43 – 50.
[51] M. R. Ariyanayagam, A. H. Fairlamb, *Mol. Biochem. Parasitol.* **2001**, *115*, 189 – 198.
[52] R. N. Vogt, D. J. Steenkamp, *Biochem. J.* **2003**, *371*, 49 – 59.
[53] A. H. Fairlamb, A. Cerami, *Annu. Rev. Microbiol.* **1992**, *46*, 695 – 729.
[54] H. F. Gilbert, *Adv. Enzymol. Relat. Areas Mol. Biol.* **1990**, *63*, 69 – 172.
[55] M. Moutiez, D. Meziane-Sherif, M. Aumercier, C. Sergheraert, A. Tartar, *Chem. Pharm. Bull.* **1994**, *42*, 2641 – 2644.
[56] C. Fraser-L'Hostis, F. Defrise-Quertain, D. Coral, J. Deshusses, *Biol. Chem.* **1997**, *378*, 1039 – 1046.
[57] L. Flohé, P. Steinert, H. J. Hecht, B. Hofmann, *Methods Enzymol.* **2002**, *347*, 244 – 258.
[58] H. Budde, L. Flohé, H. J. Hecht, B. Hofmann, M. Stehr, J. Wissing, H. Lunsdorf, *Biol. Chem.* **2003**, *384*, 619 – 633.
[59] E. Nogoceke, D. U. Gommel, M. Kiess, H. M. Kalisz, L. Flohé, *Biol. Chem.* **1997**, *378*, 827 – 836.
[60] M. Dormeyer, N. Reckenfelderbäumer, H. Lüdemann, R. L. Krauth-Siegel, *J. Biol. Chem.* **2001**, *276*, 10602 – 10606.
[61] M. Ouellette, E. Hettema, D. Wust, F. Fase-Fowler, P. Borst, *EMBO J.* **1991**, *10*, 1009 – 1016.
[62] D. Légaré, B. Papadopoulou, G. Roy, R. Mukhopadhyay, A. Haimeur, S. Dey, K. Grondin, C. Brochu, B. P. Rosen, M. Ouellette, *Exp. Parasitol.* **1997**, *87*, 275 – 282.
[63] D. Légaré, D. Richard, R. Mukhopadhyay, Y. D. Stierhof, B. P. Rosen, A. Haimeur, B. Papadopoulou, M. Ouellette, *J. Biol. Chem.* **2001**, *276*, 26301 – 26307.
[64] S. Yan, F. Li, K. Ding, H. Sun, *J. Biol. Inorg. Chem.* **2003**, *8*, 689 – 697.
[65] R. Mukhopadhyay, S. Dey, N. Xu, D. Gage, J. Lightbody, M. Ouellette, B. P. Rosen, *Proc. Natl. Acad. Sci. USA* **1996**, *93*, 10383 – 10387.
[66] S. K. Shahi, R. L. Krauth-Siegel, C. E. Clayton, *Mol. Microbiol.* **2002**, *43*, 1129 – 1138.
[67] A. Boveris, H. Sies, E. E. Martino, R. Docampo, J. F. Turrens, A. O. Stoppani, *Biochem. J.* **1980**, *188*, 643 – 648.
[68] E. Tetaud, C. Giroud, A. R. Prescott, D. W. Parkin, D. Baltz, N. Biteau, T. Baltz, A. H. Fairlamb, *Mol. Biochem. Parasitol.* **2001**, *116*, 171 – 183.
[69] S. R. Wilkinson, D. J. Meyer, J. M. Kelly, *Biochem. J.* **2000**, *352*, 755 – 761.
[70] H. Hillebrand, A. Schmidt, R. L. Krauth-Siegel, *J. Biol. Chem.* **2003**, *278*, 6809 – 6815.
[71] S. R. Wilkinson, D. Horn, S. R. Prathalingam, J. M. Kelly, *J. Biol. Chem.* **2003**, *278*, 31640 – 31646.
[72] S. R. Wilkinson, S. O. Obado, I. L. Mauricio, J. M. Kelly, *Proc. Natl. Acad. Sci. USA* **2002**, *99*, 13453 – 13458.
[73] R. L. Krauth-Siegel, S. K. Meiering, H. Schmidt, *Biol. Chem.* **2003**, *384*, 539 – 549.
[74] a) L. Thomson, A. Denicola, R. Radi, *Arch. Biochem. Biophys.* **2003**, *412*, 55 – 64; b) M. Trujillo, H. Budde, M. D. Pineyro, M. Stehr, C. Robello, L. Flohé, R. Radi, *J. Biol. Chem.* **2004**, *279*, 34175 – 34182.
[75] T. Irsch, R. L. Krauth-Siegel, *J. Biol. Chem.* **2004**, *279*, 22209 – 22217.
[76] S. E. Austin, M. O. Khan, K. T. Douglas, *Drug Des. Discov.* **1999**, *16*, 5 – 23.
[77] R. L. Krauth-Siegel, G. H. Coombs, *Parasitol. Today* **1999**, *15*, 404 – 409.
[78] S. Müller, G. H. Coombs, R. D. Walter, *Trends Parasitol.* **2001**, *17*, 242 – 249.
[79] S. Müller, E. Liebau, R. D. Walter, R. L. Krauth-Siegel, *Trends Parasitol.* **2003**, *19*, 320 – 328.
[80] B. A. Arrick, O. W. Griffith, A. Cerami, *J. Exp. Med.* **1981**, *153*, 720 – 725.
[81] P. Kapoor, M. Sachdev, R. Madhubala, *Trop. Med. Int. Health* **2000**, *5*, 438 – 442.
[82] S. L. Oza, M. R. Ariyanayagam, N. Aitcheson, A. H. Fairlamb, *Mol. Biochem. Parasitol.* **2003**, *131*, 25 – 33.
[83] S. Chen, C.-H. Lin, C. T. Walsh, J. K. Coward, *Bioorg. Med. Chem. Lett.* **1997**, *7*, 505 – 510.
[84] K. Amssoms, S. L. Oza, E. Ravaschino, A. Yamani, A. Lambeir, P. Rajan, G. Bal, J. Rodriguez, A. H. Fairlamb, K. Augustyns, A. Haemers, *Bioorg. Med. Chem. Lett.* **2002**, *12*, 2553 – 2556.
[85] For a review, see: A. Schmidt, R. L. Krauth-Siegel, *Curr. Top. Med. Chem.* **2002**, *2*, 1239 – 1259.
[86] C. H. Williams, Jr in *Chemistry and Biochemistry of Flavoenzymes, Vol. 3* (Ed.: F. Müller), CRC Press, Boca Raton, FL, **1992**, pp. 121 – 211.
[87] B. N. Leichus, M. Bradley, K. Nadeau, C. T. Walsh, J. S. Blanchard, *Biochemistry* **1992**, *31*, 6414 – 6420.
[88] R. Zheng, N. Cenas, J. S. Blanchard, *Biochemistry* **1995**, *34*, 12697 – 12703.
[89] H. Bauer, V. Massey, L. D. Arscott, R. H. Schirmer, D. A. Ballou, C. H. Williams, Jr, *J. Biol. Chem.* **2003**, *278*, 33020 – 33028.
[90] V. S. Stoll, S. J. Simpson, R. L. Krauth-Siegel, C. T. Walsh, E. F. Pai, *Biochemistry* **1997**, *36*, 6437 – 6447.

 © 2005 Wiley-VCH Verlag GmbH & Co. KGaA, Weinheim

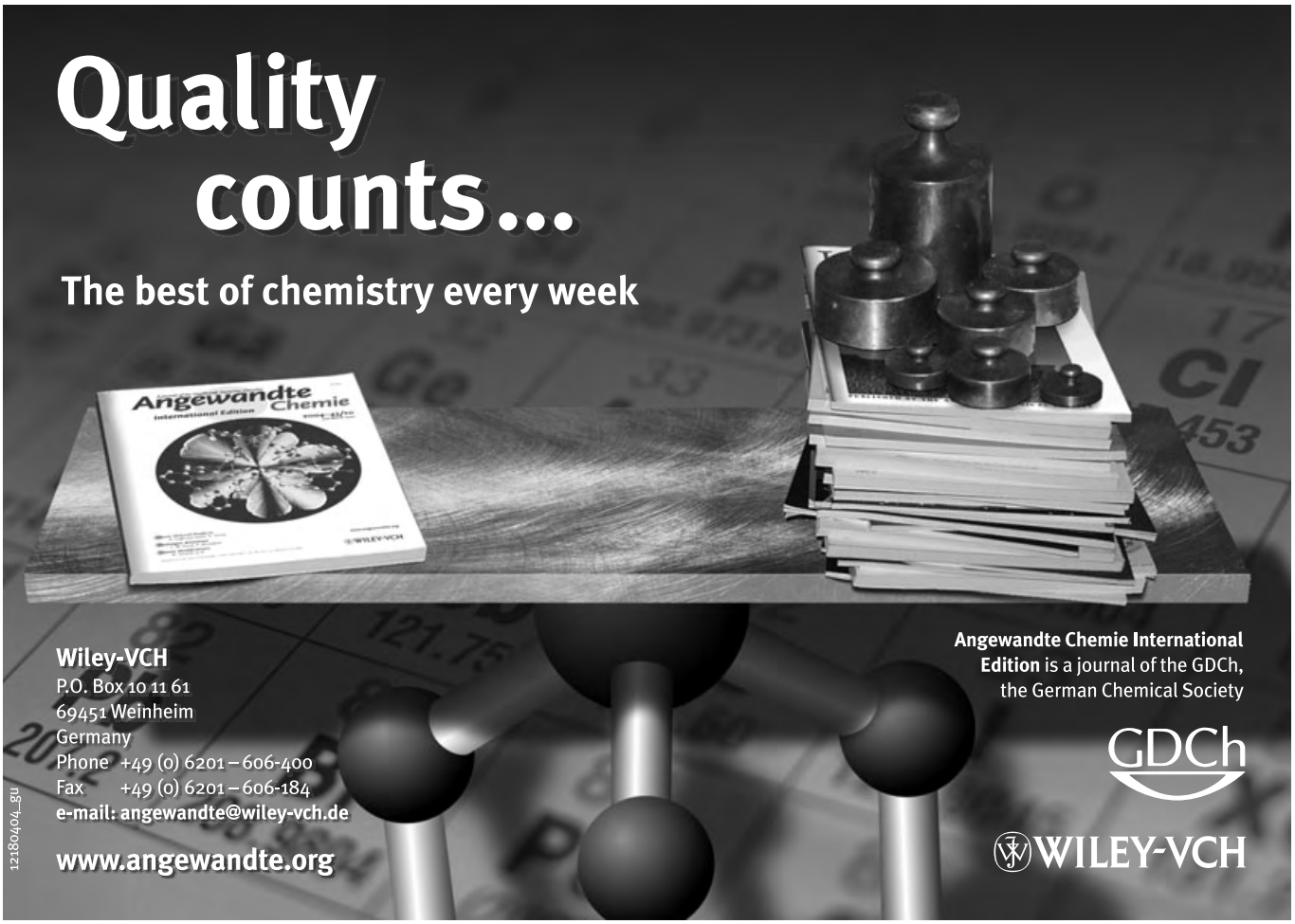
[91] E. M. Jacoby, I. Schlichting, C. B. Lantwin, W. Kabsch, R. L. Krauth-Siegel, *Proteins* **1996**, *24*, 73 – 80.
[92] J. Kuriyan, X. P. Kong, T. S. Krishna, R. M. Sweet, N. J. Murgolo, H. Field, A. Cerami, G. B. Henderson, *Proc. Natl. Acad. Sci. USA* **1991**, *88*, 8764 – 8768.
[93] W. N. Hunter, S. Bailey, J. Habash, S. J. Harrop, J. R. Helliwell, T. Aboagye-Kwarteng, K. Smith, A. H. Fairlamb, *J. Mol. Biol.* **1992**, *227*, 322 – 333.
[94] C. B. Lantwin, I. Schlichting, W. Kabsch, E. F. Pai, R. L. Krauth-Siegel, *Proteins* **1994**, *18*, 161 – 173.
[95] S. Bailey, K. Smith, A. H. Fairlamb, W. N. Hunter, *Eur. J. Biochem.* **1993**, *213*, 67 – 75.
[96] C. S. Bond, Y. Zhang, M. Berriman, M. L. Cunningham, A. H. Fairlamb, W. N. Hunter, *Structure Fold. Des.* **1999**, *7*, 81 – 89.
[97] J. A. Ponasik, C. Strickland, C. Faerman, S. Savvides, P. A. Karplus, B. Ganem, *Biochem. J.* **1995**, *311*, 371 – 375.
[98] H. K. Smith, M. Bradley, *J. Comb. Chem.* **1999**, *1*, 326 – 332.
[99] Z. Li, M. W. Fennie, B. Ganem, M. T. Hancock, M. Kobašlija, D. Rattendi, C. J. Bacchi, M. C. O'Sullivan, *Bioorg. Med. Chem. Lett.* **2001**, *11*, 251 – 254.
[100] S. Bonse, C. Santelli-Rouvier, J. Barbe, R. L. Krauth-Siegel, *J. Med. Chem.* **1999**, *42*, 5448 – 5454.
[101] T. J. Benson, J. H. McKie, J. Garforth, A. Borges, A. H. Fairlamb, K. T. Douglas, *Biochem. J.* **1992**, *286*, 9 – 11.
[102] M. O. Khan, S. E. Austin, C. Chan, H. Yin, D. Marks, S. N. Vaghjiani, H. Kendrick, V. Yardley, S. L. Croft, K. T. Douglas, *J. Med. Chem.* **2000**, *43*, 3148 – 3156.
[103] S. Girault, S. Baillet, D. Horvath, V. Lucas, E. Davioud-Charvet, A. Tartar, C. Sergheraert, *Eur. J. Med. Chem.* **1997**, *32*, 39 – 52.
[104] S. Girault, T. E. Davioud-Charvet, L. Maes, J. F. Dubremetz, M. A. Debreu, V. Landry, C. Sergheraert, *Bioorg. Med. Chem.* **2001**, *9*, 837 – 846.
[105] B. Bonnet, D. Soullez, E. Davioud-Charvet, V. Landry, D. Horvath, C. Sergheraert, *Bioorg. Med. Chem.* **1997**, *5*, 1249 – 1256.
[106] P. A. Karplus, R. L. Krauth-Siegel, R. H. Schirmer, G. E. Schulz, *Eur. J. Biochem.* **1988**, *171*, 193 – 198.
[107] R. H. Schirmer, J. G. Müller, R. L. Krauth-Siegel, *Angew. Chem.* **1995**, *107*, 153 – 157; *Angew. Chem. Int. Ed. Engl.* **1995**, *34*, 141 – 154.
[108] H. Gallwitz, S. Bonse, A. Martinez-Cruz, I. Schlichting, K. Schumacher, R. L. Krauth-Siegel, *J. Med. Chem.* **1999**, *42*, 364 – 372.
[109] S. Bonse, J. M. Richards, S. A. Ross, G. Lowe, R. L. Krauth-Siegel, *J. Med. Chem.* **2000**, *43*, 4812 – 4821.
[110] C. J. Hamilton, A. Saravanamuthu, A. H. Fairlamb, I. M. Eggleston, *Bioorg. Med. Chem.* **2003**, *11*, 3683 – 3693.
[111] N. Cenas, D. Bironaité, E. Dickancaite, Z. Anusevicius, J. Sarlauskas, J. S. Blanchard, *Biochem. Biophys. Res. Commun.* **1994**, *204*, 224 – 229.
[112] G. B. Henderson, P. Ulrich, A. H. Fairlamb, I. Rosenberg, M. Pereira, M. Sela, A. Cerami, *Proc. Natl. Acad. Sci. USA* **1988**, *85*, 5374 – 5378.
[113] M. C. Jockers-Scherübl, R. H. Schirmer, R. L. Krauth-Siegel, *Eur. J. Biochem.* **1989**, *180*, 267 – 272.
[114] K. Blumenstiel, R. Schöneck, V. Yardley, S. L. Croft, R. L. Krauth-Siegel, *Biochem. Pharmacol.* **1999**, *58*, 1791 – 1799.
[115] L. Salmon-Chemin, E. Buisine, V. Yardley, S. Kohler, M. A. Debreu, V. Landry, C. Sergheraert, S. L. Croft, R. L. Krauth-Siegel, E. Davioud-Charvet, *J. Med. Chem.* **2001**, *44*, 548 – 565.
[116] K. Augustyns, K. Amssoms, A. Yamani, P. K. Rajan, A. Haemers, *Curr. Pharm. Des.* **2001**, *7*, 1117 – 1141.
[117] C. D'Silva, S. Daunes, *Expert Opin. Invest. Drugs* **2002**, *11*, 217 – 231.
[118] R. L. Krauth-Siegel, O. Inhoff, *Parasitol. Res.* **2003**, *90*, 77 – 85.
[119] C. J. Hamilton, A. Saravanamuthu, I. M. Eggleston, A. H. Fairlamb, *Biochem. J.* **2003**, *369*, 529 – 537.
[120] D. J. Hammond, S. L. Croft, J. Hogg, W. E. Gutteridge, *Acta Trop.* **1986**, *43*, 367 – 378.
[121] K. Chibale, H. Haupt, H. Kendrick, V. Yardley, A. Saravanamuthu, A. H. Fairlamb, S. L. Croft, *Bioorg. Med. Chem. Lett.* **2001**, *11*, 2655 – 2657.
[122] C. Chan, H. Yin, J. Garforth, J. H. McKie, R. Jaouhari, P. Speers, K. T. Douglas, P. J. Rock, V. Yardley, S. L. Croft, A. H. Fairlamb, *J. Med. Chem.* **1998**, *41*, 148 – 156.
[123] D. Horvath, *J. Med. Chem.* **1997**, *40*, 2412 – 2423.
[124] a) R. H. Schirmer, T. Schöllhammer, G. Eisenbrand, R. L. Krauth-Siegel, *Free Radical Res. Commun.* **1987**, *3*, 3 – 12; b) M. Bilzer, R. L. Krauth-Siegel, R. H. Schirmer, T. P. Akerboom, H. Sies, G. E. Schulz, *Eur. J. Biochem.* **1984**, *138*, 373 – 378..
[125] K. Becker, R. H. Schirmer, *Methods Enzymol.* **1995**, *251*, 173 – 188.
[126] O. Inhoff, J. M. Richards, J. W. Briet, G. Lowe, R. L. Krauth-Siegel, *J. Med. Chem.* **2002**, *45*, 4524 – 4530.
[127] T. Nozaki, J. C. Engel, J. A. Dvorak, *Am. J. Trop. Med. Hyg.* **1996**, *55*, 111 – 117.
[128] J. D. Maya, S. Bollo, L. J. Nunez-Vergara, J. A. Squella, Y. Repetto, A. Morello, J. Perie, G. Chauviere, *Biochem. Pharmacol.* **2003**, *65*, 999 – 1006.
[129] A. Argyrou, G. Sun, B. A. Palfey, J. S. Blanchard, *Biochemistry* **2003**, *42*, 2218 – 2228.
[130] N. K. Cenas, G. A. Rakauskiene, J. J. Kulys, *Biochim. Biophys. Acta* **1989**, *973*, 399 – 404.
[131] B. K. Kubata, Z. Kabututu, T. Nozaki, C. J. Munday, S. Fukuzumi, K. Ohkubo, M. Lazarus, T. Maruyama, S. K. Martin, M. Duszenko, Y. Urade, *J. Exp. Med.* **2002**, *196*, 1241 – 1251.
[132] A. Nordhoff, PhD Thesis, Universität Heidelberg, **1995**.
[133] P. A. Karplus, E. F. Pai, G. E. Schulz, *Eur. J. Biochem.* **1989**, *178*, 693 – 703.
[134] P. Campbell, D. Butler (Eds.), *Nature* **2004**, *430*, 923 – 946.
[135] *Antimalarial Chemotherapy. Mechanisms of action, resistance and new directions in drug discovery*, (Ed.: P. J. Rosenthal), Humana Press, Totowa, **2001**.
[136] R. G. Ridley, *Nature* **2002**, *415*, 686 – 693.
[137] J. Wiesner, R. Ortmann, H. Jomaa, M. Schlitzer, *Angew. Chem.* **2003**, *115*, 5432 – 5451; *Angew. Chem. Int. Ed.* **2003**, *42*, 5274 – 5293.
[138] K. Rieckmann, Q. Cheng, *Trends Parasitol.* **2002**, *18*, 293; G. C. Coles, *Trends Parasitol.* **2002**, *18*, 293 – 294.
[139] I. A. Clark, W. B. Cowden in *Oxidative Stress* (Ed.: H. Sies), Academic Press, London, **1985**, pp. 131 – 149.
[140] S. Müller, T. W. Gilberger, Z. Krnajski, K. Lüersen, S. Meierjohann, R. D. Walter, *Protoplasma* **2001**, *217*, 43 – 49.
[141] K. Becker, S. M. Kanzok, R. Iozef, M. Fischer, R. H. Schirmer, S. Rahlfs, *Eur. J. Biochem.* **2003**, *270*, 1057 – 1064.
[142] R. M. Luond, J. H. McKie, K. T. Douglas, M. J. Dascombe, J. Vale, *J. Enzyme Inhib.* **1998**, *13*, 327 – 345.
[143] G. Giribaldi, D. Ulliers, F. Mannu, P. Arese, F. Turrini, *Br. J. Haematol.* **2001**, *113*, 492 – 499.
[144] A. Irmler, A. Bechthold, E. Davioud-Charvet, V. Hofmann, R. Reau, S. Gromer, R. H. Schirmer, K. Becker in *Flavins and Flavoproteins, Vol. 14* (Eds.: S. Chapman, R. Perham, N. Scrutton), Agency for Scientific Publications, Berlin, **2002**, pp. 803 – 808.
[145] H. Ginsburg, J. Golenser, *Redox Rep.* **2003**, *8*, 276 – 279.
[146] S. M. Kanzok, R. H. Schirmer, I. Türbachova, R. Iozef, K. Becker, *J. Biol. Chem.* **2000**, *275*, 40180 – 40186.
[147] H. Sies, *Eur. J. Biochem.* **1993**, *215*, 213 – 219.
[148] K. Becker, S. Rahlfs, C. Nickel, R. H. Schirmer, *Biol. Chem.* **2003**, *384*, 551 – 566.

 © 2005 Wiley-VCH Verlag GmbH & Co. KGaA, Weinheim

[149] S. M. Kanzok, S. Rahlfs, K. Becker, R. H. Schirmer, *Methods Enzymol.* **2002**, *347*, 370 – 381.
[150] S. Rahlfs, R. H. Schirmer, K. Becker, *Cell. Mol. Life Sci.* **2002**, *59*, 1024 – 1041.
[151] Z. Krnajski, T. W. Gilberger, R. D. Walter, S. Müller, *Mol. Biochem. Parasitol.* **2001**, *112*, 219 – 228.
[152] C. H. Williams, L. D. Arscott, S. Müller, B. W. Lennon, M. L. Ludwig, P. F. Wang, D. M. Veine, K. Becker, R. H. Schirmer, *Eur. J. Biochem.* **2000**, *267*, 6110 – 6117.
[153] Z. Krnajski, T. W. Gilberger, R. D. Walter, A. F. Cowman, S. Müller, *J. Biol. Chem.* **2002**, *277*, 25970 – 25975.
[154] R. P. Hirt, S. Müller, T. M. Embley, G. H. Coombs, *Trends Parasitol.* **2002**, *18*, 302 – 308.
[155] Z. Krnajski, R. D. Walter, S. Müller, *Mol. Biochem. Parasitol.* **2001**, *113*, 303 – 308.
[156] S. Rahlfs, K. Becker, *Eur. J. Biochem.* **2001**, *268*, 1404 – 1409.
[157] S. Kawazu, K. Komaki, N. Tsuji, S. Kawai, N. Ikenoue, T. Hatabu, H. Ishikawa, Y. Matsumoto, K. Himeno, S. Kano, *Mol. Biochem. Parasitol.* **2001**, *116*, 73 – 79.
[158] K. Lüersen, R. D. Walter, S. Müller, *Biochem. J.* **2000**, *346*, 545 – 552.
[159] S. Meierjohann, R. D. Walter, S. Müller, *Biochem. J.* **2002**, *363*, 833 – 838.
[160] P. M. Färber, L. D. Arscott, C. H. Williams, Jr, K. Becker, R. H. Schirmer, *FEBS Lett.* **1998**, *422*, 311 – 314.
[161] G. N. Sarma, S. N. Savvides, K. Becker, M. Schirmer, R. H. Schirmer, P. A. Karplus, *J. Mol. Biol.* **2003**, *328*, 893 – 907.
[162] E. Liebau, B. Bergmann, A. M. Campbell, P. Teesdale-Spittle, P. M. Brophy, K. Lüersen, R. D. Walter, *Mol. Biochem. Parasitol.* **2002**, *124*, 85 – 90.
[163] K. Fritz, S. Rahlfs, P. Harwaldt, R. H. Schirmer, W. Kabsch, K. Becker, *Proc. Natl. Acad. Sci. USA* **2003**, *100*, 13821 – 13826.
[164] S. Rahlfs, C. Nickel, M. Deponte, R. H. Schirmer, K. Becker, *Redox Rep.* **2003**, *8*, 246 – 250.
[165] S. Rahlfs, M. Fischer, K. Becker, *J. Biol. Chem.* **2001**, *276*, 37133 – 37140.
[166] R. Iozef, S. Rahlfs, T. Chang, H. Schirmer, K. Becker, *FEBS Lett.* **2003**, *554*, 284 – 288.
[167] H. Atamna, H. Ginsburg, *Eur. J. Biochem.* **1997**, *250*, 670 – 679.
[168] R. Munday, C. C. Winterbourn, *Biochem. Pharmacol.* **1989**, *38*, 4349 – 4352.
[169] P. Wardman, C. von Sonntag, *Methods Enzymol.* **1995**, *251*, 31 – 45.
[170] R. L. Krauth-Siegel, J. G. Müller, F. Lottspeich, R. H. Schirmer, *Eur. J. Biochem.* **1996**, *235*, 345 – 350.
[171] H. Sztajer, B. Gamain, K. D. Aumann, C. Slomianny, K. Becker, R. Brigelius-Flohé, L. Flohé, *J. Biol. Chem.* **2001**, *276*, 7397 – 7403.
[172] Z. A. Wood, L. B. Poole, P. A. Karplus, *Science* **2003**, *300*, 650 – 653.
[173] E. Davioud-Charvet, M. J. McLeish, D. M. Veine, D. Giegel, L. D. Arscott, A. D. Andricopulo, K. Becker, S. Müller, R. H. Schirmer, C. H. Williams, Jr, G. L. Kenyon, *Biochemistry* **2003**, *42*, 13319 – 13330.
[174] U. Benatti, L. Guida, A. De Flora, *Biochem. Biophys. Res. Commun.* **1984**, *120*, 747 – 753.
[175] A. Schönleben-Janas, P. Kirsch, P. R. Mittl, R. H. Schirmer, R. L. Krauth-Siegel, *J. Med. Chem.* **1996**, *39*, 1549 – 1554.
[176] E. Davioud-Charvet, S. Delarue, C. Biot, B. Schwöbel, C. C. Böhme, A. Müssigbrodt, L. Maes, C. Sergheraert, P. Grellier, R. H. Schirmer, K. Becker, *J. Med. Chem.* **2001**, *44*, 4268 – 4276.
[177] H. Zappe, MD Thesis, Universität Heidelberg, **1980**.
[178] R. H. Schirmer, B. Coulibaly, A. Stich, M. Scheiwein, H. Merkle, J. Eubel, K. Becker, H. Becher, O. Müller, T. Zich, W. Schiek, B. Kouyaté, *Redox Rep.* **2003**, *8*, 272 – 275.
[179] S. N. Savvides, M. Scheiwein, C. C. Böhme, G. E. Arteel, P. A. Karplus, K. Becker, R. H. Schirmer, *J. Biol. Chem.* **2002**, *277*, 2779 – 2784.
[180] M. Schirmer, M. Scheiwein, S. Gromer, K. Becker, R. H. Schirmer in *Flavins and Flavoproteins, Vol. 13* (Eds.: S. Ghisla, P. Kroneck, P. Macheroux, H. Sund), Agency for Scientific Publications, Berlin, **1999**, pp. 857 – 862.
[181] R. H. Schirmer, H. Bauer, K. Becker in *Wiley Encyclopedia of Molecular Medicine, Vol. 5* (Ed.: T. E. Creighton), Wiley, New York, **2002**, pp. 1471 – 1475.
[182] S. Müller, T. W. Gilberger, P. M. Färber, K. Becker, R. H. Schirmer, R. D. Walter, *Mol. Biochem. Parasitol.* **1996**, *80*, 215 – 219.
[183] Z. Krnajski, T. W. Gilberger, R. D. Walter, S. Müller, *J. Biol. Chem.* **2000**, *275*, 40874 – 40878.
[184] T. W. Gilberger, R. D. Walter, S. Müller, *J. Biol. Chem.* **1997**, *272*, 29584 – 29589.
[185] V. N. Gladyshev, K. T. Jeang, T. C. Stadtman, *Proc. Natl. Acad. Sci. USA* **1996**, *93*, 6146 – 6151.
[186] H. Bauer, S. Gromer, A. Urbani, M. Schnölzer, R. H. Schirmer, H. M. Müller, *Eur. J. Biochem.* **2003**, *270*, 4272 – 4281.
[187] P. Harwaldt, S. Rahlfs, K. Becker, *Biol. Chem.* **2002**, *383*, 821 – 830.
[188] T. W. Gilberger, R. H. Schirmer, R. D. Walter, S. Müller, *Mol. Biochem. Parasitol.* **2000**, *107*, 169 – 179.
[189] P. M. Färber, K. Becker, S. Müller, R. H. Schirmer, R. M. Franklin, *Eur. J. Biochem.* **1996**, *239*, 655 – 661.
[190] S. N. Savvides, P. A. Karplus, *J. Biol. Chem.* **1996**, *271*, 8101 – 8107.
[191] C. C. Böhme, L. D. Arscott, K. Becker, R. H. Schirmer, C. H. Williams, Jr, *J. Biol. Chem.* **2000**, *275*, 37317 – 37323.
[192] M. A. Keese, R. Saffrich, T. Dandekar, K. Becker, R. H. Schirmer, *FEBS Lett.* **1999**, *447*, 135 – 138.
[193] H. Y. Long, B. Lell, K. Dietz, P. G. Kremsner, *Parasitol. Res.* **2001**, *87*, 553 – 555.
[194] A. Nordhoff, C. Tziatzios, J. A. van den Broek, M. K. Schott, H. R. Kalbitzer, K. Becker, D. Schubert, R. H. Schirmer, *Eur. J. Biochem.* **1997**, *245*, 273 – 282.
[195] M. Mayer, *Dtsch. Med. Wochenschr.* **1919**, *45*, 1052 – 1053.
[196] P. Guttmann, P. Ehrlich, *Berl. Klin. Wochenschr.* **1891**, *28*, 953 – 956.
[197] J. L. Vennerstrom, M. T. Makler, C. K. Angerhofer, J. A. Williams, *Antimicrob. Agents Chemother.* **1995**, *39*, 2671 – 2677.
[198] H. Atamna, M. Krugliak, G. Shalmiev, E. Deharo, G. Pescarmona, H. Ginsburg, *Biochem. Pharmacol.* **1996**, *51*, 693 – 700.
[199] J. Golenser, J. Miller, D. T. Spira, N. S. Kosower, J. A. Vande Waa, J. B. Jensen, *Trop. Med. Parasitol.* **1988**, *39*, 273 – 276.
[200] Y. Zhang, I. König, R. H. Schirmer, *Biochem. Pharmacol.* **1988**, *37*, 861 – 865.
[201] F. Turrini, H. Ginsburg, F. Bussolino, G. P. Pescarmona, M. V. Serra, P. Arese, *Blood* **1992**, *80*, 801 – 808.
[202] S. Krieger, W. Schwarz, M. R. Ariyanayagam, A. H. Fairlamb, R. L. Krauth-Siegel, C. Clayton, *Mol. Microbiol.* **2000**, *35*, 542 – 552.
[203] J. F. Morrison, C. T. Walsh, *Adv. Enzymol. Relat. Areas Mol. Biol.* **1988**, *61*, 201 – 301.
[204] A. Nordhoff, R. H. Schirmer, *Naturwiss. Rundsch.* **1995**, *48*, 336 – 343.
[205] F. Q. Schafer, G. R. Buettner, *Free Radical Biol. Med.* **2001**, *30*, 1191 – 1212.
[206] S. Gromer, S. Urig, K. Becker, *Med. Res. Rev.* **2004**, *24*, 40 – 89.
[207] B. W. Lennon, C. H. Williams, Jr, *Biochemistry* **1996**, *35*, 4704 – 4712.
[208] S. M. Kanzok, A. Fechner, H. Bauer, J. K. Ulschmid, H. M. Müller, J. Botella-Munoz, S. Schneuwly, R. H. Schirmer, K. Becker, *Science* **2001**, *291*, 643 – 646.

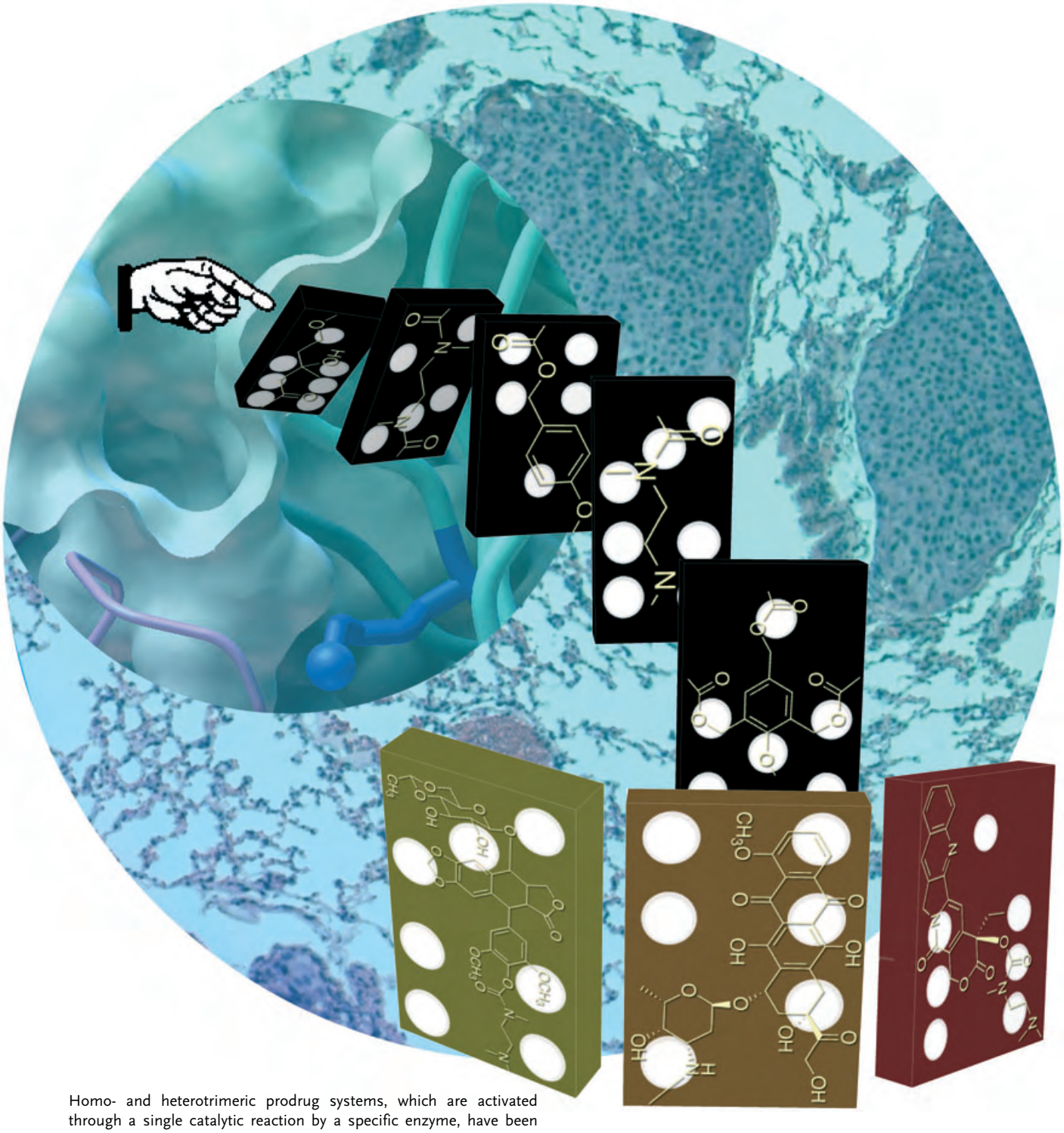
 © 2005 Wiley-VCH Verlag GmbH & Co. KGaA, Weinheim

[209] E. N. Iheanacho, N. H. Hunt, R. Stocker, *Free Radical Biol. Med.* **1995**, *18*, 543 – 552.
[210] D. Shenton, G. Perrone, K. A. Quinn, I. W. Dawes, C. M. Grant, *J. Biol. Chem.* **2002**, *277*, 16853 – 16859.
[211] E. S. Arnér, A. Holmgren, *Eur. J. Biochem.* **2000**, *267*, 6102 – 6109.
[212] A. Holmgren, *Annu. Rev. Biochem.* **1985**, *54*, 237 – 271.
[213] I. A. Cotgreave, R. Gerdes, I. Schuppe-Koistinen, C. Lind, *Methods Enzymol.* **2002**, *348*, 175 – 182.
[214] H. Ostergaard, C. Tachibana, J. R. Winther, *J. Cell. Biol.* **2004**, *166*, 337 – 345.
[215] Z. Bozdech, H. Ginsburg, *Malar. J.* **2004**, *3*, 23 – 30.
[216] B. Biteau, J. Labarre, M. B. Toledano, *Nature* **2003**, *425*, 980 – 984.
[217] T. S. Chang, W. Jeong, H. A. Woo, S. M. Lee, S. Park, S. G. Rhee, *J. Biol. Chem.* **2004**, *279*, 50994 – 51001.
[218] A. Saravanamuthu, T. J. Vickers, C. S. Bond, M. R. Peterson, W. N. Hunter, A. H. Fairlamb, *J. Biol. Chem.* **2004**, *279*, 29493 – 29500.
[219] C. Biot, H. Bauer, R. H. Schirmer, E. Davioud-Charvet, J. Med. Chem. **2004**, *47*, 5972 – 5983.
[220] A. Argyrou, J. S. Blanchard, *Prog. Nucleic Acid Res. Mol. Biol.* **2004**, *78*, 89 – 142.
[221] B. Coulibaly, J. Eubel, S. Gromer, R. H. Schirmer in *Health Research in Developing Countries* (Eds.: H. Becher, B. Kouyaté), Springer, Heidelberg, **2005**, pp.285 – 292.



 © 2005 Wiley-VCH Verlag GmbH & Co. KGaA, Weinheim

Communications



Homo- and heterotrimeric prodrug systems, which are activated through a single catalytic reaction by a specific enzyme, have been prepared to release anticancer drugs. For more information about the knock-on (domino) effect of the bioactivation of the prodrug platform, see the Communication by D. Shabat et al. on the following pages.

© 2005 Wiley-VCH Verlag GmbH & Co. KGaA, Weinheim
DOI: 10.1002/anie.200461657

Prodrug Dendrimers

Single-Triggered Trimeric Prodrugs**

*Keren Haba, Mikhail Popkov, Marina Shamis, Richard A. Lerner, Carlos F. Barbas III, and Doron Shabat**

Of the various approaches designed to minimize undesirable properties of drugs while retaining therapeutic activity, the chemical approach of drug derivatization offers the highest flexibility and has been demonstrated to improve drug efficacy.[1] The term "prodrug" indicates that chemical derivatization has been used to alter the physicochemical properties of a drug. The prodrug is converted in vivo by metabolic processes or environmental conditions into the active form. Several anticancer prodrugs have been designed for selective activation in malignant tissues by a specific enzyme secreted within the proximity of the tumor.[2] The amount of drug activated at the targeted tissue is dependent on the rate and concentration of the specific enzyme. To overcome this limitation, our group[3,4] and two others[5,6] have designed dendritic units that are able to release several drug molecules with a single enzymatic cleavage. We have also demonstrated the potential of the dendritic platform with the first bioactivation of dimeric prodrugs.[7] Here we report the advantages of a trimeric prodrug system relative to a conventional monomeric system.

Our prodrug system is based on an AB_3 dendritic unit (Figure 1) in which three drug molecules B are linked to one enzymatic substrate A. The trigger is activated upon enzymatic cleavage and is designed to release the three drug molecules through a mechanism based on self-cyclization and triple quinone methide rearrangement (see Supporting Information for the detailed mechanism). Although a similar conceptual molecule was described previously, it was not examined as a prodrug system.[5]

To evaluate the self-cyclization and triple quinone methide rearrangement, we constructed a model system from three molecules of *p*-nitroaniline to mimic the drug units and a *tert*-butoxycarbonyl (Boc) protecting group to mimic the enzymatic substrate. Cleavage of the Boc group should trigger the release of the *p*-nitroaniline moieties as shown in Figure 2. Initially, we set out to examine whether the release could occur under physiological conditions. The Boc group was removed with anhydrous hydrogen chloride, and the product was then incubated in phosphate buffered saline (PBS) solution at pH 7.4. The progress of the reaction was monitored by HPLC by following the formation of *p*-nitroaniline. Figure 3 shows that free *p*-nitroaniline was rapidly generated after the cleavage of the Boc protecting group. No release was observed when the Boc group remained attached to the platform.

This experiment proved that the triple quinone methide rearrangement could indeed take place under physiological conditions. With this information in hand, we synthesized a trimeric prodrug system in which three molecules of the anticancer drug camptothecin (pro-tCPT) were linked through a retro-aldol, retro-Michael trigger to a substrate for the catalytic antibody 38C2. This antibody catalyzes aldol and retro-aldol reactions by using the enamine mechanism of natural aldolases and has been used for the selective activation of prodrugs.[8–13] Furthermore, we synthesized a

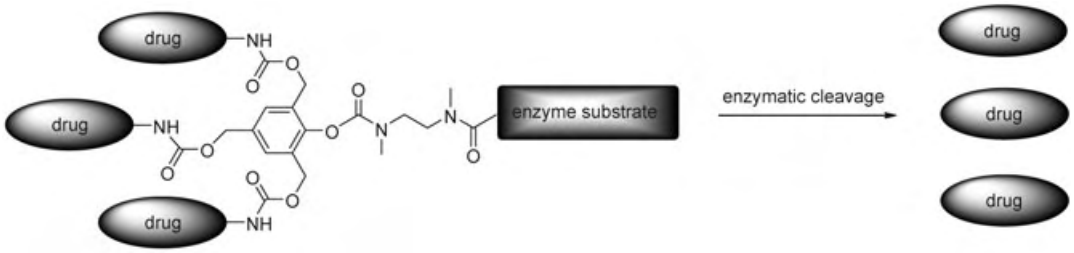


Figure 1. General structure of a single-triggered trimeric prodrug.

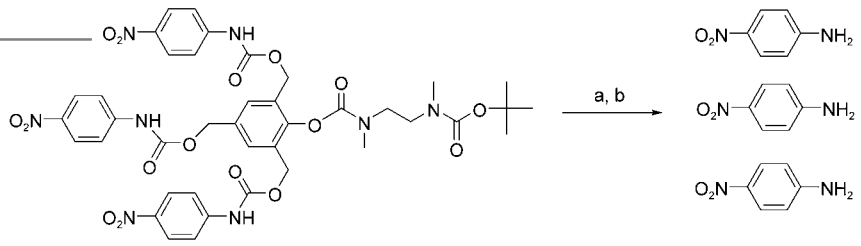


Figure 2. Cleavage of a Boc group triggers the release of *p*-nitroaniline from the trimeric platform. a) HCl; b) PBS, pH 7.4.

[*] K. Haba, M. Shamis, Dr. D. Shabat
Department of Organic Chemistry
School of Chemistry, Faculty of Exact Sciences
Tel Aviv University
Tel Aviv 69978 (Israel)
Fax: (+972) 3-640-9293
E-mail: chdoron@post.tau.ac.il
Dr. M. Popkov, Prof. R. A. Lerner, Prof. C. F. Barbas III
The Skaggs Institute for Chemical Biology
Departments of Molecular Biology and Chemistry
The Scripps Research Institute
10550 North Torrey Pines Road
La Jolla, CA 92037 (USA)

[**] D.S. thanks the Israel Science Foundation for financial support. We thank Dr. Michael Meijler for his helpful comments. K.H. and M.P. contributed equally to this work.

Supporting information for this article is available on the WWW under http://www.angewandte.org or from the author.

 © 2005 Wiley-VCH Verlag GmbH & Co. KGaA, Weinheim

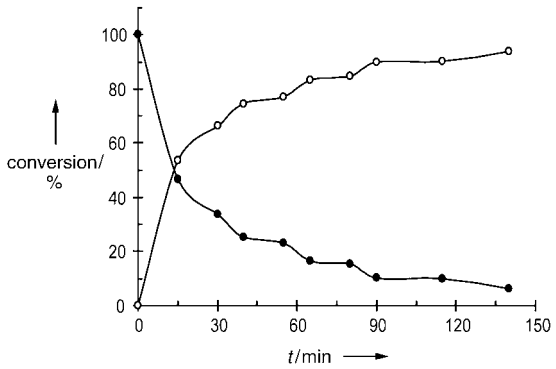


Figure 3. Release (% conversion) of *p*-nitroaniline from the trimeric platform, ○ = *p*-nitroaniline, ● = starting material.

monomeric CPT prodrug (pro-mCPT) with an identical linker (Figure 4 a). Both prodrugs were activated upon incubation with the antibody 38C2, and the release of CPT was confirmed by HPLC analysis (data not shown).

Next, we examined whether the trimeric prodrug system had an advantage over the monomeric system in a cell-growth inhibition assay. We evaluated the ability of the prodrugs to inhibit cell proliferation in the presence of catalytic antibody 38C2 using three different cell lines: the human T-lineage acute lymphoblastic leukemia (ALL) cell line MOLT-3, the human erythroleukemia cell line HEL, and the human acute myeloid leukemia (AML) cell line HL-60. The results are summarized in Table 1 and the data from the MOLT-3 cell

Table 1: IC_{50} values [nM] from cell-growth inhibition assays.

Drug/Prodrug	MOLT-3		HL-60		HEL	
	IC_{50}[a]	IC_{50}[b]	IC_{50}[a]	IC_{50}[b]	IC_{50}[a]	IC_{50}[b]
CPT	2.2	2.0	9.0	7.5	13	11
pro-mCPT	100	15	150	31	400	100
pro-tCTP	80	2.7	100	7.5	200	19

[a] Cells were incubated in medium with drug/prodrug. [b] Cells were incubated in medium with drug/prodrug and 1-μM catalytic antibody 38C2.

line are presented in Figure 4 b. The trimeric prodrug is more potent then the monomeric drug when incubated with the antibody. This behavior is as expected because triple the amount of CPT is released relative to the amount released from an equivalent concentration of the monomeric prodrug.

In the trimeric system, one cleavage by the antibody releases three times the amount of CPT as a cleavage in the monomeric prodrug system. We selected one cell line (MOLT-3 leukemia) for further studies with fixed concentrations of the prodrug and varying concentrations of antibody 38C2. To have equal amounts of CPT, the concentration of the monomeric prodrug was three times that of the trimeric prodrug (36 nM and 12 nM for the monomeric and trimeric prodrugs, respectively). The results are shown in Figure 5. The trimeric prodrug inhibited cell growth up to three times more effectively than the monomeric prodrug in the concentration range of 15–150 nM of the antibody. In other words, the

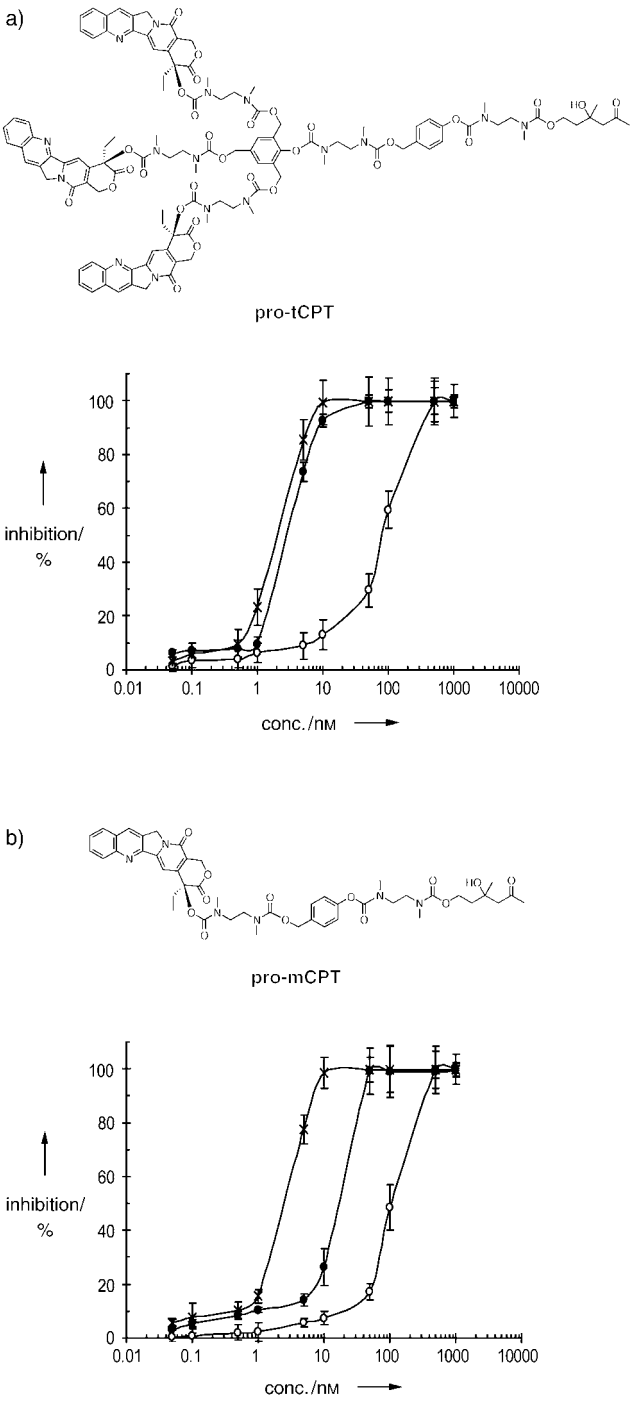


Figure 4. Molecular structures of the single-triggered CPT trimeric prodrug (pro-tCPT) and the classic CPT monomeric prodrug (pro-mCPT), which both have identical triggers, and the growth inhibition assays of human MOLT-3 leukemia cell line with the prodrugs in the presence and absence of catalytic antibody 38C2. a) pro-tCPT: ○ = pro-tCPT, ○ = pro-tCPT + 38C2, × = CPT; b) pro-mCPT: ○ = pro-mCPT, ● = pro-mCPT + 38C2, × = CPT.

concentration of antibody needed to inhibit the cell growth by 50% with pro-tCPT is about three times less than that needed with pro-mCPT. Note that the cytotoxicity of the platform degradation products in cell-growth inhibition was previously evaluated. The degradation products were found to have

 © 2005 Wiley-VCH Verlag GmbH & Co. KGaA, Weinheim

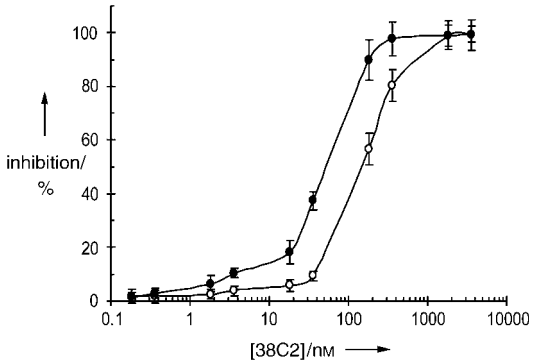


Figure 5. Growth inhibition assay of the human MOLT-3 leukemia cell line at a fixed concentration of the prodrug and upon variation of the concentration of the catalytic antibody 38C2. Cells were incubated for 72 h. ○ = 36-nM pro-mCPT, ● = 12-nM pro-tCPT.

negligible or no toxicity at all within the concentration range for the drug in the cell assay.[5]

It is also possible to incorporate three different drug molecules on the same prodrug platform. This would effectively allow triple-drug therapy in a single molecule. We prepared a heterotrimeric system with the anticancer drugs CPT, doxorubicin, and etoposide by using the retro-aldol, retro-Michael trigger activated by antibody 38C2 (Figure 6). Upon single-activation cleavage by the catalytic antibody, it was anticipated that this prodrug system should almost simultaneously release three different chemotherapeutic drugs at the same location. HPLC analysis confirmed the release of the drugs in the presence of antibody 38C2.

The heterotrimeric prodrug system was also evaluated in a cell-growth inhibition assay (Figure 7). The prodrug was incubated with MOLT-3 leukemia cells in the presence and in the absence of catalytic antibody 38C2. The inhibition of cell growth by the heterotrimeric prodrug was increased approximately 15-fold upon activation by antibody 38C2. We

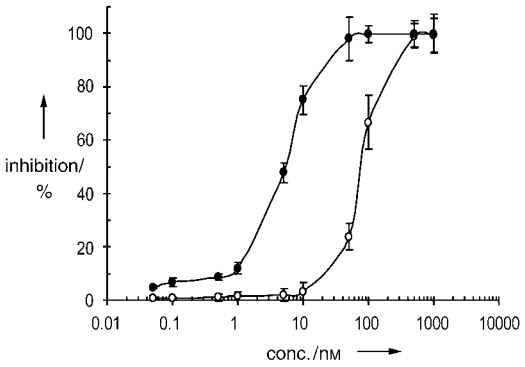


Figure 7. Growth inhibition assay of the human MOLT-3 leukemia cell line. Cells were incubated for 72 h. a) ● = heterotrimeric prodrug (pro-HT) + 1-μM catalytic antibody 38C2; b) ○ = pro-HT.

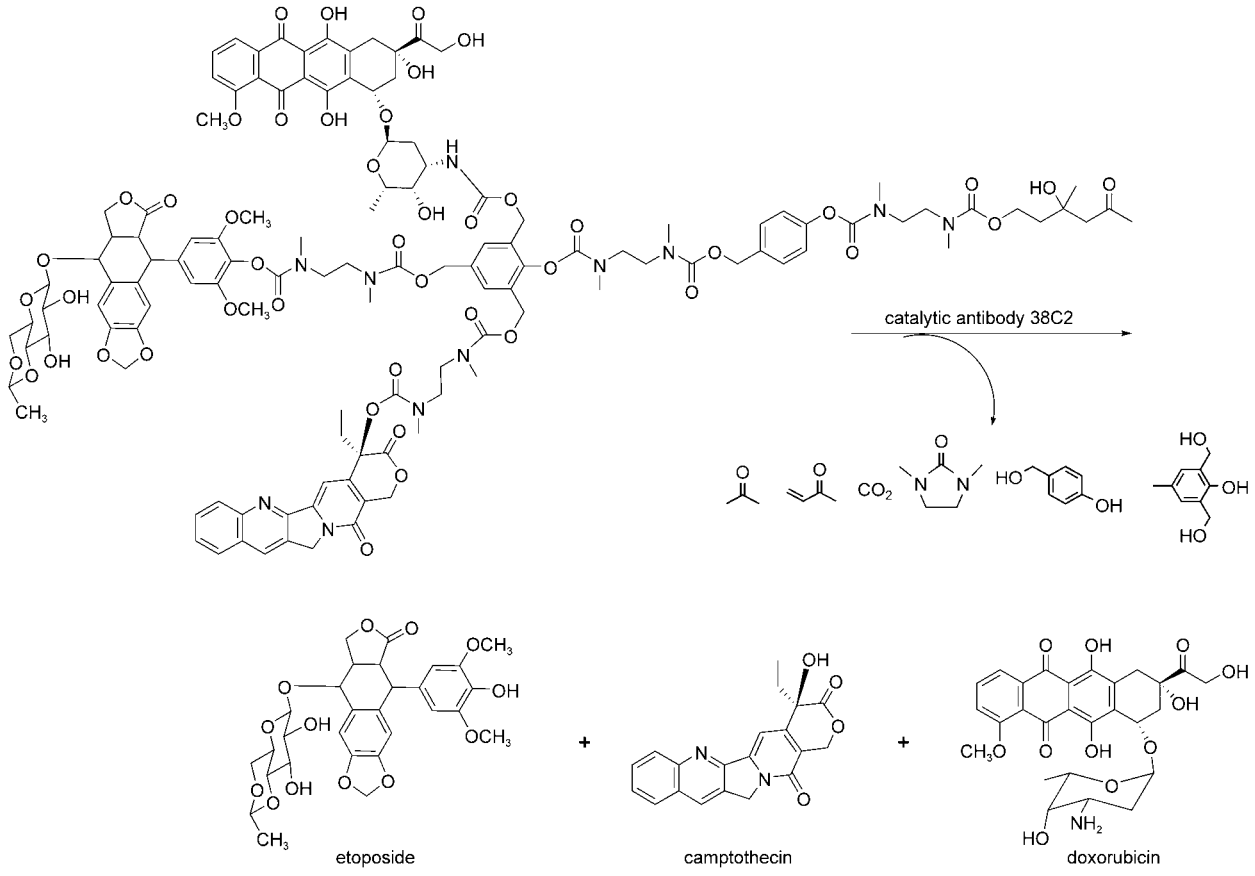


Figure 6. Single-triggered heterotrimeric prodrug system with the anticancer drugs CPT, doxorubicin, and etoposide, and a retro-aldol, retro-Michael substrate.

 © 2005 Wiley-VCH Verlag GmbH & Co. KGaA, Weinheim

previously reported that a heterodimeric prodrug system was more effective in the inhibition of cell growth than two monomeric prodrugs.[7] Single-triggered heterotrimeric prodrugs may offer additional synergy in chemotherapy.

Dendritic prodrugs that are activated through a single catalytic reaction by a specific enzyme could offer significant advantages in the inhibition of tumor growth, especially if the targeted or secreted enzyme exists at relatively low levels in the malignant tissue. We have prepared the first example of a single-triggered trimeric prodrug system with the anticancer drug CPT and activated by catalytic antibody 38C2. We anticipate that single-triggered dendritic prodrugs will be exploited to further improve selective chemotherapeutic approaches in cancer therapy.

Received: August 15, 2004

Keywords: aldol reaction · catalytic antibodies · dendrimers · drug delivery · prodrugs

[1] F. M. de Groot, E. W. Damen, H. W. Scheeren, *Curr. Med. Chem.* **2001**, *8*, 1093.
[2] K. D. Bagshawe, C. J. Springer, F. Searle, P. Antoniw, S. K. Sharma, R. G. Melton, R. F. Sherwood, *Br. J. Cancer* **1988**, *58*, 700.
[3] D. Shabat, B. List, R. J. Amir, M. Shamis, N. Pessah (Ramot at Tel Aviv University Ltd., Israel; The Scripps Research Institute), PCT Int. Appl., **2004**, p. 153.
[4] R. J. Amir, N. Pessah, M. Shamis, D. Shabat, *Angew. Chem. Angew Chem.* **2003**, *115*, 4632; *Angew. Chem. Int. Ed.* **2003**, *42*, 4494.
[5] F. M. de Groot, C. Albrecht, R. Koekkoek, P. H. Beusker, H. W. Scheeren, *Angew. Chem.* **2003**, *115*, 4628; *Angew. Chem. Int. Ed.* **2003**, *42*, 4490.
[6] M. L. Szalai, R. M. Kevwitch, D. V. McGrath, *J. Am. Chem. Soc.* **2003**, *125*, 15688.
[7] M. Shamis, H. N. Lode, D. Shabat, *J. Am. Chem. Soc.* **2004**, *126*, 1726.
[8] C. Rader, J. M. Turner, A. Heine, D. Shabat, S. C. Sinha, I. A. Wilson, R. A. Lerner, C. F. Barbas, *J. Mol. Biol.* **2003**, *332*, 889.
[9] D. Shabat, C. Rader, B. List, R. A. Lerner, C. F. Barbas III, *Proc. Natl. Acad. Sci. USA* **1999**, *96*, 6925.
[10] D. Shabat, H. Lode, U. Pertl, R. A. Reisfeld, C. Rader, R. A. Lerner, C. F. Barbas III, *Proc. Natl. Acad. Sci. USA* **2001**, *98*, 7528.
[11] S. C. Sinha, L. S. Li, G. P. Miller, S. Dutta, C. Rader, R. A. Lerner, *Proc. Natl. Acad. Sci. USA* **2004**, *101*, 3095.
[12] J. Wagner, R. A. Lerner, C. F. Barbas III, *Science* **1995**, *270*, 1797.
[13] A. Cordova, K. D. Janda, *J. Am. Chem. Soc.* **2001**, *123*, 8248.

 © 2005 Wiley-VCH Verlag GmbH & Co. KGaA, Weinheim

Temperature-Dependent Magnetism

Unusual Magnetic Properties of the Edge-Sharing Bioctahedral Dirhenium(IV) Complex of Pyridine-2-thiolate**

Keisuke Umakoshi, Noriko Misasa, Chikako Ohtsu, Takashi Kojima, Maxim Sokolov, Makoto Wakeshima, Yukio Hinatsu, and Masayoshi Onishi**

Since the discovery of the $^3(\delta\delta^*)$ excited triplet state in a dimolybdenum(III) complex,[1] much effort has been devoted to the development of edge-sharing bioctahedral (ESBO) dimolybdenum(III) and ditungsten(III) complexes.[2] In ESBO complexes with a d^3–d^3 electron configuration, it is expected that the order of the molecular orbitals associated with metal–metal bonding is σ, π, δ*, δ, π*, and σ* in increasing in energy owing to mixing of the δ orbital with p orbitals on the bridging atoms.[3] The δ and δ* orbitals of diphosphine- or thiolato-bridged dimolybdenum and ditungsten complexes, however, are close in energy. The temperature-dependent magnetic properties of these complexes are consistent with the thermal population of the accessible excited triplet state.[1,2] Although several ESBO dirhenium(IV) complexes have also been synthesized to date, they are all diamagnetic.[4,5] Herein, we report the first μ-oxo-μ-thiolato ESBO dirhenium(IV) complex, which exhibits temperature-dependent magnetic properties that indicate the existence of a $^3(\delta\delta^*)$ excited state. We have also synthesized its one-electron reduced complex, and the structures and magnetic properties of Re_2^{IV} and $Re_2^{III,IV}$ complexes are compared.

It is known that the reaction of quadruply metal–metal-bonded dirhenium(III) complexes $(n\mathrm{Bu_4N})_2[\mathrm{Re_2X_8}]$ (X = Cl, Br) with pyridine-2-thiol (Hpyt) affords $[\mathrm{Re_2(pyt)_4X_2}]$ complexes that have a lantern structure with the retention of the metal–metal quadruple bond.[6] When the oxorhenium(V) complex $[\mathrm{ReOCl_3(PPh_3)_2}]$ was chosen as the starting material,

[*] Prof. Dr. K. Umakoshi, N. Misasa, C. Ohtsu, T. Kojima, Prof. Dr. M. Onishi
Department of Applied Chemistry
Faculty of Engineering
Nagasaki University
Bunkyo-machi, Nagasaki 852-8521 (Japan)
Fax: (+81) 95-819-2672
E-mail: kumks@net.nagasaki-u.ac.jp
onishi@net.nagasaki-u.ac.jp

Dr. M. Sokolov
Institute of Inorganic Chemistry
pr. Lavrentyeva 3, Novosibirsk 630090 (Russia)

Dr. M. Wakeshima, Prof. Dr. Y. Hinatsu
Division of Chemistry
Graduate School of Science
Hokkaido University
Kita-ku, Sapporo 060-0810 (Japan)

[**] This work was supported by a Grant-in-Aid for Scientific Research (No. 15550053) to K.U. We thank Mr. Eiji Yamaguchi and Miss Hikari Hamasaki for assistance.

Supporting information for this article is available on the WWW under http://www.angewandte.org or from the author.

 © 2005 Wiley-VCH Verlag GmbH & Co. KGaA, Weinheim DOI: 10.1002/anie.200460532

the edge-sharing bioctahedral (ESBO) dirhenium(IV) complex $[Re_2Cl_2O(pyt)_4]$ (**1a**) with a Re_2OS framework was obtained as the major product.[7] The asymmetric structure of the neutral complex **1a** is shown in Figure 1a. The coordination environments of the two Re atoms are different; the Re1 atom is surrounded by a Cl_2N_2OS atom set, whereas the Re2 atom is surrounded by an NOS_4 atom set. The Re–Re distance and Re-S-Re and Re-O-Re angles are 2.5333(6) Å, 64.64(8)°, and 82.4(3)°, respectively. The metal–metal bond may be best described as a double bond (see below). It is noteworthy that the C–S distance (1.81(1) Å) in the pyt ligand containing the η^2-S atom is slightly longer than those (1.70(2)–1.74(1) Å) in the other three pyt ligands, which act as μ_2-S,N (η^1-S:η^1-N) bridges. It is also worth mentioning that the Re1–O1 and Re2–O1 distances differ considerably, whereas the Re1–S1 and Re2–S1 distances are comparable. A similar tendency was also observed for the minor isomer **1b**, though the Re1–O1 and Re2–O1 distances are much more similar in the one-electron reduced species, [PPN]-**2a** or $[Et_4N]$-**2a** (see below).

The structure of the linkage isomer (**1b**) obtained as the minor product is very similar to that of **1a** (Figure 1b).[7] The only difference in the structures of **1a** and **1b** is the direction of the pyt ligand chelating the Re2 atom; the N atom in the pyt ligand is *trans* to the bridging O atom in complex **1b**. The Re–Re distance and the Re-S-Re and Re-O-Re angles are 2.5419(6) Å, 64.44(7)°, and 82.8(3)°, respectively. The Re–S, Re–Cl, Re–N, and Re–O distances are very similar to those of **1a**.

The major isomer **1a** exhibits two reversible one-electron redox waves at −0.18 V ($Re_2^{III,IV}/Re_2^{IV}$) and +0.93 V ($Re_2^{IV}/Re_2^{IV,V}$) versus Ag/AgCl in CH_2Cl_2, indicating that the Re_2^{IV} state is stable in a wide potential range. The reduction of **1a** by hydrazine monohydrate in the presence of [PPN]Cl in CH_2Cl_2 under an argon atmosphere at ambient temperature afforded $[PPN][Re_2^{III,IV}Cl_2O(pyt)_4]$ ([PPN]-**2a**), which was crystallized by the diffusion of hexane vapor into the solution. The tetraethylammonium salt, $[Et_4N][Re_2^{III,IV}Cl_2O(pyt)_4]$ ($[Et_4N]$-**2a**), can also be obtained in a similar manner by using $[Et_4N]$Cl instead of [PPN]Cl. The X-ray structural analyses confirmed that both salts consist of a $[PPN]^+$ ion (Figure 2) or a $[Et_4N]^+$ ion and the complex anion in a 1:1 ratio.[7] The Re–Re distances in [PPN]-**2a** (2.5491(4) Å) and

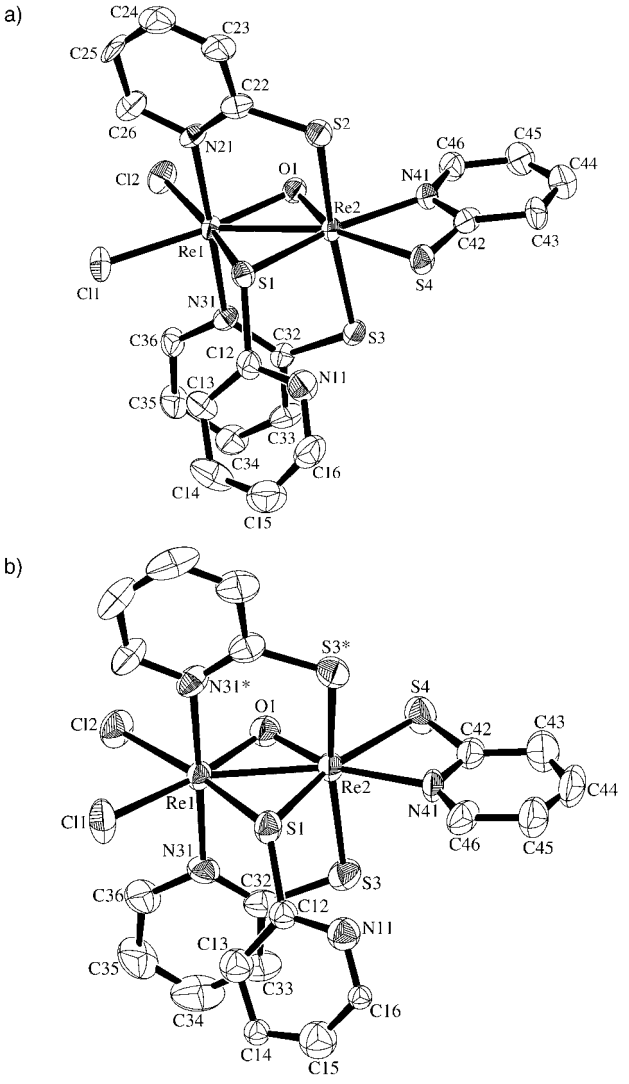


Figure 1. a) Molecular structure of the major isomer **1a** (50% probability ellipsoids). Selected bond lengths [Å] and angles [°]: Re1-Re2 2.5333(6), Re1-O1 1.977(9), Re1-S1 2.371(3), Re1-Cl1 2.390(3), Re1-Cl2 2.410(3), Re1-N21 2.16(1), Re1-N31 2.13(1), Re2-O1 1.868(8), Re2-S1 2.367(3), Re2-S2 2.358(4), Re2-S3 2.345(3), Re2-S4 2.450(3), Re2-N41 2.14(1); Re1-S1-Re2 64.64(8), Re1-O1-Re2 82.4(3). b) Molecular structure of the minor isomer **1b** (50% probability ellipsoids). Selected bond lengths [Å] and angles [°]: Re1-Re2 2.5419(6), Re1-O1 1.969(8), Re1-S1 2.366(3), Re1-Cl1 2.394(3), Re1-Cl2 2.413(3), Re1-N31 2.162(6), Re2-O1 1.872(7), Re2-S1 2.401(3), Re2-S3 2.337(2), Re2-S4 2.454(3), Re2-N41 2.148(8); Re1-S1-Re2 64.44(7), Re1-O1-Re2 82.8(3).

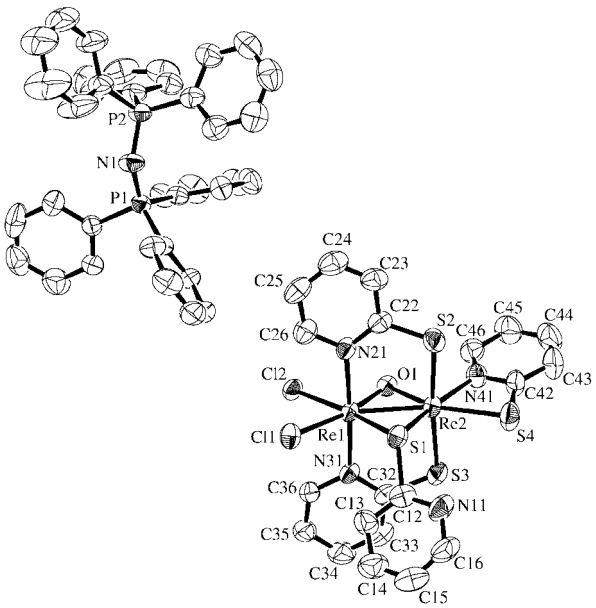


Figure 2. Molecular structure of $[PPN][Re_2Cl_2O(pyt)_4]$ ([PPN]-**2a**) (50% probability ellipsoids). Selected bond lengths [Å] and angles [°]: Re1-Re2 2.5491(4), Re1-O1 1.936(5), Re1-S1 2.362(2), Re1-Cl1 2.441(2), Re1-Cl2 2.431(2), Re1-N21 2.170(6), Re1-N31 2.153(6), Re2-O1 1.911(5), Re2-S1 2.359(2), Re2-S2 2.409(2), Re2-S3 2.379(2), Re2-S4 2.481(2), Re2-N41 2.132(7); Re1-S1-Re2, 65.36(5); Re1-O1-Re2, 83.0(2).

 © 2005 Wiley-VCH Verlag GmbH & Co. KGaA, Weinheim

$[Et_4N]$-**2a** (2.5452(8) Å) have not changed significantly upon reduction from that in **1a** (2.5333(6) Å), which is in contrast to the case in which the Re–Re distance lengthens by 0.06 Å upon one-electron reduction of the ESBO dirhenium(IV) complex $[Re_2(\mu\text{-}O)_2(Metpa)_2](PF_6)_4$ (Metpa = [(6-methyl-2-pyridyl)methyl]bis(2-pyridylmethyl)amine).[5] Thus, the Re–Re distance in **1a** is relatively insensitive towards reduction. That the change in the number of electrons in δ and/or δ* orbitals by redox reaction has little influence on the metal–metal distance has also been reported for the oxidation (corresponding to the removal of an electron from δ* orbital) of some lantern-type dirhodium(II) complexes with an $\sigma^2\pi^4\delta^2\pi^{*4}\delta^{*2}$ electron configuration.[8]

The ^{1}H NMR spectra of Re_2^{IV} complexes **1a** and **1b** exhibit 16 distinct, sharp resonances between $\delta = +20$ and -40 ppm at 20 °C (see Figure S2 in the Supporting Information). As is the case for the complexes with a singlet ground state and those with a thermally accessible triplet excited state,[9] the ^{1}H NMR chemical shifts are temperature dependent (Figure 3). These observations prompted us to measure the

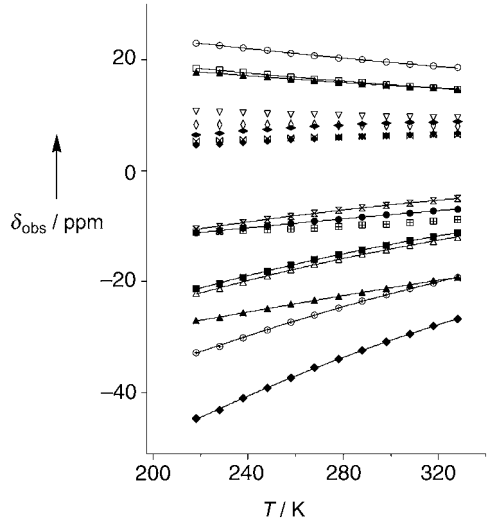


Figure 3. Temperature dependence of the proton chemical shifts in **1a**. All proton signals are derived from aromatic protons of pyridinethiolate ligands in different positions. The different symbols are experimental values; the solid lines are calculated from Equation (2) with the parameters listed in Table 1.

magnetic susceptibility of **1a** and its one-electron reduced species [PPN]-**2a** for comparison (Figure 4). Although the magnetic susceptibility data of [PPN]-**2a** indicate Curie–Weiss type magnetic behavior, the complex **1a** shows temperature-dependent behavior; the magnetic susceptibility (χ) increases with decreasing temperature and the curve tends to flatten below 100 K. A rapid increase of χ is observed below 20 K, which may be attributable to paramagnetic impurities. Cotton and co-workers reported the energy levels of d^3–d^3 dimers by fitting the van Vleck formula to the magnetic susceptibilities.[1,2] However, the χ–T curve of **1a**, which shows a constant paramagnetism below 100 K, does not obey their model. This constant contribution to χ can be accounted for by the van Vleck constant paramagnetism, and χ is given by

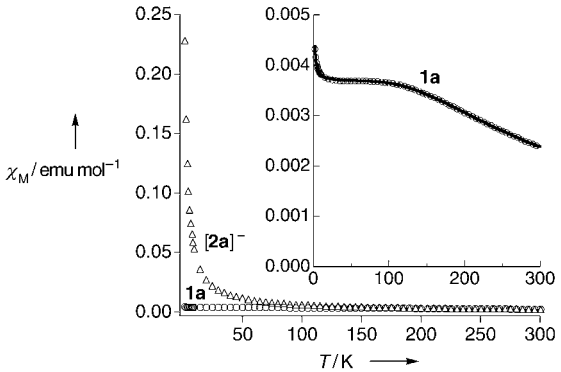


Figure 4. Plots of χ versus T for complexes **1a** (○) and [PPN]-**2a** (△) in the temperature range 2–300 K. Inset: Experimental values (○); the line is obtained from Equation (1) with the parameters listed in the text.

Equation (1), in which μ_B, E_1, and g_J are the Bohr magneton, the energy level of the first excited-state $^3B_{1u}$ ($J = 1$), and the Landé g factor, respectively, and α_0 (fixed to be 0) and α_1 is the constant derived from the van Vleck constant paramagnetism. The χ_{TIP} contribution to χ corresponds to a temperature-independent paramagnetism, and the nC/T accounts for the presence of small amounts of a paramagnetic impurity assumed to be a Re^{III} monomer with $S = 3/2$ in a proportion n. The best least-squares fit of Equation (1) to the susceptibility data leads to the following parameters: $g_J = 1.41(24)$, E_1 {$= E(^3B_{1u})$} $= 355(19)$ cm^{-1}, $\chi_{TIP} = 3.666(3) \times 10^{-3}$ emu mol^{-1}, $n = 0.075(1)$ %, $\alpha_1 = -0.0135(2)$ emu mol^{-1}.

$$\chi = (1-n)N\frac{\alpha_0 + \left\{\frac{2g_J^{\,2}\mu_B^{\,2}}{k_BT} + \alpha_1\right\}\exp\left(-\frac{E_1}{k_BT}\right)}{1+3\exp\left(-\frac{E_1}{k_BT}\right)} + \chi_{TIP} + n\frac{C}{T} \qquad (1)$$

The energy gap between the ground state and the triplet excited state can also be estimated by variable-temperature NMR studies.[9] The determination of the hyperfine coupling constant (A), the diamagnetic chemical shift (δ_{dia}) for the proton sites, the singlet–triplet energy separation (E_1), and the constant α_1 derived from the van Vleck constant paramagnetism, were initially attempted by a fit of the temperature dependence of the observed ^{1}H NMR chemical shifts, δ_{obs} (H_{obs}) to Equation (2), which also takes into account a contribution of the van Vleck constant paramagnetism.

$$H_{obs} = H_{dia} + \frac{H_0 A}{g_J\mu_B\gamma_H/2\pi}\bullet\frac{\left(\frac{2g_J^{\,2}\mu_B^{\,2}}{k_BT} + \alpha_1\right)\exp\left(-\frac{E_1}{k_BT}\right)}{1+3\exp\left(-\frac{E_1}{k_BT}\right)} \qquad (2)$$

However, we found that the hyperfine coupling constant A and the constant α_1 are strongly correlated, and the magnitude of these two parameters had a substantially smaller effect on the shape of the fitting curve as long as the product of the two parameters is almost constant. Because

 © 2005 Wiley-VCH Verlag GmbH & Co. KGaA, Weinheim

it is difficult to determine A and α_1 a priori from the NMR data, the α_1 value was fixed to be $-0.0135\,\mathrm{emu\,mol^{-1}}$ as estimated from the susceptibility data. The g_J value was also fixed to be 1.41 in the curve fitting. The reliable parameters were obtained from 10 of the 16 resonances (Table 1). The

Table 1: Calculated magnetic and electronic parameters for **1a**.

Resonance	δ_{dia} [ppm]	A [MHz]	E_1 [cm^{-1}]
H1	27.1(4)	0.224(2)	314(19)
H2	22.5(4)	0.186(1)	277(21)
H3	20.9(3)	0.158(1)	301(20)
H9	−18.3(11)	−0.278(5)	215(31)
H10	−14.3(3)	−0.220(4)	367(19)
H12	−34.8(18)	−0.505(7)	227(30)
H13	−34.6(15)	−0.507(5)	249(27)
H14	−32.0(4)	−0.418(8)	397(16)
H15	−41.9(13)	−0.673(5)	289(21)
H16	−64.6(20)	−0.890(6)	270(22)

solid lines in Figure 3 show fitting curves obtained by using Equation (2) with the parameters listed in Table 1. Because the variable-temperature NMR data for the six remaining resonances could not be well fitted, probably due to the small change of H_{obs} in the range of temperature measured, the experimental data are plotted without fitting curves in Figure 3. The average S–T gap, E_1(av), estimated from the variable-temperature NMR studies is 291 cm^{-1}, and is thus very close to the value obtained from the susceptibility data.

These results indicate that the energy gap between the ground state and the triplet excited state in **1a** is smaller than those in diphosphine- or thiolato-bridged dimolybdenum(III) and ditungsten(III) complexes (Figure 5).[1,2] In this model, the

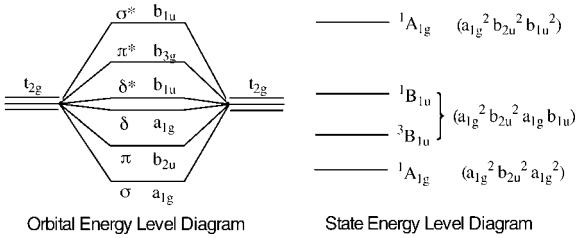


Figure 5. Qualitative orbital and state energy level diagrams for the case where $E(\delta) < E(\delta^*)$.

δ and δ* orbitals have very similar energies and the resulting $^3(\delta\delta^*)$ and $^1(\delta\delta^*)$ excited states are thermally accessible, though we could not estimate the energy level of the latter with sufficient reliability. The very close energies of the δ and δ* orbitals in **1a**, found for first time for an ESBO dirhenium(IV) system, may indicate that the metal–metal bond is best described as a double bond. The view is consistent with the description of the bond order for the diphosphine- or thiolato-bridged dimolybdenum(III) and ditungsten(III) complexes.[1,2]

In conclusion, a pair of ESBO dirhenium complexes in neighboring oxidation states, $[Re_2^{IV}Cl_2O(pyt)_4]$ and [PPN] $[Re_2^{III,IV}Cl_2O(pyt)_4]$, have been prepared. The X-ray structural analyses of these complexes revealed that the addition of an electron to the Re_2^{IV} complex does not influence the Re–Re distance in this system. Although the di-μ-oxo ESBO dirhenium complexes are diamagnetic, temperature-dependent magnetic behavior was observed for the μ-oxo-μ-thiolato Re_2^{IV} complex for the first time. The magnetic behavior of **1a** can essentially be understood by considering the model to be similar to those of diphosphine- or thiolato-bridged dimolybdenum(III) and ditungsten(III) complexes, though the van-Vleck constant paramagnetism should be taken into account probably due to the spin-orbit coupling in the third-row transition-metal ions.

Experimental Section

1a and 1b: A mixture of $[ReOCl_3(PPh_3)_2]$ (248 mg, 0.30 mmol) and pyridine-2-thiol (71 mg, 0.64 mmol) in 1,4-dioxane (100 mL) was refluxed for 12 h under an argon atmosphere. The dark brown solution was cooled to room temperature and filtered. The filtrate was concentrated to dryness.[10] The dark brown solid was dissolved in dichloromethane (15 mL) and precipitated again by addition of *n*-hexane (50 mL) into the solution. The precipitate was filtered, washed with diethyl ether, and dried in vacuo. Then about half of the solid was dissolved in dichloromethane, and the solution was loaded onto a silica gel column (40 × 3 cm) and eluted with dichloromethane. The second purple fraction (minor isomer, **1b**) and the third deep blue fraction (major isomer, **1a**) were collected and concentrated to dryness. The bluish-purple solid (**1b**) and the deep blue solid (**1a**) were washed with diethyl ether and then dried in vacuo. The same procedure of column chromatography was repeated again. Total yield of **1a**, 68 mg (51%); **1b**, 3 mg (2%). Crystals suitable for X-ray structural analysis were obtained by recrystallization from CH_2Cl_2 for **1a** and from CH_2Cl_2–CH_3CN for **1b**. Elemental analysis calcd (%) for $C_{20}H_{16}Cl_2N_4ORe_2S_4$: C 26.69, H, 1.79, N 6.23, S 14.25, Cl 7.88; found: **1a** [**1b**]: C 26.62 [26.84], H 1.72 [1.82], N 6.05 [6.35], S 14.53 [14.19], Cl 8.02 [7.84]; FAB-MS (*m*/*z*): 901 [*M*+H]; ^{1}H NMR (400 MHz, $CDCl_3$, 20 °C, TMS): **1a**: δ = 19.76 (d), 15.71 (t), 15.52 (d), 9.80 (dd), 8.44 (d), 8.15 (dd), 6.23 (2H), −6.46 (d), −8.17 (d), −9.72 (d), −13.87 (t), −14.69 (t), −21.60 (t), −22.99, −31.64 ppm; **1b**: δ = 19.93 (d), 17.30 (d), 15.92 (d), 15.14 (d), 14.97, 11.07 (d), 8.03 (dd), 5.69 (t), 2.08, 1.03, −10.70, −15.34, −17.54, −24.30, −28.13, −39.36 ppm.

[PPN]-2a: An excess amount of $N_2H_4{\cdot}H_2O$ (ca. 40 μL) was added to a solution of **1a** (161 mg, 0.18 mmol) and bis(triphenylphosphoranylidene)ammonium chloride ([PPN]Cl; 103 mg, 0.18 mmol) in dichloromethane (20 mL). The solution was stirred for 1 h at 20 °C under an argon atmosphere and filtered. To the filtrate was added *n*-hexane (2 mL) and the solution was left overnight. Brown crystals were collected, washed with *n*-hexane, and then dried in vacuo. Yield 211 mg (82%). Elemental analysis calcd (%) for $C_{56}H_{46}Cl_2N_5OP_2Re_2S_4$: C 46.76, H 3.22, N 4.87, S 8.91, Cl 4.93; found: C 46.69, H 3.39, N 5.03, S 9.25, Cl 4.88.

Received: May 1, 2004
Revised: October 8, 2004
Published online: December 13, 2004

Keywords: bridging ligands · magnetic properties · metal–metal interactions · mixed-valent compounds · rhenium

 © 2005 Wiley-VCH Verlag GmbH & Co. KGaA, Weinheim

[1] F. A. Cotton, M. P. Diebold, C. J. O'Connor, G. L. Powell, *J. Am. Chem. Soc.* **1985**, *107*, 7438 – 7445.
[2] a) P. A. Agaskar, F. A. Cotton, K. R. Dunbar, L. R. Falvello, C. J. O'Connor, *Inorg. Chem.* **1987**, *26*, 4051 – 4057; b) F. A. Cotton, L. M. Daniels, K. R. Dunbar, L. R. Falvello, C. J. O'Connor, A. C. Price, *Inorg. Chem.* **1991**, *30*, 2509 – 2514; c) F. A. Cotton, J. L. Eglin, C. A. James, R. L. Luck, *Inorg. Chem.* **1992**, *31*, 5308 – 5315.
[3] a) S. Shaik, R. Hoffmann, C. R. Fisel, R. H. Summerville, *J. Am. Chem. Soc.* **1980**, *102*, 4555 – 4572; b) H. B. Bürgi, G. Anderegg, P. Bläuenstein, *Inorg. Chem.* **1981**, *20*, 3829 – 3834.
[4] a) G. Böhm, K. Wieghardt, B. Nuber, J. Weiss, *Inorg. Chem.* **1991**, *30*, 3464 – 3476; b) S. Ikari, T. Ito, W. McFarlane, M. Nasreldin, B.-L. Ooi, Y. Sasaki, A. G. Sykes, *J. Chem. Soc. Dalton Trans.* **1993**, 2621 – 2628.
[5] H. Sugimoto, M. Kamei, K. Umakoshi, Y. Sasaki, M. Suzuki, *Inorg. Chem.* **1996**, *35*, 7082 – 7088.
[6] R. M. Tylicki, W. Wu, P. E. Fanwick, R. A. Walton, *Inorg. Chem.* **1995**, *34*, 988 – 991.
[7] CCDC-236276, CCDC-236277, CCDC-236278, and CCDC-236279 contain the supplementary crystallographic data for this paper. These data can be obtained free of charge via www.ccdc.cam.ac.uk/conts/retrieving.html (or from the Cambridge Crystallographic Data Centre, 12, Union Road, Cambridge CB2 1EZ, UK; fax: (+44) 1223-336-033; or deposit@ccdc.cam.ac.uk).
[8] T. Kawamura, M. Maeda, M. Miyamoto, H. Usami, K. Imaeda, M. Ebihara, *J. Am. Chem. Soc.* **1998**, *120*, 8136 – 8142.
[9] a) G. C. Campbell, J. F. Haw, *Inorg. Chem.* **1988**, *27*, 3706 – 3709; b) F. A. Cotton, J. L. Eglin, B. Hong, C. A. James, *J. Am. Chem. Soc.* **1992**, *114*, 4915 – 4917; c) F. A. Cotton, H. Chen, L. M. Daniels, X. Feng, *J. Am. Chem. Soc.* **1992**, *114*, 8980 – 8983; d) C. Cremer, P. Burger, *J. Am. Chem. Soc.* **2003**, *125*, 7664 – 7677.
[10] The ^{1}H NMR spectrum of the hexane extract of the solid exhibits the signals of O=PPh_3 and PPh_3 in about a 1:2 ratio. The delay of the workup of the reaction mixture increases the amount of O=PPh_3 and thus the O=PPh_3/PPh_3 ratio. The reaction stoichiometry is $2[ReOCl_3(PPh_3)_2] + 4\,Hpyt \rightarrow [Re_2Cl_2O(pyt)_4] + O{=}PPh_3 + 3\,PPh_3 + 4\,HCl$. The triphenylphosphine ligand in the starting material acts as a reducing agent in the reaction.

 © 2005 Wiley-VCH Verlag GmbH & Co. KGaA, Weinheim

Particle Design

Generation of Monodisperse Particles by Using Microfluidics: Control over Size, Shape, and Composition**

Shengqing Xu, Zhihong Nie, Minseok Seo, Patrick Lewis, Eugenia Kumacheva, Howard A. Stone, Piotr Garstecki, Douglas B. Weibel, Irina Gitlin, and George M. Whitesides**

Herein we describe a versatile new strategy for producing monodisperse solid particles with sizes from 20 to 1000 μm. The method involves the formation of monodisperse liquid droplets by using a microfluidic device and shaping the droplets in a microchannel and then solidifying these drops in situ either by polymerizing a liquid monomer or by lowering the temperature of a liquid that sets thermally. This method has the following features: 1) It produces particles with an exceptionally narrow range of sizes.[1] 2) A new level of control over the shapes of the particles is offered. 3) The mechanism for droplet formation allows the use of a wide variety of materials including gels, metals, polymers, and polymers doped with functional additives. 4) The procedure can be scaled up to produce large numbers of particles.

A number of methods exist for making inorganic and organic particles with narrow polydispersity. Inorganic colloids are typically prepared by precipitation reactions from organometallic precursors.[2,3] Polymer colloids with sizes from 20 nm to approximately 1 μm are usually prepared by a variation of emulsion polymerization techniques.[4] Larger beads are accessible through miniemulsion polymerization,[5]

[*] Dr. S. Xu, Z. Nie, M. Seo, P. Lewis, Prof. Dr. E. Kumacheva
Department of Chemistry
University of Toronto
80 Saint George Street, Toronto M5S 3H6, Ontario (Canada)
Fax: (+1) 416-978-3576
E-mail: ekumache@chem.utoronto.ca
Dr. P. Garstecki, Dr. D. B. Weibel, I. Gitlin, Prof. Dr. G. M. Whitesides
Department of Chemistry and Chemical Biology
Harvard University
12 Oxford Street, Cambridge, MA 02139-4307 (USA)
Fax: (+1) 617-495-9852
E-mail: gwhitesides@gmwgroup.harvard.edu
Prof. Dr. H. A. Stone
Division of Engineering and Applied Sciences
Harvard University
308 Pierce Hall, Cambridge, MA 02139-4307 (USA)

[**] E.K. acknowledges the Canada Research Chair Fund. Work by P.G., D.B.W., I.G., and G.M.W. was supported by the NIH (GM65364), DoE (DE-FG02-OOER45852), and DARPA, and they used the MRSEC Shared Facilities supported by the NSF under Award No. DMR-9809363. H.A.S. thanks Unilever and Harvard MRSEC (DMR-0213805) for support. P.G. acknowledges the Foundation for Polish Science for a postdoctoral fellowship. D.B.W. thanks the NIH for a postdoctoral fellowship (GM067445). We thank Professor W. C. W Chan for help with the synthesis of CdSe QDs.

Supporting information for this article is available on the WWW under http://www.angewandte.org or from the author.

 © 2005 Wiley-VCH Verlag GmbH & Co. KGaA, Weinheim DOI: 10.1002/anie.200462226

membrane emulsification,[6] and multistage processes.[7,8] Most of these methods are specific to a particular material. A technique sufficiently general to be applicable to a range of materials and allow the production of monodisperse colloids with control over size and shape has not been demonstrated and would be widely useful.

We have used a new type of microfluidic flow-focusing device (MFFD)[11] to generate droplets of different sizes and shapes and narrow dispersity, and these droplets were solidified in situ. The MFFDs were prepared in either poly(dimethylsiloxane) or polyurethane by using soft lithography;[9,10] an appropriate choice of the material of fabrication allowed us to produce water-in-oil or oil-in-water dispersions. Our experiments suggest that the hydrodynamic mechanism behind the stable and controllable breakup of liquid threads in these MFFDs is largely insensitive to the composition of the dispersed phase. We exploited this property to produce metal particles, microgels, and polymer particles that contain liquid crystals, fluorescent dyes, and inorganic nanoparticles. Control of both the shape and size of the solidified beads was also demonstrated; spheres, disks, ellipsoids, and rods were produced by controlling the volume of the individual drops and the cross-sectional area of the microchannel.

Figure 1a shows the design of the MFFD. A pressure gradient along the long axis of the device forced two immiscible liquids through the orifice of MFFD. The continuous phase was supplied from two sides of the device; the liquid stream comprising the dispersed phase was supplied from a central channel (Figure 1a). The continuous phase surrounds the inner, immiscible liquid so that the inner thread becomes unstable and breaks in the orifice in a periodic manner to release droplets into the outlet channel. We showed recently that the narrow size distribution of gaseous bubbles generated in a similar MFFD is a consequence of the controlled progression of the capillary instability.[12] Owing to viscous retardation in the confinement of the orifice, the velocity of collapse of the thread is reduced[13] and is controlled by the rate of flow of the continuous phase. As a result, the breakup process is much slower than the rates at which the shape of the interface and the liquid pressure fields equilibrate. This mechanism of droplet formation is different to the usual breakup of liquid jets. In contrast to the capillary instability in an unbounded fluid, the breakup in a MFFD produces extremely monodisperse droplets. Furthermore, there are obvious differences with the ink-jet printing technologies that also produce droplets with uniform size distributions. Breakup in ink-jet printers is governed by the competition between surface tension and inertial forces rather than viscous forces, and it occurs in an atmosphere of gas rather than in coflowing, immiscible liquids as in the case of MFFD.

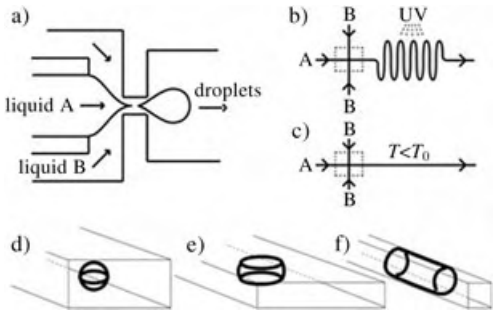


Figure 1. a) A representation of the flow-focusing geometry used in the microfluidic droplet generator. The two immiscible liquids A and B are forced into the narrow orifice where the inner liquid core breaks to release monodisperse droplets into the outlet channel. b), c) Representations of the devices used for producing photochemically and thermally solidified particles. The dashed rectangles mark the flow-focusing device shown in part a). The channels used for photochemical cross-linking were elongated to allow longer durations of exposure of the droplets to UV light. For thermal setting experiments, the flow-focusing region was kept at a temperature exceeding the gelling (or solid–liquid phase transition) temperature (T_0). The outlet channel was cooled to a temperature below T_0, and the droplets solidified as they traveled down the channel. d)–f) Representations of the shapes of drops in the microfluidic channel. If the volume of the droplet exceeds that of the largest sphere which could be accommodated in the channel, the droplet is deformed into a disk (e) or an ellipsoid or rod (f).

We obtained particles by solidifying these droplets either photochemically (by photopolymerization of monomer fluids, see Figure 1b) or thermally (Figure 1c). The volume of the droplets (V) was controlled by the flow rates of the continuous and dispersed phases. The diameter of an undeformed (regular) spherical droplet is given by $d_S = (6V/\pi)^{1/3}$ (Figure 1d). Nonspherical droplets form when d_S is larger than at least one of the dimensions of the outlet channel. In such channels, because of confinement, breakup is not followed by shape relaxation of droplets into spheres. In wide channels, $w > d_S$, (w = width) of height $h < d_S$, the drops assume a discoid shape (Figure 1e) with circular interfaces with the top and bottom walls of the channel. The diameter, d_D, of these interfaces is set by the height of the channel and the volume of the droplet. For channels with small aspect ratios (h/d_D), the droplets have a cylindrical geometry (the curvature at the liquid–liquid interface can be neglected), and the volume of these droplets is $d_D \approx 2(V/\pi h)^{1/2}$. If both the height and the width of the channel are smaller than d_S, the droplet makes contact with all of the channel walls and assumes a rodlike morphology (Figure 1f). The length l_R of elongated liquid plugs yields $l_R \approx V/wh$. The two aspect ratios (h/l_R and w/l_R) can be controlled independently by changing the volume of the droplet and the ratio of the height to the width of the channel.

Polymerization produced monodisperse solid particles from tripropyleneglycol diacrylate (TPGDA), dimethacrylate oxypropyldimethylsiloxane (DMOS), divinylbenzene (DVB), ethyleneglycol diacrylate, and pentaerythritol triacrylate in aqueous suspensions with sodium dodecylsulfate (SDS, 2 wt%) as a surfactant. Monomers were mixed with a photoinitiator, 1-hydroxycyclohexylphenyl ketone (4 wt%), and photopolymerized in a wavy channel (Figure 1b) by illumination with UV light (400 W, $\lambda = 330$–380 nm). The polymerization time was typically between 15 and 800 s. The diameter of the microspheres (controlled by the rates of flow of the water and droplet phases and the geometry of the MFFD) was between 20 and 200 μm. Figure 2a shows a typical SEM image of spherical polyTPGDA beads polymerized in the MFFD; a colloidal crystal formed by these microspheres is illustrated in Figure 2b. We also prepared

 © 2005 Wiley-VCH Verlag GmbH & Co. KGaA, Weinheim

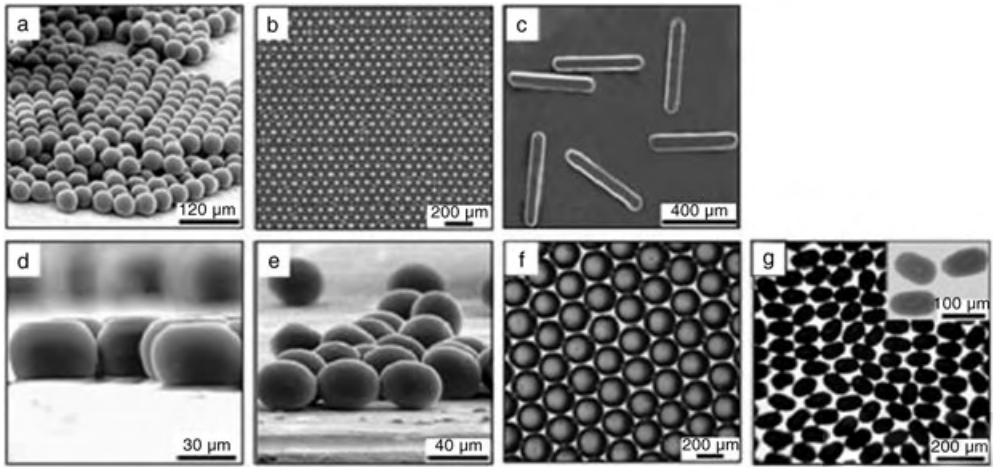


Figure 2. Optical microscopy images of polyTPGDA particles: a) microspheres, b) crystal of microspheres, c) rods, d) disks, and e) ellipsoids. Optical microscopy images of f) agarose disks and g) bismuth alloy ellipsoids produced using thermal solidification; inset: micrograph of the bismuth alloy ellipsoids at higher magnification.

polymeric rods, disks, and ellipsoids by trapping the non-spherical confined monomer droplets (shown in Figure 1e and f) in the solid state. We obtained disks and rods with aspect ratios as large as 1/3 and 1/12 (Figure 2c and d, respectively). Ellipsoids were formed at high flow rates of the continuous phase (Figure 1b).

The conversion of monomer to polymer was close to 100%. Generally, the dimensions of polymer microspheres were 5–10% smaller than the corresponding droplets owing to monomer shrinkage during photopolymerization. A thin wetting layer of the continuous phase prevented clogging of the channels by the solid particles. The rate of microbead production was up to 250 particles s^{-1}. The polydispersity (defined as the standard deviation in the particle diameter divided by the mean particle diameter) of polymerized particles was 1.5% and was similar to the polydispersity of the corresponding spherical droplets.

Figure 3a shows the variation in V with the ratio of the flow rates of the aqueous phase to the monomer phase. Increasing the ratio of flow rates to a value greater than 82 produced smaller, spherical droplets of DVB and TPGDA (filled symbols). Figure 3b–d demonstrates the size distribution of polyTPGDA spheres, disks, and rods. Particle polydispersity in all cases was less than 1.6% (for disks and rods the standard deviation σ of the diameter and length was divided by the mean values of the droplet diameter and length, respectively).

We also obtained particles by thermally-induced gelation or liquid–solid phase transition by operating at a temperature within the fluid-focusing orifice, T_{FF}, that is greater than the temperature for gelation or the liquid–solid phase transition, T_0, and by cooling the outlet channel to a temperature, $T < T_0$, to solidify the droplets (the configuration in Figure 1c). The particles were prepared from two materials: an aqueous solution of agarose ($T_0 = 37\,^{\circ}C$) and a low-melting bismuth alloy ($T_0 = 47\,^{\circ}C$). In both cases we used a continuous phase composed of a 3 wt% solution of surfactant, sorbitan monooleate (span 80), in hexadecane. Figure 2f illustrates agarose disks whose height was predetermined by the height of the channel (30 and 60 μm). By varying the flow rates of the continuous and dispersant phase, disks with diameters from 50 to 250 μm were obtained. The polydispersity of the disks

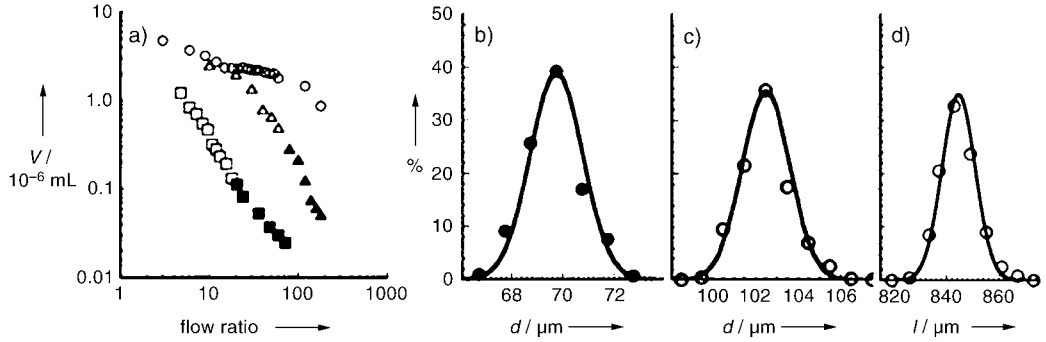


Figure 3. a) A log–log plot of the volume of the droplets versus the ratio of the rates of flow of the aqueous and monomer phases (water:monomer): dimethacrylate oxypropyldimethylsiloxane (circles); divinyl benzene (triangles); TPGDA (squares). The rate of flow of the monomer was 0.04 mL h^{-1}. Open symbols represent disks, filled symbols correspond to spheres. b) and c) Distribution of diameters (d) of poly(TPGDA) spheres and disks, respectively, and d) length (l) of rods. The experimental points were fitted with a Gaussian distribution. The resulting polydispersities are 1.5% for spheres, 1.1% for disks, and 1% for rods.

 © 2005 Wiley-VCH Verlag GmbH & Co. KGaA, Weinheim

did not exceed 3%. Figure 2g shows bismuth alloy ellipsoids made in the MFFD geometry illustrated in Figure 1c. The width and the height of the channel were 60 and 60 μm, respectively. The mean width of these ellipsoids was 58 μm (polydispersity 3.2%) and their length was 94 μm (polydispersity 7.8%). The rate of making both agarose and solder particles was controlled by the flow rates applied to the system and ranged between 100 and 1000 particles s^{-1}.

We also produced multicomponent polymer-based beads that include copolymer particles, fluorescent particles containing dyes or nanoparticles, polymer liquid crystals, and microporous particles. Fluorescent microspheres (Figure 4a)

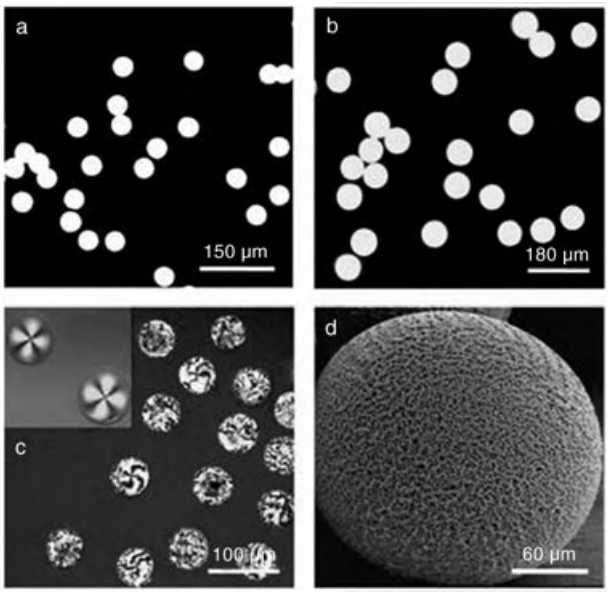


Figure 4. Microspheres labeled with a) NBD dye (NBD = 4-amino-7-nitrobenzo-2-oxa-1,3-diazole, λ_{ex} = 488 nm) and b) CdSe quantum dots (λ_{ex} = 502 nm). c) Polarization microscopy image of 4-cyano-4′-pentylbiphenyl polyTPGDA microspheres. Inset shows particle morphology at low polymerization rate (see text). d) SEM image of a porous polyTPGDA microsphere.

were synthesized by copolymerizing methyl acrylate, which was covalently attached to UV, visible, or near-IR dyes, with TPGDA[14] or by polymerizing TPGDA admixed with 4-nm-diameter CdSe quantum dots (Figure 4b).[15] Other types of hybrid microspheres were obtained by polymerizing monomers mixed with metal or magnetic nanoparticles. We synthesized liquid crystal (LC) polymer microbeads by polymerizing TPGDA admixed with 4-cyano-4′-pentylbiphenyl (5–20 wt%) (Figure 4c). When the polymerization was fast, the LC mixed uniformly with polyTPGDA; when slow, the LC segregated into the core of the microsphere (Figure 3c, inset). Porous microspheres were synthesized by mixing dioctyl phthalate with TPGDA (1/4 wt ratio), followed by polymerization, and subsequent removal of the porogen with acetone (Figure 4d). The mean size of the pores was 0.90 μm.

A single device can produce 10^5–10^6 particles per hour. To increase throughput, we envision making beads by positioning several flow-focusing devices on a single chip. The use of a high-flux UV lamp and more-efficient photoiniators will allow the length of the outlet channel required for polymerization to be decreased. Thereby, it should be straightforward to fit more than 10 devices onto a single 2 × 3-inch substrate. Given that a single MFFD device produces approximately 100–1000 particles sec^{-1}, a multidevice chip will produce about 10^6–10^8 particles h^{-1}.

In summary, the strategy described in the present work has four significant advantages: 1) it offers extensive control over the size and polydispersity of the particles, 2) particles with various shapes can be generated, 3) a range of materials can be applied, including heterogeneous multiphase liquids and suspensions, and 4) useful quantities of particles (up to 10^8 particles h^{-1}) can be produced. Control over the composition of the particles gives access to a variety of material properties. Optically and magnetically functionalized polymeric beads result from polymerization of monomer droplets doped with dyes, semiconductor quantum dots, magnetic nanoparticles, and liquid crystals. This work provides a route to materials for a systematic study of entropically ordered mixtures of particles with different shapes.[16–18]

We believe that the hydrodynamic mechanism governing the breakup of the continuous liquid stream into monodisperse droplets and the processes of thermal solidification and polymerization should both be applicable to the controlled formation of submicron particles.

Received: October 6, 2004
Published online: December 21, 2004

Keywords: copolymerization · gels · microfluidics · monodisperse particles · polymers

[1] According to the standards of the National Institute of Standards and Technology (NIST): "a particle distribution may be considered monodisperse if at least 90% of the distribution lies within 5% of the median size" (*Particle Size Characterization*, Special Publication 960–961, January 2001). To determine the standard deviations, we fit the experimental histograms of the size of the particles with Gaussian distributions. The standard deviations were typically on the order of 1–2% of the mean size, complying with the NIST definition of monodispersity (95% of the particles are within two standard deviations of the mean size).
[2] P. Jiang, J. F. Bertone, V. L. Colvin, *Science* **2001**, *291*, 453–457.
[3] B. T. Holland, C. F. Blanford, A. Stein, *Science* **1998**, *281*, 538–540.
[4] *Colloidal Polymers* (Ed.: A. Elaissari), Marcel Dekker, New York, **2003**.
[5] M. Antonietti, K. Landfester, *Prog. Polym. Sci.* **2002**, *27*, 689–757.
[6] S. Omi, G.-H. Ma, M. Nagai, *Macromol. Symp.* **2000**, *151*, 319–330.
[7] S. T. Eckersley, A. Rudin, *Prog. Org. Coat.* **1994**, *23*, 387–402.
[8] J. S. Song, F. Tronc, M. A. Winnik, *J. Am. Chem. Soc.* **2004**, *126*, 6562–6563.
[9] Y. Xia, G. M. Whitesides, *Angew. Chem.* **1998**, *110*, 568–594; *Angew. Chem. Int. Ed.* **1998**, *37*, 550–575.
[10] D. C. Duffy, J. C. McDonald, O. J. A. Schueller, G. M. Whitesides, *Anal. Chem.* **1998**, *70*, 4974–4984.
[11] S. L. Anna, N. Bontoux, H. A. Stone, *Appl. Phys. Lett.* **2003**, *82*, 364–366.

 © 2005 Wiley-VCH Verlag GmbH & Co. KGaA, Weinheim

[12] P. Garstecki, H. A. Stone, G. M. Whitesides, unpublished results.
[13] P. S. Hammond, *J. Fluid Mech.* **1983**, *137*, 363 – 384.
[14] H. Pham, I. Gourevich, J. Oh, J. Jonkman, E. Kumacheva, *Adv. Mater.* **2004**, *16*, 516 – 520.
[15] M. A. Hines, P. Guyot-Sionnest, *J. Phys. Chem. B* **1996**, *100*, 468 – 471.
[16] M. Adams, Z. Dogic, S. L. Keller, S. Fraden, *Nature* **1998**, *393*, *349–352.*
[17] H. N. W. Lekkerkerker, A. Stroobants, *Nature* **1998**, *393*, *305–307.*
[18] M. D. Eldridge, P. A. Madden, D. Frenkel, *Nature* **1993**, *365*, 35 – 37.

 © 2005 Wiley-VCH Verlag GmbH & Co. KGaA, Weinheim

Reactive Intermediates

Gas-Phase Synthesis of $[Ag_4H]^+$ and Its Mediation of the C–C Coupling of Allyl Bromide**

*George N. Khairallah and Richard A. J. O'Hair**

The formation of carbon–carbon bonds mediated by metal surfaces and nanoparticles continues to attract considerable attention.[1,2] Recent work on the interaction of allyl halides (C_3H_5X) with a range of metal surfaces revealed different reactivity that depends on both the metal as well as the halide.[3,4] Of all the metal surfaces examined, silver surfaces appear to be the most effective at mediating carbon–carbon bond coupling of allyl halides to give 1,5-hexadiene. Two distinct pathways have been observed:[4a] 1) dissociative adsorption of C_3H_5X to give surface-bound allyl groups, which then undergo coupling, and 2) a coupling reaction between C_3H_5X and a surface-bound allyl group. Surface defects play a significant role in the selectivity of 1,5-hexadiene formation which increases from 20% to greater than 60% when chlorine atoms are preadsorbed on silver surfaces.[4b] Also of interest are the largely forgotten results of Tamura and Kochi,[5] who synthesized silver nanoparticles over 30 years ago and showed that they reacted with allyl bromide to give 1,5-hexadiene and silver bromide [Eq. (1)]. Here we describe the gas-phase assembly of the subvalent silver hydride cluster $[Ag_4H]^+$[6] and its subsequent ion–molecule reactions with allyl bromide.

$$Ag_x + x\,CH_2{=}CHCH_2Br \rightarrow (AgBr)_x + x/2\,CH_2{=}CH(CH_2)_2CH{=}CH_2 \quad (1)$$

$[Ag_4H]^+$ was "synthesized" in the gas phase by collision-induced dissociation (CID) of a silver–amino acid precursor in a quadrupole ion trap (QIT) mass spectrometer.[7] The precursor was the silver ion cluster $[(M + Ag\text{-}H)_3 + Ag]^+$ (M = *N*,*N*-dimethylglycine), which was formed through electrospray ionization (ESI) of a mixture of silver nitrate ($AgNO_3$) and the amino acid.[8] A total of three stages of CID (MS^4) with consecutive neutral losses of 101 Th ($-C_4H_7NO_2$; Th = Thomson) and 103 Th ($-C_4H_9NO_2$) yielded $[Ag_4H]^+$ in high abundance. Other silver clusters such as $[Ag_n]^+$ ($n = 3, 5, 7$) and $[Ag_nH]^+$ ($n = 2, 6$) have been formed in related CID reactions of $[(M + Ag\text{-}H)_m + Ag]^+$ clusters (M = glycine or *N*,*N*-dimethylglycine). These reactions represent the first gas-phase assembly of silver clusters mediated by simple biomolecules.[9,10] Interestingly, the anionic amino acid ligands act as the reductants; this is in contrast to the condensed-phase assembly of silver clusters and nanoparticles on biomolecular templates which requires the addition of reductants.[11]

The ion–molecule reactions of these silver clusters with the allyl halides, $CH_2{=}CHCH_2X$ (X = Cl, Br, and I) were examined.[12,13] $[Ag_4H]^+$ ($m/z = 433$)[14] exhibits the highest selectivity for C–C bond coupling with allyl bromide, $CH_2{=}CHCH_2Br$ (Figure 1). The first molecule of allyl bromide reacts with $[Ag_4H]^+$ by a metathesis reaction to yield $[Ag_4Br]^+$ ($m/z = 511$)[14] as the major ionic product (Figure 1a and Equation (2)). $[Ag_4Br]^+$ subsequently reacts with a second molecule of allyl bromide to form the ion $[Ag_4Br_2(C_3H_5)]^+$ ($m/z = 633$)[14] (Figure 1b, Equation (3)). Reaction of $[Ag_4Br_2(C_3H_5)]^+$ with a third molecule of allyl bromide results in the formation of the silver organometallic ion $[Ag(C_3H_5)_2]^+$ ($m/z = 189$)[14] in combination with the neutral cluster $[Ag_3Br_3]$[15] (Figure 1c, Equation (4)). Overall, these equations combine to give a rare example of a metal-mediated C–C bond-coupling reaction [Eq. (5)] in the gas phase.[16]

$$[Ag_4H]^+ + CH_2{=}CHCH_2Br \rightarrow [Ag_4Br]^+ + CH_2{=}CHCH_3 \quad (2)$$

$$[Ag_4Br]^+ + CH_2{=}CHCH_2Br \rightarrow [Ag_4Br_2(C_3H_5)]^+ \quad (3)$$

$$[Ag_4Br_2(C_3H_5)]^+ + CH_2{=}CHCH_2Br \rightarrow [Ag(C_3H_5)_2]^+ + [Ag_3Br_3] \quad (4)$$

$$[Ag_4H]^+ + 3\,CH_2{=}CHCH_2Br \rightarrow [Ag(C_3H_5)_2]^+ + [Ag_3Br_3] + CH_2{=}CHCH_3 \quad (5)$$

Additional CID studies and DFT (density functional theory) calculations[17] were carried out to gain further support that C–C bond coupling had occurred. CID of $[Ag(C_3H_5)_2]^+$ results in only the formation of Ag^+ [Eq. (6)]. No formation of $[Ag(C_3H_5)]^+$ through the loss of an allyl radical is observed. These results suggest that C–C bond coupling has occurred, however no information about the

[*] Dr. G. N. Khairallah, Prof. R. A. J. O'Hair
School of Chemistry
University of Melbourne
Victoria 3010 (Australia)
Fax: (+613) 9347-5180
E-mail: rohair@unimelb.edu.au

[**] This work was supported by the Australian Research Council (Grant No. DP0344145). We thank the Melbourne Advanced Research Computing Centre (MARCC) and the Victorian Institute for Chemical Sciences, High Performance Computing Facility for their generous allocation of computer time, and Tom Waters for helpful discussions.

Supporting information for this article is available on the WWW under http://www.angewandte.org or from the author.

 © 2005 Wiley-VCH Verlag GmbH & Co. KGaA, Weinheim DOI: 10.1002/anie.200461328

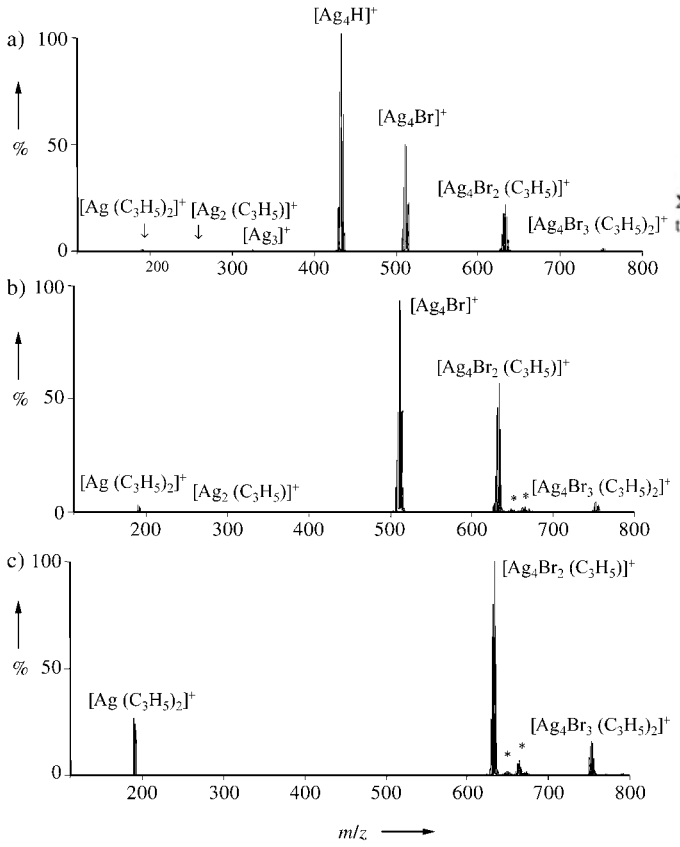


Figure 1. Ion–molecule reactions of allyl bromide with the following mass-selected ions: a) $[Ag_4H]^+$ ($m/z = 433$) to produce $[Ag_4Br]^+$ ($m/z = 511$), b) $[Ag_4Br]^+$ ($m/z = 511$) to produce $[Ag_4Br_2(C_3H_5)]^+$, and c) $[Ag_4Br_2(C_3H_5)]^+$ ($m/z = 633$) to produce $[Ag(C_3H_5)_2]^+$ ($m/z = 189$). The presence of H_2O and MeOH adducts is marked with asterisks. All spectra shown were acquired after a reaction time of 30 ms and a constant pressure of approximately 1×10^{-7} Torr of the neutral reagent C_3H_5Br.

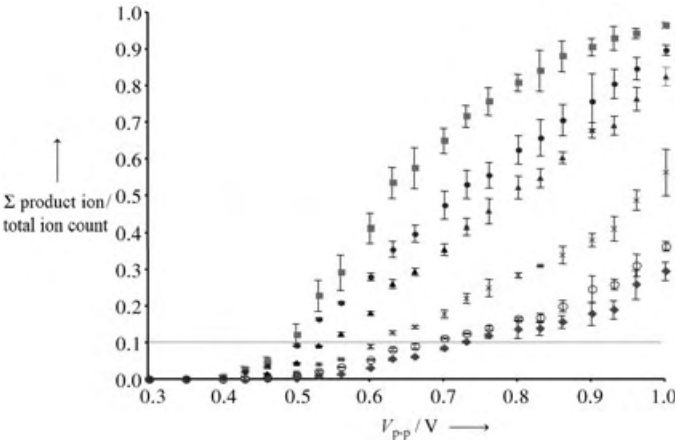


Figure 2. Energy-resolved CID spectra of various isomeric $[Ag(C_6H_{10})]^+$ ions. Plot of reaction extent (Σ product ions/total ion count) versus activation voltage ($V_{p\text{-}p}$) for the elimination of C_6H_{10} ligands from the complexes $[Ag(L)]^+$ (L = 1,3-hexadiene (■), 1,4-hexadiene (▲), 2,4-hexadiene (×), 1,5-hexadiene (○), cyclohexane (●), and the $[Ag(C_3H_5)_2]^+$ ion formed (◆; see Figure 1c and Equation (4)). The horizontal line corresponds to the 10% arbitrary threshold at which the reactivity of each of the isomeric $[Ag(C_6H_{10})]^+$ ions can be compared. The error bars represent the standard deviation of the three independent measurements for each $[Ag(C_6H_{10})]^+$ ion.

structure of the $(C_3H_5)_2$ ligand is provided. Although there are many ligands with a molecular formula of C_6H_{10} that could fragment by the loss of a ligand [Eq. (6)], previous condensed-phase studies suggest that the most likely coupled product is 1,5-hexadiene.[4,5] Thus, energy-resolved CID[18] was used to gain insight into the nature of the coupled product by comparing the energy-resolved CID spectrum of the product of [Eq. (5)] to those of authentic ion structures formed independently by ESI-MS.[19] Figure 2 shows the energy-resolved CID spectra of six $[Ag(C_3H_5)_2]^+$ systems: 1) the ion of "unknown" structure formed through the reaction depicted in [Eq. (5)], 2) the $[Ag(1,5\text{-hexadiene})]^+$ ion with an authentic structure, 3) the isomeric $[Ag(1,3\text{-hexadiene})]^+$ ion, 4) the isomeric $[Ag(1,4\text{-hexadiene})]^+$ ion, 5) the isomeric $[Ag(2,4\text{-hexadiene})]^+$ ion, and 6) the isomeric $[Ag(\text{cyclohexene})]^+$ ion. It is clear that the energy-resolved CID spectrum of $[Ag(C_3H_5)_2]^+$ formed by [Eq. (5)] closely matches that of the authentic $[Ag(1,5\text{-hexadiene})]^+$ ion. Moreover, the $[Ag(L)]^+$ ions (L = 1,3-hexadiene, 1,4-hexadiene, 2,4-hexadiene, cyclohexene) all require less energy to dissociate, suggesting that these ligands have lower Ag^+ binding energies.[19–22] Assuming that the 10% threshold in Figure 2 is an indicator of the relative binding energies, this suggests a relative Ag^+ binding order 1,3-hexadiene ≈ cyclohexene < 1,4-hexadiene < 2,4-hexadiene < 1,5-hexadiene. Although we have not quantified the experimental binding energies, these gas-phase results are consistent with equilibrium constants of silver–diene complexes determined by GC which show that the most stable complexes are those in which the two double bonds are separated by two methylene units.[23,24]

$$[Ag(C_3H_5)_2]^+ \rightarrow Ag^+ + (C_3H_5)_2 \qquad (6)$$

To gain further insight into these isomeric $[Ag(L)]^+$ complexes (L = 1,3-hexadiene, 1,4-hexadiene, 2,4-hexadiene, 1,5-hexadiene, cyclohexene), we carried out further DFT calculations.[17,22] Although the ranking of the relative binding energies of the ligands (1,3-hexadiene (33.6 kcal mol^{-1}) < 2,4-hexadiene (35.2 kcal mol^{-1}) < 1,4-hexadiene (45.1 kcal mol^{-1}) < cyclohexene (47.0 kcal mol^{-1}) < 1,5-hexadiene (52.1 kcal mol^{-1})) is different to that of Figure 2, both experiment and theory suggest that Ag^+ binds strongest to 1,5-hexadiene and that the product of the reactions described in [Eqs. (2)–(4)] is $[Ag(1,5\text{-hexadiene})]^+$.[21] Further calculations allow us to evaluate the overall energetics associated with the reactions described in [Eqs. (2)–(4)] by estimating the overall energy of the reaction in Equation (5) for the case where the product is $[Ag(1,5\text{-hexadiene})]^+$. The overall reaction sequence is determined to be exothermic by −166.3 kcal mol^{-1} from the DFT data, consistent with the formation of the $[Ag(1,5\text{-hexadiene})]^+$ product ion through ion–molecule reactions at the near room temperature conditions of the QIT.[7b]

 © 2005 Wiley-VCH Verlag GmbH & Co. KGaA, Weinheim

The gas-phase reactivity of the silver $[Ag_4H]^+$ cluster appears to represent a simple molecular model for the C–C bond coupling of allyl bromide mediated by silver surfaces[4] and nanoparticles.[5] Remarkably, the hydrogen defect plays a significant role in initiating the reaction sequence by [Eq. (2)] as the "pure" $[Ag_3]^+$ and $[Ag_5]^+$ silver clusters do not react with allyl bromide to promote C–C bond coupling. This appears to be consistent with the observation that chlorine surface defects play a role in the selectivity for 1,5-hexadiene formation on silver surfaces.[4b] Further work is underway to examine other aspects of metal-mediated C–C bond coupling reactions in the gas phase.

Received: July 16, 2004
Revised: September 17, 2004
Published online: December 23, 2004

Keywords: C–C coupling · gas-phase reactions · ion–molecule reactions · mass spectrometry · silver

[1] Selected reviews on C–C bond-formation reactions: a) F. Zaera, *Catal. Lett.* **2003**, *91*, 1; b) B. E. Bent, *Chem. Rev.* **1996**, *96*, 1361; c) F. Zaera, *Chem. Rev.* **1995**, *95*, 2651.

[2] M. Moreno-Manas, R. Pleixtas, *Acc. Chem. Res.* **2003**, *36*, 638.

[3] a) L. Bugyi, A. Oszko, F. Solymosi, *Surf. Sci.* **2002**, *519*, 139; b) H. Celio, K. C. Scheer, J. R. White, *J. Am. Chem. Soc.* **2001**, *123*, 2990; c) D. Chrysostomou, F. Zaera, *J. Phys. Chem. B* **2001**, *105*, 1003.

[4] a) H. Celio, J. M. White, *J. Phys. Chem. B* **2001**, *105*, 3908; b) K. Kershen, H. Celio, I. Lee, J. M. White, *Langmuir* **2001**, *17*, 323.

[5] M. Tamura, J. M. Kochi, *Bull. Chem. Soc. Jpn.* **1972**, *45*, 1120.

[6] The only experimentally known gas-phase silver hydride ion is the $[Ag_2H]^+$ ion: R. A. Flurer, K. L. Busch, *J. Am. Chem. Soc.* **1991**, *113*, 3656.

[7] All CID and ion–molecule reactions were carried out on a Finnegan LCQ QIT as described previously: a) T. Waters, R. A. J. O'Hair, A. G. Wedd, *J. Am. Chem. Soc.* **2003**, *125*, 3384; Work by Gronert has shown that the ions in a LCQ QIT are essentially at room temperature: b) S. Gronert, *J. Am. Soc. Mass Spectrom.* **1998**, *9*, 845.

[8] ESI of solutions containing a mixture of silver nitrate ($AgNO_3$) and simple amino acids such as glycine or *N,N*-dimethylglycine (M) yields a range of amino acid–silver ion clusters of the type $[(M + Ag\text{-}H)_n + Ag]^+$, with the most intense signals for $n = 3$ and 4. These samples were prepared by dissolving the amino acid and Ag^+ in a ratio of 3:1 to a final concentration of the amino acid of approximately 1 mM in a mixture of 50:50:1 methanol:water: acetic acid. The mixture was introduced into the ESI chamber with a flow rate of 3 $\mu L\,min^{-1}$, a spray voltage of 4.0–5.0 kV, and a capillary temperature of 170–200 °C. The nitrogen sheath pressure was in the range 30–60 psi, and the capillary and tube lens offset voltages were adjusted before each experiment to optimize the signal of the cluster of interest. Isotopic clusters of Ag and the amino acid were selected with a window width of 8–16 Th and then subjected to CID with an activation amplitude of 0.8–1.3 V, an activation (Q) of 0.25–0.4 V, and an activation time of 30 ms. All of the fragmentation reactions were confirmed by their relative masses and isotope distributions that also exclude the loss of Ag or the formation of multiply charged species. Neutral losses of AgH, $[Ag_2]$, and $[Ag_4]$ also occur during the MS^n experiments.

[9] The gas-phase synthesis of $[Ag_n]^+$ and $[Ag_mH]^+$ species by the combination of ESI and CID appears to require 1) the formation of cationic silver salt precursors, $[Ag(AgX)_n]^+$, through ESI and 2) favourable redox properties of the ligand X to facilitate reduction of Ag^+ under CID conditions. The presence of both the amine and the deprotonated carboxylate groups in glycine and *N,N*-dimethylglycine appears to be unique in meeting both of these requirements. Thus, the methyl ester of glycine fails to form large clusters (first requirement). Whereas silver acetate forms $[Ag(AgOAc)_n]^+$ clusters by means of ESI, they fragment only through the evaporation of AgOAc (failure of the second requirement). Adenine forms a range of clusters with silver nitrate under ESI conditions, but these do not readily assemble silver clusters, $[Ag_n]^+$, under CID conditions: A. K. Vrkic, T. Taverner, P. F. James, R. A. J. O'Hair, *Dalton Trans.* **2004**, 197.

[10] Large Ag clusters have been formed by means of MALDI: S. Keki, L. S. Szilagyi, J. Torok, G. Deak, M. Zsuga, *J. Phys. Chem. B* **2003**, 4818.

[11] Silver nanoparticles and colloids have been formed from a wide range of processes, including the recent use of biological templates. For DNA templates, see: a) J. T. Petty, J. Zheng, N. V. Hud, R. M. Dickson, *J. Am. Chem. Soc.* **2004**, *126*, 5207; For peptides, see: b) R. R. Naik, S. J. Stringer, G. Agarwal, S. E. Jones, M. O. Stone, *Nat. Mater.* **2002**, *1*, 169.

[12] A number of gas-phase reactions of mass-selected silver cluster ions have been examined, although not for allyl or alkyl halides: a) S. W. Buckner, J. R. Gord, B. S. Freiser, *J. Chem. Phys.* **1988**, *88*, 3678; b) P. Sharpe, C. J. Cassady, *Chem. Phys. Lett.* **1992**, *191*, 111; c) P. Sharpe, J. M. Campbell, C. J. Cassady, *Organometallics* **1994**, *13*, 3077; d) M. A. Cheeseman, J. R. Eyler, *J. Phys. Chem.* **1992**, *96*, 1082; e) M. P. Irion, P. Schnabel, A. Selinger, *Ber. Bunsen-Ges.* **1990**, *94*, 1291; f) T. H. Lee, K. M. Ervin, *J. Phys. Chem.* **1994**, *98*, 10023; g) Y. D. Kim, G. Gantefor, *Chem. Phys. Lett.* **2004**, *383*, 80; h) L. D. Socaciu, J. Hagen, J. Le Roux, D. Popolan, T. M. Bernhardt, L. Woste, S. Vajda, *J. Chem. Phys.* **2004**, *120*, 2078; i) M. Schmidt, A. Masson, C. Brechignac, *Phys. Rev. Lett.* **2003**, *91*, 243401.

[13] For a report on the gas-phase reactions of Ag^+ with alkyl halides, see: a) R. W. Jones, R. H. Staley, *J. Phys. Chem.* **1982**, *86*, 1669. Under our QIT conditions, Ag^+ reacts with allyl bromide to yield $[Ag(C_3H_4)]^+$, $[Ag(C_3H_5Br)]^+$, $[Ag(C_3H_5Br)_2]^+$, $C_3H_5^+$, and $C_6H_9^+$. The formation of $C_6H_9^+$ is likely to arise from ion–molecule reactions between $C_3H_5^+$ and C_3H_5Br, for example, see: b) T. Gäumann, Z. Zhu, M. C. Kida, J. M. Riveros, *Helv. Chim. Acta* **1990**, *73*, 2218.

[14] m/z value of the most intense peak in the cluster.

[15] The $[Ag_3Br_3]$ cluster is known to be a stable species in the gas phase, see: J.-M. L'Hermite, F. Rabilloud, P. Labastie, F. Spiegelman, *Eur. Phys. J. D* **2001**, *16*, 77–80.

[16] For a recent demonstration of a gas-phase Gilman reaction, see: a) P. F. James, R. A. J. O'Hair, *Org. Lett.* **2004**, *6*, 2761; Of direct relevance is the C–C coupling of allyl chloride mediated by coordinatively unsaturated iron–carbonyl cations. See: b) H. Mestdagh, C. Rolando, *J. Am. Chem. Soc.* **1989**, *111*, 3476.

[17] Geometry optimization and frequency calculations were carried out at the B3LYP level of theory followed by a single-point energy calculation at the MP2 level. The basis sets used were 6-31G(d) for C and H and the LanL2DZ effective core potential (ECP) of Hay and Wadt for Ag and Br. Our previous study[9] has shown that this level of theory is a useful compromise between accuracy and computational resources. Calculations were carried out by using Gaussian 03 (Revision A.1), M. J. Frisch, G. W. Trucks, H. B. Schlegel, G. E. Scuseria, M. A. Robb, J. R. Cheeseman, J. A. Montgomery, Jr., T. Vreven, K. N. Kudin, J. C. Burant, J. M. Millam, S. S. Iyengar, J. Tomasi, V. Barone, B. Mennucci, M. Cossi, G. Scalmani, N. Rega, G. A. Petersson, H. Nakatsuji, M. Hada, M. Ehara, K. Toyota, R. Fukuda, J. Hasegawa, M. Ishida, T. Nakajima, Y. Honda, O. Kitao, H. Nakai, M. Klene, X. Li, J. E. Knox, H. P. Hratchian, J. B. Cross, C. Adamo, J. Jaramillo, R. Gomperts, R. E. Stratmann, O.

 © 2005 Wiley-VCH Verlag GmbH & Co. KGaA, Weinheim

Yazyev, A. J. Austin, R. Cammi, C. Pomelli, J. W. Ochterski, P. Y. Ayala, K. Morokuma, G. A. Voth, P. Salvador, J. J. Dannenberg, V. G. Zakrzewski, S. Dapprich, A. D. Daniels, M. C. Strain, O. Farkas, D. K. Malick, A. D. Rabuck, K. Raghavachari, J. B. Foresman, J. V. Ortiz, Q. Cui, A. G. Baboul, S. Clifford, J. Cioslowski, B. B. Stefanov, G. Liu, A. Liashenko, P. Piskorz, I. Komaromi, R. L. Martin, D. J. Fox, T. Keith, M. A. Al-Laham, C. Y. Peng, A. Nanayakkara, M. Challacombe, P. M. W. Gill, B. Johnson, W. Chen, M. W. Wong, C. Gonzalez, J. A. Pople, Gaussian, Inc., Pittsburgh, PA, **2003**.

[18] For a discussion of energy-resolved CID in QITs to measure threshold activation voltages, see: A. Colorado, J. Broadbelt, *J. Am. Soc. Mass Spectrom.* **1996**, *7*, 1116.

[19] The "authentic" $[Ag(L)]^+$ complexes (L = 1,3-hexadiene, 1,4-hexadiene, 2,4-hexadiene, 1,5-hexadiene, cyclohexene) were all formed individually by ESI-MS by mixing silver nitrate with the ligand (purchased from Aldrich and used as received) in methanol and directly injecting the resultant solution into the mass spectrometer. The energy-resolved CID spectra shown in Figure 2 are an average of three independent sets of experiments carried out on different days. These energy-resolved CID spectra are used in a qualitative sense to identify the nature of the ligand and not to establish precise Ag^+ binding energies, which would ideally be determined through guided ion beam experiments (see: *Encyclopedia of Mass Spectrometry*, *Vol. 1* (Ed.: P. B. Armentrout), Elsevier, Amsterdam, **2003**, pp. 426–434). Collisional activation experiments in quadrupole ion-trap instruments depend on a number of factors such as ion mass and ion density, resonance excitation time, trapping well depth, and activation voltages. The estimation of absolute collision energies is likely to be further complicated by other factors such as lifetime effects, kinetic shifts, differing excitation efficiencies, and the possibility that some fragmentation reactions may suffer from reverse activation barriers. Nonetheless, every effort has been taken to ensure that each of the different $[Ag(L)]^+$ complexes experiences similar conditions in the QIT (starting number density of ions, helium pressure, and background allyl bromide pressure). All $[Ag(L)]^+$ complexes were mass-selected with a window of 5 Th to include both silver isotopes and were subjected to CID over a 10 ms timeframe. The ion counts of both the precursor and product ions were integrated to include both isotopes.

[20] The isomeric $[Ag(L)]^+$ complexes (L = 1,3-hexadiene, 1,4-hexadiene, 2,4-hexadiene, 1,5-hexadiene, cyclohexene) also exhibit different bimolecular reactivity towards neutral reagents such as water and methanol (data not shown).

[21] Our results highlight the need for further experimental work to establish a gas-phase silver ion affinity scale. For limited data on gas phase Ag^+ binding energies, see: a) B. C. Gui, A. W. Castleman, *Chem. Phys. Lett.* **1991**, *181*, 16; b) H. T. Deng, P. Kebarle, *J. Phys. Chem. A* **1998**, *102*, 571.

[22] These experiments are complicated by the fact that 1,3-hexadiene, 1,4-hexadiene, and 2,4-hexadiene exist as mixtures of *cis* and *trans* isomers (as supplied by Aldrich). These *cis* and *trans* isomers are likely to have different Ag^+ binding energies. Furthermore, the ratios of $[Ag(\textit{cis}\text{-}L)]^+$ versus $[Ag(\textit{trans}\text{-}L)]^+$ isomers formed by ESI-MS are unknown. In the DFT calculations, we surveyed all *cis* and *trans* isomers of the $[Ag(L)]^+$ complexes, but only calculated the binding energy for the most stable complexes.

[23] M. A. Muhs, F. T. Weiss, *J. Am. Chem. Soc.* **1962**, *84*, 4697.

[24] The fact that silver ions form complexes with π donors with different binding energies has been extensively used in various types of chromatography. For a review, see: C. M. Williams, L. N. Mander, *Tetrahedron* **2001**, *57*, 425.

 © 2005 Wiley-VCH Verlag GmbH & Co. KGaA, Weinheim

Single-Molecule Magnets

The Effect of the f–f Interaction on the Dynamic Magnetism of a Coupled $4f^8$ System in a Dinuclear Terbium Complex with Phthalocyanines**

Naoto Ishikawa, Satoshi Otsuka, and Youkoh Kaizu**

The observation of long magnetic relaxation times of bis(phthalocyaninato)terbium at high temperatures has led to a new category of magnets at the single-molecular level that are based on lanthanide complexes.[1] The relaxation times determined by alternating current (ac) magnetic susceptibility measurements for the Tb^{III} complex $[Pc_2Tb]^-$ (Pc denotes the dianion of phthalocyanine) are, for example, 0.16 ms at 40 K and 1.6 s at 8 K.[2] These temperatures are considerably higher than those reported for the transition-metal clusters known as "single-molecule magnets" (SMMs).[8,9] The long relaxation times of the Tb–Pc complex at high temperatures result from the characteristic ligand-field-splitting pattern of the $J = 6$ ground multiplet of the Tb^{III} ion with a $4f^8$ electronic configuration.[3–7] The ligand-field potential of pseudo-D_{4d} symmetry made by the two Pc macrocycles lifts the 13-fold degeneracy and yields a situation in which the lowest substates with $J_z = \pm 6$ are greatly separated (by about 400 cm^{-1}) from the rest of the substates.[8,9] This splitting pattern causes a low transition rate between the lowest substates and thus slow relaxation is observed.

The phthalocyaninato ligand is known to form other sandwich-type complexes that are composed of three Pc ligands and two lanthanide ions. These complexes are often referred to as triple deckers. The lanthanide ions are placed along the fourfold symmetry axis with a metal–metal interatomic distance of about 3.6 Å. If Tb^{III} ions are placed at the lanthanide sites, the resultant complex can be viewed as a system in which two $4f^8$ systems, each having relaxation times of the order of a millisecond to a second, are coupled by an f–f interaction.[10] Such a system is in fact hard to find and, to the best of our knowledge, has not been reported with any other lanthanide complex. In this sense, the bis-Tb complex provides us with a rare opportunity to carry out experimental studies on the dynamic magnetism of coupled 4f electronic systems.

[*] Dr. N. Ishikawa, S. Otsuka, Prof. Dr. Y. Kaizu
Department of Chemistry
Tokyo Institute of Technology
O-okayama, Meguro-ku, Tokyo 152-8551 (Japan)
Fax: (+81) 3-5734-2759
E-mail: ishikawa@chem.titech.ac.jp
ykaizu@chem.titech.ac.jp

[**] We thank Prof. Dr. Shin-ya Koshihara, Department of Materials Science, Tokyo Institute of Technology, for granting machine time on the magnetometer, and Dr. Tadahiko Ishikawa for assistance with data collection. This work was supported by a Grant-in-Aid for Science Research No. 15550046 from the Ministry of Education, Science, Sports, and Culture of Japan.

 DOI: 10.1002/anie.200461546 © 2005 Wiley-VCH Verlag GmbH & Co. KGaA, Weinheim

Herein we present the first report on the dynamic magnetism of a coupled $4f^8$ system. The effect of the f–f interaction on the temperature and frequency dependence of the ac magnetic susceptibility will be clarified by the comparison of experimental data for isostructural bis-Tb and mono-Tb complexes.

Concerning the nature of the f–f interaction in the triple-decker Pc complexes, Ishikawa et al. previously reported the analysis of the NMR spectra and the temperature dependence of the static magnetic susceptibilities of the dinuclear complexes of heavy lanthanides (Tb, Dy, Ho, Er, Tm, and Yb) and concluded that the interaction was essentially dominated by the magnetic dipolar term in all six cases.[10–12] In the case of the bis-Tb complex, the magnetic dipolar interaction between the Tb ions leads to a parallel or ferromagnetic arrangement of magnetic moments at low temperatures.[11]

We have prepared a homodinuclear complex [Tb, Tb] (Figure 1) and two heterodinuclear complexes [Y, Tb] and

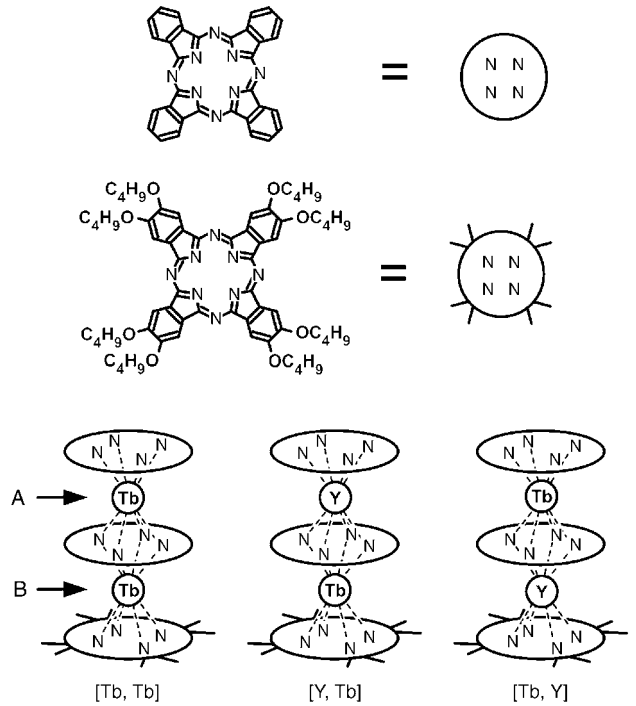


Figure 1. Structures of [Tb, Tb], [Y, Tb], and [Tb, Y]. A and B indicate the two different metal coordination environments, see text.

[Tb, Y], in which one Tb ion is replaced by a diamagnetic Y^{III} center. The compounds were synthesized by using a previously reported method.[10,11] The ac magnetic susceptibility measurements were carried out on a Quantum Design MPMS-XL magnetometer.

Figure 2 shows the temperature dependence of ac susceptibilities of the three complexes diluted in a diamagnetic [Y, Y] matrix with a concentration of 5%. The mono-Tb complexes exhibit a decrease in χ_M'/χ_M values and nonzero χ_M''/χ_M values as the temperature is lowered. The χ_M''/χ_M peaks for the 997-Hz field are observed at 7 K and 18 K for the [Y, Tb] and [Tb, Y] complexes, respectively. The difference in the temperature ranges in which the relaxation

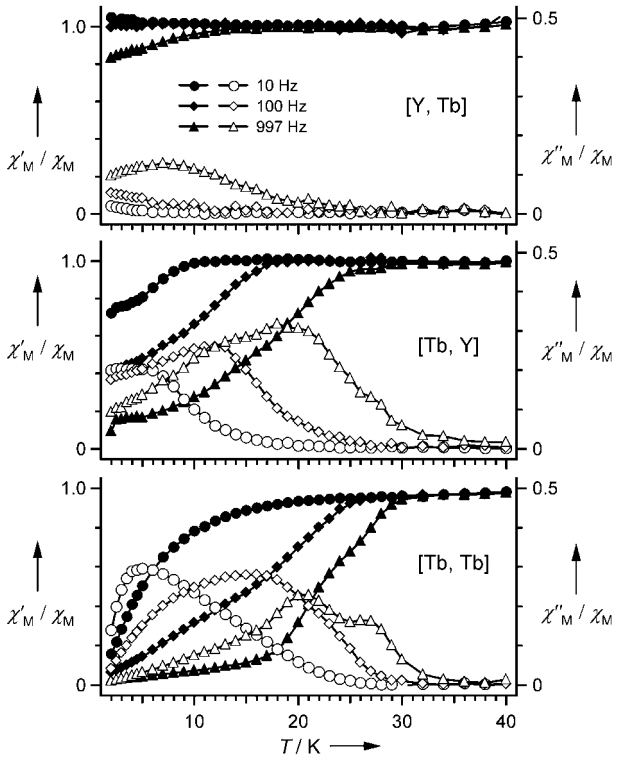


Figure 2. Plots of χ_M'/χ_M (closed symbols) and χ_M''/χ_M (open symbols) against temperature T, in which χ_M' is the in-phase ac magnetic susceptibility, χ_M'' is the out-of-phase ac magnetic susceptibility, and χ_M is the dc molar magnetic susceptibility, for a powder sample of [Y, Tb] (top), [Tb, Y] (middle), and [Tb, Tb] (bottom).

phenomena are observed reflects the difference in the ligand-field potential between the two lanthanide sites.

The bis-Tb complex [Tb, Tb] shows the relaxation phenomenon at a higher temperature range than those of the mono-Tb complexes (Figure 2, bottom). This result means that the f–f interaction increases the magnetization relaxation time of [Tb, Tb]. Even more interestingly, the χ_M''/χ_M plot for the 997-Hz field contains two peaks at 27 K and 20 K. It appears that the χ_M''/χ_M peaks of mono-Tb complexes are shifted to higher temperatures in the bis-Tb complex. We have proved experimentally that this is in fact the case.

Figure 3 shows the ac susceptibility data taken under a nonzero dc magnetic field. As the dc field increases, the χ_M''/χ_M peaks of the [Y, Tb] and [Tb, Y] complexes shift to higher temperatures. The shift reaches its maximum at a dc field of about 2000 Oe. In contrast, in the [Tb, Tb] complex the positions of the two χ_M''/χ_M peaks do not change. Most importantly, the positions of the shifted peaks of both the mono-Tb complexes almost coincide with the two peaks of the bis-Tb complex. This result clearly indicates that the two peaks of [Tb, Tb] at 27 and 20 K actually correspond to the Tb^{III} ions at sites A and B (see Figure 1), respectively.

The shift of the χ_M''/χ_M peak position of the mono-Tb complexes with an increase in the dc field should be closely related to the difference of the ground-state eigenfunctions that are between the zero-field and highfield limits. As previously reported, the lowest substates of the mono-Tb

 © 2005 Wiley-VCH Verlag GmbH & Co. KGaA, Weinheim

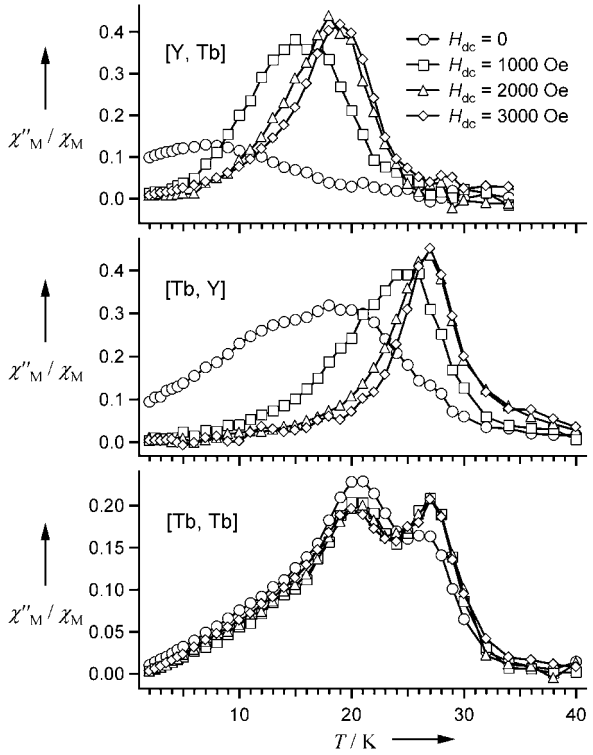


Figure 3. Plots of χ_M''/χ_M against temperature T of [Y, Tb] (top), [Tb, Y] (middle), and [Tb, Tb] (bottom) measured in a 5G ac magnetic field of 997 Hz with dc field H_{dc} of indicated magnitudes.

complexes are described predominantly by the two functions $|+6\rangle$ and $|-6\rangle$,[10,11] which correspond to the eigenfunctions at the highfield limit. In the absence of a magnetic field, the zero field eigenfunctions are $\{|+6\rangle \pm |-6\rangle\}/2^{1/2}$,[10,11] due to the presence of the nonzero off-diagonal matrix elements of the ligand-field potential, which indirectly couples $|+6\rangle$ and $|-6\rangle$.[13,14] As the magnetic field increases, the eigenfunctions vary as $\{\cos\theta\,|+6\rangle - \sin\theta\,|-6\rangle\}$ and $\{\sin\theta\,|+6\rangle + \cos\theta\,|-6\rangle\}$ with θ changing from $\pi/4$ to zero. The relaxation time to reach the equilibrium state is accordingly changed from the zero-field to the highfield limit.

In the case of the [Tb, Tb] complex, the eigenfunctions are expressed by the products of two basis functions, namely $\Phi^A\Phi^B$, in which A and B refer to the two Tb ions. The appropriate choice for the basis function Φ^X (X = A or B) is either $|+6\rangle$ or $|-6\rangle$, even in the zero-field case, because the magnetic dipolar interaction between the two Tb ions gives different diagonal energies to $|+6\rangle^A\ |J_z\rangle^B$ and $|-6\rangle^A\ |J_z\rangle^B$ (and to $|J_z\rangle^A\ |+6\rangle^B$ and $|J_z\rangle^A\ |-6\rangle^B$), in which J_z is either 6 or -6.[11,15] Consequently, the admixture of $|+6\rangle$ and $|-6\rangle$ that is seen in the mono-Tb case does not occur in the bis-Tb case. This explains the small dc-field dependence on the ac susceptibility observed for the [Tb, Tb] complex.

In conclusion, we have obtained the following information on the dynamical magnetism of the coupled $4f^8$ system. 1) Under a zero dc field, the magnetic relaxation time of the bis-Tb complex at a given temperature increases compared to the mono-Tb complexes. 2) The double-peak appearance of the χ_M''/χ_M plot of the [Tb, Tb] complex indicates that the relaxation processes in the two $4f^8$ systems occur somewhat independently of each other, at least in the temperature range above 20 K, although the two systems are certainly coupled by an f–f interaction. 3) The two χ_M''/χ_M peaks of [Tb, Tb] at 27 and 20 K correspond to the relaxations that occur at sites A and B, respectively. 4) The upward temperature shift of the χ_M''/χ_M peaks observed for the mono-Tb complexes corresponds to the resolution of the admixing of $|+6\rangle$ and $|-6\rangle$ states. In contrast, the f–f interaction in the [Tb, Tb] complex prevents the admixture of $|+6\rangle^X$ and $|-6\rangle^X$ states (X is either A or B) at the zero-field limit, which results in the greatly reduced dc-field dependence of the ac susceptibility.

Received: August 5, 2004
Published online: December 21, 2004

Keywords: lanthanides · magnetic properties · sandwich complexes · single-molecule magnets · terbium

[1] N. Ishikawa, M. Sugita, T. Ishikawa, S. Koshihara, Y. Kaizu, *J. Am. Chem. Soc.* **2003**, *125*, 8694.
[2] N. Ishikawa, M. Sugita, T. Ishikawa, S. Koshihara, Y. Kaizu, *J. Phys. Chem. B* **2004**, *108*, 11265.
[3] R. Sessoli, H.-L. Tsai, A. R. Schake, S. Wang, J. B. Vincent, K. Folting, D. Gatteschi, G. Christou, D. N. Hendrickson, *J. Am. Chem. Soc.* **1993**, *115*, 1804.
[4] R. Sessoli, D. Gatteschi, A. Caneschi, M. A. Novak, *Nature* **1993**, *365*, 141.
[5] G. Christou, D. Gatteschi, D. N. Hendrickson, R. Sessoli, *MRS Bull.* **2000**, *25*, 66.
[6] D. Gatteschi, R. Sessoli, *Angew. Chem.* **2003**, *115*, 278; *Angew. Chem. Int. Ed.* **2003**, *42*, 268.
[7] W. Wernsdorfer, N. Aliaga-Alcalde, D. N. Hendrickson, G. Christou, *Nature* **2002**, *416*, 408.
[8] N. Ishikawa, M. Sugita, T. Okubo, N. Tanaka, T. Iino, Y. Kaizu, *Inorg. Chem.* **2003**, *42*, 2440.
[9] N. Ishikawa, *J. Phys. Chem. A* **2003**, *107*, 9543.
[10] N. Ishikawa, T. Iino, Y. Kaizu, *J. Phys. Chem. A* **2002**, *106*, 9543.
[11] N. Ishikawa, T. Iino, Y. Kaizu, *J. Am. Chem. Soc.* **2002**, *124*, 11440.
[12] N. Ishikawa, T. Iino, Y. Kaizu, *J. Phys. Chem. A* **2003**, *107*, 7879.
[13] A ligand-field potential of D_{4d} symmetry is expanded by three Stevens operators, O_2^0, O_4^0, and O_6^0, which have only diagonal elements. As the symmetry is lowered to C_4, as in the present case, contributions from the terms O_4^4 and O_6^4 become nonzero. These additional terms comprise off-diagonal elements, which couple $|J_z\rangle$ and $|J_z-4\rangle$ states. Therefore, $|+6\rangle$ and $|-6\rangle$ states are admixed indirectly through the nonzero $\langle 6\,|\,H_{LF}\,|\,2\rangle$, $\langle 2\,|\,H_{LF}\,|\,-2\rangle$, and $\langle -2\,|\,H_{LF}\,|\,6\rangle$ matrix elements, in which H_{LF} is the operator for the C_4 ligand-field potential.
[14] A. Abragam, B. Bleaney, *Electron Paramagnetic Resonance*, Clarendon, Oxford, **1970**, chap. 18.
[15] The diagonal matrix elements for the magnetic dipolar interaction H_{dd} between the two Tb ions are estimated as: $\langle ++\,|\,H_{dd}\,|\,++\rangle = \langle --\,|\,H_{dd}\,|\,--\rangle = -\langle +-\,|\,H_{dd}\,|\,+-\rangle = -\langle -+\,|\,H_{dd}\,|\,-+\rangle = -2(g_J J_z \beta)^2/{r_{AB}}^3 \approx -1.5\ \mathrm{cm}^{-1}$, in which $g_J = 3/2$, $J_z = 6$, $r_{AB} \approx 3.6$ Å, and β is Bohr magneton. Here, $|++\rangle = |+6\rangle^A\,|+6\rangle^B$, $|+-\rangle = |+6\rangle^A\,|-6\rangle^B$, and so on.

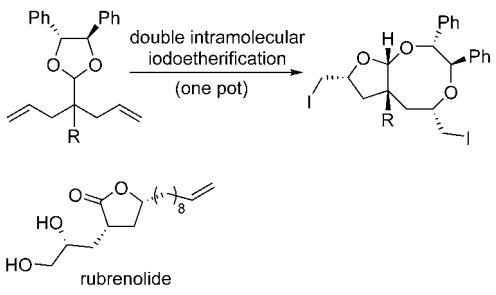
 © 2005 Wiley-VCH Verlag GmbH & Co. KGaA, Weinheim

Asymmetric Synthesis

A Double Iodoetherification of σ-Symmetric Diene Acetals for Installing Four Stereogenic Centers in a Single Operation: Short Asymmetric Total Synthesis of Rubrenolide**

Hiromichi Fujioka, Yusuke Ohba, Hideki Hirose, Kenichi Murai, and Yasuyuki Kita**

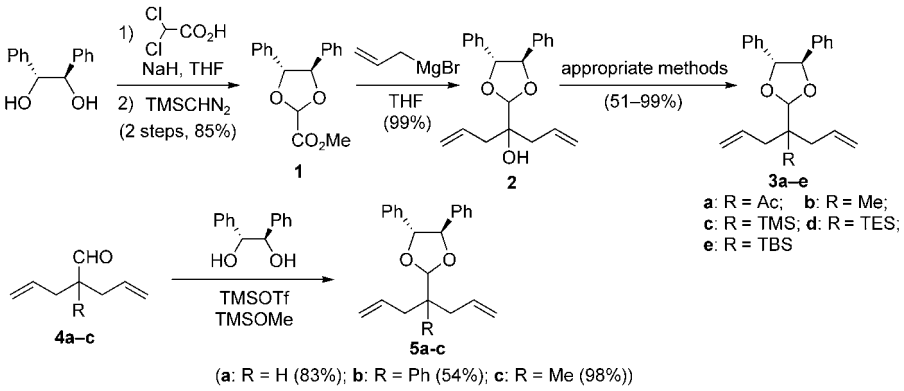
Many biologically active natural products contain multiple chiral centers and occur in their optically active form, and therefore the development of methodologies that can lead to multiple chiral centers is desirable in synthetic organic chemistry. Recently, we developed the intramolecular haloetherification of chiral ene acetals from (*R*,*R*)-hydrobenzoin in which two new chiral centers are formed at remote positions.[1] As an extension of this remote asymmetric induction method we studied the reaction of acyclic σ-symmetric diene acetals, and found an unprecedented double intramolecular haloetherification leading to the formation of four asymmetric centers in a single operation (Scheme 1).



Scheme 1. Double intramolecular haloetherification of acyclic σ-symmetric diene acetals leading to the formation of four asymmetric centers.

Although there are several reports on the discrimination of acyclic σ-symmetric dienes by intramolecular halolactonization,[2] no domino-type reaction has been reported. Furthermore, the reaction was applied to a short asymmetric synthesis of rubrenolide.

The chiral diene acetals (**2** and **3**) with oxygen-containing functional groups, such as hydroxy, ether, and ester groups, were prepared as shown in Scheme 2: 1) reaction of (*R*,*R*)-hydrobenzoin and dichloroacetic acid in the presence of NaH is followed by the formation of the ester to afford **1**; 2) reaction of allylmagnesium bromide with **1** leads to the hydroxy diene acetal **2**; and 3) protection of the *tert*-hydroxy function of **2** by appropriate methods leads to **3**. The chiral

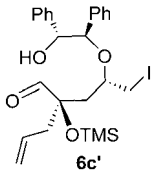


a: R = Ac; **b**: R = Me; **c**: R = TMS; **d**: R = TES; **e**: R = TBS

Scheme 2. Preparation of various acyclic diene acetals. TBS = *tert*-butyldimethyl silyl, TES = triethylsilyl, Tf = trifluoromethanesulfonate, TMS = trimethylsilyl.

diene acetals (**5**) with a hydrogen, phenyl, and methyl substituent were prepared by acetalization of the diallyl aldehyde **4** with (*R*,*R*)-hydrobenzoin.[3]

We first studied the reactivity of substrate **3c** by treatment with *N*-iodosuccinimide (NIS; 2.5 equivalents) and methanol (5.0 equivalents) in acetontrile at −40–0 °C.[1] However, no reaction occurred and the starting material **3c** was recovered. When the reaction was carried out at room temperature, the product obtained resulted from the attack of the methanol on the olefin in an intermolecular fashion. We then changed the nucleophile from methanol to water. The reaction proceeded smoothly to give **6c** (R = OTMS) as the major product in a yield of 73%. Other stereoisomers were obtained as a mixture in an approximate yield of 10% (Scheme 3).



6c'

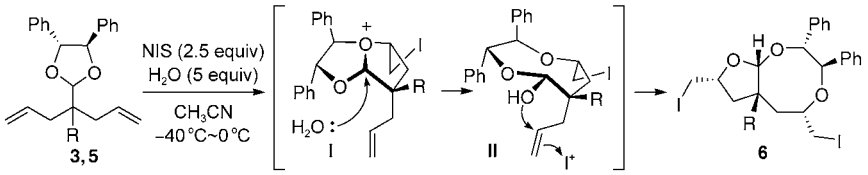
To our surprise, the hydroxy aldehyde **6c′** was not detected, which we predicted from the occurrence of intermediate II.[4] Even the use of 0.5 equivalents of NIS did not give **6c′** at all, and **3c** and **6c** were obtained. The structure of **6c** was determined as follows: The relationship of the substituents on the five-membered ring was determined by NOE interaction experiments between two protons (H_a and H_b) and the methyl group of the trimethylsilyl (TMS) functional group. The complete structure of the product, including the absolute configuration of all of the asymmetric

[*] Prof. Dr. H. Fujioka, Y. Ohba, H. Hirose, K. Murai, Prof. Dr. Y. Kita
Graduate School of Pharmaceutical Sciences
Osaka University
1-6, Yamadaoka, Suita, Osaka 565-0871 (Japan)
Fax: (+81) 6-6879-8229
E-mail: fujioka@phs.osaka-u.ac.jp
kita@phs.osaka-u.ac.jp

[**] This work was supported by Grants-in-Aid for Scientific Research [(S) and (C)] from the Ministry of Education, Culture, Sports, Science, and Technology, Japan. The authors gratefully thank Prof. B. Zwanenburg and Dr. L. Thijs for the generous gift of the mixture of natural rubrenolide and rubrynolide.

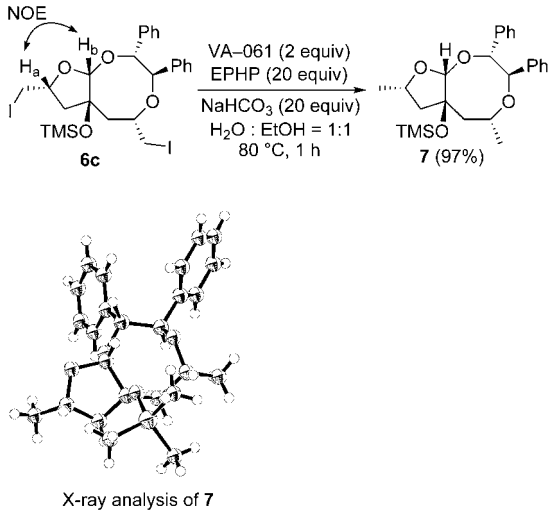
Supporting information for this article is available on the WWW under http://www.angewandte.org or from the author.

 © 2005 Wiley-VCH Verlag GmbH & Co. KGaA, Weinheim DOI: 10.1002/anie.200461584



Scheme 3. Domino-type intramolecular iodoetherification of **3c**.

carbon centers, was unambiguously determined by X-ray crystallographic analysis[5] of the dimethyl compound **7** by radical reduction using 2,2′-azobis[2-(2-imidazolin-2-yl)propane] (VA-061)[6] of **6c** (Scheme 4).



Scheme 4. Radical reduction of **6c**. VA-061 = 2,2′-azobis[2-(2-imidazolin-2-yl)propane], EPHP = 1-ethylpiperidine hypophosphite.

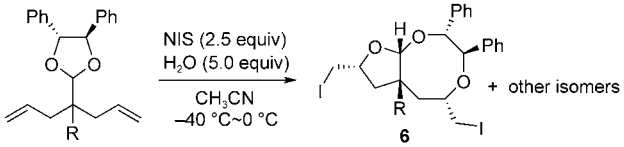
A mechanistic rationale is shown in Scheme 3. The hemiacetal intermediate II was obtained via the oxonium cation intermediate I. The hemiacetal structure of an eight-membered ring usually opens to give the hydroxy aldehyde, such as **6c′**. However, in this case, another olefin unit is present at the proper position. The second intramolecular iodoetherification then occurred faster than the opening of the eight-membered ring to give **6c** in good yield.

This unprecedented double intramolecular iodoetherification proved to be a general reaction. That is, various diene acetals **3b–e**, which have an ether group next to the acetal function, and **5a–c**, which have a hydrogen, methyl, and phenyl substituent next to the acetal function, respectively, afforded the double intramolecular iodoetherification products **6c–h** as major products in fair to good yields (Table 1).

Dreiding models and the X-ray crystal structure of **7** have led to the proposed conformation of the oxocyclic compounds **6c–h**. Their conformations show that the environments of the two iodomethyl functions (a) and (b) are completely different and that the iodomethyl group (b) bearing the eight-membered acetal ring is less hindered, so we expected it to be more reactive. We then examined this observation using compound **6c**. As expected, nucleophiles predominantly attacked at the iodomethyl group (b) bearing the eight-membered acetal ring (Scheme 5).

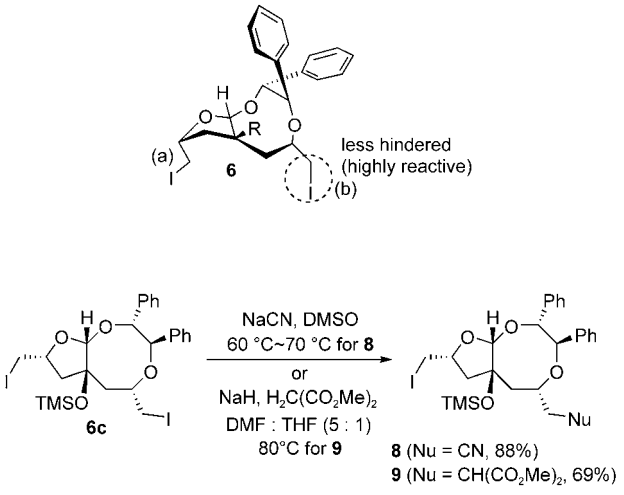
The utility of this domino-type reaction was shown with a short asymmetric synthesis of rubrenolide (Scheme 6). Rubrenolide was isolated from the trunk wood of the Amazonian tree *Nectandra rubra* of the Lauraceae family. It has a remote asymmetric center in addition to a γ-lactone ring with two asymmetric centers.[7] Although one asymmetric synthesis has already been reported,[8] we have developed a shorter asymmetric synthesis. The intramolecular iodoetherification of the diene acetal **5a**, obtained by acetalization of the aldehyde **4a** with (*R*,*R*)-hydrobenzoin, afforded **6f** in 62% yield. Although the mixture contained 18% of other stereoisomers, **6f** was readily purified by column chromatography on silica gel (hexane/ethyl acetate = 20:1). Hydrolysis of **6f** by treatment with 2,3-dichloro-5,6-dicyano-1,4-benzoquinone (DDQ) [9] followed by oxidation

Table 1: Intramolecular iodoetherification of various diene acetals.



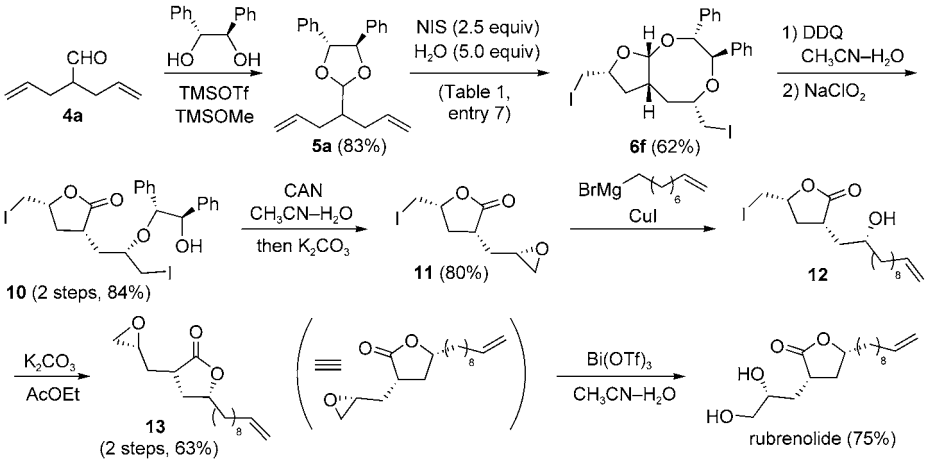
Entry	Diene acetal	*t* [h]	Total yield [%]	d.r.[a]	Major product
1	**2**	–	decomp	–	
2	**3a** (R = OAc)	–	decomp	–	
3	**3b** (R = OMe)	12	38	n.d.[b]	
4	**3c** (R = OTMS)	1.5	82	8/1	**6c**
5	**3d** (R = OTES)	3.5	58	11/1	**6d**
6	**3e** (R = OTBS)	3	84	11/1	**6e**
7	**5a** (R = H)	3	80	3.5/1	**6f**
8	**5b** (R = Ph)	3	72	2/1	**6g**
9	**5c** (R = Me)	13	72	1.5/1	**6h**

[a] Major diastereomer/other diastereomers. [b] Not determined.



Scheme 5. Regioselective nucleophilic addition to **6c**.

 © 2005 Wiley-VCH Verlag GmbH & Co. KGaA, Weinheim



Scheme 6. Asymmetric total synthesis of rubrenolide.

with $NaClO_2$ gave the lactone **10**. Cleavage of the carbon–oxygen bond of the hydrobenzoin unit by ammonium cerium nitrate (CAN)[10] followed by treatment with K_2CO_3 afforded the epoxide **11**. The introduction of the alkenyl unit to the epoxide by a copper-assisted Grignard reagent gave the hydroxylactone **12**. To our surprise, treatment of **12** with K_2CO_3 caused recyclization of the lactone ring and epoxide formation to give the epoxide **13**. Opening of the epoxy ring of **13** by $Bi(OTf)_3$[11] smoothly proceeded to give (+)-rubrenolide. Optical rotation studies and ^{1}H NMR, ^{13}C NMR, and IR spectroscopic analysis of the product with an authentic sample of (+)-rubrenolide were in good agreement.[12]

In conclusion, we have found unprecedented double intramolecular haloetherifications of σ-symmetric diene acetals. The reactions proceed in a highly diastereoselective manner to give tetrahydrofuran units with multiple chiral centers in a one-pot operation. Furthermore, a short asymmetric synthesis of (+)-rubrenolide was carried out as an application of the methodology. Since tetrahydrofuran moieties with multiple chiral centers are found in a large number of biologically active natural products, this method could prove to be a highly useful tool.

Experimental Section

Intramolecular iodoetherification reaction of **5a**: *N*-iodosuccinimide (NIS; 351 mg, 1.6 mmol) was added to a solution of **5a** (100 mg, 0.31 mmol) in CH_3CN (0.62 mL) at −40 °C under nitrogen, and the mixture was stirred for 30 min at the same temperature. Water (0.028 mL, 1.6 mmol) was added to the resulting mixture, which was allowed to warm to 0 °C over 40 min. A saturate aqueous $Na_2S_2O_3$ solution was added to the mixture, which was then extracted with diethyl ether. The organic layer was washed with brine, dried over $MgSO_4$, and evaporated in vacuo. The residue was purified by column chromatography on silica gel using hexane/ethyl acetate (20:1) to give **6f** (114 mg, 0.19 mmol, 62%) and a diastereoiomeric mixture (33 mg, 0.056 mmol, 18%).

6f: $[\alpha]_D^{24}$ +65.4 (c = 1.1, $CHCl_3$); IR (KBr): no OH, no CO; ^{1}H NMR (300 MHz, $CDCl_3$) δ: 1.98–2.03 (2H, m), 2.10–2.23 (1H, m), 2.40–2.42 (2H, m), 3.00–3.07 (3H, m), 3.28 (1H, dd, J = 9.3, 4.5 Hz), 4.03–4.21 (2H, m), 4.32 (1H, d, J = 8.4 Hz), 4.44 (1H, d, J = 8.4 Hz), 5.89 (1H, d, J = 4.5 Hz), 6.72–6.79 (4H, m), 7.04–7.19 ppm (6H, m); ^{13}C NMR (75 MHz, $CDCl_3$) δ = 6.3, 32.5, 35.4, 38.2, 65.3, 76.7, 77.4, 87.8, 127.0, 127.1, 127.8, 127.9, 128.0, 128.1, 128.3, 128.4, 128.5, 128.6, 128.7, 138.7, 139.4, 178.0 ppm; FAB-HRMS: calcd for $C_{22}H_{25}O_3I_2$: m/z 590.9906 (M^++H); found: 590.9875.

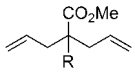
Received: August 9, 2004
Published online: December 21, 2004

Keywords: asymmetric synthesis · chiral auxiliaries · domino reactions · natural products · synthetic methods

[1] a) H. Fujioka, H. Kitagawa, Y. Nagatomi, Y. Kita, *J. Org. Chem.* **1996**, *61*, 7309–7315; b) H. Fujioka, N. Matsunaga, H. Kitagawa, Y. Nagatomi, Y. Kita, *Tetrahedron Lett.* **1996**, *37*, 2245–2248.

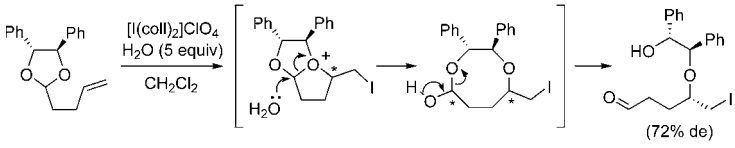
[2] For asymmetric desymmetrization of acyclic σ-symmetric dienes, see a) S. Takano, C. Murakata, Y. Imamura, N. Tamura, K. Ogasawara, *Heterocycles* **1981**, *16*, 1291–1294; b) T. Yokomatsu, H. Iwasawa, S. Shibuya, *J. Chem. Soc. Chem. Commun.* **1992**, 728–729; c) T. Yokomatsu, H. Iwasawa, S. Shibuya, *Tetrahedron Lett.* **1992**, *33*, 6999–7002; d) O. Kitagawa, T. Hanano, K. Tanabe, M. Shiro, T. Taguchi, *J. Chem. Soc. Chem. Commun.* **1992**, 1005–1007; e) O. Kitagawa, S. Momose, Y. Fushimi, T. Taguchi, *Tetrahedron Lett.* **1999**, *40*, 8827–8831.

[3] Diallyl aldehyde **4a** (R = H) and phenyl aldehyde **4b** (R = Ph) are known compounds (for **4a**, see: B. B. Snider, B. R. Smith, *Tetrahedron* **2002**, *58*, 25–34; for **4b**, see: W. A. Nugent, J. Feldman, J. C. Calabrese, *J. Am. Chem. Soc.* **1995**, *117*, 8992–8998). Diallylmethyl aldehyde (**4c**, R = Me) was prepared from the known diallyl ester **15b** (obtained by methylation of **15a**; see above reference for **4a**) first by reduction of the ester and then oxidation with pyridinium dichromate.



15a: R=H
15b: R=Me

[4] In our previous work (Ref. [1]), alcohols were used as nucleophiles, whereas here the use of water instead afforded the hydroxyaldehyde by intramolecular haloetherification followed by opening of the eight-membered hemiacetal ring (coll = 2,4,6-collidine, H. Fujioka, H. Kitagawa, Y. Kita, unpublished results).



[5] CCDC-244868 contains the supplementary crystallo-graphic data for this paper. These data can be obtained free of charge from www.ccdc.cam.ac.uk/conts/retrieving.html (or from the Cambridge Crystallographic Data Centre, 12 Union Road, Cambridge CB2 1EZ, UK; fax: (+44) 1223-336-033; or e-mail: deposit@ccdc.cam.ac.uk.

[6] a) Y. Kita, H. Namubu, N. G. Ramesh, G. Anilkumar, M. Matsugi, *Org. Lett.* **2001**, *3*, 1157–1160; b) H. Namubu, G. Anilkumar, M. Matsugi, Y. Kita, *Tetrahedron* **2003**, *59*, 77–85. For the reduction of the radical using VA-061 in water including its use for this transformation, see H. Namubu, A. H. Alinejad, K. Hata, H. Fujioka, Y. Kita, *Tetrahedron Lett.*, in press.

 © 2005 Wiley-VCH Verlag GmbH & Co. KGaA, Weinheim

[7] For isolation and structure elucidation, see: a) N. C. Franca, O. R. Gottlieb, D. T. Coxon, W. D. Ollis, *An. Acad. Bras. Cienc.* **1971**, *43*, 123–235; b) N. C. Franca, O. R. Gottlieb, D. T. Coxon, W. D. Ollis, *J. Chem. Soc. Chem. Commun.* **1972**, *9*, 514–515; c) N. C. Franca, O. R. Gottlieb, D. T. Coxon, *Phytochemistry* **1977**, *16*, 257–262; for the total synthesis, see e) S. K. Taylor, J. A. Hopkins, K. A. Spangenberg, D. W. McMillen, J. B. Grutzner, *J. Org. Chem.* **1991**, *56*, 5951–5955.

[8] For the asymmetric total synthesis, see: a) T. Saito, L. Thijs, G.-J. Ettema, B. Zwanenburg, *Tetrahedron Lett.* **1993**, *34*, 3589–3592; b) L. Thijs, B. Zwanenburg, *Tetrahedron* **2004**, *60*, 5237–5252. Although the wrong stereochemical structure of rubrenolide was originally proposed, the correct one is reported by Zwanenburg et al.

[9] J. M. G. Fernándes, C. O. Mellet, A. M. Marín, J. Fuentes, *Carbohydr. Res.* **1995**, *274*, 263–268.

[10] W. S. Trahanovsky, L. B. Young, G. L. Brown, *J. Org. Chem.* **1967**, *32*, 3865–3868.

[11] Although the use of $BiCl_3$ has been reported (I. Mohammadpoor-Baltork, S. Tangestaninejad, H. Aliyan, V. Mirkhani, *Synth. Commun.* **2000**, *30*, 2365–2374), $Bi(OTf)_3$ was also effective.

[12] Authentic rubrenolide was obtained by separation of a mixture donated by Prof. B. Zwanenburg and Dr. L. Thijs, according to Ref. [8b]. The synthetic rubrenolide has a $[\alpha]_D^{25}$ value of $+20.5$ ($c = 0.29$, $CHCl_3$), while the $[\alpha]_D^{20}$ value of the authentic sample (Ref. [7c]) is $+21.2$ ($CHCl_3$).

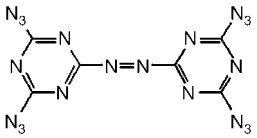
 © 2005 Wiley-VCH Verlag GmbH & Co. KGaA, Weinheim

Carbon Nitrides

Preparation of Nitrogen-Rich Nanolayered, Nanoclustered, and Nanodendritic Carbon Nitrides**

My Hang V. Huynh, Michael A. Hiskey,* Jose G. Archuleta, and Edward L. Roemer*

Carbon nitrides are of current interest due to their novel mechanical, optical, and tribological properties including low density, surface roughness, wear resistance, chemical inertness, and biocompatibility.[1–4] These superhard diamondlike materials promise a variety of technological and biological applications, for example, biocompatible coatings on biomedical implants,[5–6] battery electrodes,[7–8] gas-separation systems,[9] corrosion protection,[10] and humidity and gas sensors.[11] As these applications are primarily governed by the particle size, material texture, and nitrogen content, an extensive effort has focused on the discovery of precursors along with appropriate methods to control the size, regulate the texture, and increase the nitrogen content of carbon nitrides. We report here three novel nitrogen-rich nanolayered, nanoclustered, and nanodendritic carbon nitrides that were prepared from 4,4′,6,6′-tetra(azido)azo-1,3,5-triazine (TAAT), a member of a unique class of high-nitrogen C,N-containing energetic materials.



TAAT
m.p. 200 °C (decomp.)

Gillan reported the preparation of single-textural carbon nitrides C_3N_4 (60.9 wt % N, $\rho = 1.82\ g\,cm^{-3}$) and C_3N_5 (66.0 wt % N, $\rho = 1.82\ g\,cm^{-3}$) by pyrolyses of 2,4,6-tri-(azido)-1,3,5-triazine (TAT) at 85 °C.[12] Although pressurization was not required for making C_3N_4, 6 atm of N_2 was needed in the preparation of C_3N_5. Other preparative methods using 1,3,5-triazine-[4,13,14] and 2,5,8-heptazine-based[3,15–17] compounds as precursors have involved either applied pressure, high temperature, shock compression, or combinations of at least two of these conditions; however, the products obtained were nitrogen-poor materials, occasionally contaminated with hydrogen-incorporating byproducts. Our preparative protocols using TAAT yield three novel morphologies of nitrogen-rich carbon nitrides C_2N_3 (63.6 wt % N, $\rho = 1.32 \pm 0.01\ g\,cm^{-3}$) and C_3N_5 (66.0 wt % N, $\rho = 0.44 \pm 0.01$ and $1.08 \pm 0.01\ g\,cm^{-3}$). The pyrolyses are simple, occur under mild conditions (i.e., low temperature and without applied pressure), and require no vacuum systems, extraction, carbonization, or purification. TAAT was proposed as one of the intermediates in the decomposition of TAT,[12] and we recently developed a three-step synthetic pathway for this material.[18]

Nitrogen-rich C_2N_3 was prepared under a nitrogen atmosphere.[19] A 1.0 g crystalline sample of TAAT was loaded into a 50-mL stainless steel bomb, which was heated to 160 °C over 3 h and held at this temperature for an additional 4 h. The temperature was then increased to 185 °C over 5 h and maintained at this temperature overnight to yield glassy nanolayered C_2N_3 carbon nitride with a density of $1.32 \pm 0.01\ g\,cm^{-3}$. The glassy nanolayer was characterized by IR spectroscopy, gas pycnometry (GP), elemental analysis, thermogravimetric analysis (TGA),[20] and SEM imaging (Figure 1).

The interlinked three-dimensional network of glassy pockets shown in Figure 1 (right) suggested that the conversion to C_2N_3 involved a series of phase transitions (i.e., plastic, liquid, and solid). When the temperature was first raised from room temperature to 160 °C, TAAT became viscous, as indicated by the plastic property illustrated in Figure 2, and then gradually liquefied as the temperature approached 185 °C. The softening of TAAT to a viscous liquid

[*] Dr. M. H. V. Huynh, Dr. M. A. Hiskey, J. G. Archuleta, E. L. Roemer
Dynamic Experimentation Division
DX-2: Materials Dynamics Group, MS C920
Los Alamos National Laboratory
Los Alamos, NM 87545 (USA)
Fax: (+1) 505-667-0500
E-mail: huynh@lanl.gov
hiskey@lanl.gov

[**] This work was supported at Los Alamos by the joint program of the Department of Defense and the Department of Energy for the preparation and characterization of new energetic materials.

 DOI: 10.1002/anie.200461758 © 2005 Wiley-VCH Verlag GmbH & Co. KGaA, Weinheim

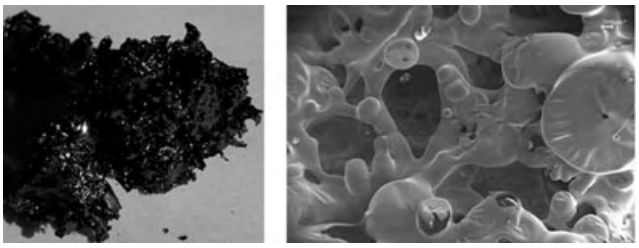


Figure 1. Glassy nanolayered C_2N_3: Photograph (left) and SEM image (×16000, right).

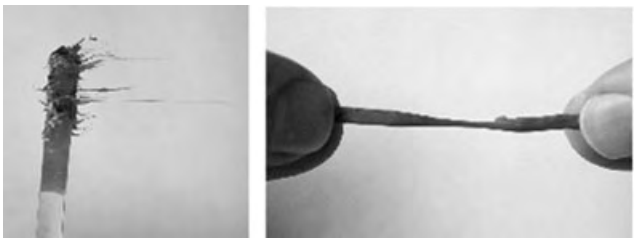


Figure 2. Photographs of TAAT with a trace of chloroform.

at 150 °C can be visually observed by using a Mel-Temp apparatus.

At 185 °C, liquid TAAT slowly decomposed to form glassy nanolayered carbon nitride, presumably by extrusion of nitrogen gas that was trapped inside the product. Slow release of the nitrogen gas over an extended period results in pockets interconnected by gossamer tunnels (Figure 1, right). From our previous study,[18] TAAT is a viscous material either at a temperature of 150 °C or when a trace of solvent remains in the sample. This plastic property makes TAAT the unique precursor for glassy nanolayered carbon nitride.

Nitrogen-rich C_3N_5 was prepared by two different heating protocols in the 50-mL stainless steel bomb. Under a nitrogen atmosphere, 1.0 g of crystalline TAAT was heated to 160 °C over 3 h and held at that temperature for an additional 4 h. The temperature was then increased to 200 °C over 5 h and maintained at this temperature overnight to produce a very low density carbon nitride ($\rho = 0.44 \pm 0.01\ g\,cm^{-3}$) with a novel tunnel-like structure constituted of spherical/elliptical nanoclusters. This nanoclustered C_3N_5 carbon nitride was characterized by IR spectroscopy, GP, elemental analysis, TGA,[21] and SEM imaging (see Figure 3).

During the course of heating for 4 h at 160 °C followed by 5 h at 200 °C, crystalline TAAT underwent a phase change from viscous plastic to liquid. At 200 °C, the liquefied TAAT

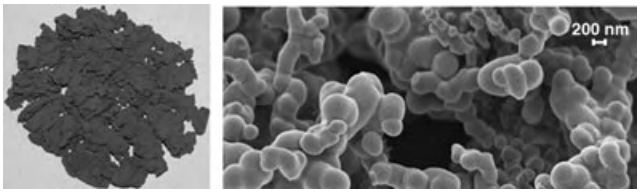


Figure 3. Spherical/elliptical nanoclustered C_3N_5: Photograph (left) and SEM image (×10000, right).

decomposed to give spherical/elliptical nanoclusters and nitrogen gas as byproduct. This suggested that the relatively slow decomposition had thrust nitrogen gas directly into the winding hollow tunnels.

In the second heating protocol, the crystalline TAAT was heated to 205 °C over 4 h and then maintained at this temperature overnight. The unprecedented denser nanodendritic C_3N_5 carbon nitride ($\rho = 1.08 \pm 0.01\ g\,cm^{-3}$) was obtained. Interlinked segments whose diameters ranged from 10 to 100 nm were characterized by IR spectroscopy, GP, elemental analysis, TGA,[22] and SEM imaging (Figure 4).

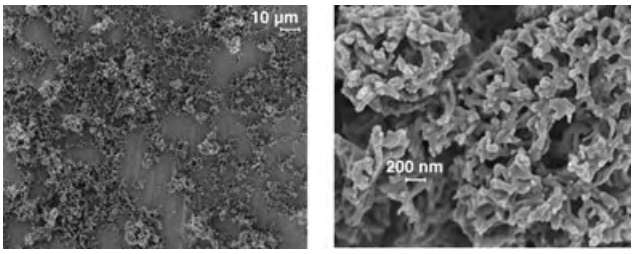


Figure 4. SEM images of nanodendritic C_3N_5: ×500 (left) and ×20000 (right).

During the period of four hours heating from room temperature to 205 °C, rapid release of N_2 from crystalline TAAT was accompanied by conversion of TAAT into an irregular framework of interlocking fragments without completely undergoing any phase transition. This faster decomposition gave a nearly $2^1/_2$-times denser C_3N_5 with much smaller particle sizes.

Unlike many other organic compounds, such as mesocarbon microbeads,[23,24] mesophase pitch-based carbon fibers,[25–27] non-azido-substituted triazines[4,13,14] and non-azido-substituted heptazines,[3,15–17] TAAT[18] and other poly-azido compounds containing only C and N atoms[28,29] are ideal precursors for nitrogen-rich carbon nitrides because of their clean and thermodynamically favorable decomposition, which presumably extrudes nitrogen gas as the only byproduct [Eqs. (1) and (2)].

$$C_6N_{20} \xrightarrow{\Delta} 3\,C_2N_3 + 5.5\,N_2 \quad (1)$$

$$C_6N_{20} \xrightarrow{\Delta} 2\,C_3N_5 + 5\,N_2 \quad (2)$$

The glassy/sturdy C_2N_3 carbon nitride in Figure 1 and the powder/soft C_3N_5 carbon nitrides in Figures 3 and 4 have revealed that the textures, nitrogen contents, and densities of these nitrogen-rich carbon nitrides are highly dependent on the temperatures at which decomposition occurs. The nanoclusters in Figure 3 and the nanodendrites in Figure 4 have shown that the morphologies of C_3N_5 are governed by the heating patterns, while the sizes of nanoparticles are inversely proportional to the heating time. The pyrolyses of TAAT to three novel nitrogen-rich carbon nitrides have illustrated that mutual manipulation of the unique viscosity and rate of

 © 2005 Wiley-VCH Verlag GmbH & Co. KGaA, Weinheim

decomposition played an essential role in controlling the nature of the pyrolized products.

Received: August 22, 2004
Published online: December 21, 2004

Keywords: azides · carbon · nanostructures · nitrides · nitrogen

[1] F. Z. Cui, D. J. Li, *Surf. Coat. Technol.* **2000**, *131*, 481 – 487, and references therein.
[2] W. Long, Y. Shun, Y. Bing, *Rare Met. Mater. Eng.* **2002**, *31*, 96 – 100, and references therein.
[3] E. K. Wilson, *Chem. Eng. News* **2004**, *82* (22), 34 – 35, and references therein.
[4] E. Kroke, M. Schwarz, *Coord. Chem. Rev.* **2004**, *248*, 493 – 532, and references therein.
[5] D. J. Li, L. F. Niu, *Bull. Mater. Sci.* **2003**, *26*, 371 – 375.
[6] D. J. Li, S. J. Zhang, L. F. Niu, *Appl. Surf. Sci.* **2001**, *180*, 270 – 279.
[7] D. Y. Zhong, G. Y. Zhang, S. Liu, E. G. Wang, Q. Wang, H. Li, X. J. Huang, *Appl. Phys. Lett.* **2001**, *79*, 3500 – 3502.
[8] M. Kawaguchi, *Adv. Mater.* **1997**, *9*, 615 – 625, and references therein.
[9] J. N. Armor in *Materials Chemistry*, *An Emerging Discipline*, *Vol. 245* (Eds.: L. V. Interrante, L. A. Caspar, A. B. Ellis), American Chemical Society, Washington, DC, **1995**, ch. 13 (Advances in Chemistry Series).
[10] I. Widlow, Y. W. Chung, *Braz. J. Phys.* **2000**, *30*, 490 – 498.
[11] W. Kulisch, C. Popov, L. Zambov, *New Diamond Front. Carbon Technol.* **2001**, *11*, 53 – 76.
[12] E. G. Gillan, *Chem. Mater.* **2000**, *12*, 3906 – 3912.
[13] D. R. Miller, J. J. Wang, E. G. Gillan, *J. Mater. Chem.* **2002**, *12*, 2463 – 2469, and references therein.
[14] J. J. Wang, D. R. Miller, E. G. Gillan, *Carbon* **2003**, *41*, 2031 – 2037, and references therein.
[15] T. Komatsu, *J. Mater. Chem.* **2001**, *11*, 802 – 805.
[16] E. Kroke, M. Schwarz, E. Horath-Bordon, P. Kroll, B. Noll, A. D. Norman, *New J. Chem.* **2002**, *26*, 508 – 512.
[17] B. Jürgens, E. Irran, J. Senker, P. Kroll, H. Müller, W. Schnick, *J. Am. Chem. Soc.* **2003**, *125*, 10288 – 10300.
[18] M. H. V. Huynh, M. A. Hiskey, R. Gilardi, E. L. Hartline, D. P. Montoya, *Angew. Chem.* **2004**, *116*, 5032 – 5036; *Angew. Chem. Int. Ed.* **2004**, *43*, 4924 – 4928.
[19] All preparations were carried out at an initial atmospheric pressure of 580 torr (11.2 psi or 0.76 atm) and a relative humidity of less than 15% at Los Alamos (New Mexico, USA) at an elevation of 7500 ft. Preparation of each type of carbon nitride was repeated in triplicate with temperatures maintained within ±2 °C.
[20] Characterization of glassy nanolayered C_2N_3: IR (Nujol): $\tilde{\nu}$ = 1456 (vs), 1367 (vs), 1342 (vs), 1303 (vs), 1080 (vs), 848 (s), 804 (vs), 398 cm^{-1} (vs), presumably due to aromatic ring modes and aromatic C–N and C–C bonds; GP: $\rho = 1.32 \pm 0.01\ g\,cm^{-3}$; elemental analysis (%): found: C 36.34, H 0.58, N, 63.07; TGA: robust up to ca. 670 °C.
[21] Characterization of nanoclustered C_3N_5 carbon nitride: IR (Nujol): $\tilde{\nu}$ = 1641 (vs), 1565 (vs), 1461 (vs), 1307 (vs), 1244 (vs), 968 (s), 814 (vs), 374 cm^{-1} (vs), presumably due to conjugated C=N/C=C species, aromatic ring modes, and aromatic C–N and C–C bonds; GP: $\rho = 0.44 \pm 0.01\ g\,cm^{-3}$; elemental analysis (%): found: C 33.18, H 0.63, N 65.89; TGA: robust up to ca. 650 °C.
[22] Characterization of nanodendritic C_3N_5 carbon nitride: IR (Nujol): $\tilde{\nu}$ = 1640 (vs), 1564 (vs), 1461 (vs), 1304 (vs), 1246 (vs), 968 (s), 815 (vs), 378 cm^{-1} (vs), presumably due to conjugated C=N/C=C species, aromatic ring modes, and aromatic C–N and C–C bonds; GP: $\rho = 1.08 \pm 0.01\ g\,cm^{-3}$; elemental analysis (%): found: C 33.26, H 0.29, N 65.70; TGA: robust up to ca. 650 °C.
[23] Y. G. Wang, Y. Korai, I. Mochida, K. Nagayama, H. Hatano, N. Fukuda, *Carbon* **2001**, *39*, 1627 – 1634.
[24] Y. C. Chang, H. J. Sohn, C. H. Ku, Y. G. Wang, Y. Korai, I. Mochida, *Carbon* **1999**, *37*, 1285 – 1297.
[25] H. Yang, S. H. Yoon, Y. Korai, I. Mochida, O. Katou, *Carbon* **2003**, *41*, 397 – 403.
[26] E. Mora, C. Blanco, R. Santamaria, M. Granda, M. Menendez, *Carbon* **2003**, *41*, 445 – 452.
[27] I. Mochida, S. H. Yoon, Y. Korai, *Chem. Rec.* **2002**, *2*, 81 – 101, and references therein.
[28] D. R. Miller, D. C. Swenson, E. G. Gillan, *J. Am. Chem. Soc.* **2004**, *126*, 5372 – 5373.
[29] H. J. Marcus, A. Remanick, *J. Org. Chem.* **1963**, *28*, 2372 – 2375.

 © 2005 Wiley-VCH Verlag GmbH & Co. KGaA, Weinheim

Radicals

Nonsolvated, Aggregated 1,1-Dilithiosilane and the Derived Silyl Radicals**

Dmitry Bravo-Zhivotovskii, Ilya Ruderfer, Semyon Melamed, Mark Botoshansky, Boris Tumanskii, and Yitzhak Apeloig**

Dedicated to Professor Josef Michl on the occasion of his 65th birthday

The chemistry of the potentially synthetically versatile geminal 1,1-dilithiosilyl compounds [R_2SiLi_2] is still in its infancy, in contrast to the chemistry of monosilyllithium compounds [R_3SiLi], which have been studied intensively.[1] Several [R_2SiLi_2] compounds have been reported,[2,3] although only a few of them have been isolated and characterized by X-ray crystallography (all in solvated form).[2e,f,3c] The aggregation behavior and the structures of dilithiosilanes in weakly solvating media are unknown. Only limited structural information is also available for geminal

[*] Dr. D. Bravo-Zhivotovskii, I. Ruderfer, S. Melamed, Dr. M. Botoshansky, Dr. B. Tumanskii, Prof. Y. Apeloig
Department of Chemistry and
the Lise Meitner-Minerva Center for Computational Quantum Chemistry
Technion-Israel Institute of Technology
Haifa 32000 (Israel)
Fax: (+972) 4829-4601
E-mail: chrbrzh@tx.technion.ac.il
chrapel@tx.technion.ac.il

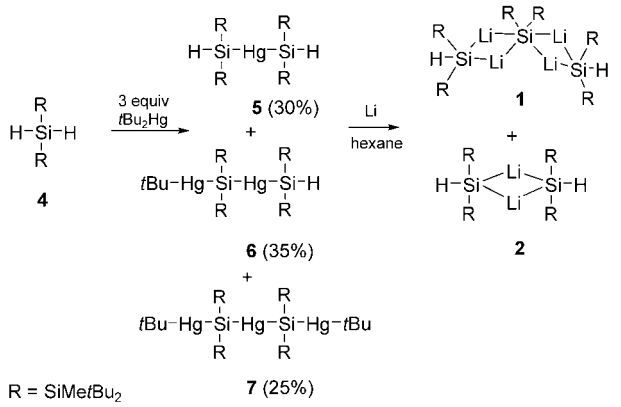
[**] This research was supported by the Israel Science Foundation, administered by the Israel Academy of Sciences and Humanities, the Fund for the Promotion of Research at the Technion, and the Minerva Foundation in Munich. B.T, M.B., and D.B.-Z. are grateful to the Ministry of Immigrant Absorption, State of Israel, for a Kamea scholarship.

Supporting information for this article is available on the WWW under http://www.angewandte.org or from the author.

 DOI: 10.1002/anie.200461765 © 2005 Wiley-VCH Verlag GmbH & Co. KGaA, Weinheim

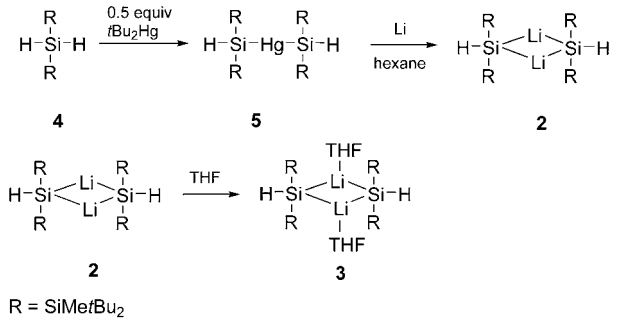
organodilithium compounds $[R_2CLi_2]$,[4] although they have already found interesting synthetic applications.[5] Such structural information is important because the chemistry of organolithium and silyllithium reagents is solvent dependent.[6,7]

Herein we report the preparation and the X-ray molecular structure analysis of the first unsolvated aggregates of the *gem*-dilithiosilane $[(R_2SiLi_2)(R_2HSiLi)_2]$ ($R = SiMe_2tBu$; **1**, Scheme 1), the hydridosilyllithium $[(R_2HSiLi)_2]$ ($R =$



Scheme 1. Synthesis of the aggregated *gem*-dilithiosilane **1**.

$SiMe_2tBu$; **2**, Scheme 2),[8] and the THF solvate of **2** (**3**, Scheme 2).[8] Compound **1** is also the first known example of a hexacoordinated silicon atom with an $\{R_2SiLi_4\}$ core. We also report the photochemical generation and characterization by EPR spectroscopy of a novel family of silyl radicals,[9] in which the silyl radical center is part of a silyllithium aggregate, and that photolysis of **1** yields a triplet-state silyl biradical.[10]



Scheme 2. Synthesis of the aggregated hydridosilyllithium **2** and its THF solvate **3**.

Silyllithium aggregate $[(R_3SiLi)_n]$ can be synthesized by lithiation, in hexane, of the corresponding silylmercury compounds $[Hg(SiR_3)_2]$,[11] which, in turn, are prepared by reaction of hydridosilanes with $[Hg(tBu)_2]$.[12] By analogy, silyldimercury compounds of the type -Hg-SiR_2-Hg- may serve as precursors to *gem*-dilithium compounds. Treatment of dihydridosilane **4** with three equivalents of $[Hg(tBu)_2]$ leads to a product mixture containing (based on ^{29}Si NMR spectroscopy) the silylmercury compounds **5**, **6**, and **7** (Scheme 1). Lithiation of this mixture in hexane yields the novel unsolvated aggregate **1** as the major (60%) product and the silyllithium dimer **2** as the minor product (25%). Compound **1** was isolated as green crystals suitable for X-ray crystallography upon crystallization from hexane.[13,14]

Treatment of **4** with only half an equivalent of $[Hg(tBu)_2]$ leads exclusively to **5** (Scheme 2). Lithiation of **5** in hexane resulted in the formation of the hydridosilyllithium dimer **2**, which was crystallized from hexane as colorless crystals.[13,15] Dissolving **2** in THF leads to **3**, which was also isolated by crystallization from hexane. The molecular structure of **3**[13,16] is similar to that of the recently reported compound $[(R_2HSiLi)_2(thf)_2]$ ($R = SiMe_2tBu$).[8]

ORTEP drawings of the molecular structures of **1** and **2** are shown in Figures 1 and 2, respectively. Compound **1** is the

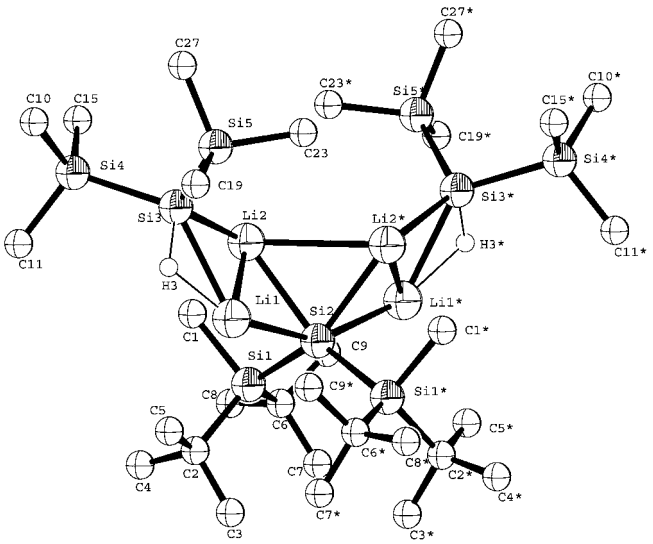


Figure 1. ORTEP diagram of the aggregated *gem*-dilithiosilane **1**. Hydrogen atoms, except for Si–H, and some of the carbon atoms have been omitted for clarity. Selected bond lengths [pm] and bond and dihedral angles [°]: Si2-Li1 264.1(10), Si2-Li2 261.3(8), Si3-Li2 267.1(9), Si3-Li1 268.2(9), Li1-Li2 264.7(13), Li2-Li2* 315.9(16), Li1-H3 190.0(5), Si3-H3 147.0(5), C1-Li2 257.9(10), Si1-C1 192.3(5), Si2-Si1 235.79(15), Si2-Si1* 235.79(15), Si3-Si4 239.33(17); Si1-Si2-Si1* 125.74(10), Si1-Si2-Li2 84.04(19), Si1*-Si2-Li2 146.14(19), Li1-Si2-Li1* 151.2(4), Li2-Si2-Li1-Si3 11.7, H3-Si3-Li1-Li2 159.6, Li1-Li2-Li*2-Li1* 114.2.

first known unsolvated *gem*-dilithiosilane. Its structure is best described as a co-aggregate of the *gem*-dilithiosilane $[(R_3Si)_2SiLi_2]$ with two molecules of the hydridosilyllithium $[(R_3Si)_2HSiLi]$. The central silicon atom (Si2) in **1** is six-coordinate and is bonded to four Li atoms, with Si2–Li bond lengths of 264 and 261 pm. These can be compared to the slightly shorter Si–Li bond lengths of 258 and 260 pm in $[\{(Me_3Si)_3SiLi\}_2]$.[11c] The two spiro four-membered $\{Si_2Li_2\}$ rings, which are slightly nonplanar (with a Si–Li–Si–Li dihedral angle within each ring of 11.7°), form an angle of 70.6° (Figure 1). The four Li atoms are arranged in a transoid open chain with a Li1-Li2-Li2*-Li1* dihedral angle of 114° and bond lengths Li1–Li2 (and Li2*–Li1*) = 265 pm and Li2–Li2* = 316 pm. The Li1···Li1* distance is 511 pm. This

 © 2005 Wiley-VCH Verlag GmbH & Co. KGaA, Weinheim

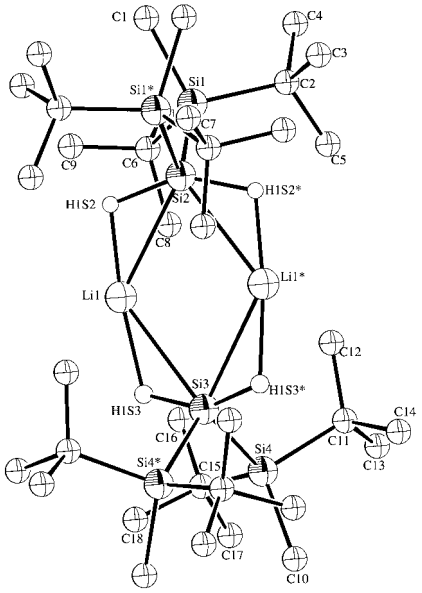


Figure 2. ORTEP diagram of the unsolvated hydridosilyllithium dimer **2**. Hydrogen atoms, except for Si–H, have been omitted for clarity. Selected bond lengths [pm] and bond and dihedral angles [°]: Si2-Li1 269.8(7), Si2-Li1* 269.8(7), Si3-Li1 276.7(7), Si3-Li1* 276.7(7), Li1-Li1* 300.3(16), Si2-H1S2 151.0(6), Si3-H1S3 145.0(5), Li1-H1S3 196.0(5), Li1-H1S2 184.0(5), Si1-Si2 238.35(10), Si1-C1 189.6(4), Si1-C6 192.5(4); Si1*-Si2-Si1 111.13(7), Si1*–Si2-Li1 124.23(18), Si1-Si2-Li1 112.15(17), Li1-Si2-Li1* 67.6(3), Si1*-Si2-H1S2 100(2), Si1-Si2-H1S2 98(2), Li1-Si3-Li1-*Si2 0.0, H1S2-Li1-Si2-Li1* 164.7, H1S3-Li1-Si3-Li1* 160.7.

open-chain arrangement is unique, as silyllithium and alkyllithium aggregates usually adopt polycyclic-type arrangements of the lithium atoms.[11d,17] The Si···Si distance within each of the spiro four-membered rings in **1** is 457 pm, similar to that in dimer **2** and much longer than a normal covalent Si–Si bond (235 pm). The Si–Li bond lengths in **1** (261–267 pm) are somewhat shorter than those in **2** (270 and 277 pm), while the Li1···Li2 distance in **1** (265 pm) is significantly shorter than that in **2** (300 pm).

Dimer **2** exhibits the usual structure of aggregated silyllithium compounds carrying bulky substituents.[11a–c] The four-membered ring in **2** is planar and the bond lengths within the $\{Si_2Li_2\}$ ring are in the range found for other silyllithium dimers.[11a–c]

In both **1** and **2** the Si–H bonds participate in agostic-type interactions with lithium atoms to form two {SiHLi} rings. Similar agostic interactions have been reported for $[(R_2HSi\text{-}Li)_2(thf)_2]$ ($R = SiMe_2tBu$).[8] The two Li atoms (Li2 and Li2*) in **1** that do not interact with the Si–H hydrogen atoms interact instead with the hydrogen atoms of the methyl groups of the tBu_2MeSi substituents (C1 and C1* in Figure 1), thereby forcing a rotation of the tBu_2MeSi groups on Si2 to an unfavorable, sterically hindered conformation in which the *t*Bu groups are oriented towards each other. This orientation causes an increase in the Si1–Si2–Si1* bond angle to 125°. The Si4–Si3–Si5 bond angle of 119.8° in the $[(R_3Si)_2HSiLi]$ fragments of **1** (Figure 1) and the Si1–Si2–Si1* bond angle of 111.5° in **2** (Figure 2) are significantly smaller.

The ^{29}Si NMR chemical shift of the central, hexacoordinated Si2 atom in **1** is $\delta = -251$ ppm; this signal is shifted to lower field by 41 ppm relative to that of the central silicon atom of the THF solvate $[(iPr_3Si)_2SiLi_2(thf)_4]$ ($\delta = -292$ ppm).[3] However, it is strongly shifted to higher field compared to that of Si3 of **1** ($\delta = -182$ ppm) and the anionic silicon atoms in **2** ($\delta = -171$ and -176 ppm) and **3** ($\delta = -189$ ppm), which exhibit normal chemical shift values for silyl anions.[8,11c]

UV irradiation ($\lambda = 300$ nm) of **1**, **2**, or **3** in hexane leads to the observation by EPR spectroscopy of several novel silyl radicals as well as a biradical, all with unprecedented structures. Irradiation of a solution of **3** in hexane at 220 K yields a septet EPR signal (Figure 3 a), which results from the splitting of the main line by two equivalent ^7Li nuclei ($I = 3/2$)

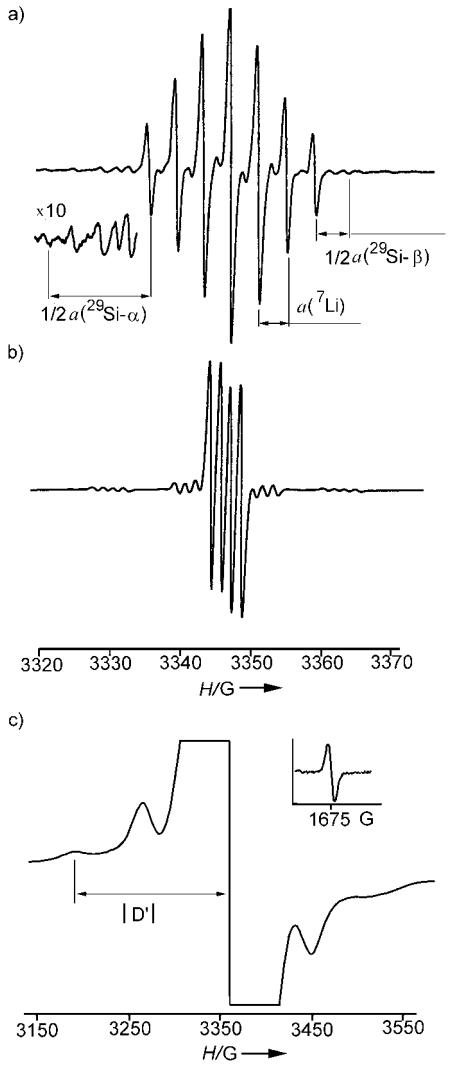
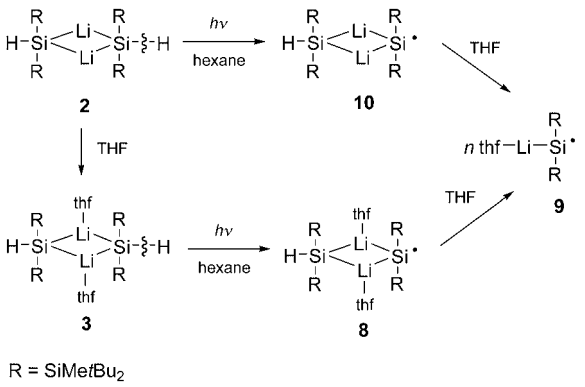


Figure 3. a) The EPR spectrum of silyl radical **8** observed during UV irradiation of **3** in hexane at 220 K. b) The EPR spectrum of silyl radical **9** observed after addition of THF to a solution of **8** or **10** in hexane. The EPR spectrum of **9** has the following parameters: $g = 2.0067$, $a(\alpha\text{-}^{29}Si) = 33.25$ G, $a(\beta\text{-}^{29}Si) = 9.5$ G, $a(^7Li) = 1.5$ G. c) The EPR spectrum observed during UV irradiation of **1** in frozen hexane at 150 K. It is a superposition of the spectra of biradical **13** and of an unassigned silyl radical. The insert shows the forbidden $\Delta M_s = 2$ resonance.

 © 2005 Wiley-VCH Verlag GmbH & Co. KGaA, Weinheim

with a hyperfine coupling (hfc) constant $a(2\,^{7}\mathrm{Li})$, of 4.17 G. The *g*-factor of the signal is 2.0073 and the hfc constants with the ^{29}Si atoms are $a(\alpha\text{-}^{29}\mathrm{Si}) = 30.0$ G and $a(2\beta\text{-}^{29}\mathrm{Si}) = 9.0$ G. The hyperfine structure of the EPR signal and the aggregated structure of the precursor **3** allow us to confidently assign this signal to radical **8** (Scheme 3), which is the first known example of a silyl radical that is part of a silyllithium aggregate skeleton.



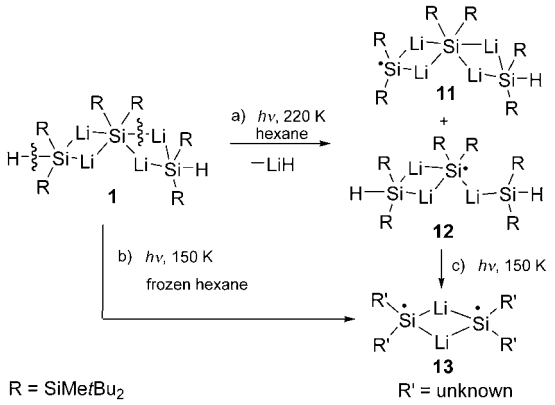
Scheme 3. Generation of radicals **8** and **10** centered on a silicon atom that is part of a silyllithium aggregate skeleton. The cleavage of the silyllithium aggregate in **8** and **10** by THF leads to formation of **9**.

Addition of THF to a solution of radical **8** in hexane gives a new, stable, silicon-centered radical with a quartet EPR signal (Figure 3b). This signal was assigned to the monomeric, lithium-substituted silyl radical **9**,[18] thus indicating that addition of THF cleaves the $\{Si_2Li_2\}$ skeleton of **8** (Scheme 3).

Irradiation of the unsolvated dimer **2** leads to a more complex EPR spectrum,[19] which is a superposition of two multiplet signals: one signal is a septet with $a(2\,^{7}\mathrm{Li}) = 6.6$ G, and the second is a multiplet resulting from the interaction of the unpaired electron with two nonequivalent lithium atoms ($a(^{7}\mathrm{Li}) = 6.0$ G and $a(^{7}\mathrm{Li}) = 7.9$ G).[19] Addition of THF to this solution also results in the formation of radical **9**. Therefore, we assume that the observed septet signals can be assigned to radical **10**, which is the unsolvated form of radical **8** (Scheme 3). The radical with two different $a(^{7}\mathrm{Li})$ splittings has not yet been fully identified.

The photochemistry of **1** leads to even more intriguing novel radicals. Thus, irradiation of a solution of **1** in hexane at 220 K leads to a complex EPR spectrum[19] that is a superposition of several EPR signals.[19] One of these signals has a septet pattern, similar to **10** but with $a(2\,^{7}\mathrm{Li}) = 6.6$ G, and we assigned it to radical **11** (Scheme 4, path a). The second of the observed signals belongs to a novel silyl radical with a splitting pattern resulting from interaction of the unpaired electron with *three* nonequivalent lithium atoms with hfc constants of 4.4, 7.1, and 15.3 G, as confirmed by a computer simulation of the EPR spectrum (using the SimFonia software).[19] This analysis indicates that the electron spin is centered on the central Si atom of **1** and we tentatively assign these signals to the radical **12** shown in Scheme 4.

UV irradiation of a frozen hexane solution (150 K) of **1** (Scheme 4, path b) or of the frozen solution obtained after



Scheme 4. Generation of silyl biradical **13**.

irradiation of **1** at 220 K (Scheme 4, path c) results in a characteristic EPR signal of a triplet biradical[10] with four sidebands from $\Delta M_s = 1$ transitions and a signal at half-field (1675 G) resulting from the forbidden $\Delta M_s = 2$ transition (Figure 3c). The zero-field splitting parameter $|D'|$ of 172 G indicates a substantial interaction between the two radical centers of the biradical. The distance between the two spin centers, calculated on the basis of $|D'|$, is 435 pm.[20] This distance is similar to that between Si(2) and Si(3) in **1** and **2** (457 pm). We therefore assumed that the unpaired electrons of the biradical are centered on the silicon atoms of a $\{(R'_2Si)_2Li_2\}$ fragment with a geometry similar to that in **1** and **2**, and we can assign the biradical structure **13** shown in Scheme 4. The typical, broadened EPR lines of biradicals means that we cannot extract more information, such as the hfc constant, and, as a result, the nature of the substituents R′ in **13** is not known.

In conclusion, we have prepared and structurally characterized the first nonsolvated, aggregated *gem*-dilithiosilanes. These aggregated silyllithium compounds were found to be photolytic precursors for the generation of previously unknown intriguing silyl radicals, as well as of a silyl biradical, in which the spins are centered on silicon atoms that are part of silyllithium aggregates. We are continuing to study the photochemistry and other reactions of the intriguing novel silyllithium compounds **1** and **2**.

Experimental Section

Standard Schlenk techniques were used for all syntheses and sample manipulations.

1: $[Hg(t\mathrm{Bu})_2]$ (27.4 g, 87 mmol) was added under argon to **4** (10.0 g, 29.0 mmol) in three equal portions while heating the mixture to 120 °C. A new portion of $[Hg(t\mathrm{Bu})_2]$ was added only after evolution of isobutene from the reaction mixture had ceased (approximately every 4 h). After evaporation of the volatile compounds, hexane (100 mL) and Li powder (7.0 g, 1.0 mol) were added and the mixture was stirred at room temperature for 6 h. The mixture was then decanted from the lithium powder. Crystallization from hexane gave 6.1 g (5.8 mmol) of **1** as green crystals (60% yield based on **4**). ^{7}Li NMR (194.3 MHz, C_6D_6, 25 °C, LiCl in methanol): $\delta = 5.4$, 4.2 ppm; ^{29}Si NMR (99.4 MHz, C_6D_6, 25 °C, TMS): $\delta = 27.4$, 23.8, 22.1 ($Si(t\mathrm{Bu})_2\mathrm{Me}$), −182 ($SiHSi_2Li_2$), −251 ppm ($Si_2SiLi_4$).

2: $[Hg(t\mathrm{Bu})_2]$ (2.3 g, 7 mmol) was added under argon to **4** (5 g, 14 mmol), and the mixture was then heated to 120 °C for approx-

 © 2005 Wiley-VCH Verlag GmbH & Co. KGaA, Weinheim

imately 4 h. The heating was terminated after evolution of isobutene from the reaction mixture had ceased. After evaporation of the volatile compounds, hexane (50 mL) and Li powder (7.0 g, 1.0 mol) were added and the mixture was stirred at 60 °C for 1 h. The mixture was then decanted from the lithium powder. Crystallization from hexane gave 3.6 g (5.1 mmol) of **2** as colorless crystals (70% yield based on **4**). ^{7}Li NMR (194.3 MHz, hexane with C_6D_6 capillary, 25 °C, LiCl in methanol): $\delta = 4.4$ ppm; ^{29}Si NMR (99.4 MHz, hexane with C_6D_6 capillary, 25 °C, TMS): $\delta = 22.6$, 21.6 ((tBu$_2$Me*Si*)$_2$SiHLi), −170.8, −176.5 ppm ((tBu$_2$MeSi)$_2$*Si*HLi).

3: Compound **2** (1 g, 1.4 mmol) was dissolved in THF (10 mL). Removal of the THF and recrystallization from hexane gave 0.9 g (1.1 mmol) of **3** as colorless crystals. ^{1}H NMR (500 MHz, C_6D_6, 25 °C, TMS): $\delta = 3.52$ (8H, thf), 1.42 (8H, thf), 1.14 (36H, $(CH_3)_3C$), 0.44 ppm (6H CH_3Si) ppm; the Si-H proton was not identified; ^{7}Li NMR (194.3 MHz, C_6D_6, 25 °C, LiCl in methanol): $\delta = 2.1$ ppm; ^{13}C NMR (125 MHz, C_6D_6, 25 °C, TMS): $\delta = 68.7$ and 25.3 (thf), 30.7 ($(CH_3)_3C$), 20.7 ($(CH_3)_3C$), −2.5 ppm (CH_3Si); ^{29}Si NMR (99.4 MHz, C_6D_6, 25 °C, TMS): $\delta = 21.1$ ((tBu$_2$Me*Si*)$_2$SiHLi), −188.8 ppm ((tBu$_2$MeSi)$_2$*Si*Li).

Received: August 23, 2004
Published online: December 21, 2004

Keywords: aggregation · EPR spectroscopy · lithium · radicals · silicon

[1] a) P. Lickiss, C. Smith, *Coord. Chem. Rev.* **1995**, *145*, 75 – 124; b) K. Tomao, A. Kawachi, *Adv. Organomet. Chem.* **1995**, *38*, 1 – 58; c) J. Belzner, U. Dehnert, in *The Chemistry of Organic Silicon Compounds*, *Vol. 2* (Eds.: Z. Rappoport, Y. Apeloig), Wiley, Chichester, **1998**, pp. 779 – 825; d) A. Sekiguchi, V. Y. Lee, M. Nanjo, *Coord. Chem. Rev.* **2000**, *210*, 11 – 45.

[2] a) J.-H. Hong, P. Boudjouk, S. Castellino, *Organometallics* **1994**, *13*, 3387 – 3389; b) U. Bankwitz, H. Sohn, D. R. Powell, R. West, *J. Organomet. Chem.* **1995**, *499*, C7 – C9; c) S.-B. Choi, P. Boudjouk, *Tetrahedron Lett.* **2000**, *41*, 6685 – 6688; d) H. Sohn, *J. Organomet. Chem.* **2004**, *689*, 134 – 138; e) R. West, H. Sohn, U. Bankwitz, J. Calabrese, Y. Apeloig, T. Mueller, *J. Am. Chem. Soc.* **1995**, *117*, 11608 – 11609; f) S.-B. Choi, P. Boudjouk, P. Wei, *J. Am. Chem. Soc.* **1998**, *120*, 5814 – 5815. Several disodium and dipotassium silole derivatives are also known: g) W.-C. Joo, J.-H. Hong, S.-B. Choi, H.-E. Son, C. H. Kim, *J. Organomet. Chem.* **1990**, *391*, 27 – 36; h) W. P. Freeman, T. D. Tilley, G. P. A. Yap, A. L. Rheingold, *Angew. Chem.* **1996**, *108*, 960 – 962; *Angew. Chem. Int. Ed. Engl.* **1996**, *35*, 882 – 884; i) Y. Liu, T. C. Stringfellow, D. Ballweg, I. A. Guzei, R. West, *J. Am. Chem. Soc.* **2002**, *124*, 49 – 57.

[3] a) S. K. Mehrotra, H. Kawa, J. R. Baran, Jr., M. M. Ludvig, R. J. Lagow, *J. Am. Chem. Soc.* **1990**, *112*, 9003 – 9004; b) N. Tokitoh, K. Hatano, T. Sadahiro, R. Okazaki, *Chem. Lett.* **1999**, *28*, 931 – 932; c) A. Sekiguchi, M. Ichinohe, S. Yamaguchi, *J. Am. Chem. Soc.* **1999**, *121*, 10231 – 10232.

[4] Several molecular structures of 1,1-dilithioalkanes with oxygen, nitrogen, or aromatic substituents have been reported. These aggregates are formed by the strong interaction of Li with the substituents, rather than interactions between Li and the central carbon atoms of neighboring molecules. For a review see: C. Strohmann, D. Schildbach, in *The Chemistry of Organolithium Compounds* (Eds.: Z. Rappoport, I. Marek), Wiley, Chichester, **2004**, pp. 941 – 996.

[5] I. Marek, J. F. Normant, *Chem. Rev.* **1996**, *96*, 3241 – 3268.

[6] M. Schlosser, in *Organometallics in Synthesis: a Manual* (Ed.: M. Schlosser), Wiley, Chichester, **2002**, pp. 5 – 352.

[7] G. Korogodsky, M. Bendikov, D. Bravo-Zhivotovskii, Y. Apeloig, *Organometallics* **2002**, *21*, 3157 – 3161; D. Bravo-Zhivotovskii, G. Korogodsky, Y. Apeloig, *J. Organomet. Chem.* **2003**, *686*, 58 – 65; R. Balasubramanian, J. Oliver, *J. Organomet. Chem.* **1980**, *197*, C7 – C11.

[8] The preparation and X-ray analysis of another THF-solvated hydridosilyllithium $[(R_2HSiLi)_2(thf)_2]$ (R = SiMe$_2t$Bu) was reported recently: T. Iwamoto, J. Okita, C. Kabuto, M. Kira, *J. Am. Chem. Soc.* **2002**, *124*, 11604 – 11605.

[9] For reviews on silyl radicals see: C. Chatgilialoglu, *Chem. Rev.* **1995**, *95*, 1229 – 1251; C. Chatgilialoglu, C. Schiesser, in *The Chemistry of Organic Silicon Compounds*, *Vol. 3* (Eds.: Z. Rappoport, Y. Apeloig), Wiley, Chichester, **2001**, pp. 341 – 390.

[10] The first triplet silyl biradical was reported only recently: I. Toulokhonova, T. Stringfellow, S. Ivanov, A. Masunov, R. West, *J. Am. Chem. Soc.* **2003**, *125*, 5767 – 5773.

[11] a) M. Yuzefovich, M. Bendikov, D. Bravo-Zhivotovskii, D. Bläser, R. Boese, Y. Apeloig, *Angew. Chem.* **2001**, *113*, 3106 – 3109; *Angew. Chem. Int. Ed.* **2001**, *40*, 3016 – 3020; b) M. Naio, A. Sekiguchi, H. Sakurai, *Bull. Chem. Soc. Jpn.* **1999**, *72*, 1387 – 1393; c) K. Klinkhammer, *Chem. Eur. J.* **1997**, *3*, 1418 – 1431; d) A. Sekiguchi, M. Nanjo, C. Kabuto, H. Sakurai, *Organometallics* **1995**, *14*, 2630 – 2632; e) H. Gilman, F. K. Cartledge, *J. Organomet. Chem.* **1965**, *3*, 255 – 257; f) N. Vyazankin, G. Razuvaev, E. Gladyshev, S. Korneva, *J. Organomet. Chem.* **1967**, *7*, 353 – 357.

[12] G. Razuvaev, N. Vyazankin, *Pure Appl. Chem.* **1969**, *41*, 353 – 374.

[13] CCDC-247482 (**1**), -247483 (**2**), and -247484 (**3**) contain the supplementary crystallographic data for this paper. These data can be obtained free of charge via www.ccdc.cam.ac.uk/conts/retrieving.html (or from the Cambridge Crystallographic Data Centre, 12, Union Road, Cambridge CB21EZ, UK; fax: (+44) 1223-336-033; or deposit@ccdc.cam.ac.uk)..

[14] Crystallographic data for **1**: $C_{27}H_{64}Li_2Si_{4.5}$, $M_r = 529.07$, monoclinic, space group $C2/c$, $a = 27.500(5)$, $b = 12.626(3)$, $c = 23.480(5)$ Å, $\alpha = 90$, $\beta = 118.86(2)$, $\gamma = 90°$, $V = 7140(3)$ Å^3, $Z = 8$, Nonius Kappa CCD diffractometer, Mo K_α radiation (0.71073 Å), 220 K, $2\theta_{max} = 50.04°$, $R = 0.0625$ ($I > 2\sigma I$), $wR2 = 0.0954$ ($I > 2\sigma I$), $R_w = 0.2137$ (all data), GOF = 0.759.

[15] Crystallographic data for **2**: $C_{36}H_{86}Li_2Si_6$, $M_r = 701.47$, monoclinic, space group $C2/c$, $a = 23.8790(11)$, $b = 14.1750(6)$, $c = 15.3980(11)$ Å, $\alpha = 90.0000(14)$, $\beta = 114.9070(19)$, $\gamma = 90.0000(15)°$, $V = 4727.2(4)$ Å^3, $Z = 4$, Nonius Kappa CCD diffractometer, Mo K_α radiation (0.71073 Å), 220 K, $2\theta_{max} = 50.2°$, $R = 0.0565$ ($I > 2\sigma I$), $wR2 = 0.1221$ ($I > 2\sigma I$), $R_w = 0.1562$(all data), GOF = 0.8. As shown in Figure 2, the Si–H hydrogen atoms are disordered and occupy two sites, each with a refined occupancy ratio of 50:50.

[16] The X-ray molecular structure of **3** will be reported elsewhere.

[17] W. Ilsley, T. F. Schaaf, M. Glick, J. P. Oliver, *J. Am. Chem. Soc.* **1980**, *102*, 3769 – 3773.

[18] An analogous Li-substituted silyl radical with R$_3$Si=*i*Pr$_3$Si was previously observed in the photolysis of the corresponding silylmercury compound: D. Bravo-Zhivotovskii, M. Yuzefovich, N. Sigal, K. Klinkhammer, B. Tumanskii, A. Shames, Y. Apeloig, *Angew. Chem.* **2002**, *114*, 671 – 673; *Angew. Chem. Int. Ed.* **2002**, *41*, 649 – 651.

[19] The Supporting Information consists of the EPR spectra observed during irradiation of **1** and **2** and the simulated (using the SimFonia software) EPR spectra of silyl radicals substituted by two or three Li atoms.

[20] Assuming that the spin–spin dipole interaction $|D'|$ is approximately given by the equation $|D'| = (3/2 g^2 b^2 r^{-3})$, where g is the EPR g-factor, b is the Bohr magneton, and r is the average distance between the two unpaired electrons; see: J. Wertz, J. Bolton, *Electron Spin Resonance*, McGraw-Hill, New York, **1972**, chap. 10.

 © 2005 Wiley-VCH Verlag GmbH & Co. KGaA, Weinheim

Molecular Devices

Catalytic Nanomotors: Remote-Controlled Autonomous Movement of Striped Metallic Nanorods**

*Timothy R. Kline, Walter F. Paxton, Thomas E. Mallouk, and Ayusman Sen**

Powering nanoscale machinery by nanosized motors that move by in situ conversion of stored chemical energy is one of the most interesting challenges facing nanotechnology. Such a procedure would circumvent the need for an external macroscopic power source. In nature, nanoscale motors typically operate by energy derived from the enzymatic catalysis of spontaneous reactions.[1,2] At the nanoscale, interfacial forces dominate over inertia and, in principle, can be harnessed to move nanoobjects. Indeed, we have recently described the autonomous, non-Brownian movement of platinum/gold (Pt/Au) nanorods with spatially defined zones that catalyze the spontaneous decomposition of hydrogen peroxide (H_2O_2) to oxygen (O_2) in aqueous solutions at the platinum end of the rods.[3] These rods are moved by an interfacial tension gradient resulting from the dissolution of the less polar oxygen in the medium around the platinum end. The sustained catalytic reaction results in the interfacial tension gradient being continuously re-established as the rod moves.

While the above system displayed autonomous movement, the direction of movement was subject to random fluctuations. Directed motion is needed for catalytic nanomotors to be useful in a number of potential applications. Herein, we present a method for controlling the directionality of nanorods by using an external magnetic field. Striped nanorods with platinum, nickel, gold, nickel, and gold segments were employed (Figure 1). The platinum segment serves as a catalyst for the decomposition of hydrogen peroxide, whereas the ferromagnetic nickel segments can be magnetized and used to control the direction of rod movement. Whitesides and coworkers have shown that electroplating nickel segments shorter than the diameter of the rod, results in a rod that could be magnetized transversely rather than longitudinally.[4,5] Furthermore, the nickel segments in our striped nanorods are single domains because their lengths are less than the critical domain size (150 nm).[6]

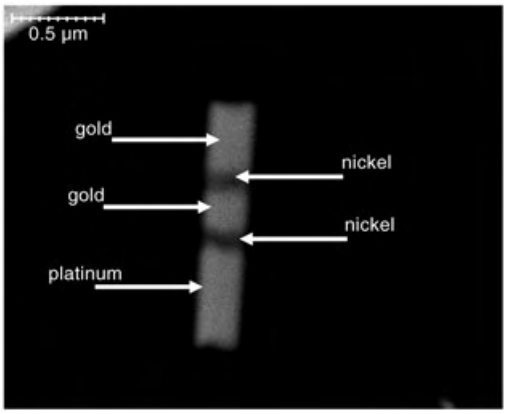


Figure 1. An SEM image at 35000× magnification of 1.5 μm × 400 nm striped metallic rod. Respective segment sizes (nm): Au, 350; Ni, 100; Au, 200; Ni, 100; Pt, 550.

After fabrication and magnetization of the nickel segments, the rods were imaged by scanning electron microscopy (SEM; Figure 1). Dark-field microscopy was used to observe rod movement in dilute solutions of hydrogen peroxide.[3] We remotely controlled the direction in which the rods moved with a NeFeB magnet that had a field strength of approximately 550 G with respect to the sample, if it is assumed there is a constant field strength for the very small area of observation under the microscope objective (ca. 100 μm). When a magnetic field is applied, a majority of the rods orient themselves perpendicular to the magnetic field lines and move the platinum end forward (Figure 2). This ability to influence rod orientation is expected at 550 G because the rods have a calculated magnetic moment of 1.3×10^{-15} A m^2, which is comparable to that observed for magnetotactic bacteria.[7] At this field strength, the calculated magnetic torque (ca. 7.0×10^{-17} N m) exceeds the rotational thermal energy (2×10^{-21} N m) in the observation plane by over four orders of magnitude.[8]

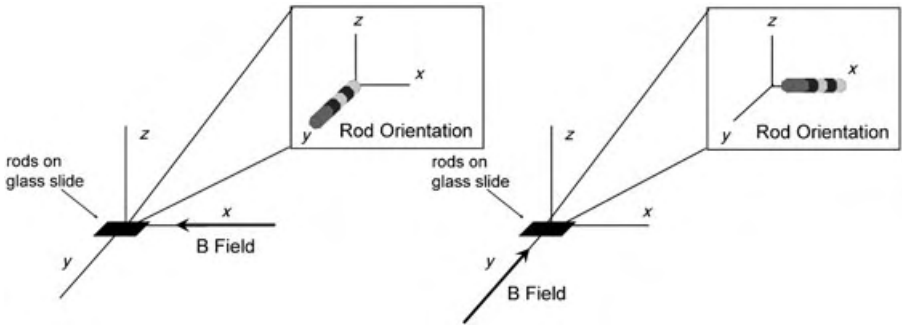


Figure 2. Rod orientation in an applied field, where the Cartesian coordinate axis to the left of the rod represents a sample of rods on the microscope stage and the arrow represents the location of the magnet in the *xy*-plane of the microscope stage.

We measured three different parameters to demonstrate the non-Brownian nature of the movement and, more

[*] T. R. Kline, W. F. Paxton, Prof. Dr. T. E. Mallouk, Prof. Dr. A. Sen
Department of Chemistry
The Pennsylvania State University
University Park, PA 16802 (USA)
Fax: (+1) 814-863-5319
E-mail: asen@chem.psu.edu

[**] Supported by the Penn State Center for Nanoscale Science (NSF-MRSEC).

Supporting information for this article is available on the WWW under http://www.angewandte.org or from the author.

 © 2005 Wiley-VCH Verlag GmbH & Co. KGaA, Weinheim DOI: 10.1002/anie.200461890

importantly, to show that the magnetic field served to only align the rods and not to statistically alter the speed (see Table 1). The first parameter measured is directionality. Directionality is defined as the cosine of the angle between the direction that a rod is pointed and the actual direction that the rod moves. A value of 1 (cos 0°) indicates a rod is moving in the same direction that it was originally pointed, whereas a rod moving orthogonal or in the opposite direction would have a value of 0 and −1, respectively. The directionality was determined for two time intervals: 0.1 and 2 seconds.

Table 1: Data for Pt/Ni/Au/Ni/Au striped nanorods in pure water and hydrogen peroxide with and without an applied magnetic field.[a]

H_2O_2 [wt%]	Magnetic field	Axial velocity [$\mu m\,s^{-1}$]	Directionality (0.1 s)	(2 s)	Rot. [$°^2 s^{-1}$]
5%	off	3.1(8)	0.5(1)	0.6(2)	2000
5%	on	2.4(7)	0.4(1)	0.85(6)	70
0%	on	0.2(2)	0.05(4)	0.3(2)	60
0%	not magnetized	0.1(2)	0.01(6)	0.1(2)	700

[a] The size of the data sets from top to bottom are 22, 19, 21, 20 rods, respectively.

The second parameter, axial velocity, is defined as the product of the directionality (over a 0.1 s interval) and the center-to-center displacement of the rod. The axial velocity essentially drops to zero for rods in pure water, thus demonstrating that only Brownian motion is exhibited. Since Brownian motion also results in a center-to-center displacement, axial velocity rather than speed (displacement/time) is a better measure of movement.

The final parameter measured was the rotational diffusion coefficient D(rot), which is defined as the square of the displacement angle divided by the time interval (1 s). Rods in the applied magnetic field have a lower rotational diffusion coefficient than in the absence of the field (Table 1).

Table 1 shows that axial velocity values are essentially unaltered by the presence of a magnetic field, thereby demonstrating that the field serves to only align the rods and not add an additional driving force for motion. In addition, axial velocity drops almost to zero without hydrogen peroxide present because only the catalytic decomposition of hydrogen peroxide serves to move these rods in solution.

The values of directionality over a short time interval (0.1 s) can be used to distinguish between Brownian and non-Brownian motion. Directionality values at the longer time interval (2 s) helps to distinguish between non-Brownian motion in the absence and presence of an applied magnetic field (Table 1). The directionality is 0.01 for Brownian motion in pure water over a 0.1 s interval, but increases to 0.5 in 5 wt% hydrogen peroxide. The increase in directionality results because the Brownian component of translational velocity becomes less important as the propulsive component increases. At this short time interval, however, it is difficult to quantitatively discern the effect of an applied magnetic field on the catalytically driven movement of the rods. We were able to see the longer term effects of rod orientation in the magnetic field by increasing the time interval from 0.1 to 2 s. Table 1 shows that the directionality of rods in 5 wt% hydrogen peroxide increases from 0.6 to 0.85 when the magnetic field is applied.

The final parameter, the rotational diffusion coefficient, clearly shows that the transverse rotation for rods in 5 wt% hydrogen peroxide ($2000°^2 s^{-1}$) is substantially quenched upon the application of a magnetic field ($70°^2 s^{-1}$; Table 1). Brownian nonmagnetized rods have a high rotational diffusion coefficient ($700°^2 s^{-1}$) versus Brownian magnetized rods ($60°^2 s^{-1}$) in the field. Thus, the magnetic field serves to orient magnetized rods with and without hydrogen peroxide. In the absence of an applied magnetic field, the rotational diffusion coefficient is higher for catalytically driven rods than for rods undergoing Brownian motion in pure water ($700°^2 s^{-1}$). The latter observation is not surprising because, unlike catalytically driven rods, there is not enough energy to cause large transverse rotations with the Brownian rods leading to a smaller rotational diffusion coefficient. We measured rotational diffusion coefficients for time intervals less than 1 s (not tabulated) and observed an approximate decrease of two orders of magnitude in the rotational diffusion coefficient for the rods in a magnetic field over the range of 0.1 to 1 second. On the other hand, there was no significant change in the rotational diffusion coefficient from 0.1 to 1 second for the rods without an applied field because these rods are merely moving by the catalytic decomposition of hydrogen peroxide with no source of control over their transverse rotation. Rods in pure water also showed a negligible change in rotational diffusion coefficient over the same time range.

The change in directionality for non-Brownian rods in the magnetic field in a two-second interval is shown in Figure 3 (see the Supporting Information). The magnetic field is applied along the "y"-axis, thereby orienting the rods to move horizontally ("x"-axis) over the three-second observation period. Figure 3 also supports the assertion that the magnetic field only orients the rods and not drive them. For example, the direction traveled by one of the rods is opposite to that of the other two. Thus, upon applying a magnetic field the rods will orient, but they will continue traveling in whatever direction the platinum segment was facing before the field was applied. Also, the rods are not appreciably drawn to the magnet, as indicated by relatively horizontal paths. Figure 4 shows the trajectory path of a nanorod spelling PSU and demonstrates the micrometer-scale control over the rods in the presence of a magnetic field while they are moving autonomously in 5% hydrogen peroxide.

In conclusion, we have presented a method to control the direction in which catalytically driven metallic nanorods move. The magnetic field does not influence the rod speed, rather it serves only to direct the nanorods by orienting their net magnetic moments (comparable to magnetotactic bacteria) parallel to the field. The application of the magnetic field results in higher directionality and substantially lower transverse rotation. In principle, tethering these magnetically controlled, catalytically driven "nano/microengines" to other objects using known procedures would result in new classes of nano/micromachines.

 © 2005 Wiley-VCH Verlag GmbH & Co. KGaA, Weinheim

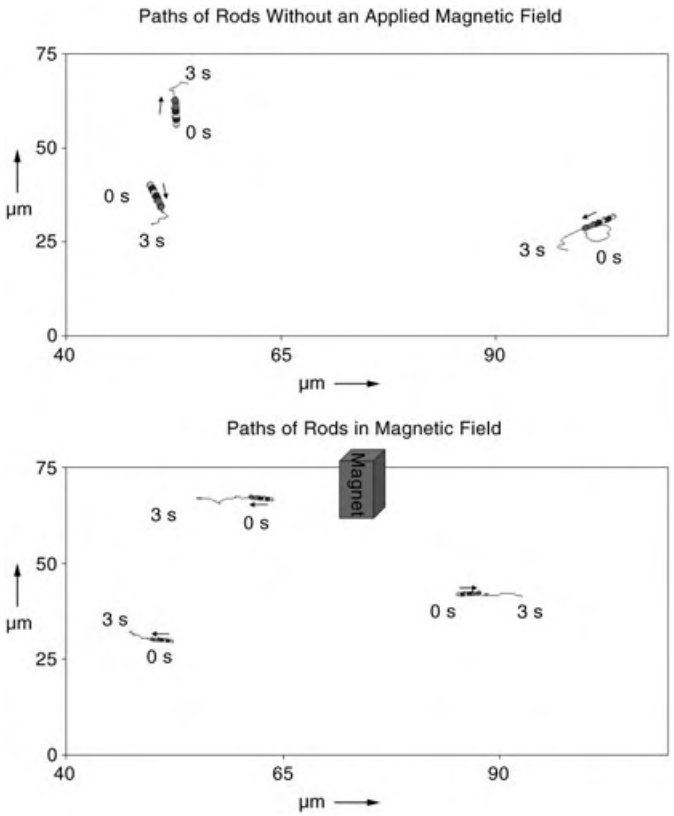


Figure 3. Trajectory paths of rods traveling in a non-oriented fashion before applying a magnetic field (top), where the arrow denotes the direction of the rod along the trajectory, and the same rods traveling in oriented direction in the presence of a field (bottom); the field is a stack of magnets located in the "*y*" direction along the microscope stage.

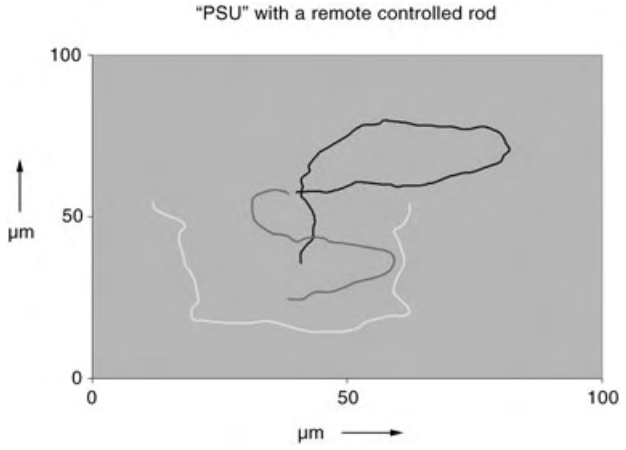


Figure 4. The trajectory path of a Pt/Ni/Au/Ni/Au nanorod spelling the letters "PSU" in 5 wt% H_2O_2.

Experimental Section

The platinum/nickel/gold/nickel/gold (Pt/Ni/Au/Ni/Au) rods were fabricated by using an electrochemical technique with a 0.2-μm pore diameter Whatman Anodisc membrane serving as a sacrificial template.[9] Silver (200 nm) was evaporated onto one side of the Whatman Anodisc membrane. First, the pores were wetted by applying a current density of 0.5 mA cm^{-2} using a Parr 173 potentiostat from Princeton Applied Research. Then the metals were electroplated in succession using commercially available electroplating solutions from Technic. After electroplating, the rods were freed by dissolving the sacrificial silver anode in 5 M nitric acid and the membrane in 5 M sodium hydroxide. Then they were ultracentrifuged and washed four times with water of an approximately neutral pH value to produce the free rods (Figure 1). All SEM images were obtained on a JEOL JSM 5400 instrument at 20 kV. The nickel segments of the rods were magnetized with a NdFeB magnet, as demonstrated previously,[4] and dilute solutions of hydrogen peroxide added to dilute suspensions of the rods. Approximately twenty rods were tracked for each data set in Table 1. Tracking of the rods was done according to the method employed earlier.[3] The magnetic field strength at a certain distance from the stack of NdFeB magnets was determined with a gaussmeter. The stack of magnets was then held in the respective "*x*" or "*y*" directions from the sample on the microscope stage, and this designation is used in assigning rod orientation.

Received: September 3, 2004
Revised: October 29, 2004
Published online: December 21, 2004

Keywords: colloids · homogeneous catalysis · magnetic properties · molecular devices · nanotechnology

[1] R. K. Soong, G. D. Bachand, H. P. Neves, A. G. Olkhovets, C. D. Montemagno, *Science* **2000**, *290*, 1555 – 1558.
[2] D. Pantaloni, C. Le Clainche, M.-F. Carlier, *Science* **2001**, *292*, 1502 – 1506.
[3] W. F. Paxton, K. C. Kistler, C. C. Olmeda, A. Sen, S. K. St. Angelo, Y. Cao, T. E. Mallouk, P. E. Lammert, V. H. Crespi, *J. Am. Chem. Soc.* **2004**, *126*, 13424 – 13431.
[4] J. C. Love, A. R. Urbach, M. G. Prentiss, G. M. Whitesides, *J. Am. Chem. Soc.* **2003**, *125*, 12696 – 12697.
[5] A. R. Urbach, J. C. Love, M. G. Prentiss, G. M. Whitesides, *J. Am. Chem. Soc.* **2003**, *125*, 12704 – 12705.
[6] M. S. Wei, S. Y. Chou, *J. Appl. Phys.* **1994**, *10*, 6679 – 6681.
[7] H. Lee, A. M. Purdon, V. Chu, R. M. Westervelt, *Nano Lett.* **2004**, *4*, 995 – 998.
[8] The magnetic moment of the Pt/Ni/Au/Ni/Au rods was calculated from the bulk magnetic moment of nickel per gram (54 emu g^{-1}) and the mass of nickel incorporated into each nanorod (2.4×10^{-14} g). The rotational thermal energy in the observation plane was estimated from the equipartition theorem ($1/2\,kT$).
[9] B. R. Martin, D. J. Dermody, B. D. Reiss, M. Fang, L. A. Lyon, M. J. Natan, T. E. Mallouk, *Adv. Mater.* **1999**, *11*, 1021 – 1025.

 © 2005 Wiley-VCH Verlag GmbH & Co. KGaA, Weinheim

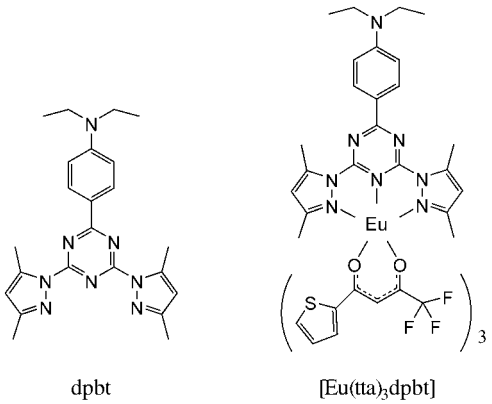
Lanthanide Luminescence

Efficient Two-Photon-Sensitized Luminescence of a Europium(III) Complex**

Li-Min Fu, Xiao-Fan Wen, Xi-Cheng Ai, Yang Sun, Yi-Shi Wu, Jian-Ping Zhang, and Yuan Wang**

The luminescence of lanthanide(III) coordination complexes is unique in their high color purity, long lifetimes, and insensitivity to environmental quenching.[1] These advantages have attracted intensive research efforts in the development of photosensitized and electrochemically driven luminescent materials[2] and luminescent biolabels.[3] Whereas the poor absorptivity of lanthanide ions owing to the parity-forbidden nature of the inner-shell f–f transition is readily overcome by the introduction of chelating chromophores with large extinction coefficients, it has long been a challenge to extend the wavelength range of photosensitization which is inherently hampered by the restriction of ligand-to-metal excitation energy transfer (EET) from the triplet excited state of the ligand.[4] Very recently, we successfully extended the sensitization wavelength up to 460 nm by incorporating a novel ligand, 2-(*N*,*N*-diethylanilin-4-yl)-4,6-bis(3,5-dimethylpyrazol-1-yl)-1,3,5-triazine (dpbt), into a europium(III)–thenoyltrifluoroacetonato (tta) complex, $[Eu(tta)_3dpbt]$ (Scheme 1). The luminescence of the Eu^{III} ion in this complex, with a quantum yield of 0.52 ($\lambda_{em} = 614$ nm), was sensitized by efficient EET from the lowest singlet excited state (S_1) of dpbt to the Eu^{III} center.[5] The *N*,*N*-diethylaniline group in dpbt functions as an electron donor (D) and the dipyrazolyltriazine moiety acts as an electron acceptor (A). Therefore, dpbt is a polar chromophore that shows D–A character, which is known to be the structural basis for an efficient two-photon absorber.[6]

As a newly emerging frontier with important application prospects, two-photon excitation (TPE) of a light-harvesting chromophore and subsequent EET to another functional chromophore in close proximity has been brought into practice by the use of femtosecond-pulsed laser sources.[7]



Scheme 1. Structures of the ligand dpbt and the $[Eu(tta)_3dpbt]$ complex.

Recently, the TPE–EET strategy has found an increasing number of applications. For instance, in photosynthetic pigment–protein complexes, two-photon-excited carotenoids transfer excitation energy to fluorescent (bacterio)chlorophylls—this was used to detect the optically forbidden excited states of carotenoids which play key roles in the photochemistry of photosynthetic carotenoids.[8] In a newly reported porphyrin-centered dendritic complex, porphyrin was activated by fluorescence resonance energy transfer (FRET) from the covalently bonded TPE peripheral chromophores and sensitized the production of singlet oxygen, which is crucial in photodynamic therapy.[7a] Lanthanide(III) ions directly coordinated to proteins, nucleic acids, and biologically relevant chromophores have been shown to act as luminescent biolabels upon TPE sensitization.[9] Here, TPE–EET provides a new way for extending the wavelengths needed for sensitization which may lead to less-harmful and deep-penetrating bioimaging applications.

Intrinsic biological fluorophores directly chelated to lanthanide ions generally have low efficiencies of two-photon sensitization owing to their low two-photon-absorption cross sections: for example, the two-photon-absorption cross sections of amino acids such as tyrosine residues in a Tb^{III}–protein complex lie between 0.4–7.4 GM in the spectral region of 502–566 nm.[9c,10] This low efficiency may be an inherent restriction for the intrinsic TPE sensitizers. Herein, we report the efficient TPE–EET sensitization of Eu^{III} luminescence in the $[Eu(tta)_3dpbt]$ complex. The two-photon-absorption cross sections of dpbt in both the free form and when chelated to Eu^{III} were measured over the spectral region of 730–830 nm by the use of femtosecond laser pulses: the maximal values are 185 and 157 GM for dpbt and $[Eu(tta)_3dpbt]$, respectively. This Eu complex displays both efficient two-photon sensitization and high-purity red emission.

In Figure 1 we see that the fluorescence excitation spectrum of dpbt in toluene is identical to the one-photon-absorption spectrum. This suggests that the absorption band between 300 nm and 400 nm results mainly from the absorptive transition from the ground state (S_0) to the S_1 state, which undergoes efficient vibrational relaxation upon one-photon excitation. Importantly, the absorption/excitation and the

[*] Dr. L.-M. Fu, Prof. Dr. X.-C. Ai, Dr. Y. Sun, Y.-S. Wu, Prof. Dr. J.-P. Zhang
State Key Laboratory for Structural Chemistry of Unstable and Stable Species
Institute of Chemistry
Chinese Academy of Sciences
Beijing 100080 (China)
Fax: (+86) 10-8261-6163
E-mail: jpzhang@mail.iccas.ac.cn
X.-F. Wen, Prof. Dr. Y. Wang
College of Chemistry and Molecular Engineering
Peking University
Beijing 100871 (China)
Fax: (+86) 10-6276-5769
E-mail: wangy@pku.edu.cn

[**] We are grateful for the Grants-in-Aid from the NSFC (grants 20273077, 20433010, 90206011, and 29925308) and the Major State Basic Research Development Program (G2000077503).

 DOI: 10.1002/anie.200462382 © 2005 Wiley-VCH Verlag GmbH & Co. KGaA, Weinheim

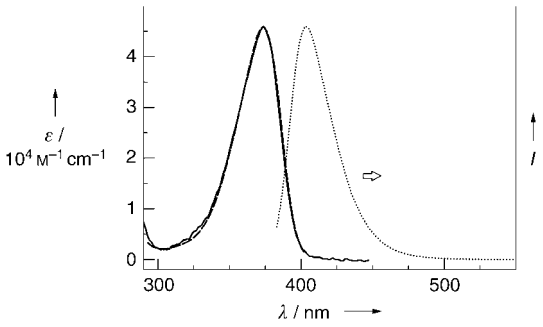


Figure 1. Room temperature UV/Vis absorption (——), fluorescence excitation (– – –; $\lambda_{em} = 405$ nm), and fluorescence emission (•••••; $\lambda_{ex} = 375$ nm) spectra for dpbt in toluene (7.2×10^{-6} M). Spectra are normalized to the absorption maximum.

fluorescence spectra display a perfect mirror-image relationship, which indicates little change in the molecular configurations of a dpbt molecule in either the S_0 or S_1 states. This structural rigidity meets the requirement for an efficient two-photon absorber.

Spectroscopic data (linear absorption and fluorescence) for dpbt in six organic solvents of different polarities are provided in Table 1. Upon increasing the solvent polarity, the

Table 1: Absorption and fluorescence maximal wavelengths (λ_A and λ_F), Stokes shift $\Delta\lambda$, and fluorescence quantum yields (Φ_F) of dpbt dissolved in organic solvents with a polarity factor $P(\varepsilon)$.

Solvent	$P(\varepsilon)$[a]	λ_A [nm]	λ_F [nm]	$\Delta\lambda$ [nm][b]	Φ_F
n-hexane	0.229	368	375	7	0.81[c]
toluene	0.343	374	405	31	0.75
diethyl ether	0.526	370	404	34	0.67
tetrahydrofuran	0.687	378	422	44	0.27
ethanol	0.886	384	440	56	0.02
N,*N*-dimethylformamide	0.922	381	444	63	0.03

[a] Polarity factor is defined as $P(\varepsilon) = (\varepsilon - 1)/(\varepsilon + 2)$, where ε is the dielectric constant. [b] Stokes shift is defined as $\Delta\lambda = \lambda_F - \lambda_A$. [c] Poor solubility in this solvent.

absorption and the fluorescence maximal wavelengths show systematic bathochromic shifts and the Stokes shift increases in parallel, whereas the fluorescence quantum yield drops significantly. This spectroscopic behavior reflects the intramolecular charge transfer (CT) character of the S_1 state[11,12] and is strongly supported by a theoretical calculation on the molecular orbitals. The promotion of an electron in dpbt from the HOMO into the LUMO (see Figure 2) results in a significant change of the electron-density distribution over the diethylaniline and the dipyrazoletriazine moieties. Therefore, the corresponding optical excitation clearly has a photon-induced CT character, and a significant change in the static dipole moment may be expected. Furthermore, the dipole moment obtained from the absorption spectrum of dpbt (Figure 1) corresponding to the $S_1 \leftarrow S_0$ transition is about 6.9 D. Thus, the strong CT character of the S_1 state and the considerably large transition dipole moment suggest a

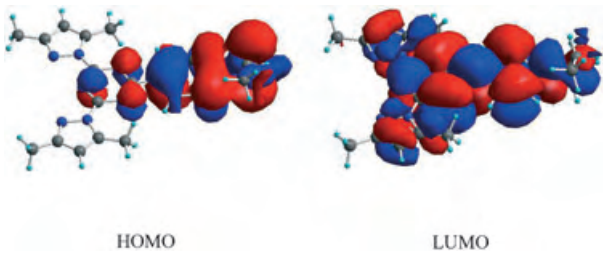


Figure 2. Frontier orbitals of HOMO and LUMO for dpbt. The geometry optimization and the frontier orbital population analysis were performed at the B3LYP/6-31G level. All calculations were carried out by using the GAUSSIAN03 program package.[13]

significant contribution of this state to the process of two-photon absorption.[6c,8c]

In Figure 3, the band at $\lambda = 402$ nm is assigned to the absorptive transition of the ligand-centered S_1 state of dpbt in the [Eu(tta)$_3$dpbt] complex. This transition is red-shifted by

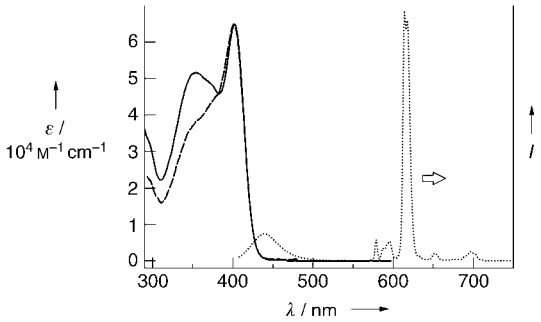


Figure 3. Room temperature UV/Vis absorption (——), fluorescence excitation (– – –; $\lambda_{em} = 614$ nm), and fluorescence emission (•••••; $\lambda_{ex} = 402$ nm) spectra of [Eu(tta)$_3$dpbt] in toluene (4.3×10^{-6} M). Spectra are normalized to the absorption maximum.

approximately 30 nm with respect to free dpbt (Figure 1) and is accounted for by the strong polarization effect of the Eu^{III} ion field on the S_1 state. Furthermore, the transition dipole moment estimated from the dpbt-centered absorption band in Figure 3 is 8.2 D, which is slightly larger than that of free dpbt. The agreement between the fluorescence excitation spectrum and the linear absorption spectrum in the dpbt-centered $S_1 \leftarrow S_0$ spectral region suggests efficient dpbt-to-Eu^{III} excitation energy transfer. However, the tta-centered absorption at 350 nm and the UV absorption at 280 nm show relatively low one-photon-sensitization efficiencies.

Figure 4 shows the excitation power dependence of TPE-sensitized luminescence intensity for both dpbt and [Eu(tta)$_3$dpbt] in toluene. In both cases, the experimental points fit nicely to a linear relationship with a similar slope of 1.98 ± 0.04. This value indicates that the excitation power dependence is quadratic and, therefore, confirms the TPE origin of the luminescence. The excitation power dependence was examined for all the other near-infrared excitation wavelengths used in the subsequent determination of the two-photon-absorption cross section and it was found that

 © 2005 Wiley-VCH Verlag GmbH & Co. KGaA, Weinheim

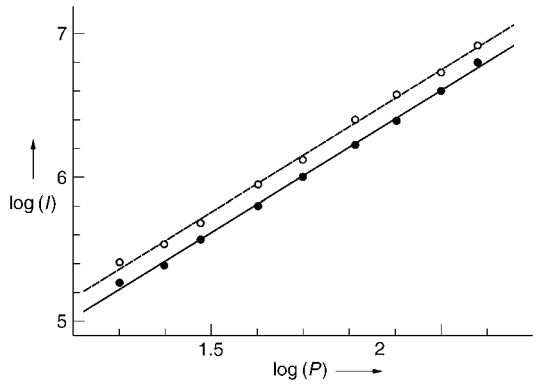


Figure 4. TPE-sensitized luminescence intensity (I) versus the incident laser power (P) for dpbt (○; $\lambda_{ex}=745$ nm, $\lambda_{em}=405$ nm) and [Eu(tta)$_3$dpbt] (●; $\lambda_{ex}=799$ nm, $\lambda_{em}=614$ nm) in toluene. The slopes found from the linear fitting (—— and – – –) are both 1.98 ± 0.04.

they all maintain the quadratic dependence with slopes of 1.95–2.05.

The maximal two-photon-absorption cross sections of dpbt and [Eu(tta)$_3$dpbt] are 185 GM at 735 nm and 157 GM at 808 nm, respectively (see Figure 5). The value of the Eu

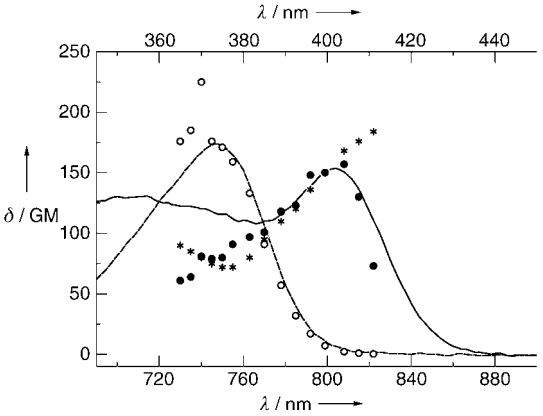


Figure 5. Two-photon-absorption cross sections (δ) for [Eu(tta)$_3$dpbt] (●; $\lambda_{em}=614$ nm) and dpbt (○; $\lambda_{em}=405$ nm) in toluene (1×10^{-4} M). Solid and dash lines are the corresponding one-photon-absorption spectra, whose wavelengths are shown as the upper abscissa, and the peak intensities are arbitrarily scaled. δ values for Rhodamine B in methanol (asterisk) taken from ref. [15] are shown for comparison. 1 GM $=10^{-50}$ cm^4 s photon^{-1} molecule^{-1}.[14]

complex is comparable to those of Rhodamine B in the same spectral range[15] and is one or two orders of magnitude larger than native biological fluorophores such as green fluorescent protein[10] and tyrosine residues.[9c] Besides the high luminescence quantum yield following one-photon-sensitization for [Eu(tta)$_3$dpbt] ($\Phi=0.52$ at $\lambda_{em}=614$ nm),[5] this complex is unique also with regards to the high efficiency of two-photon sensitization and in the high purity of the red emission.

The TPE-sensitized luminescence from [Eu(tta)$_3$dpbt] at 614 nm was mainly attributed to the ligand dpbt rather than tta because in the spectral region below 380 nm (Figure 5), the two-photon-excitation spectrum deviates significantly from the wavelength-doubled one-photon absorption of tta. Most importantly, for both dpbt and [Eu(tta)$_3$dpbt], the experimental points of two-photon-excitation spectra agree with the wavelength-doubled linear absorption spectra of dpbt. Moreover, for both dpbt and [Eu(tta)$_3$dpbt] in toluene, one- and two-photon-induced luminescence spectra show no appreciable differences in the positions and shapes of the bands (data not shown). These results suggest that the S_1 state is both one- and two-photon allowed, which is normally seen for polar chromophores that undergo a significant change of static dipole moments and have large transition dipole moments upon optical excitation.[6c,16] We have previously shown that the one-photon sensitization of [Eu(tta)$_3$dpbt] by visible light is dominated by efficient dpbt(S_1)-to-Eu^{III} energy transfer.[5] It is then most likely that the same mechanism of energy transfer is in operation for the present two-photon-sensitized Eu^{III} luminescence in the [Eu(tta)$_3$dpbt] complex.

To summarize, efficient two-photon sensitization of Eu^{III} luminescence in [Eu(tta)$_3$dpbt] has been demonstrated in the present work. The two-photon-absorption cross sections for dpbt and [Eu(tta)$_3$dpbt] in toluene were determined over the spectral range of 730–830 nm by using femtosecond laser pulses and the maximal values obtained are 185 and 157 GM, respectively. Complex [Eu(tta)$_3$dpbt] combines the advantages of two-photon sensitization and high-purity red emission and, therefore, points to a new direction for the synthesis of luminescent biolabels for less harmful and better quality bioimaging and for other biochemical applications.

Experimental Section

The ligand dpbt and the complex [Eu(tta)$_3$dpbt] were synthesized essentially according to the methods that we reported recently.[5] All the spectroscopic measurements described below were performed at room temperature.

UV/Vis absorption and photoluminescence measurements were carried out on an absorption spectrometer (U-3310, Hitachi) and a fluorescence spectrophotometer (F-2500, Hitachi), respectively. Luminescence quantum yields (Φ_F) of dpbt and [Eu(tta)$_3$dpbt] were determined by following the method described by Demas and Grosby,[17] for which anthracene ($\Phi_F\approx0.36$)[18] and 4-dicyanomethylene-2-methyl-6-*p*-dimethylaminostyryl-4*H*-pyran (DCM; $\Phi_F\approx0.71$),[19] respectively, were used as the references. Ligand dpbt and complex [Eu(tta)$_3$dpbt] were dissolved in toluene, anthracene was dissolved in cyclohexane, and DCM was dissolved in absolute ethanol, all at a concentration of approximately 5×10^{-6} M. The two-photon-absorption cross sections of dpbt and [Eu(tta)$_3$dpbt] were determined by the method of two-photon-induced fluorescence by using Rhodamine B as a standard with known two-photon-absorption cross sections.[15] The output from a mode-locked Ti:Sapphire laser (730–830 nm, ≈80 fs, 82 MHz; Tsunami, Spectra Physics) was focused into a quartz cuvette with an optical path length of 10 mm. The intensity of the incident laser beam was adjusted by using a variable neutral density filter. The two-photon-induced fluorescence was collected and sent to a polychromator (Spectropro-550i, Acton) equipped with a liquid-nitrogen-cooled CCD detector (SPEC-10-400B/LbN, Roper Scientific). To reject the interference of stray laser light, a 10-mm-long sample of a saturated aqueous solution of $CuSO_4$ was placed in front of the entrance slit. Ligand dpbt and complex [Eu(tta)$_3$dpbt] were dissolved in toluene at a concentration of 10^{-4} M, and Rhodamine B was dissolved in ethanol at the same concentration. Spectral response of the spectrograph including filters was calibrated with a standard blackbody lamp. In our experiments, the sample and

 © 2005 Wiley-VCH Verlag GmbH & Co. KGaA, Weinheim

the reference pigments were dissolved in different solvents. The two-photon-absorption cross sections (δ) were obtained according to [Eq. (1)],[15,20] in which subscripts S and R denote the sample and the reference, respectively, F represents the intensity of two-photon-induced fluorescence, Φ is the fluorescence quantum yield, c denotes the concentration, and n represents the refractive index of the solvents:

$$\delta_S = \frac{F_S}{F_R}\left[\frac{\Phi_R c_R n_S}{\Phi_S c_S n_R}\right]\delta_R \quad (1)$$

Received: October 21, 2004
Published online: December 15, 2004

Keywords: energy transfer · europium · luminescence · sensitizers · two-photon excitation

[1] a) H. Maas, A. Currao, G. Calzaferri, *Angew. Chem.* **2002**, *114*, 2607 – 2608; *Angew. Chem. Int. Ed.* **2002**, *41*, 2495 – 2497; b) J. C. G. Bünzli, C. Piguet, *Chem. Rev.* **2002**, *102*, 1897 – 1928.
[2] a) K. Kuriki, Y. Koike, Y. Okamoto, *Chem. Rev.* **2002**, *102*, 2347 – 2356; b) J. Kido, Y. Okamoto, *Chem. Rev.* **2002**, *102*, 2357 – 2368; c) J. Bender, P. S. Corbin, C. L. Fraser, D. H. Metcalf, F. S. Richardson, E. L. Thomas, A. M. Urbas, *J. Am. Chem. Soc.* **2002**, *124*, 8526 – 8527; d) M. H. V. Werts, R. T. F. Jukes, J. W. Verhoeven, *Phys. Chem. Chem. Phys.* **2002**, *4*, 1542 – 1548; e) N. M. Shavaleev, L. P. Moorcraft, S. J. A. Pope, Z. R. Bell, S. Faulkner, M. D. Ward, *Chem. Eur. J.* **2003**, *9*, 5283 – 5291.
[3] a) G. Vereb, E. Jares-Erijman, P. R. Selvin, T. M. Jovin, *Biophys. J.* **1998**, *74*, 2210 – 2222; b) H. L. Handl, J. Vagner, H. I. Yamamura, V. J. Hruby, R. J. Gillies, *Anal. Biochem.* **2004**, *330*, 242 – 250; c) M. Santos, B. C. Roy, H. Golcoechea, A. D. Campiglia, S. Mallik, *J. Am. Chem. Soc.* **2004**, *126*, 10738 – 10745.
[4] a) F. J. Steemers, W. Verboom, D. N. Reinhoudt, E. B. van der Tol, J. W. Verhoeven, *J. Am. Chem. Soc.* **1995**, *117*, 9408 – 9414; b) M. Latva, H. Takalo, V. M. Mukkala, C. Matachescu, J.-C. Rodriguez-Ubis, J. Kankare, *J. Lumin.* **1997**, *75*, 149 – 169.
[5] C. Yang, L.-M. Fu, Y. Wang, J.-P. Zhang, W.-T. Wong, X.-C. Ai, Y.-F. Qiao, B.-S. Zou, L.-L. Gui, *Angew. Chem.* **2004**, *116*, 5120 – 5123; *Angew. Chem. Int. Ed.* **2004**, *43*, 5010 – 5013.
[6] a) M. Albota, D. Beljonne, J. L. Brédas, J. E. Ehrlich, J. Y. Fu, A. A. Heikal, S. E. Hess, T. Kogej, M. D. Levin, S. R. Marder, D. McCord-Maughon, J. W. Perry, H. Röckel, M. Rumi, G. Subramaniam, W. W. Webb, X. L. Wu, C. Xu, *Science* **1998**, *281*, 1653 – 1656; b) L. Ventelon, S. Charier, L. Moreaux, J. Mertz, M. Blanchard-Desce, *Angew. Chem.* **2001**, *113*, 2156 – 2159; *Angew. Chem. Int. Ed.* **2001**, *40*, 2098 – 2101; c) B. Dick, G. Hohlneicher, *J. Chem. Phys.* **1982**, *76*, 5755 – 5760; d) B. A. Reinhardt, L. L. Brott, S. J. Clarson, A. G. Dillard, J. C. Bhatt, R. Kannan, *Chem. Mater.* **1998**, *10*, 1863 – 1874.
[7] a) W. R. Dichtel, J. M. Serin, C. Edder, J. M. J. Fréchel, M. Matuszewski, L. S. Tan, T. Y. Ohulchanskyy, P. N. Prasad, *J. Am. Chem. Soc.* **2004**, *126*, 5380 – 5381; b) J. B. Shear, *Anal. Chem.* **1999**, *71*, 598A-605A.
[8] a) B. P. Krueger, J. Yom, P. J. Walla, G. R. Fleming, *Chem. Phys. Lett.* **1999**, *310*, 57 – 64; b) P. J. Walla, J. Yom, B. P. Krueger, G. R. Fleming, *J. Phys. Chem. B* **2000**, *104*, 4799 – 4806; c) J. Zimmermann, P. A. Linden, H. M. Vaswani, R. G. Hiller, G. R. Fleming, *J. Phys. Chem. B* **2002**, *106*, 9418 – 9423.
[9] a) G. Piszezek, B. P. Maliwal, I. Gryczynski, J. Dattelbaum, J. R. Lakowicz, *J. Fluoresc.* **2001**, *11*, 101 – 107; b) G. Piszczek, I. Gryczynski, B. P. Maliwal, J. R. Lakowicz, *J. Fluoresc.* **2002**, *12*, 15 – 17; c) G. F. White, K. L. Litvinenko, S. R. Meech, D. L. Andrews, A. J. Thomson, *Photochem. Photobiol. Sci.* **2004**, *3*, 47 – 55.
[10] C. Xu, W. Zipfel, J. B. Shear, R. M. Williams, W. W. Webb, *Proc. Natl. Acad. Sci. USA* **1996**, *93*, 10763 – 10768.
[11] J. E. Rogers, J. E. Slagle, D. G. McLean, R. L. Sutherland, B. Sankaran, R. Kannan, L. S. Tan, P. A. Fleitz, *J. Phys. Chem. A* **2004**, *108*, 5514 – 5520.
[12] B. R. Cho, K. H. Son, S. H. Lee, Y. S. Song, Y. K. Lee, S. J. Jeon, J. H. Choi, H. Lee, M. Cho, *J. Am. Chem. Soc.* **2001**, *123*, 10039 – 10045.
[13] Gaussian 03 (Revision B.1), M. J. Frisch, G. W. Trucks, H. B. Schlegel, G. E. Scuseria, M. A. Robb, J. R. Cheeseman, J. A. Montgomery, Jr., T. Vreven, K. N. Kudin, J. C. Burant, J. M. Millam, S. S. Iyengar, J. Tomasi, V. Barone, B. Mennucci, M. Cossi, G. Scalmani, N. Rega, G. A. Petersson, H. Nakatsuji, M. Hada, M. Ehara, K. Toyota, R. Fukuda, J. Hasegawa, M. Ishida, T. Nakajima, Y. Honda, O. Kitao, H. Nakai, M. Klene, X. Li, J. E. Knox, H. P. Hratchian, J. B. Cross, C. Adamo, J. Jaramillo, R. Gomperts, R. E. Stratmann, O. Yazyev, A. J. Austin, R. Cammi, C. Pomelli, J. W. Ochterski, P. Y. Ayala, K. Morokuma, G. A. Voth, P. Salvador, J. J. Dannenberg, V. G. Zakrzewski, S. Dapprich, A. D. Daniels, M. C. Strain, O. Farkas, D. K. Malick, A. D. Rabuck, K. Raghavachari, J. B. Foresman, J. V. Ortiz, Q. Cui, A. G. Baboul, S. Clifford, J. Cioslowski, B. B. Stefanov, G. Liu, A. Liashenko, P. Piskorz, I. Komaromi, R. L. Martin, D. J. Fox, T. Keith, M. A. Al-Laham, C. Y. Peng, A. Nanayakkara, M. Challacombe, P. M. W. Gill, B. Johnson, W. Chen, M. W. Wong, C. Gonzalez, J. A. Pople, Gaussian, Inc., Pittsburgh, PA, **2003**.
[14] W. M. McClain, *Acc. Chem. Res.* **1974**, *5*, 129 – 135.
[15] C. Xu, W. W. Webb, *J. Opt. Soc. Am. B* **1996**, *13*, 481 – 491.
[16] L. Porrès, O. Mongin, C. Katan, M. Charlot, T. Pons, J. Mertz, M. Blanchard-Desce, *Org. Lett.* **2004**, *6*, 47 – 50.
[17] J. N. Demas, G. A. Crosby, *J. Phys. Chem.* **1971**, *75*, 991 – 1024.
[18] I. B. Berlman, *Handbook of Fluorescence Spectra of Aromatic Molecules, 2nd ed.*, Academic Press, New York, **1971**.
[19] P. R. Hammond, *Opt. Commun.* **1979**, *29*, 331 – 334.
[20] M. Rumi, J. E. Ehrlich, A. A. Heikal, J. W. Perry, S. Barlow, Z. Hu, D. McCord-Maughon, T. C. Parker, H. Rökel, S. Thayumanavan, S. R. Marder, D. Beljonne, J. L. Brédas, *J. Am. Chem. Soc.* **2000**, *122*, 9500 – 9510.

 © 2005 Wiley-VCH Verlag GmbH & Co. KGaA, Weinheim

Oligoaniline Complexes

Self-Assembly and Electrical Conductivity Transitions in Conjugated Oligoaniline–Surfactant Complexes**

*Zhixiang Wei, Teija Laitinen, Bernd Smarsly, Olli Ikkala, and Charl F. J. Faul**

Building well-ordered two- and three-dimensional nanostructures in a facile way is essential for the next generation of electrical, optical, and magnetic materials and devices.[1] Molecular self-assembly[2] is a versatile method to prepare such structures by binding mutually repulsive groups with attractive interactions, for example, ionic interactions, hydrogen bonding, van der Waals forces, and metal coordination.[3] Besides precise control over the structures, self-assembly can also lead to properties that can be controlled by external conditions.[4] Conjugated oligomers have been used for electroactive materials and devices,[5] and here we show that conjugated aniline tetramers and octamers are able to form well-defined 2D self-assembled columnar structures upon ionic complexation with di(*n*-alkyl) phosphate surfactants. This behavior is in contrast to the corresponding polyaniline (PANI) complexes that form 2D hexagonally arranged assemblies. Importantly, order–disorder transitions are observed as reversible transitions in electrical conductivity as a function of temperature. Therefore, this self-assembly strategy allows for responsive electroactive properties of conjugated materials.

PANI salts, which are both electrically conducting conjugated polymers and polyelectrolyte complexes, can form lamellar or hexagonal nanostructures through ionic self-assembly with surfactants or hydrogen-bonded amphiphiles.[6] However, as with most self-assembled polyelectrolyte complexes, the arrangements of polyaniline chains within the self-assembled conducting domains are often disordered as a result of coiling and the polydispersity of the chains. It was demonstrated with polybenzylglutamates and related polymers that polydispersity can affect the overall structure: polydispersity leads to nematic order, whereas monodispersity leads to smectic order.[7]

Oligoanilines with well-defined chain lengths are model compounds for the electronic, magnetic, optical, and structural properties of PANI.[8] For instance, the conductivity values for the complexes of tetrameric and octameric anilines with HCl are approximately 3×10^{-3} and $1\,S\,cm^{-1}$, respectively.[9,10] More importantly, as their assembly can be precisely controlled owing to their monodispersity and better solubility, they may also exhibit novel properties.[11]

Phenyl-capped tetraaniline (TANI) and phenyl-capped octaaniline (OANI) were prepared by using slight modifications of reported methods[10,12] (see Supporting Information for details). Polyaniline ($M_w = 28000$) was provided by PANIPOL Ltd. and was synthesized by a conventional method.[13] The surfactant di(undecenyl) phosphate (ωC11) was prepared according to a general procedure employed for the synthesis of di(*n*-alkyl) phosphates.[14] Bis(2-ethylhexyl) phosphate (BEHP) was obtained from Aldrich. The complexes of oligoaniline and PANI with the phosphate surfactants were prepared by dissolving TANI, OANI, or PANI and the surfactants in a common solvent (usually formic acid, but chloroform for the complexes of TANI) followed by film casting. Different molar ratios (x) of surfactant to aniline groups were used, and the complexes are denoted as [TANI(BEHP)$_x$] as an example. The nominally fully doped case corresponds to $x = 0.5$ in which all the imine nitrogen atoms have been protonated by the acid. The structures of the oligoanilines and their complexes are shown in Figure 1.

In the case of TANI complexes, the most distinct effect is that upon addition of BEHP or ωC11 surfactants, the originally crystalline TANI oligomers became softened but were still birefringent, which indicates liquid crystallinity. WAXS (wide-angle X-ray scattering) investigations of [TANI(BEHP)$_x$], $x = 0.25$, 0.42, and 0.5, reveal a narrow scattering peak near $2\theta = 4.1°$ and up to five equally spaced higher order reflections which indicate highly ordered lamellar structures with a spacing of $d_1 = 2.22$ nm (see Supporting Information for 1D WAXS and SAXS (small-angle X-ray scattering) diffractograms). Increasing the molar ratio of surfactant to aniline groups, x, caused only a slight increase in the spacing. Furthermore, two much broader peaks are present at 25° ($d = 0.35$ nm) and 20° ($d = 0.45$ nm). These are attributed to the van der Waals distances between the aromatic rings of TANI (stack height calculated to be at least 16 nm in the case of [TANI(BEHP)$_{0.5}$]) and between the aliphatic chains of the dopants, respectively.[6]

1D SAXS analyses at room temperature indicated a richer supramolecular structure beyond the plain lamellar order, as demonstrated in Figure 2 for [TANI(BEHP)$_{0.5}$]. To assign the reflections, efforts were made to align the structures by

[*] Dr. Z. Wei, Dr. B. Smarsly, Dr. C. F. J. Faul[+]
Max Planck Institute of Colloids and Interfaces
Research Campus Golm
14424 Potsdam (Germany)
E-mail: charl.faul@bristol.ac.uk

T. Laitinen, Prof. O. Ikkala
Helsinki University of Technology
Department of Engineering Physics and Mathematics and
Center for New Materials
P.O. Box 2200, 02015 HUT, Espoo (Finland)

[+] New address: School of Chemistry
Inorganic and Materials Chemistry Section
University of Bristol
Bristol BS8 1TS (UK)
Fax: (+44) 117-929-0509

[**] This work was supported as part of the European Science Foundation Collaborative Research (EUROCORES) Programme on Self-Organised NanoStructures (SONS). The MPG and the Academy of Finland are acknowledged. PANIPOL Ltd is acknowledged for providing polyaniline, and VTT Microelectronics is acknowledged for the permission to use their impedance analyzers. Tapio Mäkelä, Mari Tiitu, Teemu Ruotsalainen, and Dr. Evgeny Polushkin are acknowledged for discussions and experimental assistance. The work was partly carried out in the Centre of Excellence of Finnish Academy (Bio- and Nanopolymers Research Group, 77317).

Supporting information for this article is available on the WWW under http://www.angewandte.org or from the author.

 DOI: 10.1002/anie.200460928 © 2005 Wiley-VCH Verlag GmbH & Co. KGaA, Weinheim

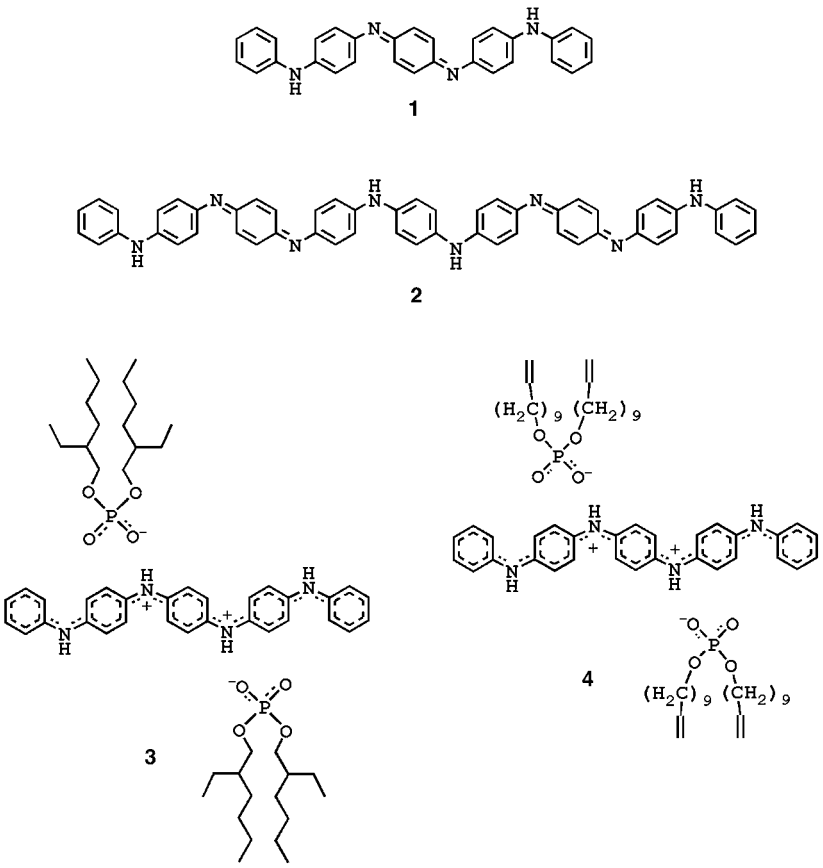


Figure 1. TANI (**1**), OANI (**2**), [TANI(BEHP)$_{0.5}$] (**3**), and [TANI(ωC11)$_{0.5}$] (**4**).

shearing the samples manually. This produced materials that were oriented to some degree. Figure 2A shows a typical 2D SAXS pattern of a manually oriented sample of [TANI(BEHP)$_{0.5}$] in which the reflections are no longer radially averaged (isotropic Debye–Scherrer patterns) but are concentrated in certain directions. Even if complete orientation with spotlike reflections was not achieved, the data quality is still sufficient to extract the angle φ from the arclike reflections (see Figure 2B for the definition of φ). For better visualization, the observed SAXS reflections are illustrated in Figure 2B (only one quadrant is shown). On the basis of a careful analysis of the anisotropic SAXS patterns, nine reflections could be determined with sufficient accuracy; that is, the position of the reflections (see the 1D pattern, Figure 2C) and the corresponding angle φ. The angles φ could only be determined with an accuracy of about 10–15°, which limits the accuracy of the structure model. Reflection i is quite broad and probably results from a superposition of two interferences. Reflection g does not show a significant degree of preferred orientation, which, however, could be a result of the limited resolution of our detector device for low scattering intensities. Hence, the main reflections can be classified into three groups with respect to the angle φ (see Table 1).

Interestingly, several families of reflections can be identified in the 2D SAXS patterns. Within a

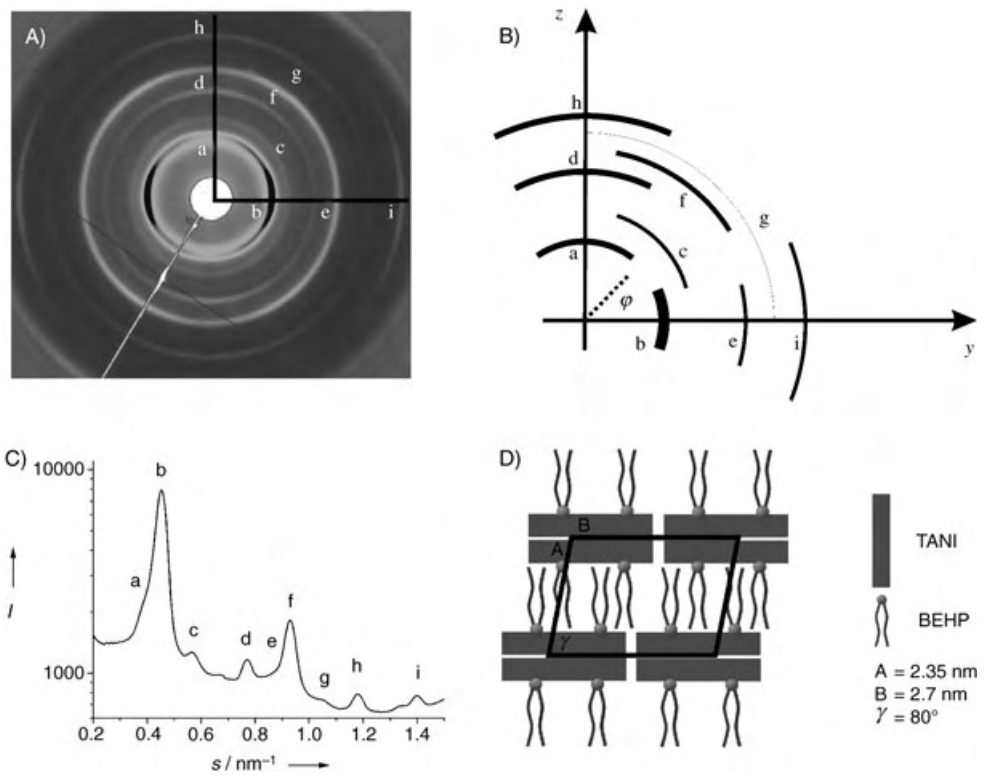


Figure 2. A) 2D SAXS pattern of an oriented sample of [TANI(BEHP)$_{0.5}$]. B) Diagram of the anisotropic scattering patterns. C) Radially averaged 1D pattern of part (A). D) Representation of the 2D columnar phase and possible packing of [TANI(BEHP)$_{0.5}$] units within the unit cell.

 © 2005 Wiley-VCH Verlag GmbH & Co. KGaA, Weinheim

Table 1: Assignment of the observed SAXS reflections.

Reflections	s [nm^{-1}]	φ_{exp} [°]	$\varphi_{theoretical}$ [°]	Indexation
a	0.375	80–90	81	(01)
b	0.454	0–10	0	(10)
c	0.57	40–50	49	(11)
d	0.76	80–90	81	(02)
e	0.89	0–10	0	(20) (+(1–2))
f	0.92–0.95	55–65	66	(12) (+(2–1))
g	1.03–1.05	n.a.	49	(21)
h	1.18	80–90	81	(03)
i	1.34	0–10	0	(30) (+(13))

certain variance, $\varphi = 80$–$90°$ for reflections a, d, and h, whereas for b and e $\varphi = 0°$. Also for i we found $\varphi = 0°$, but this reflection is superimposed with another reflection. Hence, a reasonable interpretation is that b and e belong to a (hk0) family and a, d, and h belong to the (001) family. In general, unambiguous assignments are difficult owing to the limited number of reflections and the experimental uncertainty in φ. However, as only one type of reflection is observed on the y axis (multiples of the first interference), this indicates that the present system can be regarded as a 2D mesostructure. Therefore it seems legitimate to assume that the reflections on the y axis correspond to the (h0) lattice planes of a 2D structure that lacks mesoscale periodicity in the third dimension. Within this model, the reflections in the z direction reduce to the (01) family. Furthermore, as a common feature of mesostructures in general, the symmetry of these morphologies is quite low so that usually the first-order reflections are indeed observable.

On the basis of these assumptions, the positions of all reflections can be reasonably well indexed to a 2D unit cell in the form of a parallelogram with parameters $\gamma = 80°$, $A = 2.35$ nm, and $B = 2.7$ nm (see Table 1 for the indexation). Several reflections cannot be assigned as distinguishable interferences (e.g. (1–2)) because the corresponding positions probably coincide with other reflections. This effect could explain the observation that several arcs in the 2D pattern apparently smear into a ring, which would simply be a consequence of the superposition of different reflections. In particular, this structure model accounts well for the angles φ of the off-axis reflections, c and f, which is crucial for a reasonable structure model.

Whereas, theoretically, for nonrectangular lattices, the (01) reflections cannot be located on the z axes, in the present case, the slight deviation from a rectangular lattice ($\approx 10°$) is difficult to detect in the 2D SAXS patterns.

In essence, this unit cell can be regarded as a slightly distorted 2D rectangular lattice and is similar to the columnar phases recently reported by Tschierske and co-workers for calamitic bolaamphiphiles.[15] The A parameter of the unit cell also fits very well with an interdigitated arrangement of the surfactant tails, whereas the B parameter fits with the calculated length of the salt form of a TANI molecule (see Figure 2D and Supporting Information). Furthermore, from the volume (2.22 nm^3) of a unit cell of 0.35-nm thickness (corresponding to the π–π stacking distance), the number of molecules was calculated and corresponds to the presence of two complexed TANI units (the volume of a [TANI-(BEHP)$_{0.5}$] unit is 1.10 nm^3 from calculations performed with CeriusII software).

Even if this interpretation allows the reflections to be indexed in a reasonable manner, owing to the limited number of reflections this structure analysis cannot be regarded as unambiguous. From the evaluation of 1D SAXS data, the second phosphate surfactant ωC11 forms quantitatively similar structures upon complexation with tetraaniline.

The driving force for the 2D columnar structures in [TANI(BEHP)$_x$] and [TANI(ωC11)$_x$] was next addressed. TANI is a rigid molecule as a result of its conjugated structure. Upon complexation with the phosphoric acid surfactant, it can be regarded as a supramolecule in which the soft alkyl side chains are attached to the hard TANI backbone by ionic bonds. Liquid crystallinity is therefore expected as already seen in the case of perylenediimide-based materials[16] or other rigid-core materials that contain several incompatible molecular parts.[15] Although the columnar structure is reminiscent of smectic phases found for calamitic structures, the arrangement of the molecules is slightly different as very efficient stacking of the TANI molecules in [TANI(BEHP)$_x$] and [TANI(ωC11)$_x$] is observed as a result of the strong π–π interactions (WAXS studies). These systems can therefore be seen to represent the noncovalent analogues of semifluorinated rodlike systems, with strong segregation within the molecule driving the formation of the 2D columnar phase structures. The ordering of tetraaniline within the self-assembled layers is also supported by the crystalline structure of the surfactant-free analogue, HCl-doped tetraaniline ([TANI(HCl)$_{0.5}$]). A spacing $d = 2.58$ nm, nearly the same as that of [TANI(BEHP)$_{0.5}$], was also observed, as determined by the length of the TANI molecule.

The previous discussion showed that the 2D columnar phase structure in the oligoaniline–phosphate surfactant complexes is ascribed to the monodispersity of both of the building blocks; that is, the main chains and the surfactants. As PANI is polydisperse, stacking of its surfactant complexes is therefore not expected. Interestingly, [PANI(BEHP)$_{0.5}$] self-assembles to form a highly ordered hexagonal structure, unlike the rectangular columnar phase of the corresponding oligomeric [TANI(BEHP)$_{0.5}$]. The different self-assembly of PANI and TANI may be ascribed to their different conformations. PANI displays a coil-like conformation, which therefore takes more "lateral" space and thus forms hexagonal structures in the direction of the chains. The possibility of π–π stacking (and therefore an added driving force to form side-by-side arrangements) is therefore reduced considerably. TANI, on the other hand, is rodlike and short and thus takes much less lateral space with consequent higher possibilities for π–π stacking. Such conclusions are supported by the complexes of the rigid rodlike conjugated polymer poly(2,5-pyridinediyl) (PPY) and PANI with camphor sulfonic acid (CSA) and hexylresorcinol (Hres): [PPY(CSA)$_{0.5}$(Hres)$_{1.0}$] forms a lamellar self-assembly, whereas the corresponding PANI complexes form a cylindrical self-assembly.[6b,17]

Surprisingly, a mixture of both lamellar and hexagonal structures are observed in [OANI(BEHP)$_{0.5}$], as shown in

 © 2005 Wiley-VCH Verlag GmbH & Co. KGaA, Weinheim

Figure 3A, even if no clear macroscopic phase separation was observed by means of an optical microscope (after annealing at high temperatures). The *d* spacing of the hexagonal structure is 2.89 nm, which is very similar to the value found

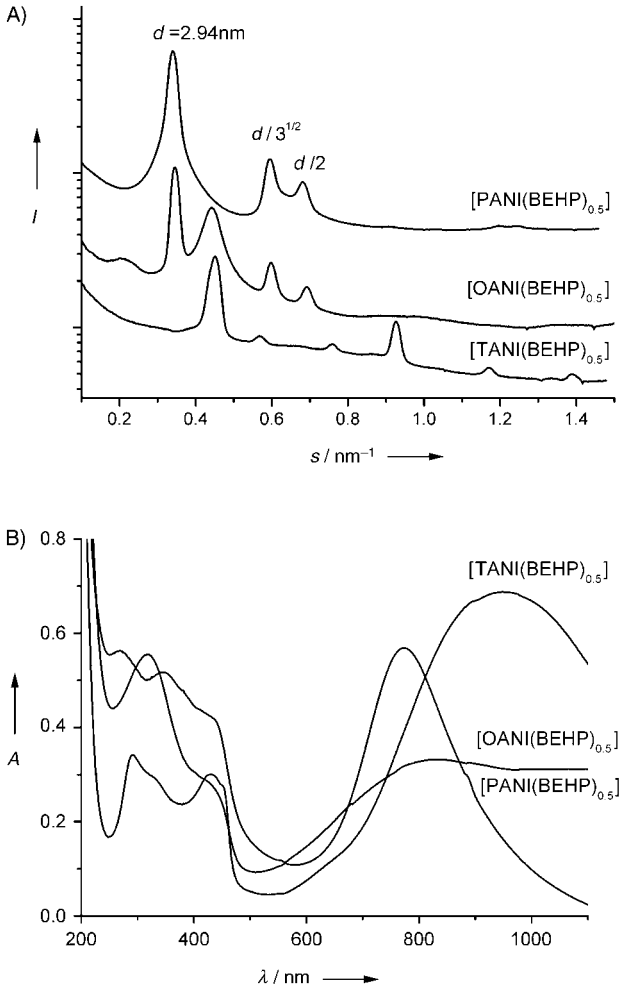


Figure 3. The effect of aniline chain length in [PANI(BEHP)$_{0.5}$], [OANI(BEHP)$_{0.5}$], and [TANI(BEHP)$_{0.5}$]. A) SAXS. B) UV/Vis spectra.

for [PANI(BEHP)$_{0.5}$] (2.94 nm), whereas the other structure has a *d* spacing of 2.25 nm, which is nearly the same as the value found in [TANI(BEHP)$_{0.5}$] (2.22 nm). This observation may indicate that OANI is a limiting case in which the coexistence of the behavior of a rodlike molecule (similar to TANI) and a coil-like conformation (similar to PANI) is found. Furthermore, another strong peak that corresponds to a *d* spacing of 4.88 nm is observed. This is slightly longer than the length calculated for the phenyl-capped octaaniline molecules (4.48 nm in the doped state, see Supporting Information). If the effect of the molecular stacks separated by surfactants is considered, the length corresponds to the expected length of the complexes.

The UV/Vis spectra of BEHP-doped complexes for aniline chains of different lengths are shown in Figure 3B. All spectra show three absorption maxima at approximately $\lambda = 300$, 400, and > 700 nm, which are ascribed to the π–π^* transition of the benzenoid ring (300 nm) and the absorption band of polarons.[18] However, their positions and relative strengths are totally different. The polaron absorption maximum of TANI is located at approximately $\lambda = 950$ nm and extends to higher wavelengths, whereas that of PANI is located at about $\lambda = 775$ nm and tails off beyond that value. This suggests that the tetraaniline chains are in an extended rodlike conformation, whereas polyaniline chains are coiled. The corresponding maximum of the OANI complex is located at $\lambda = 830$ nm and extends to higher wavelength, and the behavior is, once again, between that of TANI and PANI. Therefore, in conclusion, TANI is in a rodlike conformation, PANI is in a coiled conformation, and OANI is a limiting case with a combination of the two behaviors.

Both [TANI(ωC11)$_x$] and [TANI(BEHP)$_x$] lose birefringence upon heating beyond 70–80 °C and 80–95 °C, respectively (see the Supporting Information for representative differential scanning calorimetry (DSC) curves). This indicates that the complexes are disordered at high temperatures. This is also supported by SAXS which revealed no pronounced scattering peaks at elevated temperature. These transitions show a very interesting connection to the electrical conductivity. We made an initial effort to analyze the electrical conductivities of the oligomer–surfactant complexes by using the standard four-wire method. However, the complexes did not display linear voltage–current relationships and therefore were not purely Ohmically conducting; that is, they were not purely electronic conductors. Thus, ac-impedance spectroscopy was employed by using an impedance analyzer (HP 4192LF) at frequencies from 0.01 to 1000 kHz. The dc conductivities were determined by using standard procedures.[19]

The complexes [TANI(ωC11)$_x$] showed pronounced conductivity transitions as a function of temperature (see Figure 4A). At room temperature, the conductivity of [TANI(ωC11)$_{0.42}$] is of the order of 3×10^{-3} S cm^{-1}. An increase in the temperature to beyond 70 °C leads to an abrupt drop in the conductivity by three orders of magnitude. The transition is reversible in consecutive cooling and heating cycles with some hysteresis observed. A slightly larger transition was observed for $x = 0.5$. For smaller values of x, such as $x = 0.25$ or 0.33, the drop in conductivity is significantly smaller. For $x = 1.0$, no transition was observed. Smaller thermal conductivity switching was also observed in [TANI(BEHP)$_x$] complexes, but not for the OANI or PANI complexes.

To explain the conductivity transition, the question was posed whether tetraaniline was dedoped upon heating. The UV/Vis spectra at different temperatures were thus measured and showed that there was little decrease in the polaron absorption (Figure 4B) which indicates no dedoping. However, the conductivity of [TANI(ωC11)$_x$] can be correlated with the extent of order found within the self-assembled material. Figure 4B shows that the integrated intensity of the first diffraction peak of the columnar structures decreased upon increasing the temperature past 70 °C, which corresponds to the order–disorder transition temperature. Similar temperature-dependent behavior is observed for the conduc-

 © 2005 Wiley-VCH Verlag GmbH & Co. KGaA, Weinheim

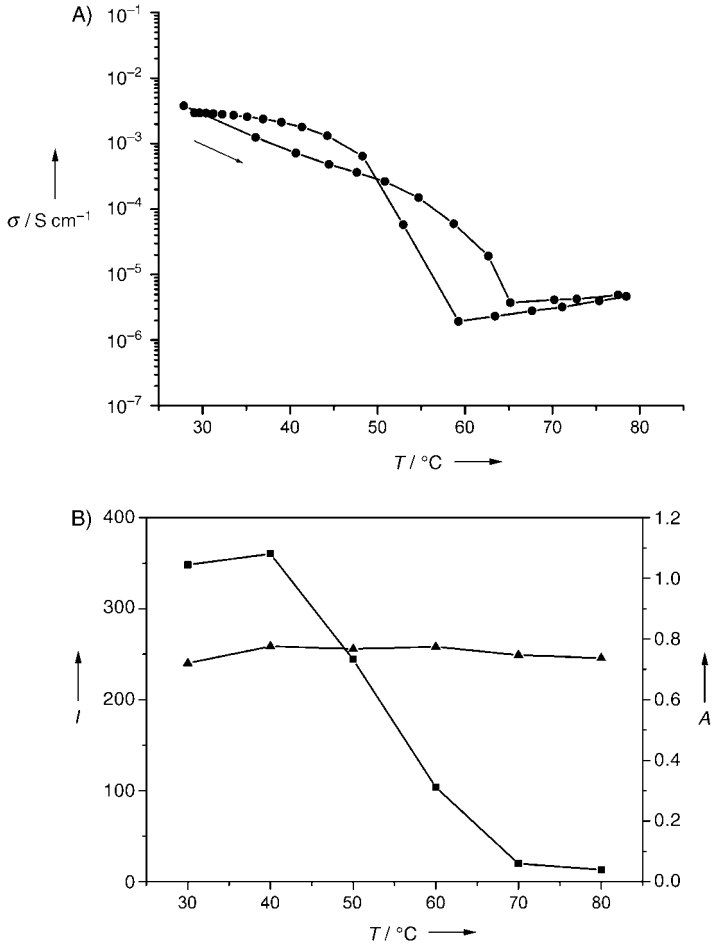


Figure 4. Correlation between conductivity and self-assembly for [TANI(ωC11)$_{0.42}$]. A) The dc conductivity as a function of temperature (temperature sweep: 1 °C min^{-1}). B) Integrated X-ray scattering peak height of the first-order reflection ($s = 0.42$ nm^{-1}) and the UV/Vis absorption at the polaron peak maximum as a function of temperature ■ = SAXS, ▲ = UV/Vis.

tivity as seen in Figure 4 A. This indicates that the conductivity switching for [TANI(ωC11)$_x$] can be assigned to the order–disorder transition from an ordered 2D columnar structure to a disordered state. In this transition, the degree of organization between the conducting layers decreases and the disorder limits the carrier mobility of the interchain electron transfer, which thus leads to a dramatic decrease in the electrical conductivity.[20] A similar but much smaller effect is observed for [TANI(BEHP)$_x$] and we are at present trying to explain the difference between the two complexes.

In summary, a 2D rectangular columnar structure based on oligoanilines was prepared by using double-tail phosphate surfactants. In this structure, the conducting layers of oligoanilines are segregated by the insulating layers of the dialkyl phosphates. The oligoaniline molecules, owing to their monodispersity, form well-ordered infinite 2D columnar stacks within the conducting layers. Upon heating, the tetraaniline complexes showed an order–disorder transition from this 2D phase structure to a disordered state: This transition corresponds to a large reversible change in the electrical conductivity. This research shows that functional and externally controllable electroactive nanostructures can be obtained by an ionic self-assembly process.

Received: June 10, 2004
Revised: September 29, 2004
Published online: December 21, 2004

Keywords: conducting materials · liquid crystals · nanostructures · self-assembly · surfactants

[1] a) S. W. Lee, C. Mao, C. E. Flynn, A. M. Belcher, *Science* **2002**, *296*, 892; b) A. Bachtold, P. Hadeky, T. Nakanish, C. Dekker, *Science* **2001**, *294*, 1317; c) S. Fan, M. G. C. Hapline, N. R. Franklin, T. W. Tombler, A. M. Cassell, H. Dai, *Science* **1999**, *283*, 512.

[2] a) G. M. Whitesides, J. P. Mathias, C. T. Seto, *Science* **1991**, *254*, 1312; b) G. M. Whitesides, B. Grzybowski, *Science* **2002**, *295*, 2418.

[3] a) O. Ikkala, G. ten Brinke, *Science* **2002**, *295*, 2407; b) C. F. J. Faul, M. Antonietti, *Adv. Mater.* **2003**, *15*, 673; c) V. Percec, M. Glodde, T. K. Bera, Y. Miura, I. Shiyanovskaya, K. D. Singer, V. S. K. Balagurusamy, P. A. Heiney, I. Schnell, A. Rapp, H.-W. Spiess, S. D. Hudson, H. Duan, *Nature* **2002**, *419*, 384; d) G. M. Whitesides, B. Grzybowski, *Science* **2002**, *295*, 2418; e) T. Kato, *Science* **2002**, *295*, 2414.

[4] J. Ruokolainen, R. Mäkinen, M. Torkkeli, T. Mäkelä, R. Serimaa, G. ten Brinke, O. Ikkala, *Science* **1998**, *280*, 557.

[5] a) *Electronic Materials: The Oligomer Approach*, (Eds.: G. Wegner, K. Müllen), Wiley-VCH, Weinheim, **1996**; b) C. Joachim, *Nanotechnology* **2002**, *13*, R1.

[6] a) W.-Y. Zheng, R.-H. Wang, K. Levon, Z. Y. Rong, T. Taka, W. Pan, *Macromol. Chem. Phys.* **1995**, *196*, 2443; b) A. Pron, P. Rannou, *Prog. Polym. Sci.* **2002**, *27*, 135; c) H. Kosonen, J. Ruokolainen, M. Knaapila, M. Torkkeli, K. Jokela, R. Serimaa, G. ten Brinke, W. Bras, A. P. Monkman, O. Ikkala, *Macromolecules* **2000**, *33*, 8671; d) B. Dufour, P. Rannou, D. Djurado, H. Janeczek, M. Zagorska, A. de Geyer, J.-P. Travers, A. Pron, *Chem. Mater.* **2003**, *15*, 1587.

[7] a) S. M. Yu, V. P. Conticello, G. Zhang, C. Kayser, M. J. Fournier, T. L. Mason, D. A. Tirrell, *Nature* **1997**, *389*, 167; b) H. Schlaad, B. Smarsly, M. Losik, *Macromolecules* **2004**, *37*, 2210.

[8] a) J. Libert, J. Cornil, D. A. dos Santos, J. L. Bredas, *Phys. Rev. B* **1997**, *56*, 8638; b) A. G. MacDiarmid, Y. Zhao, J. Feng, *Synth. Met.* **1999**, *100*, 131.

[9] W. Zhang, J. Feng, A. G. MacDiarmid, A. J. Epstein, *Synth. Met.* **1997**, *84*, 119.

[10] F.-L. Lu, F. Wudl, M. Nowak, A. J. Heeger, *J. Am. Chem. Soc.* **1986**, *108*, 8311.

[11] a) S. Quillard, B. Corraze, M. Poncet, J.-Y. Mevellec, J.-P. Buisson, M. Evain, W. Wang, A. G. MacDiarmid, *Synth. Met.* **2003**, *137*, 921; b) X. Chen, S. Liu, Y. Song, S. Dong, *Chem. Lett.* **2002**, 552.

[12] J. Gao, K. Li, W. Zhang, C. Wang, Z. Wu, Y. Ji, Y. Zhou, M. Shibata, R. Yosomiya, *Macromol. Rapid Commun.* **1999**, *20*, 560.

[13] Y. Cao, A. Andreatta, A. J. Heeger, P. Smith, *Polymer* **1989**, *30*, 2305.

[14] a) T. Kunitake, Y. Okahata, *Bull. Chem. Soc. Jpn.* **1978**, *51*, 1877; b) D. Ganeva, C. F. J. Faul, C. Götz, R. D. Sanderson, *Macromolecules* **2003**, *36*, 2862.

[15] a) M. Prehm, S. Diele, M. K. Das, C. Tschierske, *J. Am. Chem. Soc.* **2003**, *125*, 614; b) X. H. Cheng, M. K. Das, S. Diele, C. Tschierske, *Angew. Chem.* **2002**, *114*, 4203; *Angew. Chem. Int.*

 © 2005 Wiley-VCH Verlag GmbH & Co. KGaA, Weinheim

Ed. **2002**, *41*, 4031; c) M. Prehm, X. H. Cheng, S. Diele, M. K. Das, C. Tschierske, *J. Am. Chem. Soc.* **2002**, *124*, 12072.
[16] a) Y. Guan, Y. Zakrevskyy, J. Stumpe, M. Antonietti, C. F. J. Faul, *Chem. Commun.* **2003**, 894; b) Y. Zakrevskyy, C. F. J. Faul, Y. Guan, J. Stumpe, *Adv. Funct. Mater.* **2004**, *14*, 835.
[17] M. Knaapila, M. Torkkeli, L. E. Horsburgh, L.-O. Pålsson, K. Jokela, R. Serimaa, G. ten Brinke, A. P. Monkman, O. Ikkala, *Appl. Phys. Lett.* **2002**, *81*, 1489.
[18] a) A. G. MacDiarmid, A. J. Epstein, *Synth. Met.* **1994**, *65*, 103; b) L. Dai, J. Lu, B. Matthews, A. W. H. Mau, *J. Phys. Chem. B* **1998**, *102*, 4049.
[19] A. K. Jonscher, *Dielectric Relaxation in Solids*, Chelsea Dielectric, London, **1983**.
[20] K. Lee, A. J. Heeger, *Synth. Met.* **2002**, *128*, 279.

 © 2005 Wiley-VCH Verlag GmbH & Co. KGaA, Weinheim

Natural Products Synthesis

Biomimetic Total Synthesis of Gambogin and Rate Acceleration of Pericyclic Reactions in Aqueous Media**

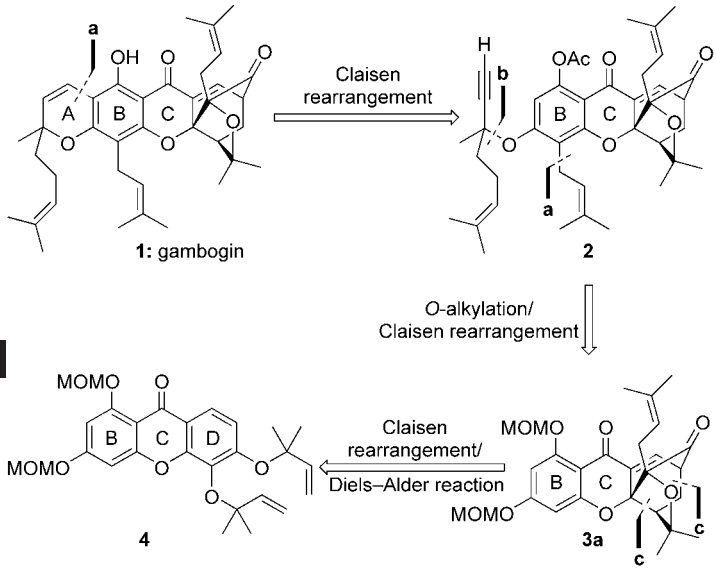
K. C. Nicolaou, Hao Xu, and Markus Wartmann*

Gambogin (**1**, Scheme 1) has an unusual molecular architecture and exhibits cytotoxic properties against the Hela and HEL cell lines (MIC: 6.25 and 3.13 $\mu g\,mL^{-1}$, respectively).[1] Isolated from the gamboge resin of *Garcina hamburyi* in 1996, this naturally occurring substance provides an intriguing synthetic challenge and an opportunity for the development of new synthetic technology and biological tools. Herein we report a biomimetic[2] total synthesis of gambogin[3] and the observation of dramatic rate accelerations of the Claisen rearrangement and the Claisen/Diels–Alder cascade reaction[4] in protic solvents, most notably in water.

[*] Prof. Dr. K. C. Nicolaou, H. Xu
Department of Chemistry and
The Skaggs Institute for Chemical Biology
The Scripps Research Institute
10550 North Torrey Pines Road, La Jolla, CA 92037 (USA)
Fax: (+1) 858-784-2469
E-mail: kcn@scripps.edu
and
Department of Chemistry and Biochemistry
University of California, San Diego
9500 Gilman Drive, La Jolla, CA 92093 (USA)
Dr. M. Wartmann
Novartis Institutes for BioMedical Research
Basel (Switzerland)

[**] We thank Dr. D. H. Huang and Dr. G. Siuzdak for NMR spectroscopic and mass spectrometric assistance, respectively. We thank Robert Reuter (Novartis) for the biological evaluations of gambogin and its analogues. Financial support for this work was provided by grants from the National Institutes of Health (USA) and the Skaggs Institute for Chemical Biology, and a fellowship from the Skaggs Institute for Research (to H.X.).

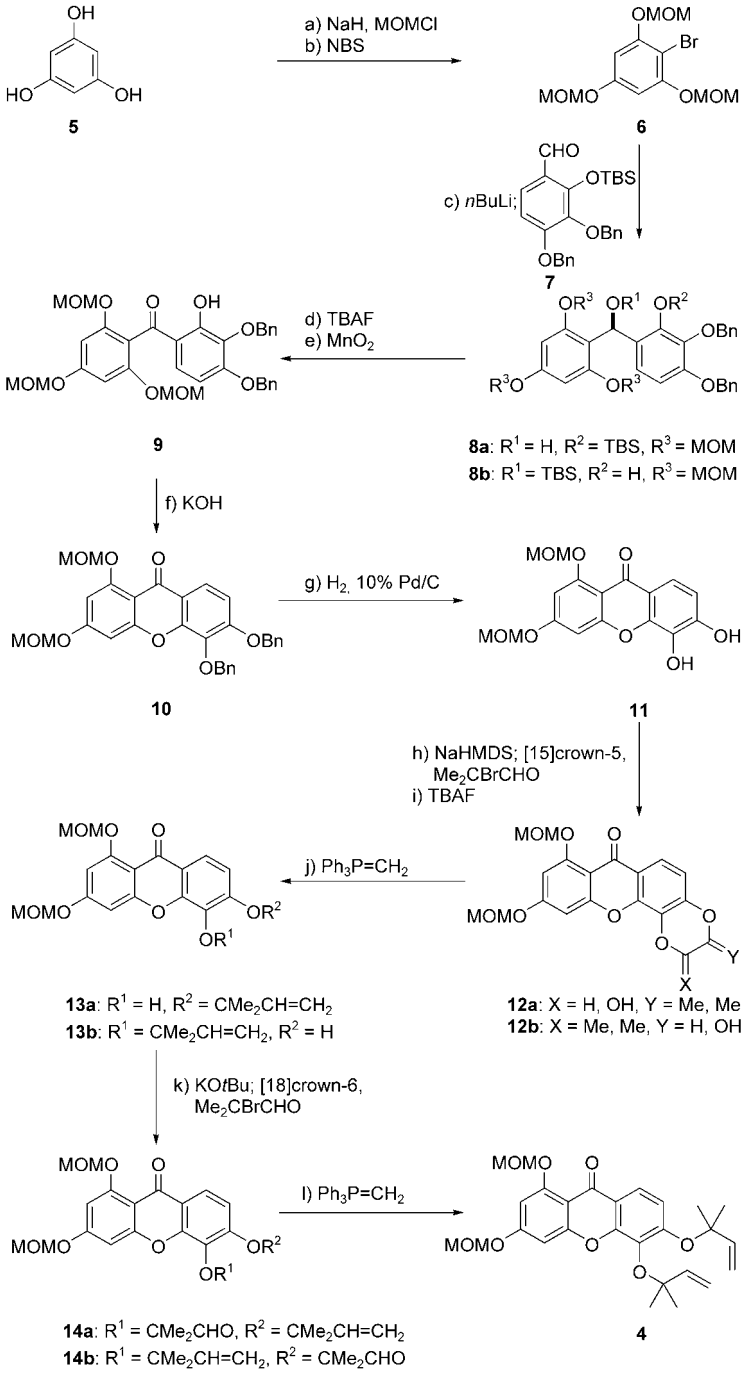
Our retrosynthetic plan for the molecule of gambogin (**1**), whose resemblance to forbesione and lateriflorone[5] influenced our thinking, is shown in Scheme 1. Thus, applying a retro-Claisen rearrangement[6] on ring A (benzopyran ring, mixture of diastereomers) unraveled the acetylenic benzenoid compound **2**, which could be derived from **3a** through *O*-alkylation and, yet again, a Claisen rearrangement. Finally, the cagelike trioxatetracyclo[7.4.1.0^{2,7}.0^{2,11}]tetradecane system[7] was dismantled as previously[5] to the BCD tricycle **4**, whose construction from readily available starting materials was reasonably anticipated. Most significantly, the synthetic plan that emerged from this analysis offered us the opportunity to investigate the possibility of accelerating pericyclic reactions such as the Claisen and Diels–Alder reactions beyond their previously defined boundaries.



Scheme 1. Retrosynthetic analysis of gambogin (1): a) Claisen rearrangement; b) *O*-alkylation; c) Diels–Alder reaction.

The required intermediate **4** was synthesized as summarized in Scheme 2. Phloroglucinol (**5**) was protected with three MOM groups, and the resulting compound was brominated with NBS to afford intermediate **6** in 62% overall yield. Lithiation of **6**, followed by trapping of the generated anion with fully functionalized benzaldehyde **7**[5b,c] in diethyl ether generated bis-aromatic system **8a** in 85% yield. However, when THF was used as the solvent in large-scale operations for solubility considerations, a spontaneous silyl group migration[8] took place, affording **8b** cleanly and in 85% yield. Desilylation of **8a** or **8b** with TBAF and subsequent oxidation with MnO_2 furnished ketone **9** in 68% overall yield. Ketone **9** was heated at reflux in a solution of KOH (EtOH/H_2O) which induced an intramolecular conjugate addition/elimination[9] to afford tricyclic system **10**. Subsequent hydrogenolysis of the two benzyl groups of **10** in THF led to the highly oxygenated xanthone **11** in 76% overall yield. Lactolization of the catechol system of **11** through our previously reported method[5b,c] (KO*t*Bu, [18]crown-6) failed to produce the desired lactols (**12a**/**12b**) in high yield. The procedure was

 © 2005 Wiley-VCH Verlag GmbH & Co. KGaA, Weinheim DOI: 10.1002/anie.200462211



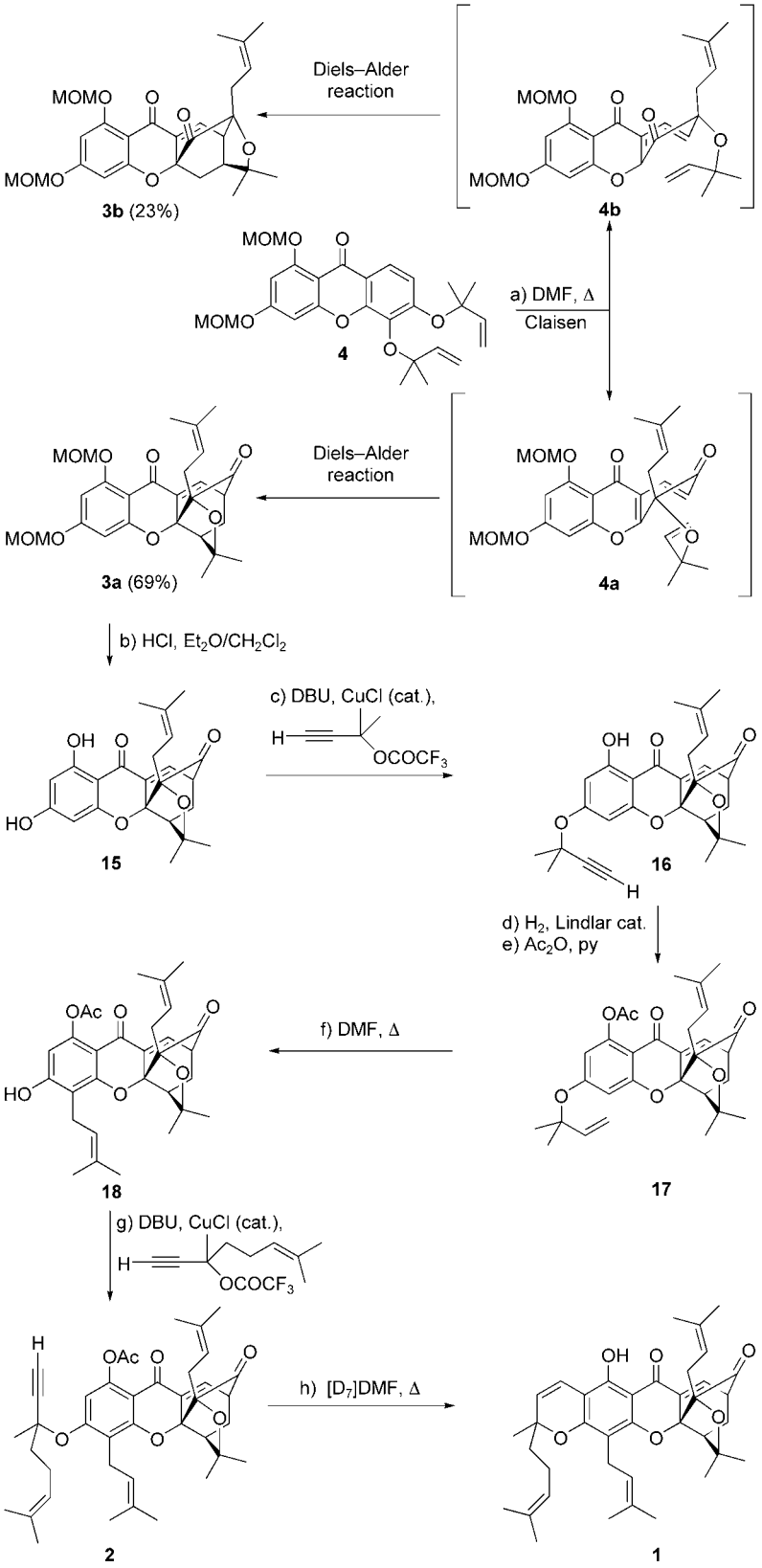
Scheme 2. Synthesis of advanced intermediate **4**: a) NaH (4.0 equiv), MOMCl (3.5 equiv), DMF, 0→25 °C, 2 h, 65%; b) NBS (1.05 equiv), CH_2Cl_2, 25 °C, 1 h, 95%; c) *n*BuLi (1.08 equiv), THF or diethyl ether, −78 °C, 2 h; then **7** (1.0 equiv), −78→0 °C, 0.5 h, 85%; d) TBAF (1.1 equiv), THF, 0 °C, 15 min, 90%; e) MnO_2 (10.0 equiv), CH_2Cl_2, 25 °C, 12 h, 75%; f) NaOH (5.0 equiv), EtOH, 90 °C, 24 h, 80%; g) Pd/C (10 wt%), H_2 (1 atm), THF, 25 °C, 2 h, 95%; h) NaHMDS (2.2 equiv), THF, 0 °C, 30 min; then concentrated and suspended in MeCN; then [15]crown-5 (2.2 equiv), 15 min, bromoisobutyraldehyde (4.0 equiv), 0→25 °C, 30 min; i) TBAF (1.2 equiv), THF, 0 °C, 15 min, 71% over two steps; j) $CH_3P^+Ph_3Br^-$ (3.5 equiv), NaHMDS (3.5 equiv), THF, 0 °C, 1 h; then **12** was added to the generated ylide, 0→25 °C, 0.5 h, 80%; k) KO*t*Bu (1.2 equiv), THF, 0 °C, 30 min; then concentrated and suspended in MeCN; then [18]crown-6 (1.2 equiv), 15 min, bromoisobutyraldehyde (4.0 equiv), 0→25 °C, 2 h, 85%; l) $CH_3P^+Ph_3Br^-$ (1.5 equiv), NaHMDS (1.5 equiv), THF, 0 °C, 1 h; then **14** was added to the generated ylide, 0→25 °C, 0.5 h, 87%. MOM = methoxymethyl, DMF = *N*,*N*-dimethylformamide, NBS = *N*-bromosuccinimide, TBAF = tetra-*n*-butylammonium fluoride, HMDS = hexamethyldisilazane.

modified so as to include NaHMDS and [15]crown-5 instead. The disodium salt of **11**, generated by addition of NaHMDS, was first suspended and then completely dissolved in acetonitrile after addition of [15]crown-5 and sonication. Treatment of this solution with freshly prepared bromoisobutyraldehyde[10] afforded a mixture of regioisomeric TMS-protected lactols (≈1:1) at 0 °C in only 20 min. The unexpected silylation of the lactol moiety might be rationalized by envisioning an intermolecular lactol anion attack of the hexamethyldisilazane generated in situ owing to the enhanced nucleophilicity of the former. Desilylation (TBAF) followed by reaction of the resulting lactols (**12a**/**12b**) with methylene phosphorane provided regioisomeric olefins **13a** and **13b** (≈1:1, 57% over three steps). The original KO*t*Bu/[18]crown-6 protocol proved successful in the second alkylation. Thus, a Wittig olefination sequence converted **13a**/**13b**, via aldehydes **14a**/**14b**, into the desired diolefin **4** in 74% overall yield.

Upon heating in DMF at 120 °C, the xanthone derivative **4** smoothly underwent the expected Claisen/Diels–Alder cascade sequence through the presumed intermediates **4a** and **4b** (Scheme 3) to furnish **3a** and **3b** in 69% and 23% yield, respectively. The structural assignments of these compounds were supported by NOE studies. Removal of the MOM groups from the desired isomer **3a** was smoothly effected through the action of HCl (1.0 M in CH_2Cl_2/Et_2O (1:1)), which generated catechol **15** in 85% yield. As one of the phenolic groups in **15** was deactivated owing to internal hydrogen bonding, we were able to effect selective monopropargylation of the other with $CH{\equiv}CC(Me)_2OCOCF_3$ in the presence of DBU and CuCl[11] in 60% yield (85% based on 70% conversion). Further selective reduction and acetylation furnished olefin **17**, whose Claisen rearrangement proceeded regioselectively and in 69% overall yield from **16**, to afford the prenylated aromatic system **18** as a single isomer. A second propargylation, this time with CH≡CC(Me)-$[CH_2CH_2CH{=}CC(Me)_2]OCOCF_3$,[12] was applied to convert **18** into **2** cleanly, albeit in relatively low conversion as a result of the steric hindrance encountered in the transition state (26% yield; 88% based on 30% conversion). Finally, heating of propargyl ether **2** in [D_7]DMF at 140 °C led directly to gambogin (**1**) as a yellow foam in 65% yield.[13] The high temperature employed in the last operation was apparently sufficient encouragement for the acetate group to depart. Three gambogin analogues (**20a**–**c**) were synthesized through the same strategy (Scheme 4).

The conversion of aryl ether **17** into the prenylated aromatic system **18** provided a good opportunity to investigate solvent effects on the rate of the Claisen rearrangement. Previous work in this field,[14] including ours,[6a] was suggestive of the requirement of heating up to 180 °C in aprotic

 © 2005 Wiley-VCH Verlag GmbH & Co. KGaA, Weinheim

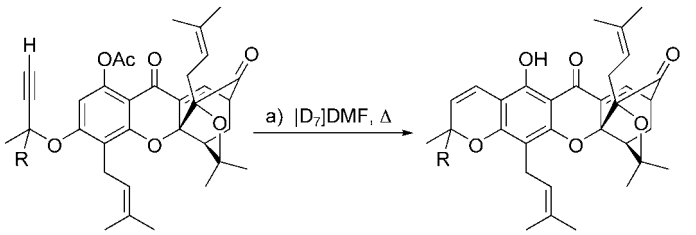


solvents such as DMF or *N*,*N*-diethylaniline, although temperatures as low as 60 °C were successfully employed by Grieco and co-workers[14f] for a Claisen rearrangement of an aliphatic system. The theoretical studies of Jorgensen and Severance,[15] in particular, were encouraging to us, for they pointed to a favorable hydrogen-bonding effect in protic solvents on the rate of pericyclic reactions such as the one under investigation. Table 1 summarizes the results of this study in which various solvents and temperatures were employed. As expected, in [D_6]benzene, there was no detectable reaction of **17** after 4 h at 100 °C, nor did the substrate react in ethanol or trifluoroethanol at 25 °C after the same period of time. In [D_7]DMF, however, we began to observe conversion of **17** into **18** through the Claisen rearrangement at 50 °C (4.5 h, 25 % conversion), whereas at 100 °C, the reaction was complete within 0.5 h. The same accelerating effect was noticed in methanol at 50 °C (4.5 h, 50 % conversion) and 100 °C (0.5 h, 100 % conversion). The addition of water to the latter solvent ($MeOH/H_2O = 2:1$) resulted in an even faster reaction (50 °C: 3.5 h, 100 % conversion or 100 °C: 0.25 h, 100 % conversion), whereas an increase in the water content of the solvent mixture to 1:1 provided similar rate acceleration (50 °C: 2.5 h, 100 % conversion or 100 °C: 0.25 h, 100 % conversion). Further addition of water was detrimental owing to precipitation of the substrate. The highest rate acceleration, however, was observed in trifluoroethanol/H_2O (1:1) (25 °C: 75 h, 100 % conversion or 40 °C: 65 h, 100 % conversion) and ethanol/H_2O (1:1) (25 °C: 72 h, 100 % conversion or 40 °C: 60 h, 100 % conversion). The ability to carry out this type of Claisen rearrangement at ambient temperature is unprecedented and is expected to expand the scope of this process to include otherwise fragile substrates and/or products.

Encouraged by these results, we proceeded to explore the effect of the same solvents on the Claisen/Diels–Alder cascade sequence involved in the conversion of **4** into **3a** (and **3b**, see Scheme 3). Table 2 exhibits the findings of this study. Thus, in [D_6]benzene, there was no reaction at 100 °C after 4 h, and no detectable reactions occurred in ethanol, trifluoroethanol or [D_7]DMF at 65 °C after 4 h. In [D_7]DMF at 100 °C,

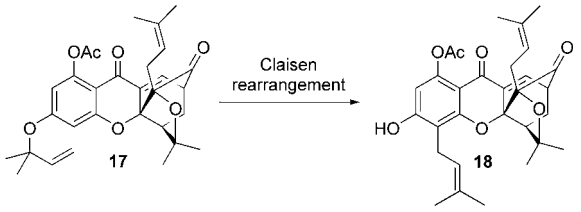
Scheme 3. Total synthesis of gambogin (**1**): a) DMF, 120 °C, 1 h, **3a** (69 %) and **3b** (23 %); b) HCl (1.0 M) in Et_2O/CH_2Cl_2 (1:1), 25 °C, 24 h, 85 %; c) propargyl alcohol (1.4 equiv), DBU (1.4 equiv), TFAA (1.4 equiv), MeCN, 0 °C, 30 min; DBU (1.5 equiv), CuCl (0.1 % equiv), 15 min; then TFA propargyl ester, 0 °C, 5 h, 60 % (85 % based on 70 % conversion); d) Lindlar catalyst (10 wt %), H_2 (1 atm), EtOAc (contaminated with 0.02 % quinoline), 25 °C, 1 h, 95 %; e) Ac_2O (10.0 equiv), py (10.0 equiv), 4-DMAP (1.0 equiv), CH_2Cl_2, 25 °C, 8 h, 85 %; f) DMF, 120 °C, 0.5 h, 85 %; g) propargyl alcohol (1.4 equiv), DBU (1.4 equiv), TFAA (1.4 equiv), MeCN, 0 °C, 30 min; DBU (1.5 equiv), CuCl (0.1 % equiv), 15 min; then TFA propargyl ester, 0 °C, 5 h, 26 % (88 % based on 30 % conversion); h) [D_7]DMF, 140 °C, 2 h, 65 %. DBU = 1,8-diazabicyclo[5, 4, 0]undec-7-ene, TFAA = trifluoracetic anhydride, py = pyridine, 4-DMAP = 4-dimethylaminopyridine.

 © 2005 Wiley-VCH Verlag GmbH & Co. KGaA, Weinheim



Scheme 4. Synthesis of analogues **20a–c** of gambogin: a) [D_7]DMF, 140 °C, 2 h, 65 %.

Table 1: Solvent effects on the rate of the Claisen rearrangement of **17** into **18**.[a]



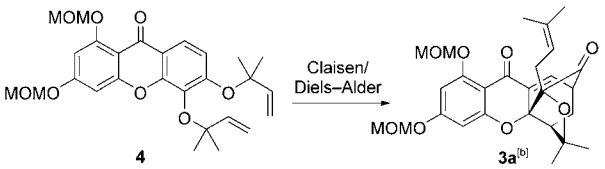
Entry	Solvent	*T* [°C]	*t* [h]	Conversion [%]
1	[D_6]benzene	100	4	0
2	EtOH	25	4	0
3	TFE[b]	25	4	0
4	[D_7]DMF	50	4.5	25
5	[D_7]DMF	100	0.5	100
6	MeOH	50	4.5	50
7	MeOH	100	0.5	100
8	MeOH/H_2O (2:1)	50	3.5	100
9	MeOH/H_2O (2:1)	100	0.25	100
10	MeOH/H_2O (1:1)	50	2.5	100
11	MeOH/H_2O (1:1)	100	0.25	100
12	TFE/H_2O (1:1)	25	75	100
13	TFE/H_2O (1:1)	40	65	100
14	EtOH/H_2O (1:1)	25	72	100
15	EtOH/H_2O (1:1)	40	60	100

[a] The reactions were carried out on a 0.1–1.0-mmol scale and monitored by disappearance of starting material by TLC and ^{1}H NMR spectroscopy. [b] TFE = trifluoroethanol.

however, the reaction started to proceed (2 h, 75 % conversion). In methanol, although there was no reaction at 65 °C after 4 h, the sequence was complete after only 1 h at 100 °C. An increase in the amount of water in the methanolic solvent (MeOH/H_2O 2:1→1:1→1:2) caused a rather dramatic effect in rate acceleration (100 % conversion at 100 °C after 0.5–1 h, Table 2, entries 9, 11, and 15, or 100 % conversion at 65 °C after 3.5–4.5 h, Table 2, entries 8, 10, and 14). This remarkable effect was also observed more or less unchanged in ethanol/water (1:1) and trifluoroethanol/water (1:1) mixtures (Table 2, entries 12 and 13).

The explanation for the observed rate acceleration of both the Claisen rearrangement and the Diels–Alder reaction constituting the cascade sequence in the conversion of **4** into **3a** can be found in previous theoretical as well as experimental work.[14,16] For the Claisen rearrangement, the model[14g] shown in Figure 1, as developed by Jorgensen and

Table 2: Solvent effects on the rate of the Claisen/Diels–Alder cascade of **4** into **3a**.[a]



Entry	Solvent	*T* [°C]	*t* [h]	Conversion [%]
1	[D_6]Benzene	100	4	0
2	EtOH	65	4	0
3	TFE	65	4	0
4	[D_7]DMF	65	4	0
5	[D_7]DMF	100	2.0	75
6	MeOH	65	4	0
7	MeOH	100	1.0	100
8	MeOH/H_2O (2:1)	65	4.5	100
9	MeOH/H_2O (2:1)	100	1.0	100
10	MeOH/H_2O (1:1)	65	4.0	100
11	MeOH/H_2O (1:1)	100	0.5	100
12	TFE/H_2O (1:1)	65	4.0	100
13	EtOH/H_2O (1:1)	65	4.0	100
14	MeOH/H_2O (1:2)	65	3.5	100
15	MeOH/H_2O (1:2)	100	0.5	100

[a] The reactions were carried out on a 0.1–1.0-mmol scale and monitored by disappearance of starting material by TLC and ^{1}H NMR spectroscopy. [b] The ratio of the two products **3a**:**3b** (see Scheme 3) stayed constant (≈3:1) during the course of the reactions.

Severance[15] based on Monte Carlo calculations, postulates one hydrogen bond from the solvent to one of the lone pairs of electrons of the ethereal oxygen atom in the ground state **4** and two hydrogen bonds from two solvent molecules to both lone pairs of electrons of the oxygen atom in the transition state **4-TS**, by virtue of the distortion of conjugation as the reaction begins to occur, a condition that results in catalysis. This bifurcated-hydrogen-bond hypothesis has found corroboration in the X-ray crystal structures of chorismate mutase isolated from *Bacillus subtilis* (BsCM)[17] and *Escherichia coli* (EcCM),[18] the enzyme that catalyzes the Claisen rearrangement[19] of the chorismate anion to the prephenate anion. Thus, whereas the polar aprotic solvent DMF can only accelerate the nonsynchromic, semi-zwitterionic[20] Claisen rearrangement by stabilizing its polar transition state, the protic solvents, because of their hydrogen-bond-donor abilities[21] (most notably water), are able to provide additional stabilization of the transition state and thus promote the dramatic acceleration effects observed.[22] It was interesting to note that a further increase in the water content in these alcoholic solvents resulted in the precipitation of the substrate and shut-down of the reaction, presumably as a result of the insufficient solvation that accompanied the observed precipitation of the reacting substrate. The concurrent acceleration of the Diels–Alder component of the cascade is due, as explained by Breslow and co-workers,[16,23] to the hydrophobic effect[24] and the unique internal pressure of water rather than simple polarity or hydrogen-bonding phenomena. It was interesting to note that at no temperature in any solvent system could we detect any of the postulated intermediate dienone **22**, leading us to conclude that the Diels–Alder[25]

 © 2005 Wiley-VCH Verlag GmbH & Co. KGaA, Weinheim

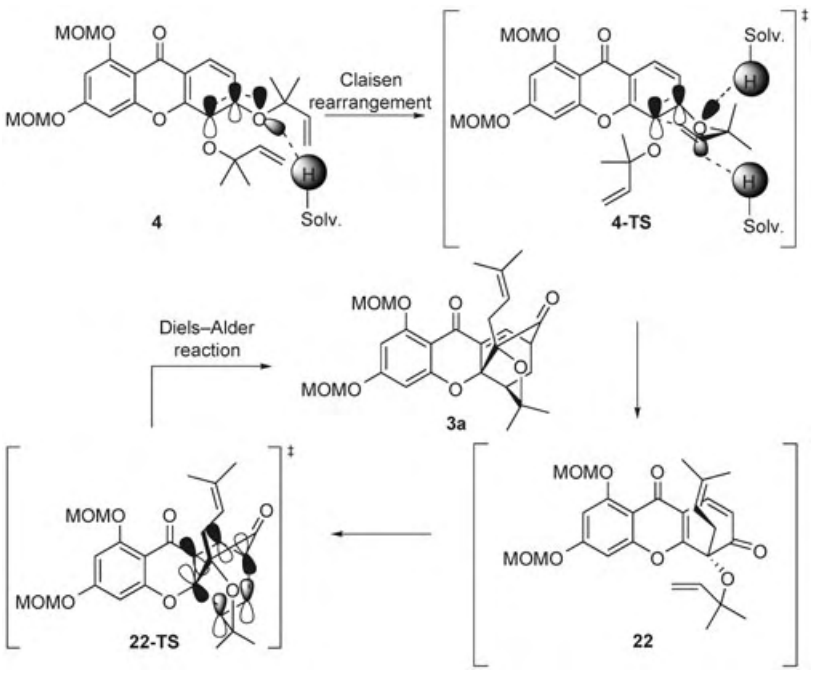


Figure 1. Molecular-orbital rationale for the acceleration of the Claisen/Diels–Alder cascade reaction (**4**→**3a**) by protic solvents.

intramolecular collapse was the faster of the two pericyclic reactions involved in this cascade. To the best of our knowledge, this is the first example of a Claisen/Diels–Alder cascade sequence accelerated by water.

The synthesized compounds **20a–c**, except for **20a**, which are diastereomeric mixtures, like gambogin **1** itself, were tested for their cytotoxicity against human epidermoid cancer cell line KB-31 and its taxol-resistant mutant cell line KB-8511. The results are shown in Table 3. Both the methyl- and isopentyl-substituted analogues **20a** and **20c** exhibited

Table 3: Cytotoxicity of gambogin (**1**) and its analogues (**20a–c**).[a]

Entry	Compound	IC_{50} [μM]	
		KB-31	KB-8511
1	**1**	9.35	>10
2	**20a**	8.41	>10
3	**20b**	>10	>10
4	**20c**	6.01	>10

[a] The antiproliferative effects of the tested compounds were assessed in human epidermoid cancer cell lines: the parent cell line (KB-31) and the taxol-resistant (due to Pgp-overexpression) cell line (KB-8511).

slightly higher potencies than the natural compound **1** against KB-31, while the ethyl derivative **20b** was less active. All compounds, including gambogin itself, failed to exhibit significant cytotoxicity against the taxol-resistant mutant cell line KB-8511 at concentrations below 10 μM. The chemistry described herein may provide entries to biologically active molecules of the gambogin type and stimulate further studies in the reaction process development.

Received: October 5, 2004

Keywords: Claisen rearrangement · Diels–Alder reaction · natural products · rate acceleration · total synthesis

[1] J. Asano, K. Chiba, M. Tada, T. Yoshii, *Phytochemistry* **1996**, *41*, 815–820.
[2] For a number of biologically active, phloroglucinol-derived natural products, see: a) M. Tada, K. Chiba, H. Yamada, H. Maruyama, *Phytochemistry* **1991**, *30*, 2559–2562; b) M. Nagai, M. Tada, *Chem. Lett.* **1987**, 1337–1340.
[3] An elegant total synthesis of gambogin was recently reported: E. J. Tisdale, I. Slobodov, E. A. Theodorakis, *Proc. Natl. Acad. Sci. USA* **2004**, *101*, 12030–12035; for other related publications from this group, see: a) E. J. Tisdale, C. Chowdhury, B. G. Vong, H. Li, E. A. Theodorakis, *Org. Lett.* **2002**, *4*, 909–912; b) E. J. Tisdale, B. G. Vong, H. Li, S. H. Kim, C. Chowdhury, E. A. Theodorakis, *Tetrahedron* **2003**, *59*, 6873–6887; c) E. J. Tisdale, I. Slobodov, E. A. Theodorakis, *Org. Biomol. Chem.* **2003**, *1*, 4418–4422.
[4] For recent reviews on biomimetic and cascade-type strategies in total synthesis, see: a) K. C. Nicolaou, S. A. Snyder, T. Montagnon, G. E. Vassilikogiannakis, *Angew. Chem.* **2002**, *114*, 1742–1773; *Angew. Chem. Int. Ed.* **2002**, *41*, 1668–1698; b) K. C. Nicolaou, T. Montagnon, S. A. Snyder, *Chem. Commun.* **2003**, 551–564.
[5] For previous total syntheses of natural products with trioxatetracyclo [7.4.1.$0^{2,7}$.$0^{2,11}$]tetradecane-type structures from this group, see: a) K. C. Nicolaou, J. Li, *Angew. Chem.* **2001**, *113*, 4394–4398; *Angew. Chem. Int. Ed.* **2001**, *40*, 4264–4268; b) K. C. Nicolaou, P. K. Sasmal, H. Xu, K. Namoto, A. Ritzén, *Angew. Chem.* **2003**, *115*, 4357–4361; *Angew. Chem. Int. Ed.* **2003**, *42*, 4225–4229; c) K. C. Nicolaou, P. K. Sasmal, H. Xu, *J. Am. Chem. Soc.* **2004**, *126*, 5493–5501.
[6] For recent examples of Claisen rearrangements in organic synthesis, see: a) K. C. Nicolaou, J. A. Pfefferkorn, A. J. Roecker, G.-Q. Cao, S. Barluenga, H. J. Mitchell, *J. Am. Chem. Soc.* **2000**, *122*, 9939–9953, and references therein; b) S. Yamaguchi, M. Ishibashi, K. Akasaka, H. Yokoyama, M. Miyazawa, Y. Hirai, *Tetrahedron Lett.* **2001**, *42*, 1091–1093; c) I. Iwai, J. Ide, *Chem. Pharm. Bull.* **1963**, *11*, 1042–1049; d) J. Hlubucek, E. Ritchie, W. C. Taylor, *Tetrahedron Lett.* **1969**, *10*, 1369–1370; e) W. K. Anderson, E. J. LaVoie, P. G. Whitkop, *J. Org. Chem.* **1974**, *39*, 881–884.
[7] For the Claisen-rearrangement-based hypothesis regarding the biosynthesis of *Garcina* family natural products, see: a) A. J. Quillinan, F. Scheinmann, *J. Chem. Soc. Perkin Trans. 1* **1972**, 1382–1387; b) A. J. Quillinan, F. Scheinmann, *J. Chem. Soc.* **1971**, 966–967.
[8] J. Mulzer, B. Schöllhorn, *Angew. Chem.* **1990**, *102*, 433–434; *Angew. Chem. Int. Ed. Engl.* **1990**, *29*, 431–432.
[9] S. Horne, R. Rodrigo, *J. Org. Chem.* **1990**, *55*, 4520–4522.
[10] A. L. J. Bechwith, C. B. Thomas, *J. Chem. Soc. Perkin Trans. 2* **1973**, 861–872.
[11] J. D. Godfrey, Jr., R. H. Mueller, T. C. Sedergran, N. Soundararajan, V. J. Colandrea, *Tetrahedron Lett.* **1994**, *35*, 6405–6408.
[12] P. H. Kahn, J. Cossy, *Tetrahedron Lett.* **1999**, *40*, 8113–8114.
[13] We thank Professor M. Tada (Tokyo University of Agriculture and Techonology, Japan) for sending us the ^{1}H NMR and ^{13}C NMR spectra of natural gambogin for comparison.
[14] For Claisen rearrangements accelerated in protic solvents, see: a) J. F. Kincaid, D. S. Tarbell, *J. Am. Chem. Soc.* **1939**, *61*, 3085–3089; b) W. N. White, D. Gwynn, R. Schlitt, C. Girard, W. Fife, *J. Am. Chem. Soc.* **1958**, *80*, 3271–3277; c) H. L. Goering, R. R. Jacobson, *J. Am. Chem. Soc.* **1958**, *80*, 3277–3285; d) R. M.

 © 2005 Wiley-VCH Verlag GmbH & Co. KGaA, Weinheim

Coates, B. D. Rogers, S. J. Hobbs, D. P. Curran, D. R. Peck, *J. Am. Chem. Soc.* **1987**, *109*, 1160 – 1170; e) J. J. Gajewski, J. Jurayj, D. R. Kimbrough, M. E. Gande, B. Ganem, B. K. Carpenter, *J. Am. Chem. Soc.* **1987**, *109*, 1170 – 1186; f) P. A. Grieco, E. B. Brandes, S. McCann, J. D. Clark, *J. Org. Chem.* **1989**, *54*, 5849 – 5851; g) B. Ganem, *Angew. Chem.* **1996**, *108*, 1014 – 1023; *Angew. Chem. Int. Ed. Engl.* **1996**, *35*, 936 – 945.

[15] D. L. Severance, W. L. Jorgensen, *J. Am. Chem. Soc.* **1992**, *114*, 10966 – 10968.

[16] For Diels–Alder reactions accelerated in water, see: a) R. Breslow, *Acc. Chem. Res.* **2004**, *37*, 471 – 478; b) D. Rideout, R. Breslow, *J. Am. Chem. Soc.* **1980**, *102*, 7816 – 7817; c) U. Lindstroem, *Chem. Rev.* **2002**, *102*, 2751 – 2771; d) Y. Harano, H. Sato, F. Hirata, *J. Am. Chem. Soc.* **2000**, *122*, 2289 – 2293; e) P. A. Grieco, K. Yoshida, P. Garner, *J. Org. Chem.* **1983**, *48*, 3137 – 3139; f) P. A. Grieco, M. D. Kaufman, *J. Org. Chem.* **1999**, *64*, 6041 – 6048; g) S. Otto, J. B. F. N. Engberts, J. C. T. Kwak, *J. Am. Chem. Soc.* **1998**, *120*, 9517 – 9525; h) J. F. Blake, W. L. Jorgensen, *J. Am. Chem. Soc.* **1991**, *113*, 7430 – 7432.

[17] Y. M. Chook, J. V. Gray, H. Ke, W. N. Lipscomb, *J. Mol. Biol.* **1994**, *240*, 476 – 500.

[18] A. Y. Lee, P. A. Karplus, B. Ganem, J. Clardy, *J. Am. Chem. Soc.* **1995**, *117*, 3627 – 3628.

[19] For the biological catalysis of the Claisen and Diels–Alder reactions, see: a) D. Hilvert, K. W. Hill, K. D. Nared, M. T. M. Auditor, *J. Am. Chem. Soc.* **1989**, *111*, 9261 – 9262; b) V. E. Gouverneur, K. N. Houk, B. de Pascual-Teresa, B. Beno, K. D. Janda, R. A. Lerner, *Science* **1993**, *262*, 204 – 208; c) J. A. Xu, Q. L. Deng, J. G. Chen, K. N. Houk, J. Bartek, D. Hilvert, I. A. Wilson, *Science* **1999**, *286*, 2345 – 2348; d) S. Laschat, *Angew. Chem.* **1996**, *108*, 313 – 315; *Angew. Chem. Int. Ed. Engl.* **1996**, *35*, 289 – 291; e) D. Y. Jackson, M. N. Liang, P. A. Bartlett, P. G. Schultz, *Angew. Chem.* **1992**, *104*, 196 – 197; *Angew. Chem. Int. Ed. Engl.* **1992**, *31*, 182 – 183; f) D. Hilvert, K. D. Nared, *J. Am. Chem. Soc.* **1988**, *110*, 5593 – 5594.

[20] For a discussion of the transition state of the Claisen rearrangement, see: a) T. H. Lowry, K. S. Richardson, *Mechanism and Theory in Organic Chemistry, 3rd ed.*, Harper & Row, New York, **1987**, chap. 10; b) J. J. Gajewski, N. D. Conrad, *J. Am. Chem. Soc.* **1979**, *101*, 2747 – 2748; c) J. J. Gajewski, *Acc. Chem. Res.* **1980**, *13*, 142 – 148.

[21] For a discussion on hydrogen-bond donors and acceptors, see: G. R. Desiraju, T. Steiner, *The Weak Hydrogen Bond in Structural Chemistry and Biology*, Oxford University Press, New York, **1999**, chap. 1 and 2.

[22] Another critical factor for the rate acceleration of the Claisen-rearrangement step is the hydrophobic effect; see: J. J. Gajewski, *Acc. Chem. Res.* **1997**, *30*, 219 – 225.

[23] For a mechanism discussion of simple organic reactions accelerated in water, see: a) R. Breslow, *Acc. Chem. Res.* **1991**, *24*, 159 – 164; b) E. T. Kool, R. Breslow, *J. Am. Chem. Soc.* **1988**, *110*, 1596 – 1597; c) R. Breslow, Z. Zhu, *J. Am. Chem. Soc.* **1995**, *117*, 9923 – 9924; d) R. Breslow, K. Groves, M. U. Mayer, *J. Am. Chem. Soc.* **2002**, *124*, 3622 – 3635.

[24] For a review of hydrophobic effects, see: a) A. Ben-Naim, *Hydrophobic Interactions*, Plenum, New York, **1980**, p. 303; b) C. Tanford, *The Hydrophobic Effect*, *2nd ed.*, Wiley, New York, **1980**, chap. 1.

[25] For a review of inverse-electron-demand Diels–Alder reactions, see: D. L. Boger, *Chem. Rev.* **1986**, *86*, 781 – 793, and references therein.

[26] We thank Professor K. B. Sharpless and Professor M. G. Finn for helpful discussions on the rate-acceleration phenomena in water.

 © 2005 Wiley-VCH Verlag GmbH & Co. KGaA, Weinheim

Asymmetric Catalysis

A Novel Dinuclear Chiral Niobium Complex for Lewis Acid Catalyzed Enantioselective Reactions: Design of a Tridentate Ligand and Elucidation of the Catalyst Structure**

Shū Kobayashi, Kenzo Arai, Haruka Shimizu, Yoichi Ihori, Haruro Ishitani, and Yasuhiro Yamashita*

Development of chiral catalysts for asymmetric reactions is one of the most important tasks in organic synthesis.[1] While various types of catalysts have been developed, exploitation of novel catalysts, especially those based on unusual metals and novel ligands, applicable to new enantioselective reactions, is still very important. Herein we describe the first highly enantioselective niobium(v) Lewis acid catalyst.

Niobium lies below vanadium in Group 5 and is expected to have high Lewis acidity,[2] there are only a few reports of chiral niobium catalysts, which have been used in asymmetric Diels–Alder reactions and oxidations.[3,4] This situation is in remarkable contrast to many asymmetric transformation catalyzed by the neighboring Group 4 metal complexes of titanium[5] and zirconium.[6] To prepare an efficient chiral pentavalent niobium(v) catalyst for activation of aldehydes or imines, we designed tridentate ligands **4a–d** (see Equation (1)),[7] which were synthesized according to conventional methods).[8]

Ligands **4a–d** were combined with niobium alkoxides ($Nb(OR)_5$), and were employed as catalysts for the Mannich-type reaction of imines **1** with silicon enolates **2** [Eq. (1)].[9]

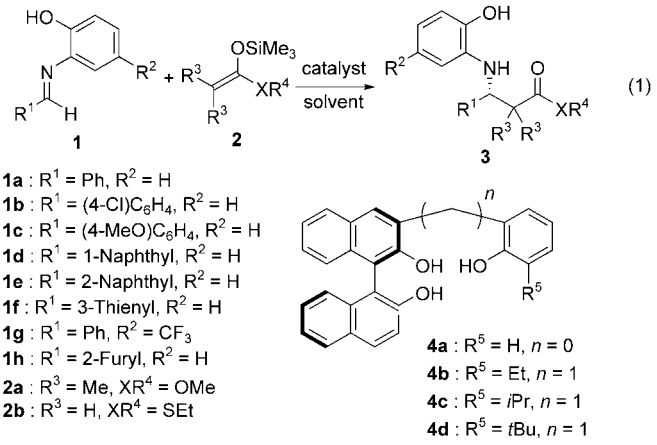
For the reaction of **1a** with **2a**, several reaction parameters were examined, and the results are summarized in Table 1. It was found that *N*-methylimidazole (NMI) was effective as an additional ligand.[10] Among the chiral ligands screened, **4c** gave the best enantioselectivity (Table 1, entry 3). The selectivity was further improved in a toluene–CH_2Cl_2 (1:1) mixed solvent system (Table 1, entry 6) and in the presence of 3-Å or 4-Å molecular sieves (MS 3Å or MS 4Å; Table 1, entries 7 and 8). We also examined several niobium alkoxides. When $Nb(OMe)_5$ was combined with ligand **4c**, the desired Mannich-type adduct was obtained in 86% yield with 99% *ee* (Table 1, entry 10). It is noteworthy that almost complete selectivity has been achieved using this novel chiral niobium catalyst.

[*] Prof. Dr. S. Kobayashi, K. Arai, H. Shimizu, Y. Ihori, Dr. H. Ishitani, Dr. Y. Yamashita
Graduate School of Pharmaceutical Sciences
The University of Tokyo
Hongo, Bunkyo-ku, Tokyo 113-0033, Japan
Fax: (+81)3-5684-0634
E-mail: skobayas@mol.f.u-tokyo.ac.jp

[**] This work was partially supported by CREST, SORT, and ERATO, Japan Science Technology Corporation (JST) and a Grant-in-Aid for Scientific Research from Japan Society of the Promotion of Sciences (JSPS).

Supporting information for this article is available on the WWW under http://www.angewandte.org or from the author.

 DOI: 10.1002/anie.200462204 © 2005 Wiley-VCH Verlag GmbH & Co. KGaA, Weinheim



(1)

Table 1: Effect of binol derivatives on the reaction of **1a** with **2a** [Eq. (1)].[a]

Entry	$Nb(OR)_5$	Binol	Additive[b]	Yield [%]	*ee* [%]
1	OEt	**4a**	none	64	14
2	OEt	**4b**	none	71	35
3	OEt	**4c**	none	73	67
4	OEt	**4d**	none	34	6
5[c]	OEt	**4c**	none	37	82
6[d]	OEt	**4c**	none	84	85
7[d]	OEt	**4c**	MS 3Å	84	92
8[d]	OEt	**4c**	MS 4Å	74	88
9[d,e]	OEt	**4c**	MS 3Å	87	95
10[d,e]	OMe	**4c**	MS 3Å	86	99
11[d,e]	O*n*Pr	**4c**	MS 3Å	80	90
12[d,e]	O*i*Bu	**4c**	MS 3Å	28	73

[a] The reactions were carried out using 10 mol% of $Nb(OR)_5$, 10–12 mol% of the binol derivative, and 10–12 mol% of NMI in CH_2Cl_2 at 0°C for 18 h. [b] Molecular sieves (100 mg/0.6 mmol substrate) were used. [c] In toluene. [d] In toluene:CH_2Cl_2 = 1:1. [e] −20°C, 48 h.

Table 2: Substrate generality [Eq. (1)].[a]

Entry	Imine	Si enolate	Product	Yield [%]	*ee* [%]
1[b,d]	**1a**	**2a**	**3a**	86	99
2[c,d]	**1a**	**2a**	**3a**	69	96
3[e]	**1b**	**2a**	**3b**	82	98
4[f]	**1c**	**2a**	**3c**	79	96
5	**1d**	**2a**	**3d**	40	95
6	**1e**	**2a**	**3e**	77	98
7	**1f**	**2a**	**3f**	85	93
8[f]	**1g**	**2a**	**3g**	75	91
9[f]	**1a**	**2b**	**3h**	69[g]	84
10	**1b**	**2b**	**3i**	44	88
11[f]	**1h**	**2b**	**3j**	70	87

[a] The reactions were performed using 10 mol% of $Nb(OMe)_5$, 12 mol% of **4c**, 12 mol% of NMI, and MS 3Å (100 mg/0.6 mmol substrate) at −20°C for 48 h. [b] 5 mol% of the catalyst was used. [c] 2 mol% of the catalyst was used. [d] MS 3Å (50 mg/0.4 mmol substrate) was added. [e] −10°C, 18 h. [f] −10°C, 48 h. [g] Determined by ^1H NMR spectroscopy.

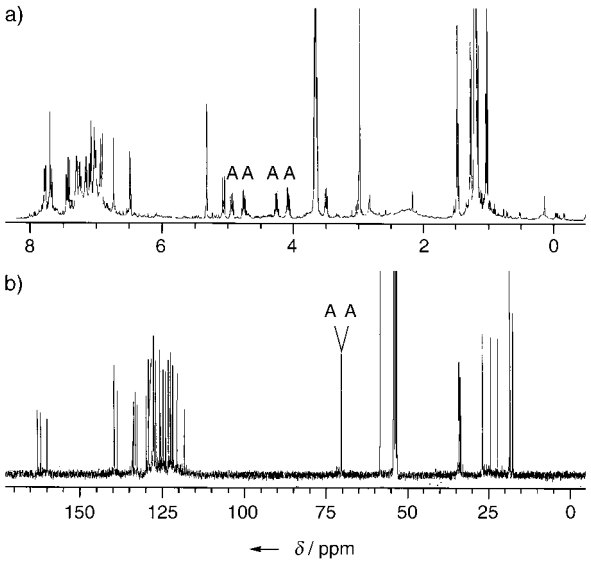


Figure 1. a) ^1H and b) ^{13}C NMR spectra of a catalyst solution of $Nb(OEt)_5$, **4c**, and NMI in CD_2Cl_2. **A**: OCH_2CH_3.

Several other substrates were tested, and the results are summarized in Table 2. Various imines reacted with **2a** in toluene-CH_2Cl_2 (1:1) between at −10 and −20°C to afford the corresponding Mannich-type adducts in high yields with excellent enantioselectivities. When silicon enolate **2b** was used, the enantioselectivities were good but slightly decreased (Table 2, entries 9–11). The catalyst loading could be reduced from 10 mol% to 5 mol% and 2 mol% without significant loss of the yield and selectivity.[11]

We next turned our attention to the structure of the chiral catalyst. Analysis of the ^1H and ^{13}C NMR spectra of $Nb(OEt)_5$, **4c**, and NMI in CD_2Cl_2 revealed the presence of a single species, in which Nb and **4c** were a 1:1 molar ratio (Figure 1). Since two sets of resonances (**A** in Figure 1) were observed for -OEt, structure **5** was tentatively assigned as a single unit of the catalyst (Figure 2). Since niobium complexes are known to form dimeric structures easily,[12] we then investigated the nonlinear effect (NLE)[13] in the Mannich-type reaction to confirm whether a dimeric structure existed. We conducted the reaction using the ligand with low enantiomeric excess (23% *ee*, 45% *ee*, 73% *ee*), and observed a significant positive NLE (■ in Figure 3). We prepared optically pure *R* and *S* chiral niobium catalysts, then mixed them together to form the catalysts with low enantiomeric excess, and conducted the

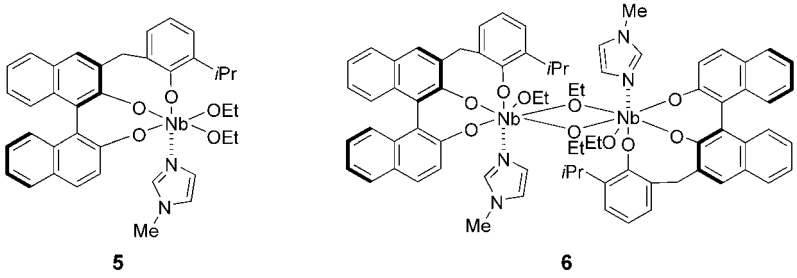


Figure 2. Possible structures of the highly selective Nb catalyst in solution.

 © 2005 Wiley-VCH Verlag GmbH & Co. KGaA, Weinheim

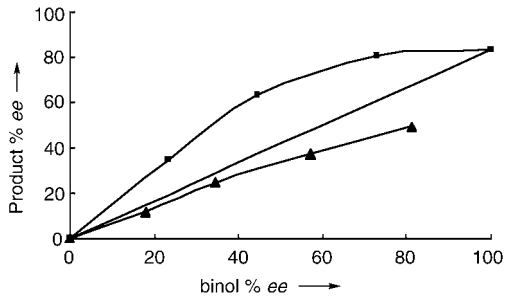


Figure 3. Nonlinear effect. The reactions were performed using **1a** and **2a** as substrates in CH_2Cl_2 at −20 °C in the presence of the Nb catalyst (10 mol %),—— linear, ■ low *ee* value binol ligand, ▲ mixed catalyst solution.

same Mannich-type reaction. Interestingly, in this case a slightly negative nonlinear effect was observed (▲ in Figure 3). These results suggest that a dimeric species such as **6** is formed by combining $Nb(OR)_5$, **4c**, and NMI, and that the *R*,*S* heterodimeric species might be less reactive than the *R*,*R* and *S*,*S* homodimeric species. It is also assumed that no ligand exchange occurred after formation of the dimeric species.

Single crystals of a Nb complex suitable for X-ray analysis were obtained by the addition of petroleum ether to a combination of $Nb(OEt)_5$, **4c**, and NMI in toluene. Crystals formed gradually, and the X-ray structure obtained is shown in Figure 4.[14] Surprisingly, crystal structure **7** was different from the assumed structure in solution (**6**). Characteristic features of **7** are a Nb-(μ_2-O)-Nb unit, and that the binol moiety of **4c** is bound in a bidentate fashion to one niobium

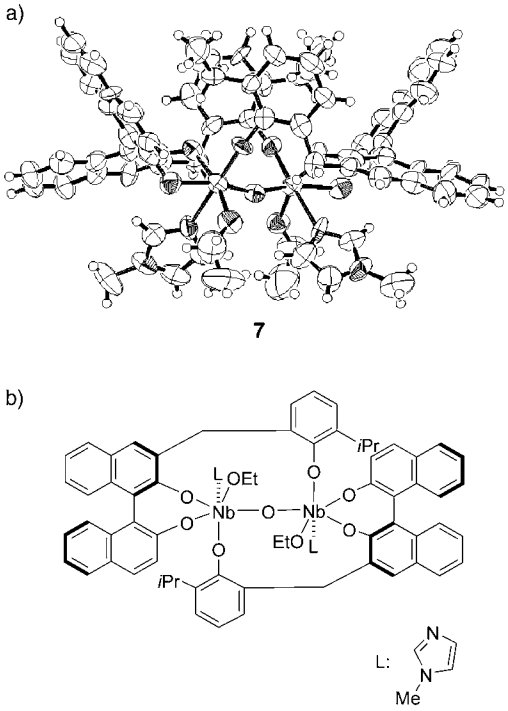


Figure 4. a) Crystal structure and b) structural formula of the niobium complex **7**.

atom while the oxygen atom of the pendent phenol moiety is bonded to the other niobium atom (bridged structure).

Crystals of **7** thus obtained were also analyzed by ^1H and ^{13}C NMR spectroscopy in CD_2Cl_2 (Figure 5). Of note is that

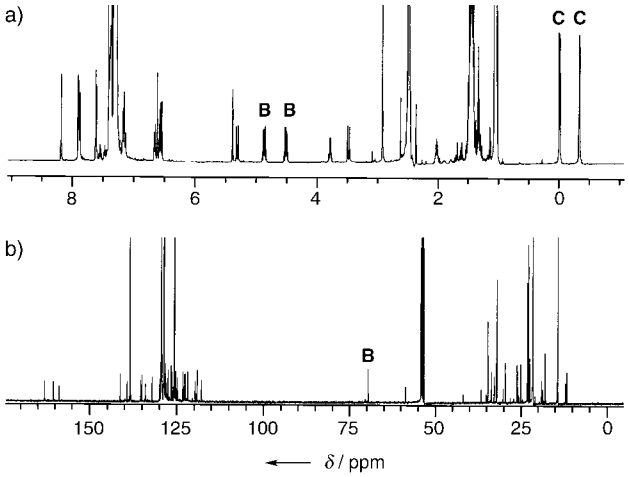


Figure 5. a) ^1H and b) ^{13}C NMR spectra of **7** in CD_2Cl_2. **B**: OCH_2CH_3, **C**:$(CH_3)_2CH$.

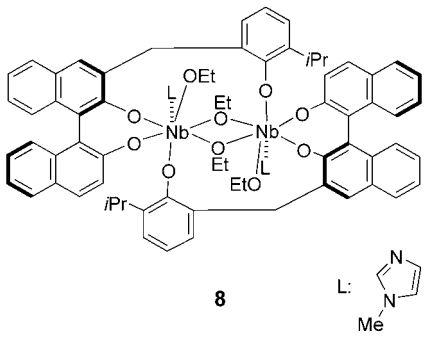
the spectra are quite different from those of the assumed complex **6** (Figure 1). The principle differences are the number of the ethoxy moieties (**B** in Figure 5) and the chemical shifts of the methyl groups in the isopropyl substituents (**C** in Figure 5) in the ^1H NMR spectrum. The chemical shifts of the methyl groups in **7** are at around $\delta = 0$ ppm, while the chemical shifts of the methyl groups in the assumed complex **6** are observed at around $\delta = 1.2$ ppm. Aromatic shielding effects might be the cause of the significant upfield shift.

Chiral Nb complex **7** displayed lower catalytic activity in the Mannich-type reaction of imine **1a** with silicon enolate **2a** (9 mol % based on Nb atom) of **7**, in dichloromethane at −20 °C for 18 h). The desired product was obtained in 21 % yield with 61 % *ee*, while the same product was obtained in 74 % yield with 83 % *ee* in the presence of 10 mol % of the chiral niobium catalyst prepared in situ.

Since the NLE experiments suggested that no ligand exchange occurred after formation of the dimeric species, we propose **8** as the most plausible structure of the highly enantioselective Nb complex (Figure 6). We assume that **7** was formed from **8** during the crystallization. A key to understanding the mechanism for the formation of **7** from **8** is the origin of the oxygen atom between the niobium atoms in **7**. Contamination of a small amount of water might form **7** from **8**, but this possibility was ruled out by several control experiments. A possible mechanism is the cleavage of the C–O bond of the bridging ethoxy group of **8**, followed by the Nb-O-Nb bond formation accompanied with generation and elimination of diethyl ether. The highly strained structure of **8** might induce the formation of **7**. Further investigations to obtain clear evidence for this mechanism are now in progress.

In summary, we have developed a novel dinuclear chiral niobium catalyst, in which tridentate ligands have been shown

 © 2005 Wiley-VCH Verlag GmbH & Co. KGaA, Weinheim



8

Figure 6. The most plausible structure of the highly selective niobium catalyst in solution.

to be effective. In the presence of a catalytic amount of this complex, asymmetric Mannich-type reactions proceeded smoothly to afford the desired adducts in high yields with high enantioselectivities. A crystal structure of a chiral binuclear niobium complex, which contains a Nb-(μ_2-O)-Nb unit and a tridentate binol derivative (**4c**) chelates one Nb atom while bridging to another, has been revealed. Furthermore, the most plausible structure of the highly selective niobium complex has been proposed.

Received: October 5, 2004
Published online: December 21, 2004

Keywords: asymmetric catalysis · chirality · Lewis acids · Mannich reaction · niobium

[1] a) *Catalytic Asymmetric Synthesis*, *2nd ed.*, (Ed.: I. Ojima), Wiley, New York, **2000**; b) *Comprehensive Asymmetric Catalysis* (Eds.: E. N. Jacobsen, A. Pfaltz, H. Yamamoto), Springer, Heidelberg, **1999**.

[2] For examples using $NbCl_5$ as a Lewis acid, see: a) H. Maeta, T. Nagasawa, Y. Handa, T. Takei, Y. Osamura, K. Suzuki, *Tetrahedron Lett.* **1995**, *36*, 899; b) K. Suzuki, T. Hashimoto, H. Maeta, T. Matsumoto, *Synlett* **1992**, 125; c) T. Hashimoto, H. Maeta, T. Matsumoto, M. Morooka, S. Ohba, K. Suzuki, *Synlett* **1992**, 340; d) C. K. Z. Andrade, N. R. Azevedo, *Tetrahedron Lett.* **2001**, *42*, 6473; e) C. K. Z. Andrade, G. R. Oliveira, *Tetrahedron Lett.* **2002**, *43*, 1935; f) J. Howarth, K. Gallespie, *Tetrahedron Lett.* **1996**, *37*, 6011; g) M. Yamamoto, M. Nakazawa, K. Kishikawa, S. Kohmoto, *Chem. Commun.* **1996**, 2353; h) S. Arai, Y. Sudo, A. Nishida, *Synlett* **2004**, 1104.

[3] J. Howarth, K. Gillespie, *Molecules* **2000**, *5*, 993. The highest enantioselectivity obtained is 55% *ee*.

[4] Oxidation reactions using chiral Nb catalysts are also reported, see a) S. L. Colletti, R. L. Halterman, *J. Organomet. Chem.* **1993**, *455*, 99; b) T. Miyazaki, T. Katsuki, *Synlett* **2003**, 1046.

[5] K. Mikami, M. Terada, in *Lewis Acids in Organic Synthesis*, *Vol. 2* (Ed.: H. Yamamoto), Wiley-VCH, Weinheim, **2000**, chap. 16.

[6] S. Yamasaki, M. Kanai, M. Shibasaki, *Chem. Eur. J.* **2001**, *7*, 4066.

[7] For examples of asymmetric reactions using multidentate binol (2,2′-dihydroxy-1,1′-binaphthyl) derivatives as effective ligands, see: a) H. Ishitani, T. Kitazawa, S. Kobayashi, *Tetrahedron Lett.* **1999**, *40*, 2161; b) S. Matsunaga, J. Das, J. Roels, E. M. Vogl, N. Yamamoto, T. Iida, K. Yamaguchi, M. Shibasaki, *J. Am. Chem. Soc.* **2000**, *122*, 2252; c) N. Kumagai, S. Matsunaga, T. Kinoshita, S. Harada, S. Okada, S. Sakamoto, K. Yamaguchi, M. Shibasaki, *J. Am. Chem. Soc.* **2003**, *125*, 2169.

[8] Details are given in the Supporting Information. For the synthesis of **4a**, see: K. Ishihara, H. Yamamoto, *J. Am. Chem. Soc.* **1994**, *116*, 1561.

[9] a) Review, see: S. Kobayashi, M. Ueno in *Comprehensive Asymmetric Catalysis* (Eds.: E. N. Jacobsen, A. Pfaltz, H. Yamamoto), Springer, Heidelberg, **1999**, supplement 1, p. 143; See also b) H. Ishitani, M. Ueno, S. Kobayashi, *J. Am. Chem. Soc.* **1997**, *119*, 7153; c) H. Ishitani, M. Ueno, S. Kobayashi, *J. Am. Chem. Soc.* **2000**, *122*, 8180; d) S. Xue, S. Yu, Y. Deng, W. D. Wulff, *Angew. Chem.* **2001**, *113*, 2331; *Angew. Chem. Int. Ed.* **2001**, *40*, 2271; e) A. G. Wenzel, E. N. Jacobsen, *J. Am. Chem. Soc.* **2002**, *124*, 12964; f) K. Ishihara, M. Miyata, K. Hattori, T. Tada, H. Yamamoto, *J. Am. Chem. Soc.* **1994**, *116*, 7153; g) T. Akiyama, J. Itoh, K. Yokota, K. Fuchibe, *Angew. Chem.* **2004**, *116*, 1592; *Angew. Chem. Int. Ed.* **2004**, *43*, 1566.

[10] We have already found that NMI is an effective additional ligand in zirconium-catalyzed enantioselective reactions. See, for example, ref. [9b,c].

[11] Recently, several "direct" asymmetric Mannich-type reactions have been reported; however, to our knowledge, there is no example using simple esters as nucleophiles. In the present method, highly enantioselective reactions of simple ester enolates with imines have been achieved. For "direct" Mannich-type reactions, see a review: a) A. Córdova, *Acc. Chem. Res.* **2004**, *37*, 102; For selected examples, see also: b) W. Notz, K. Sakthivel, T. Bui, G. Zhong, C. F. Barbas III, *Tetrahedron Lett.* **2001**, *42*, 199; c) K. Juhl, N. Gathergood, K. A. Jørgensen, *Angew. Chem.* **2001**, *113*, 3083; *Angew. Chem. Int. Ed.* **2001**, *40*, 2995; d) A. Córdova, W. Notz, G. Zhong, J. M. Betancort, C. F. Barbas III, *J. Am. Chem. Soc.* **2002**, *124*, 1842; e) A. Córdova, S.-i. Watanabe, F. Tanaka, W. Notz, C. F. Barbas III, *J. Am. Chem. Soc.* **2002**, *124*, 1866; f) A. Córdova, C. F. Barbas III, *Tetrahedron Lett.* **2002**, *43*, 7749; g) S.-i. Watanabe, A. Córdova, F. Tanaka, C. F. Barbas III, *Org. Lett.* **2002**, *4*, 4519; h) S. Matsunaga, N. Kumagai, S. Harada, M. Shibasaki, *J. Am. Chem. Soc.* **2003**, *125*, 4712; i) Y. Hayashi, W. Tsuboi, M. Shoji, N. Suzuki, *J. Am. Chem. Soc.* **2003**, *125*, 11208; j) Y. Hayashi, W. Tsuboi, I. Ashimine, T. Urushima, M. Shoji, K. Sakai, *Angew. Chem.* **2003**, *115*, 3805; *Angew. Chem. Int. Ed.* **2003**, *42*, 3677; k) S. Matsunaga, T. Yoshida, H. Morimoto, N. Kumagai, M. Shibasaki, *J. Am. Chem. Soc.* **2004**, *126*, 8777; For examples using modified esters, see: l) L. Bernardi, A. S. Gothelf, R. G. Hazell, K. A. Jørgensen, *J. Org. Chem.* **2003**, *68*, 2583; m) M. Marigo, A. Kjærsgaard, K. Juhl, N. Gathergood, K. A. Jørgensen, *Chem. Eur. J.* **2003**, *9*, 2359; n) D. Uraguchi, M. Terada, *J. Am. Chem. Soc.* **2004**, *126*, 5356, and references therein.

[12] For review, see: R. C. Mehrotra, A. K. Rai, P. N. Kapoor, R. Borha, *Inorg. Chim. Acta* **1976**, *16*, 237.

[13] C. Girard, H. B. Kagan, *Angew. Chem.* **1998**, *110*, 3088; *Angew. Chem. Int. Ed.* **1998**, *37*, 2922.

[14] CCDC-251938 contains the supplementary crystallographic data for this paper. These data can be obtained free of charge via www.ccdc.cam.ac.uk/conts/retrieving.html (or from the Cambridge Crystallographic Data Centre, 12 Union Road, Cambridge CB21EZ, UK; fax: (+44) 1223-336-033; or deposit@ccdc.cam.ac.uk).

Natural Product Synthesis

Spirocycloisomerization of Tethered Alkylidene Glycocyamidines: Synthesis of a Base Template Common to the Palau'amine Family of Alkaloids**

*Hugo Garrido-Hernandez, Masakazu Nakadai, Marc Vimolratana, Qingyi Li, Thomas Doundoulakis, and Patrick G. Harran**

In 1993 Scheuer, Kinnel, and co-workers described the structural elucidation of palau'amine (**1**), an antimicrobial principle isolated from extracts of the marine sponge *Stylotella aurantium*.[1] This substance inhibits both bacterial and fungal growth. It has the additional ability to block stimulated T-cell proliferation in vitro, yet remains relatively innocuous toward resting lymphocytes. The mechanism(s) underlying this immunosuppressive property is not known. As a step toward the preparation of molecules useful for its exploration, we describe herein a new spirocyclization process—one with potential to support a synthesis of palau'amine as well as its constitutional relatives axinellamine (**2**)[2] and massadine (**3**)[3].

Polycyclic bisguanidines **1**–**3** are members of a larger alkaloid family whose precise biosynthetic origin is a subject of speculation.[1b,4,5] Until recently, imidazole **4** was considered likely feedstock for the group.[4a,c] New observations challenge that idea.[6] However, from the synthetic perspective,[7] casting structures **1**–**3** in terms of **4** remains a useful exercise. Substructure **4** can be traced twice within polycycles **1**–**3** (Scheme 1). In each instance, the monomers are oriented head-to-head with bonds a and b forming a common embedded cyclopentane. The relative stereochemistries of substituents that emanate from this core differ in **1**–**3**. Such spatial variations offer a rationale for how conserved events, initiated oxidatively after or during formation of the cyclopentane ring, could diverge to the observed ring systems—those similarly constituted but alternately linked.[4a] We report herein a core substrate type prone to form bond a in a spirocyclization applicable to all three targets.

Scheme 2 details how the reaction could operate in the palau'amine case. This specific example parallels the general biosynthetic postulates of Al-Mourabit and Potier.[4a] The natural product is thought to be accessible from intermediate **5**, in which reductions at C20 and C6 and a net dehydration to install the C6 diaminal would be required to produce **1**.[8] The guanidine units in **5** are now both part of glycocyamidine[9] rings. The right-hand spirocycle is reminiscent of an intermediate proposed in the oxidative synthesis of dibromophakellin from dihydrooroidin by Büchi and Foley.[5] Analogously, albeit at a higher oxidation state, this portion of the palau'amine structure could arise from internal trapping of C-acyl iminium ion **6** (as indicated). Notably, ion **6** may be in equilibrium with fragmented species **7**, itself another C-acyl iminium ion. The latter could be formed by the action of chloronium ion on pseudosymmetric bisalkylidene **8**. If this were possible, hypohalite oxidations of **8** could initiate the formation of two rings and four new stereocenters in a single operation (**8**→**5**).

The stereochemical outcome of such a process depends on several factors. However, our initial goal was to validate the construction itself. Spirocyclization within intermediate **7** requires its tethered heterocycles to stack in parallel, which forces both the external electrophile and internal nucleophile to approach from trajectories peripheral to this self-assembled unit (**A**/**B**). Carbon–carbon bond formation would necessarily intervene. The reactivity sought is analogous to that observed in the oxidation of 1,5-cyclooctadiene with halogen to give bicyclooctane products (**9**→**10**, Scheme 2).[10] In that case, the olefins are spatially constrained and communicate transannularly during the reaction. In our case, substrate conformation would be relied upon to dictate comparable results.

We first needed to assess the behavior of an isolated alkylidene glycocyamidine toward electrophilic halogen. Heterocycle **11**[11] was condensed with isobutyraldehyde in the presence of *N*,*N*-dimethylethylene diamine monotosylate as catalyst[12] to afford alkylidene **13** (Scheme 3). When this material was treated with *t*BuOCl in glacial AcOH, epimeric vicinal chloroacetoxylation products **14** were produced efficiently. Angular acetates **14** are themselves unstable, although methanolysis affords isolable congeners **15**—materials that have been fully characterized. These results confirm a desired "enamine" type reactivity of the alkylidene in **13** towards hypohalite.[13]

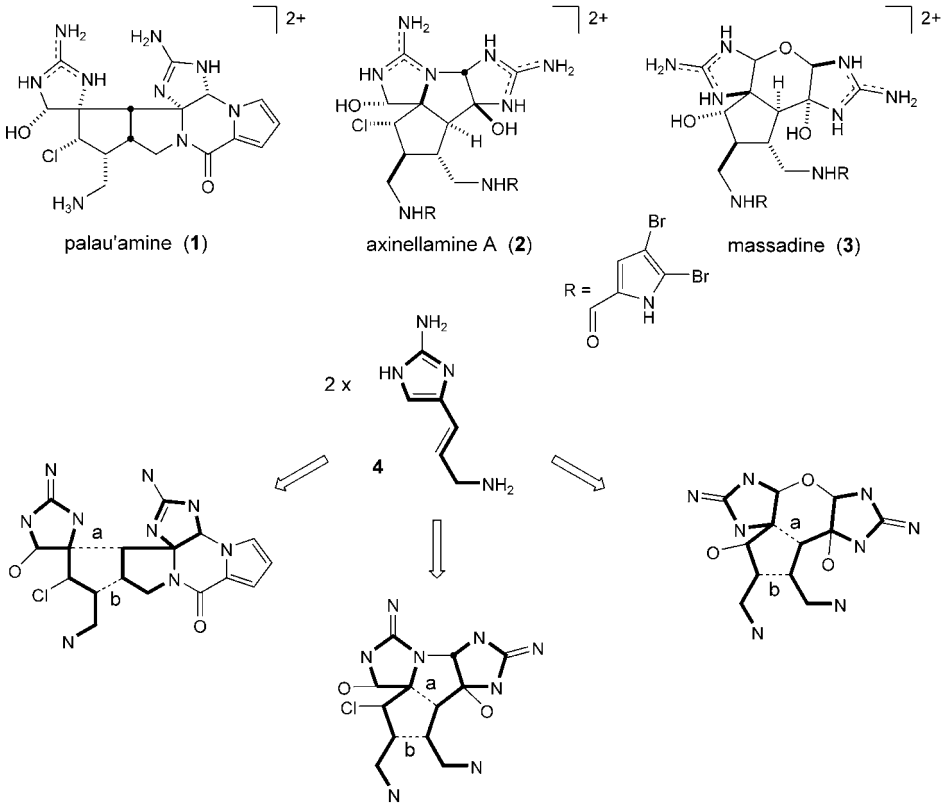
We next examined if similar chemistry executed on a dimeric substrate would result in spirocyclization. The original plan was to retain the substitution pattern of **13** in this dimer. The condensation of **11** with dialdehydes was unproductive. However, we did observe that glycocyamidine **12** could be dehydrogenated to alkylidene **13** with SeO_2[14] (Scheme 3). Performing this reaction twice on tethered bisglycocyamidine **16** appeared a means to access target **17** (Scheme 4 A). A synthesis of **16** was developed that begins with 1,4-dibromo-2-butyne and elaborates symmetrically in two directions.[15] Interestingly, with **16** in hand, it was apparent that the properties of this molecule were not those intended. The substance readily formed insoluble aggregates. Under conditions in which dehydrogenation to **17** was possible, both materials were almost completely insoluble. Conversion was low and the isolation of even small quantities

[*] H. Garrido-Hernandez, M. Nakadai, M. Vimolratana, Q. Li, T. Doundoulakis, Prof. P. G. Harran
Department of Biochemistry
University of Texas Southwestern Medical Center at Dallas
Dallas, TX 75390-9038 (USA)
Fax: (+1) 214-648-6455
E-mail: pharra@biochem.swmed.edu

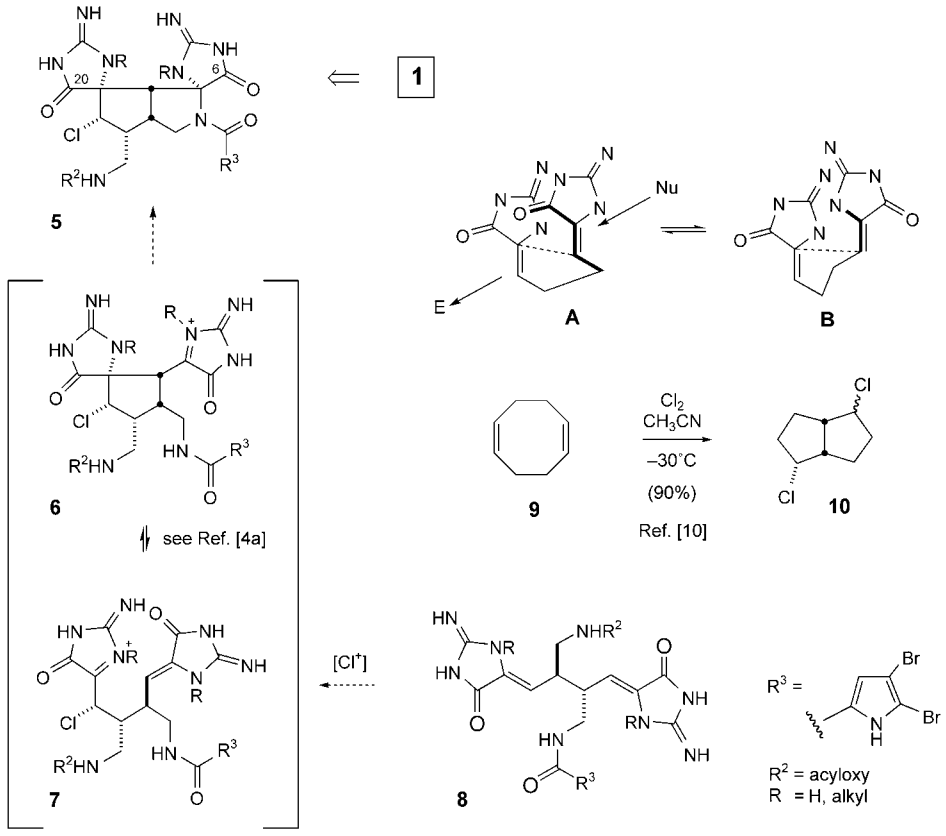
[**] Funding provided by the NIH (RO1-GM60591), the Robert A. Welch Foundation, and unrestricted research awards from AstraZeneca, Eli Lilly, and Pfizer. M.N. acknowledges the JSPS for a postdoctoral fellowship. P.H. is a fellow of the Alfred P. Sloan Foundation. We are grateful to Dr. Radha Akella (Department of Biochemistry, UTSW) for her expert crystallographic analyses and insight.

Supporting information for this article is available on the WWW under http://www.angewandte.org or from the author.

 DOI: 10.1002/anie.200462069 © 2005 Wiley-VCH Verlag GmbH & Co. KGaA, Weinheim

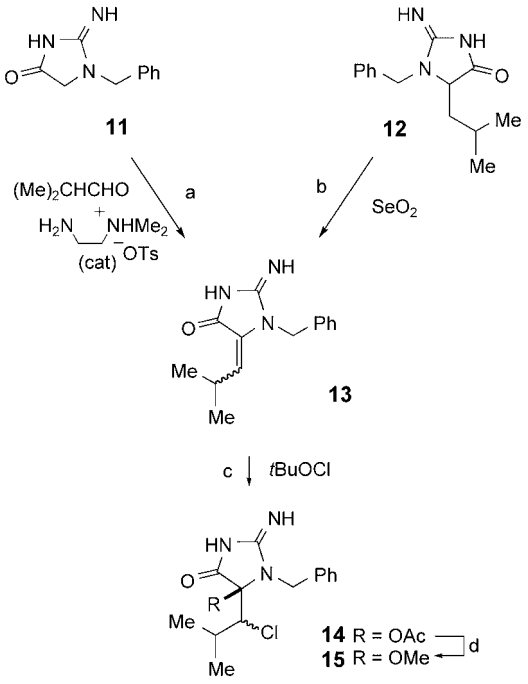


Scheme 1. Palau'amine (**1**) and its constitutional relatives axinellamine A (**2**) and massadine (**3**) can be viewed as dimeric composites of conserved subunit **4.**[4a]



Scheme 2. Retrosynthesis of palau'amine identifies a core spirocyclization relevant to structural types **1**–**3**.

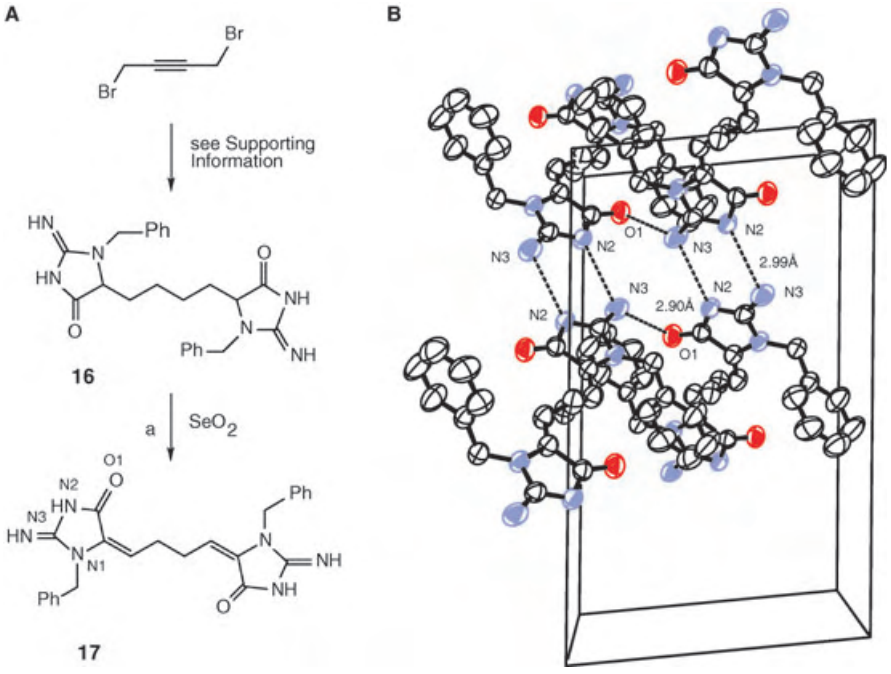
 © 2005 Wiley-VCH Verlag GmbH & Co. KGaA, Weinheim



Scheme 3. Regioselective vicinal chloroacetoxylation of an alkylidine glycocyamidine. Reaction conditions: a) isobutyraldehyde (1.2 equiv), *N*,*N*-dimethylethylene diamine (30 mol%), *p*TsOH (30 mol%), DMF, microwave heating (150°C), 50 min (41%, *E*/*Z* = 5:1); b) SeO_2, *t*BuOH, 75°C, 2 h (75%); c) *t*BuOCl (1.1 equiv, neat), glacial AcOH, room temperature, 1 h (>80%-^{1}H NMR); d) silica gel, MeOH, room temperature, 6 h (95%). Ts = toluene-*p*-sulfonyl; DMF = *N*,*N*-dimethylfomamide.

of **17** in pure form was a painstaking exercise. Compound **17** has the functionality to test our key idea, but is otherwise a poor model. The goal was a substrate whose heterocyclic termini could associate internally to facilitate the cyclization illustrated in Scheme 2. Treatment of **17** with hypochlorite initiated no such event,[16] probably reflecting, as does its solubility profile, an unwanted preference for bimolecular association. The arrangement of **17** in the crystalline state supports this idea. The unit cell contains four molecules of **17** (8 asymmetric units, space group $C2_1/c$), each in extended conformation with their glycocyamidine rings interacting bimolecularly through multiple H bonds (Scheme 4B).[17]

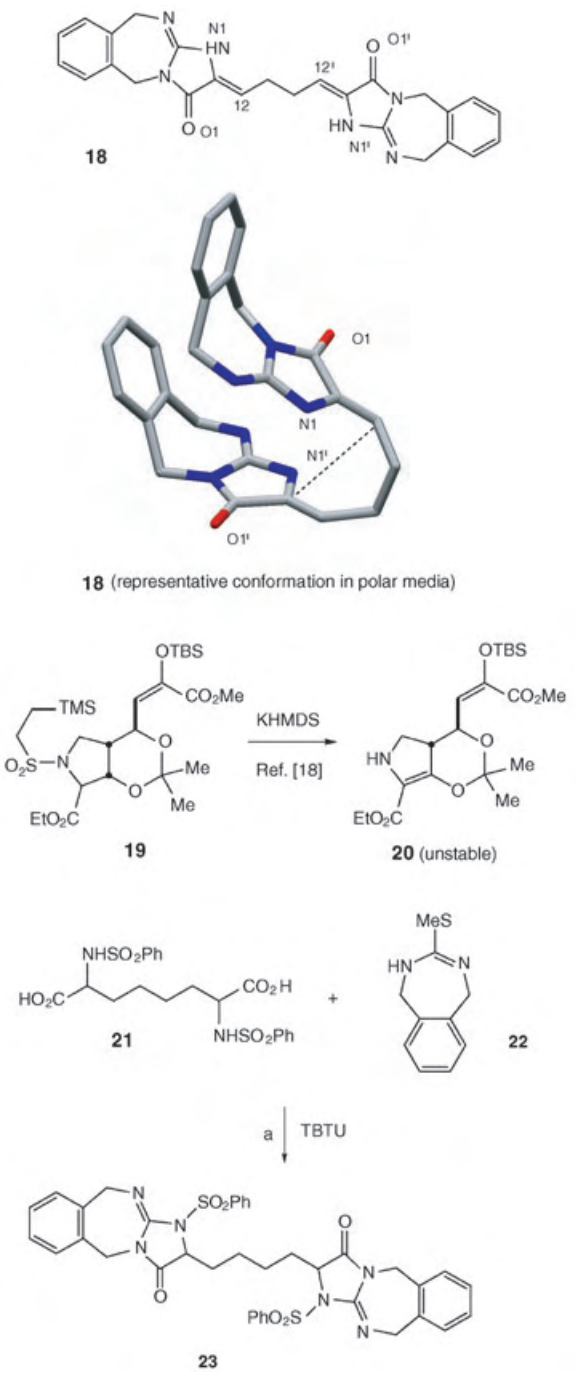
Another design was needed—one in which the guanidine units are more properly managed. As a means to disrupt bimolecular hydrogen bonding, we considered repositioning the N1 benzyl unit on each heterocycle to N2. Alone, the change was synthetically awkward, but the incorporation of both N2 and N3 into a 2,4-benzodiazepine appeared workable. Compound **18** (Scheme 5) became the target. Computer simulations suggested this molecule would adopt compact globular forms in polar solvents, positioning the alkylidene units appropriately for subsequent oxidative spirocyclization. With N1 unsubstituted, *Z*-alkylidene geometry in **18** was expected to be thermodynamically favored. How to install this unsaturation was the pivotal question. We eventually adopted an approach based on basic degradation of sulfonamides. Overman and Trenkle had shown that a potassium enolate of **19** fragments with loss of the 2-trimethylsilylethylsulfinate ion, affording an imine product that tautomerizes to enamine **20** in situ.[18] A related transformation, executed twice on bissulfonamide **23**, was considered a method to produce **18**. Whereas the ring system in **23** was unknown, it could be prepared concisely. The route used to synthesize **16** was adapted to access the 2,7-diaminosuberic acid derivative **21**.[15] Condensing this material with a twofold excess of *o*-xylyldiamine-derived methylisothiourea **22**[19] provided **23** directly. The *seco* amides presumably formed transiently in the reaction cyclized spontaneously, with ejection of methanethiol at each end of the molecule.



Scheme 4. Bisalkylidene **17** forms highly insoluble aggregates and proves to be an intractable model system. A) Reaction conditions: a) SeO_2 (1.4 equiv), *t*BuOH, 70°C, 4 h (5–7%). B) X-ray crystallography indicates the glycocyamidine rings in **17** associate bimolecularly through extensive hydrogen bonds. Partial unit-cell occupancy is shown (space group $C2_1/c$) in ORTEP format (50% probability thermal ellipsoids, hydrogen atoms omitted for clarity).

With **23** available, we examined its response to base. Exposure to KHMDS caused degradation. However, when the compound was treated with DBU in DMF, monoalkylidene **26** formed rapidly (Scheme 6). This material was isolated without incident. When **26** was reexposed to DBU, two new products emerged in high yield. Surprisingly, neither was found to be bisalkylidene **18**. Rather, they proved to be geometric isomers of spirocycloisomerization product **24**.[17] When the reaction was per-

 © 2005 Wiley-VCH Verlag GmbH & Co. KGaA, Weinheim



Scheme 5. Compound **18** is designed to have a diminished hydrogen bonding capability, which allows the structure to adopt conformations more readily that facilitate the intended carbon–carbon bond formation. Reaction conditions for the formation of **23**: a) TBTU, $(i\text{Pr})_2\text{NEt}$, **22** (2.2 equiv), CH_2Cl_2, RT (35%). TBTU = 2-(1*H*-benzotriazol-1-yl)-1,1,3,3-tetramethyluronium tetrafluoroborate; KHMDS = potassium hexamethyldisilazide.

formed in [D_7]DMF and monitored periodically by ^{1}H NMR spectroscopy (Scheme 6 inset), a progression of events became evident. Within 10 minutes, DBU converted **23** into **26**. During the next hour, a second olefinic triplet (δ = 5.23 ppm) became more prominent, although concurrently with signals corresponding to rearrangement products **24**. The system siphoned completely to the latter within 10 h.

We noted that the ratio of isomers **24** changed during the experiment. It was likewise possible that the second alkene signal reflected equilibration of **26** with an isomeric monoalkylidene and that target bisalkylidene **18** was not observed, or perhaps even formed, under these conditions. To address this question, we synthesized nonsymmetric monosulfonamide **25**[15] and subjected it to identical elimination conditions. Like **23**, **25** rapidly converted into a monoalkylidene (namely, **27**). Notably, carbamate **27** was inert to further degradation and did not equilibrate with a second product over time, which implies the second olefinic signal in the original experiment is itself reflective of symmetric bisalkylidene **18**.

This is precisely the behavior we had hoped to see. Whereas **18** was designed to participate in a spirocyclization initiated by hypohalite, the molecule is apparently so well-poised for the reaction that a proton is sufficient provocation. Compound **18** cannot be isolated, and available data does not distinguish whether carbon–carbon bond formation occurs through: 1) **C** directly, perhaps catalyzed by salt **28**; 2) imino tautomer **D**; or 3) inner salt **E**, the product of net proton transfer from C12 to C12′ within **D**. Nevertheless, the outcome validates the central tenet of our approach to **1**–**3** (Scheme 1 and Scheme 2). Moreover, the markedly different reactivities of bisalkylidenes **17** and **18**, with the former showing no inclination to cycloisomerize (Scheme 4), suggest the propensity for cyclization is tunable. In substrates substituted appropriately to complete the natural products, there should be ample opportunity to initiate analogous spirocyclization through chlorination (or oxygenation in the case of **3**). Attempts to synthesize such substrates while attending to stereochemical parameters associated with the larger problem are ongoing.

Received: September 22, 2004
Published online: December 28, 2004

Please note: Minor changes have been made to this manuscript since its publication in *Angewandte Chemie* Early View. The Editor.

Keywords: cyclization · guanidines · heterocycles · natural products · total synthesis

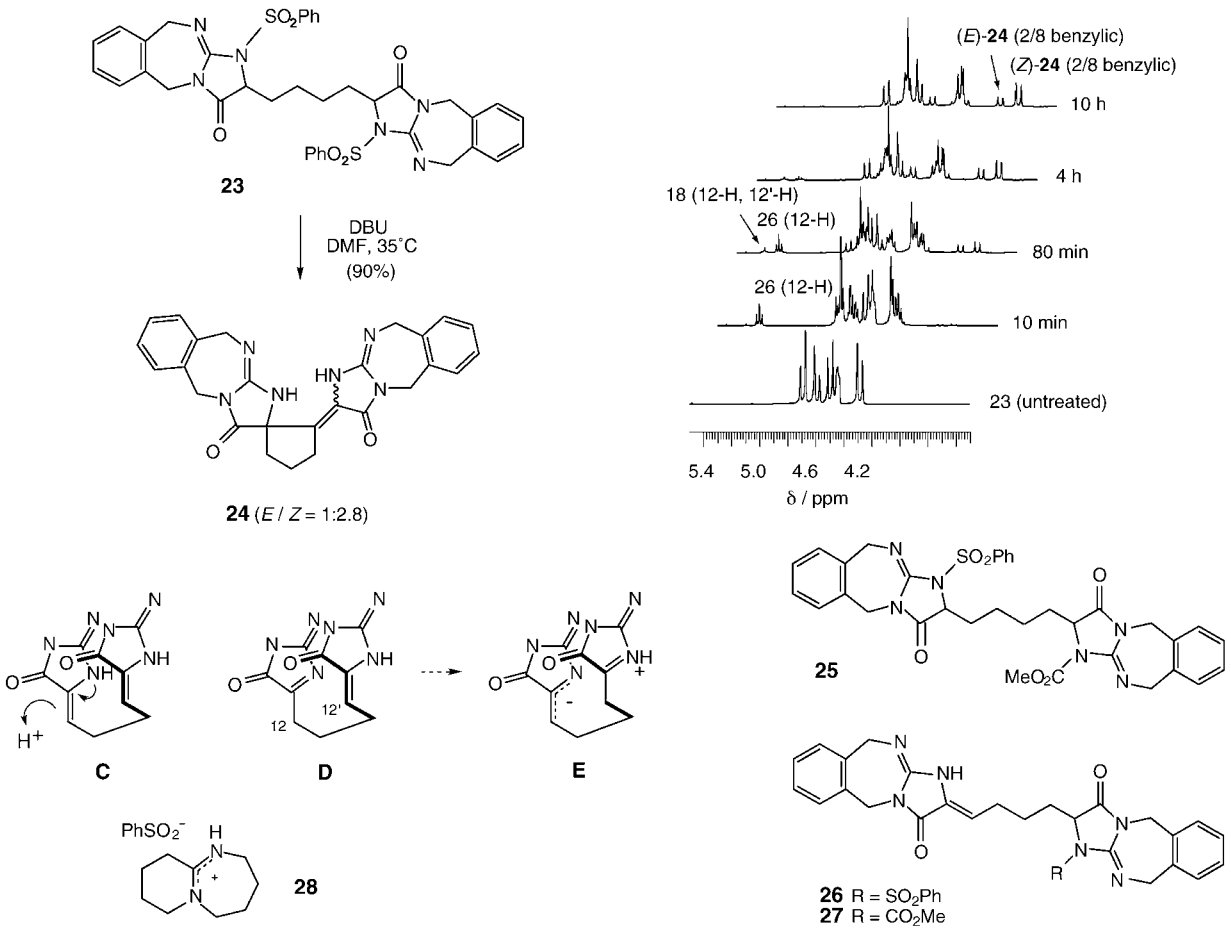
[1] a) R. B. Kinnel, H.-P. Gehrken, P. J. Scheuer, *J. Am. Chem. Soc.* **1993**, *115*, 3376–3377; b) R. B. Kinnel, H.-P. Gehrken, R. Swali, G. Skoropowski, P. J. Scheuer, *J. Org. Chem.* **1998**, *63*, 3281–3286.

[2] S. Urban, P. de Almeida Leone, A. R. Carroll, G. A. Fechner, J. Smith, J. N. A. Hooper, R. J. Quinn, *J. Org. Chem.* **1999**, *64*, 731–735.

[3] S. Nishimura, S. Matsunaga, M. Shibazaki, K. Suzuki, K. Furihata, R. W. M. van Soest, N. Fusetani, *Org. Lett.* **2003**, *5*, 2255–2257.

[4] a) A. Al-Mourabit, P. Potier, *Eur. J. Org. Chem.* **2001**, 237–243; b) H. Hoffman, T. Lindel, *Synthesis* **2003**, 1753–1783; c) P. Andrade, R. Willoughby, S. A. Pomponi, R. G. Kerr, *Tetrahedron Lett.* **1999**, *40*, 4775–4778; d) P. S. Baran, D. P. O'Malley, A. L. Zografos, *Angew. Chem.* **2004**, *116*, 2728–2731; *Angew. Chem. Int. Ed.* **2004**, *43*, 2674–2677.

 © 2005 Wiley-VCH Verlag GmbH & Co. KGaA, Weinheim



Scheme 6. Elimination of phenylsulfinic acid (2 equiv net) from **23** initiates a high-yielding spirocycloisomerization in situ. Real-time monitoring of the reaction by ^{1}H NMR spectrosopy (DBU (2.2 equiv), one portion at $t = 0$ min, 70 μM in [D_7]DMF, 400 MHz, 35 °C) implicates the successive intermediacy of **26** and **18**. DBU = 1,8-diazabicyclo[5.4.0]undec-7-ene.

[5] L. H. Foley, G. Büchi, *J. Am. Chem. Soc.* **1982**, *104*, 1776–1777.
[6] N. Travert, A. Al-Mourabit, *J. Am. Chem. Soc.* **2004**, *126*, 10252–10253.
[7] As **1**–**3** are currently inaccessible, there has been considerable attention paid to the synthetic problem; for a review see reference [4b]. More recent contributions include: a) J. D. Katz, L. E. Overman, *Tetrahedron* **2004**, *60*, 9559–9568; b) P. S. Baran, A. L. Zografos, D. P. O'Malley, *J. Am. Chem. Soc.* **2004**, *126*, 3726–3727; c) S. G. Koenig, S. M. Miller, K. A. Leonard, R. S. Loewe, B. C. Chen, D. J. Austin, *Org. Lett.* **2003**, *5*, 2203–2206.
[8] L. E. Overman, B. N. Rogers, J. E. Tellew, W. C. Trenkle, *J. Am. Chem. Soc.* **1997**, *119*, 7159–7160.
[9] Glycocyamidine nomenclature refers to cyclic anhydrides of α-guanidino carboxylic acids; the prototype is derived from glycine: C. Lempert, *Chem. Rev.* **1959**, *59*, 667–736; the equivalent IUPAC designation is 2-amino-1*H*-5-imidazolone.
[10] S. Uemura, S. Fukuzawa, A. Toshimitsu, M. Okano, *J. Org. Chem.* **1983**, *48*, 270–273.
[11] F. Kienzle, A. Kaiser, M. S. Chodnekar, *Eur. J. Med. Chem.* **1982**, *17*, 547–556.
[12] S. Saito, M. Nakadai, H. Yamamoto, *Synlett* **2001**, 1245–1248.
[13] For related observations, see: a) T. Fukuyama, B. D. Robins, R. A. Sachleben, *Tetrahedron Lett.* **1981**, *22*, 4155–4158; b) R. Furstoss, R. Tadayoni, G. Esposito, J. Lacrampe, A. Heumann, B. Waegell, *Can. J. Chem.* **1976**, *54*, 3569–3579.
[14] K. C. Nicolaou, N. A. Petasis, *Selenium in Natural Products Synthesis*, CIS, Philadelphia, **1984**, Chap. 3.
[15] See Supporting Information.
[16] Treatment of **17** with *t*BuOCl in AcOH/CF_3CH_2OH provides vicinal bifunctionalization products in low yields, analogous to those generated from monomer **13** (Scheme 3) under similar conditions.
[17] Crystallographic data (excluding structure factors) for **17** and (*Z*)-**24** have been deposited with the Cambridge Crystallographic Data Centre as supplementary publication nos. CCDC 250890 and CCDC 250891. These data can be obtained free of charge via www.ccdc.cam.ac.uk/conts/retrieving.html (or from the Cambridge Crystallographic Data Centre, 12, Union Road, Cambridge CB21EZ, UK; fax: (+44) 1223-336-033; or deposit@ccdc.cam.ac.uk)..
[18] W. C. Trenkle, Ph.D. Thesis, University of California, Irvine, **2000**, UMI no. 9950654.
[19] H. R. Rodriguez, B. Zitko, G. Desteve, *J. Org. Chem.* **1968**, *33*, 670–676.

 © 2005 Wiley-VCH Verlag GmbH & Co. KGaA, Weinheim

Platinum Anions

Dibariumplatinide: $(Ba^{2+})_2Pt^{2-}\cdot 2e^-$ and Its Relation to the Alkaline-Earth-Metal Subnitrides**

*Andrey Karpov, Ulrich Wedig, Robert E. Dinnebier, and Martin Jansen**

Dedicated to Professor Arndt Simon on the occasion of his 65th birthday

Among the transition elements, gold and platinum are unique in that their first electron affinities are positive and of a magnitude comparable to those of typical non-metals. For instance, platinum with an electron affinity of 2.13 eV[1] even surpasses that of oxygen (1.46 eV),[1] while gold (2.31 eV)[1] approaches the value as determined for iodine (3.06 eV).[1] These experimental data are mirrored by calculations[2] demonstrating the 6s states of gold and platinum to experience the strongest relativistic stabilization and orbital contraction of all stable elements. The implications of these atomic properties for the chemistry of the respective elements have been addressed extensively,[3] while the number of observations adding experimental evidence is growing steadily. For gold, the large band gap of the long-known CsAu[4] has been attributed to relativistic effects. More recently, the intrinsic stability of the Au^- ion, for example, as a solvated anion in a liquid electrolyte[5] or as a particle diffusing through an insulating ionic solid,[6] has been demonstrated. Also, striking parallels to the chemistry of halogens have been uncovered, such as the close crystal chemical correspondences of auride and halide compounds,[7] and the disproportionation of elemental gold in basic media.[8] For platinum, only recently evidence for its capability to exist as an anion has been provided: Cs_2Pt,[9] forming red transparent crystals, shows full charge separation, and thus is composed of the ions Cs^+ and Pt^{2-}. Treating platinum with barium, which is less electropositive than cesium, again induces charge transfer, which now, however, is incomplete. Thus, in BaPt[10] platinum bears a charge of approximately −1 and, because of its open-shell character, forms infinite chains of homoatomic bonds. Offering more electrons by increasing the Ba/Pt ratio should render platinum less capable to forming Pt–Pt bonds. In agreement with this expectation, in the structures of Ca_3Pt_2[11] and Ba_3Pt_2[12] platinum pairs can be identified.[13] The bonds within the dumbbells, however, are weak and are easily expanded while adapting to the packing requirements. Extending this work, we now have managed to synthesize Ba_2Pt, a platinide with an even higher barium content, which indeed contains isolated platinide ions.

Ba_2Pt was synthesized from the elements, sealed in tantalum ampoules, at 1223 K in argon. The as obtained micro-crystalline samples (EDX: Ba/Pt = 2.1(2)) are shiny-black, sensitive to air and moisture. The melting point is at about 1100 K. The compound exhibits temperature independent diamagnetism ($\chi_{mol}(273\,K) = -75\times10^{-11}\,m^3mol^{-1}$). The electrical conductivity is of metallic character ($\rho(273\,K) = 0.17\,m\Omega\,cm$; $\rho(273\,K)/\rho(5\,K) = 1.37$). According to laboratory X-ray powder data the product is single phasic.[14] All reflections can be indexed assuming a trigonal crystal system, and the intensities are well reproduced by supposing the $CdCl_2$[15] type of structure. However, the *c/a* ratio corresponds to a cubic cell, within the limits of experimental error. To distinguish whether the $CdCl_2$ or the closely related cubic PrI_2-V[16] structure type is the correct one, we have recorded high-resolution synchrotron data (Figure 1). Subsequent Rietveld profile refinement clearly showed line splittings, and the trigonal $CdCl_2$ structure type being the correct one.[17]

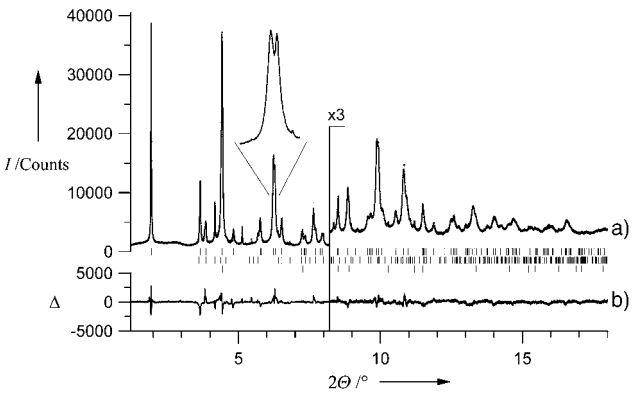


Figure 1. Scattered synchrotron X-ray intensity for Ba_2Pt as a function of diffraction angle 2Θ. Shown are the observed pattern (gray points), the best Rietveld-fit profile (line a), the difference curve between observed and calculated profile (line b), and the reflection markers (vertical bars: Ba_2Pt (top), BaH_2 (middle), and BaO (bottom)). The higher angle data starting at $2\Theta = 8.2°$ is enlarged by a factor of 3.

The resulting structure, is given in Figure 2. Ba_2Pt is the first example of a solid composed of two metals that adopts the $CdCl_2$ structure which is otherwise preferably found for ionic compounds with either a polarizable anion or cation. This strong indication for Ba_2Pt being a basically polar compound is corroborated by the observed bonding separations. Adding the effective radius of the Pt^{2-} ion, as derived[18] from Cs_2Pt[19] to the tabulated value for the Ba^{2+} ion[19] results in 303 pm which is in fair agreement with the observed Ba–Pt separation (315 pm). The distortion of the $PtBa_6$ octahedra (shrunk along one of the threefold axes) is due to the ratio $r(Pt^{2-})/r(Ba^{2+})$ of 1.04 which is not the ideal for an octahedral coordination (see Table 1). The interlayer Ba–Ba separations are enlarged in comparison to those in the elemental metal.

[*] Dipl.-Chem. A. Karpov, Dr. U. Wedig, Priv.-Doz. Dr. R. E. Dinnebier, Prof. Dr. M. Jansen
Max-Planck-Institut für Festkörperforschung
Heisenbergstrasse 1
70569 Stuttgart (Germany)
Fax: (+49) 711-689-1502
E-mail: m.jansen@fkf.mpg.de

[**] We thank Claus Muehle for his support of the experimental work, Roland Eger for hydrogen analysis, and the Fonds der Chemischen Industrie for continuous financial support. Special thanks to Andy Fitch (ESRF) for his help during synchrotron data collection.

 © 2005 Wiley-VCH Verlag GmbH & Co. KGaA, Weinheim DOI: 10.1002/anie.200462055

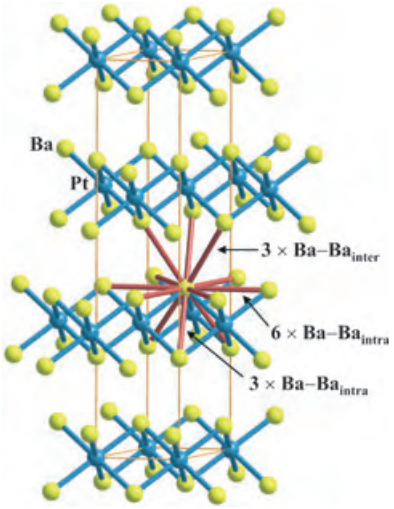


Figure 2. Perspective representation of the crystal structure of Ba_2Pt (blue spheres: platinum atoms; yellow spheres: barium atoms; orange lines: unit cell-edges).

These structural features justify the assignment of the charges as $(Ba^{2+})_2Pt^{2-}\cdot 2e^-$, in a first approximation.

From this scenario it is clear that Ba_2Pt has to be classified as another representative of the family of subvalent alkali and alkaline-earth compounds. This class of solids that has continued to arouse curiosity since the discovery of the first representatives,[20] is meanwhile well investigated,[21] and, furthermore, soundly based for structural and bonding concepts have been elaborated.[22] However, to date, one aspect appears not to be fully settled. The metal–metal separations in the interslab region are rather long, and moreover show variations from one compound to the other, which are hard to rationalize. One explanation, based on the low work function of these compounds and their characteristics as void metals, suggests Ba_2N, Ba_3N, and Cs_3O being expanded owing to the pressure of their conduction electron gases, in the metallic region.[23] Though providing just one more example, the features of Ba_2Pt are suited to shed some new light on this problem. To exclude ambiguities originating from different topologies, we restrict our considerations to $CdCl_2$ type representatives. Out of these, we disregard Tl_2O, Ag_2F, Ti_2O,and M_2C (M = rare-earth element) because of the totally different sets of valence orbitals available. The relevant structural data of the remaining alkaline-earth subnitrides, of Cs_2O and of Ba_2Pt are compiled in Table 1. The distortions of the octahedra, as expressed by the differences in the intraslab distances correlate with the deviations of their $r(X)/r(M)$ ratios from the value for an ideal octahedron (0.414), which lends support to regarding these parts of the structures constituted of the respective ions. Except for Cs_2O, in each case the interslab M–M separation $M–M_{inter}$ is significantly longer than in the pristine element M. The factors to be considered in trying to explain the trends are sizes of the cores M^{2+} and M^+, electrostatic M–M repulsion, metal-core polarizability, next-but-one-neighbor M–X Coulomb attraction, a reduction of the Coulomb interaction by the excess electrons in the interslab region, and the metallic bonding mediated by the excess electrons. These various interactions are of quite different effectiveness and thus have to be weighted, appropriately. Doubling the charge of M quadruples the interslab Coulomb repulsion. This would explain the conspicuously short interslab separations in Cs_2O. The increase of the interslab separation from calcium to barium can be partially attributed to the growing diameter of the M^{2+} cores, while the superproportional component to this increase might result from the diminishing M–X next-but-one-neighbor electrostatic attraction. The difference between Ba_2N and Ba_2Pt, finally, reflects the increase in metallic bonding in Ba_2Pt owing to the higher number valence electrons available.

To check the charge distribution suggested, particularly the role of platinum, and the relation of Ba_2Pt to the subnitrides, LMTO-TB-ASA band structure calculations[28] (LDA-functional,[29] relativistic partial waves) were performed for Ba_2Pt and Ba_2N. In both cases the polarization of the Ba core has been considered by including the 5p shell in the valence space, and the description of the interslab region has been improved by using nonstandard radii[30] of the atomic spheres. Owing to the polarization of the Ba core, the Ba 5p bands below −1 Ry are split significantly in Ba_2N. In Ba_2Pt such an extreme splitting is not observed (Figure 3), because of the softer anion. In this case dynamic correlation contributions have to be assumed.[9] Above −0.5 Ry, the densities of states of both Ba_2Pt and Ba_2N are very similar (Figure 3), showing a lower part describing the ionic layers and an upper delocalized part (Ba_2Pt: above −0.28 Ry; Ba_2N: above −0.19 Ry). The delocalized part is mainly built from

Table 1: Overview of selected crystallographic data and interatomic distances [ppm] of M_2X compounds crystallizing in the $CdCl_2$ structure type.

Compound	a	c/a	$(M–M_{intra})$; $(M–M)_{norm}$[a]	$(M–M_{intra})$; $(M–M)_{norm}$[a]	$(M–M_{inter})$; $(M–M)_{norm}$[a]	$(M–X)$; $(M–X)_{norm}$[b]	$r_{cryst}(X)/r_{cryst}(M)$
Cs_2O[24]	425.6(4)	4.46	383(2); 0.72	425.6(4); 0.80	419(2); 0.78	286(1); 0.93	0.70
Ca_2N[25]	361.58(5)	5.25	326.0(1); 0.83	361.6(1); 0.92	436.0(1); 1.10	243.4(1); 0.97	1.20
Sr_2N[25]	386.25(3)	5.36	351.4(2); 0.82	386.3(1); 0.90	473.9(1); 1.10	261.1(1); 0.97	1.04
Ba_2N[26]	401.7(3)	5.59	374.4(5); 0.84	401.7(3); 0.90	509.6(1); 1.15	274.6(3); 0.96	0.92
Ba_2Pt	456.42(1)	4.84	434.0(1); 0.98	456.4(1); 1.03	471.9(1); 1.06	314.9(1); 1.04[c] 0.87[d]	1.03

[a] $(M–M)_{norm} = (M–M)_{(M_2X)}/(2\times r_{met})$, where r_{met} are tabulated atomic radii in metals.[27] [b] $(M–X)_{norm} = (M–X)_{(M_2X)}/(r_{cryst}(M)+r_{cryst}(X))$; r_{cryst} are tabulated crystal radii for CN = 6,[19] except for N^{3-} where $r_{cryst}(CN=6)$ was estimated as $1.04\times r_{cryst}(CN=4)$.[27] [c] $(Ba–Pt)_{norm} = (Ba–Pt_{(Ba_2Pt)})/(r_{cryst}(Ba^{2+}{}_{CN=6}) + r_{cryst}(Pt^{2-}{}_{CN=6}))$; $r_{cryst}(Pt^{2-}{}_{CN=6}) = 154$ pm was derived[18] from Cs_2Pt (ECoN(Pt) = 6.5) [d] $(Ba–Pt)_{norm} = ((Ba–Pt)_{(Ba_2Pt)})/(r_{met}(Ba)+r_{met}(Pt))$. CN = coordination number, ECoN = effective coordination number.[18]

 © 2005 Wiley-VCH Verlag GmbH & Co. KGaA, Weinheim

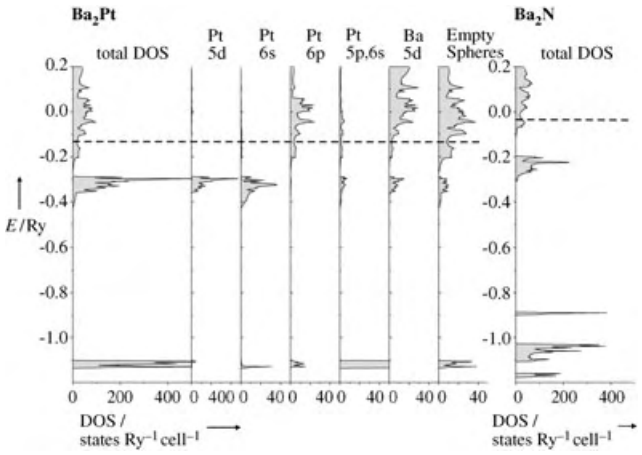


Figure 3. Total and partial densities of states (DOS; LMTO-TB-ASA) of Ba_2Pt (left). Total DOS of Ba_2N (right). The dashed line marks the Fermi level.

the orbitals of the empty spheres, which is also reflected by the electron distribution calculated for these bands (Figure 4). It should be noted that the electron density between the layers is very low. For this reason the domains of the electron localization function (ELF)[31] in the interslab region (Figure 4), which also are found in Sr_2N,[32] should be discussed cautiously. What can be stated from the ELF unambiguously is the ionic nature of the atoms, both in Ba_2Pt and Ba_2N, and the significant polarization of the ions. The ionicity of the layers is confirmed by COHP[33] calculations, which show in the valence region only a negligible antibonding contribution of +0.01 Ry for the Ba–Pt interaction.

The following partial charges are obtained from the topological analysis of the electron density according to Bader[34] in both, Ba_2Pt and Ba_2NPt: −1.8, N: −1.9, Ba: +0.9. The total electron density, however, does not contain any information on the local or delocalized character of any electrons. That is why with the Bader analysis the electrons in the interslab regions are added to the atomic basins, especially to those of Ba. From the integration of the DOS in the upper valence region (see above) we know that there are two delocalized electrons in Ba_2Pt and one delocalized electron in Ba_2N per formula unit, which must be subtracted from the partial charges. That is why the formal descriptions $(Ba^{2+})_2Pt^{2-}\cdot 2e^-$ and $(Ba^{2+})_2N^{3-}\cdot e^-$ are justified.

The larger volume of the Pt^{2-} ion compared to the N^{3-} ion (basin volumes from Bader analysis: 44.8 Å^3 (Pt) and 19.7 Å^3 (N)) is reflected only by a larger *a* parameter. The *c* parameter, and connected with this the interslab distance, in Ba_2Pt shrinks compared to Ba_2N, because the number of delocalized electrons in Ba_2Pt is doubled.

Ba_2Pt is another example for compounds containing platinum in a negative oxidation state with striking similarities to main-group elements. With increasing Ba/Pt ratio, going along from BaPt through Ba_3Pt_2 to Ba_2Pt, and thus with increasing number of valence electrons, the anionic subunits show decreasing covalent interaction, and are isolated ions in Ba_2Pt. In contrast to Cs_2Pt, the Ba compounds contain excess electrons, which are responsible for their metallic behavior.

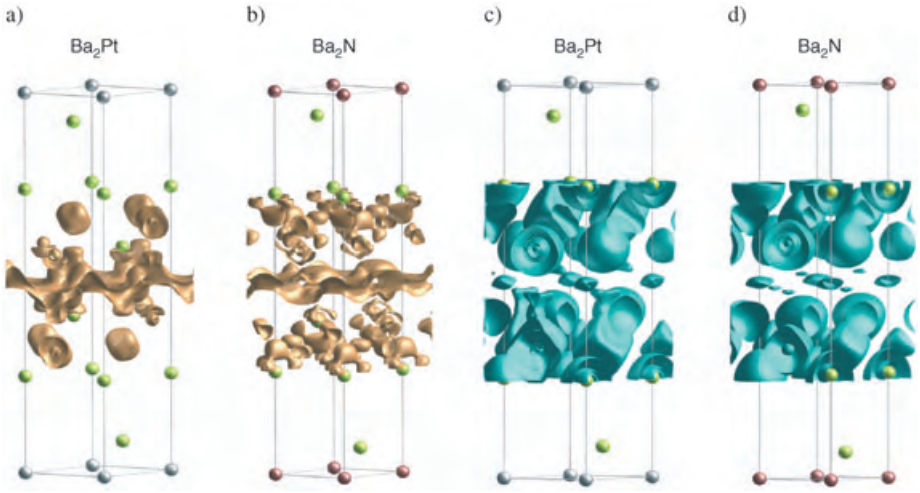


Figure 4. Electron densities computed from the highest occupied bands in a) Ba_2Pt ($\rho = 0.003\,e^-\,Bohr^{-3}$) and in b) Ba_2N ($\rho = 0.002\,e^-\,Bohr^{-3}$). Isosurfaces of the electron-localization function of c) Ba_2Pt and d) Ba_2N (both $\eta = 0.34$). Green spheres Ba, silver spheres Pt, purple spheres N.

Experimental Section

Ba_2Pt was prepared by reaction of barium (Sigma-Aldrich, 99.99%) with platinum sponge (MaTeck, 99.9%, dried and degassed before use at 673 K in the dynamic vacuum of 10^{-9} bar) in a 2.4:1 ratio. The mixture (≈0.5 g) was sealed under Ar in a tantalum tube, annealed at 1223 K for 2 days, and then cooled to room temperature with a rate of 10 K h^{-1}. The shiny-black product was isolated and handled under strictly inert conditions (Schlenk technique or glove box). Metal element analyses were performed using a scanning electron microscope (XL 30 TMP, Philips), equipped with an integrated energy dispersive X-ray (EDX) spectroscopy system. The hydrogen content was measured by oxidizing the sample mixed with V_2O_5 in an O_2 stream[35] and titration the evolved water pulse-coulometrically according to the Karl Fischer method.[36] Differential scanning calorimetry (DSC) was performed with a computer-controlled DSC sensor (DSC 404 C Pegasus, Netzsch). Temperature-dependent resistivity data was obtained for a pressed pellet connected to four probes of the resistivity measurement apparatus using the van der Pauw method[37] in the temperature range 5–290 K. Magnetization was measured using a SQUID magnetometer (MPMS 5.5, Quantum Design) in the temperature range 5–330 K at $H = 1$ T.

Received: September 21, 2004
Published online: December 21, 2004

Keywords: band structure calculation · barium · platinum · relativistic effects · structure elucidation

 © 2005 Wiley-VCH Verlag GmbH & Co. KGaA, Weinheim

[1] T. Andersen, H. K. Haugen, H. Hotop, *J. Phys. Chem. Ref. Data* **1999**, *28*, 1511 – 1533.
[2] J. P. Desclaux, *At. Data Nucl. Data Tables* **1973**, *12*, 311 – 406.
[3] P. Pyykkö, J. P. Desclaux, *Acc. Chem. Res.* **1979**, *12*, 276 – 281; P. Pyykkö, *Chem. Rev.* **1988**, *88*, 563 – 594.
[4] A. Sommer, *Nature* **1943**, *152*, 215; W. E. Spicer, A. H. Sommer, J. G. White, *Phys. Rev.* **1959**, *115*, 57 – 62.
[5] A.-V. Mudring, M. Jansen, J. Daniels, S. Krämer, M. Mehring, J. P. P. Ramalho, A. H. Romero, M. Parrinello, *Angew. Chem.* **2002**, *114*, 128 – 132; *Angew. Chem. Int. Ed.* **2002**, *41*, 120 – 124; P. D. C. Dietzel, M. Jansen, *Chem. Commun.* **2001**, 2208 – 2209.
[6] C. Feldmann, M. Jansen, *Angew. Chem.* **1993**, *105*, 1107 – 1108; *Angew. Chem. Int. Ed. Engl.* **1993**, *32*, 1049 – 1050; C. Feldmann, M. Jansen, *J. Chem. Soc. Chem. Commun.* **1994**, 1045 – 1046; A. Pantelouris, G. Küper, J. Hormes, C. Feldmann, M. Jansen, *J. Am. Chem. Soc.* **1995**, *117*, 11749 – 11753; C. Feldmann, M. Jansen, *Z. Anorg. Allg. Chem.* **1995**, *621*, 201 – 206.
[7] C. Feldmann, M. Jansen, *Z. Anorg. Allg. Chem.* **1995**, *621*, 1907 – 1912.
[8] A.-V. Mudring, M. Jansen, *Angew. Chem.* **2000**, *112*, 3194 – 3196; *Angew. Chem. Int. Ed.* **2000**, *39*, 3066 – 3067; A.-V. Mudring, J. Nuss, U. Wedig, M. Jansen, *J. Solid State Chem.* **2000**, *155*, 29 – 36.
[9] A. Karpov, J. Nuss, U. Wedig, M. Jansen, *Angew. Chem.* **2003**, *115*, 4966 – 4969; *Angew. Chem. Int. Ed.* **2003**, *42*, 4818 – 4821.
[10] A. Karpov, J. Nuss, U. Wedig, M. Jansen, *J. Am. Chem. Soc.* **2004**, *126*, 14123 – 14128.
[11] A. Palenzona, *J. Less-Common Met.* **1981**, *78*, P49-P53.
[12] A. Karpov, U. Wedig, M. Jansen, *Z. Naturforsch. B* **2004**, *59*, 1387 – 1394.
[13] In the system Ba–Pt two other alloys containing more platinum, $BaPt_2$ and $BaPt_5$, are also known.[38]
[14] The first samples synthesized were contaminated with small amounts of BaH_2 and BaO. Such a sample was used for the synchrotron experiment.[17] After barium metal was purified by heating in a closed Ta ampoule at 1173 K for 12 h in dynamic vacuum, followed by distillation at 1100 K, a hydrogen free product was obtained. The hydrogen analysis yielded 0.03(2) wt% of H, which is on the detection limit.
[15] L. Pauling, J. L. Hoard, *Z. Kristallogr.* **1930**, *74*, 546 – 551.
[16] E. Warkentin, H. Bärnighausen, *Z. Anorg. Allg. Chem.* **1979**, *459*, 187 – 200.
[17] Crystal structure data of Ba_2Pt: rhombohedral, space group $R\bar{3}m$ (No. 166), $a = 456.42(1)$, $c = 2209.12(5)$ pm, Pt in 3*a* (0,0,0), Ba in 6*c* (0,0,*z*) with $z = 0.25528(5)$, $V = 398.55(1) \times 10^6$ pm^3, $\rho_{calcd} = 5.872$ g cm^{-3}, $Z = 3$. Device for X-ray diffraction experiments: ID31 beamline at the European Synchrotron Radiation Facility (ESRF), Si(111) monochromator, 9-Ge(111) crystal analyzers, $\lambda = 24.804$ pm, 9 scintillation counters, $T = 298$ K, $1.0° < 2\Theta < 18.0°$ in steps of $0.002° 2\Theta$, glass capillary of 0.2 mm diameter. Structure determination process: Data reduction and background modelling by using the GUFI program,[39] three phases Rietveld refinement[40] using Ba_2N[26] as a starting model with barium hydride and barium oxide as impurity phases by using the GSAS program package,[41] $R_p = 0.053$, $R_{wp} = 0.072$, $R_F = 0.034$, $R_F^2 = 0.054$, number of reflections 131, number of variables 30. Further details on the crystal structure investigations may be obtained from the Fachinformationszentrum Karlsruhe, 76344 Eggenstein-Leopoldshafen, Germany (fax: (+49) 7247-808-666; e-mail: crysdata@fiz-karlsruhe.de), on quoting the depository number CSD-414463.
[18] R. Hoppe, *Z. Kristallogr.* **1979**, *150*, 23 – 52.
[19] R. D. Shannon, C. T. Prewitt, *Acta Crystallogr. Sect. B* **1969**, *25*, 925 – 946; R. D. Shannon, *Acta Crystallogr. Sect. A* **1976**, *32*, 751 – 767.
[20] E. Rengade, *C. R. Hebd. Seances Acad. Sci.* **1909**, *148*, 1199 – 1202.
[21] A. Simon, *Z. Anorg. Allg. Chem.* **1973**, *395*, 301 – 319; A. Simon, E. Westerbeck, *Z. Anorg. Allg. Chem.* **1977**, *428*, 187 – 198; A. Simon, *Z. Anorg. Allg. Chem.* **1977**, *431*, 5 – 16.
[22] A. Simon, *Struct. Bonding (Berlin)* **1979**, *36*, 81 – 127; A. Simon, *Coord. Chem. Rev.* **1997**, *163*, 253 – 270.
[23] U. Steinbrenner, A. Simon, *Z. Anorg. Allg. Chem.* **1998**, *624*, 228 – 232.
[24] K. R. Tsai, P. M. Harris, E. N. Lassettre, *J. Phys. Chem.* **1956**, *60*, 338 – 344.
[25] O. Reckeweg, F. J. DiSalvo, *Solid State Sci.* **2002**, *4*, 575 – 584.
[26] O. Seeger, Ph.D. Thesis, University of Tübingen, Germany, **1994**.
[27] U. Müller, *Anorganische Strukturchemie*, B. G. Teubner, Stuttgart, **1996**, pp. 46 – 50.
[28] R. W. Tank, O. Jepsen, A. Burkhardt, O. K. Andersen, TB-LMTO-ASA-Program, Version 4.7, Max-Planck-Institut für Festkörperforschung, Stuttgart, **1998**.
[29] U. von Barth, L. Hedin, *J. Phys. C* **1972**, *5*, 1629 – 1642.
[30] Radii of the muffin tin spheres (/Bohr) Ba_2Pt: Pt: 3.890, Ba: 3.025, E(0,0,1/2): 4.090, E1(0,0,3/8): 2.019, E2(0,0,1/8): 1.952; Ba_2N: N: 2.407, Ba: 3.612, E(0,0,1/2): 3.543, E1(0,0,1/8): 1.995.
[31] A. Savin, A. D. Becke, J. Flad, R. Nesper, H. Preuß, H. G. von Schnering, *Angew. Chem.* **1991**, *103*, 421 – 424; *Angew. Chem. Int. Ed. Engl.* **1991**, *30*, 409 – 412; A. Savin, O. Jepsen, J. Flad, O. K. Andersen, H. Preuß, H. G. von Schnering, *Angew. Chem.* **1992**, *104*, 186 – 188; *Angew. Chem. Int. Ed. Engl.* **1992**, *31*, 187 – 188.
[32] W. Bronger, R. Kniep, M. Kohout, *Z. Anorg. Allg. Chem.* **2004**, *630*, 117 – 121.
[33] R. Dronskowski, P. E. Blöchl, *J. Phys. Chem.* **1993**, *97*, 8617 – 8624.
[34] R. F. W. Bader, *Atoms in Molecules: a Quantum Theory*, Oxford University Press, Oxford, **1990**.
[35] R. Eger, H. Mattausch, A. Simon, *Z. Naturforsch. B* **1993**, *48*, 48 – 51.
[36] K. Fischer, *Angew. Chem.* **1935**, *48*, 394 – 396.
[37] L. J. van der Pauw, *Philips Res. Rep.* **1958**, *13*, 1 – 9; J. P. Suchet, *Electrical Conduction in Solid Materials* in *International Series of Monographs in the Science of the Solid State* (Gen. Ed.: B. R. Pamplin), Pergamon, Oxford, **1975**.
[38] H. Schulz, K. Ritapal, W. Bronger, W. Klemm, *Z. Anorg. Allg. Chem.* **1968**, *357*, 299 – 313.
[39] R. E. Dinnebier, GUFI a program for measurement and evaluation of powder pattern, Version 5.0, Heidelberger Geowiss. Abh. 68, Heidelberg, **1997**.
[40] H. M. Rietveld, *Acta Crystallogr.* **1967**, *23*, 151 – 152; H. M. Rietveld, *J. Appl. Crystallogr.* **1969**, *2*, 65 – 71.
[41] A. C. Larson, R. B. von Dreele, GSAS, General Structure Analysis System, Los Alamos National Laboratory Report LAUR 86 – 748, Los Alamos National Laboratory, Los Alamos, NM (USA), **2002**.

 © 2005 Wiley-VCH Verlag GmbH & Co. KGaA, Weinheim

Chirality Switching

Field-Induced Switching of Chirality in Undulated Ferroelectric and Antiferroelectric SmCP Phases Formed by Bent-Core Mesogens**

Ramaiahgari Amaranatha Reddy, Martin W. Schröder, Michael Bodyagin, Horst Kresse, Siegmar Diele, Gerhard Pelzl, and Wolfgang Weissflog*

Chirality is a fundamental property of matter. In most cases chirality is an inherent molecular property, but it can also occur in solid crystals even though the constituent moieties are nonchiral, for example, as a consequence of a spontaneous discrimination during the crystallization process. Chirality in liquid systems formed by nonchiral molecules seems to be impossible because of the mobility of the particles. However, there are new kinds of mesophases formed by nonchiral bent-core molecules which are also able to exhibit phase chirality. The molecules can be packed in a polar fashion because of their bent shape and give rise to a long-range correlation of the lateral dipoles and therefore to a macroscopic polarization in the smectic (SmC) layers.[1] In the most widely studied SmCP phase (P = polar), the polar packed molecules are tilted with respect to the normal of the layer. As first shown by Link et al.[2] four structures can be distinguished depending on the stacking of the molecules in adjacent smectic layers (Figure 1). The molecules can have either a synclinic or an anticlinic interlayer correlation which is indicated in the phase symbol SmCP by the subscripts S and A after C. The polar order is specified by the suubscripts A and F, where A corresponds to an antiferroelectric structure and F designates a ferroelectric structure (the possible phase symbols are thus SmC_AP_A, SmC_SP_A, SmC_AP_F, and SmC_SP_F).[2] The polar packing as well as the tilt of the molecules in the SmCP phases are two steps of symmetry breaking which create a layer chirality without any molecular chirality. As seen in Figure 1, two equivalent layer structures with antiparallel polar axes exist for a given tilt direction which are mirror images of each other. The opposite handedness is depicted by filled (black) or open (white) molecule symbols. All layers of a macroscopic domain in the SmC_AP_A and SmC_SP_F structures have the same layer chirality (homochiral state) whereas the chirality alternates from layer to layer in the SmC_SP_A and SmC_AP_F structures (racemic state).

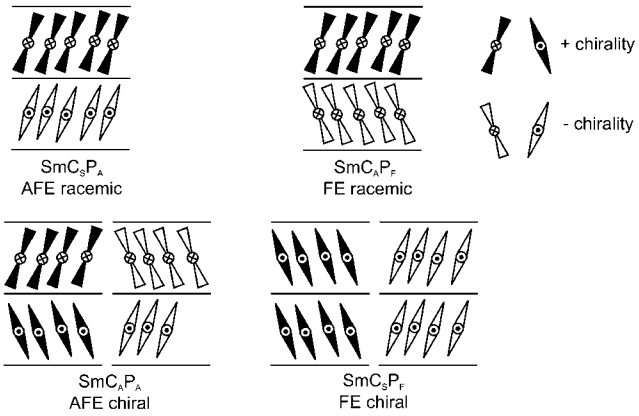


Figure 1. Possible orientations of the tilt and polar axes of bent-core molecules in adjacent layers that lead to chiral or racemic ferroelectric and antiferroelectric SmCP phases. Filled and open molecule symbols designate layers of opposite chirality.

To avoid bulk polarization an antiferroelectric ground state exists in most cases where the polarization alternates in adjacent layers.[3] The antiferroelectric states can be switched to the corresponding ferroelectric states (Figure 1). This field-induced reorientation takes place through rotation of the director around the normal to the layer on the tilt cone such as occurs in ferro- and antiferroelectric phases of calamitic compounds. The chirality of the layers is preserved during this switching process and is also the case for a switch between two ferroelectric states. Recently, it was found that the polar switching in "banana phases" can also take place by another mechanism, which is based on the collective rotation of the molecules around their long axes (Figure 2a). In polar smectic A (SmAP) phases[4,5] and in B_{1rev} phases formed by SmAP-like layer fragments[6] this mechanism is the only possibility for polar switching. There are a few examples that this switching mechanism can also occur in tilted $SmCP_A$ phases[7–9] as well as in B_{1rev} phases with SmCP-like layer fragments,[6] mostly under special experimental conditions. Nakata et al.[8] and Bedel et al.[9] were able to detect this switching mechanism above a critical electric field. Schröder et al.[7] observed this kind of polar switching only on very slow increase or decrease of the electric field. It should be emphasized that the field-induced switching in tilted

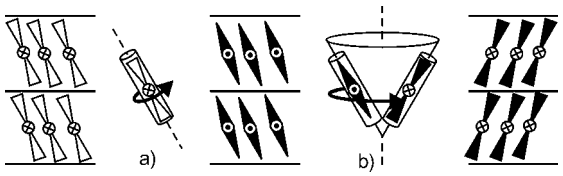


Figure 2. Mechanisms of polar switching a) by collective rotation of the molecules around their long axes and b) by rotation of the director around the tilt cone. Filled and open molecule symbols designate layers of opposite chirality.

[*] Dr. R. Amaranatha Reddy, M. W. Schröder, M. Bodyagin, Prof. Dr. H. Kresse, Dr. S. Diele, Prof. Dr. G. Pelzl, Prof. Dr. W. Weissflog
Institut für Physikalische Chemie
Martin-Luther-Universität Halle-Wittenberg
Mühlpforte 1, 06108 Halle/Saale (Germany)
Fax: (+49) 345-552-7157
E-mail: pelzl@chemie.uni-halle.de

[**] This work was supported by the Deutsche Forschungsgemeinschaft (Graduiertenkolleg 894 "Selbstorganisation durch koordinative und nichtkovalente Wechselwirkungen" and the Fonds der Chemischen Industrie.

Supporting information for this article is available on the WWW under http://www.angewandte.org or from the author.

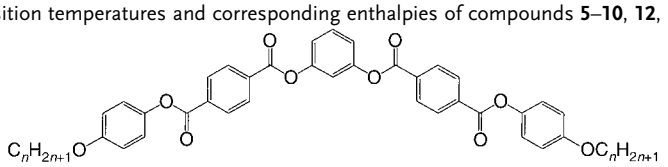
 © 2005 Wiley-VCH Verlag GmbH & Co. KGaA, Weinheim DOI: 10.1002/anie.200461490

"banana phases" by rotation around the long axes is accompanied by an inversion of the layer chirality.

Herein we focus mainly on the switching of chirality by external electric fields. We investigated eight homologues of a new series of bent-core mesogens in which the outer linking groups are reversed compared to isomeric compounds reported in the literature.[10] We found that all the homologues form a polar tilted smectic C (SmCP) phase with undulated smectic layers. From electrooptical experiments it follows that the short-chain members possess an antiferroelectric ground state while the long-chain members are ferroelectric. It is the first example where the switching process is changed from an antiferroelectric to a ferroelectric one with increasing chain length. Furthermore, for the first time, we found a clear dependence of the switching mechanism on the experimental conditions, that is, on the frequency and the temperature. At higher frequencies or lower temperatures, the polar switching of the ferroelectric phase takes place in the usual way, that is, by the rotation of the director around the tilt cone. This switching process retains the chirality of the layer and reverses only the polarity of the layer (see Figure 2b). The other type of polar switching takes place through collective rotation of the molecules around their long axes at sufficiently low frequencies or high temperatures. This process, which was first observed for the ferroelectric tilted "banana phases", reverses the polarity of the layer and is now accompanied by an inversion of the macroscopic chirality (see Figure 2a). Interestingly, both switching mechanisms compete at intermediate frequencies. By using polarizing microscopy an irreversible field-induced inversion of chirality could be clearly visualized in a texture which exhibits circular domains of opposite handedness. It should be noted that rotation around the long axes is probably the only mechanism of polar switching in the antiferroelectric phase of the short-chain homologues.

All members **5**–**10**, **12**, and **16** of the series have been prepared by esterification of resorcinol with the corresponding 4-(4-*n*-alkyloxyphenoxycarbonyl)benzoic acids in the presence of *N*,*N*'-dicyclohexylcarbodiimide (DCC) and 4-(*N*,*N*-dimethylamino)pyridine (DMAP) as the catalyst in dichloromethane (for the reaction pathway and analytical data for compound **12**, see the Supporting Information). The transition temperatures together with the enthalpy values are recorded in Table 1. Compounds **5**–**9** show similar optical textures, thus indicating they have the same phase. Cooling the isotropic liquid of any of these compounds results in the mesophase growing with ribbonlike textures together with the helical filaments (Figure 3a). However, the textural features observed for the higher homologues, namely, compounds **10**–**16**, are completely different to that of the first group, thus indicating a different mesophase. The mesophases of these longer chain compounds only show a spherulytic texture as shown in Figure 3b.

Table 1: Transition temperatures and corresponding enthalpies of compounds **5**–**10**, **12**, and **16**.[a]



Compound	*n*	Transition (*T* [°C]) [δH [kJ mol^{-1}]]	Transition (*T* [°C]) [δH [kJ mol^{-1}]]
5	5	Cr→Sm$\tilde{C}$P$_A$ (168.5) [92.2]	Sm$\tilde{C}$P$_A$→I (163.5) [18.8]
6	6	Cr→Sm$\tilde{C}$P$_A$ (166.5) [70.9]	Sm$\tilde{C}$P$_A$→I (168.0) [20.6]
7	7	Cr→Sm$\tilde{C}$P$_A$ (161.5) [79.3]	Sm$\tilde{C}$P$_A$→I (165.0) [11.6]
8	8	Cr→Sm$\tilde{C}$P$_A$ (160.0) [68.7]	Sm$\tilde{C}$P$_A$→I (168.0) [21.5]
9	9	Cr→Sm$\tilde{C}$P$_A$ (157.5) [83.9]	Sm$\tilde{C}$P$_A$→I (165.5) [20.7]
10	10	Cr→Sm$\tilde{C}$P$_F$ (154.5) [86.7]	Sm$\tilde{C}$P$_F$→I (164.0) [21.7]
12	12	Cr→Sm$\tilde{C}$P$_F$ (152.0) [79.7]	Sm$\tilde{C}$P$_F$→I (162.0) [23.6]
16	16	Cr→Sm$\tilde{C}$P$_F$ (151.0) [110.4]	Sm$\tilde{C}$P$_F$→I (160.5) [24.3]

[a] Abbreviations: Cr = crystalline solid, Sm$\tilde{C}$P$_A$ = antiferroelectrically switchable undulated tilted smectic phase, Sm$\tilde{C}$P$_F$ = ferroelectrically switchable undulated tilted smectic phase, I = isotropic liquid.

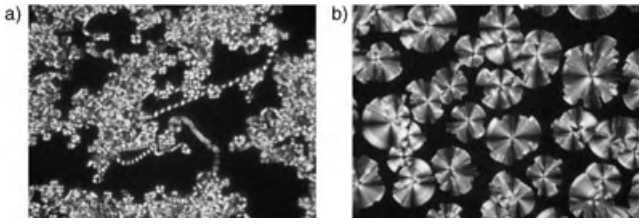


Figure 3. Optical photomicrographs of a) the Sm$\tilde{C}$P$_A$ phase of compound **8** at 167 °C and b) the Sm$\tilde{C}$P$_F$ phase of compound **12** at 161 °C.

The compounds under discussion are interesting from a structural point of view. X-ray powder diffraction patterns recorded with a Guinier film camera show strong layer reflections indicating that the basic structure is smectic. In addition, satellites of weak intensity could be clearly seen behind the layer reflections which suggests the presence of an undulated layer structure. The XRD powder pattern obtained for the mesophase of compound **6** is shown as an example in the Supporting Information. Satellites of weak intensity are obtained for the complete homologous series (see the Supporting Information). The undulation period increases from 100 to 150 Å with increasing chain length. The X-ray diffraction pattern of a partially aligned sample of the mesophase (see the Supporting Information) allows a tilt angle of about 20° to be estimated for compound **12** (designated as Sm$\tilde{C}$P, where the symbol ~ indicates the periodic in-plane density wave according to the recommendation in ref. [11]). This value is relatively small compared with the tilt angle of smectic phases of other bent-core compounds. A wide-angle diffuse maximum obtained at 4.7 Å indicates the absence of any long-range positional order. As shown by Coleman et al.,[12] the modulated layer structure formed by bent-core molecules is generated by splayed polarization with domains of alternate tilt and polarization periodically arranged. This is another way to avoid bulk polarization.

In addition to the structural features, the electrooptical behavior is also particularly interesting. On applying a triangular-wave electric field[13] to the mesophase of com-

 © 2005 Wiley-VCH Verlag GmbH & Co. KGaA, Weinheim

pound **7**, two polarization current peaks per half period were recorded which indicates an antiferroelectric ground state (see the Supporting Information). The calculated polarization value is about 520 $nC\,cm^{-2}$. However, the field-induced circular domains in which the extinction crosses are aligned along the directions of the crossed polarizers do not change on reversal of the field. At first sight, these observations could indicate a racemic ground state for the mesophase. However, no relaxation of the extinction crosses could be seen on terminating the applied field, apart from a small change in the birefringence. If the effect arose from a racemic nature of the domains, the texture should have shown a striped pattern parallel to the smectic layers as a result of an alternating chirality.[2] Instead we only observe a smooth fan-shaped texture (see the Supporting Information). Therefore, these observations suggest that the chirality of the layer switches by collective rotation of molecules around their long axes on reversing the applied field. A similar switching behavior could be observed for the homologues (**5**, **6**, **8**, and **9**) exhibiting antiferroelectric switching. On the basis of these experimental observations, mesophases of these compounds have been designated as the $SmC\tilde{P}_A$ phase.

The mesophase of compounds with longer aliphatic chains (**10**, **12**, and **16**) shows a different and interesting electro-optical switching behavior. A ferroelectric switching current response could be observed in the mesophase of compound **12** (see the Supporting Information); this result was also confirmed by applying a modified triangular wave (the plateau is introduced at zero voltage), which shows only a single polarization peak per half period. Therefore, we designated this phase as $SmC\tilde{P}_F$. A texture with spherulytic patterns appeared on cooling the mesophase of compound **12** under a polarizing microscope, and application of an electric field afforded a texture with bright and dark domains which depends on the polarity of the applied field. The texture remains unchanged on terminating the field, thus indicating bistable switching. Circular domains with extinction crosses could be obtained on increasing the voltage above a threshold value ($E > E_{th}$). These domains show bistable (ferroelectric) switching and the extinction crosses remain unchanged after removing the applied field. These bistable states are stable for several hours (Figures 4 and 5a), thus confirming the ferroelectric ground state of this mesophase. We strongly believe that the appearance of switching chiral domains at higher electric fields (triangular wave) is the consequence of the suppression of the undulated structure of the ground state, as observed for several other compounds.[12] The field-induced SmC_sP_F phase is stable on sudden removal of the field. However, the switching circular domains disappear slowly when the applied field is slowly reduced, which indicates a transition back to the undulated ground state. The switching mechanism of the ferroelectric $SmC\tilde{P}$ phase clearly depends on the frequency and on the temperature, which contrasts the behavior of the antiferroelectric $SmC\tilde{P}$ phase of the short-chain members.

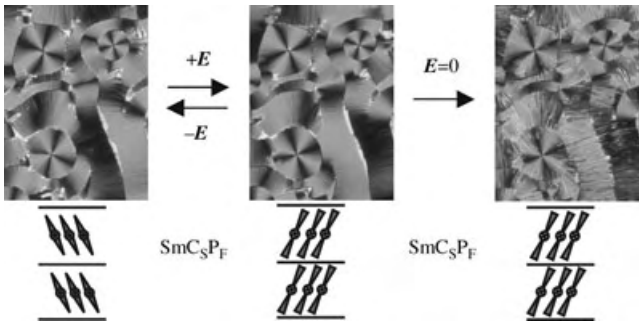


Figure 4. Bistable (ferroelectric) switching states obtained for the mesophase of compound **12** ($\pm 40\ V\,\mu m^{-1}$, 30 Hz at 149 °C), which are stable for several hours.

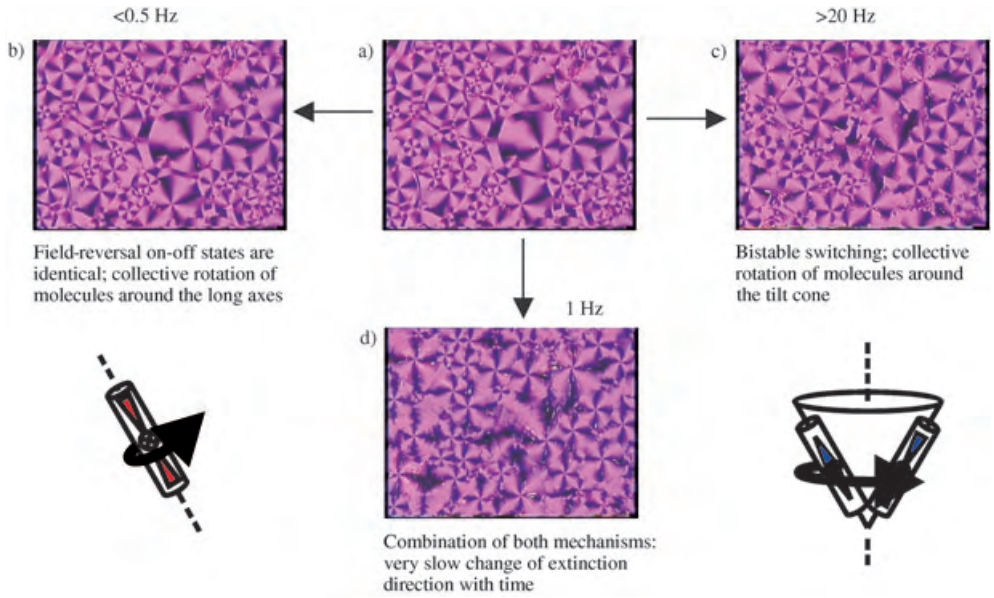


Figure 5. Frequency-dependent switching mechanism under a triangular-wave field for the $SmC\tilde{P}_F$ phase of compound **12** at 148 °C and $\pm 40\ V\,\mu m^{-1}$. Red and blue molecule symbols designate layers of opposite chirality.

 © 2005 Wiley-VCH Verlag GmbH & Co. KGaA, Weinheim

No change in the position of the extinction crosses and no change of the birefringence could be seen by reversing the polarity of the applied field at lower frequencies (< 0.2 Hz), although the optical effect and a current response could be clearly detected. These findings indicate that a reversal of the polarization takes place through the collective rotation around the long molecular axes. This kind of switching not only reverses the polarity but also the chirality of the layer. This result means that the chirality of the whole domain is inverted in the case of ferroelectric phases (Figure 5b).

At higher frequencies (≥ 20 Hz) a fast bistable switching is observed where the extinction crosses rotate clockwise or anticlockwise depending on the handedness of the circular domains (Figure 5c). This observation indicates that reversal of the polarization occurs by rotation of the director around the tilt cone. In this case, the chirality of the layer is retained and only the direction of polarization is reversed, as in SmC* phases.

Interestingly, at intermediate frequencies (> 0.5 Hz) a switching process could be clearly seen which takes place in the frequency of the applied a.c. field (Figure 5d), and simultaneously a very slow rotation of the extinction crosses (clockwise or anticlockwise) could be observed. These two results indicate a combination of both switching mechanisms.

No optical switching could be seen in the temperature interval 5 °C below the clearing temperature irrespective of the frequency, which suggests switching by a rotation around the molecular long axes. Bistable switching domains slowly appeared on further cooling the sample, which indicates switching around the tilt cone. The temperature dependence could be explained if we assume that the viscosity χ_α (related to the rotation around the long axes) is lower than the viscosity χ_φ (related to the rotation around a tilt cone) for a given field $\boldsymbol{E}$ and a given polarization $\boldsymbol{P}$ at higher temperature, whereas at lower temperatures the situation is opposite.

We also observed the inversion of the macroscopic chirality under the influence of an a.c. field over time. As seen from Figure 6, the texture consists of circular domains of opposite handedness; there are domains which have both an outer and inner part (indicated by arrows) with opposite handedness. If a sufficiently high voltage (a.c. field) is applied for some time (see snapshots after 30, 60, and 95 seconds) it can be seen that the inner domain with opposite chirality grows at the cost of the outer one. After about 60 s, the nucleation of a new domain begins in the center of the growing inner domain, again with opposite handedness. In this way, the field-induced change of chirality can be directly visualized. In this context it should be noted that an irreversible changeover of a homochiral into a racemic structure was reported in a $SmCP_A$ phase [14] by application of a triangular electric field.

In conclusion, we have presented a new homologous series of bent-core mesogens where all members form a polar tilted smectic C phase with an undulated layer structure. We have found for the first time that the polar structure is changed from antiferroelectric to ferroelectric with increasing

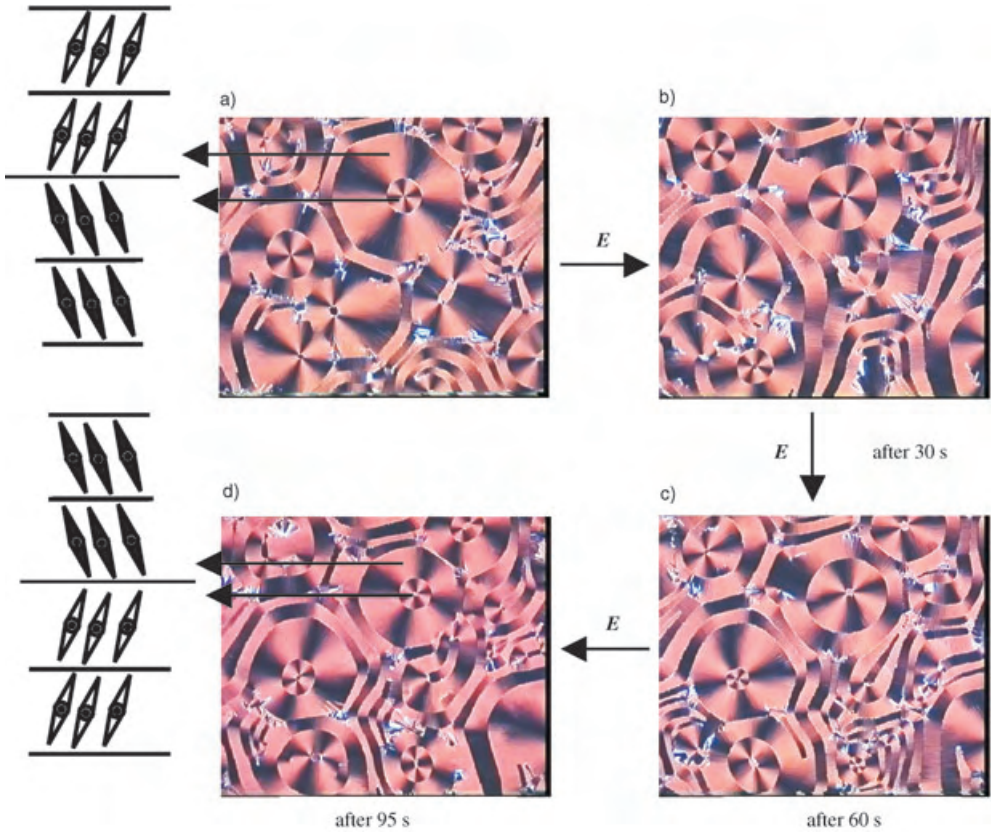


Figure 6. Visualization of the inversion of macroscopic chirality with time under a triangular-wave field in the $Sm\tilde{C}P_F$ phase of compound **12**; $\pm 40\ V\,\mu m^{-1}$, 30 Hz at 148 °C. Filled and open molecule symbols designate layers of opposite chirality.

 © 2005 Wiley-VCH Verlag GmbH & Co. KGaA, Weinheim

chain length. This observation can be explained in terms of interlayer interactions: they could be stronger for short-chain members which would clearly favor the formation of an antiferroelectric polar structure. Another remarkable feature is the occurrence of two different mechanisms of polar switching. In the case of ferroelectric phase, the switching mechanism clearly depends on the experimental conditions. At low temperatures and high frequencies the polar switching is based on the rotation of the director around the tilt cone. At a high temperature and a low frequency the polar switching takes place through rotation of the long molecular axes. Furthermore, we were able to change the chirality of circular domains irreversibly by application of an a.c. field.

Received: July 30, 2004
Published online: December 21, 2004

Keywords: chirality · electrooptical switching · ferroelectric structures · mesophases · phase transitions

[1] T. Niori, T. Sekine, J. Watanabe, T. Furukawa, H. Takezoe, *J. Mater. Chem.* **1996**, *6*, 1231.
[2] D. R. Link, G. Natale, R. Shao, J. E. Maclennan, N. A. Clark, E. Körblova, D. M. Walba, *Science* **1997**, *278*, 1924.
[3] G. Pelzl, S. Diele, W. Weissflog, *Adv. Mater.* **1999**, *11*, 707.
[4] A. Eremin, S. Diele, G. Pelzl, H. Nadasi, W. Weissflog, J. Salfetnikova, H. Kresse, *Phys. Rev. E* **2001**, *64*, 051707.
[5] R. Amaranatha Reddy, B. K. Sadashiva, *J. Mater. Chem.* **2004**, *14*, 1936.
[6] J. Szydlowska, J. Mieczkowski, J. Matraszek, D. W. Bruce, E. Gorecka, D. Pociecha, D. Guillon, *Phys. Rev. E* **2003**, *67*, 031702.
[7] M. W. Schröder, S. Diele, G. Pelzl, W. Weissflog, *ChemPhysChem* **2004**, *5*, 99.
[8] M. Nakata, R.-F. Shao, W. Weissflog, H. Takezoe, N. A. Clark, *Poster at the Ferroelectric Liquid Crystal Conference*, Dublin, **2003**.
[9] J. P. Bedel, J. C. Rouillon, J. P. Marcerou, H. T. Nguyen, M. F. Achard, *Phys. Rev. E* **2004**, *69*, 061702.
[10] D. Shen, A. Pegenau, S. Diele, I. Wirth, C. Tschierske, *J. Am. Chem. Soc.* **2000**, *122*, 1593; R. Amaranatha Reddy, B. K. Sadashiva, *Liq. Cryst.* **2003**, *31*, 1031.
[11] M. Baron, *Pure Appl. Chem.* **2001**, *73*, 845.
[12] D. A. Coleman, J. Fernsler, N. Chattham, M. Nakata, Y. Takanishi, E. Korblova, D. R. Link, R.-F. Shao, W. G. Jang, J. E. Maclennan, O. Mondainn-Monval, C. Boyer, W. Weissflog, G. Pelzl, L.-C. Chien, J. Zasadzinski, J. Watanabe, D. M. Walba, H. Takezoe, N. A. Clark, *Science* **2003**, *301*, 1204.
[13] K. Miyasato, S. Abe, H. Takezoe, A. Fukuda, E. Kuze, *Jpn. J. Appl. Phys.* **1983**, *22*, L661.
[14] G. Heppke, A. Jàkli, S. Rauch, H. Sawade, *Phys. Rev. E* **1999**, *60*, 5575.

 © 2005 Wiley-VCH Verlag GmbH & Co. KGaA, Weinheim

Heterogeneous Catalysis

Preferential Oxidation of CO in H_2 by Aqueous Polyoxometalates over Metal Catalysts**

*Won Bae Kim, Tobias Voitl, Gabriel J. Rodriguez-Rivera, Steven T. Evans, and James. A. Dumesic**

Production of H_2 for fuel cells is usually accomplished by a multistep process, which starts with catalytic reforming of hydrocarbons[1] or oxygenated hydrocarbons over metal catalysts[2,3] to produce a mixture of H_2, CO, and CO_2. These reformate gases are subsequently treated by several steps, such as water–gas shift (WGS) ($CO + H_2O \rightarrow CO_2 + H_2$)[4,5] and preferential oxidation of CO in the H_2-rich gas stream (PROX; $CO + 1/2\,O_2 \rightarrow CO_2$),[6,7] for applications involving proton-exchange membrane (PEM) fuel cells, this oxidation of CO is necessary owing to the strong poisoning effects of CO on Pt-based anodes.[8] While these methods for removing CO from H_2 gas stream are well established, they suffer from several limitations. For example, the WGS reaction is slow at the low temperatures (e.g., 500 K) required to achieve favorable thermodynamics for this reaction,[9] and PROX requires the injection of O_2 (or air) into the H_2 gas stream and consumes a fraction of the H_2 as well. Moreover, these processes for CO conversion often involve the use of platinum or platinum-alloy catalysts, which are expensive and compete with fuel-cell electrodes for the limited supply of this precious metal, compared with the abundant holdings of gold in the world.[10]

Recently, we reported the discovery of a room-temperature process for production of electrical energy using a fuel cell containing a carbon anode and operating with an aqueous solution of a polyoxometalate (POM) compound that had been reduced with pure CO over gold-nanotube catalysts.[11] This process for the oxidation and utilization of CO involves the reaction of CO and liquid water with a reducible POM, such as $[H_3PMo_{12}O_{40}]$, which serves as an oxidizing agent for reaction of CO with liquid water and as an energy-storage agent for electrons; the process takes advantage of the high catalytic activities of gold for CO oxidation,[12–14] especially in the presence of liquid water, as shown experimentally using gold-nanotube membrane catalysts[15] and as predicted by density functional theory calculations.[16,17] A representative

[*] W. B. Kim, T. Voitl, G. J. Rodriguez-Rivera, S. T. Evans, Prof. J. A. Dumesic
Chemical and Biological Engineering Department
University of Wisconsin
Madison, WI 53706 (USA)
Fax: (+1) 608-262-5434
E-mail: dumesic@engr.wisc.edu

[**] This work was supported by the National Science Foundation and Daimler-Chrysler, and the U.S. Department of Energy. Fellowships were provided by the Camille and Henry Dreyfus Foundation and the Graduate Engineering Scholars program. We thank the World Gold Council for providing gold catalysts, and we thank M. Mavrikakis, J. K. Nørskov, and Bjerne S. Clausen for valuable discussions.

 © 2005 Wiley-VCH Verlag GmbH & Co. KGaA, Weinheim DOI: 10.1002/anie.200461601

stoichiometric reaction for this process is shown in Equation (1).

$$CO_{(g)} + H_2O_{(l)} + [PMo_{12}O_{40}]^{3-}_{(aq)} \rightarrow CO_{2(g)} + 2\,H^{+}_{(aq)} + [PMo_{12}O_{40}]^{5-}_{(aq)} \quad (1)$$

The aqueous solution of protons and reduced POM formed in this reaction can be delivered to a PEM fuel cell to generate electrical energy by using a carbon anode, thereby regenerating the POM in its initial oxidized state.[11] The POM species thus functions as a redox shuttle, thereby eliminating the need to convert CO with H_2O into gaseous H_2 and CO_2 for the production of electrical energy.

Herein, we demonstrate that this new process for CO oxidation using aqueous POM solutions can be carried out at high rates at room temperature over various metal catalysts, such as nanoparticles of Au, Pt, Pd, and Ir supported on carbon. Importantly, we show that catalysts containing Au nanoparticles are unique because they selectively and rapidly catalyze the oxidation of CO, in H_2-rich gas mixtures containing CO concentrations from 0.1 to 10%, using a reversible POM oxidant, in contrast to the irreversible O_2 oxidant that is employed in the conventional PROX process. Accordingly, our room-temperature process using aqueous POM solutions can be employed effectively for PROX applications without consuming significant amounts of H_2, which is of particular importance in the production and purification of H_2 for the PEM fuel-cell applications.

Rates of CO oxidation by aqueous POM at 298 K are presented in Figure 1 for different supported metal catalysts. All catalysts tested herein showed a monotonic increase of turnover frequency (TOF, s^{-1}) with respect to CO pressure from 3.4 to 15.8 bar, the TOF in this study is defined as the number of CO_2 molecules produced per second normalized by the number of surface metal sites (see caption of Figure 1). All reaction kinetics measurements were made repeatedly, under conditions where the rates were not limited by mass-transport effects, by working at initial conversions of POM lower than 20% (i.e., less than 1 electron transferred per POM) and by decreasing the amount of catalyst and the metal loading until the measured rate per gram of catalyst became independent of the amount of catalyst and the metal loading (i.e., 1 wt%). The values of TOF measured at 3.4 and 15.8 bar of CO pressure are compared over the different metals in Figure 1, showing that the TOF for oxidation of pure CO decreases in the order Pd > Au > Pt > Ir > Rh > Ru at the higher pressure of CO (15.8 bar), with a negligible rate for Ag/C catalyst. The Au/C catalyst showed the highest TOF compared to the other metals at the lower CO pressure of 3.4 bar.

High catalytic activity for oxidation of CO by aqueous POM solutions may be related to low binding energy for the adsorption of OH groups on the metal surface (as given in Figure 1 (black bars) by the energy change for the dissociative adsorption of water to give adsorbed OH species and gaseous H_2), combined with sufficiently high binding energies for the adsorption of CO and H-atoms (as given in Figure 1 (light and dark gray bars) by the energy changes for the molecular and dissociative adsorption of CO and H_2, respectively).[18,19] A low value (that is, a positive energy change) of the binding energy for OH species is desirable to ensure that the surface of the metal does not become oxidized and thereby poisoned by the aqueous POM solution. Thus, metals such as Au, Pd, and Pt display high activities because they bind OH species sufficient weakly. A sufficiently high binding energy (that is, a negative energy change) for CO and H-atoms is required for these species to interact with the metal surface during the steps that eventually lead to the formation of protons and electrons. Thus, Ag shows very low catalytic activity because of the very weak interactions of adsorbed CO and H atoms with this metal. Finally, very high (negative) binding energies of CO on the metal surface may be undesirable, since such high values could lead to poisoning of the surface by strongly adsorbed CO at room temperature. Thus, the weaker binding of CO on Au compared to Pt may explain the higher catalytic activity of Au.

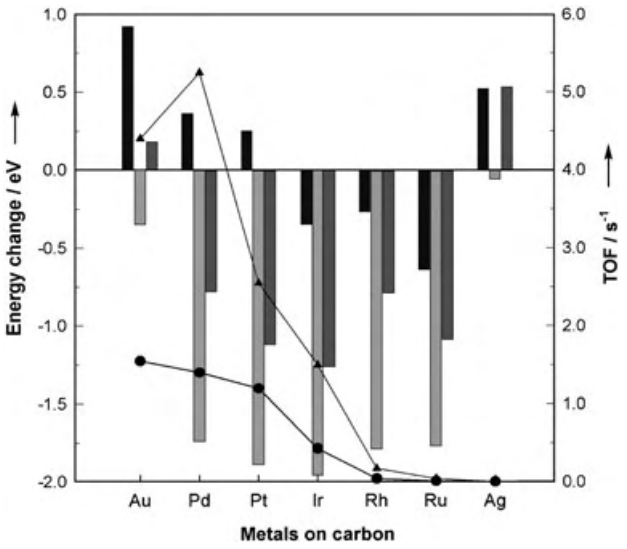


Figure 1. Rate of CO oxidation by aqueous $[H_3PMo_{12}O_{40}]$ (0.05 M) over carbon-supported metal catalysts, (●) TOF at 3.4 bar, (▲) TOF at 15.8 bar, and associated energy changes: (black bar) energy change for dissociative adsorption of water ($H_2O \rightarrow OH_{ads} + 0.5\,H_2$), (light gray bar) energy change for adsorption of CO, (dark gray bar) energy change for dissociative adsorption of H_2 ($H_2 \rightarrow 2\,H_{ads}$). Values for energy changes were determined by DFT calculations for stepped surfaces.[19] To determine the TOF value, the number of surface sites for Au/C was estimated from the TEM-determined metal particle size, for Pd/C, Pt/C, Ir/C, Rh/C, and Ru/C the number of surface sites was measured by CO adsorption at 298 K, and for Ag/C the number of surface sites was determined by O_2 adsorption at 423 K as is established elsewhere.[22] The metal dispersion (the number of surface metal atoms normalized by the total number of metal atoms) is 0.12 for Au/C, 0.39 for Pt/C, 0.23 for Pd/C, 0.13 for Ir/C, 0.18 for Rh/C, 0.55 for Ru/C, and 0.09 for Ag/C.

The metal loadings of the supported Au, Pd, Pt, and Ir catalysts were determined by inductively coupled plasma (ICP) analysis before and after their use for CO oxidation in aqueous POM solutions. The gold loading of the Au/C catalyst remained unchanged after exposure to reaction conditions, and dissolved gold species were not observed in the aqueous solution within the detection limit of the ICP

 © 2005 Wiley-VCH Verlag GmbH & Co. KGaA, Weinheim

analysis (≈1 ppm). Moreover transmission electron microscopy (TEM) measurements did not show any changes in average metal particle sizes upon exposure of supported gold catalysts to reaction conditions. We observed 10–20% loss of the initial catalytic activity after first use, but stable activity was maintained, at levels of at least 50% of the initial activity, after exposure of the catalyst to 0.05 M POM solution for 3 months. In contrast, Pd was leached from Pd/C into the aqueous solution under the reaction conditions, which led to dissolved species, such as Pd^{2+}, that might serve as a homogeneous catalyst.[20] Slow leaching of metal may take place upon exposure of carbon-supported Pt and Ir catalysts to reaction conditions, ICP analyses detected 10–20 ppm of Pt and 5 ppm of Ir species in 0.05 M POM solutions contacted for 24 h with the Pt/C and Ir/C catalysts, respectively.

Rates of CO versus H_2 oxidation by aqueous POM solution were measured on Au/C, Pt/C, Pd/C, and Ir/C catalysts using pure CO and pure H_2 gases (Figure 2 A), as well as gas mixtures containing 10% CO in H_2 (Figure 2 B) and 1% CO in H_2 (Figure 2 C). The rate of CO oxidation over Au/C was at least 10-times faster than the rate of H_2 oxidation when both gases were passed separately, whereas Pt/C showed a much higher rate of H_2 oxidation than CO oxidation. For a CO:H_2 gas mixture containing 10% CO (Figure 2 B), the rate of CO oxidation was approximately 0.8 s^{-1} on Au/C, and the rate of H_2 oxidation was negligible. The other catalysts also showed an inhibition of the rate of H_2 oxidation by CO when 10% CO in H_2 was used compared to using pure H_2. When the concentration of CO was decreased to 1% CO in H_2 (Figure 2 C), the Au catalyst maintained its effectiveness for PROX, showing a value for the rate ratio (defined as TOF(CO)/TOF(H_2)) of about 9. In contrast, the other catalysts showed low ratios for the rate of CO versus H_2 oxidation under these conditions.

The rate ratio of 9 for the Au catalyst using the 1% CO in H_2 gas mixture corresponds to a first-order rate constant of CO oxidation that is 900-times higher than the rate constant for H_2 oxidation at 14.8 bar, assuming that the rates are proportional to the respective reactant pressures. These results indicate that our process for CO oxidation using aqueous POM solutions with gold catalysts can be used to remove CO efficiently from H_2 gas streams even at room temperature without significant consumption of H_2. Indeed, for a lower CO concentration of 0.1% CO in H_2, the ratio of the rate of CO versus H_2 oxidation was 0.10–0.15 at total pressures of the gas mixture from 14.8 to 49.3 bar, corresponding to a first-order rate constant (see Figure 3 B) that is still at least 100 times faster for CO than for H_2 oxidation. The TOF for CO oxidation is not affected by the presence of H_2, and the rate is first order with respect to CO pressure, that is, all the TOF for CO data in Figure 3 A fall on the same line regardless of whether measurements were made using pure CO or using gas mixtures of CO in H_2. In contrast, the TOF for H_2 oxidation is suppressed by the presence of CO, showing a significant decrease of the rate from the case using pure H_2 to when using 99.9% H_2 (with 0.1% CO), and the TOF decreases further when using 99% H_2 (with 1% CO; Figure 3 A). Note, when the gas mixture containing 90% H_2 with 10% CO is employed, there is no measurable rate of H_2 oxidation over the gold catalyst (see Figure 2 B).

It is clear from Figure 2 and Figure 3 that Au/C catalyzes the selective oxidation of CO (compared to H_2) by aqueous POM solutions, and the presence of CO inhibits the oxidation of H_2. In contrast, the rate of H_2 oxidation over Pt/C is faster than the rate of CO oxidation, and although the presence of CO inhibits the oxidation of H_2, metals such as Pt, Pd, and Ir are not effective catalysts for selective oxidation of CO, although these metals show high activity for the oxidation of CO without H_2.

Figure 4 shows a possible reaction scheme for CO oxidation by an oxidized POM species in aqueous condition on a gold catalyst (the structure of the POM anion is a simplified representation of the Keggin structure[21] in which one PO_4 tetrahedron is surrounded by 12 MoO_6 octahedra). Carbon monoxide and water adsorb, albeit weakly, on the gold surface. In contrast, dissociative adsorption of H_2 on gold is energetically unfavorable compared to the adsorption of CO and is accompanied by a high energy barrier.[18] The results in Figure 2 and Figure 3 indicate that this more favorable adsorption of CO inhibits the activation of H_2 on

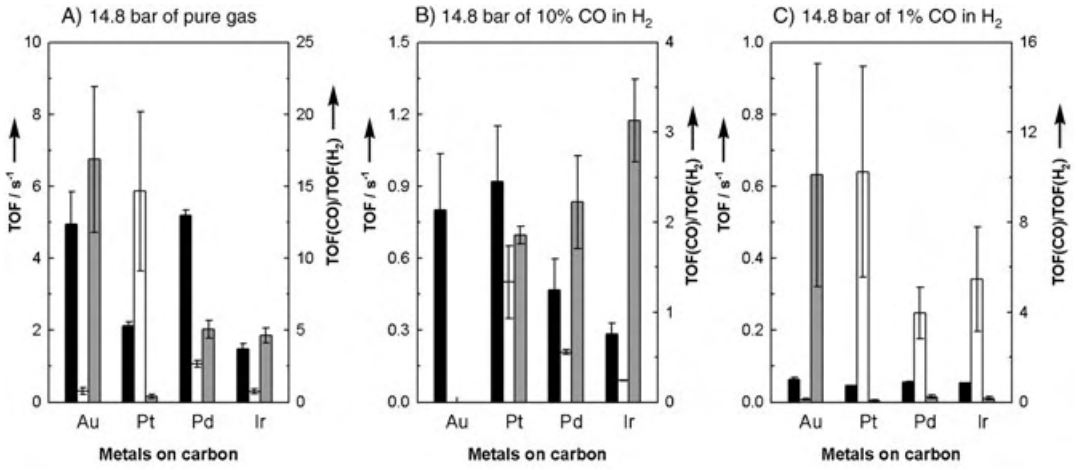


Figure 2. Rates of CO and H_2 oxidation with aqueous [$H_3PMo_{12}O_{40}$] (0.05 M) over carbon-supported metal catalysts in different gas mixtures. (Black bar) CO oxidation, (white bar) H_2 oxidation, (gray bar) ratio of rates for CO versus H_2 oxidation (TOF(CO)/TOF(H_2)).

 © 2005 Wiley-VCH Verlag GmbH & Co. KGaA, Weinheim

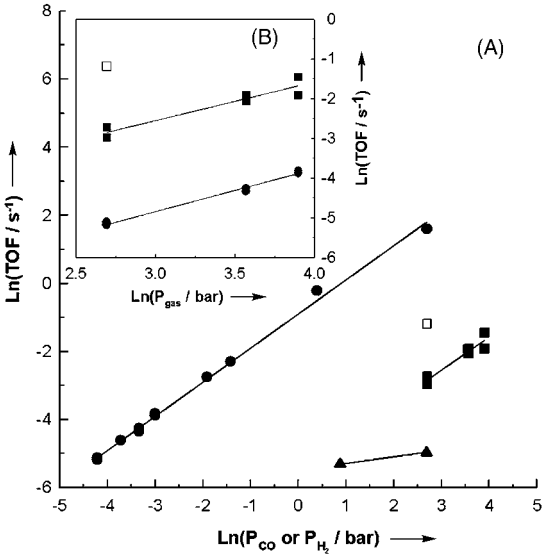


Figure 3. Rates of CO and H_2 oxidation with aqueous $[H_3PMo_{12}O_{40}]$ (0.05 M) over 0.8% Au/C. A) (●) TOF for CO with respect to CO pressure in measurements using pure CO and gas mixtures of CO (10%, 1%, and 0.1%) in H_2, (□) TOF for H_2 using pure H_2, (■) TOF for H_2 with respect to pressure of H_2 in 99.9% H_2 with 0.1% CO and (▲) in 99% H_2 with 1% CO. B) (●) TOF for CO and (■) TOF for H_2 with respect to the total pressure of 0.1% CO:H_2 mixture, (□) TOF of H_2 using pure H_2.

dissociates eventually to produce CO_2, which results in the formation of a proton in liquid water and transfer of an electron to the gold surface, this electron is subsequently transported to a reducible POM species.

Experimental Section

In a typical experiment, a batch reactor loaded with 20 cm^3 of 0.05 M POM ($[H_3PMo_{12}O_{40}]$, purchased from Aldrich) solution and catalyst was purged three times with CO and then filled with CO at specific pressures. The reactor was a stainless steel vessel (approximately 350 cm^3 volume), in which the POM solution and catalyst were placed in a glass liner with a magnetic stirrer. For the oxidation of CO in H_2, the reactor was purged three times with N_2 and then filled with a CO:H_2 mixture. Gas-phase products were analyzed at specific times by releasing pressure to an online gas chromatograph equipped with a thermal conductivity detector. The rate of H_2 oxidation was measured by monitoring the color change of the POM solution using a UV/Vis spectrometer operating at 500 nm.

CO and mixtures of CO:H_2 were supplied from AGA. Carbon-supported gold catalyst (Au/C) was supplied from the World Gold Council (Type D, Lot No. 4D), which was characterized by the supplier as 0.8 wt% Au with an average Au particle diameter of 10.5 nm. Catalysts consisting of 1 wt% Pt/C and 1 wt% Pd/C were purchased from Aldrich and 1 wt% Ir/C was purchased from Alfa. A catalyst containing 1 wt% Rh on carbon (Vulcan carbon) was prepared using a solution reduction method of $RhCl_3$ by $NaBH_4$, followed by rinsing with deionized water and drying in a vacuum desiccator. Preparations of 1 wt% Ru and Ag on carbon were carried out by impregnation of $RuCl_3$ and $AgNO_3$, followed by reduction at 623 K with flowing H_2. All catalysts were characterized by ICP to determine the actual metal loadings on the catalysts.

Received: August 10, 2004
Published online: December 23, 2004

Keywords: carbon monoxide · gold · heterogeneous catalysis · hydrogen · polyoxometalates

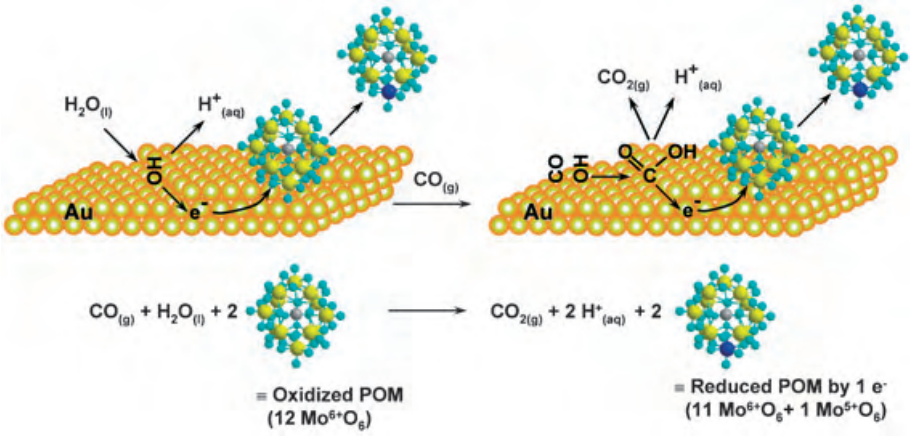


Figure 4. Reaction schematic for oxidation of CO using aqueous polyoxometalate ($[H_3PMo_{12}O_{40}]$) solutions over gold catalysts. The POM reduced by 1 electron is represented by showing 1 Mo atom in the distinct blue color of the reduced compound, the other Mo centers are yellow, O turquoise, P gray. See text for details.

the gold surface for reaction with the POM species when the CO is present in concentrations higher than about 0.1%. The adsorbed water molecule dissociates heterolytically in the presence of liquid water,[16,17] forming a hydroxy group adsorbed on the metal surface and hydrogen atom that is subsequently oxidized by transfer of an electron into the metal and formation of a proton stabilized in liquid water. The electron is then transported through the metal to the reducible POM species present on the metal. The adsorbed hydroxy species interacts with adsorbed CO to form an intermediate surface species, such as adsorbed COOH, which

[1] J. R. Rostrup-Nielsen, T. Rostrup-Nielsen, *CATTECH* **2002**, *6*, 150.
[2] R. D. Cortright, R. R. Davda, J. A. Dumesic, *Nature* **2002**, *418*, 964.
[3] G. W. Huber, J. W. Shabaker, J. A. Dumesic, *Science* **2003**, *300*, 2075.
[4] Q. Fu, H. Saltsburg, M. Flytzani-Stephanopoulos, *Science* **2003**, *301*, 935.
[5] R. R. Davda, J. A. Dumesic, *Angew. Chem.* **2003**, *115*, 4202; *Angew. Chem. Int. Ed.* **2003**, *42*, 4068.
[6] Y.-F. Han, M. J. Kahlich, M. Kinne, R. J. Behm, *Phys. Chem. Chem. Phys.* **2002**, *4*, 389.
[7] A. Wootsch, C. Descorme, D. Duprez, *J. Catal.* **2004**, *225*, 259.
[8] B. C. H. Steele, A. Heinzel, *Nature* **2001**, *414*, 345.
[9] C. V. Ovesen, P. Stoltze, J. K. Nørskov, C. T. Campbell, *J. Catal.* **1992**, *134*, 445.
[10] D. Cameron, R. Holliday, D. Thompson, *J. Power Sources* **2003**, *118*, 298.
[11] W. B. Kim, T. Voitl, G. J. Rodriguez-Rivera, J. A. Dumesic, *Science* **2004**, *305*, 1280.

 © 2005 Wiley-VCH Verlag GmbH & Co. KGaA, Weinheim

[12] M. Haruta, T. Kobayashi, H. Sano, N. Yamada, *Chem. Lett.* **1987**, *2*, 405.
[13] M. Valden, X. Lai, D. W. Goodman, *Science* **1998**, *281*, 1647.
[14] M. Daté, M. Okumura, S. Tsubota, M. Haruta, *Angew. Chem.* **2004**, *116*, 2181; *Angew. Chem. Int. Ed.* **2004**, *43*, 2129.
[15] M. A. Sanchez-Castillo, C. Couto, W. B. Kim, J. A. Dumesic, *Angew. Chem.* **2004**, *116*, 1160; *Angew. Chem. Int. Ed.* **2004**, *43*, 1140.
[16] S. K. Desai, M. Neurock, *Phys. Rev. B* **2003**, *68*, 075420.
[17] S. Desai, M. Neurock, *Electrochim. Acta* **2003**, *48*, 3759.
[18] S. Kandoi, A. A. Gokhale, L. C. Grabow, J. A. Dumesic, M. Mavrikakis, *Catal. Lett.* **2004**, *93*, 93.
[19] T. Bligaard, J. K. Nørskov, S. Dahl, J. Matthiesen, C. H. Christensen, J. Sehested, *J. Catal.* **2004**, *224*, 206.
[20] V. A. Golodov, B. S. Jumakaeva, *J. Mol. Catal.* **1986**, *35*, 309.
[21] G. M. Brown, M.-R. Noe-Spirlet, W. R. Busing, H. A. Levy, *Acta Crystallogr. B* **1977**, *B33*, 1038.
[22] S. Lambert, C. Cellier, P. Grange, J.-P. Pirard, B. Heinrichs, *J. Catal.* **2004**, *221*, 335.

 © 2005 Wiley-VCH Verlag GmbH & Co. KGaA, Weinheim

Surface Chemistry

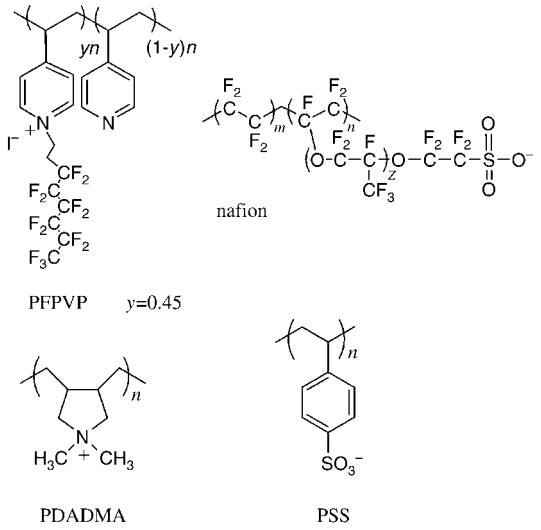
Hydrophobic and Ultrahydrophobic Multilayer Thin Films from Perfluorinated Polyelectrolytes**

*Rana M. Jisr, Hassan H. Rmaile, and Joseph B. Schlenoff**

Interest in surfaces exhibiting large water contact angles is stimulated both by important technological implications and by novel aspects of surface physics. Since wetting can be controlled by a single monolayer of material, novel materials or surface treatments can yield a fascinating range of properties. Such treatments, which are capable of generating particularly hydrophobic surfaces, include conventional coating processes such as spraying or dipping,[1a] vacuum deposition techniques,[1b] and such surface-modification technologies as diffusion,[1c] laser and plasma processes,[1d] chemical plating,[1e] grafting[1f] or bonding hydrogel encapsulation,[1g] and bombardment with high-energy particles.[1h]

The use of the layer-by-layer sequential adsorption[2] method for the assembly of an ultrathin film has very recently been reported for making ultrahydrophobic surfaces.[3,4] These studies address the critical issue of inducing surface roughness, which is required for true ultrahydrophobic behavior.[5–15] Soeno et al.[3] described a multilayered polyelectrolyte/silica nanoparticle system which was heated to sinter the particles and burn off the polymer, then treated with a fluorosilane to induce the required hydrophobicity. Zhai et al.[4] reported the formation of a pH-sensitive multilayer which undergoes a porosity-inducing phase transition in acidic solutions. Additional treatment steps, including cross-linking, deposition of silica nanoparticles, fluorosilane treatment, and thermal annealing, yielded stable ultrahydrophobic materials. Although the targeted surface properties were obtained, multiple processing steps are not desirable. Herein, we describe a multilayering process that uses both fluorinated polyanions and polycations, with a roughening step, by utilizing a naturally occurring nanorod that can be inserted conveniently into the layering sequence.

The polyelectrolytes used were nafion (Scheme 1), which is a commercially available sulfonated fluorinated material, and a polycation synthesized from poly(vinylpyridine) and a fluorinated alkyl iodide. Polyelectrolyte components were deposited on silicon wafers under ambient conditions using dilute solutions/dispersions. Although fluorinated solvents, such as trifluoroethanol, were useful for dispersing the polyelectrolytes, we were interested in employing more common solvents as vehicles for manipulating all the components. Methanol was effective in this respect. Figure 1 shows the layer-by-layer build-up of the fluorinated polyelectrolytes. The regular growth of the multilayer alleviated our concerns that the polyelectrolytes, probably existing as micellar, nanoparticulate dispersions rather than true solutions, might not produce acceptable multilayering behavior. Some curvature of the build-up curve hints at exponential growth (a topic of recent interest[16,17]), but the fact that such curvature is so slight suggests it might result from increasing surface roughness, which was found to be 2.9, 3.2, 4.8, 5.7, 7.0, and 10 nm root-mean-square (RMS) for 10, 20, 30, 40, 50, and 60 layers, respectively.



Scheme 1. Structures of the polyelectrolytes.

[*] R. M. Jisr, H. H. Rmaile,[+] Prof. J. B. Schlenoff
Department of Chemistry and Biochemistry and
Center for Materials Research and Technology (MARTECH)
The Florida State University
Tallahassee, FL 32306-4390 (USA)
Fax: (+1) 850-644-8281
E-mail: schlen@chemmail.chem.fsu.edu
[+] Current address:
Hercules Inc.
Wilmington, DE (USA)

[**] We thank the National Science Foundation for support of this work.

 © 2005 Wiley-VCH Verlag GmbH & Co. KGaA, Weinheim DOI: 10.1002/anie.200461645

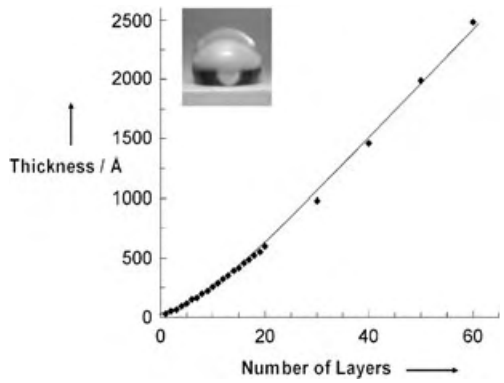


Figure 1. Layer-by-layer build-up of nafion/PFPVP on polished Si(100). The refractive index was measured to be 1.40. The insert shows a droplet of water on the final multilayer.

The contact angles on the fluorinated multilayers, as well as some more common multilayer systems, are summarized in Table 1. Two techniques for measuring the contact angle were employed. The "sessile drop" method involves the use of a telescope (Rame–Hart Inc.) to manually estimate the angle made by a 10-μL drop dispensed on the surface. This method gives a value akin to an advancing contact angle θ_a. Rectangular pieces of a completely coated silicon wafer were also employed to determine the dynamic contact angles (DCA) by using the Wilhelmy plate method.[18] In this method a plate is dipped slowly into water and then withdrawn. After correction for buoyancy, the respective advancing and receding θ_r angles are calculated, which are subject to less operator interpretation than the sessile drop instrument.[19] While the fluorinated surfaces give large advancing contact angles (some larger than for teflon), the value of θ_r is much smaller for smooth hydrophobic surfaces than ultrahydrophobic (rough and hydrophobic) surfaces (Table 1).

Table 1: Water contact angles, both static and dynamic, on various multilayer surfaces.

System	Dynamic contact angle [°]		Static contact angle [°]
	advancing	receding	
blank	21	19	0
$(PDADMA/PSS)_{10}PSS$	41	19	15
$(PDADMA/PSS)_{11}PDADMA$	57	23	35
$PEI(PFPVP/nafion)_{10}PFPVP$	114	28	114
$PEI(PFPVP/nafion)_{11}nafion$	102	37	104
$PDAMA(PSS/PDADMA)_3$-$(clay/PDADMA)_3$ $(nafion/PFPVP)_4PFPVP$	156, 154[a]	143, 142[a]	168, 168[a]

[a] Value measured after 2 months of immersion in water.

Measurements of both θ_a and θ_r, in particular the difference (or hysteresis) between them, are essential for verifying true ultrahydrophobic behavior.[20–22] In the wetting state described by Wenzel,[23,24] a water droplet penetrates the roughness features of the surface and becomes pinned to the surface. Although such a surface might exhibit a large θ_a value, that of θ_r is usually much smaller. By contrast, Cassie and Baxter[25,26] considered a water droplet that rides over the uppermost features of a hydrophobic surface, essentially remaining in contact with air. This surface may exhibit very small contact angle hysteresis, with the result that water droplets roll easily. In a recent critical evaluation of the "superhydrophobic" or "ultrahydrophobic" surface literature, Chen et al. provide numerous examples of systems that are poorly defined because they fail to clearly present contact angle hysteresis.[14] Even very recent work falls short in this respect.[27] Following the recommendation of Chen et al.,[14] we reserve the term "ultrahydrophobic" for those surfaces exhibiting both large water contact angles and small hysteresis between θ_a and θ_r.

It is interesting to note that extremely large contact angles and surface roughness are not prerequisites for ultralyophobicity in non-aqueous liquids (exhibiting "lyophobic" behavior).[14] Ultrahydrophobicity, however, appears to require surface roughness, although the length scales are not well understood. Regularly patterned pillars, produced by lithography, with diameters of approximately 10 μm and about the same spacing generated ultrahydrophobic surfaces.[20,22] In contrast, Zhai et al.[4] focused on reproducing the "lotus effect,"[28] whereby micrometer-sized surface features are decorated with nanometer-sized wax particles. Similarly, we sought to create surface roughening on two length scales—micrometer and nanometer—but using particles inserted as layers in the multilayering process.

Clay minerals constitute one of the many different types of particles that have been employed in the layer-by-layer assembly process.[29] However, most clays are platelike and have been shown to deposit parallel to the substrate during multilayering, thus leading occasionally to short-range order. Such tiling would not be optimum for surface roughness. For this purpose we employed attapulgite, a clay mineral with an unusual needlelike morphology.[30] Attapulgite (also known as Palygorskite or Fuller's Earth) is magnesium aluminum silicate clay of very fine particle size.[31,32] The average particle length is between 1 to 2 μm, with widths from 10 to 50 nm. As such, attapulgite represents an intriguing, naturally occurring nanorod. By using the multilayering design (the detailed sequence is summarized in Table 1) we deposited three strata. The first, adjacent to the substrate, consisted of a few layer pairs of poly(diallyldimethylammonium)/poly(4-styrenesulfonate) (PDADMA/PSS) deposited from a 0.8 M salt solution. This served as an initial "bed" for the particles. The next stratum alternated clay particles (which bear a negative surface charge) with PDADMA to produce roughness. The final stratum comprised the fluorinated polyelectrolytes. The entire process was performed under ambient conditions in common solvents. No annealing steps were required.

This tri-strata approach (one of many similar variations) produced ultrahydrophobic surfaces, as indicated by a small hysteresis between θ_a and θ_r (Table 1). Several experimental refinements were needed. Optimally, the clay nanorods must protrude from the surface so that droplets are able to ride over them in a manner similar to that reported by Cassie and Baxter. This arrangement is contrary to the expected fate of individual objects of high aspect ratio, which would tend to lie

 © 2005 Wiley-VCH Verlag GmbH & Co. KGaA, Weinheim

flat on the surface. Thus, sonicating a dispersion of the clay in water for 24 h proved counterproductive. There is also the possibility that the clay nanorods would bundle together along their long axes instead of forming "spiky" aggregates. The attapulgite dispersion appears to have cooperated in this respect, as seen in Figure 2, which shows aggregates on the

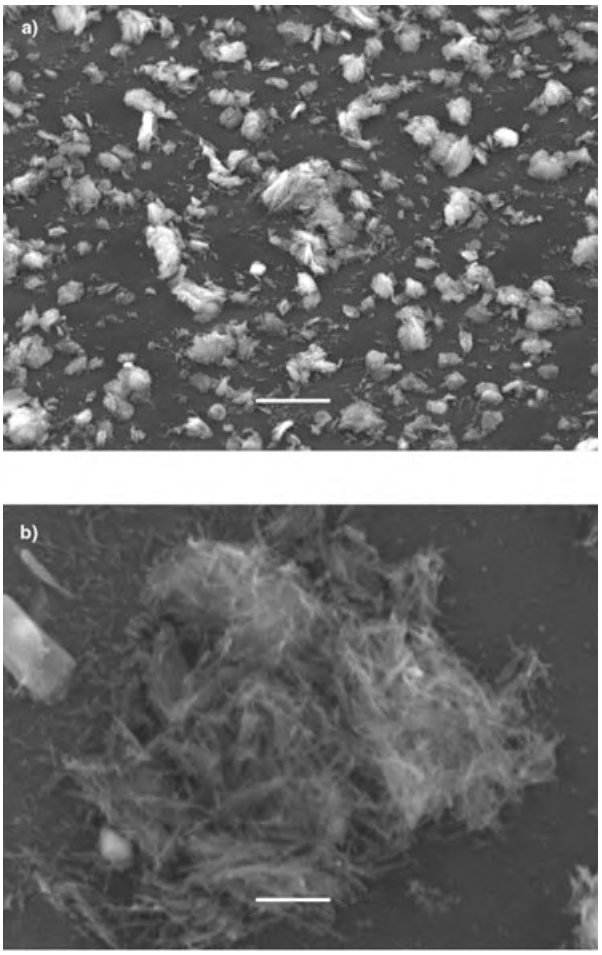


Figure 2. Scanning electron micrographs of the polyelectrolyte–clay ultrahydrophobic multilayer $(PSS/PDADMA)_3(clay/PDADMA)_3$-nafion/$PFPVP)_4PFPVP$. a) Scale bar = 20 μm and b) scale bar = 2 μm scale. The SEM stage was tilted 50°.

micrometer scale of disordered clay particles of nanometer dimensions. The separation between the larger aggregates is also on the order of a few micrometers. It is not possible to discern from the micrographs whether the polyelectrolytes deposit as a continuous coating on the particles, but hydrophobic material is clearly sufficiently well dispersed to make the surface homogeneously ultrahydrophobic. Heterogeneity was more of a problem from the roughening perspective: for example, if salt was added to the PDADMA solution used to generate the PDADMA/clay stratum, the density of the agglomerates on the surface was lower (as seen by SEM and also the surface appears less hazy to the eye). Water exhibited a large contact angle to the surface coated with the fluorinated stratum, but only localized areas gave a small contact angle hysteresis, and the DCA traces were very ragged, thus indicating multiple pinnings of the receding water front. A multilayer nanocomposite (Figure 2) with uniform (over the whole 2.5-cm diameter wafer) ultrahydrophobic behavior and a surface rms roughness of 3.2 μm was obtained with salt present in the clay suspensions and no salt in the PDADMA for the PDADMA/clay stratum.

Immobile droplets (Figure 3) were very hard to obtain. Attempts were made to level the substrate, but a slope of only a degree or so exceeded the critical angle for rolling.[33] In fact,



Figure 3. Water drop on the surface of the ultrahydrophobic multilayer surface from Figure 2. The diameter of the drop is about 2 mm.

we believe that the droplet shown in Figure 3 has been loosely pinned by a defect. This surface remained ultrahydrophobic after being immersed in water for more than two months—neither static nor dynamic contact angles changed over this time period (Table 1). The thermal stability of the multilayer from Figure 2 was assessed by heating it at 120 °C for 24 h in air. There were no changes in the contact angles.

The contact angle is exquisitely dependent on the hydrophilicity of the top layer. The ultrahydrophobic film from Figure 2 was transformed into an ultrahydrophilic surface by coating it with 2.5 additional layer pairs of a 1 mM solution of PAA-*co*-PAEDAPS/PFPVP (that is, with $(PAA\text{-}co\text{-}PAEDAPS/PFPVP)_2PAA\text{-}co\text{-}PAEDAPS$; PAA-*co*-PAEDAPS is a statistical copolymer of 75 mol % poly(acrylic acid) and 25 mol % poly((3-[2-(acrylamido)-ethyldimethylammonio]-propane sulfonate), a zwitterion).[34] It is very hydrophilic. The rough multilayer terminated with this polymer had a contact angle of 0° (too small to measure).

In conclusion, we have demonstrated a facile method of generating ultrahydrophobic surfaces from a novel combination of fluorinated polyelectrolytes and natural nanorods. Several issues remain to be addressed. Of interest is the critical spacing between roughness features that characterizes a transition between a pinning (Wenzel) and a free-rolling (Cassie–Baxter) ultrahydrophobic surface. Any characteristic distances will be averages, as the deposition of nanorod agglomerates is random.

 © 2005 Wiley-VCH Verlag GmbH & Co. KGaA, Weinheim

Experimental Section

Poly(4-vinylpyridine) (M_W 300000) was alkylated to a level of 45 ± 3% with 1,1,1,2,2,3,3,4,4,5,5,6,6-tridecafluoro-8-iodooctane (TDFI, $C_8H_4F_{13}I$) to give the fluorinated polycation PFPVP by using a 1:1 (v/v) mixture of DMF and nitromethane. Multilayers were prepared from this and nafion (Aldrich) using 1 mM solutions of the polyelectrolyte (based on the repeat unit) in methanol. The polished Si(100) wafers were exposed to polyelectrolyte solutions for 10 min with stirring, with 3 intermediate rinses in methanol for 30 s. Some substrates were primed with one layer of polyethyleneimine (PEI). The clay solution consisted of 0.2 wt% attapulgite (Attagel 50, Englehard Inc.) in distilled water. The immersion time for each clay layer was 1 h, followed by 3 rinses in distilled water.

The thickness of the film was measured with an ellipsometer (Gaertner L116S) or a profilometer (KLA Tencor P15). The profilometer was also used for measuring the rms surface roughness and thickness of the ultrahydrophobic film. Atomic force microscopy (Dimension 3100, Digital Instruments) was used to determine the surface roughness of the nafion/PFPVP films. The contact angle was measured by the sessile drop method (Rame-Hart telescope) or by a dynamic contact angle instrument (Cahn Instruments). Care was taken to coat the rectangular Si wafer substrates for DCA uniformly. The following shorthand for multilayers is used: $(A/B)_x$ where A is the starting cationic polyelectrolyte contacting the substrate, B is the anionic polyelectrolyte, and x is the number of layer pairs. In $(A/B)_xA$, A would be the terminating polymer. The salt MY (cation M^+ and anion Y^-) plays an important role in the build-up process and is represented by $(A/B)_x@c$MY, where c is the molarity of the salt (MY) in the polymer solution.

Received: August 13, 2004
Published online: December 23, 2004

Keywords: clays · polyanions · polycations · self-assembly · surface chemistry

[1] a) D. Qian, C. Nakamura, T. Wakayama, J. Miyake, *J. Porphyrins Phthalocyanines* **2003**, *7*, 415–419; b) J. J. Senkevich, R. G. Yang, M. T. Lu, *Colloids Surf. A* **2002**, *207*, 139–145; c) O. M. Jensen, G. O. Mouritsen, H. G. Peters, *J. Chem. Phys.* **2004**, *120*, 9729–9744; d) J. S. Pelt, M. E. Ramsey, R. Magana, Jr., E. Poindexter, Jr., M. P. de Boer, D. A. LaVan, M. T. Dugger, J. H. Smith, S. M. Durbin, *Proc. SPIE-Int. Soc. Opt. Eng.* **1999**, *3874*, 76–84; e) K. Tadanaga, N. Katata, T. Minami, *J. Am. Ceram. Soc.* **1997**, *80*, 1040–1042; f) Z. Zhao, J. Li, P. Qin, D. Zhang, C. Chen, *Polym. Prepr. Am. Chem. Soc. Div. Polym. Chem.* **2004**, *45*, 48–49; g) J. O. Karlsson, P. Gatenholm, *Macromolecules* **1999**, *32*, 7594–7598; h) B. Sang, K. Kushiya, D. Okumura, O. Yamase, *Sol. Energy Mater. Sol. Cells* **2001**, *67*, 237–245.

[2] *Multilayer Thin Films—Sequential Assembly of Nanocomposite Materials* (Eds.: G. Decher, J. B. Schlenoff), Wiley-VCH, Weinheim, Germany, **2003**.

[3] T. Soeno, K. Inokuchi, S. Shiratori, *Appl. Surf. Sci.* **2004**, *237*, 539–543.

[4] L. Zhai, F. Ç. Cebeci, R. E. Cohen, M. F. Rubner, *Nano Lett.* **2004**, *4*, 1349–1353.

[5] A. Marmur, *Langmuir* **2004**, *20*, 3517–3519.

[6] A. Lafuma, D. Quéré, *Nat. Mater.* **2003**, *2*, 457–460.

[7] T. Onda, S. Shibuichi, N. Satoh, K. Tsujii, *Langmuir* **1996**, *12*, 2125–2127.

[8] S. Pilotek, H. K. Schmidit, *J. Sol-Gel Sci. Technol.* **2003**, *26*, 782–792.

[9] J. P. Youngblood, T. J. McCarthy, *Macromolecules* **1999**, *32*, 6800–6806.

[10] Z. Yoshimitsu, A. Nakajima, T. Watanabe, K. Hashimoto, *Langmuir* **2002**, *18*, 5818–5822.

[11] J. Genzer, K. Efimenko, *Science* **2000**, *290*, 2130–2133.

[12] N. J. Shirtcliffe, G. McHale, M. I. Newton, C. C. Perry, *Langmuir* **2003**, *19*, 5626–5631.

[13] P. S. Swain, R. Lipowsky, *Langmuir* **1998**, *14*, 6772–6780.

[14] W. Chen, A. Fadeev, M. C. Hsieh, D. Öner, J. Youngblood, T. J. McCarthy, *Langmuir* **1999**, *15*, 3395–3399.

[15] A. Nakajima, K. Hashimoto, T. Watanabe, *Monatsh. Chem.* **2001**, *132*, 31–41.

[16] Ph. Lavalle, C. Gergely, F. J. G. Cuisinier, G. Decher, P. Schaaf, J. C. Voegel, C. Picart, *Macromolecules* **2002**, *35*, 4458–4465.

[17] D. M. Delongchamp, M. Kastantin, P. T. Hammond, *Chem. Mater.* **2003**, *15*, 1575–1586.

[18] J. Wilhelmy, *Ann. Phys.* **1863**, *119*, 177–183.

[19] R. J. Good, *J. Adhes. Sci. Technol.* **1992**, *6*, 1269–1302.

[20] D. Öner, T. J. McCarthy, *Langmuir* **2000**, *16*, 7777–7782.

[21] D. Quéré, A. Lafuma, J. Bico, *Nanotechnology* **2003**, *14*, 1109–1112.

[22] G. McHale, N. J. Shirtcliffe, M. I. Newton, *Analyst* **2004**, *129*, 284–287.

[23] R. N. Wenzel, *J. Phys. Colloid Chem.* **1949**, *53*, 1466–1467.

[24] R. N. Wenzel, *Ind. Eng. Chem.* **1936**, *28*, 988–994.

[25] A. B. D. Cassie, S. Baxter, *Trans. Faraday Soc.* **1944**, *40*, 546–551.

[26] A. B. D. Cassie, *Discuss. Faraday Soc.* **1948**, *3*, 11–16.

[27] L. Feng, Y. Song, J. Zhai, B. Liu, J. Xu, L. Jiang, D. Zhu, *Angew. Chem.* **2003**, *115*, 824–826; *Angew. Chem. Int. Ed.* **2003**, *42*, 800–802.

[28] P. Gould, *ASM News Quarterly* **2003**, *6*, 44–48.

[29] *Multilayer Thin Films—Sequential Assembly of Nanocomposite Materials* (Eds.: G. Decher, J. B. Schlenoff), Wiley-VCH, Weinheim, Germany, **2003**, pp. 207–236.

[30] W. S. W. McCarter, K. A. Krieger, H. Heinemann, *Ind. Eng. Chem.* **1974**, *51*, 311–320.

[31] C. E. Marshall, O. G. Caldwell, *J. Phys. Colloid Chem.* **1947**, *51*, 311–320.

[32] Our attapulgite, mined just a few miles from the Florida State University, was a gift from Engelhard Industries of Quincy, FL.

[33] M. Miwa, A. Nakajima, A. Fujishima, K. Hashimoto, T. Watanabe, *Langmuir* **2000**, *16*, 5754–5760.

[34] D. S. Salloum, S. G. Olenych, T. C. S. Keller, J. B. Schlenoff, *Biomacromolecules* **2004**, *ASAP.*

 © 2005 Wiley-VCH Verlag GmbH & Co. KGaA, Weinheim

Cluster Chemistry

The First Trimetallic Pd/Tl/Co Carbonyl Cluster, Trigonal $[Pd_9\{\mu_3\text{-}TlCo(CO)_3L\}(\mu_2\text{-}CO)_6(\mu_3\text{-}CO)_3L_6]$: Ligand-Stabilization of the Trigonal-Bipyramidal $[TlCo(CO)_3L]$ Entity**

*Evgueni G. Mednikov, Charles G. Fry, and Lawrence F. Dahl**

Dedicated to Professor R. Bruce King on the occasion of his 66th birthday

In the course of our exploration of reactivities of carbonyl/phosphine clusters of palladium with thallium(I) complexes,[1] we have isolated approximately 40% yield) and crystallographically and spectroscopically characterized a remarkable 11-metal-atom pseudo-C_{3v} cluster, $[Pd_9\{\mu_3\text{-}TlCo(CO)_3L\}(\mu_2\text{-}CO)_6(\mu_3\text{-}CO)_3L_6]$, (L = PEt_3) (**1**), from reactions of $[Pd_4(CO)_5L_4]$ (**2**) and/or $[Pd_{10}(CO)_{12}L_6]$ (**3**) with $[TlCo(CO)_4]$. Its unusual solid-state molecular geometry was ascertained from a low-temperature X-ray diffractometry study. Cluster **1** furnishes the first crystallographic example of a trigonal-bipyramidal $[TlCo(CO)_3L]$ entity of thallium(I) which in **1** is stabilized as a ligand by tripalladium coordination; otherwise it would be unstable. The only other isolated non-phosphite L derivative of $[TlCo(CO)_4]$ is $[TlCo(CO)_3PPh_3]$,[2a] but even this molecular thallium(I) product was found to readily disproportionate into thallium(III) $[Tl\{Co(CO)_3PPh_3\}_3]$ and thallium metal.[2] Spectroscopic measurements including a multinuclear NMR ($^{205,203}Tl$, ^{31}P, ^{13}C, ^{1}H) investigation coupled with solid-state/solution IR and UV/Vis spectra have provided considerable insight concerning the indicated dynamic behavior of the entire $[TlCo(CO)_3PEt_3]$ ligand of **1** in solution.

Thallium(I) tetracarbonylcobaltate was initially prepared in 1942[3a] and 30 years later reliably introduced in synthetic organometallic chemistry by Robinson and co-workers[3b,c] as "a convenient and versatile source of the tetracarbonylcobaltate anion." They also showed from an X-ray diffraction study that crystalline $[TlCo(CO)_4]$ possesses an ionic NaCl-like cubic structure with the shortest Tl···Co separations being 3.55(1) Å.[3c] To date, the role of this compound has not been extended markedly beyond its proposed use in reactions with organic and organometallic halides; these reactions predictably result in the generation of carbon–cobalt or metal–cobalt bonds, respectively, along with formation of thallium(I) halides arising from complete breakdown of ion-pair $Tl^+[Co(CO)_4]^-$ interactions.[4] Although $[TlCo(CO)_4]$ has fulfilled the same role as the widely used $[NaCo(CO)_4]$, it may have additional synthetic potential owing to the filled $Tl^I 6s^2$ atomic orbital. To our knowledge, **1** is the first example where the donor ability of this so-called "inert" electron pair of Tl^I has been realized with simultaneous retention of the Tl–Co bond, in this case through its triply bridging coordination to a triangular Pd_3 face of the octahedral unit of the Pd_9 core (see below).

Both the composition and atomic arrangement of **1** in the solid state were unambiguously established from a low-temperature single-crystal CCD X-ray crystallographic analysis[5a,b] which revealed two closely resembling independent molecules of pseudo C_{3v} symmetry in the unit cell.[5c] The overall geometry of **1** can be described as a distorted Pd_6 octahedron with three $Pd(\mu_2\text{-}CO)_2L$ fragments that each edge-bridge one triangular Pd_3 face of the Pd_6 octahedron (Figure 1). Its salient structural feature is the additional attachment of a trigonal-bipyramidal $[\mu_3\text{-}TlCo(CO)_3L]$ ligand to one Pd_3 triangle. The principal pseudo threefold axis passes through the P, Co, and Tl atoms and the centers of two

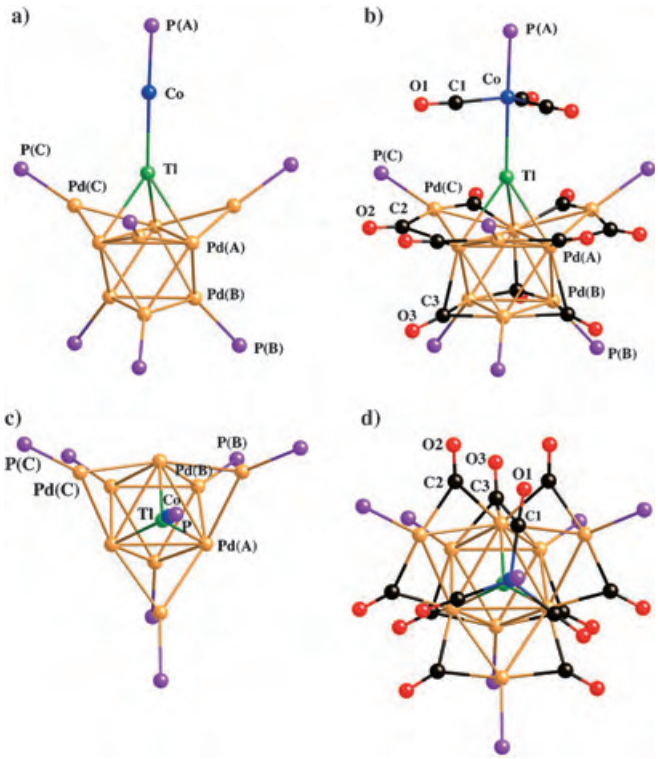


Figure 1. Side (a,b) and top views (b,c) of C_{3v} geometry of **1**: without CO ligands (a,c), and with CO ligands (b,d). The ethyl substituents are omitted for clarity.

[*] Dr. E. G. Mednikov, Dr. C. G. Fry, Prof. L. F. Dahl
Department of Chemistry
University of Wisconsin-Madison
1101 University Avenue, Madison, WI 53706 (USA)
Fax: (+1) 608-262-6143
E-mail: dahl@chem.wisc.edu

[**] This research was supported by the National Science Foundation. The CCD area detector system was purchased, in part, from NSF grant, CHE-9310428. The Varian Inova-500 NMR spectrometer was purchased, in part, from NSF grant, CHE-9629688, and the Bruker AC-300 NMR spectrometer, in part, by funds from NSF CHE-9208963 and NIH SIO RR 08389-01. Color figures were prepared with Crystal Maker, Interactive Crystallography Software; David C. Palmer (Begbroke Park, Bldg 5, Sandy Lake, Yarnton OX5 1PF (UK)). We thank Dr. Ilia Guzei (UW-Madison) for helpful crystallographic advice and Dr. Irina Toulokhonova (UW-Madison) for NMR assistance, Dr. Gordon Shaw III (UW-Madison) for measurement of the UV/Vis spectrum and Dr. Sergei Ivanov (Los Alamos National Laboratory) for valuable discussions. L = PEt_3.

 © 2005 Wiley-VCH Verlag GmbH & Co. KGaA, Weinheim DOI: 10.1002/anie.200461124

opposing triangular faces of the Pd_6 octahedron. The nine palladium atoms in **1** can be classified into three different types (A–C): namely, the three Pd(A) atoms of the "inner" Pd_3 triangle to which the $TlCo(CO)_3L$ ligand is attached, the three edge-bridging Pd(C) atoms, and the three Pd(B) atoms of the "outer" opposite (staggered) Pd_3 triangle in the Pd_6 octahedron (Figure 1a). Of the seven phosphorus atoms, three are coordinated to the edge-bridging Pd(C) atoms, three to the Pd(B) atoms, and the remaining one (located on the pseudo threefold axis) to the cobalt atom (Figure 1a,c). The 12 carbonyl ligands are distributed as follows: three terminal ones are connected to the cobalt atom, six doubly bridging ones are linked to the six Pd(C)–Pd(A) edges, and three triply bridging ones cap asymmetrically three alternate triangular faces of the Pd_6 octahedron (Figure 1b,d). Mean distances and ranges of individual connectivities for both independent molecules under pseudo C_{3v} symmetry are given in Table 1.

Table 1: Selected mean interatomic distances for the two independent molecules of **1** under pseudo C_{3v} symmetry.

Bonding connectivity	N[a]	1st molecule		2nd molecule	
		Mean [Å]	Range [Å]	Mean [Å]	Range [Å]
Tl-Pd(A)	3	2.76	2.747(1)–2.775(1)	2.77	2.761(1)–2.798(1)
Tl···Pd(C)	3	3.33	3.262(1)–3.433(1)	3.28	3.197(1)–3.342(1)
Tl-Co	1	2.64	2.638(1)	2.64	2.643(1)
Pd(A)-Pd(C)	6	2.72	2.711(1)–2.733(1)	2.72	2.694(1)–2.728(1)
Pd(A)-Pd(A)	3	3.05	3.017(1)–3.089(1)	3.07	3.023(1)–3.088(1)
Pd(A)-Pd(B)	6	2.77	2.751(1)–2.788(1)	2.75	2.734(1)–2.785(1)
Pd(B)-Pd(B)	3	2.80	2.774(1)–2.821(1)	2.81	2.782(1)–2.820(1)
Pd(B)-P(B)	3	2.31	2.307(2)–2.329(2)	2.31	2.301(2)–2.315(2)
Pd(C)-P(C)	3	2.32	2.311(2)–2.331(2)	2.32	2.305(2)–2.321(2)
Co-P(A)	1	2.20	2.196(2)	2.20	2.199(2)
Pd(A)-(μ_2-CO)	6	2.09	2.070(6)–2.106(6)	2.09	2.076(5)–2.103(5)
Pd(C)-(μ_2-CO)	6	2.03	2.022(5)–2.032(5)	2.03	2.022(5)–2.051(5)
Pd(A)-(μ_3-CO)	3	2.31	2.262(5)–2.361(5)	2.32	2.304(5)–2.338(5)
Pd(B)-(μ_3-CO)	6	2.12	2.097(5)–2.134(5)	2.12	2.100(5)–2.144(5)
Co-CO	3	1.77	1.765(6)–1.776(6)	1.77	1.760(6)–1.771(6)
C-O	3	1.15	1.147(7)–1.158(7)	1.16	1.154(7)–1.165(6)
μ_2-C-O	6	1.16	1.151(7)–1.166(7)	1.16	1.148(6)–1.167(6)
μ_3-C-O	3	1.17	1.166(6)–1.175(6)	1.16	1.158(6)–1.168(6)

[a] N denotes the number of symmetry-equivalent connectivities under C_{3v} symmetry.

In marked distinction from the known Tl–Pd clusters, $[TlPd_6(CO)_6(PEt_3)_6]^+$[1a] and $[Tl_2Pd_{12}(CO)_9(PEt_3)_9]^{2+}$,[1b] in which each thallium(I) is coordinated to six palladium atoms in a conspicuously irregular manner with relatively long Tl–Pd bonds,[1c] the thallium(I) atom of the $TlCo(CO)_3PEt_3$ ligand in each of the two independent molecules of **1** is symmetrically coordinated to the three Pd(A) atoms with relatively short mean Tl–Pd(A) bonds of 2.76 and 2.77 Å. The much longer mean separations of 3.28 and 3.33 Å for the distances between Tl^I and the Pd(C) atoms of the edge-bridging Pd(μ_2-$CO)_2L$ fragments are considered to be nonbonding (or weak secondary bonding) connectivities (Figure 1a).

In cobalt carbonyl chemistry, the $TlCo(CO)_3L$ ligand of **1** represents the first X-ray characterized example of a trigonal-bipyramidal geometry about the central cobalt atom containing thallium(I) and phosphorus atoms (see below). The Tl-Co-P fragment in each independent molecule deviates only slightly (1.8° and 3.7°) from linearity, while the angular displacement of the Tl–Co bond from being perpendicular to the plane of the $Pd(A)_3$ triangle is 5.9° and 8.9°. The Tl–Co bond length is identical in the two independent molecules (2.64 Å) and compares favorably with the three Tl^{III}–Co bonds of 2.66 Å (average) found in the trigonal-planar $[Tl\{Co(CO)_4\}_3]$, which is the only reported structurally characterized compound containing discrete Tl–Co bonds.[6]

Table 1 shows that the Pd(A)–Pd(A) separations of the thallium-capped triangular face of the Pd_6 octahedron are 0.26 Å longer (average for both independent molecules) than the Pd(B)–Pd(B) separations of the opposite triangular face. This marked elongation may be attributed to the composite geometrical effect of the μ_3-$TlCo(CO)_3L$ and the three edge-bridging Pd(μ_2-$CO)_2L$ ligations.

$^{31}P\{^1H\}$ NMR temperature-dependent spectra of **1** acquired at 11.74 T in $[D_8]$toluene solution[7] are shown in Figure 2. At room temperature (RT) three signals are displayed with an expected integral ratio of 3:3:1 in accordance with the solid-state structure. The observed and assigned signals at RT are as follows: a) a relatively narrow singlet (33 Hz) at 3.62 ppm attributed to the three P(B) nuclei; (b) a broad singlet (53 Hz) at 2.11 ppm attributed to the three P(C) nuclei;[8] and (c) a very broad doublet ($\approx$360 Hz) at 96 ppm with $^2J_{P(A)\text{-}Tl} = 1800$ Hz unambiguously assigned to the P(A) atom axially coordinated to the cobalt atom. Upon the cooling of the toluene solution to −85 °C, the singlet at 2.11 ppm splits into a doublet with $^3J_{P(C)\text{-}Tl} = 180$ Hz, whereas the broad doublet arising from the cobalt-attached P(A) nucleus becomes narrowed by a factor of three to 105 Hz while its $^2J_{P(A)\text{-}Tl}$ coupling and chemical shift remain virtually unchanged, as shown in Figure 2. The narrowing observed with decreasing temperature follows the expected behavior for a spin $^1/_2$ nucleus J-coupled to a nucleus with a large electric quadrupolar moment.[9a] The splitting of the $\delta = 2.11$ ppm resonance, on the other hand, strongly suggests that the molecule is undergoing dynamic behavior.

A room-temperature $^{13}C\{^1H\}$ NMR spectrum (Figure 3), displays signals (in addition to those observed, but not shown in Figure 3, for -CH_2- and -CH_3)[7] for all three types of CO carbon atoms: at $\delta = 247$ ppm for bridging μ_3-CO and 238 ppm assigned to μ_2-CO carbonyl groups coordinated to palladium atoms, and at $\delta = 212$ ppm for the three terminal, cobalt-bonded CO ligands. A decrease of the temperature to −60 °C broadens the $\delta = 212$ ppm signal to near coalescence, while further cooling to −85 °C splits it into a doublet ($^2J_{C\text{-}Tl} \approx$ 640 Hz). The size of this two-bond coupling is sensitivity to geometrical changes occurring in the sample arising from the dynamic behavior indicated by these data. The two-bond

 © 2005 Wiley-VCH Verlag GmbH & Co. KGaA, Weinheim

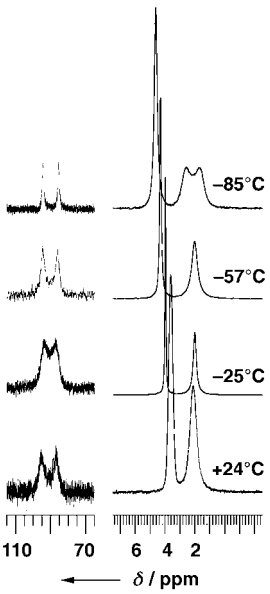


Figure 2. $^{31}P\{^1H\}$ spectra acquired at 202.5 MHz: number of transients = 100 to 400, repetition delay = 2 s, acquisition time = 0.64 s, line broadening = 3 Hz. The spectrum sections plotted for $\delta = 115$–65 ppm are vertically increased 70-fold.

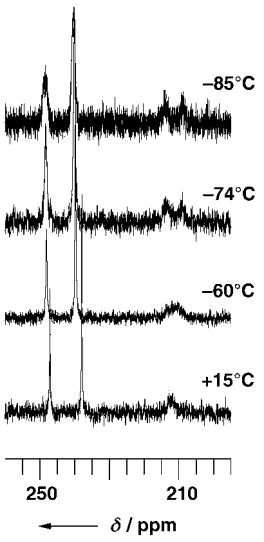


Figure 3. $^{13}C\{^1H\}$ spectra acquired at 125.8 MHz: number of transients = 1200 to 1800, repetition delay = 3 s, acquisition time = 0.95 s, line broadening = 4 Hz.

^{205,203}Tl-Co-^{31}P *J*-coupling, on the other hand, was observed to be essentially independent of these changes. The other carbonyl groups must have small two-bond *J*-coupling to the ^{205,203}Tl nuclei.

Extensive attempts to observe ^{205}Tl (or ^{203}Tl) signals at −85 °C over a wide range of chemical shifts, from −6000 ppm to +7500 ppm (relative to the ^{205}Tl signal readily observed in one scan from a 50 mM solution of $TlNO_3$ in D_2O used as a standard), were unsuccessful. Either the dynamic behavior observed in the ^{31}P and ^{13}C NMR spectra is in the broad coalescence region for ^{205,203}Tl, or the scalar-coupling broadening of the ^{205,203}Tl nuclei from the ^{59}Co nucleus is still large at −85 °C. Both may be present, as could other broadening mechanisms (beyond that expected from multiple ^{31}P splittings).[9b] The combination of these broadening mechanisms presumably prevents observation of ^{205,203}Tl resonances, even after 1000 scans.

The ^{31}P and ^{13}C NMR spectra provide strong evidence that **1** is undergoing dynamic behavior in toluene solution. This behavior is consistent with a model involving reversible dissociation/association of the $TlCo(CO)_3L$ ligand from/to the Pd_9 core of **1** [Eq. (1)].

$$[Pd_9\{TlCo(CO)_3L\}(CO)_9L_6] \rightleftharpoons [Pd_9(CO)_9L_6] + [TlCo(CO)_3L] \quad (1)$$

At room temperature, the reversible conversion of these species is presumed to be fast on the NMR timescale. This proposed model of the rapid reversible dissociation/association of $[TlCo(CO)_3L]$ from the Pd_3 triangle of **1** in toluene appears to account for the temperature-dependent NMR data, even though it is surprising that the ^2J ^{31}P(A)-Co-Tl coupling constant and the ^{31}P(A) chemical shift remain essentially unchanged. The fact that the ^{31}P(A)-Tl ^2J coupling and chemical shift are not influenced by the temperature variation provides definitive NMR evidence that the cobalt-attached P(A) atom is not dissociating from the cobalt atom. The model rationalizes the changed ^{13}C signal of the three cobalt-attached carbonyl ligands, as well as the observed changes with the ^{31}P(C)-Tl ^3J coupling constants. The ^{31}P(B)-Tl ^3J value must be small.

Although the ^{31}P and ^{13}C NMR studies indicate that in solution the coordination of the $[TlCo(CO)_3L]$ ligand ($L = PEt_3$) to the triangular $Pd(A)_3$ face of the Pd_9 core is relatively weak, it must be, however, sufficiently strong to prevent disproportionation of this ligand into the corresponding Tl^{III} derivative and thallium metal [Eq (2)].

$$3\,[TlCo(CO)_3L] \rightarrow [Tl\{Co(CO)_3L\}_3] + 2\,Tl_{(S)} \quad (2)$$

The reaction in Equation (2) has been shown[2a] to be typical for $L = PR_3$ with basicities close to and higher than that for PPh_3. In fact, no alkyl phosphine derivatives of $[TlCo(CO)_3(PR_3)]$ have been isolated to date.

An IR spectrum (THF) of **1** exhibited two characteristic terminal-carbonyl bands at 1974 (wm) cm^{-1} (A_1 mode) and 1910 (s) cm^{-1} (E mode) in accordance with the C_{3v} trigonal-bipyramidal geometry of $[TlCo(CO)_3L]$[2a,c] being maintained in solution. A solid-state IR spectrum (nujol) of **1** displayed analogous CO bands at 1974 (wm) 1912 (sh), and 1906 (s) cm^{-1} and thereby ruled out the occurrence of a possible disproportionation reaction [Eq. (2)] in THF solution.

While the NMR spectroscopic observations provide strong evidence for the dynamic behavior of **1** consistent with the proposed equilibrium process shown in Equation (1): namely the IR data show that this dynamic process in weakly polar THF solution is strongly weighted to one side of the equation, the left-hand side must be highly populated, to > 95 %; otherwise, the species on the right-hand side would be observed in the IR spectrum.[10]

 © 2005 Wiley-VCH Verlag GmbH & Co. KGaA, Weinheim

A UV/Vis absorption spectrum of **1** (toluene) exhibited two electronic bands at approximately 314 and 428 nm. The 428 nm (visible-range) band may be a consequence of the expected strong ion-pair Tl–Co bonding interaction between Tl^{I} and $[Co(CO)_3L]^-$. Our assignment is based upon a detailed investigation of UV/Vis absorption spectra of $[TlCo(CO)_4]$ in different solvents by Schramm and Zink[4b] which led to their hypothesis that the presence of a band at wavelengths greater than 350 nm is indicative of $Tl^+[Co(CO)_4]^-$ ion-pair interactions; in particular, they observed that the UV/Vis absorption spectrum of $[TlCo(CO)_4]$ in toluene exhibits two characteristic bands at 283 and 435 nm.

Compound **1** (with $L = PEt_3$) can be prepared from either $[Pd_4(CO)_5L_4]$ (**2**) and/or $[Pd_{10}(CO)_{12}L_6]$ (**3**) with $[TlCo(CO)_4]$ in THF, C_6H_6, or C_7H_8 solutions at room or elevated temperatures. In the case of only **2** being involved in the reaction, an excess of the undesired phosphine L ligand would be generated, which in turn would trigger the formation of $[Tl\{Co(CO)_3L\}_3]$ and thallium metal by the disproportionation reaction [Eq. (2)], as ideally formulated in Equation (3).

$$27\,[Pd_4(CO)_5L_4] + 36\,[TlCo(CO)_4] \rightarrow 12\,[Pd_9\{TlCo(CO)_3L\}(CO)_9L_6] + 8\,[Tl\{Co(CO)_3L\}_3] + 16\,Tl_{(s)} + 63\,CO \quad (3)$$

On the other hand, the reaction with only **3** as the other reactant would instead give rise to the formation of palladium metal owing to the deficiency of L, as ideally formulated in Equation (4).

$$7\,[Pd_{10}(CO)_{12}L_6] + 6\,[TlCo(CO)_4] \rightarrow 6\,[Pd_9\{TlCo(CO)_3L\}(CO)_9L_6] + 16\,Pd_{(s)} + 36\,CO \quad (4)$$

To optimize the yield of **1**, we set the mole ratio Pd/L of the reactants to be 9/7, and thereby combined both Equations (3) and (4) to give the idealized stoichiometry in Equation (5) for the reaction. This reaction[11] was carried

$$9\,[Pd_{10}(CO)_{12}L_6] + 16\,L + 10\,[TlCo(CO)_4] \rightarrow 10\,[Pd_9\{TlCo(CO)_3L\}(CO)_9L_6] + 28\,CO \quad (5)$$

out in two stages: 1) an initial reaction of **3** and L under CO with formation in situ of a required ratio of **2** and **3**;[12] and 2) a subsequent reaction of this mixture with a stoichiometric amount of $[TlCo(CO)_4]$.[3c]

Received: June 30, 2004
Revised: October 24, 2004
Published online: December 23, 2004

Keywords: cluster compounds · cobalt · palladium · structure elucidation · thallium

[1] a) E. G. Mednikov, L. F. Dahl, *Dalton Trans.* **2003**, 3117; b) S. A. Ivanov, R. V. Nichiporuk, E. G. Mednikov, L. F. Dahl, *Dalton Trans.* **2002**, 4116; c) the mean Tl–Pd separations in the $[TlPd_6(CO)_6(PEt_3)_6]^+$ and $[Tl_2Pd_{12}(CO)_9(PEt_3)_9]^{2+}$ clusters are 2.96 Å (range, 2.881(1)–3.127(1) Å)[1a] and 2.91 Å (range, 2.847(1)–3.042(1) Å),[1b] respectively.

[2] a) S. E. Pedersen, W. R. Robinson, *Inorg. Chem.* **1975**, *14*, 2360; b) J. M. Burlitch, T. W. Theyson, *J. Chem. Soc. Dalton Trans.* **1974**, 828; c) D. J. Patmore, W. A. G. Graham, *Inorg. Chem.* **1968**, *7*, 771.

[3] a) W. Hieber, U. Teller, *Z. Anorg. Allg. Chem.* **1942**, *249*, 48; b) S. E. Pedersen, W. R. Robinson, D. P. Schussler, *J. Organomet. Chem.* **1972**, *43*, C44; c) D. P. Schussler, W. R. Robinson, W. F. Edgell, *Inorg. Chem.* **1974**, *13*, 153.

[4] The different degrees of interaction between Tl^+ and $[Co(CO)_4]^-$ ions were attributed to the changes in dielectric constants and coordinating abilities in various solvents: a) W. F. Edgell, W. R. Robinson, A. Barbetta, D. P. Schussler, unpublished results, mentioned in ref. [3c]; b) C. Schramm, J. I. Zink, *J. Am. Chem. Soc.* **1979**, *101*, 4554.

[5] a) X-Ray data for crystal of **1** were collected at 100(2) K on a Bruker SMART CCD-1000 area-detector diffractometer with graphite-monochromated $Mo_{K\alpha}$ radiation ($\lambda = 0.71073$ Å) from a sealed-tube generator. The crystal structure was determined from direct methods. Least-squares refinements (based on F^2) were carried out with SHELXTL.[5b] CCDC-240814 (**1**) contains the supplementary crystallographic data for this paper. These data can be obtained free of charge via www.ccdc.cam.ac.uk/conts/retrieving.html (or from the Cambridge Crystallographic Data Centre, 12 Union Road, Cambridge CB2 1EZ, UK; fax: (+44) 1223-336-033; or deposit@ccdc.cam.ac.uk). $[Pd_9\{TlCo(CO)_3PEt_3\}(CO)_9(PEt_3)_6]$: $M_r = 2384.07$, monoclinic, $P2_1/c$, $a = 14.584(1)$, $b = 44.101(2)$, $c = 23.589(1)$ Å, $\alpha = \gamma = 90$, $\beta = 91.388(1)°$, $V = 15166.9(9)$ Å^3, $Z = 8$; $F(000) = 9216$; $\rho_{calcd} = 2.088$ Mg m^{-3}. 146406 reflections were obtained over $1.96 \le \theta \le 56.6°$. Empirical absorption correction (SADABS) was applied ($\mu(Mo_{K\alpha}) = 4.605$ mm^{-1}, max./min. transmission, 0.7697/0.4045). Full-matrix least-squares refinement (on F^2) of 37250 independent merged reflections $R(\text{int}) = 0.0443$ with 1515 parameters (21 restraints) converged at $wR_2(F^2) = 0.0860$ for all data; $R_1(F) = 0.0315$ for $I > 2\sigma(I)$; max./min. residual electron density, 1.90/−1.16 e Å^{-3}; GoF (on F^2) = 0.884. Hydrogen atoms were included in structure factor calculations at idealized positions and were allowed to ride on attached carbon atoms with relative isotropic displacement coefficients. All non-hydrogen atoms, except carbon atoms of disordered CH_2 and CH_3 groups, were refined anisotropically; b) all crystallographic software and sources of the scattering factors are contained in the SHELXTL (version 5.1; G. Sheldrick) program library, Bruker Analytical X-Ray Systems, Madison, WI; c) Superposition of the refined positional parameters for the corresponding 11 metal atoms in the two crystallographically independent molecules showed their geometries to be nearly equivalent, as evidenced by the weighted rms deviation of 0.091 Å for the optimal superimposed fit.[5b] Hence, it was necessary to determine that they are not related to each other by a higher symmetry space group. Structural tests, performed by the checkcif@iuer.org service with check CIF/PLATON, provided convincing evidence that the uniquely determined centrosymmetric monoclinic $P2_1/c$ space group was indeed correctly chosen.

[6] J. W. van Hal, L. B. Alemany, K. H. Whitmire, *Inorg. Chem.* **1997**, *36*, 3152.

[7] NMR spectra were obtained for C_7D_8 solutions of **1** under N_2 atmosphere on Bruker AC-300 or Varian UNITY-500 and INOVA-500 spectrometers. The ^1H, $^{13}C\{^1H\}$, and $^{31}P\{^1H\}$ spectra were referenced, respectively, to TMS by the ^1H signal of residual protons of $[D_8]$toluene at 2.09 ppm, to TMS by the methyl ^{13}C signal of $[D_8]$toluene at 20.4 ppm, and to 85 % H_3PO_4 in D_2O as an external standard (at 300 MHz). At 500 MHz, the unified-scale method of referencing ["*NMR Nomenclature. Nuclear Spin Properties and Conventions for Chemical Shifts*"

 © 2005 Wiley-VCH Verlag GmbH & Co. KGaA, Weinheim

(IUPAC Recommendations 2001): R. K. Harris, E. D. Becker, S. M. Cabral de Menezes, R. Goodfellow, P. Granger, *Pure Appl. Chem.* **2001**, *73*, 1795–1818] was used for referencing ^{13}C, ^{31}P, ^{205}Tl, and ^{203}Tl from the ^{1}H-TMS reference. ^{1}H NMR (300 MHz, ambient temperature): $\delta_1 = 0.81$ ppm (dt, 9H, CH_3, $^{3}J_{H\text{-}H} = 7.8$ Hz, $^{3}J_{H\text{-}P} = 15.7$ Hz); $\delta_2 = 0.94$ ppm (dt, 27H, CH_3, $^{3}J_{H\text{-}H} = 7.5$ Hz, $^{3}J_{H\text{-}P} = 15.0$ Hz); $\delta_3 = 1.06$ ppm (dt, 27H, CH_3, $^{3}J_{H\text{-}H} = 7.6$ Hz, $^{3}J_{H\text{-}P} = 15.2$ Hz); $\delta_4 = 1.42$ ppm (qn, 6H, CH_2, $^{3}J_{H\text{-}H} = {}^{2}J_{H\text{-}P} = 7.9$ Hz); $\delta_5 = 1.56$ ppm (qn, 18H, CH_2, $^{3}J_{H\text{-}H} = {}^{2}J_{H\text{-}P} = 7.4$ Hz); $\delta_6 = 1.74$ ppm (qn, 18H, CH_2, $^{3}J_{H\text{-}H} = {}^{2}J_{H\text{-}P} = 7.4$ Hz) with intensity ratios of $\delta_1/\delta_2/\delta_3/\delta_4/\delta_5/\delta_6/ = 1.04/3.00/2.98/0.67/1.94/1.94$ (versus theoretical ones of 1.00/3.00/3.00/0.67/2.00/2.00). ^{1}H (500 MHz, −25 °C): $\delta_1 = 0.81$ ppm (dt, 9H, CH_3, $^{3}J_{H\text{-}H} = 7.8$ Hz, $^{3}J_{H\text{-}P} = 15.7$ Hz); $\delta_2 = 0.94$ ppm (dt, 27H, CH_3, $^{3}J_{H\text{-}H} = 7.5$ Hz, $^{3}J_{H\text{-}P} = 14.6$ Hz); $\delta_3 = 1.06$ ppm (dt, 27H, CH_3, $^{3}J_{H\text{-}H} = 7.6$ Hz, $^{3}J_{H\text{-}P} = 14.6$ Hz); $\delta_4 = 1.36$ ppm (qn, 6H, CH_2, $^{3}J_{H\text{-}H} = {}^{2}J_{H\text{-}P} = 7.7$ Hz); $\delta_5 = 1.58$ ppm (qn, 18H, CH_2, $^{3}J_{H\text{-}H} = {}^{2}J_{H\text{-}P} = 7.4$ Hz); $\delta_6 = 1.74$ ppm (qn, 18H, CH_2, $^{3}J_{H\text{-}H} = {}^{2}J_{H\text{-}P} = 7.4$ Hz) with intensity ratios of $\delta_1/\delta_2/\delta_3/\delta_4/\delta_5/\delta_6/ = 1.09/2.98/3.13/0.77/1.95/2.01$ (versus theoretical ones of 1.00/3.00/3.00/0.67/2.00/2.00). ^{1}H (500 MHz, −85 °C): $\delta_1 = 0.80$ ppm (barely resolved dt); $\delta_2 = 0.93$ ppm (barely resolved dt); $\delta_3 = 1.01$ ppm (barely resolved dt); $\delta_4 = 1.25$ ppm (broad single peak, half-width at half height = 17 Hz); $\delta_5 = 1.57$ ppm (broad single peak, half-width at half height = 19 Hz); $\delta_6 = 1.71$ ppm (broad single peak, half-width at half height = 17 Hz). $^{13}C\{^{1}H\}$ (125.797 MHz at 15 °C): $\delta = 7.91$ (s, 3C, CH_3); 8.29 (s, 9C, CH_3); 8.64 (s, 9C, CH_3); 16.14 (d, 9C, CH_2, $^{1}J_{C\text{-}P} = 18.6$ Hz); 16.71 (d, 9C, CH_2, $^{1}J_{C\text{-}P} = 14.1$ Hz); 22.08 (d, 3C, CH_2, $^{1}J_{C\text{-}P} = 22.0$ Hz); 212 (s, 3C, terminal CO); 238 (s, 6C, μ_2-CO); 247 ppm (s, 3C, μ_3-CO). $^{31}P\{^{1}H\}$ (202.513 MHz), RT: $\delta = 2.11$ (s, 3P, P(C)), 3.62 (s, 3P, P(B)), 96 ppm (d, 1P, $^{2}J_{P\text{-}Tl} = 1800$ Hz, P(A)); −85 °C: $\delta_1 = 2.14$ (d, 3P, P(C), $^{3}J_{P(C)\text{-}Tl} = 180$ Hz), $\delta_2 = 4.63$ (s, 3P, P(B)), $\delta_3 = 95$ ppm (d, 1P, $^{2}J_{P\text{-}Tl} = 1800$ Hz) with ratio of intensities $\delta_1/\delta_2/\delta_3 = 3.0/3.0/1.0$.

[8] The three P(C) nuclei in the non-dissociated structure of **1** (in solution) should be comparatively closer to the Tl atom (i.e., the mean nonbonding P(C)···Tl separation in the solid-state structure is 5.06 Å versus the mean P(B)···Tl separation of 6.77 Å). In addition, each P(C) atom may interact with Tl not only by ^{3}J coupling through the P(C)-Pd(C)-Pd(A)-Tl bonding chain but also more directly by ^{2}J coupling through a P(C)-Pd(C)···Tl shorter link including secondary bonding interactions.

[9] a) "Chemical and Biochemical Applications" by R. G. Kidd in *NMR of Newly Accessible Nuclei*, *Vol. 1* (Ed.: P. Laszlo), Academic Press, New York, **1983**, pp. 123–125; b) Quadrupolar coupling with the ^{59}Co nucleus ($I = 7/2$, 100 %; $Q = 42.0$ fm^2) can broaden the thallium line shape through scalar coupling relaxation, but not through the commonly understood method of direct splitting of the resonance by scalar coupling. ^{59}Co has a very large electric quadrupole moment (147× that of ^{2}H) and should therefore self-decouple unless the ^{59}Co nucleus is in a very symmetric bonding arrangement (either tetrahedral or octahedral). Self-decoupling occurs when the relaxation time for transitions between the available spin states (namely, eight for ^{59}Co with $I = 7/2$) will be so fast that other nuclei will only see the "average" spin state from ^{59}Co. Since the ^{59}Co nucleus in **1** has a trigonal-bipyramidal ligand environment, its relaxation should be very fast such that it should have no direct coupling (splitting of resonances) with other nuclei. Other nuclei, even so, can be broadened by a scalar coupling relaxation mechanism with cobalt that typically will increase the transverse relaxation rate (decrease the line width) as the temperature is decreased. This narrowing of the resonances as the temperature is decreased are clearly observed in the ^{31}P spectra of Figure 2. The same narrowing is not observed in the ^{13}C spectra of Figure 3, however. In this case, the line widths in the ^{13}C NMR spectrum are dominated by exchange broadening.

[10] The fact that IR frequencies are very fast ($\approx 10^{13}$ s^{-1}) implies that the solution IR carbonyl spectrum should give rise to the superposition of vibrational signals from all species (as though static) generated in solution. The presence of two observed frequencies at 1912 and 1906 cm^{-1} in the solid state versus one at 1910 cm^{-1} in THF may be readily attributed to factor-group splitting of the E vibrational mode under the monoclinic crystal packing environment. Hence, the remarkable agreement in the solution/solid-state IR spectra of the corresponding terminal and bridging carbonyl frequencies provides no observable evidence for a rapid detachment/reattachment process of either the entire $[TlCo(CO)_3PEt_3]$ ligand or its PEt_3 group; in either case the cobalt-attached terminal carbonyl frequencies would be noticeably shifted.

[11] Reactions were carried out by standard Schlenk techniques on a preparative vacuum line under nitrogen atmosphere. All solvents were deoxygenated by the bubbling of N_2 through them for at least 20 min at room temperature. IR spectra were recorded on a Mattson Polaris FT-IR spectrometer by use of CaF_2 windows or a nitrogen-purged CaF_2 cell. $[TlCo(CO)_4]$ was prepared according the procedure of Schussler et al.[3c] The synthesis of $[Pd_{10}(CO)_{12}L_6]$ (**3**) is analogous to that of $[Pd_{10}(CO)_{12}(PnBu_3)_6]$;[12] compound **3** was purified by recrystallization from C_6H_6/heptane. A typical procedure for the preparation of **1**: a solution of $[Pd_{10}(CO)_{12}(PEt_3)_6]$ (0.400 g; 0.190 mmol) and PEt_3 (0.05 mL; 0.344 mmol) in toluene (8 mL) was stirred for about 10 min at RT under CO. The atmosphere was changed to N_2, after which $[TlCo(CO)_4]$ (0.135 g; 0.360 mmol) was added under continued stirring for 45 min. at 70 °C. The resulting deep-brown-yellowish solution was filtered to remove a black precipitate, heptane (6 mL) was added to the filtrate, and the solution was kept overnight at −20 °C. Black crystals of **1**, (0.113 g) were collected (from the solution which also contained a small amount of light amorphous brown precipitate) and then were washed with hexane. The solution was filtered, heptane (30 mL) was added to the filtrate, and an additional 0.092 g of crystals of **1** were separated by the above procedure, in this case without formation of any amorphous precipitate. Total yield of **1** was 0.205 g (41 % on the basis of Pd). IR spectra in Nujol: 1974 (wm), 1912 (sh), 1906 (s), 1878 (s), 1852 (m), 1835 (sh w), 1794 (m), 1761 (ms) cm^{-1}; in THF solution: 1974 (wm), 1910 (s), 1881 (s), 1852 (mw), 1801 (ms), 1770 (s) cm^{-1}. Single crystals of **1** were obtained by vapor diffusion of pentane into toluene solution of **1**; one of size $0.24 \times 0.09 \times 0.06$ mm^3 was used for the X-ray diffraction study.

[12] For such a Pd/L ratio with the PEt_3 ligand under CO atmosphere, it was shown that only palladium clusters of nuclearity $n = 4$ and 10 exist: E. G. Mednikov, N. K. Eremenko, *Izv. Acad. Nauk Ser. Khim.* **1982**, 2540; [*Bull. Acad. Sc. USSR Div. Chem. Sc.* **1982**, *31*, 2240 (Engl. Transl.)].

 © 2005 Wiley-VCH Verlag GmbH & Co. KGaA, Weinheim

Noncovalent Interactions

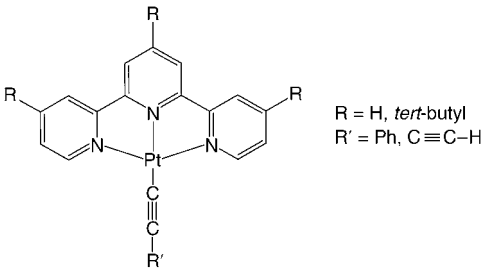
Polymer-Induced Self-Assembly of Alkynylplatinum(II) Terpyridyl Complexes by Metal···Metal/π···π Interactions**

*Cong Yu, Keith Man-Chung Wong, Kenneth Hoi-Yiu Chan, and Vivian Wing-Wah Yam**

The intriguing structures and bonding properties of square-planar platinum(II) complexes have attracted long-standing interest,[1] and more-so recently with the growing interest in the spectroscopic properties associated with this class of compounds.[2–9] These complexes are known to display a strong tendency towards the formation of highly ordered extended linear chains or oligomeric structures in the solid state.[1e,2,4,5a] A particularly interesting class of platinum(II) complexes is the polypyridyl complexes. The extent of the d^8–d^8 metal–metal interaction and the π–π stacking of the polypyridyl ligand have led to the observation of interesting spectroscopic and luminescence properties,[2–5] and recent reports based on the utilization of these observations for molecular recognition, chemosensing, and optoelectronic applications have also been published.[5,6c,10]

Recently, we reported the synthesis of a butadiynylplatinum(II)–terpyridyl complex and showed that changing the solvent composition from pure acetonitrile to an acetonitrile/diethyl ether mixture resulted in the complex changing from its monomeric state to an aggregated state in solution, and drastic changes in the solution color were observed.[5] Since the platinum(II) complex ion carries a positive charge, to maintain a charge balance and a neutral environment, its aggregation may also induce a reorganization of the counteranion. Similarly, assembly of the counteranions in an orderly manner may also influence the self-assembly of the positively charged platinum(II) units by an aggregation process. An example of an ordered array of counteranions is the class of polyelectrolyte anions, where negatively charged functional groups are connected to a polymer chain.[11] Polyelectrolyte anions include important macromolecules such as nucleic acids and many types of synthetic polymers, and herein we report the use of a polycarboxylate in the self-assembly of platinum(II) complexes. We found that the polymer itself could, upon deprotonation, induce the self-assembly of the terpyridylplatinum(II) complexes, without the need to change the solvent composition, thus giving rise to remarkable UV/Vis and luminescence changes.

Poly(acrylic acid) was obtained by acid hydrolysis of poly[1-(ethoxy)ethyl acrylate], which was prepared by atom-transfer radical polymerization (ATRP) of the corresponding monomer.[12] Three alkynylplatinum(II) complexes, [Pt(tpy)(C≡C–C≡CH)]OTf (**1**),[5] [Pt(tpy)(C≡C–Ph)]OTf (**2**),[6c] and [Pt(*t*Bu$_3$-tpy)(C≡C–C≡CH)]OTf (**3**)[5] (tpy = 2,2′:6′,2″-terpyridine; OTf = trifluoromethanesulfonate; *t*Bu$_3$-tpy = 4,4′,4″-tri-*tert*-butyl-2,2′:6′,2″-terpyridine), were tested in this investigation (Scheme 1). Addition of complex



Scheme 1. Structure of the platinum(II) complexes.

1 or **2** to a solution of poly(acrylic acid) in the presence of tetrabutylammonium hydroxide (TBAH) as a base in an organic medium resulted in a remarkable change in the color and the UV/Vis absorption spectra (Figure 1). A color change of the solution of complex **1**, from light-yellow to pink/red occurred, and, along with a decrease in the intensity of the absorbance bands at 338 and 408 nm, a new band appeared at 543 nm. Similar observations were found for complex **2**, with a decrease in the intensity of the absorbance bands at about 330 and 430 nm and the formation of new bands at about 480 and 580 nm. The solutions were found to be very stable, with

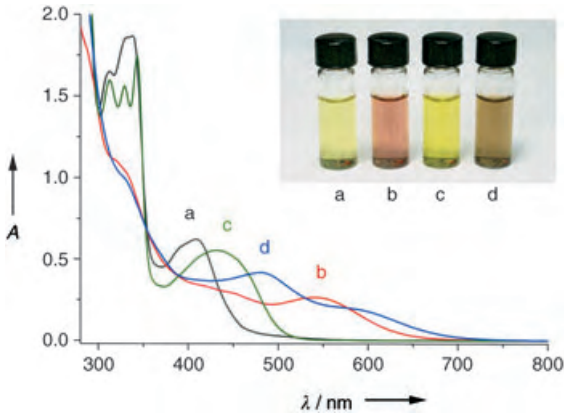


Figure 1. UV/Vis absorbance changes of the complex (0.15 mM) in a mixture of MeOH and CH_3CN (2:1, v/v) upon addition of poly(acrylic acid) (0.45 mM carboxylic acid unit) and TBAH (0.45 mM): a) **1**; b) **1** + poly(acrylic acid) + TBAH; c) **2**; d) **2** + poly(acrylic acid) + TBAH. Inset: photographs of the solution mixtures (a)–(d).

[*] Dr. C. Yu, Dr. K. M.-C. Wong, K. H.-Y. Chan, Prof. Dr. V. W.-W. Yam
Centre for Carbon-Rich Molecular and Nanoscale Metal-Based Materials Research
and the Department of Chemistry
The University of Hong Kong
Pokfulam Road, Hong Kong (P. R. China)
Fax: (+852) 2857-1586
E-mail: wwyam@hku.hk

[**] V.W.-W.Y. acknowledges support from the University Development Fund of The University of Hong Kong, the University of Hong Kong Foundation for Educational Development and Research Limited, and the Research Grants Council of Hong Kong Special Administrative Region, China (Project No. HKU 7022/03P). K.H.-Y.C. acknowledges the receipt of a postgraduate studentship administered by the University of Hong Kong. Dr. W.-K. Chan and his students are thanked for their assistance in the use of the gel-permeation chromatography (GPC) system.

 DOI: 10.1002/anie.200461261 © 2005 Wiley-VCH Verlag GmbH & Co. KGaA, Weinheim

no precipitate formation after standing at ambient temperature for several days. Addition of a solution of complexes **1** or **2** in acetonitrile to either a methanolic solution of poly(acrylic acid) or TBAH alone did not yield any observable changes in the UV/Vis absorption spectra, thereby indicating that the changes are associated with the presence of both poly(acrylic acid) and a base, that is, the deprotonation of poly(acrylic acid) to the anionic polyacrylate.

On the basis of our previous work[5] and other related studies,[3,4] the newly formed bands of complexes **1** and **2** at longer wavelength were assigned as metal-metal-to-ligand charge-transfer (MMLCT) transitions resulting from the aggregation of these complexes, presumably through metal···metal and/or π···π interactions. These results suggest that the electrostatic binding of the positively charged platinum(II) complex ions to the negatively charged polymer chain brings the platinum(II) complex ions into close proximity with each other and thus induces their aggregation (Figure 2). The

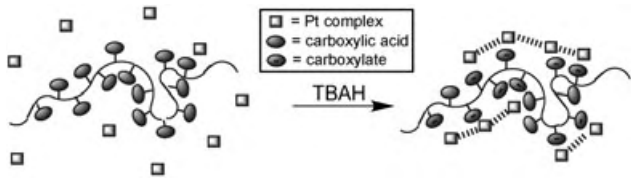


Figure 2. Aggregation of the platinum(II) complex ions in the presence of a base and a polycarboxylic acid.

decrease in the absorbance intensity in the 330–430 nm region, which is typical of a metal-to-ligand charge transfer (MLCT) transition of a monomeric terpyridylplatinum(II) complex, further supports the conversion of the monomeric complex into an aggregated form.

Addition of complex **3** to a solution of poly(acrylic acid) in the presence of TBAH did not yield any observable color change. Apparently, the bulky *tert*-butyl groups on the terpyridine ring in **3** prevent aggregation of the complex from taking place. A number of small carboxylic acids were also tested, including monocarboxylic acids (acetic acid, acrylic acid, isobutyric acid), dicarboxylic acids (fumaric acid, maleic acid, oxalic acid, malonic acid, succinic acid, glutaric acid), and a tricarboxylic acid (citric acid). No observable color change was observed upon mixing complex **1** or **2** (0.15 mM) with such small mono-, di-, or tricarboxylic acids in the presence of TBAH at different complex/carboxylic acid group/base molar ratios (1/3/3, 2/3/3, and 3/3/3). This result strongly suggests that the aggregation of the metal complex is induced only by the polyacrylate and not by the smaller carboxylates. The observed differences in behavior between poly(acrylic acid) and the smaller carboxylic acids are presumably a result of the high density of negative charge.

The aggregation process was found to be fully reversible. Thus, addition of HCl to a solution of **1** in the aggregated state converted the red solution back into the yellow solution characteristic of the original monomeric state, by protonation of the polyanion to form the polyacid. Addition of TBAH to the yellow solution caused the solution to become red again. The corresponding changes in the UV/Vis absorption spectra confirmed the reversible interconversion between the aggregated state and the monomeric state upon repeated addition of acid and base. In addition, positive-ion ESI-MS experiments confirmed that no change or degradation of the platinum(II) complexes occurred and their identity remained intact during the process of adding acid and base.

It is interesting to note that when the metal complex loading per polymer chain was lowered, that is, when more poly(acrylic acid) was added, no induction of complex aggregation was observed. For example, the UV/Vis absorption spectra for a mixture containing complex **1** (0.15 mM), poly(acrylic acid) (22.5 mM carboxylic acid unit), and TBAH (0.45 mM) [complex/carboxylic acid unit/base = 1/150/3 in $MeOH/CH_3CN$ (2:1, v/v)] was very similar to that of a solution of complex **1** (0.15 mM) in the same solvent. As the concentration of the poly(acrylic acid) was gradually reduced, the MMLCT band began to appear and became more intense (Figure 3, left). Since the concentration of the base remained constant throughout the experiments, the use of a higher

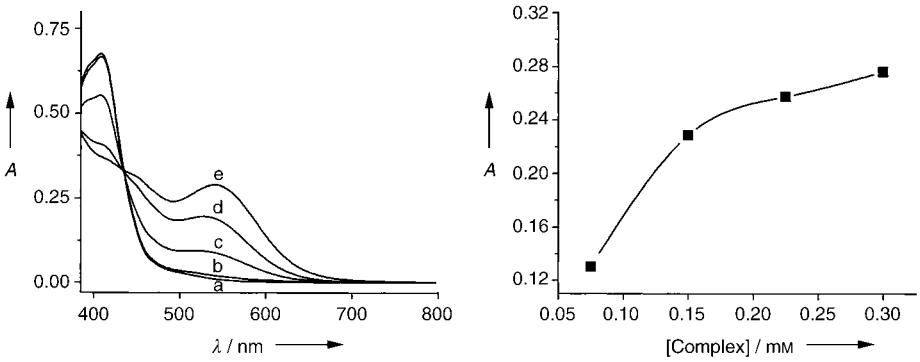


Figure 3. Left: Curve a: complex **1** (0.15 mM) in $MeOH/CH_3CN$ (2:1, v/v); curves b–e: complex **1** (0.15 mM) + poly(acrylic acid) (22.5, 15, 7.5, 0.45 mM carboxylic acid unit, respectively) + TBAH (0.45 mM) in $MeOH/CH_3CN$ (2:1, v/v). Right: complex **1** + poly(acrylic acid) (0.225 mM carboxylic acid unit) + TBAH (0.225 mM) in $MeOH/CH_3CN$ (2:1, v/v).

poly(acrylic acid) concentration would give rise to a lower average number of deprotonated carboxylic acid groups on each polymer chain, thus rendering them widely spaced and isolated, which, in turn, would lead to the platinum complexes bound to the anionic carboxylate groups also becoming more isolated from each other and thus preventing aggregate formation.

When the concentration of the polymer and base was kept constant and the concentration of the complex was increased, the MMLCT band intensity at peak maximum (543 nm) increased gradually (Figure 3, right), which suggests that a

 © 2005 Wiley-VCH Verlag GmbH & Co. KGaA, Weinheim

higher degree of ordering occurs at higher concentrations of the complex. With the concentration of complex **1** fixed and equimolar amounts of the carboxylic acid unit and base added, the absorbance of the MMLCT band of the complex at 543 nm reached a maximum at a complex/carboxylic acid unit/base molar ratio of 1/3/3; further increase of the poly(acrylic acid) and base concentration caused a decrease in the absorbance. In addition, concomitant with the color and absorbance changes, a new emission band, attributed to a ^{3}MMLCT emission, appeared at about 800 nm (Figure 4), and

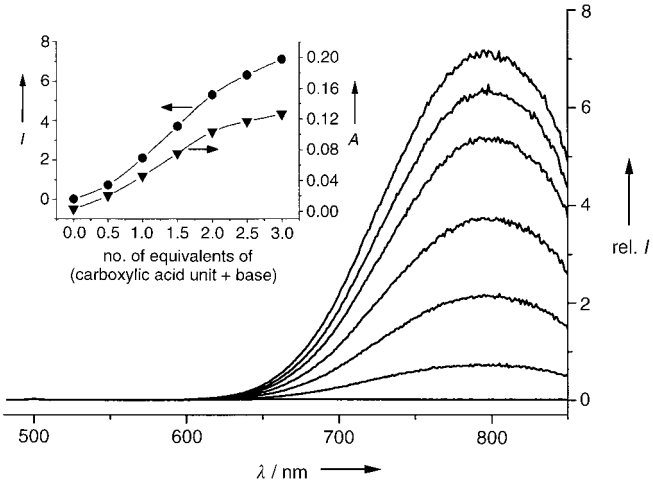


Figure 4. Emission enhancement of **1** (0.075 mM) upon addition of equimolar amounts of carboxylic acid unit and base. Inset: Plot of the emission intensity at 800 nm or absorbance at 543 nm versus the ratio of the polymer and base added. The emission intensities are expressed in arbitrary units.

again reached maximum intensity at the complex/carboxylic acid unit/base molar ratio of 1/3/3. This new emission band disappeared completely when HCl was added to the solution and could be regenerated by adding TBAH. Similar results were observed with complex **2**, with an emission maximum at about 840 nm. These results indicate that the availability of too many polymer binding sites reduces the tendency of the complex to aggregate. More importantly, the same trend in the changes of the UV/Vis absorbance and emission intensity suggests that they have a similar origin—the self-assembly of the complex molecules into the aggregated state. Further support for such a ^{3}MMLCT transition came from solid-state emission studies,[5,6c] as well as the observation of an excitation band at about 543 nm in the excitation spectrum of complex **1** monitored at the ^{3}MMLCT emission band.

In conclusion, we have demonstrated for the first time that a polyelectrolyte, namely poly(acrylic acid), upon deprotonation can indeed induce self-assembly of terpyridylplatinum(II) complexes, and, in turn, induce remarkable UV/Vis and emission intensity changes. It is possible that the UV/Vis and emission properties could be finely tuned by selection of other suitable metal complexes, optimization of assay conditions, and varying the structure of the polyelectrolyte. We envisage that such changes in the electronic absorption and luminescence properties may be exploited for probing conformational and microenvironmental changes in polymers and biomolecules.

Experimental Section

The monomer 1-(ethoxy)ethyl acrylate was prepared from the addition reaction of ethyl vinyl ether with acrylic acid.[12e] CuCl complexed with *N*,*N*′,*N*′,*N*″,*N*″-pentamethyldiethylenetriamine (PMDETA) was used as the catalyst, with methyl 2-bromopropionate as the initiator and toluene as the solvent. The molecular weight of the resulting polymer before deprotection was determined by GPC (calibration standard: poly(methyl methacrylate) (PMMA); eluent: *N*-methylpyrrolidone (NMP); $M_n = 8612$, $M_w = 10971$, PDI = 1.27), which gave an average of about 59 carboxylic acid functional groups on each polymer chain.

Received: July 10, 2004
Revised: October 14, 2004
Published online: December 23, 2004

Keywords: noncovalent interactions · platinum · polyelectrolytes · self-assembly · UV/Vis spectroscopy

[1] a) *Extended Linear Chain Compounds*, *Vol. 1* (Ed.: J. S. Miller), Plenum, New York, **1982**; b) J. S. Miller, A. J. Epstein, *Prog. Inorg. Chem.* **1976**, *21*, 1; c) M. Atoji, J. W. Richardson, R. E. Rundle, *J. Am. Chem. Soc.* **1957**, *79*, 3017; d) P. M. Kiernan, A. Ludi, *J. Chem. Soc. Dalton Trans.* **1978**, 1127; e) R. S. Osborn, D. Rogers, *J. Chem. Soc. Dalton Trans.* **1974**, 1002.

[2] a) V. M. Miskowski, V. H. Houlding, *Inorg. Chem.* **1989**, *28*, 1529; b) V. M. Miskowski, V. H. Houlding, *Inorg. Chem.* **1991**, *30*, 4446; c) V. H. Houlding, V. M. Miskowski, *Coord. Chem. Rev.* **1991**, *111*, 145.

[3] a) H. K. Yip, C.-M. Che, Z. Y. Zhou, T. C. W. Mak, *J. Chem. Soc. Chem. Commun.* **1992**, 1369; b) J. A. Bailey, V. M. Miskowski, H. B. Gray, *Inorg. Chem.* **1993**, *32*, 369; c) M. G. Hill, J. A. Bailey, V. M. Miskowski, H. B. Gray, *Inorg. Chem.* **1996**, *35*, 4585.

[4] a) J. A. Bailey, M. G. Hill, R. E. Marsh, V. M. Miskowski, W. P. Schaefer, H. B. Gray, *Inorg. Chem.* **1995**, *34*, 4591; b) R. Büchner, C. T. Cunningham, J. S. Field, R. J. Haines, D. R. McMillin, G. C. Summerton, *J. Chem. Soc. Dalton Trans.* **1999**, 711.

[5] V. W.-W. Yam, K. M.-C. Wong, N. Zhu, *J. Am. Chem. Soc.* **2002**, *124*, 6506.

[6] a) G. Arena, G. Calogero, S. Campagna, L. M. Scolaro, V. Ricevuto, R. Romeo, *Inorg. Chem.* **1998**, *37*, 2763; b) S. W. Lai, M. C. W. Chan, K.-K. Cheung, C.-M. Che *Inorg. Chem.* **1999**, *38*, 4262; c) V. W.-W. Yam, R. P.-L. Tang, K. M.-C. Wong, K.-K. Cheung, *Organometallics* **2001**, *20*, 4476; d) D. R. McMillin, J. J. Moore, *Coord. Chem. Rev.* **2002**, *229*, 113; e) V. W.-W. Yam, K. M.-C. Wong, N. Zhu, *Angew. Chem.* **2003**, *115*, 1438; *Angew. Chem. Int. Ed.* **2003**, *42*, 1400.

[7] a) J. A. Zuleta, C. A. Chesta, R. Eisenberg, *J. Am. Chem. Soc.* **1989**, *111*, 8916; b) J. A. Zuleta, M. S. Burbery, R. Eisenberg, *Coord. Chem. Rev.* **1990**, *97*, 47; c) W. Paw, R. J. Lachicotte, R. Eisenberg, *Inorg. Chem.* **1998**, *37*, 4139.

[8] a) M. Hissler, W. B. Connick, D. K. Geiger, J. E. McGarrah, D. Lipa, R. J. Lachicotte, R. Eisenberg, *Inorg. Chem.* **2000**, *39*, 447; b) C. E. Whittle, J. A. Weinstein, M. W. Geore, K. S. Schanze, *Inorg. Chem.* **2001**, *40*, 4053; c) S. C. Chan, M. C. W. Chan, Y. Wang, C. M. Che, K. K. Cheung, N. Zhu, *Chem. Eur. J.* **2001**, *7*, 4180; d) W. Lu, M. C. W. Chan, N. Zhu, C. M. Che, Z. He, K. Y. Wong, *Chem. Eur. J.* **2003**, *9*, 6155.

 © 2005 Wiley-VCH Verlag GmbH & Co. KGaA, Weinheim

[9] a) C. E. Buss, C. E. Anderson, M. K. Pomije, C. M. Lutz, D. Britton, K. R. Mann, *J. Am. Chem. Soc.* **1998**, *120*, 7783; b) C. E. Buss, K. R. Mann, *J. Am. Chem. Soc.* **2002**, *124*, 1031.
[10] a) A. J. Goshe, I. M. Steele, B. Bosnich, *J. Am. Chem. Soc.* **2003**, *125*, 444; b) V. Adamovich, J. Brooks, A. Tamayo, A. M. Alexander, P. I. Djurovich, B. W. D. Andrade, C. Adachi, S. R. Forrest, M. E. Thompson, *New J. Chem.* **2002**, *26*, 1171.
[11] a) *Handbook of Polyelectrolytes and Their Applications* (Eds.: S. K. Tripathy, J. Kumar, H. S. Nalwa), American Scientific, Stevenson Ranch, **2002**; b) F. M. Gray, *Polymer Electrolytes*, The Royal Society of Chemistry, Cambridge, **1997**; c) H. Dautzenberg, W. Jaeger, J. Kötz, B. Philipp, Ch. Seidel, D. Stscherbina, *Polyelectrolytes: Formation, Characterization and Application*, Hanser, Munich, **1994**.
[12] a) K. Matyjaszewski, J. Xia, *Chem. Rev.* **2001**, *101*, 2921; b) D. A. Shipp, J.-L. Wang, K. Matyjaszewski, *Macromolecules* **1998**, *31*, 8005; c) K. A. Davis, K. Matyjaszewski, *Macromolecules* **2000**, *33*, 4039; d) S. Lu, Q.-L. Fan, S.-Y. Liu, S.-J. Chua, W. Huang, *Macromolecules* **2002**, *35*, 9875; e) H. Zhang, E. Ruckenstein, *Macromolecules* **1998**, *31*, 7575.

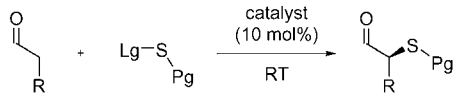
 © 2005 Wiley-VCH Verlag GmbH & Co. KGaA, Weinheim

Asymmetric Catalysis

Enantioselective Organocatalyzed α Sulfenylation of Aldehydes**

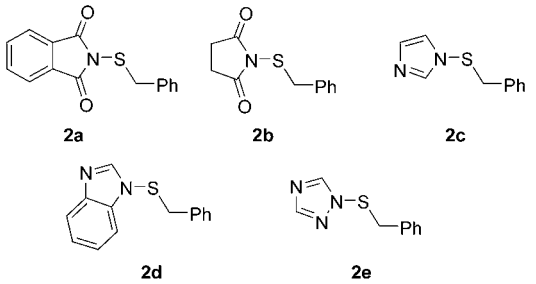
*Mauro Marigo, Tobias C. Wabnitz, Doris Fielenbach, and Karl Anker Jørgensen**

Optically active α-heterosubstituted aldehydes are versatile building blocks for the synthesis of chiral molecules that bear heteroatom functionalities. Recent advances in the synthesis of these molecules have been focused on the development of direct organocatalytic procedures[1] that avoid metal catalysts and reagents. Organocatalyzed additions of simple carbonyl compounds to diazocarboxylates and nitrosobenzene allow the incorporation of nitrogen-[2] and oxygen-containing[3] α substituents into aldehydes and ketones with excellent levels of stereoselectivity. Very recently, organocatalyzed substitution reactions of *N*-halosuccinimides and related electrophiles have been developed for the α halogenation of aldehydes and ketones.[4] In contrast, the analogous asymmetric introduction of sulfur-based substituents has not been reported, in spite of the synthetic potential of α-sulfenylated aldehydes and the merits of organocatalytic processes, which circumvent the undesired association of sulfur reagents with metal catalysts. To date, all practical methods for the preparation of chiral α-sulfenylated aldehydes have been multistep procedures that involve chiral auxiliaries.[5] According to our knowledge, no catalytic processes are available for the preparation of these useful optically active building blocks. Herein, we report the first direct organocatalyzed enantioselective α sulfenylation of aldehydes [Eq. (1)].



(1)

In analogy to organocatalyzed halogenation reactions, sulfenylations are substitution reactions, which are inherently more difficult to perform enantioselectively than addition processes as a result of the more flexible nature of the transition state. Therefore, the design of a suitable leaving group (Lg) is crucial. Furthermore, a second substituent that can serve as a protecting group (Pg) needs to be chosen for sulfenylation reactions. To provide for facile product elaboration, *S*-benzyl-protected α-sulfenylated aldehydes were chosen as synthetic targets, as there are well-established methods for the cleavage of this protecting group.[6] Similarly, the development of a practical sulfenylation process called for a leaving group that could be separated readily from the product after the reaction. Additionally, the protonated nucleofuge should be a neutral species that does not affect the equilibrium of enamine formation or deactivate the amine catalyst. In line with these considerations, initial experiments were carried out for the α sulfenylation of isovaleraldehyde (**1a**) with the reagents shown in Scheme 1, all of which



Scheme 1. Sulfenylation reagents with different leaving groups tested in the organocatalyzed enantioselective α sulfenylation of isovaleraldehyde (**1a**).

contain weakly basic heterocyclic nitrogen-centered nucleofuges, in the presence of different pyrrolidine derivatives. Whereas the phthalimide and succinimide reagents **2a** and **2b** underwent only sluggish conversion, and the imidazole-derived electrophile **2c** turned out to be unstable, the desired α-sulfenylated product was obtained from isovaleraldehyde in good yield with the reagents **2d** and **2e**. Finally, the novel triazole derivative 1-benzylsulfanyl-1,2,4-triazole (**2e**) was

[*] M. Marigo, Dr. T. C. Wabnitz, Dr. D. Fielenbach, Prof. Dr. K. A. Jørgensen
The Danish National Research Foundation: Center for Catalysis
Department of Chemistry, Aarhus University
8000 Aarhus C (Denmark)
Fax: (+45) 8919-6199
E-mail: kaj@chem.au.dk

[**] This work was made possible by a grant from The Danish National Research Foundation. M.M. and T.C.W. thank the EU (HMPT-CT-2001-00317) for financial support.

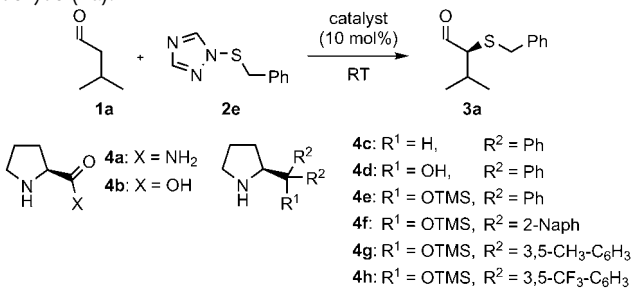
Supporting information for this article is available on the WWW under http://www.angewandte.org or from the author.

 © 2005 Wiley-VCH Verlag GmbH & Co. KGaA, Weinheim DOI: 10.1002/anie.200462101

chosen as the electrophilic sulfur source,[7] as it exhibited the highest level of reactivity.

Systematic studies of a model system comprising isovaleraldehyde (**1a**), the sulfur electrophile **2e**, and 10 mol% of a chiral secondary amine organocatalyst at ambient temperature are summarized in Table 1. With the L-proline-derived

Table 1: Organocatalyzed enantioselective α sulfenylation of isovaleraldehyde (**1a**).[a]



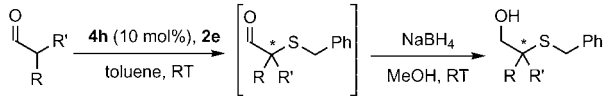
Entry	4	Solvent	Yield [%][b]	*ee* [%][c]
1	**a**	DMSO	–[d,e]	–
2	**a**	Et_2O	5	18
3	**a**	CH_2Cl_2	7	22
4	**a**	toluene	30	25
5	**b**	toluene	16	0
6	**c**	toluene	56[e]	52[f]
7	**d**	toluene	–[d]	–
8	**e**	toluene	90	77
9	**f**	toluene	75[e]	84
10	**g**	toluene	73[e]	90
11	**h**	toluene	90	98
12[g]	**h**	toluene	90	96
13[h]	**h**	toluene	90	90

[a] Compound **2e** (0.27 mmol) was added to **1a** (0.25 mmol) and **4** (0.025 mmol) in the solvent (0.5 mL), and the mixture was stirred at room temperature. [b] Based on NMR spectroscopic analysis of the crude reaction mixture after 3 h. [c] The *ee* value was determined by GC on a chiral phase (chrompak CP-chiralsil dex CB column) and verified by HPLC (chiralpak AD column) after reduction of **3a** to the corresponding alcohol. [d] Compound **3a** was not formed. [e] The α,α-disulfenylated aldehyde by-product was detected in the crude reaction mixture in >10% yield. [f] After 24 h at room temperature: 25% *ee*. [g] After 1 h in the presence of $LiClO_4$ (30 mol%). [h] After 1 h in the presence of *o*-nitrobenzoic acid (10 mol%). DMSO = dimethyl sulfoxide, Naph = naphthyl, TMS = trimethylsilyl.

amide **4a**, only traces of the product **3a**, but large amounts of the α,α-disulfenylated aldehyde, were observed in DMSO (Table 1, entry 1). In less polar solvents, such as toluene, the desired product **3a** was generated in low yield with low enantioselectivity in the presence of **4a** (Table 1, entries 2–4). Whereas L-proline (**4b**) was ineffective (Table 1, entry 5), the chiral pyrrolidine derivative **4c** increased the rate and enantioselectivity of the reaction (Table 1, entry 6), although it slowly racemized the product upon prolonged reaction times and led to α,α disulfenylation. To minimize such undesired interactions between the organocatalyst and the reaction product, we attempted the reaction in the presence of a catalyst with increased steric bulk. No reaction occurred with α,α-diphenyl-L-prolinol (**4d**; Table 1, entry 7), probably as a result of the reaction of **2e** with the hydroxy group[7] and/or formation of an unreactive hemiaminal by reaction with the aldehyde. However, trimethylsilyl protection of the free hydroxy moiety of **4d** restored reactivity and enhanced selectivity (Table 1, entry 8). Further improvements were made through variation of the aryl substituents in the catalyst structure. The silylated L-prolinol derivatives **4f–h** with sterically demanding aryl substituents furnished the product with high enantiomeric excess (Table 1, entries 9–11). The fluorinated derivative **4h** was identified as the best of these catalysts, as it gave **3a** in 90% yield and with 98% *ee*, with only traces of concomitant α,α-disulfenylation and no product racemization (Table 1, entry 11). However, the reaction rate was found to be strongly dependent on the purity of the reagent **2e**, which slowly degraded upon storage. Nevertheless, in cases of slow conversion the turnover could be increased by adding salts such as $LiClO_4$ to the reaction mixture, with only a minor decrease in enantiomeric excess (Table 1, entry 12). Protic acids also accelerated the reaction, but led to a more pronounced loss of enantiomeric excess (Table 1, entry 13).[8]

Under the optimized conditions, a series of aldehydes **1a–g** underwent enantioselective α sulfenylation in the presence of **2e** as the *S*-benzyl-protected sulfur donor and **4h** as the catalyst. To facilitate workup, the reaction products were isolated as the alcohols **5** after in situ reduction of the aldehyde moiety with $NaBH_4$.[9] The reduction of the α-sulfenylated aldehyde **3a** to the alcohol **5a** showed that this process occurs without loss of enantiomeric excess. Simple aliphatic aldehydes **1a–c** (Table 2, entries 1–3), as well as those containing a phenyl group or an additional double bond (Table 2, entries 4 and 5), underwent the desired reaction, and the optically active α-sulfenylated alcohols **5a–e** were obtained in good yields and with excellent enantioselectivities. Similarly, the sterically encumbered aldehyde **1f** was transformed smoothly into the corresponding chiral alcohol **5f** with very high enantioselectivity (Table 2, entry 6). Furthermore, the method could be extended to the construction

Table 2: Organocatalyzed enantioselective α sulfenylation of aldehydes.[a]



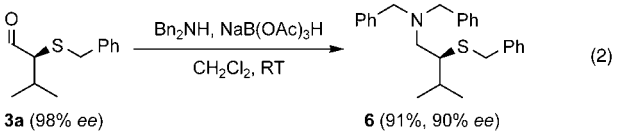
Entry	1/5	R	R′	Yield of 5 [%][b]	*ee* [%][c]
1	**a**	*i*Pr	H	81	98
2	**b**	Me	H	60	95
3	**c**	Et	H	85	96
4	**d**	Bn	H	94	97
5	**e**	allyl	H	64	96
6	**f**	*t*Bu	H	83	95
7[d]	**g**	Ph	Me	84	61

[a] Compound **2e** (0.33 mmol) was added to **1** (0.25 mmol) and **4h** (0.025 mmol) in toluene (0.5 mL), and the mixture was stirred at room temperature for 3 h. [b] Yield of the isolated product after column chromatography. [c] The *ee* value was determined by HPLC of the alcohols **5** on a chiral phase (see Supporting Information). [d] After 16 h with catalyst **4e** (10 mol%) and *o*-nitrobenzoic acid (10 mol%). Bn = benzyl.

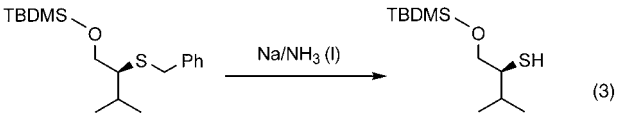
 © 2005 Wiley-VCH Verlag GmbH & Co. KGaA, Weinheim

of quaternary stereocenters starting from α,α-disubstituted aldehydes, such as 2-phenyl propanal (**1g**). In this case, the optically active α-sulfenylated alcohol **5g** was obtained in high yield and with good enantioselectivity when **4e** was used as the catalyst (Table 2, entry 7).

As well as reduction to the α-sulfenylated alcohols **5**, the optically active α-sulfenylated aldehydes **3** also undergo reductive amination with dibenzylamine and sodium triacetoxyborohydride. By using this procedure, the chiral α-sulfenylated amine **6** was obtained directly from the aldehyde **3a** with only a minor loss of enantiomeric excess [Eq. (2)]. Moreover, after protection of the hydroxy group as a *tert*-butyldimethylsilyl (TBDMS) ether, the benzyl sulfide moiety could be cleaved reductively with $Na/NH_3(l)$. Thus, the free thiol **8** was formed from **7** in good yield [Eq. (3)]. These transformations underline the synthetic versatility of optically active α-sulfenylated aldehydes in the preparation of chiral sulfur-containing compounds.



3a (98% *ee*) **6** (91%, 90% *ee*) (2)



7 **8** (65%) (3)

The absolute configuration of the optically active α-sulfenylated alcohols **5a** and **5b** was determined to be *S* by comparison of their optical rotation with values reported in the literature.[5f,10] This configuration is in agreement with *Si*-face attack of the sulfur-centered electrophile on the *E*-configured enamine intermediate. The *Re* face of the enamine is shielded effectively by the aryl and silyl substituents of the catalyst **4h**. A model for this mode of attack is depicted in Figure 1.

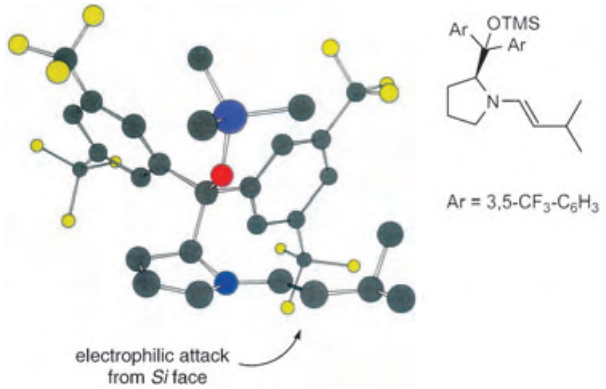


Figure 1. Postulated *Si*-face attack of the electrophile on the *E* enamine formed from isovaleraldehyde (**1a**) and catalyst **4h**.

In summary, a novel class of organocatalysts in the form of sterically encumbered chiral pyrrolidine derivatives without additional free heteroatom functionalities has been developed. These compounds were found to be highly efficient organocatalysts for the direct enantioselective α sulfenylation of aldehydes, which is one of the first examples of an asymmetric intermolecular substitution reaction mediated by a secondary amine. This procedure constitutes the first enantioselective catalytic preparation of α-sulfenylated aldehydes and, to the best of our knowledge, the first successful use of electrophilic sulfur sources in asymmetric catalysis. The optically active products were obtained in high yields with excellent enantioselectivities and underwent further facile modifications. Further exploration of the new class of chiral organocatalysts described are now in progress in our laboratory.

Received: September 24, 2004

Keywords: aldehydes · asymmetric catalysis · enantioselectivity · organocatalysis · sulfenylation

[1] For some recent reviews, see, for example: a) P. I. Dalko, L. Moisan, *Angew. Chem.* **2001**, *113*, 3840; *Angew. Chem. Int. Ed.* **2001**, *40*, 3726; b) B. List, *Tetrahedron* **2002**, *58*, 5573; c) R. O. Duthaler, *Angew. Chem.* **2003**, *115*, 1005; *Angew. Chem. Int. Ed.* **2003**, *42*, 975; d) P. Merino, T. Tejero, *Angew. Chem.* **2004**, *116*, 3055; *Angew. Chem. Int. Ed.* **2004**, *43*, 2995; e) B. List, *Acc. Chem. Res.* **2004**, *37*, 548; f) W. Notz, F. Tanaka, C. F. Barbas III, *Acc. Chem. Res.* **2004**, *37*, 580; g) P. I. Dalko, L. Moisan, *Angew. Chem.* **2004**, *116*, 5248; *Angew. Chem. Int. Ed.* **2004**, *43*, 5138.

[2] a) A. Bøgevig, K. Juhl, N. Kumaragurubaran, W. Zhuang, K. A. Jørgensen, *Angew. Chem.* **2002**, *114*, 1868; *Angew. Chem. Int. Ed.* **2002**, *41*, 1790; b) B. List, *J. Am. Chem. Soc.* **2002**, *124*, 5656; c) H. Vogt, S. Vanderheiden, S. Bräse, *Chem. Commun.* **2003**, 2448; d) N. Kumaragurubaran, K. Juhl, W. Zhuang, A. Bøgevig, K. A. Jørgensen, *J. Am. Chem. Soc.* **2002**, *124*, 6254.

[3] a) G. Zhong, *Angew. Chem.* **2003**, *115*, 4379; *Angew. Chem. Int. Ed.* **2003**, *42*, 4247; b) S. P. Brown, M. P. Brochu, C. J. Sinz, D. W. C. MacMillan, *J. Am. Chem. Soc.* **2003**, *125*, 10808; c) Y. Hayashi, J. Yamaguchi, K. Hibino, M. Shoji, *Tetrahedron Lett.* **2003**, *44*, 8293; d) A. Córdova, M. Enqvist, I. Ibrahem, J. Casas, *J. Am. Chem. Soc.* **2004**, *126*, 8914; e) N. Momiyama, H. Torii, S. Saito, H. Yamamoto, *Proc. Natl. Acad. Sci. USA* **2004**, *101*, 5374; f) W. Wang, J. Wang, H. Lia, L. Liao, *Tetrahedron Lett.* **2004**, *45*, 7235; g) A. Bøgevig, H. Sundéen, A. Córdova, *Angew. Chem.* **2004**, *116*, 1129; *Angew. Chem. Int. Ed.* **2004**, *43*, 1109; h) Y. Hayashi, J. Yamaguchi, T. Sumaiya, M. Shoji, *Angew. Chem.* **2004**, *116*, 1132; *Angew. Chem. Int. Ed.* **2004**, *43*, 1112; i) Y. Hayashi, J. Yamaguchi, T. Sumiya, K. Hibino, M. Shoji, *J. Org. Chem.* **2004**, *69*, 5966; j) A. Córdova, H. Sundén, A. Bøgevig, M. Johansson, F. Himo, *Chem. Eur. J.* **2004**, *10*, 3673.

[4] a) M. P. Brochu, S. P. Brown, D. W. C. MacMillan, *J. Am. Chem. Soc.* **2004**, *126*, 4108; b) N. Halland, A. Braunton, S. Bachmann, M. Marigo, K. A. Jørgensen, *J. Am. Chem. Soc.* **2004**, *126*, 4790; c) M. Marigo, S. Bachmann, N. Halland, A. Braunton, K. A. Jørgensen, *Angew. Chem.* **2004**, *116*, 5623; *Angew. Chem. Int. Ed.* **2004**, *43*, 5507.

[5] See, for example: a) J.-H. Youn, R. Herrmann, I. Ugi, *Synthesis* **1987**, 158; b) G. Poli, L. Belvisi, L. Manzoni, C. Scolastico, *J. Org. Chem.* **1993**, *58*, 3165; c) D. Enders, T. Schäfer, O. Piva, A. Zamponi, *Tetrahedron* **1994**, *50*, 3349; d) K. Chibale, S. Warren, *Tetrahedron Lett.* **1994**, *35*, 3991; e) D. Enders, T. Schäfer, W.

 © 2005 Wiley-VCH Verlag GmbH & Co. KGaA, Weinheim

Mies, *Tetrahedron* **1998**, *54*, 10239; f) D. A. Evans, K. R. Campos, J. S. Tedrow, F. E. Michael, M. R. Gagné, *J. Am. Chem. Soc.* **2000**, *122*, 7905.
[6] T. W. Greene, P. G. M. Wuts, *Protective Groups in Organic Synthesis*, 3rd ed., Wiley, New York, **1999**, p. 458.
[7] For a study of electrophilic sulfur reagents that contain nitrogen nucleofuges, see: D. N. Harpp, K. Steliou, T. H. Chan, *J. Am. Chem. Soc.* **1978**, *100*, 1222.
[8] These additives accelerate enamine formation, but they can racemize tertiary α-sulfenylated aldehydes.
[9] The optically active α-sulfenylated aldehyde **3a** slowly racemized during column chromatography on silica gel.
[10] L. N. Owen, M. B. Rahman, *J. Chem. Soc. C* **1971**, 2432.

 © 2005 Wiley-VCH Verlag GmbH & Co. KGaA, Weinheim

Nanoporous Materials

A Self-Ordered, Crystalline–Glass, Mesoporous Nanocomposite for Use as a Lithium-Based Storage Device with Both High Power and High Energy Densities**

Haoshen Zhou, Donglin Li, Mitsuhiro Hibino, and Itaru Honma*

Lithium-based storage devices with both high power and high energy densities are necessary for electric devices, especially for electric vehicles (EV) and other mobile or portable electric devices.[1] Herein we introduce a new concept to design a novel electrode material having a self-ordered, crystalline-glass, mesoporous nanocomposite (CGMN) structure for such industrial needs. The 5-nm frameworks of the CGMN are assembled in a compact arrangement from electrode-active nanocrystals with a small quantity of glass phase. The 4-nm uniform mesochannels of the CGMN can be filled with electrolyte solution during use to provide electrolyte and lithium-ion pathways throughout the material. In addition, the high surface area of the CGMN reduces the effective specific current density, and the three-dimensional glass network in the framework of the CGMN is able to incorporate a high content of electronic conductive oxides above the percolation-threshold value to form an electronic path, and to add lithium ions as a network modifier during the first insertion process to form an ionic path. The experimental results show that the specific capacities (energy density) at high current densities (power density) can be improved several hundred fold when the CGMN replaces TiO_2 powder as the electrode of a lithium-based storage device.

An electric vehicle (EV) powered by a rechargeable battery is an ideal solution to reduce environmental pollution as it is a clean energy source. However, the power densities of rechargeable batteries are still too low to support such industrial needs, even though their energy densities are high. The development of such an energy-storage device with both high power and high energy densities has been widely studied.[1] There are two typical approaches in this field: one is to increase the energy density of the capacitor, which is often studied by measurement of the electrical double-layer capacity (EDLC), and the other is to improve the specific capacity of the rechargeable battery by a rapid charge–discharge process, especially for lithium-based rechargeable batteries. Recently, a great deal of effort has been spent on improving the energy density of the EDLC by increasing the effective surface area of carbon-based materials,[2] although the resulting densities are still too low. In the second approach there are four main problems that have to be solved:[3,4] a) the particle size needs to be decreased to reduce the required diffusion length in the active materials; b) the effective specific current density needs to be reduced in the rapid charge–discharge process; c) a high cycle performance needs to be achieved even during the rapid charge–discharge process; and d) the electronic conductivity of the electrode materials needs to be increased.

The diffusion of lithium ions is very complex because the nature of the electrolyte phase, the solid–liquid interface, the tortuosity, and the size of the nanoparticles have to be considered.[5] Herein we only consider the the overall process by assuming that the diffusion coefficient is independent of these factors, which means that the diffusion length, L, can be estimated as $\sqrt{D\tau}$,[6] where D and τ are the diffusion coefficient and time, respectively. The value of τ decreases rapidly at high charge–discharge current, so the effective specific capacity rate will depend on the volume ratio $[r^3-(r-L)^3]/r^3$, where r is the radius of the active particle (Figure 1a). The required diffusion length L should be larger than r (namely, $L(=\sqrt{D\tau}) \geq r$) to obtain the maximum specific capacity. If we assume that the rapid charge–discharge process is complete within one minute and that D is of the order of $10^{-16}\,cm^2\,s^{-1}$ [5] in the solid state, particles with a size of $2r$ should be about 2 nm. If it is assumed that a particular material is constructed in a compact manner from nanoparticles with a size of 2 nm, most of the pores in the material should be micropores with a pore size in the range of 0.5 to 1.0 nm, and therefore much of the internal surface area of the solid will not be accessible to electrolyte solutions containing the large organic solvent molecules usually used to dissolve the lithium ions. Herein, we report the synthesis of a novel, self-ordered, mesoporous nanocomposite (CGMN) to satisfy such needs.

[*] Dr. H. Zhou, Dr. D. Li, Dr. M. Hibino, Dr. I. Honma
Institute of Energy Technology
National Institute of Advanced Industrial Science and Technology (AIST)
Umezono 1-1-1, Tsukuba, 305-8568 (Japan)
Fax: (+81) 298-615-829
E-mail: hs.zhou@aist.go.jp

[**] H.Z. thanks Mr. Mitsuhiro Ichihara for his help with the TEM observations, as well as the Japanese Society for the Promotion of Science (JSPS) and the National Institute of Advanced Industrial Science and Technology (AIST) for partially funding this research. D.L. acknowledges the financial support of a JSPS Fellowship for work carried out at the Institute of Energy Technology.

Supporting information for this article is available on the WWW under http://www.angewandte.org or from the author.

 DOI: 10.1002/anie.200460937 © 2005 Wiley-VCH Verlag GmbH & Co. KGaA, Weinheim

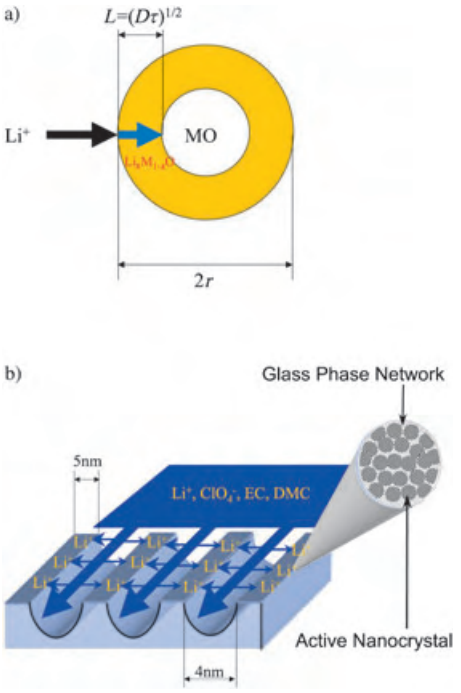


Figure 1. a) A schematic representation of the effective diffusion length in electrode-active materials. The area marked in yellow shows the volume reacting with Li^+ ions in the charge/discharge period τ in a diffusion-controlled process. b) A schematic representation of the reduced diffusion length in a rechargeable battery containing a self-ordered CGMN.

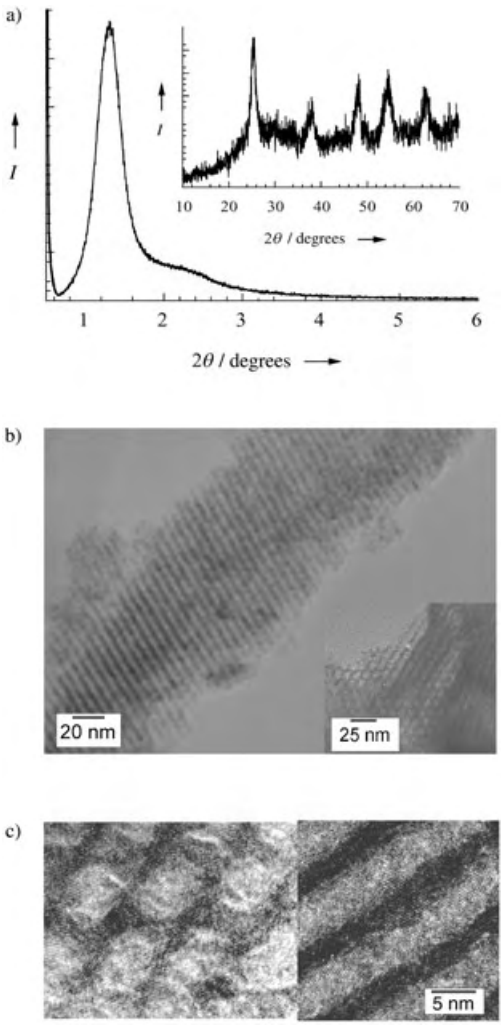


Figure 2. a) The small-angle X-ray diffraction (SAXRD) patterns and wide-angle X-ray diffraction (WAXRD) patterns of TiO_2–P_2O_5 CGMN (inset). b) TEM images of the self-ordered mesoporous structure. c) High-resolution TEM images of the TiO_2–P_2O_5 CGMN perpendicular to (left), and along the direction of (right), the nanochannels.

Self-ordered mesoporous materials were first reported in 1992,[7] and have since found applications in catalysis, absorbents, separation technology, gas sensors, solar cells, and electronics.[8–10] The framework of the self-ordered, mesoporous metal oxide is generally in an amorphous state because the crystallization of the metal oxide at high temperatures causes the collapse of the self-ordered, mesoporous structure. However, most cathode- and anode-active oxides with stable charge–discharge performance are active in the crystalline phase, such as $LiMn_{2-x}M_xO_4$ (M = transition metal)[11] in the spinel phase, $LiMPO_4$ (M = Mn, Fe, Co, Ni)[11] with an olivine structure, TiO_2 with an anatase structure, and TiS_2, $LiCoO_2$, and $LiMnO_2$ with a layer structure.[11] Recently, we designed and synthesized a CGMN with a high thermal stability that contains a homogeneous, nanocrystalline metal oxide assembled in the framework.[12] Herein, we have chosen TiO_2 as the nanocrystalline transition-metal oxide for potential application as the anode of a lithium-based rechargeable battery.[13–15] In addition, a phosphate-based glass was selected as the glass phase to construct TiO_2–P_2O_5 (CGMN).[12]

The TiO_2–P_2O_5 CGMN is a two-dimensional, hexagonal mesostructure with a unit cell length of 11 nm (Figure 2a). It contains uniform pores with a diameter of 4 nm (see TEM image in Figure 2b) and a framework of 5-nm width that are co-assembled with 3–5-nm nanocrystalline anatase TiO_2 particles (see WAXRD image in the inset of Figure 2a and the high-resolution TEM image in Figure 2c). Such a CGMN has five novel characteristics—uniform nanochannels, a uniform nanoframework, a high surface area, a glass-phase buffer layer, and an electronic network path—that suggest its possible use as an electrode to overcome the main problems for a lithium-based storage device with both high power and high energy densities.

The first two novel characteristics of the CGMN are the uniform nanochannel and the framework with an electrode-active nanocrystal. A uniform channel 4 nm wide is large enough to be easily accessed by an electrolyte solution that includes large organic molecules such as ethylene carbonate (EC) or dimethoxyl carbonate. Li^+ ions and counteranions such as ClO_4^- can be transported inside the CGMN and react with the nanocrystalline metal-oxide framework, which is assembled from 3–5 nm TiO_2 anatase nanocrystals. In this case, the required diffusion length for the lithium ions could be reduced to half of the frame-wall thickness, about 2 nm (Figure 1b). This arrangement guarantees that a rapid charge–discharge process will be complete in a very short period of time, which results in a high specific capacity even at

 © 2005 Wiley-VCH Verlag GmbH & Co. KGaA, Weinheim

a high charge–discharge current. The charge–discharge profiles of the TiO_2–P_2O_5 CGMN at different current densities are shown in Figure 3a. Both the discharge and charge processes show similar specific capacities of about 260 mA h g^{-1} at a current density of 10 A g^{-1}. We assume that TiO_2 is the only active material, even though acetylene/black carbon (AB) and P_2O_5 are present in the electrode materials, since the specific capacities of pure AB and pure P_2O_5 are too small to be measured at a current density of 10 A g^{-1}.[16] The insertion and extraction process can be described by $TiO_2 + x(Li^+ + e^-) \rightleftharpoons Li_xTiO_2$.[13,15] The specific capacity of traditional anatase (TiO_2) dramatically decreases at a high current density because the over-potential from the various polarizations is very large at high current density.

We also investigated traditional anatase (TiO_2) which was purchased in powder (PP) form with a particle size of several hundred nanometers. The specific capacity of this powder was less than 1 mA h g^{-1} at 10 A g^{-1}. A mesoporous TiO_2 powder (MP), which was synthesized by the method of Stucky and coworkers,[17] had an activity of about 18 mA h g^{-1} at 10 A g^{-1} (Figure 3c). In our CGMN system we find a specific capacity of 260 mA h g^{-1} for anatase TiO_2 at a current density of 10 A g^{-1}. This extremely large value corresponds to $x = 0.76$ for Li_xTiO_2, which is much larger than the highest value ($x = 0.5$; 167.5 mA h g^{-1}) previously reported for anatase Li_xTiO_2.[15] It has been reported recently that there are two reduction/oxidation models for self-ordered, mesoporous TiO_2:[18] one is the traditional insertion/extraction of Li^+ ions into Li_xTiO_2, and the other is surface storage of Li, which has been observed in mesoporous, nanosheet, and nanorod TiO_2,[18] although the exact mechanism is still unknown. In the cyclic voltammogram (CV) of the TiO_2–P_2O_5 CGMN, the peaks of both Li^+ ion insertion/extraction and surface storage of Li are observed at 1.7/1.9 eV and 1.5/1.6 eV (Li^+/Li), respectively (Figure 3b). It is therefore reasonable for the total specific energy capacity of the TiO_2–P_2O_5 CGMN to be much larger than the maximum value of $x = 0.5$ for insertion of Li^+ ions into anatase TiO_2.

The third novel characteristic of the CGMN is its high surface area (about 280 $m^2 g^{-1}$),[12] which reduces the specific current density from I/A_{area} to I/S_{area}, where A_{area} and S_{area} are the areas of the nickel-mesh electrode and the surface area of the TiO_2–P_2O_5 CGMN, respectively. If it is considered that A_{area} (0.25 cm^2) and S_{area} (2.8×10^3 cm^2 for 1 mg of the TiO_2–P_2O_5 CGMN) differ by a factor of 10^4, the effective current density (I/S_{area}) is about 10^{-4} of the practical applied current density of an electrode (I/A_{area}); this is why the specific capacity remains very high even at the high charge–discharge

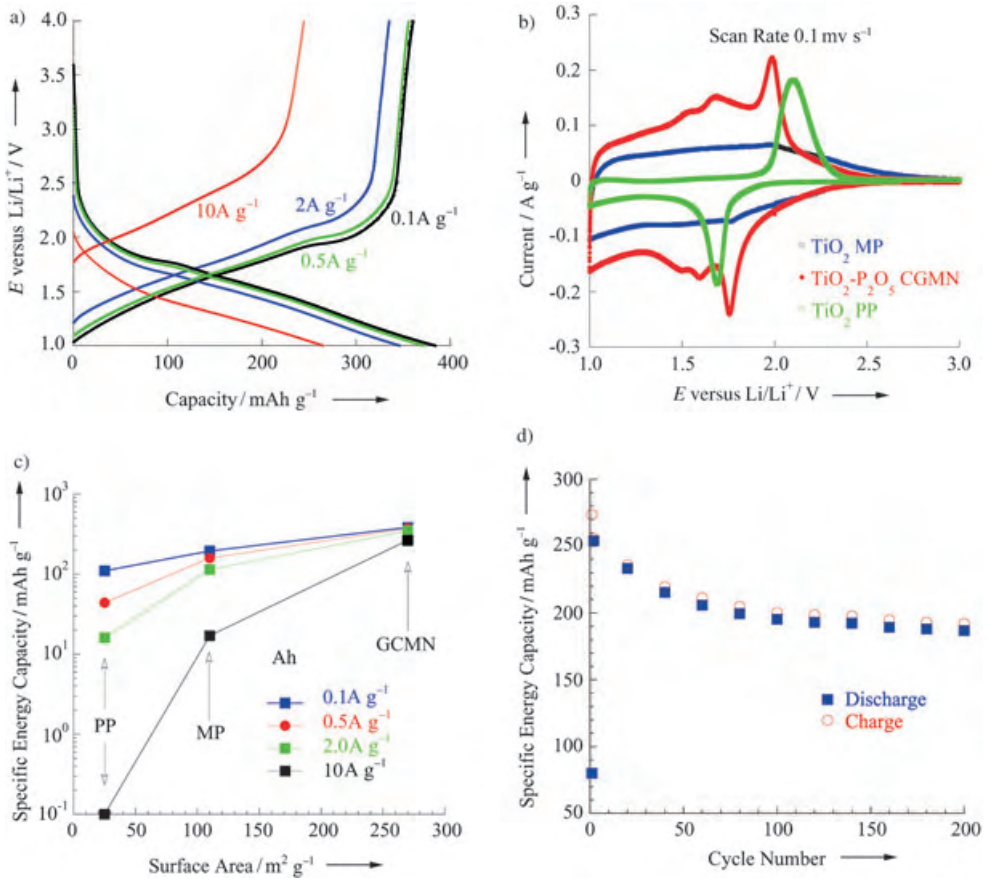


Figure 3. a) The second cycle charge–discharge profiles of the TiO_2–P_2O_5 CGMN in the potential range from 1.0 to 4.0 V (versus Li^+/Li) with current densities of 0.1, 0.5, 2, and 10 A g^{-1} based on active TiO_2. b) The cyclic voltammetry (CV) curves of the TiO_2–P_2O_5 CGMN, TiO_2 MP, and TiO_2 PP at a scan speed of 0.1 mv s^{-1} in a potential window from 1.0 to 3.5 eV (versus Li^+/Li). c) The relationship between specific energy capacity and the surface area at current densities of 10, 2, 0.5, and 0.1 A g^{-1}. d) The performance cycle of discharge and charge capacities of TiO_2–P_2O_5 CGMN at a current density of 10 A g^{-1}.

 © 2005 Wiley-VCH Verlag GmbH & Co. KGaA, Weinheim

current density for the TiO_2-P_2O_5 CGMN with a high surface area (Figure 3c). It is also the reason why the specific capacity dramatically decreases at high charge–discharge current density for TiO_2 PP with a low surface area of about 25 $m^2 g^{-1}$ (Figure 3c). The high specific capacity at a high charge–discharge current density is therefore a result of the decrease in the required diffusion length (about 2 nm) and of the decrease in the effective current density (I/S_{area}).

The fourth novel characteristic is that the P_2O_5-glass phase forms a buffer layer between active nanocrystalline TiO_2 blocks that helps to relax the stress because of the insertion and extraction of lithium ions and thereby improves the performance cycle under rapid charge–discharge conditions. Lithium insertion and extraction generally results in a small change in the crystalline lattice length. This small change destroys both the nanoarchitecture and the crystalline structure, and results in poor performance after a number of charge–discharge cycles.[4] Our TiO_2–P_2O_5 CGMN gives good performance up to 200 cycles, with a specific capacity of about 195 mA h g^{-1} (see Figure 3d), and has a high coulomb efficiency of 96%. The specific capacity remains at about 150 mA h g^{-1}, with a high coulomb efficiency of 93%, up to the 800th cycle.

The final and very important characteristic of the CGMN is that the P_2O_5-glass phase can also act as a host for electronic conductive oxide dopants to build up an ideal electronic path throughout the material. Recently, a large number of binary and ternary glasses with electronic and ionic conductivities (containing transition-metal oxides) have been investigated for possible practical applications as solid-state lithium-ion batteries and integrated microbatteries,[19,20] We have doped metal oxides (M_xO_y; Li_2O, NiO, CuO, Fe_2O_3, MnO_2, SnO_2, WO_3) into P_2O_5 to form ternary M_xO_y–P_2O_5 composites containing some residual TiO_2-glass network.[12] The incorporation of an electronically conductive oxide, such as CuO or SnO_2, into the three-dimensional network of the P_2O_5-glass phase, to form a multicomponent P_2O_5–CuO–TiO_2 or P_2O_5–SnO_2–TiO_2 glass path inside the TiO_2–P_2O_5–CuO or TiO_2–P_2O_5–SnO_2 CGMN respectively, improved the electronic conductivity of TiO_2–P_2O_5 CGMN. According to inductively coupled plasma (ICP) analysis, the incorporation ratio of CuO or SnO_2 into P_2O_5 was about 0.20 and 0.44, respectively. These values are high enough to form an electronically conductive CuO or SnO_2 path in the P_2O_5-glass network with a percolation-threshold value in the range 0.13–0.18.[21] We also synthesized a TiO_2–SiO_2 CGMN system.[12] The experimental results show this system has a worse performance than TiO_2–P_2O_5 CGMN,[16] which indicates that SiO_2-glass networks are poorer electronic conductors than a P_2O_5-glass network. CuO or SnO_2 is incorporated into the P_2O_5-glass phase as a result of the interaction of the P=O bond, in the form of PO_4 anions, with metal ions.[12,22] Moreover, during the discharge process, when lithium ions insert into the active materials, some lithium ions also diffuse into the glass networks to form multicomponent Li_2O–CuO–P_2O_5–TiO_2 and Li_2O–SnO_2–P_2O_5–TiO_2 glassy network systems. In fact, according to recent results,[20] ternary and multicomponent glasses show both an electronic conductive path, because of the presence of transition-metal oxides, and an ionic path, arising from the alkali-metal oxides. Both these factors improve the lithium storage performance. For example, the specific capacity of a TiO_2–P_2O_5 CGMN (65 mA h g^{-1}) at a current density of 20 A g^{-1} is improved significantly to 195 mA h g^{-1} for TiO_2–P_2O_5–SnO_2 CGMN and 270 mA h g^{-1} for TiO_2–P_2O_5–CuO (Figure 4a). The charge–discharge profiles of the TiO_2–P_2O_5–SnO_2 CGMN at current densities of 10 A g^{-1}, 20 A g^{-1}, and 50 A g^{-1} are 230 mA h g^{-1}, 195 mA h g^{-1}, and 178 mA h g^{-1}, respectively (Figure 4a).

The relationship between the specific capacities of discharge and the current densities of the TiO_2 PP, TiO_2 MP, TiO_2–P_2O_5 CGMN, TiO_2–P_2O_5–CuO CGMN, and TiO_2–P_2O_5–SnO_2 CGMN are shown in Figure 4b. The specific capacity of traditional TiO_2 anatase particles at 10 A g^{-1} is increased several hundred times upon incorporation into a TiO_2–P_2O_5 CGMN. Furthermore, the specific capacity of the TiO_2–P_2O_5 CGMN at 20 A g^{-1} is further improved by a factor of about four or five upon formation of a TiO_2-P_2O_5-CuO CGMN or TiO_2-P_2O_5-SnO_2 CGMN.

The energy density E and power density P in a constant-current charge–discharge can be written as: $E = \int_0^{\tau_d} \frac{IV}{m} dt = \frac{I}{m} V_{av} \tau_d$ and $P = \frac{1}{\tau_d} \int_0^{\tau_d} \frac{IV}{m} dt = \frac{I}{m} V_{av}$, where, I, V, and m are the current, cell voltage, and mass of active material, respectively. τ_d and V_{av} are the average discharge (or charge) time and average potential, respectively. For the power-density and energy-density calculations, we assume that the TiO_2–P_2O_5 CGMN will be used as the anode with V_2O_5[3] as the cathode (ca. 3.5 V versus Li/Li^+, 250 mA h g^{-1} at 10 A g^{-1}). These equations give a value of V_{av} of 1.65 V. The weight, including all other parts of the battery such as the current collector, electrolytes, and chassis, is assumed to be five times that of the active materials. The calculated[23] energy densities and power densities of these CGMN lithium-based storage devices are higher than the targets of PNGV (the Partnership for a New Generation of Vehicle)[1] (Figure 4c).

The experimental results described here show that the five novel characteristics—uniform nanochannels, uniform nanoframework, high surface area, glass-phase buffer layer, and electronic network path—of this GCMN suggest its suitability for the development of high power and high energy density lithium-based storage devices. These results are interesting with respect to both fundamental research and potential applications. We first introduced a lithium-ion pathway through the nanochannels and an electronic pathway through the three-dimensional, glass-phase network by assembling nanocrystals into the electrode materials to give a GCMN structure that is able to undergo a rapid charge–discharge process, which differs from the traditional concept of lithium-ion insertion/extraction into bulk crystalline materials. We hope this concept can be extended to electrode-active materials such as Si and Sn, for the anode, and LiM_2O_4 (M = transition metal) and $LiMPO_4$ (M = Mn, Fe, Co, Ni, etc) for the cathode, by functionalization with Si, Sn, LiM_2O_4, and $LiMPO_4$ CGMNs. This will be of benefit not only to the EV industry, but also to any other mobile or portable electronic device, for saving charging time.

 © 2005 Wiley-VCH Verlag GmbH & Co. KGaA, Weinheim

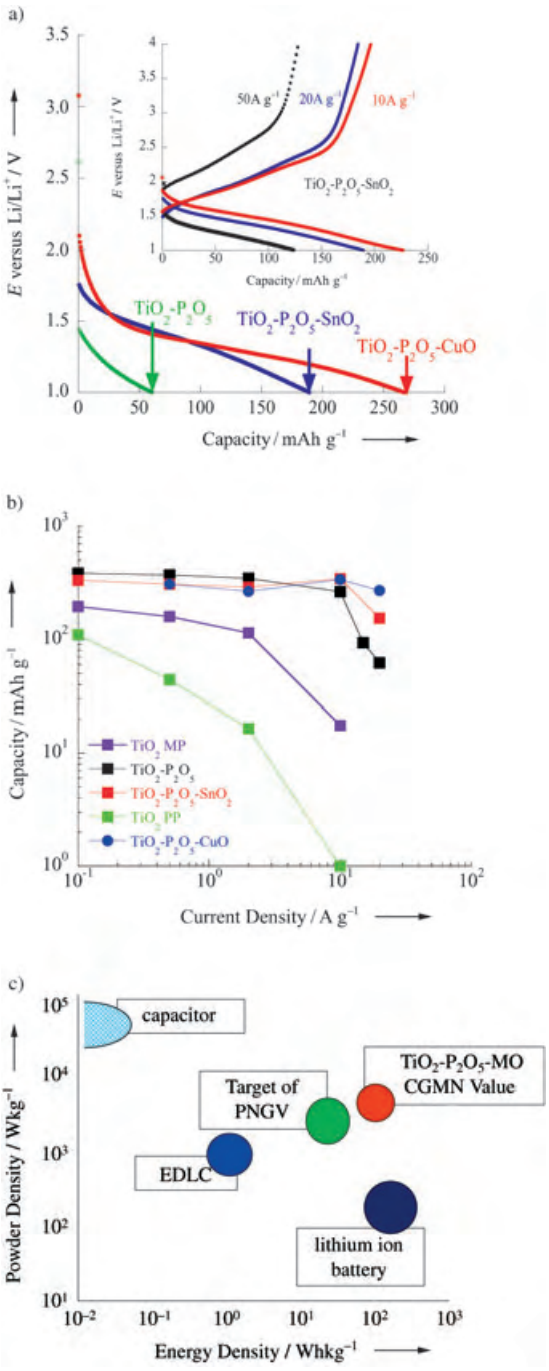


Figure 4. a) The charge–discharge profiles of the TiO_2–P_2O_5 CGMN, TiO_2–P_2O_5–SnO_2 CGMN and TiO_2–P_2O_5–CuO CGMN at 20 $A\,g^{-1}$. The inset shows that the specific capacity of the TiO_2–P_2O_5–SnO_2 CGMN at current densities of 10 $A\,g^{-1}$, 20 $A\,g^{-1}$, and 50 $A\,g^{-1}$ is 230, 195, and 178 $mAh\,g^{-1}$, respectively. b) The relationship between the specific discharge capacities and the current densities of TiO_2–P_2O_5 CGMN, TiO_2–P_2O_5–SnO_2 CGMN, and TiO_2–P_2O_5–CuO CGMN. c) A Regone plot showing the position of the power and energy densities of CGMN, including all components, as an energy-storage device, relative to EDLC, a capacitor, a traditional rechargeable lithium battery, and the PNGV target.

Experimental Section

Titanium tetraisopropoxide (TTIP, 2.5 g) was added to a solution of triblock copolymer $HO(CH_2CH_2O)_{20}(CH_2CH(CH_3)O)_{70}(CH_2CH_2O)_{20}H$ (P123; 0.8–1.2 g) in ethanol (8–10 g). The mixture was stirred for 10 mins and 0.5 N HCl (1 g) added to form a transparent solution. $PO(C_2H_5)_3$ (1 g) was then added to this solution. In the case of doped materials, 10 mol % $CuCl_2$ or $SnCl_4$ was added with stirring. The multicomponent mixtures were stirred in a sealed bottle for 20 h. The transparent sols were then gelled in an open petri dish at room temperature in air for 5 days to give a transparent gel that was then dried at 80 °C for 7 days. The as-synthesized samples were calcined at 400 °C for 6 h to remove any organic species and afforded inorganic amorphous solids. These products were subsequently annealed at 500 °C for 1–2 h under air to form the desired nanocomposites.

Powder X-ray diffraction (XRD) patterns were recorded on a MacScience-M03XHF22 diffractometer using $Cu_{K\alpha}$ irradiation. The nitrogen adsorption/desorption isotherm curve was recorded at 77 K on a Belsorpt-23SA volumetric adsorption analyzer. The BET surface area was calculated from the adsorption/desorption isotherm curve. TEM studies were carried out at 200 Kev on a Hitachi-800 instrument. Inductively coupled plasma analyses were performed on a Therm Jarrell Ash IRIS/AP instrument.

For electrochemical measurement, the samples were heated at 120 °C in a vacuum for 5 h to remove adsorbed water on the surface of the mesopore. They were then mixed and ground with 5 wt % teflon (poly(tetrafluoroethylene)) powder as a binder and 45 wt % acetylene back carbon (AB) powder as the conductive assistant materials. The mixture was spread and pressed on a 0.25 cm^2 nickel mesh (100 mesh) as the working electrode (WE). The reference (RE) and counter electrode (CE) were prepared by spreading and pressing lithium metals on such a nickel mesh. The electrolyte was 1 M $LiClO_4$ in EC + DMC (EC/DMC = 1/1 v/v). Cell assembly was carried out in a glove box under an argon atmosphere. The charge-discharge performance of the material was investigated in such a three-electrode cell using lithium metal as the counter and reference electrodes.

Cyclic voltametry studies were performed over a potential range of 1.0 to 3.5 V (Li^+/Li) at scan rates of 0.1, 0.5, 2, 10, and 50 $mv\,s^{-1}$. Galvanostatic discharge-charge was performed in a potential range of 1.0 to 4.0 V (Li^+/Li) under constant currents of 0.1, 0.5, 2, 10, 20, and 50 $A\,g^{-1}$. The circuit was kept open for 10 min after each discharge and charge. The weight was based on the active materials (TiO_2, excluding P_2O_5 and AB), unless otherwise noted. The TiO_2 content is about 85 wt % in TiO_2–P_2O_5 CGMN.

Received: June 11, 2004
Revised: August 26, 2004
Published online: December 21, 2004

Keywords: conducting materials · lithium storage · materials science · mesoporous materials · nanostructures

[1] B. Scrosati, *Nature* **1995**, *373*, 557; R. F. Nelson, *J. Power Sources* **2000**, *91*, 2.
[2] K. Sawai, T. Ohzuku, *J. Electrochem. Soc.* **1997**, *144*, 988.
[3] T. Kudo, Y. Ikeda, T. Watanabe, M. Hibino, M. Miyayama, H. Abe, K. Kajita, *Solid State Ionics* **2002**, *152–153*, 833.
[4] M. Hibino, H. Kawaoka, H. S. Zhou, I. Honma, *J. Power Sources* **2003**, *124*, 143; H. Kawaoka, M. Hibino, H. S. Zhou, I. Honma, *J. Power Sources* **2004**, *125*, 85.
[5] L. Kavan, J. Prochazka, T. M. Spitler, M. Kalbac, M. Zukalova, T. Drezen, M. Gratzel, *J. Electrochem. Soc.* **2003**, *150*, A1000.
[6] J. Bard, L. R. Faulkner, *Electrochemical Methods*, Wiley, New York, **1980**.
[7] C. T. Kresge, M. E. Leonowicz, W. J. Roth, J. C. Vartuli, J. S. Beck, *Nature* **1992**, *359*, 710.
[8] M. E. Davis, *Nature* **2002**, *417*, 813; A. Stein, *Adv. Mater.* **2003**, *15*, 763; R. D. Miller, *Science* **1999**, *286*, 421; U. Bach, D. Lupo, P.

 © 2005 Wiley-VCH Verlag GmbH & Co. KGaA, Weinheim

Comte, J. E. Moster, F. Weissortel, J. Salbeck, H. Spreitzer, M. Gratzel, *Nature* **1998**, *395*, 583.
[9] T. Yamada, H. S. Zhou, H. Uchida, M. Tomida, Y. Ueno, T. Ichino, I. Honma, K. Asai, T. Katsube, *Adv. Mater.* **2002**, *14*, 812; Y. Ueno, T. Horiuchi, M. Tomita, O. Niwa, H. S. Zhou, T. Yamada, I. Honma, *Anal. Chem.* **2002**, *74*, 5257.
[10] H. S. Zhou, S. Zhu, M. Hibino, I. Honma, M. Ichihara, *Adv. Mater.* **2003**, *15*, 2107.
[11] M. Winter, J. O. Besenhard, M. E. Spahr, P. Novak, *Adv. Mater.* **1998**, *10*, 725; M. Wakihara, O. Yamamoto, *Lithium Ion Batteries*, Wiley-VCH, Weinheim, **1988**.
[12] D. Li, H. S. Zhou, I. Honma, *Nature Mater.* **2004**, *3*, 65.
[13] L. Kavan, M. Gratzel, S. E. Gilbert, C. Klemenz, H. J. Scheel, *J. Am. Chem. Soc.* **1996**, *118*, 6716.
[14] J. M. Tarascon, M. Armand, *Nature*, **2001**, *414*, 359; S. Y. Huang, L. Kavan, I. Exnar, M. J. Gratzel, *J. Electrochem. Soc.* **1995**, *142*, L142.
[15] M. Wagemaker, A. P. M. Kentgens, F. M. Mulder, *Nature* **2002**, *418*, 397.
[16] H. S. Zhou, D. Li, M. Hibino, I. Honma, unpublished results.
[17] P. Yang, D. Zhao, D. I. Margolese, B. F. Chmelka, G. D. Stucky, *Nature* **1998**, *396*, 152; P. Yang, D. Zhao, D. I. Margolese, B. F. Chmelka, G. D. Stucky, *Chem. Mater.* **1999**, *11*, 2813.
[18] L. Kavan, J. Rathousky, M. Gratzel, V. Shklover, A. Zukal, *J. Phys. Chem. B* **2000**, *104*, 12012; L. Kavan, J. Rathousky, M. Gratzel, V. Shklover, A. Zukal, *Microporous Mesoporous Mater.* **2001**, *44–45*, 653; L. Kavan, M. Kalbac, M. Zukalova, I. Exnar, V. Lorenzen, R. Nesper, M. Gratzel, *Chem. Mater.* **2004**, *16*, 477; X. Gao, H. Zhu, G. Pan, S. Ye, Y. Lan, F. Wu, D. Song, *J. Phys. Chem. B* **2004**, *108*, 2868; M. Wagemaker, G. J. Kearley, A. A. VanWell, H. Mutka, F. M. Mulder, *J. Am. Chem. Soc.* **2003**, *125*, 840.
[19] M. M. El-Desoky, *Mater. Chem. Phys.* **2002**, *73*, 259; L. Bih, M. El Omari, J. M. Reau, A. Nadiri, A. Yacoubi, M. Haddad, *Mater. Lett.* **2001**, *50*, 308.
[20] J. E. Garbarczyk, M. Wasiucionek, P. Machowski, W. Jakubowski, *Solid State Ionics* **1999**, *119*, 9; L. Bih, M. El Omari, J. M. Reau, M. Haddad, D. Boudlich, A. Yacoubi, A. Nadiri, *Solid State Ionics* **2000**, *132*, 71.
[21] D. S. McLachlan, M. Blaszkiewicz, R. E. Newnham, *J. Am. Ceram. Soc.* **1990**, *73*, 2187.
[22] The typical small-angle X-ray diffraction (SAXRD) peaks from the hexagonal mesoporous structure and the broad wide-angle X-ray diffraction (WAXRD) peaks of TiO_2 anatase nanocrystals are still clearly present after incorporation of CuO or SnO_2 into the P_2O_5-glass phase. We did not observe any compounds with the structure $Ti_{1-x}Cu_{2x}O_2$ or $Ti_{1-x}Sn_xO_2$ in the TiO_2–P_2O_5–CuO or TiO_2–P_2O_5–SnO_2 CGMNs, respectively.
[23] B. E. Conway, *Electrochemical Supercapacitors*, Kluwer Academic Publishers, Plenum, New York, **1999**.

 © 2005 Wiley-VCH Verlag GmbH & Co. KGaA, Weinheim

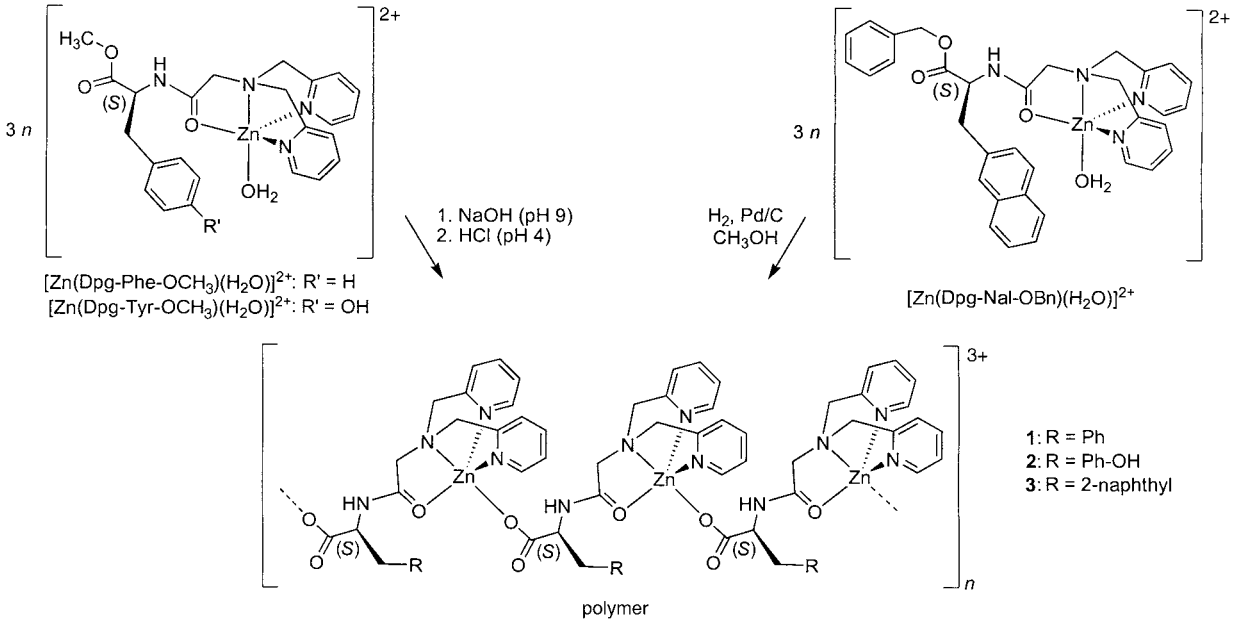
Coordination Polymers

The Deposition of Metallopeptide-Based Coordination Polymers on Graphite Substrates: Effects of Side-Chain Functional Groups and Local Surface Structure**

Slobodan Novokmet, Mohammad S. Alam, Viatcheslav Dremov, Frank W. Heinemann, Paul Müller, and Ralf Alsfasser**

Coordination polymers have attracted much attention in the development of new functional materials[1] owing to their many interesting properties such as zeolitic behavior,[2] conductivity,[3] luminescence,[4] magnetism,[5] spin-crossover,[6] and nonlinear optical effects.[7] Stimulated by possible applications, scientists have made impressive progress in the so-called crystal engineering of solid materials.[8] Yet the equally important controlled assembly of metal-organic polymers on solid surfaces is in its infancy.[9] A central focus of this research must be the investigation of elementary structure-formation processes on substrate surfaces. With a series of structurally similar polymers containing different aromatic amino acid building blocks, we were able to study both the effects of substituents and local surface properties on the deposition of coordination polymers on highly ordered pyrolytic graphite (HOPG).

Scheme 1 illustrates our synthetic approach. Cleavage of the methyl ester or benzyl ester protecting groups in zinc complexes of dipicolylglycyl (Dpg) peptides results in the formation of a free carboxylate function, which binds to the metal ion under slightly acidic conditions. The coordination polymers that form precipitate from aqueous solutions. We have already reported on the synthesis and structure of $[\{Zn(Dpg\text{-}Phe\text{-}O)\}_n](CF_3SO_3)_n$ (**1**; Phe = phenylalanine).[10] Here we present two new compounds, $[\{Zn(Dpg\text{-}Tyr\text{-}O)\}_n](CF_3SO_3)_n$ (Tyr = tyrosine, **2**) and $[\{Zn(Dpg\text{-}Nal\text{-}O)\}_n](CF_3SO_3)_n$ (Nal = 2-naphthylalanine, **3**). Ortep plots of their structures are given in Figures 1 and 2. The cationic polymers in **1**–**3** are very similar. In all cases right-handed antiparallel-packed helices are found, in which three zinc complex fragments make up each turn. Only the pitch increases from 14.80 Å in **1** to 14.83 Å in **2** and 15.06 Å in **3**, most likely as a consequence of the larger aryl substituents.



Scheme 1. Synthesis of the homochiral helical coordination polymers **1**–**3**.

The structural similarity of **1**–**3** was a desired feature since it enabled us to compare the effects of different aromatic side chains on the deposition of helical coordination polymers on HOPG by scanning tunneling microscopy (STM). It turned out that the phenylalanine and napthylalanine derivatives **1** and **3** do not form sufficiently stable patterns. Only the tyrosine derivative **2** gave satisfactory results. The phenolic tyrosyl OH groups seem to be necessary for a sufficient grip on the substrate surface. Samples of **2** on HOPG were

[*] M. S. Alam, Dr. V. Dremov, Prof. Dr. P. Müller
Physikalisches Institut III
Universität Erlangen-Nürnberg
Erwin-Rommel-Strasse 1, 91058 Erlangen (Germany)
Fax: (+49) 9131-15-249
E-mail: phm@physik.uni-erlangen.de
Priv.-Doz. Dr. R. Alsfasser
Institut für anorganische Chemie
Universität Freiburg
Albertstrasse 21, 79104 Freiburg (Germany)
Fax: (+49) 761-203-6012
E-mail: ralf.alsfasser@ac.uni-freiburg.de
S. Novokmet, Dr. F. W. Heinemann
Institut für anorganische Chemie
Universität Erlangen-Nürnberg
Egerlandstrasse 1, 91058 Erlangen (Germany)

[**] We gratefully acknowledge support from the SFB 583.

 DOI: 10.1002/anie.200461274 © 2005 Wiley-VCH Verlag GmbH & Co. KGaA, Weinheim

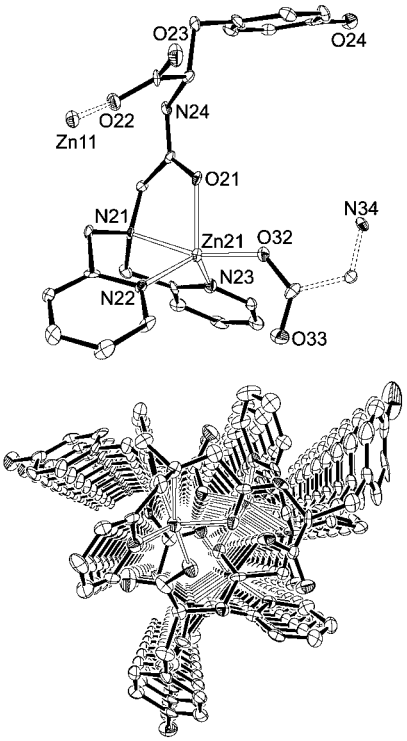


Figure 1. Top: Ortep plot (ellipsoids at 30% probability) of a single cation in **2**; shown is the second complex in the trimeric asymmetric unit. Bottom: View along the 100 axis of the helical polymer.

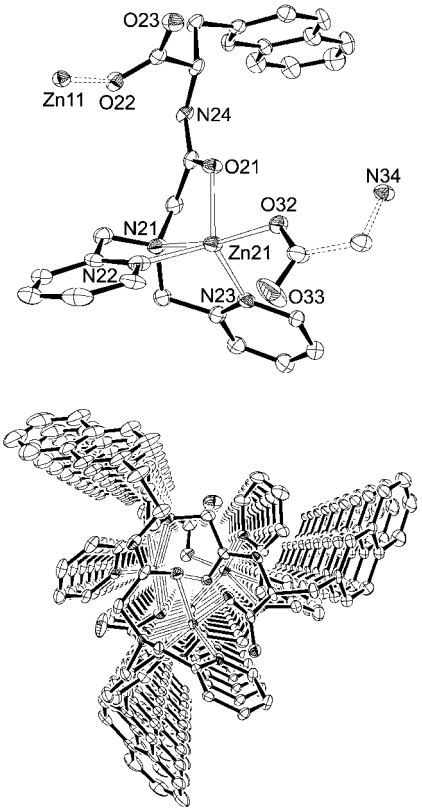


Figure 2. Top: Ortep plot (ellipsoids at 30% probability) of a single cation in **3**; shown is the second complex in the trimeric asymmetric unit. Bottom: View along the 100 axis of the helical polymer.

conveniently prepared by allowing 10^{-9} M aqueous solutions of pH 5 to 6 to evaporate under air. Figure 3 shows that the polymer adopts two different structures depending on the local environment. A double-helical plait is formed on

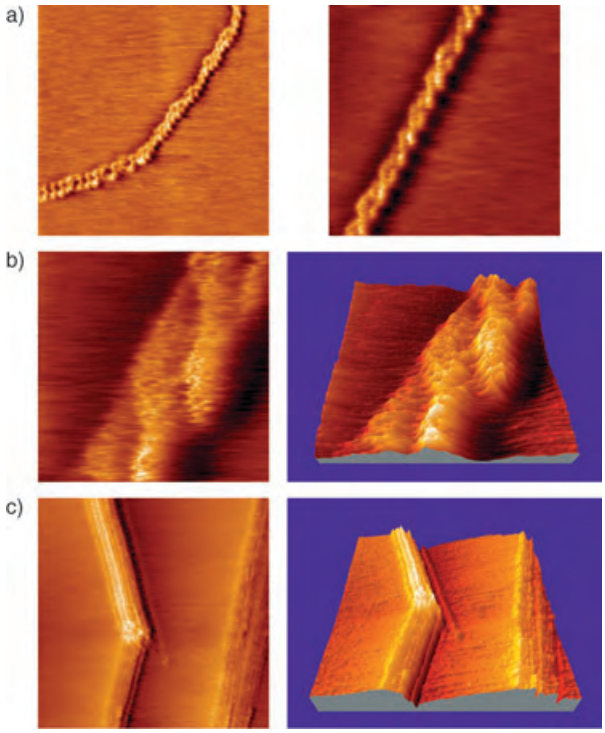


Figure 3. STM topographies (HOPG) showing a) the formation of double-helical superstructures on two different undisturbed surface areas (left: 108×108 nm^2; right: 42×42 nm^2); b) a 10×10 nm^2 detail of a double-helix (left: 2D, right: 3D); and c) the aggregation of linear polymer strands at steps on the surface (left: 2D, right: 3D; 100×100 nm^2).

undisturbed flat surface areas (Figure 3a and b). The distance between two crossing points is approximately 6 nm. Each of the two intertwined strands has a diameter of roughly 13.8 Å, indicating that it consists of a single helical coordination polymer. Interestingly, the double-helical superstructure has a left-handed chirality that is opposite to the right-handed molecular helicity. Double helices most probably form because a flat surface does not provide any means of stabilization for the polymer, and intermolecular interactions are dominant. However, the macromolecules show a preference for steps, which may be regarded as one-dimensional distortions. Figure 3c shows that the polymer **2** nicely decorates a step and even follows a sharp kink. The structure has changed drastically, presumably as a consequence of stronger interactions with the distorted surface. Linearly stretched polymer strands are formed. Single strands are not resolved in Figure 3c but the width of approximately 11 nm indicates that roughly eight helices are packed together, most likely in the same antiparallel fashion as that observed in the crystal structure.

In a few cases we were able to map single linear polymer strands with high magnification (Figure 4a). Again, the width

 © 2005 Wiley-VCH Verlag GmbH & Co. KGaA, Weinheim

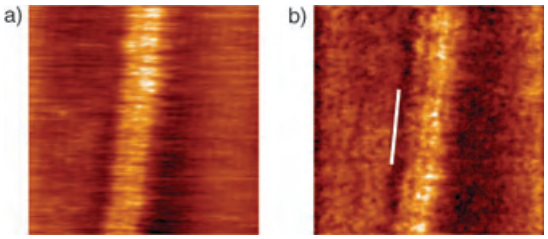
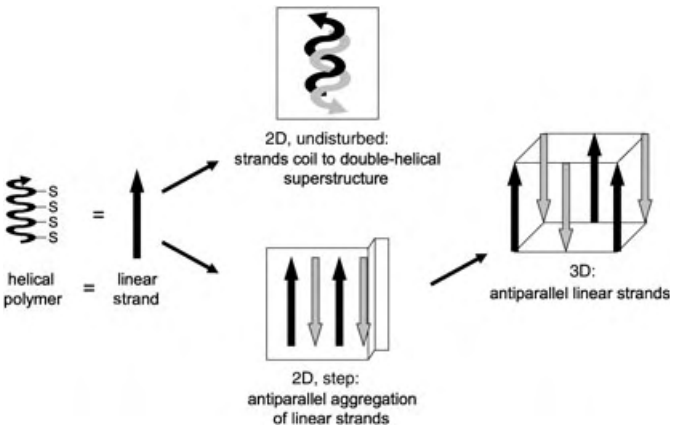


Figure 4. Topography and CITS image of a linear polymer strand recorded simultaneously. $V = 72.9$ mV, tunneling current = 0.2 nA. a) Topography (5×5 nm^2), b) current image (5×5 nm^2) at -135 mV.

of the structure conforms to the diameter of a single molecular strand. Figure 4b depicts a CITS image recorded simultaneously. CITS (current imaging tunneling spectroscopy) records tunneling current–voltage characteristics at every point of the topography map. The tip-to-sample distance is defined by the topography parameters. CITS reveals a three-dimensional data set of current and bias voltage vs. position. Usually cross sections at some selected bias points are plotted as current images. The current contrast changes significantly when at certain bias values new molecular energy levels come into play, thus enhancing the information obtained from topography alone. Figure 4b is a current image taken at a tunneling bias of -135 mV. One clearly recognizes a periodicity along the strand which conforms to the length of a single molecule (14.85 Å, see the scale bar in Figure 4b).

As a control, we prepared and investigated samples of the amino acid ligand alone under conditions similar to those employed with the polymer solution. The structures formed are completely different from those of the coordination polymer. Linear arrangements of single or multiple strands of molecules are observed. Helical topologies are not detected. For these low concentrations the surface is rather empty. Effects resulting from the self-organization of dense molecular layers are certainly not expected.[11]

Scheme 2 summarizes our findings. On undisturbed surfaces two right-handed homochiral helical coordination polymers self-assemble to form a left-handed double-helical superstructure. In contrast, steps on the surface induce the formation of linearly stretched helical single strands which aggregate to two-dimensional ribbons. The latter structure resembles a two-dimensional slice through the three-dimensional crystal structure of **2** and indicates that crystal growth starts at surface irregularities. These results shed first light on some elementary steps during the pattern formation of metal-organic polymers on solid substrate surfaces.



Scheme 2. Structure-formation processes in the coordination polymer **2**. Linear strands are made up of from helical chains. On undisturbed surfaces these strands coil to form a double-helical superstructure. Steps in the surface result in an antiparallel aggregation of linear strands. Layers of such sheets build a three-dimensional crystal.

Experimental Section

$[Zn(Dpg\text{-}Nal\text{-}OBn)(H_2O)](CF_3SO_3)_2$ and $[Zn(Dpg\text{-}Tyr\text{-}OCH_3)(H_2O)](CF_3SO_3)_2$: Solid $Zn(CF_3SO_3)_2$ was added in one portion to a stirred solution of the designated ligand in CH_3CN. The solution was stirred overnight and the solvent was removed under vacuum. Addition of CH_2Cl_2 resulted in the formation of a cloudy solution, which was left in a refrigerator at $-20\,^\circ$C overnight in order to complete the precipitation of unchanged $Zn(CF_3SO_3)_2$. Filtration and removal of all solvent under vacuum provided the product as a white solid.

$[Zn(Dpg\text{-}Tyr\text{-}OCH_3)(H_2O)](CF_3SO_3)_2$**:** 1.56 g (4.30 mmol) $Zn(CF_3SO_3)_2$, 1.87 g (4.30 mmol) Dpg-Tyr-OCH_3, 100 mL CH_3CN, 50 mL CH_2Cl_2. Yield: 2.80 g, 3.43 mmol, 79.80 %. Elemental analysis (%) calcd. for $C_{26}H_{28}F_6N_4O_{11}S_2Zn$ (816.03 g mol^{-1}): C 38.27, H 3.46, N 6.87, S 7.86; found: C 39.26, H 3.59, N 6.66, S 7.63; FAB-MS (nitrobenzyl alcohol): $m/z = 649$ $[M^+ - CF_3SO_3 - H_2O]$; ^{1}H NMR (300 MHz, CD_3OD): $\delta = 2.58$ (dd, 1H, $^\beta CH_2$), 2.95 (dd, 1H, $^\beta CH_2$), 3.58 (s, 3H, OCH_3), 3.61 (d, 1H, $C(O)CH_2$), 3.73 (d, 1H, $C(O)CH_2$), 4.39–4.54 (m, 5H, $pyCH_2$, $^\alpha CH$), 6.50 (m, 2H, $H2{,}6_{PhOH}$), 6.69 (m, $H3{,}5_{PhOH}$), 7.66 (m, 4H, $H3{,}5_{py}$), 8.13 (m, 2H, $H4_{py}$), 8.54 (m, 1H, $H5_{py}$), 8.60 ppm (m, 1H, $H6_{py}$).

$[Zn(Dpg\text{-}Nal\text{-}OBn)(H_2O)](CF_3SO_3)_2$: 1.33 g (3.67 mmol) $Zn(CF_3SO_3)_2$, 2.00 g (3.67 mmol) Dpg-Nal-OBn, 100 mL CH_3CN, 100 mL CH_2Cl_2. Yield: 3.00 g, 3.24 mmol, 88.26 %. Elemental analysis (%) calcd. for $C_{36}H_{34}F_6N_4O_{10}S_2Zn$ (926.19 g mol^{-1}): C 46.68, H 3.70, N 6.05, S 6.92; found: C 46.82, H 3.36, N 6.27, S 7.63; FAB-MS (nitrobenzyl alcohol): $m/z = 757$ $[M^+ - CF_3SO_3 - H_2O]$; ^{1}H NMR (300 MHz, $CDCl_3$): $\delta = 2.95$ (m, 1H, $^\beta CH_2$), 3.24–3.37 (m, 6H, $^\beta CH_2$, $C(O)CH_2$, *n* H_2O), 3.53 (d, 1H, $pyCH_2$), 3.75–3.96 (m, 2H, $pyCH_2$), 4.21 (d, 1H, $pyCH_2$), 4.96–5.07 (m, 3H, $^\alpha CH$, CH_2Bn), 6.80–7.84 (m, 18H, $5 \times H_{Bn}$, $7 \times H_{naphtyl}$, $H3{,}4{,}5_{py}$), 8.50 (d, 1H, $H6_{py}$), 8.70 (d, 1H, $H6_{py}$), 9.05 ppm (d, 1H, NH).

2: $[Zn(Dpg\text{-}Tyr\text{-}OCH_3)(H_2O)](CF_3SO_3)_2$ (1.00 g, 1.23 mmol) was dissolved in 30 mL H_2O. The pH was adjusted to 9.00 with 1 M NaOH. Consumption of base was monitored with a pH meter, and 1 M NaOH was used to keep the pH approximately constant at 9. The mixture was stirred at room temperature until the pH remained constant (ca. 2 d). Lowering the pH to 4 with 0.2 M HCl was followed by the immediate precipitation of the product $\mathbf{2}\cdot 3H_2O$, which was collected on a sintered glass filter and dried under vacuum (0.50 g, 0.77 mmol, 62.35 %). Elemental analysis (%) calcd. for $(C_{24}H_{23}F_3N_4O_7SZn)_3\cdot 3H_2O$ (1953.9 g mol^{-1}): C 44.22, H 3.87, N 8.59, S 4.92; found: C 44.15, H 3.75, N 8.54, S 4.96; FAB-MS (nitrobenzyl alcohol): $m/z = 483$ $[M^+ - CF_3SO_3]$; ^{1}H NMR (300 MHz, CD_3OD): $\delta = 3.03$ (dd, 1H, $^\beta CH_2$), 3.24 (dd, 1H, $^\beta CH_2$), 3.75 (s, 2H, $C(O)CH_2$), 3.95–4.39 (m, 4H, $pyCH_2$), 4.78 (m, 1H, $^\alpha CH$), 6.63 (m, 2H, $H2{,}6_{PhOH}$), 7.11 (m, 2H, $H3{,}5_{PhOH}$), 7.41–7.56 (m, 4H, $H3{,}5_{py}$), 8.05 (m, 2H, $H4_{py}$), 8.22 (br. s, 1H, 1 $H6_{py}$), 8.81 ppm (d, 1H, $H6_{py}$).

3: $[Zn(Dpg\text{-}Nal\text{-}OBn)(H_2O)](CF_3SO_3)_2$ (1.68 g, 1.81 mmol) was dissolved in 150 mL absolute CH_3OH. Palladium/charcoal was added as a catalyst. Hydrogen was passed over the stirred solution for 6 h at 70 °C. The mixture was filtered through celite and the solvent

 © 2005 Wiley-VCH Verlag GmbH & Co. KGaA, Weinheim

removed by rotary evaporation. After the residue had been washed with diethyl ether and dried under vacuum, the product **3**·4 H_2O was obtained as a white powder (1.15 g, 1.68 mmol, 92.62 %). Elemental analysis (%) calcd. for $(C_{28}H_{25}F_3N_4O_6SZn)_3 \cdot 4H_2O$ (2003.91 g mol^{-1}): C 48.60, H 4.03, N 8.10, S 4.63; found: C 48.67, H 3.96, N 8.14, S 4.48; FAB-MS (nitrobenzyl alcohol): $m/z = 667$ [M^+], 517 [$M^+ - CF_3SO_3$]; ^{1}H NMR (300 MHz, CD_3CN): $\delta = 3.00$ (dd, 1 H, $^{\beta}CH_2$), 3.36–3.68 (m, 4 H, $^{\beta}CH_2$, C(O)CH_2, pyCH_2), 3.95–4.23 (m, 3 H, pyCH_2), 4.92 (m, 1 H, $^{\alpha}$CH), 7.27–7.69 (m, 11 H, $H_{naphtyl}$, H3,5$_{py}$), 7.96 (m, 1 H, H4$_{py}$), 8.05 (m, 1 H, H4$_{py}$), 8.22 (d, 1 H, NH), 8.38 (d, 1 H, H6$_{py}$), 8.60 ppm (d, 1 H, H6$_{py}$).

X-ray structure analyses: Colorless needles of [{Zn(Dpg-Tyr-O)}$_3$]$(CF_3SO_3)_3 \cdot 8.5\,CH_3OH \cdot H_2O$ (**2**) were obtained after slow diffusion of diethyl ether into a solution of the product in CH_3OH over a period of several weeks at room temperature. Colorless crystals of [{Zn(Dpg-Nal-O)}$_3$]$(CF_3SO_3)_3 \cdot 2.5\,CH_3OH$ (**3**) were obtained in an analogous fashion. Suitable single crystals were embedded in protective perfluoropolyether oil, and data were collected at 100 K on a Bruker-Nonius KappaCCD diffractometer using $Mo_{K\alpha}$ radiation ($\lambda = 0.71073$ Å, graphite monochromator). Images were recorded using φ- and ω-rotations with a rotation angle of 1.0° for **2** and 1.4° for **3,** and an irradiation time of 100 s per frame for **2** and 210 s per frame for **3**. Lorentz, polarization, and semiempirical absorption corrections (SADABS on the basis of multiple scans) were applied. The structures were solved by direct methods and refined using full-matrix least-squares procedures on F^2 (SHELXTL NT 6.12). All non-hydrogen atoms were refined anisotropically (with the exception of some disordered CH_3OH molecules in **3** which were refined isotropically). All hydrogen atoms were geometrically positioned with isotropic displacement parameters being 1.2 or 1.5 times U(eq) of the corresponding C, N, or O atom. Compound **2** crystallizes with 8.5 molecules CH_3OH and one H_2O per formula unit. Some of the CH_3OH molecules in **2** are disordered and have been refined using similarity restraints. Compound **3** crystallizes with 2.5 molecules CH_3OH per formula unit. These solvate molecules and two of the CF_3SO_3 anions of **3** are disordered and were refined using a number of restraints. Selected crystallographic data for **2**: $C_{80.5}H_{108}F_9N_{12}O_{30.5}S_3Zn_3$; orthorhombic $P2_12_12_1$ (no. 19), $a = 14.834(2)$, $b = 22.470(4)$, $c = 29.320(4)$ Å; $Z = 4$; $V = 9773(3)$ Å^3; $\rho_{calcd} = 1.492$ g cm^{-3}, $\mu = 0.895$ mm^{-1}, $T_{min} = 0.743$, $T_{max} = 1.000$, 51406 measured reflections (7.1° = 2θ = 51.4°), 16501 unique reflections, 9940 observed reflections [$I > 2\sigma(I)$], 1312 parameters, $wR_2 = 0.1727$ (all data), $R_1 = 0.0764$ [$I > 2\sigma(I)$]. Selected crystallographic data for **3**: $C_{86.5}H_{85}F_9N_{12}O_{20.5}S_3Zn_3$; monoclinic $P2_1$ (no. 4), $a = 15.065(2)$, $b = 13.053(2)$, $c = 24.108(2)$ Å, $\beta = 93.30(1)$°, $Z = 2$; $V = 4732.8(9)$ Å^3; $\rho_{calcd} = 1.462$ g cm^{-3}, $\mu = 0.912$ mm^{-1}, $T_{min} = 0.804$, $T_{max} = 1.000$, 105250 measured reflections (6.4° = 2θ = 54.0°), 20414 unique reflections, 14676 observed reflections [$I > 2\sigma(I)$], 1305 parameters, $wR_2 = 0.1627$ (all data), $R_1 = 0.0598$ [$I > 2\sigma(I)$]. CCDC 243711 (**2**) and CCDC 243712 (**3**) contain the supplementary crystallographic data for this paper. These data can be obtained free of charge via www.ccdc.cam.ac.uk/conts/retrieving.html (or from the Cambridge Crystallographic Data Centre, 12, Union Road, Cambridge CB21EZ, UK; fax: (+44) 1223-336-033; or deposit@ccdc.cam.ac.uk)

STM measurements: The STM imaging was carried out under ambient conditions using a home-built, low-drift microscope equipped with RHK1000 control electronics or with a commercial Nanoscope III system. A drop of the aqueous 10^{-9} M sample solution was placed onto a freshly cleaved HOPG surface. Sections without molecules clearly showed monoatomic resolution of the graphite structure. Typically, tunneling currents between 10 and 200 pA were employed. The bias voltage was ±72.9 mV. The scan frequency was varied between 2 to 5 Hz. Resolution was 256 × 256 points for topography, and 128 × 128 in the CITS measurements. In most cases, Pt/Ir(10 %) tips were used.

Received: July 12, 2004
Revised: September 28, 2004
Published online: December 28, 2004

Keywords: coordination polymers · materials science · peptides · scanning probe microscopy · zinc

[1] C. Janiak, *Dalton Trans.* **2003**, 2781.
[2] a) M. Eddaoudi, J. Kim, N. Rosi, D. Vodak, M. O'Keeffe, O. M. Yaghi, *Science* **2002**, *295*, 469; b) B. L. Chen, M. Eddaoudi, S. T. Hyde, M. O'Keeffe, O. M. Yaghi, *Science* **2001**, *291*, 1021; c) M. Eddaoudi, D. Moler, H. Li, T. M. Reineke, M. O'Keeffe, O. M. Yaghi, *Acc. Chem. Res.* **2001**, *34*, 319; d) J. S. Seo, D. Whang, H. Lee, S. I. Jun, J. Oh, Y. J. Jeon, K. Kim, *Nature* **2000**, *404*, 982.
[3] J. Hjelm, R. W. Handel, A. Hagfeldt, E. C. Constable, C. E. Housecroft, R. J. Foster, *J. Phys. Chem. B* **2003**, *107*, 10431.
[4] a) J.-C. Dai, X.-T. Wu, Z.-Y. Fu, C.-P. Cui, S.-M. Hu, W.-X. Du, L.-M. Wu, H.-H. Zhang, R.-Q. Sun, *Inorg. Chem.* **2002**, *41*, 1391; b) C. Seward, W.-L. Jia, R.-Y. Wang, G. D. Enright, S. Wang, *Angew. Chem.* **2004**, *116*, 2993; *Angew. Chem. Int. Ed.* **2004**, *43*, 2933.
[5] L. Li, Z. Liu, S. S. Turner, D. Liao, Z. Jiang, S. Yan, *Eur. J. Inorg. Chem.* **2003**, 62.
[6] O. Sato, *Acc. Chem. Res.* **2003**, *36*, 692.
[7] O. R. Evans, W. Lin, *Acc. Chem. Res.* **2002**, *35*, 511.
[8] B. Moulton, M. J. Zaworotko, *Chem. Rev.* **2001**, *101*, 1629.
[9] a) D. Wouters, U. S. Schubert, *Angew. Chem.* **2004**, *116*, 2534; *Angew. Chem. Int. Ed.* **2004**, *43*, 2480; b) C. Safarowsky, L. Merz, A. Rang, P. Broekman, B. A. Hermann, C. A. Schalley, *Angew. Chem.* **2004**, *116*, 1311; *Angew. Chem. Int. Ed.* **2004**, *43*, 1291; c) U. S. Schubert, C. Eschbaumer, *Angew. Chem.* **2002**, *114*, 3016; *Angew. Chem. Int. Ed.* **2002**, *41*, 2892; d) A. Dmitriev, H. Spillmann, N. Lin, J. V. Barth, K. Kern, *Angew. Chem.* **2003**, *115*, 2774; *Angew. Chem. Int. Ed.* **2003**, *42*, 2670; e) P. Messina, A. Dmitriev, N. Lin, H. Spillmann, M. Abel, J. V. Barth, K. Kern, *J. Am. Chem. Soc.* **2002**, *124*, 14000; f) A. Semenov, J. P. Spatz, M. Möller, J.-M. Lehn, B. Sell, D. Schubert, C. H. Weidl, U. S. Schubert, *Angew. Chem.* **1999**, *111*, 2701; *Angew. Chem. Int. Ed.* **1999**, *38*, 2547.
[10] N. Niklas, F. Hampel, R. Alsfasser, *Chem. Commun.* **2003**, 1586.
[11] Y. J. Zhang, M. Jin, R. Lu, Y. Song, L. Jiang, Y. Zhao, T. J. Li, *J. Phys. Chem. B* **2002**, *106*, 1960.

 © 2005 Wiley-VCH Verlag GmbH & Co. KGaA, Weinheim

Asymmetric Organocatalysis

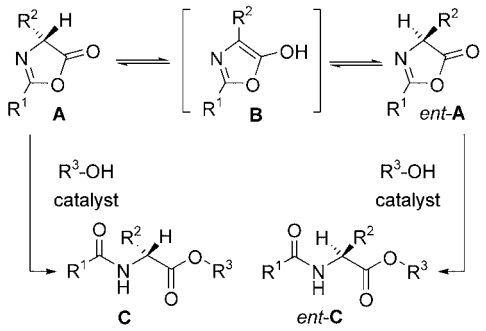
Highly Efficient Dynamic Kinetic Resolution of Azlactones by Urea-Based Bifunctional Organocatalysts**

Albrecht Berkessel, Felix Cleemann, Santanu Mukherjee, Thomas N. Müller, and Johann Lex*

Dedicated to Professor Günter Helmchen

Enantiomerically pure α-amino acids are extremely valuable chemicals in their own right. They are also the monomers of peptides/peptoids and serve as starting materials in the preparation of a wealth of enantiomerically pure pharmaceuticals, organocatalysts, ligands for transition-metal catalysts, and many other types of chiral compounds.[1–4] Besides proteinogenic α-amino acids, which are readily available from natural sources, there is an increasing demand for enantiomerically pure non-natural α-amino acids, such as *tert*-leucine.[5]

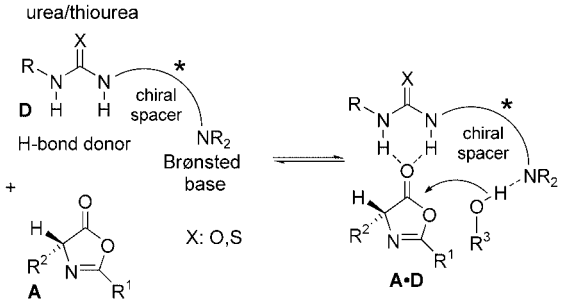
For the preparation of pure enantiomers from racemic mixtures, dynamic kinetic resolution (DKR) is an extremely attractive method, because it enables the transformation of the entire racemate into the desired enantiomer.[6,7] Azlactones of the general formula **A** (Scheme 1) are readily available and configurationally labile α-amino acid derivatives.[8] They are readily prepared by the Erlenmeyer azlactone synthesis or from amino acids by N-acylation (e.g. with benzoyl chloride) followed by cyclization–dehydration in the presence of a condensation agent (e.g. acetic anhydride).[12] The alcoholytic ring opening of azlactones leads to *N*-acyl amino acid esters (such as **C**, *ent*-**C**; Scheme 1).



Scheme 1. Basis of the dynamic kinetic resolution of azlactones **A**.

Lipases have been used for the rather efficient enzymatic DKR of azlactones[13–16] (note that no genuine "azlactonase" is known). Seebach et al. reported that titanium taddolates, present in stoichiometric or substoichiometric amounts, effect the DKR of azlactones (up to 72% *ee*).[17] Hua and co-workers used the cyclic dipeptide *cyclo*-[(*S*)-His-(*S*)-Phe] as an organocatalyst for the alcoholytic DKR of the phenylalanine azlactone (up to 39% *ee*).[18] All these methods suffer from either narrow substrate scope or very long reaction times (ranging from days to weeks), or both. Fu and co-workers showed that the DKR of azlactones can also be effected by alcoholysis in the presence of a planar-chiral DMAP derivative.[19] They reported *ee* values in the range of 50–60% for a number of azlactones. In the case of the alanine azlactone, 78% *ee* was observed with 2-propanol as the nucleophile; however, the reaction rate was relatively low.[19]

Recently, bifunctional organocatalysts of type **D** were used successfully by Takemoto and co-workers for the enantioselective Michael addition of malonates to nitroolefins and for the aza-Henry reaction.[20,21] We reasoned that this structural motif would be efficient in the DKR of azlactones: A substrate–catalyst interaction is expected to occur by hydrogen bonding of the quasi Lewis acidic urea moiety to the azlactone carbonyl group (Scheme 2).[22–24] In the supramolecular aggregate **A**·**D**, the azlactone **A** is activated both towards racemization (by enolization) and nucleophilic ring opening.[22,23] The nucleophilicity of the alcohol reagent is increased by hydrogen bonding to the Brønsted basic group of the catalyst **D**, and the alcohol molecule is steered to the carbon atom of the azlactone carbonyl group. It was expected that alcoholytic ring opening would proceed faster in one of the two possible diastereomeric supramolecular aggregates **A**·**D** that result from the binding of **A** or *ent*-**A** to the chiral catalyst **D**.



Scheme 2. Interactions in the azlactone–catalyst aggregate **A**·**D** and the mechanism of alcoholysis. X = O, S.

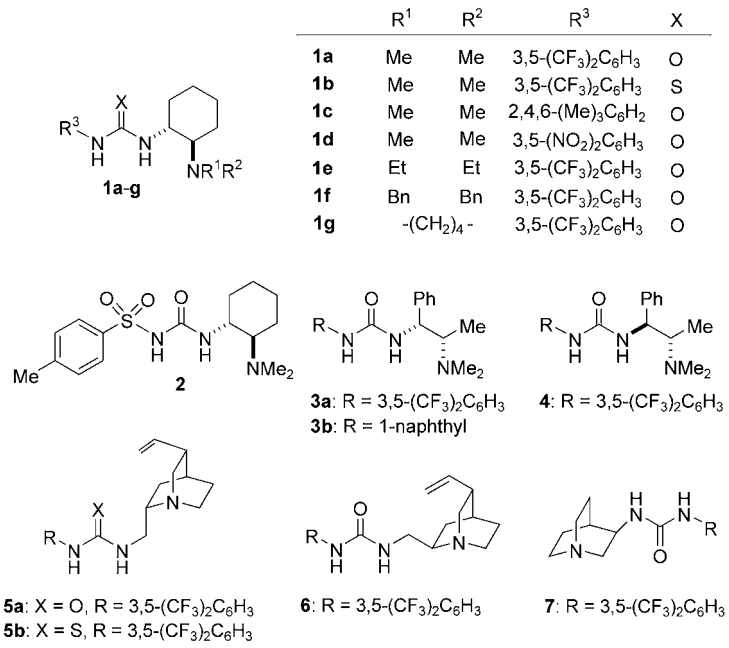
As potential bifunctional catalysts **D**, we synthesized the conjugates **1**–**7** shown in Scheme 3 from ureas/thioureas and tertiary amines.[25] The X-ray crystal structure of the urea catalyst **1a** shows that intermolecular hydrogen bonds exist between the urea N–H groups and the urea oxygen atom of a neighboring molecule of **1a** (Figure 1).[26,27] The urea moiety of **1a** is planar, and the planes of the urea moieties of

[*] Prof. Dr. A. Berkessel, Dipl.-Chem. F. Cleemann, S. Mukherjee, Dipl.-Chem. T. N. Müller, Dr. J. Lex
Institut für Organische Chemie
Universität zu Köln
Greinstrasse 4, 50939 Köln (Germany)
Fax: (+49) 221-470-5102
E-mail: berkessel@uni-koeln.de

[**] This work was supported by the Fonds der Chemischen Industrie, in particular through a doctoral fellowship to F.C. The authors thank Degussa AG, Hanau for generous gifts of amino acids. Samples of compounds **2** and **10**–**13** were kindly provided by Katrin Roland, Burkhard Koch, Marc Brandenburg, and Stefan Schnippering.

Supporting information for this article is available on the WWW under http://www.angewandte.org or from the author.

 DOI: 10.1002/anie.200461442 © 2005 Wiley-VCH Verlag GmbH & Co. KGaA, Weinheim



Scheme 3. Conjugates **1**–**7** formed from ureas/thioureas and tertiary amines as potential bifunctional catalysts **D**. Bn = benzyl.

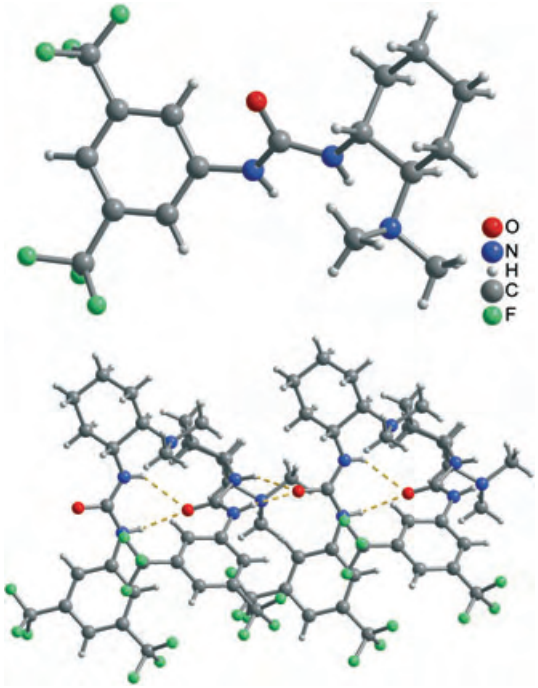


Figure 1. X-ray crystal structure of the bifunctional organocatalyst **1a**; top: molecular structure of **1a**; bottom: packing of **1a** in the crystal, intermolecular H bonding between neighboring molecules of **1a**.

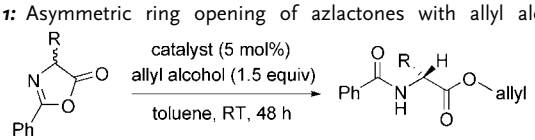
neighboring molecules of **1a** intersect at an angle of about 80°. There is no intramolecular H bond to the N atom of the tertiary amine. Thus, the H-bonding behavior of **1a**, as revealed by its crystal structure, corresponds to the design features summarized in Scheme 1 for a bifunctional organocatalyst.

The viability of the general concept of a bifunctional quasi Lewis acid–Brønsted base catalyst was reflected in the catalytic performance of **1a**: Initial experiments with the phenylalanine-derived azlactone **8a** and methanol as the nucleophile afforded >60% *ee* in the presence of 5 mol% of the catalyst **1a.** Conversion into the *N*-benzoyl amino acid ester was complete within 24 h at room temperature in toluene as the solvent. The screening of different alcohols revealed that the conversion rates drop sharply as the steric demand of the alcohol increases; the highest rate was observed with methanol. As allyl alcohol gave the best enantioselectivity, this nucleophile was used in all further experiments. Of the solvents examined, toluene and fluorobenzene proved optimal. Consistent with our mechanistic picture (Scheme 2), no reaction occurred in solvents that act as H-bond acceptors, such as THF.

Entries 1–6 of Table 1 summarize our results for the alcoholysis of the azlactones **8a–f** derived from the aliphatic α-amino acids phenylalanine (**8a**), alanine (**8b**), valine (**8c**), leucine (**8d**), and *tert*-leucine (**8e**), and the aromatic α-amino acid phenylglycine (**8f**). In all cases, the *N*-benzoyl amino acid allyl esters **9a–f** were obtained with greater than 70% *ee* in the presence of 5 mol% of the urea catalyst **1a** at room temperature. For the valine-, leucine-, and *tert*-leucine-derived azlactones **8c–e**, 85–87% *ee* was observed (Table 1, entries 3–5). These were the highest enantioselectivities ever attained in the non-enzymatic DKR of azlactones. The conversions observed (up to 96% after a reaction time of 24 h; Table 1, entry 1) clearly reflect the dynamic character of the resolution process.

A comparison of entries 5 and 7 of Table 1 reveals that the enantioselectivity of **1b**, the thiourea analogue of the catalyst

Table 1: Asymmetric ring opening of azlactones with allyl alcohol.



Entry	Substrate	R	Catalyst	Conversion [%]	*ee* [%]
1[a]	**8a**	$PhCH_2$	**1a**	96	72
2	**8b**	Me	**1a**	43	72
3	**8c**	*i*Pr	**1a**	76	85
4	**8d**	*i*Bu	**1a**	74	85
5	**8e**	*t*Bu	**1a**	67	87
6	**8f**	Ph	**1a**	76	75
7	**8e**	*t*Bu	**1b**	69	83
8[b]	**8e**	*t*Bu	**1b**	37	88
9[c]	**8e**	*t*Bu	**1b**	16	91
10	**8e**	*t*Bu	**1c**	9	84
11	**8e**	*t*Bu	**1d**	66	86
12	**8a**	$PhCH_2$	**1e**	53	73
13	**8a**	$PhCH_2$	**1f**	<2	n.d.[d]
14[a]	**8a**	$PhCH_2$	**1g**	95	68
15	**8e**	*t*Bu	**1e**	16	73
16	**8e**	*t*Bu	**1f**	<2	n.d.[d]
17	**8e**	*t*Bu	**1g**	75	75

[a] After 24 h. [b] Reaction was carried out at 0°C. [c] Reaction was carried out at −20°C. [d] n.d. = not detected.

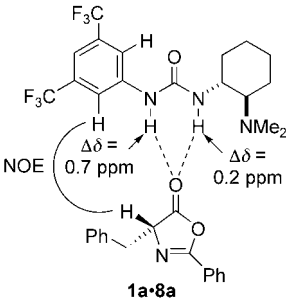
 © 2005 Wiley-VCH Verlag GmbH & Co. KGaA, Weinheim

1a, is lower than that of **1a** at room temperature. However, when the reaction temperature was decreased to −20 °C, 91 % *ee* was observed with the thiourea catalyst **1b** (Table 1, entry 9).[28] To the best of our knowledge, this level of enantioselectivity is unprecedented in the organocatalytic DKR of azlactones, and it rivals the results obtained with lipases. However, in contrast to enzymatic DKR, the organocatalytic method described herein furnishes either enantiomer of the product, as desired. A structurally diverse range of azlactones can be resolved with comparable enantioselectivities (Table 1). Furthermore, after a single recrystallization, the product *N*-benzoyl amino acid allyl esters **9a–f** were obtained with > 95 % *ee*.

In the ureas **1c** and **1d** (Scheme 3), the 3,5-bis(trifluoromethyl)phenyl group of **1a** was replaced by a mesityl and a 3,5-dinitrophenyl substituent, respectively. Very good enantioselectivities were observed with these catalysts (84 and 86 % *ee*; Table 1, entries 10 and 11). However, the reaction rate was relatively low in the case of the mesityl catalyst **1c**, thus highlighting the importance of the electron-withdrawing trifluoromethyl and nitro substituents on the aromatic ring (Table 1, entries 5, 10, and 11). In line with this argumentation, the *N*-sulfonyl urea **2** (Scheme 3) is also catalytically active and gives 70 % *ee* in the DKR of **8e** with allyl alcohol.

In compounds **1e–g**, the steric demand of the substituents on the nitrogen atom of the Brønsted basic tertiary amine was varied. An increase in the steric bulk of the substituents on the N atom from methyl to ethyl groups resulted in no significant change in enantioselectivity in the DKR of **8a** (72 % *ee* for **1a**, 73 % *ee* for **1e**; Table 1, entries 1 and 12), but led to a decrease in enantioselectivity in the DKR of **8e** (from 87 to 73 % *ee*; entries 5 and 15). The exchange of the dimethylamino group for a pyrrolidine unit (i.e. in **1g**) led to almost no change for substrate **1a** (Table 1, entries 1 and 14), but to a lower *ee* value for substrate **8e** (entries 5 and 17). The dibenzylamino derivative **1f** was virtually inactive (Table 1, entries 13 and 16). The ephedrine derivatives **3a**,**b** were catalytically active, but did not provide appreciable levels of enantioselectivity (< 40 % *ee*). However, the diastereomer **4**, derived from pseudoephedrine, afforded 78 % *ee* in the DKR of the azlactone **8e** with allyl alcohol (60 % conversion after 24 h at room temperature). We also prepared the urea/thiourea derivatives **5a**,**b**, **6**, and **7** of quinuclidine shown in Scheme 3. All showed high catalytic activity (70–96 % conversion in the methanolysis of **8a** after 24 h at room temperature), but the enantioselectivities did not exceed 45 % *ee* (DKR of **8e** with allyl alcohol).

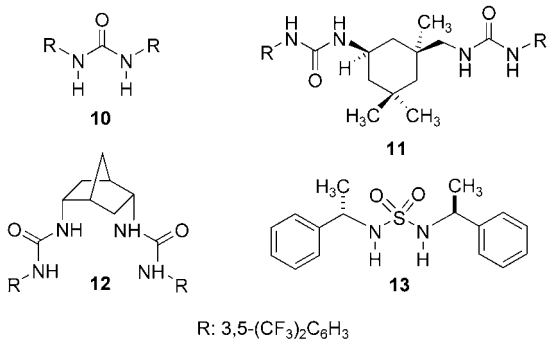
The formation of a substrate–catalyst complex (such as **1a**·**8a**, Scheme 4) was supported by NMR spectroscopic experiments: Upon addition of the racemic azlactone substrate **8a** to a solution of the catalyst **1a** in [D_8]toluene, downfield shifts of $\delta = 0.2$ and 0.7 ppm were observed for the urea N–H hydrogen atoms of the catalyst (Scheme 4). Furthermore, an *inter*molecular NOE of the azlactone 4–H resonance was observed upon irradiation at the resonance frequency of the aromatic hydrogen atoms at the 2- and 6-positions of the catalyst. The ^{1}H and ^{13}C NMR spectra of **1a**·**8a** consisted of only one set of signals, thus indicating the preferential formation of one of the two possible diastereomers of the catalyst–azlactone aggregate and confirming the rapid interconversion of the azlactone enantiomers.[29] The assignment of the *R* configuration to the stereogenic center of the azlactone **8a** in the complex **1a**·**8a** (Scheme 4) rests on the observation that (*R*)-**9a** was formed as the major enantiomer in the alcoholysis (see Table 1).



1a·8a

Scheme 4. NMR spectroscopic characteristics of the azlactone–catalyst complex **1a·8a**.

The following observations support the bifunctional activity of the urea and thiourea catalysts employed in this study (as shown for **A**·**D** in Scheme 2): Mono- and bisureas that lack the Brønsted basic amine functionality, such as **10**,[31] **11**,[32] and **12**,[32] were not catalytically active; the same holds for sulfamides such as **13**.[33] Amines that lack the urea moiety, such as triethylamine, effected a very slow conversion of the substrate azlactones. Chiral variants, such as (−)-quinine and the dimeric cinchona alkaloids $(DHQD)_2PHAL$[34] and $(DHQD)_2AQN$,[34] were also tested. In particular, $(DHQD)_2AQN$ appeared promising because this type of dimeric cinchona alkaloid had been shown by Deng and coworkers to be a highly enantioselective catalyst for the alcoholytic DKR of *N*-carbamoyl-protected amino acid *N*-carboxyanhydrides[35] and of α-aryl α-hydroxycarboxylic acid *O*-carboxyanhydrides.[36] In the present case, at best slow transformations of the substrate azlactones were observed, with low enantioselectivities (11 % *ee* in the methanolysis of **8a** with $(DHQD)_2AQN$ as the catalyst).



R: 3,5-$(CF_3)_2C_6H_3$

In summary, we have described a broadly applicable organocatalytic method for the dynamic kinetic resolution of azlactones with the highest levels of enantioselectivity reported to date. The method is based on bifunctional urea/thiourea–amine catalysts, which activate the substrate azlactones to nucleophilic attack through the formation of a hydrogen-bonded supramolecular aggregate. The catalysts

 © 2005 Wiley-VCH Verlag GmbH & Co. KGaA, Weinheim

can be prepared easily and have a modular structure. Therefore, our method should be readily adaptable for the generation of other enantiomerically pure amino acids.

Experimental Section

All commercially available chemicals and amino acids were used without further purification. L-*tert*-Leucine was obtained from Degussa AG, Hanau. Solvents were distilled prior to use and dried if necessary by using standard techniques. *N*-Benzoyl amino acids were synthesized by acylation with benzoyl chloride according to a literature procedure.[37] HPLC analysis was performed on Agilent HPLC equipment with HPLC-grade solvents from Fisher Scientific. The catalysis experiments were carried out under an inert atmosphere.

Alcoholytic DKR of azlactones: The alcohol (1.5 equiv) was added to a solution of one of the catalysts **1**–**7** (8.33 μmol, 0.05 equiv) in toluene (0.5 mL). In the case of the ureas/sulfamides **10**–**13**, NEt_3 (8.33 μmol) or 1,8-diazabicyclo[5.4.0]undec-7-ene (DBU; 0.05 equiv) were added. A solution of the azlactone **8** (167 μmol, 1.00 equiv) in toluene (0.5 mL) was added, and the homogeneous reaction mixture was stirred at ambient temperature. For analysis, 100-μL samples were withdrawn and diluted with dichloromethane (900 μL). Conversion and enantiomeric excess were determined immediately by HPLC (Daicel Chiralpak AD or Merck (S,S) Whelk O1, *n*-hexane/2-propanol). Quantification was based on UV detection at $\lambda = 230$ and 210 nm, respectively. Conversion was determined by comparison with the peak areas of stock solutions of the azlactones and the corresponding *N*-benzoyl amino acid esters in dichloromethane.

8a–f: The azlactones **8a–e** were prepared by cyclodehydration of the corresponding *N*-benzoyl amino acids with acetic anhydride according to the procedure of Goodman and Glaser.[38] The phenylglycine-derived azlactone **8f** was prepared by the cyclization of *N*-benzoyl phenylglycine in the presence of 1-ethyl-3-(3-dimethylaminopropyl)carbodiimide (EDC).[39] All analytical data were identical to those published.[19,40]

For HPLC parameters for the analysis of the *N*-benzoyl amino acid esters **9**, see Supporting Information.

Received: July 27, 2004

Keywords: amino acids · azlactones · kinetic resolution · organocatalysts · urea

[1] M. Breuer, K. Ditrich, T. Habicher, B. Hauer, M. Keßeler, R. Stürmer, T. Zelinski, *Angew. Chem.* **2004**, *116*, 806 – 843; *Angew. Chem. Int. Ed.* **2004**, *43*, 788 – 824.
[2] R. N. Patel in *Stereoselective Biocatalysis* (Ed.: R. N. Patel), Marcel Dekker, New York, **2000**, pp. 877 – 902.
[3] E. R. Jarvo, S. J. Miller, *Tetrahedron* **2002**, *58*, 2481 – 2495.
[4] H. Gröger, K. Drauz in *Asymmetric Catalysis on Industrial Scale* (Eds.: H. U. Blaser, E. Schmidt), Wiley-VCH, Weinheim, **2004**, pp. 131 – 147.
[5] A. S. Bommarius, M. Schwarm, K. Drauz, *J. Mol. Catal. B* **1998**, *5*, 1 – 11.
[6] H. B. Kagan, J. C. Fiaud, *Top. Stereochem.* **1988**, *18*, 249 – 330.
[7] a) K. Faber, *Chem. Eur. J.* **2001**, *7*, 5004 – 5010; b) H. Pellissier, *Tetrahedron* **2003**, *59*, 8291 – 8327.
[8] Oxazol-5(4*H*)-ones ("azlactones") racemize through enol formation (**B**, Scheme 1). The pK_a value of the hydrogen atom at the 4-position is about 8.9.[9] Azlactones are racemized easily by external bases, but autocatalytic racemization can also occur.[10] See reference [11] for an example of the crystallization-induced generation of a diastereomerically pure azlactone.
[9] J. De Jersey, B. Zerner, *Biochemistry* **1969**, *8*, 1967 – 1974.
[10] M. Slebioda, M. A. St-Amand, F. M. F. Chen, N. L. Benoiton, *Can. J. Chem.* **1988**, *66*, 2540 – 2544.
[11] H. T. Stock, N. J. Turner, *Tetrahedron Lett.* **1996**, *37*, 6575 – 6578.
[12] H. E. Carter, *Org. React.* **1946**, *3*, 198 – 239.
[13] S. A. Brown, M.-C. Parker, N. J. Turner, *Tetrahedron: Asymmetry* **2000**, *11*, 1687 – 1690.
[14] N. J. Turner, J. R. Winterman, R. McCague, J. S. Parratt, S. J. C. Taylor, *Tetrahedron Lett.* **1995**, *36*, 1113 – 1116.
[15] J. Z. Crich, R. Brieva, P. Marquart, R. L. Gu, S. Flemming, C. J. Sih, *J. Org. Chem.* **1993**, *58*, 3252 – 3258.
[16] R. L. Gu, I.-S. Lee, C. J. Sih, *Tetrahedron Lett.* **1992**, *33*, 1953 – 1956.
[17] a) D. Seebach, G. Jaeschke, K. Gottwald, K. Matsuda, R. Formisano, D. A. Chaplin, M. Breuning, G. Bringmann, *Tetrahedron* **1997**, *53*, 7539 – 7556; b) K. Gottwald, D. Seebach, *Tetrahedron* **1999**, *55*, 723 – 738.
[18] L. Xie, W. Hua, A. S. C. Chan, Y.-C. Leung, *Tetrahedron: Asymmetry* **1999**, *10*, 4715 – 4728.
[19] J. Liang, J. C. Ruble, G. C. Fu, *J. Org. Chem.* **1998**, *63*, 3154 – 3155.
[20] T. Okino, Y. Hoashi, Y. Takemoto, *J. Am. Chem. Soc.* **2003**, *125*, 12672 – 12673.
[21] T. Okino, S. Nakamura, T. Furukawa, Y. Takemoto, *Org. Lett.* **2004**, *6*, 625 – 627.
[22] The catalytic activity of ureas through hydrogen bonding has been shown to be comparable to the action of metal-containing Lewis acids: P. R. Schreiner, A. Wittkopp, *Org. Lett.* **2002**, *4*, 217 – 220; A. Wittkopp, P. R. Schreiner, *Chem. Eur. J.* **2003**, *9*, 407 – 414; P. R. Schreiner, *Chem. Soc. Rev.* **2003**, *32*, 289 – 296.
[23] P. M. Pihko, *Angew. Chem.* **2004**, *116*, 2110 – 2113; *Angew. Chem. Int. Ed.* **2004**, *43*, 2062 – 2064.
[24] For seminal studies on the use of chiral amidinium catalysts for stereoselective Diels–Alder reactions, see: T. Schuster, M. Bauch, G. Dürner, M. W. Göbel, *Org. Lett.* **2000**, *2*, 179 – 181; T. Schuster, M. Kurz, M. W. Göbel, *J. Org. Chem.* **2000**, *65*, 1697 – 1701.
[25] The synthesis and full characterization of the bifunctional catalysts **1a**,**c–g**, **2**, **3a**,**b**, **4**, **5a**,**b**, **6**, and **7** will be published elsewhere.
[26] Crystal data of **1a**: $C_{17}H_{21}N_3OF_6$, $M_r = 397.37$, colorless needles, $0.30 \times 0.20 \times 0.15$ mm, orthorhombic, $a = 8.849(1)$, $b = 17.212(1)$, $c = 24.025(1)$ Å, $V = 3659.2(5)$ Å^3, $T = 100(2)$ K, space group $P2_12_12_1$, $Z = 8$, $\rho_{calcd} = 1.443$ g cm^{-3}, $\mu = 0.133$ mm^{-1}. A total of 21188 reflections were measured, 7809 unique, final residuals were $R1 = 0.0979$ and w$R2 = 0.2213$ for 2669 observed reflections with $I > 2\sigma(I)$, 493 parameters, GOF = 0.961, maximum residual electron density 0.415 e Å^{-3}. Data were collected on a Nonius KappaCCD diffractometer ($2\Theta_{max} = 54°$, $Mo_{K\alpha}$ radiation ($\lambda = 0.71073$ Å), graphite monochromator, φ/ω scans. The structure was solved by using direct methods (G. M. Sheldrick, SHELXS-97, Program for the Solution of Crystal Structures, University of Göttingen, Germany, **1997**), followed by full-matrix least-squares refinement (by using all unique reflections) with anisotropic thermal parameters for non-hydrogen atoms. The positions of hydrogen atoms were refined by using a riding model (SHELXL-97). CCDC 246910 contains the supplementary crystallographic data for this paper. These data can be obtained free of charge from the Cambridge Crystallographic Data Centre via www.ccdc.cam.ac.uk/data_request/cif.
[27] For the solid-state structural features and the typical bifurcate H bonding of ureas to nucleophilic O acceptors, see: M. C. Etter, T. W. Panunto, *J. Am. Chem. Soc.* **1988**, *110*, 5896 – 5897; M. C. Etter, *Acc. Chem. Res.* **1990**, *23*, 120 – 126.
[28] The urea catalyst **1a** did not show a comparable increase in enantioselectivity with decreasing temperature: At 0 °C the product **9e** was formed with 88 % *ee* (87 % *ee* at room temperature; Table 1, entry 5).

 © 2005 Wiley-VCH Verlag GmbH & Co. KGaA, Weinheim

[29] In the HPLC analysis (see Experimental Section) of the racemic azlactones **8a–f** on a chiral stationary phase, equilibration of the azlactone enantiomers was clearly indicated by the peak forms typical for dynamic, interconverting analytes (see, for example, reference [30]).
[30] K. Cabrera, M. Jung, M. Fluck, V. Schurig, *J. Chromatogr. A* **1996**, *731*, 315 – 321.
[31] D. J. Maher, S. J. Connon, *Tetrahedron Lett.* **2004**, *45*, 1301 – 1305.
[32] The synthesis and characterization of the diureas **11** and **12** will be reported elsewhere.
[33] F. D. Greene, M. A. Berwick, J. C. Stowell, *J. Am. Chem. Soc.* **1970**, *92*, 867 – 874.
[34] $(DHQD)_2PHAL$: dihydroquinidine-(1,4-phthalazinediyl diether); $(DHQD)_2AQN$: dihydroquinidine-(anthraquinone-1,4-diyl diether).
[35] a) J. Hang, H. Li, L. Deng, *Org. Lett.* **2002**, *4*, 3321 – 3324; b) J. Hang, L. Deng, *Synlett* **2003**, 1927 – 1930.
[36] L. Tang, L. Deng, *J. Am. Chem. Soc.* **2002**, *124*, 2870 – 2871.
[37] J. P. Greenstein, M. W. Winitz, *Chemistry of the Amino Acids*, Wiley, New York, **1961**, pp. 1266 – 1268.
[38] M. Goodman, C. B. Glaser, *J. Org. Chem.* **1970**, *35*, 1954 – 1962.
[39] S. Peddibhotla, J. J. Tepe, *Synthesis* **2003**, 1433 – 1440.
[40] G. Schulz, P. Gruber, W. Steglich, *Chem. Ber.* **1979**, *112*, 3221 – 3236.

 © 2005 Wiley-VCH Verlag GmbH & Co. KGaA, Weinheim

Water Structures

Calculation of Clathrate-Like Water Clusters Including H_2O-Buckminsterfullerene**

Ralf Ludwig and Andreas Appelhagen**

The concept of buckminsterfullerene-like topology as a molecular-level structural motif has a long history in water cluster chemistry.[1] While carbon-based analogues have a well-established experimental foundation, "bucky-water" clusters remain largely conjectural species in the theoretical descriptions of pure water. Fullerene-like topologies are distinguished by the pattern of tricoordinate vertices in pentagonal and hexagonal facets that close to a convex polyhedron in three dimensions. They require exactly 12 pentagons and any number n_{hex} of hexagons to form a polyhedron of $2n_{hex}+20$ vertices. While pentagonal and hexagonal facets are well-known structural elements of all known crystalline forms of ice,[2] the intact Bucky-water polyhedra are principally recognized as elements in certain clathrate-type hydrates, such as the pentagonal dodecahedral $(H_2O)_{20}$ ($n_{hex}=0$) and tetrakaidecahedral $(H_2O)_{24}$ units ($n_{hex}=2$) of chlorine hydrate.[3]

Today, gas hydrates are among the most well-known clathrate structures. These nonstoichiometric, crystalline compounds are found in natural-gas pipelines, on the ocean floor, and in permafrost environments,[4,5] deep ice cores,[6] rock inclusions,[7] comets, and certain outer planets.[8] There are three known types of natural-gas hydrates: the two cubic structures I and II,[9] and a hexagonal structure H.[10] The type I hydrate structures is made up of pentagonal dodecahedral $(H_2O)_{20}$ and tetrakaidecahedral $(H_2O)_{24}$ cages. Type II hydrates consist of hexakaidecahedrons $(H_2O)_{28}$ and pentagonal dodecahedrons $(H_2O)_{20}$. The icosahedral $(H_2O)_{36}$ cluster is the largest constituent of structure H.

Recently, we extended a quantum statistical model of liquid water to include larger ice-like clusters, such as tetrahedral and fullerene-like clusters with up to 26 water molecules.[11] A low-energy tetrakaidecahedral $(H_2O)_{24}$ cluster leads to a new low-temperature phase that bounds both liquid and vapor regions in first-order transition lines and gives rise to a true triple point. We characterized the microstructural composition and macroscopic properties of this "Bucky-ice" phase. Although it differs significantly from physical ice I_h (for example, the melting point is 20 K too high and the molar volume is 5% too low), it manifests qualitatively correct thermodynamic features of true ice polymorphs, which suggests an important role of voluminous clusters in the liquid/solid transition region. Thus understanding the structure and stability of such water clusters is of crucial importance for studying clathrate hydrates and hydration phenomena.

The aim of this work is to investigate properties of larger water clusters including up to 60 water molecules. Some key questions will be addressed: Which of the calculated water clusters present minimum structures? How important are cooperative effects with increasing cluster size? Can hydrophobic guest molecules promote structure formation? Are larger clathrate structures than those known experimentally reasonable based on energetic considerations?

The calculated bucky-water clusters having between 20 and 60 water molecules are shown in Figure 1. The variety of water cage structures comprises the dodecahedral $(H_2O)_{20}$ cluster ($n_{hex}=0$), the tetrakaidecahedral $(H_2O)_{24}$ cluster ($n_{hex}=2$), the hexakaidecahedral $(H_2O)_{28}$ cluster ($n_{hex}=4$), the icosahedral $(H_2O)_{36}$ cluster ($n_{hex}=8$), and finally the truncated icosahedral $(H_2O)_{60}$ cluster ($n_{hex}=20$). Whereas the first represents structural elements of true gas hydrates, the

[*] Prof. Dr. R. Ludwig
Universität Rostock
Institut für Chemie
Abt. Physikalische Chemie
Dr.-Lorenz-Weg 1, 18051 Rostock (Germany)
Fax: (+49) 381-498-6524
E-mail: ralf.ludwig@chemie.uni-rostock.de
Dipl.-Chem. A. Appelhagen
Universität Dortmund
Fachbereich Chemie
Physikalische Chemie 2a
Otto-Hahn-Strasse 6, 44221 Dortmund (Germany)
Fax: (+49) 231-755-3937
E-mail: app@pc2a.chemie.uni-dortmund.de

[**] This work was supported by the Deutsche Forschungsgemeinschaft (DFG-Forschergruppe 436) and the State of Mecklenburg-Western Pomerania (Hochschulwissenschaftsprogramm). We thank the John von Neumann Institut für Computing, Jülich, for generous computer time.

Supporting information for this article is available on the WWW under http://www.angewandte.org or from the author.

 DOI: 10.1002/anie.200460899 © 2005 Wiley-VCH Verlag GmbH & Co. KGaA, Weinheim

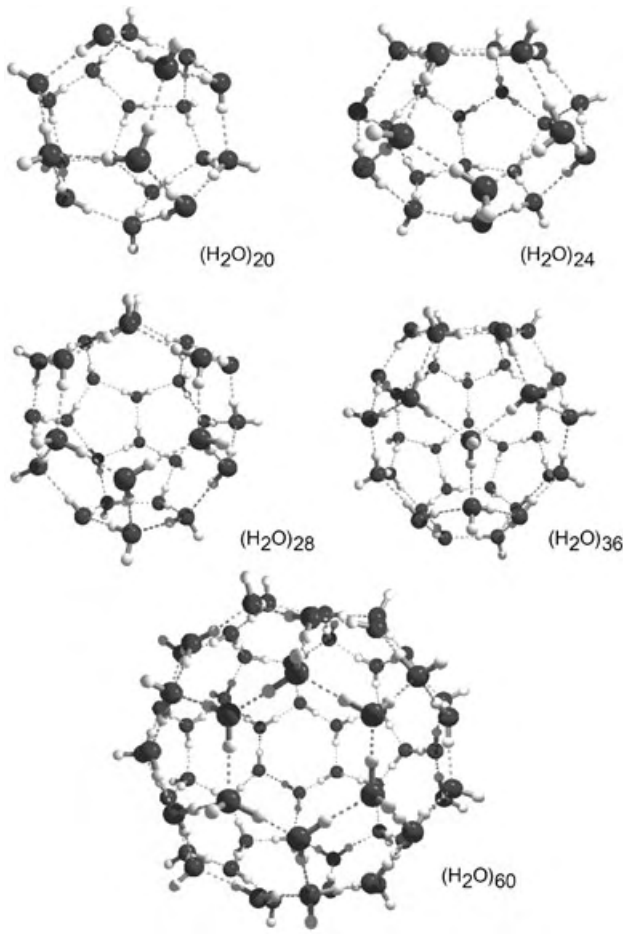


Figure 1. Optimized structures of bucky-water clusters.

largest cluster $(H_2O)_{60}$ can be regarded as a real buckminsterfullerene of water as suggested by Ermer and Eling some time ago.[12] It presents the water analogue to the famous C_{60}. A water oxygen atom is located at each of the sixty vertices, and the edges of the polyhedron are formed by hydrogen bonds between water oxygen and hydrogen atoms. As in all clathrate structures three-quarters of the OH bonds are involved in this cluster H-bonding, whereas one-quarter points outside the cage structure. To our knowledge these are the first Hartree-Fock (HF) and density-functional-theory (DFT) calculations on a buckminsterfullerene of water $(H_2O)_{60}$. Similar calculations have been performed on quasi-one-dimensional pentagon and hexagon ice nanotubes $(H_2O)_{30}$, $(H_2O)_{60}$, and $(H_2O)_{120}$ by Bai et al.[13]

Related water assemblies $(H_2O)_{40}$, $(H_2O)_{80}$, and $(H_2O)_{100}$ were found experimentally in microporous networks or in supramolecular compounds.[14,15] But these cagelike clusters have different numbers of vertices and edges than our carbon-analogue water structures. Additionally, interactions with nanoscaled cavities lead to structural motifs such as trimers, which do not occur in pure water cages.

Both molecular orbital and density-functional methods (implemented in the Gaussian 98 software package)[16] were employed. The geometries of the water clusters were fully optimized using HF and B3LYP levels of theory and a variety of basis sets. The simple water ring pentamer ($n = 5$) and ring hexamer ($n = 6$) representing the structural motifs of the polyhedrons were calculated for comparison. The B3LYP/6-311G** calculated binding energies and geometries are given in Table 1. In Figures 2 and 3 all B3LYP energies and geometries are shown as a function of the basis set. All the other calculated data are given in the Supporting Information. The large increase in energy on going from the simple cyclic clusters to the buckyball structures can be explained primarily by an increasing number of hydrogen bonds. Whereas in the two-coordinate ring clusters each monomer forms only two of the four possible H-bonds, in the three-coordinate buckyballs each water monomer has three H-bonded neighbors.

Table 1: BSSE-corrected binding energies per monomer, average distances R(O—O) and R(O—H), and angles ∢(O-H-O) for all optimized water clusters calculated at the B3LYP/6-311G** level of theory (BSSE = basis set superposition error).

Cluster	E/n [kJ mol^{-1}]	R(O—O) [pm]	R(O—H) [pm]	∢(O-H-O) [°]
$(H_2O)_5$	31.19	269.46 ± 0.45	98.79 ± 0.02	3.19 ± 0.76
$(H_2O)_6$	32.40	268.41 ± 0.02	98.78 ± 0.00	3.07 ± 0.03
$(H_2O)_{20}$	40.86	274.27 ± 9.94	98.64 ± 1.55	2.31 ± 1.39
$(H_2O)_{24}$	42.11	273.13 ± 9.55	98.73 ± 1.55	2.02 ± 1.04
$(H_2O)_{28}$	41.11	273.90 ± 9.39	98.62 ± 0.15	3.83 ± 2.61
$(H_2O)_{36}$	41.52	273.52 ± 9.34	98.63 ± 1.48	3.93 ± 2.68
$(H_2O)_{60}$	41.73	273.14 ± 8.87	98.60 ± 1.39	5.42 ± 2.81

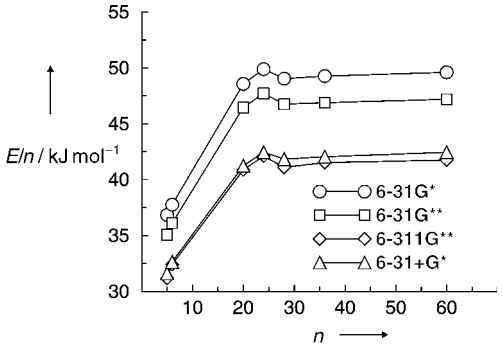


Figure 2. BSSE-corrected binding energies per monomer in the clusters $(H_2O)_n$, E/n, calculated at the B3LYP level of theory for four basis sets.

The energy per H-bond is larger for the ring structures, because favorable unstrained, nearly linear O-H-O alignments permit strong intermolecular electronic delocalization ("charge transfer"), leading to a strong cooperative enhancement of H-bonding. The formation of three-coordinate structures is effectively opposed by unfavorable reductions in average H-bond strength as well as vibrational entropy loss.[17,18] A comparison of the three-coordinate clathrate structures shows that the energy per monomer slightly increases going from $(H_2O)_{20}$ to $(H_2O)_{60}$. The tetrakaidehedral $(H_2O)_{24}$ is an exception from this rule since it shows a particular stability. This energetic behavior is reflected in the B3LYP cluster geometries (Figure 3). Thus the ring structures give the shortest intermolecular distances R(O—O) and the

 © 2005 Wiley-VCH Verlag GmbH & Co. KGaA, Weinheim

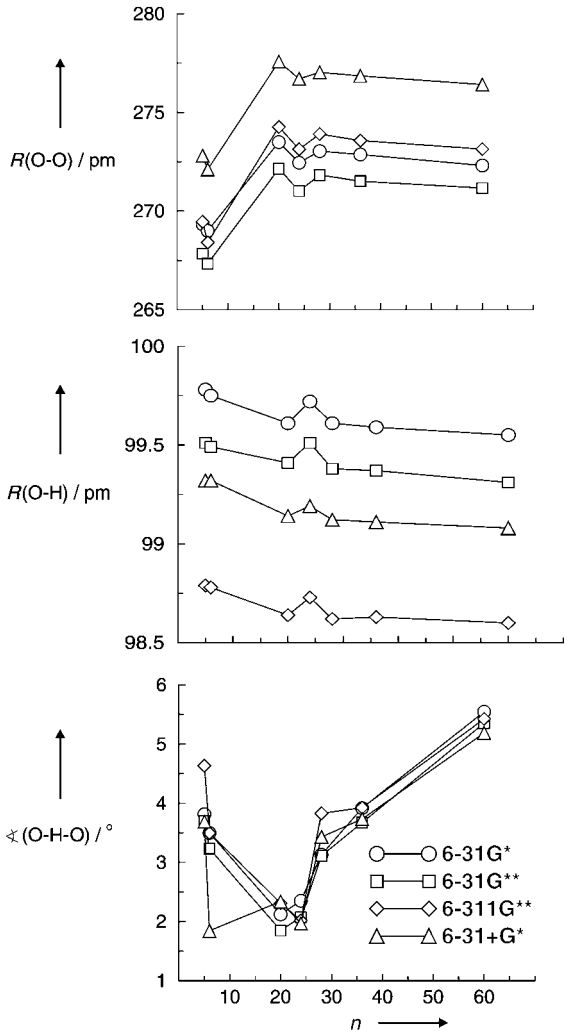


Figure 3. Optimized average distances R(O–O) and R(O–H) and angles ∢(O-H-O) for water clusters calculated at the B3LYP level of theory for four basis sets.

longest intramolecular bonds R(O–H). For the cage structures we can notice that R(O–O) slightly decreases as a consequence of cooperative enhancement and increasing H-bond strength with larger cluster size. Again the tetrakaidecahedral $(H_2O)_{24}$ shows its exceptional stability. It has the shortest intermolecular distances R(O–O), the longest bonds R(O–H), and the smallest H-bond angles ∢(O-H-O) of all cage structures (Figure 3). In general it can be concluded that in clathrate-like structures cooperativity is already at a maximum with the tetrakaidecahedral $(H_2O)_{24}$ structure. The H-bonds of the $(H_2O)_{24}$ cluster appear slightly less bent than in most of the other water clusters. However, the most surprising result is that the buckminsterfullerene of water, $(H_2O)_{60}$, can compete energetically with all smaller clathrate structures. It represents a true minimum structure on the potential energy surface, as proven by frequency calculations.

The bucky-water clusters can be easily calculated up to $(H_2O)_{36}$. This is the size up to which water cages exist in true clathrate hydrates. Larger clusters such as $(H_2O)_{40}$, $(H_2O)_{50}$, and $(H_2O)_{60}$ tend to collapse. This is not surprising, because water prefers to be coordinated in a tetrahedral fashion as known from studies on ice I_h[19] and liquid water.[20] When the cluster collapses, some water molecules gain four rather than three H-bonds, thus increasing the total H-bond contribution per monomer. However, the formation of the buckminsterfullerene of water can be supported by using hydrophobic guest molecules. They act like a bubble inside a ball and prevent the collapse of the host structure. Here, we copied nature where small hydrophobic gas molecules such as methane are required for the formation of $(H_2O)_{20}$, $(H_2O)_{24}$, $(H_2O)_{28}$, and $(H_2O)_{36}$ cages in gas hydrate structures at low temperatures and high pressures. The choice of the guest molecule depends on the size of the water structure. Whereas adamantane may be sufficiently large to support $(H_2O)_{36}$, it is too small to strengthen large cages such as $(H_2O)_{40}$, $(H_2O)_{50}$, and $(H_2O)_{60}$. For the buckminsterfullerene of water, for example, the tetra(*tert*-butyl)phosphonium ion or the carbon analogue C_{60} are possible guest molecules. In principle both particles are large enough to support the voluminous water cage. The guest molecules were chosen primarily for their size and shape, and not for their stability and solubility in water. However, it is well known that the tetra(*tert*-butyl)phosphonium ion exists in aqueous solution, and even buckminsterfullerene C_{60} is soluble in water. The latter can be dispersed in water (> 2 mM)[21] by transfer from an organic solvent using sonication without required stabilizers or chemical modification.[22] The hydration of any of these guest molecules is not known experimentally.

In the optimization procedure the bucky-water remains stable and keeps its shape only if C_{60} is used as the guest molecule (Figure 4). The slightly smaller size and in particular

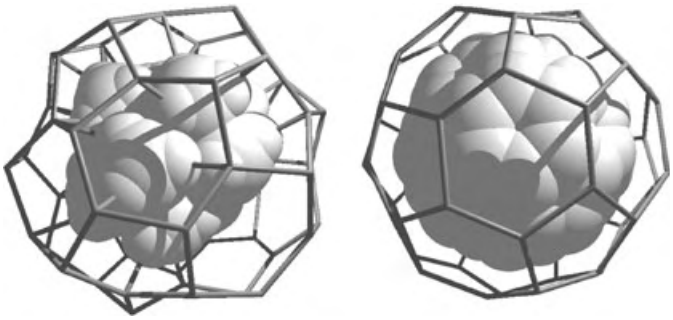


Figure 4. Optimized structures of tetra(*tert*-butyl)phosphonium@$(H_20)_{60}$ (left) and C_{60}@$(H_20)_{60}$ (right).

the positive charged surface of the tetra(*tert*-butyl)phosphonium ion leads to strong distortions of the $(H_2O)_{60}$ structure. Although all pentamer and hexamer ring motifs are preserved, the bucky-water structure shrinks because of strong interactions of about 243 kJ mol^{-1} (HF/6-31G*) and 289 kJ mol^{-1} (B3LYP/6-31G*) between the water oxygen atoms and the cation. In contrast, only weak interactions between the water molecules and C_{60} are observed. For C_{60}@$(H_2O)_{60}$ this interaction is only 20% of that in tetra(*tert*-butyl)phosphonium@$(H_2O)_{60}$, specifically in the range between 50 (HF/6-31G) and 71 kJ mol^{-1} (B3LYP/6-31G*). For comparison, the dispersion energy in a CH_4@$(H_2O)_{20}$

 © 2005 Wiley-VCH Verlag GmbH & Co. KGaA, Weinheim

cluster was calculated to be 29 kJ mol^{-1} (MP2/6-31G*//HF/6-31G*).[23]

The interaction between the water protons and the C_{60} π system has been reported.[20] In smaller water cages that include guest molecules with a significant dipole moment (e.g. THF) the water protons change their direction from pointing away to pointing into the water cage. This phenomenon is not observed here for strongly hydrophobic interactions. This finding is in perfect agreement with recent molecular dynamics simulations (MD) of C_{60} in water.[24,25] The water molecules were found to be located approximately 3.2 Å from the carbon buckyball, and their plane is tangential to the buckyball surface at the buckyball–water interface. In addition the authors could show that the surrounding water did not affect the breathing mode of the buckyball. Apparently there is no significant interaction between the water molecules and C_{60}.

Our calculations show the typical preferential orientation of water in the hydration shell of a nonpolar solute. Placing a solute molecule in liquid water leads to a rearrangement of the random H-bond network. Besides making some space for the guest molecule, water tries to strengthen its network around the nonpolar solute. This is accomplished best when water assumes straddling positions.[20] The water molecule is aligns with its three tetrahedral directions tangential to the surface of the occupied space in order to preserve the maximum number of H-bonds. However, the number of hydrogen bonds per water molecule decreases from the idealized four in bulk water to three at the buckyball–water interface; this is in good agreement with the numbers 3.79 and 2.75 obtained from MD simulations, respectively.[24,25] The accordance with these results should not be overestimated because simple force fields are used in MD calculations. On the other hand, entropic effects are considered in this method.

We do not think (as discussed in literature) that the negatively charged surface of C_{60} dispersed in water arises from the adsorption of hydroxide ions, which has been observed for other hydrophobic surfaces in water. Instead, our calculations suggest that charge transfer between the water oxygen atoms and C_{60} can be one reason for the negatively charged surface of C_{60}. Fullerenes are strong electron acceptors.[26] For the C_{60}–γ-cyclodextrin complex, Yoshida et al.[27] reported that charge transfer occurs between C_{60} and γ-cyclodextrin and that the ether and alcohol oxygen atoms are the electron donors. We come to similar conclusions. Within the $C_{60}@(H_2O)_{60}$ structure (Figure 5) the carbon buckyball has a slightly negative charge (0.54 e at HF/6-31G* and 0.21 e at B3LYP 6-31G*).

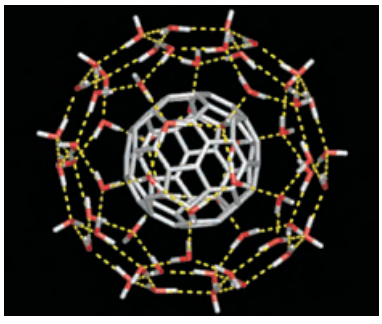


Figure 5. Fully optimized structure of $C_{60}@(H_2O)_{60}$.

Overall it can be concluded that the calculated buckminsterfullerene of water, $(H_2O)_{60}$, represents a true minimum structure. The large volume and an entropic penalty of the water cage is compensated by favorable binding energies caused by cooperative effects. The water buckyball can be further strengthened by the insertion of hydrophobic guest molecules. It can be considered to be the perfect hydration shell for a larger hydrophobic molecule such as its carbon analogue C_{60}.

Experimental Section

Ab initio calculations were performed at the restricted Hartree–Fock (RHF) and density functional (B3LYP) levels with the Gaussian 98 program.[16] The following basis sets were used: 3-21G, 6-31G*, 6-31G**, 6-311G**, and 6-31+G*. Locating the minima of the water clusters usually required a few hundred optimization steps. The basis set superposition error (BSSE)-corrected binding energies per molecule and the geometries of the water clusters are given in the Supporting Information. Selected data is given in Table 1 and shown in Figures 2 and 3. Frequencies and zero-point energies could be calculated only at the RHF/3-21G level of theory due to computational limitations.

We are aware that water clusters $(H_2O)_{20}$, $(H_2O)_{24}$, and $(H_2O)_{28}$ were previously calculated at the Hartree–Fock level of theory using the basis sets 3-21G,[28] 6-31G*,[23,29] 6-31+G*,[30] and 6-31G**.[31] To our knowledge the electronic correlation effect is taken into account in three studies with density functional theory (B3LYP/cc-pVVDZ,[32] (B3LYP/6-311++G**[33] and ab initio plane wave molecular dynamics[34]) computations for the dodecahedron $(H_2O)_{20}$ and tetrakaidecahedron $(H_2O)_{24}$ only. Here we want to emphasize that we optimized water clusters that are twice as large as those, and that we calculated all structures at the Hartree–Fock and the B3LYP level throughout. Calculations at the same level of theory allow a reliable comparison of all water clusters taken into consideration including $(H_2O)_{60}$.

Received: June 7, 2004
Revised: October 18, 2004
Published online: December 23, 2004

Keywords: clathrate hydrates · density functional calculations · hydrogen bonds · water clusters

[1] G. A. Jeffrey, *An Introduction to Hydrogen Bonding*, Oxford University Press, New York, **1997**, chaps. 8, 9.
[2] G. A. Jeffrey, in ref. [1], p. 143. Pentagonal elements occur in ices III, V, IX. Ice V most resembles clathrate hydrate host lattices of the type studied here.
[3] L. Pauling, R. E. Marsh, *Proc. Natl. Acad. Sci. USA* **1952**, *49*, 112–118; G. A. Jeffrey, ref. [1], chap. 9.
[4] R. K. McMullan, G. A. Jeffrey, *J. Chem. Phys.* **1965**, *42*, 2725–2732; F. Hollander, G. A. Jeffrey, *J. Chem. Phys.* **1977**, *66*, 4699–4705.
[5] J. M. Brooks, H. B. Cos, W. R. Bryant, M. C. Kennicut, R. G. Mann, T. S. McDonald, *Org. Geochem.* **1986**, *20*, 221–234.
[6] T. Hondoh, H. Anzail, A. Goto, S. Mae, A. Higashi, C. C. Langway, Jr., *J. Inclusion Phenom.* **1990**, *8*, 17–24.
[7] J. C. Seitz, J. D. Pasteris, B. Wopenka, *Geochim. Cosmochim. Acta* **1987**, *51*, 1651–1664.
[8] J. I. Lunine, D. J. Stevenson, *Astrophys. J. Suppl. Ser.* **1985**, *58*, 493–531.

 © 2005 Wiley-VCH Verlag GmbH & Co. KGaA, Weinheim

[9] J. A. Ripmeester, J. S. Tse, C. I. Ratcliffe, B .M. Powell, *Nature* **1987**, *325*, 135 – 136.
[10] D. W. Davidson, S. K. Garg, S. R. Gough, Y. P. Handa, C. I. Ratcliffe, J. A. Ripmeester, J. S. Tse, W. F. Lawson, *Geochim. Cosmochim. Acta* **1986**, *50*, 619 – 623.
[11] R. Ludwig, F. Weinhold, *J. Chem. Phys.* **1999**, *110*, 508 – 515.
[12] O. Ermer, A. Eling, *J. Chem. Soc. Perkin Trans. 2* **1994**, 925 – 944.
[13] J. Bai, C.-R. Su, R. D. Parra, X. C. Zang, H. Tanaka, K. Koya, J.-M. Li, *J. Chem. Phys.* **2003**, *118*, 3913 – 3916.
[14] A. Müller, E. Krickemeyer, H. Bögge, M. Schmidtmann, B. Botar, M. O. Talismanova, *Angew. Chem.* **2003**, *115*, 2085 – 2090; *Angew. Chem. Int. Ed.* **2003**, *42*, 2131 – 2136.
[15] A. Müller, M. Henry, *C. R. Chim.* **2003**, *6*, 1201 – 1208.
[16] Gaussian 98 (Revision A.7), M. J. Frisch, G. W. Trucks, H. B. Schlegel, G. E. Scuseria, M. A. Robb, J. R. Cheeseman, V. G. Zakrzewski, J. A. Montgomery, R. E. Stratmann, J. C. Burant, S. Dapprich, J. M. Millam, A. D. Daniels, K. N. Kudin, M. C. Strain, O. Farkas, J. Tomasi, V. Barone, M. Cossi, R. Cammi, B. Mennucci, C. Pomelli, C. Adamo, S. Clifford, J. Ochterski, G. A. Petersson, P. Y. Ayala, Q. Cui, K. Morokuma, D. K. Malick, A. D. Rabuck, K. Raghavachari, J. B. Foresman, J. Cioslowski, J. V. Ortiz, B. B. Stefanov, G. Liu, A. Liashenko, P. Piskorz, I. Komaromi, R. Gomperts, R. L. Martin, D. J. Fox, T. Keith, M. A. Al-Laham, C. Y. Peng, A. Nanayakkara, C. Gonzalez, M. Challacombe, P. M. W. Gill, B. G. Johnson, W. Chen, M. W. Wong, J. L. Andres, M. Head-Gordon, E. S. Replogle, J. A. Pople, Gaussian, Inc., Pittsburgh, PA, **1998**..
[17] F. Weinhold, *J. Mol. Struct.* **1997**, *398–399*, 181 – 197.
[18] F. Weinhold, *J. Chem. Phys.* **1998**, *109*, 367 – 372; F. Weinhold, *J. Chem. Phys.* **1998**, *109*, 373 – 384.
[19] D. Eisenberg, W. Kauzmann, *The Structure and Properties of Water*, Oxford University Press, New York, **1969**.
[20] F. H. Stillinger, *Science* **1980**, *209*, 451 – 457.
[21] G. V. Andrievsky, V. K. Klochkov, A. Bordynh, G. I. Dovbeshko, *Chem. Phys. Lett.* **2002**, *364*, 8 – 17.
[22] G. V. Andrievsky, V. K. Klochkov, E. L. Karyakina, N. O. Mchedlov-Petrossyan, *Chem. Phys. Lett.* **1999**, *300*, 392 – 396.
[23] A. Khan, *J. Chem. Phys.* **1999**, *110*, 11 884 – 11 889.
[24] E. M. Kotsalis, R. L. Jaffe, J. H. Walther, T. Werder, P. Koumoutsakos (Center for Turbulence Research), *Ann. Res. Briefs* **2001**, 283 – 291.
[25] J. H. Walther, T. Halicioglu, R. Jaffe, P. Koumoutsakos, *J. Chem. Phys. B* **2001**, *105*, 9980 – 9987.
[26] M. S. Dresselhaus, G. Dresselhaus, P. C. Eklund, *Science of Fullerenes and Carbon Nanotubes*, Academic Press, San Siego, **1996**.
[27] Z. Yoshida, H. Takekuma, S. Takekuma, Y. Matsubara, *Angew. Chem.* **1994**, *106*, 1658 – 1660; *Angew. Chem. Int. Ed. Engl.* **1994**, *33*, 1597 – 1599.
[28] I. Ida, K. Endo, *J. Comput. Chem.* **2002**, *23*, 1071 – 1075.
[29] A. Khan, *J. Phys. Chem. A* **2001**, *105*, 7429 – 7434.
[30] R. V. Bolosludov, Y. Kawazoa, V. R. Bolosludov, F. A. Kuznetzov in *Proceedings of the Fourth International Conference on Gas Hydrates*, Yokohama, **2002**, p. 683.
[31] S. Maheshwary, N. Patel, N. Sathymurthy, A. D. Kulkarni, S. R. Gadre, *J. Phys. Chem. A* **2001**, *105*, 10 525 – 10 537.
[32] J. L. Kuo, C. V. Ciobanu, L. Ojamämae, I. Shavitt, S. J. Singer, *J. Chem. Phys.* **2003**, *118*, 3583 – 3588.
[33] K. Laasonen, M. L. Klein, *J. Phys. Chem.* **1994**, *98*, 10 079 – 10 083.
[34] V. Chihaia, S. Adams, W. Kuhs, *Chem. Phys.* **2004**, *297*, 271 – 287.

 © 2005 Wiley-VCH Verlag GmbH & Co. KGaA, Weinheim

Catalyst Development

Very Stable and Highly Regioselective Supported Ionic-Liquid-Phase (SILP) Catalysis: Continuous-Flow Fixed-Bed Hydroformylation of Propene**

Anders Riisager, Rasmus Fehrmann, Stephan Flicker, Roy van Hal, Marco Haumann, and Peter Wasserscheid**

In the last decade the application of ionic liquids in catalysis[1] has been the subject of intensive research in academia and industry.[2] A major reason for the growing interest is the use of ionic liquids as alternative solvents[3] for many transition-metal-catalyzed reactions. In particular, liquid–liquid biphasic processes having an organic product phase have been examined since the ionic catalyst phase often induces excellent catalyst immobilization and also has low miscibility with the organic reaction products. However, implementation of these strategies in industrial processes is still hampered by the fact that the biphasic methodologies rely on relatively large amounts of ionic liquids. Even though ionic liquids have become commercially available[4] they are still relatively expensive compared to traditional solvents.

In many cases, liquid–liquid biphasic catalysis makes use of only a fraction of the ionic-liquid solvent and of the catalyst dissolved therein. In the case of a fast chemical reaction and relatively slow mass transfer (caused by the relatively high viscosity of the ionic liquid) the concentration of the reactant in the bulk ionic-liquid phase is reduced significantly, and the reaction occurs primarily at the interphase or in the diffusion layer of the ionic-liquid catalyst phase rather than in the bulk solvent. An ideal catalyst system would thus consist of a bulk catalyst phase the same size as the diffusion layer. In this way the solubilized catalyst complex and the ionic liquid are all available. In addition, application of solid catalysts is pre-

[*] Dr. A. Riisager, Prof. R. Fehrmann, Dr. S. Flicker
Department of Chemistry and
Interdisciplinary Research Center for Catalysis (ICAT)
Technical University of Denmark
Building 207, 2800 Kgs. Lyngby (Denmark)
Fax: (+45) 4525-2235
E-mail: ar@kemi.dtu.dk

Dipl.-Chem. R. van Hal, Dr. M. Haumann, Prof. P. Wasserscheid
Lehrstuhl für Chemische Reaktionstechnik
Universität Erlangen-Nürnberg
Egerlandstrasse 3, 91058 Erlangen (Germany)
Fax: (+49) 9131-852-7421
E-mail: wasserscheid@crt.cbi.uni-erlangen.de

[**] This work was supported by the ConNeCat project "Smart ligands—smart solvents" financed by the German Federal Ministry for Education and Research (BMBF). Financial support (M.H.) by the Deutsche Forschungsgemeinschaft (DFG) and by The Foundation of Technical Chemistry, Technical University of Denmark (FTIR equipment) are gratefully acknowledged. The authors thank Dr. A. Kustov (Department of Chemistry, Technical University of Denmark) and Prof. O. B. Lapina (Boreskov Institute of Catalysis, Novosibirsk, Russia) for their contributions to this work.

Supporting information for this article is available on the WWW under http://www.angewandte.org or from the author.

 DOI: 10.1002/anie.200461534 © 2005 Wiley-VCH Verlag GmbH & Co. KGaA, Weinheim

ferred from a technical standpoint due to easy product separation and the potential for developing a continuous-flow fixed-bed process.

Recently we and others introduced "heterogenized" versions of homogeneous ionic-liquid catalyst systems, described as supported ionic-liquid-phase (SILP) catalyst systems, for olefin hydroformylation[5–7] (Rh-catalyzed), hydrogenation[8] (Rh-catalyzed), Heck reactions[9] (Pd-catalyzed), and hydroamination[10] (Rh-, Pd-, and Zn-catalyzed). In these systems the catalysts are composed of a transition-metal complex dissolved in a thin film of the ionic liquid, which is held on a porous solid with high surface area by physisorption, tethering, or covalent anchoring. The SILP catalyst concept results in a very efficient use of the ionic liquid and relatively short diffusion distances for the reactants compared to those in conventional two-phase systems with an ionic-liquid catalyst phase. In addition, the negligible vapor pressure, large liquid range, and thermal stability of ionic liquids ensure that the solvent is retained on the support in its fluid state even at elevated temperatures; this makes SILP catalysts highly suitable for continuous processes. Moreover, the solvent properties of the ionic liquid are tuneable by the choice of the cation/anion combination. Further advantages of the SILP concept are, for example, compatibility with hydrolytically labile catalyst complexes and possible catalyst activation by interaction with the ionic liquid.[11]

In rhodium-catalyzed olefin hydroformylation, Mehnert et al.[7] examined the liquid-phase reaction of 1-hexene in a batch reactor using unselective (*n*/*iso* ratios of 0.4–2.4) SILP catalyst systems. The catalysts were composed of monophosphines (PPh_3 and TPPTS) dissolved in [bmim]X (bmim = 1-*n*-butyl-3-methylimidazolium, X = PF_6 or BF_4) on a 1-*n*-butyl-3-[3-(triethoxysilanyl)propyl]imidazolium-modified silica gel support (average of 0.4 imidazolium fragments per nm^2, corresponding to the involvement of approximately 35% of the silanol groups of the support). The SILP catalysts were found to have higher activity than analogous biphasic systems; however, a significant amount of the metal catalyst leached into the product phase at high conversions (rhodium loss of up to 2.1 mol%), due to depletion of the ionic-liquid phase from the support. Importantly, even at lower conversion pronounced catalyst deactivation was observed during recycling, which was independent of the presilylation of the support.[12] This deactiviation shortened the lifetime and limited the applicability of the catalysts significantly.

Recently we have described a selective (*n*/*iso* ratios up to 23.7, that is, 96.0% linearity) SILP catalyst for the Rh-catalyzed gas-phase hydroformylation of propene in a fixed-bed reactor.[6] The rhodium catalyst contains the bisphosphine ligand sulfoxantphos **1** and is dissolved in either a halogen-containing or halogen-free ionic liquid ([bmim]X (X = PF_6 or n-$C_8H_{17}OSO_3$)). These ionic catalyst solutions were physisorbed on the unmodified silica support. However, these systems were also deactivated after prolonged use (reaction time > 24 h) regardless of the type of ionic liquid, the loading α (defined as the volume of the ionic liquid divided by the pore volume,) and the ligand/rhodium ratio.

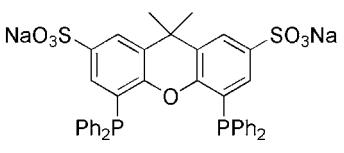
Very recently, Han et al.[13] demonstrated an interesting variation of the SILP concept. They immobilized Pd nanoparticles with a lactate-based ionic liquid on molecular sieves and used the resulting systems for the liquid-phase hydrogenation of cyclohexene and 1-hexene.

In this communication we demonstrate the first use of a SILP catalyst system in which the catalyst remains active, highly selective, and stable over extended periods in a continuous gas-phase process. The catalysts are composed of Rh-**1** in [bmim][n-$C_8H_{17}OSO_3$] on a partly dehydroxylated silica support (hereafter referred to as Rh-**1**/IL/SiO_2). Moreover, we propose an explanation for the deactivation phenomena previously observed with analogous nondehydroxylated SILP silica catalysts. Our proposal is based on FTIR studies of the catalyst conducted in situ (syngas atmosphere at elevated temperature), as well as characterization of the support by MAS ^{31}P NMR spectroscopy and temperature-programmed desorption of ammonia (NH_3-TPD).

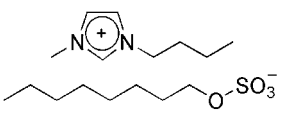
In our previous studies of silica-based Rh-**1** SILP catalysts on nondehydroxylated supports in the continuous-flow hydroformylation of propene (reaction times of 4–5 h),[6] we found that the catalyst performance was strongly influenced by the ligand/rhodium ratio and the loading of the ionic liquid, but less affected by the choice of ionic liquid (except for the catalyst preformation, which appears to depend on the solubility of the ligand and precursor). High selectivities (*n*/*iso* > 20) were obtained only for Rh-**1**/IL/SiO_2 catalyst systems with an L/Rh ratio of more than 10; this is in contrast to analogous reactions performed with an ionic-liquid catalyst solution without a support where high selectivities were observed even at **1**/Rh ratios of 2.[14] The results clearly indicate a significant effect of the inorganic support. Accordingly, we devised a suitable preparation for the support (catalysts with an untreated support were not stable beyond 12–24 h).

In our continuous-flow gas-phase hydroformylation of propene with a reaction time of 60 h, we applied a partially dehydroxylated silica support (heating at 500°C in air for 15 h). In the earlier work[6] support pretreatment implied only drying the support in vacuo (110°C, 24 h). The thermal pretreatment proved to be a crucial parameter for obtaining Rh-**1** silica-based catalysts with high stability during prolonged reactions (Figure 1).

The catalytic performance and catalyst stability, however, still proved to be significantly influenced by the catalyst composition, (loading α and **1**/Rh ratio; Figures 2 and 3). In reactions with catalysts having various **1**/Rh ratios we found that catalysts with low ligand contents (**1**/Rh = 3 and 5) were initially very active compared to the catalyst with **1**/Rh = 10 but less selective (Figure 2). In addition, the catalysts with low ligand content were deactivated relatively quickly within the first 24 h; the turnover frequency (TOF) dropped to 4–5 h^{-1}, and the selectivity fell to *n*/*iso* = 1–1.3). In contrast, the



sulfoxantphos **1**



[bmim][n-$C_8H_{17}OSO_3$]

 © 2005 Wiley-VCH Verlag GmbH & Co. KGaA, Weinheim

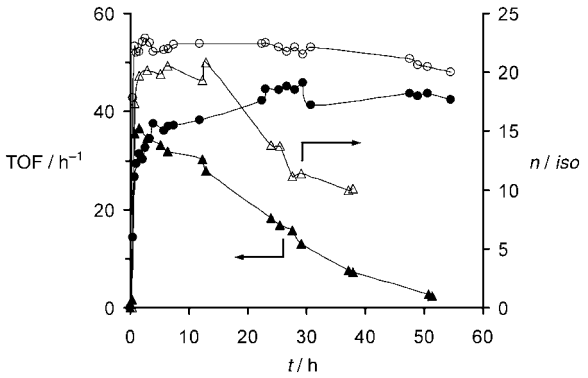


Figure 1. Hydroformylation of propene on untreated (△, ▲) and partly dehydroxylated supports (○,●). Plots of activity (mol butanal (mol Rh)$^{-1}$ h^{-1}, closed symbols) and selectivity (*n*/isobutanal, open symbols) of Rh-**1**/[bmim][*n*-$C_8H_{17}OSO_3$] on silica ($\alpha = 0.1$, **1**/Rh = 10) as function of reaction time.

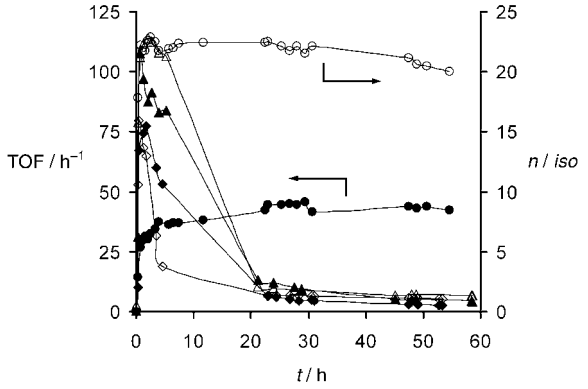


Figure 2. Hydroformylation of propene with catalysts having different amounts of ligand. Plots of activity (mol butanal (mol Rh)$^{-1}$ h^{-1}, closed symbols) and selectivity (*n*/isobutanal, open symbols) of Rh-**1**/[bmim][*n*-$C_8H_{17}OSO_3$] on silica ($\alpha = 0.1$). Results for catalysts with **1**/Rh = 3 (◇, ◆), **1**/Rh = 5 (△, ▲), and **1**/Rh = 10 (○, ●) are shown.

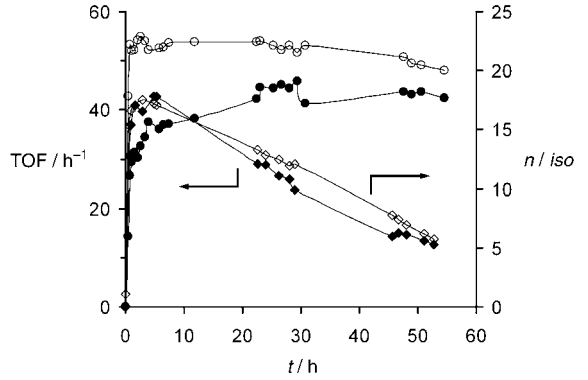


Figure 3. Hydroformylation of propene with catalysts having different loadings α. Plots of activity (mol butanal (mol Rh)$^{-1}$ h^{-1}, closed symbols) and selectivity (*n*/isobutanal, open symbols) of Rh-**1**/[bmim][*n*-$C_8H_{17}OSO_3$] on silica (**1**/Rh = 10). Results for catalysts with $\alpha = 0$ (◇, ◆) and $\alpha = 0.1$ (○, ●) are shown.

catalyst with **1**/Rh = 10 retained the initial catalytic performance over at least 60 h (TOF = 44 h^{-1}, TON ≈ 2600, *n*/*iso* > 20).

These results clearly indicate that a large excess of ligand is required for a stable SILP catalytic system. Even when the support is pretreated, reactions presumably occur between the ligand and the support, rendering some of the ligand inaccessible for complex formation. Evidence for the interaction of the ligand and the support was provided by solid-state MAS ^{31}P NMR spectra of Rh-**1**/IL/SiO_2 (**1**/Rh = 10) recorded prior to reaction (see the Supporting Information). Here, the signals measured could be assigned to free ligand ($\delta = -13$ ppm, 27%), surface-bonded ligand ($\delta = -21$ ppm, 54%), and complexed ligand ($\delta = 31$ ppm, 19%).

Moreover, in studies with catalysts having different loadings of the ionic liquid ($\alpha = 0$–0.5), the catalyst systems containing no ionic liquid were deactivated rapidly; after a reaction time of 60 h only 30% of the initial activity and selectivity remained (Figure 3). The slow deactivation of the other catalysts can be explained by the slow surface diffusion of the ligand from the initial Rh-coordinated active state to the surface-bonded state, in which the metal atom is less coordinated to the ligand but possibly more strongly coordinated to the support and thus less active and selective. Evidently the SILP catalysts require a certain amount of ionic-liquid solvent—not only for high selectivities (*n*/*iso* > 20) as previously seen—but also for stability over longer periods during continuous processes. Further, since the *n*/*iso* selectivity in hydroformylation reactions is known to depend on the amount of ligand available for coordination,[15] the simultaneous decrease in selectivity along with activity lends additional support to the hypothesis that deactivation is closely related to a gradual degradation and removal of ligand from the catalyst complex system.

To further explain the observed results, we studied the catalyst in situ under conditions closely related to the reaction conditions by FTIR spectroscopy (Figure 4). The FTIR spectra of the system Rh-**1**/IL/SiO_2 (**1**/Rh = 10; 100 °C) show the relatively fast transformation of the red dimeric catalyst precursor [{Rh(μ-CO)(**1**)(CO)}$_2$] (**2**)[16]—characterized by a broad band for the terminal CO stretch at $\tilde{\nu}$(CO) = 1990 cm^{-1}—to the light-yellow monomeric compound

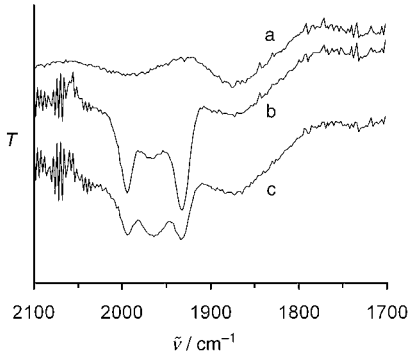


Figure 4. Part of an FTIR spectra of Rh-**1**/IL/SiO_2 catalysts (**1**/Rh = 10, $\alpha = 0.5$) at 100 °C after: a) 15 min in nitrogen, b) 15 min in syngas, and c) 30 min in syngas.

 © 2005 Wiley-VCH Verlag GmbH & Co. KGaA, Weinheim

[$HRh(CO)_2$(**1**)] (Scheme 1), which has two isomeric forms, **3**-ea ($\tilde{\nu}$(CO) = 1994, 1948 cm^{-1}) and **3**-ee ($\tilde{\nu}$(CO) = 2035 (w), 1964 cm^{-1}) coexisting in dynamic equilibrium. Reexposure of the **3**-ea/**3**-ee mixture to nitrogen slowly regenerates the dimer **2** reversibly, while air treatment leads to irreversible degradation of the complex and presumably to the oxidation of excess ligand. This is supported by a significant change in the color of the sample along with the appearance of a new broad CO band at $\tilde{\nu}$(CO) = 1972 cm^{-1}.

Importantly, the complex formation in the SILP Rh-**1**/IL/SiO_2 catalysts with **1**/Rh = 10 (Scheme 1) is very similar to that previously reported for Rh-**1** and analogous rhodium–xanthene-based systems[16] in organic and ionic-liquid solvents (Table 1). Thus, it seems reasonable to conclude that complex formation in the SILP catalyst systems takes place in the ionic-liquid solvent, and consequently that the examined SILP hydroformylation reactions are indeed homogeneously catalyzed.

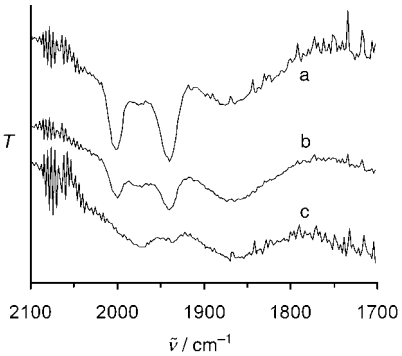
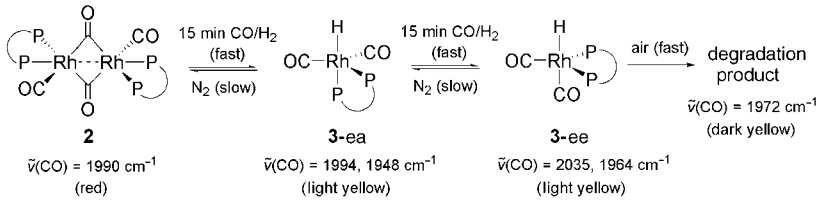


Figure 5. Part of an FTIR spectra of Rh-**1**/IL/SiO_2 catalysts (α = 0.1, 100 °C, after 15 min in syngas) containing different ligand/Rh ratios: a) **1**/Rh = 10, b) **1**/Rh = 5, and c) **1**/Rh = 3.



Scheme 1. Formation of Rh complexes in the Rh-**1**/IL/SiO_2 catalyst systems (**1**/Rh = 10) at 100 °C during various gas treatments.

Table 1: Comparison of $\tilde{\nu}$(CO) bands of [$HRh(CO)_2$(L)] complexes in different systems.

	Solvent	ea isomer $\tilde{\nu}$(CO) [cm^{-1}]	ee isomer $\tilde{\nu}$(CO) [cm^{-1}]
SILP (Rh-**1**/IL/SiO_2)	[bmim][*n*-$C_8H_{17}OSO_3$]	1994, 1948	2035, 1964
[$RhH(CO)_2$(**1**)][16b]	[bmim][PF_6]	1985, 1935	2032, 1967
[$RhH(CO)_2$(xantphos)][16b]	benzene	1991, 1941	2036, 1969
[$RhH(CO)_2$(thixantphos)][16b]	cyclohexane	1999, 1953	2040, 1977

The FTIR spectra of the analogous catalysts with **1**/Rh = 3 and 5 show that degraded catalysts formed irreversibly regardless of the gas treatment. The decrease in the intensity of the two characteristic absorption bands was more pronounced for catalysts with **1**/Rh = 3 than for catalysts having **1**/Rh = 5 (Figure 5). For catalysts with **1**/Rh = 10 no loss in intensity was observed. This clearly suggests that catalysts with **1**/Rh = 10 contain a sufficient amount of ligand to stabilize the monomeric, catalytically active monomers. Since this is in excellent accordance with the relative catalyst stabilities measured, the stability of the SILP catalyst is directly related to the degradation of the catalytically active complex, which in turn is correlated to the amount of ligand available for complex formation.

The proportion of acidic OH groups (mostly Brønsted sites) on the partly dehydroxylated silica support used was evaluated by NH_3-TPD to be 69 μmol OH g^{-1}, which corresponds to 26 % of the original content present in the untreated support (see the Supporting Information for details). This is in relatively good agreement with the remaining fraction of 35 % Si-OH groups (Q3, $\delta \approx -100$ ppm) relative to Si-O-Si groups (Q4, $\delta \approx -111$ ppm) determined by solid-state MAS ^{29}Si NMR spectroscopy for analogous samples (see the Supporting Information). Therefore, it seems reasonable to assume that the pretreatment decreases the amount of acidic OH groups on the support only by dehydroxylation of surface silanol groups and not by, for example, inducing structural changes in the support. This is further affirmed by the identical T_{max} values obtained for ammonia desorption and by the practically unchanged BET surface area and pore volume after dehydroxylation.

The amount of ligand **1** present in the Rh-**1**/IL/SiO_2 system during catalysis was determined for L/Rh = 3 to be 58 μmol **1** g^{-1}; for L/Rh = 5, 97 μmol **1** g^{-1} support; and for L/Rh = 10, 194 μmol **1** g^{-1} support. These values can be correlated to the measured OH content of the support, by assuming that the ligand bonds irreversibly to one acidic OH group on the surface of the support. Hence, very little ligand should be available for complex formation in the case of a catalyst with L/Rh = 3, 30 % of the ligand should still be available with L/Rh = 5 (i.e. effective **1**/Rh ratio = 1.5), and 65 % of the ligand should still be available with L/Rh ratio = 10 (effective **1**/Rh = 6.5). Consequently, highly selective and stable catalyst systems can be obtained only when the amount of ligand is sufficient to compensate for the loss induced by the surface bonding, that is, when the effective **1**/Rh ratio is greater than 1. This is in excellent agreement with the experimental data, thus underlining the importance of the acidic OH groups of the support for the long-term stability of SILP Rh–phosphine catalysts.

This paper describes important progress in the very promising field of SILP catalysis. We demonstrate for the first time the long-term stability of Rh-**1**/[bmim][*n*-$C_8H_{17}OSO_3$] catalysts supported on partly dehydroxylated silica in the selective, continuous, gas-phase hydroformylation of propene. Clear spectroscopic evidence also indicates that the catalysis in the supported ionic-liquid layer is homogeneous. Moreover, decreasing the number of surface silanol

 © 2005 Wiley-VCH Verlag GmbH & Co. KGaA, Weinheim

groups on the support material by thermal treatment is a crucial parameter in the preparation of stable hydroformylation systems that are selective and active for at least 60 h on stream.

We have found that the effect of the support is directly related to the irreversible reaction of the ligand with the acidic silanol surface groups before and during catalysis. Therefore, the prerequisites for active, highly selective, and long-term stable SILP catalysts are not only the ionic-liquid solvent but also a relatively large excess of phosphine ligand to compensate for some detrimental surface reactions.

We hope that the knowledge gained in this work will lead to the development of new SILP catalysts for hydroformylations, hydrogenations, and C–C coupling reactions. The combination of well-defined catalyst complexes, nonvolatile ionic liquids, and porous solid supports offers many advantages over traditional catalysis with water (SAPC) or with organic solvents with low vapor pressure (SLPC) on supports,[17] which are clearly limited by solvent volatility.[18] We therefore consider the SILP catalysis concept to be a significant contribution to the development of highly selective, heterogenized homogeneous catalysts.

Experimental Section

The SILP catalysts were prepared according to our previously reported method[6] by impregnation of the partly dehydroxylated silica support with an anhydrous methanolic solution of the ionic liquid [bmim][*n*-$C_8H_{17}OSO_3$][19] containing the catalyst precursor [Rh(acac)$(CO)_2$] (Aldrich, 98%) and bisphosphine ligand **1**[20] under argon atmosphere using standard Schlenk techniques. The partial dehydroxylation of the support (silica gel 100, Merck) was performed by heating at 500°C in air for 15 h followed by storage in vacuo over P_4O_{10} prior to use (BET surface area: 304 $m^2 g^{-1}$, pore volume: 1.01 $cm^3 g^{-1}$, mean pore diameter (monomodal): 132 Å).

The continuous-flow gas-phase hydroformylation of propene was performed at a total pressure of 10 bar (C_3H_6:CO:H_2 = 1:1:1) and T = 100°C with differential conversion (< 10% conversion) using a microcatalytic flow system. The solid SILP catalyst was used as a fixed bed in a stainless-steel tubular reactor, as previously described.[5,6] The activity (TOF) and selectivity (*n*/*iso*) of the catalysts were determined directly from online FID-GC measurements (Shimadzu GC-9A, Nukol capillary columm, 15 m × 0.53 mm ID, Supelco Inc.) of the reaction products by comparison with authentic samples of aldehydes.

FTIR spectra of the catalysts were recorded on a Perkin Elmer Paragon 1000 FTIR spectrophotometer. Samples were prepared as KBr catalyst wafers by pressing catalyst onto the KBr and mounted for measurements in situ under various gas atmospheres at 100°C in a stainless-steel variable-temperature transmittance IR cell (Infraspac LB-100, Infraspac Ltd, Novosibirsk, Russia; Si optical windows) having gas inlet and outlet ports and an adjustable sample holder. With this setup each recording could be corrected for background absorbance without changing the atmosphere.

Experimental details and data from MAS ^{31}P and ^{29}Si NMR spectroscopy and NH_3-TPD measurements are available in the Supporting Information.

Received: August 4, 2004
Published online: December 21, 2004

[1] List of reviews: a) J. D. Holbrey, K. R. Seddon, *Clean Prod. Proc.* **1999**, *1*, 223–236; b) T. Welton, *Chem. Rev.* **1999**, *99*, 2071–2083; c) P. Wasserscheid, W. Keim, *Angew. Chem.* **2000**, *112*, 3926–3946; *Angew. Chem. Int. Ed.* **2000**, *39*, 3772–3789; d) J. Dupont, C. S. Consorti, J. Spencer, *J. Braz. Chem. Soc.* **2000**, *11*, 337–344; e) R. Sheldon, *Chem. Commun.* **2001**, 2399–2407; f) C. M. Gordon, *Appl. Catal. A* **2001**, *222*, 101–117; g) D. Zhao, M. Wu, Y. Kou, E. Min, *Catal. Today* **2002**, *74*, 157–189; h) H. Olivier-Bourbigou, L. Magna, *J. Mol. Catal. A: Chem.* **2002**, *182/183*, 419–437; i) J. Dupont, R. F. de Souza, P. A. Z. Suarez, *Chem. Rev.* **2002**, *102*, 3667–3692; j) H. Zhao, S. V. Malhotra, *Aldrichimica Acta* **2002**, *35*, 75–83.
[2] R. D. Rogers, K. R. Seddon, *Science* **2003**, *302*, 792–793, and references therein.
[3] a) *Ionic Liquids in Synthesis*, *1st ed.* (Eds.: P. Wasserscheid, T. Welton), VCH-Wiley, Weinheim, **2003**; b) J. S. Wilkes, *J. Mol. Catal. A: Chem.* **2004**, *214*, 11–17.
[4] Selection of ionic liquid suppliers: a) Solvent Innovation (www.solvent-innovation.com); b) Sigma-Aldrich (www.sigma-aldrich.com); Fluka (www.fluka.com); c) Merck (www.merck.-com); d) Acros Organics (www.acros.com); e) Wako (www.wako-chem.co.jp); f) Strem (www.strem.com).
[5] A. Riisager, K. M. Eriksen, P. Wasserscheid, R. Fehrmann, *Catal. Lett.* **2003**, *90*, 149–153.
[6] a) A. Riisager, P. Wasserscheid, R. van Hal, R. Fehrmann, *J. Catal.* **2003**, *219*, 252–255; b) A. Riisager, R. Fehrmann, P. Wasserscheid, R. van Hal in *Ionic Liquids III: Fundamentals, Progress, Challenges, and Opportunities* (Eds.: R. Rogers, K. R. Seddon), ACS, Washington DC, **2004**, in press.
[7] C. P. Mehnert, R. A. Cook, N. C. Dispenziere, M. Afeworki, *J. Am. Chem. Soc.* **2002**, *124*, 12932–12933.
[8] a) C. P. Mehnert, E. J. Mozeleski, R. A. Cook, *Chem. Commun.* **2002**, 3010–3011; b) A. Wolfson, I. F. J. Vankelecom, P. A. Jacobs, *Tetrahedron Lett.* **2003**, *44*, 1195–1198.
[9] H. Hagiwara, Y. Sugawara, K. Isobe, T. Hoshi, T. Suzuki, *Org. Lett.* **2004**, *6*, 2325–2328.
[10] S. Breitenlechner, M. Fleck, T. E. Müller, A. Suppan, *J. Mol. Catal. A: Chem.* **2004**, *214*, 175–179.
[11] P. Wasserscheid, M. Eichmann, *Catal. Today* **2001**, *66*, 309–316.
[12] C. P. Mehnert, R. A. Cook, E. J. Mozeleski, N. C. Dispenziere, M. Afeworki, *Supported ionic liquid catalysis for hydroformylation and hydrogenation reactions*, 226th ACS National Meeting, New York, USA, **2003**.
[13] J. Huang, T. Jiang, H. Gao, B. Han, Z. Liu, W. Wu, Y. Chang, G. Zhao, *Angew. Chem.* **2004**, *116*, 1421–1423; *Angew. Chem. Int. Ed.* **2004**, *43*, 1397–1399.
[14] R. van Hal, P. Wasserscheid, unpublished results.
[15] *Rhodium Catalyzed Hydroformylation*, (Eds.: P. W. N. M. van Leeuwen, C. Claver), Kluwer, Dordrecht, **2000**.
[16] a) A. J. Sandee, V. F. Slagt, J. N. H. Reek, P. C. J. Kamer, P. W. N. M. van Leeuwen, *Chem. Commun.* **1999**, 1633–1634; b) S. M. Silva, R. P. J. Bronger, Z. Freixa, J. Dupont, P. W. N. M. van Leeuwen, *New J. Chem.* **2003**, *27*, 1294–1296.
[17] a) K. T. Wan, M. E. Davis, *Nature* **1994**, *370*, 449–450; b) *Applied Homogeneous Catalysis with Organometallic Compounds*, *1st ed.* (Eds.: B. Cornils, W. A. Herrmann), VCH, Weinheim, **1996**.
[18] A. Beckmann, F. J. Keil, *Chem. Eng. Sci.* **2003**, *58*, 841–847.
[19] P. Wasserscheid, R. van Hal, A. Bösmann, *Green Chem.* **2002**, *4*, 400–404.
[20] M. S. Goedheijt, P. C. J. Kamer, P. W. N. M. van Leeuwen, *J. Mol. Catal. A: Chem.* **1998**, *134*, 243–249.

Keywords: catalyst development · hydroformylation ionic liquids · phosphine ligands · rhodium

 © 2005 Wiley-VCH Verlag GmbH & Co. KGaA, Weinheim

Natural Product Synthesis

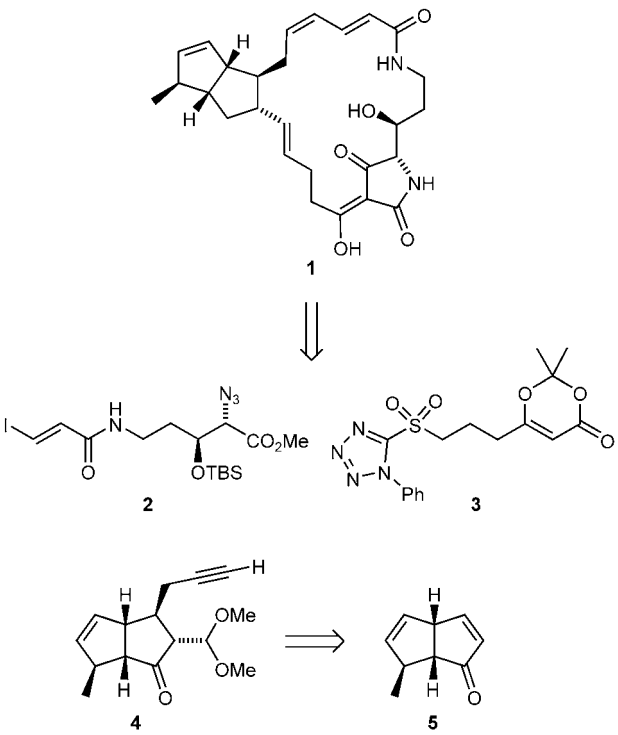
Enantioselective Total Synthesis of Cylindramide**

Nicolai Cramer, Sabine Laschat, Angelika Baro, Harald Schwalbe, and Christian Richter*

Dedicated to Professor Franz Effenberger on the occasion of his 75th birthday

Marine organisms produce a tremendous variety of bioactive secondary metabolites,[1] which are often used as lead structures in the development of novel pharmaceuticals. In 1993 Fusetani et al. isolated cylindramide (**1**) from the marine sponge *Halichondria cylindrata*, and it was found to exhibit pronounced cytotoxicity against B16 melanoma cells.[2] Cylindramide belongs to the class of complex tetramic acid lactams, which also includes structurally related compounds such as discodermide from the Caribbean marine sponge *Discodermia dissoluta*,[3] alteramide A from a bacterium *Alteromonas* sp. associated with the sponge *Halichondria okadai*,[4] aburatubolactam A isolated from a cultured broth of a *Streptomyces culture* stemming from a mollusk,[5] maltophilin produced by *Stenotrophomonas maltophilia*,[6] and geodin A magnesium salt, which was recently isolated from the Southern Australian marine sponge *Geodia*.[7] Besides the tetramic acid unit, a substituted bicyclo[3.3.0]octane skeleton is the characteristic feature of these macrocyclic compounds. However, to our knowledge, syntheses of this type of macrocycles have not yet been reported, with exception of one model study[8] and two total syntheses of the related ikarugamycin, in which the bicyclooctane moiety is replaced by a decahydroindacene framework.[9,10]

Our synthetic strategy was based on the retrosynthetic degradation of cylindramide (**1**) into the three fragments **2**–**4** (Scheme 1). The pentalene derivative **4** should be accessible from pentalenone **5** by a tandem process consisting of a Michael addition and an electrophilic trapping reaction. It should be possible to couple hydroxyornithine **2** and phenyltetrazolyl (PT) sulfone **3** to pentalene **4** by Sonogashira coupling and Julia–Kocienski olefination, respectively. After macrocyclization, the formation of the tetramic acid unit should conclude the synthesis.



Scheme 1. Retrosynthesis of cylindramide (**1**).

The generation of building block **2** (Scheme 2) started with a Wittig olefination of the Boc-protected β-aminoaldehyde **6**[11] to give derivative **7**, which was converted into alcohol **8** by Sharpless asymmetric dihydroxylation and subsequent regioselective nosylation.[12] A sequence of nucleophilic substitution with tetramethylguanidinium azide ($TMGN_3$),[13] protection of the OH function, and removal of the Boc protecting group afforded α-azidoester **9**. Following the method of Shioiri et al.,[14] we finally coupled derivative **9** with β-iodoacrylic acid **10** to give fragment **2** in 83% yield.

Sulfone **3** was prepared from precursor 2,2,5-trimethyl-4*H*-1,3-dioxin-4-one (**11**)[15] (Scheme 3). Alkylation, ozonolysis, and reductive workup gave alcohol **13**. The phenyltetrazolthiol was introduced by a Mitsunobu reaction, and the resulting intermediate **14** oxidized to PT-sulfone **3** with H_2O_2 in the presence of a Mo catalyst.[16]

Enantiopure bicyclo[3.3.0]octanonacetal **15**, which is available in five steps by transannular Pd-catalyzed coupling of cycloocta-1,5-diene followed by enzymatic resolution,[17] served as the starting material for the pentalene unit. We employed the IBX method of Nicolaou et al.[18] to oxidize ketone **15** affording enone **16** in 63% yield (Scheme 4).

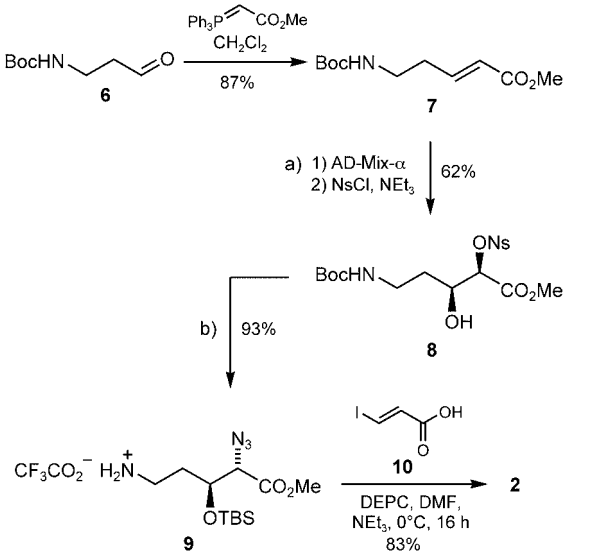
The 1,4-addition of Me_2CuLi to enone **16** and trapping with Comins reagent (**17**)[19] resulted, however, in a mixture of vinyl triflate **19** (47%) and ketone **18** (39%). Fortunately, the latter could be converted into the desired triflate **19** in 72%

[*] Dipl.-Chem. N. Cramer, Prof. S. Laschat, Dr. A. Baro
Institut für Organische Chemie
Universität Stuttgart
Pfaffenwaldring 55, 70569 Stuttgart (Germany)
Fax: (+49) 711-685-4285
E-mail: sabine.laschat@oc.uni-stuttgart.de
Prof. H. Schwalbe, Dr. C. Richter
Institut für Organische Chemie und Chemische Biologie
Zentrum für Biomolekulare Magnetische Resonanz
Johann Wolfgang Goethe-Universität Frankfurt
Marie-Curie-Strasse 11, 60439 Frankfurt am Main (Germany)

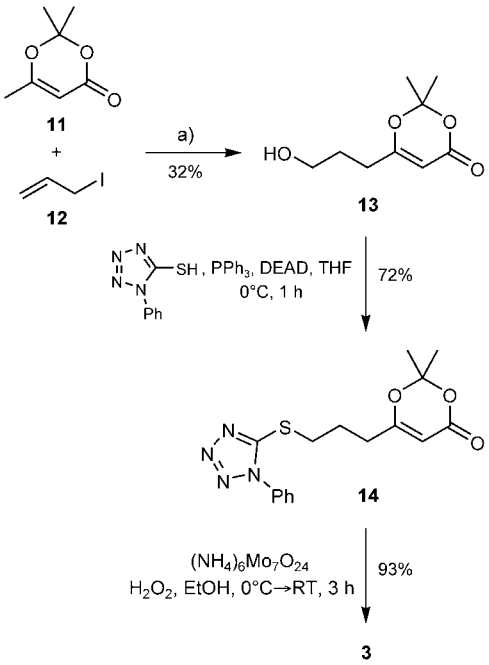
[**] This work was supported by the Deutsche Forschungsgemeinschaft, the Ministerium für Wissenschaft, Forschung und Kunst des Landes Baden-Württemberg, and the Fonds der Chemischen Industrie (fellowship for N.C.). We thank Dipl.-Chem. N. Steinke and M. Buchweitz for their assistance, Prof. N. Fusetani and Dr. S. Matsunaga for reference spectra, and the Amersham Buchler company for chemicals.

Supporting information for this article is available on the WWW under http://www.angewandte.org or from the author.

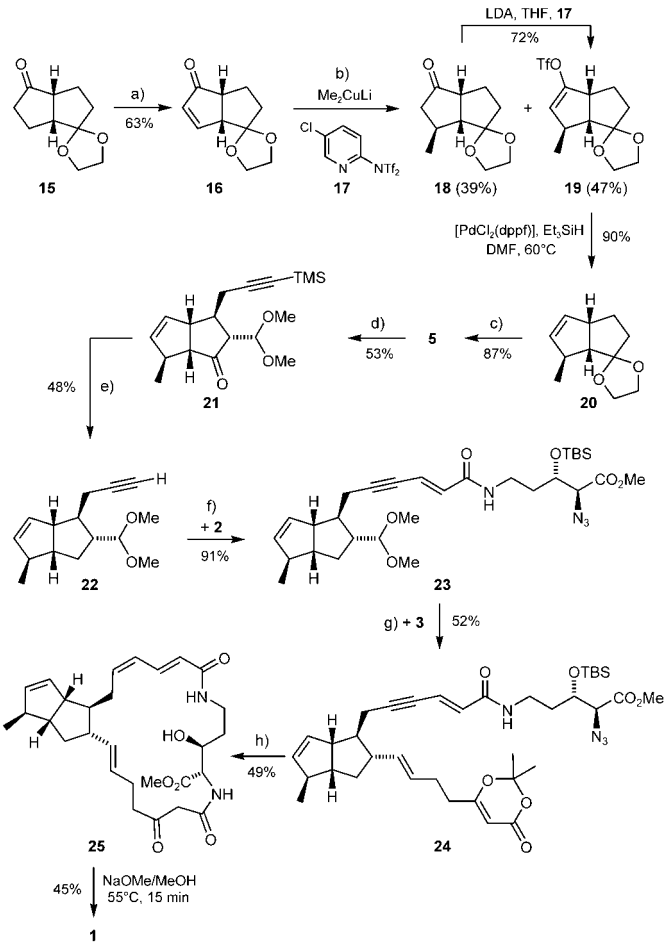
 © 2005 Wiley-VCH Verlag GmbH & Co. KGaA, Weinheim DOI: 10.1002/anie.200461823



Scheme 2. Reagents and conditions: a) 1. AD-mix-α, *t*BuOH/H_2O, $MeSO_2NH_2$, 0 °C, 1 d, 95 %, 96 % *ee*, 2. NsCl (1 equiv), NEt_3, CH_2Cl_2, 0 °C, 12 h, 65 %; b) 1. tetramethylguanidinium azide ($TMGN_3$) (6 equiv), DMF, 50 °C, 15 h, 96 %, 85:15 d.r., 2. TBSCl, DMAP, DMF, 97 %, 3. TFA, CH_2Cl_2, 0 °C, 1 h, quant. Boc = *tert*-butoxycarbonyl, DEPC = diethyl cyanophosphonate, DMAP = 4-dimethylaminopyridine, DMF = dimethylformamide, Ns = 4-nitrobenzenesulfonyl, TFA = trifluoroacetic acid, TBS = *tert*-butyldimethylsilyl.



Scheme 3. Reagents and conditions: a) 1. LDA, DMPU, THF, **11**, 0 °C, 1 h, **12**, −40 °C→RT, 16 h, 50 %; 2. O_3, $MeOH/CH_2Cl_2$/pyridine (3:3:1), −78 °C, then $NaBH_4$, 64 %. DEAD = diethylazodicarboxylate, DMPU = *N*,*N*′-dimethyl-*N*,*N*′-propylene urea.



Scheme 4. Reagents and conditions: a) LDA, THF, TMSCl, −78 °C→0 °C, 4-methoxypyridin-*N*-oxide (MPO), IBX, DMSO, CH_2Cl_2, RT, 45 min, 63 %; b) Me_2CuLi, THF, **17**, −78 °C→0 °C; c) 1. PPTS, acetone, H_2O, reflux, quant., 2. LDA, THF, TMSCl, −78 °C→0 °C, then MPO, IBX, DMSO, CH_2Cl_2, RT, 30 min, 87 %; d) TMS-C≡CCH_3, *t*BuLi, TMEDA, THF, −40 °C, 1 h, CuI, TMSCl, THF, −78 °C, **5**, 2 h, then $BF_3{\cdot}OEt_2$, $HC(OMe)_3$, CH_2Cl_2, −20 °C, 1 h, 53 %; e) 1. $NaBH_4$, MeOH, 0 °C, 2. $(Im)_2CS$ (5 equiv), DMAP (5 equiv), DCE, reflux, 16 h, 3. Bu_3SnH, AIBN, toluene, 110 °C, 45 min, 57 % over 3 steps, 4. EtOH, H_2O, $AgNO_3$, 0 °C, 3 h, KCN, 30 min, 85 %; f) **2**, $[Pd(PPh_3)_4]$, CuI, NEt_3, THF, 91 %; g) 1. PPTS, acetone, H_2O, reflux, 2. **3** (3 equiv), NaHMDS, DME, −55 °C→RT, 52 %; h) 1. PPh_3, THF, H_2O, RT, 24 h, 2. toluene, 2.5×10^{-4} M, reflux, 10 h, 82 %, 3. H_2, $Pd/BaSO_4$, quinoline, EtOH, 66 % (referred to recovered starting material), 4. HF/MeCN, RT, 3 h, 91 %. AIBN = azobisisobutyronitrile, DCE = dichloroethane, DME = dimethoxyethane, dppf = 1,1′-bis(diphenylphosphanyl)ferrocene, PPTS = pyridinium *p*-toluenesulfonate, NaHMDS = sodium hexamethyldisilazide, TMEDA = *N*,*N*,*N*′,*N*′-tetramethylethylenediamine, TMS = trimethylsilyl.

yield by a second deprotonation with LDA and reaction with **17**. Pentalenacetal **20**, prepared from **19** in 90 % yield by Pd-catalyzed reduction using Et_3SiH,[20] was deprotected and transformed into the pentalenone **5** in 87 % yield. After reaction of **5** with TMS-protected propynyl cuprate[21] and subsequent addition of orthoformate and $BF_3{\cdot}OEt_2$, the pentalene derivative **21** was isolated in 53 % yield as a single diastereoisomer, as supported by NMR and GC data. Compound **21** was reduced with $NaBH_4$ to give a 1:1 mixture of diastereomeric alcohols. Despite the steric hindrance of the convex bicyclo[3.3.0]octane moiety, Barton deoxygenation followed by desilylation to **22** (48 % yield) was successful.

After all the required coupling components were available, we followed our strategy to create the macrocycle.

 © 2005 Wiley-VCH Verlag GmbH & Co. KGaA, Weinheim

Sonogashira coupling[22] of pentalene **22** with iodoacrylate **2** provided the enyne **23** in 91% yield. The dimethyl acetal group was hydrolyzed to give the corresponding intermediate aldehyde, which was olefinated with sulfone **3** under Julia–Kocienski conditions[16] giving the *E*-alkene **24** (52%).[23] Cyclization to the macrolactam could be realized in 82% yield by Staudinger reduction of the azide function, subsequent dilution in toluene (2.5×10^{-4} M), and heating the dilute solution at reflux. The Lindlar reduction of the enyne moiety to yield the *Z*,*E*-diene turned out to be difficult. Only incomplete conversion resulted in 66% yield for the desired diene, whereas overreduction was observed at longer reaction times. Removal of the silyl protecting group afforded the macrocyclic β-hydroxy ester **25** in 91% yield. Brief heating of **25** with NaOMe in MeOH[24] finally gave the target macrolactam **1** with partial epimerization (3:1). The major diastereomer (2*S*,3*S*)-**1** could be isolated in pure form by reversed-phase chromatography, and the spectroscopic data of synthetic cylindramide (**1**, major diastereomer) are in accordance with those of the natural product.[25]

In summary, the described convergent route was used for the first total synthesis of the cytotoxic tetramic acid lactam **1** in 29 steps and in 1.0% overall yield, with a longest linear sequence of 18 steps. The synthetic strategy should allow access to the other interesting tetramic acid natural products mentioned in the introduction.

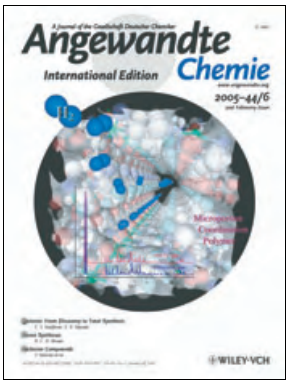
Received: August 30, 2004
Published online: December 28, 2004

Keywords: macrolactams · tetramic acid · total syntheses

[1] Review: R. J. Capon, *Eur. J. Org. Chem.* **2001**, 633 – 645.
[2] S. Kanazawa, N. Fusetani, S. Matsunaga, *Tetrahedron Lett.* **1993**, *34*, 1065 – 1068.
[3] S. P. Gunasekera, M. Gunasekera, P. McCarthy, *J. Org. Chem.* **1991**, *56*, 4830 – 4833.
[4] H. Shigemori, M.-A. Bae, K. Yazawa, T. Sasaki, J. Kobayashi, *J. Org. Chem.* **1992**, *57*, 4317 – 4320.
[5] M.-A. Bae, K. Yamada, Y. Ijuin, T. Tsuji, K. Yazawa, Y. Tomono, D. Uemura, *Heterocycl. Commun.* **1996**, *2*, 315 – 318.
[6] M. Jakobi, G. Winkelmann, D. Kaiser, C. Kempter, G. Jung, G. Berg, H. Bahl, *J. Antibiot.* **1996**, *49*, 1101 – 1104.
[7] R. J. Capon, C. Skene, E. Lacey, J. H. Gill, D. Wadsworth, T. Friedel, *J. Nat. Prod.* **1999**, *62*, 1256 – 1259.
[8] R. K. Boeckman, R. B. Perni, *J. Org. Chem.* **1986**, *51*, 5486 – 5489.
[9] R. K. Boeckman, C. H. Weidner, R. B. Perni, J. J. Napier, *J. Am. Chem. Soc.* **1989**, *111*, 8036 – 8037.
[10] L. A. Paquette, D. Macdonald, L. G. Anderson, J. Wright, *J. Am. Chem. Soc.* **1989**, *111*, 8037 – 8039.
[11] S.-G. Shin, T. Obara, S. Segami, Y. Yonezawa, *Tetrahedron Lett.* **1987**, *28*, 3827 – 3830.
[12] P. R. Fleming, K. B. Sharpless, *J. Org. Chem.* **1991**, *56*, 2869 – 2875.
[13] The replacement of ONs with the N_3 group proceeded with partial epimerization. The mixture of diastereomers (85:15) of both TBS-protected azides, however, could be separated by chromatography.
[14] S. Takuma, K. Hamada, T. Shioiri, *Chem. Pharm. Bull.* **1982**, *30*, 3147 – 3153.
[15] H. Graalfs, R. Fröhlich, C. Wolff, J. Mattay, *Eur. J. Org. Chem.* **1999**, 1057 – 1073.
[16] P. R. Blakemore, *J. Chem. Soc. Perkin Trans. 1* **2002**, 2563 – 2585.
[17] a) Y.-W. Zhong, X.-S. Lei, G.-Q. Lin, *Tetrahedron: Asymmetry* **2002**, *13*, 2251 – 2255; b) K. Lemke, S. Ballschuh, A. Kunath, F. Theil, *Tetrahedron: Asymmetry* **1997**, *8*, 2051 – 2055.
[18] K. C. Nicolaou, D. L. F. Gray, T. Montagnon, S. T. Harrison, *Angew. Chem.* **2002**, *114*, 1038 – 1042; *Angew. Chem. Int. Ed.* **2002**, *41*, 996 – 1000.
[19] D. L. Comins, A. Dehghani, *Tetrahedron Lett.* **1992**, *33*, 6299 – 6302.
[20] W. J. Scott, J. K. Stille, *J. Am. Chem. Soc.* **1986**, *108*, 3033 – 3040.
[21] E. J. Corey, H. A. Kirst, *Tetrahedron Lett.* **1968**, 5041 – 5043.
[22] K. Sonogashira in *Metal-Catalyzed Cross-Coupling Reactions* (Eds.: F. Diederich, P. J. Stang), Wiley-VCH, Weinheim, **1997**, pp. 203 – 230.
[23] Based on the NMR spectra and gas chromatograms, epimerization in the conversion of **23** to **24** can be excluded.
[24] R. N. Lacey, *J. Chem. Soc.* **1954**, 850 – 854.
[25] In the ^{13}C NMR spectra the missing C=O signals of the tetramic acid unit of synthetic cylindramide (**1**) indicates the presence of complex tautomer equilibria. Broadening of some ^{1}H NMR signals indicates that compound **1** complexes metal ions. This interpretation is supported by FAB mass spectra, in which $[M-H+2Na]^+$ adducts with high intensity are observed. Tautomer equilibria and metal-ion complexation are currently under investigation.

 © 2005 Wiley-VCH Verlag GmbH & Co. KGaA, Weinheim

Cover Picture



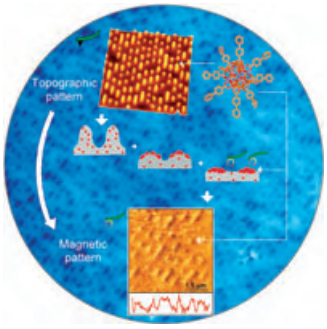
Yoshiki Kubota,* Masaki Takata, Ryotaro Matsuda, Ryo Kitaura, Susumu Kitagawa, Kenichi Kato, Makoto Sakata, and Tatsuo C. Kobayashi

Fundamental structural information on hydrogen molecules adsorbed in nanochannels is required for the rational synthetic design of novel metal–organic porous materials as hydrogen-storage materials. The cover picture shows the charge-density distribution of hydrogen molecules adsorbed in the nanochannels of a copper coordination polymer. The hydrogen molecules are located in the pocket cavities of the suitably sized nanochannels. More details can be found in the Communication by Y. Kubota et al. on page 920 ff.



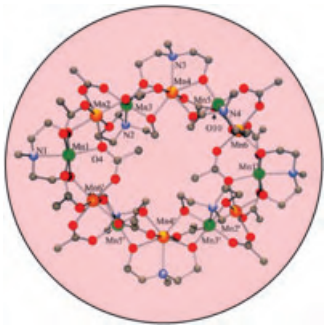
History of Chemistry

The 60th anniversary of the publication of Woodward's synthesis of quinine is marked by T. S. Kaufman and E. A. Rúveda in their Review on page 854 ff. An overview is given of the history of quinine, from its discovery to the three modern total syntheses.



Nanotechnology

The fabrication of patterns of magnetic bits on a polymer surface is described by J. Veciana, F. Biscarini, and co-workers in their Communication on page 887 ff. This approach yields a system for permanent information storage with magnetic readout.



Single-Molecule Magnets

G. Christou and co-workers report on one of the rare single-molecule magnets with a cyclic structure on page 897 ff. The compound, a Mn_{12} cluster, has a high ground-state spin of 7.

Contents

VIP ***The following Communications have been judged by at least two referees to be "very important papers" and will be published online at www.angewandte.org soon:***

Liang Deng, Hoi-Shan Chan, Zuowei Xie:*
Synthesis, Reactivity, and Structural Characterization of the First 14-Vertex Carborane

Xuejun Liu, Gaosheng Chu, Robert A. Moss, Ronald R. Sauers,* Ralf Warmut*:*
Fluorophenoxycarbene inside a Hemicarcerand: A Bottled Singlet Carbene

Silvio Aime, Carla Carrera, Daniela Delli Castelli, Simonetta Geninatti Crich, Enzo Terreno:*
Light-On/Light-Off of Cells Labeled with MRI-PARACEST Agents

Zulfiya Orynbayeva, Sofiya Kolusheva, Etta Livneh, Alexandra Lichtenshtein, Ilana Nathan, Raz Jelinek:*
Visualization of Membrane Processes in Living Cells by Surface-Attached Chromatic Polymer Patches

Gábor Bunkóczi, László Vértesy, George M. Sheldrick:*
The Antiviral Antibiotic Feglymycin: First Direct-Methods Solution of a 1000+ Equal-Atom Structure

Dieter Enders, Christoph Grondal:*
Direct Organocatalytic de novo Synthesis of Carbohydrates

Meeting Reviews

Polyoxometalate Nanostructures, Superclusters, and Colloids: From Functional Clusters to Chemical Aesthetics — *P. Kögerler and L. Cronin* ____ **844–846**

Books

Bioconjugation Protocols — Christof M. Niemeyer — *reviewed by H.-B. Kraatz* ____ **847**

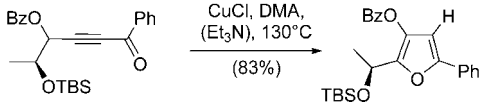
An Introduction to Plastics — Hans-Georg Elias — *reviewed by B. Voit* ____ **848**

Highlights

Cycloisomerization

R. C. D. Brown* ____ **850–852**

Developments in Furan Syntheses



Diversely substituted furans can be prepared from alkynones and alkynoate esters by means of mechanistically novel cycloisomerization and reductive cyclization processes, respectively. Even tetrasubstituted furans can be prepared by cycloisomerization of alkynones, or from allenyl ketones through a Pd-catalyzed cross-coupling-cyclization approach (see scheme; DMA = *N*,*N*-dimethylacetamide).

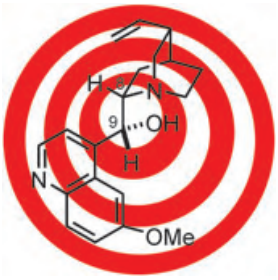
Reviews

Natural Products Synthesis

T. S. Kaufman,* E. A. Rúveda **854–885**

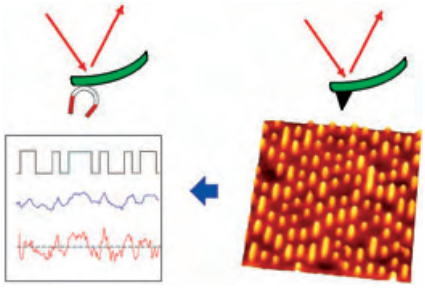
The Quest for Quinine: Those Who Won the Battles and Those Who Won the War

Tonic for the troops: The year 2004 marks the 60th anniversary of Woodward's total synthesis of quinine (see picture), which for a long time had been the only useful treatment for malaria. Quinine proved to be an attractive and elusive synthetic target since Perkin's attempts in 1856, which gave birth to industrial organic synthesis and the dye industry. This Review highlights the history of the isolation, structural elucidation, and synthesis of quinine.



© 2005 Wiley-VCH Verlag GmbH & Co. KGaA, Weinheim

Communications



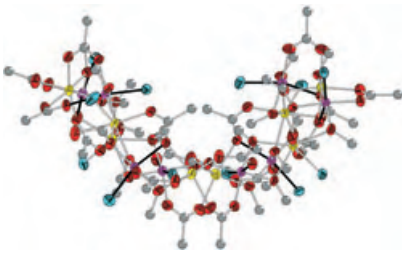
An attractive read: Magnetic Mn_{12} clusters are patterned by molding a dispersion in a polymer matrix onto a structured master (e.g., a DVD). The protrusions of the polymer replica surface disappear on exposure to solvent vapor, and the clusters concentrate on the surface at the positions of the original protrusions. The cluster distribution produces a magnetic contrast, which can be imaged by magnetic force microscopy (see picture).

Nanotechnology

M. Cavallini, J. Gomez-Segura, D. Ruiz-Molina, M. Massi, C. Albonetti, C. Rovira, J. Veciana,* F. Biscarini* ——— **888 – 892**

Magnetic Information Storage on Polymers by Using Patterned Single-Molecule Magnets

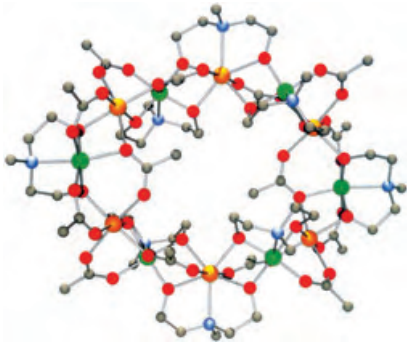
Saddle seen: The use of the potentially tetradentate triethanolamine ($teaH_3$) ligand provides a useful route to three new structural types in mixed-valent manganese cluster chemistry, which include near-rectangular and closed-sinusoidal (saddle-shaped; see structure: Mn^{III} purple, Mn^{II} yellow, O red, N blue, C gray) topologies. Further, two of these complexes are also new single-molecule magnets (SMMs).



Single-Molecule Magnets

M. Murugesu, W. Wernsdorfer, K. A. Abboud, G. Christou* — **892 – 896**

New Structural Motifs in Manganese Single-Molecule Magnetism from the Use of Triethanolamine Ligands



Loopy about magnetism: The use of *N*-methyldiethanolamine ($mdaH_2$) leads to new Mn_{12} and Mn_4 single-molecule magnets (SMMs) with $S = 7$ and $S = 9$ ground-state spins, respectively. The Mn_{12} species (see structure: Mn^{III} green, Mn^{II} orange, O red, N blue, C gray) is a rare example of an SMM with a loop structure. Its unusual $S = 7$ ground state for an $Mn^{III}_6Mn^{II}_6$ species is rationalized by DFT calculations.

Single-Molecule Magnets

D. Foguet-Albiol, T. A. O'Brien, W. Wernsdorfer, B. Moulton, M. J. Zaworotko, K. A. Abboud, G. Christou* ——— **897 – 901**

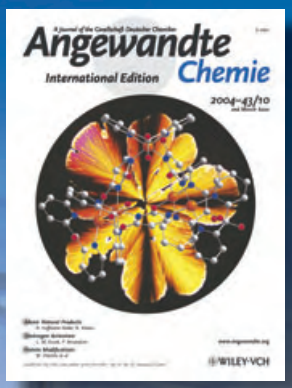
DFT Computational Rationalization of an Unusual Spin Ground State in an Mn_{12} Single-Molecule Magnet with a Low-Symmetry Loop Structure

For the USA and Canada:
ANGEWANDTE CHEMIE International Edition (ISSN 1433-7851) is published weekly by Wiley-VCH PO Box 191161, D 69451 Weinheim, Germany. Air freight and mailing in the USA by Publications Expediting Inc. 200 Meacham Ave., Elmont, NY 11003. Periodicals postage paid at Jamaica NY 11431. US POSTMASTER: send address changes to *Angewandte Chemie*, Wiley-VCH, 111 River Street, Hoboken, NJ 07030. Annual subscription price for institutions: US$ 4948.00/4498.00 (valid for print and electronic / print or electronic delivery); for individuals who are personal members of a national chemical society, or whose institution already subscribes, or who are retired or self-employed consultants, print only: US$ 394.00. Postage and handling charges included. All Wiley-VCH prices are exclusive VAT.

 © 2005 Wiley-VCH Verlag GmbH & Co. KGaA, Weinheim

The best in chemistry –

for more than a hundred years



A Journal of the Gesellschaft Deutscher Chemiker

Angewandte
International Edition **Chemie**

www.angewandte.org

1888: ***The beginning of a success story***

Constant Innovations

1962: *First issue of the International Edition*
1976: *Graphical abstracts*
1979: *Cover pictures*
1988: *Centenary of Angewandte*
1989: *Routine use of color*
1991: *New section: Highlights*
1992: *Computerized editorial tracking system*
1995: *Internet service for readers*
1998: *Regular press service; full-text online*
2000: *New section: Essays; EarlyView: Communications available online ahead of the printed version*
2001: *New section: Minireviews*
2002: *Online submission of manuscripts*
2003: *Weekly publication; new section: News; new layout*
2004: *Backfiles (1962-1997); ManuscriptXpress: Online system for authors and referees*



Angewandte's advisors...

Frans C. De Schryver
Katholieke Universiteit Leuven

» *Over the years* ***Angewandte Chemie*** *has been a beacon for sound, exciting, and novel chemistry and has built its well-deserved reputation on nonsubjective, thorough, but constructive refereeing and a highly professional layout. I am sure that the new initiatives will further strengthen its leadership with the help of scientists and the outstanding staff.* «

Angewandte Chemie International Edition *is a journal of the German Chemical Society (GDCh)*

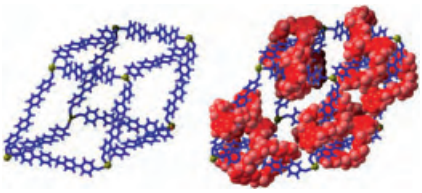
GDCh

WILEY InterScience® DISCOVER SOMETHING GREAT

WILEY-VCH

1613412_gu

Circles cubed: The title materials can be prepared by self-assembly and are similar to conventional metal–organic framework materials, but with every linker being a [2]rotaxane made from pyridinium axles and crown-ether wheels (see structures; left: a single "cube" unit of the 3D network with the crown-ether wheels removed, right: the same framework with crown-ether wheels included; Sm ions gold).

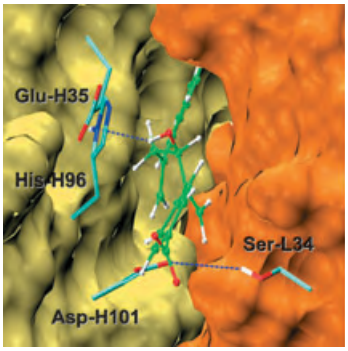


Supramolecular Chemistry

D. J. Hoffart, S. J. Loeb* ——— **901 – 904**

Metal–Organic Rotaxane Frameworks: Three-Dimensional Polyrotaxanes from Lanthanide-Ion Nodes, Pyridinium *N*-Oxide Axles, and Crown-Ether Wheels

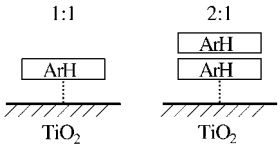
Stabilizing the transition state of a reaction is not the only consideration in the design of catalytic antibodies. The energetics of the substrate–catalyst complex preceding the transition state also play a role. The picture shows such a complex for an oxy-Cope rearrangement in the active site of the antibody catalyst AZ-28 in its germline form.



Catalytic Antibodies

S. Martí, J. Andrés, V. Moliner,* E. Silla, I. Tuñón,* J. Bertrán ——— **904 – 909**

Towards a Rational Design of Antibody Catalysts through Computational Chemistry

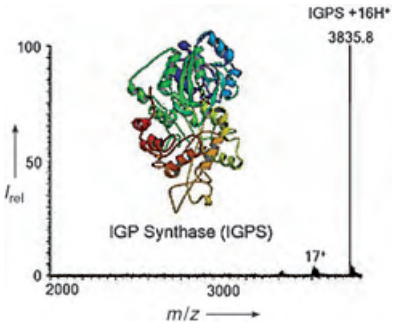


The coloration of TiO_2 upon contact with solutions of aromatic hydrocarbons is explained by the formation of 1:1 and 2:1 complexes (see picture) by physical adsorption. UV/Vis spectra and calculations indicate that these complexes are based on a charge-transfer interaction.

Physisorption on TiO_2

Y. S. Seo, C. Lee, K. H. Lee, K. B. Yoon* ——— **910 – 913**

1:1 and 2:1 Charge-Transfer Complexes between Aromatic Hydrocarbons and Dry Titanium Dioxide



It's a phase it's going through: Electrosonic spray ionization shows better desolvation efficiency than electrospray ionization and usually gives single-charge states when used to ionize noncovalent complexes of large biomolecules. The binary and ternary complexes of imidazole-3-glycerol phosphate synthase (IGPS) with its inhibitors appear to retain their native solution-phase conformations upon transfer into the gas phase (see picture).

Analytical Techniques

J. M. Wiseman, Z. Takáts, B. Gologan, V. J. Davisson, R. G. Cooks* — **913 – 916**

Direct Characterization of Enzyme–Substrate Complexes by Using Electrosonic Spray Ionization Mass Spectrometry

 © 2005 Wiley-VCH Verlag GmbH & Co. KGaA, Weinheim

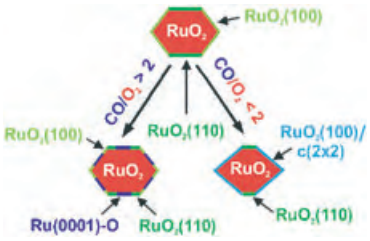
Contents

Heterogeneous Catalysis

J. Aßmann, D. Crihan, M. Knapp, E. Lundgren, E. Löffler, M. Muhler,* V. Narkhede, H. Over,* M. Schmid, A. P. Seitsonen, P. Varga ——— **917 – 920**

Understanding the Structural Deactivation of Ruthenium Catalysts on an Atomic Scale under both Oxidizing and Reducing Conditions

Performance enhancement: The surface-science approach coupled with industrial catalyst research offers a synergistic strategy to improve the performance of industrial catalysts. The poorly understood microscopic processes that determine the structural deactivation of ruthenium-based catalysts during CO oxidation have been elucidated (see scheme). Based on these results measures are proposed to improve the performance of ruthenium catalysts.

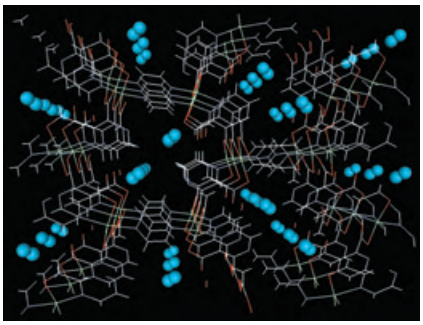


Inclusion Compounds

Y. Kubota,* M. Takata, R. Matsuda, R. Kitaura, S. Kitagawa, K. Kato, M. Sakata, T. C. Kobayashi ——— **920 – 923**

Direct Observation of Hydrogen Molecules Adsorbed onto a Microporous Coordination Polymer

Trapped hydrogen molecules in the nanochannels of a copper coordination polymer were successfully observed by the synchrotron powder-diffraction method. The adsorbed molecules are located near one corner of the rectangular nanochannels, and the pockets of the pore walls are suited to the size of the hydrogen molecules (see picture). These results could provide guidelines for the design of hydrogen-storage materials.

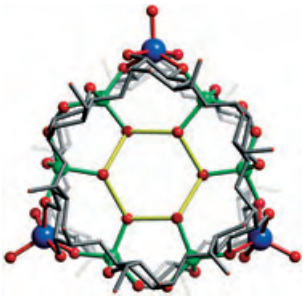


Supramolecular Chemistry

A. Geißelmann, P. Klüfers,* C. Kropfgans, P. Mayer, H. Piotrowski ——— **924 – 927**

Carbohydrate–Metal Interactions Shaped by Supramolecular Assembling

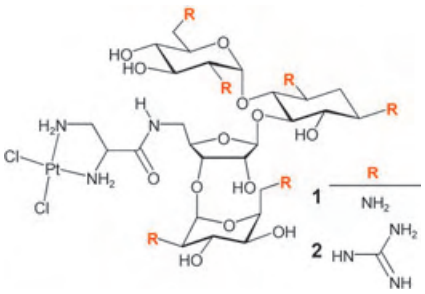
Cyclodextrin ligands: Carbohydrates can be used as framework molecules that provide patterns of metal-binding oxygen atoms. The divalent forms of the biologically important metals iron and manganese can be part of such assemblies (see structure: Fe blue, O red, counterion green, hydrogen bonds between water molecules yellow). The assemblies are stabilized by favorable contributions other than the carbohydrate–metal interaction.



RNA-Selective Pt^{II} Conjugates

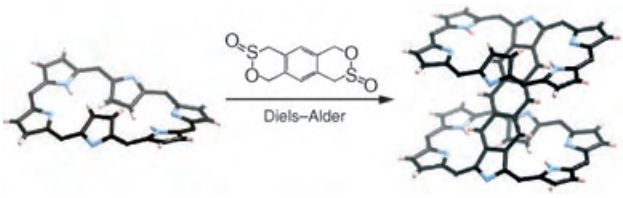
J. Boer, K. F. Blount, N. W. Luedtke, L. Elson-Schwab, Y. Tor* ——— **927 – 932**

RNA-Selective Modification by a Platinum(II) Complex Conjugated to Amino- and Guanidinoglycosides



Revving up the RNA response: Binding of the anticancer drug cisplatin (*cis*-Pt) to nucleic acids is believed to favor DNA over RNA. To "reverse" the nucleic acid selectivity of *cis*-Pt, amino- and guanidinoglycoside–Pt^{II} conjugates (**1** and **2**) have been synthesized and evaluated. The conjugates generate site-specific, RNA-selective, covalent cross-links to the HIV-1 Rev response element.

© 2005 Wiley-VCH Verlag GmbH & Co. KGaA, Weinheim

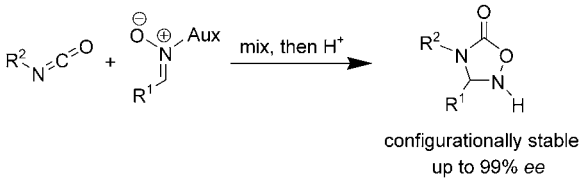


An expanded porphyrin with six pyrrole units, a *meso*-aryl hexaphyrin, acts as a dienophile in Diels–Alder reactions with *o*-xylylene. Consecutive double cycloadditions of the hexaphyrin with a bis-*o*-xylylene equivalent leads to an anthracene-bridged hexaphyrin dimer (see scheme), whose unique Z-shaped structure has been elucidated by X-ray crystallographic analysis.

Expanded Porphyrins

H. Hata, H. Shinokubo,*
A. Osuka* ——— **932 – 935**

Anthracene-Bridged Z-Shaped [26]Hexaphyrin(1.1.1.1.1.1.1) Dimer from the Regioselective Diels–Alder Reaction of a Hexaphyrin with Bis-*o*-xylylene Equivalents

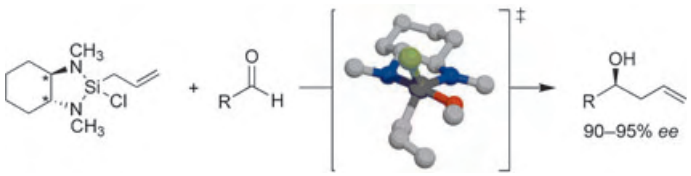


An intriguing scaffold for drug development, 1,2,4-oxadiazolidinones are obtained in enantiomerically pure form by a simple reaction and purification protocol (see scheme). These heterocycles, including the previously unknown N2-unsubstituted parent structures, were shown to be configurationally stable under a variety of conditions.

Asymmetric Heterocycle Synthesis

T. Ritter, E. M. Carreira* ——— **936 – 938**

1,2,4-Oxadiazolidinones as Configurationally Stable Chiral Building Blocks



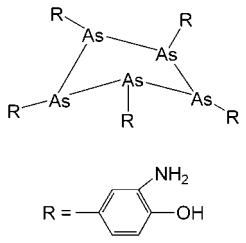
Explaining the experiment: The transition states for a concerted asymmetric allylation (see scheme) were studied by theoretical methods. The apical attack of the aldehyde oxygen atom on Si accompanied by minimization of electrostatic repulsion in the trigonal-bipyramidal transition state leads to high stereoselectivity.

Allylation Transition States

X. Zhang, K. N. Houk,*
J. L. Leighton ——— **938 – 941**

Origins of Stereoselectivity in Strain-Release Allylations

Elusive molecular structure revealed: The primary components of the historically important pharmaceutical compound salvarsan (arsphenamine, Ehrlich 606) have been shown by ESI mass spectrometry to be cyclopolyarsines $[RAs]_n$ (see structure; $n = 3$–6 and R = 3-amino-4-hydroxyphenyl).



Molecular Structure

N. C. Lloyd, H. W. Morgan, B. K. Nicholson,*
R. S. Ronimus ——— **941 – 944**

The Composition of Ehrlich's Salvarsan: Resolution of a Century-Old Debate

 © 2005 Wiley-VCH Verlag GmbH & Co. KGaA, Weinheim

Contents

Photocycloaddition

J. W. Boyd, N. Greaves, J. Kettle, A. T. Russell,* J. W. Steed ____ **944 – 946**

Alkene–Arene *meta* Photocycloadditions with a Four-Carbon-Atom Tether: Efficient Approach toward the Polycyclic Ring Systems of Aphidicolin and Stemodinone

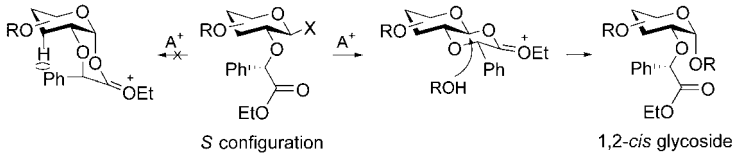


At the end of its tether! The fusion of a six-membered ring onto the four-carbon-atom tether of substrate **1** provides an efficient approach toward the polycyclic ring systems of the natural products aphidicolin and stemodinone. The reaction represents a unique example of a preference for product formation from an *endo* exciplex in an intramolecular system (*exo*:*endo* **2**:**3** = 1.0:1.2).

Anomeric Selectivity

J.-H. Kim, H. Yang, G.-J. Boons* ____ **947 – 949**

Stereoselective Glycosylation Reactions with Chiral Auxiliaries

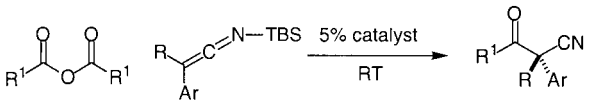


Good neighbors: A chiral auxiliary is used for the first time to control the anomeric selectivity of glycosylation reactions. In this approach, upon treatment with an activator A^+, neighboring-group participation of an (*S*)-ethoxycarbonylbenzyl auxiliary at C2 leads to the formation of 1,2-*cis* glycosides, probably via a *trans*-fused ethyloxonium ion intermediate (see scheme).

Asymmetric Synthesis

A. H. Mermerian, G. C. Fu* ____ **949 – 952**

Nucleophile-Catalyzed Asymmetric Acylations of Silyl Ketene Imines: Application to the Enantioselective Synthesis of Verapamil

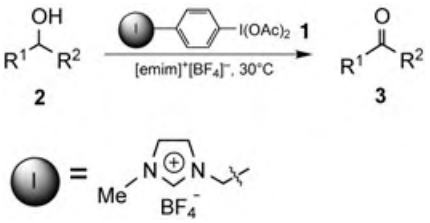


All-carbon quaternary stereocenters are generated with good enantioselectivity through a nucleophile-catalyzed acylation reaction of silyl ketene imines (see scheme, TBS = *tert*-butyldimethylsilyl). The method is applied to the first catalytic asymmetric synthesis of the drug verapamil.

Oxidation Reagents

W. Qian, E. Jin, W. Bao, Y. Zhang* ____ **952 – 955**

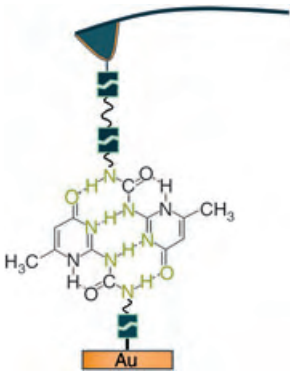
Clean and Highly Selective Oxidation of Alcohols in an Ionic Liquid by Using an Ion-Supported Hypervalent Iodine(III) Reagent



Alcohol consumption: The $PhI(OAc)_2$-derived hypervalent iodine reagent **1** acts as an oxidant in the conversion of primary and secondary alcohols **2** into carbonyl compounds **3** with good to excellent yields (see scheme). The bromide ion remaining from the preparation of $[emim]^+[BF_4]^-$ (emim = 1-ethyl-3-methylimidazolium tetrafluoroborate) acts as a catalyst in the reaction. Primary alcohols are oxidized without any detectable overoxidation.

© 2005 Wiley-VCH Verlag GmbH & Co. KGaA, Weinheim

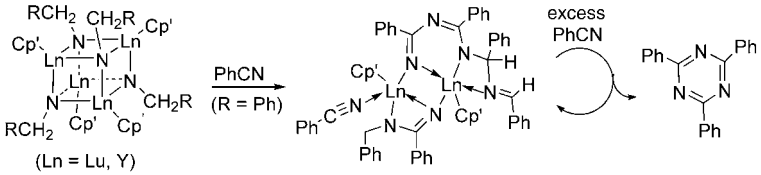
Breaking point: The unbinding behavior of single supramolecular polymers formed through quadruple hydrogen bonds between 2-ureido-4(1H)-pyrimidinone (UPy) units was studied by AFM-based single-molecule force spectroscopy. The interactions between individual UPy moieties and the stretching of polyethylene glycol (PEG) spacers in reversible supramolecular polymer chains were unveiled by AFM force-displacement measurements.



Supramolecular Polymers

S. Zou, H. Schönherr,*
G. J. Vancso* ——— 956 – 959

Stretching and Rupturing Individual Supramolecular Polymer Chains by AFM



1 2

Highly reactive imido ligands, even when in a bridging mode as in **1**, distinguish lanthanide–imido complexes from their d-block counterparts. For example, imido species **1** can undergo nucleophilic addition to benzonitrile to give **2**. Catalytic cyclotrimerization of benzonitrile occurs in the presence of **1** or **2** by a unique combination of C–N bond-formation, hydrogen-transfer, and C–N bond-cleavage reactions (see scheme). Cp′ = η^5-$C_5Me_4SiMe_3$

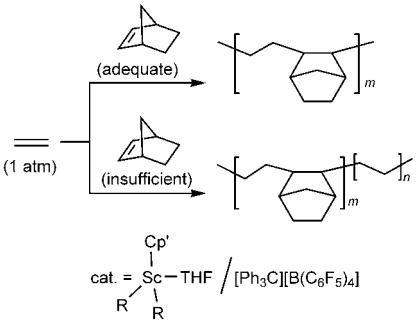
Cyclotrimerization

D. Cui, M. Nishiura, Z. Hou* 959 – 962

Lanthanide–Imido Complexes and Their Reactions with Benzonitrile

---

Rare activity of an active rare-earth-metal catalyst is observed in the alternating copolymerization of ethylene and norbornene. The reaction yields exclusively the alternating copolymer in the presence of both monomers and affords poly(ethylene-*alt*-norbornene)-*b*-polyethylene block copolymers when a relatively small quantity of norbornene is used under a constant flow of ethylene (see scheme).

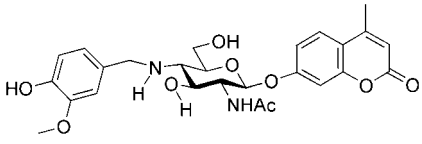


Polymerization Catalysts

X. Li, J. Baldamus, Z. Hou* 962 – 965

Alternating Ethylene–Norbornene Copolymerization Catalyzed by Cationic Half-Sandwich Scandium Complexes

---



1

Lysozyme makes its choice: Hen egg-white lysozyme selects the optimal binder from a collection of aromatic motifs that mimic a carbohydrate unit upon exposure to a dynamic library of potential ligands that are directed towards its active site by a low-affinity scaffold. The structure of one of the selected members **1** is shown.

Combinatorial Chemistry

S. Zameo, B. Vauzeilles,*
J.-M. Beau* ——— 965 – 969

Dynamic Combinatorial Chemistry: Lysozyme Selects an Aromatic Motif That Mimics a Carbohydrate Residue

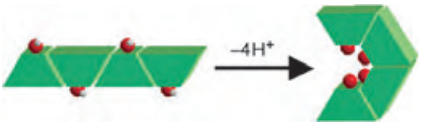
© 2005 Wiley-VCH Verlag GmbH & Co. KGaA, Weinheim

Contents

Oligoamide Conformations

D. Kanamori, T.-a. Okamura, H. Yamamoto, N. Ueyama* — **969 – 972**

Linear-to-Turn Conformational Switching Induced by Deprotonation of Unsymmetrically Linked Phenolic Oligoamides



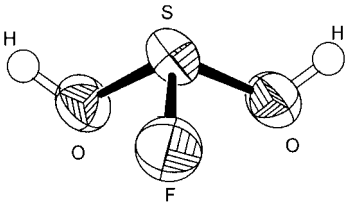
Proton-triggered conformational switching: Unsymmetrically linked phenolic oligoamides fold into a turn conformation from a linear conformation following the deprotonation of the phenol groups (see scheme). Deprotonation induces a rearrangement of the hydrogen-bonding mode within each unit from OH···O=C (linear) to NH···O(oxyanion) such that all of the phenolate O^- atoms are directed toward the inside of the turn.

Superacid Systems

A. Kornath,* R. Seelbinder, R. Minkwitz — **973 – 975**

Synthesis of Fluorodihydroxysulfonium Hexafluoroantimonate $[FS(OH)_2]^+[SbF_6]^-$

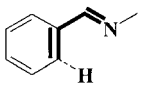
Audience participation: Fluorosulfinic acid, which is not known in its free state, was isolated in its protonated form as the $[FS(OH)_2]^+[SbF_6]^-$ salt. It was prepared by addition of SO_2 to the superacid HF/SbF_5. SO_2 has been used as a solvent for HF/SbF_5 superacid systems for over 40 years. Only now is it shown that when SO_2 is added to HF/SbF_5 the $[FS(OH)_2]^+$ ion (see structure) is formed in an equilibrium with the SO_2SbF_5 adduct.



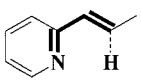
C–H Activation

H.-F. Klein,* S. Camadanli, R. Beck, D. Leukel, U. Flörke — **975 – 977**

Cyclometalation of Substrates Containing Imine and Pyridyl Anchoring Groups by Iron and Cobalt Complexes



1



2

Steric control dictates the cyclometalation of aromatic substrates containing imine anchoring groups upon reaction with basic iron or cobalt complexes. As structural isomers, the azadiene systems **1** and **2** undergo regiospecific activation of the (vinylic or aromatic) C–H bond of the CH group that has switched places with the N atom.

Deadline for recruitment adverts

10/2005	February 10	Publication date: February 25
11/2005	February 17	Publication date: March 4

Angewandte Chemie International Edition
Advertising Sales Department:
Marion Schulz
Phone: 0 62 01 – 60 65 65
Fax: 0 62 01 – 60 65 50
E-Mail: MSchulz@wiley-vch.de

Place an advert in the printed version and have it made available online for 1 month, free of charge!

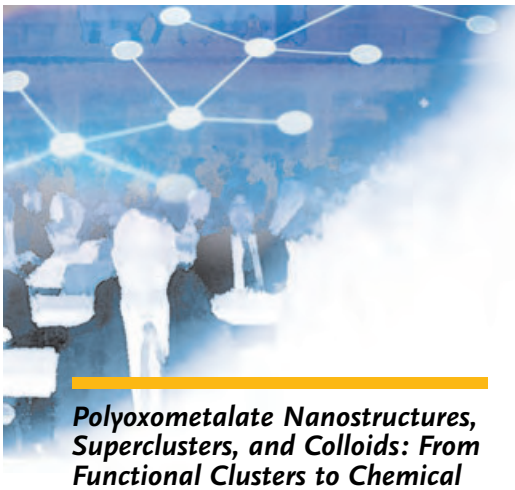
Service

Keywords — **978**

Authors — **979**

Vacancies — **841**

Preview — **981**



Polyoxometalate Nanostructures, Superclusters, and Colloids: From Functional Clusters to Chemical Aesthetics**

Paul Kögerler and Leroy Cronin

It has often been stated that polyoxometalates (POMs) represent a class of molecules of almost unrivaled versatility, which results from their enormous structural diversity, range of sizes, tunable redox properties, and fascinating catalytic activity. These properties were very much in evidence at a recent four-day "International Symposium on Nano-structures and Physicochemical Properties of Polyoxometalate Superclusters and Related Colloid Particles" in Kanagawa (Japan), organized by T. Yamase, M. T. Pope, and A. Müller with the support of the JSPS, CREST, the Rigaku Corporation, and the Chemical Society of Japan. The previous conference in this series had taken place in 1999 at the Universität Bielefeld (Germany). POMs represent unique polymerizable entities that are often based on common structural fragments, or building blocks. This research area has undergone an important transition from classical structural and coordination chemistry towards the chemistry of "smart", "functional" materials, which may even have properties of artificial cells/porous capsules. There has been a dramatic increase in the number of interdisciplinary projects in a reasonably short period of time. The field also continues to surprise with new findings at a fundamental scientific level which open avenues for future research.[1–7]

The diverse and exciting nature of this field became apparent immediately from the opening lecture of F. Sécheresse (Université Versailles St-Quentin, France), who described interesting developments in the synthesis of discrete polyoxomolybdates and polyoxotungstates. In particular the careful use of simple, directing building blocks based on Mo^{V} dimers of the form $[Mo_2O_2(\mu\text{-}E)_2(H_2O)_6]^{2+}$ (E = S or O) to produce an impressive array of larger cluster structures was demonstrated.[1] Sécheresse then described effectively how POM-based building blocks (this time lanthanide-functionalized ε Keggin anions) can be taken to the next level by linking complete molecular cluster anions with carboxylate ligands to networks of different topologies and dimensionalities, as well as strategies for the formation of "superclusters" by carefully considering how POM-based building blocks can be connected geometrically and chemically.

This concept was also a focus of M. T. Pope's (Georgetown University, USA) review of general routes to ever larger POMs by using lacunary fragments. Pope also proposed the development of large clusters based on reduced polytungstate moieties, thereby applying concepts that are successfully used in polyoxomolybdate chemistry.[2] P. Gouzerh (Université Pierre et Marie Curie, France) extended the discussions on polytungstate-based moieties by presenting the special abilities of the hexavacant $\{P_2W_{12}\}$ anion. This species readily cocondenses with 3d cations to form large and symmetrical assemblies of $\{P_2W_{12}\}$ fragments that are supported by a $\{M_4O_6\}$ core ($M = Fe^{III}$).

The self-assembly of a range of polytungstate clusters was also explored by U. Kortz (Universität Bremen, Germany), who showed some exciting new approaches to polytungstate systems by using novel linking groups, including a polyoxotungstate wheel $[\{\beta\text{-}Ti_2SiW_{10}O_{39}\}_4]^{24-}$. In this case the use of Ti^{4+} to connect the $\{W_{10}\}$-based building blocks is key.[3] Recent developments in polyoxoniobate chemistry were presented by M. Nyman (Sandia National Laboratories, USA), who demonstrated how this field could be expanded from the $\{Nb_6O_{19}\}$ Lindqvist ion to a variety of Keggin-based compounds, despite the considerable challenges faced in determining the correct conditions for the formation and isolation of these materials.

In one of several highlights of the conference C. Hill (Emory University, USA) presented a route to break through the "oxo wall" and stabilize a single $(H_2O)Pt{=}O$ moiety by using electron-withdrawing $\{PW_9\}$ building blocks as ligands to sandwich the Pt=O moiety. The resulting complex is the first discrete metal–oxo complex of a late transition metal (Figure 1).[4] Because such species are thought to represent intermediates in O_2 activation at platinum surfaces, this finding is of significant consequence and will surely spark extensive follow-up work.

The nanoscopic nature of POM-based clusters and their great potential as mesoporous materials were discussed by T. Yamase (Tokyo Institute of Technology, Japan), who showed how the photoreduction-induced self-assembly of molybdenum blue type polyoxomolybdates can be controlled by the incorporation of different Ln^{3+} ions into the reaction system. This process leads to the formation of nanowheel structures

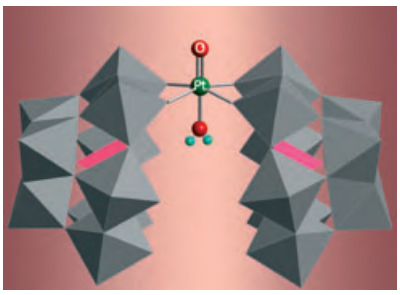


Figure 1. The structure of $[O{=}Pt^{IV}(H_2O)(PW_9O_{34})]^{16-}$. The $[PW_9O_{34}]^{9-}$ ligands are represented by gray polyhedra (Pt green, O red, H blue-green).[4]

[*] Dr. P. Kögerler
Ames Laboratory and
Department of Physics and Astronomy
Iowa State University
Ames, IA 50011 (USA)
E-mail: kogerler@ameslab.gov
Dr. L. Cronin
Department of Chemistry
The University of Glasgow
Glasgow, G12 8QQ (UK)
Fax: (+44) 141-330-4888
E-mail: L.Cronin@chem.gla.ac.uk

[**] International Symposium on Nano-structures and Physicochemical Properties of Polyoxometalate Superclusters and Related Colloid Particles, Shonan Village Center, Kanagawa (Japan), November 21–25, 2004.

 © 2005 Wiley-VCH Verlag GmbH & Co. KGaA, Weinheim DOI: 10.1002/anie.200462662

of the type described by Müller and coworkers, but also mediates the self-assembly of nanotubes comprised of stacked $\{Mo_{154}\}$ wheels, as well as the self-assembly of ellipsoidal Japanese-rice-cake-shaped nanorings.[5] The formation of Mo-based nanotubes is extraordinary, and the possibility of generating very long tubes from solution is tantalizing. The development of multifunctional and nanoporous materials was also explored in some detail (Hill, Yamase, Sécheresse, Errington, Aida), as well as the development of sophisticated catalysts (Hill, Mizuno).

The utilization of POM-based building blocks in the area of hybrid, conducting, and magnetic materials was discussed; it was illustrated how POMs can be very effectively incorporated into hybrid architectures with organic donors, such as tetrathiafulvalene, nitroxide radicals, and organometallic units (Ouahab). A notable development in this field was presented by E. Coronado (Universidad de Valencia, Spain) in the form of a hybrid material that demonstrates metallic conductivity down to 2 K and comprises a complex of the organic radical bis(ethylenedioxo)tetrathiafulvalene (BEDO-TTF) and the $\{BW_{12}\}$ Keggin anion. This result certainly shows the potential the field of POM-based hybrid materials holds for novel material properties.[6] In a further discussion L. Cronin (University of Glasgow, UK) presented several new POM architectures and routes to hybrid materials. Some of these POMs may be used in the development of POM-based components for molecular electronics and functional nanoscopic systems.

Polyoxometalates also serve as versatile frameworks for the generation of large and sometimes highly symmetrical spin arrays. Indeed, the interest in functionalized POMs that serve as novel magnetic molecules and materials is growing rapidly. P. Kögerler (Iowa State University and Ames Laboratory, USA) presented the latest developments in understanding the complex and rich magnetic behavior associated with, for example, magnetically substituted keplerate clusters, such as $\{Mo_{72}Fe_{30}\}$. H. Nojiri (Tohoku University, Japan) expanded on this topic and described the manipulation of the magnetic states of spin-frustrated clusters by pulsed magnetic fields.

The development of POM-based colloids and nanoparticles was also an important theme, as many of the participants are already able to synthesize molecular metal-oxide-like fragments effectively; POM-protected nanoparticles were also described (Tong, Cronin). T. Liu (Brookhaven National Laboratory, USA) suggested that the aggregation of cluster anions to giant vesicles in aqueous solution represents a "second solute state". He has examined the assembly of giant molybdenum blue type wheels as well as keplerate spheres to partially monodisperse anionic spherical vesicles containing approximately 1000 monomers.[7] This phenomenon will certainly attract much attention in the future. In surface studies of POM clusters there have also been developments; indeed, the structure, stability, and stoichiometry of transition-metal oxides on surfaces is a tremendously interesting research area (Klemperer, Errington, Tong, Cronin), which is central to understanding many chemical processes.

The complex and demanding general structural analysis of nanometer-sized POMs by crystallographic techniques was described by H. Bögge (Universität Bielefeld), who outlined the various approaches to determine the structure of these sometimes protein-sized molecules. M. Henry (Université Louis Pasteur, France) expanded on the area of structural studies by discussing structural, computational, and NMR spectroscopic studies. The examination of confined water clusters and patches was also an important topic (Müller, Henry, Ozeki). Henry, inspired by the dramatically beautiful functional clusters of Müller, summed up some of the perspectives and expectations for this field in what must be the quote of the conference, with the phrase: "… these clusters exist in the hyper-super-supra-molecular-bio-nano-world of polyoxometalates!" A. Müller (Universität Bielefeld), whose research group produced, for example, the giant wheels (molybdenum blue), the $\{Mo_{368}\}$ nanohedgehog, and nanosized porous spherical clusters (keplerates), took the audience through an inspiring, colorful, and sometimes philosophical journey in describing how these ring species and the keplerates can serve as comparatively stable platforms for chemistry at the level of nanoparticles: For example, control over the molecular porosity of keplerates enables the stabilization of water clusters of different sizes inside these spherical polyoxomolybdate hosts. He then suggested that the keplerates could be described as artificial cells[8] and outlined perspectives for nanotechnology (Figure 2). The related POM

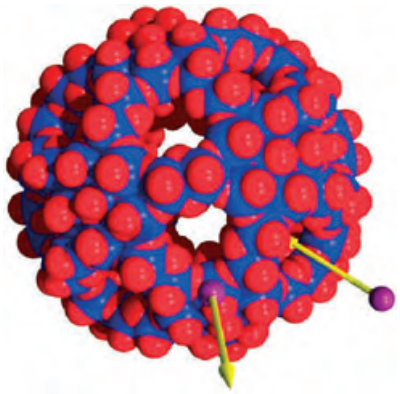


Figure 2. Schematic space-filling representation of the temperature-dependent reversible equilibrium of Li^+-ion binding observed for a keplerate species, a model of an "artificial cell" (Mo blue, O red, Li purple).[8]

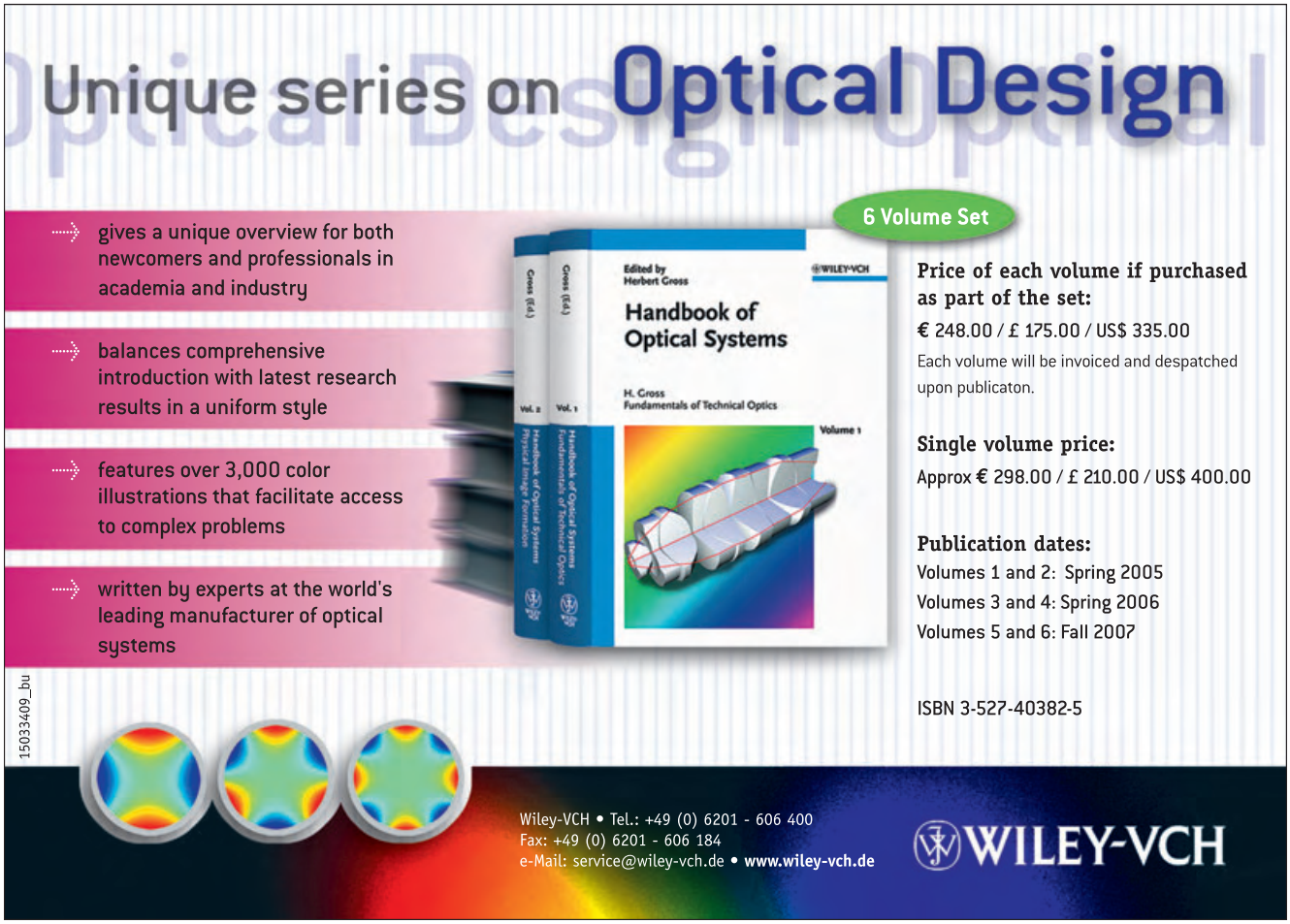
chemistry allows access to different areas of chemistry that were simply not available before, such as the generation of protein-sized clusters, the formation of inorganic "cells", and the examination of confined molecules in porous nanometer-sized capsules; a new type of "super-supramolecular chemistry" that can be extended down many avenues is also now possible.

The most satisfying aspect of this conference was the truly diverse and interdisciplinary nature of the work presented, yet almost all topics discussed were unified by the themes of utilizing POM-based building blocks and the quest to design architectures to produce functionality. It was also interesting to see how conceptual cross-fertilization in polyoxotungstate and polyoxomolybdate chemistry is providing inspiration. POM chemistry is an extraordinary area of science which touches an almost unprecedented number of other fields of chemistry and has provided many highlights in the past, both in the

 © 2005 Wiley-VCH Verlag GmbH & Co. KGaA, Weinheim

academic and the public arenas. Based on this symposium, the future of polyoxometalate chemistry as a multifaceted and interdisciplinary subject shines bright, and is sure to deliver further inspiration and highlights.

[1] F. Sécheresse, E. Cadot, "Sulfur-containing Keggin anions and cyclic polyoxothioanions", NATO Science Series II: Mathematics, Physics and Chemistry **2003**, *98* (Polyoxometalate Molecular Science), 253 – 271.
[2] A. Müller, S. Roy, *Coord. Chem. Rev.* **2003**, *245*, 153 – 166.
[3] F. Hussain, B. S. Bassil, L.-H. Bi, M. Reicke, U. Kortz, *Angew. Chem.* **2004**, *116*, 3567 – 3571; *Angew. Chem. Int. Ed.* **2004**, *43*, 3485 – 3488.
[4] T. M. Anderson, W. A. Neiwert, M. L. Kirk, P. M. B. Piccoli, A. J. Schultz, T. F. Koetzle, D. G. Musaev, K. Morokuma, R. Cao, C. L. Hill, *Science* **2004**, *306*, 2074 – 2077.
[5] T. Yamase, P. Prokop, Y. Arai, *J. Mol. Struc.* **2003**, *656*, 107 – 117.
[6] E. Coronado, C. Giménez-Saiz, C. J. Gómez-García, S. C. Capelli, *Angew. Chem.* **2004**, *116*, 3084 – 3087; *Angew. Chem. Int. Ed.* **2004**, *43*, 3022 – 3025.
[7] T. Liu, E. Diemann, H. Li, A. Dress, A. Müller, *Nature* **2003**, *426*, 59 – 62.
[8] A. Müller, D. Rehder, E. T. K. Haupt, A. Merca, H. Bögge, M. Schmidtmann, G. Heinze-Brückner, *Angew. Chem.* **2004**, *116*, 4566 – 4570; *Angew. Chem. Int. Ed.* **2004**, *43*, 4466 – 4470.



 © 2005 Wiley-VCH Verlag GmbH & Co. KGaA, Weinheim

cycloisomerization

Developments in Furan Syntheses**

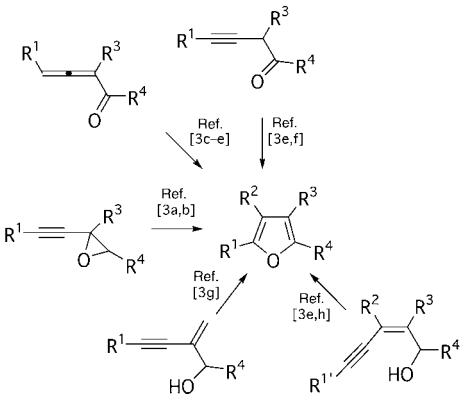
*Richard C. D. Brown**

Keywords:
alkynes · allenes · cycloisomerization · heterocycles · synthetic methods

The synthesis of furans has attracted tremendous interest for well over a century,[1] reflecting both the importance of these heterocycles in natural and synthetic substances[2] and the requirement for more selective and versatile approaches for their synthesis. In particular, the development of routes that allow the facile assembly of substituted furans under mild conditions from simple readily available starting materials remains an important objective.

Classical approaches to substituted furans have involved the cyclocondensation of dicarbonyl compounds or equivalents, or the substitution of an existing furan ring.[1] Alternative strategies have explored the cycloisomerization of alkyne- and allene-containing compounds (Scheme 1).[1a,b,3,4] However, there are some limitations, including ease of access to allenyl substrates that contain sensitive functional groups and the inability to prepare 3,4-substituted furans by the direct cycloisomerization of allenes.

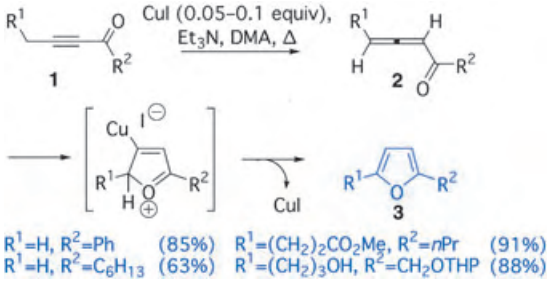
Alkynes are typically considered to be more attractive starting materials than allenes, and recently some ingenious methods to effect propargyl–allenyl interconversion and subsequent heterocyclization have been reported.[5–9] One such approach was based on the finding that the readily accessible alkynones **1** underwent cycloisomerization to furans



Scheme 1. Cycloisomerization methods for the synthesis of substituted furans.[3]

3 in the presence of a copper catalyst and an amine base (Scheme 2).[5,6] The reaction is believed to proceed through the intermediacy of allenyl isomers **2**, which were previously known to undergo cyclization in the presence of a number of transition metals,[3] including Cu^{I}.[3d]

Subsequent studies involving 4-thio- and 4-acyloxybut-2-ynones, **4** and **5** ($R^1 \neq H$), resulted in the discovery of novel routes to di- and tri-substituted furans **7** and **9**, involving mechanistically novel 1,2-shifts of the heteroatom-containing groups (Scheme 3).[7,8] The proposed reaction pathway involves propargyl–allenyl isomerization followed by formation of aromatic thiirenium ions **6** or dioxolenylium zwitterions **8**, which may then cyclize by an Ad_N-E (nucleophilic addition–elimination) mechanism. The role of Cu^{I} in the overall process is not fully understood, but evidence suggests that it may facilitate more than one step. The results presented suggest that the 1,2-acyloxy-migration–cycloisomerization sequence may be less effective for acetylenic ketones with enolizable α protons (e.g. $X = O_2CR^2$, $R^3 = Me$), although, curiously, this is not the case for sulfanyl analogues.[8]



Scheme 2. Cu^{I}-catalyzed cycloisomerization of alkynones to provide 2-monosubstituted and 2,5-disubstituted furans. DMA = *N*,*N*-dimethylacetamide, THP = tetrahydropyranyl.

Tetrasubstituted furans **12** are also available through a complementary Ag^{I}-catalyzed cycloisomerization of 2-acetoxybut-3-yn-1-ones **10** (Scheme 4).[7] The modified approach made use of a formal 1,3-acyloxy shift to provide a tetrasubstituted allene **11** that underwent the cycloisomerization sequence with concomitant 1,2-migration of the acyloxy group at ambient temperature.

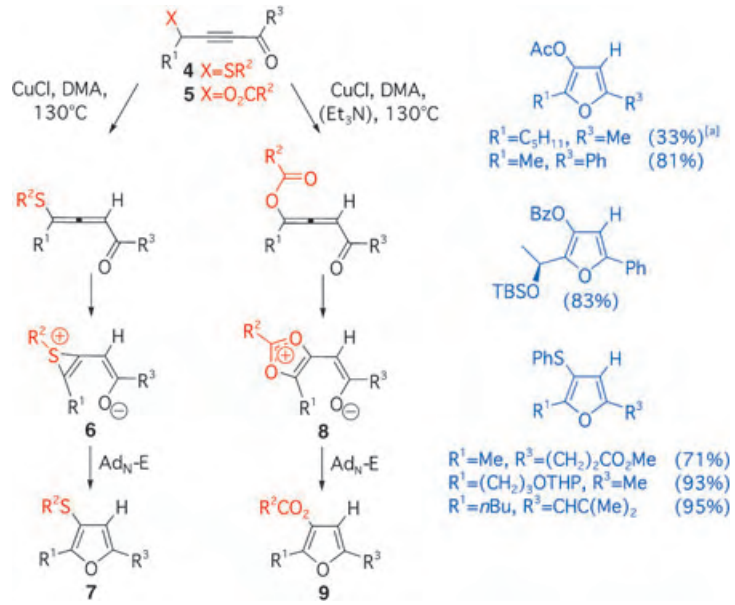
The sequence has been extended to substrates **13**, which contains sulfonyloxy and phosphatyloxy groups, to provide products with the potential for further elaboration in metal-catalyzed cross-coupling processes (Scheme 5). Interestingly, isolation of the allenyl intermediates **14** and **16** provided further support for the proposed mechanism.

The scope of these fascinating cycloisomerization processes remains to be fully explored, but the major appeal lies in the use of alkynyl substrates and the

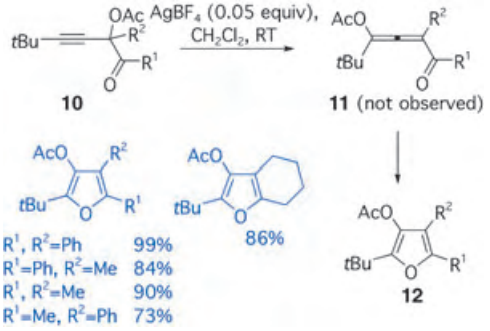
[*] Dr. R. C. D. Brown
School of Chemistry
University of Southampton
Highfield, Southampton, SO17 1BJ (UK)
Fax: (+44) 23-8059-6805
E-mail: rcb1@soton.ac.uk

[**] The Royal Society is gratefully acknowledged for a University Research Fellowship, and Dr. Bruno Linclau is thanked for helpful comments.

© 2005 Wiley-VCH Verlag GmbH & Co. KGaA, Weinheim
DOI: 10.1002/anie.200461668



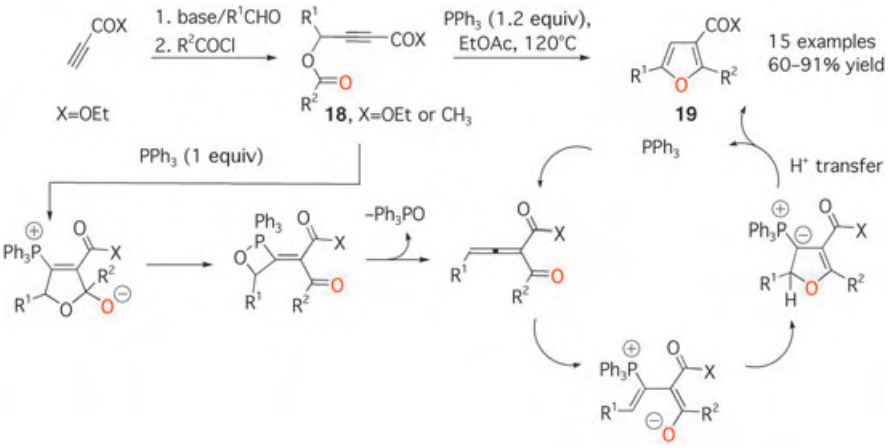
Scheme 3. Novel 1,2-migrations of thio and acyloxy groups in the synthesis of 3-thio-substituted furans **7** and 3-acyloxy-substituted furans **9** by Cu^{I}-catalyzed cycloisomerization. [a] Isolated as a 6.7:1 mixture of isomers. Bz = benzoyl, TBS = *tert*-butyldimethylsilyl.



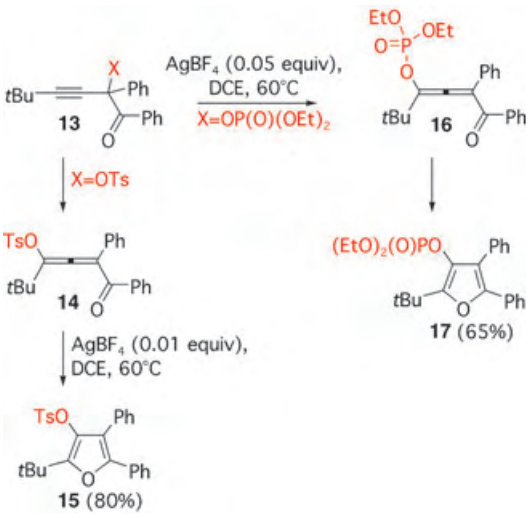
Scheme 4. Cycloisomerization approach to tetrasubstituted furans.

initial indications of excellent functional-group compatibility.

Another mechanistically intriguing and potentially powerful approach to the synthesis of substituted furans **19** involved reductive cyclization of γ-acyloxy butynoates **18** (Scheme 6).[9] Reductive cyclization of butynoates and one example of that of a butynone (**18**, X = Me) were reported to occur in the presence of 1.2 equivalents of PAr_3 at temperatures ranging from ambient to 120 °C, depending on the electrophilicity of the acyloxy group. ^{18}O-enriched material was used to corroborate the proposed mechanism by demonstrating that the isotopic label is retained in the product. On the basis of the proposed mechanism, it appears that the scope of the process may extend to alkynes bearing other electron-withdrawing groups, although direct exposure of monoactivated allenes to the reaction conditions did not give furans.



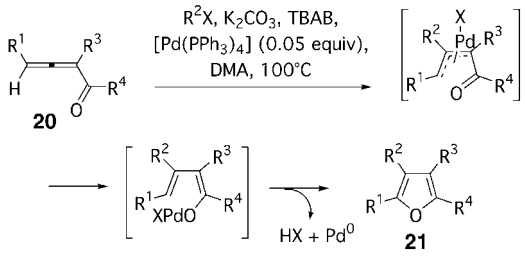
Scheme 6. Phosphine-mediated reductive cyclocondensation of γ-acyloxy butynoates to furans. Red atom labels indicate ^{18}O-enriched sites.



Scheme 5. Synthesis of sulfonyloxy-substituted and phosphatyloxy-substituted furans **15** and **17**. DCE = 1,2-dichloroethane, Ts = *p*-toluenesulfonyl.

Tetrasubstituted furans can now also be prepared directly from allenyl ketones by means of a palladium(0)-catalyzed coupling–cyclization reaction (Scheme 7).[10] The range of 1,2-allenyl ketone substrates **20** investigated was restricted to simple aryl, allyl, and alkyl substituted species, although the metal-catalyzed coupling–cyclization reaction conditions should be compatible with a much wider variety of functionality.

The strategies described above constitute significant new synthetic routes



Scheme 7. Pd-catalyzed cross-coupling–cyclization to give highly substituted furans. TBAB = tetrabutylammonium bromide.

 © 2005 Wiley-VCH Verlag GmbH & Co. KGaA, Weinheim

to diversely substituted furans from acetylenic and allenic compounds. Beneficial aspects, including good functional-group tolerance, predictable regioselectivity, the ability to synthesize highly substituted furans, and the use of more easily accessible acetylenic compounds, add to the practical attraction of these heterocyclization processes.

Published Online: December 23, 2004

[1] For reviews of furan synthesis, see: a) "*Hetarenes and Related Ring Systems: Fully Unsaturated Small-Ring Heterocycles and Monocyclic Five-Membered Hetarenes with One Heteroatom*": B. König, *Methoden Org. Chem. (Houben-Weyl) 4th ed. 1952–*, *Vol. 9*, **2001**, pp. 183–286; b) X. L. Hou, H. Y. Cheung, T. Y. Hon, P. L. Kwan, T. H. Lo, S. Y. Tong, H. N. C. Wong, *Tetrahedron* **1998**, *54*, 1955; c) L. D. Krasnoslobodskaya, Y. L. Gol'dfarb, *Russ. Chem. Rev.* **1969**, *38*, 389.

[2] a) B. A. Keay, P. W. Dibble in *Comprehensive Heterocyclic Chemistry II*, *Vol. 2* (Eds.: A. R. Katritzky, C. W. Rees, E. F. V. Scriven), Elsevier, Oxford, **1997**, pp. 395–436; b) D. M. X. Donnelly, M. J. Meegan, in *Comprehensive Heterocyclic Chemistry*, *Vol. 4* (Eds.: A. R. Katritzky, C. W. Rees), Pergamon, Oxford, **1984**, pp. 657–712.

[3] For selected examples of cycloisomerization approaches to substituted furans, see: a) A. S. K. Hashmi, P. Sinha, *Adv. Synth. Catal.* **2004**, *346*, 432; b) D. Miller, *J. Chem. Soc. C* **1969**, 12; c) J. A. Marshall, E. D. Robinson, *J. Org. Chem.* **1990**, *55*, 3450; d) A. S. K. Hashmi, *Angew. Chem.* **1995**, *107*, 1749; *Angew. Chem. Int. Ed. Engl.* **1995**, *34*, 1581; e) A. S. K. Hashmi, L. Schwarz, J. H. Choi, T. M. Frost, *Angew. Chem.* **2000**, *112*, 2382; *Angew. Chem. Int. Ed.* **2000**, *39*, 2285; f) Y. Fukuda, H. Shiragami, K. Utimoto, H. Nozaki, *J. Org. Chem.* **1991**, *56*, 5816; g) J. A. Marshall, C. A. Sehon, *J. Org. Chem.* **1995**, *60*, 5966; h) B. Seiller, C. Bruneau, P. H. Dixneuf, *Tetrahedron* **1995**, *51*, 13089.

[4] For an example of Pd-catalyzed addition–cycloisomerization sequence to give furans, see: B. M. Trost, M. C. McIntosh, *J. Am. Chem. Soc.* **1995**, *117*, 7255.

[5] A. V. Kel'in, V. Gevorgyan, *J. Org. Chem.* **2002**, *67*, 95.

[6] For the related cyclizations of alkynyl imines to pyrroles, see: a) J. T. Kim, V. Gevorgyan, *Org. Lett.* **2002**, *4*, 4697; b) A. V. Kel'in, A. W. Sromek, V. Gevorgyan, *J. Am. Chem. Soc.* **2001**, *123*, 2074.

[7] A. W. Sromek, A. V. Kel′in, V. Gevorgyan, *Angew. Chem.* **2004**, *116*, 2330; *Angew. Chem. Int. Ed.* **2004**, *43*, 2280.

[8] J. T. Kim, A. V. Kel'in, V. Gevorgyan, *Angew. Chem.* **2003**, *115*, 102; *Angew. Chem. Int. Ed.* **2003**, *42*, 98.

[9] C.-K. Jung, J.-C. Wang, M. J. Krische, *J. Am. Chem. Soc.* **2004**, *126*, 4118.

[10] S. M. Ma, J. L. Zhang, L. H. Lu, *Chem. Eur. J.* **2003**, *9*, 2447.

 © 2005 Wiley-VCH Verlag GmbH & Co. KGaA, Weinheim

Natural Products Synthesis

The Quest for Quinine: Those Who Won the Battles and Those Who Won the War

Teodoro S. Kaufman and Edmundo A. Rúveda*

Keywords:
alkaloids · asymmetric synthesis · history of chemistry · quinine · structural determination



© 2005 Wiley-VCH Verlag GmbH & Co. KGaA, Weinheim
DOI: 10.1002/anie.200400663

For a long time, the synthesis of quinine constituted an elusive target. In 2004, which marked the 60th anniversary of the publication of the approach used by Woodward and Doering to synthesize quinine, two new stereocontrolled total syntheses of the natural product were accomplished. Together with the well-publicized first stereocontrolled total synthesis of quinine by Stork in 2001, these publications evidence the revival of interest of organic chemists in the synthesis of this compound, once considered a miracle drug. The recently disclosed syntheses of quinine also testify in a remarkable manner the huge progress made by organic synthesis during the last three decades since the first series of partially controlled syntheses of quinine by the group of Uskokovic. Following an account of the historical importance of quinine as an antimalarial drug and a brief description of the experiments which contributed to its isolation and structural elucidation, the first reconstructions of quinine and the total syntheses of the natural product are discussed.

From the Contents

1. Introduction 855
2. Quina: Bark from the New World That Cures Malaria 856
3. The Search for the Active Component in the Cinchona Bark 857
4. The First Synthetic Approach to Quinine: Birth of a New Industry 858
5. The Structure of Quinine 860
6. Rabe Provides the First Steps and the Synthesis of Quinine Seems To Become Simpler 864
7. The Much Awaited Total Synthesis of Quinine 865
8. Mastering the C8–N Strategy: The First Total Synthesis of Quinine and Variation on the Theme 869
9. After 55 Years: A Modern, Stereocontrolled Synthesis of Quinine 873
10. The Resurrection of the C8–N Strategy: A Catalytic Enantioselective Total Synthesis of Quinine 875
11. Another C8–N Strategy: The Latest Total Synthesis of Quinine 877
12. Concluding Remarks 878

1. Introduction

The year 2004 marks the 60th anniversary of the first communication by Woodward and Doering of their formal total synthesis of quinine,[1a] the most celebrated cinchona alkaloid that was claimed as "*the drug to have relieved more human suffering than any other in history*".[2] In its time, this epoch-making publication seemed to have ended the almost 100-year era of man trying to master this single natural product, which for centuries constituted the only effective remedy to malaria. The authors were therefore acclaimed as heroes.

Malaria is a life-threatening disease producing a debilitating condition which is caused by several species of the parasite *Plasmodium*. These parasites enter red blood cells, feed upon the protein therein, and destroys them. *Plasmodium* is transferred from an infected person to a healthy individual by the females of several species of *Anopheles* mosquitoes, which use human blood as a means to provide nourishment for their developing eggs.[3]

The parasite lodges in the mosquito's salivary gland and moves into the blood stream of the victim when it is bitten. The most conspicuous symptom of malaria is an intermittent fever that is associated with discrete stages of the life cycle of *Plasmodium*. Patients normally recover but they are weakened by the experience, being left listless and anemic. Repeated attacks can be observed many months or years after the initial infection because a form of the parasite becomes lodged in the person's liver. One form of malaria, caused by *P. falciparum*, can be quickly fatal, even to otherwise healthy individuals, because it can produce blood clots in the brain.

Malaria has affected mankind since the beginnings of recorded history and probably before.[4] Although malaria was associated with marshy areas since Hippocrates' time and was described by Thomas Sydenham around 1680,[5] its cause was unknown until 1880 when the French physician Alphonse Laveran discovered the parasite in patients' blood. Laveran, as well as the Italian physiologist Camilo Golgi, the British bacteriologist Sir Ronald Ross (who by the turn of the century discovered the role of the mosquito vector in the transmission of the disease), and the Swiss chemist Paul Hermann Müller (the inventor of DDT), were each honored with the Nobel Prize for their important contributions to the increased knowledge and better control of malaria.[6]

[*] Prof. T. S. Kaufman, E. A. Rúveda
Instituto de Química Orgánica de Síntesis (CONICET-UNR)
Universidad Nacional de Rosario
Suipacha 531, S2002LRK Rosario (Argentina)
Fax: (+54) 341-437-0477
E-mail: tkaufman@fbioyf.unr.edu.ar

 DOI: 10.1002/anie.200400663 © 2005 Wiley-VCH Verlag GmbH & Co. KGaA, Weinheim

Malaria has been designated as "*the most significant disease for world civilization over the past three millennia*";[7] the disease is still rampant in many countries, particularly those in Africa south of the Sahara. Even today, despite over 100 years of continuous research and a plethora of antimalarial drugs,[8] malaria remains a major disease, which affects approximately 40 percent of the world's population.[9] The World Health Organization (WHO) reported that there are between 300 and 500 million new cases worldwide each year and the disease claims between 1.5 and 2.7 million lives annually, mostly children.[10]

From a chemical perspective, what also marks Woodward's synthesis out as an important landmark is that it can be considered as the dawn of what was called "the Woodwardian era" of organic chemistry and the first of an impressive series of outstanding and increasingly daring accomplishments in the total synthesis of natural products. The 1944 publication by Woodward and Doering was the beginning of a series of events which would add excitement to the discipline of organic synthesis and give strong impulse to its subdiscipline of natural products synthesis. It was also the origin of the longstanding misunderstanding that Woodward and Doering were the first in achieving the total synthesis of quinine, a polemical controversy that persists even now.[11,12]

2. Quina: Bark from the New World That Cures Malaria

Malaria was brought to the New World by Europeans.[13] Ironically, the New World almost immediately exported the most efficient treatment to Europe for this disease, a supply that was set to continue for approximately 300 years afterwards.

The cinchona alkaloids are found in the bark of cinchona and Remijia species, which are evergreen trees originally part of the high forest (1500–2700 m) of the eastern slopes of the Andes mountains from Venezuela to Bolivia. Natives called the cinchona tree "quina-quina" ("bark of barks" in the native indian tongue) and seemed to have been aware of its antipyretic properties (it was also known as "ganna perides" or "fever stick"); they used the bark to treat fevers a long time before the arrival of the Spanish. Jesuits, particularly Father Antonio de la Calancha in Perú and Cardinal Juan de Lugo in Europe, are credited with the introduction of cinchona bark into medical use in Europe around 1640, after the perhaps serendipitous discovery[14] of its antimalarial properties in Peru (hence it was also known as Jesuit's bark, Cardinal's powder, Popish powder, etc.).[15] This fortuitous discovery seems to have taken place while the Count of Chinchon was Viceroy of this part of the Spanish colonies; according to a widespread legend, his wife, the Countess of Chinchon, was miraculously cured from malaria after being treated with a remedy made from cinchona bark specially brought to Lima from Loxa (now Loja, Ecuador).[16]

The Jesuits must also be credited with the spread of this remedy in Europe since Rome was the malaria capital of the world in the middle 17th century. A decisive contribution was also made by Robert Talbor, an English apothecary who cured many noblemen and several members of European royal families (including King Charles II of England and the son of King Louis XIV of France) from malaria. While Europe was involved in a controversy regarding the use of the new medicine, Talbor used a curative secret formula—which was shown after his death to be based on cinchona bark. The bark was officially introduced into the London Pharmacopoeia in 1677, and by 1681 it was universally accepted as an antimalarial substance.[17] The valuable properties of the medicine raised demand for the bark, which culminated in the installation of a Spanish-owned commercial monopoly and the beginning of the slow extinction of the natural cinchona forests because of overharvesting.[18] Such was the demand for the drug that there was always a shortage of cinchona bark in Europe, which for more than 200 years was imported from South America at great expense.[19]

Mankind seems to have learned a lesson from cinchona depredation: in recent times, it was realized that world demand for the powerful antitumor compound paclitaxel could result in extinction of its natural source, the Pacific yew tree. Pharmaceutical companies redirected their research towards the synthesis of semisynthetic derivatives and analogues; 150–200 years ago such environmental concerns did not exist.[20]



Teodoro S. Kaufman graduated in biochemistry (1982) and pharmacy (1985) from the National University of Rosario (Argentina) and received his PhD in 1987 under the guidance of Prof. Edmundo A. Rúveda. After a two-year post-doctoral training with Prof. Robert D. Sindelar at The University of Mississippi (USA), he returned to the National University of Rosario in 1989 as an Assistant Professor. He is a member of the Argentine National Research Council and Vice-Director of the Institute of Synthetic Organic Chemistry. His research interests include heterocyclic chemistry and the synthesis of natural products.



Edmundo A. Rúveda graduated in pharmacy (1956) and biochemistry (1960) from the National University of Rosario (Argentina) and completed his PhD in 1963 with Prof. Venancio Deloufeu. He moved to England for post-doctoral studies with Prof. Alan Battersby (1964–1965) before returning to Argentina as Associate Professor and then Full Professor (1974) at the University of Buenos Aires. In 1975, after a short period in the pharmaceutical industry, he became Associate Director of the Institute of Chemistry at the University of Campinas (Brazil). In 1980 he returned as the Director of the Institute of Synthetic Organic Chemistry to the National University of Rosario, from which he has recently retired.

© 2005 Wiley-VCH Verlag GmbH & Co. KGaA, Weinheim

3. The Search for the Active Component in the Cinchona Bark

Written records of the use of plants as medicinal agents date back thousands of years. The oldest records come from Mesopotamia and date from about 2600 BC. These records indicate that instead of only one- or two-plant-based medicines finding their way into popular use, there were in fact many in use (up to 1000 in Mesopotamia).[21]

During the middle of the 18th century chemists began to take renewed interest in herbal remedies, including the cinchona bark. They became convinced that the dried and powdered herb contained an "active principle"—a definite chemical compound that was responsible for the plant's curative properties—a pure extract of which would provide an even better cure. A direct consequence of this reasoning was that in the early 1800s the active principles from plants began to be isolated. It was at this point that the effectiveness of medicinal natural products commenced to be attributed to science and not to magic or witchcraft.

During this age of discovery, reputed scientists of several European laboratories started to study cinchona bark. The concentration of the active principle of the bark differed according to its natural source and it seems that some degradation always occurred during the trip overseas to Europe, a feature that also encouraged adulteration. Therefore, their aim was to gain a better knowledge about its constituents, in particular its active principle, and detect the more frequent adulterations of this valuable product imported from overseas.[22]

In 1746 the Count Claude Toussaint Marot de la Garaye obtained a crystalline substance in France from the bark which he termed "sel essentiel de quinquina". A few years later, the two French chemists Buquet and Cornette introduced a new "sel essentiel de quinquina"; however, both proved to be the inactive calcium salt of quininic acid. In another failure, the Swedish physician Westerling announced in 1782 the discovery of the active principle, which he called "vis coriaria" and later shown to be "cinchotannic acid".[22b]

Antoine François Fourcroy systematically analyzed the bark by extracting it with water, alcohol, acids, and alkaline solutions. In 1790 he was finally able to obtain a dark red, resinous, odorless, and tasteless mass, which he called "chinchona red". Fourcroy claimed this to be the essential pharmacologic constituent of the bark; however, in contradiction to his affirmations, it was demonstrated that "chinchona red" was unable to cure malaria. Fourcroy also observed that the water placed in contact with the bark gave litmus a blue color—then a known property of alkalis—and that a green precipitate was produced when the infusion of the bark was treated with lime water. This French scientist was very close to entering the history books as the first to isolate quinine, but, surprisingly, he decided to abandon his research on the bark. Perhaps as a premonition, he commented that "*doubtlessly, this research work will lead some day to the discovery of a febrifuge for the periodic fever that, once identified, will be extracted from different plants*".[22b,38]

At the beginning of the 19th century the problem of the nature of the active principle of the Peruvian bark, as it was then called, still remained unsolved. In 1811 the Portuguese navy surgeon Bernardo Antonio Gomes extracted the bark of the gray variety with alcohol, added water and a small amount of potassium hydroxide, and observed the separation of a few crystals. Gomes called this substance cinchonine, which had been previously isolated by Duncan in Edinburgh from certain varieties of quina trees. Interestingly, it seems that the botanist Aylmer B. Lambert was also able to prepare the same compound; however, neither of them suspected the alkaline (alkaloidal) nature of the substance.

In 1817 the German Chemist Friedrich Wilhelm Sertürner[23] reported that morphine forms salts in the presence of acids, an observation that led him to the isolation of this important alkaloid. Driven by Sertürner's findings, Joseph Louis Gay-Lussac commissioned his colleague Pierre Jean Robiquet of the Ecole de Pharmacie of Paris with the task of searching for useful applications of the reported strategy. Robiquet's co-worker Pierre Joseph Pelletier was selected to conduct this study in collaboration with Joseph Bienaimé Caventou, a young student of pharmacology, and quickly led to the isolation of emetine (1817), strychnine (1818), brucine (1819), and veratrine (1919),[24] as well as other substances which the German chemist Wilhelm Meissner in 1819 termed alkaloids.[25]

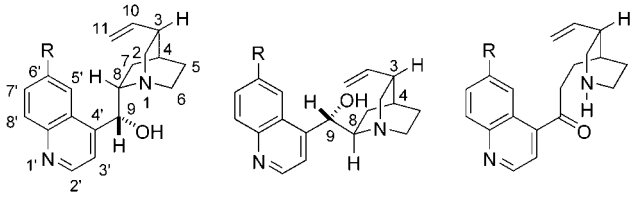
In 1820 Pelletier and Caventou, experts in the isolation of alkaloids, began to work with the yellow bark of cinchona, known to be more effective against malaria than the gray bark employed by Gomes.[26] The alcoholic extract did not produce a precipitate when diluted with water and basified with potassium hydroxide; instead, a pale yellow gummy mass formed. The compound, which was extraordinarily bitter in taste, was soluble in water, alcohol, and diethyl ether. The latter feature was a key difference between its behavior and that of Gomes' material. Pelletier and Caventou cleverly demonstrated that the cinchonine isolated by Gomes was a mixture of two alkaloids which they named as quinine and cinchonine, thus successfully crowning a 70 year search.[27] Their original samples are now exhibited in London's Science Museum. The isolation of quinine allowed the quantitative evaluation of the quality of quina bark, the administration of a pure compound as a specific treatment for malaria, and the development of more accurate dose regimes.

Being pharmacists, neither of the Frenchmen risked demonstrating the curing ability of the newly isolated natural product; perhaps prophetically, they just mentioned that "*some skilful physician … joining prudence to sagacity … will conduct the appropriate clinical trials*".[27] These physicians quickly appeared and demonstrated that quinine was notably effective against the malarial fever, while cinchonine was inactive. The distinguished physiologist Francois Magendie gained broad experience in administering quinine to his patients and, by 1821, provided instructions for its use in the *Formulaire pour la préparation et L'emploi de plusieurs nouveaux médicaments.* In 1834 the surgeon of the French army, François Clément Maillot, who had previously used cinchona bark in Corsica, made successful trials of quinine with the troops in Argel and Ajaccio. Pure quinine rather than the powdered bark soon became the drug of choice for treating malaria.[5,28]

 © 2005 Wiley-VCH Verlag GmbH & Co. KGaA, Weinheim

Pelletier and Caventou did not patent their invention, but instead were generously rewarded by their country with high positions and honors. The Academy of Sciences of Paris awarded the scientists the Montyon Prize, and Pelletier became the associate director of the Ecole de Pharmacie in 1832 as well as being appointed member of the French Académie des Sciences in 1840. Pelletier and Caventou established a factory in Paris for the extraction of quinine, an activity that is often mentioned as the beginning of the modern pharmaceutical industry.

The isolation of quinine paved the way for a series of new and interesting discoveries. In 1821 Robiquet isolated caffeine



cinchonidine, R= H
quinine, R= OMe

cinchonine, R= H
quinidine, R= OMe

cinchotoxine, R= H
quinotoxine, R= OMe

following the hypothesis that quinine should be present in the coffee tree, since this belongs to the the same family (the Rubiaceae) as the cinchona trees. Other alkaloids were later isolated from cinchona species: quinidine was isolated in 1833 by Delondre and Henry,[29] while in 1844 Winckler isolated what Pasteur termed in 1851 cinchonidine.[30] An additional 25 alkaloids related to quinine had been isolated by 1884 and an additional 6 were added between 1884 and 1941.[31]

Pasteur, the versatile French scientist, produced several "toxines" (cinchotoxine, quinotoxine—initially known as quinicine) by reaction of the natural bases with weak or diluted acids.[26e] His observations would prove to be of key importance 50 years later during the development of the first series of serious attempts to synthesize quinine; their importance can still be noticed today through the development of new approaches to the C8–N connection (see below). He also demonstrated the usefulness of quinotoxine as a resolving agent for racemic mixtures of acids.[26d,e]

4. The First Synthetic Approach to Quinine: Birth of a New Industry

By the 1800s the French, British, and Dutch all had colonies in malaria-infested areas. After the isolation of quinine by Pelletier and Caventou and the subsequent successful medical experiments demonstrating that this alkaloid was indeed the active antimalarial principle contained in the quina bark, demand for it started to rise. In the middle of the 19th century, both the alkaloid as well as the bark were always in short supply, since they were the only effective known treatment against malaria. It was regarded so critical strategically that it could determine the size and prosperity of an empire.[32] Two alternatives were considered possible to secure a continuous and abundant supply of quinine: the establishment of new plantations in areas other than South America and/or the chemical synthesis of quinine through the use of the then new science of organic chemistry.

Examples of the first alternative (the story of which can be likened to that of rubber, wherein Sir Henry Wickham transferred seeds to Ceylon in the 1890s) include the several expeditions of Justus Hasskarl, Richard Spruce, Robert Cross, and Clemens Markham, as well as others representing European powers, in the search for plants, seedlings, and seeds of cinchona.[33] Most of the attempts at cultivating the cinchona tree as a source of quinine sound today either hilarious or tragic. They all met with failure because of a range of diverse factors that reveal the deep lack of precise botanical knowledge about cinchona and its biology. The French had little or no success, but the English partially succeeded in establishing cinchona plantations in Ceylon (modern day Sri Lanka) and India, which provided for their colonial army.[34] In a strange twist of fate, this strategy actually culminated in the establishment of productive Dutch plantations of cinchona in Java (Dutch East Indies, now Indonesia).[35] These Dutch plantations were made possible thanks to a small amount of seeds cheaply sold to the Dutch by a British trader, Charles Ledger,[36] in Peru and they constituted the basis of the Dutch control of the cinchona trade up to world war II. In these plantations the bark was removed in a controlled way and a continuous supply of quinine was obtained, much of which was supplied to those involved in colonial expansion.

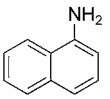
The second strategy proved to be a much more demanding task. The indefatigable pursuit of synthetic quinine eventually resulted in it playing an important historical role in organic chemistry, both as a demanding target for structure elucidation and chemical synthesis. August Wilhelm von Hofmann, the German Director appointed to the recently founded Royal College of Chemistry, was the first to talk about the challenge of its synthesis. In a 1849 public address to the Royal College of Chemistry, Hofmann stated his intention of synthesizing the lucrative quinine as a way to demonstrate the ability of organic chemistry to solve social needs. In his words "*… it is obvious that naphthalidine [now α-naphthylamine], differing only by the elements of two equivalents of water might pass [into quinine] simply by an assumption of water. We cannot of course, expect to induce the water to enter merely by placing it in contact, but a happy experiment may attain this end by the discovery of an appropriate metamorphic process …*".[37]

The race for synthetic quinine was heating up by the middle of the 19th century. French scientists kept close track of developments across the English Channel, and in 1850 the French Society of Pharmacy made a call to the chemists in the following way: "*… during a long time, there has been an important problem to find a substitute for quinine with its same therapeutic effects … Therefore, we make a call … offering the amount of 4000 francs to the … discoverer of the way to prepare synthetic quinine*".[38] Participants were notified of the January 1, 1851 deadline and the requirement of submitting at least half a pound of the synthetic substance. Needless to say, nobody claimed the prize.

 © 2005 Wiley-VCH Verlag GmbH & Co. KGaA, Weinheim

Chemical synthesis was in its infancy at this time. The main reservoir of chemicals was obtained from coal and the petrochemical industry, both being important sources of starting materials for various scientific problems. Carbonization of coal to provide gas for lighting and heating (mainly hydrogen and carbon monoxide) also gave a brown tar rich in aromatic compounds such as benzene, pyridine, phenol, aniline, and thiophene. Scientific research in this field was often a matter of trial and error based on intuition. Furthermore, there were no appropriate concepts for structure—these ideas came a decade later with the invention of structural theory by Butlerov, Couper, Kekulé, and van't Hoff. Indeed, the tetravalency of carbon atoms was proposed in 1858 and Kekule's theory on the structure of the benzene nucleus was formulated in 1865.[39]

The theory of types was proposed in 1838 by Dumas as a method to explain the combining power of carbon and became the predominant way of thinking among the most prominent chemists.[40] Type formulas intended to indicate the chemical similarity of compounds, but they were by no means structural formulas. However, this theory had strong supporters and contributors such as Alexander Williamson[41] and August Wilhelm von Hofmann. Following previous work of Wurtz, Hofmann prepared primary, secondary, and tertiary amines in 1851 as well as quaternary ammonium salts and classified them as belonging to the new ammonia type after recognizing that these compounds were related to ammonia. The theory of types successfully predicted the existence of acid anhydrides, which had been discovered in 1852 by Charles Gerhardt—the chief exponent of the new type theory.[42] Therefore, nobody was surprised to hear Hofmann's proposal of synthesizing quinine by hydration of naphthylamine [Eq. (1)], an abundant by-product from the British coal and gas industry.

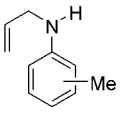


naphthalidine
(α-naphthylamine)

$$2\ C_{10}H_9N + 2\ H_2O \longrightarrow C_{20}H_{22}N_2O_2 \qquad (1)$$

The molecular formula postulated by Hofmann for quinine ($C_{20}H_{22}N_2O_2$) had two hydrogen atoms less than the correct formula ($C_{20}H_{24}N_2O_2$), which was established in Göttingen in 1854 by Adolf Strecker.[43] The establishment of the correct molecular formula for the natural product stimulated the beginning of the experimental phase of Hofmann's project, which was still guided by the simple atom-counting strategy. It is worth noting that urgent utilitarian objectives drove Hofmann's interest in this specific project: quinine was then a miracle drug and the economic support of the Royal College had started to decline because of the impatience on the part of its rich sponsors. They began to worry about the lack of results from their investments and strongly debated the true virtues of applied organic chemistry and its ability to produce something useful. This adverse climate was perceived by Hofmann as constituting a risk to the novel style and dynamics he had begun to impart to the College. On the other hand, organic synthesis was embryonic at that time, and Hofmann's proposal was daring.

During the Easter vacation of 1856, with the correct molecular formula of quinine in his hands and following his mentor's ideas, William H. Perkin decided to "reproduce" quinine. The 18-year-old disciple of Hofmann confidently began the quest by carrying out simple experiments, such as attempting a potassium dichromate mediated oxidative dimerization of "*N*-allyltoluidine" [Eq. (2)], in his home-



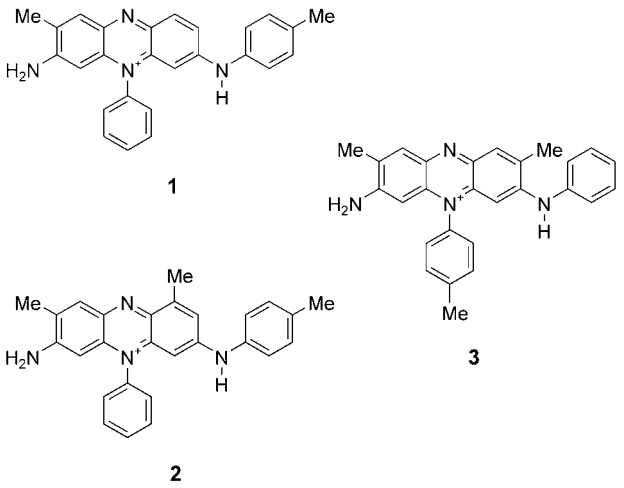
N-allyltoluidine

$$2\ C_{10}H_{13}N + 3\ [O] \longrightarrow C_{20}H_{24}N_2O_2 + H_2O \qquad (2)$$

made laboratory in Shadwell, East London.[44] Since *N*-allyltoluidine is structurally nothing like half a quinine molecule, this attempt was utterly futile and he did not succeed. Undeterred, however, like a true Prince of Serendip—a prepared mind in search of unanticipated wonders—he must have observed something in the noxious, black coal tar derivative formed, which spurred him into next trying to similarly oxidize "aniline". Assuming that the primitive and useless atom-counting rule employed by young Perkin still governed his experiments, it is certain that his main objective was no longer the originally sought cinchona alkaloid.[45] Although Perkin did not produce quinine, he discovered to his amazement that after a series of clever manipulations his experiment produced a new dye and that this new dye was resistant to fade or run when subjected to washing or when exposed to sunlight. The compound was termed aniline purple and later called mauve by French designers, before becoming known as mauveine. The exact structure of the products resulting from the chemical transformations made by Perkin was studied more than one century later by employing modern high-field NMR techniques; these showed that mauveine has two major constituents: components A (**1**) and B (**2**), which differ from the previously postulated structure **3**.[46]

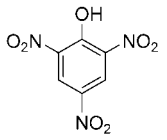
Colored substances were highly valued and much sought after as raw materials. Therefore, against Hofmann's recommendation, and in spite of a lukewarm response from local dyers, with the financial aid of his father (a builder) whom he managed to persuade to join the venture, Perkin developed the processes for the mass-production and use of his new dye. In 1857 he opened his factory at Greenford Green, not far from London, for commercialization of his discovery. Thus, young Perkin began work in the world's first large-scale organic chemical factory.[47] When Queen Victoria and Empress Eugenie publicly flaunted mauve dresses, his new dye became so popular that the period became known as the Mauve Decade. Moreover, the British post issued a penny stamp which became known as "penny mauve" or "penny lilac" and remained in use until 1901.

 © 2005 Wiley-VCH Verlag GmbH & Co. KGaA, Weinheim

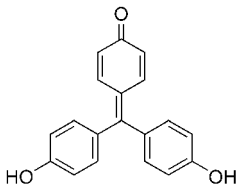


Before Perkin's discovery, all commercial dyes had been obtained from nature by crushing and squeezing insoluble dyes from vegetables, insects, and invertebrates, while employing poorly understood chemical methods for their manipulation. Natural colors were expensive and lacked the brightness we are accustomed to today. With the exception of indigo, they slowly faded on exposure to light or after successive washings. Perkin's aniline purple imparted a bright magenta appearance to diverse yarns which did not fade with time and exposure to other stress factors.[48]

Although picric acid had been produced in Lyon since 1849 and Runge had prepared aurin in 1834,[49] Perkin's



picric acid



aurin

discovery is considered to be a unique event that gave birth to the industry of the aniline dyes,[50] and Perkin's mauveine was one of the first industrial fine-chemicals. This dye was also the source of his personal fortune and an important stimulus for research towards a better understanding of the structure of molecules and their properties.[37] Perkin's industrial preparation of mauveine also signals the beginning of industrial organic synthesis. Many of the modern chemical and pharmaceutical giants such as BASF, Hoechst (now Aventis), Ciba–Geigy (now Novartis), and ICI (parts of which are now Astra–Zeneca and Syngenta) began as aniline dye companies. They later diversified to other products such as fragrances, agrochemicals, and pharmaceuticals. Dyes were employed in the 1880s to visualize pathogenic microorganisms and, by the end of the 19th century, synthetic dyes were being used and had fully replaced natural dyes.[47b,51] Dye research also led to the introduction of sulfonamides in 1936, but ironically, not one of these companies had synthesized quinine in their more than century lifetimes.

The history of chemical synthesis is replete with stories of both luck and perseverance. Similar to Friedrich Wöhler's accidental synthesis of urea[52] and Roy J. Plunkett's discovery of teflon,[14] Perkin's experiment was designed to produce a quite different product. Like his colleagues, Perkin's genius was not to throw away the reaction product but, prompted by unusual observations, to examine its properties. This he did by dissolving the dark and seemingly useless product in alcohol and then dipping pieces of silk into the resultant purple solution.

The key factors determining Perkin's success from his initial failure were the arrival of Hofmann in England, with the aim of creating a school of chemists, as well as Hofmann's contagious enthusiasm for research and his interest in high-impact research subjects, such as the study of organic bases found in coal tar. Also, Perkin's previous experience with dyes was important, as well as his motivation and personal characteristics as a passionate young scientist, with an interest in experimental research, and who relished taking the initiative. No less important was the fact that Perkin was a curiosity-driven person, who was gifted with powerful observational skills.

Paradoxically, the lack of a structural theory made a great contribution by allowing the design and execution of what nowadays could be considered a senseless and futile project condemned to failure before the start. Finally, the purity of the starting "aniline" also played a key role in Perkin's favor. Since the starting benzene was a coal tar derivative it was contaminated with toluene, which upon nitration and subsequent reduction gave a complex mixture of aniline and toluidines. As recognized even by early chemists involved with mauveine, the presence of *o*- and *p*-toluidine were vital for the formation of the most effective dye.

5. The Structure of Quinine

The three most important techniques currently for the elucidation of the structure of natural products are mass spectrometry, nuclear magnetic resonance (NMR) spectroscopy, and X-ray crystallography. The structures of most natural products can be determined with relative ease with the first two techniques, and although X-ray crystallography is a more powerful tool, it requires that the compound in question be capable of producing good-quality crystals.

Quinine is of not too structurally complex and, despite the fact that these techniques are not infallible, today's organic chemists could hardly spend more than a few days determining the structure of the natural product accurately. Modern chemists, however, can hardly imagine how difficult this task was before the advent of these powerful analytical methods. During the late 19th and early 20th century analytical methods were scarce and "wet" chemical analysis was used routinely. Much of the organic chemistry of that time involved the exploration of chemical structures, and destructive approaches such as derivatization, degradation (a method that literally analyzed—breaking down a compound under a

 © 2005 Wiley-VCH Verlag GmbH & Co. KGaA, Weinheim

known set of conditions, such as boiling the compounds in question with concentrated acids or caustic alkalis), and combustion were used to garner structural evidence.[53]

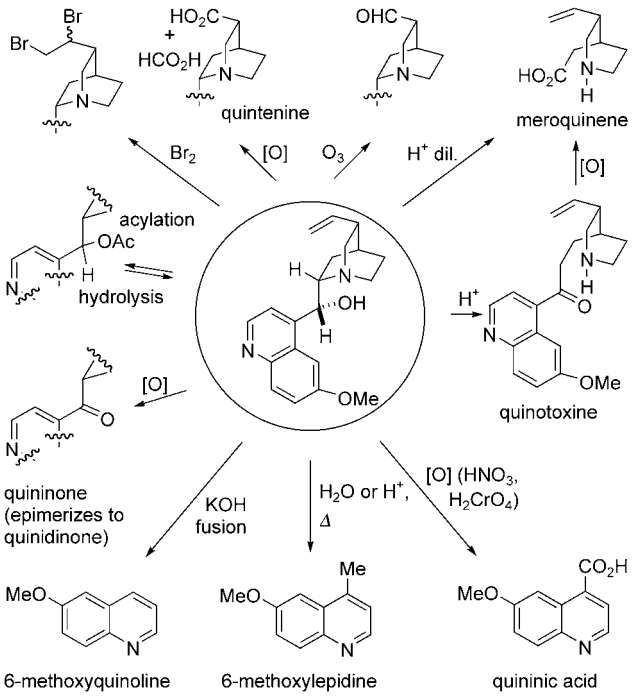
After Perkin's naive experiment and useful failure, there were no other serious attempts to synthesize quinine for the next 50 years. However, before the turn of the century, and with the new concepts of structural theory, organic chemists realized that the structure of quinine was more complex than previously thought and that complete structural elucidation ought to be the first stage in a stepwise rational approach towards the total synthesis of this alkaloid.

The structural elucidation of quinine, now a classic in organic chemistry,[54] was a formidable task and an extraordinary challenge at the time. Interestingly, however, it started with small advances such as Pasteur's demonstrations in 1853 that quinine was levorotatory and could be converted into the corresponding toxine by dilute acid,[55] before Strecker established the empirical formula of the natural product as $C_{20}H_{24}N_2O_2$ in 1854.[43] The whole effort directed towards the structural elucidation of quinine lasted more than 50 years, including a 20 year period of very intense activity in the laboratories of many prominent European chemists. This complex investigation, which also involved the related alkaloids cinchonine, cinchonidine, and quinidine, is one of the most illustrative examples of the joint use of functional group reactions, chemical degradation, and chemical intuition. The benefits of this research widely surpassed its original purpose, since the body of results which culminated in the structural determination of quinine and related alkaloids contributed much to our present chemical knowledge on pyridine and quinoline derivatives.[56]

The simplicity of the experiments is amazing; for example, initial ones carried out by Strecker himself,[43] and also by Skraup, demonstrated the tertiary nature of both nitrogen atoms.[57] Conventional acetylation followed by mild basic hydrolysis of the resultant monoacetyl derivative to regenerate quinine suggested the presence of a hydroxy group, a deduction which was confirmed by its conversion into the corresponding chloride with PCl_5.[58]

The presence of the vinyl group was deduced from experiments undertaken by Skraup, Königs, Hesse, and others, who observed that the alkaloid was easily attacked by permanganate, gave other characteristic reactions of alkenes, such as adding halogens and hydracids,[59] was ozonolyzed to the corresponding aldehyde,[60] and oxidatively degraded to a carboxylic acid known as quintenine with the release of formic acid (Scheme 1).[61] Cinchonine gave the same reactions, an observation which proved important for the joint structural elucidation of the four important cinchona alkaloids: quinine, quinidine, cinchonine, and cinchonidine.

Clues on the nature of the aromatic moiety of quinine were gained by degradative fusion with potassium hydroxide, which furnished 6-methoxyquinoline.[62] Meanwhile, experiments from the laboratories of Königs, Baeyer, and others leading to quinoline, lepidine[63] and 6-methoxylepidine (from cinchonine and quinine), cinchoninic acid (from cinchonine and cinchonidine),[64] and quininic acid (from quinine and quinidine)[65] provided insights on the attachment point of the non-aromatic portion of the molecule.



Scheme 1. Some of the reactions that provided clues to the structure of quinine.

Degradation experiments dilute acid conducted by Königs in 1894 allowed the isolation of a monocyclic structure to which the name meroquinene (μερος = part in Greek) was given.[66] This proved to be a key piece of knowledge for the establishment of the structure of the non-aromatic (quinuclidine) portion of quinine and it became an important fragment in future synthetic efforts. Since degradation of quinine, quinidine, cinchonine, and cinchonidine produced the same meroquinene[66,67] and oxidation of this product gave D-β-cincholoiponic acid,[68] the conclusion was drawn that the relative configuration at C3 and C4 was the same in the four alkaloids. Partial epimerization to α-cincholoiponic acid, however, clouded an otherwise clear stereochemical proof (Scheme 2).[69]

Another critical step in the determination of the chemical structure of quinine was the acquisition of quinotoxine,[55,70] a product already obtained by Pasteur in 1853 after exposure of quinine to a slightly acidic medium.[26e] This reaction and other characteristic chemical transformations, in which assistance of the quinoline moiety was fundamental, would prove to be of compelling importance during the early design of synthetic routes towards the natural product.

A series of papers published by G. Rohde and W. von Miller between 1894 and 1900[71] on the chemistry of quinotoxine suggested that the non-aromatic part of quinine could have a tertiary nitrogen atom as the bridgehead of a bicyclic structure. This proposal was rapidly accepted by Königs because it explained many previous observations from his research.[72] Before his death in 1906, Königs consolidated the structural knowledge on quinine.[67] In 1907 the German chemist Paul Rabe, who worked for almost 40 years on structural and synthetic aspects of quinine, demonstrated that

 © 2005 Wiley-VCH Verlag GmbH & Co. KGaA, Weinheim



Extract from the tribute to Paul Rabe by Henry Albers and Wilhelm Hochstätter in *Chemischen Berichten* **1996**, *99*, XCI–CXI:

Paul Rabe was born in the town of Hoym, on August 24, 1869, son of the pharmacist Ludwig Rabe and his wife Antonie (née Faaß). When Rabe was 11, he entered the Gymnasium at the nearby city of Quedlinburg. He lived these years happily and without deprivations or worries under the intelligent guidance of his "Pensionmutter", the wife of preacher Hohmann, who instilled him her faith in God. Home and school influences, as well as education based on the high values of the classics, inclined Rabe towards science. School friendships were not a random encounter for him; he cultivated them until his death.

In 1890, after passing the Bachelor test, he decided to study chemistry. There can be little doubt, and this was later confirmed by subsequent conversations with colleagues, that his fathers pharmacy had left a lasting impression, which tipped the scales in his choice of career. Here Rabe met some of the most important chemists of his time. First, he spent two semesters at the Institute of his future teacher, Ludwig Knorr, who had just taken over the Professorship at Jena; then, he spent two semesters in Berlin, where the Director was A. W. von - Hofmann, and finally, in 1892, he went back to the University of Jena. Here, in July 1894, he started his Doctorate under the supervision of Knorr on the topic of antipyrin. In February of the following year he was promoted to Dr. Phil. Up until 1897 he was employed as an Assistant in Knorr's laboratory, but then started his career as an independent scientist, working on the isomers of benzylidene bis(acetoacetate), which led him to his "Habilitation" in May 1900. The next steps of his scientific career included his promotion to Assistant Professor in 1904, to Chief of the Division of Organic Chemistry in 1911, and finally on October 1, 1912, he was transferred from the main University to the Deutsche Technische Hochschule of Prague as Ordinary Professor, with duties concentrating on the experimental chemistry of organic materials.

In later years, Rabe recounted with fondness the days he spent in Prague, where under the monarchy of the Habsburgs he learned the rules of etiquette of the noblemen of the Viennese castles who wore two-cornered hats and ornamental swords as ensignia of rank, and where his future wife, Else Hess, was born. However, he siezed the opportunity to return to a prosperous German institute, when in October 1914 the senate of the free and Hanseatic city of Hamburg invited him to be the Director of the State Laboratory of Chemistry a few months before the outbreak of the First World War. Their four children were born in Hamburg, and the parents completely devoted themselves to their upbringing. They were not, however, spared the cruel hand of fate: they suffered the tragic loss of their eldest daughter and the untimely death of their only son during the Second World War. Therefore, Paul Rabe and his wife found refuge in their faith in God, and gave all their love to both of their remaining daughters, their son in law, and their grandchildren. The Rabe's beautiful house in Parkalle became the home for a troop of students, who came to participate in the warmth and wisdom of these adored people. The "Rabenvater" and "Rabenmutter", as they were jokingly known, in truth formed the hub of the working group since 1919, after the foundation of Hamburg University. The students flocked around their adored teacher and his wife, who brought warmth to any occasion. She guided special occasions with a steady hand and understood intuitively how to educate effectively. Every one who crossed the path of this extraordinary woman felt inspired. Else Rabe, who died on December 28, 1962, also thought along those lines.

Rabe was a classic scientist in the sense of William Ostwald. Science represented for him the pure quest for knowledge, far from any utilitarian deviations. His devotion to science was high and he always pursued the search of knowledge through experimental results and high-level research, never speculating about monetary profits. This attitude greatly influenced his publication standards, and placed severe limits to what he considered of novelty and publishable. If he did not feel confident enough with a result, then he would wait to secure the data, because he felt the danger of someone else publishing the results before him was less than having to publish a correction or have a correction pointed out to him.—In his function as teacher he placed a great emphasis on experimental chemistry—which included inorganic and organic chemistry—for which he prepared with extreme care.

Paul Rabe felt a strong connection with this large city, and thanks to his efforts, after the establishment of the University of Hamburg in 1919, the State Laboratory of Chemistry became an Institute of the University in 1921; besides his chair in organic and inorganic Chemistry, Rabe also directed the State Research Office. The newly established School of Mathematics and Natural Sciences appointed him as its first Dean, and he found many good friends among his colleagues. His coworkers, K. Kindler, H. Schmalfuß, E. Jantzen, H. Albers diversified from Rabe's original research subjects and extended the "Privatlabor" work through their own research and teaching at the Institute and in universities abroad. They and numerous other students could count on the care and ever watchful participation of their teacher.

Rabe's high-point as a scientist was reached on February 24, 1931, when one of his immediate collaborators brought to him one gram of fully synthetic hydroquinine. The ensuing party, which celebrated this extraordinary accomplishment, was unforgettable for all of the participants.

As far as it is known, Rabe did not participate in politics; he was moderately against National Socialism and in the winter semester of 1934/35 he even removed a notice from the notice board notifying of a boycott against Jewish students at his Institute. This behavior led to his premature retirement from his workplace; the authorities of the University of Hamburg, who had extended his appointment as Director of the Institute until 1939, decided his retirement should be effective from March 31, 1935, by enforcing the January 1935 enactment establishing the retirement age of university professors as 65.

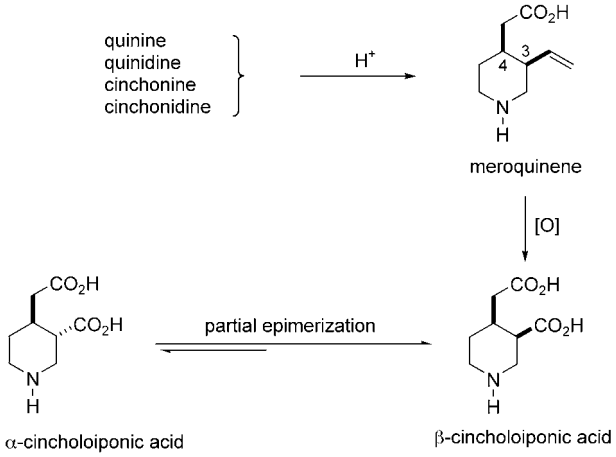
Undeterred by this insulting procedure he continued his research work, now with very limited resources and, as in the old times when he was younger, with himself working at the bench. The outbreak of the war in 1939 challenged him with preserving his life and his family wellbeing; his house, severely damaged by the continuous bombings, was always full of people even worse affected. He bore everything with the calm composure of a philosopher.—

During the period 1942–1944 he returned to supervising young coworkers, when he was invited by his former students to the Institute of Organic Chemistry of the Technical University of Danzig as an old "chief" with laboratory experience and wisdom in life. Again, the "Rabenvater", as he was soon also jokingly known here, bestowed love and kindness on his extended family, which also included new Danziger colleagues.—

During the hard years after the end of the war, his friends and students tried to ameliorate the hunger and cold of the Rabes; some of them visited, bringing potatoes and cabbages in their rucksacks, instead of

 © 2005 Wiley-VCH Verlag GmbH & Co. KGaA, Weinheim

flowers. In 1946, he became afflicted by an eye illness, which interrupted his desk work. An operation two years later partially restored his sight; deeply happy again he enjoyed walking and appreciating the beauty of nature, and content that he could once again share in the chemical literature. When Rabe was 80, in recognition of his long-standing work on cinchona alkaloids, the School of Medicine of the University of Hamburg awarded him the title of Doctor in Medicine, *honoris causa*. The German Society of Pharmacy also appointed him as an honorary member. At his 83th birthday, still active and spiritual, he rejoiced with family, friends, and students. However, his health rapidly deteriorated; a few days later, his strength suddenly left him, and with serene clarity he died on August 28, 1952. His last words were "nun est es aus" (it is over now).

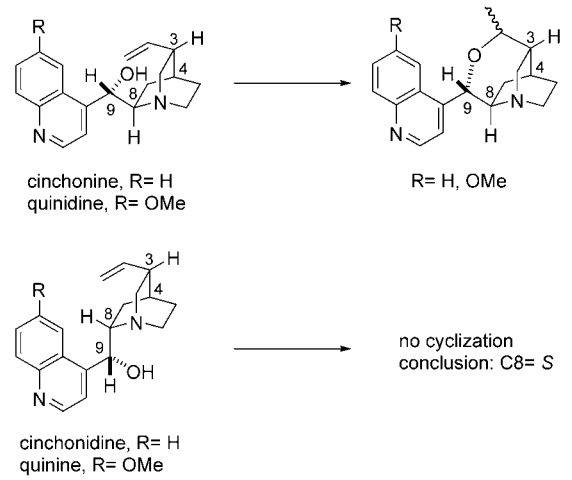


Scheme 2. The cinchona alkaloids and their configuration at C3 and C4.

the alcohol function in the alkaloids was secondary, and established its exact location by oxidation of cinchonine to cinchoninone.[73] Finally, by an irony of destiny, a short time after Perkin's death Rabe was able to suggest the correct connectivity of quinine in 1908.[73,74] As a result of the evaluation of a set of results from simultaneous studies carried out on the other alkaloids, this work allowed chemical structures to be proposed for them. Some stereochemical issues, however, would have to wait another three and a half decades to be definitively and unambiguously clarified.

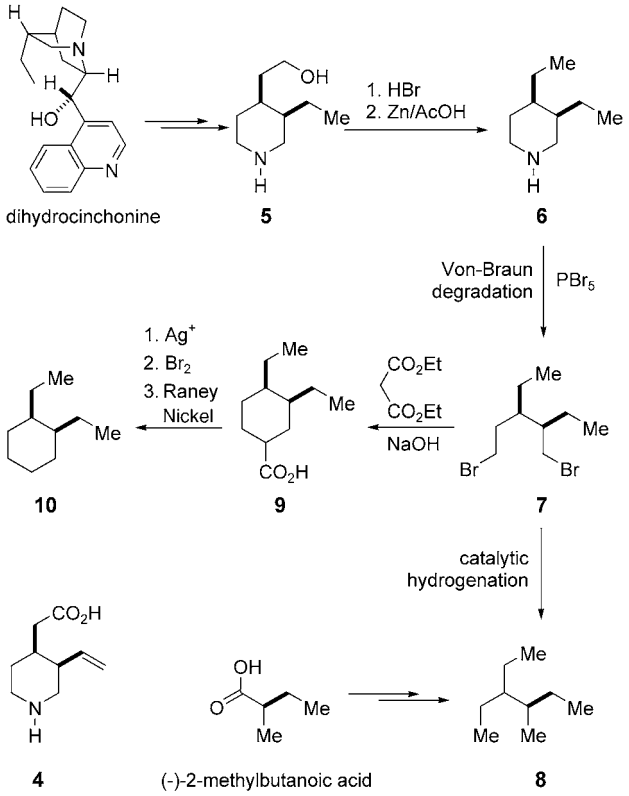
With the clues discovered in the 1920s that the C3 and C4 configuration was the same for the the four alkaloids, the C8 configuration was solved by evaluating the ability of quinine and its congeners to cyclize to oxepanes (Scheme 3).[75] The inability of quinine and cinchonidine to cyclize, whereas quinidine and cinchonine did, suggested that the C8 configuration of the former compound was what we now call *S*.[76] The C9 configuration of the cinchona alkaloids was rationalized in 1932.[77]

In 1944 Vladimir Prelog, who would go on to develop a long-standing experimental interest in stereochemistry, succeeded in unambiguously establishing both the *cis* relationship at the C3 and C4 centers and the absolute configuration of meroquinene (**4**), and hence of the quinuclidine moiety of



Scheme 3. Probing the C8 configuration of the quinine alkaloids.

the cinchona alkaloids, through clever chemical manipulations of a meroquinene derivative to simple hydrocarbons (Scheme 4).[78] Cinchonine was reduced to dihydrocinchonine and, in turn, this was degraded[79] to alcohol **5**; the alcohol was then transformed into 3,4-diethylpiperidine (**6**), which furnished dibromide **7** after a von Braun degradation with PBr_5. Catalytic hydrogenation of **7** gave (−)-3-ethyl-4-methylhexane (**8**), from which the absolute configuration of meroquinene was deduced by comparison with (−)-**8** (which was prepared from (−)-ethylmethylacetic acid of known absolute



Scheme 4. Prelog's unequivocal determination of absolute and relative configuration at C3 and C4.

 © 2005 Wiley-VCH Verlag GmbH & Co. KGaA, Weinheim

configuration, secured by correlation with glyceraldehyde.[78b] On the other hand, malonic ester synthesis from **7** to furnish homochiral acid **9**, followed by decarboxylation, provided an optically inactive 1,2-diethylcyclohexane (**10**), thus providing conclusive proof of the relative *cis* arrangement of the C3 and C4 centers.[78a]

6. Rabe Provides the First Steps and the Synthesis of Quinine Seems To Become Simpler

At the beginning of the 20th century structural determination was in its infancy and final proof of the structure of simple degradation products was thought to require unambiguous synthesis of the compound with the suspected structure. In a few cases this could be done by synthesis of the natural product itself (for example, camphor),[80] followed by comparison with an authentic sample of the natural product.[81] Thus, synthesis, with complementary analysis, was often a matter of utilitarian necessity rather than the creative, elegant art form revealed by the work of many of the great synthetic chemists who characterize the second half of that century.

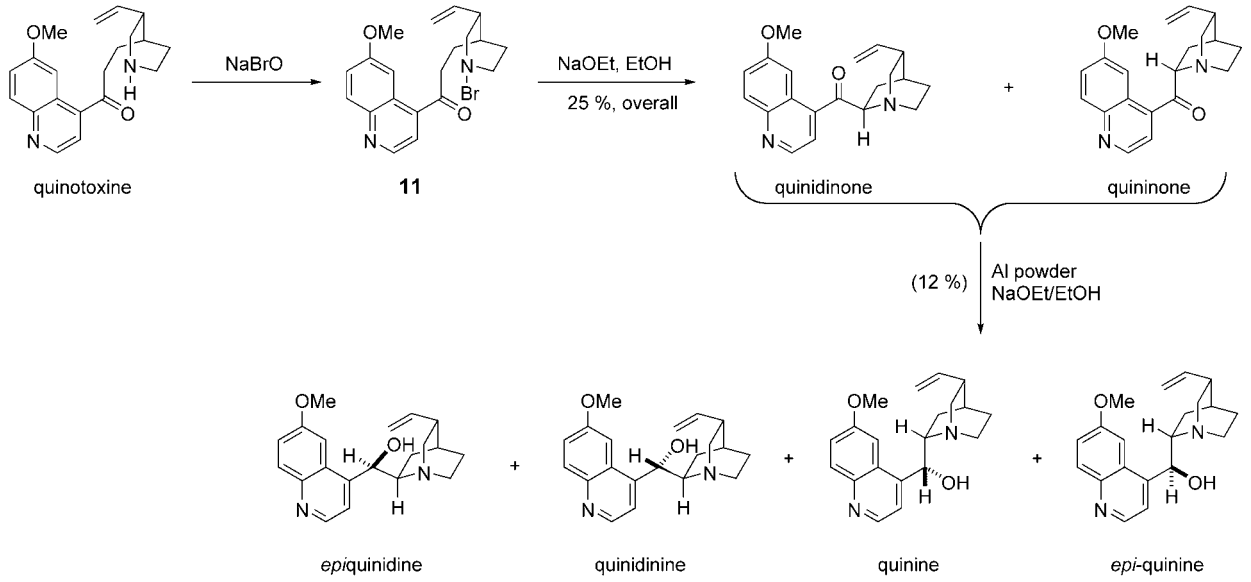
Just as countless shoeboxes filled with rattling gears and levers may testify to the fact that dismantling a clock is never as daunting as putting it back together, the reassembling (total synthesis) of quinine, even with the aid of more powerful tools than those at Perkin's disposal, would require decades of tenacious efforts.

At the beginning of the 20th century a number of research groups were making progress towards the synthesis, or at least the reconstruction, of quinine, and the research group of Rabe was publishing perhaps the most important results in this area. In 1908 Rabe reduced cinchonidinone to cinchonine, thus achieving a new and important breakthrough,[74a] while in 1909 he described the cleavage of cinchona ketones by the action of sodium ethoxide and alkyl nitrites which led to quinoline-4-carboxylic acid and meroquinene derivatives.[67b] In 1911 he succeeded in converting cinchotoxine into cinchonidinone by treatment of the former with hypobromous acid, followed by cyclodehydrobromination of the resultant *N*-bromo derivative with sodium ethoxide.[82] The same sequence yielded dihydrocinchonine when applied to dihydrocinchotoxine.[82b] In addition, in 1913, Rabe demonstrated the smooth condensation of aliphatic esters with ethyl cinchoninate to give β-ketoesters, from which quinoline-4-ketones were readily available by hydrolysis and decarboxylation.[83]

Without complete knowledge of the stereochemistry of quinine, Rabe chose to attempt its reconstruction from quinotoxine, a 3,4-disubstituted piperidine.[55] In 1918, in a very laconic publication entitled "*Uber die Partialle Synthese des Chinins*",[84] Rabe and Kindler outlined a synthetic sequence for the reconstruction of quinine and quinidine from quinotoxine (Scheme 5). This sequence was analogous to one previously employed, and involved the construction of the C8–N bond (C8–N approach) through the intermediacy of *N*-bromo compound **11**.[82] Reduction of the resultant quininone with aluminum powder in ethanol containing sodium ethoxide afforded a mixture of quinine (12%) and quinidine (6%).[85] This transformation was the first major step towards the synthesis of quinine since the famous failure of Perkin 50 years before.

Rabe's efforts in this field reached a high point in 1931 with the publication of the total synthesis of dihydroquinine,[86] then a major and highly acclaimed achievement, which employed the same strategy used in the 1918 report for the final steps. Taken together, these results suggested that the total synthesis of quinine could be accomplished from quinotoxine by using Rabe's protocol.

Unfortunately, however, perhaps because of wartime pressures, Rabe's procedure from his 1918 report was not cautiously reviewed and his claims were not fully substantiated. The key procedure for the reduction of quininone to quinine with aluminum powder was detailed 14 years later,[85] by the reduction of dihydrocinchoninone to dihydrocincho-

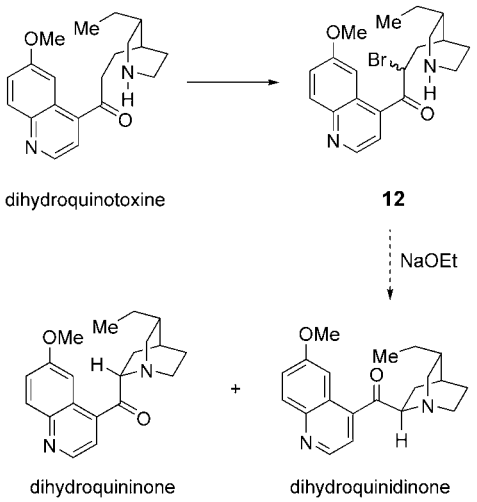


Scheme 5. Apparent course of synthesis of quinine developed by Rabe and Kindler in 1918.

 © 2005 Wiley-VCH Verlag GmbH & Co. KGaA, Weinheim

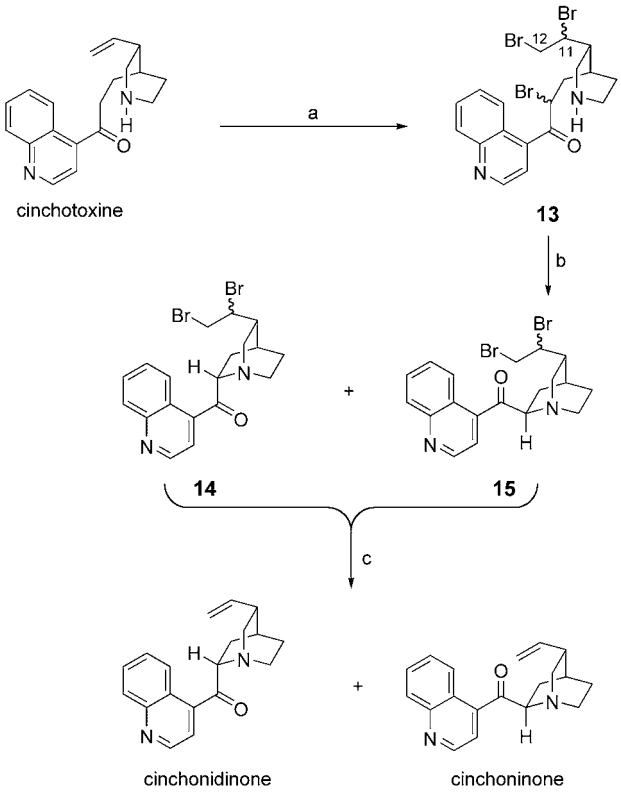
nine, which is known to have the same configuration at C8 and C9 as quinidine. Furthermore, Rabe commented in 1918 that his method "ist noch nicht eingehend beschrieben worden" (is not described yet in detail).[84] This would prove to be of paramount importance in one of the most important chapters of the history of the synthesis of quinine, which was written during the second World War. In the words of Professor Gilbert Stork *"[Paul Rabe] simply did not sufficiently document what he reported having done that one could be sure to do the relevant chemical transformations exactly the way he did them"*.[87] Moreover, Rabe's protocol proceeded without addressing the stereochemical problem, which means that a "total synthesis" along his synthetic scheme would always produce a mixture of isomers that required painstaking separation.

Interestingly, some years before Rabe's reconstruction of quinine, the research group of Kaufmann brominated dihydroquinotoxine with bromine in 48% hydrobromic acid to obtain mainly dihydroquinidinone after treatment of the α-bromoketone **12** with an alkaline alkoxide (Scheme 6). The same operation was carried out on dihydrocinchotoxine and provided dihydrocinchonidinone.[88] Their approach was proved correct three decades later, but during his time this procedure was regarded, unfortunately, as useful only for compounds devoid of a reactive vinyl group.



Scheme 6. The approach used by Kaufmann et al. for the synthesis of dihydroquininone and dihydroquinidinone.

Despite the poor resources available, the research groups of Kaufmann as well as Rabe were certainly very close to reconstructing quinine. In 1946 Woodward et al. transformed 11,12-dibromoquininone into quininone[89] by debromination with sodium iodide, and in a 1948 publication[90] Ludwiczakówna demonstrated that tribromides **13** resulting from the bromination of cinchotoxine with bromine in 48% hydrobromic acid could be cyclized with sodium ethoxide in ethanol to give good yields of a mixture of 11,12-dibromo ketones **14** and **15** (Scheme 7). These compounds could be debrominated with sodium iodide to yield cinchonidinone and cinchoninone. Furthermore, quininone and quinidinone were obtained when



Scheme 7. "Extended" Kaufmann approach to cinchoninone and cinchonidinone. Reagents and conditions: a) 48% HBr, Br_2, 70°C (97%); b) 1. NaEtO, EtOH; 2. HCl (81%); c) NaI, EtOH, reflux, 50 h (90%).

quinotoxine was submitted to the same procedure, and these steps became a complementary alternative to Rabe's approach. Interestingly, participation of α-haloketones such as those synthesized as intermediates by Kaufmann et al. in the Rabe-type cyclization of quinotoxine to quininone and quinidinone was decisively demonstrated by Gutzwiller and Uskokovic in 1973.[91] The feasibility of the protocol by Kaufmann et al., however, has never been tested in a total synthesis of quinine.

7. The Much Awaited Total Synthesis of Quinine

Chemistry blossomed between the two World Wars, and occurred at an ever-accelerating pace of discovery. Work done in chemical physics and physical chemistry did much to transform notions of how molecules are held together, how bonds are formed and broken, and how reactions occur. This more mathematically rigorous treatment of bonding and reactivity, particularly in the wake of quantum mechanics, gave novel theoretical grounding to structure theory and to the search for definitive structures of natural products. This search had begun in the 19th century and had continued unabated and largely unchanged by the reconceptualizations of chemical bonding during the 1920s and 1930s.

Organic synthesis made interesting progress; however, the lack of appropriate theoretical interpretation of reactions somehow slowed further advances. The gap between theoret-

 © 2005 Wiley-VCH Verlag GmbH & Co. KGaA, Weinheim

ical chemistry and organic chemistry is clearly illustrated in a textbook of the period: "*No doubt the ultimate goal toward which organic chemistry is striving is that state in which fundamental laws and theories will have been developed to such an extent that it will be possible, in advance of experimental trial, to deduce a satisfactory method for the synthesis of any compound and to predict all its properties. Owing to the complex structure of most organic molecules, however, it seems probable that such a Utopian state is impossible of achievement and that organic chemists must content themselves with the more modest aim of augmenting what Gilbert Lewis gallantly calls their "uncanny instinct" by such exact science as they may find applicable*".[92]

At the age of 20, and after a meteoric 4-year stay at MIT—where he earned his BSc in 1936 and a PhD the next year—the child prodigy Robert Burns Woodward started working in 1937 as a post-doctoral fellow and later as a member of the Society of Fellows in the Department of Chemistry at Harvard University. He remained there for the next 42 years to become one of the preeminent organic chemists of the 20th century. Woodward made great contributions to the strategy of synthesis, to the deduction of difficult structures, to the invention of new chemical methods, and also to theoretical aspects.

During his successful scientific career he received numerous awards as well as the 1965 Nobel Prize for Chemistry for "*his outstanding achievements in the art of organic chemistry*". More than 400 graduate and postdoctoral students trained in his laboratories.

Many interesting natural products had been conquered by synthesis before 1940, such as tropinone (Willstätter: 1901; greatly improved by Robinson in 1917), camphor (Komppa: 1903; Perkin: 1904), α-terpineol (Perkin: 1904), haemin (Fischer: 1929), equilenin (Bachmann: 1939) and pyridoxine (Folkers: 1939).[11a,93] However, Woodward's explosive entry into the arena of natural product synthesis changed the history of this field, which would never be the same again.

The accomplishments of Woodward in his time were amazing; their spectacular nature not only stems from the relevance of the chosen synthetic targets, but also from the originality in his way of attacking the synthetic problems, the elegant solutions he provided to complex challenges, and the simplicity of the methods involved in applying those solutions. The catalogue of Woodward's achievements in the total synthesis of natural products include quinine [(±)-homomeroquinene (**17**) or (+)-quinotoxine, 1944], patulin (1950),[94] cholesterol and cortisone (1952),[95] lanosterol (1954),[96] lysergic acid and strychnine (1954),[97] reserpine (1958),[98] ellipticine (1959),[99] chlorophyll *a* (1960),[100] tetracycline (1962),[101] colchicine (1965),[102] cephalosporin C (1966),[103] prostaglandin F_{2a} (1973),[104] and his paramount achievement: the synthesis of vitamin B_{12} (1973, with A. Eschenmoser).[105] The total synthesis of erythromycin A was published in 1981,[106] after his death.

Woodward's genius contributed to the deduction of the structures of penicillin (1945),[107] patulin (1949),[108] strychnine (1947),[109] oxytetracycline (1952),[110] carbomycin (magnamycin, 1953),[111] cevine (1954),[112] gliotoxin (1958),[113] calycanthine (1960),[114] oleandomycin (1960),[115] streptonigrin (1963),[116] and tetrodotoxin (1964),[117] as well as others.[118] He unveiled the family of macrolide antibiotics, for which he also proposed a mode of formation in nature[119]—as he had done with the first proposal of the cyclization of squalene in cholesterol biosynthesis.[120]

The scientific world first knew Woodward through a series of publications (1940–1942) highlighting the correlation of ultraviolet spectra with molecular structure.[121] Those publications show his reduction of the ultraviolet spectra of many organic compounds to a few numerical relationships and demonstrate his remarkable powers of analysis and passion for scientific order. They also show how he readily adopted any seemingly relevant new technique that might improve his grasp of the chemistry of natural products. These correlations, his first chemical achievement, became known as the "Woodward rules" or sometimes as the "Woodward–Fieser rules" in acknowledgment of Louis and Mary Fieser's reformulation of them. Thus, at 24 years of age Woodward was able to accurately point out the mistaken findings of others by means of a general rule relating structural features to UV spectra. In the words of Lord Todd: "*He was one of those very rare people who possessed that elusive quality of genius … it seemed to me to herald a breakthrough in the use of spectroscopy in the study of molecular structure*".[122]

The Woodward rules, which foreshadowed Woodward's later work with Roald Hoffmann (leading to the Woodward–Hoffmann rules),[123] were a result of his early recognition that physical methods had far greater power than chemical reactions to reveal structural features. These rules were only the beginning of his championing the development of spectroscopic techniques, which have empowered chemists and greatly eased the problem of structure determination.[124]

At the beginning of the 1940s, and with a towering career in front of him,[125a] Woodward was the right person to complete Perkin's work, and WWII played its role in accelerating the process. During WWII quinine supplies, which were considered critical for the allied forces, suddenly became scarce, thus causing thousands of soldiers to die after becoming infected with malaria during the campaigns in Africa and the Pacific. The cinchona plantations established in Java by the Dutch were the major sources of the European reserves of quinine, which were stored in Amsterdam. However, the German capture of Holland in 1940 and the Japanese military invasion of Java in 1942 abruptly cut these vital supplies.

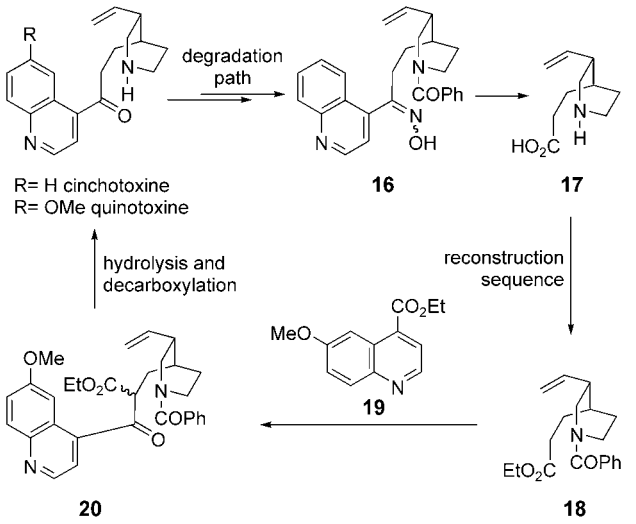
In an expedition to Colombia, Ecuador, Peru, and Bolivia between 1943 and 1944, the botanist Raymond Fosberg and his co-workers collected and secured 12.5 million pounds of cinchona bark for the allied forces. In a desperate effort, cinchona seeds were also brought from the Philippines, germinated in Maryland (USA), and planted in Costa Rica.[126] The sudden cut in supply of quinine caused justified alarm and triggered the initiation of research programs directed towards the development of new antimalarial drugs.[127]

Edwin Land, a Harvard graduate and the founder in 1937 of the Polaroid Company, used quinine iodosulfate (herapathite) for the manufacture of light polarizers and became one of the first businessmen involved in the desperate search for

 © 2005 Wiley-VCH Verlag GmbH & Co. KGaA, Weinheim

quinine or a substitute that would keep his company in business.[128] Woodward was a consultant to Land's company from 1940 and, in 1942, when Land required a quinine substitute, Woodward quickly solved his problem. This association was fruitful, since Land also agreed to financially assist Woodward's own synthetic project on quinine, which had been conceived a few years before while he was still a student.

At this time, others were working in closely related areas. Vladimir Prelog published his first paper in 1921, at the age of only 15, and began his first independent research around 1930 on quinine. His synthesis of quinuclidine in 1937 was a highlight, eventually leading to his interest in stereochemistry, the field in which Prelog became renowned and for which he was awarded the Nobel Prize for Chemistry in 1975.[129] In 1943 Prelog made a notable step forward when he degraded cinchotoxine to optically active homomeroquinene (**17**) and reconstructed quinotoxine with the aid of the degradation product (Scheme 8).[130] The first part of his procedure was



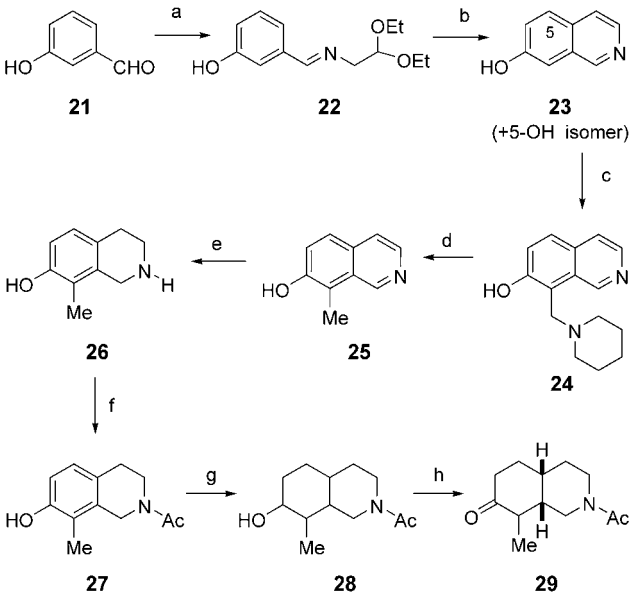
Scheme 8. The degradation and reconstruction of quinotoxine by Prošstenik and Prelog.

smoothly carried out through a Beckmann degradation through the intermediacy of oxime **16**, while reconstruction entailed transformation of homomeroquinene into protected derivative **18** followed by its Rabe condensation with ethyl quininate (**19**) to furnish β-ketoester **20**, which was conveniently converted into quinotoxine by hydrolysis and decarboxylation. Since Rabe has claimed success in converting quinotoxine into quinine, this step forward simplified the problem of a formal total synthesis of quinine to that of the total synthesis of enantiomerically pure homomeroquinene (**17**); it also strengthened Rabe's hypothesis that a route to quinine through quinotoxine was feasible.

The main challenge offered by the synthesis of the required homomeroquinene derivative was the correct introduction of the differentially substituted side chains, which ought to have a *cis* configuration. Although the syntheses were planned in advance, before the birth of of what we now call "retrosynthetic analysis", there was no rational and systematic approach to the design of synthetic strategies, and in the 1940s conformational analysis did not exist. The old masters in chemistry treated each synthetic target individually and obscurely related the final product to an appropriate starting material; therefore, success or failure was greatly influenced by their initial guesses.

Woodward's thinking was guided by his deep knowledge of chemistry and chemical literature as well as by a great deal of chemical intuition. The genius of his contribution to the homomeroquinene/quinine synthesis challenge was in his unusual and novel treatment of that problem and consisted of installing an extra ring to secure the appropriate configuration of adjacent centers.[125] In a timely fashion, this ring was opened to reveal new and distinct functionalities. Like an artist's personal signature, Woodward recurrently used this feature with increasing mastery in the subsequent and more demanding syntheses of reserpine, vitamin B_{12}, and erythromycin A.[98,104,105]

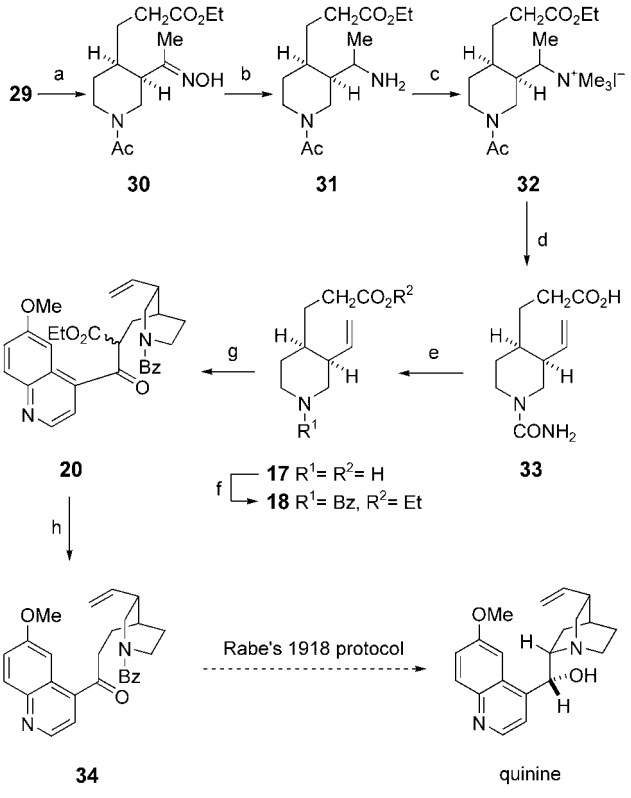
Woodward ingeniously visualized that the basic homomeroquinene skeleton could be accessed from an isoquinoline (Scheme 9). Synthetic routes and protocols for the preparation of such compounds were available from the beginning of the century,[131] but truly innovative research cannot be planned to the last detail. Therefore, in practice these basic ideas necessitated slightly more effort than initially thought to yield the expected product and demanded a considerable number of synthetic steps, which were carefully carried out by the enthusiastic scientist and outstanding experimentalist William von Eggers Doering.



Scheme 9. The approach to quinine by Woodward and Doering: Preparation of the homomeroquinene derivative. Reagents and conditions: a) $H_2NCH(OEt)_2$ (94%); b) 1. 80% H_2SO_4; 2. NaOH, crystallization then H^+ (64%); c) piperidine, HCHO, EtOH (61%); d) NaOMe, MeOH, 220°C, 16 h (65%); e) H_2, Pt, AcOH; f) Ac_2O (95%); g) H_2, Raney nickel, EtOH, 150°C, 205 bar, 16 h [1:1 *cis*(crystalline)/*trans*(oil)]; h) $H_2Cr_2O_7$, AcOH; Et_2O/H_2O, diastereomer separation (28%).

 © 2005 Wiley-VCH Verlag GmbH & Co. KGaA, Weinheim

During the synthesis, 3-hydroxybenzaldehyde (**21**, accessible in two steps from 3-nitrobenzaldehyde) was transformed into isoquinolin-7-ol (**23**) via Schiff base **22** by employing the Pomerantz–Fritsch isoquinoline synthesis.[131] This starting isoquinoline was converted into its 8-methyl derivative **25** through the intermediacy of piperidine **24**.[132] In turn, **25** was partially catalytically hydrogenated to the tetrahydroisoquinoline **26**, which was isolated as its *N*-acetyl derivative **27**, while a second catalytic hydrogenation furnished **28** as a complex diastereomeric mixture.[133] This mixture was simplified by oxidation to the related ketones, with concomitant epimerization of the tertiary carbon center next to the carbonyl group. Separation of the diastereomers was aided by the lucky formation of the hydrate of compound **29** with a *cis* ring junction: ring opening of the latter through preferential nitrosation of the tertiary carbon atom next to the carbonyl group furnished the oxime **30** (Scheme 10). Conservation of the crucial *cis* geometry of the substituents on the piperidine ring in **30** marked the success of the strategy for building both adjacent side chains. Reduction of **30** provided amine **31**. Exhaustive methylation of **31** afforded **32** and then a Hofmann elimination was employed to install the vinyl moiety and generate the intermediate product protected as a uramido derivative (**33**) to facilitate its isolation. The uramido derivative **33** was finally subjected to an acid hydrolysis to regenerate homomeroquinene (**17**).[134] Since Prelog had earlier prepared quinotoxine from homomeroquinene, and assuming the validity of Rabe's protocol to access quinine from quinotoxine, Woodward's synthesis of homomeroquinene meant that all the stepping stones for a formal total synthesis of quinine appeared to have now been bridged. However, his synthetic homomeroquinene (**17**) was racemic, thus prompting Woodward to go one step further and include a resolution in his synthesis. This was achieved by conveniently protecting **17** as its known *N*-benzoyl ethyl ester **18**, thus setting the stage for a Rabe condensation, which he carried out following the method developed by Prelog by using the readily available ethyl quininate **19**.[135]



Scheme 10. The approach used by Woodward and Doering to synthesize quinine: Completion of the synthesis. Reagents and conditions: a) EtO-N=O, NaOEt, EtOH (68%); b) H_2, Pt, AcOH, 1–3 bar; c) MeI, K_2CO_3 (91% overall); d) 1. 60% KOH, 180°C, 1 h; 2. KCNO (40%); e) 1. dilute HCl, EtOH, reflux (100%); f) PhCOCl, K_2CO_3 (96%); g) ethyl quininate (**19**), NaOEt, 80°C; h) 1. 6 N HCl, reflux (50%); 2. resolution with D-dibenzoyl tartrate (11%). Bz = benzoyl.

Subsequent hydrolysis and decarboxylation of the resultant β-ketoester **20** gave DL-quinotoxine derivative **34**, which was hydrolyzed to DL-quinotoxine and the latter carefully resolved with D-dibenzoyl tartaric acid.[136] Finally, after little over a year of feverish work, on April 11, 1944 Woodward and Doering obtained a precious 30 mg of synthetic D-quinotoxine which—with Rabe's procedure being repeatable—could be considered the first entry into synthetic quinine. Woodward had crossed the finish line that he had first spotted so many years previously and this accomplishment somehow turned him into a veritable demigod in his field.

In the middle of WWII, and with natural quinine supplies cut by enemy forces, news on this breakthrough rapidly found its way from the University laboratory to the national press. Thus, The New York Times enthusiastically hailed the achievement in its May 4 edition with the heavyweight title "*Synthetic Quinine Produced, Ending Century Search*". In the article that followed below, it remarked the accomplishment of "*the duplication of the highly complicated chemical architecture of the quinine molecule*" that had been achieved, a feat that was considered "*as one of the greatest scientific achievements in a century*".[137] The Science News Letter[138] also echoed this praise by highlighting that this accomplishment, highly useful to the war effort, was done "*… without the help of a tree*"; the same journal commented that "*starting with five pounds of chemicals they obtained the equivalent of 40 mg of quinine*". A cartoon in the May 28 issue of the Oregon Journal commented on the good news, which also appeared in the June 5 issue of the well-known magazine Life, wherein it was covered under the title of "*Quinine: Two Young Chemists End a Century's Search by Making Drug Synthetically from Coal Tar*".[139]

In contrast to Perkin's attempt ending in mauveine, which met with commercial success, Woodward's synthesis of quinine was not amenable to large-scale commercial production. In spite of the hype and wishful thinking surrounding the synthesis, which gave Woodward immense popularity, commercial production of quinine by the newly devised strategy would have cost approximately 200 times more than its natural equivalent if, indeed, it was feasible. Moreover, it would have taken years of research to optimize the process and reduce the prices down to reasonable levels, and by that time alternative synthetic drugs could have been made available for treatment.

Quinine has five stereogenic centers, two of which (the quinuclidine nitrogen atom and C4) constitute a single

 © 2005 Wiley-VCH Verlag GmbH & Co. KGaA, Weinheim

asymmetric unit because of their bridgehead location. The Woodward–Doering synthetic scheme successfully built two of them selectively by laborious diastereomer separations and chemical resolution. Despite the complexity of the synthetic route, it was carried out with conventional reactions and reagents that were available to any chemist of that time, protecting groups were hardly used, and one third of the reactions were run at room temperature. The synthesis suffered from low yields and lacked stereocontrol at every center, particularly because of the anticipated need to separate the four diastereomers resulting from the use of Rabe's 1918 protocol in which quinotoxine was transformed into quinine. However, the synthesis was completed in a few months,[140] was Woodward's first total synthesis, captured admiration and public imagination, and represented in its time an important and unmatched accomplishment, which remained as a scientific milestone. Indirectly, the Woodward–Doering synthesis of quinine signaled the way organic synthesis would head in the next few decades. It is not too far from the truth to state that many modern synthetic medicines owe their being to the impulse given to the field by complex challenges such as that of quinine.

Woodward tackled increasingly daring synthetic targets throughout his career and demonstrated that an understanding of chemical reaction mechanisms made it possible to plan and successfully execute extended sequences of reactions to build up complex compounds in the laboratory. Stereocontrol was of little concern in the days when the synthesis of quinine was carried out, mainly because chemists lacked many of the currently available synthetic tools, including the physical and chemical concepts that form the basis of stereochemical control. Moreover, stereochemistry was then not deeply considered in synthetic designs and some chemists even expressed a lack of interest in the challenge.

The couple of publications reporting the experimental details on the synthesis of D-quinotoxine, which appeared in 1944 and 1945 under the same title ("*The Total Synthesis of Quinine*"),[1] meticulously informed the reader about the series of synthetic manipulations leading to D-quinotoxine, in what could be termed a formal total synthesis of quinine. However, experimental evidence on the synthesis of the natural product from synthetic D-quinotoxine was not provided, merely relying on Rabe's 1918 paper and procedure, which for some reason they qualified as "established".[141] Nevertheless, and perhaps because of anxiety caused by wartime needs, the series of chemical transformations reported in the 1944 and 1945 publications by Woodward and Doering started the legend that quinine had finally been completely synthesized.

Unfortunately, Rabe's method would prove to be unreliable, thus necessitating the need for additional time and efforts before the claim could be made for the achievement of the first total synthesis of quinine. It is noteworthy, however, that as part of his effort to convert quinine into valuable quinidine, Woodward shortly afterwards disclosed a very efficient method for accessing quininone from quinine by reaction of the former with potassium *tert*-butoxide and benzophenone, and the reduction of the ketone with sodium isopropoxide to afford a mixture of quinine (ca. 30%) and quinidine (ca. 60%).[89] Thus, cyclization of quinotoxine to quininone remained the weakest link in the chain of reactions from isoquinolin-7-ol to quinine in the Woodward–Rabe approach.

8. Mastering the C8–N Strategy: The First Total Synthesis of Quinine and Variation on the Theme

Cinchona alkaloids, mainly quinine and quinidine, are of high industrial importance. Approximately 300–500 tons per annum are produced commercially by extraction of the bark from various cinchona species that are now widely cultivated. About 40% of the quinine goes into the production of pharmaceuticals, while the remaining 60% is used by the food industry as the bitter principle of soft drinks, such as bitter lemon and tonic water. Quinine is employed for the treatment of chloroquine-resistant malaria, while quinidine is still prescribed in human therapeutics as an antiarrhythmic to regulate heartbeat.

Derivatives of the cinchona alkaloids also serve as highly versatile chiral auxiliaries in asymmetric synthesis, and are perhaps the most remarkable example of a specific class of chiral catalysts. The key structural feature responsible for their synthetic utility is the presence of the tertiary quinuclidine nitrogen atom, which renders them effective ligands for a variety of metal-catalyzed processes. In addition, the nucleophilic quinuclidine nitrogen atom can also be used directly as a reactive center for enantioselective catalysis. The cinchona alkaloids have proven to be useful in an astonishing variety of important enantioselective transformations, including the Sharpless asymmetric dihydroxylation reactions, enantioselective Diels–Alder reactions, hydrocyanations, [2+2] cycloadditions, Michael additions, SmI_2-mediated reductions, dehydrohalogenations, and hydrogenations.[142] In addition, examples of quinine as a chiral resolving agent are numerous[143] and new examples are still being reported at a steady rate. The recent use of quinine and quinidine for the chromatographic and electrophoretic separation of enantiomers[144] suggests that interesting applications of cinchona alkaloids will keep on growing. Industrial preparation of active pharmaceutical ingredients such as the antidepressant oxitriptan, the widely used anti-inflammatory and analgesic naproxen, and the calcium antagonist diltiazem have been described in which cinchona alkaloids were employed as resolving agents.[145]

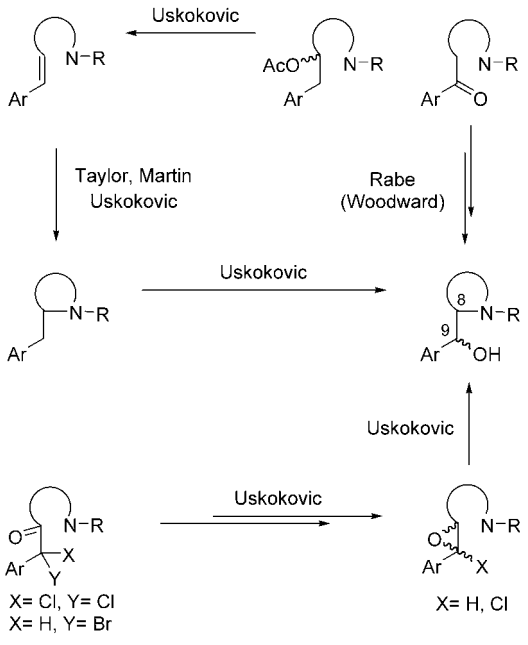
The regular use of analytical instruments introduced after WWII produced a second revolution in organic chemistry which paralleled that first revolution made by structural theory almost one century before. This enabled limits to be set on what claims chemists could make about chemical structures and stabilized their concepts of both chemical structures and reaction mechanisms. In addition, the popularization of preparative thin-layer chromatography and column chromatography greatly eased separations, while gas chromatographic techniques facilitated analysis of minute amounts of samples and made estimations of purity easier.

 © 2005 Wiley-VCH Verlag GmbH & Co. KGaA, Weinheim

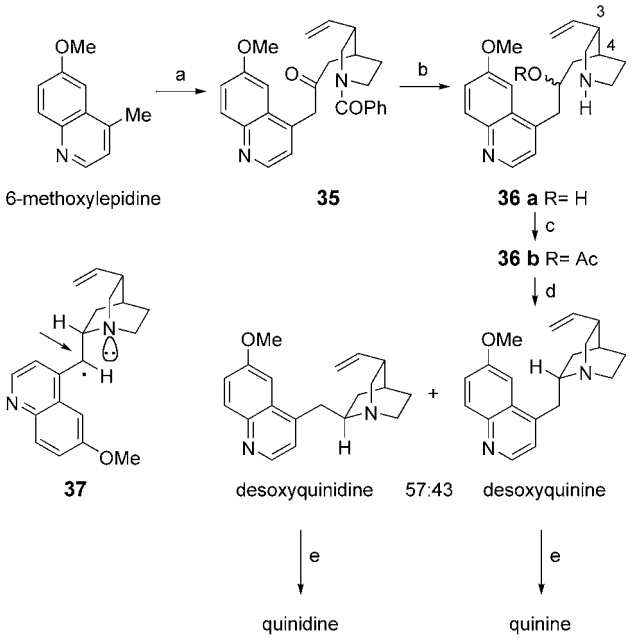
In the beginning of the 1960s, almost two decades after Woodward's acclaimed achievement, a group of Hoffman–La Roche (Nutley, New Jersey) researchers became interested in the synthesis of cinchona alkaloids. An extensive series of experiments was carried out under the leadership of Milan R. Uskokovic in which literature procedures were repeated and new protocols devised for accessing the pharmaceutically important cinchona alkaloids. The team developed new syntheses of homomeroquinene, which it used for the preparation of quinotoxine by either employing Rabe's condensation with ethyl quininate (Schemes 8 and 10) or by reaction with 6-methoxy-4-quinolyllithium (**52**).[146] In turn, this accomplishment allowed Uskokovic's group to demonstrate that the nitrogen atom of quinotoxine could be chlorinated with sodium hypochlorite and that α-chloro derivatives, analogous to the bromoketone **12** previously prepared by Kaufmann (Scheme 6), could become intermediates in the Rabe-type conversion of quinotoxine into quininone and quinidinone. The yield for this conversion was more than 70% when a strong acid was employed instead of the base treatment reported by Rabe and when the ketones were transformed into either a 1:1 mixture of quinine and quinidine or selectively into quinidine by reduction with diisobutylaluminum hydride (DIBAL-H).[91,147] This research made it evident that Rabe's original procedure was unsuitable for producing quinine, unless it was substantially modified.

Researchers at Hoffmann–La Roche came closer to a stereoselective total synthesis of quinine in the 1970s after concentrated efforts on mastering the C8–N approach for the formation of the quinuclidine ring. In 1970 they disclosed a total synthesis of quinine, which was the first of a series of total syntheses of this natural product based on such an approach to be published during that decade (Scheme 11). The weak point of this approach was its characteristic poor stereocontrol, which led to the generation of stereoisomers at C8. Furthermore, some modified protocols incurred the formation of undesired stereoisomers during the installation of the functional group at C9, thus limiting the attractiveness and usefulness of the method. This study, however, resulted in the development of considerably more efficient strategies that allowed a better control of the configuration at two of the stereogenic carbon atoms in the quinuclidine portion of the molecule.

The initial strategies used by Uskokovic and co-workers (Scheme 12) were similar to that of Woodward and Rabe in the sense that they used the C8–N approach and the pivotal intermediate was a meroquinene derivative. However, better steric control at key stages and the use of more efficient transformations improved the overall yield compared to that obtained by Woodward's route.



Scheme 11. Synthetic variations of the C8–N approach used during the 1970s.



Scheme 12. Synthesis of quinine by Uskokovic and co-workers in 1970. Reagents and conditions: a) 1. LDA, −78 °C; 2. *N*-benzoylmeroquinene methyl ester (**41b**; 78%); b) DIBAL-H (85%); c) $BF_3{\cdot}Et_2O$, AcOH (96%); d) NaAcO, AcOH/benzene (via **44b**; 79%); e) KO*t*Bu, $^1O_2$, *t*BuOH, DMSO (40%). LDA = lithium diisopropylamide.

During the synthesis, the lithium anion of 6-methoxylepidine[148] was condensed with racemic *N*-benzoylmeroquinene methyl ester (**41b**) and the resultant ketone **35** was reduced to alcohols **36a** with DIBAL-H, which also removed the *N*-benzoyl protecting group. The racemic mixture of diastereomeric alcohols **36a** was resolved with D-dibenzoyltartaric acid and the required 3*R*,4*S* enantiomer was transformed into the related acetates **36b** by a $BF_3{\cdot}Et_2O$ catalyzed acetylation. Finally, construction of the quinuclidine ring proceeded by conjugate addition of the piperidine nitrogen atom to vinylquinoline intermediate **44b** (see Scheme 13),[149] which was formed in situ by elimination of the acetate to yield a mixture of the previously known desoxyquinine and desoxyquinidine in a ratio of 57:43 (Scheme 12).[150] The

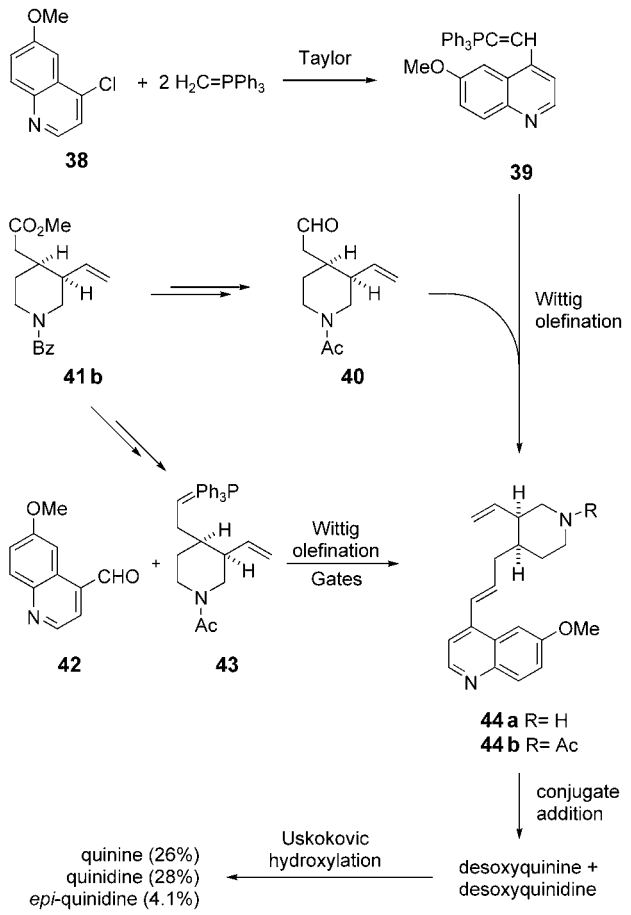
 © 2005 Wiley-VCH Verlag GmbH & Co. KGaA, Weinheim

most interesting step of the synthesis was the last one, which was based on an important observation previously made within Uskokovic's group: In an extraordinary example of 1,2-asymmetric induction not involving a carbonyl group, the necessary functional group was cleanly introduced at C9 with the correct configuration (and a stereoselectivity of approximately 5:1) by an autooxidation with oxygen catalyzed by potassium *tert*-butoxide. Almost equal amounts of quinine and quinidine were produced, when it was used directly on the mixture of C8 isomers. Dimethyl sulfoxide was employed to reduce in situ the intermediate hydroperoxides formed.[151] From an industrial viewpoint, the synthesis was considered satisfactory when the comparatively higher commercial value of quinidine with respect to quinine was taken into account. The autooxidation was an efficient transformation and its fortuitous stereochemical result constituted a remarkable step forward. The reaction outcome (selective access to *erythro* amino alcohols) was attributed to the "*preferred backside attack of the oxygen radical anion on the intermediate radical … in order to avoid the repulsive force of the quinuclidino nitrogen free electron pair*" (see **37** in Scheme 12).[152] This strategy would be employed as the final step of a much improved and more controlled synthesis 30 years later. Before Uskokovic's synthesis of quinine,[153] there was no truly dependable published protocol for completing the last crucial steps of the synthesis of the natural product.

In 1974 Taylor and Martin disclosed their approach to quinine from 4-chloro-6-methoxyquinoline (**38**), via olefin **39**, which acted as a nonisolable transient intermediate (Scheme 13).[154] Their procedure became a method for the direct introduction of alkyl and alkenyl groups into heterocyclic nuclei and involved the nucleophilic displacement of a suitable leaving group on the heterocycle by a Wittig reagent, followed by the transformation of the resultant heterocyclic ylide into alkyl- or alkenyl-substituted heterocycles by hydrolysis or reaction with aldehydes, respectively.[154]

The synthetic sequence towards quinine, which can be considered a new route to olefin **44b**, has the same drawbacks with the formation of diastereomers as the protocol developed by Uskokovic and co-workers. The sequence consisted of the preparation of ylide **39** and its olefination with *N*-acetylpiperidineacetaldehyde derivative **40**, which was easily prepared from the known *N*-benzoylmeroquinene methyl ester **41b**. Hydrolysis of the *N*-acetyl protecting group (**44b** → **44a**) occurred with concomitant spontaneous intramolecular Michael addition of the piperidine nitrogen atom to the double bond generated in the Wittig reaction to produce the expected mixture of desoxyquinine and desoxyquinidine. Interestingly, this mixture could be induced to revert to the starting olefin by refluxing it with acetic anhydride. The diastereomers of this hard-to-separate mixture were, nevertheless, individually oxidized by using the procedure developed by Uskokovic and co-workers and the resultant alkaloids isolated as the corresponding tartrates.

A previous sequence published in 1970 by Gates et al.[155] (which was disclosed simultaneously with that of Gutzwiller and Uskokovic[153]), also entailed the preparation of olefin **44b**; however, in this case phosphorane **43**, which is derived

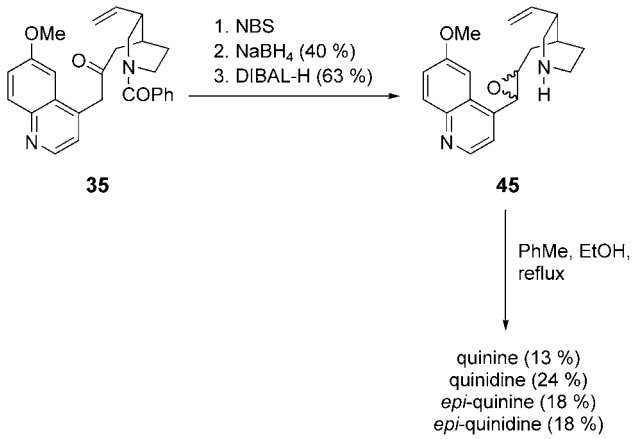


Scheme 13. Syntheses of quinine by the research groups of Taylor and Gates.

from meroquinene alcohol,[156] and aromatic aldehyde **42** were employed in a Wittig reaction and the *cis*/*trans* mixture of olefins so obtained equilibrated with acetic acid to afford exclusively the more stable *trans* alkene (Scheme 13). Gates et al. did not devise a protocol for the required construction of the alicyclic moiety, and considered his route explicitly as a partial synthesis of quinine. The key meroquinene bromide employed was produced by functional group transformations of meroquinene derivatives obtained by degradation of quinidinone, or by employing Uskokovic's synthesis.[147b]

In a modification of his previous synthesis Uskokovic and co-workers also performed the key C8–N ring-closing reaction through the ring opening of an epoxide (Scheme 14), which allowed the simultaneous installation of the secondary alcohol at C9.[91] This alternative sequence, which would become relevant two decades later as a strategy for the fully controlled access to quinine, started with known ketone **35**, which was prepared in enantiomerically pure form by employing the semisynthetic, optically active meroquinene. Installation of the epoxide was carried out by benzylic bromination with *N*-bromosuccinimide (NBS), followed by reduction of the α-bromoketone to a mixture of bromohydrins as well as spontaneous cyclization. Unfortunately, the transformation took place in a disappointing 40% yield and all four possible epoxides were formed. DIBAL-H assisted

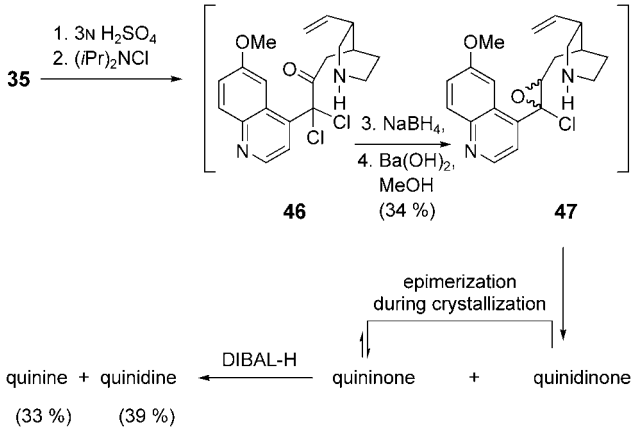
 © 2005 Wiley-VCH Verlag GmbH & Co. KGaA, Weinheim



Scheme 14. Synthesis of quinine by the amino epoxide ring closing approach by Uskokovic and co-workers (1970).

reductive removal of the *N*-benzoyl protecting group to give **45** then set the stage for the nucleophilic ring opening and cyclization, which as expected produced mixtures of the four possible diastereomers at C8 and C9. Thus, this initial version of the amino epoxide ring opening approach proved inefficient and lacked the elegance of the auto-oxidation procedure for functionalization at C9.

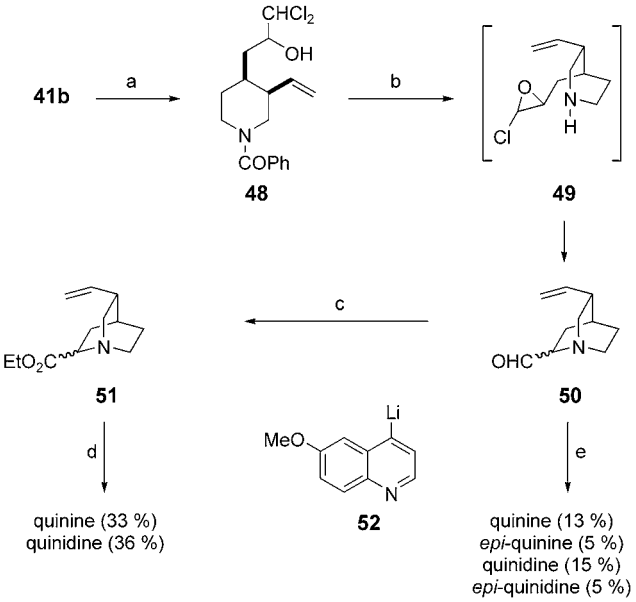
In a further modification of the basic strategy,[152] the formation of the crucial C8–N bond was achieved with concomitant installation of the carbonyl group at C9, through the cyclization of aminochloroepoxide **47** (Scheme 15).[157]



Scheme 15. Synthesis of cinchona alkaloids by the amino chloroepoxide ring-closing approach by Uskokovic and co-workers.

Reminiscent of the amino-epoxide approach, chloroepoxide **47** was prepared by benzylic chlorination of **35** followed by sodium borohydride reduction of the resultant ketone **46** with spontaneous formation of an oxirane. The *N*-benzoyl protecting group was then removed hydrolytically with barium hydroxide; under these conditions cyclization took place to furnish a spontaneously equilibrating mixture of quininone and quinidinone. Fractional crystallization provided crystals of the less-soluble quinidinone, while the quininone, which remained in the mother liquor, was epimerized to quinidinone and formed in a yield of 80% of the original mixture. Gutzwiller and Uskokovic later demonstrated that the highly diastereoselective DIBAL-H mediated reduction of the carbonyl group could be modified by altering the reaction conditions to provide either a roughly 1:1 mixture of quinine and quinidine or allow preferential access to quinidine.[152]

Despite mastering the "historical" C8–N approach for construction of the quinuclidine bicycle, and having limited success with the autooxidation strategy or the highly diastereoselective DIBAL-H mediated reduction of carbonyl compounds for functionalization at C9, by the end of the 1970s chemists were still unable to appropriately control the transformations leading to all the stereocenters, particularly the C8 center. The Uskokovic team had no better luck when in 1978 they disclosed two slightly different syntheses of quinine by using the novel C9–C4′ approach (Scheme 16).[158]



Scheme 16. Synthesis of quinine by the C9–C4′ coupling approach by Uskokovic and co-workers (1978). Reagents and conditions: a) 1. DIBAL-H; 2. PhCOCl; 3. Cl_2HCLi (59%); b) KOH, benzene; c) 1. $AgNO_2$; 2. $EtOH/H^+$; d) 1. **52**, Et_2O, −78°C (30–40%); 2. DIBAL-H (59%); e) **52**, Et_2O, −78°C.

This new route was the first departure from the C8–N approach, which had reigned supreme for 70 years. Problems with low yields and control of the configuration at C8 in the key quinuclidine intermediates, however, remained as major drawbacks. Certain characteristics from previous syntheses emanating from this research group are clearly seen in the new strategy, such as the aminochloroepoxide cyclization employed for accessing the key quinuclidine intermediates **50** and **51**,[159] which were prepared and used as diastereomeric mixtures. This approach can, therefore, be considered as a crypto-C8–N approach. Aldehyde **50** was highly unstable and needed to be employed immediately after its preparation, while ester **51** was more stable and amenable for use.

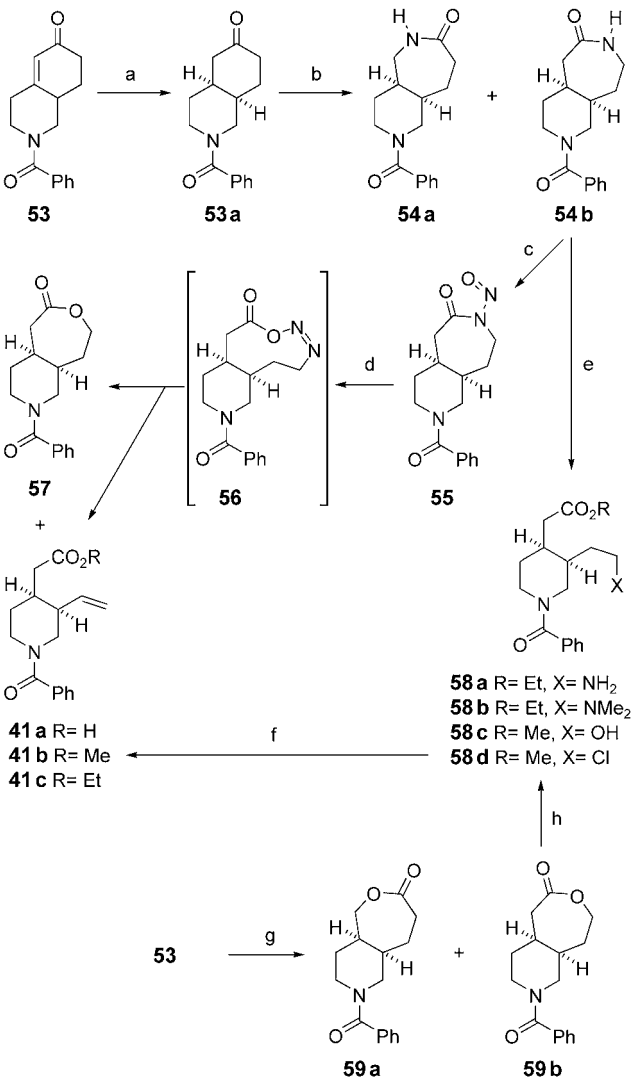
All of the syntheses of quinine performed during the 1970s by the C8–N approach relied heavily on protected

 © 2005 Wiley-VCH Verlag GmbH & Co. KGaA, Weinheim

meroquinene derivatives, which became interesting synthetic targets during the 1970s and afterwards.[160] Enantiomerically pure meroquinene derivatives, were employed in the syntheses of Gates, Taylor, and that of Uskokovic (employing opening of the aminoepoxide); however, they were semisynthetically obtained by degradation of quinidinone.[156]

Uskokovic et al. disclosed their first synthesis of *N*-benzoylmeroquinene (**41a**) by a sequence vaguely reminiscent of Woodward's (Scheme 17) for his preparation of homomeroquinene (**17**).[160i,j] The cumbersome approach started with the catalytic hydrogenation of *N*-benzoylhexahydroisoquinolone (**53**), which provided a *cis*/*trans* mixture of octahydro derivatives in which the required *cis* diastereomer **53a** was favored.[161] A Schmidt rearrangement of **53a** furnished a mixture of lactams **54a**,**b**, which were separated. Lactam **54b** was in turn transformed into a mixture of lactone **57** and meroquinene **41a**[162] via the nitrosoderivative **55** and the rearranged diazolactone **56**.[163] A less-effective sequence involving ethanolysis of **54b**, with reductive methylation of the resultant amino ester **58a** to the *N*,*N*-dimethylamino derivative **58b**, followed by pyrolysis of its *N*-oxide, was also disclosed as an approach to the related ester **41c**. An alternative approach to **41c** was also problematic: Baeyer–Villiger oxidation of **53a** to lactones **59a**,**b** and ring opening with concomitant esterification of the lactones, followed by substitution of the hydroxy group of the resultant **58c** by chloride (**58d**) and dehydrohalogenation provided another access to racemic **41b** (Scheme 17). Although the isoquinolone **53a** was successfully resolved, thus providing a potential route to optically active meroquinene, the number of hard-to-separate mixtures which characterized this protocol deterred it from being used as a source of the optically active **41b**.

A better and more practicable synthesis of **41a** was achieved from pyridine derivative **60**, which is easily available from β-collidine (Scheme 18). Hydrogenation of the heterocycle to *cis*-**61** (*rac*-cincholoipon methyl ester), originally synthesized stereospecifically by Stork et al. in 1946,[164] was followed by its resolution with (+)-tartaric acid and the ingenious application of a Hofmann–Löffler–Freytag remote halogenation[165] on the appropriate enantiomer **61a**. Protection of the nitrogen atom furnished **58d**. Dehydrochlorination to form **41a** completed this concise sequence. A Japanese team synthesized meroquinene, thus claiming a formal total synthesis of (±)-quinine.[160k,l]



Scheme 17. Synthesis of *N*-benzoylmeroquinine (**41a**) by Uskokovic and co-workers. Reagents and conditions: a) H_2, Rh/Al_2O_3, HCl/EtOH; b) NaN_3, PPA, 60°C,16 h (100%, **54a**:**54b** = 1:2); c) N_2O_4 (100%); d) 125°C (**41a** = 48%; **57** = 30%); e) 1. 5% HCl, EtOH (65%); f) from **58a**: 1. HCHO, HCO_2H; 2. H_2O_2; 3. Δ (85%); from **58d**: 1. NaOH, MeOH (99%); 2. KO*t*Bu, DMSO, 70°C, 7 h (85%); g) mCPBA, $NaHCO_3$, RT, 24 h (94%); h) 1. MeOH, HCl (36%); 2. CCl_4, PPh_3, DMF, RT, 21 h (18%). PPA = polyphosphoric acid, *m*CPBA = *meta*-chloroperoxybenzoic acid.

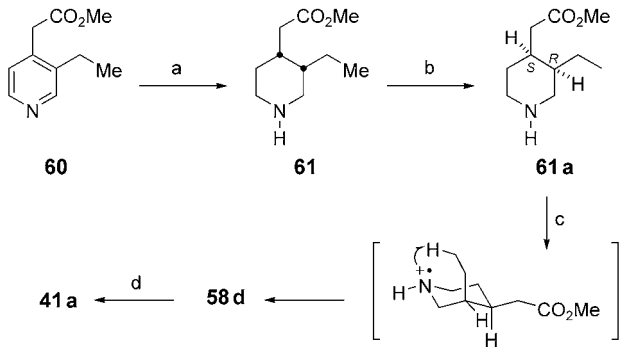
9. After 55 Years: A Modern, Stereocontrolled Synthesis of Quinine

Professor Gilbert Stork of Columbia University has been one of the most prominent leaders in the field of organic synthesis for over half a century. In the 1940s and 1950s he introduced the concept of stereoselective organic synthesis through the Stork–Eschenmoser hypothesis for polycyclic terpenoids and steroid synthesis, which enabled the stereorational total synthesis of cantharidin[164b] and, before that, of *rac*-cincholoipon.[164a,166] Among other outstanding accomplishments, Stork created a number of fundamental synthetic methods which enriched the synthetic chemist's arsenal, such as enamine and silyl enol ether carbon–carbon bond-forming methodologies and radical cyclizations.[166b]

Stork proudly confessed that it was the structure of quinine that he first saw in *Chemical Abstracts* while an undergraduate at the University of Florida which started his fascination with the challenges of organic synthesis.[166b] He began his quest for a stereochemically controlled total synthesis of quinine just two years after Woodward and Doering announced their success, and published his above-mentioned stereoselective synthesis of racemic ethyl cincholoiponate, a dihydromeroquinene derivative.[164]

His early efforts became entangled in a stereochemical thicket and a quarter of a century had to pass before he could

 © 2005 Wiley-VCH Verlag GmbH & Co. KGaA, Weinheim

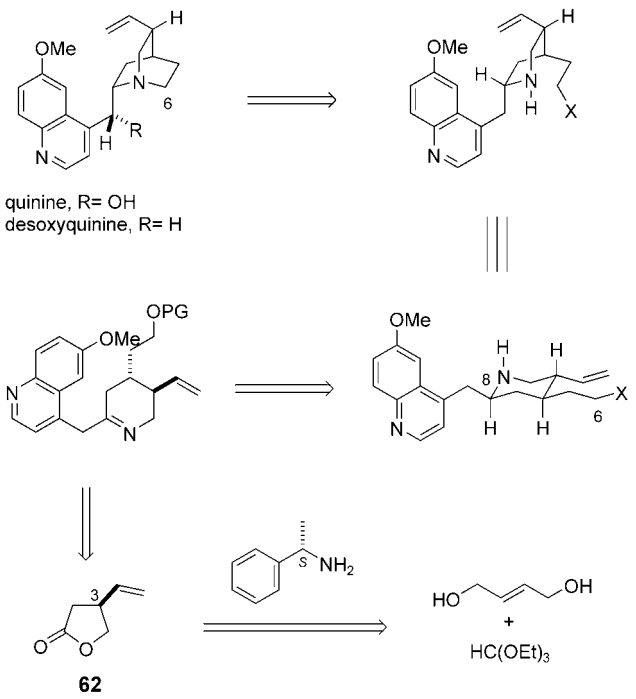


Scheme 18. Synthesis of meroquinine from **60**. Reagents and conditions: a) H_2, dilute HCl, PtO_2, 70 atm, 60 °C (88 %); b) resolution with L-tartaric acid (25 %); c) 1. NCS, Et_2O, 92 %; 2. F_3CCO_2H, *hν*, 200 W, 50 min (84 %); d) 1. NaOH, MeOH, RT (99 %); 2. KO*t*Bu, benzene/DMSO, 70 °C, 7 h (88 %). NCS = *N*-chlorosuccinimide.

make substantial further progress. He worked on and off on the problem, but in the eyes of many competitors he seemed to have abandoned this natural product as a synthetic target. Fortunately for science, however, Stork's ability to synthesize complex molecules was once more reiterated through his well-publicized report of a highly stereoselective total synthesis of quinine, which included the stereospecific installation of the C8 stereocenter.

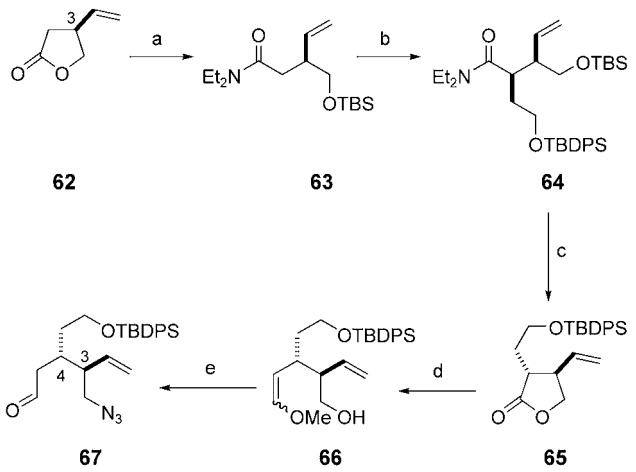
Before Stork's intervention, Rabe's route had long dominated the synthetic approaches to quinine because of the remarkable structural simplification involved in the C8–N coupling. To avoid the pitfalls of this strategy and achieve his goal, Stork had to take a novel and previously unexplored approach, which consisted of performing a C6–N connection (Scheme 19). His route also benefited from the advances made in terms of reagents, reactions, and conformational analysis during the preceding decades when the synthesis of quinine was an almost unattainable target. The key feature of his synthetic design was the observation that the C6–N strategy generated a trisubstituted piperidine—a compound that at first sight looks to have structural complexity similar to that of quinine. Thinking retrosynthetically, however, the synthetic problem has been simplified by considering that the related tetrahydropyridine would be a good precursor to this compound. This route looks feasible if stereospecific reduction of the tetrahydropyridine from its less-hindered face is accomplished. This compound is also an excellent choice as an intermediate, since its preparation requires placement of only two adjacent side chains with the appropriate configuration, thereby greatly reducing the burden of the synthetic problem.

The starting material for the synthesis of the non-aromatic quinine framework was Taniguchi's lactone (**62**), which is easily available from but-2-ene-1,4-diol and triethyl orthoformate.[167] Appropriate choice of the optically active α-phenethylamine enables selection of one of the intermediate diastereomeric amides and thus gives access to either one of both enantiomeric lactones. The precursor of the quinuclidine ring **67** containing nine carbon atoms was efficiently obtained through a series of carefully planned chemical manipulations.[168] In an unforeseen complication, the lactone had to be opened with a nucleophile to generate the related amide **63**



Scheme 19. Retrosynthetic approach to quinine by Stork et al. PG = protecting group.

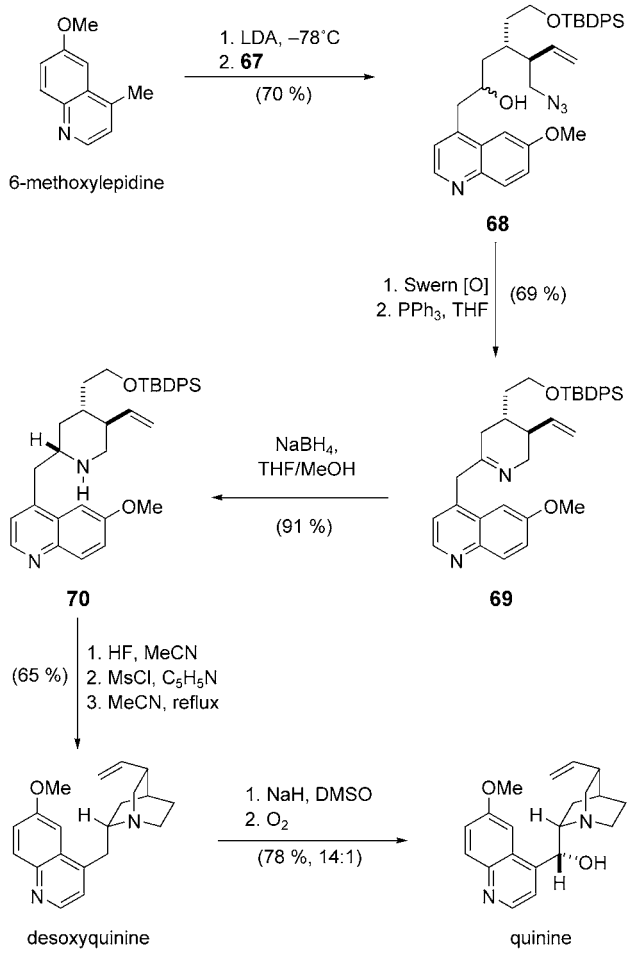
for the proper introduction of the required C_2 side chain (**64**). Ring closure of **64** to give lactone **65** was followed by reduction to the corresponding lactols and subsequent Wittig homologation to give **66** (Scheme 20). This procedure left a primary alcohol suitable for the introduction of a nitrogen atom by means of a Mitsunobu-type azidation.[169] Reminiscent of the first synthesis of quinine by Uskokovic et al., Stork et al. coupled the 6-methoxylepidine anion with aldehyde **67**



Scheme 20. Synthesis of quinine by Stork et al. by chemical manipulation of Taniguchi's lactone. Reagents and conditions: a) 1. Et_2NAlMe_2; 2. TBSCl, imidazole (79 %); b) 1. LDA, −78 °C; 2. $ICH_2CH_2OTBDPS$ (79 %, 20:1); c) 1. PPTS, EtOH; 2. xylene (93 %), d) 1. DIBAL-H; 2. $Ph_3PCH(OMe)$ (93 %); e) 1. $(PhO)_2P(O)N_3$; PPh_3, DEAD; 2. 5 N HCl (74 %). DEAD = diethylazodicarboxylate, PPTS = pyridinium *p*-toluenesulfonate, TBS = *tert*-butyldimethylsilyl, TBDPS = *tert*-butyldiphenylsilyl.

 © 2005 Wiley-VCH Verlag GmbH & Co. KGaA, Weinheim

and oxidized the resultant mixture of alcohols **68** to the corresponding ketone. A Staudinger reaction, which took place with concomitant cyclization, was implemented to produce tetrahydropyridine derivative **69** (Scheme 21).[170]



Scheme 21. Synthesis of quinine by Stork et al.: The final steps. Ms = methanesulfonyl.

The key enantiospecific reduction of the tetrahydropyridine with sodium borohydride was then performed. This procedure, which entails an axial addition of a hydride ion to an iminium intermediate, gave **70**,[171] with all three stereocenters of the quinuclidine ring with the correct configuration. This was probably a consequence of the formation of the conformationally favored chair form of **69** in which the side chains adopt equatorial dispositions. Subsequent transformation of the silyl ether into a suitable leaving group was then followed by intramolecular cyclization to furnish, specifically and exclusively, desoxyquinine, which was finally converted into quinine by the elegant autooxidation described by Uskokovic et al. The use of sodium hydride and dimethyl sulfoxide as the solvent conferred improved selectivity (14:1) to this transformation.

Interestingly, the groundbreaking synthesis Stork et al. uses less catalytic reactions than the sequence developed by Woodward et al., employs carbon–carbon bond forming reactions rather than chemical degradation for the synthesis of the alicyclic moiety, and resorts to the different stabilities of a pair of silyl ethers for the differentiation of two primary alcohols. The sequence is extremely simple in its design and amazingly efficient, such that it was likened to a ballet: "*An inexperienced observer of a great performance might leave with a view that there are no new steps. But one schooled in the field will see the exquisite choreography, the remarkable timing, the efficiency of execution, and the economy of movement—and leave inspired*".[172]

Paralleling Woodward's success, and despite of its lack of value as a commercial source of quinine, the synthesis received worldwide attention and important media coverage. Among the scientific community members, chemistry masters considered Stork's contribution as an "*absolute classic*",[87] and "*a work of tremendous historical value*". Another opinion was that "*the Stork paper is written with an insight and historical perspective (as well as correcting some myths) rarely seen in the primary chemical literature, and should be required reading for all students of organic chemistry*".[173]

10. The Resurrection of the C8–N Strategy: A Catalytic Enantioselective Total Synthesis of Quinine

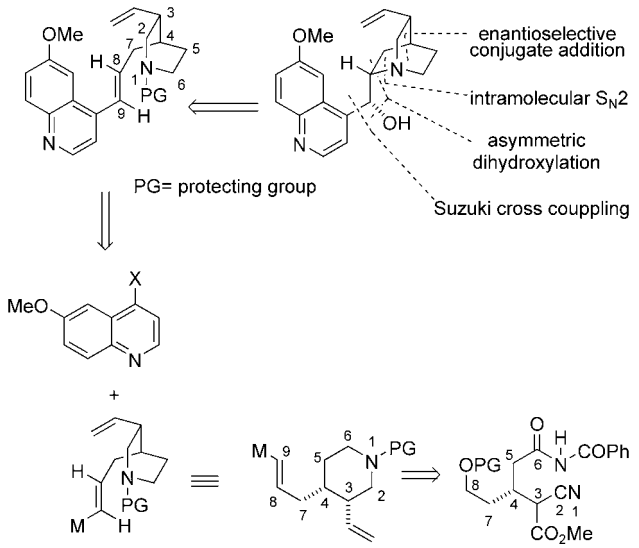
The C8–N strategies devised by Uskokovic and coworkers,[91,147a] Taylor and Martin,[154] and Gates et al.[155] in the 1960s and 1970s for the formation of quinuclidine relied on conjugate addition of an amine to a vinylquinoline or the related epoxide or chloroepoxide. The first of these transformations produced diastereomeric mixtures, because of the unselective addition of the amine to the olefin. The lack of stereocontrol at C8 in the protocols of Taylor and Martin as well as Gates et al. resulted because the epoxides could not be synthesized stereoselectively from vinyl arenes; this problem also caused the syntheses to lack stereocontrol at the C9 position.[174] The demands of such a strategy could not be fulfilled with the resources of the arsenal of chemical transformations available. The reagents required did not become available until one decade later.

One of the most intensively studied areas of current research is the selective synthesis of optically active compounds. Numerous chiral auxiliaries and catalysts have been developed which approach or sometimes even match the selectivity observed in enzymatic reactions. These catalysts not only accelerate chemical reactions, but can also exert remarkable kinetic control over product distribution. The novel term "chemzyme" was coined by Corey and Reichard[175] to collectively designate those chiral chemical catalysts exhibiting enzyme-like features and complete selectivity. Many useful chemzymes have been developed during the last decade.

Professor Eric N. Jacobsen from Harvard University, who has emerged as an outstanding chemist in the area of designing and discovering selective catalysts for use in organic synthesis, published, with his research group, a new breakthrough: a catalytic and highly stereocontrolled total synthesis of quinine and quinidine.[176] His strategy enabled the

 © 2005 Wiley-VCH Verlag GmbH & Co. KGaA, Weinheim

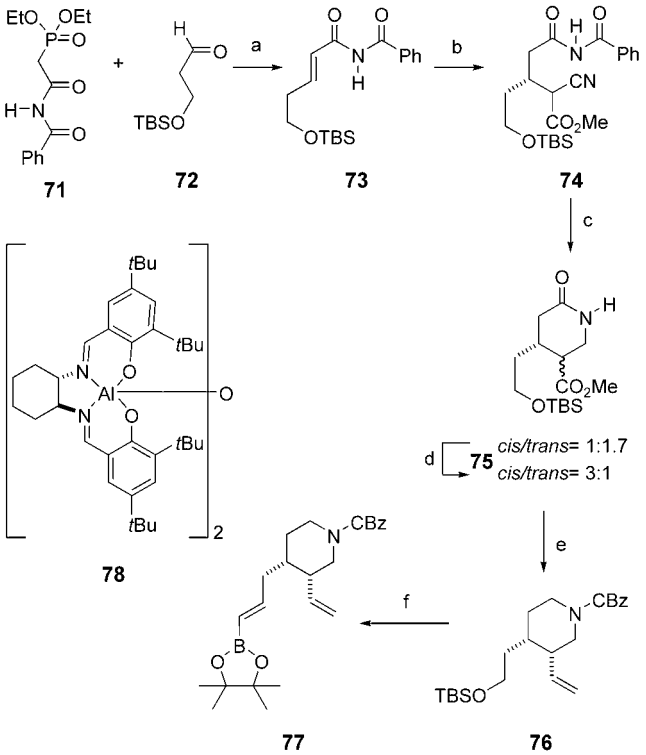
simultaneous control of the configuration at the C8 and C9 stereocenters in the final product and allowed either one of the two commercially important cinchona alkaloids to be selectively secured, simply by changing the nature of the chiral catalyst employed in this key step. The fundamental part of his strategy is a modern and stereocontrolled version of the aminoepoxide cyclization conceptually established by Gutzwiller and Uskokovic in the 1970s.[91] Interestingly, the catalysts used are cinchona alkaloid derivatives, as the crucial step is a modification of the well-known Sharpless asymmetric dihydroxylation (Scheme 22).



Scheme 22. Retrosynthetic analysis of quinine by Jacobsen and co-workers.

The overall strategy of Jacobsen and co-workers hinges upon four fundamental C–C, C–N, and C–O bond-forming reactions: a catalytic enantioselective conjugate addition to establish the C4 stereocenter, a convergent catalytic Suzuki cross-coupling reaction to join the quinoline ring to a chiral alicyclic unit, an asymmetric dihydroxylation for the construction of the C8 and C9 stereocenters, and an intramolecular amino epoxide S_N2-type cyclization for the stereospecific synthesis of the quinuclidine bicycle with the correct configuration at C8.

The alicyclic fragment required for the Suzuki cross-coupling reaction was readily accessed by following the sequence depicted in Scheme 23. Olefination of protected aldehyde **72** with imidophosphonate **71**[177] proceeded with high *trans* selectivity to give **73**.[178] Enantioselective conjugate addition of methyl cyanoacetate to **73** in the presence of (*S,S*)-(salen)–aluminum complex **78** (salen = *N,N*′-bis(salicylidene)ethylenediamine dianion)[179] gave **74**, and a hydrogenative lactamization with a Raney nickel catalyst afforded **75**. The inconvenient *cis/trans* diastereomeric mixture (1:1.7) of esters obtained was transformed into a more desirable 3:1 *cis/trans* mixture by a clever selective deprotonation/reprotonation sequence. After a transformation of the functional groups a Wittig olefination was performed,[180] which installed the required vinyl moiety of **76**. Removal of the silyl protecting

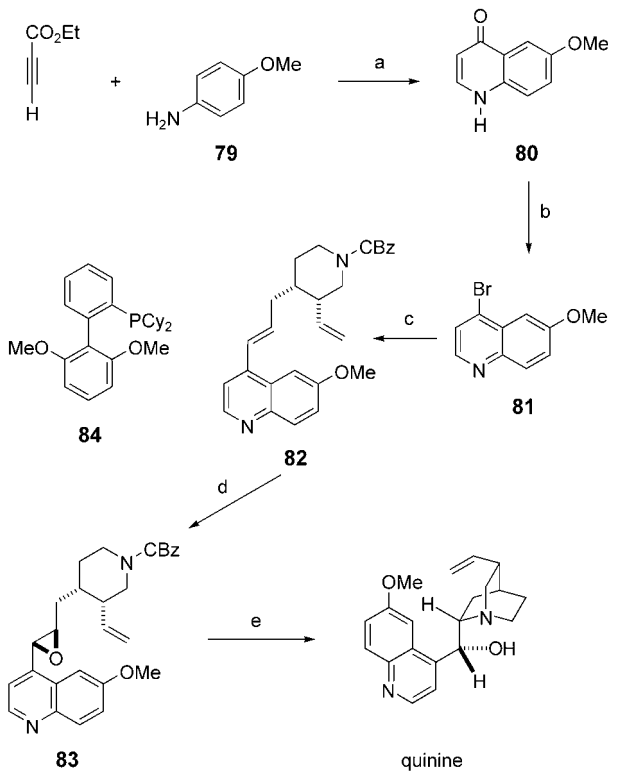


Scheme 23. Synthesis of quinine by Jacobsen and co-workers: Construction of the alicyclic fragment. Reagents and conditions: a) *n*BuLi, THF, −78 °C–0 °C (84%, $E/Z > 50:1$); b) $NCCH_2CO_2Me$, (*S,S*)-**78** (5 mol%), *t*BuOH, C_6H_{12}, RT (91%); c) Raney Ni, H_2, toluene/MeOH (3:1), 44 bar, 80 °C, 12 h (89%); d) 1. LDA, THF, −78 °C; 2. 5% H_2O/THF, −78 °C; e) 1. $LiAlH_4$, THF; 2. CBz_2O, Et_3N, CH_2Cl_2 (51%); 3. chromatographic separation of diastereomers; 4. TPAP, NMO, CH_2Cl_2; $Ph_3P^+MeBr^-$, KO*t*Bu, THF, 0 °C (73%); f) 1. TBAF, THF; 2. TPAP, NMO, CH_2Cl_2 (86%); 3. Cl_2CHB(pinacolate), $CrCl_2$, LiI, THF (79%, $E/Z > 20:1$). CBz_2O = dibenzyl dicarbonate, NMO = *N*-methylmorpholine-*N*-oxide, TBAF = tetrabutylammonium fluoride, TPAP = tetrapropylammonium perruthenate.

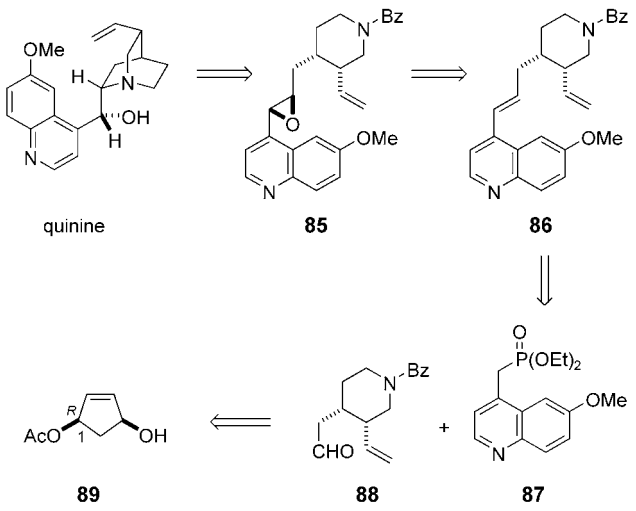
group, followed by oxidation of the resultant alcohol to the corresponding aldehyde and olefination with dihalomethylboron pinacolate under Takai conditions selectively furnished the necessary (*E*)-vinyl component **77**.[181] On the other hand, preparation of the appropriately substituted bromoquinoline **81**, previously employed for the synthesis of quinine,[44b] was straightforward, and achieved by condensation of *p*-anisidine (**79**) with methyl propiolate, followed by microwave-assisted bromination of the resultant **80** with concomitant aromatization.[182] The two fragments were joined through a Suzuki cross-coupling reaction in the presence of ligand **84** to give vinyl quinoline **82** (Scheme 24). This latter compound is reminiscent of **44b**, a common intermediate in earlier quinine and quinidine constructions (Scheme 13).

A Sharpless asymmetric dihydroxylation procedure using the AD-mix-β reagent mixture[183] allowed convenient access to the required epoxide functionality (**83**) through an intermediate halohydrin,[184] while microwave-assisted nucleophilic attack of the oxirane by the deprotected secondary amine[185] completed the correct installation of the quinuclidine core and the synthesis of quinine.[186]

 © 2005 Wiley-VCH Verlag GmbH & Co. KGaA, Weinheim



Scheme 24. Synthesis of quinine by Jacobsen and co-workers. Reagents and conditions: a) 1. MeOH, RT, 12 h; 2. Dowtherm A, 250 °C, 30 min (63 %); b) Ph_3PBr_2, MeCN, microwaves, 170 °C,15 min (86 %); c) **77**, $Pd(OAc)_2$, **84** (2.5 mol %), K_3PO_4, H_2O, THF, 16 h, RT (89 %, $E/Z > 20:1$); d) 1. AD-mix-β, $MeSO_2NH_2$, *t*BuOH, H_2O, 0 °C (88 %, d.r. > 96:4); 2. $MeCH(OMe)_3$, PPTS (cat.), CH_2Cl_2; 3. MeCOBr, CH_2Cl_2; 4. K_2CO_3, MeOH (81 %); e) 1. Et_2AlCl, benzenethiol, 0 °C–RT; 2. microwaves, 200 °C, 20 min (68 %). Cy = cyclohexyl.



Scheme 25. Retrosynthetic analysis of quinine by Kobayashi and co-workers.

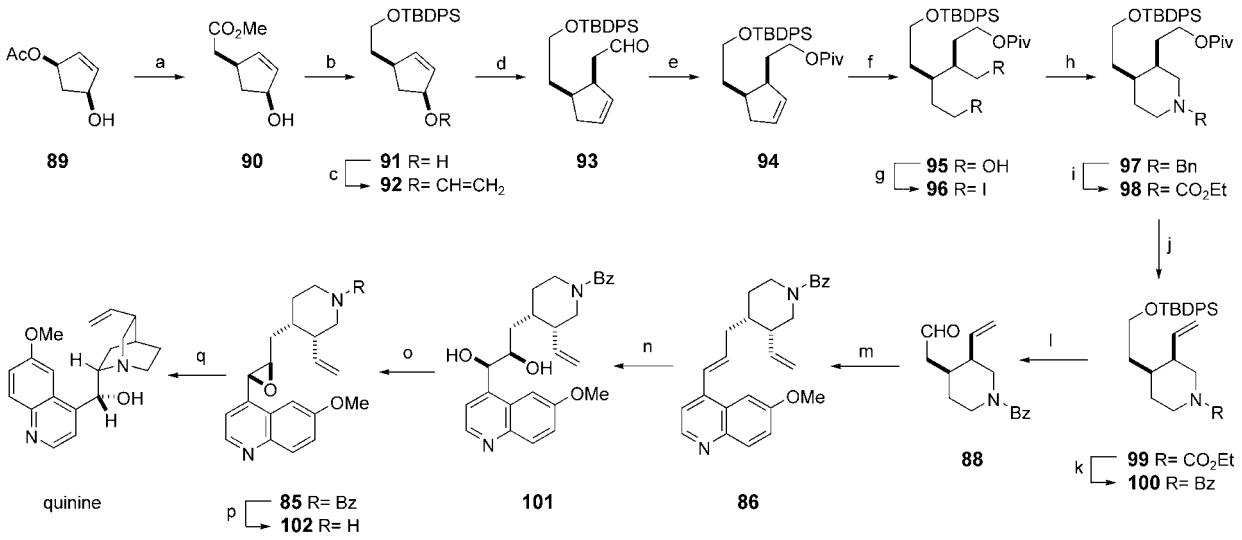
11. Another C8–N Strategy: The Latest Total Synthesis of Quinine

More recently, however, a Japanese research group headed by Kobayashi disclosed a total synthesis of quinine.[187] Their route follows a more classical synthetic approach and is strongly based on previous experience accumulated during the research of Uskokovic et al.,[91,147a] Taylor and Martin,[154] and Jacobsen and co-workers.[176] Its novelty, however, resides in its original and highly stereocontrolled synthesis of the meroquinene moiety. Their retrosynthetic analysis of the natural product (Scheme 25) shows that the epoxide **85**, analogous to **83** and reminiscent of **45**, is formed, which in turn is assumed to come from *E*-olefin **86**, similar to **82** and **44b**.[153b,154,155] Formation of the critical C–C double bond leading to **86** through the use of organophosphorous reagents is the key step for joining the known alicyclic fragment **88** to the aromatic moiety **87**. The synthesis of **88**[160] employs the readily available 1*R* enantiomer of monoacetate **89**,[188] which contains all of the five carbon atoms required to build the piperidine ring of **88**.

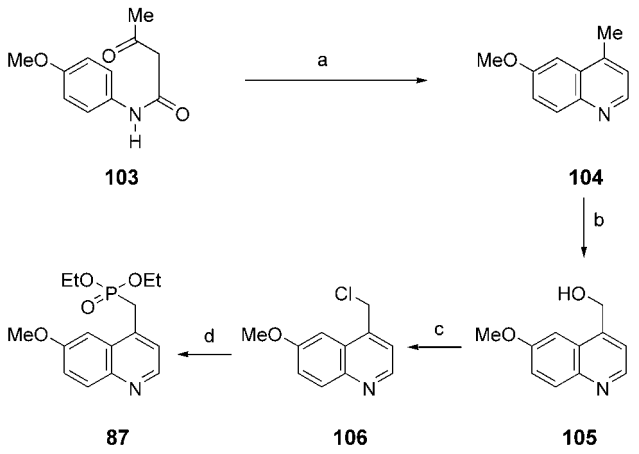
Reaction of allylic monoacetate **89**[189] with dimethyl malonate under palladium catalysis furnished ester **90** as a single enantiomer in almost quantitative yield (Scheme 26).[190] Reduction of the ester and selective protection of the resulting primary alcohol provided intermediate **91** in 63 % yield. Pivalate **94** was then synthesized by employing a sequence involving formation and Claisen rearrangement of the vinyl ether **92** derived from **91**, followed by reduction of aldehyde **93**, and conventional protection of the resulting alcohol with pivaloyl chloride. Ozonolysis of **94** with a reductive work up led to diol **95**, and subsequent formation of the corresponding diiodide **96** under Mitsunobu conditions set the stage for the construction of the piperidine ring of **97** by dialkylation of benzylamine. Replacement of the *N*-benzyl group of **97** with CO_2Et (**98**) afforded the characteristic vinyl group of the meroquinene aldehyde fragment. This was achieved by selective deprotection of the pivalic acid ester, followed by phenylselenenylation of the free primary alcohol with Grieco's reagent,[191] its subsequent oxidation to the corresponding selenoxide and final elimination to give good yields of **99**. A second replacement of the *N*-protecting group to give **100** was implemented by hydrolysis of the carbamate and benzoylation of the resulting free secondary amine. These successive changes in the nitrogen protecting group are necessary because selenoxide elimination apparently cannot be carried out on benzoyl derivatives. Finally, mild desilylation of **100** liberated the remaining primary alcohol, which was smoothly oxidized to the anticipated key intermediate **88**. The aromatic component **87** was prepared from keto amide **103** (Scheme 27).[192] Cyclization with sulfuric acid and subsequent dehydration with phosphorous oxychloride provided **104**. Functionalization of the methyl group with *m*CPBA afforded **105**,[193] and finally phosphorylation with the aid of thionyl chloride and intermediacy of the related chloride **106** afforded **87**.

The aldehyde **88** was coupled with the phosphonate **87** by using sodium hydride as the base and the product **86** submitted to Sharpless' asymmetric dihydroxylation with AD-mix-β to furnish **101**.[142a,183] Analogous to the protocol of Jacobsen and co-workers, diol **101** was converted into the

 © 2005 Wiley-VCH Verlag GmbH & Co. KGaA, Weinheim



Scheme 26. Synthesis of quinine by Acharya and Kobayashi. Reagents and conditions: a) 1. $CH_2(CO_2Me)_2$, *t*BuOK, $[Pd(PPh_3)_4]$ (cat.); 2. KI, DMF, 125 °C (70%); b) 1. $LiAlH_4$; 2. TBDPSCl, imidazole (63%); c) $H_2C{=}CHOEt$, $Hg(OAc)_2$ (cat.); d) 190 °C; e) 1. $NaBH_4$; 2. *t*BuCOCl, Et_3N, CH_2Cl_2 (66%); f) 1. O_3, *n*PrOH, [78 °C; 2. $NaBH_4$ (81%); g) I_2, PPh_3, imidazole (88%); h) $BnNH_2$, dioxane (98%); i) $ClCO_2Et$, PhMe (99%); j) 1. NaOEt, EtOH; 2. *o*-NO_2-C_6H_4SeCN; PBu_3, THF; 3. 35% H_2O_2, THF (77%); k) 1. MeLi, 0 °C; 2. BzCl (61%); l) 1. TBAF; 2. PCC (80%); m) **87**, NaH, THF, RT (82%); n) AD-mix-β, 0 °C; o) $MeC(OMe)_3$, PPTS (cat.), CH_2Cl_2, TMSCl, K_2CO_3, MeOH (95%); p) DIBAL-H, PhMe; q) DMF, 160 °C (66% from **85**). PCC = pyridinium chloroformate, piv = pivaloyl, Bn = benzyl.



Scheme 27. Synthesis of key intermediate **87** by Kobayashi et al. Reagents and conditions: a) 1. H_2SO_4; 2. $POCl_3$; 3. Zn, AcOH (72%); b) *m*CPBA, CH_2Cl_2, RT; 2. Ac_2O, RT; 3. K_2CO_3, MeOH (43%); c) $SOCl_2$, CH_2Cl_2, reflux (71%); d) H-P(=O)$(OEt)_2$, *n*BuLi, THF (70%).

related epoxide **85**,[184] which was reductively deprotected with DIBAL-H to provide the last intermediate **102**. Unlike the procedure of Jacobsen and co-workers in which microwaves were used, the synthesis was completed by nucleophilic ring opening of the epoxide under purely thermal conditions and furnished quinine in a yield of 66% from oxirane **85**. Compound **45**, an epoxide similar to **85** and **83**, has been previously synthesized nonstereoselectively by Uskokovic et al. Both the Jacobsen and Kobayashi research groups solved the selectivity problem associated with the amino epoxide cyclization by making the "correct" oxirane.

12. Concluding Remarks

More than 85 years have passed since Rabe's claim to have reconstructed quinine and sixty years since Woodward and Doering shocked the world with their claim to have accomplished the first total synthesis of quinine. We are also approaching the 150th anniversary of Perkin's historic experiment. So, what does the resurgence of the interest in quinine manifested through the recent total syntheses by the research groups of Stork, Jacobsen, and Kobayashi mean?

In recent years the chemical community has witnessed the power of total synthesis through the syntheses of scarcely available and structurally complicated targets such as paclitaxel, palytoxin, and the ecteinascidins,[194] to name but a few of the successfully completed ventures. Why should the relatively simple quinine, now clinically overshadowed by synthetic antimalarial drugs, no longer a miracle drug, and more than abundantly available for its main use to be in the preparation of tonic water, be catching the attention of renowned chemists?

Organic chemistry has evolved into a well-established branch of science and has become such a sophisticated and demanding area that the synthesis of natural products is no longer just oriented towards proof of structure, but to the testing of new reagents, reactions, concepts, and strategies. Factors such as atom economy, stereocontrol, overall simplicity, and environmental impact have become the new principles orienting the development of this discipline.

Unlike any other endeavor, quinine has been a long-sought synthetic target, with an aura of elusiveness. Perhaps the most important reasons behind the recent syntheses of quinine are those confessed to by Stork himself: "*the value of a quinine synthesis has essentially nothing to do with quinine*

 © 2005 Wiley-VCH Verlag GmbH & Co. KGaA, Weinheim

… it is like the solution to a long-standing proof of an ancient theorem in mathematics: it advances the field".

In this context, the distinguished achievement made by Jacobsen and co-workers is highly symbolic: it comes almost 60 years after the accomplishment of Woodward and Doering. Both syntheses of quinine were carried out by employing "state of the art" chemical knowledge, chemical thinking, and chemical reagents, and both resorted to the same, almost one century old C8–N approach. Although all of the chemicals and all the reactions were available to both scientists, they both developed unique strategies towards the natural product.

Every scientific achievement must be judged by the standards of its time. There is a clear evolution from the protocol of Woodward to those of Kobayashi and Jacobsen through those of Uskokovic, Gates, Taylor, and Stork and provides clear proof of lessons learned in synthetic methodology and strategy over the intervening years. They are also strong signals that the total synthesis of natural products, considered by many as the most demanding form of organic chemical research, which Woodward enriched and stimulated so profoundly in the past, did indeed become a major endeavor in organic chemistry.[195,196] Organic synthesis is still developing and has a bright, strong, and promising future. Thus, one thing is assured: although Kobayashi et al. have described the most recent and perhaps one of the most efficient total syntheses of quinine, it will not be the last.

Addendum

In addition to being the 60th anniversary of the first paper by Woordard and Doering on quinine, 2004 also marks the 25th year since Robert B. Woordward's untimely and unfortunate death. A short and useful account on Woodward's personal and professional life can be found in ref. [197].

The authors gratefully acknowledge Fundación Antorchas, CONICET, ANPCyT, and SECyT-UNR.

Received: February 28, 2004

[1] a) R. B. Woodward, W. E. Doering, *J. Am. Chem. Soc.* **1944**, *66*, 849; b) R. B. Woodward, W. E. Doering, *J. Am. Chem. Soc.* **1945**, *67*, 860; c) an educational discussion of this synthesis is found in R. E. Ireland, *Organic Synthesis*, Prentice-Hall, Englewood Cliffs, NJ, **1969**, pp. 123–139.

[2] D. A. Casteel in *Burger's Medicinal Chemistry and Drug Discovery, 5th Ed., Vol. 5* (Ed.: M. E. Wolff), Wiley, New York, **1997**, Chap. 59, p. 16.

[3] a) P. Manson-Bahr, *Int. Rev. Trop. Med.* **1963**, *2*, 329; b) I. Sherman, *Malaria: Parasite Biology, Pathogenesis, and Protection*, ASM, Washington, **1998**.

[4] L. J. Bruce-Chwatt, *History of Malaria from Prehistory to Erradication*, in *Malaria. Principles and Practice of Malariology, Vol. 1* (Eds.: W. Wernsdorfer, I. McGregor), Churchill Livingstone, Edinburgh, **1988**, pp. 1–59.

[5] J. Kreier, *Malaria*, *Vol. 1*, Academic Press, New York, **1980**.

[6] The four scientists received the Nobel Prize for Medicine or Physiology: Sir Ronald Ross (1902) *"for his work on malaria, by which he has shown how it enters the organism and thereby has laid the foundation for successful research on this disease and methods of combating it"*; Camillo Golgi (1906, shared with Santiago Ramón y Cajal) *"in recognition of their work on the structure of the nervous system"*; Charles Louis Alphonse Laveran (1907) *"in recognition of his work on the role played by protozoa in causing diseases"*; and Paul Hermann Müller (1948) *"for his discovery of the high efficiency of DDT as a contact poison against several arthropods"*.

[7] a) R. E. McGrew, *Encyclopedia of Medical History*, McGraw Hill, New York, **1985**, p. 166; b) deadly fevers—most probably malaria—have been recorded since the beginning of the written word; for example, references can be found in the Vedic writings of 1600 BC in India and by Hippocrates some 2500 years ago.

[8] J. Wiesner, R. Ortmann, H. Jomaa, M. Schlitzer, *Angew. Chem.* **2003**, *115*, 5432; *Angew. Chem. Int. Ed.* **2003**, *42*, 5274.

[9] For a discussion on the recent status of the malaria problem, see E. Marshall, *Science*, **2000**, *290*, 428.

[10] World Health Organization, *Report 2000, World Health in Statistics*, Annex, Table 3, Geneva, **2000**.

[11] a) K. C. Nicolau, D. Vourloumis, N. Winssinger, P. S. Baran, *Angew. Chem.* **2000**, *112*, 46; *Angew. Chem. Int. Ed.* **2000**, *39*, 44, and references therein; b) K. C. Nicolau, E. J. Sorensen, *Classics in Total Synthesis: Targets, Strategies, Methods*, VCH, Weinheim, Germany, **1996**; c) K. C. Nicolau, S. A. Snyder, *Classics in Total Synthesis II: More Targets, Strategies, Methods*, Wiley-VCH, Weinheim, Germany, **2003**.

[12] See, for example: a) *The Columbia Encyclopedia*, *6th Ed.*, Columbia University Press, New York, **2000**, p. 2344: *"Chemical synthesis [of quinine] was achieved in 1944 by R. B. Woodward, and W. E. Doering"*; b) *The Encyclopaedia Britannica*, *15th Ed., Vol. 9*, Chicago, **1997**, p. 862: "*[quinine's] total laboratory synthesis in 1944 is one of the classical achievements of synthetic organic chemistry*"; c) *The Grolier Library of Scientific Biography, Vol. 10*, Grolier Educational, Danbury, **1997**, p. 167: "*In 1944 Woodward, with William von Eggers Doering, synthesized quinine from the basic elements. This was a historic moment…*"; d) *The Pharmaceutical Century, Ten Decades of Drug Discovery, Chem. Eng. News Suppl.*, American Chemical Society, Washington, **2000,** p. 58: "*In 1944, William E. Doering and Robert B. Woodward synthesized quinine—a complex molecular structure—from coal tar*".

[13] R. S. Desowitz, *Who Gave Pinta To The Santa Maria?: Tracking the Devastating Spread of Lethal Tropical Diseases into America*, Harcourt Brace, New York, **1998**.

[14] R. M. Roberts, *Serendipity: Accidental Discoveries in Science*, Wiley, New York, **1989**.

[15] J. J. Arango, *J. Linn. Soc. London, Bot.* **1949**, *53*, 272.

[16] For a fascinating account on the background of quinine, see: M. B. Kreig, *Green Medicine*, McNally Rand, New York, **1964**, pp. 165–206.

[17] B. B. Simpson, M. Conner-Ogorzaly, *Economic Botany, Plants in Our World*, McGraw-Hill, New York, **1986**.

[18] M. Honigsbaum, *The Fever Trail: In Search of the Cure for Malaria*, Macmillan, New York, **2001**.

[19] During the period 1772–1786 cinchona bark was so expensive that it served as a distinguished gift; the Spanish presented the bark to the Empress of Hungary, the Pope Clemens XIV, the Duke of Parma, the Electress of Baviera, and the General Commissioner of the Sacred Places in Jerusalem.

[20] a) K. C. Nicolau, R. K. Gay, *Angew. Chem.* **1995**, *107*, 2047; *Angew. Chem. Int. Ed. Engl.* **1995**, *34*, 2079; b) S. Borman, *Chem. Eng. News* **1992**, 30.

[21] M. Wahlgren, P. Perlmann, *Malaria: Molecular and Clinical Aspects*, Harwood Academic Publishers, Netherlands, **1999**, pp. 3–18.

 © 2005 Wiley-VCH Verlag GmbH & Co. KGaA, Weinheim

[22] For a captivating account on the fascinating history of cinchona, see: a) H. Hobhouse, *Seeds of Change*, Harper and Row, New York, **1985**, pp. 3–40; b) A. C. Wootton, *Chronicles of Pharmacy*, *Vol. 2*, Milford House, Boston, **1972**.
[23] a) F. W. Sertürner, *Trommsdorff's J. der Pharmazie*, **1805**, *13*, 234; b) F. W. Sertürner, *Gilberts Ann. Phys.* **1817**, *55*, 56.
[24] a) F. Magendie, P. J. Pelletier, *J. Gen. Med. Chirurgie Pharm.* **1817**, *59*, 223; b) P. J. Pelletier, J. B. Caventou, *Ann. Chim. Phys.* **1819**, *12*, 113; c) P. J. Pelletier, J. B. Caventou, *Ann. Chim. Phys.* **1818**, *8*, 323; d) P. J. Pelletier, J. B. Caventou, *Ann. Chim. Phys.* **1819**, *10*, 144; e) P. J. Pelletier, J. B. Caventou, *Ann. Chim. Phys.* **1819**, *10*, 117; f) G. E. Dann, *Einführung in die Pharmaziegeschichte*, Wissenschaftliche Verlagsgesellschaft, Stuttgart, **1975**, pp. 82–83.
[25] M. Hesse, *Alkaloide*, Wiley-VCH, Weinheim, **2000**.
[26] a) From 38 known cinchona species, only 4 are of commercial interest: *C. calisaya*, *C. ledgeriana*, *C. succirubra*, and *C. officinalis*; they have different quinine content, from 7 to 15% and their complex taxonomy was not stabilized until the 1990s; b) the term cinchona was coined by the Swedish botanist Linnaeus in 1742, perhaps to honor the Countess of Chinchon after hearing the tale of her cure from malaria. In 1866 the International Botanical Congress opted to keep the error in the spelling. The first botanical description of the tree made by Linnaeus was based on drawings of the French geographer and explorer Charles Marie de La Condamine, member of the French Geodesic Expedition of 1735; c) after the isolation of quinine, the industrial procedure adopted for its mass production consisted of extracting pulverized bark with toluene in the presence of alkali, back-extracting the alkaloids from toluene into diluted sulfuric acid, then carefully neutralizing, and collecting the crystals of quinine sulfate. d) The availability of quinine in a pure state allowed a better study of the alkaloid. Pasteur tried to employ the natural product as a resolving agent. e) Pasteur reported the formation of quinotoxine, with the aid of which he carried out the first resolution ever made, see: L. Pasteur, *Compt. Rend.* **1853**, *37*, 110 and L. Pasteur, *Liebigs Ann. Chem.* **1853**, *88*, 209.
[27] a) P. J. Pelletier, J.-B. Caventou, *Ann. Chim. Phys.* **1820**, *15*, 291; b) P. J. Pelletier, J.-B. Caventou, *Ann. Chim. Phys.* **1820**, *15*, 337; c) P. J. Pelletier, J.-B. Caventou, *Analyse Chimique des Quinquina* (Ed.: L. Colas), Paris, **1821**.
[28] A. Butler, T. Hensman, *Educ. Chem.*, **2000**, 151.
[29] a) A. Delondre, H. Henry, *J. Pharm.* **1833**, *19*, 623; b) A. Delondre, H. Henry, *J. Pharm.* **1834**, *20*, 157; c) J. van Hejningen, *Liebigs Ann. Chem.* **1849**, *72*, 302; d) J. van Hejningen, *Pharm. Zentralhalle* **1849**, 465.
[30] F. L. Winckler, *Jahresbericht* **1847**, 620.
[31] R. B. Turner, R. B. Woodward, *The Chemistry of the Cinchona Alkaloids* in *The Alkaloids*, *Vol. 3* (Ed.: R. H. F. Manske), Academic Press, New York, **1953**, Chap. 16; b) L. Andersson, *A Revision of the Genus Cinchona (Rubiaceae-Cinchoneae)*, The New York Botanic Garden Press, New York, **1998**.
[32] a) In the 1850s the East India Company alone spent £100000 annually on cinchona bark, but even with this level of expenditure it could not keep the colonists healthy. b) Nearly half of the admissions to St Thomas's Hospital in London in 1853 were smitten with the "ague". c) John Eliot Howard became an expert on the chemistry of quinine, with his expertise recognized by his appointment as Fellow of the Royal Society; his factory produced more than 4 tons of quinine in 1854. d) During the American Civil War, more soldiers died of malaria than in battle in the southern states. e) Malaria decimated military strength in many battles during the 18th and the early 19th century; for example, thousands of British troops succumbed to it while fighting Napoleon in 1809. f) Without antimalarial drugs, the political shape of the world might have been very different from what we see today; access to dependable sources of reasonably priced quinine decisively helped European exploration of Africa and its colonialization. The great explorer David Livingstone called quinine "*the most constipating of drugs*". It causes constipation, but indeed, without quinine he and others would probably have succumbed to malaria much sooner than he did. g) The building of the Panama Canal came to a halt in 1889 when malaria and yellow fever struck.
[33] For example, the Frenchman Charles Marie de La Condamine sailed the Amazon river with cinchona seedlings, but his boat was wrecked where the Amazon flows into the Atlantic Ocean. His countryman and colleague of the French Geodesic Expedition, the Botanist Joseph de Jussieu collected plant samples and seeds, which were stolen in Buenos Aires a short time before his planned departure to Europe. The Botanist Weddel obtained some specimens of *Cinchona calisaya*, which he gave to the Dutch, who planted them in the Ciboda Gardens in Java.
[34] P. Blanchard, *Markham in Peru: The Travels of Clements R. Markham*, University of Texas, Austin, **1991**, p. 1852–1853.
[35] N. Taylor, *Cinchona in Java: The Story of Quinine*, Greenberg, New York, **1945**.
[36] C. Ledger, *Am. J. Pharm.* **1881**, *53*, 1; b) G. Gramiccia, *The Life of Charles Ledger (1818–1905): Alpacas and Quinine*, MacMillan Press, Basingstoke, **1988**; c) H. Hobhouse, *Seeds of Change. Five Plants that Transformed the World*, Papermac, London, **1992**.
[37] a) S. Garfield, *Mauve: How One Man Invented a Color That Changed the World*, Norton, New York, **2000**; b) A. W. Hofmann, *Report of the Royal College of Chemistry*, **1849**.
[38] M. Silverman, *Magic in a Bottle*, MacMillan, New York, **1944**.
[39] a) A. Kekulé, *Bull. Soc. Chim. Fr.* **1865**, *3*, 98; b) A. Kekulé, *Ann. Chem. Pharm.* **1866**, *137*, 129; c) J. H. Van't Hoff, *Ber. Dtsch. Chem. Ges.* **1876**, *9*, 1881; d) A. Kekulé, *Ann. Chem. Pharm.* **1872**, *162*, 77.
[40] J. Hudson, *The History of Chemistry*, Chapman and Hall, New York, **1992**, pp. 110–118.
[41] a) A. W. Williamson, *J. Chem. Soc.* **1852**, *4*, 106; b) A. W. Williamson, *J. Chem. Soc.* **1852**, *4*, 229.
[42] C. Gerhardt, *Ann. Chim. Phys.* **1853**, *37*, 285.
[43] A. Strecker, *Liebigs Ann. Chem.* **1854**, *91*, 155.
[44] For a retrospective personal account, see: a) W. H. Perkin, *J. Chem. Soc.* **1896**, *69*, 596; b) H. Armstrong, *J. Chem. Soc.* **1896**, *69*, 637.
[45] For an interesting discussion on serendipity and science, see: S. L. Glashow, *Contrib. Sci.* **2002**, *2*, 251.
[46] a) O. Meth-Cohn, M. Smith, *J. Chem. Soc. Perkin Trans. 1* **1994**, 5; b) O. Meth-Cohn, A. S. Travis, *Chem. Br.* **1995**, 547; c) O. Fischer, E. Hepp, *Ber. Dtsch. Chem. Ges.* **1888**, *21*, 2617; d) O. Fischer, E. Hepp, *Ber. Dtsch. Chem. Ges.* **1893**, *26*, 1194; e) O. Fischer, E. Hepp, *Liebigs Ann. Chem.* **1892**, *272*, 306; f) R. Nietzki, *Ber. Dtsch. Chem. Ges.* **1896**, *29*, 1442; g) small-scale syntheses of mauveine were reported by: R. L. Scaccia, D. Coughlin, D. W. Ball, *J. Chem. Educ.* **1998**, *75*, 769 and by T. M. Brown, C. J. Cooksey, A. T. Dronsfield, *Educ. Chem.* **2000**, *37*, 75.
[47] For an historical account on the early industrial chemistry, see: a) A. S. Travis, *The Rainbow Makers. The Origin of the Synthetic Dyestuff Industry in Western Europe*, Lehigh University Press, Bethlehem, **1993**; b) J. W. Stadelhofer, H. Vierrath, O. P. Krätz, *Chem. Ind.* **1988**, 515.
[48] For an image of a piece of silk dyed with an original batch of mauveine prepared by Perkin himself, see: H. S. Rzepa, *Molecules* **1998**, *3*, 94.
[49] W. V. Farrar, *Endeavour* **1974**, *33*, 149.

 © 2005 Wiley-VCH Verlag GmbH & Co. KGaA, Weinheim

[50] a) H. Caro, *Ber. Dtsch. Chem. Ges.* **1892**, *25*, 955; b) V. Deulofeu, *Cienc. Invest.* **1956**, *12*, 387.
[51] R. E. Rose, *J. Chem. Educ.* **1926**, *3*, 973.
[52] F. Wohler, *Ann. Phys. Chem.* **1828**, *12*, 253.
[53] a) W. A. Smit, A. F. Bochkov, A. Caple, *Organic Synthesis, The Science behind the Art*, The Royal Society of Chemistry, Cambridge, **1998**; b) J. A. Berson, *Chemical Creativity*: *Ideas from the Work of Woodward, Hückel, Meerwein and Others*, Wiley-VCH, Weinheim, **1999**; c) J. A. Berson, *Chemical Discovery and the Logician's Program*, *A Problematic Pairing*, Wiley-VCH, Weinheim, **2003**; d) J. A. Berson, *Angew. Chem.* **2000**, *112*, 3173; *Angew. Chem. Int. Ed.* **2000**, *39*, 3045; .
[54] a) R. Verpoorte in *The Cinchona Alkaloids* in *The Monoterpene Indole Alkaloids* (Ed.: J. E. Saxton), Wiley, New York, **1994**, Chap. 12, p. 647; b) G. Grethe, M. R. Uskokovic in *The Chemistry of Heterocyclic Compounds Vol. 23* (Ed.: J. E. Saxton), Wiley-Interscience, New York, **1983**, p. 279; c) G. Grethe, M. R. Uskokovic in *The Alkaloids*, *Vol. 14* (Ed.: R. H. F. Manske), Academic Press, New York, **1973**, pp. 181 – 223.
[55] The structure of quinotoxine was first documented by Rabe in 1909, see: P. Rabe, *Liebigs Ann. Chem.* **1909**, *365*, 366.
[56] E. C. Taylor, *Heterocyclic Chemistry* in *Foundations of Modern Organic Chemistry Series*, Prentice-Hall, Englewood Cliffs, NJ, **1968**.
[57] Z. H. Skraup, F. Konek von Norwall, *Ber. Dtsch. Chem. Ges.* **1893**, *26*, 1968; b) Z. H. Skraup, F. Konek von Norwall, *Monatsh. Chem.* **1894**, *15*, 37.
[58] a) O. Hesse, *Liebigs Ann. Chem.* **1880**, *205*, 314; b) W. J. Comstock, W. Königs, *Ber. Dtsch. Chem. Ges.* **1880**, *13*, 285; c) W. Königs, W. J. Comstock, *Ber. Dtsch. Chem. Ges.* **1884**, *17*, 1986; d) W. Königs, W. J. Comstock, *Ber. Dtsch. Chem. Ges.* **1885**, *18*, 1223; e) W. Königs, W. J. Comstock, *Ber. Dtsch. Chem. Ges.* **1892**, *25*, 1539.
[59] a) W. Zorn, *J. Prakt. Chem.* **1873**, *8*, 279; b) O. Hesse, *Liebigs Ann. Chem.* **1874**, *174*, 340; c) Z. H. Skraup, *Liebigs Ann. Chem.* **1880**, *201*, 324; d) W. J. Comstock, W. Königs, *Ber. Dtsch. Chem. Ges.* **1887**, *20*, 2510; e) Z. H. Skraup, *Monatsh. Chem.* **1891**, *12*, 431; f) E. Lippmann, F. Fleissner, *Monatsh. Chem.* **1891**, *12*, 327; g) E. Lippmann, F. Fleissner, *Monatsh. Chem.* **1891**, *12*, 661; h) A. Schubert, Z. H. Skraup, *Monatsh. Chem.* **1891**, *12*, 667; i) A. Christensen, *J. Prakt. Chem.* **1901**, *63*, 330; j) A. Christensen, *J. Prakt. Chem.* **1903**, *68*, 430; k) A. Christensen, *J. Prakt. Chem.* **1904**, *69*, 193.
[60] L. Seekles, *Rec. Trav. Chim.* **1923**, *42*, 69.
[61] a) E. Caventou, E. Willm, *Liebigs Ann. Chem.* **1870**, *7* (suppl), 247; b) Z. H. Skraup, G. Vortmann, *Liebigs Ann. Chem.* **1879**, *197*, 235; c) O. Hesse, *Ber. Dtsch. Chem. Ges.* **1881**, *14*, 1892; d) G. Kerner, *Jahresbericht* **1869**, 718; e) Z. H. Skraup, *Liebigs Ann. Chem.* **1879**, *199*, 348; f) G. Frost, C. Böhringer, *Ber. Dtsch. Chem. Ges.* **1882**, *15*, 1659; g) Z. H. Skraup, *Monatsh. Chem.* **1895**, *16*, 159; h) Z. H. Skraup, *Ber. Dtsch. Chem. Ges.* **1895**, *28*, 12.
[62] a) Z. H. Skraup, *Monatsh. Chem.* **1883**, *4*, 699; b) Z. H. Skraup, *Monatsh. Chem.* **1885**, *6*, 762.
[63] a) H. Wiedel, *Monatsh. Chem.* **1882**, *3*, 79; b) S. Hoogewerff, W. A. Van Dorp, *Rec. Trav. Chim.* **1883**, *2*, 10; c) O. Fischer, *Jahresbericht* **1885**, 1014; d) W. Pfitzinger, *J. Prakt. Chem.* **1902**, *66*, 263; e) A. Mengel, W. Königs, *Ber. Dtsch. Chem. Ges.* **1904**, *37*, 1322; f) W. Königs, A. Mengel, *Ber. Dtsch. Chem. Ges.* **1904**, *37*, 1328; g) A. Baeyer, *Ber. Dtsch. Chem. Ges.* **1879**, *12*, 460; h) A. Baeyer, *Ber. Dtsch. Chem. Ges.* **1879**, *12*, 1320; i) A. Baeyer, V. Drewsen, *Ber. Dtsch. Chem. Ges.* **1883**, *16*, 2207.
[64] a) H. Weidel, *Liebigs Ann. Chem.* **1874**, *173*, 76; W. Königs, *Ber. Dtsch. Chem. Ges.* **1879**, *12*, 97; c) Z. H. Skraup, *Ber. Dtsch. Chem. Ges.* **1879**, *12*, 330.
[65] a) Z. H. Skraup, *Ber. Dtsch. Chem. Ges.* **1879**, *12*, 1104; b) Z. H. Skraup, *Monatsh. Chem.* **1881**, *2*, 587.
[66] a) W. Königs, *Ber. Dtsch. Chem. Ges.* **1894**, *27*, 900; b) W. Königs, *Ber. Dtsch. Chem. Ges.* **1894**, *27*, 1501.
[67] a) W. Königs, *Liebigs Ann. Chem.* **1906**, *347*, 172; b) P. Rabe, *Liebigs Ann. Chem.* **1909**, *365*, 353.
[68] Z. Skraup, *Monatsh. Chem.* **1888**, *9*, 783; b) Z. H. Skraup, *Monatsh. Chem.* **1889**, *10*, 39; c) W. Königs, *Ber. Dtsch. Chem. Ges.* **1895**, *28*, 3150; d) W. Königs, *Ber. Dtsch. Chem. Ges.* **1895**, *28*, 1986; e) H. Schniderschitsch, *Monatsh. Chem.* **1889**, *10*, 54.
[69] W. Königs, *Ber. Dtsch. Chem. Ges.* **1895**, *30*, 1326.
[70] a) P. Rabe, *Liebigs Ann. Chem.* **1906**, *350*, 180; b) P. Rabe, *Liebigs Ann. Chem.* **1909**, *365*, 377; c) P. Rabe, A. McMillan, *Ber. Dtsch. Chem. Ges.* **1910**, *43*, 3308.
[71] a) W. von Miller, G. Rohde, *Ber. Dtsch. Chem. Ges.* **1894**, *27*, 1187; b) W. von Miller, G. Rohde, *Ber. Dtsch. Chem. Ges.* **1894**, *27*, 1280; c) W. von Miller, G. Rohde, *Ber. Dtsch. Chem. Ges.* **1895**, *28*, 1056; d) W. von Miller, G. Rohde, *Ber. Dtsch. Chem. Ges.* **1900**, *33*, 3214.
[72] W. Königs, *Ber. Dtsch. Chem. Ges.* **1890**, *23*, 2669.
[73] P. Rabe, E. Ackerman, W. Schneider, *Ber. Dtsch. Chem. Ges.* **1907**, *40*, 3655.
[74] a) P. Rabe, *Ber. Dtsch. Chem. Ges.* **1908**, *41*, 62; b) Rabe's original numbering of the cinchona alkaloids skeleton is used today.
[75] J. Kenner, *Ann. Rep. Chem. Soc.* **1922**, *19*, 157.
[76] a) O. Hesse, *Liebigs Ann. Chem.* **1893**, *276*, 88; b) Z. H. Skraup, *Monatsh. Chem.* **1901**, *22*, 1097; c) P. Rabe, B. Böttcher, *Ber. Dtsch. Chem. Ges.* **1917**, *50*, 127; d) E. Jungfleisch, E. Léger, *Ann. Chim.* **1920**, *14*, 59; e) E. Léger, *Bull. Soc. Chim.* **1938**, *5*, 183; f) M. Pfannl, *Monatsh. Chem.* **1911**, *32*, 241; g) T. A. Henry, W. Solomon, E. M. Gibbs, *J. Chem. Soc.* **1935**, 966; h) T. Dománski, J. Suszko, *Rec. Trav. Chim.* **1935**, *54*, 481.
[77] W. Leithe, *Ber. Dtsch. Chem. Ges.* **1932**, *65*, 660; b) K. Freundenberg, *J. Am. Chem. Soc.* **1932**, *54*, 234.
[78] a) V. Prelog, E. Zalan, *Helv. Chim. Acta* **1944**, *27*, 535; b) V. Prelog, E. Zalan, *Helv. Chim. Acta* **1944**, *27*, 545.
[79] A. Kaufmann, E. Rothlin, P. Brunnschweiler, *Ber. Dtsch. Chem. Ges.* **1916**, *49*, 2302.
[80] S. F. Thomas in *The Total Synthesis of Natural Products*, *Vol. 2* (Ed.: J. ApSimon), Wiley, New York, **1973**, pp. 149 – 154.
[81] This approach is often still used today and has been important in reassigning a host of structures recently, see for example: a) L. Hanus, S. Abu-Lafi, E. Fride, A. Breuer, Z. Vogel, D. E. Shalev, I. Kustanovich, R. Mechoulam, *Proc. Natl. Acad. Sci. USA* **2001**, *98*, 3662; b) J. Desire, J. Prandi, *Carbohydr. Res.* **1999**, *317*, 110; c) T. Akihisa, Y. Kimura, T. Tamura, *Phytochemistry*, **1998**, *47*, 1107; d) H. R. Sonawane, A. V. Pol, P. P. Moghe, A. Sudalai, S. S. Biswas, *Tetrahedron Lett.* **1994**, *35*, 8877; e) K. Mori, N. Murata, *Liebigs Ann. Chem.* **1994**, 637; f) D. Tanner, P. G. Andersson, L. Tedenborg, P. Somfai, *Tetrahedron* **1994**, *50*, 9135; g) N. Valls, M. Vallribera, M. Font-Bardía, X. Solans, J. Bonjoch, *Tetrahedron: Asymmetry* **2003**, *14*, 1241; h) M. Y. Rios, G. Delgado, R. A. Toscano, *Tetrahedron* **1998**, *54*, 3355; i) P. Hanhinen, M. Lounasmaa, *J. Nat. Prod.* **2001**, *64*, 686; j) Z. Xiong, E. J. Corey, *J. Am. Chem. Soc.* **2000**, *122*, 4831; k) N. Toyooka, A. Fukutome, H. Nemoto, J. W. Daly, T. F. Spande, H. M. Garraffo, T. Kaneko, *Org. Lett.* **2002**, *4*, 1715; l) H. Kigoshi, M. Kita, S. Ogawa, M. Itoh, D. Uemura, D. *Org. Lett.* **2003**, *5*, 957; m) A. K. Ghosh, G. Gong, *J. Am. Chem. Soc.* **2004**, *126*, 3704.
[82] a) P. Rabe, *Ber. Dtsch. Chem. Ges.* **1911**, *44*, 2088; b) P. Rabe, *Angew. Chem.* **1913**, *26*, 543.
[83] P. Rabe, R. Pasternack, *Ber. Dtsch. Chem. Ges.* **1913**, *46*, 1032.
[84] P. Rabe, K. Kindler, *Ber. Dtsch. Chem. Ges.* **1918**, *51*, 466; this article briefly mentions that the conditions for the transformation of quinotoxine to quininone (now known to be quinidi-

 © 2005 Wiley-VCH Verlag GmbH & Co. KGaA, Weinheim

none) were the same as those used for the related conversion of cinchotoxine into cinchoninone seven years before (see ref. [82]).
[85] P. Rabe, *Liebigs Ann. Chem.* **1932**, *492*, 242.
[86] P. Rabe, W. Huntenberg, A. Schultze, G. Volger, *Ber. Dtsch. Chem. Ges.* **1931**, *64*, 2487.
[87] P. Ball, *Chem. Br.* **2001**, *October 26*.
[88] a) A. Kaufmann, M. Huber, *Ber. Dtsch. Chem. Ges.* **1913**, *46*, 2913; b) A. Kaufmann, P. Haensler, *Ber. Dtsch. Chem. Ges.* **1917**, *50*, 702.
[89] R. B. Woodward, N. L. Wendler, F. J. Brutshy, *J. Am. Chem. Soc.* **1945**, *67*, 1425.
[90] R. Ludwiczakówna, *Rocz. Chem.* **1948**, *22*, 138; *Chem. Abstr.* **1949**, *44*, 7628.
[91] J. Gutzwiller, M. R. Uskokovic, *Helv. Chim. Acta* **1973**, *56*, 1494.
[92] a) A. E. Remick, *Electronic Interpretation of Organic Chemistry*, Wiley, New York, **1943**, p. iii; b) L. B. Slater, *Stud. Hist. Phil. Sci.* **2002**, *33*, 1.
[93] a) S. Turner, *The Design of Organic Synthesis*, Elsevier, Amsterdam, **1976**; b) I. Fleming, *Selected Organic Syntheses*, Wiley, London, **1977**.
[94] R. B. Woodward, G. Singh, *J. Am. Chem. Soc.* **1950**, *72*, 1428.
[95] R. B. Woodward, F. Sondheimer, D. Taub, K. Heusler, W. M. McLamore , *J. Am. Chem. Soc.* **1952**, *74*, 4223.
[96] R. B. Woodward, A. A. Patchett, D. H. R. Barton, D. A. H. Ives, R. B. Kelly, *J. Am. Chem. Soc.* **1954**, *76*, 2852.
[97] a) E. C. Kornfield, E. J. Fornefeld, G. B. Kline, M. H. Mann, R. G. Jones, R. B. Woodward, *J. Am. Chem. Soc.* **1954**, *76*, 5256; b) R. B. Woodward, M. P. Cava, W. D. Ollis, A. Hunger, H. U. Daeniker, K. Schenker, *J. Am. Chem. Soc.* **1954**, *76*, 4749; c) R. B. Woodward, M. P. Cava, W. D. Ollis, A. Hunger, H. U. Daeniker, K. Schenker, *Tetrahedron* **1963**, *19*, 247.
[98] a) R. B. Woodward, F. E. Bader, H. Bickel, A. J. Frey, R. W. Kierstead, *J. Am. Chem. Soc.* **1956**, *78*, 2023; b) R. B. Woodward, F. E. Bader, H. Bickel, A. J. Frey, R. W. Kierstead, *J. Am. Chem. Soc.* **1956**, *78*, 2657; c) R. B. Woodward, F. E. Bader, H. Bickel, A. J. Frey, R. W. Kierstead, *Tetrahedron* **1958**, *2*, 1.
[99] R. B. Woodward, G. A. Iacobucci, F. A. Hochstein, *J. Am. Chem. Soc.* **1959**, *81*, 4434.
[100] a) R. B. Woodward, W. A. Ayer, J. M. Beaton, F. Bickelhaupt, R. Bonnett, P. Buchschacher, G. L. Closs, H. Dutler, J. Hannah, F. P. Hauck, S. Itô, A. Langermann, E. Le Goff, W. Leimgruber, W. Lwowski, J. Sauer, Z. Valenta, H. Volz, *J. Am. Chem. Soc.* **1960**, *82*, 3800; b) R. B. Woodward, *Pure Appl. Chem.* **1961**, *2*, 383; c) R. B. Woodward, W. A. Ayer, J. M. Beaton, F. Bickelhaupt, R. Bonnett, P. Buchschacher, G. L. Closs, H. Dutler, J. Hannah, F. P. Hauck, S. Itô, A. Langermann, E. Le Goff, W. Leimgruber, W. Lwowski, J. Sauer, Z. Valenta, H. Volz, *Tetrahedron* **1990**, *46*, 7599.
[101] L. H. Conover, K. Butler, J. D. Johnston, J. J. Korst, R. B. Woodward, *J. Am. Chem. Soc.* **1962**, *84*, 3222.
[102] R. B. Woodward, *The Harvey Lectures*, *Vol. 31*, Academic Press, New York, **1965**.
[103] a) R. B. Woodward, K. Heusler, J. Gosteli, P. Naegeli, W. Oppolzer, R. Ramage, S. Rangeanathan, H. Vorbruggen, *J. Am. Chem. Soc.* **1966**, *88*, 852; b) R. B. Woodward, *Science* **1966**, *153*, 487.
[104] R. B. Woodward, J. Gosteli, I. Ernest, R. J. Friary, G. Nestler, H. Raman, R. Sitrin, C. Suter, J. K. Whitesell, *J. Am. Chem. Soc.* **1973**, *95*, 6853.
[105] R. B. Woodward, *Pure Appl. Chem.* **1968**, *17*, 519; b) R. B. Woodward, *Pure Appl. Chem.* **1971**, *25*, 283; c) R. B. Woodward, *Pure Appl. Chem.* **1973**, *33*, 145; d) A. Eschenmoser, C. E. Wintner, *Science* **1977**, *196*, 1410; e) A. Eschenmoser, *Pure Appl. Chem.* **1963**, *7*, 297; f) A. Eschenmoser, *Pure Appl. Chem.* **1971**, *15*, 69; g) A. Eschenmoser, *Naturwissenschaften* **1974**, *61*, 513.
[106] a) R. B. Woodward, E. Logusch, K. P. Nambiar, K. Sakan, D. E. Ward, B. W. Au-Yeung, P. Balaram, L. J. Browne, P. J. Kard, C. H. Chen, *J. Am. Chem. Soc.* **1981**, *103*, 3210; b) R. B. Woodward, B. W. Au-Yeung, P. Balaram, L. J. Browne, D. E. Ward, P. J. Card, C. H. Chen, *J. Am. Chem. Soc.* **1981**, *103*, 3213; c) R. B. Woodward, E. Logusch, K. P. Nambiar, K. Sakan, D. E. Ward, B. W. Au-Yeung, P. Balaram, L. J. Browne, P. J. Card, C. H. Chen, *J. Am. Chem. Soc.* **1981**, *103*, 3215.
[107] R. B. Woodward in *The Chemistry of Penicillin* (Eds.: H. T. Clarke, J. R. Johnson, R. Robinson), Princeton University Press, Princeton, NJ, **1949**, p. 443.
[108] R. B. Woodward, G. Singh, *J. Am. Chem. Soc.* **1949**, *71*, 758.
[109] a) R. B. Woodward, W. J. Brehm, A. L. Nelson, *J. Am. Chem. Soc.* **1947**, *69*, 2250; b) R. B. Woodward, W. J. Brehm, *J. Am. Chem. Soc.* **1948**, *70*, 2107.
[110] a) M. Schach von Wittenau, R. K. Blackwood, L. H. Conover, R. H. Glauert, R. B. Woodward, *J. Am. Chem. Soc.* **1965**, *87*, 134; b) F. A. Hochstein, C. R. Stephens, L. H. Conover, P. P. Regna, R. Pasternack, K. J. Brunings, R. B. Woodward, *J. Am. Chem. Soc.* **1952**, *74*, 3708.
[111] a) P. P. Regna, F. A. Hochstein, R. L. Wagner, Jr, R. B. Woodward, *J. Am. Chem. Soc.* **1953**, *75*, 4625; b) R. B. Woodward, *Angew. Chem.* **1957**, *69*, 50.
[112] B. Riniker, J. Kalvoda, D. Arigoni, A. Fürst, O. Jeger, A. M. Gold, R. B. Woodward, *J. Am. Chem. Soc.* **1954**, *76*, 313.
[113] M. R. Bell, J. R. Johnson, B. S. Wildi, R. B. Woodward, *J. Am. Chem. Soc.* **1958**, *80*, 1001.
[114] R. B. Woodward, N. Yand, T. J. Katz, *Proc. Chem. Soc. London* **1960**, 76.
[115] F. A. Hochstein, H. Els, W. D. Celmer, B. L. Shapiro, R. B. Woodward, *J. Am. Chem. Soc.* **1960**, *82*, 3225.
[116] V. Rao Koppaka, K. Biemann, R. B. Woodward, *J. Am. Chem. Soc.* **1963**, *85*, 2532.
[117] a) R. B. Woodward, *Pure Appl. Chem.* **1964**, *9*, 49; b) R. B. Woodward, J. Zanos Gougoutas, *J. Am. Chem. Soc.* **1964**, *86*, 5030.
[118] a) R. B. Woodward, F. J. Brutschy, H. Baer, *J. Am. Chem. Soc.* **1948**, *70*, 4216; b) R. B. Woodward, E. G. Kovach, *J. Am. Chem. Soc.* **1950**, *72*, 1009; c) R. B. Woodward, B. Witkop, *J. Am. Chem. Soc.* **1949**, *71*, 379; d) C. Djerassi, M. Gorman, S. C. Pakrashi, R. B. Woodward, *J. Am. Chem. Soc.* **1956**, *78*, 1259; e) R. B. Woodward, B, Witkop, *J. Am. Chem. Soc.* **1948**, *70*, 2409; f) R. B. Woodward, R. B. Loftfield, *J. Am. Chem. Soc.* **1941**, *63*, 3167; g) R. B. Woodward, P. Yates, *J. Am. Chem. Soc.* **1963**, *85*, 551.
[119] R. B. Woodward, L. S. Weiler, P. C. Dutta, *J. Am. Chem. Soc.* **1965**, *87*, 4662.
[120] R. B. Woodward, K. Bloch, *J. Am. Chem. Soc.* **1953**, *75*, 2023.
[121] a) R. B. Woodward, *J. Am. Chem. Soc.* **1941**, *63*, 1123; b) R. B. Woodward, A. F. Clifford, *J. Am. Chem. Soc.* **1941**, *63*, 2727; c) R. B. Woodward, *J. Am. Chem. Soc.* **1942**, *64*, 72; d) R. B. Woodward, *J. Am. Chem. Soc.* **1942**, *64*, 76.
[122] A. Todd, *A Time to Remember*, University Press, New York, **1983**.
[123] a) R. B. Woodward, R. Hoffmann, *The Conservation of Orbital Symmetry*, VCH, Weinheim, 1970; b) R. B. Woodward, R. Hoffmann, *Angew. Chem.* **1969**, *81*, 797; *Angew. Chem. Int. Ed. Engl.* **1969**, *8*, 781.
[124] a) For an account on the ferrocene controversy with Geoffrey Wilkinson, see: T. M. Zydowsky, *Chem. Intell.* **2000**, *6*, 29; b) P. Laszlo, R. Hoffmann, *Angew. Chem.* **2000**, *112*, 127; *Angew. Chem. Int. Ed.* **2000**, *39*, 123.
[125] a) O. T. Benfey, P. J. T. Morris, *Robert Burns Woodward: Architect and Artist in the World of Molecules*, Chemical

Heritage Foundation, Philadelphia, **2001**; b) G. Stork, *Nature* **1980**, *284*, 383.

[126] F. R. Fosberg, *Econ. Bot.* **1947**, *1*, 330.

[127] The quinine supply, principally from the bark of the cinchona tree grown in Java, was interrupted during WWI, and the Germans mounted a research program to find and synthesize useful substitutes. Chloroquine and atabrine (mepacrine), a compound with some chemical similarities to quinine, resulted from these investigations. In spite of its side effects and tendency to impart a sickly color to the skin, atabrine was the standard american antimalarial drug during WWII.

[128] V. K. McElheny, *Insisting on the Impossible, the Life of Edwin Land*, Perseus Book Group, New York, **1998**.

[129] a) D. Arigoni, J. D. Dunitz, A. Eschenmoser, *Vladimir Prelog, Biographical Memoirs of Fellows*, Royal Society of London, **2000**, *46*, pp. 443–464; b) the Nobel Prize was awarded to Prelog "*for his research into the stereochemistry of organic molecules and reactions*".

[130] a) M. Proštenik, V. Prelog, *Helv. Chim. Acta* **1943**, *26*, 1965; b) Prelog's reconstitution of quinotoxine was based on the assumption that the Rabe protocol was suitable for the synthesis of quinine.

[131] a) P. Fritsch, *Liebigs Ann. Chem.* **1895**, *286*, 10; b) C. Pomeranz, *Monatsh. Chem.* **1893**, *14*, 116.

[132] J. W. Cornforth, R. Robinson *J. Chem. Soc.* **1942**, 682.

[133] R. P. Linstead, W. E. Doering, S. B. Davis, P. Levine, R. R. Whetstone, *J. Am. Chem. Soc.* **1942**, *64*, 1985.

[134] a) C. E. Fawsitt, *Z. Physik. Chem.* **1902**, *41*, 610; b) C. E. Fawsitt, *J. Chem. Soc.* **1905**, *87*, 494.

[135] a) A. Pictet, R. R. Misner, *Ber. Dtsch. Chem. Ges.* **1912**, *45*, 1800; b) A. Kaufmann, H. Peyer, *Ber. Dtsch. Chem. Ges.* **1912**, *45*, 1805.

[136] a) W. T. Haskins, C. S. Hudson, *J. Am. Chem. Soc.* **1939**, *61*, 1266; b) C. L. Butler, L. H. Cretcher, *J. Am. Chem. Soc.* **1933**, *55*, 2605.

[137] W. M. Lawrence, *The New York Times*, May 4, **1944**.

[138] H. Manchester, *Sci. News Lett.* **1944**, 378.

[139] The hype of that glorious moment was such that over four days Woodward and Doering re-enacted each step of their synthesis in front of a photographer, showing glassware, apparatus, crystalline products, and even molecular models of the intermediates. The journalist Gerard Piel, who covered this accomplishment, perhaps influenced by Woodward, developed an active interest in science and went on to found the modern journal *Scientific American*.

[140] W. E. Doering, "*I get sick thinking of the details, but we worked fourteen months—February first, 1943, to April eleventh, 1944, at eleven AM sharp—Boy what a moment!*", quoted in *New Yorker,* **1944**, *May 13*, 20.

[141] In the 1945 fullpaper, Woodward and Doering state: "*It was then found that it was possible to effect the reconversion first to cinchotoxine, and later of quinotoxine, into cinchonine and quinine. Quinotoxine was converted by action of sodium hypobromite into N-bromoquinotoxine, which was cyclized by alkali, with loss of hydrogen bromide, to give quininone. Reduction of the ketone with aluminum powder and ethanol in the presence of sodium ethoxide gave a mixture of stereoisomeric alcohols, from which both quinine and quinidine were isolated*"; later in the paper, they add: "*There remained the task of carrying out a total synthesis of quinine. The problem had been simplified by the work described above to one of the synthesis of quinotoxine. Further, at the outset of our work, it seemed highly probable, in view of the conversion by Rabe of homocincholoipon (dihydrohomomeroquinene) to dihydroquinotoxine, that homomeroquinene would be transformable to quinotoxine, and accordingly our efforts were directed to the synthesis of [homomeroquinene]. This further simplification of the synthetic objective was subsequently established by Prelog, who prepared homomeroquinene by degradation of natural cinchonine, and converted it, by Rabe's method, to quinotoxine*".

[142] a) H. C. Kolb, M. S. Van Nieuwenhze, K. B. Sharpless, *Chem. Rev.* **1994**, *94*, 2483; b) O. Raint, H. B. Kagan, *Tetrahedron Lett.* **1988**, *30*, 7403; c) S. Kobayashi, Y. Tsuchiya, T. Mukaiyama, *Chem. Lett.* **1991**, 541; d) H. Wynberg, *Top. Curr. Stereochem.*, Wiley, New York, **1986**, p. 87; e) S. Takeuchi, Y. Ohgo, *Chem. Lett.* **1988**, 403; f) A. Sera, K. Takagi, H. Katayama, H. Yamada, K. Matsumoto, *J. Org. Chem.* **1988**, *53*, 1157; g) H. U. Basler, S. K. Boyer, U. Pittelkow, *Tetrahedron: Asymmetry* **1991**, *2*, 721; h) H. Wynberg, A. G. J. Staring, *J. Chem. Soc. Chem. Commun.* **1984**, 1181; i) N. Künzle, A. Szabo, M. Schürch, G. Wang, T. Mallat, A. Baiker, *Chem. Commun.* **1998**, 1377.

[143] a) J. Jacques, A. Collet, S. H. Wilen, *Enantiomers, Racemates and Resolution*, Wiley, New York, **1981**, pp. 254, 257; b) for a review on the use of cinchona alkaloids in asymmetric synthesis, see: K. Kacprzak, J. Gawronski, *Synthesis* **2001**, 961; c) about 25% of the resolutions recorded in the chemical literature have been carried out with cinchona alkaloids.

[144] a) P. Salvador, C. Rosini, D. Pini, C. Bertucci, P. Altemura, G. Uccello-Baretta, A. Rafaelli, *Tetrahedron* **1987**, *43*, 4969; b) S. Schefzick, W. Lindner, K. B. Lipkowitz, M. Jalaie, *Chirality* **2000**, *12*, 7; c) R. Bhushan, M. Arora, *Biomed. Chromatogr.* **2001**, *15*, 433; d) A. M. Stalcup, K. H. Gahm, *J. Microcolumn Sep.* **1996**, *8*, 145.

[145] a) *Pharmaceutical Substances: Syntheses, Patents, Applications, 4th Edition* (Eds.: A. Kleemann, J. Engel, B. Kutscher, D. Reichert), Georg Thieme Verlag, New York, **2001**; b) *Chirality in Industry. II. Development in the Commercial Manufacture and Applications of Optically Active Compounds* (Eds.: A. N. Collins, G. N. Sheldrake, J. Crosby), Wiley, Chichester, **1997**.

[146] H. Gilman, T. S. Soody, *J. Org. Chem.* **1958**, *23*, 1584.

[147] a) G. Grethe, J. Gutzwiller, H. L. Lee, M. R. Uskokovic, *Helv. Chim. Acta* **1972**, *55*, 1044; b) G. Grethe, H. L. Lee, T. Mitt, M. R. Uskokovic, *Helv. Chim. Acta* **1973**, *56*, 1485.

[148] K. N. Campbell, I. J. Schaffner, *J. Am. Chem. Soc.* **1945**, *67*, 86.

[149] W. E. Doering, R. A. N. Weil, *J. Am. Chem. Soc.* **1947**, *69*, 2461.

[150] a) W. Koenigs, *Ber. Dtsch. Chem. Ges.* **1896**, *29*, 372; b) P. Rabe, E. Kuliga, O. Marschall, W. Naumann, W. F. Russell, *Liebigs Ann. Chem.* **1910**, *373*, 85.

[151] a) O. L. Russell, E. G. Janzen, A. G. Bemis, E. J. Geels, A. J. Moye, S. Mak, E. T. Strom, *Oxidation of Hydrocarbons in Basic Solutions*, *Adv. Chem. Ser.* **1965**, *51*, 112; b) G. A. Russell, A. G. Bemis, E. J. Geels, E. G. Janzen, A. J. Moye, *Advances in—Chemistry Series*, *No. 75*, American Chemical Society, Washington, **1968**, p. 174.

[152] J. Gutzwiller, M. R. Uskokovic, *J. Am. Chem. Soc.* **1978**, *100*, 576.

[153] a) J. Gutzwiller, M. R. Uskokovic, *J. Am. Chem. Soc.* **1970**, *92*, 203; b) J. Gutzwiller, M. R. Uskokovic, *J. Am. Chem. Soc.* **1970**, *92*, 204.

[154] a) E. C. Taylor, S. F. Martin, *J. Am. Chem. Soc.* **1972**, *94*, 6218; b) E. C. Taylor, S. F. Martin, *J. Am. Chem. Soc.* **1974**, *96*, 8095; c) E. C. Taylor, S. F. Martin, *J. Am. Chem. Soc.* **1974**, *96*, 2874.

[155] M. Gates, B. Sugavanam, W. L. Schreiber, *J. Am. Chem. Soc.* **1970**, *92*, 205.

[156] W. E. Doering, J. D. Chanley, *J. Am. Chem. Soc.* **1946**, *68*, 586.

[157] a) A. Kirmann, P. Duhamel, R. Nouri-Bimorghi, *Bull. Soc. Chim. Fr.* **1964**, 3264; b) P. Duhamel, L. Duhamel, J. Gralak, *Bull. Soc. Chim. Fr.* **1970**, 3641.

[158] a) G. Grethe, H. L. Lee, T. Mitt, M. R. Uskokovic, *J. Am. Chem. Soc.* **1978**, *100*, 581; b) G. Grethe, H. L. Lee, T. Mitt, M. R. Uskokovic, *J. Am. Chem. Soc.* **1978**, *100*, 589.

[159] a) G. Grethe, H. L. Lee, T. Mitt, M. R. Uskokovic, *J. Am. Chem. Soc.* **1971**, *93*, 5904; b) G. Grethe, H. L. Lee, T. Mitt,

 © 2005 Wiley-VCH Verlag GmbH & Co. KGaA, Weinheim

M. R. Uskokovic, *Synth.Commun.* **1972**, *2*, 55; c) R. L. Augustine, S. F. Wanat, *Synth. Commun.* **1971**, *1*, 241.
[160] a) A. Barco, S. Benetti, C. Risi, G. P. Pollini, R. Romagnoli, G. Spalluto, V. Zanirato, *Tetrahedron* **1994**, *50*, 2583; b) B. Danieli, G. Lesma, M. Mauro, G. Palmisano, D. Passarella, *Tetrahedron: Asymmetry* **1990**, *1*, 793; c) S. Hanessian, A.-M. Faucher, S. Léger, *Tetrahedron* **1990**, *46*, 231; d) S. R. Wilson, M. J. Di Grandi, *J. Org. Chem.* **1991**, *56*, 4767; e) R. T. Brown, J. Leonard, *Tetrahedron Lett.* **1978**, *19*, 1605; f) S. E. Yoo, K. Y. Yi, S.-H. Lee, N. Jeong, *Synlett* **1990**, 575; g) S. Takano, M. Takahashi, S. Hatake-Yama, K. Ogasawara, *J. Chem. Soc. Chem. Commun.* **1979**, 556; h) R. L. Funk, J. D. Munger, Jr, *J. Org. Chem.* **1984**, *49*, 4319; i) M. Uskokovic, C. Reese, H. L. Lee, G. Grethe, J. Gutzwiller, *J. Am. Chem. Soc.* **1971**, *93*, 5902; j) M. R. Uskokovic, T. Henderson, C. Reese, H. L. Lee, G. Grethe, J. Gutzwiller, *J. Am. Chem. Soc.* **1978**, *100*, 571; k) T. Imanishi, T. Inoue, Y. Wada, M. Hanaoka, *Chem. Pharm. Bull.* **1982**, *30*, 1925; l) T. Imanishi, T. Inoue, Y. Wada, M. Hanaoka, *Chem. Pharm. Bull.* **1983**, *31*, 1551; m) R. T. Brown, J. Leonard, *J. Chem. Soc. Chem. Commun.* **1978**, 725.
[161] R. L. Augustine, *J. Org. Chem.* **1958**, *23*, 1853.
[162] E. H. Whie, *J. Am. Chem. Soc.* **1955**, *77*, 6014.
[163] a) R. Huisgen, J. Reinertshofer, *Liebigs Ann. Chem.* **1952**, *575*, 174; b) R. Huisgen, J. Reinertshofer, *Liebigs Ann. Chem.* **1952**, *575*, 197.
[164] a) G. Stork, S. M. McElvain, *J. Am. Chem. Soc.* **1946**, *68*, 1053; b) G. Stork, E. E. Van Tamelen, L. J. Friedman, A. W. Burgstahler, *J. Am. Chem. Soc.* **1951**, *73*, 4501.
[165] M. E. Wolff, *Chem. Rev.* **1963**, *63*, 55.
[166] a) The *cis* configuration of the 3,4-disubstituted piperidine was confirmed more than 20 years after its synthesis by Stork, see: R. J. Sundberg, F. Hollcomb, *J. Org. Chem.* **1969**, *34*, 3273; b) for a summary of the major achievements in regio- and stereocontrolled synthesis by Stork's research group, see: G. Stork, *Med. Res. Rev.* **1999**, *19*, 370.
[167] a) F. Ishibashi, E. Taniguchi, *Bull. Chem. Soc. Jpn.* **1988**, *61*, 4361; b) K. Kondo, E. Mori, *Chem. Lett.* **1974**, 741.
[168] a) G. Stork, D. Niu, R. A. Fujimoto, E. R. Koft, J. M. Balkovec, J. R. Tata, G. R. Dake, *J. Am. Chem. Soc.* **2001**, *123*, 3239; b) for a discussion of Stork's synthesis of quinine, see: G. Appendino, F. Zanardi, G. Casiraghi, *Chemtracts: Org. Chem.* **2002**, *15*, 175; c) for an interesting comment on Stork's synthesis, see: S. M. Weinreb, *Nature* **2001**, *411*, 429.
[169] a) B. Lal, B. M. I. Pramanik, M. S. Manhas, A. K. Bose, *Tetrahedron Lett.* **1977**, *18*, 1977; b) D. L. Hughes, *Org. Prep. Proced. Int.* **1996**, *28*, 129.
[170] a) N. Knouzi, M. Vaultier, R. Carrie, *Bull. Soc. Chim. Fr.* **1985**, 815; b) for a related sequence, see: W. H. Pearson, S. C. Bergmeier, J. P. Williams, *J. Org. Chem.* **1992**, *57*, 3977.
[171] a) J. Valls, E. Toromanoff, *Bull. Soc. Chim. Fr.* **1961**, 758; b) E. Toromanoff, *Bull. Soc. Chim. Fr.* **1966**, 3357; c) P. Deslongchamps, *Stereoelectronic Effects in Organic Chemistry*, Pergamon, New York, **1983**, p. 211.
[172] A. M. Rouhi, *Chem. Eng. News* **2001**, *79*(19), 54 – 55.
[173] *Chem. Eng. News* **2001**, *79*(19), 56.
[174] Gutzwiller and Uskokovic were able to produce an inseparable mixture of *N*-benzoyl-8-chloroquinotoxines by chlorination of *N*-benzoylquinotoxine. Reduction with $NaBH_4$ stereoselectively afforded the corresponding *threo* chlorohydrins, which upon treatment with KOH gave a mixture of *N*-benzoyl-*cis*,*erythro*-epoxides. Since they were the wrong diastereomeric epoxides, their cyclization furnished *epi*-quinine and *epi*-quinidine (50% yield from the chlorohydrins) and only traces of quinine and quinidine.
[175] E. J. Corey, G. A. Reichard, *Tetrahedron Lett.* **1989**, *30*, 5297.
[176] I. T. Raheem, S. N. Goodman, E. N. Jacobsen, *J. Am. Chem. Soc.* **2004**, *126*, 706.
[177] S. N. Goodman, E. N. Jacobsen, *Adv. Synth. Catal.* **2002**, *344*, 953.
[178] J. E. Baldwin, P. G. Bulger, R. Marquez, *Tetrahedron* **2002**, *58*, 5441.
[179] M. S. Taylor, E. N. Jacobsen, *J. Am. Chem. Soc.* **2003**, *125*, 11204.
[180] S. V. Ley, J. Norman, W. P. Griffith, S. P. Marsden, *Synlett* **1994**, 639.
[181] K. Takai, N. Shinomiya, H. Kaihara, N. Yoshida, T. Moriwake, *Synlett* **1995**, 963.
[182] K. C. Nicolau, J. L. Gross, M. A. Kerr, *J. Heterocycl. Chem.* **1996**, *33*, 735.
[183] K. B. Sharpless, W. Amberg, Y. L. Bennani, G. A. Crispino, J. Hartung, K. Jeong, H. Kwong, K. Morikawa, Z. Wang, D. Xu, X. Zhang, *J. Org. Chem.* **1992**, *57*, 2768.
[184] H. C. Kolb, K. B. Sharpless, *Tetrahedron* **1992**, *48*, 10515.
[185] A. Murai, T. Tsujimoto, *Synlett* **2002**, 1283.
[186] The use of microwaves resulted in shorter reaction times, see: a) R. T. Brown, D. Curless, *Tetrahedron Lett.* **1986**, *27*, 6005; b) A. Solange, *Tetrahedron* **1994**, *50*, 3327; c) B. Lygo, J. Crosby, R. Terence, P. G. Wainwright, *Tetrahedron Lett.* **1997**, *38*, 2343.
[187] J. Igarashi, M. Katsukawa, Y.-G. Wang, H. P. Acharya, Y. Kobayashi, *Tetrahedron Lett.* **2004**, *45*, 3783.
[188] a) T. Sugai, K. Mori, *Synthesis* **1988**, 19; b) K. Laumen, M. P. Schneider, *J. Chem. Soc. Chem. Commun.* **1986**, 1298.
[189] a) Y. Kobayashi, *Curr. Org. Chem.* **2003**, *7*, 133; b) Y. Kobayashi, *Trends*, *Org. Chem.* **1998**, *7*, 27; c) D. R. Deardorff, R. G. Linde, A. M. Martin, M. J. Sjulman, *J. Org. Chem.* **1989**, *54*, 2759.
[190] H. P. Acharya, Y. Kobayashi, *Tetrahedron Lett.* **2004**, *45*, 1199.
[191] P. A. Grieco, S. Gilman, M. Nishizawa, *J. Org. Chem.* **1976**, *41*, 1485.
[192] K. N. Campbell, R. S. Tipson, R. C. Elderfield, B. K. Campbell, M. A. Clapp, W. J. Gensler, D. Morrison, W. J. Moran, *J. Org. Chem.* **1946**, *11*, 803.
[193] R. Unno, H. Michishita, H. Inagaki, Y. Suzuki, Y. Baba, T. Jomori, M. Moku, T. Nishikawa, M. Isobe, *Bioorg. Med. Chem.* **1997**, *5*, 903.
[194] a) R. W. Armstrong, J.-M. Beau, S. H. Cheon, W. J. Christ, H. Fujioka, W.-H. Ham, L. D. Hawkins, H. Jin, S. H. Kang, Y. Kishi, M. J. Martinelli, W. W. McWhorter, Jr, M. Mizuno, M. Nakata, A. E. Stutz, F. X. Talamas, M. Taniguchi, J. A. Tino, K. Ueda, J.-I. Uenishi, J. B. White, M. Yonaga, *J. Am. Chem. Soc.* **1989**, *111*, 7525; b) R. W. Armstrong, J.-M. Beau, S. H. Cheon, W. J. Christ, H. Fujioka, W.-H. Ham, L. D. Hawkins, H. Jin, S. H. Kang, Y. Kishi, M. J. Martinelli, W. W. McWhorter, Jr, M. Mizuno, M. Nakata, A. E. Stutz, F. X. Talamas, M. Taniguchi, J. A. Tino, K. Ueda, J.-I. Uenishi, J. B. White, M. Yonaga, *J. Am. Chem. Soc.* **1989**, *111*, 7530; c) E. M. Suh, Y. Kishi, *J. Am. Chem. Soc.* **1994**, *116*, 11295; d) E. J. Corey, D. Gin, R. S. Kania, *J. Am. Chem. Soc.* **1996**, *118*, 9202; e) K. C. Nicolaou, Z. Yang, J.-J. Liu, H. Ueno, P. G. Nantermet, R. K. Guy, C. F. Claiborne, J. Renaud, E. A. Couladouros, K. Paulvannan, E. J. Sorensen, *Nature*, **1994**, *367*, 630; f) K. C. Nicolaou, P. G. Nantermet, H. Ueno, R. K. Guy, E. A. Couladouros, K. Paulvannan, E. J. Sorensen, *J. Am. Chem. Soc.* **1995**, *117*, 624; g) K. C. Nicolau, J.-J. Liu, Z. Yang, H. Ueno, E. J. Sorensen, C. F. Claiborne, C.-K. Hwang, M. Nakada, P. G. Nantermet, *J. Am. Chem. Soc.* **1995**, *117*, 634; h) K. C. Nicolaou, Z. Yang, J.-J. Liu, P. G. Nantermet, C. F. Claiborne, J. Renaud, R. K. Guy, K. Shibayama, *J. Am. Chem. Soc.* **1995**, *117*, 645; i) K. C. Nicolaou, H. Ueno, J.-J. Liu, P. G. Nantermet, Z. Yang, J. Renaud, K. Paulvannan, R. Chadha, *J. Am. Chem. Soc.* **1995**, *117*, 653; j) K. C. Nicolaou, R. K. Guy, *Angew. Chem.* **1995**, *107*, 653; *Angew. Chem. Int. Ed. Engl.* **1995**, *34*, 2079; ; k) R. A. Holton, C. Somoza, K. B. Kim, F. Liang, R. J. Biediger, P. D. Boatman, M. Shindo, C. C. Smith, S. Kim, H. Nadizadeh, Y. Suzuki, C.

Tao, P. Vu, S. Tang, P. Zhang, K. K. Murthi, L. N. Gentile, J. H. Liu, *J. Am. Chem. Soc.* **1994**, *116*, 1597; l) R. A. Holton, K. B. Kim, C. Somoza, F. Liang, R. J. Biediger, P. D. Boatman, M. Shindo, C. C. Smith, S. Kim, H. Nadizadeh, Y. Suzuki, C. Tao, P. Vu, S. Tang, P. Zhang, K. K. Murthi, L. N. Gentile, J. H. Liu, *J. Am. Chem. Soc.* **1994**, *116*, 1599.

[195] a) M. Freemantle, *Chem. Eng. News*, **2004**, *March 1*, 33; b) S. J. Mickel, G. H. Sedelmeier, D. Niederer, R. Daeffler, A. Osmani, K. Schreiner, M. Seeger-Weibel, B. Bérod, K. Shaer, R. Gamboni, *Org. Process Res. Dev.* **2004**, *8*, 92; c) S. J. Mickel, G. H. Sedelmeier, D. Niederer, F. Schuerch, D. Grimler, G. Koch, R. Daeffler, A. Osmani, H. Hirni, K. Shaer, R. Gamboni, *Org. Process Res. Dev.* **2004**, *8*, 101; d) S. J. Mickel, G. H. Sedelmeier, D. Niederer, F. Schuerch, G. Koch, E. Kuesters, R. Daeffler, A. Osmani, M. Seeger-Weibel, E. Schmid, A. Hirni, K. Shaer, R. Gamboni, *Org. Process Res. Dev.* **2004**, *8*, 107; e) S. J. Mickel, G. H. Sedelmeier, D. Niederer, F. Schuerch, M. Seeger-Weibel, K. Schreiner, R. Daeffler, A. Osmani, D. Bixel, O. Loiseleur, J. Cercus, H. Stettler, K. Shaer, R. Gamboni, *Org. Process Res. Dev.* **2004**, *8*, 113; f) S. J. Mickel, D. Niederer, R. Daeffler, A. Osmani, E. Kuesters, E. Schmid, K. Schaer, R. Gamboni, *Org. Process Res. Dev.* **2004**, *8*, 122.

[196] a) The multigram total synthesis of the novel anticancer agent and polyketide lactone (+)-discodermolide is one of the most recent proofs of the power of modern synthetic chemistry and the industrial use of reagents and reactions developed by academic research; as in the case of quinine, it also shows that "*if a new drug candidate is sufficiently valuable, synthetic chemists will rise to the challenge of developing a viable synthetic approach no matter how complex the structure*".[195a] b) The supply of (+)-discodermolide needed for development cannot be met through the isolation and purification from its natural source, a sponge that must be harvested using manned submersibles; furthermore, attempts to reproducibly isolate a discodermolide-producing microorganism for fermentation have not been successful to date. A chemical synthesis was, therefore, considered as the best option for accessing multigram quantities of this compound.

[197] G. B. Kaufmann, *Chem. Educator* **2004**, *9*, 172.

Life's Simple Pleasures!



No need to waste precious time looking for the right information – Register now for the free **Wiley-VCH Alerting Service.**

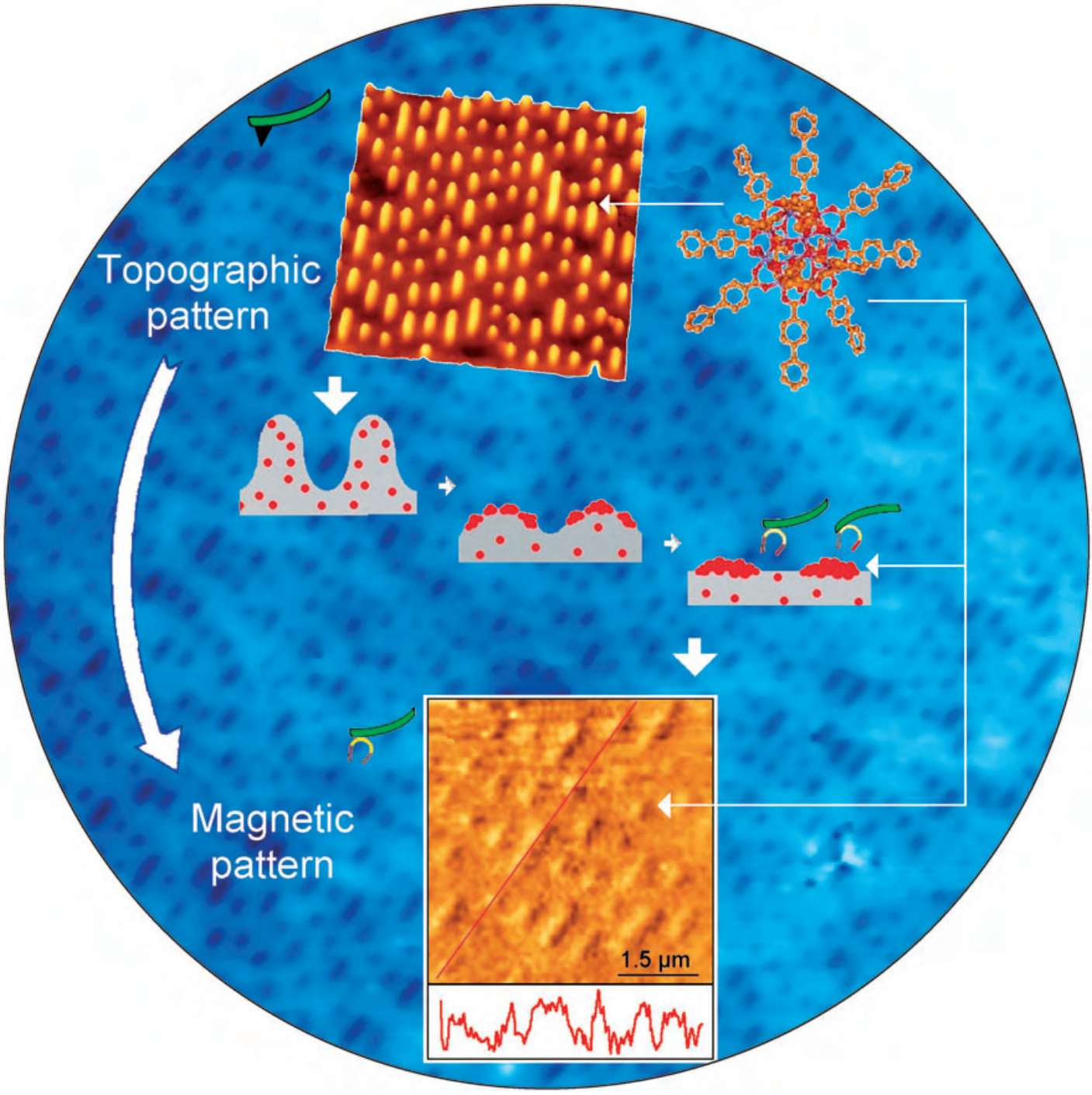
It's simple – and it's fast.

To receive regular news per e-mail tailored precisely to your needs and interests, just fill in the registration form at **www.wiley-vch.de/home/pas/**

WILEY-VCH

 © 2005 Wiley-VCH Verlag GmbH & Co. KGaA, Weinheim

Communications



A molecule-based magnetic material with a paramagnetic response at room temperature has been used to fabricate patterns of magnetic bits on a polycarbonate surface. This system can be used effectively as a permanent information-storage medium with magnetic readout. For more information see the Communication by J. Veciana, F. Biscarini, and co-workers on the following pages.

© 2005 Wiley-VCH Verlag GmbH & Co. KGaA, Weinheim
DOI: 10.1002/anie.200461554

Nanotechnology

Magnetic Information Storage on Polymers by Using Patterned Single-Molecule Magnets**

Massimiliano Cavallini, Jordi Gomez-Segura, Daniel Ruiz-Molina, Massimiliano Massi, Cristiano Albonetti, Concepció Rovira, Jaume Veciana, and Fabio Biscarini**

Nanoscopic magnetic materials are of increasing interest because of their potential use for ultrahigh-density information storage, quantum computing, sensing, and biomedical applications.[1–3] Herein we demonstrate that, while working in the paramagnetic regime, it is possible to encode and read out information from domains of Mn_{12} molecules patterned on a polymer surface across a large area. The patterns are fabricated by molding a dispersion of Mn_{12} molecules in a polycarbonate matrix on a structured master, then exposing the polymer replica to the vapor of an organic solvent. The protrusions of the replica surface disappear upon exposure to the solvent, and the Mn_{12} molecules concentrate on the surface at the positions of the original protrusions. The distribution of Mn_{12} molecules at the polymer surface gives rise to a magnetic contrast, which can be imaged by magnetic force microscopy. Information can be transferred from a recorded digital video disk (DVD), functioning as the master, to a magnetically readable flexible medium.

The search for increasingly small, lighter, and cheaper nanoscopic magnetic materials faces the challenge of overcoming anomalies such as dipolar interactions, matrix effects, domain wall rearrangements, and percolation effects, which degrade the observable magnetic properties. Thus, there is a worldwide effort aimed at developing new and enhanced nanostructured magnetic materials. An emerging family that is being explored is molecule-based magnets, because they possess several attractive attributes: 1) they have homogeneous and precisely defined sizes; 2) their chemical and topological structure can be tailored by chemical design; 3) they are soluble in common solvents and hence can be easily processed for applications; and 4) they can be considered as the ultimate limit for storing high densities of information data.[4] Mn_{12} clusters have a large-spin ground state with appreciable magnetic anisotropy, which results in a barrier for the spin reversal.[5–8] As a consequence, interesting magnetic properties such as out-of-phase ac magnetic susceptibility signals and stepwise magnetization hysteresis loops, caused by individual molecules rather than by long-range orderings, are observed below the blocking temperature (T_B).[9] However, if a truly molecular magnetic device is to be achieved, addressing properly oriented individual magnetic molecules or their aggregates, as well as increasing their critical temperatures of such molecule-based materials, are required. The first successful attempts toward the development of functional molecule-based magnetic devices focused on the deposition and addressing of Mn_{12} clusters on different surfaces. Mn_{12} clusters have been organized into multilayered films by the Langmuir–Blodgett technique or self-assembly on functionalized surfaces.[10] Deposition of isolated or small aggregates of such molecules onto a polycarbonate surface[11] and the self-assembly of thiol-substituted Mn_{12} clusters on thin Au films[12] have also been achieved. Nevertheless, no control of the position and distance between Mn_{12} molecules was attained in either case. Recently, we used a stamp-assisted self-organization method to successfully pattern Mn_{12} molecules into 50-nm-diameter dots with a characteristic length scale less than 200 nm,[13] which demonstrates the possibility of addressing organized clusters on the surface of a silicon wafer.

Herein, we report a reliable and simple methodology to pattern magnetic Mn_{12} molecules on a polycarbonate (PC) film, and show that it is possible to map (read) the patterned domains on the film surface while working in the paramagnetic regime. We used the complex $[Mn_{12}O_{12}(O_2CC_{12}H_9)_{16}(H_2O)_4]$ (**1**), whose synthesis has been previously described.[14] Frequency-dependent out-of-phase ac signals and hysteresis in the magnetization versus external field are seen for solid samples of complex **1**, which indicates that this complex behaves as a single-molecule magnet with a T_B value of 4–6 K and as a paramagnet at higher temperatures.[14] A consistent magnetic behavior is observed for the same complex dispersed in thin films of polycarbonate.[11] In the work described herein, the films are prepared by casting a solution of complex **1** and polycarbonate in CH_2Cl_2 onto a blank DVD support that acts as a structured master (Figure 1 a).[15] On the basis of the similarity of the conditions used in the process reported in ref. [11], we infer that the magnetic behavior of complex **1** should remain unchanged.

Once the solvent is evaporated, the replica is removed from the master, which results in a stable, flexible, and transparent film of a solid solution of complex **1** in polycarbonate. The film surface, imaged by atomic force microscopy (AFM), exhibits an inverted pattern with respect to the DVD master, with parallel lines 300-nm wide and 120-nm deep and a periodicity between grooves of 740 nm (Figure 1 b). A representative topographical profile along line 1 in Figure 1 b is shown in Figure 1 d. In a second step, the film is exposed to a saturated atmosphere of CH_2Cl_2 vapor that swells the film and solvates the polymer chains, thus decreasing the glass transition temperature of the polymer below

[*] Dr. M. Cavallini, Dr. M. Massi, Dr. C. Albonetti, Dr. F. Biscarini
CNR-Istituto per lo Studio dei Materiali Nanostrutturati
Sez. di Bologna
Via P. Gobetti 101, 40129 Bologna (Italy)
Fax: (+39) 051-639-8539
E-mail: f.biscarini@ism.bo.cnr.it
J. Gomez-Segura, Dr. D. Ruiz-Molina, Prof. C. Rovira, Prof. J. Veciana
CSIC-Institut de Ciencia de Materials de Barcelona
Campus Universitari de Bellaterra
08193 Cerdanyola (Spain)
Fax: (+34) 93-580-5729
E-mail: vecianaj@icmab.es

[**] This work was supported by the European Commission under projects IST-NANOMAGIQC and NMP-IP-500355 NAIMO, the European Science Foundation under Eurocore SONS program FUNSMARTS, and the Dirección General de Investigación (Spain) under project NanoMultiFun.

 © 2005 Wiley-VCH Verlag GmbH & Co. KGaA, Weinheim

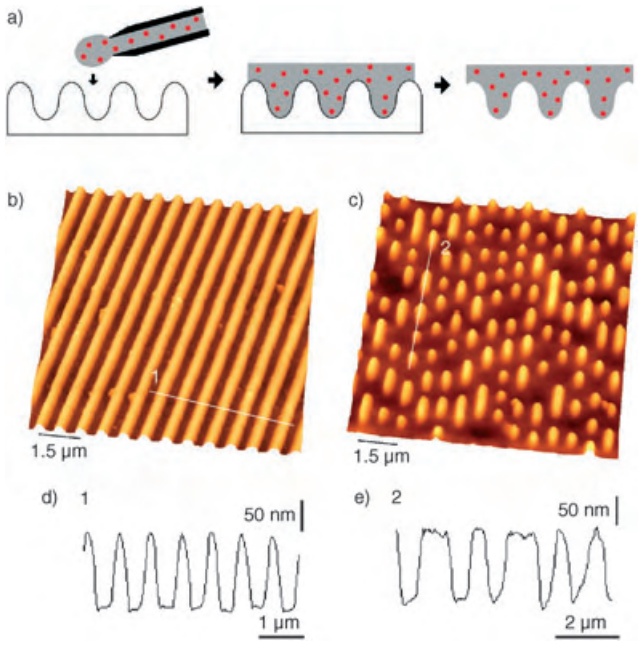


Figure 1. a) Schematic representation of the experimental process followed to obtain a DVD replica made of a solid solution of Mn_{12} complex and PC. b) AFM image of a Mn_{12}–PC replica exhibiting a sequence of grooves replicating the blank DVD master. The distance between grooves is 740 nm and their depth and width are 120 and 300 nm, respectively. c) AFM image of a Mn_{12}–PC replica of a recorded DVD, which exhibits a structured sequence of bits of information as protrusions. One bit corresponds to a protrusion 300 nm wide, 400 nm long, and 120 nm high. d) Topographical line profile along the white line 1 drawn in (b). e) Topographical line profile along the white line 2 drawn in (c).

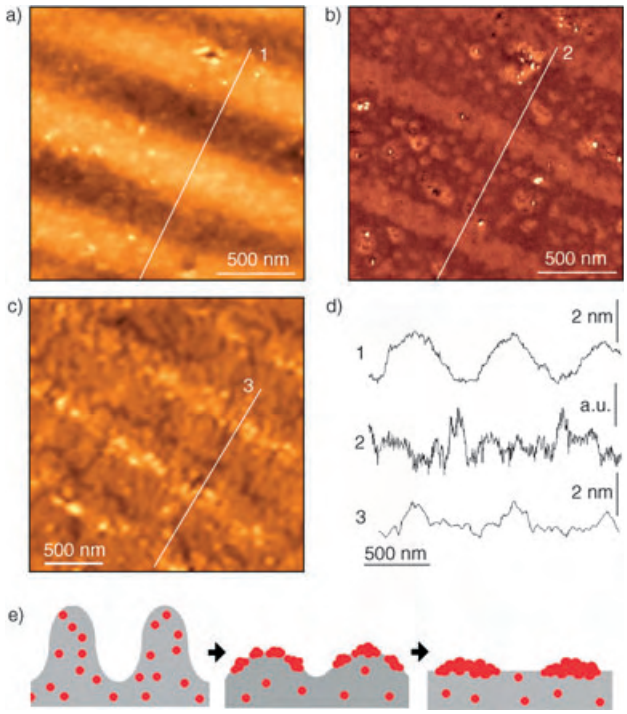


Figure 2. a) AFM topography image of a molded film of Mn_{12}–PC, as in Figure 1 b, after treatment with CH_2Cl_2 solvent vapor for 120 s. The height of the protrusions has decreased by more than 96% compared to its original value of 120 nm. b) AFM phase-contrast image of the replica surface depicted in (a) showing the inhomogeneous distribution of the Mn_{12} solute at the surface. Darker areas are solute-rich regions. c) AFM image of the film after treatment with CH_2Cl_2 vapor for 180 s. d) Profiles along the white lines shown in the topographic (lines 1 and 3) and phase-contrast (line 2) images. e) Schematic representation of the smoothening and Mn_{12} aggregation processes occurring during the CH_2Cl_2 solvent vapor treatment.

room temperature. Under these conditions, the structured film surface experiences a smoothening driven by the minimization of the surface tension, which leads to the progressive deletion of the topographic reliefs. The time needed for a complete smoothening depends on experimental parameters such as solvent nature, temperature, and initial surface roughness.

Topographic AFM images of the molded replica after exposure to CH_2Cl_2 vapor for 120 and 180 s are shown in Figure 2. The protrusions decrease from 120 nm (root-mean-square (rms) roughness 56 nm) to less than 5 nm after solvent exposure for 120 s (Figure 2 a and first profile in Figure 2 d), and by more than 99% (rms roughness <1 nm) after 180 s (Figure 2 c and third profile in Figure 2 d). An extensive film rupture occurs by nucleation and growth of nanosized pores upon longer exposure times (not shown). Interestingly, the corresponding AFM phase-contrast images show that the Mn_{12} clusters concentrate preferentially in the regions where the protrusions were originally formed, while they are absent from the grooves (Figure 2 b and second profile in Figure 2 d). This evidence shows that the lateral (in-plane) diffusion of Mn_{12} clusters, which were initially dissolved in the polymer solid solution, is marginal during the smoothening process. Other concurrent mechanisms may be linked to convective or diffusive mass transport toward the sharper protrusions, driven by a faster solvent evaporation rate at the loci with smaller curvature.[16]

These results encouraged us to further advance this approach by focusing on Mn_{12} molecular clusters patterned into domains with controlled shapes and positions on the polymer surface, since these domains of Mn_{12} molecules can be used as magnetic bits. With this aim, we molded a Mn_{12}–PC film replica of a recorded DVD. AFM imaging of the replica surface reveals an ordered array of 120-nm-thick protrusions of variable length ranging from 380 to 1500 nm, aligned along lines (tracks) with an intertrack distance of 740 nm (Figure 1 c). A representative topographical profile along a sector (line 2 in Figure 1 c) is shown in Figure 1 e.

The Mn_{12}–PC replica was then exposed to CH_2Cl_2 vapor, and the process was interrupted just before the rupture of the film surface took place. At this stage, the original protrusions that replicate the topographic indentations of the coded DVD have almost disappeared (topographic rms roughness is <1 nm), as is apparent from Figure 3 a and 3 e. The local magnetic response of the surface film was investigated by magnetic force microscopy (MFM), which revealed the formation of a spatially distributed magnetic pattern that closely follows the original topographic indentations of the recorded DVD (Figure 3 b). Again, the preferential concen-

 © 2005 Wiley-VCH Verlag GmbH & Co. KGaA, Weinheim

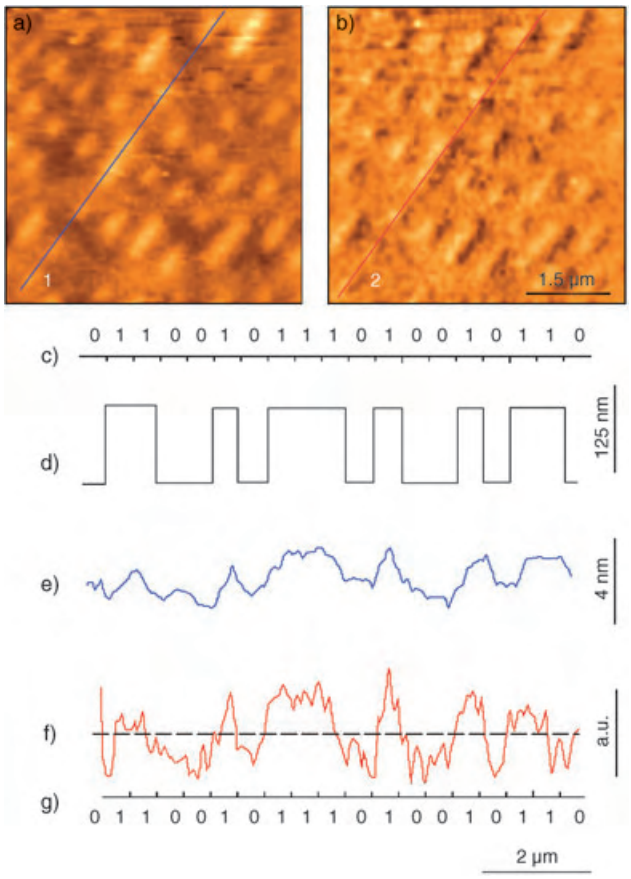


Figure 3. a) AFM topography image of a DVD replica after solvent exposure (rms roughness is 1 nm). b) Magnetic mapping of (a) with MFM. The image (phase shift during second pass) was acquired by a two-pass mode using a cobalt-coated magnetic tip. The lift height was 30 nm. c) Sequence of bits that is represented by the topographic sequence along the track marked by line 1 in (a). d) Idealized representation of the corresponding topographical line profile of the track in the replica before exposure to solvent. e) Topographical line profile of the track after exposure to solvent. f) Magnetic contrast along line 2 in (b). The mean signal line (-----) is a guide to the eye. g) Sequence of magnetic bits extracted from (f), which shows a perfect correspondence with the original sequence in (c).

tration of Mn_{12} clusters corresponding to the protrusions of the polymer film surface occurs as previously described. Each sequence of magnetic domains, composed of aggregates of Mn_{12} molecules, represents magnetically readable information that, overall, replicates the information that was originally accessible by optical readout in the DVD. The magnetic response of the domains of Mn_{12} molecules, which are paramagnetic at room temperature, to MFM can be ascribed to the strong magnetic contrast with the diamagnetic polymeric surroundings. Similar magnetic responses have been previously observed for other paramagnetic organic molecules on diamagnetic surfaces.[11,17] Figure 3d is an idealized representation of the topographical profile of the replica along the track marked by line 1 in Figure 3a before exposure to solvent. The corresponding logic sequence of bits for an optical readout is shown in Figure 3c. Figure 3f shows the line profile of the magnetic force along the same track with a signal-to-noise ratio of 2:1, which makes it possible to resolve the sequence of magnetic bits represented in Figure 3g (line 2 in Figure 3b). The sequence of magnetic bits perfectly reproduces the original sequence of optical DVD bits.

In summary, we have developed a simple process that is able to fabricate patterns of magnetic bits on a polymer surface, on the basis of a molecule-based magnetic material with a paramagnetic response at room temperature. We demonstrated that this system can be effectively used as a permanent information storage medium with magnetic readout. The patterning process can be scaled down to smaller length scales and higher densities by improving the resolution of the master, or by patterning the solute/polymer mixture by using a higher-resolution fabrication technique, for example, nanoimprint lithography. This technique may lead to the fabrication of magnetic Mn_{12} domains with features a few tens of nanometers in size,[18] which corresponds to a few molecular diameters (end-to-end distance is 4 nm). Finally, the patterning and addressing of molecular materials across multiple length scales is one of the most important issues in nanotechnology. Extension of this work could lead to the development of next-generation storage media based on a variety of molecular responses,[19] for example: charge storage; conformational, orientational, or positional shifting; phase transitions or reorganization; and optical anisotropy changes and fluorescence switching.

Experimental Section

Sample preparation: Pellets of poly(bisphenol A carbonate) (PC) with Mn_{12} single-molecule magnets (4% by weight) was dissolved in CH_2Cl_2, and the solution was cast on a master. The DVD masters were covered with a 100-nm-thick Au film. Circular samples of 1 cm diameter and 20 µm thickness were fabricated.

AFM/MFM measurements: AFM/MFM was carried out in air in intermittent-contact mode for imaging. For MFM measurements, cobalt-coated tips (MDT, Moscow, Russia) were used with the instrument operated in a two-pass mode: in the first pass the topography was measured in intermittent-contact mode; in the second pass the cantilever was lifted to a selected height with respect to the topography line, and the phase shift was measured as the tip followed the stored topography line. The magnetic signal was resolved as phase shift during the second pass. The magnetic contrast was comparable to that of MFM images reported earlier.[11,17] The typical lift height was 30 nm which, when compared to sample roughness (< 1 nm), was sufficient to avoid topographic artifacts in the magnetic signal. Imaging samples using a nonmagnetic tip did not yield any contrast in the second-pass mode, and neither did a magnetic tip on samples made of polycarbonate alone.

Received: August 5, 2004

Keywords: cluster compounds · magnetic properties · nanotechnology · polymers · single-molecule studies

[1] D. D. Awschalom, J. M. Kikkawa, *Phys. Today* **1999**, *52*, 33–38.
[2] H. Ohno, D. Chiba, F. Matsukura, T. Omiya, E. Abe, T. Dietl, Y. Ohno, K. Ohtani, *Nature* **2000**, *408*, 944–946.
[3] R. L. Edelstein, C. R. Tamanaha, P. E. Sheehan, M. M. Miller, D. R. Baselt, L. J. Whitman, R. J. Colton, *Biosens. Bioelectron.* **2000**, *14*, 805–813.
[4] J. S. Miller, A. J. Epstein, *MRS Bull.* **2000**, *11*, 21–28.

 © 2005 Wiley-VCH Verlag GmbH & Co. KGaA, Weinheim

[5] D. Ruiz-Molina, G. Christou, D. N. Hendrickson, *Mol. Cryst. Liq. Cryst.* **2000**, *343*, 17 – 27.
[6] R. Sessoli, D. Gatteschi, A. Caneschi, M. A. Novak, *Nature* **1993**, *365*, 141 – 143.
[7] J. R. Friedman, M. P. Sarachick, J. Tejada, R. Ziolo, *Phys. Rev. Lett.* **1996**, *76*, 3830 – 3833.
[8] J. M. Hernandez, X. X. Zhang, F. Luis, J. Bartolomé, J. Tejada, R. Ziolo, *Europhys. Lett.* **1996**, *35*, 301 – 306.
[9] D. Gatteschi, R. Sessoli, *Angew. Chem.* **2003**, *115*, 278 – 309; *Angew. Chem. Int. Ed.* **2003**, *42*, 268 – 297.
[10] a) M. Clemente-León, H. Soyer, E. Coronado, C. Mingotaud, C. J. Gómez-García, P. Delhaes, *Angew. Chem.* **1998**, *110*, 3053 – 3056; *Angew. Chem. Int. Ed.* **1998**, *37*, 2842 – 2845; b) G. C. Condorelli, A. Motta, I. L. Fragala, F. Giannazzo, V. Rainieri, A. Caneschi, D. Gatteschi, *Angew. Chem.* **2004**, *116*, 4173 – 4176; *Angew. Chem. Int. Ed.* **2004**, *43*, 4081 – 4084; c) a. N. Abdi, J. P. Bucher, P. Rabu, O. Toulemonde, M. Drillon, P. Gerbier, *Jnl. Appl. Phys.* **2004**, *95*, 7345 – 7347; d) J. S. Steckel, N. S. Persky, C. R. Martinez, C. L. Barnes, E. A. Fry, J. Kulkarni, J. D. Burgess, R. B. Pacheco, S. L. Stoll, *Nano Lett.* **2004**, *4*, 399 – 402; correction: S. L. Stoll, *Nano. Lett.* **2004**, *4*, 1167.
[11] D. Ruiz-Molina, M. Mas-Torrent, J. Gómez, A. I. Balana, N. Domingo, J. Tejada, M. T. Martínez, C. Rovira, J. Veciana, *Adv. Mater.* **2003**, *15*, 42 – 45.
[12] A. Cornia, A. C. Fabretti, M. Pacchioni, L. Zobbi, D. Bonacchi, A. Caneschi, D. Gatteschi, R. Biagi, U. Del Pennino, V. De Renzi, L. Gurevich, H. S. J. Van der Zant, *Angew. Chem.* **2003**, *115*, 1683 – 1686; *Angew. Chem. Int. Ed.* **2003**, *42*, 1645 – 1648.
[13] M. Cavallini, F. Biscarini, J. Gómez-Segura, D. Ruiz, J. Veciana, *Nano Lett.* **2003**, *3*, 1527 – 1530.
[14] D. Ruiz-Molina, P. Gerbier, E. Rumberger, D. B. Amabilino, I. A. Guzei, K. Folting, J. C. Huffman, A. Rheingold, G. Christou, J. Veciana, D. N. Hendrickson, *J. Mater. Chem.* **2002**, *12*, 1152 – 1161.
[15] Y. Xia, E. Kim, X.-M. Zhao, J. A. Rogers, M. Prentiss, G. M. Whitesides, *Science* **1996**, *273*, 347 – 349.
[16] R. D. Deegan, O. Bakajin, T. F. Dupont, G. Huber, S. R. Nagel, T. A. Witten, *Nature* **1997**, *389*, 827 – 829.
[17] H. Nishide, T. Ozawa, M. Miyasaka, E. Tsuchida, *J. Am. Chem. Soc.* **2001**, *123*, 5942 – 5946.
[18] M. D. Austin, S. Y. Chou, *Appl. Phys. Lett.* **2002**, *81*, 4431 – 4433.
[19] M. Cavallini, F. Biscarini, S. Léon, F. Zerbetto, G. Bottari, D. A. Leigh, *Science* **2003**, *299*, 531 – 531.

 © 2005 Wiley-VCH Verlag GmbH & Co. KGaA, Weinheim

Single-Molecule Magnets

New Structural Motifs in Manganese Single-Molecule Magnetism from the Use of Triethanolamine Ligands**

*Muralee Murugesu, Wolfgang Wernsdorfer, Khalil A. Abboud, and George Christou**

Single-molecule magnets (SMMs) are molecules with a large barrier (vs kT) to magnetization relaxation, and consequently display magnetization versus applied-field hysteresis loops at low enough temperatures, the diagnostic property of a magnet.[1] Such molecules derive their properties from a combination of a large ground-state spin (S) value and a significant magnetoanisotropy of the Ising (easy-axis) type. SMMs thus offer a molecular approach to nanoscale magnetic materials, and their potential applications include information storage at the molecular level and use as quantum bits (qubits) in quantum computation.

Manganese carboxylate chemistry has been the main source of new SMMs during the last several years,[2] and we are therefore seeking to develop new synthetic methodology to manganese clusters of various nuclearities and structural types. In earlier work, we showed how the tridentate (N,O,O) chelate, pyridine-2,6-dimethanol ($pdmH_2$) provided access to $[Mn_4(O_2CMe)_2(pdmH)_6]^{2+}$ ions with $S = 9$,[2b,c] $[Mn_9(O_2CEt)_{12}(pdm)(pdmH)_2(L)_2]$ with $S = 11/2$,[2h] and $[Mn_{25}O_{18}(OH)_2(N_3)_{12}(pdm)_6(pdmH)_6]^{2+}$ with $S = 51/2$,[2q] all of which are SMMs. As an extension to this work, we have recently been exploring reactions with the related molecule triethanolamine ($teaH_3$) to see what kind of manganese clusters might result from the use of this potentially tetradentate (N,O,O,O) chelate, which is also more flexible than $pdmH_2$. There are only a very few reported examples of manganese compounds obtained with $teaH_3$.[3] We herein report the results of our study, which has produced new Mn_6, Mn_8, and Mn_{16} clusters.

We have investigated many reactions between $teaH_3$ and a number of manganese carboxylate sources, by using different molar ratios and under a variety of conditions, and three new manganese clusters are described herein. The reaction of $[Mn_3O(O_2CCHPh_2)_6(py)_3](ClO_4)$ (py = pyridine) with $teaH_3$ in a 1:2 ratio in MeCN yielded the mixed-valent (Mn^{III}_2, Mn^{II}_4) complex $[Mn_6(teaH)_2(teaH_2)_2(O_2CCHPh_2)_8]\cdot 4MeCN$ (**1**·4MeCN) in 42% yield. This complex crystallizes in the triclinic $P\bar{1}$ space group. The centrosymmetric structure[4]

[*] Dr. M. Murugesu, Dr. K. A. Abboud, Prof. Dr. G. Christou
Department of Chemistry
University of Florida
Gainesville, FL 32611-7200 (USA)
Fax: (+1) 352-392-8757
E-mail: christou@chem.ufl.edu
Dr. W. Wernsdorfer
Laboratoire Louis Neel CNRS
38042 Grenoble Cedex 9 (France)

[**] This work was supported by the National Science Foundation.

 © 2005 Wiley-VCH Verlag GmbH & Co. KGaA, Weinheim DOI: 10.1002/anie.200461703

(Figure 1) contains a central planar Mn_4 rhombus (Mn1, Mn2 and their symmetry partners); each of the two doubly deprotonated $teaH^{2-}$ groups act as a tetradentate chelate to Mn1 and Mn1′, and provide edge-bridging atoms O1 and O5, and capping atom O3 (and their symmetry partners); O2 is the protonated O atom. This central rhombus is very similar to that in $[Mn_4(O_2CMe)_2(pdmH)_6]^{2+}$[2b,c] (and also the very similar hmp^- analogue, where hmp^- is the anion of 2-hydroxypyridine[5]) except that the Mn^{II} and Mn^{III} sites are interchanged. A further two Mn^{II} ions (Mn3 and Mn3′) in **1** are each connected to the central rhombus by two carboxylate groups and an alkoxide O atom (O8) of a singly deprotonated $teaH_2^-$ group, which is also acting as a tridentate chelate to Mn3; atoms O9 and O13 are both protonated. The Mn^{III} ions show Jahn–Teller (JT) distortions (elongations), shown as the solid black bonds in Figure 1.

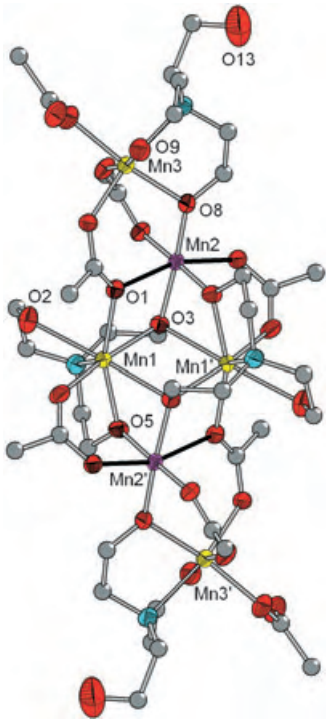


Figure 1. ORTEP representation of complex **1** with the thermal ellipsoids set at 50% probability. H atoms have been omitted for clarity. Solid black lines indicate the Mn^{III} Jahn–Teller elongation axes; Mn^{III} purple, Mn^{II} yellow, O red, N blue, C gray.

The reaction of $[Mn_{12}O_{12}(O_2CCH_2tBu)_{16}(H_2O)_4]$ with approximately 8 equivalents of $teaH_3$ in CH_2Cl_2 led to large dark brown crystals of the mixed-valent (Mn^{III}_4, Mn^{II}_4) complex $[Mn_8(O_2CCH_2tBu)_{12}(teaH)_4]\cdot 2\,CH_2Cl_2$ (**2**·2 CH_2Cl_2) in 58% yield. The structure[6] consists of an unusual Mn_8 near rectangle lying on C_2 rotation axis which passes through Mn1 and Mn5 (Figure 2). The octahedrally coordinated Mn^{II} and Mn^{III} ions alternate around the rectangle. Each Mn_2 pair is bridged by a combination of carboxylate groups and an alkoxide O atom of doubly deprotonated $teaH^{2-}$ groups; the protonated O atoms are O17 and O18. Four carboxylate groups bridge in a rare η^1,η^2,μ_3 mode, whereas the rest are in

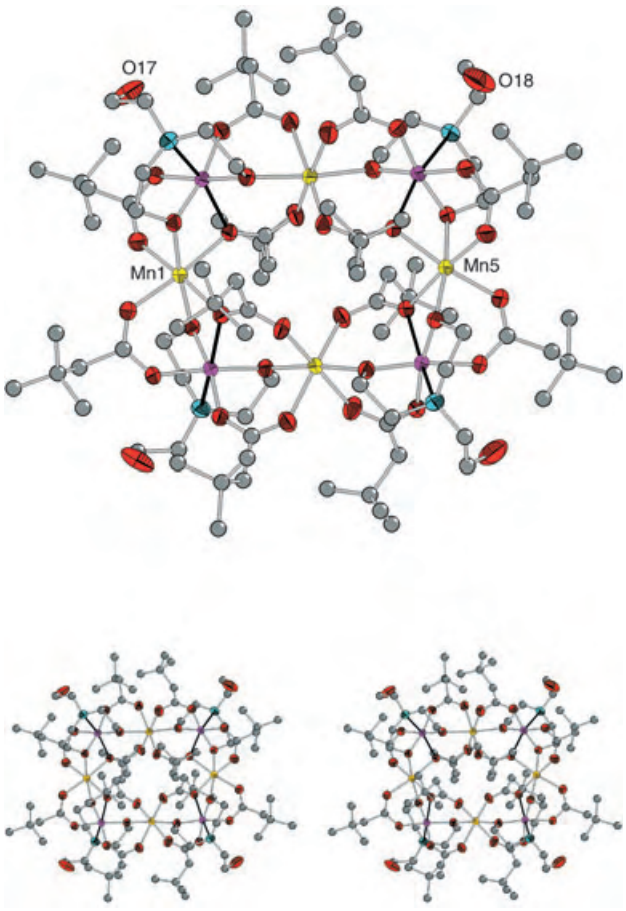


Figure 2. ORTEP representation and stereopair of complex **2** with the thermal ellipsoids set at 50% probability. H atoms have been omitted for clarity. Solid black lines indicate the Mn^{III} Jahn–Teller elongation axes. Color code as in Figure 1.

the common η^1,η^1,μ mode. The $teaH^{2-}$ groups bind as tridentate chelates to the corner (Mn^{III}) ions of the rectangle, and bridge to the adjacent Mn^{II} ions. In every case, the Mn^{III} JT elongation axes contain the $teaH^{2-}$ N atom.

The reaction between $Mn(O_2CMe)_2\cdot 4H_2O$, $teaH_3$, and NEt_3 in a 1:1:1 ratio in MeCN led to the formation of dark brown rectangular blocks of the mixed-valent (Mn^{III}_8, Mn^{II}_8) complex $[Mn_{16}(O_2CMe)_{16}(teaH)_{12}]\cdot 16\,MeCN$ (**3**·16 MeCN) in 60% yield. The same reaction but using $NnBu_4MnO_4$ instead of NEt_3 led to same product in lower yield (30%). The structure[7] comprises an Mn_{16} loop of alternating Mn^{II} and Mn^{III} ions with a saddle-shaped or closed sinusoidal conformation (Figure 3). Although involving a bigger loop size, the structure of **3** has similarities to that of **2**; again, eight of the mono-protonated $teaH^{2-}$ groups bind one each to the Mn^{III} ions in a tridentate chelate fashion, and bridge with their alkoxide O atoms to adjacent Mn^{II} ions; the protonated (alcohol) arms are unbound. The remaining four $teaH^{2-}$ groups bind one each to every other Mn^{II} ion around the loop in a tetradentate chelate fashion (i.e. including the protonated alcohol arm) giving seven-coordinate, distorted pentagonal-bipyramidal geometry. Each Mn_2 pair is thus again bridged by a combination of carboxylate groups and an alkoxide O atom. This is similar to the situation in Ni_{12}[8] and

 © 2005 Wiley-VCH Verlag GmbH & Co. KGaA, Weinheim

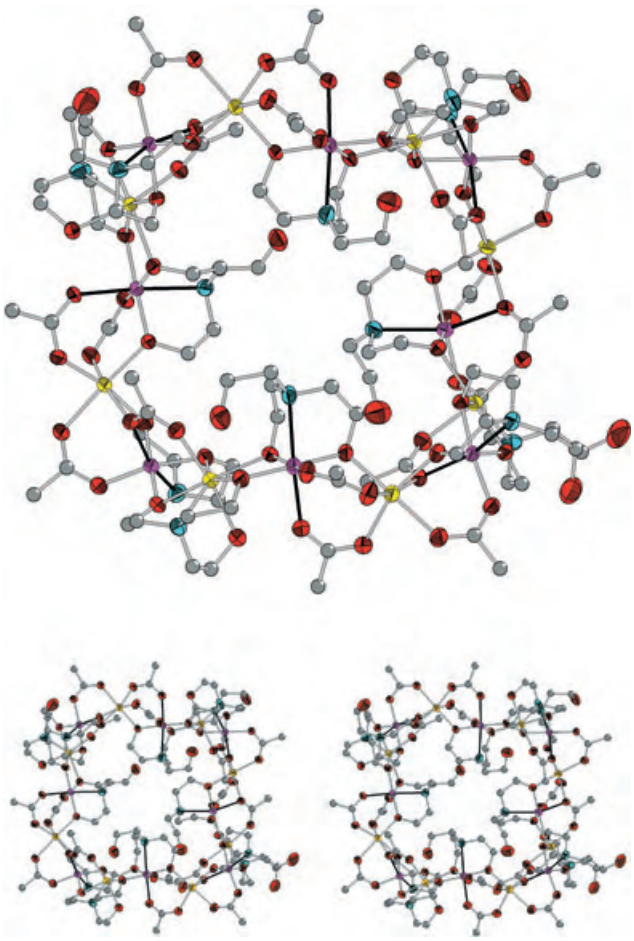


Figure 3. ORTEP representation and stereopair of complex **3** with the thermal ellipsoids set at 50% probability. H atoms have been omitted for clarity. Solid black lines indicate the Jahn–Teller axes. Color code as in Figure 1.

Fe_{16}[9] wheel-like complexes, the latter employing a triolate ligand. Side-views emphasizing the planar and saddle-shaped cores of **2** and **3**, are shown in Figure 4.

In all three compounds, the oxidation state assignments were made by examination of bond lengths, bond valence sum calculations, and detection of Mn^{III} JT elongation axes. JT elongated Mn^{III}–O bonds for **1**–**3** are in the ranges 2.183(4)–2.395(6) Å (**1**), 2.182(3)–2.412(3) Å (**2**), and 2.210(2)–2.438(3) Å (**3**), significantly longer than the other Mn^{III}–O bonds (1.875(4)–1.985(4) (**1**), 1.876(2)–1.962(3) (**2**), and 1.875(2)–1.979(3) Å (**3**).

The magnetic properties of **1**–**3** were investigated by solid-state magnetic susceptibility (χ_M) measurements in the 5.0–300 K range in a DC field of 1000 Oe (0.1 Tesla); the resulting data are shown in Figure 5 as $\chi_M T$ vs T plots. All three compounds show a decreasing $\chi_M T$ value with decreasing temperature, which indicates that antiferromagnetic exchange interactions dominate within the molecules. The $\chi_M T$ values at 5.0 K are 10.1 (for **1**), 4.0 (**2**), and 41.4 $cm^3 K mol^{-1}$ (**3**); this suggests the complexes all have non-zero ground-state spin (S) values, with that for **3** being particularly large. To determine the ground-state S values, magnetization (M) measurements were carried out in the 1.8–

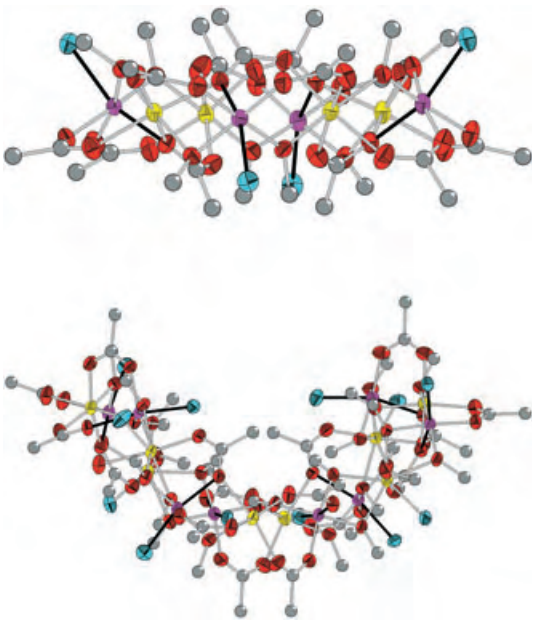


Figure 4. Side views of complexes **2** (top) and **3** (bottom) emphasizing the different conformations. Color code as in Figure 1.

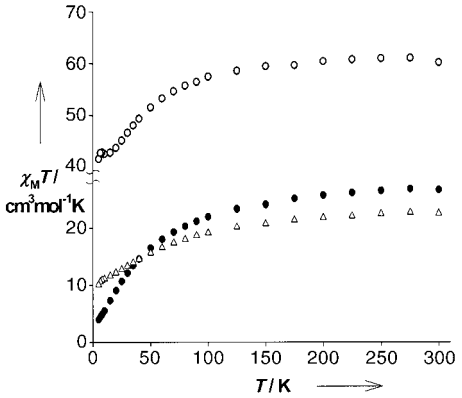


Figure 5. Plot of $\chi_M T$ versus T for complexes **1** (△), **2** (●), and **3** (○).

4 K temperature and 0.1–3 T field ranges. Only low fields were used to try to avoid problems with low-lying excited states, which are expected for high-nuclearity clusters with a high density of spin states and/or when Mn^{II} ions are present, which give weak exchange interactions. We have described such problems in detail elsewhere.[2d,r] The data were fitted by a matrix-diagonalization method to a model that assumes only the ground state is populated, includes axial zero-field splitting ($D\hat{S}_z^2$), and performs a full powder average.[2c] Good fits were obtained for **1** with $S=5$, $g=1.79(1)$, $D=-0.20(1)$ cm^{-1}, and for **3** with $S=10$, $g=2.00(1)$, $D=-0.060(4)$ cm^{-1}. No acceptable fit for **2** could be obtained: however, its low $\chi_M T$ value (Figure 4) suggests a small ground-state spin, of $S=3$ or less.

As described elsewhere,[2d,r] more reliable conclusions about the S value can be reached by AC magnetic susceptibility measurements, which also can detect the slow magnetization relaxation suggestive of SMMs. For **1** and **3**, fre-

 © 2005 Wiley-VCH Verlag GmbH & Co. KGaA, Weinheim

quency-dependent tails were observed below approximately 3 K in the out-of-phase AC susceptibility (χ_M'') versus T signal, the maxima of which lie below the temperature limit of our SQUID instrument (1.8 K), but no tail was seen for **2**. Corresponding frequency-dependent decreases in the in-phase AC susceptibility (χ_M'), plotted as ($\chi_M'T$ vs T), were observed for **1** and **3**, but not for **2** (Figure 6). In addition, the

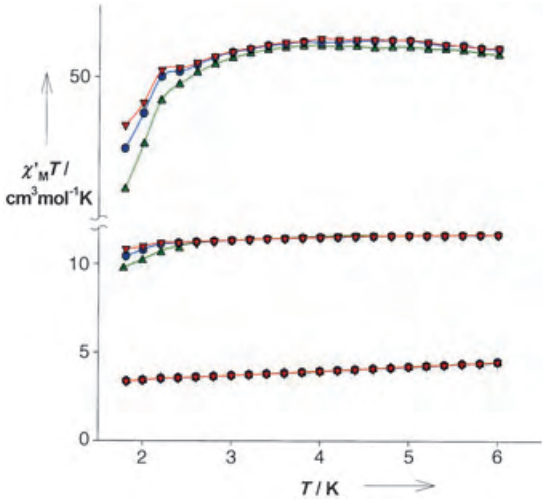


Figure 6. In-phase AC susceptibility signals (χ_M', plotted as $\chi_M'T$ vs T) at 1000 (▲), 250 (●) and 50 (▼) Hz for **1** (middle), **2** (bottom), and **3** (top).

$\chi_M'T$ versus T plots change with temperature, confirming the presence of low-lying excited states, and extrapolation of the plots to 0 K (from regions not affected by the decreases arising from slow relaxation) gives values of approximately 11 (for **1**), 3 (**2**), and 49 cm^3 K mol^{-1} (**3**). These are consistent with the values expected for $S = 5$, 2, and 10, respectively, and $g = 2.0$ or slightly below (as expected for Mn^{III}). The AC data thus confirm the ground-state S values deduced form the magnetization fits for **1** and **3**. In addition, the $S = 2$ value for **2** is consistent with antiferromagnetic interactions between adjacent Mn^{II} and Mn^{III} ions around the ring, which would give a predicted $S = 8-6 = 2$ ground state.

Complexes **1** and **3** were confirmed to be SMMs by magnetization versus DC-field scans on single crystals using an array of micro-SQUIDs.[10] These gave hysteresis loops, the diagnostic behavior of magnets, below 0.5 K for **1** and 0.8 K for **3** (Figure 7), whose coercivities increase with decreasing temperature, as expected for SMMs. Further, the loops of **1** show the steps characteristic of quantum tunneling of magnetization (QTM), whereas those of **3** do not, as is usually the case for larger SMMs since they are more susceptible to step-broadening effects from low-lying excited states, intermolecular interactions, and distributions of local environments owing to ligand and solvent disorder.[2g,p,q]

In summary, the use of $teaH_3$ has provided a useful route to three new structural types in mixed-valent manganese cluster chemistry, which include near-rectangular and closed-sinusoidal (saddle-shaped) topologies. Further, two of these complexes are also new SMMs. Complexes **2** and **3** are the

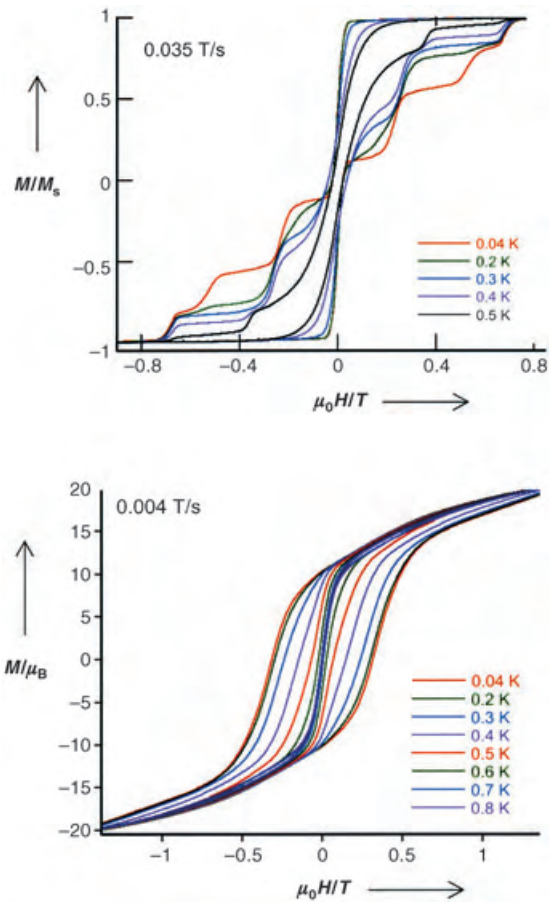


Figure 7. Magnetization (M) versus field ($\mu_0 H$ in tesla) hysteresis loops for single crystals of **1**·4 MeCN (top) and **3**·16 MeCN (bottom) at the indicated temperatures. For **1**·4 MeCN, M is normalized to its saturation value, M_s. For **3**·16 MeCN, the M value per molecule (M/μ_B) was determined from quantitative meaasurements.

first examples of mixed-valent Mn wheels, with **3** also being the largest single-stranded manganese loop known to date; the recently reported Mn_{22} is not a single-stranded loop.[2p] The Mn_{16} complex **3** joins the Ni_{12} complex $[Ni_{12}(chp)_{12}(O_2CMe)_{12}(thf)_6(H_2O)_6]$ ($chp^- = 6$-chloro-2-pyridonate)[8] and $[Mn_{12}(O_2CMe)_{14}(mda)_8]$ ($mda^{2-} = N$-methyldiethanolamine)[1a] as the only single-stranded wheel/loop SMMs known to date. This is despite the relatively frequent occurrence of this structural topology.[11] Finally, the present results illustrate once again the versatility and aesthetic beauty of manganese carboxylate chemistry.

Experimental Section

1: A solution of $teaH_3$ (0.075 g, 0.5 mmol) in MeCN (5 mL) was added to a stirred solution of $[Mn_3O(O_2CHPh_2)_6(py)_3](ClO_4)$ (0.27 g, 0.25 mmol) in MeCN (35 mL). The resultant dark brown solution was stirred for a further 15 min, filtered, and the filtrate left undisturbed at ambient temperature. After two weeks, X-ray quality brown crystals had formed and were collected by filtration, washed with MeCN, and dried in vacuo. Yield, 42%. The crystallographic sample was maintained in contact with mother liquor to prevent solvent loss and identified crystallographically as **1**·4 MeCN. Elemental analysis (%) calcd for **1**·4 MeCN: C 62.38, H 5.52, N 4.04; found: C

 © 2005 Wiley-VCH Verlag GmbH & Co. KGaA, Weinheim

62.01, H 5.54, N 3.82. Selected IR data (KBr): $\nu = 3427$ (br), 2889 (br), 1575 (m), 1497 (s), 1451 (s), 1386 (m), 1068 (s), 1032 (s), 899 (s), 743 (s), 702 (m), 664 cm^{-1} (w).

2: A solution of $teaH_3$ (0.075 g, 0.5 mmol) in CH_2Cl_2 (10 mL) was added to a stirred solution of $[Mn_{12}O_{12}(O_2CCH_2tBu)_{16}(H_2O)_4]$ (0.17 g, 0.06 mmol) in CH_2Cl_2 (35 mL). The resultant dark brown solution was stirred for a further 15 min, filtered, and the filtrate left undisturbed at ambient temperature. After one week, X-ray quality dark brown crystals had formed and were collected by filtration, washed with CH_2Cl_2, and dried in vacuo. Yield, 58%. The crystallographic sample was maintained in contact with mother liquor to prevent solvent loss and identified crystallographically as $\mathbf{2}\cdot 2\,CH_2Cl_2$. Elemental analysis (%) calcd for $\mathbf{2}\cdot CH_2Cl_2$: C 46.70, H 7.51, N 2.25; found: C 46.63, H 7.60, N 2.27. Selected IR data (KBr): $\nu = 3446$ (br), 2953 (s), 2866 (m), 1615 (s), 1585 (s), 1383 (s), 1297 (m), 1236 (w), 1089 (m), 910 (w), 897 (w), 730 (w), 593 cm^{-1} (m).

3: A solution of NEt_3 (0.075 mL, 0.5 mmol) in MeCN (5 mL) was added to a stirred, pale yellow-brown solution of $Mn(O_2CMe)_2\cdot 4\,H_2O$ (0.123 g, 0.5 mmol) and $teaH_3$ (0.075 g, 0.5 mmol) in MeCN (35 mL). The resulting dark brown solution was stirred for a further 15 min, filtered, and the filtrate left undisturbed at ambient temperature. After two days, X-ray quality dark brown crystals had formed and were collected by filtration, washed with MeCN, and dried in vacuo. Yield, 60%. The crystallographic sample was maintained in contact with mother liquor to prevent solvent loss and identified crystallographically as $\mathbf{3}\cdot 16\,MeCN$. Dried material is hygroscopic, and analyzed as $\mathbf{3}\cdot 6\,H_2O$. Elemental analysis (%) calcd for $\mathbf{3}\cdot 6\,H_2O$: C 33.78, H 5.88, N 4.54; found: C 33.72, H 5.80, N 4.44. Selected IR data (KBr): $\nu = 3410$ (br), 2850 (b), 1575 (m), 1409 (m), 1339(w), 1085 (m), 1036 (m), 903 (m), 746 (w), 662 (m), 572 cm^{-1} (s).

Received: August 18, 2004
Published online: December 28, 2004

Keywords: cluster compounds · magnetic properties · manganese · N, O ligands · single-molecule magnets

[1] a) D. Foguet-Albiol, T. A. O'Brien, W. Wernsdorfer, B. Moulton, M. J. Zaworotko, K. A. Abboud, G. Christou, *Angew. Chem.* **2005**, *117*, 919; *Angew. Chem. Int. Ed.* **2005**, *44*, 897; b) A. J. Tasiopoulos, W. Wernsdorfer, K. A. Abboud, G. Christou, *Angew. Chem.* **2004**, *116*, 6498; *Angew. Chem. Int. Ed.* **2004**, *43*, 6338; c) R. Sessoli, H.-L. Tsai, A. R. Schake, S. Wang, J. B. Vincent, K. Folting, D. Gatteschi, G. Christou, D. N. Hendrickson, *J. Am. Chem. Soc.* **1993**, *115*, 1804; d) R. Sessoli, D. Gatteschi, A. Caneschi, M. A. Novak, *Nature* **1993**, *365*, 141.

[2] a) R. Sessoli, H. Tsai, A. R. Schake, S. Wang, J. B. Vincent, K. Folting , D. Gatteschi, G. Christou, D. N. Hendrickson, *J. Am. Chem. Soc.* **1993**, *115*, 1804; b) E. K. Brechin, J. Yoo, M. Nakano, J. C. Huffman, D. N. Hendrickson, G. Christou, *Chem. Commun.* **1999**, 783; c) J. Yoo, E. K. Brechin, A. Yamaguchi, M. Nakano, J. C. Huffman, A. L. Maniero, L.-C. Brunel, K. Awaga, H. Ishimoto, G. Christou, D. N. Hendrickson, *Inorg. Chem.* **2000**, *39*, 3615; d) M. Soler, W. Wernsdorfer, K. Folting, M. Pink, G. Christou, *J. Am. Chem. Soc.* **2004**, *126*, 2156; e) W. Wernsdorfer, N. Aliaga-Alcalde, D. N. Hendrickson, G. Christou, *Nature* **2002**, *416*, 406; f) D. Price, S. Batten, B. Moubaraki, K. Murray, *Chem. Commun.* **2002**, 762; g) E. Brechin, C. Boskovic, W. Wernsdorfer, J. Yoo, A. Yamaguchi, C. Sanudo, T. Concolino, A. Rheingold, H. Ishimoto, D. Hendrickson, G. Christou, *J. Am. Chem. Soc.* **2002**, *124*, 9710; h) C. Boskovic, W. Wernsdorfer, K. Folting, J. C. Huffman, D. N. Hendrickson, G. Christou, *Inorg. Chem.* **2002**, *41*, 5107; i) N. E. Chakov, K. A. Abboud, L. N. Zakharov, A. L. Rheingold, D. N. Hendrickson, G. Christou, *Polyhedron* **2003**, *22*, 1759; j) J. T. Brockman, K. A. Abboud, D. N. Hendrickson, G. Christou, *Polyhedron* **2003**, *22*, 1765; k) M. Soler, W. Wernsdorfer, K. A. Abboud, J. C. Huffman, E. R. Davidson, D. N. Hendrickson, G. Christou, *J. Am. Chem. Soc.* **2003**, *125*, 3576; l) M. Soler, W. Wernsdorfer, K. A. Abboud, D. N. Hendrickson, G. Christou, *Polyhedron* **2003**, *22*, 1777; m) A. Morello, O. N. Bakharev, H. B. Brom, L. J. de Jongh, *Polyhedron* **2003**, *22*, 1745; n) E. Brechin, M. Soler, G. Christou, M. Helliwell, S. Teat, W. Wernsdorfer, *Chem. Commun.* **2003**, 1276; o) C. J. Milios, C. P. Raptopoulou, A. Terzis, F. Lloret, R. Vicente, S. P. Perlepes, A. Escuer, *Angew. Chem.* **2004**, *116*, 212; *Angew. Chem. Int. Ed.* **2004**, *43*, 210; p) M. Murugesu, J. Raftery, W. Wernsdorfer, G. Christou, E. K. Brechin, *Inorg. Chem.* **2004**, *43*, 4203; q) M. Murugesu, M. Habrych, W. Wernsdorfer, K. A. Abboud, G. Christou, *J. Am. Chem. Soc.* **2004**, *126*, 4766; r) E. C. Sañudo, W. Wernsdorfer, K. A. Abboud, G. Christou, *Inorg. Chem.* **2004**, *43*, 4137 – 4144.

[3] a) B. Pilawa, M. Keleman, S. Wanka, A. Geisselmann, A. Barra, *Europhys. Lett.* **1998**, *43*, 7; b) L. Wittick, K. Murray, B. Moubaraki, S. Batten, L. Spiccia, K. Berry, *Dalton Trans.* **2004**, 1003.

[4] a) Crystal structure data for $\mathbf{1}\cdot 4\,MeCN$: $C_{144}H_{154}Mn_6N_8O_{28}$, $M_r = 2774.39$, triclinic, space group $P\bar{1}$, $a = 14.7173(9)$, $b = 14.8251(9)$, $c = 17.6759(11)$ Å, $\alpha = 90.389(2)$, $\beta = 109.950(2)$, $\gamma = 108.101(2)°$, $V = 3418.2(4)$ Å^3, $T = 173$ K, $Z = 1$, 25657 reflections collected, 11970 unique ($R_{int} = 0.0773$), $R1 = 0.0952$, $wR2 = 0.1414$, using 8832 reflections with $I > 2\sigma(I)$. The asymmetric unit consists of half the Mn_6 and 2 MeCN molecules. b) CCDC-225868, CCDC-247748, and CCDC-225869 contain the supplementary crystallographic data for this paper. These data can be obtained free of charge via www.ccdc.cam.ac.uk/conts/retrieving.html (or from the Cambridge Crystallographic Data Centre, 12, Union Road, Cambridge CB2 1EZ, UK; fax: (+44) 1223-336-033; or deposit@ccdc.cam.ac.uk).

[5] J. Yoo, A. Yamaguchi, M. Nakano, J. Krzystek, W. Streib, L. Brunel, H. Ishimoto, G. Christou, D. Hendrickson, *Inorg. Chem.* **2001**, *40*, 4604.

[6] Crystal structure data for $\mathbf{2}\cdot 2\,CH_2Cl_2$: $C_{98}H_{188}Cl_4Mn_8N_4O_{36}$, $M_r = 2579.8$, monoclinic, space group $C2/c$, $a = 26.2251(14)$, $b = 18.4264(10)$, $c = 25.8724(12)$ Å, $\alpha = 90$, $\beta = 99.4770(10)$, $\gamma = 90°$, $V = 12328(12)$ Å^3, $T = 173$ K, $Z = 4$, 37856 reflections collected, 13813 unique ($R_{int} = 0.0676$), $R1 = 0.0521$, $wR2 = 0.1338$, using 7094 reflections with $I > 2\sigma(I)$. The asymmetric unit consists of half a Mn_8 cluster and a disordered CH_2Cl_2 molecule.[4b]

[7] Crystal structure data for $\mathbf{3}\cdot 16\,MeCN$: $C_{136}H_{252}Mn_{16}N_{28}O_{68}$, $M_r = 4246.7$, triclinic, space group $P\bar{1}$, $a = 20.2034(17)$, $b = 21.6675(18)$, $c = 24.124(2)$ Å, $\alpha = 105.025(2)$, $\beta = 100.393(2)$, $\gamma = 104.126(2)°$, $V = 9550.6(14)$ Å^3, $T = 173$ K, $Z = 2$, 85365 reflections collected, 42222 unique ($R_{int} = 0.0531$), $R1 = 0.0468$, $wR2 = 0.1089$, using 22696 reflections with $I > 2\sigma(I)$. The asymmetric unit consists of a Mn_{16} and 16 MeCN molecules.[4b]

[8] a) C. Cadiou, M. Murrie, C. Paulsen, V. Villar, W. Wernsdorfer, R. E. P. Winpenny, *Chem. Commun.* **2001**, 2666; b) L. Jones, A. Batsanov, E. Brechin, D. Collison, M. Helliwell, T. Mallah, E. McInnes, S. Piligkos, *Angew. Chem.* **2002**, *114*, 4494; *Angew. Chem. Int. Ed.* **2002**, *41*, 4318.

[9] L. Jones, A. Batsanov, E. Brechin, D. Collison, M. Helliwell, T. Mallah, E. McInnes, S. Piligkos, *Angew. Chem.* **2002**, *114*, 4494; *Angew. Chem. Int. Ed.* **2002**, *41*, 4318.

[10] W. Wernsdorfer, *Adv. Chem. Phys.* **2001**, *118*, 99.

[11] A. Dolbecq, F. Secheresse, *Adv. Inorg. Chem.* **2002**, *53*, 1 – 41.

 © 2005 Wiley-VCH Verlag GmbH & Co. KGaA, Weinheim

Single-Molecule Magnets

DFT Computational Rationalization of an Unusual Spin Ground State in an Mn_{12} Single-Molecule Magnet with a Low-Symmetry Loop Structure**

*Dolos Foguet-Albiol, Ted A. O'Brien, Wolfgang Wernsdorfer, Brian Moulton, Michael J. Zaworotko, Khalil A. Abboud, and George Christou**

Single-molecule magnets (SMMs) represent a molecular approach to nanoscale magnetic materials. They are molecules possessing a large barrier (versus kT) to magnetization relaxation, and thus display magnetization versus applied-field hysteresis loops at low enough temperatures, the diagnostic property of a magnet.[1] SMMs derive their properties from a combination of a large ground-state spin (S) value and a significant magnetoanisotropy of the Ising (easy-axis) type.

Deprotonated pyridine-2,6-dimethanol ($pdmH_2$) has proven a versatile N,O,O chelating and bridging ligand in our manganese-cluster chemistry. It has been found as a chelate in species such as $[PtCl_2(pdmH_2)]$,[2] $[TcOCl(pdmH)_2]$,[3] and $[\{MoO_2(pdm)\}_n]$.[4] In manganese chemistry, the alkoxide arms also act as bridging groups yielding polynuclear clusters such as $[Mn_4(O_2CMe)_2(pdmH)_6]^{2+}$ with $S = 9$,[5] $[Mn_9(O_2CEt)_{12}(pdm)(pdmH)_2(L)_2]$ with $S = 11/2$,[6] and $[Mn_{25}O_{18}(OH)_2(N_3)_{12}(pdm)_6(pdmH)_6]^{2+}$ with $S = 51/2$.[7] All these complexes are SMMs. Recently, we have been exploring the products from reactions employing *N*-methyldiethanolamine ($mdaH_2$). This is also a N,O,O chelate, but is more flexible than $pdmH_2$ and we anticipated that it might lead to new types of manganese clusters; we were unaware of any use of $mdaH_2$ in manganese chemistry. We herein report the synthesis and properties of Mn_4 and Mn_{12} clusters with this ligand, and show that they are new SMMs. Further, the Mn_{12} cluster has an unusual ground-state spin value for a loop structure, and we provide rationalization for this using DFT calculations.

The reactions of $mdaH_2$ have been investigated with a variety of Mn carboxylate sources and under a variety of conditions. The reaction between $Mn(O_2CMe)_2{\cdot}4H_2O$, $mdaH_2$,and NEt_3 in a 1:1:1 molar ratio in MeCN resulted in the formation of $[Mn_{12}(O_2CMe)_{14}(mda)_8]{\cdot}MeCN$ (**1**·MeCN) in 55% yield. In contrast, when the same reaction was carried out with the bulkier benzoate group by using $Mn(O_2CPh)_2{\cdot}4H_2O$, the crystalline product was $[Mn_4(O_2CPh)_4(mda)_2(mdaH)_2]{\cdot}CH_2Cl_2{\cdot}Et_2O$ (**2**·CH_2Cl_2·Et_2O) in 16% yield. The crystal structure of complex **1**[8] consists of a Mn_{12} loop with crystallographic *Ci* symmetry that is mixed-valent ($Mn^{II}_6Mn^{III}_6$) and possesses a chair conformation (Figure 1, top). All the manganese centers are six-coordinate except Mn^{II} ions Mn4 and Mn4′, which have a very distorted pentagonal-bipyramidal coordination sphere. Six mda^{2-} ligands each chelate a Mn^{III} ion, and the two alkoxide O atoms bridge to the adjacent Mn^{II} ions. The other two mda^{2-} groups chelate Mn^{II} ions and bridge by their alkoxide O atoms to Mn^{III} ions. As a result, the mda^{2-} groups alternate between being axial and equatorial with respect to

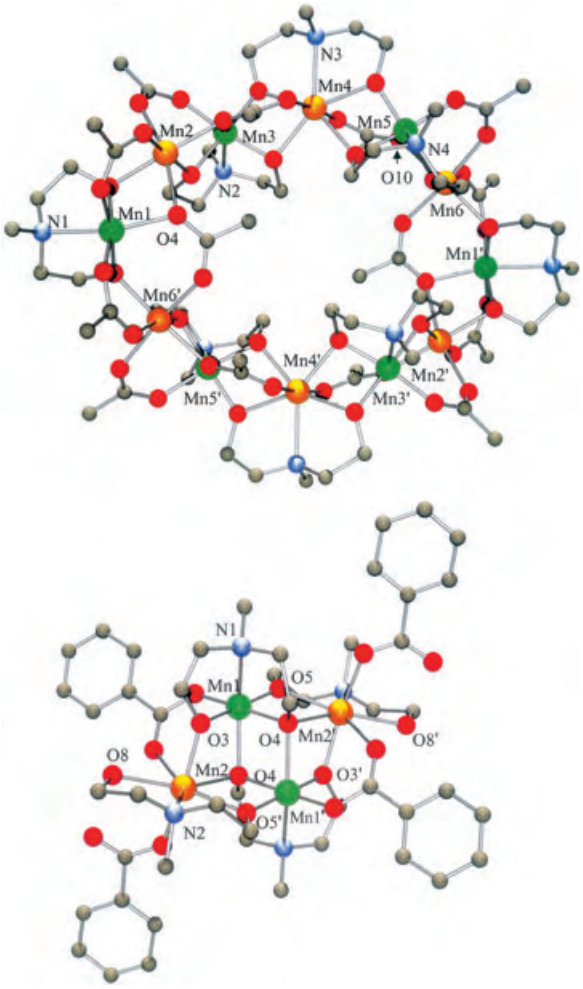


Figure 1. PovRay plot of complexes **1** (top) and **2** (bottom). Color scheme: Mn^{III} green, Mn^{II} orange, O red, N blue, C gray. H atoms have been omitted for clarity.

[*] D. Foguet-Albiol, Dr. K. A. Abboud, Prof. Dr. G. Christou
Department of Chemistry
University of Florida
Gainesville, FL 32611-7200 (USA)
Fax: (+1) 352-392-8757
E-mail: christou@chem.ufl.edu
Dr. W. Wernsdorfer
Laboratoire Louis Néel-CNRS, BP-166
Grenoble, Cedex 9 (France)
Dr. T. A. O'Brien
Department of Chemistry
Indiana University-Purdue University Indianapolis
Indianapolis, IN 46202-3274 (USA)
Dr. B. Moulton, Prof. Dr. M. J. Zaworotko
Department of Chemistry
University of South Florida, Tampa, FL 33620 (USA)

[**] This work was supported by the U.S. National Science Foundation (Grant CHE-0414155).

 DOI: 10.1002/anie.200461820 © 2005 Wiley-VCH Verlag GmbH & Co. KGaA, Weinheim

the plane of the Mn_{12} loop. Each Mn_2 pair is additionally bridged by an acetate group in its familiar η^1,η^1,μ (*syn*,*syn*) binding mode on the outside of the loop, whereas the final two acetate groups bridge in a rarer η^1,η^2,μ_3 mode on the inside of the loop. The Mn^{II}/Mn^{III} oxidation state assignments were established by consideration of bond lengths, bond-valence sum (BVS) calculations[9] and the presence of Jahn–Teller (JT) distortions at six of the Mn ions, as expected for high-spin Mn^{III} in near-octahedral geometry; the JT axes all contain the mda^{2-} N atoms.

The structure of **2**[8] is similar to that of $[Mn_4(O_2C\text{-}Me)_2(pdmH)_6]^{2+}$[5] and consists of a Mn_4 planar rhombus that can be described as two edge-fused Mn_3 triangular units (Figure 1, bottom). Inspection of structural parameters, BVS calculations, and detection of Mn^{III} JT elongation axes at Mn1/Mn1′ identifies Mn1/Mn1′ as Mn^{III} and Mn2/Mn2′ as Mn^{II} centers. Each Mn^{III} ion is chelated by a tridentate mda^{2-} group, one of whose alkoxide O atoms (O3) bridges to Mn2, and the other (O4) to Mn1′ and Mn2′. The two $mdaH^-$ groups also each bind in a tridentate fashion, with one of their alkoxide O atoms (O5) doubly bridging to Mn2′ but the other (O8) being protonated, terminally bound to Mn2, and forming a hydrogen bond to the unbound O atom of the monodentate benzoate ligand. This situation was confirmed by the BVS for O8 being 1.15, as expected for a protonated O atom whose bound H^+ ion is not located. Finally, two additional benzoate groups, each bridging a Mn^{II}/Mn^{III} pair, complete the ligation, making Mn1 six coordinate and Mn2 seven coordinate. Mn1 and Mn1′ display JT elongations along the O4-Mn1-N1 and O4′-Mn1′-N1′ axes.

Solid-state DC magnetic susceptibility (χ_M) measurements were made on **1** and **2** in a 0.1 tesla field in the 5.00–300 K range. The obtained data are shown as $\chi_M T$ versus T plots in Figure 2, and indicate that both **1** and **2** have relatively large ground-state spin values. These values were determined by fits of magnetization (M) data collected in the 1.8–10 K and 0.1–3 T ranges: the fits are shown in Figure 3, and the fit parameters were $S=7$, $g=1.91$, and $D=-0.37$ K for **1**, and $S=9$, $g=1.78$, and $D=-0.22$ K for **2**. When data collected at fields higher than 3 T were used, the fits were poor, suggesting the presence of low-lying excited states, as expected for species containing Mn^{II} ions, which give weak exchange interactions. The use of low-field data to avoid this common problem has been described elsewhere.[10,11] The $S=9$ ground state of **2** is as expected for all the exchange interactions in the cluster being ferromagnetic, as found in other compounds with a related core.[5] The $S=7$ ground state of **1**, however, is most unusual for an Mn^{II}_6,Mn^{III}_6 species.

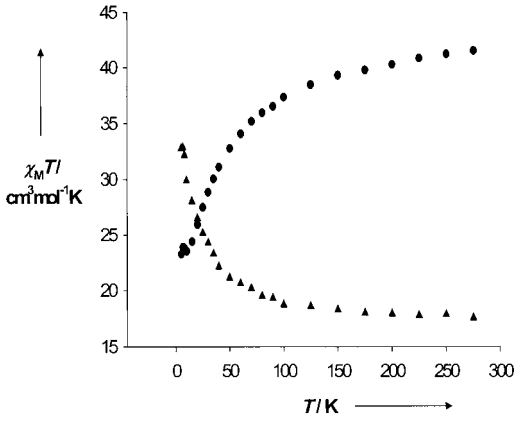


Figure 2. $\chi_M T$ versus T plots for complexes **1** (●) and **2** (▼).

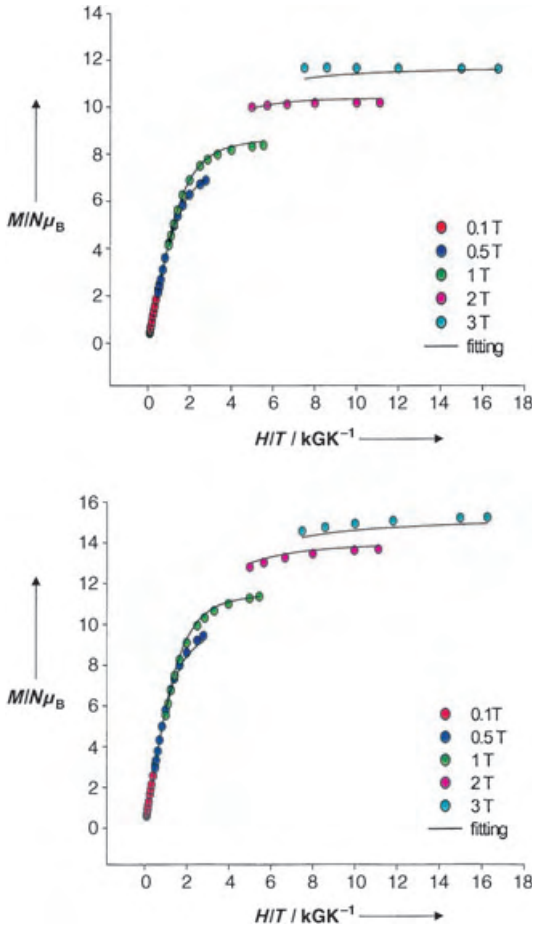


Figure 3. Magnetization (M) versus field (H) and temperature (T) data, plotted as reduced magnetization ($M/N\mu_B$) versus H/T, for complexes **1** (top) and **2** (bottom) at applied fields of 0.1, 0.5, 1.0, 2.0 and 3.0 T and in the 1.8 to 10 K temperature range. The solid lines are the fits of the data; see the text for the fit parameters.

Since **1** and **2** have significant ground-state S values, AC susceptibility measurements were performed in the 1.8–10 K range with a 3.5 G AC field oscillating at 50–1500 Hz to determine if they might be SMMs. Indeed, frequency-dependent tails were seen of out-of-phase (χ_M'') signals whose maxima lie below the operating minimum temperature of our SQUID instrument (1.8 K). In addition, the in-phase (χ_M') signals support the S values obtained for **1** and **2** from the above magnetization fits. Confirmation that **1** and **2** are SMMs was obtained from magnetization (M) versus applied DC field scans on single crystals down to 0.04 K, these scans displayed hysteresis, the diagnostic property of a magnet (Figure 4). The hysteresis loops for **1** show the characteristic steps arising from quantum tunneling of the magnetization (QTM), with the step sizes increasing with decreasing scan rates, as expected for SMMs. The loops for **2** are similar, but

 © 2005 Wiley-VCH Verlag GmbH & Co. KGaA, Weinheim

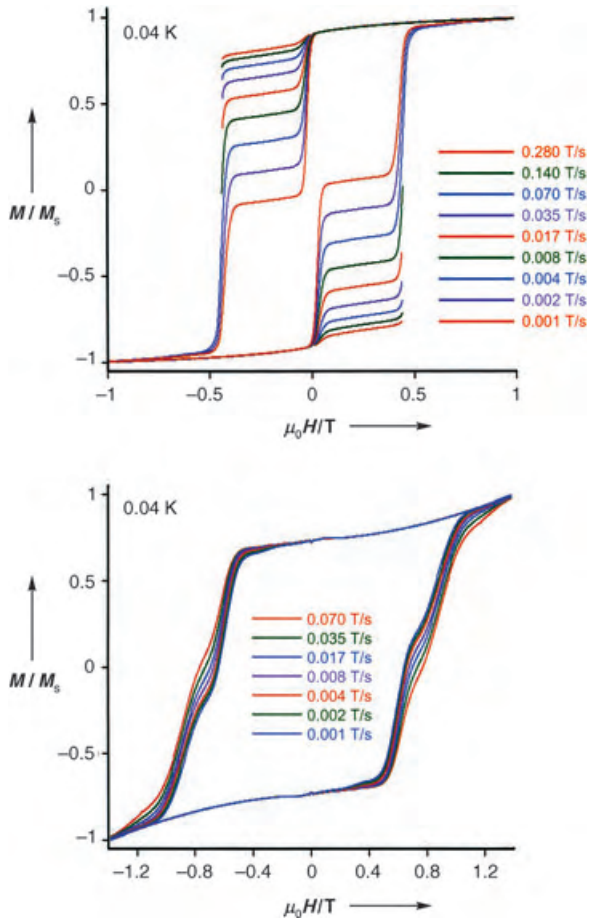


Figure 4. Magnetization (*M*) versus field (*H*) hysteresis loops for complexes **1** (top) and **2** (bottom) at 0.04 K and at the indicated scan rates; the magnetization is normalized to its saturation value (M_S).

have an unusual background slope owing to the presence of two molecules with different orientations in the unit cell. The field was applied along the easy axis (*z* axis) of one molecule and thus approximately transverse to the easy axis of the other; these field orientations should give a step-like hysteresis loop and a linear slope from the two molecules, respectively, and a combination of the two results is thus observed. Complex **1** is a rare example of a SMM with a single-strand loop structure, with only a Mn_{16} complex with $S = 10$[1a] and a Ni_{12} complex with $S = 12$[12] being reported to date.

Magnetization decay studies were carried out at different temperatures, and the resulting relaxation time (τ) versus T data used to construct τ versus $1/T$ Arrhenius plots. The effective barriers to relaxation (U_{eff}) can be obtained from the slopes in the thermally activated regions and the pre-exponential factors (τ_0) from the intercepts. These were $U_{eff} = 11$ K and $\tau_0 = 7 \times 10^{-7}$ s for **1**, and $U_{eff} = 15.3$ K and $\tau_0 = 3 \times 10^{-7}$ s for **2**. At very low temperatures, both compounds display the temperature-independent relaxation characteristic of QTM.

The $S = 7$ ground state of **1** is unusually intermediate in magnitude for a single-stranded Mn^{II}_6,Mn^{III}_6 loop complex: antiferromagnetic or ferromagnetic Mn^{II}/Mn^{III} exchange interactions would be expected to give $S = 3$ or 27 ground states, respectively, so it is clear that there must be both types of interaction within low-symmetry **1**. Since a quantitative rationalization of the *S* values of low-symmetry, high-nuclearity clusters is rarely available, and yet is crucial to our full understanding of their magnetic properties, we have carried out DFT calculations on **1**.

The entire complex is too large to be considered with DFT, so several smaller model clusters were constructed; a similar approach has been used by others for a number of complexes.[13] The six symmetry-inequivalent Mn ions were divided into two clusters of three, the first including Mn3, Mn4, and Mn5 and the second including Mn2, Mn1, and Mn6′. In defining the model clusters, ligands bridging metal centers had to be made terminal. To do so, carboxylate ligands were protonated to give $MeCO_2H$ ligands, with the H^+ ion added outside the cluster at a distance of 1.0 Å along the line connecting the O atom and the metal. Only the oxygen-donor site was retained for mda^{2-} ligands bridging between the different clusters, along with the first carbon atom of the corresponding ethylene chain. The second carbon atom was replaced with a hydrogen atom at a bond length scaled to 1.1 Å, giving an MeO^- ligand. In this way, the model clusters had neutral charge, as does the parent complex, and a reasonable simulation of the ligand field of each Mn was maintained.

With the above-described alterations, Mn3, Mn4, and Mn5 are included in the model complex $[Mn^{II}Mn^{III}_2(O_2CMe)_2(HO_2CMe)_2(mda)_3]$. Similarly, Mn2, Mn1, and Mn6′ are included in the model complex $[Mn^{II}_2Mn^{III}(O_2CMe)_3(HO_2CMe)_4(OMe)_2(mda)]$. Finally, the connections between the units, Mn2–Mn3 and Mn5–Mn6, are each modeled with the dinuclear complex $[Mn^{II}Mn^{III}(O_2CMe)(HO_2CMe)_3(OMe)_2(mda)]$; although this formula is identical for both connections, the structural parameters are not, and retain the same values as those in the Mn2–Mn3 and Mn5–Mn6 subunits of complex **1**.

Atomic spin densities were monitored in the calculations to ensure the correct spin components were obtained for each cluster. Values of 4.77, 3.71, and 3.71 were obtained for the high-spin component of the $Mn^{II}Mn^{III}_2$ cluster, for example. The energies of these components were then used to find the exchange parameters (Table 1). It is clear that all the *J* values are weak, in the range $4.0 > J > -4.6$ cm^{-1}. This range is fully consistent with values for $Mn^{II}Mn^{III}$ exchange parameters,

Table 1: Exchange parameters (*J*), using the $\hat{\mathcal{H}} = -2J\hat{S}_i\hat{S}_j$ convention, from DFT calculations on complex **1**.

Interactions	*J*
Mn4–Mn5, Mn4′–Mn5′[a]	+4.0
Mn3–Mn4, Mn3′–Mn4′[a]	+3.5
Mn2–Mn3, Mn2′–Mn3′[b]	−4.6
Mn5–Mn6, Mn5′–Mn6′[b]	−2.5
Mn1–Mn2, Mn1′–Mn2′[c]	−1.4
Mn1–Mn6′, Mn1′–Mn6[c]	+0.0[d]

[a] Model complex $[Mn^{II}Mn^{III}_2(O_2CMe)_2(HO_2CMe)_2(mda)_3]$. [b] Model complex $[Mn^{II}Mn^{III}(O_2CMe)(HO_2CMe)_3(OMe)_2(mda)]$. [c] Model complex $[Mn^{II}_2Mn^{III}(O_2CMe)_3(HO_2CMe)_4(OMe)_2(mda)]$. [d] Small ferromagnetic value (+0.02 cm^{-1}) calculated for this parameter.

 © 2005 Wiley-VCH Verlag GmbH & Co. KGaA, Weinheim

which are always weak and either side of zero, depending on the bridges.[14] The ferromagnetic ($J > 0$) parameters correspond to Mn_2 pairs bridged by two mono-atomic alkoxide bridges, whereas all the other bridging types are antiferromagnetic; this is the same pattern as in dinuclear $Mn^{II}Mn^{III}$ complexes.[14] Within the uncertainty of the DFT calculation, the Mn1–Mn6′ and Mn1′–Mn6 interactions are calculated to be 0.0 cm^{-1}: in fact, they are almost certainly either very weakly positive or negative. Since the spin of each half of the molecule is calculated to be $S = 7/2$, positive Mn1–Mn6′ and Mn1′–Mn6 interactions would give a ground-state spin of $S = 0$ while negative Mn1–Mn6′ and Mn1′–Mn6 interactions give $S = 7$, for the complete molecule (Figure 5). On the basis of

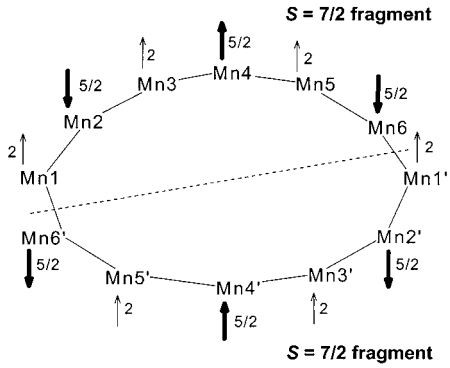


Figure 5. Depiction of the spin alignments in the $S = 7$ ground state of complex **1** as predicted by the DFT calculations, with the Mn1–Mn6′ and Mn1′–Mn6 interactions antiferromagnetic. The Mn labeling scheme is the same as that in Figure 1 (top). The dashed line separates the two $S = 7/2$ fragments that are coupled by the interactions between Mn1–Mn6′ and Mn1′–Mn6; if these interactions are antiferromagnetic (negative J values), the resultant spin of the complete molecule is $S = 7$.

the magnetization data described above, complex **1** clearly does not have an $S = 0$ ground state, and we thus conclude that the ground state is $S = 7$, resulting from the spin alignments in Figure 5. Weakly antiferromagnetic Mn1–Mn6′ and Mn1′–Mn6 interactions are in fact consistent with the nature of the bridging ligands at these sites.[14] The conclusion that $S = 7$ is also in complete agreement with the magnetization fits and in-phase AC data.

In summary, the use of $mdaH_2$ has led to new Mn_{12} and Mn_4 SMMs with $S = 7$ and $S = 9$ ground-state spins, respectively. The Mn_{12} species is a very rare example of a SMM with a loop structure,[1a,21] and its unusual $S = 7$ ground state for an $Mn^{III}_6Mn^{II}_6$ species has been rationalized by DFT calculations to be due to the variety of exchange interactions present.

Experimental Section

1·MeCN: Method A: $mdaH_2$ (0.23 mL, 1.0 mmol) and NEt_3 (0.28 mL, 1.0 mmol) were added to a stirred solution of $Mn(O_2CMe)_2{\cdot}4H_2O$ (0.50 g, 1.0 mmol) in MeCN (30 mL), which caused a rapid color change to dark brown. The resulting dark brown solution was stirred for 1 h, and then layered with diethyl ether. After several days, dark red crystals of **1**·MeCN were collected by filtration, washed with Et_2O (2×15 mL), and dried in air. The yield was 55%. Elemental analysis (%) calcd for $C_{72}H_{136}Mn_{12}N_{10}O_{44}$ (**1**·MeCN): C 33.92, H 5.42, N 4.87; found: C 34.33, H 5.72, N 4.48.

Method B: $mdaH_2$ (0.29 mL, 1.0 mmol), NaO_2CMe_2 (0.42 g, 2.0 mmol) and NEt_3 (0.35 mL, 1.0 mmol) were added to a stirred solution of $MnCl_2{\cdot}4H_2O$ (0.50 g, 1.0 mmol) in MeCN (30 mL), which caused a rapid color change to dark brown. The resulting dark brown solution was stirred for 1 h and then layered with diethyl ether. After several days, dark red crystals of **1**·MeCN were collected by filtration, washed with ether and dried in air; yield 46%. The material was spectroscopically identical with the material from Method A.

2·CH_2Cl_2·Et_2O: $mdaH_2$ (0.17 g, 1.0 mmol) was added to a stirred solution of $Mn(O_2CPh)_2{\cdot}4H_2O$ (0.50 g, 1.0 mmol) in MeCN (30 mL) and NEt_3 (0.21 mL, 1.0 mmol), which caused a rapid color change to dark brown. The resulting dark brown solution was stirred for 1 h and the resulting precipitate was collected by filtration, washed with MeCN, dissolved in CH_2Cl_2 (50 mL), filtered, and the filtrate layered with diethyl ether. After several days, light brown crystals of **2** were collected by filtration, washed with diethyl ether (2×15 mL), and dried in air; yield 16%. Elemental analysis (%) calcd for $C_{58}H_{90}Cl_4Mn_4N_4O_{18}$ (**2**·CH_2Cl_2·Et_2O): C 48.99, H 5.82, N 4.76; found: C 48.99, H 5.44, N 4.56.

Density functional theory (DFT) calculations were carried out using the B3LYP functional[15] implemented in the Gaussian 98 program,[16] with the all-electron Dunning–Huzinaga double-ζ basis for light atoms[17] and the Los Alamos effective core potential plus double-ζ valence basis set for manganese atoms.[18] The procedure given in ref. [19] was used to obtain starting orbitals for the DFT calculations. The exchange constants were found by fitting calculated energies and spin couplings to the Heisenberg Hamiltonian.[19,20]

Received: August 29, 2004
Published online: December 28, 2004

Keywords: cluster compounds · density functional calculations · magnetic properties · manganese · single-molecule magnets

[1] a) M. Murugesu, W. Wernsdorfer, K. A. Abboud, G. Christou, *Angew. Chem.* **2005**, *117*, 914; *Angew. Chem. Int. Ed.* **2005**, *44*, 892; b) A. J. Tasiopoulos, W. Wernsdorfer, K. A. Abboud, G. Christou, *Angew. Chem.* **2004**, *116*, 6498; *Angew. Chem. Int. Ed.* **2004**, *43*, 6338; c) G. Christou, D. Gatteschi, D. N. Hendrickson, R. Sessoli, *MRS Bull.* **2000**, *25*, 66; d) R. Sessoli, H.-L. Tsai, A. R. Schake, S. Wang, J. B. Vincent, K. Folting, D. Gatteschi, G. Christou, D. N. Hendrickson, *J. Am. Chem. Soc.* **1993**, *115*, 1804; e) R. Sessoli, D. Gatteschi, A. Caneschi, M. A. Novak, *Nature* **1993**, *365*, 141.

[2] F. D. Rochon, A. L. Beauchamp, C. C. Bensimon, *Can. J. Chem.* **1996**, *74*, 2121.

[3] F. D. Rochon, R. Melanson, P. C. Kong, *Inorg. Chim. Acta* **1997**, 254, 303.

[4] J. M. Berg, R. H. Holm, *Inorg. Chem.* **1983**, *22*, 1768.

[5] a) E. K. Brechin, J. Yoo, M. Nakano, J. C. Huffman, D. N. Hendrickson, G. Christou, *Chem. Commun.* **1999**, 783–784; b) J. Yoo, E. K. Brechin, A. Yamaguchi, M. Nakano, J. C. Huffman, A. L. Maniero, L.-C. Brunel, K. Awaga, H. Ishimoto, G. Christou, D. N. Hendrickson, *Inorg. Chem.* **2000**, *39*, 3615.

[6] C. Boskovic, W. Wernsdorfer, K. Folting, J. C. Huffman, D. N. Hendrickson, G. Christou, *Inorg. Chem.* **2002**, *41*, 5107.

[7] M. Murugesu, M. Habrych, W. Wernsdorfer, K. A. Abboud, G. Christou, *J. Am. Chem. Soc.* **2004**, *126*, 4766.

[8] Crystal structure data for **1**·MeCN: $C_{72}H_{136}Mn_{12}N_{10}O_{44}$, $M_r = 2505.19$, triclinic, space group $P\bar{1}$, $a = 13.1062(13)$, $b = 13.2707(13)$, $c = 17.2424(17)$ Å, $\alpha = 107.223(2)$, $\beta = 109.214(2)$, $\gamma = 99.260(2)°$, $V = 2591.6(4)$ Å^3, $T = 100(2)$ K, $Z = 2$, $\rho_{calcd} = 1.605$ g cm^{-3}, 17243 reflections collected, 8624 unique ($R_{av} = 0.0868$), $R1 = 0.0486$, w$R2 = 0.0891$, using 5470 reflections with

 © 2005 Wiley-VCH Verlag GmbH & Co. KGaA, Weinheim

$I > 2\sigma(I)$. Crystal structure data for **2**·CH_2Cl_2·Et_2O: $C_{58}H_{90}Cl_4Mn_4N_4O_{18}$, $M_r = 1492.90$, Monoclinic, space group $P2_1/n$, $a = 18.069(2)$, $b = 8.3713(11)$, $c = 23.707(3)$ Å, $\alpha = 90°$, $\beta = 102.096(3)$, $\gamma = 90°$, $V = 3506.3(8)$ Å^3, $T = 173$ K, $Z = 1$, $\rho_{calcd} = 1.414$ g cm^{-3}, 18497 reflections collected, 8624 unique ($R_{av} = 0.0868$), $R1 = 0.0718$, w$R2 = 0.1839$, using 18497 reflections with $I > 2\sigma(I)$. CCDC-248525 and CCDC-248526 contain the supplementary crystallographic data for this paper. These data can be obtained free of charge via www.ccdc.cam.ac.uk/conts/retrieving.html (or from the Cambridge Crystallographic Data Centre, 12 Union Road, Cambridge CB21EZ, UK; fax: (+44) 1223-336-033; or deposit@ccdc.cam.ac.uk).

[9] a) Bond valence sum (BVS) calculations for the Mn ions of **1** gave values of 2.83 (for Mn1), 1.90 (Mn2), 2.95 (Mn3), 1.74 (Mn4), 2.96 (Mn5) and 1.83 (Mn6), and for the Mn ions of **2** gave values of 3.01 (for Mn1) and 1.86 (Mn2); b) W. Liu, H. H. Thorp, *Inorg. Chem.* **1993**, *32*, 4102; c) Brown, I. D. Altermatt, *Acta Crystallogr. Sect. B* **1985**, 244.

[10] M. Soler, W. Wernsdorfer, K. Folting, M. Pink, G. Christou, *J. Am. Chem. Soc.* **2004**, *126*, 2156–2165.

[11] E. C. Sañudo, W. Wernsdorfer, K. A. Abboud, G. Christou, *Inorg. Chem.* **2004**, *43*, 4137.

[12] C. Cadiou, M. Murrie, C. Paulsen, V. Villar, W. Wernsdorfer, R. E. P. Winpenny, *Chem. Commun.* **2001**, 2666.

[13] a) J. Cano, P. Alemany, S. Alvarez, M. Verdaguer, E. Ruiz, *Chem. Eur. J.* **1998**, *4*, 476; b) E. Ruiz, J. Cano, S. Alvarez, P. Alemany, *J. Am. Chem. Soc.* **1998**, *120*, 11122; c) E. Ruiz, J. Cano, S. Alvarez, P. Alemany, *J. Comput. Chem.* **1999**, *20*, 1391; d) E. Ruiz, A. Rodriguez-Fortea, J. Cano, S. Alvarez, *J. Comput. Chem.* **2003**, *24*, 982; e) R. Carrasco, J. Cano, T. Mallah, L. F. Jones, D. Collison, E. K. Brechin, *Inorg. Chem.* **2004**, *43*, 5410.

[14] L. Que, A. E. True, *Prog. Inorg. Chem.* **1990**, *38*, 97.

[15] A. D. Becke, *J. Chem. Phys.* **1993**, *98*, 5648; C. Lee, W. Yang, R. G. Parr, *Phys. Rev. B* **1988**, *37*, 785.

[16] Gaussian 98 (Revision A.7), M. J. Frisch, G. W. Trucks, H. B. Schlegel, G. E. Scuseria, M. A. Robb, J. R. Cheeseman, V. G. Zakrzewski, J. A. Montgomery, R. E. Stratmann, J. C. Burant, S. Dapprich, J. M. Millam, A. D. Daniels, K. N. Kudin, M. C. Strain, O. Farkas, J. Tomasi, V. Barone, M. Cossi, R. Cammi, B. Mennucci, C. Pomelli, C. Adamo, S. Clifford, J. Ochterski, G. A. Petersson, P. Y. Ayala, Q. Cui, K. Morokuma, D. K. Malick, A. D. Rabuck, K. Raghavachari, J. B. Foresman, J. Cioslowski, J. V. Ortiz, B. B. Stefanov, G. Liu, A. Liashenko, P. Piskorz, I. Komaromi, R. Gomperts, R. L. Martin, D. J. Fox, T. Keith, M. A. Al-Laham, C. Y. Peng, A. Nanayakkara, C. Gonzalez, M. Challacombe, P. M. W. Gill, B. G. Johnson, W. Chen, M. W. Wong, J. L. Andres, M. Head-Gordon, E. S. Replogle, J. A. Pople, Gaussian, Inc., Pittsburgh, PA, **1998**..

[17] T. H. Dunning, P. J. Hay in *Modern Theoretical Chemistry* (Ed.: H. F. Schaefer III), Plenum, New York, **1976**, 1–28.

[18] P. J. Hay, W. R. Wadt, *J. Chem. Phys.* **1985**, *82*, 270.

[19] E. R. Davidson, A. E. Clark, *J. Phys. Chem. A* **2002**, *106*, 7456.

[20] T. A. O'Brien, E. R. Davidson, *Int. J. Quantum Chem.* **2003**, *92*, 294.

[21] Note added in proof (December 13, 2004): Complex **1** has recently been reported by others: E. M. Rumberger, L. N. Zakharov, A. L. Rheingold, D. N. Hendrickson, *Inorg. Chem.* **2004**, *43*, 6531.

 © 2005 Wiley-VCH Verlag GmbH & Co. KGaA, Weinheim

Supramolecular Chemistry

Metal–Organic Rotaxane Frameworks: Three-Dimensional Polyrotaxanes from Lanthanide-Ion Nodes, Pyridinium *N*-Oxide Axles, and Crown-Ether Wheels**

*Dennis J. Hoffart and Stephen J. Loeb**

The dynamic nature of mechanically interlocked molecules has been shown to be particularly useful for the construction of molecular machines.[1] A great deal of information about the potential for the fabrication of nanoscale devices from these units has been gleaned from studies of their fundamental properties in solution.[2] The incorporation of these individual molecular components into the repeating framework of crystalline materials provides a simple method for imposing the type of higher order required for future applications.[3]

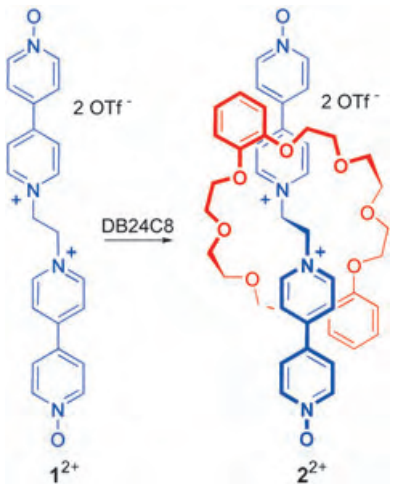
A simple interlocked unit from which various types of molecular machines have been constructed is the [2]rotaxane. We have recently shown that a [2]pseudorotaxane comprising a dipyridinium axle and a dibenzo-[24]crown-8 ether (DB24C8) wheel[4] could be used to construct solid-state materials in the form of coordination polyrotaxanes in which every bridging ligand is a [2]rotaxane.[5] These materials contained varying degrees of porosity as there was no detectable interpenetration of nets[6] even though the metal–metal distances are over 22 Å.[7] Unfortunately, regardless of the metal to ligand ratio, a two-dimensional (2D) square net was the highest order attainable with this dynamic ligand and d block transition-metal ions. It was rationalized that a three-dimensional (3D) network was simply not possible owing to the crowding occurring on placing six of these sterically demanding ligands around a single metal ion. To circumvent this problem the dipyridinium ligand was extended by forming the bis(*N*-oxide) analogue, axle $\mathbf{1}^{2+}$. This new axle was prepared from the reaction of 4,4′-bipyridine mono-*N*-oxide with 1,2-dibromoethane and subsequent anion exchange to triflate utilizing the same conditions used to make the bis(4,4′bipyridinium)ethane axle.[4b,8] Scheme 1 shows the conversion of the new bis(*N*-oxide) axle $\mathbf{1}^{2+}$ into a [2]pseudorotaxane, $\mathbf{2}^{2+}$ employing DB24C8 as the wheel. In MeCN, $\mathbf{1}^{2+}$ has an association constant, K_a, of $1125\,\text{M}^{-1}$ with DB24C8 as measured by ^{1}H NMR spectroscopy.[9]

[*] D. J. Hoffart, Prof. S. J. Loeb
Department of Chemistry and Biochemistry
University of Windsor
Windsor, ON N9B 3P4 (Canada)
Fax: (+1) 519-973-7098
E-mail: loeb@uwindsor.ca

[**] We thank NSERC of Canada for financial support of this research. DJH thanks the University of Windsor's Centre for Catalysis and Materials Research and ORDCF for the award of a graduate scholarship. Dr. Jorge Tiburcio is thanked for his help with powder XRD measurements.

Supporting information for this article is available on the WWW under http://www.angewandte.org or from the author.

 DOI: 10.1002/anie.200461707 © 2005 Wiley-VCH Verlag GmbH & Co. KGaA, Weinheim



Scheme 1. The formation of a [2]pseudorotaxane ligand from a pyridinium *N*-oxide axle and a dibenzo-[24]crown ether wheel.

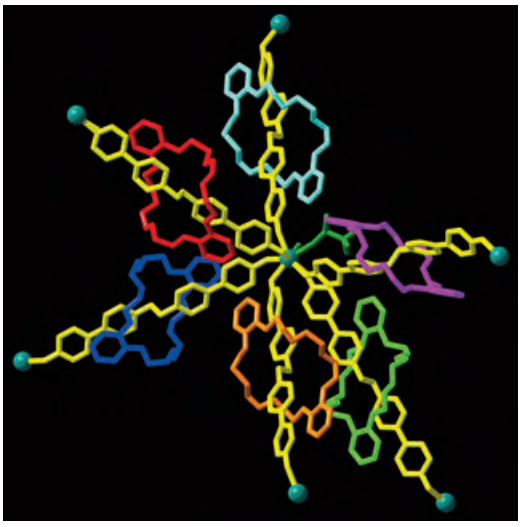


Figure 1. A ball-and-stick representation of the metal–ligand coordination sphere around Sm^{III} in $\mathbf{3}^{8+}$; solvent, noncoordinating anions and hydrogen atoms have been removed for clarity. Key: $\mathbf{1}^{2+}$ axle is shown in yellow; DB24C8 wheels are shown in red, blue, orange, light green, purple, cyan; coordinated water and triflate anion are shown in dark green; Sm metal ions are shown in gray.

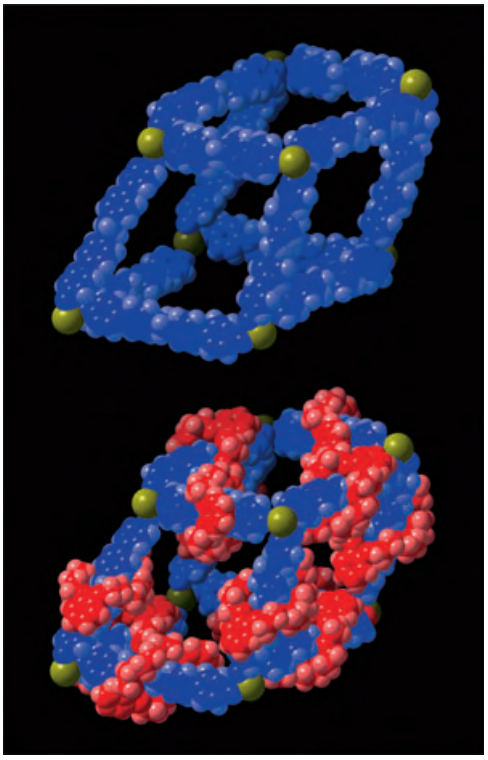


Figure 2. Top: A space-filling model showing a single "cube" unit of the 3D network for $\mathbf{3}^{8+}$ with the molecules of DB24C8 removed for clarity. Bottom: The same framework with the DB24C8 units included. Key: The 3D metal–ligand framework is shown in blue; the molecules of DB24C8 are shown in red; the Sm metal ions in gold.

The only 3D metal containing polyrotaxane reported to date is that of Kim and co-workers.[10] Under hydrothermal conditions, cyano functional groups on a [2]pseudorotaxane, constructed from a diaminoalkane axle and a cucurbituril wheel, were converted into carboxylate groups in the presence of $Tb(NO_3)_3$. Herein, we report that the *N*-oxide version of our [2]pseudorotaxane motif,[4] $\mathbf{2}^{2+}$, can be employed in simple room-temperature, metal–ligand self-assembly (crystal engineering) reactions using lanthanide ions[11] to form two distinctly different types of 3D, metal–organic framework materials containing [2]rotaxanes.

Three equivalents of $\mathbf{1}[OTf]_2$ (OTf = triflate, $[CF_3SO_3]^-$) were mixed with nine equivalents of DB24C8 and one equivalent of $[M(OTf)_3]$ (M = Sm, Eu, Gd, Tb) in MeCN. X-ray quality crystalline material[12] was produced in moderate yield (≈50% on average). Figure 1 shows that the use of Ln^{III} ions as nodes results in an eight-coordinate metal center with a square antiprismatic geometry comprising six [2]rotaxane ligands, one water molecule, and one coordinated $[OTf]^-$ ion.

Figure 2 shows how propagation of the eight-coordinate units results in 3D, metal–organic frameworks $[M(H_2O)(OTf)(\mathbf{2})_3][Cl][OTf]_7$ (M = Sm (**3**), Eu (**4**), Gd (**5**), Tb (**6**); for the source of the Cl ion see ref. [12]) in which every bridging ligand is a [2]rotaxane. The "square" sides of the α-polonium type net are defined by Sm···Sm separation of approximately 23.5 Å. The cavity has a volume of about 10000 $Å^3$, however this space is filled by the interpenetration of a parallel net. (See Supporting Information for diagrams depicting single interpenetration of the two lattices). The longer *N*-oxide axle results in an elongation of the metal–metal separation which creates an expanded cavity which can now accommodate the girth of the [2]rotaxane ligand. Of note is that only a single interpenetration occurs within such a large volume.

Although an isomorphous series (Sm, Eu, Gd, Tb) of 3D polyrotaxanes could be produced with eight-coordinate metal centers, we found that changing to a metal ion with a slightly smaller radius, Yb^{III} (2.40 Å versus 2.51 Å for Tb, 2.59 Å for Sm), yielded another 3D polyrotaxane but with a distinctly different solid-state structure. Large crystals of $[Yb(OTf)(\mathbf{2})_3][Cl][OTf]_7$ (**7**) were isolated in moderate yield from the slow

 © 2005 Wiley-VCH Verlag GmbH & Co. KGaA, Weinheim

diffusion of a solution of $Yb(OTf)_3$ into a solution of the [2]pseudorotaxane ligand $\mathbf{2}(OTf)_2$ at room temperature. The Yb^{III} center adopts a seven-coordinate pentagonal bipyramidal geometry, with five *N*-oxide rotaxanes occupying the equatorial sites of the pentagonal plane and one further [2]rotaxane and a single triflate ion positioned in the axial sites. The metal core and ligand set for $\mathbf{7}^{8+}$ are shown in Figure 3.

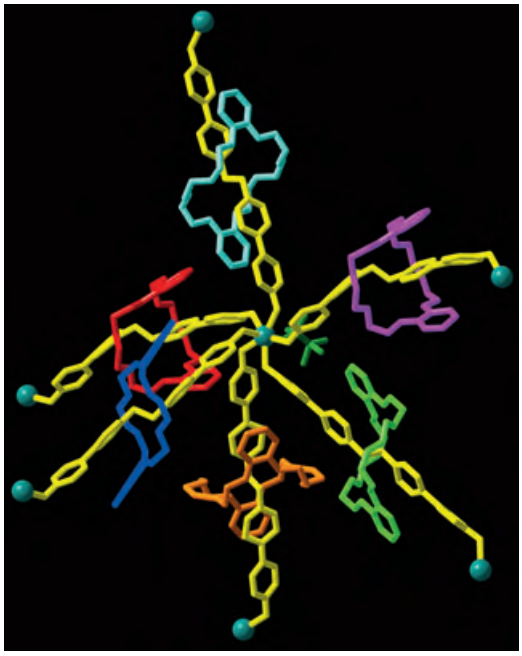


Figure 3. A ball-and-stick representation of the metal–ligand coordination sphere around Yb^{III} in $\mathbf{7}^{8+}$; solvent, noncoordinating anions, and hydrogen atoms have been removed for clarity. Key: $\mathbf{1}^{2+}$ axle is shown in yellow; DB24C8 wheels are shown in red, blue, orange, light green, purple, cyan; coordinated triflate anion is shown in green; Yb metal ions shown in gray.

The planar tessellation of a five-coordinate node into a 2D network is formally impossible, but this is what in fact occurs. Each *N*-oxide ligand can "bend" at the Yb-O-N linkage and this results in a [3/4,5] net comprising alternating triangles and squares linked through five-connected nodes.[13] Until very recently,[14] this 2D pattern was unknown in chemical systems. Figure 4 shows the tiling in the pentagonal plane. This network propagates one step further into a full 3D metal–organic framework by pillaring to adjoining layers through the sixth [2]rotaxane in the apical position. This results in a previously unknown topology and takes the form of a [3/4/6,6] 6-connected net comprised of triangles, squares, and hexagons. The square cavities are used for interpenetration of these nets in a manner conceptually similar to those of **3**–**6**. Interpenetration is not possible through the more crowded triangular cavities. (See Supporting Information for diagrams depicting the full 3D structure and associated interpenetration of the lattices).

Both sorts of materials (**3**–**6** and **7**) show similar stability as determined by thermogravimetric analysis (TGA) and powder X-ray diffraction (PXRD) measurements.[15] Solvents

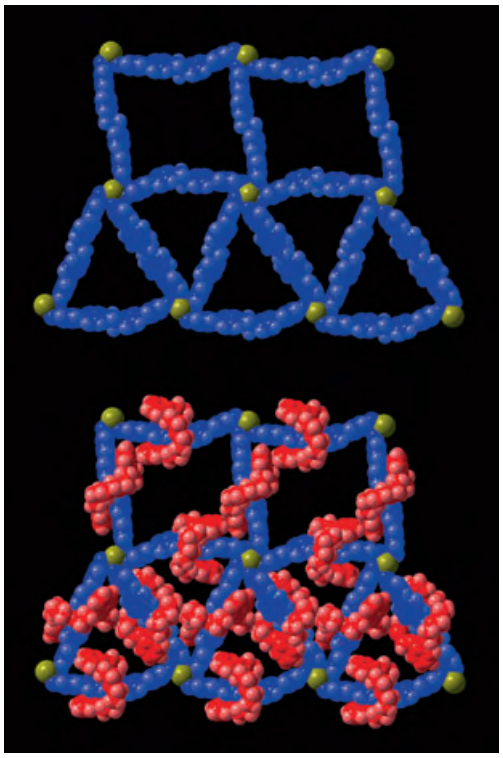


Figure 4. Top: A space-filling model of $\mathbf{7}^{8+}$ showing the 2D pentagonal network [3/4,5] plane with the molecules of DB24C8 removed for clarity. The apical [2]rotaxane has also been removed for clarity. Bottom: The same framework with the DB24C8 molecules shown. Key: The 3D metal–ligand framework is shown in blue; the molecules of DB24C8 are shown in red; the Yb metal ions in gold.

of crystallization (MeCN, H_2O) were easily lost at temperatures ranging from 25–80 °C followed by phase stability until approximately 240 °C. PXRD patterns of the desolvated materials were consistent with retention of the 3D framework. Release of the trapped crown ether was only observed at >240 °C, which also indicates that the 3D metal ligand framework is intact until this temperature. Thus, although the [2]rotaxanes are initially formed with weak noncovalent interactions, a strong metal–ligand bond must be broken to release the interlocked macrocycle from the metal–organic skeleton.

From these results, we can conclude that 1) the design of soft materials with interlocked components (metal–organic rotaxane frameworks: MORFs) can be expanded to include pyridinium *N*-oxide axles and crown-ether wheels, 2) it is possible to create fully 3D structures in which every linker is a pyridinium-based rotaxane, and 3) interpenetration of these rotaxane nets is a possibility since the openings created are large enough for these uncommonly "wide" ligands to fit through the pores.

Received: August 18, 2004
Revised: October 28, 2004
Published online: December 28, 2004

Keywords: coordination polymers · crown compounds · lanthanides · rotaxanes · self-assembly

 © 2005 Wiley-VCH Verlag GmbH & Co. KGaA, Weinheim

[1] a) J. F. Stoddart, *Acc. Chem. Res.* **2001**, *34*, 410; b) A. R. Pease, J. O. Jeppesen, J. F. Stoddart, Y. Luo, C. P. Collier, J. R. Heath, *Acc. Chem. Res.* **2001**, *34*, 433; c) J.-P. Collin, C. Dietrich-Buchecker, P. Gaviña, M. C. Jiminez-Molero, J.-P. Sauvage, *Acc. Chem. Res.* **2001**, *34*, 477; d) A. N. Shipway, I. Willner, *Acc. Chem. Res.* **2001**, *34*, 421.

[2] a) V. Balzani, A. Credi, F. M. Raymo, J. F. Stoddart, *Angew. Chem.* **2000**, *112*, 3484; *Angew. Chem. Int. Ed.* **2000**, *39*, 3348; b) R. Ballardini, V. Balzani, A. Credi, M. T. Gandolfi, M. Venturi, *Acc. Chem. Res.* **2001**, *34*, 445.

[3] a) M. Albrecht, M. Lutz, A. L. Spek, G. van Koten, *Nature* **2000**, *406*, 970; b) O. M. Yaghi, M. O'Keefe, N. W. Ockwing, H. K. Chae, M. Eddaoudi, J. Kim, *Nature* **2003**, *423*, 705.

[4] a) S. J. Loeb, J. A. Wisner, *Angew. Chem.* **1998**, *110*, 3010; *Angew. Chem. Int. Ed. Engl.* **1998**, *37*, 2838; b) S. J. Loeb, J. A. Wisner, *Chem. Commun.* **1998**, 2757.

[5] G. J. E. Davidson, S. J. Loeb, *Angew. Chem.* **2003**, *115*, 78; *Angew. Chem. Int. Ed.* **2003**, *42*, 74.

[6] M. Zaworotko, *Chem. Commun.* **2001**, 1.

[7] N. G. Pschirer, D. M. Ciurtin, M. D. Smith, U. H. F. Bunz, H-C. zur Loye, *Angew. Chem.* **2002**, *114*, 663; *Angew. Chem. Int. Ed.* **2002**, *41*, 583.

[8] M. I. Attalla, N. S. McAlpine, L. A. Summers, *Z. Naturforsch. B* **1984**, *39*, 74.

[9] This value compares well to that of the precursor bis(pyridine) axle which, in MeCN, has $K_a \approx 900\,\mathrm{M}^{-1}$ with DB24C8.

[10] a) E. Lee, J. Heo, K. Kim, *Angew. Chem.* **2000**, *112*, 2811; *Angew. Chem. Int. Ed.* **2000**, *39*, 2699; b) K. M. Park, D. Whang, E. Lee, J. Heo, K. Kim, *Chem. Eur. J.* **2002**, *8*, 498.

[11] For examples of crystal engineering with Ln^{III} ions and pyridine-*N*-oxides see: D. Long, A. J. Blake, N. R. Champness, C. Wilson, M. Schröder, *Chem. Eur. J.* **2002**, *8*, 2026.

[12] Crystal data[16] for **3**: $C_{152}H_{163.75}Cl_{0.5}F_{25.5}N_{14.75}O_{64}S_{8.5}Sm$, $M_r = 4147.7$, orange prisms, ($0.36 \times 0.34 \times 0.26$ mm) triclinic, $P\bar{1}$, $a = 17.5661(13)$, $b = 23.4327(13)$, $c = 27.0910(17)$ Å, $\alpha = 78.0860(10)$, $\beta = 80.5090(10)$, $\gamma = 74.0460(10)°$, $V = 10421.2(12)$ Å^3, $Z = 2$, $\rho_{calcd} = 1.322\,\mathrm{g\,cm^{-3}}$, $\mu = 0.476\,\mathrm{mm^{-1}}$, min/max trans. = 0.8888, $2\theta_{max} = 45.0°$, $Mo_{K\alpha}\lambda = 0.71073$ Å, $T = 100.0(2)$ K, 66987 total reflections (R(int) = 0.0483), $R1 = 0.1248$, $wR2 = 0.3293$ [$I > 2\sigma I$], $R1 = 0.1421$, $wR2 = 0.3522$ [all data], GoF (F^2) = 1.579, $N_o/N_v/N_r = 27216/3064/376$. Data for analogous compounds **4** (Eu), **5** (Gd), and **6** (Tb) were not of sufficient quality to render a full structure solution but unit cells and partial solutions verified that these are isomorphous with **3.** **7**: $C_{160}H_{175.5}ClF_{24}N_{19}O_{59.5}S_8Yb$, $M_r = 4237.7$, yellow prisms, $0.24 \times 0.20 \times 0.18$ mm) triclinic, $P\bar{1}$, $a = 20.495(3)$, $b = 22.701(3)$, $c = 27.435(3)$ Å, $\alpha = 84.146(3)$, $\beta = 78.935(3)$, $\gamma = 67.636(3)°$, $V = 11579(3)$ Å^3, $Z = 2$, $\rho_{calcd} = 1.215\,\mathrm{g\,cm^{-3}}$, $\mu = 0.579\,\mathrm{mm^{-1}}$, min/max trans. = 0.7412, $2\theta_{max} = 50.0°$, $Mo_{K\alpha}\lambda = 0.71073$ Å, $T = 100.0(2)$ K, 40594 total reflections (R(int) = 0.0980), $R1 = 0.1417$, $wR2 = 0.3729$ [$I > 2\sigma I$], $R1 = 0.1841$, $wR2 = 0.4003$ [all data], GoF (F^2) = 1.438, $N_o/N_v/N_r = 40594/2444/294$. The presence of chloride ion in these structures is attributed to small amounts of this anion in the bulk sample of axle $\mathbf{1}^{2+}$ since during work up $\mathbf{1}^{2+}$ is subjected to column chromatography in which one of the solvents is aqueous NH_4Cl before anion exchange to OTf. Crystals of **3**–**7** were frozen in paratone oil inside a cryoloop. Reflection data were integrated from frame data obtained from hemisphere scans on a Brüker APEX diffractometer with CCD detector. Decay was monitored by 50 standard data frames measured at the beginning and end of data collection. Diffraction data and unit-cell parameters were consistent with assigned space groups. Lorentzian polarization corrections and empirical absorption corrections, based on redundant data at varying effective azimuthal angles, were applied to the data sets. The structures were solved by direct methods, completed by subsequent Fourier syntheses and refined with conjugate-gradient least-squares methods against $|F^2|$ data. For both compounds a chloride anion was located and refined instead of one of the triflate anions. All non-hydrogen atoms were refined anisotropically. Hydrogen atoms were treated as idealized contributions. Scattering factors and anomalous dispersion coefficients are contained in the SHELXTL 5.03 program library (G. M. Sheldrick, Madison, WI). CCDC-247756 and CCDC-247757 (**3** and **7**) contain the supplementary crystallographic data for this paper. These data can be obtained free of charge from The Cambridge Crystallographic Data Centre via www.ccdc.cam.ac.uk/data_request/cif.

[13] A. F. Wells, *Three-Dimensional Nets and Polyhedra*, Wiley, New York, **1977**.

[14] a) J.-R. Li, X.-H. Bu, R.-H. Zhang, *Inorg. Chem.* **2004**, *43*, 237; b) X.-H. Bu, W. Weng, W. Chen, R.-H. Zhang, *Inorg. Chem.* **2002**, *41*, 413.

[15] TGA were performed on a Mettler Toledo TGA/SDTA85 Instrument under He(g) atmosphere at scan rate of 5°C/min. PXRD measurements were recorded on a Brüker D8 Discover diffractometer with an AXS HI-STAR area detector using $Cu_{K\alpha}$ radiation.

[16] Ball-and-stick and space-filling diagrams were prepared using DIAMOND-Visual Crystal Structure Information System CRYSTAL IMPACT, Postfach 1251, 53002 Bonn.

 © 2005 Wiley-VCH Verlag GmbH & Co. KGaA, Weinheim

Catalytic Antibodies

Towards a Rational Design of Antibody Catalysts through Computational Chemistry**

Sergio Martí, Juan Andrés, Vicent Moliner, Estanislao Silla, Iñaki Tuñón,* and Juan Bertrán*

Pauling's seminal idea concerning enzymatic catalysis is that an enzyme lowers the energy of the transition state (TS).[1] Evidence in support of this proposal is the fact that stable

[*] Dr. S. Martí, Prof. J. Andrés, Dr. V. Moliner
Departament de Ciències Experimentals
Universitat Jaume I
Box 224, Castellón (Spain)
Fax: (+34) 964-728-066
E-mail: moliner@exp.uji.es
Prof. E. Silla, Dr. I. Tuñón
Departament de Química Física/IcMol
Universidad de Valencia
46100 Burjasot (Spain)
Fax: (+34) 963-544-564
E-mail: ignacio.tunon@uv.es
Prof. J. Bertrán
Departament de Química
Universitat Autònoma de Barcelona
08193 Bellaterra (Spain)

[**] This research was supported by DGI project BQU2003-04168-C03, BANCAIXA project P1A99-03, and Generalitat Valenciana projects GV04B-21 and GV04B-131. We acknowledge the Servei d'Informàtica of the Universitat Jaume I for providing us with computer capabilities. We thank Professor Ian H. Williams for valuable discussions.

 © 2005 Wiley-VCH Verlag GmbH & Co. KGaA, Weinheim DOI: 10.1002/anie.200461325

compounds that resemble the TS, transition state analogues (TSAs), are competitive inhibitors of enzymes.[2] One approach to TSA design is to establish the nature of the enzymatic TS and to synthesize chemically stable analogues with similar features.[3] Raso and Stollar pioneered the use of TSAs as haptens in immunization processes to synthesize new catalysts: catalytic antibodies (CAs).[4] The study of processes associated with the activity of CAs provides opportunity to examine and understand enzyme catalysis and vice versa. In-depth knowledge of enzyme activity can be used to improve the specificity, selectivity, and efficiency of these new catalysts.[5] CAs are especially interesting as catalysts for those reactions for which no enzyme is known.[6]

The simplest kinetic scheme used to understand enzymatic and CA processes is that proposed by Michaelis and Menten, which proceeds with the formation of a substrate–catalyst complex (the Michaelis complex, MC) before the product-forming step during which the catalyst is recovered.[7] In the simplest version the reaction takes place through a single TS [Eq. (1)].

$$E + S \rightleftharpoons MC \rightarrow TS \rightarrow P + E \quad (1)$$

The activation free energy of the catalyzed reaction step can be related to that of a counterpart uncatalyzed process through the binding energies of the MC and the TS [Eq. (2)].

$$\Delta G^{\ddagger}_{cat} = \Delta G^{\ddagger}_{uncat} + \Delta G^{TS}_{bind} - \Delta G^{MC}_{bind} \quad (2)$$

Here $\Delta G^{\ddagger}_{cat}$ and $\Delta G^{\ddagger}_{uncat}$ are the free energies of activation for the catalyzed and the uncatalyzed reactions, while ΔG^{TS}_{bind} and ΔG^{MC}_{bind} reflect the affinities of the protein for the TS and the MC, respectively. According to this scheme, the catalytic power of enzymes comes from the larger affinity of the enzyme for the TS than for the MC, since $\Delta G^{TS}_{bind} - \Delta G^{MC}_{bind}$ is a negative quantity. Antibodies are synthesized on the basis of their affinity for a TSA (ΔG^{TSA}_{bind}), a quantity expected to be correlated to the binding energy of the true TS of the reaction to be catalyzed (ΔG^{TS}_{bind}). Thus, CAs are expected to provide a lower activation free energy.

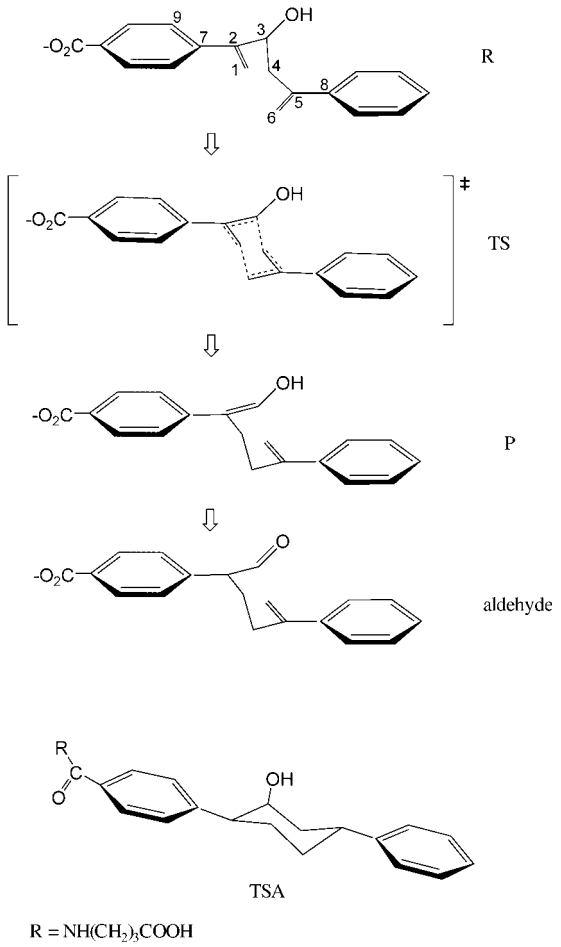
However, initial expectations for CAs as catalysts have not been fully met. First of all, CAs are not as efficient as the enzymes. Second, not all antibodies that stabilize TSAs are catalysts of the reaction. Finally, there are cases where after a process of maturation (which results in an increased affinity of the CA for the TSA) a paradoxical decrease in the catalytic power is observed, relative to the initial or germline CA.[8]

Different arguments have been proposed to explain these findings. The fact that CAs present modest rate enhancements relative to those of enzymes could be due to the low affinity between the CA and the TSA that can be developed by the immune system. This affinity is apparently not enough to result in the TS affinity required for a substantial increase of the reaction rate. During the process of maturation, the TSA–CA affinity (in terms of the dissociation constants calculated for the TSA) increases to ca. 10^{-10} while the TS–enzyme affinity increases to 10^{-23}.[7] Secondly, even when the CA–TSA affinity could be improved enough, to date it has been difficult to elicit antibodies that are as effective at differentiating the ground state from the TS.[7] In this regard, Schultz et al. have stressed the lack of flexibility of the catalytic antibodies.[9] The introduction of somatic mutations, which lead to an increase in binding affinities, can cause a significant restriction in the relative orientation of the substrate, thereby decreasing the rate constant.[9] The increased binding affinity of the affinity-matured antibody stabilizes the substrate in a catalytically unfavorable conformation. Thus, it would be possible to rationalize why some CAs do not act as catalysts. Finally, as also suggested by Bartlett and Mader,[7] it is not possible to devise very accurate TSAs; that is, the TSA cannot be similar enough to the true TS. As a consequence, an improvement in ΔG^{TSA}_{bind} would not be directly translated into an improvement in ΔG^{TS}_{bind}. All these problems arise because of an important issue of timescales. In its continuous processes of evolution, nature has brought forth countless mechanisms for complex biochemical reactions, but the biological selection process that produces the antibody differs from that governing enzyme evolution by an enormous factor: a timescale of weeks in the former in contrast to a process occurring over millions of years in the latter.

The methods and techniques of computational chemistry provide excellent tools for obtaining molecular details of catalytic processes.[10–13] In this paper we use these tools to show that developing a good catalyst requires consideration of both the TS and the MC. With the aim of increasing the stability of the TSs, scientists design CAs based on their affinity to TSAs. In this process the effect of the CA on the reactant state is completely lost. We suggest that CAs usually present low catalytic efficiency (relative to that of enzymes) and even inverse correlations between maturation process and catalytic power. This can be explained not only because the TSA does not properly represent the TS, but mainly because the MC is not considered in the improvement process. Enzymes and CAs have evolved with different purposes: the former to decrease the activation free energy of the reaction, and the latter to increase the binding energy for the TSA (and for the TS). In the first case the target is the difference between the binding energy of the TS and the MC, ($\Delta G^{TS}_{bind} - \Delta G^{MC}_{bind}$), while in the second case attention is focused on ΔG^{TSA}_{bind} (which is related to ΔG^{TS}_{bind}), and the MC is not considered at all.

CAs have been produced for a plethora of chemical reactions including hydrolytic reactions, sigmatropic rearrangements, and cycloadditions, carbon–carbon bond-forming reactions, and redox reactions.[14] In this study we have selected an oxy-Cope rearrangement catalyzed by AZ-28 and related antibodies.[15] Apart from the advantages of this system from the computational point of view,[16] no enzyme is known for this reaction. The monoclonal AZ-28 catalyzes the unimolecular rearrangement of a substituted hexadiene to the corresponding aldehyde (see Scheme 1). The immune system provides a large number of different germline antibodies as an initial response to a foreign molecular structure. In this process the antigen is the TSA, depicted in Scheme 1. Once a germline antibody is selected from the pool based on its affinity for an antigen, an additional process of affinity maturation follows, in which random somatic mutations are

 © 2005 Wiley-VCH Verlag GmbH & Co. KGaA, Weinheim



Scheme 1. Schematic diagram of the molecular mechanism of the oxy-Cope reaction and detail of the TSA.

selected to obtain a high-affinity antibody. In the case of the AZ-28, it was found that the matured AZ-28 presented a 40-fold higher affinity for the TSA but afforded a 30-fold lower rate enhancement than its germline precursor.[8] Analysis of the effects of individual amino acid mutations indicated that the SerL34Asn substitution was largely responsible for the decrease in catalytic efficiency during affinity maturation.[8] We can now explain why the affinity-matured antibody is less efficient than its precursor germline antibody.

The mechanism of catalysis of the antibody-catalyzed oxy-Cope rearrangement has been theoretically study by Kollman et al.[17] using ab initio molecular orbital calculations and classical molecular dynamics simulations, and recently by Houk et al.[18] by means of gas-phase density functional theory calculations and flexible docking. In this paper we describe the application of a hybrid quantum mechanics/molecular mechanics (QM/MM) methodology already tested in our group on similar enzymatic pericyclic reactions.[19] As a first result of our study, free energy profiles for the AZ-28 catalytic antibody in its germline and matured form are plotted in Figure 1. The profiles indicate an associative mechanism described by two TSs; the first and rate-limiting step is formation of the C1–C6 bond, and the second step is breaking

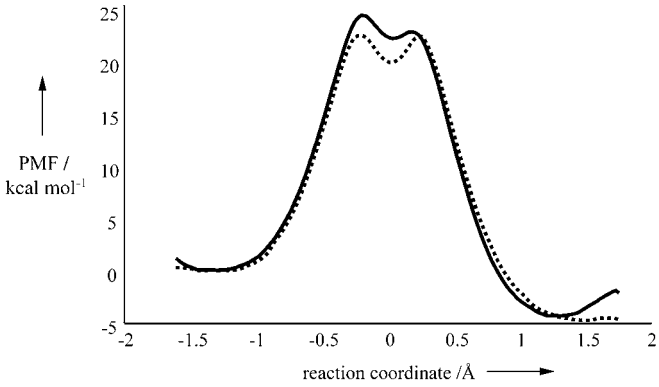


Figure 1. Free energy profiles in terms of the potential mean fore (PMF) for the AZ-28 catalytic antibody in its germline (dotted line) and matured forms (solid line) for the R-to-P transformation (see Scheme 1). The reaction coordinate is the antisymmetric combination of the interatomic distances of the forming and breaking bonds, C1···C6 and C3···C4, respectively. For details see ref. [19].

of the C3–C4 bond.[20] The oxy-Cope rearrangement catalyzed by the matured AZ-28 involves a slightly higher barrier than that catalyzed by its germline counterpart. Our calculations render a difference in the free energy barriers of 1.9 kcal mol^{-1}, which can be directly compared with the experimental result of 2.2 kcal mol^{-1}, obtained by Schultz et al.[8] This agreement allows us to be confident in our calculations and consequently to analyze the origin of this difference in free energy barriers by means of theoretical simulations.

Molecular simulations provide us with a detailed knowledge of chemical processes in terms of structures and energies. In Figure 2 we present some snapshots representative of the averaged structures of TSA, TS, and MC obtained from the QM/MM MD trajectories of the oxy-Cope rearrangement in the active sites of the germline and matured antibodies.[21] Some key residues and interactions are also depicted. The first conclusion that can be extracted from the analysis of the structures is that the cavity in the matured antibody is narrower than that in its germline counterpart. The compression between the light and heavy chains can be measured by the distance between the carboxylate OD1 or OD2 oxygen atoms of H101 and terminal hydrogen atom of L34 residues (HG1 for Ser or HD21 for Asn), located in the outer part of the catalytic cavity. Thus, the germline antibody presents a distance of about 4.3 Å, while in the matured antibody this distance is significantly shorter, 2.2 Å. Therefore, it is evident that the germline CA has a larger cavity than the matured CA for accommodating the TS and the MC, in accordance with Schultz's experimental results.[9]

Following with the analysis of Figure 2, the observed pattern of interactions in the CA–substrate complex reveals important differences. Starting from the TSAs, the hydroxy substituent of the cyclohexyl ring is hydrogen-bonded to Glu35 in both CAs (2.25 and 1.98 Å for the germline and the matured antibodies, respectively). Other TSA–CA interactions are also shorter for the matured antibody than for the germline counterpart, reflecting improved matching with the

 © 2005 Wiley-VCH Verlag GmbH & Co. KGaA, Weinheim

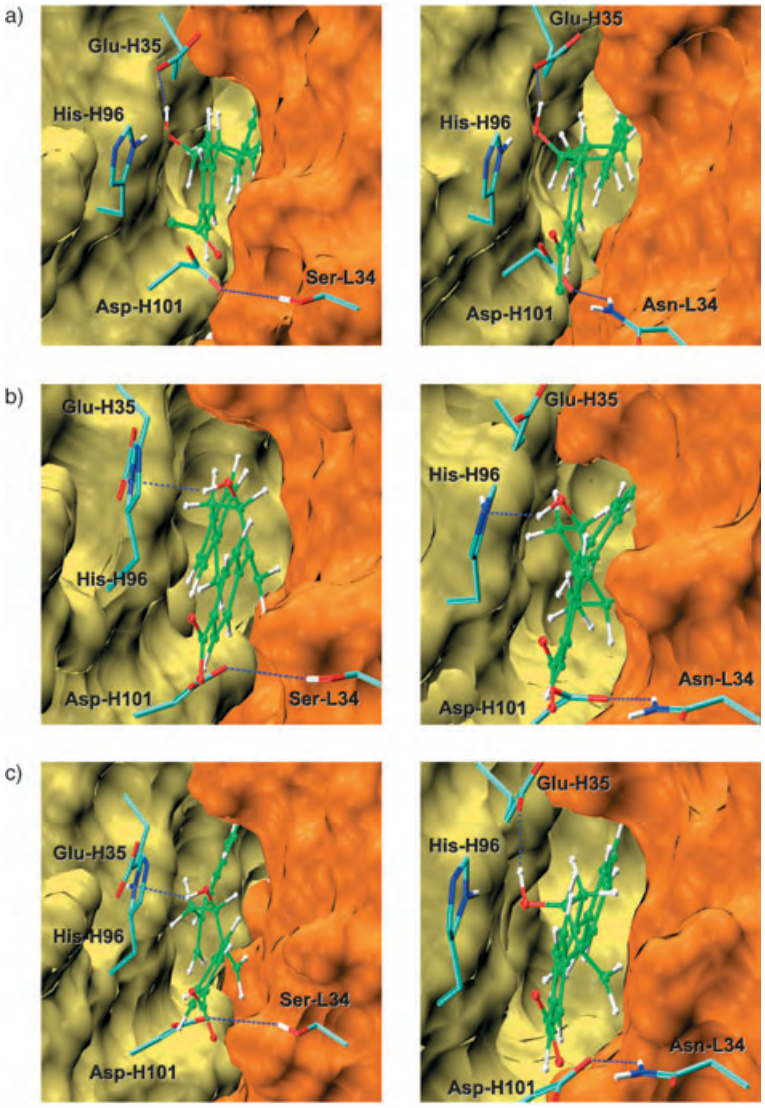


Figure 2. Detail of the averaged structures of the a) TSA, b) TS, and c) MC of the oxy-Cope rearrangement in the active site of the germline (left) and matured AZ28 antibodies (right). The heavy and light chains are shown in yellow and orange, respectively.

substrate after the maturation process. Another observed feature is the relative position of the cyclohexane ring (which is always in a chairlike conformation) with respect to the two aryl substituents. The observation that the cyclohexane ring is almost perpendicular to the substituents is in agreement with X-ray diffraction analysis.[9] Nevertheless, an important difference with the X-ray structure is the position of substrate in the antibody cavity. During our MD simulations the substrate moves inside the cavity, changing the initial hydrogen bond between the hydroxy group and the Glu50 through a bridging water molecule into a new interaction with the Glu35 located on the inside of the cavity. Packing effects in the X-ray diffraction structures could account for this difference.

In the case of TS–CA complexes, the first observation is the different orientation of the hydroxy substituent with respect to that in the TSA–CA complexes. The hydroxy group is now hydrogen-bonded to the His96 (2.84 and 2.79 Å for the germline and the matured antibodies, respectively). The dramatic change in the pattern of interactions on going from the TSA to the TS is due to the different hybridization of the C2 and C5 atoms. These carbon atoms present sp^2 and sp^3 hybridizations in TSs and TSAs, respectively, defining an important change in the orientation of the reactive ring. As a result the hydroxy substituent cannot interact with the same residues in the TS and the TSA, as commented above. The new interaction is established by means of rotation around the C2–C3 bond. As previously postulated in the literature, the hydrogen bond between the hydroxy group and His96 may enhance the rate of the process by increasing the electron density on the hydroxy oxygen atom.[14,22] In order to estimate quantitatively this prediction, Baumann et al.[22] and Haeffner et al.[23] have calculated the effect of some substituents on the rates and mechanisms of oxy-Cope rearrangements by means of simple molecular models in the gas phase with a density functional theory based method. These results confirm that the greater the electron density on the hydroxy group, the lower the barrier height. From these observations it is obvious that the use of a TSA that better resembles the TS would be the first step to designing a more efficient CA. Some strategies that work in this sense have already been postulated,[24,25] but it is not the aim of this study.

Regarding the MC structures, it is amazing that while the pattern of interactions of the germline CA remains almost invariable with respect to its TS (2.71 Å for the hydrogen bond between the hydroxy group and His96), the orientation and interactions of the MC in the matured cavity change dramatically; the MC assumes a conformation close to that of the initial TSA (the hydroxy group is now hydrogen-bonded to Glu35, with an average distance of 2.16 Å, and not to His96). The shorter intermolecular distances between the matured CA and the substrate cause the MC to be trapped in a conformation resembling the TSA rather than the TS, thus making the reaction less favorable. This observation can be tested by the values of the reaction coordinate of the MCs (−1.56 for the matured and −1.47 for the germline antibodies, see Figure 1), as well as the distance C1–C6 of the forming bond (3.10 and 3.03 Å for the matured and germline, antibodies, respectively). In both cases, the germline CA presents values closer to the TS than the matured antibody does.

To gain deeper insight into the different behavior of the germline and matured CAs, we determined the energy of the interaction between the substrates and the antibodies (Table 1).[26] From the values listed, it can be observed firstly

 © 2005 Wiley-VCH Verlag GmbH & Co. KGaA, Weinheim

Table 1: Interaction energy differences [kcal mol^{-1}] of matured and germline AZ-28 antibodies with different substrates.

Substrate	E_{int} (matured)	E_{int} (germline)	ΔE_{int}
TSA	−232.4	−228.3	−4.0
TS	−199.0	−193.6	−5.3
MC	−197.6	−190.2	−7.4

that TSA interacts better with the matured CAs than with the germline CAs, and secondly that the TSA species present larger interaction energies than the TSs and MCs. Both results are quite logical when one considers the nature of the affinity maturation process. From the mechanistic point of view, the comparison between the stabilization of the TS and the MC by the catalytic antibody on going from the germline to the matured forms allows us to conclude that the maturation process produces a larger effect in the MC (−7.4 kcal mol^{-1}) than in the TS (−5.3 kcal mol^{-1}). The difference between these values (2.1 kcal mol^{-1}) is almost equivalent to the differences in free energy barriers obtained both experimentally (2.2 kcal mol^{-1}) and theoretically (1.9 kcal mol^{-1}). Nevertheless, we must bear in mind that the estimated free energy barriers plotted in Figure 1 are only related to the MC-to-TS step of Equation (2). The fact that the equilibrium constant of the MC formation was proved experimentally to be almost equal for the germline and the mature CAs[8] is not in agreement with the different interaction energies given in Table 1 for the MC complex. This means that although entropic and other enthalpic terms make different contributions to the substrate binding energy in the germline and mature antibodies, the similarity between free energy barriers and the interaction energies suggests that the source of the different catalytic efficiencies may be attributed to the larger CA–MC interaction in the mature CA. The analysis of the interaction energy shows that this term is mainly electrostatic in nature.

From these results, it is clear that our methodology explains the difference in CA activity for the germline and matured antibodies. Combining the results of different mutations, it has been demonstrated experimentally that the particular AsnL34Ser mutation in the matured CA lowers the free energy barrier by 1.0 kcal mol^{-1}.[8] The effect of this mutation can be analyzed by means of our computational methodology by introducing it in the MC–CA complex of the matured antibody. Hybrid QM/MM molecular dynamics simulations started from different MC structures with the matured antibody, in which the Asn-L34 residue was changed to Ser, have shown a spontaneous opening of the cavity after 0.5–1 ns. This effect is accompanied by a change in the pattern of interactions, establishing the same pattern as that observed in the germline CA. In particular, the hydrogen bond between the hydroxy substituent and Glu35 is broken, and a new interaction is established with His96. The generation of a free energy profile for this new CA yields an activation free energy of 23.7 kcal mol^{-1}, which is 0.7 kcal mol^{-1} lower than that of the matured antibody and in good agreement with the decrease in the barrier observed by Schultz et al.[8] While the matured antibody displays an enhancement in the affinity for the TS, a single mutation can improve its catalytic power by changing the interaction with the MC. In this way, the target quantity in Equation (2), $\Delta G^{TS}_{bind} - \Delta G^{MC}_{bind}$, is optimized. The biological selection of enzymes by evolution can be imitated by antibodies.

It has always been the ambition of research chemists to imitate nature in its magnificent methods for generating complex chemical structures with corresponding chemical reactivity. The present work shows how computational techniques can be crucial to approaching nature's power in evolution. The rational design of a CA requires an in-depth knowledge of enzyme catalysis. First of all, the choice of an appropriate stable TSA, as close as possible to the TS of the reaction to be catalyzed, is crucial to obtaining an efficient CA. In addition, a favorable balance of interactions between the antibody and the relevant structures that the substrate adopts along the full chemical process: the MC and the TS. In improving the activity of a CA the interesting mutations are those that stabilize both the TS and the MC but, as a general feature for all catalysts, the stabilization of the MC must not be too strong. As pointed out in the Sabatier principle,[27] the interactions of the catalyst–substrate complex must be strong enough to favor its formation but not so strong that the catalyst becomes an inhibitor. The maturation process succeeds in stabilizing the TSA and to some extent the TS but not in controlling the relative stabilization of the TS with respect to the MC. We have shown in this paper that computational chemistry enables the study and prediction of which mutations can stabilize the TS relative to the MC, improving the design of the CAs. The combination of theoretical and experimental studies appears to be essential to improving the efficiency of new semisynthetic biological catalysts, thus imitating nature in enzyme evolution.

Received: July 15, 2004
Revised: November 3, 2004
Published online: December 28, 2004

Keywords: catalytic antibodies · computer chemistry · enzyme models · oxy-Cope rearrangement

[1] L. Pauling, *Chem. Eng. News* **1946**, *24*, 1375–1377; L. Pauling, *Am. Sci.* **1948**, *36*, 51; L. Pauling, *Nature* **1948**, *161*, 707–709.
[2] R. Wolfenden, *Acc. Chem. Res.* **1972**, *5*, 10–18; R. Wolfenden, M. J. Snider, *Acc. Chem. Res.* **2001**, *34*, 938–945.
[3] V. I. Schramm, *Acc. Chem. Res.* **2003**, *36*, 588.
[4] V. Raso, B. D. Stollar, *Biochemistry* **1975**, *14*, 584–591.
[5] P. G. Schultz, R. A. Lerner, *Science* **1995**, *269*, 1835–1842.
[6] P. G. Schultz, R. A. Lerner, *Acc. Chem. Res.* **1993**, *26*, 391–395.
[7] M. M. Mader, P. A. Bartlett, *Chem. Rev.* **1997**, *97*, 1281–1301.
[8] H. D. Ulrich, E. Mundorff, B. D. Santarsiero, E. M. Driggers, R. C. Stevens, P. G. Schultz, *Nature* **1997**, *389*, 271–275.
[9] E. C. Mundorff, M. A. Hanson, A. Varvak, H. Ulrich, P. G. Schultz, R. C. Stevens, *Biochemistry* **2000**, *39*, 627–632.
[10] J. Villà, A. Warshel, *J. Phys. Chem. B* **2001**, *105*, 7887–7907.
[11] T. C. Bruice, *Acc. Chem. Res.* **2002**, *35*, 139–148.
[12] S. J. Benkovic, S. Hammes-Schiffer, *Science* **2003**, *301*, 1196–1202.
[13] M. García-Viloca, J. Gao, M. Karplus, D. G. Truhlar, *Science* **2004**, *303*, 186–195.

 © 2005 Wiley-VCH Verlag GmbH & Co. KGaA, Weinheim

[14] P. G. Schultz, J. Yin, R. A. Lerner, *Angew. Chem.* **2002**, *114*, 4607 – 4618; *Angew. Chem. Int. Ed.* **2002**, *41*, 4427 – 4435.
[15] A. P. Marchand, R. E. Lehr, *Pericyclic Reactions*, Academic Press, New York, **1977**.
[16] From a computational point of view, the fact that no covalent bonds exist between the substrate and the catalytic antibody allows a clear separation between the QM region and the MM region. Problems arising from frontier treatments are thus avoided. This kind of system also permits a clear analysis of the different interaction energy terms between both subsystems.
[17] T. Asada, H. Gouda, P. Kollman, *J. Am. Chem. Soc.* **2002**, *124*, 12535 – 12542.
[18] K. A. Black, A. G. Leach, M. Y. S. Kalani, K. N. Houk, *J. Am. Chem. Soc.* **2004**, *126*, 9695 – 9708.
[19] For a general review of the methodology we are currently applying to study enzyme reactions see ref. [28]. Based on the original idea of the hybrid quantum mechanical/molecular mechanical methods,[29] in this particular antibody-catalyzed oxy-Cope rearrangement, free energy profiles (in terms of potential of mean force) were obtained with the umbrella-sampling approach[30] implemented in the Dynamo program.[31] We sampled all the degrees of freedom but the distinguished reaction coordinate (the antisymmetric combination of the interatomic distances of the forming and breaking bonds, C1···C6 and C3···C4 as depicted in Scheme 1) by means of a series of molecular dynamic simulations. Umbrella sampling was used to place the system at an adequate value of the reaction coordinate (ζ_0) and then molecular dynamics simulations were run. The fluctuations of the reaction coordinate are finally pieced together by means of the weighted histogram analysis method (WHAM)[30] obtaining the full distribution function and thus the free energy profile. The system consisted of a cubic box with sides of 79.5 Å in which the CA and 15492 water molecules (50167 atoms in total) were all treated using the OPLS force field,[32] plus the substrate (39 atoms) which was was treated by AM1 semiempirical Hamiltonian. Periodic boundary conditions were used in all calculations. Because of its size, only those CA atoms within 30 Å of the substrate center of mass were allowed to move (~11500 atoms, model dependent), and the positions of the remaining atoms were frozen.
[20] We have also explored the potential energy surface of the reaction by means of gas-phase calculations with density functional theory methods (B3LYP/6-31G*) as implemented in the Gaussian03 package of programs.[33] Our results render two mechanisms, depending on the orientation of the hydroxy substituent (inwards or outwards the cyclohexane ring). Both mechanisms involve a cyclohexanediyl intermediate in one step. Gas-phase AM1 calculations have been also carried out in order to test the suitability of the semiempirical method to be used in the QM/MM calculations. The same molecular mechanisms were obtained although slightly higher energy barriers were observed for the rate-limiting steps, that is, the first step (ca. 1.5–4.5 kcal mol^{-1}). We also obtained the PMF values in aqueous solution using the same QM/MM simulation protocol than for the antibody-catalyzed reaction. In this case, the calculated free energy barrier was 2.5 kcal mol^{-1} higher than the experimental value.[8] We think that this is a reasonable estimation of the expected error in the catalytic free energy barriers.
[21] Once the full PMF values were obtained for the oxy-Cope rearrangement (Figure 1) MD trajectories of 1 ns were carried out in the region of the MC and TS (with constraints applied just in the reaction coordinate of the latter), as well as for the TSA–CA complexes. The values mentioned in the text come from the averaged distances obtained in these long QM/MM trajectories.
[22] H. Baumann, P. Chen, *Helv. Chim. Acta* **2001**, *84*, 124 – 140.
[23] F. Haeffner, K. N. Houk, Y. R. Reddy, L. A. Paquette, *J. Am. Chem. Soc.* **1999**, *121*, 11880 – 11884.
[24] M. Barbany, H. Gutiérrez-de-Terán, F. Sanz, J. Villà, A. Warshel, *ChemBioChem* **2003**, *4*, 277 – 285.
[25] Critical analysis of antibody catalysis: D. Hilvert, *Annu. Rev. Biochem.* **2000**, *69*, 751 – 793.
[26] A similar treatment was previously run for the [3,3] sigmatropic rearrangement catalyzed by chorismate mutase.[34] This is based in the decomposition of the total potential energy as the sum of the QM energy, the QM/MM interaction energy, and the MM energy: $E = E_{QM} + E_{QM/MM} + E_{MM}$. A note of caution has to be considered concerning the accuracy of the reported data in Table 1. Thus, although the reported interaction energies are listed with one decimal place, the overall expected relative accuracy is not that high, since the standard deviations are on the order of unity (in kcal mol^{-1}).
[27] P. Sabatier, *Ber. Dtsch. Chem. Ges.* **1911**, *44*, 1984.
[28] S. Martí, M. Roca, J. Andrés, V. Moliner, E. Silla, I. Tuñón, J. Bertrán, *Chem. Soc. Rev.* **2004**, *33*, 98 – 107.
[29] A. Warshel, *Proc. Natl. Acad. Sci. USA* **1978**, *75*, 5250 – 5254.
[30] G. M. Torrie, J. P. Valleau, *J. Comput. Phys.* **1977**, *23*, 187 – 199.
[31] M. J. Field, M. Albe, C. Bret, F. Proust-de Martin, A. Thomas, *J. Comput. Chem.* **2000**, *21*, 1088 – 1100.
[32] W. D. Cornell, P. Cieplak, C. I. Bayly, I. R. Gould, K. M. Merz, Jr., D. M. Ferguson, D. C. Spellmeyer, T. Fox, J. W. Caldwell, P. A. Kollman, *J. Am. Chem. Soc.* **1995**, *117*, 5179 – 5197.
[33] Gaussian 03 (Revision A.1), M. J. Frisch, G. W. Trucks, H. B. Schlegel, G. E. Scuseria, M. A. Robb, J. R. Cheeseman, V. G. Zakrzewski, J. A. Montgomery, Jr., R. E. Stratmann, J. C. Burant, S. Dapprich, J. M. Millam, A. D. Daniels, K. N. Kudin, M. C. Strain, O. Farkas, J. Tomasi, V. Barone, M. Cossi, R. Cammi, B. Mennucci, C. Pomelli, C. Adamo, S. Clifford, J. Ochterski, G. A. Petersson, P. Y. Ayala, Q. Cui, K. Morokuma, D. K. Malick, A. D. Rabuck, K. Raghavachari, J. B. Foresman, J. Cioslowski, J. V. Ortiz, B. B. Stefanov, G. Liu, A. Liashenko, P. Piskorz, I. Komaromi, R. Gomperts, R. L. Martin, D. J. Fox, T. Keith, M. A. Al-Laham, C. Y. Peng, A. Nanayakkara, C. Gonzalez, M. Challacombe, P. M. W. Gill, B. Johnson, W. Chen, M. W. Wong, J. L. Andres, C. Gonzalez, M. Head-Gordon, E. S. Replogle, J. A. Pople, Gaussian, Inc., Pittsburgh, PA, **2003**.
[34] S. Martí, J. Andrés, V. Moliner, E. Silla, I. Tuñón, J. Bertrán, M. J. Field, *J. Am. Chem. Soc.* **2001**, *123*, 1709.

 © 2005 Wiley-VCH Verlag GmbH & Co. KGaA, Weinheim

Physisorption on TiO_2

1:1 and 2:1 Charge-Transfer Complexes between Aromatic Hydrocarbons and Dry Titanium Dioxide**

*You Seok Seo, Changhoon Lee, Kee Hag Lee, and Kyung Byung Yoon**

The unique properties of TiO_2 have made it a popular material for various extensive applications in, for example, solar cells,[1] water splitting,[2] water treatment,[3] photocatalysts,[4,5] superhydrophilic coatings,[5] sensors,[6] and batteries.[7] Since the first step in these applications involves the interaction between the TiO_2 surface and the adsorbate, understanding the nature of the interactions at the interface is essential for understanding the known properties and for exploring new applications.

Two types of interactions have been observed so far: coordinative covalent bonding (CCB)[8–15] between the adsorbates and the Ti^{IV} ions on TiO_2 surfaces and the physical adsorption (PA). The CCB-type interactions give rise to ligand-to-metal charge-transfer (LMCT) interactions between the adsorbates and Ti^{IV} ions, owing to the low-lying empty t_{2g} orbitals of the Ti^{IV} centers in octahedral environments. Indeed, those relatively electron-rich adsorbates having functional groups such as enediol (notably catechol,[8] ascorbic acid,[9] dopamine,[10] and alizarin[8c]), carboxylate (notably 4-(methylsulfanyl)benzoic acid[11] and sulfanylacetic acid[12]), nitrile (notably ferricyanide[13]), and alcohol (notably 4-hydroxybiphenyl[14]) groups display LMCT bands in the visible region. The less electron-rich adsorbates such as thiocyanate showed the corresponding LMCT band in the UV region.[15]

In contrast to the well-studied CCB-type interaction, however, nothing is known about the nature of interaction between the physically adsorbed molecules and TiO_2. Stemming from our interests on the charge-transfer (CT) interactions between the zeolite framework and intercalated guest molecules,[16] we have conducted a series of experiments to study the interaction between TiO_2 and the adsorbates. As a result, we have discovered that pure polycyclic hydrocarbon arenes (ArHs) readily form 1:1 and 2:1 CT complexes with dry TiO_2 surfaces.

When dry TiO_2 (anatase, average diameter = 50 nm) particles were suspended in dilute CH_2Cl_2 solutions of phenanthrene (**1**), chrysene (**2**), anthracene (**3**), pyrene (**4**), and benzo[*a*]pyrene (**5**, Figure 1) in a dry box, the TiO_2 particles immediately picked up pale brownish colors. The added amounts of ArHs correspond to 2–20% surface coverage of TiO_2 based on the monomeric forms. Upon removal of the solvent by evacuation in the dry box, the colors intensified significantly. The colored TiO_2 particles bleached back to colorless when they were washed with CH_2Cl_2, and the UV/Vis spectra of the rinses were identical to those of the pure ArHs (see the Supporting Information), indicating that the color generation is a reversible process, and the coloration is not the result of the degradation of the ArHs upon contact with TiO_2. On the contrary, coloration did not occur with dried SiO_2 and $BaSO_4$, emphasizing that the coloration is unique to TiO_2. The diffuse reflectance spectra of the colored, dry TiO_2 particles revealed the presence of new absorption bands whose onsets progressively red-shifted with decreases in the calculated vertical ionization potential (IP_V) of ArH (Table 1, Figure 2a).

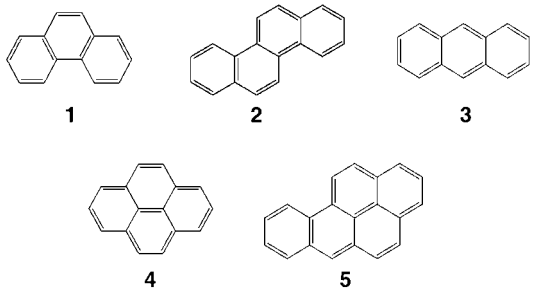


Figure 1. Structures of the aromatic hydrocarbons used in this study.

Deconvolution of the spectra (see the Supporting Information) revealed a new absorption in the case of phenanthrene (**1**) and two new absorption bands in the cases of more electron-rich arenes (Figure 2b). The two new absorption bands are designated as high-energy bands (HEBs) and low-energy bands (LEBs), respectively, and their energies at the absorption maximums ($E(\lambda_{max})$) are listed in Table 1. The new absorption band from **1** is classified as LEB based on the trend of other ArHs and by assuming that its HEB has shifted to the shorter wavelength UV region. The HEBs are unequivocally assigned as CT bands between ArH and TiO_2 based on the Mulliken linear relationship[17] between the calculated IP_V(ArH) and $E(\lambda_{max})$ as shown in Figure 3a.

LEBs were assigned as the CT bands between the arene dimers[18] and TiO_2, based on the following reasoning and evidence. First, it is well established that polycyclic ArHs readily form dimers $(ArH)_2$s on the hydrophilic solid surfaces when the surface coverage exceeds 1%.[19] Indeed, the diffuse reflectance spectra of the adsorbed ArHs on $BaSO_4$ were broader when the surface coverage was higher than 3%, and the onsets significantly red-shifted with respect to the

[*] Y. S. Seo, Prof. Dr. K. B. Yoon
Center for Microcrystal Assembly and
Department of Chemistry
Sogang University
Seoul 121-742 (Korea)
Fax: (+82) 2-706-4269
E-mail: yoonkb@sogang.ac.kr
C. Lee, Prof. Dr. K. H. Lee
Department of Chemistry and
Research Institute of Basic Science
Wonkwang University
Iksan, Jeonbuk 570-749 (Korea)

[**] We thank the Ministry of Science and Technology, Korea (Creative Research Initiatives Program) and Wonkwang University (2003) for supporting this work.

Supporting information for this article is available on the WWW under http://www.angewandte.org or from the author.

 © 2005 Wiley-VCH Verlag GmbH & Co. KGaA, Weinheim DOI: 10.1002/anie.200461972

Table 1: IP_V and IP_A values of monomeric and dimeric arenes and energies of new absorption bands [eV].[a]

ArH	IP_V(ArH)	IP_A(ArH)		$IP_V[(ArH)_2]$	$IP_A[(ArH)_2]$	$E(\lambda_{max})$[a]	
	Calcd[b]	Calcd[b]	Expt[c]	Calcd[b]	Calcd[b]	HEB	LEB
1	8.08	7.89	7.89[d]	7.96	7.58		3.35
2	7.81	7.62	7.60[e]	7.50	7.21	3.41	2.99
3	7.65	7.51	7.44[d]	7.29(7.1)[f]	6.99(6.89)[f]	3.24	2.83
4	7.63	7.48	7.43[d]	7.27	6.99	3.23	2.84
5	7.33	7.16	7.12[d]	6.92	6.49	2.97	2.41

[a] Energy of new absorption bands at the absorption maximum. [b] Calculated values. [c] Experimentally determined values. [d] From ref. [21]. [e] From ref. [22]. [f] From ref. [23].

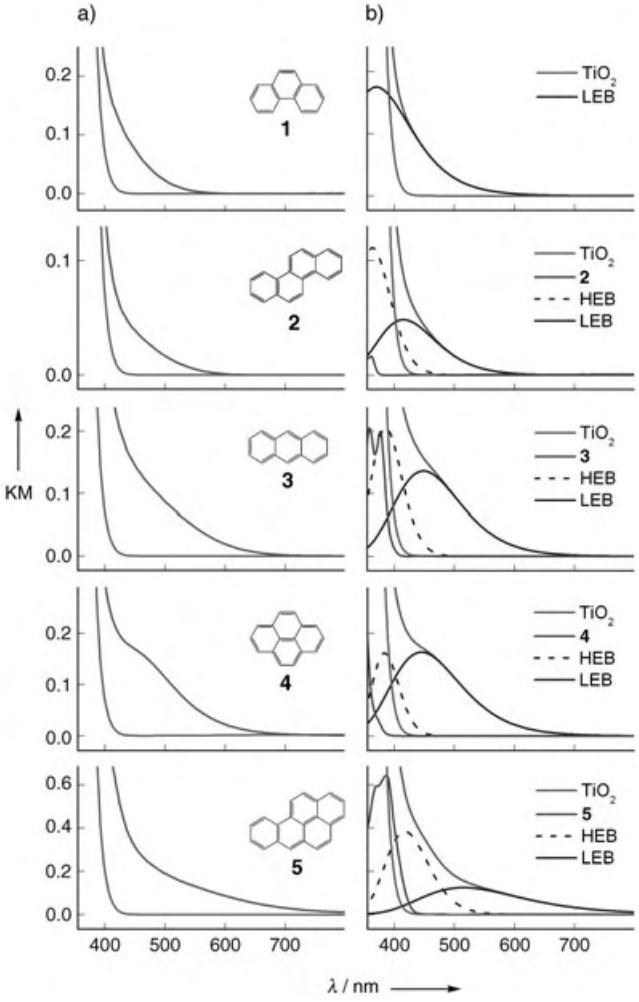


Figure 2. a) Diffuse reflectance UV/Vis spectra of TiO_2 (green curve) and arene-adsorbed TiO_2 (red curve) for each arene as indicated and b) the corresponding deconvoluted spectra. KM in the ordinate stands for the Kubelka–Munk value.

corresponding spectra in CH_2Cl_2 (see the Supporting Information), which is a characteristic feature of arene dimers. Furthermore, in the case of anthracene (**3**), the fluorescence spectrum on $BaSO_4$ displayed an excimer emission band at 420 nm (see the Supporting Information), which is another characteristic feature of the presence of $\mathbf{3}_2$.

By the same analogy, it is most likely that both ArH and $(ArH)_2$ coexist on the hydrophilic TiO_2 surface, although the obscuring CT bands make it difficult to identify the local bands of the two species. Second, the relative intensities of the LEBs increased when the surface coverage on TiO_2 was increased from 2% to 20% (see the Supporting Information). Last, most convincingly, there also exists an excellent Mulliken linear relationship between the calculated IP_V values of arene dimers (denoted as $IP_V[(ArH)_2]$) and the $E(\lambda_{max})$ values of LEBs (Table 1) as shown in Figure 3b.

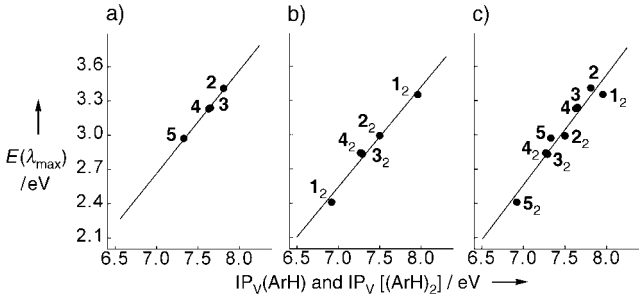


Figure 3. The Mulliken relationships between a) HEB and IP_V(ArH), b) LEB and $IP_V[(ArH)_2]$, and c) the combined values.

The formation of two CT bands also often occurs due to the transitions from the HOMOs (highest occupied molecular orbitals) and the HOMO-1s (second HOMOs) of the electron donors, respectively, to the LUMOs (lowest unoccupied molecular orbitals) of the electron acceptors. In this respect, as a possible means to check whether the two bands arise from the CT transitions from the HOMOs and HOMO-1s of ArHs, respectively, to the TiO_2 conduction band, we also obtained HOMO and HOMO-1 energy levels of the ArHs (see the Supporting Information). While the plot between HOMO energy levels and LEBs gave a linear relationship, the plot between HOMO-1 energy levels and HEBs showed no correlation whatsoever (see the Supporting Information), unambiguously showing that the HEBs do not arise due to the transition from HOMO-1 energy levels of ArH to the conduction band of TiO_2.

We therefore conclude that the arene donors form two types of CT complexes with dry TiO_2 surface, [ArH–TiO_2] and [$(ArH)_2$–TiO_2], as illustrated in Figure 4. The combined linear relationship (Figure 3c) was formulated as Equation (1),

$$E(\lambda_{max}) = 0.96\ IP_V(\text{arene}) - 4.18 \quad (1)$$

where IP_V(arene) represents both IP_V(ArH) and $IP_V[(ArH)_2]$. Interestingly, the observed correlation constant is close to 1 even though the CT interaction is heterogeneous in nature. From the energy level diagram shown in Figure 5, the average acceptor energy level of TiO_2 was deduced to be −4.45 eV, which is lower than the TiO_2 conduction band edge

 © 2005 Wiley-VCH Verlag GmbH & Co. KGaA, Weinheim

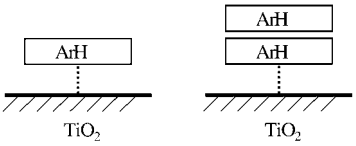


Figure 4. The two types of CT complexes formed by ArH on TiO_2.

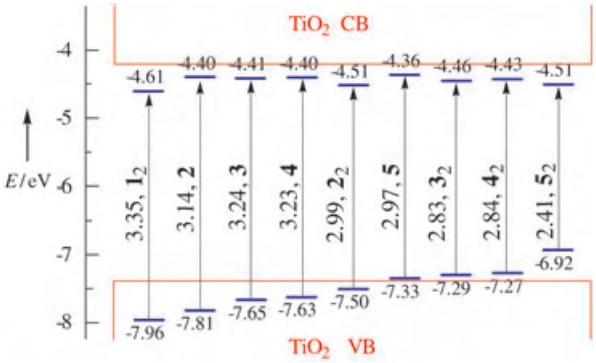


Figure 5. Energy level diagram of $IP_V(ArH)$, $IP_V[(ArH)_2]$, the conduction and valence bands of TiO_2, and the CT excitation energy.

(−4.2 eV)[20] by 0.25 eV. This indicates that the acceptor sites are mostly the defect or trap sites of the TiO_2 particles.

We also listed the calculated adiabatic ionization potentials (IP_A) of the arene monomers and dimers in Table 1. The $IP_A(ArH)$ values are very close to those determined experimentally,[21–23] thus demonstrating the reliability of our calculated IP_V and IP_A values. Although the $IP_A(ArH)$ and $IP_A[(ArH)_2]$ values also gave an excellent Mulliken plot with the $E(\lambda_{max})$ values of the LEBs and HEBs (see the Supporting Information), we used IP_V values in Figures 3 and 5, in compliance with the Mulliken CT theory.[17]

Unlike on $BaSO_4$ and SiO_2, the arenes did not fluoresce on TiO_2, most likely due to electron-transfer quenching, in support of the CT nature of the interaction. The CT bands quickly disappeared upon exposure of the colored, dry TiO_2 to moisture, indicating that moisture quickly intervenes between the hydrophilic TiO_2 surface and hydrophobic ArH or $(ArH)_2$, leading to breakage of arene–TiO_2 CT interaction (see the Supporting Information). The CT bands are also thermally and photochemically unstable most likely due to electron transfer from the arene monomers and dimers to TiO_2 (see the Supporting Information). The elucidation of the electron-transfer dynamics and the identification of the photoproducts are subjects of further study. This report thus reveals that the PA-type interaction between arenes and TiO_2 is a CT interaction in nature, suggesting that this type of interaction is general for other physically adsorbed molecules on TiO_2. The CCB- and PA-type interactions can be rephrased as inner- and outer-sphere CT interactions, respectively, according to the formulation of Kochi et al.[24] Thus, our finding leads to the conclusion that molecules form either inner- or outer-sphere CT complexes with TiO_2. Our finding also opens the possibility of using dry TiO_2 films in sensors and other useful devices.

Experimental Section

Titanium(IV) isopropoxide [$Ti(OiPr)_4$] was purchased from Across and used as received. Tetramethylammonium hydroxide (TMAOH, 25% aqueous solution), compounds **1**–**5** were purchased from Aldrich and used as received. $BaSO_4$ was purchased from Matheson, Coleman, and Bell.

Preparation of TiO_2 (anatase) nanoparticles. TMAOH (25% solution, 6.92 g, 19 mmol) was dissolved in distilled deionized water (450 g, 25 mol) contained in a 1 L beaker. $Ti(OiPr)_4$ (170.4 g, 25 mol) was dissolved in isopropyl alcohol (180 mL), and the $Ti(OiPr)_4$ solution was slowly added dropwise to the TMAOH solution while it was rigorously stirred with the aid of a magnetic stirring bar. The milky, opaque gel was heated at 100 °C for 3 h with vigorous stirring until the solution became semitransparent. After addition of 200 mL of distilled deionized water to the gel, the gel was heated (at 100 °C) and stirred further until the total volume decreased to 450 mL, and the solution became transparent. The transparent gel was then transferred to a Teflon-lined autoclave, and the gel was heated at 180 °C for 5 h. After the gel was cooled to room temperature by immersing the autoclave in cold water, the gel was passed through a Whatman filter (pore size = 2.5 μm) to remove Teflon particles and other large particles. The gel was then dried under vacuum at room temperature and the remaining white mixture of TiO_2 nanoparticles and TMAOH was ground into a fine powder with a mortar and pestle. The finely ground mixture was calcined at 450 °C for 24 h to remove TMAOH and other organic residues. The identity of the calcined powder as anatase was confirmed by its X-ray diffraction pattern measured with a Rigaku D/MAX-1C instrument (see the Supporting Information). The surface area of the anatase particles was with a Micromeritics ASAP 2000 as 48 $m^2 g^{-1}$. The scanning electron microscope (SEM) image of the calcined TiO_2 particles showed the grains were ≈50 nm in diameter and that they exist as agglomerates (see the Supporting Information).

Formation of arene–TiO_2 CT complexes. The calcined anatase particles (50 g) were introduced into a cylindrical glass flask equipped with a vacuum adaptor, and the particles were evacuated at 200 °C for 12 h at $< 10^{-5}$ torr. The airtight glass container was then transferred into a dry box charged with high-purity argon and stored as such in the dry box. Typically, an aliquot of the anatase particles (1.3 g) was transferred into a 10-mL vial, and CH_2Cl_2 (2 mL) was introduced into the vial. The roomlight around the dry box was turned off, and most of the windowpane of the dry box was covered with black cloth. A weak red lightbulb was turned on around the uncovered windowpane of the dry box. Anthracene (3 mg, 1.68×10^{-5} mol) was then introduced into the vial under the weak red light, and the heterogeneous mixture was shaken for 10 min with the help of a small shaker placed inside the dry chamber. Since thermal degradation of the arene proceeded slowly even at room temperature and in the dark, the period of shaking was limited to 10 min, during which the degree of thermal degradation of arene was negligible. The solvent was then removed from the vial by applying vacuum in the dry box. The colored anatase particles were then transferred into a flat fused-silica cell (thickness = 2 mm, diameter = 19 mm) equipped with an inner joint. The tightly capped cell was removed from the dry box, and the diffuse reflectance spectrum of the colored anatase was quickly measured on a Shimadzu 3101-PC spectrophotometer equipped with an integrating sphere. Adsorption of other arene donors onto the anatase particles and the spectral measurements of the CT colors were carried out similarly. The procedure was repeated using inert $BaSO_4$ powder (0.7 g) as the solid support to obtain the local bands of the arene donors.

Calculation of IP(ArH) and IP[$(ArH)_2$] values. Theoretical studies have verified that arenes readily associate as dimers.[25] For instance, the exhaustive relaxed potential energy surface (PES) scans, combined with full geometry optimizations carried out at the MP2/6-31G and MP2/6-31+G levels, predicted that anthracene forms crossed (C), parallel-displaced (PD), and two T-shaped (T edge and T point) structures.[26] However, the force-field calculations predicted

 © 2005 Wiley-VCH Verlag GmbH & Co. KGaA, Weinheim

only the C dimer of D_{2d} symmetry.[27] The dimer PES obtained by interacting multipolar multicenter distributions on the monomers and the valence-bond-based structures gave three structurally different dimers (PD, T edge, and T point) for the neutral and four dimers (sandwich-staggered (SS), sandwich-eclipsed (SE), PD long axis, and PD short axis) for the cationic dimers.[21]

The semiempirical AM1 method[26] was used to describe the ionization energies of the organic monomers and dimers for **1**–**5**. Both vertical and adiabatic IP(ArH) and IP[$(ArH)_2$] values were obtained by subtracting the potential energies of the most stable monomer and dimer from the corresponding cationic forms of monomer and dimer in the same geometry and from the most stable forms of the cationic monomer and dimer, respectively. No constraints were applied in the AM1 geometry optimizations.

Received: September 13, 2004
Published online: December 28, 2004

Keywords: arenes · charge transfer · physisorption · surface chemistry · titanium dioxide

[1] A. Hagfeldt, M. Grätzel, *Acc. Chem. Res.* **2000**, *33*, 269.
[2] A. Fujishima, K. Honda, *Nature* **1972**, *238*, 37.
[3] O. Legrini, E. Oliveros, A. M. Braun, *Chem. Rev.* **1993**, *93*, 671.
[4] M. A. Fox, M. T. Dulay, *Chem. Rev.* **1993**, *93*, 341.
[5] A. Fujishima, T. N. Rao, D. A. Tryk, *J. Photochem. Photobiol. C* **2000**, *1*, 1.
[6] N.-L. Wu, S.-Y. Wang, I. A. Rusakova, *Science* **1999**, *285*, 1375.
[7] M. Wagemaker, A. P. M. Kentgens, F. M. Mulder, *Nature* **2002**, *418*, 397.
[8] a) Y. Wang, K. Hang, N. A. Anderson, T. Lian, *J. Phys. Chem. B* **2003**, *107*, 9434; b) P. C. Redfern, P. Zapol, L. A. Curtiss, T. Rajh, M. C. Thurnauer, *J. Phys. Chem. B* **2003**, *107*, 11419; c) T. Rajh, L. X. Chen, K. Lukas, T. Liu, M. C. Thurnauer, D. M. Tiede, *J. Phys. Chem. B* **2002**, *106*, 10543; d) P. Persson, R. Bergström, S. Lunell, *J. Phys. Chem. B* **2000**, *104*, 10348.
[9] a) A. P. Xagas, M. C. Bernard, A. Hugot-Le Goff, N. Spyrellis, Z. Loizos, P. Falaras, *J. Photochem. Photobiol. A* **2000**, *132*, 115; b) T. Rajh, J. M. Nedeljkovic, L. X. Chen, O. Poluektov, M. C. Thurnauer, *J. Phys. Chem. B* **1999**, *103*, 3515.
[10] N. M. Dimitrijevic, Z. V. Saponjic, D. M. Bartels, M. C. Thurnauer, D. M. Tiede, T. Rajh, *J. Phys. Chem. B* **2003**, *107*, 7368.
[11] a) T. Tachikawa, S. Tojo, M. Fujitsuka, T. Majima, *Langmuir* **2004**, *20*, 4327; b) T. Tachikawa, S. Tojo, M. Fujitsuka, T. Majima, *J. Phys. Chem. B* **2004**, *108*, 5859.
[12] T. Rajh, M. C. Thurnauer, P. Thiyagarajan, D. M. Tiede, *J. Phys. Chem. B* **1999**, *103*, 2172.
[13] a) E. Vrachnou, M. Grätzel, A. J. McEvoy, *J. Electroanal. Chem. Interfacial Electrochem.* **1989**, *258*, 193; b) H. Lu, J. N. Prieskorn, J. T. Hupp, *J. Am. Chem. Soc.* **1993**, *115*, 4927; c) M. Khoudiakov, A. R. Parise, B. S. Brunschwig, *J. Am. Chem. Soc.* **2003**, *125*, 4637; d) M. Yang, D. W. Thompson, G. J. Meyer, *Inorg. Chem.* **2002**, *41*, 1254; e) Y.-X. Weng, Y.-Q. Wang, J. B. Asbury, H. N. Ghosh, T. Lian, *J. Phys. Chem. B* **2000**, *104*, 93.
[14] T. Tachikawa, S. Tojo, M. Fujitsuka, T. Majima, *Langmuir* **2004**, *20*, 2753.
[15] P. V. Kamat, *Langmuir* **1985**, *1*, 608.
[16] a) K. B. Yoon in *Handbook of Zeolite Science and Technology* (Eds.: S. M. Auerbach, K. A. Carrado, P. K. Dutta), Marcel Dekker, **2003**, 591–720; b) K. B. Yoon, *Chem. Rev.* **1993**, *93*, 321.
[17] R. S. Mulliken, *J. Am. Chem. Soc.* **1952**, *74*, 811.
[18] The lowest energy forms were assumed.
[19] a) R. Dabestani, K. J. Ellis, M. E. Sigman, *J. Photochem. Photobiol. A* **1995**, *86*, 231; b) W. E. Ford, P. V. Kamat, *J. Phys. Chem.* **1989**, *93*, 6423.
[20] A. Hagfeldt, M. Grätzel, *Chem. Rev.* **1995**, *95*, 49.
[21] B. Bouvier, V. Brenner, P. Millié, J. M. Soudan, *J. Phys. Chem. A* **2002**, *106*, 10326.
[22] J. W. Hager, S. C. Wallace, *Anal. Chem.* **1988**, *60*, 5.
[23] M. Shahbaz, I. Akiyama, P. R. LeBreton, *Biochem. Biophys. Res. Commun.* **1981**, *103*, 25.
[24] S. M. Hubig, R. Rathore, J. K. Kochi, *J. Am. Chem. Soc.* **1999**, *121*, 617.
[25] a) T. Chakraborty, E. C. Lim, *J. Phys. Chem.* **1993**, *97*, 11151; b) T. Matsuko, K. Kosugi, K. Hino, M. Nishiguchi, K. Ohashi, N. Nishi, H. Sekiya, *J. Phys. Chem. A* **1998**, *102*, 7598.
[26] C. Gonzalez, E. C. Lim, *J. Phys. Chem. A* **2000**, *104*, 2953.
[27] R. P. White, J. A. Niesse, H. R. Mayne, *J. Chem. Phys.* **1998**, *108*, 2208.

 © 2005 Wiley-VCH Verlag GmbH & Co. KGaA, Weinheim

Analytical Techniques

Direct Characterization of Enzyme–Substrate Complexes by Using Electrosonic Spray Ionization Mass Spectrometry**

*Justin M. Wiseman, Zoltán Takáts, Bogdan Gologan, V. J. Davisson, and R. Graham Cooks**

Numerous reports have cited the use of electrospray ionization (ESI) mass spectrometry to characterize intact, multiply-charged proteins and protein complexes.[1–4] Herein we describe the application of a variant method, electrosonic spray ionization (ESSI),[5] to monitor dynamic changes associated with formation of binary and ternary complexes, such as enzyme–substrate and enzyme–substrate–inhibitor systems. The basis for the experiment is that the gentle ESSI ionization method preserves solution protein and protein complex structures and tags each protein with a charge state that is characteristic of its conformation. In the course of the study, we show that noncovalent solution interactions between the enzyme imidazole-3-glycerol phosphate synthase (IGP synthase) and the substrate/inhibitor are preserved in the gas-phase ions. This enzyme contains two distinct active sites, the glutaminase domain and the synthetase domain located some 30 Å apart. The observations indicate the capacity of this method to preserve native-like protein

[*] J. M. Wiseman, Z. Takáts, B. Gologan, Prof. R. G. Cooks
Department of Chemistry
Purdue University
West Lafayette, IN 47907 (USA)
Fax: (+1) 765-494-0239
E-mail: cooks@purdue.edu
Prof. V. J. Davisson
Department of Medicinal Chemistry and Molecular Pharmacology
Purdue University
West Lafayette, IN 47907 (USA)

[**] This work is supported by Inproteo (Indianapolis, IN) and NIH grant GMRO1 GM 67195. The authors also gratefully acknowledge Rebecca S. Myers for providing sample materials and for helpful discussions.

 DOI: 10.1002/anie.200461672 © 2005 Wiley-VCH Verlag GmbH & Co. KGaA, Weinheim

conformations, and also to detect minor alterations in the protein structure induced by ligand binding as well as major alterations associated with denaturation.

Many regulatory events in living systems are governed by protein interactions involving either static or transient noncovalent macromolecular complexes. These interactions are often mediated through subtle changes of protein structure that translate into catalytic properties or signaling events within a cell.[6] These interactions between proteins and/or small-molecule metabolites generally involve changes in surface accessibility through ligand-induced conformational changes. Effectors, such as drugs or cellular second messengers, can perturb these interactions either directly or indirectly and their potency is often related to the extent to which these protein conformations are stabilized. Often indirect kinetic measurements or spectral methods must be used to deduce information regarding the dynamics of the protein–ligand or protein–protein interactions.

Since the introduction of the "soft" ionization techniques, electrospray ionization[7] (ESI) and matrix-assisted laser desorption ionization[8] (MALDI), the study of noncovalent biological complexes has been a focus of significant attention.[1,4,9–11] Electrospray ionization, in particular, allows large macromolecular assemblies to be ionized directly from solution and offers the opportunity to analyzing these complexes. Owing to multiple charging inherent in the electrospray process, these ions have relatively low mass/charge ratios and are amenable to characterization using ion-trapping instruments. There are a number of recent examples employing ESI/MS-based methods for detecting specific noncovalently bound protein assemblies and linking their solution-phase properties to those of the detected gas-phase ion.[2,4,9,12] Recently, we introduced a new electrospray variant, electrosonic spray ionization (ESSI),[5] for ionizing proteins from aqueous solutions at physiological pH values. The technique showed considerable improvement in spectral peak widths when compared to the nano-electrospray technique. Evidence was provided that the observed narrow charge-state distributions correspond to native-like solution-phase structures.[5] This result suggests a capability of ESSI for preserving intact biomolecule complexes in solution, transferring them to the gas phase, and detecting whether the native structure is retained. Herein, we test this hypothesis in a particular case of an unusual enzyme–substrate system. Direct characterization of the binary and ternary enzyme–substrate complexes is demonstrated and the solution-phase binding order is deduced from the pattern of charge states observed.

IGP synthase (IGPS) is a bifunctional enzyme of the glutamine amidotransferase family that incorporates ammonia derived from glutamine hydrolysis into the nucleotide, *N*-[(5′-phosphoribulosyl)formimino]-5-aminoimidazole-4-carboxamide ribonucleotide (PRFAR) to yield 5′-(5-aminoimidazole-4-carboxamide) ribonucleotide (AICAR) and imidazole glycerol phosphate (IGP).[13] This glutamine amidotransferase exhibits a $(\beta/\alpha)_8$ motif with the nucleotide active site formed by loop regions at the open end or top of the barrel. Such enzymes are excellent targets for genetic redesign, since the substrate specificity and catalytic function resides in the loop regions which are separated from the α helices and β strands that provide structural stability. A second active site for glutamine binding and hydrolysis (glutaminase site) resides in a separate domain juxtaposed at the bottom of the barrel some 30 Å away from the nucleotide binding site. The efficient transfer of the ammonia generated in this second active site to the nucleotide binding site requires an orchestrated signaling event that transmits binding and catalytic information across the interface of these two protein domains. However, these events have evaded any type of direct observation.

The ESSI mass spectrum of the intact 61 kDa IGPS is shown in Figure 1 and characteristically it shows a narrow charge-state distribution with the majority of the protein's

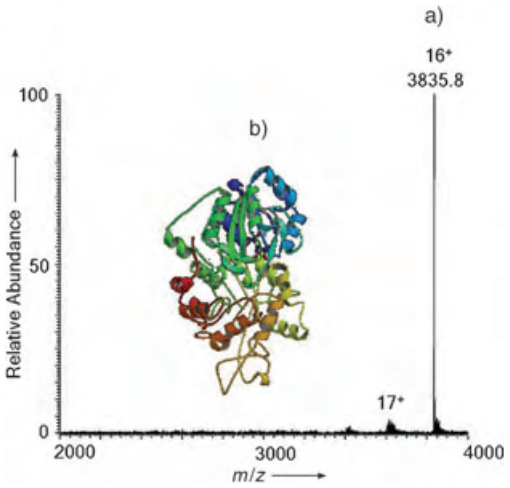


Figure 1. a) ESSI mass spectrum of imidazole-3-glycerol phosphate synthase (IGPS) in 10 mM ammonium acetate pH 7.1. b) 3D crystal structure of IGPS (http://www.rcsb.org/pdb/, Protein Data Bank Identifier (PDB ID): 1JVN[18]).

charge being collapsed into the +16 charge state. There is evidence that the observed charge state in ESI corresponds to the protein's net ionic charge in solution.[14] In addition, narrow charge-state distributions can indicate the retention of compact structures in the gas-phase that are like those of the native solution state.[11,15]

The observation of fewer charge states and, in some cases, a single charge state for a protein enhances the ability to track subtle changes occurring from perturbations of the enzyme–substrate system, as well as making it easier detect small molecular complexes.[5] Shown in Figure 2 is the ESSI mass spectrum acquired from a solution of IGPS and rPRFAR, the reduced form of PRFAR. The noncovalent complex of the enzyme and nucleotide substrate inhibitor is preserved in the gas phase and gives a single charge state, +16. In comparison, when using ESI the peaks are broader and less intense and as energy (that is, high capillary temperature and tube lens offset voltage) is added to enhance desolvation, dissociation of the complex is observed (data not shown). In Figure 2 the nucleotide inhibitor is not observed to be bound to the other higher charge states of the protein even though these appear in the mass spectrum. These charge states, +17 to +19,

 © 2005 Wiley-VCH Verlag GmbH & Co. KGaA, Weinheim

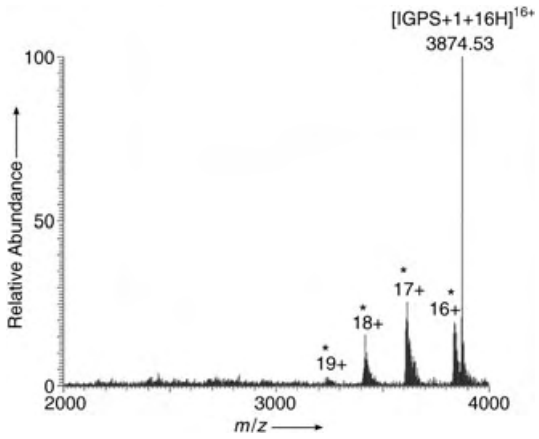


Figure 2. ESSI mass spectrum of IGPS–rPRFAR (**1**) solution containing 10 mM ammonium acetate pH 7.1 and 1 mM piperazine-*N*,*N*′-bis(2-ethane sulfonic acid) (PIPES) buffer. The (*) indicates peaks assigned to alternative conformations of the IGPS characterized by higher charge states.

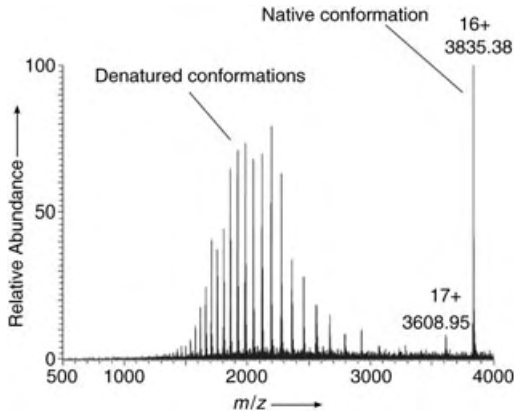


Figure 3. ESSI mass spectrum of IGPS under denaturing conditions. The presence of strong signals arising from multiple higher charge states is indicative of open denatured conformations although the single peak characteristic of the native structure is still present.

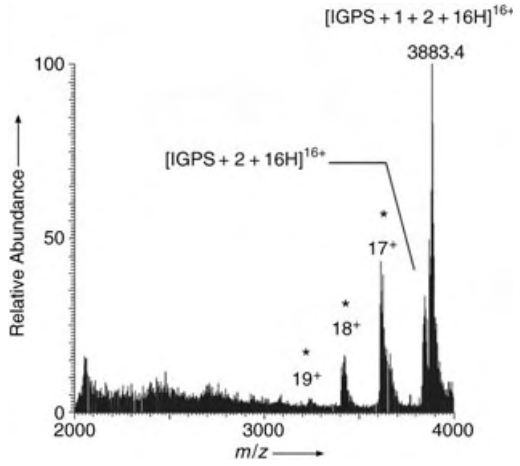


Figure 4. ESSI mass spectrum of IGPS–rPRFAR (**1**) acivicin (**2**) solution containing 10 mM ammonium acetate pH 7.1 and 1 mM PIPES buffer. The (*) indicates peaks assigned to an alternative non-native and hence nonbinding conformation(s) of the IGPS enzyme distinguished by higher charge states.

were virtually absent for the pure protein (Figure 1) and are interpreted as representing the protein in conformations that are unfavorable for substrate binding. (The unbound +16 signal marked with an asterisk is similarly assigned.) These conformations may result from binding–release events in which the released structure is altered and trapped in an unfavorable state through the course of the experiment. The following information is consistent with this interpretation. The binding of the nucleotide inhibitor induces small conformational changes within the $(\beta/\alpha)_8$ barrel of the enzyme.[13] An electrostatic gate of alternating positively and negatively charged amino acids is present in the interdomain region of the enzyme. Residues R239, E293, K360, and E465 make up this cap which facilitates ammonia tunneling within the hydrophobic core of the protein.[13] The X-ray crystal structure reveals the presence of a water-filled cavity near the interdomain region of the enzyme.[16] As substrate binding occurs in the synthase domain, a conformational reorganization of residues in the interdomain region takes place, exposing basic residues to solvent-accessible regions where they may be protonated. The increase in the number of charge states appearing in Figure 2 is tentatively associated with this conformational reorganization. This phenomenon, however, is clearly not a sign of global unfolding which gives the much broader charge-state distribution characteristic of a more open structure as is displayed in Figure 3. The observed peak broadening in Figure 2 for the asterisked charge states +16 to +19 implies the formation of a number of loose solvent or buffer adducts. Note that the spectrum shown in Figure 3 was taken from a solution containing 6 mM PIPES which is a zwitterionic, non-volatile buffer compound and presumably makes stable ion pairs which contain protonated arginine residues.

Figure 4 shows the ESSI mass spectrum of a solution containing IGPS, rPRFAR, and the glutamine amidotransferase inhibitor, acivicin. The peak at *m*/*z* 3883 corresponds to the ternary complex of IGPS, rPRFAR, and acivicin. The preservation of the products of two separate noncovalent binding events for the +16 charge state provides evidence for the existence of more and less favorable conformations in protein systems, recognized in this case by their characteristic charge states. Note that IGP synthase did not form a stable complex in the presence of acivicin alone. This is consistent with the fact that nucleotide binding induces a 200-fold shift in the apparent affinity of acivicin for IGPS.[17] As such, it is concluded that these binding events are not a result of non-specific interactions; rather, they are indicative of the interactions occurring in solution.

In conclusion, these studies reveal the feasibility of using electrosonic spray ionization (ESSI) for ionizing intact biomolecular complexes and preserving their solution-phase interactions in the gas phase. The example described herein emphasizes the advantages of ESSI in the direct characterization of proteins interacting noncovalently with multisubstrate systems. The identification of ligand binding to selected charge states highlights the potential of this ionization

 © 2005 Wiley-VCH Verlag GmbH & Co. KGaA, Weinheim

method to detect alternative protein conformations in equilibrium with the native conformation at concentrations that would evade detection by other biophysical methods.

Experimental Section

The electrosonic spray ionization source has been described in detail elsewhere.[5] The high voltage was applied to the stainless steel syringe needle used for sample infusion. The source and instrument parameters used in this study are listed in Table 1. The position of the ESSI source was carefully aligned in front of the heated capillary interface of the Finnigan LCQ Classic ion trap used in this work. The atmospheric interface potentials and lens potentials in the fore vacuum were optimized for maximum ion intensity. For this study, the ion trap was operated in high-mass mode to allow mass analysis up to 4000 Th. IGPS and rPRFAR was prepared as described in reference [14] and references therein. The purified protein was stored in 50 mM PIPES buffer until required for analysis. After purification, IGPS was buffer exchanged using Microcon YM-10 (10 kDa M_r cutoff) membrane filters (Millipore) against 0.2 M ammonium acetate pH 7.1 and reconstituted in 10 mM ammonium acetate pH 7.1 to a final concentration of approximately 1 μM. The centrifugation cycles were repeated 3×. For this study rPRFAR (**1**) a competitive nucleotide inhibitor of IGPS, and acivicin (**2**) [(*RS*,5*S*)-*R*-amino-3-chloro-4,5-dihydro-5-isoxazoleacetic acid] (Sigma), a covalent inactivator of the glutaminase function, were used as substrate analogues for IGPS.[15] Both rPRFAR and acivicin were prepared in PIPES buffer to a concentration of 6 mM. rPRFAR concentration was determined by UV-spectroscopy using an extinction coefficient of $6069\,M^{-1}\,cm^{-1}$ at 300 nm. Mixtures of the enzyme and substrate(s) were prepared to an enzyme:substrate ratio of 1:100.

Table 1: Experimental parameters used with the LCQ Classic mass spectrometer.

Parameter	Value
Sample flow rate	$3\ \mu L\,min^{-1}$
Nebulizing gas linear velocity	$350\ m\,s^{-1}$
Spray potential	3000 V
Heated capillary temperature	150 °C
Heated capillary voltage	15 V
Tube lens voltage	110 V
Octapole 1 offset	−1.3 V
Lens potential	−25.1 V
Octapole 2 offset	−3.0 V
Automatic Gain Control Target (AGC)	5E+07

Received: August 16, 2004
Revised: October 10, 2004
Published online: December 28, 2004

Keywords: electrospray ionization · mass spectrometry · noncovalent interactions · proteins

[1] a) J. A. Loo, *Mass Spectrom. Rev.* **1997**, *16*, 1; b) K. J. Lightwahl, B. L. Schwartz, R. D. Smith, *J. Am. Chem. Soc.* **1994**, *116*, 5271.
[2] F. Sobott, M. G. McCammon, C. V. Robinson, *Int. J. Mass Spectrom.* **2003**, *230*, 193.
[3] a) C. V. Robinson, *Nat. Struct. Biol.* **2002**, *9*, 505; b) H. Hernandez, C. V. Robinson, *J. Biol. Chem.* **2001**, *276*, 46685; c) T. A. Craig, L. M. Benson, A. J. Tomlinson, T. D. Veenstra, S. Naylor, R. Kumar, *Nat. Biotechnol.* **1999**, *17*, 1214; d) A. J. R. Heck, R. H. H. van den Heuvel, *Mass Spectrom. Rev.* **2004**, *23*, 368.
[4] a) T. D. Veenstra, *Biophys. Chem.* **1999**, *79*, 63; b) D. Lafitte, A. J. R. Heck, T. J. Hill, K. Jumel, S. E. Harding, P. J. Derrick, *Eur. J. Biochem.* **1999**, *261*, 337; c) A. J. R. Heck, T. J. D. Jorgensen, M. O'Sullivan, M. von Raumer, P. J. Derrick, *J. Am. Soc. Mass Spectrom.* **1998**, *9*, 1255; d) S. M. Clark, L. Konermann, *Anal. Chem.* **2004**, *76*, 1257.
[5] Z. Takáts, J. M. Wiseman, B. Gologan, R. G. Cooks, *Anal. Chem.* **2004**, *76*, 4050.
[6] M. G. McCammon, C. V. Robinson, *Curr. Opin. Chem. Biol.* **2004**, *8*, 60.
[7] J. B. Fenn, M. Mann, C. K. Meng, S. F. Wong, C. M. Whitehouse, *Mass Spectrom. Rev.* **1990**, *9*, 37. See also, J. B. Fenn, *Angew. Chem.* **2003**, *115*, 3999; *Angew. Chem. Int. Ed.* **2003**, *42*, 3871.
[8] M. Karas, F. Hillenkamp, *Anal. Chem.* **1988**, *60*, 2299. See also, K. Tanaka, *Angew. Chem.* **2003**, *115*, 3989; *Angew. Chem. Int. Ed.* **2003**, *42*, 3861.
[9] a) S. K. Chowdhury, V. Katta, B. T. Chait, *J. Am. Chem. Soc.* **1990**, *112*, 9012; b) T. J. D. Jorgensen, P. Roepstorff, A. J. R. Heck, *Anal. Chem.* **1998**, *70*, 4427.
[10] a) B. Ganem, Y. T. Li, J. D. Henion, *J. Am. Chem. Soc.* **1991**, *113*, 7818; b) T. B. Farmer, R. M. Caprioli, *J. Mass Spectrom.* **1998**, *33*, 697; c) V. Katta, B. T. Chait, *J. Am. Chem. Soc.* **1991**, *113*, 8534; d) E. N. Kitova, D. R. Bundle, J. S. Klassen, *J. Am. Chem. Soc.* **2002**, *124*, 9340; e) B. L. Schwartz, K. J. Lightwahl, R. D. Smith, *J. Am. Soc. Mass Spectrom.* **1994**, *5*, 201; f) Review: J. M. Daniel, S. D. Friess, S. Rajagopalan, S. Wendt, R. Zenobi, *Int. J. Mass Spectrom.* **2002**, *216*, 1.
[11] J. A. Loo, *Int. J. Mass Spectrom.* **2000**, *200*, 175.
[12] a) D. J. Wilson, L. Konermann, *Anal. Chem.* **2004**, *76*, 2537; b) M. G. McCammon, D. J. Scott, C. A. Keetch, L. H. Greene, H. E. Purkey, H. M. Petrassi, J. W. Kelly, C. V. Robinson, *Structure* **2002**, *10*, 851; c) T. A. Craig, T. D. Veenstra, S. Naylor, A. J. Tomlinson, K. L. Johnson, S. Macura, N. Juranic, R. Kumar, *Biochemistry* **1997**, *36*, 10482; d) V. Katta, B. T. Chait, *Rapid Commun. Mass Spectrom.* **1991**, *5*, 214; e) A. A. Rostom, P. Fucini, D. R. Benjamin, R. Juenemann, K. H. Nierhaus, F. U. Hartl, C. M. Dobson, C. V. Robinson, *Proc. Natl. Acad. Sci. USA* **2000**, *97*, 5185.
[13] R. S. Myers, J. R. Jensen, I. L. Deras, J. L. Smith, V. J. Davisson, *Biochemistry* **2003**, *42*, 7013.
[14] M. Peschke, A. Blades, P. Kebarle, *J. Am. Chem. Soc.* **2002**, *124*, 11519.
[15] a) J. A. Loo, R. R. O. Loo, H. R. Udseth, C. G. Edmonds, R. D. Smith, *Rapid Commun. Mass Spectrom.* **1991**, *5*, 101; b) I. A. Kaltashov, S. J. Eyles, *J. Mass Spectrom.* **2002**, *37*, 557.
[16] B. N. Chaudhuri, S. C. Lange, R. S. Myers, V. J. Davisson, J. L. Smith, *Biochemistry* **2003**, *42*, 7003.
[17] S. V. Chittur, T. J. Klem, C. M. Shafer, V. J. Davisson, *Biochemistry* **2001**, *40*, 876.
[18] H. M. Berman, J. Westbrook, Z. Feng, G. Gilliland, T. N. Bhat, H. Weissig, I. N. Shindyalov, P. E. Bourne, *Nucleic Acids Res.* **2000**, *28*, 235.

 © 2005 Wiley-VCH Verlag GmbH & Co. KGaA, Weinheim

Heterogeneous Catalysis

Understanding the Structural Deactivation of Ruthenium Catalysts on an Atomic Scale under both Oxidizing and Reducing Conditions**

Jens Aßmann, Daniela Crihan, Marcus Knapp, Edvin Lundgren, Elke Löffler, Martin Muhler, Vijay Narkhede, Herbert Over,* Michael Schmid, Ari P. Seitsonen, and Peter Varga*

The science and technology of catalysis are of central practical importance. About 80% of all industrial chemicals are manufactured by utilizing (heterogeneous) catalysis. Besides activity and selectivity, catalyst deactivation during use is a key issue in practical catalysis. "The importance of understanding and being able to predict loss of activity during catalyst usage must not be under-estimated"[1] since replacement of a catalyst means high operational costs. Industrially used catalysts are, however, far too complex to allow for a microscopic understanding of why a catalyst deactivates. This knowledge calls rather for the use of model catalysts (such as single-crystalline surfaces) and their investigations under well-controlled ultrahigh vacuum conditions. The trade off for this so-called surface-science approach[2] is the introduction of a pressure and a materials gap by which catalytic properties determined under well defined conditions may not be extrapolated to those at realistic reaction conditions.[3]

For a ruthenium-based catalyst, activity loss was reported for the CO oxidation reaction. In particular, under oxidizing reaction conditions the activity of supported ruthenium catalysts declines substantially.[4,5] This finding has been quite puzzling as recent investigations clearly indicate that RuO_2 is much more active than ruthenium in the oxidation of CO.[6] Since the pressure and materials gap for the CO oxidation over ruthenium are considered to be bridged[7] we can utilize the surface-science approach to clarify the microscopic processes determining the structural deactivation of ruthenium-based catalysts and how this atomic-scale knowledge is used to optimize the performance of practical ruthenium catalysts.

We concentrate herein mainly on polycrystalline RuO_2 powder which is calcined at 573 K, resulting in a specific surface area of 0.9 $m^2 g^{-1}$. Complementary data of supported ruthenium catalysts are provided in the Supporting Information. The mean diameter of the particles in the RuO_2 powder is about 1 μm. Therefore RuO_2 powder represents a natural link between single–crystal ruthenium model catalysts and ruthenium catalysts supported on SiO_2 or MgO with an active surface area of 10 $m^2 g^{-1}$.[8] Applied partial pressures of CO and O_2 are in the range of 5–35 mbar.

Figure 1a displays the conversion of CO over oxidized RuO_2 polycrystalline powder as a function of time on stream, using a stepwise temperature variation and a CO/O_2 feed ratio of 1:2. During the first temperature cycle each temperature jump is accompanied by a rapid increase of the CO conversion followed by a transient decrease of the CO conversion whose steady state is not reached within 1 h. This deactivation process occurs faster at higher temperatures, whereas the extent of deactivation increases with higher concentrations of O_2 (see Supporting Information). For all investigated CO/O_2 feed stocks it is found that the conversion

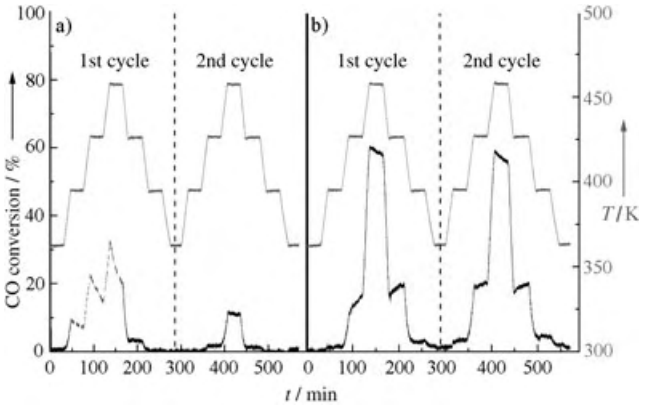


Figure 1. Conversion of CO over a) oxidized polycrystalline RuO_2 powder and b) pre-reduced polycrystalline RuO_2 powder as a function of time on stream and temperature. The applied cyclic temperature program (363 K–456 K) is shown in the gray trace (right-hand axis). The total flow rate was 50 mL min^{-1} with a CO/O_2 feed ratio of 1:2 (1.8% CO/3.6% O_2). The transient decrease of the CO conversion is indicated as a broken curve in the first cycle of Figure 1a.

[*] D. Crihan, M. Knapp, Prof. Dr. H. Over
Physikalisch-Chemisches Institut
Justus-Liebig-Universität
Heinrich-Buff-Ring 58, 35392 Giessen (Germany)
Fax: (+49) 641-99-34559
E-mail: herbert.over@phys.chemie.uni-giessen.de
Dr. J. Aßmann, Dr. E. Löffler, Prof. Dr. M. Muhler, V. Narkhede
Lehrstuhl für Technische Chemie
Ruhr-Universität Bochum
44780 Bochum (Germany)
Fax: (+49) 234-32-14115
E-mail: muhler@techem.rub.de
Dr. E. Lundgren
Department of Synchrotron Radiation Research
University of Lund, Sölvegatan 14, 22362 Lund (Sweden)
Prof. Dr. M. Schmid, Prof. Dr. P. Varga
Institut für Allgemeine Physik, TU Wien
Wiedener Hauptstrasse 8–10, 1040 Wien (Austria)
Dr. A. P. Seitsonen
Physikalisch-Chemisches Institut, Universität Zürich
Winterthurerstrasse 190, 8057 Zürich (Switzerland)

[**] H.O. and M.M. gratefully acknowledge financial support by Deutsche Forschungsgemeinschaft (DFG, SPP 1091). We acknowledge the Leibniz-Rechenzentrum in Munich for providing us with massive parallel computing time. The work in Vienna was supported by the "Fonds zur Förderung der wissenschaftlichen Forschung". E.L. thanks for financial support by the Swedish Research Council. Partial financial support is acknowledged from the European Union under contract no. NMP3-CT-2003-505670 (NANO2).

Supporting information for this article is available on the WWW under http://www.angewandte.org or from the author.

 DOI: 10.1002/anie.200461805 © 2005 Wiley-VCH Verlag GmbH & Co. KGaA, Weinheim

of CO is significantly lower when reaching 363 K for the second time, and that almost no further deactivation takes place during the second temperature cycle. The highest CO conversion is accomplished with a stoichiometric CO/O_2 gas feed.

The oxidation state of the RuO_2 powder catalyst is determined by temperature programmed reduction (TPR) in H_2 (see Figure 2 trace a). The consumption of H_2 by water

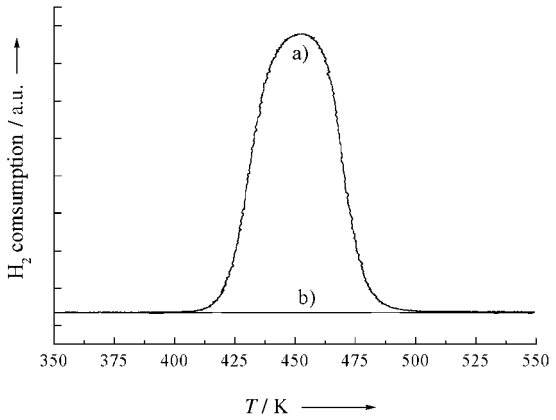


Figure 2. TPR (in H_2) profiles of polycrystalline RuO_2 after oxidizing CO at 453 K under net oxidizing conditions (CO/O_2 reactant feed ratio of 1:2) for 2 h: a) using a pre-oxidized RuO_2 catalyst; b) using a pre-reduced RuO_2 catalyst. The pre-reduced RuO_2 catalyst was prepared by purging the RuO_2 powder at 750 K in H_2 (30 mbar) for 2 h prior to the CO oxidation reaction.

formation is a direct measure of the oxygen capacity in the ruthenium particle and therefore of the O/Ru ratio. For instance, after running the RuO_2 powder catalyst with net oxidizing gas feeds at 453 K, the O/Ru ratio turns out to be 2:1, consistent with fully oxidized RuO_2.

To identify the microscopic processes that lead to the deactivation of a RuO_2-powder catalyst and also to find efficient measures to impede its deactivation we invoke the surface science approach. The initial oxidation of a macroscopic Ru(0001) single crystal proceeds by various characteristic stages.[6] First, oxygen from the gas phase adsorbs dissociatively on the Ru(0001) surface, forming distinct ordered O overlayers. All these Ru(0001)–O overlayers are inactive in the oxidation of CO molecules because of the strong O−Ru bonding. Below 500 K oxide formation does not set in, even under oxygen pressures of 10^{-2} mbar. At 650 K oxide formation proceeds in an autocatalytic process,[9] resulting in an ultra thin $RuO_2(110)$ layer on Ru(0001) (typical thickness of 1 nm). This thin $RuO_2(110)$ layer is extraordinarily active in the oxidation of CO. At higher temperatures (above 800 K) the RuO_2 film grows thicker under oxidizing conditions and is observed to roughen. CO adsorption and reaction experiments indicate that a very rough RuO_2 film on Ru(0001) is practically inactive in the oxidation of CO, that is, the RuO_2 film deactivates.

Excessive exposure of an $Ru(10\bar{1}0)$ surface to oxygen at 650 K leads also to the growth of an ultra thin RuO_2 film that is oriented along the (100) direction and which is as active as $RuO_2(110)$ in the oxidation of CO.[10] However, under oxidizing conditions and temperatures above 800 K the $RuO_2(100)$ film grows thicker and transforms irreversibly from the catalytically active $RuO_2(100)$ phase into a reconstructed $c(2\times2)$ phase which is unable to convert CO into CO_2.[11]

What is the reason for the deactivation of a rough RuO_2 film on Ru(0001), where as a flat $RuO_2(110)$ surface is extraordinarily active in the oxidation of CO? The scanning tunneling microscope (STM) images in Figure 3 visualize the

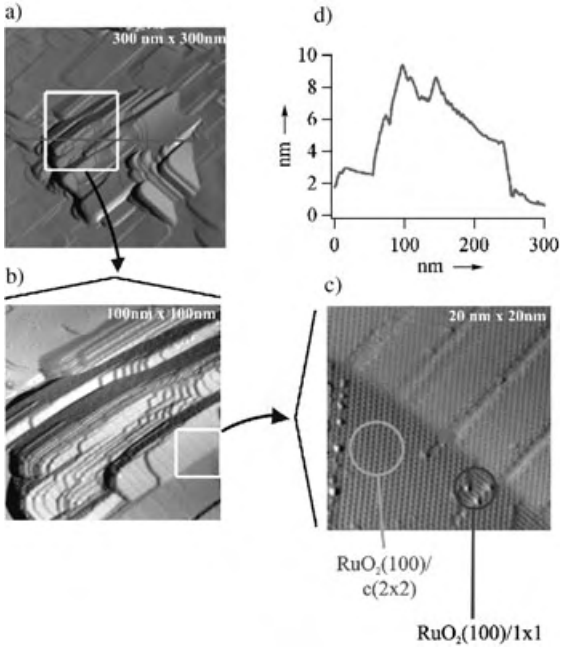


Figure 3. The initial roughening of a $RuO_2(110)$ film on Ru(0001). a) STM image (300 nm × 300 nm). b) and c) close-up images of the rough region (STM image: 100 nm × 100 nm (b), 20 nm × 20 nm (c)) indicating that the facets are oriented along the (100) direction and reconstructed into a $c(2\times2)$ phase. d) a line profile across the facetted region along the line shown in (a).

initial roughening of the $RuO_2(110)$ surface. The flat regions in Figure 3a are the catalytically active $RuO_2(110)$ areas. However, the rough part of the surface with a height of 8 nm above the flat region (Figure 3d) exposes $RuO_2(100)$ facets. Zooming into this facet we can identify (Figure 3b, c) the catalytically inactive $c(2\times2)$ regions which are separated by narrow $RuO_2(100)$ stripes. Similar STM images were reported for the growth of $RuO_2(100)$ on $Ru(10\bar{1}0)$.[11] Since the $c(2\times2)$ patches are inactive in the CO oxidation, a rough RuO_2 film on Ru(0001) becomes gradually inactive. Finally a thick RuO_2 film is completely covered by these $c(2\times2)$ domains and therefore catalytically inactive.

Under reducing reaction conditions the $RuO_2(110)$ surface will first be depleted of bridging O atoms. CO molecules adsorb strongly (binding energy = 180 kJ mol^{-1} [12]) into such bridging O vacancies, thereby stabilizing the mildly reduced $RuO_2(110)$ surface. Nevertheless, this mildly reduced $RuO_2(110)$ surface is still active in the oxidation of CO.[7] Only at temperatures above 450 K and under reducing

 © 2005 Wiley-VCH Verlag GmbH & Co. KGaA, Weinheim

reaction conditions does the mildly reduced surface decompose into a metallic and an oxide surface phase[11] until the RuO_2(110) film is buried under a catalytically inactive Ru(0001)–O layer.

Therefore, the deactivation of the RuO_2-powder catalyst under reducing reaction conditions is straight forwardly explained by the presence of catalytically inactive Ru(0001)-O domains on the surface of the catalyst (see Figure 4). To comprehend the deactivation of the RuO_2

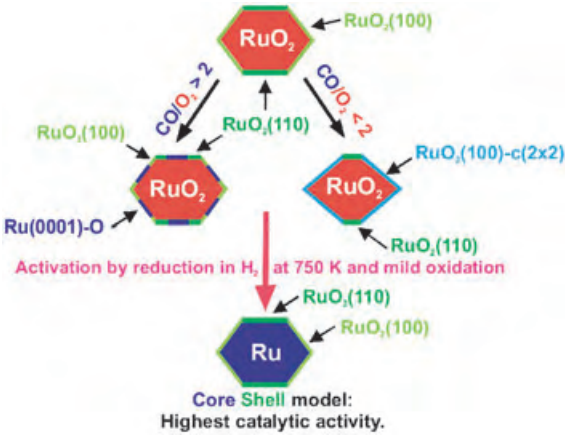


Figure 4. Core–shell model for RuO_2 powder catalysts: The degree of surface oxidation is determined by the CO/O_2 reactant feed ratio and the temperature. The inactive RuO_2(100)–c(2×2) (light blue) surface facets are formed under oxidizing conditions ($CO/O_2 < 2$), whereas low-activity metallic ruthenium surfaces (Ru(0001)–O) (dark blue) are exposed under net reducing conditions ($CO/O_2 > 2$). The most active state is an ultrathin RuO_2 (light and dark green: thickness 1–2 nm) layer supported on a metallic ruthenium core. This state is achieved by complete reduction of the RuO_2 particle followed by a mild re-oxidation below 500 K.

powder catalyst (and also supported ruthenium catalysts) under net oxidizing conditions we transfer knowledge gained from the surface-science approach across the materials and pressure gap as summarized in Figure 4. The RuO_2 particles expose preferentially (110) and (100) facets. Upon CO oxidation at net oxidizing conditions, the active RuO_2(100) facets of the RuO_2 particle transform into the inactive RuO_2(100)-c(2×2) phase. But also the RuO_2(110) facets will deactivate partly under oxidizing conditions. The RuO_2(110) facets roughen considerably, thereby forming additional RuO_2(100) facets (Figure 3) which reconstruct into the inactive c(2×2) phase. Both deactivation processes are the more efficient the higher the temperature is, consistent with the deactivation behavior of RuO_2 powder and supported ruthenium catalysts. Eventually the RuO_2 particle exposes predominantly catalytically inactive RuO_2(100)-c(2×2) facets and only small areas of active RuO_2(110) facets.

Is there any remedy to impede the deactivation of the RuO_2 powder catalyst? Again we will find the answer by transcribing the knowledge from the surface-science approach to the practical RuO_2 catalyst. We know that ultrathin RuO_2 films (thickness 1–2 nm) both on Ru(0001) and on Ru(10$\bar{1}$0) are extremely active in the oxidation of CO.[10] We know also that for reaction temperatures below 650 K these active RuO_2 films are stable under oxidizing reaction conditions. This suggests the following recipe to prepare an active and stable RuO_2 powder catalyst. First we fully reduce the RuO_2 particles to metallic ruthenium by purging the catalyst in H_2 at 750 K. Then we re-oxidize the ruthenium particles under gentle reaction conditions, say temperatures below 500 K. This procedure indeed results in a very active and also stable RuO_2 powder catalyst as indicated in Figure 1 b: Note that the conversion of CO is enhanced by a factor of three. The oxidation state of this catalyst is determined by TPR (Figure 2 trace b). Only a little oxygen is present in/on the ruthenium particle consistent with a ruthenium particle that is covered by only an ultrathin RuO_2 layer.

We can safely assume that the metallic ruthenium particles in the fully reduced RuO_2 powder catalyst, expose preferentially (0001) and (10$\bar{1}$0) facets, since those are the surfaces with lowest surface energies (see Supporting Information). Under mild reaction conditions the ruthenium particle will oxidize by growing a RuO_2(110) layer on the Ru(0001) facets and a RuO_2(100) layer on the Ru(10$\bar{1}$0) facets. This RuO_2/Ru core–shell particle (see Figure 4) reveals the highest activity in the CO oxidation (see Figure 1 b).

The stability of this RuO_2/Ru core–shell particle is controlled by kinetics. For ruthenium particles with a mean diameter of 1 μm (reduced RuO_2 powder) or for the macroscopic Ru(0001) and Ru(10$\bar{1}$0) single crystals the oxidation of ruthenium stops at a thickness of 1–2 nm as long as the temperature does not exceed 650 K. Therefore the active state of the reduced RuO_2 powder catalyst is maintained under oxidizing reaction conditions. In contrast, for supported ruthenium catalysts, the ruthenium nanoparticles with active RuO_2(110) and RuO_2(100) layers surrounding the metallic ruthenium core are instable under both reducing and oxidizing reaction conditions (see Supporting Information). Either the nanoparticle reduces, exposing inactive ruthenium domains, or it oxidizes completely, exposing predominantly inactive c(2×2) domains.[13]

The atomic-scale information of the deactivation of ruthenium-based catalysts upon CO oxidation can be utilized for practical applications. If the size of the ruthenium nanoparticles is about 3 nm (typical size of supported ruthenium catalysts[8]), the catalyst should be run under alternating reducing and oxidizing conditions about the CO/O_2 gas feed ratio of 2:1 to maintain the active RuO_2/Ru core–shell particle with its high conversion rate. The supported ruthenium catalyst is more stable if the ruthenium particles are larger. The high catalytic activity is, however, balanced by the inferior surface-to-bulk ratio of larger particles, so that an optimum particle size is expected to be in the order of 10 nm.

The deactivation of RuO_2 is not restricted to the CO oxidation reaction. The RuO_2 coated electrodes used in the electrochemical evolution of chlorine[14] may also deactivate under oxidizing conditions. In industrial chemistry ruthenium-based catalysts are currently discussed as promising candidates for a green chemistry route of the aerobic alcohol oxidation.[15,16] The deactivation of the ruthenium-based

 © 2005 Wiley-VCH Verlag GmbH & Co. KGaA, Weinheim

catalyst through full oxidation of the ruthenium particles is an important issue to be settled for future application.

Received: August 27, 2004
Revised: November 18, 2004
Published online: December 28, 2004

Keywords: catalytic activity · heterogeneous catalysis · oxidation · ruthenium · surface chemistry

[1] J. M. Thomas, W. J. Thomas, *Principles and Practice of Heterogeneous Catalysis*, VCH, Weinheim, **1996**.
[2] See for example, various articles in Frontiers in Surface and Interface Science (Eds.: C. B. Duke, E. W. Plummer), *Surf. Sci.* **2001**, 500.
[3] *Handbook of Heterogeneous Catalysis*, *Vol. 5* (Eds.: G. Ertl, H. Knözinger, J. Weitkamp), Wiley, New York, **1997**.
[4] J. T. Kiss, R. D. Gonzalez, *J. Phys. Chem.* **1984**, *88*, 892 – 903.
[5] N. W. Cant, P. C. Hicks, B. S. Lennon, *J. Catal.* **1978**, *54*, 372 – 383.
[6] H. Over, Y. D. Kim, A. P. Seitsonen, S. Wendt, E. Lundgren, M. Schmid, P. Varga, A. Morgante, G. Ertl, *Science* **2000**, *287*, 1474 – 1477.
[7] H. Over, M. Muhler, *Prog. Surf. Sci.* **2003**, *72*, 3 – 17.
[8] J. Aßmann, E. Löffler, A. Birkner, M. Muhler, *J. Catal.* **2003**, *85*, 235 – 249.
[9] H. Over, A. P. Seitsonen, *Science* **2002**, *297*, 2003 – 2004.
[10] Y. D. Kim, H. Over, G. Krabbes, G. Erk, *Topics Catal.* **2001**, *14*, 95 – 100.
[11] H. Over, M. Knapp, E. Lundgren, A. P. Seitsonen, M. Schmid, P. Varga, *ChemPhysChem* **2004**, *5*, 167 – 174.
[12] "Ruthenium Dioxide, a Versatile Oxidation Catalyst: First Principles Analysis": A. P. Seitsonen, H. Over in *High Performance Computing in Science and Engineering in Munich 2002*, Springer, Heidelberg, **2003**, pp. 171 – 180.
[13] J. Aßmann, V. Narkhede, L. Khodeir, E. Löffler, O. Hinrichsen, A. Birkner, H. Over, M. Muhler, *J. Phys. Chem. B* **2004**, *108*, 14634 – 14642.
[14] a) S. Trasatti, *Electrochim. Acta* **2000**, *45*, 2377 – 2385; b) R. Mason, A. Mills, D. Milton, *J. Less-Common Met.* **1989**, *155*, 89 – 109.
[15] K. Yamaguchi, N. Mizuno; *Angew. Chem.* **2002**, *114*, 4720 – 4724; *Angew. Chem. Int. Ed.* **2002**, *41*, 4538 – 4542.
[16] B.-Z. Zhan, M. A. White, T.-K. Sham, J. A. Pincock, R. J. Doucet, K. V. R. Rao, K. N. Robertson, T. S. Cameron, *J. Am. Chem. Soc.* **2003**, *125*, 2195 – 2199.

 © 2005 Wiley-VCH Verlag GmbH & Co. KGaA, Weinheim

Inclusion Compounds

Direct Observation of Hydrogen Molecules Adsorbed onto a Microporous Coordination Polymer**

Yoshiki Kubota, Masaki Takata, Ryotaro Matsuda, Ryo Kitaura, Susumu Kitagawa, Kenichi Kato, Makoto Sakata, and Tatsuo C. Kobayashi*

Hydrogen storage is an important technology and is indispensable for the establishment of clean hydrogen energy systems. Although various materials have been studied as hydrogen-storage materials,[1] there is yet no decisive way to store and release H_2 molecules efficiently. Adsorption of H_2 molecules in metal–organic porous materials[2,3] is one of the most promising candidates. To develop a rational synthetic strategy for novel metal–organic porous materials that can adsorb large amounts of H_2 molecules, the elucidation of the intermolecular interactions between H_2 molecules and pore walls is essential. Despite several investigations into novel metal–organic porous materials as hydrogen-storage materials,[4] little is known about the effective interaction mechanism and the fundamental structural characteristics of the adsorbed H_2 molecules. In previous work,[5] we determined the assembled structure of O_2 molecules in nanochannels by

[*] Dr. Y. Kubota
Department of Environmental Sciences
Faculty of Science, Osaka Women's University
Sakai, Osaka 590-0035 (Japan)
Fax: (+81) 72-222-4791
E-mail: kubotay@center.osaka-wu.ac.jp

Dr. M. Takata, K. Kato
Japan Synchrotron Radiation Research Institute/SPring-8
Sayo-gun, Hyogo 679-5198 (Japan)
and
CREST, Japan Science and Technology Agency

R. Matsuda, Dr. R. Kitaura,[+] Prof. Dr. S. Kitagawa
Department of Synthetic Chemistry and Biological Chemistry
Graduate School of Engineering, Kyoto University
Katsura, Kyoto 615-8510 (Japan)

Prof. Dr. M. Sakata
Department of Applied Physics, Nagoya University
Nagoya 464-8603 (Japan)

Prof. Dr. T. C. Kobayashi
Department of Physics, Okayama University
Okayama 700-8530 (Japan)

[+] Present address: Toyota Central Research and Development Laboratories, Inc.
Nagakute, Aichi 480-1192 (Japan)

[**] This study was supported by CREST, JST, and JASRI/SPring-8 Nanotechnology Support Project of the Ministry of Education, Culture, Sports, Science, and Technology of Japan (Proposal No. 2004A0217-ND1b-np/BL-No. 02B2). This research was also supported by a grant-in-aid for Scientific Research from the Ministry of Education, Culture, Sports, Science, and Technology of Japan. The authors thank Dr. H. Tanaka for the computer program ENIGMA for the MEM analysis.

Supporting information for this article is available on the WWW under http://www.angewandte.org or from the author.

 © 2005 Wiley-VCH Verlag GmbH & Co. KGaA, Weinheim DOI: 10.1002/anie.200461895

in situ synchrotron powder diffraction, which allowed a good understanding of the magnetic and adsorption behavior of O_2 molecules. Therefore the structure determination of adsorbed H_2 molecules should also provide us with much information on physicochemical properties to allow a rational design and synthesis of high-performance hydrogen-storage materials. Although the weakest X-ray scattering amplitude of hydrogen made it difficult to determine the structure, the elusive hydrogen can be observed by using a high-brilliance synchrotron light source and MEM (maximum entropy method)/Rietveld charge-density analysis.[6] These techniques are particularly suitable for systems in which the contribution from heavy elements is not dominant. In a recent study on metal hydrides,[7] the position of the hydrogen atoms was determined and the bonding between the hydrogen atom and the metal atom was revealed. Herein we report the first successful direct observation of H_2 molecules adsorbed in the nanochannels of metal–organic porous materials by in-situ synchrotron powder diffraction experiment of gas adsorption and MEM/Rietveld analysis.

The sample used in this study is $[Cu_2(pzdc)_2(pyz)]_n$ (pzdc = pyrazine-2,3-dicarboxylate, pyz = pyrazine), which has a pillared layer structure with uniform nanochannels of 4×6 Å.[2] We call it CPL-1 (coordination polymer 1 with pillared layer structure). Figure 1 shows the variation of the lattice parameters and the cell volume of CPL-1 with hydrogen gas obtained by Rietveld analysis. Significant lattice expansion occurred between 90 and 110 K. This can be considered as the H_2 molecules being adsorbed in the nanochannels of CPL-1. Changes in cell parameters are due to the slight transformation of the CPL framework to accommodate the adsorbed hydrogen molecules. The peak shifts and a slight profile broadening by the H_2 adsorption are also seen in the powder pattern at 90 K. As a reference, the powder diffraction pattern of CPL-1 without hydrogen gas was also collected. The powder patterns of CPL-1 with and without hydrogen gas at 90 K were analyzed (Figure 2).

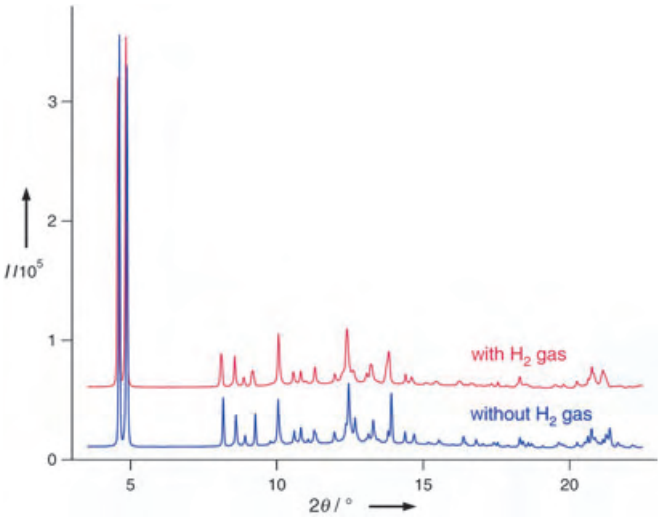


Figure 2. Synchrotron X-ray powder diffraction patterns of CPL-1 (90 K) with hydrogen gas (102 kPa) and without hydrogen gas.

The structure was analyzed by using the MEM/Rietveld method.[6] The amount of H_2 molecules adsorbed in CPL-1 at 90 K at 102 kPa was determined to be 0.3 molecules per Cu atom from the measurement of the hydrogen-adsorption isotherm. Thus, the atomic occupancy parameter of a hydro-

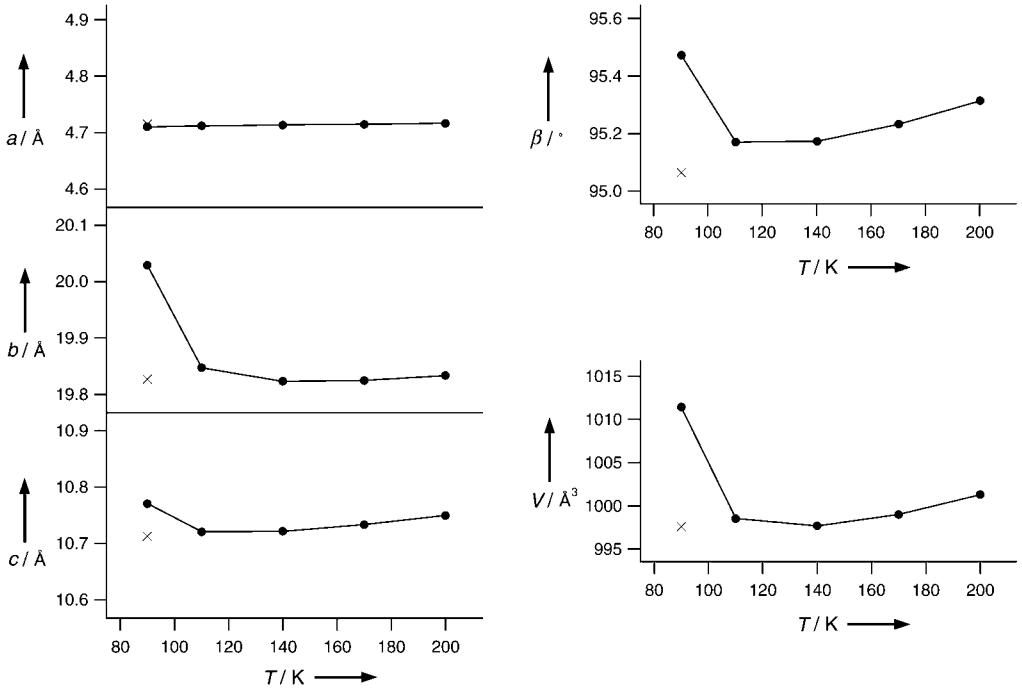


Figure 1. Variation of the lattice parameters and the cell volume of CPL-1 in hydrogen-gas adsorption. The black circles show the data with hydrogen gas and the crosses show the data without hydrogen gas.

 © 2005 Wiley-VCH Verlag GmbH & Co. KGaA, Weinheim

gen atom of a H_2 molecule was fixed as 0.3 in the Rietveld analysis. The MEM calculation was carried out by the computer program ENIGMA.[8] The reliability (R) factors based on the powder profile R_{WP} and the Bragg integrated intensities R_I for the final Rietveld analysis of CPL-1 with H_2 gas were 2.45% and 3.33%, respectively. The R factor based on the structure factors in the final MEM analysis R_F was 1.86%. The R_{WP}, R_I, and R_F for CPL-1 without H_2 gas were 2.21%, 3.89%, and 2.50%, respectively.

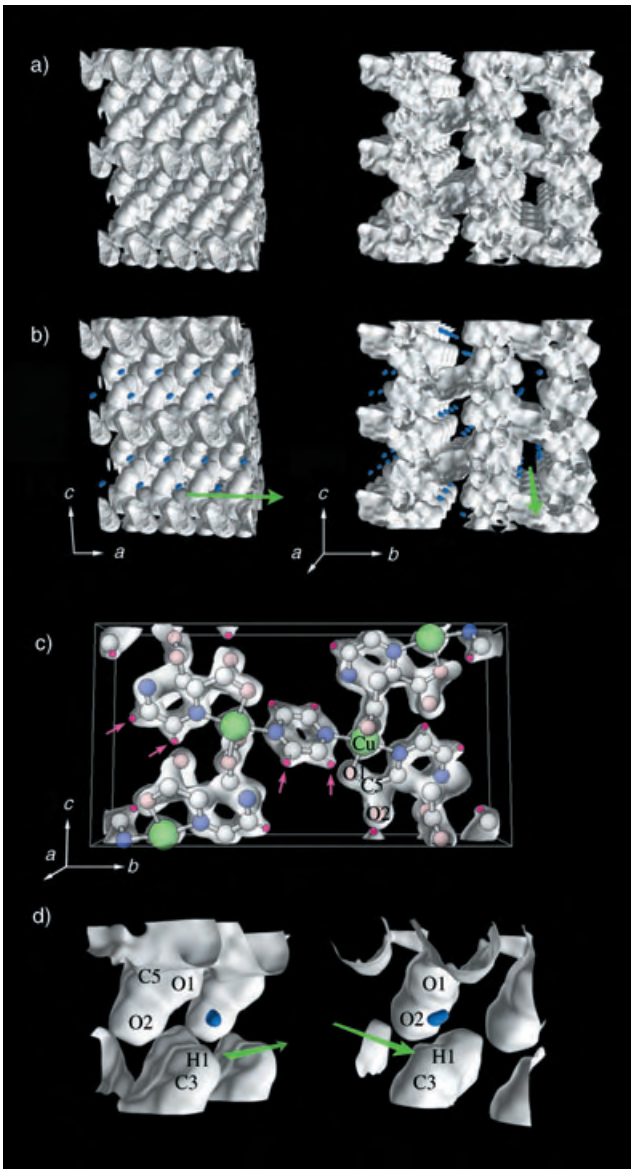


Figure 3. MEM charge-density distributions of CPL-1 at 90 K as an equidensity contour surface: a) without H_2 molecules, b) and c) with adsorbed H_2 molecules, and d) close-up views around the adsorbed H_2 molecule. The equidensity contour level is 0.11 eA^{-3} in a), b), and d) and 0.80 eA^{-3} in c). Charge densities of adsorbed H_2 molecules are colored in blue. The green arrows indicate the direction of the nanochannel of CPL-1. In c), the charge density within the unit cell is drawn and the structural model is superimposed. Arrows indicate the hydrogen atoms of pyrazine in the CPL framework. The charge density of adsorbed H_2 molecules is not seen at this level.

The MEM charge density distributions of CPL-1 with and without H_2 molecules are shown in Figure 3 as an equidensity contour surface. In the MEM charge density of CPL-1 without H_2 molecules (Figure 3a), only the nanochannel structure was clearly seen and no electron density was observed in the nanochannels, even at lower electron-density levels. On the other hand, in the MEM charge density of CPL-1 with H_2 molecules (Figure 3b), the small peak maxima of the electron densities with elongated shape distribution were observed in the nanochannels. The number of electrons around the density areas was calculated to be 0.6(1) e, which virtually agrees with the initial estimated amount of adsorbed H_2 molecules ($0.3\,e \times 2 = 0.6\,e$). Thus, we considered those to be the densities of adsorbed H_2 molecules. It should be noted that the position and the orientation of the H_2 molecules are mean values obtained by statistical analysis. The charge-density distribution of the adsorbed H_2 molecule is broader than that of the hydrogen atoms of pyrazine in the CPL framework (see Figure 3c) as a result of the large thermal motion. The position of the H_2 molecule is found to be displaced from the center of the nanochannel and is near the corner of the rectangular nanochannels. They align in a zigzag pattern to form a one-dimensional array along the nanochannels. The H_2 molecule is positioned closely to the oxygen atom (O1) of the carboxylate group (Figure 3d). The H_2 molecules seem to be trapped in the concave spaces formed by the O1 atoms and the hydrogen atoms H1 of the pyrazine molecules of the CPL framework. The determined crystal structure of CPL-1 with the adsorbed H_2 molecules is shown in Figure 4.

At lower temperature and/or higher gas pressure, more H_2 molecules are expected to be adsorbed in CPL-1. In the case of the adsorption of dilute hydrogen gas, it is interesting and

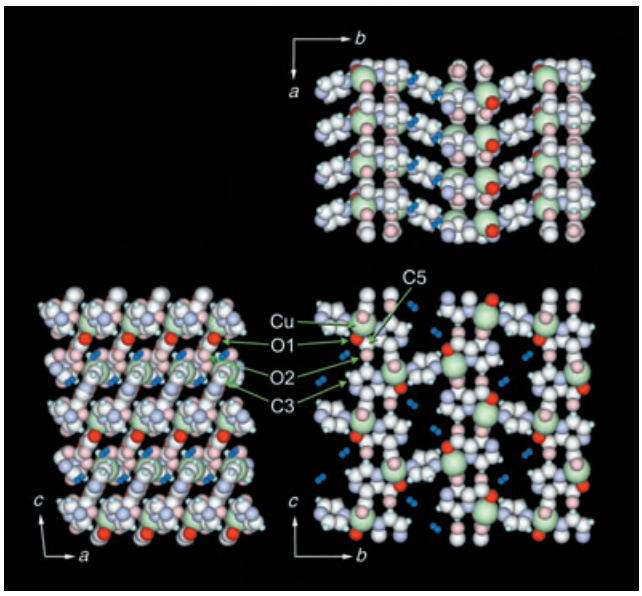


Figure 4. Crystal structure of CPL-1 with adsorbed H_2 molecules. The adsorbed H_2 molecules and the oxygen atoms (O1) of the carboxylate group in the framework are presented as blue dumbbells and red balls, respectively. The adsorbed H_2 molecules randomly occupy the site with a probability of 0.3.

 © 2005 Wiley-VCH Verlag GmbH & Co. KGaA, Weinheim

important to know where the first adsorbed H_2 molecule is located in the nanochannel, because that will give us structural information at the beginning stage of adsorption phenomena in this system. The O1 atom to which the H_2 molecule is close forms a coordination bond to the Cu^{II} ion and is slightly negatively charged. The Cu-OOC moiety is associated with an attractive interaction site for H_2 molecules.[9] Interestingly, most metal–organic porous compounds reported to date that behave as hydrogen-gas-storage materials[4] have similar metal–oxygen (M–O) bonded units. The possibility that the interaction between the hydrogen molecules and the M–O units is essential for H_2 adsorption should be examined in the next stage of this work. Moreover the pocket of the cavity formed by the carboxylate group and the pyrazine unit is suited to the size of adsorbed H_2 molecules in CPL-1. A pocket that is well-suited to the size of the adsorbed molecule *and* a functional site from the Cu–OOC moiety could have an effect on the H_2 adsorption in this system. The first direct observation of the H_2 molecules adsorbed in the nanochannels of CPL-1 could give us promising guidelines for designing hydrogen-gas-storage materials.

Experimental Section

The synthesis and crystal structure of CPL-1 are shown in the previous paper.[2] The in situ synchrotron powder diffraction experiment of hydrogen-gas adsorption was performed on the large Debye-Scherrer camera installed at SPring-8 BL02B2,[10] by using an imaging plate as a detector. The wavelength of an incident X-ray was 0.800 Å. The amount of the adsorbed gas was controlled by changing the temperature of the sample under a constant pressure of hydrogen gas (102 kPa).

The space group was assigned as $P2_1/c$. The cell parameters for CPL-1 with H_2 gas determined by the Rietveld refinement were $a =$ 4.7101(1) Å, $b = 20.0289(2)$ Å, $c = 10.7704(1)$ Å, $\beta = 95.472(2)°$. The cell parameters for CPL-1 without H_2 gas were determined as $a =$ 4.7154(1) Å, $b = 19.8268(2)$ Å, $c = 10.7124(2)$ Å, $\beta = 95.065(2)°$. CCDC-249301 (CPL-1 with adsorbed hydrogen) and CCDC-249302 (CPL-1 without adsorbed hydrogen) contain the supplementary crystallographic data for this paper. These data can be obtained free of charge via www.ccdc.cam.ac.uk/conts/retrieving.html (or from the Cambridge Crystallographic Data Centre, 12, Union Road, Cambridge CB21EZ, UK; fax: (+44) 1223-336-033; or deposit@ccdc.cam.ac.uk).

Received: September 4, 2004
Published online: November 22, 2004

Keywords: hydrogen adsorption · metal–organic frameworks · microporous materials · structure elucidation · X-ray diffraction

[1] a) H. W. Langmi, A. Walton, M. M. Al-Mamouri, S. R. Johnson, D. Book, J. D. Speight, P. P. Edwards, I. Gameson, P. A. Anderson, I. R. Harris, *J. Alloys Compd.* **2003**, *356–357*, 710–715; b) L. Schlapbach, A. Züttel, *Nature* **2001**, *414*, 353–358; c) P. Chen, Z. Xiong, J. Luo, J. Lin, K. L. Tan, *Nature* **2002**, *420*, 302–304; d) A. Züttel, S. Rentsch, P. Fischer, P. Wenger, P. Sudan, P. Mauron, C. Emmenegger, *J. Alloys Compd.* **2003**, *356–357*, 515–520; e) M. Hirscher, M. Becher, M. Haluska, A. Quintel, V. Skakalova, Y. Choi, U. Dettlaff-Weglikowska, S. Roth, I. Stepanek, P. Bernier, A. Leonhardt, J. Fink, *J. Alloys Compd.* **2002**, *330–332*, 654–658; f) M. R. Smith, Jr., E. W. Bittner, W. Shi, J. K. Johnson, B. C. Bockrath, *J. Phys. Chem. B* **2003**, *107*, 3752–3759; g) P. Sudan, A. Züttel, P. Mauron, C. Emmenegger, P. Wenger, L. Schlapbach, *Carbon* **2003**, *41*, 2377–2383.

[2] M. Kondo, T. Okubo, A. Asami, S. Noro, T. Yoshitomi, S. Kitagawa, T. Ishii, H. Matsuzaka, K. Seki, *Angew. Chem.* **1999**, *111*, 190–193; *Angew. Chem. Int. Ed.* **1999**, *38*, 140–143.

[3] a) S. Noro, S. Kitagawa, M. Kondo, K. Seki, *Angew. Chem.* **2000**, *112*, 2161–2164; *Angew. Chem. Int. Ed.* **2000**, *39*, 2082–2084; b) K. Seki, *Chem. Commun.* **2001**, *16*, 1496–1497; c) M. Eddaoudi, D. B. Moler, H. Li, B. Chen, T. M. Reineke, M. O'Keeffe, O. M. Yaghi, *Acc. Chem. Res.* **2001**, *34*, 319–330.

[4] a) J. L. C. Rowsell, A. R. Millward, K. S. Park, O. M. Yaghi, *J. Am. Chem. Soc.* **2004**, *126*, 5666–5667; b) G. Férey, M. Latroche, C. Serre, F. Millange, T. Loiseau, A. Percheron-Guégan, *Chem. Commun.* **2003**, *24*, 2976–2977; c) P. M. Forster, J. Eckert, J. Chang, S. Park, G. Férey, A. K. Cheetham, *J. Am. Chem. Soc.* **2003**, *125*, 1309–1312; d) D. N. Dybtsev, H. Chun, K. Kim, *Angew. Chem.* **2004**, *116*, 5143–5146; *Angew. Chem. Int. Ed.* **2004**, *43*, 5033–5036; e) L. Pan, M. B. Sander, X. Huang, J. Li, M. Smith, E. Bittner, B. Bockrath, J. K. Johnson, *J. Am. Chem. Soc.* **2004**, *126*, 1308–1309.

[5] R. Kitaura, S. Kitagawa, Y. Kubota, T. C. Kobayashi, K. Kindo, Y. Mita, A. Matsuo, M. Kobayashi, H. Chang, T. C. Ozawa, M. Suzuki, M. Sakata, M. Takata, *Science* **2002**, *298*, 2358–2361.

[6] a) M. Takata, E. Nishibori, M. Sakata, *Z. Kristallogr.* **2001**, *216*, 71–86; b) M. Takata, B. Umeda, E. Nishibori, M. Sakata, Y. Saito, M. Ohno, H. Shinohara, *Nature* **1995**, *377*, 46–49; c) C. Wang, T. Kai, T. Tomiyama, T. Yoshida, Y. Kobayashi, E. Nishibori, M. Takata, M. Sakata, H. Shinohara, *Nature* **2000**, *408*, 426–427.

[7] a) T. Noritake, M. Aoki, S. Towata, Y. Seno, Y. Hirose, E. Nishibori, M. Takata, M. Sakata, *Appl. Phys. Lett.* **2002**, *81*, 2008–2010; b) S. Yamamura, S. Kasahara, M. Takata, Y. Sugawara, M. Sakata, *J. Phys. Chem. Solids* **1999**, *60*, 1721–1724.

[8] H. Tanaka, M. Takata, E. Nishibori, K. Kato, T. Iishi, M. Sakata, *J. Appl. Crystallogr.* **2002**, *35*, 282–286.

[9] When H_2 was introduced below its boiling point (20.3 K) to the sample, the liquid H_2 filled up in the cavity and no information on the attractive sites was obtained. In the structural determination described herein, a low pressure and high temperature allowed a H_2 loading per unit that was low enough to explore a specific attractive site among the functional groups in the cavity.

[10] M. Takata, E. Nishibori, K. Kato, Y. Kubota, Y. Kuroiwa, M. Sakata, *Adv. X-Ray Anal.* **2002**, *45*, 377–384.

 © 2005 Wiley-VCH Verlag GmbH & Co. KGaA, Weinheim

Supramolecular Chemistry

Carbohydrate–Metal Interactions Shaped by Supramolecular Assembling**

Andreas Geißelmann, Peter Klüfers, Claudia Kropfgans, Peter Mayer, and Holger Piotrowski*

The most abundant biomolecules, the carbohydrates, can form stable complexes with metal ions in aqueous solution, provided that (multiple) deprotonation of the sugars is supported by a sufficient degree of Lewis acidity of the metal center. The first transition row of the periodic table contains the most important biometals. Of these, all divalent ions except copper(II) are so weakly acidic that stable carbohydrate complexes are known only in higher oxidation states (Mn, Fe, Co) or in the presence of ancillary ligands (Ni). Both iron and manganese, in their higher oxidation states +III (Mn and Fe) and +IV (Mn), are sufficiently acidic to stabilize multiply deprotonated carbohydrate ligands which, in turn, form complexes of such a high stability that precipitation of even some of the least soluble (hydr)oxides, namely, $Fe(OH)_3$/FeO(OH), $Mn(OH)_3$/MnO(OH), and MnO_2, is prevented in the presence of some carbohydrates. Hence the monosaccharide mannose, being a particularly well-suited ligand in terms of the O_5 pattern of its β-furanoside isomer, forms dinuclear Fe_2^{III}, Mn_2^{III}, and $Mn^{III}Mn^{IV}$ complexes in the neutral or alkaline pH region with two entirely deprotonated mannosefuranose anions as the only ligands.[1,2] Deprotonated carbohydrate ligands are apparently present in the active centers of carbohydrate-directed metal enzymes as well. The most important example, economically, is xylose isomerase which is used to convert D-glucose into D-fructose on a commercial scale.[3,4] The active site contains two metal ions (manganese, magnesium, or cobalt) which are divalent, and thus are of lower Lewis acidity. With the exception of the enzyme's pocket, an aqueous carbohydrate chemistry of divalent manganese, as well as divalent iron, ions does not appear to exist in terms of stable, structurally characterized complexes. The addition of iron(II) or manganese(II) salts, for example, to aqueous alkaline carbohydrate solutions, results in precipitation of the respective hydroxide only—compare this behavior with that of copper(II), the strongest Lewis acid among the M^{2+} ions of the first transition row which forms deep blue complexes in alkaline solutions of various carbohydrates, such as monosaccharides[5] and glycosides including cyclodextrins.[6]

Herein we demonstrate that the formation of supramolecular assemblies, other than the preorganized pattern of ligands in the active site of an enzyme, can add additional stability to the carbohydrate complexes of the divalent ions of iron and manganese. The supramolecular aspects of carbohydrate–metal chemistry appeared in outline during a particularly simple observation: with α-cyclodextrin (α-CD), the cyclic α-1,4-linked hexamer of glucose, clear solutions form instead of a hydroxide precipitate when lithium salts are added to $Fe(OH)_2$/α-CD/NaOH slurries—or, more directly, when lithium hydroxide is used instead of sodium hydroxide. Crystallization and X-ray analysis of the individual compounds revealed the same structure for iron(II) and manganese(II). Figure 1 (left) shows the structural principles for the iron compound $Li_5[Li_6(H_2O)_6Fe_3(H_2O)_3(\alpha\text{-}CDH_{-7.5})_2H_{-2}]\cdot 56\,H_2O$ (**1a**); a very similar molecular structure is observed with manganese(II).[7] Three five-coordinate iron centers form aqua–bis(diolato) moieties—which are not stable as complexes with isolated glucose residues, such as, with glucose itself or an alkylglucopyranoside as the ligand. In **1a** however, the glucose units are not isolated but there are several stabilizing structural fragments which are all formed according to the rules of pattern recognition, that is, according to principles of supramolecular chemistry.[8]

To unravel the various factors which contribute cooperatively to the overall stability of the assembly in **1a**, a step-by-step approach has been chosen which, of course, may not reflect the true formation mechanism. A structural description may thus start with three iron(II) atoms that assemble two CD tori to a $(CD)_2$ double torus. The six diol functions of one torus now face the six diol groups of the other, and, after 12-fold deprotonation, three of the six diol pairs bind the iron(II) atoms to give three bis(diolato)iron centers. The deprotonated sites are stabilized by shortening some of the intramolecular O2···O3′ hydrogen bonds of each torus. Since the typical hydrogen-bonded O2···O3′ distance between the glucose units of an α-CD torus is about 2.8 Å, those glucose units that do not bind to iron are tilted towards one of their two neighboring iron-bonding glucose units to shorten the respective hydrogen bond. This feature is depicted in Figure 2: the upper non-iron-binding glucose shortens the O···O distance to the left diolate, the lower to the right one. The remaining two hydroxy functions of the non-metallized glucoses reorientate their hydrogen bonds. The intratorus hydrogen bonds are lost and a new, short, intertorus bond is established. Considering both the short O···O separation and the balance of charges, monodeprotonation of this site should be assumed (Figure 2). Having established these three hydrogen bonds per non-metallized glucose pair, two optimal binding sites for lithium counterions result in this part of the double torus, that is, six sites in the entire assembly. These sites resemble O_3 basal planes of LiO_4 tetrahedra. The remaining coordination sites at Li point inside the double

[*] Prof. Dr. P. Klüfers, Dr. C. Kropfgans, Dr. P. Mayer
Department Chemie und Biochemie
Ludwig-Maximilians-Universität
Butenandtstrasse 5–13, 81377 München (Germany)
Fax: (+49) 89-2180-77407
E-mail: kluef@cup.uni-muenchen.de
Dr. A. Geißelmann
Degussa AG
Rodenbacher Chaussee 4, 63457 Hanau (Germany)
Dr. H. Piotrowski
Lohmann Therapie-Systeme AG
Lohmannstrasse 2, 56626 Andernach (Germany)

[**] Polyol metal complexes, Part 50. This work was supported by the Deutsche Forschungsgemeinschaft and the Fachagentur Nachwachsende Rohstoffe. Part 49: S. Herdin, P. Klüfers, T. Kunte, H. Piotrowski, *Z. Anorg. Allg. Chem.* **2004**, *630*, 701–705.

 © 2005 Wiley-VCH Verlag GmbH & Co. KGaA, Weinheim DOI: 10.1002/anie.200460079

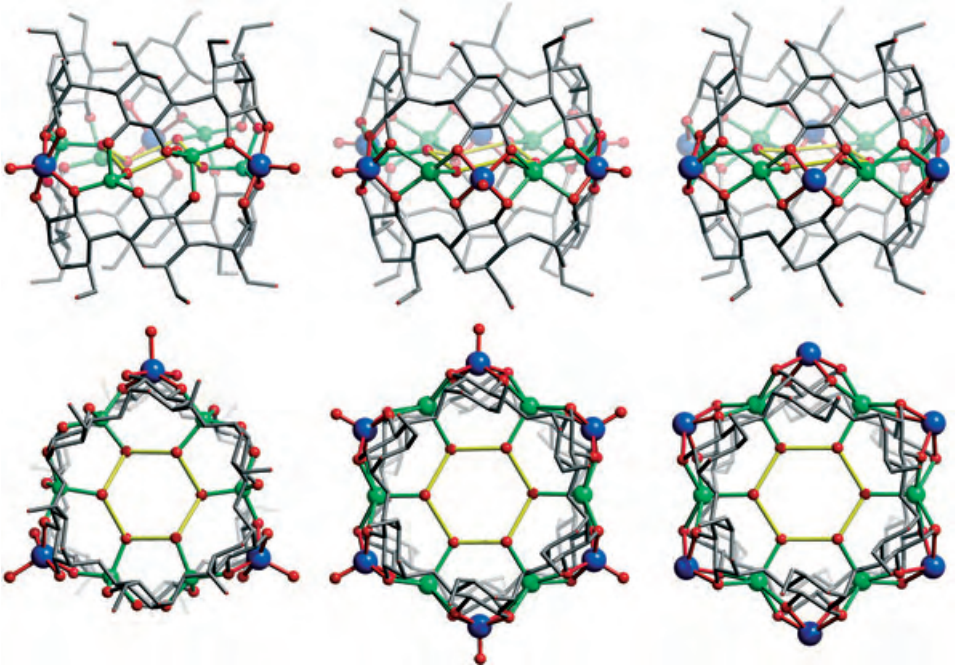


Figure 1. X-ray crystal structures of the C_3-symmetric ferrate(II) unit in **1a** (left), the C_3-symmetric oxo-vanadate(IV) unit in **2** (middle), and the C_2-symmetric, electroneutral bismuth(III) aggregate in **3** (right). Top: view onto the cylinder; bottom: view through the cylinder. Blue Fe, V, or Bi; red O; green counterion; yellow bonds represent hydrogen bonds between water molecules. For comparison, all structures are drawn to the same scale.

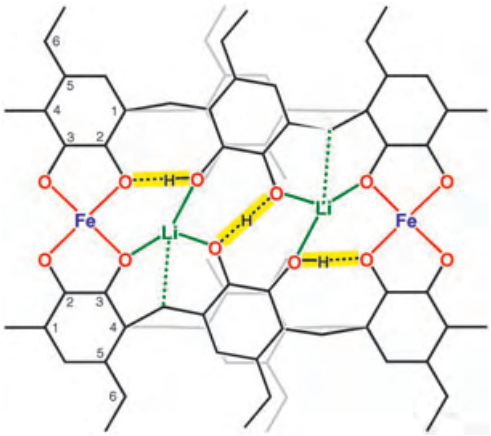


Figure 2. Hydrogen bonds in the cylinder wall in **1a**: shown here is the front part of the cylinder shown in Figure 1, top left. The two middle glucose units are tilted out of their undistorted position, which is show in gray. O—O separations in the highlighted hydrogen bonds are between 2.45 and 2.55 Å. Glucose-atom-numbering scheme also shown on the left side; in this scheme, centers without a number are oxygen atoms.

torus. Owing to the aqueous reaction medium, these positions are occupied by six water molecules, which, because of the overall dimensions of α-cyclodextrin, find themselves at an optimum distance to establish a homodromic $(H_2O)_6$ cycle (yellow hexagon in Figure 1 a, homodromic = hydrogen bonds all run in the same direction). Owing to its chairlike structure, the water hexamer resembles the basic building block of cubic ice I_c. Along with other water oligomers, the chair hexamer has been recognized as one of the more stable conformations of this basic motif.[9,10] As a result, there are many factors that, though too small to establish isolated structural fragments of a similar kind, such as diolato ferrates derived from simple diols or highly lithiated α-CD salts, nevertheless contribute to the total energy of the entire supramolecular assembly. These factors are: 1) aqua–diolato–ferrate(II) formation, 2) intramolecular hydrogen-bond strengthening, 3) counterion aggregation, 4) counterion hydration, and 5) formation of a cooperative hydrogen-bond system in the cyclic water hexamer. From the viewpoint of carbohydrate–iron complexation, points 2–5 represent a supramolecular support that resembles the three-dimensional pre-orientation of the ligating protein side-chains in a metal enzyme, such as xylose isomerase.

The significance of the supramolecular contributions is particularly clear if the scope of the investigation is extended to stronger Lewis acidic metal ions that stabilize deprotonated diol functions more efficiently. Though supramolecular support is not necessary for carbohydrate complexation in these cases, the respective α-CD complexes show in their cooperative features a surprising persistency, which strongly underlines the significance of the supramolecular factors mentioned. As a result, metal ions of very different kinds lose their individuality of behavior when forming an assembly with α-CD tori. This principle is demonstrated by two metals of otherwise different chemistry, one a hard Lewis acid and the other a soft Lewis acid: oxo-vanadium(IV) and bismuth(III).

Owing to their higher Lewis acidity than iron, metal-bonding and the formation of intramolecular hydrogen bonds do not compete in the case of oxo-vanadium(IV) ions, VO^{2+}.

 © 2005 Wiley-VCH Verlag GmbH & Co. KGaA, Weinheim

Hence each of the six facing bis(diol) moieties of a hypothetical $(\alpha\text{-CD})_2$ double torus transforms into a bis(diolato)oxo-vanadium center on the reaction of α-CD, an oxovanadium salt, and sodium hydroxide. Blue crystals of $Na_6[Na_6(H_2O)_6(VO)_6(\alpha\text{-CDH}_{-12})_2]\cdot 59\,H_2O$ (**2**) contain double-toroidal anions (Figure 1; middle). Again, the principle of pattern recognition is adequate to comprehend the structure. As a result of the entire deprotonation and metalation of each of the diol functions, no intramolecular hydrogen bonding has to be considered—and hence no deformation of the tori with respect to a glucose tilt such as that shown in Figure 2. Instead, between the glucose units, that is, between each of the bis(diolato)vanadium moieties, an almost square O_4 pattern is present, which is optimally suited to coordinate a larger counterion than the lithium-binding O_3 pattern in **1**. Six sodium ions are thus found per double torus. The side of the square is not long enough to accommodate the sodium ions into the square plane, thus they are located outside the plane. Of the two possible orientations (inside and outside the double torus), the inside-the-double-torus arrangement is realized and the homodromic hexaqua cycle can form as well. Note that in **1** the stabilizing factors may partly be compensated by the energy that is required for the glucose tilt described above. With **2**, we do not find any destabilizing contributions of steric origin.

As the energy gain from counterion binding and the fitting of the hexaqua hexagon may be substantial, the structure of the electroneutral bismuth compound $[Na_6(H_2O)_6Bi_6(\alpha\text{-CDH}_{-12})_2]\cdot 47\,H_2O$ (**3**) is as expected (Figure 1, right). Owing to its +III oxidation state, a stereochemically active lone pair takes the place of the oxo ligand in **2** and the aqua ligand in **1**. The larger bismuth atoms stretch the double torus to a greater degree than the smaller iron and vanadium atoms. Thus the cone angle of each α-CD torus is smaller and the hexaqua hexagon is pulled flatter, but despite these marginal differences the similarity of the two structures **2** and **3** is striking and demonstrates their conditioning by supramolecular control.

The structures of compounds **2** and **3** demonstrate particularly that use of the principle of pattern recognition in synthetic work opens the door to a variety of low-dimensional oxo-metal compounds. The use of carbohydrates in bioinorganic chemistry as decisive building blocks could thus make a contribution to materials science. Although α-cyclodextrin molecules are not strictly rigid,[11] double tori composed of them appear as reliable building units with predictable binding properties for this new class of compounds. The rules of metal assembling through carbohydrate-based nucleation, however, are still largely unexplored; even in cyclodextrin–metal chemistry there are open questions. A problem regarding the planned synthesis of these materials is presented by the preparation of **1**–**3**: what are the products of the reaction of oxo-vanadium and bismuth salts with α-cyclodextrin and lithium hydroxide? We will contribute descriptions of how nature accommodates a mismatch of one component in due course.

In conclusion, the synthetic principles reported herein open avenues towards molecular materials of the oxo-metalate class based on a biomolecule backbone. Supramolecular and bioinorganic chemistry interact in this approach to provide a new synthetic strategy towards nanometer-scaled metalates for materials science.

Experimental Section

All compounds were prepared from alkaline aqueous solutions. Details for the synthesis of **1a** are given as an example. To prevent formation of iron(III), all operations were carried out under nitrogen. A suspension of iron(II) chloride tetrahydrate (0.255 g, 1.28 mmol) and α-cyclodextrin (0.629 g, 0.647 mmol) in water (5 mL) was slowly dropped into a suspension of lithium hydroxide monohydrate (1.355 g, 32.3 mmol) and α-cyclodextrin (0.605 g, 0.622 mmol) in water (5 mL). A clear, pale blue solution formed. On controlled diffusion of acetone vapors into the filtered solution, needles of **1a** formed in the course of 3 days. Colorless crystals of $Li_7[Li_6(H_2O)_6Mn_3(H_2O)_3(\alpha\text{-CDH}_{-7.5})_2H_{-4}]\cdot 41\,H_2O\cdot 2.5\,EtOH$ (**1b**) are prepared by a similar procedure. For the manganese preparations, successful exclusion of oxygen is monitored with particular ease as the presence of even traces of oxygen lead to the solutions turning intensely blue owing to the formation of trivalent manganese. Compounds **2** and **3** are prepared similarly except that no inert gas is needed.

Received: March 22, 2004
Published online: January 3, 2005
Publication delayed at authors request.

Keywords: bismuth · cyclodextrins · iron · manganese · vanadium

[1] J. Burger, C. Gack, P. Klüfers, *Angew. Chem.* **1995**, *107*, 2950–2951; *Angew. Chem. Int. Ed. Engl.* **1995**, *34*, 2647–2649.
[2] A. Geißelmann, P. Klüfers, B. Pilawa, *Angew. Chem.* **1998**, *110*, 1181–1184; *Angew. Chem. Int. Ed. Engl.* **1988**, *27*, 1119–1121.
[3] H. Häusler, A. E. Stütz, *Top. Curr. Chem.* **2001**, *215*, 77–114.
[4] S. H. Bhosale, M. B. Rao, V. V. Deshpande, *Microbiol. Rev.* **1996**, *60*, 280–300.
[5] P. Klüfers, T. Kunte, *Eur. J. Inorg. Chem.* **2002**, *6*, 1285–1289.
[6] P. Klüfers, H. Piotrowski, J. Uhlendorf, *Chem. Eur. J.* **1997**, *3*, 601–608.
[7] Stoe IPDS, $Mo_{K\alpha}$. **1a**: $C_{72}H_{233}Fe_3Li_{11}O_{125}$, $M_r = 3343.432\ g\,mol^{-1}$, almost colorless needles, $1.30\times0.05\times0.05\ mm^3$, trigonal, $P321$, $a = 29.322(3)$, $c = 15.8374(13)$ Å, $V = 11792.7(19)$ Å^3, $Z = 3$, $\rho = 1.4124(2)\ g\,cm^{-3}$, $T = 200(2)$ K, $\mu(Mo_{K\alpha}) = 0.395\ mm^{-1}$, θ range: 1.4–20.7°, 32193 reflections, 8062 independent and used in refinement, 3936 with $I \geq 2\sigma(I)$, $R_{int} = 0.1564$, mean $\sigma(I)/I = 0.2348$, 468 parameters, $R(F_{obs}) = 0.0933$, $R_w(F^2) = 0.2346$, $S = 0.885$, Flack parameter: 0.01(5), min. and max. residual electron density: −0.487, 0.790 e Å^{-3}. **1b**: $C_{77}H_{228}Li_{13}Mn_3O_{118.5}$, $M_r = 3305.610\ g\,mol^{-1}$, colorless platelet, $0.46\times0.39\times0.06\ mm^3$, orthorhombic, $P2_12_12_1$, $a = 15.632(3)$, $b = 25.561(4)$, $c = 35.086(5)$ Å, $V = 14019(4)$ Å^3, $Z = 4$, $\rho = 1.5662(4)\ g\,cm^{-3}$, $T = 200(2)$ K, $\mu(Mo_{K\alpha}) = 0.393\ mm^{-1}$, θ range: 1.7–24.0°, 45176 reflections, 19395 independent and used in refinement, 11327 with $I \geq 2\sigma(I)$, $R_{int} = 0.0531$, mean $\sigma(I)/I = 0.1032$, 904 parameters, $R(F_{obs}) = 0.0758$, $R_w(F^2) = 0.2261$, $S = 0.968$, Flack parameter: −0.01(2), min. and max. residual electron density: −0.757, 0.978 e Å^{-3}. To obtain electroneutrality, two deprotonated sites are required for **1a** and four for **1b**, which, however, have not been located. The metal-bonded aqua ligands and the O6 hydroxy groups appear as candidates. **2**: $C_{72}H_{226}Na_{12}O_{131}V_6$, $M_r = 3770.013\ g\,mol^{-1}$, blue prism, $0.34\times0.22\times0.10\ mm^3$, trigonal, $P312$ (close to $P622$, twin refinement with trigonal symmetry, [010] considered as the twin axis), $a = 17.8985(13)$, $c =$

 © 2005 Wiley-VCH Verlag GmbH & Co. KGaA, Weinheim

31.066(3) Å, $V = 8618.8(12)$ Å^3, $Z = 2$, $\rho = 1.4527(2)$ g cm^{-3}, $T = 200(2)$ K, $\mu(Mo_{K\alpha}) = 0.457$ mm^{-1}, θ range: 1.5–23.9°, 53404 reflections, 8842 independent and used in refinement, 5616 with $I \geq 2\sigma(I)$, $R_{int} = 0.0960$, mean $\sigma(I)/I = 0.1041$, 348 parameters, $R(F_{obs}) = 0.0909$, $R_w(F^2) = 0.2733$, $S = 0.988$, Flack parameter: −0.03(7), min. and max. residual electron density: −0.637, 1.640 e Å^{-3}. **3**: $C_{72}H_{202}Bi_6Na_6O_{113}$, $M_r = 4268.13$ g mol^{-1}, colorless prism, $0.25 \times 0.23 \times 0.15$ mm^3, orthorhombic, $C222_1$, $a = 40.292(8)$, $b = 25.814(4)$, $c = 15.442(2)$ Å, $V = 16061(5)$ Å^3, $Z = 4$, $\rho = 1.7651(5)$ g cm^{-3}, $T = 293(2)$ K, $\mu(Mo_{K\alpha}) = 6.676$ mm^{-1}, θ range: 3.7–24.1°, 48016 reflections 12159 independent and used in refinement, 11523 with $I \geq 2\sigma(I)$, $R_{int} = 0.0799$, mean $\sigma(I)/I = 0.0464$, 460 parameters, $R(F_{obs}) = 0.0423$, $R_w(F^2) = 0.1126$, $S = 1.047$, Flack parameter: −0.020(7), min. and max. residual electron density: −1.938, 1.139 e Å^{-3}. CCDC 234016 (**1a**), CCDC 234017 (**1b**), CCDC 234018 (**2**), and CCDC 234015 (**3**) contain the supplementary crystallographic data for this paper. These data can be obtained free of charge from The Cambridge Crystallographic Data Centre via www.ccdc.cam.ac.uk/data_request/cif.

[8] J.-M. Lehn, *Supramolecular Chemistry*, VCH, Weinheim, **1995**.

[9] F. N. Keutsch, R. J. Saykally, *Proc. Natl. Acad. Sci. USA* **2001**, *98*, 10533 – 10540.

[10] E. Whalley, *J. Phys. Chem.* **1983**, *87*, 4174 – 4179.

[11] G. A. Jeffrey, W. Saenger, *Hydrogen Bonding in Biological Structures*, Springer, Berlin, **1991**.

 © 2005 Wiley-VCH Verlag GmbH & Co. KGaA, Weinheim

RNA-Selective Pt^{II} Conjugates

RNA-Selective Modification by a Platinum(II) Complex Conjugated to Amino- and Guanidinoglycosides**

*Jürgen Boer, Kenneth F. Blount, Nathan W. Luedtke, Lev Elson-Schwab, and Yitzhak Tor**

Binding of the anticancer drug cisplatin (*cis*-Pt) to nucleic acids is believed to favor DNA over RNA.[1] Covalent modification of DNA produces intrastrand cross-links (at GpG, ApG, and GpNpG; N = A, C, G, or T),[2] and interstrand cross-links (at GG).[3] Cisplatin reacts with other cellular components including proteins,[4] phospholipids,[5] and small molecules.[6] To enhance DNA targeting, numerous conjugates have been prepared in which the *cis*-Pt moiety has been tethered to high-affinity nucleic acid ligands (for example, acridine, ethidium bromide, peptides, and short oligonucleotides).[7] As part of our program aimed at advancing RNA as a drug target,[8] we have become interested in devising methods to "reverse" the nucleic acid selectivity of *cis*-Pt. Since RNA–protein complexes serve key functions in the life cycle of many retroviruses, RNA-selective delivery of reactive Pt^{II} complexes may provide a novel mechanism for the inactivation of pathogen-specific RNA.

HIV-1 replication is critically dependent on the nuclear export of intron-containing viral RNA by the Rev protein.[9] The high-affinity Rev binding site within the Rev response element (RRE) is located at a G-rich bulge that is present in the minimized construct RRE JW shown in Figure 1.[10] Rev–RRE recognition has served as an important paradigm for exploring the competitive inhibition of RNA–protein interactions.[11] Aminoglycoside antibiotics,[12] guanidinoglycosides,[13] and other small molecules that exhibit RNA over DNA selectivity have been shown to bind to the RRE and displace Rev through noncovalent interactions.[14] We hypothesized that, by using Pt^{II} derivatives to covalently cross-link aminoglycosides and guanidinoglycosides to the RRE, viral RNA could be permanently damaged. Toward this end, we have developed RNA-selective Pt^{II} conjugates. Herein we report the synthesis and RRE selectivity of two conjugates that, to our knowledge, represent the first examples of RNA-selective cross-linking agents.

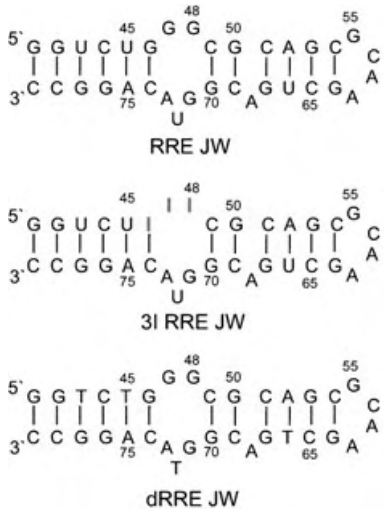


Figure 1. Secondary structures of the RRE constructs used. RRE JW is a minimized all-ribo Rev-binding RRE construct.[10] All-ribo 3I RRE JW contains three inosine (I) residues substituting the corresponding G residues. dRRE JW is an all-deoxyribo DNA analogue of RRE JW. The numbering used is in accordance with ref. [10].

Several criteria have guided the design of the glycoside–Pt^{II} conjugates: a) Established RNA-selective scaffolds (for example, aminoglycosides or guanidinoglycosides) are chosen to secure preferential RNA over DNA binding; b) the polycationic scaffold is modified by substitution of a hydroxy group, rather than a chargeable group that is likely to be

[*] Dr. J. Boer, Dr. K. F. Blount, N. W. Luedtke, L. Elson-Schwab, Prof. Dr. Y. Tor
Department of Chemistry and Biochemistry
University of California, San Diego
La Jolla, CA 92093-0358 (USA)
Fax: (+1) 858-534-0202
E-mail: ytor@ucsd.edu

[**] K.F.B. and J.B. contributed equally to this work. We thank the National Institutes of Health (Grant nos.: AI47673 to Y.T. and GM065652 to K.B.), the Universitywide AIDS Research Program (Grant no.: ID01-SD-027), and the Deutsche Forschungsgemeinschaft (postdoctoral fellowship to J.B.) for support.

Supporting information for this article is available on the WWW under http://www.angewandte.org or from the author.

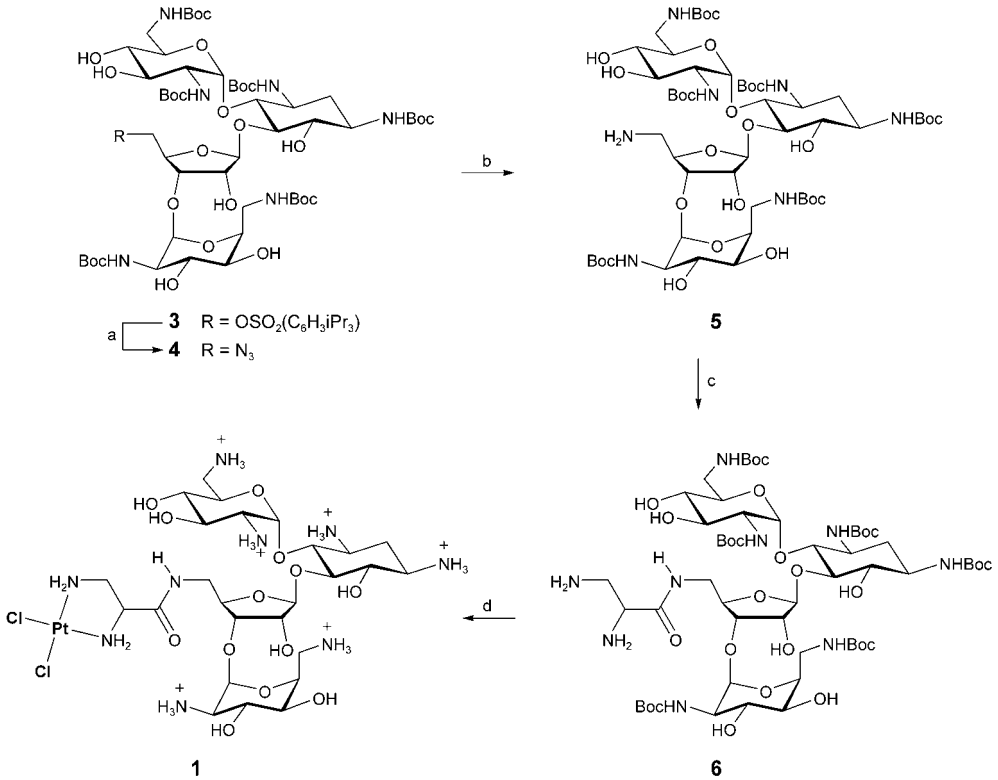
 DOI: 10.1002/anie.200461182 © 2005 Wiley-VCH Verlag GmbH & Co. KGaA, Weinheim

essential for RNA binding; c) a short linker between the Pt center and the RNA ligand is chosen to ensure enough conformational flexibility while maintaining proximity of the reactive metal center to the RNA-selective scaffold; and d) a chelating diamine is selected to secure Pt^{II} coordination to the RNA-selective binder. With these considerations in mind, Pt^{II} conjugates of neomycin B (**1**, Scheme 1) and guanidinoneomycin B (**2**, Scheme 2) were selected as our first-generation RNA-selective modifiers.

The synthesis of both derivatives starts with 5″-2,4,6-triisopropylbenzenesulfonate *N*-Boc-protected neomycin **3**.[15] Treatment of **3** with excess sodium azide affords the desired monoazide **4** in 89% yield (Scheme 1).[16] Catalytic hydrogenation of **4** quantitatively gives the corresponding amine **5**, which is coupled to N^{α},N^{β}-di-Fmoc-(*S*)-2,3-diaminopropionic acid by using TBTU and HOBT. Cleavage of the Fmoc groups under basic conditions affords the neomycin derivative **6**, which presents a bidentate coordination site for platinum. Treatment with potassium tetrachloroplatinate in DMF/H_2O leads to the formation of the fully protected aminoglycoside conjugate. Deprotection with 2 M HCl in dioxane/water affords the desired Pt^{II} derivative **1** as the chloride salt in 95% yield (from **6**).[16]

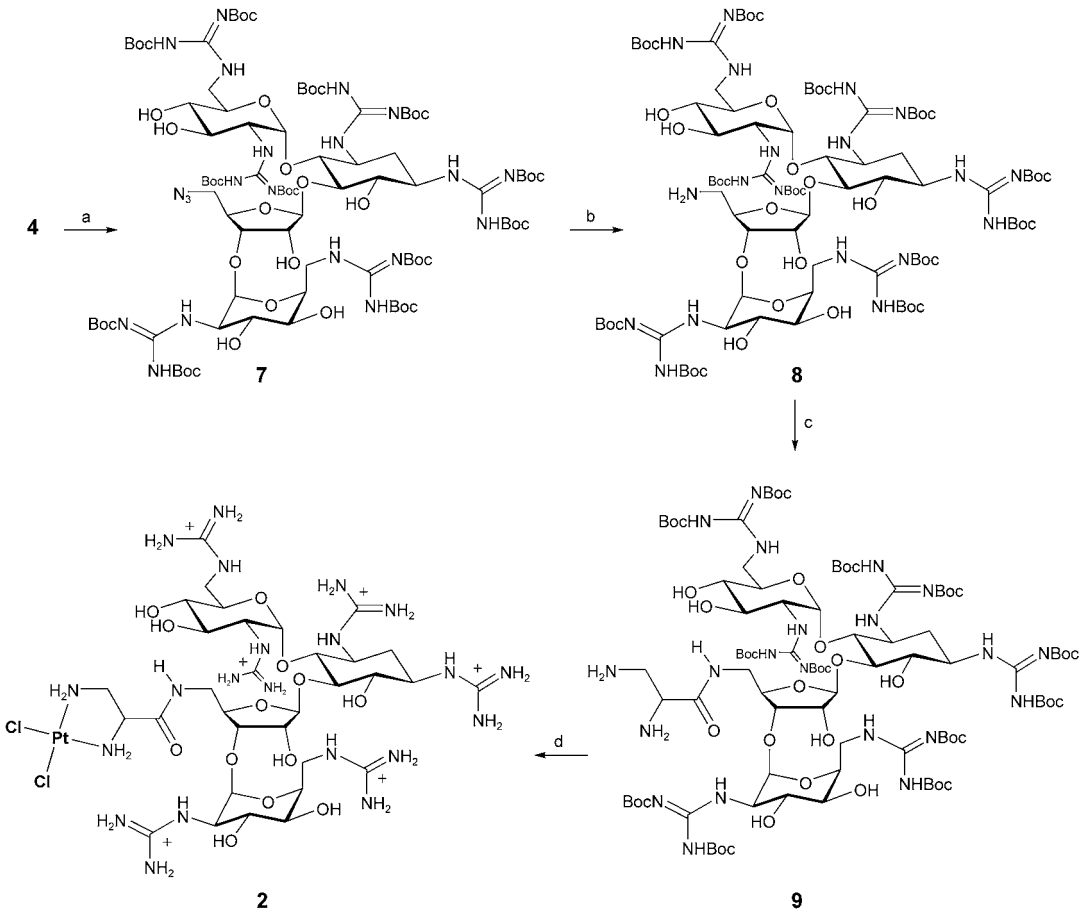
The 5″-azido neomycin derivative **4** is a common precursor for the synthesis of the neomycin–Pt^{II} and guanidinoneomycin–Pt^{II} conjugates, **1** and **2**, respectively. Thus, after removal of the six Boc protecting groups in **4** with 50% TFA/CH_2Cl_2, the crude 5″-azido neomycin is dissolved in MeOH/NEt_3 and treated with excess *N*,*N*′-di-Boc-*N*″-triflylguanidine, a powerful guanidinylating reagent.[17,18] Excess reagent is readily removed, and the desired Boc-protected perguanidinylated 5″-azido neomycin **7** is obtained in excellent yield (99%; see Scheme 2). Reduction to the corresponding amine under Staudinger conditions provides **8** in 75% yield.[19] Condensation of the free amine with N^{α},N^{β}-di-Fmoc-(*S*)-2,3-diaminopropionic acid by using TBTU/HOBT, followed by deprotection of the Fmoc groups with piperidine, gives **9** in 63% yield for the two steps. The reaction of the free chelating 1,2-diamino group with potassium tetrachloroplatinate in a two-phase $CHCl_3/H_2O$ system, followed by TFA-mediated deprotection of the Boc groups, leads to the desired guanidinylated aminoglycoside–Pt^{II} conjugate **2** as the TFA salt in 94% yield.[20]

To explore the ability of **1** and **2** to form covalent cross-links with RRE JW, denaturing polyacrylamide gel shift electrophoresis (DPAGE) has been utilized. Upon titration of RRE JW with **1** and **2**, DPAGE shows multiple retarded bands, a result indicating that the Pt^{II} conjugates covalently bind the RRE (Figure 2a).[21] Addition of neomycin B, the parent aminoglycoside, produces no such effect (Figure 2b).[21] The reaction of **1** and **2** with the RRE is rapid and the adducts formed are stable under these denaturing conditions (Figure 2b).[22] According to DPAGE analysis, both conjugates covalently modify the RRE with comparable efficiencies (Figure 2a). Importantly, covalent modification takes place even in the presence of a vast excess of calf thymus DNA (CT DNA; Figure 2c). Approximately 5000-fold nucleotide excess of CT DNA must be added to prevent covalent-adduct formation between the platinated glycosides **1** and **2** and the RRE (Figure 2c). This competition experi-



Scheme 1. Synthesis of **1**: a) NaN_3, DMF/H_2O, 89%; b) H_2, Pd/C, 99%; c) 1. N^{α},N^{β}-di-Fmoc-(*S*)-2,3-diaminopropionic acid, TBTU, HOBT, 2,4,6-collidine, DMF; 2. piperidine, DMF, 80%; d) 1. K_2PtCl_4, DMF/H_2O; 2. 2 M HCl/dioxane, 95%. Boc = *tert*-butoxycarbonyl, DMF = *N*,*N*-dimethylformamide, Fmoc = 9-fluorenylmethoxycarbonyl, HOBT = 1-hydroxy-1*H*-benzotriazole, TBTU = benzotriazol-1-yl-N-tetramethyluronium tetrafluoroborate.

 © 2005 Wiley-VCH Verlag GmbH & Co. KGaA, Weinheim



Scheme 2. Synthesis of **2**: a) 1. TFA/CH_2Cl_2; 2. *N*,*N*′-di-Boc-*N*″-triflylguanidine, Et_3N, MeOH, 99%; b) Ph_3P, THF/H_2O, 75%; c) 1. N^{α},N^{β}-di-Fmoc-(*S*)-2,3-diaminopropionic acid, TBTU, HOBT, 2,4,6-collidine, DMF/$CHCl_3$; 2. piperidine, DMF, 63%; d) 1. K_2PtCl_4, H_2O/CH_2Cl_2, nBu_4NCl; 2. TFA/CH_2Cl_2, 94%. TFA = trifluoroacetic acid.

ment indicates a significant preference of these Pt^{II}–glycoside conjugates for the RRE over CT DNA.

To explore the nature of the modification induced by the platinated conjugates, nonlabeled RRE JW (20 μM) was incubated with **1** (1.5 equiv) for 4 h, and the desalted reaction mixture was analyzed by MALDI-TOF mass spectrometry (Figure 3a,b). Under these conditions, the primary species observed (*m*/*z* 11914) represents a 1:1 covalent adduct, **1**·RRE, with both chloride ions displaced (expected *m*/*z* 11911).[23] Smaller amounts of both unmodified RRE JW (*m*/*z* 11023) and doubly conjugated (**1**)$_2$·RRE (*m*/*z* 12806; expected *m*/*z* 12800) are also observed (Figure 3b). As shown in Figure 3c, a similar reactivity pattern is established for the guanidinoneomycin–Pt^{II} conjugate **2** under the same conditions, where the dominant species observed is the singly conjugated product **2**·RRE (*m*/*z* 12164; expected *m*/*z* 12164). As with **1**, small amounts of the unmodified RRE JW and doubly modified product (**2**)$_2$·RRE (*m*/*z* 13304; expected *m*/*z* 13303) are detected (Figure 3c). In contrast, treatment of **1** with 3I RRE JW or dRRE JW (see Figure 1 for sequences) under similar conditions does not yield a significant fraction of covalent adducts (not shown). Since neomycin displays lower affinity to these analogous nucleic acids than to RRE JW,[16] a correlation between specific binding and conjugation is implied.[24] When it is taken into account that MALDI-TOF mass spectrometry is a strongly denaturing technique, these mass spectral data confirm the specific covalent-adduct formation of platinated glycosides to the all-ribo RRE JW.[25]

To identify the modification site of the Pt^{II} conjugates **1** and **2** within RRE JW, the mixtures represented by the spectra in Figures 3b and c were 5′-^{32}P-labeled and fractionated by using preparative 20% DPAGE. A representative purification gel is shown in Figure 3d. Whereas the **1**·RRE adduct ran as primarily one shifted band, addition of **2** to the RRE yielded two separable bands (marked **2**·RRE_a and **2**·RRE_b). Once labeled and isolated, these platinated RRE adducts were characterized by alkaline hydrolysis mapping (Figure 4). Covalent binding of the platinated glycosides to the RRE not only increases the mass of the RNA but also considerably diminishes its overall negative charge. This reduces the mobility of each hydrolyzed RNA fragment that contains the Pt^{II} conjugate, whereas unmodified RNA fragments migrate identically to the hydrolyzed control. Thus, a discontinuity in the ladder points to the site of RNA–ligand conjugation. For **1**, this binding site is localized at the 3′-side of the tetraloop, a fact suggesting coordination to A_{62}, A_{63}, and G_{64} (Figure 4a). This putative binding site is consistent with the coordination to purines that is seen for *cis*-Pt binding to DNA.[2a] Interestingly, a distinct gap is observed in the

 © 2005 Wiley-VCH Verlag GmbH & Co. KGaA, Weinheim

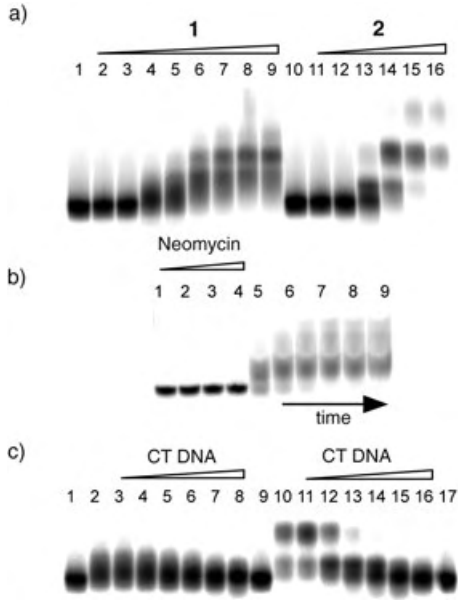


Figure 2. DPAGE radiogram with 25 nM 5′-^{32}P-labeled RRE JW.[16] a) Lane 1: RNA only; lanes 2–9: increasing concentrations of **1** (0.050, 0.10, 0.50, 1.0, 2.5, 5.0, 7.5, and 10 μM, respectively); lane 10: RNA only; lanes 11–16: increasing concentrations of **2** (0.050, 0.10, 0.50, 1.0, 2.5, and 5.0 μM, respectively). b) Lanes 1–4: RNA with increasing concentrations of neomycin B (0.625, 1.25, 12.5, and 125 μM, respectively); lanes 5–9: RNA with 625 nM of **1** after incubation (after 0.5, 1, 2, 3, 4 and 5 h, respectively). c) Lane 1: RNA only; lanes 2–8: RRE JW with 1 μM **1** and increasing concentrations of calf thymus DNA (0, 8.5, 85, 425, 850 μM, 4.25 and 8.5 mM base pairs, respectively); lane 9: RNA only; lanes 10–17: RRE JW with 1 μM **2** and increasing calf thymus DNA (0, 8.5, 85, 425, 850 μM, 4.25 and 8.5 mM base pairs, respectively).

hydrolytic map of **2**·RRE$_b$ (Figure 4a), a result that suggests an intramolecular cross-link between nucleosides at the boundaries of the gap, as has been previously observed for other RNA–RNA cross-links.[26] These results suggest the formation of an intramolecular cross-link between approximately G_{48} and G_{67}. This is consistent with the known propensity of *cis*-Pt to form cross-strand purine–purine cross-links.[2a] Examination of the NMR spectrum of the RRE reveals that the N7 positions of these two nucleotides are favorably placed for forming this interstrand cross-link (Figure 4c).[27]

In summary, new Pt^{II} conjugates of neomycin B and guanidinoneomycin B are found to generate site-specific, RNA-selective, covalent cross-links to the RRE. The use of RNA-selective scaffolds, such as aminoglycosides or guanidinoglycosides, is demonstrated to impart the necessary RNA selectivity upon the *cis*-Pt moiety. This observation serves as an important precedent for the selective covalent modification of therapeutically relevant RNA targets.

Experimental Section

RNA: Oligonucleotides were purchased from Dharmacon Research, deprotected, and purified by using standard protocols. A solution of calf thymus DNA was purchased from Gibco BRL (catalogue no.: 15633-019) and quantified by using an average extinction

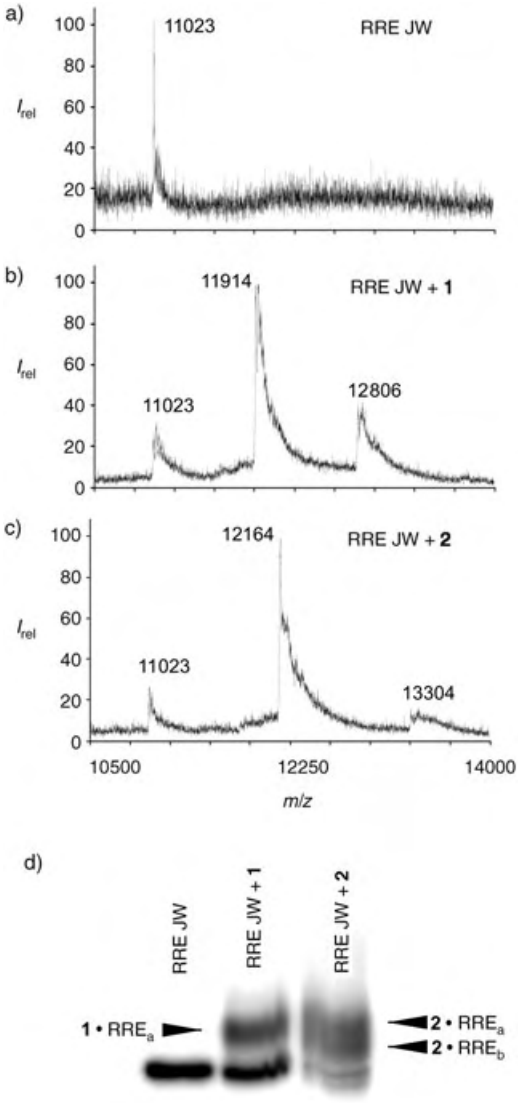


Figure 3. MALDI-TOF MS analysis of 20 μM RRE JW a) alone, b) with 30 μM of **1**, and c) with 20 μM of **2**. See the Experimental Section for procedures. d) Denaturing gel purification of 5′-^{32}P-labeled RRE JW and RRE JW adducts. The two adducts isolated are indicated (**2**·RRE$_a$ and **2**·RRE$_b$).

coefficient of 6550 cm^{-1}M^{-1} per base. The extinction coefficient for all RRE JW constructs was calculated as 371 000 cm^{-1}M^{-1}.

DPAGE analysis: For evaluating the cross-linking ability of **1** and **2**, RNA was prefolded by being heated to 65 °C for 5 minutes and then cooled to room temperature for 20 min. A final concentration of 25 nM prefolded RRE JW containing a trace of 5′-^{32}P-labeled RRE JW (≈5000 cpm) was then incubated with the indicated amount of **1** or **2** in 10 mM sodium phosphate buffer (pH 7.0) containing 100 mM sodium perchlorate. Where appropriate, calf thymus DNA was added to the folded RRE JW prior to the addition of **1** or **2**. After 2 h at room temperature, cross-linking reactions were diluted with an equal volume of formamide loading dye, heated to 90 °C for 3 min, and loaded immediately onto a 20% denaturing polyacrylamide gel.

MALDI-TOF MS experiments: A solution of RRE JW (75 μL of a 40 μM solution) in 10 mM tris(hydroxymethyl)aminomethane (Tris; pH 7.5) with 50 mM NaCl was heated to 65 °C for 5 min and cooled at room temperature for 20 min. This solution was diluted with

 © 2005 Wiley-VCH Verlag GmbH & Co. KGaA, Weinheim

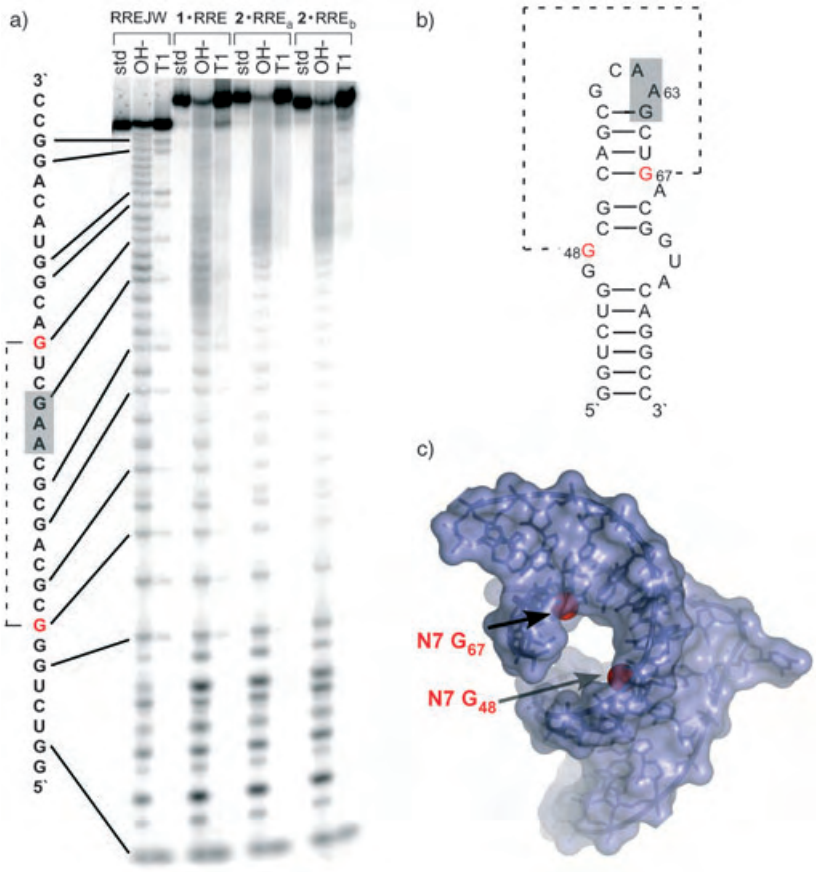


Figure 4. Alkaline hydrolytic footprint of RRE JW and its platinated adducts.[16] a) "std" lanes are untreated RNA, "OH^-" lanes show RNA after alkaline hydrolysis, and "T1" lanes show RNA after cleavage by ribonuclease T1 under denaturing conditions. The conjugation site of **1** is shaded. An interstrand cross-link (dotted line) is observed between approximately G_{48} and G_{67} (shown in red). b) Conjugation sites are shown in the context of the secondary structure of RRE JW. c) The three-dimensional structure of the RRE reveals that the N7 positions of G_{48} and G_{67} (red space-filling representation) are near each other in space and well-positioned for forming an interstrand cross-link.

phosphate/perchlorate buffer (75 μL) to yield final concentrations of 10 mM sodium phosphate (pH 7.4), 100 mM sodium perchlorate, and either 30 μM **1** or 20 μM **2**. These reaction mixtures were incubated at room temperature for 4 h, at which point they were desalted by passing through a G-25 spin column (Amersham–Pharmacia) that had been equilibrated with water. After desalting, the reactions were lyophilized overnight and resuspended in water (20 μL). To confirm the addition of platinated conjugates, an aliquot was fractionated on a 20% DPAGE gel and visualized with Stains-all (Acros). For MALDI-TOF MS analysis, 2 μL of each sample was combined with 1 μM ammonium citrate buffer (PE Biosystems), 1 μL of 75 μM DNA standard (5′-AGGCATGCAAGCTTGAGTATTCTAT-3′), and 6 μL of saturated 3-hydroxypiccolinic acid. After desalting with an ion-exchange resin (PE Biosystems), the sample was spotted onto a gold-coated MALDI plate and dried on a 55 °C heat block. MALDI-TOF spectra were collected on a PE Biosystems Voyager-DE STR MALDI-TOF spectrometer in positive-ion, delayed-extraction mode. By calibrating all spectra relative to the +1 and +2 ions of the internal DNA standard, the observed mass of RRE JW and its adducts should have a resolution of ±4 mass units.

Footprinting analysis: **1**·RRE and **2**·RRE (3 μL) from the MALDI-TOF MS analysis described above were labeled with T4 polynucleotide kinase (New England Biolabs) and purified by using standard protocols.[16] Purified RNA adducts were resuspended in water (50 μL). Alkaline hydrolysis reactions were conducted in a 50 mM sodium bicarbonate buffer (pH 9.0; total volume 8 μL) and contained 5′-^{32}P-labeled RRE JW (≈60000 cpm). These reactions were heated to 90 °C for 6.5 min and immediately quenched on ice for 10 min. Following a brief spin, samples were 1:1 diluted with formamide loading dye and 1.5 μL were loaded onto a 20% polyacrylamide gel. Ribonuclease T1 reactions contained 38000 cpm of each RRE JW adduct and 1 unit of ribonuclease T1 (Boehringer Mannheim) in a solution of 20 mM sodium citrate (pH 5.0), 1 mM ethylenediaminetetraacetate (EDTA), 3 M urea, and 0.04 μg μL^{-1} yeast torula RNA (Ambion). These reactions were incubated at 65 °C for 30 minutes, then diluted into an equal volume of formamide loading dye and separated with 20% denaturing polyacrylamide gels. All gels were run for approximately 3 h at 15 W and analyzed by using a Molecular Dynamics Storm Phosphorimager.

Received: July 3, 2004
Published online: January 3, 2005

Keywords: aminoglycosides · antiviral agents · drug design · platinum · RNA

[1] E. R. Jamieson, S. J. Lippard, *Chem. Rev.* **1999**, *99*, 2467–2498.
[2] a) A. M. J. Fichtinger-Schepman, J. L. van der Veer, J. H. J. den Hartog, P. H. M. Lohman, J. Reedijk, *Biochemistry* **1985**, *24*, 707–713; b) A. Eastman, *Biochemistry* **1986**, *25*, 3912–3915.
[3] H. Huang, J. Woo, S. C. Alley, P. B. Hopkins, *Bioorg. Med. Chem.* **1995**, *3*, 659–669.
[4] R. N. Bose, *Mini-Rev. Med. Chem.* **2002**, *2*, 103–111.
[5] G. Speelmans, R. W. Staffhorst, K. Versluis, J. Reedijk, B. de Kruijff, *Biochemistry* **1997**, *36*, 10545–10550.
[6] T. Ishikawa, F. Ali-Osman, *J. Biol. Chem.* **1993**, *268*, 20116–20125.
[7] Selected examples: a) B. E. Bowler, L. S. Hollis, S. J. Lippard, *J. Am. Chem. Soc.* **1984**, *106*, 6102–6104; b) B. D. Palmer, H. H. Lee, P. Johnson, B. C. Baguley, G. Wickham, L. P. G. Wakelin, W. D. McFadyen, W. A. Denny, *J. Med. Chem.* **1990**, *33*, 3008–3014; c) D. Gibson, K. F. Gean, J. Katzhendle, R. Ben-Shoshan, A. Ramu, I. Ringel, *J. Med. Chem.* **1991**, *34*, 414–420; d) J. Whittaker, W. D. McFadyen, G. Wickham, L. P. Wakelin, V. Murray, *Nucleic Acids Res.* **1998**, *26*, 3933–3939; e) L. C. Perrin, C. Cullinane, W. D. McFayden, D. R. Phillips, *Anti-Cancer Drug Des.* **1999**, *14*, 243–252; f) Y. S. Chen, M. J. Heeg, P. G. Brauschweiger, W. H. Xie, P. G. Wang, *Angew. Chem.* **1999**, *111*, 1882–1884; *Angew. Chem. Int. Ed.* **1999**, *38*, 1768–1769; g) M. S. Robillard, A. R. P. M. Valentijn, N. J. Meeuwenoord, G. A. van der Marel, J. H. van Boom, J. Reedijk, *Angew. Chem.* **2000**, *112*, 3226–3229; *Angew. Chem. Int. Ed.* **2000**, *39*, 3096–3099; h) Y. Mikata, Y. Shinohara, K. Yoneda, Y. Nakamura, I. Brudzinska, T. Tanase, T. Kitayama, R. Takagi, T. Okamoto, I. Kinoshita, M. Doe, C. Orvig, S. Yano, *Bioorg. Med. Chem. Lett.* **2001**, *11*, 3045–3047; i) S. K. Sharma, L. W. McLaughlin, *J. Am. Chem. Soc.* **2002**, *124*, 9658–9659; j) M. S. Robillard, N. P. Davies, G. A. van der Marel, J. H. van Boom, J. Reedijk, V. Murray, *J. Inorg. Biochem.* **2003**, *96*, 331–338; k) R. J. Heetebrij, M. de Kort, N. J. Meeuwenoord, H. den Dulk, G. A. van der

 © 2005 Wiley-VCH Verlag GmbH & Co. KGaA, Weinheim

Marel, J. H. van Boom, J. Reedijk, *Chem. Eur. J.* **2003**, *9*, 1823 – 1827.
[8] a) Y. Tor, *ChemBioChem* **2003**, *4*, 998 – 1007; b) N. W. Luedtke, Y. Tor in *Small Molecule DNA and RNA Binders: From Synthesis to Nucleic Acid Complexes* (Eds.: M. Demeunynck, C. Bailly, D. Wilson), Wiley-VCH, Weinheim, **2003**, pp. 18 – 40.
[9] a) V. W. Pollard, M. H. Malim, *Annu. Rev. Microbiol.* **1998**, *52*, 491 – 532; b) A. D. Frankel, J. A. T. Young, *Annu. Rev. Biochem.* **1998**, *67*, 1 – 25.
[10] J. L. Battiste, H. Mao, N. S. Rao, R. Tan, D. R. Muhandiram, L. E. Kay, A. D. Frankel, J. R. Williamson, *Science*, **1996**, *273*, 1547 – 1551.
[11] N. W. Luedtke, Y. Tor, *Biopolymers* **2003**, *70*, 103 – 119.
[12] M. L. Zapp, S. Stern, M. R. Green, *Cell* **1993**, *74*, 969 – 978.
[13] N. W. Luedtke, T. J. Baker, M. Goodman, Y. Tor, *J. Am. Chem. Soc.* **2000**, *122*, 12035 – 12036.
[14] K. Li, T. M. Davis, C. Bailly, A. Kumar, D. W. Boykin, W. D. Wilson, *Biochemistry* **2001**, *40*, 1150 – 1158.
[15] a) K. Michael, H. Wang, Y. Tor, *Bioorg. Med. Chem.* **1999**, *7*, 1361 – 1371; b) S. R. Kirk, N. W. Luedtke, Y. Tor, *J. Am. Chem. Soc.* **2000**, *122*, 980 – 981.
[16] See the Supporting Information for detailed experimental procedures and additional data.
[17] T. J. Baker, N. W. Luedtke, Y. Tor, M. Goodman, *J. Org. Chem.* **2000**, *65*, 9054 – 9058.
[18] We have found it is beneficial to install the guanidinium groups at early stages of the synthetic scheme.
[19] Attempts to reduce the azide by catalytic hydrogenation, a method that was successfully employed for **4**, led to several by-products.
[20] Both cisplatin conjugates were fully characterized by ESI mass spectrometry and 1D and 2D ^{1}H and ^{13}C NMR spectroscopy, as well as by ^{195}Pt NMR spectroscopy.[16] Importantly, the ^{195}Pt NMR spectra show a single peak at $\delta = -2360$ and -2361 ppm, for **1** and **2**, respectively; this indicates a $[Cl_2PtN_2]$ coordination sphere.
[21] Noncovalent complexes are denatured under such conditions and yield no gel-mobility shift. See, for example, Figure 2b which illustrates the case with neomycin B (a molecule that is known to associate with the RRE noncovalently).
[22] Note that displacement experiments with BODIPY-labeled neomycin and CN^--treated **1** and **2** indicate that these derivatives have approximately the same affinity to the RRE JW compared to the nonmodified parent compounds (neomycin B and guanidinoneomycin B, respectively).[16] This indicates that the conjugated metal center does not significantly alter the RNA-binding characteristics of the glycoside skeleton.
[23] The unmodified RNA (*m*/*z* 11023) plus **1** (964 for $C_{26}H_{53}N_9O_{13}PtCl_2$) minus two chloride ions (70) yields an expected mass of *m*/*z* 11917. Since the aminoglycoside carries six positive charges under the acidic conditions of the matrix used, six fewer protons are required to form a single-charged positive ion of the Pt-conjugated RRE JW. For an oligonucleotide of this size, MALDI-TOF MS can be expected to show an accuracy of ± 4 amu. As such, good agreement between the expected and experimentally observed mass is established.
[24] Similar mass spectral characterization of **2** with the RRE reveals its binding and covalent modification are slightly less specific than those of **1**. This agrees with a previous determination of the RRE-binding specificity of amino- and guanidinoglycosides[13] and underscores the link between specific binding and platinum conjugation to the RNA.
[25] Since the mass spectra indicate that both chloride ions are displaced, a similar mechanism to the coordination of *cis*-Pt to DNA is implied.
[26] L. Wang, D. E. Ruffner, *Nucleic Acids Res.* **1997**, *25*, 4344 – 4361.
[27] J. A. Ippolito, T. A. Steitz, *J. Mol. Biol.* **2000**, *295*, 711 – 717.

 © 2005 Wiley-VCH Verlag GmbH & Co. KGaA, Weinheim

Expanded Porphyrins

Anthracene-Bridged Z-Shaped [26]Hexaphyrin(1.1.1.1.1.1) Dimer from the Regioselective Diels–Alder Reaction of a Hexaphyrin with Bis-*o*-xylylene Equivalents

Hiroshi Hata, Hiroshi Shinokubo, and Atsuhiro Osuka**

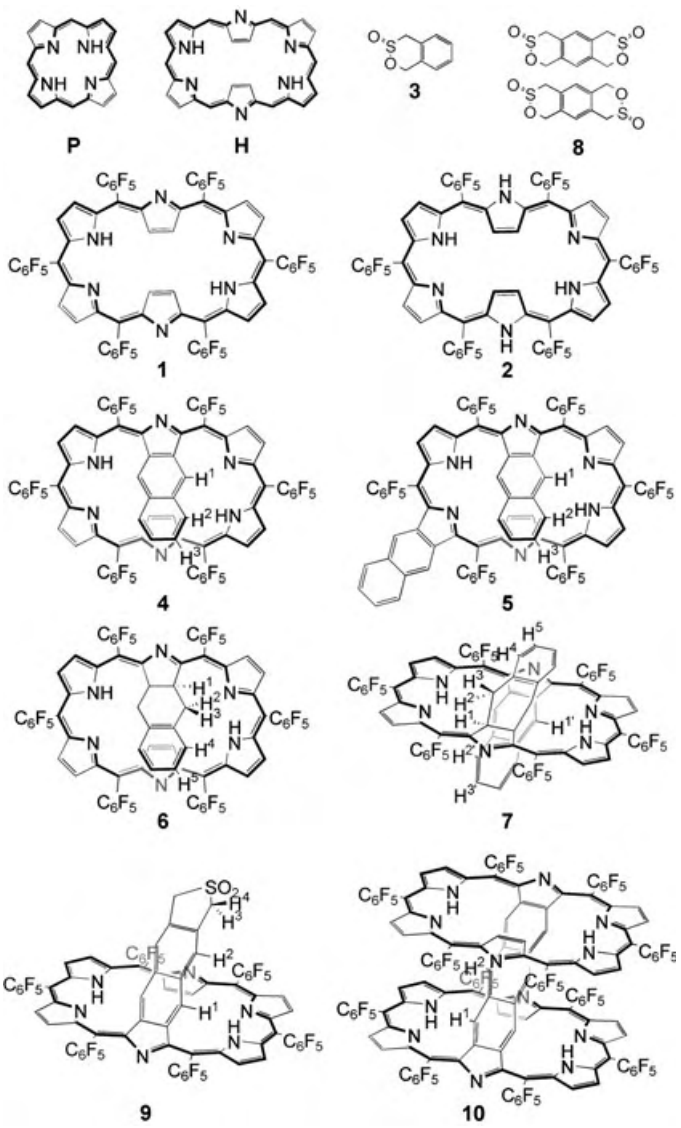
Expanded porphyrins which are porphyrin analogues with more than five pyrrolic subunits have recently attracted much attention because of their interesting structural and functional features and unique metal-coordination properties.[1] However, until now, there have been only a few reports on the chemical transformation of expanded porphyrins.[2] Herein, we report the Diels–Alder reaction of [26]hexaphyrin **1** with *o*-xylylene as the first example of a concerted cycloaddition of *meso*-aryl-substituted expanded porphyrins. Porphyrin (**P**) has an 18-π-aromatic electronic system and the peripheral diagonal double bonds are partially isolated from this aromatic conjugation. This situation explains the reactivity of the peripheral double bonds of **P** in cycloaddition reactions.[3] In this regard, [26]hexaphyrin(1.1.1.1.1.1) (**H**)[4] may also potentially undergo related cycloaddition reactions because the diagonal and inverted pyrrolic double bonds do not participate in the aromatic circuit.

A solution of hexakis(pentafluorophenyl)-substituted [26]hexaphyrin(1.1.1.1.1.1) **1** (5 mM) and benzosultine **3**[5] (1.3 equiv) in benzene was heated at reflux for 24 h under nitrogen atmosphere. After cooling the reaction mixture to room temperature, 2,3-dichloro-5,6-dicyano-1,4-benzoquinone (DDQ, 5 equiv) was added, and the resulting mixture was stirred for a further 12 h. Separation by column chromatography through silica gel provided naphthohexaphyrin **4** (55%) and bisnaphthohexaphyrin **5** (4.6%). FAB mass spectrometry revealed a molecular weight of 1560 for **4** which indicates the addition of one *o*-xylylene unit to **1**. The ^{1}H NMR spectrum of **4** exhibited a symmetric feature involving four doublets at $\delta = 9.12$, 9.07, 8.88, and 8.84 ppm (all $J = 4.6$ Hz) owing to the outer β-pyrrolic protons, a singlet at $\delta = -0.07$ ppm for the inner NH protons, and a singlet at $\delta = -2.50$ ppm for the inner β-pyrrolic protons. Characteristically, the protons of the fused naphthalene ring appeared at $\delta = 5.55$ (H^3), 3.53 (H^2), and 1.31 ppm (H^1). The observed

[*] H. Hata, Prof. Dr. H. Shinokubo, Prof. Dr. A. Osuka
Department of Chemistry
Graduate School of Science
Kyoto University
Sakyo-ku, Kyoto 606-8502 (Japan)
and
CREST
Japan Science and Technology Agency (JST)
Fax: (+81) 75-753-3970
E-mail: hshino@kuchem.kyoto-u.ac.jp
osuka@kuchem.kyoto-u.ac.jp

Supporting information for this article is available on the WWW under http://www.angewandte.org or from the author.

 © 2005 Wiley-VCH Verlag GmbH & Co. KGaA, Weinheim DOI: 10.1002/anie.200462231



phyrin **2** (10%). Oxidation of **6** with DDQ gave **4** quantitatively. The ^{1}H NMR spectrum of **6** exhibits peaks at $\delta = -6.07$ (H^1), -5.10 (H^2), -3.79 (H^3), 4.06 (H^4), and 5.64 ppm (H^5) owing to the protons in the fused tetrahydronaphthalene moiety. The structure of **6** was confirmed further by X-ray crystallographic analysis (Figure 1).[7]

We carried out theoretical calculations at the B3LYP/6–31G* level on hexaphyrin **1** and **6′**, a cycloadduct between **1** and 1,3-butadiene. Figure 2 illustrates the LUMOs for **1** and **6′** and shows clear differences in their distributions. The LUMO of hexaphyrin **1** develops at both the inner and outer double bonds. However, the LUMO of **6′** has very small coefficients at the inverted β-pyrrolic double bond. This result leads to the following predictions: 1) the initial Diels–Alder reaction can occur at either inner or outer double bonds[8] and 2) the second cycloaddition never takes place at the other side of the inner double bond once one of the inner double bonds has reacted with a 1,3-diene. The preferential formation of **4** suggests that the inner inverted β-pyrrolic double bonds are the most reactive and that the second prediction is indeed consistent with the formation of **5**. Interestingly, however, the [26]hexaphyrin aromatic system is restored in the oxidized adduct **4** because the DFT calculation predicts that the LUMO of **4′** develops significantly at the inverted β-pyrrolic double bond, as in **1** (Figure 2). Thus, we examined the reactivity of **4** toward *o*-xylylene and obtained the bis-*o*-xylylene adduct **7** as a major product in 33% yield. The ^{1}H NMR spectrum of **7** exhibits peaks at $\delta = -8.00$ (H^{1}), -4.06 (H^{2}), -3.27 (H^{3}), 2.98 (H^{4}), and 5.20 ppm (H^{5}) owing to the protons in the fused tetrahydronaphthalene moiety and at $\delta = 0.95$ ($H^{1'}$), 3.47 ($H^{2'}$), and 5.54 ppm ($H^{3'}$) in the fused naphthalene moiety. Curiously, the adduct **7** could not be oxidized with DDQ even under rather forcing conditions. Importantly, the regioselectivity during the addition of the second *o*-xylylene unit can be controlled by the oxidation state of the initial addition site, probably through electronic communication along the hexaphyrin macrocycle.

substantial highfield shifts can be ascribed to the diamagnetic ring current of [26]hexaphyrin and a bent orientation of the fused naphthalene ring with respect to the hexaphyrin plane. These data correspond with the structure of **4**, which results from the Diels–Alder reaction at the inner β-pyrrolic double bond in **1**. The strong ring current as suggested from these data indicates that the aromatic character is preserved in **4**. The ESI mass spectrum of **5** showed a peak for its parent ion at $m/z =$ 1661, which indicates the addition of two *o*-xylylene units to **1**. The ^{1}H NMR spectrum of **5** showed two different sets of signals for the protons on the fused naphthalene rings, and as these were observed at high and low fields, the adduct **5** is assigned to have both inner and outer fused naphthalene rings.[6] When the reaction was stopped before the oxidation with DDQ, the initial adduct **6** was isolated in 43% yield along with the recovery of **1** (28%) and reduced [28]hexaphyrin **2** (10%). Oxidation of **6** with DDQ gave **4** quantitatively. The ^{1}H NMR spectrum of **6** exhibits peaks at $\delta = -6.07$ (H^1), -5.10 (H^2), -3.79 (H^3), 4.06 (H^4), and 5.64 ppm (H^5) owing to the protons in the fused tetrahydronaphthalene moiety. The structure of **6** was confirmed further by X-ray crystallographic analysis (Figure 1).[7]

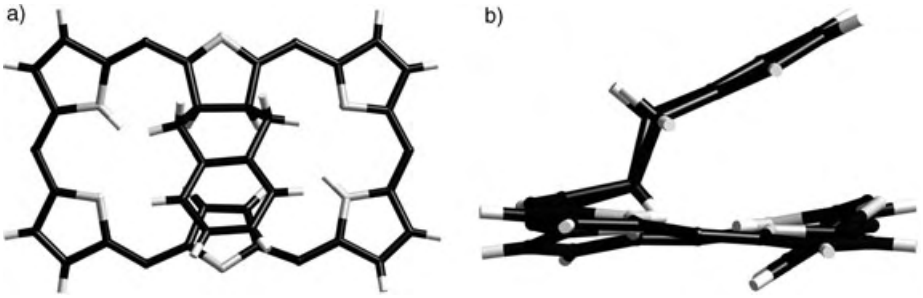


Figure 1. X-ray crystal structure of **6**. a) Top view and b) side view. *meso*-Pentafluorophenyl substituents are omitted for clarity.

It then occurred to us that the use of benzodisultine **8**[9] as a diene toward **1** may lead to the formation of a hexaphyrin dimer in which two hexaphyrin rings are bridged by an anthracene spacer. With this expectation, a solution of **1** (20 mM) and **8** (18 mM) in benzene was heated at 80 °C for 48 h and then subjected to oxidation with DDQ at room

 © 2005 Wiley-VCH Verlag GmbH & Co. KGaA, Weinheim

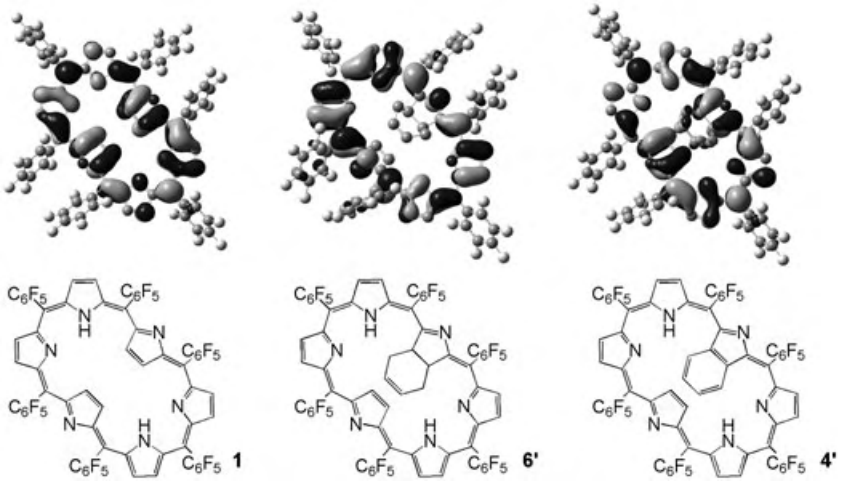


Figure 2. DFT calculations of hexaphyrin **1**, cycloadduct **6′**, and the oxidized adduct **4′**. LUMOs of **1** (left), **6′** (middle), and **4′** (right).

temperature. Two adducts, **9** (24%) and **10** (20%), were isolated along with some unconverted starting material **1** (21%). The FAB mass spectrum of **9** showed a peak for the parent ion at $m/z = 1650$ (calcd for $C_{76}H_{20}F_{30}N_6SO_2$: 1650), and its ^{1}H NMR spectrum exhibited a symmetric structure similar to that of **4** with additional AB-quartet signals at $\delta =$ 3.17 and 3.00 ppm (H^3 and H^4) with $J = 15$ Hz. The IR spectrum of **9** showed bands at $\tilde{\nu} = 1333$ and 1135 cm^{-1} which were assigned to transitions in the sulfone functionality. Thermal rearrangement of sultine to sulfone in the initial Diels–Alder adduct can explain the formation of **9**. The naphthosulfolene-fused hexaphyrin structure of **9** was confirmed by X-ray crystallographic analysis (Figure 3).[10] The fused sulfolene–naphthalane moiety is bent toward the hexaphyrin core with a dihedral angle of approximately 43.0°, and this structure explains the highfield shift of the fused naphthosulfolene moiety.

The product **10** displayed its parent-ion peak at $m/z =$ 3043.1875 (high resolution ESI-MS: calcd for $C_{142}H_{31}N_{12}F_{60}$: 3043.1831 [$(M+H)^+$]). The ^{1}H NMR spectrum of **10** supports its symmetric zigzag structure with the protons at the anthracene bridge appearing upfield as singlets at $\delta = 0.37$ (4H) and 0.10 ppm (2H). Indeed, the zigzag structure of **10** has been elucidated by X-ray diffraction studies with the fused anthracene unit bridging two hexaphyrin units with a dihedral angle of 42.7° (Figure 4).[11] Obviously, Diels–Alder reactions occurred consecutively at both diene moieties of bis-*o*-xylylene with two hexaphyrin molecules to give rise to the unique Z-shape double-decker structure of **10** with an interplanar distance of the hexaphyrins of 6.34 Å.

The absorption spectra of **4, 5**, and **10** are shown along with that of **1** in Figure 5. The Soret-like bands of **4** and **5** are broadened and red-shifted, which probably reflect the perturbations imposed by the fused naphthalene. On the other hand, the absorption spectrum of **10** exhibits a blue-shifted Soret-like band at $\lambda_{max} = 545$ nm with a full width at half maximum (fwhm) of 3220 cm^{-1}, which is rather broad relative to that for **1** (1590 cm^{-1}). These observations may be accounted for in terms of exciton coupling between the two hexaphyrin chromophores arranged in a face-to-face fashion[12] and hence suggest that **10** is a useful platform to study the excitonic interaction between aromatic [26]hexaphyrins.



Figure 4. X-ray crystal structure of **10**. *meso*-Pentafluorophenyl groups are omitted for clarity.

In summary, the Diels–Alder reaction of **1** with *o*-xylylene occurs selectively at the inner C–C double bond to provide novel aromatic ring-fused hexaphyrins. Furthermore, the use of benzodisultine as a bis-*o*-xylylene equivalent furnished the anthracene-bridged double-decker hexaphyrin **10**. This is the first example of a concerted cycloaddition reaction that involves the peripheral double bond of *meso*-aryl-substituted expanded porphyrins. Explorations of cycloaddition reactions of other expanded porphyrins with 1,3-dienes or 1,3-dipolarophiles are ongoing in our laboratory.

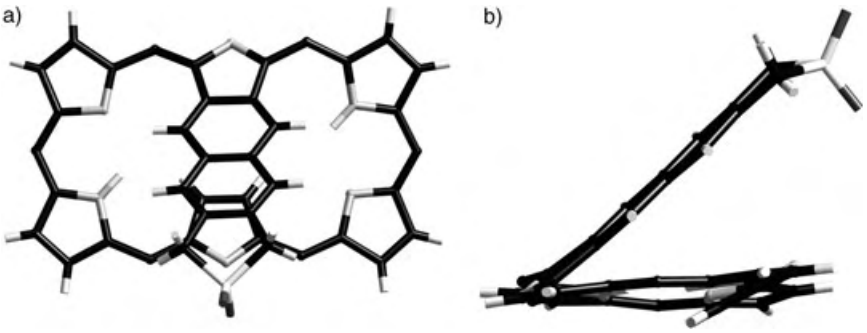


Figure 3. X-ray crystal structure of **9**. a) Top view and b) side view. *meso*-Pentafluorophenyl substituents are omitted for clarity.

Received: October 7, 2004
Published online: December 28, 2004

 © 2005 Wiley-VCH Verlag GmbH & Co. KGaA, Weinheim

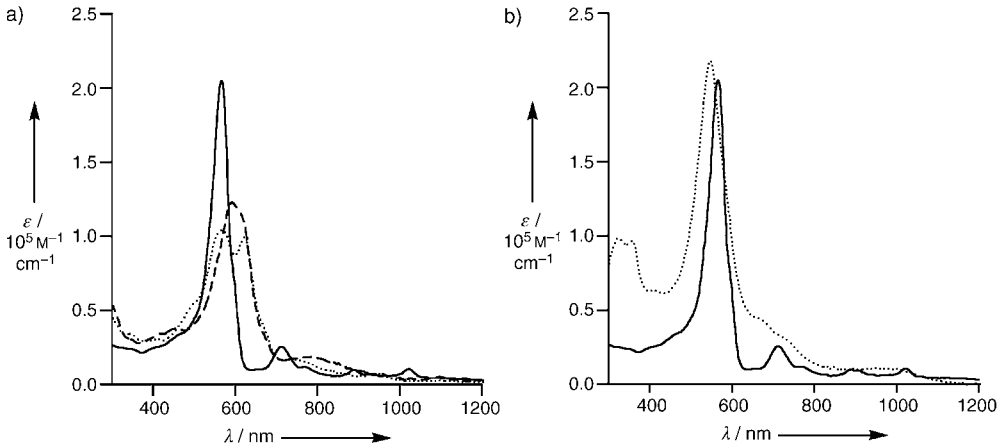


Figure 5. UV/Vis spectra of a) **1** (——), **4** (••••), and **5** (– – –), and b) **1** (——) and **10** (••••).

Keywords: cycloaddition · diene ligands · heterocycles · macrocycles · porphyrinoids

[1] a) J. L. Sessler, A. Gebauer, S. J. Weghorn in *The Porphyrin Handbook*, *Vol. 2* (Eds.: K. M. Kadish, K. M. Smith, R. Guilard), Academic Press, San Diego, **1999**, chap. 9, pp. 5; b) J. L. Sessler, S. J. Weghorn, *Expanded, Contracted & Isomeric Porphyrins*, Pergamon, Oxford, **1997**; c) E. Vogel, *J. Heterocycl. Chem.* **1996**, *33*, 1461; d) A. Jasat, D. Dolphin, *Chem. Rev.* **1997**, *97*, 2267; e) T. D. Lash, *Angew. Chem.* **2000**, *112*, 1833; *Angew. Chem. Int. Ed.* **2000**, *39*, 1763; f) J.-i. Setsune, S. Maeda, *J. Am. Chem. Soc.* **2000**, *122*, 12405; g) H. Furuta, H. Maeda, A. Osuka, *Chem. Commun.* **2002**, 1795; h) T. K. Chandrashekar, S. Venkatraman, *Acc. Chem. Res.* **2003**, *36*, 676; i) J. L. Sessler, D. Seidel, *Angew. Chem.* **2003**, *115*, 5292; *Angew. Chem. Int. Ed.* **2003**, *42*, 5134; j) A. Ghosh, *Angew. Chem.* **2004**, *116*, 1952; *Angew. Chem. Int. Ed.* **2004**, *43*, 1918.

[2] a) Y. Tanaka, W. Hoshino, S. Shimizu, K. Youfu, N. Aratani, N. Maruyama, S. Fujita, A. Osuka, *J. Am. Chem. Soc.* **2004**, *126*, 3046; b) M. Suzuki, S. Shimizu, J.-Y. Shin, A. Osuka, *Tetrahedron Lett.* **2003**, *44*, 4597.

[3] a) A. C. Tomé, P. S. S. Lacerda, M. G. P. M. S. Neves, J. A. S. Cavaleiro, *Chem. Commun.* **1997**, 1199; b) A. C. Tomé, P. S. S. Lacerda, A. M. G. Silva, M. G. P. M. S. Neves, J. A. S. Cavaleiro, *J. Porphyrins Phthalocyanines* **2000**, *4*, 532; c) J. A. S. Cavaleiro, M. G. P. M. S. Neves, A. C. Tomé, *ARKIVOC* **2003**, *14*, 107; d) J. Flemming, D. Dolphin, *Tetrahedron Lett.* **2002**, *43*, 7281.

[4] a) J.-Y. Shin, H. Furuta, K. Yoza, S. Igarashi, A. Osuka, *J. Am. Chem. Soc.* **2001**, *123*, 7190; b) R. Taniguchi, S. Shimizu, M. Suzuki, J.-Y. Shin, H. Furuta, A. Osuka, *Tetrahedron Lett.* **2003**, *44*, 2505; c) M. G. P. M. S. Neves, R. M. Martins, A. C. Tomé, A. J. D. Silvestre, A. M. S. Silva, V. Félix, M. G. B. Drew, J. A. S. Cavaleiro, *Chem. Commun.* **1999**, 385.

[5] a) M. D. Hoey, D. C. Dittmer, *J. Org. Chem.* **1991**, *56*, 1947; b) J. L. Segure, N. Martin, *Chem. Rev.* **1999**, *99*, 3199.

[6] We could not determine the exact structure of compound **5**. The position at which the outer naphthalene ring is fused to the hexaphyrin core is still ambiguous.

[7] Crystal data for **6** ($C_{74}H_{22}F_{30}N_6$): $M_W = 1564.98$, monoclinic $P2_1/n$ (No. 14), $a = 19.68(3)$, $b = 13.79(2)$, $c = 26.23(3)$ Å, $\beta = 95.76(4)°$, $V = 7081(13)$ Å^3, $T = 123$ K, $\rho_{calcd} = 1.468$ g cm^{-3}, $Z = 4$. 61481 reflections were measured, and $R = 0.096$, w$R = 0.124$ for 17777 reflections with $[I > 3\sigma(I)]$, $GOF = 1.399$. CCDC-248442 (**6**), CCDC-248443 (**9**), and CCDC-248444 (**10**) contain the supplementary crystallographic data for this paper. These data can be obtained free of charge from The Cambridge Crystallographic Data Centre via www.ccdc.cam.ac.uk/data_request/cif.

[8] The preference for the inner double bond in the initial addition step may be explained in terms of the steric factor of the outer pentafluorophenyl groups.

[9] A.-T. Wu, W.-D. Liu, W.-S. Chung, *J. Chin. Chem. Soc.* **2002**, *49*, 77.

[10] Crystal data for **9** ($C_{78}H_{22}F_{30}N_6Cl_4SO_2$): $M_W = 1818.89$, triclinic $P\bar{1}$ (No. 2), $a = 15.582(8)$, $b = 15.939(7)$, $c = 16.93(1)$ Å, $\alpha = 79.58(4)$, $\beta = 64.89(4)$, $\gamma = 66.46(4)°$, $V = 3489(3)$ Å^3, $T = 123$ K, $\rho_{calcd} = 1.731$ g cm^{-3}, $Z = 2$. 64912 reflections were measured, and $R = 0.085$, w$R = 0.136$ for 8104 reflections with $[I > 3\sigma(I)]$, $GOF = 1.272$.

[11] Crystal data for **10** ($C_{158}H_{30}N_{12}F_{60}O_{10}$): $M_W = 3395.95$, triclinic $P\bar{1}$ (No. 2), $a = 10.278(6)$, $b = 18.118(9)$, $c = 18.80(1)$ Å, $\alpha = 97.95(5)$, $\beta = 94.19(5)$, $\gamma = 93.79(4)°$, $V = 3447(3)$ Å^3, $T = 123$ K, $\rho_{calcd} = 1.636$ g cm^{-3}, $Z = 1$. 31007 reflections were measured, and $R = 0.084$, w$R = 0.097$ for 3567 reflections with $[I > 3\sigma(I)]$, GOF = 1.186.

[12] a) M. Kasha, H. R. Rawls, M. A. El-Bayoumi, *Pure Appl. Chem.* **1965**, *11*, 371; b) A. Osuka, K. Maruyama, *J. Am. Chem. Soc.* **1988**, *110*, 4454.

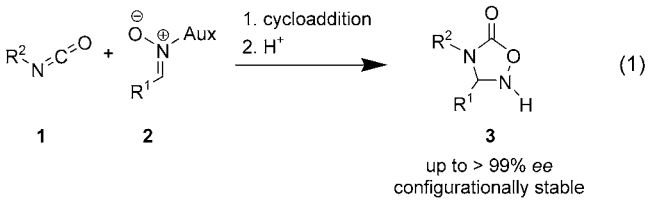
 © 2005 Wiley-VCH Verlag GmbH & Co. KGaA, Weinheim

Asymmetric Heterocycle Synthesis

1,2,4-Oxadiazolidinones as Configurationally Stable Chiral Building Blocks**

*Tobias Ritter and Erick M. Carreira**

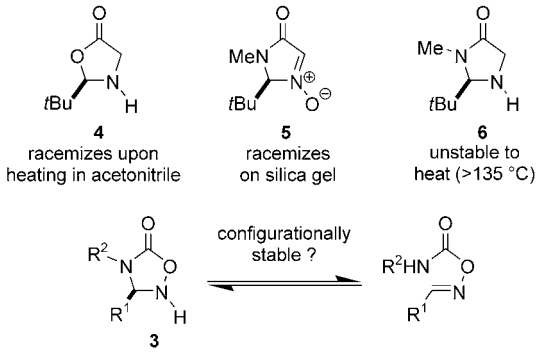
Heterocycles are ubiquitous in drug discovery and development by virtue of the fact that they can serve as scaffolds incorporating multiple points of diversification and thereby facilitate library synthesis. Nonaromatic heterocycles can impart added benefits in drug design, because they define out-of-plane vectors from a central core. One of the more recent examples of such a scaffold is the antibacterial linezolid, an optically active oxazolidinone.[1,2] Chiral 1,2,4-oxadiazolidinones **3** [Eq. (1)] constitute a structurally intriguing scaffold,



(1)

which bear structural similarity to oxazolidinones. However, they have rarely been employed as biologically active agents and then only in racemic form.[3] Their absence in the medicinal chemistry literature likely stems from the lack of synthetic methodology for their preparation in enantiomerically pure form and, consequently, the fact that it is unclear whether they would be configurationally stable. In this communication we document the convenient asymmetric synthesis of a wide range of substituted 1,2,4-oxadiazolidinones by cycloaddition. Access to the enantiomerically pure compounds allows us to ascertain for the first time the configurational stability of this class of compounds, including that of the unsubstituted, previously unknown parent heterocycle **3**.

The cycloaddition of isocyanates and nitrones was first reported by Goldschmidt and Beckmann in 1890, but it was not until almost 100 years later (1987) that the structure of the cycloadducts was firmly established as 1,2,4-oxadiazolidinones.[4] In order to exploit these heterocycles as potentially useful, versatile building blocks, two key criteria must be met: 1) methodology must be available for the convenient synthesis of oxadiazolidinones in optically active form,[5] and 2) the heterocycle **3** (intermediates and end products) must be configurationally stable. Examination of related heterocycles casts into question the configurational stability, especially under acidic and alkaline conditions (Scheme 1). In this



Scheme 1. Configurational stabiliy of heterocycles related to oxadiazolidinones.

respect, oxazolidinone **4** racemizes upon heating in acetonitrile[6] and the cyclic nitrone **5** was found to undergo rapid racemization during chromatography on silica gel through putative ring opening to the acyl imminium ion and subsequent recyclization.[7] The imidazolidinone scaffold **6** was reported to undergo degradation to the Schiff base upon vacuum distillation (135 °C, 0.05 torr).[8]

Our recent work in alkynylzinc additions to mannosyl- and erythrosyl- (Aux^1 and Aux^2, respectively) derived nitrones[9] led us to explore these substrates[10] in the cycloaddition reaction for the preparation of oxadiazolidinones. The starting nitrones are conveniently accessed from readily available starting materials (mannose, hydroxylamine, aldehyde) in three steps.[11]

Simply mixing a range of commercially available isocyanates **1** with mannosyl-derived nitrones **2** in CH_2Cl_2 led to smooth cycloaddition at 23 °C to afford oxadiazolidinones **7** in 69–87 % yield [Eq. (2), Table 1]. The diastereoselectivity of the cycloaddition ranges from 4:1 to 12:1 for the products isolated directly upon evaporation of the solvent. We were pleased to observe that simple trituration of the products with methanol generally furnished the desired substituted 1,2,4-oxadiazolidinones in up to >99:1 d.r. in analytically pure form. Electron-deficient and -rich aromatic and heteroaromatic nitrones, alkenylnitrones, as well as alkylnitrones participate in this cycloaddition, with the *C*-alkylnitrones most and the electron-deficient aromatic least reactive. Electron-deficient isocyanates react more readily than those substituted with electron-releasing groups, consistent with frontier orbital control. Reactions of substrates that are less reactive can be carried out successfully in refluxing acetonitrile.

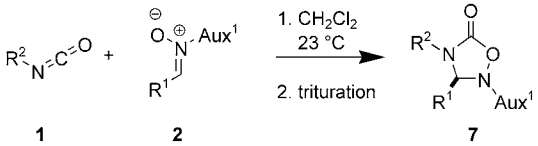
The enantiomeric oxadiazolidinones can be accessed by using the erythrose-derived auxiliary [Eq. (3)] and removing the auxiliary from the heterocyclic product [Eq. (4)]. In analogy to the cycloadditions described above, concentration

[*] T. Ritter, Prof. Dr. E. M. Carreira
Laboratorium für Organische Chemie, ETH Hönggerberg
8093 Zürich (Switzerland)
Fax: (+41) 1-632-1328
E-mail: carreira@org.chem.ethz.ch

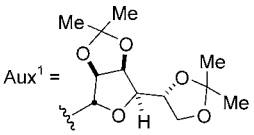
[**] We thank the Swiss National Science Foundation and F. Hoffmann-LaRoche AG for support of this research, the Fonds der Chemischen Industrie for a Kekulé Fellowship (T.R.), and Prof. Andrea Vasella for helpful discussions.

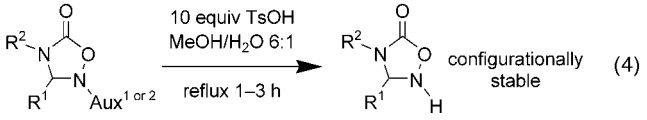
Supporting information for this article is available on the WWW under http://www.angewandte.org or from the author.

 © 2005 Wiley-VCH Verlag GmbH & Co. KGaA, Weinheim DOI: 10.1002/anie.200461934



(2)





(4)

auxiliaries is removed in the aqueous workup, leading to the isolation of the N2-unsubstituted heterocycles in >99% *ee* as determined by HPLC.

The results in Table 2 make apparent that the optically active oxadiazolidinones are stable towards acid, even when

Table 1: Diastereoselective nitrone cycloaddition [Eq. (2)].[a]

R^1	R^2	d.r. (crude prod.)	d.r. (isolated prod.)	Yield [%][b]
p-$C_6H_4NO_2$	*p*-$C_6H_4NO_2$	11:1	>99:1	84
p-C_6H_4Br		10:1	>99:1	87
p-$C_6H_4CF_3$	*p*-$C_6H_4CF_3$	10:1	>99:1	85
Ph	*p*-C_6H_4F	8:1	>99:1	83
p-C_6H_4OMe		12:1	>99:1	81
p-C_6H_4OMs		8:1	>99:1	84
3-Py	*p*-C_6H_4F	8:1	>99:1	80
2-C_4H_3S		8:1	19:1	79[c]
2-furyl	Ph	7:1	13:1	82[c]
E-styryl		10:1	>99:1	76
p-$C_6H_4NO_2$	Bz	5:1	24:1	71
1-Naph		10:1	>99:1	79
p-C_6H_4Br	Bn	7:1	>99:1	74[d]
p-C_6H_4OMe		10:1	>99:1	76[c]
Me	*p*-$C_6H_4NO_2$	4:1	>99:1	69
Cy		5:1	19:1	84
*t*Bu	*p*-C_6H_4OMe	6:1	>99:1	70
	2,6-$Cl_2C_6H_3$	6:1	>99:1	70

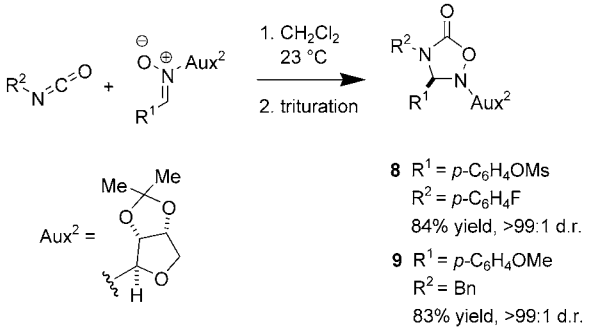
[a] Reaction conditions: CH_2Cl_2, 23 °C. Abbreviations used: Cy = cyclohexyl, Ms = methanesulfonyl, Naph = naphthyl, Py = pyridyl. [b] Yield of the isolated, analytically pure material. [c] Reaction conducted at reflux. [d] Reaction conducted in acetonitrile at reflux.

Table 2: Cleavage of the chiral auxiliary [Eq. (4)].

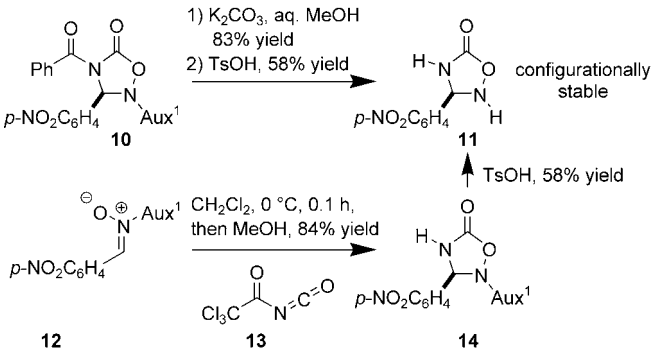
R^1	R^2	Yield [%]	*ee* [%]
from Aux^1			
p-C_6H_4OMe	Bn	88	>99
p-C_6H_4OMs	*p*-C_6H_4F	87	>99
p-C_6H_4OMs	*p*-C_6H_4F[a]	87	>99
Ph	*p*-C_6H_4F	81	>99
3-Py	*p*-C_6H_4F	65	>99
Me	*p*-$C_6H_4NO_2$	65	>99
1-Naph	H[b]	35	>99
from Aux^2			
p-C_6H_4OMe	Bn	86	>99
p-C_6H_4OMs	*p*-C_6H_4F	91	>99

[a] Reaction conditions: MeOH/aq HCl conc. 5:1, 15 h, 23 °C. [b] Reaction conditions: 40 °C, 6 h.

conc. aq. HCl in MeOH is used.[12] Additionally, the heterocycles have also been shown to be stable under alkaline conditions. Thus, as exemplified for **10**, cleavage of the *N*-benzoyl group with K_2CO_3 in aq. MeOH leads to monosubstituted oxadiazolidinone **11** in >99% *ee* after auxiliary removal (Scheme 2).



(3)



Scheme 2. Synthesis of oxadiazolidinone **11**.

of the reaction mixture and simple trituration of the resulting solids (MeOH) generally affords the desired heterocycles in analytically pure form (>99:1 d.r.).

Auxiliary removal is readily accomplished under acidic conditions (0.5 M toluenesulfonic acid (TsOH), aq. MeOH) [Eq. (4)]. We found that in the course of this reaction the isopropylidene protecting groups on the auxiliary first undergo hydrolysis followed by release of the heterocycle. Consequently, the water-soluble carbohydrate remnant of the

Trichloroacetyl isocyanate (**13**) participates in rapid cycloaddition (6 min) with the least reactive nitrone investigated (**12**). An added advantage is that product **14** is produced directly, since the trichloroacetyl group is cleaved during workup. Subsequent acid treatment affords **11**. These observations collectively underscore the fact that the oxadiazolidinones are inherently configurationally stable, even in their least substituted form.

 © 2005 Wiley-VCH Verlag GmbH & Co. KGaA, Weinheim

In conclusion, we report the first general synthesis of enantiomerically pure oxadiazolidinones including the previously unknown optically active N2-unsubstituted parent structures. The salient features of this process include the convenient experimental protocol (simple dissolution of the two reactants in CH_2Cl_2) and the isolation of analytically pure products upon trituration with methanol in up to >99:1 d.r. Of additional importance, we document that this class of optically active heterocycles is configurationally stable. These compounds should find application as building blocks for pharmaceutical and other biologically relevant substances in industry and academia.

Received: September 9, 2004
Published online: December 28, 2004

Keywords: asymmetric synthesis · cycloaddition · heterocycles · isocyanates · nitrones

[1] For a review on linezolid, see M. R. Barbachyn, C. W. Ford, *Angew. Chem.* **2003**, *115*, 2056; *Angew. Chem. Int. Ed.* **2003**, *42*, 2010.
[2] A related chiral heterocyclic core can be found in HIV protease inhibitors, see G. V. De Lucca, P. Y. S. Lam, *Drugs Future* **1998**, *23*, 987.
[3] For application as microbiocides, see: Merck Patent Gesellschaft mit beschränkter Haftung (DE), US 6455529 B1, **2002**; b) For application as adhesion receptor antagonists see: Du Pont Merck Pharma (US), US 5610294, **1997**; c) For application as retroviral protease inhibitors, see: Syngenta Crop Protection, US2004/0063937, **2004**.
[4] a) H. Goldschmidt, *Ber. Dtsch. Chem. Ges.* **1890**, *23*, 2746; b) E. Beckmann, *Ber. Dtsch. Chem. Ges.* **1890**, *23*, 3319; c) A. M. T. Bell, J. Bridges, R. Cross, C. P. Falshaw, B. F. Taylor, G. A. Taylor, I. C. Whittaker, M. J. Begley, *J. Chem. Soc. Perkin Trans. 1* **1987**, 2593; d) For a review on nitrone cycloadditions including isocyanates as reaction partners, see: D. S. C. Black, R. F. Crozier, V. C. Davis, *Synthesis* **1975**, *7*, 205.
[5] In a study of asymmetric cycloaddition involving nitrones and olefins, brief mention of the cycloaddition reaction with phenylisocyanate is described. At best a 2:1 ratio of diastereomers was obtained, and attempts to remove the phenethyl auxiliary led to destruction of the heterocycle, see: C. Belzecki, I. Panfil, *J. Chem. Soc. Chem. Commun.* **1977**, 303.
[6] D. Blaser, D. Seebach, *Liebigs Ann. Chem.* **1991**, 1067.
[7] S. W. Baldwin, A. Long, *Org. Lett.* **2004**, *6*, 1653.
[8] R. Fitzi, D. Seebach, *Tetrahedron* **1988**, *44*, 5277.
[9] R. Fässler, D. E. Frantz, J. Oetiker, E. M. Carreira, *Angew. Chem.* **2002**, *114*, 3180; *Angew. Chem. Int. Ed.* **2002**, *41*, 3054.
[10] For the development of the chiral mannose-derived nitrones, see: A. Vasella, *Helv. Chim. Acta* **1977**, *60*, 1273.
[11] A. Basha, R. Henry, M. A. McLaughlin, J. D. Ratajczyk, S. J. Wittenberger, *J. Org. Chem.* **1994**, *59*, 6103.
[12] The configurational stability of these heterocycles may be related to the low basicity of the N2 nitrogen. Preliminary investigations with the oxadiazolidinone derived from *p*-fluorophenyl isocyanate and *p*-mesyloxyphenyl-derived nitrone provide an estimate of the pK_a as ≤ 2 for the corresponding conjugate acid.

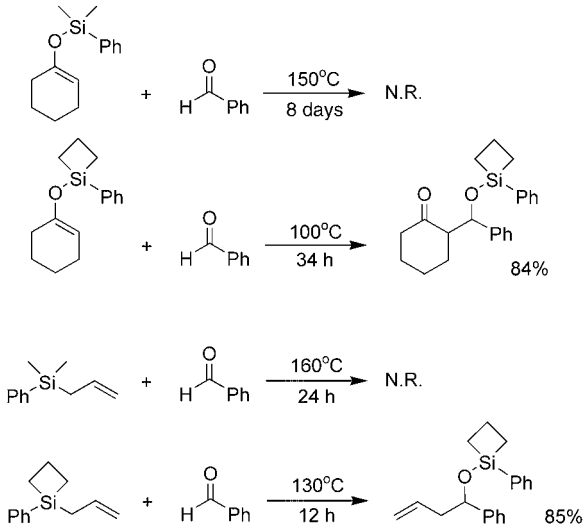
 © 2005 Wiley-VCH Verlag GmbH & Co. KGaA, Weinheim

Allylation Transition States

Origins of Stereoselectivity in Strain-Release Allylations**

Xiyun Zhang, Kendall N. Houk, and James L. Leighton*

A decade ago, the research groups led by Myers and Denmark discovered independently that enol silacyclobutanes could undergo aldol-like reactions with benzaldehyde, while no reaction was observed with the corresponding acyclic enol silanes (Scheme 1).[1] Later, Utimoto et al. reported similar results for carbonyl allylations (Scheme 1).[2]



Scheme 1. Reactions of acyclic and cyclic silanes reported by the research groups of Myers, Denmark, and Utimoto.[1,2] N.R. = no reaction.

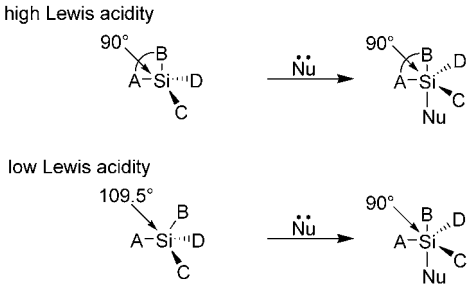
The phenomenon responsible for this unusual reactivity was termed "strain-release Lewis acidity" by Denmark.[3] Scheme 2 contrasts cyclic and acyclic tetrahedral silanes.

[*] Dr. X. Zhang, Prof. Dr. K. N. Houk
Department of Chemistry and Biochemistry
University of California, Los Angeles
Los Angeles, CA 90095 (USA)
Fax: (+1) 310-206-1843
E-mail: houk@chem.ucla.edu
Prof. Dr. J. L. Leighton
Department of Chemistry
Columbia University
New York, NY 10027 (USA)

[**] We are grateful to the National Institute of General Medical Sciences, National Institutes of Health, for financial support of this research.

Supporting information (ChemDraw structures of 12 transition states for allylation of formaldehyde, relative energies of **TS1**–**4**, **TS1-e**/**a**, and **TS2-e**/**a** from calculations with different methods and basis sets, and Cartesian coordinates of **TS1**–**4**, **TS1-e**/**a**, and **TS2-e**/**a**) for this article is available on the WWW under http://www.angewandte.org from the author.

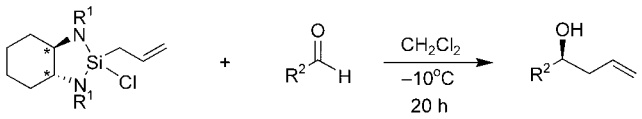
 © 2005 Wiley-VCH Verlag GmbH & Co. KGaA, Weinheim DOI: 10.1002/anie.200462130



Scheme 2. "Strain-release Lewis acidity" proposed by Denmark et al.[3]

The latter has relatively low Lewis acidity. However, when incorporated into a four-membered ring, a silane exhibits much higher Lewis acidity; nucleophilic attack on the strained silane produces a pentavalent, trigonal-bipyramidal silane intermediate in which the unstrained silacyclobutane spans apical and equatorial positions.

Recently, a new silane reagent has been developed for the asymmetric allylation of aldehydes based upon this concept (Scheme 3).[4] The novel *N*,*N*′-bis-4-bromobenzyldiazasilane



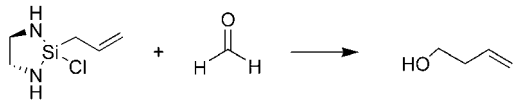
1: $R^1 = CH_2C_6H_4$-*p*-Br, 95–98% *ee*
2: $R^1 = CH_3$, 90–95% *ee*

aliphatic, aromatic, and conjugated aldehydes

Scheme 3. Enantioselective aldehyde allylation by the silane reagents developed by Leighton and Kubota.[4]

reagent (*R*,*R*)-**1** is crystalline and easy to prepare. Ring-strain-release Lewis acidity still remains in such five-membered silacycles due to the long Si–N bonds and short C–N bonds. (*R*,*R*)-**1** has been used for the allylation of aliphatic, aromatic, and conjugated aldehydes. Yields range from 61 to 93%, and the enantioselectivities are always excellent (95–98% *ee*). Interestingly, without the benzyl substituents, (*R*,*R*)-**2** still gives 90–95% *ee* (Scheme 3).

The mechanism and stereoselectivity of asymmetric aldehyde allylations employing the strain-release-activated silane reagents has been studied with computational methods. Optimizations in the gas-phase and frequency calculations were carried out using HF/6-31G* and B3LYP/6-31G* as implemented in Gaussian 98.[5] These give very similar geometries. Single-point energies were computed at HF, B3LYP, and MP2 levels employing the 6-31G* and 6-311++G** basis sets.[6] Calculations using MP2/6-311++G**//HF/6-31G* give reaction barriers ($\Delta E_a^{\ddagger}$, $\Delta E_b^{\ddagger}$) and stereoselectivity ($\Delta\Delta E_{ab}^{\ddagger}$) that agree with the experimental results. B3LYP gives qualitatively similar results but underestimates the stereoselectivity.



Scheme 4. The simplified computational model.

A simplified model used for the initial computational mechanistic studies is shown in Scheme 4. An achiral backbone was used but held in the gauche conformation present in the actual (*R*,*R*) reagent. This means if the two equatorial H atoms were replaced with other substituents, the two backbone C atoms would have *R* chirality. No constraint was applied in the transition-state optimizations. Formaldehyde was used as the model aldehyde. Calculations indicate that the neutral trigonal-bipyramidal silane intermediates, with formaldehyde at either apical or equatorial position, are not energy minima. Optimizations at HF, B3LYP, and MP2 levels lead to dissociation to the reactants. Thus, the reaction occurs in a single concerted step.

With the diazasilane ring spanning one apical and one equatorial position, there are 12 possible chairlike transition states for the model reaction, including four with apical aldehyde, four with apical allyl, and four with apical chlorine.[6] Boatlike transition states were calculated to be 10 kcal mol^{-1} higher in energy. Experimentally, the *cis*-crotyl version of the diazasilane reagent gives the *syn* product, and the *trans*-crotyl diazasilane reagent gives *anti*.[7]

The calculations show that only the four transition states with apical aldehyde, **TS1**–**TS4**, are true saddle points (Figure 1). This places electronegative atoms, N and O, in

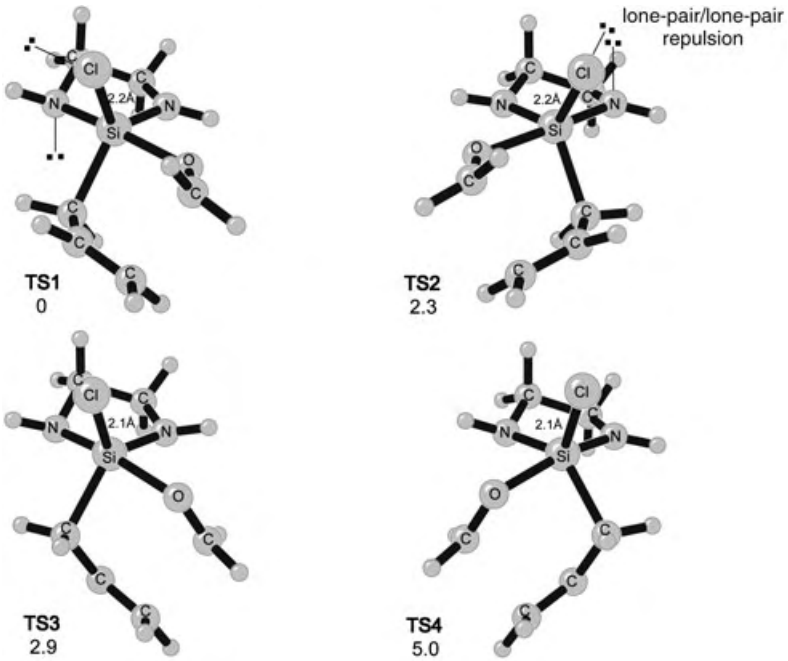


Figure 1. Transition-state geometries from HF/6-31G* optimizations and relative energies [kcal mol^{-1}] from MP2/6-311++G** single-point energy calculations for a simplified model (Scheme 4). Nonlabeled atoms are hydrogen; the Si–Cl distances are given in Å.

 © 2005 Wiley-VCH Verlag GmbH & Co. KGaA, Weinheim

apical positions. **TS1** is the lowest energy transition state. IRC calculations performed on **TS1** confirm that **TS1** is a transition state for formaldehyde allylation. The activation barrier is only 11.8 kcal mol^{-1}. This agrees with the ease of reaction even at reduced temperatures (−10 °C).[4] The reagent with a six-membered diazasilane ring does not react even at 50 °C.[8] Our calculations show that when the diazasilane ring is six-membered instead of five-membered, the reaction barrier increases to 22.9 kcal mol^{-1}. With the five-membered-ring reagent, the transition state achieves an N-Si-N angle of 89°, while this becomes 98° for the transition state with the six-membered ring; the substantial strain lowers the activation barrier by 11.1 kcal mol^{-1}.

The actual reagent, (*R*,*R*)-**2**, has substituents at both nitrogen atoms as well as a cyclohexane ring fused to the ethylene backbone (Scheme 3). Recalculations of **TS1** and **TS2** (Figure 1) for the actual reagent with acetaldehyde gave the four transition states in Figure 2. Equatorial substitution

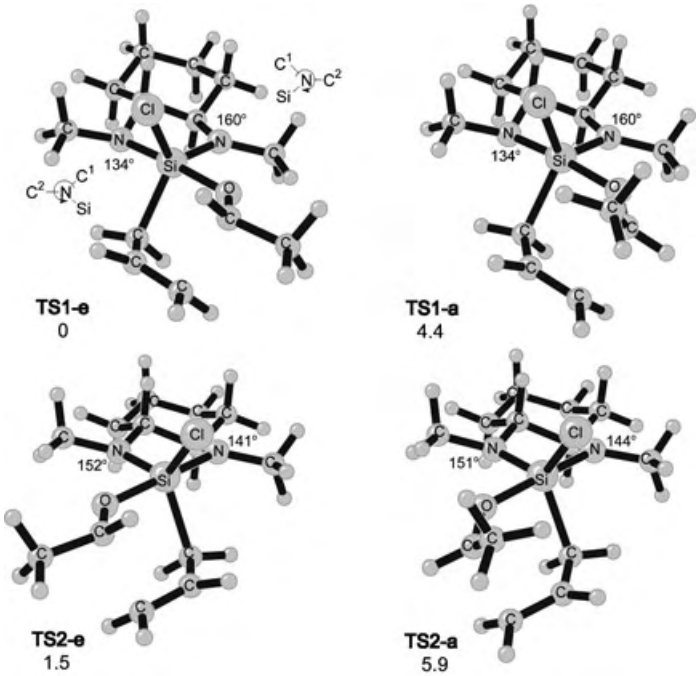


Figure 2. Transition-state geometries from HF/6-31G* optimizations and relative energies [kcal mol^{-1}] from MP2/6-311++G** single-point energy calculations for the reaction of (*R*,*R*)-**2** with acetaldehyde. Nonlabeled atoms are hydrogen; C^1-N-C^2-Si improper torsions are given in degrees.

(**TS1-e** and **TS2-e**) is more favored than axial substitution (**TS1-a** and **TS2-a**) by 4.4 kcal mol^{-1}, typical for the Zimmerman–Traxler-type chair six-membered ring. **TS2-e** is higher in energy than **TS1-e** by 1.5 kcal mol^{-1}, similar to the energy difference for the simplified model (Figure 1). The pyramidalization of nitrogen atoms was measured as the C^1-N-C^2-Si improper torsions (120° for a perfect pyramidal NH_3 or 180° for a planar nonpyramidal N). Figure 2 shows that pyramidalization is greater at the apical N atom than equatorial.

The origins of stereoselectivity can be explained using the simple models in Figure 1. **TS3** and **TS4** are higher in energy than **TS1** and **TS2** due to the unfavorable electron repulsion between the formaldehyde oxygen atom and the chlorine atom in **TS3** and **TS4**, and the favorable arrangement of an oxygen lone-pair *anti* to the Si–Cl bond in **TS1** and **TS2**. This is essentially an anomeric effect, which is demonstrated by the 0.1 Å longer Si–Cl bond in **TS1** and **TS2**.[9] **TS1** is the lowest energy transition state because the apical N (directly opposite the aldehyde) is pyramidalized to have its lone pair facing downward and minimize N lone-pair and Cl lone-pair repulsion. In **TS2**, the apical N (directly opposite the aldehyde) is also pyramidalized, but its lone pair is directed upward, and therefore there is unfavorable N lone-pair and Cl lone-pair repulsion in **TS2**. To verify this reasoning, we replaced chlorine with a methyl group and found that no selectivity is predicted. The importance of nitrogen pyramidalization was already noted by Denmark and Fu in the development of their 2,2′-bispyrrolidine-based bisphosphoramide catalysts for aldehyde allylations.[10] Asymmetric allylation controlled by nitrogen pyramidalization was also employed by Williams and co-workers for the development of the C28–C41 fragment in the total synthesis of phorboxazole A.[11]

In summary, the transition states for the stereoselective strain-release allylations have been located. The model based on these transition states suggests the components important for the stereoselectivity of diazasilane reagents: 1) attack of aldehyde oxygen on an apical position of the Si center (*anti* to an N); 2) an antiperiplanar arrangement of an O lone-pair and the Si–Cl bond in the chair transition state; 3) location of the chlorine with the lone pair *anti* to the lone-pair of apical N. Studies of acylhydrazone allylations by Leighton's oxazasilane reagents are in progress.[12]

Received: September 27, 2004
Published online: December 28, 2004

Please note: Minor changes have been made to this manuscript since its publication in *Angewandte Chemie* Early View.
The Editor.

Keywords: allylation · computer chemistry · reaction mechanisms · silanes · stereoselectivity

[1] a) A. G. Myers, S. E. Kephart, H. Chen, *J. Am. Chem. Soc.* **1992**, *114*, 7922–7923; b) S. E. Denmark, B. D. Griedel, D. M. Coe, *J. Org. Chem.* **1993**, *58*, 988–990; c) S. E. Denmark, B. D. Griedel, D. M. Coe, M. E. Schnute, *J. Am. Chem. Soc.* **1994**, *116*, 7026–7043.

[2] K. Matsumoto, K. Oshima, K. Utimoto, *J. Org. Chem.* **1994**, *59*, 7152–7155.

[3] S. E. Denmark, R. T. Jacobs, G. Dai-Ho, S. Wilson, *Organometallics* **1990**, *9*, 3015–3019.

[4] a) K. Kubota, J. L. Leighton, *Angew. Chem.* **2003**, *115*, 976–978; *Angew. Chem. Int. Ed.* **2003**, *42*, 946–948.

[5] Gaussian 98 (Revision A.7), M. J. Frisch, G. W. Trucks, H. B. Schlegel, G. E. Scuseria, M. A. Robb, J. R. Cheeseman, V. G. Zakrzewski, J. A. Montgomery, R. E. Stratmann, J. C. Burant, S. Dapprich, J. M. Millam, A. D. Daniels, K. N. Kudin, M. C. Strain, O. Farkas, J. Tomasi, V. Barone, M. Cossi, R. Cammi, B. Mennucci, C. Pomelli, C. Adamo, S. Clifford, J. Ochterski, G. A. Petersson, P. Y. Ayala, Q. Cui, K. Morokuma, D. K. Malick,

 © 2005 Wiley-VCH Verlag GmbH & Co. KGaA, Weinheim

A. D. Rabuck, K. Raghavachari, J. B. Foresman, J. Cioslowski, J. V. Ortiz, B. B. Stefanov, G. Liu, A. Liashenko, P. Piskorz, I. Komaromi, R. Gomperts, R. L. Martin, D. J. Fox, T. Keith, M. A. Al-Laham, C. Y. Peng, A. Nanayakkara, C. Gonzalez, M. Challacombe, P. M. W. Gill, B. G. Johnson, W. Chen, M. W. Wong, J. L. Andres, M. Head-Gordon, E. S. Replogle, J. A. Pople, Gaussian, Inc., Pittsburgh, PA, **1998**.

[6] See the Supporting Information.

[7] B. M. Hackman, P. J. Lombardi, J. L. Leighton, *Org. Lett.* **2004**, *6*, 4375–4377.

[8] J. W. A. Kinnaird, P. Y. Ng, K. Kubota, X. Wang, J. L. Leighton, *J. Am. Chem. Soc.* **2002**, *124*, 7920–7921.

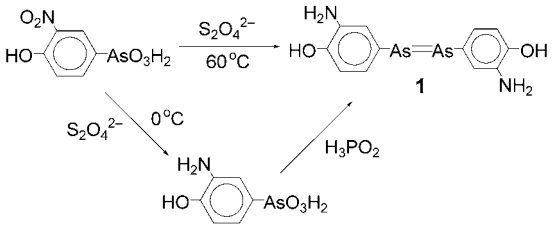
[9] a) This was suggested by B. T. King at the 227th ACS National Meeting, Anaheim, CA, USA, **2004**; b) For reviews of the anomeric effect, see A. J. Kirby, *The Anomeric Effect and Related Stereoelectronic Effects at Oxygen*, Springer, Berlin, **1983**.

[10] S. E. Denmark, J. Fu, *J. Am. Chem. Soc.* **2001**, *123*, 9488–9489.

[11] D. R. Williams, A. A. Kiryanov, U. Emde, M. P. Clark, M. A. Berliner, J. T. Reeves, *Proc. Natl. Acad. Sci. USA* **2004**, *101*, 12058–12063.

[12] a) R. Berger, P. M. A. Rabbat, J. L. Leighton, *J. Am. Chem. Soc.* **2003**, *125*, 9596–9597; b) R. Berger, K. Duff, J. L. Leighton, *J. Am. Chem. Soc.* **2004**, *126*, 5686–5687.

 © 2005 Wiley-VCH Verlag GmbH & Co. KGaA, Weinheim



Scheme 1. Two routes to salvarsan (**1**). The initial route of Ehrlich and Bertheim involves simultaneous reduction of the nitro group and As^V (top arrow).[3] Christiansen's two-step process of sequential reductions is shown below. [4]

Molecular Structure

The Composition of Ehrlich's Salvarsan: Resolution of a Century-Old Debate**

Nicholas C. Lloyd, Hugh W. Morgan, Brian K. Nicholson, and Ron S. Ronimus*

In 1910, Ehrlich introduced the compound 3-amino-4-hydroxyphenylarsenic(I) (salvarsan, arsphenamine, or Ehrlich 606) as a remedy for syphilis, a disease caused by the spirochaete bacterium *Treponema pallidum.* His methodical search for a specific curative for an identified disease can be regarded as the introduction of targeted chemotherapy.

Despite its long history and importance, the actual structure of salvarsan is still debated.[1,2] Ehrlich synthesized the compound by the reaction of 3-nitro-4-hydroxyphenylarsonic acid with dithionite.[3] This simultaneously reduced the NO_2 group to NH_2 and As^V to As^I to give a material of formula 3-H_2N-4-HOC_6H_3As (Scheme 1). The product was isolated as the hydrated hydrochloride salt of formula 3-H_2N-4-$HOC_6H_3As{\cdot}HCl{\cdot}H_2O$. This synthesis was not always reproducible, and inevitably gave rise to sulfur-containing impurities, which may have accounted for the variable toxicity of different batches of salvarsan.[5] A two-step process that involved initial reduction of the NO_2 group by sodium dithionite followed by reduction of As^V with hypophosphorous acid was subsequently shown by Christiansen to lead to sulfur-free material (Scheme 1).[4]

By analogy with azo compounds, Ehrlich assigned structure **1** to the free base of salvarsan. Although As=As bonds are now known to be found only in sterically crowded molecules,[6] the As=As form is repeatedly cited, with textbooks and reviews still giving structure **1**.[1,2] Various suggestions for the true structure of salvarsan have been proposed, including large polycyclic molecules[7] and polymers,[8] but lack strong supporting data.

We now report the first definitive evidence for the composition of salvarsan based on electrospray ionization mass spectrometric data. Salvarsan was synthesized by using a modification of the two-step synthesis first described by Christiansen.[4] The compound was isolated as the hydrochloride, giving consistent yields of a pale-yellow material that was analyzed as the monohydrate, corresponding exactly to Ehrlich's original reports.[9] We also isolated the mixed $H_2PO_2^-/H_2PO_3^-$ salt form (^{31}P NMR spectroscopic data) by direct precipitation from the reaction mixture.

^{1}H and ^{13}C NMR spectroscopic data were recorded for salvarsan, but were not particularly useful for structural assignment; ESI MS proved much more practical for this purpose. A typical spectrum is shown in Figure 1. Although there are many peaks, they can be readily assigned. Three clear series can be identified (Table 1). The first of these is the major one and consists of $[(RAs)_n + H]^+$ peaks (R = 3-H_2N-4-HOC_6H_3) for $n = 3$–8. Peaks corresponding to $n = 3$ and $n = 5$ are clearly dominant in this series. A lesser series comprises ions generated by loss of R^- from $(RAs)_n$, that is, $[R_{n-1}As_n]^+$ for $n = 4$–8. There are also minor peaks, which can be assigned to species $[(RAs)_n + O + H]^+$ arising from mild oxidation, presumably through the insertion of an oxygen atom into the As_n ring. There is a significant peak ($[R_2As]^+$) which connotes a fragmentation product of the cyclic polyarsines (see below). Peaks corresponding to $[RAs(OH)_2 + H]^+$ and $[RAs(OH)]^+$ arise from complete oxidative cleavage of As–As bonds.

The small peak at m/z 459 is a doubly charged ion (as determined by the spacing in the high-resolution isotope

[*] N. C. Lloyd, Prof. H. W. Morgan, Prof. B. K. Nicholson, Dr. R. S. Ronimus
Departments of Chemistry and Biological Sciences
University of Waikato
Private Bag 3105, Hamilton (New Zealand)
Fax: (+64) 7-838-4219
E-mail: b.nicholson@waikato.ac.nz

[**] We thank the Marsden Fund, administered by the Royal Society of New Zealand, for financial support.

 DOI: 10.1002/anie.200461471 © 2005 Wiley-VCH Verlag GmbH & Co. KGaA, Weinheim

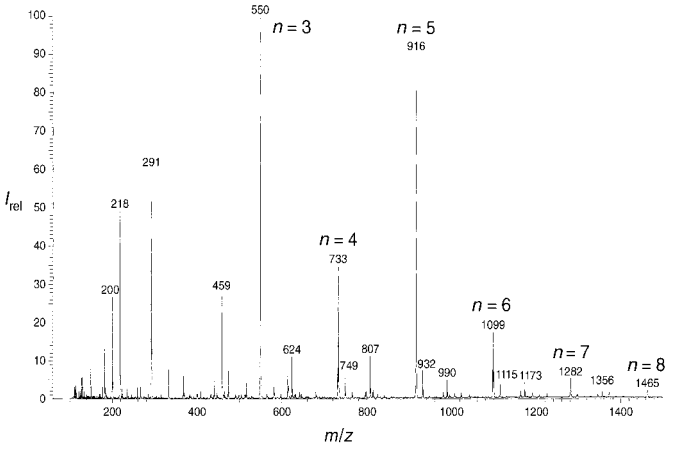


Figure 1. The ESI mass spectrum of salvarsan in H_2O. Ions derived from the different cycloarsines, $(RAs)_n$, are indicated as values of *n*. Assignment of other ions is given in Table 1.

Table 1: ESI mass spectral data for an aqueous solution of salvarsan.

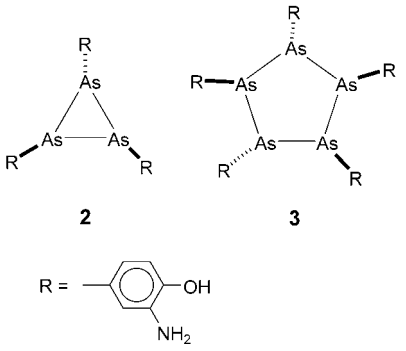
m/z	I_{rel} [%]	Assignment[a]
1465	2	$[(RAs)_8+H]^+$
1356	2	$[(RAs)_8-R^-]^+$
1282	4	$[(RAs)_7+H]^+$
1173	2	$[(RAs)_7-R^-]^+$
1115	3	$[(RAs)_6O+H]^+$
1099	18	$[(RAs)_6+H]^+$
990	3	$[(RAs)_6-R^-]^+$
932	5	$[(RAs)_5O+H]^+$
916	90	$[(RAs)_5+H]^+$
807	10	$[(RAs)_5-R^-]^+$
749	5	$[(RAs)_4O+H]^+$
733	43	$[(RAs)_4+H]^+$
624	10	$[(RAs)_4-R^-]^+$
550	100	$[(RAs)_3+H]^+$
458.5	30	$[(RAs)_6+2H]^{2+}$
291	61	$[R_2As]^+$
218	50	$[RAs(OH)_2+H]^+$
200	25	$[RAs(OH)]^+$

[a] R = 3-NH_2-4-HOC_6H_3-; see Figure 1

pattern) and can be attributed to $[(RAs)_5+2H]^{2+}$. Similarly, there is a small overlapping contribution to the $[(RAs)_3+H]^+$ peak at *m/z* 550 from doubly protonated $[(RAs)_6+2H]^{2+}$ ions. There were no features in any of the mass spectra of the type expected for higher-molecular-mass polymeric compounds.

All the evidence indicates that salvarsan in solution consists of cyclic species $(RAs)_n$, with $n=3$ (**2**) and $n=5$ (**3**) as the preferred sizes. We are confident that the ESI MS data provide an accurate profile of the components of salvarsan in solution, and that the species observed are not artifacts generated in the mass spectrometer, for the following reasons:

1) In many other areas it has been demonstrated that ESI MS provides an accurate guide to solution speciation, as the chemical ionization process is mild and does not lead to significant fragmentation.[10] Ions present in solution are transferred directly into the source. This is why ESI is so much more informative than EI, FAB, or MALDI in speciation studies.
2) The overall ESI MS profile does not change significantly with varying skimmer cone voltage (20–100 V), with varying pH, or with the different electrospray desolvation mechanisms of the two different instruments used. If the smaller rings were fragmentation products of larger molecules, then the distribution of peaks would change markedly under the different conditions. Furthermore, when fragmentation of the specific rings was deliberately induced in MS/MS experiments, the observed processes involved elimination of R, R_2As, and R_3As fragments, with no sign at all of conversion from larger into smaller rings.



Whereas the ESI MS results are believed to give a true qualitative reflection of the composition of salvarsan, quantitative allocation to different ring sizes is less certain, as the ion signal reflects ease of chemical ionization as well as relative abundance.[10] However, each molecule in the series is chemically ionized (protonated) on the same type of NH_2 group. Therefore, a moderate correlation between signal intensity and the amount present should exist. Certainly it appears that $(RAs)_3$ and $(RAs)_5$ are the predominant molecules in the mixture, with significant $(RAs)_4$ and $(RAs)_6$ present, and only minor representation from larger ring sizes.

It is pertinent to ask why elucidation of the structure of salvarsan has proved so difficult, as it has been established that other organoarsenic(I) compounds such as $(PhAs)_n$ and $(MeAs)_n$ can form rings ($n=5$ and 6 for $(PhAs)_n$, and $n=5$ together with a polymeric ladder form for $(MeAs)_n$).[1] This is a result of its resilient physical features—the material is a mixture of compounds; it does not crystallize in a form suitable for X-ray crystallographic analysis; it is not volatile, so it cannot be examined by traditional mass spectrometric methods; it is readily oxidized in solution (particularly at neutral or higher pH values[11]); and it has strong hydrogen bonding functional groups, which will complicate cryoscopic mass measurements (salvarsan forms gels in aqueous solutions at critical concentrations and pH values[4,12]).

We have attempted to separate salvarsan into its constituent ring species with HPLC experiments. However, these

 © 2005 Wiley-VCH Verlag GmbH & Co. KGaA, Weinheim

have so far been unsuccessful, presumably because of the high reactivity and hydrogen bonding properties of the compound.

The $(RAs)_n$ rings formed by salvarsan are of interest, especially the trimer, as an As_3 ring does not seem to have been confirmed before, although examples of both $(RP)_3$ and $(RSb)_3$ are known.[13] It is striking that the trimer and pentamer appear to be the main forms when R = 4-hydroxy-3-aminophenyl, whereas the hexamer and pentamer are the only characterized examples for R = phenyl.[1,7] (We note that West and co-workers found a peak corresponding to $[(PhAs)_3]^+$ in the EI mass spectrum of $(PhAs)_n$, but concluded it to be a fragmentation ion rather than a true component of the mixture.[14])

It has been accepted that salvarsan in the clinically administered form differs from the active form in vivo. Oxidation is needed to activate the compound.[15] This was earlier assumed to give rise to what was originally formulated as the oxide (RAs = O), but is undoubtedly $RAs(OH)_2$ or a condensation product thereof.[12] In essence, salvarsan $(RAs)_n$ appears to serve as a slow-release source of $RAs(OH)_2$. This oxidation process was confirmed by our ESI MS results. Peaks at *m*/*z* 218 and 200 can be assigned to $[RAs(OH)_2+H]^+$ and $[RAs(OH)]^+$, respectively (Figure 1). As the sample was exposed to air, these signals increased in intensity at the expense of those from the various $[(RAs)_n+H]^+$ species, until after a few hours they completely dominated the spectrum.

In conclusion, we have demonstrated for the first time that salvarsan consists of small rings $(RAs)_n$, particularly **2** and **3**, rather than the commonly written form **1**. Although this assignment is based mainly on ESI mass spectrometry of the mixture because the properties of the compound have so far precluded separation into components, we are confident that this work has provided an accurate description of the dominant structures of salvarsan.

Experimental Section

ESI mass spectra were recorded on VG Platform and Finnegan LCQ mass spectrometers. For the former, the compounds were dissolved in the appropriate solvent and injected through a Rheodyne injector equipped with a 10-mL sample loop. A flow rate of 0.02 mL min^{-1} and a source temperature of 60 °C was used. Nitrogen was used as both the nebulizing and drying gas. For the LCQ instrument, the sample was directly injected at 5 μL min^{-1} with a syringe pump. The capillary temperature was set at 100 °C. Nitrogen was used as the drying gas, and argon for collisionally induced fragmentation. NMR spectroscopic data were recorded with a Bruker Avance 300 spectrometer. 3-Nitro-4-hydroxyphenylarsonic acid (roxarsone) was purchased from Aldrich.

Preparation of 3-amino-4-hydroxyphenylarsonic acid (adapted from the method of Fargher[16]): 3-Nitro-4-hydroxyphenylarsonic acid (13.1 g, 0.05 mol) was dissolved in a solution of aqueous NaOH (1M, 100 mL) and cooled to 0 °C in an ice/salt bath. Sodium dithionite ($Na_2S_2O_4$) (30.25 g) was added in one portion with vigorous stirring. The solution effervesced. As soon as the color changed from orange to pale yellow, concentrated aqueous HCl (12 mL) was added. This mixture was held at < 0 °C until all frothing ceased and the product precipitated from solution. The precipitate was filtered and washed twice with ice-cold water to give crude 3-amino-4-hydroxyphenylarsonic acid (6.50 g, 56 %) as a cream-colored solid. This was dried under vacuum for 24 h.

Purification of 3-amino-4-hydroxyphenylarsonic acid (adapted from the method of Christiansen[4]): The crude product (6.0 g) obtained above was dissolved in dilute aqueous HCl (H_2O (25 mL), concd HCl (2 mL)), and the solution was stirred with decolorizing charcoal for 15 min. The mixture was filtered, and a solution of sodium acetate (25 %) was added to the filtrate until the solution was no longer acidic to Congo Red. The solution was cooled to 4 °C for 20 min. The resulting precipitate was collected by filtration and dried under vacuum to yield 3-amino-4-hydroxyphenylarsonic acid (4.7 g, 78 %) as an off-white microcrystalline solid. ^{1}H NMR ([D$_6$]DMSO): δ = 6.97, 6.81 ppm; ^{13}C NMR: δ = 114.5, 115.0, 119.0, 122.6, 137.8, 148.3 ppm; ESI MS (H_2O): positive ion *m*/*z* 234 $[M+H]^+$, 449 $[2M-H_2O+H]^+$, 664 $[3M-2H_2O+H]^+$; negative ion *m*/*z* 232 $[M-H]^-$, 465 $[2M-H]^-$, 698 $[3M-H]^-$. Elemental analysis calcd for $C_6H_8AsNO_4$: C 30.90, H 3.43, N 6.01 %; found: C 30.76, H 3.41, N 6.32 %.

Preparation of salvarsan (3-amino-4-hydroxyphenylarsenic(I)) (adapted from the method of Christiansen[4]): All solvents and solutions were degassed and the reaction was carried out under nitrogen. 3-Amino-4-hydroxyphenylarsonic acid (2.3 g, 0.01 mol) was dissolved in a solution of hypophosphorous acid (14 mL, 50 %) in water (73 mL). An aqueous solution of KI (1 mL, 3 %) was added, and the solution was heated gradually to 55 °C and held between 55 and 60 °C for 90 min. The mixture was cooled to 10 °C and poured with vigorous stirring into a cold mixture of HCl/H_2O (1:1, 164 mL). Salvarsan precipitated as a pale yellow gelatinous solid, which was collected and dried under vacuum as the hydrochloride. Elemental analysis calcd for $C_6H_6AsNO{\cdot}HCl{\cdot}H_2O$: C 30.37, H 3.80, N 5.91 %; found: C 30.66, H 3.70, N 5.62 %. Alternatively, ethanol was added to the cooled reaction mixture after the heating step with vigorous stirring, until a precipitate formed. The solid was collected and dried as above, and was characterized as a mixed hypophosphite/phosphite salt of 3-amino-4-hydroxyphenylarsenic(I). ^{31}P NMR (D_2O): δ = 9.7 ppm (t, $^1J_{H\text{-}P}$ = 536 Hz) $H_2PO_2^-$, δ = 4.1 ppm (d, $^1J_{H\text{-}P}$ = 648 Hz) HPO_3^{2-} (≈5:1). Elemental analysis calcd for $C_6H_6AsNO{\cdot}H_2PO_2{\cdot}H_2O$: C 26.97, H 4.12, N 5.24 %; found: C 27.50, H 3.92, N 5.14 %.

Received: July 29, 2004
Revised: October 8, 2004
Published online: December 29, 2004

Keywords: arsenic · arsphenamine · mass spectrometry · salvarsan · structure elucidation

[1] O. M. N. Dhubhghaill, P. J. Sadler, *Struct. Bonding (Berlin)* **1991**, *78*, 129.
[2] A. Lykknes, L. Kvittingen, *J. Chem. Educ.* **2003**, *80*, 497; A. S. Levanson, *J. Chem. Educ.* **1977**, *54*, 98.
[3] P. Ehrlich, A. Bertheim, *Ber. Dtsch. Chem. Ges.* **1912**, *45*, 756. See also W. G. Christiansen, *J. Am. Chem. Soc.* **1921**, *43*, 2202; for a review, see: S. Riethmiller, *Bull. Hist. Chem.* **1999**, *24*, 28.
[4] W. G. Christiansen, *J. Am. Chem. Soc.* **1920**, *42*, 2402.
[5] W. G. Christiansen, *J. Am. Chem. Soc.* **1922**, *44*, 847; H. King, *J. Chem. Soc.* **1921**, *119*, 1107; H. King, *J. Chem. Soc.* **1921**, *119*, 1415; R. G. Fargher, F. L. Pyman, *J. Chem. Soc.* **1920**, *117*, 370.
[6] B. Twamley, C. D. Sofield, M. M. Olmstead, P. P. Power, *J. Am. Chem. Soc.* **1999**, *121*, 3357.
[7] L. R. Smith, J. L. Mills, *J. Organomet. Chem.* **1975**, *84*, 1; T. Klapotke, *Biol. Met.* **1988**, 69; C. Elschenbroich, A. Salzer, *Organometallics: a Concise Introduction*, *2nd ed.*, VCH, Weinheim, **1992**, p.158.
[8] M. Ya. Kraft, E. B. Agracheva, *Dokl. Akad. Nauk Az. SSR* **1955**, *100*, 279 (CAN 50:8273); M. Ya. Kraft, I. A. Bashchuk, *Dokl. Akad. Nauk Az. SSR* **1949**, *65*, 509 (CAN 45:16367).

 © 2005 Wiley-VCH Verlag GmbH & Co. KGaA, Weinheim

[9] P. Ehrlich, A. Bertheim, US Patent 986148, **1911**, (CAN 5:10870).
[10] R. B. Cole, *Electrospray Ionization Mass Spectrometry*, Wiley, New York, **1997**; W. Henderson, B. K. Nicholson, L. J. McCaffrey, *Polyhedron* **1998**, *17*, 4291; R. Colton, A. D'Agostino, J. C. Traeger, *Mass Spectrom. Rev.* **1995**, *14*, 79; N. B. Cech, C. G. Enke, *Mass Spectrom. Rev.* **2001**, *20*, 362.
[11] C. Voegtlin, H. W. Smith, *J. Pharmacol. Exp. Ther.* **1920**, *16*, 199; R. P. Hogan, H. Eagle, *J. Pharmacol. Exp. Ther.* **1944**, *80*, 93.
[12] G. O. Doak, H. G. Steinman, H. Eagle, *J. Am. Chem. Soc.* **1941**, *63*, 99; P. V. Ioannou, *Appl. Organomet. Chem.* **2000**, *14*, 261.
[13] C. Frenzel, E. Hey-Hawkins, *Phosphorus Sulfur Silicon Relat. Elem.* **1998**, *143*, 1; H. J. Breunig, R. Rosler, E. Lork, *Organometallics* **1998**, *17*, 5594.
[14] P. S. Elmes, S. Middleton, B. O. West, *Aust. J. Chem.* **1970**, *23*, 1559.
[15] C. Voegtlin, *Physiol. Rev.* **1925**, *5*, 63; H. Eagle, G. O. Doak, *Pharm. Rev.* **1951**, 107.
[16] R. G. Fargher, *J. Chem. Soc.* **1919**, *115*, 982.

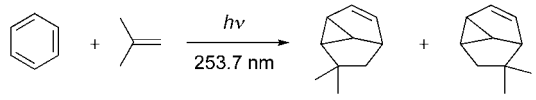
 © 2005 Wiley-VCH Verlag GmbH & Co. KGaA, Weinheim

Photocycloaddition

Alkene–Arene *meta* Photocycloadditions with a Four-Carbon-Atom Tether: Efficient Approach toward the Polycyclic Ring Systems of Aphidicolin and Stemodinone**

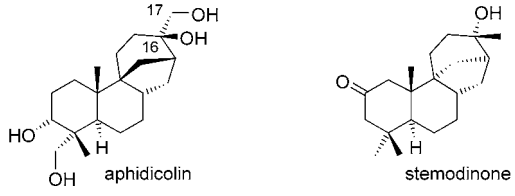
Joseph W. Boyd, Nicola Greaves, Jason Kettle, Andrew T. Russell, and Jonathan W. Steed*

Since its contemporaneous discovery in 1966 by Bryce-Smith, Gilbert, and Orger at Reading, and Wilzbach and Kaplan at Illinois, the photochemical *meta* cycloaddition of alkenes to arenes has provided considerable inspiration for mechanistic and synthetic studies (Scheme 1).[1–4] Extensive experimental and theoretical investigations of this reaction over the ensuing 38 years have greatly advanced the understanding of its mechanism and synthetic potential,[3–5] although much remains to be addressed. In 1969, Morrison and Ferree reported the first example of the intramolecular variant of this reaction.[6]



Scheme 1. Alkene–arene *meta* cycloaddition with characteristic regioisomeric cyclopropane products.[3]

We speculated that use of this reaction might give a rapid entry into the aphidicolin/stemodin ring system and hence facilitate the synthesis of analogue structures.[7] Aphidicolin and its prodrugs, 17-glycinate HCl salt and 16-fluoroaphidicolin, have shown good activity against a range of tumor types,[7] and the use of aphidicolin and its hydroxylated analogues against *leishmanial* parasites has also been discussed.[8]



To apply this reaction to these targets, we had to assess several selectivity issues including the mode of cycloaddition (*ortho*/*meta*), the regio- and stereoselectivity, and the effect of tether length. With regard to the skeleton of aphidicolin (Figure 1), although a *meta* cycloaddition is expected to be the favored mode and while an electron-donating methoxy group can be employed to control the regiochemistry of the addition,[9] a number of studies have emphasized the strong preference for product formation through an *exo* rather than an *endo* exciplex.[3,4] This preference suggests that the biologically potent aphidicolin system might be difficult to access.

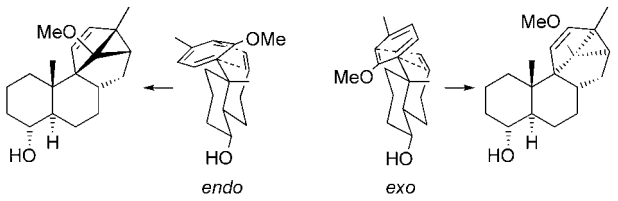


Figure 1. Stereochemical outcome of cycloadditions from *endo* and *exo* exciplexes.

[*] J. W. Boyd, Dr. A. T. Russell
School of Chemistry
University of Reading
Whiteknights, Reading RG6 6AD (UK)
Fax: (+44) 118-378-6331
E-mail: a.t.russell@reading.ac.uk
N. Greaves
Department of Chemistry
University of Salford
Salford M5 4WT (UK)
Dr. J. Kettle
AstraZeneca
Mereside, Alderley Edge
Macclesfield, Cheshire SK10 4TG (UK)
Dr. J. W. Steed
Department of Chemistry
University of Durham
South Road, Durham DH1 3LE (UK)

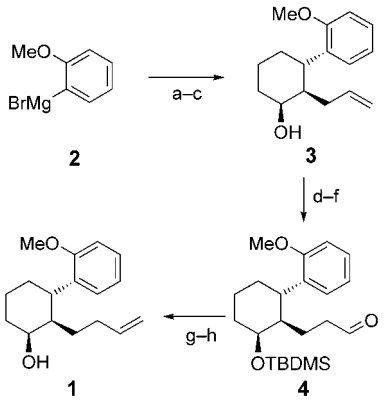
[**] Dedicated to Professor Andrew Gilbert on the occasion of his retirement. The authors would like to thank Mr. Peter Heath (Reading) for the NMR spectral characterization and AstraZeneca for a studentship to N.G. and for financial assistance from the AstraZeneca Strategic Fund.

 © 2005 Wiley-VCH Verlag GmbH & Co. KGaA, Weinheim DOI: 10.1002/anie.200461661

Besides these considerations, simple substrates which feature tethers with four linking units (e.g. CH_2 groups) are reported to have very poor quantum yields (e.g. 6-phenylhex-1-ene, $\varphi < 0.005$,[10] whereas for *cis*-6-phenylhex-2-ene, $\varphi = 0.26$).[6,11] During a study of tandem Norrish Type I intramolecular alkene–arene photocycloaddition reactions, De Keukeleire and He described a highly *exo*-selective reaction that proceeded in 42% yield, whereas DeLong and Wender noted a highly *exo*-selective cycloaddition with 68% yield of product at 60% conversion for four-atom tethers.[12] What appears to distinguish these two examples, which together represent the most efficient cycloadditions of this type, is some restriction of the conformational freedom of the tether. Given that 1) the four-unit tether illustrated in Figure 1 allows the system to adopt a geometry that is suitable for the formation of an *endo* exciplex (favored for most intermolecular cases)[3,4] without undue strain and 2) that the presence of the necessary fused six-membered ring should reduce the conformational freedom of the tether, we felt that such reactions might be successful.

Thus, we synthesized and photolyzed compound **1**. Chlorotrimethylsilane-accelerated, copper-catalyzed addition of **2** to cyclohexenone[13] afforded the expected silyl enol ether in 68% yield. Generation of the corresponding lithium enolate, by treatment with methyl lithium, was followed by alkylation with allyl iodide. Then, to avoid any complications from Norrish-type reactions, the ketone was stereoselectively reduced with L-selectride (lithium tri-*sec*-butylborohydride) to give the axial alcohol **3** as a crystalline solid in an overall yield of 77% (Scheme 2).[14]

The initial hope of preparing **1** by alkylation with homoallyl iodide was compromised by its low reactivity and a severe allergic reaction to the reagent by one of us. Thus we elected to homologate **3** as shown in Scheme 2. The axial alcohol was protected by treatment of **3** with *tert*-butyldimethylsilyl (TBDMS) triflate, then hydroboration of the double bond with 9-BBN followed by a two-step oxidation reaction afforded aldehyde **4** in 91% overall yield. A Wittig reaction (86%) and subsequent fluoride-mediated cleavage of the silyl ether (94%) completed the sequence.



Scheme 2. Synthesis of substrate **1**. Reagents and conditions: a) CuCN (4%), TMSCl, DMPU, THF, cyclohex-2-enone, 68%; b) MeLi, THF, allyl iodide, −78°C, 79%; c) L-selectride, THF, −78°C, 97%; d) TBDMSOTf, 2,6-lutidine, CH_2Cl_2, 0°C, 98%; e) 9-BBN then NaOH (3 N), 30% H_2O_2, THF, 94%; f) Dess–Martin periodinane, CH_2Cl_2, 99%; g) H_3CPPh_3Br, MeLi, THF, 0°C, 86%; h) TBAF, THF, 50°C, 94%. TMS = trimethylsilyl, DMPU = *N*,*N*′-dimethyl-*N*,*N*′-propylene urea, TBDMS = *tert*-butyldimethylsilyl, 9-BBN = 9-Borabicyclo[3.3.1]nonane, TBAF = tetra-*n*-butylammonium fluoride.

Comparison of the fluorescence quenching of **1** with that of its saturated analogue **5** (formed by quantitative hydrogenation of **1** over 10% Pd/C) revealed a fairly strong interaction between the excited-singlet state S_1 of the arene and the alkene (Figure 2). Therefore, a solution of **1** in

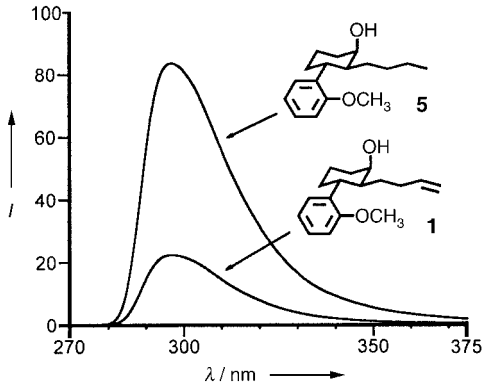
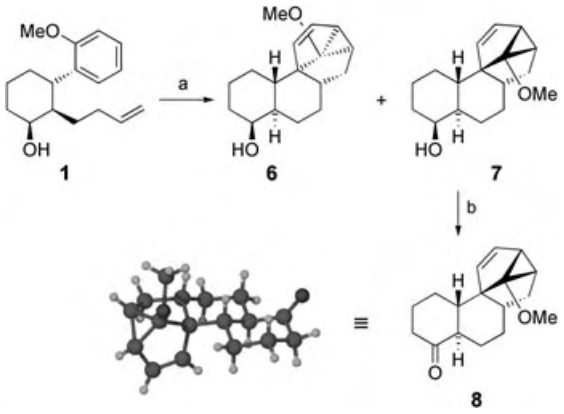


Figure 2. Fluorescence quenching of **1** and **5** in cyclohexane (4 mM) upon irradiation at $\lambda = 267$ nm.

cyclohexane (0.45 mM) was photolyzed in a falling-film photoreactor[15] at $\lambda = 253.7$ nm for 1.5 h. Such photolysis afforded a 1.0:1.2 mixture of two main photoadducts **6** and **7** in a remarkable 90% yield (Scheme 3). The structure of the



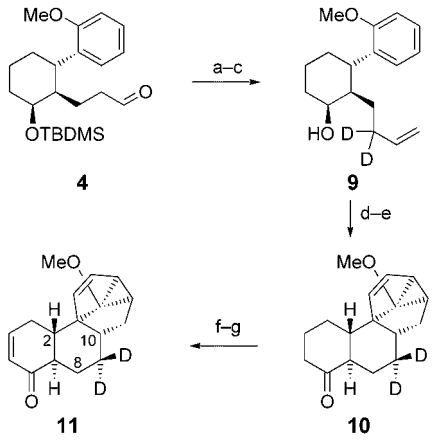
Scheme 3. *Endo*-selective intramolecular photochemical cycloaddition of **1**. Reagents and conditions: a) *hν* ($\lambda = 253.7$ nm), cyclohexane, 90% (**6**:**7**, 1.0:1.2); b) Dess–Martin periodinane, CH_2Cl_2, 81%.

major product **7** was solved by a single-crystal X-ray structure of the ketone derivative **8** and shown to arise from an *endo* conformation analogous to that shown in Figure 1.[16] The product **7** also exhibits the correct relative stereochemistry for aphidicolin.

Owing to the poor dispersal of resonances, we were unable to directly assign the structure and stereochemistry of **6** by NMR spectroscopic techniques. Taking advantage of the

 © 2005 Wiley-VCH Verlag GmbH & Co. KGaA, Weinheim

homologation sequence we had developed to prepare **1** (Scheme 2), the aldehyde **4** was dideuterated by using sodium deuteromethoxide in deuterated methanol and then converted into **9** as shown in Scheme 4. Photolysis of **9** followed



Scheme 4. Structural assignment of **6**. Reagents and conditions: a) sodium [D_3]methoxide, [D_4]MeOH; b) H_3CPPh_3Br, MeLi, THF, 0 °C, 77%; c) TBAF, THF, 50 °C, 96%; d) *hν* ($\lambda = 253.7$ nm), cyclohexane, 73% (then separate); e) PCC, CH_2Cl_2, 73%; f) LDA, THF, PhSeCl, −78 °C, 61%; g) H_2O_2 (27.5%), THF, 0 °C, 94%. PCC = pyridinium chlorochromate, LDA = lithium diisopropylamide.

by oxidation of the product with pyridinium chlorochromate[17] afforded ketone **10**, which on desaturation to **11** by the Sharpless–Reich protocol[18] allowed the relative stereochemistry at C-10 to be established by NOE measurements with irradiation of H-2 and H-8(axial) that showed a significant enhancement at H-10 (Scheme 4). Thus, **1** exhibited a rare high regioselectivity of cyclopropane formation[3,19] to give **6** starting from a conformation that is analogous to the *exo* arrangement shown in Figure 1 and proceeding by an *exo* exciplex to give a relative stereochemistry that is appropriate for the stemodinone ring system (Scheme 3).

In summary, an intramolecular alkene–arene *meta* photocycloaddition has been carried out on **1** in a high yielding reaction despite the presence of a four-carbon-atom tether. Furthermore, this is a unique example of such a reaction proceeding with a preference for an *endo* exciplex in an intramolecular case. Taken with De Keukeleire's and Wender's examples, these results show that with careful design of the tether, the restriction of three-linking-unit tethers in this type of reaction is no longer valid. The products of these reactions hold promise of a rapid entry into the aphidicolin/stemodinone ring systems and to yield biologically active analogues.

Received: August 15, 2004
Revised: October 2, 2004
Published online: January 5, 2005

Keywords: cycloaddition · fused-ring systems · natural products · photochemistry · polycycles

[1] D. Bryce-Smith, A. Gilbert, B. H. Orger, *Chem. Commun.* **1966**, 512.
[2] K. E. Wilzbach, L. Kaplan, *J. Am. Chem. Soc.* **1966**, *88*, 2066.
[3] J. Cornelisse, *Chem. Rev.* **1993**, *93*, 615.
[4] a) P. A. Wender, L. Siggel, J. M. Nuss in *Comprehensive Organic Synthesis*, *Vol. 5* (Eds.: B. M. Trost, I. Fleming), Pergamon, Oxford, **1991**, pp. 645–673; b) N. Hoffmann, *Synthesis* **2004**, 481.
[5] S. Clifford, M. J. Bearpark, F. Bernardi, M. Olivucci, M. A. Robb, B. R. Smith, *J. Am. Chem. Soc.* **1996**, *118*, 7353.
[6] H. Morrison, W. I. Ferree, *Chem. Commun.* **1969**, 268.
[7] a) M. Toyota, M. Ihara, *Tetrahedron* **1999**, *55*, 5641; b) F. Bilodeau, L. Dube, P. Deslongchamps, *Tetrahedron* **2003**, *59*, 2781; c) M. Toyota, M. Sasaki, M. Ihara, *Org. Lett.* **2003**, *5*, 1193.
[8] O. Kayser, A. F. Kiderlen, S. Bertels, K. Siems, *Antimicrob. Agents Chemother.* **2001**, *45*, 288.
[9] P. A. Wender, J. J. Howbert, *J. Am. Chem. Soc.* **1981**, *103*, 688.
[10] A. Gilbert, *Pure Appl. Chem.* **1980**, *52*, 2669.
[11] a) W. I. Ferree, J. B. Grutzner, H. Morrison, *J. Am. Chem. Soc.* **1971**, *93*, 5502; b) H. A. Neijenesch, E. J. Ridderikhoff, C. A. Ramsteijn, J. Cornelisse, *J. Photochem. Photobiol. A* **1989**, *48*, 317.
[12] a) D. De Keukeleire, S-L He, *J. Chem. Soc. Chem. Commun.* **1992**, 419; b) M. DeLong, Ph. D. Thesis, Stanford University, 1992.
[13] S-e. Yoo, K. Y. Yi, *Synlett* **1990**, 697.
[14] Compound **3** was photolyzed by using 253.7-nm radiation to give three main cycloadducts, which were derived exclusively from *exo* transition states as expected. For studies of compounds related to **3**, see; a) H. M. Barentsen, E. G. Talman, D. P. Piet, J. Cornelisse, *Tetrahedron* **1995**, *51*, 7469; b) H. M. Barentsen, A. B. Sieval, J. Cornelisse, *Tetrahedron* **1995**, *51*, 7495.
[15] A falling-film reactor (Photochemical Reactors Ltd.) equipped with a 15-W low-pressure mercury lamp was used for irradiations.
[16] CCDC-246803 (**8**) contains the supplementary crystallographic data for this paper. These data can be obtained free of charge from The Cambridge Crystallographic Data Centre via www.ccdc.cam.ac.uk/data_request/cif.
[17] E. J. Corey, J. W. Suggs, *Tetrahedron Lett.* **1975**, *16*, 2647.
[18] a) H. J. Reich, I. L. Reich, J. M. Renga, *J. Am. Chem. Soc.* **1973**, *95*, 5813; b) K. B. Sharpless, R. F. Lauer, A. Y. Teranishi, *J. Am. Chem. Soc.* **1973**, *95*, 6137.
[19] a) D. C. Blakemore, A. Gilbert, *Tetrahedron Lett.* **1995**, *36*, 2307; b) D. M. Amey, A. Gilbert, D. T. Jones, *J. Chem. Soc. Perkin Trans. 2* **1998**, 213; c) P. A. Wender, T. W. von Geldern, B. H. Levine, *J. Am. Chem. Soc.* **1988**, *110*, 4858.

 © 2005 Wiley-VCH Verlag GmbH & Co. KGaA, Weinheim

Anomeric Selectivity

Stereoselective Glycosylation Reactions with Chiral Auxiliaries**

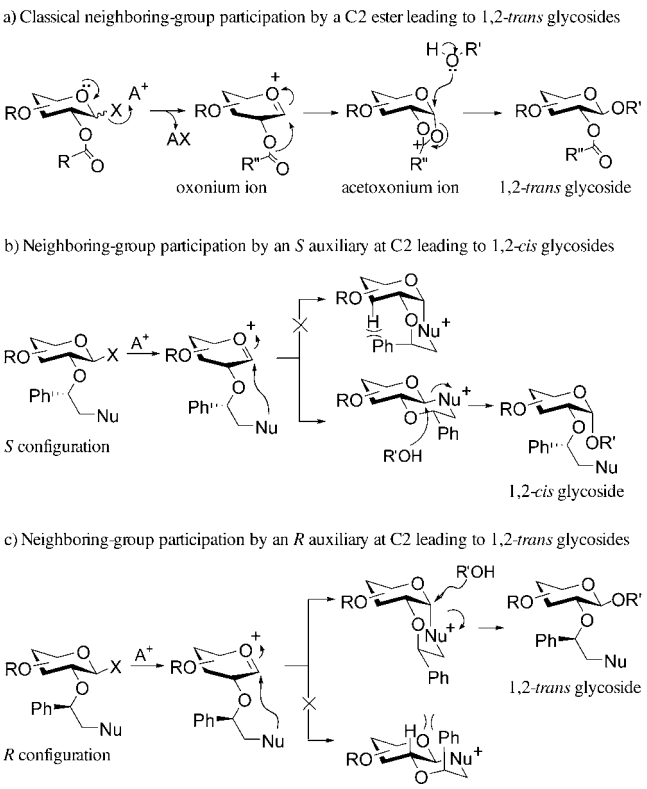
*Jin-Hwan Kim, Hai Yang, and Geert-Jan Boons**

In memory of Professor Jacques van Boom

It is now well recognized that protein- and lipid-bound saccharides play essential roles in many molecular processes that have an impact on eukaryotic biology and disease.[1–3] Examples of such processes include fertilization, embryogenesis, neuronal development, hormone activities, and the proliferation of cells and their organization into specific tissues. The interactions of saccharides with proteins or lipids are also important in health science and are involved in the invasion and attachment of pathogens, inflammation, metastasis, blood-group immunology, and xenotransplantation. A major obstacle to advances in glycobiology is the lack of pure and structurally well-defined carbohydrates and glycoconjugates. These compounds are often found in low concentrations and in microheterogeneous forms, thus greatly complicating their isolation and characterization. In many cases, well-defined oligosaccharides can only be obtained by organic synthesis.[4]

Although much progress has been made in methods for oligosaccharide synthesis, the construction of complex carbohydrates remains time consuming.[5] One-pot multistep glycosylations[6,7] and polymer-supported syntheses[8–10] are two approaches being applied to streamline the preparation of complex oligosaccharides. The usefulness of these methods is, however, compromised by the fact that many glycosylations give mixtures of the two possible anomers. If these anomers are not separated after each glycosylation, complex mixtures of products are obtained that cannot be used for biological studies. Routine oligosaccharide synthesis will only be possible when robust stereoselective glycosylations become available.

The most reliable method for stereoselective glycosidic-bond formation is based on the neighboring-group participation of a 2-*O*-acyl functionality (Scheme 1a).[11] In these reactions, a promoter activates an anomeric leaving group, thereby resulting in its departure and the formation of an oxonium ion. Subsequent neighboring-group participation of a 2-*O*-acyl protecting group will give a more stable acetoxonium ion. An alcohol can attack the anomeric center of an acetoxonium ion from only one face, to provide a 1,2-*trans* glycoside. Thus, β-linked products will be obtained in the case of glucosyl-type donors, whereas mannosides will give α-glycosides. The introduction of 1,2-*cis* glycosidic linkages, such as α-glucosides and α-galactosides, requires glycosyl donors with a non-assisting functionality at the C2 position. Invariably, these glycosylations lead to mixtures of anomers.[12] In general, reasonable anomeric selectivities will only be obtained by extensive optimization of reaction conditions such as solvent, temperature, promoter, leaving group, and protecting-group pattern. Thus, the stereoselective formation of 1,2-*cis* glycosides is the principal challenge in complex oligosaccharide synthesis.



Scheme 1. Conventional and new approaches for stereoselective glycosylation. A = activating group, Nu = nucleophile, X = leaving group.

We describe herein a novel strategy for stereoselective glycosylations in which a chiral auxiliary at the 2-position of a glycosyl donor is used (Scheme 1b,c). The auxiliary is a substituted ethyl moiety that contains a nucleophilic group. Upon formation of an oxonium ion, participation of the nucleophilic moiety of the auxiliary should lead to the formation of either a *trans*- or a *cis*-decalin system. It was expected that the use of an auxiliary with *S* stereochemistry would lead only to the formation of the *trans* decalin, since the alternate *cis*-fused system would place the phenyl substituent in an axial position and induce unfavorable steric interactions (Scheme 1b). Subsequent displacement of the anomeric moiety of the *trans*-decalin intermediate would then lead to the formation of a 1,2-*cis* glycoside. Alternatively, the use of an auxiliary with *R* stereochemisty would lead to the formation of a 1,2-*trans* glycoside, because in this case the

[*] Dr. J.-H. Kim, H. Yang, Prof. Dr. G.-J. Boons
Complex Carbohydrate Research Center
University of Georgia
315 Riverbend Road, Athens, GA 30602 (USA)
Fax: (+1) 706-542-4412
E-mail: gjboons@ccrc.uga.edu

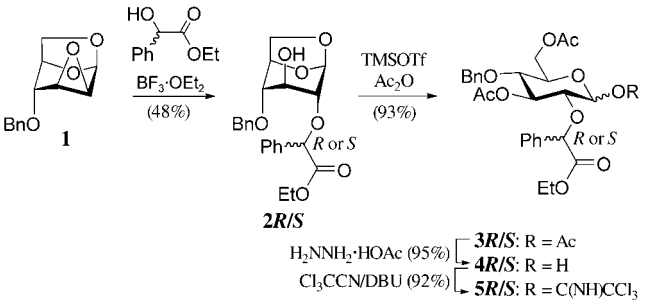
[**] This work was supported by the National Cancer Institute of the National Institutes of Health (Grant: RO1 CA88986).

Supporting information for this article is available on the WWW under http://www.angewandte.org or from the author.

 DOI: 10.1002/anie.200461745 © 2005 Wiley-VCH Verlag GmbH & Co. KGaA, Weinheim

trans-decalin system would experience unfavorable steric interactions, and therefore glycosylation would only take place from the *cis*-decalin intermediate (Scheme 1c).

Ethyl mandelate was explored as a first-generation chiral auxiliary (Scheme 2). This derivative was deemed attractive because both enantiomers are



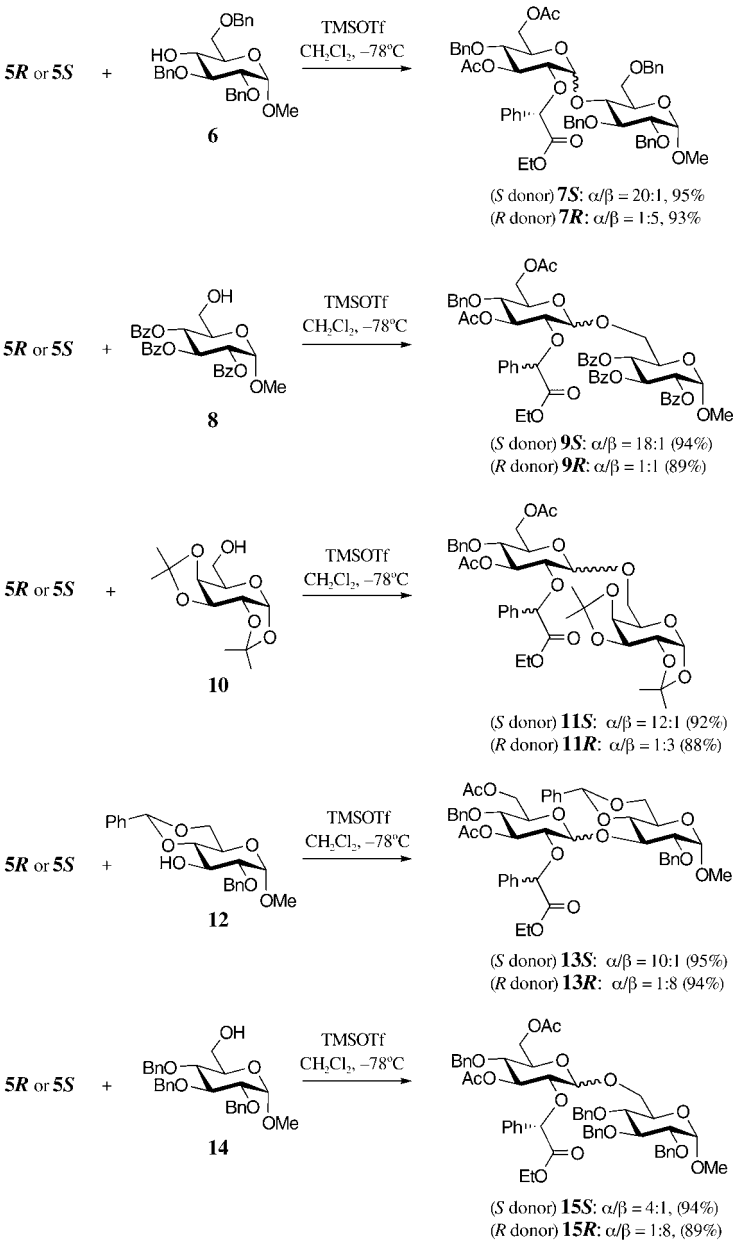
Scheme 2. Preparation of glycosyl donors **5*R*** and **5*S***. Bn = benzyl, DBU = 1,8-diazabicyclo[5.4.0]undec-7-ene, TMSOTf = trimethylsilyl trifluoromethanesulfonate.

readily available, esters are well established as appropriate participating functionalities in glycosylations, and the benzylic nature of the auxiliary should make its removal possible under reductive conditions.

Glycosyl donors **5*R*** and **5*S***, containing an (*R*)- or (*S*)-ethoxycarbonylbenzyl moiety, could be prepared by an efficient procedure from the readily available epoxide **1**.[13] Thus, the reaction of **1** with ethyl (*R*)-mandelate in the presence of $BF_3{\cdot}Et_2O$ led to a *trans*-diaxial opening of the epoxide to give **2*R*** in a yield of 48%. Next, acetolysis of the 1,6-anhydro bridge of **2*R*** with acetic anhydride and TMSOTf gave compound **3*R*** in an almost quantitative yield. The anomeric acetyl group of **3*R*** was selectively removed with hydrazine acetate to give hemiacetal **4*R***, which was converted into trichloroacetimidate **5*R*** by using standard conditions.[14] Glycosyl donor **5S** was prepared by a similar protocol with ethyl (*S*)-mandelate as the starting material.

With glycosyl donors **5*R*** and **5*S*** in hand, attention was focused on the glycosylation of a range of different glycosyl acceptors. Thus, coupling of **5*S*** with **6** by using a catalytic amount of TMSOTf in dichloromethane at −78 °C gave disaccharide **7*S***, mainly as the α-glycoside, in an almost quantitative yield (Scheme 3). At this low temperature, the reaction was completed within 15 minutes, which indicates that the glycosyl donor **5*S*** is highly reactive. Dilution of the reaction mixture led to a small increase in anomeric selectivity, whereas higher reaction temperatures led to decreases in selectivity. As expected, coupling of **1*R*** with **6** under similar reaction conditions gave **7*R*** mainly as the β anomer.

The fact that an inversion of configuration at the asymmetric center of the auxiliary led to a reversal of the stereochemical outcome of the glycosylation provides strong



Scheme 3. Stereoselective glycosylation with glycosyl donors **5*R*** and **5*S***. Bz = benzoyl.

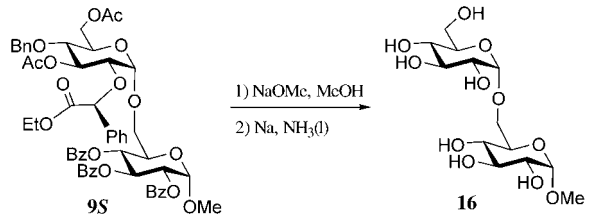
support for the proposed mode of participation as outlined in Scheme 1.

To demonstrate the generality of the approach, a range of glycosyl acceptors were glycosylated with **5*R*** and **5*S***. As can be seen in Scheme 3, glycosylations of **5*S*** with glycosyl acceptors that have either a primary or a secondary hydroxy group gave disaccharides with high α-anomeric selectivity. In each case, the use of glycosyl donor **5*R*** led to a reversal of anomeric selectivity and mainly β-linked disaccharides were isolated, albeit with somewhat lower selectivity than that observed with **5*S***.

The results of the glycosylations indicate that the use of ethyl mandelate as an auxiliary at the 2-position provides a reliable approach for the synthesis of α-linked glycosides. To

 © 2005 Wiley-VCH Verlag GmbH & Co. KGaA, Weinheim

be useful for target synthesis, it is important that the auxiliary can be removed under mild conditions. The auxiliary was designed as a substituted benzyl ether, and thus should be removable by a catalytic hydrogenation over Pd or by Birch reduction. Indeed, saponification of the benzoyl and acetyl esters of **9*S*** by treatment with NaOMe in methanol followed by removal of the benzyl ethers and the auxiliary by using sodium in liquid ammonia led to the clean formation of the deprotected compound **16** (Scheme 4).



Scheme 4. Deprotection of disaccharide **9*S***.

Although the glycosylations with **5*S*** led to disaccharides with high α-anomeric selectivity, the ultimate goal is the development of an auxiliary that gives only one of the two possible anomers in each glycosylation. The small amount of unwanted anomer that is formed probably results from glycosylation of the oxonium ion. In this respect, participation by an ethoxycarbonylbenzyl moiety is probably slower than that of a conventional acyl functionality because the formation of the six-membered ring is slower than that of the five-membered ring. Thus, it is expected that a second-generation auxiliary could be obtained by improving the nucleophilicity of the auxiliary or reducing the flexibility of the rotatable bonds.

In summary, it has been shown for the first time that the anomeric selectivity of a glycosylation can be controlled by a chiral auxiliary. This new method for anomeric control is particularly suited for the introduction of α-glucosides. However, it is expected that other glycosides can easily be installed by a similar approach. For example, the use of the readily available 1,6:2,3-dianhydro-β-D-talopyranoside[15] as the starting material, instead of epoxide **1**, would lead to a galactosyl donor. Furthermore, preliminary studies have shown that the methodology is also compatible with other protecting-group patterns. It is to be expected that a systematic optimization of the structure of the auxiliary will lead to a stereospecific glycosylation protocol. Only such a method will make it possible for the potential of polymer-supported[8–10] and one-pot multistep oligosaccharide[6,7] syntheses to be realized, so that these methods can be used in a routine manner for a large number of oligosaccharide targets.

Received: August 20, 2004
Published online: January 3, 2005

Keywords: anomeric control · carbohydrates · chiral auxiliaries · glycosides · glycosylation

[1] P. M. Rudd, T. Elliott, P. Cresswell, I. A. Wilson, R. A. Dwek, *Science* **2001**, *291*, 2370.
[2] A. Varki, *Glycobiology* **1993**, *3*, 97.
[3] R. A. Dwek, *Chem. Rev.* **1996**, *96*, 683.
[4] C. R. Bertozzi, L. L. Kiessling, *Science* **2001**, *291*, 2357.
[5] P. Sears, C. H. Wong, *Science* **2001**, *291*, 2344.
[6] K. M. Koeller, C. H. Wong, *Chem. Rev.* **2000**, *100*, 4465.
[7] N. L. Douglas, S. V. Ley, U. Lucking, S. L. Warriner, *J. Chem. Soc. Perkin Trans. 1* **1998**, 51.
[8] O. J. Plante, E. R. Palmacci, P. H. Seeberger, *Science* **2001**, *291*, 1523.
[9] P. H. Seeberger, W. C. Haase, *Chem. Rev.* **2000**, *100*, 4349.
[10] D. Kahne, *Curr. Opin. Chem. Biol.* **1997**, *1*, 130.
[11] G.-J. Boons, *Contemp. Org. Synth.* **1996**, *3*, 173.
[12] A. V. Demchenko, *Synlett* **2003**, 1225.
[13] J. Xue, Z. W. Guo, *Tetrahedron Lett.* **2001**, *42*, 6487.
[14] R. R. Schmidt, *Angew. Chem.* **1986**, *98*, 213; *Angew. Chem. Int. Ed. Engl.* **1986**, *25*, 212.
[15] N. R. Williams, *Adv. Carbohydr. Chem. Biochem.* **1970**, *25*, 109.

 © 2005 Wiley-VCH Verlag GmbH & Co. KGaA, Weinheim

Asymmetric Synthesis

Nucleophile-Catalyzed Asymmetric Acylations of Silyl Ketene Imines: Application to the Enantioselective Synthesis of Verapamil**

*Ara H. Mermerian and Gregory C. Fu**

Generating enantiomerically enriched nitriles in which the cyano group is bound to an all-carbon quaternary stereocenter (e.g. **1**) is an important challenge in synthetic organic chemistry and is owed in part to the biological activity of such compounds.[1] We have recently turned our attention to the development of catalytic asymmetric methods that address this challenge[2,3] by focusing on reactions of nitrile anions.[4] Such species are, of course, ambident nucleophiles that are capable of reacting at nitrogen centers to afford an N-substituted ketene imine or at carbon atoms to furnish a C-substituted nitrile [Eq. (1)].[5]

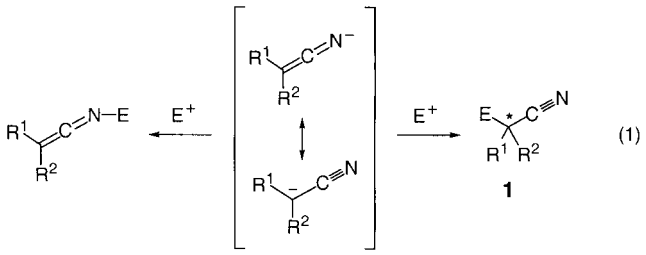
We recently described the application of a new dual-activation strategy to catalytic enantioselective intermolecu-

[*] A. H. Mermerian, Prof. Dr. G. C. Fu
Department of Chemistry
Massachusetts Institute of Technology
Cambridge, MA 02139 (USA)
Fax: (+1) 617-324-3611
E-mail: gcf@mit.edu

[**] Support has been provided by the National Institutes of Health (National Institute of General Medical Sciences: R01-GM57034; National Cancer Institute: training grant CA009112), Merck, and Novartis. Funding for the MIT Department of Chemistry Instrumentation Facility has been furnished in part by NSF CHE-9808061 and NSF DBI-9729592.

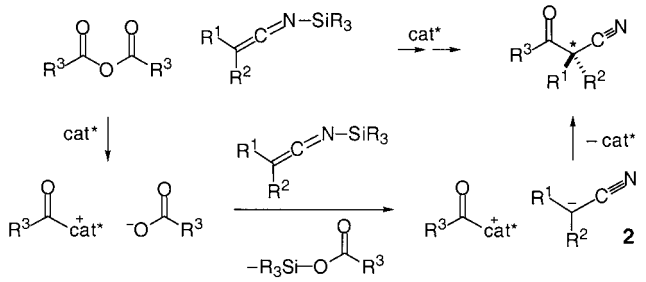
Supporting information for this article is available on the WWW under http://www.angewandte.org or from the author.

 DOI: 10.1002/anie.200461886 © 2005 Wiley-VCH Verlag GmbH & Co. KGaA, Weinheim



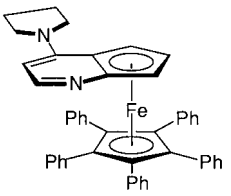
(1)

lar C acylations of silyl ketene acetals.[6] Naturally, we have been interested in determining if this approach is general and can be employed for reaction partners other than silyl ketene acetals. For example, we were intrigued by the possibility of synthesizing enantioenriched target molecules such as **1** through the treatment of silyl ketene imines with anhydrides[7] through the chiral-nucleophile-catalyzed pathway outlined in Scheme 1.



Scheme 1. Proposed pathway for a chiral-nucleophile-catalyzed asymmetric synthesis of all-carbon quaternary stereocenters through the acylation of silyl ketene imines.

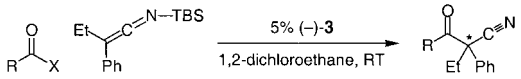
Silyl ketene imines are readily generated through the reaction of a nitrile with a Brønsted base and a silylating agent.[5] At room temperature in the absence of a catalyst, silyl ketene imines are essentially inert to a variety of acylating agents. However, in the presence of the chiral PPY (4-(pyrrolidino)pyridine) derivative **3**[8] (5%), they



undergo C acylation to furnish α-cyano carbonyl compounds (Table 1).[9] Reactions of cyanoformates or chloroformates proceed with low enantioselectivity (Table 1, entries 1 and 2, respectively), whereas acylations by anhydrides can lead to substantial values of *ee* (Table 1, entries 3 and 4). Very bulky anhydrides do not react at room temperature (Table 1, entry 5). To the best of our knowledge, these are the first examples of nucleophile-catalyzed reactions of silyl ketene imines.

With an interesting new catalytic and enantioselective C–C bond-forming process in hand, we turned our attention to the determination of the scope of the reaction. With respect to the alkyl substituent on the ketene imine, the acylations proceed with good *ee* values for a variety of groups (Table 2, entries 1–4), although the sterically demanding cyclopentyl-substituted compound reacts with somewhat diminished stereoselectivity (Table 2, entry 5).[10]

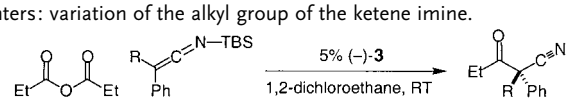
Table 1: Reaction of acylating agents with a silyl ketene imine in the presence of a chiral PPY derivative.



Entry	RCOX	*ee* [%][a]	Yield [%][a]
1	$MeO_2C(CN)$	< 5	81
2	$tBuCH_2O_2CCl$	7	61
3	Ac_2O	72	64
4	$(EtCO)_2O$	81	85
5	$(iPrCO)_2O$	–	< 5

[a] Average of two runs. TBS = *tert*-butyldimethylsilyl.

Table 2: Catalytic asymmetric synthesis of all-carbon quaternary stereocenters: variation of the alkyl group of the ketene imine.

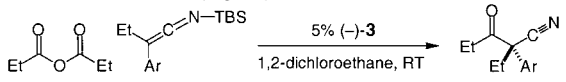


Entry	R	*ee* [%][a]	Yield [%][a]
1	Me	81	89
2	Et	81	85
3	CH_2CHMe_2	83	93
4	CH_2CMe_3	81	52
5	cyclopentyl	69	53

[a] Average of two runs.

We have also examined the scope of this process with respect to the aryl substituent on the ketene imine.[11] Increasing the electron-rich nature of the aromatic ring has no effect on the values of the *ee* (Table 3, entry 1 versus entry 2), whereas the introduction of an electron-withdrawing group leads to a loss in enantioselectivity (Table 3, entry 1 versus entry 3). Reactions of more-hindered aryl or heteroaryl (Table 3, entries 4 and 5) ketene imines furnish values for *ee* that are comparable to the phenyl-substituted substrate (Table 3, entry 1).

Table 3: Catalytic asymmetric synthesis of all-carbon quaternary stereocenters: variation of the aryl group of the ketene imine.

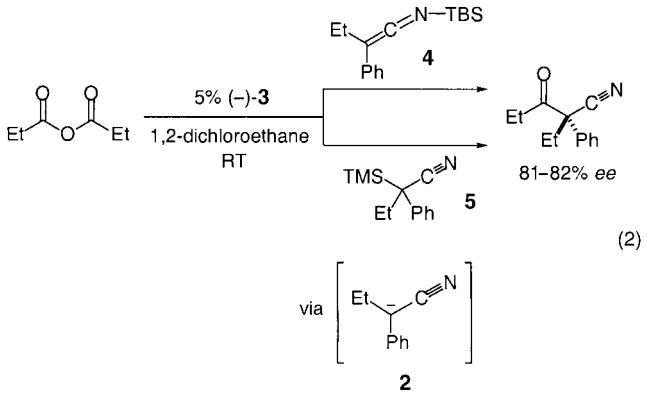


Entry	Ar	*ee* [%][a]	Yield [%][a]
1	Ph	81	85
2	4-$(MeO)C_6H_4$	81	65
3	4-$(F_3C)C_6H_4$	53	50
4	1-naphthyl	80	78
5	3-thienyl	77	72

[a] Average of two runs.

 © 2005 Wiley-VCH Verlag GmbH & Co. KGaA, Weinheim

In analogy with the chemistry of silyl ketene acetals,[6] we believe that these acylations of silyl ketene imines proceed through the pathway depicted in Scheme 1, wherein the carboxylate ion desilylates the imine to generate a nitrile anion **2** as the key reactive nucleophile.[12] On the basis of this mechanistic hypothesis, we predicted that **4** and **5** [Eq. (2),



(2)

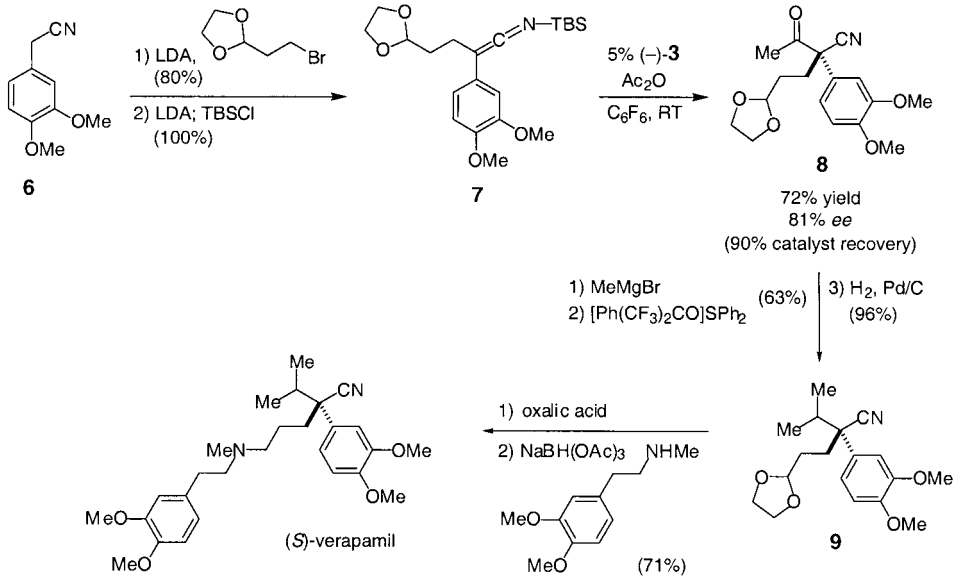
TMS = trimethylsilyl] should react with an anhydride in the presence of catalyst **3** to furnish the target α-cyano carbonyl compound with the same sense and level of enantioselectivity. As illustrated in Equation (2) this prediction has indeed been borne out experimentally and is consistent with a common intermediate, that is, a silicon-free nitrile anion **2**, for the two acylation processes.

To demonstrate the utility of our catalytic asymmetric method for the generation of cyano-substituted, all-carbon quaternary stereocenters, we applied the method to the enantioselective synthesis of the drug verapamil (Scheme 2), the enantiomers of which have significantly different biological activity.[1,13,14] Alkylation of nitrile **6** with 2-(2-bromoethyl)-1,3-dioxolane, both of which are commercially available, followed by formation of the silyl ketene imine, furnishes **7** in 80% yield (over two steps). Asymmetric C acylation catalyzed by (–)-**3** generates **8**, which bears the target quaternary stereocenter, in 81% *ee*.[15] A two-step olefination reaction followed by a hydrogenation reaction affords intermediate **9**. The aldehyde is deprotected and then subjected to reductive amination, which provides (*S*)-verapamil in 25% overall yield from **6**.

In conclusion, we have described a new nucleophile-catalyzed reaction, the acylation of silyl ketene imines, and we have established that it can produce all-carbon quaternary stereocenters with good enantioselectivity. Our mechanistic data are consistent with a dual-activation pathway in which a nitrile anion intermediate undergoes asymmetric acylation. We have applied our method to the first catalytic asymmetric synthesis of the drug verapamil.[16] Ongoing studies are directed at providing further evidence for the generality of this dual-activation strategy in asymmetric catalysis.

Received: September 3, 2004
Published online: January 3, 2005

Keywords: acylation · asymmetric synthesis · cyanides · homogeneous catalysis · total synthesis



Scheme 2. Catalytic asymmetric synthesis of (*S*)-verapamil. LDA = lithium diisopropylamide.

[1] As an example, the drug verapamil, which is the oldest known calcium-channel blocker, belongs to this category. For reviews of verapamil, see: a) L. M. Prisant, *Heart Dis.* **2001**, *3*, 55–62; b) R. N. Brogden, P. Benfield, *Drugs* **1996**, *51*, 792–819.

[2] As noted in a recent review, "only a few catalytic asymmetric C–C bond-forming reactions have been shown to be useful for constructing all-carbon quaternary stereocenters." See: C. J. Douglas, L. E. Overman, *Proc. Natl. Acad. Sci. USA* **2004**, *101*, 5363–5367.

[3] For examples of catalytic asymmetric methods for the synthesis of cyano-substituted, all-carbon quaternary stereocenters, see:

 © 2005 Wiley-VCH Verlag GmbH & Co. KGaA, Weinheim

a) M. Sawamura, H. Hamashima, Y. Ito, *J. Am. Chem. Soc.* **1992**, *114*, 8295 – 8296; b) M. S. Taylor, E. N. Jacobsen, *J. Am. Chem. Soc.* **2003**, *125*, 11 204 – 11 205.

[4] a) For a review of cyclization reactions of nitrile anions, see: F. F. Fleming, B. C. Shook, *Tetrahedron* **2002**, *58*, 1 – 23; b) For a recent example of a catalytic asymmetric acylation process that involves a nitrile anion intermediate, see: D. A. Nicewicz, C. M. Yates, J. S. Johnson, *Angew. Chem.* **2004**, *116*, 2706 – 2709; *Angew. Chem. Int. Ed.* **2004**, *43*, 2652 – 2655.

[5] For early studies of the silylation of nitrile anions, see: a) G. A. Gornowicz, R. West, *J. Am. Chem. Soc.* **1971**, *93*, 1714 – 1720; b) D. S. Watt, *Synth. Commun.* **1974**, *4*, 127 – 132.

[6] A. H. Mermerian, G. C. Fu, *J. Am. Chem. Soc.* **2003**, *125*, 4050 – 4051.

[7] We are aware of very few studies of reactions of silyl ketene imines with electrophiles. See: a) P. Cazeau, J.-P. Llonch, F. Simonin-Dabescat, E. Frainnet, *J. Organomet. Chem.* **1976**, *105*, 145 – 156; b) P. Cazeau, J.-P. Llonch, F. Simonin-Dabescat, E. Frainnet, *J. Organomet. Chem.* **1976**, *105*, 157 – 160; c) S. Meier, E.-U. Würthwein, *Chem. Ber.* **1990**, *123*, 2339 – 2347.

[8] For leading references, see: G. C. Fu, *Acc. Chem. Res.* **2004**, *37*, 542 – 547.

[9] For a few examples of total syntheses that employ such α-cyano carbonyl compounds (wherein the α position is an all-carbon quaternary stereocenter) as intermediates, see: a) F. E. Ziegler, C. A. Metcalf III, A. Nangia, G. Schulte, *J. Am. Chem. Soc.* **1993**, *115*, 2581 – 2589; b) D. G. Batt, N. Takamura, B. Ganem, *J. Am. Chem. Soc.* **1984**, *106*, 3353 – 3354; c) R. V. Stevens, F. C. A. Gaeta, D. S. Lawrence, *J. Am. Chem. Soc.* **1983**, *105*, 7713 – 7719; d) R. M. Coates, S. K. Shah, R. W. Mason, *J. Am. Chem. Soc.* **1982**, *104*, 2198 – 2208.

[10] Notes: a) Solvents such as Et_2O, CH_2Cl_2, and toluene furnish 5–10% lower *ee* values; b) A decrease in reaction temperature results in a decrease in enantioselectivity; c) After an extended reaction time, the *ee* value of the product is unchanged, which is consistent with irreversible C–C bond formation.

[11] If both substituents on the silyl ketene imine are alkyl groups, no acylation is observed under our standard conditions. We believe that the key reactive intermediate in processes catalyzed by **3** is a nitrile anion (intermediate **2** in Scheme 1), the formation of which is facilitated by the presence of an anion-stabilizing aromatic substituent on the silyl ketene imine.

[12] For recent discussions of acylation reactions of nitrile anions, see: a) F. F. Fleming, Z. Zhang, P. Knochel, *Org. Lett.* **2004**, *6*, 501 – 503; b) A. R. Katritzky, A. A. A. Abdel-Fattah, M. Wang, *J. Org. Chem.* **2003**, *68*, 4932 – 4934.

[13] a) J. A. Longstreth in *Clinical Pharmacology*, Dekker, New York, **1993**, pp. 315 – 336; b) *The Merck Index*, *13th ed.*, Merck, Whitehouse Station, **2001**, pp. 1771 – 1772.

[14] For leading references regarding the synthesis of nonracemic verapamil, see: R. M. Bannister, M. H. Brookes, G. R. Evans, R. B. Katz, N. D. Tyrrell, *Org. Process Res. Dev.* **2000**, *4*, 467 – 472.

[15] Use of C_6F_6 rather than 1,2-dichloroethane as the solvent leads to improved enantioselectivity. This solvent effect on *ee* values appears to be general. For example, for the reaction illustrated in entry 1 of Table 2, the product is generated in 90% *ee* when C_6F_6 is employed as the solvent.

[16] Brunner reported a method that furnishes a precursor to verapamil in up to 11% *ee*: H. Brunner, H. Zintl, *Monatsh. Chem.* **1991**, *122*, 841 – 848.

 © 2005 Wiley-VCH Verlag GmbH & Co. KGaA, Weinheim

Oxidation Reagents

Clean and Highly Selective Oxidation of Alcohols in an Ionic Liquid by Using an Ion-Supported Hypervalent Iodine(III) Reagent

*Weixing Qian, Erlei Jin, Weiliang Bao, and Yongmin Zhang**

The oxidation of alcohols to carbonyl compounds plays an important role in organic synthesis, not only in the laboratory but also at the industrial level. Numerous methods are available to accomplish this conversion under various reaction conditions.[1] The demands in recent years for environmentally benign and eco-conscious chemical processes are encouraging chemists to search for clean, high-yielding, highly selective, and economical oxidation methods.[2] In the last decade, in particular, there has been increasing interest in the oxidizing properties of organohypervalent iodine reagents.[3] The extensively studied pentavalent iodine reagents, for example, Dess–Martin periodane (DMP)[4] and its direct precursor *o*-iodoxybenzoic acid (IBX),[5] oxidize alcohols efficiently to carbonyl compounds in organic solvents such as DMSO, CH_2Cl_2, and acetone. Despite their utility and popularity, these iodine(v) oxidants are potentially explosive.[2e] Thus, the readily available and stable iodine(III) oxidants such as iodosobenzene PhIO and diacetoxyiodobenzene $PhI(OAc)_2$ attract much attention. An effective and convenient polymer-supported $PhI(OAc)_2$ reagent was demonstrated by Tohma et al. for the oxidation of alcohols in aqueous media with a potassium bromide catalyst, but primary alcohols were further oxidized to carboxylic acids.[2e] Adam et al. employed Cr^{III}–salen complexes (salen = *N*,*N*′-bis[(2-hydroxyphenyl)methylene]-1,2-ethanediimine) for the selective catalytic oxidation of allylic alcohols to enones by PhIO and $PhI(OAc)_2$ in dichloromethane.[6] However, in view of the carcinogenicity of chromium compounds, environmental and health concerns greatly limit their use. Although the dehydrogenating properties of PhIO and $PhI(OAc)_2$ have been demonstrated in a few cases, only a limited number of clean and selective catalytic oxidations of alcohols to carbonyl compounds have been reported.[7]

Recently, much attention has been focused on the use of ionic liquids as environmentally benign reaction media. Various chemical reactions can be performed in ionic liquids.[8] This fact is attributed to some intriguing properties of ionic liquids, such as high thermal stability, negligible vapor pressure, high loading capacity, and tunable polarity. In view of these distinct advantages, ionic liquids have become an

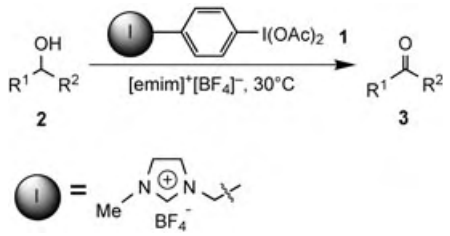
[*] Prof. W. Qian, E. Jin, Prof. W. Bao, Prof. Y. Zhang
Department of Chemistry
Zhejiang University, Xi Xi Campus
Hangzhou, Zhejiang 310028 (P. R. China)
Fax: (+86) 571-8880-7077
E-mail: yminzhang@mail.hz.zj.cn

Supporting information for this article is available on the WWW under http://www.angewandte.org or from the author.

 © 2005 Wiley-VCH Verlag GmbH & Co. KGaA, Weinheim DOI: 10.1002/anie.200461889

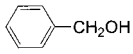
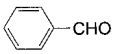
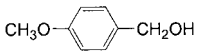
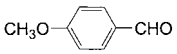
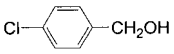
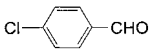
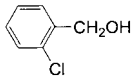
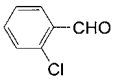
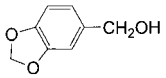
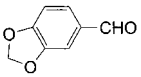
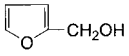
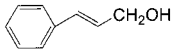
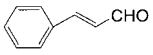
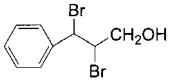
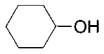
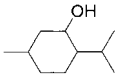
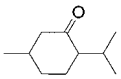
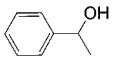
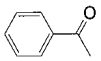
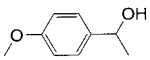
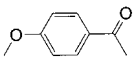
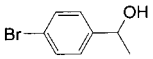
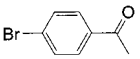
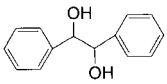
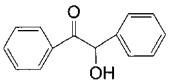
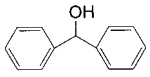
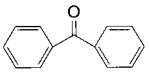
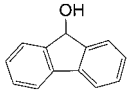
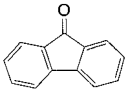
exciting area of research. More recently, ionic liquid formulations have been expanded to include ions with structurally and functionally complex side chains—the so-called "task-specific ionic liquids".[9] Miao and Chan employed ionic liquids as soluble supports for a Suzuki coupling reaction.[10] In comparison with traditional polymer supports or soluble polyethylene glycol (PEG), which has some limitations in loading capacity and solubility,[11] these low-molecular-weight ionic liquids have larger loading capacity and tunable solubility. Herein we report the preparation of 1-(4-diacetoxyiodobenzyl)-3-methylimidazolium tetrafluoroborate ([dibmim]$^+$[BF_4]$^-$; **1**) and its application in the oxidation of alcohols.

Compound **1** was readily synthesized by reaction of 1-methylimidazole with 4-bromomethyliodobenzene and then oxidation with peracetic acid (30% H_2O_2 and acetic anhydride). The oxidation of alcohols using [dibmim]$^+$[BF_4]$^-$ as an oxidant was conducted in the ionic liquid [emim]$^+$[BF_4]$^-$ (1-ethyl-3-methylimidazolium tetrafluoroborate; Scheme 1) in the presence of a low concentration of bromide ions under mild conditions (30 °C, a 1:1.4 ratio of substrate **2**:oxidant **1**; (Table 1).



Scheme 1. Selective oxidation by [dibmim]$^+$[BF_4]$^-$ (**1**) in [emim]$^+$[BF_4]$^-$ of alcohol substrates (**2**) to give carbonyl compounds (**3**).

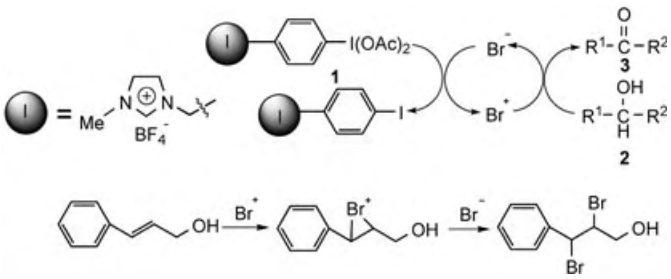
Table 1: Oxidation of alcohols with [dibmim]$^+$[BF_4]$^-$ in [emim]$^+$[BF_4]$^-$.

Entry	Substrate		Product		t [h]	Yield [%][a]
1		**2a**		**3a**	3	92[b]
2		**2b**		**3b**	3	95
3		**2c**		**3c**	3	91
4		**2d**		**3d**	3	89
5		**2e**		**3e**	3	57
6		**2f**		**3f**	3	94[b]
7		**2g**		**3g**	4	< 5
				**3g′**		93
8		**2h**		**3h**	16	95
9		**2i**		**3i**	18	75[c]
10		**2j**		**3j**	4	90[b]
11		**2k**		**3k**	5	94
12		**2l**		**3l**	5	96
13		**2m**		**3m**	2	93
14		**2n**		**3n**	9	98[c]
15		**2o**		**3o**	12	98[c]

[a] Yields of isolated product after chromatographic purification unless otherwise noted. [b] Yields were determined by ^{1}H NMR spectrometry. [c] Ten drops of acetonitrile were added to increase the solubility of substrates.

 © 2005 Wiley-VCH Verlag GmbH & Co. KGaA, Weinheim

A variety of primary and secondary alcohols were oxidized to carbonyl compounds in moderate to excellent yields at room temperature. The reactions were performed in a flask without any particular precautions. Under these conditions primary alcohols (Table 1, entries 1–6) were oxidized in less than four hours to the corresponding aldehydes in 57–95% yields without any noticeable overoxidation to the carboxylic acids. Secondary alcohols (Table 1, entries 8–15) were oxidized to the corresponding ketones over longer reaction times except for entry 13. The oxidation was relatively sluggish (16–18 h) and needed two equivalents of oxidant for the unactivated, alicyclic substrates (Table 1, entries 8 and 9). Notably, cinnamyl alcohol (Table 1, entry 7) was mainly converted into the double-bond addition product. It has been suggested that the oxidation of alcohols is catalyzed by a small amount of bromide ion remaining in the $[emim]^+[BF_4]^-$.[12] A possible mechanism for the oxidation of alcohols with $[dibmim]^+[BF_4]^-$ is described in Scheme 2. The



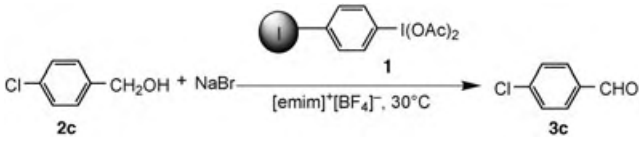
Scheme 2. A possible mechanism for the oxidation of substrates by $[dibmim]^+[BF_4]^-$.

bromide ion present in the $[emim]^+[BF_4]^-$ seems to be oxidized by $[dibmim]^+[BF_4]^-$ to form a highly active intermediate Br^+ ion, probably in the form of acetyl hypobromite or the bromate(I) complex reported by Kirschning and coworkers,[13] which reacts with alcohols to produce the corresponding carbonyl compounds with regeneration of the bromide ion.[14] The Br^+ ion attacks a C=C bond of a substrate preferentially, so the main product from the oxidation of cinnamyl alcohol is 2,3-dibromo-3-phenylpropanol.

The ionic liquid $[emim]^+[BF_4]^-$ used in the above reactions was prepared by the metathesis of 1-ethyl-3-methylimidazolium bromide with sodium tetrafluoroborate in acetone. However, this method did not remove the bromide ion completely if no further purification procedure was applied. Although the oxidation reaction proceeded in high yield, we were concerned about whether the change in concentration of the bromide ion would lead to overoxidation. Therefore, we investigated the influence of bromide ion concentration on the oxidation result. First, the concentration of bromide ion in $[emim]^+[BF_4]^-$ was measured by Volhard's procedure (Table 2, entry 2) to be 1.82–1.94% (w/w). The ionic liquid $[emim]^+[BF_4]^-$ was then thoroughly purified through method B reported by Park and Kazlauskas.[12] In the following experiment sodium bromide was taken as the source of the bromide ion.

The oxidation of 4-chlorobenzyl alcohol (**2c**) was examined as a standard substrate while varying the bromide ion concentration from 0 to 10% (w/w). The reaction was performed in a mixture of purified ionic liquid $[emim]^+[BF_4]^-$ (1.50 g), alcohol (0.5 mmol), and oxidant (0.7 mmol). We were pleased to find that alcohol **2c** was oxidized to aldehyde **3c** in 72–93% yield (Table 2). A low

Table 2: The influence of the bromide ion concentration on oxidation.



Entry	Conc. of Br^- [% (w/w)]	*t* [h]	Yield [%]
1	0.0	24	84
2	ca. 1.9	3	91
3	0.5	3	72
4	1.0	3	92
5	2.0	3	93
6	5.0	3	91
7	10.0	3	83

concentration of bromide ions (Table 2, entry 3, 0.5%) was unfavorable since it slowed down the reaction rate; the reaction was very slow in the absence of bromide ions (Table 2, entry 1). However, when 10% of bromide ion (equal to 0.193 g NaBr) was added to 1.50 g of purified $[emim]^+[BF_4]^-$, the solid could not dissolve in the ionic liquid completely, which made the solution too thick to stir efficiently and resulted in a decreased yield. No further oxidation of 4-chlorobenzaldehyde to the corresponding carboxylic acid was observed even after the reaction times were prolonged to 24 hours. We think that in this system the ionic liquid $[emim]^+[BF_4]^-$ plays a very important role in preventing aldehydes from overoxidation to carboxylic acids.[15]

To evaluate the performance of $[dibmim]^+[BF_4]^-$ we compared it with the widely used oxidant $PhI(OAc)_2$ in $[emim]^+[BF_4]^-$. The results (Table 3) show that the yields of alcohols using $[dibmim]^+[BF_4]^-$ are higher than those with $PhI(OAc)_2$ in the same reaction time. For the primary alcohols (Table 3, entries 1 and 2) with $PhI(OAc)_2$ as the oxidant, an electron-donating group on the aryl ring gives satisfactory yields, but an electron-withdrawing group greatly decreases the yields. Poor yields are obtained in the oxidation of secondary alcohols, which means not only electronic effects

Table 3: Comparison of $[dibmim]^+[BF_4]^-$ with $PhI(OAc)_2$ in $[emim]^+[BF_4]^-$.

Entry	Substrate	Product	*t* [h]	Yield with $PhI(OAc)_2$ [%]	Yield with $[dibmim]^+[BF_4]^-$ [%]
1	**2b**	**3b**	3	73	95
2	**2c**	**3c**	3	37	91
3	**2k**	**3k**	5	32	94
4	**2l**	**3l**	5	22	96
5	**2n**	**3n**	9	11[a]	98[a]

[a] Ten drops of acetonitrile were added to increase the solubility of the substrates.

 © 2005 Wiley-VCH Verlag GmbH & Co. KGaA, Weinheim

(Table 3, entries 3 and 4) but also steric effects (Table 3, entry 5) significantly influence the reaction. However, both primary and secondary alcohols with electron-donating or -withdrawing groups give excellent yields with [dibmim]$^+$[BF_4]$^-$ as the oxidant. Pausacker measured the oxidation rates of isohydrobenzoin by aryl iodosoacetates in acetic acid and found that electron-donating groups present in the aryl moiety decrease the reaction rate, but electron-withdrawing groups increase the rate.[16] The imidazolium cation will act as an electron-withdrawing group in the [dibmim]$^+$[BF_4]$^-$ oxidant, and hence greatly enhance the reaction rate. Therefore, higher yields can be obtained in a shorter reaction time.

In conclusion, we have demonstrated that the dehydrogenating properties of [dibmim]$^+$[BF_4]$^-$ can be used for the oxidation of alcohols to carbonyl compounds. The main features of this process are: 1) a high degree of selectivity for the oxidation of primary alcohols to carbonyl compounds in an ionic liquid; 2) easy workup and environmentally benign—the ion-supported hypervalent iodine(III) reagent can be recovered and reused after oxidation with peracetic acid; and 3) notably, the aldehydes do not undergo further oxidation to carboxylic acids even at longer reaction times. Studies on applications of [dibmim]$^+$[BF_4]$^-$ in other reactions are in progress.

Received: September 3, 2004
Published online: January 3, 2005

Keywords: alcohols · hypervalent compounds · iodine · ionic liquids · oxidation

[1] a) J. Muzart, *Chem. Rev.* **1992**, *92*, 113 – 140; b) R. C. Larock, *Comprehensive Organic Transformations*, *2nd ed.*, Wiley, New York, **1999**; c) V. R. Choudhary, P. A. Chaudhari, V. S. Narkhede, *Catal. Commun.* **2003**, *4*, 171 – 175.

[2] a) I. E. Marko, P. R. Giles, M. Tsukazaki, S. M. Brown, C. J. Urch, *Science* **1996**, *274*, 2044 – 2046; b) K. Sato, M. Aoki, J. Takagi, R. Noyori, *J. Am. Chem. Soc.* **1997**, *119*, 12386 – 12387; c) I. E. Marko, M. Tsukazaki, P. R. Giles, S. M. Brown, C. J. Urch, *Angew. Chem.* **1997**, *109*, 2297 – 2299; *Angew. Chem. Int. Ed. Engl.* **1997**, *36*, 2208 – 2210; d) M. Zhao, J. Li, E. Mano, Z. Song, D. M. Tschaen, E. J. J. Grabowski, P. J. Reider, *J. Org. Chem.* **1999**, *64*, 2564 – 2566; e) H. Tohma, S. Takizawa, T. Maegawa, Y. Kita, *Angew. Chem.* **2000**, *112*, 1362 – 1364; *Angew. Chem. Int. Ed.* **2000**, *39*, 1306 – 1308; f) S. Velusamy, T. Punniyamurthy, *Org. Lett.* **2004**, *6*, 217 – 219; g) B. Z. Zhan, M. A. White, T. K. Sham, J. A. Pincock, R. J. Doucet, K. V. Ramana Rao, K. N. Robertson, T. S. Cameron, *J. Am. Chem. Soc.* **2003**, *125*, 2195 – 2199.

[3] a) P. J. Stang, V. V. Zhdankin, *Chem. Rev.* **1996**, *96*, 1123 – 1178; b) A. Varvoglis, *Hypervalent Iodine in Organic Synthesis*, Academic Press, London, **1997**; c) T. Wirth, U. H. Hirt, *Synthesis* **1999**, 1271 – 1287; d) R. M. Moriarty, O. Prakash, *Org. React.* **1999**, *54*, 273 – 418; e) V. V. Zhdankin, P. J. Stang, *Chem. Rev.* **2002**, *102*, 2523 – 2584.

[4] a) D. B. Dess, J. C. Martin, *J. Org. Chem.* **1983**, *48*, 4155 – 4156; b) D. B. Dess, J. C. Martin, *J. Am. Chem. Soc.* **1991**, *113*, 7277 – 7287; c) S. D. Meyer, S. L. Schreiber, *J. Org. Chem.* **1994**, *59*, 7549 – 7552.

[5] a) M. Frigerio, M. Santagostino, S. Sputore, G. Palmisano, *J. Org. Chem.* **1995**, *60*, 7272 – 7276; b) E. J. Corey, A. Palani, *Tetrahedron Lett.* **1995**, *36*, 3485 – 3488.

[6] a) W. Adam, F. G. Gelalcha, C. R. Saha-Moller, V. R. Stegmann, *J. Org. Chem.* **2000**, *65*, 1915 – 1918; b) W. Adam, S. Hajra, M. Herderich, C. R. Saha-Moller, *Org. Lett.* **2000**, *2*, 2773 – 2776.

[7] a) A. De Mico, R. Margarita, L. Parlanti, A. Vescovi, G. Piancatelli, *J. Org. Chem.* **1997**, *62*, 6974 – 6977; b) R. S. Varma, R. Dahiya, R. K. Saini, *Tetrahedron Lett.* **1997**, *38*, 7029 – 7032.

[8] a) T. Welton, *Chem. Rev.* **1999**, *99*, 2071 – 2084; b) P. Wasserscheid, W. Keim, *Angew. Chem.* **2000**, *112*, 3926 – 3945; *Angew. Chem. Int. Ed.* **2000**, *39*, 3772 – 3789; c) J. S. Wilkes, *Green Chem.* **2002**, *4*, 73 – 80; d) P. Wasserscheid, T. Welton, *Ionic Liquids in Synthesis*, Wiley-VCH, Weinheim, **2003**; e) M. J. Earle, S. P. Katdare, K. R. Seddon, *Org. Lett.* **2004**, *6*, 707 – 710.

[9] a) A. E. Visser, R. P. Swatloski, W. M. Reicher, R. Mayton, S. Sheff, A. Wierzbicki, J. H. Davis, R. D. Rogers, *Chem. Commun.* **2001**, 135 – 136; b) E. D. Bates, R. D. Mayton, I. Ntai, J. H. Davis, Jr., *J. Am. Chem. Soc.* **2002**, *124*, 926 – 927.

[10] W. Miao, T. H. Chan, *Org. Lett.* **2003**, *5*, 5003 – 5005.

[11] a) S. V. Ley, A. W. Thomas, H. Finch, *J. Chem. Soc. Perkin Trans. 1* **1999**, 667 – 671; b) W. Miao, T. H. Chan, *Org. Lett.* **2003**, *5*, 5003 – 5005.

[12] S. Park, R. J. Kazlauskas, *J. Org. Chem.* **2001**, *66*, 8395 – 8401.

[13] a) H. Monenschein, G. Sourkouni-Argirusi, K. M. Schubothe, T. O'Hare, A. Kirschning, *Org. Lett.* **1999**, *1*, 2101 – 2104; b) A. Kirschning, *Eur. J. Org. Chem.* **1998**, 2267 – 2274.

[14] Many reports about the oxidation of organic compounds by hypohalite salts or halogens have been published: a) A. R. Katritzky, O. Meth-Cohn, C. W. Rees in *Comprehensive Organic Functional Group Transformations*, *Vol. 5*, Pergamon, New York, **1995**; b) R. C. Larock, *Comprehensive Organic Transformations*, Wiley, New York, **1999**; c) J. Palou, *Chem. Soc. Rev.* **1994**, *23*, 357 – 361; d) P. L. Anelli, C. B. Fernando, S. Quici, *J. Org. Chem.* **1987**, *52*, 2559 – 2562; e) J. Yoshida, R. Nakai, N. Kawabata, *J. Org. Chem.* **1980**, *45*, 5269 – 5273; f) D. Pletcher, N. Tomov, *J. Appl. Electrochem.* **1977**, *7*, 501 – 504; g) T. Shono, Y. Matsumura, J. Hayashi, M. Mizoguchi, *Tetrahedron Lett.* **1979**, *20*, 165 – 168, and references therein.

[15] K. R. Seddon, A. Stark, *Green Chem.* **2002**, *4*, 119 – 123.

[16] K. H. Pausacker, *J. Chem. Soc.* **1953**, 107 – 109.

 © 2005 Wiley-VCH Verlag GmbH & Co. KGaA, Weinheim

Supramolecular Polymers

Stretching and Rupturing Individual Supramolecular Polymer Chains by AFM**

Shan Zou, Holger Schönherr, and G. Julius Vancso**

Dedicated to Professor Helmut Ringsdorf on the occasion of his 75th birthday

Inspired by nature, supramolecular chemistry utilizes multiple, reversible cooperative intermolecular interactions, such as hydrogen bonding, to fabricate self-organized structures with a very rich structural hierarchy.[1] The corresponding intermolecular interactions (forces)[2] govern the interplay of order and mobility,[3] as well as the properties and functionality (recognition, reaction, transport, regulation etc.) in such systems.[3,4]

In recent years, supramolecular polymers[5,6] (also called reversible polymers) comprised of bifunctional monomeric units that are reversibly aggregated through relatively strong noncovalent interactions were described.[6–9] A prime example are the supramolecular polymers formed through self-complementary recognition of the quadruple hydrogen-bonded 2-ureido-4[1H]-pyrimidinone (UPy) motif, introduced by Sijbesma, Meijer et al.[6,10,11] Owing to the highly dynamic character of the aggregation, these materials show a truly unique combination of tunable properties, such as viscosity, composition, or effective chain length on one hand, and short equilibration times on the other hand.[6] Even though these properties are a direct consequence of the presence of multiple weak interactions, typically the equilibrium complexation constants and complex lifetimes serve as measures for the strength of the interactions.[12] Recently, theoretical work by van der Gucht et al.[13] shed some light on the forces between surfaces in the presence of reversible polymers. From an experimental point of view, however, little is known about the actual underlying inter- and intramolecular forces.[14]

AFM-based single-molecule force spectroscopy (SMFS)[15–18] appears to be suitable to address interaction forces and to directly probe individual supramolecular polymer chains. As illustrated in Scheme 1, such experiments involve the probing of a dynamic "macromolecule" that comprises reversibly aggregated self-complementary building blocks. As we will show herein, the interactions between individual surface-immobilized UPys[19] and the stretching of reversible supramolecular polymer chains were probed in AFM force-displacement (fd) measurements in hexadecane (HD) and DMSO/propan-2-ol mixtures. Our results open the pathway to elucidate the properties of these dynamic, reversibly aggregated polymers as a function of various external parameters on the molecular scale.

The systematic investigation of the single-chain mechanical properties of supramolecular UPy polymers was based on the measurement of the individual molecular interactions present in these supramolecular polymers. For this purpose, we first prepared the monolayer architecture **3** on Au(111), which comprised surface-immobilized ω-hydroxy PEG chains, by coupling UPy isocyanate **2** to the terminal alcohol functionalities of a layer of **1** (Scheme 1).[20] Similar to **5**,[19] this architecture ensures that the UPy units are available for complexation in a solution-like environment, as indicated by differential pulse voltammetry experiments with the ferrocenyl-labeled UPy derivative **6** (see Supporting Information). Layers of **3** thus expose chemically accessible UPy units tethered by PEG spacers to gold surfaces. As the mechanical properties of these spacers are known,[21] we can identify and verify the stretching of single macromolecules in SMFS measurements.

Force displacement curves were measured in HD between **3**, which was immobilized on Au(111), and AFM tips that were functionalized with **5**. The data were converted into force–extension curves and fitted with the m-FJC model (Figure 1; see also the Experimental Section, Equation (1)). The observed stretching is attributed to the stretching of the PEG segment of **3**. The Kuhn length of PEG was found to be 0.65 ± 0.08 nm and the segment elasticity is 6.2 ± 0.6 nN nm^{-1}. These fit parameters agree well with reported data[21] and thus confirm the successful stretching of single PEG chains. The observed extensions agree favorably with the contour length of the linker ($\approx 12 \pm 3$ nm; PEG chain is 9.5 ± 1.0 nm). As single PEG chains are stretched, the rupture forces of a single UPy–UPy complex can be directly determined as 180 ± 21 pN in HD ($T = 301$ K, loading rate: 35 nN s^{-1}, see also Supporting Information).

To probe the single-chain mechanical properties of UPy-based supramolecular polymers, AFM measurements were carried out with tips and substrates that were both modified with the short-chain UPy disulfide **5** in the presence of bis(UPy) **4** in HD (10^{-3} mM). Owing to the high complexation constant of $\geq 10^9$ M^{-1} and a complex lifetime greater than 1 s,[11b,12] bis(UPy) forms supramolecular polymers with an effective degree of polymerization of approximately 40 in solution.[22] Figure 2 shows a typical force–extension curve measured under these experimental conditions.

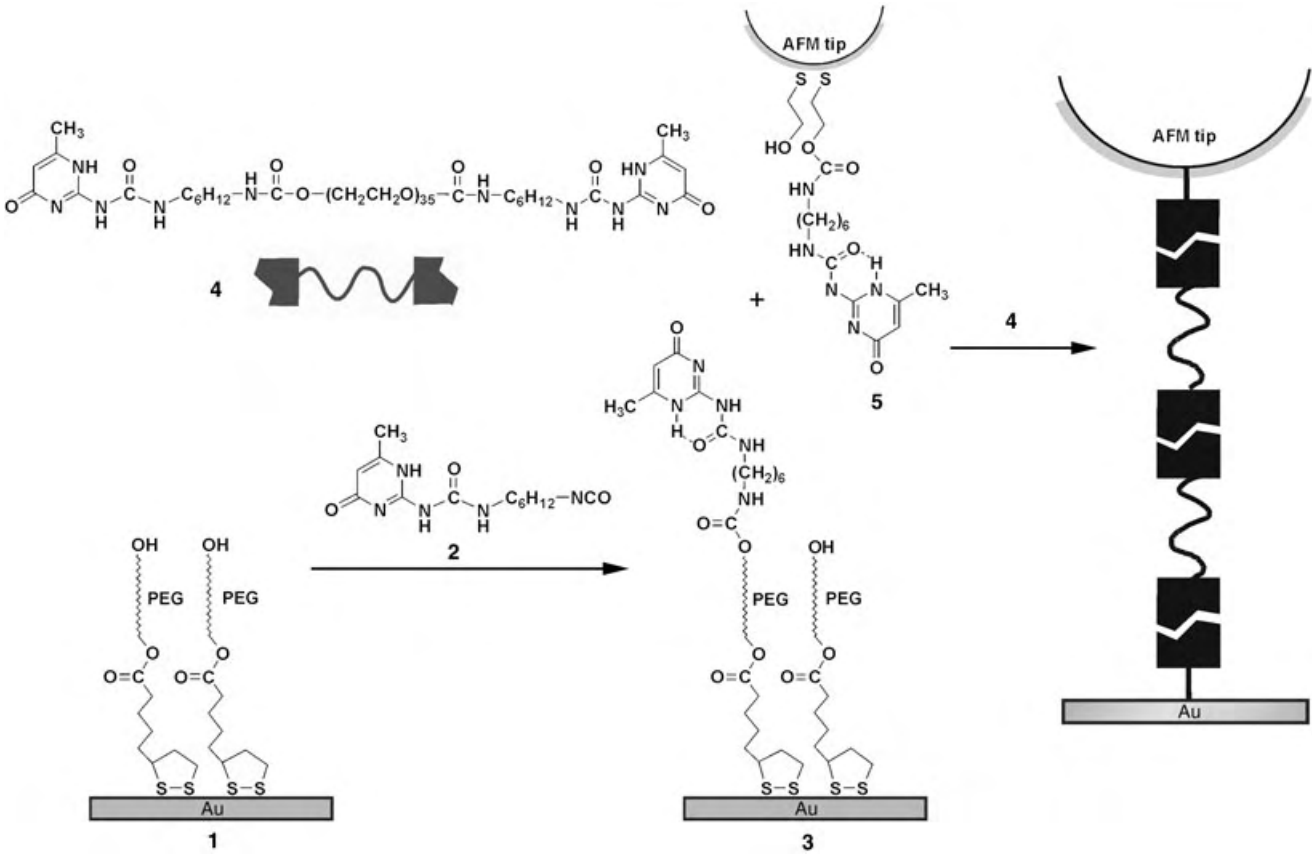
A significant restoring force is observed only for extensions greater than 50 nm. Fits to Equation (1) yielded values for the Kuhn length of 0.68 ± 0.08 nm and a segment elasticity of 7.6 ± 2.5 nN nm^{-1}. The elasticity parameters are within the error margins for the data measured for a single PEG chain

[*] S. Zou, Dr. H. Schönherr, Prof. Dr. G. J. Vancso
University of Twente
MESA+ Institute for Nanotechnology and Faculty of Science and Technology
Materials Science and Technology of Polymers
P. O. Box 217, 7500 AE Enschede (The Netherlands)
Fax: (+31) 53-489-3823
E-mail: h.schonherr@utwente.nl
g.j.vancso@utwente.nl

[**] This work was supported by the MESA+ Institute for Nanotechnology (MESA+ Strategic Research Orientation Nanolink) of the University of Twente. The authors thank Dr. W. K. den Otter for the discussion on modeling of the degree of polymerization in solution and are indebted to Dr. Phil Williams for enlightening discussions.

Supporting information for this article is available on the WWW under http://www.angewandte.org or from the author.

 © 2005 Wiley-VCH Verlag GmbH & Co. KGaA, Weinheim DOI: 10.1002/anie.200460963



Scheme 1. Molecular thin layers of ω-hydroxy-terminated PEG are obtained by self-assembly of disulfide **1** from solution in chloroform onto Au(111) surfaces, followed by reaction with isocyanate **2** to form a layer **3** that exposes UPy moieties. Supramolecular polymers, which are formed by self-complementary association of the telechelic PEG derivative **4** in hexadecane solution, can be probed by AFM (right) by utilizing gold-coated AFM tips that are functionalized with a self-assembled monolayer of the asymmetrically substituted UPy disulfide **5** in hexadecane.

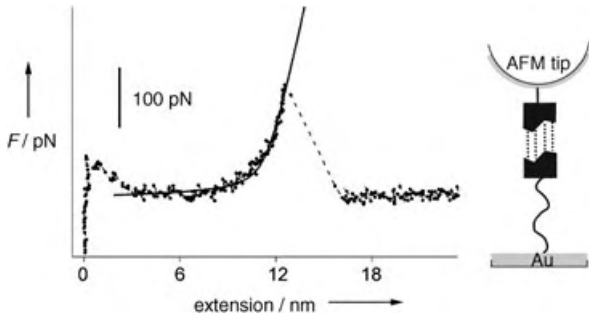


Figure 1. Force–extension curve measured between a gold-coated AFM tip, which is functionalized with a SAM of UPy disulfide **5**, and a Au(111) sample that is functionalized with a layer of **3** in hexadecane. The fit of the data to the m-FJC model is shown as a solid line.

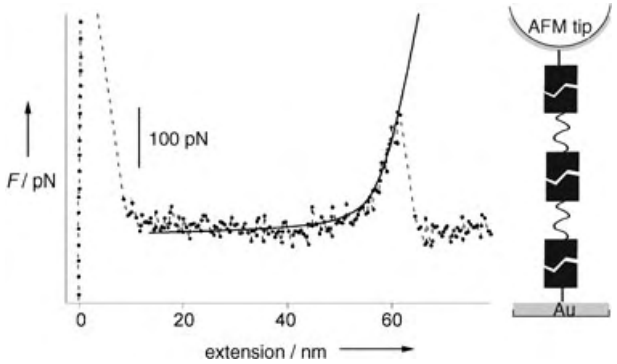


Figure 2. Force–extension curve measured between a gold-coated AFM tip and a Au(111) sample that are both functionalized with layers of **5** in the presence of the bifunctional bis(UPy) derivative **4** in hexadecane. The fit of the data to the m-FJC model is shown as a solid line.

which thus indicates that also in the current experiment a single PEG "chain" is being stretched. The significantly longer stretching length (≫ contour length of a single PEG segment) indicates that indeed supramolecular polymers were stretched, which appears to be reasonable if the lifetimes of UPy complexes in HD are considered. By contrast, fd curves recorded in 15% DMSO in propan-2-ol showed a markedly different stretching length distribution. In this case, only very short chains were stretched, in a similar fashion to the data observed for the dimer experiment in HD. A very similar reduction in stretching length was observed in blocking experiments with a trifluoromethyl-functionalized UPy derivative (see Supporting Information).

The mean value of the rupture forces observed for the supramolecular polymers in HD of 172 ± 23 pN lies within the error margins for the rupture force of the dimeric complex. Our data suggests, however, that the rupture forces decrease

 © 2005 Wiley-VCH Verlag GmbH & Co. KGaA, Weinheim

slightly with increasing lengths of the stretched supramolecular polymer chains (see Supporting Information). This observation is in agreement with the theory developed by Evans et al.,[23,24] who predict a decrease in the magnitude of the single-complex rupture force with increasing spacer length and an increasing number of consecutive bonds along one molecule.[25]

Stretching lengths of more than 150 nm were detected in HD (Figure 3a) which corresponds to a "degree of polymerization" of up to 15, assuming a "monomer length" of 12 nm. The probability of stretching a supramolecular polymer chain that bridges the gap between the substrate and the tip appears to be an exponential function of the chain length (Figure 3a, inset). In the presence of DMSO, the hydrogen bonds are disrupted[6,10] and consequently the stretching and rupture of long supramolecular polymers is not observed (Figure 3b).

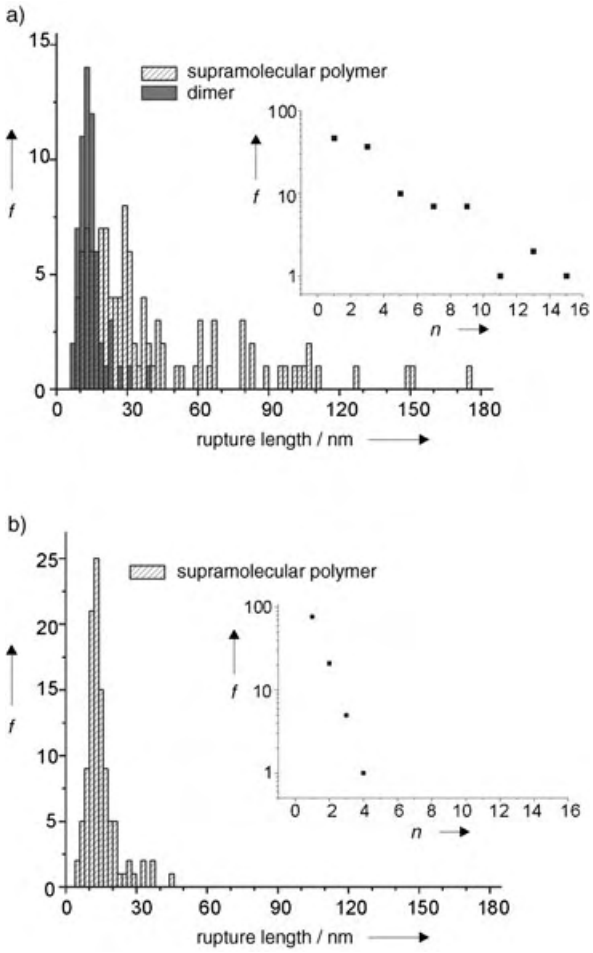


Figure 3. a) Histogram of extension lengths observed for the dimeric interactions and the supramolecular polymers in hexadecane. Inset: Frequency of extension events (f) versus the number of repeat units (n) in stretched supramolecular polymers calculated on the basis of the length of one repeat unit. b) Histogram of extension lengths observed for the supramolecular polymers in 15% DMSO in propan-2-ol. Inset: Frequency of extension events versus the number of repeat units n in stretched supramolecular polymers.

We observed in the AFM experiments that the chain lengths obtained for supramolecular polymers are shorter than predicted. However, independent of the length, an exponential decay of the distribution of effective length versus the degree of polymerization is expected on the basis of the model.[22] The sampling of the rupture length in the AFM experiment may lead to an underestimate because the attachment sites for the UPy telechelic derivatives on the AFM tip are not restricted to the very end of the tip, while the supramolecular polymer "chain" may also be attached to the substrate at a location outside the tip–sample contact area. Furthermore, possible effects of the tip–substrate gap distance (the polymer may form after the tip and the substrate may become detached) and the rate of the loading have not yet been addressed systematically. A systematic investigation of the frequency of successful stretching events probed versus independently adjusted tip–sample separation distances and equilibration times would open the path to elucidate the kinetics of polymerization at a single-molecule level.

In conclusion, the AFM data show that supramolecular polymers can indeed be investigated on the single-molecule level. In PEG-based telechelic bis(UPy) materials, the individual reversible linking sites along a supramolecular polymer chain, that is, the complexes based on self-complementary recognition of 2-ureido-4[1H]-pyrimidinone, act as independent bonds in series. As the material properties including viscosity, composition, or chain length are functions of various external parameters and stimuli, which can be investigated in situ, highly useful information for the design and construction of nanometer scale devices and stimuli-responsive systems will now become directly accessible from SMFS experiments.

Experimental Section

Materials: Isocyanate **2**[19] was coupled to PEG derivative **1**, which was immobilized through disulfide moieties to Au(111) (5-mM $CHCl_3$ solution, RT),[18,19] to yield surface-immobilized **3** (Scheme 1). Bis(pyrimidinone) **4** was synthesized according to a procedure adapted from Ref. [26] (for details see Supporting Information). AFM: The AFM measurements were carried out with a NanoScope IIIa multimode AFM (Digital Instruments, Santa Barbara, CA) utilizing a liquid cell and functionalized tips prepared as described previously (see also Supporting Information).[18] The temperature inside the liquid cell was 28 °C. The cantilever spring constants were calibrated by using the thermal noise method.[27] The fd curves were fitted by using IGOR PRO software (version 4.07) to the modified freely jointed chain model (m-FJC), [Eq. (1)], with the extension of the polymer chain x, applied force F, Kuhn length I_K, contour length $L_{contour}$, number of segments n, segment elasticity K_S, Boltzmann constant k_B, and temperature T.[15]

$$x(F) = \left[\coth\left(\frac{FI_K}{k_B T}\right) - \frac{k_B T}{FI_K}\right]\left[L_{contour} + \frac{n}{K_S}F\right] \quad (1)$$

Received: June 15, 2004
Revised: August 31, 2004
Published online: December 28, 2004

Keywords: atomic force microscopy · hydrogen bonds · single-molecule studies · supramolecular chemistry · surface chemistry

 © 2005 Wiley-VCH Verlag GmbH & Co. KGaA, Weinheim

[1] a) J.-M. Lehn, *Supramolecular Chemistry: Concepts and Perspectives*, VCH, Weinheim, **1995**; b) *Supramolecular Materials and Technologies* (Ed.: D. N. Reinhoudt), Wiley, New York, **1999**.

[2] J. N. Israelachvili, *Intermolecular and Surface Forces: With Applications to Colloidal and Biological Systems*, Academic Press, New York, **1992**.

[3] H. Ringsdorf, B. Schlarb, J. Venzmer, *Angew. Chem.* **1988**, *100*, 117; *Angew. Chem. Int. Ed. Engl.* **1988**, *27*, 113.

[4] a) A. D. Buckingham, A. C. Legon, S. M. Roberts, *Principles of Molecular Recognition*, Blackie, London, **1993**; b) *The Lock and Key Principle: The State of the Art* (Ed.: J.-P. Behr), Wiley, Chichester, **1994**; c) G. Cooke, V. M. Rotello, *Chem. Soc. Rev.* **2002**, *31*, 275; d) J.-M. Lehn, *Science* **2002**, *295*, 2400; e) D. N. Reinhoudt, M. Crego-Calama, *Science* **2002**, *295*, 2403.

[5] J.-M. Lehn, *Macromol. Chem. Macromol. Symp.* **1993**, *69*, 1.

[6] R. P. Sijbesma, F. H. Beijer, L. Brunsveld, B. J. B. Folmer, J. H. K. K. Hirschberg, R. F. M. Lange, J. K. L. Lowe, E. W. Meijer, *Science* **1997**, *278*, 1601.

[7] P. S. Corbin, S. C. Zimmerman, *J. Am. Chem. Soc.* **1998**, *120*, 9710.

[8] B. Gong, Y. Yan, H. Zeng, E. Skrzypczak-Jankunn, Y. W. Kim, J. Zhu, H. Ickes, *J. Am. Chem. Soc.* **1999**, *121*, 5607.

[9] S. Boileau, L. Bouteiller, F. Lauprêtre, F. Lortie, *New J. Chem.* **2000**, *24*, 845.

[10] a) F. H. Beijer, H. Kooijman, A. L. Spek, R. P. Sijbesma, E. W. Meijer, *Angew. Chem.* **1998**, *110*, 79; *Angew. Chem. Int. Ed.* **1998**, *37*, 75; b) F. H. Beijer, R. P. Sijbesma, H. Kooijman, A. L. Spek, E. W. Meijer, *J. Am. Chem. Soc.* **1998**, *120*, 6761.

[11] a) L. Brunsveld, B. J. B. Folmer, E. W. Meijer, R. P. Sijbesma, *Chem. Rev.* **2001**, *101*, 4071; b) A. T. ten Cate, R. P. Sijbesma, *Macromol. Rapid Commun.* **2002**, *23*, 1094.

[12] S. H. M. Söntjens, R. P. Sijbesma, M. H. P. van Genderen, E. W. Meijer, *J. Am. Chem. Soc.* **2000**, *122*, 7487.

[13] J. van der Gucht, N. A. M. Besseling, G. J. Fleer, *J. Chem. Phys.* **2003**, *119*, 8175.

[14] For a very recent report, see: F. R. Kersey, G. Lee, P. Marszalek, S. L. Craig, *J. Am. Chem. Soc.* **2004**, *126*, 3038.

[15] For reviews, see: a) T. Hugel, M. Seitz, *Macromol. Rapid Commun.* **2001**, *22*, 989; b) A. Janshoff, M. Neitzert, Y. Oberdörfer, H. Fuchs, *Angew. Chem.* **2000**, *112*, 3346; *Angew. Chem. Int. Ed.* **2000**, *39*, 3212; c) W. Zhang, X. Zhang, *Prog. Polym. Sci.* **2003**, *28*, 1271.

[16] a) M. Rief, F. Oesterhelt, B. Heymann, H. E. Gaub, *Science* **1997**, *275*, 1295; b) J. E. Bemis, B. B. Akhremitchev, G. C. Walker, *Langmuir* **1999**, *15*, 2799; c) H.-J. Butt, M. Kappl, H. Müller, R. Raiteri, W. Meyer, J. Rühe, *Langmuir* **1999**, *15*, 2559; d) H. Li, W. A. Linke, A. F. Oberhauser, M. Carrion-Vazquez, J. G. Kerkvliet, H. Lu, P. E. Marszalek, J. M. Fernandez, *Nature* **2002**, *418*, 998; e) T. Gutsmann, G. E. Fantner, J. H. Kindt, M. Venturoni, S. Danielsen, P. K. Hansma, *Biophys. J.* **2004**, *86*, 3186.

[17] R. Merkel, P. Nassoy, A. Leung, K. Ritchie, E. Evans, *Nature* **1999**, *397*, 50.

[18] a) H. Schönherr, M. W. J. Beulen, J. Bügler, J. Huskens, F. C. J. M. van Veggel, D. N. Reinhoudt, G. J. Vancso, *J. Am. Chem. Soc.* **2000**, *122*, 4963; b) S. Zapotoczny, T. Auletta, M. R. de Jong, H. Schönherr, J. Huskens, F. C. J. M. van Veggel, D. N. Reinhoudt, G. J. Vancso, *Langmuir* **2002**, *18*, 6988; c) T. Auletta, M. R. de Jong, A. Mulder, F. C. J. M. van Veggel, J. Huskens, D. N. Reinhoudt, S. Zou, S. Zapotoczny, H. Schönherr, G. J. Vancso, L. Kuipers, *J. Am. Chem. Soc.* **2004**, *126*, 1577.

[19] S. Zou, Z. Zhang, R. Förch, W. Knoll, H. Schönherr, G. J. Vancso, *Langmuir* **2003**, *19*, 8618.

[20] The presence of the UPy moieties in the PEG layers and the molecular recognition of labeled self-complementary UPys in solution were assessed by spectroscopic and electrochemical means (see Supporting Information).

[21] a) F. Oesterhelt, M. Rief, H. E. Gaub, *New J. Phys.* **1999**, *1*, 6.1; b) F. Kienberger, V. P. Pastushenko, G. Kada, H. J. Gruber, C. Riener, H. Schindler, P. Hinterdorfer, *Single Mol.* **2000**, *1*, 123.

[22] See the Supporting Information.

[23] a) E. Evans, K. Ritchie, R. Merkel, *Biophys. J.* **1995**, *68*, 2580; b) E. Evans, K. Ritchie, *Biophys. J.* **1997**, *72*, 1541.

[24] E. Evans, P. Williams, in *Physics of Biomolecules and Cells*, Ecoles des Houches d'Eté LXXV, (Eds.: H. Flyvbjerg, F. Julicher, P. Ormos, F. David), EDP Sciences, Springer, Berlin, **2002**, p. 145.

[25] E. Evans, *Annu. Rev. Biophys. Biomol. Struct.* **2001**, *30*, 105.

[26] B. J. B. Folmer, R. P. Sijbesma, R. M. Versteegen, J. A. J. van der Rijt, E. W. Meijer, *Adv. Mater.* **2000**, *12*, 874.

[27] J. L. Hutter, J. Bechhoefer, *Rev. Sci. Instrum.* **1993**, *64*, 1868.

 © 2005 Wiley-VCH Verlag GmbH & Co. KGaA, Weinheim

Cyclotrimerization

Lanthanide–Imido Complexes and Their Reactions with Benzonitrile**

*Dongmei Cui, Masayoshi Nishiura, and Zhaomin Hou**

Transition-metal–imido complexes have received much current interest because of the ability of the M=N group to undergo a wide range of reactions[1] such as metathesis of imines, aldehydes, and carbodiimides,[2] metallacycle formation with alkenes and alkynes,[3] hydroamination of alkynes and allenes,[4] and C–H bond activation.[5] In contrast to the extensive studies on the rich chemistry of transition-metal–imido complexes, reports on well-defined lanthanide–imido complexes are scarce[6] and the reactions of lanthanide–imido complexes have remained almost unexplored to date. This is mainly due to the lack of suitable complexes for reactivity studies.[7]

During our recent studies on lanthanide–polyhydrido complexes,[8] we found that reactions of the tetranuclear lanthanide polyhydrido complexes [{Cp′Ln(μ-H)$_2$}$_4$(thf)]

[*] Dr. D. Cui, Dr. M. Nishiura, Prof. Dr. Z. Hou
Organometallic Chemistry Laboratory
RIKEN (The Institute of Physical and Chemical Research)
Hirosawa 2-1, Wako, Saitama 351-0198 (Japan)
Fax: (+81) 48-462-4665
E-mail: houz@riken.jp
and
PRESTO
Japan Science and Technology Agency (JST) (Japan)

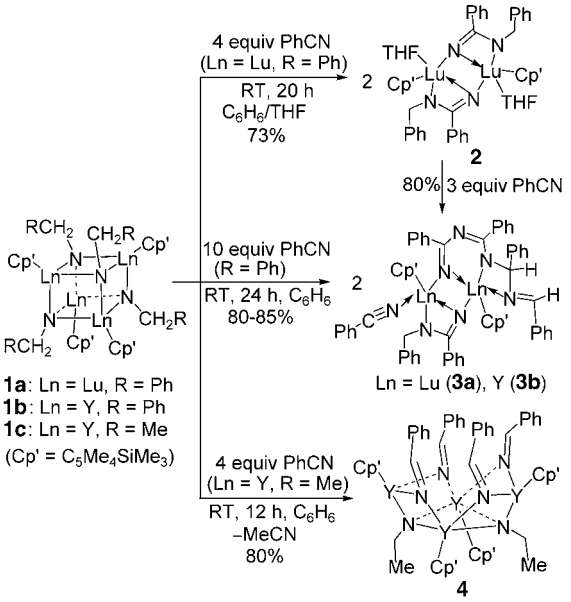
[**] This work was partly supported by a Grant-in-Aid for Scientific Research on Priority Areas (No. 14078224, "Reaction Control of Dynamic Complexes") from the Ministry of Education, Culture, Sports, Science, and Technology of Japan. We are also grateful to the Japan Society for the Promotion of Science (JSPS) for a Postdoctoral Fellowship for D.C.

Supporting information for this article is available on the WWW under http://www.angewandte.org or from the author.

 DOI: 10.1002/anie.200461939 © 2005 Wiley-VCH Verlag GmbH & Co. KGaA, Weinheim

($Cp' = \eta^5$-$C_5Me_4SiMe_3$; Ln = Lu, Y) with nitriles RCN can offer a convenient route to the corresponding imido complexes [{Cp′Ln(μ_3-NCH_2R)}$_4$] by double addition of the Ln–H units across the C≡N bond.[8a] The imido species formed in this way have a methylene substituent at the N atom and adopt a novel Ln_4N_4 cubane core structure with μ_3-N-Ln bridges, a structural feature that has not been observed previously. Here we report that this new class of imido complexes can show unprecedented reactivity. They not only exhibit strong nucleophilicity but can also transfer α-hydrogen atoms.

Reaction of benzylimido–lutetium complex [{Cp′Lu(μ_3-NCH_2Ph)}$_4$] (**1a**) with 4 equivalents of benzonitrile at room temperature in toluene gave the benzamidinate dianion complex **2** in 73% yield after recrystallization from THF (Scheme 1).[9] X-ray analysis showed that **2** has a dimeric structure (Figure 1) in which the two Lu atoms are bridged by the ketimido nitrogen atom (Lu–N 2.149(4), 2.326(4) Å), and the amido nitrogen atom is bonded terminally to one Lu atom (Lu–N 2.352(4) Å). The formation of **2** apparently proceeded by nucleophilic addition of the imido unit to the C≡N group of benzonitrile, which demonstrates that a lanthanide–imido bond, even in a bridging form, is very reactive. This is in contrast with what was observed previously for bonds between transition metals and bridging imido ligands, which are usually robust and unreactive.[1–5] Moreover, the resultant product **2** represents the first metal complex of an amidinate dianion, in contrast to the well-known complexes of various metals with amidinate monoanions [RNC(R′)NR]$^-$ as ligands.[10]



Scheme 1. Nucleophilic addition and hydrogen transfer of lanthanide–imido complexes to benzonitrile.

Interestingly, the reaction of the ethylimido complex [{Cp′Y(μ_3-NCH_2CH_3)}$_4$] (**1c**) with benzonitrile did not afford an insertion product, but instead gave the mixed benzaldiminato/ethylimido complex **4** (Scheme 1). X-ray analysis established that **4** adopts a tetranuclear crownlike core structure, in which the four Y atoms are unsymmetrically bridged by four μ_2-benzaldiminato and two μ_3-ethylimido ligands (Y–N(μ_2-iminato) 2.298(7)–2.532(7) Å, Y–N(μ_3-imido) 2.116(6)–2.418(6) Å, mean C–N(iminato) 1.248(10) Å, mean C–N(imido) 1.473(7) Å; Figure 1). In this reaction, four molecules of benzonitrile were hydrogenated to give four benzaldiminato species by abstraction of four methylene hydrogen atoms from two of the four ethylimido units in **1c** with the release of two molecules of acetonitrile, while the other two ethylimido units remained unchanged. Such formation of an iminato species through hydrogen transfer from an imido species to a nitrile is, as far as we are aware, unprecedented.

When 10 equivalents of benzonitrile were allowed to react with the benzylimido complexes **1a** and **1b**, the benzonitrile tetramerization products **3a** and **3b** were obtained, respectively (Scheme 1). The reaction of the benzamidinate dianion complex **2** with 3 equivalents of benzonitrile also afforded **3a** in high yield, and this suggests that **2** is an intermediate in the formation of **3a** from **1a**. The structures of **3a** and **3b** were confirmed by X-ray analysis (Figure 1).

Although the formation of **2** from **1a** is straightforward, the formation of **3a** from **2** apparently requires both the insertion of two molecules of benzonitrile into a Lu–amido bond in **2** and hydrogen transfer from the methylene group to the two incoming benzonitrile molecules. The formation of **3a**

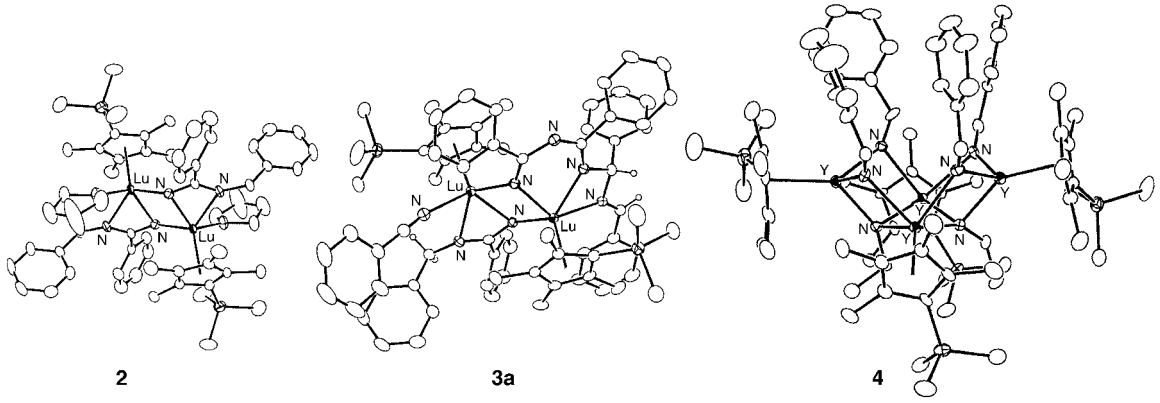
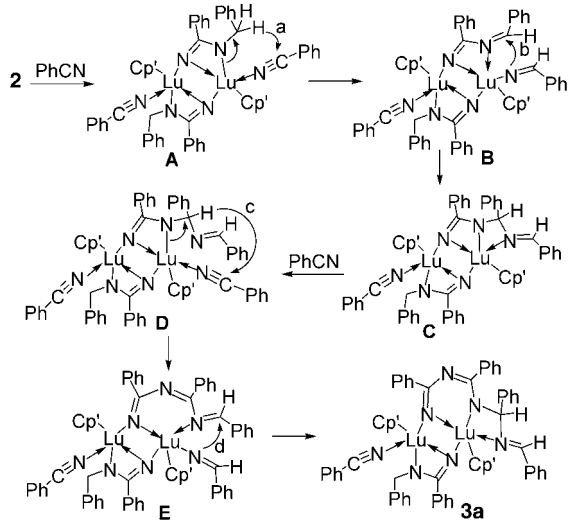


Figure 1. X-ray crystal structures of **2**, **3a**, and **4** with 30% probability ellipsoids. Hydrogen atoms and lattice solvent molecules are omitted for clarity.

 © 2005 Wiley-VCH Verlag GmbH & Co. KGaA, Weinheim

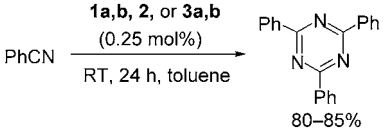
from **2** could be explained by the reaction steps shown in Scheme 2. The coordination of one molecule of benzonitrile to each Lu atom in **2** should yield **A**. Hydrogen transfer from a methylene group to coordinated PhCN in **A** (step a)[11]



Scheme 2. Possible mechanism for the formation of **3a**.

should afford **B**. Nucleophilic addition of the newly formed benzaldiminato unit to the aldimine group (step b) could yield **C**, which on coordination of one molecule of PhCN gives **D**. Migration of the methine hydrogen atom to the PhCN unit in **D** (step c) followed by addition of the resulting aldiminato unit to the aldimine group in **E** (step d) should give **3a**.

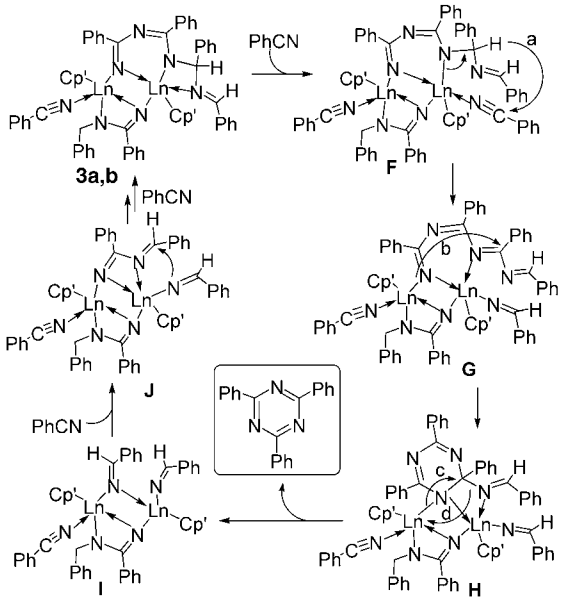
It is also noteworthy that only one of the two benzamidinate dianion units in **2** formally participated in the reaction with benzonitrile. No reaction was observed between the remaining benzamidinate dianion unit and the benzonitrile ligand in **3a** or **3b** even at elevated temperatures (80 °C). Surprisingly to us, when an excess of benzonitrile was added to a solution of **3a** or **3b** in toluene, the benzonitrile cyclotrimerization product 2,4,6-triphenyl-1,3,5-triazine was formed selectively, while **3a** (or **3b**) was recovered. The polyhydrido complexes $[\{Cp'Ln(\mu\text{-}H)_2\}_4(thf)]$ **1a** and **1b** and benzamidinate dianion complex **2** also showed similar catalytic activity for the cyclotrimerization of benzonitrile (Scheme 3). Here, the formation of **3a** (or **3b**) was also observed after completion of the reaction which strongly suggests that **3a** (or **3b**) is the true catalytic species. The formation of 2,4,6-triphenyl-1,3,5-triazine, a cyclic benzonitrile trimer, from **3a** or **3b** (containing a linear benzonitrile tetramer as a ligand) clearly must involve both cyclization



Scheme 3. Catalytic cyclotrimerization of benzonitrile.

(intramolecular C–N bond formation) and C–N bond cleavage.

A possible mechanism for the catalytic cyclotrimerization of benzonitrile by **3a** or **3b** is shown in Scheme 4. The coordination of one molecule of benzonitrile to a metal center in **3a** or **3b** could give **F**. Methine hydrogen transfer (step a) to coordinated benzonitrile would afford **G**. Intramolecular nucleophilic addition of the amido unit to the newly formed imine moiety (step b) could yield **H**. Aromatization of the resultant six-membered ring in **H** through step c (Ln–N bond cleavage and C=N bond formation) and step d (C–N bond cleavage and Ln–N bond formation) should release the triazine and generate **I**. An insertion of benzonitrile into **I** would give **J**, which resembles intermediate **B** in Scheme 2, and could regenerate **3a** or **3b** as described above.



Scheme 4. Possible mechanism for the catalytic cyclotrimerization of benzonitrile.

In summary, tetranuclear μ_3-N-bridged lanthanide–imido complexes **1a–c** undergo not only nucleophilic addition but also hydrogen-transfer reactions with benzonitrile to afford a new series of structurally characterizable multinuclear lanthanide complexes **2–4** that have novel structures. The combination of C–N bond-formation, hydrogen-transfer, and C–N bond-cleavage steps constitutes a unique catalytic cycle for the cyclotrimerization of benzonitrile.[12] This work demonstrates for the first time that lanthanide–imido complexes can show rich and unique chemistry that differs from that of d-block transition metal analogues.

Received: September 10, 2004
Published online: December 21, 2004

Keywords: cyclotrimerization · hydrogen transfer · lanthanides · N ligands · nitriles

 © 2005 Wiley-VCH Verlag GmbH & Co. KGaA, Weinheim

[1] Recent reviews on early-transition-metal–imido complexes: a) A. P. Duncan, R. G. Bergman, *Chem. Rec.* **2002**, *2*, 431 – 445; b) P. Mountford, *Chem. Commun.* **1997**, 2127 – 2134.

[2] For examples, see: a) T. Ong, G. A. Yap, D. S. Richeson, *Chem. Commun.* **2003**, 2612 – 2613; b) R. L. Zuckerman, S. W. Krska, R. G. Bergman, *J. Am. Chem. Soc.* **2000**, *122*, 751 – 761; c) R. L. Zuckerman, R. G. Bergman, *Organometallics* **2000**, *19*, 4795 – 4809; d) W. Wang, J. H. Espenson, *Organometallics* **1999**, *18*, 5170 – 5175; e) S. Y. Lee, R. G. Bergman, *J. Am. Chem. Soc.* **1996**, *118*, 6396 – 6406.

[3] a) R. L. Zuckerman, R. G. Bergman, *Organometallics* **2001**, *20*, 1792 – 1807; b) P. J. Walsh, F. J. Hollander, R. G. Bergman, *J. Am. Chem. Soc.* **1988**, *110*, 8729 – 8731; c) J. L. Polse, R. A. Anderson, R. G. Bergman, *J. Am. Chem. Soc.* **1998**, *120*, 13405 – 13414; d) P. L. McGrane, M. Jensen, T. Livinghouse, *J. Am. Chem. Soc.* **1992**, *114*, 5459 – 5460.

[4] For recent examples, see: a) Y. Li, Y. Shi, A. L. Odom, *J. Am. Chem. Soc.* **2004**, *126*, 1794 – 1803; b) C. Cao, Y. Shi, A. L. Odom, *J. Am. Chem. Soc.* **2003**, *125*, 2880 – 2881; c) L. Ackermann, R. G. Bergman, R. Loy, *J. Am. Chem. Soc.* **2003**, *125*, 11956 – 11963.

[5] a) H. M. Hoyt, M. E. Michael, R. G. Bergman, *J. Am. Chem. Soc.* **2004**, *126*, 1018 – 1019; b) J. L. Bennett, P. T. Wolczanski, *J. Am. Chem. Soc.* **1997**, *119*, 10696 – 10719.

[6] a) G. R. Giesbrecht, J. C. Gordon, *Dalton Trans.* **2004**, *16*, 2387 – 2393; b) D. J. Beetstra, A. Meetsma, B. Hessen, J. H. Teuben, *Organometallics* **2003**, *22*, 4372 – 4374; c) J. C. Gordon, G. R. Giesbrecht, D. L. Clark, P. J. Hay, D. W. Keogh, R. Poli, B. L. Scott, J. G. Watkin, *Organometallics* **2002**, *21*, 4726 – 4734; d) H.-S. Chan, H.-W. Li, Z. Xie, *Chem. Commun.* **2002**, 652 – 653; e) S. Wang, Q. Yang, T. C. W. Mak, Z. Xie, *Organometallics* **1999**, *18*, 5511 – 5517; f) Z. Xie, S. Wang, Q. Yang, T. C. W. Mak, *Organometallics* **1999**, *18*, 1578 – 1579; g) A. A. Trifonov, M. N. Bochkarev, H. Schumann, J. Loebel, *Angew. Chem.* **1991**, *103*, 1170 – 1171; *Angew. Chem. Int. Ed. Engl.* **1991**, *30*, 1149 – 1150.

[7] The deprotonation approaches used successfully for the generation of transition-metal–imido species[1–5] did not seem to work well for the analogous lanthanide–imido complexes.[6] When main group metal–alkyl compounds, such as RLi or AlR_3, were used as a base to deprotonate primary amido–lanthanide complexes, the main group metal ions were often incorporated into the resultant imido products.[6c,d]

[8] a) D. Cui, O. Tardif, Z. Hou, *J. Am. Chem. Soc.* **2004**, *126*, 1312 – 1313; b) O. Tardif, D. Hashizume, Z. Hou, *J. Am. Chem. Soc.* **2004**, *126*, 8080 – 8081; c) O. Tardif, M. Nishiura, Z. Hou, *Organometallics* **2003**, *22*, 1171 – 1173; d) Z. Hou, Y. Zhang, O. Tardif, Y. Wakatsuki, *J. Am. Chem. Soc.* **2001**, *123*, 9216 – 9217.

[9] The products reported in this paper have all been fully characterized. See Supporting Information for experimental details.

[10] L. Bourget-Merle, M. F. Lappert, J. R. Severn, *Chem. Rev.* **2002**, *102*, 3031 – 3065.

[11] The formation of **4** in the reaction of **1c** with PhCN should proceed by a similar hydrogen-transfer process.

[12] Although benzonitrile cyclotrimerization is known, the mechanistic aspects of this process are not well understood. For examples, see: a) J. H. Forsberg, V. T. Spaziano, T. M. Balasubramanian, G. K. Liu, S. A. Kinsley, C. A. Duckworth, J. J. Poteruca, P. S. Brown, J. L. Miller, *J. Org. Chem.* **1987**, *52*, 1017 – 1021; b) F. Xu, J. H. Sun, H. B. Yan, Q. Shen, *Synth. Commun.* **2000**, *30*, 1017 – 1022.

 © 2005 Wiley-VCH Verlag GmbH & Co. KGaA, Weinheim

Polymerization Catalysts

Alternating Ethylene–Norbornene Copolymerization Catalyzed by Cationic Half-Sandwich Scandium Complexes**

*Xiaofang Li, Jens Baldamus, and Zhaomin Hou**

Cationic alkyl–rare-earth-metal complexes (i.e., Group 3 and the lanthanides) have recently attracted much interest as homogeneous polymerization catalysts.[1–10] A number of cationic alkyl–rare-earth-metal complexes supported by various ancillary ligands such as deprotonated aza crowns,[2] benzamidinates,[3] β-diketiminates,[4] anilido imines,[5] amide-functionalized triazacyclononanes,[6] phosphides,[7] cyclopentadienyls,[8] and crown ethers[9] have been synthesized and their reactivity has been studied. Despite these extensive efforts, however, the olefin-polymerization chemistry of the cationic alkyl–rare-earth-metal complexes is still limited solely to that of ethylene,[2–10] whereas the development of active rare-earth-metal catalysts for the efficient polymerization/copolymerization of higher olefins has remained a challenge.

The copolymer of ethylene with a cyclic olefin such as norbornene (COC) is one of the most important high-performance polymer materials with many desirable properties. Since Kaminsky et al. first described the copolymerization of ethylene (E) with norbornene (NB) by using zirconocene-based catalysts in 1991,[11] extensive studies have been carried out in this area. Most of the catalysts reported so far are complexes based on transition metals such as those of Group 4 and Group 10,[12] whereas no rare-earth-metal complex has been previously used for the copolymerization of ethylene with norbornene.[13]

Herein we report an excellent cationic half-sandwich scandium catalyst for the copolymerization of ethylene with norbornene. This catalyst not only represents the first example of a rare-earth-metal catalyst for ethylene–norbornene copolymerization, but it also shows several unique characteristics, such as extremely high activity for the alternating ethylene–norbornene copolymerization and unprecedented formation of novel poly(ethylene-*alt*-norbornene)-*b*-polyethylene block copolymers.

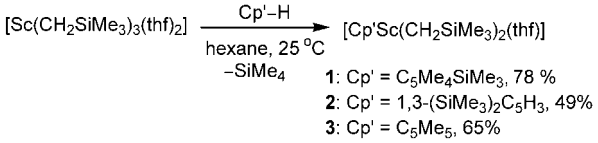
[*] Dr. X. Li, Dipl.-Chem. J. Baldamus, Prof. Dr. Z. Hou
Organometallic Chemistry Laboratory
RIKEN (The Institute of Physical and Chemical Research)
Hirosawa 2-1, Wako, Saitama 351-0198 (Japan)
and
PRESTO, Japan Science and Technology Agency (JST; Japan)
Fax: (+81) 48-462-4665
E-mail: houz@riken.jp

[**] This work was partly supported by a Grant-in-Aid for Scientific Research on Priority Areas (No. 14078224, "Reaction Control of Dynamic Complexes") from the Ministry of Education, Culture, Sports, Science, and Technology of Japan.

Supporting information for this article is available on the WWW under http://www.angewandte.org or from the author.

 © 2005 Wiley-VCH Verlag GmbH & Co. KGaA, Weinheim DOI: 10.1002/anie.200461971

The acid–base reaction between the scandium–tris(alkyl) complex $[Sc(CH_2SiMe_3)_3(thf)_2]$ and the cyclopentadiene ligands Cp′H easily afforded the corresponding mono(cyclopentadienyl)scandium–bis(alkyl) complexes $[Cp'Sc(CH_2SiMe_3)_2(thf)]$ ($Cp' = SiMe_3C_5Me_4$ (**1**); 1,3-$(SiMe_3)_2C_5H_3$ (**2**); C_5Me_5 (**3**); Scheme 1). The X-ray crystal structure of **2** is shown in Figure 1.



Scheme 1. Synthesis of mono(cyclopentadienyl)scandium–bis(alkyl) complexes.

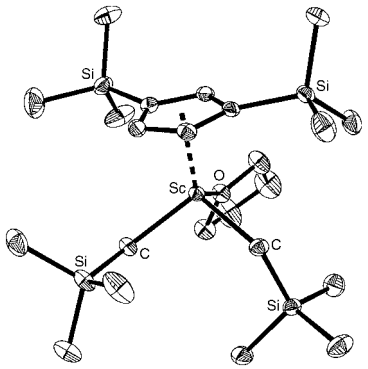


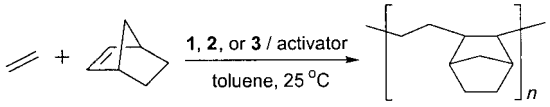
Figure 1. ORTEP drawing of **2** with ellipsoids shown at the 30% level of probability. Hydrogen atoms are omitted for clarity.

Treatment of complexes **1**–**3** with 1 equivalent of $[Ph_3C][B(C_6F_5)_4]$ (**A**) in C_6D_6 at 25 °C led to the immediate formation of $Ph_3CCH_2SiMe_3$ and a cationic scandium alkyl species assignable to $[Cp'Sc(CH_2SiMe_3)(thf)_x][B(C_6F_5)_4]$, as monitored by ^1H NMR spectroscopy. However, attempts to isolate such a cationic Sc species were not successful because of its extremely high reactivity (i.e., instability). Nevertheless, the in situ generated cationic scandium species showed high activity for ethylene polymerization ($\approx 10^5$ g(mol of Sc)$^{-1}$ h^{-1} atm^{-1}; Table 1, entry 1). These species were also active for norbornene polymerization, though the activity was very low ($\approx 10^2$ g(mol of Sc)$^{-1}$ h^{-1} atm^{-1}; Table 1, entry 2). More remarkably, in the presence of both ethylene and norbornene, extremely rapid copolymerization of the two monomers took place ($\approx 10^6$ g(mol of Sc)$^{-1}$ h^{-1} atm^{-1}) to yield the alternating ethylene–norbornene copolymers with a norbornene content of up to around 43 mol% (Table 1, entries 3–5).

Among complexes **1**–**3**, **1** showed the highest activity under the examined conditions. As an activator, $[PhMe_2NH][B(C_6F_5)_4]$ (**B**) was also effective for this copolymerization (Table 1, entry 6), whereas the use of $B(C_6F_5)_3$ (**C**) led to only a trace amount of norbornene incorporation into the polymer product (Table 1, entry 7).[14] In contrast, the neutral bis(alkyl) complexes **1**–**3** alone showed no activity for either norbornene homopolymerization or ethylene–norbornene copolymerization, although they were active for ethylene homopolymerization. None of the boron compounds were active towards ethylene or norbornene. These results clearly indicate that the cationic half-sandwich scandium–alkyl species play a critical role in this ethylene–norbornene copolymerization.

On the basis of the results described above, the **1**/**A** system was chosen to examine the ethylene–norbornene copolymerization under various conditions. The copolymerization can be carried out over a wide range of temperatures (0–70 °C; Table 2, entries 1–4). The activity of the catalyst increased at elevated temperatures, but the molecular weight of the resultant polymer decreased when the polymerization temperature was raised, thus suggesting that chain transfer should occur more rapidly at higher temperatures. Consistent with the above observation that the copolymerization of the two monomers is much faster than the homopolymerization of either monomer, a strong dependence of the activity of the catalyst on the monomer concentration (or the ethylene/norbornene molar ratio in the reaction solution) was observed (Table 2, entries 2, 5–9). Under appropriate conditions (with respect to the ethylene/norbornene molar ratio), the catalytic activity reached as high as 25.2×10^6 g of copolymer (mol of

Table 1: Copolymerization of ethylene with norbornene by half-sandwich scandium catalysts.[a]



Entry	Compound	Activator[b]	$p_{ethylene}$ [atm]	NB [mmol]	Yield [g]	Activity[c]	Product[d]	NB cont.[d] [mol%]	M_n[e] ($\times 10^4$)	PDI[f]	T_g[f] [°C]
1	**1**	**A**	1	0	0.03	0.4	PE		n.d.[g]	n.d.	n.d.
2[h]	**1**	**A**	0	20	0.02	0.0005	P(NB)	100	n.d.	n.d.	n.d.
3	**1**	**A**	1	20	0.67	8.0	P(E-*alt*-NB)	41.2	11.0	1.79	126
4	**2**	**A**	1	20	0.47	5.6	P(E-*alt*-NB)	36.1	4.9	1.89	105
5	**3**	**A**	1	20	0.20	2.4	P(E-*alt*-NB)	42.9	5.8	2.22	101
6	**1**	**B**	1	20	1.18	14.2	P(E-*alt*-NB)	43.6	12.1	2.78	110
7	**1**	**C**	1	20	0.06	0.7	PE		n.d.	n.d.	n.d.

[a] Conditions: Sc (1 μmol), activator (1 μmol), toluene (40 mL), $T = 25$ °C; $t = 5$ min, unless otherwise noted. [b] **A** = $[Ph_3C][B(C_6F_5)_4]$, **B** = $[PhMe_2NH][B(C_6F_5)_4]$, **C** = $B(C_6F_5)_3$. [c] 10^6 g of copolymer (mol of Sc)$^{-1}$ h^{-1} atm^{-1}. [d] NB content determined by ^{13}C NMR spectroscopy. [e] M_n is the number-averaged molecular mass determined by GPC with polystyrene standards. [f] Measured by differential scanning calorimetry (DSC; PDI = polydispersity index). [g] n.d. = not determined. [h] Conditions: Sc (21 μmol), activator (21 μmol), toluene (10 mL), $T = 25$ °C; $t = 2$ h.

 © 2005 Wiley-VCH Verlag GmbH & Co. KGaA, Weinheim

Table 2: Alternating copolymerization of ethylene and norbornene by **1**/**A**.[a]

Entry	NB [mmol]	T [°C]	V [mL]	Yield [g]	Activity[b]	NB cont. [mol%][c]	M_n[d] ($\times 10^4$)	PDI[d]	T_g[e] [°C]
1	20	0	40	0.35	4.2	35.7	12.1	1.49	104
2	20	25	40	0.67	8.0	41.2	11.0	1.79	126
3	20	50	40	0.81	9.7	42.5	8.0	1.81	119
4	20	70	40	0.97	11.6	43.2	4.0	2.33	127
5	30	25	40	2.10	25.2	44.2	8.5	2.19	118
6	40	25	40	0.31	3.7	45.5	7.4	1.80	120
7	20	25	60	0.62	7.4	35.8	15.4	1.65	105
8	20	25	20	1.29	15.5	46.4	6.5	1.92	134
9	20	25	10	0.37	4.4	48.1	3.2	2.08	128

[a] Conditions: **1** (1 μmol), **A** (1 μmol), toluene (V mL), $p_{ethylene} = 1$ atm, $t = 5$ min. [b] 10^6 g of copolymer (mol of Sc)$^{-1}$ h^{-1} atm^{-1}. [c] NB content determined by ^{13}C NMR spectroscopy. [d] PDI determined by GPC with polystyrene standards. [e] Measured by DSC.

catalyst)$^{-1}$ h^{-1} atm^{-1} (Table 2, entry 5). To our knowledge, this is the highest activity ever reported for the copolymerization of ethylene and norbornene.[12]

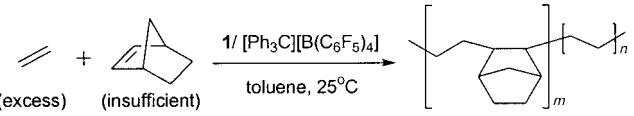
The ^{13}C{^{1}H} NMR spectra of the copolymers show eight singlets at $\delta = 47.99$, 47.37, 42.19, 41.68, 33.14, 30.87, 30.50, and 30.18 ppm, as expected for an alternating ethylene–norbornene copolymer.[12d,e] The copolymers are amorphous and most of them have glass-transition temperature (T_g) values in the range of 118–134 °C. The gel-permeation chromatography (GPC) curves of the copolymers are all unimodal with relatively narrow molecular distributions (1.49–2.78), consistent with the predominance of a single homogeneous catalytic species. Solvent-fractionation experiments reveal negligible quantities of homopolymer impurities.[15]

More remarkably, the alternating ethylene–norbornene copolymerization system presented here could be applied to the preparation of poly(ethylene-*alt*-norbornene)-*b*-polyethylene block copolymers by use of an insufficient amount of norbornene monomer in the copolymerization as successive ethylene insertion can occur after all of the norbornene monomer has been consumed. As shown in Table 3, when the copolymerization reaction of 10 mmol of norbornene with ethylene (1 atm) in the presence of 21 μmol of **1**/**A** was quenched after 0.3 min, pure alternating ethylene–norbornene copolymer with a norbornene content of 45.6 mol% (equivalent to 53.4% conversion of added norbornene) was obtained (Table 3, entry 2). However, when the reaction time was extended to 1.0, 3.5, and 5.0 min under a constant flow of ethylene (1 atm), all of the norbornene was consumed and poly(ethylene-*alt*-norbornene)-*b*-polyethylene block copolymers, which had norbornene contents of 32.1, 25.6, and 19.9 mol% (Table 3, entries 3–5, respectively) were obtained as the major product together with a small amount of homopolyethylene in the case of longer reactions.[16] The new block copolymers showed values for both the glass-transition temperature (110–114 °C) and the melting point (126–128 °C; Table 3, entries 4 and 5) that correspond to the amorphous poly(ethylene-*alt*-norbornene) segment and the crystalline polyethylene segment, respectively.

In summary, the cationic half-sandwich scandium–alkyl species [Cp′Sc(CH_2SiMe_3)(thf)$_x$][B(C_6F_5)$_4$], generated in situ by reaction of **1**, **2**, or **3** with 1 equivalent of an activator such as **A**, act as excellent catalysts for the alternating copolymerization of ethylene and norbornene. Successive norbornene insertion is sluggish in the present catalyst system, possibly due to steric hindrance. However, the insertion of a norbornene monomer into a Sc–CH_2CH_2R bond and that of an ethylene monomer into a Sc–norbornyl bond could be very fast, and the former could be even more preferred to successive ethylene insertion when a sufficient quantity of norbornene is present. These unique properties lead to rapid and exclusive formation of the alternating ethylene–norbornene copolymer under appropriate ethylene/norbornene molar ratios and also leads to unprecedented formation of poly(ethylene-*alt*-norbornene)-*b*-polyethylene block copolymers when the quantity of the norbornene monomer is low. This work demonstrates, for the first time, that a cationic rare-earth-metal–alkyl species can serve as an excellent catalyst for the copolymerization of ethylene and a cyclic olefin. Further studies on the polymerization/copolymerization of other monomers by this and related rare-earth-metal catalysts are in progress.

Received: September 13, 2004
Published online: December 23, 2004

Table 3: Synthesis of poly(ethylene-*alt*-norbornene)-*b*-polyethylene by **1**/**A**.[a]



Entry	NB [mmol]	t [min]	THF-sol[b]	Yield [g] tol-sol[c]	tol-insol[d]	Major product	NB cont. [mol%][e]	M_n[f] ($\times 10^4$)	PDI[f]	T_g[g] [°C]	T_m[g] [°C]
1	0	5.0	0	0	1.57	PE		12.8	3.05		130
2	10	0.3	0.68			P(E-*alt*-NB)	45.6	3.2	1.42	111	n.o.[h]
3	10	1.0	0.12	1.18	trace	P(E-*alt*-NB)-*b*-PE	32.1	6.7	1.29	118	n.o.[h]
4	10	3.5	trace	1.77	0.07	P(E-*alt*-NB)-*b*-PE	25.6	16.6	1.36	114	128
5	10	5.0	trace	2.12	0.22	P(E-*alt*-NB)-*b*-PE	19.9	18.9	1.40	110	126

[a] Conditions: **1** (21 μmol), **A** (21 μmol), $p_{ethylene} = 1$ atm, toluene (40 mL), $T = 25$ °C. [b] THF-soluble portion: P(E-*alt*-NB) without PE block. [c] THF-insoluble, toluene-soluble portion: P(E-*alt*-NB)-*b*-PE. [d] THF-insoluble, toluene-insoluble portion: homo-PE. [e] NB content determined by ^{13}C NMR spectroscopy. [f] Determined by GPC with polystyrene standards. [g] Measured by DSC. [h] n.o. = not observed.

 © 2005 Wiley-VCH Verlag GmbH & Co. KGaA, Weinheim

Keywords: alkyl complexes · copolymerization · cyclopentadienyl ligands · scandium

[1] a) Z. Hou, Y. Wakatsuki, *Coord. Chem. Rev.* **2002**, *231*, 1–22; b) W. E. Piers, D. J. H. Emslie, *Coord. Chem. Rev.* **2002**, 131–155; c) J. Okuda, *Dalton Trans.* **2003**, 2367–2378; d) Z. Hou, *Bull. Chem. Soc. Jpn.* **2003**, *76*, 2253–2266; e) J. Gromada, J.-F. Carpentier, A. Mortreux, *Coord. Chem. Rev.* **2004**, *248*, 397–410.

[2] L. Lee, D. J. Berg, F. W. Einstein, R. J. Batchelor, *Organometallics* **1997**, *16*, 1819–1821.

[3] a) S. Bambirra, D. van Leusen, A. Meetsma, B. Hessen, J. H. Teuben, *Chem. Commun.* **2003**, 522–523; b) S. Bambirra, M. W. Bouwkamp, A. Meetsma, B. Hessen, *J. Am. Chem. Soc.* **2004**, *126*, 9182–9183.

[4] a) L. W. M. Lee, W. E. Piers, M. R. J. Elsegood, W. Clegg, M. Parvez, *Organometallics* **1999**, *18*, 2947–2949; b) P. G. Hayes, W. E. Piers, R. McDonald, *J. Am. Chem. Soc.* **2002**, *124*, 2132–2133.

[5] a) T. M. Cameron, J. C. Gordon, R. Michalczyk, B. L. Scott, *Chem. Commun.* **2003**, 2282–2283; b) P. G. Hayes, G. C. Welch, D. J. H. Emslie, C. L. Noack, W. E. Piers, M. Parvez, *Organometallics* **2003**, *22*, 1577–1579.

[6] a) S. Bambirra, D. van Leusen, A. Meetsma, B. Hessen, J. H. Teuben, *Chem. Commun.* **2001**, 637–638; b) C. G. J. Tazelaar, S. Bambirra, D. van Leusen, A. Meetsma, B. Hessen, J. H. Teuben, *Organometallics* **2004**, *23*, 936–939; c) S. Hajela, W. P. Schaefer, J. E. Bercaw, *J. Organomet. Chem.* **1997**, *532*, 45–53.

[7] K. Izod, S. T. Liddle, W. Clegg, *Chem. Commun.* **2004**, 1748–1749.

[8] a) C. J. Schaverien, *Organometallics* **1992**, *11*, 3476–3478; b) S. Arndt, T. P. Spaniol, J. Okuda, *Organometallics* **2003**, *22*, 775–781; c) L. D. Henderson, G. D. MacInnis, W. E. Piers, M. Parvez, *Can. J. Chem.* **2004**, *82*, 162–165.

[9] a) S. Arndt, T. P. Spaniol, J. Okuda, *Chem. Commun.* **2002**, 896–897; b) S. Arndt, P. M. Zeimentz, T. P. Spaniol, J. Okuda, M. Honda, K. Tatsumi, *Dalton Trans.* **2003**, 3622–3627.

[10] S. Arndt, T. P. Spaniol, J. Okuda, *Angew. Chem.* **2003**, *115*, 5229–5233; *Angew. Chem. Int. Ed.* **2003**, *42*, 5075–5079.

[11] W. Kaminsky, A. Bark, M. Arndt, *Makromol. Chem. Macromol. Symp.* **1991**, *47*, 83–93.

[12] For examples, see: a) D. Ruchatz, G. Fink, *Macromolecules* **1998**, *31*, 4669–4673; b) B. Y. Lee, Y. H. Kim, Y. C. Won, J. W. Han, W. S. Suh, I. S. Lee, Y. K. Chung, K. H. Song, *Organometallics* **2002**, *21*, 1500–1503; c) A. L. McKnight, R. M. Waymouth, *Macromolecules* **1999**, *32*, 2816–2825; d) P. Altamura, A. Grassi, *Macromolecules* **2001**, *34*, 9197–9200; e) K. Nomura, M. Tsubota, M. Fujiki, *Macromolecules* **2003**, *36*, 3797–3799; f) I. Tritto, C. Marestin, L. Boggioni, M. C. Sacchi, H.-H. Brintzinger, D. R. Fetto, *Macromolecules* **2001**, *34*, 5770–5777; g) Y. Yoshida, J. Saito, M. Mitani, Y. Takagi, S. Matsui, S. Ishii, T. S. Nakano, N. Kashiwa, T. Fujita, *Chem. Commun.* **2002**, 1298–1299; h) G. M. Benedikt, E. Elce, B. L. Goodall, H. A. Kalamarides, L. H. McIntosh, L. F. Rhodes, K. T. Selvy, *Macromolecules* **2002**, *35*, 8978–8988; i) X. F. Li, K. Dai, W. P. Ye, L. Pan, Y. S. Li, *Organometallics* **2004**, *23*, 1223–1230.

[13] The homopolymerization of norbornene with low activity by Sm or Yb amido complex/MAO (MAO is methylaluminoxane) was described previously. See: M. Karl, S. W. Massa, K. Harms, S. Agarwal, R. Maleika, W. Stelter, A. Greiner, W. Heitz, B. Neumüller, K. Dehnicke, *Z. Anorg. Allg. Chem.* **1999**, *625*, 1301–1309.

[14] $B(C_6F_5)_3$ is a weaker activator than $[Ph_3C][B(C_6F_5)_4]$ or $[PhMe_2NH][B(C_6F_5)_4]$ for the generation of a cationic species. The reaction of $[(C_5Me_5)ScMe_2(OPtBu_3)]$ with 1 equivalent of $B(C_6F_5)_3$ in toluene was reported to give a contact ion pair, $[(C_5Me_5)ScMe(OPtBu_3)][MeB(C_6F_5)_3]$, which exhibits a significant $Sc\cdots MeB(C_6F_5)_3$ interaction. See reference [8c].

[15] The alternating ethylene–norbornene copolymers were soluble in toluene, whereas homopolyethylene and homopolynorbornene were insoluble.

[16] The three polymer products P(E-*alt*-NB), P(E-*alt*-NB)-*b*-PE, and PE could be easily separated by solvent fractionation: P(E-*alt*-NB) ($M_n < 4 \times 10^4$) was soluble in THF; P(E-*alt*-NB)-*b*-PE was insoluble in THF but soluble in toluene; PE was insoluble in both THF and toluene.

 © 2005 Wiley-VCH Verlag GmbH & Co. KGaA, Weinheim

Combinatorial Chemistry

Dynamic Combinatorial Chemistry: Lysozyme Selects an Aromatic Motif That Mimics a Carbohydrate Residue**

Sandrine Zameo, Boris Vauzeilles, and Jean-Marie Beau**

Dedicated to Professor Julius Rebek, Jr. on the occasion of his 60th birthday

In a series of recent developments, dynamic combinatorial chemistry (DCC)[1] has proved its capacity to select potent enzyme inhibitors.[2] The success of these preliminary validation studies was mainly based on the use of a previously known high-affinity scaffold[2a,c,d,f] that could reversibly self-assemble with several complementary building blocks. This process results in the formation of a dynamic library of potential ligands in which the target of interest, which acts as a thermodynamic trap, can select its best binder. When the experimental conditions are properly chosen,[3] binding leads to an amplification of this particular compound which can be detected by an appropriate analytical method such as HPLC.

In these early studies, the products that were selected bore very close similarities, both in structure and affinity, to previously known inhibitors of the target enzymes. We were curious to challenge this process with an enzyme for which a scaffold with relatively poor binding properties would hopefully direct members of the dynamic combinatorial library (DCL) towards the active site. Such situations are frequently found in glycobiology, an area of research that is rapidly

[*] S. Zameo, Dr. B. Vauzeilles, Prof. J.-M. Beau
Université Paris-Sud
Laboratoire de Synthèse de Biomolécules associé au CNRS
Institut de Chimie Moléculaire et des Matériaux
91405 Orsay Cedex (France)
Fax: (+33) 1-6985-3715
E-mail: jmbeau@icmo.u-psud.fr

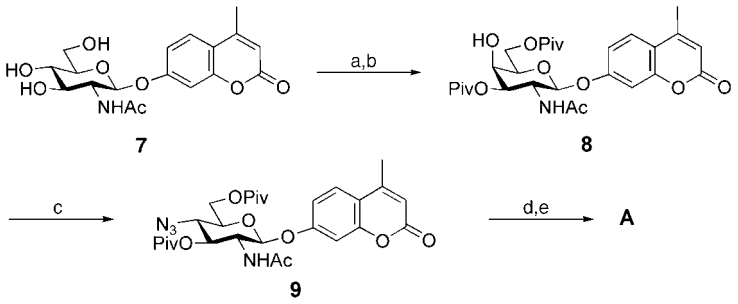
[**] We gratefully acknowledge the Conseil Général de l'Essonne for financial support of this study and GlaxoSmithKline for their interest.

Supporting information for this article is available on the WWW under http://www.angewandte.org or from the author.

 DOI: 10.1002/anie.200462150 © 2005 Wiley-VCH Verlag GmbH & Co. KGaA, Weinheim

becoming fundamental in the post-genomic era.[4] Indeed, many carbohydrate-binding proteins including enzymes (termed Group II proteins)[5] comprise shallow carbohydrate-binding sites that result in relatively weak carbohydrate–protein interactions with dissociation constants often in the millimolar range. We therefore decided to assess the capacity of DCC to probe such low energy interactions and selected for an initial proof-of-principle study a well-known and readily available Group II glycosidase, namely hen egg-white lysozyme (HEWL). Involved in peptidoglycan degradation, HEWL is known to cleave *N*-acetyl-glucosamine oligomers (chito-oligosaccharides) into their smaller units, which, up to the tetramer, behave as competitive inhibitors.[6] The affinity of *N*-acetyl-D-glucosamine (D-GlcNAc) for the HEWL-binding site lies in the 20–50 mM range, whereas chitobiose and chitotriose display higher affinities.[7] On the basis of this knowledge, we designed a DCL of potential HEWL binders starting with a D-GlcNAc (or D-Glc) motif as a scaffold and by using the generation of imines to introduce diversity (Scheme 1). This reversible connecting system, which functions under mild conditions, has previously been reported to be suitable for the formation of DCLs.[2a,c,d,8]

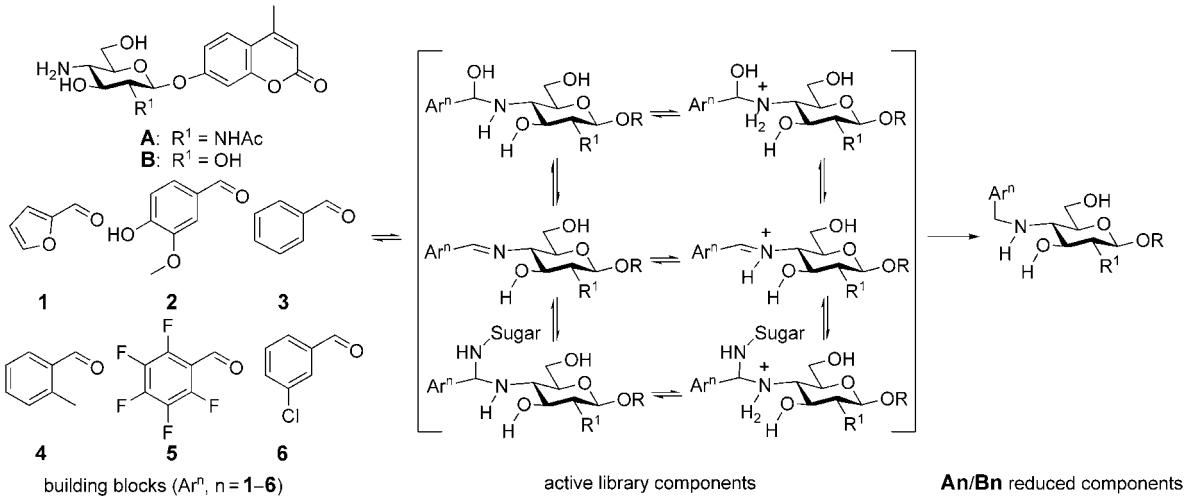
Two amino-derived carbohydrate compounds (amines **A** and **B** in the D-GlcNAc and D-Glc series, respectively) and six differently substituted aromatic aldehydes (**1**–**6**) were selected.[9] A 4-methylumbelliferyl chromophore was introduced at the anomeric position of the carbohydrate building blocks **A** and **B** to allow equal HPLC detection of the different library products at a specific near-UV wavelength ($\lambda = 322$ nm). The aromatic motifs may "mimic", after imine formation, a second carbohydrate ring and potentially interact with complementary aromatic residues of the binding site. Stacking interactions between aromatic residues of the amino acid side chains and the hydrophobic faces of carbohydrates are a common feature of almost every carbohydrate–protein complex studied until present.[5a,10]



Scheme 2. Synthesis of carbohydrate scaffold **A**. a) PivCl, pyridine, CH_2Cl_2, 0 °C, 2 h (78%); b) 1) Tf_2O, pyridine, CH_2Cl_2, −15 °C, 1 h; 2) $NaNO_2$, DMF, 20 °C, 16 h; 3) $NaHCO_3$, H_2O, 20 °C, 5 min (64%); c) 1) Tf_2O, pyridine, CH_2Cl_2, −15 °C, 1 h; 2) NaN_3, Bu_4NHSO_4, DMF, 20 °C, 16 h (61%); d) MeONa, MeOH, 20 °C, 5 d (84%); e) H_2, Pd/C (5%), MeOH, 20 °C, 4 h (90%). Piv = pivaloyl, Tf = trifluoromethylsulfonate, DMF = *N*,*N*-dimethylformamide.

Amine **A** was synthesized from *N*-acetyl-D-glucosamine following the sequence presented in Scheme 2. The 4-methylumbelliferyl glycoside **7** was obtained by Roy's procedure[11] and by using Horton's chloride.[12] Regioselective pivaloylation of hydroxyl groups at the 3 and 6 positions,[13] followed by epimerization at C-4[14] furnished the D-galacto derivative **8**. Triflate formation and nucleophilic substitution by sodium azide provided the azido intermediate **9**, which after deprotection of the hydroxyl groups and catalytic hydrogenation afforded amine **A**. A similar sequence was applied to the preparation of amine **B** from D-galactose (see Supporting Information).

When a mixture of amines **A** and **B** (0.4 mM) were equilibrated with aldehydes **1**–**6** (0.4 mM each) at room temperature in an aqueous phosphate buffer solution (pH 6.2) in the presence of sodium cyanoborohydride (3.6 mM), slow formation of the amines through reduction of the iminium species was observed. After 24 h, the twelve expected products could be detected by reverse-phase HPLC (Figure 1 a). Equilibration of the same library in the presence of HEWL (0.4 mM) induced a detectable change in the distribution of the amines in the mixture with enrichment of



Scheme 1. Structures of the building blocks and components of the dynamic combinatorial library (DCL).

 © 2005 Wiley-VCH Verlag GmbH & Co. KGaA, Weinheim

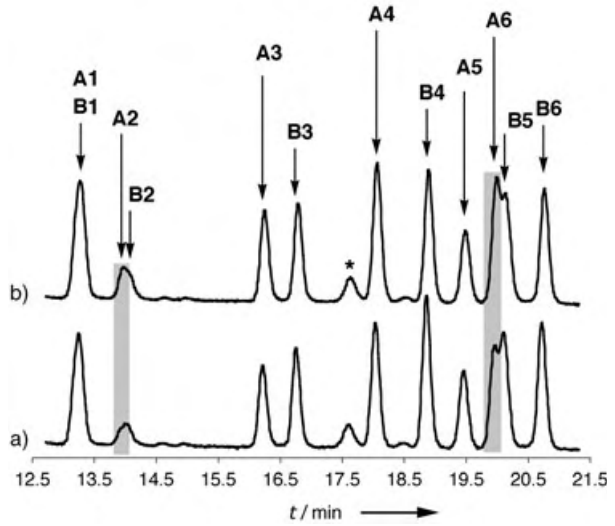


Figure 1. Selected portion of HPLC chromatograms of the DCL made from amines **A** and **B**, and aldehydes **1**–**6** over 24 h: a) in the absence of HEWL and b) in the presence of HEWL (1 equiv). (* indicates residual 4-methylumbelliferone).

amines **A2** and, to a lesser extent, **A6** (resulting from reductive alkylation of amine **A** with aldehydes **2** and **6**, respectively; see Figure 1b). Although HPLC–MS analysis easily confirmed the structures, amplification of the active components becomes difficult to evaluate when a strong overlap occurs (see, for instance, amines **A1** and **B1** in Figure 1), and this difficulty increases with the size of the library.[9,15] We therefore constructed and analyzed sublibraries with amines **A** and **B**. As expected from the previous experiments, amplification of amines **A2** and **A6** was observed when comparing libraries synthesized from **A** in the presence (Figure 2b) and in the absence (Figure 2a) of HEWL. No amplification was detected in the presence of HEWL in the sublibrary that was based on amine **B** (see Supporting Information). This clearly indicates that the enzyme selects amine **A** as a scaffold rather than amine **B**. When the reaction was performed at a higher concentration of HEWL (1.2 mM), the amplification was significantly enhanced (Figure 2c). Also, the addition of chitotriose, a good HEWL inhibitor, led to a reduction (0.4 mM chitotriose, not shown) or disappearance (1.2 mM chitotriose, Figure 2d) of the amplification effect.

All these simple experiments clearly indicate an amplification of the library members selected through interaction with the HEWL active site. Interaction of scaffold **A** with the active site rather than scaffold **B** further indicates that the 2-acetamido group is an essential feature for recognition of the library members by HEWL.[7b,16] The active site of the enzyme is a cleft composed of six carbohydrate-binding subsites (A to F[17] or −4 to +2[18]). Subsites −4, −2, and +1 are D-GlcNAc-binding sites which are sensitive to the acetamido substituent by strict hydrogen-bonding and hydrophobic interactions, whereas the three other sites are not.[17] As chitotriose is known to tightly bind to the −4 to −2 subsites,[17] the extra stabilization of the precursors of amines **A2** and **A6** above

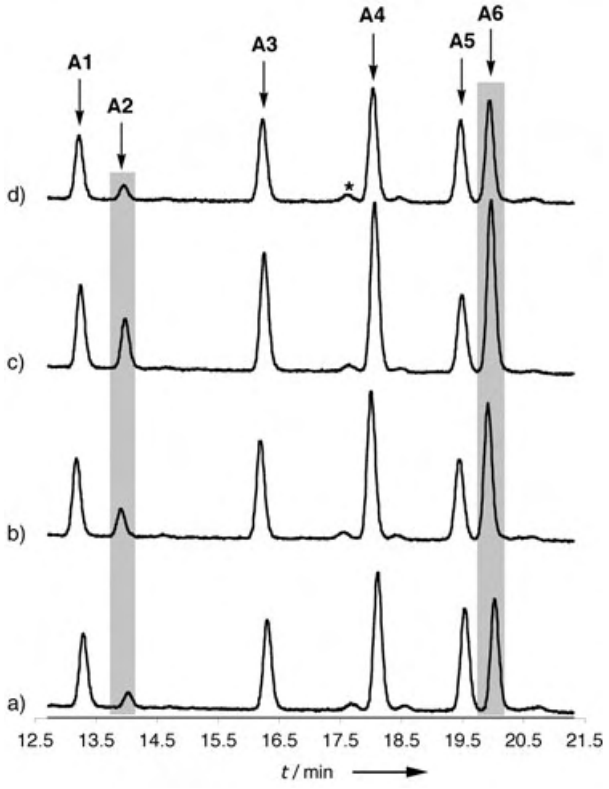
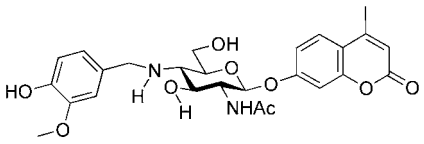


Figure 2. Selected portion of HPLC chromatograms showing the products of the DCL prepared from amine **A** and aldehydes **1**–**6** over 24 h: a) in the absence of HEWL, b) in the presence of 1 equivalent of HEWL, c) in the presence of 3 equivalents of HEWL, and d) in the presence of 1 equivalent of HEWL and 3 equivalents of chitotriose. (* indicates residual 4-methylumbelliferone).

suggests that the D-GlcNAc scaffold may occupy subsite −2 with the selected aromatic motif occupying subsite −3.

If this reasoning is correct, amines **A2** or **A6** may display inhibitory activities which are comparable to that of chitobiose.[19] To test this hypothesis, the most amplified compound (amine **A2**, Scheme 3) was synthesized separately,[20] and its



A2

Scheme 3. Amine **A2**, which results from reductive alkylation of amine **A** with aldehyde **2**.

inhibitory activity was measured and compared with the chito-oligomers. We used the lysis rate of *Micrococcus lysodeikticus*, a Gram-positive bacteria that is very sensitive to HEWL,[21] as a measure of the enzyme activity. Lineweaver–Burk analysis is presented in Figure 3. The inhibition constants (K_i) measured for *N*-acetyl-D-glucosamine and chitotriose were the same as those reported (not shown).[7] The value found for chitobiose was in the range reported (0.6 mM instead of 0.2 mM reported, see Supporting Informa-

 © 2005 Wiley-VCH Verlag GmbH & Co. KGaA, Weinheim

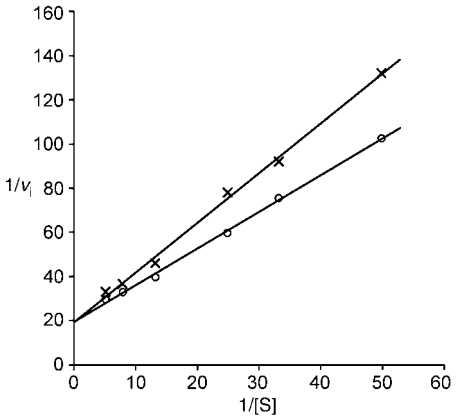


Figure 3. Lineweaver–Burk analysis (double reciprocal plot) of the observed initial lysis rate (V_i) as a function of the concentration of *Micrococcus lysodeikticus* ([S]) in the absence (○) and in the presence (×) of amine **A2** (214 μM).

tion). The inhibition assays carried out with amine **A2** (Figure 3) yielded a competitive type of inhibition with a K_i value that was similar to the value observed for chitobiose ($K_i = 0.6$ mM).

These results indicate an additional binding effect from the aromatic motifs, with amine **A2** being around 100-fold more active than the starting *N*-acetyl-D-glucosamine. With the peptidoglycan substrate, HEWL subsite −3 hosts a carbohydrate moiety (a *N*-acetylmuramic acid unit) which is known to interact with complementary aromatic residues through stacking interactions.[17] The K_i values, which are similar for **A2** and chitobiose, suggest that the enzyme selects from the DCL an aromatic motif with a precise substitution pattern that best fits in subsite −3.

We have shown that hen egg-white lysozyme selects from a dynamic library of potential active-site ligands an optimal binder, which comprises an aryl group that mimics a carbohydrate unit. In such a dynamic combinatorial assay, the system has shown its capacity to discriminate subtle affinity variations induced by the different substitutions on the aromatic moiety of the aldehydes. Further structural studies to confirm this hypothesis and experiments to develop and extend this approach are currently in progress in our group.

Experimental Section

Preparation of a DCL from amines **A** and **B** and aldehydes **1**–**6**: Stock solutions of amines **A** (12 mM) and **B** (2.4 mM) were prepared in distilled water. Solutions of aldehydes (0.6 mM) in phosphate buffer (30 mM, pH 6.2) and sodium cyanoborohydride (36 mM) in distilled water were prepared just prior to use. Solutions of amine **A** (16.7 μl), amine **B** (83.5 μl), and the aldehydes (333 μl) were introduced into an Eppendorf tube, which was equipped with a small magnetic stirrer bar, and the volume was adjusted to 450 μl with distilled water. After stirring, a 225-μl aliquot of the mixture was removed and introduced into an Eppendorf tube that contained HEWL (1.5 mg, 1 equiv). Both Eppendorf tubes were stirred for 30 min before solutions of sodium cyanoborohydride (25 μl) were added. The resulting mixtures (250 μl) were equilibrated at room temperature for 24 h. 20-μl aliquots were removed from these solutions and guanidine thiocyanate (4.7 mg), a good denaturant of HEWL, was added prior to HPLC analysis to ensure the release of any bound ligand from the active site. This treatment was also applied in the control experiment without HEWL. After 1 h, acetic acid (20 μl) was added, and the solution was diluted with methanol (120 μl). Analytical chromatography was performed on a JASCO LC-1500 system equipped with a Phenomenex LUNA C18 (2) 5μ reversed-phase HPLC column (150 × 4.60 mm) with UV/Vis detection at $\lambda = 322$ nm. A binary solvent gradient (solvent A: 0.1% trifluoroacetic acid in 95:5 H_2O/CH_3CN, solvent B: 0.1% trifluoroacetic acid in 95:5 CH_3CN/H_2O) was optimized to separate most of the DCL compounds: from 90:10 A/B to 70:30 A/B over 20 min, with a flow rate of 0.8 mL min^{-1}. HPLC peaks were assigned by means of LC–MS analysis. Some products were synthesized and characterized separately to validate their assignments on the chromatograms.

Received: September 29, 2004
Published online: January 11, 2005

Keywords: carbohydrates · combinatorial chemistry · enzyme inhibitors · molecular recognition · reduction

[1] J.-M. Lehn, *Chem. Eur. J.* **1999**, *5*, 2455; I. Huc, R. Nguyen, *Comb. Chem. High Throughput Screening* **2001**, *4*, 109; S. J. Rowan, S. J. Cantrill, G. R. L. Cousins, J. K. M. Sanders, J. F. Stoddart, *Angew. Chem.* **2002**, *114*, 938; *Angew. Chem. Int. Ed.* **2002**, *41*, 898.

[2] a) I. Huc, J.-M. Lehn, *Proc. Natl. Acad. Sci. USA* **1997**, *94*, 2106; b) T. Bunyapaiboonsri, O. Ramström, S. Lohman, J.-M. Lehn, L. Peng, M. Goeldner, *ChemBioChem* **2001**, *2*, 438; c) M. Hochgürtel, H. Kroth, D. Piecha, M. W. Hofmann, C. Nicolau, S. Krause, O. Schaaf, G. Sonnenmoser, A. V. Eliseev, *Proc. Natl. Acad. Sci. USA* **2002**, *99*, 3382; d) M. Hochgürtel, R. Biesinger, H. Kroth, D. Piecha, M. W. Hofmann, S. Krause, O. Schaaf, C. Nicolau, A. V. Eliseev, *J. Med. Chem.* **2003**, *46*, 356; e) T. Bunyapaiboonsri, H. Ramström, O. Ramström, J. Haiech, J.-M. Lehn, *J. Med. Chem.* **2003**, *46*, 5803; f) M. S. Congreve, D. J. Davis, L. Devine, C. Granata, M. O'Reilly, P. G. Wyatt, H. Jhoti, *Angew. Chem.* **2003**, *115*, 4617; *Angew. Chem. Int. Ed.* **2003**, *42*, 4479.

[3] Z. Grote, R. Scopelliti, K. Severin, *Angew. Chem.* **2003**, *115*, 3951; *Angew. Chem. Int. Ed.* **2003**, *42*, 3821; P. T. Corbett, S. Otto, J. K. M. Sanders, *Chem. Eur. J.* **2004**, *10*, 3139.

[4] R. U. Lemieux, *Acc. Chem. Res.* **1996**, *29*, 373; R. A. Dwek, *Chem. Rev.* **1996**, *96*, 683; C. Bertozzi, L. L. Kiessling, *Science* **2001**, *291*, 2357; P. M. Rudd, R. A. Dwek, *Crit. Rev. Biochem. Mol. Biol.* **1997**, *32*, 1; H. J. Gabius, *Biochim. Biophys. Acta* **2002**, *1572*, 165; H. Kogelberg, D. Solis, J. Jiménez-Barbero, *Curr. Opin. Struct. Biol.* **2003**, *13*, 646.

[5] a) F. A. Quiocho, N. K. Vyas in *Bioorganic Chemistry: Carbohydrates* (Ed.: S. M. Hecht), Oxford University Press, Oxford, **1999**, pp. 441–457; b) P. Sears, C.-H. Wong, *Angew. Chem.* **1999**, *111*, 2446; *Angew. Chem. Int. Ed.* **1999**, *38*, 2300.

[6] J. A. Rupley, *Proc. R. Soc. London, Ser. B* **1967**, *167*, 416.

[7] a) F. W. Dahlquist, L. Jao, M. Raftery, *Proc. Natl. Acad. Sci. USA* **1966**, *63*, 26; b) D. M. Chipman, N. Sharon, *Science* **1969**, *165*, 454.

[8] H. Li, P. Williams, J. Micklefield, J. M. Gardiner, G. Stephens, *Tetrahedron* **2004**, *60* , 753.

[9] For clarity, only six out of the thirty-six aromatic aldehydes that were tested are shown in this work (see Supporting Information).

[10] C.-H. Wong, *Acc. Chem. Res.* **1999**, *32*, 376.

[11] D. Carrière, S. J. Meunier, F. D. Tropper, S. Cao, R. Roy, *J. Mol. Catal. A* **2000**, *154*, 9.

 © 2005 Wiley-VCH Verlag GmbH & Co. KGaA, Weinheim

[12] D. Horton, *Org. Synth.* **1966**, *46*, 1.
[13] L. Lay, F. Nicotra, L. Panza, G. Russo, E. Adobati, *Helv. Chim. Acta* **1994**, *77*, 509.
[14] F. Santoyo-Gonzalez, C. Uriel, J. A. Calvo-Asin, *Synthesis* **1998**, 1787.
[15] Out of thirty-six aromatic aldehydes tested (see Supporting Information), the product derived from aldehyde **2** was the most amplified by the enzyme.
[16] A. Neuberger, B. M. Wilson, *Nature* **1967**, *215*, 524.
[17] C. C. F. Blake, D. F. Koenig, G. A. Mair, A. C. T. North, D. C. Phillips, V. R. Sarma, *Nature* **1965**, *206*, 757; L. N. Johnson, D. C. Phillips, *Nature* **1965**, *206*, 761; C. C. F. Blake, L. N. Johnson, G. A. Mair, A. C. T. North, D. C. Phillips, V. R. Sarma, *Proc. R. Soc. London Ser. B* **1967**, *167*, 378; K. Maenaka, M. Matsushima, H. Song, F. Sunada, K. Watanabe, I. Kumagai, *J. Mol. Biol.* **1995**, *247*, 281.
[18] G. J. Davies, K. S. Wilson, B. Henrissat, *Biochem. J.* **1997**, *321*, 557; D. J. Vocadlo, G. J. Davies, R. Laine, S. G. Withers, *Nature* **2001**, *412*, 835.
[19] It should, however, be noted that the true binders are one of the two hemiaminals, the aminal, the imine, or their protonated species and that the corresponding reduced compound may have much poorer binding properties.
[20] The imine was preformed in methanol (amine **A**, aldehyde **2**, MeOH, 3 Å molecular sieves, 48 h) and then reduced ($NaBH_4$, 16 h, 83%).
[21] D. Shugar, *Biochim. Biophys. Acta* **1952**, *8*, 302; A. L. N. Prasad, G. Litwack, *Anal. Biochem.* **1963**, *6*, 328.

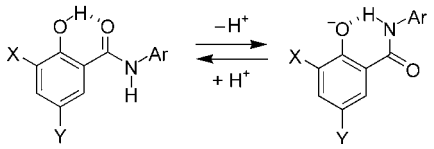
 © 2005 Wiley-VCH Verlag GmbH & Co. KGaA, Weinheim

Oligoamide Conformations

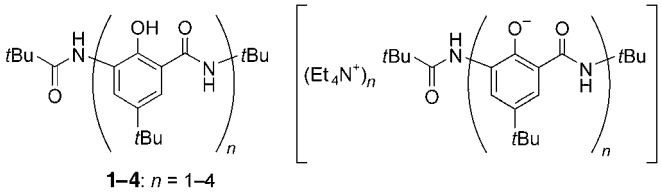
Linear-to-Turn Conformational Switching Induced by Deprotonation of Unsymmetrically Linked Phenolic Oligoamides**

*Daisuke Kanamori, Taka-aki Okamura, Hitoshi Yamamoto, and Norikazu Ueyama**

Aromatic oligoamide compounds attract much attention because they form highly ordered structures with intramolecular hydrogen bonds.[1–8] In particular, control of conformational switching within a molecule could lead to the development of molecular machines.[9–11] Salicylamide derivatives are well known to form a highly ordered, planar conformation through hydrogen bonds.[12,13] A rearrangement of the intramolecular hydrogen bond induced by deprotonation of the phenolic OH group was suggested previously[14] and established in our recent study on the crystal structures of protonated and deprotonated salicylamide derivatives (Scheme 1).[15] From these findings, we believe that oligoamide compounds that comprise a salicylamide moiety in a repeating unit have the potential to exhibit conformational switching with the rearrangement of the intramolecular hydrogen bond as the driving force of conformational switching.[9,10] Herein, we report the synthesis and structure determinations of unsymmetrically linked phenolic oligoamides (**1**–**4**) that comprise a salicylamide skeleton in a repeating unit as novel aromatic oligoamide compounds that undergo a conformational switch.



Scheme 1. Conformational switching of a salicylamide derivative by deprotonation and protonation. Ar = 2-chlorophenyl, X = Br, Y = Cl.



1–4: *n* = 1–4

The crystal structures of protonated and deprotonated monomer models, namely, **1′** and $(\mathbf{1}'-H^+)^-Me_4N^+$, which differ from **1** by the replacement of the *t*BuCO group by MeCO, are shown in Figure 1. In **1′**, the phenol OH group forms intramolecular NH···OH and OH···O=C hydrogen bonds with average short distances for O11-N1 and O11-O2 of 2.622 and 2.486 Å, respectively. In the case of $(\mathbf{1}'-H^+)^-Me_4N^+$, the phenolate oxygen anion forms double intramolecular NH···O(oxyanion) hydrogen bonds with short distances for O11-N1 and O11-N2 of 2.605(2) and 2.643(2) Å. The *C*-terminal *N*-*tert*-butylcarbamoyl substituent forms two different types of hydrogen bonds which means that the deprotonation of the phenol OH group induces a conformational change (≈180° rotation about the C12–C2 bond) that leads from a linear-to-turn conformational switching in longer oligoamides. This type of conformational switching was established in our previous study with other salicylamide derivatives (Scheme 1).[15] Intermolecular interactions were found in **1′** only as NH···O=C hydrogen bonds.

Molecular structures of the dimer in protonated and deprotonated forms, **2** and $(\mathbf{2}-2H^+)^{2-}(Et_4N^+)_2$, are shown in Figure 2. In **2**, each phenol OH group forms intramolecular NH···OH and OH···O=C hydrogen bonds that result in an intramolecular NH···OH···O=C-NH···OH···O=C hydro-

[*] D. Kanamori, Dr. T.-a. Okamura, Dr. H. Yamamoto, Prof. N. Ueyama
Department of Macromolecular Science
Graduate School of Science
Osaka University
Toyonaka, Osaka, 560-0043 (Japan)
Fax: (+81) 6-6850-5474
E-mail: ueyama@chem.sci.osaka-u.ac.jp

[**] D.K. expresses his special thanks to the Center of Excellence (21COE) program "Creation of Integrated EcoChemistry of Osaka University".

Supporting information for this article is available on the WWW under http://www.angewandte.org or from the author.

 DOI: 10.1002/anie.200461842 © 2005 Wiley-VCH Verlag GmbH & Co. KGaA, Weinheim

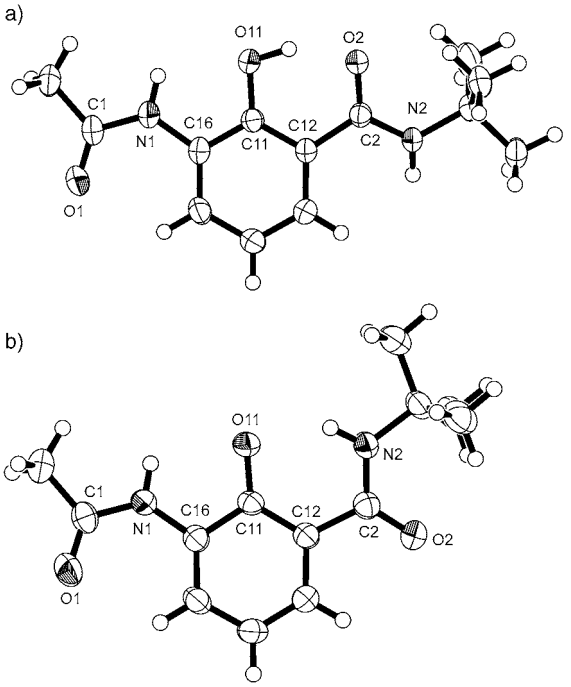


Figure 1. Molecular structures of a) **1′** (one of the two crystallographically independent molecules is shown) and b) $(\mathbf{1}'-H^+)^-Me_4N^+$. Displacement ellipsoids are drawn at the 50% probability level; the tetramethylammonium cation is omitted for clarity in (b). Selected bond lengths, short contacts [Å], and torsion angles [°] for **1′**: C11–O11 1.3606(16), O11···N1 2.606(1), O11···O2 2.481(1), C1-N1-C16-C11 170.71(15), N2-C2-C12-C11 −167.69(14). Selected bond lengths, short contacts [Å], and torsion angles [°] for $(\mathbf{1}'-H^+)^-$: C11–O11 1.297(2), O11···N1 2.605(2), O11···N2 2.643(2), C1-N1-C16-C11 173.43(14), N2-C2-C12-C11 7.2(2).

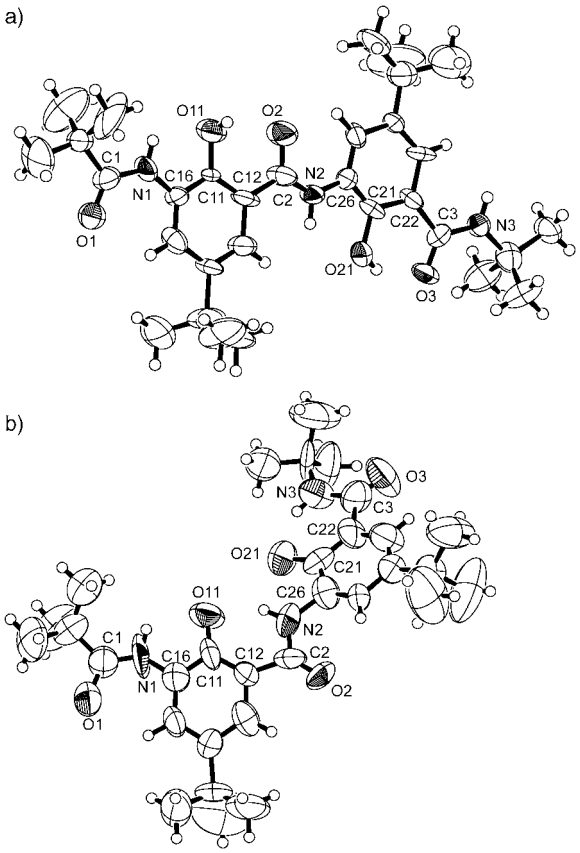


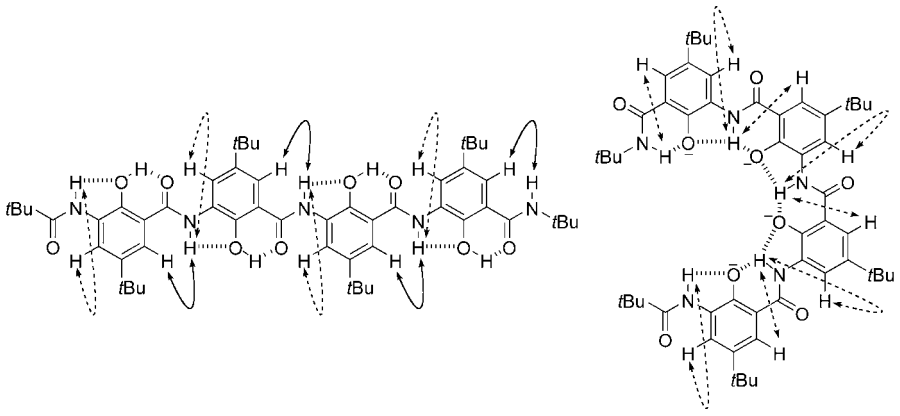
Figure 2. Molecular structures of a) **2** and b) $(\mathbf{2}-2H^+)^{2-}(Et_4N^+)_2$. Displacement ellipsoids are drawn at the 50% probability level; solvent molecules and tetraethylammonium cations are omitted for clarity. Selected bond lengths, short contacts [Å], and torsion angles [°] for **2**: C11–O11 1.332(9), C21–O21 1.414(10), O11···N1 2.584(9), O11···O2 2.472(9), O21···N2 2.584(9), O21···O3 2.462(8), C1-N1-C16-C11 172.8(9), N2-C2-C12-C11 −172.2(10), C2-N2-C26-C21 178.4(10), N3-C3-C22-C21 −175.0(8). Selected bond lengths, short contacts [Å], and torsion angles [°] for $(\mathbf{2}-2H^+)^{2-}$: C11–O11 1.268(14), C21–O21 1.339(13), O11···N1 2.50(1), O11···N2 2.64(1), O21···N2 2.72(1), O21···N3 2.58(1), C1-N1-C16-C11 −176(2), N2-C2-C12-C11 −22(2), C2-N2-C26-C21 153.2(14), N3-C3-C22-C21 7(2).

gen-bonded chain. A similar mode of hydrogen bonding was reported for 3,3′,5,5′,6-pentachloro-2′-hydroxysalicylanilide.[16] In $(\mathbf{2}-2H^+)^{2-}(Et_4N^+)_2$, both of the phenolate oxygen anions form double intramolecular NH···O(oxyanion) hydrogen bonds. The NH group in the bridging amide group is involved in a bifurcated intramolecular NH···O(oxyanion) hydrogen bond. This type of intramolecular hydrogen bond is classified as a three-center hydrogen bond and is reported to be strong.[17] Three-center hydrogen-bonded structures are also known to be almost planar.[3,6,17] However, the crystal structure of $(\mathbf{2}-2H^+)^{2-}(Et_4N^+)_2$ has a slightly distorted structure that is different from other oligoamides. Because the optimized structure of simplified $(\mathbf{2}-2H^+)^{2-}$ is planar,[18] this slight distortion may be caused by its packing structure. The difference in the hydrogen-bonding mode between the hydroxyl or phenoxyl group and the neighboring substituents on the *C*-terminal side gives a linear-to-turn conformational switch. Intermolecular hydrogen bonds are formed in the protonated form **2** as NH···O=C hydrogen-bonded chains and not in $(\mathbf{2}-2H^+)^{2-}(Et_4N^+)_2$. This behavior is similar to that of the monomeric protonated pair, **1′** and $(\mathbf{1}'-H^+)^-Me_4N^+$.

Structures of the oligoamides in solution were determined by ^1H NMR spectroscopy of samples dissolved in $CDCl_3$ and CD_3CN (5 mM). Chemical shifts of OH and NH groups indicate hydrogen-bond formation. Dilution experiments from 40 to 1 mM for all oligoamides resulted in no significant changes in the chemical shifts for the OH and NH groups (within 0.04 ppm) which indicates that intermolecular hydrogen bonds are not formed.[3] In the protonated forms of all the oligoamides, the signals for the phenol OH groups were observed at significantly low field ($\delta = 12.49$–13.36 ppm) which suggests the formation of OH···O=C hydrogen bonds. The signals for the NH protons of the *N*-terminal and bridging amide groups were observed at $\delta = 8.24$–8.25 and $\delta = 8.99$–9.06 ppm, respectively. These NH signals were shifted slightly downfield relative to the NH protons in benzanilide ($\delta =$ 7.76–7.86 ppm),[19] which indicates the formation of NH···OH hydrogen bonds in the *N*-terminal and bridging amide groups. The amide NH protons in the *C*-terminal amide groups were observed at $\delta = 6.13$ ppm, where signals for non-hydrogen-bonded NH groups of benzamide derivatives are usually observed. NOE correlations between amide NH protons and aryl protons are useful in elucidating the conformations of aromatic amide compounds, including salicylamide derivatives.[20] The NH protons, except in the

 © 2005 Wiley-VCH Verlag GmbH & Co. KGaA, Weinheim

N-terminal amide group, show NOE correlations with neighboring aromatic protons in each unit. If all oligoamides display a similar mode of hydrogen bonding in solution as that found in the crystal structures of **1′** and **2**, these results are reasonable. The proposed structure of **4** is depicted in Scheme 2 with arrows representing the observed NOE correlations. The similarities in the ^{1}H NMR spectroscopic results of all the oligoamides show that the longer oligoamides also have linear conformations with the same hydrogen-bonding mode in the protonated forms as shown for **1′** and **2**.



Scheme 2. Proposed structures of **4** (linear) and the anionic part of $(\mathbf{4}-4\,H^+)^{4-}$ (turn) in solution. Arrows represent NOE correlations (----- represent correlations that are present only in [D_6]DMSO).

For the deprotonated forms of all the oligoamides, the signals for the NH protons were largely shifted downfield relative to the corresponding protons in the protonated forms which suggests strong NH···O(oxyanion) hydrogen-bond formation. The NH protons in the bridging amide groups showed the largest downfield shift relative to other NH protons in each oligoamide. As established in the crystal structure of $(\mathbf{2}-2\,H^+)^{2-}(Et_4N^+)_2$, the NH proton in the bridging amide group forms a bifurcated NH···O(oxyanion) hydrogen bond. The bifurcated hydrogen bond is stronger and shifts the signal for NH more downfield than a single hydrogen bond would do.[21] No NOE correlations were observed for any of the NH protons in $CDCl_3$ or CD_3CN. The results also show that the amide NH protons do not direct to aromatic protons but rather to phenolate oxygen anions. The proposed structure of the anion part of $(\mathbf{4}-4\,H^+)^{4-}(Et_4N^+)_4$ is depicted in Scheme 2. The similarities in the ^{1}H NMR spectroscopic results for the longer oligoamides to those for $(\mathbf{1}'-H^+)^-Me_4N^+$ and $(\mathbf{2}-2\,H^+)^{2-}(Et_4N^+)_2$ indicate that the other oligoamides also adopt the turn conformation in the deprotonated form with the same hydrogen-bonding mode.

Even in a strong intermolecular hydrogen-bonding solvent, [D_6]DMSO,[22] the overall conformations of protonated and deprotonated forms are maintained because the observed additional NOE correlations between the NH and aryl protons are very weak.

In terms of the close proximity of the phenol oxygen atoms, the turn conformation in the deprotonated form resembles the conformation of benzoxazine oligomers[23] and calixarenes, although the conformations of the latter are observed for the protonated form. Because the pK_a values of each phenol OH group of these oligoamides are lowered by the intramolecular NH···O(oxyanion) hydrogen bonds,[14,24,25] the OH protons can completely dissociate, unlike the case of calixarenes.[26,27] Our results indicate that as a consequence of lowering the basicity, intramolecular NH···O(oxyanion) hydrogen bonds enable phenolate anions to position themselves close to each other. Charge delocalization of phenolate anions supported by the results of cyclic voltammograms that reveal that all phenolate anions are in a mixed-valence state also means a lowering of the basicity (see Supporting Information).

In conclusion, conformational switching in the unsymmetrically linked phenolic oligoamides, monomer **1** to tetramer **4**, was established in both the solid (for monomers and dimers) and solution states. The deprotonation of a hydroxyl group in each unit induces a rearrangement of the hydrogen-bonding mode within the unit from OH···O=C to NH···O(oxyanion), which leads to linear-to-turn conformational switching.

Experimental Section

X-ray crystal structure analysis: The data were collected at 200 K on a Rigaku RAXIS-RAPID Imaging Plate diffractometer ($Mo_{K\alpha}$ radiation; $\lambda = 0.71069$ Å for **1′** and 0.71075 Å for others). The structures were solved by direct methods (SIR92[28] for **1′** and $(\mathbf{1}'-H^+)^-Me_4N^+$ and SIR2002[29] for **2** and SHELXS-97[30] for $(\mathbf{2}-2\,H^+)^{2-}(Et_4N^+)_2$) and refined by full-matrix least-squares on F^2. The non-hydrogen atoms were refined anisotropically. The coordinates of OH and NH protons in **1′** were refined by using fixed thermal factors, and the rests were included in calculated positions. Crystal data for $C_{13}H_{18}N_2O_3$ (**1′**): $0.35\times0.35\times0.35$ mm^3, monoclinic, $P2_1/a$ (#14), $a = 16.4062(10)$, $b = 9.9004(7)$, $c = 16.5488(14)$ Å, $\beta = 92.1580(10)°$, $V = 2686.1(3)$ Å^3, $Z = 8$, $\rho_{calcd} = 1.238$ g cm^{-3}, $\mu(Mo_{K\alpha}) = 0.88$ cm^{-1}, $M_w = 250.29$. 6124 reflections and 349 variables were used to solve the structure, $R_1 = 0.044$, $wR_2 = 0.113$, GOF $(F^2) = 1.00$. Crystal data for $C_{17}H_{21}N_3O_3$ ($(\mathbf{1}'-H^+)^-Me_4N^+$): $0.40\times0.20\times0.10$ mm^3, monoclinic, $P2_1/n$ (#14), $a = 6.890(5)$, $b = 15.33(2)$, $c = 18.05(2)$ Å, $\beta = 93.41(8)°$, $V = 1904(4)$ Å^3, $Z = 4$, $\rho_{calcd} = 1.128$ g cm^{-3}, $\mu(Mo_{K\alpha}) = 0.77$ cm^{-1}, $M_w = 323.43$. 4350 reflections and 209 variables were used to solve the structure, $R_1 = 0.042$, $wR_2 = 0.095$, GOF $(F^2) = 0.81$. Crystal data for $C_{35}H_{55}N_3O_6$ (**2**·Et_2O): $0.30\times0.10\times0.10$ mm^3, monoclinic, *Cc* (#9), $a = 16.720(3)$, $b = 10.2219(16)$, $c = 23.907(3)$ Å, $\beta = 93.248(11)°$, $V = 4079.4(11)$ Å^3, $Z = 4$, $\rho_{calcd} = 0.999$ g cm^{-3}, $\mu(Mo_{K\alpha}) = 0.68$ cm^{-1}, $M_w = 613.83$. 7681 reflections and 427 variables were used to solve the structure, $R_1 = 0.077$, $wR_2 = 0.163$, GOF $(F^2) = 0.85$. Crystal data for $C_{49}H_{86}N_6O_5$ ($(\mathbf{2}-2\,H^+)^{2-}(Et_4N^+)_2$·$CH_3CN$): $0.20\times0.20\times0.20$ mm^3, monoclinic, $P2_1/c$, $a = 15.223(12)$, $b = 17.143(13)$, $c = 19.901(14)$ Å, $\beta = 101.44(3)°$, 5090(7) Å^3, $Z = 4$, $\rho_{calcd} = 1.095$ g cm^{-3}, $\mu(Mo_{K\alpha}) = 0.71$ cm^{-1}, $M_w = 839.24$. 8946 reflections and 542 variables were used to solve the structure, $R_1 = 0.095$, $wR_2 = 0.128$, GOF $(F^2) = 0.74$. CCDC 247765–CCDC 247768 contain the supplementary crystallographic data for this paper. These data can be obtained free of charge

 © 2005 Wiley-VCH Verlag GmbH & Co. KGaA, Weinheim

from the Cambridge Crystallographic Data Centre via www.ccdc.cam.ac.uk/data_request/cif.

Received: August 31, 2004
Revised: October 23, 2004
Published online: December 28, 2004

Keywords: amides · conformation analysis · hydrogen bonds · protonation

[1] I. Huc, *Eur. J. Org. Chem.* **2004**, 17 – 29.
[2] H. Jiang, C. Dolain, J.-M. Léger, H. Gornitzka, I. Huc, *J. Am. Chem. Soc.* **2004**, *126*, 1034 – 1035.
[3] Z.-Q. Wu, X.-K. Jiang, S.-Z. Zhu, Z.-T. Li, *Org. Lett.* **2004**, *6*, 229 – 232.
[4] X. Yang, L. Yuan, K. Yamato, A. L. Brown, W. Feng, M. Furukawa, X. C. Zeng, B. Gong, *J. Am. Chem. Soc.* **2004**, *126*, 3148 – 3162.
[5] H. Jiang, J.-M. Léger, I. Huc, *J. Am. Chem. Soc.* **2003**, *125*, 3448 – 3449.
[6] J. Zhu, R. D. Parra, H. Zeng, E. Skrzypczak-Jankun, X. C. Zeng, B. Gong, *J. Am. Chem. Soc.* **2000**, *122*, 4219 – 4220.
[7] B. Gong, *Chem. Eur. J.* **2001**, *7*, 4337 – 4342.
[8] J. T. Ernst, J. Becerril, H. S. Park, H. Yin, A. D. Hamilton, *Angew. Chem.* **2003**, *115*, 553 – 557; *Angew. Chem. Int. Ed.* **2003**, *42*, 535 – 539.
[9] C. Dolain, V. Maurizot, I. Huc, *Angew. Chem.* **2003**, *115*, 2844 – 2846; *Angew. Chem. Int. Ed.* **2003**, *42*, 2738 – 2740.
[10] E. Kolomiets, V. Berl, I. Odriozola, A.-M. Stadler, N. Kyritsakas, J.-M. Lehn, *Chem. Commun.* **2003**, 2868 – 2869.
[11] M. Barboiu, J.-M. Lehn, *Proc. Natl. Acad. Sci. USA* **2002**, *99*, 5201 – 5206.
[12] E. Steinwender, W. Mikenda, *Monatsh. Chem.* **1990**, *121*, 809 – 820.
[13] M. Kondo, *Bull. Chem. Soc. Jpn.* **1972**, *45*, 2790 – 2793.
[14] W. L. Mock, D. C. Y. Chua, *J. Chem. Soc. Perkin Trans. 2* **1995**, 2069 – 2074.
[15] D. Kanamori, T. Okamura, H. Yamamoto, S. Shimizu, Y. Tujimoto, N. Ueyama, *Bull. Chem. Soc. Jpn.* **2004**, *77*, 2057 – 2064.
[16] A. C. Sindt, M. F. Mackay, *Acta Crystallogr. Sect. B* **1979**, *35*, 2103 – 2108.
[17] R. D. Parra, H. Zeng, J. Zhu, C. Zheng, X. C. Zeng, B. Gong, *Chem. Eur. J.* **2001**, *7*, 4352 – 4357.
[18] Structural optimization was performed using the Gaussian03 program at RHF/6-311 + G(d,p) level. The simplified $(\mathbf{2}-2H^+)^{2-}$ anion has no counter cation (Et_4N^+) nor *tert*-butyl groups at the *para* position relative to the phenolate oxygen atom, but has methyl groups at the N and C termini in place of *tert*-butyl groups. (Gaussian 03, Revision A.1, M. J. Frisch, G. W. Trucks, H. B. Schlegel, G. E. Scuseria, M. A. Robb, J. R. Cheeseman, J. A. Montgomery, Jr., T. Vreven, K. N. Kudin, J. C. Burant, J. M. Millam, S. S. Iyengar, J. Tomasi, V. Barone, B. Mennucci, M. Cossi, G. Scalmani, N. Rega, G. A. Petersson, H. Nakatsuji, M. Hada, M. Ehara, K. Toyota, R. Fukuda, J. Hasegawa, M. Ishida, T. Nakajima, Y. Honda, O. Kitao, H. Nakai, M. Klene, X. Li, J. E. Knox, H. P. Hratchian, J. B. Cross, C. Adamo, J. Jaramillo, R. Gomperts, R. E. Stratmann, O. Yazyev, A. J. Austin, R. Cammi, C. Pomelli, J. W. Ochterski, P. Y. Ayala, K. Morokuma, G. A. Voth, P. Salvador, J. J. Dannenberg, V. G. Zakrzewski, S. Dapprich, A. D. Daniels, M. C. Strain, O. Farkas, D. K. Malick, A. D. Rabuck, K. Raghavachari, J. B. Foresman, J. V. Ortiz, Q. Cui, A. G. Baboul, S. Clifford, J. Cioslowski, B. B. Stefanov, G. Liu, A. Liashenko, P. Piskorz, I. Komaromi, R. L. Martin, D. J. Fox, T. Keith, M. A. Al-Laham, C. Y. Peng, A. Nanayakkara, M. Challacombe, P. M. W. Gill, B. Johnson, W. Chen, M. W. Wong, C. Gonzalez, and J. A. Pople, Gaussian, Inc., Pittsburgh PA, **2003**.)
[19] E. Miyazawa, T. Sakamoto, Y. Kikugawa, *J. Chem. Soc. Perkin Trans. 2* **1998**, 7 – 12.
[20] H. Suezawa, M. Hirota, T. Yuzuki, Y. Hamada, I. Takeuchi, M. Sugiura, *Bull. Chem. Soc. Jpn.* **2000**, *73*, 2335 – 2339.
[21] V. Bertolasi, P. Gilli, V. Ferretti, G. Gilli, K. Vaughan, *New J. Chem.* **1999**, *23*, 1261 – 1267.
[22] D. T. McQuade, S. L. McKay, D. R. Powell, S. H. Gellman, *J. Am. Chem. Soc.* **1997**, *119*, 8528 – 8532.
[23] G. R. Goward, D. Sebastiani, I. Schnell, H. W. Spiess, H.-D. Kim, H. Ishida, *J. Am. Chem. Soc.* **2003**, *125*, 5792 – 5800.
[24] A. Onoda, Y. Yamada, J. Takeda, Y. Nakayama, T. Okamura, M. Doi, H. Yamamoto, N. Ueyama, *Bull. Chem. Soc. Jpn.* **2004**, *77*, 321 – 329.
[25] N. Ueyama, M. Inohara, A. Onoda, T. Ueno, T. Okamura, A. Nakamura, *Inorg. Chem.* **1999**, *38*, 4028 – 4031.
[26] S. Shinkai, K. Araki, P. D. J. Grootenhuis, D. N. Reinhoudt, *J. Chem. Soc. Perkin Trans. 2* **1991**, 1883 – 1886.
[27] P. D. J. Grootenhuis, P. A. Kollman, L. C. Groenen, D. N. Reinhoudt, G. J. Van Hummel, F. Ugozzoli, G. D. Andreetti, *J. Am. Chem. Soc.* **1990**, *112*, 4165 – 4176.
[28] A. Altomare, M. C. Burla, M. Camalli, M. Cascarano, C. Giacovazzo, A. Guagliardi, G. Polidori, *J. Appl. Crystallogr.* **1994**, *27*, 435.
[29] M. C. Burla, M. Camalli, B. Carrozzini, G. L. Cascarano, C. Giacovazzo, G. Polidori, R. Spagna, *J. Appl. Crystallogr.* **2003**, *36*, 1103.
[30] G. M. Sheldrick, SHELXS-97, Program for the Refinement of Crystal Structures, University of Göttingen, Göttingen (Germany), **1997**.

 © 2005 Wiley-VCH Verlag GmbH & Co. KGaA, Weinheim

Superacid Systems

Synthesis of Fluorodihydroxysulfonium Hexafluoroantimonate $[FS(OH)_2]^+[SbF_6]^-$**

Andreas Kornath, Raphael Seelbinder, and Rolf Minkwitz*

Reactions of sulfur dioxide in the superacids HSO_3F/SbF_5 and HF/SbF_5 are well investigated by NMR and vibrational spectroscopy.[1,2] In the case of superacid HSO_3F/SbF_5 the formation of the 1:1 adduct SO_2SbF_5 was detected by NMR and Raman spectroscopy [Eq. (1)].

$$SO_2 + SbF_5 \rightleftharpoons OSOSbF_5 \quad (1)$$

If a stronger base than sulfur dioxide is present in the solution only the protonated species of the base and SO_2 are detected. In the case of HF/SbF_5 only marginal differences in proton-transfer tendency, that is the H_0 values, have been observed with SO_2 as the solvent.[2] In spite of this fact, the presence of sulfur dioxide has no effect on reactions in superacidic systems and it was therefore used as a solvent for salts isolated from superacidic solutions.[3–5]

The apparent inactivity of sulfur dioxide in superacids is surprising, since SO_2 cannot be claimed as inert. As already mentioned, SO_2 reacts easily with SbF_5 to form SO_2SbF_5. In solutions with CH_3F and MF_5 (M = Sb, As), SO_2 reacts to give $[CH_3SO_2]^+[MF_6]^-$ salts (M = As, Sb), which are used as methylating agents.[6] Especially this reaction leads to doubts about SO_2 not being protonated in superacids. Therefore we thoroughly investigated the solutions of SO_2 in HF/SbF_5 and DF/SbF_5 by Raman spectroscopy in a sapphire reactor with concentrations of SbF_5 in the range of 1–20 mol% and equivalent amounts of SO_2 in HF and in DF. At high concentrations of SbF_5 (15–20 mol%) a reaction was observed on warming the solution from −90 °C to −25 °C. The solution was then cooled to −90 °C and a colorless solid precipitated. Its Raman spectrum was measured in the presence of the solution (Figure 1). Beside the vibrations of SO_2SbF_5 at 1313 and 1100 cm^{-1}, which are described in literature, new Raman lines appeared which indicated the formation of $[H_2SO_2F]^+$ and $[D_2SO_2F]^+$ ion, respectively (Table 1). Broad Raman lines at 3296, 3128 cm^{-1} can be attributed to OH stretching vibrations and those at 2402(sh), 2294 cm^{-1} to OD stretching vibrations. Further Raman lines occur between 910 and 1272 cm^{-1} which is the typical region for SO stretching modes and between 823 and 878 cm^{-1}, the region for SF stretching modes.

[*] Dr. A. Kornath, Dipl.-Chem. R. Seelbinder, Prof. Dr. R. Minkwitz
Department of Chemistry, Inorganic Chemistry
University of Dortmund
Otto-Hahn-Strasse 6, 44227 Dortmund (Germany)
Fax: (+49) 231-755-3797
E-mail: kornath@chemie.uni-dortmund.de

[**] This work was supported by the Deutsche Forschungsgemeinschaft.

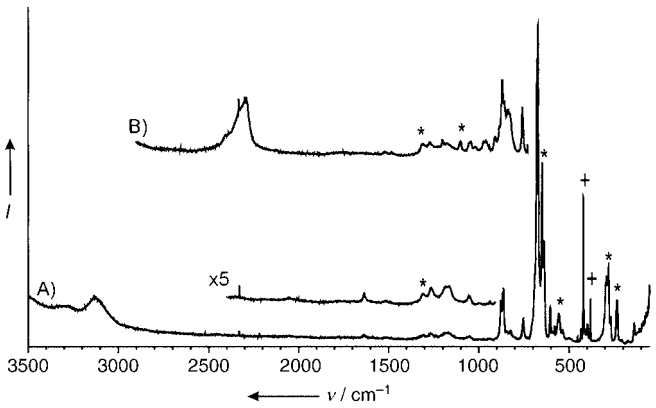


Figure 1. Raman spectra of the reaction solution at −90 °C after the reaction of SO_2 with XF/SbF_5 (X = H, D): (+) sapphire reactor, (*) SO_2SbF_5, A) $SO_2 + HF/SbF_5$, Inset: fivefold expansion of a region of (A), B) $SO_2 + DF/SbF_5$.

Table 1: Raman frequencies [cm^{-1}] of the solid.[a]

$SO_2 + HF/SbF_5$ −90 °C	$SO_2 + DF/SbF_5$ −90 °C	Assignment
3296		ν (OX)
3124		
	2402	
	2293	
1634		δ (SOH)
1273	1272	ν (SO_2)
	1199	
1177	1174	
1053		
	1041	
	963	
938		
	910	
878		ν (SF)
864	869	
843	838	
823		

[a] Spectra taken in the presence of the reaction solution in the sapphire tube after the reaction of SO_2 with XF/SbF_5 (X = H, D).

After removal of the volatile compounds from the solution at −80 °C an extremely moisture sensitive solid with amorphous and crystalline domains remains which decomposes between −75 and −70 °C. A Raman spectroscopy characterization of the isolated solid was not successful, because it decomposed in the laser beam at −78 °C and at lower temperatures strong fluorescence occurred.

In the crystalline part of the solid, $[H_2SO_2F]^+[SbF_6]^-$ was identified by single-crystal X-ray diffraction.[8] The structure of the cation is shown in Figure 2. In the $[H_2SO_2F]^+[SbF_6]^-$ salt, two S–O bonds with lengths of 153.7(7) and 152.2(8) pm are observed, these lengths are in the region typical for SO single bonds (Table 2). The S–F separation of 154.7(7) pm is in the typical region of S–F bonds. The S–F and S–O bonds have similar bond lengths, thus crystallographic disorder, which is often found in $[SO_2F]^-$ salts, could be assumed.[9] This assumption can be rejected on taking the environment of the

 DOI: 10.1002/anie.200461847 © 2005 Wiley-VCH Verlag GmbH & Co. KGaA, Weinheim

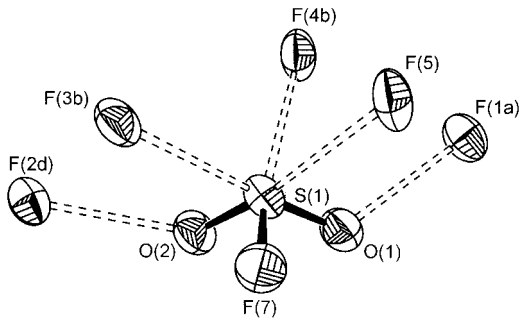
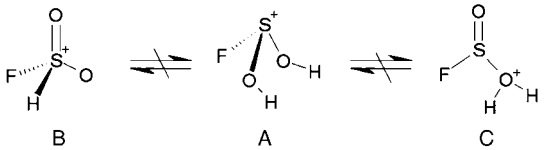


Figure 2. $[H_2SO_2F]^+$ ion and selected interionic contacts [pm]: O(1)···F(1a) 253(1), O(2)···F(2d) 258(1), S(1)···F(3b) 273(1); S(1)···F(4b) 281(1); S(1)···F(5) 281(1). Symmetry operations: a = 1 + *x*, *y*, *z*; b = −*x*, $^1/_2$ + *y*, $^1/_2$ − *z*; c = −x, −*y*, −*z*; d = *x*, $^{-1}/_2$ − *y*, $^{-1}/_2$ + *z*. Thermal ellipsoids are set at 50% probability.

Table 2: Bond lengths [pm] und selected angles [°] of $[H_2SO_2F]^+[SbF_6]^-$.

Bond lengths		Bond angles	
S(1)–O(1)	152.2(8)	O(1)-S(1)-O(2)	98.6(4)
S(1)–O(2)	153.7(7)	O(1)-S(1)-F(7)	99.0(4)
S(1)–F(7)	154.7(7)	O(2)-S(1)-F(7)	100.1(4)
Sb(1)–F(6)	185.2(6)	F(1)-Sb(1)-F(2)	178.6(3)
Sb(1)–F(5)	186.8(6)	F(3)-Sb(1)-F(2)	90.5(3)
Sb(1)–F(3)	186.3(6)	F(3)-Sb(1)-F(1)	88.5(3)
Sb(1)–F(4)	186.8(7)	F(3)-Sb(1)-F(4)	88.8(3)
Sb(1)–F(1)	188.3(6)	F(5)-Sb(1)-F(4)	88.3(3)
Sb(1)–F(2)	189.5(6)	F(5)-Sb(1)-F(3)	177.1(3)
		F(6)-Sb(1)-F(4)	178.5(3)

oxygen and fluorine atoms of the cation into account. The oxygen atoms have O···F contacts to the anions of 253(1) and 258(1) pm, lengths which are in the range of short hydrogen bonds, like those found, for example, in $[H_3SO_4]^+[SbF_6]^-$ salts.[10] The shortest F···F separation between anion and cation on the other hand is 281(1) pm. Because of the steric demand of the free electron pair at the sulfur atom, the F-S-O angles are compressed to 100.1(4), 99.0(4)°, and the O-S-O angle to 98.6(4)°, from the ideal tetrahedral arrangement. The positions of the protons were not found, but of the three possible $[H_2SO_2F]^+$ isomers, species B and C can be excluded [Eq. (2)].



(2)

For isomer B an S–H stretching mode should be observed in the Raman spectrum, which usually occurs as a line of medium intensity. In case of the isomer C the two S–O bonds should have significantly different bond lengths.

The $[SbF_6]^-$ ion is a weakly distorted octahedron with Sb–F bond lengths between 185.2(6) and 189.5(6) pm. The F-Sb-F angles are between 88.3(3) and 92.0(3)°, and between 177.1(3) and 178.6(3)°. Two fluorine atoms of the anion take part in the hydrogen bridges and three other fluorine atoms form intermolecular contacts to the sulfur atom of the cation.[11] The S···F separations between 273(1) and 281(1) pm are 14–17% under the sum of the van der Waals radii. The three S···F contacts together with the S–O and S–F bonds result a distorted octahedral geometry about the sulfur atom that is typical for sulfonium salts.[12,13]

The reaction of SO_2 in superacid HF/SbF_5 can be described by Equation (3) and Equation (4):

$$SO_2 + 2\,HF + SbF_5 \xrightarrow{-90\,^\circ C} [H_2F]^+[SbF_6]^- + SO_2 \quad (3)$$

$$[H_2F]^+[SbF_6]^- + SO_2 \xrightarrow{-25\,^\circ C} SO_2SbF_5 + 2\,HF \rightleftharpoons [FS(OH)_2]^+[SbF_6]^- \quad (4)$$

Sulfur dioxide does not only react, as assumed up to now, under formation of the SO_2SbF_5 adduct. It also adds HF and is then protonated to form $[FS(OH)_2]^+[SbF_6]^-$, a salt of the protonated fluorosulfinic acid, which is not known in its isolated form.

Probably $[FS(OH)_2]^+[SbF_6]^-$ has been detected during earlier Raman spectroscopy investigations of solutions of SO_2 in HSO_3F/SbF_5 but was not identified.[1] A Raman line at 830 cm^{-1} was assigned as the S–F vibration of fluorosulfuric acid and its unusual position was explained by solvent effects. However, this vibration can be assigned to the $[FS(OH)_2]^+$ ion whose other vibrations are overlaid by those of the fluorosulfuric acid.

Received: August 31, 2004
Published online: December 28, 2004

Keywords: fluorosulfinic acid · Raman spectroscopy · structure elucidation · sulfur dioxide · superacid systems

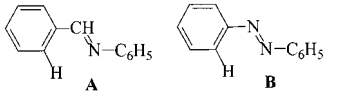
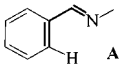
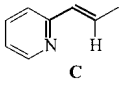
[1] A. Commeyras, G. A. Olah, *J. Am. Chem. Soc.* **1969**, *91*, 2929.
[2] J. Sommer, P. Canivet, S. Schwartz, P. Rimmelin, *Nouv. J. Chim.* **1981**, *5*, 45.
[3] R. Minkwitz, S. Schneider, *Angew. Chem.* **1999**, *111*, 749; *Angew. Chem. Int. Ed.* **1999**, *38*, 714.
[4] R. Minkwitz, S. Schneider, *Z. Anorg. Allg. Chem.* **1998**, *624*, 1989.
[5] R. Minkwitz, S. Schneider, *Angew. Chem.* **1999**, *111*, 229; A *ngew. Chem. int. Ed.* **1999**, *38*, 210.
[6] R. Minkwitz, D. Bernstein, H. Preut, *Z. Anorg. Allg. Chem.* **1991**, *606*, 157.
[7] D. M. Byler, D. F. Shriver, *Inorg. Chem.* **1976**, *15*, 32.
[8] Crystal structure analysis of $[FS(OH)_2]^+[SbF_6]^-$ at 173 K: monoclinic, space group *P*21/*c* (No. 14), *a* = 523,1(1), *b* = 820,3(2) *c* = 1621,6(3) pm, β = 91,73(3) *Z* = 4, *V* = 695,5(3) × 10^6 pm^3 , ρ_{calcd} = 3,064 g cm^{-3}, crystal dimension: 0.1 × 0.15 × 0.2 mm^3, 2θ/ω scans, $2\theta_{max}$ = 54.92°, *T* = 120(2) K, reflections collected 3160, 1335 independent reflections, σ limit 2.0, $\mu(Mo_{K\alpha})$ = 5.433 mm^{-1}, structure solution: Patterson method, difference Fourier synthesis; SHELXS-86, SHELXL-93, PARST, PLATON, MISSYM, DENZO, SCALEPACK,[14–18] 101 free parameters, *R* = 0.0563, *wR2* = 0.1387, $R = \Sigma\,||F_0| - |F_c||/\Sigma\,|F_0|$, structure refinement: full-matrix least-squares analysis on F^2, largest difference peak and hole = 1.496/ −1.363 e$Å^{-3}$. Further details on the crystal structure investigation may be obtained from the Fachinformationszentrum

 © 2005 Wiley-VCH Verlag GmbH & Co. KGaA, Weinheim

Karlsruhe, D-76344 Eggenstein-Leopoldshafen (Fax: (+40) 7247-808-666; E-mail: crysdata@fiz-karlruhe.de) on quoting the depository number CSD-414424.
[9] U. Kessler, L. van Wullen, M. Jansen, *Inorg. Chem.* **2001**, *40*, 7040.
[10] R. Minkwitz, R. Seelbinder, R. Schöbel, *Angew. Chem.* **2002**, *114*, 119; *Angew. Chem. Int. Ed.* **2002**, *41*, 111.
[11] A. Bondi, *J. Phys. Chem.* **1964**, *68*, 441.
[12] R. Minkwitz, A. Kornath, H. Preut, *Z. Naturforsch. B* **1992**, *47*, 594.
[13] N. W. Alcock, *Adv. Inorg. Chem. Radiochem.* **1973**, *15*, 1.
[14] G. M. Sheldrick, SHELXL-93, Universität Göttingen, **1993**.
[15] G. M. Sheldrick, SHELXL-86, Universität Göttingen, **1986**.
[16] G. M. Sheldrick, SHELXTL Plus Version 3.4, An integrated System for Solving, Refining and Displaying Crystal Structures from Diffraction Data, Universität Göttingen, **1993**.
[17] M. Nardelli, *Comput. Chem.* **1983**, *7*, 95.
[18] Y. LePage, *J. Appl. Crystallogr.* **1987**, *20*, 264.

 © 2005 Wiley-VCH Verlag GmbH & Co. KGaA, Weinheim

Table 1: Isoelectronic compounds with exchange of N for CH (**A**, **B**), structural isomers (**A**, **C**) with azadiene topology, and reagents to effect cyclometalation.

Substrate	Reagent
 **A** **B**	$[MnCH_3(CO)_4]$[3]
 **A**	$[Fe(PMe_3)_4]$ $[Fe(CH_3)_2(PMe_3)_4]$ $[CoCH_3(PMe_3)_4]$
 **C**	$[CoCH_3(PMe_3)_4]$

C–H Activation

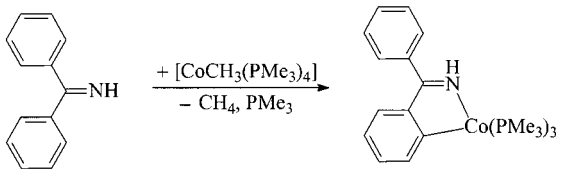
Cyclometalation of Substrates Containing Imine and Pyridyl Anchoring Groups by Iron and Cobalt Complexes

Hans-Friedrich Klein, Sebnem Camadanli, Robert Beck, Diana Leukel, and Ulrich Flörke*

Cyclometalations transform barely activated or nonactivated C–H bonds of coordinated ligands into C–metal bonds. Metallacyclic species are known for almost all transition elements, and the majority of them contain five-membered rings.[1] The first examples of cyclometalation were observed for azobenzene (**B**) with nickel, palladium, and platinum.[2] Bruce et al. applied the reaction to Schiff bases of benzaldehyde (**A**) and also described examples with manganese, rhenium, ruthenium, and rhodium (Table 1).[3] If, in the series azobenzene, benzalaniline, and stilbene, N atoms are replaced by CH groups,[4] then elevated temperatures are required for cyclometalation to occur. The reaction with benzalaniline must be run in THF or toluene at reflux, and stilbene does not react.

We have recently been able to effect cyclometalation reactions for the first time at basic cobalt and iron centers by using imine and pyridyl anchoring groups. Phenyl ketimines and benzaldimines react smoothly under particularly mild conditions[5] as well as their isoelectronic structural isomers having an azadiene topology, the 2-vinylpyridines (**C**, Table 1). The new, stable, and structurally characterized compounds containing N,C-metallacycles can be viewed as models for the organometallic intermediates in ruthenium- and rhodium-catalyzed C–C coupling reactions between aromatic imines and olefins utilized in organic synthesis.[6] In these reactions typically conducted in refluxing toluene the metalated species[7] are not isolated but are converted into metal-free products in a catalytic process.

After simply combining the phenyl ketimines, benzaldimines, or 2-vinylpyridine with cobalt or iron complexes at −70 °C, we observed a color change indicating that the reaction was already occurring; for methyl complexes this was accompanied by evolution of gas (methane, GC). The mixture was warmed to 20 °C to give complete conversion and moderate to high yields of crystalline product (Table 2). Thus benzophenone imine was smoothly *ortho*-metalated with methyltetrakis(trimethylphosphane)cobalt [Eq. (1)].



(1)

1

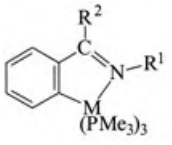
The green crystals of **1** obtained from pentane decompose at 106 °C under argon; at 20 °C in air the crystal surface remains unchanged for at least 15 minutes. NMR spectra obtained from $[D_8]$THF solutions are compatible with a trigonal-bipyramidal configuration around cobalt and a C-axial/N-equatorial coordination of the (2-iminobenzoyl)-phenyl ligand. In the IR spectrum the ν(NH) band is observed with a hypsochromic shift of 45 cm^{-1} indicating coordination through the N atom (Table 2).

The X-ray crystal structure of **1**[9] confirms this configuration at cobalt. Bond lengths and angles in the molecule remain within the range of expected values. The sum of the internal bond angles of the chelate ring (542.6°) indicates little strain (planar five-membered ring: 540°). This is also reflected by the positions of the next-neighbor atoms at the metal

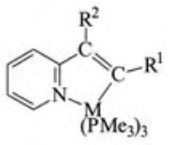
[*] Prof. Dr. H.-F. Klein, S. Camadanli, Dr.-Ing. R. Beck, Dipl.-Ing. D. Leukel
Eduard-Zintl-Institut für Anorganische und Physikalische Chemie
Technische Universität Darmstadt
Petersenstrasse 18, 64287 Darmstadt (Germany)
Fax: (+49) 6151-16-4173
E-mail: hfklein@ac.chemie.tu-darmstadt.de
Dr. U. Flörke
Anorganische und Analytische Chemie
Universität Paderborn
Warburger Strasse 100, 33098 Paderborn (Germany)

 DOI: 10.1002/anie.200460978 © 2005 Wiley-VCH Verlag GmbH & Co. KGaA, Weinheim

Table 2: Syntheses[8] and properties of metallacyclic compounds of cobalt and iron.



1–5



6, 7

	R^1	R^2	M	Yield [%]	Color	Decomp. [°C]	$\tilde{\nu}$ [cm^{-1}]
1	H	C_6H_5	Co	76	green	<106	3301 (N-H)
2	H	C_6H_5	FeH	78	violet	<105	3281 (N-H)
3	CH_3	H	$FeCH_3$	65	violet	<115	1180 δ($FeCH_3$)
4	H	$C(CH_3)_3$	Co	42	green	<112	3358 (N-H)
5	H	$C(CH_3)_3$	FeH	48	violet	<118	3335 (N-H),1795 (Fe-H)
6	H	H	Co	41	green	<78	–
7	H	C_6H_5	Co	62	green	<97	–

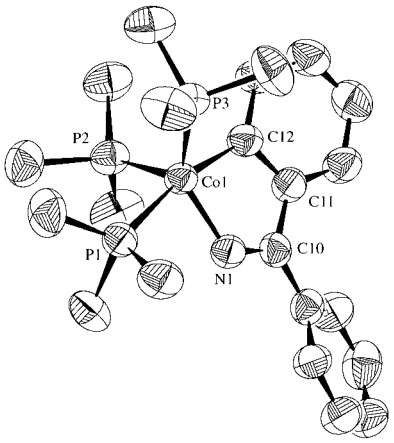
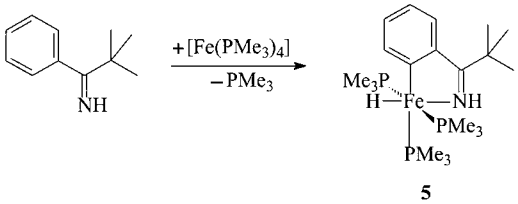


Figure 1. X-ray crystal structure of **1**. Selected distances [Å] and angles [°]: Co1–N1 1.882(5), Co1–C12 1.959(6), Co1–P1 2.2178(18), Co1–P2 2.1858(19), Co1–P3 2.189(2), N1–C10 1.337(8); N1-Co1-C12 80.6(2), C12-Co1-P1 168.15(19), C10-N1-Co1 121.5(4).

center, which show no gross deviation from ideal trigonal-bipyramid coordination (Figure 1).

When an equimolar mixture of tetrakis(trimethylphosphane)iron and (2,2-dimethyl-1-phenyl)propylidenimine[10] in pentane was warmed from −70 °C to 20 °C, the initial orange mixture turned dark red. Through oxidative addition the hydridoiron(II) complex **5** formed [Eq. (2)].

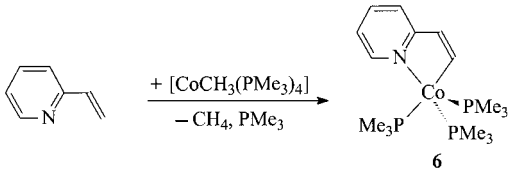


(2)

5

Violet crystals of **5** are stable up to 118 °C under argon. According to NMR spectra in [D_8]THF[11] the iron center has an octahedral coordination environment made up of three PMe_3 groups in meridional positions, the N,C-chelate ligand, and a hydrido ligand *trans* to the imine donor of the chelate. The methyliron compound **3** shows the same configuration in solution, except that the Fe–H group of **5** is replaced by a Fe–CH_3 group. Compounds **5** and **4** are isoelectronic by the analogy of Co and Fe-H.

Combining 2-vinylpyridine with methyltetrakis(trimethylphosphane)cobalt in THF resulted in evolution of gas and a color change from orange–red to green. According to Equation (3) the metallacyclic complex **6** formed.



(3)

6

Dark green crystals of **6** were grown from pentane at −20 °C; their surface planes reflect incident daylight as red light. At 78 °C under argon these dichroitic properties were lost, and thermal decomposition commenced. When air was admitted, the crystals rapidly deliquesced and underwent oxidative decomposition already at 20 °C. Both the NMR spectra in [D_8]THF and the crystal structure of **6**[12] (Figure 2)

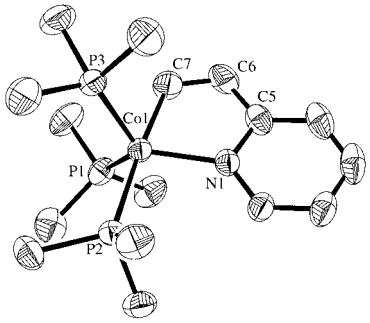


Figure 2. X-ray crystal structure of **2**. Selected distances [Å] and angles [°]: Co1–C7 1.913(2), Co1–N1 2.006(2), Co1–P1 2.1526(7), Co1–P2 2.2030(7), Co1–P3 2.1575(7), C6–C7 1.337(3); N1-Co1-C7 80.5(1), P2-Co1-C7 175.50(8).

show molecular complex entities in which the C-donor function is axial and the N-donor function is equatorial. The chelate and the metal center form a planar five-membered ring with a typical bite angle at the cobalt atom (N1-Co-C7 80.5(1)°).

The IR spectra of by-products give no evidence for isomers. Also, in the course of the analogous formation of **7** neither of the two aromatic C–H groups available for the

 © 2005 Wiley-VCH Verlag GmbH & Co. KGaA, Weinheim

formation of six-membered metallacycles were activated in competition with the vinyl group.

This result demonstrates that in structural isomers containing a 1,4-interchanged azadiene topology (Table 1) activation occurs at the formally interchanged C–H group, which may be aromatic or vinylic. Furthermore these findings are in accord with the notion[13] that the N-donor function is coordinated first, followed by activation and regiospecific cleavage of the most suitable ligand C–H bond. The M–H function thus formed either remains in the final product, as observed after reaction at the iron(0) center, or when there is an adjacent M–CH_3 unit, it is eliminated as methane as in all the other cyclometalation reactions described here. As the metals retain their low oxidation states in the products and since the effects of donor ligands are similar before and after reaction, except for the chelate effect, it should be possible to perform a second C–H activation. Subsequent elimination accompanied by C–C coupling would facilitate a catalytic reaction mode. Experiments with this aim are currently under way.

Received: June 16, 2004
Revised: October 18, 2004
Published online: January 11, 2005

Keywords: C–H activation · cobalt · cyclometalation · iron · N ligands

[1] a) I. Omae, *Chem. Rev.* **1979**, *79*, 287–321; b) A. D. Ryabov, *Chem. Rev.* **1990**, *90*, 403–424.
[2] G. W. Parshall, *Acc. Chem. Res.* **1970**, *3*, 139–144.
[3] M. I. Bruce, *Angew. Chem.* **1977**, *89*, 75–89; *Angew. Chem. Int. Ed. Engl.* **1977**, *16*, 73–86.
[4] H. B. Bürgi, J. D. Dunitz, *Helv. Chim. Acta* **1971**, *54*, 1255–1260.
[5] When $Na_2[PdCl_4]$ in methanol is used, cyclopalladation of Schiff bases proceeds already at 20 °C: S. Trofimenko, *Inorg. Chem.* **1973**, *12*, 1215–1221.
[6] F. Kakiuchi, S. Murai, *Acc. Chem. Res.* **2002**, *35*, 826–834.
[7] The structure of a cyclometalated 2-vinylpyridine at a ruthenium(II) center has been described by J. N. Coalter, W. E. Streib, K. G. Caulton, *Inorg. Chem.* **2000**, *39*, 3749–3756.
[8] General procedure: Solutions of the iron complexes in pentane or of $[CoCH_3(PMe_3)_4]$ in THF on a scale of about 3 mmol were combined with equimolar amounts of the imine in the same solvent and stirred at −70 °C. The reaction mixture was allowed to warm to 20 °C and stirred for 3 h at 20 °C. The volatiles were removed in vacuo, and the residue was extracted with fresh pentane over a glass-sinter disc (G3). When the solution was cooled, crystals formed. The solution was decanted off, and the crystals were washed with cold pentane and dried in vacuo to afford analytically pure materials **1**–**7** (Table 2).
[9] Crystal data for **1**: $C_{22}H_{37}CoNP_3$, $M_r = 467.4$; crystal size: $0.20 \times 0.25 \times 0.35$ mm, orthorhombic, space group $Pna2_1$, $a = 16.815(4)$, $b = 9.473(3)$, $c = 15.676(5)$ Å, $V = 2497.0(13)$ Å^3, $Z = 4$, $\rho_{calcd} = 1.243\ g\,cm^{-3}$, $F(000) = 922$; 2974 reflections with $2.84° < 2\theta < 49.98°$, Stoe-Stadi-4 diffractometer, $Mo_{K\alpha}$ radiation, no absorption correction, graphite monochromator, structure solution using Patterson and Fourier methods, refinement from 2974 independent reflections ($R_{int} = 0.0925$) for 244 parameters based on F^2 with SHELXL97, $R = 0.0460$, $wR2 = 0.1073$ (all data). Max./min. residual electron densities $0.593/-0.373\ e\,Å^{-3}$. All non-hydrogen atoms were refined anisotropically; the hydrogen atoms were set at calculated positions.
[10] F. J. Weiberth, S. S. Hall, *J. Org. Chem.* **1987**, *52*, 3901–3904.
[11] **5**: ^1H NMR (500 MHz, [D$_8$]THF, 25 °C, TMS): $\delta = -17.5$ (dt, $^{cis}_2J(P_AH) = 80$ Hz, $^{cis}_2J(P_BH) = 22$ Hz, 1H, FeH), 0.88 (br s, 18H, P_ACH_3), 1.40 (d, $^3J(PH) = 4.5$ Hz, 9H, P_BCH_3), 1.46 (s, 9H, CCH_3), 6.70–7.90 (m, 4H, H_{Ar}), 9.13 ppm (s, 1H, NH); ^{31}P NMR (202 MHz, [D$_8$]THF, 25 °C, H_3PO_4): $\delta = 18.2$ (d, $^2J(PP) = 37$ Hz, 2P), 23.7 ppm (t, $^2J(PP) = 37$ Hz, 1P).
[12] a) Crystal data for **6** ($C_{16}H_{33}CoNP_3$): $M_r = 391.3$; crystal size: $0.40 \times 0.35 \times 0.25$ mm, monoclinic, space group $P2_1/c$, $a = 14.753(2)$, $b = 14.528(2)$, $c = 9.9920(14)$ Å, $\beta = 102.975(2)°$, $V = 2086.9(5)$ Å^3, $Z = 4$, $\rho_{calcd} = 1.245\ g\,cm^{-3}$, $F(000) = 832$; 23679 reflections with $2.84° < 2\theta < 56.78°$, Bruker AXS SMART APEX CCD[14] diffractometer, $Mo_{K\alpha}$ radiation ($\mu = 1.047\ mm^{-1}$), graphite monochromator, semiempirical absorption correction using equivalent reflections (SADABS[14]). Structure solution using direct methods,[14] refinement[14] from 5022 independent reflections ($R_{int} = 0.050$) for 199 parameters based on F^2, $R1$ ($I > 2\sigma(I)$) = 0.038, $wR2$ (all data) = 0.092. Max./min. residual electron densities $0.49/-0.22\ e\,Å^{-3}$. All non-hydrogen atoms were refined anisotropically, hydrogen atoms with riding model at idealized positions and isotropic parameters $U_{iso}(H) = 1.2\,U_{eq}(C)$ or $1.5\,U_{eq}(-CH_3)$. b) CCDC-240668 and −239924 (**1** and **6**) contain the supplementary crystallographic data for this paper. These data can be obtained free of charge via www.ccdc.cam.ac.uk/conts/retrieving.html (or from the Cambridge Crystallographic Data Centre, 12, Union Road, Cambridge CB2 1EZ, UK; fax: (+44) 1223-336-033; or deposit@ccdc.cam.ac.uk).
[13] J. F. van Baar, K. Vrieze, D. J. Stufkens, *J. Organomet. Chem.* **1975**, *85*, 249–263.
[14] Bruker (2002). SMART (Version 5.62), SAINT (Version 6.02), SADABS, SHELXTL (Version 6.10). Bruker AXS Inc., Madison, Wisconsin, USA.

 © 2005 Wiley-VCH Verlag GmbH & Co. KGaA, Weinheim